

# Polystyrenes of known structure: Part 3. Polymers with long-chain branching

J. Pannell

*Imperial Chemical Industries Limited, Plastics Division,  
Welwyn Garden City, Herts. UK  
(Received 13 April 1971, revised 19 July 1971)*

The melt- and solution viscosity behaviour of some polystyrenes with long-chain branching is described. These polymers, which were prepared by reacting chloromethylated polystyrene with potassium polystyryl, are distinguishable from the comb-shaped polystyrenes previously described in having longer branches and lower branching frequencies. (The number-average molecular weight of the branches is greater than  $4.6 \times 10^4$  and in some cases greater than that of the backbone.) Their low shear melt viscosities and intrinsic viscosities in tetrahydrofuran and cyclohexane are above those of the backbone polymer and increase as the branch length increases for a given branching frequency, the rate of increase being greater the lower the branching frequency. In each solvent the intrinsic viscosities of the branched polymers are below those of linear polymers of comparable molecular weights. The melt viscosities of the majority of the branched polymers are also below those of linear polymers of the same molecular weights, but for a few, those with the longest branches in the series with the lowest branching frequency, the opposite is true.

Another outcome of this work is the finding that for these branched polymers the low-shear melt viscosities and the intrinsic viscosities in solution are given by:

$$\text{viscosity} \propto \langle S_0^2 \rangle^a$$

where  $\langle S_0^2 \rangle$  is the theoretical mean square unperturbed radius of gyration. The exponents  $a$  for the branched polymers in the melt and in tetrahydrofuran differ from those for linear polystyrenes for which a similar relation holds, but are about equal for branched and linear polystyrenes in cyclohexane.

The behaviour shown by the branched polystyrenes described here is considered in relation to the behaviour of the comb-shaped polystyrenes reported earlier and that of the branched polystyrenes studied by Decker and by Fujimoto *et al.*

## INTRODUCTION

This paper gives details of some of the properties of polystyrenes with long-chain branching. In particular the effect of altering the length of the branches and the branching frequency on the melt and intrinsic viscosity behaviour of these polymers is described and an attempt is made to correlate this behaviour with the theoretical unperturbed dimensions of the molecules by analogy with linear polymers. For convenience polystyrenes with long-chain branching are defined as those in which the number-average molecular weight,  $M_n^b$ , of the branches is greater than  $4.6 \times 10^4$  to distinguish them from the comb-shaped polymers (for which  $M_n^b < 4.6$

$\times 10^4$ ) described in an earlier paper<sup>1</sup>. The polymers with long-chain branching may also be distinguished from the comb-shaped polymers by their lower branching frequencies and by their behaviour, both in solution and in the melt.

By considering the results obtained in these laboratories together with those obtained by Fujimoto *et al.*<sup>2</sup> on branched polystyrenes a fairly wide perspective is obtained of the effect of changes in branch length and branching frequency on melt viscosity behaviour and to a lesser extent on the solution viscosity behaviour also.

Although the reaction used in the preparation of the polymers described here is basically the same as that employed for the comb-shaped polymers,

potassium polystyryl rather than lithium polystyryl was used in the coupling reaction with chloromethylated polystyrene in order to avoid the possible complication of crosslinking which can conceivably occur when using lithium polystyryl<sup>1</sup>. All reactions were carried out in a sealed apparatus and steps were taken to exclude all impurities which would terminate the living polymer. In spite of these precautions, however, the product after coupling always consisted of a mixture of the branched polymer and the linear polymer formed by termination of the living polymer and this was clearly shown by gel permeation chromatography (g.p.c.).

## EXPERIMENTAL

### Preparation of linear and branched polystyrenes

Three apparatuses were developed for the preparation of linear and branched polystyrenes. The first of these, A1, was referred to in Part 1<sup>3</sup> and was used initially to prepare linear polymers on a  $5-6 \times 10^{-2}$  kg scale for subsequent characterization and chloromethylation and for the reaction of potassium polystyryl with <sup>14</sup>C-labelled CO<sub>2</sub>. It was later modified for the preparation of branched polymer. The second apparatus, A2, was designed to prepare up to six branched polymers from a single batch of living polymer, each branched polymer therefore having the same branch length but different branching frequencies and/or different backbones. The third apparatus, A3, was a smaller version of A2 and was used for the preparation of a single branched polymer on a smaller scale than was convenient in apparatus A1. All reagents, including the initiator ( $\alpha$ -phenyl isopropyl potassium), styrene, methanol and chloromethylated polystyrene solution were contained in break seal ampoules on the apparatus. The procedure used for the preparation of living polymer was similar in all three apparatuses and was briefly described in Part 1<sup>3</sup>. The bulk of the living polymer was coupled with the chloromethylated polystyrene to give branched polymer but part of it was terminated with methanol and used to characterize the branches.

### Materials

*$\alpha$ -Phenyl isopropyl potassium.* This initiator was originally prepared from methyl  $\alpha$ -phenyl isopropyl ether by a modified form of the procedure described by Ziegler and Dislich<sup>4</sup> using benzene rather than aliphatic hydrocarbons as the reaction medium, but later it was obtained as a suspension in heptane from a commercial source<sup>5</sup>. In the former case it was dissolved in tetrahydrofuran (THF) and the solution was cooled to precipitate the unwanted potassium methoxide and filtered. The commercial material was also dissolved in THF but because of the presence of some solid material, thought to be unreacted potassium, the solution was allowed to settle before use.

*Styrene.* This was freed of phenolic inhibitor by treatment with caustic soda solution, followed by

washing with water. After drying over sodium sulphate it was vacuum distilled from calcium hydride and stored over calcium hydride at 253K until required. Transfer to the ampoules was carried out on a vacuum line.

*Tetrahydrofuran.* This was refluxed over KOH to remove the inhibitor (hydroquinone) and dried and stored in the dark over sodium wire. Final purification was done by distillation from the sodium naphthalene complex in a stream of pure argon.

*Chloromethylated polystyrene solution.* The dry polymer was pumped continuously for several days on a vacuum line and THF distilled onto it. The solution was then taken through several freeze-thaw cycles to complete the outgassing and then sealed into the ampoules.

### Gel permeation chromatography

The products obtained after coupling were injected into a Waters Associates' Gel Permeation Chromatograph. The solvent used was toluene at room temperature, and the polymer samples, at 0.25% (w/w) concentration were injected for 1 min. Four columns in series were used, 10<sup>7</sup>A, 10<sup>5</sup>A, 10<sup>4</sup>A and 250 A, using the Waters designation, and the plate count for the combination, determined by injecting *o*-dichlorobenzene, was 1241 plates per foot. The chromatograms of the mixtures of branched and linear polymers were used, in conjunction with those obtained for the linear polymers alone, in determining the composition of these mixtures. The procedure for doing this and details of the g.p.c. elution behaviour of these branched polymers will be given in a later paper<sup>6</sup>.

## RESULTS AND DISCUSSION

Osmotic pressure measurements on and g.p.c. analysis of the products obtained in the reaction of potassium polystyryl with chloromethylated polystyrene showed that in all cases the final polymer consists of two components. The high molecular weight component was assumed to be the branched polymer obtained by coupling and the low molecular weight component was clearly linear homopolymer, formed by termination of the living polymer. A clear cut separation of the branched and linear components by fractionation of the mixtures was not possible because of overlap of the molecular weight distributions of the two components, and so none was attempted. Because of this the melt and intrinsic viscosities of the branched components in the mixtures were obtained by difference and it is shown here how this was done, knowing the weight fractions of the two components in the mixtures and the properties of the mixtures and the linear homopolymers. The latter were isolated separately in the sequence of operations in the synthesis of the branched polymers.

Determination of the composition of two component mixtures by g.p.c.

Determination of the composition of a mixture by g.p.c. depends on resolving the composite chromatogram of this mixture into its two components and measuring the area contributed by each component. The ratio of the area contributed by each component to the total area under the chromatogram is equal to the weight fraction of that component in the mixture. Resolution of the chromatograms of the mixtures examined here was readily achieved since (a) there was a region in each in which the two components did not overlap and (b) the chromatograms of the linear components alone could be obtained. Additional details will be given in a later paper dealing with the g.p.c. study of these branched polystyrenes<sup>6</sup>. Figure 1 shows two examples of this analysis of chromatograms of mixtures containing branched and linear polymers. Results given elsewhere<sup>6</sup> show that the compositions of mixtures of linear polymers determined from the chromatograms by this method agree to better than 7% with the compositions given by direct weighing.

Melt viscosity-composition correlation for blends of branched and linear polystyrenes

Since all the branched polystyrenes prepared were mixed in varying proportions with the linear precursors in the reaction products and since no attempt was made to separate the two components by fractionation, it was necessary to establish how the melt viscosity of such blends depends on their composition before the melt viscosity of the branched

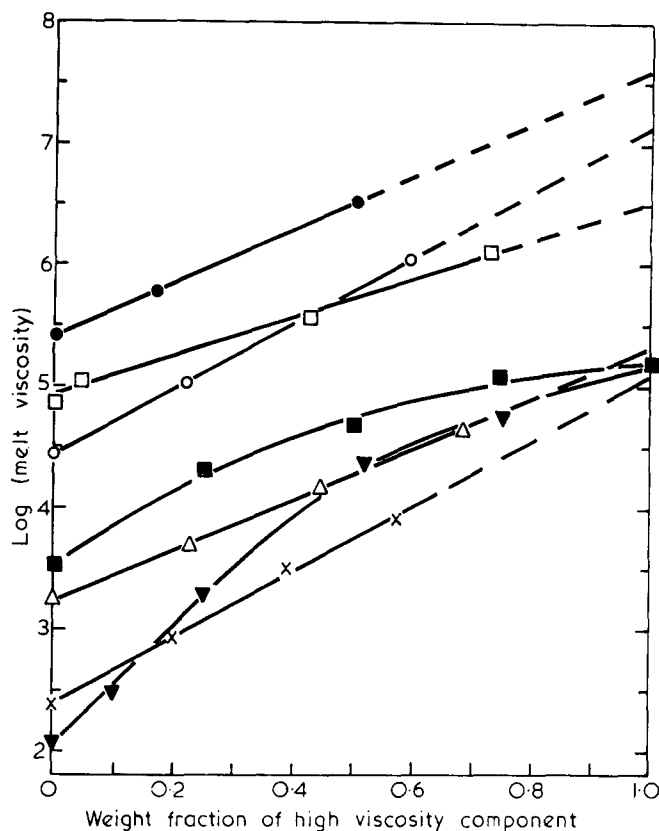


Figure 2 Correlation between the melt viscosity and composition for blends of two polymers. The straight lines, described by a logarithmic additivity rule (equation 1), represent the behaviour of blends of linear and branched polymers, while the curves are for blends of two linear polymers. ● Blends of B104I and B104; ○ blends of B103L and B103; □ blends of B115L and B115; X, blends of B118L and B118; △ blends of B105L and B105 under shear (shear stress  $7 \times 10^3 \text{ Nm}^{-2}$ ) ▼ blends of B114L and U25; ■ blends of U14 and U25

component alone could be determined. Additional blends of the branched and linear polymers were prepared by dissolving weighed amounts of the reaction product and the linear precursor polymer in THF, followed by precipitation into methanol or water and drying. A knowledge of the weight fractions of the branched and linear components in these blends depends ultimately on the composition of the reaction product as determined by g.p.c.

Figure 2 shows examples of how the melt viscosity of these blends varies with the weight fraction of the high viscosity component, which in this case is the branched polymer. The variation of the melt viscosity with composition for some blends of linear polymers is also shown. It is clear that over the range of composition of blends of branched and linear polymers covered, there is a linear relation between  $\log \eta$  and the weight fraction of the branched component and the melt viscosity of the latter is obtained by linear extrapolation. That is, the melt viscosity  $\eta$  of blends of branched and linear polystyrenes is given by the logarithmic additivity rule

$$\log \eta = w_1 \log \eta_1 + w_2 \log \eta_2 \quad (1)$$

where  $\eta_1$  and  $\eta_2$  are the melt viscosities of the linear and branched components respectively and  $w_1$  and

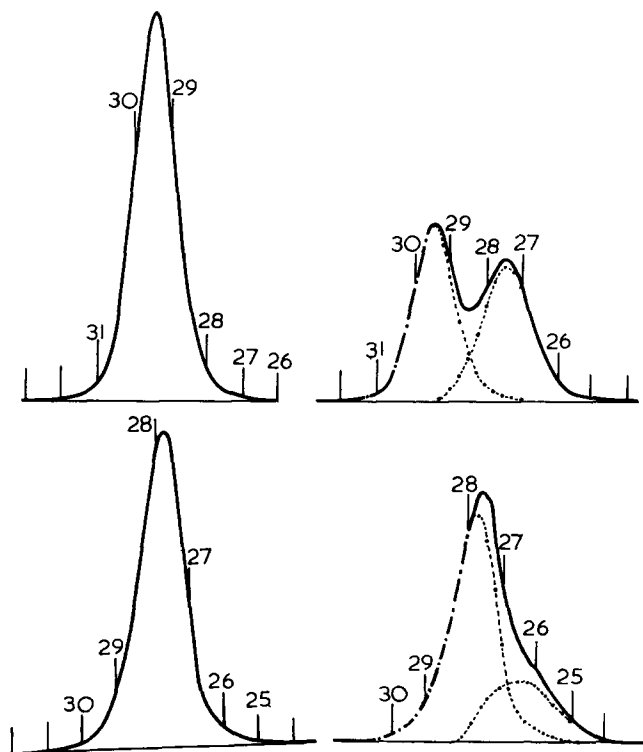


Figure 1 Examples of the chromatograms obtained by g.p.c. on the product of the reaction between chloromethylated polystyrene and potassium polystyryl and on the linear polymer formed by termination of the latter. The fraction of the total area contributed by each component in the composite chromatogram is equal to its weight fraction in the mixture

$w_2$  their weight fractions in the blend. Equation (1) has been found to apply not only to measurements of the low shear melt viscosities of these polymer blends but also to viscosities measured under shear (up to a shear stress in the region of  $6 \times 10^4 \text{ N m}^{-2}$ ). This is illustrated in Figure 2 for blends of B105 and B105L, the melt viscosities of which were measured at a shear stress of  $7 \times 10^3 \text{ N m}^{-2}$ .

It is of some interest to note that Kataoka and Ueda<sup>1</sup> obtained a more complex empirical equation for the low-shear melt viscosity of blends of linear polymers :

$$\log \eta_B = \frac{v_1(1-a)}{(1-av_1)} + \frac{v_2}{(1-av_2)} \log \eta_2 \quad (2)$$

where  $v_1$  and  $v_2$  are the volume fractions of the two components in the blend and  $a$  is a constant independent of composition. This equation may be reduced to equation (1) by substituting weight fractions for volume fractions and putting  $a = 0$ .

#### Intrinsic viscosity-composition correlation for blends of branched and linear polystyrenes

The average intrinsic viscosity of an unfracti- onated polymer is usually taken as the arithmetic

sum of contributions from individual fractions, i.e.

$$[\eta] = \sum_i w_i [\eta]_i \quad (3)$$

where  $[\eta]$  is the intrinsic viscosity of the whole polymer and  $[\eta]_i$  and  $w_i$  the intrinsic viscosity and weight fraction, respectively, of the  $i$ th fraction. The same relation is used here in calculating the intrinsic viscosities of the branched components in the mixtures of linear and branched polymers, knowing the viscosities of the mixtures and the linear polymers and the weight fractions of the two components from the g.p.c. data.

All measurements made on the mixtures of branched and linear polymers, on the linear component (branches) and on the backbone polymer are given in Table 1. The melt and intrinsic viscosities and the weight average molecular weights computed for the branched polymers alone are given in Table 2.

#### Molecular weights of branched polymers

Since no attempt was made to separate the branched polymers from their linear precursors, no direct measurements of their molecular weights

Table 1 Measured data on the polymers obtained in the preparation of branched polystyrenes

Backbone polymer	Two-component mixture from coupling reaction					Linear precursor (branches)				
	Mixture	$\eta_0^*$	$[\eta]_{\text{THF}}^\dagger$	$[\eta]_{\text{CH}}^\dagger$	Wt fraction of branched component from g.p.c.	Polymer	$M_n \times 10^{-4}$	$\eta_0^*$	$[\eta]_{\text{THF}}^\dagger$	$[\eta]_{\text{CH}}^\dagger$
$\bar{M}_n = 18.1 \times 10^4$ $\eta_0 = 1.63 \times 10^4$ $[\eta]_{\text{Tot}} = 70.2^b$ $[\eta]_{\text{CH}} = 33.7^a$ $\bar{p} = 2.55$	B114	$4.89 \times 10^3$	63.42	31.6	0.666	B114.L	4.65	$1.15 \times 10^2$	28.4	19.4
	B118	$8.20 \times 10^3$	63.3	31.4	0.607	B118.L	6.03	$2.43 \times 10^2$	35.67	21.4
	B116.1	$1.16 \times 10^4$	62.9	32.4	0.649	B116.L	8.01	$2.88 \times 10^2$	36.9	23.3
	B121	$2.80 \times 10^4$	74.9	35.9	0.372	B121.L	11.12	$6.80 \times 10^3$	55.5	30.3
	B120	$4.82 \times 10^4$	85.0	39.2	0.270	B120.L	15.74	$1.01 \times 10^4$	69.4	34.6
	B130	$9.24 \times 10^4$	93.9	38.5	0.368	B130.L	17.52	$1.88 \times 10^4$	70.7	33.9
	B122	$1.98 \times 10^5$	109.7	46.5	0.243	B122.L	24.23	$6.57 \times 10^4$	94.1	42.3
	B115.1	$1.79 \times 10^5$	107.5	46.8	0.178	B115.L	26.6	$7.19 \times 10^4$	96.3	43.7
	B110.4	$1.00 \times 10^4$	63.98	32.5	0.667	B110.L	5.67	$3.47 \times 10^4$	31.83	22.5
	B116.3	$3.28 \times 10^4$	75.38	34.4	0.763	B116.L	8.01	$2.88 \times 10^2$	36.9	22.3
$\bar{M}_n = 12.16 \times 10^4$ $\eta_0 = 2.02 \times 10^3$ $[\eta]_{\text{THF}} = 48.1$ $[\eta]_{\text{CH}} = 29.5^a$ $\bar{p} = 5.73$	B123	$7.85 \times 10^4$	92.7	39.0	0.542	B123.L	11.43	$5.03 \times 10^3$	53.3	29.4
	B108.2	$9.41 \times 10^4$	89.45	42.6	0.449	B108.L	13.60	$1.20 \times 10^4$	65.4	33.8
	B131	$8.05 \times 10^5$	136.6	52.5	0.654	B131.L	19.56	$2.51 \times 10^4$	69.7	36.9
	B124.2	$1.82 \times 10^5$	106.9	42.7	0.263	B124.L	21.35	$6.17 \times 10^4$	86.65	38.9
	B115.2	$7.41 \times 10^5$	149.8	56.2	0.522	B115.L	26.60	$7.19 \times 10^4$	96.3	43.7
	B109.F	$2.00 \times 10^4$	77.8	-	1.00	B109.L	2.31	-	77.8	-
	B109.1	$1.66 \times 10^4$	78.3	34.9	0.685	B110.L	5.67	$3.47 \times 10^2$	31.83	22.5
	B107.1	$4.71 \times 10^4$	64.6	35.9	0.658	B107.L	7.83	$5.05 \times 10^2$	45.3	25.8
	B105	$1.28 \times 10^5$	101.4	40.5	0.682	B105.L	9.46	$1.40 \times 10^3$	45.9	26.4
	B108.1	$1.09 \times 10^5$	97.3	40.8	0.428	B108.L	13.60	$1.20 \times 10^4$	65.4	33.8
$\bar{M}_n = 15.5 \times 10^4$ $\eta_0 = 9.55 \times 10^3$ $[\eta]_{\text{THF}} = 61.4$ $[\eta]_{\text{CH}} = 33.2$ $\bar{p} = 8.87$	B103	$1.16 \times 10^6$	149.6	51.4	0.594	B103.L	20.61	$2.73 \times 10^4$	79.6	39.2
	B106	$1.11 \times 10^6$	162.7	56.1	0.255	B106.L	36.75	$3.30 \times 10^5$	122.2	47.1
	B104	$3.34 \times 10^6$	206.4	59.4	0.508	B104.L	41.77	$2.58 \times 10^5$	114.2	48.8
	B111	-	75.7	-	0.734	B111.L	4.96	$1.15 \times 10^2$	31.55	-
	B112	$1.53 \times 10^4$	75.8	31.6	0.600	B112.L	4.98	$1.70 \times 10^2$	29.0	19.5
	B107.5	$5.74 \times 10^4$	98.2	38.3	0.679	B107.L	7.83	$5.05 \times 10^2$	45.3	25.8
	B108.4	$1.93 \times 10^5$	115.4	51.0	0.520	B108.L	13.60	$1.20 \times 10^4$	65.4	33.8
	B115.4	$1.28 \times 10^6$	171.5	57.4	0.581	B115.L	26.60	$7.19 \times 10^4$	96.3	45.7
	B112L									
	B107.L									

\* Melt viscosities ( $\text{N s m}^{-2}$ ) were measured in a melt penetrometer at 460K

† Intrinsic viscosities ( $\text{dm}^3/\text{kg}$ ) were obtained using a dilution viscometer: (i) in THF at 298K, (ii) in cyclohexane at 308K

<sup>a</sup> Intrinsic viscosities estimated from  $\log[\eta]_{\text{CH}} - \log \bar{M}_n$  relationship

<sup>b</sup> Intrinsic viscosity in toluene at 298K

Table 2 Derived results for branched polystyrenes

Inverse branching frequency, $\lambda$	Parent mixture	Derived viscosities $\ddagger$ of branched polymers			Calculated molecular weights*	
		$[\eta]_{\text{THF}}$	$[\eta]_{\text{CH}}$	$\eta_0$	$M_n^B \times 10^{-5}$	$M_w^B \times 10^{-5}$
682	B114	81.0	38.0	$4.36 \times 10^4$	3.00	3.18
	B118	81.4	37.7	$7.85 \times 10^4$	3.35	3.63
	B116.1	77.0	38.0	$8.81 \times 10^4$	3.85	4.28
	B121	107.2	45.2	$3.52 \times 10^5$	4.64	5.32
	B120	127.0	51.5	$3.23 \times 10^6$	5.82	6.91
	B130	132.0	46.8	$1.48 \times 10^6$	6.28	7.52
	B122	150.7	61.5	$6.17 \times 10^6$	7.99	9.87
	B115.1	150.8	60.9	$1.22 \times 10^7$	8.59	10.69
202	B110.4	80.0	37.6	$5.43 \times 10^4$	4.50	4.91
	B116.3	87.4	38.2	$1.41 \times 10^5$	5.86	6.48
	B123	125.8	47.1	$7.95 \times 10^5$	7.82	8.78
	B108.2	118.9	53.6	$1.17 \times 10^6$	9.08	10.25
	B131	172.3	61.5	$5.25 \times 10^6$	12.53	14.31
	B124.2	166.3	53.7	$3.80 \times 10^6$	13.56	15.50
	B115.2	208.2	67.7	$1.00 \times 10^7$	16.60	19.05
168	B109.F†	77.8	36.1	$2.00 \times 10^4$	3.60	3.73
	B110.1	99.4	40.6	$1.00 \times 10^5$	6.58	7.01
	B107.1	100.0	41.2	$4.84 \times 10^5$	8.49	9.12
	B105	129.5	47.1	$1.00 \times 10^6$	9.94	10.74
	B108.1	140.0	50.5	$2.24 \times 10^6$	13.61	14.81
	B103	197.5	59.7	$1.53 \times 10^7$	19.83	21.71
	B106	280.5	82.8	$3.89 \times 10^7$	35.15	37.63
	B104	295.0	72.0	$3.89 \times 10^7$	38.60	42.58
	B111	92.0			4.40	4.66
	109	B112	106.7	39.5	$3.09 \times 10^5$	11.43
B107.5		123.3	44.2	$5.31 \times 10^5$	16.76	17.43
B108.4		161.4	66.8	$2.48 \times 10^6$	25.64	26.80
B115.4		225.5	67.4	$1.03 \times 10^7$	51.86	54.08

\*The molecular weights  $M_n^B$  and  $M_w^B$  are calculated from equations (2) and (A1) respectively, given in Part 2<sup>1</sup>. Backbone and branches assumed to be monodisperse

†The only sample where it was possible to separate the linear precursor (branches) from the branched polymer. The viscosities are the measured, not derived, values

‡Intrinsic viscosities (dm<sup>3</sup>/kg) in (a) THF at 298K and (b) cyclohexane (CH) at 308K.

Melt viscosities (N s m<sup>-2</sup>) at 460 K

could be made. The molecular weights given in Table 2 and used throughout this paper are therefore the calculated values. The number average molecular weight  $M_n^B$  is computed from the known (measured) molecular weights of the backbone and branches and the number of chloromethyl groups in the backbone before coupling (see Table 1). This assumes that quantitative coupling occurs between the chloromethyl group in the backbone and the potassium polystyryl (branch precursor). Weight average molecular weights,  $M_w^B$ , are calculated from the ratio  $M_w^B/M_n^B$ , an expression for which was derived by Orofino<sup>8</sup> and given in the Appendix to the previous paper on comb-shaped polystyrenes<sup>1</sup>.

From the measurements of the molecular weights of the linear polystyrenes, used for the backbones and the branches in this work, it was clear that these polymers possess relatively narrow molecular weight distributions, with the ratio  $M_w/M_n$  generally lower than 1.2 (see results in Table 2 of the paper on linear polystyrenes<sup>3</sup>), and this has been confirmed by gel permeation chromatography. Application of Orofino's equation to the branched polymers considered here shows that the ratio  $M_w^B/M_n^B$  for them

depends much more on the corresponding ratio for the backbone polymer than on that of the branches. Uncertainty in the ratio  $M_w^B/M_n^B$  for the branches produces a relatively much smaller error in  $M_w^B$  than a similar uncertainty in the ratio  $M_w^L/M_n^L$  for the backbone e.g. a 20% change in the ratio  $M_w^L/M_n^L$  for the backbone changes the value of  $M_w^B$  by the same amount, for all the branched polymers, whereas a 20% change in  $M_w^B/M_n^B$  for the branches changes the value of  $M_w^B$  by about 3%. The weight average molecular weights given in Table 2 for the branched polymers shown have been calculated on the assumption that the backbone and branches are monodisperse. It is noteworthy that even when the backbone and branches are monodisperse, the branched polymer has a finite molecular weight distribution by virtue of the statistical spread in the number of branches. This distribution (as reflected in the ratio  $M_w^B/M_n^B$ ) becomes wider as the average branching frequency decreases.

In Table 3 the inverse branching frequency  $\lambda$  is defined as the average number of repeat units of backbone per branch

$$\lambda = M_n^L/M_o \bar{p} \quad (4)$$

where  $M_n^b$  and  $M_o$  are the molecular weights of the backbone polymer and repeat unit (monomer) respectively, and  $\bar{p}$  is the average number of branches per backbone. This way of expressing the branching frequency has the advantage of making comparisons of the degree of branching independent of the actual total length of the backbone molecule. It also enables comparisons to be made more readily with other published data on branched polymers of similar or dissimilar chemical types.

#### Effect of branching on the melt- and intrinsic viscosities of polystyrene

Because the molecular weight of the backbone polymer is different for each series of branched polymers, when the data in Table 2 are plotted in the conventional way as  $\log(\text{viscosity})$  versus  $\log(\text{molecular weight})$ , the four separate curves obtained each originate from a different point on the straight line plot (of slope 3.4) for linear polymers. As a result it is difficult to see clearly the changes in the melt- and intrinsic viscosities which occur when the branching frequency is altered. To overcome this disadvantage of the conventional plot, the data are presented here as plots of  $(\log \eta_0^b - \log \eta_0^L)$  or  $(\log [\eta]^b - \log [\eta]^L)$  against  $(\log M_w^b - \log M_w^L)$  in Figures 3, 4 and 7, where  $B$  and  $L$  refer to the branched polymer and the linear backbone respectively, and  $\eta_0$ ,  $[\eta]$  and  $M_w$  have their usual meaning. This way of presenting the results is equivalent to translating the usual  $\log(\text{viscosity})$  versus  $\log M_w$  plots for each series of branched polymers to a common origin on the straight line describing the variation of viscosity with molecular weight for linear polymers above the critical chain length.

**Intrinsic viscosity behaviour.** The effect of branching on the intrinsic viscosity behaviour of polystyrene in two solvents, tetrahydrofuran at 298 K and cyclohexane at 308 K, is shown in Figures 3 and 4 respectively. Although concerned primarily with the results for the polymers with long-chain branching, also included in Figures 3 and 4 are the results for the two series of comb-shaped polymers, each with a fixed branching frequency<sup>1</sup>. Figure 3 shows that in THF (a good solvent for linear polystyrenes), the intrinsic viscosity behaviour of the branched polymers studied is described by a family of curves, each curve representing the

variation in viscosity with variation in branch length at a particular frequency of branching. The pattern of variation is the same at all frequencies of branching but the overall change in intrinsic viscosity in a given range of molecular weights decreases as the branching frequency increases. It is apparent in Figure 4 that the polymers with long-chain branching exhibit the same type of behaviour in cyclohexane (a  $\theta$ -solvent for linear polystyrenes) as in THF, but the two series of comb-shaped polymers depicted show anomalous behaviour in cyclohexane by comparison. This parallels the behaviour of branched polymers in the melt, where the comb-shaped variety also show a different behaviour from the polymers with long-chain branching.

The behaviour of comb-shaped polystyrenes in cyclohexane at 308K was shown to be consistent with the finding by Decker<sup>9</sup> that the measured  $\theta$ -temperature of these polymer molecules in cyclohexane is lower than that of linear polystyrenes and depends on the molecular weight of the branches. The results of Decker do not extend to

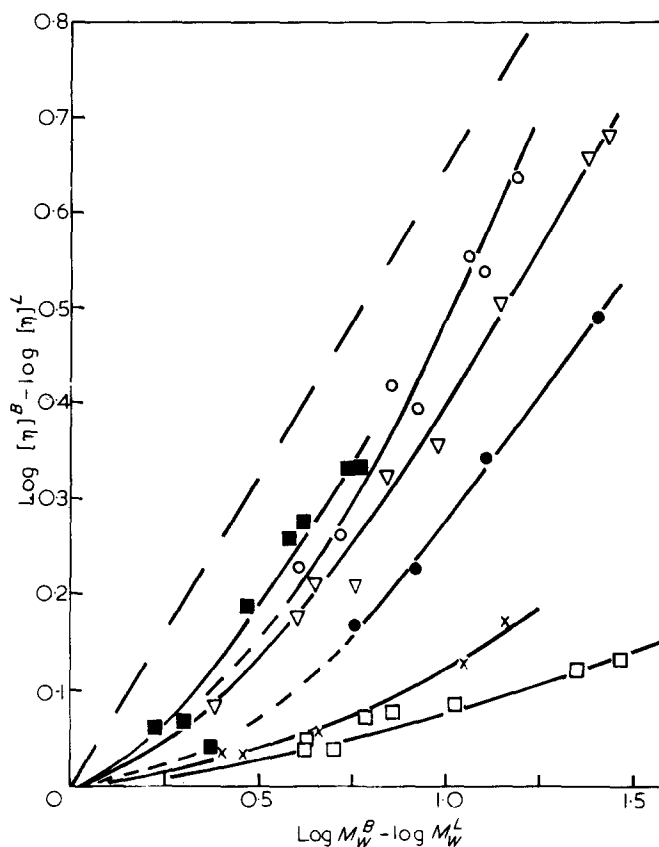


Figure 3 Variation of  $(\log [\eta]^B - \log [\eta]^L)$  with  $(\log M_w^B - \log M_w^L)$  in tetrahydrofuran at 298 K for six series of branched polystyrenes. In each series the branching frequency is fixed while the branch length is varied. The curves shown here are the  $\log [\eta]$  versus  $\log M_w$  plots for each series of polymers shifted to a common origin on the same plot, given by the broken line, for linear polymers.

- 2 branches per backbone ( $\lambda=682$ )
  - 5.78 branches per backbone ( $\lambda=202$ )
  - ▽ 8.87 branches per backbone ( $\lambda=168$ )
  - 18.7 branches per backbone ( $\lambda=109$ )
  - × 33 branches per backbone ( $\lambda=33$ )
  - 71 branches per backbone ( $\lambda=15$ )
- } Series of polymers with long-chain branching
- } Series of comb-shaped polymers<sup>1</sup>

Table 3 Comparison of range of variables covered in present study, by Fujimoto *et al.*<sup>2</sup> and in previous study<sup>1</sup>

	Polystyrenes with long-chain branching (present study)	Branched polystyrenes (Fujimoto <i>et al.</i> <sup>2</sup> )	Comb-shaped polystyrenes (Part 2 <sup>1</sup> )
$\lambda^1$	682-109	152-17.5	110-2.3
$M_n^b$	$4.65 \times 10^4$ - $41.8 \times 10^4$	$6.5 \times 10^4$ - $35.8 \times 10^4$	$0.52 \times 10^4$ - $4.5 \times 10^4$

<sup>1</sup>  $\lambda$  = Number of backbone repeat units per branch.

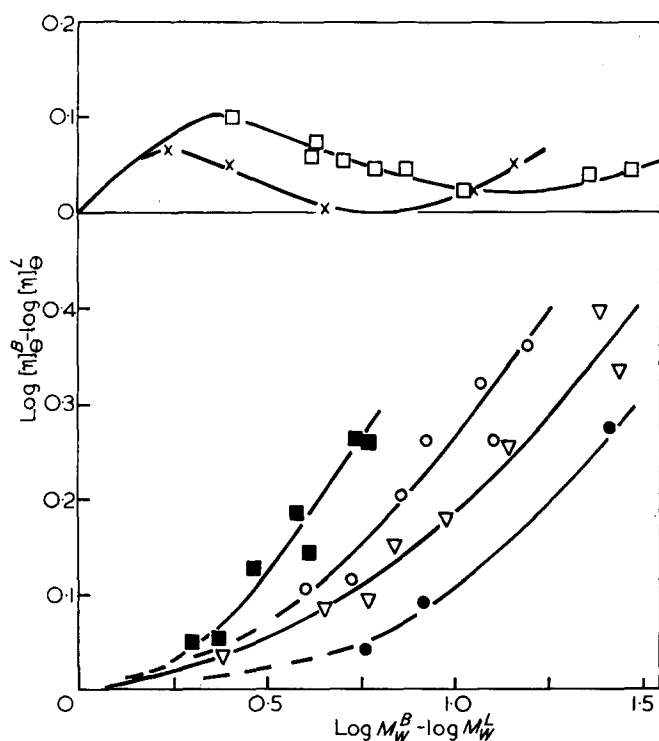


Figure 4 Variation of  $(\log [\eta]^B - \log [\eta]^L)$  with  $(\log M_w^B - \log M_w^L)$  in cyclohexane at 308 K for branched polystyrenes. Explanation of this plot and the symbols used are as in Figure 3. In contrast to the results in tetrahydrofuran, the comb-shaped polymers show a different behaviour from the polymers with long-chain branching in cyclohexane

polymers with branches with molecular weights in excess of  $3.6 \times 10^4$  but from the upward trend apparent in these results, when the molecular weight of the branches reaches about  $6-7 \times 10^4$  the  $\theta$ -temperature should be quite close to that of linear polymers. Whether the  $\theta$ -temperature continues to increase or settles around 308K with further increase in the length of the branches (i.e. long-chain branching) remains to be determined.

The dependence of the intrinsic viscosity of these polymers with long-chain branching on their actual size in solution is not known at present since no actual measurements of their size have been made. It has been found useful, however, to consider the intrinsic viscosities in relation to the calculated  $\theta$ -point dimensions of the molecules. By assuming that the type of branched polymer under consideration here obeys random flight statistics, Orofino<sup>10</sup> derived an equation for the mean square  $z$ -average radius of gyration  $\langle S_0^2 \rangle$  in terms of the degrees of polymerization of the backbone, branches and branched polymer and the average number of branches per backbone. This equation was given in the Appendix to Part 2<sup>1</sup>. In using Orofino's equation to calculate the radii of gyration of the polystyrenes with long-chain branching, the approximation has been made that the backbone and the branches are both homogeneous in chain length (see section on molecular weights). The results of these calculations are shown in Figure 5 for each series of polymers with a fixed frequency of branching, including two

series of comb-shaped polymers (33 and 71 branches per backbone respectively), after shifting the curves to a common origin on the straight line plot for linear polymers. The similarity between Figures 3 and 5 suggests that the intrinsic viscosities of these branched polymers in a good solvent (THF) are related to the theoretical unperturbed dimensions and indeed plots of  $\log [\eta]_{\text{THF}}$  against  $\log \langle S_0^2 \rangle$  produce straight lines, within experimental error, for all series of branched polymers except the series of comb-shaped polymers with 71 branches. This is shown in Figure 6. For the series of comb-shaped polymers with 71 branches per backbone no such correlation is evident because of the scatter in the data. The four series of polymers with long-chain branching also give a correlation between  $\log [\eta]_{\text{CH}}$  and  $\log \langle S_0^2 \rangle$ , where  $[\eta]_{\text{CH}}$  is the intrinsic viscosity in cyclohexane at 308K, but this is not so for the comb-shaped polymers.

This dependence of the intrinsic viscosity on the theoretical unperturbed dimensions shown by the polymers with long-chain branching (and by the series of comb-shaped polymers with 33 branches per backbone in THF) is also shown by linear polymers. According to the Fox-Flory theory of intrinsic viscosity of linear polymers

$$[\eta] \propto \langle S_0^2 \rangle^a \quad (5)$$

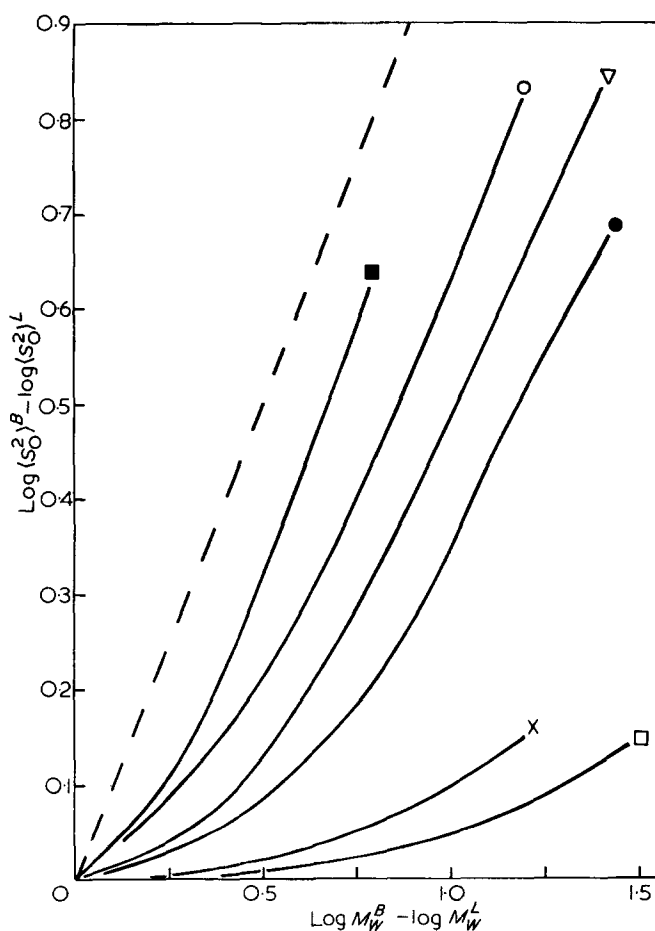


Figure 5 Variation of  $(\log \langle S_0^2 \rangle^B - \log \langle S_0^2 \rangle^L)$  with  $(\log M_w^B - \log M_w^L)$  for the series of branched polymers depicted in Figures 3 and 4. Here  $\langle S_0^2 \rangle^B$  is the mean square unperturbed radius of gyration of a branched polymer, calculated from Orofino's equation (equation A3, ref. 1)

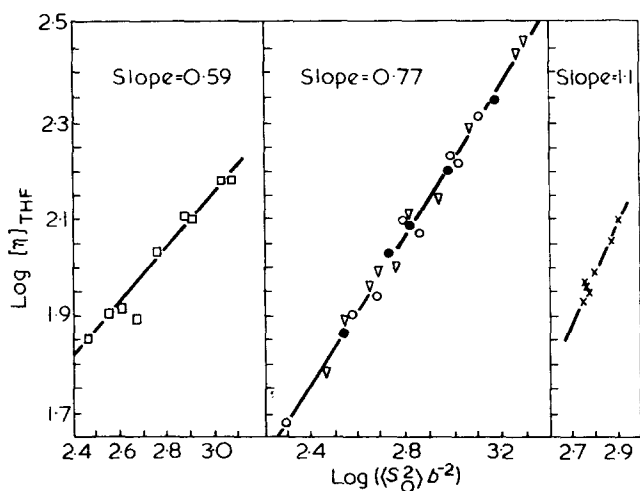


Figure 6 Logarithmic plot of the variation of the intrinsic viscosity in tetrahydrofuran at 298K with the calculated mean square unperturbed radius of gyration for branched polystyrenes. The symbols represent the same series of polymers as in Figure 3. The slope of the same plot for linear polystyrenes in THF at 298K is 0.65

where  $a$  is the exponent in the Mark-Houwink relation. In a  $\theta$ -solvent,  $a = 0.5$  and in a good solvent  $a > 0.5$ . For linear polystyrenes in THF at 298 K,  $a = 0.65$ . In THF the slope of the  $\log [\eta]_{\text{THF}}$  versus  $\log \langle S_0^2 \rangle$  plot for branched polymers appears to show some dependence on the branching frequency, e.g. the series of polymers with the lowest branching frequency gives a line with a slope of 0.59, the comb-shaped polymers with 33 branches a line of slope 1.15 and all branched polymers with an intermediate branching frequency a line with a slope of 0.77 (see Figure 6). In cyclohexane at 308K no such dependence of the slope of the  $\log [\eta]$  versus  $\log \langle S_0^2 \rangle$  plot on branching frequency is observed, all polymers falling on or near a line with a slope of about 0.5. For linear polymers the difference  $a'$  between the Mark-Houwink exponent in a good solvent and its value in a  $\theta$ -solvent is related, to a good approximation, to the expansion  $\alpha^3$  of the polymer molecule over its  $\theta$ -point dimensions when dissolved in the good solvent by

$$\alpha^3 \propto M^{a'} \quad (6)$$

By analogy with linear polymers, therefore, the variation in the slopes of the  $\log [\eta]_{\text{THF}}$  versus  $\log \langle S_0^2 \rangle$  plots for the branched polymers could be taken to mean that the expansion of a branched polymer molecule in a good solvent over the dimensions it would be expected to have if it behaved as a random coil in a  $\theta$ -solvent, is greater or less than that exhibited by linear polymers, this depending on the branching frequency. More results on branched polymers will be needed to verify this interpretation. In particular it will be necessary to show whether or not cyclohexane at 308K is a  $\theta$ -solvent (or near  $\theta$ -solvent) for polystyrenes with long-chain branching, i.e. that the  $\theta$ -temperature in cyclohexane is around 308K and is independent of the length of the branches (cf. the results on comb-shaped polystyrenes by Decker, mentioned earlier).

**Melt viscosity behaviour.** The melt viscosity results given in Table 2 for the polystyrenes with long-chain branching are plotted and shown in Figure 7. It is clear from the Figure that four distinct curves are obtained, each characterized by a different branching frequency. At each branching frequency the melt viscosity increases above the viscosity of the backbone polymer as the length of the branches is increased. This behaviour is different from that shown by the two series of comb-shaped polystyrenes with fixed branching frequencies<sup>1</sup>. For these polymers a minimum is exhibited in the  $\log \eta_0$  versus  $\log M_w$  plot, that is the initial effect of adding short branches is to depress the melt viscosity below that of the backbone; the viscosity continues to decrease as the branch length increases, reaches a minimum and then rises with further increase in the length of the branches. The two groups of polymers do, however, differ not only in the range of branch lengths covered but also in the degree of branching – the comb-shaped polymers have higher branching frequencies than the polymers with long-chain branching.

It is also apparent in Figure 7 that the transposed  $\log \eta_0$  versus  $\log M_w$  curves show a progressive

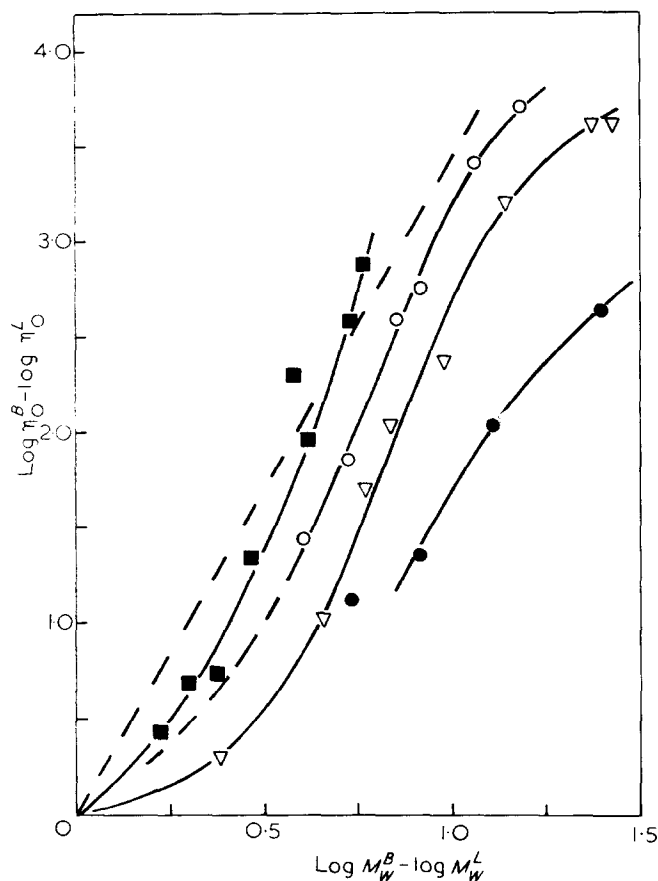


Figure 7 Variation of  $(\log \eta_0^B - \log \eta_0^L)$  with  $(\log M_w^B - \log M_w^L)$  for the four series of polymers with long-chain branching, where  $\eta_0$  is the low shear melt viscosity at 460 K. The curves shown here are the usual  $\log \eta_0$  versus  $\log M_w$  plots for each series of polymers shifted to a common origin on the straight line obtained for linear polymers, which is shown by the broken line of slope 3.4. Symbols as in Figure 3



displacement away from the  $(\log \eta_0^b - \log \eta_0^l)$  axis as the branching frequency is increased and that the melt viscosities of nearly all the polymers with long-chain branching are below the values for linear polystyrenes of the same molecular weights. The exceptions to this are the branched polymers with the longest branches in the series with the lowest branching frequency.

It was mentioned in the paper on comb-shaped polystyrenes that in the region of chain entanglements, the zero shear melt viscosities of linear polystyrenes are related to the mean square radii of gyration of the polymer molecules in a  $\theta$ -solvent by

$$\eta_0 \propto \langle S_0^2 \rangle^{3.4} \quad (7)$$

where the exponent 3.4 is the slope of the  $\log \eta_0$  versus  $\log M$  plot in the region of chain entanglements. Figure 8 shows the result of plotting  $\log \eta_0$  against  $\log \langle S_0^2 \rangle$  for the polystyrenes with long-chain branching, where  $\langle S_0^2 \rangle$  is the mean square radius of gyration calculated from Orofino's equation (see section on intrinsic viscosity behaviour). It is apparent that, apart from a few polymers with the highest molecular weights, the melt viscosities of these branched polymers are given by

$$\eta_0 \propto \langle S_0^2 \rangle^{4.8} \quad (8)$$

where 4.8 is the slope of the straight line shown in Figure 8. This shows that in the range of branching frequencies covered here, the melt viscosities of the majority of the polymers with long-chain branching show a more pronounced dependence on the theoretical  $\theta$ -point dimensions than linear polymers. Figure 8 also shows that for a given  $\langle S_0^2 \rangle$  a polymer with long-chain branching has a higher melt viscosity, i.e. is more entangled in the melt, than a linear polymer. The opposite is true of the comb-shaped polystyrenes<sup>1</sup>.

The only other systematic investigation of the effects of branching on the melt viscosity behaviour of polystyrene so far reported is that by Fujimoto *et al.*<sup>2</sup> and some of their results are reproduced in Figure 9. In their work the viscoelastic properties were studied as a function of the branching frequency with the branch- and backbone lengths held constant. Four series of polymers were studied, each series being characterized by a different branch length. As is seen in Figure 9, the low shear melt viscosity shows a slow increase as the branching frequency increases in all four series of polymers. In the case of the comb-shaped polymers described in the previous paper in this series the melt viscosity decreased as the branching frequency increased for a fixed branch length. In order to make a direct comparison between the results obtained by Fujimoto *et al.* and our own on polystyrenes with long-chain branching, a series of curves are shown in Figure 9 depicting the way in which the melt viscosity varies with increasing branch length for a fixed branching frequency. These curves show a progressive displacement away from the line for linear polymers with increasing branching frequency similar to that shown by the polymers with long-chain branching described here.

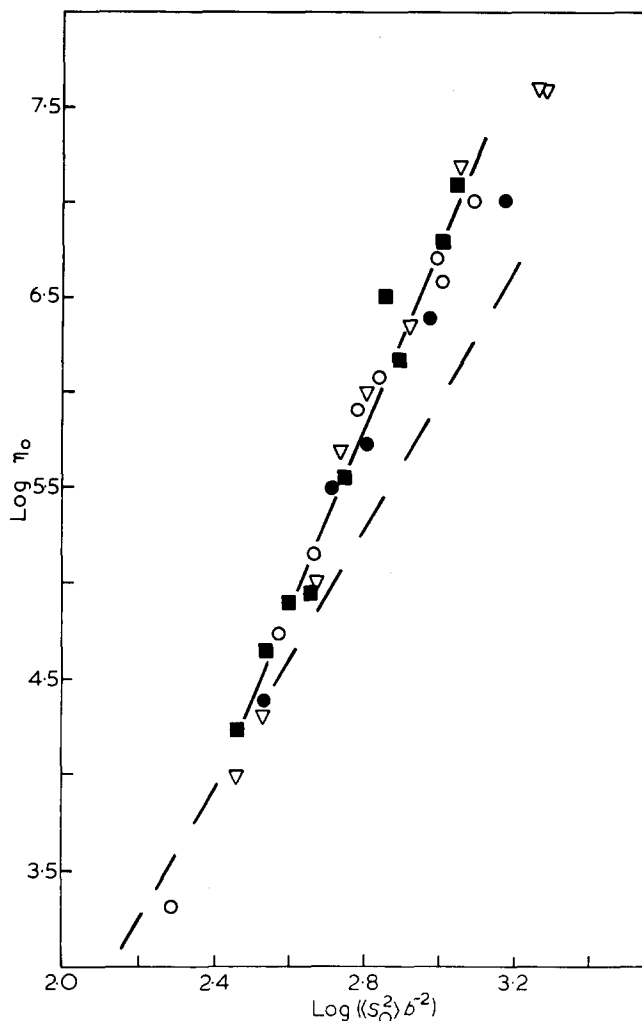


Figure 8 Logarithmic plot of the variation of the low shear melt viscosity with the theoretical mean square unperturbed radius of gyration for the polystyrenes with long-chain branching. For a given  $\langle S_0^2 \rangle$ , the branched polymers have higher melt viscosities than linear polymers, i.e. are more entangled in the melt in this range of branching frequencies. The plot for linear polymers beyond the critical chain length is shown by the broken line. Symbols as in Figure 3

The ranges of variables covered by Fujimoto *et al.* are given in Table 3, where it is seen that the molecular weights of the branches in the polymers prepared by Fujimoto *et al.* fall in the range covered in our polymers with long-chain branching whereas the branching frequencies covered overlap those of the two groups of branched polymers prepared in these laboratories. The results obtained on the branched polystyrenes by Fujimoto *et al.* can be considered, therefore, to be an extension, into a region of higher branching frequencies (low  $\lambda$ ), of our results on polymers with long-chain branching. They may also be regarded, in part, as an extension into a region of longer branches (i.e.  $M_n > 4.6 \times 10^4$ ), of our results on comb-shaped polymers. For the latter, where  $M_n^b < 4.6 \times 10^4$ , minima were observed in the  $\log \eta_0$  versus  $\log M_w$  plots for the series with fixed branching frequencies and variable branch length. The curves in Figure 9 depicting the variation of melt viscosity with branch length seem unlikely, on continuation into the region where  $M_n^b < 4.6 \times 10^4$ , to pass through the point representing the backbone polymer without first passing through minima, at least at the higher branching frequencies.

The dependence of the low shear melt viscosity on the theoretical unperturbed dimensions (calculated from Orofino's equation) of the polymers prepared by Fujimoto *et al.* is shown in Figure 10. To a first approximation a straight line with a slope of 5.1 can be drawn through the points shown in Figure 10 showing that the melt viscosities of these branched polymers also show a more pronounced dependence on the theoretical  $\theta$ -point dimensions than linear polymers. This result is similar to that obtained with our polystyrenes with long-chain branching (Figure 8) although the slope of the  $\log \eta_0$  versus  $\log \langle S_0^2 \rangle$  plot for the latter is somewhat lower (4.8). It is apparent in Figure 10 that in the range of branching frequencies covered by Fujimoto *et al.*, a branched polymer may have a higher or a lower melt viscosity (i.e. it may be more or less entangled) than a linear polymer with the same unperturbed dimensions, this depending on the branch length. The low-shear melt viscosities of our polystyrenes with long-chain branching are all higher than those of linear polymers with the same theoretical unperturbed dimensions.

Closer inspection of the plot of  $\log \eta_0$  versus  $\log \langle S_0^2 \rangle$  for the polymers prepared by Fujimoto *et al.* (Figure 10) reveals that, while most of the above conclusions remain valid, several straight lines close together, rather than a single line are actually required. Each of these lines represents the variation of  $\log \eta_0$  with  $\log \langle S_0^2 \rangle$  for a fixed branching frequency and each has a different slope, this ranging from 5.6 for the polymers with the highest branching frequency to 4.8 for the polymers with the fewest branches.

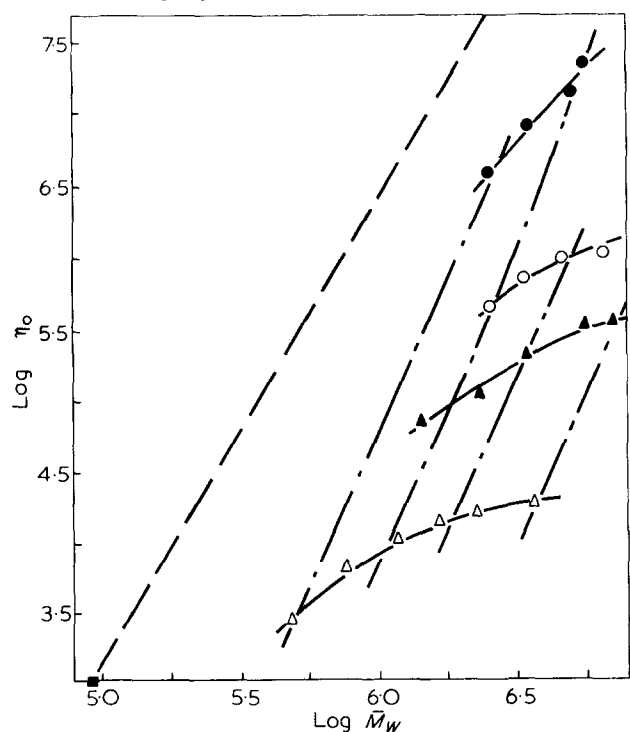


Figure 9 Logarithmic plot showing the variation of the low-shear melt viscosity with molecular weight for the branched polystyrenes prepared by Fujimoto *et al.*<sup>2</sup> In each series of polymers the branch length and backbone were fixed in length but the branching frequency was varied. From these results it is also possible to show how the melt viscosity varies with branch length for a fixed branching frequency, and this is depicted for several branching frequencies by the broken curves. ● J-series; ○ I-series; ▲ H-series; ▲ F-series; ■ common linear backbone. Reprinted from *Macromolecules* (1970, 3,57) by permission of the American Chemical Society

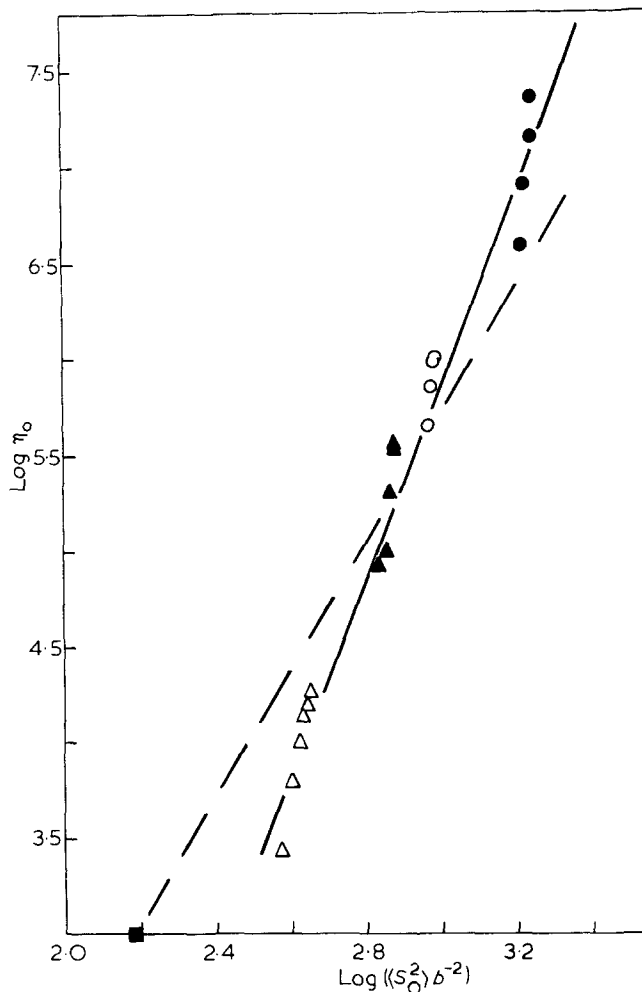


Figure 10 Logarithmic plot of the variation of the low-shear melt viscosity with the theoretical mean square unperturbed radius of gyration for the branched polystyrenes prepared by Fujimoto *et al.* Although a single straight line of slope 5.1 is drawn through all the points shown, several lines are probably required with slopes ranging from 4.8 for the polymers with the lowest branching frequency to 5.6 for those with the highest frequency

Although a fairly wide range of branching frequencies has now been covered in our studies of branched polystyrene and those of Fujimoto *et al.* there is a region of very low degrees of branching in which no studies of branched polystyrene have so far been reported in the literature. It is possible, however, to gain some idea of the likely behaviour in this region of lower branching frequencies from the trends in the melt viscosity behaviour exhibited by our polystyrenes with long-chain branching. For example, it is seen in Figure 7 that the melt viscosity increases more rapidly with increasing branch length as the branching frequency decreases and this trend is expected to continue when the degree of branching is reduced below that of the polystyrenes considered in this paper. This will result in many of the branched polymers with very low branching frequencies having melt viscosities which are higher than those of linear polymers of the same molecular weights. (This is true of only a few of the branched polystyrenes depicted in Figure 7). That is, the branch length beyond which the melt viscosity of the branched polymer exceeds that of a linear polymer of the same

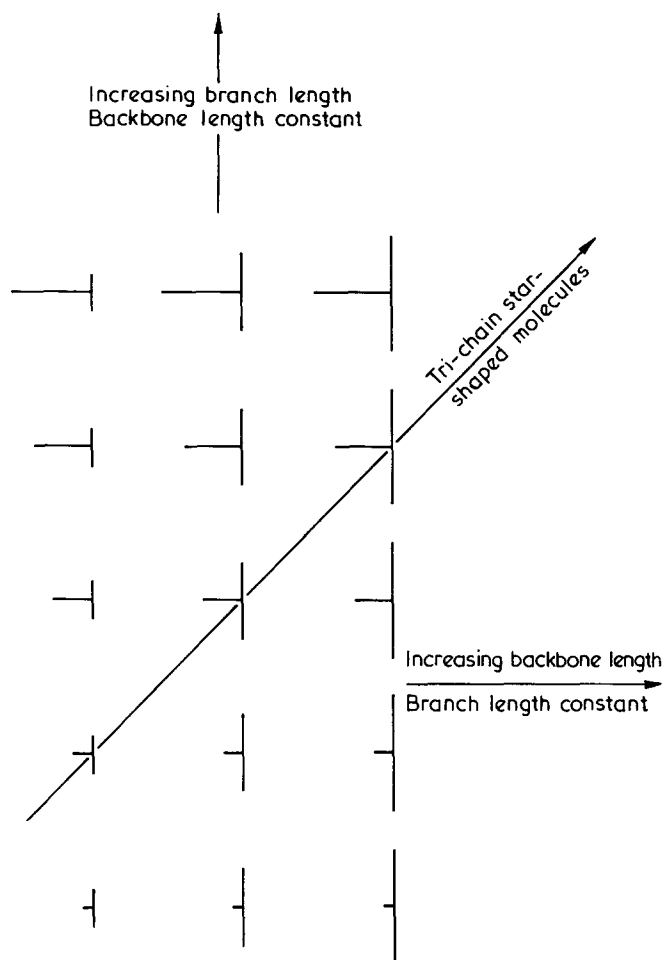


Figure 11 Schematic representation of series of branched polymers with a single branch of variable length attached at the mid-point of a linear backbone. Each series of polymers shown is one of a number of series in which a branch of variable length is attached at random to a linear backbone

molecular weight is expected to decrease with decrease in branching frequency in this region. The limiting behaviour for the type of branched polymer considered here (in which the branches are all attached to a common linear backbone) will probably be that exhibited by a series of polymers with just one branch (of variable length) per backbone molecule.

Some results of studies of the melt viscosity behaviour of two other chemically different polymers lend some support to these views about the likely behaviour of polystyrenes with low levels of branching, namely those on some randomly branched poly(vinyl acetates) by Long *et al.*<sup>11,12</sup> and those on some star-shaped polybutadienes by Kraus and Gruver<sup>13</sup>. Nearly all the branched poly(vinyl acetates) referred to, in which the branches have the same average molecular weight as the backbone (which is beyond the critical molecular weight for the onset of entanglements for linear polymers), have higher melt viscosities than those of linear poly(vinyl acetates) of the same molecular weights and lower branching frequencies ( $\lambda \geq 1300$  backbone repeat units per branch) than the branched polystyrenes described in this paper ( $\lambda \leq 682$ ). In the case of the polybutadienes two series of star-shaped polymers were studied – one series with three arms of equal length (tri-chain) and one series with four arms of

equal length (tetra-chain). The molecular weight beyond which the low shear melt viscosities of tetra-chain star-shaped polymers exceed those of linear polymers of comparable molecular weights is around  $1 \times 10^5$ . For the tri-chain polymers it is lower, in the region of  $6 \times 10^4$ . Above these molecular weights the slope of the  $\log \eta_0$  versus  $\log M_w$  curves increases rapidly, the melt viscosity of the star-shaped molecules eventually becoming at least two orders of magnitude greater than that of linear polymers. It may be seen in Figure 11 that a star-shaped polymer with three arms of equal length may be considered to be one member of a series of polymers in which a single branch of variable length is attached at the mid-point of a linear backbone molecule. Such a series of polymer molecules is itself one of a number of series in which a branch of variable length is attached at random to a linear backbone. Hence the polymers in these series will exhibit the behaviour shown in the melt by tri-chain star-shaped polymer molecules, that is they will have higher or lower melt viscosities than linear polymers of comparable molecular weights, this depending on the lengths of the backbone and branch.

#### ACKNOWLEDGEMENTS

The author is grateful to Dr J. C. Greaves and Dr P. A. Small for useful discussions in the preparation of this paper and to Mr A. Titterton for valuable assistance in the experimental work.

#### REFERENCES

- 1 Pannell, J. *Polymer* 1971, **12**, 558
- 2 Fujimoto, T., *et al. Macromolecules* 1970 **3**, 57
- 3 Pannell, J. *Polymer* 1971, **12**, 547
- 4 Ziegler, K. and Dislich, H. *Chem. Ber.* 1957, **90**, 1107
- 5 Orgmet Inc., Hampstead, New Hampshire, USA
- 6 Pannell, J., *Polymer* 1972, **13**, in the press
- 7 Kataoka, T. and Ueda, S. *J. Polym. Sci. (A-1)* 1967, **5**, 3071
- 8 Orofino, T. A. *Polymer* 1961, **2**, 295
- 9 Decker, D. *Makromol. Chem.* 1969, **125**, 136
- 10 Orofino, T. A. *Polymer* 1961, **2**, 305
- 11 Long, V. C. *PhD Thesis*, University of Michigan, 1958
- 12 Long, V. C., *et al. Polymer* 1964 **5**, 517
- 13 Kraus, G. and Gruver, J. T. *J. Polym. Sci. (A)* 1965, **3**, 105

#### Note added in proof

Since the paper on comb-shaped polystyrenes<sup>1</sup> was published a paper has appeared (Candau, F. and Franka, E. *Makromol. Chem.* 1971, **149**, 41) in which it is shown that for comb-shaped polystyrenes the  $\theta$ -temperature in cyclohexane depends on the branching frequency as well as on the branch length. As the branching frequency increases the  $\theta$ -temperature decreases and this decrease is most pronounced for the polymers with the shortest branches. In the results presented by Decker<sup>9</sup> no variation of  $\theta$ -temperature with branching frequency was apparent but it now seems likely, because of the narrow range of branching frequencies covered by Decker, that such variation was masked by a bigger variation of  $\theta$ -temperature with change of branch length. The discussion of the solution behaviour of comb-shaped polystyrenes in the present paper is not affected by the new results of Candau and Franka.

#### Erratum

Part 1<sup>3</sup>, (*Polymer* 1971, **12**, 547) Table 3. The figure for sample U31 in column 5 should read 9.20, not 8.32 as shown.

# High-density polyethylene : thermal history and melting characteristics

W. G. Harland, M. M. Khadr and R. H. Peters

*Department of Polymer and Fibre Science, University of Manchester Institute of Science and Technology, Manchester, M60 1QD, UK*

*(Received 12 March 1971; revised 13 July 1971)*

The melting characteristics of high-density polyethylene have been shown to be dependent on molecular weight and molecular weight distribution as well as on annealing and crystallizing history. The phenomenon of double melting endotherms is explained on the basis of a molecular weight fractionation process occurring during annealing and crystallization in which there is preferential crystallization of low or high molecular weight species according to the temperature. Reference is made to other polymers exhibiting similar behaviour.

## INTRODUCTION

It has frequently been reported that polyethylenes that have been isothermally crystallized or annealed, subsequently quench cooled, and remelted in instruments for differential thermal analysis or differential scanning calorimetry give rise to two endotherms<sup>1-7</sup>. For a given polymer sample the phenomenon has a number of well-defined characteristics. Firstly, the areas of the peaks and the peak temperatures are dependent on the crystallizing or annealing temperature. Secondly, prolonged annealing or crystallizing causes the high-temperature peak to increase in area and the peak moves to higher temperatures. Thirdly, the low-temperature peak either decreases in area and moves to lower temperatures and eventually disappears, or increases in area and joins the high-temperature peak. The direction of movement depends on the temperature of crystallizing or annealing; relatively high temperatures favour the former change. The growth and movement of a low-temperature peak to high temperatures has not been reported until now for high-density polyethylene, but there is a number of references to this behaviour with other polymers, notably poly(ethylene terephthalate)<sup>8-10</sup>, nylon-6,6<sup>11-13</sup>, and isotactic polystyrene<sup>13,14</sup> after annealing or crystallizing in a relatively low range of temperatures. Cold drawing also induces similar melting behaviour with these polymers<sup>12,13</sup> and, as will be shown in a subsequent paper, in high-density polyethylene as well.

The phenomenon seems to exist with most polymers, and various explanations have been advanced; secondary crystallization<sup>2</sup>, differences in degree of crystalline perfection<sup>4</sup>, crystallization in

two different lattice structures<sup>12</sup>, partial melting followed by recrystallization followed by complete melting<sup>7</sup>, sporadic and predetermined nucleation<sup>6</sup>, and conversion of chain-folded crystallites to chain-extended type<sup>10,13</sup>. However, a factor common to all polymers that has been largely overlooked is molecular weight distribution, and it is the purpose of this paper to show that many of the unusual aspects of double melting endotherms are explicable in terms of a process of molecular weight fractionation which occurs both during annealing and crystallizing. Differences exist between different polymer types, but these appear to be of degree rather than kind, and are explicable in terms of differences in their abilities to reach equivalent extents and degrees of crystalline perfection within the time scale of the experimental procedures.

## EXPERIMENTAL

### *Polymer samples*

The following samples of high-density polyethylene were supplied by Shell Plastics Laboratory, Carrington.

1. Two commercial polyethylenes with the following properties:

Code	U1(60 004)	U2(65 045)
$\overline{M}_v$	$1.2 \times 10^5$	$6.0 \times 10^4$
$\overline{M}_v/\overline{M}_n$	10	-
Density, g/ml	0.960	0.965
Melt index, g/10 min at 190°C	0.40	4.50

2. Six polyethylenes with narrow molecular weight distribution (*MWD*) specially prepared with a vanadium–aluminium alkyl catalyst system. These samples may be identified in the text since values of  $\overline{M}_v$  and  $\overline{M}_v/\overline{M}_n$  are quoted.

3. Various fractions of the above six polyethylenes. Each of the polyethylenes were separated into 8 or 9 fractions by an elution-column method<sup>15</sup>. The estimates of  $\overline{M}_v/\overline{M}_n$  referred to above were obtained from the fractionation data. The fractions were a combination of several smaller consecutive fractions obtained from the column, a few of which were separately recovered to provide samples of narrower distribution.

*Determination of intrinsic viscosity and molecular weight*

Intrinsic viscosities were determined from measurements of relative viscosity in decalin at 120°C and viscosity-average molecular weights were calculated from the expression<sup>16</sup>:

$$[\eta] = 2.76 \times 10^{-4} (\overline{M}_v)^{0.78}$$

*Melting, crystallization and annealing*

Melting, crystallizing and annealing were done on samples of known weight (3–4 mg) in a Perkin-Elmer differential scanning calorimeter (model DSC-1), under dry nitrogen (18 ml/min). The instrument was calibrated with five pure substances whose known melting points covered the range 95.0–166.0°C. Thermogram area was converted to heat of fusion by standardization against zone-refined benzoic acid (33.9 cal/g). Degrees of crystallinity were derived from the heats of fusion and a value for crystalline polyethylene of 66 cal/g. The instrument was calibrated at weekly intervals. An empty aluminium pan was used as reference.

Polymer samples were first heated at 160°C for 10 min to destroy their previous morphology. The following thermal treatments then followed.

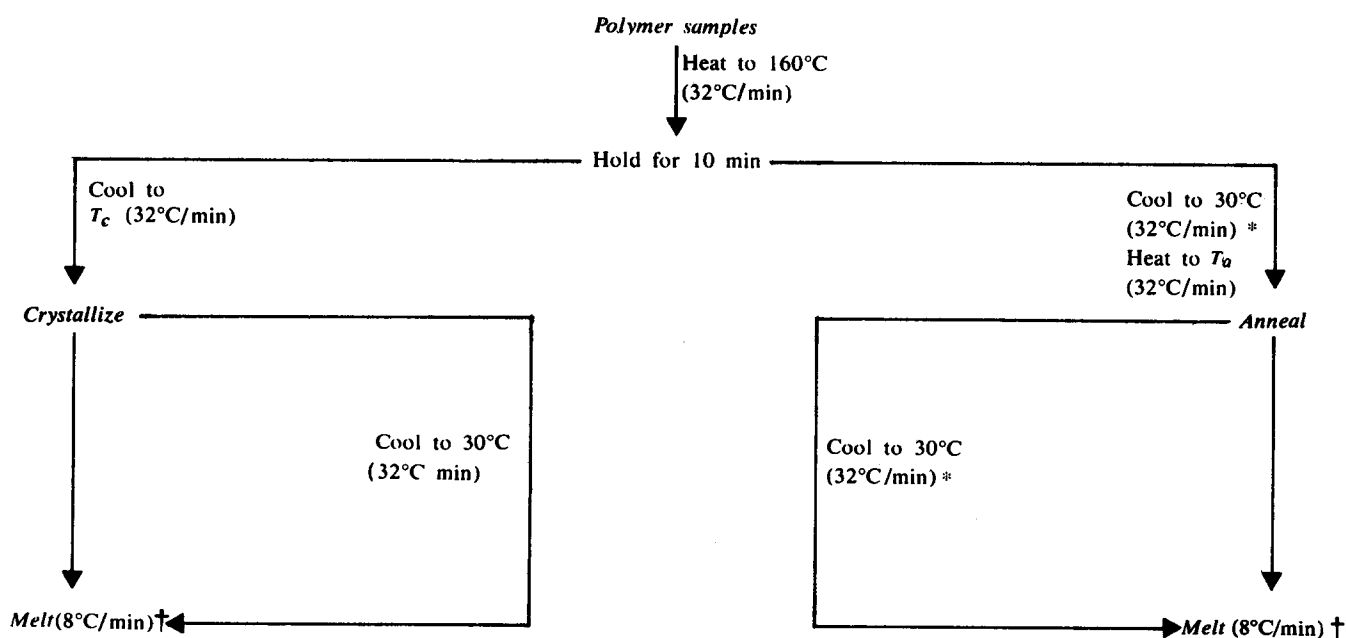
RESULTS AND DISCUSSION

The processes of crystallizing from a melt and the annealing of initially solid samples have been investigated and compared. Temperature, duration of annealing and crystallization, molecular weight and *MWD* have been varied.

*Temperature of crystallizing and annealing*

It is known from dilatometric studies<sup>17,18</sup>, that annealing in a narrow temperature range just below the melting point melts a fraction of the crystalline content. Partial melting and partial crystallization may readily be detected with the differential scanning calorimeter by annealing or crystallizing the polymer isothermally in the instrument; the temperature is then raised in order to melt the crystalline fraction, the quantity of which existing at the particular temperature may be calculated from the endotherm. Figure 1 shows the results of the procedure using a high-density polyethylene of  $M = 1.2 \times 10^5$  which had been annealed and crystallized for 10 min. The Figure also shows the percentage crystallinity obtained after subsequent quench-cooling and remelting.

Partial melting and partial crystallization processes have been used to explain the phenomenon of double endotherms. It has been argued that prolonging either of these processes will increase the perfection of the crystalline fraction and hence raise its melting point to a higher value than that of the crystalline fraction produced by subsequent quench-cooling. Partial melting or crystallization may also be used to explain the effects of changing the annealing or crystallizing temperature a few degrees; a smaller or larger crystalline fraction remains, and hence the size of the crystalline fraction produced by subsequent quench-cooling also varies; the relative areas and peak temperatures of the two endotherms obtained after remelting change accordingly. It will



$T_c$ , crystallization temperature;  $T_a$ , annealing temperature.

\* Designated 'quench-cooling' in the text.

† Similar results are obtained at scanning speeds of 4, 16 and 32°C/min

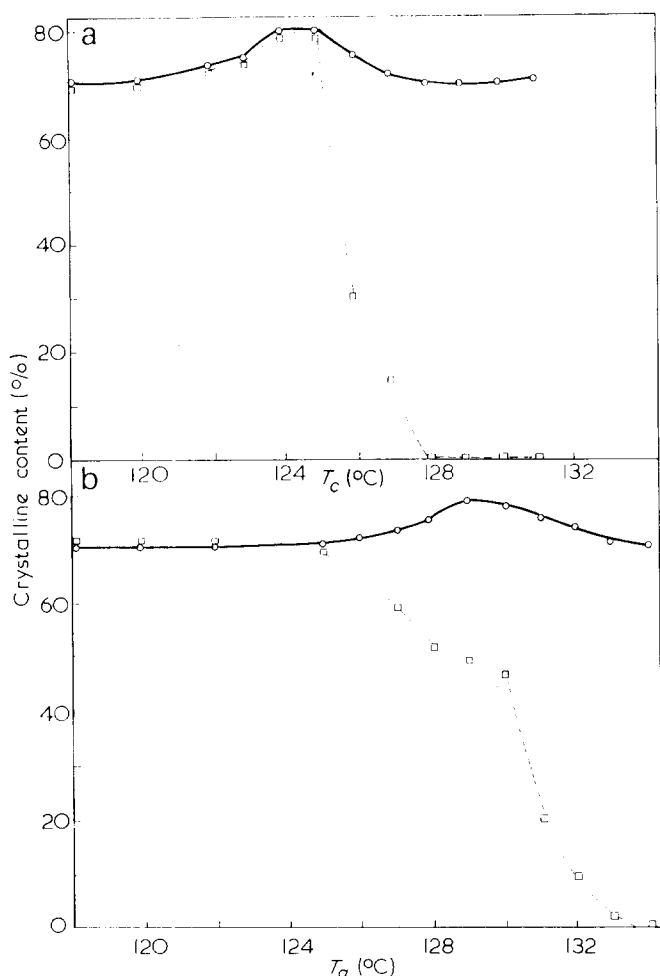


Figure 1 Percentage crystalline contents after (a) crystallizing and (b) annealing for 10 minutes at various temperatures. Values obtained from melting endotherms of polyethylene ( $\bar{M}_v = 1.2 \times 10^5$ ) before (□) and after (○) quench-cooling

be seen, however, that this explanation is inadequate to account for all experimental observations.

Figure 1 shows that after annealing or crystallizing, followed by quench-cooling, the total crystallinity passes through maxima at certain temperatures. The temperature at which maximum crystallinity is obtained is about 5°C lower for crystallizing than for annealing; this difference is, of course, accountable for by the degree of supercooling needed to effect nucleation, but it also provides an alternative means of producing double endotherms with some polymers. For example, if a polymer is partly crystallized from the melt and then the temperature is slowly raised, melting occurs (endotherm obtained), and athermal nucleation resulting from the persistence of chain alignment may cause further material to crystallize at a higher temperature where maximum extent of crystallization occurs in annealing (exotherm obtained), and this material will melt at slightly higher temperatures (endotherm obtained). Whether or not all these processes are observable depends on the difference between the two maximum temperatures and the rate at which the temperature is raised relative to the rate of re-crystallization. This behaviour has been observed in these laboratories with the polymer poly(hexamethylene terephthalate).

It may be seen from Figure 1 that melting and partial crystallization occur in the ranges 125–133°C and 125–128°C respectively. If the two processes are compared in these ranges, it will be seen from Figure 2 that quench-cooling and remelting can produce a double endotherm with a sample that has been annealed for 10 min and possibly less but, if the same sample is crystallized from the melt, crystallizing times in excess of 30 min and up to 3 h are required. The difference is not as great as first appears since a fair comparison may only be made at temperatures such that the crystalline fractions existing at annealing and crystallizing temperatures are comparable in size. Examination of Figures 2(a), (b) and (c) shows that roughly this condition is met when crystallizing at 126°C and annealing at 132°C. Under these conditions and after quench-cooling, remelting gives a double endotherm after 30–90 min crystallizing and 10–30 min of annealing.

Explanations will follow later, but the most significant observation from Figures 2(a), and (c) is that a crystalline fraction may exist at certain annealing and crystallizing temperatures for at least 10 and 30 min respectively, and hence have an opportunity to increase in fold length and in degree of crystalline perfection, and yet there is obtained only a single endotherm after quench-cooling and remelting. It would seem, therefore, that the phenomenon of double endotherms is dependent on another parameter in addition to those of temperature and time.

#### Effect of molecular weight and MWD

It is important to recognise that molecular weight and its distribution are important parameters and that the temperature ranges within which fractional

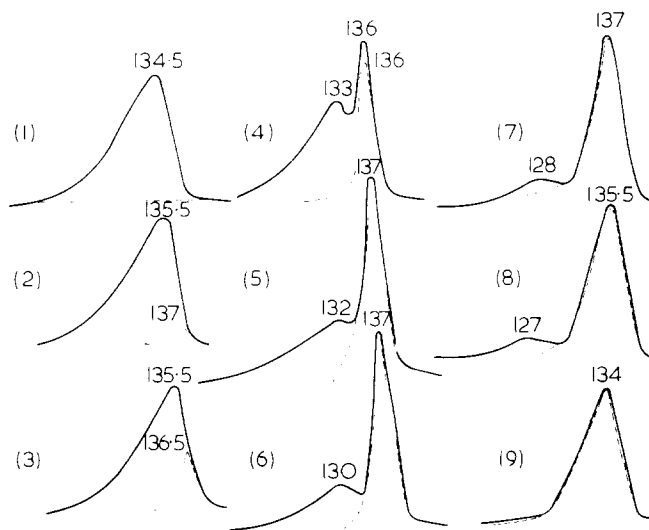


Figure 2(a) Melting endotherms of polyethylene ( $\bar{M}_v = 1.2 \times 10^5$ ) after annealing at various temperatures for 10 min. (1) 134°C; (2) 133°C; (3) 132°C; (4) 131°C; (5) 130°C; (6) 129°C; (7) 127°C; (8) 126°C; (9) 124°C. Peak temperatures indicated (°C). — anneal., quench-cool, melt; - - - - anneal, melt

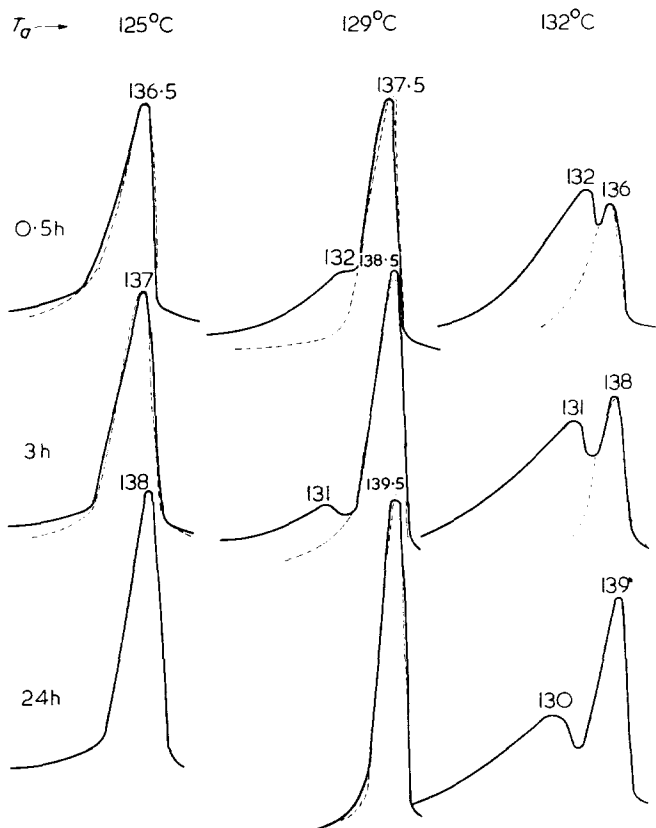


Figure 2(b) Melting endotherms of polyethylene ( $M_v = 1.2 \times 10^5$ ) after annealing at various temperatures for different times. Peak temperatures indicated ( $^{\circ}\text{C}$ ). — anneal, quench-cool, melt; - - - anneal, melt

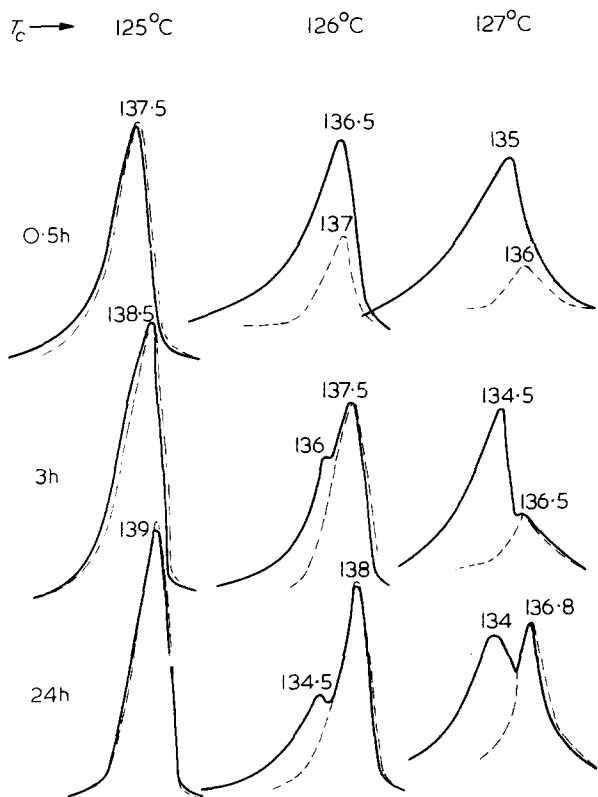


Figure 2(c) Melting endotherms of polyethylene ( $\bar{M}_v = 1.2 \times 10^5$ ) after crystallizing at various temperatures for different times. Peak temperatures indicated ( $^{\circ}\text{C}$ ). — crystallize, quench-cool, melt; - - - crystallize, melt

crystallization and partial melting occur are dependent on them; Figure 3 illustrates the point with respect to annealing. It is probably for this reason that it is sometimes reported that a sample of a given molecular weight exhibits a double melting endotherm while one of a different molecular weight does not<sup>6</sup>; this is a consequence of making comparisons at the same temperature of crystallizing or annealing. Figure 4 shows that the level of temperature and the range of temperature within which double endotherms may be obtained after annealing is dependent on molecular weight and *MWD* respectively. It is particularly important to note that the effect of narrowing the *MWD* is to narrow the temperature range of annealing that will produce double endotherms. The fractions used to produce some of the data are of unknown homogeneity and were obtained by combining several consecutive very small fractions from the column. Some of these sub-fractions were annealed over a range of temperatures for times up to several hours, and in some instances cooling and remelting gave only a single endotherm, notably when the fractions were extremely small and therefore likely to have a very narrow *MWD*.

The rate of crystallization<sup>19</sup> and the melting point<sup>20</sup> of high-density polyethylene are known to be molecular weight dependent, and melting point is dependent also, and to a greater extent, on the size and degree of order of crystalline regions. These parameters of the system make it possible to explain changes that occur during prolonged annealing on the basis that : quench-cooling a polymer melt to room temperature produces a crystalline and amorphous fraction each of which is a random mixture of the species of different molecular weight present in the sample; the crystalline phase contains a wide

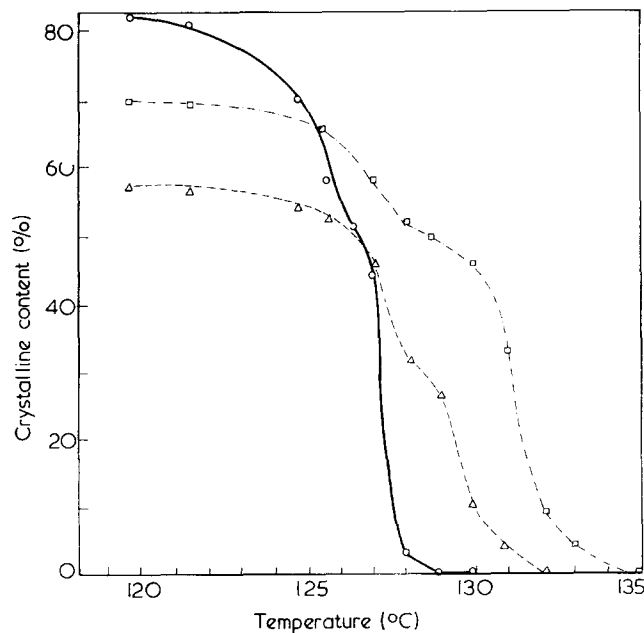


Figure 3 Percentage crystalline content remaining after annealing different polyethylenes for 10 min at various temperatures. O,  $\bar{M}_v = 1.8 \times 10^4$  fraction.  $\Delta$ ,  $\bar{M}_v = 25 \times 10^4$  fraction.  $\square$ ,  $\bar{M}_v = 12 \times 10^4$ ;  $\bar{M}_v/\bar{M}_n = 10$

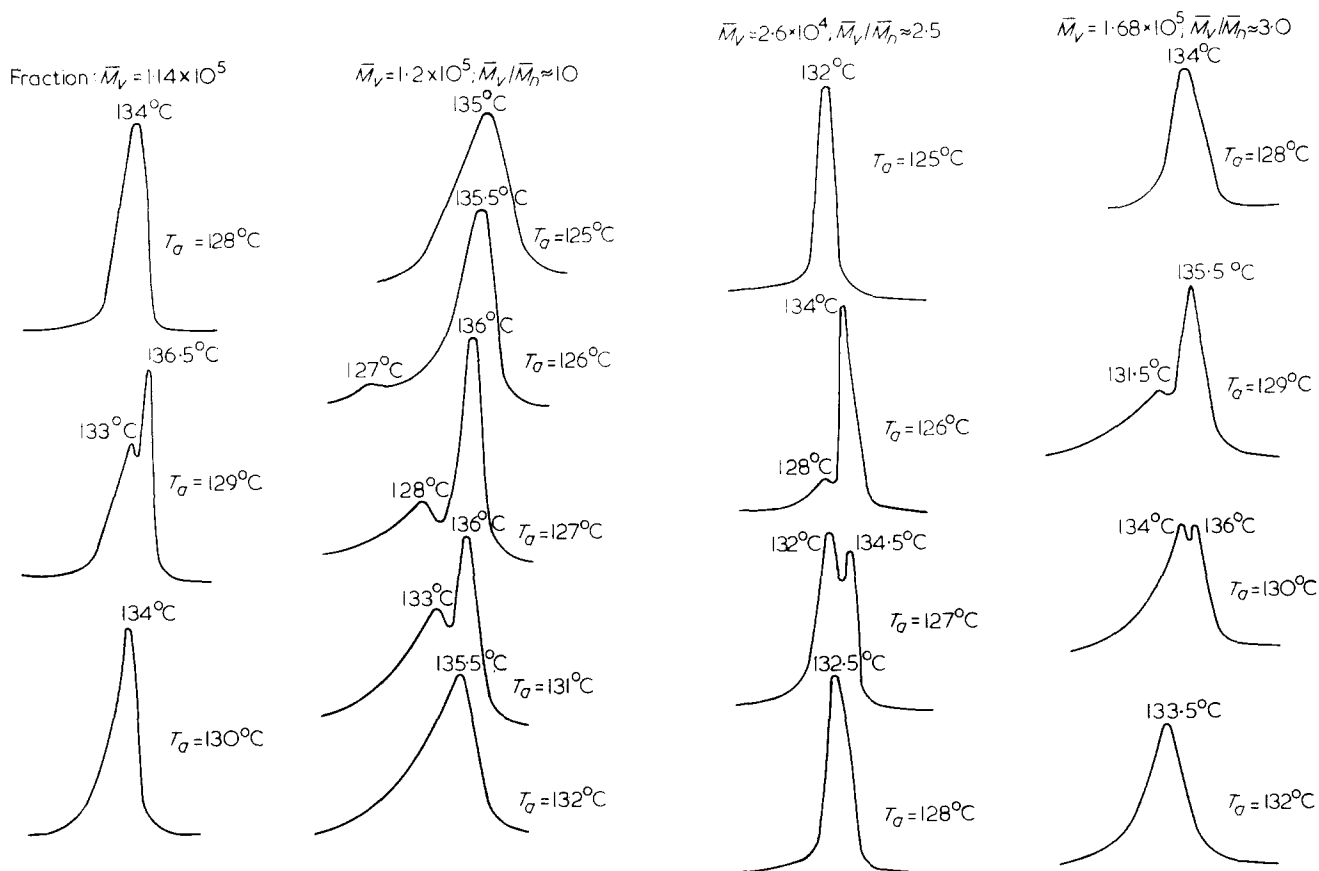


Figure 4 Melting endotherms of polyethylenes differing in molecular weight and MWD after being annealed for 10 min at various temperatures and quench-cooled

spectrum of degrees of order; at the annealing temperature a fraction of the crystalline content comprising the less stable crystalline regions melts; and during the course of annealing a fractionation process takes place, in which, at any instant the polymer joining the crystalline phase is the fraction of highest molecular weight present in the amorphous/molten phase. Such a fractionation process will lower the average molecular weight of the amorphous/molten phase, such that the crystalline fraction produced by quench-cooling will have an increasing content of chain-end defects and will have a melting point which progressively decreases with duration of annealing. Consequently with increasing duration of annealing the corresponding endotherm moves to lower temperatures. At the same time more polymer crystallizes at the annealing temperature and therefore less can crystallize during quench-cooling; hence the endotherm decreases in area and ultimately disappears. Although the fractionation process will at first increase and then subsequently decrease the average molecular weight of the crystalline fraction present at the annealing temperature, the melting point of this fraction will be largely independent of changes in molecular weight since newly crystallized polymer will adopt the fold length of pre-existing crystalline fraction, which is increasing with duration of annealing, and which will determine melting point. A similar argument holds for partial crystallization from the melt. The general behaviour is shown in Figures 2(b), (c) and 5

and the disappearance of the low-temperature peak is illustrated for the case of annealing at 129°C.

Justification for the concept of fractionation advanced here, namely that at any instant polymer of highest molecular weight joins the crystalline phase, may be found in the work of Mandelkern<sup>19</sup>, which shows that for isothermal crystallization in the range 125–130°C the rate of crystallization increases with molecular weight up to a value of the latter, which is dependent on the temperature, and lies in the range  $3 \times 10^4$  to  $10^5$ ; at higher values of molecular weight the rate was found to decrease. Since the samples used in the present work have viscosity-average values of up to  $1.2 \times 10^5$ , fractionation will at first be confounded by the simultaneous crystallization of high molecular weight polymer with some of lower molecular weight. However, even with some cross-fractionation taking place there will soon be established a significant lowering of the average molecular weight of the amorphous/molten phase present at crystallizing and annealing temperatures, and this difference will increase with time.

Confirmation of the fractionation principle has been sought by comparing the increase in crystallinity of a range of unfractionated samples of increasing average molecular weight but of similar distribution, that have been crystallized and annealed at different temperatures for 3h. The data are given in Table 1 and they show that in the range of interest (125–132°C), there is a positive tendency for high molecular weight polymer to crystallize to



the largest extent. The reverse effect at lower temperatures will be dealt with in the next section.

It is now possible to comment further on the observation made in the previous section that small crystalline fractions may exist for appreciable time at certain crystallizing and annealing temperatures and yet a double endotherm is not obtained after quench-cooling and remelting, and secondly to comment on the relatively long time of crystallizing that is apparently needed to create a double endotherm.

With regard to the first observation, it should be noted that existence of a small crystalline fraction corresponds to a situation where only a comparatively small extent of fractionation has occurred, and therefore the molecular weight of the crystalline fraction produced by quench-cooling will not have changed sufficiently for it to have a melting point differing significantly from that of the crystalline fraction existing at the annealing or crystallizing temperature.

As to the second point it will be noted by reference to *Table 1* that the efficiency of fractionation is greater the higher the temperature of crystallizing or annealing. Since a comparison is being made of crystallizing at 126°C and annealing at 132°C it is to be expected that fractionation will be more efficient in the latter case and therefore double endotherms will be produced in relatively short times. Confirmation of this explanation may be gained by observing the melting points of the two crystalline fractions as a function of crystallizing and annealing time. Such a comparison is shown in *Figure 5* for crystallizing at 126°C and annealing at 132°C; data are also included for annealing at 129°C. *Figure 5* shows that the extent of separation of melting points that determine double endotherms is far greater at a temperature of 132°C than at 126°C, and is even greater at 129°C. The last fact

Table 1 Increase in percentage crystallinity

T <sub>c</sub> or T <sub>a</sub>	After crystallizing for 3 h				After annealing for 3 h			
	1 <sup>a</sup>	2 <sup>b</sup>	3	4 <sup>d</sup>	1 <sup>a</sup>	2 <sup>b</sup>	3 <sup>c</sup>	4 <sup>d</sup>
115	3.0	1.0	1.0	0.5	0.8	0.0	0.0	0.0
120	7.0	3.5	2.5	1.3	4.2	2.4	0.8	0.1
124	16.5	12.5	7.5	6.6	11.5	7.2	3.5	1.9
125	11.5	15.7	14.0	13.6	17.3	12.3	9.8	7.5
126	1.5	12.0	18.0	17.0	18.1	15.2	13.3	10.8
127	0.8	6.5	12.8	18.5	17.0	16.5	15.7	14.6
128	0.5	4.0	10.4	19.6	4.9	17.9	16.8	16.2
129	0.0	1.5	8.0	17.0	1.0	6.7	18.6	17.9
130	—	—	—	—	0.8	2.7	14.1	19.6
132	0.0	0.0	3.0	8.5	0.1	0.9	5.6	10.8

<sup>a</sup>M<sub>v</sub> = 2.6 × 10<sup>4</sup>; M<sub>v</sub>/M<sub>n</sub> = 2.5

<sup>b</sup>M<sub>v</sub> = 5.3 × 10<sup>4</sup>; M<sub>v</sub>/M<sub>n</sub> = 2.0

<sup>c</sup>M<sub>v</sub> = 11.4 × 10<sup>4</sup>; M<sub>v</sub>/M<sub>n</sub> = 2.0

<sup>d</sup>M<sub>v</sub> = 16.8 × 10<sup>4</sup>; M<sub>v</sub>/M<sub>n</sub> = 2.0

arises from the greater rate of additional crystallization occurring at that temperature. Movements of the high-temperature peaks are not so temperature dependent as the low-temperature peaks which bears out the suggestion made earlier that in this case melting point is largely dependent on increasing fold length; the minor differences possibly reflect the effect of the varying efficiency of fractionation on the average molecular weight of the crystalline fraction.

Annealing and crystallizing at low temperatures

*Table 1* shows that at temperatures below 125°C the extent of further crystallization increases with decreasing molecular weight. This result may be attributed to the greater mobility of the smaller molecules, and leads to the conclusion that annealing or crystallizing at relatively low temperatures will lead to the formation of a new crystalline fraction initially of low molecular weight, therefore containing a high concentration of chain-end defects, and hence having a low melting point. This fraction will increase in size, average molecular weight, degree of perfection and melting point with duration of thermal treatment. This behaviour has been observed with a high-density polyethylene of M<sub>v</sub> 6 × 10<sup>4</sup>, and unknown distribution, which had been very rapidly cooled from the melt to obtain the relatively low crystalline content of 60%. Very long times of annealing at 110°C were required to produce the effect and, as may be seen from *Figure 6*, it is not very marked.

This behaviour contrasts strongly with similar experiments conducted with poly(ethylene terephthalate)<sup>8-10</sup>, nylon-6,6<sup>11-13</sup>, and isotactic polystyrene<sup>13-14</sup>, where a low-temperature endotherm is readily produced, whose peak temperature changes like that of high-density polyethylene, but which grows in size while the area of the high-temperature peak steadily diminishes to zero. The high-temperature endotherm is considered by Ikeda<sup>9</sup> to represent melting of a crystalline form resulting from recrystallization during the heating programme of the d.s.c. or d.t.a. instrument, and the

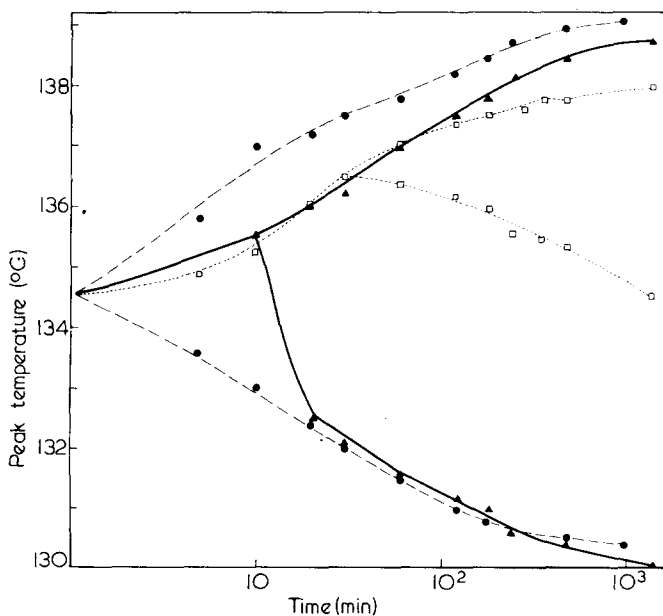


Figure 5 Peak temperature versus time for polyethylene (M<sub>v</sub> = 1.2 × 10<sup>5</sup>) after crystallizing and annealing at different temperatures. .... crystallize at 126°C; - - anneal at 129°C, — anneal at 132°C

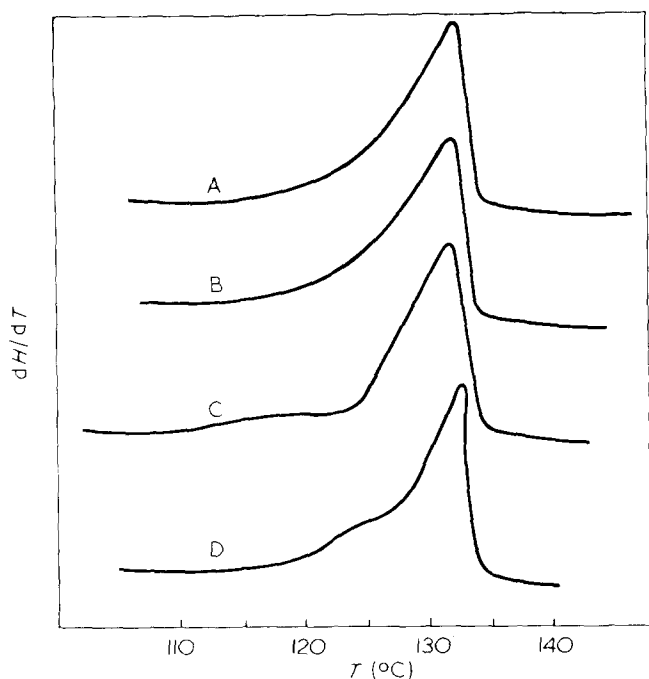


Figure 6 Melting endotherms of polyethylene ( $\bar{M}_v = 6 \times 10^4$ ) obtained after annealing for A.0; B.1; C.16; D.65h and quench-cooling

low-temperature endotherm to melting of the chain-folded crystalline form produced during the initial cooling step which has been annealed sufficiently to limit its extent of recrystallization. This approach explains why one peak apparently grows at the expense of the other. Several other investigations<sup>10,13</sup>, however, dispute that annealing results in a chain-folded crystalline structure and claim that there is conversion of chain-folded to chain-extended structures.

It is not the the purpose of the present report to give support to one view or the other concerning the effect of annealing on the final crystalline form of the above polymers, but it is appropriate to comment on their different behaviour to that of high density polyethylene and to pose the question, 'Is molecular weight fractionation involved?'

In the last analysis double endotherm phenomena are observed because semi-crystalline polymers may be obtained in a metastable state, and because non-equilibrium techniques such as differential thermal analysis permit the intermediate stages of annealing treatments to be studied. Quench-cooled polymer in particular is remote from thermodynamic equilibrium, and there are good reasons for expecting that the quench-cooled states of nylon-6,6, poly(ethylene terephthalate,) and isotactic polystyrene are more unstable than that of high-density polyethylene. No relatively difficult molecular adjustments are needed for the

crystallization of high-density polyethylene; however, when chain units are bulky and cumbersome as in poly(ethylene terephthalate) and isotactic polystyrene, and when as in the three polymers in question consecutive carbon atoms do not carry the same atomic groupings, then more time is required for segments to rotate and position themselves in equilibrium lattice positions, with the result that the overall rate of crystallization and degree of crystalline perfection is relatively low.

The influence of chain length on rate of crystallization must surely be common to all polymers; hence it is difficult to conceive that the greater mobility of low molecular weight species will be without significance when such polymers as poly(ethylene terephthalate); nylon-6,6, and isotactic polystyrene are annealed at low temperature. The effect of  $MWD$  will be to cause the low-temperature peak to move to higher temperatures – as is observed – and while this movement can and has been interpreted in terms of changes in degree and type of crystalline perfection, it should be noted that the changes are invariably accompanied by appreciable increases in crystalline content; this additional growth from amorphous regions, at least, is not likely to be exempt from the influence of molecular weight. While molecular weight fractionation probably occurs during the annealing of these polymers it is not claimed that it is the sole or even major process responsible for the observed phenomena.

#### REFERENCES

- 1 Clampitt, B. H. *Analyt. Chem.* 1963, **35**, 577
- 2 Holden, H. W. *J. Polym. Sci.* 1964, **6**, 53
- 3 Gray, A. P. and Casey, K. *J. Polym. Sci. (B)* 1964, **2**, 381
- 4 Mandelkern, L., Fatou, J. G., Denison, R. and Justin, J. *J. Polym. Sci. (B)* 1965, **3**, 803
- 5 Mandelkern, L. and Allou, A. L. *J. Polym. Sci.* 1966, **4**, 447
- 6 Hoashi, K. and Machizuki, T. *Makromol. Chem.* 1967, **100**, 78
- 7 Bair, H. E., Salovey, R. and Huseby, T. W. *Polymer*, 1967, **8**, 9
- 8 Roberts, R. C. *Polymer* 1969, **10**, 117
- 9 Ikeda, M., *Kobunshi Kagaku* 1968, **25**, 87
- 10 Nealy, D. L., Davis, T. G. and Kibler, C. J. personal communication
- 11 Hybart, F. J. and Platt, J. D. *J. Appl. Polym. Sci.* 1967, **11**, 1449
- 12 Bell, J. P., Slade, P. E. and Dumbleton, J. H. *J. Polym. Sci.* 1968, **6**, 1773
- 13 Bell, J. P. and Dumbleton, J. H. *J. Polym. Sci.* 1969, **7**, 1033
- 14 Pelzbauer, Z. and Manley, R. St. John *J. Polym. Sci. (A-2)*, 1970, **8**, 649
- 15 Francis, P.S., Cooke, R. C. and Elliott, J. H. *J. Polym. Sci.* 1958, **31**, 453
- 16 Duch, E. and Kùchler, B. *Z. Electrochem.* 1956, **60**, 218
- 17 Fischer, E. W. and Schmidt, G. F. *Angew. Chem.* 1962, **1**, 488
- 18 Gubler, M., Rabesiaka, J. and Kovacs, A. J. 'Polymer Single Crystals' (Ed. P.H. Geil) Interscience, New York, 1963
- 19 Mandelkern, L., Fatou, J.G. and Ohno, K. *J. Polym. Sci.* 1968, **6**, 615
- 20 Fatou, J. G. and Mandelkern, L. *J. Phys. Chem.* 1965, **69**, 417

# Electron microscopy of sym-SBS block polymers

P. R. Lewis

*Department of Metallurgy, University of Manchester, Manchester M13 9PL, UK*

and C. Price

*Department of Chemistry, University of Manchester, Manchester M13 9PL, UK*

*(Received 3 June 1971)*

Binary ABA block copolymers where the central block is elastomeric possess a range of characteristic textures when observed as osmium tetroxide stained thin films (40 nm) in the electron microscope. A study of low styrene content samples (~25%) prepared from dilute solution indicated three basic morphologies: an irregular phase structure, arrays of linear and hexagonally-packed circular styrene domains. The observed texture was a function of rate of preparation, decreasing rates resulting in greater domain ordering. Domains varied in size from 10 to 24 nm with corresponding spacings in the range 10–45 nm. Grain structure was only clearly observed in arrays of circular domains but quasi-spherulitic patterns occurred in linear morphologies. Coherent and random multilayers were also observed, in some cases giving rise to Moiré fringes. Comparison of observed and calculated area fractions from dilute solution characterization implied a rod-like domain structure, although significant errors were introduced by strains in the thin films.

## INTRODUCTION

Triplex block copolymers of styrene and butadiene or isoprene (SBS or SIS) have recently attracted a great deal of attention, particularly as the high rubber content materials present the attractive possibility of non-vulcanized crosslinked elastomers<sup>1</sup>. Owing to the combination of a very low entropy of mixing and a small, positive heat of mixing, phase separation is usually the thermodynamically most stable condition for homopolymer pairs<sup>2</sup>, and by an extension of the argument, the equivalent block copolymers. When the components are chemically distinct species, it is possible to preferentially stain the system and examine the phase structure microscopically. It has been confirmed by using osmium tetroxide as staining agent for polybutadiene or polyisoprene when the thin sample had either been cut from a bulk specimen<sup>3,4</sup> or cast as a film from dilute solution<sup>5,6</sup>.

The present paper describes work we have been conducting on symmetrical-SBS block polymers which had been prepared anionically, characterized in dilute solution and examined using several techniques. Among the primary objectives of our investigation were the effects of processing conditions and primary chain variables on morphology. A previous paper presented morphological evidence for bulk samples using low-angle X-ray diffraction<sup>7</sup>.

Direct visual examination of structure is often preferable however, owing to the greater amount of detail one can obtain. Two electron optical preparation techniques are currently available for block copolymers: ultramicrotomy and thin film casting. In this publication, we present the evidence of copolymer morphology as shown by *in situ* grown ultrathin films examined by transmission electron microscopy.

## EXPERIMENTAL

### *Samples*

Copolymer samples, designated S<sub>1</sub> and S<sub>2</sub>\* were characterized using a combination of dilute solution techniques. The composition of the copolymers was established by ultra-violet (u.v.) and infra-red (i.r.) spectroscopy and showed a common butadiene content of 46% *cis*, 46% *trans* and 8% vinyl units. Styrene was present to the extent of 26 and 23 wt.% ( $\bar{x}_w$ ), respectively. Sample S<sub>1</sub> was fractionated from 1% benzene by stepwise addition of methanol and the fractions were studied by light scattering in

\*Corresponding to trade names KRATON 1101 and 1102, respectively. Samples were kindly supplied by Dr G. Holden of Shell Chemical Company, Torrance, California, USA.

cyclohexane solution. The precipitation curve correlated very well with that obtained in a chromatographic gradient elution experiment. Apparent weight-average molecular weights were practically identical with true values owing to the low spread of composition. Heterogeneity parameters ( $P$  and  $Q$ ) as defined by Benoit<sup>8</sup> were  $-2800$  and  $90$  respectively. This conclusion was corroborated independently by studying two samples in different solvents. Gel permeation chromatographic (g.p.c.) studies of  $S_1$  and  $S_2$  and  $S_1$  fractions indicated the presence of 2% and 8% homopolystyrene and styrene-butadiene (SB) block polymer respectively in the unfractionated samples. The molecular weights were equivalent to the styrene block and half the overall molecular weight in the corresponding triplex polymer. Weight- and number-average molecular weights ( $\bar{M}_w, \bar{M}_n$ ) for  $S_1$  and  $S_2$  were 102 000 and 84 000, and 91 000 and 75 000 respectively. The number-average molecular weights have been corrected for the impurities mentioned above. The overall distributions for  $S_1$  and  $S_2$  were relatively sharp ( $\bar{M}_w/\bar{M}_n = 1.21$ ) and skewed towards low molecular weights. The distributions of the  $S_1$  fractions decreased in width from  $\bar{M}_w/\bar{M}_n = 1.2$  to 1.1 for decreasing molecular weight. The corresponding styrene block molecular weights ( $\bar{M}_w$ ) for  $S_1$  and  $S_2$  were 13 300 and 11 300 respectively (Table 1)<sup>9</sup>.

#### Specimen preparation

Three different methods of film casting were employed. The first involved straightforward application of Kato's method<sup>10</sup>. A drop of 10% (w/w) benzene solution of the polymer was placed on a 200-mesh grid mounted on a glass slide and allowed to evaporate isothermally. Complete evaporation occurred rapidly, leaving a film coating the surface of the grid. In an attempt to improve the technique, a slightly modified version of the procedure recommended by Hall was used<sup>11</sup>. A small volume ( $\sim 0.01$  ml) of the solution was pipetted onto a clean water surface, the solvent evaporating almost immediately to leave a film floating on the surface. The water in the bath was slowly removed, the film eventually being caught on a number of grids placed at the bottom of the vessel. The grids were cut free and air-dried at room temperature. Contrast in the films was achieved by staining in osmium tetroxide ( $\text{OsO}_4$ ) vapour. The grids were suspended above a 1% aqueous osmium tetroxide solution in a closed container for 0.5 h. Both preparation techniques proved unsatisfactory for obtaining uniform films thin enough for electron microscopic examination, although textural details could occasionally be resolved. Casting from a water surface invariably gave films which broke during drying, an effect which may be due to crazing induced by small quantities of absorbed water.

The last technique, eventually adopted for all specimens, involved casting a thin film on a mercury surface. 0.08 ml of a 0.1% benzene solution was accurately diluted to 10 ml and filtered to remove suspended matter. The solution was poured into a small Petri dish (4.75 cm diameter), the bottom of which was just covered by freshly distilled and

cleaned mercury. Controlled evaporation was achieved by simply adjusting a small watch-glass covering the mouth of the dish. The experiments were performed in a darkened fume cupboard, the updraught providing a reasonably low, controllable evaporation rate ( $< 1 \text{ cm}^3/\text{h}$ ) at room temperature. A typical film was mounted by drawing tweezer-held grids, shiny surface down, over the surface at a slightly acute angle. Negative staining was carried out as before. All solvents used (benzene, cyclohexane) were distilled Analar grade, the initial concentration of polymer being chosen to give a film thickness of 40 nm. An AEI EM6G electron microscope operated at 100 kV was used to examine the thin films. An objective lens aperture of  $50 \mu\text{m}$  was used to enhance contrast and the microscope had previously been calibrated at various magnifications using diffraction grating replicas.

#### RESULTS

Films prepared by the drop method produced textures of the kind shown in Figure 1. A similar morphology was obtained by casting from a water surface. Phase contrast is poor and there is little evidence of regularity either in domain size or shape or interdomain distance. Measured dimensions lay in the region 10–16 nm and 10–26 nm respectively for a  $S_1$  sample prepared from benzene solution.

By slowing down the rate of solvent removal and casting from mercury, comparatively regular hexagonal arrays of domains were observed in all films. Figure 2 and inset show representative arrays of  $S_1$  and  $S_2$  samples. Contrast is much enhanced and many textural details may be distinguished. Long-range order in the array is not as perfect as first sight would suggest; the plate exhibits a line defect (an extra array line) emanating from the five-coordinate point  $5/3^*$ . The defect width is large judging from

\* Array domains are numbered horizontally and vertically from the bottom right-hand corner of the Figure.

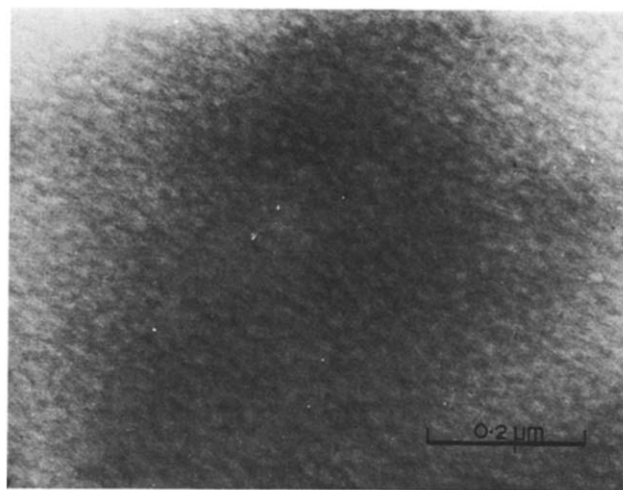


Figure 1 Irregular texture in  $S_1$  film prepared from benzene under flash conditions

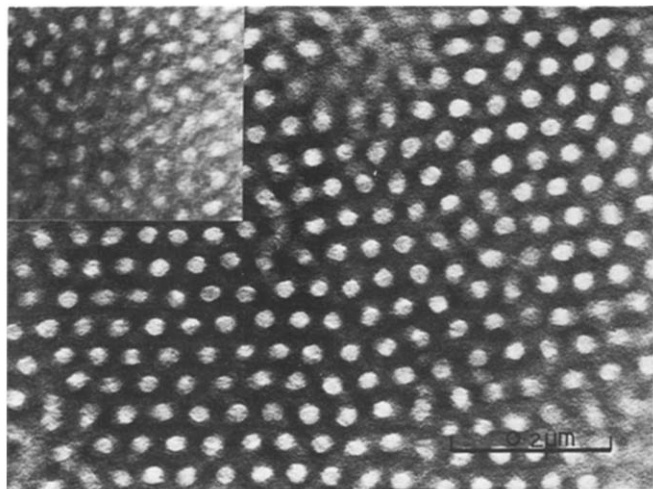


Figure 2 Ordered array of domains in  $S_1$  film prepared from benzene at slow evaporation rate. Inset shows  $S_2$  film at same scale

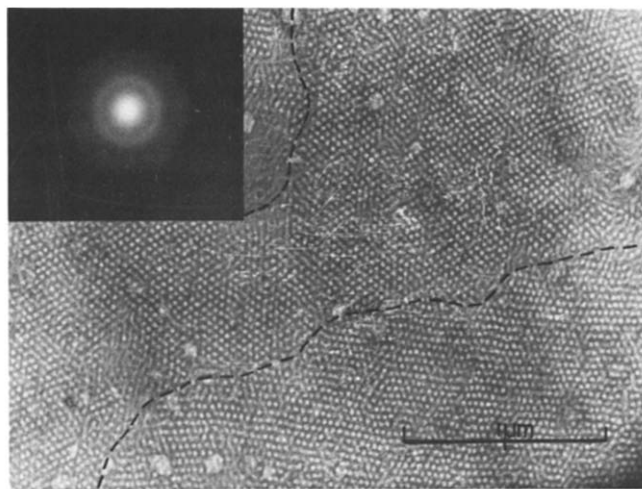


Figure 3 Randomly oriented grain structure in  $S_2$  film. Electron diffraction pattern at upper left showing amorphous halos

the decrease in shear angle from the bottom to the top of the plate ( $\sim 10-5^\circ$ ). Although matrix staining is fairly uniform, minor features are discernible. These include 'ghost' domains of lower optical density not apparently part of the overall array (e.g. at 4.5/3 or 4.5/6), and large areas of penumbra as in the middle of the plate. Certain array-domains are of equally low density (e.g. at 6/1), some showing a blurring effect towards the edge (particularly evident in the inset plate) and others showing asymmetric internal fringes indicative of slight beam astigmatism (e.g. at 4/12). Domain sizes ( $D$ ) and inter-domain distances ( $d_{int}$ ) lay in the range 19–21, 13–15 nm and 42–44, 33.5–35.5 nm for  $S_1$  and  $S_2$  respectively.

At larger fields of view, grain structure was clearly visible in all the films of hexagonal arrays examined. Figure 3 for example, shows parts of three grains with boundaries as indicated in a  $S_2$  film. The inset shows the electron diffraction pattern for the array. Four diffuse halos at 0.81 (low intensity), 1.14, 2.06 and 10 Å were observed, confirming the non-crystalline nature of the chain assembly already suspected both from chemical and wide-angle X-ray studies. Although at some points (e.g. middle lower border) the boundary is of negligible thickness, considerable areas of random blurring occur similar to that noted in Figure 2. In order to gain a meaningful estimate of grain size, a representative area, 79  $\mu\text{m}^2$  of film was micrographed at low magnification in mosaic. The composite plate covered five grains completely and fragments of fifteen others. Analysis by the method of Jeffries<sup>12</sup> gave an average grain area ( $\bar{A}$ ) of 5.05  $\mu\text{m}^2$  and hence an average grain size ( $\bar{A}$ )<sup>1/2</sup> of 2.25  $\mu\text{m}$ .  $\bar{A}$  agreed well with an independent planimetric estimate of 4.1  $\mu\text{m}^2$ . Minimum and maximum grain areas and widths were 2.8, 7.7  $\mu\text{m}^2$  and 0.425, 5.1  $\mu\text{m}$  respectively. Areas of penumbra similar to that noted in Figure 3 extended over a considerable proportion of the mosaic ( $\sim 20\%$ ). Although the staining level was relatively low, a vague linear structure could be discerned both at the borders and interior of the region. The effect was

confined to grain boundaries and no significant penumbra occurred within grains. Moiré fringes, and phase inversion effects bordered the inter-grain/penumbra region to a small extent. Neglecting grain boundaries of shallow depth, defects of the type noted in Figure 2 were randomly distributed through grains in the density range 0.5–1.2  $\mu\text{m}^{-2}$ . In some cases, the defects bridged entire grains in width. Other defects noted were two-dimensional sections of screw dislocations and negative Volterra dislocations of the sixth type<sup>13</sup>.

Relative grain orientation was assessed by measuring the angles subtended by the symmetry axes with a base line. Within sampling error, the grains were randomly oriented within the 0–30° sector. Other sources of error included distortion due to defects and strain effects. It was observed that severe distortion from the ideal 60°/60°/60° pattern occurred throughout the film. Measurement of inter-domain spacings showed a degree of strain not exceeding about 20% (usually less) along a single strain axis corresponding to the minimum trihedral angle. Grain orientation was thus measured along the axis subject to least angular distortion, namely that approximately perpendicular to the strain axis. Figure 2 shows a similar uniaxial strain at a slight clockwise angle ( $\sim 10^\circ$ ) to the side of the plate.

A selection of  $S_1$  fractions were cast as thin films to explore the correlation between styrene block molecular weight ( $\bar{M}_w$ )<sub>s</sub> and domain size ( $D$ ) suggested by  $S_1$  and  $S_2$  (Table 1). Although there were clear differences in  $D$  and  $d_{int}$  between the various samples, there appeared to be no simple correlation with the characterization data. The values in general fell between those for  $S_1$  and  $S_2$ , those for  $F_7$  (thirteen fractions were produced in all) being reported in Table 1. The bracketed values are for linear arrays as discussed in more detail below. In some cases (e.g.  $F_{11}$ ,  $F_{13}$ ) only linear arrays were obtained but this may be but a reflection of the lack of exact control over rate of preparation. Measurements of  $d_{int}$  were made on least distorted films by averaging along coherent array axes. A sam-

Table 1 Characterization data of SBS copolymers

Sample	$M_w$	$(\bar{x}_w)_s$ and $(\phi_s)$	$(M_w)_s$	$d_{int}$ (nm)	$D$ (nm)	$\phi_A$
S <sub>1</sub> (B)	102 000	0.26 (0.238)	13 300	42–44 (35–39)	19–21 (18–20)	0.195 (0.510)
S <sub>1</sub> (C)				43–45	19–22	0.215
F <sub>7</sub> (B)	131 000	0.24 (0.22)	15 700	41.5–43.5 (16–22)	18–24 (13–16)	0.220 (0.760)
F <sub>11</sub> (B)	113 500	0.24 (0.22)	13 600	(36–40) (14–16)	(14.5–16.5) (7.5–9.5)	(0.420) (0.570)
S <sub>2</sub> (B)	91 000	0.23 (0.21)	11 300	33.5–35.5 (26–34)	13–15 (14–18)	0.150 (0.530)

ple of twenty was chosen in best cases, lower if substantial disorder occurred. A similar sample was used for obtaining the range of domain sizes. The area fraction ( $\phi_A$ ) was calculated using the equation  $\phi_A = 0.905 (D/d_{int})^2$ . Although benzene was the principal solvent used for casting, the suggestion that solvent type could affect phase texture<sup>14</sup> prompted us to use cyclohexane for a series of experiments. With the possible exception of multilayer formation (see below), the morphologies were identical with those produced from benzene. Table 1 also includes characterization data together with the volume fraction of styrene ( $\phi_s$ ) calculated from the weight fraction ( $\bar{x}_w$ ), assuming the densities of polybutadiene and polystyrene to be 0.93 and 1.04 respectively.

Although most films exhibited distinct hexagonal arrays, multilayer effects were evident in certain samples. Figure 4 shows such a film (S<sub>1</sub>) where long-range order seems to be absent although a few signs of regularity are evident. The inset shows at high magnification part of the same film where it is clear that two coherent superimposed layers are present (three domains of the upper array are arrowed). The

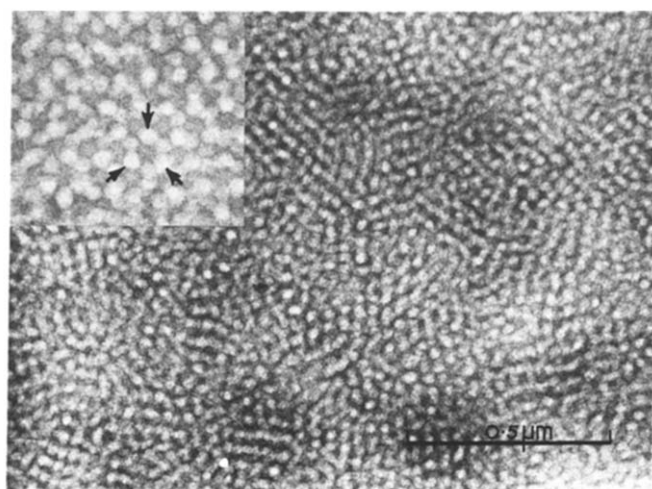


Figure 4 Multilayer growth in S<sub>1</sub> film produced at a slow evaporation rate from cyclohexane. Inset shows detail of film with coherent packing ( $\times 1.67$ )

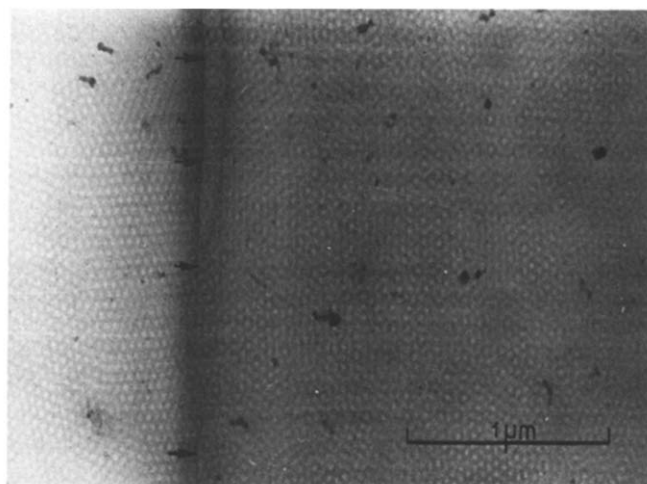


Figure 5 Moiré fringe pattern created by random film overlap in S<sub>1</sub> sample prepared from benzene

domains of the lower array possess a lower optical density and lie at interstitial points of the upper array, similar to the ghost domains noted in Figure 2. A related phenomenon is shown in the above Figure (Figure 5), where it is apparent that two layers have been fortuitously superposed during specimen preparation. The edge of the overlying film can be seen at left (marked by arrows: the second diffuse edge was produced by shadowing during photographic development to enhance the contrast of the single layer).

The Moiré fringe effect at right, consisting of irregularly spaced rings and lines, was observed in a number of samples. The effect is due to optical confusion between two independent superimposed arrays which have been rotated  $\theta$  degrees with respect to one another. The fringe diameter ( $F$ ) is related to the inter-domain spacing by the equation

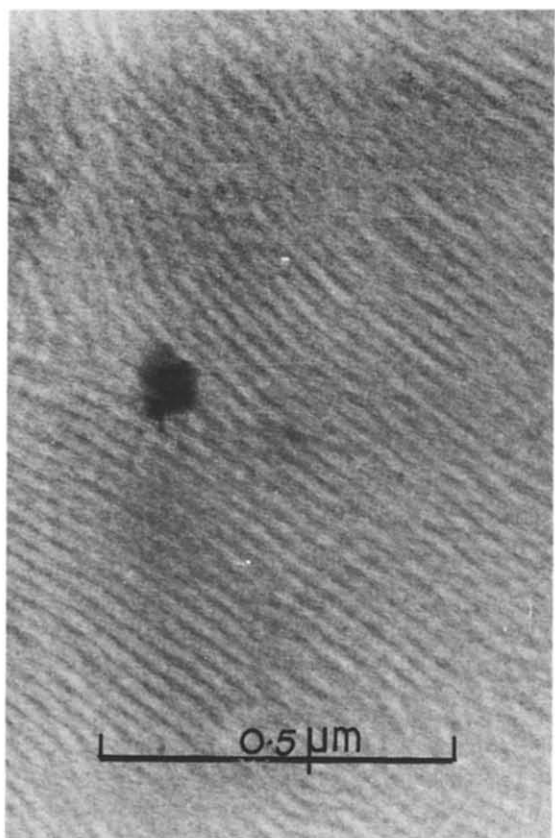
$$F = d_{int}/2\sin\theta/2$$

Decreasing angles give honeycomb patterns with steadily increasing cell size, although owing to the long-range distortions common in these films, irregularity in the fringe pattern was the rule rather than the exception. Shift along any axis of symmetry without rotation produces parallel structures of the same spacing as the original array. Figure 5 shows the Moiré pattern with a cell size of  $2d_{int}$  (85 nm), where the angle of incidence is  $30^\circ$ .

At intermediate evaporation rates ( $>1\text{cm}^3/\text{h}$ ), linear arrays with varying degrees of curvature were observed. Figure 6a shows a typical quasi-‘spherulitic’ structure (the size of the ‘spherulite’ in the top centre is  $\sim 1\ \mu\text{m}$ ) in an S<sub>1</sub> sample where the degree of curvature is very high<sup>15</sup>, while Figure 6b shows a portion of more regular structure surrounded by a disordered phase array (F<sub>7</sub>). Degenerate linear arrays of the type shown in Figure 7 were observed in some samples, particularly the high S<sub>1</sub> fractions. The g.p.c. distribution for this sample (F<sub>12</sub>) possessed a twin-peak, from which it was inferred that it consisted of a mixture of SBS and SB polymer. In several areas of the array, the spacing and domain diameters are about half that visible in the rest of the array. A similar effect is seen in Figure 8c in a somewhat



a



b

Figure 6 (a) Quasi-'spherulitic' structure in  $S_1$  array of linear domains. Mercury stains are prominent on the film surface. (b) Regular linear array in  $S_1$  fraction ( $F_7$ ) encircled by curvilinear morphology. Mercury blot is present at middle left. Both samples prepared from benzene at intermediate evaporation rate

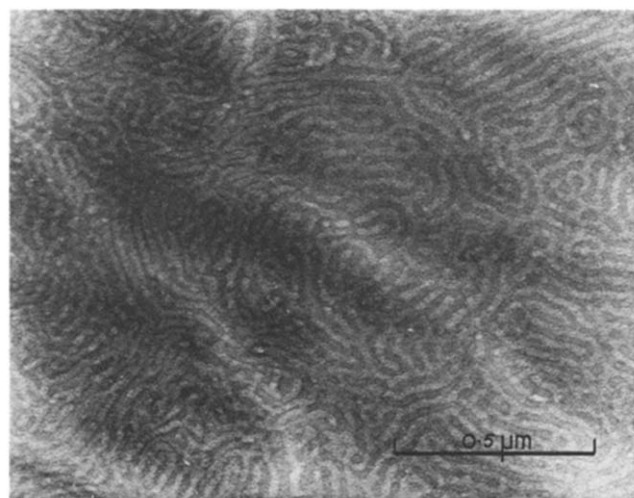


Figure 7 Degenerate linear array prepared at intermediate rates of evaporation. Doubly spaced texture present at left of plate.  $S_1$  fraction containing SB and SBS species ( $F_{12}$ )

more regular structure, which also includes domain terminations and subdivisions. Multilayers were evident, whether coherent (Figures 8a and 8b) or otherwise (Figure 8d). The latter Figure also shows a marked irregular variation in spacing. Quantitative analysis was made on those arrays possessing the least degree of curvature and disorder (parentheses, Table 1). Area fractions were calculated using the equation  $\phi_A = D/d_{int}$ .

Among the most important artefacts introduced by the casting technique was retention of mercury particles (e.g. Figures 5 and 6) which volatilized under the impact of the beam leaving slight stains (e.g. Figure 3). In general the films proved quite stable to electron bombardment although film movement was visible during examination. Small degrees of strain were also induced in a large number of films probably during sample preparation as noted in Figure 3. Arrays of circular domains were much more susceptible to strain than linear arrays. Visual recognition of phase structure was optimized by slightly underfocusing micrographs.

## DISCUSSION

The most immediate problem as presented by the block polymer morphologies is clearly the identification of the three-dimensional phase structure. Two types of evidence are available. The volume fraction of styrene may be calculated by two independent routes, in the first place from characterization data (column 3) and secondly, from measured area fractions (column 7) assuming a particular domain structure (sphere, rod, lamella). Secondly, we have direct evidence of three-dimensional structure from the films themselves. With one exception ( $F_7$ ), comparison of the volume fractions for the samples tabulated indicates a rod-like structure for both types of array, the observed volume fractions lying an average of ~20% above and below  $\phi_s$  for linear and circular structures respectively. A similar discrepancy for circular arrays was noted by Fischer<sup>5</sup>. The alternative possibilities of

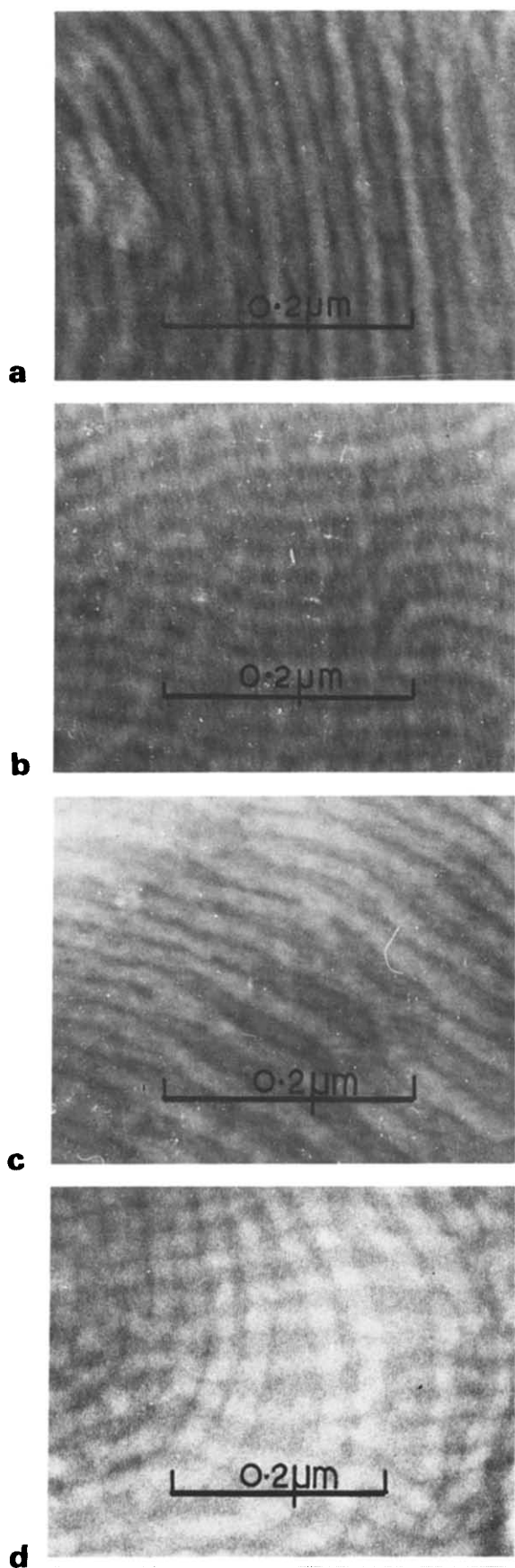


Figure 8 (a) Linear array in SB polymer (F13); (b) multilayer array in SBS polymer (F11) showing domain termination and breaks; (c) domain division and combination effects leading to double spacing in F11 film; (d) incoherent multilayer in S1 film showing spacing variation. (All samples prepared at intermediate rates from benzene)

arrays of lamellae or spheres give much greater disagreement.

The direct evidence from the film is not as straightforward, however. In particular, the presence of ghost domains in regular circular arrays (Figure 2) and the existence of coherent multilayers (Figure 4) suggest spherical rather than cylindrical domains. The latter for example, could be interpreted in terms of a close-packed structure (f.c.c. or h.c.p.) viewed at right angles to the (111) plane. The slightly higher observed volume fraction may be significant, although the difference lies well within the error in magnification accepted for the electron microscope ( $\pm 5\%$ ) and the error escalation inherent in the calculation of volume fraction. Apart from a defocusing effect, an attempt to examine domain shape by tilting a monolayer sample through  $6^\circ$  to the beam axis proved inconclusive in that very little change was observed. The ambiguity may lie in the extremely thin nature of the films, which at 40 nm (or  $\sim 80$  nm for the multilayer) is comparable with domain size. In the case of the multilayer, there is also the remote but possible chance of accidental superposition. The contradictory nature of the two strands of evidence prompts a closer examination of possible sources of error, which include strain in the film, staining effects, incomplete phase separation and the effects of irradiation in the electron beam.

Small amounts of fortuitously induced strain were particularly noted in hexagonal circular arrays (e.g. Figure 3) and depending on its nature, would be expected to decrease substantially the observed area fraction of styrene. Thus for simple elongation, pure shear and uniform two-dimensional extension

$$\frac{\phi_A}{\phi'_A} = \phi_A + (1 - \phi_A)\lambda^n$$

where  $\phi_A$  is the area fraction for the strained film,  $\lambda$  the overall elongation ratio and  $n = 1/2, 1$  and  $2$  respectively. Thus a strain of 10% would result in observed percentile changes of 4, 7 and 14% respectively. Excluding fortuitous strains which could be easily detected, a uniform two-dimensional dilation of 60% would be needed to account for the observed volume fraction of an S1 sample if the domains were spherical. Unique surface forces are present during film formation but it is not known what effect these would have on structure. Low strains were easily introduced into films of circular arrays, presumably during pick-up onto the grids, but in one case strains of the order of 300% occurred in a microfilament owing to vacuole formation<sup>16</sup>. Little is known either about staining effects (e.g. masking) or incomplete phase separation, although both could lead to differences in observed area fractions. Penumbra regions detected in various films could not always be assigned to flash preparation conditions as in Figure 1. Although no degradation occurred during film examination, rippling effects were observed, in some cases leading to severe contraction of films as shown in Figure 5b (Table 1). The effect is probably thermal in origin. Similar effects have been noted in thin films of natural rubber<sup>17</sup>.

The evidence from electron micrographs of grown thin films at present indicates a common domain



assignment of cylinders viewed edge-on and end-on for linear and circular arrays respectively. The slight differences in dimensions (Table 1) may be attributed to the different behaviour of the two types of thin film, although in view of what has been said above, the possibility of spherical domains cannot be totally excluded for circular arrays. A similar ambiguity for solvent-cast thick films was discussed previously with regard to the low-angle X-ray evidence<sup>7</sup>. On the other hand, the conclusions concerning grain size and orientation correlate well with the relatively sharp, isotropic X-ray patterns obtained. One of the main problems which must be faced when comparing the two types of evidence is the great wealth of structural detail provided by electron microscopy, information which may be totally lost owing to the averaging effect associated with X-ray techniques. The variation of  $d_{int}$  for example, in Figures 7 and 8 clearly demonstrates this point. A related problem is the extent to which growth is affected by surface forces, quite apart from the effect they may have on structural dimensions. Ultramicrotomy may be one way of circumventing the problem since bulk specimens can be examined at various orientations. One is still faced with the possibility of relaxation of the elastomeric phase however, just as with as-grown thin films. Keller and co-workers for example, observed a significant difference in  $d_{int}$  between sections cut parallel and perpendicular to an SBS sample composed of cylinders<sup>18</sup>. An examination of high styrene-low butadiene samples of constant composition but varying block structure by Matsuo *et al.* also indicated discrepancies between observed and calculated volume fractions (Table 2 of ref. 4).

The phenomenon of ordered, regular growth of two-phase materials is well-established for non-polymeric materials including organic and metallic eutectic/eutectoid systems<sup>19</sup>. A number of interesting parallels may be drawn between polymeric and small-molecule systems (e.g. the features shown in Figure 8), but the principal difference lies in observed phase dimensions. For block polymers, the dimensions are several orders of magnitude lower, the explanation lying in the linear nature of polymer chains. It can be shown that the surface density of interfacial S/B junctions assuming complete phase separation is given by the expression  $\chi = kD(\bar{M}_w)_s$ , where  $k = N\rho_s/4$  for cylindrical domains and  $N$  is Avogadro's number. For constant molecular weight,  $\chi$  will approach a close-packed value with increasing

domain size. The domain cannot increase in size above the excluded volume cut-off, and in general might be expected to be much lower owing to the effect on interfacial surface tension. Such a restriction is absent in small-molecule systems. Owing to the extremely large interfacial areas present in block polymers, surface forces are likely to play a controlling but at present undetermined role in domain formation. Typical  $\chi$  values for SBS samples with cylindrical domains were  $2.4 \times 10^5$  and  $2.0 \times 10^5$  chains per  $\mu\text{m}^2$  for  $S_1$  and  $S_2$  respectively.

#### ACKNOWLEDGEMENTS

We would like to thank Dr G.W. Lorimer and Professor R.B. Nicholson of the Department of Metallurgy, University of Manchester for the use of an electron microscope, assistance in electron optical examination and many stimulating and useful discussions. We would also like to express our appreciation to Professor J.A. Chapman and Mr S. M. W. Grundy for help in the initial stages of our work. One of us (P.R.L.) would like to acknowledge the tenureship of an SRC research studentship while this work was carried out.

#### REFERENCES

- 1 Holden, G., Bishop, E.T. and Legge, H.R. *J. Polym. Sci. (C)* 1969, **26**, 37
- 2 Gee, G. *Q. Rev.* 1947, **1**, 265
- 3 Hendus, H., Illers, K. and Ropte, E. *Kolloid-Z.* 1967, **216**, 110
- 4 Matsuo, M., Sagae, S. and Asai, H. *Polymer* 1969, **10**, 79
- 5 Fischer, E. *J. Macromol. Sci.* 1968, **A2**, 1285
- 6 Lewis, P.R. and Price, C. *Nature* 1969, **223**, 494
- 7 Lewis, P.R. and Price, C. *Polymer* 1971, **12**, 258
- 8 Bushuk, W. and Benoit, H. *Can. J. Chem.* 1958, **36**, 1616
- 9 Lewis, P.R. and Price, C. to be published
- 10 Kato, K. *J. Polym. Sci. (B)* 1966, **4**, 35
- 11 Hall, C.E. 'Introduction to Electron Microscopy', McGraw-Hill, New York, 1966, p 278
- 12 Jeffries, Z., Kline, A.H. and Zmimer, E.B. *Trans. Am. Inst. Mech. Eng.* 1916, **57**, 596
- 13 Traube, H. and Essmann, U. *Phys. Stat. Sol.* 1968, **25**, 373
- 14 Beecher, J.F., Marker, L., Bradford, R.D. and Aggarwal, S.L., *J. Polym. Sci. (C)* 1969, **26**, 117
- 15 Robinson, R. *Discuss. Faraday Soc.* 1958, **25**, 29
- 16 Price, C. and Lewis, P.R. *Lab. Pract.* 1970, **19**, 599
- 17 Andrews, E.H. *Proc. R. Soc.* 1962, **A270**, 232
- 18 Dlugosz, J., Keller, A. and Pedemonte, E. *Kolloid-Z.* 1970, **242**, 1125
- 19 Hunt, J.D. and Jackson, K.A. *Trans. Am. Inst. Mech. Eng.* 1966, **236**, 843

# Peak resolution and X-ray crystallinity determination in heat-treated cellulose triacetate

A. M. Hindeleh\* and D. J. Johnson

*Textile Physics Laboratory, Department of Textile Industries,  
University of Leeds, Leeds LS2 9JT, UK  
(Received 4 May 1971)*

X-ray diffraction traces of cellulose triacetate fibres heat-treated in the range 220 – 290°C were resolved by a computational method which fits Gaussian or Cauchy functions to the peak profiles. A polynomial background is fitted at the same time so that the total area formed by the resolved peaks is a parameter for estimating crystallinity and the area under the background is a parameter for estimating the non-crystalline or disordered component. This measure of actual crystallinity is shown to be dependent upon the function chosen for the peak profile. After appropriate corrections, crystallite widths were obtained and compared with fibril widths measured on electron micrographs. Cauchy resolution data overestimate crystallite size whilst Gaussian resolution data underestimate it. In all cases the crystallites from fibres annealed at 290°C have greatly increased widths compared with crystallites from fibres annealed at 220°C or 250°C.

## INTRODUCTION

In an earlier paper we have discussed measurements of relative crystallinity in heat-treated cellulose triacetate by a correlation method<sup>1</sup>. A clearly marked transition in crystallinity index was observed at 172°C and at annealing temperatures above this value the increase in crystallinity was inversely correlated with tenacity. The basis of the correlation-crystallinity method is the X-ray scattering law, termed the 'law of conservation of intensity' by Vainshtein<sup>2</sup>, which states that total scatter in reciprocal space from equivalent regions with perfect lattice order (crystalline), imperfect lattice order (paracrystalline), and complete disorder (amorphous) is identical. For a random system of atoms which may or may not be ordered :

$$\begin{aligned} \int_0^\infty I(s) \, dv_s &= 4\pi \int_0^\infty I(s) \, s^2 \, ds \\ &= 4\pi \int_0^\infty \bar{f}^2 \, s^2 \, ds \end{aligned} \quad (1)$$

$$\bar{f}^2 = \Sigma N_i f_i^2 / \Sigma N_i$$

where  $f_i$  is the scattering factor of an atom of type  $i$ ,  $N_i$  is the number of atoms of type  $i$ , and  $s$  is the reciprocal space vector,  $|s| = 2\sin\theta/\lambda$ . For a system of molecules with cylindrical symmetry the three dimensional case can be simplified if we consider only equatorial X-ray scatter, then

$$2\pi \int_0^\infty I(s) \, s \, ds = 2\pi \int_0^\infty \bar{f}^2 \, s \, ds \quad (2)$$

In our earlier paper<sup>1</sup> we showed that complete randomization of fibres was difficult without introducing errors due to cutting or grinding and that rotation is adequate for the purpose of relative crystallinity. We now propose to investigate the possibility of defining a non-relative or actual measure of crystallinity based on the above expressions for the equatorial scatter from fibrous specimens of cellulose triacetate heat-treated above the transition temperature of 172°C.

## MEASUREMENT OF ACTUAL CRYSTALLINITY

The classical method of measuring actual crystallinity is to draw a line through the minima of the diffraction peaks and divide the X-ray scatter into a crystalline fraction

$$X_{cr} = \int_0^\infty I_{cr}(2\theta) \, d(2\theta),$$

and an amorphous fraction

$$X_{am} = \int_0^\infty I_{am}(2\theta) \, d(2\theta).$$

Modern theory has introduced the concept of lattice imperfections which give rise to a defect phase. Hosemann has demonstrated by means of optical transforms how imperfections in lattice order may be described in terms of distortions of the first and second kind<sup>3</sup>. With distortions of the first kind, long range lattice order is preserved and a series of orders of a particular reflection shows no increased line broadening, only a fall off in intensity; with distortions of the second kind, long range order is lost and an increase in the order of a reflection gives rise

\*Present address: Department of Physics, University of Jordan, Amman, Jordan

to both increased line broadening and fall off in intensity. In either case if a line is drawn between the minima we have a finite background which is a function not only of the degree of partial disorder but also of the peak overlap, and cannot be considered simply as a background due to total disorder.

In an attempt to measure crystallinity by an improved method which takes into account lattice imperfections, Ruland<sup>4</sup> has made use of equation (1) with the addition that if  $I_{cr}$  is the intensity in the crystalline phase

$$4\pi \int_0^\infty I_{cr}(s) s^2 ds = X_{cr} 4\pi \int_0^\infty \bar{f}^2 s^2 D ds$$

Where  $X_{cr}$  is the crystalline fraction and  $D$  is the disorder function of the form  $\exp(-ks^2)$ . The crystalline fraction can then be determined from

$$X_{cr} = \frac{\int_{s_0}^{s_p} I_{cr}(s) s^2 ds}{\int_{s_0}^{s_p} I(s) s^2 ds} \times \frac{\int_{s_0}^{s_p} \bar{f}^2 s^2 D ds}{\int_{s_0}^{s_p} \bar{f}^2 s^2 D ds}$$

where  $s_p$  and  $s_0$  are the upper and lower limits of integration. As  $k$  and hence  $D$  are varied,  $X_{cr}$  should be constant over different ranges of integration. This is found to be the case for  $k=4$  in polypropylene, and gives values of  $X_{cr}$  between 0.14 and 0.65. The method requires the separation of  $s^2 I_{cr}(s)$ ; this is again done by drawing a line underneath the minima and must arbitrarily exclude a part of the scatter due to distortions of both kinds. Consequently Ruland's conclusion that the results are in favour of a two-phase crystalline non-crystalline system can be anticipated.

Buchanan and Miller<sup>5</sup> have discussed in great detail the separation of size broadening and distortion broadening from line profiles of isotactic polystyrene after correction for instrumental broadening. A background curve which again follows the diffraction minima is said to involve 'a certain amount of guesswork'; not surprisingly, the corrected line-profile data are found to support a microstrain theory rather than a paracrystalline theory.

It is obvious that if we are to achieve a realistic measure of actual crystallinity then a method must be found for separating resolved line profiles from a background all of which are determined on a sound mathematical basis. The classical expression for a symmetrical line profile in X-ray diffraction is

$$I = I_{max} F(kx)$$

where  $F(kx)$  is  $\exp(-k^2x^2)$  i.e. Gaussian

$$\text{or } \frac{1}{1 + k^2x^2} \text{ i.e. Cauchy.}$$

In many cases line-broadening corrections can in fact be made on the assumption of Gaussian profiles but more realistic profiles have been obtained by assuming a Cauchy function for particle size broadening and a Gaussian function for distortion broadening<sup>6</sup>.

We have already discussed the general application of a computer program<sup>7</sup> based on a minimization

procedure due to Powell<sup>8</sup>. This program fits a function for the sum of line profiles of Gaussian, Cauchy, or part Gaussian part Cauchy shape, together with a polynomial background, to the experimental X-ray diffraction data corrected and normalized according to equation (2). Tests showed that the program was capable of accurately resolving closely overlapping peaks of a similar or of a disparate nature together with a polynomial background initially given zero parameters.

## EXPERIMENTAL

### X-ray diffraction

Cellulose triacetate yarn of 150 denier 36 filaments produced by Société Rhodiaceta was annealed at constant length in a nitrogen atmosphere, at temperatures controlled to  $\pm 1^\circ\text{C}$  in the range 180–290°C, for 30 min. Equatorial X-ray diffraction traces were recorded with a modified Hilger and Watts Y115 diffractometer and a Y90 constant-output generator; the diffractometer employs a scintillation counter whose output is fed through a single-channel pulse-height analyser to a counter or, via a ratemeter, to a chart recorder.

A correction program for use on the University's KDF 9 computer was written and established. The program corrects for air scatter, polarization, and Compton scatter; it also allows for various Lorentz correction factors to be chosen. The corrected trace is then normalized to a convenient standard area according to equation (2). A subsidiary experiment showed that the choice of Lorentz factor including a recent factor due to Cella *et al.*<sup>9</sup> has no significant effect on peak widths where the width is of the order of  $2^\circ$ , but has a significant effect on peak height.

Corrected data were then analysed by the resolution program which outputs data for each peak and the background remaining after the appropriate function has been fitted. The positions of equatorial peaks were assumed from Dulmage's orthorhombic unit cell<sup>10</sup>.

### Electron microscopy

Specimens for electron microscopy were cut into short lengths, suspended in water and dispersed by ultrasonic irradiation. The breakdown products were concentrated, drops placed on carbon-coated grids in the usual way, then negatively stained with phosphotungstic acid. The grids were examined and images recorded in a Philips EM300 electron microscope.

## RESULTS

### Peak resolution

An uncorrected diffractometer trace of cellulose triacetate yarn heat-treated at 290°C is given in *Figure 1*. The corrected trace on the  $2\theta$  scale is given in *Figure 2*. The resolution of the corrected trace into eleven Gaussian peaks and a polynomial background is illustrated, again on the  $2\theta$  scale, in *Figure 3*. An initial resolution was carried out for eight peaks but an improvement in the sum of

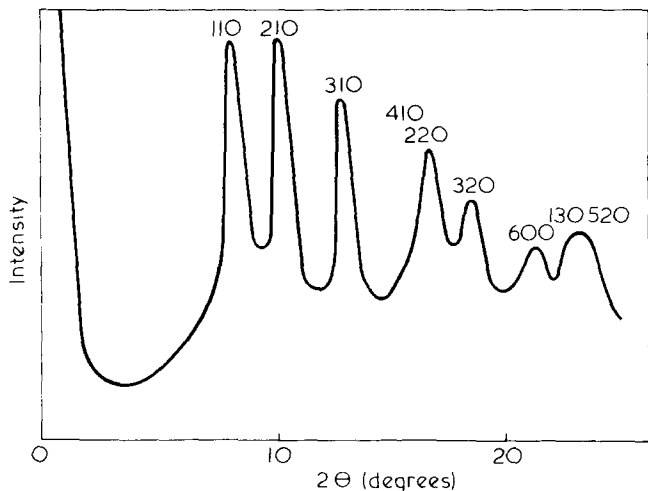


Figure 1 Uncorrected diffractometer trace of cellulose triacetate yarn heat-treated to 290°C

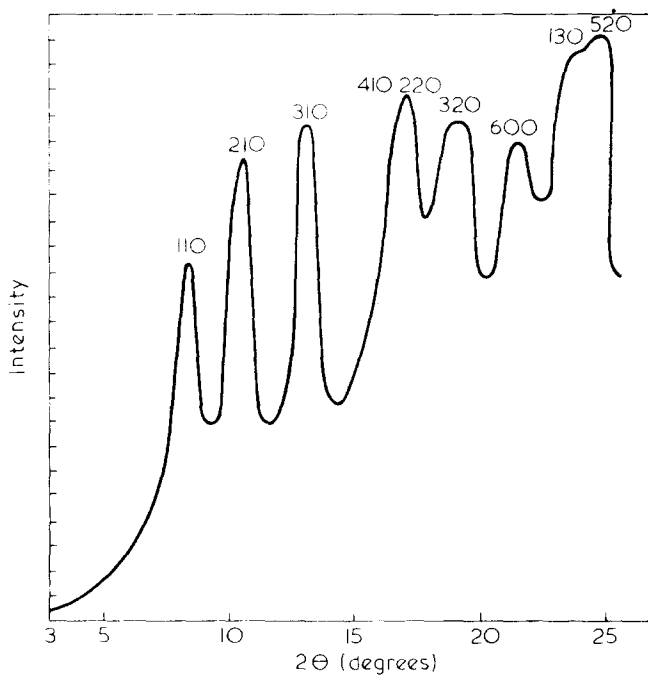


Figure 2 Corrected trace of Figure 1

squares could only be achieved by including the additional peaks 200, 400 020 and the two separate peaks 410,220 rather than a single peak at an intermediate position. In the final stages of computation for resolution the positions of the peaks, initially constrained, became additional iterative parameters so that a mathematically improved fit could be made.

Table 1 gives full details of the parameters for the resolved peaks from the 290°C specimen. The mathematical positions of the peaks are all less than 2% different from those given by Dulmage and the peaks contribute 94% to the total scatter. In our earlier publication<sup>1</sup> this specimen was considered to be 100% crystalline and was the  $C_{max}$  standard of the correlation crystallinity method.

When the corrected trace for the same specimen was analysed in terms of Cauchy line profiles the results showed that, as might be expected, all the main peaks were narrower; surprisingly the total

contribution of the peaks was only 1% greater at 95%. The widths of the main peaks for both Gaussian and Cauchy analyses are given in Table 2.

Similar results for cellulose triacetate yarn annealed at 250°C and 220°C are given in Tables 3 and 4. The difference in crystallinity between the Gaussian and Cauchy analysis is more marked for these specimens and there are large differences between the peak widths at the lower temperature. Correlation crystallinities ( $CI$ ) of 72 and 48 were recorded earlier for these specimens<sup>1</sup>.

Electron microscopy

The breakdown products of all three heat-treated specimens were essentially fibrillar. Figure 4 is a typical example of fibrils from the specimen annealed at 220°C. The enhancement effect of defocusing phase contrast, which has been studied in this laboratory in relation to fibrils from other textile fibres<sup>11</sup>, can cause uncertainties in the size of periodic structures such as a bundle of fine fibrils. In this particular image, recorded close to true focus, there is little defocusing phase contrast and fibrils can be measured with widths in the range 30 to 70 Å.

Table 1 Peak resolution of cellulose triacetate annealed at 290°C. Gaussian profiles

Peak	Theoretical $2\theta$	Experimental $2\theta$	Amplitude	Width $d\ 2\theta$
200	7.21	7.34	8.5	2.16
110	8.45	8.29	60.0	1.00
210	10.49	10.46	82.3	1.49
310	13.28	13.15	87.9	1.62
400.020	14.92	14.73	40.0	0.41
410	16.40	16.02	57.8	2.00
220	16.97	17.00	57.4	0.99
320	18.80	18.91	98.4	2.60
600	21.80	21.29	57.4	1.32
130	23.35	23.47	53.6	3.94
520	23.80	24.30	64.5	2.99

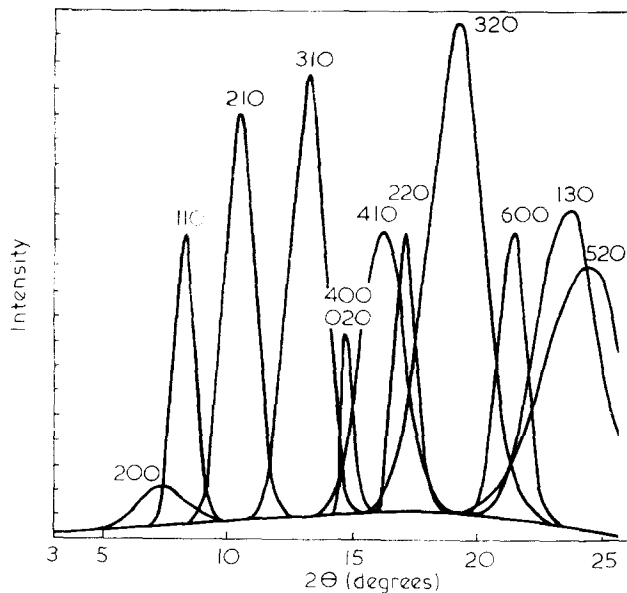


Figure 3 Corrected trace of Figure 2 resolved into eleven Gaussian peaks and a polynomial background

Table 2 Peak resolution and crystallinity of cellulose triacetate annealed at 290°C

Crystallinity:		Gaussian 94%		Cauchy 95%		Correlation method <sup>1</sup>		100%	
Peak	Width (2θ°)		L(Å)		L(Å)		L(Å)		
	Gaussian	Cauchy	r	c	r	c	r	c	
110	1.00	0.67	97	334	167				
210	1.49	1.06	62	136	91				
310	1.62	0.95	57	162	103				
410	2.00	1.80	46	64	51				
220	0.99	0.88	100	186	114				

r=resolution; c= correction

Table 3 Peak resolution and crystallinity of cellulose triacetate annealed at 250°C

Crystallinity :		Gaussian 52%		Cauchy 59%		Correlation method <sup>1</sup>		72%	
Peak	Width (2θ°)		L(Å)		L(Å)		L(Å)		
	Gaussian	Cauchy	r	c	r	c	r	c	
110	1.54	1.29	60	100	72				
210	2.06	1.36	44	93	68				
310	1.36	1.08	68	131	89				
410	4.50	2.74	21	38	34				
220	2.25	2.00	41	58	46				

r= resolution; c= correction

Table 4 Peak resolution and crystallinity of cellulose triacetate annealed at 220°C

Crystallinity :		Gaussian 49%		Cauchy 56%		Correlation method <sup>1</sup>		48%	
Peak	Width (2θ°)		L(Å)		L(Å)		L(Å)		
	Gaussian	Cauchy	r	c	r	c	r	c	
110	3.52	1.56	25	76	59				
210	4.64	2.17	19	50	41				
310	1.69	1.57	54	76	58				
410	3.12	6.05	29	16	15				
220	3.15	3.19	29	32	28				

r=resolution;c=correction

Similar fibrils were found from the specimen heated at 250°C. Figure 5 shows a typical fibrillar bundle with slight defocusing phase contrast and fibrils with widths again in the range 30–70 Å. These fibrils are very similar to those obtained from native celluloses such as cotton and ramie.

The fibrils obtained from cellulose triacetate heat-treated at 290°C are somewhat different. Figure 6 is a good example of the increased size of the fibrils which appear to have crystallized together into bundles which may be as much as 400 Å in width. Measurements on individual fibrils were made from several micrographs giving a normal distribution with a mean of 130 Å and a standard deviation of 30 Å.

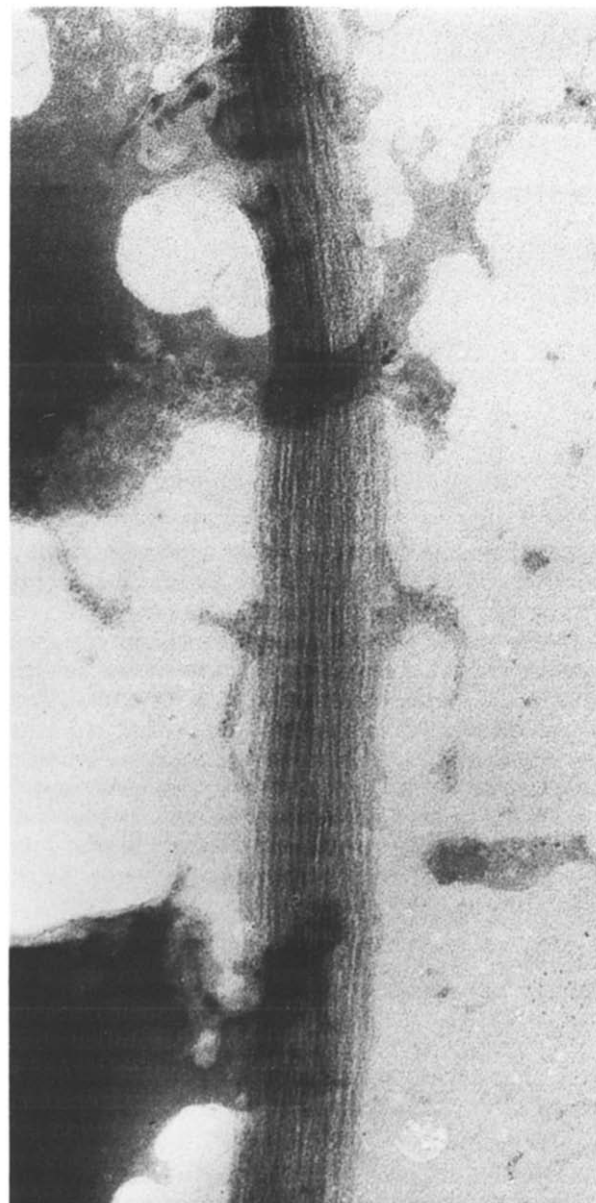


Figure 4 Fibrils from cellulose triacetate heat-treated at 220°C X 150 000

#### Crystallite size

Before evaluating crystallite size it is necessary to correct peak widths for instrumental broadening. Three correction methods are generally used; the deconvolution procedure discussed by Stokes<sup>12</sup> is considered most accurate and makes no assumptions about line profiles. However, since we have necessarily assumed either Gaussian or Cauchy line profiles, it would seem more appropriate to apply the corrections for Gaussian or Cauchy instrumental profiles. The usual corrections which approximate to the deconvolution procedure discussed by Jones<sup>13</sup> are:

$$\beta^2 = B^2 - b^2 \text{ (Gaussian)}$$

$$\beta = B - b \text{ (Cauchy)}$$

where  $\beta$  relates to the corrected profiles,  $B$  to the observed profile corrected for geometrical factors, and  $b$  to the instrumental profile. Although integral breadths are used in most analytical work our

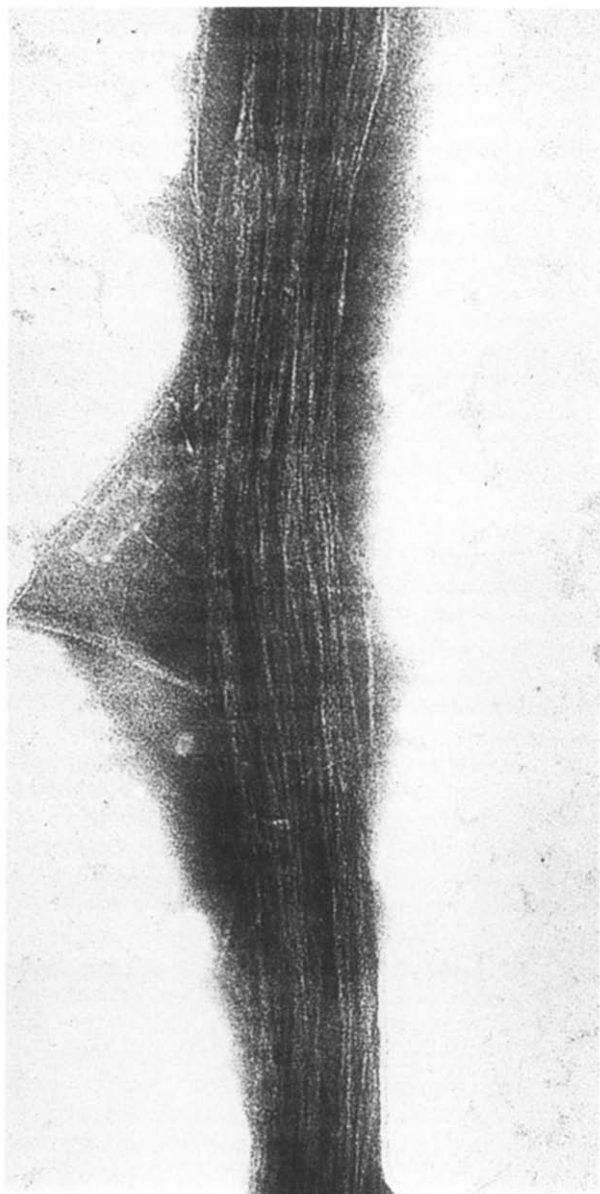


Figure 5 Fibrils from cellulose triacetate heat-treated to 250 C. X 150 000

resolution programme evaluates data according to line breadths at half-peak intensity; consequently this is the line-breadth measure used here.

The corrected line breadths were evaluated for an instrumental breadth of  $0.4^\circ$  using Gaussian corrections for the Gaussian resolution, and both Cauchy and Gaussian corrections for the Cauchy resolution. If we assume that the corrected profiles have size broadening only, then the crystallite size normal to the planes ( $hkl$ ) is given by:

$$L(hkl) = \frac{1}{\beta} = K\lambda/\cos\theta d(2\theta)$$

the usual Scherrer equation with  $K = 1$  and  $d(2\theta)$  the breadth of the curve in terms of  $2\theta$ . The values of  $L(hkl)$  are given in Tables 2,3 and 4;  $r$  refers to the resolution,  $c$  to the correction applied. The narrow profiles of the  $290^\circ\text{C}$  heat-treated cellulose triacetate are affected much more by the instrumental correction than the broader peaks of the fibres heated at lower temperatures, but in all cases the Cauchy resolution followed by a Cauchy correction appears to give crystallite size values which are too great.

#### Crystallite distortion

If the crystallites in cellulose triacetate have no distortions, or distortions of the first kind only, then the pseudo-orders 110, 210, 310, 410 should have the same width in a direction normal to 110, i.e.

$L(110):$	$L(210):$	$L(310):$	$L(410)$
1:	1.05:	1.15:	1.25.

Inspection of Tables 2,3 and 4 shows that there is no regular increase in  $L(h10)$ . The Gaussian resolution of  $290^\circ\text{C}$  cellulose triacetate shows a monotonic decrease in  $L(h10)$  whilst there is a similar decrease for the other specimens, except for the peak 310 which may be unduly influenced by the inclusion of the doublet 400 020. In all cases it would appear that distortions of the second kind are present even in the most crystalline cellulose triacetate. No reliance can be placed on the similar widths of 110 and 220 peaks in the  $290^\circ\text{C}$  and  $250^\circ\text{C}$  specimens since the presence of overlapping peaks limits the accuracy of resolution in the region of 220.

Since three true orders of reflection are needed to deconvolute size and distortion profiles by most methods based on theories of microstrain or paracrystalline distortion broadening<sup>5</sup>, we must consider here the use of the pseudo-order  $h10$ .



Figure 6 Fibrils from cellulose triacetate heat-treated at 290 C. X 90 000

The only set of resolved breadths which is suitable for analysis is that relating to the Gaussian resolution of the 290°C cellulose triacetate specimen. If we consider that the breadth is divided into components due to size broadening  $\beta_s$  and distortion broadening  $\beta_d$ , then a Gaussian correction can be applied of the form,

$$\beta^2 = \beta_s^2 + \beta_d^2$$

If  $\beta_s = 1/L$  and  $\beta_d = 4e \sin\theta/\lambda$ , where  $e$  is the microstrain distortion  $\Delta d(hkl)/d(hkl)$  discussed by Wilson<sup>14</sup>, then from a plot of  $\beta^2(h10)$  against  $(2\sin\theta/\lambda)^2$ , the intercept  $1/L$  and the slope  $2e$  can be found. Hence for the 290°C specimen  $L = 105 \text{ \AA}$  and  $e = 0.03$ . If we consider the reflections 110 and 220,  $L = 97 \text{ \AA}$ ,  $e = 0$  for the 290°C specimen, and  $L = 76 \text{ \AA}$ ,  $e = 0.05$  for the 250°C specimen.

We may note that  $e$  can be related to an average measure of distortions of the second kind  $\langle g_r^2 \rangle^{1/2}$  by  $e = 1.25 \langle g_r^2 \rangle^{1/2}$ . Then  $\langle g_r^2 \rangle^{1/2} = 0.025$  (2.5%) which compares reasonably with values found for drawn polyethylene (3.0%) and polyethylene crystals (2.0%)<sup>16</sup>.

## CONCLUSIONS

The results of the investigation are summarized in Table 5. The difficulty of resolving many overlapping reflections in X-ray diffraction traces of crystalline cellulose triacetate has been overcome in so far as it is now possible to make a mathematically optimized fit to given profile functions and an unconstrained polynomial background. However the actual crystallinities measured here are still relative in the sense that they refer to the function attributed to the line profiles. The Cauchy resolution data appear to overestimate crystallite size if we compare  $L(110)$  with the electron microscope results on mean fibril width. With the exception of the 250°C sample, the Gaussian resolution tends to underestimate the crystallite size, consequently it would seem that a profile intermediate between the two would be more appropriate. It is intended to investigate profiles of part Gaussian part Cauchy form with a fibrous material giving fewer overlapping equatorial peaks.

It is difficult in this case to estimate the effect of paracrystallinity but it would appear that distortions of the second kind are present in all specimens. In fibrous materials such as isotactic polystyrene, where several true orders of a particular reflection can be

Table 5 Summary of results

Specimen	Resolution	Cryst.	Non-cryst.	CI	$L(\text{\AA})$	$\bar{F}(\text{\AA})$
290°C	Gaussian	94	6	100	100	130
	Cauchy	95	5		165	
250°C	Gaussian	52	48	72	60	50
	Cauchy	59	41		70	
220°C	Gaussian	49	51	48	25	40
	Cauchy	56	44		60	

CI = Correlation crystallinity index<sup>1</sup>.

$L$  = Crystallite size normal to (110) planes

$\bar{F}$  = Mean fibril width from electron microscope observations

observed, the resolution of the peaks and background by a mathematical method would seem to be an improvement on graphical methods and could lead to more reliable estimates of crystallite size and lattice distortion.

## ACKNOWLEDGEMENT

The authors would like to thank Mr B. Ballance for investigating the effect of Lorentz factors on peak widths.

## REFERENCES

- Hindeleh, A. M. and Johnson, D. J. *Polymer* 1970, **11**, 666
- Vainshtein, B. K. 'Diffraction of X-rays by chain molecules', Elsevier Publishing Co., London, 1966, p 178
- Hosemann, R. and Bagchi, S. N. 'Direct Analysis of Diffraction by Matter', North Holland Publishing Co., Amsterdam, 1962, p 656
- Ruland, W. *Acta Cryst.* 1961, **14**, 1180
- Buchanan, D. R. and Miller, R. L. *J. Appl. Phys.* 1966, **37**, 4003
- Schoening, F. R. L. *Acta Cryst.* 1965, **18**, 975
- Hindeleh, A. M. and Johnson, D. J. *J. Phys. (D: Appl. Phys.)* 1971, **4**, 259
- Powell, M. J. D. *Computer J.* 1964, **7**, 155
- Cella, R. J., Lee, B. and Hughes, R. E. *Acta Cryst.* 1970, **A26**, 118
- Dulmage, W. J. *J. Polym. Sci.* 1957, **26**, 277
- Johnson, D. J. *J. Roy. Microscop. Soc.* 1968, **88**, 39
- Stokes, A. R. *Proc. Phys. Soc.* 1948, **A61**, 382
- Jones, F. W. *Proc. Roy. Soc.* 1938, **A116**, 16
- Wilson, A. J. C. 'X-ray optics', Methuen & Co., London, 1949, p 5
- Buchanan, D. R., McCullough, R. L. and Miller, R. L. *Acta Cryst.* 1966, **20**, 922
- Hoseman, R., Cackovič, H. and Wilke, N. *Naturwiss.* 1967, **54**, 278

# Conformational studies of poly(L-tyrosine) in solvent mixtures of dimethylsulphoxide with water and trimethylphosphate

E. M. Bradbury, C. Crane-Robinson, V. Giancotti\* and R. M. Stephens

*Biophysics Laboratories, Physics Department, Portsmouth Polytechnic, Portsmouth PO1 2DZ, UK  
(Received 29 April 1971)*

The conformational behaviour of poly(L-tyrosine) has been studied in dimethylsulphoxide/water and dimethylsulphoxide/trimethylphosphate solvent systems. The evidence provided by nuclear magnetic resonance and infra-red spectroscopy shows that the conformation of the polymer in dimethylsulphoxide is most probably the random coil. Addition of 20% D<sub>2</sub>O or 50% trimethylphosphate to the dimethylsulphoxide/poly(L-tyrosine) solution results in a conformational transition of the polymer which can be followed by both infra-red and nuclear magnetic resonance spectroscopy and changes in optical rotation. The evidence supports the conclusion that this transition is to a largely, though not fully, right-handed  $\alpha$ -helical conformation.

## INTRODUCTION

Poly(L-tyrosine) has been studied extensively in aqueous solutions using the techniques of optical rotatory dispersion (o.r.d.) and circular dichroism (c.d.)<sup>1,2</sup> and a transition in the Cotton effect parameters was observed on increasing the pH to a value of about 11.2 and above, the region of phenolic ionization. This transition was interpreted, not without reservation, as resulting from a right-handed  $\alpha$ -helix to random coil conformational change. The ambiguities in the interpretation of the o.r.d. and c.d. data stem from the presence of side chain chromophores which contribute Cotton effects overlapping those from the peptide chromophore. Furthermore it is suggested that in the helical polymer, tyrosyl-tyrosyl interactions are present. More recently Patrone *et al.*<sup>3</sup> have studied the same transition in aqueous solution using, with other techniques, o.r.d. and infra-red (i.r.) spectroscopy and find that whereas their o.r.d. data are consistent with those already published the i.r. spectra clearly show that a transition occurs between the random coil conformation and the antiparallel  $\beta$ -structure at pH values between 11.25 and 11.5.

The conformation of poly(L-tyrosine) has also been studied in non-aqueous solvents. Coombes *et al.*<sup>4</sup> questioning earlier work<sup>5</sup> concluded that in pyridine and dimethylformamide, in which the phenolic groups are non-ionized, the polymer is in the helical conformation. In dimethyl sulphoxide

(DMSO) Fasman<sup>6</sup> assumed poly(L-tyrosine) to be helical by analogy with poly(L-glutamic acid) which shows  $b_0 = -560^\circ$  in this solvent. A monotonic change of  $b_0$  over a range of copolymers of L-glutamic acid and L-tyrosine was therefore interpreted as indicating a right-hand helix sense for poly(L-tyrosine). The present work, however, indicates that this solvent supports the random coil conformation of poly(L-tyrosine). Two recent papers<sup>7,8</sup> give strong evidence for a helical conformation in trimethylphosphate (TMP) a solvent having the advantage of excellent transmission in the 6  $\mu$ m region of the infra-red and in the ultra-violet.

We have used nuclear magnetic resonance (n.m.r.) in addition to other spectroscopic techniques in an attempt to help understand further the conformation of poly(L-tyrosine) in the non-ionized form. The solvent systems used are DMSO-water and DMSO-TMP.

## MATERIALS AND METHODS

The sample of poly(L-tyrosine) (Pilot Chemicals, Lot T24) showed an intrinsic viscosity of 0.84 dl/g in 0.2 M NaCl at pH = 12. The molecular weight calibration of Idelson and Blout<sup>9</sup> for poly(L-glutamic acid), also in the random coil form, suggests that the molecular weight is greater than 50 000 and the sample can thus be regarded as a high polymer. The integrity of the sample was further checked by preparing the ordered conformation in aqueous solution at pH 11.2 in 0.2 M NaCl. The sample as purchased was dissolved at pH 12.5, dialysed against 10<sup>-2</sup> N HCl and lyophilized. Adding

\*CNR Postdoctoral Fellow on leave from: Istituto di Chimica, Universita degli Studi, Trieste, Italy.



alkali to pH 11.2 brought this lyophilized sample into solution. The optical rotation was then found to be in close accord with that published previously<sup>1</sup>.

DMSO for optical rotation was a BDH product 'special for spectroscopy' and was used without further purification. DMSO  $d_4$  (99.5% $d$ ) for n.m.r. and i.r. spectroscopy was an SIC product and was used directly from fresh 1 ml ampoules. TMP was a BDH product and was distilled at 93°C under 25 mmHg. The D<sub>2</sub>O was an ICI product of 99.5% $d$  isotopic purity.

All polymer solutions were prepared by dissolving the polymer in DMSO and then adding the appropriate amount of water or TMP. Most of the experiments were carried out on material that had first been dialysed against acid and then lyophilized<sup>1</sup>. This procedure was not found to affect the spectral properties in the solvent systems used and several measurements were subsequently made on untreated polymer.

### SPECTROSCOPY

Ultra-violet absorption spectra were recorded at 24°C on a Perkin-Elmer 402 spectrophotometer in 1 mm cells at polymer concentrations between 0.06 and 0.09% w/v. Optical rotation was measured on a Bendix Polarmatic 62 spectropolarimeter, using fused and jacketed quartz cells of path lengths 0.1 and 10 mm at concentrations of between 0.2 and 2% w/v. Infra-red spectra were obtained with a Grubb Parsons 'Spectromaster' using barium fluoride cells and polymer concentrations of 3–5% w/v. High temperature i.r. spectra were obtained using a Research and Industrial Instruments high temperature cell heated by water circulated from a Haake thermostat bath. Wavelength calibration was controlled by switching to single beam operation whilst scanning and obtaining a portion of the atmospheric water band close to 6  $\mu$ m. N.m.r. spectra were obtained at 220 MHz using a Varian HR-220 spectrometer and at 100 MHz using Jeolco 4H-100 and Varian HA 100 spectrometers. Internal TMS reference was used throughout.

### RESULTS

In order to establish that the polymer exists in the un-ionized phenolic form in the solvent systems studied, spectra were obtained in the ultra-violet and these are shown in *Figure 1*. In TMP, DMSO and DMSO–water the spectra show no sign of the peak at 294 nm characteristic of the ionized form (pH 13.5 in water<sup>1</sup>) and are in good agreement with those published for the polymer in TMP<sup>7,8</sup>.

For poly(L-tyrosine) in DMSO Fasman<sup>6</sup> obtained a  $b_0$  value of +494°. In the same solvent at 22°C our polymer gave  $b_0 = +300^\circ$  and on the addition of 20% water this changed to +570°, suggesting a conformational change. Since the contributions of side-chain chromophores to this parameter are by no means fully understood, we preferred simply to monitor the rotation at a single wavelength for following conformational changes. A wavelength of 345 nm represents a compromise between high

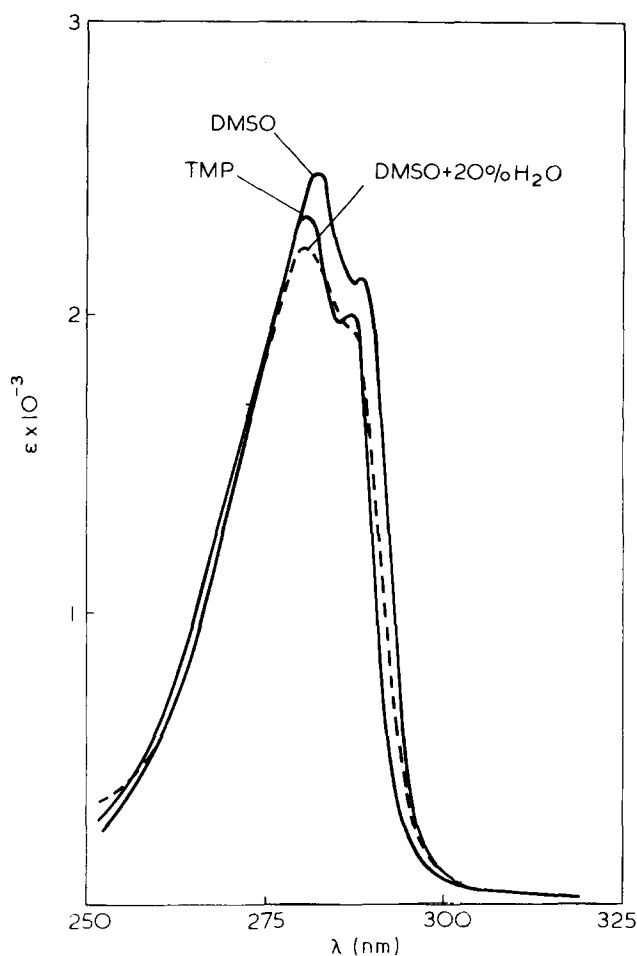


*Figure 1* Ultra-violet absorption spectra of poly(L-tyrosine) in different solvents

rotational sensitivity and adequate optical transmission. *Figure 2* shows the effect of water addition at 22 and 60°C. That a conformational transition is being observed is suggested by the sharpness of the rotational changes and by the fact that at room temperature up to 6% water has no effect upon the rotation. At water contents above 25% the polymer precipitates. A somewhat broader transition is observed at 60°C and is fully reversible; recoiling solutions from 60 to 22°C reproduced the room temperature curve. Since TMP is thought to promote the helical conformation of poly(L-tyrosine)<sup>7,8</sup>, mixtures of TMP and DMSO were studied at 345 nm and the results are given in *Figure 3*. A transition similar to that already seen on water addition to DMSO solutions is observed and the bulk of the rotational change occurs over a narrow range of solvent composition suggesting a conformational change and therefore that in DMSO the polymer is not helical.

Infra-red spectroscopy has been of increasing use in conformational studies of polypeptides in recent years and we have studied both films and solutions of poly(L-tyrosine).

Films of poly(L-tyrosine) are expected to be in a regular conformation. Damle<sup>7</sup> has shown that films cast from TMP or pyridine show parallel dichroism of amide I and perpendicular dichroism of amide II, concluding that the polypeptide is helical. We have observed similar dichroisms in films cast from pyridine and DMSO. Accurate measurement of the

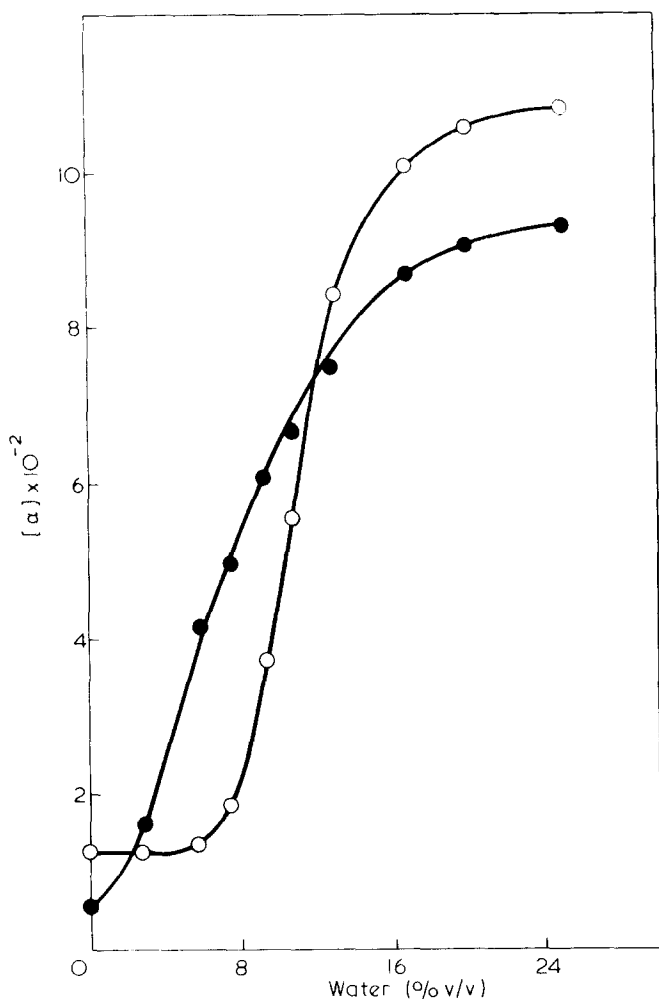


Figure 2 Optical rotation (345 nm) of poly(L-tyrosine) in DMSO-H<sub>2</sub>O solvent system : O, 22°C; ● 60°C

amide I position in films cast from pyridine, TMP and DMSO gave a value of  $1657\text{ cm}^{-1}$  in all three cases and we conclude this to be the characteristic frequency of this vibration in helical poly(L-tyrosine). Further evidence for this correlation comes from electron diffraction studies in this laboratory<sup>10</sup> of films of poly(L-tyrosine) which show the presence of a  $1.5\text{ \AA}$  meridional reflection characteristic of the  $\alpha$ -helix. The amide II band is quite distinct in these films, although of irregular shape and lies at  $1544\text{ cm}^{-1}$ . Figure 4 shows the  $6\mu\text{m}$  region of solutions of poly(L-tyrosine) in TMP and TMP/DMSO  $d_6$  1:1. The spectra are virtually identical and amide I appears as a sharp band at  $1657\text{ cm}^{-1}$ . Damle<sup>7</sup> has concluded that the polymer is helical in TMP solution and it is likely therefore that it is also helical in the 1:1 mixture with DMSO. Figure 5 shows the spectra of poly(L-tyrosine) dissolved in DMSO  $d_6$  and DMSO  $d_6$ /20% D<sub>2</sub>O. The spectrum of the polymer in the mixed solvent is very similar to that already described, showing a sharp amide I band at  $1658\text{ cm}^{-1}$  and a distinct amide II band at  $1543\text{ cm}^{-1}$ . We conclude that the polymer is largely helical in this mixed solvent. The spectrum in pure DMSO  $d_6$  is, however, very different; the maximum of the broad amide I band lies at  $1663\text{ cm}^{-1}$  and amide II is very indistinct. Although the amide I frequency is unusually high this appears to be the spectrum of a random coil con-

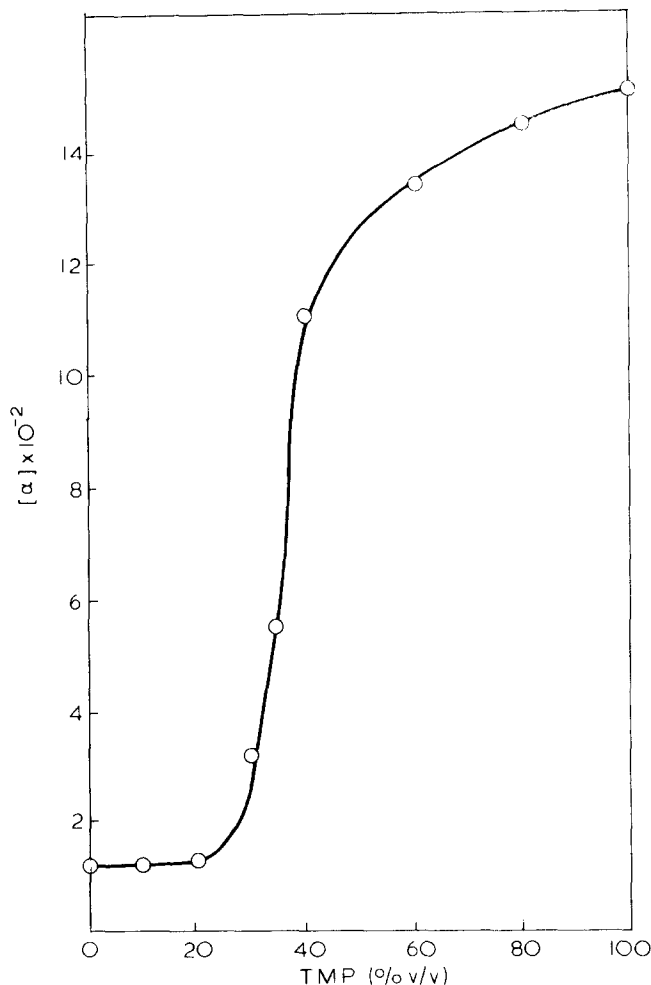


Figure 3 Optical rotation (345 nm) of poly(L-tyrosine) in DMSO-TMP solvent system at 24°C

formation. These i.r. results are thus in good accord with the proposal that poly(L-tyrosine) is random coil in DMSO and addition of 20% D<sub>2</sub>O or 50% TMP causes transition to the helical form.

All the i.r. spectra, with the exception of that in pure DMSO show a shoulder on the low frequency side of amide I that can be assigned to a small proportion ( $\approx 15\%$ ) of  $\beta$ -material. On the assumption that this is due to low molecular weight fractions, attempts were made to separate the higher molecular weights by precipitation and by dialysis, but without success. The proportion of  $\beta$ -material remained approximately constant. That poly(L-tyrosine) readily takes up the  $\beta$ -conformation has been pointed out by Patrone *et al.*<sup>3</sup>.

In an attempt to assess the validity of these conclusions drawn on the basis of i.r. frequencies we have studied several other polypeptides in DMSO  $d_6$  solution. Values of  $b_0$  and amide I positions are given in Table 1. It is known that L-aspartate polymers in the random coil form in trifluoroacetic acid (TFA) give anomalously high  $b_0$  values in the range  $-150^\circ$  to  $-260^\circ$ <sup>11</sup>. Similarly high values for these polymers in DMSO are also taken as an indication of the random coil form. A sample of very low molecular weight poly(*O*-methyl-DL-serine) was found to dissolve in DMSO  $d_6$  and the amide I and II region of the i.r. spectrum was found to be very similar indeed to that of poly(L-tyrosine) in DMSO

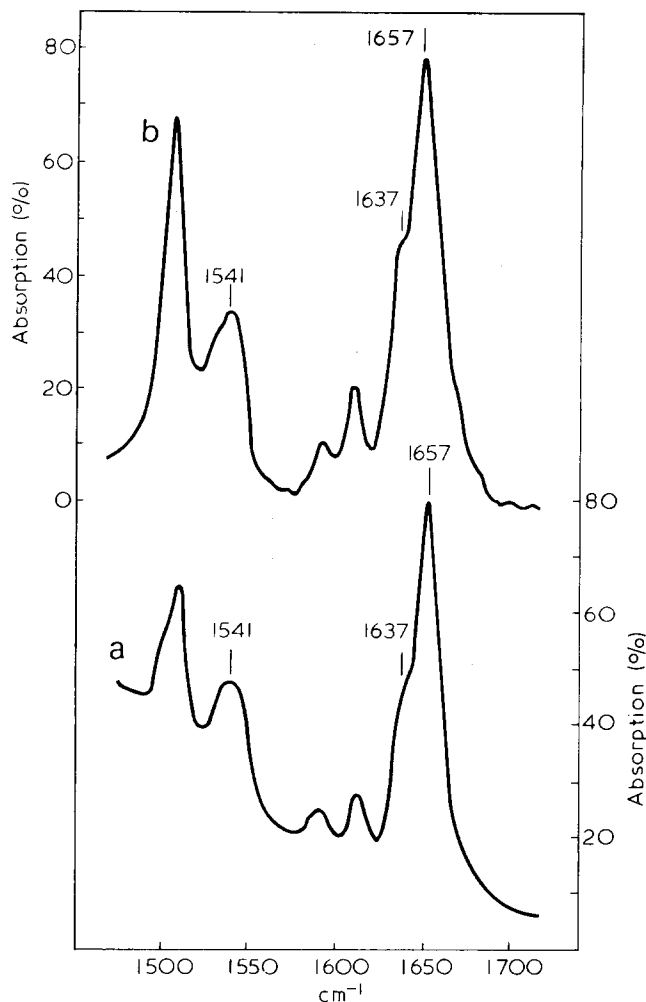


Figure 4 Infra-red spectra of poly(L-tyrosine) in solution in : (a) trimethylphosphate; (b) trimethylphosphate-dimethylsulphoxide  $d_6$  (1:1 v/v)

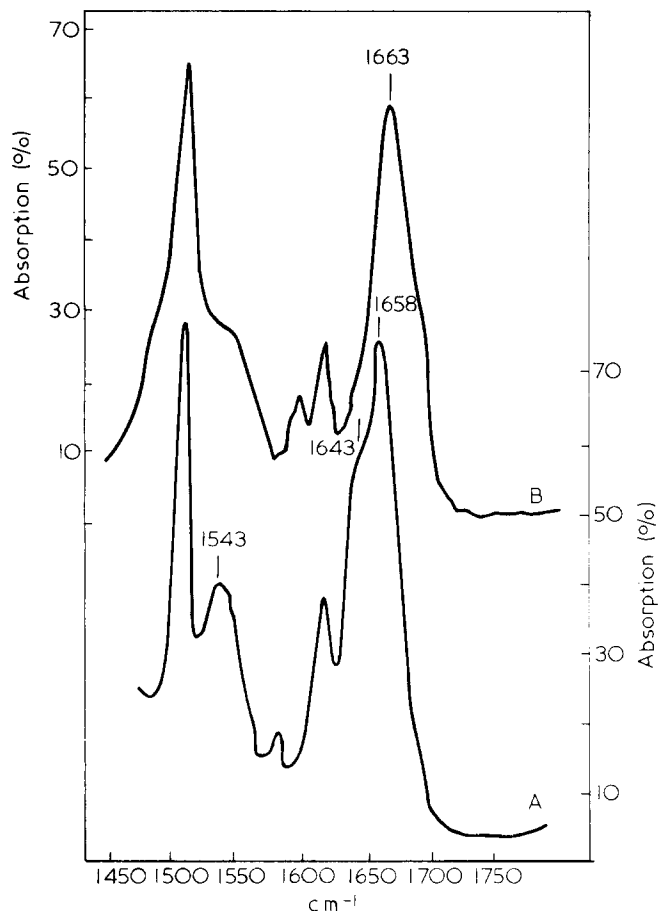


Figure 5 Infra-red spectra of poly(L-tyrosine) in solution in : (A) dimethylsulphoxide  $d_6$  - 20%  $D_2O$ . (B) dimethylsulphoxide  $d_6$

Table 1 Values of  $b_0$  and amide I positions

Polymer	Solvent	$b_0$ ( $\lambda_0 = 212\text{nm}$ )	Conformation	Amide I
Poly( $\beta$ -n-propyl-L-aspartate)	DMSO	$-160^\circ$	Random coil	$1675\text{ cm}^{-1}$
Poly( $\beta$ -benzyl-L-aspartate)	DMSO	$-130^\circ$	Random coil	$1673\text{ cm}^{-1}$
Poly(O-methyl-DL-serine)	DMSO	-	Random coil	$1666\text{ cm}^{-1}$
Poly(L-tyrosine)	DMSO	-	Random coil (?)	$1663\text{ cm}^{-1}$
Poly( $\gamma$ -benzyl-L-glutamate)	DMSO	$-570^\circ$	Helical	$1652\text{ cm}^{-1}$
Poly(L-glutamic acid)	DMSO	$-770^\circ$	Helical	$1654\text{ cm}^{-1}$
Poly( $\epsilon$ -carbobenzoxy-L-lysine)	DMSO	$-623^\circ$	Helical	$1650\text{ cm}^{-1}$
Poly(L-tyrosine)	DMSO + 20% $D_2O$	-	Helical (?)	$1657\text{ cm}^{-1}$
Poly(L-tyrosine)	DMSO : TMP (1:1)	-	Helical (?)	$1657\text{ cm}^{-1}$
Poly(L-tyrosine)	TMP	-	Helical	$1657\text{ cm}^{-1}$
Poly(L-tyrosine)	solid form	-	Helical	$1657\text{ cm}^{-1}$

$d_6$  with an amide I band at  $1666\text{ cm}^{-1}$ . L-Serine polymers have been found<sup>12</sup> not to take up helical conformations on adding chloroform to TFA solutions but to precipitate in the form of anti-parallel  $\beta$ -sheets and only the random coil form has been observed in solution. The i.r. spectrum of this polymer in DMSO  $d_6$  shows no peak at  $1635\text{ cm}^{-1}$  indicating the absence of  $\beta$ -structures. It is inferred from this that the poly(O-methyl-DL-serine) is also in the random coil form in DMSO  $d_6$  solution and the

very sharp n.m.r. spectra observed support this. For the random coil form of polypeptides in DMSO  $d_6$  therefore, the amide I positions are found in the range  $1666$  to  $1675\text{ cm}^{-1}$ . Several polypeptides that take up the right-handed  $\alpha$ -helical form in DMSO  $d_6$  have also been studied and the  $b_0$  values and amide I positions are also given in Table 1. The range of values found are in good agreement with the frequency range observed for helical polypeptide in the solid state and in chloroform solution of

1650–1658  $\text{cm}^{-1}$ <sup>13</sup> These data lend support to the suggestion that in DMSO  $d_6$  poly(L-tyrosine) is in the random coil form while in 80% DMSO : 20% D<sub>2</sub>O, 50% DMSO : 50% TMP and in TMP the polymer is most probably helical. The question then arises as to the helix sense.

The left-handed sense has been proposed by Applequist and Mahr<sup>14</sup> on the basis of dipole moment measurements. The minimum energy calculations of Ooi *et al.*<sup>15</sup> indicate that there is a preference for the right-handed sense and their proposed side-chain conformation led them to re-evaluate the dipole moment data and conclude that such measurements cannot, in this case, determine the helix sense unambiguously. The helix sense of poly(L-tyrosine) is thus a matter of considerable interest and i.r. spectroscopy can under certain circumstances give an indication of helix sense. Miyazawa *et al.*<sup>16</sup> have calculated that the left-handed form of polypeptides should show an amide I band 8  $\text{cm}^{-1}$  to higher frequencies of the right-handed form and this has been borne out by experiment both in solution and in the solid state using L-aspartate esters<sup>17</sup>. Thus left-handed poly( $\beta$ -benzyl-L-aspartate) in chloroform solution shows an amide I band at 1668  $\text{cm}^{-1}$  and at 1666  $\text{cm}^{-1}$  in films<sup>17</sup>. The right-handed form occurs in mixed alkyl/aryl esters and shows an amide I band at 1658–1659  $\text{cm}^{-1}$  films<sup>17</sup>. *Para* substitution of poly( $\beta$ -benzyl-L-aspartate) with chloro or methyl also induces the right-handed form and in chloroform solution the amide I band of these polymers lies at 1656  $\text{cm}^{-1}$  to 1657  $\text{cm}^{-1}$ <sup>18</sup>. Right-handed poly(phenethyl-L-aspartate) in chloroform solution also shows an amide I frequency of 1657  $\text{cm}^{-1}$ <sup>18</sup>. The sum total of the evidence is thus that a frequency of 1657–1658  $\text{cm}^{-1}$  for helical poly(L-tyrosine) is strongly suggestive of the right-handed helix sense. Damle<sup>7</sup> in a footnote to his paper gives amide I frequencies of films of helical poly(L-tyrosine) as  $1661 \pm 1 \text{ cm}^{-1}$ , concluding that this could indicate a left-handed helical sense. We can offer no explanation for these differences in the observed frequencies but would not have postulated the right hand sense had we observed amide I frequencies in the range 1661–1662  $\text{cm}^{-1}$ .

Additional information on the conformational behaviour of poly(L-tyrosine) has been obtained from n.m.r. studies. The 220 MHz spectrum in DMSO  $d_6$  and the changes on the addition of D<sub>2</sub>O and TMP are shown in Figures 6, 7 and 8. In DMSO  $d_6$  the peak assignments (ppm from TMS) are 7.96 ppm amide NH; 6.94 ppm aromatic *H meta* to hydroxyl; 6.59 ppm aromatic *H ortho* to hydroxyl; 4.43 ppm,  $\alpha\text{CH}$ ; 2.62 and 2.86 ppm  $\beta\text{CH}_2$  protons. It is immediately apparent that the spectrum is very sharp in DMSO, the line widths of the aromatic protons being  $\sim 3 \text{ Hz}$ , a value similar to that found for other polypeptides in TFA. Addition of TMP or 20% D<sub>2</sub>O brings about several changes in the spectrum. Firstly, marked line broadening is observed, the amide proton NH peak in particular becoming too broad to be observed. The *meta* aromatic protons show greater dipolar broadening than the *ortho* probably due to their closer proximity to the main chain. Both observations suggest a change to a more rigid conformation of the polypeptide backbone.

Secondly, several peaks show a chemical shift transition (see Figure 9) the form of which closely parallels the optical rotation changes. This is strikingly clear with the  $\alpha\text{CH}$  peak, particularly when the optical and n.m.r. data are compared for the room temperature and 55°C measurements, leaving no doubt that the same conformational changes are being observed by both techniques. The measurements at elevated temperature were made to enable the  $\alpha\text{CH}$  peak to be observed at higher D<sub>2</sub>O contents than is possible at room temperature. This is due to the large upfield shift of the water peak with increasing temperature. On the addition of  $\sim 20\%$  D<sub>2</sub>O the  $\alpha\text{CH}$  peak shifts upfield by  $\sim 0.3 \text{ ppm}$  and this can be compared with the value of  $\sim 0.5 \text{ ppm}$  well established for helix formation in polypeptides dissolved in chloroform/trifluoroacetic acid mixtures (see Bradbury *et al.*<sup>19</sup>). In water/methanol a similar shift is observed<sup>20</sup> although in water alone the shift is of much lower magnitude<sup>21,22</sup>.

Close inspection of the spectra in Figures 6 and 8 shows that the  $\alpha\text{CH}$  undergoes a marked broadening in the centre of the transition and appears to have a double peak character. This

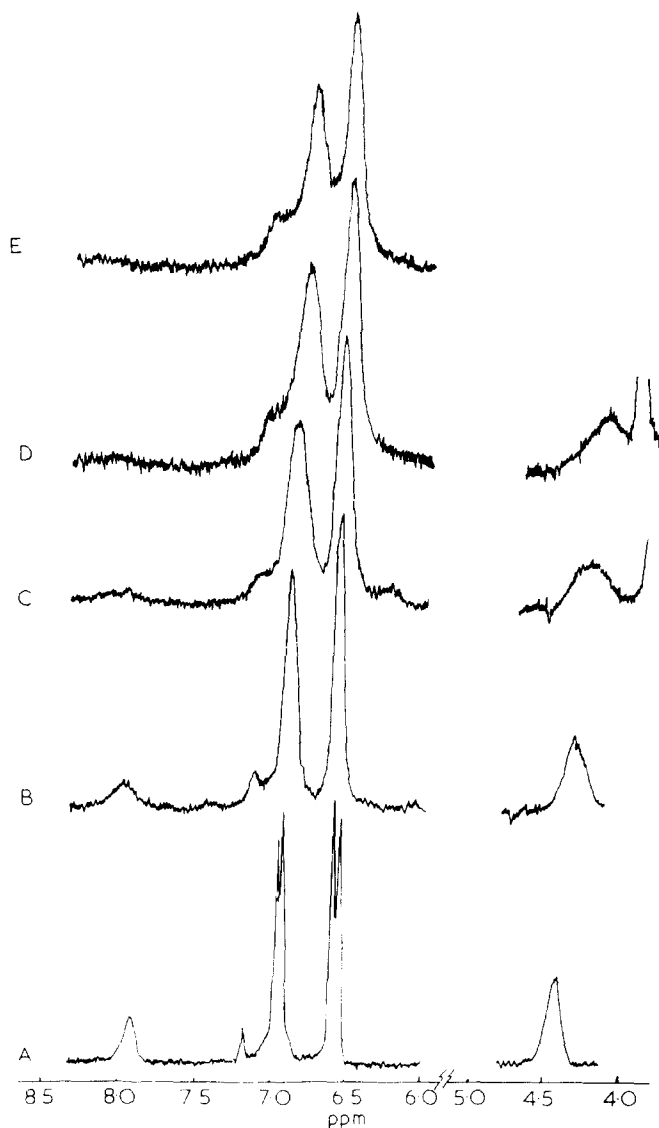


Figure 6 220 MHz proton magnetic resonance spectra 4.0–8.5 ppm of poly(L-tyrosine) in DMSO  $d_6$ /D<sub>2</sub>O solvent system at 22°C. % D<sub>2</sub>O: A,0; B,9; C,11; D,15; E,22

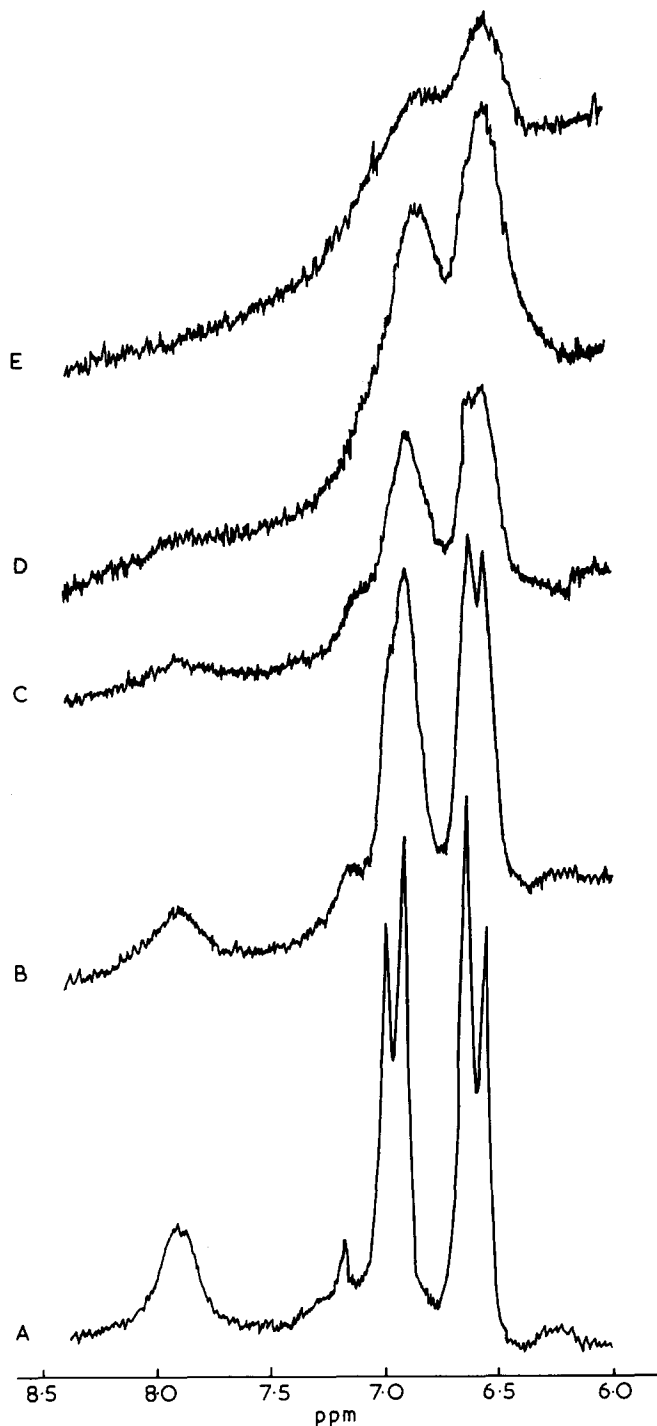


Figure 7 100 MHz proton magnetic resonance spectra 6.0–8.5 ppm of poly(L-tyrosine) in DMSO  $d_6$ /TMP solvent system at 29°C. % TMP : A,0; B,20; C,25; D,30; E,60.

behaviour is frequently observed in the spectra of polypeptides undergoing helix  $\rightarrow$  coil transition. Although there are several explanations of this behaviour evidence<sup>23</sup> now supports the proposal of Ullman<sup>24</sup> that it results from polydispersity in the sample. The existence of this behaviour for poly(L-tyrosine) strongly suggests that a coil  $\rightarrow$  helix transition is taking place on the addition of D<sub>2</sub>O or TMP to DMSO solutions.

The behaviour of the sidechain proton resonances on adding D<sub>2</sub>O or TMP to the DMSO solutions are of interest. The  $\beta$ -protons show marked changes in chemical shift and width over the composition range corresponding to the conformational transition. In

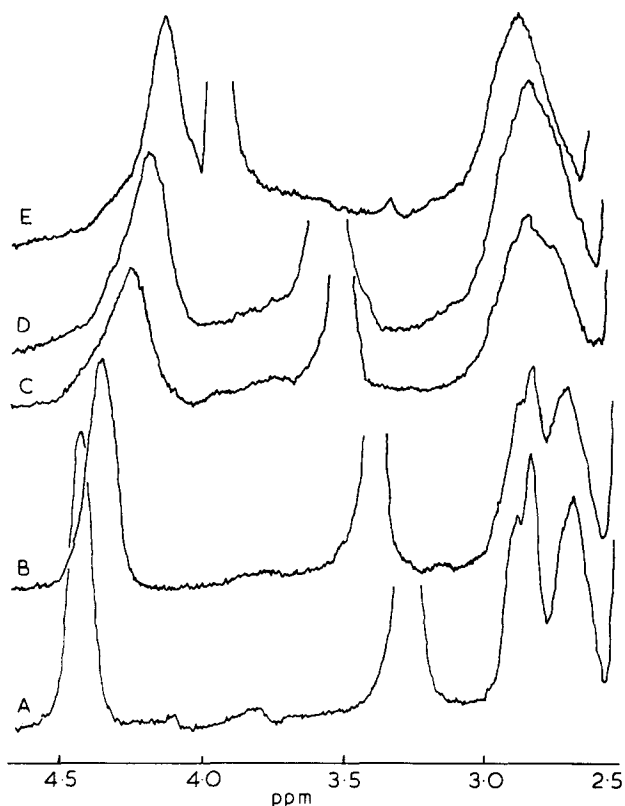


Figure 8 220 MHz spectra, 2.50 to 4.50 ppm, of poly(L-tyrosine) in DMSO/D<sub>2</sub>O mixtures at 55°C. A, pure DMSO ; B, 3.9% D<sub>2</sub>O; C, 5.7% D<sub>2</sub>O; D, 6.7% D<sub>2</sub>O; E, 18.7% D<sub>2</sub>O

pure DMSO  $d_6$  the AB part of an ABX system is observed having  $\Delta \sim 0.20$  ppm. Addition of D<sub>2</sub>O has little effect upon the low field doublet; however, the upfield doublet moves downfield ( $\Delta$  being reduced) and also shows greater broadening than does the lowfield doublet. Although no detailed interpretation of these changes in structural terms is possible, it does indicate a large change in molecular symmetry in the region of the  $\beta$ CH<sub>2</sub> group as the D<sub>2</sub>O is added.

The *ortho* and *meta* proton resonances show different behaviour through the D<sub>2</sub>O and TMP induced transition. Except for small broadening effects the *ortho* proton peak is found to undergo only a very small change in chemical shift. For the *meta* proton resonance peak larger effects are observed. There is a more marked broadening, possibly changes in peak shape and an upfield shift of 0.15 ppm. Since the mobilities of the *ortho* and *meta* protons in the ring are the same the differences observed for the *meta* protons must be attributed to their closer proximity to the polypeptide backbone. Possibly the transition from a flexible random coil to a more rigid conformation leads to the *meta* protons being more efficiently relaxed by their proximity to the asymmetry of a helical conformation. The presence of tyrosyl-tyrosyl interactions has been suggested for helical poly(L-tyrosine) from optical spectroscopic studies. Regular interactions between aromatic rings which exists for the helical but not the random coil conformation might be expected to be detected in a difference in the magnetic environment of the aromatic protons and hence a chemical shift difference on going through the transition from the random coil to the more ordered form. As the behaviour of the *meta* protons resonances is made more complicated by the

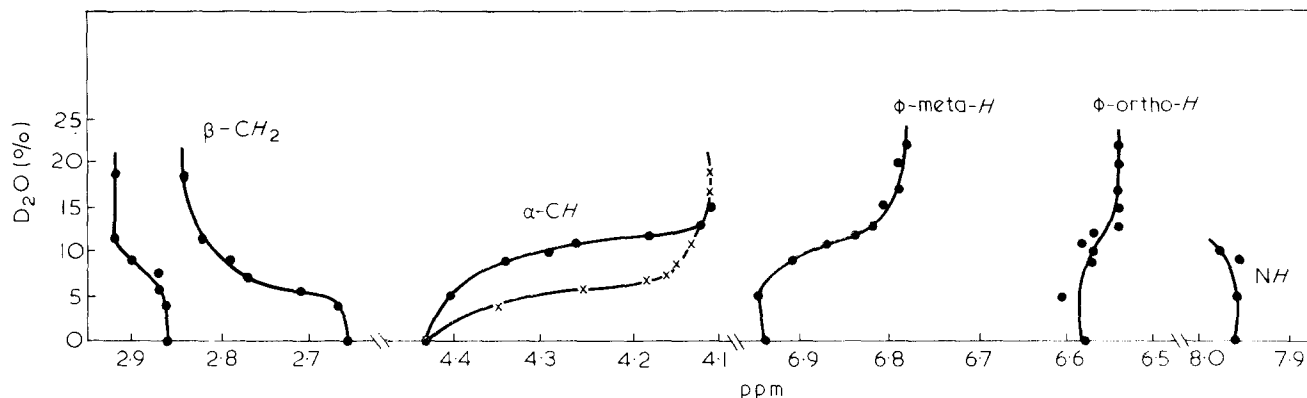


Figure 9 Chemical shift values for poly(L-tyrosine) in DMSO /D<sub>2</sub>O mixtures at ● 22°C; X 55°C

presence of the adjacent  $\beta\text{CH}_2$  and the closer proximity of the polypeptide backbone the effect of the interactions of aromatic rings should be sought in the behaviour of the resonances of the *ortho* protons. There is little, however, in this behaviour to suggest the presence of aromatic ring interactions. The *ortho* protons resonance peak shows a very small chemical shift difference and the small broadening to be expected for a transition of the polypeptide to a more rigid conformation. It should be noted, however, that the time scale of the optical spectroscopic techniques is very much shorter than for magnetic resonance techniques and interactions may exist for a sufficiently short time to be observable by o.r.d. and c.d. but not by n.m.r.

The complete shift data presented in Figure 9 clearly shows evidence for a change in conformation of poly(L-tyrosine) as 20% D<sub>2</sub>O is added to a DMSO *d*<sub>6</sub> solution. The sum total of the spectroscopic evidence strongly indicates that this transition is from the random coil to a helical conformation. The same changes are observed as TMP is added to a DMSO *d*<sub>6</sub> solution. It is not possible to state with complete surety that transition to a 100% helical form is achieved with our polymer sample in these solvent systems. Whilst the n.m.r. peak positions, in particular the  $\alpha\text{CH}$  show little change as greater than 15% D<sub>2</sub>O is added and the optical rotation behaves similarly, neither measurement has an absolute calibration appropriate to the system, as for example is possible with many polypeptides using the  $b_0$  parameter. Comparison of the width of the  $\beta\text{CH}_2$  and  $\alpha\text{CH}$  peaks in DMSO *d*<sub>6</sub>/20% D<sub>2</sub>O with that of fully helical poly( $\gamma$ -benzyl-L-glutamate) of similar molecular weight suggests that the polymer is largely but not fully helical. Thus although a limiting conformation is clearly obtained in 20% D<sub>2</sub>O and 50% TMP, the present evidence does not constitute definitive proof of a fully helical structure.

## CONCLUSIONS

The spectroscopic evidence presented above shows that poly(L-tyrosine) in DMSO *d*<sub>6</sub> is in the random coil conformation. Addition of 20% D<sub>2</sub>O or TMP results in a conformational transition to a largely though probably not a fully helical conformation. The i.r. frequencies for the amide I of the ordered form lie in the range of frequencies found for a right-handed  $\alpha$ -helix.

## ACKNOWLEDGEMENTS

This work was supported by the Science Research Council of Great Britain. One of us (V.G.) is grateful to Consiglio Nazionale delle Ricerche, Roma, (Italy) for a Fellowship.

We are grateful to the NMR laboratory of CNR, Arco Felice, Naples, Italy for several spectra and to Dr E. Patrone for a copy of his manuscript prior to publication.

## REFERENCES

- 1 Fasman, G. D., Bodenheimer, E. and Lindblow, C. *Biochemistry* 1964, **3**, 1665
- 2 Beychok, S. and Fasman, G. D. *Biochemistry* 1964, **3**, 1675
- 3 Patrone, E., Conio, G. and Brighetti, S. *Biopolymers* 1970, **9**, 897
- 4 Coombes, J. D., Katchalski, E. and Doty, P. *Nature* 1960, **185**, 534
- 5 Downie, A. R., Elliott, A. and Hanby, W. E. *Nature* 1959, **183**, 110
- 6 Fasman, G. D. *Nature* 1962, **193**, 681
- 7 Damle, V. N. *Biopolymers* 1970, **9**, 937
- 8 Quadrioglio, F., Ius, A. and Crescenzi, V. *Makromol. Chem.* 1970, **136**, 241
- 9 Idelson, M. and Blout, E. R. *J. Am. Chem. Soc.* 1958, **80**, 4631
- 10 Baldwin, J. and McLuckie, I. personal communication
- 11 Bradbury, E. M., Downie, A. R., Elliott, A. and Hanby, W. E. *Proc. R. Soc. (A)* 1960, **259**, 110
- 12 Bradbury, E. M., Elliott, A. and Hanby, W. E. *J. Mol. Biol.* 1962, **5**, 487
- 13 Bamford, C. H., Elliott, A. and Hanby, W. E. 'Synthetic Polypeptides', Academic Press, New York, 1956, p 157
- 14 Applequist, J. and Mahr, T. G. *J. Am. Chem. Soc.* 1966, **88**, 5419
- 15 Ooi, T., Scott, R. A., Vanderkooi, G. and Scheraga, H. A. *J. Chem. Phys.* 1967, **46**, 4410
- 16 Miyazawa, T., Fukushima, K., Sugano, S. and Masuda, Y. 'Conformation of Biopolymers', (Ed. G. N. Ramachandran), Vol. 2, Academic Press, New York, 1967
- 17 Bradbury, E. M., Carpenter, B. G. and Stephens, R. M. *Biopolymers* 1968, **6**, 905
- 18 Hashimoto, M. and Arakawa, S. *Bull. Chem. Soc. Japan* 1967, **40**, 1698
- 19 Bradbury, E. M., Crane-Robinson, C., Goldman, H. and Rattle, H. W. E. *Nature*, 1968, **217**, 812
- 20 Boublik, M., Bradbury, E. M., Crane-Robinson, C. and Rattle, H. W. E. *Eur. J. Biochem.* 1970, **12**, 258
- 21 Markley, J. L., Meadows, D. H. and Jardetzky, O. *J. Mol. Biol.* 1967, **27**, 25
- 22 Bradbury, E. M., Crane-Robinson, C., Goldman, H. and Rattle, H. W. E. *Biopolymers* 1968, **6**, 851
- 23 Bradbury, E. M., Crane-Robinson, C. and Rattle, H. W. E. *Polymer* 1970, **11**, 277
- 24 Ullman, R. *Biopolymers* 1970, **9**, 471

# Interchain force field and elastic constants of polytetrafluoroethylene

J. F. Twisleton and J. W. White

Physical Chemistry Laboratory, Oxford University, South Parks Road, Oxford, OX1 3QZ, UK

(Received 7 June 1971)

Neutron inelastic scattering spectroscopy has been used to determine the phonon dispersion curve for longitudinal lattice vibrations perpendicular to the chain axes in hexagonal polytetrafluoroethylene at 25°C. By the nature of the method measurements are confined to the microcrystalline regions of the polymer and in addition to providing information about the intermolecular force field it is possible to calculate the crystalline elastic constant,  $C_{11}$ , perpendicular to the chains as  $18.2 + 0.2 \times 10^{10}$  dyne  $\text{cm}^{-2}$ .

We report here a measurement of the  $[10\bar{1}0]$  phonon dispersion curve for lattice vibrations perpendicular to the chain axes in hexagonal polytetrafluoroethylene (PTFE). This leads to the elastic stiffness constant  $C_{11}$  for the basal plane of the crystal and can be used to obtain parameters of the intermolecular force field. The method of cold neutron inelastic scattering used<sup>1-3</sup> ensures that the stiffness measured is that of crystalline regions in the polymer and it is expected that this value of the modulus will be larger than that for bulk polymer<sup>3</sup>.

No measurements of this quantity have been reported using any other method presumably owing to experimental difficulties<sup>4</sup>.

For the fibre axis direction the interchain force field has been probed by laser Raman scattering below and above the 19°C phase transition<sup>5</sup>. Elastic moduli along the chain direction have also been calculated<sup>5-6</sup> and measured<sup>4</sup>. Neutron inelastic scattering<sup>7</sup> has confirmed the calculated dispersion curve for the  $\nu_8$  (chain longitudinal acoustic) branch in this direction. The present measurements in the perpendicular direction have used fibres and polycrystalline material, characterized by neutron diffraction. The  $a$  and  $c$  parameters were in agreement with accepted<sup>8</sup> values (5.66 and 19.5 Å respectively) and the crystallinity was greater than 95% in each case. The anisotropy and hexagonal symmetry of the system allow separate assignments to be made of phonon singularities in the neutron coherent scattering spectra for both isotropic, polycrystalline and fibre specimens.

Neutron scattering experiments were performed on the 6H cold neutron spectrometer<sup>9</sup> and a rebuilt version of the 4H5, cold neutron scattering apparatus<sup>10</sup> at AERE, Harwell. The large solid angle counter bank of the 6H instrument was used for high intensity but relaxed momentum resolution studies and the phonon arc<sup>10</sup> of 4H5 for high momentum resolution in the scattered neutron wave vector. In the spectrometers, the neutron beam incident on the

sample has a well defined wavevector modulus  $|\mathbf{k}_0|$ , ( $\Delta\lambda/\lambda$  5%) but a divergence of  $\pm 1^\circ$ . The beam is therefore quite bright and the scattered intensity correspondingly large. The resolution obtained for the total momentum transfer,  $\mathbf{Q} = \mathbf{k} - \mathbf{k}_0$  can be chosen to suit the mosaic spread of the scatterer by opting for either large or small scattered angular resolution detectors. This combination of properties has been most valuable for optimizing coherent scattering measurements from our polymers where 'mosaic' spread may be as high as  $30^\circ$ .

In a typical experiment at lower scattering angular resolution the time of flight spectra of scattered neutrons are recorded simultaneously in counters at thirteen different scattering angles between  $7^\circ$  and  $90^\circ$  to the incident beam (*Figure 1* shows the spectra at some of these angles). For incident  $5.0 \text{ \AA}$  neutrons the momentum transfer  $\mathbf{Q}$  approached that for the prismatic  $[1010]$  Bragg reflection of polytetrafluoroethylene at high scattering angles. The momentum transfer conditions prevailing for coherent inelastic scattering<sup>12</sup> were

$$\mathbf{Q} = 2\pi\boldsymbol{\tau} - \mathbf{q} \quad (1)$$

where  $\boldsymbol{\tau}$  is the reciprocal lattice vector for the  $[10\bar{1}0]$  planes and  $\mathbf{q}$  is the momentum of a phonon annihilated in the scattering. All phonons satisfying the condition may contribute to the scattering spectrum but because of the limited range of momentum transfer attainable with cold neutron up scattering (energy gain) and because of the neutron structure factors of hexagonal polytetrafluoroethylene, a simplification of the observations occurs.

The intensity of coherent inelastic scattering is given by the square of the modulus of the dynamical structure factor  $g_j(\mathbf{Q})$

$$g_j(\mathbf{Q}) = \sum_D \left( \frac{\mathbf{k}}{2NM_D\omega_j} \right)^{1/2} \cdot b_D |C_{jD}(\mathbf{Q})| \exp[2\pi i(\mathbf{Q} \cdot \mathbf{R}_D)] \quad (2)$$

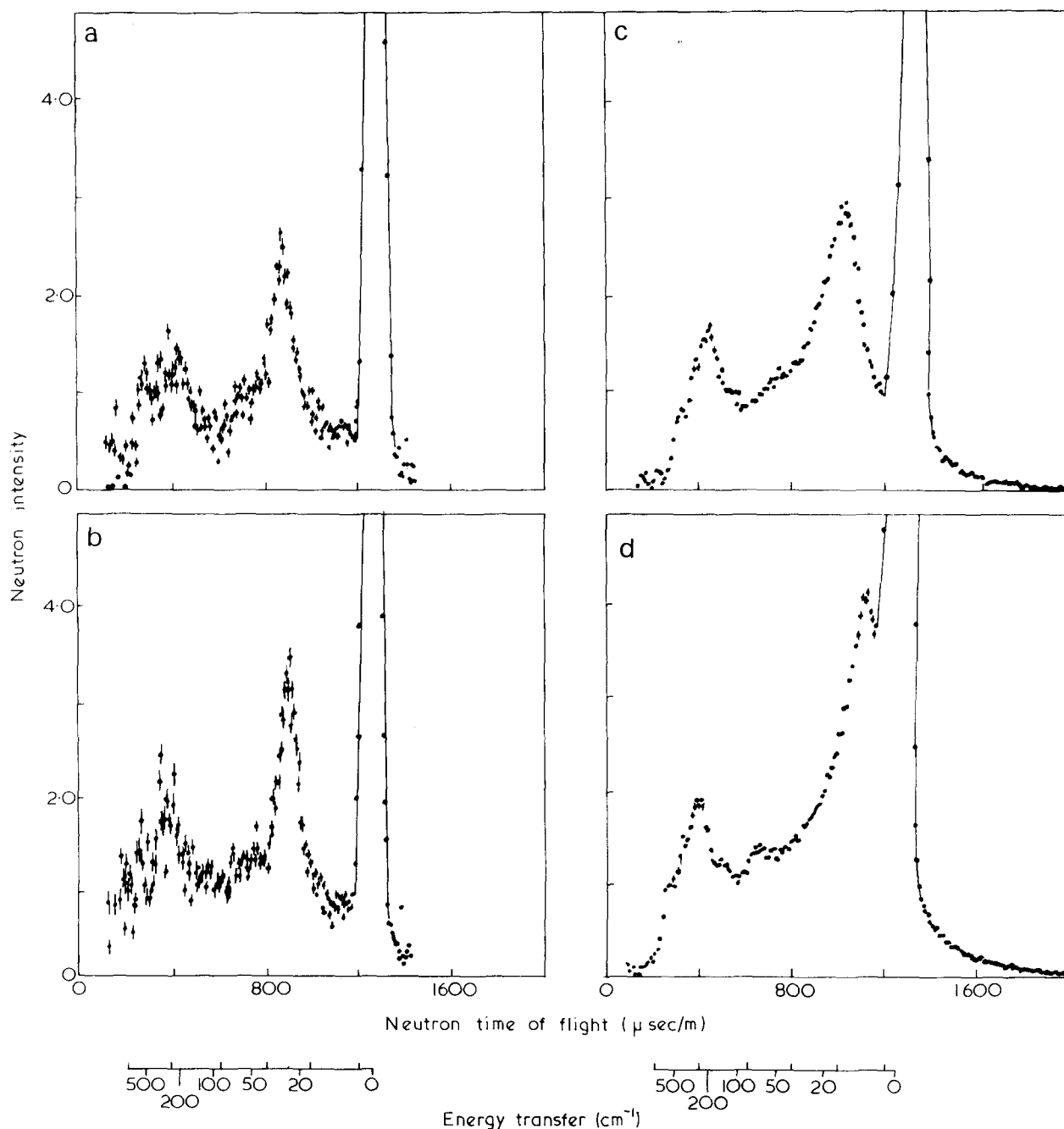


Figure 1 Time of flight spectra for polycrystalline, hexagonal polytetrafluoroethylene at scattering angles (a)  $27^\circ$ , (b)  $36^\circ$ , (c)  $45^\circ$  and (d)  $54^\circ$  to the incident  $5.0 \text{ \AA}$  neutron beam at 296 K. The phonon cut-off is at  $\sim 900 \mu\text{sec}$  for scattering at  $\theta = 36^\circ$ .

where  $b_v$  is the scattering length,  $\mathbf{R}_v$  the atomic position and  $\mathbf{C}_{jv}$  the amplitude of motion, in the  $j$ th vibrational mode of atom  $v$ , mass  $M_v$ , in a crystal vibration of wave vector,  $\mathbf{q}$ , determined by equation (1).  $N$  is the total number of atoms in the unit cell. For acoustic vibrations the effect of the last term is to enhance the scattered intensity when  $\mathbf{Q}$  approaches  $2\pi\tau$  for a strongly reflecting set of planes.

The optic modes of vibration are conversely affected. The remaining scalar product term determines the relative intensities of the transverse and longitudinal acoustic modes near a strong Bragg reflection as in our experiments. The effect of this term is to give the longitudinal phonon maximum enhancement when  $\mathbf{Q}$ ,  $\mathbf{q}$  and  $2\pi\tau$  are collinear, at which point the transverse modes are suppressed.

For a constant  $|\mathbf{Q}|$  experiment the resulting energy spectrum has a low frequency cut-off corresponding to the longitudinal acoustic mode of wave vector  $2\pi|\tau| - |\mathbf{Q}|$ . This is a consequence of the nature of the dispersion relationship  $\omega(\mathbf{q})$  which is a rising function of  $\mathbf{q}$  for acoustic modes. As for the contribution of the transverse modes, they have a cut-on at lower frequencies in the spectrum rising continuously from zero and hence have no distinguishable features. The possibility of the transverse features obscuring the longitudinal cut-off may be eliminated by a theoretical treatment<sup>2</sup>.

The steps taken in characterizing the coherent features in PTFE time of flight spectra are then as follows: (a) the anisotropy and high symmetry of the unit cell lead to a diffraction picture with only one



strong reflection at low momentum transfers. This corresponds to the inter-chain spacing; (b) acoustic phonons are only observable when excited in the region of a strong Bragg reflection and there is but one here; (c) the longitudinal phonons are alone characterized by a singularity, on account of the scalar product term in equation (2). This applies especially when the basis has the high symmetry exhibited here.

The time of flight spectra of PTFE powder and fibres were measured in the hexagonal phase at 25°C. A wide range of reciprocal space was covered in experiments at wavelengths between 3.5 and 6 Å. A strong coherent feature appeared which moved to lower frequency with increasing scattering angle (Figure 1), ( $Q$  increasing in equation (1)). This feature evolves into the  $[10\bar{1}0]$  Bragg peak at higher angles and is identified as the longitudinal cut-off, which is convoluted with a Gaussian resolution function. Differing neutron flight paths from the large samples are an important contribution to this function. The peak maximum is taken as the longitudinal edge and  $q_{\min}$  evaluated from equation (1).

The phonon frequencies and wavevectors are plotted on the dispersion curve (Figure 2). It can be seen

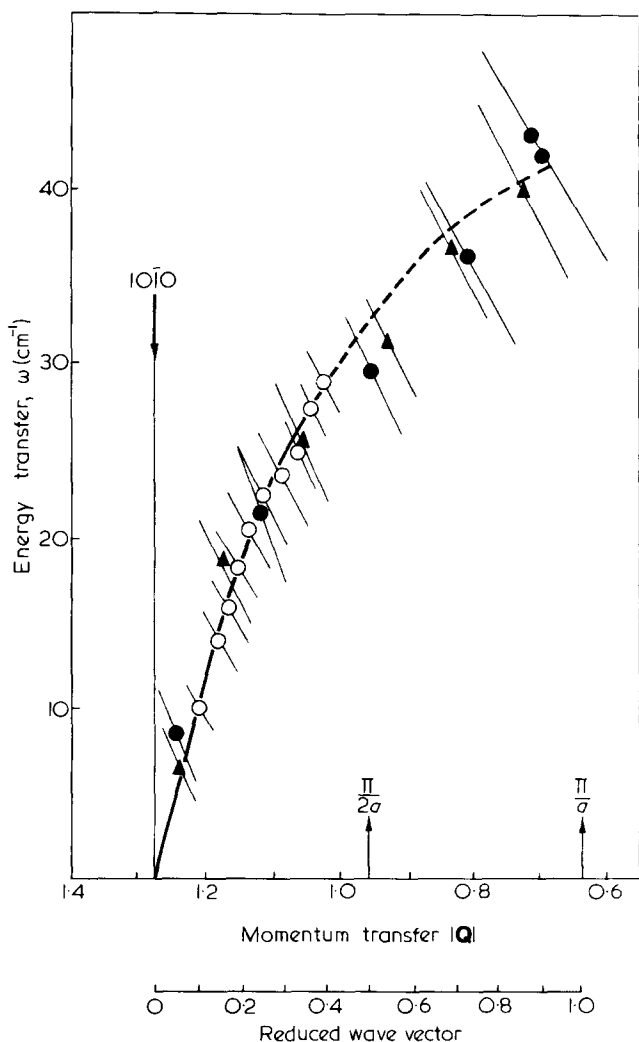


Figure 2 Dispersion curve for the longitudinal acoustic mode along  $[10\bar{1}0]$  in hexagonal polytetrafluoroethylene. Polycrystalline data : ●, 4.1 Å; ▲, 5.0 Å data. Fibre specimen : ○, 0.5-8 Å data.

that the phonon of zero frequency (elastic scattering) occurs at an extrapolated  $|Q|$  value equal to  $2\pi\tau$  for the  $[10\bar{1}0]$  reflection and it is on this basis that the phonon branch is assigned. Maximum possible error bars are shown on instrumental  $(Q, \omega)$  tracks, which fall at an acute angle to the dispersion surface for constant scattering angle experiments. From the sharpness of the phonon cut-offs (Figure 1) it can be seen that confidence in the experimental points is rather greater than the error bars indicate. The phonon peaks at higher scattering angles appear broader than at low angles (high energy transfers) because of the non-linear energy scale.

Within present experimental momentum and energy resolution the points from the fibre experiments (with  $Q$  in the basal plane) and the polycrystalline sample were superimposable. This confirms the exclusion of contributions from intramolecular and transverse modes. There is some evidence to suggest that the curve has an inflection near the half zone point. Further data to investigate this suggestion of long range forces are being gathered. The dispersion curve approaches the zone edge at  $42 \pm 2 \text{ cm}^{-1}$ .

From the slope at low  $|q|$  we find that the high frequency velocity of sound is  $2.77 \pm 0.10 \times 10^5 \text{ cm sec}^{-1}$  ( $2.77 \times 10^3 \text{ M sec}^{-1}$ ) whereas for the chain axis it is  $9.74 \pm 0.10 \times 10^5 \text{ cm sec}^{-1}$  ( $9.74 \times 10^3 \text{ M sec}^{-1}$ ). Using a crystalline density of  $2.342 \text{ g cm}^{-3}$  the corresponding values of  $C_{11}$  and  $C_{33}$  are  $18.2 \pm 0.2 \times 10^{11} \text{ dyne cm}^{-2}$  and  $222 \pm 1 \times 10^{10} \text{ dyne cm}^{-2}$ . The ratio ( $\approx 1/12$ ) is much greater than for polyethylene for which neutron scattering (on deuterio-polyethylene) gives a ratio of about  $1/20^{2,3}$ .

#### ACKNOWLEDGEMENTS

We thank Mr H. Willis (ICI Plastics, Welwyn) for a sample of high crystallinity unsintered Fluon and Dr H. W. Starkweather (E. I. du Pont de Nemours, Wilmington, USA) for a sample of Teflon fibres.

#### REFERENCES

- 1 Cocking, S. J. and Guner, Z. 'Inelastic Scattering of Neutrons in Solids and Liquids', IAEA, Vienna, 1963, Vol 1, p 237
- 2 Twisleton, J. F. Thesis, Oxford University, 1970; Twisleton, J. F. and White, J. W. 'Inelastic Scattering of Neutrons', IAEA, Grenoble, 1972
- 3 Holliday, L. and White, J. W. *Pure Appl. Chem.* 1971, **27**, No. 2
- 4 Sakurada, I., Ito, T. and Nakamae, K. *J. Polym. Sci. (C)* 1966, **27**, 15, 75
- 5 Koenig, J. L. and Boerio, F. J. *J. Chem. Phys.* 1969, **50**, 2823
- 6 Shimanouchi, T., Asahina, M. and Enomoto, S. *J. Polym. Sci.* 1962, **59**, 93
- 7 LaGarde, V., Prask, H. and Trevino, S. *Discuss. Faraday Soc.* 1969, **48**, 15
- 8 Clarke, E. S. and Muus, L. T. *Z. Phys. Chem.* 1962, **117**, 119
- 9 Bunce, L. J., Harris, D. H. C. and Stirling, G. C. *AERE Res. Rep.* R-6246, 1970
- 10 Harris, H. H. C., Cocking, S. J., Egelstaff, P. A. and Webb, F. J. 'Inelastic Scattering of Neutrons in Solids and Liquids', IAEA, Vienna, 1963, Vol 1, p 107
- 11 Pyn, R. and Squires, G. 'Inelastic Scattering of Neutrons in Solids and Liquids', IAEA, Copenhagen, 1968, Vol 1, p 215
- 12 Lomer, W. M. and Low, G. G. E. 'Thermal Neutron Scattering', (Ed. Egelstaff, P. A.) Academic Press, London and New York, 1965, Ch 1

## Modifications to the morphology of poly(*m*-phenylene adamantane-1,3-dicarboxamide) fibres

D. E. Montgomery, K. Tregonning and P. R. Blakey  
 Department of Textile Industries, University of Bradford Bradford 7, UK  
 (Received 4 August, 1971; revised 17 September 1971)

The introduction of orientation and crystallinity into thermally stable fibres has a significant effect upon the physical properties of these fibres. For example, orientation in aromatic polyamides produces high values of initial modulus and tenacity and these high values are more readily maintained at elevated temperatures in crystalline fibres than in amorphous fibres<sup>1</sup>.

Thermally stable fibres have recently been produced<sup>2</sup> from poly(*m*-phenylene adamantane-1,3-dicarboxamide)[poly(*m*-PAD), *Figure 1*] and a report is given here of attempts to introduce morphological changes, in the form of increased orientation and crystallinity, into these amorphous poly(*m*-PAD) fibres.

The effect of the various treatments upon the supermolecular structure of the fibres could be followed by noting the changes occurring in both the X-ray diffraction pattern and also the stress-strain curves obtained from the fibres.

### PRODUCTION OF FIBRES

#### *Extrusion*

A small-scale wet spinning machine was used to produce fibres by the extrusion of a solution of poly(*m*-PAD) in dimethylformamide containing 5% (w/w) lithium chloride. A 25% (w/w) solution of poly(*m*-PAD) in dimethylformamide (containing 5% LiCl) was extruded through a five-hole spinneret into a bath containing 60% (w/w) dimethylformamide in water at 16°C. The polymer had an inherent viscosity of 1.48 dl/g when measured (Sewell, J.H. personal communication) at 27°C as a 0.5% (w/v) solution in sulphuric acid of density 1.84 g/ml. After coagulation, the five filaments were washed in a second bath containing water at 60°C before being packaged on a modified Leesona 950 take-up machine. The packaged filaments were further washed in distilled water and then dried in a forced-draught oven.

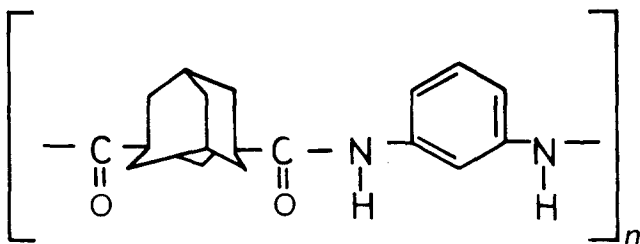


*Figure 1* Poly(*m*-phenylene adamantane-1,3-dicarboxamide)

#### *Drawing*

Optimum drawing conditions were determined on an Instron tensile tester. Specially designed jaws were used to hold short lengths of fibre in intimate contact with a hot plate mounted on the Instron cross-head. The fibres were then drawn against the hot-plate at various rates and temperatures and the optimum conditions were deduced from reinforcement data collected from the stress-strain traces. These data were then confirmed by drawing longer lengths of fibre on a small-scale continuous drawing machine and measuring the tensile properties of the fibres produced. Good fibres were produced at a temperature of 325°C and a draw rate of 100 000% min<sup>-1</sup>.

### RESULTS OF MORPHOLOGICAL CHANGES

#### *Heat treatment*

The as-spun fibres were uniform and free of voids; typical stress-strain characteristics are illustrated in *Figure 2*. The X-ray diffraction pattern (*Figure 3*) showed that the fibres were unoriented and of very low crystallinity.

Many polymers crystallize when exposed to temperatures between the glass transition temperature

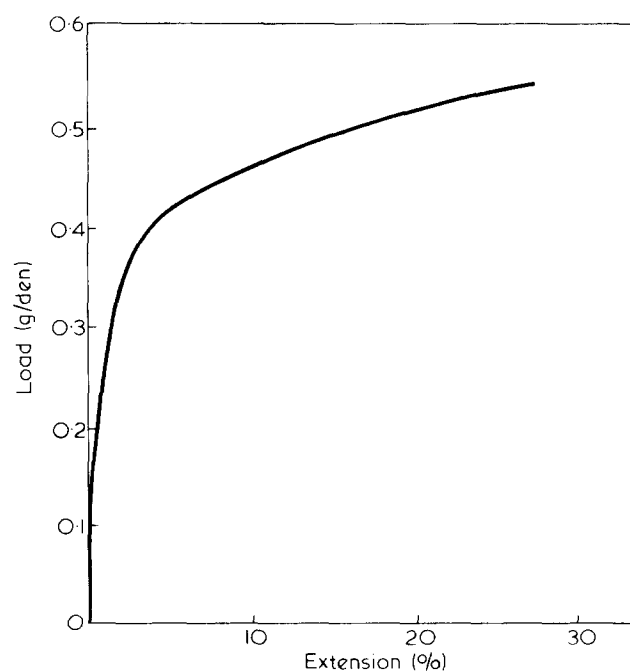


*Figure 2* Stress-strain curve given by amorphous fibre

and the melting point<sup>3</sup> but this was not found to be the case with poly(*m*-PAD). As-spun fibres heated to 330°C ( $T_g$  311–317°C) gave an X-ray diffraction pattern which is unchanged from that of the as-spun fibres. At temperatures above 330°C the fibres degraded rapidly and meaningful comparisons become difficult to make.

Drawing over a hot plate by the technique described previously gave fibres with a tenacity of 3.7 g/den, an initial modulus of 77 g/den and a break elongation of 10%; this is reflected in the X-ray pattern (Figure 4) which shows a certain degree of orientation. These drawn fibres, however, still show very little crystallinity.

#### Solvent treatment

Crystallinity may also be induced in polymeric materials by exposure to suitable organic liquids in the vapour phase<sup>4,5</sup> and attempts were made to

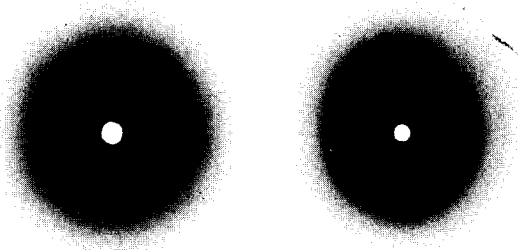


Figure 3

Figure 4

Figure 3 Untreated, as-spun fibre

Figure 4 Fibre drawn  $\times 7.6$  at 325°C

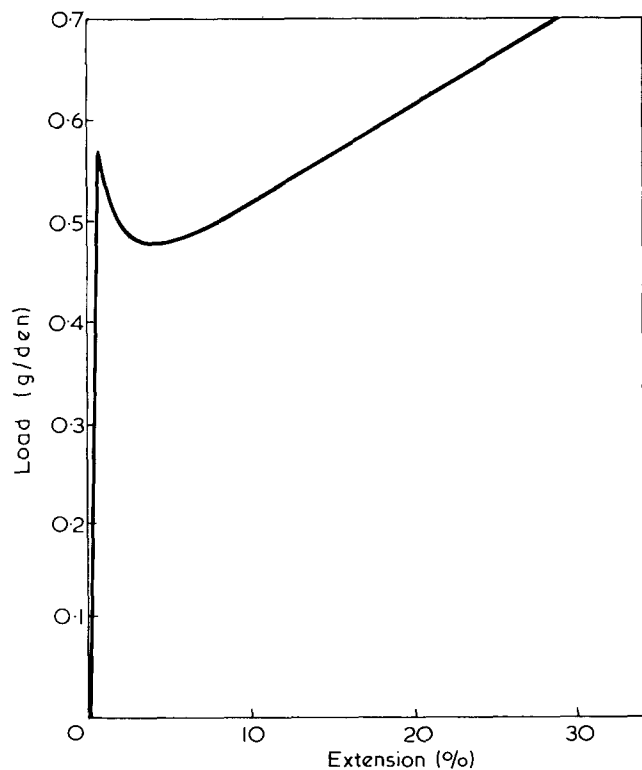


Figure 5 Stress-strain curve given by crystalline fibre

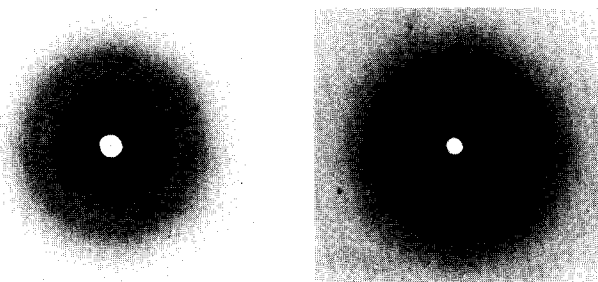


Figure 6

Figure 7

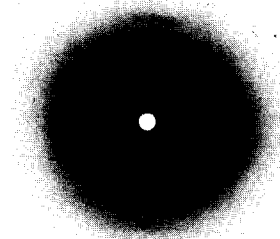


Figure 8

Figure 6 Undrawn fibre, exposed to dimethylformamide vapour

Figure 7 Undrawn fibre, exposed to dimethylacetamide vapour

Figure 8 Drawn fibre, then exposed to dimethylformamide vapour

crystallize poly(*m*-PAD) fibres in this way. Dimethylformamide was placed in the bottom of an empty desiccator and as-spun fibres were placed in the top, so that they were exposed to the dimethylformamide vapour. After about an hour, the fibres, which were initially opaque, had become translucent and when tested later on the Instron tensile tester, the stress-strain curves were found to be completely different in character to those of the original fibres, as Figure 5 shows. The fibres now exhibited cold drawing and Figure 6 indicates that crystallinity had been introduced.

The introduction of crystallinity was not specific to dimethylformamide. Exposure to dimethylacetamide for a similar length of time also induced crystallinity, as Figure 7 shows, but it is evident that the crystal structure is different in this case.

Having shown that crystallinity could be induced in as-spun fibres attempts were then made to crystallize drawn fibres. Orientation had the effect of increasing significantly the rate at which the crystallizing process took place and the crystalline fibres shown in Figure 8 were produced within a matter of seconds of being exposed to dimethylformamide.

#### ACKNOWLEDGEMENTS

We would like to acknowledge the financial assistance supplied by the Ministry of Technology (and later the Ministry of Defence) for part of this work.

#### REFERENCES

- 1 Du Pont, Br. Pat. 877 885 (1961)
- 2 N R D C, Pat. Appln 5359/70 (1970)
- 3 Scott, N.D. *Polymer* 1960, **1**, 114
- 4 Sheldon, R.P. and Blakey, P.R. *Nature* 1962, **195**, 172
- 5 Conciatori, A.B. Chenevey, C.E., Bohrer, T.C. and Prince A. E. *J. Polym. Sci. (C)* 1967, **19**, 49

# Refractive index increments of polymers in solution:

## 1. General theory

J. W. Lorimer\*

*Department of Chemistry, University of Western Ontario,  
London 72, Ontario, Canada  
(Received 3 May 1971)*

Methods for calculation of refractive index increments of polymers in solution from the properties of the pure polymer and solvent and a suitable theory of polarization are developed. Volume changes on mixing the components, the effects of polydispersity, and the value of partial specific refractions are discussed rigorously. The general methods are used to derive a new equation for the refractive index increment from the polarization theory of Onsager and Böttcher. Errors in the Lorenz-Lorentz equation for the refractive increment are predicted to depend on the refractive index of the solvent, in agreement with experiment. Tests of the new equation, using existing experimental data, show that its accuracy is greater than the Lorenz-Lorentz equation, but is limited by a lack of knowledge of molecular parameters for the solvent and polymer.

Specific refractive index increments  $\nu = dn/dc$  of polymers in solution have been studied extensively in connection with light-scattering measurements, where  $\nu^2$  appears in the equation for calculating molecular weight, and with optical methods of measuring diffusion and sedimentation. Experimental values of  $\nu$  and their interpretation have been reviewed up to 1964 by Huglin<sup>1, 2</sup>. In a number of recent papers equations have been developed to calculate  $\nu$  and its temperature dependence from the properties of the pure polymer and solvent<sup>3-6</sup> and to estimate refractive indices and partial specific volumes of polymers in solution<sup>7</sup>. It has also been suggested that measurements of  $\nu$ , along with suitable equations, could be used to investigate inter- and intra-molecular interactions such as helix-coil transitions, micelle formation and changes in solvation<sup>7</sup>. Although knowledge of  $\nu$  as a function of molecular weight and polydispersity is necessary for the correct interpretation of scattering measurements on polymers of low molecular weight<sup>8, 9</sup>, only rough estimates<sup>2, 10</sup> and a few measurements<sup>1, 7</sup> of this dependence have been made. The variation of specific refraction with molecular weight has been used as a method of estimating the number of end-groups in a polymer<sup>11</sup>.

Most equations for  $\nu$  are based ultimately on equations for specific refraction, of which a large number have

been proposed. The most widely used<sup>7, 12-15</sup> are those of Gladstone and Dale, Eykman, and Lorenz and Lorentz. Although the Gladstone-Dale equation is a special case of Lorenz-Lorentz equation<sup>13, 15</sup>, and the Eykman equation is empirical<sup>13, 14</sup>, these two equations frequently give surprisingly good agreement with experimental data, as shown, for example, by the recent precise measurements of Bodmann<sup>12</sup>. Most equations proposed for  $\nu$  do not take lack of volume additivity of polymer and solvent into account, although Heller<sup>7</sup> has proposed an approximate way of doing this, and Bodmann<sup>12</sup> has approached the problem through partial specific refractions. Bodmann's work has also indicated that the Lorenz-Lorentz equation is not completely satisfactory, a feature that has been recognized in other areas<sup>13, 16, 17</sup> and on theoretical grounds<sup>13, 18</sup>.

In this paper, we first discuss the general problem of calculating refractive index increments from the properties of the pure polymer and solvent. Effects due to excess volumes and polydispersity and relation of the theory to partial specific refractions<sup>12, 19</sup> will be treated rigorously. Finally, new equations for the refractive index increment will be deduced from the polarizability theory of Onsager<sup>18</sup> and Böttcher<sup>13</sup> and will be applied to experimental data. In Part 2, the dependence of  $\nu$  on molecular weight, and the necessary modification of the light-scattering equations will be discussed<sup>8</sup>. A subsequent paper<sup>9</sup> will deal with the application of the general theory to a complex case, the solution properties of the polymeric titanium oxide trimethylsilyloxides.

\* Part of this work was carried out while on sabbatical leave at Dept. of Chemistry, University of Southampton, Southampton SO9 5NH, UK.

## REFRACTIVE INDICES OF MIXTURES

General equations for specific refractive index increments will be derived from equations for the refractive index of mixtures, which have been reviewed extensively<sup>4, 13-15</sup>. Two general approaches have been used in deducing these equations, which we shall call the specific refraction and immersed particle methods.

The first method defines a specific refraction as some function

$$R_i = f(n_i)v_i = K_i g_i(n_i, u_i) \quad (1)$$

of the refractive index  $n_i$ , specific volume  $v_i$  and molecular parameter  $u_i$  for each component  $i$ , where  $K_i$  is assumed to be independent of temperature and pressure. The many functions  $f(n_i)$  that have been proposed<sup>4, 13-15, 17</sup> may be classified as empirical, with  $g_i = 1$ , or as arising from the polarizability theories of Lorenz and Lorentz<sup>13</sup> (for which  $g_i = 1$  as well) or of Onsager<sup>18</sup> and Böttcher<sup>13</sup> (for which  $g_i \neq 1$ ). The only exception is the empirical function of Rosen<sup>17, 20</sup>, which has the form  $R = f(n)v = Kg(v, u)$ . We shall emphasize those functions that result from theories of polarizability, although equations based on any function of the form (1) can be derived easily by the methods given below.

Both the Lorenz-Lorentz and Onsager-Böttcher equations are derived by calculating, from electrostatic theory, the local electric field at a polarizable molecule in a continuous dielectric, and are expected to apply to systems containing small molecules and ions<sup>13</sup>, and to polymers in which the refractive index is determined by the properties of the chain segments, and not by overall configuration. Nose<sup>21</sup> has shown that this is a good approximation, by calculating the refractive index of polymers from assigned segment refractions.

The Lorenz-Lorentz specific refraction is<sup>13</sup>

$$R_i = (n_i^2 - 1)v_i/(n_i^2 + 2) = 4\pi N_A \alpha_i / 3M_i \quad (2)$$

where  $\alpha_i$  is the molecular polarizability and  $M_i$  the molecular weight of component  $i$  and  $N_A$  Avogadro's constant. The Onsager-Böttcher correction to equation (2) is<sup>13</sup>

$$g_i(n_i, u_i) = 9n_i^2/(n_i^2 + 2) [2n_i^2(1 - u_i) + 1 + 2u_i] \quad (3)$$

so that

$$R_i = (n_i^2 - 1)v_i/(n_i^2 + 2) = 4\pi N_A \alpha_i g_i(n_i, u_i) / 3M_i \quad (4)$$

The quantity  $u_i = \alpha_i/a_i^3$  can be used to define a refractive index  $n_i^*$ :

$$u_i = (n_i^{*2} - 1)/(n_i^{*2} + 2), \quad n_i^{*2} = (1 + 2u_i)/(1 - u_i) \quad (5)$$

This is the maximum allowed value of  $n_i$  since<sup>13</sup>  $u_i$  is the molecular polarization of a uniform dielectric sphere of radius  $a_i$ . Values of  $a_i$  correspond closely, in the few cases investigated<sup>13</sup>, to radii of freely-rotating molecules at 0K. We assume that  $u_i$  is a characteristic parameter, independent of molecular weight, for a given polymer, i.e.,  $u_i$  is determined by the nature of the repeating unit, and any effects due to overall chain configuration alter  $\alpha_i$  and  $a_i^3$  by the same factor.

The superiority of equation (4) has been demonstrated in several areas<sup>13</sup>, although it is undoubtedly an approximate answer to the complex problem of polarizability in liquids<sup>22</sup>. The Onsager-Böttcher equation does not seem to have been used previously for polymers, except in one case. Oster<sup>23</sup> attributed the equation

$$(n_i^2 - 1)(2n_i^2 + 1)/9n_i^2 = K_i'$$

to Onsager, where  $K_i'$  depends only on the nature of the molecule, and suggested its use in light scattering. Equations (3) and (4) show that Oster's equation is the special case  $u_i = 0$ , or  $n_i^* = 1$ , so that it cannot be valid except for the trivial case  $n_i = 1$ , where  $g_i = 1$ .

For the simple case  $g_i = 1$ , mixture rules are constructed from equation (1) by taking, for a mixture of  $q$  components,

$$R = \sum_{i=1}^q w_i R_i \quad (6)$$

where  $w_i = m_i/m$  is the mass fraction and  $m_i$  the mass of component  $i$ , and

$$m = \sum_{i=1}^q m_i$$

Equation (2) shows that equation (6) assumes that the polarizabilities of the pure components are unchanged on mixing<sup>7, 13</sup>. Since  $w_i v_i / v = V_i / V = \phi_i$ , the volume fraction of component  $i$  calculated as the ratio of the volume  $V_i$  of the pure component to the volume  $V$  of the mixture, equations (1) and (6) give

$$f(n) = \sum_{i=1}^q \phi_i f(n_i) \quad (7)$$

The specific form of equation (7) for the Lorenz-Lorentz equation is the well-known expression:

$$(n^2 - 1)/(n^2 + 2) = \sum_{i=1}^q \phi_i (n_i^2 - 1)/(n_i^2 + 2) \quad (8)$$

For the Onsager-Böttcher theory, the equation for the mixture is more complex, since the local field at a molecule depends on  $n_i$  and  $u_i$ , and on the refractive index  $n$  of the mixture as well. It is found that<sup>13</sup>

$$(n^2 - 1)/n^2 = (12\pi N_A / V) \times \sum_{i=1}^q \alpha_i m_i / M_i [2n^2(1 - u_i) + 1 + 2u_i] \quad (9)$$

Substitute from equation (4) for  $\pi N_A \alpha_i / M_i$  to obtain

$$R = \sum_{i=1}^q w_i R_i G_i \quad (10)$$

where

$$G_i = (n/n_i)^2 (n_i^2 + 2)(2n_i^2 + n_i^{*2}) / (n^2 + 2)(2n^2 + n_i^{*2}) \quad (11)$$

or, on introduction of volume fractions,

$$f(n) = \sum_{i=1}^q \phi_i f(n_i) G_i \quad (12)$$

or

$$(n^2 - 1)/n^2 = \sum_{i=1}^q \phi_i (n_i^2 - 1)(2n_i^2 + n_i^{*2}) / n_i^2 (2n^2 + n_i^{*2}) \quad (13)$$

None of the above equations assumes that the volume of the mixture is equal to the sum of the volumes of the pure components; i.e.

$$\sum_i \phi_i \neq 1.$$

The second method of deducing a refractive index rule for a mixture is to calculate the dielectric constant  $\epsilon$  (and hence the refractive index through  $\epsilon = n^2$ ) for a medium in which a small number of spheres of slightly different dielectric constant is immersed. The equation

for the mixture is thus found directly, and volume additivity is assumed. The original calculation is due to Rayleigh (see<sup>24</sup>), with subsequent versions by Wiener<sup>25</sup>, Heller<sup>25</sup>, Debye<sup>25</sup>, Onsager<sup>18</sup> and Böttcher<sup>24</sup>. Wiener also introduced a shape factor, but his equation for spherical particles and all the other equations become identical for small differences between the refractive indices of particles and medium. These equations are applicable to suspensions of colloidal spheres, so that their application to polymer solutions is probably unwarranted unless the molecular weight is very high or the solvent is very poor. Refractive index increments derived by this method have been discussed by Heller<sup>25</sup>, and will not be considered further here.

### SPECIFIC REFRACTIVE INDEX INCREMENTS

The specific refractive index increment of component  $i$  is  $dn/dc_i$  where  $c_i = m_i/V$  is the concentration of component  $i$  in mass per unit volume. If component 1 is the solvent, and the solute is polydisperse, the total solute concentration is

$$c_s = \sum_{i=2}^q m_i/V = \sum_{i=2}^q c_i = \sum_{i=2}^q \beta_i c_s \quad (14)$$

where  $\beta_i$  is the relative mass fraction of component  $i$  in the solute, and is a constant for a given component in a given distribution of solute components. Thus, the overall specific refractive increment is

$$dn/dc_s = \sum_{i=2}^q (dn/dc_i)(dc_i/dc_s) = \sum_{i=2}^q \beta_i dn/dc_i \quad (15)$$

and the overall partial specific volume of the solute is

$$\bar{v}_s = (\partial V/\partial m_s)_{m_1} = \sum_{i=2}^q (\partial V/\partial m_i)(\partial m_i/\partial m_s) = \sum_{i=2}^q \beta_i \bar{v}_i \quad (16)$$

where  $\bar{v}_i = (\partial V/\partial m_i)_{m_j}$  is the partial specific volume of component  $i$ .

If  $v_i$  is the specific volume of pure component  $i$ , then  $\phi_i = c_i v_i$ , and  $\partial \phi_i/\partial c_i = v_i$ . For the solvent,

$$\partial \phi_1/\partial c_s = -(V_1/V^2)\partial V/\partial c_s = -(\phi_1/V)\partial V/\partial c_s \quad (17)$$

But,

$$\begin{aligned} \partial V/\partial c_s &= (\partial V/\partial m_s)(\partial m_s/\partial c_s) = \bar{v}_s \partial(c_s V)/\partial c_s \\ &= \bar{v}_s (V + c_s \partial V/\partial c_s) \end{aligned}$$

Solve for  $\partial V/\partial c_s$  and substitute in equation (17) to obtain

$$\partial \phi_1/\partial c_s = -\phi_1 \bar{v}_s / (1 - c_s \bar{v}_s) \quad (18)$$

The general equation (12) can now be differentiated with respect to  $c_s$  to give, using equations (15) and (18),

$$\begin{aligned} (\partial f/\partial n)(\partial n/\partial c_s) &= \sum_{i=2}^q \beta_i v_i f(n_i) G_i - \phi_1 \bar{v}_s f(n_1) G_1 / (1 - c_s \bar{v}_s) + \\ &\quad \sum_{i=2}^q \beta_i \phi_i f(n_i) (\partial G_i/\partial n) (\partial n/\partial c_i) + \\ &\quad \phi_1 f(n_1) (\partial G_1/\partial n) (\partial n/\partial c_s) \quad (19) \end{aligned}$$

This equation may be simplified greatly by taking an infinitely dilute solution, where  $\phi_i = 0$ ,  $i = 2, \dots, q$ ,  $\phi_1 = 1$ ,  $G_1 = 1$ ,  $n = n_1$ . This is the state to which most experimental measurements correspond, and will be adopted throughout the remainder of this paper. With  $\nu$  the limiting refractive index increment at infinite dilution, equation (19) becomes

$$\begin{aligned} \nu [\partial f/\partial n - f(n_1) \partial G_1/\partial n]_{n_1} + \bar{v}_s f(n_1) &= \sum_{i=2}^q \beta_i v_i f(n_i) G_i \\ &= \sum_{i=2}^q \beta_i R_i G_i \quad (20) \end{aligned}$$

The term on the right hand side is, by equation (10), the number average of the product  $R_i G_i$  for the solute. If  $v_i$  and  $n_i$  are independent of molecular weight and equal to  $v_s$  and  $n_s$  respectively, this quantity is simply  $R_s G_s$ .

If  $G_i = 1$ ,  $i = 1, \dots, q$ , equation (20) is further simplified to

$$\nu (\partial f/\partial n)_{n_1} + \bar{v}_s f(n_1) = \sum_{i=2}^q \beta_i R_i \quad (21)$$

If  $R_i$  is the same for all species, equation (21) is equivalent to an equation deduced by Mächtle and Fischer<sup>6</sup>. Their deduction is restricted to infinite dilution, and does not include the terms for finite concentrations given in equations (17) to (19) above.

The explicit equations for the refractive index increment at infinite dilution are found by substituting  $f(n) = (n^2 - 1)/(n^2 + 2)$  and  $G_i$  from (11) into equations (20) and (21). This gives

$$\nu = \frac{n_1^3}{2} \left( \frac{2n_1^2 + n_1^{*2}}{2n_1^4 + n_1^{*2}} \right) \left\{ \sum_{i=2}^q \beta_i v_i \left( \frac{n_i^2 - 1}{n_i^2} \right) \left( \frac{2n_i^2 + n_i^{*2}}{2n_1^2 + n_i^{*2}} \right) - \bar{v}_s \left( \frac{n_1^2 - 1}{n_1^2} \right) \right\} \quad (22)$$

for the Onsager-Böttcher equation, and

$$\nu = [(n_1^2 + 2)^2/6n_1] \left\{ \sum_{i=2}^q \beta_i v_i (n_i^2 - 1)/(n_i^2 + 2) - \bar{v}_s (n_1^2 - 1)/(n_1^2 + 2) \right\} \quad (23)$$

for the Lorenz-Lorentz equation. These equations may be written in several different forms. One useful form is obtained by rearrangement:

$$\begin{aligned} (2\nu/n_1^3) \left( \frac{2n_1^4 + n_1^{*2}}{2n_1^2 + n_1^{*2}} \right) (2n_1^2 + n_s^{*2}) + (2n_1^2 + n_s^{*2}) \bar{v}_s (n_1^2 - 1)/n_1^2 \\ = v_s \left( \frac{n_s^2 - 1}{n_s^2} \right) (2n_s^2 + n_s^{*2}) \quad (24) \end{aligned}$$

for the Onsager-Böttcher case, and

$$\begin{aligned} 6n_1 \nu / (n_1^2 + 2)^2 + \bar{v}_s (n_1^2 - 1)/(n_1^2 + 2) \\ = v_s (n_s^2 - 1)/(n_s^2 + 2) = R_s \quad (25) \end{aligned}$$

for the Lorenz-Lorentz case. The left hand side of equation (24) or (25) contains only properties of the solvent and the measurable quantities  $\nu$  and  $\bar{v}_s$  while the right hand side contains the measurable quantities  $v_s$ ,  $n_s$  and  $n_s^*$  which are characteristic of the pure polymer only. In these equations, it has been assumed that  $n_i$  (but not necessarily  $v_i$ ) is independent of molecular weight, although in fact the dependence of both these quantities on molecular weight is usually of the same order of magnitude. Bodmann<sup>12</sup> has derived equation (25) in an apparently different way (see below), and used it to test the validity of the Lorenz-Lorentz equation. The left hand side of equation (25) showed a small but significant variation with  $n_1$  for both poly(methyl methacrylate) (PMMA) and polystyrene in a number of solvents. Since the differences between equations (24) and (25) are small, it is convenient to calculate corrections to the Lorenz-Lorentz equation. To do this, define  $\delta$  as the difference between the right and left sides of equation (25), and assume that equation (24) agrees exactly with experiment.

From equations (20) and (21), with  $n_i$  independent of molecular weight, we find readily that

$$\delta = R_s(1 - G_s) - \nu f(n_1)(\partial G_1/\partial n)n_1 \quad (26)$$

The explicit correction terms are

$$R_s(1 - G_s) = \frac{2R_s(n_s^2 - n_1^2)(n_s^* - n_1^*n_s^2)}{n_s^2(n_1^2 + 2)(2n_1^2 + n_s^{*2})} \quad (27)$$

and

$$-\nu f(n_1)(\partial G_1/\partial n)n_1 = 4\nu(n_1^2 - 1) \times \frac{(n_1^* - n_1^{*2})/n_1(n_1^2 + 2)(2n_1^2 + n_1^{*2})}{(n_1^* - n_1^{*2})/n_1(n_1^2 + 2)(2n_1^2 + n_1^{*2})} \quad (28)$$

Methods for estimating  $n_1^*$  and  $n_s^*$  and calculating these correction terms will be discussed below. Note that the corrections disappear only if  $n_1 = n_s = 1$ , which is, of course, the conditions under which equations (22) and (23) are identical, if  $n_i$  is independent of molecular weight. If  $n_1 = n_s$ , the correction equation (27) is zero, but both equations (22) and (23) give a finite value of  $\nu$  which is proportional to the difference  $v_s - \bar{v}_s$  between the specific volume of the pure polymer and the partial specific volume at infinite dilution. In general, if  $n_1^2 n_s^2 > n_s^{*2}$ , and if  $\nu > 0$ , the correction term equation (27) is negative if  $n_s > n_1$ , positive if  $n_s < n_1$ , positive if  $n_s < n_1$ . Also,  $n_1^{*2} < n_1^2$ , in general, so that the correction term equation (28) is always positive in practice.

#### ADDITIVITY OF VOLUMES

If additivity of volumes of polymer and solvent holds strictly then  $v_i = \bar{v}_i$  and equations (22) and (23) become, with  $n_i$  independent of molecular weight,

$$\nu = (v_s n_1 / 2n_s^2)(n_s^2 - n_1^2) \left( \frac{2n_1^2 + n_1^{*2}}{2n_1^2 + n_s^{*2}} \right) \left( \frac{2n_s^2 n_1 + n_s^{*2}}{2n_1^2 + n_1^{*2}} \right) \quad (29)$$

and

$$\nu = v_s(n_s^2 - n_1^2)(n_1^2 + 2)/2n_1(n_s^2 + 2) \quad (30)$$

Equation (30) has been deduced by Heller<sup>7</sup>, who assumed volume additivity. He then replaced  $v_s$  by  $\bar{v}_s$ , and  $n_s$  by  $\bar{n}_s$ , and assumed that the specific refractions for the pure polymer and for the solute at infinite dilution were equal:

$$R_s = v_s(n_s^2 - 1)/(n_s^2 + 2) = \bar{v}_s(\bar{n}_s^2 - 1)/(\bar{n}_s^2 + 2) \quad (31)$$

Here,  $\bar{n}_s$  is a refractive index (called  $n_2^*$  by Heller) chosen so that equations (30) and (31) are satisfied simultaneously. From measured values of  $v_s$ ,  $n_s$  and  $\nu$ , Heller used equations (30) and (31) to evaluate  $\bar{v}_s$  and  $\bar{n}_s$  by successive approximations. However, since there are two equations in the two unknowns, explicit equations may be found by direct solution. The result for the partial specific volume is

$$\bar{v}_s = R_s(n_1^2 + 2)/(n_1^2 - 1) - 6n_1\nu/(n_1^2 - 1)(n_1^2 + 2) \quad (32)$$

This equation is much easier to use than Heller's method and gives values identical to those<sup>7</sup> derived by successive approximations. However, it is found by comparison that equation (32) is just equation (25), i.e. Heller's two assumptions are equivalent to a rigorous treatment which allows for non-additivity of volume. It will be noted that there is no need for the quantity  $\bar{n}_s$ , which has no physical significance.

The accuracy of equation (32) is limited by the accuracy of the Lorenz-Lorentz equation. In fact, data given by

Heller<sup>7</sup> and by Rietveld<sup>26</sup> agree with the conclusions of Bodmann<sup>12</sup>, that the Lorenz-Lorentz equation gives results accurate to 1 or 2% only, in general. Equation (24) should provide a more accurate method of determining partial specific volumes from measured values of  $\nu$ ,  $n_1$ ,  $n_s$  and  $v_s$  if  $n_1^*$  and  $n_s^*$  can be estimated.

#### PARTIAL SPECIFIC REFRACTIONS

Bodmann<sup>12</sup> has introduced the concept of partial specific refractions  $\bar{R}_i$  through the equation

$$R = \sum_{i=1}^q w_i \bar{R}_i \quad (33)$$

and has deduced, by a complicated procedure, a practical equation for the calculation of  $\bar{R}_s$  for a solute from a given theoretical equation for  $R$  and experimental values of  $\nu$ ,  $n_1$  and  $\bar{v}_s$ . Partial molar refractions seem to have been introduced first by Guggenheim<sup>19</sup>, whose treatment is simpler than Bodmann's. We note that  $mR$  is an extensive quantity (homogeneous of degree one in the masses of the components). Euler's theorem on homogeneous functions then gives at once

$$mR = \sum_{i=1}^q m_i \bar{R}_i \quad (34)$$

with

$$\bar{R}_i = [\partial(mR)/\partial m_i]_{m_j} \quad (35)$$

Equations (33) and (34) are identical. For a polydisperse solute,

$$\begin{aligned} \bar{R}_s &= \sum_{i=2}^q [\partial(mR)/\partial m_i](\partial m_i/\partial m_s)_{m_1} \\ &= \sum_{i=2}^q \beta_i \bar{R}_i \end{aligned} \quad (36)$$

For a mixture, equation (10) gives

$$mR = f(n)V = \sum_{i=1}^q m_i R_i G_i$$

Differentiation of the first part of this equation gives

$$\bar{R}_i = f(n)\bar{v}_i + (\partial f/\partial n)(\partial n/\partial c_i)(1 - c_i\bar{v}_i) \quad (37)$$

Differentiation of the second part gives

$$\bar{R}_i = R_i G_i + \sum_{i=1}^q \phi_i f(n_i)(\partial G_i/\partial n)(\partial n/\partial c_i)(1 - c_i\bar{v}_i) \quad (38)$$

Now pass to infinite dilution, where  $\phi_i = c_i = 0$ ,  $i = 2, \dots, q$ ,  $\phi_1 = 1$ ,  $n = n_1$ , equate equations (37) and (38) and use equation (36) to obtain

$$\begin{aligned} R_s &= \nu(\partial f/\partial n)_{n_1} + \bar{v}_s f(n_1) \\ &= \sum_{i=2}^q \beta_i R_i G_i + \nu f(n_1)(\partial G_1/\partial n)n_1 \end{aligned} \quad (39)$$

which is equation (20). Partial molar refractions, therefore, yield no new results, but provide a convenient notation and nomenclature, and an alternative way of deducing rigorous equations for the refractive increment. Thus, equations (25) and (39) show that  $\bar{R}_s = R_s$  for the Lorenz-Lorentz equation, as shown by Bodmann<sup>12</sup>. For the Onsager-Böttcher equation, the partial specific refraction is not independent of the solvent, and is given by a complicated expression which can be rearranged to give equation (22).

## DISCUSSION OF EXPERIMENTAL DATA

The parameter  $n_1^*$  for the solvent can be estimated from the variation of refractive index and density  $\rho_1 (=1/v_1)$  with temperature, at constant pressure. Differentiation of equation (4) for component 1 gives, if  $\alpha_1$  and  $u_1$  are independent of density the result

$$n_1^{*2} = 2n_1^3 [2n_1\rho_1\partial n_1/\partial\rho_1 - (n_1^2 - 1)] / [n_1(n_1^2 - 1) - 2\rho_1\partial n_1/\partial\rho_1] \quad (40)$$

after algebraic rearrangement. Böttcher<sup>27</sup> has deduced a similar equation, but in a form suitable for calculating the parameter  $a_1$ .

In practice, very precise data are required to evaluate  $\rho_1\partial n_1/\partial\rho_1$ , and calculation shows that the error in  $n_1^{*2}$  is about 7 times that in  $\rho_1\partial n_1/\partial\rho_1$ , and that the resulting error in equation (24) is about half that in  $n_1^{*2}$ . No data of sufficient precision are available for polymers or for tetrahydrofuran. Of the other solvents used by Bodmann<sup>12</sup>, benzene, toluene, chloroform and cyclohexane give reasonable values of  $n_1^*$  from experimental data<sup>28, 29</sup>, but data for other solvents used by him give values of  $n_1^*$  less than unity. One reason for this is apparent from data for water, where  $\rho_1\partial n_1/\partial\rho_1$  is strongly dependent on temperature. Precise data for other liquids at more than two temperatures are not available, in general. Furthermore,  $n_1^*$  should exhibit dispersion. As an approximate solution to this problem, we assume that the ratio  $n_1^*/n_1$  is independent of wavelength, and derive the values  $n_1^*/n_1 = 1.1126$  for benzene, 1.1021 for toluene, 1.2747 for chloroform and 1.2710 for cyclohexane. The average of these is 1.1901, and we use this value for the other solvents, although it is somewhat lower than the few values that have been reported (1.578 for water, by the above method<sup>27</sup>; 1.545 for CS<sub>2</sub> and 1.546 for CCl<sub>4</sub> from dielectric data<sup>30</sup>).

To test the Onsager-Böttcher equation for specific refractive index increments, we use the precise data of Bodmann<sup>12</sup>, and calculate the difference  $\delta$  between the Lorenz-Lorentz partial specific refractivities for the pure

polymer and the polymer in solution. The correction equation (28) is then calculated, and subtracted from  $\delta$  to give the correction equation (27). Equation (27) is then used to calculate  $n_s^*$  for the polymer. These values are all given in Table 1 for PMMA and polystyrene at 25°C, two different wavelengths, and in a number of solvents. The original data<sup>12</sup> are not repeated here.

The calculated values of  $n_s^*$  are constant to within the error expected from the error in  $\delta$  (at least<sup>12</sup>  $\pm 0.0003$ ) for each of the four cases in Table 1, except for two cases for PMMA in benzene and toluene, which give values less than unity. In these two cases,  $n_1^2 \div n_2^2$ , and errors in the calculated value of  $n_2^*$  are very large. In general, Table 1 shows that the correction equations (27) and (28) can account for the deviations of the Lorenz-Lorentz equation (25) from experiment. Accurate, direct calculation of the correction  $\delta$  is not possible, since the two terms which make up  $\delta$  are of the same order of magnitude and frequently of opposite sign, and the magnitude of each term is sensitive to the value of the parameters  $n^*$ , which are known only approximately. The average value of  $n_s^*/n_s$  in Table 1 is 1.19, standard error 0.05. This suggests that the general approximation  $n_i^*/n_i = \gamma$ , with  $\gamma = 1.2$ , can be used if no other data are available. With this approximation, each side of equation (24) can be calculated, and the results for the cases listed in Table 1 are given in Table 2. The greatest difference in the values for the left hand side of equation (24) is 0.6% for PMMA and 0.8% for polystyrene, compared with the Lorenz-Lorentz values<sup>12</sup> 0.9 and 1.3%, respectively. The standard errors for the left side of equation (24) are estimated to be 0.008 for PMMA and 0.006 for polystyrene; for the right side, the errors listed in Table 2 correspond to errors in  $v_s$  of 0.005 for PMMA and 0.003 cm<sup>3</sup>/g for polystyrene. Error calculations were based on these errors in  $v_s$ , assumed errors in  $n_s$  of 0.005 for PMMA and 0.001 for polystyrene, and error estimates of Bodmann<sup>12</sup> for  $\nu$  and  $\bar{v}_s$ . The two sides of equation (24) agree to within experimental error, but variations in the value of the left side appear to lie outside the expected error. In view of the

Table 1 Corrections to the Lorenz-Lorentz equation for refractive index increments

System	436 nm					546 nm				
	$n_1$	$\delta/10^3$ (cm <sup>3</sup> /g)	$-10^3\nu f\partial G/\partial n$ eq. (28)	$10^3R_s(1-G_s)$ by diff.	$n_s^*$ eq. (27)	$n_1$	$\delta/10^3$ (cm <sup>3</sup> /g)	$-10^3\nu f\partial G/\partial n$	$10^3R_s(1-G_s)$	$n_s^*$
PMMA in:										
acetone	1.3645	0.6	2.9	-2.3	1.86	1.3577	-0.6	2.7	-3.3	1.66
ethyl acetate	1.3778	1.2	2.9	-1.7	1.81	1.3714	-0.2	2.7	-2.9	1.77
n-butyl acetate	1.4007	1.0	2.8	-1.8	1.90	1.3936	-0.3	2.6	-2.9	1.74
THF	1.4138	1.0	2.7	-1.7	1.89	1.4068	-0.3	2.5	-2.8	1.72
dioxan	1.4290	1.3	2.4	-1.1	1.96	1.4216	0.0	2.2	-2.2	1.75
chloroform	1.4527	2.9	1.5	1.4	1.83	1.4436	1.5	1.4	0.1	2.12
toluene	1.5133	2.7	0.6	2.1	—	1.4962	1.3	0.9	0.4	1.48
benzene	1.5195	2.9	0.2	2.7	—	1.5016	1.5	0.6	0.9	1.74
Average and std. error					1.88 ± 0.05					1.75 ± 0.18
$n_s^*/n_s$					1.25					1.17
Polystyrene in:										
MEK	1.3848	-4.0	5.8	-9.8	1.86	1.3779	-2.5	5.3	-7.8	1.88
dioxan	1.4290	-3.2	6.1	-9.3	1.86	1.4216	-1.7	5.4	-7.1	1.90
cyclohexane	1.4333	-3.3	3.9	-7.2	1.95	1.4257	-2.1	2.9	-5.0	1.98
toluene	1.5133	0.6	7.1	-6.5	1.85	1.4962	1.6	6.5	-4.9	1.92
benzene	1.5195	0.6	6.7	-7.3	1.75	1.5016	0.4	6.2	-5.8	1.83
Average and std. error					1.85 ± 0.07					1.90 ± 0.04
$n_s^*/n_s$					1.14					1.19



Table 2 Test of equation (24) with  $n_i^*/n_i=1.2$  (units:  $\text{cm}^3/\text{g}$ )

System	436 nm		546 nm	
	Left side	Right side	Left side	Right side
PMMA in:				
acetone	3.642	3.655	3.562	3.568
ethyl acetate	3.635		3.558	
n-butyl acetate	3.640		3.561	
THF	3.642		3.564	
dioxan	3.638		3.560	
chloroform	3.622		3.544	
toluene	3.630		3.551	
benzene	3.626		3.548	
Average and standard error	3.634 $\pm 0.008$	$\pm 0.02$	3.556 $\pm 0.007$	$\pm 0.02$
Polystyrene in:				
MEK	5.332	5.308	5.116	5.108
dioxan	5.325		5.109	
cyclohexane	5.329		5.116	
toluene	5.291		5.078	
benzene	5.292		5.079	
Average and standard error	5.314 $\pm 0.021$	$\pm 0.01$	5.100 $\pm 0.020$	$\pm 0.01$

approximation for  $n_i^*$ , such variations are hardly surprising. Even with the approximation, equation (24) is superior to the Lorenz-Lorentz equation.

Other assumed values of  $\gamma$  can be used, but calculations show that it is not satisfactory to take  $n_i^*$  as a constant for all components. In general,  $\gamma > 1.2$  gives poorer constancy of the left side of equation (24), while  $\gamma < 1.2$  gives greater constancy, but greater differences between the two sides of the equation. The value  $\gamma = 1.2$  appears to be a reasonable compromise. For estimation of  $\bar{v}_s$  and  $\nu$ , errors of about 1% and several %, respectively, are to be expected in the worst cases, and it is important to use the most reliable value of  $n_i^*$  that is available.

#### ACKNOWLEDGEMENTS

The research for this paper was supported, in part, by the Defence Research Board of Canada and the National

Research Council of Canada. The author also wishes to thank the British Council for a travel grant, and Dr D. E. G. Jones for his critical comments.

#### REFERENCES

- Huglin, M. B. *J. Appl. Polym. Sci.* 1965, **9**, 3963
- Huglin, M. B. *J. Appl. Polym. Sci.* 1965, **9**, 4003
- Chiang, R. *J. Polym. Sci. (C)* 1965, **8**, 295
- Wigand, G. and Veith, H.-J. *Plaste Kaut.* 1969, **9**, 671
- Kalz, G. *Plaste Kaut.* 1970, **5**, 331
- Mächtle, W. and Fischer, H. *Angew. Makromol. Chem.* 1969, **7**, 147
- Heller, W. *J. Polym. Sci. (A-2)* 1966, **4**, 209
- Lorimer, J. W. and Jones, D. E. G. *Polymer* 1972, **13**, 52
- Jones, D. E. G. and Lorimer, J. W. *Polymer* 1972 (in the press)
- Stacy, C. J. and Arnett, R. L. *J. Polym. Sci. (A)* 1964, **2**, 167
- Bodmann, O. *Makromol. Chem.* 1969, **122**, 210
- Bodmann, O. *Makromol. Chem.* 1969, **122**, 196
- Böttcher, C. J. F. 'Theory of Electric Polarisation', Elsevier Publishing Co., Amsterdam, 1952, sections 40, 44, 48, 49
- Partington, J. R. 'An Advanced Treatise on Physical Chemistry. Vol. IV. Physico-chemical Optics', Longmans, Green and Co., London, 1963, sections 2, 10, 14
- Heller, W. *J. Phys. Chem.* 1965, **69**, 1123
- Coumou, J. D., Mackor, E. L. and Hijmans, J. *Trans. Faraday Soc.* 1964, **60**, 1539
- Parfitt, G. D. and Wood, J. A. *Trans. Faraday Soc.* 1968, **64**, 805
- Onsager, L. *J. Am. Chem. Soc.*, 1936, **58**, 1486
- Guggenheim, E. A. 'Thermodynamics', North-Holland Publishing Co., Amsterdam, 1949, p 172
- Rosen, J. S. *J. Chem. Phys.* 1949, **17**, 1192
- Nose, S. *J. Polym. Sci. (C)* 1964, **2**, 1127
- Brown, W. F., Jr. in 'Encyclopedia of Physics' (S. Flügge, Ed.), Springer Verlag, Berlin, 1956, Vol 17, p 118
- Oster, G. *Chem. Rev.* 1948, **43**, 319
- Böttcher, C. J. F. 'Theory of Electric Polarisation', Elsevier Publishing Co., Amsterdam, 1952, section 64
- Heller, W. *Phys. Rev.* 1945, **68**, 5
- Rietveld, B. J. *J. Polym. Sci. (A-2)* 1970, **8**, 1837
- Böttcher, C. J. F. *Rec. Trav. chim.* 1946, **65**, 14
- Timmermans, J. 'Physico-chemical Constants of Pure Organic Compounds', Elsevier Publishing Co., Amsterdam, 1950
- Rossini, F. D. *et al.* 'Selected Values of Physical and Thermodynamic Properties of Hydrocarbons and Related Compounds', API Project 44, Carnegie Press, Pittsburgh, 1953
- Böttcher, C. J. F. *Rec. Trav. chim.* 1943, **62**, 325

# Refractive index increments of polymers in solution:

## 2. Refractive index increments and light-scattering in polydisperse systems of low molecular weight\*

J. W. Lorimer† and D. E. G. Jones‡

Department of Chemistry, University of Western Ontario,  
London 72, Ontario, Canada  
(Received 3 May 1971)

Theoretical equations are deduced which predict that the specific refractive index of a polymer in solution is  $\nu = \nu_\infty + \nu_0/\bar{M}_n$ , where  $\bar{M}_n$  is the number average molecular weight, and  $\nu_\infty$  and  $\nu_0$  depend on the refractive index,  $n_1$ , of the solvent, on the specific refractivity of the pure polymer, and on the specific volume of the polymer in solution. These equations are used to show that the true weight average molecular weight and second virial coefficient, as obtained from light scattering, can be obtained from the observed values of these quantities only if  $\bar{M}_n$  and the dependence of  $\nu$  on  $\bar{M}_n$  are known. The difference between the true and observed values can be very pronounced for values of  $\bar{M}_n$  less than about  $10^3$ .

Mixtures of two polymers whose refractive increments depend on molecular weight are also considered. Methods of distinguishing the effects of polydispersity of composition from effects due to the dependence of the average  $\nu$  on the average molecular weight are discussed for mixtures of components whose individual properties are unknown.

### INTRODUCTION

Light-scattering measurements are used widely to obtain weight-average molecular weights and second virial coefficients of polymers in solution, and general treatments, based on fluctuation theory, have been proposed<sup>1,2</sup> which can be used for the interpretation of experimental measurements. In all applications of these general treatments, it is assumed that the refractive index increment which occurs therein is independent of molecular weight. This assumption is not valid in systems of sufficiently low degree of polymerization.

To deduce correct equations for light-scattering in polydisperse systems of low molecular weight, a general theory of the dependence of both refractive index and specific volume becomes necessary, since these quantities, along with the refractive index of the solvent, determine the magnitude of the refractive index increment in

solution. General equations for the refractive index increment have been deduced<sup>3</sup> in Part 1, and in this paper, their specific forms for polymers and mixtures of polymers of low molecular weight are deduced. A subsequent paper<sup>4</sup> describes the application of these equations to a complex case.

### REFRACTIVE INDEX AND MOLECULAR WEIGHT IN A HOMOLOGOUS SERIES

We assume that a polymeric solute molecule  $i$  has a molecular optical polarizability  $\alpha_i$  that is a linear function of the degree of polymerization  $r$ :

$$4\pi N_A \alpha_i / 3 = P_0 + rP_r, \quad r = 0, 1, 2 \dots \quad (1)$$

where  $N_A$  is Avogadro's constant and  $P_0$ ,  $P_r$  are the molar polarizabilities of the two end-groups and the repeating unit, respectively, each multiplied by  $3/4\pi$ . The molecular weight of molecule  $i$  is

$$M_i = M_0 + M_r r, \quad r = 0, 1, 2 \dots \quad (2)$$

where  $M_0$ ,  $M_r$  are the formula weights of the two end-groups and the repeating unit, respectively. Equations (1) and (2) give

$$4\pi N_A \alpha_i / 3 = a_0 + P_\infty M_i \quad (3)$$

\* An abstract of this work was presented at the IUPAC Symposium on Macromolecules, Leiden, The Netherlands, 31 Aug.-4 Sept. 1970.

† Part of this work was carried out while on sabbatical leave at Dept. of Chemistry, University of Southampton, Southampton SO9 5NH, UK.

‡ Present address: Department of Chemistry, University of Otago, Dunedin, New Zealand.

where

$$a_0 = M_0(P_0/M_0 - P_r/M_r) \quad (4)$$

$$P_\infty = P_r/M_r \quad (5)$$

If the Lorenz-Lorentz equation holds, the molar polarization is<sup>5</sup>, for component  $i$ ,

$$[R]_i = (n_i^2 - 1)v_i M_i / (n_i^2 + 2) = 4\pi N_A \alpha_i / 3 \quad (6)$$

where  $n_i$  is the refractive index and  $v_i$  the specific volume of component  $i$ . The Onsager-Böttcher correction to this equation is<sup>5</sup>

$$[R]_i = (4\pi N_A \alpha_i / 3) g_i \quad (7)$$

where

$$g_i = 9n_i^2 / (n_i^2 + 2) [2n_i^2(1 - u_i) + 1 + 2u_i] \quad (8)$$

with  $u_i$  a molecular parameter which has been discussed<sup>3</sup> in Part 1. Equation (1), with the polarizability expressed in the Lorenz-Lorentz form, equation (6), has been used to correlate the molar refractions of a number of homologous series<sup>6,7</sup>, while equation (3) with equation (6) has been used by Bodmann<sup>8</sup>, who attributes departures from linearity in  $M_i$  to departures from a true homologous series. For the Lorenz-Lorentz case, the specific refraction of component  $i$  is

$$R_i = (n_i^2 - 1)v_i / (n_i^2 + 2) = a_0 / M_i + R_\infty \quad (9)$$

Clearly,  $R_\infty = P_\infty$ , in this case, is the specific refraction for the infinite polymer. For the Onsager-Böttcher case, equations (3), (6)-(8) give

$$(n_i^2 - 1)v_i M_i = 9n_i^2(a_0 + R_\infty M_i) / (1 - u_i)(2n_i^2 + n_i^{*2}) \quad (10)$$

where<sup>3</sup>

$$n_i^{*2} = (1 + 2u_i) / (1 - u_i) \quad (11)$$

#### SPECIFIC VOLUME AND MOLECULAR WEIGHT IN A HOMOLOGOUS SERIES

In analogous manner, we assume that the molar volume is a linear function of the degree of polymerization:

$$v_i M_i = V_0 + V_r r, \quad r = 0, 1, 2 \dots \quad (12)$$

where  $V_0$ ,  $V_r$  are the molar volumes of the end-groups and of a repeating unit. For many homologous series<sup>7</sup>, further terms in the degree of polymerization must be added, but except for the first few members of series with small repeating units, equation (12) is a good approximation. Combination of equations (2) and (12) gives

$$v_i = b_0 / M_i + v_\infty \quad (13)$$

where

$$b_0 = M_0(V_0/M_0 - V_r/M_r) \quad (14)$$

$$v_\infty = V_r/M_r \quad (15)$$

Clearly,  $v_\infty$  is the specific volume of the infinite polymer.

If  $\beta_i = m_i/m_s$  is the relative mass fraction of component  $i$  in a polydisperse component of mass  $m_s$ , the specific volume of this component is

$$v_s = b_0/\bar{M}_n + v_\infty \quad (16)$$

where

$$\bar{M}_n = \sum_{i=2}^q \beta_i / M_i \quad (17)$$

is the number-average molecular weight of the component. It is to be noted that two samples of a polydisperse component made up of members of a homologous series can, in general, have different number- and weight-average molecular weights, but the specific volume is determined by the number-average molecular weight alone. Equation (16) has been deduced for polymer melts by Fox and Loshaek<sup>9</sup> (see also ref. 10), who also showed that it agreed well with experimental data for a number of polymers. It is also clear from their treatment that the number-average molecular weight is appropriate, although they did not specify which average was to be used.

It is assumed that equation (16) is valid for the partial specific volume  $\bar{v}_s$  of a polydisperse solute as well as for the specific volume  $v_s$  of the molten solute. In general, these two values differ, and it is to be expected that  $b_0$  and  $v_\infty$  are functions of the nature of the solvent, for a given polymer. To emphasize this, we write for the partial specific volume

$$\bar{v}_s = \bar{b}_0/\bar{M}_n + \bar{v}_\infty \quad (18)$$

Equation (18) has also been proposed empirically<sup>11</sup> from data on poly(methyl methacrylate) and polystyrene, again without specifying which average molecular weight is involved. Statistical mechanical calculations<sup>12</sup> also support equation (18), but add a small term  $\kappa RT$  to  $\bar{b}_0$ , where  $\kappa$  is the isothermal compressibility of the solvent at temperature  $T$ , and  $R$  is the gas constant.

#### SPECIFIC REFRACTIVE INDEX INCREMENTS

Substitution of equations (9), (10) and (18) in equations (22) and (23) of Part 1<sup>3</sup> give equations for  $\nu$ , the specific refractive increment at infinite dilution. The resulting equations are

$$(2\nu/n_1^3)(2n_1^4 + n_1^{*2}) / (2n_1^2 + n_1^{*2}) = [R_\infty / (1 - u_s)(2n_1^2 + n_s^{*2}) - \bar{v}_\infty(n_1^2 - 1)/n_1^2] + [a_0 / (1 - u_s)(2n_1^2 + n_s^{*2}) - \bar{b}_0(n_1^2 - 1)/n_1^2] / \bar{M}_n \quad (19)$$

for the Onsager-Böttcher case, and

$$6n_1\nu / (n_1^2 + 2)^2 = [R_\infty - \bar{v}_\infty(n_1^2 - 1)/(n_1^2 + 2)] + [a_0 - \bar{b}_0(n_1^2 - 1)/(n_1^2 + 2)] / \bar{M}_n \quad (20)$$

for the Lorenz-Lorentz case. In equation (19),  $n_s^*$ , and hence  $u_s$ , have been assumed to be independent of molecular weight<sup>3</sup>, and become the solute parameters  $n_s^*$  and  $u_s$ .

Both equations (19) and (20) are of the form

$$\nu = \nu_\infty + \nu_0/\bar{M}_n \quad (21)$$

for the solute, and

$$\nu_i = \nu_\infty + \nu_0/M_i \quad (22)$$

for each component, where  $\nu_\infty$  is the value of  $\nu_i$  at infinite molecular weight, and  $\nu_0$  is related to  $a_0$  of equation (3) and to  $\bar{b}_0$  of equation (18). Both  $\nu_\infty$  and  $\nu_0$  are functions of the nature of the solvent and the nature of the homologous series.

The methods used to deduce equation (20) have also been used to estimate the effect of molecular weight on  $\nu$ <sup>13-15</sup>, but direct confirmation from experimental data has been limited to poly(ethylene glycol) and *p*-oligophenylenes (see ref. 16 for data) and to poly-

(propylene glycol)<sup>17</sup>. It is doubtful that the *p*-oligophenylenes constitute a true homologous series, but equation (21) is in reasonable agreement with experiment even in this case. In general, calculation<sup>13-15</sup> and experiment<sup>15</sup> show that the term in  $\bar{M}_n$  is usually not important for values of  $\bar{M}_n$  greater than  $5-10 \times 10^3$ . Dependence of  $\nu$  on molecular weight will be greater for polymers with large values of  $a_0$  and  $b_0$ , i.e. polymers with end-groups and repeating units that differ greatly in molar refraction and in molar volume. Larger effects can be expected, therefore, in condensation polymers compared to addition polymers with roughly the same repeating units.

According to equation (20),  $6n_1\nu/(n_1^2+2)^2$  is approximately linear in  $(n_1^2-1)/(n_1^2+2)$  for a given polymer with a given  $\bar{M}_n$ , since  $\bar{v}_\infty$  and  $\bar{b}_0$  vary only a few % in different solvents, in several cases<sup>11, 15</sup>. Rearrangement of equation (20) shows that  $\nu$  is also approximately linear in  $n_1^2$ , since the factor  $6n_1/(n_1^2+2)$  varies only about 2% over the range  $n_1=1.3$  to  $1.7$ , which covers most common solvents. In fact, this range of  $n_1$  is so small that plots of  $\nu$  against  $n_1$  or against  $n_1^2$  are both linear. This observation has been considered to be a consequence of the Gladstone-Dale equation<sup>13, 16, 18, 19</sup> but obviously has a much more general basis. The dependence of  $\nu$  on refractive index of the solvent is more complex for the Onsager-Böttcher equation (19), but can be calculated if  $n_i^2$  is known with sufficient accuracy<sup>3</sup>.

#### THE LIGHT-SCATTERING EQUATION

The turbidity  $\tau$  for a polydisperse non-electrolyte in a single solvent is given by<sup>1, 2</sup>

$$\tau/H' = \sum_{i=2}^q x_i M_i (\partial n / \partial x_i)^2 - \frac{1}{2} \sum_{i,j=2}^q \beta_{ij} (\partial n / \partial x_i) (\partial n / \partial x_j) x_i x_j \quad (23)$$

where

$$H' = 32\pi^3 n_1^3 / 3 N_A c_1 \lambda^4 \quad (24)$$

with  $N_A$  Avogadro's constant,  $\lambda$  the wavelength of light in vacuum,  $c_1$  the concentration of solvent in mass per unit volume. The molecular weight of solute component  $i$  is  $M_i$ , and its concentration is  $x_i = m_i/m_1$ , where  $m_1$  is the mass of the solvent. The quantity

$$\beta_{ij} = M_j (\partial \ln \gamma_i / \partial x_j)_{x_i},$$

where  $\gamma_i$  is the activity coefficient of component  $i$ , is the first term in a Taylor expansion of  $\ln \gamma_i$  in the concentration. In terms of the concentrations  $c_i = m_i/V$  in mass per unit volume,  $x_i = c_i/c_1$ , and

$$x_i \partial n / \partial x_i = c_i \nu_i (1 - c_i \bar{v}_i) \quad (25)$$

The terms in equation (23) are correct to quadratic terms in  $x_i$  so that  $c_i \bar{v}_i$  in equation (25) may be dropped. This is equivalent to evaluating the terms in equation (23) at infinite dilution of solute.

Equation (23), for the case in which  $\nu_i$  is independent of molecular weight, becomes, using equation (25),

$$c_1 H' \nu^2 c_s / \tau = 1 / \bar{M}_w + 2A_2 c_s \quad (26)$$

where the weight-average molecular weight is

$$\bar{M}_w = \sum_{i=2}^q c_i M_i / c_s \quad (27)$$

with  $c_s = \sum_{i=2}^q c_i$  the total solute concentration, and the second virial coefficient is

$$A_2 = \frac{1}{4} \sum_{i,j} \beta_{ij} c_i c_j / \bar{M}_w^2 c_s^2 c_1 \quad (28)$$

We therefore rewrite equation (23), using equation (25), in the form

$$c_1 H' \nu^2 c_s / \tau = (1/M_{\text{obs}}) \left[ 1 - \left( \frac{1}{2} M_{\text{obs}} \nu^2 c_1 c_s \right) \sum_{i,j} \beta_{ij} \nu_i \nu_j c_i c_j \right]^{-1} \quad (29)$$

where

$$M_{\text{obs}} = \sum_{i=2}^q c_i \nu_i^2 M_i / c_s \nu^2 \quad (30)$$

Expansion of equation (29), with retention of the first two terms only, gives

$$c_1 H' \nu^2 c_s / \tau = 1/M_{\text{obs}} + 2A_{\text{obs}} c_s \quad (31)$$

where

$$A_{\text{obs}} = \left( \frac{1}{4} M_{\text{obs}}^2 \nu^2 c_s^2 c_1 \right) \sum_{i,j} \beta_{ij} \nu_i \nu_j c_i c_j \quad (32)$$

Equations (30) and (31) must now be combined with equation (22) so that the observed molecular weight, equation (30), and second virial coefficient, equation (32), may be used to obtain correct values of  $\bar{M}_w$  and  $A_2$ . Substitution of equation (22) in equation (30) gives, using equations (21) and (27),

$$M_{\text{obs}} = (\nu_\infty / \nu)^2 [\bar{M}_w + 2\nu_0 / \nu_\infty + (\nu_0 / \nu_\infty)^2 / \bar{M}_n] = \bar{M}_n + (\nu_\infty / \nu)^2 (\bar{M}_w - \bar{M}_n) \quad (33)$$

The observed molecular weight is equal to the weight-average molecular weight only when  $\nu = \nu_\infty$ . In general, both the number-average molecular weight and the dependence of  $\nu$  on molecular weight must be known in order to obtain  $\bar{M}_w$  from  $M_{\text{obs}}$ , and  $M_{\text{obs}}$  can be larger or smaller than  $\bar{M}_w$ , depending on whether  $\nu$  increases or decreases with molecular weight.

Substitution of equation (22) into equation (32) gives:

$$A_{\text{obs}} = \left( \frac{1}{4} M_{\text{obs}}^2 \nu^2 c_s^2 c_1 \right) \sum_{i,j} \beta_{ij} (\nu_\infty + \nu_0 / M_i) (\nu_\infty + \nu_0 / M_j) c_i c_j = (A_2 \nu_\infty^2 \bar{M}_w^2 / \nu^2 M_{\text{obs}}^2 c_1) \times [1 + B \sum \beta_{ij} c_i c_j (1/M_i + 1/M_j + \nu_0 / \nu_\infty M_i M_j)] \quad (34)$$

where

$$4B = \nu_0 / \nu_\infty c_s^2 \bar{M}_w A_2.$$

The main difference between  $A_{\text{obs}}$  and  $A_2$  is contained in the term in front of the term in square brackets. The sums inside the square brackets can only be evaluated approximately. To do this, we use the expression of Flory and Krigbaum<sup>20</sup> for the second virial coefficient of a random polymer chain:

$$A_2 = (J / N_A c_s^2 \bar{M}_w^2) \sum_{i,j} F(J \xi_{ij}^3) c_i c_j M_i M_j \quad (35)$$

where

$$J = (\psi_1 - \kappa_1) v_s^2 / V_1 \quad (36)$$

with  $\psi_1$ ,  $\kappa_1$  enthalpy and entropy parameters characteristic of the polymer,  $v_s$  the specific volume of the polymer, and  $V_1$  the molar volume of the solvent. The function  $F(J \xi_{ij}^3)$  contains the quantities  $\xi_{ij}$  in its argument, which are related to the excluded volume of an  $ij$  pair. In the present case,  $v_s$  is an increasing

function of molecular weight, and calculations show<sup>20</sup> that  $F(J\xi_{ij}^3)$  is a decreasing function of molecular weight. A reasonable approximation for the range of molecular weights over which  $\nu_i$  is not constant is thus to take  $JF(J\xi_{ij}^3)$  constant. According to equations (35) and (28), this means that  $\beta_{ij} = 4A_2M_iM_jc_1$ , and equation (34) becomes

$$A_{\text{obs}}/A_2 = (\nu_\infty \bar{M}_w / \nu M_{\text{obs}})^2 \times [1 + (2\nu_0/\nu_\infty \bar{M}_w)(1 + \nu_0/2\nu_\infty \bar{M}_w)] \quad (37)$$

Once  $\bar{M}_w$  is known,  $A_2$  can be obtained from  $A_{\text{obs}}$  and equation (36).

Figure 1 shows the dependence of  $M_{\text{obs}}$  and  $A_{\text{obs}}$  on the refractive index of the solvent for a polymer with  $\bar{M}_w = 2\bar{M}_n = 2000$ ,  $v_s^\infty = \bar{v}_s^\infty = 0.9 \text{ cm}^3/\text{g}$ ,  $n_s^\infty = 1.60$ ,  $a_0 = 10$ ,  $b_0 = 100 \text{ cm}^3/\text{mol}$ . The values of  $\nu$  and  $\nu_\infty$  become zero, in general, at different values of the refractive index of the solvent, resulting in a marked dependence of both  $M_{\text{obs}}$  and  $A_{\text{obs}}$  on  $n_1$ .

## MIXTURES OF POLYMERS

The dependence of the observed molecular weight on the refractive index of the solvent, as deduced above, resembles the dependence of the observed molecular weight of a homopolymer mixture or of a copolymer on the refractive index of the solvent, as deduced by Bushuk and Benoit<sup>21</sup>. It is of interest to extend the theory to include mixtures with refractive index increments that depend on molecular weight.

Consider a mixture of polydisperse solutes of types A and B, with relative mass fractions  $w_A$ ,  $w_B = 1 - w_A$ . For each of the  $q' - 1$  members of type A (component 1 is the solvent),

$$\nu_i = \nu_\infty^A + \nu_0^A/M_i, \quad i = 2, \dots, q' \quad (38)$$

and a similar equation holds for the remaining  $q - q'$  members of type B. The observed refractive index increment is then

$$\bar{\nu} = \sum_{i=2}^{q'} \beta_i (\nu_\infty^A + \nu_0^A/M_i) + \sum_{i=q'+1}^q \beta_i (\nu_\infty^B + \nu_0^B/M_i) \\ = \bar{\nu}_\infty + \bar{\nu}_0/\bar{M}_n \quad (39)$$

where

$$\bar{\nu}_0 = x_A \nu_0^A + x_B \nu_0^B \quad (40)$$

$$\bar{\nu}_\infty = w_A \nu_\infty^A + w_B \nu_\infty^B \quad (41)$$

$$\bar{M}_n^A = w_A / \sum_{i=2}^{q'} \beta_i / \bar{M}_i \quad (42)$$

and  $x_A$ ,  $x_B$  are the mole fractions of A and B, and a similar equation holds for  $\bar{M}_n^B$ . From equations (30), (38) and (39), the observed molecular weight is given by:

$$\bar{\nu}^2 M_{\text{obs}} = \sum_{i=2}^q \nu_i^2 c_i M_i / c_s \\ = (\nu_\infty^A)^2 w_A (\bar{M}_n^A - \bar{M}_n^A) + (\nu_\infty^B)^2 w_B (\bar{M}_n^B - \bar{M}_n^B) + \\ (\nu_0^A)^2 w_A \bar{M}_n^A + (\nu_0^B)^2 w_B \bar{M}_n^B \quad (43)$$

where  $c_s = c_A + c_B$  is the total solute concentration, and the weight-average molecular weight of A is

$$\bar{M}_w^A = \sum_{i=2}^{q'} c_i M_i / c_A \quad (44)$$

$\bar{M}_w^B$  is defined in the same manner. Equation (43) may be expressed in a form analogous to equation (33):

$$\bar{\nu}^2 M_{\text{obs}} = \bar{\nu}^2 \bar{M}_n^* + \bar{\nu}_\infty^2 (\bar{M}_w - \bar{M}_n^*) + 2(P - R)(\nu_\infty^A - \nu_\infty^B) \bar{\nu}_\infty + \\ (Q - S)(\nu_\infty^A - \nu_\infty^B)^2 + 2R(\nu_0^A - \nu_0^B) \bar{\nu} + \\ S(\nu_0^A - \nu_0^B)^2 \quad (45)$$

where

$$\bar{M}_n^* = w_A \bar{M}_n^A + w_B \bar{M}_n^B \quad (46)$$

and  $\bar{M}_w$  and  $\bar{\nu}$  are defined similarly. The form of equation (45) follows by noting that equation (43) is a quadratic function of the refractive index increments. The parameters are found by substituting for  $\bar{\nu}$ ,  $\bar{\nu}_\infty$  and  $\bar{M}_n^*$  in equation (45), equating the resulting equation to equation (43), and comparing coefficients of like powers of the various refractive index increments. These parameters are measures of the heterogeneity of the mixture, and are given by:

$$P = w_A w_B (\bar{M}_w^A - \bar{M}_w^B) \\ Q = w_A w_B (w_B \bar{M}_n^A + w_A \bar{M}_n^B) \\ R = w_A w_B (\bar{M}_n^A - \bar{M}_n^B) \\ S = w_A w_B (w_B \bar{M}_n^A + w_A \bar{M}_n^B) \quad (47)$$

Equation (45) contains  $\bar{M}_n^*$ , which is not directly measurable from the properties of the mixture alone. If  $w_A \bar{M}_n^A$  and  $w_B \bar{M}_n^B$  are not widely different,  $\bar{M}_n^*$  is much closer to  $\bar{M}_n$  than to  $\bar{M}_w$ . For  $\nu_0^A = \nu_0^B = 0$ , equation (45) reduces to the equation of Bushuk and Benoit. The factor of 2 in this equation conforms to their usage. Comparison of equation (45) with equation (33) shows that the simplest mixture gives additional terms in the expression for  $M_{\text{obs}}$ . Since the total refractive index  $\bar{\nu}$  can approach zero while  $\bar{\nu}_\infty$ ,  $\bar{\nu}_\infty^A - \bar{\nu}_\infty^B$  and  $\bar{\nu}_0^A - \bar{\nu}_0^B$  remain finite, these terms alone can cause the observed molecular weight to become very large in an appropriate solvent<sup>21</sup>.

If the properties of each component of the mixture are known, the behaviour of equation (45) as a function of the refractive index of the solvent can be found. As an example, take  $\bar{M}_n^A = 5000$ ,  $\bar{M}_n^B = 2000$ ,

$$\bar{M}_w^A / \bar{M}_n^A = \bar{M}_w^B / \bar{M}_n^B = 2.$$

For polymer A,  $v_s^\infty = \bar{v}_s^\infty = 0.8 \text{ cm}^3/\text{g}$ ,  $n_s^\infty = 1.50$ ,  $a_0 = 20$ ,  $b_0 = 200 \text{ cm}^3/\text{mol}$ . For polymer B, the parameters are those used to derive Figure 1. For a mixture with  $w_A = w_B = 0.5$ ,  $2P = R = 1500$ ,  $Q = S/2 = 875$ ,

$$\bar{M}_w = 2\bar{M}_n^* = 3500,$$

$\bar{M}_n = 1429$ ,  $\bar{M}_w / \bar{M}_n = 2.35$ . In Figure 2, the observed molecular weight, calculated from equations (45) and (19), is plotted as a function of  $n_1$ , the refractive index of the solvent. As in Figure 1, it is apparent that the mixture terms become less important as the value of  $n_1$  differs more from the refractive index of either solute component. If the assumption  $\bar{M}_n = \bar{M}_n^*$  is made, the correct  $\bar{M}_w$  can be estimated from measurements of  $M_{\text{obs}}$  as a function of  $n_1$ .

Comparison of Figures 1 and 2 shows the striking difference in the dependence of  $M_{\text{obs}}$  on  $n_1$ , especially near the value of  $n_1$  for which  $\bar{\nu}$  becomes zero. In principle, this dependence can be used to detect the presence of two components with different refractive index increments. A simple mixture and a copolymer cannot be distinguished however, since equations of the same form hold for a copolymer<sup>21</sup>.

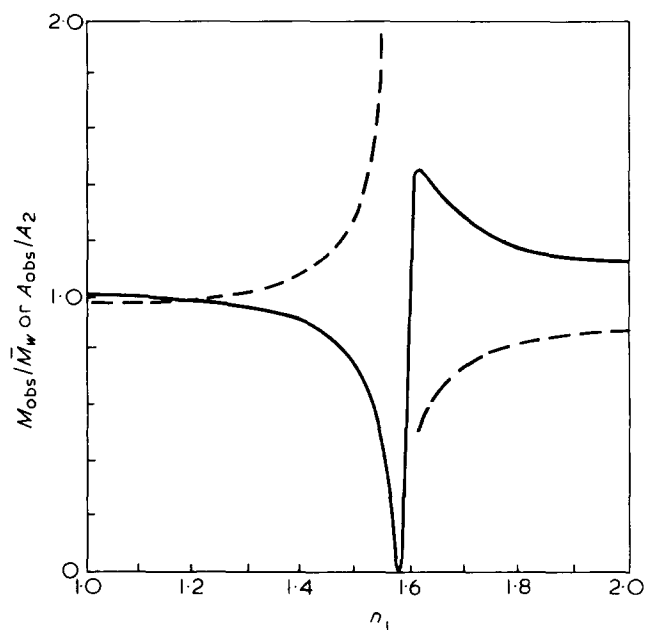


Figure 1  $M_{obs}/\bar{M}_w$  as a function of refractive index of solvent,  $n_1$ , ----;  $A_{obs}/A_2$  as a function of  $n_1$ , ——. The polymer has  $\bar{M}_w = 2\bar{M}_n = 2000$ , and other parameters as given in the text

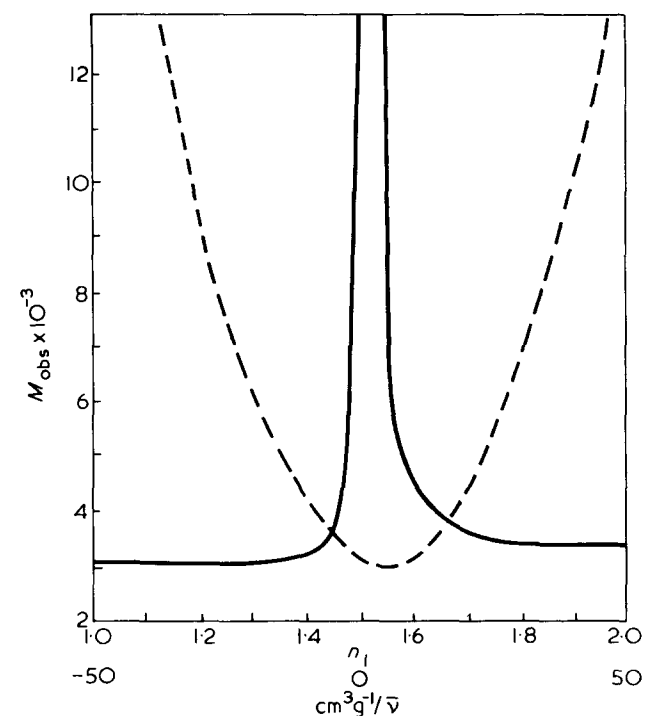


Figure 2 Observed molecular weight of a mixture with parameters as given in the text as a function of a refractive index of solvent,  $n_1$ , —; and as a function of average refractive index increment,  $\bar{v}$ , ----. The dashed curve is parabolic. The correct weight average molecular weight is  $\bar{M}_w = 3500$

If the properties of the individual components of the mixture (or copolymer) are unknown, treatment of experimental data using equation (45) to find the parameters (47) is difficult, since the roughest approximation gives  $\bar{v}^2 M_{obs}$  as a quadratic function of the refractive index of the solvent. A useful approximation is to assume that  $\bar{v}_\infty/\bar{v}$ ,  $\nu^A - \nu^B$  and  $\nu_\infty^A - \nu_\infty^B$  vary much less than  $\bar{v}$  or  $\bar{v}_\infty$  over the range of values of  $n_1$  that is en-

countered in practice. For the example given above,  $\nu^B - \nu^A$  and  $\nu_\infty^B - \nu_\infty^A$  vary from 0.07 to 0.09 and  $\bar{v}_\infty/\bar{v}$  varies from 0.06 to 1.0 over the range  $n_1 = 1.8$  to 1.3, while  $\bar{v}$  varies from 0.2 to -0.3. According to equation (45),  $M_{obs}$  is then a quadratic function of  $1/\bar{v}$ , of the form:

$$M_{obs} = A + B/\bar{v} + C/\bar{v}^2 \quad (48)$$

For the example given above,  $A = 2.87 \times 10^3$  g/mol, and the average values of  $B$  and  $C$  are  $-48.0 \times 10^3$  cm<sup>3</sup>/mol and  $5.6 \times 10^3$  cm<sup>6</sup> g<sup>-1</sup> mol<sup>-1</sup>, respectively. If the data for the example are fitted by quadratic least squares<sup>22</sup> to equation (48), the values

$$A = 3.21 \times 10^3, \quad B = -49.0 \times 10^3, \quad C = 7.0 \times 10^3$$

are found, in reasonable agreement. Figure 2 also shows  $M_{obs}$  as a function of  $1/\bar{v}$ . The least squares curve is indistinguishable from the plotted points on the scale of the Figure. A similar approximation should also hold for the simpler case  $\nu_0^A = \nu_0^B = 0$ , but if the data of Bushuk and Benoit<sup>21</sup> are fitted to equation (48) by least squares, the values of the coefficients  $A$ ,  $B$  and  $C$  differ considerably from their estimates. The standard error of estimate is also large, and emphasizes that highly precise scattering data are necessary if a mixture is to be analysed by any of the above methods.

#### ACKNOWLEDGEMENTS

The research for this paper was supported, in part, by the Defence Research Board of Canada and the National Research Council of Canada. We wish to thank the Government of Ontario for a graduate fellowship to D. E. G. J., and the British Council for a travel grant to J. W. L.

#### REFERENCES

- 1 Kirkwood, J. G. and Goldberg, R. J. *J. Chem. Phys.* 1950, **18**, 54
- 2 Stockmayer, W. J. *J. Chem. Phys.* 1950, **18**, 58
- 3 Lorimer, J. W. *Polymer* 1972, **13**, 46
- 4 Jones, D. E. G. and Lorimer, J. W. *Polymer* (in the press)
- 5 Böttcher, C. J. F. 'Theory of Electric Polarisation', Elsevier Publishing Co., Amsterdam, 1952, sections 40, 44
- 6 Partington, J. R. 'An Advanced Treatise on Physical Chemistry. Vol. IV. Physico-chemical Optics', Longmans, Green and Co., London, 1963, section 10
- 7 Li, K., Arnett, R. L., Epstein, M. B., Ries, R. B., Bitler, L. P., Lynch, J. M. and Rossini, F. D. *J. Phys. Chem.* 1956, **60**, 1400
- 8 Bodmann, O. *Makromol. Chem.* 1969, **122**, 210
- 9 Fox, T. G. and Loshaek, S. *J. Polym. Sci.* 1955, **15**, 371
- 10 Fox, T. G. and Flory, P. J. *J. Appl. Phys.* 1950, **21**, 581
- 11 Schulz, G. V. and Hoffmann, M. *Makromol. Chem.* 1957, **23**, 220
- 12 Kobatake, Y. and Inagaki, H. *Makromol. Chem.* 1960, **40**, 118
- 13 Stacy, C. J. and Arnett, R. L. *J. Polym. Sci. (A-2)* 1964, **2**, 167
- 14 Heller, W. *J. Polym. Sci. (A-2)* 1966, **4**, 209
- 15 Huglin, M. B. *J. Appl. Polym. Sci.* 1965, **9**, 4003
- 16 Huglin, M. B. *J. Appl. Polym. Sci.* 1965, **9**, 3963
- 17 Meyerhoff, G. and Moritz, U. *Makromol. Chem.* 1967, **109**, 143
- 18 Bodmann, O. *Makromol. Chem.* 1969, **122**, 196
- 19 Wigand, G. and Veith, H.-J. *Plaste Kaut.* 1969, **9**, 671
- 20 Flory, P. J. and Krigbaum, W. R. *J. Chem. Phys.* 1950, **18**, 1086
- 21 Bushuk, W. and Benoit, H. *Can. J. Chem.* 1958, **36**, 1616
- 22 Hamilton, W. C. 'Statistics in Physical Science', Ronald Press Co., New York, 1964, section 5-6

# Preparation and properties of networks containing chloroprene

J. Ashworth, C. H. Bamford and E. G. Smith

*Department of Inorganic, Physical and Industrial Chemistry, Donnan Laboratories, University of Liverpool, PO Box 147, Liverpool L69 3BX, UK (Received 1 June 1971)*

The free-radical solution polymerization of chloroprene (CP) photoinitiated by manganese carbonyl  $[\text{Mn}_2(\text{CO})_{10}]$  in the presence of organic halides has been studied and found to obey conventional steady-state kinetics with  $k_p k_t^{-1/2} = 0.012 \text{ mol}^{-1/2} \text{ l}^{1/2} \text{ s}^{-1/2}$ . Use of a preformed polymer, poly(vinyl trichloroacetate) (PVTCA), as the halide component of the initiator enabled the nature of the termination reaction to be deduced from measurements of gel times; it appears that termination occurs predominantly by combination at 25°C. Autoacceleration, which accompanies gelation, sets in before the gel point is reached, and becomes more pronounced with increasing crosslink density.

With the aid of the above kinetic data it was possible to prepare crosslinked systems of known constitution based on PCP and PVTCA. Electron microscope studies showed the existence of two-phase systems in which the domains of polychloroprene are much smaller and far more uniform than in a comparable blend of the component polymers. The structure of these materials is discussed.

## INTRODUCTION

We have already described<sup>1-4</sup> a synthetic route to block and graft copolymers and networks based on initiating systems typically composed of an organic halide and an organometallic derivative of a transition metal in a low oxidation state. This technique is of rather wide applicability and allows statistical control of the mean crosslink density and length, the ratio of branches to crosslinks in networks, and related relevant quantities in graft and block copolymers.

As part of a study of the properties of materials prepared in this way we have examined<sup>5</sup> the networks poly(vinyl trichloroacetate) (PVTCA) + poly(methyl methacrylate) (PMMA) and poly(vinyl trichloroacetate) + polystyrene (PS). Dilatometric observations showed the existence of two glass-transition temperatures, indicating the presence of two separate phases. In the case of the systems containing polystyrene, the coefficients of cubical expansion were consistent with almost complete separation of the two polymer species. However, with the poly(methyl methacrylate) systems the slope of the volume-temperature plot between the two transition temperatures was larger than anticipated on this basis and it was proposed that the two phases consist of poly(methyl methacrylate) and a mixture of this polymer and poly(vinyl trichloroacetate), respectively. The latter phase was considered to exhibit a single glass transition. Geometrical constraints imposed by the network structure must be one important factor determining the morphology of such systems.

Direct ultramicroscopic investigations of the morphology of the networks was not possible since no suitable staining technique could be devised. It was therefore thought desirable to use a diene as crosslinking monomer to enable the osmium tetroxide fixation technique described by Kato<sup>6</sup> to be employed. Further, systems of this type might provide information in the fields of thermoplastic elastomers and high impact plastics.

Chloroprene (CP) appeared to be the most suitable monomer. Both butadiene and isoprene polymerize very slowly in solution, on account of high termination and low propagation velocity coefficients<sup>7</sup>. They have the additional disadvantage of being non-solvents for PVTCA. Little quantitative information on the kinetics of free-radical solution polymerization of chloroprene is available in the literature so that it was necessary to determine the kinetic parameter  $k_p k_t^{-1/2}$  ( $k_p$ ,  $k_t$  are the velocity coefficients of propagation and termination, respectively) and also the incidence of combination in the termination reaction. For these purposes photoinitiation by manganese carbonyl in the presence of a suitable organic halide was used<sup>4, 8</sup>. (Chloroprene itself does not behave as an active halide in the reaction.) Reasons have been advanced in an earlier publication<sup>4</sup> for believing that the rate of initiation by this system is independent of the nature of the monomer; consequently comparison of the rates of polymerization of chloroprene and methyl methacrylate ( $k_p k_t^{-1/2} = 0.055 \text{ mol}^{-1/2} \text{ l}^{1/2} \text{ s}^{-1/2}$  at 25°C) allowed  $k_p k_t^{-1/2}$  for chloroprene to be estimated. The nature of the termination reaction was investigated by

using PVTCA as the halide, and comparing the gel time with that for methyl methacrylate (for which the fraction of combination in termination is known<sup>4</sup> to be 0.34 at 25°C).

The work on chloroprene polymerization and the ultramicroscopic examination of PVTCA + PCP networks are the subjects of the present paper.

## EXPERIMENTAL

### Materials

Manganese carbonyl  $[\text{Mn}_2(\text{CO})_{10}]$  was purified by sublimation in vacuum and was stored in the dark.

Chloroprene is extremely reactive towards oxygen, forming unstable peroxides which subsequently dissociate and initiate polymerization. To obtain kinetically pure material it was necessary to ensure the absence of oxygen at all stages of purification.

The stabilizer (t-butyl) catechol) was removed by several washings with dilute sodium hydroxide, followed by distilled water. After standing over molecular sieves for several hours the chloroprene was transferred to a vessel fitted with a break-seal. These processes were carried out in a glove-box purged with nitrogen. The vessel containing the monomer was evacuated and sealed off, and any peroxides present were decomposed by irradiating the liquid with light of wavelength 365 nm. Finally, the container was attached to the vacuum line, and the desired amount of chloroprene was distilled directly into the reaction vessels through the break-seal.

The purification of methyl methacrylate and the preparation of poly(vinyl trichloroacetate) have been described in an earlier paper<sup>9</sup>. Analar ethyl trichloroacetate, required for the determination of  $k_p k_t^{-1/2}$  for chloroprene, was used without further purification.

### Apparatus and techniques

Polymerizations were carried out in a laboratory illuminated by inactive (sodium) light.

Photo-initiation was effected by a parallel beam of light, with wavelength predominantly 435.8 nm. The optical apparatus, and the dilatometric technique used for following polymerization have been described in detail elsewhere<sup>1</sup>. In experiments involving gelation a portion of the capillary of the dilatometer adjacent to the light beam was blackened to prevent destruction of the meniscus by gelation.

Gel times were measured in Pyrex vacuum viscometers of the type described by Bamford and Dewar<sup>10</sup>.

A JEM7 electron microscope, operating with an accelerator voltage of 80 kV, was used to obtain electron micrographs of thin films and sections.

*Thin films.* Cast films of suitable thickness for direct examination by electron microscopy were prepared by two methods.

In the first method, a drop of a solution of polymer in benzene (0.4% w/v) was placed on a microscope grid and allowed to dry. The film formed had a somewhat irregular thickness of the order of 2  $\mu\text{m}$ .

Alternatively, freshly cleaved mica sheet was coated with a fine carbon deposit by means of a vacuum evaporator. It was then covered with a solution of the polymer in benzene (0.04% w/v), and the solvent was

evaporated. The polymer film was carefully floated off the mica by bringing the edge into contact with a clean water surface. The floating film was separated into convenient portions and lifted on to grids; observation of the films was greatly facilitated by the carbon support. Film thicknesses obtained by this technique were calculated to be of the order of 100 nm.

Thin films of the PVTCA/PCP network (I) (Table 1) were prepared by both methods. A film of a blend of PVTCA + PCP (100:16 w/w) was obtained by the first method.

Specimens were stained for periods of 1 and 4 h by exposure to the vapour of a 1% aqueous solution of osmium tetroxide contained in a closed vessel. The longer period produced a considerable improvement in contrast.

In order to check that the casting procedure did not introduce artifacts which might have been interpreted as structural details a film of PVTCA was prepared by the first method. No structure was discernible after prolonged exposure to osmium tetroxide vapour.

*Ultra-thin sections.* A small piece of the PVTCA/PCP network II (Table 1) from which excess monomer and solvent had been removed in vacuum, was stained in a 1% aqueous osmium tetroxide solution for 24 h then stuck to a block of Araldite resin. The specimen was trimmed to a small area and faced in an LKB ultra-microtome. After restaining the face, sections 80 nm in thickness were cut.

## RESULTS AND DISCUSSION

### Determination of $k_p k_t^{-1}$ for chloroprene

The polymerization of chloroprene (80% v/v in benzene) at 25°C was photo-initiated ( $\lambda = 435.8 \text{ nm}$ ) by manganese carbonyl in the presence of ethyl trichloroacetate. Rates of initiation  $\mathcal{I}$  were determined by comparable experiments with methyl methacrylate. Figure 1 shows that the

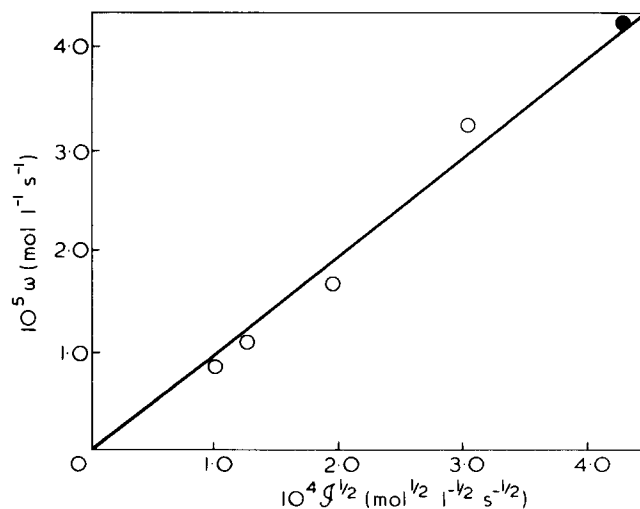


Figure 1 Proportionality between rate of polymerization of chloroprene  $\omega$  and square root of rate of photo-initiation  $\mathcal{I}^{1/2}$  at 25°C. [Chloroprene] = 8.16 mol l<sup>-1</sup>; solvent = benzene.  $10^4 [\text{Mn}_2(\text{CO})_{10}]$  (mol l<sup>-1</sup>): ○ 5.14, ● 10.28. [Ethyl trichloroacetate] = 0.032 mol l<sup>-1</sup>,  $\lambda = 435.8 \text{ nm}$



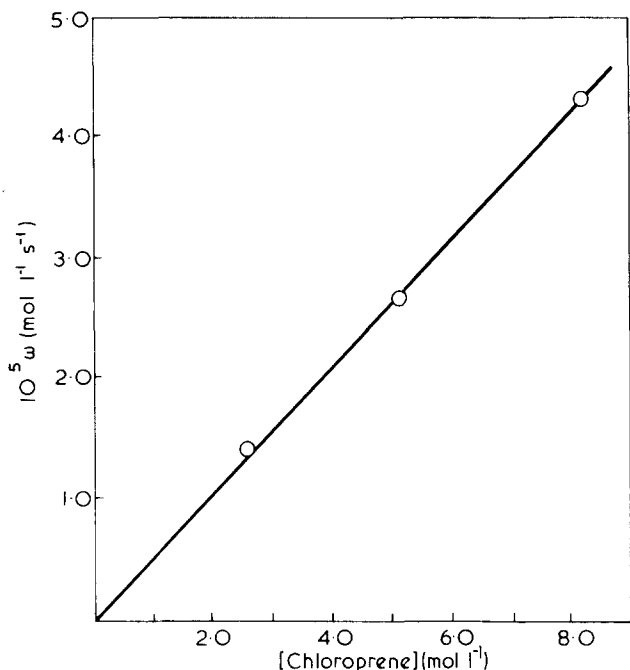


Figure 2 Proportionality between rate of polymerization of chloroprene and chloroprene concentration at 25°C. Solvent = benzene.  $10^4[\text{Mn}_2(\text{CO})_{10}] = 10.28 \text{ mol l}^{-1}$ ,  $\lambda = 435.8 \text{ nm}$ . [Ethyl trichloroacetate] =  $0.032 \text{ mol l}^{-1}$

rate of polymerization  $\omega$  is proportional to the square root of the rate of initiation over the range studied. At constant rate of initiation the rate of polymerization is proportional to the monomer concentration  $[M]$  (Figure 2). The reaction therefore appears to follow conventional free-radical kinetics expressed by:

$$\omega = k_p k_t^{-1/2} [M] \mathcal{I}^{1/2} \quad (1)$$

$\mathcal{I}$  being independent of the monomer concentration under our conditions. From the data in Figure 1 we find that

$$k_p k_t^{-1/2} = 0.012 \pm 0.001 \text{ mol}^{-1/2} \text{ l}^{1/2} \text{ s}^{-1/2} \quad (2)$$

#### Termination reaction in chloroprene polymerization

Use of a polymeric halide such as PVTCA in association with an organometallic derivative (e.g.  $\text{Mn}_2(\text{CO})_{10}$ ) leads ultimately to gelation if termination occurs at least partly by radical combination. Under the simplest conditions, application of gel theory leads to the following expression for the gel time  $t_g^0$

$$\frac{1}{t_g^0} = \frac{\mathcal{I} \bar{P}_w}{c} \frac{k_{tc}}{k_{tc} + k_{td}} \quad (3)$$

in which  $\bar{P}_w$ ,  $c$  represent the weight-average degree of polymerization and base-molar concentration of the prepolymer and  $k_{tc}$ ,  $k_{td}$  are the velocity coefficients for termination by combination and disproportionation, respectively. In practice,  $t_g^0$  may differ from the observed gel time  $t_g$  on account of the occurrence of transfer processes, initiator consumption, and radical wastage arising from ring-formation<sup>1,2</sup>. Methods for calculating  $t_g^0$  from  $t_g$  have been described in an earlier publication<sup>2</sup>. In correcting for initiator consumption it was assumed that the rate of free-radical generation is twice the rate of

consumption of  $\text{Mn}_2(\text{CO})_{10}$ <sup>11</sup>. Chain-transfer was supposed to be negligible in the chloroprene system; for methyl methacrylate the transfer constant to monomer was taken as  $2 \times 10^{-5}$  at 25°C. According to equation (3) a plot of  $1/t_g^0$  against  $\mathcal{I}$  for constant  $c$  should be linear with slope

$$\frac{\bar{P}_w}{c} \frac{k_{tc}}{k_{tc} + k_{td}}$$

Thus if  $\bar{P}_w/c$  is known,  $k_{tc}/(k_{tc} + k_{td})$  may be calculated. Alternatively, if  $t_g^0$  is determined for a monomer for which the nature of the termination reaction is known, application of equation (3) gives  $\bar{P}_w/c$  and hence leads to a value of  $k_{tc}/(k_{td} + k_{tc})$  for the monomer under investigation. We have adopted the latter procedure, with methyl methacrylate as the reference monomer. From a plot of  $1/t_g^0$  against  $\mathcal{I}$  for methyl methacrylate we find that

$$\bar{P}_w/c = (5.56 \pm 0.72) \times 10^4 \text{ mol}^{-1} \quad (4)$$

A plot of  $1/t_g^0$  against  $\mathcal{I}$  for chloroprene in benzene solution (80% v/v) is shown in Figure 3 for a value of  $c$  ( $0.046 \text{ mol l}^{-1}$ ) equal to that in the methyl methacrylate experiments. From equations (3) and (4) we find that for chloroprene at 25°C

$$\frac{k_{tc}}{k_{tc} + k_{td}} = 1.00 \pm 0.13 \quad (5)$$

Thus the termination reaction in chloroprene polymerization is effectively a combination process, and networks prepared as described earlier will contain few branches.

#### Autoacceleration in the formation of networks containing chloroprene

During the preparation of these networks it was found that for reactions taken beyond the gel time the con-

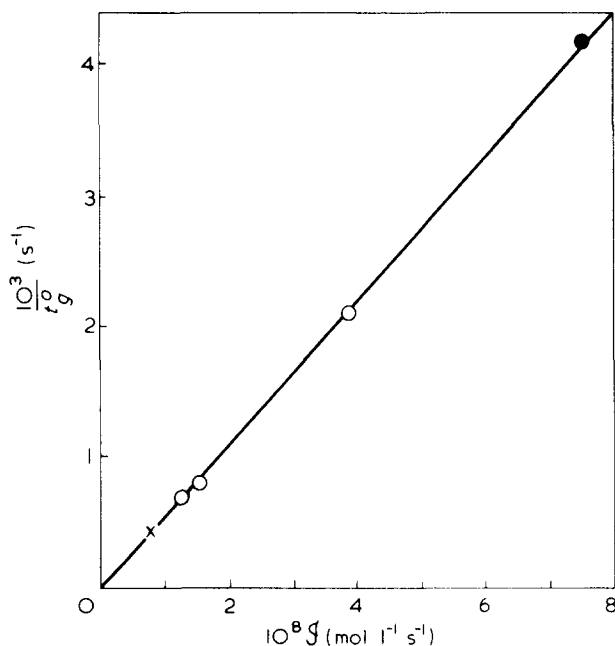


Figure 3 Dependence of corrected gel time  $t_g^0$  on  $\mathcal{I}$  at 25°C. [Chloroprene] =  $8.16 \text{ mol l}^{-1}$ ; solvent = benzene;  $10^4[\text{Mn}_2(\text{CO})_{10}]$  (mol l<sup>-1</sup>): ×, 2.57; ○, 5.14; ●, 10.28. [PVTCA] =  $0.046 \text{ mol l}^{-1}$

versions were much higher than predicted by equation (1). From the dilatometric plots shown in Figure 4 it will be seen that autoacceleration sets in before the gel point is reached. On the other hand, with methyl methacrylate as monomer, there is no detectable autoacceleration until reaction has proceeded for considerably longer than  $t_g$ , and the effect is much less marked than with chloroprene (see Figure 5). It has previously been reported<sup>5</sup> that styrene also shows considerable autoacceleration under similar conditions. The autoacceleration is clearly a manifestation of the Trommsdorf-Norrish effect, arising

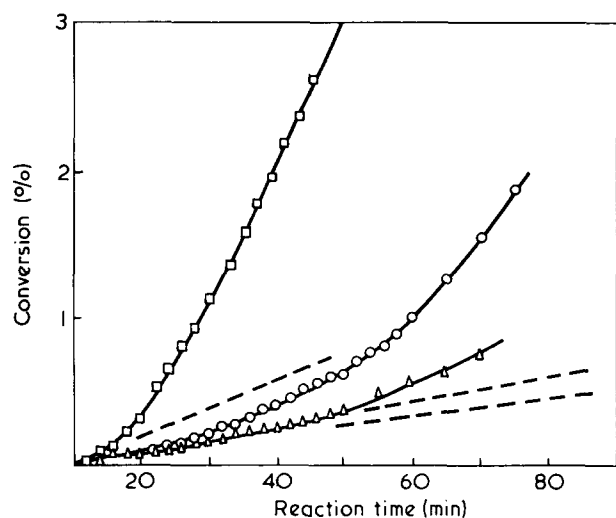


Figure 4 Autoacceleration during network formation with chloroprene at 25°C. [Chloroprene]=8.16 mol l<sup>-1</sup>; solvent=benzene; [PVTCA]=0.046 mol l<sup>-1</sup>. 10<sup>9</sup>  $\mathcal{J}$  (mol l<sup>-1</sup> s<sup>-1</sup>): □, 76; ○, 15; △, 7.5. Measured gel times (min): □, 4; ○, 20; △, 44. 10<sup>4</sup>[Mn<sub>2</sub>(CO)<sub>10</sub>] (mol l<sup>-1</sup>): □, 10.28; ○, 5.14; △, 2.57. ---- represents calculated initial rates of conversion

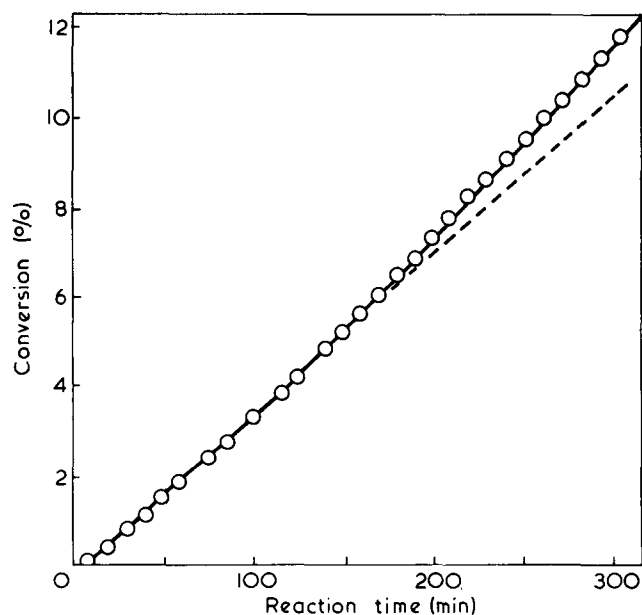


Figure 5 Autoacceleration during network formation with methyl methacrylate at 25°C. [MMA]=7.5 mol l<sup>-1</sup>; solvent=benzene. [PVTCA]=0.092 mol l<sup>-1</sup>. 10<sup>8</sup>  $\mathcal{J}$ =3.8 mol l<sup>-1</sup> s<sup>-1</sup>. 10<sup>4</sup>[Mn<sub>2</sub>(CO)<sub>10</sub>]=5.14 mol l<sup>-1</sup>. Measured gel time=55 min

from a reduced velocity coefficient of chain termination. The results obtained with the three monomers suggest that a low value of  $k_p k_t^{-1/2}$ , which would lead to shorter crosslinks under comparable conditions and so give 'tighter' gels, might favour autoacceleration.

The occurrence of autoacceleration is useful in systems of this type in which monomers with low values of  $k_p k_t^{-1/2}$  are polymerized, since it allows appreciable conversions to be obtained in relatively short times. If most of the autoacceleration takes place in the early stages of reaction, as appears to be the case in the polymerization represented by □ in Figure 4, its broadening effect on the molecular weight distribution might be less than would appear at first sight.

In view of the uncertainties introduced by the pronounced autoacceleration in systems containing chloroprene, the mean crosslink length in network II was calculated from the consumption of chloroprene and the number of chains started (i.e.  $\mathcal{J} \times$  reaction time), rather than from  $k_p k_t^{-1/2}$ .

### Electron microscopy

Specimens suitable for examination by electron microscopy were obtained both by thin-film casting from benzene solution and by cutting ultrathin sections by microtomy as described above.

The preparative experimental details for the networks are summarized in Table 1, together with compositions and structural parameters derived as already explained. A blend of PVTCA and PCP was also examined; a mixture of the homopolymers was cast on a grid as a film from benzene solution.

Table 1 Network preparation and parameters  
Polymerization temperature: 25°C. Diluent: benzene

Polymerization	I	II
Initial [Mn <sub>2</sub> (CO) <sub>10</sub> ] (mol l <sup>-1</sup> )	5.14 × 10 <sup>-4</sup>	6.4 × 10 <sup>-4</sup>
[PVTCA] (g/l)	10	12.5
[M] (mol l <sup>-1</sup> )	8.16	7.65
Observed gel time (min)	44	3-4
Reaction time (min)	25	35
10 <sup>9</sup> $\mathcal{J}$ (mol l <sup>-1</sup> s <sup>-1</sup> )	7.5	110
10 <sup>2</sup> [ΔM] (mol l <sup>-1</sup> )	1.29 (calc)	43
% Chloroprene in network (w/w)	10.4	75.5
Mean no. of crosslinked units per weight-average prepolymer chain	0.57	11.7-8.8
$\bar{P}_n$ crosslinks	2290	3720

Figures 6 and 7 show typical electron micrographs of two films of polymer I (Table 1) cast on a mica surface and a grid respectively, as already described. Both specimens exhibit phase separation, the dark areas in the Figures corresponding to regions rich in chloroprene. The thinner film (Figure 6) shows a relatively regular distribution of rubber domains; the thickness of the film is probably of the order of the domain size and less than the average inter-domain separation so that Figure 6 is likely to represent a single layer of domains. Figure 7, which refers to a thicker specimen, presumably corresponds to a superposition of structures such as those in Figure 6. Figure 8 was obtained from a section of network II (Table 1), containing a much higher proportion of polychloroprene. The distribution is much less regular than that in Figure 6; this may, in part, be the result of damage during sectioning. Dis-

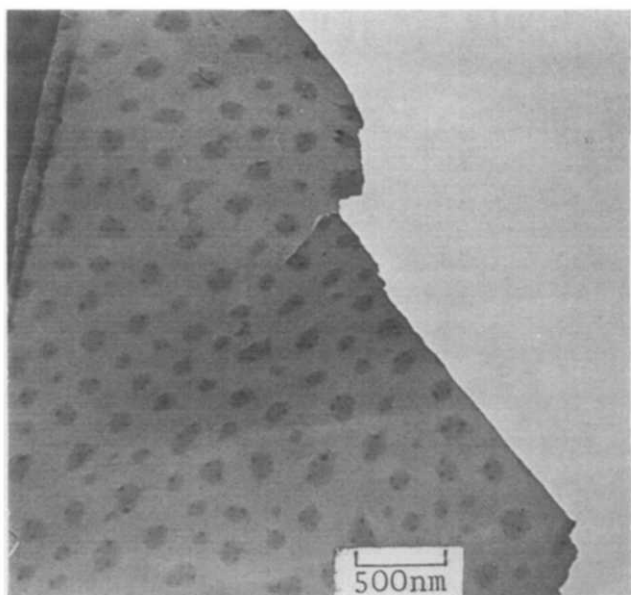


Figure 6 Electron micrograph of film prepared by the second method, thickness  $\sim 100\text{nm}$ ; network I (Table 1)

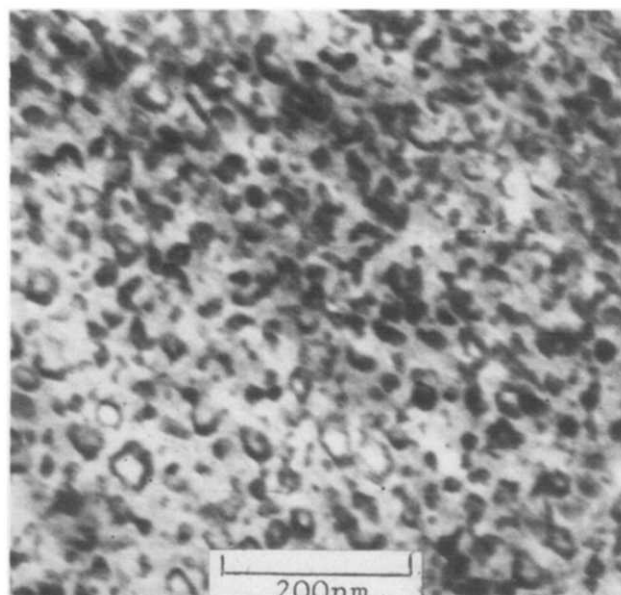


Figure 8 Electron micrograph of section of network II (Table 1), thickness  $\sim 80\text{nm}$

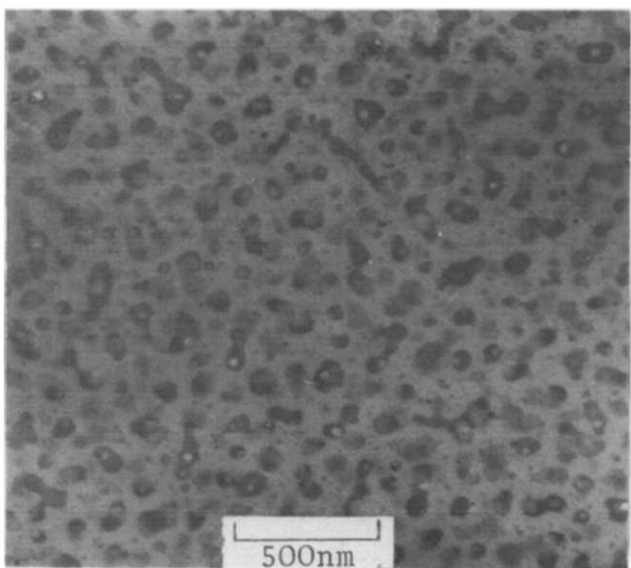


Figure 7 Electron micrograph of film prepared by the first method; thickness  $\sim 2\mu\text{m}$ ; network I (Table 1)

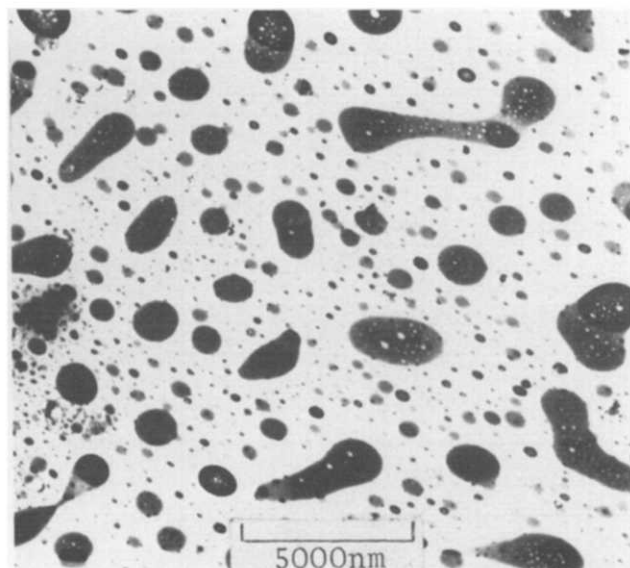


Figure 9 Electron micrograph of film of blend of PVTCA and PCP (100 : 16 w/w) cast as in the first method; thickness  $\sim 2\mu\text{m}$

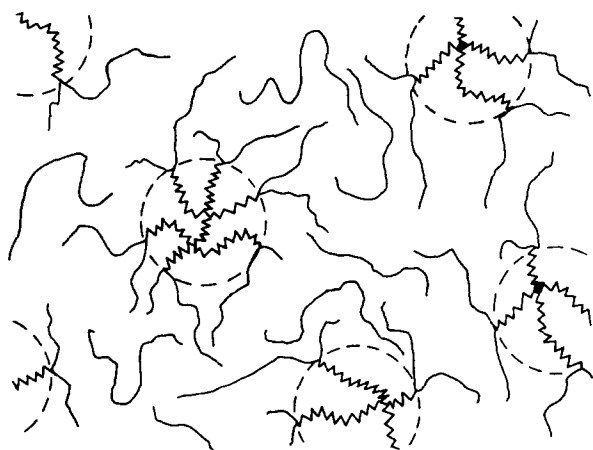
tion on drying may also be important, since the specimen has a comparatively high crosslink density.

Figure 9 shows the structure of the film cast from the blend under comparable conditions and resembles electron micrographs obtainable from many other polymer blends<sup>12</sup>. Comparison of Figures 6, 7 and 9 shows that only in the blend are large rubber domains ( $\sim 2000\text{nm}$ ) in evidence. The networks appear to have domains which are much smaller ( $\sim 150\text{nm}$ ) and more nearly uniform in size and shape.

We now consider the separation of the domains in Figure 6. This appears to have an average value of approximately  $200\text{nm}$ ; since it is greater than even the fully extended length of an average PVTCA chain, the rubber domains cannot be connected by single PVTCA

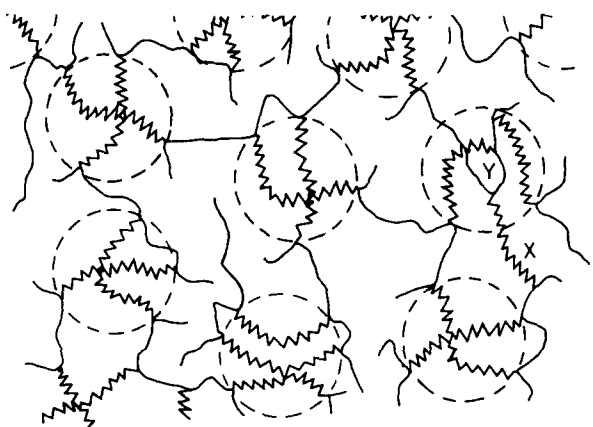
molecules. The degree of crosslinking in the polymer of Figure 6 is low, and the material must therefore contain a high proportion of unreacted PVTCA. We propose that domains of polychloroprene are formed by agglomeration of crosslinks of this polymer, with a large degree of exclusion of the attached PVTCA, which therefore assumes the form of external branches and loops. The result is effectively a rubber particle with attached PVTCA chains which can act as stabilizers when the material is suspended in a matrix of PVTCA.

From Figure 6 we see that the average diameter of the domain is of the order  $150\text{nm}$ . If the domains are spherical with this diameter, each will contain approximately 7000 polychloroprene molecules ( $\bar{P}_n = 2290$ ) if no PVTCA is incorporated. Further, the domain diameter



**a**

Figure 10a Schematic representation of specimen I (Table 1).  
 -----, PCP chain; ———, PVTCA chain



**b**

Figure 10b Schematic representation of specimen II (Table 1).  
 X and Y represent PCP and PVTCA chains trapped in the 'wrong' phases. -----, PCP chain; ———, PVTCA chain

is similar in magnitude to the unperturbed mean end-to-end distance of a polychloroprene molecule with  $\bar{P}_n = 2290$ , so that most molecules could have their terminal groups on the surface of a domain. From Table 1 it follows that the total concentration of PVTCA units reacting (in 25 min) is  $7.5 \times 10^{-9} \times 1500 = 1.12 \times 10^{-5} \text{ bmol l}^{-1}$ , and since the concentration of PVTCA is  $4.6 \times 10^{-2} \text{ bmol l}^{-1}$  the probability of a given unit entering into reaction is only  $2.43 \times 10^{-4}$ . Consequently the majority of the copolymer molecules produced will be H-shaped, with only a minor amount of more complex copolymers. These considerations lead us to believe that the picture of domain formation already proposed is quantitatively satisfactory; a schematic drawing of the morphology is given in Figure 10a.

Growth of a domain to greater sizes would appear to necessitate incorporation of PVTCA. The behaviour of the blend of the two polymers (Figure 9) shows that they are incompatible, so that continued growth, beyond that illustrated in Figure 10a would be thermodynamically unfavourable.

The situation is naturally more complicated with specimen II (Table 1), which was prepared with a much higher degree of crosslinking. According to Figure 8 the domains are more irregular and somewhat smaller, but the inter-domain separation is greatly reduced. We therefore believe that the basic domain structure is similar to that in Figure 10a, but that the domains must now be linked together, predominantly by PVTCA (Figure 10b), but perhaps also by some polychloroprene (X, Figure 10b). Geometrical constraints may necessitate the trapping of some PVTCA in rubber domains (Y, Figure 10b).

If the suggestions advanced above are correct, it follows that in these systems the domain size should be mainly determined by the mean crosslink length, while the domain separation should depend on the degree of crosslinking. We intend to discuss these matters in future publications, together with the properties of these two-phase systems.

#### ACKNOWLEDGEMENTS

We wish to thank I.C.I. Ltd for a support grant to J.A. and Unilever Research Ltd for financial support of E.S. We are grateful to BP Chemicals International Ltd for generous gifts of chloroprene.

#### REFERENCES

- 1 Bamford, C. H., Dyson, R. W. and Eastmond, G. C. *J. Polym. Sci. (C)* 1967, **16**, 2425
- 2 Bamford, C. H., Dyson, R. W., Eastmond, G. C. and Whittle, D. *Polymer* 1969, **10**, 759
- 3 Bamford, C. H., Eastmond, G. C. and Whittle, D. *Polymer* 1969, **10**, 771
- 4 Bamford, C. H., Dyson, R. W. and Eastmond, G. C. *Polymer* 1969, **10**, 885
- 5 Bamford, C. H., Eastmond, G. C. and Whittle, D. *Polymer* 1971, **12**, 247
- 6 Kato, K. *J. Electron Microsc. 1965*, **14** (3), 219; *Polym. Lett.* 1966, **4**, 35
- 7 Brandrup, J. and Immergut, E. H. (Eds) 'Polymer Handbook', Interscience, New York, 1966
- 8 Bamford, C. H., Crowe, P. A. and Wayne, R. P. *Proc. R. Soc. (A)* 1965, **284**, 455
- 9 Bamford, C. H., Eastmond, G. C. and Robinson, V. J. *Trans. Faraday Soc.* 1965, **60**, 751
- 10 Bamford, C. H. and Dewar, M. J. S. *Proc. R. Soc. (A)* 1948, **192**, 309
- 11 Kwok, J. *PhD Thesis*, University of Liverpool, 1971
- 12 Matsuo, M., Nozaki, C. and Jyo, Y. *Polym. Eng. Sci.*, 1969, **9** (3), 197

# Low-angle X-ray diffraction studies of reduced and silver-stained $\alpha$ -keratin

G. A. Wilson\*

*Textile Physics Laboratory, Department of Textile Industries, The University, Leeds 2, UK*

*(Received 31 March 1971; revised 11 June 1971)*

When the cystine in Lincoln wool fibres is reduced and the fibres subsequently 'stained' with silver nitrate, the low-angle X-ray diffraction pattern becomes considerably enhanced, and to a good approximation represents the regular distribution of silver atoms throughout the fibre. This regular distribution of silver atoms is equivalent to the distribution of cystine, since if the reduced cystine is blocked by alkylation before staining, the silver uptake is low and the only enhancement which occurs is a very small intensification of the low-angle equatorial reflections. The precise nature of the enhanced diffraction patterns varies considerably with the prior reduction treatment and it is possible to distinguish between matrix and microfibril fractions of cystine. When the microfibril cystine is labelled the low-angle meridional reflections contract in spacing and this is accompanied by a similar change in fibre length. There is no apparent change in the high-angle, helical pattern, however, which leads to the conclusion that the ordered keratin protein chains are made up of alternating helical and non-helical sections. A model for the matrix is also proposed, consisting of short, randomly orientated  $\alpha$ -helical segments, which become orientated about the fibre axis where they form the surfaces of the microfibrils. A possible mode of interaction between the matrix and microfibrils is also suggested.

## INTRODUCTION

The low-angle X-ray diffraction of  $\alpha$ -keratin impregnated with heavy metals after reduction of the disulphide bonds has been reported by several workers<sup>1-4</sup>. Both the equatorial reflections (at approximate Bragg spacings of 80 Å ( $e_1$ ), 45 Å ( $e_2$ ) and 27 Å ( $e_3$ )) and the meridional reflections (as orders of a macroperiod of 198 Å) have been shown to be enhanced.

The equatorial patterns of wool fibres obtained using silver nitrate and phenyl mercuric hydroxide as the heavy metal reagents have been related to the histological distribution of the stains throughout the fibre<sup>3</sup>. The matrix-microfibril contrast observed in the transmission electron microscope<sup>3, 6</sup> has suggested a fine structure of 'holes' arranged in an electron-dense medium<sup>5</sup> and this structure has been related to the spacings and intensities of  $e_1$ ,  $e_2$  and  $e_3$ . The 'holes' have been equated with the

microfibrils, and hence it has been concluded that the stain is entering, preferentially, the matrix. The fact that the observed effects take place after prior reduction of the disulphide bonds to thiol groups suggests that the binding site for the heavy atom is at a sulphur atom, and thus a cystine-rich matrix is implied.

The interpretation of the changes in the meridional X-ray diffraction patterns produced by heavy atoms has been made difficult by the fact that previous workers have not only used different metals but also different reduction treatments prior to staining. This paper examines the effect of different prior reduction treatments on the X-ray diffraction of silver-stained keratin.

## EXPERIMENTAL

Lincoln wool samples were prepared in which (i) 40% of the wool cystine was reduced with thioglycollic acid (termed 'most reactive' cystine); (ii) the 'most reactive'

\* Present address: School of Biological Sciences, The University, Bradford 7, Yorkshire, UK.

cystine was reduced as above, alkylated with ethylene dibromide, and the remaining 'least reactive' cystine reduced with tetra(hydroxy methyl) phosphonium chloride (THPC); (iii) 80% of the cystine was reduced with THPC; and (iv) all the cystine was reduced and alkylated with ethylene dibromide by two reduction-alkylation cycles (using thioglycollic acid and THPC as the two respective reducing agents).

The samples were all stained in solutions of silver nitrate, and X-ray photographs were taken of the washed and dried samples.

Parallel experiments were carried out on single fibres and tests were made for fibre contraction at each stage of the reaction sequence.

Lincoln wool was prepared for analysis by Soxhlet extraction followed by a dilute ( $6 \times 10^{-4}$  N) hydrochloric acid wash to remove any metal ions and reduce the ash content of the wool<sup>7</sup>, and finally washing in conductivity water to the isoelectric point of wool (pH = 5.1).

Low-angle X-ray photographs were taken using a 'pin-hole' camera designed in this laboratory<sup>8</sup>. Nickel filtered  $\text{CuK}\alpha$  ( $\lambda = 1.54 \text{ \AA}$ ) radiation was used and was generated from a Hilger Y-25 100  $\mu\text{m}$  microfocus tube operating at about 35 kV and 2.5 mA.

High-angle photographs using  $\text{CuK}\alpha$  radiation were taken on simple glass-capillary collimated cameras, also designed in this laboratory<sup>9</sup>. The source of X-rays was a Hilger and Watts Y-90 X-ray generator, working at 34 kV and 14 mA. A nickel filter was employed as before, and silver foil was inserted in the centre of each sample in order to measure the exact reflection spacings.

The X-ray photographs were analysed on a Joyce Loebel Automatic Recording Microdensitometer Model Mk IIIC. All traces were corrected for background scatter by comparison with a trace at an angle of  $45^\circ$  to the equator.

The reduction procedure with 0.45 M thioglycollic acid followed by a standard wash to yield samples of known constant thiol content (equivalent to 40% reduction), and the silver nitrate staining procedure at pH 5.4, were both developed in this laboratory<sup>3</sup>. Uptakes of silver were measured gravimetrically against blank samples.

Reduction with 4% (w/v) THPC at pH 5.4<sup>10</sup> yielded a sample with 80% of the cystine converted to thiols. In the case where the sample had already been reduced by thioglycollic acid and subsequently alkylated, all the remaining cystine was reduced. Before further reaction THPC reduced samples were quickly washed in successive changes of conductivity water for 10 min.

The alkylation procedure with 0.05 M ethylene dibromide at pH 8 has been described elsewhere<sup>11</sup>.

The thiol contents of all the samples were measured by gravimetric uptake of phenyl mercuric hydroxide<sup>3</sup>, and by measurement of the remaining cystine after alkylation of the thiols, by the Shin O'Hara method<sup>12</sup>. This was compared with the cystine content of untreated wool, which was found to be 860  $\mu\text{mol/g}$ , in agreement with the analyses of other workers<sup>3, 13</sup>.

## RESULTS AND DISCUSSION

### Specificity of silver nitrate for reduced cystine

The silver uptakes for all the samples considered are shown in Table 1. It should be noted that the uptakes are

Table 1 Uptakes of silver after reduction of cystine in Lincoln wool

Reduction treatment	Thiol content ( $\mu\text{mol/g}$ wool)	Silver uptake ( $\mu\text{mol/g}$ wool)
0.45M thioglycollic acid (pH 6)	340	1220
0.2M THPC (pH 5.4)	700	2120
0.45M thioglycollic acid (pH 6) alkylation with $(\text{CH}_2)_2\text{Br}_2$ further reduction with 0.2M THPC (pH 5.4)	580	1470
Complete reduction and alkylation	0	310

Table 2 Intensity distribution of the low-angle equatorial reflections  $e_1$ ,  $e_2$ ,  $e_3$  at approximate respective Bragg spacings 80  $\text{\AA}$ , 42  $\text{\AA}$ , 27  $\text{\AA}$  in silver-stained Lincoln wool

Treatment	Intensity ratio $I_{e_1} : I_{e_2} : I_{e_3}$	Approximate enhancement (intensity ratio $I_{e_2} : I_{9.8 \text{\AA}}$ )*
Untreated sample	10 : 0.75 : 1	0.4 : 1
'Most reactive' cystine silver stained	14 : 3.75 : 1	50 : 1
'Least reactive' cystine silver stained	3 : 1.9 : 1	50 : 1
80% of cystine silver stained	14.5 : 3 : 1	50 : 1
All of cystine reduced and alkylated before silver staining	14 : 1.2 : 1	1 : 1

\* Intensity of  $e_2$  compared with that of the main equatorial high-angle helical reflection at a Bragg spacing of 9.8  $\text{\AA}$

far too high to be accounted for by a stoichiometric 1 : 1 reaction with thiols. Most of the reaction appears to take place with these groups, however, as the introduction of an alkylation step between the reduction and staining reactions considerably decreases the metal uptake.

The low-angle X-ray diffraction patterns of the samples, with the exception of that of the reduced and alkylated sample, become considerably intensified with respect to the high-angle coiled coil diffraction after staining (Table 2). To a good approximation, therefore, they describe the distributions of silver atoms in the different samples. The low-angle diffraction pattern of the reduced and alkylated sample, however, shows no enhancement along the meridian after staining (densitometer traces showed the meridional pattern to be identical to that obtained from untreated Lincoln wool), and very little along the equator (Table 2). Thus the enhanced diffraction patterns may be assumed to be due to silver atoms located at cystine residues, and hence describe the distribution of cystine throughout Lincoln wool fibres.

### Low-angle X-ray diffraction of the reduced and stained samples

The low-angle X-ray diffraction photograph of the sample in which the 'most reactive' cystine has been reduced and labelled with silver is shown in Figure 1, and that of the sample in which the 'least reactive' cystine has been reduced and labelled is shown in Figure 2.

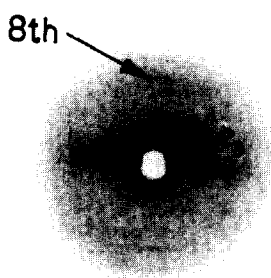


Figure 1 Low-angle X-ray diffraction photograph of Lincoln wool that has been silver stained after reduction of the 'most reactive' cystine

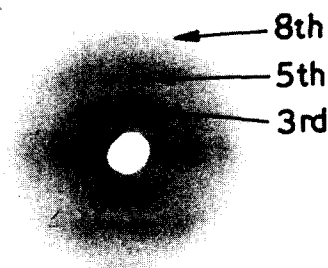


Figure 2 Low-angle X-ray diffraction photograph of Lincoln wool that has been silver stained after the 'most reactive' cystine has been blocked and the 'least reactive' cystine reduced

Important differences are apparent, both along the equator and the meridian. These are discussed in detail below.

*The equatorial diffraction.* The intensities of the low-angle equatorial reflections are summarized in Table 2. The equatorial diffraction of the sample in which the 'most reactive' cystine has been reduced prior to staining is identical to that found by other workers<sup>1,3</sup>. This type of pattern, taken in conjunction with the observation in such samples of matrix-microfibril contrast in the transmission electron microscope, is generally interpreted as being produced by scatter from a system of 'holes' (microfibrils) embedded in an electron dense (i.e. silver dense) medium (the matrix). This type of scatter is characterized by a high intensity of  $e_1$  due to external interference between microfibrils, and  $e_2$  and  $e_3$  representing the scatter from a single cylinder, radius  $37.5 \text{ \AA}$ , having an intensity ratio  $I_{e_2} : I_{e_3} \sim 4 : 1$ . When, however, the 'least reactive' cystine is labelled, the relative intensity of  $e_1$  becomes much lower, and  $I_{e_2} : I_{e_3} \sim 2 : 1$ .

These differences may be explained, qualitatively at least, by postulating that when the 'least reactive' cystine is reduced and stained, considerable quantities of silver enter the microfibril. The effect of this will be to randomize the histological distribution of silver, and hence

lower the intensity of the external interference giving rise to  $e_1$ . By drawing an analogy with untreated Lincoln wool, where  $I_{e_2} : I_{e_3} \sim 1 : 1$ , the observed lowered intensity ratio from 4 : 1 to 2 : 1 may be similarly explained. The theory explaining the low-angle equatorial diffraction of untreated Lincoln wool is based on the scatter from regularly distributed protofibrils (3-strand coiled coils) inside the microfibril<sup>14</sup>. In the usual stained specimens as typified by Figure 1, the electron density difference between the matrix and microfibrils is so large that the arrangement of protofibrils inside the microfibrils becomes unimportant and may be neglected. However, if the stain enters the microfibrils in large quantities, the density difference between the microfibrils and matrix will become equalized, and essentially the same diffraction conditions as those for untreated Lincoln wool will occur, i.e. the low-angle equatorial diffraction will be based largely on the arrangement of protofibrils. The effect of this in the stained sample will presumably be to lower the intensity ratio  $I_{e_2} : I_{e_3}$ .

These results suggest, therefore, that the 'most reactive' cystine is located mainly in the matrix, and the 'least reactive' cystine in the microfibril.

*The meridional diffraction.* When the 'most reactive' cystine is labelled the 8th order meridional reflection alone appears to be notably enhanced (Figure 1). When, however, the 'least reactive' cystine is labelled the 3rd, 5th and 8th orders are enhanced, with the 3rd order particularly strong (Figure 2).

This last feature of the meridional diffraction confirms the results of workers using mercury compounds as the stains<sup>2,4</sup> and provides a simple explanation for the non-correlation of their results with those of workers using silver compounds. Evidently the prior reduction treatment is extremely important in determining which reflections are enhanced on staining. The 5th order enhancement has also been reported previously, but this has been associated with a lysine repeat<sup>15,16</sup>. It is quite possible that this repeat is present in addition to that attributed to cystine in the present paper.

The intensity ratios of the meridional reflections of all three enhanced diffraction patterns are shown in Table 3. It will be noted that when enhanced, the intensity ratio of the 3rd and 5th orders is constant, but the relative intensity of the 8th order varies with the exact chemical treatment, being strongest when the 'most reactive' cystine has been labelled, and weakest when the 'least reactive' cystine has been labelled. It would appear that the intensity of the 8th order is associated with 'most reactive' (or matrix) cystine, and the 3rd and 5th orders with 'least reactive' (or microfibril) cystine.

Table 3 Relative intensities of enhanced meridional reflections in silver-stained Lincoln wool

Treatment	Intensity ratio $I_{3rd} : I_{5th} : I_{8th}$
'Least reactive' cystine silver stained	10 : 2 : 1.5
80% cystine silver stained	10 : 2 : 4
'Most reactive' cystine silver stained	10* : — : > 10

\* In this sample the 5th order is very weak and has not been measured. Also there appears to be very little enhancement of the 3rd order

**Table 4** Bragg spacings of the meridional reflections enhanced when the 'least reactive' cystine in Lincoln wool is silver stained

Order	Bragg spacing (Å)	
	Untreated Lincoln wool	'Least reactive' cystine silver stained
3rd	65.8	61.65
5th	39*	36.80
8th	24.4	23.20
Macroperiod (Å)	198	185

\* A very weak reflection which is only occasionally observed in untreated specimens<sup>8, 26</sup>

The shapes of the 3rd and 5th order reflections are different (Figure 2). The 3rd order, like the 8th, is a sharp meridional arc, but the 5th order splits into three distinct reflections which form a rudimentary layer line. In the light of work on collagen<sup>17</sup>, and more recently on untreated  $\alpha$ -keratin<sup>8</sup>, this would suggest that the microfibril cystine itself is subdivided into cystine in two different structural positions (although of similar reactivity to reducing agents).

When only the 8th order reflection is enhanced, its Bragg spacing is the same as in untreated specimens at 24.4 Å. When the 3rd, 5th and 8th orders are enhanced, however, the spacings all contract by 6.5% and the macroperiod falls from 198 to 185 Å (Table 4).

This change in low-angle spacing is accompanied by a contraction in fibre length of 6.3% (average of five single fibres) which occurs only at the final silver staining stage. No contraction is observed for samples which do not show spacing changes. Thus there is a direct correlation between change in X-ray spacing and change in fibre length.

As the contraction in length occurs at the final silver staining reaction, it would suggest that the contraction takes place in the parts of the protein chain where the silver is being attached, rather than continuously along its length. This contention is supported by a study of the high-angle pattern. The high-angle X-ray diffraction of keratin is generally accepted as being that given by a 2- or 3-strand coiled coil<sup>18, 19</sup>. (Recently, other  $\alpha$ -helical forms have been shown to be possibilities<sup>20-23</sup>, but this is irrelevant to the following argument.) In particular, the strong meridional reflection at 5.15 Å represents the pitch of an  $\alpha$ -helix which has been twisted to form one strand of a coiled coil. A regular contraction would presumably cause a decrease in the spacing of the reflection (for example, compare the fact that when wool is extended by 20%, the 5.15 Å reflection increases in spacing by 2%<sup>24</sup>) but accurate measurement showed that the reaction sequence had caused no change. However, further consideration of the high-angle pattern, and this reflection in particular, suggests that the implied irregular coiled coil contraction is not taking place either. There is no sign of any disorder which would arise from an irregular contraction of the coiled coil. Although to establish the fact completely it would be necessary to measure quantitatively intensity changes in the 5.15 Å reflection which result from silver staining—a very difficult task owing to the presence of the silver swamping the natural diffraction pattern—the results do suggest that there is no contraction in the coiled coil,

helical regions of the fibre. This, in turn, leads to the deduction that the contraction is taking place in non-helical regions which alternate in series with the coiled coil (or other  $\alpha$ -helical regions). If this is so, it may reasonably be assumed that the non-helical regions are stabilized to a large extent by disulphide bonds, and the cleavage of these bonds by reduction, and the subsequent reaction with silver nitrate, cause these regions to contract.

The very great intensity of the 3rd order reflection suggests that the major repeat of one helical plus one non-helical region is 66 Å. This agrees with analyses of other workers studying the 3rd order reflection in untreated keratin<sup>8, 25</sup>, who suggest that it arises from a major discontinuity at this spacing. This discontinuity has been linked by these workers with the anti-helical amino acids<sup>25</sup> or, more specifically, cystine residues<sup>8</sup>. The present results are in full accord with the latter postulate.

The much weaker 5th order reflection (suggesting a 39.5 Å repeat) is not considered to be associated with helical-non-helical discontinuities. However, as it always has the same comparative intensity as the 3rd order, it appears to represent a repeat which is part of the same chain.

It is difficult to envisage how regular contractions at 66 Å intervals could bring about a regular contraction of the 39.5 Å spacing. One possibility is that in untreated specimens this repeat is slightly irregular. The reflection is extremely weak and does not index satisfactorily on a macroperiod of 198 Å, its actual Bragg spacing being recorded as 39 Å<sup>8, 26</sup>. These characteristics would be expected if the cystine residues giving rise to the repeat were occasionally spaced at intervals shorter than the theoretical 39.5 Å. The contraction of non-helical regions every 66 Å could then be envisaged as making the spacing more regular, as well as decreasing its overall value. This explanation would also account for the fact that other workers who have recorded intensification of the 3rd order after labelling cystine with mercury compounds but no change in spacing have not reported any intensification of the 5th order<sup>2, 4</sup>.

## CONCLUSIONS

### *The structure of the matrix*

The broad halo (Bragg spacing=25 Å) observed in X-ray diffraction studies of silver-stained fibres and the sharp diffraction ring (Bragg spacing=21 Å) observed in X-ray diffraction patterns of the silver-stained keratogenous zone of developing fibres have been interpreted as indicating matrix order<sup>27, 28</sup>. In the latter studies<sup>28</sup> electron micrographs revealed the presence of silver globules of the same order of size, between the microfibrils, and it was also reported that after keratinization but before dehydration the diffraction ring became broader. These results were interpreted in terms of the matrix originally being a globular entity which becomes distorted on keratinization owing to oxidation of cysteine to cystine.

More recently, very wide angle studies have suggested that the matrix consists of short, randomly orientated  $\alpha$ -helical segments<sup>3, 8</sup>, and the 25 Å halo has been related to the length of a segment<sup>8</sup>. A closer examination of this



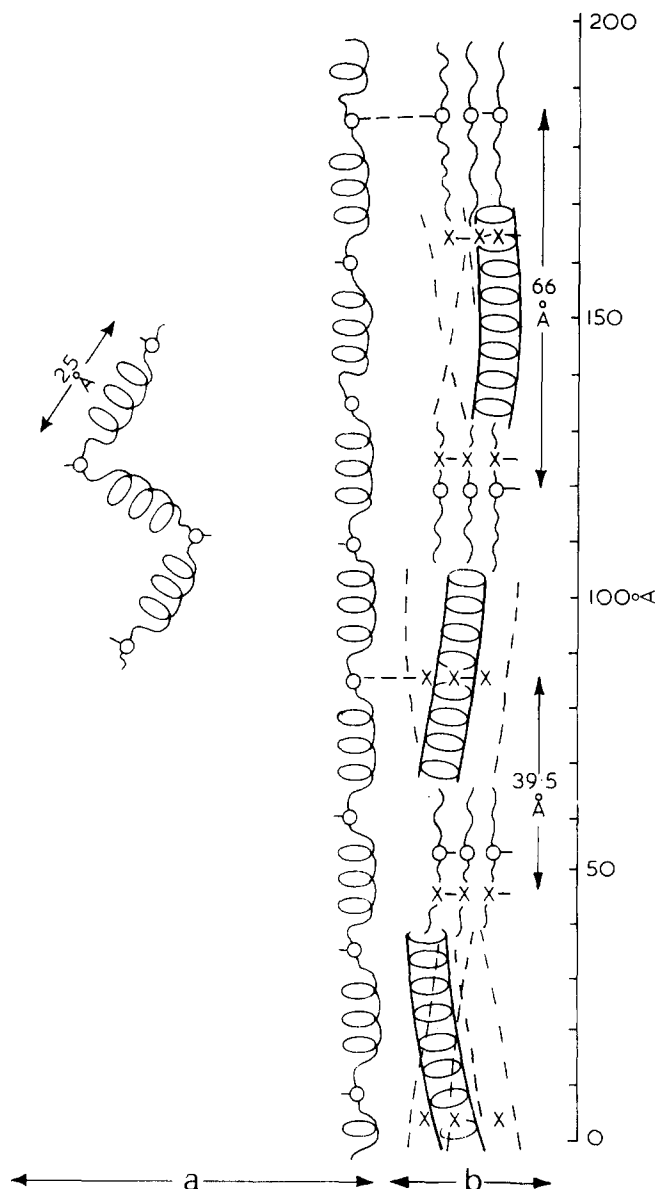


**Figure 3** The molecular configuration of  $\alpha$ -keratin. (a) Proposed structure for the matrix, consisting of short units of helical plus non-helical material, about 25 Å long. Cystine (half-cystine represented by  $\circ$ ) is located in the non-helical segments and the disulphide bonds between the units produce a 'rigid' structure. The units are orientated randomly except where they form the surface of the microfibril. Here they become orientated along the fibre axis. (b) Shows one protofibril on the periphery of a microfibril. It consists of a 3-strand coiled coil, interspersed at regular intervals by non-helical sections. The basic unit of one helical plus one non-helical segment is 66 Å long. The non-helical sections all contain cystine and there is a 66 Å cystine (half-cystine represented by  $\circ$ ) repeat. The other cystine repeat (half-cystine represented by  $\times$ ) is shown as 39.5 Å but may be irregular. This cystine may be located either in the coiled coil or non-helical segments. Possible disulphide links with the matrix to form 'rigid' parts of the structure are shown

halo has revealed it to be more intense and of slightly greater spacing along the meridian<sup>8</sup>, suggesting the segments to be partly orientated about, and extended along the fibre axis. These deductions are in full agreement with a recently derived mechanical model for the matrix<sup>29</sup>.

In this type of model (Figure 3a) it is easy to envisage how the 25 Å meridional reflection, which has been

associated in the present work with a regular matrix repeat, could arise from complete orientation of the matrix segments about the fibre axis. This would most likely occur at the surfaces of the microfibrils (a possibility suggested by early workers on the X-ray diffraction of silver-stained keratin<sup>1</sup>), to enable maximum disulphide crosslinking between the matrix and microfibrils.

#### The structure of the protofibrils

Correlation of the 'least reactive' cystine with microfibril cystine and co-ordination of the data obtained from the diffraction pattern of the sample in which this fraction has been labelled with silver lead to a general model for the microfibril sub-units or protofibrils (Figure 3b). The helical regions in this Figure are shown as 3-strand coiled coils, and the non-helical regions are shown to have a finite length, so that they contain some cystine residues which form part of the 39 Å repeat. This has been done because it is well known that cystine is not readily incorporated into  $\alpha$ -helical structures. It is possible that the non-helical regions form a fairly large proportion of the protofibrils. Optical transform results show that 60 Å lengths of coiled coil will yield well-ordered helical reflections, although if the length is reduced to 27 Å they become diffuse<sup>25</sup>.

The idea of alternating helical and non-helical regions has been the basis of various mechanical models<sup>29, 30</sup>, and also some recent models derived from chemical studies<sup>31-33</sup>. It represents a significant departure, however, from recent X-ray diffraction models such as the segmented rope model, where the coiled coil is continuous and the coiling takes place at specific residues<sup>23, 25</sup>, and the straight  $\alpha$ -helix models<sup>20-22</sup>. These models have been derived because the experimental data from diffraction patterns do not fit exactly the theoretical continuous coiled coil diffraction. Models similar to that presented in this paper may explain the discrepancies equally well.

#### The unified structure

If the possible disulphide bonds are drawn between the matrix and microfibril to give the unified model (Figure 3), then it is immediately apparent that only a few may be so formed. Presumably the other cystine residues of the matrix and microfibrils are used for the internal crosslinking and stabilization of their respective structures. Thus some parts of the protofibrils are stiffened by covalent crosslinks with the matrix, and others are not. This type of model has also been deduced from a study of the mechanical properties of reduced and methylated fibres<sup>34</sup>.

The proposed structure is attractive in that it incorporates the features of three different mechanical models mentioned above. It is also consistent with current chemical evidence, and the previous apparently contradictory reports from X-ray diffraction observations concerning the regular distribution of cystine in  $\alpha$ -keratin are easily explained.

#### ACKNOWLEDGEMENTS

The above work was carried out under a Research Studentship sponsored by the Science Research Council to whom the author is indebted for their financial support. The author would also like to acknowledge the

considerable help and advice given by Mr H. J. Woods, and especially for his critical help in preparing the manuscript.

#### REFERENCES

- 1 Simpson, W. S. and Woods, H. J. *Nature* 1960, **185**, 157
- 2 Dobb, M. G., Fraser, R. D. B. and Macrae, T. P. *3rd Congr. Int. de la Rech. Text. Lainiere*, Inst. Text. de France, 1965, Vol 1, p 13
- 3 Bailey, C. J. *PhD Thesis*, University of Leeds, 1966
- 4 Spei, M., Heidemann, G. and Zahn, H. *Naturwiss.* 1968, **7**, 346
- 5 Fraser, R. D. B., Macrae, T. P. and Miller, A. J. *J. Mol. Biol.* 1964, **10**, 147
- 6 Dobb, M. G. *PhD Thesis*, University of Leeds, 1963
- 7 Cockburn, R. *PhD Thesis*, University of Leeds, 1954
- 8 Tyson, C. N. *PhD Thesis*, University of Leeds, 1969
- 9 Forrester, M. M. *MSc Thesis*, University of Leeds, 1958
- 10 Kulkarni, V. G. *PhD Thesis*, University of Leeds, 1969
- 11 Maclaren, J. A. and Sweetman, B. J. *Aust. J. Chem.* 1966, **19**, 2355
- 12 Block, R. J. 'A Laboratory Manual of Analytical Methods in Protein Chemistry' (Ed. P. Alexander and R. J. Block) Pergamon Press, Oxford, 1960, Vol 2, p 1
- 13 O'Donnell, I. J. and Thompson, E. O. P. quoted in *Adv. Protein Chem.* 1965, **20**, 232
- 14 Bailey, C. J., Tyson, C. N. and Woods, H. J. *3rd Congr. Int. de la Rech. Text. Lainiere*, Inst. Text. de France, 1965, Vol 1, p 21
- 15 Heidemann, G. and Halboth, H. *Nature* 1967, **213**, 71
- 16 Spei, M., Heidemann, G. and Halboth, H. *Nature*, 1968, **217**, 247
- 17 Bear, R. S. *Adv. Protein Chem.* 1952, **7**, 69
- 18 Crick, F. H. C. *Acta Cryst.* 1953, **6**, 685
- 19 Fraser, R. D. B., Macrae, T. P. and Miller, A. J. *J. Mol. Biol.* 1965, **14**, 432
- 20 Parry, D. A. D. 'Fibrous Proteins' (Ed. W. G. Crewther) Butterworths, Sydney, 1967, p 287
- 21 Parry, D. A. D. *J. Theor. Biol.* 1969, **24**, 73
- 22 Parry, D. A. D. and Suzuki, E. *Biopolymers* 1969, **7**, 199
- 23 Parry, D. A. D. *J. Theor. Biol.* 1970, **26**, 429
- 24 Astbury, W. T. and Woods, H. J. *Phil. Trans. R. Soc.* 1933, **A232**, 333
- 25 Fraser, R. D. B. and Macrae, T. P. *J. Mol. Biol.* 1961, **3**, 640
- 26 Onions, W. J., Woods, P. B. and Woods, H. J. *Nature* 1960, **185**, 157
- 27 Jeffrey, J. M., Sikorski, J. and Woods, H. J. *Proc. Int. Wool Text. Conf., Aust.* 1956, **F**, 130
- 28 Fraser, R. D. B., Macrae, T. P. and Rogers, G. E. *Nature* 1962, **193**, 1052
- 29 Menefee, E. *Text. Res. J.* 1968, **38**, 1149
- 30 Skertchly, A. R. B. *Nature* 1964, **202**, 161
- 31 Corfield, M. C., Fletcher, J. C. and Robson, A. 'Fibrous Proteins' (Ed. W. G. Crewther), Butterworths, Sydney, 1967, p 289
- 32 Crewther, W. G., Gillespie, J. M., Harrap, B. S., O'Donnell, I. J. and Thompson, E. O. P. *3rd Congr. Int. de la Rech. Text. Lainiere*, Inst. Text. de France, 1965, Vol 1, p 303
- 33 Crewther, W. G. and Harrap, B. S. *J. Biol. Chem.* 1969, **242**, 4310,
- 34 Crewther, W. G. *Text. Res. J.* 1965, **35**, 867

# Orientation of the methylene groups in poly(ethylene terephthalate)

I. H. Hall

*Physics Department, University of Manchester Institute of Science and Technology, Sackville Street, Manchester M60 1QD, UK*  
(Received 19 May 1971)

Diffraction studies have led to the conclusion that the molecular chains in oriented, crystalline, poly(ethylene terephthalate) are highly extended and to the expectation that the methylene groups are oriented so that their planes are almost normal to the chain axis. Polarized infra-red studies contradict this expectation. Calculations are presented which show that it is impossible to change the chain conformation, whilst maintaining the chain repeat distance, in a way which will tilt the methylene groups sufficiently to satisfy the infra-red data. However, it has been assumed, both in these calculations and in the infra-red studies, that the methylene group is unstrained. A published electron-diffraction study indicates that it might be very highly strained, and this strain is considered to be a possible cause of the discrepancy.

## INTRODUCTION

The chain conformation and crystalline structure of poly(ethylene terephthalate) (PET) was first determined by Daubeny, Bunn and Brown<sup>1</sup> (DBB), using X-ray diffraction techniques. It has also been determined by Tomashpol'skii and Markova<sup>2</sup> (TM) using electron diffraction techniques. The DBB structure has been refined by Arnott and Wonacott<sup>3</sup>. Neither Daubeny *et al.* nor Arnott and Wonacott located the hydrogen atoms; Tomashpol'skii and Markova, however, have done so.

These three structures are all in close agreement, showing that the PET molecule is in a fairly extended conformation, and leading to the expectation that the methylene groups would be nearly normal to the chain axis of the molecule. (Information from the three structures is summarized in *Table 1*.)

The results of certain infra-red studies<sup>4, 5</sup> have caused this conclusion to be questioned. From the structure determinations the infra-red absorption bands due to both symmetric and antisymmetric vibrations of the CH<sub>2</sub> bonds would be expected to be strong for radiation plane-polarized perpendicular to the chain axis. The opposite effect has been observed experimentally by Liang<sup>4</sup> and Manley and Williams<sup>5</sup>, and the latter authors postulate rotation around certain valence bonds additional to that in the structure determined by diffraction methods, in order to give an inclination which satisfies the infra-red results.

However, unless the repeat distance along the molecular chain is to vary, compensating rotations must be applied to other valence bonds. In this note it is shown that if

this repeat distance is maintained, then it is impossible to alter the chain conformation to give the required inclination. This is true even if severe strain is allowed in bond lengths and angles along the chain, and if the requirement of centro-symmetry in the chain conformation (assumed in both diffraction and infra-red studies) is dropped. The repeat distance determined by Daubeny *et al.* is assumed, but this is unlikely to be in serious error.

It is also shown, from an analysis of the TM structure (the only one which attempts to locate the hydrogen atoms), that the methylene groups are highly strained, and this strain is considered to be a possible way of reconciling the infra-red and diffraction data.

## CALCULATION OF THE INCLINATION OF THE METHYLENE GROUP TO THE CHAIN AXIS

A schematic diagram of the PET molecule is given in *Figure 1*. The atoms in this diagram are numbered and, for both brevity and clarity, will be referred to by these numbers in the following text. The length PQ constitutes one repeat unit, and in the subsequent calculations it will be assumed that the DBB value (10.75 Å) is the correct value of this length. The evidence for the unit cell determined by Daubeny *et al.* was very conclusive and this cell has been confirmed by the independent investigation of Tomashpol'skii and Markova. Thus this assumption is very likely to be correct.

The maximum possible angle of inclination between the methylene groups and chain axis that can be obtained by rotation around valence bonds keeping PQ constant is calculated. The calculations are considered in three

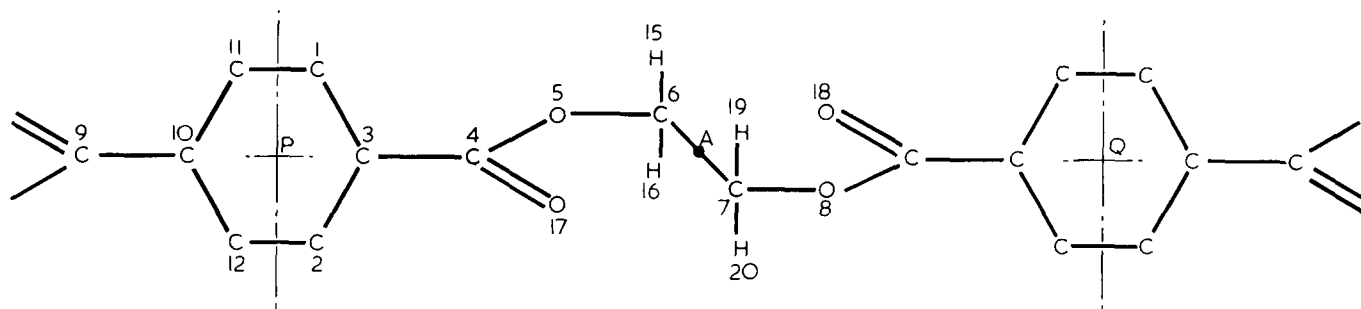


Figure 1 Molecule of poly(ethylene terephthalate)

Table 1 Values of bond length and bond angles

Bond description	Length (Å)			
	(1)	(2)	(3)	(4)
11-1	1.40	1.41	1.31	1.28
12-2	1.40	1.41	1.31	1.28
1-3	1.40	1.41	1.45	1.41
2-3	1.40	1.34	1.35	1.38
3-4	1.49	1.48	1.45	1.46
4-5	1.36	1.36	1.53	1.38
5-6	1.43	1.45	1.42	1.44
6-7	1.54	1.48	1.53	1.52
6-16	1.07			1.13
6-15	1.07			1.16

Bond description	Angle (degrees)			
	(1)	(2)	(3)	(4)
11-1-3	120	121	114	115
12-2-3	120	122	122	118
2-3-1	120	117	123	126
1-3-4	120	118	107	110
3-4-5	114	110	110	121
4-5-6	111	114	116	121
5-6-7	110	104	101	114
7-6-16	110			107
7-6-15	110			125
5-6-16	110			137
5-6-15	110			107

Bond description refers to Figure 1

(1) Normally assumed value for length and angle of this bond

(2) Calculated from coordinates of Daubeny *et al.*

(3) Given by Arnott and Wonacott

(4) Calculated from coordinates of Tomashpol'skii and Markova

parts. In the first part normal values of bond angles and lengths (column (1) of Table 1) are assumed and it is further assumed that the molecular conformation is centro-symmetric (as was assumed in the diffraction studies). The maximum possible inclination of the plane of the methylene group to the chain axis is then calculated. In the second part the effect of strain in bond lengths and angles along the molecular chain is considered, and in the third part the constraint of centro-symmetry is removed, but that of normal bond lengths and angles re-imposed.

In order to define the inclination of the methylene group to the chain axis, three orthogonal directions were chosen: a line through the centres of the hydrogen atoms (15 and 16 in Figure 1), a line normal to the plane containing the centres of the atoms in this group, and a line in this plane perpendicular to the line joining 15 and 16. The angles between these lines and the chain axis

are designated  $\alpha$ ,  $\beta$  and  $\gamma$  respectively. The polarization of the absorption band due to the symmetric vibration will be controlled by  $\gamma$ , and that due to the asymmetric vibration by  $\alpha$ . The results of the infra-red studies require that each of these angles be less than  $54^\circ 44'$ .

#### Normal bond lengths and angles and centro-symmetry

If bond lengths and angles are fixed, the molecule can change conformation by rotation about bonds, and the following rotations are available: (i) rotation of 4-5 about 3-4 as axis; (ii) rotation of 5-6 about 4-5 as axis; (iii) rotation of 6-7 about 5-6 as axis. Assuming centro-symmetry, there is no further freedom of rotation.

The coordinate system used is shown in Figure 2. The centre of the benzene ring is taken as the origin of coordinates, and its plane as the  $X-Z$  plane. The  $Z$ -axis is co-linear with bond 3-4. The coordinates of 4 may thus be determined.

Rotation of 4-5 about 3-4 is equivalent to a rotation of axes about the  $Z$ -axis, and so cannot affect the conformation. Thus a rotation angle is chosen so that 5 lies in the  $X-Z$  plane, and its coordinates determined.

On rotation of 5-6 about 4-5, 6 will describe a circle, and the location of 6 on this circle can be expressed in terms of a suitably defined torsion angle  $\theta$ . Thus the coordinates of 6 may be expressed as a function of  $\theta$ . Similarly, rotation of 6-7 about 5-6 will cause the centre of symmetry A to describe a circle, and A may be located in terms of a torsion angle  $\phi$ . The coordinates of A may therefore be expressed as a function of  $\theta$  and  $\phi$ , and its distance from P calculated in terms of these variables. Since  $PA = 5.375 \text{ \AA}$  (half the repeat distance),  $\phi$  may be expressed as a function of  $\theta$  and its value determined for any value of  $\theta$ .

For a given value of  $\theta$ , the coordinates of 5, 6 and 7 can now be calculated. Since normal values of bond lengths and angles are assumed, the plane containing the  $\text{CH}_2$  bonds will bisect the angle between bonds 5-6 and 6-7 and the angles  $\alpha$ ,  $\beta$ , and  $\gamma$  may be determined.

By repeating the calculation for different values of  $\theta$ , the smallest possible values of  $\alpha$  and  $\gamma$  can be found.

#### Strained bond lengths and angles and centro-symmetry

To study the effect of strain in bond angles and lengths, the above calculation was repeated using values of angles and lengths slightly different from those normally assumed. Only bonds on the chain axis were strained; the strain in pendant bonds was not considered.

*No centro-symmetry but normal bond lengths and angles*

The calculation is easily extended to take account of the non-symmetrical case. As already described, the location of A can be expressed in terms of  $\theta$  and  $\phi$ , although PA no longer equals 5.375 Å. The conformation of the remainder of the molecule is most easily determined by proceeding along the chain from P in a left-hand direction in *Figure 1*. The coordinates of 9 can be calculated directly. Rotation of 8-9 about 9-10 is no longer equivalent to a rotation of coordinate axes and so the coordinates of 8 must be expressed in terms of a torsion angle. Two further torsion angles are required to locate atom 7 and the equivalent point to A (A') to the left of P. The length of AA' must equal 10.75 Å, and the direction cosines of the bond 6-A must be the same as those of A'-7. Thus 5 torsion angles are required to specify the chain conformation, and 3 conditions must be satisfied, i.e. only two torsion angles are independent. An arbitrary pair of values was chosen for these, the atomic coordinates determined as described above, and the values of  $\alpha$ ,  $\beta$  and  $\gamma$  calculated for each of the methylene groups. It transpired that solutions to the various equations existed only for a certain range of these torsion angles (i.e. with angles outside this range there was no conformation satisfying the imposed constraints), and the minimum values of  $\alpha$  and  $\gamma$  occurring in this range was determined.

## RESULTS OF CALCULATIONS

*Normal bond lengths and angles and centro-symmetry*

The angles  $\alpha$ ,  $\beta$  and  $\gamma$  defining the inclination of the methylene groups to the chain axis are plotted in *Figure 3* as a function of  $\theta$ . It is seen that the minimum values of  $\alpha$  did not occur at the same value of the torsion angle  $\theta$  as the minimum in  $\gamma$ , and that neither angle approaches anywhere near the values required to explain the observed dichroism.

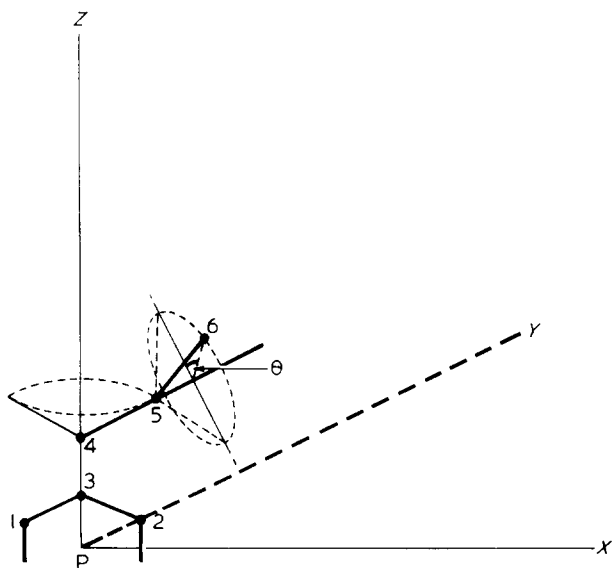


Figure 2 Coordinate system

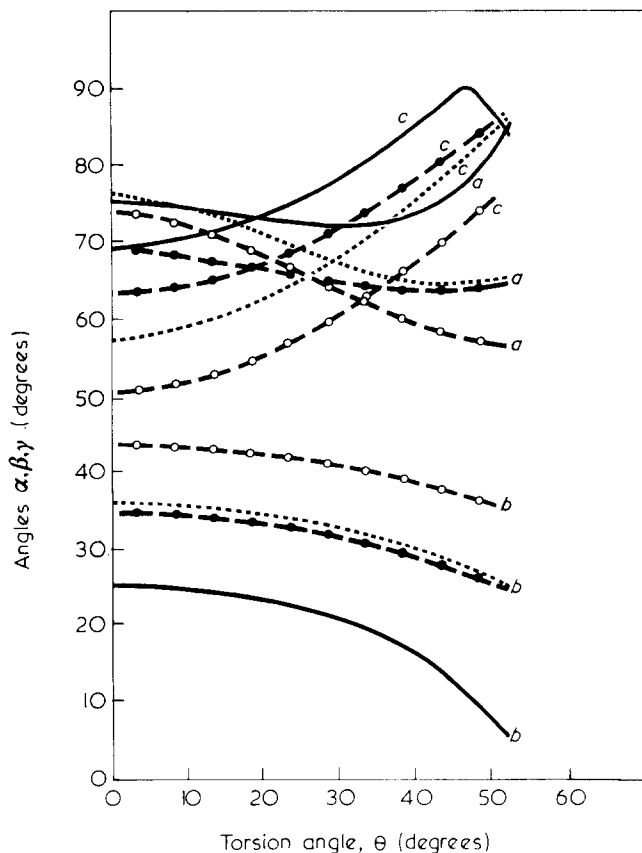


Figure 3 Inclination of methylene group to chain axis. — No strain; ... 10% strain in bond 3-4; ● 10% strain in bond angle 3-4-5; ○ 10% strain in 3-4 and 10° strain in 3-4-5

*Strained bond lengths and angles and centro-symmetry*

The angles  $\alpha$ ,  $\beta$  and  $\gamma$  were most sensitive to strain in the length of bond 3-4 and in the angle of the bond 3-4-5, and are plotted as functions of  $\theta$  for both of these strains in *Figure 3*. The Figure shows that even with a 10% strain in 3-4, or a 10° strain in 3-4-5  $\alpha$  and  $\gamma$  do not simultaneously approach the values required to explain the observed dichroism. The case in which the above strains are applied simultaneously is also plotted in this Figure. At small  $\theta$  the angle  $\gamma$  is seen to approach the range of values required to explain the dichroism, but  $\alpha$  remains outside the range for all  $\theta$ . Similar results are obtained (though not plotted) if 3-4 is strained still further whilst maintaining the strains in 3-4-5, or if 4-5 or 5-6 are strained by 5 or 10% whilst maintaining the strain in 3-4 and 3-4-5. No combination of strains was found which reduced the minimum in  $\alpha$  below 55°.

Hence even if very severe strains are introduced into the bond lengths and angles, the molecule still cannot take up a conformation that will explain the observed dichroism, provided the repeat length is maintained at the crystallographically determined value.

*No centro-symmetry but normal bond lengths and angles*

When the constraint of centro-symmetry was removed, but no strain allowed in any bonds or angles, the minimum value of  $\alpha$  became 64.7°. However, the two methylene groups now had different inclinations, and the value of

$\alpha$  for the other was increased to  $84.2^\circ$  in this particular conformation. The values of  $\gamma$  were  $79.4^\circ$  and  $85.6^\circ$  for each of the groups. The conformation for which  $\gamma$  was a minimum was centro-symmetrical with  $\gamma=69.0^\circ$  and  $\alpha=75.5^\circ$ . It is therefore clear that a non-centro-symmetric conformation will not allow the methylene groups to be tilted sufficiently to satisfy the infra-red data. The two sets of calculations also indicate that a combination of strain and asymmetry is unlikely to be satisfactory.

### Conclusions from calculations

It can therefore be concluded (if the long spacing from the diffraction data is correct) that modifications to the chain conformation will not tilt the methylene groups sufficiently to satisfy the infra-red evidence. However, in reaching this conclusion it has been explicitly assumed that the methylene bonds are unstrained. This assumption has also been made implicitly by the infra-red workers in their interpretation of the diffraction data. Since such strain is the only remaining means of reconciling the two sets of data, evidence for its existence will now be considered.

### EVIDENCE OF STRAIN IN METHYLENE GROUPS

Since the TM structure is the only one to locate the H atoms, this is the only one from which evidence of strain can be sought. Tomashpol'skii and Markova consider the positions established for the hydrogens in the methylene group to be particularly reliable, but do not consider the question of strain. However, it is possible to study this from the atomic coordinates given by them.

From column (4) of *Table 1* it is clear that the bond angles 7–6–15 and 5–6–16 are highly strained, and these angles control the orientation of the methylene group. The angles  $\alpha$ ,  $\beta$  and  $\gamma$  calculated from the atomic coordinates are  $52^\circ$ ,  $46^\circ$  and  $69^\circ$  respectively. If it is assumed that the group is in the unstrained position, and  $\alpha$ ,  $\beta$  and  $\gamma$  calculated from the TM chain conformation, their values become  $80^\circ$ ,  $21^\circ$  and  $72^\circ$  respectively. Thus the strain in the methylene group changes its inclination to the chain axis considerably, and in a direction which helps to reconcile the diffraction and infra-red data, although the angles  $\gamma$  and  $\alpha$  are still too large to provide a complete explanation of the disagreement.

The results therefore strongly suggest the possibility of strain in the methylene group, but there is no readily apparent cause of such strain. (If normal van der Waals radii are assumed the hydrogen atoms will pack comfortably in their unstrained positions.) Another puzzling feature is that the distance between the centres of the protons is very small—only about 1 Å. The evidence of strain is therefore indicative rather than conclusive and further work to confirm the location of the protons is necessary.

Such work should take account of the fact that these protons are in an environment of oxygen atoms. Consider two neighbouring chains (called *I* and *J*) along the *b*-axis of the unit cell. On each chain the pair of hydrogen atoms 15 and 16 (see *Figure 1*) has the oxygen atoms 17 and 8 as nearest neighbours, and the pair 19 and 20 has 18 and 5 as nearest neighbours (excepting, of course, the carbons to which they are bonded). The chains pack so that the hydrogen atoms 19 and 20 on *J* face 15 and 16

on *I*, the four atoms being very nearly co-planar. Thus oxygen atoms 18 on *J* and 8 on *I* are close below this group of four hydrogens, and oxygen atoms 17 on *I* and 5 on *J* are close above.

The chain along the *a*-axis of the unit cell from *I* packs so that the oxygen atom 5 is adjacent to the four hydrogens, and similarly the chain along the *a*-axis from *J* packs with oxygen atom 17 adjacent to them.

The close proximity of these oxygen atoms might cause strain; on the other hand they might confuse the interpretation of either the electron diffraction or the infra-red data.

### TILT OF CHAIN AXIS TO FIBRE AXIS

It has been assumed in the discussion hitherto, that the chain axis and fibre axis are coincident. Daubeny *et al.* showed that if oriented PET is annealed at  $210^\circ\text{C}$  and allowed to contract freely, then the chain axis becomes tilted with respect to the fibre axis. The tilt was given as  $5^\circ$  in a direction such that the  $(\bar{2}30)$  plane remains vertical and the inclination of the (001) plane to the fibre axis is increased. Tomashpol'skii and Markova used a lower annealing temperature ( $180^\circ\text{C}$ ) and found a tilt of  $3^\circ$  but did not give its direction.

Manley and Williams subjected the PET to cold drawing and then gave an unspecified heat treatment. It is not possible therefore, to determine whether this tilting occurred in their test-pieces, but it is unlikely to cause sufficient change in the orientation of the methylene groups to have a significant effect on the infra-red results.

### CONCLUSIONS

There are three possible causes of the disagreement between the results of X-ray and infra-red studies of the chain conformation of poly(ethylene terephthalate): (i) the X-ray structure is incorrect; (ii) the infra-red data are misinterpreted; (iii) the methylene groups are highly strained.

It has been shown that provided the long spacing determined by X-ray diffraction is correct (and this is very unlikely to be incorrect), then chain conformations which tilt the methylene groups sufficiently to satisfy the infra-red data are impossible. Previously published electron-diffraction studies have been analysed and these indicate considerable strain in the methylene group. However, the cause of this strain is puzzling; it is unlikely to be due to the locations of the surrounding atoms. Further work is therefore necessary to confirm the locations of the protons if this disagreement is to be resolved.

### REFERENCES

- 1 Daubeny, R., Bunn, C. W. and Brown, C. J. *Proc. R. Soc. (A)* 1954, **226**, 531
- 2 Tomashpol'skii, Y. Y. and Markova, G. S. *Polym. Sci. USSR*, 1964, **6**, 316
- 3 Arnott, S. and Wonacott, A. J. *Polymer* 1966, **7**, 157
- 4 Liang, C. Y. 'Newer Methods of Polymer Characterisation', Wiley, New York, 1964, p 85
- 5 Manley, T. R. and Williams, D. A. *Polymer* 1969, **10**, 339

# Melting of low molecular weight poly(ethylene oxide)

D. R. Beech\*, C. Booth and D. V. Dodgson†

Department of Chemistry, University of Manchester, Manchester M13 9PL, UK

and R. R. Sharpe and J. R. S. Waring

ICI Ltd, Dyestuffs Division, Hexagon House, Blackley, Manchester, UK

(Received 16 April 1971)

The melting behaviour of fractions of poly(ethylene oxide) of narrow molecular weight distribution and of molecular weight of 20 000 or less has been studied. Fractions of molecular weight 4000 or less have one melting transition; those with molecular weight of 6000 or greater may have two melting transitions. Consideration of the influence of molecular weight and crystallization temperature on the melting transitions, of the low-angle scattering of X-rays, and of calculations based upon Flory's theory of melting enables us to ascribe the transitions to the melting of extended-chain or of variously folded-chain lamellar crystals. The end interfacial free energy ( $\sigma_e$ ) of extended-chain crystals of poly(ethylene oxide) is found to increase within the range 1 to 4 kcal/mol as the molecular weight increases. It is suggested that this increase in  $\sigma_e$  is related to an increase in polydispersity of molecular weights in the fractions.

## INTRODUCTION

Poly(ethylene oxide) is particularly useful for a study of the properties of crystalline polymers of low molecular weight. A wide range of samples of narrow molecular weight distribution are readily available. Their chain structure is linear and high crystallinities can be achieved, and their melting and crystallization temperatures are in the convenient range of 30 to 70°C.

Several studies of the melting of very low molecular weight poly(ethylene oxide) samples have been made<sup>1-3</sup>. It has also been reported<sup>4, 5</sup> that poly(ethylene oxide) of molecular weight near 6000 has two melting transitions. This observation is in keeping with the results of low-angle X-ray scattering and density measurements<sup>6, 7</sup> which indicate a complex morphology in such polymers.

Here we present an experimental and theoretical study of the melting of well characterized fractions of low molecular weight poly(ethylene oxide), with emphasis placed upon the detection and interpretation of multiple melting, and supplemented by low-angle X-ray scattering studies of selected samples.

## EXPERIMENTAL

### Preparation and characterization

Samples of poly(ethylene oxide), from a variety of commercial sources (see Table 1), were fractionated by

\* Present address: Materials Science Unit, Turner Dental School, University of Manchester.

† Present address: Donnan Laboratories, University of Liverpool, PO Box 147, Liverpool L69 3BX, UK.

Table 1 Characteristics of the poly(ethylene oxide) fractions

Fraction	Source	$M_n$		$[\eta]$ (dl/g)	$M_w/M_n$
		Osmometry	Analysis		
1000	A	1040	1070	—	1.06
1500	A	1580	—	0.062	1.05
2000	B	2030	1910	—	1.05
4000	A	4070	—	0.118	1.05
6000M	C	6100	—	0.186	1.11
6000	A	6100	6040	—	1.23
10000	B	—	—	0.295	1.2
20000	C	—	—	0.374	1.2

A. Shell Chemical Co. Ltd, Shell Centre, London, SW1

B. Hoechst Chemicals Ltd, Hoechst House, Salisbury Road, Hounslow, Middlesex

C. Union Carbide Ltd, Chemicals Division, 8 Grafton Street, London W1

precipitation from dilute solution in benzene by addition of iso-octane. Fractions, comprising about half the original sample, were freeze-dried from benzene before use.

Number-average molecular weights ( $M_n$ ) were measured by means of a Mechrolab Vapour Pressure Osmometer and by end-group analysis<sup>8</sup>. Intrinsic viscosities in benzene at 25°C were measured as described earlier<sup>9</sup>. Molecular weight distributions were investigated by means of a Waters Gel Permeation Chromatograph. Tetrahydrofuran at 45°C was a suitable solvent for samples with  $M_n \leq 6000$ . Samples of higher molecular weight were insufficiently soluble in tetrahydrofuran for purposes of gel permeation chromatography, and either 2-ethoxyethanol at 90°C or dimethylacetamide at 90°C was preferred. Four columns, ranging from  $5 \times 10^6$  Å to 700 Å nominal pore size, were used at a flow rate of

1 cm<sup>3</sup>/min. Correction for adventitious dispersion was made by the method of Aldhouse and Stanford<sup>10</sup>. In this method the variance of the observed chromatogram is taken to be the sum of the variances due to the polydispersity of the sample and due to adventitious dispersion. The adventitious dispersion is characterized by the variance ( $\sigma^2$ ) of a hypothetical monodisperse polymer sample. For the set of columns used here we found  $\sigma = 10.5 - 0.047v$  where  $v$  is the elution volume in cm<sup>3</sup>. Calibration was by plotting  $\log_{10} M_n$  against the observed peak maxima.

In Table 1 we list the molecular characteristics of the samples. It is convenient to denote samples by their nominal molecular weights. Most fractions had hydroxyl terminal groups; the exception was 6000M which was prepared from a methoxide initiator and had some methoxy terminal groups.

### Dilatometry

Small samples (<200 mg), moulded in high vacuum, were placed in glass dilatometers, outgassed and confined with mercury. The dilatometers were immersed in boiling water for 15 minutes and transferred to a bath held (to  $\pm 0.01^\circ\text{C}$ ) at the appropriate crystallization temperature,  $T_c$ . Thermal equilibrium was established within 2 min. Various times were allowed for crystallization and the melting behaviour of both completely and partly crystallized samples was studied.

Crystallization was stopped and melting was effected by transferring the dilatometer to a bath held not more than  $1^\circ\text{C}$  below the lowest transition temperature to be observed, and then raising the temperature by 2 to  $6^\circ\text{C}/\text{h}$ . The expansion was followed by means of a cathetometer. The melting point,  $T_m$ , was taken to be that temperature at which detectable crystallinity disappeared; a subsidiary melting transition was defined by

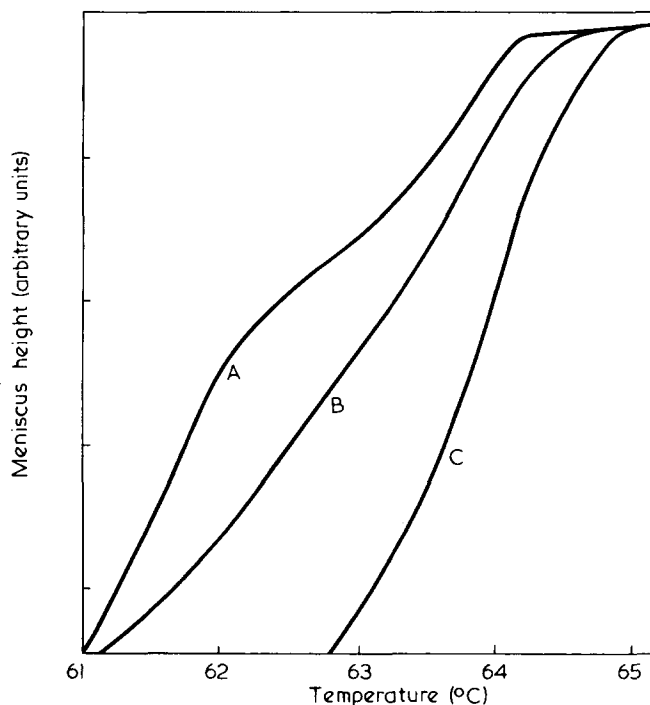


Figure 1 Dilatometer meniscus height (arbitrary units) against temperature ( $^\circ\text{C}$ ) for poly(ethylene oxide) fraction 6000M crystallized at various temperatures ( $T_c$ ). A:  $T_c = 54.1^\circ\text{C}$ ; B:  $T_c = 54.8^\circ\text{C}$ ; C:  $T_c = 55.5^\circ\text{C}$

the appropriate point of inflexion in the melting curve (see, for example, Figure 1). The starting temperatures were sufficiently close to the melting points that no change in melting behaviour was observed if the sample was held at the starting temperature for several days, i.e. annealing and recrystallization were absent. The heating rates were chosen to avoid superheating which was detectable at  $12^\circ\text{C}/\text{h}$ . Similar melting curves to those obtained here for 6000M have been recorded for heating rates of  $1^\circ\text{C}/\text{day}^5$ .

### Low-angle X-ray scattering

A Rigaku-Denki slit collimated low angle camera was used, with copper  $K_\alpha$  radiation supplied from a Philips 'Fine Focus' tube (36 kV, 20 mA) via a nickel filter. The diffraction pattern was recorded on film mounted 25.5 cm from the sample. The backstop strip, visible in Figure 2, was 0.075 cm wide.

Poly(ethylene oxide) samples (dimensions  $2.5 \times 1.0 \times 0.1$  cm) were prepared on Melinex polyester film by melting and then recrystallizing on a microscope hot stage<sup>11</sup>. The Melinex film was removed before the sample was exposed.

## RESULTS

Single melting transitions were found for samples with  $M_n \leq 4000$ , but two melting transitions were found for samples of higher molecular weight at certain crystallization temperatures (Figure 1). The molecular weight above which two transitions can be found is not well defined; we note that two melting transitions have been found (Pickles, C. J., personal communication) in other samples of poly(ethylene oxide) of molecular weight near 4000.

Melting temperatures are listed in Tables 2 and 3. In these tables high and low crystallinity corresponds to about 100% and to 10–15% of realizable crystallinity, as judged by the volume contraction at the crystallization temperature. The melting points are not greatly affected by changes in crystallization temperature and crystallinity. However, the crystallization temperature has a marked effect upon the relative proportions of the two crystalline forms of the higher molecular weight polymers (Table 3). An increase in  $T_c$  is accompanied by an increase in the proportion of the higher melting form and, on occasion, by the appearance or disappearance of a transition; this is illustrated in Figure 1.

Low-angle X-ray scattering from samples 1500 and 4000 is indicative of lamellar crystals with thicknesses very close to the extended lengths of the polymer chains. Skoulios *et al.*<sup>6</sup> have shown this to be so for several samples of poly(ethylene oxide) of molecular weight less than  $M_n = 3300$ . The single melting points for our fractions with  $M_n \leq 4000$  (Table 2) are consistent with this simple crystal morphology.

Fractions with  $M_n \approx 6000$  have one melting transition when  $T_c > 55^\circ\text{C}$ . Low-angle X-ray scattering from such samples [Figure 2(a)] corresponds to a repeat distance of about 390 Å, which is close to the extended chain length. Two melting transitions are observed for fractions of  $M_n \approx 6000$  when  $T_c < 55^\circ\text{C}$ . Low-angle X-ray scattering from these samples [Figure 2(b)] is indicative of lamellar



Table 2 Effect of molecular weight and crystallization conditions on the melting of poly(ethylene oxide)

Fraction	High crystallinity		Low crystallinity	
	$T_c$ (°C)	$T_m$ (°C)	$T_c$ (°C)	$T_m$ (°C)
1000	34.8	39.1	36.8	39.0
	36.1	39.1		
1500	43.3	49.0	44.9	48.7
	44.8	49.0		
	45.9	49.0		
2000	45.2	53.8	46.9	53.6
	46.3	53.8		
	48.3	53.8	48.3	53.6
4000	43.2	61.4	49.2	60.6
	49.6	61.3		
	50.9	61.4	49.9	60.6
	52.4	61.6		
	53.4	61.5		

Table 3 Effect of molecular weight and crystallization conditions on the melting of poly(ethylene oxide)

Fraction	High crystallinity		Low crystallinity	
	$T_c$ (°C)	$T_m$ (°C)	$T_c$ (°C)	$T_m$ (°C)
6000M	45.5	62.4, 64.4	45.5	62.3, 63.7
	49.7	62.4, 64.5		
	53.0	62.5, 64.2		
	54.1	62.3, 64.2		
	54.8	abs., 64.4		
	55.5	abs., 64.9		
6000	48.0	61.0, 64.1	48.0	— 63.0
	49.2	61.1, 64.1		
	49.6	61.0, 64.1		
	50.9	61.0, 64.1		
	54.1	abs., 63.5		
	54.8	abs., 63.6		
	55.2	abs., 63.8		
	55.2	abs., 63.8		
10000	35.4	64.3, abs.	54.5	63.9, 64.9
	44.8	64.0, 65.0		
	49.9	64.3, 65.1		
	53.6	64.3, 65.3		
	55.4	64.3, 65.2		
	57.5	64.3, 65.3		
20000	30.0	65.6, abs.	51.1	65.0, 65.5
	44.1	65.7, abs.		
	51.1	65.8, 66.4		
	54.8	65.9, 66.7		
	57.5	65.9, 66.7		

crystals with thickness about half of the polymer chain length. Close examination of the original negative of Figure 2(b) reveals lines of low intensity equidistant between the more intense lines and due to the extended-chain crystals which are also present. It was noted that long exposure times (>15 h) were needed to record the scattering from extended-chain crystals of 6000M: exposure for 2 h gave a blank film when  $T_c=55.5^\circ\text{C}$  and a pattern characteristic of folded-chain crystals only when  $T_c=53.0^\circ\text{C}$ . The density of the crystalline polymer is high when  $T_c$  is high<sup>7</sup>, so it is presumed that the low intensity is due to imperfection in the end surfaces of the extended chain crystals (see the discussion). On the basis of the X-ray evidence we attribute the lower transition to the melting of once-folded-chain crystals and the higher transition to the melting of extended-chain crystals\*.

\* Our interpretation of X-ray data for poly(ethylene oxide) of molecular weight 6000 and higher differs from that of Arlie *et al.*<sup>7</sup> and Spegt<sup>12</sup>. We have been aided by the availability of melting data and of X-ray studies over a wide range of exposure times.

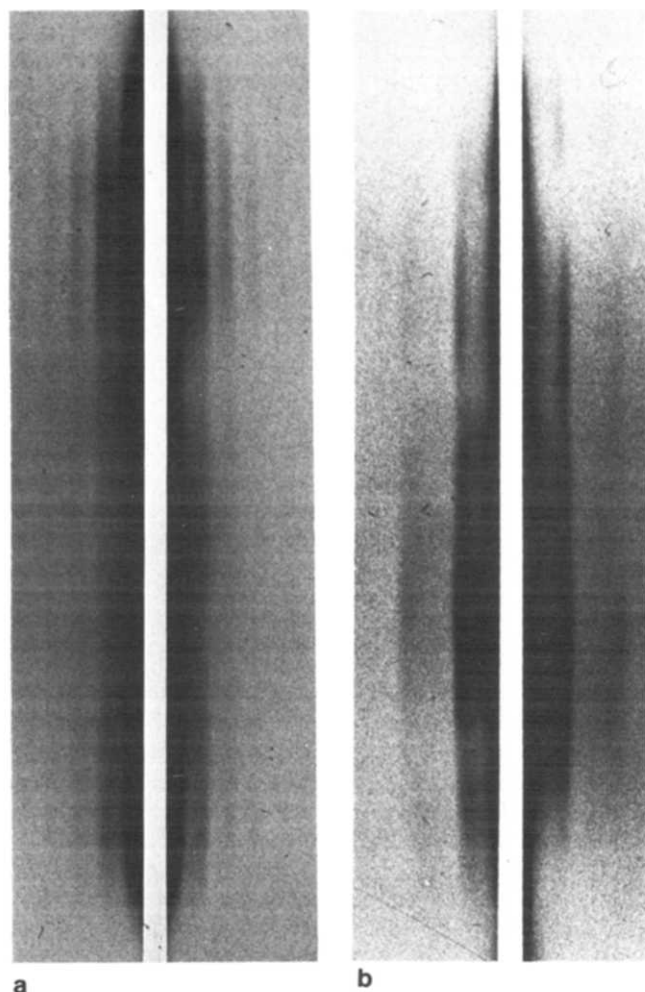


Figure 2 Low-angle X-ray scattering from poly(ethylene oxide) fraction 6000M crystallized at temperature  $T_c$  and exposed for 18 h: (a)  $T_c=55.5^\circ\text{C}$ ; (b)  $T_c=53.0^\circ\text{C}$

The fact that lower melting (less stable) folded-chain crystals are formed simultaneously with more stable extended-chain crystals when  $T_c < 55^\circ\text{C}$  indicates a preference for folded-chain crystallization in a rate controlled crystallization process under these conditions. It is consistent with this idea that the proportion of folded-chain crystals increases as the crystallization temperature decreases, i.e. as the crystallization rate increases. We also note that the folded-chain crystals can be entirely converted to extended-chain crystals by annealing at a suitable temperature, e.g. 6000M crystallized at  $53.4^\circ\text{C}$  to 15% crystallinity and held at  $61.4^\circ\text{C}$  for one week showed little increase in crystallinity and only one melting transition at  $64.9^\circ\text{C}$ .

The various melting transitions found for samples 10 000 and 20 000 presumably correspond to differing folded-chain morphologies. Arlie *et al.*<sup>7</sup> and Spegt<sup>12</sup> have recorded X-ray scattering for similar samples which indicate discontinuous variations in lamellar thickness and are attributed to differing extents of chain folding.

We conclude that poly(ethylene oxide) fractions of molecular weight ( $M_n$ ) less than 4000 crystallized in extended-chain lamellar crystals; that fractions of  $M_n$  near 6000 may crystallize in both extended- and chain-folded crystals; and that fractions of higher molecular weight probably form folded-chain crystals only.

## THEORY

The melting points of extended-chain crystals formed from mono-disperse polymers can be calculated from the theory of Flory<sup>13</sup> or of Flory and Vrij<sup>14</sup>, depending upon whether the ends of the molecules are paired<sup>14</sup> or not<sup>13</sup>. The melting points of polydisperse polymers, such as our fractions, can be evaluated by appropriate extension of these theories. Flory<sup>13</sup> has discussed the case of polymers with most probable molecular weight distributions. Here we present equations and calculations for polymers having exponential<sup>15</sup> molecular weight distributions of varying widths. In view of the impropriety of the end-paired model for polymers with molecular weight distributions of finite width we restrict our discussion to the theory of Flory<sup>13</sup>.

It is assumed that lamellar crystals of thickness  $\zeta$  chain units are formed. A restriction upon the selection of units to incorporate into the crystals is that the ends of the molecules are excluded. The probability that a sequence of  $\zeta$  chain units, chosen from a polydisperse polymer, does not contain a chain end is

$$\int_{\zeta}^{\infty} w(x) \left( \frac{x-\zeta+1}{x} \right) dx \quad (1)$$

where  $w(x)$  is the weight fraction of molecules of length  $x$  units. We assume that  $w(x)$  is given by the Schulz-Zimm<sup>15</sup> expression

$$w(x) = \frac{b^{(a+1)}}{a!} x^a e^{-bx} \quad (2)$$

where  $b = a/x_n$ ,  $a = x_n/(x_w - x_n)$  and is integral in equation (2) and  $x_n$  and  $x_w$  are the number- and weight-average chain lengths (in chain units) respectively.

Following Flory<sup>13</sup> we combine this probability with terms arising from the disordering of the polymer on melting to obtain the entropy of fusion and, ultimately, the free energy of fusion of  $N$  polymer molecules.

$$\frac{\Delta F_f}{Nx_n} = (1-\lambda)\Delta f + RT \left[ \frac{1}{x_n} \ln \lambda + \frac{1-\lambda}{\zeta} (\ln D + \ln I) \right] \quad (3)$$

In equation (3),  $(1-\lambda)$  is the degree of crystallinity of the polymer sample;  $\Delta f$  is the free energy of fusion per chain unit of bulk polymer and is given, at temperature  $T$ , by

$$\Delta f = \Delta h (1 - T/T_m^0) \quad (4)$$

where  $\Delta h$  is the enthalpy of fusion of bulk polymer per chain unit and  $T_m^0$  is the thermodynamic melting point of the polymer (i.e. the equilibrium melting point of the polymer as  $x$  and  $\zeta$  tend to infinity);  $\ln D = -2\sigma_e/RT$ , where  $\sigma_e$  is the end interfacial free energy of the lamellar crystal, and

$$I = \frac{b^{(a+1)}}{a!} \int_{\zeta}^{\infty} x^{(a-1)} e^{-bx} (x-\zeta+1) dx \quad (5)$$

The melting point  $T_m$  corresponding to a crystal of lamellar thickness  $\zeta$  is given by the conditions

$$\left( \frac{\partial \Delta F_f}{\partial \lambda} \right)_{\zeta} = 0 \text{ and } \lambda = 1 \quad (6)$$

and is given by

$$T_m = T_m^0 \left( 1 - \frac{2\sigma_e}{\Delta h \zeta} \right) / \left[ 1 + \frac{RT_m^0}{\Delta h} \left( \frac{1}{x_n} - \frac{\ln I}{\zeta} \right) \right] \quad (7)$$

This formulation leaves open the method of evaluation of  $\zeta$ . It has been assumed<sup>2,3</sup> that  $\zeta$  is determined by the condition of equilibrium between crystal and melt, but we discount this for our systems since we find two melting points, due to differing morphologies, in poly(ethylene oxides) of molecular weight greater than 4000. It has also been suggested<sup>16</sup> that  $\zeta$  may be determined by a three-dimensional nucleation process, but we discount this for our fractions on the basis of calculations of  $\zeta$  and  $T_m$ , for values of  $\sigma_e$  in the range 1–5 kcal/mol, which show  $\zeta$  to be substantially less than  $x_n$  and  $T_m$  to vary markedly with  $T_c$ . Neither of these predictions is confirmed by the results presented earlier. In calculations we have adopted values of  $\zeta$  such that  $x_n > \zeta > 0.9x_n$ , as indicated for extended chain crystals by X-ray and density measurements<sup>6,7,12</sup>.

## COMPARISON OF THEORY AND EXPERIMENT

We have calculated values of the melting points of poly(ethylene oxide) by numerical solution of equation (7) with the following values of the parameters:  $T_m^0 = 76^\circ\text{C}^{17}$ ;  $\Delta h = 2 \text{ kcal/mol}^{2,18}$ ;  $\sigma_e$  in the range 1–5 kcal/mol;  $M_n > 1000$ ;  $M_w/M_n < 2$ ;  $\zeta \sim x_n$ .

In Table 4 we present results which show that calculated melting points of extended-chain crystals of low molecular weight poly(ethylene oxide) are greatly influenced by the width of the molecular weight distribution. It is clear that the finite width of the molecular weight distribution must be properly accounted for in a comparison of theory with experimental data on conventional polymer fractions.

In Table 5 we present calculated melting points of samples of poly(ethylene oxide) similar in molecular constitution to those we have investigated in our experiments. Since the end interfacial free energy of these polymers is not known we have covered a wide range of values of  $\sigma_e$ . Comparison of the experimental results for mature crystals (Tables 2 and 3) with these and other calculations enables us to estimate values of  $\sigma_e$  for our

Table 4 Variation of calculated melting point of poly(ethylene oxide) [ $T_m$  (°C)] with polydispersity:  $\sigma_e = 1.5 \text{ kcal/mol}$ ;  $\zeta = x_n$

$M_n$	$M_w/M_n$				
	1.0	1.05	1.2	1.5	2.0
1000	33.6	37.7	40.3	42.2	43.5
2000	52.5	56.2	57.7	58.7	59.5
6000	67.0	69.2	69.8	70.2	70.4

Table 5 Variation of calculated melting point of poly(ethylene oxide) [ $T_m$  (°C)] with end interfacial free energy:  $\zeta = x_n$

$M_n$	$M_w/M_n$	$\sigma_e$ (kcal/mol)			
		1.0	2.0	3.0	4.0
1000	1.05	45.0	30.4	15.7	—
1500	1.05	54.8	44.9	35.0	25.1
2000	1.05	59.9	52.4	44.9	37.4
4000	1.05	67.8	64.0	60.2	56.4
6000	1.10	70.8	68.2	65.4	63.1
10000	1.20	—	—	70.0	68.4
20000	1.20	—	—	73.0	72.2

Table 6 End interfacial free energy ( $\sigma_e$ ) for extended-chain crystals of poly(ethylene oxide)

$M_n$	$M_w/M_n$ (approx.)	Deviation, $S_w$ (chain units)	$\sigma_e$ (kcal/mol)
1000	1.05	5	1.4
1500	1.05	8	1.6
2000	1.05	10	1.8
4000	1.05	21	2.7
6000M	1.10	45	3.4
6000	1.20	67	3.6

crystalline samples. These results are given in Table 6; it is found that  $\sigma_e$  increases markedly as the molecular weight increases.

We suggest that the increase in  $\sigma_e$  with increasing molecular weight is due to an increase in roughness of the end surface of the crystal, which is due to the increase in the absolute spread of molecular weights which accompanies an increase in molecular weight at constant (or increasing) values of  $M_w/M_n$ . A better parameter than  $M_w/M_n$  with which to describe the width of the molecular weight distribution in this context is the deviation  $S_w$  given by

$$S_w^2 = x_w(x_z - x_w) \quad (8)$$

or, for an exponential distribution, by

$$S_w = x_n(a+1)^{1/2}/a \quad (9)$$

This parameter is the standard deviation of a normal weight distribution of molecular weights, and for the narrow molecular weight distributions under discussion, the distinction between exponential and normal distributions is not important. Values of  $S_w$ , together with values of  $\sigma_e$  calculated for crystals of thickness  $\zeta = x_n$ , are given in Table 6. We would expect the roughness of the end surface of the crystal to bear a direct relation to the deviation  $S_w$ . In Figure 3 we plot  $\sigma_e$  against  $S_w$  (using the values of Table 6). We find a limiting value of  $\sigma_e$  near 1 kcal/mol for monodisperse samples of poly(ethylene oxide) and a limiting value near 4 kcal/mol for samples of poly(ethylene oxide) of high polydispersity. Calculations for crystals of thickness  $\zeta = 0.9x_n$  give very similar results for polydisperse polymers.

Folded-chain crystals are detected in samples of poly(ethylene oxide) of  $M_n > 4000$ , ultimately ( $M_n > 6000$ ) to the exclusion of extended-chain crystals. Melting points of extended-chain crystals of poly(ethylene oxide) 10 000 and 20 000 are included in Table 5. The end interfacial free energy for such crystals should be near 4 kcal/mol. It can be seen that calculated values of  $T_m$  with  $\sigma_e = 4$  kcal/mol exceed the highest measured value (Table 3) by about 4°C. This is in keeping with the conclusions of Arlie *et al.*<sup>7</sup> and Spegt<sup>12</sup> that poly(ethylene oxide) of molecular weight 10 000 and greater forms only folded-chain crystals. The calculated melting point of a crystal of poly(ethylene oxide) with  $M_n = 6000$ ,  $M_w/M_n = 1.2$ ,  $\sigma_e = 4.0$  kcal/mol and  $\zeta = x_n/2$  is 53.6°C. The corresponding experimental value for the chain-folded (lower melting) crystals of sample 6000 is 61.0°C (Table 3). It is clear that  $\sigma_e$  for chain-folded crystals of poly(ethylene oxide) 6000 is substantially lower than that for crystals of similar thickness ( $x_n/2$ ) but with all chains emerging from the surface. This is to be expected since the folding of chains, quite apart from the introduction of chain-fold surface, will reduce the surface roughness due to the spread in effective molecular

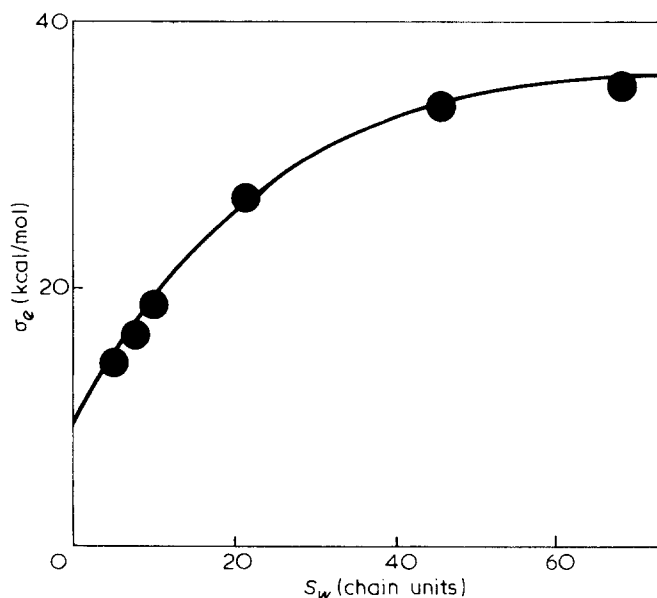


Figure 3 Surface free energy ( $\sigma_e$ , kcal/mol) against deviation ( $S_w$ , chain units) of the molecular weight distribution for extended-chain crystals of poly(ethylene oxide) fractions of low molecular weight

length by a factor of two. However, it is equally clear from the experimental results for poly(ethylene oxide) 6000 that the end interfacial free energy of its folded-chain crystals is not sufficiently reduced below that of the extended-chain crystal as to render it more thermodynamically stable.

#### ACKNOWLEDGEMENTS

We thank Mr D. J. Roy and Miss G. Patfield for assistance with the characterization of the polymers. D. R. Beech and D. V. Dodgson acknowledge receipt of Science Research Council Studentships.

#### REFERENCES

- Spegt, P. A., Terrisse, J., Gilg, B. and Skoulios, A. E. *Makromol. Chem.* 1967, **107**, 29
- Braun, W., Hellwege, K. H. and Knappe, W. *Kolloid-Z.* 1967, **215**, 10
- Hay, J. N., Sabir, M. and Stephen, R. L. T. *Polymer* 1969, **10**, 187
- Kobayashi, T., Sakijama, M. and Seki, S. *Int. Symp. Macromol. Chem., Tokyo* 1966
- Devoy, C. J. *PhD Thesis*, University of Manchester, 1966
- Arlie, J. P., Spegt, P. A. and Skoulios, A. E. *Makromol. Chem.* 1966, **99**, 160
- Arlie, J. P., Spegt, P. A. and Skoulios, A. E. *Makromol. Chem.* 1967, **104**, 212
- Price, C. C. and St. Pierre, L. E. *J. Am. Chem. Soc.*, 1956, **78**, 3432
- Beech, D. R. and Booth, C. J. *Polym. Sci. (A-2)* 1969, **7**, 575
- Aldhouse, S. T. E. and Stanford, D. M. *5th Int. Gel Permeation Chromatog. Seminar, London* 1968
- Hay, J. N. *J. Sci. Instr.* 1964, **41**, 456
- Spegt, P. A. *Makromol. Chem.* 1970, **140**, 167
- Flory, P. J. *J. Chem. Phys.* 1949, **17**, 223
- Flory, P. J. and Vrij, A. *J. Am. Chem. Soc.* 1963, **85**, 3548
- Schulz, G. V. *Z. Phys. Chem.* 1939, **B43**, 25; Zimm, B. H. *J. Chem. Phys.* 1948, **16**, 1093
- Mandelkern, L., Fatou, J. G. and Howard, C. J. *Phys. Chem.* 1964, **68**, 3386
- Beech, D. R. and Booth, C. J. *Polym. Sci. (B)* 1970, **8**, 731
- Beaumont, R. H., Clegg, B., Gee, G., Herbert, J. B. M., Marks, D. J., Roberts, R. C. and Sims, D. *Polymer* 1966, **7**, 401

# Temperature scanning studies of polyolefin solutions

H. P. Schreiber

Canadian Industries Ltd, Central Research Laboratory, McMasterville, Quebec,  
Canada  
(Received 26 April 1971)

Double endotherms, indicative of recrystallization (annealing) during solution, have been observed in temperature scans of the solution process for linear polyethylenes in various common solvents. The effectiveness of recrystallization during solution varies inversely with the cooling rate used to crystallize the polymer from solution. An analogy is drawn between the dependence of recrystallization processes on crystallization rate, and the dependence of isothermal crystallization rates on solution temperature. A fractionation effect occurs during the recrystallization of linear polyethylenes. This complicates further the recrystallization behaviour in the polymer and is a source for the dependence of its solution processes on the thermodynamics of polymer/solvent interaction. The results draw attention to the need for careful selection of solvents and processing variables in solutions used for molecular structure determinations. Failure to take into account recrystallization phenomena also questions the validity of some literature values for the free energy of mixing parameter  $\chi$  in polyethylene/solvent systems, and emphasizes the need for accurate redetermination of this parameter.

## INTRODUCTION

The investigations of Blackadder and Schleinitz<sup>1</sup>, and Koenig and Carrano<sup>2,3</sup> have indicated the usefulness of differential thermal analysis (d.t.a.) in studies of crystallization and solution processes involving polyethylene. The method is capable of providing a permanent record of crystallization and solution temperatures, of the energy changes accompanying these phase transitions and of the dependence of the parameters on controlled thermal history. The above-noted publications, along with the literature dealing with the kinetics of crystallization of the polymer from solution, and with morphological effects arising from changes in solution and crystallization temperatures, have prompted a re-examination of data obtained some time ago, in the course of d.t.a. studies of polyolefin solution processes.

Our work was undertaken in an effort to account for anomalous, temperature-dependent values of  $\bar{M}_w$  for polyethylenes<sup>4</sup>, based on light-scattering results in  $\alpha$ -chloronaphthalene ( $\alpha$ -CN) solutions. Specifically, an effort was made to substantiate the suggestion made in that work<sup>4</sup> that crystallites or ordered aggregates of polymer, persisting in solution well above the temperature for optical clarification, could account for the anomalous molecular weight data. Whilst the persistence of crystalline particles in polyethylene solutions is now generally accepted<sup>5,6</sup>, our temperature scan experiments only inferred their existence without offering final proof: they were therefore not prepared for publication. The

reason for presenting the results now is that they represent a useful complement to the data offered in refs. 1, 2 and 3. The present purpose is to show that the dissolution of a polyethylene crystal suspension at a controlled heating rate is strongly dependent on the cooling path chosen for the preparation of the suspension; that a fractionation process occurs during solution along the selected heating path and that the fractionation appears to be dependent on polymer/solvent interaction effects. The results call for more accurate evaluation of thermodynamic interaction parameters for polyethylene/solvent systems.

## EXPERIMENTAL

### Apparatus

Two d.t.a. cells were constructed for the present work. The analytic cell, used in the great majority of experiments, is illustrated in *Figure 1*. Some 12 in. in height and 3 in. in diameter, it has provision in the top portion for connections with vacuum pumps and N<sub>2</sub> cylinders. A Teflon plug, supported on glass projections, isolated a volume of about 15 ml which contained the materials under study. The rather tight-fitting plug served to reduce vapour space, to fix the sensing probe in the tip of the analytic cell, and to support a glass-rod stirrer connected to a 60 rev/min synchronous (Bodine) motor. In order to gain maximum sensitivity in experiments, the thermal probes were in direct contact with test solutions.

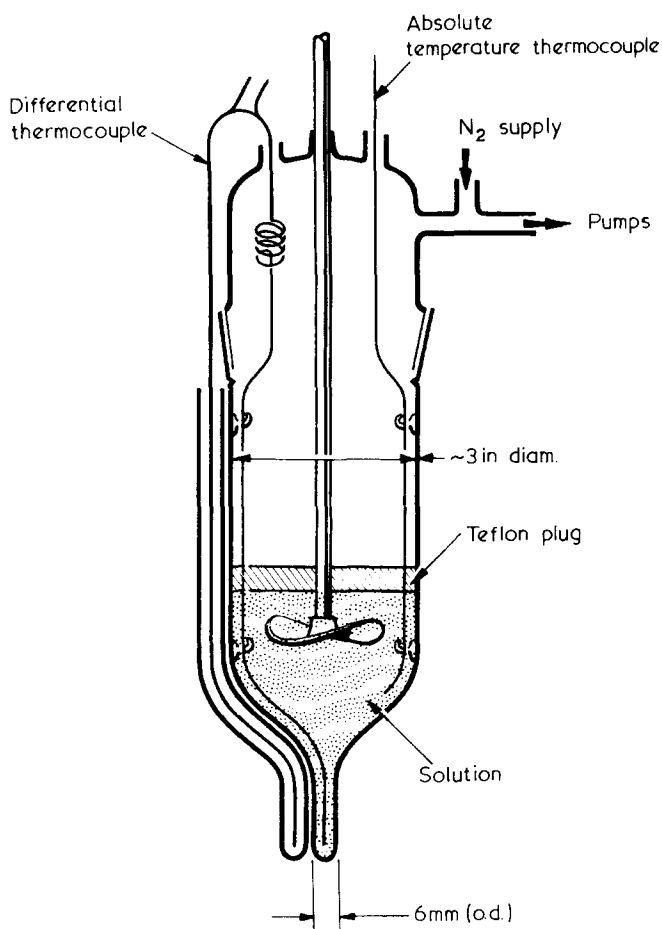


Figure 1 Analytic scanning cell

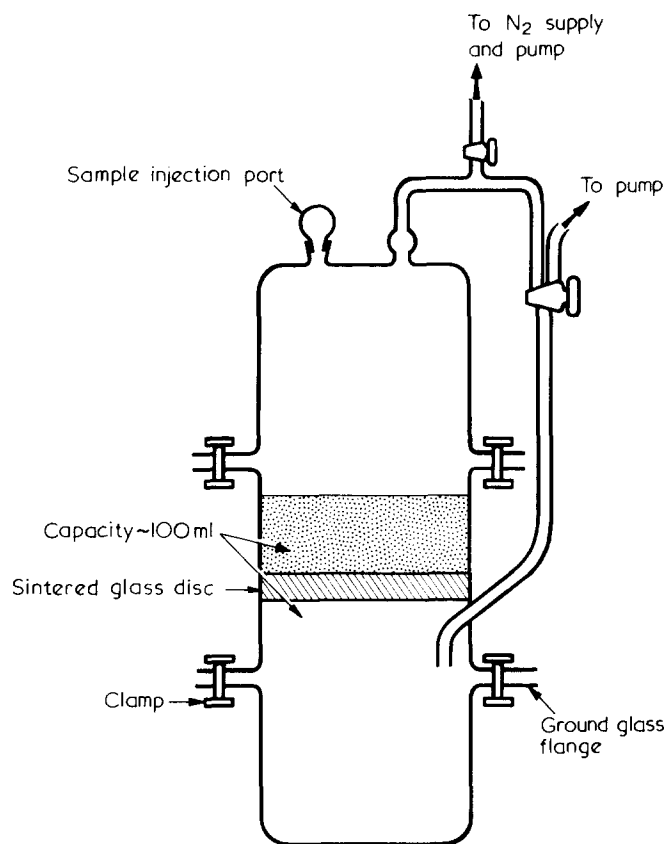


Figure 2 Fractionation cell

Pallador\* junctions were employed, the sensing probe being located in the tip of the cell, as shown, while the reference junction was placed in a glass tube of the same geometry as the sensing tip, and in contact with the cell wall. Silicone oil (viscosity 800 cP at 30°C) was used in the reference tube to provide an environment of approximately equal thermal conductivity as that in the cell. Smooth, reproducible base-line traces were generated by this system in cell calibration experiments using pure solvents. The thermocouples, connected to a Liston-Becker model 14 breaker-amplifier, provide  $3 \mu\text{V}/\text{in}$  sensitivity for recording temperature differences in scanning experiments. The absolute temperature of the system was recorded similarly, using as a reference conductivity water at its triple-point.

A larger cell, referred to as the 'fractionation cell' was also used in a number of cases. This unit is shown in Figure 2. The two dome-shaped pieces and the central cylindrical section were clamped together at the ground-glass flanges, providing a volume of nearly  $100 \text{ cm}^3$  between the upper flange and a coarse, sintered glass disc cemented against the wall of the cylindrical section. Connections to vacuum and  $\text{N}_2$  lines permitted control of the environment in contact with the fluid and allowed suction to be applied in order to separate dissolved and undissolved polymer fractions under selected isothermal conditions. The cell, mounted in an eccentrically rotating arm, allowed the solution to be agitated gently during the

experiment. No provision for temperature sensing existed in the fractionation cell; for this reason it could be used only in conjunction with the analytical cell. Since fractionation in the cell occurred only after several hours of annealing under isothermal conditions, it is reasonable to assume that the measured temperature conditions in the analytic unit also applied to the larger cell.

The two cells were housed in an oil bath, the temperature of which was controlled by heater banks. Continuous heating was supplied by 500 W heaters, while a second group of heaters, totalling 700 W, was connected to variable resistors, the settings of which were programmed by a clock-driven servo-mechanism. The arrangement provided linear heating and cooling rates of  $1^\circ\text{--}6^\circ\text{C}/\text{min}$  in the range  $30^\circ\text{--}130^\circ\text{C}$ . Calibration experiments defined heating conditions needed to maintain constant temperatures ( $\pm 0.2^\circ\text{C}$ ) at any point within this range. More rapid cooling of the analytic cell was obtained by lifting the cell out of the bath, following attainment of the high-temperature limit of an experiment. The resulting cooling rate of  $\sim 18^\circ\text{C}/\text{min}$  was found to be nearly linear to  $70^\circ\text{C}$ , i.e. well below the crystallization temperature range in the systems studied.

### Materials

Two whole linear polyethylenes (Marlex 50 coded LPE-1, LPE-2) were used in most of the work described. In addition, four fractions (F1-F4), prepared from the higher molecular weight sample by fractional precipitation<sup>7</sup> were also used. Molecular weights were obtained

\* Johnson-Matthey-Mallory Co. alloys of platinum/rhodium, gold/palladium. The couples have a sensitivity about equal to standard chromel/alumel in the temperature range of concern.

Table 1 Molecular properties of polyethylenes used

Sample	$\bar{M}_w \times 10^{-3}$	$M_w/M_n$
LPE-1	95	14
LPE-2	76	11
F1	180	2.8
F2	29	2.4
F3	15.5	2.2
F4	4.9	~2.1

by light-scattering in  $\alpha$ -CN at 140°C, as described earlier<sup>4</sup>, and from terminal unsaturation using infra-red spectra. Characterization data are given in Table 1.

The solvents were tetrahydronaphthalene (tetralin),  $\alpha$ -chloronaphthalene ( $\alpha$ -CN), *p*-xylene and decalin. All were fresh, Fisher reagent grade materials, used without further purification.

### Procedure

The experimental procedures reflected limitations of d.t.a. already noted in the reports of earlier workers<sup>1-3</sup>. Solutions were prepared *in situ*, using the analytic cell. The solution temperature was 140°C for  $\alpha$ -CN, tetralin and decalin, 125°C when *p*-xylene was the solvent. A small amount of thermal stabilizer [0.1% of 4,4'-thio-bis(3-methyl-6-*t*-butylphenol)] was added to prevent oxidative changes during work periods. As a further precaution, all work was performed under a N<sub>2</sub> atmosphere.

The concentration range in these experiments extended from about 0.3–3.0 wt. % polymer. At concentrations below about 0.6% the phase-separation effects already noted by others<sup>1-3</sup> were observed, when the temperature was in or below the crystallization range. This violates the principle of thermal analysis which requires conduction to be the sole mechanism of heat transport. High-speed stirring, possibly effective in overcoming this difficulty, was avoided to guard against frictional heating in the relatively viscous polymer solutions. The compromise of gentle stirring at 60 rev/min extended the useful operating range to near the 0.4% level. Reproducible, smooth d.t.a. signals were recorded without the need of stirring at polymer concentrations above about 0.7%, once again in agreement with the findings of Blackadder, Koenig and their collaborators.

Following dissolution of the polymer, crystal suspensions were grown along one of three arbitrary but reproducible cooling paths, corresponding to 1.2°, 3.0° and ~18°C/min. No attempt was made to grow crystals isothermally, as in the many kinetic studies of the crystallization process from solutions<sup>8-10</sup>. The primary intention was to study the effects of typical thermal history cycles on the re-resolution behaviour of the polymer. Following the attainment of room temperature, the opaque suspensions were allowed to digest for roughly 1 h, whereupon re-resolution was effected by heating at a linear rate of 1.2°C/min. This heating rate was followed in all experiments, with the exception of those involving isothermal annealing periods, as specified elsewhere in the text.

## RESULTS AND DISCUSSION

### Solution behaviour in tetralin

The re-resolution behaviour of polyethylene crystal suspensions in tetralin, and its dependence on crystallization path, is shown in Figure 3a. A number of work parameters defined from the endotherms are shown in Figure 3b. In the case of double peaks,  $T'_s$  and  $T''_s$  represent the lower and higher peak temperatures respectively, while  $A'_s$ ,  $A''_s$  and  $A_t$  are the areas under the low and high  $T$  endotherms and the sum of the two. The endotherms shown are for 1% solutions of LPE-1, and are typical generically of the whole polymers and of the high molecular weight fractions.

The endotherm patterns were found to be highly reproducible internally, identical cooling–heating cycles repeated several times on a given fluid always producing the same signal. The absolute magnitude of the signals was found to be linearly dependent on concentration as shown in Table 2, and the slower cooling paths produced somewhat greater endothermic effects than the rapid cooling mode. The dissolution temperatures show a very mild dependence on concentration, notably in the > 2% range. Similar behaviour has been reported earlier<sup>1,2</sup>.

Ideal solution conditions for polyethylene crystal suspensions would require heating along a zero entropy-production path<sup>11</sup>, creating neither superheating effects nor morphological rearrangements. Prior experience of Blackadder<sup>1</sup>, Koenig<sup>2,3</sup> and Peterlin<sup>12</sup> shows that at heating rates less than about 3°C/min, substantial

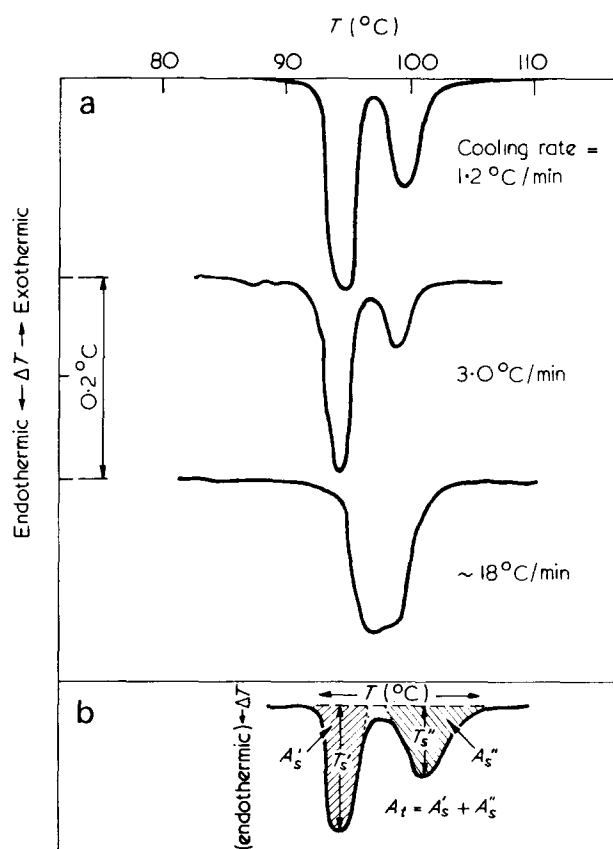


Figure 3 (a) Solution endotherms for linear polyethylene in tetralin: dependence on crystallization rate. All solution concentrations are 1.00% polymer. (b) Parameters drawn from solution endotherms (model endotherm shown)

Table 2 Concentration effects on endotherm parameters  
All results for LPE-1 in tetralin; heating rate=1.2°C/min

Cooling rate	Conc. (c) (wt. %)	$T'_s$	$T''_s$	$A_t$	$A_t/c$
		(°C)	(°C)	(arb. units)	
1.2°C/min	0.240	94.8	99.3	0.127	0.528
	0.470	94.3	99.1	0.257	0.547
	1.142	95.6	99.7	0.617	0.540
	2.185	96.5	100.5	1.232	0.564
	3.006	96.0	100.4	1.613	0.536
18°C/min	0.240	96.3	0.099	0.412	
	0.470	96.5	0.197	0.421	
	1.142	97.1	0.470	0.412	
	2.185	97.6	0.883	0.405	
	3.006	98.0	1.284	0.427	

recrystallization and annealing occurs during the solution of polyethylenes. The present endotherms therefore must be interpreted as reflecting the occurrence of recrystallization during solution. Clearly the extent of morphological rearrangement is strongly dependent on the cooling path chosen for the formation of the crystal suspension. Suspensions grown by the slower cooling modes produce sufficient morphological effect during the dynamic heating scan to generate the distinct double endotherms shown. As might be expected, the relative magnitudes of  $A'_s$  and  $A''_s$  shift toward  $A''_s$  for the slower cooling mode. The resolution of peaks is not seen when the present heating scan is applied to quenched suspensions. In discussing the traces of Figure 3 it is also to be noted that to the unaided eye, suspension clarification (i.e. solution) occurs at or near a temperature intermediate between  $T'_s$  and  $T''_s$  in the slow-cooled systems (for tetralin, this temperature is 97°C).

The complex endotherms of Figure 3 invite speculation on the type of crystal structures involved in the solution process. Two distinct morphological groups seem to be present, each dissolving in its characteristic temperature range, centred on  $T'_s$  and  $T''_s$ . The present data do not permit specifying how these morphological groups differ, but the bulk of existing literature (*loc. cit.*) would suggest that lamellar thicknesses and fold periods will depend strongly on the cooling path chosen for crystallization. Judging from the shift in areas under the endotherms, the number of more highly perfected structures dissolving in the higher temperature environment varies inversely with the cooling rate, much as the number of crystal nuclei acting as initiation centres for isothermal crystallization varies with dissolution temperature<sup>5, 6, 13</sup>. Carrying further the analogy with isothermal crystallization, recrystallization during solution must be regarded as a kinetic process, so that the traces in Figure 3 are not necessarily equilibrium representations of the crystallization tendency. Also, the failure of the quenched system to show a distinct pair of endotherms simply may be the result of too rapid a traversal of the critical temperature range for recrystallization to occur on the (relatively) few highly perfected nuclei of this system.

An attempt was made, accordingly, to specify the kinetic basis of the recrystallization process. To do so, 2.0% solutions of the whole polyethylenes in tetralin were crystallized as noted, then heated at the usual scanning rate to 97°C—the midpoint between  $T'_s$  and  $T''_s$  for the system. The (apparently) clarified solutions were annealed at 97°C for various periods of time, whereupon the scan continued at the usual rate of 1.2°C/min. The

results of the experiment are given graphically in Figure 4 and more completely in Table 3, emphasis being placed on the area parameter  $A''_s$  which is most sensitive to variations in the annealing period.

Figure 4 shows clearly that an apparent equilibrium value of  $A''_s$  (~1.0 area units) is in fact attained only following lengthy annealing of systems crystallized on the slow-cooling path. The tabulated results indicate the great increase in the annealing period required to approach the same value of  $A''_s$  in systems crystallized along the 3.0°C cooling path, while in the quenched systems only the 900 min annealing period was sufficient to produce a small second endotherm on resumption of the scan above 97°C. For practical reasons, annealing was not carried beyond 900 min, so that the given datum is the only indication of a peak resulting from recrystallization in quenched systems. Table 3 also lists temperature values for endotherms relating to the solution of slow-cooled suspensions. The  $T'_s$  column is, basically, an index of reproducibility in the analysis, while  $T''_s$  shows a moderate increase with annealing period, with a final value ( $\sim 100.6 \pm 0.2^\circ\text{C}$ ) attained after about 2 h annealing.

Table 3 Effect of annealing on high temperature peak for LPE-1/tetralin

2.0% polymer solutions. Anneal  $T = 97 \pm 0.2^\circ\text{C}$

Cool rate (°C/min)	Anneal time (min)	$A''_s$	$T'_s$ (°C)	$T''_s$ (°C)
1.2	0*	0.415	95.1	99.3
	30	0.560	94.9	99.7
	60	0.725	95.2	100.1
	120	0.850	94.9	100.5
	240	0.910	95.0	100.7
	480	0.970	95.1	100.6
	900	0.995	95.1	100.8
3.0	0*	0.260	—	—
	30	0.335	—	—
	60	0.380	—	—
	120	0.470	—	—
	240	0.575	—	—
	480	0.640	—	—
	900	0.790	—	—
~18	900	0.275	—	—

\* Arbitrary definition. Finite time is spent in the vicinity of the annealing temperature during an uninterrupted scan.

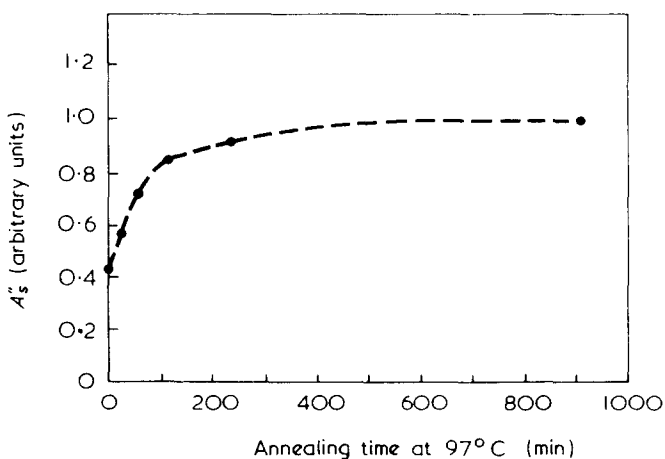


Figure 4 Approach to equilibrium of area under high temperature endotherm signal for 2.0% LPE-1 in tetralin (cooling rate 1.2°C/min)

In usual analyses of time-dependent, isothermal crystallization indexes (e.g. dilatometric data<sup>13, 14</sup>) concepts of the Avrami equation<sup>15</sup> are applied. In the present case, the fractional value of the area  $A_s^r$  should be related to annealing (recrystallization) time via,

$$1 - (A_s^r)_t / (A_s^r)_\infty = \exp(-kt^n) \quad (1)$$

Appropriate graphical representation of the data for slow-cooled suspensions was found to yield the expected linear sections, roughly superimposable by a shift in the time axis, and with  $3 \leq n \leq 4$ . This is consistent with heterogeneously nucleated, three-dimensional crystallization processes<sup>10, 13</sup>. Present results are too scanty to pursue this analysis in a formal manner. Assuming, however, that the increase in  $A_s^r$  resulting from annealing of the quenched suspensions follows a similar path, it is possible to define the half-times for  $(A_s^r)_\infty$ , and this parameter can be compared with half-times for isothermal crystallization from solutions of polyethylene conditioned at various (solution) temperatures. A useful set of results for comparison is given by Mandelkern<sup>16</sup> for a very similar polyethylene (Marlex 50) crystallized from dilute solutions in  $\alpha$ -chloronaphthalene:

Cooling rate (this work)	$t_{1/2}$ (min)	Solution $T$ (ref. 16)
1.2°C/min	13	96.5°C
3.0°C/min	150	100.5°C
18°C/min	1100	103°C

The comparison appears to confirm the kinetic similarity of reported isothermal crystallization behaviour and of the recrystallization during solution studied here. The effects on recrystallization rates of an increase in the cooling rate leading to the formation of crystal suspensions, is analogous to the effect of an increase in solution temperature on isothermal crystallization rates. The work of Keller and co-workers<sup>5, 6</sup> would relate each of these effects to a decrease of 2–4 orders of magnitude in the number of persisting nucleation centres available for crystallization or recrystallization.

#### Molecular weight dependence of solution processes in tetralin

In order to clarify further the complex solution behaviour of polyethylene crystal suspensions, the effect of molecular composition was studied in tetralin solutions of the materials listed in *Table 1*, along with 1:1 blends of fractions F1 and F4. In all cases the polymer concentration was 1.00 ( $\pm 0.08\%$ ). A 'standard scan' was performed, i.e. suspensions were formed and dissolved at equivalent cooling and heating rates of 1.2°C/min. The parameters from the dissolution endotherms for these experiments are reported in *Table 4*.

An increase in the relative importance of the higher-temperature endotherm is evident as the average molecular weight of the polymer increases (see *Table 1*). The standard scan failed to produce a higher temperature peak for the low molecular weight ( $M_v = 5000$ ) fraction F4; also, the signal generated by the F1/F4 blend is quantitatively accounted for by the high molecular weight component F1. Tentatively it can be concluded that the number of crystal nuclei persisting in tetralin solution

beyond the apparent clarification temperature of 97°C must increase with the molecular weight of the polymer, in addition to being a function of the cooling path. Furthermore, the real importance of molecular weight dependence is somewhat played down by the reported data which describe non-equilibrium solution conditions. Koenig and Carrano<sup>2, 3</sup> have reported that the rate of recrystallization (annealing) processes during solution of polyethylene increases with decreasing molecular weight; thus, the data in *Table 5* presumably diminish the molecular weight effect by reporting on the situation at different relative approaches to equilibrium.

In further studies of molecular weight effects use was made of the fractionation cell. It was noted in preliminary work with the larger cell that annealing periods at 97°C produced a quantity of gel-like material, which escaped attention in work with the smaller, less-readily scrutinized analytic cell. Experiments were carried out therefore in which suspensions prepared along the 1.2°C cooling path were heated to 97°C, annealed at that temperature for 6–8 h (sufficiently long to establish equilibrium morphological conditions, according to the results of the preceding section), and were then fractionated by applying mild suction to the lower section of the cell (viz. *Figure 2*). The polymer contained in the 'sol' and 'gel' fractions separated by this procedure was recovered (methanol addition to tetralin solutions) and analysed by intrinsic viscosity measurements. This phase of the work was restricted to the whole polymers, fractions F1, F4 and the 1:1 blend of these fractions. Results are given in *Table 5*.

The effectiveness of material recovery following fractionation is documented in the final columns of *Table 5*. The  $M_v$  of each starting polyethylene sample was calculated from the respective  $M_v$  values and weight fractions of the sol and gel components, and found to agree quantitatively with the experimental  $M_v$  values in every case. The dominant feature of the Table, however, is that only the 'gel' fraction reflects the changing molecular weight average. The molecular weight of the components

*Table 4* Solution endotherm parameters for linear polyethylene samples

Sample	$T_s^r$ (°C)	$T_s^c$ (°C)	$A_s^r$	$A_s^c$	$A_s^r/A_s^c$
LPE-1	94.1	99.1	0.350	0.145	0.293
LPE-2	94.3	100.0	0.316	0.137	0.303
F1	95.1	99.3	0.336	0.218	0.394
F2	94.4	98.2	0.368	0.105	0.285
F3	94.4	97.8	0.332	0.065	0.196
F4	94.0	—	0.185	0	0
F1:F4 (1:1)	95.0	99.8	0.271	0.116	0.294

*Table 5* Fractionation of polyethylene 'solutions' in tetralin following annealing at 97°C

1% solutions used in all cases, annealing times at 97°C in the range 6–8 h

Polymer	'Sol fraction' $M \times 10^{-3}$	'Gel fraction' $M_v \times 10^{-3}$	Overall $M_v \times 10^{-3}$	
			Expt.	Calc.
LPE-1	14.3	127	95.0	99.7
LPE-2	12.9	93	76.0	78.6
F1	15.5	205	180	187
F4	4.9	—	4.9	4.9
F1/F4 (1:1)	7.0 (16.1)*	196	95.5	97.5

\* Calculated  $M_v$  of constituents contributed by F1 only



actually in solution at 97°C is effectively constant, and independent of that average. This is true also of the blended fractions; the low molecular weight fraction F4 enters solution quantitatively during the annealing period (hence also its failure to produce a recrystallization endotherm, as noted in the context of Table 4); hence from the composition of the gel and sol components of the F1/F4 blend, it was possible to compute  $M_v$  for the solvated component originating in F1. This value, bracketed in Table 5, helps to establish an apparent 'critical' molecular weight of  $M_v \approx 14\,000$ , which seems to characterize an equilibrium capability of tetralin to dissolve polyethylene at a temperature corresponding to visual clarification in temperature-scanning (dynamic) experiments.

The above observations are consistent qualitatively with those of Blackadder and Schleinitz<sup>1</sup>, who followed the distribution of dissolved and recrystallized polyethylene in *p*-xylene as a function of isothermal (93°C) annealing time, without however specifying the molecular weights of the solvated and solid-state components. Furthermore, the data elaborate on the complex processes leading to the solution endotherms discussed above, and to their sensitivity on the selected crystallization path. Since recrystallization during solution and during isothermal annealing apparently requires the solvent to disassociate soluble chain molecules from the recrystallizable components, it seems reasonable to suppose that this disassociation will take place more rapidly as the chain size distribution in crystallites becomes narrower. Intuitively, the limiting case would involve crystallites grown under thermodynamically ideal conditions (infinitely slow cooling). Here crystallites

would tend to have minimum size distributions of constituent chain molecules, and little delay would be expected in attaining equilibrium distributions of chains in the solvated and crystalline state. Under experimental cooling conditions, however, increasing randomness in the chain size distributions within crystallites may be envisaged as the cooling rate is increased. This factor would slow the disassociation step and thus complicate the kinetics of attaining equilibrium endotherm patterns. Finally, the data raise the possibility that the critical  $M_v$  value is not characteristic of the polymer alone, but rather that it is a function of polymer/solvent interaction. This point is considered briefly below.

#### Solvent dependence of solution processes

Ample evidence now exists<sup>1,13,17</sup> to the effect that thermodynamic properties of polyethylene crystals (e.g. fold energies, fusion enthalpies) do not depend on the solvent environment from which they are formed. Nevertheless, the solution process and the accompanying recrystallization (annealing) effects discussed here are clearly dependent on the solvent environment. Qualitative evidence of this is shown in Figure 5, which compares the solution endotherms of LPE-1 (1.00% concentrations) in tetralin and  $\alpha$ -CN. For each case the 'standard scan' is represented and as noted before, each of the solution endotherms is closely reproduced by repeated 'standard scan' cycles. The general outline of the endotherms is similar, of course, but the  $\alpha$ -CN system is shifted some 10°C towards higher solution temperatures, and there is a marked increase in the relative importance of  $A''$ . Evidently  $\alpha$ -CN is a less effective solvent for the polyethylene than tetralin; the increase in relative size of the higher temperature peak suggests more drastic morphological effects during solution, either because of a larger number of nucleation sites in the system or (and) because of a reduction in the fraction of polymer chains which can be maintained in solution following the generation of the lower temperature endotherm.

A more quantitative view of the role played by polymer/solvent interactions was sought by repeating the fractionation experiments described above. Solutions of the whole polymers in xylene, tetralin, decalin and  $\alpha$ -CN were subjected to a 'standard scan' to define the respective annealing temperatures; 1.00% solutions were then crystallized at 1.2°C/min cooling rate in the fractionation cell, heated at 1.2°C/min to the appropriate annealing temperature, and fractionated after ~8 h annealing. Molecular weight determinations on the recovered polymers are given in Table 6 along with the pertinent temperature and weight fraction data.

The fractionation effectiveness during annealing at temperatures which correspond to the same relative solution state, is a distinct function of the solvent.

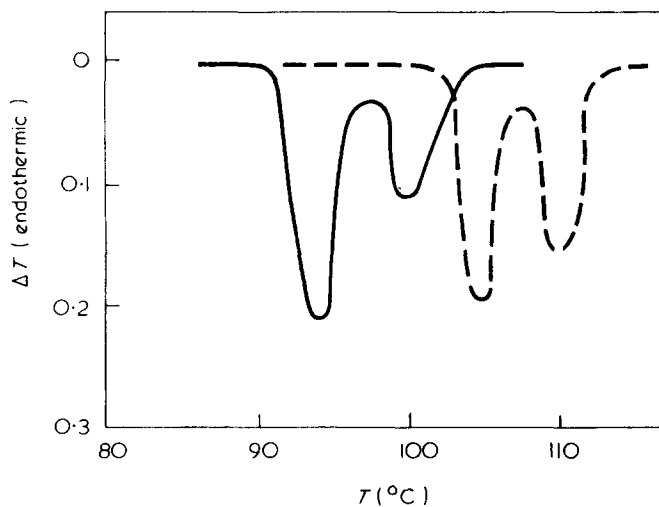


Figure 5 Solution endotherms for LPE-1 in (—) tetralin and (---)  $\alpha$ -chloronaphthalene. 1.00% polymer concentrations. Scan rate = 1.2°C/min

Table 6 Solvent dependence of polyethylene solution effects

Solvent	Anneal $T$ (°C)	LPE-1				LPE-2			
		Wt.%		$M_v \times 10^{-3}$		Wt.%		$M_v \times 10^{-3}$	
		Sol'n	Crystal	Sol'n	Crystal	Sol'n	Crystal	Sol'n	Crystal
$\alpha$ -CN	107	21	79	10.3	130.4	17	83	8.9	92.7
Xylene	97	24	76	14.0	124.5	19	81	13.3	90.7
Tetralin	97	24	76	14.3	127.0	18	82	12.8	93.0
Decalin	92	29	71	18.7	140.1	22	78	19.9	93.1

$\alpha$ -CN is the least effective, being incapable of maintaining in equilibrium solution polymer chains having  $M_v \gtrsim 10\,000$ ; tetralin and xylene are about equivalent in dissolving chains with  $M_v \lesssim 13\,000$ , while the equilibrium solution capability of decalin extends to about  $M_v \simeq 18\text{--}20\,000$ . An immediate consequence of this evidence is to seek a relationship between the  $M_v$  values and thermodynamic interaction effects for the polymer/solvent systems.

The most commonly used parameter of polymer/solvent interaction is the free energy of mixing parameter  $\chi$  drawn from lattice theories, and more recently, from corresponding-states theories of polymer solutions<sup>18-20</sup>. Efforts to relate  $\chi$  with the molecular weights of polymer dissolving at the pertinent annealing temperatures in the given systems encounter difficulties similar to those noted by Devoy *et al.*<sup>13</sup> in their attempts to relate polyethylene crystallization kinetics with polymer/solvent interactions: insufficiently accurate interaction data.

Paradoxically, some frequently used literature values of the interaction parameters for polyethylene/solvent systems may be in considerable error precisely because of the complex solution effects described here. The data given by Coran and Anagnostopoulos<sup>21</sup> illustrate the problem particularly well. These authors determined  $\chi$  from a simplified version of the familiar Flory expression, having the form:

$$1/T_m - 1/T_m^\circ = R/\Delta H_u(V_u/V_l)(1 - \chi) \quad (2)$$

where  $T_m$  and  $T_m^\circ$  are the depressed melting point of polymer in excess solvent and the melting temperature of pure polymer,  $\Delta H_u$  is the fusion enthalpy per mole of polymer repeat units,  $V_u$  is the volume per mole of repeat units and  $V_l$  is the molar volume of solvent. The critical experimental evaluation is that of  $T_m$ ; this was determined by heating crystals of polymer in excess solvent at a rate of  $1^\circ\text{C}/\text{min}$  on the hot stage of an optical microscope. The temperature at which spherulites disappeared (viewed between crossed polaroids) was equated with  $T_m$ . The  $T_m$  values for decalin, tetralin and xylene, given in ref. 21 are within  $1^\circ\text{C}$  of the corresponding annealing temperatures given in Table 6. Adopting the techniques of ref. 21, we have measured a  $T_m = 107^\circ\text{C}$  for  $\alpha$ -CN, in exact accord with the annealing temperature listed in Table 6. This quantitative agreement is not surprising considering the very similar solution paths used in our very differently oriented sets of experiments. It is clear, however, that these temperatures, and by inference the temperatures quoted for additional solvents by Coran and Anagnostopoulos<sup>21</sup>, do not correspond to equilibrium 'melting' temperatures (i.e. solution temperatures) of the polymer in excess of the given solvents. Consequently their use in equation (2) must underestimate  $\chi$ , to a degree dependent at least on the molecular weight of the polymer, and (presumably) on the thermal history of crystal preparation. The fact that a reasonably linear relationship was defined by plotting  $\chi$  values of ref. 21 against the  $M_v$  of polymer in equilibrium solution at the respective  $T_m$  values is therefore to be considered as fortuitous. Greater reliability in measurements of  $\chi$  values will be necessary to clarify the question of solvent influence on fractionation

effects during the crystallization and solution of polymers such as the present polyethylenes. Gas-liquid chromatography is currently being considered for application in this regard<sup>22</sup>.

## CONCLUSION

It is concluded that the solution of linear polyethylenes along standard heating paths is subject to variations arising from the crystallization history of the material and from a fractionation effect, the nature of which reflects both the molecular structure of the polymer and the thermodynamics of polymer/solvent interaction. The importance of these effects should be borne in mind in the selection of solvents and the handling of polymer solutions intended for the characterization of polymer molecular structure. The present elaboration on the complexities of dynamic polymer solution processes also questions the validity of some literature values for the free-energy of mixing parameter  $\chi$ , thereby illustrating further the need for suitable experimental procedures in testing the predictions of theories for the behaviour of polymer solutions.

## ACKNOWLEDGEMENTS

The author is indebted to Dr P. Kruus and Dr G. J. Erskine, sometime Research Associates in these laboratories, for assistance in the performance of much of the experimental work.

## REFERENCES

- Blackadder, D. A. and Schleinitz, H. M. *Polymer* 1966, **7**, 603
- Koenig, J. L. and Carrano, A. J. *Polymer* 1968, **9**, 359
- Koenig, J. L. and Carrano, A. J. *Polymer* 1968, **9**, 401
- Schreiber, H. P. and Waldman, M. H. *J. Polym. Sci. (A)* 1964, **2**, 1655
- Blundell, D. J., Keller, A. and Kovacs, A. J. *J. Polym. Sci. (B)* 1966, **4**, 481
- Blundell, D. J. and Keller, A. *J. Macromol. Sci. (B)* 1968, **2**, 332
- Blackmore, W. R. and Alexander, W. *Can. J. Chem.* 1961, **39**, 1888
- Keller, A. *Phil. Mag.* 1957, **2**, 1171
- Fischer, E. W. *Z. Naturforsch. (A)* 1957, **12**, 753
- Mandelkern, L. 'Crystallization of Polymers', McGraw-Hill, New York, 1964
- Wunderlich, B. *Polymer* 1964, **5**, 611
- Peterlin, A. and Meinel, G. *J. Polym. Sci. (B)* 1964, **2**, 751
- Devoy, G., Mandelkern, L. and Bourland, L. *J. Polym. Sci. (A-2)* 1970, **8**, 869
- Marker, L., Hay, P. M., Tilley, G. P., Early, R. M. and Sweeting O. J. *J. Polym. Sci.* 1959, **38**, 33
- Avrami, M. *J. Chem. Phys.* 1939, **7**, 1103; 1940, **8**, 212
- Mandelkern, L. *S.P.E. JI* (Jan.) 1959, **15**, 1
- Sharma, R. K. and Mandelkern, L. *Macromolecules* 1970, **3**, 758
- Flory, P. J. 'Principles of Polymer Chemistry', Cornell Univ. Press, Ithaca, 1953
- Patterson, D. *J. Polym. Sci. (C)* 1968, **16**, 3379
- Eichinger, B. E. and Flory, P. J. *Trans. Faraday Soc.* 1968, **64**, 2555
- Coran, A. Y. and Anagnostopoulos, C. E. *J. Polym. Sci.* 1962, **57**, 13
- Tewari, Y. B., Patterson, D., Schreiber, H. P. and Guillet, J. E. *Macromolecules* 1971, **4**, 356

# Thermally stable fibres from an adamantane polymer

E. Dyson, D. E. Montgomery and K. Tregonning\*

School of Textiles, University of Bradford, Bradford, BD7 1DP, UK  
(Received 26 May 1971; revised 26 July 1971)

The thermal stability of fibres from poly(*m*-phenylene adamantane-1,3-dicarboxamide) is described in terms of the mechanical properties at, and after exposure to, elevated temperatures. It is shown that fibres from this polymer have sufficiently good retention of tenacity and modulus when exposed to elevated temperatures in air to warrant further development work.

## INTRODUCTION

The recent growth of the aerospace industry has fostered a demand for fibres which retain their tensile properties at high temperatures and special structures have been employed in polymer synthesis to obtain thermally stable polymers which exhibit fibre-forming properties. One approach to this problem has been to incorporate aromatic rings in the polymer chain. In addition to producing a stiffer and more dimensionally stable polymer, it has been known for some time that replacement of aliphatic units by aromatic rings in linear polymers produces materials of greater thermal stability. This approach tends to raise both the glass transition temperature and in most cases the melting point of a polymer.

Several experimental fibres have been produced which retain useful tensile properties at temperatures up to 300°C. Much of the research on such materials has been directed towards wholly aromatic polyamides incorporating arylene units<sup>1-3</sup> because although the heterocyclics, for example, are often potentially superior to the aromatic polyamides as thermally stable fibre forming polymers, there are considerable financial and technical difficulties impeding their production on a large scale. The polymers are relatively expensive to produce and in most cases are insoluble. Thus it is necessary for a precursor to be extruded and cyclization (which can be a lengthy process) to be carried out as a separate operation after spinning. Commercial interest has, therefore, been lacking as regards heterocyclic fibres, although such polymers have been used in other high temperature applications, for example as films<sup>4</sup>.

Another series of polymers with thermal stability potential are condensation polymers based on the adamantane system (see *Figure 1a*), which has a rigid symmetrical structure of high thermal and chemical stability. Adamantane is a by-product of the oil industry,

and it would seem that if polymers based on the adamantane system prove suitable for use as thermally stable fibre-forming polymers, these could be of commercial interest.

Condensation of adamantane-1,3-dicarbonyl chloride with diamines yields a series of polyamides<sup>5</sup> the general formula of which is illustrated in *Figure 1b*.

The thermal properties of some of these polymers have been reported and as might be expected those polymers containing aromatic rings are more thermally stable than those containing aliphatic units.

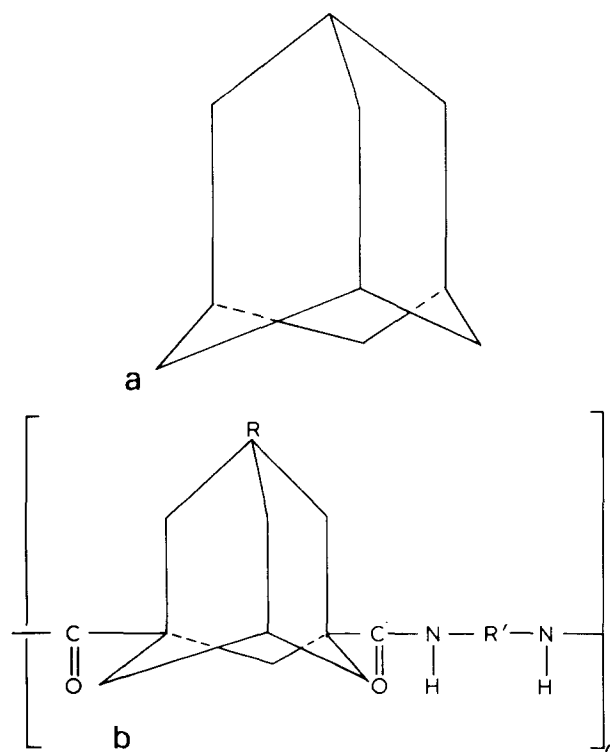


Figure 1 (a) Adamantane and (b) polyamides incorporating adamantane

\* Present address: UK Atomic Energy Authority, Dounreay, Caithness, Scotland, UK.

The work reported in this paper concerns the properties of fibres from the polymer shown in Figure 2, poly(*m*-phenylene adamantane-1,3-dicarboxamide), and an evaluation of its high temperature performance. According to Flavell<sup>5</sup> this polymer has a softening point of 294°C and suffers no weight loss below 380°C. A  $T_g$  of 311–317°C has been measured by Sewell<sup>6</sup> from thermogravimetric analysis which indicated no weight loss below 400°C in air at a heating rate of 32°C/min, but a 0.86% weight loss in air if a temperature of 325°C is maintained for 2 h. It seems reasonable to expect, therefore, that if filaments could be produced having acceptable textile properties at room temperature, then their high temperature properties would be of interest.

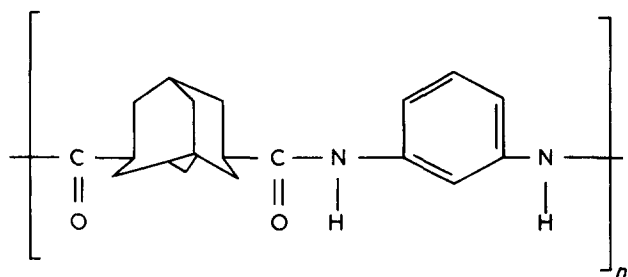


Figure 2 Poly(*m*-phenylene adamantane-1,3-dicarboxamide)

## EXPERIMENTAL AND RESULTS

### Fibre production

A 25% w/w spinning solution was prepared by dissolving the polymer in dimethylformamide containing 5% lithium chloride. The solution was filtered through cotton wadding and transferred to the extrusion unit of a small-scale wet-spinning machine. Extrusion took place through a spinneret having five holes of 75 μm diameter into a spin bath containing 60% w/w dimethylformamide in water at 10°C. After coagulation the filaments were passed through a hot water bath to remove residual solvent and were then packaged before being washed in distilled water and dried in a forced-draught oven.

The fibres had the following properties at this stage:

$[\eta]$	1.5 dl/g in conc. H <sub>2</sub> SO <sub>4</sub> (density 1.84 g/ml) at 27°C
tenacity	0.62 g/den
extension at break	72.2%
initial modulus	19.9 g/den
sonic modulus	30.0 g/den
appearance	dumbbell section with complete absence of voids

### Preparation of drawn fibres

The initial drawing experiments were of a discontinuous nature and were performed by drawing short samples in an Instron tensile tester whilst they were in contact with a hot plate. The information obtained was then used to choose suitable drawing conditions for a small-scale continuous drawing machine. A full description of these techniques will be published later. The filaments on which high temperature tests were conducted were drawn using the following conditions.

Temperature	325°C
Input velocity	24.6 m/min
Take-up velocity	147.0 m/min

equivalent to a draw ratio of ~6.0 : 1 and a draw rate of 220 000 % min<sup>-1</sup>.

The five filaments were separated and drawn individually. They were then packaged by hand and stored in a desiccator prior to testing. Separate denier determinations were made on 90 cm lengths of each of the drawn filaments (using a microtorsion balance) and their room temperature tensile properties were determined in the usual way.

The drawn fibres had the following properties:

denier	7.3
tenacity	4.0 g/den
extensibility	25.2%
initial modulus	51.1 g/den

X-ray analysis revealed that minimum crystallinity had been introduced by drawing<sup>7</sup>.

The tensile properties of the drawn fibres were determined at temperatures between ambient and 310°C and the room temperature tensile properties of the drawn fibres were determined after exposure in air to temperatures between 200°C and 325°C for periods of time between 18 min and 100 h.

### Tests at elevated temperatures

A heating chamber was used with the Instron tensile tester to determine the tensile properties in air at elevated temperatures, the results being shown in Figure 3. The tests were made at an extension rate of 20 % min<sup>-1</sup> with a gauge length of 2.5 cm. Each sample was exposed to the chosen temperature for 3 min prior to testing and tenacity, extensibility, and initial modulus were measured. The tension in the fibre prior to test was also noted.

At 300°C and above, high shrinkage tension precluded meaningful measurement of extensibility and initial modulus.

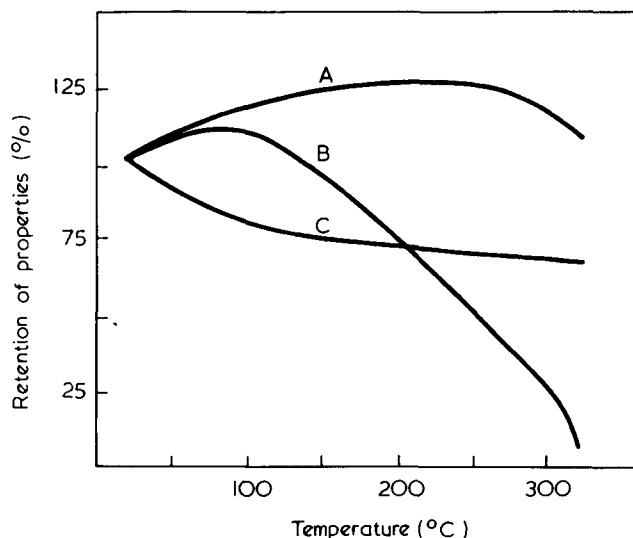


Figure 3 Tensile properties of drawn fibres at various temperatures, room temperature values taken as 100%. A, break extension; B, tenacity; C, initial modulus

### Heating ageing and free shrinkage

For the heat ageing experiments, fibres were wrapped around glass microscope slides under a small tension and secured at each end with Bostik 1160 high temperature adhesive, so that no shrinkage was possible. The samples were exposed in air to various temperatures for periods of time up to 100h, a forced-draught oven providing the heat source. Although an inert atmosphere such as nitrogen is often used for these tests, it was felt that an oxidative atmosphere would provide more useful information, and not enough fibre was available for both types of test.

When the fibres were removed from the oven, any discoloration was noted, and the normal testing procedure was used to determine the tensile properties at room temperature, although in this case a 5cm gauge length was used. Results for the percentage strength retention plotted against exposure time for various temperatures are shown in *Figure 4*, and similar plots for retention of initial modulus and extensibility are shown in *Figures 5* and *6*.

The effect of temperature on free shrinkage was determined by loosely wrapping 50cm lengths of fibre onto 0.75 in. diameter stainless-steel tubes. The tubes were then stood on end in the forced-draught oven so that the fibres would meet minimum restriction to shrinkage. The fibres were exposed for 20 min at each temperature and after removal their lengths were measured, the results being given in *Figure 7*.

### DISCUSSION

The limit of stability of poly(*m*-PAD) fibre undergoing short exposures in air to elevated temperatures is well illustrated by the shrinkage data and the tensile properties at elevated temperatures. It would appear that the effects of disorientation became marked between 250°C and 300°C. However, even were it possible to minimize these effects by, for example, the introduction of a higher degree of crystallinity, an upper limit of 325°C for quite short exposures would have to be imposed. After 18 min exposure to this temperature the fibre was appreciably discoloured and as can be seen from *Figures 4*, *5* and *6* retention of tenacity, initial

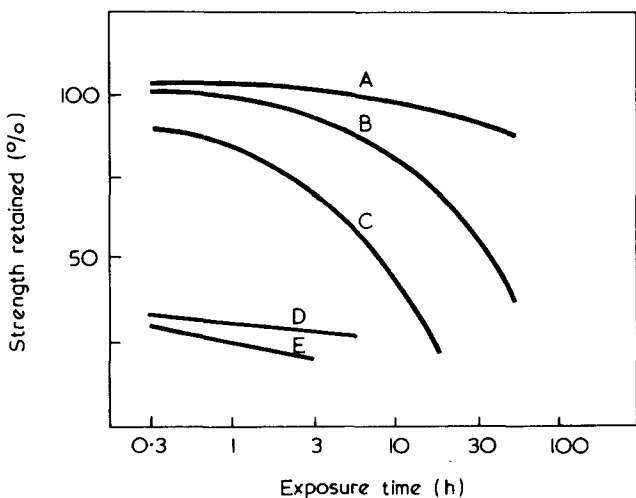


*Figure 4* Percentage of room temperature tenacity retained after exposure to various temperatures for a range of times. A, 200°C; B, 250°C; C, 275°C; D, 300°C; E, 325°C

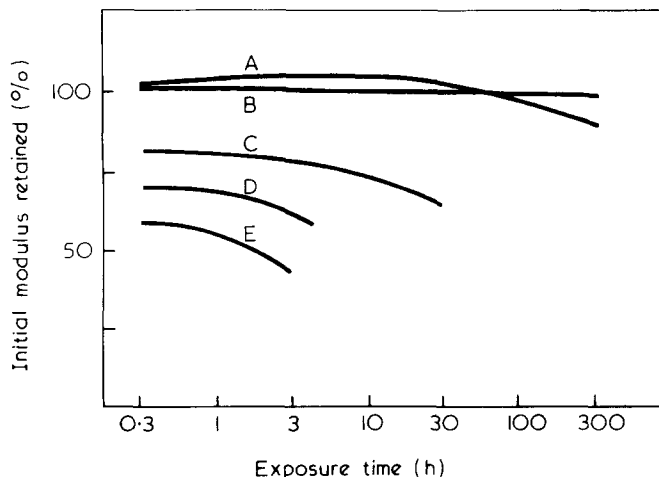


*Figure 5* Percentage of room temperature initial modulus retained after exposure to various temperatures for a range of times. A, 200°C; B, 250°C; C, 275°C; D, 300°C; E, 325°C

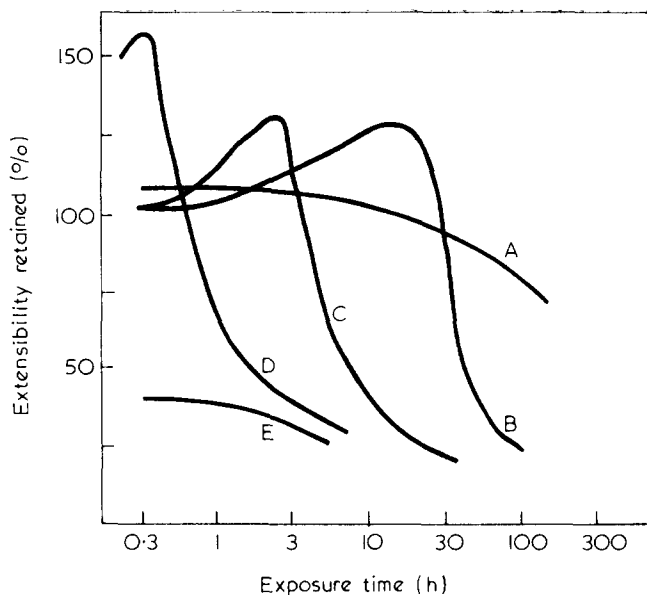


*Figure 6* Percentage of room temperature extensibility retained after exposure to various temperatures for a range of times. A, 200°C; B, 250°C; C, 275°C; D, 300°C; E, 325°C

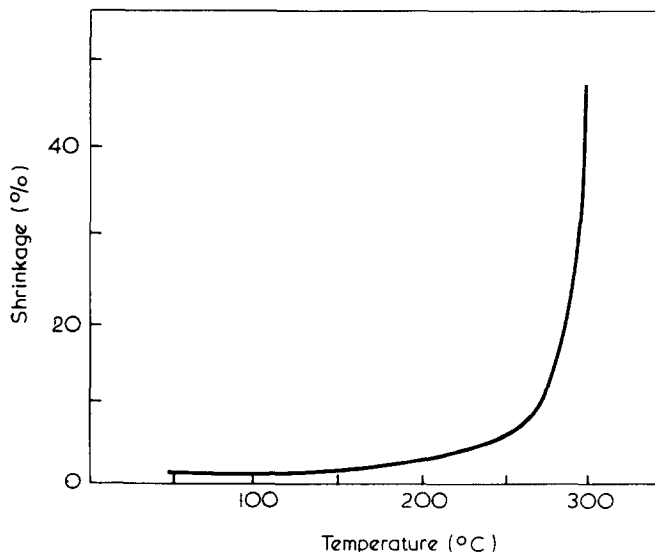


*Figure 7* Percentage shrinkage after exposure to various temperatures for 20 min

modulus and extensibility was low, indicating the effects of thermal degradation.

Figure 6 probably best illustrates the usefulness of poly(*m*-PAD) fibre at a particular temperature. For each temperature (except 200°C) the percentage of room temperature extensibility retained increases gradually with time up to a point which is different for each temperature, it then falls more rapidly to a value which is too low for use. The point at which the percentage extensibility retained exhibits a maximum coincides with observed onset of discoloration.

Table 1 below compares the 50% strength loss temperature of poly(*m*-PAD) fibres with other experimental and commercially available fibres and it can be seen that poly(*m*-PAD) behaves reasonably well. One might also expect the introduction of crystallinity to increase the 50% strength loss temperature to a more favourable value.

Table 1 Comparison of the 50% strength loss temperatures of some selected experimental and commercial fibres

Fibre	50% strength loss temperature (°C)
Nylon-6,6 tyre cord yarn	145
Nomex <sup>8</sup>	280
Poly( <i>m</i> -PAD)	240
Polyimide <sup>9</sup>	280
Aromatic copolyamide <sup>3</sup>	260
Oxadiazole-amide copolymer <sup>3</sup>	250

## CONCLUSIONS

Fibres with a tenacity of 4.0 g/den, an initial modulus of 51.1 g/den and an extensibility of 25.2% have been produced from poly(*m*-phenylene adamantane-1,3-dicarboxamide) by wet spinning from dimethylformamide and then hot drawing at 325°C.

Elevated temperature and heat ageing tests have been conducted on these fibres and the results are reasonably

encouraging. The fibres retain almost 50% of their room temperature tenacity when tested at 250°C and show little change in their physical properties after exposure to a temperature of 250°C for several hours. Indeed the initial modulus remains unchanged after exposure to this temperature for 100 h. However, at temperatures above 250°C the fall in tensile properties is fairly rapid and is probably due to a combination of disorientation and degradation.

It is possible that some improvement in the high temperature performance of poly(*m*-PAD) fibres may be obtained by the introduction of a higher degree of crystallinity.

## ACKNOWLEDGEMENTS

The work described in this paper represents part of a programme being carried out under a research agreement between the Ministry of Aviation Supply and the University of Bradford. The authors acknowledge the financial support afforded by this agreement and the continuous encouragement of the staff of the Materials Department, Royal Aircraft Establishment, especially J. H. Sewell.

## REFERENCES

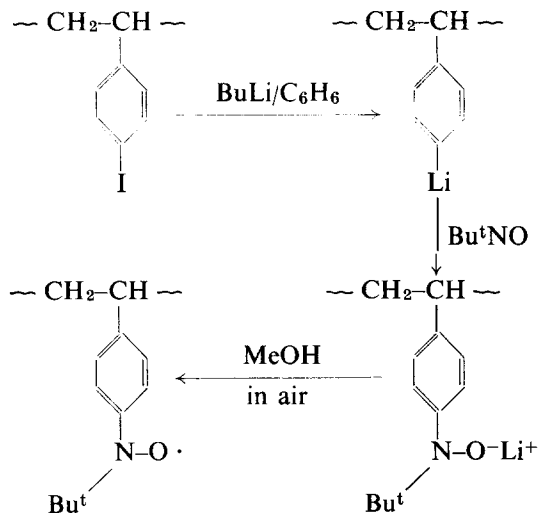
- Hill, R. and Walker, E. E. *J. Polym. Sci.* 1948, 3, 609
- Weiss, J., Morgan, H. S. and Lilyquist, M. R. *J. Polym. Sci. (C)* 1967, 19, 29
- Preston, J. and Black, W. B. *J. Polym. Sci. (C)* 1967, 19, 17
- Kapton Technical Bulletin, Du Pont
- Flavell, W. *Chem. Ind.* 1969, p 397
- Sewell, J. H., Royal Aircraft Establishment, personal communication
- Montgomery, D. E., Tregonning, K. and Blakey, P. R. *Polymer* 1972, 13, 43
- Du Pont Technical Information Bulletin N-201
- Irwin, R. S. and Sweeny, W. *J. Polym. Sci. (C)* 1967, 19, 41

## Electron spin resonance studies of spin-labelled polymers: Part 2. Preparation and characterization of spin-labelled polystyrene

A. T. Bullock, G. G. Cameron and P. Smith

Department of Chemistry, University of Aberdeen, Old Aberdeen, AB9 2UE (UK)  
(Received 27 October 1971)

The line widths of the electron spin resonance (e.s.r.) spectra of nitroxide radicals can yield the correlation time for rotational diffusion of the radical. By attaching a stable nitroxide group to a macromolecule line width measurements can give useful information on the motion or conformation of the macromolecule in various environments. This spin-labelling technique was originally applied to biological macromolecules<sup>1</sup>. More recently it has been extended to synthetic polymers. From line width measurements of a toluene solution of polystyrene labelled at random with phenyl nitroxide groups (~one label per 1000 monomer units) the correlation times and activation energy for segmental rotation were derived<sup>2</sup>. The labelled polystyrene was prepared by a modified version of the synthesis described by Drefahl *et al.*<sup>3</sup> This route, which has also been used to prepare polystyrene labelled with *t*-butyl nitroxide groups (unpublished), is inconvenient in several respects. For example, the mercurated polymer is rather insoluble and the intermediate nitroso polystyrene is unstable. In this communication we describe a more convenient synthesis of *t*-butyl nitroxide polystyrene based on the following reaction sequence:



Lithiated polystyrene was prepared by the method of Braun<sup>4</sup>. The iodination step was modified to yield a polymer containing 4–6% iodine corresponding to one iodine atom per 20–30 monomer units. 500 mg of iodinated

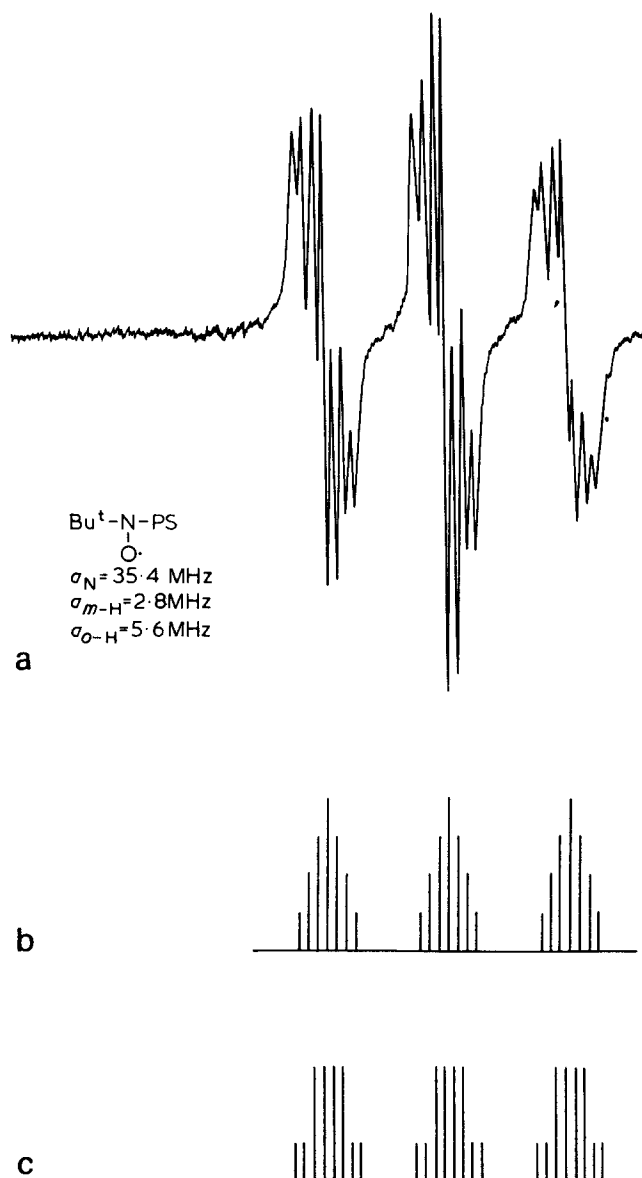


Figure 1 (a) The e.s.r. spectrum of spin-labelled polystyrene (mol. wt. 2000) in toluene solution (1%); (b) stick spectrum for *t*-butyl nitroxide in *o*- or *p*-position; (c) stick spectrum for *t*-butyl nitroxide in *m*-position

polystyrene dissolved in 40 ml benzene were added dropwise with rapid stirring into an excess of butyl lithium in benzene (800 mg in 12 ml) under nitrogen at room temperature. The addition took 2–3 h after which an excess of 2-methyl-2-nitrosopropane in benzene was injected into the resulting solution of lithiated polystyrene. It is important to ensure that the lithiation step is conducted with slow addition of the iodinated polymer and a large excess of butyl lithium, otherwise there is a risk that crosslinking of the polymer will occur via a Wurtz-type reaction. A convenient preparation of 2-methyl-2-nitrosopropane was described recently<sup>5</sup>. The reaction product was precipitated in excess methanol under aerobic conditions which preclude the need to isolate and oxidize the intermediate hydroxylamine. The spin-labelled polymer was purified by two further precipitations in methanol from chloroform. Elemental analysis showed the residual iodine content to be <0.5%.

The parent polystyrenes had molecular weights of 126 000 and 2000. The latter was a narrow fraction supplied by Waters Associates for gel permeation chromatography calibration. The spectra of the solid polymers were closely similar to that of the phenyl nitroxide polystyrene<sup>2</sup>. *Figure 1a* shows the spectrum of the labelled narrow fraction recorded at room temperature from a 1% solution in toluene. Each multiplet comprises seven lines in approximate intensity ratio 1:2:3:4:3:2:1, with a separation of 2.8 MHz between adjacent lines. This fine structure is consistent with interaction of the unpaired electron with one pair of equivalent protons having  $a_H = 2.8$  MHz and with another pair having  $a_H = 5.6$  MHz, while  $a_N = 35.4$  MHz. From data on small aryl nitroxides the coupling constants of protons in the *ortho*- and *para*-positions (to the nitroxide group) are known to be equal and approximately twice the coupling constants of *meta*-protons<sup>6</sup>.

On this basis, the 'stick' spectrum in *Figure 1b* was constructed for nitroxide substitution in the styrene ring at the positions *ortho*- or *para*- to the carbon atom of the backbone, while *Figure 1c* corresponds to nitroxide substitution in the *meta*-position. *Figure 1b* fits the observed spectrum closely while *Figure 1c* does not. From steric considerations it seems unlikely that *ortho*-substitution has occurred. The conclusion that these polymers are labelled exclusively in the *para*-position is in accord with Braun's observation that iodination also occurs exclusively at this point in the molecule<sup>4</sup>.

We have observed that the correlation times for a polystyrene sample labelled with phenyl nitroxide and *t*-butyl nitroxide groups are the same. The results of these e.s.r. studies will be published in detail in due course.

#### ACKNOWLEDGEMENTS

P.S. gratefully acknowledges the award of a studentship from Imperial Chemical Industries Ltd. We are grateful to the Science Research Council for an equipment grant.

#### REFERENCES

- 1 Ingham, J. D. *Rev. Macromolec. Chem. (C)* 1968, **2**, 279
- 2 Bullock, A. T., Butterworth, J. H. and Cameron, G. G. *Eur. Polym. J.* 1971, **7**, 445
- 3 Drefahl, G., Hörhold, H.-H. and Hofmann, K. D. *J. Prakt. Chem.* 1968, **37**, 137
- 4 Braun, D. *Makromol. Chem.* 1959, **30**, 85
- 5 Calder, A., Forrester, A. R. and Hepburn, S. P. *Organic Syntheses* in press
- 6 Forrester, A. R., Hay, J. M. and Thomson, R. H. 'Organic Chemistry of Stable Free Radicals', Academic Press, London and New York, pp 202–203



# Book Reviews

## Essential fiber chemistry

Mary E. Carter

Marcel Dekker, New York, 1971, 216 pp, £9.40

In this book the author has set out to provide a sound understanding of the chemistry of ten commercial fibres: cotton, rayon, cellulose acetate, wool, polyamides, acrylics, poly(ethylene terephthalate), polyolefins, polyurethanes and glass. This she has done admirably but as she states in the preface, the depth of treatment for any one fibre cannot be great. However, a surprisingly large amount of information is included and there are very many appropriate references for further reading. Many patent references are included. One chapter is devoted to each of these fibres and the treatment is well balanced. The polymerization and production of synthetic fibres and the preparation of natural fibres are discussed fairly briefly. The author concentrates on the chemical modification of the fibres. In some cases, for example with the polyolefins, perhaps there is too much emphasis on modification (19 pages) compared to that on synthesis and production (3 pages). For each synthetic fibre I would have liked to see a little information on the source and synthesis of the monomers used for its production. Also I would have liked to see more comparison of the properties of the fibres with a discussion of their price and suitability for various applications. Perhaps that could not be expected in a book entitled 'Essential fibre chemistry'.

The publishers state that the book is intended for chemists in research and development in natural and synthetic fibres. It will be most useful to them as an introduction to a more detailed study of any one of these fibres. It will be invaluable for anyone wanting a general appreciation of the chemistry of fibres. It fills a gap and I certainly intend to use the book as a text for my lectures to BSc and MSc students. The book is well produced, easy to read and well illustrated. I recommend it but it is expensive at £9.40.

F. J. Hybart

## Rubber technology and manufacture

Edited by C. M. Blow

Butterworths, London, 1971, 527 pp, £9.00

'This is all ye know on earth, and all ye need to know' This misquotation came to mind on looking through this book. The quote naturally applies only to the limited sector of knowledge with which the book deals but seems a fair, if enthusiastic, summing up of it.

The book has a clearly defined area of knowledge to encompass. It is not one otherwise covered in an up-to-date way and of practical value to supplement the education of a chemistry, physics, or engineering first degree to an entrant to the rubber industry. It attempts to provide more specialized knowledge in each of the three disciplines and a cross-reference to the useful technology in the other two. It unquestionably succeeds for the chemist. It is progressively less satisfactory in providing more specialized knowledge on elastomers for the physicist and engineer. Dr Blow recognises this limitation in a book already of 527 pages and refers to the physics and engineering texts complementary to it.

It is not primarily a reference book. Hopefully, the new graduate will read it all. He can start at any chapter which particularly attracts his interest. From Dr Blow's present interest in postgraduate courses, he no doubt has had in mind that the book will be the one text book needed in a one-year MSc course specializing in elastomer technology.

It has two other readership aims, in which it also generally succeeds. One is as a refresher volume for people like me, whose general knowledge needs rubbing up. It also does act as a reference book. Dr Blow has taken considerable effort to produce a method of providing reference to selected books for general reading and a method of subject and author indexing with the idea that these will actually be used.

This book will remain the authoritative text in the UK for

several years to come. It has been produced by the authoritative body, the Institution of the Rubber Industry, which will see that it remains authoritative through the setting of the technical standards and related examinations of the Institution. Dr Blow has enlisted 31 contributors. Not a single one has had an academic career. A number have just retired from eminent positions in industry in this country, the USA, and in European countries. It seems so sensible to gain their wealth of experience while it is still fresh and valuable to the entrant to the industry.

Emphasis in the book is on the technology of materials and their conversion to rubber products. This includes a background to the exciting history of the industry and a perspective of the materials equally important to the polymers which go into rubber products. Both these topics are sadly lacking in the typical educational course and in university research studies. The later chapters deal with the general processing operations of the industry, mastication and mixing, extruding, calendering, moulding and the like. These are followed by useful synopses of the manufacture of the main types of product, tyres, belting, hose, footwear, rubber/metal units, sports goods, cables and other industrial products. Test procedures and standard test methods rightly merit good cover.

Dr Blow and the Institution of the Rubber Industry are to be congratulated and well merit our thanks for this effort.

W.F. Watson

## IUPAC 22nd International Congress of Pure and Applied Chemistry

1969 Plenary Lectures, Sydney

Butterworths, London, 1971, 287 pp, £7.50

It is almost impossible to review this book in a short article. It consists of the plenary lectures delivered to the IUPAC Conference in Sydney in 1969. The range of topics is very wide, the speakers being chosen for their pre-eminence in their chosen topics. Some of the lectures are synoptic treatments of the subject over a long period of years. Some deal with quite specific fields in an up-to-date review of recent developments. Another group deals with the special problems involving even the relevant details of experimental work. The book as a whole will not be of interest to any one reader, but, on the other hand, the articles are not designed to cover the requirements of a general reader: but this is the feature that makes the book quite different from others and makes it quite unique in its own special way.

For the general reader, most of the articles are reasonably easily comprehended but the special section on 50 years of Valence Theory will naturally be more easily readable by those who work in this field. The authors, Mulliken, Daudel, Van Fleck and Coulson give quite unique accounts of the way they see the subject has developed. To the more general reader, this is probably one of the most valuable perspectives that has been given in this part of chemistry. Then there are three lectures dealing with water and its interaction with surfaces. Maybe the most interesting is by Derjaguin who deals with the subject in a general way and then gives a much more detailed account of the production of anomalous water. In polymer chemistry, Wichterle looks into the future trying to decide in what fields practicable new polymers might be produced, but also looking critically into those systems and reactions which need not lead into the production of new articles of this kind. This kind of survey is particularly useful to rationalize false hopes and to define regions into which future progress might be made.

Although most of the articles deal with various parts of fundamental chemistry, there is an extremely useful and practical article by I. E. Newnham on Minerals, their prospecting, processing and production. There is, therefore, in this volume something of interest to most chemists and for others who are not experts in the field dealt with often a sufficiently broad review to make the articles of more general interest. The standard of the production of the book is very high indeed, but so equally is its price.

H. W. Melville

### Block polymers

Edited by S. L. Aggarwal

Plenum Press, New York, 1970, 339 pp, \$16.00

The book contains a collection of papers which were presented at a symposium on Block Copolymers held at the meeting of the American Chemical Society in New York City, in September 1969. A number of other contributions from selected authors have been added to the volume so as to make the coverage more comprehensive. Since the aim has been to cover all aspects of the subject, contributions include work on synthesis, molecular characterization, solution behaviour and bulk properties.

Interest in this class of materials has grown rapidly since it was realized that it was possible by anionic techniques to prepare block copolymers with controlled structures. It is fitting therefore that the first two papers by M. Morton, and J. Prud'homme and S. Bywater respectively deal with various problems encountered in the synthesis of well-defined polymers. The topic is also treated, in a somewhat forceful manner, by A. Gourdenne. Taken together these three papers lay down in a concise and clear fashion the guide-lines which must be followed if a specific, readily characterizable product is to be obtained by an anionic route. A number of other papers also touch on synthetic problems. These include reports of a detailed study of some segmented polyurethanes, work on the synthesis and properties of siloxane block copolymers, and a study of cationic polymerization.

Microphase separation in block copolymers is known to lead to many interesting properties. A paper by T. Inoue *et al.* attempts to provide a semi-quantitative framework for the factors leading to and governing the type of two-phase behaviour obtained. However, in order to fully rationalize the interrelationship between primary chain structure and properties detailed morphological studies are required. A number of papers are presented which attempt to bridge this difficult gap. It should be noted, however, that since publication of the book there have been some important advances in the study of domain morphology and therefore in this respect the book has become slightly dated.

On the whole the strength of the book lies in the variety of block systems to which it gives coverage. Thus in addition to the now traditional styrene and butadiene or isoprene systems these include reports of block polymers based on ethylene oxide-styrene, siloxanes, propylene sulphide, imino ethers, and  $\alpha$ -methyl styrene-isoprene.

As a source book of general information on block copolymers it can be readily recommended to workers in the field.

C. Price

### Ablative plastics

Edited by G. F. D'Alelio and J. A. Parker

Marcel Dekker, New York, 1971, 488 pp, \$26.50

This book provides another example of the current practice for papers presented to special sections of American Chemical Society meetings to be collected for publication in one authoritative volume. In this case the 21 papers were (with one exception) read at a Symposium in San Francisco in 1968, published subsequently in full in the *Journal of Macromolecular Science (A)* 1969, 3, 327-802, and are now issued in book form under the editorship of Professor G. F. D'Alelio of the University of Notre Dame, Indiana, and Dr J. A. Parker of the Ames Research Centre, Moffett Field, California, both well-known for their work in polymer chemistry. The papers are printed exactly as in the Journal, even to typographical errors, and apart from a brief introduction by the editors are not considered collectively or critically. The 32 contributors represent USA university, industry, government, space agency and armed forces laboratories, and their papers provide an overall picture of the findings arising in this specialized field.

The precise study and development of ablative plastics, whereby in their use thermal energy is expended via the formation of char surfaces and sacrificial loss of material so as to afford protection under hyperthermal and hypersonic conditions, commenced little more than twelve years ago, being promoted largely by the

requirements of sophisticated rocketry and space technology. The papers collected in this volume deal with the provision and behaviour of a wide range of heat-resistant polymers (phenolic, epoxy, polyphenylene, polyamide, polyimide and related heterocyclic polycondensates, silicones, etc.) and derived composites, detailed attention being paid to the effects of chemical and mechanical structure and environmental conditions.

Specific factors investigated involve the heat capacity of the materials and products of degradation, thermal resistance, endothermal reactions, phase changes, heat transfer and radiation at and from boundary layers, gas evolution and the formation of the strong char surfaces essential for adequate insulation and retention of mechanical strength. Polymer synthesis and structure, characterization, processability, and fabrication receive considerable attention throughout, particularly with regard to thermal resistance, behaviour of composites, and the provision of evaluation tests designed to give reliable indication of ultimate performance.

Although the book is primarily on a specialized subject, it will be of interest generally to those concerned with polymer chemistry, physics and engineering, especially as the numerous tables and figures provide much useful information. The title of 'Ablative plastics' implies heat-erodable carbonaceous coatings but attention is given generally to polymer structure/property relationships, to polymer processing and engineering, even to economic considerations. Each paper has a useful summary and list of references while author and subject indexes cover the book as a whole. It should be pointed out, however, that these papers, which deal entirely with USA investigations, were all prepared during 1968 so that the subject as presented in this book is of necessity three years out of date.

It is well-produced and for those who do not have easy access to the *Journal of Macromolecular Science* for 1969, will have considerable appeal, albeit at a cost of \$26.50, about £11.00 sterling.

R.J.W. Reynolds

#### Conference Announcement

2-7 July 1972

#### IUPAC International Symposium on Macromolecules

HELSINKI, Finland

The main topics of the symposium are :

1. Polymerization and copolymerization reactions
2. Solution properties and characterization methods of polymers
3. Bulk properties of polymers
4. Degradation and decomposition of polymers
5. Polysaccharides and their derivatives

The programme will consist of a number of main lectures given by invited speakers and short communications submitted by the participants.

Further details and registration forms, which should be returned by 31 March 1972, may be obtained by writing to the Symposium Office, International Symposium on Macromolecules, P O Box 28, SF 00131, Helsinki 13, Finland.

# Effect of stereostructure on glass transition temperatures of poly(methyl methacrylate)

S. Bywater and P. M. Toporowski

Division of Chemistry, National Research Council of Canada,  
Ottawa K1A 0R9, Canada  
(Received 23 June 1971)

The volume-temperature curves of a number of poly(methyl methacrylate) fractions produced by various forms of catalysis have been investigated. It was confirmed that the isotactic samples have a much lower  $T_g$  than has conventional polymer. The highly syndiotactic polymer, however, was found to have a  $T_g$  not markedly different from that observed for conventional polymer in contrast with earlier published reports. The latter polymers show a more marked  $\beta$  transition.

## INTRODUCTION

The development of techniques for the preparation of regular forms of some polymers has generated interest in the effect of configuration on physical properties. One of the simplest properties is the glass transition temperature. The first report of regular forms of poly(methyl methacrylate)<sup>1,2</sup> included data showing that  $T_g$  of the iso- and syndio-forms are markedly different. The isotactic polymer was reported to have a  $T_g \sim 45^\circ\text{C}$  and the syndio-polymer one of  $\sim 115^\circ\text{C}$ . A highly isotactic polymer is relatively easy to prepare using phenyl magnesium bromide initiated polymerization in toluene, but the preparation of a highly syndiotactic polymer presents more problems and we have found that most of the methods recommended in the literature give polymers which are no more than  $\sim 80\%$  syndiotactic (dyads). The  $T_g$  of syndiotactic polymer is thus usually determined by extrapolation of data obtained on polymers of mixed structure. Values obtained in this manner have indicated a  $T_g$  of around  $160^\circ\text{C}$ <sup>3</sup>. A Ziegler-type catalyst used at low temperature according to a method described by Abe *et al.*<sup>4</sup> is the only system we can confirm producing a highly syndiotactic polymer ( $>95\%$ ). We have, therefore, investigated this polymer together with those of different tacticity.

## EXPERIMENTAL

Since only small amounts of polymer were available, the specific volume-temperature curves of the polymers were measured using a density gradient technique described by Gordon and Macnab<sup>5</sup>. Its modification was described by Cowie and Toporowski<sup>6</sup>. The gradient was produced by layering aqueous sodium nitrate solutions of approximate densities 1.09 and 2.70. The polymer films of  $\sim 1$  mm diameter and  $\sim 0.3$  mm thickness were prepared by compressing a small amount of powdered polymer

Table 1 Preparation method and stereostructure of the samples

Sample	Catalyst	Solvent	Temperature			
			( $^\circ\text{C}$ )	<i>i</i>	<i>h</i>	<i>s</i>
PGR-2	PhMgBr	Toluene	0	96	4	—
DPHL-GIB	DPHLi*	Toluene	-30	78	16	6
G5-A1	BuLi	Toluene	-30	51	19	30
$\Delta 4:2$	Radical	Aqueous	25	6	36	58
MTS1A	MgEt <sub>2</sub>	THF	-78	4	20	76
Z4-A2 <sub>x</sub>	Ziegler	Toluene	-90	—	5	95

\* DPHLi=1,1-diphenylhexyllithium, the product of addition of n-butyl lithium to 1,1-diphenylethylene

between two stainless-steel rods in a 1 mm glass capillary. The capillary tube could be pumped from both ends to remove trapped air. The specimen was moulded by heating until the polymer became transparent followed by chilling with the application of slight pressure\*. The pellet is easily removed and was washed with dilute detergent solution and degassed before use. Before density determinations were made, the sample was annealed at the highest temperature to be used in the measurements. The temperature was changed at a rate of  $\sim 10^\circ\text{C}/\text{h}$ .

A number of samples were studied. All were fractionated samples of sufficiently high molecular weight ( $>2 \times 10^5$ ) that the  $T_g$  observed would correspond closely to the value expected for infinitely high molecular weight polymers. Their preparation and analysis is given in Table 1. Nuclear magnetic resonance (n.m.r.) spectroscopic determinations of tacticity were carried out in chlorobenzene at  $135^\circ\text{C}$  on a Varian HR-100 spectrometer using repeated slow scans over the methyl region. The highly stereoregular forms showed no evidence of

\* We are indebted to Professor G. Allen of the University of Manchester for the description of this technique

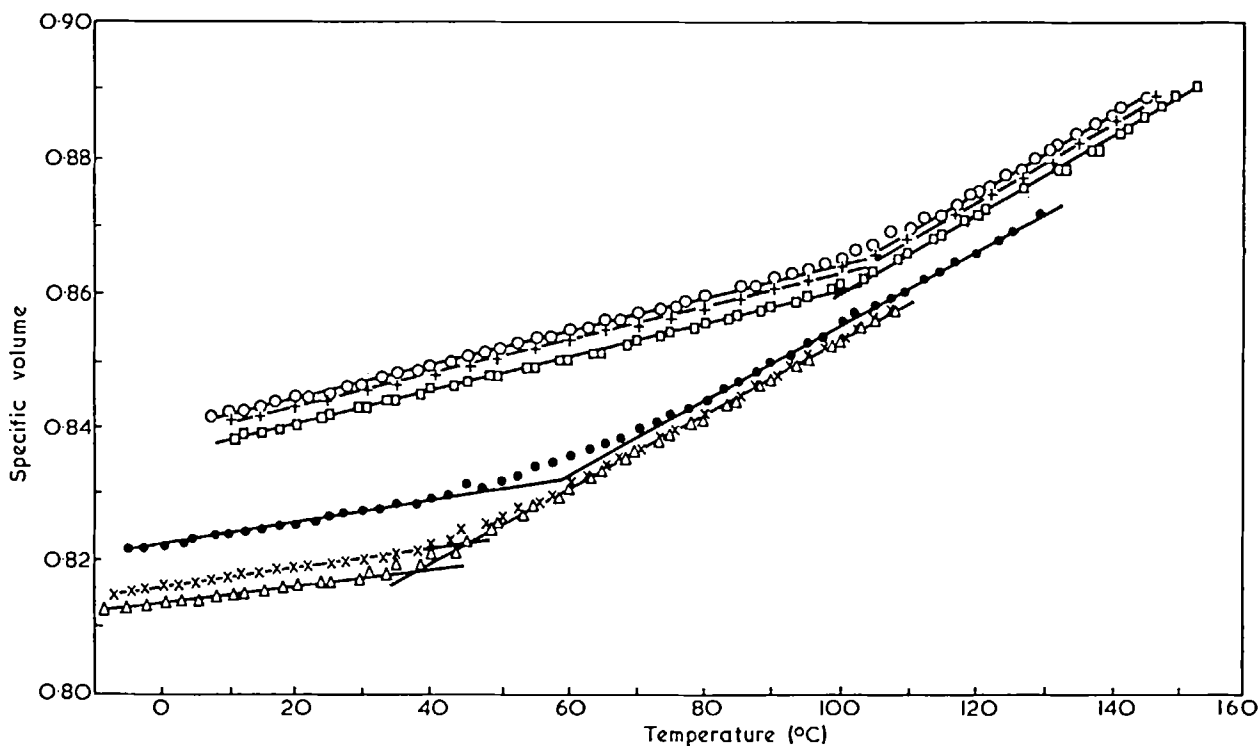


Figure 1 Volume-temperature curves for poly(methyl methacrylate) fractions of different stereostructure as determined by the density gradient technique.  $\circ$ , Z4-A2x; +, MTS-1A;  $\square$ ,  $\Delta 4:2$ ;  $\bullet$ , G5-A1;  $\times$ , DPHL-G1B;  $\triangle$ , PGR-2

crystallinity when examined after the experiments by X-ray diffraction. For the highly isotactic sample this was confirmed from the volume measurements, no evidence of the melting transition at 150°C being evident. Regular forms of this polymer appear to crystallize only under rather extreme conditions of annealing or solvent treatment.

## RESULTS AND DISCUSSION

The volume-temperature curves are shown in Figure 1. According to these results, extrapolated values of  $T_g$  for the syndiotactic polymer do not appear to give correct results, the difference from conventional polymers being at most a few degrees. The n.m.r. determinations indicate that polymer G5A1 has a short block structure with  $l_i \sim 7$  and  $l_s \sim 5$  monomer units. Only a single broad transition has been indicated. It would be possible to interpret the results in terms of two transitions, one about the value for isotactic polymers and one about 70°C. The experimental accuracy is not sufficient to distinguish between these possibilities. It has been suggested<sup>7,8</sup> that other apparently stereo-block poly(methyl methacrylates) produced by similar catalysts are, in fact, mixtures of largely isotactic and syndiotactic polymers. A mixture of isotactic and syndiotactic polymers (60:40) does give a similar volume-temperature curve to that observed for polymer G5A1. The possibility cannot therefore be excluded that this polymer also is a mixture of two stereoregular forms.

The results are summarized in Table 2. The expansion coefficients ( $dV/dt$ ) can be compared with literature values. The values for the isotactic polymer,  $\alpha_i = 5.5 \times 10^{-4}$ ,  $\alpha_g = 1.1 \times 10^{-4}$  of Goode and co-workers<sup>9</sup> determined

Table 2 Summarized experimental results (density gradient column)

Sample	$P_i$	$T_g$ (°C)	$10^4 \alpha_i$	$10^4 \alpha_g$	$10^4 \Delta \alpha$	$T_g \Delta \alpha$	$V_g$
PGR-2	0.98	38	5.6	1.3	4.3	0.131	0.818
DPHL-GIB	0.86	44	5.6	1.45	4.15	0.131	0.822
G5-A1	0.60	58	5.6	1.7	3.9	0.129	0.832
$\Delta 4:2$	0.24	101	5.8	2.5	3.3	0.124	0.860
MTS:1A	0.12	103	5.85	2.55	3.3	0.124	0.865
Z4-A2x	0.02	105	5.85	2.55	3.3	0.125	0.866

dilatometrically are comparable although their  $\alpha_g$  is about 20% lower than the present value. For conventional polymer values of  $\alpha_i$  of 5.0 to  $5.2 \times 10^{-4}$  are common<sup>10-12</sup> with  $\alpha_g$  values of 1.9 to  $2.3 \times 10^{-4}$ . Once again, the present values are rather higher especially for  $\alpha_i$ . Table 2 also gives values of the product  $T_g \Delta \alpha$ , the Simha-Boyer constant<sup>13</sup> symptomatic of an iso-free volume transition. It is reasonably constant over the series. As noted by these authors this result could be expected from both thermodynamic and dynamic theories of the glass transition. Karasz and MacKnight<sup>14</sup> have used the Gibbs-DiMarzio theory to interpret the difference in  $T_g$  values in terms of a larger difference in energy levels between rotational isomers in syndiotactic chains. The results could be equally well interpreted in terms of higher energy barriers to rotation in this stereostructure. There is evidence from n.m.r. line-width studies<sup>15</sup> and measurements of dielectric relaxation<sup>16,17</sup> in solution, that the isotactic form has a more dynamically flexible main chain. Estimations of the cohesive energy density of the two regular forms<sup>18</sup> indicate little difference so intermolecular interactions in the solid do not seem to be an important source of differing behaviour.

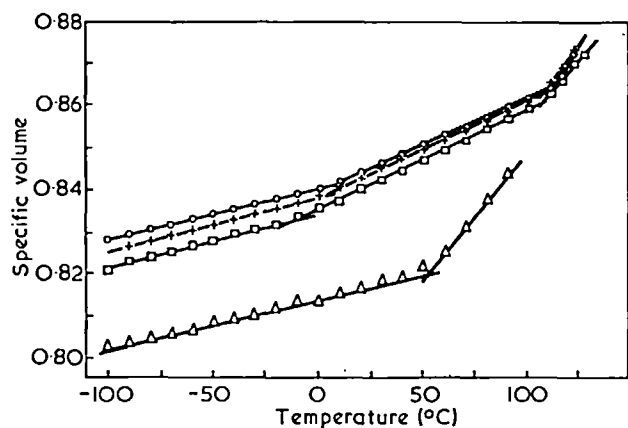


Figure 2 Volume-temperature curves for poly(methyl methacrylate) fractions of different stereostructure as determined with a Perkin-Elmer TMS-1 instrument. O, Z4-A2x; +, MTS:1A; □, Δ4:2; △, PGR-2

As seen from Table 2, the expansion coefficients of syndiotactic and isotactic polymers are noticeably different in the immediate region below  $T_g$ . This behaviour is evident also in previously reported data on isotactic and conventional polymers<sup>9-12</sup>. Since the expansion coefficients would be expected to become roughly equal at lower temperatures, it may be surmised that predominantly syndiotactic polymers show a larger sub-glass transition in the temperature range below that investigated. In order to check this point, some of the samples were studied using a Perkin-Elmer Thermomechanical Analyzer. This instrument measures sample length over a wide range of temperatures. Slightly larger samples were used ( $2 \times 3$  mm) and the scan rate used was  $2-5^\circ\text{C}/\text{min}$ . The length measurements were converted to effective volumes and normalized to specific volumes at room temperature as determined by the density gradient technique. The results are shown in Figure 2. Predominantly syndiotactic polymers show a substantial change of expansion coefficient between 0 and  $-10^\circ\text{C}$  to give an  $\alpha$  value virtually identical to the isotactic sample below this temperature. This change should correspond to the  $\beta$  transition usually attributed to  $-\text{COOCH}_3$  side-chain rotation and which gives a loss-maximum at  $\sim 25^\circ\text{C}$  at  $1\text{ Hz}$ <sup>19</sup> in shear measurements. The isotactic glass shows no appreciable change in expansion coefficient at least down to  $-80^\circ\text{C}$  which seems too low a temperature for the  $\beta$  transition. The difference in temperature of the loss-maximum between stereoisomers for the  $\beta$  transition is relatively small<sup>17</sup>. These observations can be correlated with the observation that side-

chain rotation is considerably less excited in the isotactic form<sup>19, 20</sup>. The larger  $\Delta\alpha$  observed at  $T_g$  for this structure could then be caused by both complete side-chain and main chain rotation becoming effective at  $T_g$  as has been previously suggested<sup>19</sup>.

The glass temperatures as measured on the thermo-mechanical analyser are somewhat higher than those obtained using the density gradient technique. This could be caused by plasticization by water in the latter experiments, an effect noted by previous authors<sup>21</sup>. The effect is small ( $\sim 5^\circ\text{C}$ ) except for the isotactic sample where it seems to be closer to  $12^\circ\text{C}$ . The accuracy of the measurements with the TMS-1 instrument is, however, limited by the fact that reliable length measurements above  $T_g$  are virtually impossible to obtain. As the modulus decreases, results depend on the weight applied to the sample. Although true expansion coefficients above  $T_g$  were not obtained, those below are reasonably reproducible and lower than observed in density gradient experiments, but only by 10%.

## REFERENCES

- 1 Fox, T. G., Garrett, B. S., Goode, W. E. *et al.* *J. Am. Chem. Soc.* 1958, **80**, 1768
- 2 Stroupe, J. D. and Hughes, R. E. *J. Am. Chem. Soc.* 1958, **80**, 2341
- 3 Thompson, E. V. *J. Polym. Sci. (A-2)* 1966, **4**, 199
- 4 Abe, H., Imai, K. and Matsumoto, M. *J. Polym. Sci. (B)* 1965, **3**, 1053
- 5 Gordon, M. and Macnab, I. A. *Trans. Faraday Soc.* 1953, **49**, 31
- 6 Cowie, J. M. G. and Toporowski, P. M. *J. Macromol. Sci. (B)* 1969, **3**, 81
- 7 Liquori, A. M., Anzuino, G., D'Alagni, M. *et al.* *J. Polym. Sci. (A-2)* 1968, **6**, 509
- 8 Miyamoto, T. and Inagaki, H. *Polym. J.* 1970, **1**, 46
- 9 Goode, W. E., Owens, F. H., Fellmann, R. P. *et al.* *J. Polym. Sci.* 1960, **46**, 317
- 10 Loshaek, S. *J. Polym. Sci.* 1955, **15**, 391
- 11 Wittmann, J. C. and Kovacs, A. J. *J. Polym. Sci. (C)* 1965, **16**, 4443
- 12 Heydemann, P. and Guicking, H. D. *Kolloid Z.* 1963, **193**, 16
- 13 Simha, R. and Boyer, R. F. *J. Chem. Phys.* 1962, **37**, 1003
- 14 Karasz, F. E. and MacKnight, W. J. *Macromolecules* 1968, **1**, 537
- 15 Brownstein, S. and Wiles, D. M. *Can. J. Chem.* 1966, **44**, 153
- 16 Pohl, H. A., Bacskai, R. and Purcell, W. P. *J. Phys. Chem.* 1960, **64**, 1701
- 17 Pohl, H. A. and Zabusky, H. H. *J. Phys. Chem.* 1962, **66**, 1390
- 18 Cowie, J. M. G. *Polymer* 1969, **10**, 708
- 19 Heijboer, J. 'Physics of Non-crystalline Solids', North Holland, Amsterdam, 1965, p 231
- 20 Mikhailov, G. P. and Borisova, T. I. *Polym. Sci. USSR* 1961, **2**, 387
- 21 McLoughlin, J. R. and Tobolsky, A. V. *J. Colloid Sci.* 1952, **7**, 555

# Segregation and conformational transition in triblock copolymers: Part 2. Light-scattering studies

A. Dondos, P. Rempp and H. C. Benoit

*Centre de Recherches sur les Macromolécules, CNRS, 6 Rue Boussingault,  
67 Strasbourg, France  
(Received 16 June 1971)*

From light-scattering experiments carried out on a polystyrene (PS) sample, a poly(methyl methacrylate) (PMMA) sample, on a random copolymer of styrene and MMA and on an anionically prepared triblock copolymer PMMA-PS-PMMA, all of the same molecular weight, in various solvents over a range of temperature (18–65°C) it was shown that a conformational transition occurs for the triblock copolymer. At lower temperatures segregation occurs and the second virial coefficient  $A_2$  is the weighted average between the  $A_{2A}$  and  $A_{2B}$  values for the corresponding homopolymers (PS and PMMA). At higher temperatures contacts between chemically unlike parts of the molecule become possible, and the additivity rules are no more valid for  $A_2$ , as well as for the expansion coefficient. This change from a segregated to a 'pseudo-gaussian' conformation involves a change in specific volume of the molecule, and it therefore brings with it an abnormal variation of the refractive index increment, which has been investigated on the same light-scattering diagrams.

## INTRODUCTION

Investigations on the conformational behaviour of block copolymers in dilute solutions have led many authors to the conclusion that in two-block copolymers segregation always occurs<sup>1-4</sup>: the two blocks have distinct locations, and heterocontacts, i.e. contacts between an A segment and a B segment of the same molecule are very few. This general phenomenon is due to incompatibility between chemically unlike blocks<sup>5</sup>, and it is in fact an intramolecular phase separation. The case of ABA triblock copolymers is somewhat more complex, because in many cases a transition was observed<sup>6,7</sup> on studying the temperature dependence of their intrinsic viscosities. It was assumed that below the transition temperature,  $T_c$ , phase separation is the rule, whereas when temperature increases above  $T_c$  the number of heterocontacts is no longer negligible, and it increases with temperature, yielding more extended conformations. Some authors<sup>8,9</sup> who studied triblock copolymers and who denied the existence of segregation may well have worked under experimental conditions which did not allow real intramolecular phase separation to occur. One of the most valid arguments in favour of segregation at temperatures below  $T_c$  is the fact that the location of  $T_c$  itself depends upon the solvent<sup>6</sup>. In a solvent in which

the incompatibility between the corresponding homopolymers is high,  $T_c$  is also high. In good solvents for both polymers, the critical demixion volume between the homopolymers is smaller<sup>10</sup>, and in those solvents  $T_c$  is also found to be lower.

The main experimental technique which was used to study segregation is measurement of the limiting viscosity number  $[\eta]$ . Radii of gyration are not of great help, because the overall dimensions of a two-block copolymer containing 50% of each constituent could not be very different for segregated conformations<sup>11</sup>.

The purpose of this paper is to bring new arguments in favour of segregation in block copolymers, based upon precise measurements of the second virial coefficient, in various solvents, over a range of temperature including  $T_c$ . These measurements were carried out by light-scattering.

## EXPERIMENTAL

A triblock methyl methacrylate-styrene-methyl methacrylate (PMMA-PS-PMMA) copolymer was prepared anionically, using the standard experimental techniques. Sodium- $\alpha$ -methylstyrene tetramer was used as initiator, and 1,1-diphenylethylene was added to the 'living' poly-

Table 1 Molecular weights and refractive index increment  $dn/dc$  for triblock copolymer in various solvents

Solvent	$M_w$	$dn/dc$
THF	425000	0.1460
Dioxane	445000	0.1300
$\text{CHCl}_3$	455000	0.1110
<i>p</i> -xylene	495000	0.0601
Benzene	520000	0.0562

styrene prior to the addition of methyl methacrylate, to prevent side reactions onto the ester functions to occur<sup>12</sup>. The molecular weight of the central polystyrene block is 230 000; the molecular weight of the copolymer itself, measured by light-scattering in tetrahydrofuran (THF) is 425 000. It contains 53% of styrene, as shown by refractive index measurements, as well as by elemental analysis.

Light-scattering measurements were carried out in several other solvents. From the obtained results, summarized in Table 1, it can be assumed that there are some fluctuations in composition within the sample<sup>13</sup>,

most likely due to the presence of some two-block copolymer molecules amongst the triblock molecules. But we shall not take these fluctuations into account, and, following the conclusions of Leng and Benoit<sup>13</sup> we shall consider the value of  $M_w$  measured in THF, the solvent in which the  $dn/dc$  value is the highest, to be the true weight average molecular weight of the copolymer.

A polystyrene homopolymer and a poly(methyl methacrylate) homopolymer were both prepared anionically.

Their molecular weights, measured by light-scattering amounted to 400 000 and 435 000 respectively. Gel permeation chromatography experiments showed that their molecular weight distributions were narrow.

A random copolymer of styrene and methyl methacrylate was prepared by radical copolymerization of an azeotrope mixture of the monomers (52 mol.% styrene/48 mol.% MMA). The sample was fractionated and a fraction exhibiting a weight-average molecular weight of 394 000 was used in the present work.

To carry out measurements of the second virial coefficient a FICA light-scattering apparatus was used. It was fitted with a thermostat, and the temperature of

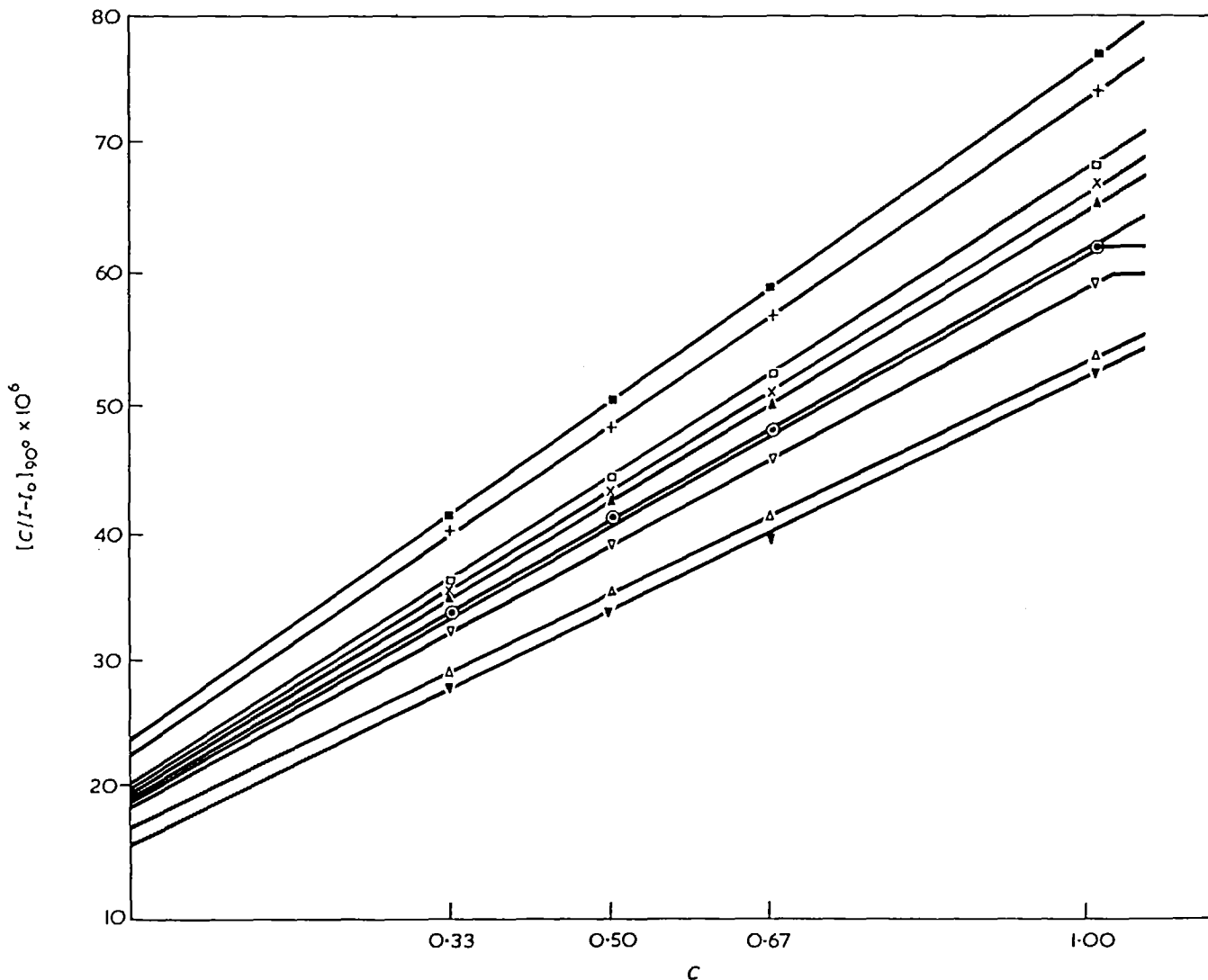


Figure 1 Plot of  $[C/(I-I_0)]$  at fixed angle ( $90^\circ$ ) against  $C$  for the triblock copolymer in benzene solution at various temperatures. ■, 20°C; +, 24.5°C; □, 32°C; ×, 34°C; ▲, 36.5°C; ○, 40°C; ●, 42.5°C; ▽, 45°C; △, 56°C; ▼, 60.5°C

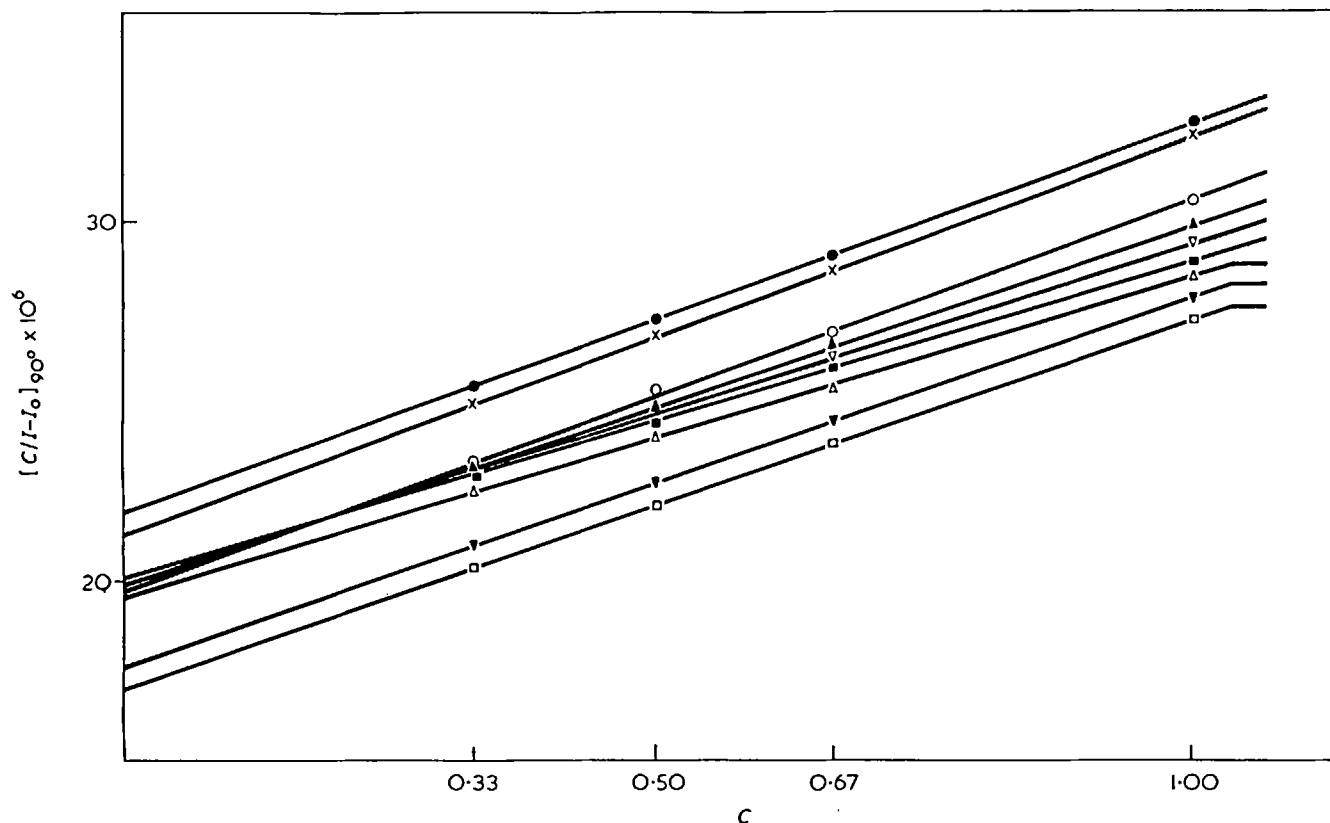


Figure 2 Plot of  $[C/(I-I_0)]_{90^\circ}$  against  $C$  for the triblock copolymer PMMA-PS-PMMA in *p*-xylene at various temperatures. The intensities  $I$  and  $I_0$  for solution and solvent are measured at  $90^\circ$ . ●,  $20^\circ\text{C}$ ; ×,  $30^\circ\text{C}$ ; ▲,  $37^\circ\text{C}$ ; ○,  $38^\circ\text{C}$ ; ▽,  $43^\circ\text{C}$ ; ■,  $45.5^\circ\text{C}$ ; △,  $48^\circ\text{C}$ ; ▼,  $53.5^\circ\text{C}$ ; □,  $59^\circ\text{C}$

the cells was maintained constant within  $\pm 0.2^\circ\text{C}$ ; the range of temperature covered by our measurements extended from 18 to  $65^\circ\text{C}$ . The cells were fitted with ground stopcocks to prevent evaporation of the solvent. A series of 4 concentrations were prepared, made free of dust by centrifugation in a Pirouette-Phywe centrifuge, and filled into the cells. These solutions were used throughout a series of light-scattering experiments carried out at different temperatures. Account was taken of the expansion of the solvent (i.e. the dilution of the solution) with increasing temperature.

Series of such curves, obtained in two solvents, benzene and *p*-xylene, are shown in Figures 1 and 2. The scattered intensities were measured at  $90^\circ$  and were not extrapolated to zero angle, which does not introduce any appreciable difference on the  $A_2$  value. This procedure is justified by the fact that the radius of gyration of all the molecules investigated was of the order of 200–250 Å, which is low enough to justify the use of the 'small molecule approximation'.

Furthermore in the case of the triblock copolymer in dilute *p*-xylene solution (Figure 2) the dissymmetry of scattered intensity is so small that it can hardly be measured.

## RESULTS AND DISCUSSION

### Second virial coefficient

It should be recalled first that the second virial coefficient  $A_2$  measured for linear macromolecules in dilute solution is dependent upon molecular weight and upon the segment–segment interaction coefficient  $Z$ . According

to several authors<sup>14,15</sup> one can express  $A_2$  as the sum of two terms: one depends solely upon the unperturbed dimensions, and the other is a function of the long-range interactions which induce expansion of the chain. According to Kurata *et al.*<sup>15</sup>:

$$A_2 = \frac{1.65 \times 10^{23}}{6^{3/2}\phi} \frac{K_0}{M^{1/2}} + \frac{0.958 \times 10^{23}}{6^{3/2}\phi} \frac{K_0}{M^{1/2}} \left(\frac{3}{2\pi}\right)^{3/2} Z$$

$$\text{or } M^{1/2}A_2 = BK_0 + DK_0 \cdot Z$$

where

$$K = \frac{[\eta]_0}{M^{1/2}} = 6^{3/2} \cdot \phi \cdot \left(\frac{\overline{R}_0^2}{M}\right)^{3/2}$$

In this expression, valid even for rather high values of  $A_2$ :

- $\phi$  is the universal Flory constant,
- $K_0$  is the unperturbed dimensions parameter of the chain ratio of the intrinsic viscosity at  $\theta$  point  $|\eta|_\theta$ , to the square root of molecular weight  $M$ ,
- $\overline{R}_0^2$  is the unperturbed mean square radius of gyration,
- $Z$  is the long-range interaction parameter.

For a copolymer one can write<sup>11</sup>:

$$Z = C_1 Z_{AA} + C_2 Z_{BB} + C_3 Z_{AB}$$

where  $Z_{AA}$ ,  $Z_{BB}$  and  $Z_{AB}$  are the interaction parameters, for each type of contact: between two A segments, between two B segments, between one A and one B segment, and  $C_1$ ,  $C_2$ ,  $C_3$  are the probability of occurrence of each type of contact.

If segregation occurs, since in the present case  $Z_{AB}$  is obviously not zero, the probability factor  $C_3$  is very close to zero. On the other hand, as shown in earlier papers, when segregation occurs, the unperturbed dimensions of



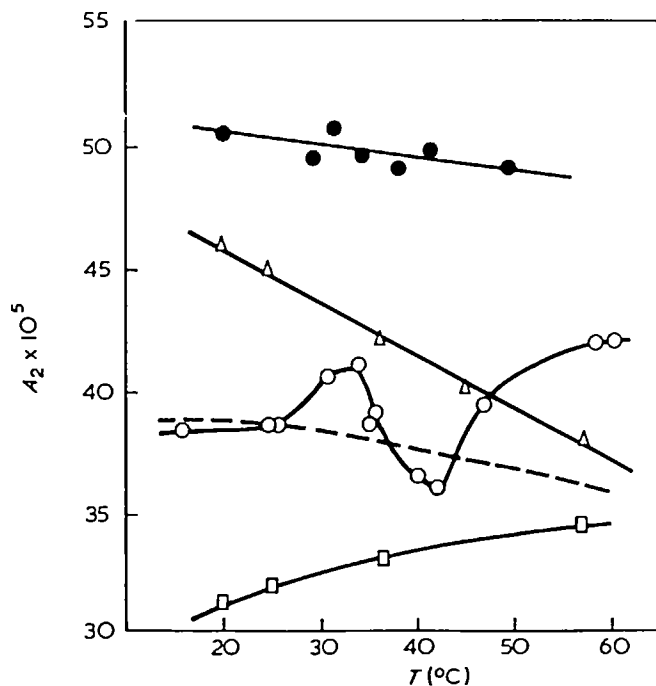


Figure 3 Plot of the temperature variation of the second virial coefficient  $A_2$  in the THF solution. ●, Random copolymer; △, PS; □, PMMA; ○, triblock copolymer. ----, see text

the copolymer are approximately equal to the weighted average of the unperturbed dimensions of the corresponding homopolymers<sup>8,16</sup>.

These assumptions can be written:

$$Z = xZ_{AA} + (1-x)Z_{BB}$$

$$K_{\theta} = xK_{\theta A} + (1-x)K_{\theta B}$$

It follows for  $A_2$

$$M^{1/2}A_2 = [xK_{\theta A} + (1-x)K_{\theta B}][B + D(xZ_{AA} + (1-x)Z_{BB})]$$

which can be rearranged to:

$$A_2 = xA_{2A} + (1-x)A_{2B} +$$

$$[x(1-x) \cdot D(Z_{BB} - Z_{AA}) \cdot (K_{\theta A} - K_{\theta B})] \frac{1}{M^{1/2}}$$

In this expression the third term is very small, and can be neglected in first approximation. Following this rather crude calculation in the case of segregation, the  $A_2$  coefficient should be the weighted average between those of the corresponding homopolymers A and B, of same molecular weight as the copolymer.

If heterocontacts are numerous both our hypotheses are wrong. The  $K_{\theta}$  value for the copolymer is higher than the weighted average between the corresponding homopolymers, as was shown from measurements carried out on random copolymers<sup>17,18</sup>. Still more important is the fact that the value of  $Z$  does not reduce to two terms involving A-A and B-B contacts, solely. Therefore it can be expected that the  $A_2$  value for the copolymer should be higher than the weighted average between the two  $A_2$  values for the homopolymers of the same molecular weight as the copolymer.

Let us now compare these assumptions with our experimental results.

In Figure 3 the  $A_2$  values are plotted against temperature for the 4 polymeric compounds investigated: polystyrene, poly(methyl methacrylate), random copolymer

and triblock copolymer, all of approximately equal molecular weights. The solvent is THF. As expected, the  $A_2$  coefficient for the random copolymer is higher than the  $A_2$  values for PS or PMMA, over the entire range of temperature, owing to the influence of the  $Z_{AB}$  factor. Looking at the results on the triblock copolymer, we can see that in the lower temperature range the  $A_2$  value is close to the weighted average between the  $A_{2A}$  and  $A_{2B}$  values (indicated by the broken line in Figure 3) whereas in the higher temperature range the value of  $A_2$  is bigger than both  $A_{2A}$  and  $A_{2B}$ . In the intermediate range of temperature the  $A_2$  coefficient of the triblock copolymer varies in a rather strange fashion, with two

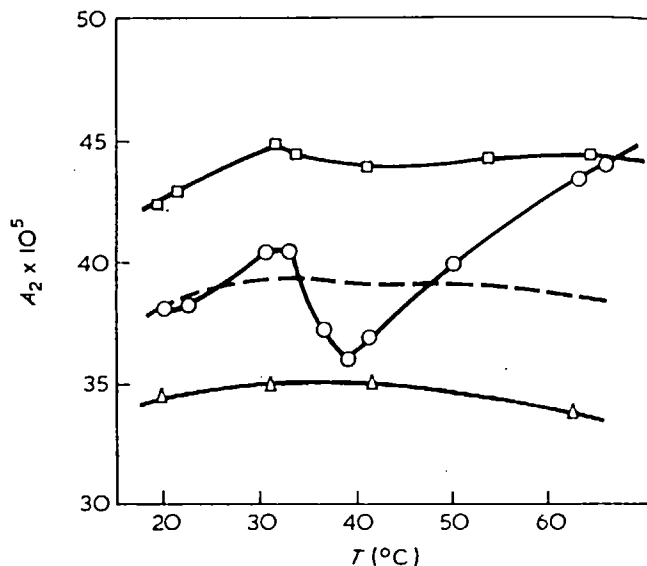


Figure 4 Plot of the temperature variation of the second virial coefficient  $A_2$  in dioxan. △, PS; □, PMMA; ○, triblock copolymer. ----, see text

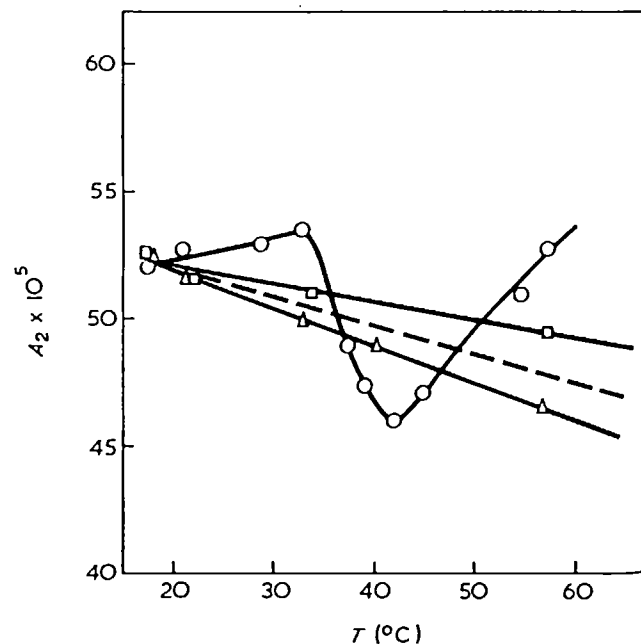


Figure 5 Plot of the temperature variation of the second virial coefficient  $A_2$  in chloroform. △, PS; □, PMMA, ○, triblock copolymer. ----, see text

extremes, and we would not yet consider attempting an explanation for this behaviour. But it should be emphasized that the same type of curve has been found for the same triblock copolymer by  $[\eta]$  measurements in the same solvent and at approximately the same temperature.

Even if it is difficult to explain the shape of these curves in the intermediate range it seems well established that at low temperature the molecule is segregated and tends to a non-segregated or 'gaussian' conformation when the temperature increases.

One should realize that, even if the absolute values of the second virial coefficient are usually not known with great precision, we are using here the same samples in the same machine, which increases considerably the precision on a relative scale.

These experiments have been repeated, increasing or decreasing the temperature; the results are exactly the same, even after a few days.

Similar results are shown for other solvents, including dioxane (Figure 4), chloroform (Figure 5) and benzene (Figure 6). The same transition appears for  $A_2$  in all cases. Obviously at lower temperatures the  $A_2$  is always located in-between the corresponding values for the homopolymers, whereas at higher temperatures conformational changes have occurred, yielding an increase of  $A_2$ , far above the average value between  $A_{2A}$  and  $A_{2B}$ .

The temperature dependence of  $A_2$  in *p*-xylene is shown in Figure 7. Here the  $A_2$  values for PMMA are not experimentally accessible because of lack of solubility. But the transition can be seen distinctly, and it is located somewhat higher (38°C) than in other solvents. This is not surprising, because it has been shown<sup>10,19</sup> that *p*-xylene is one of the solvents in which the PS and PMMA homopolymers are most incompatible. It is in this solvent that the critical volume for phase separation as determined by Kern<sup>10</sup> reaches its highest value. If a small amount of a good solvent such as chloroform is added the corresponding increase of  $A_2$  is accompanied by a lowering of the transition temperature by about 5°C. This can be explained by saying that heterocontacts are easier to form.

Another way of showing the results is to plot  $A_2$  against the amount of added chloroform (Figure 8) at two different temperatures; the curve obtained at 20°C is linear and the conformations are always segregated. The curve obtained over the same amount of added chloroform, but at 37.5°C is similar to that obtained for  $A_2$  against  $T$  in any solvent. It is therefore possible to obtain this conformational change not only by changing the temperature, but also by changing the composition of the solvent.

#### Thermal dependence of $[C/(I-I_0)]_0$

From these experiments by light-scattering, we have also observed a curious effect, which seems to be related to the conformational transition and which deserves mention.

Let us consider the value of  $C/(I-I_0)$ , extrapolated to zero concentration,  $[C/(I-I_0)]_0$ , as a function of temperature (Figures 9, 10 and 11). An abnormal behaviour is found for the triblock copolymer in the region of the critical temperature. Homopolymers do not show any effect of this type. Since molecular weight cannot change (there is no aggregation) it must be one of the factors relating  $[C/(I-I_0)]_0$  to molecular weight which exhibits

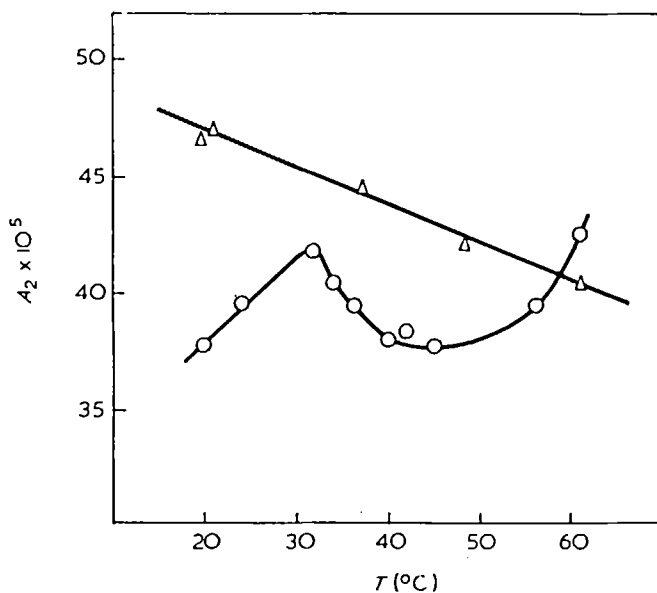


Figure 6 Plot of the temperature variation of the second virial coefficient  $A_2$  in benzene.  $\Delta$ , PS;  $\circ$ , triblock copolymer

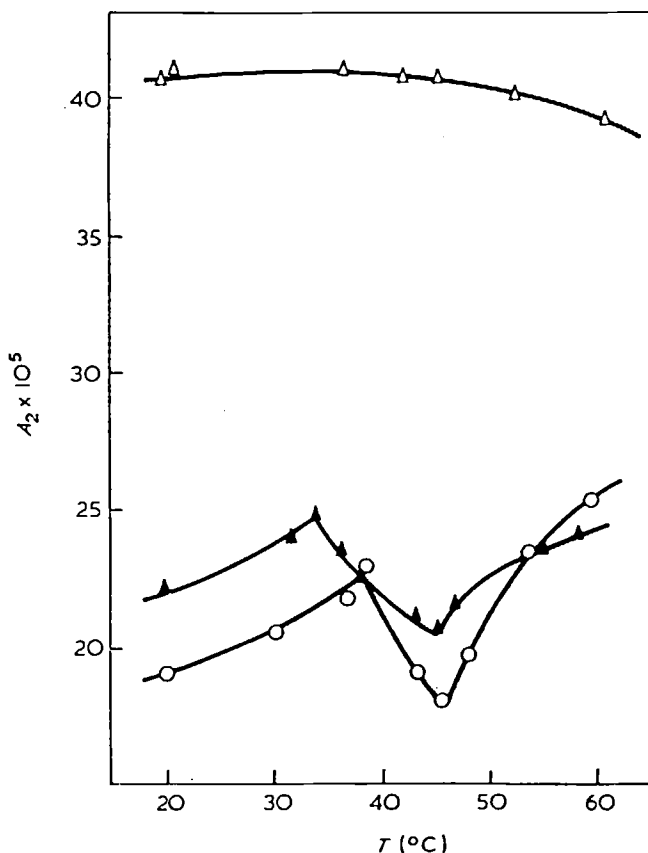


Figure 7 Temperature variation of  $A_2$ . In pure *p*-xylene:  $\circ$ , triblock copolymer PMMA-PS-PMMA;  $\Delta$ , PS. In *p*-xylene containing 3.85% chloroform:  $\blacktriangle$ , triblock copolymer

an irregular variation. The only variable is the refractive index increment  $dn/dc$ .

Two explanations can be found for this result. If the structure of the molecule is changed, the internal field at the different monomer position varies and so does the  $dn/dc$  factor. Since effects of this kind have never been found in polymeric materials this seems to be rather

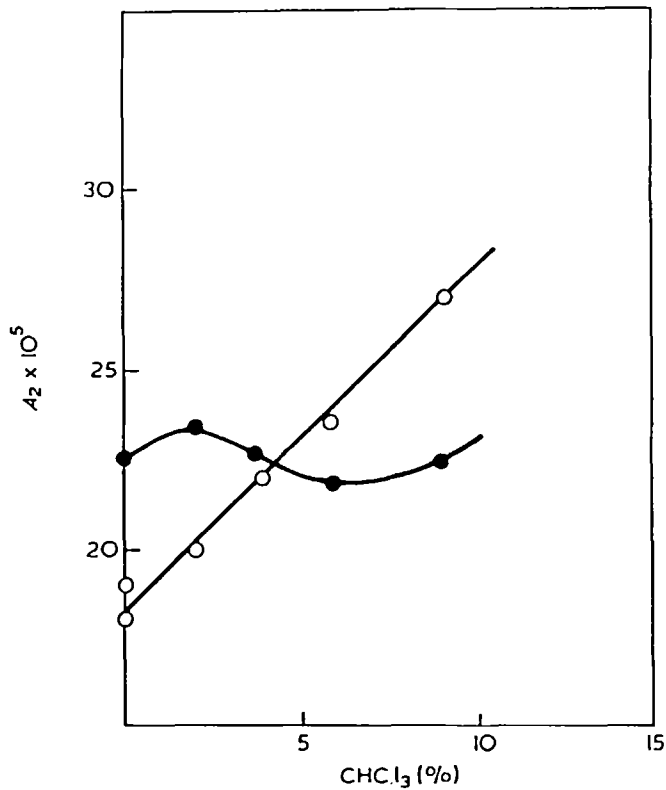


Figure 8 Variation of  $A_2$  of triblock copolymer measured in chloroform containing *p*-xylene against the percentage of chloroform.  $\circ$ , 20°C;  $\bullet$ , 37.5°C

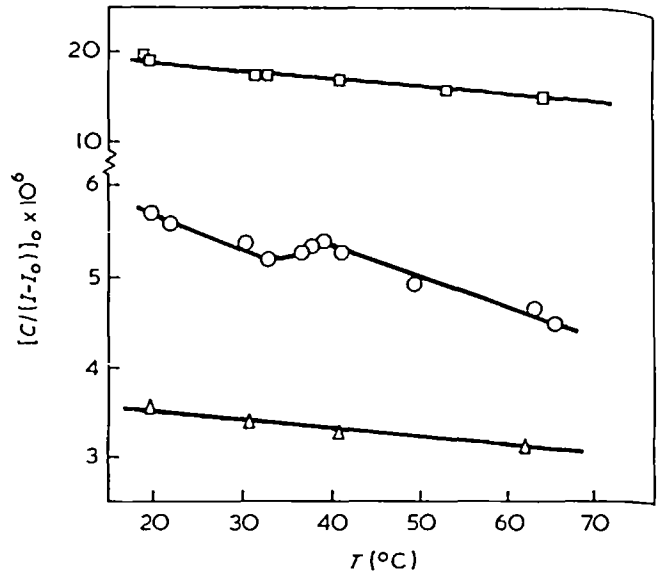


Figure 10 Plot of  $[C/(I-I_0)]_0$  against temperature for PS ( $\Delta$ ) for PMMA ( $\square$ ) and for the triblock copolymer ( $\circ$ ) in dioxan

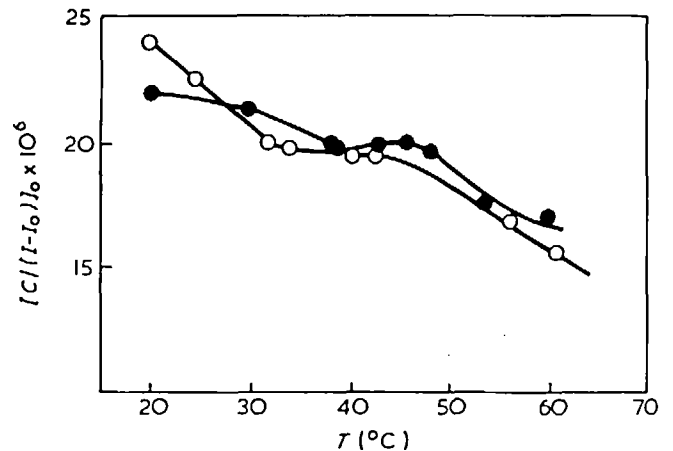


Figure 11 Plot of  $[C/(I-I_0)]_0$  (extrapolated to zero concentration) for the triblock copolymer in benzene ( $\circ$ ) and *p*-xylene ( $\bullet$ )

improbable<sup>20</sup>, but it would be very interesting if it were true.

A second explanation, which is more trivial, could be found by saying that this reflects only a volume change during the conformational transition. Since in many transitions one observes a change of specific volume it is quite normal that in the transition described above one observes also a small volume change, yielding a change in the index of refraction increment<sup>20</sup>. This abnormal variation is not very large, and we are presently trying to measure it directly in order to confirm our hypothesis. It is difficult to predict the extent of variation from a theoretical point of view. Since all the classical theories of solution properties of polymers are based on the assumption of constant volume, only the more recent theories based on equations of state could be used.

#### CONCLUSIONS

New arguments have been presented, confirming the results previously described on conformation of triblock

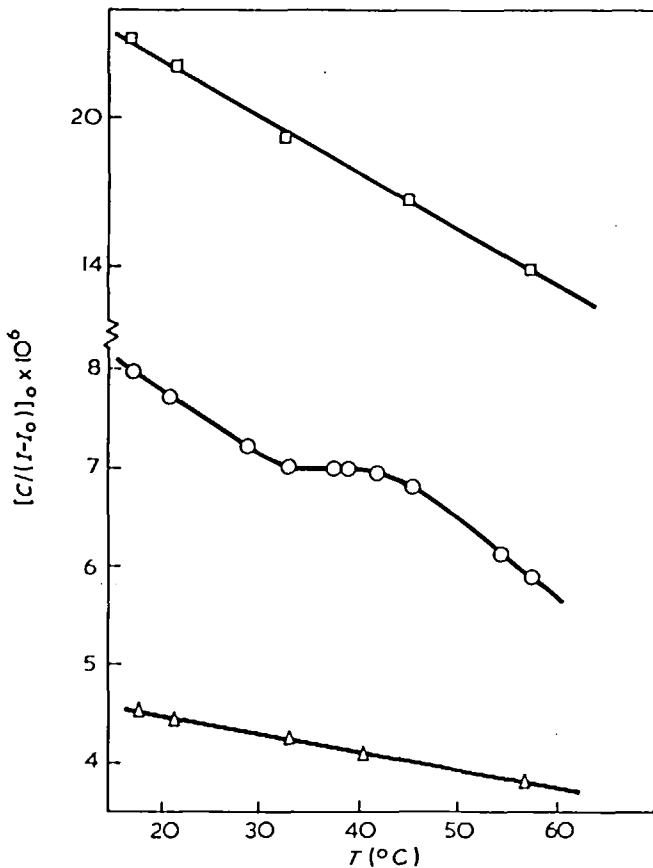


Figure 9 Temperature variation of  $[C/(I-I_0)]_0$  (extrapolated to zero concentration). Solvent: chloroform.  $\square$ , PMMA;  $\Delta$ , PS;  $\circ$ , triblock copolymer

copolymers. At low temperature segregation is observed, as in two-block copolymers. As temperature increases one is obliged, in order to account for the results, to assume formation of heterocontacts. This formation of heterocontacts brings with it a change in conformation which has still to be studied carefully.

The rules of additivity are valid for  $K_\theta$  as well as for the viscosity expansion coefficient  $\alpha_\eta$ , and for the second virial coefficient  $A_2$  in the case of segregation without heterocontact interactions. These rules are not valid above the transition temperature  $T_c$  (or, better, above the transition domain) and this is a proof of the existence of contacts between chemically unlike segments of the same molecule, at higher temperature. This conformational change depends upon the solvent, and in that respect our results confirm what has been already reported.

#### ACKNOWLEDGEMENT

The triblock copolymer was kindly synthesized for us by Dr D. J. Worsfold of NRC, Ottawa (Canada). We wish to express here our appreciation for his help.

#### REFERENCES

- 1 Burnett, G. M., Meares, P. and Paton, C. *Trans. Faraday Soc.* 1962, **58**, 737
- 2 Krause, S. *J. Phys. Chem.* 1964, **68**, 1948
- 3 Dondos, A., Rempp, P. and Benoit, H. C. *Makromol. Chem.* 1969, **130**, 233
- 4 Eskin, V. E. and Korotkina, O. Z. *Vysokomol. Soedin. (A)* 1970, **12**, 2216
- 5 Dobry, A. and Boyer-Kawenoki, F. *J. Polym. Sci.* 1947, **2**, 90
- 6 Dondos, A. *Makromol. Chem.* 1971, **147**, 123
- 7 Mayer, R. Thesis, Univ. Strasbourg, 1971
- 8 Cramond, D. N. and Urwin, J. R. *Eur. Polym. J.* 1969, **5**, 35
- 9 Utracki, L. A., Simha, R. and Fetters, L. J. *J. Polym. Sci. (A-2)* 1968, **6**, 2051
- 10 Kern, R. *J. Polym. Sci.* 1956, **21**, 19
- 11 Froelich, D. and Benoit, H. C. *Makromol. Chem.* 1966, **92**, 224
- 12 Freyss, D., Leng, M. and Rempp, P. *Bull. Soc. Chim. Fr.* 1964, p 221
- 13 Leng, M. and Benoit, H. C. *J. Chim. Phys.* 1961, **58**, 480
- 14 Kurata, M. and Stockmayer, W. H. *Fortschn. Hochpolym. Forsch.* 1963, **3**, 196
- 15 Kurata, M., Fukatsu, M., Sotobayashi, H. and Yamakawa, H. *J. Chem. Phys.* 1964, **41**, 139
- 16 Kotaka, T., Ohnuma, H. and Inagaki, H. *Polymer* 1969, **10**, 517
- 17 Dondos, A. and Benoit, H. C. *Makromol. Chem.* 1968, **118**, 165
- 18 Mohite, R. B., Gundiah, S. and Kapur, S. L. *Makromol. Chem.* 1967, **108**, 52
- 19 Hugelin, C. and Dondos, A. *Makromol. Chem.* 1969, **126**, 206
- 20 Heller, W. *J. Polym. Sci. (A-2)* 1966, **4**, 209

# Laser-Raman spectrum of polyethylene: Part 1. Structure and analysis of the polymer

M. J. Gall\*, P. J. Hendra\*, C. J. Peacock†, M. E. A. Cudby‡ and H. A. Willis‡

(Received 30 April 1971)

The Raman spectra of several different samples of polyethylene are reported. It appears that the spectra are sensitive to crystallinity and to the presence of impurities such as vinyl groups. The possible effect of the presence of *gauche* CH<sub>2</sub> groups are considered. There is definite evidence that Raman spectroscopy has value as an analytical technique for polyethylenes.

## INTRODUCTION

The infra-red spectrum of polyethylene has been known for many years and has been analysed by many workers with a view to assigning fundamental modes<sup>1-4</sup>, the examination of effects due to crystallinity<sup>5-8</sup>, chain branching<sup>9-11</sup>, and chain folding<sup>12-14</sup>. The Raman spectrum has been reported by a number of authors<sup>15-19</sup> using both discharge sources and more recently lasers. The quality of their data has varied considerably and as a result this has led to a number of different assignments of bands to fundamental modes. These are commented upon in recent reviews<sup>20, 21</sup>. We have studied a series of polyethylene samples in different forms in order to investigate the effects of crystallinity, molecular weight and chain-folding on the observed Raman spectrum. We have also considered the vibrational analysis of this polymer but in this paper we confine our attention to the structural and analytical aspects of the spectra.

## EXPERIMENTAL

Raman spectra were recorded on a Spex 1401 Ramalog instrument with a Spectra Physics Model 140 Ar<sup>+</sup> laser (~700 mW in the 5145 Å line) and on a Cary 81L with a Spectra Physics Model 125 He/Ne laser (~50 mW in the 6328 Å line).

\* Department of Chemistry, University of Southampton, Southampton, SO9 5NH, UK

† Department of Chemistry, University of Lancaster, Bailrigg, Lancaster, UK

‡ ICI Ltd, Plastics Division, Welwyn Garden City, Herts, UK

The following polyethylene samples were examined and are numbered throughout this paper as follows: (1) a solid paraffin-wax-like sample of low molecular weight (mol. weight ~800); (2) a sample of 'low density' polyethylene (mol. wt. 10<sup>4</sup>-10<sup>5</sup>, crystallinity 60-70%); (3) sample 2 made into a transparent film by the rapid quench method<sup>22</sup>; (4) a 'high density' sample, made by the Phillips process (mol. wt. 10<sup>4</sup>-10<sup>5</sup>, crystallinity 80-90%); (5) sample 4 made into a single crystal mat by isothermal crystallization from xylene solution; (6) sample 4 made into the extended chain form by heating at 250°C for 2 hours under 5000 kg/cm<sup>2</sup> pressure; (7) another 'high density' sample, made by a Ziegler catalyst process, and of high molecular weight (mol. wt. ~10<sup>6</sup>, crystallinity ~80%).

None of these samples showed orientation effects when their Raman scattering was analysed. Also, electron micrographs showed that no ordering occurred with dimension larger than the wavelengths of visible light. Sample (4) was also examined as a melt (see below).

## RESULTS

Typical spectra obtained on the Spex 1401 instrument with the Ar<sup>+</sup> laser are given in *Table 1*. We will consider the spectra by frequency regions and comment upon analytically interesting features. The vibrational assignment is considered in Part 2 of this series (*Spectrochim. Acta* 1972, 28A, in press).

It is immediately apparent from *Table 1* that the spectra are sensitive to crystallinity but an experimental complication must be borne in mind. If we are comparing the intensities of two Raman bands, and their relative intensities appear to be sensitive to crystallinity, the symmetry of the bands must be considered. If one band

Table 1 The observed Raman spectra from non-oriented polyethylene samples\*

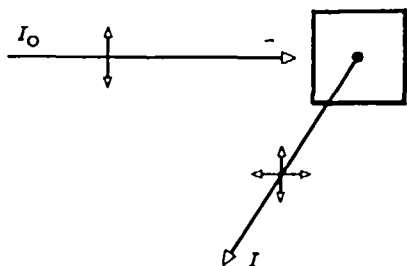
Frequency $\Delta\nu$ (cm <sup>-1</sup> )	Sample Number						
	1	2	3	4	5	6	7
3085	0.7			vw		vw	
3005	1	vw	vw	vw		vw	vw
2970	1	vw	2	vw		vw	
2932	19	23	32	18	25	10	13
2905 sh	38	43	50	38	52	22	25
2884	100	100	100	100	100	100	100
2848	62	72	90	61	49	48	58
2725	5	4	3	3	3	4	4
2660	0.5	0.6	vw	vw		0.5	0.7
2617	vw	vw	vw	vw		vw	0.6
2595	0.7	0.5	vw	vw		vw	0.9
2430	vw	vw	vw	vw		vw	vw
2185	0.8	0.6	0.6	vw		0.7	0.9
1672	0.5						
1655	0.6						
1645	4			vw		vw	
1461	16	17	8	9	9	10	9
1440	30	30	12	17	19	19	19
1418	15	9	3	9	11	14	10
1370	2	2	1	1	1	1	2
1306 sh	3	5	2	2	vw		1
1296	40	36	16	26	41	34	40
1274 sh	1	1	0.8	0.5	1	1	1
1170	4	3	1	3	2	5	7
1131	19	14	7	13	21	25	26
1080	2	3	2	1	1		2
1063	24	20	9	14	18	22	22
912	0.9						
892	3	1	1	vw			0.6
800-880	~0.9	vw	0.5				
725	vw	0.5	0.5	vw			0.5

\* Peak heights relative to the most intense band but arbitrarily at 100. Bands of intensity less than 0.5% recorded as vw. Limit of detection generally ~0.05%. Spex 1401: exciting line 5145 Å

is known to arise from a totally symmetric mode and the other from a vibration of lower symmetry, then the first will be polarized and the other second completely depolarized in a truly random sample. As the crystallinity of polyethylene rises its turbidity also increases. As a consequence of this the polarization of the laser source tends to be destroyed. In normal measurements (i.e. without polarization analyser) one observes the total scattered radiation polarized both parallel and perpendicular to the electric vector of the source. One can define an observed intensity ratio

$$R_{\text{obs}} = \frac{I_{\text{totally sym}}}{I_{\text{lower sym}}}$$

In the case of a transparent specimen  $R_{\text{obs}}$  tends to exceed the value characteristic of a turbid specimen<sup>23</sup>. Clearly our samples lie between the two extremes but do tend in general to cause a very considerable degree of scrambling. Thus considerable care is required if useful correlations between spectral intensity and crystallinity are to be proposed.



### Frequency region below $\Delta\nu=1000\text{ cm}^{-1}$

The region  $\Delta\nu=700$  to  $950\text{ cm}^{-1}$  is shown in Figure 1. There is a band at  $\Delta\nu=725\text{ cm}^{-1}$  and a series of weak features in the region  $\Delta\nu=800$  to  $900\text{ cm}^{-1}$ , which appear most strongly in the spectrum of the least crystalline samples and are absent from that of the most crystalline. These features have also been observed in fibres<sup>24</sup> and oriented samples (see Part 2). Raman active bands are not expected in this region for an infinite sequence of *trans*-methylene groups<sup>25</sup>. However, if there are methylene units in a *gauche* relationship to each other Raman active modes arising from CH<sub>2</sub> twisting and rocking together with C-C stretching and bending are expected in this part of the spectrum<sup>25</sup>. In shorter sequences of *trans* methylene groups terminated by methyl groups a band at  $\Delta\nu=890\text{ cm}^{-1}$  is observed<sup>19</sup>. This feature decreases in intensity as molecular weight increases. It is found with similar relative intensity in sample 1 and the pure hydrocarbon n-C<sub>42</sub>H<sub>86</sub> (mol. wt. = 590).

It is well-known that polyethylene chain folds in single crystals at intervals of between 100–200 Å<sup>26</sup>. Further, it is presumed that this also occurs in bulk specimens. The orientation of CH<sub>2</sub> units in the fold between two adjacent planar zig-zag sequences is not known for certain. It is clear however that some *gauche* methylene groups must exist. However, in the amorphous regions, i.e. those between the crystallites, non-planar arrays must be present with their *gauche* methylene groups. The observa-

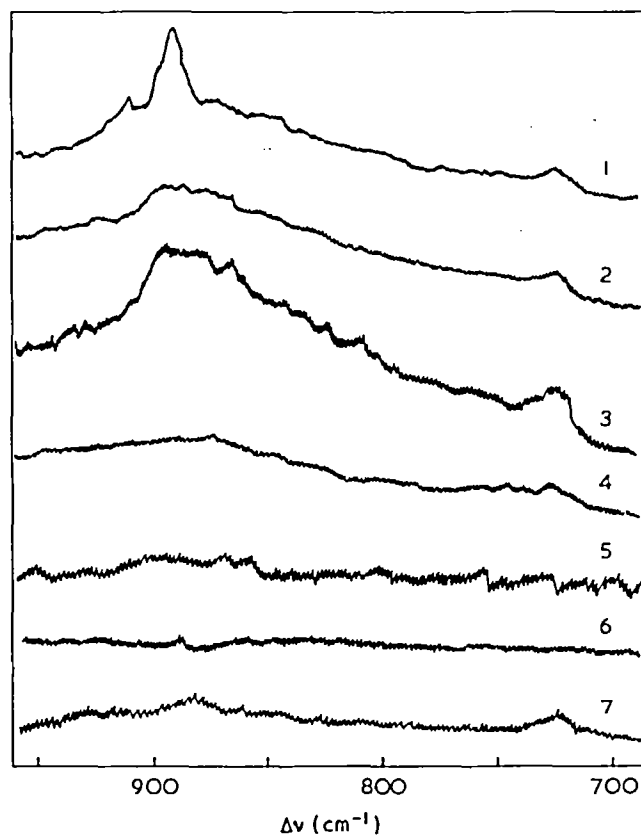


Figure 1 Raman spectra of polyethylene samples, No. 1–7 inclusive, in the region  $\Delta\nu=700$  to  $950\text{ cm}^{-1}$ . Intensities have been normalized with respect to the band at  $\Delta\nu=1296\text{ cm}^{-1}$

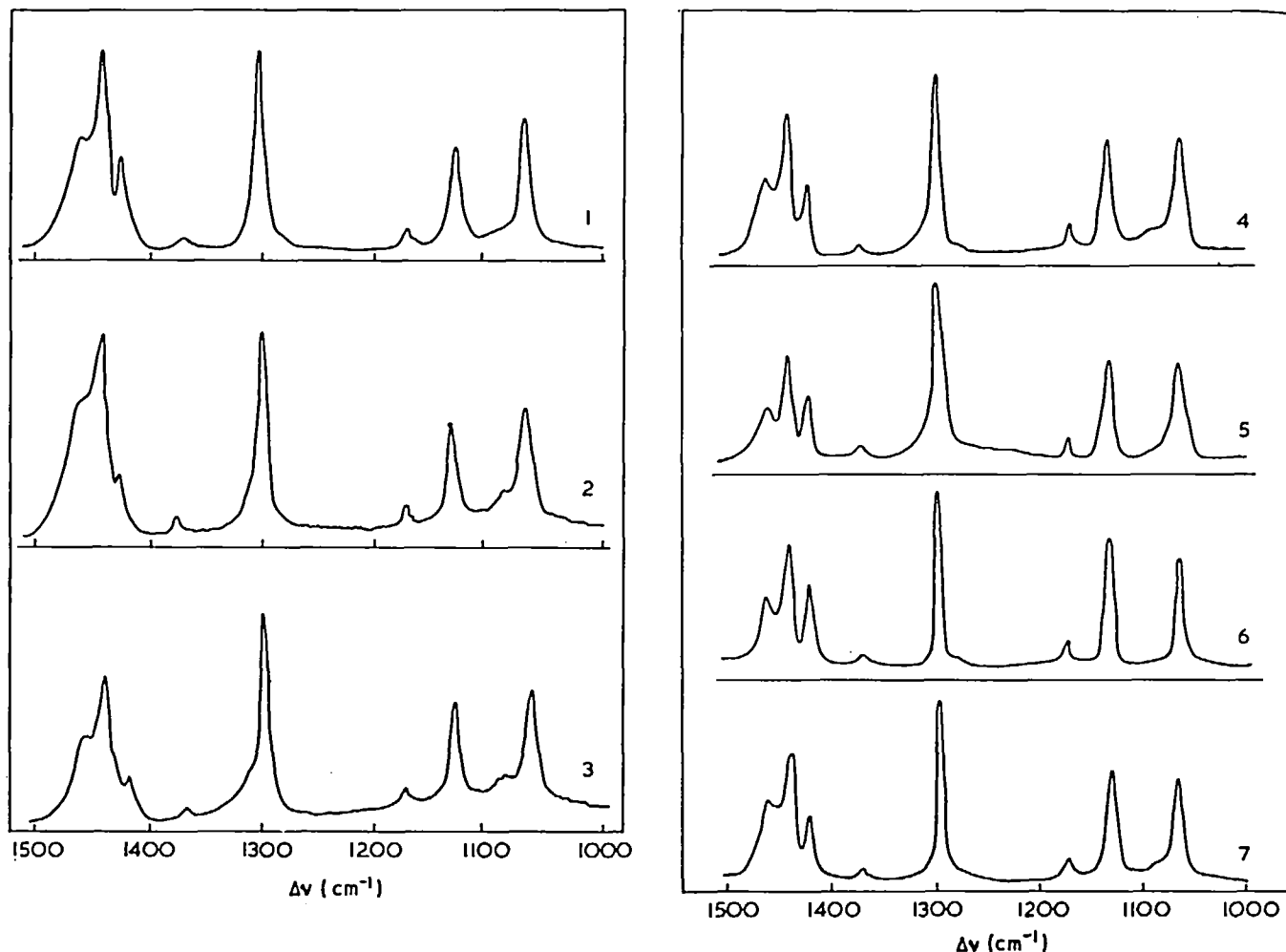


Figure 2 Raman spectra of polyethylene samples, No. 1-7 inclusive, in the region  $\Delta\nu=1000$  to  $1500\text{cm}^{-1}$ . Intensities have been normalized with respect to the band at  $\Delta\nu=1296\text{cm}^{-1}$

tion of bands between  $\Delta\nu=700$  and  $900\text{cm}^{-1}$  therefore does not enable us to discriminate between these two effects but it simply indicates the existence of *gauche* methylene groups.

#### The region $\Delta\nu=1000\text{--}1500\text{cm}^{-1}$

Spectra are illustrated in Figure 2. It can be seen that the half-width of the three bands between  $\Delta\nu=1400$  and  $1500\text{cm}^{-1}$  decreases with increasing crystallinity. Beside the well-established bands<sup>15-19</sup> at  $\Delta\nu=1063$ ,  $1131$ ,  $1170$ ,  $1296$ ,  $1370$ ,  $1418$ ,  $1440$  and  $1461\text{cm}^{-1}$  other features were observed at  $\Delta\nu=1080$ ,  $1280$  and  $1306\text{cm}^{-1}$ . Of these the band at  $\Delta\nu=1280\text{cm}^{-1}$  seems to be a feature common to all the spectra, whereas the bands at  $\Delta\nu=1080$  and  $1306\text{cm}^{-1}$  decrease in relative intensity with increasing crystallinity of sample. These last two bands have been found in the infra-red spectrum<sup>2, 7, 12, 22</sup> and have been assigned to modes of methylene groups in a *gauche* relationship to their neighbours. It is worthwhile at this stage to carefully compare the spectra of extended chain polyethylene and that of the single crystal mat (samples 6 and 5 respectively). It is known that the former is highly crystalline, thus differences in their spectra should

arise primarily from chain-folding. However, the differences appear to be very slight. In these samples it would be reasonable to expect the presence of some *gauche* methylene units which would give rise to the very weak features seen at  $\Delta\nu=1080$  and  $1306\text{cm}^{-1}$ . The extended chain specimen (sample 6) may well contain 5% of methylene groups in the *gauche* orientation in defect and amorphous regions. On the other hand, the single crystal mat, which is probably completely crystalline, must contain between 5 and 15% of *gauche* methylene groups due to the chain folds. As a corollary to this, samples 1, 2, 3, 4, and 7 must contain appreciable amounts of *gauche* oriented methylene groups from the intensity of the bands at  $\Delta\nu=1080$  and  $1306\text{cm}^{-1}$  in their spectra. Although no standards exist at present perhaps the relative intensity of these features could be used in the future to quantitatively determine the ratio of *gauche* to *trans* oriented methylene groups in polyethylene samples.

#### The region $\Delta\nu=1600$ to $1700\text{cm}^{-1}$

Weak features due to vinyl and vinylidene groups can be seen in this region for some samples; these are illus-

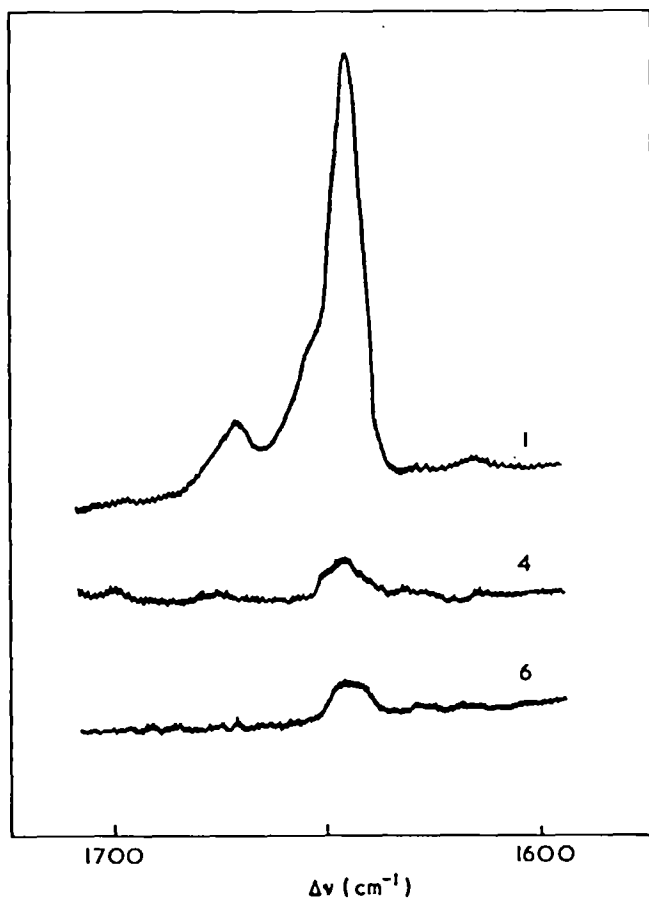


Figure 3 Raman spectra of polyethylene samples, No. 1, 4 and 6, in the region  $\Delta\nu=1600$  to  $1700\text{cm}^{-1}$ . Intensities have been normalized with respect to the band at  $\Delta\nu=1296\text{cm}^{-1}$

trated in Figure 3. Group frequency correlations exist for some substituted olefins<sup>27</sup> and these are used below.

Sample No.	Raman shift ( $\text{cm}^{-1}$ )	Group
1, 4, 5	1645	R-CH=CH <sub>2</sub>
1	1655	$\begin{array}{c} \text{R} \\ \diagdown \\ \text{C}=\text{CH}_2 \\ \diagup \\ \text{R}' \end{array}; \quad \begin{array}{c} \text{R} \\ \diagdown \\ \text{C}=\text{C} \\ \diagup \\ \text{R}' \end{array}$
1	1672	$\begin{array}{c} \text{R}' \\ \diagdown \\ \text{C}=\text{C} \\ \diagup \\ \text{H} \end{array}$

#### The C-H stretching region

Bands due to C-H stretching fundamentals and also some overtones and combinations are normally seen between  $\Delta\nu=2700$  and  $3100\text{cm}^{-1}$ . As we shall show in the second paper of this series this region is difficult to characterize in terms of correlations between fundamentals and Raman features. As a result it is not possible to explain spectral changes occurring with crystallinity. It seems, however, that the observed relative intensities of the bands at  $\Delta\nu=2848$  and  $2884\text{cm}^{-1}$  are sensitive to crystallinity.

Table 2 Raman spectrum of high density polyethylene melt. 5145 Å excitation; Spex 1401; spectral slit  $5\text{cm}^{-1}$ ; sample temperature;  $145\pm 5^\circ\text{C}$

$\Delta\nu$ ( $\text{cm}^{-1}$ )	Relative Intensity (peak heights)	Width at half height ( $\text{cm}^{-1}$ )	$\rho\rho$ (peak areas) Uncertainty $\pm 0.07$
2923	55	25	0.05
2895	62	30	0.25
2853	100	25	0.05
1445	22	35	0.78
1305	15	35	0.80
1085	6	30	0.71

#### Raman spectrum of molten polyethylene

It is worth considering the spectrum of molten polyethylene because in this state the stereoregular planar zig-zag configuration is thought not to be retained<sup>28</sup>. The Raman spectrum of molten 'low density' polyethylene has been studied some years ago by Brown<sup>16</sup>. We have examined the 'high density' polyethylene as a melt at  $145^\circ\text{C}$  and obtained very similar results. They are given in Table 2, along with the observed depolarization ratios. Part of the spectrum is shown in Figure 4, where it may be seen to show similarities to that of liquid n-cetane ( $\text{C}_{16}\text{H}_{34}$ ) at room temperature. This latter sample probably contains only molecules in a state of conformational randomness on the basis of Schaufele's study<sup>29</sup> of a large series of normal hydrocarbons. By observing the change and disappearance of the Raman active accordion mode he concluded that the amount of *trans* conformations is vanishingly small in the liquid state for normal hydrocarbons larger than n-octane.

The broadness of the peaks in the polyethylene spectrum would indicate that the methylene units are adopting a series of different orientations with respect to one another. It is interesting that there are bands centred at  $\Delta\nu=1085$  and  $1305\text{cm}^{-1}$ —frequencies that have already been associated, directly or indirectly with *gauche* methylene units<sup>25</sup> in the solid state.

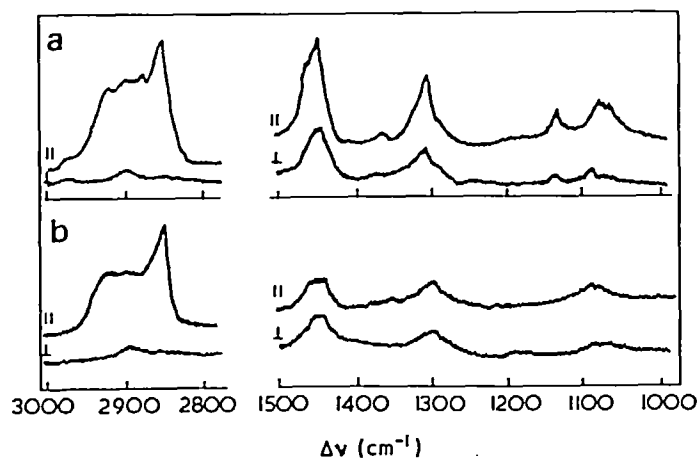


Figure 4 Raman spectra of (a) n-cetane at  $23^\circ\text{C}$  and (b) polyethylene (sample No. 4) at  $145^\circ\text{C}$ . || and  $\perp$  denote the relative polarization orientations of the excitation and analysed scattering. The intensity scale for the C-H stretching region is 2.5 times that of the remainder



Thus, to conclude, it would seem that the Raman spectra of the various polyethylenes and normal paraffin samples examined are sensitive to crystallinity and give indications of the presence, where appropriate, of vinyl and related groups and non-*trans* CH<sub>2</sub>-CH<sub>2</sub> sequences. It is possible that this technique may be developed as a quantitative method for analysing the ratio of *gauche* to *trans* dimethylene conformers in this type of specimen.

#### REFERENCES

- 1 Krimm, S., Liang, C. Y. and Sutherland, G. B. B. M. *J. Chem. Phys.* 1956, **25**, 549
- 2 Krimm, S. *Fortschr. Hochpolym. Forsch.* 1960, **2**, 51
- 3 Zbinden, R. 'Infrared Spectroscopy of High Polymers', Academic Press, New York, 1964
- 4 Nielsen, J. R. and Holland, R. F. *J. Mol. Spectrosc.* 1961, **6**, 394
- 5 Miller, R. G. J. and Willis, H. A. *J. Polym. Sci.* 1956, **19**, 485
- 6 Zachmann, H. G. and Stuart, H. A. *Makromol. Chem.* 1961, **44/46**, 622
- 7 Okada, T. and Mandelkern, L. *J. Polym. Sci. (A-2)* 1967, **5**, 239
- 8 Read, B. E. and Stein, R. S. *Macromolecules* 1968, **1**, 116
- 9 Willbourn, A. H. *J. Polym. Sci.* 1959, **34**, 569
- 10 Harvey, M. C. and Ketley, A. D. *J. Appl. Polym. Sci.* 1961, **5**, 247
- 11 Wood, D. L. and Luongo, J. P. *Mod. Plastics* 1961, **38**, 132
- 12 Koenig, J. L. and Witenhafer, D. E. *Makromol. Chem.* 1966, **99**, 193
- 13 Tasumi, M. and Krimm, S. *J. Polym. Sci. (A-2)* 1968, **6**, 995
- 14 Bank, M. I. and Krimm, S. *J. Polym. Sci. (A-2)* 1969, **7**, 1785
- 15 Nielsen, J. R. and Woollett, A. H. *J. Chem. Phys.* 1957, **26**, 1391
- 16 Brown, R. G. *J. Chem. Phys.* 1963, **38**, 221
- 17 Boerio, F. J. and Koenig, J. L. *J. Chem. Phys.* 1970, **52**, 3425
- 18 Hendra, P. J. *J. Mol. Spectrosc.* 1968, **28**, 119
- 19 Snyder, R. G. *J. Mol. Spectrosc.* 1969, **31**, 464
- 20 Cudby, M. E. A., Willis, H. A., Hendra, P. J. and Peacock, C. J. *Chem. Ind.* 1971, p 531
- 21 Gilson, T. R. and Hendra, P. J. 'Laser-Raman Spectroscopy', J. Wiley, London, 1970
- 22 Gall, M. J., Hendra, P. J., Peacock, C. J. and Watson, D. S. *Appl. Spectrosc.* 1971, **25**, 423
- 23 Gall, M. J. *Spectrochim. Acta*, 1971, in press
- 24 Carter, V. J. *J. Mol. Spectrosc.* 1970, **34**, 356
- 25 Snyder, R. G. *J. Chem. Phys.* 1967, **47**, 1316
- 26 Miller, R. L. 'High Polymers' (Ed. R. A. V. Raff and K. W. Doak), Interscience, New York, 1965, Vol XX, Part I, p 633
- 27 Bellamy, L. J. 'Advances in Infrared Group Frequencies', Methuen, London, 1968
- 28 Billmeyer, F. W. 'Textbook of Polymer Science', Interscience, New York, 1962
- 29 Schaufele, R. F. *J. Chem. Phys.* 1968, **49**, 4168

# Filler reinforcement in silicone polymers

D. K. Thomas and B. B. Moore

Materials Department, RAE Farnborough, Hampshire, UK  
(Received 21 June 1971)

Criteria have been established for identifying fillers which are potentially highly reinforcing in silicone rubber from the way in which they influence the steady-state viscosity of silicone oils. The results show that acidic fillers, such as the widely used fumed silicas, can lead to significant amounts of scission in methyl silicone oils, and it is likely that the same reaction will occur during the vulcanization of silicone rubber.

## INTRODUCTION

In order to produce rubber vulcanisates with an adequate level of mechanical properties it is often necessary to incorporate reinforcing fillers at the compounding stage. This is particularly necessary with non-crystallizing rubbers and especially so with silicone rubbers. Silicone gum vulcanisates are extremely soft and weak and if it were not for the remarkable enhancement in strength resulting from the introduction of fine silica they would be of very limited use in mechanical applications. The enhancement of mechanical properties achieved by the introduction of finely divided silica in silicone rubbers is far in excess of that observed in any other commercially available rubber. For example the ultimate tensile strength, as determined at a strain rate of 20 in/min, can be raised by a factor of about 40 by the introduction of fine silica; this compares with a factor of about 10 achieved with carbon black in a non-crystallizing rubber such as styrene-butadiene rubber, and about 1.6 with carbon black in a crystallizing rubber such as natural rubber.

Experience has shown that silica-filled silicone rubber can revert to soft, weak materials when exposed to high temperatures in confined conditions, and there is evidence<sup>1</sup> to show that this reversion is due largely to hydrolytic scission in the main chain polymer. The fine silica used for reinforcement will certainly contain considerable physically adsorbed and some chemically combined water, and the release of this water at high temperature in a confined condition will produce an environment conducive to reversion. For this reason there is a considerable incentive to finding alternative fillers for silicone rubbers which will not have the same affinity for water as the highly reinforcing fine silicas.

The prime objective of the present work was to determine whether there were some special features associated with the behaviour of fine silica which made it particularly, or uniquely, effective as a filler for silicone rubber.

In view of the difficulties associated with the dispersion of finely divided materials in solid polymers and possible complications arising during the curing process, it was decided to work with fluid polymers. Poly(dimethyl silicone) oils are available in a range of viscosities (i.e. molecular weights) and should serve as excellent model systems for the high molecular weight poly(dimethyl silicone) gum stocks which form the basis for a wide range of silicone rubbers.

## EXPERIMENTAL

### Materials

The silicone oil used throughout was a poly(dimethyl silicone) of the MS200 series having a viscosity of 30 000 cS at 25°C supplied by Midland Silicones Ltd. The fillers used, together with their known characteristics, are shown in Table 1.

Table 1 Particulate fillers used

Filler type	Name	Ultimate particle size (nm)	Surface area (m <sup>2</sup> /g)	Slurry pH
Fumed silica	Aerosil K3	10-40	175±25	4.3
	Aerosil 2491	5-20	300±30	4.3
	Aerosil 380	3-15	380±40	4.3
Precipitated silica	Hysil 233	22	140-160	7.0
	Quso G32	13	300	8.5
	Quso H40	16	200	4.0
Channel black	Royal Spectra	10	1125	2.8
	No 999	16	275	5.8
	Peerless Mk II	26	430	2.3
Furnace black	Raven R150	18	187	8.2
	Raven 40	24	102	8.2
	Conductex SC	17	200	8.2
	Statex	54	33	9.5
	Witcoblak F-4	30	80	8.2
Magnesia	Levissima	—	—	10.4

All experiments with dry silicone rubbers were done in a methyl vinyl silicone (ICI grade E302) vulcanized with 2,5-dimethyl-2,5-di-*t*-butyl peroxyhexane.

*Measurement of pH*

The pH of aqueous slurries of the fine particle fillers was measured according to ASTM D1512-60 standard test, using a pH meter equipped with glass and calomel electrodes.

*Dispersion of fillers*

Known weights of filler were mixed into known weights of oil by means of a spatula. Following introduction of the filler stirring was continued mechanically, the speed of stirring being gradually increased over a period of 3 h. The time of stirring was dictated largely by the volume fraction of filler being introduced. As a result of prolonged mechanical mixing a considerable amount of air usually became trapped within the mixture and this was removed by continuous evacuation for periods up to 8 h.

*Measurement of viscosity*

The viscosities of filler/oil mixtures were measured with a Ferranti variable shear viscometer in the temperature range from 30 to 130°C. This instrument is of the rotating cylinder type; three shear rates are available for each combination of inner and outer cylinders, corresponding to the three speeds of rotation of the outer cylinder. With any one mixture readings of viscosity were taken at 20° intervals between 30 and 130°C, the measurements being made at three shear rates at each temperature. For systems containing Aerosil K3, Hysil 233, Magnesia, and Witcoblak F-4, speeds 1, 2, and 3 of the outer cylinder corresponded to shear rates of 0.78, 3.28, and 9.1 sec<sup>-1</sup> respectively, whilst for all other systems the values were 0.31, 1.29, and 3.59 sec<sup>-1</sup>.

*Compounding of dry rubbers*

Rubber, filler, and vulcanizing agent were mixed on a 6 × 2 in laboratory roll mill. Vulcanization of thin sheets for mechanical testing was carried out under pressure for 1 h at 160°C. The sheets were not post-cured.

*Mechanical testing of rubbers*

Two types of mechanical test were carried out on filled vulcanisates; first the normal test to failure in uniaxial tension at a strain rate of 20 in/min and second a stepwise loading experiment giving an equilibrium, or near equilibrium stress-strain curve. In both cases tests were carried out at room temperature.

*Recovery of oils*

In certain cases where there were indications of chemical reaction between particulate filler and oil it was deemed necessary to recover the oil from the mixture for further study. To facilitate separation, benzene or toluene was added to the mixture; this dissolved in the methyl silicone oil and reduced the viscosity of the suspension sufficiently for centrifuging out the filler.

Each mixture was centrifuged until a clear liquid layer was obtained. This could take a few hours in the case of

coarse fillers, or a few days with the finer fillers. With the finest fillers a complete separation was impossible.

The benzene or toluene was removed from the clear liquid layer by distillation, the last traces being taken off under reduced pressure.

RESULTS AND DISCUSSION

*Viscosity-concentration relations*

All the fillers used in this work showed a much greater influence on the viscosity of silicone oil than would be predicted on the basis of the Einstein hydrodynamic law<sup>2</sup> (see Figure 1). Even at low volume fractions of filler, i.e.  $V_f < 0.03$ , departures are large, sometimes extremely large. The simplest explanation for this behaviour would be that the effective volume fraction ( $V_{f(ett)}$ ) is much larger than the nominal value ( $V_{f(nom)}$ ) because of association of filler particles with the silicone oil and/or aggregation of filler particles to give network-like structures. The oil-filler associates or filler aggregates then behave according to the Einstein law at low concentrations.

In hydrodynamic terms, the increased viscosity of a suspension is due to the perturbation of flow of the dispersion medium around the suspended particles, and current theories of intrinsic viscosity assume that in dilute suspensions the total effect is equal to the sum of the effects caused by individual particles. Applying these ideas to the results of the present work it is possible to calculate the effective 'hydrodynamic' volume at low concentration by substituting values for specific viscosity in the equation

$$\eta_{sp} = 2.5 V_{f(ett)} \tag{1}$$

In systems containing highly reinforcing fillers it is found that the values calculated for  $V_{f(ett)}$  are extremely high, even in the limit of infinite dilution. Typically, with fumed silica (Aerosil K3) the limiting value for the ratio  $V_{f(ett)}/V_{f(nom)}$  at 130°C is 80; it rises rapidly with increasing concentration, reaching a value of 130 at  $V_{f(nom)} = 0.01$  and shear rate 3.59 sec<sup>-1</sup>. These results show that the simple view of isolated, and essentially

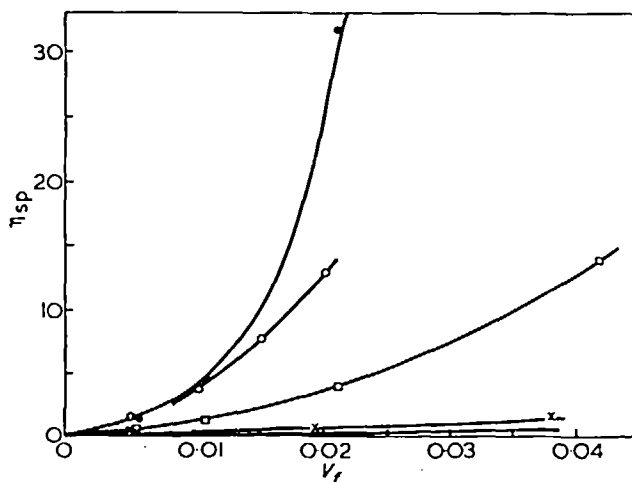


Figure 1 Viscosity at 30°C, shear rate 1. ● Royal spectra; ○, Aerosil K3; □, Conductex; ×, Hysil 233; —, Einstein for rigid spheres

spherically symmetrical oil-filler associates cannot be sustained even at high dilution. At  $V_{f(\text{nom})}=0.01$  a value of 130 for the ratio  $V_{f(\text{eff})}/V_{f(\text{nom})}$  means that the oil-filler particles occupy a volume greater than that of the whole system of filler+oil. It would seem necessary, therefore, to accept that even at the lowest concentrations, network-like aggregates of filler, rather than isolated particles, must be involved.

The variation of specific viscosity with concentration in these filled systems is interesting because of its similarity to that shown by polymer/low molecular weight solvent systems. A Huggins type equation<sup>3</sup> is found to describe the variation of specific viscosity with volume concentration over the whole range covered, and it is only in those systems where a chemical reaction between filler and oil is thought to occur that this relation breaks down. It is interesting to pursue the analogy with polymer-solvent systems. For polymers in solution the Huggins equation is:

$$\frac{\eta_{sp}}{c} = [\eta] + \frac{1}{2}k[\eta]^2c \quad (2)$$

where  $\eta_{sp}$  is the specific viscosity,  $[\eta]$  the limiting viscosity number,  $c$  the concentration of solute in g/100 ml of solvent, and  $k$  the Huggins constant. For polymers the quantity  $[\eta]$  is related to molecular weight, i.e. molecular size, at infinite dilution, and the constant  $k$  is thought to be related more to molecular shape than size.

The relation found to apply to the filler-silicone oil systems is:

$$\frac{\eta_{sp}}{V_f} = \alpha + \frac{1}{2}k'\alpha^2V_f \quad (3)$$

where  $V_f$  is the volume fraction of filler in the mixture and  $\alpha$  and  $k'$  are constants for a given filler under conditions of constant temperature and shear rate. The closeness with which this relation is followed is shown by the results in Figure 2 for carbon black (Conductex SC) in 30 000 cS silicone oil. By analogy with equation (2)  $\alpha$  will be related to the size of the solvated filler aggregate at infinite dilution, and  $k'$  will be determined primarily by its shape. Values of  $\alpha$  and  $k'$  obtained for the various fillers at the maximum and minimum temperatures and shear rates are shown in Table 2. The calculated values for

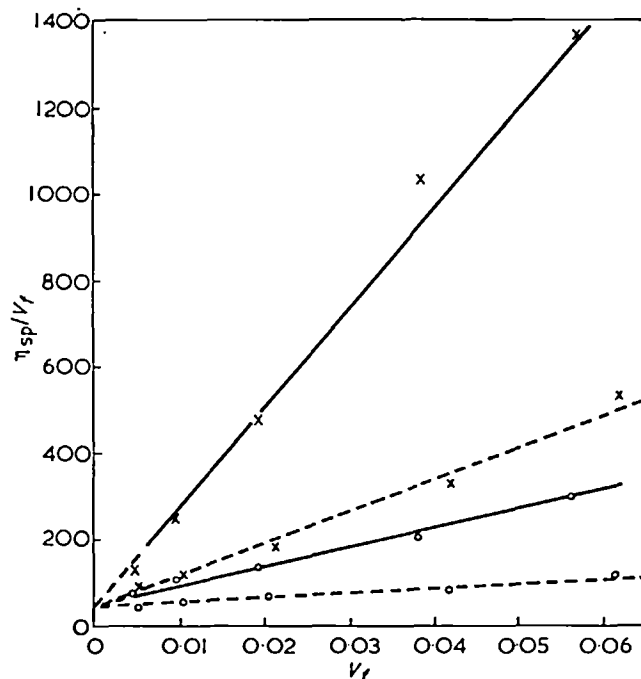


Figure 2 Conductex furnace black in 30 000 cS oil. x, speed 1; o, speed 3; —, 130°C; ----, 30°C

$\alpha$  show two interesting features: (a) the values for fumed silicas are very much higher than those for any other filler (compare Aerosil K3 and 2491 with the others); and (b) the values for fumed silicas are sensitive to changes in temperature within the range studied, whereas those for all other fillers are not. From the point of view of establishing a simple practical criterion for the identification of potentially reinforcing fillers for silicone rubber the abnormally high  $\alpha$ -values and characteristic effect of temperature on  $\alpha$ -value in fumed silicas is encouraging. It would appear that a fine particle filler possessing a high  $\alpha$ -value (say  $>100$ ) which increases with temperature will be highly reinforcing in silicone rubber vulcanisates.

Table 2 Values of  $\alpha$  and  $k'$  derived from the Huggins equation

Filler	$\alpha$ -value				$k'$ value			
	30°C		130°C		30°C		130°C	
	0.78 sec <sup>-1</sup>	9.1 sec <sup>-1</sup>	0.78 sec <sup>-1</sup>	9.1 sec <sup>-1</sup>	0.78 sec <sup>-1</sup>	9.1 sec <sup>-1</sup>	0.78 sec <sup>-1</sup>	9.1 sec <sup>-1</sup>
Aerosil K3	120	120	190	190	0.52	0.10	0.51	0.10
Hysil 233	39	39	39	39	0.02	0.02	0.14	0.06
Magnesia	45	45	45	45	0.52	0.11	1.62	0.18
Witcoblak F-4	40	40	40	40	1.10	0.15	3.8	0.66
	30°C		130°C		30°C		130°C	
	0.31 sec <sup>-1</sup>	3.59 sec <sup>-1</sup>	0.31 sec <sup>-1</sup>	3.59 sec <sup>-1</sup>	0.31 sec <sup>-1</sup>	3.59 sec <sup>-1</sup>	0.31 sec <sup>-1</sup>	3.59 sec <sup>-1</sup>
Statex	50	50	50	50	1.2	0.07	6.4	0.90
Conductex SC	40	40	40	40	2.3	0.35	7.3	1.41
Quso G32	20	20	20	20	2.5	2.5	2.5	2.5
Raven R150	8	8	8	8	27.7	8.6	83.0	15.6
Aerosil 2491	300	300	380	380	0.11	0.003	0.31	0.31

Pursuing the analogy between  $\alpha$  in filler-oil and  $[\eta]$  in polymer-solvent systems leads to the view that very large  $\alpha$ -values are associated with a large effective volume of filler in suspension in the oil. It is known that fine fumed silicas aggregate in the dry state, and the very large effective volumes observed at low concentration in silicone oil could result from aggregation to rather open network-type structures. These aggregates because of their large effective surface area and three-dimensional structure will immobilize large volumes of oil by association and trapping. At relatively low nominal concentration these large asymmetric solvated structures will interact and something akin to a continuous swollen network, i.e. gel, structure could be formed. The observed increase in  $\alpha$  with temperature for the fumed silicas is consistent with this view.

Fillers other than fumed silicas, i.e. precipitated silicas, carbon blacks, and magnesia, have relatively low and sometimes very low  $\alpha$ -values, the highest value observed being about 40% of that shown by a fumed silica (Aerosil K3). Undoubtedly these fillers aggregate and become associated with oil, but their failure to give large  $\alpha$ -values could be attributed to an inability to aggregate to network-type structures.

From the  $k'$  values at a given shear rate and temperature in Table 2 two kinds of behaviour can be distinguished. For example, at 30°C and low shear rate (0.31–0.78 sec<sup>-1</sup>) there is a group consisting of the two fumed silicas and the coarse precipitated silica (Hysil 233) which show  $k'$  values significantly below 1.0, and a group containing a fine precipitated silica (Quso G32) and all the carbon blacks which have  $k'$  values significantly greater than 1.0. In polymer-solvent systems at a given level of molecular weight  $k$  is known to decrease with branching in the polymer, i.e.  $k$  decreases as the molecule becomes more compact or symmetrical. Values of  $k'$  in the range 1.1 to 27.7 observed for fine carbon blacks at 30°C must represent a very high degree of asymmetry in the aggregates, since values of  $k$  for polymers in solution are of the order of 0.3.

It has been proposed that one criterion for reinforcement should be that  $\alpha$  exceeds 100. It does not follow that all highly reinforcing fillers necessarily have high  $\alpha$ -values. Perhaps a high  $k'$  value, i.e.  $k' > 1.0$ , although coupled with only a moderate  $\alpha$ -value, could also serve as a criterion for reinforcement. To test this hypothesis fillers having high  $\alpha$ -low  $k'$  and low  $\alpha$ -high  $k'$  were compounded by conventional techniques with a commercial methyl vinyl silicone gum stock. The vulcanisates were tested at a strain rate of 20 in/min in uniaxial tension at room temperature and the results are shown in Table 3.

The highly reinforcing effect of Quso G32 and Conductex SC makes it clear that a high  $k'$  value (i.e.  $k' > 1.2$

Table 3 Mechanical tests on filled silicone rubbers at room temperature

Filler	Wt.% of filler	Ultimate tensile strength (lbf/in <sup>2</sup> )	100% modulus (lbf/in <sup>2</sup> )	Ultimate strain (%)
Aerosil K3	40	817	191	480
Quso G32	30	752	229	285
Witcoblak F-4	30	433	80	—
Conductex SC	40	867	146	328
Magnesia	40	352	77	474

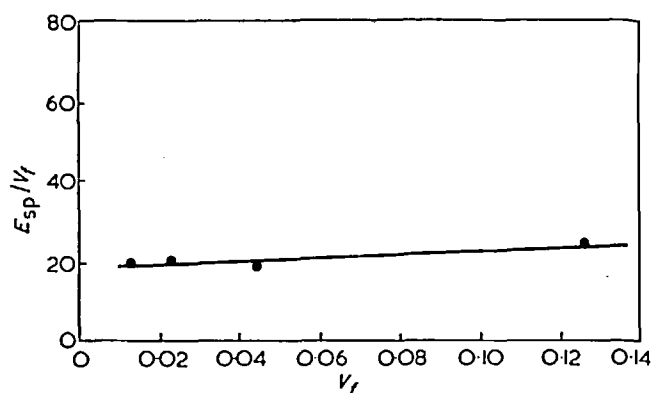


Figure 3 Aerosil K3 in methyl vinyl silicone rubber

Table 4 Variation of  $\log \eta$  with  $1/T$  for filled silicone oil

Group (i)	Group (ii)	Group (iii)
Magnesia	Aerosil K3	Conductex SC
Witcoblak F-4	Aerosil 380	Statex
Hysil 233	Aerosil 2491	Raven R150
Quso G32	Quso H40	Raven 40
	Royal Spectra	
	999 Channel	
	Peerless Mk II	

at 30°C and shear rate 0.31 sec<sup>-1</sup>) can serve as a criterion for reinforcement, even though associated with a relatively low  $\alpha$ -value. It is interesting to note that Conductex SC carbon black is used where high electrical conductivity is required and it is, therefore, a filler which might be expected to form highly asymmetric aggregates.

The ability of a Huggins type equation to describe the dependence of specific viscosity on volume concentration has been demonstrated for a wide variety of fillers in silicone oil. The same analysis has been extended to a fine fumed silica (Aerosil K3) in a silicone rubber vulcanisate up to a filler loading of 25 parts by weight, and it can be seen that the same equation applies (see Figure 3). Values of tensile modulus ( $E$ ) used in this instance were equilibrium values obtained from stepwise loading tests, and this was done in order to be consistent with the viscosity measurements which were always made under steady-state conditions.

#### Effect of temperature on viscosity

Increasing temperature in the range from 30 to 130°C produces a decrease in the viscosity of filler-oil systems. However, the form of variation depends upon filler type. Three kinds of behaviour were observed: (i)  $\log \eta$  vs.  $1/T$  is linear, the slope is independent of filler loading and is the same as that for pure oil; (ii) slope of  $\log \eta$  vs.  $1/T$  is dependent on filler concentration and is greater than that for pure oil; departures from linearity often occur at temperatures above 100°C; (iii)  $\log \eta$  vs.  $1/T$  is strictly linear over the whole temperature range, the slope depends on filler loading and is less than that for pure oil. All the fillers studied can be placed in one or other of these categories (see Table 4), and typical examples are shown in Figure 4.

The behaviour of materials in group (i) is what would be expected from steady-state viscosity measurements on solvated aggregates under conditions where there is little or no interaction between individual aggregates. The fillers in group (ii) are those which give low slurry pH values (see *Table 1*), and the fall off in viscosity at high temperature, in some cases to values below that for pure oil, is attributed to scission of the siloxane chain in an acidic environment. Confirmation of the occurrence of main chain scission in the oil was obtained by recovering the oil from certain filler-oil mixtures by a centrifuging technique. The results of measurements on recovered oils are shown in *Table 5*. An identical treatment produced no change in the viscosity of pure oil.

In no case was it thought that all the fine particles had been removed, but even so substantial falls were observed in the viscosity of the recovered oil. This scission of dimethyl silicone oil, induced by heating to a temperature of 130°C in the presence of an acidic filler, has important implications for the processing of dry silicone rubbers. These rubbers are usually compounded with high loadings of fumed silica and vulcanized by heating with an organic peroxide in the temperature range from 130 to 160°C. Since the chemical structure of silicone rubber is similar to that of the oil used in this work there seems no reason to doubt the occurrence of main chain scission during vulcanization. This could account, in fact, for the much improved resistance to heat ageing of silicone rubbers when compounded with fumed silicas, since chain scission would offset the effect of oxidative crosslinking

*Table 5* Viscosity measurements on recovered silicone oil

Filler	Concentration	Viscosity of oil at 30°C and 3.58 sec <sup>-1</sup>		
		Original value (P)	Recovered oil (P)	% decrease
Peerless Mk II Carbon	2% by wt.	244	147	39
Royal Spectra Carbon	4% by wt.	244	182	25
Aerosil 2491 Silica	4% by wt.	244	205	16

which normally occurs in methyl silicone vulcanisates. Chain scission during vulcanization could also account for the relatively disappointing performance of Aerosil-filled silicone rubber in long term room temperature compression set tests. It is significant that Hysil 233 (a neutral filler which does not degrade silicone oil) when incorporated in silicone rubber gives a vulcanisate with superior room temperature set properties.

Fillers in group (iii), i.e. those showing a lower temperature dependence of viscosity than pure oil, offer interesting possibilities for the reinforcement of silicone rubbers in that they may give vulcanisates in which certain important properties, such as tensile or shear modulus and tear strength, may be less sensitive to temperature than is the case with current silica-filled materials.

#### *Effect of shear rate on viscosity*

An increase of shear rate always leads to a decrease in the steady-state viscosity of filler-oil systems, the magnitude of the change depending on the temperature and filler type. The effects of shear rate are least at 30°C and greatest at 130°C, and this is consistent with the view that one is dealing, as in the case of polymer-solvent systems and dilute suspensions, with a dispersed phase which is asymmetric and whose disposition will be determined by the relative effects of Brownian motion and shear orientation. At low temperatures asymmetric aggregates will be highly oriented in the direction of the shearing force even at the lowest shear rates and the steady-state viscosity will therefore be fairly insensitive to an increase in shear rate. At high temperatures aggregates will have greater thermal energy and will take up a more random orientation. In these circumstances an increase in shear rate could have a large effect on the observed viscosity. It is only in the case of spherically symmetrical aggregates or particles that steady-state viscosity will be completely independent of shear rate. The closest approach to this type of behaviour in the present work is shown by Hysil 233. The data in *Table 6* show the effect of limited changes in shear rate on the viscosities observed at a single concentration and over a range of temperature with a number of different fillers. These results are typical of those obtained over the whole concentration range with these fillers.

#### CONCLUSIONS

The effect of a wide variety of fine particle fillers on the viscosity of dimethyl silicone oil can be described by a

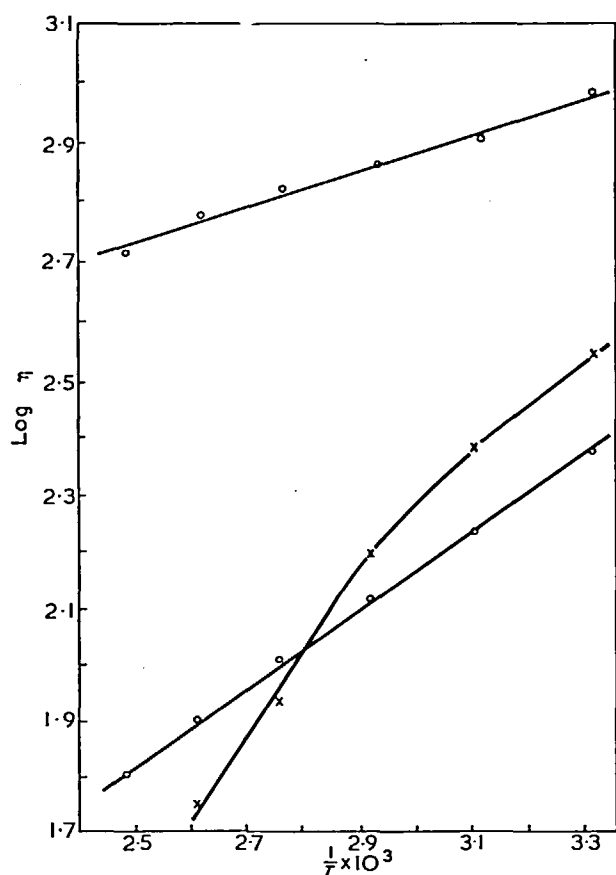


*Figure 4* Viscosities measured at a shear rate of 3.587 sec<sup>-1</sup>. ●, Pure oil; ×, 1% Peerless Mk II; ○, 8% Conductex SC

Table 6 Effect of shear rate on viscosity ( $P$ ) at a filler loading of 2% by weight

Shear rate (sec <sup>-1</sup> )	Filler type	T (°C)					
		30	50	70	90	110	130
0.31	Aerosil 2491	1962	1623	1365	1160	999	874
1.29		1211	937	756	619	524	445
3.59		966	730	575	402	388	322
0.31	Quso G32	384	294	223	169	134	107
1.29		372	269	202	154	120	94
3.59		362	261	196	150	116	90
0.31	Conductex SC	535	392	330	312	268	232
1.29		430	322	258	215	180	150
3.59		379	286	224	181	150	124
0.78	Hysil 233	384	256	192	144	112	80
3.28		348	243	177	139	112	88
9.1		330	235	179	140	108	89

Huggins type equation. This allows each filler, at a given temperature and shear rate, to be characterized by the quantities  $\alpha$  and  $k'$  in the equation:

$$\frac{\eta_{sp}}{V_f} = \alpha + \frac{1}{2}k'\alpha^2V_f$$

The initial aim of this work, which was to establish a simple and quick method for screening potentially reinforcing fillers for silicone rubber, has been achieved in that reinforcement seems to be associated with a high value for  $\alpha$  and/or a high value for  $k'$ . The criteria which could be laid down on the evidence of the present work are that a filler having an  $\alpha$ -value in excess of 100, and/or a  $k'$  value in excess of 1.2 as measured at 30°C and shear rate 0.31 sec<sup>-1</sup>, is potentially highly reinforcing in silicone rubber.

An important fact which emerges from this work is that acidic fillers such as fumed silicas and channel blacks will cause appreciable chain scission when heated to 130°C in silicone oil. This must also occur in dry rubbers and should be borne in mind when selecting fillers for use in silicone rubber which is vulcanized, post cured, and often used, at temperatures far in excess of 130°C. The ability of certain fillers such as Conductex Sc and Statex, to give rise to systems in which the viscosity is less sensitive to temperature than the pure oil is also interesting. If this is carried over to the dry rubber it will lead to vulcanisates in which some important mechanical properties are less variable with temperature than is the case with current silica filled materials.

The mechanism of filler reinforcement in rubbers is still a contentious matter, but the results presented for

silicone polymers fit into a fairly simple physical picture based on aggregation of filler and immobilization of polymer by association and trapping. The close similarity which exists between the behaviour of fine particle fillers in silicone oil and that of polymers in low molecular weight solvents in respect of the dependence of specific viscosity on concentration, and the effect of shear rate and temperature on viscosity, coupled with the fact that all fillers studied, whether acidic, neutral, or basic, show the same form of behaviour in silicone oil, makes it seem unnecessary to invoke any degree of chemical bonding between silica filler and silicone rubber in order to account for the reinforcement observed in these systems.

A consistent explanation for the effect of finely divided fillers on silicone polymers would seem to be given in terms of aggregation of filler particles, immobilization of polymer by association with filler and trapping within the network-like aggregate to give a large effective volume, and the formation of extremely asymmetric aggregates, again giving a large effective volume fraction. In all of this the interactions would be of a secondary nature and would be influenced by temperature and shear stress. In other words much of what we regard as reinforcement in silicone rubbers will be time dependent, and apart from the obvious effect on equilibrium modulus the benefits of fillers will be seen primarily in the dynamic applications of rubber. It is interesting to note that the high tensile strength observed in Aerosil-filled silicone rubber when tested at a strain rate of 20 in/min is largely lost if the test is carried out at a very slow rate. In order to achieve an effectively very low strain rate a silicone rubber containing 20 parts of Aerosil K3 was strained at a rate of 0.25 in/min at 100°C. Under these conditions the rubber had an ultimate tensile strength of 160 lbf/in<sup>2</sup> and a breaking strain of 240%, a gum vulcanisate tested under the same conditions gave an ultimate tensile strength of 125 lbf/in<sup>2</sup> and breaking strain of 190%.

#### ACKNOWLEDGEMENTS

Crown Copyright and published by permission of the Controller, HMSO.

#### REFERENCES

- 1 Thomas, D. K. *Polymer* 1966, 7, 99
- 2 Einstein, A. *Annln. Phys.* 1906, 19, 289
- 3 Huggins, M. L. *J. Am. Chem. Soc.* 1942, 64, 2716

# An etch method for microscopy of rubber-toughened plastics

C. B. Bucknall, I. C. Drinkwater and Wendy E. Keast

*Department of Materials, Cranfield Institute of Technology,  
Cranfield, Bedford, UK  
(Received 7 July 1971; revised 18 August 1971)*

Microtomed blocks of acrylonitrile-butadiene-styrene (ABS), high-impact polystyrene (HIPS), and high-impact poly(2,6-dimethyl-1,4-phenylene oxide) (PPO) were etched with a mixture of chromic and phosphoric acids, and examined in optical and scanning-electron microscopes. Replicas of the etched surfaces were examined by electron microscopy. These techniques reveal details of orientation in injection mouldings, of internal structure in composite rubber particles, and of crazing and shear band formation. The etch method avoids the specimen distortion inherent in sectioning.

## INTRODUCTION

Etch methods have received comparatively little attention from microscopists working on rubber-toughened plastics. There are two previous publications on the subject: Spit<sup>1</sup> demonstrated the composite nature of the rubber particles in HIPS (high-impact polystyrene) by means of gas discharge etching; and Keskkula and Traylor<sup>2</sup> obtained improved electron micrographs of the same features with the aid of isopropanol etching. Most laboratories have preferred to concentrate upon sectioning techniques, and Kato's method<sup>3-6</sup> of osmium staining the rubber particles prior to ultra-sectioning has become a standard procedure for electron microscope studies of structure. Both Kato's method and Traylor's method<sup>7</sup> for preparing optical micrographs gave excellent results.

However, sectioning methods suffer from one major disadvantage: the sections are distorted by the knife during the sectioning operation. This distortion can be tolerated in studies of particle size and structure, but presents serious difficulties in studies of orientation, which require accurate information about particle shape. Evans *et al.*<sup>8</sup> working on hot-drawn HIPS, found that both isopropanol etching of microtomed surfaces and fractography avoid the problem of distortion, and selected the isopropanol method because particle shapes could not be distinguished on fractographs when the draw ratio was greater than two. The isopropanol etch gives unsatisfactory results at high draw ratios, but has a much greater range than fractography.

The chromic acid etch method described in the present paper was developed in order to overcome the difficulties experienced with isopropanol etching at high draw ratios. The acid solution oxidizes the rubber particles in the surface preferentially, leaving the plastics matrix relatively unaffected. The etch is equally effective at all draw ratios, since it distinguishes regions with different chemical

resistance, unlike isopropanol, which is a differential swelling agent.

## METHOD

Specimens were trimmed to shape, and sectioned in an ultramicrotome equipped with a glass knife, to produce a perfectly flat surface for examination. The microtomed blocks were then immersed for periods between 15 sec and 3 min in a bath containing 400 ml of H<sub>2</sub>SO<sub>4</sub>, 130 ml of H<sub>3</sub>PO<sub>4</sub>, 125 ml of H<sub>2</sub>O, and 20 g of CrO<sub>3</sub>, at a temperature of 70°C.

After washing and drying, specimens were examined directly under a metallurgical microscope. Specimens for scanning electron microscopy were coated with a thin layer of platinum/gold in order to eliminate charging, and examined directly. Specimens for electron microscopy were prepared by a two-stage replica process: the etched surface was given four coats of a 5% aqueous solution of poly(vinyl alcohol) (PVA); the PVA replica formed in this way was allowed to dry thoroughly, stripped, coated with a thin layer of carbon, and shadowed with platinum; finally, the PVA layer was dissolved away in distilled water, and the carbon replica produced was submitted to electron microscopy.

Attempts to improve upon the results by altering the concentrations of the ingredients of the etch were unsuccessful. Unwanted changes in composition occur over a period of about a week, probably owing to uptake of water from the atmosphere, and it was found necessary to prepare fresh etch solution each week, especially for use with acrylonitrile-butadiene-styrene (ABS).

Control of etch conditions, including both etching time and etch composition, is more important for ABS than for HIPS, because the matrix of ABS is more easily attacked by the oxidizing acid solution. Specimens of HIPS give good results even with stale etch, or with etching times of an hour or more.



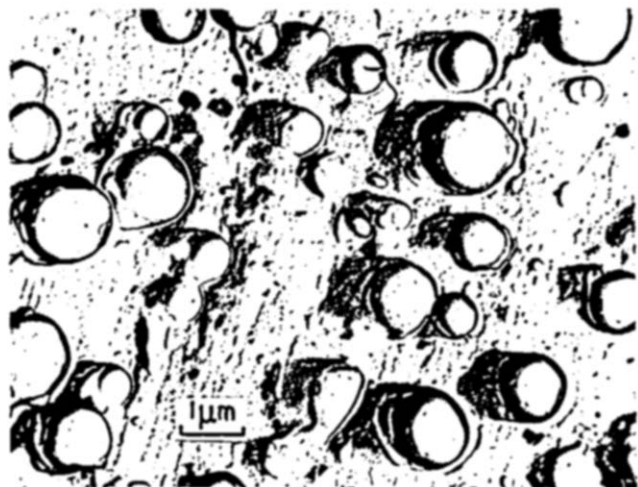


Figure 1 Compression-moulded ABS polymer: 20 second etch. Electron micrograph of replica. ( $\times 8300$ )

## RESULTS

The etch method has proved successful for studying both morphology and deformation mechanisms in rubber-toughened plastics. Representative results are shown in Figures 1-5.

### Morphology

Figure 1 is an electron micrograph of a compression-moulded sheet of ABS. The replica shows that the material contains a moderate concentration of spherical rubber particles up to  $1.5\ \mu\text{m}$  in diameter, which are preferentially attacked by the etch. The shape of the particles indicates that the sheet is isotropic in the plane of the etched surface. The large particle size and moderate rubber concentration suggest that the polymer was made by a mass or suspension process, rather than the emulsion process used more generally for ABS. Etching of emulsion-grade ABS produces a large number of inter-connected etched channels running deep into the surface; this type of etched surface does not replicate satisfactorily, but does provide an ideal base for electroplating<sup>9, 10</sup>.

The sub-inclusions within the rubber particles of HIPS, ABS, and related plastics have the same composition as the matrix, and are therefore resistant to the etch. The consequences of this resistance are illustrated in Figure 2a, which is a scanning electron micrograph of a lightly-etched specimen of HIPS. Near the original microtomed surface, the rubber component of the particles has been removed by the acid, leaving the polystyrene sub-inclusions proud. An unetched region of the composite rubber particle lies beneath the sub-inclusions visible in the micrograph.

Figure 2b shows a replica of a similar specimen. During the first stage of replication, polystyrene sub-inclusions became attached to the PVA, and were subsequently encapsulated by the carbon layer. Consequently, they were retained on the carbon throughout the water wash, and appeared in the electron microscope as electron-dense spheres. The shape and size distribution of the sub-inclusions is well illustrated in this photograph.

Figure 3 illustrates the use of etching in the study of orientation in rubber toughened plastics. The specimen

is an injection-moulded bar of HIPS, sectioned parallel to the flow direction and normal to the moulded surface. The pattern of orientation is readily observable, although the rubber particles in the microtomed surface were barely discernable under the optical microscope before the specimen was etched. Figure 3a shows that the rubber particles are highly oriented near the mould surface, where the HIPS is cooled rapidly in contact with the cold mould, and become progressively more spherical away from the mould surface, where the rate of cooling is much lower. These effects are well known; the advantage of the etch technique is that it offers a quick and reliable method for observing orientation, and one that could be adopted for routine quality control.

Below the surface region shown in Figure 3a is the zone illustrated in Figure 3b, in which the rubber particles are aligned in long strings lying parallel to the flow direction. Zones of this type, which were first observed by Kato<sup>11</sup> in ABS, appear to be formed in regions of high shear rate during moulding. Shear rates are lower nearer the mould surface because of cooling effects<sup>12</sup>.

Many rubber-toughened plastics are unsuitable for optical microscopy because the rubber particle size is below the limit of resolution. Even in these cases, however, an examination under the optical microscope is

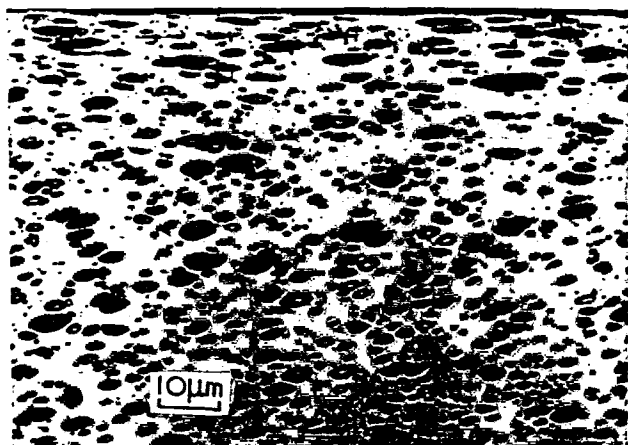


a

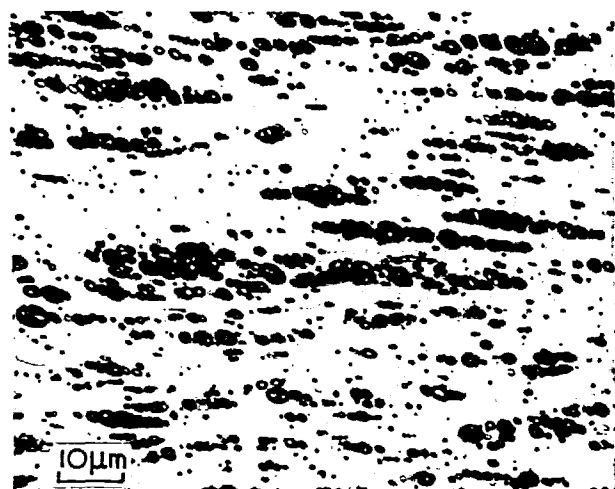


b

Figure 2 Internal structure of composite rubber particles in HIPS: 30 second etch. (a) Scanning electron micrograph showing polystyrene sub-inclusions ( $\times 20\ 500$ ); (b) electron micrograph of polystyrene sub-inclusions adhering to replica ( $\times 16\ 700$ )



a



b

Figure 3 Injection-moulded HIPS bar, sectioned normal to moulded surface and parallel to flow direction: 1 minute etch. (a) Oriented surface layer; (b) zone of maximum shear rate. Optical micrographs ( $\times 830$ )

often useful as a screening test, in selecting specimens for replication or scanning electron microscopy. Etched specimens are unsuitable for oil-immersion techniques, but ordinary objectives give good results at high magnifications, as the specimens are flat, and free from the problems of wrinkling and depth of focus encountered with sections.

Apart from the difficulty of observing small particles, the main problem in optical microscopy of etched specimens arises with pigmented materials. Pigment particles cause excessive scattering of light, resulting in loss of contrast in the final image. This can be improved if viewed by polarized light. However, results are still not as successful as for unpigmented materials and photography is difficult.

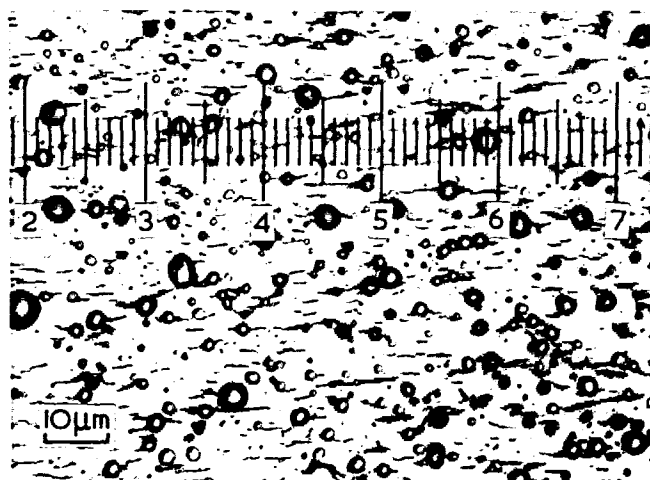
#### Deformation mechanisms

Research continues into the deformation mechanisms responsible for rubber-toughening. Bucknall and Smith<sup>13</sup> concluded from an optical microscope study that crazing is the dominant mechanism of toughening in HIPS and related polymers, and their conclusions are supported by later observations<sup>6, 14</sup>. More recently, McGarry and co-workers<sup>15</sup> have shown that shear bands also contribute

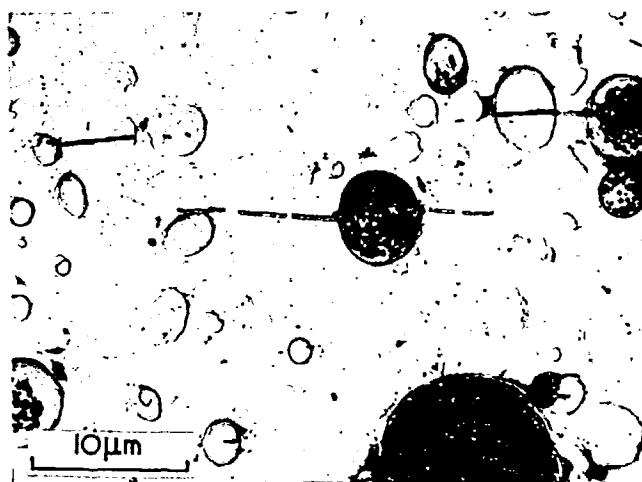
to toughening in certain rubber-toughened plastics. Sharply-bounded shear bands have been observed in a range of glassy polymers, usually as a result of compression<sup>16-19</sup>. McGarry's work suggests that toughness is enhanced by the interaction of crazes and shear bands, and underlines the importance of developing adequate microscopy techniques for studying the interaction.

The resistance of the matrix polymer to etching is lowered within both crazes and shear bands. This can be seen in high-impact PPO (a solution-mixed blend of HIPS and poly(2,6-dimethyl-1,4-phenylene oxide) (PPO)). Figure 4a is an optical micrograph of this material crazed in uniaxial tension; the size and distribution of the crazes are clearly observable. Figure 4b is an electron micrograph of a similar area in HIPS. The crazes in both specimens lie normal to the applied stress, and approximately equatorial to the rubber particles. Figure 4b shows sub-inclusions picked up from incompletely-etched rubber particles, as in Figure 2b. One of the larger rubber particles was completely etched, and it can be seen that the associated craze is in contact with the particle at all points on the equator.

Comparable observations of shear bands are shown in Figure 5. The specimen is a compression-moulded bar of high-impact PPO, which was subjected to plane-strain



a



b

Figure 4 Crazes formed under uniaxial tension (vertical direction). (a) Optical micrograph of high-impact PPO specimen: 1 minute etch ( $\times 830$ ); (b) electron micrograph of replica of HIPS specimen: 30 second etch ( $\times 3333$ )

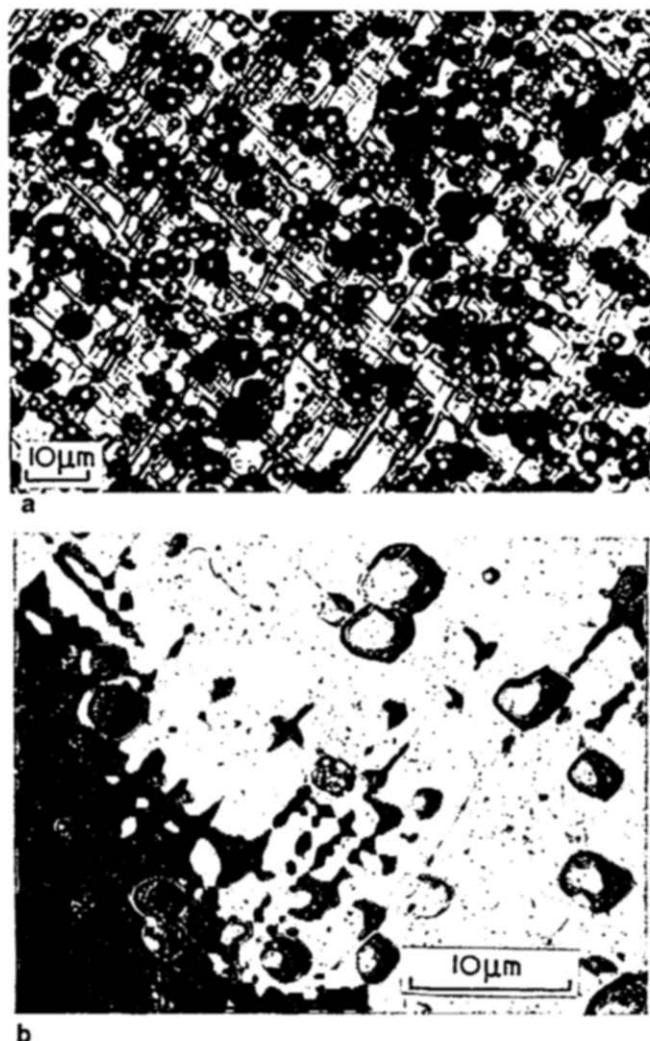


Figure 5 Shear bands in high-impact PPO (compression direction vertical). (a) Optical micrograph: 10 minute etch ( $\times 830$ ); (b) electron micrograph of replica: 1 minute etch ( $\times 3333$ )

compression, and sectioned normal to the direction of zero strain. Both the optical and electron micrographs show two sets of parallel shear bands, each at a little less than  $45^\circ$  to the compression axis. This study appears to be the first in which microscopic shear bands have been observed in rubber-toughened plastics. An additional feature shown in the electron micrograph is the distortion of the rubber particles from their original spherical shape. The distorted particles emphasize the inhomogeneity of the strain, and provide some indication of its magnitude within the shear bands.

#### EVALUATION OF ETCH METHOD

The availability of both etching and sectioning techniques presents the microscopist with a choice. The two methods are complementary: there are certain problems in which sectioning gives better results than etching, and *vice versa*, and there is a considerable area of overlap. The advantages of the etch technique are as follows: (a) knife distortion and damage of the type observed on sections is eliminated, so that the method can be applied to studies of particle shape and orientation, and to measurement of the size and distribution of crazes and shear bands; (b) the operations of microtoming and etching

are straightforward, and can be completed in a few minutes; (c) highly oriented specimens present no particular problems; (d) specimens can be examined by optical, electron, and scanning electron microscopy, using standard procedures; (e) particle shapes and deformation mechanisms can be studied over a comparatively wide area in a short time, using optical or scanning-electron microscopy; and (f) specimens are flat enough to permit optical microscopy at high magnifications. The disadvantages of the technique are: (i) optical microscopy, and photomicrography in particular, are difficult with pigmented specimens because scattered light reduces contrast; (ii) replica methods give poor results with ABS emulsion polymers because the etch produces interconnected channels below the surface; (iii) care is necessary in peeling PVA replicas from etched ABS surfaces, in order to avoid distortion caused by interfacial adhesion (the problem does not arise with HIPS); (iv) etching destroys the internal structures of crazes, shear bands, and rubber particles, which are better studied in ultrathin sections, although additional information about composite rubber particles can be obtained using the etch method.

Some of the disadvantages listed, especially the problem of adhesion between PVA and etched ABS, could probably be overcome by using a different etch solution. There is a need for a range of etch solutions, each matched to a particular rubber-modified polymer. For particle shapes studies, the requirement is that the etch should degrade the rubber destructively, without degrading or activating the plastics matrix; for studies of crazes and shear bands, on the other hand, a limited amount of reaction between the etch and the matrix polymer is probably necessary.

#### ACKNOWLEDGEMENTS

The authors thank the Science Research Council and the General Electric Company for grants in support of this work, and Mr A. A. Chambers for experimental assistance with the scanning electron microscopy.

#### REFERENCES

- 1 Spit, B. J. *Polymer* 1963, 4, 109
- 2 Keskkula, H. and Traylor, P. A. *J. Appl. Polym. Sci.* 1967, 11, 2361
- 3 Kato, K. *J. Electron Microsc.* 1965, 14, 220
- 4 Kato, K. *Polym. Eng. Sci.* 1967, 7, 38
- 5 Kato, K. *Kolloid-Z. Z. Polym.* 1967, 220, 24
- 6 Matsuo, M. *Polym. Eng. Sci.* 1967, 7, 38
- 7 Traylor, P. A. *Anal. Chem.* 1961, 33, 1629
- 8 Evans, L. J., Bucknall, C. B. and Hall, M. M. *Plastics and Polymers* 1971, 39, 118
- 9 Atkinson, E. B., Brooks, P. R., Lewis, T. D., Smith, R. R. and White, K. A. *Trans. J. Plastics Inst.* 1967, 35, 549
- 10 Kato, K. *Polymer* 1967, 8, 33
- 11 Kato, K. *Polymer* 1968, 9, 225
- 12 Pearson, J. R. A. 'Mechanical Principles of Polymer Melt Processing', Pergamon, Oxford, 1966, p 129
- 13 Bucknall, C. B. and Smith, R. R. *Polymer* 1965, 6, 437
- 14 Bucknall, C. B. and Clayton, D. *Nature (Phys. Sci.)* 1971, 231, 107
- 15 McGarry, F. J. *Proc. R. Soc. (A)* 1970, 319, 59
- 16 Whitney, W. J. *J. Appl. Phys.* 1963, 34, 3633
- 17 Argon, A. S., Andrews, R. D., Godrick, J. A. and Whitney, W. J. *J. Appl. Phys.* 1968, 39, 1899
- 18 Bowden, P. B. and Jukes, J. A. *J. Mater. Sci.* 1968, 3, 183
- 19 Bowden, P. B. and Raha, S. S. *Phil. Mag.* 1970, 22, 463

# Interaction of poly(vinyl pyrrolidone) with phenolic cosolutes

P. Bandyopadhyay\* and F. Rodriguez

*School of Chemical Engineering, Olin Hall, Cornell University,  
Ithaca, NY 14850, USA*

*(Received 10 May 1971; revised 10 June 1971)*

Complexes between poly(vinyl pyrrolidone) and phenolic materials can be important in such drug applications as slow-release formulations, reduced physiological shock, and detoxification. Hydroquinone serves as a model compound for the phenobarbital type of drug. The interaction of poly(vinyl pyrrolidone) with hydroquinone is manifested by a turbidity which develops in aqueous solutions at low concentrations. Also, the intrinsic viscosity of the polymer is reduced by the addition of hydroquinone and other phenols. Near the turbidity point, the behaviour is similar to that in a  $\theta$ -solvent. Crosslinked polymer in equilibrium with an aqueous hydroquinone solution lowers the concentration in a manner correlated by the Langmuir equation. The interaction by all criteria is much weaker in isopropyl alcohol than in water, and too small to be measured in dimethyl sulphoxide.

## INTRODUCTION

Association complexes between polymers and small molecules are frequently encountered<sup>1</sup>. Complex formation between two small molecules occurs less frequently. Thermodynamically, one can rationalize the situation by considering the relative enthalpy and entropy factors involved. Since complexes, almost by definition, are bound by weak interactions, the enthalpy contribution can be expected to be favourable but slight. However, the loss of translational and rotational entropy in the complexed state is so great that it overwhelms the enthalpy contribution and makes the complex unstable. If a polymer is involved as half of the complex, there already are restrictions on translational and rotational entropy so that the loss of such freedom does not constitute a bar to complex stability<sup>2</sup>.

The complexes between water-soluble polymers and small molecules typical of pharmaceutical systems have been studied from several viewpoints<sup>3-7</sup>. A problem of practical importance is the phase separation which may occur when polymers are included in formulations as emulsifiers, humectants, or lubricants. Another problem is the change in effectiveness which may occur when a drug or antibiotic is complexed. In some cases, a slowly decomposing complex which allows a slow release of a drug into the system may be very desirable to prevent shock to a physiological system and to decrease the frequency of dose application. One of the best known complexes with altered properties is that between iodine

and poly(vinyl pyrrolidone). The oral toxicity of the complex is far less than that of free iodine, but the effectiveness as an antiseptic solution is retained<sup>1</sup>.

An interesting and vital role can be played by polymers in mitigating the effects of toxins in the human body and, perhaps, in aiding their removal. Schreiner<sup>8</sup>, in his annual review of dialysis of poisons and drugs, points out that the poisoning of human beings can be accidental, suicidal, homicidal, or homicidal on a grand scale, that is, by chemical warfare. The two major methods of dealing with such poisons is to remove them as quickly as possible either by diuresis, usually encouraged or forced, or by dialysis using an artificial kidney machine to dialyse the poison from the blood.

The problem of detoxification has been studied using mathematical models<sup>9</sup>. One conclusion from such studies is the importance of binding of toxins in the blood phase. A binding polymer which would compete effectively with adipose tissue for the toxin would make dialysis much more efficient and cut down the time it takes to reduce the concentration of free toxin in the blood to a safe level.

Among the poisons commonly encountered, the barbiturates form a class which continues to grow. In 1964, 20% of the deaths due to acute poisoning involved barbiturates<sup>8</sup>. Rucdy and Chernecki<sup>10</sup> found that poly(vinyl pyrrolidone) with a molecular weight of 10 000 would bind significant amounts of phenobarbital. As a practical demonstration they observed rabbits who were fed phenobarbital or secobarbital. Those who received poly(vinyl pyrrolidone) intravenously had a higher respiratory rate after a few hours than the control group. In this case, the polymer-phenobarbital complex was small enough to be excreted normally.

\* Present address: New England Laminates Co. Inc., Stamford, Conn., USA

## EXPERIMENTAL

The polymers and solvents used are summarized in Table 1. The various cosolutes employed were conventional laboratory-grade chemicals used without further purification. The two crosslinked polymers differed mainly in particle size. Polyclar AT is a fine powder whereas AT-717 is comprised of large granules about 1 mm in diameter.

Viscosity was measured in Ubbelohde viscometers at 30°C. Cloud points were estimated by titration of a polymer solution with a 3 wt. % hydroquinone solution (about 0.03 mol/l). Approximately 50 ml of the polymer solution was stirred in a beaker by a magnetic bar on an illuminated stirring platform. The end-point did not appear to be sensitive to stirring rate, volume of solution, or rate of addition. There was little ambiguity in the end-point and no fading. The technique is essentially the turbidometric method used by previous workers<sup>5</sup>.

Equilibration data were obtained by mixing about 1 g of a crosslinked poly(vinyl pyrrolidone) with 50 ml water or other solvent and varying amounts of hydroquinone. For Agent AT-717 (Table 1) in water or isopropyl alcohol, the particles could be filtered off and the

concentration of hydroquinone in the supernatant liquid determined gravimetrically. However, the Polyclar AT powder was not easily filtered nor was the dimethyl sulphoxide easily evaporated. In these cases small amounts of the supernatant liquid were removed and the hydroquinone concentration evaluated in an ultra-violet spectrophotometer (Perkin-Elmer Model 202) after diluting down to the linear region. The results of the equilibration can be correlated by a form of the Langmuir isotherm<sup>7</sup>:

$$1/\rho = 1/n + 1/(Kn\alpha) \quad (1)$$

where  $\rho$  = molar ratio of hydroquinone to polymer (in monomer units)

$\alpha$  = free concentration of hydroquinone at equilibrium, mol/l

$1/(n)$  = monomer units associated with 1 molecule of hydroquinone at saturation

$K$  = 'binding constant' (a measure of strength of binding), 1/mol

Since the molecular weight of the monomer unit of the polymer is 111 and the molecular weight of hydroquinone is 110, the ratio on a molar basis is almost the same as the ratio on a weight basis. The greatest advantage of this equilibrium measurement over the membrane dialysis technique used by previous workers is the shortened time-scale permitted. With crosslinked polymer, a single day in gently rocked container assures equilibrium. Dialysis usually requires on the order of several days. Also, the crosslinked polymer permits the use of much higher cosolute concentrations than a dialysis method.

Table 1 Materials used in study

Material	Grade	Supplier	Intrinsic viscosity at 30°C in water (dl/g)
Poly(vinyl pyrrolidone)	K-30	GAF Corp.	0.23
Poly(vinyl pyrrolidone)	K-90	GAF Corp.	1.72
Poly(vinyl pyrrolidone)	K-115	GAF Corp.	2.4
Poly(vinyl pyrrolidone)	Polyclar AT	GAF Corp.	Crosslinked fine powder
Poly(vinyl pyrrolidone)	Agent AT-717	GAF Corp.	Crosslinked granules
Hydroquinone	'Photopurified'	Mallinckrodt	—
Isopropyl alcohol	Analytical reagent	Mallinckrodt	—
Dimethyl sulphoxide	'Practical'	Eastman	—

## RESULTS AND DISCUSSION

## Preliminary experiments

A number of cosolutes were screened for their effect on the viscosity,  $\eta$ , of a 0.5% g/dl solution of the K-90 polymer (Table 2). Both the organic acids and the phenols lower the viscosity appreciably. There is no clear-cut pattern among the results for the acids, but among the phenols it is apparent that the effect is increased with increased number of hydroxyl groups. The *p*- and *m*-dihydroxybenzenes are much more effective than the *o*-derivative. Endres and Hoermann<sup>11</sup> found a similar

Table 2 Viscosity reduction by phenolic cosolutes

Cosolute	Structure as benzene derivative	Mol.wt.	Conc. (mol/l) $\times 10^3$	Ratio of specific viscosities $\eta_{sp}/\eta_{sp}^*$		pH
				Measured	Literature†	
Cyclohexanol	—	100	20	0.98	—	6.3
Anisole	methoxy	108	18	0.97	—	6.8
Phenol	hydroxy	94	21	0.91	0.93	5.9
<i>m</i> -Cresol	1-hydroxy-2-methyl	108	18	0.87	—	6.9
Benzoic acid	carboxy	122	16	0.85	0.91	3.1
Pyrocatechol	1,2-dihydroxy	110	18	0.85	—	5.3
Salicylic acid	1-carboxy-2-hydroxy	138	14	0.83	—	2.5
Phthalic acid	1,2-dicarboxy	166	12	0.81	0.92	2.4
Pyromellitic acid	1,2,4,5-tetracarboxy	290	6.9	0.81	—	—
Hydroquinone	1,4-dihydroxy	110	18	0.75	—	5.7
Pyrogallol	1,2,3-trihydroxy	126	16	0.72	—	5.6
Resorcinol	1,3-dihydroxy	110	18	0.66	0.66	6.4
Hydrochloric acid	—	—	—	0.95	—	1.7

† Conditions: 0.5 g/dl, K-90 in water at 30°C (specific viscosity,  $\eta_{sp}^* = 1.175$ ); 0.2 g/dl cosolute. Literature values interpolated from ref. 7

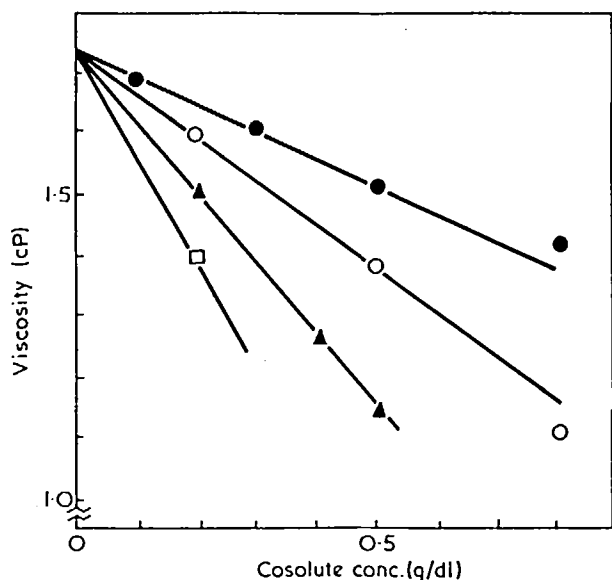


Figure 1 Variation in viscosity of a K-90 poly(vinyl pyrrolidone) solution (0.5 g/dl) by the addition of various phenols at 30°C. ●, Phenol; ○, pyrocatechol; ▲, hydroquinone; □, resorcinol

situation for the interaction of protein with phenols. They hypothesized that hydrogen bonding between one hydroxyl with the oxygen of the adjacent hydroxyl competed effectively with the intermolecular hydrogen bonding between phenol and protein. In the case of the phenols, the effect on viscosity appears to be linear with concentration (Figure 1). In separate experiments in which the temperature was varied between 30° and 40°C, the relative viscosity (solution viscosity divided by viscosity of water) remained constant for polymer solutions with and without phenol indicating no ready dissociation. Four of the cosolutes were reported by Molyneux and Frank<sup>7</sup> so that a comparison of the viscosity ratio is possible. Phenol and resorcinol give good checks (Table 2) but the acids do not.

#### Cloud point

In the range of interest for this study, the point of incipient precipitation for two grades of polymer was found to be a linear function of the polymer concentration (Figure 2). The lower molecular weight polymer required more hydroquinone to cause turbidity. On the other hand, temperature does not play a major role. For example, at a concentration of 0.66 g/dl for the K-90 polymer, raising the temperature from 25°C to 37°C raises the hydroquinone concentration required for turbidity only by a factor of 1.010. All of these hydroquinone concentrations are well below the solubility of hydroquinone itself in water at 25°C which is over 6 g/dl.

#### Changes in viscosity with concentration and molecular weight

The typical behaviour of poly(vinyl pyrrolidone) on dilution corresponds to the Huggins equation<sup>12</sup>:

$$\eta_{sp}/c = [\eta] + k'[\eta]^2c \quad (2)$$

where  $\eta_{sp}$  = specific viscosity

$[\eta]$  = intrinsic viscosity, dl/g

$c$  = concentration, g/dl

It can be seen in Figure 3 that a 'normal value' of  $k' = 0.4$  is found when the reduced viscosity  $\eta_{sp}/c$  is plotted at a constant concentration of hydroquinone. A very abnormal plot would obviously result if the ratio of hydroquinone to polymer were held constant. Another possibility that suggests itself in view of the linearity of the cloud point plot (Figure 2) is to keep the hydroquinone concentration in a fixed ratio to the cloud point concentration for each particular polymer concentration. At the higher hydroquinone concentrations this would lead to a  $k'$  of about zero. The conclusion one reaches is that only a part of

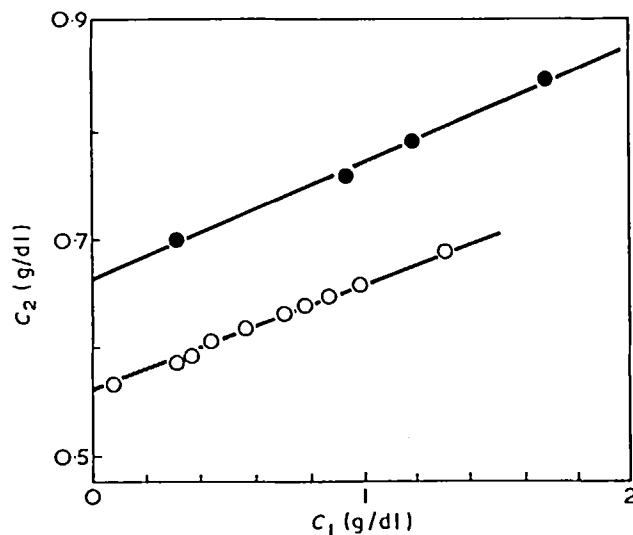


Figure 2 Effect of adding hydroquinone ( $c_1$ ) to aqueous solutions of poly(vinyl pyrrolidone) ( $c_2$ ) on turbidity. ●, K-30:  $c_2 = 0.665 + 0.105c_1$ ; ○, K-90:  $c_2 = 0.565 + 0.095c_1$ . (Results were obtained at 23°C but curves at 37°C are almost identical.)

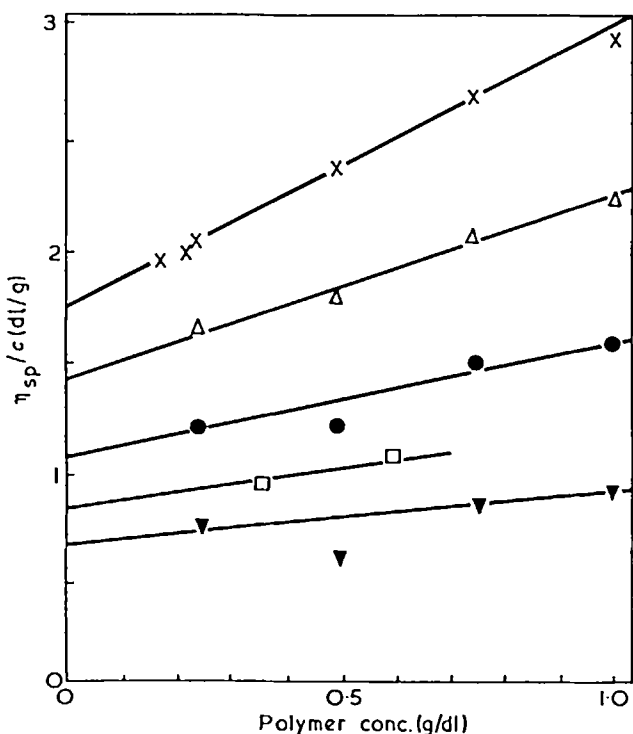


Figure 3 Behaviour of specific viscosity with concentration for K-90 as represented by the Huggins equation (equation 2) with  $k' = 0.40$ . ×, 0; Δ, 0.2; ●, 0.4; □, 0.5; ▼, 0.6 g/dl hydroquinone

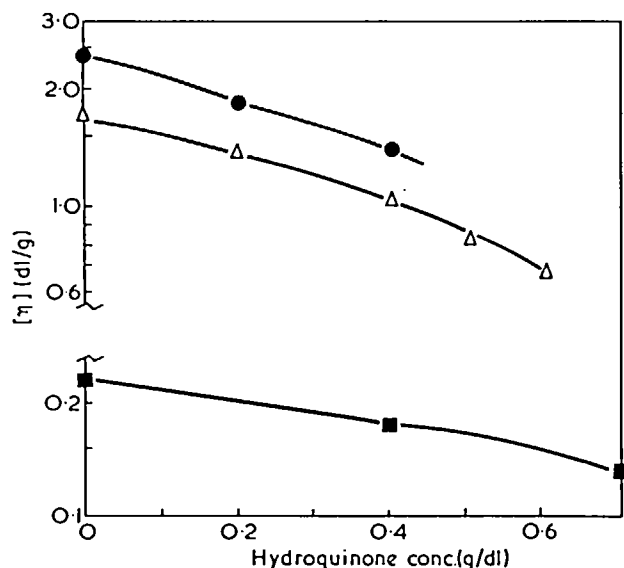


Figure 4 Variation of intrinsic viscosity with hydroquinone concentration for polymers of different molecular weight: ●, K-115; △, K-90; ■, K-30

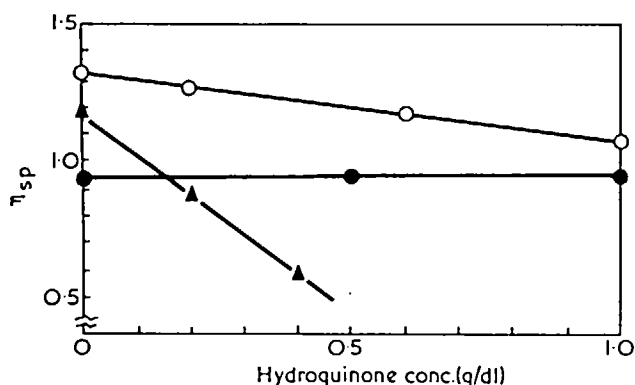


Figure 5 Variation of specific viscosity with hydroquinone concentration for K-90 (0.5 g/dl) in various solvents at 30°C. ○, isopropyl alcohol; ●, dimethyl sulphoxide; ▲, water

hydroquinone is actually combined with the polymer in dilute solutions. If this were not the case, then a high concentration of polymer would deplete the hydroquinone concentration and the effective molecular size, that is, the reduced viscosity, would rise more rapidly than usual. This conclusion is reinforced by the equilibrium experiments with crosslinked polymer discussed later.

The Huggins constant  $k'$  changed with molecular weight but not very much with hydroquinone concentration. The high molecular weight polymer K-115 gave  $k'=0.35$  while the low molecular weight K-30 had  $k'=0.6$ . As is usual with viscometric data, there is more scatter in the values of  $k'$  than there is in the values of the intrinsic viscosity.

The decrease in intrinsic viscosity with addition of hydroquinone can be carried slightly beyond the cloud point (Figure 4) since the actual measurements are made at finite concentrations where the cloud point concentration is higher than that for infinite dilution. The decrease is quite gradual even to the cloud point. The cloud point should represent a case of a  $\theta$ -solvent. Elias<sup>13</sup> found that

poly(vinyl pyrrolidone) in an acetone-water  $\theta$ -solvent at 25°C corresponded to the equation:

$$[\eta]_{\theta} = K_{\theta} M_w^{1/2}, \quad K_{\theta} = 7.2 \times 10^{-4} (\text{dl/g})(\text{mol/g})^{1/2} \quad (3)$$

Going on the assumption that  $M_v$  is about  $0.85 M_w$ , and that  $M_v$  can be obtained from a Mark-Houwink equation, the points for intrinsic viscosity against molecular weight do indeed come close to the prediction by Elias (Figure 5). The Mark-Houwink equation used is<sup>14</sup>:

$$[\eta] = 1.4 \times 10^{-4} M_v^{0.70} \quad (4)$$

On the basis of equilibrium studies reported later, it would appear that 1 mol of hydroquinone is associated with about 3 mol of monomeric repeat units in the polymer. If this is true also at the cloud point, it is of interest to note that polymer does not seem unduly expanded by accommodating the cosolute. The unperturbed dimensions can be calculated<sup>15</sup> from  $K_{\theta}$  by:

$$(\bar{r}_0^2/M)^{1/2} = (K_{\theta}/\Phi)^{1/3} \quad (5)$$

where  $\Phi$  is a universal constant equal to  $2.1 \times 10^{21}$  when  $r$  is in cm,  $M$  in g/mol, and  $[\eta]$  in dl/g. If the hydroquinone were being accommodated by inclusion within a helical polymer coil, one would expect the value of  $(\bar{r}_0^2/M)^{1/2}$  to be appreciably larger than it is when the  $\theta$ -solvent is a water-acetone mixture as used by Elias.

#### Viscosity changes in isopropyl alcohol and in dimethyl sulphoxide

Since the polymer is soluble in a variety of solvents, we can explore the complexing with hydroquinone under other conditions. Isopropyl alcohol and dimethyl sulphoxide are over twice as viscous as water at 30°C (Table 2). However, the alcohol is a better solvent than water and dimethyl sulphoxide is a poorer one judging from the intrinsic viscosity for a specific polymer sample (Table 3). Hydroquinone has no discernible effect on viscosity of the dimethyl sulphoxide solution and only a small effect on the alcoholic solution (Figure 5). We can conclude then that the interaction between poly(vinyl pyrrolidone) and hydroquinone is conditioned to a large extent by the presence of water. For example, we might envisage the water molecules as forming a bridge between the polymer and the hydroquinone molecules. If we picture the alcohol molecules as attaching to the polymer by their polar hydroxyl groups, the polymer surface becomes converted to a surface of non-polar methyl groups with very small likelihood of binding to the hydroquinone.

The dielectric constant does not seem to be a useful correlating parameter to explain the behaviour of viscosity. Neither the series of three intrinsic viscosities nor the series of viscosity-lowering by hydroquinone fall in the same order as the series of dielectric constants (Table 3).

Table 3 Solvent parameters

Solvent	Viscosity at 30°C (cP)	Intrinsic viscosity of K-90 at 30°C (dl/g)	Dielectric constant at 30°C
Water	0.8004	1.72	78
Isopropyl alcohol	1.77	2.0	18
Dimethyl sulphoxide	1.87	1.4	45

## Equilibrium measurements

When crosslinked poly(vinyl pyrrolidone) was placed in contact with dimethyl sulphoxide solutions of hydroquinone, there was no discernible interaction. This is consistent with the previous observation that hydroquinone has no effect on the viscosity of a polymer solution in the same solvent. In water and in isopropyl alcohol there is an interaction apparent from the plot of the Langmuir equation (Figure 6). The data for water with two grades of crosslinked poly(vinyl pyrrolidone) yield essentially the same result. Considering the fact that hydroquinone decreases the viscosity of aqueous polymer solutions much more than it does alcoholic solutions, it is surprising that the complexing behaviour is so similar for the two solvents (Figure 7). Both solvents give intercepts corresponding to about 2.5 monomer units in the polymer per mol of complexed hydroquinone at the limit of high hydroquinone concentrations.

Molyneux and Frank used an equilibrium dialysis method to study the complexing of phenols by poly(vinyl pyrrolidone)<sup>7</sup>. An aqueous polymer solution in a cellulose casing is suspended in water. The cosolute concentration originally is the same on both sides of the membrane. After equilibrium is attained the difference in cosolute concentration between polymer and water solutions divided by the polymer concentration is  $\rho$  in the Langmuir equation (equation 1). The free cosolute concentration at equilibrium is  $\alpha$  in the same equation.

For hydroquinone in water at 30°C, Molyneux and Frank measured a  $K$  of 38 l/mol assuming that  $1/n$  was 10 mol vinyl pyrrolidone/mol hydroquinone. The present work yields  $K=14$  l/mol and  $1/n=2.4$ . It can be argued that the new value for  $1/n$  is more reliable than the old since the old one was extrapolated from data at low hydroquinone concentrations (or possibly assumed from data with other phenols). The highest hydroquinone concentration used by Molyneux and Frank in their dialysis experiments was about 0.01 mol/l. The lowest concentration in the present work was twice that. Thus it seems likely that a good part of the difference is due to the concentration ranges used. Another difference is that the present work uses crosslinked polymer instead of the soluble material used previously. The value of  $K$  is derived from the slope of the plot and the value of  $1/n$ . The present slope is 0.17 mol/l compared to

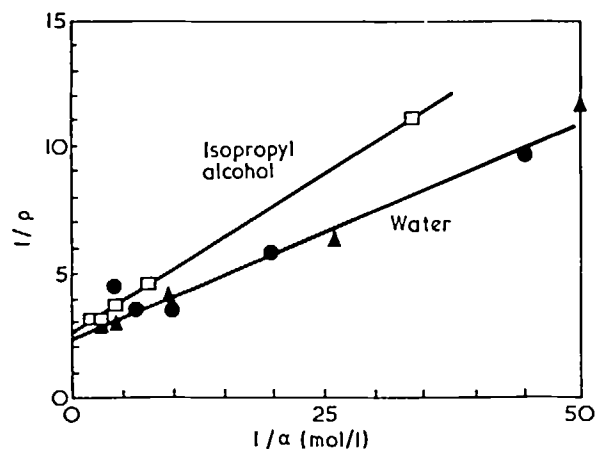


Figure 6 Langmuir isotherms (equation 1) for Agent AT-717 (●) and Polyclar AT (▲, □) at 23°C. The binding strength is somewhat lower in isopropyl alcohol than in water

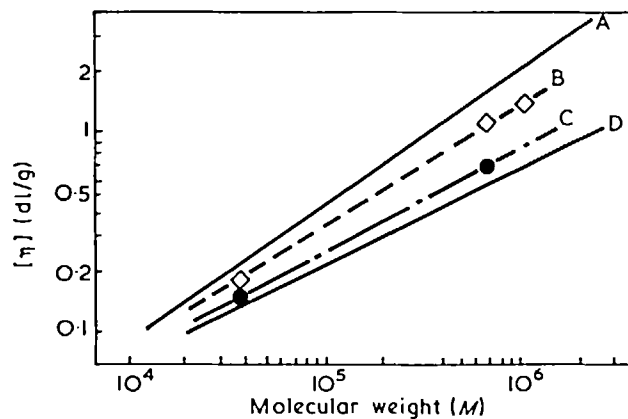


Figure 7 Effect of addition of hydroquinone to aqueous solutions of poly(vinyl pyrrolidone) on shifting the Mark-Houwink curve in the direction of the curve by Elias in a  $\theta$ -solvent (curve D) at 30°C. A, no hydroquinone; B, 0.4 g/l hydroquinone; C, 0.6 g/l hydroquinone

Molyneux and Frank's value of 0.26 mol/l. If their value of the slope (possibly more reliable than the present work) is combined with the new value of  $1/n=2.4$ , we calculate  $K=9.2$  l/mol.

The equilibration results in isopropyl alcohol are quite different from those of Molyneux and Frank in method. Where they found  $1/n$  to be ten times that in water, the present work indicates  $1/n$  in isopropyl alcohol to be about the same as in water.

Since alcohol and water complex the hydroquinone and dimethyl sulphoxide does not, it seems necessary to have protons available in the solvent. Apparently this is not a necessary condition for dissolving the polymer in the solvent. Both the alcohol and dimethyl sulphoxide are solvents of interest in pharmaceutical applications. The present work points up the fact that complex formation is affected strongly by the choice of solvent and that the binding of small molecules by polymers cannot be generalized easily.

## REFERENCES

- 1 Morawetz, H. 'Macromolecules in Solution', Interscience, New York, 1965, Ch 8
- 2 Bailey, F. E. Jnr and Lundberg, R. D. 'Association Complexes of Polymers', Gordon Conference, Santa Barbara, California, 1964
- 3 Breuninger, W. B. and Goettsch, R. W. *J. Pharm. Sci.* 1965, 54, 1487
- 4 Guttman, D. and Higuchi, T. *J. Am. Pharm. Assoc.* 1956, 45, 659
- 5 Kabedi, B. N. and Hammarlund, E. R. *J. Pharm. Sci.* 1966, 55, 1069
- 6 Patel, N. K. and Foss, N. E. *J. Pharm. Sci.* 1965, 54, 1495
- 7 Molyneux P. and Frank, H. P. *J. Am. Chem. Soc.* 1961, 83, 3169, 3175
- 8 Schreiner, G. E. *Trans. Am. Soc. Artif. Organs* 1970, 16, 544
- 9 Bischoff, K. B. and Dedrick, R. L. *J. Pharm. Sci.* 1968, 57, 1346
- 10 Ruedy, J. and Chernecki, W. *Can. J. Physiol. Pharm.* 1968, 46, 829
- 11 Endres, H. and Hoermann, H. *Angew. Chem. (Int. edn)* 1963, 2, 254
- 12 Flory, P. J. 'Principles of Polymer Chemistry', Cornell University Press, Ithaca, 1953, Ch 7
- 13 Elias, H-G. *Makromol. Chem.* 1961, 50, 1
- 14 Scholtan, W. *Makromol. Chem.* 1951, 7, 209
- 15 Flory, P. J. 'Principles of Polymer Chemistry', Cornell University Press, Ithaca, 1953, Ch 14



# The precipitation chromatographic column: theory, critique and method of design

Donald L. MacLean and James L. White

*Department of Chemical and Metallurgical Engineering, University of Tennessee,  
Knoxville, Tennessee 37916, USA  
(Received 18 June 1971)*

A new theory of the Baker-Williams precipitation chromatograph is presented. Both differential mass transfer and cell models have been described and the latter has been developed in some detail and calculations carried out. The influence of solvent gradient, temperature gradient and initial polymer sample size are considered.

## INTRODUCTION

The fractionation of polymers based upon the variation of solubility with molecular weight has been utilized since the recognition of the macromolecular hypothesis<sup>1</sup> and indeed batch fractionations have been a useful technique for the polymer chemist interested in characterizing materials of importance.<sup>2-5</sup> The liquid chromatographic technique based upon adsorption mechanisms was, after its renaissance in the 1930s, applied though with only mediocre success to synthetic polymers<sup>6-9</sup>. The first successful chromatographic techniques, those of Desreux<sup>10</sup> and especially that of Baker and Williams<sup>11</sup> were based rather on the variation of solubility with molecular weight, solvent composition and temperature. Desreux essentially fractionated polymer samples by selective extraction using a mixture of solvents with a gradient of improving solvent quality. Baker and Williams<sup>11</sup> constructed a column packed with glass beads along which they placed a temperature gradient with the higher temperatures at the top where the polymer sample to be fractionated was placed in a finely divided form. A mixture of two solvents (one good and one bad) was added to the column with a gradient of improving solvent quality as the experiment continued. These researchers found the low molecular weight polymer to be eluted first followed by the high molecular weight species. Baker and Williams and later experimenters<sup>12-16</sup> have used this instrument to determine molecular weight distributions and to obtain sizeable quantities of fractions for physical measurements. Some question has been raised about the necessity and efficiency of using a temperature gradient at all<sup>15,16</sup>. Reasonable fractionations can in many instances be obtained through simple gradient extraction, or as it is sometimes called, elution fractionation. Recently other types of large-scale polymer fractionation apparatus based on thermodynamic phase separation have been described<sup>17,18</sup>.

A qualitative explanation of the operation of this column called a Baker-Williams column or a precipitation chromatograph was given by Baker and Williams<sup>11</sup> themselves. These authors suggested that the initial poor solvent dissolves only the low molecular weight polymer which percolates down the column until the lower temperature induces its precipitation. The improved solvent now entering the column dissolves intermediate molecular weight species which begin to traverse downward. This fraction also precipitates when reaching lower temperatures. However, the low molecular weight species precipitated from the original poor solvent is redissolved by the better solvent and again proceeds down the column. The continually improving solvent entering the top of the column now dissolves the higher molecular weight species which begin their descent. One can now see that low molecular weight polymer will elute from the column followed by intermediate and high molecular weight species.

The ideas of Baker and Williams cited in the above paragraph have been generally accepted by later researchers. The first attempt to develop a quantitative theory of separation in this instrument was by Caplan.<sup>12</sup> Indeed it was Caplan, who introduced the descriptive term *precipitation chromatography* on the basis of these considerations. While Caplan has the right physical 'feel' of the problem and seems to recognize some of the difficulties arising from applying classical chromatography theory, he does not follow through and develop a rational scheme to handle these difficulties. Instead he intuitively applies a simplified form of the ternary phase equilibrium equations of the Meyer-Flory-Huggins theory of polymer solutions<sup>19,20</sup> coupled with an intuitive notion of the variation of solvent quality along the length of the column. A second attempt at analysis which was more in line with classical chromatography theory was published by Schulz *et al.*<sup>21</sup> who attempt to set up and solve differential mass balances. A similar approach was later

taken by Smith<sup>22</sup>. However, both of these papers make oversimplifications. In particular neither of these groups is able to cope with the implications of the variation of the gel fraction along the length of the column and proceed by making questionable approximations of this quantity.

In this paper, we describe two improved theories of the precipitation chromatograph. One of these will be developed in considerable detail. This paper represents a continuation of our efforts to put the theory of column separations of macromolecules on a stronger basis<sup>23</sup>.

### PHASE EQUILIBRIA IN POLYMER SOLUTIONS

Before proceeding with the detailed analysis of the column operation, we must first discuss phase equilibrium in polymer solutions. The phenomenon of phase equilibrium for heterogeneous polymers in mixed solvents is the basis of fractionation in the Baker-Williams instrument. The ternary system polymer/solvent 1/solvent 2 is the simplest situation for which the column may be operated and indeed understood. Generally phase equilibrium in such a ternary system is represented in terms of triangular diagram<sup>20, 24, 25</sup> indicated in *Figure 1*. The composition of a solution with volume fractions of species 1, 2 and polymer of  $\phi_1, \phi_2, \phi_p$  is indicated by the intersection of the perpendiculars from value  $\phi_1$  on the  $2p$  axis,  $\phi_2$  on the  $1p$  axis and  $\phi_p$  on the  $12$  axis. There have been remarkably few experimental studies of phase equilibrium in polymer solutions with mixed solvents<sup>26-30</sup>. Generally for systems of the type which we have interest in (polymer/solvent/non-solvent), the two phase region has the form shown in *Figure 1*.

In the absence of experimental data, we turn to statistical thermodynamic theories. Flory<sup>31</sup> seems to have been the first to give serious consideration to the problem of phase separation in polymer solutions, and the interaction of solvent quality and molecular weight on the criterion of its occurrence and the character of the separated phases. This analysis was based upon the Meyer-Flory-Huggins solution theory. These concepts were extended in succeeding years to heterogeneous homopolymers and mixed solvents<sup>19, 20, 21, 32-35</sup> at least for the case in which there were no specific favoured associations. Somewhat complex though still tractable expressions were obtained. In particular the distribution of polymer of species  $i$ , containing  $m_i$  lattice site occupying units, between solution and swollen precipitate phases is:

$$\ln \frac{\phi_i}{\phi_i^0} = -m_i [ (-\chi_{13} + \chi_{23} - \chi_{12})(\phi_2 - \phi_2^0) + (1 - 2\chi_{13})(\phi_p - \phi_p^0) + \chi_{12}(\phi_2^0 - \phi_2^0) + (\phi_p/m_n - \phi_p/m_n) + \chi_{13}(\phi_p^0 - \phi_p^0) + (\chi_{13} - \chi_{23} + \chi_{12})(\phi_2\phi_p - \phi_2^0\phi_p^0) ] \quad (1)$$

Here the  $\chi_{ij}$  are interaction parameters representing dimensionless site interaction energy differences<sup>19</sup>.  $\phi_i$  is the volume fraction of species  $i$  in the liquid,  $\phi_i^0$  is its volume fraction in the gel, and  $\phi_p$  is the total volume fraction of polymer in the liquid. In more recent years, there have been attempts to remove the 'no-association' restriction but the resulting phase equilibrium relationships have been considerably complicated<sup>36</sup>. Generally it is found that the Meyer-Flory-Huggins theory predictions of partition following phase separation to be

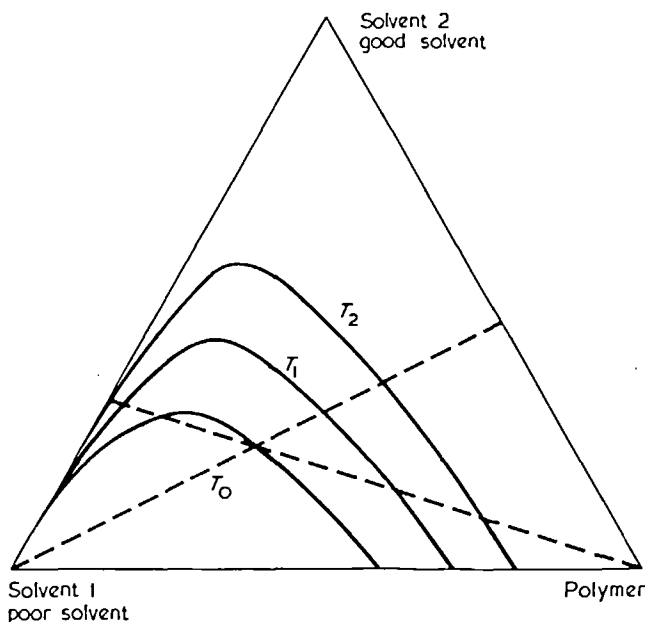


Figure 1 Triangular phase diagram

qualitatively valid. The ability to fractionate on the basis of molecular weight is verified, but the quantitative details are not satisfactorily explained.

### ANALYSIS OF COLUMN PROCESSES

There have been three general approaches to theoretically analysing chromatographic separations. These are the application of differential mass balances as devised by Wilson<sup>37</sup>, Thomas<sup>38</sup> and Lapidus and Amundson<sup>39</sup> among others; division of the column into a series of discrete perfectly mixed stages and application of finite difference methods as described by Martin and Synge<sup>40</sup>; and stochastic process methods as devised by Giddings and Eyring<sup>41, 42</sup>. However, these techniques are restricted to application to adsorptions and molecular sieving processes. We shall look at the appropriate developments for applying the first two of these techniques to precipitation chromatography.

#### Differential mass balance

Consider a column (see *Figure 2*) which stretches from the origin along the  $z$ -direction. In a thickness  $\Delta z$  there will be a volume fraction  $\beta$  of stationary glass beads,  $\alpha$  of mobile fluid phase and  $\gamma$  precipitated gel of polymer and solvent components. In particular:

$$\alpha + \beta + \gamma = 1 \quad (2)$$

Generally  $\beta$  will be constant through the length of the column, but  $\alpha$  and  $\gamma$  will vary with position and time. If a solvent flow rate  $Q$  (volume/time) is pushed through the column then a balance over species  $i$  at time  $t$  will lead to:

$$Qc_i|_{z+\Delta z, t} - Qc_i|_{z, t} = - \left[ \frac{\partial}{\partial t}(\alpha c_i) + \frac{\partial}{\partial t}(\gamma \bar{c}_i) \right] A \Delta z \quad (3)$$

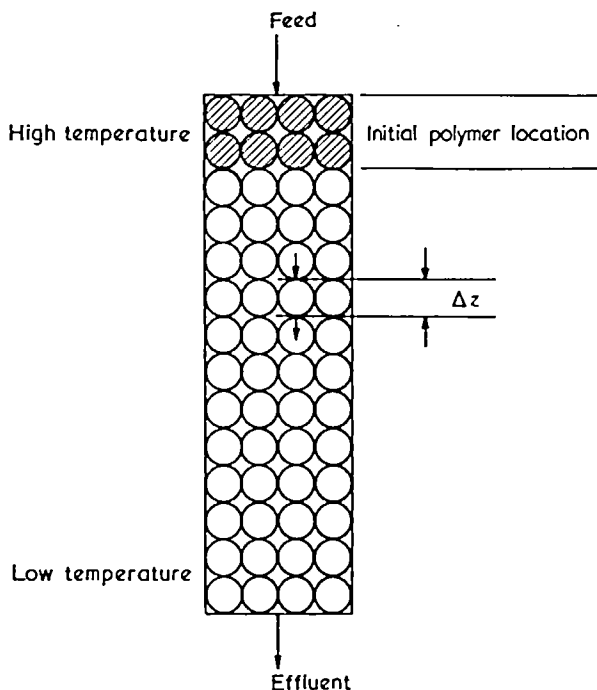


Figure 2 Precipitation chromatograph

where  $c_i$  and  $\bar{c}_i$  are the concentrations of  $i$  in the sol and gel phases and  $A$  the cross-sectional area of the column. Equation (3) is equivalent to:

$$\frac{\partial c_i}{\partial t} + \frac{Q}{\alpha A} \frac{\partial c_i}{\partial z} = \frac{\partial \ln \alpha}{\partial t} (\bar{c}_i - c_i) - \gamma \frac{\partial \bar{c}_i}{\partial t} \quad (4)$$

where equation (1) has been used ( $\partial \alpha / \partial t = -\partial \gamma / \partial t$ ). In the derivation of equation (3), we have neglected axial dispersion processes, radial concentration gradients and indeed radial processes in general. Equation (3) should perhaps be thought of as a non-homogeneous first-order partial differential equation containing two unknown quantities  $\bar{c}_i$  and  $\alpha$  which relate to the characteristics of the gel that forms when  $c_i$  becomes greater than some threshold concentration  $c_{i,sat}$ , a quantity varying with time (because of the elution gradient) and position (because of both the elution and temperature gradients) in the column.

We may use equation (4) to directly solve the column elution problem for the special case of elution fractionation, i.e. columns without temperature gradients<sup>15</sup>. Here the eluting solvent entering the column dissolves each species to an extent  $c_i$ , which then directly flow through the column without formation of gel. The right-hand side of equation (4) is zero, and it may be directly solved to give:

$$c_i(z, t) = c_{i0} \left( t - \frac{(z - \Delta)}{\alpha U} \right) \quad (5)$$

where  $c_{i0}(t)$  represents the concentration of species  $i$  in the mobile phase entering the column at time  $t$ . The problem of analysing the column simply reduces now to determination of  $c_{i0}(t)$ . If one is willing to presume equilibrium in the polymer layer at the top of the column,  $c_{i0}(t)$  may be determined directly from phase equilibrium data.

The more general problem involving temperature gradients in the column leads to significantly greater

difficulties. For here we must come face to face with knowing  $\bar{c}_i$  and the gel fraction  $\gamma$ . In essence one may proceed as follows. Equation (5) remains valid along the path of the percolating fluid in the column until  $c_{i0}$  exceeds  $c_{i,sat}$ . At this point gel begins to form,  $\gamma$  takes on non-zero values and  $\alpha$  decreases. If equilibrium is assumed, then application of the lever rule to the phase diagram will yield the relative amounts of the two phases. If  $\bar{c}_i$  is the apparent concentration at  $z$  and  $t$  then:

$$\begin{aligned} (1 - \beta) \bar{c}_i(t, z) &= \alpha c_i + \gamma \bar{c}_i \\ &= (1 - \beta - \gamma) c_i + \gamma \bar{c}_i \end{aligned} \quad (6)$$

where for a ternary system one may consider  $\alpha/(1 - \beta)$  and  $\gamma/(1 - \beta)$  to be determined from application of the lever rule to Figure 1. This becomes conceptually more complicated as the number of components increases, but the essentials remain the same.

The reader may see at this point that unless the variation of  $\gamma$  with distance and time be specified in a simple analytical form even the equilibrium theory described above becomes too difficult to handle with the differential mass balance approach. If rates of dissolution and precipitation be included, the problem becomes all that more difficult. We turn next to what we believe is a more tractable approach.

#### Discrete stages

An alternative approach to this problem makes use of the representation of the column as a series of discrete mixing cells. This technique was devised by Martin and Synge<sup>40</sup> and the basis of its applicability may perhaps best be seen in Aris and Amundson's<sup>43</sup> analysis of axial dispersion processes occurring in packed columns. The precipitation chromatographic column is considered to be divided into a series of perfectly mixed cells representing portions of the column beginning with the top of the column. The eluting fluid moves first into the cell which consists of the polymer to be fractionated and then successively through the 1st, 2nd, 3rd, and  $(n - 1)$ th and  $n$ th cells each of which is maintained at a successively lower temperature,  $T_0, T_1, T_2, T_3 \dots T_n$ . Let us first consider the special case when only one polymer species is involved. When the composition gradient has increased the solvent power of the eluent to the extent that it dissolves the polymer in cell 0, a saturated solution with concentration  $c_i(1, 0)$  and volume fraction in solution  $\phi_i(1, 0)$  is formed which flows during a period  $t_1$  into cell 1. This yields a cell at temperature  $T_1$  containing a solution which is saturated at a higher temperature,  $T_0$ . At temperature  $T_1$ , this solution is supersaturated and precipitation proceeds yielding a gel phase with concentration,  $\bar{c}_i(2, 1)$ , volume fraction  $\phi_i(2, 1)$  and gel fraction  $\gamma(2, 1)$ . The average volume fraction of  $i$  in the cell is  $\phi_i'(2, 1)$ . If  $\alpha(2, 1)$  is the remaining void fraction and  $c_i(2, 1)$  the concentration of the solution phase in the cell, then:

$$\begin{aligned} \alpha(1, 0) [\phi_i(1, 0) - \phi_i(1, 1)] + (1 - \beta) \phi_i'(1, 1) \\ = (1 - \beta) \phi_i'(2, 1) = \alpha(2, 1) \phi_i(2, 1) + \gamma(2, 1) \phi_i(2, 1) \end{aligned} \quad (7)$$

where  $\phi_i'(1, 1)$  which is shown for the purpose of illustration is zero.

$\phi_i(1, 0)$  and  $\alpha(1, 0)$  can be found from the known concentrations in the first cell using phase equilibrium data as is indicated in Figure 1 and the lever rule. Once

$\phi_i(1, 0)$  and  $\alpha(1, 0)$  are found the procedure is repeated for the phase equilibrium data at temperature  $T_1$  to find the quantities on the right hand side of equation (7). During period 2 additional eluent flows into the column and the new solution phase in cell 0 moves into cell 1 displacing  $\alpha(2, 1)$   $\phi_i(2, 1)$  from cell 1 into cell 2. For cell 1:

$$\alpha(2, 1)[\phi_i(2, 0) - \phi_i(2, 1)] + (1 - \beta)\phi_i'(2, 1) = (1 - \beta)\phi_i'(3, 1) = \alpha(3, 1)\phi_i(3, 1) + \gamma(3, 1)\bar{\phi}_i(3, 1) \quad (8)$$

Since the solvent power is now greater, part and perhaps all of gel in cell 1 will dissolve. For cell 2 we must write:

$$\alpha(2, 1)[\phi_i(2, 1) - \phi_i(2, 2)] + [1 - \beta]\phi_i'(2, 2) = (1 - \beta)\phi_i'(3, 2) = \alpha(3, 2)\phi_i(3, 2) + \gamma(3, 2)\bar{\phi}_i(3, 2) \quad (9)$$

where  $\phi_i(2, 2)$  will be zero. The quantities on the right hand side will be computed from the diagram. If  $\phi_i(3, 2)$  is less than  $\phi_{i,sat}(3, 2)$  then

$$\begin{aligned} \phi_i(3, 2) &= \phi_i'(3, 2) \\ \alpha(3, 2) &= 1 - \beta \\ \gamma(3, 2) &= 0. \end{aligned} \quad (10)$$

This procedure may be repeated. Generally for the  $J$ th cell and the  $M$ th time period we may write:

$$\begin{aligned} \alpha_{\min}(M-1)[\phi_i(M-1, J-1) - \phi_i(M-1, J)] + (1 - \beta)\phi_i'(M-1, J) &= (1 - \beta)\phi_i'(M, J) \\ &= \alpha(M, J)\phi_i(M, J) + \gamma(M, J)\bar{\phi}_i(M, J) \end{aligned} \quad (11)$$

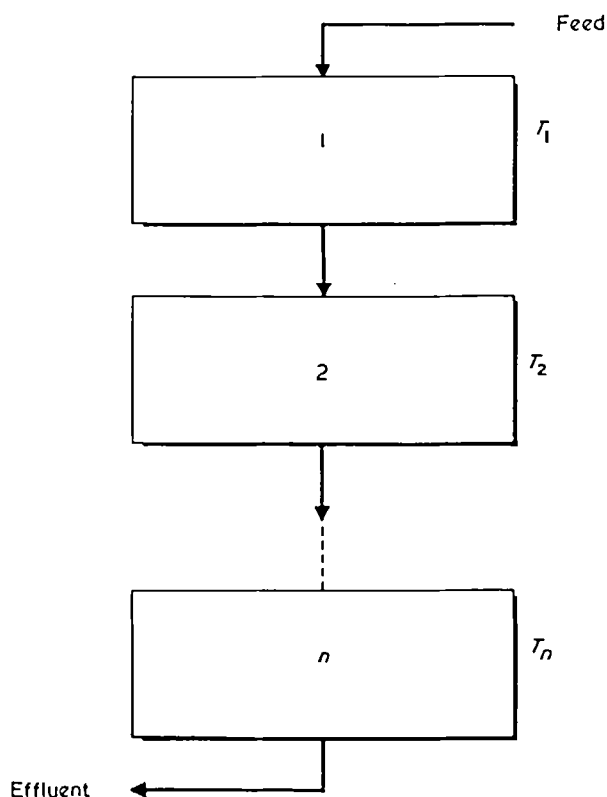


Figure 3 Discrete stage or mixing cell model of a precipitation chromatograph

where  $\gamma(M, J)$  may be zero and  $\alpha_{\min}(M-1)$  is the minimum cell liquid fraction at time increment  $(M-1)$ . Equation (11) is valid for  $n$  components and  $J$  cells.

It should be seen that this procedure is an awkward one and not really suitable for classical mathematical analysis or 'hand' calculations. It is, however, of a form that has long been treated by the digital computer and this tool has been utilized in our calculations. Computer simulation becomes especially necessary as it is realized that: (i) a sizeable number of cells will probably prove necessary to give a reasonable approximation; (ii) a multi-component and not a ternary system must be considered in analysis of polydisperse systems which is after all the primary application; and (iii) the phase diagram that must be used in each stage is different because of the temperature variation and the average solvent composition in each cell varies with time. A suitable computer programme which applies to multi-component systems has been developed. It is summarized in Figure 4. Details are given by MacLean<sup>41</sup>.

### SAMPLE CALCULATIONS

Fractionation of polymer systems with the precipitation chromatograph have been computed by the techniques outlined in the previous section. The phase equilibrium relationship has been constructed using the Meyer-Flory-Huggins theory, in particular utilizing equation (1). We have chosen a system involving a good solvent which interacts with a second poor solvent in the same way as the molecules of the second solvent interact with the polymer. In particular, we take

$$\chi_{1p} = 0 \quad \chi_{12} = \chi_{2p} = 0.50 + \frac{283}{T} \quad (12)$$

where  $T$  is in Kelvins. Thus '1' designates the better solvent '2' the poorer solvent. The physical description of the column is modelled closely upon the original Baker-Williams column. In particular a 35 cm long column was used. The temperature ranged from 333K to 283K and a 5 ml/h flow rate through a 2 cm diameter column was considered. For modelling purposes the column was divided into 10 equal sized cells with all the polymer initially in the first cell.

Three basic parameters were considered in our study: (i) the quantity of polymer placed in the column; (ii) the solvent gradient; and (iii) the temperature gradient. The results are shown in Figures 5 to 10.

#### Effect of quantity of polymer

At initial values of polymer volume fraction greater than about 0.20 no separation was noticed and Figures 5 and 6 show that better separation occurred with lower polymer volume fractions.

#### Solvent gradient

With linear solvent gradient of the form:

$$\phi_{1\text{feed}}(M, t + \Delta t) = \phi_{1\text{feed}}(M, t) + B\Delta t \quad (13)$$

and constant temperature levels better separation occurs with smaller values of  $B$ . This may be seen in Figures 5 and 6. However, the best separation occurred with a

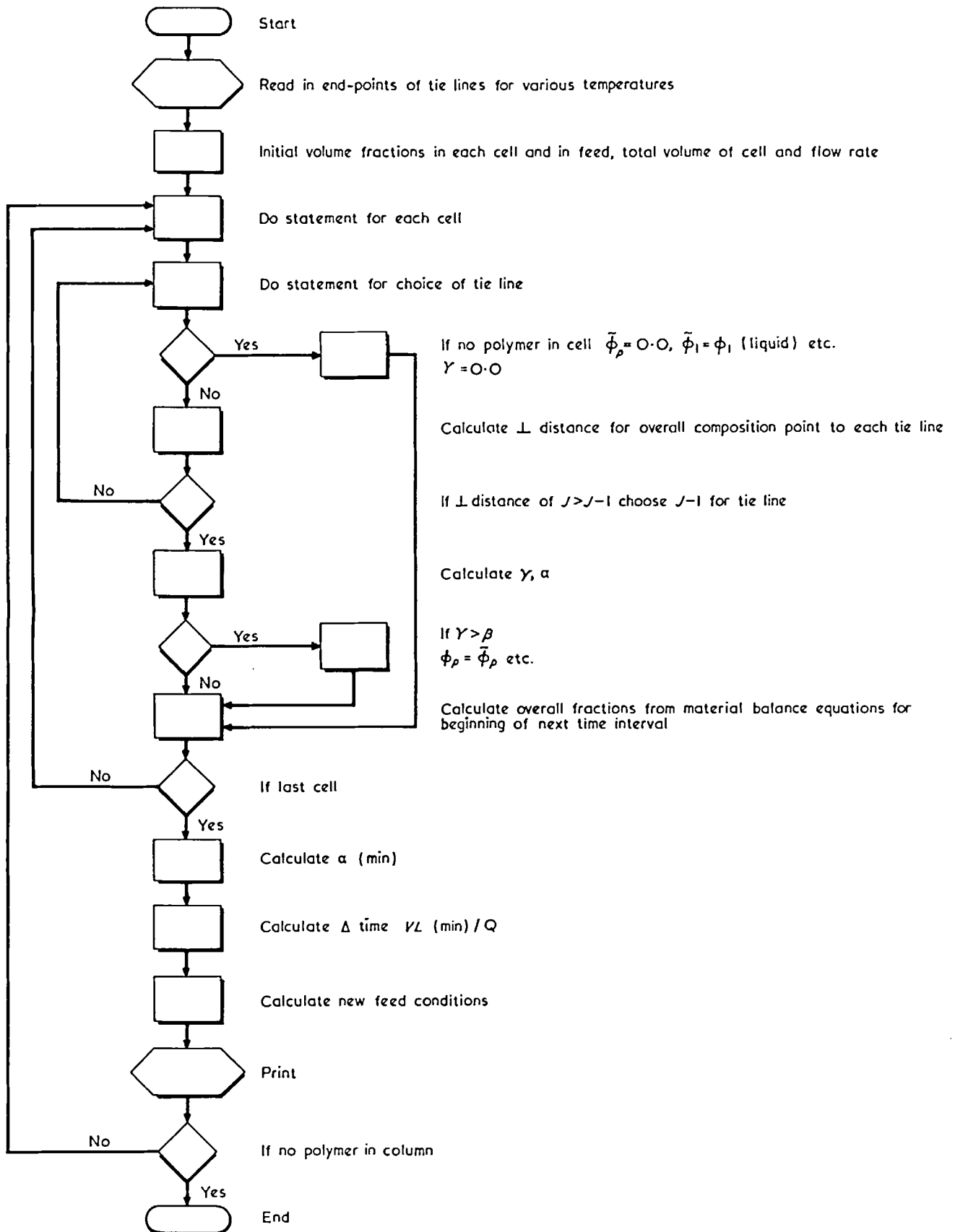


Figure 4 Simplified computer diagram for mixing cell model

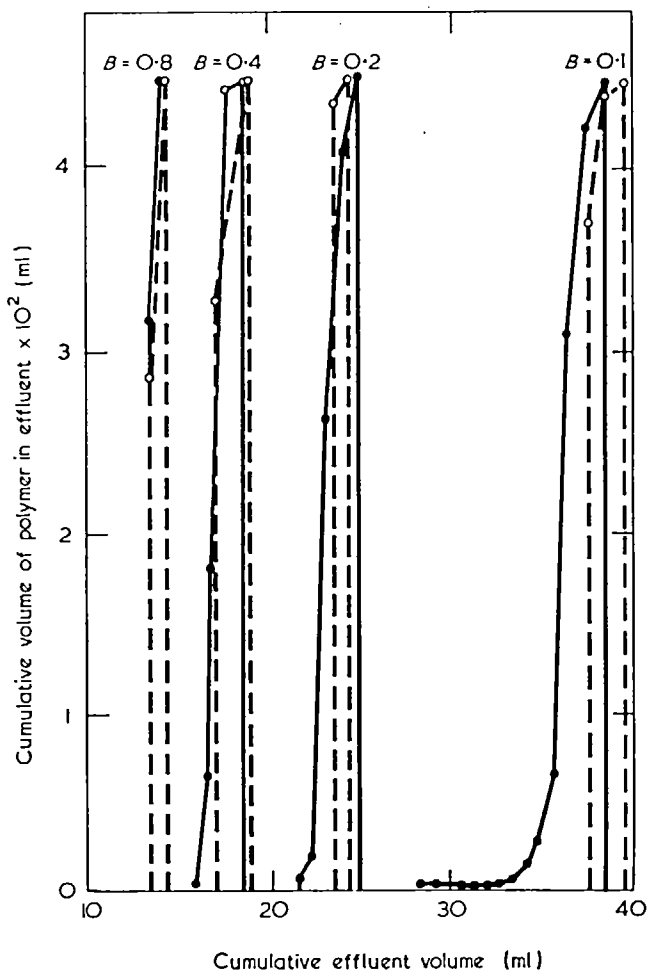


Figure 5 Effect of linear solvent and temperature gradient for initial polymer volume fraction of 0.05.  $B$  = slope of solvent gradient.  $\circ$ ,  $m_i=1000$ ;  $\bullet$ ,  $m_i=100$

solvent gradient of  $B$  equal to  $1.0 \text{ sec}^{-1}$ , with  $\phi_{1\text{feed}}$  less than 0.35. When  $\phi_{1\text{feed}}$  is greater than 0.35, the best value of  $B$  is 0.05. This means that just before dissolution the solvent gradient should be changed from a high to a low value. This is shown in Figure 7. When the solvent gradient becomes large, the small differences in dissolution composition for the different polymer species are overshoot. Too large solvent gradients would thus seem to be self defeating.

Temperature gradient

Both linear and logarithmic temperature gradients have been considered. These have the form:

$$T(z) = T_0 + (T_L - T_0) \frac{z}{L} \quad (14a)$$

$$T(z) = T_0 + (T_L - T_0) \ln \left[ k_1 \frac{z}{L} + k_2 \right] \quad (14b)$$

The form of the temperature gradient was found to have little effect on the fractionations produced by the column as seen by comparing Figures 7 and 8.

While the shape of the temperature gradient is of little importance, its presence is. Figure 9 shows the

column for isothermal conditions with all cells at the temperature of the first cell, fifth cell, and the tenth or last cell. This shows that the best separation of all those investigated occurs with the column operated isothermally at a high temperature while the separation for the columns operated isothermally at a lower temperature is nearly the same as with the temperature gradient. The reason for the superiority of the high constant temperature model can be seen in Figures 11 and 12. These Figures calculated from the Meyer-Flory-Huggins theory and thus limited to systems which can be qualitatively represented by it show that at the higher temperatures a greater difference in the binodals of the two polymer species exists than at a lower temperature. The lower temperature region can be envisioned as a bottleneck where the smaller polymer species are slowed down until the larger polymer molecules almost overtake them. This can also be seen in Figure 10 where a reverse temperature gradient is used and the fractionation is about the same as the low temperature isothermal run.

DISCUSSION

It was found that while the Baker and Williams mechanism for precipitation chromatography should be valid

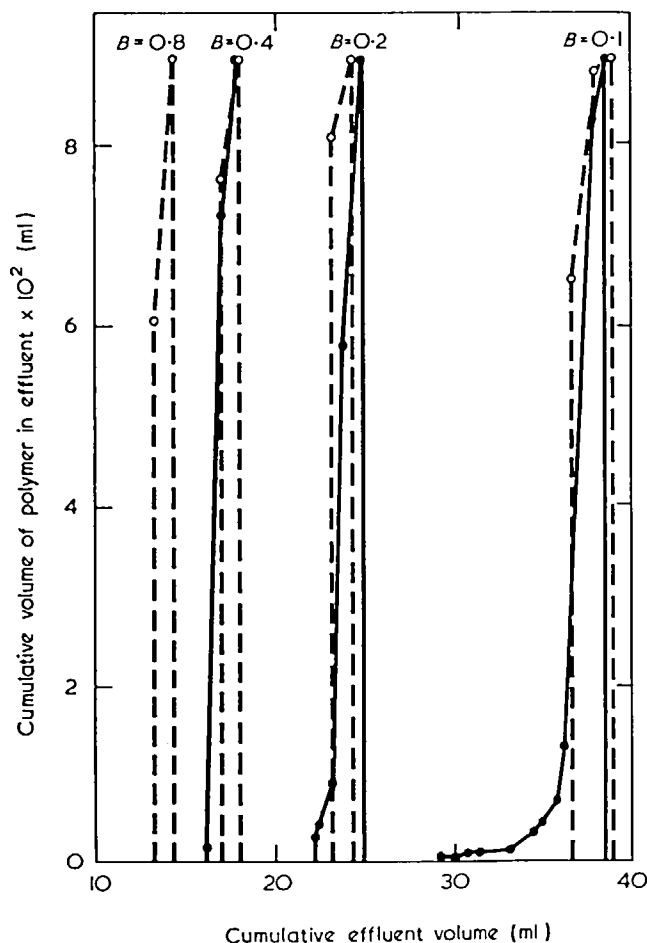


Figure 6 Effect of linear solvent and temperature gradient for initial volume fraction of 0.10.  $B$  = slope of solvent gradient.  $\circ$ ,  $m_i=1000$ ;  $\bullet$ ,  $m_i=100$

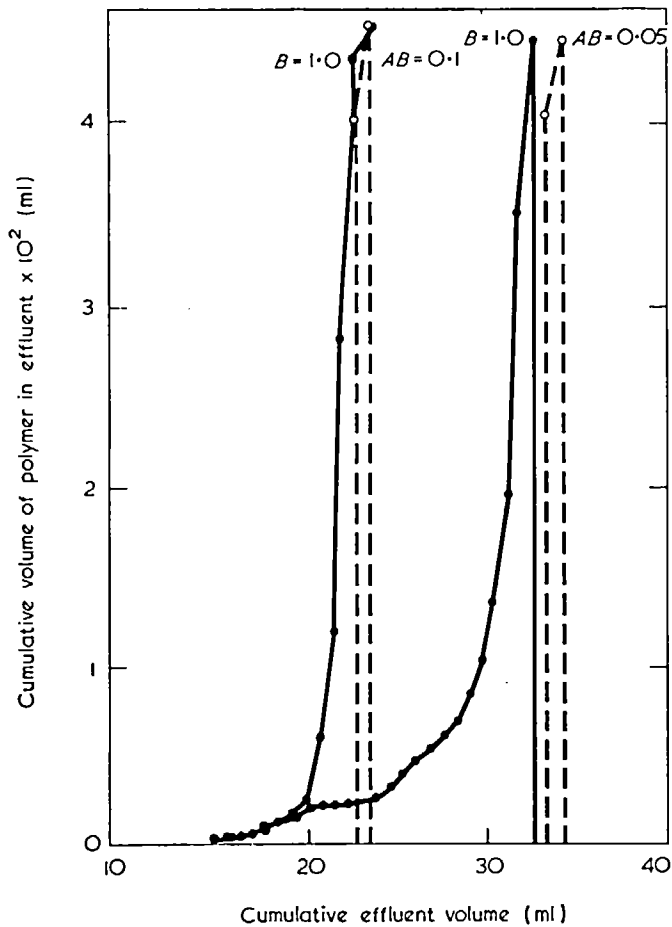


Figure 7 Effect of '2 slope' solvent gradient with linear temperature gradient for initial volume fraction of 0.05.  $B$  = first slope of solvent gradient;  $AB$  = second slope of solvent gradient.  $\circ$ ,  $m_i = 1000$ ;  $\bullet$ ,  $m_i = 100$

additional dispersion will be caused by the lack of equilibrium between the polymer solution and gel which will certainly exist throughout the length of the column. Some experimental studies of rates of dissolution have appeared<sup>48</sup> but little or nothing on the reverse problem of rates of coagulation and precipitation from solution. We intend to treat this problem further at a later time.

A second feature of interest is that if we had utilized the Kilb-Bueche<sup>49</sup> theory of solutions of copolymers, the procedures of this paper would allow predictions of separation on the basis of composition as well as molecular weight. Thus attempting to separate a polydisperse copolymer with compositional heterogeneity on a precipitation chromatograph should lead to rather complicated results. This phenomenon has been observed at various times by polymer chemists.

### CONCLUSIONS

Two new theoretical models of the Baker-Williams precipitation chromatograph have been developed. These are based upon mixing cell and differential mass balance concepts. The mixing cell model is applicable to multi-component systems and has been simulated on a digital

the improved separation over the Desreux constant temperature method was not found in the sample calculations for equilibrium conditions using the ternary Flory-Huggins relations and equation (1) to provide the equilibrium data. Our use of theoretical phase equilibrium data points to a need for further experimental work on phase equilibrium of polymers in mixed solvents especially the effect of temperature and molecular weight. These experimental data could then be used directly with our mixing cell model.

It should be noted that this mixing cell theory is capable of predicting dispersion just as in the original Martin-Syngé<sup>40</sup> theory of the adsorption chromatograph. Dispersion was found to be greater for the lower molecular weight species and increased as the amount of polymer and solvent gradient decreased. Studies of the mixing cell theory<sup>43, 45</sup> indicate that the source of dispersion predicted in this theory is due solely to hydrodynamic mixing patterns in the column and in terms of the differential mass transfer balance theory is equivalent to an axial Peclet number of two. This, however, is known to misrepresent the hydrodynamic dispersion in liquid chromatography<sup>46</sup>, and specific molecular weight effects have been observed indicating greater dispersion with higher molecular weight polymer species<sup>47</sup>. Furthermore

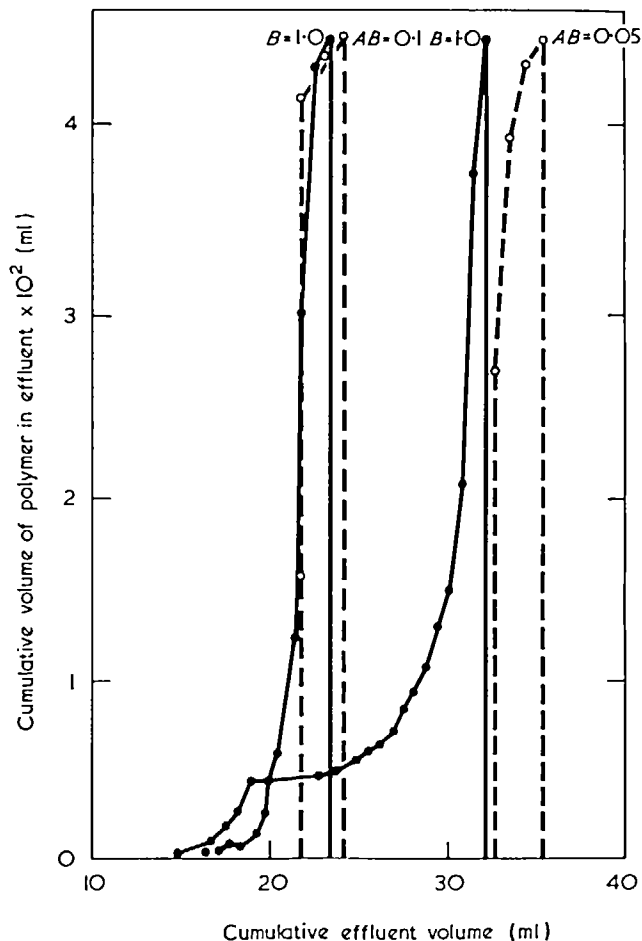


Figure 8 Effect of '2 slope' solvent gradient and log temperature gradient for initial polymer volume fraction of 0.05.  $B$  = first slope of solvent gradient;  $AB$  = second slope of solvent gradient.  $\circ$ ,  $m_i = 1000$ ;  $\bullet$ ,  $m_i = 100$

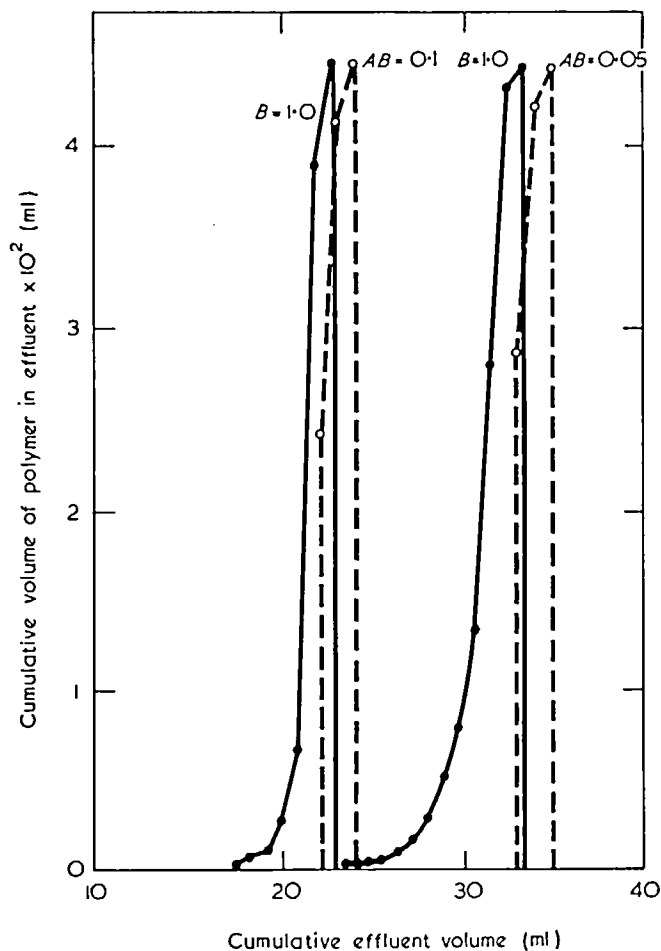
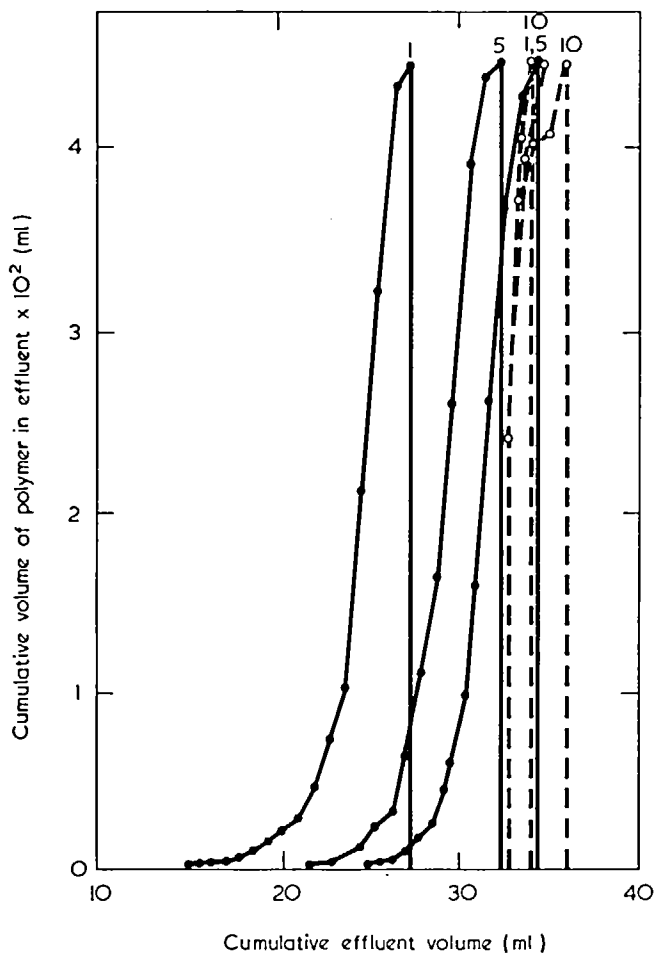


Figure 9 Isothermal column fractionization using '2 slope' solvent gradient ( $B=1$ ,  $AB=0.05$ ). 1, 330.5K; 5, 310.5K; 10, 285.5K.  $\circ$ ,  $m_i=1000$ ;  $\bullet$ ,  $m_i=100$

Figure 10 Reversed temperature gradient with '2 slope' solvent gradient for initial volume fraction of 0.05.  $B$ =first slope of '2 slope' solvent gradient;  $AB$ =second slope of '2 slope' solvent gradient.  $\circ$ ,  $m_i=1000$ ;  $\bullet$ ,  $m_i=100$

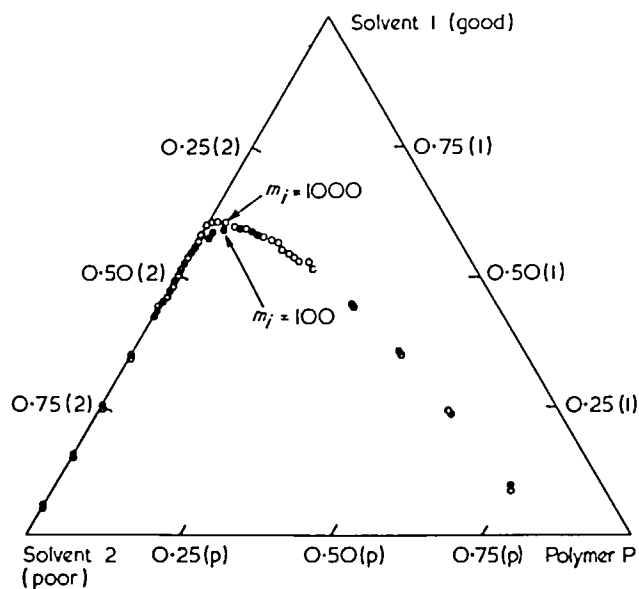
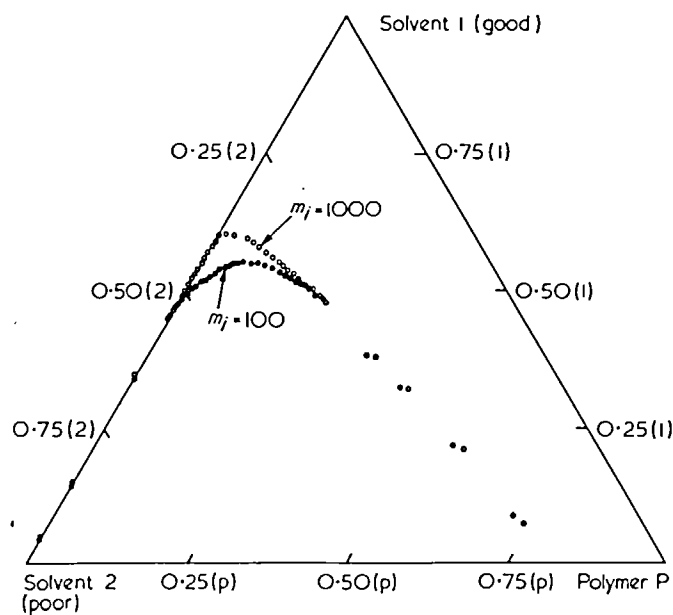


Figure 11 Phase diagram for cell 1 (330.5K)

Figure 12 Phase diagram for cell 10 (285.5K)



computer. This model in contrast to previous models fully allows for the variation of gel volume axially within the column. Sample calculations have been made using the Meyer-Flory-Huggins relation for ternary phase equilibria and the effects of initial amount of polymer, solvent gradient, and temperature gradient have been explored. Based on sample calculations a high constant temperature fractional solution method with a 'two slope', solvent gradient, a high slope initially and a low slope beginning just before dissolution is recommended for design. Also the amount of polymer should be kept low.

#### ACKNOWLEDGEMENTS

This work was supported in part by National Science Foundation Grant GK11035.

#### REFERENCES

- 1 Staudinger, H. and Bondy, H. F. *Annu. Phys.* 1931, **488**, 153; *Ber. Dtsch. Chem. Ges.* 1930, **63**, 734
- 2 Flory, P. J. *J. Am. Chem. Soc.* 1943, **65**, 372; *Ind. Eng. Chem.* 1946, **38**, 417
- 3 Johnson, B. L. *Ind. Eng. Chem.* 1948, **40**, 351
- 4 Johnson, B. L. and Wolfangel, R. L. *Ind. Eng. Chem.* 1949, **41**, 1580
- 5 Vanko, J. A. *J. Polym. Sci.* 1948, **3**, 576
- 6 Mark, H. and Saito, G. *Monatshft. Chem.* 1936, **68**, 237
- 7 Cajelli, G. *Rubber Chem. Technol.* 1939, **12**, 762
- 8 Landler, I. C. *R. Hebd. Seanc. Acad. Sci.* 1947, **225**, 629
- 9 Claesson, S. *Ark. Kem. (A)* 1949, **26**, 1
- 10 Desreux, V. *Rev. Trav. Chim.* 1949, **68**, 789
- 11 Baker, C. A. and Williams, R. J. P. *J. Chem. Soc.* 1956, p 2352
- 12 Caplan, S. *J. Polym. Sci.* 1959, **35**, 409
- 13 Hulme, J. M. and McLeod, L. A. *Polymer* 1962, **3**, 153
- 14 Smith, W. V. and Thiruvengeda, S. *Rubber Chem. Technol.* 1970, **43**, 1439
- 15 Elliott, J. H. in 'Polymer Fractionation', (Ed. M. J. R. Cantow) Academic Press, New York, 1967, Ch B2
- 16 Porter, R. S. and Johnson, J. F. in 'Polymer Fractionation' (Ed. M. J. R. Cantow), Academic Press, New York, 1967, Ch B3
- 17 Blair, D. E. *J. Appl. Polym. Sci.* 1970, **14**, 2469
- 18 Englebert, A. and Tompa, H. *Polymer* 1970, **11**, 507
- 19 Flory, P. J. 'Principles of Polymer Chemistry', Cornell, Ithaca, 1953
- 20 Tompa, H. 'Polymer Solutions', Butterworth, London, 1956
- 21 Schulz, G. V., Deussen, P. and Scholz, A. R. *Makromol. Chem.* 1963, **69**, 47
- 22 Smith, W. V. *J. Polym. Sci. (A-2)* 1970, **8**, 207
- 23 White, J. L. and Kingry, G. W. *J. Appl. Polym. Sci.* 1970, **14**, 2723
- 24 Tompa, H. *Trans. Faraday Soc.* 1949, **45**, 1142
- 25 Hougen, O. A., Watson, K. W. and Ragatz, R. 'Chemical Process Principles', Wiley, New York, 1954, Vol 1
- 26 Bronsted, J. N. and Volquartz, K. *Trans. Faraday Soc.* 1940, **36**, 619
- 27 Gee, G. *Trans. Faraday Soc.* 1944, **40**, 468
- 28 Powers, P. O. *Ind. Eng. Chem.* 1950, **42**, 2558
- 29 Gavoret, and Magat, M. *J. Chim. Phys.* 1949, **47**, 355; *J. Chem. Phys.* 1949, **17**, 999
- 30 Schulz, G. V. and Jirgenson, B. Z. *Phys. Chem. (B)* 1940, **46**, 105
- 31 Flory, P. J. *J. Chem. Phys.* 1942, **10**, 51
- 32 Flory, P. J. *J. Chem. Phys.* 1944, **12**, 425
- 33 Gee, G. *Trans. Faraday Soc.* 1944, **40**, 463
- 34 Scott, R. L. and Magat, M. *J. Chem. Phys.* 1945, **13**, 172
- 35 Scott, R. L. *J. Chem. Phys.* 1949, **17**, 268
- 36 Yamamoto, M., White, J. L. and MacLean, D. L. *Polymer* 1971, **12**, 290
- 37 Wilson, J. N. *J. Am. Chem. Soc.* 1940, **62**, 1583
- 38 Thomas, H. C. *J. Am. Chem. Soc.* 1944, **66**, 1664; *Ann. N.Y. Acad. Sci.* 1948, **49**, 161
- 39 Lapidus, L. and Amundson, N. R. *J. Phys. Chem.* 1952, **56**, 984
- 40 Martin, A. J. P. and Synge, R. L. M. *Biochem. J.* 1941, **35**, 1358
- 41 Giddings, J. C. and Eyring, H. *J. Phys. Chem.* 1955, **59**, 416
- 42 Giddings, J. C. 'Dynamics of Chromatography', Marcel Dekker, New York, 1965, Vol 1
- 43 Aris, R. and Amundson, N. *Am. Inst. Chem. Eng. J.* 1957, **3**, 280
- 44 MacLean, D. L. *PhD Dissertation*, University of Tennessee, 1971
- 45 van Decmter, J. J., Zuiderweg, F. J. and Klinkenberg, A. *Chem. Eng. Sci.* 1956, **5**, 271
- 46 Miller, S. F. and King, C. J. *Am. Inst. Chem. Eng. J.* 1966, **12**, 767
- 47 Billmeyer, F. W. and Kelley, R. N. *J. Chromatog.* 1968, **34**, 322
- 48 Uberreiter, F. and Asmussen, F. *J. Polym. Sci.* 1962, **57**, 187, 199
- 49 Kilb, R. W. and Bueche, A. M. *J. Polym. Sci.* 1958, **28**, 285

# Melting and transition phenomena in some polyester-urethanes

K. Onder, R. H. Peters and L. C. Spark

*Department of Polymer and Fibre Science, University of Manchester Institute of Science and Technology, Sackville Street, Manchester M60 1QD, UK  
(Received 16 March 1971; revised 30 July 1971)*

A series of poly(ethylene adipates) with molecular weights between 1800 and 15 000 were prepared, and were extended by reaction with di-isocyanates. In one series of extended polymers the different polyesters were all extended with tolylene di-isocyanate whilst in a second series a polyester of molecular weight 3000 was extended with 4 different di-isocyanates. The glass transition temperatures and melting points of all polymers were studied. The variation of  $T_g$  of homopolymers with molecular weight was not adequately represented by the usual equations and it was concluded that the OH end groups are tied into the structure. On the other hand the variation of  $T_m$  with molecular weight obeyed the Flory equation and leads to a value for the heat of fusion similar to that obtained by Edgar and Ellery by the copolymer method. The observed values of  $T_g$  and  $T_m$  of the copolymers did not agree with values calculated by random copolymer theory. In the case of melting points it is likely that the discrepancy arose from the disparate nature of the ethylene adipate, crystallizable, units and the di-isocyanate, non-crystallizable, units; the latter distorted the structure so badly that a number of neighbouring crystallizable units were prevented from crystallizing.

## INTRODUCTION

The properties of a polymer depend on molecular weight, chemical nature of the units composing the polymer, the morphology in the solid state, etc. As part of a programme designed to elucidate the relations between properties, polymers and their composition, a range of polymers and copolymers of poly(ethylene adipate) were prepared. The work reported here is concerned essentially with two kinds of materials, namely poly(ethylene adipates) of (a) different molecular weights and (b) low molecular weight joined together by reaction with di-isocyanates. With the latter 'extended' polymers, the material produced could be regarded essentially as a crystalline polymer in which the chain regularity was broken up at a limited number of points. It was considered of interest to ascertain to what extent the polymer properties could usefully be modified by such changes.

## EXPERIMENTAL

### Materials

The di-isocyanates as received were all purified prior to use and their purity was estimated by reaction with *n*-butylamine.

Hexamethylene di-isocyanate (HDI) (supplied by Mobay Chemical Co.) was fractionally distilled giving a liquid (b.p. 89°C at 0.9 mmHg; purity 99.1%).

4,4'-Diphenylmethane di-isocyanate (MDI) (supplied by Du Pont) was flash distilled under reduced pressure by dropping the warm molten material onto the hot distillation flask. (B.p. 107°C at 0.1 mmHg; m.p. 40°C; purity 98.7%.)

1,5-Naphthalene di-isocyanate (NDI) (supplied by Du Pont) was recrystallized from Analar benzene under direct dry gas<sup>1</sup>. (M.p. 132°C; purity, 98.0%.)

Toluene-2,4-di-isocyanate (supplied by Du Pont) was fractionally distilled. (B.p. 97°C at 0.1 mmHg; purity 99.8%.)

Dimethyl adipate and ethylene glycol were fractionally distilled. (B.p. 58°C at 0.25 mmHg and 79°C at 4 mmHg respectively.)

### Preparation of polymers

*Polyethylene adipate.* Poly(ethylene adipate) (PEA) samples were prepared by ester interchange using dimethyl adipate and ethylene glycol. The latter were heated together in the presence of calcium acetate and antimony trioxide as catalysts at 160–180°C in a current of dry nitrogen. After 3–5 h when the methanol had ceased distilling over, a vacuum was applied and the temperature was raised to 230°C to distil off ethylene glycol. The quantity of the latter controlled the molecular weight of the product. The resulting polymer was washed in water to remove the catalyst, dissolved in acetone and filtered into ethanol to reprecipitate the polymer.

*Extended polymers.* For extension of low molecular weight samples of PEA, the latter in nitrobenzene were reacted at 105°C with 75% of the di-isocyanate required to combine with the hydroxyl end-groups of the polymer in the presence of a catalyst (triethylene diamine and dibutyl tin dilaurate). After a period of 1–2 h had elapsed, the remainder of the di-isocyanate was added over the course of several hours. By this controlled addition of the di-isocyanate, allophanate links were avoided and a linear polymer was obtained. The polymers were purified by precipitation in ethanol followed by solution in chloroform and reprecipitation in ethanol.

#### Molecular weight determination

*Polyethylene adipate.* Results were obtained (a) by end-group analysis using the succinate method<sup>2</sup>, (b) from the intrinsic viscosity in chloroform solution at 25°C with the aid of the equation given by Chang et al.<sup>3</sup>

$$[\eta] = 2.0 \times 10^{-4} (M_v)^{0.77} \quad (1)$$

On the assumption that the most probable distribution of molecular weights existed even though a small quantity of the low molecular weight fraction might have been lost in purification, the number average value was calculated by the factor<sup>4</sup>:

$$[(1+a)\Gamma(1+a)]^{1/a} \quad (a=0.77 \text{ in this case})$$

and (c) by vapour pressure osmometry in chloroform, or for the higher molecular weight materials in benzene at 65°C.

The results for the series of samples used in this work are given in Table 1. When the molecular weight was required in subsequent calculations, it was considered that the end-group determination was the most reliable.

Table 1 Number-average molecular weights of poly(ethylene adipate)

Polymer	End group	Viscosity	Vapour pressure osmometry
P1	1 850	1 790	—
P2	3 050	2 890	2 800
P3	5 100	4 750	—
P4	7 000	6 150	—
P5	8 500	8 040	8 730
P6	12 000	9 900	—
P7	—	—	18 400

Table 2 Number-average molecular weights of extended polymers

Mol. wt. of PEA	Isocyanate concn.	Molar	$M_n$ (viscosity)	$M_n$ (vapour pressure osmometry)
P2 3 000	HDI	0.0532	22 800	24 500
P2 3 000	MDI	0.0532	30 200	19 100
P2 3 000	NDI	0.0532	24 500	—
P2 3 000	TDI	0.0532	24 500	30 000
P1 1 850	TDI	0.0847	28 700	19 000
P2 3 000	TDI	0.0532	25 400	30 000
P3 5 100	TDI	0.0338	34 600	23 900
P4 7 000	TDI	0.0240	38 000	—
P5 8 500	TDI	0.0198	39 800	21 100

The maximum molecular weight obtained by ester interchange was about 12 000. To obtain a product with a value greater than this, sample P3 was successively fractionated to give sample P7; sample P7 possessed a higher molecular weight than the others but naturally is expected to have a narrower distribution.

*Extended polymers.* Absolute measurements were not satisfactory since their molecular weights are too large for end-group analysis, almost too high for vapour pressure yet too low for membrane osmometry. In the latter kind of measurement, it was found that even with the 'Mechrolab' rapid-acting osmometer, too much polymer diffused through the membrane to allow reliable measurements to be made. Most reliance was therefore placed on results calculated using equation (1); even so it must be observed that the constants in this equation are those for PEA and will not strictly apply to the data obtained using the extended polymer. The molecular weights must therefore be taken as a guide (Table 2). Nevertheless, even though the agreement between viscosity and vapour pressure osmometry data is poor, the polymers possess molecular weights of at least 20 000, a magnitude which is sufficient for the material to be in the range in which molecular weight changes have little effect on the properties of the polymer.

#### Measurement of melting points and glass transition temperatures

The thermal transitions of the polymers were examined by means of a Perkin-Elmer DSC1 differential scanning calorimeter (d.s.c.): prior to starting the run, the samples of polymer were melted at 80°C for 10 min followed by quenching in ethanol cooled with solid carbon dioxide to minimize the extent of crystallization. The samples were scanned at a heating rate of either 2 or 4°C per minute, the temperature being raised sufficiently high to observe crystallization and melting phenomena. To obtain the values of the glass transition temperatures, the conventional construction was used.

Later in the investigation when a Du Pont Differential Thermal Analyser became available, this was used to determine more accurately the melting points of the polymers where fast heating rates were essential to reduce the possibility of recrystallization occurring. In the customary manner, the temperature of the sample at the peak of the melting endotherm was taken to be the melting temperature.

Glass transition temperatures were also determined dilatometrically. The dilatometer consisted of a glass bulb of 2–3 ml capacity fitted by means of a ground joint to a length of precision glass tubing (1 mm bore). 1–2 g of polymer was used, the confining fluid being a silicone (M.S. 200 of freezing point –85°C). The polymer was melted and quenched as for the thermal measurements. The position of the liquid in the meniscus was followed whilst the temperature was raised at about 4°/h. Measurements were not continued above –20°C since crystallization commenced with most polymers at this temperature. The data yielded good straight lines whose intersection gave  $T_g$  to within 0.5°C.

Because even the homopolymers crystallize slowly relative to the rate of cooling during quenching, it is considered that the observed transitions are truly representative of the polymers in the amorphous state and

Table 3 Glass transition temperatures of PEA

Polymer	$M_n$	$T_g$ (dil.) (°C)	$T_g$ (d.t.a.) (°C)	$x$ bonds per chain	kJ mol <sup>-1</sup>
P1	1 850	-52.5	-52	108	4.05
P2	3 050	-50.0	-51	178	3.84
P3	5 100	-48.5	-48	296	3.71
P4	7 000	-47.5	—	407	3.66
P5	8 500	-47.0	-47.0	494	3.64
P6	12 000	-46.6	—	698	3.60
P7	18 000	-46.0	-46.0	1046	3.57

Table 4 Glass transition temperatures of extended polymers

Polymer	$T_g$ (dil.) (°C)	$T_g$ (d.t.a.) (°C)
P2-HDI	-45.5	-44
P2-MDI	-36.5	-38
P2-NDI	-36.0	-37
P2-TDI	-38.25	-39
P1-TDI	-35.5	-29
P2-TDI	-38.25	-39
P3-TDI	-40.5	-40
P4-TDI	-41.0	-42
P5-TDI	-42.0	-42

are not significantly affected by the presence of crystallized material. This opinion is substantiated by the occurrence of crystallization when the samples were heated above  $T_g$ , especially in the dilatometer experiments in which the onset of crystallization was observed at temperatures as low as  $-20^\circ\text{C}$ .

The results for all the polymers are shown in Tables 3 and 4. The agreement between the values obtained from the two methods appears satisfactory until it is recalled that different heating rates have been used. Application of the W.L.F. equation suggests that the results from the faster method (d.s.c.) should be about  $4^\circ\text{C}$  higher than those from the slower. However, the glass transition in most of these polymers ranges over some  $8^\circ\text{C}$ . The determination of transition temperatures is different, dilatometry assigning values to the middle of the range, whereas d.s.c. determines the temperature at the low end of the transition range. This difference in method accounts for some  $2.5^\circ\text{C}$  difference in the values of  $T_g$  and it is considered that this value and the  $4^\circ\text{C}$  suggested from the W.L.F. equation agree within experimental error. It was however felt that the dilatometric data are the more reliable.

Melting points were determined by differential thermal analysis (d.t.a.) after the polymers had been crystallized for 6 or 8 days at a temperature chosen on the basis of the rates of crystallization which had previously been determined. The time allowed for crystallization was of a length several times the times of half crystallization. The melting points of samples treated in this way approximate to the thermodynamic melting point.

## RESULTS AND DISCUSSION

### Glass transition temperatures

Changes in  $T_g$  with molecular weight of the homopolymers. The figures show the expected trend of increase in  $T_g$  with increasing molecular weight. The simplest

descriptions of such data are those derived by Fox and Flory<sup>5</sup> and Ueberreiter and Kanig<sup>6</sup>.

The equation derived by the former workers relates  $T_g$  at a given molecular weight  $M$  to that at infinite molecular weight,  $T_{g\infty}$  by:

$$T_g = T_{g\infty} - \frac{A}{M} \quad (2)$$

whereas the latter workers have given a reciprocal relation:

$$\frac{1}{T_g} = \frac{1}{T_{g\infty}} + \frac{B}{M} \quad (3)$$

$A$  and  $B$  being empirical constants.

Fox and Loshaek<sup>7</sup> have shown how both equations are approximate forms for high molecular weights of a more precise equation derived from considerations of free volume and some data concerning the specific volumes of polystyrene. The experimental data are plotted according to equations (2) and (3) (Figure 1); the relation is linear for those polymers which lie in the higher molecular weight range but neither equation is obeyed by the polymers of the lower molecular weights. Extrapolation of the straight line portions of both graphs gives a value of  $-45.0^\circ\text{C}$  for  $T_{g\infty}$ . Regression lines for all seven points have been calculated from the data, giving mean deviations of  $0.2$  and  $0.4^\circ\text{C}$  values which are within experimental error; even so the data clearly lie on curves suggesting that for low molecular weights the approximations involved in deriving equations (2) and (3) are not valid.

Bueche<sup>8</sup> shows how, from the value of  $A$  in equation (2), the additional free volume associated with a chain end may be calculated. Inserting the experimental data from the high molecular weight region of PEA (where equations (2) and (3) apply), a very small volume, about  $6A^3$  is obtained, which may be compared with  $80A^3$  for polystyrene<sup>8</sup> or  $75A^3$  for poly(methyl methacrylate) (PMMA) (calculated from Fig. 3 of ref. 10). This small free volume is a reflection of the fact that there is a drop in  $T_g$  of only  $5^\circ\text{C}$  for a change in  $M_n$  from  $\infty$  to 3000; this value is to be compared with the corresponding

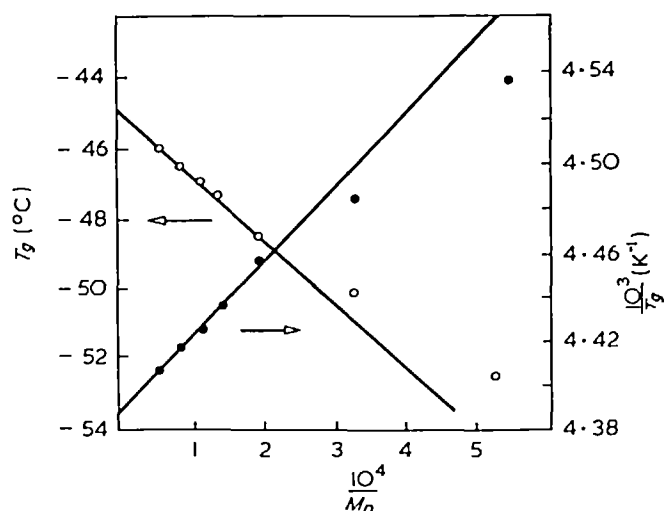


Figure 1 Glass transition temperature and molecular weight, plotted according to (O) equation (2), and (●) equation (3)

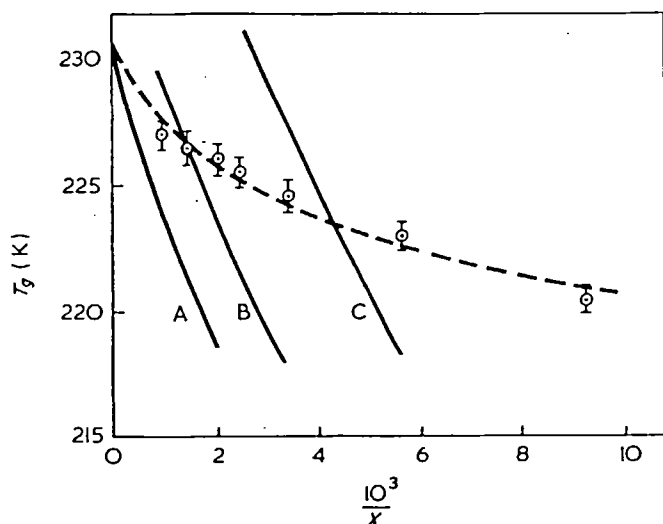


Figure 2 Glass transition temperature and molecular weight, with lines calculated for equation (4) using three fixed flex energies ( $\epsilon$ ) and a variable flex energy. A,  $\epsilon = -3500 \text{ J mol}^{-1}$ ; B,  $\epsilon = -3600 \text{ J mol}^{-1}$ ; C,  $\epsilon = -3750 \text{ J mol}^{-1}$  (calculated from equation (4).) ---- experimental  $\pm 0.5 \text{ K}$ .  $\epsilon = -[3500 + 28300(2/x)] \text{ J mol}^{-1}$

reduction in the  $T_g$  of the polystyrene and PMMA of  $\sim 50^\circ\text{C}$ .

Two explanations for this are possible: either the polymer chain as a whole is so flexible, as the low  $T_g$  indicates, that the ends add little to chain mobility; or the end groups in this polymer are not as mobile as in many other polymers.

An alternative basis for the deviation of the  $T_g$  with molecular weight is a statistical one in which the number of arrangements of the chain segments are enumerated and the total energy calculated in terms of the flex energy  $\epsilon$ , i.e. the additional energy which is required by each bond in the chain which is not in the position of lowest energy. The calculations define  $T_g$  as that temperature at which only one state of the system exists. An equation relating  $T_g$  to molecular size may then be derived<sup>9</sup>:

$$\frac{2\exp\left(-\frac{\epsilon}{kT_g}\right)}{1 + 2\exp\left(-\frac{\epsilon}{kT_g}\right)} \times \frac{\epsilon}{kT_g} + \ln\left[1 + 2\exp\left(-\frac{\epsilon}{kT_g}\right)\right] = \frac{x}{x-2} \left[ \frac{v \ln v}{1-v} - \frac{\ln 2x}{x} + x - 1 \right] \quad (4)$$

where  $x$  is number of atoms in chain,  $v$  is fraction of vacant sites, i.e. fractional free volume.

The experimental results are plotted in Figure 2 together with theoretical curves for three selected values of  $\epsilon$ ; the comparison indicates that the equation does not adequately represent the observations. This is in contrast to analyses on various polymers where good agreement is claimed<sup>10</sup>.

The values calculated from the practical data (Table 3) show that  $\epsilon$  cannot be treated as a constant but rather  $\epsilon$  increases as the number of chain ends increases (i.e. as the molecular weight decreases). However, if we wish to apply equation (4) to PEA,  $\epsilon$  must be taken to be the average of the energies of all the bonds in the chain.

For a polymer such as PEA which carries at its ends hydroxyl groups capable of forming hydrogen bonds, it is possible that the flex energy may be made up of two contributions, namely  $\epsilon_1$  from the main chain and  $\epsilon_2$  from each end. The flex energy in equation (4) will then be given as:

$$\epsilon = \epsilon_1 + \frac{2\epsilon_2}{x} \quad (5)$$

where  $\epsilon$  is averaged over all the bonds in the chain. The values of  $\epsilon$  have been calculated by trial and error from the data assuming the usual value for  $v$  of 0.025: a plot of  $\epsilon$  against  $1/x$  is a good straight line, showing that equation (5) is a good representation of the data. The value of  $\epsilon_1$  turns out to be  $3.5 \text{ kJ mol}^{-1}$ , whereas  $\epsilon_2$  is of the order of magnitude of a hydrogen bond at  $28.3 \text{ kJ mol}^{-1}$ . Over the range of values of the flex energy,  $\epsilon_1$  is of the correct order of magnitude for a polymer possessing a low  $T_g$  and may be compared with 3.16, 5.98 and  $6.02 \text{ kJ mol}^{-1}$  (0.76, 1.33 and  $1.44 \text{ kcal mol}^{-1}$ ) for polyisobutylene, polystyrene and PMMA respectively<sup>11</sup>. The value of  $\epsilon_1$  leads to a  $T_g$  for PEA of infinite molecular weight of  $-42.5^\circ\text{C}$ . The theoretical curve using values of  $\epsilon$  calculated from equation (5) is shown in Figure 2 to represent the experimental data very satisfactorily.

This kind of analysis falls in line with intuitive ideas, namely that the flex energy of an aliphatic polyester chain is low, but that if the end-groups are capable of forming hydrogen bonds with neighbouring chains or other end-groups presumably in the 'amorphous' regions, the increase in free volume is less than anticipated. It would seem that either approach ('free volume' or 'flex energy') manifest the same result; in the former, the interactions of the end-groups show up as making a small contribution, whereas with the latter, the interactions show up as a substantial increase in the average flex energy. A somewhat similar effect has been observed<sup>12</sup> in a series of polystyrenes having trichloro-triphenylmethyl end-groups in which  $T_g$  actually increases with decreasing molecular weight.

'Extended' polymers. The experimental results are shown in Tables 3 and 4. Since these materials have molecular weights of 20 000 or more, the values of  $T_g$  should be compared with  $-45^\circ\text{C}$  or  $-46^\circ\text{C}$  which would be given by the homopolymer of corresponding molecular weight. The polymers are of two types, namely those in which the same PEA was extended with different isocyanates to examine the effects of different types of modifying units, and those where poly(ethylene adipates) of different molecular weights were used to yield polymers whose concentration of modifying units was varied.

For the former series, the presence of one di-isocyanate unit for every 180 segments in the chain can raise the  $T_g$  by as much as  $7-9^\circ\text{C}$  even though at first sight the introduction of rogue groups, by virtue of the increased free volume, might be expected to give the opposite result. Increases in  $T_g$  are noticeable when the di-isocyanate introduces a rigid ring, e.g. naphthalene, but not where size and flexibility are similar to the ethylene adipate units. This last point is exemplified by the hexamethylene groups in HDI whose introduction does not modify  $T_g$ . There are therefore two competing factors, namely the introduction of rigid rings which

reduces chain flexibility, thereby increasing  $T_g$ , and the introduction of the large bulky groups which will presumably increase the amount of free volume available and hence cause a lowering of the  $T_g$ . It is impossible to predict the changes observed but it is clear that here the introduction of these small quantities of rigid groups raises the  $T_g$ .

In the second series, the average lengths of the PEA segments were different with the result that the  $T_g$  varied continuously with composition; and extrapolation of the data to zero TDI concentration is not inconsistent with a  $T_g$  of about  $-46^\circ\text{C}$  for the homopolymer of molecular weight  $\sim 20\,000$ .

Only qualitative comments can be made on these data. In copolymers in which the two comonomers are randomly distributed (and of not too dissimilar chemical character, e.g. styrene and butadiene) an equation of the form<sup>13, 14</sup>:

$$A_1c_1(T_g - T_{g1}) + A_2c_2(T_g - T_{g2}) = 0 \quad (6)$$

is applicable. In this equation  $A_1$  and  $A_2$  are constants and  $c_1$ ,  $c_2$  are the weight fractions of the two comonomers.  $T_{g1}$  and  $T_{g2}$  are the glass transition temperatures of the two homopolymers. This equation implies that  $T_g$  of the copolymer is intermediate between those of the parent homopolymers, though a few exceptional cases have been observed<sup>15, 16</sup>. Assuming that the polyurethanes studied here are random copolymers of PEA and TDI units, the present results were found to fit equation (6). However, the numerical values which had to be assigned to  $T_{g2}$  and to  $(A_1/A_2)$  appear to have no physical significance. The most probable reason for this would seem to be that because of the small range of molar concentrations covered the lengthy extrapolation to a molar fraction of 1.0 is extremely unreliable and magnifies experimental errors even when the data are plotted in the linear fashion proposed by Wood<sup>14</sup>. It is also possible that despite the low molar concentration of TDI and the wide molecular weight distribution of the parent polyester, the polyurethanes are not sufficiently random for equation (6) to apply.

### Melting points

The observed melting points of the homopolymers after being crystallized for 6 days (Tables 5 and 6) increase with molecular weight, becoming approximately constant once a value of 12 000 is exceeded. A satisfactory straight line is obtained when the data are plotted according to the Flory equation (Figure 3):

$$\frac{1}{T_m} - \frac{1}{T_{m\infty}} = \frac{R}{\Delta H} \times \frac{2}{x}$$

where  $T_m$  is the melting point of a polymer of number average DP of  $x$ ,

$T_{m\infty}$  is the melting point of a polymer of infinite DP,

$\Delta H$  is the heat of fusion.

By extrapolation,  $T_{m\infty}$  is found to be  $60^\circ\text{C}$ ; the heat of fusion is  $18.4\text{ kJ mol}^{-1}$ . This latter value may be compared with Edgar and Ellery's value of  $15.9\text{ kJ mol}^{-1}$  ( $3800\text{ cal mol}^{-1}$ )<sup>17</sup> which was determined from the depression of the melting point when copolymerized with poly(ethylene terephthalate). Agreement is satisfactory when it is remembered that the copolymer

Table 5 Melting points of PEA crystallized for 6 days at  $T_x$

Polymer	$T_x$ ( $^\circ\text{C}$ )	$T_m$ ( $^\circ\text{C}$ )
P1	46	50
P2	48	54
P3	48	55
P4	50	57
P5	50	57
P6	51	58
P7	51	59

Table 6 Melting points of extended polymers. Crystallized for 8 days at  $T_x$

Polymer	$T_x$ ( $^\circ\text{C}$ )	$T_m$ ( $^\circ\text{C}$ )
P2-HDI	42.5	50
P2-MDI	40	45
P2-NDI	40	45
P2-TDI	40	44
P1-TDI	33	38
P2-TDI	40	44
P3-TDI	44	50
P4-TDI	45	51.5
P5-TDI	45	53

method generally leads to a low value for the heat of fusion.

The homopolymers P6 and P7 had molecular weights which were sufficiently high to allow the method of Hoffman and Weeks<sup>18</sup> to be used to determine the thermodynamic melting temperature  $T_m^0$ , which was found to be  $63^\circ\text{C}$ .

The melting points of the 'extended' polymers were lower than that of PEA of comparable molecular weight ( $59\text{--}60^\circ\text{C}$ ). Even the flexible HDI unit lowered the melting point by  $9^\circ\text{C}$ , showing some serious distortion of the structure. The introduction of the units from MDI, NDI and TDI cause considerable reductions in melting temperature. The melting points of these polymers correspond to those of homopolymers of lower molecular weight than that of the parent polyester (2000 for the HDI urethane and 1200 for the others compared with 3000 of the parent polymer) and it is tempting to use

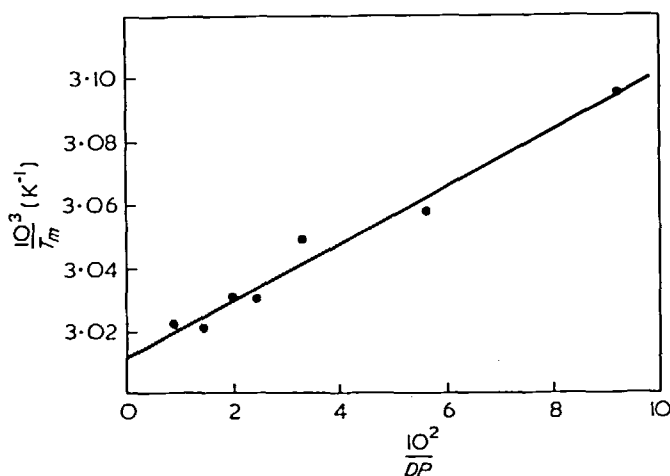


Figure 3 Melting points of homopolymers

the difference as a parameter related to the reduction of crystallite size caused by presence of the isocyanate units.

Again, the data are plotted (Figure 4) according to the random copolymer equation (7)\*:

$$\frac{1}{T_m} - \frac{1}{T_m^0} = \frac{R}{\Delta H} \ln X \quad (7)$$

where  $X$  is the molar fraction of crystallizable units. The intercept of the best line drawn through the five copolymer points corresponds to a melting point of 57.2°C for the homopolymer, compared with the observed value of 59°C for high molecular weight PEA crystallized under comparable conditions. However, the slope of the line leads to the very low value of 3.8 kJ mol<sup>-1</sup> for the heat of fusion, indicating that the introduction of the di-isocyanate residue is more damaging to the structure than is anticipated by random copolymer theory<sup>19</sup>.

The copolymer method is renowned for giving low values for the heat of fusion. Mandelkern has attributed the discrepancy to the experimental difficulty of determining the temperature at which the last crystallite has melted and has shown how this will lead to a low heat of fusion, though the relation between  $1/T_m$  and  $\ln X$  remains linear.

Here it seems unlikely that this explanation is appropriate for the following reasons. If the points in Figure 4 were to be interpreted empirically it would probably be better to draw a curve rather than a straight line through

\* In the derivation of this equation<sup>19</sup>, the copolymer is treated as an ideal binary mixture.

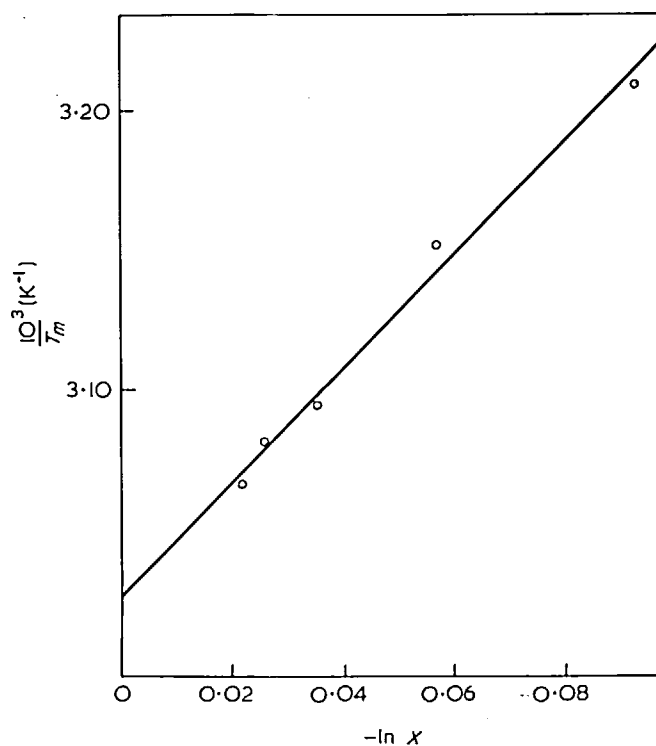


Figure 4 Melting points of copolymers

the points. Secondly, probably because the molar concentration of non-crystallizing groups does not exceed 10%, the melting peaks for the copolymers are only a little broader than the peaks for the homopolymers so it would be expected that errors arising from incorrect measurement of the true  $T_m$  would be similar for both the co- and homo-polymers, yet the variation of melting point with molecular weight of the latter leads to a satisfactory heat of fusion.

The large difference in size and character between the crystallizing and non-crystallizing units in these copolymers suggests another possibility. If the presence of a TDI or other di-isocyanate unit renders a number of adjacent PEA units non-crystallizable, then appropriate allowance must be made in the calculation of  $X$ , the mole fraction of crystallizable units, for use in equation (7). By varying the number of polymer units which are rendered non-crystallizable by each TDI unit, a family of  $1/T_m \ln X$  curves may be drawn, Figure 4 being the limiting curve. Because of the non-linearity, particularly in those cases where a large disrupting effect is assumed, quantitative analysis is not possible. However, as an indication of the magnitude of the effect, a heat of fusion of about 18 kJ mol<sup>-1</sup> is obtained from the initial slope of the graph when it is assumed that each TDI unit renders 6 PEA units non-crystallizable.

The curvature of the lines suggests that these polyurethanes are not sufficiently like the ideal random copolymer for equation (7) to apply. This is not surprising when it is realized that for the case under consideration some 40% of the molecules in the parent polyester are shorter than the length of the chain which is prevented from crystallizing by the isocyanate. Consequently as the number of TDI units in the chain increase, they will not be able to exert their full disruptive effect, causing an increase in the apparent heat of fusion.

A converse effect has been noted in the classical work of Evans *et al.*<sup>20</sup> who found that for certain copolyesters the depression of the melting point was less than expected, and attributed this to the occurrence of a limited amount of co-crystallization.

## CONCLUSIONS

As far as the homopolymers are concerned, both melting and glass transition temperatures have been shown, as anticipated, to depend on molecular weight. From the variation of melting point the heat of fusion agrees satisfactorily with the value given by other workers using a different method. However, the glass transition temperature does not change very much as the molecular weight is changed leading to either an abnormally small free volume associated with the chain ends or, on the thermodynamic interpretation, the necessity to assume that the chain ends are bonded into the structure. It must be remembered that these are hydroxyl ended polymers and the environment at the ends will be very different from that in e.g. PMMA where the original form of Gibbs' equation has been found to be adequate<sup>10</sup>.

The insertion of di-isocyanate units into the polyester again affects both melting and transition temperatures, though a given di-isocyanate may affect the crystalline and amorphous regions differently, e.g. HDI is almost as effective as TDI in damaging the crystalline structure

and lowering the melting point, but only small changes of the transition temperatures are observed. It is interesting to speculate on the possibility of the converse occurring; is it possible to find copolymerizing or extending materials which are a good geometric fit in the crystal lattice but which are very different in flexibility from the parent polymer, and, if so, how would the properties of the copolymer differ from these of the homopolymer?

Resulting from the method of preparation, these copolymers are more in the nature of block than random copolymers, but because the maximum molar concentration of the di-isocyanate relative to the ester is only 10% it was thought that they may behave as random copolymers. However, these polymers do not follow the pattern of behaviour predicted for random copolymers. From the data available, the changes in transition temperature, i.e. the situation in the amorphous regions, cannot be interpreted but it is likely that the anomalous depression of melting point (indicated by the very low calculated heat of fusion) is connected with the influence of the di-isocyanate on the behaviour of neighbouring 'crystallizable' units—a feature ignored in copolymer theory.

#### ACKNOWLEDGEMENT

K. O. wishes to thank Sümerbank of Ankara, Turkey for financial support during the course of this work.

#### REFERENCES

- 1 Vogel, A. I. 'Practical Organic Chemistry', 3rd edn, Longmans, London, 1956
- 2 Sorensen, W. R. and Campbell, T. W. 'Preparative Methods of Polymer Chemistry', Interscience, New York, 1961
- 3 Chang, P. S., Zavaglia, E. A. and Billmeyer, F. W. *Off. Dig. J. Paint Technol. Eng.* 1965, 37, 235
- 4 Schaeffgen, J. R. and Flory, P. J. *J. Am. Chem. Soc.* 1948, 70, 2709
- 5 Fox, T. G. and Flory, P. J. *J. Appl. Phys.* 1950, 21, 581
- 6 Ueberreiter, K. and Kanig, G. *J. Colloid Sci.* 1952, 7, 569
- 7 Fox, T. G. and Loshaek, S. *J. Polym. Sci.* 1955, 15, 371
- 8 Bucche, F. 'Physical Properties of Polymers', Interscience, New York, 1962, p 114
- 9 Gibbs, J. H. *J. Chem. Phys.* 1956, 25, 185
- 10 Beevers, R. B. and White, E. F. T. *Trans. Faraday Soc.* 1960, 56, 744; Pezzin, G., et al. *Eur. Polym. J.* 1970, 6, 1053
- 11 Gibbs, J. H. and DiMarzio, E. A. *J. Chem. Phys.* 1958, 28, 373
- 12 Ueberreiter, K. and Rohde-Liebenau, U. *Makromol. Chem.* 1961, 49, 164
- 13 DiMarzio, E. A. and Gibbs, J. H. *J. Polym. Sci.* 1959, 40, 121
- 14 Wood, L. A. *J. Polym. Sci.* 1958, 28, 319
- 15 Beevers, R. B. and White, E. F. T. *Trans. Faraday Soc.* 1960, 56, 1529
- 16 Loshaek, S. *J. Polym. Sci.* 1955, 15, 391
- 17 Edgar, O. B. and Ellery, E. *J. Chem. Soc.* 1952, p 2636
- 18 Hoffman, J. D. and Weeks, J. J. *J. Res. Natl Bur. Stand. (A)* 1961, 66, 13
- 19 Mandelkern, L. 'Crystallization of Polymers', McGraw-Hill, New York, 1964, p 79; Baker, C. H. and Mandelkern, L. *Polymer* 1966, 7, 7
- 20 Evans, R. D., Mighton, H. R. and Flory, P. J. *J. Am. Chem. Soc.* 1951, 72, 2018



# Book Reviews

## **NMR: Basic principles and progress** **Vol. 4: Natural and synthetic high polymers** *Edited by P. Diehl, E. Fluck and R. Kosfeld* Springer-Verlag, Berlin, 1971, 309 pp, \$17.60

This volume represents the proceedings of an NMR colloquium held at Aachen in April 1970. Thirteen of the seventeen papers are in English (the remainder being in German) and the first seven, comprising nearly half the book, concern the theory and experimental study of tacticity and sequence heterogeneity of synthetic polymers, largely by means of high resolution  $^1\text{PMR}$  spectroscopy at 220 MHz. The introductory chapter is by Frank Bovey. Although not everyone prominent in this field has contributed these chapters nevertheless represent a very useful compilation of 'almost up to the minute' data for all directly concerned with research in this field. Several mentions of the potential of  $^{13}\text{C}$  spectroscopy are made and enough spectra are shown to whet the appetite for this approach to polymer structure. This section of the book concludes with a chapter by Tosi on copolymer statistics.

The volume is No. 4 of a series having the title 'NMR: Basic principles and progress' and this first part is very much in the 'Progress' bracket.

There are several contributions on the NMR of solids and three excellent chapters by Slichter, Kosfeld and Connor are broad in scope and of a review nature, representing the 'Basic principles' part. These are of interest to a wider range of reader than is the first half of the book. Although the principal importance and appeal of the volume rests largely on these two major sections there are also other chapters not fitting too closely to the main themes, but being 'the book of the conference' such a mixed bag is not surprising. Thus infa-red (Shimanouchi), electron spin resonance (Fischer) and dielectric relaxation (Williams) are covered in single chapters, as are high resolution NMR of proteins (Hill) and broad line work on cellulose (Forslind). The last two chapters are the only ones concerned with natural polymers. With the exception of the chapter on dielectric relaxation these topics seem somewhat out of place.

The quality of production is high and there are few misprints, although on page 130 Prof. Corradine of Naples is unfortunately thanked for 'unvaluable help'.

C. Crane-Robinson

## **Synthetic polymer membranes**

*Robert E. Kesting*

McGraw-Hill, New York, 1971, 307 pp, £9.00

Polymeric barriers that have been restructured prior to use in membrane separation processes, is the author's definition given in the preface and so a large proportion of this book (some 170 pages) is devoted to a detailed discussion of the formation and structure of actual membranes. These have been dealt with in five classes: dense membranes, porous membranes, porous phase inversion membranes, membranes formed *in situ*, and ion-exchange membranes. The membrane classes have in turn been considered under different sub-headings according to the method of formation, the physical properties and the fine structure. This portion of the book is probably the most valuable as it represents the first reasonably complete summary of current knowledge about membrane structure and fabrication methods. Apart from a short introductory section the rest of the work is concerned with membrane characterization, some of the theories and concepts of the function of membranes as diffusion media and permselective barriers, and finally with a few details of the industrial and medical applications.

Although some interesting quantitative information is given the method of treatment throughout the book is mainly practical and descriptive rather than theoretical and mathematical. A few mathematical derivations and statements have been included, however, but due to the looseness of definitions and incomplete

statements of assumptions these represent a rather less successful part of the book and in many cases understanding can only be achieved by reference to the original papers. Thus on page 37 it is not at all clear why the pore radius products  $r_1r_2$  and  $r_2r_3$  should be equal, on page 249 there is no stated relationship that leads to the disappearance of  $J_a$  and  $J_b$  while the reader cannot begin to understand the comparisons of the different theories of reverse osmosis without definition of the symbols  $D'$  and  $\Delta\pi$  and without a statement about the presence or absence of permselectivity in equation (17).

A subject index containing about 500 entries has been included but no author index is given. This is a pity and in fact the Loeb Sourirajan membranes mentioned on the dust cover are not listed in the subject index. A thorough reading of the appropriate chapter revealed one or two mentions of these authors but the reviewer was not certain at the end how these membranes were prepared. A useful help for locating information is given, however, by a very full summary (one page or more) included at the end of each chapter.

The author uses a wordy and sometimes imprecise style of writing that makes the book somewhat longer than it need be and occasionally hides the meaning. The description, for instance, of the mechanism of the formation of ionotropic gels on page 104 is obscure. In these days of edited editions of collective multi-author works, however, the author is to be congratulated for undertaking alone the task of gathering and classifying the extensive knowledge of polymer membranes that is presented.

The book is well produced and an interesting feature is the inclusion of several very beautiful scanning electron microscope photographs showing the three-dimensional porous structure of some membranes.

Everyone concerned with membrane separation processes will want to have access to this book but at a cost of almost 3p per page it is rather expensive for purchase by individual research workers and technologists. Its unique character as a source book on membrane fabrication and structure will, however, make it a necessity for many libraries.

G. S. Park

### Conference Announcement

#### **6th Biennial Polymer Symposium**

Ann Arbor, 12-15 June 1972

The 6th Biennial Polymer Symposium, sponsored by the Division of Polymer Chemistry of the American Chemical Society will be held from 12 to 15 June, 1972 at the Macromolecular Research Center, University of Michigan, Ann Arbor, Michigan, USA.

The registration fee for the entire conference will be \$20.00 for American Chemical Society members, \$25.00 for non-members, and \$3.00 for students; the single-day fee for non-students will be \$8.00. These fees will cover both the technical sessions and a social gathering scheduled for the evening of June 12th. Registration forms and detailed information will be mailed in April to all members of the American Chemical Society Divisions of Polymer Chemistry, Rubber Chemistry, and Organic Coatings and Plastics. Others interested in attending can obtain the same material by writing to the University of Michigan, Extension Service Conference Department, 412 Maynard Street, Ann Arbor, Michigan 48104, USA.

# Equilibrium ring concentrations and the statistical conformations of polymer chains: Part 7. Cyclics in poly(1,3-dioxolane)

J. M. Andrews and J. A. Semlyen

*Department of Chemistry, University of York, Heslington, York YO1 5DD, UK  
(Received 2 August 1971)*

Cyclic oligomers  $[\text{CH}_2\text{OCH}_2\text{CH}_2\text{O}]_x$  with  $x=2-9$  were found to be present in poly(1,3-dioxolane) samples prepared by monomer-polymer equilibrations using boron trifluoride diethyl etherate as catalyst. The molar cyclization equilibrium constants  $K_x$  for cyclics  $[\text{CH}_2\text{OCH}_2\text{CH}_2\text{O}]_x$  with  $x=1-8$  were measured for an undiluted and a solution equilibrate at 333K. The  $K_x$  values for the cyclics with  $x \geq 5$  were in agreement with those calculated by the Jacobson-Stockmayer theory, using a rotational isomeric state model to describe the statistical conformations of the corresponding chains and assuming that the chains obey Gaussian statistics.

## INTRODUCTION

The measurement of cyclic concentrations in polymeric equilibrates provides a powerful method for studying the statistical conformations of chain molecules over a range of molecular weights and in a variety of different environments. The potential of the method has already been demonstrated by theoretical and experimental studies of cyclic concentrations in polysiloxane equilibrates<sup>1-4</sup>. Here, we report the results of an investigation into the concentrations of cyclic oligomers in a polyether. Molar cyclization equilibrium constants for cyclics  $[\text{CH}_2\text{OCH}_2\text{CH}_2\text{O}]_x$  in poly(1,3-dioxolane) have been determined for monomer-polymer equilibrates in the bulk polymer and in solution in dichloroethane at 333K. The experimental values are compared with those predicted by the Jacobson and Stockmayer<sup>5</sup> theory for cyclics formed from chains in random-coil conformations.

## EXPERIMENTAL

### *Polymerizations*

1,3-Dioxolane and dichloroethane were dried by refluxing over sodium wire and calcium hydride respectively. The monomer and solvent were fractionally distilled and stored under dry nitrogen. Boron trifluoride diethyl etherate and diethylamine were obtained from BDH. They were used as supplied.

The bulk polymerization was carried out by adding 0.435 g boron trifluoride diethyl etherate to 207.6 g 1,3-dioxolane. The solution polymerization was carried out by adding 0.463 g boron trifluoride diethyl etherate to 104.9 g 1,3-dioxolane dissolved in 187.1 g dichloroethane. The reactants were maintained initially at 273K

so that the polymerizations proceeded in a controlled manner. The temperature was then raised slowly to 333K and held at this temperature for several days to ensure that equilibrium had been attained. The polymeric products were quenched by adding small amounts of diethylamine.

### *Extraction of oligomers*

100 ml dichloromethane were added to the quenched undiluted equilibrate and oligomers were extracted from this and from the quenched solution equilibrate using the following procedure. 1500 ml methanol were added and the mixture was heated to dissolve the polymer. The mixture was then allowed to cool overnight to 273K. The supernatant liquid was decanted off and filtered. Methanol was removed from the filtrate using a rotary evaporator and the material remaining was weighed. Two more extractions were carried out in a similar way. Analysis of a further extract showed negligible amounts of oligomers. Equilibrium monomer concentrations were determined by drying and weighing the oligomeric extracts and polymeric residues and subtracting these weights from the initial weights of 1,3-dioxolane used.

### *Instrumental methods*

Polymeric products were analysed using a gel permeation chromatograph fitted with a Waters Model R4 differential refractometer detector<sup>6</sup>. Volatile oligomeric extracts were analysed using a Pye-Unicam (Series 104) gas-liquid chromatograph fitted with a heated dual flame-ionization detector<sup>7</sup>. Response factors for cyclics on the gas-liquid chromatograph were determined using oligomeric fractions obtained by the molecular distil-

lation of cyclic extracts. Gas-liquid chromatography was found to be suitable for the analysis of cyclics  $[\text{CH}_2\text{OCH}_2\text{CH}_2\text{O}]_x$  up to  $x=9$ , and n-hexadecane was used as an internal standard.

Mass spectra were obtained using a combined AEI M.S.12 mass spectrometer/Pye-Unicam (Series 104) gas-liquid chromatograph. Nuclear magnetic resonance spectra were measured on a Varian 60 MHz instrument. Infra-red spectra were obtained using a Unicam SP 200G spectrophotometer.

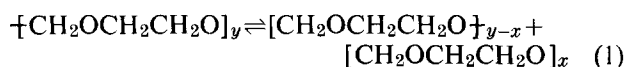
## RESULTS AND DISCUSSION

### Identification of cyclic oligomers

Other workers<sup>8-10</sup> have demonstrated that under the influence of boron trifluoride diethyl etherate an equilibrium is set up between 1,3-dioxolane and poly(1,3-dioxolane) in both the undiluted polymer and in solution. Analysis of low molecular weight extracts showed that cyclic oligomers  $[\text{CH}_2\text{OCH}_2\text{CH}_2\text{O}]_x$  with  $x=2-9$  were present as 2.2% by weight in the undiluted equilibrate and as 2.4% by weight in the solution equilibrate. The identities of the cyclic dimer and cyclic trimer were established by mass spectrometry. The cyclic oligomers  $[\text{CH}_2\text{OCH}_2\text{CH}_2\text{O}]_x$  with  $x=4-9$  were identified by their gas-liquid chromatographic retention times. The nuclear magnetic resonance spectra and infra-red spectra of oligomeric fractions corresponded to those expected for mixtures of the cyclics  $[\text{CH}_2\text{OCH}_2\text{CH}_2\text{O}]_x$ .

### Theoretical molar cyclization equilibrium constants

The equilibrium between cyclic and linear molecules in poly(1,3-dioxolane) may be represented as follows:



Although the molecular weight distributions of the chains in the equilibrates were not characterized, gel permeation chromatographic tracings suggested that it is reasonable to assume a most probable distribution of chain lengths for the linear polymer. Hence, experimental molar cyclization equilibrium constants  $K_x$  for  $x$ -meric cyclics were calculated using Flory's relationship<sup>11</sup>:

$$K_x = [\text{CH}_2\text{OCH}_2\text{CH}_2\text{O}]_x / (1 - 1/\bar{y})^x \quad (2)$$

where  $\bar{y}$  represents the average number of monomeric units in the chain molecules. Gel permeation chromatography was used to estimate  $\bar{y}$  for the undiluted equilibrate ( $\bar{y} \sim 400$ ) and the solution equilibrate ( $\bar{y} \sim 20$ ).

Chains in the undiluted and solution equilibrates of poly(1,3-dioxolane) at 333K should adopt random-coil conformations unperturbed by excluded volume effects; and, if the chains are of sufficient length and flexibility to obey the Gaussian expression for the density  $W_x(\mathbf{r})$  of their end-to-end vectors  $\mathbf{r}$  in the region  $\mathbf{r}=\mathbf{0}$ , the Jacobson-Stockmayer theory<sup>2, 5</sup> provides the following expression for the  $K_x$  values for unstrained cyclics  $[\text{CH}_2\text{OCH}_2\text{CH}_2\text{O}]_x$  formed by the forward step of equation (1) with zero enthalpy change

$$K_x = (3/2\pi \langle r_x^2 \rangle_0)^{3/2} (1/2xN_A) \quad (3)$$

where  $\langle r_x^2 \rangle_0$  is the unperturbed mean-square distance between the ends of the  $x$ -meric chains and  $N_A$  is the Avogadro constant. The symmetry number  $2x$  in equation

(3) arises because in the equilibration reaction the cyclics open at only two of the bonds in each monomeric unit. Molar cyclization equilibrium constants for cyclics  $[\text{CH}_2\text{OCH}_2\text{CH}_2\text{O}]_x$  were calculated by equation (3) using the rotational isomeric state model described in the following section to compute the required mean-square end-to-end distances of the corresponding chain molecules.

### Rotational isomeric state model for poly(1,3-dioxolane)

A section of the poly(1,3-dioxolane) chain is shown in Figure 1. The lengths of the skeletal carbon-oxygen and carbon-carbon bonds were assigned the values 1.43 Å and 1.53 Å respectively and all bond angles were taken to be tetrahedral. Rotational isomeric states about each skeletal bond were chosen at 0° (*trans*), 120° (*gauche*+) and 240° (*gauche*-). The mutual interdependence of adjacent bond rotational states was taken into account by means of five matrices referring to pairs of bonds as shown in Figure 1. Each statistical weight parameter used in these matrices is related to the difference in energy  $\Delta E$  between its associated conformation and the all-*trans* conformation by the Boltzmann factor  $\exp(-\Delta E/RT)$  where  $R$  is the gas constant. The matrices are as follows

$$\mathbf{U}_a = \begin{bmatrix} 1 & \sigma & \sigma \\ 1 & \psi\sigma & \omega\sigma \\ 1 & \omega\sigma & \psi\sigma \end{bmatrix} \quad (4)$$

$$\mathbf{U}_b = \begin{bmatrix} 1 & \sigma' & \sigma' \\ 1 & \psi'\sigma' & \omega'\sigma' \\ 1 & \omega'\sigma' & \psi'\sigma' \end{bmatrix} \quad (5)$$

$$\mathbf{U}_c = \begin{bmatrix} 1 & \sigma & \sigma \\ 1 & \psi'\sigma & \omega'\sigma \\ 1 & \omega'\sigma & \psi'\sigma \end{bmatrix} \quad (6)$$

$$\mathbf{U}_d = \begin{bmatrix} 1 & \sigma'' & \sigma'' \\ 1 & \psi''\sigma'' & \omega''\sigma'' \\ 1 & \omega''\sigma'' & \psi''\sigma'' \end{bmatrix} \quad (7)$$

$$\mathbf{U}_e = \begin{bmatrix} 1 & \sigma'' & \sigma'' \\ 1 & \psi''\sigma'' & \omega''\sigma'' \\ 1 & \omega''\sigma'' & \psi''\sigma'' \end{bmatrix} \quad (8)$$

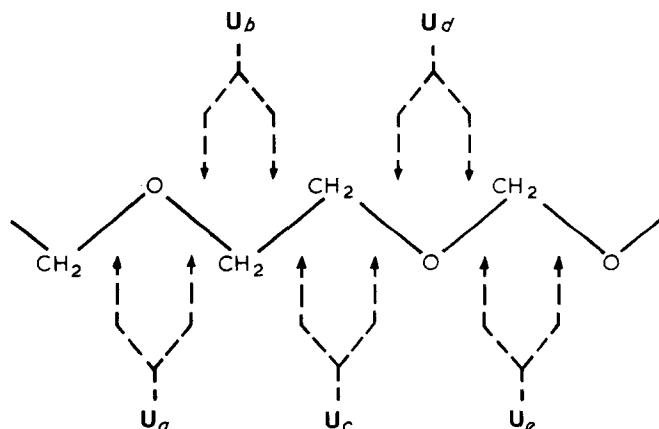


Figure 1 Section of the poly(1,3-dioxolane) chain in the all-*trans* conformation. The statistical weight matrices  $\mathbf{U}_a$ ,  $\mathbf{U}_b$ ,  $\mathbf{U}_c$ ,  $\mathbf{U}_d$ ,  $\mathbf{U}_e$ , take account of the mutual interdependence of rotational states about the pairs of bonds shown

Sections of the poly(1,3-dioxolane) chain have a similar structure to sections of poly(oxyethylene) and poly(oxyethylene) chains. Thus, three of the statistical weight matrices (viz.  $U_b$ ,  $U_c$ ,  $U_e$ ) and all the statistical weight parameters except  $\psi$  and  $\omega$  were taken from Flory and Mark's analysis<sup>12, 13</sup> of these polyethers. A consideration of the non-bonded interactions involved led to the conclusion that  $\psi \approx 1$  and  $\omega \approx 0$ . The statistical weight parameters for poly(1,3-dioxolane) at 333K are listed in Table 1. Using these parameters, the characteristic ratio  $\langle r^2 \rangle_0 / 5x\bar{l}^2$  was calculated to be 4.4. This value is close to Gorin and Monnerie's experimental values<sup>15</sup> of 3.9 at 318K and 4.2 at 280K.

#### Comparison of experiment with theory

Experimental molar cyclization equilibrium constants for cyclics in the undiluted equilibrate (containing 81% linear polymer) and the solution equilibrate (containing 14% linear polymer) are plotted as  $\log K_x$  against  $\log x$  in Figure 2. The experimental values (which are believed to be correct to within  $\pm 10\%$  for  $x=2-5$  and to a somewhat greater degree of uncertainty for  $x > 5$ ) are compared with those calculated by equation (3) by substituting values of  $\langle r_x^2 \rangle_0$  computed for  $\text{[CH}_2\text{OCH}_2\text{CH}_2\text{O]}_x$  chains. The latter were calculated by the exact mathematical methods of Flory and Jernigan<sup>18, 19</sup> using the rotational isomeric state model described above.

The plot of  $\log K_x$  against  $\log x$  for cyclics in poly(1,3-dioxolane) is strikingly similar to that for cyclics in equilibrates of polydimethylsiloxane<sup>1, 3</sup> and nylon-6<sup>20</sup>. Although the experimental  $K_x$  values for the cyclic dimer and trimer fall far below the calculated values, there is close agreement between experiment and theory for cyclics with 25 or more skeletal bonds and the limiting slope of  $-2.5$  predicted by the Jacobson-Stockmayer<sup>5</sup> theory is attained for  $x > 5$ . This result shows that 1,3-dioxolane chains adopt random-coil conformations in both the undiluted and solution equilibrates. Furthermore 1,3-dioxolane chains with as few as 25 skeletal bonds obey the Gaussian relationship for the probability of intramolecular cyclization.

Further studies on the concentrations of cyclics in poly(1,3-dioxolane) samples prepared under a variety of conditions are in progress.

Table 1 Statistical weight parameters for poly(1,3-dioxolane)

Interacting atoms or groups	Number of bonds apart	Distance between their centres (Å)	Statistical weight parameter*	Value at 333K
CH <sub>2</sub> ...CH <sub>2</sub>	3	2.81	$\sigma$	0.26
O...O	3	2.84	$\sigma'$	1.9
CH <sub>2</sub> ...O	3	2.75	$\sigma''$	9.7
CH <sub>2</sub> ...O	4	3.54	$\psi$	1
CH <sub>2</sub> ...O	4	3.38	$\psi'$	1
CH <sub>2</sub> ...CH <sub>2</sub>	4	3.32	$\psi''$	1
CH <sub>2</sub> ...O	4	2.35	$\omega$	0
CH <sub>2</sub> ...O	4	2.46	$\omega'$	0.6
CH <sub>2</sub> ...CH <sub>2</sub>	4	2.37	$\omega''$	0

\* The values assigned to these parameters by Gorin and Monnerie<sup>14, 15</sup> were not used, because these authors used semi-empirical equations to describe the attractions and repulsions between non-bonded atoms in the chain. This approach has been shown<sup>16, 17</sup> to give values of the parameters for polyethers that are not in agreement with those deduced experimentally.

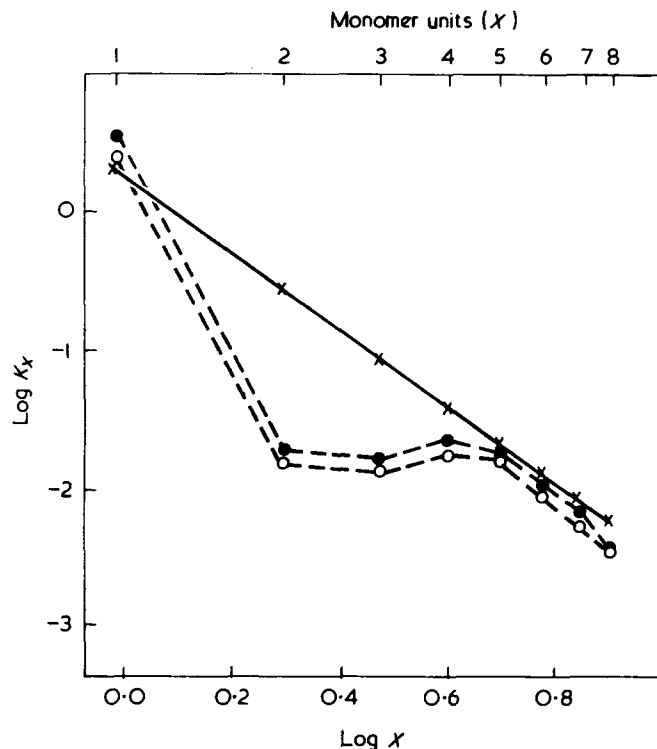


Figure 2 Experimental molar cyclization equilibrium constants  $K_x$  (in mol/l) in undiluted (○) and solution (●) equilibrates of poly(1,3-dioxolane) at 333K compared with values calculated (×) by the Jacobson-Stockmayer theory

#### ACKNOWLEDGEMENTS

We are indebted to the Courtaulds' Educational Trust Fund for a Research Scholarship (to J.M.A.). We gratefully acknowledge computational facilities at the University of York.

#### REFERENCES

- Brown, J. F. and Slusarczuk, G. M. *J. Am. Chem. Soc.* 1965, **87**, 931
- Flory, P. J. and Semlyen, J. A. *J. Am. Chem. Soc.* 1966, **88**, 3209
- Semlyen, J. A. and Wright, P. V. *Polymer* 1969, **10**, 543
- Wright, P. V. and Semlyen, J. A. *Polymer* 1970, **11**, 462
- Jacobson, H. and Stockmayer, W. H. *J. Chem. Phys.* 1950, **18**, 1600
- Wright, P. V. *D.Phil. Thesis*, University of York, 1970
- Andrews, J. M. and Semlyen, J. A. *Polymer* 1971, **12**, 642
- Yamashita, Y., Okada, M., Suyama, K. and Kasahara, H. *Makromol. Chem.* 1968, **114**, 146
- Yamashita, Y., Asakura, T., Okada, M. and Ito, K. *Makromol. Chem.* 1969, **129**, 1
- Gorin, S. and Monnerie, L. *Bull. Soc. Chim. France* 1966, **2**, 2047
- Flory, P. J. 'Principles of Polymer Chemistry', Cornell University Press, New York, 1953
- Flory, P. J. and Mark, J. E. *Makromol. Chem.* 1964, **11**, 75
- Mark, J. E. and Flory, P. J. *J. Am. Chem. Soc.* 1965, **87**, 1415
- Gorin, S. and Monnerie, L. *J. Chim. Phys.* 1968, **65**, 2079
- Gorin, S. and Monnerie, L. *J. Chim. Phys.* 1968, **65**, 2084
- Brant, D. A., Flory, P. J. and Semlyen, J. A. unpublished results
- Flory, P. J. 'Statistical Mechanics of Chain Molecules', Interscience, New York, 1969
- Flory, P. J. *Proc. Natl. Acad. Sci., USA* 1964, **51**, 1060
- Flory, P. J. and Jernigan, R. L. *J. Chem. Phys.* 1965, **42**, 3509
- Semlyen, J. A. and Walker, G. R. *Polymer* 1969, **10**, 597

# The measurement of molecular orientation in drawn poly(vinyl chloride) by broad line nuclear magnetic resonance

M. Kashiwagi\* and I. M. Ward

Department of Physics, University of Leeds, Leeds 2, UK  
(Received 22 June 1971)

Measurements have been made of the anisotropy of the proton magnetic resonance second moment at liquid nitrogen temperatures, for a series of drawn poly(vinyl chloride) samples. The data were used to calculate orientation functions which characterize the molecular orientation. This was done on an aggregate model, where the polymer is regarded as an aggregate of transversely isotropic units whose structure is postulated on considerations based on the structure of crystalline poly(vinyl chloride). The orientation functions for the drawn samples are shown to be consistent with those obtained from pseudo-affine deformation of the aggregate units in the drawing process, and there is a good correlation with birefringence data. The relevance of these results to other deformation studies is discussed.

## INTRODUCTION

In a recent publication we described the use of broad line nuclear magnetic resonance to determine molecular orientation in an amorphous polymer, poly(methyl methacrylate)<sup>1</sup>. The present note describes a limited investigation on poly(vinyl chloride) which demonstrates the applicability of the technique to this polymer also.

Previous broad line nuclear magnetic resonance (n.m.r.) studies of poly(vinyl chloride) have been limited to an examination of the isotropic polymer<sup>2</sup>. It was shown that the half-width of the proton resonance signal was unchanged from 15°C to 75°C. Recent measurements of the n.m.r. relaxation times by pulse techniques<sup>3</sup> have confirmed that  $T_2$  is constant over the temperature range from -200°C to 75°C, the relaxation processes occurring at higher temperatures. It can therefore be concluded that at liquid nitrogen temperatures, where the present measurements were undertaken, there are no appreciable molecular motions, and that the rigid lattice second moment is being determined.

## EXPERIMENTAL

The oriented poly(vinyl chloride) samples were in the form of sheets, prepared by drawing 3.3 mm thick isotropic sheets of a commercial polymer ('Darvic' sheet, manufac-

tured by Imperial Chemical Industries Ltd.) in a tensometer at selected temperatures and strain rates. Only three samples were selected for detailed examination, and their specifications are given in *Table 1*.

It can be seen that the dimensional changes are close to those for uniaxial drawing. It will therefore be assumed that the drawn samples are transversely isotropic.

The n.m.r. measurements were undertaken using a Robinson oscillating detector<sup>4</sup> at a frequency of 25 MHz, a narrow band amplifier, and a phase sensitive detector. A Time Average Computer was incorporated to give improved signal/noise ratios. To obtain accurate second moment values a modulation field of large amplitude (peak-to-peak amplitude 3.2 G) was applied. The Andrew correction was used in calculating the second moment. The radio-frequency field was at the highest level possible without introducing signal saturation. All measurements were made at -196°C to ensure that rigid lattice second moments were being observed.

*Table 1* Specification of poly(vinyl chloride) samples

Sample	Draw temperature (°C)	Strain rate (min <sup>-1</sup> )	Draw ratio*			Birefringence × 10 <sup>3</sup>
			$\lambda_1$	$\lambda_2$	$\lambda_3$	
A	90	1	1.79	0.70	0.76	1.7
B	80	0.05	2.20	0.70	0.69	2.4
C	80	0.1	2.58	0.60	0.63	3.1

\* On leave from Toray Industries, Inc., Basic Research Laboratories, Tebiri, Kamakura, 248 Japan

\*  $\lambda_1$ =along draw direction;  $\lambda_2$ =along normal to sheet;  $\lambda_3$ =perpendicular to the draw direction in the plane of the sheet

## THEORY

In the present study of poly(vinyl chloride) we used exactly the same procedure as was proposed for poly(methyl methacrylate) in the previous publication<sup>1</sup>. It is assumed that the drawn polymer possesses uniaxial orientation, and can be regarded as an aggregate of units of structure each of which also possesses transverse isotropy. The second moment  $\langle \Delta H^2 \rangle$  when the steady magnetic field makes an angle  $\gamma$  with the draw direction is given by the equation

$$\langle \Delta H^2 \rangle = \frac{4G}{N} \sum_{l=0,2,4} a_l S_l P_l(\cos\gamma) \overline{P_l(\cos\Delta)}$$

where  $G = 3/2I(I+1)g^2\mu_n^2$ ,  $I$  is the nuclear spin number,  $g$  the nuclear  $g$ -factor,  $\mu_n$  the nuclear magneton,  $N$  the number of magnetic nuclei over which the sum is taken and  $a_0 = 1/5$ ,  $a_2 = 2/7$  and  $a_4 = 18/35$ . The quantities  $P_l$  are Legendre polynomials and  $\Delta$  is the angle between the symmetry axis of the units and the draw direction. The orientation functions,  $\overline{P_l(\cos\Delta)}$ , define the distribution of units about the draw direction. The quantities  $S_l$  are the lattice sums.

As in the study of poly(methyl methacrylate) it will be assumed that the magnetic anisotropy arises from the intramolecular interactions only, and because the units of structure possess transverse isotropy, that only the

$S_0$ ,  $S_2$  and  $S_4$  lattice sums concern us. Moreover, it will also be assumed, as in the previous publication, that the intermolecular interactions are isotropic and must be determined on the basis of the best fit to the experimental data.

The intramolecular interactions were calculated assuming that the local conformation of the molecule in the amorphous specimens which we studied is identical to that in the crystalline regions of crystalline syndiotactic poly(vinyl chloride). The chain conformation adopted was proposed by Natta and Corradini<sup>5</sup> and is shown in diagrammatic form in Figure 1. The positions of the hydrogen atoms were calculated assuming that the C-H bond length is 1.094 Å, the C-C bond length 1.54 Å and, for simplicity of calculation that both the H-C-H and the H-C-Cl angles are 109°28'. The positions of the hydrogen atoms obtained are shown in Table 2, and the computed intramolecular lattice sums in Table 3. As has been emphasized, the intermolecular interactions are assumed to be isotropic and will therefore give rise to an additional term in the  $S_0$  lattice sum, to be found from the experimental data.

## RESULTS AND DISCUSSION

## Calculation of orientation distribution functions

The orientation functions  $\overline{P_2(\cos\Delta)}$  and  $\overline{P_4(\cos\Delta)}$  were calculated from the n.m.r. data by a similar method to that proposed for poly(methyl methacrylate). The true value of the isotropic lattice sums term  $S'_0$  differs from the approximate value  $S_0$  based on intramolecular interactions only, by a correction term  $\delta$ . The best fit to the experimental data is obtained, regarding  $\overline{P_2(\cos\Delta)}$ ,  $\overline{P_4(\cos\Delta)}$  and  $\delta$  as independent parameters. The measured n.m.r. anisotropy of each sample together with the least squares fit is shown in Figure 2.

Table 4 shows the values of  $\overline{P_2(\cos\Delta)}$ ,  $\overline{P_4(\cos\Delta)}$ ,  $\overline{\cos^2\Delta}$ ,  $\overline{\cos^4\Delta}$ , the isotropic second moment obtained from  $S'_0$ , and the root-mean-square deviation of the experimental points from the predicted curve. It can be seen that the predicted isotropic second moment is constant within experimental error.

Table 2 Atomic coordinates of syndiotactic poly(vinyl chloride)

Atom	$x$ (Å)	$y$ (Å)	$z$ (Å)
H <sub>1</sub>	0.8931	-0.6316	0
H <sub>2</sub>	-0.8931	-0.6316	0
H <sub>3</sub>	0.8931	1.5208	1.2573
H <sub>4</sub>	0.8931	-0.6316	2.5145
H <sub>5</sub>	-0.8931	-0.6316	2.5145
H <sub>6</sub>	-0.8931	1.5208	3.7118

Repeat unit = 5.029 Å

C-H = 1.094 Å; C-C = 1.54 Å; C-C-C = 109°28'; H-C-H = 109°28'; H-C-Cl = 109°28' (for simplification of calculation)

Table 3 Intramolecular lattice sums for syndiotactic poly(vinyl chloride)

$S_0$	$S_2$	$S_4$
0.10683	-0.01412	0.03200

Number of hydrogen atoms = 6

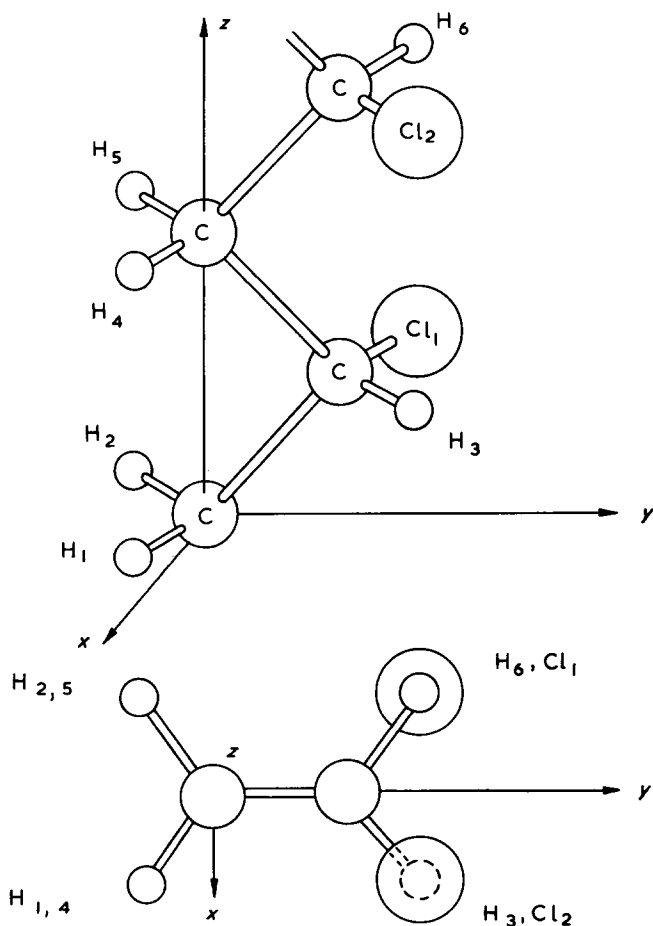


Figure 1 Diagrammatic sketch of chain conformation of syndiotactic poly(vinyl chloride)

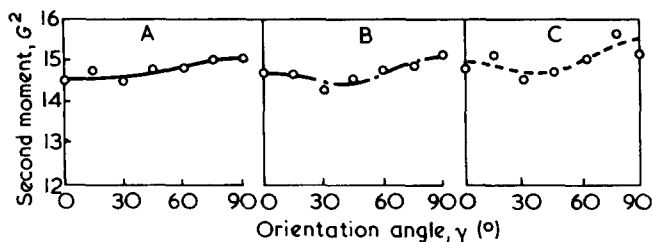


Figure 2 Variation of second moment against orientation angle  $\gamma$  for various samples (A, B, C) of poly(vinyl chloride). The lines represent the least squares fit to the experimental data, which are shown as open circles (O)

#### Comparison of n.m.r. anisotropy with optical measurements

The n.m.r. anisotropy will now be compared with the optical anisotropy obtained from birefringence measurements.

On the aggregate model<sup>6</sup>, the birefringence  $\Delta n$  of a uniaxially oriented polymer is given by

$$\Delta n = \Delta n_{\max} \overline{P_2(\cos \Delta)}$$

where  $\Delta n_{\max}$  is the maximum birefringence for a completely oriented polymer and  $\Delta$  is the angle between the draw direction and the symmetry axis of the polarizable unit of structure. Thus, if the optical and mechanical anisotropy relate to the orientation of similar units of structure, there should be a good correlation between the optical birefringence and the values of  $\overline{P_2(\cos \Delta)}$  obtained from the n.m.r. measurements.

The data obtained in the present work are shown in Figure 3. It can be seen that there is a good correlation. Furthermore, the values of  $\overline{\cos^2 \Delta}$  and  $\overline{\cos^4 \Delta}$  obtained from the n.m.r. measurements are shown in Figure 4 together with a theoretical curve predicted on the basis of the pseudo-affine deformation scheme. The latter scheme proposes that during the drawing process the unique axes of the units of structure undergo the same changes of direction as lines connecting pairs of material parts in a body undergoing uniaxial deformation, without change of volume. It can be seen that the experimental points lie on the theoretical curve to a very good approximation.

These results suggest firstly that the birefringence is a good measure of molecular orientation in uniaxially drawn poly(vinyl chloride) and secondly that the distribution of molecular orientation is close to that predicted by the pseudo-affine deformation scheme. This does not mean, however, that the measured values of  $\overline{\cos^2 \Delta}$  and  $\overline{\cos^4 \Delta}$  correspond to these predicted by the pseudo-affine deformation scheme, assuming uniaxial drawing and

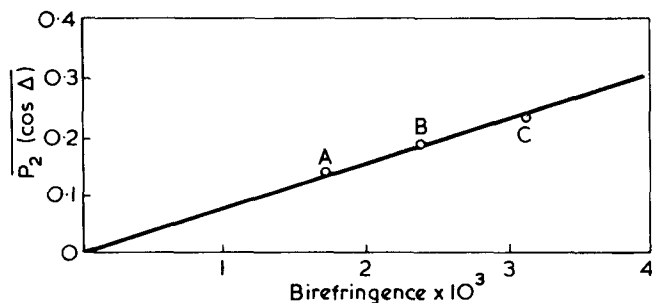


Figure 3 Variation of  $\overline{P_2(\cos \Delta)}$  obtained from n.m.r. measurements with birefringence. Open circles (O) are experimental values; the aggregate theory would predict a straight line through the origin

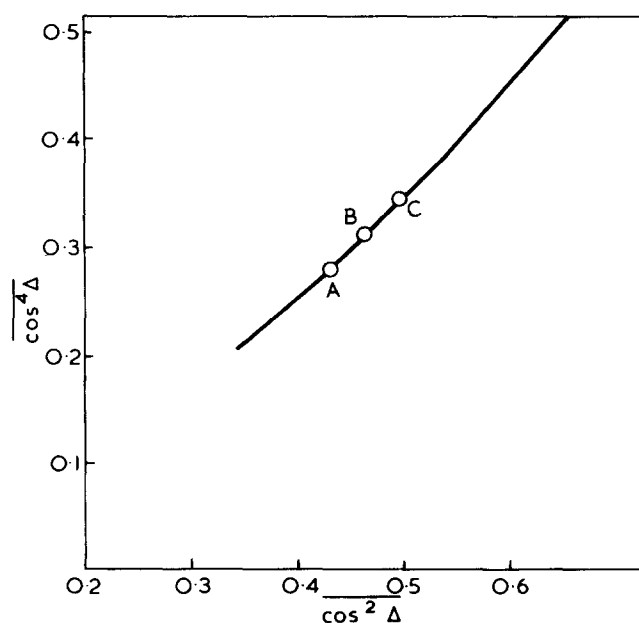


Figure 4 Comparison of measured values of  $\overline{\cos^4 \Delta}$  and  $\overline{\cos^2 \Delta}$  with the line predicted on the basis of the pseudo-affine deformation scheme

using the values of draw ratio  $\lambda$  given in Table 1. In Table 4, the measured draw ratios are compared with an 'effective' draw ratio based on the measured values of the orientation functions. The values of the 'effective' draw ratios are very much lower than the measured values, showing that deformation processes during drawing at high temperatures are much more complex than predicted by the pseudo-affine deformation scheme. For purposes of predicting properties such as the subsequent deforma-

Table 4 Orientation distribution functions obtained from the n.m.r. measurements

Sample	$\overline{P_2(\cos \Delta)}$	$\overline{P_4(\cos \Delta)}$	$\overline{\cos^2 \Delta}$	$\overline{\cos^4 \Delta}$	Isotropic* second moment, $G^2$	Root mean square deviation, $G^2$	Measured draw ratio, $\lambda_1$	'Effective' draw ratio
A	0.1415	0.0127	0.4277	0.2837	14.8	0.10	1.79	1.26
B	0.1869	0.0397	0.4579	0.3159	14.7	0.12	2.20	1.36
C	0.2362	0.0495	0.4908	0.3463	15.0	0.25	2.58	1.47

\* Intramolecular interactions:  $12.7 G^2$

tion behaviour at room temperature it may, however, still be of value to characterize the drawn polymer in terms of an 'effective' draw ratio because this gives a good first-order representation of the state of orientation, providing a consistent prediction of  $\overline{P_2(\cos\Delta)}$  and  $\overline{P_4(\cos\Delta)}$  in terms of a single parameter. This approach was originally proposed for poly(ethylene terephthalate)<sup>7, 8</sup> and was subsequently used with some success in studies of deformation bands in poly(vinyl chloride) by Rider and Hargreaves<sup>9</sup>. The present study gives good support for the latter work in this respect.

The data in Figure 3 predict a maximum birefringence  $\Delta n_{\max}$  for poly(vinyl chloride) of  $12.6 \times 10^{-3}$ . Rider and Hargreaves attempted to obtain  $\Delta n_{\max}$  on the basis of the pseudo-affine deformation scheme. It can be seen from the present work that because of the large discrepancy between the measured draw ratio and the 'effective' draw ratio this is a somewhat uncertain exercise and Rider and Hargreaves were aware of this difficulty. Their value of  $7.2 \times 10^{-3}$  obtained by assuming that the measured and 'effective' draw ratios are identical at 20°C differs markedly from the value of  $12.6 \times 10^{-3}$  predicted by the n.m.r. data. Both these values are very much less than the values of  $27 \times 10^{-3}$  and  $85 \times 10^{-3}$  proposed by Shindo *et al.*<sup>10</sup> on the basis of measurements of dichroism

and stress-optical data respectively, on dehydrohalogenated poly(vinyl chloride).

It is intended to undertake further work in this area, combining studies of deformation bands in poly(vinyl chloride) with measurements of molecular orientation by n.m.r. and laser-Raman spectroscopy in an attempt to resolve some of these problems.

#### REFERENCES

- 1 Kashiwagi, M., Folkes, M. J. and Ward, I. M. *Polymer* 1971, **12**, 697
- 2 Odajima, A., Sohma, T. and Koike, M. *J. Phys. Soc. Japan* 1957, **12**, 272
- 3 McCall, D. W. and Falcone, D. R. *Trans. Faraday Soc.* 1970, **66**, 262
- 4 Robinson, F. N. H. *J. Sci. Instrum.* 1959, **36**, 481
- 5 Natta, G. and Corradini, P. *J. Polym. Sci.* 1956, **20**, 251
- 6 Ward, I. M. *Proc. Phys. Soc.* 1962, **80**, 1176
- 7 Brown, N., Duckett, R. A. and Ward, I. M. *J. Phys. (D: Appl. Phys.)* 1968, **1**, 1369
- 8 Richardson, I. D., Duckett, R. A. and Ward, I. M. *J. Phys. (D: Appl. Phys.)* 1970, **3**, 649
- 9 Rider, J. G. and Hargreaves, E. *J. Phys. (D: Appl. Phys.)* 1970, **3**, 993
- 10 Shindo, Y., Read, B. E. and Stein, R. S. *Makromol. Chem.* 1968, **118**, 272



# Copolymerization behaviour of some *N*-vinyl monomers

I. Negulescu, D. Feldman and Cr. Simionescu

Department of Chemistry, Polytechnic Institute of Jassy, Jassy, Romania  
(Received 29 December 1970)

The simple molecular orbital method is employed to show that *N*-vinylpyrrolidone and *N*-vinylcarbazole, monomers which possess the common group  $\text{CH}_2=\text{CH}-\text{N}<$ , must have almost the same  $Q$  and  $e$  parameters of the Alfrey-Price treatment. In terms of these parameters, the reactivity ratios of *N*-vinylpyrrolidone and *N*-vinylcarbazole with some monomers in radical copolymerization are neighbouring and in good agreement with the experimental ones.

## INTRODUCTION

Alfrey and Price<sup>1, 2</sup> have proposed an empirical formula which attempts to express the reactivity of any radical and monomer pair in terms of two parameters related only to the individual monomers. The parameters for a monomer, once determined, can then be used in the calculation of reactivity ratios for the copolymerization of this monomer with any other monomer. These two parameters are designed by  $Q$  and  $e$ , where the parameter  $Q$  is assumed to denote the general reactivity of the monomer, while  $e$  is assumed to indicate its polar properties. According to the  $Q, e$  scheme, the corresponding reactivity ratios are:

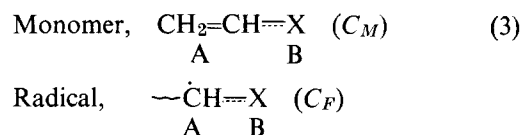
$$\begin{aligned} r_1 &= Q_1/Q_2 \exp[-e_1(e_1 - e_2)] \\ r_2 &= Q_2/Q_1 \exp[-e_2(e_2 - e_1)] \end{aligned} \quad (1)$$

These formulae have been found to be useful in the prediction of reactivity ratios, although the assumptions on which the derivation is based are questionable<sup>3</sup>. Values of free radical reactivity ratios correlated with the  $Q, e$  scheme have been tabulated for almost one thousand monomer pairs<sup>4, 5</sup>. The parameter  $Q$  should be related to the increase in  $\pi$  electron energy in going from  $\text{C}=\text{C}-\text{X}$  to  $\text{C}-\dot{\text{C}}-\text{X}$ , and the parameter  $e$ , being attributed to the charge-donating and charge-attracting properties of both the monomer and radical, should be related to electron affinities and ionization potential of the monomer and radical; the electron-donating properties should be related to the ionization potential of the species while the electron-withdrawing properties (or electron affinities) should be related to the energy of the lowest empty orbital of the monomer and the energy of the singly occupied orbital of the radical<sup>6</sup>. The specific reactivity  $Q$  of the monomer has been considered by Evans and co-workers, thus<sup>7</sup>:

$$Q = \exp[K((C_F - C_M)/RT)] \quad (2)$$

where  $T$  is the absolute temperature of the system,  $R$  is the gas constant, and  $C_F, C_M$  represent the stabilization energies when the conjugation across the single bond

takes place between  $\pi$  electrons localized in the two parts A and B in a monomer and a radical.



The formula which expresses the  $e$  value has been given by Alfrey and Price<sup>1</sup> as:

$$e = q'/(rDkT)^{1/2} \quad (4)$$

where  $r$  is the distance of separation in the activated complex,  $D$  is the effective dielectric constant and  $q'$  is related to the final charge at the carbon atoms to be attacked in a monomer or a radical. It was assumed<sup>8</sup> that the final charge can be expressed in terms of the total  $\pi$  electron density  $q_r$  at the position of attack in a monomer or a radical as shown in equation (5):

$$q' = q_r^{-N/n} \quad (5)$$

where  $N$  is the total number of  $\pi$  electrons and  $n$  is the number of atoms in the conjugated system. Qualitative correlations between copolymerization data and molecular orbital (*MO*) calculations have been presented in relation to values of localization energies<sup>7, 9, 10</sup> and resonance-stabilization energies,  $\Delta E_{rs}$ <sup>7-9, 11-13</sup>.

In the present paper the validity of the theory is further tested by reference to the radical copolymerization of some *N*-vinyl compounds, i.e. *N*-vinylpyrrolidone and *N*-vinylcarbazole.

## EXPERIMENTAL

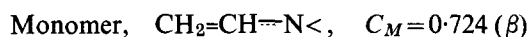
The solvent (benzene, 'Reactivul'—Bucharest) and the monomer (styrene, industrial polymerization purity) were distilled under reduced pressure in order to free them from inhibitor. *N*-vinylcarbazole (Dr Schuchardt, München) and azodiisobutyronitrile (Fluka), were purified by recrystallizing twice from methanol. Mixtures of the monomers in various chosen proportions and solvent (the molar ratio between solvent and monomer

mixture was maintained at 1 : 1 for the styrene-vinylpyrrolidone system and 2 : 1 for the system with vinylcarbazole) were introduced into glass ampoules and 1% (based on the monomer mixture) of azodiisobutyronitrile was added. The ampoules were sealed under slight nitrogen pressure after being alternately evacuated and filled with nitrogen several times. They were then kept, while occasionally shaken, in a water bath thermostated at  $60 \pm 0.1^\circ\text{C}$ , for the time necessary to obtain a conversion of a few per cent; the time required increased with increasing vinylpyrrolidone and vinylcarbazole content in the monomer mixture. The contents of the ampoules were poured into methanol (or into octane in the case of vinylpyrrolidone). The copolymers were collected by filtration and after prolonged methanol or *n*-octane washing (respectively) were then dried under vacuum for 24 h. Unreacted and unwashed vinylcarbazole monomer was extracted from the copolymers with methanol. The conversion was calculated from the weight of polymer obtained from a known amount of reaction mixture. Kjeldahl's method gave the best results for the determination of the nitrogen content in copolymers.

## RESULTS AND DISCUSSION

The *N*-vinyl group,  $\text{CH}_2=\text{CH}-\text{N}<$ , is common to *N*-vinylpyrrolidone (NVP), *N*-vinylcarbazole (NVC), *N*-vinylurethane (NVU) and *N*-vinyl-*N'*-ethylurea (NVUr); since this group will dominate the copolymerization behaviour, and considering that the influences of the various *N*-substituents are almost identical, the behaviour of these compounds in copolymerization reactions shall also be rather similar. First, if the  $\pi$  electron density at the N in the *N*-vinyl group,  $q^{\text{N}}$ , pyrrolidone,  $q^{\text{P}}$ , and carbazole,  $q^{\text{C}}$  are compared, their values are found to be close to one another:  $q^{\text{N}}=1.67$ ;  $q^{\text{C}}=1.63$ ;  $q^{\text{P}}=1.74$ . Further a comparison made between the effects of the insertion of the vinyl group on *MO* energies in benzene and carbazole (the latter is supposed to be more conjugate than pyrrolidone, urethane and urea), and shows that little modification is required for the latter.

As a result of these comparisons, it was concluded that the *N*-vinyl group could be considered in isolation from the rest of the molecule, and all the calculations were subsequently made with *MO* parameters of this group. With  $k=0.47$ ,  $\beta=-20\text{ kcal/mol}^8$ ,  $T=333\text{K}$  and  $C_M$ ,  $C_F$  from the following scheme:



substituted in equation (2), the theoretical  $Q$  value is found to be 23.300 or, relative to styrene ( $Q_{\text{st}}=80.811$ )<sup>8</sup>,  $Q_1=0.288$ . The *MO* parameters were calculated using the simple LCAO *MO* method (neglecting overlap integrals). The Coulomb integral of a carbon atom being

Table 1 Parameters  $k_x$  and  $l_{\text{C-X}}$  in the Coulomb integral and resonance integral<sup>15</sup>

Heteroatom X		$k_x$	$l_{\text{C-X}}$
Nitrogen	-N<	0.6	1.00
	-NH-	1.0	1.00
Oxygen	=O	2.0	1.41
Carbon adjacent to heteroatom		0.1	1.00

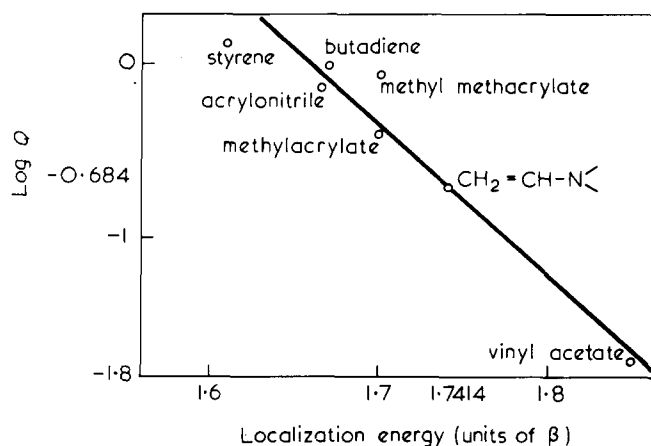


Figure 1 Comparison of parameter  $Q$  with localization energy<sup>6</sup>

$\alpha$ , the Coulomb integrals of heteroatoms were expressed as  $\alpha+k_x\beta$ , where  $\beta$  is the resonance integral of  $\text{C}=\text{C}$  in benzene. A carbon atom adjacent to a heteroatom was assumed to have a Coulomb integral of  $\alpha+0.1k_x\beta$  due to the inductive effect of the heteroatom. The resonance integral between C and the heteroatom X was written as  $\beta_{\text{C-X}}=l_{\text{C-X}}\beta$ , where  $l_{\text{C-X}}$  is a parameter depending on the nature of the C-X bond. Typical values employed for the parameters  $k_x$  and  $l_{\text{C-X}}$  are shown in Table 1<sup>15</sup>.

If, for the purpose of calculating  $C_F$ ,  $k_x$  is considered to be zero for the carbon adjacent to heteroatom N, then  $C_F=0.923(\beta)$  and equation (2) gives  $Q'=11.25$  or, relative to styrene,  $Q_2=0.139$ ; this value corresponds well with the values calculated by Young<sup>4</sup> from experimental data for NVP ( $Q_{\text{NVP}}=0.140$ ), NVU ( $Q_{\text{NVU}}=0.120$ ) and NVUr ( $Q_{\text{NVUr}}=0.130$ ). With regard to Levinson's relationships between  $Q$  and localization energy<sup>6</sup>, the plot of localization energy against  $\log Q$  (Figure 1), gives for the former [ $L\beta=1.767(\beta)$ , calculated for the *N*-vinyl group] an average value between  $Q_1$  and  $Q_2$ , namely  $Q_m=0.210$ .

Inserting the appropriate values ( $r=2.5\text{ \AA}$ ,  $D=20 \times 4.77 \times 10^{-10}\text{ e.s.u.}$ )<sup>8</sup> in equation (4), with  $T=333\text{K}$ , one obtains  $e_{\text{calc.}}=0.68$ . The relative value of  $e$ ,  $e'_{\text{calc.}}=-1.48$ , was obtained from the following equation:

$$e'_{\text{calc.}}=-e_{\text{calc.}}-0.8 \quad (6)$$

this value is in agreement with the plot of  $e$  against the average electron affinity of Levinson<sup>6</sup>.

As the data existing in the literature are very varied with respect to the conditions of synthesis (temperature, initiator, solvent, conversion), from one author to another, the theoretical values obtained can be tested experimentally. Thus, two *N*-vinyl derivatives, NVP and NVC, were copolymerized with styrene as reference monomer at  $T=333\text{K}$ , and the results are listed in Table 2.

From Figure 2 it is seen that the points for the NVC-styrene system correspond very well to the monomer-polymer composition curves of the NVP-styrene system. Data for the runs with the lowest conversion were examined by the Fineman-Ross method<sup>16</sup> and the plots were used to determine the reactivity ratios in the usual manner, e.g. in Figures 3 and 4,  $F(f-1)/f$  is plotted against  $F^2/f$ , where  $F$  is the initial molar ratio of the two monomer concentrations and  $f$  is the same ratio in

Table 2 Copolymerization of (A) NVP and (B) NVC with styrene at  $T=333\text{K}$ 

A: N-vinylpyrrolidone (1)-styrene(2) system

Feed composition (mol.%)		Conv. (%)	Copolymer composition (mol.%)		
$M_1$	$M_2$		%N	$m_1$	$m_2$
90.93	9.06	4.65	4.77	36.39	63.61
90.04	9.96	2.08	4.62	34.91	65.09
87.47	12.53	2.68	4.32	32.89	67.11
83.35	16.67	5.00	3.60	27.24	72.76
81.72	18.28	2.90	3.66	27.69	72.31
54.28	45.72	3.55	1.70	12.78	87.22
50.73	49.26	8.10	3.34	25.32	74.68
33.45	66.55	7.40	1.65	12.27	87.73
22.20	77.80	4.10	0.52	3.86	96.14
11.61	88.49	3.25	0.25	1.88	98.12
9.75	90.25	5.70	0.31	2.31	97.69

B: N-vinylcarbazole(1)-styrene(2) system

Feed composition (mol.%)		Conv. (%)	Copolymer composition (mol.%)		
$M_1$	$M_2$		%N	$m_1$	$m_2$
82.24	17.76	3.40	3.53	23.58	76.42
75.11	24.89	3.28	2.46	21.72	78.29
66.55	33.45	4.85	2.15	18.50	81.50
58.16	41.84	3.90	1.90	15.99	84.01
50.00	50.00	5.50	1.41	11.51	88.49
40.98	59.02	2.25	1.22	9.78	90.22
25.54	74.46	3.45	0.77	5.98	94.02
9.03	90.97	6.53	0.32	2.43	97.57

the copolymer. Inserting the reactivity ratios obtained ( $r_1=0.012 \pm 0.003$ ,  $r_2=6.5 \pm 0.2$  for the NVP (1)-styrene(2) system, and  $r_1=0.062 \pm 0.009$ ,  $r_2=5.6 \pm 0.5$  for the NVC (1)-styrene(2) system) in equation (7),  $Q$  and  $e$  values are obtained from

$$e_1 = e_2 \pm (-\ln r_1 r_2)^{1/2} \quad (7)$$

$$Q_1 = Q_2 / r_2 [-e_2(e_2 - e_1)]$$

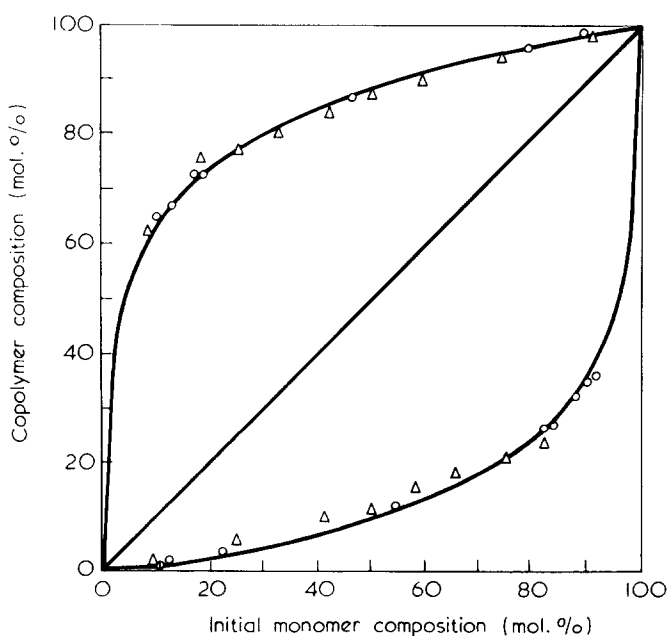


Figure 2 Monomer-polymer composition curves for the copolymerization of N-vinyl derivatives with styrene at 333K.  $\circ$ , NVP-styrene system;  $\triangle$ , NVC-styrene system; A, the curve of styrene; B, the curve of vinylpyrrolidone

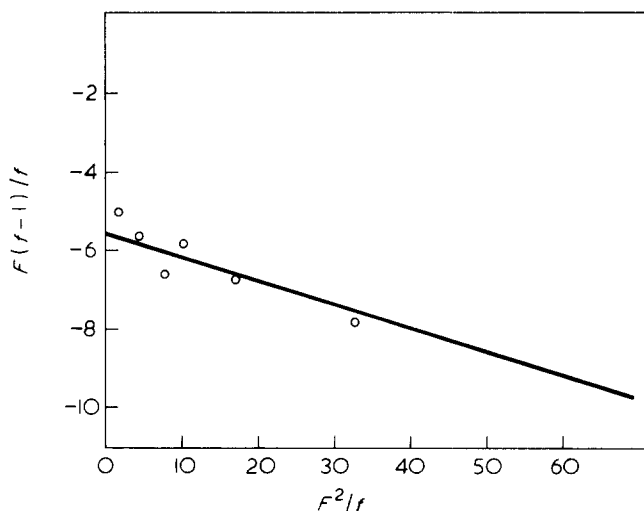


Figure 3 Fineman-Ross plot for the copolymerization of NVP (1) with styrene (2)

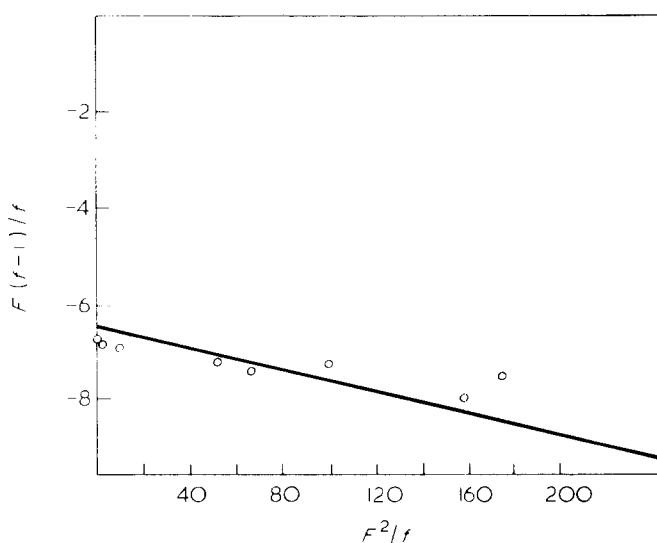


Figure 4 Fineman-Ross plot for the copolymerization of NVC (1) with styrene (2)

The resultant  $Q$  and  $e$  data are collected in Table 3 together with the values theoretically calculated for comparison.

The agreement with experiment observed in Table 3 seems to be satisfactory; it follows that the behaviour of these two monomers must also be nearly the same for the other systems. Results are listed in Table 4.

## CONCLUSIONS

The  $MO$  method has the very important advantage of requiring few empirical parameters; whereas the Alfrey-Price method requires two empirical parameters for each monomer, the  $MO$  method in general requires only two parameters for each type of atom attached to the vinyl group. Thus, it may be stated that the agreement between the theoretically calculated  $Q$  and  $e$  parameters and Alfrey and Price's values is good, even if the  $MO$  calculations were not made for the whole molecule, and it is

Table 3 Comparison between theoretical and experimental  $Q$  and  $e$  parameters for *N*-vinylpyrrolidone and *N*-vinylcarbazole

$Q, e$	Theoretical	Experimental	
	$\text{CH}_2=\text{CH}-\text{N}<$	NVC	NVP
$Q$	0.288* 0.210†	0.28	0.25
$e$	-1.48	-1.49	-1.25

\* Calculated with equation (2)

 † From the plot  $\log Q$  vs.  $L_\beta$ 

 Table 4 Comparison between reactivity ratios of *N*-vinylpyrrolidone and *N*-vinylcarbazole with different monomers

Monomer (2)	<i>N</i> -vinylcarbazole (1)			Ref.
	$r_1$	$r_2$	$T$ (°C)	
Styrene	$0.062 \pm 0.009$	$5.6 \pm 0.5$	60	—
	$0.012 \pm 0.002$	$5.5 \pm 0.8$	70	17
Vinyl acetate	$2.68 \pm 0.1$	$0.126 \pm 0.032$	65	18
	$3.02 \pm 0.24$	$0.152 \pm 0.018$	100	18
Methyl methacrylate	$0.20 \pm 0.03$	$2.0 \pm 0.3$	70	17

Monomer (2)	<i>N</i> -vinylpyrrolidone (1)			Ref.
	$r_1$	$r_2$	$T$ (°C)	
Styrene	$0.012 \pm 0.003$	$6.5 \pm 0.2$	60	—
	$0.045 \pm 0.05$	$15.7 \pm 0.5$	50	19
	0.11	9.0	80	4
Vinyl acetate	$3.30 \pm 0.15$	$0.205 \pm 0.015$	50	19
Methyl methacrylate	$0.05 \pm 0.00$	$4.7 \pm 0.5$	50	19

possible to hope that  $MO$  calculation may make it possible to estimate the  $Q, e$  parameters and to predict reactivity ratios for new monomers [simpler by correlation with equation (7)], while the Alfrey-Price method is limited to only these molecules for which the said parameters have been experimentally determined.

## REFERENCES

- 1 Alfrey, T. Jnr and Price, C. C. *J. Polym. Sci.* 1947, 2, 101
- 2 Price, C. C. *J. Polym. Sci.* 1948, 3, 772
- 3 Mayo, F. and Walling, C. *Chem. Rev.* 1950, 46, 191
- 4 Young, L. J. *J. Polym. Sci.* 1961, 54, 411
- 5 Ham, G. E. 'Copolymerization', Interscience, New York, 1966
- 6 Levinson, G. S. *J. Polym. Sci.* 1962, 60, 43
- 7 Evans, M. G., Gerhely, J. and Seaman, E. C. *J. Polym. Sci.* 1948, 3, 866
- 8 Hayashi, K., Yonezawa, T., Okamura, S. and Fukui, K. *J. Polym. Sci. (A-1)* 1963, 4, 1405
- 9 Fueno, K., Tsureta, T. and Furukawa, J. *J. Polym. Sci.* 1959, 40, 487
- 10 Okamura, S., Katagiri, K. and Yonezawa, T. *J. Polym. Sci.* 1960, 42, 535
- 11 Yonezawa, T., Hayashi, K., Nagata, C., Okamura, S. and Fukui, K. *J. Polym. Sci.* 1954, 14, 312
- 12 Hayashi, T., Yonezawa, T., Nagata, C., Okamura, S. and Fukui, K. *J. Polym. Sci.* 1956, 20, 537
- 13 Kawabata, N., Tsuruta, T. and Furukawa, J. *Makromol. Chem.* 1962, 51, 80
- 14 Coulson, C. A. and Streitwieser, A. Jnr. 'Dictionary of  $\pi$  Electron Calculations', Pergamon Press, Oxford, 1965.
- 15 Butler, G. B. and O'Driscoll, K. F. 'Reviews in Macromolecular Chemistry', Marcel Dekker, New York, 1967
- 16 Fineman, M. and Ross, S. D. *J. Polym. Sci.* 1950, 5, 259
- 17 Alfrey, T. Jnr and Kapur, S. *J. Polym. Sci.* 1949, 4, 215
- 18 Ushakov, S. N. and Nikolaev, A. F. *Dokl. Akad. Nauk SSSR, Ser. Chim.* 1956, 1, 79
- 19 Bork, J. F. and Coleman, L. E. *J. Polym. Sci.* 1960, 43, 413

# Production of organometallic polymers by the interfacial technique:

## 24. Kinetics of polycondensation and thermal properties of poly-[oxy(dicyclopentadienylzirconium)-oxycarbonylferrocenylcarbonyl]

C. E. Carraher Jr. and J. T. Reimer

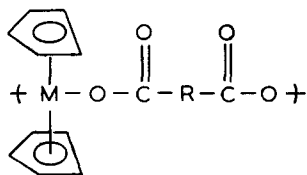
*Department of Chemistry, University of South Dakota, Vermillion, South Dakota 57069, USA*

*(Received 22 July 1971; revised 8 October 1971)*

Poly[oxy(dicyclopentadienylzirconium)oxycarbonylferrocenylcarbonyl] is synthesized using the interfacial technique. Polycondensation is first order with respect to the  $\text{Cp}_2\text{ZrCl}_2$ , zero order with respect to the 1,1'-ferrocene dicarboxylate and pseudo first order overall. A kinetic model using a modified Langmuir adsorption isotherm model is presented which is in agreement with the experimental findings. The product exhibits moderate thermal stability in both air and nitrogen. It undergoes oxidative degradation in air.

### INTRODUCTION

We have been interested in the synthesis of polymers containing organometallic moieties in their backbone<sup>1-4</sup>. Recently we reported the synthesis, via the interfacial and solution methods<sup>5</sup>, of Group IVB polyesters of the form:



This represented the initial synthesis of such polyesters via any method. We now report the synthesis of a similar polyester containing both iron and zirconium in the polymer backbone.

The possible advantages of including Fe and Zr in a polymer are clearly evident. For instance zirconium compounds similar to those employed in this study are known to exhibit catalytic activity in certain systems. One such system is the Ziegler catalysts system. The iron is contained in a ferrocene moiety. Such ferrocene moieties are known to be good ultra-violet absorbers. The actual use of ferrocene derivatives in industry is well known and

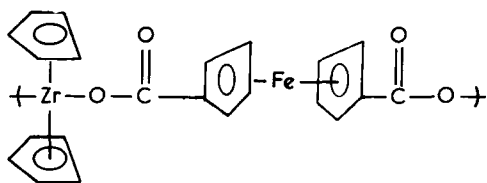
has been recently reviewed<sup>6</sup>. Also the incorporation of ferrocene moieties into polymers has been recently reviewed<sup>7</sup>.

### EXPERIMENTAL

Dicyclopentadienylzirconium dichloride (Alfa Inorganics, Inc., Beverly, Mass.) and 1,1'-ferrocene dicarboxylic acid (Research Organic/Inorganic Chem. Corp., Sun Valley, Calif.) were used as received. The salt of 1,1'-ferrocene dicarboxylic acid was generated by addition of an equivalent amount of sodium hydroxide in water.

The reaction procedure has been described in detail elsewhere<sup>5</sup>. Briefly, aqueous solutions of disodium 1,1'-ferrocene dicarboxylate were added to rapidly stirred organic solutions containing  $\text{Cp}_2\text{ZrCl}_2$ . The polycondensations were conducted in a one pint Kimax emulsifying jar placed on a Waring Blendor (Model 1043). The reactants were added through a large-mouthed funnel placed through a hole in the jar cap. Addition is such that 100 ml of a solution can be added in about a second so that the rate of addition of one phase to the second is rapid, minimizing any reaction time error owing to a variance in the time needed for addition of the two phases. Polyester precipitates rapidly from the reaction mixture as a 'rust' red solid.

Infra-red spectra were obtained on samples using Perkin-Elmer 237B and Beckman IR-12 spectrophotometers. The spectra and elemental analysis are in agreement with the repeating structure illustrated below:



Solubility studies were conducted in small test tubes containing about 0.001 g of material with 2 ml of liquid over an observation period of two weeks. The polyester exhibited poor solubility characteristics being insoluble or unstable in most solvents tried. For instance the product appeared to be soluble in triethyl phosphate but on careful recovery (using a series of acetone and ethyl ether washes coupled with the use of a vacuum oven at a temperature less than 40°C and a pressure of about 20 mmHg) it was found that reaction with the solvent occurred. So far no suitable solvent has been found. Thus no solution characterization is reported. The products are probably of high molecular weight since the analogous titanium, zirconium and hafnium polyesters (non-iron containing products) are generally of high molecular weight with weight-average degrees of polymerization via light-scattering photometry of  $10^3$  to  $10^4$ .

Thermal gravimetric analysis (t.g.a.) was carried out on a du Pont 950 TGA. Differential scanning calorimetry (d.s.c.) was carried out employing a du Pont 900 DSC cell fitted on a du Pont Thermal Analyzer console using a linear baseline compensator to insure a constant energy baseline. A Mettler H20T semi-micro balance was used for weighing the d.s.c. samples. Measurements were obtained on samples contained in open aluminium cups to allow the free flow away from the solid of volatilized materials thus closely simulating the conditions under which the t.g.a. studies were conducted. Air and nitrogen flows of about 0.3 l/min were used. Samples were ground to a fine powder to aid in obtaining reproducible results.

## RESULTS AND DISCUSSION

### Kinetic study of the polycondensation of $Cp_2ZrCl_2$ with disodium 1,1'-ferrocene dicarboxylate

Table 1 contains some results obtained from the condensing of  $Cp_2ZrCl_2$  with disodium 1,1'-ferrocene dicarboxylate. Yield increases as reaction time increases; we attempted a kinetic treatment of the data.

Rate studies involving interfacial polycondensation systems are not numerous for several reasons. One concerns the difficulty of removing the polymer from the reaction zone at a constant or known rate. Reproducible polymer removal can be achieved by using rapidly stirred systems. Another difficulty concerns the theoretical treatment of concentrations of the reactants present in the two immiscible phases. A third difficulty is the heterogeneity of the interfacial system which complicates the gathering and interpretation of data. In the condensing of  $Cp_2ZrCl_2$  with disodium 1,1'-ferrocene dicarboxylate rates and concentrations of reactants are based on the amount of polymer formed. This is believed to be valid for this

system since an investigation of the species present in each phase does not indicate the presence of any (detectable by infra-red spectroscopy) side products.

The kinetic data are in agreement with a first order rate expression as depicted by equation (1) (see Figure 1). By varying the amounts of reactants it is tentatively concluded that rate is primarily dependent on the concentration of the  $Cp_2TiCl_2$  but not greatly dependent on the concentration of the acid salt (Table 1). This is in agreement with the rate expression given in equation (2).

$$\text{Rate} = k(A)^n(B)^m \quad \text{or} \quad k(A)^{m+n} \quad (1)$$

$$\text{Rate} = K[Cp_2TiCl_2] \quad (2)$$

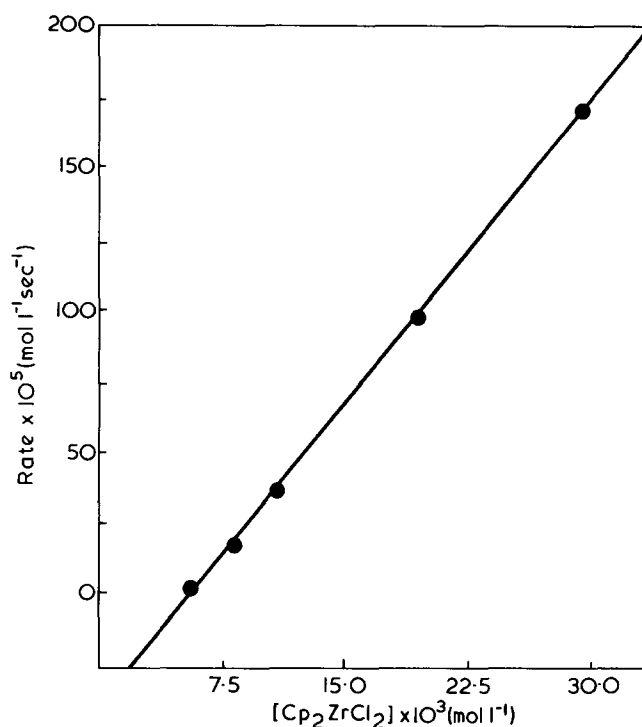


Figure 1 First order kinetic plot for the interfacial condensation of dicyclopentadienylzirconium dichloride with disodium 1,1'-ferrocene dicarboxylate. Reaction conditions: 28°C; 17 000 rev/min stirring load (no load) with 0.00125 moles of disodium 1,1'-ferrocene dicarboxylate in 10 ml of  $H_2O$  added to rapidly stirred solutions containing 0.00125 moles of  $Cp_2ZrCl_2$  in 30 ml of  $CHCl_3$

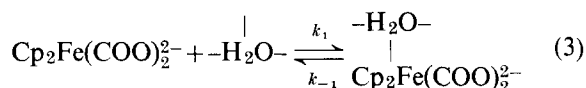
Table 1 Product yield as a function of reactant concentration and reaction yield\*

Moles of ferrocene salt	Moles of $Cp_2ZrCl_2$	Volume of $H_2O$ (ml)	Reaction time (sec)	Yield (%)
0.00125	0.00125	10	5	14
0.00125	0.00125	10	10	43
0.00125	0.00125	10	30	66
0.00125	0.00125	10	40	74
0.00125	0.00125	10	60	85
0.00125	0.00125	30	20	61
0.00125	0.00125	30	20	72
0.00375	0.00125	30	20	61
0.000625	0.000625	30	20	33
0.00125	0.000625	30	20	34

\* Reaction conditions:  $Cp_2ZrCl_2$  was contained in 30 ml  $CHCl_3$  whereas disodium 1,1'-ferrocene dicarboxylate was contained in water. Reactions were conducted at 28°C with a stirring rate of 17 000 rev/min (no load).

The reaction is pseudo first order. Previous studies have shown that the rate of polyester formation is dependent on the nature of both reactants. Also the intercept of the plot of rate vs. concentration is not zero (Figure 1).

Thus the reaction expression given in equation (2) is pseudo first order. The following model is offered as a reasonable interpretation of the  $K$  value and is offered as a basis for further study. The model is based on the Langmuir adsorption isotherm treatment. For reasons which become apparent later the model will treat the 1,1'-ferrocene dicarboxylate dianion (which will be shortened to  $\text{Cp}_2\text{Fe}(\text{COO})_2^{2-}$ ) as the species which is adsorbed. The simplest situation exists when  $\text{Cp}_2\text{Fe}(\text{COO})_2^{2-}$  molecules occupy single sites on the aqueous interface surface, indicated by  $-\text{H}_2\text{O}-$ . The adsorption and desorption process may be represented as:



Langmuir's kinetic description of the adsorption-desorption process is well known. For solutions we can substitute for gas pressure a concentration term designated as  $s$ . We can assume for calculation's sake that reaction rate is proportional to  $F$  and to the first power of  $\text{Cp}_2\text{ZrCl}_2$  yielding the following expression where  $f_1$  and  $f_2$  are functions.

$$\text{Rate} = f_1(F) \cdot f_2 \text{Cp}_2\text{ZrCl}_2 = f_1 \frac{(k_1/k_{-1})s}{1 + (k_1/k_{-1})s} \cdot f_2 [\text{Cp}_2\text{ZrCl}_2] \quad (4)$$

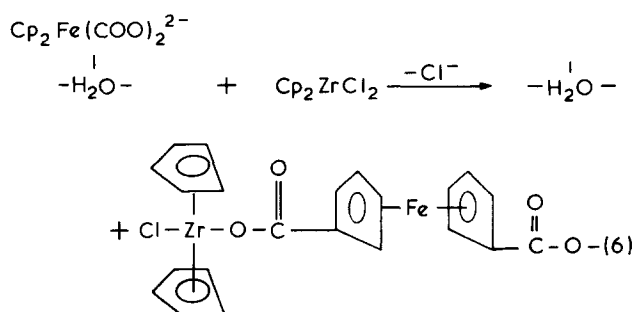
If  $f_1$  and  $f_2$  are simple, involving only proportionality constants, and  $s$  be necessarily understood to be proportional to  $\text{Cp}_2\text{Fe}(\text{COO})_2^{2-}$  then equation (4) can be re-written as:

$$\text{Rate} = \frac{K_1 [\text{Cp}_2\text{Fe}(\text{COO})_2^{2-}] [\text{Cp}_2\text{TiCl}_2]}{1 + K_2 [\text{Cp}_2\text{Fe}(\text{COO})_2^{2-}]} \quad (5)$$

The mathematics invoked to derive the Langmuir adsorption isotherm describes a situation where there exists a high density population of gas molecules occupying the surface. In a similar manner it would insist on a high occupancy of the interfacial surface area by the  $[\text{Cp}_2\text{Fe}(\text{COO})_2^{2-}]$  ions. The concentration involved in the present study argue against this unless it can be shown that  $[\text{Cp}_2\text{Fe}(\text{COO})_2^{2-}]$  ions preferentially 'seek' the surface relative to occupying internal sites. While this has not yet been demonstrated the authors have measured the surface tension of the solutions used in the present study and found that the surface tension is 20% lower than that of pure water. This indicates the preferential occupancy of surface sites by the  $[\text{Cp}_2\text{Fe}(\text{COO})_2^{2-}]$  ions.

It must be noted that for equation (5) to yield a linear plot of rate vs.  $[\text{Cp}_2\text{ZrCl}_2]$  the concentration of  $[\text{Cp}_2\text{Fe}(\text{COO})_2^{2-}]$  must be approximately constant. It can be argued that the tendency to occupy surface 'lattice' sites by  $\text{Cp}_2\text{Fe}(\text{COO})_2^{2-}$  is great so the surface concentration of  $\text{Cp}_2\text{Fe}(\text{COO})_2^{2-}$  is approximately constant. This would indicate that the rate of polycondensation is first order in  $\text{Cp}_2\text{ZrCl}_2$  concentration and is independent of the  $\text{Cp}_2\text{Fe}(\text{COO})_2^{2-}$  concentration. As previously noted this is what is presently tentatively found.

In simple terms this would be in agreement with a two step process, the first step being pictured in equation (3) where the  $\text{Cp}_2\text{Fe}(\text{COO})_2^{2-}$  ion is seeking the interface between the water layer and organic layer with secondary bonding with the water being (probably including hydrogen bonding between the  $\text{Cp}_2\text{Fe}(\text{COO})_2^{2-}$  and water) responsible for the adsorption of  $\text{Cp}_2\text{Fe}(\text{COO})_2^{2-}$ . The second step consists of a bimolecular engagement between the  $\text{Cp}_2\text{Fe}(\text{COO})_2^{2-}$  and  $\text{Cp}_2\text{ZrCl}_2$  resulting in the formation of the ester linkage and regeneration of a vacant water site.



Admittedly the above is an exercise to present a description to a term (rate =  $K[A]$ , the term being  $K$ ) which is often not addressed usually because of a lack of sensing tools and theoretical models upon which to base definitive experiments. The above is an attempt to do the latter and should be viewed as such.

This type of kinetic behaviour has been found to be followed by the interfacial condensation of  $\text{Cp}_2\text{TiCl}_2$  with disodium terephthalate and is believed to be general for Ti and Zr polyester formation via the interfacial route<sup>8</sup>. A similar interfacial system involving the condensation of dihalo-organosilanes and ethylene glycol was experimentally found to be dependent on the surface area of the phases<sup>9</sup>. The relationship was not that shown in equation (2) but can be expressed as

$$\text{Rate} = k[\text{silane}][\text{glycol}]^{2/3} \quad (7)$$

which can be derived via a consideration of the surface area of the glycol phase compared with glycol concentration. Thus surface area is important and experimentally demonstrable for at least some interfacial systems. The reasons for the difference in behaviour between the two systems may be numerous. In the silane-glycol study one phase consisted solely of the glycol so an adsorption-desorption phenomenon is not critical.

The treatment must be considered with caution. More work must be done before such a treatment or any treatment can be confidently applied to the present system. Even though other expressions can be derived which are consistent with the kinetic data the present treatment holds some particular merit. It is derived using a model which is consistent with interface systems and utilizes concepts which seem reasonable when considering such systems.

#### Thermal characterization

This section presents some thermal characteristics (via d.s.c., t.g.a. and visual observation) of the polyester. Such products might be expected to offer some degree of

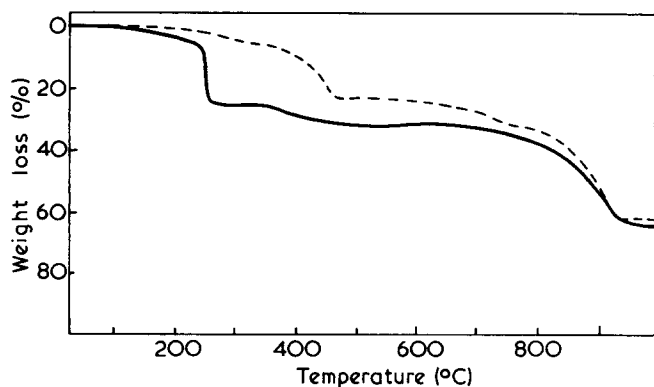


Figure 2 T.g.a. plot for the product formed from the condensation of  $\text{Cp}_2\text{ZrCl}_2$  with disodium 1,1'-ferrocene dicarboxylate in air (—) and nitrogen (-----) with a gas flow of 0.3l/min at a heating rate of 20°C/min

thermal stability, at least under inert gas purges because of the presence of (potentially) a high degree of polar bonding between portions of one or more chains. The oxidative stability will be dependent on the availability of 'out-lying' orbitals to oxygen which is more easily (and accurately) experimentally tested than theorized.

Figure 2 presents some representative t.g.a. thermograms. It exhibits moderately good thermal stability in both air and nitrogen yielding less than 30% weight loss to about 800°C. As expected the thermal stability is greater in nitrogen than in air. The decrease in weight at 270°C in air is unusual because of its rapidity. This type of rapid loss was also observed for the polyester formed from  $\text{Cp}_2\text{TiCl}_2$  and disodium terephthalate in air. D.s.c. thermograms appear in Figure 3<sup>8</sup>. There is a large, sharp exothermic peak at 270 to 280°C which corresponds to the rapid loss of weight but as previously noted is unusual because of the sharpness of the exotherm. The products remain solid in air and nitrogen up to 1000°C (via visual observation).

Oxidation of Group IVB organometallic compounds is not widely studied<sup>10</sup>. The mechanism(s) of polymer degradation is clearly different in nitrogen and air. The degradations occurring in air are all exothermic whereas the degradations occurring in nitrogen are generally endothermic. The occurrence of highly exothermic

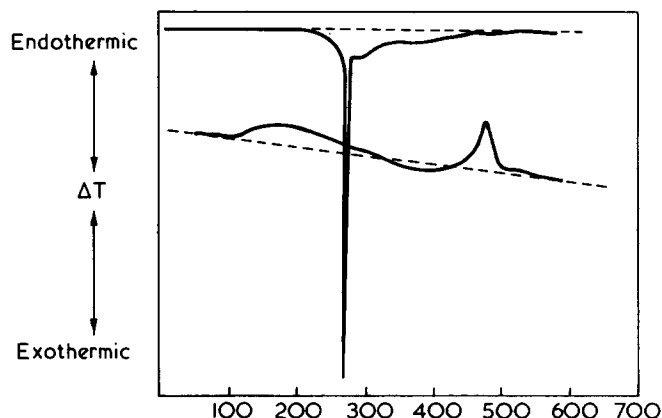


Figure 3 D.s.c. plot for the product formed from the condensation of  $\text{Cp}_2\text{ZrCl}_2$  with disodium 1,1'-ferrocene dicarboxylate in air (upper plot) and nitrogen (lower plot) at a gas flow of 0.3l/min and a heating rate of 20°C/min with 0.0010g samples. The y axis setting in air was 5°C/in (0.20 mV/in) while the y axis setting in nitrogen was 0.10°C/in (0.0040 mV/in). ----- represents  $\Delta T=0$

degradations in air is unusual for hydrocarbon products but is more usual for heteroatomed products<sup>11</sup>. Such exothermic areas results from crosslinkage or oxidation reactions<sup>11</sup>. The former is not responsible for the highly exothermic nature of the air degradations since similar (non-oxidative) crosslinking should also occur in nitrogen, which is not found. Thus oxidation is primarily responsible for the degradation of the product in air to 600°C.

#### REFERENCES

- 1 Carraher, C. and Winter, D. *Makromol. Chem.* 1971, **141**, 237, 259
- 2 Carraher, C. and Scherubel, G. *J. Polym. Sci. (A-1)* 1971, **9**, 983
- 3 Carraher, C. *Macromolecules* 1971, **4**, 263
- 4 Carraher, C. and Dammeier, R. *Makromol. Chem.* 1971, **141**, 245, 251
- 5 Carraher, C. *J. Polym. Sci. (C)* 1971, **31**, 338
- 6 Neuse, E. and Rosenberg, H. 'Metallocene Polymers', Marcel Dekker, New York, 1970
- 7 Pittman, C. *J. Paint Technol.* 1967, **39**, 585
- 8 Carraher, C. *J. Polym. Sci. (A-1)* 1971, **9**, 3661
- 9 Carraher, C. *J. Polym. Sci. (A-1)* 1969, **7**, 2351
- 10 Brilkina, T. and Shushunov, V. 'Reactions of Organometallic Compounds with Oxygen and Peroxides', CRC Press, Cleveland, Ohio, 1969
- 11 Ehlers, G. and Fisch, K. 'International Symposium on Polymer Characterization', Interscience, New York, 1969



# Methyl group motion in poly(propylene oxide), polypropylene and poly(methyl methacrylate)

J. S. Higgins, G. Allen and P. N. Brier

*Chemistry Department, University of Manchester, Manchester M13 9PL, UK  
(Received 10 August 1971)*

Incoherent inelastic neutron scattering spectroscopy has been used to measure the fundamental torsional frequencies of methyl groups in poly(propylene oxide) and poly(methyl methacrylate). From these frequencies barriers hindering internal rotation were calculated for each methyl group in the approximation of a rigid 3-fold rotor attached to an asymmetric frame. The values of  $V_3$  so obtained are compared with activation energies for methyl group relaxation obtained primarily from n.m.r.  $T_1$  and  $T_{1\rho}$  measurements. The barrier to internal rotation makes the main contribution to the relaxation process. Consideration of quantum mechanical tunnelling allows alternative estimates of  $V_3$  from the relaxation studies; these values are in reasonable agreement with the values calculated from the torsional frequencies.

## INTRODUCTION

The dynamical physical properties of polymers are determined by the frequency spectra of their chain motions. Dielectric, mechanical and nuclear magnetic resonance (n.m.r.) spin-lattice relaxation experiments are the principal techniques used to investigate molecular motion in polymers. Loss maxima and  $T_1$  minima are observed when the time scales of the various conformational changes pass through the time scale of the dynamical experiment. An important aspect of these experiments is to identify the molecular motion causing each of the observed losses. A major loss phenomenon is always observed at the rubber-glass transition temperature corresponding to the freezing in of main-chain motion of the polymer molecules. Below the glass transition temperature, subsidiary loss maxima are found which in many cases can be assigned to side-group motions. Such assignments can be made with confidence from the evidence provided by selective chemical substitution (or deuterium substitution in the case of proton n.m.r. studies). If the relaxation phenomena are treated as rate processes, the temperature dependence of the frequencies of maximum loss allows an activation energy,  $E_a$ , to be calculated<sup>1,2</sup> for each motion from a simple Arrhenius plot. The magnitudes of the activation energies found in this way suggest that the observed side-group motion is predominantly a torsional motion, and that the hindering barrier is largely intramolecular in character.

In the case of torsional motion of side groups, vibrational spectroscopy can provide useful additional information. In contrast to the relaxation experiments

which essentially measure bulk properties of the sample and from these deduce average transition rates over the potential barrier hindering the motion, vibrational spectroscopy observes directly transitions between energy levels in the minima of molecular potential curves. The spacings of these torsional vibrational levels are determined by the shape and height of the potential barrier. In favourable cases, where the side group is symmetric, for example  $\text{CH}_3$ ,  $\text{C}_6\text{H}_5$  etc., and hence the potential barrier to internal rotation is a symmetric function of the torsional angle, reasonable assumptions concerning the shape of the barrier enable its height to be estimated from the spectroscopic observation of the fundamental torsional frequency<sup>3,4</sup>.

The activation energy from the dynamical experiments and the barrier height from the spectroscopic measurements will be comparable if: (i) the motion causing the dynamical loss is due to side-group reorientation about its symmetry axis; (ii) the hindering potential is predominantly intramolecular in origin and hence the usual assumption of a sinusoidal barrier shape for the spectroscopic measurements is a good approximation (for condensed phases this approximation should be treated with some caution); (iii) the relaxation measurements are measuring transitions over the barrier and not a tunnelling process through the barrier. In the latter case a barrier height can be calculated for the relaxation measurements by an alternative procedure (see below).

The torsional modes of all symmetrical side groups attached to polymer chains are active in the infra-red and Raman spectra, but in practice the respective changes in dipole moment and polarization are so small that the

corresponding bands are very weak and extremely difficult to identify. Inelastic incoherent neutron scattering spectroscopy<sup>5, 6</sup>, however, is particularly well suited to the observation of torsional motion and vibration, because selection rules do not apply. In neutron spectroscopy a mono-energetic beam of neutrons is scattered by a molecular target and detected at one or more angles of scatter. At each angle of scatter an energy analysis yields a spectrum analogous to a Raman spectrum. Peaks occur in the inelastic spectrum corresponding to neutrons gaining or losing quanta of molecular rotational or vibrational energy. In contrast to optical spectroscopy, the intensity of the vibrational band is proportional to the square of the amplitude of motion of the nuclei in the normal mode of vibration. Furthermore, because the incoherent scattering cross-section of protons is very much larger than that for any other nucleus, modes involving the motion of protons dominate the inelastic spectrum. Consequently torsional modes of groups containing protons are relatively intense. Identification of the torsional frequency is further assisted by the fact that if, for example, in a CH<sub>3</sub> group the protons are replaced by deuterium, the scattering involving modes of vibration of that group is reduced by two orders of magnitude.

This paper reports the use of inelastic incoherent neutron spectroscopy to study the torsional motions in side-groups in poly(propylene oxide), poly(methyl methacrylate), poly( $\alpha$ -chloro methacrylate) and poly(methyl methacrylate-COOC D<sub>3</sub>).

## EXPERIMENTAL

### Neutron inelastic scattering

The neutron spectra described here were obtained using the 6H long wavelength inelastic neutron spectrometer at AERE, Harwell<sup>7</sup>. In this apparatus bursts of low energy neutrons ( $\lambda=4.2$  Å or  $E=4.5$  meV in these experiments) are produced by mechanical selection using twin-phased rotors. High energy neutrons and  $\gamma$ -rays are removed by cooled crystal transmission filters. Scattered neutrons are detected over 9 angles of scatter ranging from 18° to 90°, and analysis is in terms of time-of-flight over a measured path length of 1.2 metres from the sample to the counter banks. The measured energy resolution in these experiments was about 12% and remained constant across the energy range involved.

The sample is cycled with a blank cell and a vanadium standard during the experiment, providing internal calibration of flight paths and detector efficiencies and allowing corrections to be made for background scattering (including cell scattering where these are used).

The initial spectra which are produced at each angle of scatter are time-of-flight cross-sections,  $\partial^2\sigma/\partial\Omega\partial\tau$  against  $\tau$ , where  $\tau$  is the time of flight in  $\mu\text{s/m}$  and  $\partial\Omega$  is an element of solid angle around the direction  $\Omega$ .

From the time-of-flight cross-section the so-called scattering law,  $S(\mathbf{K}, \omega)$ , can be obtained. This is a function of the scattering system only and is independent of the particular neutron experiment performed to obtain it.

In this case:

$$S(\mathbf{K}, \omega) = \frac{\hbar}{b^2} \frac{\mathbf{k}_0}{\mathbf{k}} \frac{\tau^3}{m} \frac{\partial^2 \sigma}{\partial \Omega \partial \tau}$$

$m$  is the neutron mass,  $b$  is the 'scattering length' for the neutron-nucleus interaction (in this case dominated by

the <sup>1</sup>H nuclei),  $\hbar\omega$  is the energy transfer involved in the scattering event,  $\mathbf{k}$  and  $\mathbf{k}_0$  are the initial and final wave vectors of the neutron,  $\hbar\mathbf{K} = \hbar(\mathbf{k} - \mathbf{k}_0)$  is the momentum transferred to the neutron. This momentum transfer may be substantial and increases with increasing incident neutron energy and scattering angles.

Considerable information about the dynamics of the scattering system may be contained in the dependence of the scattered spectra on the momentum transfer, particularly in the energy transfer region well below the vibrational energies, the so-called quasi-elastic region. This aspect of neutron scattering technique has important application for polymer systems, but discussion will be deferred until a later paper. Another consequence of these large momentum transfers is that dispersion effects may become important in neutron spectra, leading to broadening and shifting of band centres as the scattering angle is increased. Fortunately, it is likely that the dispersion curves for torsional motions of symmetric side-groups are essentially flat so that the bands should remain sharp and unshifted over increasing scattering angle. (This was confirmed; see Figures 2 and 3.)

Neutron results at several angles of scatter allow an extrapolation to be made to zero momentum transfer. The result of this extrapolation is the generalized frequency function:

$$p(\omega) = \omega^2 \lim_{K \rightarrow 0} \left[ \frac{S(\mathbf{K}, \omega)}{K^2} \exp(\hbar\omega/2k_B T) \right]$$

It has been shown<sup>6, 9, 10</sup> that it is this function that should be used if a comparison is to be made between neutron and optical spectra. Since the extrapolation should remove small effects of dispersion and produce a useful averaging of the results at various scattering angles, the frequency function has been quoted for each of the samples described below.

### Internal rotation barriers from vibrational spectroscopy

The potential function  $V(\phi)$  for hindered internal rotation of a three-fold symmetric top about its axis of symmetry (in this case the bond joining the side group to the main chain) is assumed to be of the form:

$$V(\phi) = \frac{V_3}{2} (1 - \cos 3\phi)$$

If there is very little mixing of the side-group torsion with the other normal modes of the polymer chain, the torsional wave equation is then of the form:

$$\left[ \frac{1}{F} \frac{\partial^2}{\partial \phi^2} - V(\phi) \right] \psi_{v\sigma}(\phi) = E_{v\sigma} \psi_{v\sigma}(\phi)$$

where  $F$  is a factor containing the reduced moment of inertia of the side group with respect to the rest of the molecule, determined by the molecular geometry.  $E_{v\sigma}$  are the torsional energy levels characterized by a vibrational quantum number,  $v$ , and an index  $\sigma$ . The index  $\sigma$  specifies the periodicity of the eigen-functions  $\psi_{v\sigma}$ . For a three-fold symmetric top  $\sigma=0$  or  $\pm 1$  and the eigen-functions have A or E species symmetry respectively. The energy difference between levels with the same quantum number,  $v$ , but different  $\sigma$  is due to tunnelling through the barrier and is small for the lowest torsional levels in a potential of moderate height. From the spectroscopic observation of the transition from  $v=0 \rightarrow v=1$ , the height of the barrier ( $V_3$ ) can be calculated<sup>4</sup>.

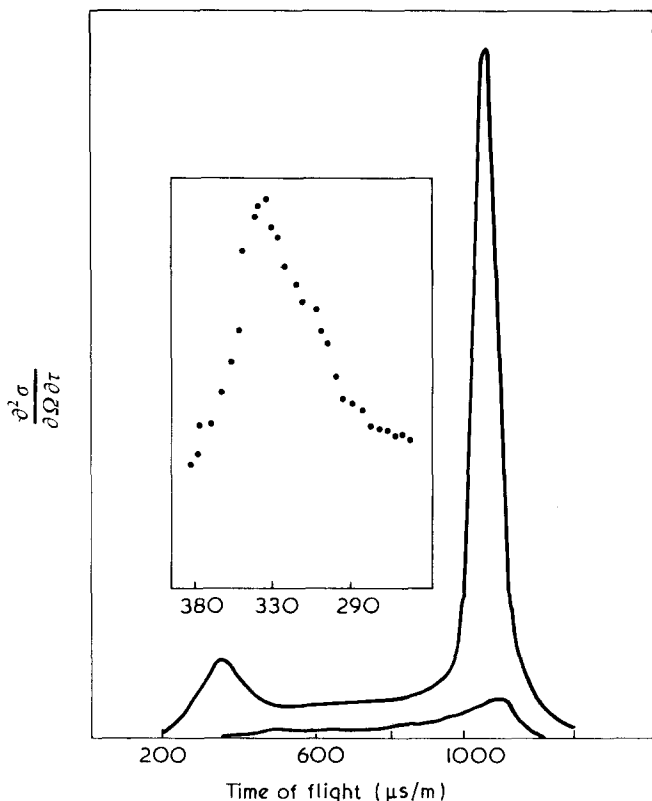


Figure 1 Time-of-flight spectrum at  $90^\circ$  scatter from poly(methyl methacrylate- $\text{COOCD}_3$ ) swollen with  $\text{CDCl}_3$ . The lower spectrum is the scattering from the same volume of  $\text{CDCl}_3$  as used in swelling the sample. Inset is the region between 250 and 450  $\mu\text{s/m}$  on an expanded scale

### Materials

Perspex was used as the sample of poly(methyl methacrylate). The relative proportions of triad sequences, as assessed by n.m.r. spectroscopy of polymer solution was: syndio, 61%; hetero, 31%; iso, 8%.

Poly(methyl methacrylate- $\text{COOCD}_3$ ) was prepared from its monomer  $\text{CH}_2 : \text{C}(\text{CH}_3)\text{COOCD}_3$  using azobisbutyronitrile at  $40^\circ\text{C}$  as a free radical initiator. The ratio of syndiotactic sequences was slightly higher than in Perspex.

Poly( $\alpha$ -chloro methacrylate) was kindly donated by Dr J. B. Rose of ICI Plastics Division. It was not possible to estimate the stereoregular nature of the material. It was, however, an amorphous polymer prepared by free radical polymerization and thus it is probably predominantly syndiotactic.

Films of Perspex were obtained by a hot pressing technique. Films of poly(methyl methacrylate- $\text{COOCD}_3$ ), and poly( $\alpha$ -chloro methacrylate) were obtained by flotation off mercury using  $\text{CDCl}_3$  as a solvent.

The poly(propylene oxide) and poly(propylene oxide- $\text{CD}_3$ ) were similar to the sample used in a previous investigation by Blears *et al.*<sup>11</sup> The polymers were 15–20% crystalline as determined by dilatometry. Samples for neutron scattering were pressed into thin films.

The thin film thicknesses were chosen to give approximately 10% scatter of the incident neutron beam (this is a compromise between reducing multiple scattering effects and wasting valuable neutron flux).

The acrylic polymers were self-supporting and were held in aluminium rings during the experiments. In these

cases the blank position was an empty ring and the background effects subtracted were largely due to scatter from the sample changer, monitors and helium atmosphere surrounding the samples.

Samples of the acrylic polymers were also swollen with an equal volume of deuterated chloroform (to investigate the effect of separating the polymer molecules with 'invisible' solvent molecules). These samples were in the form of gums and were held between thin aluminium sheets clamped with O-ring seals. For these spectra the blanks were similar aluminium cans containing an equal thickness of  $\text{CDCl}_3$ . Figure 1 shows the scattering from swollen Perspex, with, underneath, the spectrum from the corresponding blank. It is clear that the can and solvent background is very small. It is estimated that subtraction of the background will introduce errors of less than 5% in  $p(\omega)$  in the final spectra.

The poly(propylene oxide) samples, which were rubbery, were supported in thin aluminium sheets, the blank in these cases being similar aluminium sheets.

## RESULTS

### Acrylic polymers

Figure 1 shows the time-of-flight spectrum for the swollen sample of poly(methyl methacrylate- $\text{OCD}_3$ ) recorded at  $90^\circ$  angle of scatter. The large peak at  $\sim 1100 \mu\text{s/m}$  corresponds to the neutrons scattered with approximately zero energy change, i.e. the quasi-elastic peak. The remaining part of the spectrum corresponds to the neutrons gaining energy from molecular modes—the inelastic region. Inset in Figure 1 the inelastic spectrum of the swollen sample is shown on an expanded scale. The large inelastic feature at about 330  $\mu\text{s/m}$  corresponds to a neutron energy gain of about  $350 \text{ cm}^{-1}$ . Figure 2 shows

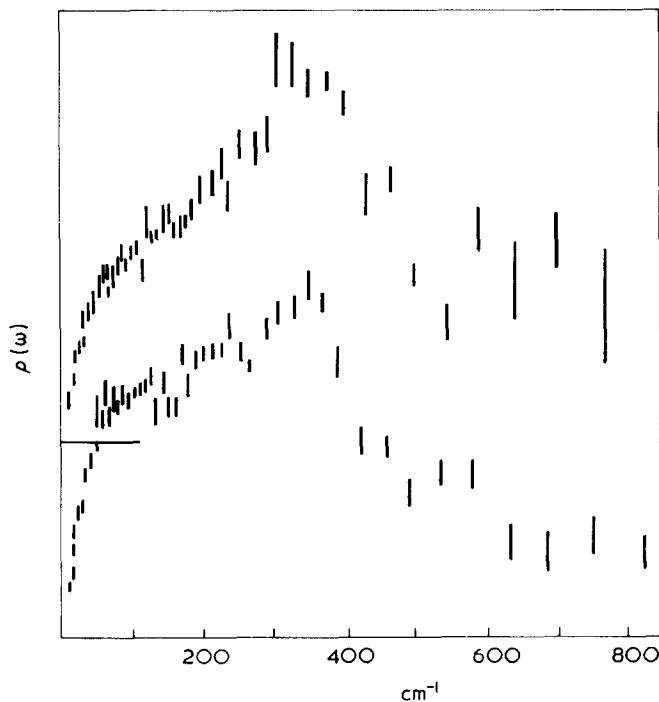


Figure 2  $p(\omega)$  function for swollen poly(methyl methacrylate  $\text{COOCD}_3$ ). The length of the vertical lines is a measure of the error

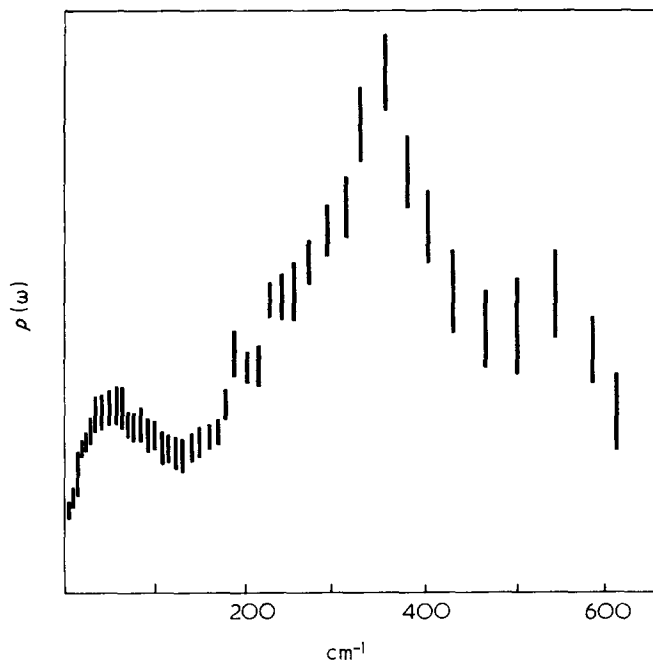


Figure 3  $p(\omega)$  for Perspex (upper spectrum) and Perspex swollen with  $\text{CDCl}_3$

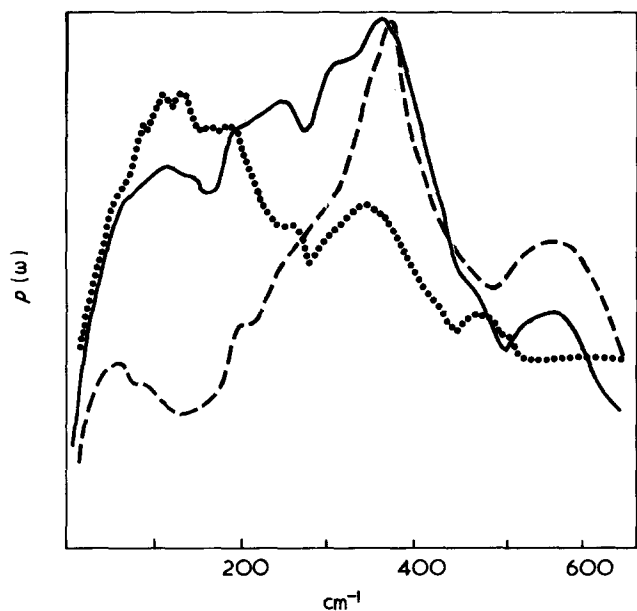


Figure 4  $p(\omega)$  for three Perspex samples. —, Perspex; --- poly(methyl methacrylate- $\text{COOCd}_3$ ); ... poly( $\alpha$ -chloro methacrylate)

the effect of extrapolation over the nine scattering angles to produce the frequency function at zero momentum transfer for this sample. The good agreement of the band position in Figures 1 and 2 is strong evidence that dispersion effects are relatively small in the observed spectra. Similar agreement was obtained for the other acrylic samples. The extrapolation has somewhat sharpened the band at  $350\text{ cm}^{-1}$  and resolved another at  $550\text{ cm}^{-1}$  which cannot clearly be seen in the  $90^\circ$  data.

The effect of swelling the sample is shown in Figure 3. The molecules of  $\text{CDCl}_3$ , essentially 'invisible' to the neutrons, separate the polymer chains, and bring about a 'sharpening' of the spectrum. The region between  $100$  and  $400\text{ cm}^{-1}$  appears continuous for the poly(methyl

methacrylate) sample, but after swelling, is resolved into three bands centred at  $\sim 100$ ,  $240$  and  $350\text{ cm}^{-1}$ .

In Figure 4 the frequency functions for the three swollen samples of acrylic polymers are compared. The ordinate is in absolute units (within experimental errors) so that the effects of substitution for the  $\alpha$ - and ester-methyl groups are seen quantitatively from the relative intensities at each frequency.

The spectrum of these acrylic samples divides into three principal regions—the three bands seen in Figure 3 for the unsubstituted sample. Comparison of the three spectra assigns the energy transfer at  $350\text{ cm}^{-1}$  to the presence of an  $\alpha$ -methyl group in the polymer repeat unit. The band at  $100\text{ cm}^{-1}$  is associated with the ester methyl group since it is observed only in the spectrum of Perspex and poly( $\alpha$ -chloro methacrylate).

The band at  $240\text{ cm}^{-1}$  is probably due to the small percentage of isotactic sequences in poly(methyl methacrylate). Figure 5 compares  $p(\omega)$  for a predominantly isotactic sample of poly(methyl methacrylate) with the corresponding  $p(\omega)$  for the commercial sample and it will be noted that in the isotactic sample the peak at  $350\text{ cm}^{-1}$  is absent, but instead there is a peak at  $250\text{ cm}^{-1}$  of comparable intensity. An isotactic sample of poly(methyl methacrylate- $\text{COOD}_3$ ) is now required to enable a more precise value of this frequency to be obtained for the isotactic stereoisomer.

#### Poly(propylene oxide)

Figure 6 compares the frequency functions of poly(propylene oxide) and poly(propylene oxide- $\text{CD}_3$ ). The sharp, intense band at  $230\text{ cm}^{-1}$  is completely removed by deuterium substitution of the methyl group, indicating that this spectral feature is peculiar to the methyl group alone. Comparison of data taken at different angles of scatter shows once again (Figure 6) that dispersion effects are small. The weak shoulder observed at  $163\text{ cm}^{-1}$  probably also disappears on deuteration of the methyl group, but this cannot be asserted with confidence.

## DISCUSSION

#### Barriers to internal rotation

From the inelastic incoherent scattering spectrum the torsional frequencies of the methyl group in poly(methyl methacrylate) and poly(propylene oxide) can be identified in terms of the following criteria: (a) the torsional mode is expected to occur in the region below  $400\text{ cm}^{-1}$  and the intensity of the inelastic band should be high due to the large amplitude of motion of the protons; (b) selective substitution of chlorine or deuterium in the methyl group removes the  $\text{CH}_3$  band; (c) the relative intensities of higher transition  $V=2 \rightarrow 1$ ,  $3 \rightarrow 2$  etc. will be low compared with the fundamental transition  $V=1 \rightarrow 0$ .

In our experiments with poly(methyl methacrylate) we have found the spectral frequencies to be independent of swelling. The bands sharpen but do not move in position, so that it is reasonably certain that the bands we are looking at are intramolecular in origin. The assignment of the observed bands to torsional frequencies is given in Table 1 and values of  $V_3$  have been calculated on the assumption that the  $\text{CH}_3$  group is an independent rotor attached to a polymer chain of infinite mass.

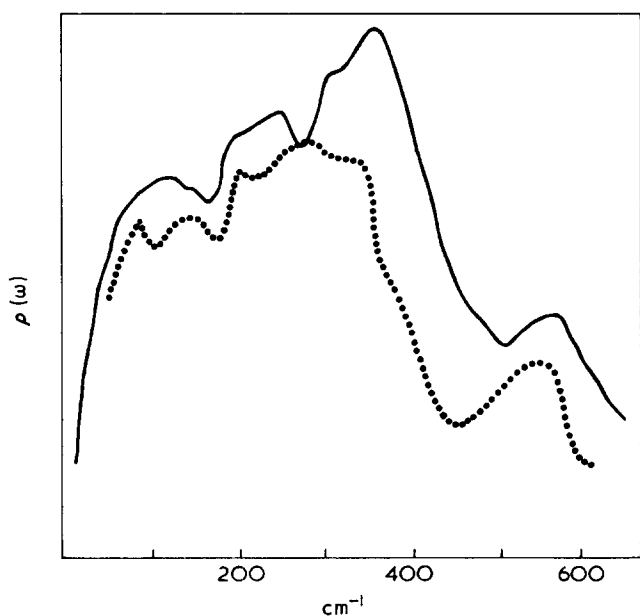
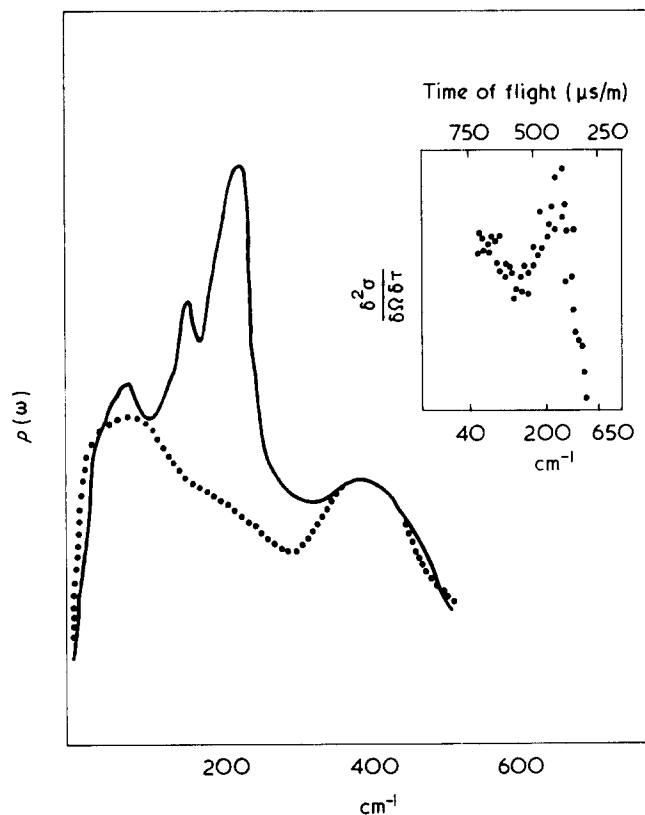
Table 1 Values of  $V_3$  calculated from torsional frequencies

	$\nu_{\text{tor}}$ ( $\text{cm}^{-1}$ )	$V_3$ ( $\text{kJ mol}^{-1}$ )
$\text{CH}_3$ in PPO	228	13.8
$\alpha\text{-CH}_3$ in PMMA: predominantly syndiotactic	350	34.3
isotactic	(240)	(16.7)
$\text{OCH}_3$ in PMMA	100	4.2

In assessing the reliability of these values, we must take into account: (i) that the spectra are recorded in the condensed phase and the influence of intermolecular interactions. However, the torsional frequencies of methyl groups in simple molecules only move  $5\text{--}10\text{cm}^{-1}$  on transferring from vapour to the liquid phase<sup>5</sup>; (ii) the lack of precise geometrical data. In calculating the structure factor we have assumed  $r_{\text{CH}}=1.08\text{ \AA}$ ,  $r_{\text{CC}}=1.54\text{ \AA}$ , and tetrahedral angles; (iii) the experimental error in  $\nu_{\text{tor}}$ , which is  $\sim \pm 10\text{cm}^{-1}$ .

The most difficult problem is to estimate the uncertainty in  $V_3$  arising from the separation of the contribution to the total Hamiltonian from internal rotation, i.e. coupling with other vibrational modes etc. Factors (i), (ii) and (iii) are most probably adequately covered by assigning an error of 20% to the values of  $V_3$  quoted above. In order to estimate the errors arising from the separation of the internal rotation contribution to the Hamiltonian it would be necessary to perturb the very low lying frequencies of the polymer molecule by isotopic substitution. Unfortunately the synthesis of suitable molecules is a major undertaking, and in any case, it is doubtful whether a sufficient perturbation could be obtained to fully analyse the effects of coupling on the torsional frequencies.

The most interesting feature of the values quoted for  $V_3$  is the surprisingly high value  $V_3=34.3\text{ kJ mol}^{-1}$  found for the  $\alpha\text{-methyl}$  group in predominantly syndiotactic poly(methyl methacrylate).  $V_3=13.8$  must be regarded as a more normal value for a methyl group with an aliphatic main chain, since the torsional frequency quoted for polypropylene<sup>16</sup> is  $210\text{cm}^{-1}$ , and although there are

Figure 5  $p(\omega)$  for Perspex (—) and isotactic Perspex (.....)Figure 6  $p(\omega)$  for poly(propylene oxide) (—) and poly(propylene oxide- $\text{CD}_3$ ) (.....). Inset time-of-flight spectrum at  $81^\circ$  scattering angle between  $40$  and  $650\text{cm}^{-1}$  for poly(propylene oxide)

complications because of the highly crystalline nature of this polymer, the literature indicates that the torsional frequency in the amorphous phase must lie very close to  $210\text{cm}^{-1}$ . The corresponding value for  $V_3$  for polypropylene is  $12.6\text{ kJ mol}^{-1}$ .

Another feature which merits further investigation (if our tentative assignment of  $\nu_{\text{tor}}$  for isotactic poly(methyl methacrylate) proves to be correct) is the marked difference in  $V_3$  for the  $\alpha\text{-CH}_3$  groups in iso- and syndiotactic sequences of poly(methyl methacrylate). Such a large difference has never been reported for stereoisomers of small molecules and we have not observed corresponding effects in other polymers arising from variations in stereoregular character. Nevertheless, there may be smaller changes in other polymers which are difficult to observe because of the widths of the torsional bands of the limited resolution of the neutron spectrometer.

#### Relaxation phenomena associated with methyl group re-orientation

*Poly(propylene oxide) and polypropylene.* Dielectrical, mechanical and n.m.r. (including  $T_1$  and  $T_{1\rho}$ ) relaxation studies have been made for poly(propylene oxide) samples<sup>2,11</sup> similar to the ones used in this work. The results are summarized in Figure 7. It is clear that the  $\gamma$ -loss peak is observed both in n.m.r. and mechanical and dielectric measurements, and studies of  $T_1$  values for deuterated samples undoubtedly prove that this loss mechanism is associated with methyl group re-orientation. Furthermore dilution of the polymer sample with  $\text{CS}_2$  does not shift the location of the  $T_1$  minimum associated with methyl group re-orientation, which suggests

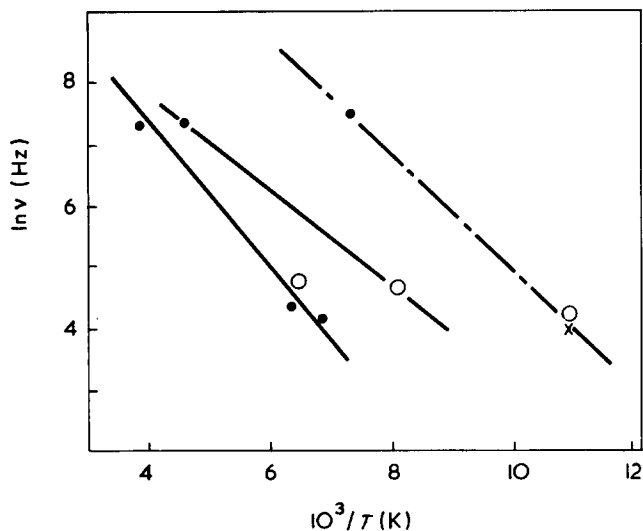


Figure 7 Logarithm of loss frequency maxima,  $\nu$  against inverse temperature for relaxation studies of poly(propylene oxide)<sup>2,11,17</sup> and poly(methyl methacrylate)<sup>13</sup>. ●,  $T_1$  measurements; ○,  $T_{1\rho}$  measurements; ×, mechanical; —, syndiotactic poly(methyl methacrylate); - - -, isotactic poly(methyl methacrylate); - · - ·, poly(propylene oxide)

that the motion is predominantly intramolecular in character. Thus it is reasonable to assign the relaxation process to the torsional motion of the methyl group about its  $C_3$  axis. The activation energy measured from the relaxation data for this loss mechanism is  $15.9 \pm 1.7$  kJ mol<sup>-1</sup>. It is interesting to note that the activation energy and  $V_3$  are very similar in magnitude, and so it is likely that the barrier to internal rotation is largely responsible for the magnitude of the activation energy.

In a recent detailed study of spin-lattice relaxation in polypropylene over a range of n.m.r. frequencies, Noack *et al.*<sup>12</sup> found that the activation energy for the methyl group reorientation is 12.1 kJ mol<sup>-1</sup>. Again there is close agreement between the activation energy and the value for  $V_3$  obtained from vibrational spectroscopy.

**Poly(methyl methacrylate).** The poly(methyl methacrylate) used in the present neutron scattering studies is predominantly syndiotactic. For the syndiotactic polymer, activation energy of the  $\alpha$ -methyl group reorientation is 23–25 kJ mol<sup>-1</sup>, determined by n.m.r.,  $T_1$  and  $T_{1\rho}$  measurements<sup>13</sup>. Again the origin of this loss mechanism is assigned as a hindered internal rotation of the methyl group. All the data available are plotted in Figure 7. In this case the activation energy is somewhat lower than the value of  $V_3$  for this motion obtained from our neutron scattering studies, but in view of the uncertainties in the value of  $V_3$  and the difficulty of precisely assigning the temperature of the minima in the  $T_{1\rho}$  curve, the disagreement is not definitely outside experimental error. In view of the tentative lower value of  $V_3$  for  $\alpha$ -CH<sub>3</sub> groups in isotactic sequences than in syndiotactic sequences, it is particularly interesting to note that n.m.r. studies on isotactic poly(methyl methacrylate) yield a lower value for  $E_a$  too. The value is  $E_a = 15.5$  kJ mol<sup>-1</sup> compared with  $E_a = 23$ –25 kJ mol<sup>-1</sup> for the syndiotactic material. It thus lends support to the tentative conclusion from our preliminary neutron studies.

Unfortunately the activation energy for the ester methyl group reorientation has not been determined by relaxa-

tion spectroscopy because the  $T_1$  minima are broad and lie at very low temperatures. Only the minimum in  $T_1$  has been reported. Although a direct comparison between activation energy and  $V_3$  is therefore not possible for this particular torsional motion, the low value of  $V_3 = 4.2$  kJ mol<sup>-1</sup> is consistent with the fact that the loss peaks lie at very low temperatures.

#### QUANTUM MECHANICAL TUNNELLING

The sets of eigen values for the torsional oscillation of a threefold symmetric rotor are identical in each well so that conditions are favourable for tunnelling to occur between the wells. The energy levels in fact occur in pairs and the separation of each pair of levels is a direct measure of the rate at which tunnelling occurs through the barrier. The separation is small for the lowest levels where tunnelling is a less likely process and increases for successively higher pairs.

If tunnelling is an important relaxation process, then values of  $E_a$  cannot be estimated from  $T_1$  measurements by simple Arrhenius type plots because the  $\nu - T^{-1}$  plots are no longer linear at lower temperatures (see Figure 8). Stejskal and Gutowsky<sup>14</sup> have calculated the average tunnelling frequency  $\nu_t$  for the set of eigen values as a function of temperature for a series of values of  $V_3$ . A regular set of curves is obtained which converge at an infinite temperature limit  $\nu_t = 2.5 \times 10^{12}$  Hz.

Assuming tunnelling to be the major relaxation process, values for the potential barriers,  $V_3$ , have been calculated from the  $T_1$  and  $T_{1\rho}$  data using these curves. Eisenberg<sup>15</sup> has already used this method to estimate  $V_3$  values for a variety of polymers including poly(methyl methacrylate). We have revised these estimates by including further  $T_1$  and  $T_{1\rho}$  results which are now available for poly(methyl methacrylate), poly(propylene oxide) and polypropylene. In Figure 8 the  $T_1$  and  $T_{1\rho}$  measurements from these polymers are compared to Stejskal and Gutowsky's curves.

It will be noted that a fairly consistent value of  $V_3 = 29$  kJ mol<sup>-1</sup> is obtained for the  $\alpha$ -CH<sub>3</sub> in poly(methyl

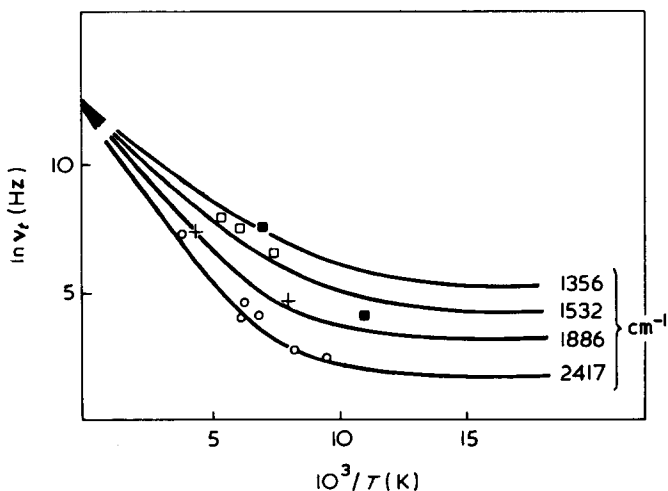


Figure 8 Curves of logarithm of tunnelling frequency  $\nu_t$  against inverse temperature<sup>14</sup> for four barrier heights. Also shown is n.m.r. relaxation data for: +, isotactic Perspex<sup>13</sup>; ○, syndiotactic Perspex<sup>13</sup>; □, polypropylene<sup>12</sup>; ■, poly(propylene oxide)<sup>2,11</sup>

Table 2 Comparison of activation energies and barriers for CH<sub>3</sub> side-group motion (kJ mol<sup>-1</sup>)

Polymer	$V_3$ (vibrational)	$E_a$ (Arrhenius)	$V_3$ (tunnelling)
Propylene	12.5 <sup>16</sup>	12.1	16.7
Propylene oxide	13.8	15.9	18.4
Methyl methacrylate			
$\alpha$ -CH <sub>3</sub>			
predominantly			
syndiotactic	34	23-25	28.9
isotactic	16.7	15.5	22.6
OCH <sub>3</sub>			
all stereo-			
isomers	4.2	very low	8.4*

\* From one datum only

methacrylate) and this value is in better agreement with the value calculated from the neutron results than the value of  $E_{act}=23-25$  kJ mol<sup>-1</sup> obtained from a simple Arrhenius plot. The value calculated on the basis of tunnelling for the isotactic sample is  $V_3=23$  kJ mol<sup>-1</sup> which compares with  $V_3=17$  from neutron scattering. Only one point is recorded for the methoxy group and this suggests  $V_3=8.8$  kJ mol<sup>-1</sup> to be compared with  $V_3=4.2$  kJ mol<sup>-1</sup> from vibrational spectroscopy. Further relaxation data are clearly required for this -CH<sub>3</sub> process.

The relaxation data for poly(propylene oxide) scatter about  $V_3=18.4 \pm 2$  kJ mol<sup>-1</sup> in Figure 7 compared with  $V_3=13.8$  kJ mol<sup>-1</sup> from vibrational spectroscopy and 15.9 kJ mol<sup>-1</sup> from the Arrhenius plot. The relatively poor fit to the  $\nu_t$ -temperature curve may reflect the inadequacy of Stejskal and Gutowsky's model of quantum mechanical -CH<sub>3</sub> tunnelling to produce a precise value of  $V_3$ .

The results for polypropylene are similarly scattered between the curves but again a value of  $V_3=17$  kJ mol<sup>-1</sup> is estimated. Based on a single relaxation datum Eisenberg estimated  $V_3=29$  kJ mol<sup>-1</sup> for the CH<sub>3</sub> group in polypropylene. This high value must be discounted in favour of  $V_3 \sim 12.5$  to 17 kJ mol<sup>-1</sup> in view of the similar results obtained for polypropylene and poly(propylene oxide) both from  $T_1$  measurements and also from neutron scattering results.

## CONCLUSION

The precise significance of the corrections for tunnelling is difficult to assess. However, inspection of the data presented in Table 2 shows that there is a correlation between values of  $V_3$  obtained from torsional frequencies

and the activation energies for the corresponding CH<sub>3</sub> group re-orientation obtained from Arrhenius plots.

There is a slightly better correlation between these values of  $V_3$  and the corresponding values extracted from the relevant data using Stejskal and Gutowsky's model for quantum mechanical tunnelling of the CH<sub>3</sub> group. Thus both analyses of the experimental results lead to the conclusion that the potential barrier hindering -CH<sub>3</sub> side-group rotation in polymer molecules is a major factor governing the frequency-temperature dependence of the corresponding relaxation phenomena observed in bulk properties of the polymers. These processes are therefore primarily intramolecular in character.

## ACKNOWLEDGEMENTS

We should like to thank the SRC for allocation of reactor time and for a fellowship for one of us (J.S.H.). We are also very grateful to the University Support Group at AERE, Harwell for their willing assistance at all times.

We are grateful to Dr J. B. Rose (ICI, Plastics Division) for the sample of poly( $\alpha$ -chloro methylacrylate) and to Mr S. M. Todd for the preparation of poly(methyl methacrylate-COOCd<sub>3</sub>).

## REFERENCES

- 1 McCrum, G., Read, B. E. and Williams, G. 'Anelastic and Dielectric Effects in Polymer Solids', Wiley, London, 1967
- 2 Connor, T. M. and Hartland, A. *Polymer* 1968, **9**, 591
- 3 Cunliffe, A. V. *J. Mol. Structure* 1970, **6**, 9
- 4 Fateley, W. G. and Miller, F. A. *Spectrochim. Acta* 1963, **19**, 611
- 5 Brier, P. N. *J. Mol. Structure* 1970, **6**, 23
- 6 Brier, P. N., Higgins, J. S. and Bradley, R. H. *J. Mol. Phys.* 1971, **21**, 721
- 7 Bunce, L. J., Harris, D. H. C. and Stirling, G. C. *UK At. Energy Auth. Rep. AERE, R6246*, 1970
- 8 Wignall, G. D. *UK At. Energy Auth. Rep. AERE, M1928*, 1967
- 9 Longster, G. R. and White, J. W. *Mol. Phys.* 1969, **17**, 1
- 10 Boutin, H. and Yip, S. 'Molecular Spectroscopy with Neutrons', Cambridge, Mass., The MIT press, 1968
- 11 Blears, D. J., Connor, T. M. and Allen, G. *Trans. Faraday Soc.* 1965, **61**, 1097
- 12 Kienzle, U., Noack, F. and von Schütz, J. *Kolloid-Z. Z. Polym.* 1970, **236** (2), 129
- 13 Connor, T. M. and Hartland, A. *Phys. Lett.* 1966, **23**, 662
- 14 Stejskal, E. O. and Gutowsky, H. S. *J. Chem. Phys.* 1958, **28**, 388
- 15 Eisenberg, A. and Reich, S. *J. Chem. Phys.* 1969, **51**, 5706
- 16 Boutin, H. and Yip, S. 'Molecular Spectroscopy with Neutrons', Cambridge, Mass., The MIT press, 1968, p 87
- 17 Crissman, J. M., Sauer, J. A. and Woodward, A. E. *J. Polym. Sci. (A-2)* 1961, p 5075

# Transient scattering from absorbing solutions

B. R. Jennings

*Physics Department, Brunel University, Uxbridge, Middlesex, UK*

and J. Schweitzer

*Physics Department, Queen Elizabeth College, University of London, London W8, UK*

*(Received 19 August 1971 ; revised 15 November 1971)*

Although light scattering has become a standard method for determining the geometric parameters of macromolecular solutes in solution, it has serious theoretical and experimental limitations when the solutions partly absorb the incident light. When subjected to pulsed electric fields, electrically anisotropic molecules orientate. This changes the scattered intensity. By making measurements of the relative scattered intensity changes as the molecules revert to a random array after the electric pulse has ceased, the molecular relaxation times, and hence the molecular dimensions, may be evaluated whether or not the material is absorbing. Typical measurements are made on vanadium pentoxide and benzopurpurine suspensions and tobacco mosaic virus solutions at a variety of wavelengths to demonstrate the method.

## INTRODUCTION

Light-scattering measurements have become a standard means of determining the molecular weight and size of macromolecules and particles in solution or suspension. The method is particularly suited to those molecules whose major dimension is similar to the wavelength ( $\lambda$ ) of the incident light. It is common to utilize the so-called 'Rayleigh-Gans-Debye' (RGD) theory<sup>1-3</sup> and to measure the scattered intensity ( $I$ ) from solutions of varying concentration ( $c$ ) at a number of angles ( $\theta$ ) to the forward direction of the incident light beam. The experimental data are usually analysed in the form of a Zimm<sup>4</sup> plot.

The Rayleigh<sup>1</sup> theory is based on the assumption that the scattering particles are transparent or non-absorbing, and are in a non-absorbing medium. In such a case, the oscillating electric vector of the incident light beam induces electric dipoles in the scattering particles. These then act as secondary sources of radiation of the same frequency as the incident light beam if, and only if, this frequency is far removed from the natural frequency of the outer bound electrons. Many polymer, and in particular biopolymer, solutions are coloured. In this case, the incident light beam is attenuated through both scattering and selective absorption. If the absorption is an inherent

property of the solute, then the frequency of the incident radiation is close to the natural frequency of the electrons and a complex refractive index must be used in the fundamental Rayleigh equation, so that the RGD theory becomes inappropriate. Attempts have been made to calculate theoretical factors which would suitably modify the RGD theory for an absorbing solute<sup>5, 6</sup>. However, they apply only for specific optical geometries and experimental conditions, such as an extremely well positioned cell in a Brice Phoenix photometer when rectangular collimating slits and square scattering cells are used for observations at 90° to the incident beam direction<sup>7</sup>. Corrections for dissymmetry measurements have also been suggested<sup>8</sup>.

Apart from the aforementioned difficulty, there are three secondary problems. Firstly, the refractive index increment ( $dn/dc$ ) ceases to be a linear function of wavelength and so must be measured under practical conditions. This increment is needed in the evaluation of the scattering data using the RGD theory<sup>9</sup>. Secondly, selective absorption may also come from the solvent or impurities in the same. The recorded intensity will not be that scattered by the solute molecules on account of the attenuation of the incident and scattered beams in the scattering cell. Putzeys and Dory<sup>5</sup> have proposed a cor-



rection factor for this, once the extinction coefficient of the sample solution has been measured at the wavelength concerned. Thirdly, with highly absorbing solutions, it may prove difficult to obtain sufficient light penetration of the cell. Dilution overcomes this problem, but also reduces the scattered intensity.

Because of these difficulties, it is unusual to undertake scattering experiments on absorbing solutions. One is faced with the problem of using the various correction factors and modifying the experimental conditions to suit them<sup>7</sup> or of working in a spectral region where the solutions absorb negligibly<sup>10</sup>. The latter case, may be impracticable or correspond to wavelengths for which the scattering is small.

There has been a growing interest of late in the electro-optical properties of molecular solutions. In general, a stable solution consists of solute molecules which are randomly distributed and orientated in the body of the solvent. Under the influence of an external electric field, polar or electrically anisotropic molecules orientate towards the applied field direction. Such alignment enables any optically anisotropic (or tensor) property, such as the refractive index<sup>11, 12</sup>, extinction coefficient<sup>12, 13</sup> or optical rotatory power<sup>14, 15</sup> of the individual molecules to be manifest. With large molecules, whose dimensions are close to that of  $\lambda$ , the polar scattering intensity diagram (of  $I$  as a function of  $\theta$ ) is not symmetric. This is accounted for in the particle scattering factor  $P(\theta)$  in conventional scattering theory<sup>9</sup>. In an electric field, particle alignment will be accompanied by changes in  $P(\theta)$  and hence in the scattered intensity at any angle of observation. In non-absorbing media, measurements of the intensity changes as a function of the applied field amplitude, frequency and shape have enabled solute dipole moments ( $\mu$ ), sizes, electric polarizabilities and rotary diffusion constants ( $D$ ) to be determined<sup>16</sup>. The latter is very dependent upon particle size, and can be determined with ease from perturbed scattering data whether or not the medium is absorbing, provided that the light scattered from the solution is measurable.

Thus, the object of this paper is to show that measurements of the changes in the scattered light intensity from macromolecular solutions under the influence of applied electric fields, affords a method of determining solute rotary diffusion constants and hence particle sizes even if the solutions are absorbing.

## OUTLINE OF METHOD

If continuous alternating current electric fields are applied to macromolecular solutions, rotary diffusion constants and molecular relaxation times ( $\tau=1/6D$ ) may be determined by observing the changes ( $\Delta I$ ) in the scattered intensity ( $I$ ) as a function of the angular frequency ( $\omega$ ) of the applied fields. Polar molecules show a dispersion of  $\Delta I$  with  $\omega$  in much the same way as the real dielectric constant does in dielectric dispersion measurements<sup>17</sup>. Measurements of  $\Delta I$  would thus be required at various  $\omega$ . As these are relative measurements, one does not need to determine the absolute scattered intensity and hence avoids all the difficulties of conventional scattering measurements mentioned above. Absorption is not a problem therefore as long as enough light is scattered to register on the photodetector. In addi-

tion, solution concentration need not be known, especially if data are extrapolated to zero concentration. Details of the apparatus and procedures for evaluation of  $D$  using continuous sinusoidal fields were reviewed by Jennings<sup>16</sup>.

A more convenient and rapid method is to use pulsed electric fields, as was first developed for d.c. fields by Stoylov and Sokerov<sup>18</sup>. Changes in the scattered intensity can be considered in three temporal regions: (a) as the pulse is switched on, (b) during the steady influence of the pulse, and (c) after the pulse has terminated. During the first region, the molecules will start to orientate towards their position of least potential energy in the field. This process will take a finite time owing to the opposition of the molecular torque due to Brownian forces and the electrostatic orienting couple. The scattered intensity will thus increase (or decrease) in a transient manner, until it reaches a steady saturation condition in region (b). The magnitude of  $\Delta I$  during regions (a) and (b) is a complicated function of the field strength and frequency, the electrical and geometrical properties of the solute molecules and the viscosity of the solvent. For absorbing solutions it will also depend upon the absorption of the incident light by the solution. After the pulse has terminated, the molecules will revert to a random array under Brownian forces alone. The corresponding transient decay in  $\Delta I$  will thus be a function of the particles' geometry and size and the solvent viscosity alone. For a monodisperse solute, it will follow the equation<sup>19</sup>:

$$\Delta I = \Delta I_0 \exp(-t/\tau) = \Delta I_0 \exp(-6Dt) \quad (1)$$

where  $\Delta I_0$  is the scattered intensity change at time  $t=0$  when the pulse is terminated. Hence, analysis of the field-free decay in the scattered intensity yields  $\tau$  and  $D$  directly. If the particle shape is known, size parameters can be derived directly from  $D$  using the Broersma<sup>20</sup> or Burgers<sup>21</sup> equation for rods, Perrin's<sup>22</sup> equations for discs or ellipsoids or the Stockmayer and Bauer<sup>23</sup> equations for flexible coils.

The use of pulsed rather than continuous electric fields has specific advantages. The method is quick as all data are obtained from a single photographic measurement. Heating and electrophoretic effects are greatly reduced. Rotary diffusion constants are obtained without knowledge of the electrical and geometrical properties of the molecules. Fields of any (reasonable) amplitude can be used; restriction to small degrees<sup>11, 16</sup> of molecular orientation is not necessary.

Details of the apparatus and method, which will not be appreciably different for absorbing systems, have appeared elsewhere<sup>16, 18</sup>.

A further improved method is to use sinusoidal pulsed fields. The scattered intensity will again follow a transient shape with the three regions described above. The method retains the advantages of the d.c. pulsed method but has three additional features. Firstly, it prevents electrophoretic effects. Secondly, it reduces the problems associated with the migration of mobile charge carriers in conducting solutions. Thirdly, by using high frequency fields, contributions from any permanent dipole orientation can be excluded and analysis made in terms of induced dipolar contributions alone.

Using this method, measurements were made on a modified<sup>16, 24</sup> Sofica photometer. A diagrammatic representation of both the optic and electronic apparatus used to

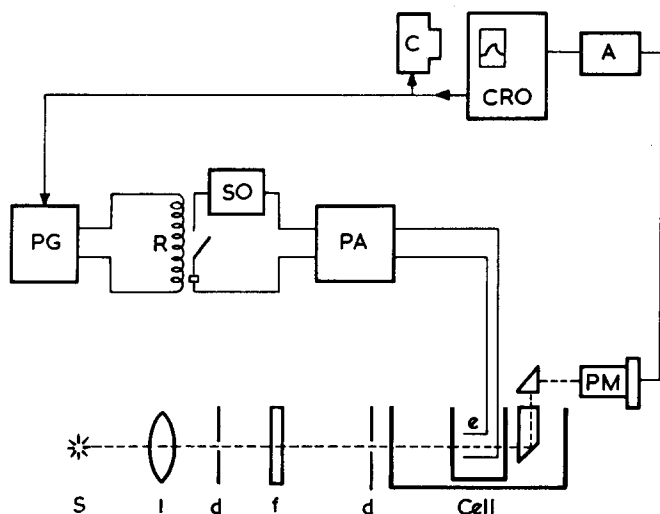


Figure 1 Schematic diagram of the apparatus for transient scattering measurements using pulsed, sinusoidal electric fields. Optical components are the source (s), lens (l), diaphragm (d) and interference filter (f). Electric components are: PM, photomultiplier; A, amplifier; CRO, oscilloscope; C, camera; PG, low voltage pulse generator; R, relay; SO, sine wave oscillator; PA, pulse amplifier

deliver the pulses and detect the resulting transients is given in Figure 1. The Sofica light source was replaced by a 500 W mercury arc powered by a stabilized d.c. supply. A low noise EMI 9635 QB photomultiplier was used to detect the transients. The electrodes, of separation 1 cm, were positioned so that the field was applied perpendicular to the incident light beam. The short bursts of sinusoidal electric field were generated as follows. The output from a low voltage, sine wave, oscillator was fed through a relay which was triggered by a low voltage pulse generator. The relay was obtained from Astralux Dynamics Ltd (of Brightlingsea, Essex), and could handle pulses longer than 1 ms with a switching time of less than 100  $\mu$ s. The output from the relay was amplified using a 150 W power amplifier with a frequency response from 30 Hz to 30 KHz supplied by Airmec-Racal Ltd (of Reading, Berkshire). Since the intensity of the scattered beam was relatively low in an absorbing spectral region, the signal to noise ratio was reduced. All measurements were made at an angle of 30° where the scattered intensity was proportionately larger than at higher angles.

REPRESENTATIVE RESULTS

As a feasibility study, three systems were investigated. Suspensions of vanadium pentoxide in methanol were studied at 546, 436 and 365 nm wavelengths. The suspensions were pale green in colour. Measurements were made at three wavelengths corresponding to different degrees of absorption. White light was used to study suspensions of benzopurpurine in methanol, which were deep orange-red in colour. Finally, aqueous solutions of tobacco mosaic virus (TMV) were examined at 436 and 310 nm wavelength. The TMV solutions exhibited negligible absorption in the visible region of the spectrum, but absorbed strongly in the ultra-violet. Measurements were thus made in the visible and ultra-violet for comparison.

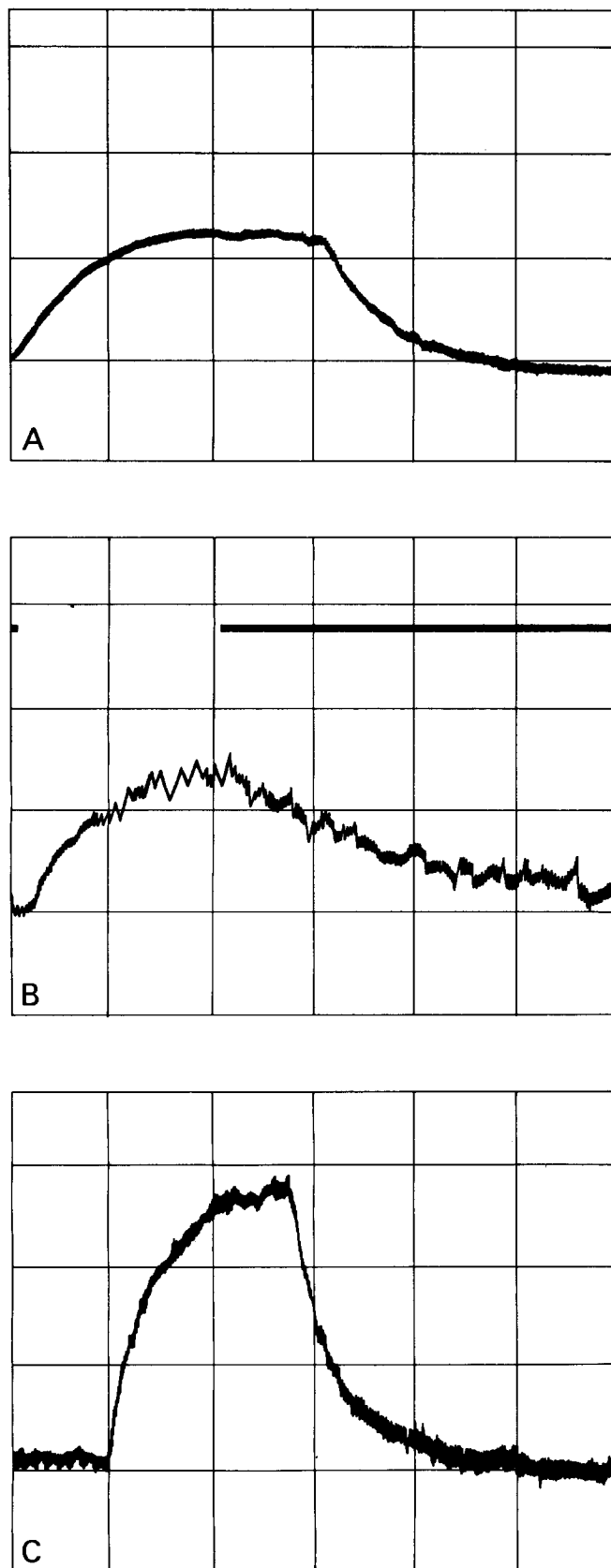


Figure 2 Typical transient scattering traces. (A), vanadium pentoxide in methanol,  $\lambda=436$  nm,  $E=635$  V/cm; (B), benzopurpurine in methanol, white light,  $E=1.13$  kV/cm; (C), TMV in water,  $\lambda=310$  nm,  $E=320$  V/cm. Time scales of 20ms, 15.5ms and 10ms per division for (A), (B) and (C) respectively. Pulsed sinusoidal fields of 5 KHz frequency were used. The field duration is indicated in frame (B) for that particular case

Typical transient responses are shown in Figure 2. The decays of these transients were analysed by plotting graphs of the natural logarithms of  $(\Delta I/\Delta I_0)$  against time. All such graphs were curved (Figures 3 and 4) indicating that more than one diffusion constant was involved (equation 1) and that the samples were all polydisperse. From the *initial slopes* of the graphs, the rotary diffusion constants listed in Table 1 were obtained. Such values of  $D$  were not truly representative of all material present in the polydisperse systems. They have been designated  $D'$  for clarity. Data for  $V_2O_5$  suspensions and TMV solutions show that within the limits of the experimental error, the same value of  $D'$  is obtained within or without the absorbing regions, thereby confirming the validity of the method. The identical decay rates for the TMV solutions is especially gratifying. The small variation between wavelengths for the  $V_2O_5$  suspensions shows no obvious wavelength dependence and is considered to be insignificant. In general, the scattered light is reduced in the absorbing region so that the noise on the traces is relatively greater. This is seen in the case of benzopurpurine, which was so strongly absorbing that white light was used to increase the scattered intensity. The error in  $D'$  was thus larger in this case. Increased noise in the absorbing region was not evidenced for the TMV solutions as the scattering was greater at lower wavelengths owing to the dependence of  $I$  on  $\lambda^{-4}$  as predicted by the Rayleigh theory.

Two further points are of interest. Firstly, an electron microscope study on the TMV sample indicated the presence of monomer, dimer and fragmentary virus particles, thereby confirming the polydisperse nature of

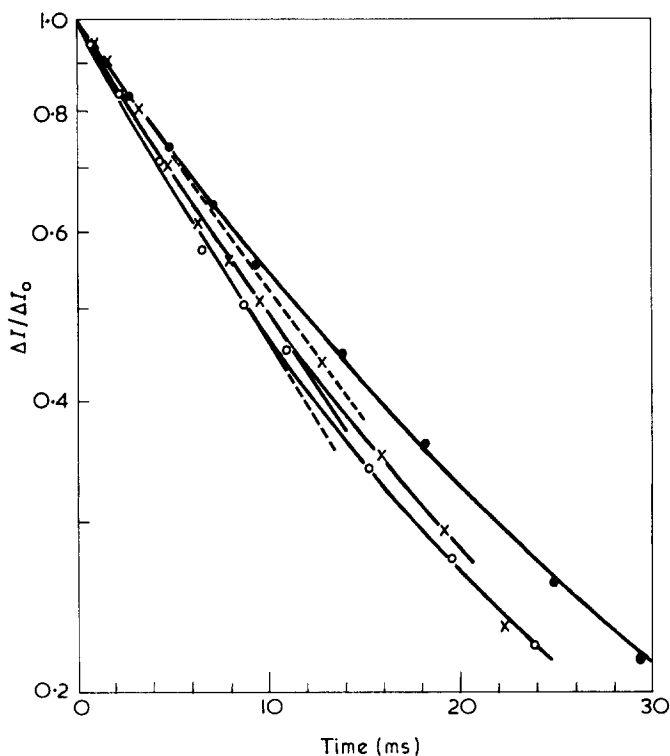


Figure 3 Decay analysis for vanadium pentoxide.  $E=635$  V/cm. ●,  $\lambda=546$  nm; ○,  $\lambda=436$  nm; ×,  $\lambda=365$  nm.

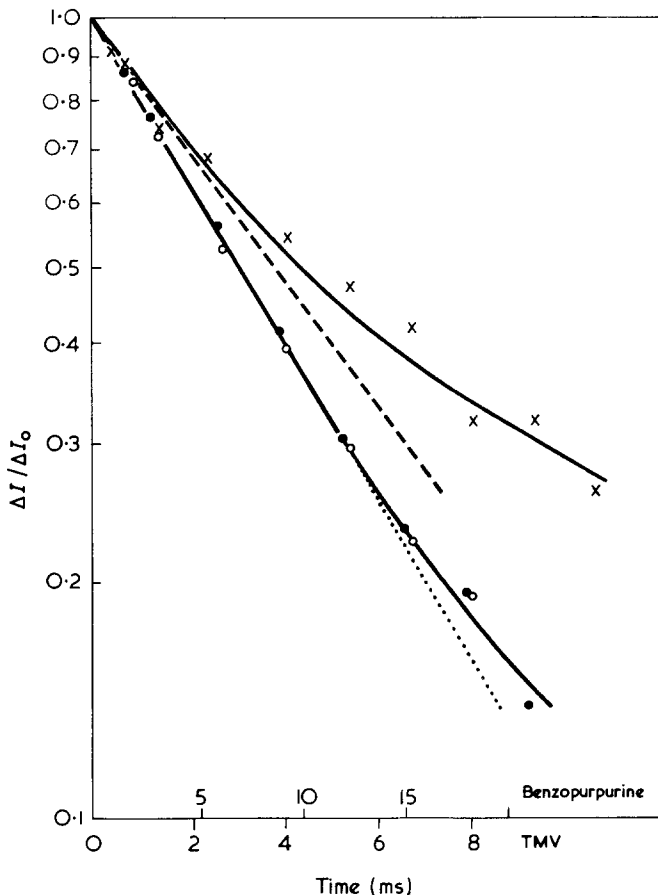


Figure 4 Decay analysis for TMV and benzopurpurine. ×, benzopurpurine in white light,  $E=1.13$  kV/cm; ○, ●, TMV at 310 and 436 nm respectively,  $E=320$  V/cm. Note the different abscissa scales

Table 1 Analysis of scattering transients

Material	Solvent	$c$ (approx) (g/ml)	$\lambda$ (nm)	$D'$ * ( $s^{-1}$ )
Vanadium pentoxide	Methanol	$5 \times 10^{-1}$	546	$11.9 \pm 1.5$
			436	$12.5 \pm 1.5$
			365	$10.5 \pm 1.5$
Benzopurpurine	Methanol	$1 \times 10^{-1}$	White light	$13.0 \pm 3.0$
Tobacco mosaic virus	Water	$1 \times 10^{-1}$	436	$37.8 \pm 3.0$
			310	$37.8 \pm 3.0$

\* Rotary diffusion constants ( $D'$ ) are from the initial slopes alone, and are not necessarily comparable directly with results for  $D$  in the literature (see text)

the material. Our value of  $D'$  is in very good agreement with that reported by Stoylov and Sokerov<sup>18</sup> at a similar field strength and for a sample of similar polydispersity. It should be noted that with polydisperse samples, the initial slope of the transient depends upon both the nature of the polydispersity distribution and the field strength. Information about the distribution of particle sizes can be determined by adjusting the field strength and pulse duration. The results presented here are not to be compared with 'weighted' or 'averaged' values of  $D$  obtained by other experimental methods which are generally

equivalent to data obtained in electric field scattering experiments at high field strengths. By demonstrating the agreement with Stoylov and Sokerov's<sup>18</sup> results, who did make a study of the field strength dependence, the present work illustrates that measurements are possible in or near an absorption band without influencing unduly the value of  $D'$ . For clarity, it is emphasized that the value of  $D'$  obtained here (to be compared with  $D \approx 300 \text{ s}^{-1}$  for TMV when obtained by methods which weight over the complete distribution) is simply a reflection of the sample polydispersity. With a monodisperse system, the decay rate would reflect a single, consistent value for  $D' = D$  whatever the field strength employed. A full study of the dependence of the initial slope of transient electro-optic decay rates has been made in this laboratory and will be published elsewhere.

Secondly,  $D$  can be determined from electrically induced transient changes in other optical properties such as the birefringence<sup>11,12</sup>, dichroism<sup>12</sup> and optical rotation<sup>15</sup>. Because these are essentially transmission methods they are inapplicable for absorbing solutions. The scattering method is superior in this respect, as long as the particles are large enough to give a dissymmetric polar scattering diagram.

#### ACKNOWLEDGEMENTS

The equipment was purchased with the aid of a Science Research Council grant. One of us (J.S.) thanks Queen Elizabeth College for a Demonstratorship, during the tenure of which this work was undertaken.

#### REFERENCES

- 1 Lord Rayleigh *Phil. Mag.* 1881, **12**, 81
- 2 Gans, R. *Ann. Phys.* 1925, **76**, 29
- 3 Debye, P. *Ann. Phys.* 1915, **46**, 809
- 4 Zimm, B. H. *J. Chem. Phys.* 1948, **16**, 1099
- 5 Putzeys, P. and Dory, E. *Ann. Soc. Sci. Brux.* 1940, Ser. 1, **60**, 37
- 6 Laver, J. L. *J. Opt. Soc. Am.* 1951, **41**, 482
- 7 Brice, B. A., Nutting, G. C. and Halwer, M. J. *Am. Chem. Soc.* 1953, **75**, 824
- 8 Frank, H. P., Ullman, R. *J. Opt. Soc. Am.* 1955, **45**, 471
- 9 Stacey, K. A. in 'Light Scattering in Physical Chemistry', Butterworths, London, 1956
- 10 Alexander, P. and Stacey, K. A. *Proc. R. Soc. (A)* 1952, **212**, 274
- 11 Benoit, H. *Ann. Phys. (Paris)*, 1951, **6**, 561
- 12 Yoshioka, K. and Watanabe, H. in 'Physical Principles and Techniques of Protein Chemistry', Part A. (Ed. S. Leach), Academic Press, New York, 1969
- 13 Baily, E. D. and Jennings, B. R. *Appl. Optics*, in press
- 14 Tinoco, I. and Hammerle, W. G. *J. Phys. Chem.* 1956, **60**, 1619
- 15 Jennings, B. R. and Baily, E. D. *Nature* 1970, **228**, 1309
- 16 Jennings, B. R. *Br. Polym. J.* 1969, **1**, 252
- 17 Takashima, S. in 'Physical Principles and Techniques of Protein Chemistry', Part A. (Ed. S. Leach), Academic Press, New York, 1969
- 18 Stoylov, S. P. and Sokerov, S. *J. Colloid Interface Sci.* 1967, **24**, 235
- 19 Eigen, M. and De Maeyer, L. in 'Technique of Organic Chemistry', Part I (Eds. S. Friess, E. Lewis and A. Weissberger), Interscience, New York, 1963, Vol 8
- 20 Broersma, S. J. *Chem. Phys.* 1960, **32**, 1626
- 21 Burgers, J. M. *Verhandel-Koninkl. Ned. Akad. Wetenschap* 1938, **16**, 113
- 22 Perrin, F. *J. Phys. Rad.* 1934, **5**, 497
- 23 Stockmayer, W. H. and Bauer, M. J. *Am. Chem. Soc.* 1964, **86**, 3485
- 24 Jennings, B. R. and Plummer, H. *J. Colloid Interface Sci.* 1968, **27**, 377

# Tensile failure properties of some branched polyurethane elastomers

R. E. Whittaker

*Shoe and Allied Trades Research Association, Kettering, Northants, UK  
(Received 30 July 1971)*

Earlier papers have shown that the energy input to break obtained from tensile stress-strain curves for a crosslinked amorphous vulcanized rubber is exponentially related to the reciprocal of absolute temperature. These earlier investigations also showed that for both amorphous and crystalline rubbers the energy input to break over a range of temperature was related by a square law to the strain at break. This paper demonstrates that these relationships are obeyed by a series of branched polyurethane elastomers. By multiplying the strains at break on the energy input to break/strain at break graph by the parameter  $V_e$ , the number of network chains per unit volume, the results for various degrees of branching are made coincident. When compared with earlier results from cross-linked rubber, it is found that a unique relationship involving only one numerical constant can be derived which is applicable to amorphous, crystalline and branched polymers at different degrees of crosslinking, whether filled or unfilled.

## INTRODUCTION

Harwood *et al.*<sup>1-3</sup> have found in recent years that quantitative failure relationships can be obtained for amorphous rubbers between the energy input to break and hysteresis at break and secondly between the energy input and strain at break in a uniaxial tensile stress-strain test.

These failure relationships have also been applied to amorphous rubbers filled with carbon black when it was shown that under conditions of constant energy input, both the strains at break and the hysteresis at break of the filled rubbers could be corrected and unified with the gum rubber by use of a hydrodynamic factor. A recent paper<sup>4</sup> has shown a correlation between these relationships and parameters from cut growth and fatigue theory.

Another investigation<sup>5</sup> showed that a strain-crystallizing rubber such as natural rubber diverged from the hysteresis failure law between 80 and 130°C. This divergence is due to the material between these two temperatures being in neither a uniformly crystalline nor totally amorphous state. Natural rubber was, however, found to obey the failure relationship between energy input to break and strain at break. This latter relationship was also obeyed<sup>5</sup> by several dicumyl peroxide-cured natural rubber vulcanisates of differing crosslink densities. Under conditions of constant energy input to break, the strains at break of the different crosslinked mixes, when corrected by a parameter from rubber elasticity theory became coincident.

Whittaker<sup>6</sup> has recently shown that a similar correlation on the energy input to break/strain at break relationships can be obtained for sulphur-cured vulcanisates of

styrene-butadiene rubber (SBR) taken to different degrees of crosslinking. The hysteresis at break failure criterion was found, however, to be markedly dependent on the degree of crosslinking.

The paper extends these earlier studies by considering the failure properties of a range of polyurethane elastomers where the degree of branching associated with the polyol component is varied.

## CAST POLYURETHANE ELASTOMERS

The elastomers used in this study were identical with those previously considered by Buist *et al.*<sup>7,8</sup>. A usual procedure for the preparation of cast polyurethane elastomers with a lightly crosslinked structure is to use formulations containing at least one component with more than two reactive end-groups, such as the reaction of a diisocyanate with a lightly branched, or mixture of linear and branched, polyester or polyether. The properties of the elastomers are determined mainly by the chain structure and degree of branching of the polymeric intermediate and by the stoichiometric balance of the components.

Processing characteristics and properties of the products can be varied by use of more than one polyol component. This allows not only the degree of branching associated with the polyol component to be varied but by varying order of interaction of the polyols with the diisocyanate it is possible to vary processing factors such as temperature of reaction, viscosity and cure of casting mix; this also facilitates the incorporation of fillers. In addition to using polymeric polyol components, low

molecular weight polyols may be included and branching can be introduced by use of a polyol such as glycerol or trimethylolpropane<sup>7, 8</sup>. This system was adopted for the cast polyurethane mixes used in this investigation which are shown in *Table 1*.

Daltorol PR1\* is a slightly branched polyester based on adipic acid and Suprasec PR\* is toluene diisocyanate (TDI). The reaction of Daltorol PR1 with somewhat less than an equivalent of Suprasec PR yields a soft elastomer but by including trimethylolpropane in the formulation, the hardness and tensile strength can be increased. Small amounts of trimethylolpropane increase resilience but high proportions give resinous products of low resilience and low ultimate elongation rather than elastomers.

The procedure used for preparation of the polyurethane sheets was to add trimethylolpropane to Daltorol PR1 at the start of the dehydration stage. The dehydration was carried out in the normal manner but because of the more exothermic reaction obtained with the trimethylolpropane process, the mixtures were cooled to about 40°C at the end of the dehydration period before additions of the Suprasec PR. The sheets were prepared by a simple casting technique.

## EXPERIMENTAL

The test pieces used in the investigation were in the form of rings with inner diameters of 23 mm and wall thickness 2 mm cut by a rotating cutter from rubber sheets approximately 2.5 mm thickness. The samples were extended on an Instron Tensile Tester over a temperature range 21–110°C. The rate of strain was 250% per minute in every case.

The experimental procedure to determine the energy input and hysteresis at break was to obtain, at each temperature, three tensile stress-strain curves up to failure on new samples. A fourth sample was then extended and the crosshead reversed at just below the average breaking stress of the three tensile curves. The energy input was obtained from the area under the extension curve and the hysteresis from the area between the extension and retraction curves directly by use of an integrator unit attached to the Instron Tester.

## RESULTS

### Effect of temperature

The tensile strength and hysteresis of all the mixes were found to be very low. The hysteresis ratio at break (ratio of hysteresis at break to energy input to break) at 21°C was found to be 10.9% for mix D and approximately 4% for

*Table 1* Formulations of cast elastomers used

Compound	A	B	C	D
Daltorol PR1	100	100	100	100
Trimethylolpropane	3.5	7.0	10	13
Suprasec PR (TDI)	16.2	22.9	29.0	34.9
Cure (hours at 110°C)	3	3	3	3

\* Registered ICI Ltd Trade Names

mixes A and B. The hysteresis was negligible at temperatures above 50°C and hence a full study on the effect of branching in polyurethanes on the energy at break/hysteresis at break failure criterion could not be carried out.

The effect of temperature on energy input to break for all the mixes is shown in *Figure 1* where the average value of energy input to break for each of the four rubbers is plotted on semi-logarithmic paper against the reciprocal of absolute temperature.

Earlier studies<sup>2, 6</sup> on optimum crosslinked amorphous rubbers showed that the energy input to break was related to the reciprocal of absolute temperature by an equation which was considered analogous to the van't Hoff isochore:

$$U_B = D \exp(G/T) \quad (1)$$

where  $D$  and  $G$  are constants.

Straight lines have been drawn through the experimental points in *Figure 1* and hence equation (1) is shown to be obeyed. The lines for the different compounds are also approximately parallel indicating that the constant  $G$  is independent of the degree of branching in the polyurethane and hence must be a parameter associated with the base constituents of the rubber. Similar results<sup>6</sup> were found on a series of SBR vulcanisates of differing cross-link densities.

### Failure envelope

Work on both amorphous and strain-crystallizing vulcanized rubbers has shown that the energy input to break ( $U_B$ ) is related to the strain at break ( $\epsilon_B$ ) up to the maximum extensibility of the network ( $\epsilon_B \text{ max.}$ ) by a relationship of the following form:

$$\left(\frac{294}{T}\right) U_B = A(\epsilon_B)^2 \quad (2)$$

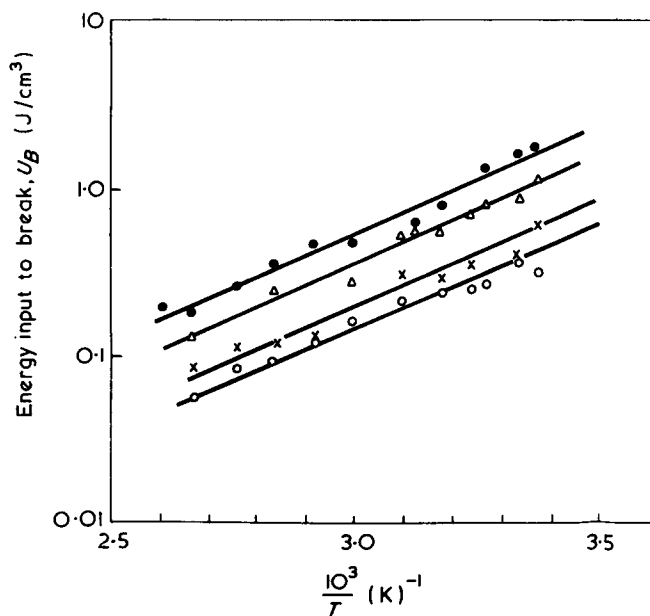


*Figure 1* Variation of energy input to break with reciprocal of absolute temperature for branched polyurethane rubbers. ○, Mix A; ×, mix B; △, mix C; ●, mix D

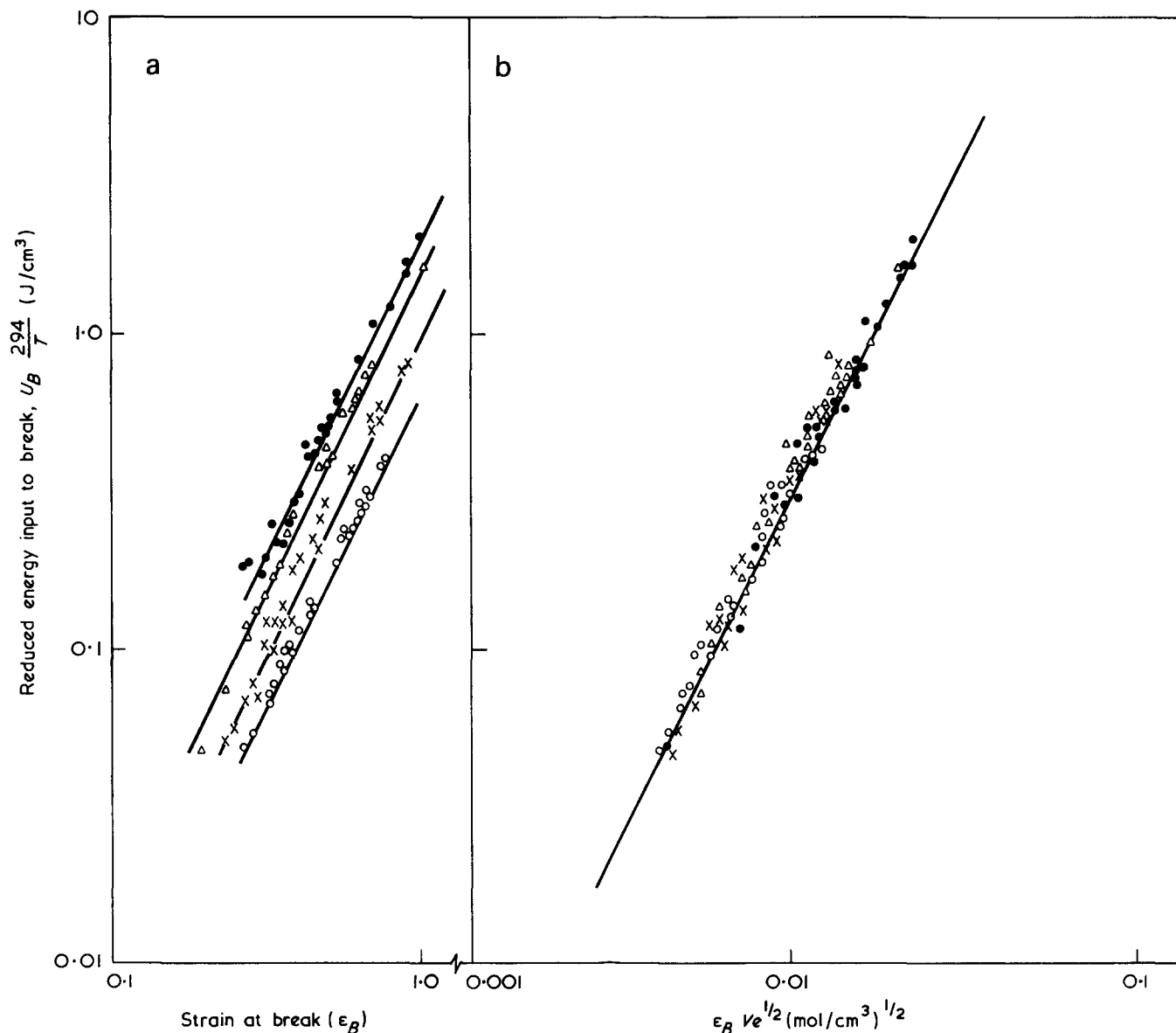


Figure 2 Variation of reduced energy input to break for branched polyurethane rubbers with (a) strain at break and (b) strain at break multiplied by  $V_e^{1/2}$ . O, Mix A; x, mix B;  $\Delta$ , mix C;  $\bullet$ , mix D

where  $A$  is a constant and  $T$  is the temperature of test. The energy is reduced by the term  $294/T$  to allow for the temperature dependence of rubberlike elasticity as predicted by the kinetic theory<sup>9</sup>. This relationship is a modification of the 'failure envelope' approach of Smith<sup>10, 11</sup> and others<sup>12</sup> who plot stress or real stress at break against the strain at break. The use of the parameter, energy input to break allows, however, a quantitative relationship between the failure parameters to be derived.

The variation of energy input to break with strain at break is shown in Figure 2a. The results as predicted by equation (2) produce a square law relationship, up to the maximum extensibility of the network ( $\epsilon_B \text{ max.}$ ), but are displaced along the strain axis.

Earlier work<sup>5, 6</sup> on natural and styrene-butadiene rubber has shown that at the same energy input to break, the strains at break are in the ratio of their respective  $V_e^{1/2}$  values provided that the strains are below the maximum extensibility of the network.  $V_e$  represents the number of network chains per unit volume of the rubber network and is usually expressed in  $\text{mol/cm}^3$ . The value of  $V_e$  can

be obtained from the equilibrium modulus  $E_e$  by the following relationship<sup>13, 14</sup>:

$$E_e = 3VeRT \quad (3)$$

where  $R$  is the gas constant.

It is usually assumed that in the case of branched polymers  $V_e$ , which represents the number of chains between effective crosslinks of vulcanized rubbers, includes chains between the branch points.

At high temperatures (about  $100^\circ\text{C}$ ), the hysteresis was negligible and hence the polyurethane rubbers were considered to be in an equilibrium condition. The modulus at these temperatures could therefore be considered as the equilibrium value and values of  $V_e$  were obtained by use of equation (3). These are shown for the four mixes in Table 2.

The strains at break of mixes A–D were multiplied by their respective  $V_e^{1/2}$  values and the resulting graph is shown in Figure 2b. The agreement between the four mixes on this type of graph is shown to be remarkably

**Table 2** Values of  $Ve^{1/2}$

Mix	$Ve^{1/2}$ (mol/cm <sup>3</sup> ) <sup>1/2</sup>
A	$1.39 \times 10^{-2}$
B	$1.66 \times 10^{-2}$
C	$2.07 \times 10^{-2}$
D	$2.36 \times 10^{-2}$

good and therefore the equation to the line for different crosslink densities can be expressed as

$$\left(\frac{294}{T}\right)U_B = BVe\epsilon_B^2 \tag{4}$$

where  $B$  is a constant.

COMPARISON WITH VULCANIZED RUBBERS

A similar graph to that shown in *Figure 2a* was found in an earlier investigation<sup>5</sup> into the failure properties of natural rubber vulcanisates and this is shown in *Figure 3a*. It is found that a square law relationship predicted by equation (2) is obeyed for three vulcanisates cured with 1, 2 and 4 phr (phr=parts per hundred) dicumyl peroxide.

Values of  $Ve$  for these mixes was obtained from the data of Porter (personal communication). In this early

investigation, agreement between the vulcanisates on this type of graph was obtained by multiplying the strains at break for the 2 and 4 phr dicumyl peroxide vulcanisates by the ratio of the respective  $Ve^{1/2}$  value to the value of  $Ve^{1/2}$  for the 1 phr dicumyl peroxide mix.

The results shown in *Figure 3b* have, however, been obtained by multiplying the strain directly by  $Ve^{1/2}$  and hence can be used as a direct comparison with branched polyurethane rubber results shown in *Figure 2b*.

A similar graph was obtained from work<sup>6</sup> on styrene-butadiene rubbers of differing crosslink densities and the composite plots for the three systems are compared in *Figure 4*. It is seen that the generalized failure relationship, equation (4), is approximately the same line for the three different polymer systems, amorphous, crystalline and branched, and is given by:

$$U_B \frac{294}{T} = (4.1 \times 10^3)Ve\epsilon_B^2 \tag{5}$$

if  $U_B$  is expressed in joules/cm<sup>3</sup>.

CONCLUSIONS

The tensile failure properties of a typical branched polyester polyurethane have been compared with earlier work on natural rubber and styrene-butadiene rubber vulcanisates.

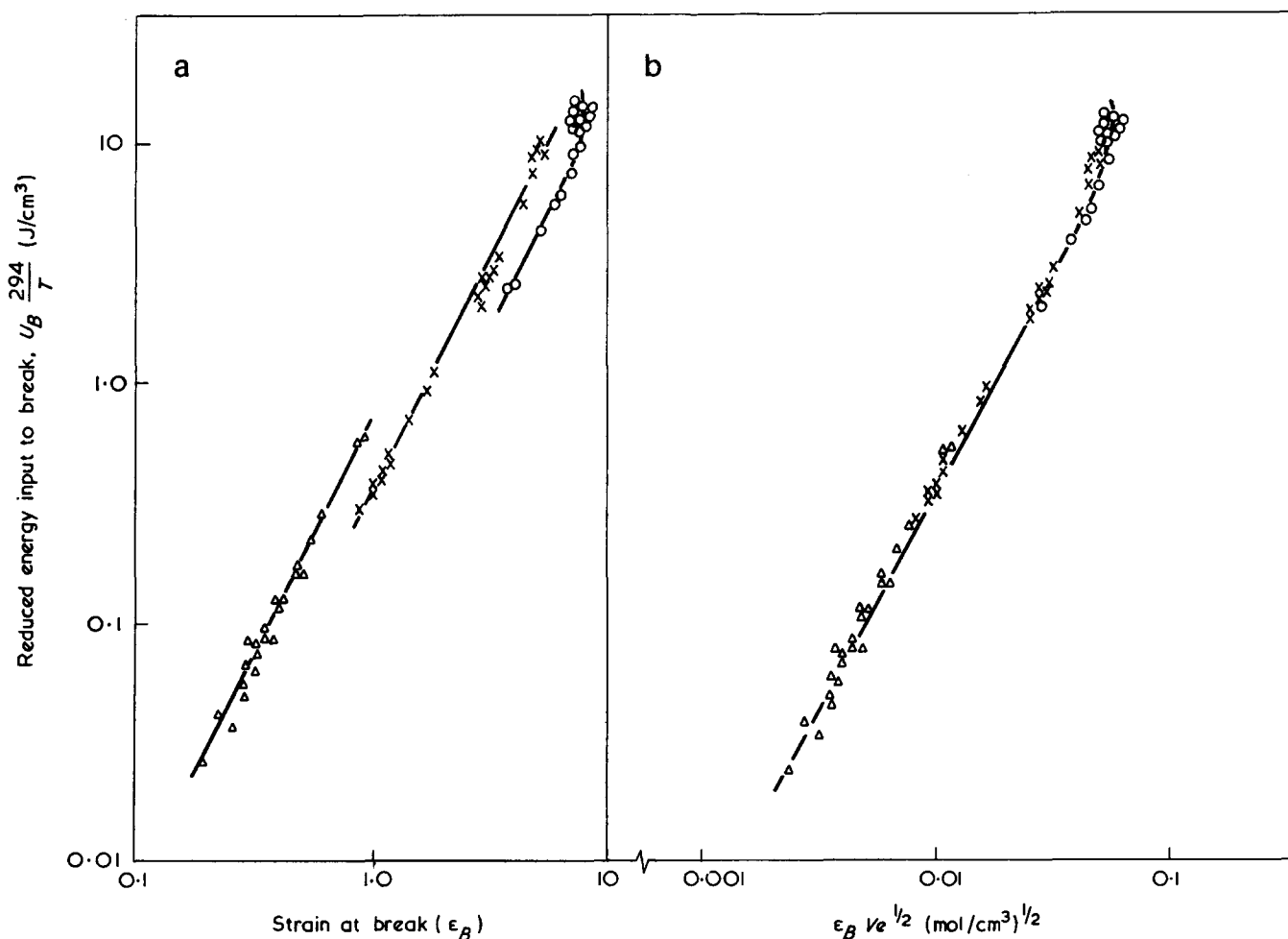


*Figure 3* Variation of reduced energy input to break for natural rubber-dicumyl peroxide cured vulcanisates from a previous study<sup>5</sup> with (a) strain at break and (b) strain at break multiplied by  $Ve^{1/2}$ . O, Natural rubber with 1 phr dicumyl peroxide; x, natural rubber with 2 phr dicumyl peroxide; Δ, natural rubber with 4 phr dicumyl peroxide



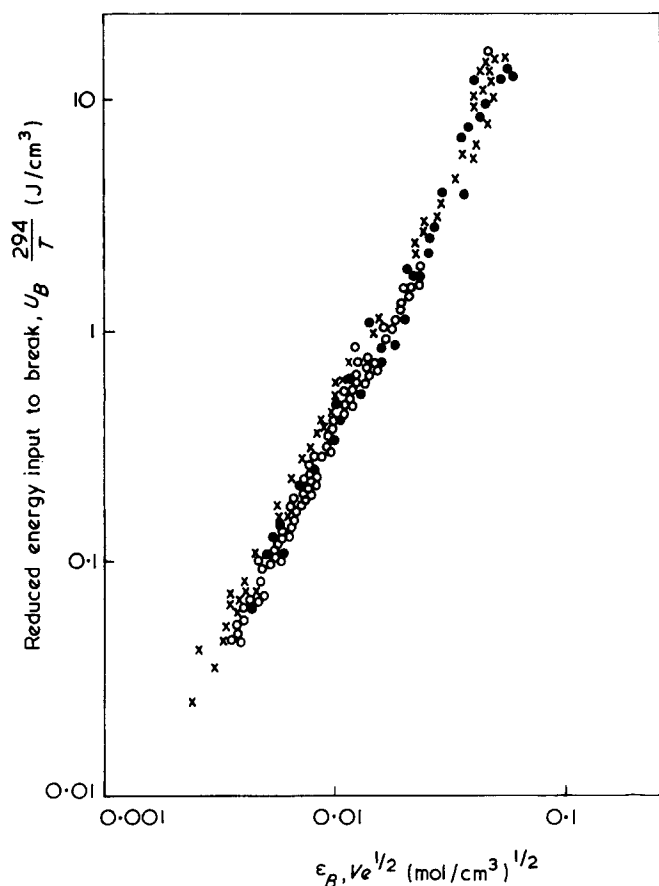


Figure 4 Variation of reduced energy input to break with strain at break multiplied by  $V_e^{1/2}$  for natural rubber-dicumyl peroxide cured vulcanisates ( $\times$ ), sulphur cured SBR vulcanisates ( $\bullet$ ) and branched polyurethane rubbers ( $\circ$ )

Although the low values of hysteresis at break excluded from the present investigation a comparison of the hysteresis properties and their effect on failure, a similar type of relationship to that found in vulcanized rubbers between energy input to break and reciprocal of absolute temperature has been established. The constant in this equation appeared to be independent of the degree of branching of the polyurethane.

The square law relationship between energy input and strain at break was found to be obeyed by polyurethane elastomers and correction by a parameter from rubber elasticity theory unified the results as found for both natural and styrene-butadiene rubber. The relationship was found, however, to be the same for the three polymer systems and hence must represent a basic material property.

The work on SBR and natural rubber showed that vulcanisates filled with various concentrations of carbon black could also be correlated on the energy input to break/strain at break graph by multiplying the strains at break of the filled vulcanisates by a hydrodynamic factor, ( $X$ ) first derived by Guth and Gold<sup>15</sup> for expressing the viscosity of a liquid containing small spherical particles to that of the liquid alone and given by:

$$X = 1 + 2.5c + 14.1c^2 \quad (6)$$

The general failure relationship then can be expressed as

$$U_B = (4.1 \times 10^3) V_e (X \epsilon_B)^2 \quad (7)$$

which is obeyed by amorphous, crystalline and branched polymers at different degrees of crosslinking, whether filled or unfilled.

#### ACKNOWLEDGEMENTS

The author is indebted to Imperial Chemical Industries Limited (Dyestuffs Division) for the provision of the polyurethane elastomers used in this investigation.

The author also wishes to thank Professor R. J. W. Reynolds (Loughborough University) for initially suggesting this research programme and to Dr C. M. Blow (Loughborough University) and Dr A. R. Payne (Director, SATRA) for their helpful advice and encouragement.

#### REFERENCES

- 1 Harwood, J. A. C., Payne, A. R. and Whittaker, R. E. Paper presented to I.R.I. Conference, 'Advances in Polymer Blends and Reinforcement', Loughborough, 1969
- 2 Harwood, J. A. C. and Payne, A. R. *J. Appl. Polym. Sci.* 1968, **12**, 889
- 3 Payne, A. R. and Whittaker, R. E. *Composites* 1970, **1**, 203
- 4 Payne, A. R. and Whittaker, R. E. *J. Appl. Polym. Sci.* 1971, **15**, 1941
- 5 Harwood, J. A. C., Payne, A. R. and Whittaker, R. E. *J. Appl. Polym. Sci.* 1970, **14**, 2183
- 6 Whittaker, R. E. to be published
- 7 Trappe, G. in 'Advances in Polyurethane Technology'. (Ed. J. M. Buist and H. Gudgeon), Maclaren, London 1968, Ch 2
- 8 Buist, J. M. and Lowe, A. *Br. Polym. J.* 1971, **3**, 104
- 9 Ferry, J. D., Fitzgerald, E. R., Grandine, L. D. and Williams, M. L. *Ind. Eng. Chem.* 1952, **44**, 703
- 10 Smith, T. L. *J. Appl. Phys.* 1964, **35**, 27
- 11 Smith, T. L. *Rubb. Chem. Technol.* 1967, **40**, 544
- 12 Kelley, F. N. *Appl. Polym. Symp. No. 1* 1965, p 299
- 13 Ferry, J. D. 'Viscoelastic Properties of Polymers', Wiley, New York, 1970
- 14 Staverman, A. J. 'Handbuch de Physik'. (Ed. S. Flugge) 1962, Vol 13, p 432
- 15 Guth, E. and Gold, O. *Phys. Rev.* 1938, **53**, 322

# Birefringence of plastically deformed poly(methyl methacrylate)

S. Raha\* and P. B. Bowden

*Department of Metallurgy and Materials Science, University of Cambridge,  
Pembroke Street, Cambridge CB2 3QZ, UK  
(Received 2 September 1971)*

The birefringence of poly(methyl methacrylate) (PMMA) has been studied for samples deformed plastically in plane strain compression. The results have been analysed in a semi-quantitative manner based on the theory of birefringence for rubbers. The results suggest that the molecular chains are bound by cohesion points which are dissociated by increasing temperature or under the influence of plastic strain. It is suggested that these cohesion points can be attributed to interactions between the dipoles of the ester side groups.

## INTRODUCTION

A reliable theory of plastic yield in amorphous polymers has yet to be established. An early theory that localized adiabatic heating caused the temperature to increase to the glass-transition temperature ( $T_G$ ) has been disproved and has been replaced by the belief that stress induces a reduction of the  $T_G$  to the test temperature<sup>1</sup>. Bryant's tensile recovery experiments<sup>2</sup> on a modacrylic fibre have been interpreted as showing a progressive reduction of the  $T_G$  with increasing strain. Andrews and Kazama<sup>3</sup> have shown that there is a stress-temperature equivalence in the creep curves of poly(vinyl chloride) (PVC). Others<sup>4, 5</sup> have preferred to consider a stress-induced increase in free volume which may be regarded either as an equivalent statement to the above or an intermediate step leading to an apparent lowering of the  $T_G$ . Attempts have been made to relate the volume increase accompanying tensile strain to an increase in free volume<sup>5</sup>. Litt and Koch<sup>6</sup> have presented evidence that an applied uniaxial stress allows internal stresses to relax in all three dimensions, both in the direction of the applied stress and perpendicular to it. The conclusion drawn was that the free volume increase at yield produced a condition analogous to that at the  $T_G$ . An apparent conflict arises in extending this simple volume expansion hypothesis to the case of compression where, on similar arguments to the tensile case, there would be a reduction in free volume. On the basis of the concavity of the curve of volume decrease with increasing compressive stress, Whitney and Andrews<sup>7</sup> have postulated that the total

volume decrease in compression contains a positive contribution from an increase of 'plastic volume', but applying their argument to the tensile case would lead to the prediction of a plastic volume decrease in tension. A consistent model embracing both tensile and compressive situations has not yet been produced but there is accumulating evidence that a state analogous to the glass transition plays a crucial role in yield. Associated with such theories should be a model of what yield entails on the molecular scale. The precise molecular motion involved is a matter of conjecture although it is evident that the movement of whole polymer chains relative to one another does not occur. The irrecoverable flow that this would imply is inconsistent with observations<sup>8</sup>; nor does it provide an adequate explanation of strain-hardening. Melt-viscosity measurements show that units of length several orders of magnitude smaller than the macromolecular chain length are the effective units in mechanical properties<sup>9</sup>, and co-operative motions between similarly short sections are generally ascribed to be the motion operative at the  $T_G$ .

Treloar<sup>10</sup> commented that the discrepancy between the theoretical and experimental stress-strain behaviour of rubber could be attributed to the breakdown of cohesion points under certain states of strain. Vincent<sup>1</sup> visualized rigid plastics as a tighter network (i.e. with more frequent cohesion points) than allowed for in normal rubber elasticity theory. The cohesion points were likely to be of secondary valence forces and as the material was stressed these bonds would be broken. As the number of effective cohesion points was reduced, the material would become 'less like diamond and more like rubber', with consequent reduction in the modulus. Bartenev and Zuyev<sup>11</sup> considered deformation in terms of a spatial network of temporary nodes and concluded that with increasing

\* Present address: ICI (India) Private Limited, ICI House, 34 Chowringhee, Calcutta 16, India

stress the probability of renewal of the temporary nodes decreased and the average number of broken nodes grew.

To these proposals should be added that unloading or stress relaxation will create the renewal of cohesion points (nodes) tending towards the thermal equilibrium value. Vincent<sup>1</sup>, and Whitney and Andrews<sup>7</sup>, among others, have noted that the stress relaxation following an interruption in loading apparently 'hardens' the material and that a second yield point may be exhibited on reloading. Nielsen<sup>12</sup> feels that the shape of the creep curve is indicative of the progressive decrease in the number of cohesion points on stretching. He reports that when creep is interrupted, the creep curve may on reloading be identical to the first curve provided a sufficiently long rest period has been allowed and after correction for the small amounts of non-recoverable deformation from the first test, suggesting that in the intervening time the number of cohesion points was restored to the equilibrium concentration.

The basis of the work to be described is a study of the structural changes associated with yield in glassy polymers. Some of the results on polystyrene and poly(methyl methacrylate) (PMMA) have already been reported elsewhere<sup>13</sup> and we shall be concerned here more specifically with the birefringence results obtained on PMMA. Measurements of birefringence during loading and after unloading were made on samples deformed in plane-strain compression over a temperature range 20°C to 190°C. These have been analysed in a semi-quantitative manner to present further evidence of the nature of cohesion points in PMMA and their breakdown at yield.

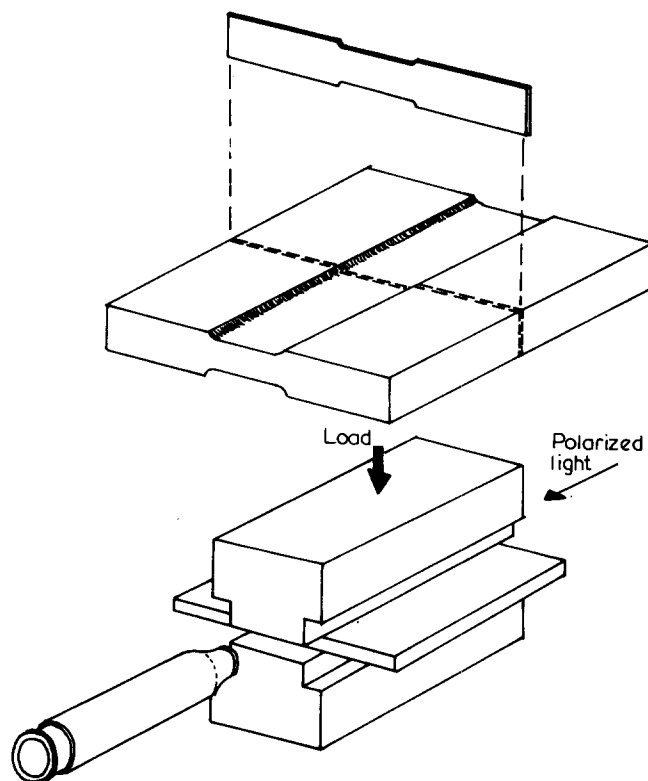


Figure 1 Experimental arrangement for plane strain compression and schematic diagram of sections cut from deformed specimens for observation in the optical microscope

## BIREFRINGENCE

The results have been analysed in terms of the theory of the birefringence of rubbers<sup>14</sup> which considers the change in angular distribution of optical anisotropic units on deformation. The theory gives the result:

$$\Delta n_{xy} = n_x - n_y = CN\alpha(\lambda_x^2 - \lambda_y^2) \quad (1)$$

where  $n_x$ ,  $n_y$  are the refractive indices in the  $x$  and  $y$  directions respectively, and  $N$  is the number of 'chains' per unit volume, a 'chain' referring to a segment between two cohesion points. The quantity  $\alpha$  is the polarizability anisotropy of a repeat unit of the molecular chain and  $\lambda_x$ ,  $\lambda_y$  are the extension ratios in the  $x$  and  $y$  directions.

The precision of the results and the assumptions involved do not justify attempts at a more rigorous analysis by considering advances from this simple theory such as applying the modified statistics for short chains<sup>15</sup>. It is appreciated that extension of such a theory to glasses is questionable, particularly for birefringence under stress where non-equilibrium distortions certainly take place in addition to the 'orientational' birefringence considered by the theory of rubbers. In the discussion below we shall show that the theory may be an adequate representation of the birefringence of drawn material in the absence of external stress. Quantitative appraisal of stress-birefringence data is precluded by the lack of an established general theory for the birefringence of glasses. Nevertheless, trends in the magnitude and sign of the birefringence under stress provide qualitative information on molecular behaviour.

## SAMPLES AND EXPERIMENTAL METHOD

Samples were cut from 1.6 mm thick sheets of commercial ICI 'Perspex'. The cut surfaces were polished to allow optical measurements by grinding on emery paper flooded with water followed by polishing on a soft cloth impregnated with 'Silvo' metal polish. Samples were annealed at 110°C for a day and cooled over the space of another day to eliminate any residual strains and absorbed moisture.

Details of the experimental arrangement have been previously described<sup>13</sup>. The arrangement is shown schematically in Figure 1. Samples of width 25 mm were compressed in plane strain between polished and lubricated parallel dies 6.35 mm wide which were longer than the specimen width. The dies could be heated to 150°C with a temperature control accurate to  $\pm \frac{1}{2}^\circ\text{C}$ . Birefringence measurements under load were made by isolating the 5461 Å line of a collimated mercury arc source and viewing through the specimen width between the dies. On compression the central region of the sample became bright and dark as successive extinctions occurred. The retardation was calculated from the order of the extinction. Intermediate measurements were made by inserting a six-order Berek compensator which was also used to check the sign of the birefringence and to measure the birefringence of samples after unloading. For measurements after unloading sections were cut out of the sample as shown in Figure 1 and then polished to a thickness of about 0.2 mm by a procedure similar to that described above.

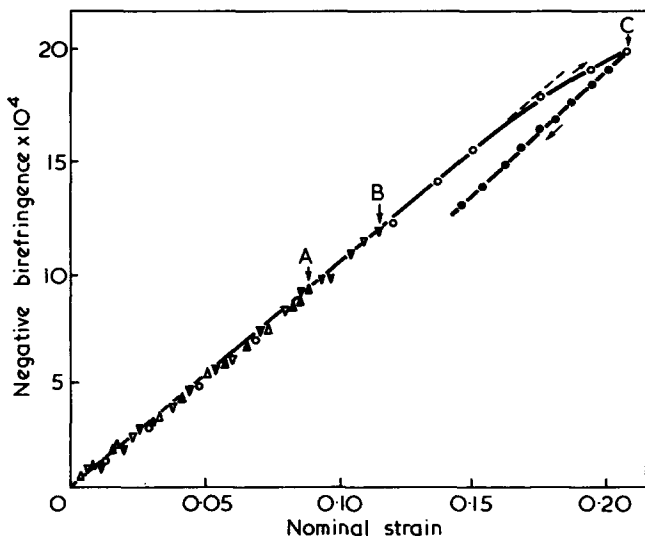


Figure 2 Relationship between (negative) birefringence and strain for PMMA during loading and unloading in plane strain compression at 22°C.  $\circ$ ,  $\Delta$ ,  $\triangle$  denote measurements during loading. Loading was interrupted at points A ( $\Delta$ ,  $\blacktriangle$ ) B ( $\nabla$ ,  $\blacktriangledown$ ) and C ( $\circ$ ,  $\bullet$ ) and the load reduced to zero

## RESULTS

Birefringence measurements were made on PMMA under load. Up to yield, the birefringence field was homogeneous. Figure 2 shows the relationship between birefringence and strain observed during loading and unloading at 22°C. A typical stress-strain cycle corresponding to the first point of interrupted loading (A in Figure 2) is shown in Figure 3. It is evident that birefringence is a univalued function of strain almost up to the yield point and is not related to stress in any obvious way. This is further borne out by interrupting the loading at some point before yield and holding the material at constant strain. Although there is a relaxation of stress there is no noticeable change in the birefringence. Similarly, although the elastic modulus increases with increase of strain-rate, the relationship between birefringence and strain under load remains the same. This relationship appears to be linear and reversible up to approximately 10% strain. As diffuse shear zones initiate from the die-corners, the birefringence field becomes inhomogeneous<sup>13</sup>. It is still possible to measure the birefringence increase with continued straining at any fixed point of the specimen. Since the variation of birefringence across the specimen is small (about 10%) the measurement of birefringence at a fixed point will remain a close approximation to the overall birefringence behaviour with continued straining beyond yield, although the absolute magnitude of the birefringence will vary from point to point until the region of the minimum of the stress-strain curve when the birefringence field becomes approximately homogeneous once again. The birefringence-strain relationship under load up to 50% nominal strain is shown in Figure 4. In the region of yield there is a marked decrease in the magnitude of the gradient  $\delta(-\Delta n)/\delta\epsilon$ . Beyond yield, the birefringence-strain path is not retraced on unloading (Figure 2), the birefringence being smaller at each strain whilst unloading.

The strain-birefringence measured under load at a constant strain rate of  $3.6 \times 10^{-4} \text{sec}^{-1}$  is shown in Figure 5 as a function of temperature. At strains below 2% the strain-optical coefficient is independent of temperature. As temperature is increased the divergence from a linear strain-birefringence relationship occurs at lower strains so that above 2% strain the negative birefringence decreases with increasing temperature.

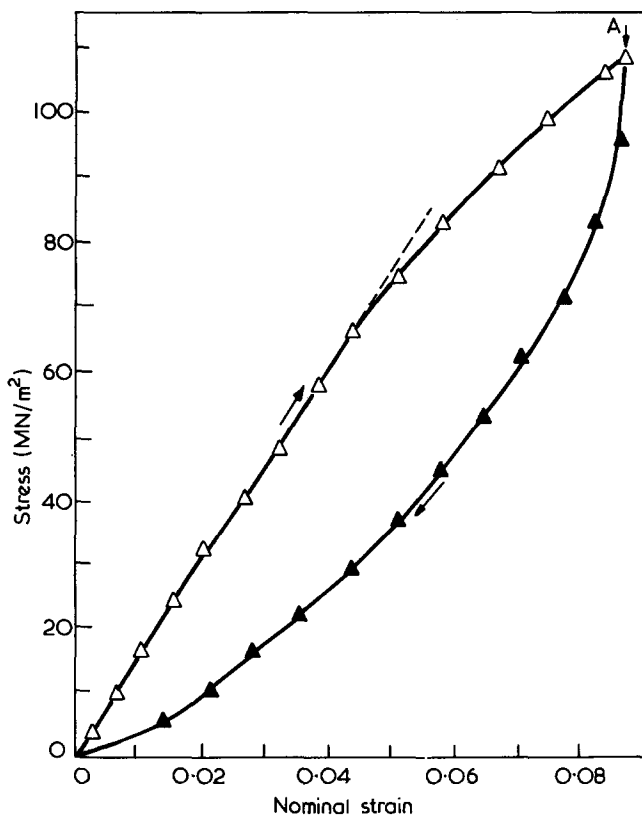


Figure 3 Stress-strain curve for PMMA deformed in plane strain compression at 22°C at a strain rate of  $5.0 \times 10^{-4} \text{sec}^{-1}$ . The specimen was loaded to the point A (below the yield point) and then unloaded at the same strain rate. Birefringence measurements during the loading and unloading portions of the curve are plotted in Figure 2

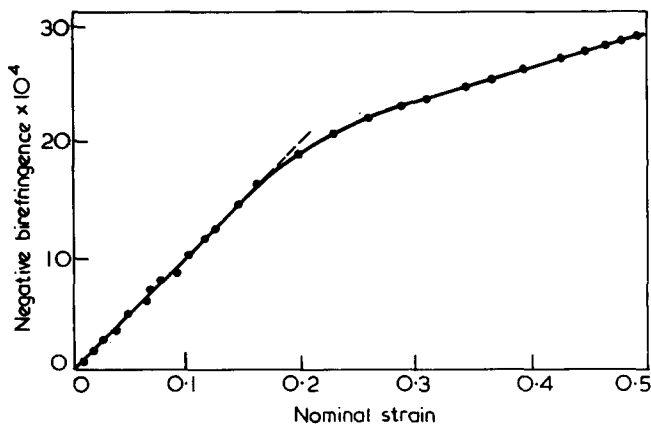


Figure 4 Relationship between (negative) birefringence and strain for a PMMA sample deformed in plane strain compression at 22°C at a strain rate of  $5.1 \times 10^{-4} \text{sec}^{-1}$ . Measurements were made under load

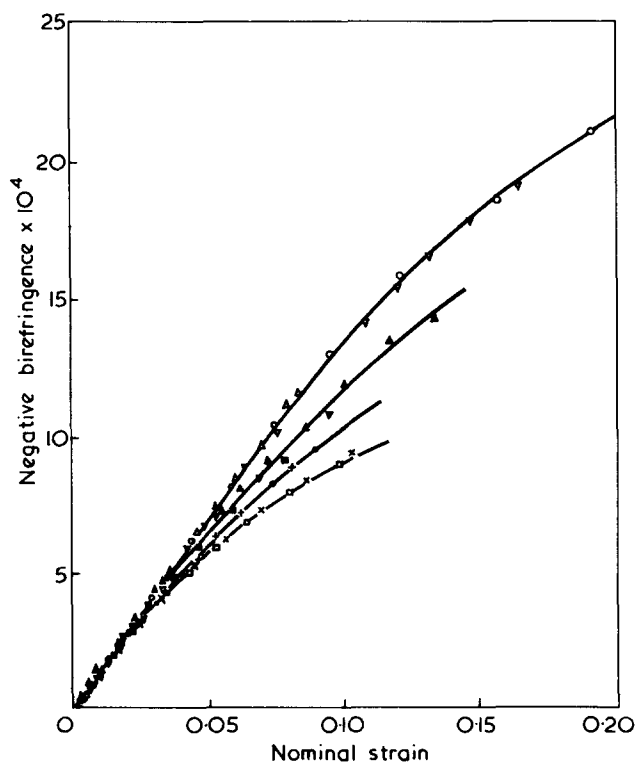


Figure 5 Birefringence of PMMA under load as a function of nominal strain at a strain rate of  $3.6 \times 10^{-4} \text{sec}^{-1}$ . Results were obtained at 20°C: ○, △, ▽; 70°C: ▲, ▼, ■; 80°C: +, ●; 90°C: □, ×. The results for 40°C and 60°C have been omitted for clarity

#### Discussion of birefringence data under load

The observation that the birefringence of PMMA under stress is a single-valued function of strain has also been made by Kolsky<sup>16</sup> from tensile experiments. Le Grand<sup>17</sup> and Read<sup>18</sup> have measured the dynamic birefringence of PMMA over the temperature range  $-130^\circ\text{C}$  to  $+140^\circ\text{C}$  and the frequency range  $3 \times 10^{-3}$  to 16 Hz. Their results show that the strain-optical coefficient at low strain is independent of temperature and frequency between 20°C and 80°C which is the approximate temperature range of our measurements. Below 20°C the strain-optical coefficient becomes increasingly negative with decreasing temperature or increasing frequency. In contrast, the stress-optical coefficient is constant up to 20°C and then becomes increasingly negative between 20°C and 80°C. This is in accordance with our results since a constant strain-optical-coefficient and a decreasing elastic modulus with increasing temperature leads immediately to an increase in the stress-optical coefficient. Above 80°C the negative stress-optical coefficient passes through a maximum and the stress-optical coefficient becomes positive above about 150°C<sup>18-20</sup>.

The variation of optical properties with temperature has been attributed to rotational isomerism within the ester side-group<sup>19,21</sup>. Read<sup>18</sup> has shown how enhanced freedom of rotation within the ester group leads to a decreasingly negative polarizability anisotropy of a repeat unit. Andrews and Hammack<sup>20</sup> stretched samples of PMMA at a temperature 'slightly higher than the  $T_G$ ' and then cooled them to ambient temperature maintaining the

stretching load. On temperature-cycling their oriented samples below the  $T_G$ , they found the birefringence of the samples to be a reversible function of temperature. Furthermore, the changes in birefringence occurred instantaneously with change of temperature with no observable time-delay effects. The instantaneous reversible nature of the birefringence rules out large-scale molecular rearrangements and suggests that the observed birefringence is a thermal equilibrium value associated with the thermal energy of the material. Clearly thermally induced side-chain rotation would be consistent with the observations. However, Andrews and Hammack's observations were on pre-oriented samples in the absence of external stress and their conclusions are not wholly relevant to the stressed condition. They indicated the disagreement of the trends in their data with other data in the literature. Checking the literature we find that the reference data were strain-birefringence measurements on PMMA samples under stress in contrast to Andrews's experiment. More precisely, Andrews's results show a gradual fall of negative birefringence with temperature increase from  $-200^\circ\text{C}$  to  $+100^\circ\text{C}$  with no indication of the region of constancy between 20°C and 80°C observed by us and by Read, nor the changes in slope of the birefringence-temperature plot below  $-100^\circ\text{C}$  observed by Trapeznikova. Andrews's birefringence measurements were made below the  $T_G$  and since the birefringence extrapolated to zero in the region of the  $T_G$  he assumed that the birefringence would become positive above the  $T_G$ . We feel that this assumption is incorrect. Moreover, it is in direct contrast to the results of Trapeznikova and Zhurina<sup>22</sup> and Peukert<sup>23</sup> who observed the positive birefringence at high temperatures only in the presence of applied stress and reported that the positive birefringence could not be 'frozen-in' on removal of the stress even with very rapid cooling. Read<sup>18</sup> has shown that even complete freedom of rotation of the ester group does not produce a positive polarizability anisotropy unless transverse isotropy of the C=O bond is assumed. We feel that the data from the two types of experiments can only be reconciled by the presumption that in the stressed condition the side-chains are distorted and that these distortions relax on removal of the stress. In a relaxed condition in the absence of external stress, as in Andrews's experiments, the observed birefringence would be independent of these distortional forces and will reflect the thermal equilibrium value associated with side-chain motion. In the following section we will show that the enhanced freedom of the ester group may be a consequence of thermal dissociation of dipole-dipole interactions which bind the ester groups. Since the conclusions of that section are relevant to birefringence observation under stress it is convenient to discuss the results of this section more fully at that stage.

#### Residual birefringence after deformation and relaxation: evidence for thermal dissociation of cohesion points

A serious complication to the analysis of the birefringence of a glass in a stressed condition is the presence of distortional or non-equilibrium situations. However, if the material is deformed beyond yield, unloaded, and allowed to relax, it is plausible that the birefringence refers to an equilibrium conformation. On this basis we have endeavoured to examine the orientational contribution to the strain-birefringence relationship in the absence

of a distortional contribution. Samples were deformed through yield to a series of strains, unloaded and allowed to relax at the temperature of deformation. The temperature range investigated was 22°C to 100°C. The time required for the birefringence to reach a constant relaxed value was found to be several minutes at 100°C, 10 h at 50°C, and approximately 100 h at 22°C. In each case measurements were made only after a time greater than these minimum times and the results were re-checked at successive intervals afterwards. To eliminate the effect of the intrinsic temperature dependence of birefringence observed by Andrews and Hammack<sup>20</sup>, all the samples were slowly cooled to room temperature (22°C) after relaxation and all the birefringence measurements were made at this same temperature on polished sections of the deformed samples.

Figure 6 shows the relationship between birefringence and strain after relaxation for samples deformed at 22°C and 100°C (cf. Figure 8). We emphasize the point that the '100°C' curve refers to samples that have been deformed at 100°C and relaxed after unloading at 100°C and have subsequently been slowly cooled to 22°C at which temperature the birefringence measurements have been made. Birefringence has been plotted against  $(\lambda_x^2 - \lambda_y^2)$  where  $\lambda_y$ ,  $\lambda_x$ , are respectively the extension ratios in the compression direction, and the direction perpendicular to this and the long axis of the dies (Figure 1). By the theory of birefringence for rubber mentioned at the beginning of the paper the birefringence in the  $x$ - $y$  plane would correspond to equation (1).

The fall in the gradient of the plot with increasing strain or temperature may be attributed to a decrease in  $\alpha$  or a decrease in  $N$ . Although Andrews and Hammack suggested that  $\alpha$  was dependent only on the temperature of birefringence measurement they did not prove conclusively that this was so. Remembering that our birefringence data refer to the same temperature of measurement we shall show that a decrease in  $\alpha$  is inconsistent with observations. If a sample deformed at 22°C is heated to 100°C, allowed to reach equilibrium and then cooled to 22°C for birefringence measurement, the birefringence falls from A to B. There is a small decrease in strain and a large decrease in (negative) birefringence. If now at 22°C the sample is re-deformed to a slightly higher residual strain, the birefringence increases to the region of C. If the birefringence changes are attributed solely to changes in  $\alpha$  then the only change that would produce a birefringence increase of the magnitude observed in traversing from B to C is rotation of the ester group as a whole. From consideration of the magnitude of the changes in strain-optical coefficient with temperature<sup>18</sup> and the changes effected by substituting bulkier side-groups for the methyl group in the side-chain<sup>19</sup> it has been shown that only limited rotation *within* the ester group exists below the glass-transition temperature and that rotation of the ester group as a whole is extremely unlikely.

On the assumption that the changes are attributable solely to changes in  $\alpha$  we are also faced with the following inconsistency. Consider two rotational isomers  $a$ ,  $b$  of which  $b$  has the lower negative polarizability anisotropy. The decrease in slope of the birefringence-strain plots with increasing strain or temperature is attributed to an increase in population of the  $b$  isomer to the  $a$  isomer. Thus in traversing the paths O to A to B, the population of  $b$  is successively increased. In traversing BC the strain is increased, yet in contradiction to our original hypothesis

we need to propose an increase in the population of  $a$  to account for the increase of birefringence.

If instead we propose a model where the density of chains  $N$  is a function of temperature and strain, a consistent picture is obtained. Since the cohesion points determining the density of chains are likely to be due to secondary valence bonds, it is plausible that they should be subject to dissociation as a result of increasing thermal energy or the distortional forces produced by continued straining. We visualize that, at a constant temperature, increased strain causes a breakdown of cohesion points so that the chain conformations correspond to a decreasing value of  $N$ . In common with the models discussed in the introduction, it is assumed that rubber-like freedom is introduced at yield, permitting the use of Treloar's theory. On unloading intermediate cohesion points reform so that on relaxation the number of cohesion points is at the thermal equilibrium value. Assuming limited chain mobility below the glass-transition temperature the chains will, however, have retained the conformation corresponding to the decreased value of  $N$ . This would have been 'frozen' by the formation of new intermediate cohesion points preventing any significant molecular rearrangement. Figure 7 shows the effect of annealing temperature on a series of residual strains after yielding at 22°C. At each temperature annealing was continued until any further strain relaxation was inappreciable. It can be seen that the extent of the recovered strain is not strongly dependent on the magnitude of the initial orientation suggesting that molecular rearrangement occurs only to a limited extent characteristic of the temperature rather than the value of the strain. Furthermore, large-scale rearrangement does not occur until the neighbourhood of the  $T_G$  (110°C). Returning to the temperature cycle of Figure 6, heating of sample A to

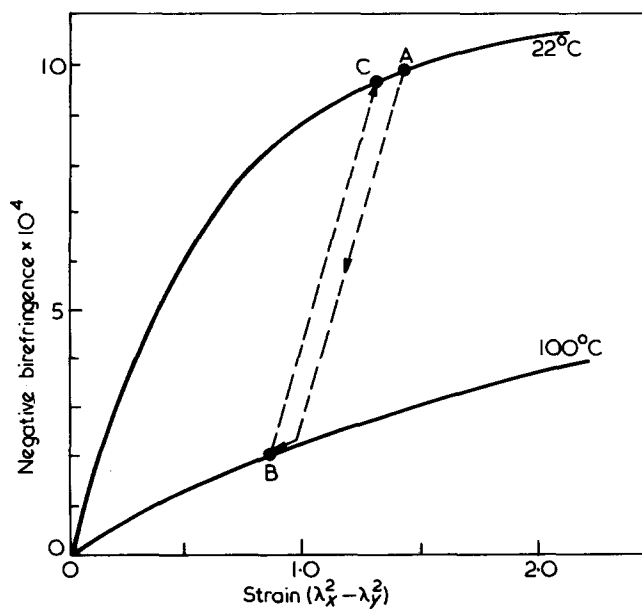


Figure 6 Residual birefringence of a sample of PMMA deformed at 22°C, heated to 100°C, cooled to 22°C and then deformed further at 22°C. The sample was initially deformed at 22°C and unloaded. The strain and birefringence then corresponded to the point A. In the unloaded state it was heated to 100°C and held at this temperature for several hours until further strain relaxation could not be detected. After slowly cooling to 22°C, the birefringence and strain corresponded to the point B. On re-deforming the sample at 22°C and unloading, the birefringence and strain were in the region of C

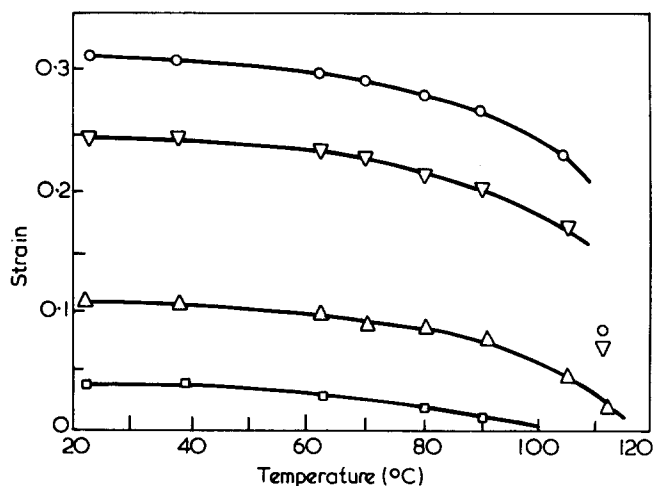


Figure 7 Effect of annealing temperature on PMMA samples deformed to a series of strains at 22°C. At each temperature the samples were annealed until further strain relaxation was inappreciable. The time required for this anneal decreased from 10h at 50°C to 0.5h at 100°C

100°C would produce chain conformations corresponding to the reduced thermal equilibrium value of cohesion points at 100°C. On cooling to 22°C new intermediate cohesion points will form so that at the time of the birefringence measurement, although the number of cohesion points is increased in the thermal equilibrium value at 22°C, the chains will have retained the conformation corresponding to the reduced value at 100°C. On subsequent deformation at 22°C the birefringence increase will be determined by the thermal equilibrium value at 22°C and will increase accordingly along BC.

#### Strain-induced dissociation of cohesion points

Stein and Norris<sup>24</sup> have presented a model in which each chain was regarded as having a limited extensibility determined by its contour length. Our results indicated that the maximum extension proposed by this model was an underestimate of the extensions attainable in PMMA but, owing to specimen damage, they were confined to too low strains to confirm this point. However, Shishkin and Milagin's data<sup>25</sup> on PMMA appear to show that extensions are possible in excess of the predictions of this model and Rider (personal communication) has shown this explicitly for PVC. In view of the probable weakness of cohesion points formed from secondary valence bonds and the distortional forces which must be set up on stretching a system of predominantly rigid links it seems likely that as the strain is increased cohesion points will break progressively, leading to an increase in the effective number of molecular chains per unit volume. This would lead to a relation of the form

$$-\frac{\delta N}{\delta \epsilon} \propto N \quad (2)$$

where  $\epsilon$  is the applied compressive strain. Longer chains will contain more links and will be capable of extending

further before the cohesion points are broken. (Strictly speaking the parameter used to describe strain should be a function such as  $|(\lambda_x - \lambda_y)|$  or  $|\epsilon|$  which is positive for both tensile and compressive strains since any plastic strain will cause a decrease in  $N$ . We have used  $\epsilon$  for convenience.)

Integrating equation (2) gives:

$$N = N_0 \exp(-k\epsilon) \quad (3)$$

where  $N_0$  is the thermal equilibrium value of chain density prior to any breakdown of cohesion points as a result of strain and  $k$  is a constant determined by the extensibility of the chains.  $N_0$  will itself be a function of temperature so equation (1) may be rewritten:

$$\Delta n_{xy} = CN_0(T) \cdot \alpha (\lambda_x^2 - \lambda_y^2) \exp(-k\epsilon) \quad (4)$$

For plane strain compression  $\lambda_y = 1 - \epsilon$  and  $\lambda_x = 1/(1 - \epsilon)$  assuming that the volume is constant. Measurements of birefringence and strain are made in the relaxed state and in this condition we could not detect any changes in volume with the accuracy of a density gradient column ( $\pm 0.1\%$  change in density). Equation (4) can be rearranged to give:

$$\log_{10} \frac{\Delta n_{xy}}{(\lambda_x^2 - \lambda_y^2)} = \log_{10}[CN_0(T) \cdot \alpha] - \frac{k}{2.3} \epsilon \quad (5)$$

Thus a plot of  $\log[\Delta n_{xy}/(\lambda_x^2 - \lambda_y^2)]$  against  $\epsilon$  should give a straight line of slope  $-k/2.3$  and intercept  $\log[C \cdot N_0(T) \cdot \alpha]$ . Figure 8 shows the experimentally determined points and Figures 9a and b are plots of  $\log[\Delta n_{xy}/(\lambda_x^2 - \lambda_y^2)]$  against  $\epsilon$  for deformations in the temperature range 22°C to 100°C.

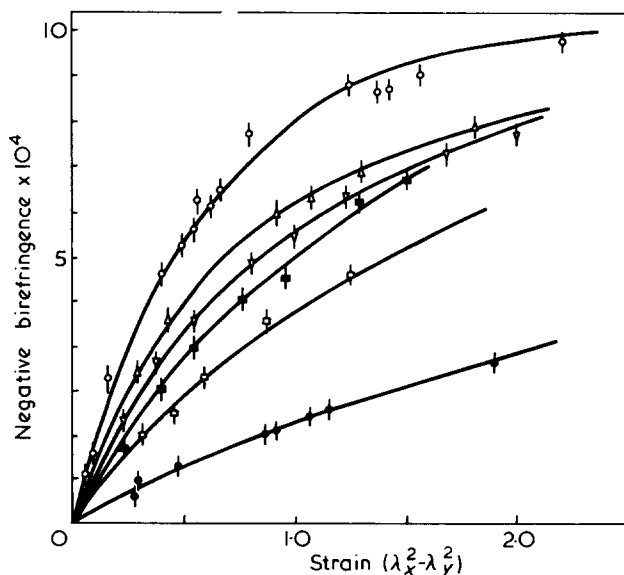
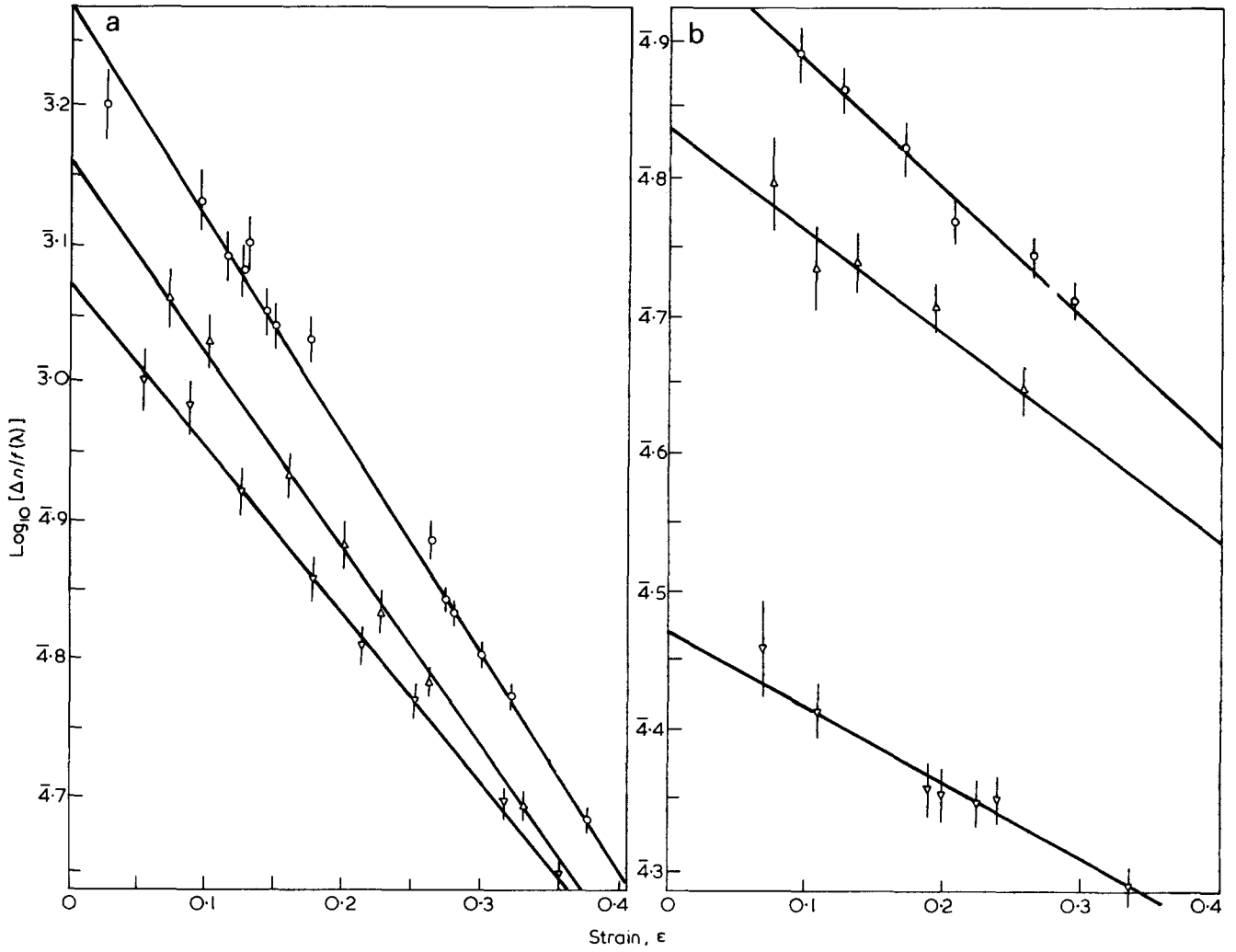


Figure 8 Relationship between residual birefringence and residual strain for PMMA after deformation and relaxation at a series of temperatures. After relaxation at the temperature of deformation all samples were slowly cooled to 22°C and birefringence and strain measurements were made at this temperature. ○, 22°C; △, 60°C; ▽, 70°C; ■, 80°C; □, 90°C; ●, 100°C



Figures 9a and b Plots of  $\log_{10}[\Delta n/f(\lambda)]$  against  $\epsilon$  for PMMA in accordance with equation (5) to determine  $CN_{0\alpha}$  and  $k$

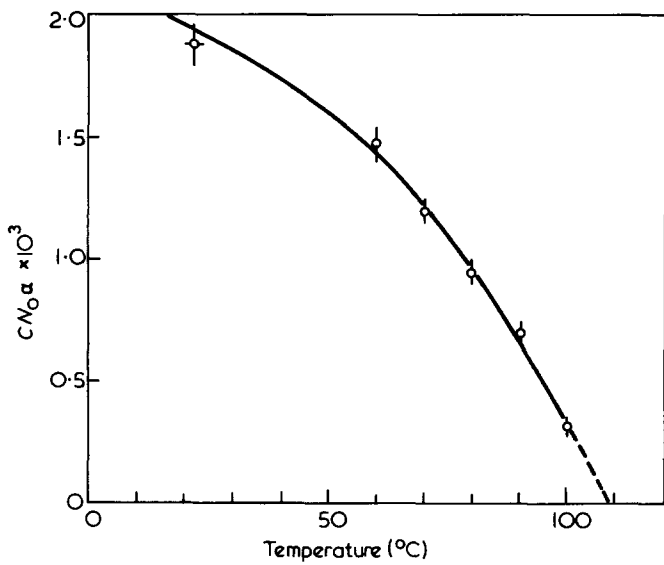


Figure 10 Temperature variation of  $CN_{0\alpha}$  calculated from the intercepts of Figure 9

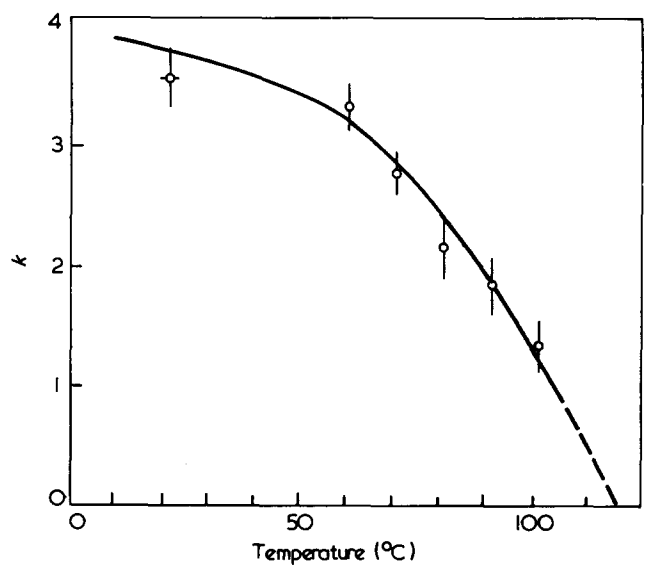


Figure 11 Temperature variation of  $k$  calculated from the gradients of Figure 10



Within experimental error the plots are linear and *Figures 10* and *11* show the variation of  $(CN_0\alpha)$  and  $k$  with temperature determined from the intercepts and slopes of *Figures 9a* and *9b*. Since  $C$  and  $\alpha$  are assumed constant at the temperature of measurement *Figure 10* reflects the variation of  $N_0$  with temperature.  $N_0$  extrapolates to zero at the glass-transition temperature ( $110^\circ\text{C}$  for this material). We anticipate that finer measurements around the  $T_G$  and above would show continued dependence of  $N_0$  on temperature as the character of the controlling cohesion points altered from secondary valence bonds to more widely spaced mechanical entanglements. The influence of mechanical entanglements is apparent even in the melt<sup>9</sup>. Though the curve drawn for  $k$  in *Figure 11* is only one of several that could have been drawn through the experimental points, it is clear that  $k$  falls steadily with temperature increase as may be expected from the increased thermal mobility of each link with increase of temperature permitting a greater degree of flexibility between cohesion points displaced by strain. The extrapolated value of zero in the region of the  $T_G$  is consistent with the well-known rubbery behaviour above the  $T_G$ .

*Thermal dissociation of cohesion points: evidence for dipole-dipole association*

The temperature dependence of  $N_0$  may be examined further. Suppose we attribute a dissociation energy  $E_a$  (per mole of repeat units) to the cohesion points. On the assumption that the thermal dissociation of the secondary bonds is governed in some way by a Boltzmann distribution of energy modes, the number of bonds with energy less than  $E_a$  is proportional to  $[1 - \exp(-E_a/RT)]$  so that:

$$N_0(T) = A' + B'[1 - \exp(-E_a/RT)] \quad (6)$$

where  $A'$  and  $B'$  are constants.  $A'$  refers to the number of points which are not subject to significant thermal influence e.g. points of mechanical entanglements and side-branching. Implicit in the foregoing discussion of strain-induced bond dissociation has been the assumption that  $A'$  is much smaller than the term containing  $B'$ . Since  $C$  and  $\alpha$  are constants, equation (6) may be rewritten:

$$CN_0(T)\alpha = A + B[1 - \exp(-E_a/RT)] \quad (7)$$

Putting  $\theta = 1/T$ , this gives:

$$\frac{\delta}{\delta\theta}(CN_0\alpha) = \frac{BE_a}{R} \exp\left(-\frac{E_a\theta}{R}\right)$$

and

$$\log_{10} \frac{\delta}{\delta\theta}(CN_0\alpha) = D - \frac{1}{2.3} \times \frac{E_a\theta}{R} \quad (8)$$

where  $D$  is a constant.

A plot of  $\log[\delta(CN_0\alpha)/\delta\theta]$  against  $\theta$  should then give a straight line of slope  $-E_a/2.3R$ . *Figure 12* shows such a plot of the experimental points. From the gradient  $E_a$  is calculated to be  $5.9(\pm 0.5)$  kcal/mol. The dissociation energy could equally have been derived from the temperature dependence of the equilibrium constant of an association-dissociation reaction. It yields an equation

identical with equation (8). Mark<sup>26</sup> lists a table of cohesive energies of secondary valence bonds determined from heats of vaporization. For the dipole-dipole interaction of  $-\text{COOCH}_3$  groups he quotes the figure of 5.6 kcal/mol.

Several assumptions have been used in these calculations and need to be clarified. Stein and Norris's suggestion<sup>24</sup> of a distribution of chain lengths is likely to be correct. Our data are insufficiently precise to distinguish between this and an 'average value' approach and, accordingly,  $N_0(T)$  must be regarded as an average over all the chains. It is unlikely that each segment of the molecular chain will be in an identical environment and one must presume a spectrum of cohesive energies in accordance with a spectrum of segmental separations of which, once again, the calculated value must be some average. Mark's dipole interaction figure<sup>26</sup> must be a similar average value. Niklas and von Schmelting<sup>27</sup> have given a more critical discussion of the possible distribution of energy modes which is likely to be more complex than a simple Boltzmann distribution. The form of equation (6) would, however, be relatively unchanged, certainly within the precision of our measurements, although constants such as  $A'$  and  $B'$  would be modified.

From the calculated values of  $(CN_0\alpha)$  and experimental values for  $C$  and  $\alpha$  in the literature,  $N_0$  may be estimated. The refractive index of Perspex for the wavelength of light used for the birefringence measurements is 1.48. From this  $C$  is calculated to be 1.67. From the limiting values of the strain-optical coefficient at low and high temperatures and the height of the strain-optical relaxation peak Read<sup>18</sup> has calculated the polarizability anisotropy at  $20^\circ\text{C}$  to be between  $-10.3 \times 10^{-25} \text{ cm}^3$  and

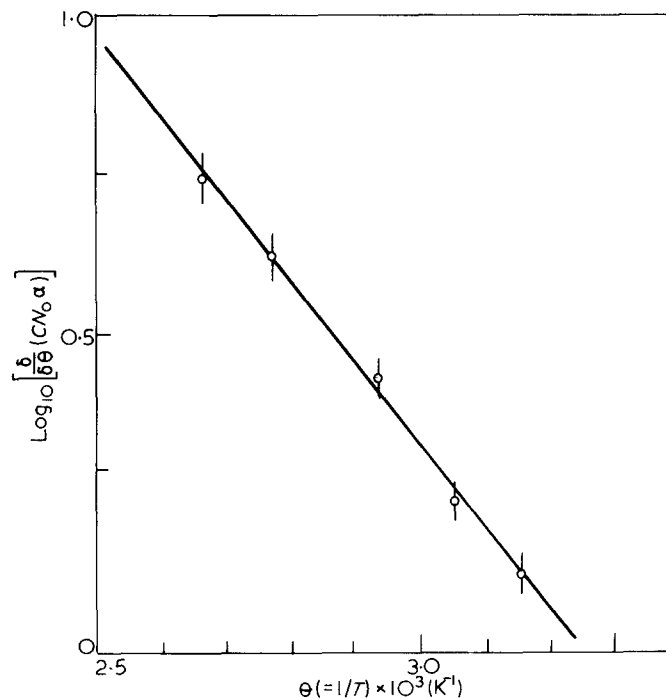


*Figure 12* Plot of  $\log_{10}[\delta(CN_0\alpha)/\delta\theta]$  in accordance with equation (8) to determine  $E_a$

$-8.7 \times 10^{-25} \text{ cm}^3$ . His calculations are based on the changes in the side-group. If we introduce the concept of an increase in chain length with increase of temperature, the mean value of  $\alpha$  is slightly raised to approximately  $10 \times 10^{-25} \text{ cm}^3$ . Substituting these values in our data for  $CN_{0\alpha}$ ,  $N_0$  is approximately  $12 \times 10^{21} \text{ cm}^{-3}$  at  $22^\circ\text{C}$  and  $1.9 \times 10^{21} \text{ cm}^{-3}$  at  $100^\circ\text{C}$ . From the measured density of  $1.19 \text{ g/cm}^3$  for PMMA this is equivalent to a chain length of six segments at  $22^\circ\text{C}$  and forty segments at  $100^\circ\text{C}$ . From the melt viscosity measurements on PMMA, mechanical entanglements are thought to be spaced by about 400 segments<sup>28</sup> so that the assumption that dissociable interaction points are the controlling parameter below the  $T_G$  is justifiable.

Shishkin and Milagin<sup>25</sup> have analysed the elastic modulus data of McLoughlin and Tobolsky<sup>29</sup> in the temperature range  $30^\circ$  to  $112^\circ\text{C}$  on the basis of a thermally activated dissociation process of secondary bonds and have found that the temperature dependence of the modulus indicates a dissociation energy of  $5.5 \text{ kcal/mol}$ . They also measured the dependence of birefringence on stretching temperature and found an activation energy of approximately  $5 \text{ kcal/mol}$ . This paper was unknown to us during the course of our work and, although our conclusions are similar, there are marked differences between our birefringence data and theirs. This may be attributable to the fact that after orientation their samples were cooled *under stress* which raises the possibility of frozen distortions or non-equilibrium structures. Andrews and Kimmel<sup>30</sup> have shown for polyacrylonitrile that there is a distinct difference in the magnitude and the temperature dependence of birefringence depending on whether the material is cooled under load or after relaxation and this is likely to be true generally. Shishkin cites unpublished work by Veselovskii and Matveev showing that the intermolecular cohesive energy of the  $-\text{COOCH}_3$  bonds determined from dielectric measurements on solutions of PMMA in toluene is  $6.4 \text{ kcal/mol}$ . In the absence of any specification by Mark of the material used to determine his figure of  $5.6 \text{ kcal/mol}$  the higher figure may be more directly relevant to PMMA.

In view of the above work and ours there seems strong evidence that intermolecular secondary valence bonding in PMMA is attributable to dipole-dipole interactions and that increased strain beyond yield or increasing temperature causes dissociation of these bonds. It is possible that the pre-yield part of the stress-strain curve is associated with the distortional extension that the chains can sustain before strain-rupture of the secondary bonds occurs. If there is no large-scale molecular rearrangement involving breakdown of the cohesive bonding the birefringence-strain curve is retraceable on unloading. At yield some limiting chain extensibility condition is reached and rupture of secondary bonds occurs. Subsequent chain conformations are retained on unloading as new intermediate cohesion points form, and the birefringence-strain path is no longer retraceable. On unloading and relaxation the oriented samples will contain the thermal equilibrium value of cohesion points. On re-loading each sample will show similar strain-birefringence curves until the limiting extensibility condition is again reached and the material will yield once again. As secondary bond rupture increases the chain length and consequently the chain extensibility (equation 2), the modulus would be expected to fall and the material will strain-soften. The extent of the strain-softening will be

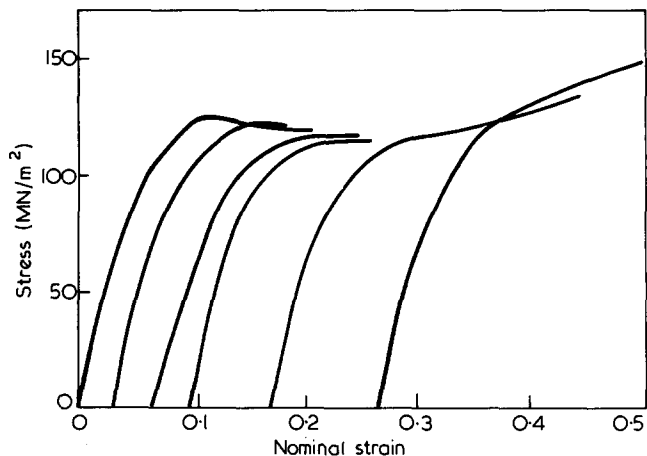


Figure 13 Stress-strain curves for a PMMA sample compressed at  $20^\circ\text{C}$ . The sample was successively loaded, unloaded and then loaded again. The unloading portions of the curves have been omitted for clarity. The strain axis refers to the strain calculated from the original undeformed thickness

determined by the counter-effect of strain-hardening due to an increased number of covalent bonds opposing the stress<sup>1</sup>, so that with increasing orientation a decreasing extent of strain-softening will be observed in practice as is shown in Figure 13.

As a check of this model it is necessary to estimate whether a sensible amount of distortional energy is available at the yield point to provoke rupture of secondary bonds. Since  $E_a$  is the dissociation energy per mole of repeat units, the energy of a single bond is  $(E_a/A)$  where  $A$  is Avogadro's number. As a simple approximation  $N_0$  chains will have associated with them  $N_0$  cohesion points so that the total energy per unit volume will be  $E_a N_0/A$ , which, for  $N_0 = 12 \times 10^{20} \text{ cm}^{-3}$  at  $22^\circ\text{C}$  is  $5 \times 10^8 \text{ erg cm}^{-3}$ . At  $22^\circ\text{C}$  the yield stress is  $13 \text{ kg mm}^{-2}$  and occurs at a strain of 15%, so the energy density is approximately  $\frac{1}{2}(13 \times 10^8 \times 0.15) \text{ erg cm}^{-3}$  which is  $10^8 \text{ erg cm}^{-3}$ . Thus the order of magnitude of the energy available at yield is consistent with the energy required for bond dissociation.

Since the model associates a distortional mode with the elastic portion of the stress-strain curve a quantitative appraisal of the birefringence-strain relationship under stress is not possible. In the absence of any data on bond polarizabilities in a stressed condition or precise information on the distortional influences on the highly polarizable side-groups it is not possible to carry out a rigorous analysis.

## CONCLUSIONS

Although several assumptions have been made in the foregoing discussion, the model of dissociable cohesion points produces a consistent picture of many of the features of the mechanical and optical behaviour of PMMA. In common with other suggestions in the literature our results support the view that these cohesion points are attributable to interactions between the dipoles

from the ester side-groups. In the undeformed condition the concentration of these interaction points is governed by thermally activated dissociation. Strain-induced rupture of the secondary bonds occurs during yield and subsequent drawing.

#### ACKNOWLEDGEMENTS

We wish to thank Professor R. W. K. Honeycombe for the provision of laboratory facilities and for his encouragement during this work which was carried out with the help of a research grant from the Science Research Council. One of us (S.R.) wishes to thank the Master and Fellows of Corpus Christi College for the award of the Plumian Research Scholarship, and ICI Plastics Division and the Science Research Council for an industrial studentship. In addition we are grateful to Professor D. W. Saunders for a valuable discussion.

#### REFERENCES

- 1 Vincent, P. I. *Polymer* 1960, **1**, 7
- 2 Bryant, G. M. *Textile Res. J.* 1961, **31**, 399
- 3 Andrews, R. D. and Kazama, Y. *J. Appl. Phys.* 1967, **38**, 4118
- 4 Newman, S. and Strella, S. *J. Appl. Polym. Sci.* 1965, **9**, 2297
- 5 Eirich, F. R. *Appl. Polym. Symp.* 1965, **1**, 271
- 6 Litt, M. H. and Koch, P. *J. Polym. Sci. (B)* 1967, **5**, 251
- 7 Whitney, W. and Andrews, R. D. *J. Polym. Sci. (C)* 1967, **16**, 2981
- 8 Vincent, P. I. *Polymer* 1960, **1**, 425
- 9 Bueche, F. 'Physical Properties of Polymers', Interscience, New York, 1962, pp 70, 74
- 10 Treloar, L. R. G. *Rubber Chem. Technol.* 1944, **17**, 813
- 11 Bartenev, G. M. and Zuyev, Yu. S. 'Strength and Failure of Viscoelastic Materials', Pergamon Press, Oxford, 1968, p 155
- 12 Nielsen, L. E. 'Mechanical Properties of Polymers', Reinhold, New York, 1962, p 59
- 13 Bowden, P. B. and Raha, S. *Phil. Mag.* 1970, **22**, 463
- 14 Treloar, L. R. G. 'Physics of Rubber Elasticity', Oxford University Press, Oxford, 1958, p 129
- 15 Volkenstein, M. V. 'Configurational Statistics of Polymeric Chains', Interscience Publishers, New York, 1963, p 391
- 16 Kolsky, H. *Trans. Soc. Glass Technol.* 1952, **36**, 56
- 17 Le Grand, D. G. *J. Polym. Sci. (A)* 1964, **2**, 931
- 18 Read, B. E. *J. Polym. Sci. (C)* 1967, **16**, 1887
- 19 Tsvetkov, V. N. and Verkhovina, L. N. *Sov. Phys.-Tech. Phys.* 1958, **3**, 87
- 20 Hammack, T. J. and Andrews, R. D. *J. Appl. Phys.* 1965, **36**, 3574
- 21 Trapasnikova, O. N. *Sov. Phys.-Solid State* 1959, **1**, 597
- 22 Trapeznikova, O. N. and Zhurina, M. N. *Zh. Fiz. Khim.* 1950, **14**, 1471
- 23 Peukert, H. *Kunststoffe* 1951, **41**, 154
- 24 Stein, R. S. and Norris, F. H. *J. Polym. Sci.* 1956, **21**, 381
- 25 Shishkin, N. J. and Milagin, M. F. *Sov. Phys.-Solid State* 1963, **4**, 1967
- 26 Mark, H. 'Physical Chemistry of High Polymeric Systems', Interscience, New York, 1940, p 112
- 27 Niklas, H. and von Schmeling, H. K. *Kunststoffe* 1963, **53**, 839
- 28 Porter, R. S. and Johnson, J. F. 'Proceedings of the 4th International Congress on Rheology', (E. H. Lee and A. L. Copley, Eds.) Interscience, New York, 1965, Part 2, p 467
- 29 McLoughlin, J. R. and Tobolsky, A. V. *J. Polym. Sci.* 1952, **7**, 555
- 30 Andrews, R. D. and Kimmel, R. M. *J. Polym. Sci. (B)* 1965, **3**, 167

# Linear, high molecular weight poly(2-alkyl-4-vinyl-6-(dialkylaminomethyl)phenols) and poly(2,6-bis(dialkylaminomethyl)-4-vinylphenols)

P. Ferruti and A. Bettelli

*Istituto Chimica Industriale del Politecnico, Piazza Leonardo da Vinci 32, 20133 Milano, Italy*  
(Received 27 July 1971)

Poly(2-alkyl-4-vinyl-6-(dialkylaminomethyl)phenols) and poly(2,6-bis(dialkylaminomethyl)-4-vinylphenols) were prepared in high yields from poly(3-alkyl-4-vinylphenols) or poly(4-vinylphenol), by a Mannich-type reaction. Some properties of the new poly(aminomethylvinylphenols) are given, and their solubility behaviour is discussed.

## INTRODUCTION

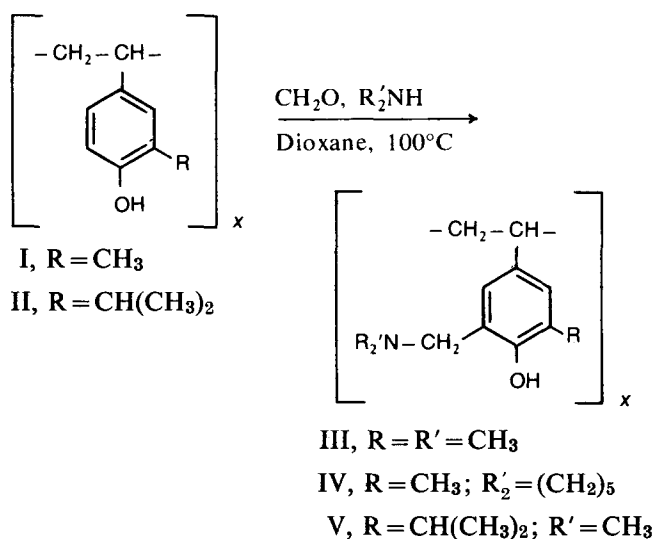
Tertiary amino polymers have potential applications in some fields of experimental surgery<sup>1</sup>. They may show pharmacological properties, owing to their ability to interact with biological macromolecules such as heparin<sup>1,2</sup>, and the *N*-oxides of many of them have been extensively studied as antisilicogenic agents, with considerable success<sup>3</sup>. Furthermore, polymers which have both a phenolic hydroxyl and an amino group in the monomeric unit may be expected to show other interesting properties. For example, they might act as chelating agents<sup>4</sup>, and probably also as macromolecular inhibitors as the related poly(4-vinylphenols) and poly(2-alkyl-4-vinylphenols) do<sup>5</sup>.

The synthesis and properties of several poly(2-alkyl-4-vinyl-6-(dialkylaminomethyl)phenols) and poly(2,6-bis(dialkylaminomethyl)-4-vinylphenols) are reported here. This work was mainly performed in order to find new polymers for biological and pharmacological purposes. It is part of an extensive research on the synthesis of tertiary amino polymers<sup>6</sup>.

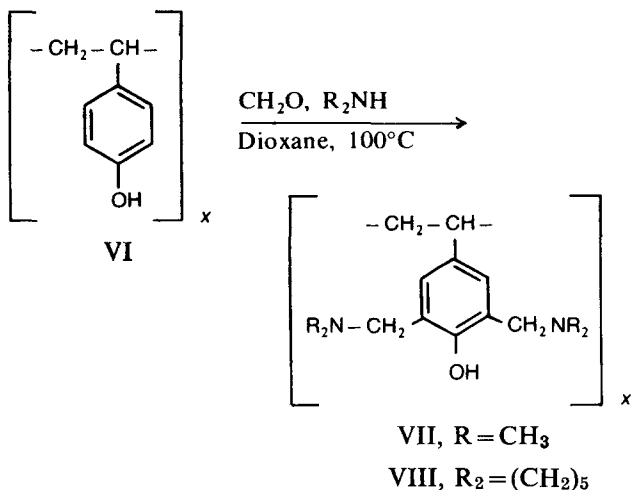
Some crosslinked polymers having the structure of poly(2-aminomethyl-4-vinylphenol) have been previously prepared<sup>4</sup> by reaction of ammonia with the corresponding chloro- or bromo-methyl derivatives. To our knowledge, however, no linear polymers such as that described in the present paper have so far been described.

## SYNTHESIS AND PROPERTIES OF THE POLYMERS

When high molecular weight poly(2-alkyl-4-vinylphenols) were allowed to react in a suitable solvent, such as dioxane, with an excess of formaldehyde and a secondary amine, a smooth Mannich reaction ensued and poly(2-alkyl-4-vinyl-6-(dialkylaminomethyl)phenols) were obtained in very high yields. The degree of substitution, as indicated by elemental analysis, was essentially complete:



Under similar conditions, poly(4-vinylphenol) (VI) gave poly(2,6-bis(dialkylaminomethyl)-4-vinylphenols):



Although we limited our investigation to dimethyl-amino- and piperidino-derivatives, the above reactions may be reasonably expected to be quite general, thus opening a facile and apparently clean route to several amino derivatives of poly(vinylphenols), which would not be easily accessible, in a pure state, by other means.

Elemental analysis and viscosity data of the new poly-(aminomethylvinylphenols) are given in Table 1. By considering the intrinsic viscosities, it does not seem probable that a significant change in the average molecular weight generally occurs during the reaction.

The poly(aminomethylvinylphenols) were white powders, with a very poor wettability with water, on whose surface, when dry, they usually floated. Some solubility data on these polymers are given in Table 2. As a rule they are insoluble in lower alcohols, with the exception of VII, but they are all soluble in aromatic hydrocarbons and chlorinated solvents.

On the other hand, the parent poly(vinylphenols)<sup>5,7</sup> were easily soluble in alcohols, but insoluble in aromatics and most chlorinated solvents. This also holds true for other similar, high molecular weight poly(vinylphenols), such as poly(3-vinylphenol)<sup>8</sup> and even poly(2-*t*-butyl-4-vinylphenol) (unpublished results), in spite of the bulkiness of the 2-substituent in the latter.

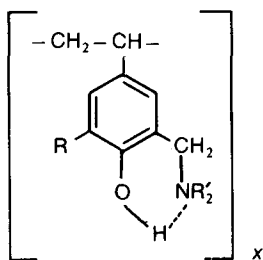
In our opinion, this different behaviour of the two classes of polymers is not probably due to steric effects only. It is known that when both the nature of the chemical groups involved and the geometry of the molecule are favourable, the formation of intramolecular hydrogen bonds commonly takes place in 2-substituted phenols<sup>9</sup>. Therefore, a strong intra-mono-molecular hydrogen bond may be expected to be formed between the phenolic hydroxyl and the tertiary amino groups in the monomeric unit of the poly(2-alkyl-4-vinyl-6-(dialkylaminomethyl)phenols):

Table 1 Elemental analysis and intrinsic viscosities of poly(2-alkyl-4-vinyl-6-(dialkylaminomethyl)phenols), and of poly(2,6-bis(dialkylaminomethyl)4-vinylphenols)

Compound	Formula of the monomeric unit	$[\eta]^*$	$[\eta]$ of the parent poly(vinylphenol) <sup>†</sup>	Elemental analysis (%)
III		0.54	0.49	Calcd: C, 75.35; H, 8.96; N, 7.32 Found: C, 75.19; H, 8.80; N, 7.30
IV		0.50	0.49	Calcd: C, 77.88; H, 9.15; N, 6.06 Found: C, 77.76; H, 9.02; N, 6.20
V		1.36	1.55	Calcd: C, 76.67; H, 9.65; N, 6.39 Found: C, 76.47; H, 9.53; N, 6.21
VII		0.35	0.32	Calcd: C, 71.75; H, 9.46; N, 11.95 Found: C, 71.90; H, 9.35; N, 11.77
VIII		0.32	0.27	Calcd: C, 76.39; H, 9.62; N, 8.91 Found: C, 76.55; H, 9.75; N, 8.87

\* In chloroform at 30°C (100 cm<sup>3</sup>/g)

† In 2-butanone at 30°C (100 cm<sup>3</sup>/g)



The same should occur also in poly(2,6-bis(dialkylaminomethyl)-4-vinylphenols), perhaps with a tautomeric shift of the hydrogen bond from one amino group to the other and *vice versa*. It is also known that for *ortho*-substituted phenols in which intramolecular hydrogen bonds are possible, intermolecular hydrogen bonding may be reduced<sup>10</sup>. Consequently, poly(dialkylaminomethylvinylphenols) may be expected to be less easily solvated than poly(vinylphenols) by hydroxylated solvents through hydrogen bond formation. For the same reason, the formation of intermolecular hydrogen bonds, such as are probably responsible for the insolubility of high molecular weight poly(vinylphenols) in aromatic and related solvents, should be consistently depressed in poly(aminomethylvinylphenols), thus allowing the latter polymers to dissolve in most of these solvents.

The poly(aminomethylvinylphenols) are very weak acids. Most of them, in fact, do not seem to react with aqueous diluted sodium hydroxide, unlikely the parent poly(vinylphenols). On the other hand, these new polymers appear to be fairly strongly basic. The latter property is of interest in view of some biological applications<sup>1, 2</sup>.

## EXPERIMENTAL

### *Poly(2-methyl-4-vinyl-6-(dimethylaminomethyl)phenol) (III)*

To a cooled solution of 7.7 g poly(2-methyl-4-vinylphenol) (I)<sup>5</sup> in 170 ml dioxane and 16 g dimethylamine, 17.2 ml of aqueous 38% formaldehyde were added dropwise while stirring. The reacting mixture was allowed to warm up spontaneously at room temperature, and then refluxed for 3 h. The mixture was poured into an excess of saturated NaCl solution; the precipitated III was collected, washed with water, dried and finally purified by dissolving it in benzene and reprecipitating in n-heptane. The yield, apart from mechanical losses, was practically quantitative.

### *Poly(2-methyl-4-vinyl-6-(piperidinomethyl)phenol) (IV)*

The same procedure as in the previous case, starting from 3.04 g of I, 70 ml dioxane, 17.4 ml piperidine and 6.8 ml formaldehyde solution was used. The polymer (IV), also obtained in essentially quantitative yield, was recovered and purified in the same way.

### *Poly(2-isopropyl-4-vinyl-6-(dimethylaminomethyl)phenol) (V)*

Starting with 1.4 g poly(2-isopropyl-4-vinylphenol) (II)<sup>5</sup>, 30 ml dioxane, 2.6 g dimethylamine and 3 ml formaldehyde solution, the same procedure was adopted. Isolation and purification were performed in a similar manner. The yield of V was essentially quantitative.

Table 2 Solubility data on poly(2-alkyl-4-vinyl-6-(dialkylaminomethyl)phenols) (III-V), and poly(2,6-bis(dialkylaminomethyl)-4-vinylphenols) (VII and VIII)\*

Solvent	Compound				
	III	IV	V	VII	VIII
n-Heptane	i	i	i	i	i
Benzene	s	s	s	s	s
Toluene	s	s	s	s	s
Dioxane	s	s	s	s	s
Chloroform	s	s	s	s	s
Carbon tetrachloride	s	s	s	s	s
Methanol	i	i	i	s	sw
95% Ethanol	i	i	i	s	i
n-Butanol	sh	sh	sh	s	sw
Acetone	s	sw	s	s	sw
2-Butanone	s	s	s	s	sw
Ethyl acetate	s	s	s	s	sw
Water	i	i	i	i	i
1% aq. acetic acid	s	s	s	s	s
5% aq. sodium hydroxide	i	i	i	s	i

\* = soluble; sh = soluble at the b.p.; sw = swells; i = insoluble

### *Poly(2,6-bis(dimethylaminomethyl)-4-vinylphenol) (VII)*

Using 4 g poly(4-vinylphenol) (VI)<sup>7</sup>, 200 ml dioxane, 17.5 g dimethylamine and 22.6 ml formaldehyde solution in a similar procedure, the mixture was finally refluxed for 12 h. The product was isolated as previously, and purified by dissolving in a little dioxane and reprecipitating with water. The yield was over 90%.

### *Poly(2,6-bis(dipiperidinomethyl)-4-vinylphenol) (VIII)*

The same method as used previously, starting with 4 g VI, 46 ml piperidine and the same quantities of dioxane and formaldehyde solution was employed. The polymer (VIII) was isolated and purified as described before. The yield was over 90%.

## ACKNOWLEDGEMENT

This work was supported by the 'Programma speciale Tecnologie Biomediche' of the Italian National Council of Researches.

## REFERENCES

- 1 Marchisio, M. A., Longo, T., Ferruti, P. and Danusso, F. *6th Congr. Eur. Soc. Exp. Surgery, Hälsingborg (Sweden), April 27-29, 1971; Eur. Surg. Res.* 1971, **3**, 240
- 2 Marchisio, M. A., Sbertoli, C., Farina, G. and Ferruti, P. *Eur. J. Pharmacol.* 1970, **12**, 236
- 3 Natta, G., Vigliani, E. C., Danusso, F., Pernis, B., Ferruti, P. and Marchisio, M. A. *Atti Accad. Naz. Lincei VIII*, 1965, **39**, 498
- 4 Packam, D. I. *J. Chem. Soc.* 1964, p 2617
- 5 Moraglio, G., Ferruti, P. and Feré, A. *Chim. Ind., Milan* 1968, **50**, 742
- 6 Danusso, F. and Ferruti, P. *Polymer* 1970, **11**, 88
- 7 Danusso, F., Ferruti, P. and Gazzaniga Marabelli, C. *Chim. Ind., Milan* 1965, **47**, 54
- 8 Ferruti, P. *Chim. Ind., Milan* 1965, **47**, 496
- 9 Rochester, C. H. in 'The chemistry of the hydroxyl group', (Ed. S. Patai) Interscience, New York, 1971, pp 360-367
- 10 'The chemistry of the hydroxyl group'. (Ed. S. Patai) Interscience, New York, 1971, p 332

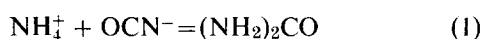
# Note to the Editor

## Preparation of carbamoylated polyethylenimine and its flocculation property\*

Norio Ise, Hiroyuki Moritani and Tsuneo Okubo

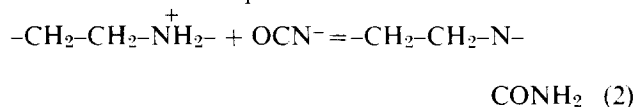
Department of Polymer Chemistry, Kyoto University, Kyoto, Japan  
(Received 3 January 1972)

In 1828 Wöhler discovered the conversion of ammonium cyanate into urea:



Cyanate ions were later found to be reactive also to primary and secondary amino cations<sup>1</sup>. Thus it is to be expected that polymers having primary and secondary amino groups such as polyethylenimine and poly(L-lysine) would react with cyanate anions to produce carbamoylated polymers.

In this work we investigated carbamoylated polyethylenimine derived from polyethylenimine and cyanate ions by an interionic reaction process:



Carbamoylated polyethylenimine (carb. PEI) was prepared by mixing poly(ethylenimine hydrochloride) (PEI·HCl) with silver cyanate or with sodium cyanate. Polyethylenimine was obtained from the Nippon Shyokubai Chemicals Co., Osaka, Japan (P-1000). The fraction of the tertiary amino groups was found to be 0.25 by acetylation. Silver cyanate was obtained by the method of Warner and Warrick<sup>2</sup>. Sodium cyanate was commercially available.

A solution of PEI·HCl (0.180 equiv./l; 1000 ml) was mixed with a slight excess of silver cyanate (27.1 g) with strong agitation and silver chloride was filtered off after centrifugation. The aqueous solution of poly(ethylenimine cyanate) (PEI·OCN) was then kept for 24 h. The solution was then frozen and dried under vacuum: a white powder (yield 95%) was obtained.

The degree of carbamoylation of the primary and secondary amino groups of PEI was 0.99 as determined by the Volhard method. The carbamoylation reaction proceeded almost quantitatively. The degree of carbamoylation could be easily changed by varying the amounts of NaOCN and AgOCN.

The results of the elemental analyses of PEI·HCl and 99% carb. PEI are shown in Table 1. The calculated values were obtained by assuming that PEI is composed of secondary amino groups (75%) and tertiary amino

Table 1 Elemental analyses of PEI·HCl and 99% carb. PEI

		H	C	N	Cl	O
PEI·HCl	obsd. (%)	8.45	35.7	17.7	32.4	0
	calcd. (%)	7.55	30.2	17.6	44.7	0
99% carb. PEI	obsd. (%)	8.74	45.6	25.1	2.23	19.0
	calcd. (%)	7.33	44.0	32.7	0	16.0

groups (25%). The agreement between observed and calculated values is reasonably good.

The infra-red (i.r.) spectra of PEI·HCl and 99% carb. PEI were taken using an infra-red spectrophotometer, model IR-27 (Shimadzu Manufacturing Co., Kyoto, Japan). The peaks of 720, 1370, 1458, 2861, and 1919 cm<sup>-1</sup> are due to ethylene groups and appeared in both samples of PEI·HCl and carb. PEI. The peaks of primary amide groups at 3050–3200, 1650 and 1640 cm<sup>-1</sup> appeared in carb. PEI, whereas they disappeared in PEI·HCl. Furthermore, the absorption band at 1655 cm<sup>-1</sup> ascribed to the secondary amide group existed in 99% carb. PEI but not in PEI·HCl. Thus, the main structure of the new polymer will be concluded to have carbamoyl groups attached to the nitrogen atom of the secondary amino group.

Carbamoylated polyethylenimines for flocculation test were prepared by mixing PEI·HCl and NaOCN as follows: PEI (product of Dow Chemical Co., Separane C-120) was diluted to 1.065 equiv./l and neutralized with 2M HCl. 0, 3.70, 11.11, 18.51, and 27.77 g of sodium cyanate (commercially pure grade) were added to five fractions of PEI·HCl solutions (250 ml for each). The degrees of carbamoylation attained after 24 h were 0, 19.9, 58.0, 94.0 and 98.0%, respectively. A suspended solution of kaolin (100 ml) and a certain amount of a carb. PEI solution of 0.1% concentration were mixed in a measuring cylinder with a stopper, and the pH of the solution was adjusted with NaOH. The resulting mixture was then suspended completely by rapidly turning the cylinder up and down 10 times. Then, the velocity of precipitation was recorded. After 10 min the transparency of the supernatant liquid at 660 nm and the precipitate volume were read. All measurements were performed at 20 ± 2°C.

Figure 1 gives the flocculation velocity of a 1% suspension of kaolin at pH 8.0. The flocculation velocity is

\* Presented in part at the 28th Annual Meeting of the Research Institute for Chemical Fibers, Japan, on 8 October 1971.

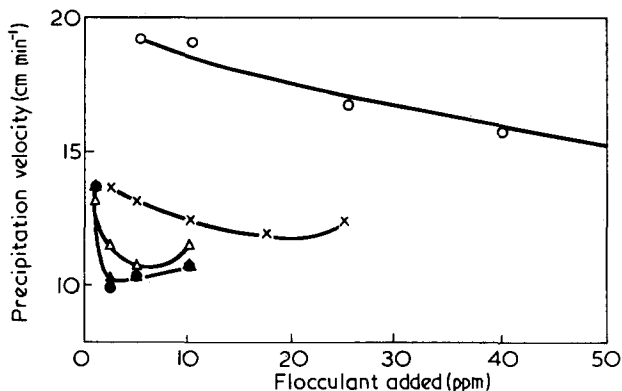


Figure 1 Precipitation velocity of aqueous 1% kaolin suspension (pH=8.0) with carb. PEI. ▲, 0%; ●, 19.9%; △, 58%; ×, 94%; ○, 98%.

clearly larger with carb. PEI than with PEI, especially when the degree of carbamoylation is over 90%. It should be noted that the increase in the flocculation velocity becomes larger when the pH of the suspension is high. For example, the velocities for the 2% kaolin suspension at pH 10.7 and at flocculant concentrations of 30–100 ppm were 2–4, 4–6, 8–14, and 19–21 cm/min for the carb. PEI with degrees of carbamoylation of 0, 19.9, 58.0 and 98.0%, respectively. It should be further noted that the flocculation velocity with polyacrylamide could not be measured because of the unclear precipitate interface under the present experimental condition.

The maximum value of the transparency did not decrease by carbamoylation of PEI (Figure 2). The amount of polymer required for the attainment of the maximum, however, increased with increasing degree of carbamoylation. For comparison, the effectiveness for the transparency of a cationic derivative of polyacrylamide (CPAAm) and polyacrylamide (PAAm) were also shown in the Figure. Both samples did not give satisfactory transparency. The fact that the efficiency for the transparency was not depressed by the carbamoylation will be attributed in part to the ionizable tertiary amino groups of carb. PEI remaining unreacted with  $\text{OCN}^-$ .

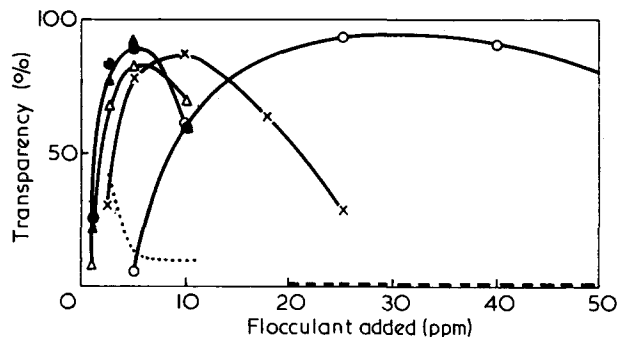


Figure 2 Transparency of supernatant liquid of aqueous 1% kaolin suspension (pH=8.0) with carb. PEI. ▲, 0%; ●, 19.9%; △, 58%; ×, 94%; ○, 98%; ---, PAAm; ·····, CPAAm

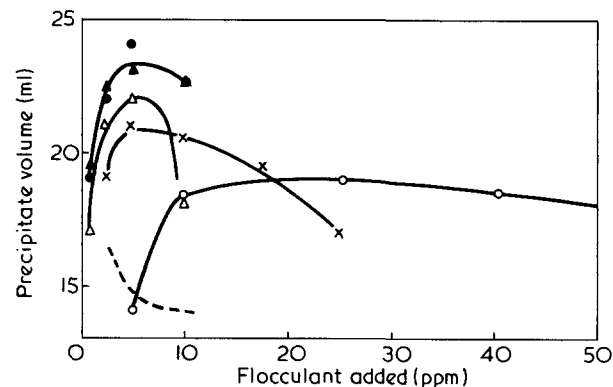


Figure 3 Precipitate volume of aqueous 1% kaolin suspension (pH=8.0) with carb. PEI. ▲, 0%; ●, 19.9%; △, 58%; ×, 94%; ○, 98%; ----, CPAAm

The volume of precipitate decreased with increasing degree of carbamoylation especially in the range larger than 0.9 as is shown in Figure 3.

A detailed account of this work will be published shortly.

#### REFERENCES

- 1 Frost, A. A. and Pearson, R. G. 'Kinetics and Mechanism', 2nd edn, John Wiley, New York, 1961
- 2 Warner, J. C. and Warrick, E. L. *J. Am. Chem. Soc.* 1935, **57**, 1491

#### Conference Announcement

### 6th Biennial Polymer Symposium

Ann Arbor, 12–15 June 1972

The 6th Biennial Polymer Symposium, sponsored by the Division of Polymer Chemistry of the American Chemical Society will be held from 12 to 15 June, 1972 at the Macromolecular Research Center, University of Michigan, Ann Arbor, Michigan, USA.

The registration fee for the entire conference will be \$20.00 for American Chemical Society members, \$25.00 for non-members, and \$3.00 for students; the single-day fee for non-students will be \$8.00. These fees will cover both the technical sessions and a

social gathering scheduled for the evening of June 12th. Registration forms and detailed information will be mailed in April to all members of the American Chemical Society Divisions of Polymer Chemistry, Rubber Chemistry, and Organic Coatings and Plastics. Others interested in attending can obtain the same material by writing to the University of Michigan, Extension Service Conference Department, 412 Maynard Street, Ann Arbor, Michigan 48104, USA.



# Polysaccharide synthesis from mono- and oligo-saccharides by the action of phosphorus pentoxide in dimethyl sulphoxide\*

Shigehiro Hiranot, Naoki Kashimura, Noboru Kosaka and Konoshin Onodera

Department of Agricultural Chemistry, Kyoto University, Kyoto, Japan  
(Received 10 August 1971)

Phosphorus pentoxide–dimethyl sulphoxide ( $P_4O_{10}$ –DMSO) was found predominantly to catalyse the polymerization reaction of carbohydrates at below  $35^\circ\text{C}$  and the oxidation reaction at  $60$ – $65^\circ\text{C}$ . A series of new synthetic polysaccharides were prepared from mono- and oligo-saccharides including 2-acetamido-2-deoxy-D-glucose and hexuronic acids in up to 48% yield by the action of  $P_4O_{10}$ –DMSO at  $10$ – $25^\circ\text{C}$ . These synthetic polysaccharides showed  $s_{20,w}$  0.68–1.34S, and the degree of polymerization fell in 1.3–4.7 monosaccharide units per polysaccharide chain on the basis of reducing end-group assay. A structural analysis by the methylation of the synthetic glucan (2) revealed  $\alpha$ -1,4- and  $\alpha$ -1,6-glucosidic linkages as main chains with various branchings. The synthetic polysaccharides contained 1.3–15.9% phosphorus, but the linkages are unknown.

## INTRODUCTION

In previous years, a number of attempts have been made to synthesize naturally occurring polysaccharides and the related polymers of increasing interest from biochemical and industrial points of view<sup>1</sup>. Fischer and Delbrück<sup>2</sup> first reported a procedure for the synthesis of an oligosaccharide from substituted monosaccharides by the action of  $P_4O_{10}$ . Since then, the simple principle in that a water molecule is eliminated with  $P_4O_{10}$  has been applied to the synthesis of various glycosides and polysaccharides from mono- and oligo-saccharides without significant success. In 1961, Micheel *et al.*<sup>3</sup> prepared a series of branched polysaccharides from mono- and oligo-saccharides by the action of  $P_4O_{10}$  in the presence of HCl or HBr as catalyst in dimethyl sulphoxide (DMSO). In the course of our studies on catalytic action of phosphorus compounds<sup>4–7</sup>, we found, in addition to the oxidation<sup>4, 8</sup>, the formation of polysaccharides (*O*-glycosides) and glycosylamines (*N*-glycosides) by the action of  $P_4O_{10}$  without any addition of catalyst in DMSO at below  $35^\circ\text{C}$ . More recently, Husemann and Müller<sup>9</sup> prepared a cellulose-like polysaccharide

from 2,3,6-tri-*O*-(*N*-phenylcarbonyl)-D-glucopyranose by the action of  $P_4O_{10}$  in DMSO– $\text{CHCl}_3$ . Independently Mizuno<sup>10</sup> confirmed  $P_4O_{10}$  as a good dehydrating agent for polysaccharide synthesis in DMSO and prepared a series of polysaccharides from monosaccharides. Partial structural analysis of the synthetic galactan and xylan indicated considerable branchings<sup>11</sup>.

The present work reports that  $P_4O_{10}$ –DMSO catalyses polycondensation and oxidation depending on the reaction temperature. The synthesis of a series of new synthetic polysaccharides is described. These are prepared from mono- and oligo-saccharides including 2-acetamido-2-deoxy-D-glucose and hexuronic acids by the action of  $P_4O_{10}$ –DMSO at  $10$ – $35^\circ\text{C}$ . Furthermore, a structural analysis by the methylation of the synthetic glucan (2) is for the first time described.

## EXPERIMENTAL

### Analytical methods

Hexoses and pentoses were analysed by the anthrone method<sup>12</sup>, hexosamine by the Elson–Morgan method<sup>13</sup>, hexuronic acids by the carbazole method<sup>14</sup>, phosphorus by the Allen method<sup>15</sup>, and reducing sugar values by both the ferricyanide<sup>16</sup> and 3,5-dinitrosalicylic acid<sup>17</sup> methods. Sedimentation patterns were obtained with a synthetic boundary cell at 59 780 rev/min with a Spinco Model E

\* Presented at the annual meeting of the Agricultural Chemical Society of Japan, Tokyo, 1–4 April 1965, and a preliminary note of the present work appeared in a footnote of ref. 4

† To whom inquiries should be addressed. Present address: Department of Agricultural Chemistry, Tottori University, Tottori, Japan

ultracentrifuge in  $\sim 1\%$  solution of the sample as dissolved in 0.15 M KCl. Sedimentation constants are expressed as  $s_{20,w}$ . Tiselius electrophoresis was carried out in two different buffer solutions at 4.0–4.5°C: (a) sodium borate (0.1 M), pH 8.98,  $\mu$  0.15, 9.8 mA; (b) acetic acid–sodium acetate (0.1 M), pH 5.0,  $\mu$  0.10, 10.0 mA. Periodate oxidation was carried out at 4.0°C in the dark<sup>18</sup>, and the periodate consumed is calculated in terms of the corresponding monosaccharide unit which is free of phosphorus. Infra-red (i.r.) spectra were recorded with a Shimadzu AR-6 spectrometer in Nujol or KBr pellet, and optical rotatory dispersion (o.r.d.) with a JASCO automatic recording spectropolarimeter with 1% solution of the sample at 17°C in water. Paper chromatography was carried out on Toyo Roshi No. 51 filter paper by descending method with a solvent: 1-butanol/ethanol/1% ammonia (4 : 1 : 5, v/v), and the alkali silver nitrate reagent was utilized for the detection of reducing sugars. Enzyme digestion was carried out with  $\alpha$ -amylase originated from *Aspergillus oryzae* (Sigma Chemical Co.) at 35°C at pH 5.5, and with  $\beta$ -amylase originated from barley malt (Sigma Chemical Co.) at 35°C at pH 5.0<sup>19</sup>.

The change of specific rotation was measured during the mild acid hydrolysis of the synthetic polysaccharides: each of the polysaccharides was dissolved in 1.0% concentration in both 0.01 N and 1.0 N HCl and the solution was hydrolysed in a boiling water bath. Specific rotation was measured with a Yanagimoto direct reading polarimeter.

#### General procedure for polysaccharide synthesis

To 50 ml of anhydrous DMSO, 10 g of  $P_4O_{10}$  were added in small portions with stirring to produce a homogeneous solution in an ice bath. To the solution was added 10 g of the corresponding carbohydrate or the mixture, and the solution was shaken at 15–35°C for 3–5 days. In some cases, 0.5 g of dried Dowex 50(H<sup>+</sup>) resin was additionally added as a catalyst to the reaction mixture at the beginning of the reaction. The reaction mixture was poured into a large volume of acetone, and the mixture was stirred to produce an amorphous product. The supernatant solution was decanted and the residue was dis-

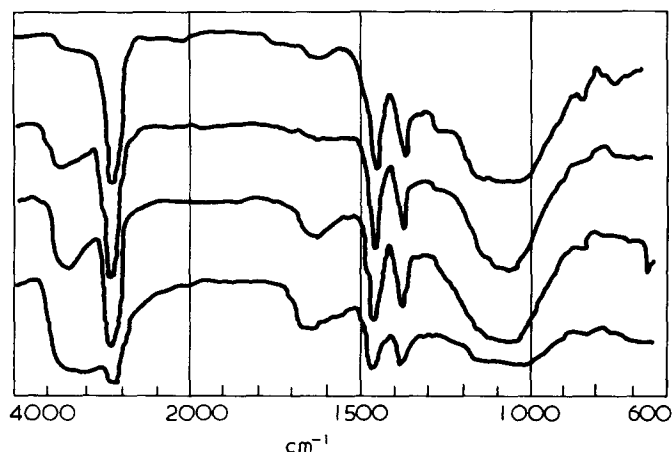


Figure 1 Infra-red spectra at each step of the methylation of synthetic glucan (2). (a) Synthetic glucan (2); (b) after Hakomori's methylation (Found: CH<sub>3</sub>O, 35.6%); (c) after Hakomori and Purdie's methylations (Found: CH<sub>3</sub>O, 38.8%); (d) after Hakomori, Purdie and Kuhn's methylations (Found: CH<sub>3</sub>O, 41.7%)

solved in  $\sim 300$  ml of ice water. The solution was dialysed against running water through a cellophane tubing for two days and concentrated *in vacuo* at below 45°C to give a syrupy product. Residual DMSO was removed from the syrup by evaporating three times after addition of 50 ml each of 1,4-dioxane. The polysaccharide thus obtained was precipitated by addition of five volumes of acetone. The mixture was kept at room temperature for 24 h. The precipitates produced were collected by centrifugation, washed with ether and dried over calcium chloride in a desiccator (see Table 1).

#### Structural analysis by the methylation of the synthetic glucan (2)

The synthetic glucan (2) (5.0 g) was dissolved in 200 ml of DMSO. The methylation was carried out by Hakomori's procedure<sup>20</sup>, twice by Purdie's procedure of continuous refluxing for 5 days<sup>21</sup>, and finally by Kuhn's procedure of treating for continuous 6 days<sup>22</sup>. Further methylation did not give the increase of methoxyl content. No OH absorption was detected in 3000–3500 cm<sup>-1</sup> region in the i.r. spectrum (see Figure 1). Yield, 4.2 g;  $[\alpha]_D^{20} + 74^\circ$  (c 1.0, methanol). Calcd for (C<sub>9</sub>H<sub>16</sub>O<sub>5</sub>)<sub>n</sub>: CH<sub>3</sub>O, 45.6%. Found: CH<sub>3</sub>O, 41.2%.

The fully methylated product (3 g) was refluxed in 200 ml of 85% HCOOH for 1 h and then refluxed in 200 ml of 0.5 N H<sub>2</sub>SO<sub>4</sub> for 17 h. After neutralizing with solid BaCO<sub>3</sub>, the filtrate was concentrated *in vacuo* to a syrup (2.8 g). Paper chromatography indicated nine spots of methylated D-glucoses. At the first step, the hydrolysate was separated into four fractions of mono-, di-, tri- and tetra-*O*-methylated D-glucoses by the preparative paper chromatography (Whatman 3MM). At the second step, the mono-*O*-methyl fraction was separated into three compounds, the di-*O*-methyl fraction into three compounds and tri-*O*-methyl fraction into two compounds, respectively by the second preparative paper chromatography (see Table 4).

**Spot 1.** The fraction was 2,3,4,6-tetra-*O*-methyl-D-glucose which was identified by mixture melting point and i.r. spectroscopy as 2,3,4,6-tetra-*O*-methyl-*N*-phenyl-D-glucopyranosylamine: m.p. 138–139°C;  $[\alpha]_D^{20} + 230^\circ$  (c 0.5, acetone); reported<sup>23</sup> m.p. 137–138°C;  $[\alpha]_D + 228$ –239.5° (acetone). Calcd for C<sub>16</sub>H<sub>25</sub>NO<sub>5</sub>: CH<sub>3</sub>O, 39.9%. Found: CH<sub>3</sub>O, 40.3%.

**Spot 2.** The fraction was 2,3,4-tri-*O*-methyl-D-glucose which was identified by mixture melting point and i.r. spectroscopy as 2,3,4-tri-*O*-methyl-*N*-phenyl-D-glucopyranosylamine: m.p. 150°C;  $[\alpha]_D^{20} - 103^\circ$  (c 0.7, ethanol); reported<sup>24</sup> m.p. 150°,  $[\alpha]_D - 103^\circ$  (ethanol). Calcd for C<sub>15</sub>H<sub>23</sub>NO<sub>5</sub>: CH<sub>3</sub>O, 31.3%. Found: CH<sub>3</sub>O, 30.6%.

**Spot 3.** The fraction was identified by mixture melting point and i.r. spectroscopy as 2,3,6-tri-*O*-methyl- $\alpha$ -D-glucopyranose: m.p. 120–122°C,  $[\alpha]_D^{20} + 83 \rightarrow +20^\circ$  (c 0.2, water); reported<sup>25</sup> m.p. 121–123°C,  $[\alpha]_D + 90 \rightarrow +70.5^\circ$  (water). Calcd for C<sub>9</sub>H<sub>18</sub>O<sub>6</sub>: CH<sub>3</sub>O, 41.9%. Found: CH<sub>3</sub>O, 41.3%.

**Spot 8.** The fraction was identified by mixture melting point, i.r. and nuclear magnetic resonance (n.m.r.) spectroscopies as 3-*O*-methyl- $\alpha$ -D-glucopyranose: m.p. 161°C,  $[\alpha]_D^{20} + 85 \rightarrow +56^\circ$  (c 0.3, water); reported<sup>26</sup> m.p. 160–161°C,

Table 1 Polysaccharide synthesis from mono- and oligo-saccharides

Synthetic polysaccharide	Carbohydrates used for polycondensation	Reaction condition		Yield (%)
		Temperature (°C)	Time (h)	
(1)	D-glucose*	20-35	120	48
(2)	D-glucose	35	120	48
(3)	D-glucose and $\alpha$ -D-glucose-1-phosphate (K salt) (1000 : 1, w/w)	30-35	120	45
(4)	D-glucose	10-15	340	0.5
(5)	2-acetamido-2-deoxy-D-glucose*	20-35	72	24
(6)	2-acetamido-2-deoxy-D-glucose	35	72	38
(7)	L-arabinose	35	72	12
(8)	D-xylose	35	72	36
(9)	D-xylose and xylan (4 : 1, w/w)	15	72	45
(10)	D-xylose and xylan (100 : 1, w/w)	15	72	39
(11)	lactose*	20-35	120	24
(12)	lactose	10-15	340	5
(13)	maltose	10-15	340	16
(14)	cellobiose	10-15	340	11
(15)	2-acetamido-2-deoxy-D-glucose and D-glucose (1 : 1, w/w)	10-15	340	14
(16)	D-glucofuranuronolactone and D-glucose (1 : 1, w/w)	10-15	340	15
(17)	2-acetamido-2-deoxy-D-glucose and D-glucofuranuronolactone (1 : 1, w/w)	10-15	340	12

\* Dry Dowex 50(H<sup>+</sup>) was used as a catalyst (see text)

$[\alpha]_D +104 \rightarrow +55^\circ$  (water).  $\delta(D_2O)3.61$  (*s* 3H, MeO-3), 5.20 (*d* 1H, H-1,  $J_{1,2}$  3.0 Hz).

Other spots could not be crystallized, but a tentative assignment of the spots was carried out by paper chromatography with the reference of reported  $R_{fg}$  values<sup>27, 28</sup> ( $R_{fg}$ : mobility rate on the paper chromatogram with reference to 2,3,4,6-tetra-*O*-methyl-D-glucose) (Table 4).

## RESULTS AND DISCUSSION

P<sub>4</sub>O<sub>10</sub>-DMSO catalyses not only the oxidation but also the polycondensation of carbohydrates. Maximum yield of the oxidation products was obtained in the reaction at 60-65°C as reported in our previous papers<sup>4, 8</sup>. On the other hand, maximum yield of the synthetic polysaccharides was obtained in the reaction at 30-35°C (see Table 1). It was found that the reaction temperature influences significantly to the type of predominant reactions. The yield of the synthetic polysaccharides was up to 48%, which is in agreement with a reported result<sup>11</sup>. Catalytic action of Dowex 50(H<sup>+</sup>) was not significant in the polymerization reaction. This indicates that P<sub>4</sub>O<sub>10</sub> may act as dehydrating agent as well as acidic catalyst. The reaction with methyl- $\alpha$ -D-glucopyranoside,  $\alpha$ -D-glucopyranose-1-phosphate and methyl-2-acetamido-2-deoxy- $\alpha$ -D-galactopyranoside did not produce the corresponding polymer. This substantiates the view that the polysaccharides have mainly glycosidic linkages.

It is of interest to examine an action of naturally occurring polysaccharides as a starter or an action of monosaccharide phosphates as an intermediate in the polycondensation reaction. The experiments were carried out in the polycondensation of D-xylose in the presence of natural xylan and in the polycondensation of D-glucose in the presence of  $\alpha$ -D-glucopyranose-1-phosphate (see Table 1). As a result, no significant action of these compounds was found in the yield and the physical properties of the products.

The synthetic polysaccharides are soluble in water and DMSO, and the 15% aqueous solution showed almost no viscosity in comparison with water.

The synthetic polysaccharides were hydrolysed with 2N H<sub>2</sub>SO<sub>4</sub> at 100°C for 8-16 h. Paper chromatographic examination indicated mainly the corresponding monosaccharide (~90%) together with one or two minor spots which are considered to be oxidized products. The detailed structure of the minor spots is unknown. Partial acid hydrolysis (1N H<sub>2</sub>SO<sub>4</sub> at 100°C for 30 min) of the synthetic glucan (2) showed more than two spots of oligosaccharides in small quantity in addition to the large amount of D-glucose. One of the spots was identical with maltose on paper chromatogram. In the case of heteropolycondensation, (15) showed an equivalent proportion of the component sugars, but the proportion was changed in (16) and (17), with which low contents of uronic acid was observed. The synthetic polysaccharides contained 1.3-20.9% phosphorus. The phosphorus could not be removed by repeating the procedure of mild methanolysis<sup>29</sup>, and the treatment was attended with partial degradation of some glycosidic linkages of the polysaccharides (see Table 2).

The synthetic polysaccharides showed relatively narrow distribution in the molecular weight from behaviour in sedimentation patterns. The  $s_{20, w}$  fell in 0.69-1.34S. Tiselius electrophoresis revealed that each of the polysaccharides consists of two or more components. These results indicate no typical difference of molecular weight with regard to the products, but there is some heterogeneous distribution of the phosphorus content. Reducing values of the products is relatively high in comparison with that of naturally occurring polysaccharides and the value indicates the degree of polymerization in 1.5-3.4.7 monosaccharide units per polysaccharide chain. The high reducing value may be due to the participation of new reducing groups produced in a small quantity during the polymerization by partial oxidation of the polymers<sup>4, 8</sup> or by decomposition of DMSO<sup>6</sup>.

The stability of the polymers towards dilute acid solutions was characteristic of pyranoside linkages more than furanoside ones or acyclic ones<sup>30-32</sup>, and the change of specific rotation during acid hydrolysis suggests occurrence of the predominance of  $\alpha$ -D- or  $\beta$ -L-configuration. Moreover, the  $\alpha$ -D-configuration was confirmed by both the positive plain curves in the o.r.d. analysis and the

Table 2 Analysis of the synthetic polysaccharides

Sample	Carbohydrate (%)				N (%)	P (%)	S <sub>20, w</sub>	Reducing sugar value*		Periodate oxidation†	[α] <sub>D</sub> <sup>20</sup> (c 1.0, water) (degrees)
	Hexose	Hexosamine	Pentose	Uronic acid				Method 1	Method 2		
(1)	69.0	—	—	—	—	7.0	0.90	14.7	9.3	1.62	+87.5
(2)	72.0	—	—	—	—	7.7	n.d.	13.2	10.4	1.12	+87.5
(3)	70.7	—	—	—	—	6.9	0.80	12.6	9.6	0.90	+88.0
(6)	—	52.6	—	—	4.13	3.6	1.34	17.6	n.d.	0.89	+27.0
(7)	—	—	65.0	—	—	12.0	0.69	13.3	n.d.	1.65	+20.0
(8)	—	—	40.0	—	—	15.9	n.d.	n.d.	6.5	n.d.	+15.0
(9)	—	—	50.0	—	—	11.0	n.d.	n.d.	n.d.	n.d.	+10.0
(10)	—	—	30.0	—	—	20.9	n.d.	n.d.	n.d.	n.d.	+8.0
(11)	76.5	—	—	—	—	4.7	1.11	n.d.	9.6	0.73	+24.0
(12)	66.8	—	—	—	—	6.4	n.d.	n.d.	n.d.	n.d.	+35.0
(13)	83.9	—	—	—	—	1.3	1.27	13.0	10.8	1.02	+95.0
(14)	47.6	—	—	—	—	3.5	1.00	20.9	n.d.	n.d.	+17.3
(15)	49.3	40.6	—	—	2.04	3.5	0.86	14.6	n.d.	n.d.	+6.1
(16)	41.5	—	—	9.4	—	6.5	0.83	15.0	n.d.	n.d.	+42.3
(17)	—	66.3	—	15.6	3.68	2.3	0.89	n.d.	n.d.	10.0	+12.0

\* Method 1, the 3,5-dinitrosalicylic acid method; method 2, the ferricyanide method

† Periodate consumed during 150h per monosaccharide unit (moles)

850 cm<sup>-1</sup> absorption in the i.r. spectra. (7) showed a positive plain curve in the o.r.d. analysis, which supports β-L-configuration (see Table 3). It is of interest to note that (1) was not hydrolysed with any of α- and β-amylases, but (2) was hydrolysed with only α-amylase. On the other hand, both the enzymes hydrolysed (13). These observations were on the basis of increase of the reducing sugar values in the reaction mixture. This indicates a structural difference between the synthetic glucans (1) and (2). (1) was prepared in the presence of Dowex 50(H<sup>+</sup>) and (2) in the absence of the reagent. The selective oxidation of primary hydroxyl groups in (1) and (2) with nitrogen dioxide<sup>33</sup> did not produce any of uronic acids, which were examined by the carbazole reaction. The iodine reaction for starch was negative for (1), (2), (3), (4), and (13).

#### Structure of the synthetic glucan (2)

Hakomori's methylation procedure did not give the fully methylated product of (2) even after twice treat-

ments (Found: CH<sub>3</sub>O, 35.6%). As shown in Figure 1, successive methylations by Hakomori, Purdie and Kuhn's procedures gave a fully methylated product, which showed almost no OH absorption. Further additional methylations did not increase the methoxyl contents. The methoxyl content as observed is ~4% less than that calculated. This may be due to the presence of oxy-methylene bridges as originated from DMSO<sup>6</sup>, partly oxidized products<sup>4, 8</sup>, and phosphorus.

The recovery of total methylated derivatives was in 54% yield. As shown in Table 4, molar ratio of tetra-, tri-, di- and mono-*O*-methyl-D-glucoses was in 4 : 5 : 2.5 : 1. In the tri-*O*-methyl fraction, the molar ratio of 2,3,4- and 2,3,6-tri-*O*-methyl-D-glucoses was in ~1 : 1. Taking α-D-anomeric configuration into consideration as described above, it is concluded that the synthetic glucan (2) has α-1,4- and α-1,6-glucosidic linkages as main chains with various branchings. Especially it is noteworthy that almost the same amount of tri-*O*-methyl fraction was tetra-*O*-methyl-D-glucose originating from the non-

Table 3 Infra-red and o.r.d. data of the synthetic polysaccharides

Sample	Nujol ∇ <sub>max</sub> (cm <sup>-1</sup> )*				o.r.d. (c 1.0, water, 17°C) (degrees)					
	COO <sup>-</sup>	-CONH-	P=O	Anomeric	700	600	500	400	350	300 nm
(1)	—	—	1240 w	850 w	+38	+72	+158	+303	+418	+638
(2)	—	—	1240 w	850 w	n.d.	—	—	—	—	—
(3)	—	—	1240 w	850 w	+31	+66	+154	+307	+430	+655
(6)	—	1640-1670 s	—	—	n.d.	—	—	—	—	—
(7)	—	—	1230 w	—	+17	+18	+33	+58	+75	+84
(8)	—	—	1240 w	—	+10	+10	+18	+29	+33	+48
(9)	—	—	1260 w	—	n.d.	—	—	—	—	—
(10)	—	—	1260 w	—	n.d.	—	—	—	—	—
(11)	—	—	—	—	+20	+25	+32	+52	+67	+100
(12)	—	—	1240 w	—	n.d.	—	—	—	—	—
(13)	—	—	—	850 w	+70	+90	+130	+210	+295	+425
(14)	—	—	1240 w	—	+2	+16	+30	+62	+93	+148
(15)	—	—	—	850 w	+5	+14	+45	+65	+76	+108
(16)	1630-1650 w	—	1240 w	850 w	+24	+39	+66	+130	+171	+249
(17)	1640-1670 s	1640-1670 s	—	850 w	n.d.	—	—	—	—	—

\* In addition to these absorptions, strong absorption of HO at 3300-3400 cm<sup>-1</sup> appeared in all samples  
s, strong; w, weak

Table 4 O-Methyl derivatives of D-glucose as isolated from the acid hydrolysate of the fully methylated product of synthetic glucan (2)

Spot	Paper chromatography (R <sub>fg</sub> )*		Assignment of O-methyl-D-glucose	Yield† (mg)	Molar ratio
	Solvent 1	Solvent 2			
1	1.00		2,3,4,6-	550	4.0
2	0.79		2,3,4-	647	5.0
3	0.72		2,3,6-		
4	0.54 (0.57)	0.65 (0.66)	2,3-‡	301	2.5
5	0.49 (0.51)	0.50 (0.51)	2,6-‡		
6	0.44 (0.46)	0.62 (0.61)	2,4-‡		
7	0.37	0.44	Not assigned	133	1.0
8	0.32		3-		
9	0.31	0.41	Not assigned		

\* R<sub>fg</sub>, mobility rate on the paper chromatograms with reference to 2,3,4-tetra-O-methyl-D-glucose. Solvent 1, 1-butanol/ethanol/1% ammonia (4 : 1 : 5, v/v). Solvent 2, 1-butanol/ethanol/water (4 : 1 : 5, v/v)

† The synthetic glucan (2) (5.0g) was used for the methylation. The recovery of the methylated fractions was in 54% yield

‡ Tentative assignment on the basis of paper chromatography

reducing end group. The presence of a large amount of the tetra-O-methyl fraction may be because of low molecular weight of the synthetic glucan. This is also in agreement with the high reducing value.

#### REFERENCES

- Goldstein, I. J. and Hullar, T. L. *Adv. Carbohydr. Chem.* 1966, **21**, 431
- Fischer, E. and Delbrück, K. *Ber. Dtsch. Chem. Ges.* 1909, **42**, 2776
- Micheel, F., Böckmann, A. and Meckstroth, W. *Makromol. Chem.* 1961, **48**, 1
- Onodera, K., Hirano, S. and Kashimura, N. *J. Am. Chem. Soc.* 1965, **87**, 4651
- Onodera, K., Hirano, S. and Fukumi, H. *Agric. Biol. Chem.* 1964, **28**, 173
- Onodera, K., Hirano, S., Kashimura, N. and Yajima, T. *Tetrahedron Lett.* 1965, p 4327
- Onodera, K., Hirano, S., Kashimura, N., Masuda, F., Yajima, T. and Miyazaki, N. *J. Org. Chem.* 1966, **31**, 1291
- Onodera, K., Hirano, S. and Kashimura, N. *Carbohydr. Res.* 1968, **6**, 276
- Husemann, E. and Müller, G. J. *Makromol. Chem.* 1966, **91**, 212
- Mizuno, T. *Nippon Nogeikagaku Kaishi* 1967, **41**, 189
- Mizuno, T. *Nippon Nogeikagaku Kaishi* 1967, **41**, 195
- Scott, T. A., Jr. and Melvin, E. H. *Anal. Chem.* 1953, **25**, 1656
- Elson, L. A. and Morgan, W. T. J. *Biochem. J.* 1933, **27**, 1824
- Dische, Z. *J. Biol. Chem.* 1947, **167**, 189
- Park, J. T. and Johnson, M. J. *J. Biol. Chem.* 1949, **181**, 149
- Bruner, R. L. *Methods in Carbohydr. Chem.* 1964, **4**, 67
- Allen, R. J. L. *Biochem. J.* 1940, **34**, 858
- Guthrie, R. D. *Methods Carbohydr. Chem.* 1962, **1**, 435
- Whelan, W. J. *Methods Carbohydr. Chem.* 1964, **4**, 252, 261
- Hakomori, S. *J. Biochem., Tokyo* 1964, **55**, 205
- Purdie, T. and Irvine, J. C. J. *Chem. Soc.* 1903, **83**, 1021
- Kuhn, R., Trischmann, H. and Löw, I. *Angew. Chem.* 1955, **67**, 32
- Onuki, M. *Nippon Nogeikagaku Kaishi* 1933, **9**, 90
- Geerdes, J. D., Lewis, B. A. and Smith, F. J. *Am. Chem. Soc.* 1957, **79**, 4209
- Irvine, J. C. and Hirst, E. I. *J. Chem. Soc.* 1922, **121**, 1213
- Irvine, J. C. and Hogg, T. P. *J. Chem. Soc.* 1914, **105**, 1386
- Durand, H. W., Dull, M. F. and Tipson, R. S. *J. Am. Chem. Soc.* 1958, **80**, 3691
- Hirst, E. L., Hough, L. and Jones, J. K. N. *J. Chem. Soc.*, 1949, p 928
- Kantor, T. G. and Schubert, M. *J. Am. Chem. Soc.* 1957, **79**, 152
- Micheel, F. and Gresser, W. *Ber. Dtsch. Chem. Ges.* 1958, **91**, 1214
- Kent, P. W. *Biochem. J.* 1953, **55**, 361
- Mora, P. T., Wood, J. W., Maury, P. and Young, B. G. *J. Am. Chem. Soc.* 1958, **80**, 693
- Schachman, H. K. *Methods Enzymol.* 1957, **4**, 32
- Gibbons, R. A. in 'Glycoproteins', (Ed. A. Gottschalk), Elsevier Publishing Co., Amsterdam, 1966, 1st edn, p 61

Note added in proof.—A further proof of polymer was obtained by the molecular weight analysis according to the Archibald method<sup>33</sup> (time=38 min, T=299°C, ω<sup>2</sup>=1.3633 × 10<sup>6</sup>). Molecular weights of (3), (6) and (11) are calculated as 7600, 16000 and 9500, respectively, by assuming the partial specific volumes<sup>34</sup> of (3) and (11) to be 0.613 and that<sup>34</sup> of (6) to be 0.666.

# Swelling of a rubber cylinder in torsion: Part 1. Theory

L. R. G. Treloar

*Department of Polymer and Fibre Science, University of Manchester Institute of Science and Technology, Sackville Street, Manchester M60 1QD, UK  
(Received 14 September 1971)*

The Flory-Huggins theory of the swelling of a crosslinked rubber by a liquid of low molecular weight is applied to the problem of a cylinder subjected to combined axial extension and torsion about the axis. Equations are developed which enable the radial distribution of stress, strain and swelling to be derived. For the case when the torsion is small an explicit (approximate) expression is obtainable for the change of swollen volume ( $\Delta V/V$ ) resulting from the torsion. The effect is a reduction of swollen volume by an amount proportional to the square of the torsion. For large torsional strains the problem can only be solved by numerical computation, using an iterative process. This is illustrated by a typical numerical example, in which the radial distributions of stress, strain and swelling are calculated and compared with the approximate distributions valid for small torsional strains.

## STATEMENT OF PROBLEM

The equilibrium degree of swelling of a crosslinked rubber immersed in an organic liquid and subjected to strain has already been examined theoretically for the case of a pure homogeneous strain of the most general type<sup>1, 2</sup>, and also for particular types of strain, such as simple extension or uniaxial compression<sup>3</sup>. Experiments involving both simple extension and uniaxial compression<sup>3</sup> have been found to give a dependence of equilibrium swelling on strain in quantitative agreement with the theory, the swelling increasing in the case of extension and decreasing in the case of compression.

The relation between swelling and strain for a rubber cylinder subjected to torsion can be treated on the same basis as that employed in the problems previously examined. Although no new physical principles are involved, the treatment is, however, considerably more complicated mathematically, owing to the fact that the state of strain is not homogeneous. As a result the equilibrium degree of swelling is likewise not homogeneous, but varies from point to point in the body. For such a system an explicit analytical solution cannot be obtained (except for the limiting case when the torsional strain is small), and numerical methods of analysis have to be employed.

The theoretical conclusions are of particular interest. Whereas for the types of strain previously examined the change in swelling due to the strain is approximately proportional to the amount of the strain, for the case of torsion the theory gives the result that the resultant

decrease of swelling is approximately proportional to the square of the torsional strain. This decrease of swelling due to torsion may be associated with the presence of normal (compressive) components of stress in the axial and radial directions which are likewise proportional to the square of the torsion<sup>2</sup>. The decrease of swelling on torsion may be regarded as analogous to the reduction of volume which accompanies the twisting of a compressible (dry) rubber, which has been shown theoretically to be proportional to the normal components of stress and hence also to the square of the torsion<sup>4</sup>.

In the present paper the theoretical treatment for a cylinder subjected to combined axial extension (or compression) and torsion about the axis is presented. Equations are derived giving the radial variation of the components of stress and of the equilibrium swelling. These equations provide the basis for the numerical computation of the overall reduction of swelling due to torsion.

An approximate form of the theory, which enables an explicit solution to be obtained for the case when the torsional strain is small, is also included.

These theoretical conclusions are compared with experimental observations in Part 2<sup>5</sup>.

## PHYSICAL BASIS AND ASSUMPTIONS

It will be assumed that the elastic properties of the rubber in the most general state of strain may be represented by the usual Gaussian network theory, according to which

the free energy  $A_e$  of the network in the strained swollen state is given by:

$$A_e = \frac{1}{2}G(\lambda_1^2 + \lambda_2^2 + \lambda_3^2 - 3) \quad (1)$$

In this expression  $\lambda_1$ ,  $\lambda_2$  and  $\lambda_3$  are the principal extension ratios, referred to the unswollen unstrained state, and:

$$G = NkT = \rho RT/M_c \quad (1a)$$

where  $N$  is the number of chains per unit volume of the unswollen rubber,  $\rho$  the density of the rubber and  $M_c$  the 'chain molecular weight'. The degree of swelling is conveniently represented in terms of the volume fraction  $v_2$  of the rubber in the swollen state. The ratio of swollen volume  $V$  to unswollen volume  $V_u$  is related to the strain parameters and to  $v_2$  thus:

$$V/V_u = \lambda_1\lambda_2\lambda_3 = 1/v_2 \quad (2)$$

In the standard theory of swelling it is assumed that both components (rubber and liquid) are incompressible and that their volumes are additive. With these assumptions the relations between the principal (tensile) stresses  $t_1$ ,  $t_2$  and  $t_3$  and the corresponding extension ratios are of the type<sup>6</sup>:

$$t_1 = \frac{A_{om}}{V_1} + Gv_2\lambda_1^2 \text{ etc.} \quad (3)$$

in which  $V_1$  is the molar volume of the swelling liquid and  $A_{om}$  is the molar free energy of dilution of the polymer molecules in the un-crosslinked state. For the latter, the Flory-Huggins relation:

$$A_{om} = RT[\ln(1 - v_2) + v_2 + \chi v_2^2] \quad (4)$$

will be used,  $\chi$  being an interaction parameter characteristic of the particular polymer-liquid system.

Since  $A_{om}$  is a function of  $v_2$ , equation (3) expresses the relation between the three variables  $t_1$ ,  $\lambda_1$  and  $v_2$ . If any two of these (e.g.  $\lambda_1$  and  $v_2$ ) are fixed, the third is therefore determined.

## METHOD OF ANALYSIS

### Geometry of strain: compatibility conditions

We shall consider a cylinder of radius  $a_0$  and length  $l_0$  in the unswollen state subjected to combined axial extension and torsion and swollen to equilibrium. If  $l$  is the axial length in the final state, the axial extension ratio  $\beta_3$  is defined as

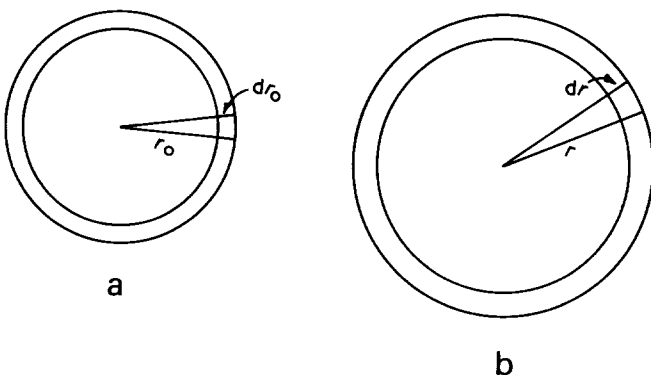


Figure 1 Coordinates in (a) unstrained unswollen and (b) strained swollen state

$l/l_0$ . The torsion  $\psi$  is defined as the angular rotation per unit axial length, measured in the final state.

It will be assumed, in accordance with the classical theory of torsion, that the state of strain in an element of the material at the radial position  $r$  is a function of  $r$  only, and independent of its axial coordinate. With this assumption the strain distribution is identical for all transverse sections of the cylinder. The dimensional changes in the transverse plane are therefore definable in terms of  $r_0$ , the radial coordinate of a point in the unswollen unstrained state, and the corresponding coordinate  $r$  in the strained swollen state (Figure 1). The strains in the transverse plane are defined by a circumferential extension ratio  $\beta_1$  and a radial extension ratio  $\beta_2$ , referred to the unswollen unstrained state. The three extension ratios  $\beta_1$ ,  $\beta_2$  and  $\beta_3$  satisfy the equations

$$\left. \begin{aligned} \beta_1 &= \frac{r}{r_0}, & \beta_2 &= \frac{dr}{dr_0}, & \beta_3 &= \frac{l}{l_0} = \text{constant} \\ & & & & \beta_1\beta_2\beta_3 &= 1/v_2 \end{aligned} \right\} \quad (5)$$

The first two of equations (5) are obvious from inspection of Figure 1.

It is important to note that  $\beta_1$ ,  $\beta_2$  and  $\beta_3$  are not the three principal extension ratios, i.e., they do not (except for  $\beta_2$ ) coincide with the principal axes of the strain ellipsoid.

The requirement of compatibility of the strains imposes restrictions on the variations of strain with radial position. Thus from equations (5):

$$\beta_2 = \frac{dr}{dr_0} = \frac{d(\beta_1 r_0)}{dr_0} = \beta_1 + r_0 \cdot \frac{d\beta_1}{dr_0}$$

whence

$$\frac{d\beta_1}{dr_0} = \frac{\beta_2 - \beta_1}{r_0} \quad (6)$$

To obtain  $d\beta_1/dr$  we put

$$\frac{d\beta_1}{dr} = \frac{d\beta_1}{dr_0} \cdot \frac{dr_0}{dr} = \frac{\beta_2 - \beta_1}{r_0} \cdot \frac{dr_0}{dr}$$

Substituting for  $r_0$  and  $dr_0/dr$  from equations (5) this gives

$$\frac{d\beta_1}{dr} = \frac{\beta_1}{r} \left( 1 - \frac{\beta_1}{\beta_2} \right) \quad (7)$$

Equation (7) implies that if the state of strain at any point is given, the rate of change of  $\beta_1$  with respect to  $r$  is determined by purely geometrical considerations.

### Stress-strain relations

We are concerned with the normal components of stress in the circumferential and radial directions. These (which are not principal stresses) will be designated by  $t_{11}$  and  $t_{22}$  respectively. Considering an element at the radial position  $r$ , the final state of strain is equivalent to a pure homogeneous strain with principal extension ratios equal to  $\beta_1$ ,  $\beta_2$  and  $\beta_3$  in the circumferential, radial and axial directions, together with a shear strain  $\gamma$ , equal to  $\psi r$ , corresponding to a sliding in the circumferential direction of planes normal to the axis of the cylinder. This system has been treated elsewhere<sup>4</sup> and leads to a stress-strain relation which, when adapted to take account of the swelling, may be written:

$$t_{11} - t_{22} = Gv_2(\beta_1^2 - \beta_2^2 + \beta_3^2\psi^2r^2) \quad (8)$$

in which  $G$  is defined by equation (1a). (This equation is obtained by putting  $G'/V_u = G$  and  $V_u/V = v_2$  in equation (4) of ref. 4).

#### Equilibrium of stresses

The conditions for equilibrium of the stresses in the transverse plane, for a cylindrical system, lead to an equation determining the radial variation of the stress component  $t_{22}$ , namely<sup>7</sup>:

$$\frac{dt_{22}}{dr} = \frac{t_{11} - t_{22}}{r} \quad (9)$$

Introducing equation (8) this becomes:

$$\frac{dt_{22}}{dr} = \frac{Gv_2}{r}(\beta_1^2 - \beta_2^2 + \beta_3^2\psi^2r^2) \quad (10)$$

#### Swelling equilibrium

Since the normal stress  $t_{22}$  is also a principal stress, equation (3) is immediately applicable. Hence

$$t_{22} = \frac{A_{0m}}{V_1} + Gv_2\beta_3^2 \quad (11)$$

#### Radial variation of $v_2$

From equation (9), giving the radial variation of  $t_{22}$ , together with equation (11), which relates the swelling parameter  $v_2$  to this stress component, it is possible to obtain the radial variation of the swelling. From equations (5) we have  $\beta_2 = 1/\beta_1\beta_3v_2$ . Insertion in equation (11) together with the Flory-Huggins expression (4) for  $A_{0m}$  gives:

$$t_{22} = \frac{RT}{V_1}[\ln(1-v_2) + v_2 + \chi v_2^2] + G/\beta_1^2\beta_3^2v_2 \quad (12)$$

Differentiation with respect to  $r$  gives:

$$\frac{dt_{22}}{dr} = \frac{RT}{V_1}\left[2\chi - \frac{1}{1-v_2}\right]v_2 \cdot \frac{dv_2}{dr} - \frac{G}{\beta_3^2}\left[\frac{1}{\beta_1^2v_2^2} \frac{dv_2}{dr} + \frac{2}{\beta_1^3v_2} \cdot \frac{d\beta_1}{dr}\right] \quad (13)$$

Introducing the expression (7) for  $d\beta_1/dr$ , and making use of equations (5), we obtain, on collecting terms:

$$\frac{dt_{22}}{dr} = \left[\frac{RT}{V_1}\left(2\chi - \frac{1}{1-v_2}\right)v_2 - G\beta_3^2\right]\frac{dv_2}{dr} - \frac{2G}{r\beta_3}(\beta_2/\beta_1 - 1) \quad (14)$$

An alternative expression for  $t_{22}$  is provided by equation (9). Equating the right-hand sides of equations (9) and (14) leads to the relation:

$$r \frac{dv_2}{dr} = \frac{t_{11} - t_{22} + 2G(\beta_2/\beta_1 - 1)/\beta_3}{(RT/V_1)[2\chi - 1/(1-v_2)]v_2 - G\beta_3^2} \quad (15)$$

Dividing numerator and denominator by  $G$  and utilizing equation (1a) we obtain finally

$$r \frac{dv_2}{dr} = \frac{(t_{11} - t_{22})/G + 2(\beta_2/\beta_1 - 1)/\beta_3}{(M_c/\rho V_1)[2\chi - 1/(1-v_2)]v_2 - \beta_2^2} \quad (16)$$

in which  $t_{11} - t_{22}$  is related to the strains through equation (10).

#### Application of foregoing relations

Let us assume that the state of strain, as defined by the parameters  $\beta_1$ ,  $\beta_2$  and  $\beta_3$ , and hence the swelling parameter  $v_2$ , at a particular radial position  $r$ , are given. The corresponding components of stress  $t_{11}$  and  $t_{22}$  are then automatically determined (equations 8 and 11). The foregoing equations are sufficient to enable the state of strain (and stress) at a neighbouring point  $r + \delta r$  to be derived. For this purpose we note that the radial variation of  $\beta_1$  is given by equation (7), and the radial variation of  $v_2$  by equation (16). We are thus able to obtain the values of  $\beta_1$  and  $v_2$  at the point  $r + \delta r$ , and hence, since  $\beta_3$  is constant, of  $\beta_2$  also. The complete state of strain at the point  $r + \delta r$  is thus determined. By repeating this procedure for successive increments  $\delta r$  it is therefore possible, in principle, to obtain the strain distribution throughout the cylinder.

The application of this principle is complicated by the necessity of satisfying certain boundary conditions. It is assumed that the axial extension ratio  $\beta_3$  and the torsion  $\psi$  are fixed. Of the three remaining parameters  $\beta_1$ ,  $\beta_2$  and  $v_2$ , any two are independently variable. Let us suppose that we arbitrarily fix  $\beta_1$  and  $\beta_2$  at the outer boundary ( $r = a$ ), where  $t_{22} = 0$ , and apply the iterative procedure outlined above to obtain the variation of these parameters for successively decreasing values of  $r$ . This will not (except by accident) satisfy the condition which must be satisfied at the axis, namely:

$$\beta_1 = \beta_2, \quad t_{11} = t_{22}$$

since at  $r = 0$  the distinction between radial and circumferential strains must vanish. This method is therefore not applicable.

If, on the other hand, we commence our calculations by assigning values of  $\beta_1 (= \beta_2)$  and hence  $v_2$  at the axis, we encounter the difficulty that  $d\beta_1/dr = 0$  (equation 6) and  $dv_2/dr = 0$  (equation 16), which implies that in the axial region the strains are constant. The above equations are therefore not applicable in the immediate vicinity of the axis.

It would appear, therefore, that the iterative procedure cannot be applied by starting directly from either the outer boundary or the axis.

#### THE AXIAL REGION

The difficulty encountered in attempting to start from the axis, may, however, be circumvented by the adoption of a special analytical treatment which takes into account the peculiar conditions of strain in the axial region. This treatment, which is only approximate, may be applied up to a certain small value of  $r$ , namely  $r = r_1$ , beyond which point numerical computation by the iterative procedure outlined above becomes practicable. The value of  $r_1$  is chosen to be sufficiently large to yield a significant difference between the radial and circumferential strains.

The analytical method makes use of the equations for the stress distribution for a rubber cylinder (i.e. unswollen) originally given by Rivlin<sup>7</sup>. In this case the variation of the radial stress  $t_{22}$  is found to be parabolic, with a maximum numerical value at  $r = 0$ . The same distribution applies to a swollen cylinder, provided that the degree of swelling is constant throughout. As already noted, however, the presence of the non-uniform strain



distribution will lead to a variation of the state of swelling with radial position, as a result of which there will be a subsequent change in the stress distribution. Nevertheless in the axial region the deviations from homogeneity in the state of swelling will be slight, and their effect on the stress distribution may be ignored, i.e., it may be assumed that in this region the variation of  $t_{22}$  with radius remains parabolic, as for a homogeneously swollen cylinder. (This assumption can always be justified if the inhomogeneity in  $t_{22}$  is sufficiently small, i.e., for sufficiently small values of  $r$ .)

A parabolic variation of  $t_{22}$  implies a parabolic variation of  $v_2$  and also of the strain parameters  $\beta_1$  and  $\beta_2$ . We may therefore write, for the axial region:

$$\beta_1 = \beta_0(1 + c_1 r^2) \quad (17a)$$

$$\beta_2 = \beta_0(1 + c_2 r^2) \quad (17b)$$

$$v_2 = v_{20}(1 + c_3 r^2) \quad (17c)$$

$$t_{22} = t_0(1 + c_4 r^2) \quad (17d)$$

where  $\beta_0$ ,  $t_0$  and  $v_{20}$  are the values of  $\beta_1$  (or  $\beta_2$ ),  $t_{22}$  (or  $t_{11}$ ) and  $v_2$  at  $r=0$ , and  $c_1$ ,  $c_2$ ,  $c_3$  and  $c_4$  are constants, as yet unspecified.

It is not necessary to know in advance the range of  $r$  over which the parabolic relations (17) are sufficiently valid. This will be apparent on examination of the results of the subsequent numerical computations.

#### EVALUATION OF CONSTANTS

The constants  $c_1$  to  $c_4$  in equation (17) are not independent, and cannot therefore be assigned arbitrary values. In fact, if one of them is arbitrarily chosen, the other three are completely determined, as will now be shown.

##### $c_1$ and $c_2$

The basis for the relation between  $c_1$  and  $c_2$  is provided by equation (7). From equation (17a) we have:

$$d\beta_1/dr = 2c_1\beta_0 r \quad (18)$$

Substitution of this result, together with the expressions (17a) and (17b) for  $\beta_1$  and  $\beta_2$ , into equation (7) gives

$$2c_1\beta_0 r^2 = \frac{\beta_0}{r}(1 + c_1 r^2) \left(1 - \frac{1 + c_1 r^2}{1 + c_2 r^2}\right) \quad (19)$$

Since we are concerned only with small differences from the axial values of  $\beta_0$  etc.,  $c_1 r^2$ ,  $c_2 r^2$ , etc., are small compared with unity. Neglecting terms containing  $c_1^2 r^4$  etc., and higher powers, equation (19) reduces to:

$$2c_1\beta_0 r^2 = \beta_0(c_2 - c_1)r^2 \quad (20)$$

$$c_2 = 3c_1$$

##### $c_1$ and $c_3$

From equations (5), with (17a) and (17b) together with (20), we have (neglecting higher-order terms):

$$\begin{aligned} 1/v_2 &= \beta_1\beta_2\beta_3 \\ &= \beta_3\beta_0(1 + c_1 r^2)(1 + c_2 r^2) \\ &= \beta_3\beta_0^2(1 + 4c_1 r^2) \end{aligned} \quad (21)$$

Similarly from equation (17c):

$$1/v_2 = (1/v_{20})(1 - c_3 r^2) = \beta_3\beta_0^2(1 - c_3 r^2) \quad (22)$$

Comparing equations (21) and (22)

$$c_3 = -4c_1 \quad (23)$$

$c_4$  and  $c_1$

From equation (17d):

$$dt_{22}/dr = 2t_0 c_4 r \quad (24)$$

while from equations (8) and (9):

$$\frac{dt_{22}}{dr} = \frac{t_{11} - t_{22}}{r} = \frac{Gv_2}{r}(\beta_1^2 - \beta_2^2 + \beta_3^2\psi^2 r^2) \quad (25)$$

Hence

$$2t_0 c_4 r^2 = Gv_2(\beta_1^2 - \beta_2^2 + \beta_3^2\psi^2 r^2) \quad (26)$$

From equations (17a) and (17b), together with equation (20):

$$\begin{aligned} \beta_1^2 - \beta_2^2 &= (\beta_1 - \beta_2)(\beta_1 + \beta_2) = -2c_1 r^2 \beta_0 \cdot 2\beta_0(1 + 4c_1 r^2) \\ \beta_1 - \beta_2 &= -4c_1 r^2 \beta_0^2 \end{aligned} \quad (27)$$

Inserting the results given by equations (23) and (27) into equation (26):

$$2t_0 c_4 r^2 = Gv_{20}(1 - 4c_1 r^2)(-4c_1 r^2 \beta_0^2 + \beta_3^2 \psi^2 r^2) \quad (28)$$

For finite values of  $\psi a$  (the shear strain at the surface) the range of  $r$  may always be chosen so that  $\psi r$  is small compared with unity, so that the product  $c_1 r^2(\psi^2 r^2)$  may be neglected. Equation (28) then gives

$$2t_0 c_4 r^2 = Gv_{20}(\beta_3^2 \psi^2 r^2 - 4c_1 r^2 \beta_0^2)$$

or

$$c_4 = \frac{G/\beta_3}{t_0}(\beta_3^2 \psi^2 / 2\beta_0^2 - 2c_1) \quad (29)$$

##### Evaluation of $c_1$

The preceding results [equations (20), (23) and (29)] give the relations between the four constants in equation (17), but are not sufficient to determine their values in terms of the parameters  $\beta_0$  and  $v_{20}$  which together with  $\beta_3$  and  $\psi$  completely define the system. To do this it is necessary to derive a fourth relation between these quantities. This is more complicated, and involves the second differential of the stress,  $d^2 t_{22}/dr^2$ . This may be obtained by double differentiation of equation (11), the result so derived being then compared with that obtained from double differentiation of equation (17d).

From equation (11):

$$\begin{aligned} \frac{dt_{22}}{dr} &= \left[ \frac{1}{V_1} \frac{dA_{0m}}{dv_2} + G\beta_2^2 \right] \frac{dv_2}{dr} + 2Gv_2\beta_2 \frac{d\beta_2}{dr} \\ \frac{d^2 t_{22}}{dr^2} &= \left[ \frac{1}{V_1} \frac{dA_{0m}}{dv_2} + G\beta_2^2 \right] \frac{d^2 v_2}{dr^2} + 2Gv_2\beta_2 \frac{d^2 \beta_2}{dr^2} \end{aligned} \quad (30)$$

+ terms involving squares and products of  $dv_2/dr$  and  $d\beta_2/dr$ .

We are interested only in the limiting value of  $\frac{d^2 t_{22}}{dr^2}$  as  $r \rightarrow 0$ , where the first derivatives of  $v_2$  and  $\beta_2$  with respect to  $r$  also tend to zero, while the second derivatives remain

finite. We may therefore neglect all higher-order terms in  $dv_2/dr$  and  $d\beta_2/dr$  in obtaining this limiting value. Thus:

$$\left(\frac{d^2 t_{22}}{dr^2}\right)_{r=0} = \left[ \frac{1}{V_1} \left(\frac{dA_{0m}}{dv_2}\right)_{v_2=v_{20}} + G\beta_0^2 \right] \left(\frac{d^2 v_2}{dr^2}\right)_{r=0} + 2Gv_{20}\beta_0 \left(\frac{d^2 \beta_2}{dr^2}\right)_{r=0} \quad (31)$$

where  $v_{20}$  and  $\beta_0$  are the values of  $v_2$  and  $\beta_2$  at  $r=0$ . The second differentials of  $v_2$  and  $\beta_2$  may be expressed in terms of the constant  $c_1$  in equation (17a), thus

$$\left. \begin{aligned} \frac{d^2 v_2}{dr^2} &= 2c_3 v_{20} = -8c_1 v_{20} \\ \frac{d^2 \beta_2}{dr^2} &= 2c_2 \beta_0 = 6c_1 \beta_0 \end{aligned} \right\} \quad (32)$$

while the Flory-Huggins equation (equation 4) gives:

$$\left(\frac{dA_{0m}}{dv_2}\right)_{v_2=v_{20}} = RT \left( 2\chi - \frac{1}{1-v_{20}} \right) v_{20} \quad (33)$$

Insertion of the above expressions into equation (31) gives:

$$\left(\frac{d^2 t_{22}}{dr^2}\right)_{r=0} = -8c_1 v_{20} \left[ \frac{RT}{V_1} \left( 2\chi - \frac{1}{1-v_{20}} \right) v_{20} + G\beta_0^2 \right] + 12c_1 G v_{20} \beta_0^2 \quad (34)$$

We have to compare this result with that obtained from equation (17d). The latter gives:

$$\left(\frac{d^2 t_{22}}{dr^2}\right)_{r=0} = 2c_4 t_0 = 2Gv_{20}\beta_0^2 (\beta_3 \psi^2 / 2\beta_0^2 - 2c_1) \quad (35)$$

from equation (29). Comparing equations (34) and (35), and collecting terms in  $c_1$ ,

$$-8c_1 \left[ \frac{RT}{V_1} \left( 2\chi - \frac{1}{1-v_{20}} \right) v_{20} + G\beta_0^2 \right] + 16c_1 G v_{20} \beta_0^2 = G\beta_3^2 \psi^2 \quad (36)$$

Dividing throughout by  $G$  and substituting the expression (1a) for  $G$ , this reduces to:

$$-8c_1 \left[ \frac{M_c}{\rho V_1} \left( 2\chi - \frac{1}{1-v_{20}} \right) v_{20} - \beta_0^2 \right] = \beta_3^2 \psi^2 \quad (37)$$

giving finally:

$$c_1 = - \frac{\beta_3^2 \psi^2 / 8}{(M_c / \rho V_1) [2\chi - 1/(1-v_{20})] v_{20} - \beta_0^2} \quad (38)$$

This result, together with equation (17) provides a complete solution to the problem.

#### MINOR MODIFICATIONS TO METHOD OF CALCULATION

The calculations may be facilitated somewhat by the introduction of certain minor modifications.

#### Integration with respect to $r^2$

Since the functions representing the radial distributions are approximately parabolic, increased accuracy (for an equivalent step length) is obtainable by adopting  $r^2$ , rather than  $r$ , as a basis for the stepwise integration. This involves converting  $dt_{22}/dr$  and  $dv_2/dr$  in equations (14) and (16) to

$dt_{22}/d(r^2)$  and  $dv_2/d(r^2)$  respectively. The modifications are obvious and need not be written out.

#### Elimination of $r_1$

Using integration with respect to  $r^2$  it was found practicable effectively to eliminate the axial region by making  $r_1^2$  equal to  $\delta(r^2)$ , the step length, i.e. making the axial region coincident with the region covered by the first step. The final results were found to be independent of the step length, to an accuracy of 5 significant figures (at least) for step lengths  $\delta(r^2)$  of  $10^{-3}$  and  $10^{-4}$ .

These modifications were used for the calculations given in the following section.

#### NUMERICAL EXAMPLE

It is assumed initially that the quantities  $\rho$ ,  $V_1$ ,  $M_c$  and  $\chi$ , which are specific to a given rubber and swelling liquid, and are obtainable from independent measurements, are given. The system is now defined by the parameters  $\beta_3$  (axial extension ratio) and  $\psi$  (torsion). To define the conditions in the axial region it is sufficient to assign a value to any one of the three variables  $v_{20}$ ,  $\beta_0$  or  $t_0$ . Let us suppose that the value of  $\beta_0$  is so chosen. The state of swelling at the axis is then determined by the relation  $v_{20} = 1/\beta_3\beta_0^2$  (equations 5), and the stress  $t_0$  is obtainable from the insertion of these values of  $\beta_0$  and  $v_{20}$  into equation (11). The constant  $c_1$  may be obtained from equation (38), and from this the remaining constants  $c_2$ ,  $c_3$  and  $c_4$  are determined by equations (20), (23) and (29). Equation (17) then enables the state of strain, the degree of swelling and the stress  $t_{22}$  to be derived up to the arbitrarily chosen value of  $r$ , i.e.  $r=r_1$ , or  $r_1^2 = \delta(r^2)$ , using the modified procedure.

From this point the calculation is pursued by the stepwise analysis shown above, until the boundary surface  $r=a$  (defined by the condition  $t_{22}=0$ ) is reached. This will be clear from Figure 2, which shows the variation of  $t_{22}$  with  $r^2$ , for different values of  $\beta_0$ , using data chosen to

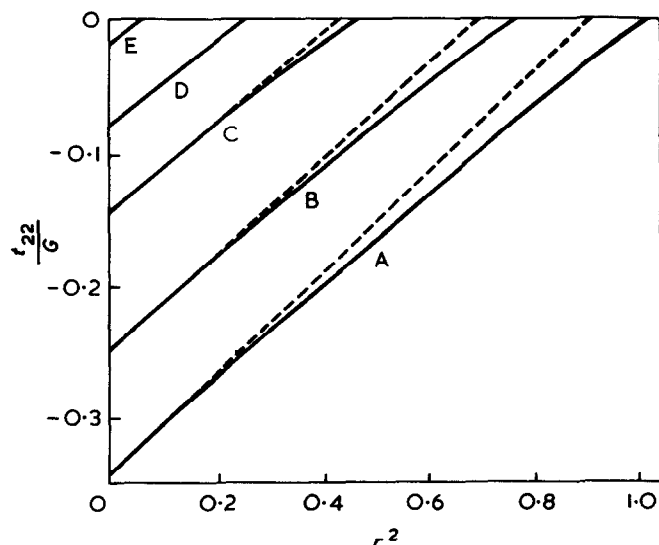


Figure 2 Variation of radial stress component  $t_{22}$  with  $r^2$  for values of axial swelling parameter  $v_{20}$ : A, 0.222; B, 0.212; C, 0.200; D, 0.192; E, 0.184. —, Numerical computation; ---, equation (17)

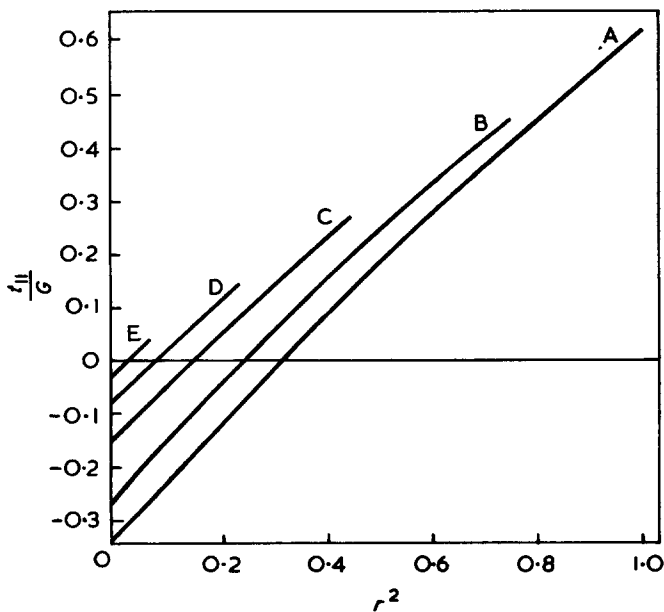


Figure 3 Variation of circumferential stress component  $t_{11}$  with  $r^2$  for values of axial swelling parameter: A, 0.222; B, 0.212; C, 0.200; D, 0.192; E, 0.184

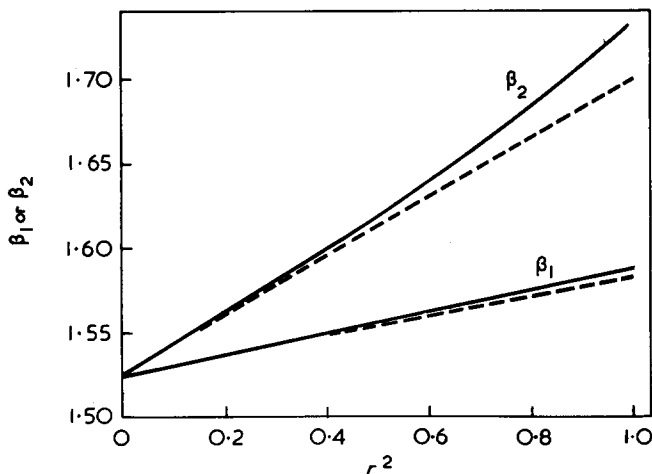


Figure 4 Variation of radial ( $\beta_2$ ) and circumferential ( $\beta_1$ ) extension ratios with  $r^2$ ,  $v_{20}=0.222$ . —, Numerical computation; ---, equations (17)

correspond to one of the experimental systems studied—a poly(*cis*-isoprene) swollen in toluene (sample A in Part 2<sup>5</sup>, to which reference should be made for details). Different values of  $\beta_0$  yield different values of  $a$ , and hence of the dimensionless parameter  $\psi a$ , which is equivalent to the shear strain at the surface, (or alternatively of  $\psi a_0$ ). The results are therefore applicable directly to any value of cylinder radius  $a_0$ .

The corresponding distributions for the circumferential stress  $t_{11}$ , the circumferential and radial strain parameters  $\beta_1$  and  $\beta_2$ , and the swelling parameter  $v_2$ , are shown in Figures 3, 4 and 5 respectively.

It has already been noted that for small values of the torsion ( $\psi a_0 \rightarrow 0$ ) all these distributions should tend to

become linear functions of  $r^2$ , this relationship being taken as a basis for the treatment of the axial region. It is satisfactory to find that this is borne out by the detailed calculations to a very close approximation, even up to comparatively large values of  $\psi a_0$ . Where appropriate, the corresponding parabolic relations (equation 17), using the calculated values of the constants  $c_1$  to  $c_4$ , are shown for comparison. The degree of agreement shown justifies the treatment applied to the axial region.

#### CHANGE OF SWELLING DUE TO TORSION

The foregoing calculations enable the final swollen volume, and hence the change of volume due to torsion, to be readily obtained. For this we are concerned with the value of the circumferential strain parameter  $\beta_1$  at the surface ( $r=a$ ). From equations (5):

$$a/a_0 = (\beta_1)_{r=a} \quad (39)$$

where  $a_0$  is the radius of the cylinder in the unstrained, unswollen state. The overall swelling ratio is therefore:

$$\frac{V}{V_u} = \frac{\pi a^2 \beta_3}{\pi a_0^2} = (\beta_3 \beta_1^2)_{r=a} \quad (40)$$

where  $V_u$  is the volume of the unswollen cylinder, per unit axial length. In this equation  $V$  is the volume in the swollen twisted state at an axial extension  $\beta_3$  and torsion  $\psi$ . To obtain the change of swollen volume due to torsion we require also the equilibrium swollen volume  $V_0$  at the same axial extension ratio  $\beta_3$  but with zero torsion. This is obtainable immediately from equation (11) on putting  $t_{22}=0$  and  $\beta_2^2 = \beta_1^2 = 1/v_2 \beta_3$  (from equations 5), and solving for  $v_2$  ( $=V_u/V_0$ ). The relative change of swelling due to torsion is then:

$$\frac{\Delta V}{V_0} = \frac{V - V_0}{V_0} \quad (41)$$

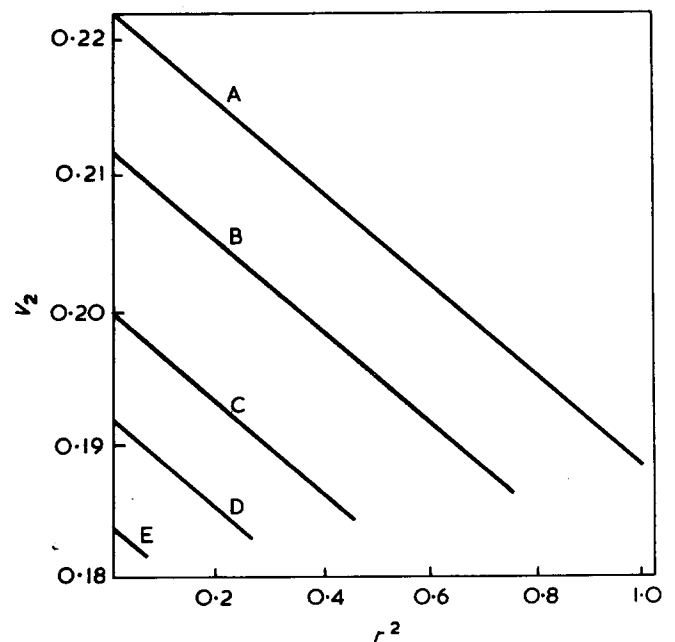


Figure 5 Variation of volume fraction of rubber ( $v_2$ ) with  $r^2$ , A,  $v_{20}=0.222$ ; B,  $v_{20}=0.212$ ; C,  $v_{20}=0.200$ ; D,  $v_{20}=0.192$ ; E,  $v_{20}=0.184$

Table 1 Change of swelling ( $\delta V/V$ ) and associated variables for following values of parameters:  $M_c/\rho V_1=92.27$ ;  $\chi=0.40$ ;  $\beta_3=1.938$ ;  $\psi=1.0$ ;  $V_0$  (calculated)=5.515

$v_{20}$	$a$	$(\beta_1)_{r=a}$	$a_0$ ( $=a/\beta_1$ )	$V/V_0$ ( $=\beta_3\beta_1^2$ )	$-\Delta V/V_0$ (%)	$\psi^2 a_0^2$
0.1813 <sub>3</sub>	0	1.6870	0	5.515	0	0
0.182	0.1270	1.6851	0.0754	5.503	0.22	0.0057
0.184	0.2540	1.6797	0.1512	5.468	0.85	0.0229
0.186	0.3361	1.6744	0.2007	5.433	1.48	0.0403
0.188	0.4019	1.6691	0.2408	5.399	2.09	0.0580
0.192	0.5087	1.6587	0.3067	5.332	3.32	0.0940
0.196	0.5969	1.6486	0.3621	5.267	4.49	0.1311
0.200	0.6740	1.6386	0.4113	5.203	5.65	0.1692
0.204	0.7434	1.6288	0.4564	5.141	6.77	0.2083
0.208	0.8072	1.6192	0.4985	5.081	7.87	0.2485
0.212	0.8667	1.6098	0.5384	5.022	8.93	0.2898
0.217	0.9361	1.5982	0.5857	4.950	10.23	0.3431
0.222	1.0013	1.5869	0.6310	4.881	11.50	0.3981

The results are given in Table 1, and are shown graphically in Figure 6.

#### APPROXIMATE FORM OF THEORY

The closeness of approach of the calculated distributions of stress and strain parameters to the approximate parabolic relations suggests a basis for a derivation of an explicit formula for the effect of torsion on swelling which would be valid for small torsional strains. Such a formula would have obvious advantages over the more exact numerical analysis in all cases where a high degree of accuracy was not essential.

In developing such a formula the changes in  $v_2$  due to the stresses induced by the torsional strain are assumed to be so small that the secondary effect of these changes on the stress distribution can be neglected. In other words, the local changes in swelling are calculated on the assumption of a strictly parabolic distribution of stress.

This treatment is analogous to that previously applied to the derivation of the volume change due to torsion in a compressible (dry) rubber<sup>4</sup>.

Consider the cylinder to be homogeneously swollen to volume fraction  $v_2$  at an axial extension ratio  $\beta_3$ . Application of torsion will produce an instantaneous gradient of stress  $dt_{22}/dr$  given by equation (10). Since the swelling is assumed homogeneous  $\beta_1=\beta_2$  and therefore

$$dt_{22}/dr = Gv_2\beta_3^2\psi^2 r \quad (42)$$

Integration subject to the boundary condition  $t_{22}=0$  when  $r=a$  yields

$$t_{22} = -\frac{1}{2}Gv_2\beta_3^2\psi^2(a^2 - r^2) \quad (43)$$

The change in the state of swelling at the radial position  $r$  is calculated on the basis of equation (11), which on substitution of equation (4) for  $A_{0m}$  and insertion of  $\beta_2^2=1/v_2\beta_3$  becomes

$$t_{22} = (RT/V_1)[\ln(1-v_2) + v_2 + \chi v_2^2] + G/\beta_3 \quad (44)$$

Since we are concerned with small values of  $t_{22}$  and small changes of  $v_2$  we shall use the differential form of equation (44), i.e.,

$$(dt_{22}/dv_2)_\beta = (RT/V_1)[2\chi - 1/(1-v_2)]v_2 \quad (45)$$

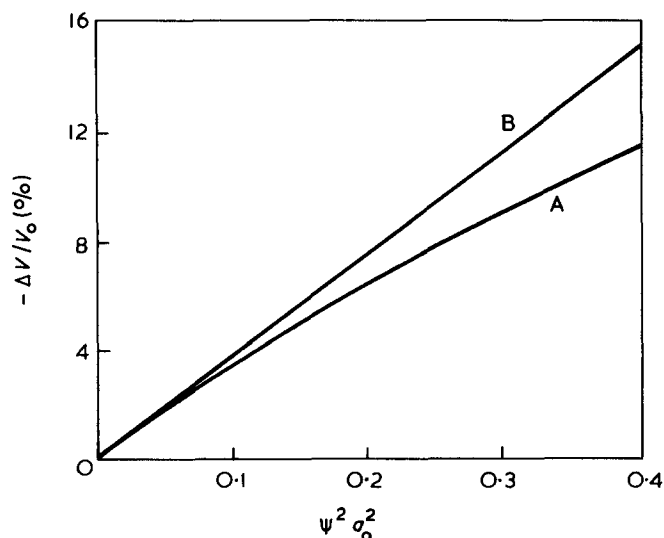


Figure 6 Dependence of reduction of volume on twisting on  $\psi^2 a_0^2$ ; A, numerical computation; B, approximate solution, equation (52a)

The change in  $v_2$  may therefore be written:

$$\delta v_2 = \left( \frac{dv_2}{dt_{22}} \right)_\beta \delta t_{22} = \frac{V_1/RT}{[2\chi - 1/(1-v_2)]v_2} \delta t_{22} \quad (46)$$

Since in the untwisted state  $t_{22}=0$ , we may equate  $\delta t_{22}$  to  $t_{22}$  in equation (43) in the calculation of the effect of the torsion on swelling. For this purpose it is convenient to consider the relative change in swollen volume  $\delta V/V$ , where  $V$  is the volume of a given element in the swollen untwisted state. With these changes, equation (46) becomes

$$\frac{\delta V}{V} = -\frac{\delta v_2}{v_2} = -\frac{V_1/RT}{[2\chi - 1/(1-v_2)]v_2^2} t_{22} \quad (47)$$

This will be written:

$$\delta V/V = -At_{22} \quad (48)$$

where

$$A = \frac{V_1/RT}{[2\chi - 1/(1-v_2)]v_2^2} \quad (48a)$$

The total change of volume due to torsion is obtained by considering a cylinder of unit axial length in the strained state. For a cylindrical shell of thickness  $dr$  and volume  $2\pi r dr$  the change of volume, as given by equations (48) and (43), is

$$\delta V = -AVt_{22} = -A2\pi r dr [-\frac{1}{2}Gv_2\beta_3^2\psi^2(a^2 - r^2)] \quad (49)$$

Integration with respect to  $r$  yields the total volume change  $\Delta V$ , namely

$$\Delta V = \int_0^a \delta V dr = A\frac{1}{4}\pi Gv_2\beta_3^2\psi^2 a^4 \quad (50)$$

Since the volume of the whole cylinder before twisting is  $\pi a^2$ , the relative change of volume due to the torsion is given by:

$$\Delta V/V = A\frac{1}{4}Gv_2\beta_3^2\psi^2 a^2 \quad (51)$$

Swelling of a rubber cylinder in torsion (1): L. R. G. Treloar

Insertion of  $A$  from equation (48a) and  $G$  from equation (1a) gives finally:

$$\frac{\Delta V}{V} = \frac{(\rho V_1/M_c)\beta_3^2\psi^2 a^2}{4[2\chi - 1/(1 - \nu_2)]\nu_2} \quad (52)$$

or, since  $a^2 = a_0^2/\nu_2\beta_3$

$$\frac{\Delta V}{V} = \frac{(\rho V_1/M_c)\beta_3\psi^2 a_0^2}{4[2\chi - 1/(1 - \nu_2)]\nu_2^2} \quad (52a)$$

The denominator of this expression is always negative. The result therefore represents a reduction of swelling due to the torsion, the amount of this reduction being proportional to the square of the torsion.

Insertion of the values of parameters given at the top of Table 1 into equation (52a) gives the result:

$$\Delta V/V = -0.3789\psi^2 a_0^2 \quad (52b)$$

This result is included in Figure 6 for comparison with the accurate computation. The approximate solution corresponds, of course, to the tangent to the exact curve at zero torsion. For a value of  $\psi^2 a_0^2$  of 0.32, which corresponds to the maximum value of torsion attained in the

experiments described in Part 2, the error involved in the use of the approximate formula would amount to 20%.

ACKNOWLEDGEMENT

The author wishes to thank Dr D. M. Heaton for a number of helpful discussions and Dr R. F. T. Stepto for advice and assistance relating to the computational aspects of the work.

REFERENCES

- 1 Treloar, L. R. G. *Proc. R. Soc. (A)* 1950, **200**, 176
- 2 Treloar, L. R. G. 'The Physics of Rubber Elasticity', Oxford University Press, 1958
- 3 Treloar, L. R. G. *Trans. Faraday Soc.* 1950, **46**, 783
- 4 Treloar, L. R. G. *Polymer* 1969, **10**, 291
- 5 Loke, K. M., Dickinson, M. and Treloar, L. R. G. *Polymer* 1972, **13**, 203
- 6 Treloar, L. R. G. 'The Physics of Rubber Elasticity', Oxford University Press, 1968, p 145
- 7 Rivlin, R. S. *Phil. Trans. R. Soc. (A)* 1949, **242**, 173

# Swelling of a rubber cylinder in torsion: Part 2. Experimental

K. M. Loke, M. Dickinson and L. R. G. Treloar

*Department of Polymer and Fibre Science, University of Manchester Institute of Science and Technology, Sackville Street, Manchester M60 1QD, UK  
(Received 14 September 1971)*

Experiments have been carried out on the effect of torsion on the swelling of a rubber cylinder in a low molecular-weight liquid, the object being to test the theory given by Treloar. Both natural rubber and a synthetic poly(*cis*-isoprene) were used, with toluene as the swelling liquid. Application of torsion resulted in a reduction in the swelling by an amount approximately proportional to the square of the torsion, as predicted theoretically. The values of this reduction, however, were less than the predicted values by amounts varying from 12% to 23%, depending to some extent on the type of rubber and on the degree of crosslinking. These discrepancies are believed to arise mainly from experimental difficulties.

## INTRODUCTION

In the previous paper<sup>1</sup> the theory of the effect of torsion on the equilibrium swelling of a crosslinked rubber was developed. It was shown that the expected effect is a *reduction* of the degree of swelling by an amount which is approximately proportional to the *square* of the torsion.

The present paper is concerned with the experimental examination of this problem in relation to the theory developed.

Since the expected effect depends on the square of the torsional strain, it is important for the purpose of obtaining an accurate result that this torsional strain shall be as large as possible. This involves considerable practical difficulty, since under conditions of prolonged loading in the highly swollen state the strength of the rubber is greatly diminished. Also, in order to avoid buckling in the twisted state it is necessary to apply some extension in the axial direction, and this further increases the total stress to be borne. In practice the maximum torsion which could be applied before the specimen ruptured corresponded to a value of the parameter  $\psi a$  (surface shear strain) of about 0.8, which yielded a change of swelling due to twist of about 8%. This, although not as large as it had been hoped to obtain, was sufficient to provide a fair basis for comparison with the theory.

The experiments were carried out on both natural rubber (smoked sheet grade 1) and 100% poly(*cis*-1,4-isoprene), swollen in toluene (Analar grade). The vulcanizates were compounded according to the recipes given in *Table 1* using cold mixing on an open mill.

The design of the test-piece and of the clamps took into account the necessity to avoid high stress concentrations in the region of the clamps. The test-piece was in the form

of a dumbbell having substantial conical ends terminated by square blocks for the application of the torsional stress (*Figure 1*). The junction between the central cylindrical portion and the conical end was rounded off to avoid a stress concentration in this region. The internal dimensions of the clamp (*Figure 2*) were larger than the corresponding dimensions of the unswollen test-piece, but smaller than its freely swollen dimensions; this, together

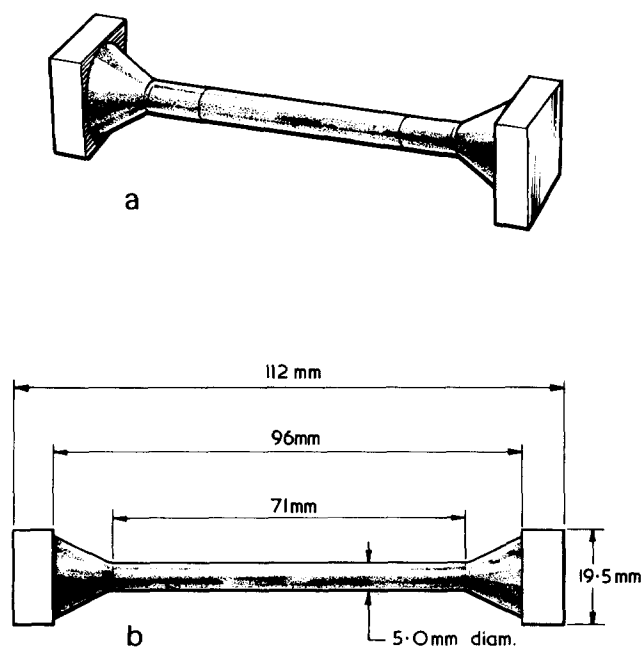


*Figure 1* Test-piece dimensions: (a) perspective; (b) elevation

with a rounding-off of the edge of the clamp from which the rubber emerged, was intended to reduce the stresses at the edge of the clamp, while retaining a positive pressure on the conical region of the sample.

The degree of swelling of the cylinder in torsion was obtained from measurements of axial length and diameter obtained by means of a Pye 2-way travelling microscope reading to 0.005 mm. The accuracy of the swelling measurement was limited by the accuracy with which the diameter of the specimen could be measured. For the highest accuracy it is desirable that this diameter should be as large as possible; however, the greater the diameter the longer is the time required to attain equilibrium swelling and the greater, therefore, the probability of fracture. The diameter chosen (5 mm) represented a practical compromise, and gave a time to reach equilibrium of between 10 and 20 hours.

The moulding presented a problem. The mould was split in the diametral plane of the cylinder. Closure of the two halves caused the trapping of a variable amount of rubber in the 'bite'; this resulted in a non-circular section of the final test-piece. To overcome this difficulty moulding was carried out by a transfer moulding process which involved injection of the rubber into the closed mould through a small hole in the end-plate, excess 'flash' being extruded through a similar hole at the other end. Even with the precaution, however, significant deviations from circularity of the cross-section were not entirely eliminated and the experimental procedure had to be designed to minimize their effects (see below).

#### METHOD OF MEASUREMENT

The specimen was mounted between clamps A and B attached to the apparatus shown in *Figure 2*. This

enabled the required amount of torsion and axial extension to be applied while the specimen was immersed in the swelling liquid. Rotation of the clamp A was effected by means of the worm-gear mechanism C, and changes in axial length by the bevel gear D, which enabled the carriage B to be shifted horizontally (by rotation of the threaded shaft F). The assembly was mounted in a metal trough filled with the swelling liquid up to a level at which the clamps were immersed. The trough was covered with a sheet of glass to reduce evaporation, and stood in an outer water bath thermostatically controlled at  $25 \pm 0.05^\circ\text{C}$ .

The measurements of axial length were obtained from reference marks 3 to 4 cm apart inscribed on the surface of the specimen as shown in *Figure 1*. A rubber embossing ink was used for the natural rubber/sulphur vulcanizates, whilst for the dicumyl peroxide cured samples of both natural rubber and Natsyn an ordinary 'biro' ink proved satisfactory.

The specimen was allowed to swell for 2 to 3 days, with periodic adjustments of axial length, in order to achieve swelling equilibrium without 'buckling' of the cylinder. This procedure was adopted after it has been found that stretching of the unswollen cylinder to the final length followed by immersion in liquid resulted in early rupture. A considerable tension was required to achieve the desired extension of the dry rubber, and in the presence of the liquid the strength was so much reduced that rupture occurred before this tension could be sufficiently relieved by swelling. In the method used here elongation proceeded concurrently with swelling and high stresses were avoided. (A similar principle was adopted by Flory and Rehner<sup>3</sup> to overcome this difficulty.)

After a final measurement of dimensions the torsion was then applied, keeping the length between clamps constant. Because of the slight irregularity in shape of the cross-section of the sample already referred to, the

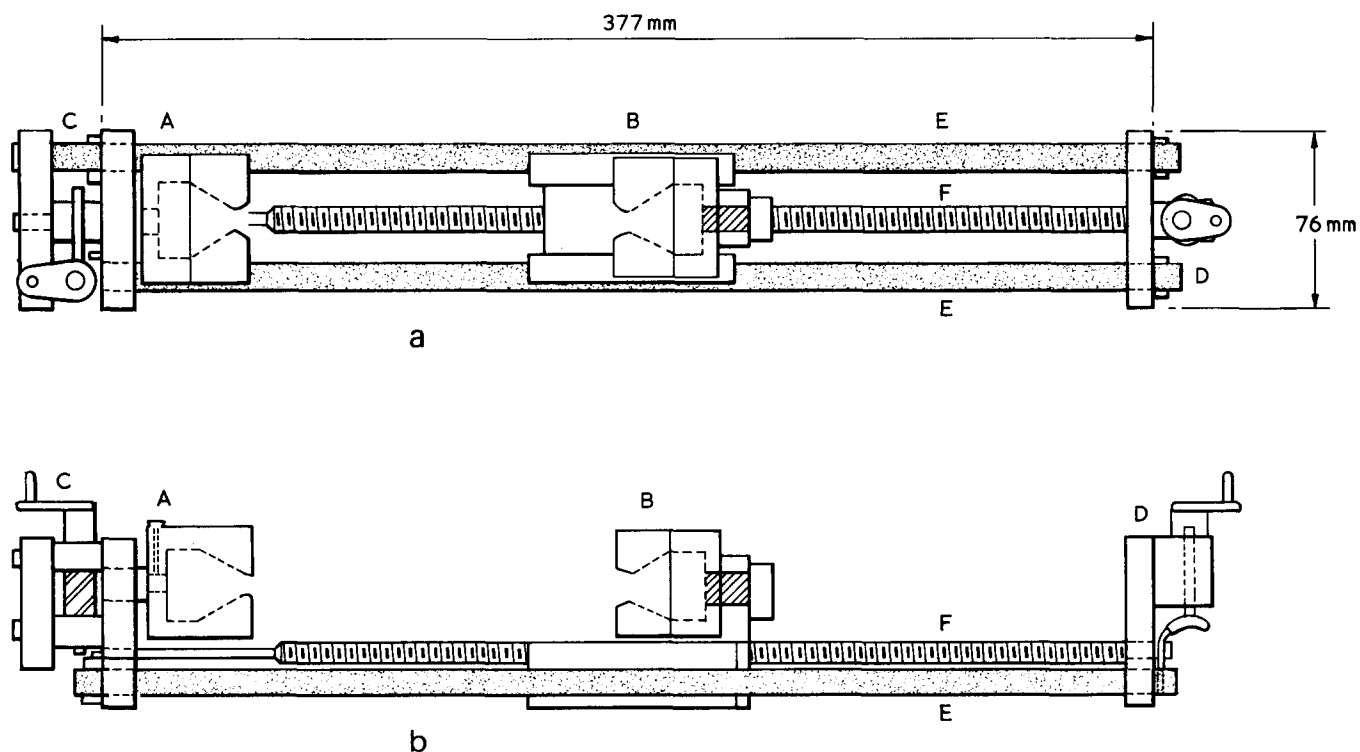


Figure 2 Apparatus for combined torsion and extension: (a) plan; (b) elevation

Table 1 Rubber compounding ingredients (parts by weight)

Sample	A	B	C	D	E	F	G
Smoked sheet, Grade 1				100	100	100	100
Natsyn	100	100	100				
Dicumyl peroxide	3.2	3.5	3.0		3.0	3.0	3.0
M.B.T.S. Vulcafor (accelerator)				0.5			
Zinc oxide		0.5		2	0.5	0.5	
Stearic acid				0.5			
Carbon black		0.25					
<i>N</i> -phenyl-2-naphthylamine (antioxidant)				0.5			
Sulphur				6			
Cure time (min) at platen temp. of 140°C	35	30	33	55	30	32	30
$M_c$ (swelling)	8891	8184	12 380	8313	11 294	11 312	14 566

swollen volume corresponding to the untwisted state was obtained from measurements of the dimensions of the swollen cylinder immediately after application of the torsion. In the time required to carry out this measurement ( $\sim 1$  min) any change of swelling would have been very small. This was confirmed by checks against the volume before twisting; the differences (volume after twisting minus volume before twisting) ranged from  $+0.039$  to  $-0.011$  cm<sup>3</sup>, with an arithmetic mean of  $+0.0141$  or  $+0.3\%$ , i.e. in the opposite sense to the subsequent change of swelling. The important consideration was that by focusing always on the same diametral section of the sample (midway between the reference marks) the effects of any irregularity of section were avoided. Measurements were made periodically until a limiting value of swelling was reached, after which the twist was removed. The sample was then allowed to swell overnight to equilibrium in the untwisted state (at constant axial length). A new twist was then applied and the above procedure repeated. The torsional strain was obtained from measurement of the axial length of one or more complete turns of twist, using the mould closure line as reference mark.

A small irreversible increase in swelling occurred over the entire period of experimentation, lasting from 10 to 14 days. However, this slight irreversibility, in which successive equilibrium volumes in the untwisted state differed by less than  $0.5\%$ , had no significant effect on the value of relative volume change obtained over a single run occupying from 8 to 13 hours.

#### CHARACTERIZATION OF SAMPLES

The mean chain molecular weight  $M_c$  may be determined from measurements of either modulus or swelling equilibrium. Since the relevant problem is concerned with swelling, it was more appropriate to use the swelling equilibrium for the purpose. The cylindrical portion of the rubber sample was cut out and free-swollen in toluene to equilibrium (2–3 days), after which it was removed, surface-dried, and weighed. Weighings were then made at 5 h intervals during drying, which required 3 days. These weighings, together with the measured densities of the dry rubber and of the toluene, enabled the volume fraction of rubber ( $v_2$ ) to be obtained (assuming additivity of volumes). The value of  $M_c$  was then calculated from the equation:

$$\ln(1 - v_2) + v_2 + \chi v_2^2 = -(\rho V_1 / M_c) v_2^{1/3} \quad (1)$$

Values calculated in this way are given in Table 1.

The successive twisted states for any one sample did not correspond to exactly the same axial length, or axial extension ratio  $\beta_3$ , between reference marks. Since the objective is to derive the effect of torsion on equilibrium swelling, at constant axial length, it was necessary to apply a correction to the measured swollen volume to obtain the equivalent degree of swelling at a fixed value of  $\beta_3$ , for which the mean over the complete range of torsion values was taken. The required correction was obtained by differentiating the following equation (equivalent to equation (11) of Part 1<sup>1</sup>) with respect to  $v_2$ :

$$\ln(1 - v_2) + v_2 + \chi v_2^2 = -\rho V_1 / M_c \beta_3 \quad (2)$$

and writing  $\delta V/V = -\delta v_2/v_2$ . This gives:

$$\delta V/V = -\frac{\rho V_1 / M_c}{[2\chi - 1/(1 - v_2)]v_2^2 \beta_3^2} \delta \beta_3 \quad (3)$$

This formula is strictly valid only for zero torsion, but was assumed to be sufficiently accurate for the present purpose, the corrections involved being quite small ( $\delta V/V \approx 0.6\%$  at most).

#### TREATMENT OF EXPERIMENTAL DATA

The experiments were carried out on 4 natural rubber vulcanizates and 3 Natsyn vulcanizates, each group comprising a range of chain molecular weights  $M_c$  (Table 1). Detailed consideration of the data, and of the methods of calculation employed, will be presented for one sample only—the Natsyn 'A' sample. Corresponding results for the remaining samples will be limited to the comparison of theoretical and experimental volume changes on twisting.

##### Derivation of $M_c$

For the Natsyn 'A' vulcanizate the measured free swelling equilibrium at 25°C corresponded to a volume fraction ( $v_2$ ) of rubber of 0.189<sub>3</sub>. The measured density of the rubber was 0.9016 g cm<sup>-3</sup>, and of the solvent 0.862. The molecular weight of toluene being 92.13, this gives a molar volume ( $V_1$ ) of 106.9. Taking  $\chi = 0.40$  (as for natural rubber in toluene<sup>2</sup>) substitution of these data in equation (1) yields the result  $M_c = 8891$ .

##### Attainment of equilibrium

Figure 3 shows the course of the volume changes subsequent to the introduction of a particular value of twist,



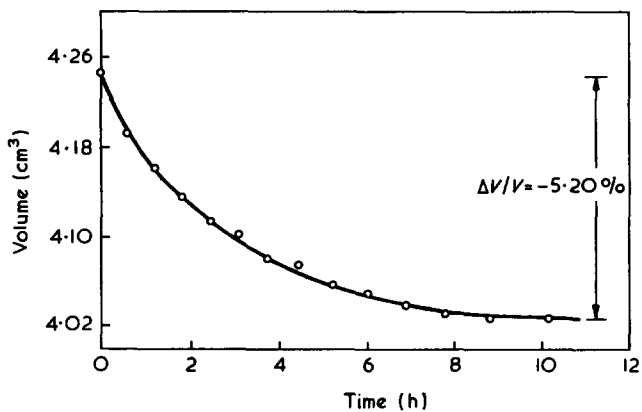


Figure 3 Change of volume with time after application of torsion. Natsyn sample A,  $\psi a_0 = 0.4383$

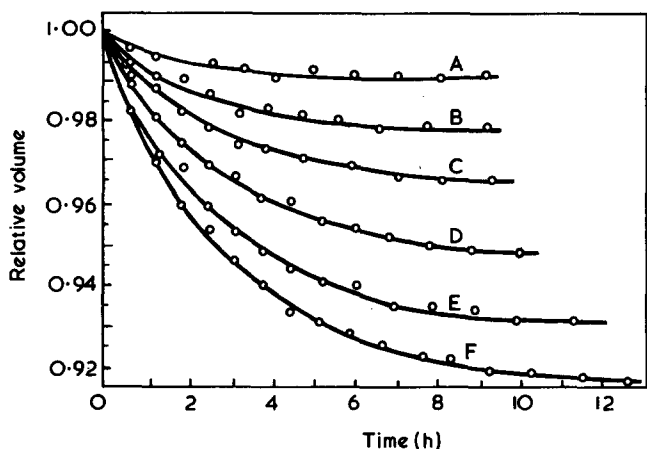


Figure 4 Relative change of volume with time for Natsyn A, for following values of  $\psi a_0$ : A, 0.1806; B, 0.2706; C, 0.3609; D, 0.4383; E, 0.5157; F, 0.5670

represented by  $\psi a_0 = 0.4383$ . The volumes shown have been corrected to take account of the small difference of axial extension ratio  $\beta_3$ , which in this case was 1.934, from the mean, 1.938, for all experiments on this sample; this correction varied from +0.0036 to +0.0038 cm<sup>3</sup> during the course of equilibrium. The total reduction of volume due to torsion amounted to 0.2207 cm<sup>3</sup> on an original volume of 4.2467 cm<sup>3</sup>, giving  $\Delta V/V_0 = -5.20\%$ , for this particular twist.

The complete set of curves for the six values of twist employed is shown in Figure 4. These have been plotted, for ease of comparison, in terms of relative volume, referred to the untwisted state.

#### Derivation of $a_0$

For comparison with the theory, which gives the change of swelling most conveniently in terms of the dimensionless parameter  $\psi a_0$ , it is necessary to determine the unswollen radius  $a_0$ . Because of the non-circularity of the cross-section this was obtained not by direct measurement of the dry rubber, but from the measured diameter in the swollen untwisted state, at the extension ratio  $\beta_3$ , together with the calculated value of  $v_2$  for this state.

Since there is the danger here of a circular argument, this procedure needs some justification. We note first that the value of  $M_c$  is determined from free swelling, hence the calculation of  $v_2$  for the swollen stress-free state is simply a conversion back to an original swelling measurement. The only truly theoretical part of the calculation is therefore the effect of the axial extension on the swelling. For the case considered the value of  $v_2$  in free swelling was 0.1893, corresponding to a change of linear dimensions in the ratio 1.742 : 1. The relatively small extension to  $\beta_3 = 1.938$  gives a calculated change of  $v_2$  to 0.1813, i.e. a reduction in  $v_2$  of 4.4%. It is only this 4.4% which relies on the applicability of the theory, and on the basis of previous experiments on simple extension<sup>4</sup> it would seem reasonable to assume that this will not be in error by more than, say, 5% of itself, or 0.2% of the whole swollen volume. This would produce an error of the same amount (0.2%) in  $a_0^2$ , which is practically negligible.

#### COMPARISON WITH THEORY

The calculated values of the change of volume due to torsion ( $\Delta V/V_0$ ) were based on the theory discussed in the

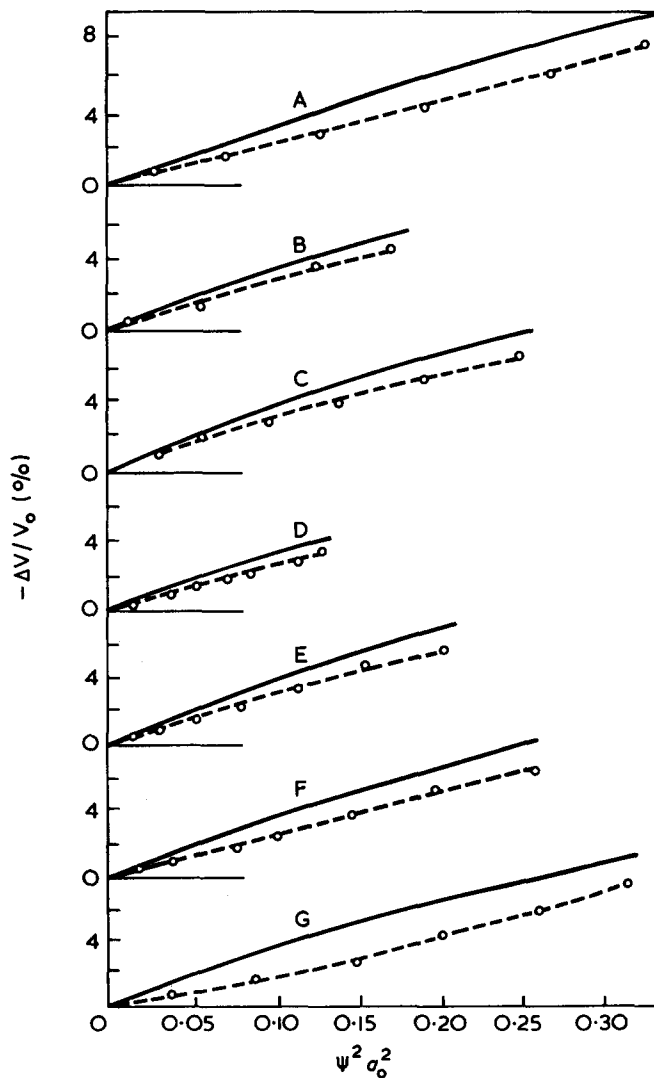


Figure 5 Relative reduction of volume due to torsion for rubbers listed in Table 1. —, Calculated; ---, observed

previous paper<sup>1</sup>. For sample A the modification referred to in Part 1, was used, in which the numerical integration was performed with respect to  $r^2$ , and the limit of the axial region ( $r_1$ ) coincided with the step length  $\delta(r^2)$ . For all the other samples the integration was performed with respect to  $r$ , using a value of  $\delta r$  of  $10^{-3}$  and a value of  $r_1$  sufficient to give a difference between  $\beta_1$  and  $\beta_2$  of  $10^{-5}$  ( $r_1 \approx 10^{-2}$ ). A check was made, however, to ensure that these two methods of calculation gave substantially identical results. The results are shown in *Figure 5* in the form of plots of  $-\Delta V/V_0$  against  $\psi^2 a_0^2$ .

The experimental results show the expected form of dependence of swelling on torsional strain, though there is a consistent quantitative discrepancy from the theoretical curves. Based on the maximum values of  $\psi a_0$ , this discrepancy ranges from  $-11.7\%$  (sample A) to  $-22.9\%$  (sample F), with a mean of  $-17.2\%$ . The discrepancy was somewhat lower for the Natsyn samples ( $-14.1\%$ ) than for the natural rubber samples ( $-19.6\%$ ). There was a slight indication of a correlation with  $M_c$ , the smaller discrepancies in either group being obtained with the samples having lower  $M_c$  values.

These discrepancies are well outside the experimental variations. There may, however, be systematic errors. One possible source of error might be the failure to attain the true swelling equilibrium after twisting. A compromise is necessary owing to the gradual upward drift in swelling referred to previously; after prolonged equilibration the initial reduction is followed by a slow increase in volume. (There is a slight indication of this in the top curve of *Figure 4*.) The total volume change may on this account be slightly underestimated. Another error might arise from the very slight residual buckling in the specimen at high twists, which could not be entirely eliminated. This also

would have the effect of reducing the true torsional strain and hence the change of volume.

More generally, it is important to bear in mind that the effect of torsion on the swelling equilibrium, in contrast to the effect of extension, is essentially a second-order effect, proportional to the *square* of the strain. As a result it is likely to be affected to a disproportionate extent by any reduction of the true elastic strain, associated with stress relaxation or irreversible structural changes, or indeed by any deviation of the material from the postulated idealized elastic structure. Any such effects would be in the direction of a reduction of the magnitude of the change in swelling, in line with the experimental deviation.

In view of these experimental difficulties the present observations cannot be regarded as providing conclusive evidence of a genuine difference between the theoretical and actual effects of torsion on the equilibrium swelling.

#### ACKNOWLEDGEMENT

The authors acknowledge with thanks the provision of maintenance grants by the Malayan Rubber Fund Board (for K.M.L.) and by the Science Research Council (for M.D.). They are also indebted to Dr M. D. Heaton and Dr R. F. T. Stepto for advice and assistance relating to the computational aspects of the work.

#### REFERENCES

- 1 Treloar, L. R. G. *Polymer* 1972, **13**, 195
- 2 Blanchard, A. F. and Wootton, P. M. *J. Polym. Sci.* 1959, **34**, 627
- 3 Flory, P. J. and Rehner, J. *J. Chem. Phys.* 1944, **12**, 412
- 4 Treloar, L. R. G. *Trans. Faraday Soc.* 1950, **46**, 783

# After-effects in polymerizations photo-initiated by manganese carbonyl + halide systems

C. H. Bamford and J. Paprotny\*

Department of Inorganic, Physical and Industrial Chemistry, Donnan Laboratories, University of Liverpool, PO Box 147, Liverpool L69 3BX, UK  
(Received 20 August 1971)

The presence of certain additives, notably cyclohexanone and acetylacetone, gives rise to relatively high and persistent dark rates of polymerization after irradiation of systems in which polymerization is photosensitized ( $\lambda=435.8\text{nm}$ ) by manganese carbonyl in association with an organic halide. These large after-effects, which are not specific to a particular monomer, occur only if the additive is present during irradiation; the presence of monomer or halide during illumination is not necessary, and the after-effect develops if these components are added subsequently. It is concluded that the after-effect arises from a species Z, produced by photochemical interaction between manganese carbonyl and the additive, which generates free radicals by reaction with the halide.

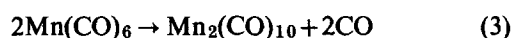
A kinetic treatment based on these ideas is developed and compared with experimental results obtained on the initiating system manganese carbonyl + ethyl trichloroacetate, with methyl methacrylate as monomer and acetylacetone as additive. Agreement may be obtained on the assumption that photolysis of the carbonyl occurs unsymmetrically, one of the resulting fragments reacting rapidly with halide to generate radicals, the other being trapped by the additive to form Z. At high concentrations of additive and small light doses the concentration of Z after irradiation approaches the total concentration of radicals formed in the light period. The presence of acetylacetone does not affect the rate of radical generation during irradiation; this observation is shown to be incompatible with a simple symmetrical primary photolytic act. The possibilities of a complex primary process are considered. Some experiments on the stability of Z in the absence of halide are discussed.

## INTRODUCTION

The mechanism of photosensitization of free-radical polymerization by manganese and rhenium carbonyls in the presence of suitable halogen compounds has been studied by Bamford *et al.*<sup>1, 2</sup>. These workers reported that under the conditions employed ( $\lambda=435.8, 365\text{nm}$  for  $\text{Mn}_2(\text{CO})_{10}$ ,  $\text{Re}(\text{CO})_{10}$ , respectively) the quantum yield of initiation during irradiation is close to unity in each case. They pointed out that this would be consistent with unsymmetrical photolytic fission of the carbonyls if only one type of fragment were able to generate radicals by interaction with the halide. Reactions (1) and (2) were proposed:



(M = Mn or Re) and it was suggested that with manganese carbonyl the species  $\text{Mn}(\text{CO})_6$  does not initiate, but forms inactive products, perhaps by reversion to  $\text{Mn}_2(\text{CO})_{10}$  by the process represented stoichiometrically, but not necessarily mechanistically, by:



On the other hand, if photolytic scission of the carbonyl molecules occurs symmetrically, the overall process would need to be 50% efficient to account for the observed quantum yield.

Bamford *et al.*<sup>2</sup> found that photoinitiation by the  $\text{Re}_2(\text{CO})_{10} + \text{CCl}_4$  system in effectively bulk methyl methacrylate is followed by a relatively high dark rate of polymerization, persisting for several hours. No such after-effect was observed with manganese carbonyl. The above mechanism can accommodate these findings if reaction (3) (with M = Re) is relatively slow, so that the concentration of  $\text{Re}(\text{CO})_6$  builds up during irradiation.

\* Present address: Silesian Institute of Technology, Gliwice, Poland

Slow generation of radicals by interaction of  $\text{Re}(\text{CO})_6$  and  $\text{CCl}_4$  then gives rise to the after-effect. Kinetic predictions based on this mechanism were shown to agree satisfactorily with the experimental observations.

Recent observations<sup>3,4</sup> have confirmed the unit quantum efficiency for photoinitiation by  $\text{Mn}_2(\text{CO})_{10}$ , and have further demonstrated<sup>4</sup> that two radicals are formed for each molecule of the carbonyl consumed. These findings are consistent with reactions (1)–(3).

It has lately become apparent that in the presence of certain solvents, notably cyclohexanone and acetylacetone, photoinitiation by the manganese carbonyl + halide system is followed by enhanced after-effects similar to those previously observed with rhenium carbonyl in bulk methyl methacrylate. The phenomenon is quite distinct from the normal photo after-effect associated with a finite (but high) rate of radical decay on interrupting illumination which, under comparable conditions, lasts for a much shorter time and is several orders of magnitude smaller<sup>5</sup>. Nor is the enhanced after-effect peculiar to methyl methacrylate.

Some interaction between a manganese species generated photolytically and the solvent therefore apparently occurs, yielding a product capable of initiating over a relatively long period. More specifically,  $\text{Mn}(\text{CO})_6$  may be trapped by reaction with a suitable solvent, and so prevented from entering into rapid destruction processes such as reaction (3). A quantitative study of the after-effect, together with data relating to the influence of the solvent on the rate of radical formation in the light, should provide information about the primary act in photolysis. This paper describes investigations carried

out to test these hypotheses. For brevity, we shall use the term after-effect to signify the type of prolonged dark reaction obtained in the presence of active solvents. Throughout the work we have used methyl methacrylate as monomer, with ethyl trichloroacetate (ETCA) as halide.

## EXPERIMENTAL

### Materials

Methyl methacrylate was purified as previously described<sup>6</sup>.

Cyclohexanone (BDH) was dried over fused magnesium sulphate and fractionally distilled in nitrogen at atmospheric pressure through a 50 cm column. The middle fraction was collected and stored under nitrogen; it was distilled in vacuum before use. Acetylacetone (Puriss, Fluka) was also distilled in vacuum. Benzene was dried over calcium hydride and distilled. AR grade acetone was used without further purification.

Manganese carbonyl was sublimed in high vacuum and stored in the dark.

### Techniques

All experiments were carried out in a laboratory illuminated by inactive (sodium) light.

The optical system consisted of a 250 W medium pressure mercury arc and two Pyrex lenses arranged to produce an approximately parallel beam of light. The latter was filtered through the pair of Wratten filters 2E and 98 to give essentially monochromatic light of wavelength 435.8 nm.

Different light intensities were obtained by insertion into the beam of blackened wire gauzes of known transmission.

The polymerization was studied dilatometrically at  $25 \pm 0.005^\circ\text{C}$ . Pyrex dilatometers of approximately 1.5 ml capacity with capillaries of 1 mm bore (Veridia) were used. Rates of polymerization  $\omega$  were calculated from the relation

$$\omega = 5.06 \times 10^{-3} R \text{ mol l}^{-1} \text{ s}^{-1} \quad (4)$$

$R$  being the rate of concentration in  $\text{cm min}^{-1}$  per ml of dilatometer volume. Reaction mixtures were thoroughly degassed by conventional freezing and melting cycles in vacuum (pressure  $< 10^{-5}$  mmHg).

Absorption spectra of degassed solutions of manganese carbonyl in cyclohexanone were measured at 450 nm by means of a Unicam SP500 spectrophotometer. Electron-spin resonance spectra at 77K were recorded with the aid of a Varian E3 spectrometer.

Viscosities of methyl methacrylate–solvent mixtures at  $25^\circ\text{C}$  were determined with an Ostwald viscometer.

## RESULTS AND DISCUSSION

### Character of the after-effect

Figure 1 shows that the dark reaction following irradiation of mixtures of manganese carbonyl, methyl methacrylate, ethyl trichloroacetate and solvent is strongly dependent on the nature of the solvent. Cyclohexanone (CH) and acetylacetone (ACAC) produce larger after-effects than any other solvent examined, while benzene and acetone are much less active in this respect.

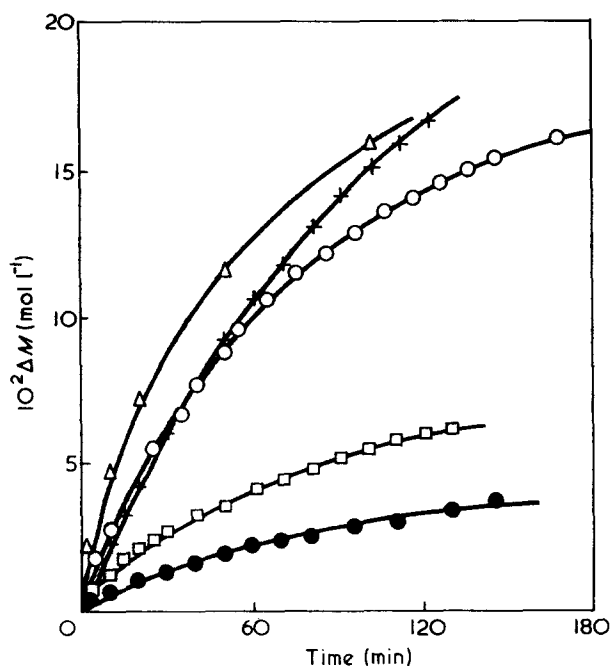


Figure 1 After-effects with different solvents and monomers M=methyl methacrylate, VC=vinyl chloride.  $[\text{ETCA}] = 6 \times 10^{-2}$  mol  $\text{l}^{-1}$ . Irradiation time 5 min,  $\lambda = 435.8 \text{ nm}$ . Concentrations given in mol  $\text{l}^{-1}$ : ●,  $[\text{M}] = 4.7$ ;  $[\text{Mn}_2(\text{CO})_{10}] = 3.0 \times 10^{-4}$ ; solvent benzene. □,  $[\text{M}] = 4.7$ ;  $[\text{Mn}_2(\text{CO})_{10}] = 2.1 \times 10^{-4}$ ; solvent acetone. ○,  $[\text{M}] = 4.7$ ;  $[\text{Mn}_2(\text{CO})_{10}] = 3.9 \times 10^{-4}$ ; solvent cyclohexanone. +,  $[\text{M}] = 4.7$ ;  $[\text{Mn}_2(\text{CO})_{10}] = 3.0 \times 10^{-4}$ ; solvent acetylacetone, experimental points, curve computed from equation (9). Δ,  $[\text{VC}] = 8.6$ ;  $[\text{Mn}_2(\text{CO})_{10}] = 6.4 \times 10^{-4}$ ; solvent cyclohexanone

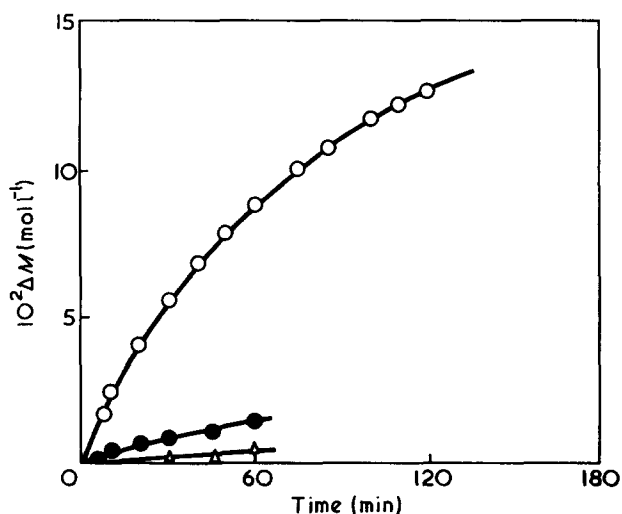


Figure 2 After-effects following irradiation (10 min,  $\lambda=435.8$  nm) of mixtures of two components, with addition of remaining components immediately after irradiation. Concentrations after mixing ( $\text{mol l}^{-1}$ ):  $\text{Mn}_2(\text{CO})_{10}$ ,  $3.42$ ; ETCA,  $6.0 \times 10^{-2}$ .  $\Delta$ , M +  $\text{Mn}_2(\text{CO})_{10}$  irradiated, ETCA + CH added; after mixing  $[\text{M}]=4.7 \text{ mol l}^{-1}$ .  $\bullet$ , M +  $\text{Mn}_2(\text{CO})_{10}$  irradiated, ETCA + M added; after mixing  $[\text{M}]=9.4 \text{ mol l}^{-1}$ .  $\circ$ , CH +  $\text{Mn}_2(\text{CO})_{10}$  irradiated, ETCA + M added; after mixing  $[\text{M}]=4.7 \text{ mol l}^{-1}$

Similar behaviour with vinyl chloride in the presence of cyclohexanone is illustrated in Figure 1. No comparable after-effect occurs with this monomer in the absence of cyclohexanone or other active solvent.

To gain some insight into the processes responsible for the after-effect we irradiated manganese carbonyl in the presence of either solvent or monomer, then added the other components in the dark. The mixture to be irradiated was contained in a vessel communicating through a glass break-seal with a second vessel connected to the dilatometer. The latter vessel contained the components to be added after irradiation. Both liquids were carefully degassed before the vessels were sealed. Results with cyclohexanone are presented in Figure 2; it is clear that the after-effect can only be obtained if the solvent is present during irradiation. On the other hand, the presence of monomer or halide during illumination appears to be inessential and the after-effect develops if these components are added subsequently. Products formed by interaction of  $\text{Mn}_2(\text{CO})_{10}$  with the halide in the light (e.g.  $\text{Mn}(\text{CO})_5\text{Cl}$ ) are therefore not responsible for the dark reaction. No observable reaction is obtained if a mixture of the carbonyl, monomer and cyclohexanone is irradiated without the halide. These experiments establish that the after-effect arises from a species Z, produced by photochemical interaction between manganese carbonyl and active solvent, which interacts with the halide to generate free-radicals. We believe that formation of Z involves interaction of a photolytic fragment from  $\text{Mn}_2(\text{CO})_{10}$  with a carbonyl group of the solvent. Although present observations suggest that solvent activity is connected with the presence of such groups, further studies on additives of different types is desirable.

To examine the possibility of thermal formation of Z, a degassed solution of carbonyl in cyclohexanone ( $[\text{Mn}_2(\text{CO})_{10}]=3 \times 10^{-4} \text{ mol l}^{-1}$ ) was heated to  $100^\circ\text{C}$  for 1 h. On cooling to  $25^\circ\text{C}$  and adding monomer and halide no after-effect was observed. However, the expected after-effect was obtained on subsequent irradiation of the

mixture. Under these conditions, therefore, Z is not formed on heating, or a negligible concentration survives; the experiment further confirms that impurities in the cyclohexanone are not responsible for the after-effect, since these should be scavenged during heating with  $\text{Mn}_2(\text{CO})_{10}$ . A similar conclusion was drawn from experiments in which manganese carbonyl was irradiated in the solvent which was then distilled off from photolysis products. This material produced normal after-effects.

It appeared likely that Z would be a rather unstable species, even in the absence of halide. To test this, experiments were carried out in which solutions of manganese carbonyl in cyclohexanone were irradiated, then added to a monomer-halide mixture after standing in the dark for predetermined intervals of time. The magnitude of the after-effect was found to decrease as the interval increased from zero to 14 h (Figure 3), indicating a slow decay of Z into non-initiating species. Calculations of the type described later show that the half-life of Z in cyclohexanone at  $25^\circ\text{C}$  is of the order 10 h.

The dependence of the after-effect on the period of illumination  $\tau$  is illustrated in Figure 4. For short irradiations, the after-effect increases with  $\tau$  but, under the conditions in Figure 4, it reaches a maximum value at  $\tau=5$  min, approximately, and decreases on longer irradiation. These unexpected observations (which are without counterpart in the rhenium carbonyl system) may be explained in a number of ways, of which destruction of Z at long  $\tau$  by photolysis seems most probable. Evidently in experiments designed to measure the rate of formation of Z,  $\tau$  should be as short as practicable.

#### Spectrophotometric observations

We have shown that Z decomposes when allowed to stand in solution in cyclohexanone in the absence of halide (Figure 3) and have suggested that Z may photolyse

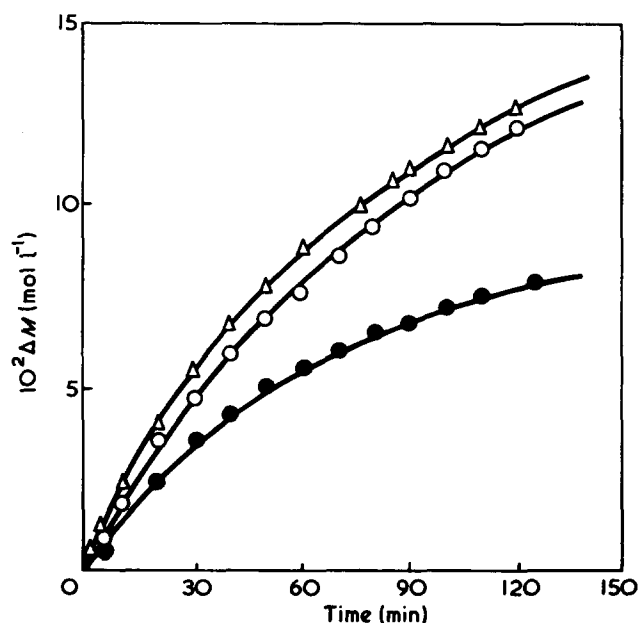


Figure 3 After-effects following irradiation (10 min,  $\lambda=435.8$  nm) of CH +  $\text{Mn}_2(\text{CO})_{10}$  with subsequent addition of M + ETCA. Concentrations after mixing ( $\text{mol l}^{-1}$ ): M,  $4.7$ ;  $\text{Mn}_2(\text{CO})_{10}$ ,  $3.0 \times 10^{-4}$ ; ETCA,  $6.8 \times 10^{-2}$ .  $\Delta$ , mixing immediately after irradiation;  $\circ$ , mixing after 4 h;  $\bullet$ , mixing after 14 h

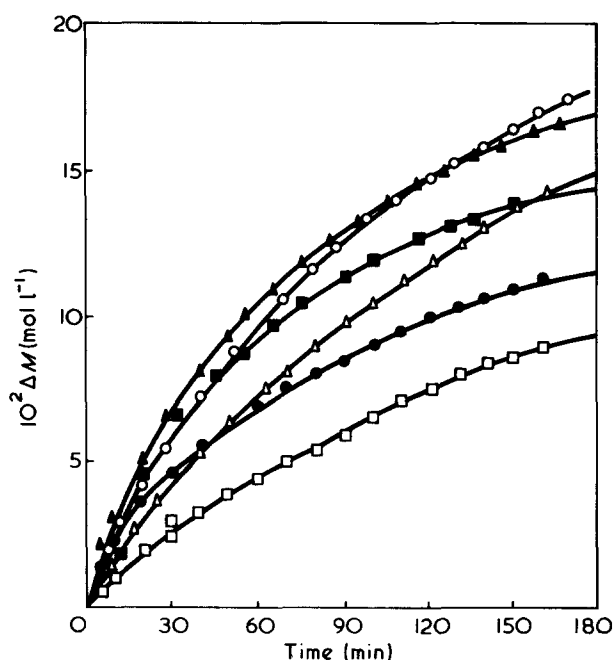


Figure 4 Dependence of after-effect on time of irradiation. Solvent CH;  $\lambda=435.8\text{nm}$ , Concentrations ( $\text{mol l}^{-1}$ ): M, 4.7;  $\text{Mn}_2(\text{CO})_{10}$ ,  $4.0 \times 10^{-4}$ ; ETCA,  $6.4 \times 10^{-2}$ . Irradiation times:  $\square$ , 10s;  $\triangle$ , 30s;  $\circ$ , 2min;  $\blacktriangle$ , 5min;  $\blacksquare$ , 10min;  $\bullet$ , 20min

during prolonged irradiation, with the implication that Z is likely to have a high extinction coefficient. It therefore seemed worthwhile to make spectrophotometric observations to ascertain whether the formation and decay of Z could be detected directly. Irradiation for 10 min was carried out with  $\lambda=435.8\text{nm}$ , and optical densities at 450 nm were measured before and after irradiation. A

degassed solution of manganese carbonyl ( $9 \times 10^{-4}\text{mol l}^{-1}$ ) in cyclohexanone, free from halide, was used in these experiments. The observations summarized in Figure 5 show that the optical density indeed increases during irradiation, and subsequently falls slowly in standing in the dark at  $25^\circ\text{C}$ . After 24 h the optical density has almost recovered its original value. A second irradiation after 50 h, approximately, produces similar (but not identical) results, so that the phenomena appear to be partly reversible.

The first decay curve in Figure 5 is not strictly first-order, but corresponds to an order approaching two initially and decreasing towards unity. Under these conditions it is not meaningful to discuss the precise value of the half-life. The maximum concentration of Z in the present experiments would be considerably higher than those in the after-effect work on account of the greater carbonyl concentration; in these circumstances the 'half-life' determined from the results in Figure 3 (10h) appears to be compatible with Figure 5.

Irradiation of manganese carbonyl in cyclohexane solution under similar conditions did not produce any measurable change in optical density.

These experiments support the proposed mechanism for the origin of the after-effect by demonstrating that the photolytic fragments derived from  $\text{Mn}_2(\text{CO})_{10}$  interact with cyclohexanone but not with cyclohexane; they are also consistent with the occurrence of photolysis of the species Z.

#### Kinetics of the after-effect

The concentration of Z formed by irradiation may be calculated from the after-effect if the kinetic mechanism of the latter is known. Equation (5) is a formal representation

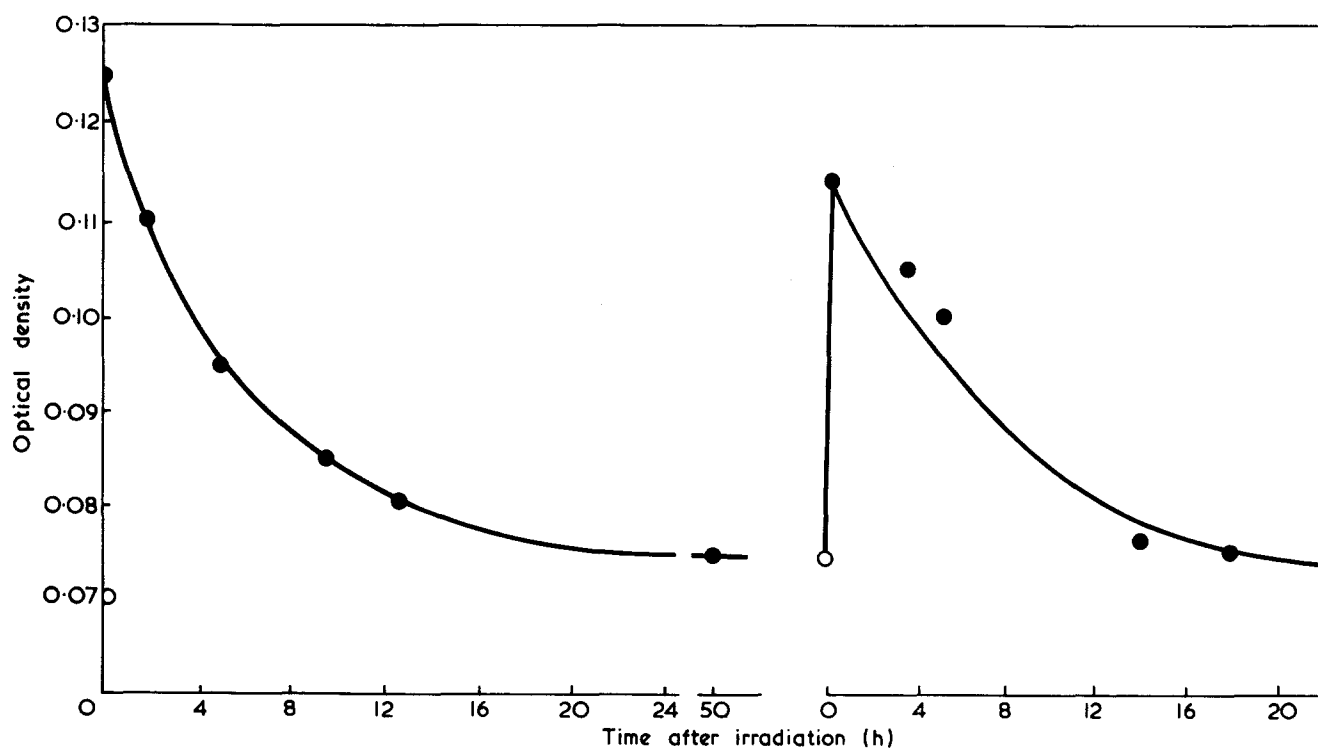
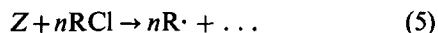


Figure 5 Changes in optical density ( $\lambda=450\text{nm}$ ) following irradiation (10min,  $\lambda=435.8\text{nm}$ ). Solvent CH;  $[\text{Mn}_2(\text{CO})_{10}] = 9.2 \times 10^{-4}\text{mol l}^{-1}$ ,  $\circ$ , Optical densities before irradiation periods;  $\bullet$ , optical densities after irradiation

of the interaction of Z and the halide (RCl) leading to the generation of radicals  $R\cdot (\equiv Cl_2\dot{C}CO_2Et)$ , which initiate polymerization of the monomer and so are responsible for the after-effect.



Here  $n$  is the number of radicals formed by reaction of one molecule of Z. At the relatively high concentration of halide used in this work, equation (5) would be expected to be first-order in  $[Z]$ , with  $[RCl]$  effectively constant during reaction. The first-order velocity coefficient  $k$  will, in general, be a function of  $[RCl]$ . Thus we may write:

$$Z_t = Z_0 e^{-kt} \quad (6)$$

where  $Z_0, Z_t$  are the concentrations of Z at zero time (the end of irradiation) and time  $t$ , respectively. No account is taken of the purely thermal decay of Z, since this process is relatively slow (see above) nor do we consider photolysis of Z. This analysis therefore applies to small light doses. The rate of radical formation by equation (5) is:

$$J_t = nkZ_t = nkZ_0 e^{-kt} \quad (7)$$

For the greater part of the after-effect, the radical concentration will be effectively that calculated from stationary state considerations, since the time scale of the after-effect greatly exceeds the half-life of a kinetic chain. For a short time after the end of irradiation the radical concentration is, of course, non-stationary, but this is not significant here since the overall conversion in the non-stationary period is very small and a small correction can readily be applied. We assume throughout this paper that all  $R\cdot (\equiv Cl_2\dot{C}CO_2Et)$ , whether formed in the light, or in the subsequent dark reaction, initiate polymerization by reaction with monomer. Thus, if  $\Delta_t$  is the magnitude of the after-effect at time  $t$  after the interruption of irradiation, i.e. the conversion occurring in the dark reaction in the specified interval, we have from equation (7)

$$\frac{d\Delta_t}{dt} = \frac{k_p[M]}{k_t^{1/2}} (nkZ_0)^{1/2} e^{-kt/2} \quad (8)$$

$k_p, k_t$  being the velocity coefficients of propagation and bimolecular termination, respectively, and  $[M]$  the monomer concentration, assumed constant. Integration of equation (8) and application of the boundary condition  $\Delta_t = 0$  when  $t = 0$  gives

$$\Delta_t = \frac{2k_p}{k_t^{1/2}} [M] \left( \frac{nZ_0}{k} \right)^{1/2} (1 - e^{-kt/2}) \quad (9)$$

For convenience in computation equation (9) may be written in the form

$$\Delta h = A(1 - e^{-Bt}) \quad (10)$$

$\Delta h$  (cm) being the change in meniscus level in the dilatometer capillary corresponding to the conversion  $\Delta_t$  (mol l<sup>-1</sup>). If  $V$  (ml) is the dilatometer volume, and the capillary has an internal diameter of 1 mm, we find from equation (4)

$$\Delta h = \Delta_t V / 0.304 \quad (11)$$

for methyl methacrylate at 25°C.

Combination of equations (9)–(11) gives

$$nZ_0 = \left\{ \frac{0.152A(k^{1/2})}{V[M](k_p/k_t^{1/2})} \right\}^2 \quad (12)$$

One of the main points of interest is a comparison between  $Z_0$  and the total concentration of radicals formed during irradiation. The latter may be estimated from the conversion during the light period, after appropriate correction for the pre-effect. (This correction is necessary since radicals are formed at a constant rate from the onset of illumination, but during the pre-effect the rate of polymerization has not attained its stationary value.) In practice, values of the contraction in the dilatometer are measured at convenient intervals and the linear portion of the contraction-time curve is extrapolated back to the beginning of irradiation; thus the corrected contraction  $a$  may be determined. If  $I$  is the rate of radical generation in the light, it is easily shown that the total concentration of radicals formed is given by:

$$I\tau = \left\{ \frac{0.304a}{V[M](k_p/k_t^{1/2})} \right\}^2 \frac{1}{\tau} \quad (13)$$

From equations (12) and (13) we obtain the simple relation:

$$\frac{nZ_0}{I\tau} = \frac{k\tau}{4} \left( \frac{A}{a} \right)^2 \quad (14)$$

If  $A, B$  are determined from after-effect data, and  $a$  is measured, equations (12), (13) (or (14)) may be used to calculate  $Z_0, I\tau$ , provided  $n$  is known. Electron spin resonance observations have shown that during reaction only a very small fraction of the total manganese is converted into  $Mn^{II}$ . Since it seems most likely that Z contains only one Mn atom, and the oxidation  $Mn^0 \rightarrow Mn^{II}$  by the halide would produce one radical, we believe that  $n = 1$ .  $A, B$  were evaluated by fitting equation (10) to the after-effect data by computer, with the aid of a program which minimized the standard deviation. The standard deviation so obtained was normally in the region of  $8 \times 10^{-4}$  mol l<sup>-1</sup>. To illustrate the closeness of the fit we show the computed curve for the experiment with acetylacetone in Figure 1. This agreement clearly supports the assumption of first-order decay of Z.

The value of the parameter  $k_p/k_t^{1/2}$  at a given temperature may be influenced by the composition of the reaction mixture in two ways. The termination reaction is diffusion-controlled, so that  $k_t$  is inversely proportional to the viscosity of the system<sup>7</sup>. Further, in the case of methyl methacrylate,  $k_p$  is increased by the presence of some additives<sup>8,9</sup>. We have looked for possible changes in  $k_p$  produced by acetylacetone by measuring rates of polymerization photoinitiated ( $\lambda = 365$  nm) by azobisisobutyronitrile over a range of intensities and composition, benzene being used as an inert additive. No effect on  $k_p/k_t^{1/2}$  attributable to acetylacetone could be observed, other than that arising from the (small) viscosity changes. Consequently values of  $k_p/k_t^{1/2}$  were derived from the figure for bulk monomer by applying the appropriate viscosity correction. For convenience the values of the parameter used subsequently are presented in Table 1 in which  $\phi_{aac}$  is the volume fraction of acetylacetone.

#### Quantitative study of the after-effect

Experiments were carried out with  $\tau = 5$  min over a range of volume fractions of acetylacetone to determine the dependence of  $Z_0$  on the concentration of acetylacetone. Experimental data were treated as described in the previous section,  $Z_0$  being calculated from equation

**Table 1** Values of  $k_p/k_t^{1/2}$  for methyl methacrylate at 25°C in mixtures containing acetylacetone

$\phi_{\text{acac}}$	0	0.1	0.2	0.3	0.4	0.5	0.75
$10^3 k_p/k_t^{1/2}$ ( $\text{mol}^{-1/2} \text{l}^{1/2} \text{s}^{-1/2}$ )	56	56.5	57	58	58.5	59	61

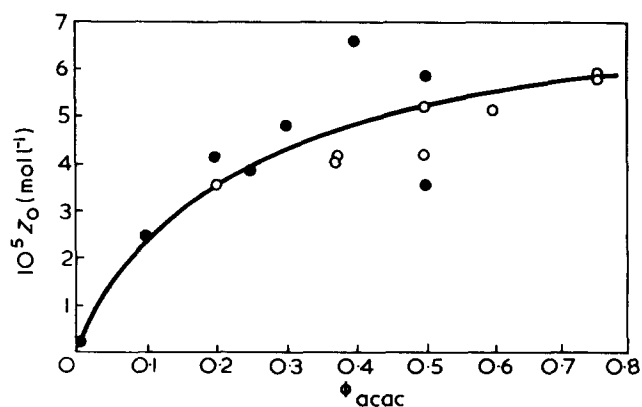
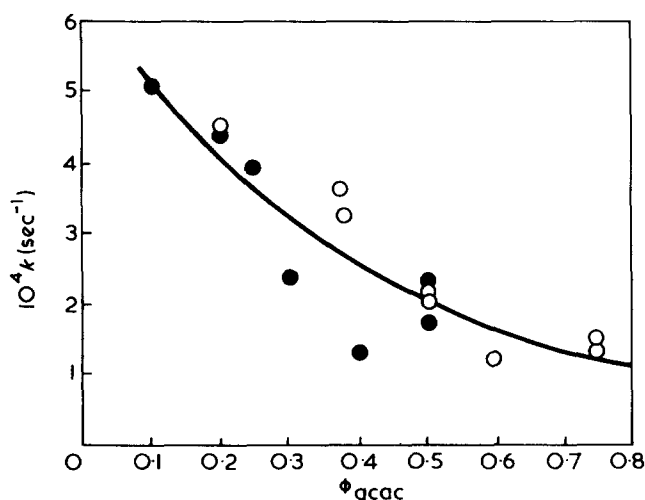
(12) with  $n=1$ . The experiments were performed at two different monomer concentrations (2.35 and 4.70 mol l<sup>-1</sup>) with addition of benzene as an inactive diluent when necessary. Results are shown in Figure 6. The calculated values of  $Z_0$  show considerable scatter; this is hardly surprising in view of the very low rates of initiation and long kinetic chain-lengths in the dark reaction, and the sensitivity of  $Z_0$  to errors in  $A$  arising from the square in equation (12). However, it is clear that increasing acetylacetone concentration is accompanied by a steady increase in  $Z_0$ , with a tendency in the latter to reach a plateau value. There is no evidence that  $Z_0$  depends significantly on  $[M]$ .

Unfortunately, the measured values of  $a$  were not very reproducible in these experiments, and this prevented meaningful application of equation (13). It appeared that  $I\tau$  was not sensitive to  $\phi_{\text{acac}}$  and had values scattered around  $10 \times 10^{-5} \text{ mol l}^{-1}$ . If this figure is accepted, it follows that at high acetylacetone concentrations the ratio  $Z_0/I\tau$  may reach 0.6 under our conditions.

Corresponding values of  $k (=2B)$  are plotted against  $\phi_{\text{acac}}$  in Figure 7, which indicates a general decrease in  $k$  with increasing acetylacetone concentration.

Since fewer chemical complications are encountered with short periods of irradiation or small light doses, the after-effect has been investigated under these conditions. Two series of experiments were carried out, one with the light intensity reduced to one-third of its previous value, with  $\tau=5$  min, the other at the higher intensity, with  $\tau=10$  s.

The results of the former series are collected in Table 2. The total concentration of radicals formed in the light ( $I\tau$ ) is sensibly independent of acetylacetone concentration, as appeared to be the case at high light intensity. Also,  $Z_0$  increases with  $\phi_{\text{acac}}$  in a similar manner (compare Figure 6), although  $Z_0/I\tau$  is generally somewhat higher. This is consistent with the view that  $Z$  may photolyse to an inactive species. Under the present conditions there appears to be no appreciable change in  $k$  as  $\phi_{\text{acac}}$  is varied, in contrast to the results shown in Figure 7.


**Figure 6** Dependence of  $Z_0$  on  $\phi_{\text{acac}}$ . Irradiation time, 5 min;  $\lambda=435.8 \text{ nm}$ . Concentrations ( $\text{mol l}^{-1}$ ):  $\text{Mn}_2(\text{CO})_{10}$ ,  $3.0 \times 10^{-4}$ ; ETCA,  $6.0 \times 10^{-2}$ ; ●, M, 4.7; ○, M, 2.35

**Figure 7** Dependence of  $k$  on  $\phi_{\text{acac}}$ . Irradiation time, 5 min;  $\lambda=435.8 \text{ nm}$ , high intensity. Concentrations ( $\text{mol l}^{-1}$ ):  $\text{Mn}_2(\text{CO})_{10}$ ,  $3.0 \times 10^{-4}$ ; ETCA,  $6.0 \times 10^{-2}$ ; ●, M, 4.7; ○, M, 2.35

Two experimental problems are encountered in measurements with short periods of irradiation. First, the conversion in the light is too small to measure directly, and secondly, traces of adventitious retarders, which may not be removed completely during the short irradiation, may vitiate the results. Consequently we decided to make separate measurements of the rate of polymerization in the light, with longer periods of illumination. The rate of polymerization became constant after illumination of the system for about 30 s, and remained effectively steady for 5 min; consumption of manganese carbonyl then produced a slow decline in rate. Rates of initiation calculated from the constant rates of polymerization are given in Table 3. These results confirm the earlier findings that the rate of radical formation in the light is sensibly independent of the acetylacetone concentration.

To eliminate the effects of impurities on the dark reaction we observed repeated after-effects in the same dilatometer, with a sufficiently long period between successive irradiations to allow the rate of reaction to decline to an insignificant value. With  $\tau=10$  s it was found that the second irradiation gave a slightly larger after-effect than the first, while the third after-effect was little different from the second. Data for the third after-effect are given in Table 4. The values of  $k$  and  $Z_0/I\tau$  are both somewhat larger than the corresponding values in Table 2, but probably not significantly so.

The results of a series of experiments designed to examine the effects of changing the manganese carbonyl concentration are presented in Table 5. The ratio  $Z_0/I\tau$  decreases with increasing  $[\text{Mn}_2(\text{CO})_{10}]$  but there is no definite trend in  $k$ .

In a further series the effect of varying the ethyl trichloroacetate concentration was investigated. According to the results in Table 6, with increasing [ETCA],  $I\tau$  increases to a small extent while both  $Z_0$  and  $Z_0/I\tau$  decrease;  $k$  also increases, but with an order in [ETCA] less than unity.

Carbon monoxide, added at pressures of 3 and 15 mmHg, was found to be without detectable influence on the rate of polymerization in the light, or on the development of the after-effect.



Table 2 After-effects at low light intensity;  $\tau=5$  min. Concentrations (mol l<sup>-1</sup>): M, 4.7; Mn<sub>2</sub>(CO)<sub>10</sub>, 3 × 10<sup>-4</sup>; ETCA, 6 × 10<sup>-2</sup>

$\phi_{acac}$	V (ml)	A (cm)	a (cm)	10 <sup>4</sup> k (=2 × 10 <sup>4</sup> B) (s <sup>-1</sup> )	10 <sup>5</sup> Z <sub>0</sub> (mol l <sup>-1</sup> )	10 <sup>5</sup> I $\tau$ (mol l <sup>-1</sup> )	Z <sub>0</sub> /I $\tau$
0	1.90	—	0.170	—	—	3.57	—
0.10	1.90	0.86	0.173	1.77	1.18	3.60	0.33
0.25	1.81	1.19	0.166	1.28	1.75	3.55	0.50
0.35	1.40	1.04	0.143	1.47	2.49	4.29	0.58
0.50	1.74	1.17	0.159	1.57	2.12	3.32	0.64

Table 3 Rates of initiation at high light intensity in methyl methacrylate + acetylacetonate systems. Concentrations (mol l<sup>-1</sup>): Mn<sub>2</sub>(CO)<sub>10</sub>, 3 × 10<sup>-4</sup>; ETCA, 6 × 10<sup>-2</sup>

$\phi_{acac}$	0	0.25	0.75
10 <sup>7</sup> I/(mol l <sup>-1</sup> s <sup>-1</sup> )	3.75	3.70	3.54

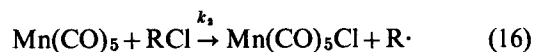
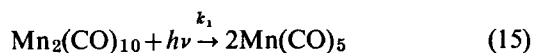
Table 4 Data on after-effect for  $\tau=10$  s, Concentrations (mol l<sup>-1</sup>): M, 4.7; Mn<sub>2</sub>(CO)<sub>10</sub>, 3 × 10<sup>-4</sup>; ETCA, 6 × 10<sup>-2</sup>;  $\phi_{acac}=0.5$

A=0.272 cm
k=2.38 × 10 <sup>-4</sup> s <sup>-1</sup>
Z <sub>0</sub> =0.27 × 10 <sup>-5</sup> mol l <sup>-1</sup>
I $\tau$ =0.36 × 10 <sup>-5</sup> mol l <sup>-1</sup> (from Table 3)
Z <sub>0</sub> /I $\tau$ =0.75

Mechanism of formation of Z

We have concluded that the species Z is formed by photoreaction between manganese carbonyl and active solvent S, and it is likely that Z is an adduct between S and a fragment resulting from the photolysis of Mn<sub>2</sub>(CO)<sub>10</sub>, e.g. S-Mn(CO)<sub>5</sub>. Two cases may be distinguished, depending on the process assumed for the photo-decomposition of Mn<sub>2</sub>(CO)<sub>10</sub>.

Symmetrical photolysis of Mn<sub>2</sub>(CO)<sub>10</sub>. The photolytic step and the radical-generating process in the light are shown in equations (15) and (16):

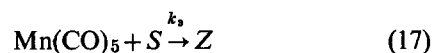


The halide concentration throughout this work was in the 'high' range, i.e. corresponding to the plateau values of the rate of polymerization<sup>1</sup>, so we are not concerned with reactions of Mn(CO)<sub>5</sub> leading to inactive species. We may

Table 6 Dependence of dark reaction on [ETCA]. High intensity,  $\tau=5$  min; concentrations (mol l<sup>-1</sup>): M, 4.7; Mn<sub>2</sub>(CO)<sub>10</sub>, 3 × 10<sup>-4</sup>;  $\phi_{acac}=0.5$

10 <sup>2</sup> [ETCA] (mol l <sup>-1</sup> )	V (ml)	A (cm)	a (cm)	10 <sup>4</sup> k (s <sup>-1</sup> )	10 <sup>5</sup> Z <sub>0</sub> (mol l <sup>-1</sup> )	10 <sup>5</sup> I $\tau$ (mol l <sup>-1</sup> )	Z <sub>0</sub> /I $\tau$
2	1.81	2.98	0.257	0.67	5.40	8.1	0.67
10	1.90	2.12	0.275	1.05	4.00	8.5	0.47
20	1.74	1.70	0.264	1.23	3.55	9.2	0.38

suppose that S competes with the halide for interaction with Mn(CO)<sub>5</sub> according to equation (17):



By assuming a stationary concentration of Mn(CO)<sub>5</sub> we find that

$$\begin{aligned} Z_0 &= 2k_1[\text{Mn}_2(\text{CO})_{10}]\tau \frac{k_3[\text{S}]}{k_2[\text{RCl}] + k_3[\text{S}]} \\ &= 2\gamma I_{\text{abs}}\tau \frac{k_3[\text{S}]}{k_2[\text{RCl}] + k_3[\text{S}]} \end{aligned} \quad (18a)$$

and

$$I\tau = 2\gamma I_{\text{abs}}\tau \frac{k_2[\text{RCl}]}{k_2[\text{RCl}] + k_3[\text{S}]} \quad (18b)$$

where  $\gamma$  is the quantum efficiency of the primary carbonyl photolysis and  $I_{\text{abs}}$  the absorbed intensity. In deriving equation (18a) no account has been taken of photolysis or decay of Z either thermally or by reaction (5). Decay is negligible during the (short) irradiation period, while at low light doses, to which this analysis mainly applies, photolysis will not be appreciable. From equation (18) we have,

$$\frac{Z_0}{I\tau} = \frac{k_3[\text{S}]}{k_2[\text{RCl}]} \quad (19a)$$

$$Z_0 + I\tau = 2\gamma I_{\text{abs}}\tau = (I\tau)_0 \quad (19b)$$

where (I $\tau$ )<sub>0</sub> is the value of I $\tau$  for [S]=0.

Table 5 Dependence of dark reaction on [Mn<sub>2</sub>(CO)<sub>10</sub>]. High intensity,  $\tau=5$  min; concentrations (mol l<sup>-1</sup>): M, 4.7; ETCA, 6 × 10<sup>-2</sup>;  $\phi_{acac}=0.5$

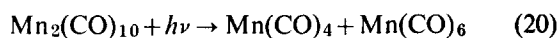
10 <sup>4</sup> [Mn <sub>2</sub> (CO) <sub>10</sub> ] (mol l <sup>-1</sup> )	V (ml)	A (cm)	a (cm)	10 <sup>4</sup> k (s <sup>-1</sup> )	10 <sup>5</sup> Z <sub>0</sub> (mol l <sup>-1</sup> )	10 <sup>5</sup> I $\tau$ (mol l <sup>-1</sup> )	Z <sub>0</sub> /I $\tau$
0.3	1.90	1.13	0.120	1.44	1.51	1.6	0.94
0.6	1.74	0.99	0.125	2.00	1.94	2.1	0.92
1.0	1.81	1.06	0.171	2.45	2.50	3.6	0.70
3.0	1.40	1.56	0.200	1.42	5.30	9.3	0.57

Although the form of the variation of  $Z_0$  with  $[S]$  (in equation 18a) is compatible with *Figure 6*, this mechanism is unsatisfactory in that equation (18b) predicts a dependence of  $I\tau$  on  $[S]$  which is not observed (*Tables 2 and 3*). Thus, unless  $k_2[\text{RCl}] \gg k_3[S]$ ,  $I\tau$  should decrease with increasing  $[S]$ ; if the inequality were to hold  $Z_0/I\tau$  would be very small (equation 19a), contrary to observation. According to equation (19b),  $Z_0 + I\tau$  should remain constant as  $[S]$  is varied and equal to the value of  $I\tau$  in pure monomer. In the experiment in *Table 4*, the expected value of  $I\tau$  on this basis would be  $(0.375 - 0.27)10^{-5} = 0.105 \times 10^{-5} \text{ mol l}^{-1}$  (see *Table 3*); the observed value  $0.36 \times 10^{-5} \text{ mol l}^{-1}$  differs from this by an amount too great to be attributable to experimental error. A similar analysis of the figures in *Table 2* leads to the same conclusion.

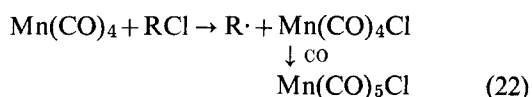
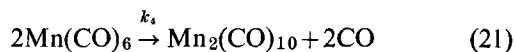
Finally, we note from equation (19a) that the ratio  $Z_0/I\tau$  would be expected to increase linearly with  $[S]$ , without approaching a finite limit. In fact, a value for the ratio exceeding unity has never been observed in any experiment. The present mechanism predicts for the experiment in *Table 4*,  $Z_0/I\tau = 0.27/0.105 = 2.58$ , whereas the observed value is 0.75.

We conclude that the simple symmetrical mode of photolysis considered does not seem compatible with the results of this work.

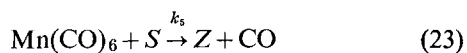
*Unsymmetrical photolysis of  $\text{Mn}_2(\text{CO})_{10}$ .* The work of Kwok to which reference has already been made<sup>4</sup> supports the type of primary act (equation 20) suggested by Bamford *et al.*<sup>1</sup>:



Kwok<sup>4</sup> further proposes that reaction (20) is followed by reactions (21) and (22):



We take these three steps as the basis of the present discussion. A possible mechanism for the formation of  $Z$  would involve an interaction between  $\text{Mn}(\text{CO})_6$  and  $S$  (presumably with evolution of  $\text{CO}$ ) which would compete with the rapid process (21):



If we assume that equation (21) is second order in  $[\text{Mn}(\text{CO})_6]$ , and that  $[\text{Mn}(\text{CO})_6]$  is stationary, we may derive:

$$Z_0 = \frac{\alpha k_5^2 [S]^2}{2k_4} \left\{ \left( 1 + \frac{4\gamma k_4 I_{\text{abs}}}{k_5^2 [S]^2} \right)^{1/2} - 1 \right\} \tau \quad (24a)$$

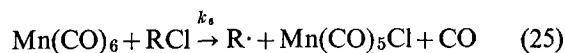
$$I\tau = \gamma I_{\text{abs}} \tau \quad (24b)$$

According to reaction (24a),  $Z_0$  increases with increasing  $[S]$ , approaching a limit  $\gamma I_{\text{abs}} \tau$ ; thus the limiting value of  $Z_0/I\tau$  at high  $[S]$  is unity. This mechanism further differs from that discussed earlier in that it predicts that  $I\tau$  should be independent of  $[S]$ . In these respects equations (24a and b) are consistent with observation.

It follows from the kinetic mechanism that as  $I_{\text{abs}}$  increases, the relative importance of reaction (21) com-

pared to reaction (23) increases, so that the ratio  $Z_0/I\tau$  should decrease. (This may, of course, be shown directly from equation (24a).) In the experiments of *Table 5*, increase in  $I_{\text{abs}}$  was brought about by increasing  $[\text{Mn}_2(\text{CO})_{10}]$  at constant incident intensity and is seen to lead to the expected reduction in  $Z_0/I\tau$ .

Equations (24a and b) do not contain the halide concentration. However, we have seen (*Table 6*) that the values of  $Z_0$ ,  $I\tau$ , and  $Z_0/I\tau$  are not independent of  $[\text{ETCA}]$ , although they are not very sensitive to it in the range studied. This may imply that a reaction between  $\text{Mn}(\text{CO})_6$  and the halide occurs to a minor extent, and competes with reaction (23). A possible reaction is:



If equation (25) is included, equations (24a and b) must be replaced by:

$$Z_0 = \frac{\alpha k_5^2 [S]^2}{2k_4} \left\{ \left( 1 + \frac{4\gamma k_4 I_{\text{abs}}}{\alpha^2 k_5^2 [S]^2} \right)^{1/2} - 1 \right\} \tau \quad (26a)$$

$$I\tau = \gamma I_{\text{abs}} \tau + Z_0(\alpha - 1) \quad (26b)$$

where

$$\alpha = 1 + k_6[\text{RCl}]/k_5[S] \quad (27)$$

If  $\alpha$  is not far from unity, equations (26a and b) explain the small trends which appear in *Table 6*. The fraction of  $\text{Mn}(\text{CO})_6$  reacting according to equation (25) is greatest when  $[S]=0$ ; even under these conditions it is probably small for the standard halide concentration used in this work ( $6 \times 10^{-2} \text{ mol l}^{-1}$ ). This will be so if  $k_6[\text{RCl}]$  is small compared to  $(\gamma k_4 I_{\text{abs}})^{1/2}$ .

In view of the experimental difficulties encountered in obtaining precise values of  $Z_0$  and  $I\tau$ , we do not think it justifiable to attempt to fit equations (26a and b) quantitatively to the results. However, for purposes of illustration we have calculated  $Z_0$ ,  $I\tau$ ,  $Z_0/I\tau$  from these equations taking  $\gamma I_{\text{abs}} = 1.2 \times 10^{-7} \text{ einstein l}^{-1} \text{ s}^{-1}$ ,  $\tau = 300 \text{ s}$ ,  $k_5^2/k_4 = 10^{-8} \text{ mol}^{-1} \text{ l s}^{-1}$ ,  $k_6/k_5 = 5$ , and the results are presented in *Figure 8*. They are in general accord with the observations at low intensity in *Table 2*; the numerical results are also in satisfactory semi-quantitative agreement with the effects produced by changes in  $[\text{Mn}_2(\text{CO})_{10}]$  (i.e.  $I_{\text{abs}}$ ) and  $[\text{ETCA}]$  shown in *Tables 5 and 6* respectively.

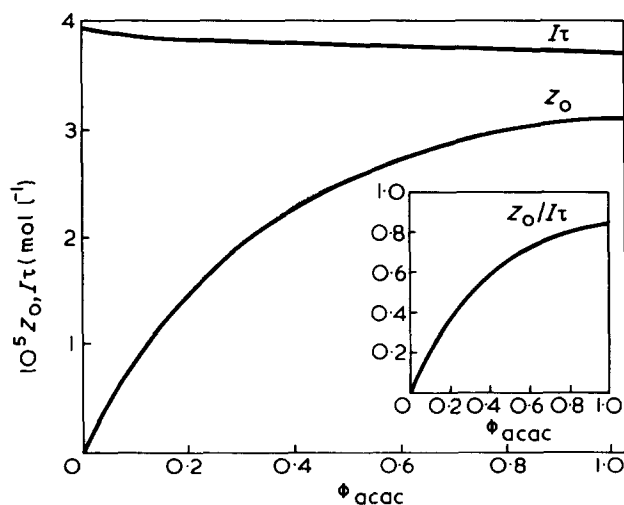


*Figure 8* Dependence of  $Z_0$ ,  $I\tau$  and  $Z_0/I\tau$  on  $\phi_{\text{acac}}$  calculated from equations (26a and b) with  $\gamma I_{\text{abs}} = 1.2 \times 10^{-7} \text{ einstein l}^{-1} \text{ s}^{-1}$ ,  $k_5^2/k_4 = 10^{-8} \text{ mol}^{-1} \text{ l s}^{-1}$ ,  $k_6/k_5 = 5$ ,  $\tau = 300 \text{ s}$

The values of the parameters chosen are appropriate to a solvent with the activity of acetylacetone. A much more active solvent may be able to compete with the halide for reaction with  $Mn(CO)_4$ . In such a case the rate of polymerization in the light may decrease with increasing  $[S]$  and the ratio  $I_0/I\tau$  could exceed unity.

The mechanism under discussion for the formation of Z following unsymmetrical splitting of  $Mn_2(CO)_{10}$  seems to agree with the majority of the salient observations. We note that it leads to an overall quantum yield for radical formation  $\gamma_0$  given by:

$$\gamma_0 = \gamma + \frac{\alpha^2 k_5^2 [S]^2}{2k_4 I_{abs}} \left( \left( 1 + \frac{4\gamma k_4 I_{abs}}{\alpha^2 k_5^2 [S]^2} \right)^{1/2} - 1 \right) \quad (28)$$

which leads to a value  $2\gamma$  as  $I_{abs}/[S]^2 \rightarrow 0$ . Since, on the basis of this mechanism,  $\gamma = 1$  at high [halide], the limiting value of  $\gamma_0$  is two.

If reaction (21) is kinetically first order in  $[Mn(CO)_6]$  (rate coefficient  $k'_4$ ) the equations assume the simpler form shown below:

$$Z_0 = \gamma I_{abs} \frac{k_5 [S]}{k_5 [S] + k'_4} \quad (29a)$$

$$I\tau = \gamma I_{abs} \tau \quad (29b)$$

$$\frac{Z_0}{I\tau} = \frac{k_5 [S]}{k_5 [S] + k'_4} \quad (29c)$$

Equation (29a) predicts a variation of  $Z_0$  with  $[S]$  similar to equation (18a) (derived for symmetrical photolysis) and is compatible with the experimental data in Figure 6 while equations (29b) and (29c) are also consistent with the results in Tables 2 and 3. However, according to equation (29c) the ratio  $Z_0/I\tau$  should not depend on  $I_{abs}$  or  $[Mn_2(CO)_{10}]$ , so that in this respect the mechanism is less satisfactory than that leading to equation (24). The accuracy of the experimental data is not sufficiently high to exclude a scheme in which both second- and first-order reactions consuming  $Mn(CO)_6$  participate. The mechanism under discussion could obviously be elaborated by inclusion of reaction (25) to obtain the observed dependence on [halide].

Hitherto we have implied that the monomer does not partake in the formation of a long-lived initiator. Inspection of Figure 2 shows that this is not strictly true; although the after-effect in bulk monomer is relatively small compared to that obtained in the presence of an active solvent, it is nevertheless much higher than the normal photochemical after-effect. Thus it is probable that a species of the type Z is formed from the monomer, in low concentration and/or of low activity. Since  $Z_0$  in acetylacetone solution is not sensitive to the monomer concentration (Figure 6), the monomer is not able to compete effectively with acetylacetone under our conditions.

### Reactions of Z

In general,  $k$  may be expected to depend on the solvent and halide concentrations. At low light intensities,  $k$  is effectively independent of  $\phi_{acac}$  (Table 2), but at high intensities  $k$  increases with decreasing  $\phi_{acac}$  (Figure 7), and also with increasing period of irradiation. The dependence on  $\tau$  is immediately apparent from a comparison of the curvatures of the plots in Figure 4; the values of  $k$  are

Table 7 Dependence of  $k$  on  $\tau$ . Additive cyclohexanone  $[Mn_2(CO)_{10}] = 4 \times 10^{-4} \text{ mol l}^{-1}$ ;  $\phi_{ch} = 0.5$

$\tau$ (s)	10	30	120	300	600	1200
$10^4 k (\text{s}^{-1})$	1.67	2.67	3.00	4.67	5.33	4.33

collected in Table 7. At high intensity  $k$  varies with [ETCA] in the expected sense (Table 6), although the dependence is less than first order.

The observations made at low light doses may be interpreted satisfactorily in terms of reactions (20), (21) and (5). With high light doses the situation is more complicated and requires further clarification, but the findings suggest that the initiator Z first formed undergoes photochemical transformation to a second species, which initiates at a rate dependent on the value of  $\phi$ . Such dependence may be readily explained. If the initiating species is represented as Y-S we may postulate the reactions:



so that, as observed, the rate of initiation becomes an inverse function of  $[S]$ . Further, this scheme predicts a dependence of  $k$  on  $[RCl]$  between zero- and first-order, as found in the high-intensity experiments. In the case of Z, direct reaction with RCl must be assumed (equation (5)), or (30b) is fast compared to the back reaction in equation (30a).

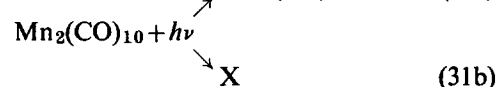
The above considerations suggest that two (or more) initiating species may be present during the dark reaction following high light doses unless effectively complete transformation of Z into one other species occurs. Computer calculations have indicated that departures from first-order decay may not be important over the range of reaction times studied and also that errors introduced into the estimation of  $Z_0$  are not large.

Other types of mechanism may be envisaged, e.g. the photochemical formation of a substance capable of catalysing radical generation from Z, but they seem less satisfactory.

There are no reasons for believing that the complications discussed above are significant at low light doses.

### General

*Alternative mechanisms.* Although unsymmetrical photolysis of  $Mn_2(CO)_{10}$  (equation (20)) offers the simplest explanation of our results, variants of the mechanism based on symmetrical photolysis (equation (15)) deserve consideration. The most attractive of these is shown in equation (31); the primary act is two-fold in nature, X being a species other than  $Mn(CO)_5$ .



For example, X may be formed by rearrangement of  $Mn_2(CO)_{10}$  to  $(CO)_5MnCOMn(CO)_4$  as suggested by

Haines *et al.*<sup>10</sup> for the thermal decomposition of manganese carbonyl. If X gives a relatively stable adduct (i.e. Z) with solvent, initiation following a subsequent dark reaction of Z with halide would be possible. It would be necessary to assume that X does not generate radicals in the absence of solvent, since we have shown that formation of Z does not reduce the rate of radical production during irradiation. Available data on initiation in the absence of solvent would be consistent with equation (31) if equation (31a) constitutes approximately 50% of the primary process, and X reverts to  $\text{Mn}_2(\text{CO})_{10}$ . In the presence of an active solvent, the limiting value of unity for the ratio  $Z_0/I\tau$  would then be obtained if the species Z contained two Mn atoms and  $n=2$  (equation (5)). Further elaboration would be required, however, to account for the dependence of  $Z_0/I\tau$  on  $[\text{Mn}_2(\text{CO})_{10}]$  (Table 5). The fortuitous equality of the rates of reactions (31a and b) is a somewhat unsatisfactory feature, particularly since it must also hold for  $\text{Re}_2(\text{CO})_{10}$ .

A mechanism in which  $(\text{CO})_5\text{MnCOMn}(\text{CO})_4$  (or  $2\text{Mn}(\text{CO})_5$  in a solvent cage) is an intermediate leading to  $\text{Mn}(\text{CO})_4 + \text{Mn}(\text{CO})_6$  is, of course, equivalent for our purposes to reaction (20).

*Delayed photogelation.* In earlier papers<sup>11</sup> we have shown that when the halide component of the initiating system is a preformed polymeric halide, combination of the propagating radicals leads to crosslinking of the chains of the preformed polymer and ultimate gelation. It is clear that the formation of the labile species Z provides a method for obtaining delayed photogelation. Irradiation

of suitable systems for periods shorter than the gel-time would be followed by further crosslinking in the dark, at a rate controllable by variations of the light dose and the reactant concentrations. We are investigating the possibilities of this process.

#### ACKNOWLEDGEMENTS

We are pleased to thank Mr A. C. Bamford, who was responsible for the computations. We are also grateful to the British Council for the award of a scholarship to one of us (J.P.).

#### REFERENCES

- 1 Bamford, C. H., Crowe, P. A. and Wayne, R. P. *Proc. R. Soc. (A)* 1965, **284**, 455
- 2 Bamford, C. H., Crowe, P. A., Hobbs, J. and Wayne, R. P. *Proc. R. Soc. (A)* 1966, **292**, 153
- 3 Bamford, C. H., Bingham, J. and Block, H. *Trans. Faraday Soc.* 1970, **66**, 2612
- 4 Kwok, J. C. *Thesis*, University of Liverpool, 1971
- 5 Bamford, C. H., Barb, W. G., Jenkins, A. D. and Onyon, P. F. 'The Kinetics of Vinyl Polymerization by Radical Mechanisms', Butterworths, London, 1958
- 6 Bamford, C. H. and Finch, C. A. *Proc. R. Soc. (A)*, 1962, **268**, 553
- 7 North, A. M. and Reed, G. A. *Trans. Faraday Soc.* 1961, **57**, 859
- 8 Bamford, C. H. and Brumby, S. *Makromol. Chem.* 1967, **105**, 122
- 9 Bamford, C. H. and Brumby, S. *Chem. Ind.* 1969, p 1020
- 10 Haines, L. I. B., Hopgood, D. and Poë, A. J. *J. Chem. Soc. (A)* 1968, p 421
- 11 See Bamford, C. H. *Eur. Polym. J. Suppl.* 1969, p 1

# Conformation and dimensions of polymethylene and polypropylene in solution

F. Heatley

Chemistry Department, University of Manchester, Manchester M13 9PL, UK  
(Received 6 August 1971)

Calculations of the characteristic ratio and its temperature dependence for polyethylene and isotactic polypropylene have been performed using a rotational isomeric model which takes account of non-staggered conformations and the interdependence of the bond rotational potentials in sequences of four chain bonds. The experimental values are shown to be reproducible satisfactorily by a set of energy parameters consistent with the similarity between steric interactions in the two polymers.

## INTRODUCTION

Recently, powerful statistical mechanical matrix methods, eminently suitable for machine computation, have been developed<sup>1</sup> to handle the problem of accounting for all of the immense number of conformations available to a macromolecule in solution.

These techniques have been applied to the calculation of conformationally averaged polymer properties such as average conformations<sup>1-3</sup>, dimensions<sup>1, 4-7</sup>, strain birefringence<sup>8</sup>, and light scattering<sup>9</sup>.

As formulated hitherto<sup>1</sup>, the method assumes that each bond exists in one of a discrete number of rotational isomers, whose energy depends not only on its own state but also on the states of adjacent bonds. Factors affecting the conformational energy but which operate over more than two chain bonds are ignored. The conformational energy is thus constructed as a sum of contributions from each bond, with each bond contribution further subdivided into contributions from interactions between vicinal groups on that bond and from interactions between those groups and groups on adjacent bonds. Hence the weighting of a given conformation in the averaging calculation is expressed as a product of statistical weights (i.e. Boltzmann factors), one for each energy contribution. A particular conformation is as usual defined as the energy zero, with a statistical weight of unity. Naturally, the calculated properties depend on the assumptions made regarding the number and interdependence of the bond rotational states, and on the magnitudes of the statistical weights. Guidance in the proper attitude to be adopted towards all these factors is obtained from three sources: (a) experimental studies of the rotational isomerism characteristics of small molecules of similar structure<sup>1, 4</sup>; (b) comparison of calculated

polymer properties with experiment<sup>1, 4, 10</sup>; and (c) conformational energy calculations<sup>1, 4, 5</sup>. It is the purpose of this paper to utilize approach (c) to re-investigate for polymethylene and polypropylene the assumptions made hitherto of a two-state<sup>7</sup> or three-state<sup>1, 4, 5</sup> rotational isomeric model for saturated carbon-carbon bonds and pairwise interdependence of bond rotational energy potentials. In the light of the modifications deemed necessary by these calculations, approaches (a) and (b) are used to correlate the experimental values of the mean-square end-to-end distance, and its temperature, dependence, for polymethylene and polypropylene with the values calculated using a consistent set of statistical weights. It is shown that an apparent conflict<sup>10, 11</sup> amongst data for polypropylene can be resolved satisfactorily.

## CONFORMATIONAL ANALYSIS OF POLYMETHYLENE

This has been done previously by Abe *et al.*<sup>4</sup> whose method and nomenclature will be broadly followed. Considering single-bond states first, *Figure 1* shows in projection the three well known<sup>12, 13</sup> staggered rotational isomers of a typical bond  $C_i-C_{i+1}$  in a polymethylene chain. The equivalent conformations designated  $g$  and  $\bar{g}$  are of higher energy than the  $t$  conformation because of the steric conflict between the proximate methylene groups  $C_{i-1}$  and  $C_{i+2}$  and they are therefore assigned a statistical weight  $\sigma < 1$ . [ $\sigma$  is defined by  $\sigma = \exp(-E_\sigma/RT)$  where  $E_\sigma = (E_g - E_t)$  is the energy difference between  $g$  and  $t$  due to the inter-methylene interaction.] Reasonable estimates of  $\sigma$  may be obtained as in previous calculations<sup>1, 4</sup> from direct measurement of  $E_\sigma$  in the lower

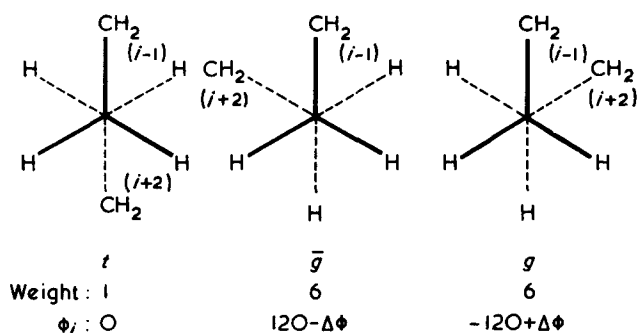


Figure 1 The staggered rotational isomers of bond  $C_i-C_{i+1}$  of polymethylene. The rotation angles are defined in Figure 3

n-alkanes by spectroscopic and electron diffraction techniques. These give an average value<sup>14</sup> of  $500 \pm 100$  cal/mol for  $E_\sigma$ .

Experiments<sup>14</sup> and calculations<sup>1,4</sup> also indicate that the  $g$  and  $\bar{g}$  energy minima do not lie exactly at the staggered rotation angles of  $\pm 120^\circ$  but are displaced by  $5-10^\circ$  towards the  $t$  conformation due to the repulsion of the methylene groups.

Two successive chain bonds can occupy any combination of the states  $t$ ,  $g$  or  $\bar{g}$  without hindrance unless the combined state is  $g\bar{g}$  or  $\bar{g}g$  in which case an interaction of the sort shown in Figure 2 occurs, with statistical weight  $\omega$  and energy contribution  $E_\omega$ . It is the role and status of this conformation which is most worthy of attention.

$E_\omega$  is undoubtedly fairly large, and so is not accessible to direct measurement like  $E_\sigma$ , since the occurrence of conformations of the lower n-alkanes containing  $\omega$  is very low. The most fruitful method of investigating this particular interaction is to use conformational energy calculations. Several sets of semi-empirical potential functions for this purpose have been described<sup>15-20</sup>; application of all these schemes to a  $g\bar{g}$  or  $\bar{g}g$  sequence yields the uniform result that if tetrahedral geometry and staggered rotation angles are maintained, the H...H steric conflict is so large ( $> 5$  kcal/mol) as to exclude this conformation from practical consideration. Indeed this conclusion is also arrived at using reasonably accurate space filling molecular models, for the  $g\bar{g}$  or  $\bar{g}g$  conformations may not be constructed without obvious large bond angle and/or torsion angle strain. The models do suggest, however, that conformations of relatively low energy exist at non-staggered rotation angles in the region of the  $g\bar{g}$  and  $\bar{g}g$  conformations. Such energy minima have been located by Abe *et al.*<sup>4</sup> for n-pentane but were not thought to be significant. The conformational state of this area has therefore been re-investigated using the potential functions given by Warshel and Lifson<sup>20</sup>. The particular value of these functions is their consistency, in that they were derived from consistent force-field calculations of many dissimilar alkane properties, including crystal structures, molecular geometries, conformations and molecular and lattice vibrations. The internal rotation potential energy  $V$  is given as a function of the rotation angles  $\Phi_i$  by:

$$V = \sum_i \frac{1}{2} V_i^0 (1 - \cos 3\Phi_i) + \sum_{j,k} 2\epsilon_{jk} \left[ \left( \frac{r_{jk}}{r} \right)^9 - \frac{3}{2} \left( \frac{r_{jk}}{r} \right)^6 \right] + \frac{e_j e_k}{r}$$

The first term represents the torsional potential energy;  $V_i^0$  is the (three-fold) barrier to rotation about bond  $i$ . The second term is the non-bonded interaction energy summed over pairs of nuclei ( $j, k$ ):  $\epsilon_{jk}$  and  $r_{jk}$  are parameters characterizing the non-bonded energy curve,  $e_j$  and  $e_k$  are the partial charges on  $j$  and  $k$  due to bond dipole moments, and  $r$  is the internuclear distance. Table 1 summarizes the structure and energy parameters used. Although confined to estimating the magnitude of the  $\omega$  interaction alone, the calculations gave results which were very similar to the much more comprehensive calculations of Abe *et al.*<sup>4</sup> for n-pentane. Thus instead of a single energy minimum at the staggered rotation angles, there are two equivalent minima in which one bond retains its staggered  $g$  or  $\bar{g}$  conformation while the other is rotated by about  $40^\circ$  back towards the  $t$  conformation. In terms of the rotation angles defined in Figure 2, neglecting  $\Delta\Phi$ , the non-staggered minima are located at about  $(-120^\circ, +80^\circ)$ ,  $(-80^\circ, +120^\circ)$ ,  $(+120^\circ, -80^\circ)$  and  $(+80^\circ, -120^\circ)$ .  $E_\omega$  is estimated to be  $\sim 2$  kcal/mol, compared to  $2.2$  kcal/mol given by Abe *et al.*<sup>4</sup>. Of course the actual value of  $E_\omega$  is subject to modification in the light of a comparison with experiment, but these calculations do suggest that it is probably low enough to require the inclusion of the non-staggered conformations in any averaging calculations. It becomes doubly important to do so when it is realized that many polymer properties are often measured at fairly high temperatures. For instance the mean-square end-to-end distances which are the subject of this paper were measured at about

Table 1 Structure and energy parameters used in conformational energy calculations

Bond lengths: C-C, 1.5 Å; C-H, 1.09 Å  
 Bond angles: C-C-C, 111°; H-C-H, 109°  
 Torsion:  $V^\circ$  for C-C bond, 1.16 kcal/mol

Non-bonded interaction	(Å)	E	
		(kcal/mol)	(e.s.u.)
H...H	3.548	$2.58 \times 10^{-3}$	0.11
C...C	3.616	$1.847 \times 10^{-1}$	
H...C	3.582	$2.184 \times 10^{-2}$	

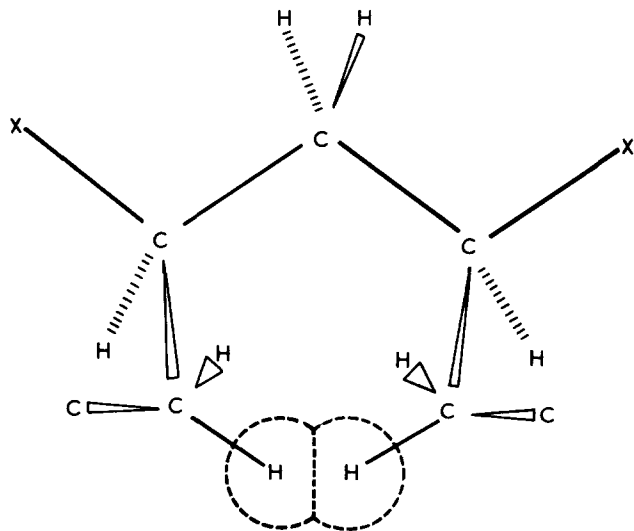


Figure 2 Diagram of the inter-proton steric-conflict in the  $\omega$  interaction

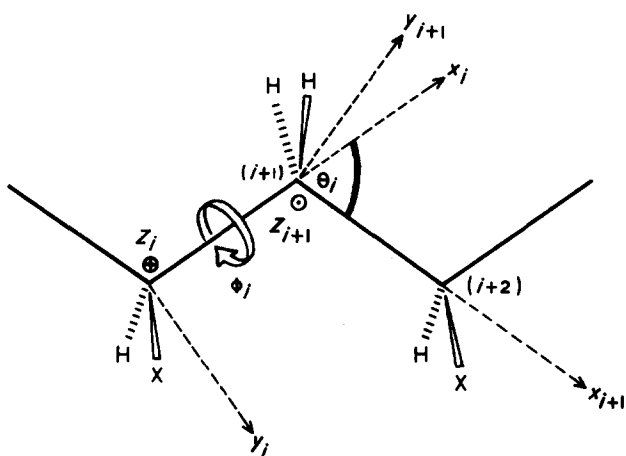


Figure 3 The coordinate reference frames on carbon atoms  $C_i$  and  $C_{i+1}$  of polymethylene ( $X=H$ ) or isotactic polypropylene ( $X=CH_3$ ). The  $z$  axes are perpendicular to the plane of the paper and complete a right-handed coordinate system

140°C (see below). A five-state scheme for each bond has therefore been adopted. The states are denoted  $t$ ,  $g$ ,  $g'$ ,  $\bar{g}$  and  $\bar{g}'$  with angles of rotation  $0$ ,  $(-120 + \Delta\Phi)$ ,  $-80$ ,  $(120 - \Delta\Phi)$  and  $+80^\circ$  respectively. A prime indicates a non-staggered conformation. For a particular bond-pair, there is a total of 21 allowed states, i.e.  $tt$ ,  $gt$ ,  $g't$ ,  $\bar{g}t$ ,  $\bar{g}'t$ ,  $tg$ ,  $tg'$ ,  $t\bar{g}$ ,  $t\bar{g}'$ ,  $gg$ ,  $g'g$ ,  $gg'$ ,  $g'g'$ ,  $\bar{g}\bar{g}$ ,  $\bar{g}'\bar{g}$ ,  $\bar{g}\bar{g}'$ ,  $\bar{g}'\bar{g}'$ ,  $g'\bar{g}$ ,  $g\bar{g}'$ ,  $\bar{g}g'$  and  $\bar{g}'g'$ .

Further calculations were carried out to test the assumption of pairwise interdependence of bond rotation potentials. It was found that in several cases the interdependence stretched over to four bonds. Thus in a four-bond sequence of the nominal  $g\bar{g}g\bar{g}$  or  $\bar{g}\bar{g}g\bar{g}$  type steric conflicts additional to the  $\eta$  and  $\omega$  interactions described above are present which are so numerous that this conformation is effectively suppressed completely. The nominal sequence  $tggg$  and  $t\bar{g}\bar{g}\bar{g}$  are only allowed in the form  $tgg'g$  and  $t\bar{g}\bar{g}'\bar{g}$  respectively, with a statistical weight close to  $\omega^2$ .

In view of considerations such as these and the obvious desirability of using a model as close as possible to the

actual polymer molecule, the  $3 \times 3$  single-bond statistical weight matrix  $U$  used elsewhere<sup>14</sup> has been recast as the  $21 \times 21$  bond-pair matrix given in Table 2. An element  $U_{ij}$  gives the weighting of a bond-pair in the conformation at the head of column  $j$  when the preceding bond-pair occupies the conformation at the left of row  $i$ . Zero elements refer to conformations which are either forbidden energetically, such as  $g\bar{g}'$ ,  $g\bar{g}$ , or do not lie at an energy minimum, even though it is of low energy, such as  $ttg't$ . The same statistical weight  $\eta$  has been used for the  $g$ ,  $\bar{g}$ ,  $g'$  and  $\bar{g}'$  conformations. Strictly a difference weight, say  $\rho$ , should be used for the primed conformations. However, if used,  $\rho$  would occur only in conjunction with  $\omega$  so any difference between  $\eta$  and  $\rho$  may be accommodated without error by re-defining  $\omega$  to take this difference into account. No loss of accuracy is occasioned by the procedure, and there are advantages to be gained by using only two parameters.

### CONFORMATIONAL ANALYSIS OF POLYPROPYLENE

Because of similarities in chemical composition and molecular geometry, the conformational analysis of polypropylene differs little from that of polymethylene. Figure 4 shows the three 'nominal' staggered conformations of the single bond  $C_i-C_{i+1}$  in Figure 3, with their rotation angles.

The  $t$  and  $g$  conformations are given equal weights of unity since the  $CH \dots CH_3$  *gauche* interaction in  $t$  is unlikely to differ significantly from the  $CH \dots CH_2$  interaction in  $g$ . The  $g^*$  conformation carries a statistical weight  $\tau < 1$  since it possesses two *gauche* interactions. The energy difference between  $g^*$  and  $t$  (or  $g$ ) in Figure 4 is approximately the same as that between  $g$  (or  $\bar{g}$ ) and  $t$  in Figure 1. However, because of the two opposed *gauche* interactions, the energy of the  $g^*$  state is not reduced by a displacement  $\Delta\Phi$  of the torsional angle as in polymethylene so  $E_\tau$  is likely to be greater than  $E_\sigma$ . A value of 1000 cal/mol has been estimated for  $E_\tau$  based on spectroscopic evidence and energy calculations. As will be shown later, the value of  $\tau$  is not critical.

Table 2 Statistical weight matrix for a bond-pair in polymethylene

	$tt$	$gt$	$g't$	$\bar{g}t$	$\bar{g}'t$	$t\bar{g}$	$t\bar{g}'$	$tg$	$tg'$	$gg$	$g'g$	$gg'$	$\bar{g}\bar{g}$	$\bar{g}'\bar{g}$	$\bar{g}\bar{g}'$	$g'\bar{g}$	$g\bar{g}'$	$\bar{g}g'$	$\bar{g}'g'$	$g'g'$	$\bar{g}'\bar{g}'$
$tt$	1	$\sigma$	0	$\sigma$	0	$\sigma$	$\sigma$	$\sigma$	$\sigma$	$\sigma^2$	0	$\sigma^2$	$\sigma^2$	0	$\sigma^2$	$\sigma^2\omega$	$\sigma^2\omega$	$\sigma^2\omega$	$\sigma^2\omega$	0	0
$gt$	1	$\sigma$	0	$\sigma$	0	$\sigma$	$\sigma$	$\sigma$	$\sigma$	$\sigma^2$	0	$\sigma^2$	$\sigma^2$	0	$\sigma^2$	$\sigma^2\omega$	$\sigma^2\omega$	$\sigma^2\omega$	$\sigma^2\omega$	0	0
$g't$	1	$\sigma$	0	$\sigma$	0	$\sigma$	$\sigma$	$\sigma$	$\sigma$	$\sigma^2$	0	$\sigma^2$	$\sigma^2$	0	$\sigma^2$	$\sigma^2\omega$	$\sigma^2\omega$	$\sigma^2\omega$	$\sigma^2\omega$	0	0
$\bar{g}t$	1	$\sigma$	0	$\sigma$	0	$\sigma$	$\sigma$	$\sigma$	$\sigma$	$\sigma^2$	0	$\sigma^2$	$\sigma^2$	0	$\sigma^2$	$\sigma^2\omega$	$\sigma^2\omega$	$\sigma^2\omega$	$\sigma^2\omega$	0	0
$\bar{g}'t$	1	$\sigma$	0	$\sigma$	0	$\sigma$	$\sigma$	$\sigma$	$\sigma$	$\sigma^2$	0	$\sigma^2$	$\sigma^2$	0	$\sigma^2$	$\sigma^2\omega$	$\sigma^2\omega$	$\sigma^2\omega$	$\sigma^2\omega$	0	0
$t\bar{g}$	1	0	$\sigma\omega$	$\sigma$	0	$\sigma$	$\sigma$	$\sigma$	$\sigma$	0	$\sigma^2\omega$	0	$\sigma^2$	0	$\sigma^2\omega$	$\sigma^2\omega$	$\sigma^2\omega$	$\sigma^2\omega$	$\sigma^2\omega$	0	0
$t\bar{g}'$	0	$\sigma\omega$	0	0	0	0	0	0	0	$\sigma^2\omega$	0	$\sigma^2\omega$	0	0	0	0	0	0	0	0	0
$tg$	1	$\sigma$	0	0	$\sigma\omega$	$\sigma$	$\sigma$	$\sigma$	$\sigma$	$\sigma^2$	0	$\sigma^2$	0	$\sigma^2\omega$	0	$\sigma^2\omega$	$\sigma^2\omega$	0	$\sigma^2\omega^2$	0	$\sigma^2\omega$
$tg'$	0	0	0	$\sigma\omega$	0	0	0	0	0	0	0	0	$\sigma^2\omega$	0	$\sigma^2\omega$	0	0	0	0	0	0
$gg$	1	$\sigma$	0	0	$\sigma\omega$	$\sigma$	$\sigma$	$\sigma$	$\sigma$	$\sigma^2$	0	$\sigma^2$	0	$\sigma^2\omega$	0	$\sigma^2\omega$	$\sigma^2\omega$	0	0	0	$\sigma^2\omega$
$g'g$	1	$\sigma$	0	0	$\sigma\omega$	$\sigma$	$\sigma$	$\sigma$	$\sigma$	$\sigma^2$	0	$\sigma^2$	0	$\sigma^2\omega$	0	$\sigma^2\omega$	$\sigma^2\omega$	0	0	0	$\sigma^2\omega$
$gg'$	0	0	0	$\sigma\omega$	0	0	0	0	0	0	0	0	$\sigma^2\omega$	0	$\sigma^2\omega$	0	0	0	0	0	0
$\bar{g}\bar{g}$	1	0	$\sigma\omega$	$\sigma$	0	$\sigma$	$\sigma$	$\sigma$	$\sigma$	0	$\sigma^2\omega$	0	$\sigma^2$	0	$\sigma^2$	0	0	$\sigma^2\omega$	$\sigma^2\omega$	$\sigma^2\omega$	0
$\bar{g}'\bar{g}$	1	0	$\sigma\omega$	$\sigma$	0	$\sigma$	$\sigma$	$\sigma$	$\sigma$	0	$\sigma^2\omega$	0	$\sigma^2$	0	$\sigma^2$	0	0	$\sigma^2\omega$	$\sigma^2\omega$	$\sigma^2\omega$	0
$\bar{g}\bar{g}'$	0	$\sigma\omega$	0	0	0	0	0	0	0	$\sigma^2\omega$	0	$\sigma^2\omega$	0	0	0	0	0	0	0	0	0
$g'\bar{g}$	1	$\sigma\omega$	0	$\sigma$	0	$\sigma$	$\sigma$	$\sigma$	$\sigma$	0	0	0	$\sigma^2$	0	$\sigma^2$	0	0	$\sigma^2\omega$	$\sigma^2\omega$	0	0
$g\bar{g}'$	1	$\sigma$	0	$\sigma\omega$	0	$\sigma$	$\sigma$	$\sigma$	$\sigma$	$\sigma^2$	0	$\sigma^2$	0	0	0	$\sigma^2\omega$	$\sigma^2\omega$	0	0	0	0
$\bar{g}'g'$	1	$\sigma$	0	0	0	$\sigma$	$\sigma$	$\sigma$	$\sigma$	$\sigma^2$	0	$\sigma^2$	0	0	0	$\sigma^2\omega$	$\sigma^2\omega$	0	0	0	0
$g'g'$	0	0	0	$\sigma\omega$	0	0	0	0	0	0	0	0	$\sigma^2\omega$	0	$\sigma^2\omega$	0	0	0	0	0	0
$\bar{g}'\bar{g}'$	0	$\sigma\omega$	0	0	0	0	0	$\sigma$	$\sigma$	$\sigma^2\omega$	0	$\sigma^2\omega$	0	0	0	0	0	0	0	0	0

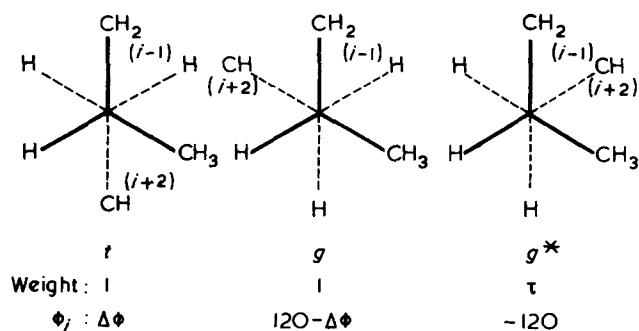


Figure 5 The staggered rotational isomers of a single bond in polypropylene. The rotation angles are for bond  $C_i-C_{i+1}$  of the isotactic dyad shown in Figure 3

The degree of interdependence of the rotational potentials of a two-bond sequence in polypropylene depends naturally on the stereochemistry. Consider first an isotactic dyad<sup>21</sup>. Of the nine possible staggered conformations of this unit only two, the  $(gt)$  and  $(tg)$  forms, are without additional steric conflicts<sup>1, 5, 22</sup>. All others contain at least one  $\omega$  interaction identical to that shown in Figure 2 with the difference that the conflicting protons may belong to a methyl group instead of to a methylene group. As in polymethylene, such conformations do not exist, and should be replaced by one or more non-staggered conformations nearby. Thus the  $tt$  and  $gg$  conformations, which contain an  $\omega$  interaction between two methyl and two methylene groups respectively, are replaced by  $t't$ ,  $tt'g'g'$  and  $gg'$  conformations where the prime again indicates a non-staggered bond. For bond  $C_i-C_{i+1}$  of the isotactic polypropylene dyad illustrated in Figure 3, the rotation angles for the  $t'$  and  $g'$  conformations are  $40^\circ$  and  $80^\circ$  respectively.

These conformations containing bonds in the  $g^*$  state depart slightly from this pattern. For the nominal  $gg^*$ ,  $g^*g$ ,  $tg^*$ , and  $g^*t$  states, energy minima for non-staggered positions of the  $g$  or  $t$  bond exist, but not for the 'twin' conformations in which the  $g^*$  bond is non-staggered. Calculations showed that although the  $\omega$ -interaction is alleviated in a  $g^*$  state, an additional conflict occurs between a methyl or methylene proton and the methine proton on the side of the polymer backbone chain opposite to that containing the  $\omega$ -interaction. This secondary interaction is strong enough to eliminate the energy minimum which would otherwise occur. Thus, the four conformations  $g'g^*$ ,  $g^*g'$ ,  $t'g^*$  and  $g^*t'$  are required.

The remaining conformation,  $g^*g^*$ , contains two  $\omega$ -interactions, neither of which can be alleviated by

moderate bond rotations. It is safe to neglect this conformation entirely.

In a sequence of two isotactic dyads, steric conflicts are encountered in conformations of the types  $(-g)(g-)$  or  $(-g^*)(g^*-)$  where the parentheses enclose the two bonds of a dyad and the hyphen represents  $t$ ,  $t'$ ,  $g$  or  $g'$  as appropriate; no difficulty arises in all other cases. In the  $(-g)(g-)$  case the conflict is an  $\omega$  interaction between two methine protons which, if the sequence is  $(tg)(gt)$  is resolvable into  $(tg)(g't)$  and  $(tg')(gt)$  conformations as before. Of the other possible sequences, those of the general type  $(gg)(gg)$ , and the conformations  $(gg)(g'g^*)$ ,  $(g^*g')(g'g^*)$  and are all precluded by the large number of irresolvable steric interactions, while those of the nominal type  $(tg)(gg)$  are allowed in the form  $(tg)(g'g)$  with statistical weight  $\omega^2$  (c.f. the  $(tggg)$  conformation of polymethylene above). The conformation  $(tg)(g'g^*)$  is also allowed with weight  $\omega^2$ .

Sequences of the type  $(-g^*)(g^*-)$  all contain a very strong methyl-methyl repulsion which is not removable, and hence these conformations may be ignored.

Tables 3 gives the  $13 \times 13$  statistical weight matrix  $U_{mm}$  for an isotactic dyad preceded by another isotactic dyad. The zero matrix elements represent conformations which are either strongly sterically hindered (see above) or do not lie at an energy minimum, e.g.  $(gt)(g't)$ .

Exactly similar considerations apply to the analysis of syndiotactic dyads. In this case the low energy conformations are  $(tt)$  and  $(gg)$ <sup>1, 5, 22</sup>. The conformational set is  $(tt)$ ,  $(gg)$ ,  $(t'g)$ ,  $(tg')$ ,  $(g't)$ ,  $(gt')$ ,  $(t'g^*)$ ,  $(g^*t')$ ,  $(g'g^*)$ ,  $(g'g')$ ,  $(gg')$  and  $(g'g')$ . Note that this set contains one more conformation  $\{(g'g')\}$  than the isotactic dyad set; this is necessary to take into account the possibility of sequences such as  $\dots(gg)(g'g')(gg)\dots$ . The  $14 \times 14$  statistical weight matrix  $U_{rr}$  for a syndiotactic dyad preceded by another is given in Table 4. The  $14 \times 13$  matrix  $U_{rm}$  for an isotactic dyad preceded by a syndiotactic is the same as  $U_{mm}$  except that row 14 identical to row 13 is added, row 12 is replaced by a row identical to row 5, and the rows are labelled as in  $U_{rr}$ . The  $13 \times 14$  matrix  $U_{mr}$  is the same as  $U_{rr}$  except that row 14 is deleted, row 12 is replaced by a row identical to row 3 and the rows are labelled as in  $U_{mm}$ .

#### CALCULATION OF UNPERTURBED MEAN-SQUARE END-TO-END DISTANCE

The treatment of this problem has been given by Flory<sup>23</sup> but since he used statistical weight matrices for single

Table 3 Statistical weight matrix for an isotactic polypropylene dyad preceded by another isotactic dyad

	$g'g$	$gg'$	$gt$	$g'g^*$	$tg$	$t't$	$tt'$	$t'g^*$	$g^*g'$	$g^*t'$	$g^*g^*$	$g't$	$tg'$
$g'g$	0	0	0	0	1	$\omega$	$\omega$	$\tau\omega$	$\tau\omega$	$\tau\omega$	0	0	1
$gg'$	0	0	$\omega$	0	1	$\omega$	$\omega$	$\tau\omega$	$\tau\omega$	$\tau\omega$	0	0	1
$gt$	$\omega$	$\omega$	1	$\tau\omega$	1	$\omega$	$\omega$	$\tau\omega$	$\tau\omega$	$\tau\omega$	0	0	1
$g'g^*$	$\omega$	$\omega$	1	$\tau\omega$	1	$\omega$	$\omega$	$\tau\omega$	0	0	0	0	1
$tg$	$\omega^2$	0	0	$\tau\omega^2$	1	$\omega$	$\omega$	$\tau\omega$	$\tau\omega$	$\tau\omega$	0	$\omega$	1
$t't$	$\omega$	$\omega$	1	$\tau\omega$	1	$\omega$	$\omega$	$\tau\omega$	$\tau\omega$	$\tau\omega$	0	0	1
$tt'$	$\omega$	$\omega$	1	$\tau\omega$	1	$\omega$	$\omega$	$\tau\omega$	$\tau\omega$	$\tau\omega$	0	0	1
$t'g^*$	$\omega$	$\omega$	1	$\tau\omega$	1	$\omega$	$\omega$	$\tau\omega$	0	0	0	0	1
$g^*g'$	0	0	$\omega$	0	1	$\omega$	$\omega$	$\tau\omega$	$\tau\omega$	$\tau\omega$	0	0	1
$g^*t'$	$\omega$	$\omega$	1	$\tau\omega$	1	$\omega$	$\omega$	$\tau\omega$	$\tau\omega$	$\tau\omega$	0	0	1
$g^*g^*$	$\omega$	$\omega$	1	$\tau\omega$	1	$\omega$	$\omega$	$\tau\omega$	0	0	0	0	1
$g't$	$\omega$	$\omega$	1	$\tau\omega$	1	$\omega$	$\omega$	$\tau\omega$	$\tau\omega$	$\tau\omega$	0	0	1
$tg'$	0	0	$\omega$	0	0	0	0	0	0	0	0	0	0



Table 4 Statistical weight matrix for a syndiotactic polypropylene dyad preceded by another syndiotactic dyad

	<i>t'g</i>	<i>tg'</i>	<i>tt</i>	<i>t'g*</i>	<i>gg</i>	<i>g't</i>	<i>gt'</i>	<i>g'g*</i>	<i>g*g'</i>	<i>g*t'</i>	<i>g*g*</i>	<i>g'g</i>	<i>gg'</i>	<i>g'g'</i>
<i>t'g</i>	$\omega$	$\omega$	1	$\tau\omega$	0	0	0	0	$\tau\omega$	$\tau\omega$	0	0	0	0
<i>tg'</i>	$\omega$	$\omega$	1	$\tau\omega$	$\omega$	0	0	0	$\tau\omega$	$\tau\omega$	0	0	$\omega$	0
<i>tt</i>	$\omega$	$\omega$	1	$\tau\omega$	1	$\omega$	$\omega$	$\tau\omega$	$\tau\omega$	$\tau\omega$	0	0	1	0
<i>t'g*</i>	$\omega$	$\omega$	1	$\tau\omega$	1	$\omega$	$\omega$	$\tau\omega$	0	0	0	0	1	0
<i>gg</i>	$\omega$	$\omega$	1	$\tau\omega$	0	$\omega^2$	0	$\tau\omega^2$	$\tau\omega$	$\tau\omega$	0	$\omega$	0	$\omega$
<i>g't</i>	$\omega$	$\omega$	1	$\tau\omega$	1	$\omega$	$\omega$	$\tau\omega$	$\tau\omega$	$\tau\omega$	0	0	1	0
<i>gt'</i>	$\omega$	$\omega$	1	$\tau\omega$	1	$\omega$	$\omega$	$\tau\omega$	$\tau\omega$	$\tau\omega$	0	0	1	0
<i>g'g*</i>	$\omega$	$\omega$	1	$\tau\omega$	1	$\omega$	$\omega$	$\tau\omega$	0	0	0	0	1	0
<i>g*g'</i>	$\omega$	$\omega$	1	$\tau\omega$	$\omega$	0	0	0	$\tau\omega$	$\tau\omega$	0	0	$\omega$	0
<i>g*t'</i>	$\omega$	$\omega$	1	$\tau\omega$	1	$\omega$	$\omega$	$\tau\omega$	$\tau\omega$	$\tau\omega$	0	0	1	0
<i>g*g*</i>	$\omega$	$\omega$	1	$\tau\omega$	1	$\omega$	$\omega$	$\tau\omega$	0	0	0	0	1	0
<i>g'g</i>	$\omega$	$\omega$	1	$\tau\omega$	0	$\omega^2$	0	$\tau\omega^2$	$\tau\omega$	$\tau\omega$	0	$\omega$	0	$\omega$
<i>gg'</i>	0	0	0	0	$\omega$	0	0	0	0	0	0	0	$\omega$	0
<i>g'g'</i>	0	0	0	0	$\omega$	0	0	0	0	0	0	0	$\omega$	0

bonds only, it will be necessary to modify the equations slightly in order to use them with matrices applying to bond pairs.

Define in the coordinate frame on the first carbon atom in bond-pair *i*,  $C_{2i}$ , a vector  $\mathbf{d}_i$  which links the outermost carbon atoms of that bond-pair. The chain vector (from the second carbon atom in the chain to the penultimate) for a chain of *n* bond-pairs is given by:

$$\mathbf{D} = \sum_{i=1}^n \mathbf{d}_i$$

The unperturbed mean-square end-to-end distance is therefore given by:

$$\begin{aligned} \langle r^2 \rangle_0 &= \langle \mathbf{D} \cdot \mathbf{D} \rangle \\ &= \sum_{i,j} \langle \mathbf{d}_i \cdot \mathbf{d}_j \rangle \\ &= \sum_i \mathbf{d}_i^2 + 2 \sum_{\substack{1 \leq i < j \leq n}} \langle \mathbf{d}_i \cdot \mathbf{d}_j \rangle \end{aligned}$$

In order to use Flory's formulation, it is necessary to write a scalar product in the second sum in the form

$$\langle \mathbf{d}_i \cdot \mathbf{d}_j \rangle = \mathbf{d}_i^{0(T)} \langle \mathbf{X}_{ij} \rangle \mathbf{d}_j^0$$

where the superscript *T* represents transposition.  $\mathbf{d}_i^0$  and  $\mathbf{d}_j^0$  are constant vectors which are independent of the conformation and  $\langle \mathbf{X}_{ij} \rangle$  is the average value of the transformation matrix which brings  $\mathbf{d}_j^0$  in the same frame as  $\mathbf{d}_i^0$ .

However, in the reference frame defined on  $C_{2i}$ ,  $\mathbf{d}_i$  will depend on  $\Phi_{2i}$ , the angle of rotation about bond  $C_{2i}-C_{2i+1}$ . It is therefore necessary to specify that  $\mathbf{d}_i$  be defined as the vector  $C_{2i} \rightarrow C_{2i+2}$  when  $\Phi_{2i} = 0$ , i.e. in the *t* conformation; this vector is denoted by  $\mathbf{d}_i^0$ .  $\mathbf{X}_{ij}$  is then given by:

$$\mathbf{X}_{ij} = \mathbf{T}_i^{0(T)} \left[ \prod_{k=i}^{j-1} (\mathbf{T}_{2k} \cdot \mathbf{T}_{2k+1}) \right] \mathbf{T}_j^0$$

$\mathbf{T}_{2k}$  is the matrix which transforms a vector in reference frame  $2k+1$  into a vector in reference frame  $2k$  and  $\mathbf{T}_i^0$  is the matrix which transforms the vector  $\mathbf{d}_i^0$  defined when bond  $2i$  is *t* into the actual vector  $\mathbf{d}_i^0$ , the reference frame being  $2i$  in both cases.

$\mathbf{T}_{2k}$  and  $\mathbf{T}_i^0$  are given by

$$\mathbf{T}_{2k} = \begin{bmatrix} \cos\theta_{2k} & \sin\theta_{2k} & 0 \\ \sin\theta_{2k} \cos\phi_{2k} & -\cos\theta_{2k} \cos\phi_{2k} & \sin\phi_{2k} \\ \sin\theta_{2k} \sin\phi_{2k} & -\cos\theta_{2k} \sin\phi_{2k} & -\cos\phi_{2k} \end{bmatrix}$$

$$\mathbf{T}_i^0 = \begin{bmatrix} 1 & 0 & 0 \\ 0 & \cos\phi_{2i} & -\sin\phi_{2i} \\ 0 & \sin\phi_{2i} & \cos\phi_{2i} \end{bmatrix}$$

Following Flory<sup>1</sup>, one can then write:

$$\begin{aligned} \langle \mathbf{d}_i \cdot \mathbf{d}_j \rangle &= Q^{-1} \cdot \mathbf{d}_i^{0(T)} \cdot \mathbf{T}_i^{0(T)} \left[ \prod_{k=1}^{j-1} (\mathbf{T}_{2k} \cdot \mathbf{T}_{2k+1}) \right] \cdot \mathbf{T}_j^0 \cdot \mathbf{d}_j^0 \\ &= Q^{-1} \cdot \mathbf{J}^* \cdot \left( \prod_{k=1}^{i-1} \mathbf{U}(k) \right) (\mathbf{E}_\nu \otimes \mathbf{d}_i^{0(T)}) \times \\ &\quad [(\mathbf{U}^{(i)} \otimes \mathbf{E}_3) \|\mathbf{T}_i^{0(T)} \cdot \mathbf{T}_{2i} \cdot \mathbf{T}_{2i+1}\|] \times \\ &\quad \left( \prod_{l=i+1}^{j-1} [(\mathbf{U}^{(l)} \otimes \mathbf{E}_3) \|\mathbf{T}_{2l} \cdot \mathbf{T}_{2l+1}\|] \right) \times \\ &\quad [(\mathbf{U}^{(j)} \otimes \mathbf{E}_3) \|\mathbf{T}_j^0\|] (\mathbf{E}_\nu \otimes \mathbf{d}_j^0) \cdot \left( \prod_{m=j+1}^n \mathbf{U}(m) \right) \cdot \mathbf{J} \end{aligned}$$

The symbol  $\otimes$  denotes the matrix direct product and  $\mathbf{E}_\nu$  is the unit matrix of dimension  $\nu$  as required to conform with  $\mathbf{U}$ . The  $1 \times \nu$  and  $\nu \times 1$  matrices  $\mathbf{J}^*$  and  $\mathbf{J}$  are defined by:

$$\mathbf{J}^* = [0 \ 0 \ 1 \ 0 \ \dots \ 0]; \quad \mathbf{J} = \begin{bmatrix} 1 \\ 1 \\ \vdots \\ 1 \end{bmatrix}$$

This  $\mathbf{J}^*$  matrix differs from that given by Flory in having the third element equal to unity, not the first, since the  $\mathbf{U}$  matrices used here have been defined such that it is row 3 which gives the statistical weights for the first bond-pair or dyad. The matrices such as  $\|\mathbf{T}_j^0\|$  are the block-diagonal matrices defined by e.g.:

$$\|\mathbf{T}_j^0\| = \begin{bmatrix} \mathbf{T}_j^0(\phi_1) & & & \\ & \mathbf{T}_j^0(\phi_2) & & \\ & & \ddots & \\ & & & \mathbf{T}_j^0(\phi_\nu) \end{bmatrix}$$

where  $\mathbf{T}_j^0(\phi_\alpha)$  is the  $\mathbf{T}_j^0$  matrix for conformation  $\alpha$  with angle of rotation  $\phi_\alpha$ .  $Q$  is the conformational partition function for the chain and is given by:

$$Q = \mathbf{J}^* \cdot \left[ \prod_{i=1}^n \mathbf{U}(i) \right] \cdot \mathbf{J}$$

$\mathbf{U}^{(i)}$  is the statistical weight matrix appropriate to the *i*th polymethylene bond-pair or polypropylene dyad as the case may be.

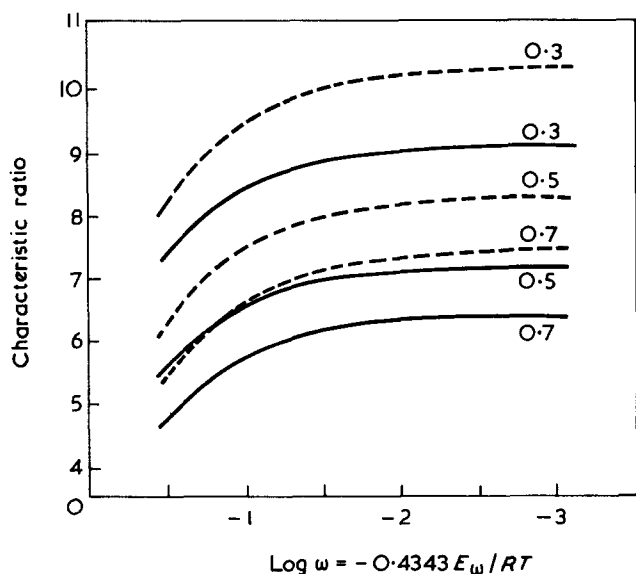


Figure 5 The characteristic ratio of polymethylene as a function of  $\omega$  for selected values of  $\sigma$  and  $\Delta\Phi$ . The values of  $\sigma$  are given for each curve. —  $\Delta\Phi=0^\circ$ ; ---  $\Delta\Phi=7.5^\circ$

For a polymer consisting of a sequence of repeating units with  $d^0 = d^1 = d^0$  the mean-square end-to-end distance is<sup>1</sup>:

$$\langle r^2 \rangle_0 = 2Q^{-1} \cdot \mathbf{J}^* \cdot [\mathbf{0} \ \mathbf{0} \ \mathbf{E}_\nu \ \mathbf{0} \ \dots \ \mathbf{0}] \left( \prod_{i=1}^{n-1} \mathcal{G}_i \right) \times \left[ \begin{array}{c} (d^2/2)\mathbf{U}^{(n)} \\ [(\mathbf{U}^{(n)} \otimes \mathbf{E}_3) \parallel \mathbf{T}_n^0 \parallel] (\mathbf{E}_\nu \otimes \mathbf{d}^0) \\ \mathbf{U}^{(n)} \end{array} \right] \cdot \mathbf{J}$$

where

$$\mathcal{G}_i = \begin{bmatrix} \mathbf{U}^{(i)} & (\mathbf{U}^{(i)} \otimes \mathbf{d}^{0(T)}) \parallel \mathbf{T}_i^0 \parallel \cdot \mathbf{T}_{2i} \cdot \mathbf{T}_{2i+1} \parallel \\ \mathbf{0} & (\mathbf{U}^{(i)} \otimes \mathbf{E}_3) \parallel \mathbf{T}_{2i} \cdot \mathbf{T}_{2i+1} \parallel \\ \mathbf{0} & \mathbf{0} \end{bmatrix} \left[ \begin{array}{c} (d^2/2)\mathbf{U}^{(i)} \\ [(\mathbf{U}^{(i)} \otimes \mathbf{E}_3) \parallel \mathbf{T}_i^0 \parallel] (\mathbf{E}_\nu \otimes \mathbf{d}^0) \\ \mathbf{U}^{(i)} \end{array} \right]$$

The symbol  $\mathbf{0}$  represents a null matrix. The characteristic ratio ( $CR$ ) is defined by  $CR = \langle r^2 \rangle / 2nl^2$  where  $l$  is the C-C bond length in the polymer backbone.

The temperature coefficient of the end-to-end distance, expressed in the usual form  $d \ln \langle r^2 \rangle / dT$  was obtained by varying the statistical weights, according to the Boltzmann equation, by small amounts about a mean value, and by use of the equation:

$$\frac{d \ln \langle r^2 \rangle}{dT} = \frac{\partial \ln \langle r^2 \rangle}{\partial \ln \sigma} \cdot \left( \frac{E_\sigma}{RT^2} \right) + \frac{\partial \ln \langle r^2 \rangle}{\partial \ln \omega} \cdot \left( \frac{E_\omega}{RT^2} \right)$$

## RESULTS AND DISCUSSION

Figure 5 shows the  $CR$  of a polymethylene chain of 256 bonds (i.e.  $n = 128$ ) as a function of  $\omega$  for a representative selection of values of  $\sigma$  and  $\Delta\Phi$ . A 256 bond chain was chosen so as to minimize computing time and yet obtain a result close to the convergence limit for an infinite chain.

Trial calculations for longer chains showed that this objective was achieved. It is seen that the calculated  $CR$  depends considerably on all three parameters. The results are similar to those calculated<sup>1,4</sup> using the three-state model, the major difference being for that given  $\sigma$ ,  $\omega$  and  $\Delta\Phi$  the present values are about 0.4 lower. This no doubt reflects the presence of more *gauche* conformations.

Figure 6 shows the temperature dependence of the mean-square end-to-end distance, expressed as  $d \ln \langle r^2 \rangle_0 / dT$ , as a function of  $\sigma$ ,  $\omega$  and  $\Delta\Phi$ . Again the behaviour is similar to that calculated with the three-state model. The temperature coefficient is negative because the 'ground state' is the extremely long all-*trans* conformation. The excited states, which are more populated as the temperature rises, are the *g* and  $\bar{g}$  states, which tend to shorten the chain. The  $CR$  increases with  $\Delta\Phi$  for much the same reason: increasing  $\Delta\Phi$  moves the *g* and  $\bar{g}$  minima towards the *t* minimum thus increasing the *t* character of the chain.

In the case of polypropylene, the chief interest lies in the dimensions of the isotactic isomer, since this is the only form whose dimensions are determined by the magnitudes of steric interactions. Earlier calculations<sup>1</sup> with the three-state rotational isomeric model have shown that irregular stereochemistry produces more or less the same randomizing influence on the overall polymer conformation as does the availability of high energy conformations. Figure 7 therefore shows the calculated  $CR$  of completely isotactic polypropylene chains as a function of  $\tau$ ,  $\omega$ , and  $\Delta\Phi$ . It is seen that the  $CR$  is quite sensitive to  $\omega$  and  $\Delta\Phi$  but much less so to  $\tau$ , particularly when  $\omega$  is large. The present results are considerably lower than those calculated using two<sup>7</sup> or three-state<sup>1,5</sup> models. For a chain with  $\tau = 0.5$ ,  $\omega = 0.1$ ,  $\Delta\Phi = 0$ , this work gives the  $CR = 5.6$ , compared with values of approximately 9 from the two-state and 7 from the three-state schemes. As for polymethylene the difference is due to the additional conformations considered in this work. In

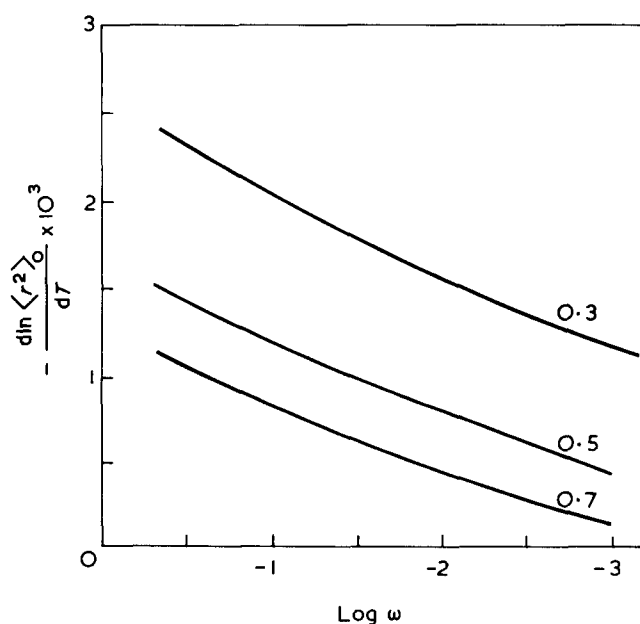


Figure 6 The temperature coefficient of the dimensions of polymethylene as a function of  $\omega$  for the values of  $\sigma$  given for each curve. The curves for  $\Delta\Phi=0$  and  $7.5^\circ$  are practically identical

contrast to polymethylene, the  $CR$  decreases as  $\Delta\Phi$  increases. This is due to the fact that in polypropylene  $\Delta\Phi$  affects the  $t$  conformation as well as the  $g$ , thus preventing the  $t$  form from propagating the chain vector in a constant direction.

Figure 8 shows the temperature coefficient of the end-to-end distance of isotactic polypropylene. It is again negative, for much the same reason as polymethylene.

In view of the close similarity between the steric interactions in polymethylene and polypropylene discussed above, the experimental values of the characteristic ratios and their temperature coefficients should be reproducible by the same set of statistical weights, allowance being made for different temperatures of measurements if necessary. The data available for  $\theta$  conditions have been collected in Table 5. The  $CR$  values were obtained from viscosity measurements using the Flory-Fox equation:

$$[\eta] = \Phi \left[ \frac{\langle r^2 \rangle}{M} \right]^{3/2} \cdot M^{1/2}$$

where  $M$  is the molecular weight.  $\Phi$  is a constant whose quoted values<sup>5</sup> range from  $2.5 \times 10^{21}$  to  $2.87 \times 10^{21}$  ( $r$  in cm,  $[\eta]$  in dl/g); the  $CR$  values in Table 5 have been recalculated using intermediate value  $\Phi = 2.6 \times 10^{21}$  given by Flory<sup>1</sup>.

The first three values of the temperature coefficient for polymethylene were obtained from stress-temperature measurements on the solid and swollen polymer; the fourth value for polymethylene and that for polypropylene were obtained from measurements of the temperature coefficient of the intrinsic viscosity.

There is good agreement amongst the data for polymethylene, but an uncomfortably wide scatter in the  $CR$  values of various polypropylene samples is evident. This is possibly due to small differences in the amount of residual syndiotactic units which are known<sup>1, 5, 7</sup> to affect the dimension critically. Only the sample used by Heatley *et al.*<sup>10</sup> was adequately characterized in this respect; nuclear magnetic resonance (n.m.r.) analysis showed this sample to contain 2% syndiotactic dyads occurring at random. Since previous calculations<sup>5</sup> using the three-state model have shown that at 2% syndiotacticity, the dimensions are determined by the conformational, not stereochemical irregularities, the  $CR$  for this sample is probably the most reliable for the purpose of determining the statistical weights. However, in view

Table 5 Experimental values of the  $CR$  and its temperature coefficient

Polymer	Temp. (°C)	$CR$	$\frac{d \ln \langle r^2 \rangle_0}{dT}$ (deg <sup>-1</sup> × 10 <sup>3</sup> )	Reference
Polymethylene	138	6.7		24, 25
	142	6.8		24, 26
	140	6.6		27, 28
	140-190		$-1.0 \pm 0.1$	29, 30
	120-170		$-1.15 \pm 0.1$	29, 30
	130-180		$-1.0 \pm 0.2$	29, 30
Polypropylene (isotactic)	110-170		$-1.2 \pm 0.2$	28
	145	5.7		31
	145	4.5		32
	145	4.6		10
	143	5.7		33
	145		$-1.6 \pm 0.2$	34

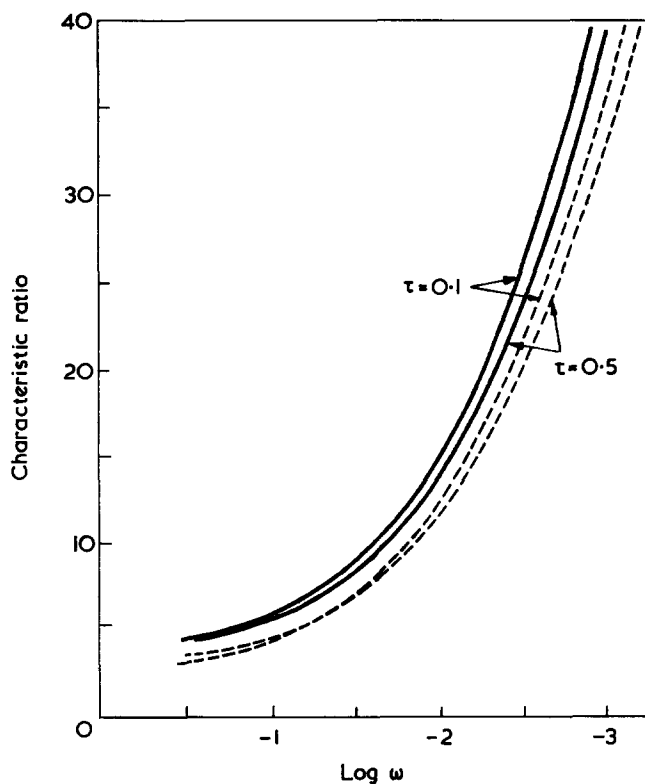


Figure 7 The characteristic ratio of isotactic polypropylene as a function of  $\omega$  for selected values of  $\tau$  and  $\Delta\omega$ . —  $\Delta\Phi = 0^\circ$ ; ---  $\Delta\Phi = 7.5^\circ$

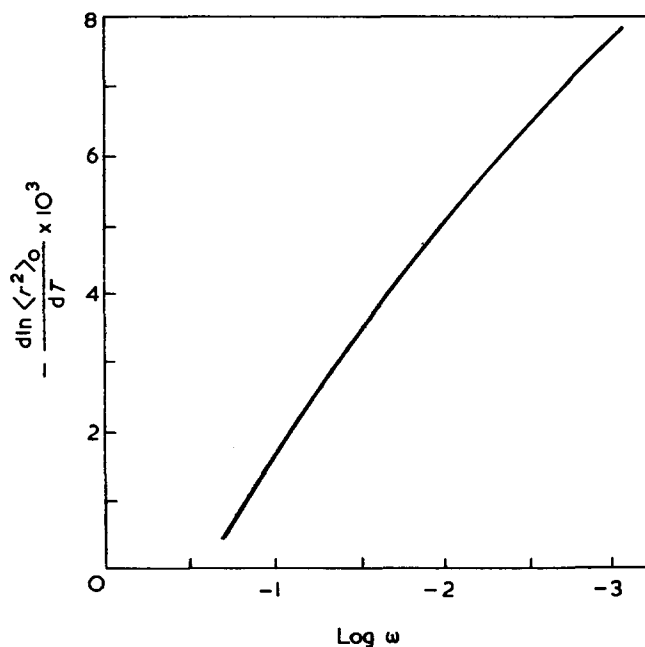


Figure 8 The temperature coefficient of the dimensions of isotactic polypropylene as a function of  $\omega$ . The curve is practically independent of  $\tau$  and  $\Delta\Phi$

of the uncertainty in  $\Phi$ , and other experimental errors, an average value of  $4.7 \pm 0.3$  will be adopted.

For polymethylene, it is found from Figures 5 and 6 that the experimental results of  $6.7 \pm 0.2$  for the  $CR$  and  $(-1.1 \pm 0.1) \times 10^{-3}$  for  $d \ln \langle r^2 \rangle_0 / dT$  are reproduced at  $\Delta\Phi = 0$  by:  $\sigma = 0.5 \pm 0.05$  and  $\omega = 0.075 \pm 0.03$ , corresponding at  $140^\circ\text{C}$  to  $E_\sigma = 580 \pm 80$  cal/mol and  $E_\omega =$

$2200 \pm 300$  cal/mol. For  $\Delta\Phi = 7.5^\circ$ , one obtains  $\sigma = 0.6 \pm 0.05$  and  $\omega = 0.16 \pm 0.04$  giving at  $140^\circ\text{C}$   $E_\sigma = 400 \pm 100$  cal/mol and  $E_\omega = 1500 \pm 300$  cal/mol.

$E_\sigma$  is about 50 and  $E_\omega$  about 200 cal/mol higher than the equivalent values obtained using the three-state scheme<sup>1,4</sup>. There is good agreement with the spectroscopic and calculated data discussed earlier.

In the case of polypropylene, the calculated dimensions and temperature coefficient are insensitive to  $\tau$ , for reasonable values of the latter, so it becomes possible to determine  $\omega$  and  $\Delta\Phi$  from the two pieces of experimental data. Best agreement is found at  $\Delta\Phi = 6 \pm 2^\circ$  and  $\omega = 0.1 \pm 0.01$ , i.e. at  $145^\circ\text{C}$ :  $E_\omega = 1950 \pm 100$  cal/mol. The small uncertainty in  $E_\omega$  is due to the sensitivity of the temperature coefficient to  $\omega$ . Additional calculations showed that for values of this magnitude, the calculated CR and its temperature coefficient were affected very little by the presence of 2% syndiotactic dyads. Hence the significance of these values of  $\Delta\Phi$  and  $E_\omega$  is real.

The value of  $\tau$  remains indeterminate within a fairly wide range. It is unlikely to be greater than  $\sigma$ , so an upper limit is 0.5. On the other hand it is unlikely to be less than  $\omega$  and a lower limit therefore is 0.1, giving

$$E_\tau = 1250 \pm 500 \text{ cal/mol}$$

There is good agreement between the values of  $E_\omega$  from polymethylene and polypropylene for  $\Delta\Phi = 5^\circ$ , justifying the rotational isomeric models employed and providing a demonstration of the basic identity between the steric interactions in the two polymers.

It has been stated<sup>11</sup> that the CR and temperature coefficient for isotactic polypropylene are not reconcilable without assuming a fairly high (>5%) degree of syndiotacticity which is moreover undetectable by n.m.r. and therefore becomes an additional quite arbitrary parameter. The results above show that stereo-irregularity need not be invoked, and support analyses<sup>10,36</sup> of polypropylene n.m.r. spectra in which all resonances, syndiotactic as well as isotactic, were detected and assigned.

The principal defect in this method of calculation is that the effect of torsional oscillations is not considered. It could possibly be incorporated by replacing the sine and cosine functions of the rotation angles in the transformation matrices by their values averaged over the torsional excited states. Such sophistication is probably unwarranted in view of the magnitude of the errors in the experimental measurements.

## REFERENCES

- 1 Flory, P. J. 'Statistical Mechanics of Chain Molecules', Interscience, New York, 1969
- 2 Flory, P. J. and Fujiwara, Y. *Macromolecules* 1969, **2**, 315
- 3 Flory, P. J. and Fujiwara, Y. *Macromolecules* 1969, **2**, 327
- 4 Abe, A., Jernigan, R. L. and Flory, P. J. *J. Am. Chem. Soc.* 1966, **88**, 631
- 5 Flory, P. J., Mark, J. E. and Abe, A. *J. Am. Chem. Soc.* 1966, **88**, 639
- 6 Fujiwara, Y. and Flory, P. J. *Macromolecules* 1970, **3**, 280
- 7 Abe, A. *Polym. J.* 1970, **1**, 232
- 8 Abe, Y., Tonelli, A. E. and Flory, P. J. *Macromolecules* 1970, **3**, 294
- 9 Tonelli, A. E., Abe, Y. and Flory, P. J. *Macromolecules* 1970, **3**, 303
- 10 Heatley, F., Salovey, R. and Bovey, F. A. *Macromolecules* 1969, **2**, 619
- 11 Flory, P. J. *Macromolecules* 1970, **3**, 613
- 12 Mizushima, S. 'Structure of Molecules and Internal Rotation', Academic Press, New York, 1954
- 13 Wilson, Jr., E. B. *Advan. Chem. Phys.* 1959, **2**, 367; *Pure Appl. Chem.* 1962, **4**, 1
- 14 Flory, P. J. 'Statistical Mechanics of Chain Molecules', Interscience, New York, 1969, p 56
- 15 Scott, R. A. and Scheraga, H. A. *J. Chem. Phys.* 1965, **42**, 2209
- 16 Allinger, N. L., Hirsch, J. A., Miller, M. A., Tyminski, I. J. and Van-Catledge, F. A. *J. Am. Chem. Soc.* 1968, **90**, 1199
- 17 McCullough, R. L. and McMahon, P. E. *Trans. Faraday Soc.* 1964, **60**, 2089
- 18 Mason, E. A. and Kreevoy, M. M. *J. Am. Chem. Soc.* 1955, **77**, 5808
- 19 Lifson, S. and Warshel, A. *J. Chem. Phys.* 1968, **49**, 5116
- 20 Warshel, A. and Lifson, S. *J. Chem. Phys.* 1970, **53**, 582
- 21 Frisch, H. L., Mallows, C. L. and Bovey, F. A. *J. Chem. Phys.* 1966, **45**, 1565
- 22 Bovey, F. A., Hood, III, F. P., Anderson, E. W. and Snyder, L. C. *J. Chem. Phys.* 1965, **42**, 3900
- 23 Flory, P. J. 'Statistical Mechanics of Chain Molecules', Interscience, New York, 1969, Ch IV
- 24 Chiang, R. *J. Phys. Chem.* 1966, **70**, 2348
- 25 Stacy, C. J. and Arnett, R. L. *J. Phys. Chem.* 1965, **69**, 3109
- 26 Nakajima, A., Hamada, F. and Hayashi, S. *J. Polym. Sci. (C)* 1966, **15**, 285
- 27 Chiang, R. *J. Phys. Chem.* 1965, **69**, 1645
- 28 Flory, P. J., Ciferri, A. and Chiang, R. *J. Am. Chem. Soc.* 1961, **83**, 1023
- 29 Ciferri, A., Hoeve, C. A. J. and Flory, P. J. *J. Am. Chem. Soc.* 1961, **83**, 1015
- 30 Chiang, R. *J. Phys. Chem.* 1966, **70**, 2348
- 31 Kinsinger, J. B. and Hughes, R. E. *J. Phys. Chem.* 1963, **67**, 1922
- 32 Incigaki, H., Miyamoto, T. and Ohta, S. *J. Phys. Chem.* 1966, **70**, 3420
- 33 Nakajima, A. and Saijyo, A. *J. Polym. Sci. (A-2)* 1968, **6**, 735
- 34 Flory, P. J. and Hamada, F. unpublished results
- 35 Brandrup, J. and Immergut, E. H. 'Polymer Handbook', Interscience, New York, 1966
- 36 Heatley, F. and Zambelli, A. *Macromolecules* 1969, **2**, 618

# Electron microscope study of freeze-etched polystyrene latex

R. Reed and J. R. Barlow

*Procter Department of Food and Leather Science, University of Leeds, Leeds LS2 9JT, UK*

*(Received 8 September 1971; revised 8 November 1971)*

Freeze-etching, which involves the freezing, fracturing and replication of samples has been used to study monosize polystyrene latex particles in the electron microscope. The temperature at which the frozen sample was fractured by cold-knife action was systematically varied whilst the effects of etching (i.e. differential removal of ice from the exposed surface) on particle size were also investigated. A theoretical treatment of the results has been developed and the particle sizes compared with those obtained by a conventional dilution-plus-drying technique. The freeze-etched particles appear to be somewhat smaller than those in conventional preparations, where size increase due to the electron beam is involved.

## INTRODUCTION

The method of freeze-etching, as introduced by Steere<sup>1</sup> and developed by Moor<sup>2</sup>, has been widely used for the preparation of biological materials in electron microscopy, when retention of the fluid contents of the sample is required. It consists of rapidly freezing a specimen to liquid air temperatures, thereby physically fixing the constituents, followed by fracturing with a cold knife and replicating the surface of fracture. Etching, i.e. the sublimation of ice from the frozen surface to reveal structural details, may also be carried out prior to replication.

This method appears well suited to the study of polymer latices and already several authors have made qualitative investigations of such systems<sup>3-7</sup>. Recently a procedure for obtaining the diameter of 'soft' lattices from freeze-etched preparations has been outlined<sup>8</sup>, and the present paper is concerned with possible modifications in particle size distributions as a function of fracture temperature and etching time.

## EXPERIMENTAL

### *Freeze-etching*

A Dow monosize polystyrene latex, of mean particle diameter  $0.109 \mu\text{m}$  and standard deviation  $0.003 \mu\text{m}$  was used. Glycerol was added as a cryoprotective until it formed 40% by volume of the liquid content. Freeze-etching procedures were essentially similar to those described earlier<sup>8</sup>, except that (i) a range of fracture temperatures from  $-80^\circ\text{C}$  to  $-150^\circ\text{C}$  was covered, and (ii) at each fracture temperature two samples were prepared, one being replicated immediately after fracture, the other being etched for 90 sec prior to replication.

### *Dilution-plus-drying technique*

The latex was diluted to about 200 ppm polymer, sprayed on to a carbon/collodion film supported on a specimen grid, dried and shadowed with platinum.

### *Electron microscope magnification calibration*

In the course of the work, the magnification given by the electron microscope was frequently calibrated using a diffraction-grating replica. This method is generally regarded as more satisfactory than using monosize polystyrene latex particles, which may suffer electron beam damage<sup>9</sup>.

## RESULTS

All plates are negative prints and, unless otherwise stated, the scale mark represents 500 nm.

### *Freeze-etched preparations*

The appearance of the latex after fracture at  $-100^\circ\text{C}$  is shown in *Figure 1* at low magnification and in *Figure 2* at higher magnification. As expected, these views correspond closely with micrographs of polystyrene latex shown previously<sup>8</sup>. There is, however, one marked difference, namely in the form of the protrusions produced when the fracture plane passes over the embedded particles of latex. In some cases the spherical form has been lost and the particles appear to have been deformed into rod-like structures which often project upwards from the fracture surface (see RP in *Figure 2*). The reasons for this type of deformation are by no means clear. The force applied by the knife itself when moving in a fixed direction does not

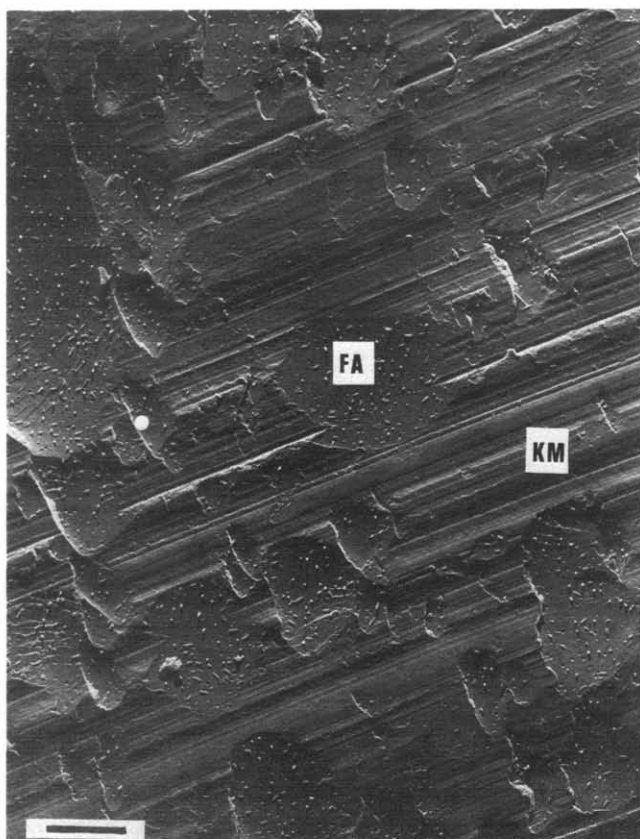


Figure 1 Latex fractured at  $-100^{\circ}\text{C}$ , low magnification view. KM=knife marks; FA=fracture area. Scale mark represents  $2\ \mu\text{m}$

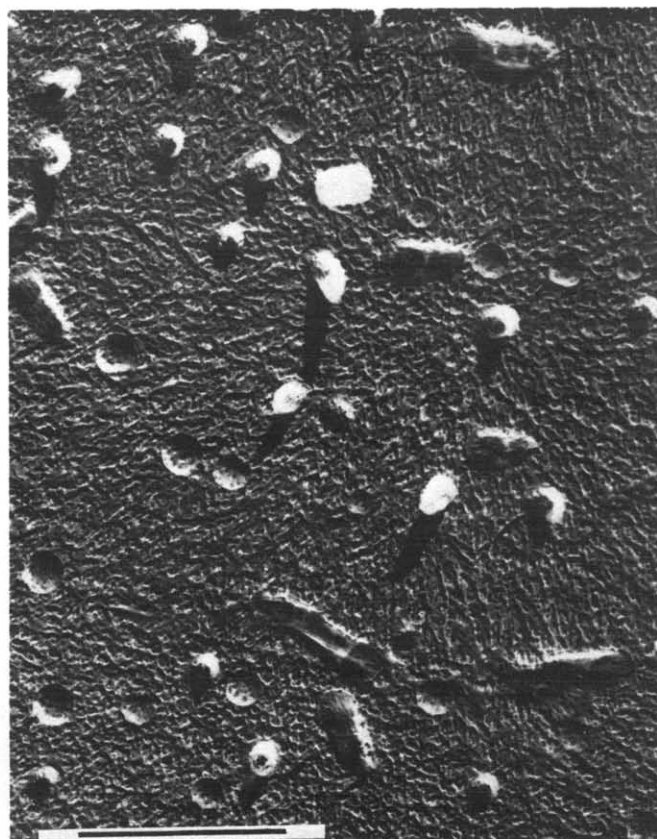


Figure 3 Latex fractured at  $-100^{\circ}\text{C}$  with subsequent etching for 90 sec

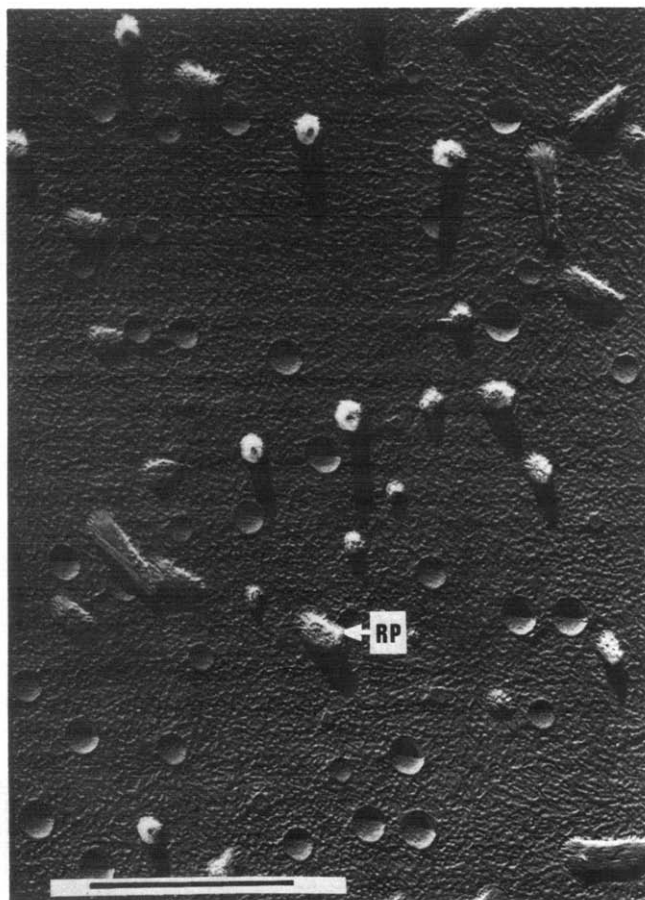


Figure 2 Latex fractured at  $-100^{\circ}\text{C}$ , high magnification view. RP=raised particle

seem entirely responsible, as the elongated particles lie in all directions in the plane of the fracture surface. Possibly the fracture forces operate some small distance ahead of the knife edge and subject the particles to deformation in various directions, the latter being determined by the anisotropy of the icy matrix surrounding the particles. Although small regions of ductility may occur occasionally in macroscopically brittle samples of polymer, its manifestation at temperatures some two hundred degrees centigrade below the glass-transition temperature is somewhat unexpected. Possibly the deformation is caused by heat and pressure changes operative over a very short period of time during the passage of the knife through the frozen specimen. Once the knife has passed beyond the strained particle, the latter quickly reverts to the rigid, frozen state.

Figure 3 shows the latex after the frozen sample (fractured at  $-100^{\circ}\text{C}$ ) has been etched for 90 sec. No major differences between this sample and that shown in Figure 2 (in which replication immediately after fracture was carried out) are apparent.

The effect of raising the temperature of fracture may be assessed by comparing Figure 4 (latex fractured at  $-80^{\circ}\text{C}$ ) with Figure 2. At  $-80^{\circ}\text{C}$  the background of the fracture surface is fairly smooth but the protrusions appear indistinct and no depressions may be detected. These observations indicate that the latex sample had probably melted and deformed somewhat during fracture by the knife, with consequent 'smearing' of fine detail. Low-magnification micrographs of fracture at  $-80^{\circ}\text{C}$  (as shown in Figure 5), confirm this view. The regions with knife marks are less distinct and individual particles may be seen in such areas, where melting has exposed them.

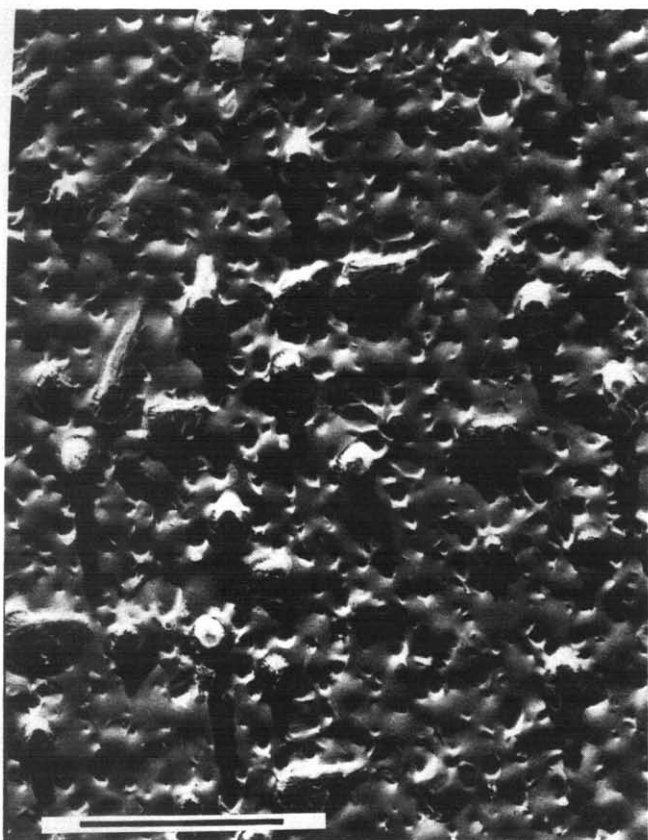


Figure 4 Latex fractured at  $-80^{\circ}\text{C}$



Figure 5 Latex fractured at  $-80^{\circ}\text{C}$ , low magnification view. Scale mark represents  $2\ \mu\text{m}$

The effects of lowering the temperature of fracture are shown in *Figure 6*, where the fracture temperature was  $-140^{\circ}\text{C}$ . Reducing the fracture temperature from  $-100^{\circ}\text{C}$  to  $-120^{\circ}\text{C}$  appeared to lead to no obvious change in particle form, but when further lowered to  $-140^{\circ}\text{C}$ , changes in the nature of the depressions were observed (compare *Figures 2* and *6*). The fracture seems to have taken a slightly different course and to have approached the latex particles in a different manner, since each circular crater is enclosed within a less distinct outer ring. The slight change in the nature of the depressions as the temperature of fracture is varied may be seen by comparing the higher magnification views shown in *Figure 7*. The fracture plane (FP in *Figure 8*) appears to be deflected slightly as it approaches the latex particle (LP), giving rise to a depression profile of the form shown in *Figures 8b* and *8c*.

So far all the micrographs, with the exception of *Figure 3*, refer to samples replicated immediately after fracture, i.e. without etching. Similar particle forms, however, were obtained even after 90 sec etching of the samples prior to replication. Hence in these polystyrene lattices, etching appears to have little effect. In one case only, when the sample was fractured at  $-130^{\circ}\text{C}$ , were differences in depression form between fractured and fractured/etched samples noted, probably due to malfunction of the temperature control device during this particular experiment.

Depression-size counts were made on micrographs of various preparations which were fractured (with and without subsequent etching) at temperatures over the range  $-80^{\circ}\text{C}$  to  $-150^{\circ}\text{C}$ , the results being shown in *Table 1*.

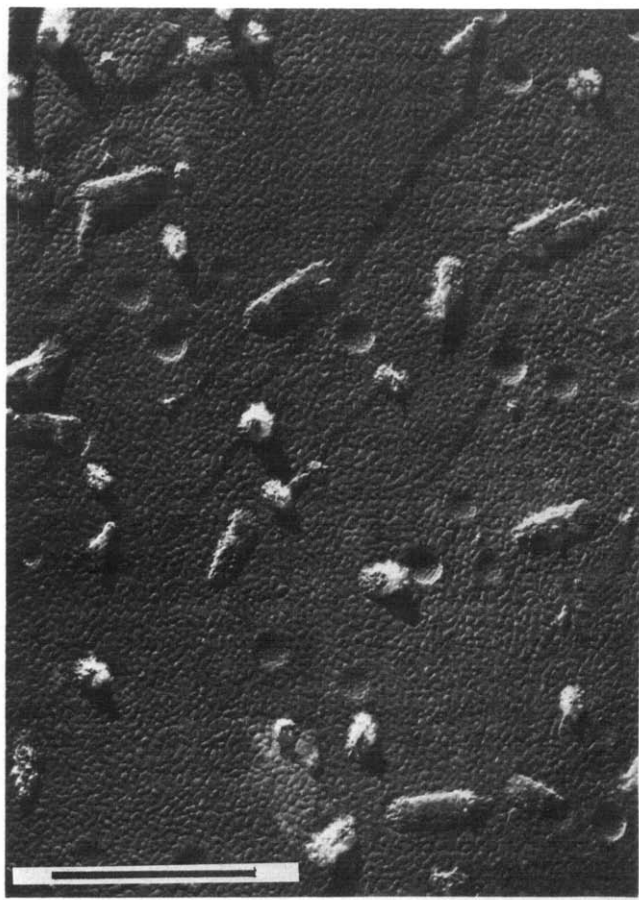


Figure 6 Latex fractured at  $-140^{\circ}\text{C}$

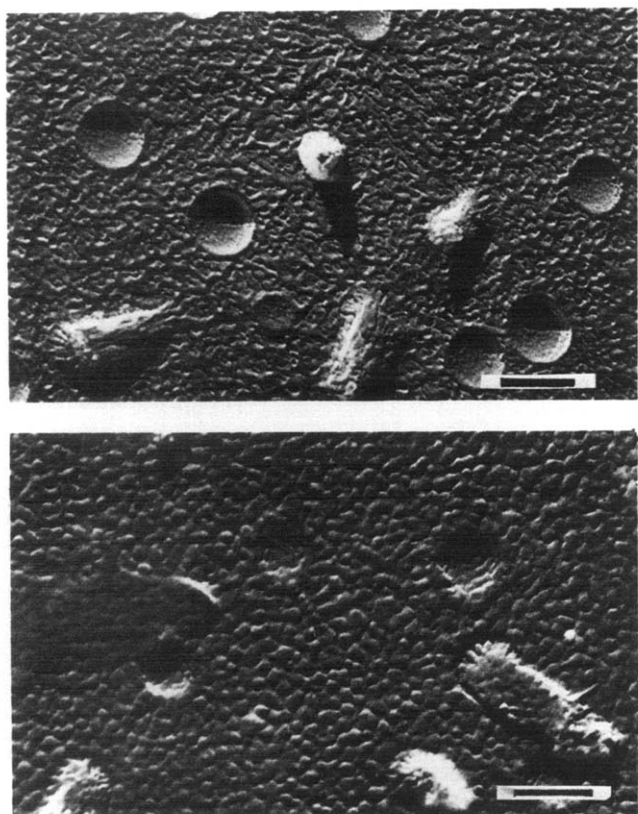


Figure 7 Comparison of depression appearance from specimens fractured at  $-100^{\circ}\text{C}$  (upper) and  $-140^{\circ}\text{C}$  (lower). High magnification view, scale mark represents 100 nm

Table 1 Depression-diameter distributions, measured on micrographs at  $\times 94\,000$  magnification

All figures are  $n_i/\sum n_i$  values, showing the fraction of the total number of particles in each diameter class

Treatment	Diameter class(mm on print)							No. of particles counted
	4	5	6	7	8	9	10	
$-90^{\circ}\text{F}^*$			0.05	0.14	0.31	0.41	0.08	195
$-90^{\circ}\text{E}^*$			0.03	0.20	0.29	0.41	0.07	143
$-100^{\circ}\text{F}$	0.06	0.08	0.09	0.11	0.24	0.33	0.09	359
$-100^{\circ}\text{E}$	0.01	0.05	0.07	0.15	0.22	0.32	0.15	206
$-110^{\circ}\text{F}$	0.07	0.08	0.10	0.13	0.21	0.39	0.03	344
$-110^{\circ}\text{E}$	0.02	0.08	0.12	0.13	0.27	0.30	0.07	348
$-120^{\circ}\text{F}$	0.03	0.05	0.12	0.13	0.29	0.34	0.04	276
$-120^{\circ}\text{E}$		0.09	0.10	0.16	0.29	0.33	0.02	283
$-130^{\circ}\text{F}\dagger$	0.01	0.06	0.09	0.19	0.34	0.30	0.03	248
$-130^{\circ}\text{E}$		0.02	0.07	0.12	0.30	0.34	0.14	233
$-140^{\circ}\text{F}\dagger$	0.03	0.08	0.13	0.18	0.35	0.24		276
$-140^{\circ}\text{E}\dagger$	0.01	0.10	0.14	0.21	0.33	0.17	0.03	208
$-150^{\circ}\text{F}\dagger$	0.08	0.08	0.12	0.17	0.28	0.26	0.02	332
$-150^{\circ}\text{E}\dagger$	0.05	0.08	0.10	0.19	0.31	0.27		313

E = Etched for 90 sec; F = fractured, no etching; \* = rough fracture, small depressions indistinguishable from background; † = irregular fracture.

#### Conventional dilution-plus-drying preparations

Figure 9 is a micrograph of polystyrene latex prepared for electron microscopic examination in the manner previously described. As is common in this type of preparation, the particles are not perfectly spherical in form and in places their surfaces appear indistinct. Such effects are ascribed to damage in the electron beam, since the build-up of contamination during electron microscope

examination is minimal when using a cold-finger anti-contamination device.

Particle diameters were measured and counted, giving a mean value of  $0.115\ \mu\text{m}$  (compared with the manufacturers stated figure of  $0.109\ \mu\text{m}$ ). The size distribution was very narrow, 77% of the particles having a diameter with the histogram class limits of  $0.111\ \mu\text{m}$  and  $0.122\ \mu\text{m}$ .

#### Magnification calibration

The magnification was found to be constant throughout the course of the experiment, to within a tolerance of  $\pm 1\%$ . A nominal magnification of  $\times 20\,000$  at which all the electron micrographs were taken, was found to be  $18\,800 \pm 200$ .

#### THEORY

A method of obtaining size distribution from freeze-etched latex preparations has been outlined previously<sup>8</sup>. When considering a monosize latex of known dimensions, it is possible to calculate the expected diameter-depression distributions using this treatment, the model on which the latter is based being shown in Figure 10. If the depressions are sized and counted (the theoretical considerations for protrusion measurement are exactly the same), the results may be tabulated in the form of a

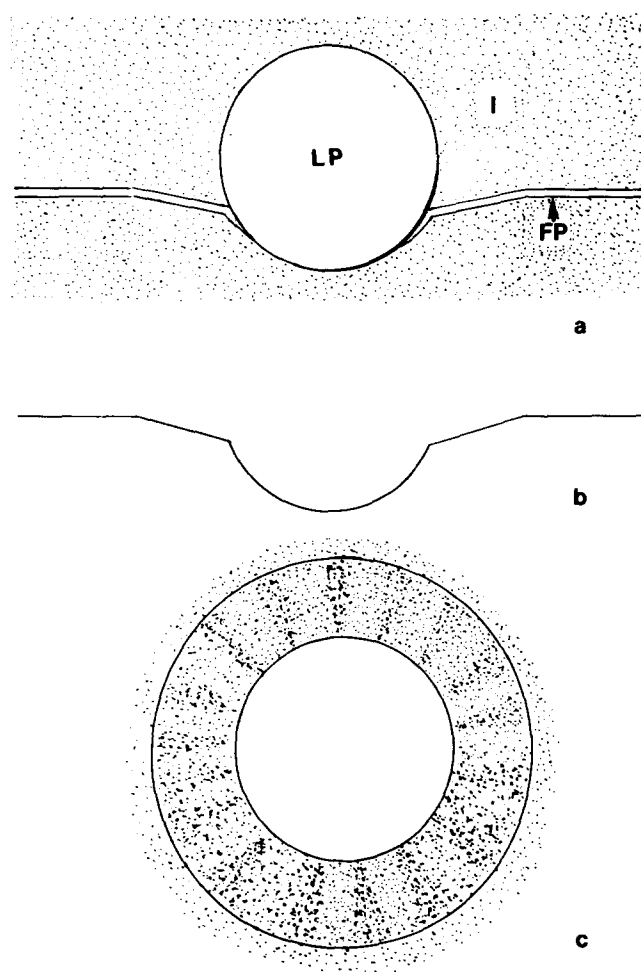


Figure 8 (a) Path of fracture plane (FP) around latex particle (LP) embedded in ice (I), at temperatures  $< -130^{\circ}\text{C}$ . (b) Cross-section of a replica of such a depression, whereas the appearance when viewed normally is shown in (c)



histogram with mean class diameters  $X_1, X_2, X_3, \dots$ , whilst the boundary limits for each of these histogram classes are  $a_1, a_2; a_2, a_3; a_3, a_4; \dots$  (see Figure 10). For a particle with true diameter  $X_1$ , it is clear that the observed diameter of the depression produced by removing the particle from the frozen matrix, will depend on the level at which the fracture plane passed round the particle. If the fracture plane lies between levels 1 and 2 (see Figure 10), the depression will have an observed diameter between  $a_1$  and  $a_2$ ; hence it will be recorded in the  $X_1$  histogram class: if the fracture plane lies between levels 2 and 3, the exposed depression will have an observed diameter between  $a_2$  and  $a_3$  and so will be recorded in the  $X_2$  histogram class. Further levels  $a_3, a_4$ , correspond to observations of particles in histogram classes  $X_3, X_4$ , etc.

Now the probability of the fracture plane encountering the latex particle between levels 1 and 2, (so giving rise to a depression of diameter  $X_1$ ) is proportional to  $y_1$ , the vertical distance between the histogram class boundaries. Hence the relative number of depressions in each histogram class is given by  $y_1 : y_2 : \dots : y_n$ , and the absolute fraction in each class by:

$$\frac{y_1}{\sum_{i=1}^{i=n} y_i} : \frac{y_2}{\sum_{i=1}^{i=n} y_i} : \dots : \frac{y_n}{\sum_{i=1}^{i=n} y_i}$$

It may be noted that provided the smallest depressions could be sized and counted, the denominator would equal  $a_1/2$ ; hence all calculations could be simplified accordingly. In practice, however, the granularity of the background prevented the registration of depressions with a diameter less than about 4 mm on the micrographs, and hence calculation of the denominator was carried out in full.

Should the particle undergo shrinkage during the freeze-etch preparation, then the depression-diameter distribution will be affected as  $y_1, y_2 \dots y_n$  will now have different values, due to the change in level of the histogram class extremes  $a_1, a_2 \dots a_n$ . In the particular latex studied, at the accurately known magnification used for each micrograph, the particles should have an observed diameter of 10.2 mm. The theoretical depression-diameter distributions, as a function of percentage shrinkage of the particles, are shown in Table 2.

The effect of etching, or removal of ice by sublimation, should also affect the observed depression-diameter distributions, as shown in Figure 11. If etching proceeds to a depth  $e$ , the chance of the fracture plane producing a

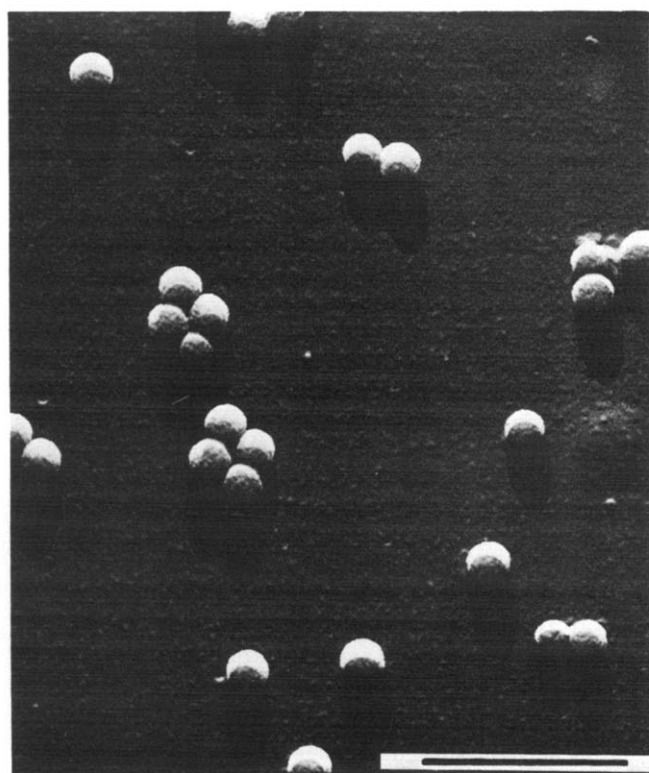


Figure 9 Latex after dilution, drying, spraying and shadowing

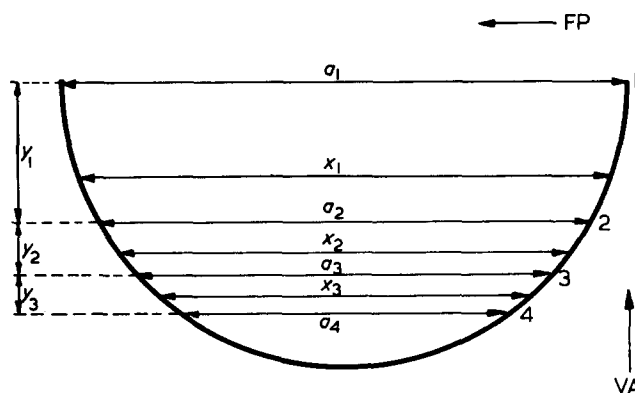


Figure 10 Relationship between level of encounter between fracture plane and latex particle with diameter of depression formed. FP=fracture plane direction; VA=vertical axis. Reproduced from *J. Appl. Polym. Sci.* 1971, 15, 1623 by permission of the publishers

Table 2 Variation in calculated depression-diameter distributions as a function of shrinkage, assuming magnification of  $\times 94\ 000$ . All values show fractions of the total number of particles in each diameter class

Shrinkage (%)	Diameter class (mm on print)								
	2	3	4	5	6	7	8	9	10
0	0.02	0.03	0.04	0.05	0.08	0.10	0.13	0.19	0.37
1	0.02	0.03	0.04	0.05	0.08	0.10	0.13	0.21	0.34
2	0.02	0.03	0.04	0.06	0.08	0.10	0.14	0.22	0.31
3	0.02	0.03	0.05	0.06	0.08	0.11	0.14	0.24	0.28
4	0.02	0.04	0.05	0.06	0.08	0.11	0.15	0.25	0.25
5	0.02	0.04	0.05	0.06	0.08	0.11	0.15	0.28	0.20
6	0.02	0.04	0.05	0.06	0.08	0.11	0.16	0.32	0.15
6.5	0.02	0.04	0.05	0.07	0.09	0.11	0.17	0.37	0.09
7	0.02	0.04	0.05	0.07	0.09	0.12	0.17	0.45	0.00

depression of observed diameter  $X_1$  is proportional to  $(y_1 - e)$  and not to  $y_1$  (as applies when etching does not occur). The calculated depression-diameter distributions, as a function of the amount of etching, are presented in Table 3, in which particle shrinkage of 6.5% is assumed.

### DISCUSSION

Although freeze-etching has proved useful for qualitative studies of polymer latices, its quantitative aspects need also to be considered. A comparison of calculated and experimentally obtained depression-diameter distributions indicates that the polystyrene particles have shrunk, since the number of depressions of diameter 10 mm is always much lower than expected. Before discussing the

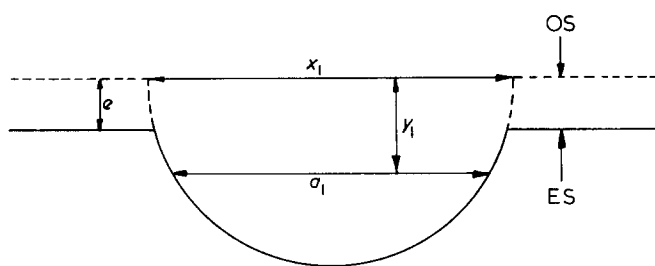


Figure 11 Effect of etching the fracture surface by an amount  $e$ . OS=original surface; ES=etched surface

Table 3 Variation in calculated depression-diameter distributions as a function of etching depth, assuming 6.5% shrinkage of particles. Assumed magnification =  $\times 94\,000$

All the values show fractions of the total number of particles in each histogram class

Depth of etching (nm)	Diameter class (mm on print)								
	2	3	4	5	6	7	8	9	10
0	0.02	0.03	0.05	0.07	0.09	0.11	0.17	0.37	0.09
2.5	0.02	0.03	0.05	0.07	0.09	0.12	0.18	0.39	0.04
5.0	0.03	0.04	0.06	0.07	0.10	0.13	0.18	0.40	0
7.5	0.03	0.04	0.06	0.08	0.10	0.14	0.20	0.36	0
10.0	0.03	0.04	0.06	0.08	0.11	0.14	0.21	0.32	0
20.0	0.04	0.06	0.09	0.11	0.14	0.19	0.28	0.10	0
50.0	0	0	0	0	0	0	0	0	0

extent of particle shrinkage it is necessary to appreciate the statistical inaccuracies in sizing and counting very small numbers of particles as involved in the present work. The exact fit of results to theoretical values is not expected, since only general trends in size distribution are obtainable. However, it is apparent from Table 2 that relatively small shrinkages can drastically affect the expected depression-diameter distributions, especially those of the larger depressions. Hence it is necessary to restrict consideration to population fractions of depressions having an observed diameter of 10 or 9 mm, as when using smaller depressions the method is too inaccurate.

From the actual results it is clear that appreciable differences in depression-diameter distributions occur. For samples fractured at  $-90^\circ\text{C}$  the uneven background made detection of very small depressions extremely difficult. Population fractions in remaining classes are, therefore, slightly raised in comparison with those of samples prepared at  $-100^\circ\text{C}$ ,  $-110^\circ\text{C}$ , or  $-120^\circ\text{C}$ . In these latter cases, although the diameter distributions show considerable variation in population fractions for the largest depressions (the value for the 10 mm class ranging, for example, from 0.02 to 0.15), the corresponding variation in particle shrinkage, as assessed from Table 2, is less than 1%. Similarly, it may be noted that the fraction of depressions having an observed diameter of 8 mm is larger than expected.

At  $-130^\circ\text{C}$  a modification in the fracture process was observed in the sample replicated without prior etching. This different mode of fracture is reflected in the depression-diameter distribution, as the maximum population fraction is now shifted downwards to the diameter class of 8 mm. Probably this is a consequence of the latex particle

being fractured at a somewhat lower level (as shown in Figure 8), giving a depression of smaller diameter.

A most interesting finding is that there appears to be little or no removal of ice during the 90 sec interval used for etching. The depression-diameter distribution is a most sensitive measure of the depth to which etching occurs, as may be seen from the marked dependence of calculated results on  $e$ . Presumably the relatively high concentration of glycerol retards the sublimation of material from the fracture surface, and consequently this phase of freeze-etch preparation may be omitted when working with polymer lattices.

The stretching of the polymer particles is a most curious phenomenon, considering the great difference between the glass transition point of the polymer and the fracture temperature of any freeze-etch preparation. Local heating of the polymer during the fracture process cannot be the whole answer, for if this were the case, one would expect the ice-glycerol fracture surface to melt and the depressions, produced on removal of a latex particle, to be filled in. As already suggested, possibly local regions of softening may arise due to pressure effects produced by the knife striking the frozen block of latex. The pressures which develop, although short-lived, are likely to be considerable because of the small area of sample over which they are generated.

These effects are also interesting in that not every particle of polystyrene showed signs of softening and deformation. If the particles were all similar in physical characteristics, one would expect them all to show signs of either softening or brittle fracture. The fact that the extent of deformation is variable indicates that in polystyrene lattices of this type, the particles are not completely homogeneous in a physico-chemical sense.

It appears, therefore, that the freeze-etch technique yields accurate results, provided standard conditions are used. The present work indicates that a fracture temperature of  $-100^\circ\text{C}$  to  $-120^\circ\text{C}$  is most suitable, to avoid either specimen melting or modification of the fracture mechanism. Etching is unnecessary and, indeed, may give rise to erroneous results if it proceeds to any appreciable extent. The degree of particle shrinkage, as a function of polymer softness, cannot be resolved until monosize lattices of soft polymers are available for investigation. It may be thought that softer compounds may undergo more severe shrinkage than polystyrene, as the effects of freezing the liquid contents of a latex, rather than the simple thermal contraction of the polymer, are responsible for the observed diminution of particle size.

## REFERENCES

- 1 Steere, R. L. *J. Biophys. Biochem. Cytol.* 1957, **3**, 45
- 2 Moor, H., Muhlethaler, K., Waldner, H. and Frey-Wyssling, A. *J. Biophys. Biochem. Cytol.* 1961, **10**, 1
- 3 Geymayer, W. F. *VI Int. Congr. Electron Microsc., Kyoto* 1966, **1**, 577
- 4 Gyorgy Bercenyi, L. *Magy. Textiltech.* 1967, **19**, 320
- 5 Geymayer, W. F. *Staub-Reinhalte Luft* 1967, **27**, 237
- 6 Kolpakov, L. V., Nikitina, S. A., Taubman, A. B., Spiridonova, V. A., et al. *Kolloid Z.* 1970, **32**, 229; *Colloid J. USSR Trans.* 1970, **32**, 187
- 7 Clark, A. W. and Branton, D. *Z. Zellforsch.* 1968, **91**, 586
- 8 Reed, R. and Barlow, J. R. *J. Appl. Polym. Sci.* 1971, **15**, 1623
- 9 Bradford, E. B. and Vanderhoff, J. W. *J. Appl. Phys.* 1955, **26**, 864
- 10 De la Court, F. H. and Vogt, H. *J. Oil Colour Chem. Assoc.* 1969, **52**, 587

# Calculation of the conformational properties of isotactic poly( $\alpha$ -olefins) in solution

P. L. Luisi

*Technisch-Chemisches Laboratorium, Eidgenössische Technische Hochschule  
Zürich, CH-8006 Zürich, Switzerland  
(Received 16 July 1971; revised March 1972)*

A method is presented for the numerical evaluation of the conformational properties of isotactic poly( $\alpha$ -olefins) in solution purposely using a simplified treatment. This is based on the numerical evaluation of the energy parameters in terms of which the conformational properties are analytically expressed by the old treatment of Volkenstein and his group. This numerical evaluation has been carried out by expressing the energy parameters in terms of conformational partition functions of couples of contiguous monomeric units, with due account of the conformational versatility of the side chain. It is found that poly(1-butene), poly(1-pentene), higher homologous poly( $\alpha$ -olefins) without branching in the side chain, as well as poly( $\alpha$ -olefins) having side-chain branching at the  $\gamma$ -position or further along the main chain, are characterized by similar conformational properties in solution, namely a characteristic ratio  $\bar{h}^2/Nl^2$  of  $\sim 10$ , and by alternating left-handed and right-handed sections composed, at room temperature, by about 5 monomeric units ( $\nu=5$ ). The branching of the side chain at the  $\alpha$  or  $\beta$  position with respect to the main chain [poly(3-methyl-1-butene) and poly(4-methyl-1-pentene)] considerably increases the values of  $\bar{h}^2/Nl^2$  and  $\nu$ . The presence of an asymmetric carbon atom in the  $\alpha$  or  $\beta$  position in the side chain further increases the stiffness of the chain in solution. It is shown that the available experimental data of  $\bar{h}^2/Nl^2$  are in fair agreement with the calculated values, and that the experimental data of optical activity are consistent with the calculated data of the conformational properties in the case of optically active poly( $\alpha$ -olefins).

## INTRODUCTION

As is well known, the macromolecules of most isotactic poly( $\alpha$ -olefins) in the solid state assume spiraled conformations<sup>1,2</sup>. When the polymers are in solution, left-handed and right-handed spiraled sections co-exist in the same macromolecule because of the low potential energy barriers hindering the rotation around carbon-carbon bonds. Left-handed and right-handed spiraled sections interconvert continuously and rapidly between each other, as the conformational reversals, which separate sections spiraled in opposite screw sense, are able to fluctuate rapidly along the main chain. According to this model, each macromolecule can exist in solution in a very large number of chain conformations, in each of which a short range conformational order is maintained<sup>3</sup>.

In this paper we are mainly interested in:  $\nu$ , the average number of monomeric units constituting a regularly spiraled section;  $n_r$ , the average number of conformational reversals;  $\omega_i$ , the molar fraction of monomeric units having the  $i$ th conformation; and  $\bar{h}^2$ , the quadratic 'unperturbed' end-to-end-distance.

The determination of the conformational properties of stereoregular poly( $\alpha$ -olefins) in solution present considerable difficulty, owing to the lack of experimental techniques which are sensitive enough to  $\nu$  (and/or to  $n_r$ ), and to the local conformational equilibria established in the monomeric units. One of the properties which is usually experimentally available is the end-to-end-distance<sup>4,5</sup>. However, this property—at least for the poly( $\alpha$ -olefins) investigated up to now—does not seem to be sensitive enough to provide details of the conformational isomerism established in the chain<sup>3,6</sup>. The conformational properties have been the subject of a very large number of investigations with mechanical statistical treatments<sup>3,7-15</sup>. However, this approach also faces serious difficulties. On the one hand, the reliability of the approximations involved in the model underlying the statistical treatments is difficult to check experimentally; and on the other hand, the conformational properties are analytically expressed in terms of energy parameters which are usually unknown, or for which, so far, no general method for their determination has been made available.

The aim of this paper is to present a method of calculat-

ing these energy parameters and hence the conformational properties as a function of the monomeric unit structure in the case of optically active and non-optically active isotactic poly( $\alpha$ -olefins); and to show that the data thus calculated are consistent at the same time with the stereochemistry of the macromolecules in solution, with the statistical treatments of the Russian school<sup>3</sup>, and with the available experimental data.

A few treatments of the conformational properties of isotactic poly( $\alpha$ -olefins) in solution have been presented in the last few years, which are certainly more elaborate than that presented here. This is, however, one of the cases in which, in our opinion, a more complex mathematical treatment does not correspond necessarily to a higher degree of reliability in the final results. Generally, the simplest possible treatment should be abandoned only when the *experimental* data show that it is obsolete. This stage has not yet been reached in the field of conformational properties of poly( $\alpha$ -olefins) in solution, where the problem is certainly not the development of more complex matrix algebra, but the scarcity of reliable experimental data with which to compare the calculated values. Furthermore, any mathematical treatment has to be based on the rotational isomeric state approximation, and on other assumptions (see discussion later in the paper) the reliability of which is still under question in the case of macromolecules in solution. Aside from this, any treatment, in order to provide semi-quantitative information, needs the use in the final analytical expressions of the values of conformational energy differences found for low molecular model compounds; and the uncertainty in these energy values is no better than 30–50%. These simple considerations, in our opinion, deprive the very complicated mathematical treatments of all the soundness that the large matrices which are used try to convey. It is also interesting to observe that most of these elaborate schemes, in order to be operative (i.e. in order to go from equations to final information) necessitate a series of *a posteriori* approximations, which often, as pointed out in some specific cases in the paper, violate important stereochemical and thermodynamic features of the chain in solution. For all these reasons, we thought it worthwhile to develop a simplified method of calculation of the conformational properties of the macromolecules in solution which, though respecting all the basic stereochemical and thermodynamic properties of the isotactic chains in solution, could be useful enough to permit a direct and transparent relation between monomer unit structure and conformational equilibrium established in the chain. The ultimate aim of this treatment is to provide the experimentalist with a series of indications that can be checked beyond the limit of the present uncertainty of the experimental data, e.g. the forecast of those polymer structures characterized by enhanced average dimensions or enhanced optical activity. These predictions can be made with the simple use of molecular models, applying the conformational analysis principles valid for low molecular weight paraffins. It will be also emphasized, that the optical activity is the experimental property that is most sensitive to the local conformational equilibrium of the isotactic chains in solution, and in this work emphasis will be given to clarify the linkage between the experimental data of optical activity and the analytical expressions which are able to interpret these data on the basis of the proposed model.

## METHOD OF CALCULATION

According to the statistical treatment developed by Volkenshtein *et al.*<sup>3, 8</sup>, the average length of the regularly spiraled section in the macromolecules of isotactic vinyl polymers in solution is given by:

$$\nu = \frac{1+p}{p} \quad (1)$$

and  $n_r$ , the probability of the conformational reversals, by  $1/\nu$ . In equation (1)  $p = \exp(-\Delta U/RT)$ , where  $\Delta U$  is defined as:

$$\Delta U = \frac{E_{ll} + E_{aa}}{2} - \frac{E_{la} + E_{al}}{2} \quad (2)$$

where  $E_{ll}$  ( $E_{aa}$ ) is the energy of a left-handed (right-handed) monomeric unit which follows a left-handed (right-handed) monomeric unit;  $E_{la}$  ( $E_{al}$ ) is the energy of a left-handed (right-handed) monomeric unit which follows a right-handed (left-handed) monomeric unit. Another way to express  $\Delta U$  is in the following<sup>3</sup>:

$$\Delta U = \frac{RT}{2} \ln \left( \frac{g_{ll}g_{aa}}{g_{la}g_{al}} \right) \quad (3)$$

where  $g_{al}$ , for instance, is the probability of a left-handed spiraled monomeric unit to follow a right-handed spiraled one. For non-optically active isotactic vinyl polymers,  $E_{ll} = E_{aa}$  ( $g_{ll} = g_{aa}$ ), whereas, for a chain considered in a given direction, usually  $E_{la} \neq E_{al}$ .

On the basis of the same statistical treatment<sup>3</sup>, the end-to-end distance is expressed by:

$$\bar{h}^2 = Nl^2 \frac{8}{3p} \quad (4)$$

which is valid for infinite ideally isotactic chains under the assumption of tetrahedral bond angles and ideal staggered bond conformations.  $N$  is the number of main chain C–C bonds and  $l$  their length. Often, reference is made to the characteristic ratio  $\bar{h}^2/Nl^2$ . An analogous treatment, leading to an equation similar to equations (1)–(4), was developed independently by Allegra *et al.*<sup>11</sup>.

Statistical treatments for isotactic vinyl polymers more sophisticated than that so far illustrated are now available. For instance, it is possible to take into account bond angles different from the ideal tetrahedral ones, and bond conformations which are not ideally staggered<sup>3</sup>. It is also possible to depart from the approximation of the infinite chain<sup>7, 12</sup> and to consider the influence of configurational irregularities in the main chain<sup>7, 13</sup>. However, the introduction of more independent parameters in the analytical expressions of the conformational properties, without a corresponding check of their numerical value in solution, would bring no real improvement in the reliability of the final calculations. At the present state of experimental knowledge, equations (1)–(4) are adequate to provide semi-quantitative information on the chain conformational equilibria in solution. The problem, in this case, is reduced to the evaluation of the energy parameter  $\Delta U$ . A rough estimation of  $\Delta U$  has been, in some cases, obtained from equation (4) and the experimental value of the characteristic ratio<sup>3</sup>. The problem, however, is to find a method which allows for the determination of  $\Delta U$  independently from the experimental data, and eventually to compare calculated and experimental values in

order to have a confirmation of the reliability of the model.

The first step for a general method to evaluate  $\Delta U$ , consistent with the approximations involved in the statistical treatment which leads to equations (1)–(4), is to consider the terms in equation (3) replaceable by the corresponding conformational partition functions.\* The terms  $g_{ll}$  and  $g_{aa}$  can be replaced by  $Q_l$  and  $Q_a$  respectively, i.e. by the conformational partition functions of a monomeric unit included in a regularly spiraled left-handed or right-handed sequence. The definition of the terms  $g_{al}$  and  $g_{la}$  in terms of conformational partition functions is less immediate. For instance,  $g_{la}$  cannot be properly replaced solely by the conformational partition function of a right-handed monomeric unit following a left-handed one, since, because of the conformational reversal, the conformational equilibrium of the latter is substantially modified with respect to the same monomeric unit when inserted in a regularly spiraled sequence. For this reason, it is more appropriate to substitute  $g_{la}$  and  $g_{al}$  with  $(Q_{la})^{1/2}$  and  $(Q_{al})^{1/2}$  respectively, where  $Q_{la}$  and  $Q_{al}$  are the conformational partition functions of a couple of monomeric units containing a conformational reversal. The problem is then reduced to evaluating the number of conformations and their statistical weight of a couple of monomeric units, the first and the last main chain bonds of which belong to regularly spiraled sequences of opposite screw senses.

With these assumptions, equation (3) is transformed to:

$$\Delta U = \frac{RT}{2} \ln \left[ \frac{Q_l \cdot Q_a}{(Q_{la} \cdot Q_{al})^{1/2}} \right] \quad (5)$$

The approximation of substituting probability terms with conformational partition functions corresponds to the assumption that only conformational energies play a determining role in establishing the energy difference between conformers, the influence of the other energy terms (vibrational, translational energy differences) being negligible. This approximation is commonly accepted in conformational analysis problems<sup>8, 18</sup>.

The determination of the conformational partition function is generally quite a difficult problem. Only in the case of paraffins is our knowledge of the conformational equilibria in the dissolved phase relatively advanced, and allows for an approximate determination of the relevant conformers and their relative statistical weight. For this reason, this paper is confined to poly( $\alpha$ -olefins).

The conformational analysis of paraffins is usually dealt within the frame of the rotational isomeric state approximation<sup>3, 7, 8, 15</sup> according to which only staggered conformations of bonds are considered. The rotamers are weighted in terms of three energy parameters,  $\sigma = \exp(-\Delta E_1/RT)$ ,  $\tau = \exp(-\Delta E_2/RT)$  and

$\omega = \exp(-\Delta E_3/RT)$ .  $\Delta E_1$  is the energy difference between a *trans* and a *gauche* conformation of bonds,  $\Delta E_2$  is the energy difference between a double *vicinal-gauche* conformation and the corresponding more stable bond conformation, and  $\Delta E_3$  is the energy excess brought about with respect to the most stable bond conformation by a  $g \pm g \mp$  conformation<sup>7, 18</sup>.  $\sigma$  and  $\tau$  refer to three bond interactions,  $\omega$  is the only available measure for long range (four bonds) interactions. Any attempt to increase the sophistication of this scheme is confronted by the poverty of reliable experimental data.

Experimental and theoretical data accumulated in recent years by independent authors agree in attributing to  $\Delta E_1$  a value of  $600 \pm 200$  cal/mol<sup>7, 20–22</sup>, to  $\Delta E_2$  a value of  $1500 \pm 500$  cal/mol<sup>23</sup>, to  $\Delta E_3$  a value of  $2500 \pm 500$  cal/mol<sup>24, 25</sup>. Values in these ranges have been used with confidence, in conformational analysis problems of paraffins, by several authors in the last few years<sup>7, 20, 26, 27</sup>.

The conformational partition functions can now be evaluated for poly( $\alpha$ -olefins) in terms of  $\sigma$ ,  $\tau$  and  $\omega$ , and numerical values can be obtained for  $\Delta U$  with the above figures for the energy parameters.

In the case of poly( $\alpha$ -olefins) other than polypropylene, the conformational versatility of the side chain must be taken into account in order to determine the conformational partition functions. In the case, for instance, of  $Q_l$  and  $Q_a$ , this can be done by assessing the main chain bonds in the proper spiraled conformation, and determining the side chain bond conformations which are consistent with the main chain bond conformations. It must be remarked, however, that such a procedure is not strictly consistent with the original statistical treatment which leads to equations (1)–(4). In this treatment, in fact, no degeneracy of the left-handed and right-handed spiraled monomeric unit as due to side chain bonds, is taken into account. On the other hand, the introduction of all those conformations in the matrix algebra would lead to an extreme complication; and the necessity of such a degree of sophistication at the present state of our knowledge is questionable. It is certainly much simpler to have a statistical treatment of general validity, referring only to the conformations of the main chain bonds in which one can introduce *a posteriori*, through equation (5), the conformational features of the actual monomeric unit; and to check the reliability of this simple model first, before going into the difficulties of a more cumbersome algebra.

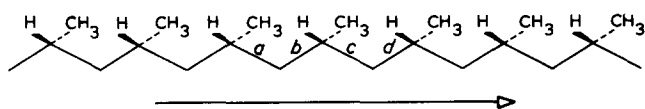
In this paper the ideally isotactic macromolecule is considered as an alternation of left-handed and right-handed sequences. This is consistent with the model developed independently by the Russian<sup>3, 8</sup> and Italian<sup>11</sup> school, and a fundamental point of this model is the proper account of the average energy spent at the junctions between helical sections of different screw sense.

In this treatment conformational irregularities in the main chain other than conformational reversals from the right-handed to the left-handed screw sense (and *vice versa*) are not taken into account. Generally they cause prohibitively high energy interactions and their statistical weight is then quite negligible. In some of the cases, however, the left  $\rightleftharpoons$  right conformational reversals take place with such high energy that other kinds of conformational transitions (as left  $\rightleftharpoons$  left or right  $\rightleftharpoons$  right) may be thought to have a comparable statistical weight. This should not affect the calculation of  $\nu$  and  $\omega$  but it may have an effect on the end-to-end distance.

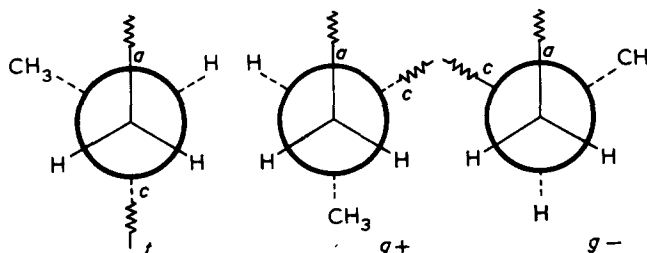
\* In this and all the other papers of our group the terms 'conformation' and 'configuration' are used according to the classical organic chemistry nomenclature<sup>16, 17</sup>. In poly( $\alpha$ -olefins) conformational problems are relative to the rotational isomerism around C–C bonds, and configuration problems to the distribution of asymmetric carbon atoms [in the main chain and/or in the lateral chain as in the case of optically active poly( $\alpha$ -olefins)]. Much confusion is present nowadays in polymer chemistry nomenclature because of the indiscriminative use of these two terms. Flory and associates, for instance, use the terms 'configurational partition functions'<sup>7, 13</sup> to indicate what, according to the classical nomenclature, should be called 'conformational partition function'. A glance at the papers presented at the last IUPAC meeting of pure and applied chemistry (Boston, 1971) is indicative of this terminology confusion.

RESULTS FOR ISOTACTIC POLY( $\alpha$ -OLEFINS)

Table 1 reports the conformational analysis at the conformational reversals for a series of isotactic poly( $\alpha$ -olefins). The statistical weight of a given conformation is evaluated in terms of  $\sigma$ ,  $\tau$  and  $\omega$  with respect to the statistical weight 1 chosen for the most stable monomeric unit conformation. The conformations having statistical weight less than  $\tau\omega$  have been neglected, except in the case of poly(3-methyl-1-butene) in the  $l \rightarrow d$  conformational reversal (Table 1). In this case, we have assumed that the conformations  $g+g+g-g-$  correspond to a statistical weight  $\omega^2$ . In Table 1, only  $tg+$  and  $tg-$  conformations are considered for each monomeric unit. For instance, conformations of the type  $\dots tttt \dots$ , which anyway have a very large energy, have not been considered, in keeping with the requirement of the statistical model that only  $tg+$  and  $g-t$  conformations are assumed by each monomeric unit<sup>3</sup>. The conformational analysis at the conformational reversals is relative to a couple of monomeric units (for instance, bonds  $a-d$ ) of the following chain configuration and in the indicated direction:



The definition of  $t$ ,  $g+$ ,  $g-$  (relative, for instance to the bond  $c$  has been taken as the following:



One can see that there are two kinds of energetically distinguishable conformational reversals. In the case of polypropylene, this was indicated many years ago by Allegra *et al.*<sup>11</sup>. We will indicate the conformational partition functions pertaining to these two types of conformational reversal as  $Q_{al}$  and  $Q_{la}$ . Obviously, this difference between  $Q_{al}$  and  $Q_{la}$  should not be taken as an indication that physically the right  $\rightarrow$  left conformational reversal is energetically favoured on the other. In a chain, each conformational reversal is either one (right  $\rightarrow$  left and left  $\rightarrow$  right) depending upon the direction along which the

chain is viewed. It is only by considering the chain in the arbitrary direction indicated above, that the energetically more favoured conformational reversal coincides with the right  $\rightarrow$  left change of the spiralization sense.

This dissymmetry in the conformational reversals does not produce dissymmetry in the calculated average conformational properties. The conformational properties, as expressed in terms of  $\Delta U$  through the equations previously discussed, refer, in fact, to an average over all the possible chain isomers; and for an isotactic macromolecule having main chain configuration opposite to that indicated in the text, the energy relation between  $Q_{al}$  and  $Q_{la}$  would be inverted. It is certainly a very interesting stereochemical feature (usually not taken in due account in other treatments) that the two kinds of conformational reversals, though having different energies, are present in the same amount in the macromolecule. To the macromolecule consisting of alternating left-handed and right-handed sequences a very large number of chain conformations are allowed, and this produces a compensation, through entropy factors, of the apparent decrease in stability brought about by the high energy conformational reversals. The probability of an average conformational reversal should be thought in terms of the free energy of the whole macromolecule, more than in terms of the actual local enthalpy.

Only in the case of polypropylene is one of the two conformational reversals 'athermal'<sup>11</sup>; in poly(1-butene) the conformational reversals involve already an energy excess  $\Delta E_2$  with respect to the regularly spiraled conformation, and in the case of poly( $\alpha$ -olefins) having a further branching in the side chain in the  $\alpha$  or  $\beta$  position, an energy excess corresponding at least to  $\Delta E_3$  is required. The importance that the entropic effects play in determining the actual  $\Delta U$  value should also be noted. In the case, for instance, of polypropylene, a couple of monomeric units can be realized in two ways in a regularly spiraled sequence. By contrast, a couple of monomeric units producing a conformational reversal can be realized in 17 ways, though with higher energy. This entropic factor contributes to lower the  $\Delta U$  value.

Table 3 gives the  $\Delta U$  values obtained with the conformational partition functions of Table 2, and on the basis of equation (5), assuming  $\Delta E_1 = 500$ ,  $\Delta E_2 = 1500$ ,  $\Delta E_3 = 2500$  cal/mol. These values are the ones more commonly employed in conformational problems of paraffins and poly( $\alpha$ -olefins)<sup>7, 18, 26, 27</sup>.

Polypropylene is the polymer structure characterized by the lowest  $\Delta U$ . The macromolecules of isotactic polypropylene in solution are then those characterized by the

Table 1 Conformational analysis at the conformational reversals in some isotactic poly( $\alpha$ -olefins)\*

No.	Conformations of main chain bonds	Polypropylene	Poly(1-butene)	Poly(1-pentene)	Poly(3-methyl-1-butene)	Poly(4-methyl-1-pentene)
1	$\dots g+t$ <i><math>g+t</math></i> <i><math>t</math></i> <i><math>g-t</math></i> $g-\dots$	$\omega$	$\omega(1+2\tau)$	$\omega(1+\tau+\sigma)^2$	$4\omega^2$	$\omega$
2	$\dots g+t$ <i><math>g+g+t</math></i> <i><math>g-t</math></i> $g-\dots$	$\tau\omega$	$2\tau\omega$	$2\tau\omega(1+\sigma)^2$	—	—
3	$\dots g+t$ <i><math>g+t</math></i> <i><math>g-g-t</math></i> $g-\dots$	$\tau\omega$	$2\tau\omega$	$2\tau\omega(1+\sigma)^2$	—	—
4	$\dots t$ <i><math>g-t</math></i> <i><math>t</math></i> <i><math>g+t</math></i> $g+t \dots$	1	$(\tau+2\omega)(1+\omega+\tau)$	$(1+\tau+\sigma)[\tau+\omega+2\omega(\sigma+\tau)]$	$2\omega$	$2\tau\omega$
5	$\dots t$ <i><math>g-t</math></i> <i><math>g-t</math></i> <i><math>t</math></i> $g+t \dots$	1	$(\tau+2\omega)(1+\omega+\tau)$	$(1+\tau+\sigma)[\tau+\omega+2\omega(\sigma+\tau)]$	$2\omega$	$2\tau\omega$
6	$\dots t$ <i><math>g-t</math></i> <i><math>g-g+t</math></i> <i><math>g+t</math></i> $\dots$	$\omega$	$\omega(1+\tau+\omega)^2$	$\omega(1+\sigma+\tau)^2$	$\omega$	$\omega$
7	$\dots t$ <i><math>g-t</math></i> <i><math>g+g+t</math></i> <i><math>g+t</math></i> $\dots$	$\tau\omega$	$\tau\omega$	$\tau\omega(1+\sigma)^2$	—	$\tau\omega$
8	$\dots t$ <i><math>g-t</math></i> <i><math>g-g-t</math></i> <i><math>g+t</math></i> $\dots$	$\tau\omega$	$\tau\omega$	$\tau\omega(1+\sigma)^2$	—	$\tau\omega$
9	$\dots t$ <i><math>g-t</math></i> <i><math>t</math></i> <i><math>g-t</math></i> $g+t \dots$	$\tau\omega$	—	—	—	—
10	$\dots t$ <i><math>g-t</math></i> <i><math>g+t</math></i> <i><math>t</math></i> $g+t \dots$	$\tau\omega$	—	—	—	—

\* Relative to the italicized couple of monomeric units (bonds  $a-d$ ) in the main chain configuration indicated in the text

Table 2 Conformational partition functions of some isotactic poly( $\alpha$ -olefins)

Polymer	$Q_l = Q_d$	$Q_{ld}^*$	$Q_{dl}^*$
Polypropylene	1	$\omega + 2\tau\omega$	$2 + \omega + 4\tau\omega$
Poly(1-butene)	$1 + \tau + \omega$	$\omega + 6\tau\omega$	$2\tau(1 + \tau + \omega) + 5\omega + 10\tau\omega$
Poly(1-pentene)	$1 + \sigma + \tau$	$\omega(1 + \sigma + \tau)^2 + 2\tau\omega(1 + \sigma)^2$	$2\tau(1 + \sigma + \tau)(1 + 2\sigma) + \omega[(1 + \sigma + \tau)^2 + 2(1 + \sigma + \tau)(1 + 2\sigma)] + 2\tau\omega(1 + \sigma)^2$
Poly(3-methyl-1-butene)	$1 + 2\omega$	$4\omega^2$	$5\omega$
Poly(4-methyl-1-pentene)	$1 + 2\omega$	$\omega + 4\tau\omega$	$\omega + 6\tau\omega$
Poly(5-methyl-1-hexene)	$2 + \sigma + 3\tau$	$\omega(2 + \sigma + 3\tau)^2$	$4\tau(2 + \sigma + 3\tau) + 2(2 + \sigma + 3\tau)(4\omega + \tau^2 + 2\omega\tau) + \omega(2 + \sigma + 3\tau)^2$

\* Sum of the relative statistical weights of the conformations 1-3 ( $Q_{ld}$ ) and 4-10 ( $Q_{dl}$ ) (see Table 1)

largest flexibility. Poly(1-butene) and poly(1-pentene) are characterized by approximately the same  $\Delta U$  value, and hence by the same conformational properties. The calculated characteristic ratio is  $\sim 10$ , whereas  $\nu$  is of the order of 5. This corresponds to a conformational reversal every 5 monomeric units. Poly(5-methyl-1-hexene), poly(6-methyl-1-heptene), and the isotactic poly( $\alpha$ -olefins) without branching in the side chain, [as poly(1-hexene), poly(1-heptene) not reported in Tables 2 and 3] have about the same  $\Delta U$  values as poly(1-butene) and poly(1-pentene), and hence the same conformational properties in solution.

When the side chain bears a substituent in  $\alpha$  or  $\beta$  position with respect to the main chain, the  $\Delta U$  value increases to about 1200–1500 cal/mol and consequently  $\nu$  reaches the value of about 10 monomeric units, and  $\bar{h}^2/Nl^2$  the value of 20–30. Examination of Table 1 indicates the reason of such an enhancement: branching in the lateral chain close to the main chain makes both types of conformational reversals take place with  $\omega$  statistical weight. Branching in  $\alpha$  of the side chain produces a larger stiffness of the chain in solution than branching in  $\beta$ .

Table 3 shows that, for the chosen values of the energy parameters, a fair agreement is obtained between the calculated and the experimentally available data of end-to-end distance. Given all the approximations involved in the evaluation of  $\Delta U$ , this quantitative agreement has to be taken with caution. However, it gives confidence that the proposed method is satisfactory in predicting the order of magnitude of the conformational properties of poly( $\alpha$ -olefins) in solution as a function of the structure of the monomeric unit.

From equations (1)–(5) and the conformational partition functions of Table 2, the conformational partition function of isotactic poly( $\alpha$ -olefins) in solution can be evaluated as a function of temperature. The calculation can be made only under the further assumption that  $\Delta E_1$ ,  $\Delta E_2$  and  $\Delta E_3$  do not change with temperature, and that the basic approximation of the model itself—the rotational isomeric state approximation and the assumption of only three conformational states for the main chain bond of the monomeric unit—are unaffected by temperature. Obviously, these can be considered as reliable approximations only by operating in a small temperature range, and towards the low temperature region.

Equations (1) and (4) predict a decrease of the  $\nu$  and  $\bar{h}^2/Nl^2$  values by increasing the temperature, a decrease which is the higher, the higher the  $\Delta U$  value. For poly(1-butene), the  $\nu$  value at 400K is reduced to 3.5 monomeric units, whereas the characteristic ratio becomes

Table 3 Conformational properties of some isotactic poly( $\alpha$ -olefins) in solution<sup>a</sup>

Polymer	$\Delta U$	$\nu$	$\bar{h}^2/Nl^2$ b,c	
			Calculated	Experimental
Polypropylene	500	3.2	6.0 4.2 (at 400K)	5.7 (at 145°C) <sup>43d</sup>
Poly(1-butene)	820	5.0	10.5	9.4 (at 45°C) <sup>44</sup>
Poly(1-pentene)	860	5.2	11.0	10 (at 31.5°C) <sup>46</sup> 9 (at 62.4°C) <sup>32</sup>
Poly(3-methyl-1-butene)	1500	13.0	30.0	—
Poly(4-methyl-1-pentene)	1200	8.0	19.0	—
Poly(5-methyl-1-hexene)	850	5.0	11.0	—

<sup>a</sup> Calculated at 300K, unless otherwise specified, with  $\Delta E_1=500$ ,  $\Delta E_2=1500$ ,  $\Delta E_3=2500$  cal/mol. Note that the temperature of the experimental data is not the same as the calculated values. We did not consider worthwhile carrying out calculations at each particular temperature, given the rough qualitative meaning that we wish to attribute to our calculations.

<sup>b</sup>  $\bar{h}^2$  indicates in this work the unperturbed mean square end-to-end distance. Other authors use the symbols  $\langle R_g^2 \rangle$  or  $\langle r_g^2 \rangle$  that we want to avoid in order not to produce confusion with the gyration radius, indicated as  $\langle r \rangle$  by many authors. In other papers the characteristic ratio is given in terms of the polymerization degree instead of the number of C–C bonds in the chain.

<sup>c</sup> The experimental values reported here have been taken from the book by Flory<sup>7</sup> and from the review by Crescenzi<sup>6</sup>. For more details about the experimental and theoretical problems connected with average dimension problems in polymers see the review by Kurata and Stockmayer<sup>42</sup>.

<sup>d</sup> A value ranging between 4.6 and 5.8 has been obtained by Nakajima and Saijyo<sup>30</sup> in the temperature range 125–183°C. The average dimensions of isotactic polypropylene have also been investigated by Parrini *et al.*<sup>44</sup>.

about 7. For poly(3-methyl-1-butene), in the same temperature range,  $\nu$  goes from 13 to 6 whereas  $\bar{h}^2/Nl^2$  goes from 30 to 14.

Lately, a series of experimental investigations have been concerned with the temperature dependence of the end-to-end distance<sup>3, 7, 26–31</sup>. Usually, reference is made to the property  $d \ln \bar{h}^2 / dT$ . In the case of isotactic poly(1-butene) and poly(1-pentene), recent viscometric measurements in  $\theta$  conditions carried out by Moraglio and coworkers<sup>28, 29</sup> indicate a value of  $d \ln \bar{h}^2 / dT$  of  $-0.8$  and  $-1.2 \times 10^{-3}$  deg<sup>-1</sup> respectively in the temperature range of 50 to about 150°C. In addition to this, Moraglio and coworkers calculated the value of this conformational property by applying good solvent theories to  $[\eta]$  in

toluene at various temperatures. Values ranging between  $-0.5$  and  $-5 \times 10^{-3} \text{ deg}^{-1}$  were obtained depending upon the theory employed<sup>28, 29</sup>. A value of  $-4 \times 10^{-3} \text{ deg}^{-1}$  over the temperature range  $125\text{--}183^\circ\text{C}$  was obtained by Japanese authors<sup>30</sup>. Equation (3), for instance for a  $\Delta U$  value of  $1000 \text{ cal/mol}$  at  $400\text{K}$ , gives a value of about  $-3 \times 10^{-3} \text{ deg}^{-1}$ . It is not easy to give an unequivocal explanation of all these different figures. Too many approximations are involved in the calculation (validity of the rotational isomeric state approximation) over a wide range of temperature; constancy of  $\Delta E_1$ ,  $\Delta E_2$ ,  $\Delta E_3$  with temperature and indetermination on their actual value; neglect in equation (3) of the role of torsional oscillations around the conformational energy minima, which, according to the Russian authors<sup>3</sup>, may bring about a substantial decrease in the  $\bar{h}^2$  (and hence in the temperature coefficient); neglect of the role of long range interactions and whole macromolecule vibrations, etc.). There are also so many approximations involved in the experimental evaluation of  $\bar{h}^2/Nl^2$ , particularly at the solid state, that the homogeneity between calculated and experimental data could be even questioned. For all these reasons we are satisfied with the agreement obtained in the present approach as far as the temperature coefficient of the average dimensions are concerned, and we do not feel inclined to follow the theory of Flory and associates\*, that attributes the lower value of the temperature coefficient of the characteristic ratio generally found in the experiments by assuming a certain amount of steric irregularities in the chains<sup>13</sup>.

#### THE CASE OF OPTICALLY ACTIVE ISOTACTIC POLY( $\alpha$ -OLEFINS)

Optically active isotactic poly( $\alpha$ -olefins) differ from their non-optically active analogues because the left-handed and right-handed spiraled conformations do not have the same energy<sup>34-37, 39</sup>. According to the statistical treatment developed by Birshtein and coworkers<sup>3, 34</sup>, their conformational properties in solution can be expressed in terms of two energy parameters:  $\Delta U$ , previously defined in the case of non-optically active polymers, and  $\Delta E$ , defined as:

$$\Delta E = RT \ln \frac{g_{ll}}{g_{aa}} \quad (6)$$

which represents the energy difference, per monomeric unit, between a regularly spiraled left-handed and right-handed sequence. The equations that, in terms of  $\Delta E$  and  $\Delta U$ , give the conformational properties of the macromolecules in solution, are:

\* With this we do not deny that configurational irregularities exist in the conventional isotactic polymers, and we do not even exclude that configurational irregularities in a chain may have some of the effect indicated by Flory, Abe and associates<sup>13, 15</sup>. Our point is that, at the present moment, all the available experimental data of the conformational properties of poly( $\alpha$ -olefins) in solution can be explained without invoking this effect, and even with a simple model like that presented here.

$$\nu_l = \frac{l+r+q}{r-q} \quad \nu_a = \frac{l+r+q}{r+q} \quad (7)$$

$$\omega_l = \frac{r+q}{2r} \quad \omega_a = \frac{r-q}{2r} \quad (8)$$

$$\frac{\bar{h}^2}{Nl^2} = \frac{8(1-g)(1-g^3) + p^2g(3+2g+3g^2)}{3p^2g(1+g)r} \quad (9)$$

where  $q = (1-g)/2$ ;  $r = (q^2 + p^2g)^{1/2}$ ;  $g = \exp(-\Delta E/RT)$ . In the above equations,  $\nu_l(\nu_a)$  is the average length, in number of monomeric units, of the regularly spiraled left-handed (right-handed) sections, and  $\omega_l(\omega_a)$  the molar fraction of monomeric units left-handed (right-handed) spiraled. We assumed in the above equations that the left-handed screw sense is the more favoured, as this is indeed the case in optically active poly( $\alpha$ -olefins) having the asymmetric carbon atom in the lateral chain in the (*S*) absolute configuration<sup>35</sup>. We will refer to this class of polymer later since they have been investigated in detail from the experimental<sup>35</sup> and theoretical<sup>14, 34, 39-41</sup> point of view.

Equation (6), on the basis of the same arguments developed in the preceding sections, can take the form:

$$\Delta E = RT \ln \frac{Q_l}{Q_a} \quad (10)$$

Equations similar to equation (10) have been considered before, in a more approximate form, for evaluating the energy difference between the two spiraled main chain conformations<sup>3, 40</sup>.

In deriving the conformational partition functions it will be assumed that the most stable left-handed and right-handed monomer unit conformations have the same statistical weight (1). This is obviously the case for non-optically active polymers, as the left-handed and right-handed conformations are related by mirror image symmetry. In the case, however, of optically active polymers, the most stable monomer unit conformations in the two opposite screw senses are diastereoisomeric conformations. Only as a first approximation can they be considered as having the same energy, even though they usually have the same number of bonds in *trans* and *gauche* conformations. In other words, in the case of optically active polymers,  $Q_l$  and  $Q_a$  should be more properly referred to as standard free energies different from one another. However, as has been previously pointed out, there is no reliable way of evaluating conformational energy differences which are not in terms of  $\sigma$ ,  $\tau$  and  $\omega$ . As a consequence of the neglect of enthalpic energy differences between the reference most stable left- and right-handed monomer unit conformations,  $\Delta E$  derives mostly from entropic effects, and the same is true for  $\Delta U$ .

Conformational analysis at the conformational reversals for a series of isotactic optically active poly( $\alpha$ -olefins) is reported in Table 4. Table 5 reports the corresponding conformational partition functions. Of these polymers, poly[(*S*)-3-methyl-1-pentene], poly[(*S*)-4-methyl-1-hexene] and poly[(*S*)-5-methyl-1-heptene] have been prepared<sup>35</sup>. No experimental data are so far available for the other two polymers.



Table 4 Conformational analysis at the conformational reversals of some isotactic optically active poly( $\alpha$ -olefins)

Conformation no.*	Poly[(S)-3-methyl-1-pentene]	Poly[(S)-4-methyl-1-hexene]†	Poly[(S)-5-methyl-1-heptene]†	Poly[(S)-3,4-dimethyl-1-pentene]	Poly[(S)-3-ethyl-5-methyl-1-hexene]
1	$\omega^2(3+\tau)$	$\omega Q_l Q_d$	$\omega Q_l Q_d$	$\omega^2$	$\tau\omega^2 + 6\omega^3$
2	$3\tau\omega^2$	$\tau\omega Q_d(Q_l + Q_d)$	$\omega\tau Q_d(Q_l + Q_d)$	$\tau\omega^2$	$\omega^2\tau$
3	$3\tau\omega^2$	$\tau\omega Q_l(Q_l + Q_d)$	$\omega\tau Q_l(Q_l + Q_d)$	$2\tau\omega^2$	$2\tau\omega^2$
4	$3\omega$	$\tau\omega Q_l(Q_l + Q_d)$	$\tau Q_l(3+4\tau)$	$4\omega^2$	$4\omega^3$
5	$3\omega$	$\tau\omega Q_d(Q_l + Q_d)$	$\tau Q_d(3+4\tau)$	—	—
6	$2\omega$	$\omega Q_l Q_d$	$\omega Q_l Q_d$	$3\omega^2$	$3\omega^2$
7	—	$\tau\omega Q_l Q_d$	$\omega\tau Q_l[3 + \sigma(1+\tau) + 4\tau]$	—	$\tau\omega^2$
8	—	$\tau\omega Q_l Q_d$	$\omega\tau Q_l Q_d$	—	—

\* The numbers refer to the conformations of the main chain bonds listed in Table 1

†  $Q_l$  and  $Q_d$  are reported in Table 5

 Table 5 Conformational partition functions of some isotactic optically active poly( $\alpha$ -olefins)

Polymer	$Q_l$	$Q_d$	$Q_{ld}^*$	$Q_{dl}^*$
Poly[(S)-3-methyl-1-pentene]	$2+2\omega$	$1+4\omega$	$3\omega^2+7\omega^2\tau$	$8\omega$
Poly[(S)-4-methyl-1-hexene]	$2+\tau+2\omega$	$1+\tau+5\omega$	$\omega Q_l Q_d + \omega\tau(Q_l + Q_d)d^2$	$\tau\omega(Q_l + Q_d)^2 + Q_l Q_d(\omega + 2\tau\omega)$
Poly[(S)-5-methyl-1-heptene]	$3+\sigma(2+\tau)+7\tau$	$3+\sigma(1+\tau)+7\tau$	$\omega Q_l Q_d + \tau\omega(Q_l + Q_d)d^2$	$\tau(3+4\tau)(Q_l + Q_d) + \omega Q_l Q_d + \omega\tau Q_l[Q_d + 2 + 4\tau + \sigma(1+\tau)]$
Poly[(S)-3,4-dimethyl-1-pentene]	$1+3\omega$	$4\omega$	$\omega^2+3\tau\omega^2$	$7\omega^2$
Poly[(S)-3-ethyl-5-methyl-1-hexene]	$1+4\omega$	$1+2\omega$	$4\tau\omega^2+6\omega^3$	$\tau\omega^2+7\omega^2$

\* Sum of the relative statistical weights of the conformations 1-3 ( $Q_{ld}$ ) and 4-8 ( $Q_{dl}$ ) of Table 4

The  $\Delta U$  value calculated for the optically active polymers (see Table 6) is in the range of that evaluated for the non-optically active ones. However, the presence of the energy parameter  $\Delta E$  makes the conformational properties of the optically active polymers remarkably different from those of the non-optically active analogous. For instance in the case of poly[(S)-4-methyl-1-hexene]  $\nu_l$  is of the order of 40-50\* monomeric units, whereas  $\nu_d$  is only  $\sim 2$  monomeric units. The macromolecules of this polymer in solution consist then of alternating long left-handed and short right-handed sequences. The number of conformational reversals is considerably lower than in the case of macromolecules of non-optically active polymers having the same  $\Delta U$  [for instance poly(4-methyl-1-pentene)]. As a consequence, a much larger end-to-end distance is obtained.

When the branching of the lateral chain is in  $\alpha$  with respect to the main chain, the stiffness of the chain reaches extremely high values e.g. poly[(S)-3-methyl-1-pentene] and poly[(S)-3,4-dimethyl-1-pentene]. The comparison between these two polymers is indicative of the effect of  $\Delta E$  on the conformational properties. The effect on  $\omega_i$  is minimal, whereas the effect on  $\bar{h}^2$  and  $\nu_l$  is very significant indeed. The comparison between poly[(S)-3-methyl-1-pentene] and poly[(S)-4-methyl-1-hexene], characterized by about the same  $\Delta E$  value, shows the effect of  $\Delta U$  on the conformational properties.

Even more noticeable, in this respect, is the comparison between poly[(S)-3-ethyl-5-methyl-1-hexene] and poly[(S)-5-methyl-1-heptene], both characterized by a minimum  $\Delta E$ . The extremely high value found for the

\* In a previous paper<sup>40</sup>, on the basis of more approximate energy parameters and partition functions, a lower value had been estimated.

conformational properties of the former polymer illustrates the high degree of cooperativity existing between the two energy parameters  $\Delta E$  and  $\Delta U$ . When a high energy is required at the conformational reversals, a minimum energy difference (of the order of 20 cal/mol) between the two spiraled screw senses is sufficient to make the macromolecules spiraled about 80% in one screw sense. However, although this example is a useful indication of the peculiarity of the conformational equilibrium established in the macromolecules of optically active vinyl polymers, the actual value of  $\Delta E$ , as given here, is quite unreliable. At these low levels of energy differences, all the approximations of the method become very critical. Poly[(S)-5-methyl-1-heptene] is an example of an optically active polymer having conformational properties in the range of those calculated for the non-optically active polymers having the same  $\Delta U$ . For poly[(S)-6-methyl-1-octene] (not reported in the Table) a  $\Delta E$  close to zero can be calculated, and in this case the difference between  $\nu_l$  and  $\nu_d$  disappears.

All these arguments make clear the importance of both energy parameters  $\Delta E$  and  $\Delta U$  in order to have a semi-quantitative idea of the actual conformational characteristics of a given chain structure. Given the close interplay between these two energy parameters, any drastic approximation in  $\Delta U$  would profoundly affect the  $\Delta E$  value, and *vice versa*.

The extremely high stiffness predicted for some of the polymers of Table 6 is due to the high  $\Delta U$  value and to the interplay between  $\Delta U$  and  $\Delta E$ . It is, however, reasonable to assume that in all the cases in which a very large  $\Delta U$  is calculated, some of the basic approximations of the method of calculation do not hold anymore. For instance, it is likely that a deviation from the ideal  $t$  and  $g$  states,

Table 6 Conformational properties of some isotactic optically active poly( $\alpha$ -olefins)\*

Polymer	$\Delta E^\dagger$	$\Delta U^\dagger$	$\nu_l$	$\nu_d$	$\omega_l$	$\bar{h}^2/Nl^2$
Poly[(S)-3-methyl-1-pentene]	390	1600	190	2	0.99	300
Poly[(S)-4-methyl-1-hexene]	360	1200	45	2	0.95	70
Poly[(S)-5-methyl-1-heptene]	60	850	6	4	0.60	11
Poly[(S)-3,4-dimethyl-1-pentene]	1700	1300	1500	1	1.00	2000
Poly[(S)-3-ethyl-5-methyl-1-hexene]	20	2200	80	22	0.78	150

\* Calculated at 300K, with  $\Delta E_1=500$ ,  $\Delta E_2=1500$ ,  $\Delta E_3=2500$  cal

† In cal/mol of monomeric unit

and/or a deviation from the ideal tetrahedral bond angles, make the conformational reversals take place with an overall lower energy. These effects would change the conformational partition functions at the conformational reversals to an extent not predictable at the present state of knowledge.

The calculated  $\nu_l$  and  $\bar{h}^2$  of optically active polymers decrease with temperature much more remarkably than those of non-optically active analogous ones. A comparative study of the calculated temperature dependence of  $\bar{h}^2/Nl^2$  and  $\nu_l$  for poly(4-methyl-1-pentene) and poly[(S)-4-methyl-1-hexene] was attempted some years ago on the basis of a more approximate approach and simpler conformational partition functions<sup>40</sup>. Equations (7)–(10) predict that for poly[(S)-4-methyl-1-hexene]  $\nu_l$  goes from 120 to  $\sim 20$  and  $\bar{h}^2/Nl^2$  from 80 to  $\sim 35$  in the temperature range 250–350K. In the case of poly[(S)-3,4-dimethyl-1-pentene] and poly[(S)-3-methyl-1-pentene], the decrease of the value of the conformational properties with temperature in the same temperature range is so significant as to resemble a phase transition. The detailed investigation of the temperature coefficient of the conformational properties for these systems should, however, take into account the length of the chain, i.e. they should be given as a function of the degree of polymerization. A calculation of the conformational properties of optically active poly( $\alpha$ -olefins) as a function of the polymerization degree has been carried out by Abe<sup>14</sup>. However, in this treatment the approximation has made the probability of high energy interaction equal to zero which would correspond to  $\Delta U \cong \infty$  in our notation. We think that this approximation leads to an unreliable physical model for the chain in solution.\* With the present model, by decreasing the temperature,  $\bar{h}^2/Nl^2$  and  $\nu$  tend to infinity and no S-shaped curve can be obtained. Since at the moment no proper analytical expressions for the conformational properties of optically active vinyl polymers as a function of the chain length are available, this problem is not discussed here.

#### OPTICAL ACTIVITY AND CONFORMATION

The molar rotation of optically active vinyl polymers can be correlated to their conformational equilibrium in solution through the relationship:

\* The unrealistic value calculated by Abe<sup>14</sup> for the optical rotation of poly[(S)-5-methyl-1-heptene] is ascribed to this approximation.

$$[\phi]_\lambda^T = M_l \omega_l + M_d \omega_d \quad (11)$$

where  $[\phi]_\lambda^T$  is the molar rotation of the polymer, referred to one monomeric unit, and  $M_l$  and  $M_d$  the average molar rotation of a left-handed and right-handed spiraled monomeric unit at the considered temperature and wavelength. The basic approximations in equation (11) are consistent with the statistical model itself, namely that only spiraled conformations can be assumed by the monomeric unit and that chain end-effects are negligible.

In principle, if one could determine accurately  $M_l$  and  $M_d$  through some independent method, one could estimate the reliability of the calculated  $\omega_l$  values ( $\omega_d = 1 - \omega_l$ ) by comparing the experimental  $[\phi]_\lambda^T$  values with those calculated from equation (11). Unfortunately, as is well known, at the present no method is available for calculating exactly *a priori* the molar rotation of a given asymmetric molecule. Only semi-empirical methods are known, and they can be useful only to obtain first approximation figures. For instance the Brewster method<sup>38</sup>, which is the one that has been extensively used for optically active poly( $\alpha$ -olefins)<sup>35</sup>, in the case of poly[(S)-4-methyl-1-hexene] predicts at the D sodium line  $M_l = +240$  and  $M_d = -300$ <sup>35</sup>. The experimental  $[\phi]_D^{25}$  is, however, +290<sup>35</sup>, i.e. higher than the calculated  $M_l$ , and so equation (11) cannot be used to obtain  $\omega_l$  values.\*

However, for the polymers for which experimental data of optical activity are available, the soundness of the calculated figures of  $\omega_l$  can be checked at least from a qualitative viewpoint by another procedure. The calculated figures predict that, in the cases in which  $\omega_l \geq 0.9$ ,  $[\phi]_D^T(\text{exp.})$  should be close to the value calculated for  $M_l$ , whereas in the case in which  $\omega_l$  is closer to 0.5,  $[\phi]_D^T$  should be close to the arithmetic average between the calculated  $M_l$  and  $M_d$  values. This is indeed what has been found. For poly[(S)-3-methyl-1-pentene] and poly[(S)-4-methyl-hexene]  $[\phi]_D^{25}$  is +160 and +290, and  $M_l + 180$  and +240 respectively<sup>35</sup>. For poly[(S)-6-methyl-1-octene] and for poly[(S)-5-methyl-1-heptene],  $[\phi]_D^{25}$  is +20 and +68, and the average between  $M_l$  and  $M_d$  is +34 and +22 respectively<sup>35</sup>.

There is another way to check the reasonability of the calculated  $\omega_l$  values on the basis of the experimental

\* It is probably worth noting that the values used by Brewster for the molar rotation of each C–C bond ( $\pm 60^\circ$ , or  $0^\circ$ ) are best-fitting values relative to a particular kind of conformational analysis (statistical weight 1 or 0 for each conformation), and that these values cannot be used with conformational analysis different from that of Brewster. The combination of the Brewster values for the molar rotation with conformational partition functions in terms of  $\sigma$ ,  $\tau$ , and  $\omega$  yields a self-inconsistent system.

$[\phi]_D^T$ . This is, to use equation (11) at two different temperatures, and calculate  $M_l$  and  $M_d$ . This has been done<sup>27, 40</sup> and the values obtained for  $M_l$  and  $M_d$ , surprisingly enough, are in fair agreement with those calculated from the Brewster method. The fact that at different temperatures equation (11) provides the expected order for  $M_l$  and  $M_d$ , indicates that  $\omega_l$  values are consistent with the temperature coefficient of optical activity of the polymers considered. According to the model so far outlined, the change of optical activity with temperature in these polymers is due to the variation of the relative percentage of left-handed and right-handed spiraled monomeric units. In particular, for the polymers listed in Table 6, increasing the temperature increases  $\omega_d$  with respect to  $\omega_l$ . The optical activity then decreases as the right-handed spiraled monomeric units have a molar rotation high and negative and those left-handed spiraled have a molar rotation high and positive<sup>34-37, 40, 41</sup>. Under the approximation that  $M_l$  and  $M_d$  are constant with temperature, the variation of optical activity with temperature can be obtained by integrating equation (11) with respect to the temperature:

$$\frac{d[\phi]_D}{dT} = (M_l - M_d) \frac{d\omega_l}{dT} \quad (12)$$

The function  $d\omega_l/dT$  is very complicated (see equation (8)). Despite this, calculation in the temperature range 300-400K indicate a monotonic, almost linear, decrease of the molar rotation with temperature, in agreement with previous experiments<sup>35-37</sup>. Since, for poly[(S)-3-methyl-1-pentene] and poly[(S)-4-methyl-1-hexene],  $(M_l - M_d)$  is a high and positive number of the order of 400-700<sup>35</sup>, and the experimental  $\Delta[\phi]_D/\Delta T$  is in the range  $-(0.4-0.7)$ ,  $\Delta\omega_l/\Delta T$  is in the range of  $10^{-3} \text{ deg}^{-1}$ . For the polymers considered, the quantity  $(\Delta[\phi]_D/\Delta T) \cdot \{1/(M_l - M_d)\}$  provides a measure of the decrease of the more favoured screw sense with temperature.

There are a few other considerations suggested by equation (12). For instance, for the polymers characterized by a very large  $\omega_l$  value at room temperature, measurements of optical activity at temperatures such that  $\omega_l = 1.0$  should provide a direct experimental measure of  $M_l$ . Theoretically, on the basis of equation (11) and the present method of calculation, this is achieved at  $T \leq 350\text{K}$  for poly[(S)-3, 4-dimethyl-1-pentene], at  $T \leq 300\text{K}$  for poly[(S)-3-methyl-1-pentene] and at  $T \leq 250\text{K}$  for poly[(S)-4-methyl-1-hexene] (namely, in an experimentally accessible range, especially if working with low molecular weight fractions). Experimentally, the check that such a limiting value is obtained for  $\omega_l$ , would be given by the fact that, by further decreasing the temperature,  $[\phi]_D$  would remain constant.

Equation (11) does not predict any sharp transition of optical activity with temperature in any of the cases listed in Table 6. This indicates that the variation of optical activity with temperature is not sensitive to changes of the stiffness of the macromolecules in solution. Optical activity depends on the relative amount of left-handed and right-handed monomeric units, and not on the average length of regularly spiraled sequences.

Finally, optical activity measurements could be also useful in obtaining information on conformational kinetics. The rate of change of  $[\phi]_D$  with time in a given temperature range is directly related, according to the present model, to the rate of main chain conformational

transitions. This concept is at the basis of a recent paper by Poul and Mazo<sup>47</sup>, in which the problem of the conformational kinetics in isotactic poly( $\alpha$ -olefins) is faced, and the possibility of a  $T$ -jump experiment, with optical activity as the monitored property, is discussed.

## CONCLUSIONS

The proposed method of calculation of  $\Delta E$  and  $\Delta U$  allows for the evaluation of the conformational properties of isotactic poly( $\alpha$ -olefins) and permits a relationship to be drawn between the monomer unit structure and the chain flexibility in solution. The method seems particularly useful for forecasting those polymer structures which may be characterized by anomalous conformational properties in solution, as in the case of optically active isotactic poly( $\alpha$ -olefins) having an asymmetric carbon atom in the  $\alpha$  or  $\beta$  position in respect to the main chain. The absolute value of the calculated figures should not be taken too literally, owing to the many approximations involved in the calculation. However, these figures are likely to be correct from a semi-quantitative viewpoint. The same method of calculation predicts values of  $\bar{h}^2/Nl^2$  that are in agreement with the available experimental data in the case of non-optically active polymers. In the case of optically active polymers, the calculated  $\omega_l$  is in agreement with the experimental data of optical activity for a number of different polymer structures. Furthermore,  $\omega_l$  and  $\omega_d$  values are consistent with the temperature coefficient of optical activity. All this confirms the soundness of the proposed model for poly( $\alpha$ -olefins) in solution, and particularly the basic concept, that these macromolecules are highly spiraled in solution. Lacking more direct experimental methods to determine  $\nu_l$ ,  $\nu_d$  and the number of conformational reversals in solution, optical activity is the only property that at the same time gives a proof of the existence of spiraled main chain conformation for poly( $\alpha$ -olefins) in solution and allows for a semi-quantitative check of their conformational properties.

The experimental determination of conformation through end-to-end distance of the extreme stiffness predicted for poly(3-methyl-1-butene), poly[(S)-3-methyl-1-pentene], poly[(S)-3,4-dimethyl-1-pentene], would be the best way to test directly the reliability of our calculation. The problem here, from the experimental point of view, lies in the very poor solubility of the above polymers and particularly of their highly isotactic fractions. An approach to this problem for these polymers can be made through the synthesis of their low molecular weight fractions at such low values of the degree of polymerization that a fair solubility is eventually obtained. Experimental work is in progress in our group to determine the end-to-end distance of poly[(S)-4-methyl-1-hexene], as this polymer offers a good compromise between solubility and calculated chain stiffness.

The method of calculation of the conformational properties here presented could, in principle, be used for polymers others than isotactic poly( $\alpha$ -olefins). For instance, it could be applied to syndiotactic poly( $\alpha$ -olefins), or to poly( $\alpha$ -olefins) with different degrees of stereoregularity. The extension of this method to other polymers, even though of vinyl type [poly(vinyl ketones), poly(vinyl ethers), etc.] is for the moment not possible. In fact, for these systems no reliable information is at hand for their conformational equilibrium in solution.

ACKNOWLEDGEMENTS

The help of Dr O. Bonsignori for evaluating the conformational partition functions and the extensive discussion with him on several aspects of this paper have been much appreciated. The interest of Professor P. Pino and his constructive criticism have been of great use to the author.

REFERENCES

- 1 Natta, G. *Makromol. Chem.* 1960, **35**, 93
- 2 Corradini, P. in 'The Stereochemistry of Macromolecules', 1968, Vol 3, p 1
- 3 Birshtein, T. M. and Ptitsyn, O. B. 'Conformation of Macromolecules', Interscience, New York, 1966
- 4 Flory, P. J. 'Principles of Polymer Chemistry', Cornell University Press, Ithaca, 1953
- 5 Morawetz, H. 'High Polymers', Wiley-Interscience, New York, 1965, Vol XXI
- 6 Crescenzi, V. in 'The Stereochemistry of Macromolecules', 1968, Vol 3, p 243
- 7 Flory, P. J. 'Statistical mechanics of chain molecules', Interscience, New York, 1969
- 8 Volkenstein, M. V. 'Configuration Statistics of Polymer Chains', Interscience, New York, 1963
- 9 Lifson, S. *J. Chem. Phys.* 1959, **30**, 964
- 10 Nagai, K. *J. Chem. Phys.*, 1962, **37**, 490
- 11 Allegra, G., Ganis, P. and Corradini, P. *Makromol. Chem.* 1963, **61**, 225
- 12 Flory, P. J. and Jernigan, R. L. *J. Chem. Phys.* 1965, **42**, 3509
- 13 Flory, P. J., Mark, J. E. and Abe, A. *J. Am. Chem. Soc.* 1966, **88**, 639
- 14 Abe, A. *J. Am. Chem. Soc.* 1968, **90**, 2205
- 15 Abe, A. *Polymer J.* 1970, **1**, 232
- 16 Klyne, W. and Prelog, W. *Experientia*, 1960, **16**, 521
- 17 Hanack, M. 'Conformation Theory', Academic Press, London and New York, 1965
- 18 Pethrick, R. A. and Wyn-Jones, E. *Q. Rev.* 1969, **23**, 301

- 19 Volkenstein, M. V. *Dokl. Akad. Nauk SSSR* 1951, **78**, 879
- 20 Flory, P. J. *J. Am. Chem. Soc.* 1967, **89**, 1798
- 21 Person, W. B. and Pimentel, G. C. *J. Am. Chem. Soc.* 1953, **75**, 532
- 22 Bartell, L. S. and Kohl, D. A. *J. Chem. Phys.* 1963, **39**, 3097
- 23 Scott, D. W., McCullough, K. D. J. P., Williamson, K. D. and Waddington, G. *J. Am. Chem. Soc.* 1951, **73**, 1707
- 24 Scott, R. A. and Sheraga, M. A. *Biopolymers* 1966, **4**, 237
- 25 Allinger, N. L., Hirsch, A., Miller, M. A., Tyminski, I. J. and Van-Catledge, F. A. *J. Am. Chem. Soc.* 1968, **90**, 1199
- 26 Abe, A., Jernigan, R. L. and Flory, P. J. *J. Am. Chem. Soc.* 1966, **88**, 631
- 27 Luisi, P. L. and Bonsignori, O. *J. Chem. Phys.* in press
- 28 Moraglio, G., Zoppi, F. and Giannotti, G. *Abstracts Int. Symp. Macromol., Leiden* 1970, p 197
- 29 Moraglio, G., Gianotti, G., Zoppi, F. and Bonicelli, U. *Eur. Polym. J.* 1971, **7**, 303
- 30 Nakajima, A. and Saijo, A. *J. Polym. Sci. (A-2)*, 1968, **6**, 735
- 31 Ciferri, A., Hoeve, C. A. J. and Flory, P. J. *J. Am. Chem. Soc.* 1961, **83**, 1015
- 32 Mark, J. E. and Flory, P. J. *J. Am. Chem. Soc.* 1965, **87**, 1423
- 33 Volkenstein, M. V. and Ptitsyn, O. B. *Zh. Tekhn. Fis.* 1955, **25**, 662
- 34 Birshtein, T. M. and Luisi, P. L. *Vysokomol. Soedin.* 1964, **6**, 1238
- 35 Pino, P., Ciardelli, F., Lorenzi, G. P. and Montagnoli, G. *Makromol. Chem.* 1963, **61**, 207
- 36 Pino, P. *Adv. Polym. Sci.* 1965, **4**, 393
- 37 Pino, P., Salvadori, P., Chiellini, E. and Luisi, P. L. *J. Pure Appl. Chem.* 1968, **16**, 469
- 38 Brewster, J. H. *J. Am. Chem. Soc.* 1969, **81**, 5475
- 39 Allegra, G., Corradini, P. and Ganis, P. *Makromol. Chem.* 1966, **90**, 60
- 40 Luisi, P. L. and Pino, P. *J. Phys. Chem.* 1968, **72**, 2400
- 41 Pino, P. and Luisi, P. L. *J. Chim. Phys.* 1968, **65**, 130
- 42 Kurata, M. and Stockmayer, W. H. *Fortschr. Hochpolym. Forsch.* 1963, **3**, 196
- 43 Kinsinger, J. B. and Hughes, R. E. *J. Phys. Chem.* 1963, **67**, 1922
- 44 Krigbaum, W. R., Kurz, J. E. and Smith, P. J. *J. Phys. Chem.* 1961, **65**, 1984
- 45 Parrini, P., Sebastiano, F. and Messina, G. *Makromol. Chem.* 1960, **38**, 27
- 46 Moraglio, G. and Brzezinski, J. *J. Polym. Sci.* 1964, **B2**, 1105
- 47 Poul, E. and Mazo, R. *Macromolecules* 1971, **4**, 424

# Note to the Editor

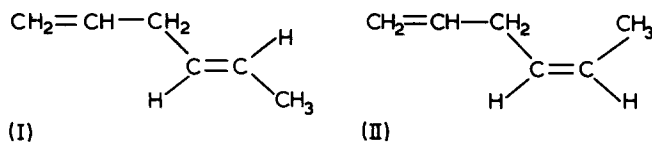
## Cis-trans isomerism in Ziegler-catalysed terpolymerization of hexa-1,4-diene with ethylene and propylene

G. A. Skinner, M. Viney and S. R. Wallis

Research and Development Laboratories, International Synthetic Rubber Company Limited, Southampton SO9 3AT, UK  
(Received 13 January 1972)

Hexa-1,*trans*-4-diene (I) is used in the preparation of ethylene-propylene terpolymers<sup>1, 2</sup> (EPDM). Of the three termonomers used commercially, namely dicyclopentadiene (DCPD), ethylidene norbornene (ENB) and hexa-1,*trans*-4-diene, the last forms a faster-curing polymer than does DCPD<sup>3</sup>. Also, compared with both DCPD and ENB, it is more efficient in terms of the degree of unsaturation present per unit weight of termonomer. A disadvantage in using hexa-1,*trans*-4-diene is that it has a relatively low level of incorporation<sup>4</sup>.

With emphasis on incorporation, a comparison was made of the polymerization behaviour of hexa-1,*trans*-4-diene<sup>5</sup> (I) and hexa-1,*cis*-4-diene<sup>6-8</sup> (II) using the Ziegler-Natta catalyst, vanadium oxychloride-ethyl aluminium sesquichloride. Using equivalent concentrations of both isomers, the only significant difference in the polymers produced was in the level of unsaturation obtained due to the higher incorporation of the *trans* isomer (see *Table 1*). Polymers prepared with the same degree of unsaturation showed a slightly different polymer plasticity owing to the effect on the molecular weight caused by the higher concentration of *cis* isomer needed to achieve the desired unsaturation level. It was shown in separate experiments that both the *cis*- and *trans*-hexadienes had similar modifying effects on the molecular weight of the polymer formed, the magnitude of the effect increasing with increase in termonomer concentration.



### EXPERIMENTAL

The polymerization conditions used have been described elsewhere<sup>9</sup>; typical results are given in *Table 1*. Gas-liquid chromatography (g.l.c.) was carried out with Perkin-Elmer F11 and Varian Autoprep 705 instruments using columns made up from 5% trityl phosphate on Chromosorb P and 30% SE-30 Silicone on Chromosorb W respectively. Infra-red (i.r.) spectra were measured for films on sodium chloride discs or aluminium plates with a specular reflectance accessory on a Unicam SP200 instrument.

#### Reaction of hexa-1,*cis*-4-diene with $\text{VOCl}_3$

$\text{VOCl}_3$  (1 mmol) was added to dry hexa-1,*cis*-4-diene<sup>5</sup> (44 mmol) in the absence of solvent at 0°C. The mixture was stirred and kept under a nitrogen atmosphere. A red solution was formed instantly. After being stirred for 1 h

Table 1 Terpolymerization of hexa-1,4-dienes with ethylene and propylene

1,4-Hexadiene isomer	Isomer concentration (mmol/l)	ETCA <sup>a</sup> (mmol/l)	Polymer yield (g/l/h)	Plasticity		Iodine No.	% Termonomer incorporation	E/P ratio <sup>c</sup>
				Hoekstra	Mooney <sup>b</sup>			
<i>Cis</i>	24.4	2.08	84.8	25	44	2.5	34	60 : 40
<i>Trans</i>	24.4	2.08	93.6	26	46	3.7	56	60 : 40
<i>Cis</i>	97.6	1.38	28.0	8	—	7.5	9	64 : 36
<i>Trans</i>	48.8	1.38	62.6	26	37	7.6	38	59 : 41

<sup>a</sup> ETCA = ethyl trichloroacetate<sup>9</sup>

<sup>b</sup> ML 1+4 at 100°C

<sup>c</sup> Ethylene/propylene ratio measured from relative intensity of 1380 and 1460 cm<sup>-1</sup> bands in i.r. spectrum

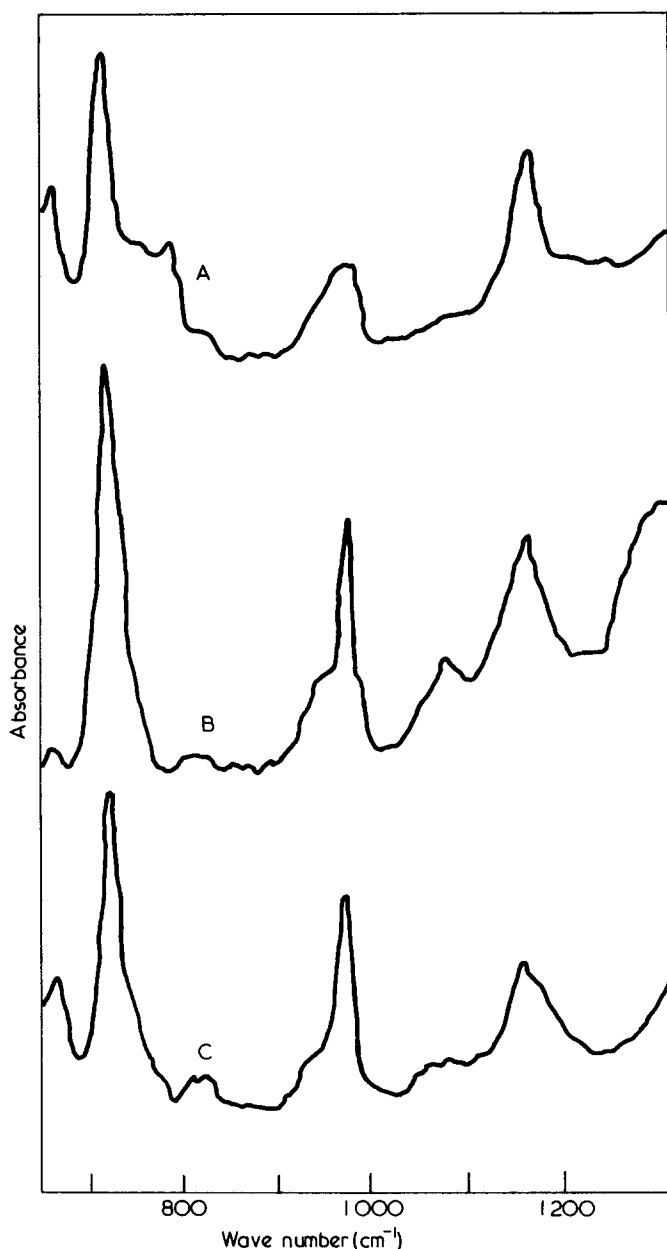


Figure 1 Infra-red spectra of (A) a typical ethylene-propylene copolymer, (B) an ethylene-propylene-hexa-1,*cis*-4-diene terpolymer of iodine number 8.7, and (C) an ethylene-propylene-hexa-1,*trans*-4-diene terpolymer of iodine number 7.6

the mixture was hydrolysed with water and the organic layer dried over sodium sulphate: it was shown by g.l.c. and i.r. analysis to be unchanged hexa-1,*cis*-4-diene.

#### Reaction of hexa-1,*cis*-4-diene with $\text{Et}_3\text{Al}_2\text{Cl}_3$

$\text{Et}_3\text{Al}_2\text{Cl}_3$  (0.5 ml) was added to dry hexa-1,*cis*-4-diene (150 ml) and the mixture heated to reflux temperature for 3 h under nitrogen, after which time the distillate was found to be unchanged hexa-1,*cis*-4-diene.

#### Reaction of hexa-1,*cis*-4-diene with $\text{VOCl}_3/\text{Et}_3\text{Al}_2\text{Cl}_3$

$\text{VOCl}_3$  (1.0 mmol) was added to dry hexa-1,*cis*-4-diene (88 mmol) at 0°C with stirring under nitrogen. On adding  $\text{Et}_3\text{Al}_2\text{Cl}_3$  (5.0 mmol) a fairly vigorous reaction took

place and the red solution was replaced by a black colloidal suspension. The mixture was stirred for 3 min at 0°C, then cooled to  $\sim -70^\circ\text{C}$  and hydrolysed with water. The organic portion was extracted with tetrahydrofuran, then washed with water to remove the solvent. Residual monomer was pumped off and found to be pure hexa-1,*cis*-4-diene by i.r. and g.l.c. analysis. The residue was a brittle polymer, soluble in chloroform. The i.r. spectrum of the polymer exhibited typical peaks<sup>10</sup> due to  $-\text{CH}_3$ ,  $-\text{CH}_2-$  at 710 w, 1380 ms, 1460 s, 2850 ssh, 2950 s  $\text{cm}^{-1}$ . In addition, a medium-weak band at 970  $\text{cm}^{-1}$  evinced the presence of a *trans* double bond (CH=CH out-of-plane deformation) and weak absorptions at 910 and 995 sh  $\text{cm}^{-1}$  due to the vinyl group were observed.

#### Reaction of hexa-1,*trans*-4-diene<sup>6-8</sup> with $\text{VOCl}_3/\text{Et}_3\text{Al}_2\text{Cl}_3$

The reaction was performed as above. The recovered monomer was shown by i.r. and g.l.c. analysis to be virtually pure hexa-1,*trans*-4-diene containing no more *cis* isomer than the starting material (1.9% *cis*). The polymer obtained had a similar i.r. spectrum to that of the previous material except that the *trans* CH=CH out-of-plane deformation vibration was rather stronger relative to the saturated  $-\text{CH}_2-$ ,  $\text{CH}_3-$  bands.

## RESULTS

It was observed that polymers prepared from both *cis*- and *trans*-hexadienes exhibit a prominent peak in the infra-red spectrum at 965  $\text{cm}^{-1}$ , assigned to the =CH out-of-plane deformation of a *trans* double bond<sup>10</sup> (see Figure 1). The peak increased in intensity as the amount of unsaturation in the terpolymer increased, no matter which isomer was used in the polymer preparation. As a result of this observation, a study was made of the action of the Ziegler catalyst and its separate components on *cis*- and *trans*-isomers of hexa-1,4-diene.

The individual  $\text{VOCl}_3$  and  $\text{Et}_3\text{Al}_2\text{Cl}_3$  components of the Ziegler catalyst did not isomerize hexa-1,*cis*-4-diene to the *trans*-diene. When both components were added to hexa-1,*cis*-4-diene (II) or to hexa-1,*trans*-4-diene (I) very similar polymers were produced with a strong absorption at 970  $\text{cm}^{-1}$  due to a *trans* double bond. In each case the recovered, unpolymerized hexa-1,4-dienes were not isomerized\*.

From these results we conclude that the *cis* double bond of the hexa-1,*cis*-4-diene monomer is isomerized to the *trans* configuration at the polymerization stage and not before. Isomerization subsequent to polymerization is also a possibility, but we have no evidence for this. The feasibility of this reaction sequence is demonstrated by the fact that when natural rubber is subjected to a catalyst prepared from  $\text{TiCl}_4\text{-EtAlCl}_2$ , *cis-trans* isomerization occurs<sup>11</sup>.

An analogy is observed in the polymerization of the *cis*- and *trans*-isomers of penta-1,3-diene with a  $\text{TiBr}_4/(\text{iBu})_3\text{Al}$  catalyst<sup>12</sup>. The penta-1,*trans*-3-diene has a faster polymerization rate than the *cis* isomer. In a comparison of the polymerization rate of these isomers using a catalyst prepared from  $\text{Ti}(\text{O}i\text{Bu})_4\text{-Et}_3\text{Al}$ <sup>13</sup> it was found that only

\* Compare ref. 5 where a transition metal/aluminium compound catalyst is used to prepare hexa-1,*cis*-4-diene of high purity

## Note to the Editor

the *trans* isomer is polymerized directly. With this system, the *cis*-isomer isomerizes on contact and reduces the rate of formation of polydiene. A similar process could explain the lower incorporation observed for the *cis*-hexa-1,4-diene.

## ACKNOWLEDGEMENTS

We thank Dr D. K. Jenkins and Dr J. M. Locke for discussions and The International Synthetic Rubber Company Limited for permission to publish the work.

## REFERENCES

- 1 Gladding, E. K., Fisher, B. S. and Collette, J. W. *Ind. Eng. Chem. (Prod. Res. Develop.)* 1962, 1, 65
- 2 Capito, J. E., Innes, F. and Allen, R. D. *J. Inst. Rubber Ind.* 1968, 2, 228
- 3 Berry, D. D. and Levine, I. J. Paper presented at the Division of Rubber Chemistry, Am. Chem. Soc. Spring Meeting, Washington D.C., May 1970
- 4 Christman, D. L. and Keim, G. J. *Macromolecules* 1968, 1, 358
- 5 Iwamoto, M., Tani, K., Igaki, H. and Yuguchi, S. *J. Org. Chem.* 1967, 32, 4148; Toyo Rayon Company Limited, Br. Pat. 1,111,508
- 6 Alderson, T., Jenner, E. L. and Lindsey, R. V. *J. Am. Chem. Soc.* 1965, 86, 5638
- 7 E. I. duPont de Nemours, U.S. Pat. 3,013,066
- 8 B. F. Goodrich Company, Br. Pat. 1,153,336
- 9 Duck, E. W. and Cooper, W. *IUPAC XXIII Int. Congr. Pure Appl. Chem., Boston*, 1971, Macromolecular Preprint, Vol 2, p 722
- 10 Bellamy, L. J. 'Infra-Red Spectra of Complex Molecules', Methuen, London, 1958
- 11 Kropacheva, E. N., Ermakova, I. I., Dolgoplosk, B. A., Koltsov, A. I. and Nel'son, K. V. *Int. Symp. Macromol. Chem., Prague*, 1965, Preprint P408
- 12 Mikhant'ev, B. I. and Shatalov, G. V. *Sb. Nauch. Rab. Aspir. Voronezh. Gos. Univ.* 1968, No. 4, 131; *Post J.* 1971, 8, 6046
- 13 Bujadoux, K., Jozefonvics, J. and Néel, J. *Eur. Polym. J.* 1970, 6, 1233

## Book Reviews

### Polymer colloids

Edited by Robert M. Fitch

Plenum Press, New York, 1971, 187 pp. £4.70

This is the proceedings of the American Chemical Society symposium on Polymer Colloids held in Chicago in September, 1970. Polymer colloids are latices prepared by emulsion polymerization, and the twelve original papers herein deal with aspects of their preparation, purification, characterization and properties. Emphasis is on the prediction and control of particle size, particle size distribution and surface charge. Overlap into those aspects of the topic with which the polymer scientist feels most affinity (i.e. the molecular composition, molecular weight and molecular weight distribution of the polymer produced and the properties of coagulated polymeric materials) is slight and is restricted to three papers.

It seems likely that well characterized polymer latices will become increasingly significant tools with which to investigate colloidal stability and related problems. These papers lend collective support to this view and certain papers, e.g. Vanderhoff *et al.* on 'clean' monodisperse latex, document significant steps towards a model colloid. The book may therefore be read with profit by colloid and polymer chemist alike, but only the specialist would want a personal copy.

C. Booth

### Progress in polymer science

Edited by A. D. Jenkins

Pergamon Press, Oxford, 1971, 303 pp. £8.50

This volume contains four substantial reviews. The first, and longest, is by F. A. Bovey on 'High resolution NMR spectroscopy of polymers'. The review is concerned largely with the structure and conformation of vinyl polymers and is, therefore, confined to spectra of polymer solutions. This is an authoritative and comprehensive account dealing both with general principles and with their application to a large number of examples.

The second review, by E. B. Bradford and L. D. McKeever of 'Block copolymers' is by comparison much more superficial. In the space of some 30 pages it reviews a variety of methods which have been used for the syntheses of block copolymers and for their structural characterization and also gives a brief account of their properties. This is a useful general introduction to a rapidly growing field.

Section 3, 'Emulsion polymerization' by the late A. E. Alexander and D. H. Napper is quite different in approach. No attempt is made to review the very large literature of emulsion polymerization. The authors accept as a working basis the general mechanism first put forward by Harkins and proceed to a critical analysis of the detailed development of a precise theory. This involves reference to the pioneer work of Smith and Ewart and of subsequent work by a number of investigators. The authors admit to a bias towards the surface and colloid aspects. It is, in fact, this bias which gives the article its greatest interest and value.

The final report is on 'Cationic polymerization' by A. Tsukamoto and O. Vogl. From this enormous field the authors have selected a number of topics in which they consider significant developments to have occurred recently. They define the period to be reviewed as the five years following from the appearance of the comprehensive review edited by Plesch in 1963. Within these terms there is a broad coverage with considerable emphasis on preparative aspects.

This latest volume in the series will be widely welcomed, especially as the contents are sufficiently homogeneous to ensure that many readers will find all the articles of interest.

G. Gee

### Gel permeation chromatography

Edited by K. H. Altgelt and L. Segal

Marcel Dekker, New York, 1971, 646 pp. \$24.75

This book is a collection of papers which were presented originally at the American Chemical Society Symposium on Gel Permeation Chromatography at Houston, Texas in February 1970. The papers have been published previously in volumes 5 and 6 of the journal *Separation Science* and consequently the book contains no information that is not available elsewhere.

The main virtue of the book is the convenience of having the set of papers bound together in one volume and arranged in four sections entitled: 'Fundamental Introduction to GPC', 'Reviews of Theory and Evaluation Methods in GPC', 'New Developments in GPC', and 'Application of GPC to Problems in Polymer and Petroleum Chemistry'. Judged on this basis, the book can be confidently recommended to laboratories who possess a GPC.

I cannot recommend the book for general purchase or for background reading about GPC since the contents are too detailed to assist the non-specialist. It is very much a book to have at the bench adjacent to a GPC instrument but not in a general library.

D. Margerison

## Note to the Editor

the *trans* isomer is polymerized directly. With this system, the *cis*-isomer isomerizes on contact and reduces the rate of formation of polydiene. A similar process could explain the lower incorporation observed for the *cis*-hexa-1,4-diene.

## ACKNOWLEDGEMENTS

We thank Dr D. K. Jenkins and Dr J. M. Locke for discussions and The International Synthetic Rubber Company Limited for permission to publish the work.

## REFERENCES

- 1 Gladding, E. K., Fisher, B. S. and Collette, J. W. *Ind. Eng. Chem. (Prod. Res. Develop.)* 1962, 1, 65
- 2 Capito, J. E., Innes, F. and Allen, R. D. *J. Inst. Rubber Ind.* 1968, 2, 228
- 3 Berry, D. D. and Levine, I. J. Paper presented at the Division of Rubber Chemistry, Am. Chem. Soc. Spring Meeting, Washington D.C., May 1970
- 4 Christman, D. L. and Keim, G. J. *Macromolecules* 1968, 1, 358
- 5 Iwamoto, M., Tani, K., Igaki, H. and Yuguchi, S. *J. Org. Chem.* 1967, 32, 4148; Toyo Rayon Company Limited, Br. Pat. 1,111,508
- 6 Alderson, T., Jenner, E. L. and Lindsey, R. V. *J. Am. Chem. Soc.* 1965, 86, 5638
- 7 E. I. duPont de Nemours, U.S. Pat. 3,013,066
- 8 B. F. Goodrich Company, Br. Pat. 1,153,336
- 9 Duck, E. W. and Cooper, W. *IUPAC XXIII Int. Congr. Pure Appl. Chem., Boston*, 1971, Macromolecular Preprint, Vol 2, p 722
- 10 Bellamy, L. J. 'Infra-Red Spectra of Complex Molecules', Methuen, London, 1958
- 11 Kropacheva, E. N., Ermakova, I. I., Dolgoplosk, B. A., Koltsov, A. I. and Nel'son, K. V. *Int. Symp. Macromol. Chem., Prague*, 1965, Preprint P408
- 12 Mikhant'ev, B. I. and Shatalov, G. V. *Sb. Nauch. Rab. Aspir. Voronezh. Gos. Univ.* 1968, No. 4, 131; *Post J.* 1971, 8, 6046
- 13 Bujadoux, K., Jozefonvics, J. and Néel, J. *Eur. Polym. J.* 1970, 6, 1233

## Book Reviews

### Polymer colloids

Edited by Robert M. Fitch

Plenum Press, New York, 1971, 187 pp. £4.70

This is the proceedings of the American Chemical Society symposium on Polymer Colloids held in Chicago in September, 1970. Polymer colloids are latices prepared by emulsion polymerization, and the twelve original papers herein deal with aspects of their preparation, purification, characterization and properties. Emphasis is on the prediction and control of particle size, particle size distribution and surface charge. Overlap into those aspects of the topic with which the polymer scientist feels most affinity (i.e. the molecular composition, molecular weight and molecular weight distribution of the polymer produced and the properties of coagulated polymeric materials) is slight and is restricted to three papers.

It seems likely that well characterized polymer latices will become increasingly significant tools with which to investigate colloidal stability and related problems. These papers lend collective support to this view and certain papers, e.g. Vanderhoff *et al.* on 'clean' monodisperse latex, document significant steps towards a model colloid. The book may therefore be read with profit by colloid and polymer chemist alike, but only the specialist would want a personal copy.

C. Booth

### Progress in polymer science

Edited by A. D. Jenkins

Pergamon Press, Oxford, 1971, 303 pp. £8.50

This volume contains four substantial reviews. The first, and longest, is by F. A. Bovey on 'High resolution NMR spectroscopy of polymers'. The review is concerned largely with the structure and conformation of vinyl polymers and is, therefore, confined to spectra of polymer solutions. This is an authoritative and comprehensive account dealing both with general principles and with their application to a large number of examples.

The second review, by E. B. Bradford and L. D. McKeever of 'Block copolymers' is by comparison much more superficial. In the space of some 30 pages it reviews a variety of methods which have been used for the syntheses of block copolymers and for their structural characterization and also gives a brief account of their properties. This is a useful general introduction to a rapidly growing field.

Section 3, 'Emulsion polymerization' by the late A. E. Alexander and D. H. Napper is quite different in approach. No attempt is made to review the very large literature of emulsion polymerization. The authors accept as a working basis the general mechanism first put forward by Harkins and proceed to a critical analysis of the detailed development of a precise theory. This involves reference to the pioneer work of Smith and Ewart and of subsequent work by a number of investigators. The authors admit to a bias towards the surface and colloid aspects. It is, in fact, this bias which gives the article its greatest interest and value.

The final report is on 'Cationic polymerization' by A. Tsukamoto and O. Vogl. From this enormous field the authors have selected a number of topics in which they consider significant developments to have occurred recently. They define the period to be reviewed as the five years following from the appearance of the comprehensive review edited by Plesch in 1963. Within these terms there is a broad coverage with considerable emphasis on preparative aspects.

This latest volume in the series will be widely welcomed, especially as the contents are sufficiently homogeneous to ensure that many readers will find all the articles of interest.

G. Gee

### Gel permeation chromatography

Edited by K. H. Altgelt and L. Segal

Marcel Dekker, New York, 1971, 646 pp. \$24.75

This book is a collection of papers which were presented originally at the American Chemical Society Symposium on Gel Permeation Chromatography at Houston, Texas in February 1970. The papers have been published previously in volumes 5 and 6 of the journal *Separation Science* and consequently the book contains no information that is not available elsewhere.

The main virtue of the book is the convenience of having the set of papers bound together in one volume and arranged in four sections entitled: 'Fundamental Introduction to GPC', 'Reviews of Theory and Evaluation Methods in GPC', 'New Developments in GPC', and 'Application of GPC to Problems in Polymer and Petroleum Chemistry'. Judged on this basis, the book can be confidently recommended to laboratories who possess a GPC.

I cannot recommend the book for general purchase or for background reading about GPC since the contents are too detailed to assist the non-specialist. It is very much a book to have at the bench adjacent to a GPC instrument but not in a general library.

D. Margerison



# Interfacial free energy of crystals of low molecular weight poly(ethylene oxide)

D. R. Beech\*, C. Booth and C. J. Pickles†

Department of Chemistry, University of Manchester, Manchester M13 9PL, UK

and R. R. Sharpe and J. R. S. Waring

ICI Ltd, Dyestuffs Division, Hexagon House, Blackley, Manchester 9, UK

(Received 22 September 1971)

The end interfacial free energies ( $\sigma_e$ ) of extended-chain and folded-chain crystals of fractions of low molecular weight poly(ethylene oxide) have been estimated from measurements of melting points and crystal lamellar thicknesses. Values of  $\sigma_e$  are in the range 1 to 4 kcal (mol of chains emerging)<sup>-1</sup>. It is found that  $\sigma_e$  for a given type of crystal increases as the molecular weight increases and that  $\sigma_e$  for a given polymer fraction decreases as the extent of folding increases. In that the extent of folding increases as the molecular weight increases, our findings imply a maximum value of  $\sigma_e$  for mature crystals of fractions of poly(ethylene oxide) at a molecular weight near 6000.

## INTRODUCTION

Samples of poly(ethylene oxide) of narrow molecular weight distribution and of low molecular weight form lamellar crystals which correspond in thickness to extended-chains, once-folded-chains, twice-folded-chains, etc.<sup>1-3</sup>. The type of crystal formed depends upon the molecular weight, the molecular weight distribution and the crystallization temperature. The molecular weight range  $M_n < 10\,000$  is most interesting since these polymers exhibit melting transitions and low-angle X-ray scattering patterns which can be assigned to the various crystal types.

Samples of poly(ethylene oxide) with  $M_n < 6000$  form, under suitable crystallization conditions, predominantly extended-chain crystals. In a previous paper<sup>1</sup> we applied Flory's theory of melting of polymers of finite molecular weight<sup>4</sup>, suitably modified to allow for the distributions of molecular weights in our samples, to measurements of the melting points of these crystals. In this way we were able to estimate that their end interfacial free energies,  $\sigma_e$ ,

increased from 1 to 4 kcal (mol of chains emerging)<sup>-1</sup> as  $M_n$  increased from 1000 to 6000.

In this paper we further modify Flory's theory to allow for multiple passing of a single molecule through a crystal, i.e. chain folding. Combination of this theory with experimental determinations of melting points and lamellar spacings enables us to estimate  $\sigma_e$  for crystals consisting predominantly of folded poly(ethylene oxide) chains.

## EXPERIMENTAL AND RESULTS

Poly(ethylene oxide) samples with number-average molecular weights in the range 3000-5000 and with terminal hydroxyl groups were prepared by use of ethylene glycol initiator and potassium hydroxide catalyst. Other samples discussed in this paper were from commercial sources<sup>1</sup>.

Methods of fractionation and characterization, of dilatometry, and of low-angle X-ray scattering have been described earlier<sup>1</sup>.

The molecular characteristics of fractions of poly(ethylene oxide) are given in Table 1. Melting temperatures and lamellar spacings are given in Table 2. (The data for fractions 6000 and 10000 derive from refs. 1 and 2.)

Melting points were measured for a range of crystallization temperatures and little variation was noted, in keeping with earlier observations<sup>1</sup>. Lamellar spacings are correlated with melting points on the basis of earlier work with fraction 6000. We assume that the higher melting points correspond to the thicker crystals. We have shown this to be so for fraction 6000<sup>1</sup>. We have not obtained such clear evidence for the other fractions discussed here. For the fractions of lower molecular weight we were able to distinguish scattering from extended-chain crystals (see Table 2) but the scattering from folded-chain crystals was obscured. The X-ray data for fraction 10000 are those of

Table 1 Characteristics of poly(ethylene oxide) fractions

Fraction	$M_n$			
	End group analysis	Vapour pressure osmometry	$[\eta]^*$ (dl/g)	$M_w/M_n$
3300	—	3400	0.110	1.08
3700	3980	3660	0.119	1.11
4300	—	4300	0.139	1.07

\* Benzene at 25°C

\* Present address: Materials Science Unit, Turner Dental School, University of Manchester

† Present address: Department of Chemistry, Stanford University, Stanford, California, USA

Table 2 Melting temperatures and lamellar spacings of poly(ethylene oxide) fractions

Fractions	$x_n$ (chain units)	$T_m$ (°C)	Lamellar spacing	
			(nm)	(chain units)
3 000	75	60.2	20	71
3 700	84	61.3	23	83
4 300	98	58.9	—	—
		61.7	27	97
6 000	136	60.1	—	—
		64.1	39	138
10 000	227	61.0	22	79
		65.2	28	100
		64.3	21	75

 Table 3 Calculated melting points of monodisperse poly(ethylene oxide).  $\sigma_e = 1.5$  kcal/mol;  $s\zeta = 0.9x$ 

$M_n$	$s$	$T_m$	
		Regular folding (equation 1)	Irregular folding (equation 2)
4 000	2	58.0	58.1
6 000	2	63.8	63.9
10 000	2	68.6	68.6
10 000	3	65.9	66.1

Arlie *et al.*<sup>2</sup>. The formal assignments of the numbers of sequences per molecule can be found (designated  $t$ ) in Table 5.

## THEORY

It is assumed that lamellar crystals of thickness  $\zeta$  chain units are formed, and that the ends of the molecules are excluded from the crystals. We assume that chains may fold so that  $s$  sequences of  $\zeta$  units each of a single molecule traverse the crystal ( $s\zeta \leq x$ , where  $x$  is the molecular length). If folding is regular, in that one sequence follows directly on another, then the probability of choosing (from a monodisperse polymer) a sequence  $\zeta$  units long which does not contain a chain end is\*:

$$I_1 = s(x - s\zeta + s)/x \quad (1)$$

If folding is irregular, in that the only restriction on choosing  $s$  sequences of length  $\zeta$  units is that they can be accommodated within length  $x$ , then the corresponding probability is:

$$I_2 = s^2(x - s\zeta + s)/[x - s(s-1)\zeta] \quad (2)$$

These probabilities can be combined<sup>1,4</sup> with terms arising from the disordering of the polymer on melting to obtain the entropy of fusion and ultimately, through the free energy of fusion, the melting point

$$T_m = T_m^0 [1 - (2\sigma_e/\Delta h\zeta)] / \{1 + (RT_m^0/\Delta h)[(1/x) - (\ln I/\zeta)]\} \quad (3)$$

where  $\Delta h$  is the heat of fusion per mol of repeat units and  $T_m^0$  is the thermodynamic melting point. For poly(ethylene oxide)  $\Delta h = 2$  kcal/mol<sup>6</sup> and  $T_m^0 = 76^\circ\text{C}$ <sup>7</sup>.

Values of  $T_m$  for monodisperse poly(ethylene oxide), calculated for  $I$  given by equations (1) and (2), are given in

\* Strictly we should allow for the length of the fold<sup>5</sup>; the refinement is not necessary in this work

 Table 4 Calculated melting points of poly(ethylene oxide)  $\sigma_e = 1.5$  kcal/mol;  $t\zeta = 0.9x_n^*$ 

$M_n$	$M_w/M_n$	$t$	$T_m$	
			Equation (4)	Equation (6)
1 000	1.05	1	36.4 (37.7)	36.5 (37.7)
6 000	1.2	1	69.3 (69.7)	69.4 (69.8)
		2	64.8 (65.7)	65.5 (66.2)
10 000	1.2	2	69.2 (69.8)	69.7 (70.1)
		3	66.4 (67.2)	67.4 (68.0)

\* Figures in parentheses are for  $t\zeta = x_n$

Table 3. We choose  $s\zeta = 0.9x$ , since density measurements<sup>2</sup> indicate that low molecular weight poly(ethylene oxide) is highly crystalline, and  $\sigma_e = 1.5$  kcal/mol, in order that predicted melting points correspond roughly with measured ones. We find little difference between values of  $T_m$  calculated for regular or irregular folding within the (reasonable) restrictions we have placed upon the parameters. Accordingly, we have adopted the simpler regular folding model for immediate use.

The effect of polydispersity is to modify the probability expression (1). We suppose that each molecule crystallizes to its maximum extent, so that short chains have a single crystalline sequence and longer chains have several regularly folded crystalline sequences. This assumption is in keeping with the high crystallinities observed<sup>2</sup> for samples of poly(ethylene oxide) of low molecular weight. The probability that a sequence  $\zeta$  units long, chosen from such a set of sequences, does not contain a chain end is:

$$I = \sum_{s=1}^{\infty} \int_{s\zeta}^{(s+1)\zeta} w(x) I_1(s, \zeta, x) dx \quad (4)$$

where  $w(x)$  is the weight fraction of molecules of length  $x$ -units, and  $I_1$  is given by equation (1). We assume that  $w(x)$  is given by the Schulz-Zimm<sup>8</sup> expression:

$$w(x) = (b^{a+1}/a!) x^a e^{-bx} \quad (5)$$

where  $b = a/x_n$ ,  $a = x_n/(x_w - x_n)$  and is integral in equation (5), and  $x_n$  and  $x_w$  are number- and weight-average chain lengths respectively.

An alternative assumption is that the number of crystalline sequences per molecule does not exceed  $t$ , the integral part of  $x_n/\zeta$ ; i.e. that the probability  $I$  is given by:

$$I = \sum_{s=1}^t \int_{s\zeta}^{(s+1)\zeta} w(x) I_1(s, \zeta, x) dx + \int_{(t+1)\zeta}^{\infty} w(x) I_1(t, \zeta, x) dx \quad (6)$$

Equation (6) was used in the earlier paper<sup>1</sup> which dealt with extended-chain crystals only, i.e.  $t = 1$ .

Examples of the values of  $T_m$  calculated by use of equations (4) or (6) in equation (3) are given in Table 4. These calculations are for values of  $t\zeta$  near  $x_n$ ,  $\sigma_e = 1.5$  kcal/mol and  $M_w/M_n = 1.05$  or  $2.0$ . We find little difference between the two models; certainly no more variation than that due to uncertainty in  $\zeta$ . Slightly lower values of  $T_m$  are predicted by the maximum crystallinity model: presumably a reflection of the lower disorder in the model crystal.

## COMPARISON OF THEORY AND EXPERIMENT

Equations (3), (4) and (5) have been used to compute melting points of samples of poly(ethylene oxide) similar in molecular constitution to those used in the experimental work. A wide range of values of  $\sigma_e$  have been used in the calculations. Comparison of predicted melting points with those found experimentally (Table 2) enable us to evaluate  $\sigma_e$  for the various types of crystal. These values are given in Table 5. We have assumed that  $t\zeta = 0.9x_n$ . This is in keeping with the lamellar spacings reported in Table 2 and the high ( $\sim 90\%$ ) crystallinity of the samples. An alternative choice of  $t\zeta = x_n$  leads to values of  $\sigma_e$  very little different from those quoted. Values of the folding parameter  $t$ , inferred from the melting and X-ray data are also given in Table 5.

In comparing the observed melting points of the lower melting crystals with calculated values we assume that the composition of the melt does not change during the melting process. In other words, we assume that differences in molecular composition of the two types of crystal are small (as might be expected if their formation is the result of rate controlled processes), and that fractionation with respect to molecular weight during the crystallization process can be ignored. These assumptions are reasonable in view of the narrow molecular weight distributions of our fractions and the fact that we are not concerned with multiple melting points at very low molecular weights when fractionation is a problem.

It has been noted earlier<sup>1</sup> that  $\sigma_e$  of predominantly extended-chain crystals increases as the molecular weight increases. Here we find the same effect for the predominantly once-folded-chain crystals ( $t=2$ ). This effect is illustrated in Figure 1. We further find (Table 5 and Figure 1) that  $\sigma_e$  of an interface which contains a high proportion of folds is markedly lower than that of an interface formed from the same polymer but from which most chains emerge (or in which most chains terminate). Moreover  $\sigma_e$  is lowest when the extent of folding is greatest. It is a consequence of these findings that the end-interfacial free energy of mature crystals of fractions of poly(ethylene oxide) will vary with molecular weight as follows: an increase from  $\sigma_e \sim 1$  kcal/mol at low molecular weight to  $\sigma_e > 3$  kcal/mol at  $M_n \sim 6000$  and then a decrease to  $\sigma_e < 2$  kcal/mol at high molecular weight, when the crystal is composed almost entirely of folded-chains.

Table 5 End interfacial free energy ( $\sigma_e$ ) of crystals of poly(ethylene oxide)

$M_n$	$M_w/M_n$	$D_w$ (chain units)	$t$	$\sigma_e$ (kcal/mol)
1 000*	1.05	5	1	1.4
1 500*	1.05	8	1	1.5
2 000*	1.05	10	1	1.7
3 300	1.1	25	1	2.2
3 700	1.1	28	1	2.3
4 000*	1.05	21	1	2.5
4 300	1.1	33	1	2.7
6 000*	1.2	67	1	3.3
3 700	1.1	28	2	1.4
4 300	1.1	33	2	1.5
6 000*	1.2	67	2	2.2
10 000*	1.2	111	2	2.7
10 000*	1.2	111	3	1.9

\* Data from ref. 1;  $\sigma_e$  calculated using equation (4) with  $t\zeta = 0.9x_n$

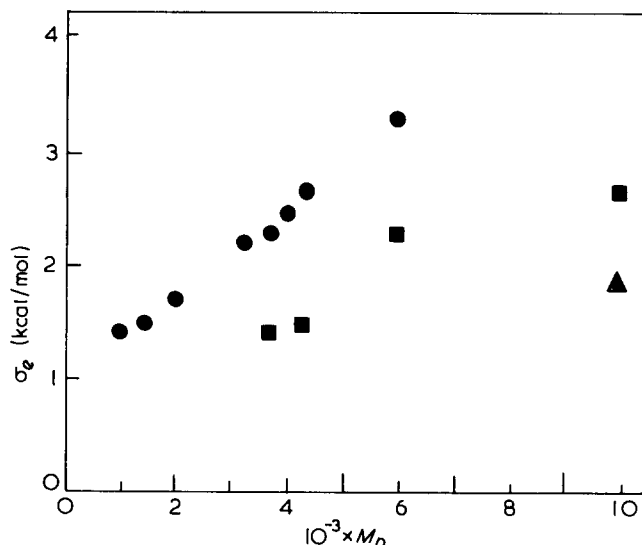


Figure 1 End interfacial free energy ( $\sigma_e$ ) versus molecular weight ( $M_n$ ) for extended-chain (●), once-folded-chain (■) and twice-folded-chain (▲) crystals of poly(ethylene oxide) fractions

The effect of folding upon  $\sigma_e$  is undoubtedly real and not a consequence of the model we have chosen to use. For example, a change in  $T_m$  of  $10^\circ$  or in  $\zeta$  of 20 nm would be required in order that  $\sigma_e$  for the extended-chain and folded-chain crystals of fraction 6000 be identical.

In the earlier paper<sup>1</sup> we suggested that the explanation of the increase in  $\sigma_e$  with increasing  $M_n$  lay in the absolute spread of molecular weights in our samples. There<sup>1</sup> we preferred to use the deviation of the weight distribution of molecular weights:  $D_w = [x_w(x_z - x_w)]^{1/2}$  to correlate with the melting point of the sample. Values of  $D_w$  for our samples are listed in Table 5. The correlation of  $\sigma_e$  with  $D_w$  is better than with  $M_n$ . It is particularly interesting that fraction 4000, which has a narrow molecular weight distribution ( $D_w = 21$ ), crystallizes in extended-chain form only whereas fraction 3700 ( $D_w = 28$ ) crystallizes in both extended-chain and once-folded-chain forms.

## ACKNOWLEDGEMENTS

We thank Messrs D. J. Roy, D. Rowlinson, J. A. Ashworth and Miss J. Swindell for assistance with characterization of the polymers. D.R.B. and C.J.P. acknowledge receipt of Science Research Council Studentships.

## REFERENCES

- Beech, D. R., Booth, C., Dodgson, D. V., Sharpe, R. R. and Waring, J. R. S. *Polymer* 1972, **13**, 73
- Arlie, J. P., Spegt, P. A. and Skoulios, A. E. *Makromol. Chem.* 1966, **99**, 160; 1967, **104**, 212
- Spegt, P. A. *Makromol. Chem.* 1970, **140**, 167
- Flory, P. J. *J. Chem. Phys.* 1949, **17**, 223
- Peterson, J. M. and Lindenmeyer, P. H. *Makromol. Chem.* 1968, **118**, 343
- Beaumont, R. H., Clegg, B., Gee, G., Herbert, J. B. M., Marks, D. J., Roberts, R. C. and Sims, D. *Polymer* 1966, **7**, 401
- Beech, D. R. and Booth, C. *J. Polym. Sci. (B)* 1970, **8**, 731
- Schulz, G. V. *Z. Phys. Chem. (B)* 1939, **43**, 25; Zimm, B. H. *J. Chem. Phys.* 1948, **16**, 1093

# Terpolymerizations involving maleic anhydride

J. C. Bevington and C. Nicora\*

Department of Chemistry, University of Lancaster, Lancaster, UK  
(Received 21 September 1971)

Tracer methods have been used to analyse terpolymers formed in radical processes. The results have been used in an attempt to compare the reactivities of styrene, methyl methacrylate and methyl acrylate towards a polymer radical having a terminal maleic anhydride unit. Anomalous results are obtained in an application of the conventional treatment.

## INTRODUCTION

Alfrey and Goldfinger<sup>1</sup> gave equations for the composition of a terpolymer, formed at low conversion, in terms of the composition of the feed and of the monomer reactivity ratios deduced from the three appropriate binary copolymerizations. Problems associated with terpolymerizations have been considered again more recently by Ham<sup>2,3</sup>, Mayo<sup>4</sup> and Jenkins<sup>5</sup>. It has been recognized that studies of terpolymerizations may be of considerable value in connection with problems such as the reactivities of monomers and of polymer radicals and also effects of penultimate groups upon reactivities of polymer radicals. This paper is concerned mainly with some radical terpolymerizations involving maleic anhydride; the original object was to compare the reactivities of monomers towards a polymer radical having a terminal maleic anhydride unit but a paper by Gaylord and Patnaik<sup>6</sup> indicates that complications may well arise in these terpolymerizations. There is also a brief report of some tests on the more general application of tracer techniques to studies of initiation of radical terpolymerizations and to analyses of terpolymers.

Monomer reactivity ratios deduced from copolymerizations have been widely used for comparison of the reactivities of monomers towards reference polymer radicals<sup>7</sup>. The procedure is unreliable for polymer radicals showing very low reactivities towards their monomers; this limitation appears to apply to the maleic anhydride polymer radical. Ham<sup>3</sup> pointed out that, in such cases, useful information may be deduced from terpolymerizations. The relative numbers (*a*, *b* and *c*) of the monomer units in a terpolymer are related to the concentrations

(*A*, *B* and *C*) of the monomers in the feed from which it is being formed<sup>1</sup>, thus:

$$a : b : c = A \left\{ \frac{A}{r_{ca}r_{ba}} + \frac{B}{r_{ba}r_{cb}} + \frac{C}{r_{ca}r_{bc}} \right\} \left\{ A + \frac{B}{r_{ab}} + \frac{C}{r_{ac}} \right\} \\ : B \left\{ \frac{A}{r_{ab}r_{ca}} + \frac{B}{r_{ab}r_{cb}} + \frac{C}{r_{cb}r_{ac}} \right\} \left\{ \frac{A}{r_{ba}} + B + \frac{C}{r_{bc}} \right\} \\ : C \left\{ \frac{A}{r_{ac}r_{ba}} + \frac{B}{r_{bc}r_{ab}} + \frac{C}{r_{ac}r_{bc}} \right\} \left\{ \frac{A}{r_{ca}} + \frac{B}{r_{cb}} + C \right\} \quad (1)$$

The various *r* terms are monomer reactivity ratios, e.g.  $r_{ab} = k_{aa}/k_{ab}$  where  $k_{aa}$  and  $k_{ab}$  are the velocity constants for reactions of the polymer radical having a terminal *A* unit with monomer molecules *A* and *B* respectively. If monomer *C* is unreactive towards the polymer radical having a terminal *C* unit, then  $r_{ca}$  and  $r_{cb}$  are small and are probably not known accurately. From equation (1), equation (2) can be derived without further assumptions.

$$a = A \frac{\left\{ \frac{RA}{r_{ba}} + \frac{B}{r_{ba}} + \frac{RC}{r_{bc}} \right\} \left\{ A + \frac{B}{r_{ab}} + \frac{C}{r_{ac}} \right\}}{b = B \left\{ \frac{RA}{r_{ab}} + \frac{B}{r_{ab}} + \frac{C}{r_{ac}} \right\} \left\{ \frac{A}{r_{ba}} + B + \frac{C}{r_{bc}} \right\}} \quad (2)$$

where  $R = r_{cb}/r_{ca} = k_{ca}/k_{cb}$ .

This equation can be used to find *R* provided that values are known for those monomer reactivity ratios which appear in it. The value of *R* immediately indicates the relative reactivities of monomers *A* and *B* towards the *C*-radical. This procedure is here tested for terpolymerizations involving maleic anhydride.

## EXPERIMENTAL

Standard procedures were used for purification of the substances involved in the work. Labelled samples of

\* Montecatini Edison SpA, Centro Ricerche, 20021 Bollate, Milan, Italy

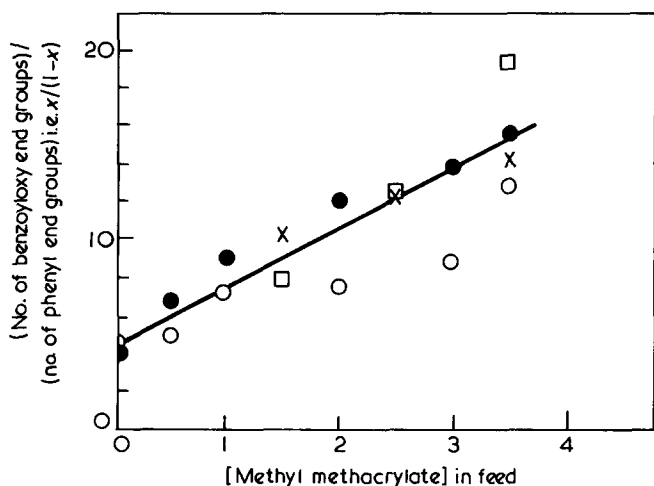


Figure 1 (No. of benzoyloxy end groups)/(no. of phenyl end groups) in terpolymers of methyl acrylate (MA), ethyl methacrylate (EMA) and methyl methacrylate (MMA) prepared at 60°C using benzoyl peroxide as initiator. Concentrations of MA and EMA fixed at 1 mol/l; concentration of MMA varied. O, benzoyl peroxide at 1 g/l; assay by gas counting; ●, benzoyl peroxide at 1 g/l; assay by scintillation counting; □, benzoyl peroxide at 3 g/l; assay by gas counting; ×, benzoyl peroxide at 3 g/l; assay by scintillation counting

methyl methacrylate and methyl acrylate were prepared by exchange between unlabelled monomer and  $^{14}\text{C}$ -methanol; styrene, labelled at the  $\beta$ -position with  $^{14}\text{C}$ , was prepared by decarboxylation of the appropriate  $^{14}\text{C}$ -cinnamic acid; 1,4- $^{14}\text{C}$ -maleic anhydride was purchased from the Radiochemical Centre, Amersham. The specific activities of the monomers lay between 0.2 and 0.3  $\mu\text{Ci/g}$ . Two types of  $^{14}\text{C}$ -benzoyl peroxide were used; R-peroxide was labelled in the rings and C-peroxide in the carboxyl groups; their specific activities were about 25  $\mu\text{Ci/g}$ .

Polymerizations were performed in vacuum dilatometers at 60°C. Polymers were recovered by precipitation in non-solvent, and purified by reprecipitation. Tests on removal of labelled contaminants gave satisfactory results. Assays were performed by gas counting<sup>8</sup> and by scintillation counting in solution using counter type 6012 (Isotope Developments Ltd) and phosphor solutions NE 211 and NE 220 (Nuclear Enterprises Ltd). Quenching in scintillation counting was allowed for by determining counting rate per mg of sample after successive additions of sample and then extrapolating to zero weight. For these measurements, dimethylformamide was used as solvent for some polymers and benzene for others; in those cases where either solvent could be used, there was good agreement between the two extrapolated values of counting rate per mg.

Different methods of calculation are needed for the two types of assay. Suppose that a terpolymer, made from a  $^{14}\text{C}$ -sample of monomer (molecular formula  $\text{C}_a\text{H}_b\text{O}_c$ ), can be represented as:



In gas counting, the counting rate refers to a standard mass of carbon so that

$$\frac{\text{counting rate for monomer}}{\text{counting rate for terpolymer}} = \frac{ax + dy + gz}{ax}$$

In scintillation counting, the counting rate refers to a standard mass of sample so that

$$\frac{\text{counting rate for monomer}}{\text{counting rate for terpolymer}} = \frac{12(ax + dy + gz) + (bx + ey + hz) + 16(cx + fy + iz)}{x(12a + b + 16c)}$$

## RESULTS

### Tests on terpolymerizations

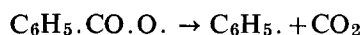
Terpolymerizations were performed at 60°C using benzoyl peroxide (at 1 g/l or at 3 g/l) with methyl acrylate (MA) at 1 mol/l, ethyl methacrylate (EMA) at 1 mol/l and methyl methacrylate (MMA) at concentrations up to 3.5 mol/l; benzene was used as diluent. For each feed, parallel experiments with ring- and carboxyl-labelled samples of peroxide were performed so that it was possible to calculate<sup>9</sup> values of the fraction  $x$  defined as:

$$\frac{\text{no. of benzoyloxy end groups}}{\text{total no. of benzoyloxy and phenyl end groups}}$$

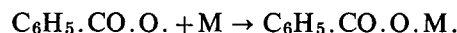
There was good agreement between the parallel experiments. Results are summarized in Figure 1. The scatter of points can be attributed to the great sensitivity of  $x/(1-x)$  to small errors in assay but it seems that the relationship

$$\frac{x}{1-x} = \frac{k_{2a}(M_a) + k_{2b}(M_b) + k_{2c}(M_c)}{k_1}$$

is obeyed,  $k_1$  being the velocity constant for the dissociation



and  $k_{2a}$ ,  $k_{2b}$  and  $k_{2c}$  the velocity constants for the reactions of monomers  $M_a$ ,  $M_b$  and  $M_c$  respectively with the benzoyloxy radical according to the general equation:



From the slope of the line in Figure 1,  $k_2/k_1$  for MMA at 60°C is 0.30 l/mol, in agreement with results from homopolymerizations<sup>10</sup>. From the intercept, the sum of the values of  $k_2/k_1$  for MA and EMA is 0.46 l/mol; from homopolymerizations, the separate values are 0.12 (for MA<sup>11</sup>) and 0.34 (for EMA<sup>7</sup>). Clearly, there is no unexpected behaviour with respect to initiation in this terpolymerization.

Terpolymers were prepared from an equimolar mixture of MA, MMA and styrene (S); three experiments were performed using, in turn, a  $^{14}\text{C}$ -sample of each monomer. In each case, the counting rate of the terpolymer was compared with that of the appropriate labelled monomer (see Table 1). From pairs of such comparisons, the composition of the copolymer was deduced (see Table 2). Using expression (1) with the following monomer reactivity ratios

$$\begin{aligned} \text{MA/MMA: } & 0.34, 1.86 \\ \text{MA/S: } & 0.17, 0.75 \\ \text{MMA/S: } & 0.47, 0.50 \end{aligned}$$

the calculated mole fractions of MA, MMA and S units in the terpolymer are 0.21, 0.36 and 0.42, respectively. The agreement with the experimental values shows that the

Table 1 Comparisons of counting rates for terpolymers of MA, MMA and S with counting rates for monomers

Labelled monomer	(Counting rate for terpolymer)/ (counting rate for monomer)	
	Gas counting	Scintillation counting
Methyl acrylate	0.135	0.172
Methyl methacrylate	0.289	0.366
Styrene	0.543	0.425

 Table 2 Compositions of terpolymers  
 Values in parentheses from results of scintillation counting; others from results of gas counting

	Pairs of labelled monomers			Average
	MA/S	MA/MMA	MMA/S	
Mole fraction MA	0.20 (0.20)	0.21 (0.20)	0.25* (0.24)	0.22
Mole fraction MMA	0.39* (0.40)	0.35 (0.36)	0.35 (0.36)	0.37
Mole fraction S	0.41 (0.40)	0.44* (0.44)	0.40 (0.40)	0.41

\* Found by difference

Table 3 Terpolymerizations involving maleic anhydride

Relative molar concentrations of monomers in feed				Relative nos. of monomer units in product			
MANH	S	MMA	MA	MANH	S	MMA	MA
1.00	1.00	0	1.00	0.86	1.00	0	0.14
0	1.00	0	1.00	0	1.00*	0	0.67*
1.00	0	1.00	1.00	0.19	0	1.00	0.40
0	0	1.00	1.00	0	0	1.00*	0.48*
1.00	1.00	1.00	0	0.91†	1.00	0.31	0
0	1.00	1.00	0	0	1.00*	1.00*	0

\* Calculated from monomer reactivity ratios quoted in the text

† Result taken from Figure 2

growth reactions can be considered as normal in this terpolymerization.

#### Systems involving maleic anhydride

Terpolymerizations with maleic anhydride (MANH) as one monomer were performed at 60°C with benzoyl peroxide as initiator and methyl ethyl ketone as diluent; the other monomers were pairs selected from S, MMA and MA. Reactions were stopped at about 5% conversion. For many of the terpolymers containing S and MANH, precipitation in methanol was satisfactory only if free MANH was present; a mixture of methanol with petroleum ether was a better precipitant. Difficulties were encountered in re-dissolving some terpolymers in methyl ethyl ketone. Copolymers of S with MANH have been reported<sup>12</sup> as easily esterified by alcohols; this reaction could lead to serious errors in the analyses of terpolymers. A suitable unlabelled terpolymer, however, acquired only a very low level of activity after precipitation and standing in <sup>14</sup>C-methanol; any esterification under these conditions can therefore be neglected.

For the system S/MMA/MANH, there was clear evidence that polymerization could occur at an appreciable rate even in the absence of added initiator and that

this unsensitized polymerization was largely photo-initiated. Tests using <sup>14</sup>C-MMA indicated no difference between the compositions of terpolymers formed in the unsensitized and sensitized processes.

Terpolymers were prepared from feeds in which the concentrations of S and MMA were fixed at 1 mol/l and that of MANH ranged from 0 to 4 mol/l. The rate of polymerization increased with rising concentration of MANH; the effect was greater than could be attributed to the additional initiation process. Compositions of the terpolymers were calculated from results of parallel experiments in which labelled samples of the three monomers were used in turn, following the general procedure outlined already. The results are shown in Figure 2. Less extensive studies were made of the other ternary systems; in each case, terpolymerizations were performed with equimolar amounts of the three monomers in the feed. Summarized results are included in Table 3. Monomer reactivity ratios for copolymerizations with MANH as the second monomer were taken as follows: S, 0.015; MMA, 3.37; MA, 2.50. These values suggest that the polystyrene radical reacts more readily with maleic anhydride than with styrene, whereas the reactions of the poly(methyl methacrylate) and poly(methyl acrylate)

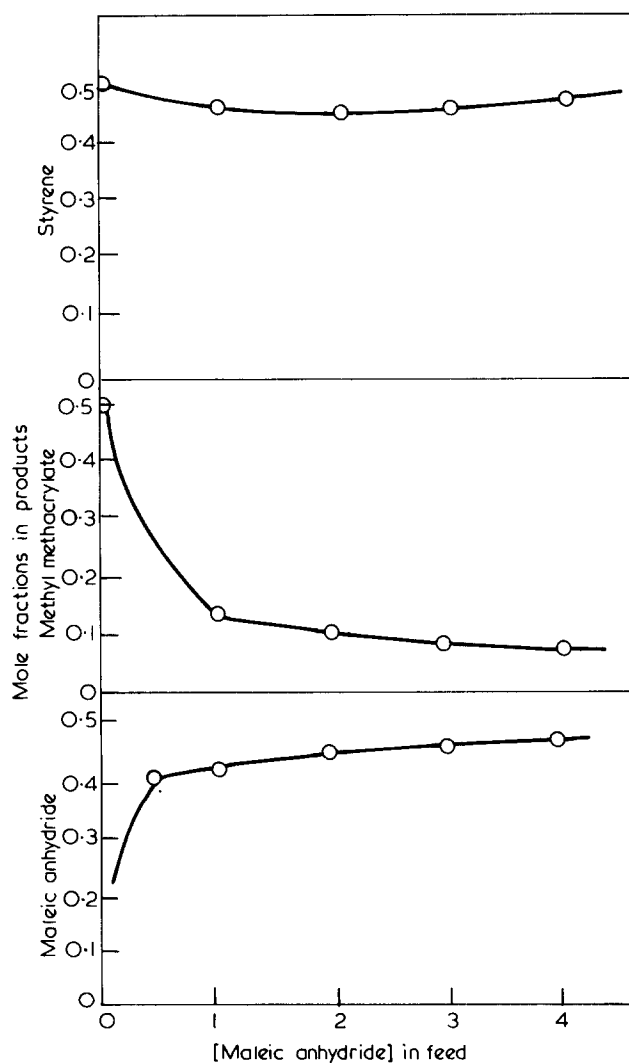


Figure 2 Terpolymerizations at 60°C with benzoyl peroxide as initiator and methyl ethyl ketone as diluent. [Styrene] and [methyl methacrylate] fixed at 1 mol/l; [maleic anhydride] varied

Table 4 Terpolymerizations of styrene, methyl methacrylate and maleic anhydride  
Concentrations of S and MMA in feed fixed at 1 mol/l

Concn. of MANH in feed (mol/l)	Relative nos. of S, MMA and MANH units in product	Ratio S/MMA units in product	Value of $k_{da}/k_{db}$ from equation (2)
0	1, 1, 0	1.0	—
1	1, 0.31, 0.91	3.2	4.2
2	1, 0.22, 1	4.5	5.4
3	1, 0.19, 0.94	5.2	6.3
4	1, 0.17, 0.98	5.9	7.4

radicals with their own monomers are favoured over their reactions with maleic anhydride.

## DISCUSSION

Little comment is needed on the results of the tests on the application of tracer techniques to terpolymerizations. For the system MA/EMA/MMA, initiation by benzoyl peroxide seems to be normal. The analyses of terpolymers of MA/MMA/S indicate that acceptable results are given by a procedure involving two labelled monomers in parallel experiments and determination of the third type of monomer unit by difference. An improvement could be effected by using one monomer labelled with  $^{14}\text{C}$  and another with  $^3\text{H}$  as was done for some copolymerizations<sup>7</sup>.

The terpolymerizations involving MANH show some interesting features. If the ratio of S to MMA in the feed is kept constant, then the ratio of S to MMA in the polymer increases markedly as the concentration of MANH in the feed is raised (see Figure 2). If penultimate group effects are absent, a copolymerization of S and MMA involves only two types of growing radicals, viz. polystyrene and poly(methyl methacrylate). If MANH is added to the system and 'normal' terpolymerization occurs, then it must be supposed that there are also polymer radicals with terminal MANH units. The variation of the S/MMA ratio with concentration of MANH would then be interpreted as showing that the poly(maleic anhydride) radical is much more reactive towards S than towards MMA. The monomer reactivity ratios for the copolymerizations S/MMA and S/MANH show that the polystyrene radical must be regarded as considerably more reactive towards MANH than towards MMA. These effects together would mean that, as MANH is added to a feed containing S and MMA, there is a strong tendency to form an alternating copolymer of S and MANH with the exclusion of MMA. The results in Table 3 indicate that addition of MANH to a S/MA feed similarly increases the S/MA ratio in the product and that therefore MA also could be regarded as less reactive than S towards the polymaleic anhydride radical.

From the results in Table 3 and taking S, MMA, MA and MANH as monomers A, B, C and D respectively, application of equation (2) leads to

$$\frac{k_{aa}}{k_{ab}} = 4.2 \text{ from the terpolymerization of A, B and D}$$

and

$$\frac{k_{aa}}{k_{ac}} = 8.6 \text{ from the terpolymerization of A, C and D}$$

According to these results, the relative reactivities of S, MMA and MA towards a poly(maleic anhydride) radical are 1, 0.24 and 0.12 respectively; Ham<sup>3</sup> deduced the values 1, 0.002 and 0.001. From the present results,  $k_{ab}/k_{ac}$  is 2.0 but application of equation (2) to the terpolymerization of MMA, MA and MANH gives a value of 13.5. A further discrepancy is revealed by using equation (2) with the set of terpolymerizations referred to in Figure 2; the value of  $k_{aa}/k_{ab}$  varies with the composition of the feed as shown in Table 4.

The discrepancies noted in the previous paragraph make it clear that equation (2) is not properly applicable to some or all of the terpolymerizations. The equation was derived on the assumption that the reactivity of a polymer radical is completely governed by the nature of the monomer unit last added. This assumption may well be in error; effects of non-terminal groups upon radical reactivity and selectivity may be pronounced but it seems unlikely that these effects could be responsible for the observed gross discrepancies. It seems much more likely that there is a fundamental error in the application of equation (2) to these systems. It is clear that they might be associated with the participation in the reactions of charge-transfer complexes of styrene with maleic anhydride. It is to be noted that Gaylord and co-workers have considered the role of such complexes in the S/MMA/MANH system<sup>6</sup> and in the sensitized radical copolymerizations of dienes with maleic anhydride<sup>13</sup>.

The conclusion that the usual treatment of terpolymerizations is invalid for the systems S/MMA/MANH and S/MA/MANH, because of the involvement of a charge transfer complex S/MANH, is confirmed by a comprehensive study of the copolymerization of S with MANH<sup>14</sup>. This binary copolymerization might be regarded as a special type of ternary polymerization in which there are growth reactions involving the two free monomers and the 1 : 1 complex. Correspondingly, the terpolymerizations considered in this paper might be thought of as processes in which growth reactions may involve four types of 'monomer', for example S, MMA, MANH and the S/MANH complex.

## ACKNOWLEDGEMENT

This work was performed while C. N. was on study leave from the Montecatini-Edison Research Centre (Bollate).

## REFERENCES

- Alfrey, T., Jr. and Goldfinger, G. *J. Chem. Phys.* 1944, **12**, 322
- Ham, G. E. *J. Polym. Sci. (A)* 1964, **2**, 2735
- Ham, G. E. *J. Polym. Sci. (A)* 1964, **2**, 4191
- Mayo, F. R. *J. Polym. Sci. (A)* 1964, **2**, 4207
- Jenkins, A. D. *Eur. Polym. J.* 1965, **1**, 177
- Gaylord, N. G. and Patnaik, B. *J. Polym. Sci. (B)* 1970, **8**, 549
- Bevington, J. C. and Malpass, B. W. *Eur. Polym. J.* 1965, **1**, 19
- Bevington, J. C., Melville, H. W. and Taylor, R. P. *J. Polym. Sci.* 1954, **12**, 449
- Allen, J. K. and Bevington, J. C. *Trans. Faraday Soc.* 1960, **56**, 1762
- Bevington, J. C. *Trans. Faraday Soc.* 1957, **53**, 997
- Bevington, J. C., Harris, D. O. and Johnson, M. *Eur. Polym. J.* 1965, **1**, 235
- Noma, K., Niwa, M. and Iwasaki, K. *Kobunshi Kagaku* 1963, **20**, 646; *Chem. Abstr.* 1964, **60**, 14618c
- Gaylord, N. G. and Maiti, S. *J. Polym. Sci. (B)* 1971, **9**, 359
- Tsuchida, E. and Tomono, T. *Makromol. Chem.* 1971, **141**, 265

# Phosphazene copolymers: Part 1. Synthesis and bulk properties

G. Allen and R. M. Mortier\*

Department of Chemistry, University of Manchester, Manchester M13 9PL, UK  
(Received 21 September 1971)

The preparation of the phosphazene copolymers:  $\text{[-NP(OR}_1\text{)}_{2-x}\text{(OR}_x\text{)}_x\text{]}_n$  where  $\text{R}_1$  is  $\text{-CH}_2\text{CF}_3$  and  $\text{R}_2$  is  $p\text{-C}_6\text{H}_4\text{C}_6\text{H}_5$ . The effect of variation of  $x$  on the thermal properties ( $T_g$ ,  $T_m$  and  $T_{dec}$ ) of the copolymers has been investigated. With  $x < 0.5$  the materials are elastomeric in nature. The copolymer having  $x = 0.15$  was investigated in some detail by means of spectroscopy, X-ray analysis and torsion pendulum studies. It is concluded that the copolymer ( $x = 0.15$ ) is a random copolymer containing crystallizable sequences of  $\text{NP(OCH}_2\text{CF}_3)_2$  units.

## INTRODUCTION

Poly(dichlorophosphazene),  $\text{[-NPCl}_2\text{]}_n$ , has been known for many years<sup>1</sup> as an elastomeric material of fairly good thermal stability but poor hydrolytic stability. Hydrolytically stable polyphosphazenes have been prepared in recent years<sup>2-5</sup> by the substitution of organo groups for chlorine in  $\text{[-NPCl}_2\text{]}_n$ . However, the majority of these poly(organophosphazenes) are highly crystalline and have lost the elastomeric nature of the chloro-polymer.

The synthesis of an elastomeric, hydrolytically stable polyphosphazene was reported recently in a preliminary communication<sup>6</sup>; the polymer had fluorinated alkoxy side groups and was prepared by reacting the sodium salts of the alcohols with  $\text{[-NPCl}_2\text{]}_n$  to give:



In an independent study, a similar elastomer



was made in our laboratory. However, these materials were solvent resistant, thus limiting characterization.

One purpose of the work described in this paper was to prepare an amorphous, elastomeric polyphosphazene which could be characterized by conventional methods. This was achieved by the synthesis of the copolyphosphazene:  $\text{[-NP(OCH}_2\text{CF}_3\text{)}_{1.85}\text{(OC}_6\text{H}_4\text{C}_6\text{H}_5\text{)}_{0.15}\text{]}_n$ .

## EXPERIMENTAL

### Preparation of hexachlorocyclotriphosphazene

A 5 litre flask was charged with *sym*-tetrachloroethane (2.2 l), phosphorus oxychloride (34 g, 0.22 mol), technical

grade ammonium chloride (118 g, 2.2 mol) and phosphorus pentachloride (460 g, 2.2 mol). The ammonium chloride and phosphorus pentachloride were ground with mortar and pestle before being added to the reaction flask. The mixture was warmed slowly with vigorous stirring until it began to reflux. After 12.5 h evolution of hydrogen chloride had ceased and the mixture was allowed to cool to room temperature.

The bulk of the solvent was distilled under reduced pressure (150 mmHg) at 90°C leaving a dark brown solution (500 ml). This solution was transferred to a 1 litre flask and the residual solvent was distilled at 40–50°C (5 mmHg). The resultant semi-solid residue was distilled at 4 mm pressure between 110° and 125°C through an air condenser. The white solid distillate was hexachlorocyclotriphosphazene containing some of the tetrameric homologue as the main impurity.

The impure product was crystallized twice from petroleum ether (b.p. 80–100°C) and sublimed at 90°C and 0.1 mmHg. The yield was 90 g, 40% overall. It had m.p. 114°C. The material was normally used immediately but when necessary it was stored under vacuum and re-sublimed immediately before use.

It should be noted that on some occasions during the vacuum distillation of the cyclic phosphazenes, overheating occurred causing the linear material present to cross-link, thus making it difficult to continue the distillation. When this occurred the material in the distillation flask was shaken with benzene to swell the crosslinked material and dissolve the cyclophosphazenes. The resultant mixture was poured into a large volume of petroleum ether (b.p. 80–100°C) to precipitate the linear phosphazenes. The solution of cyclophosphazenes was decanted and reduced in volume until crystallization began. The impure product was then recrystallized from petroleum ether (b.p. 80–100°C) and sublimed as above. The yield by this method was 80 g, 35%.

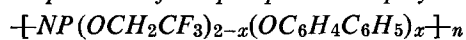
\* Present address: Department of Chemistry, University of Arizona, Tucson, Arizona 85721, USA.



*Preparation of poly(dichlorophosphazene)*

A medium-walled Pyrex tube (25 cm × 2 cm i.d.) was cleaned with chromic acid, washed with distilled water and dried at 120°C overnight. Freshly sublimed hexachlorocyclotriphosphazene (70–80 g, 0.20–0.23 mol) was ground quickly with a mortar and pestle and introduced into the tube. The tube and contents were then evacuated to 10<sup>-2</sup> mmHg for 1 hour. The tube was isolated from the vacuum and the contents were melted and then allowed to solidify. After the material had solidified the tube was opened to the vacuum for 1 hour and the de-gassing operation repeated. The tube was then sealed.

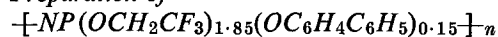
The sealed tube was placed in a furnace and heated at 250 ± 2°C for 60–80 h. When the end of the reaction was determined the tube and contents were allowed to cool to room temperature giving a pale yellow to dark brown amorphous material containing some white, crystalline cyclic chlorophosphazenes. The polymer was normally used immediately but, when necessary, it was stored in the sealed tube. When required, the tube was broken and the pieces of glass and polymer were shaken with dry benzene to give a 10–15% solution of chlorophosphazenes. The solution was filtered through glass wool to remove glass and was used immediately for the preparation of substituted polymers.

*Preparation of the phosphazene copolymers*

The quantities given here were those used for  $x=0.6$ . A solution of sodium *p*-phenylphenoxide (0.196 mol, 4.5 g sodium) in tetrahydrofuran (150 ml) was added dropwise to a stirred solution of poly(chlorophosphazenes) (38 g, 0.328 mol  $\text{NPCl}_2$ ) in benzene (250 ml). The reaction was carried out in a 1 litre flask fitted with a water condenser and silica gel drying tube, sealed stirrer and pressure equalizing dropping funnel. After completion of the addition the mixture was stirred at reflux for 1 hour when a solution of sodium 2,2,2-trifluoroethoxide (0.52 mol, 12.1 g sodium) in tetrahydrofuran (180 ml) was added. The mixture was refluxed for 38 h after completion of the addition.

The cooled reaction mixture was poured into petroleum ether (b.p. 60–80°C, 3 l) which resulted in a powdery precipitate of polymer and inorganic salts. The ether was decanted, the residual sludge was shaken with tetrahydrofuran and the mixture was poured into a large volume of water. To ensure removal of cyclic phosphazenes and inorganic salts the product was re-precipitated into petroleum ether and then water from tetrahydrofuran solutions. The rubbery product was collected and dried under vacuum. The yield was 12 g (15% based on  $\text{P}_3\text{N}_3\text{Cl}_6$ ). Intrinsic viscosities, measured in tetrahydrofuran at 25°C, and analyses of the copolymers are given below:

$x$		C (%)	H (%)	N (%)	F (%)	Cl (ppm)	$[\eta]$ (dl/g)
Theory	Expt.						
1.60	1.60	66.3	4.5	3.6	6.3	<100	2.20
1.00	1.08	55.1	3.9	4.5	17.2	<100	2.40
0.80	0.80	47.4	3.3	4.8	23.1	<100	1.95
0.60	0.64	42.6	3.3	5.2	26.7	<100	2.23
0.20	0.15	26.5	2.5	5.9	41.4	<100	1.06

*Preparation of*

A solution of sodium (4.7 g, 0.204 g atom) and *p*-phenylphenol (37.7 g, 0.222 mol), in tetrahydrofuran (170 ml) was added dropwise to a stirred solution of poly(chlorophosphazenes) (78.0 g, 0.672 mol  $\text{NPCl}_2$ ) in benzene (540 ml) contained in a 3 litre flask fitted as before. Soon after the addition was begun there was an exotherm and the mixture gelled causing the mixing to be inefficient. A slow rate of addition was therefore used and 10 h were taken to complete the addition. A further 150 ml of tetrahydrofuran were used to wash sodium *p*-phenylphenoxide, which had deposited on the wall of the flask, into the reaction mixture. The resultant mixture was stirred for 2 h at 65°C.

A solution of sodium (30 g, 1.31 g atom) in 2,2,2-trifluoroethanol (150 g, 1.50 mol) and tetrahydrofuran (400 ml) was added dropwise over 5.5 h to the stirred solution of partly substituted polymer. The reaction mixture was refluxed for 72 h and then a solution of sodium (1.0 g, 0.0435 g atom) and *p*-phenylphenol (8.1 g, 0.0476 mol) in tetrahydrofuran (30 ml) was added. The reaction was continued for 12 h when di-*n*-butyl ether (1.2 l) was added and the more volatile solvents distilled away until the reflux temperature was 110°C. The reaction mixture was refluxed for 16 h at this temperature and then allowed to cool to room temperature.

The reaction mixture was poured into a large excess of petroleum ether (b.p. 60–80°C) to give a white powdery precipitate which was filtered off and air-dried. The precipitate was shaken with acetone until most had dissolved and then added to water. The product was collected and re-precipitated into water from acetone solution. As the cyclic phosphazenes were insoluble in acetone, the small amount remaining after the initial precipitation of the product into petroleum ether was removed by dissolving the product in acetone and filtering the solution through a sintered glass filter (porosity 4). The clarified solution was poured into water and the precipitated product, a grey rubbery material, was collected and dried under vacuum.

The yield was 26 g (16% based on  $\text{P}_3\text{N}_3\text{Cl}_6$ ). The intrinsic viscosity in tetrahydrofuran at 25°C was 0.615 dl/g. The copolymer had C, 26.1%; H, 2.2%; N, 5.4%; F, 41.5%; Cl < 100 ppm giving the composition as  $\left[ \text{NP}(\text{OCH}_2\text{CF}_3)_{1.85}(\text{OC}_6\text{H}_4\text{C}_6\text{H}_5)_{0.15} \right]_n$ .

This product was the subject of detailed characterization.

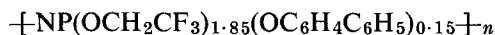
## RESULTS

*Synthesis*

Hexachlorocyclotriphosphazene ( $\text{NPCl}_2$ )<sub>3</sub> was prepared by the method of Emsley and Udy<sup>7</sup> using ammonium chloride, phosphorus pentachloride and phosphorus oxychloride in *sym*-tetrachloroethane. The material was purified by crystallization and sublimation. Poly(dichlorophosphazene) was prepared by polymerizing hexachlorocyclotriphosphazene in sealed glass tubes at 250°C. The molecular weight of the product was required to be as high as possible but it was important also that there should be no insoluble material formed. Thus, as the reaction time varied (60–80 h), the end of the reac-

tion was determined by inspecting the contents of the tube at intervals during the polymerization.

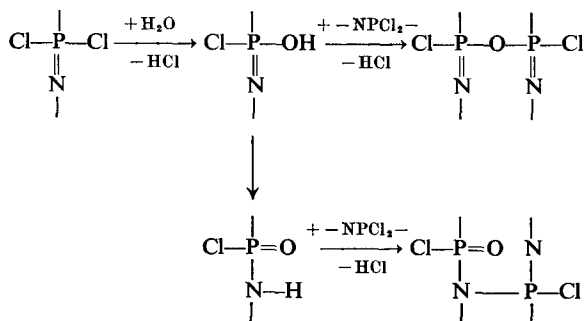
The copolymers were prepared by first reacting the chloro-polymer with sodium *p*-phenylphenoxide and then reacting the partly substituted polymer with sodium 2,2,2-trifluoroethoxide. Details of the synthesis are given above. A number of problems were associated with the preparation of



on a large scale which were not apparent when the range of copolymers was made. These problems (gelation of the reaction mixture and a longer reaction time) were a consequence of the larger scale of this particular preparation.

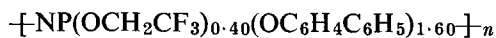
The addition of the first reactant (sodium *p*-phenylphenoxide) to the solution of poly(chlorophosphazenes) caused the reaction mixture to gel thus making the mixing inefficient. A very slow rate of addition was therefore used in order to increase the probability of obtaining a random copolymer.

The use of a longer reaction time and higher reaction temperature was essential in order that the final product should not crosslink. It was found that a residual chlorine content of  $\geq 0.1\%$  by weight in the copolymers was sufficient to cause crosslinking. The crosslinking was due to hydrolysis, possibly by the mechanisms given below. The longer reaction time and use of a high boiling solvent gave a product of lower molecular weight ( $[\eta] = 0.615 \text{ dl/g}$ ) than the smaller-scale preparations (average  $[\eta] \approx 2 \text{ dl/g}$ ). This was due to degradation of the  $\text{--P=N--}$  chain, either thermally or by the presence of the excess alkoxide.

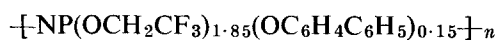


### Solubility

The copolymers were all soluble in a wide range of polar solvents (tetrahydrofuran, dimethylsulphoxide, *N,N*-dimethylformamide). Other materials were solvents only over a narrow range of copolymer compositions, e.g. the copolymer



was partly soluble in benzene, the benzene-soluble part having a higher proportion of *p*-phenylphenoxy groups than the insoluble part. Both fractions were soluble in tetrahydrofuran. Solvents for



are given in Table 1.

### Molecular weight and intrinsic viscosity

The copolymer  $x = 0.15$  was fractionated by isothermal liquid-liquid phase separation at  $25^\circ\text{C}$  by adding a 1%

Table 1 Solvents and non-solvents for  $\text{--}[\text{NP}(\text{OCH}_2\text{CF}_3)_{1.85}(\text{OC}_6\text{H}_4\text{C}_6\text{H}_5)_{0.15}]_n\text{--}$

Solvents	Non-solvents
Acetone	Water
Tetrahydrofuran	Petroleum ethers
Dimethylsulphoxide	Benzene
Cyclohexanone	Toluene
Methyl ethyl ketone	Isopropylbenzene
Dimethylacetamide	Nitrobenzene
Methanol	Chlorobenzene
Ethanol <sup>a</sup>	1,3,4-Trichlorobenzene
Dimethylformamide	Decalin
Ethyltrifluoroacetate	Dioxan
	Diethylether <sup>b</sup>
	Acetonitrile <sup>b</sup>
	Chloroform
	Carbon tetrachloride

<sup>a</sup> Partly soluble at room temperature and dissolved on warming

<sup>b</sup> Swelled but did not dissolve

Table 2 Dynamic thermogravimetry of copolyphosphazenes  $\text{--}[\text{NP}(\text{OCH}_2\text{CF}_3)_{2-x}(\text{OC}_6\text{H}_4\text{C}_6\text{H}_5)_x]_n\text{--}$

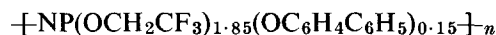
$x$	Weight loss at $500^\circ\text{C}$ (%)	Decomposition temperature ( $^\circ\text{C}$ )	Temperature of 10% loss ( $^\circ\text{C}$ )
1.60	50	355	386
1.08	80	301	371
0.80	81	259	362
0.64	85	271	365
0.15	87	264	348

brine solution to a solution of the polymer in tetrahydrofuran. Gel permeation chromatography showed that for each fraction  $M_w/M_n = 2.0 \pm 0.2$ , and for the whole polymer  $M_w/M_n = 3.7$ . The values of  $\bar{M}_n$ , determined by osmometry in cyclohexane at  $65^\circ\text{C}$ , ranged from  $3.3$  to  $0.9 \times 10^5$  and the corresponding range of intrinsic viscosity, measured in tetrahydrofuran at  $25^\circ\text{C}$  was  $1.03$  to  $0.15 \text{ dl/g}$ . The fractions separated in order of decreasing molecular weight.

Unfortunately an intrinsic viscosity-molecular weight relation could not be constructed because the chemical composition of each fraction was different;  $x$  ranged from  $0.32$  for the fraction of highest molecular weight to  $0.08$  for the lowest fraction.

### Thermal stability

The thermal stability of the copolymers was examined by thermogravimetry under dry nitrogen ( $20 \text{ ml/min}$ ) at a heating rate of  $3^\circ\text{C/min}$ . The results are given in Table 2. An isothermal method of determining the thermal stability of the copolymer



was also used. Samples of the copolymer were heated at  $155^\circ\text{C}$  under atmospheric conditions and the change in intrinsic viscosity with time was followed. These results are given in Table 3.

The dynamic  $T_g$  results show an increasing rate of percentage weight loss with increase in trifluoroethoxy content of the copolymer. This is in agreement with the

Table 3 Thermal stability of  $\text{[-NP(OCH}_2\text{CF}_3)_2\text{-}_x\text{(OC}_6\text{H}_4\text{C}_6\text{H}_5)_x\text{]}_n$  in air at 155°C

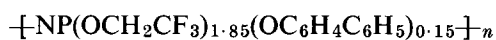
Time (h)	Intrinsic viscosity <sup>a</sup> (dl/g)	Soluble material (%)
0	0.615	100
2	0.62	95
4	0.60	93
6	0.41	95
10	0.15	98
12	0.14	97

<sup>a</sup> Measured in tetrahydrofuran at 25°C

results of Allen *et al.* who suggest the occurrence of a crosslinking mechanism during the degradation of poly(aryloxyphosphazenes), which prevents further weight loss<sup>5</sup>. The results also show decreasing thermal stability with increasing trifluoroethoxy content which confirms the better thermal stability of the *p*-phenylphenoxyphosphazene compared with the trifluoroethoxy derivative.

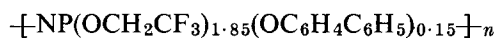
#### Polymer structure

The infra-red spectrum of

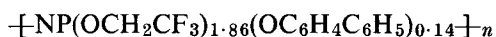


was obtained from a film of the copolymer cast onto a sodium chloride plate from acetone solution. A Perkin-Elmer Model 257 Spectrophotometer was used. The principal bands were (cm<sup>-1</sup>): 2969 (C-H, methylene); 1608, 1520, 1490 (C=C); 1457 (C-H); 1424 (P-O-C, aliphatic); 1286 (C-F); 1262 (P=N); 1210 (P-O-C, aromatic); 1177 (C-F); 1091, 971 (P-O-C, aliphatic); 947 (P-O-C, aromatic); 885 (P-O-C, aliphatic); 852, 773, 706 (C-H, aromatic). The absence of bands at wavenumbers greater than 3200 (O-H), at 2650-2680 (P-O-H) or 1225 (P=O) indicated that very little, if any, hydrolysis of the chloro-polymer had taken place.

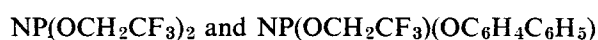
The nuclear magnetic resonance spectra (<sup>1</sup>H and <sup>19</sup>F) were obtained using a Varian HA 100 spectrometer. The proton spectrum was obtained at 100 MHz using a 10% solution of the copolymer



in D<sub>6</sub>-dimethylsulphoxide at 122°C with hexamethyldisilane as the internal reference. The spectrum consisted of a broad multiplet (2.74τ, 24H) and a broad quartet (5.74τ, 71H). Integration gave the composition of the copolymer as

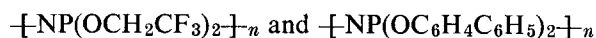


The fluorine spectrum was obtained at 94.1 MHz using a 10% solution of the copolymer in dimethylacetamide at 120°C with *m*-trifluoromethylphenol as the internal reference. The spectrum (Figure 1) consists of two triplets of intensity ratio ~8 : 1. The chemical shifts of the two triplets, relative to external trifluoroacetic acid were -3.54 ppm and -3.77 ppm. Poly[bis(2,2,2-trifluoroethoxy)phosphazene] under the same conditions gave a well-resolved triplet at -3.52 ppm, relative to external trifluoroacetic acid. The fluorine spectrum is consistent with the presence of only two types of repeat unit in the copolymer:



in the ratio 4 : 1. The broadening of the <sup>19</sup>F spectrum and of the quartet of the <sup>1</sup>H spectrum is due to coupling with phosphorus and possibly environmental differences.

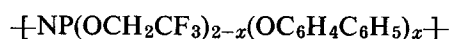
X-ray diffraction studies on a film of the copolymer  $\text{[-NP(OCH}_2\text{CF}_3)_{1.85}(\text{OC}_6\text{H}_4\text{C}_6\text{H}_5)_{0.15}\text{]}_n$  showed it to have a small degree of crystallinity. The diffraction pattern of the copolymer was compared with the patterns obtained from the two homopolymers:



The pattern of the copolymer shows four diffraction rings, all of which were found in the diffraction pattern of poly[bis(2,2,2-trifluoroethoxy)phosphazene] (Figure 2). The changes in intensity of diffuseness also compare very well with those from the trifluoroethoxy homopolymer. There are no diffraction rings in the copolymer which correspond to those found in the diffraction pattern of the *p*-phenylphenoxy homopolymer. Also, there are no diffraction rings which do not appear in the diffraction patterns of the two homopolymers. We conclude that the copolymer has a small degree of crystallinity due to crystallization of NP(OCH<sub>2</sub>CF<sub>3</sub>)<sub>2</sub> sequences.

#### Transition temperatures

The glass transitions and melting temperatures of the series of copolymers



were determined using a Du Pont 900 Differential Thermal Analyser fitted with a DSC mode. All runs were carried

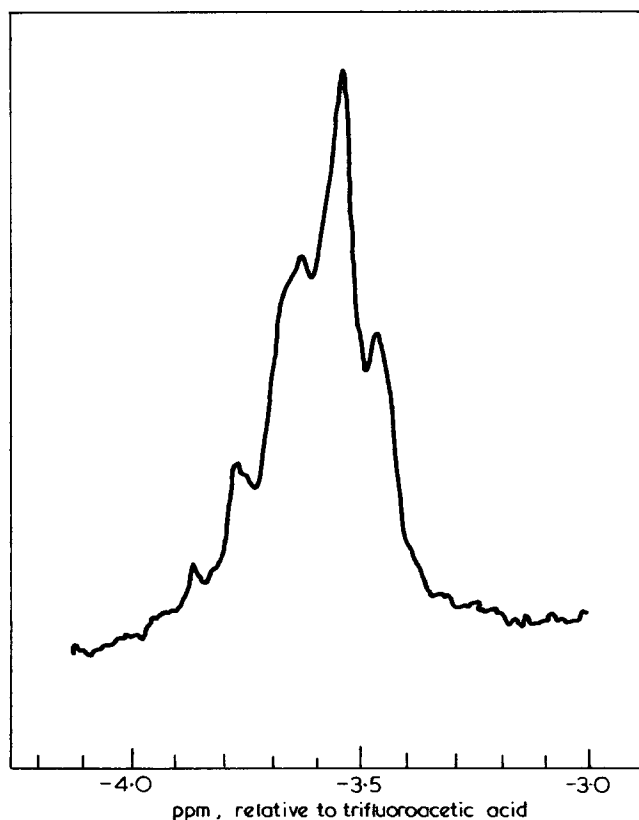
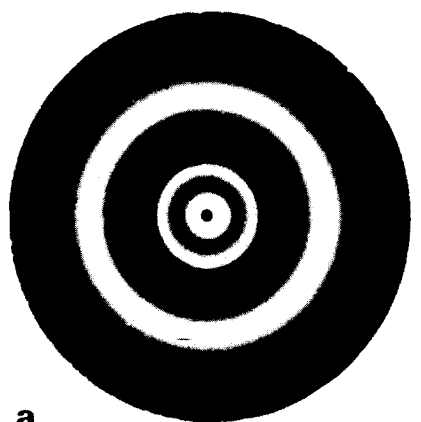


Figure 1 <sup>19</sup>F spectrum of  $\text{[-NP(OCH}_2\text{CF}_3)_{1.85}(\text{OC}_6\text{H}_4\text{C}_6\text{H}_5)_{0.15}\text{]}_n$  at 94.1 MHz in dimethylacetamide at 120°C

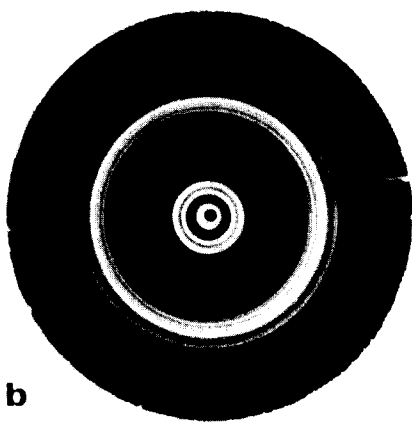
Table 4 Transition temperatures of copolyphosphazenes  $\text{[-NP(OCH}_2\text{CF}_3)_2\text{-}_x\text{(OC}_6\text{H}_4\text{C}_6\text{H}_5)_x\text{]}_n$ 

x	$T_g$ (°C)	$T_m$ (°C)			
		d.s.c.		Microscopy	
2.00	+43	160	398	> 350	
1.60	+34	61	83	195	191
1.08	+22	44	67	182	187
0.80	+12	32	55	— <sup>a</sup>	— <sup>a</sup>
0.64	-4		36	214	215
0.15	-46	39	53	167	173
0	-70		80	238	236

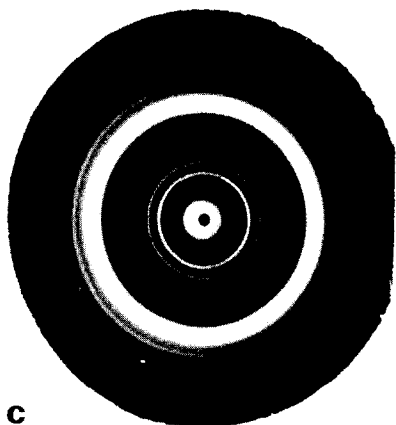
<sup>a</sup> Not detectable



a



b



c

Figure 2 X-ray diffraction photographs of polymers after heating at 120°C. (a) Copolymer; (b) poly[bis(phenylphenoxy) phosphazene]; (c) poly[bis(trifluoroethoxy) phosphazene]

out under nitrogen, at atmospheric pressure, using chromel/alumel thermocouples and a heating rate of 20°C/min. Melting points were checked using a polarizing microscope fitted with a hot stage. The results are given in Table 4.

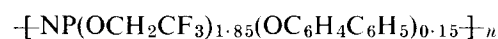
The glass transitions show a regular increase with increasing value of  $x$  and so correlate with the increased size and reduced flexibility of the  $p$ -phenylphenoxy compared with the trifluoroethoxy group. The copolymers have, in general, three melting transitions; only the upper one leads to totally amorphous material. The two lowest transitions are probably due to rearrangement of the side groups to form a second crystalline phase which melts at the highest temperature. It should be noted that only one high-temperature melting transition was observed for the copolymers.

#### Mechanical properties

Torsion pendulum experiments were carried out using a sample of a lightly crosslinked copolyphosphazene. The crosslinking resulted from the partial hydrolysis of an incompletely substituted copolymer,



This sample was used in preference to the copolymer



to improve the dimensional stability of the sample near the glass transition temperature. The polymer was compression-moulded into a bar using a force of 20 tons for 3 minutes at 175°C.

The sample was mounted in a torsional pendulum apparatus similar to that described in the ASTM index<sup>8</sup>. The period and decay of the oscillations were measured thus enabling the moduli of the sample to be calculated. The upper limit of the temperature range was determined by the loss of dimensional stability of the sample. The results are given in Figure 3.

The major loss region at -43°C corresponds to the transition which occurred at -46°C in the d.s.c. experiments (Table 4). This is the glass transition region. The loss regions which would be associated with the melting transitions could not be observed because the sample began to lose dimensional stability at temperatures above -35°C.

#### DISCUSSION

The results presented above show that it is possible to prepare amorphous, elastomeric polyphosphazenes which are soluble in a wide range of solvents. The material  $\text{[-NP(OCH}_2\text{CF}_3)_{1.85}\text{(OC}_6\text{H}_4\text{C}_6\text{H}_5)_{0.15}\text{]}_n$  is

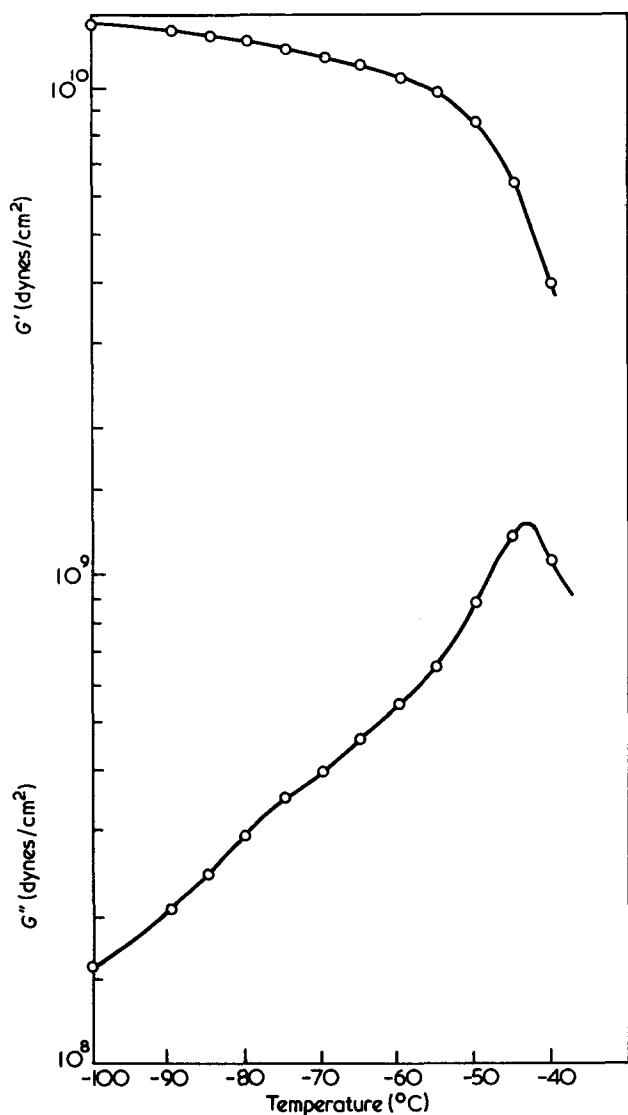


Figure 3 Torsion pendulum measurements

an elastomer ( $T_g - 45^\circ\text{C}$ ) having a small degree of crystallization ( $T_m 170^\circ\text{C}$ ). Structurally the polymer is a random copolymer having some crystallizable sequences of  $\text{NP}(\text{OCH}_2\text{CF}_3)_2$  units. There is no evidence for any units of the type  $\text{NP}(\text{OC}_6\text{H}_4\text{C}_6\text{H}_5)_2$  in the copolymer.

The thermal analysis results show that the polymer has three first order transitions at  $39^\circ$ ,  $53^\circ$  and  $167^\circ\text{C}$ , i.e. between  $50^\circ$  and  $150^\circ\text{C}$  there is a reversible transition from one crystalline phase into another. Thermal stability tests show that the long-term stability under atmospheric conditions at temperatures in excess of  $150^\circ\text{C}$  is disappointing.

#### ACKNOWLEDGEMENTS

We are indebted to Mrs S. M. Bishop for the X-ray diffraction studies; to Dr F. Heatley for assistance with the n.m.r. spectra; to ICI Ltd., Dyestuffs Division for the use of thermal analysis equipment and to Mr S. M. Todd for suggestions and helpful discussions of the chemistry involved. R. M. M. would also like to thank the Science Research Council for the award of a Research Studentship.

#### REFERENCES

- 1 Stokes, H. N. *Am. Chem. J.* 1897, **19**, 782
- 2 Mirhej, M. E. and Henderson, J. F. *J. Macromol. Chem.* 1966, **1**, 187
- 3 Allcock, H. R., Kugel, R. L. and Valan, K. J. *Inorg. Chem.* 1966, **5**, 1709
- 4 Allcock, H. R. and Kugel, R. L. *Inorg. Chem.* 1966, **5**, 1716
- 5 Allen, G., Lewis, C. J. and Todd, S. M. *Polymer* 1970, **11**, 31
- 6 Rose, S. H. *J. Polym. Sci. (B)* 1968, **6**, 837
- 7 Emsley, J. and Udy, P. *Chem. Commun.* 1967, **13**, 633
- 8 ASTM Index, D2236-67T

# Pulsed n.m.r. study of molecular motion and environment of sorbed water on cellulose

T. F. Child\*

*Unilever Research Port Sunlight Laboratory, Unilever Ltd, Port Sunlight, Wirral, Cheshire L62 4XN, UK  
(Received 18 October 1971)*

The state of sorbed water on celluloses derived from cotton and woodpulp sources has been investigated by pulsed nuclear magnetic resonance (n.m.r.) techniques. The molecular motion of sorbed water molecules was found to depend on the physical state of the cellulose, particularly on the degree of crystallinity. Temperature behaviour in the range 323K to 223K revealed a very strong interaction between cellulose and water, with a distribution of binding energies which depended on the heterogeneity of the cellulose surface. Relaxation time measurements have been made at several water contents and the results interpreted in terms of current sorption theories. In particular, the discontinuities observed by various physical measurements at a certain water content have been detected in this work and related to chain attenuation by a bridging network of water molecules.

## INTRODUCTION

Celluloses from different sources and of different crystalline contents exhibit widely different sorption behaviour<sup>1</sup>. It was the aim of this work to analyse the pulsed nuclear magnetic resonance (n.m.r.) results with particular reference to the physical state of the cellulose substrates from woodpulp and cotton sources and with a range of degree of polymerization (*DP*) from 200 to 2000. To obtain information about the sorption process, a range of water contents was considered which covered the whole range of the sorption isotherm. Temperature dependencies of the spin-lattice ( $T_1$ ) and spin-spin ( $T_2$ ) relaxation times were investigated to obtain more information about molecular motion in the system.

## EXPERIMENTAL

### Materials

Three samples of flocced, bleached sulphite woodpulp, manufactured by Rayonier Incorporated, were supplied by Unilever Chemicals Development Centre:

Woodpulp	<i>DP</i>	Water accessibility (%) <sup>2</sup>
Rayweb Q	525	77
Raybond P	1450	69
Hicolour	1000	62

\* Present address: Lever Sunlight GmbH, Zweigniederlassung Mannheim, Rhenianstrasse 76/90, 68 Mannheim 81, West Germany.

Other samples investigated were a highly crystalline fibrous cellulose obtained by controlled acid hydrolysis, Whatman CF1 (*DP* 250; water accessibility 32%), and a sample of cotton linters (*DP* 1950; water accessibility 50%). The accessibility of the celluloses to water was estimated by immersing each sample in D<sub>2</sub>O and measuring the amount of H<sub>2</sub>O in the D<sub>2</sub>O solution after exchange, by an n.m.r. method<sup>2</sup>. After correcting for the contributions from sorbed water, the H<sub>2</sub>O arising from exchange at the cellulose hydroxyls was related to accessibility by a simple calculation.

The cellulose samples were conditioned over saturated salt solutions<sup>3</sup> at 298K for at least one month and water contents were determined by Karl-Fischer titration.

### Pulsed n.m.r.

Special thin-walled n.m.r. tubes of 7.5 mm o.d. were filled to a depth of about 5 mm with cellulose and the tubes were sealed. Pulsed n.m.r. experiments were carried out using a modified version of the Bruker-Physik pulse spectrometer type B-KR 302, operating at a frequency of 60 MHz. A 'Boxcar' integrator unit was included in the pulse generator console, with read-out onto a 'Servoscribe' potentiometric recorder. Relaxation time decay and regrowth curves were observed on a Tektronix Type 549 storage oscilloscope. Temperature control was maintained to  $\pm 1$ K with a gas flow thermostat.

$T_1$  measurements were carried out with a 90°-90° pulse programme and  $T_2$  measurements were obtained using a Carr-Purcell sequence<sup>4</sup> with Gill-Meiboom<sup>5</sup> modification.

$T_1$  values for the cellulose chains were obtained with a 90°-90° sequence and the Boxcar integrator, triggered by

a third pulse, with the integrator gate set on the short induction decay characteristic of the cellulose protons. The contribution from the sorbed water was subtracted from the magnetization regrowth. Exponential curves were obtained with both  $T_1$  and  $T_2$  for the sorbed water indicating single phase behaviour. All relaxation time measurements were made at least in duplicate. The measurements should be taken as being reproducible to within  $\pm 5\%$ , although in any one run the precision was better, particularly for samples with high water content.

**RESULTS AND DISCUSSION**

The  $T_2$  behaviour of Whatman CF1 and cotton linters at different temperatures shows up a strong dependence on the cellulose fine structure, as indicated in *Figures 1 and 2*.

The  $T_1/T_2$  ratio is about 1000, and  $T_1 \gg T_2$  at high temperatures. Obviously the simple theory of Bloembergen, Purcell and Pound<sup>6</sup> (BPP) is not applicable in this case. In a system such as cellulose, with accessible and inaccessible regions, it is to be expected that the molecular motions of bound water molecules will be different, according to the binding site. In such a case, a single correlation time at a certain temperature cannot adequately describe the mobility of the system. The original BPP equations were modified by Kubo and Tomita<sup>7</sup> to allow for a distribution in correlation times,  $P(\tau)$ , in the following manner:

$$T_1^{-1} = 2A \int_0^\infty [\tau / (1 + \omega^2\tau^2) + 4\tau / (1 + 4\omega^2\tau^2)] P(\tau) \cdot d\tau$$

$$T_2^{-1} = A \int_0^\infty [3\tau + 5\tau / (1 + \omega^2\tau^2) + 2\tau / (1 + 4\omega^2\tau^2)] P(\tau) \cdot d\tau$$

where  $A$  is a constant,  $\omega$  is the nuclear angular resonance frequency and  $\tau$  is the correlation time.

The application of a log-normal distribution of correlation times, in which the logarithm of the correlation

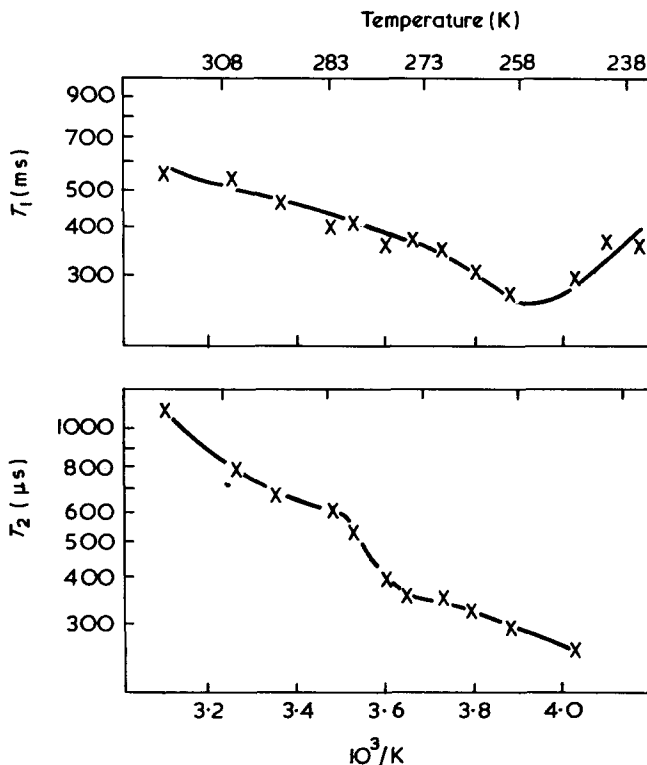


*Figure 2* Temperature dependence of  $T_1$  and  $T_2$  for water sorbed on cotton linters at 8.9% regain

time is distributed in a Gaussian fashion, results in a rise in the  $T_1$  minimum and a fall in  $T_2$ , so that the  $T_1/T_2$  ratio is greater. The temperature dependence of  $T_1$  decreases, so that the width of the minimum increases. A log-normal distribution of correlation times has been applied to several systems<sup>8,9</sup> and proved fairly satisfactory in fitting the experimental data.

*High-energy sites and nuclear transfers*

An interesting characteristic of *Figure 1*, showing the temperature dependence of  $T_2$  for water sorbed on cellulose, is that above 288K a shoulder appears, with a tendency for  $T_2$  values at higher temperatures to decrease. Similarly, for cotton linters, a discontinuity occurs at about the same temperature, although in this case  $T_2$  values continue to rise with temperature. The water dipole has a local magnetic field which is modulated by diffusional jumps from a sorption site. In other words, the intramolecular internuclear vectors may reorient only when the molecule makes a jump out of the 'well'. If this condition is fulfilled, the correlation time  $\tau$  is the jump  $\tau_d$  for translation among these sites. A collection of high-energy sites, all with the same barrier heights, is a phase in the Zimmerman and Brittin<sup>10</sup> sense (say, phase *b*). The molecules of phase *b* exchange with the normal sites (phase *a*) each time a jump out of the well is made. The lifetime in phase *b* is thus by definition the jump time  $\tau_b$ .

A trial calculation has been made by Resing<sup>11</sup> assuming 4% of high-energy or *b* sites, with activation enthalpy of  $4.52 \times 10^4 \text{ J mol}^{-1}$ , and 96% of *a* sites with activation enthalpy of  $2.51 \times 10^4 \text{ J mol}^{-1}$ . The broken curves at the left of *Figure 3a* represent the relaxation times  $T_{2b}$  and  $T_{1b}$ , which would not actually be observable because of

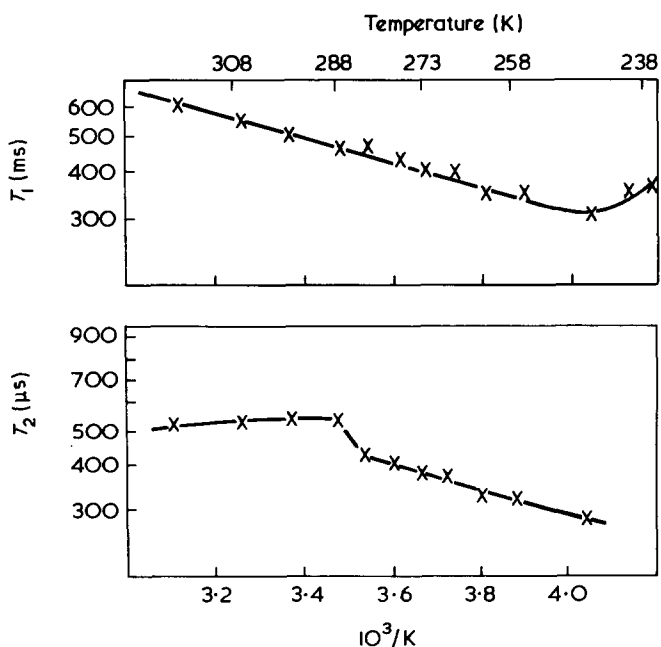


*Figure 1* Temperature dependence of  $T_1$  and  $T_2$  for water sorbed on Whatman CF1 at 7.3% regain

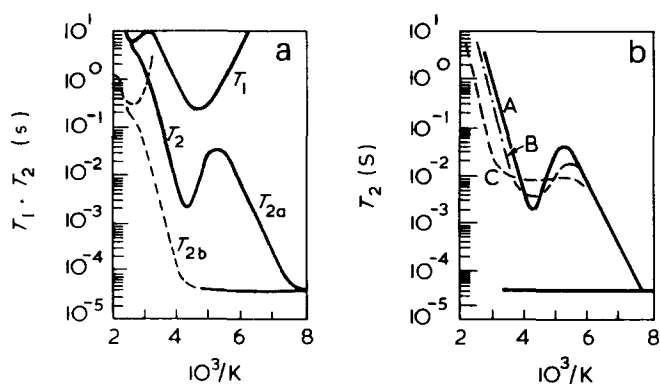


Figure 3 (a) Temperature dependence of relaxation times calculated for benzene sorbed on a hypothetical surface containing 4% high-energy sites. (b) Introduction of a distribution of barrier heights with standard deviation  $\sigma$ . (A)  $\sigma=0$ ; (B)  $\sigma=3.93 \times 10^3$  J mol<sup>-1</sup>; (C)  $\sigma=9.80 \times 10^3$  J mol<sup>-1</sup>. Reproduced from *Adv. Mol. Relaxation Processes* (1968, 1, 119) by permission of Elsevier Publishing Co., Amsterdam

fast exchange with phase *a*. In this Figure,  $T_2$  increases with increasing temperature up to a maximum and then decreases to a certain point before increasing again. The decrease represents the onset of diffusion from high-energy sites. Note that phase *b* introduces a second minimum in  $T_1$  at higher temperatures, while at very low temperatures two-phase behaviour in  $T_2$  is observed as exchange between the phases is suppressed. In this case the molecules are unable to escape from the high-energy binding sites.

If the high-energy sites have a broad distribution of barrier heights for translation, which is a reasonable supposition in a system such as cellulose, then curves of the type indicated in Figure 3b are obtained<sup>11</sup>. For a broad enough distribution the minimum turns into a plateau. This type of behaviour for  $T_2$  is very similar to that observed with Whatman CF1.

The acid-hydrolysed Whatman CF1 cellulose was fibrous and finely divided in appearance, whereas the sample of cotton linters resembled cotton-wool. Acid hydrolysis destroys the disordered regions of cellulose, so that only inert crystalline material remains. No doubt some acid attack at faults or 'soft spots' in the crystalline material produces an increase in the accessible surface area of the crystallites. The total crystalline content of the cellulose is, of course, greatly increased, which is reflected in the reduced accessibility to water, and the *DP* is reduced. The final crystalline content and *DP* will depend on the controlling conditions of the hydrolysis.

The high temperature regions of Figures 1 and 2 for  $T_2$  behaviour indicate more sites of high-binding energy in Whatman CF1 than cotton linters. The plateau in Figure 1 persists at high temperatures, whereas in Figure 2,  $T_2$  is increasing with increasing temperature, as expected from BPP theory. Presumably, with cotton linters, the barriers to diffusion from high-energy sites are soon overcome and normal temperature behaviour is obtained. In Whatman CF1, water molecules are probably sorbed mainly in those regions intermediate in order between crystalline and highly disordered. The chain motion in crystallites and their peripheries will be attenuated to an appreciable extent so that, provided accessibility is possible, such sites may prove to be deeper potential wells than sites contained

in the disordered regions. The high proportion of crystalline material in Whatman CF1 is probably the dominating factor in high temperature  $T_2$  behaviour.

#### Freezing effects

On lowering the temperature below 273K, no discontinuity appears in the  $T_1$  and  $T_2$  curves for the Whatman cellulose. The signal amplitude also remains constant, indicating that there is no freezing of sorbed water. On the other hand there is a discontinuity in the  $T_2$  curve for cotton linters at 273K. Strongly sorbed water does not freeze at 273K, so it is possible that some water sorbed on cotton linters behaves in a similar manner to bulk water. Below 243K both systems showed considerable 'freezing' of sorbed water, with the n.m.r. signal amplitude dropping almost to zero at 223K.

The 'freezing' process observed at low temperatures does not necessarily indicate ice formation as such but only a reduction in molecular mobility which produces ice-like behaviour. If ice formation occurs at higher water contents, then this is because some water molecules are sufficiently removed from the cellulose surface to be unaffected by it, allowing formation of an ice-lattice in the normal manner.

#### The $T_1$ minimum

The position of the  $T_1$  minimum indicates strong binding of water molecules with the cellulose. For the system, water in charcoal<sup>8</sup>, the  $T_1$  minimum occurred at 206K, indicating a state of water with no strong substrate interaction. The system, silica-water<sup>9</sup>, exhibited a minimum at 235K, indicating strong liquid-surface binding. In the cellulose-water system, the minimum occurs at about 253K, indicating even stronger water binding. The  $T_1$  minimum for Whatman CF1 is broader than the  $T_1$  minimum for cotton linters. This indicates a broader distribution of correlation times in the highly crystalline cellulose; an effect which may be explained by a greater surface heterogeneity of the partly hydrolysed cellulose.

At the  $T_1$  minimum  $\omega\tau_{\min} \approx 0.62$ . From this relationship, the correlation time of sorbed water molecules may be calculated at the temperature of the  $T_1$  minimum. At an operating frequency of 60 MHz, the correlation time works out at  $1.6 \times 10^{-9}$  s.

#### Comparison with other systems

Pulsed n.m.r. investigations of the silica gel-water system<sup>9, 12, 13</sup>, have indicated similar high temperature behaviour for  $T_2$ . In some respects, the two systems are related, since each sorbate is characterized by a non-uniform distribution of hydroxyl groups. These groups may be considered as the primary binding centres. Previous pulsed n.m.r. studies in the cellulose-water system have been few<sup>14, 15</sup>. However, Sasaki and co-workers<sup>14</sup> observed apparent two-phase behaviour for  $T_1$ . This indicated that sorbed water molecules could be identified as being either tightly bound or mobile. It is interesting from this work, that only single-phase behaviour for  $T_2$  was observed, although  $T_1 \gg T_2$ . Two-phase behaviour for  $T_2$  would be expected in such a system, so that unless the  $T_2$  values are almost identical



in each phase, the absence of two-phase behaviour poses some problems in interpretation.

Stejskal<sup>15</sup> showed the existence of two  $T_1$  phases at 298K over a restricted water content range. At lower water contents single phase behaviour only was observed, the shorter  $T_1$  phase having disappeared. This is unusual, since at low water contents the shorter  $T_1$  phase, representing the more tightly bound water, is expected to be more populated. This is assuming that the first sorbed molecules migrate to the strongest binding centres. There is a possibility that micropores exist in Stejskal's samples since, according to the preparative technique used, the cottons were compressed into plugs before measurements were taken. After a certain water uptake, these pores would be sufficient to produce non-exponential  $T_1$  behaviour. The conditions under which Sasaki and co-workers' samples were prepared are not known, although it is possible that sample preparation is an important factor in affecting relaxation characteristics.

In this present work, where the samples were not compressed, single phase behaviour for  $T_1$  and  $T_2$  was observed at all temperatures and water contents considered. At lower temperatures, exchange between phases will be slowed down to such an extent that observation of separate  $T_1$  values for each phase should become possible, although measurements of  $T_1$  as low as 263K revealed only single-phase behaviour.

A factor which may be important in comparing the results is that Sasaki and coworkers made measurements at 25 MHz and Stejskal at 20 MHz. Since  $T_1$  values at 60 MHz are longer, it would be expected that less chance is likely of observing water molecules in a more tightly bound phase, since the probability of exchange between phases during the  $T_1$  measurement is increased. A few measurements were made at 14 MHz to investigate any frequency dependence on  $T_1$  behaviour, but the signal/noise ratio was so poor that no conclusive results were obtained. The existence of two-phase  $T_2$  behaviour is indicated by the decrease in  $T_2$  with increasing temperature in *Figure 1*, but the actual observation and measurement of the short  $T_2$  phase was beyond the limits of detection of the spectrometer.

*Variation of  $T_1$  and  $T_2$  with water content*

The water content range investigated, from about 3% regain (weight of water sorbed/weight of dry cellulose) to 25% regain, covered the range of the sorption isotherms for most of the samples. An isotherm was obtained for each sample, although samples conditioned at 100% r.h. (over pure water) were susceptible to capillary condensation at any slight drop in temperature. As a result, the last point in the isotherms has a doubtful position with respect to water content. The isotherm at 298K for Whatman CF1 is indicated in *Figure 4*.

*Variation of  $T_1$  with water content.* *Figure 5* shows the variation of  $T_1$  with water content at 298K for each cellulose sample. Whatman CF1 and cotton linters have a higher minimum for  $T_1$  than the woodpulp celluloses Rayweb Q, Raybond P and Hicolour. The cotton and Whatman celluloses are particularly pure grades, whereas the woodpulp celluloses contain some impurities, including amounts of paramagnetic ions (iron, copper and

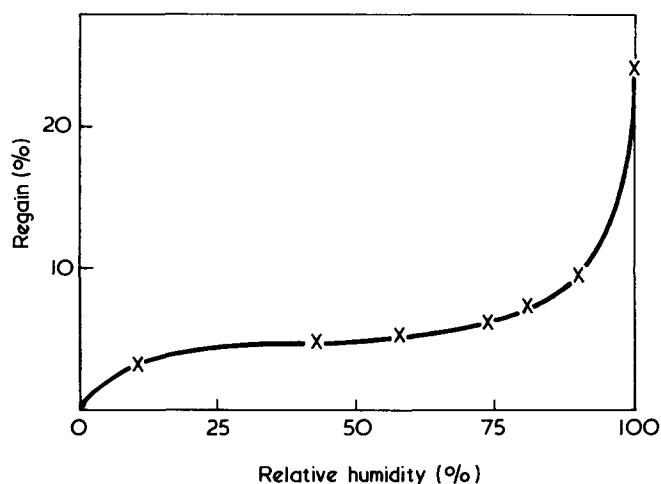


*Figure 4* Sorption isotherm for Whatman CF1 at 298K

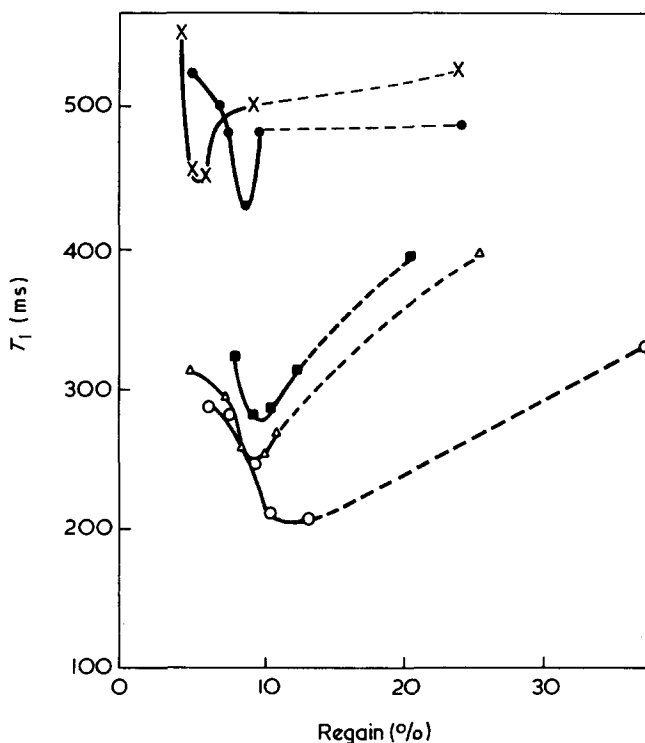


*Figure 5* Variation of  $T_1$  with water content at 298K. x, Whatman CF1; ●, Cotton linters; ■, Raybond P; Δ, Hicolour; ○, Rayweb Q

manganese), which would reduce  $T_1$  values.  $T_1$  is lowest for Rayweb Q, the most impure of the cellulose samples.

$T_1$  falls gradually from high regain values towards the minimum, but a very sharp change occurs over a 1% or 2% regain range through the minimum. Rayweb Q shows a much wider minimum. In this region, the motion of the sorbed water molecules is greatly attenuated and rapidly approaches that characteristic of solids.

If the  $T_1$  behaviour is now considered from near dryness to beyond the  $T_1$  minimum, one can envisage the first water molecules to be sorbed with long correlation times at very strong binding sites. Presumably this occurs at hydroxyl groups on the anhydroglucose ring. Chain motion will be attenuated because of interchain hydrogen

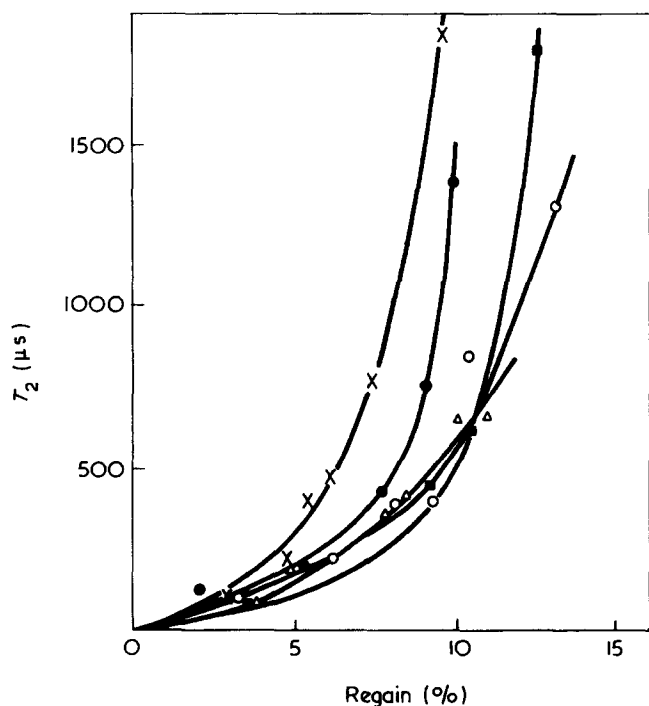


Figure 6 Variation of  $T_2$  with water content at 298 K. x, Whatman CF1; ●, Cotton linters; ■, Raybond P; △, Hicolour; ○, Rayweb Q

bonding. At regain values characterized by the  $T_1$  minimum, the average correlation time of the sorbed molecules is shortened considerably. This indicates that some form of secondary sorption is occurring, with less binding energy. The primary sorption sites could be considered almost full at this regain value. Chain motion will be increased because water molecules diffuse through the system and break intermolecular hydrogen bonds. The result is a greater mobility throughout the whole system and a gradual increase in  $T_1$  towards the higher regain values. Note that the  $T_1$  values are still much smaller than the value for bulk water.

There is correlation between position of the  $T_1$  minimum with respect to regain value and the water accessibility of the celluloses. A highly crystalline cellulose is likely to have low water accessibility. In the less accessible celluloses there will be a smaller number of primary sorption sites, so that these are soon filled and secondary sorption begins at lower regain values. The  $T_1$  minimum will therefore occur at lower regain values. This is indicated by the results in Figure 5, where the  $T_1$  minimum for Whatman CF1 (32% water accessibility) occurs at about 5.5% regain, whereas the minimum for Rayweb Q (77% water accessibility) occurs at about 12% regain.

*Variation of  $T_2$  with water content.* Figure 6 shows the fall in  $T_2$  as water content decreases.  $T_2$  does not reach zero at zero regain, but possesses a value of about 7  $\mu\text{s}$ , characteristic of dry cellulose. This approximates to the 'rigid-lattice' value. The  $T_2$  values give an 'average' indication of the state of motion in the system. At higher regains the  $T_2$  values are characteristic of more mobile water, while  $T_2$  values at low regains characterize water molecules in primary sorption sites. The curves converge in the region of primary sorption. Secondary sorption occurs sooner in Whatman CF1 and cotton linters, as

indicated by the steeper rise in  $T_2$  for these samples. This behaviour would be expected from a consideration of the  $T_1$  results. Figure 7 shows a plot for cotton linters at higher regions, indicating a lessening in the gradient of the curve at higher water contents. The curve should level-off at  $T_2$  values near bulk water. The Figure also shows that the steepest part of the curve occurs at a regain value similar to that at which the  $T_1$  minimum was observed in Figure 5. The greatest rate of attenuation in molecular motion is evidently taking place at this point.

#### Relaxation behaviour of the cellulose chains

Relaxation times characterizing the molecular motion of protons contained in the cellulose chains were also obtained. Figure 8 shows that the  $T_1$  values obtained for chain protons were identical with those obtained for

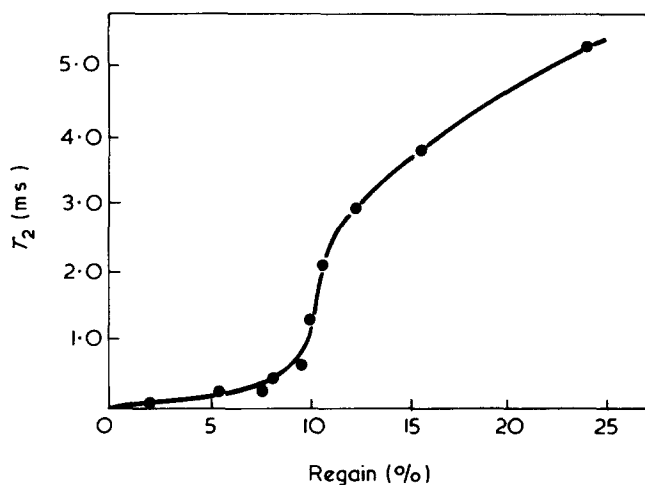


Figure 7 Variation of  $T_2$  with water content for cotton linters at 298 K

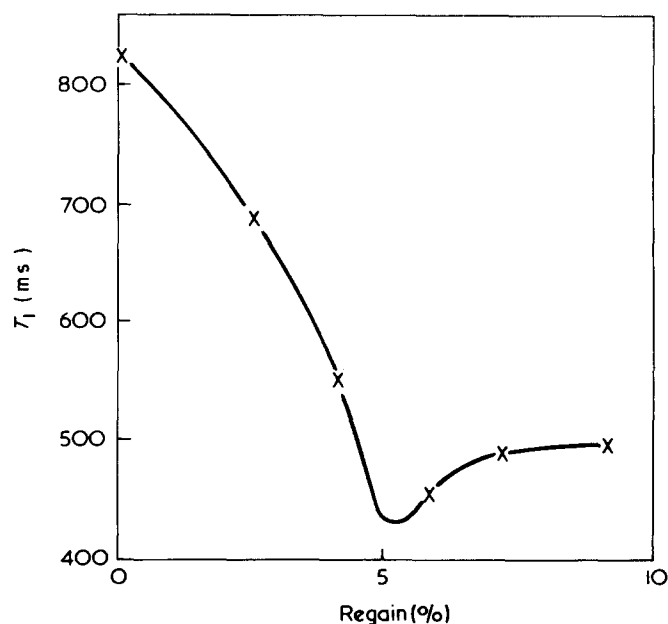


Figure 8 Water content dependence of  $T_1$  for cellulose chains in Whatman CF1 at 298 K

sorbed water within experimental error. This behaviour indicates the operation of a spin-diffusion mechanism<sup>17, 19</sup>. Protons contained in the cellulose chains cannot attain equilibrium magnetization efficiently by direct interaction with the lattice, so that the energy has to be dissipated via 'safety valves' or points along the chain where more efficient contact with the lattice is possible. Such points are probably the hydroxyl groups around the anhydroglucose ring, where the proton in the hydroxyl group is able to exchange with protons in nearby water molecules. The result is that the apparent  $T_1$  relaxation time of the protons in the cellulose chains is the same as that for the sorbed water.

#### *Correlation of results with sorption theories*

Various sorption theories have involved discussion on the first 'monolayer' of sorbed water or first 'hydrate', at a characteristic regain value. This value has also been ascribed to the condition when most of the primary sorption sites have been filled. This discontinuity in the sorption behaviour has been observed in several physical measurements, including X-ray density, refractive index, entropy and n.m.r. second moments. At a particular regain value, a maximum in density and increase in order of the system occur. Second moment results obtained by Forslind<sup>16</sup> indicated a reduction in mobility of the cellulose-water system over the regain range characteristic of the completion of the first 'monolayer'. The second moments were obtained from that part of the n.m.r. absorption curve characterizing cellulose chain motion, and it would appear that some ordering or attenuation is occurring among the chains over this range.

The pulsed n.m.r. results for  $T_1$  and  $T_2$  indicate a similar discontinuity in sorption behaviour. This is reflected in the sharp  $T_1$  minimum and steep gradient of the  $T_2$  curve over the same regain range. The actual regain range over which the discontinuity occurs will depend on the water accessibility (crystallinity) of the cellulose. A sorption mechanism is proposed here which involves chain attenuation at a certain stage in the sorption process. Initial sorption occurs at hydroxyl groups around the anhydroglucose ring and at the glycosidic oxygen atoms. These first-sorbed water molecules will replace relatively weak inter-chain hydrogen bonds with stronger water-chain hydrogen bonds, but as more water diffuses into the system, and the chains move further apart, water bridges may be formed. Primary and secondary bridges, consisting of 1 or 2 water molecules, link between the chains and tend to attenuate the chain motion. This is the point at which the discontinuities occur in the X-ray, entropy and second moment measurements. Further diffusion of water molecules through the system will eventually break the bridges and chain motion will increase. Although the mobility of the whole system has now increased considerably, sorption of water will continue until capillary water appears and the system reaches a saturated condition.

#### CONCLUSION

The heterogeneity of the cellulose surface produced a marked effect on the relaxation curves, and it was shown that for highly crystalline celluloses large numbers of high energy binding sites are present. The sorbed water on cellulose is very strongly bound, as shown by the position of the  $T_1$  minimum and the absence of freezing until about 243K. The position and shape of the  $T_1$  minimum can be related to the nature of the cellulose surface, in particular the crystalline content. Over a small regain range, strong binding of water occurs, as indicated by a sharp minimum in  $T_1$  with rapid rise to values approaching that for dry cellulose. The relaxation results can be related to a sorption theory in which, at a certain regain, water bridges are formed between cellulose chains, so as to cause a restriction in chain motion and an increase in the diffusional correlation time of the sorbed water molecule. This qualitative picture of water sorption onto cellulose facilitates correlation with observed physical measurements, although more work is required on well-characterized celluloses before a complete picture of the sorption mechanism can be presented.

#### ACKNOWLEDGEMENTS

The author should like to thank Dr D. W. Jones, Dr P. J. Anderson and Mr J. Clifford for useful discussions during the preparation of this manuscript and Mr E. G. Smith and Mr M. L. Bellis for technical assistance.

#### REFERENCES

- 1 Morton, I. E. and Hearle, J. W. S. 'Physical Properties of Textile Fibres', Butterworths, London, 1962
- 2 Child, T. F. *PhD Thesis*, Univ. of Bradford, 1971
- 3 Stokes, R. H. and Robinson, R. A. *Ind. Eng. Chem.* 1949, **41**, 2013
- 4 Carr, H. Y. and Purcell, E. M. *Phys. Rev.* 1954, **94**, 630
- 5 Meiboom, S. and Gill, D. *Rev. Sci. Instr.* 1960, **31**, 508
- 6 Bloembergen, N., Purcell, E. and Pound, R. *Phys. Rev.* 1948, **73**, 679
- 7 Kubo, R. and Tomita, K. *J. Phys. Soc., Japan* 1954, **9**, 888
- 8 Resing, H. A., Thompson, J. and Krebs, J. *J. Phys. Chem.* 1964, **68**, 679
- 9 Clifford, J. and Lecchini, S. *SCI Monogr. No. 25*, Society of Chemical Industry, London, 1966, p 174
- 10 Zimmerman, J. and Brittin, W. *J. Phys. Chem.* 1957, **61**, 1328
- 11 Resing, H. A. *Adv. Mol. Relaxation Processes* 1968, **1**, 119
- 12 Zimmerman, J. and Lasater, J. *J. Phys. Chem.* 1958, **62**, 1157
- 13 Woessner, D. *J. Chem. Phys.* 1963, **39**, 2783
- 14 Sasaki, M., Kawai, T., Hirai, A., Hashi, T. and Odajima, A. *J. Phys. Soc. Japan* 1960, **15**, 1652
- 15 Stejskal, E. O. *Rev. Sci. Instr.* 1963, **34**, 971
- 16 Forslind, E. *Report No. AD 420477*, Clearing House for Federal Scientific and Technical Information, US Dept of Commerce, 1966
- 17 Abragam, A. 'The principles of nuclear magnetism', Oxford University Press, Oxford, 1961, p 382
- 18 McCall, D. and Douglas, D. *Polymer* 1963, **4**, 433
- 19 Anderson, J. and Slichter, W. *J. Phys. Chem.* 1965, **69**, 3099

# Solution properties of poly(trimethylsiloxanotitanoxanes) (titanium oxide trimethylsilyloxides)

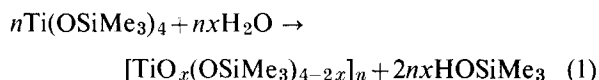
D. E. G. Jones\* and J. W. Lorimer†

Department of Chemistry, University of Western Ontario,  
London 72, Ontario, Canada  
(Received 29 September 1971)

To obtain more information on the structure of the polymeric hydrolysis products of  $\text{Ti}(\text{OSiMe}_3)_4$ , (the titanium oxide trimethylsilyloxides), measurements were made of the degrees of polymerization and hydrolysis, sedimentation, viscosity, specific volume, refractive index increment and turbidity of five hydrolysis products in cyclohexane solution. Refractive increments and turbidities were also measured for two products in carbon tetrachloride, benzene, chlorobenzene and bromobenzene. A self-consistent description of the properties of these polymers is based on repeating units containing a cube-shaped  $\text{Ti}_8\text{O}_{12}$  structure. These units undergo condensation to give two types of chains having one and two bridging oxygens, respectively, between successive repeating units. Evidence for this model is obtained from the interdependence of degrees of polymerization and hydrolysis, from sedimentation, and from the dependence of turbidity on the refractive index of the solvent. Specific volumes calculated from the model agree well with experiment. Refractions for the Ti-O bonds in metalloxane chains, calculated from the refractive index increments, indicate that formation of longer chains causes an increase in refraction towards the value for  $\text{TiO}_2$ . The distribution of metalloxane links and the high polydispersity of the products presumably arise from labile intermolecular condensation during hydrolysis.

## INTRODUCTION

The metal oxide alkoxides, or poly(alkylmetalloxanes)<sup>1</sup>, and the metal oxide trialkylsilyloxides, or poly(trialkylsiloxanometalloxanes)<sup>1</sup>, form two classes of metal-organic condensation-coordination polymers that contain metalloxane chains and organic or organosilicon groups joined by oxygen atoms to metal atoms. These polymers can be considered to arise from the modification of the three-dimensional structures of metal oxides by the introduction of organic or organosilicon groups<sup>1</sup>, and are produced by controlled hydrolysis of metal alkoxides or metal trialkylsilyloxides; for example,



The parent metal alkoxides and metal trialkylsilyloxides themselves frequently exhibit low degrees of polymerization, which are ascribed to coordinate bonding and to

changes in the coordination number of the metal atom<sup>1</sup>. The metal oxide alkoxides and trialkylsilyloxides have higher degrees of polymerization. The metal-oxygen bonds, apart from those in the metalloxane chains, are hydrolysed less readily in the oxide trialkylsilyloxides, and coordinate bonds are generally less important than in the oxide alkoxides.

Several metal oxide trialkylsilyloxides have been prepared<sup>1-7</sup>, and of these, the oxide trimethylsilyloxides<sup>2-5</sup> of  $\text{Ti}^{\text{IV}}$ ,  $\text{Zr}^{\text{IV}}$ ,  $\text{Ta}^{\text{V}}$  and  $\text{Al}^{\text{III}}$  and the oxide triethylsilyloxides<sup>6,7</sup> of  $\text{Ti}^{\text{IV}}$  have been investigated in some detail. Molecular weights and analytical data have been obtained for products of various nominal degrees of hydrolysis, and have been combined with theoretical relations<sup>8,9</sup> between the true degrees of hydrolysis and polymerization to deduce information about the structure of the polymers.

Many more metal oxide alkoxides have been prepared and investigated<sup>1,9</sup> in solution in the corresponding alcohol, but isolation of the products has not been necessary, in general, since the alcohol is the only other product of hydrolysis, and hydrolysis appears to be complete. Isolation of the oxide trialkylsilyloxides is necessary, since self-condensation of the trialkylsilanol produced on hydrolysis (see equation (1)) produces water,

\* Present address: Department of Chemistry, University of Otago, Dunedin, New Zealand.

† Part of this work was carried out while on sabbatical leave at the Department of Chemistry, University of Southampton, Southampton SO9 5NH, UK.

and thereby causes further hydrolysis. The soluble titanium oxide trimethylsilyloxides<sup>2</sup> have number-average molecular weights as high as 4000, and appeared to be promising polymers for further investigation. In this paper, measurements of a number of properties of solutions of these polymers in organic solvents are reported, and the correlation of these properties with possible polymeric structures is discussed.

## EXPERIMENTAL

Rigorous exclusion of water is necessary during measurements on the metal oxide trialkylsilyloxides. Preparation and distillations were made under dry nitrogen. Cells for optical measurements were cleaned with detergent, then rinsed, dried and stored over silica gel. All other apparatus was dried either at 150°C or in a stream of dry nitrogen, after cleaning and rinsing with double-distilled water and ethanol, and was stored in a controlled atmosphere dry box filled with dry nitrogen. Filling and transfer operations for physical measurements were also carried out in the dry box.

Titanium in titanium trimethylsilyloxide<sup>10</sup> and titanium and silicon in the oxide trimethylsilyloxides<sup>11</sup> were determined by gravimetric analysis.

Cyclohexane (BDH reagent) was percolated over silica gel to remove fluorescent impurities<sup>12</sup>, then dried azeotropically by fractional distillation in the presence of ethanol. Dioxane (Fisher reagent) was fractionally distilled over freshly cut sodium. Other solvents were Fisher spectroscopic grade, and were dried over phosphorus pentoxide before distillation. Sucrose (BDH organic analytical standard) and other solids were dried carefully.

Hexamethyldisiloxane was converted to trimethylfluorosilane in H<sub>2</sub>SO<sub>4</sub> and ammonium fluoride, neutralized and hydrolysed to give trimethylsilanol (b.p. 98.0–99.0°C at 740 mmHg<sup>13</sup>). Titanium (IV) isopropoxide was prepared from TiCl<sub>4</sub> and isopropanol by the ammonia method<sup>14</sup>, and distilled at a bath temperature of 90–100°C at 0.1 mmHg; % Ti = 16.9 (found), 16.9 [calc. for Ti(OPr<sup>i</sup>)<sub>4</sub>]. Titanium (IV) trimethylsilyloxide was prepared by interchanging freshly prepared trimethylsilanol and freshly distilled titanium (IV) isopropoxide in refluxing benzene<sup>11</sup>. The alcohol liberated was removed by azeotropic distillation at 71.9°C, and the liquid product was purified by distillation at a bath temperature of 60°C and 0.1 mmHg; % Ti = 11.9 (found), 11.9 (calc.); % Si = 27.6 (found), 27.7 [calc. for Ti(OSiMe<sub>3</sub>)<sub>4</sub>]. Vapour phase chromatography (fluorosilicone column at 40°C) showed one peak only, and only one type of methyl group was found in the 60 MHz n.m.r. spectrum in CS<sub>2</sub>. No paramagnetism was detected (Gouy balance, field 0.2 T), and there was no u.v./visible absorption spectrum beyond 350 nm. The density was  $\rho_{25}^{25} = 0.8951$ , the refractive index,  $n_{546}^{25} = 1.4321$ , and the degree of polymerization was 1.002, standard error 0.017 (by cryoscopy; see below).

Titanium oxide trimethylsilyloxides were prepared<sup>2</sup> by reacting titanium trimethylsilyloxide in dioxane (2 mol/kg of solvent) with water ( $h$  mol/mol of metal atoms) at 60°C. Volatile components<sup>2</sup> were removed under reduced pressure, finally at 160°C, 0.1 mmHg. Analytical data are given in Table 1, where the number-average degree of hydrolysis,  $\bar{x}_n$ , is found from  $w_{Si}/M_{Si} = (4 - 2\bar{x}_n)w_{Ti}/M_{Ti}$ , with  $w_j$ ,  $M_j$  the mass fraction and atomic weight of

element  $j$ . No paramagnetism was detected for the solid product with  $h = 1.5$ , and there was no u.v./visible absorption spectrum beyond 350 nm for the products with  $h = 0.1$  and 1.5 in cyclohexane. The surface tension of a solution of the  $h = 1.5$  product, 0.06 g cm<sup>-3</sup> in cyclohexane, was only 5% smaller than that of the pure solvent.

Cryoscopic molecular weights were measured using a vacuum-jacketed cell fitted with a Beckmann thermometer. The apparatus was filled with dry nitrogen, and freezing points of cyclohexane and solutions in cyclohexane of fluorene (for calibration) and of two different concentrations of each titanium oxide trimethylsilyloxide were measured from temperature–time cooling curves. Molecular weights were reproducible to about 5% for solutions of concentrations of about 2 g/kg of solvent. A special determination of the molecular weight of Ti(OSiMe<sub>3</sub>)<sub>4</sub> in cyclohexane was made using an apparatus similar to that described by Vofsi and Katchalsky<sup>15</sup>. The vacuum-jacketed cell was fitted with a polytetrafluoroethylene (PTFE)-coated magnetic stirring bar and a calibrated thermistor. Samples were transferred to previously weighed, thin-walled glass bulbs, sealed off, weighed and transferred to the cell, which contained a weighed amount of solvent and was filled with dry nitrogen. The bulb was broken by a glass plunger, and the cell was cooled at a constant rate by immersion in a stirred water bath controlled thermostatically at 3°C using a Whirlpool thermoelectric cooler. Temperature–time cooling curves were obtained on a chart recorder.

Sedimentation of the products with  $h = 1.0$  and 1.5 was studied in cyclohexane solution in a single sector cell in a Spinco Model E ultracentrifuge. The phase-plate schlieren patterns were recorded photographically at a rotor speed of 700 s<sup>-1</sup> and at 20°C. Density gradient ultracentrifugation<sup>16</sup> was attempted under the same conditions in a capillary synthetic boundary cell, and using cyclohexane–carbon tetrachloride and cyclohexane–hexachloroethane to form the density gradients. No sharp sedimentation patterns were obtained, which is to be expected with polymers of low molecular weight<sup>16</sup>.

Viscosities of solutions of several titanium oxide trimethylsilyloxides were measured at various concentrations in cyclohexane at 25.0 ± 0.1°C in a Cannon–Ubbelohde semi-micro dilution viscometer<sup>17</sup>. The openings of the viscometer were protected by drying tubes, and the efflux time for the solvent was about 400 s. The difference between the dynamic viscosity  $\eta$  and the kinematic viscosity  $\eta/\rho$ , where  $\rho$  is the density of the solution, was negligible in all cases.

Densities were measured at 25.0 ± 0.01°C in a pycnometer of the Shedlovsky–Brown type<sup>18</sup>, of volume 25 cm<sup>3</sup>, and calibrated with air-free water. For a solution of density  $\rho$  containing a solute of concentration  $c_s$  in mass per unit volume, the apparent specific volume of the solute is  $\bar{v}_s = 1/\rho_1 - (\rho/\rho_1 - 1)/c_s$ , where  $\rho_1$  is the density of the pure solvent.

Refractive index differences were measured with a Brice–Phoenix differential refractometer<sup>19</sup> calibrated at 25.0 ± 0.1°C and 546 nm with aqueous sucrose solutions. The specific refractive index increment of the solute is  $\nu = (n - n_1)/c_s$  where  $n, n_1$  are the refractive indices of the solution and solvent, respectively.

Light-scattering measurements were made using a Brice–Phoenix Model 1000D photometer, and a galvanometer.

Table 1 Titanium oxide trimethylsilyloxides

Mol H <sub>2</sub> O/mol Ti, <i>h</i>	wt.% Ti	wt.% Si	Degree of hydrolysis, $\bar{x}_n$	Molecular weight, $\bar{M}_n$	Degree of polymerization, $\bar{n}_n$	Molecular weights of components		Mass fraction of A, $w_A$	$\bar{M}_n^*$
						$\bar{M}_n^A$	$\bar{M}_n^B$		
0.1	29.9	17.4	1.50	1300	8.10	1440	1240	0.37	1310
0.3	30.4	17.0	1.52	1430	9.09	1600	1460	0.36	1510
0.5	31.5	16.5	1.55	1910	12.5	2140	1740	0.39	1900
1.0	33.6	15.7	1.60	2710	18.7	3120	2450	0.42	2730
1.5	35.0	14.6	1.64	3620	26.3	4300	3310	0.40	3710

meter of sensitivity  $0.35 \mu\text{A m}^{-1}$ . The working equations given with the instrument were corrected as described by Tomimatsu and Palmer<sup>20</sup>. The optical alignment was checked by measuring at 546 nm the angular scattering envelope between scattering angles of  $\theta = -45$  to  $-135^\circ$  at  $5^\circ$  intervals for both cyclohexane and a solution of fluorescein<sup>21</sup>,  $1 \mu\text{g cm}^{-3}$  in  $0.1 \text{ mol dm}^{-3}$  aqueous sodium acetate. A cylindrical scattering cell (Brice-Phoenix C-101) fitted with a standard taper cone and cap was used. The normalized scattering envelopes  $I_\theta \sin\theta/I_{90}(1+\cos^2\theta)$ , where  $I_\theta$  is the intensity at a scattering angle  $\theta$ , had the values 0.996, standard error 0.009, for cyclohexane, and 1.002, standard error 0.009, for fluorescein.

For measurements of turbidity, solutions were filtered into the scattering cell through a sintered glass ultrafine disc (Corning Glass 36060) mounted in a specially designed filter to which a slight pressure of inert gas could be applied. This operation was conducted in the dry box. The cell was semi-octagonal (Brice-Phoenix D-103), and was fitted with a standard taper cone and cap. After transferring the cell to the photometer, the solution was examined for dust particles with a travelling microscope, and its dissymmetry  $Z = I_{45}/I_{135}$  was measured. If  $0.95 < Z < 1.05$ , the turbidity and depolarization were measured at  $22 \pm 2^\circ\text{C}$ . In general the depolarization was identical for the solvent and for solutions of the titanium oxide trimethylsilyloxides. The cell was then returned to the dry box, and the concentration of the solution was determined by evaporation of an aliquot or by differential refractometry. The accuracy of the photometer was tested by measuring the turbidity of aqueous sucrose solutions<sup>22</sup> in the above manner. It was found necessary to add activated charcoal to these solutions before filtration in order to achieve satisfactory dissymmetries. For four concentrations of sucrose, the average difference of the measured turbidities and those given by Maron and Lou<sup>22</sup> was 0.8%.

Numerical least-square analyses (including estimated standard deviations) were carried out by standard methods<sup>23</sup>, using computer programs written in Fortran IV.

## RESULTS AND DISCUSSION

### Degree of polymerization

$\text{Ti}(\text{OSiMe}_3)_4$  is clearly monomeric in dilute cyclohexane solution. Previous measurements<sup>11</sup> by ebullioscopy gave a degree of polymerization of about 1.2, which we believe may have been due to the volatility of the solute in boiling cyclohexane. The magnetic susceptibility and u.v./visible spectrum confirm that titanium is in

the expected  $d^0$  configuration in both  $\text{Ti}(\text{OSiMe}_3)_4$  and the oxide trimethylsilyloxides.

Table 1 lists the number-average molecular weights  $\bar{M}_n$  determined from cryoscopy in cyclohexane. The values of  $\bar{x}_n$  can be used in the formula for the oxide trimethylsilyloxides to calculate formula weights (equation (1)), and these can be combined with  $\bar{M}_n$  to give the number-average degrees of polymerization,  $\bar{n}_n$ . No degrees of polymerization less than eight were found, in agreement with previous work<sup>2</sup>. The results of Table 1 fit the equation  $1/\bar{n}_n = a + b\bar{x}_n$ , with  $a = 1.050$ ,  $\sigma(a) = 0.093$ ,  $b = -0.621$ ,  $\sigma(b) = 0.059$ , where  $\sigma(x)$  is the standard error in  $x$  estimated from least squares analysis. These values are in good agreement with those of Bradley and Demas<sup>2,9</sup>:  $a = 1.027$ ,  $\sigma(a) = 0.023$ ,  $b = -0.603$ ,  $\sigma(b) = 0.018$ . The general theory of regular polymer series<sup>9</sup> gives linear relations between  $1/\bar{n}_n$  and  $\bar{x}_n$  for four different models. The model which best fits the data for the titanium oxide trimethylsilyloxides is model I, which consists<sup>9</sup> of a mixture of two types of homogeneous, linear or branched, polydisperse chains. Quantitative treatment<sup>9</sup> of the data in Table 1 indicates the two chains A and B consist of repeating units containing eight Ti and twelve O atoms. The repeating units of A-type chains are linked by single oxygen bridges between Ti atoms, while the repeating units of B-type chains are linked by two oxygen bridges. Type A chains contain a mole fraction  $\alpha = 0.44$ ,  $\sigma(\alpha) = 0.11$  of the metal atoms, and comprise a mole fraction  $\beta = 0.39$ ,  $\sigma(\beta) = 0.15$  of the molecules, in good agreement with the values found previously<sup>9</sup>:  $\alpha = 0.38$ ,  $\sigma(\alpha) = 0.04^*$ ,  $\beta = 0.34$ ,  $\sigma(\beta) = 0.06$ . These latter values are based on a larger number of samples, and will be used in further calculations.

The average degrees of polymerization of the two chains are given by<sup>9</sup>:

$$\bar{n}_A = \alpha \bar{n}_n / \beta, \quad \bar{n}_B = (1 - \alpha) \bar{n}_n / (1 - \beta) \quad (2)$$

and the calculated values of the corresponding number-average molecular weights  $\bar{M}_n^A$  and  $\bar{M}_n^B$  are listed in Table 1. The mass fraction of chains A,  $w_A$ , and the quantity:

$$\bar{M}_n^* = w_A \bar{M}_n^A + w_B \bar{M}_n^B \quad (3)$$

which arises in the theory of light-scattering<sup>24</sup> can be found readily and are also listed in Table 1.

Figure 1 gives possible structures<sup>2</sup> for the octameric unit and the chains of types A and B. These structures are

\* The standard error  $\sigma(x)$  involves  $\sigma(a/b)$ , given by  $\sigma(a/b)^2/(a/b)^2 = \sigma(a)^2/a^2 + \sigma(b)^2/b^2 - 2\rho(a,b)\sigma(a)\sigma(b)/ab$  and not the expression given elsewhere<sup>9</sup>, where  $\rho(a,b)$  is the correlation coefficient for the parameters  $a$  and  $b$ .

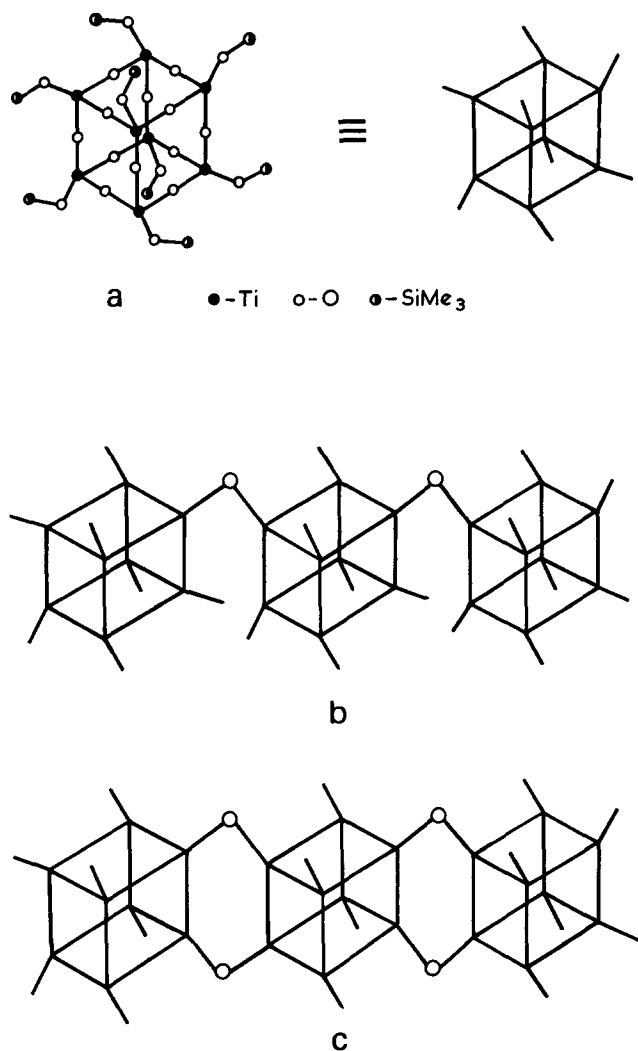


Figure 1 Possible structures of titanium oxide trimethylsilyloxides. (a)  $\text{Ti}_8\text{O}_{12}(\text{OSiMe}_3)_8$ ; (b) type A chains,  $[\text{Ti}_8\text{O}_{12}\text{O}_{1-1/n}(\text{OX})_{6+2/n}]_n$  ( $n=1, 2, \dots$ ); (c) type B chains,  $[\text{Ti}_8\text{O}_{12}\text{O}_{2-2/n}(\text{OX})_{4+4/n}]_n$  ( $n=1, 2, \dots$ ). Chains with  $n=3$  are shown in each case.  $\text{X}=\text{SiMe}_3$

analogous to structures inferred from X-ray data for some crystalline organosilsesquioxanes<sup>25</sup>, for which dodecameric molecules are also found. For the titanium oxide trimethylsilyloxides, sesquioxane structures would have the general formula  $[\text{TiO}_{3/2}\text{OSiMe}_3]_n$ ,  $n=8, 10, 12, \dots$ , and for these cyclic structures, the degree of hydrolysis would be independent of the degree of polymerization<sup>9</sup>, in contradiction to experiment. Dodecameric and larger cyclic structures cannot be ruled out, but repeating units linked by bridging oxygens must also be present. We consider the interpretation based on octameric units only to be the most probable.

The structures of all the metal oxide trimethylsilyloxides appear to be determined mainly by the coordination of the metal atom, by steric effects, and by the nature of the alkyl groups. Thus,  $[\text{Al}(\text{OSiMe}_3)_3]_2$  retains its dimeric structure in the hydrolysis products<sup>5</sup>. The effect of a 4-coordinate Al atom makes simple dimeric units joined by one or two bridging oxygens the most probable polymeric structures<sup>5</sup>. Simple structures containing one or two metal atoms per repeating unit are found in the  $\text{Ta}^{\text{V}}$  oxide trimethylsilyloxides<sup>4, 9</sup>, but octa-

meric repeating units mixed with simpler structures arise in the  $\text{Zr}^{\text{IV}}$  oxide trimethylsilyloxides<sup>3, 9</sup>. It is noteworthy that  $\text{Ti}(\text{OSiMe}_3)_4$  is a liquid at room temperature, while  $\text{Ti}(\text{OSiEt}_3)_4$  is a solid. We believe that this difference is due mainly to a higher entropy for  $\text{Ti}(\text{OSiMe}_3)_4$ , which arises from a tendency towards octahedral coordination of the Ti atoms, as found for some titanium alkoxides in solution<sup>26</sup>. The bulkier  $\text{OSiEt}_3$  groups shield the Ti atoms more effectively from interactions with oxygens on neighbouring molecules, and as a result, the titanium oxide triethylsilyloxides have simple structures, except perhaps at high degrees of hydrolysis<sup>6, 7</sup>.

The values of  $\alpha$  and  $\beta$  are not very different, and equation (2) indicates that  $\bar{n}_A = \bar{n}_B$  if  $\alpha = \beta$ . This may be the case in dioxane solution in the presence of  $\text{H}_2\text{O}$ , trimethylsilanol and hexamethyldisiloxane, and would imply an equilibrium mechanism<sup>9</sup> for the formation of the two types of polymer chain analogous to the mechanisms proposed for the rearrangement of titanium oxide triethylsilyloxides<sup>7</sup> and titanium oxide ethoxides<sup>9</sup>. Isolation of the products would upset the equilibrium slightly, so that  $\alpha \neq \beta$ . Similar rearrangements are well known in silicone polymers<sup>27</sup>. The mechanism proposed<sup>28</sup> for the formation of the organosilsesquioxanes may also apply to the titanium oxide trimethylsilyloxides, but no direct evidence is available.

#### Sedimentation

Schlieren photographs revealed two rapidly spreading peaks during the first ten minutes of experiments at a rotor speed of  $700 \text{ s}^{-1}$ . The component with the greater rate of sedimentation appeared as a shoulder on the main pattern, and the area under the peak estimated for this component was roughly half that for the other component. Further attempts at a better resolution were unsuccessful. These observations suggest that the component with the higher molecular weight has about half the mass fraction of the other component, in agreement with the data in Table 1, provided that the refractive index increments of the two components are roughly equal.

#### Viscosity

Table 2 gives the limiting viscosity number  $[\eta]$  and the interaction constant  $k$  in:

$$(\eta - \eta_1)/\eta_1 c_s = [\eta] + k[\eta]^2 c_s \quad (4)$$

where  $\eta$ ,  $\eta_1$  are the viscosities of solution and solvent, respectively, and  $c_s$  is the concentration of the solute. The variation of  $[\eta]$  with  $\bar{M}_n$  may be expressed as (see Figure 2):

$$[\eta] = a_0 + a_1 \bar{M}_n \quad (5)$$

with  $a_0 = 50$ ,  $\sigma(a_0) = 14 \text{ cm}^3 \text{ g}^{-1}$ ,  $a_1 = 0.033$ ,  $\sigma(a_1) = 0.006 \text{ cm}^3 \text{ mol}^{-1}$ , or as:

$$[\eta] = K \bar{M}_n^a \quad (6)$$

with  $K = 1.5$ ,  $\sigma(K) = 0.6 \text{ cm}^3 \text{ g}^{-1}$ ,  $a = 0.58$ ,  $\sigma(a) = 0.12$ . The dependence of  $[\eta]$  on molecular weight has been studied at low degrees of polymerization for several linear polymers. For example,  $K = 0.092 \text{ cm}^3 \text{ g}^{-1}$ ,  $a = 0.5$  for linear polystyrene<sup>29</sup> in toluene-methanol at  $25^\circ\text{C}$ . The Kirkwood-Riseman theory of viscosity of linear polymers

Table 2 Properties of titanium oxide trimethylsilyloxides in cyclohexane at 25°C

Mol H <sub>2</sub> O/mol Ti, <i>h</i>	Limiting viscosity number × 10 <sup>-2</sup> (cm <sup>3</sup> g <sup>-1</sup> )		Viscosity interaction constant		Apparent specific volume, $\bar{v}_s$ (cm <sup>3</sup> g <sup>-1</sup> )	Specific refractive index increment, $\nu$ (cm <sup>3</sup> g <sup>-1</sup> )
	$[\eta]$	$\sigma[\eta]$	<i>k</i>	$\sigma(k)$		
0.1	0.973	0.016	0.524	0.030	0.78	0.107
0.3	—	—	—	—	—	0.114
0.5	1.033	0.005	0.087	0.002	0.85	0.120
1.0	1.479	0.012	0.017	0.001	0.89	0.134
1.5	1.676	0.028	0.025	0.002	0.92	0.138

has been extended to short chains by Rossi and Perico<sup>30</sup>, who have found that  $[\eta]$  is linear in  $M$  except at very low degrees of polymerization, and over a short range of chain lengths departures from linearity will not be apparent. Despite the rigidity of the titanium oxide trimethylsilyloxides which might be expected from the presence of the metaloxane bonds, these products appear to exhibit viscosity behaviour similar to other linear chain molecules.

The interaction constants for the  $h=0.1, 0.5$  and  $1.5$  products follow the empirical equation  $1/k = a_2 + a_3 \bar{M}_n$ , with  $a_2 = -19.7$ ,  $\sigma(a_2) = 0.5$ ,  $a_3 = 0.0165$ ,  $\sigma(a_3) = 0.0002$  g<sup>-1</sup> mol (see Figure 2). The value of  $k$  for the  $h=1.0$  product is inexplicably low. Both intermolecular and hydrodynamic interactions affect the magnitude of the interaction constant<sup>31</sup>. Both  $k$  and the second virial coefficient (see below) decrease rapidly with increasing molecular weight, and it appears, therefore, that the magnitude of  $k$  is determined mainly by intermolecular interactions.

#### Apparent specific volume

The apparent specific volumes  $\bar{v}_s$  in Table 2 and Figure 3 vary with molecular weight as:

$$\bar{v}_s = \bar{v}_\infty + \bar{v}_0/\bar{M}_n \quad (7)$$

with  $\bar{v}_\infty = 0.996$ ,  $\sigma(\bar{v}_\infty) = 0.003$  cm<sup>3</sup>g<sup>-1</sup>,  $\bar{v}_0 = -281$ ,  $\sigma(\bar{v}_0) = 6$  cm<sup>3</sup>mol<sup>-1</sup>. No dependence on concentration was found. If the molar volume is an additive function of the degree of polymerization<sup>24</sup>,  $\bar{v}_0 = V_0 - M_0 V_r / M_r$ ,  $\bar{v}_\infty = V_r / M_r$ , where  $M_0$ ,  $V_0$  are the molecular weight and molar volume of the end-groups, respectively, and  $M_r$ ,  $V_r$  are the corresponding values for the repeating unit. If an octameric molecule is taken as the end group,  $M_0 = 1289$ , and  $M_r$  is the weighted average of repeating units with one and two oxygen bridges. Thus,  $M_r = 1028$ , giving  $V_0 = 1003$ ,  $\sigma(V_0) = 6$  cm<sup>3</sup>mol<sup>-1</sup>, and  $V_r = 1024$ ,  $\sigma(V_r) = 3$  cm<sup>3</sup>mol<sup>-1</sup>. Figure 1 suggests that  $V_0$  and  $V_r$  should be roughly the same. Repulsions between OSiMe<sub>3</sub> groups on adjacent repeating units, or the assumption that there are no solvation effects in cyclohexane (see below) may account for the observed difference.

The molar volume of Ti(OSiMe<sub>3</sub>)<sub>4</sub> is 452 cm<sup>3</sup>mol<sup>-1</sup> at 25°C. The radius  $R$  of a sphere with the same molecular volume (corrected for close packing), and centred on a Ti atom, is given by  $R^3 = V/4(2)^{1/2}N_A$ , where  $V$  is the molar volume, and  $N_A$  Avogadro's constant, giving  $R = 0.510$  nm. The Ti-O bond distance is about 0.20 nm, from X-ray data<sup>32</sup> on a titanium oxide ethoxide. This value is close to values given<sup>33</sup> for octahedral Ti<sup>IV</sup>-O distances (0.206 nm) and ionic Ti<sup>IV</sup>-O distances (0.196 nm in rutile), so that a contribution of 0.31 nm to  $R$  should be allowed for an OSiMe<sub>3</sub> group. The various bond lengths, corrected for

electronegativity<sup>33</sup>, are 0.177 nm for O-Si, 0.189 nm for Si-C and 0.106 nm for C-H, and the covalent radius<sup>33</sup> of H is 0.032 nm. If we assume that the bond angles at O, Si and C are tetrahedral, the total length of the OSiMe<sub>3</sub> group, projected in the direction of a Ti-O bond, is 0.315 nm, in very good agreement with the value obtained

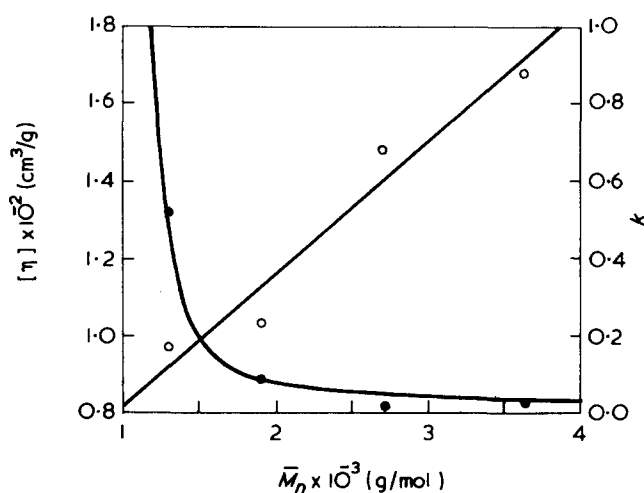


Figure 2 Limiting viscosity number,  $[\eta]$ , as a function of number-average molecular weight,  $\bar{M}_n$ .  $\circ$ , viscosity interaction constant,  $k$ , as a function of number-average molecular weight;  $\bullet$ , the lines are drawn using the least-squares parameters given in the text

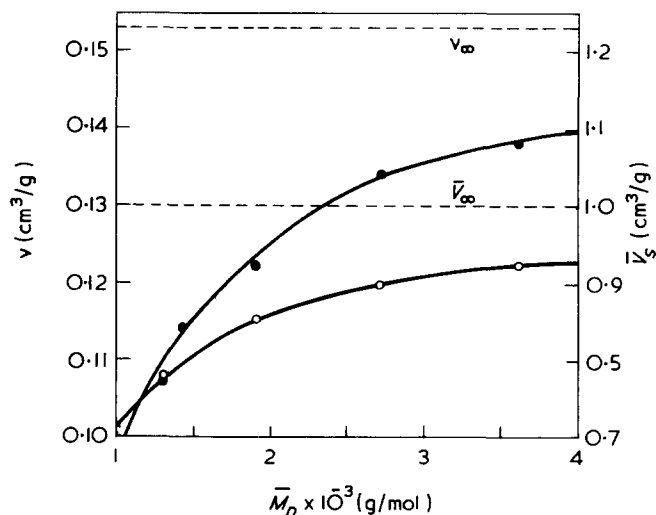


Figure 3 Apparent specific volume,  $\bar{v}_s$ , as a function of number-average molecular weight.  $\circ$ , Refractive index increment,  $\nu$ , as a function of number-average molecular weight;  $\bullet$ , the lines are drawn using the least-squares parameters given in the text



from the equivalent radius. For a cubic octamer with Ti-O-Ti bond angles of  $180^\circ$  (Figure 1), the radius swept out by the centres of the Ti atoms is 0.346 nm. The equivalent radius of the octamer is thus  $0.346 + 0.315 = 0.661$  nm, giving a molar volume of  $984 \text{ cm}^3 \text{ mol}^{-1}$ , a value that is only 2% lower than the observed value of  $V_0$ . A value of  $R = 0.665$  nm would give exact agreement. We conclude that the model based on octameric repeating units is entirely consistent with the dependence of the specific volume on molecular weight.

#### Specific refractive index increment

Table 2 and Figure 3 give values of the specific refractive index increment,  $\nu$ , for each polymer in cyclohexane, while Table 4 gives values in other solvents for the  $n = 0.5$  and  $1.5$  products. No dependence of  $\nu$  on concentration was found. In cyclohexane, the results follow the equation:

$$\nu = \nu_\infty + \nu_0/\bar{M}_n \quad (8)$$

with  $\nu_\infty = 0.156$ ,  $\sigma(\nu_\infty) = 0.002 \text{ cm}^3 \text{ g}^{-1}$ ,  $\nu_0 = -62.0$ ,  $\sigma(\nu_0) = 3.4 \text{ cm}^3 \text{ mol}^{-1}$ . For the other solvents,  $\nu_\infty$  has been estimated from equation (8) and the data in Table 3.

The general theory of refractive index increments gives, for Lorenz-Lorentz refractions<sup>24</sup>,

$$\nu_0 = (n_1^2 + 2)^2 [a_0 - \bar{v}_0(n_1^2 - 1)/(n_1^2 + 2)]/6n_1 \quad (9)$$

$$\nu_\infty = (n_1^2 + 2)^2 [R_\infty - \bar{v}_\infty(n_1^2 - 1)/(n_1^2 + 2)]/6n_1 \quad (10)$$

where  $n_1$  is the refractive index of the solvent,  $\bar{v}_0$  and  $\bar{v}_\infty$  have been defined in equation (7), and

$$a_0 = R_0 - M_0 R_r / M_r \quad (11)$$

$$R_\infty = R_r / M_r \quad (12)$$

where  $R_0$ ,  $R_r$  are the molar refractions of the end groups and repeating units, respectively. For a mixture of two polymers A and B the average values:

$$\bar{v}_\infty = w_A \nu_\infty^A + w_B \nu_\infty^B \quad (13)$$

$$\bar{v}_0 = \beta \nu_0^A + (1 - \beta) \nu_0^B \quad (14)$$

apply<sup>24</sup>. The refraction of  $\text{Ti}(\text{OSiMe}_3)_4$  is  $116.17 \text{ cm}^3 \text{ mol}^{-1}$  at  $25^\circ\text{C}$ , and bond refractions<sup>27</sup> give a refraction of  $24.46 \text{ cm}^3 \text{ mol}^{-1}$  for each  $\text{OSiMe}_3$  group. The Ti-O bond refraction is therefore  $4.58 \text{ cm}^3 \text{ mol}^{-1}$ , within the range given for various titanium-oxygen compounds by Takatani<sup>34</sup>. The experimental data in cyclohexane and equations (9) to (14) give  $R_\infty = 0.3376 \text{ cm}^3 \text{ g}^{-1}$ ,  $a_0 = -94.7 \text{ cm}^3 \text{ mol}^{-1}$ , and  $R_r = 347 \text{ cm}^3 \text{ mol}^{-1}$ .  $R_0 = 341 \text{ cm}^3 \text{ mol}^{-1}$ . For a cube-shaped octameric unit, there are eight  $\text{OSiMe}_3$  groups, eight 'normal' Ti-O bonds, and 24 Ti-O bonds in the cube, giving an average bond refraction of  $4.5 \text{ cm}^3 \text{ mol}^{-1}$  for a Ti-O bond in the  $\text{Ti}_8\text{O}_{12}$  cube. A similar calculation using  $R_r$  gives  $8.2 \text{ cm}^3 \text{ mol}^{-1}$  for the Ti-O bond refraction, which includes bridging Ti-O bonds in the average. For comparison, the principal refractive indices of  $\text{TiO}_2$  (rutile) are<sup>35</sup>  $n_e = 2.6505$ ,  $n_o = 2.9467$  at 546 nm, and the molar volume is<sup>35</sup>  $18.80 \text{ cm}^3 \text{ mol}^{-1}$ . If we take the mean refractive index as<sup>36</sup>  $(n_e^2 n_o^2)^{1/3}$ , the refraction is  $25.91 \text{ cm}^3 \text{ mol}^{-1}$ . Evidently, introduction of bridging oxygen atoms between repeating units increases the average Ti-O bond polarizability towards that found in  $\text{TiO}_2$  and is therefore an indication of greater ionic character in the bond.

Refractive index increments in solvents other than cyclohexane decrease rapidly with the refractive index of the solvent. According to equations (9) and (10),  $6n_1 \nu / (n_1^2 + 2)^2$  should be linear in  $(n_1^2 - 1)/(n_1^2 + 2)$  if  $\bar{v}_0$  and  $\bar{v}_\infty$  are independent of the nature of the solvent. Figure 4 shows clearly that this is not the case. The values of  $\nu_\infty$  and  $\bar{v}_\infty$  in cyclohexane can be used to calculate the specific refraction  $R_\infty$  for the solid polymer from equation (10), and values of  $\bar{v}_\infty$  in other solvents can then be calculated from the specific refractive index increments. These values are given in Table 4. Except for benzene, the values in all the solvents are probably the same within experimental error, and give  $\bar{v} = 0$  at a refractive index  $n_1$  of about 1.66.

#### Light-scattering

Values of  $Hc_s/\tau$  as a function of polymer concentration,  $c_s$ , are given in Figures 5 and 6, where  $H = 32\pi^3 n_1^2 \nu^2 / 3\lambda^4 N_A$ ,  $\lambda$  is the wavelength of light in vacuum (here, 546 nm),  $N_A$  is Avogadro's constant, and  $\tau$  is the turbidity in excess of the turbidity of the solvent. In Table 3, the observed molecular weights,  $M_{\text{obs}}$ , and second virial coefficients,  $A_{\text{obs}}$ , found from:

$$Hc_s/\tau = 1/M_{\text{obs}} + 2A_{\text{obs}}c_s \quad (15)$$

are given. For a single polydisperse solute, the true weight average molecular weight  $\bar{M}_w$  and second virial coefficient  $A_2$  are<sup>24</sup>:

$$\bar{M}_w = (\nu/\nu_\infty)^2 (M_{\text{obs}} - \bar{M}_n) + \bar{M}_n \quad (16)$$

$$A_2 = A_{\text{obs}} (\nu M_{\text{obs}} / \nu_\infty \bar{M}_w)^2 / [1 + (2\nu_0/\nu_\infty \bar{M}_w)(1 + \nu_0/2\nu_\infty \bar{M}_w)] \quad (17)$$

and these values are also given in Table 3. In Table 4, molecular weights in other solvents are given, along with the values of  $\bar{M}_w$  computed from equation (16). These

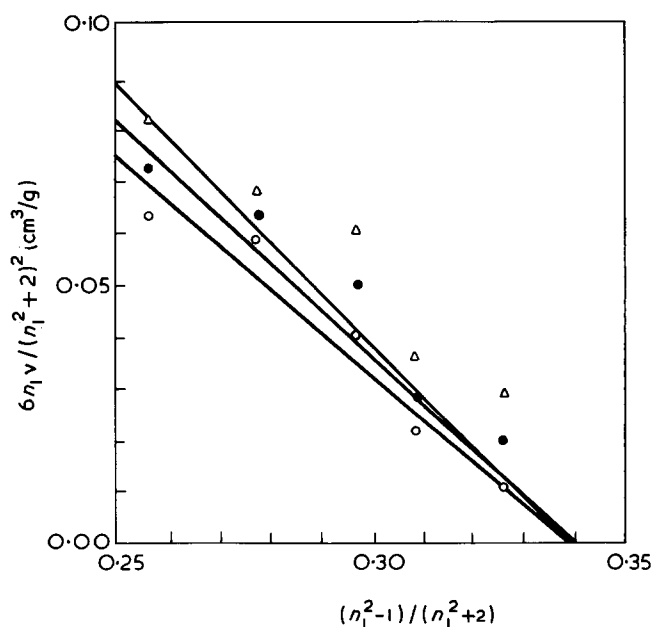


Figure 4  $6n_1 \nu / (n_1^2 + 2)^2$  as a function of  $(n_1^2 - 1)/(n_1^2 + 2)$ ;  $h = 0.5$ ,  $\circ$ ;  $h = 1.5$ ,  $\bullet$ ; infinite molecular weight,  $\triangle$ . The lines are drawn using equations (8) to (10) and the parameters found in cyclohexane

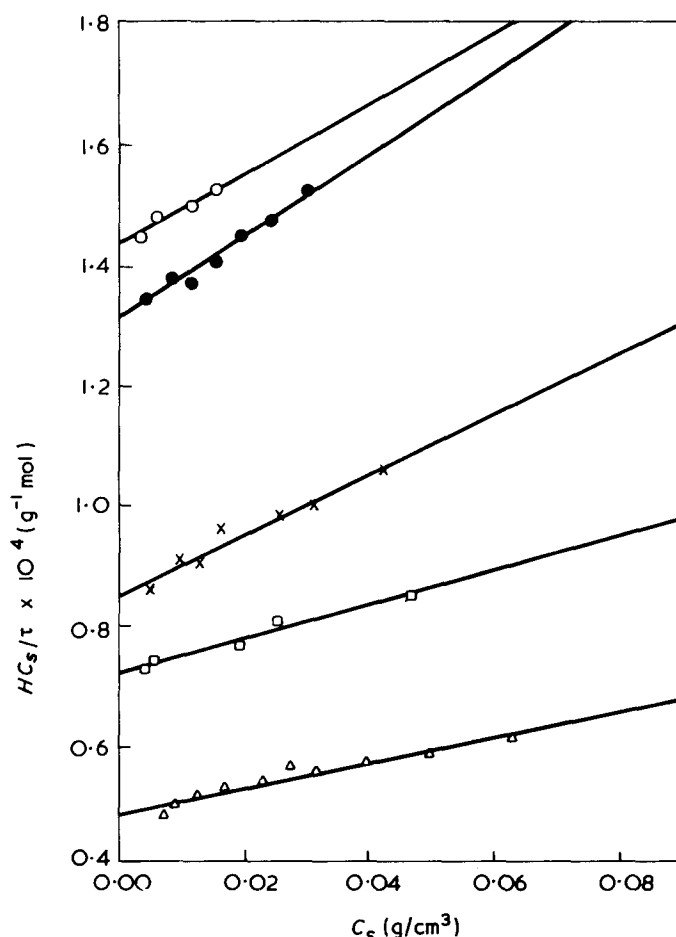


Figure 5  $Hc_s/\tau$  as a function of polymer concentration,  $c_s$ , for cyclohexane solutions of hydrolysis products with  $h = \text{mol water added/mol Ti}$ .  $\circ$ ,  $h=0.1$ ;  $\bullet$ ,  $h=0.3$ ;  $\times$ ,  $h=0.5$ ;  $\square$ ,  $h=1.0$ ;  $\triangle$ ,  $h=1.5$

Table 3 Molecular weights and virial coefficients of titanium trimethylsilyloxides in cyclohexane at 25°C

Mol H <sub>2</sub> O/mol Ti, $h$	Molecular weights $\times 10^{-3} (\text{g mol}^{-1})$			Second virial coefficients $\times 10^4 (\text{cm}^3 \text{g}^{-2} \text{mol})$		
	$M_{\text{obs}}$	$\sigma(M_{\text{obs}})$	$M_w$	$A_{\text{obs}}$	$\sigma(A_{\text{obs}})$	$A_2$
0.1	6.89	0.02	3.97	3.2	0.4	5.8
0.3	7.62	0.06	4.74	3.3	0.3	3.9
0.5	11.8	0.2	7.96	2.4	0.2	2.7
1.0	13.9	0.1	11.0	1.4	0.1	1.5
1.5	20.8	0.3	17.1	1.0	0.1	1.1

Table 4 Properties of titanium oxide trimethylsilyloxides in various solvents at 25°C

Mol H <sub>2</sub> O/mol Ti, $h$	Solvent	$n_1$ (546 nm)	Specific refractive index increment, 546 nm ( $\text{cm}^3 \text{g}^{-1}$ )		Apparent specific volume, $\bar{v}_\infty$ ( $\text{cm}^3 \text{g}^{-1}$ )	Molecular weights $\times 10^{-4} (\text{g}^{-1} \text{mol}^{-1})$		
			$\bar{v}$	$\nu_\infty$		$M_{\text{obs}}$	$\sigma(M_{\text{obs}})$	$\bar{M}_w$ (eqn. (16))
0.5	Cyclohexane	1.4265	0.122	0.156	0.996	1.18	0.02	0.796
	CCl <sub>4</sub>	1.4677	0.116	0.135	0.97	1.24	0.03	0.967
	Benzene	1.5056	0.083	0.125	0.83	1.71	0.28	0.860
	Chlorobenzene	1.5293	0.045	0.077	0.97	8.14	0.12	2.55
	Bromobenzene	1.5641	0.022	0.064	0.94	28.7	5.2	2.85
1.5	Cyclohexane	1.4265	0.138	0.156	0.996	2.08	0.03	1.71
	CCl <sub>4</sub>	1.4677	0.125	0.135	0.97	2.59	0.05	2.27
	Benzene	1.5056	0.103	0.125	0.83	3.07	0.38	2.20
	Chlorobenzene	1.5293	0.060	0.077	0.97	9.35	0.23	5.79
	Bromobenzene	1.5641	0.042	0.064	0.94	22.1	0.3	9.54

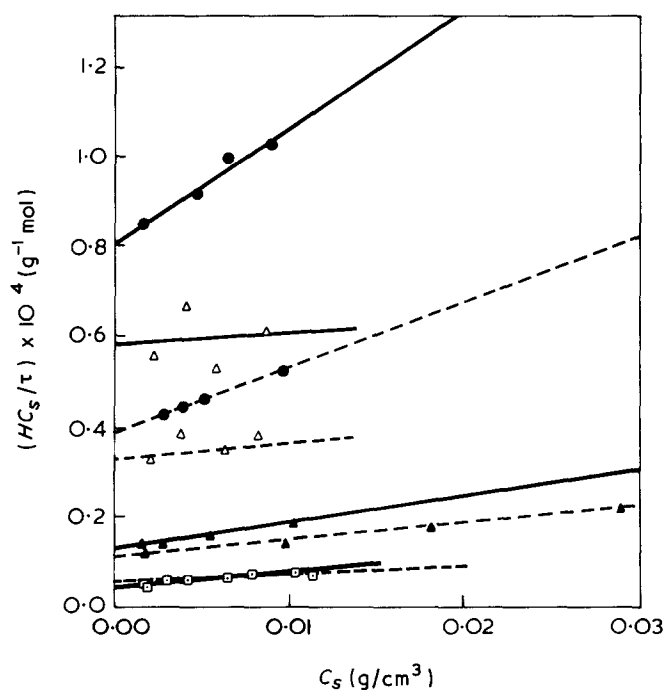


Figure 6  $Hc_s/\tau$  as a function of polymer concentration,  $c_s$ , for solutions of hydrolysis products  $h=0.5$  (—) and  $h=1.5$  (---) in various solvents;  $\bullet$ , CCl<sub>4</sub>;  $\triangle$ , benzene;  $\blacktriangle$ , chlorobenzene;  $\square$ , bromobenzene

values vary markedly with the refractive index of the solvent, and provide confirmatory evidence that more than one component is present<sup>24</sup>. For a mixture of two components,  $M_{\text{obs}}$  is given by<sup>24</sup>:

$$\bar{v}^2 M_{\text{obs}} = \bar{v}^2 \bar{M}_n^* + \bar{v}_\infty^2 (\bar{M}_w - \bar{M}_n^*) + 2(P - R)(\nu_\infty^A - \nu_\infty^B) \bar{v}_\infty + (Q - S)(\nu_\infty^A - \nu_\infty^B)^2 + 2R(\nu_\infty^A - \nu_\infty^B) \bar{v} + S(\nu_\infty^A - \nu_\infty^B)^2 \quad (18)$$

where  $\bar{M}_n^*$  has been defined in equation (3), and the parameters of heterogeneity are<sup>24</sup>:

$$\left. \begin{aligned} P &= w_A w_B (\bar{M}_w^A - \bar{M}_w^B) \\ Q &= w_A w_B (w_B \bar{M}_w^A - w_A \bar{M}_w^B) \\ R &= w_A w_B (\bar{M}_n^A - \bar{M}_n^B) \\ S &= w_A w_B (w_B \bar{M}_n^A + w_A \bar{M}_n^B) \end{aligned} \right\} \quad (19)$$

Values of  $\bar{M}_n^*$  (Table 1),  $R$  and  $S$  can be calculated readily, but  $\bar{M}_w^A$  and  $\bar{M}_w^B$  are separately unknown. The procedure<sup>24</sup> of expressing  $M_{\text{obs}}$  as a quadratic function of  $1/\bar{v}$  is too sensitive to errors in  $M_{\text{obs}}$ , and gives unreasonable values

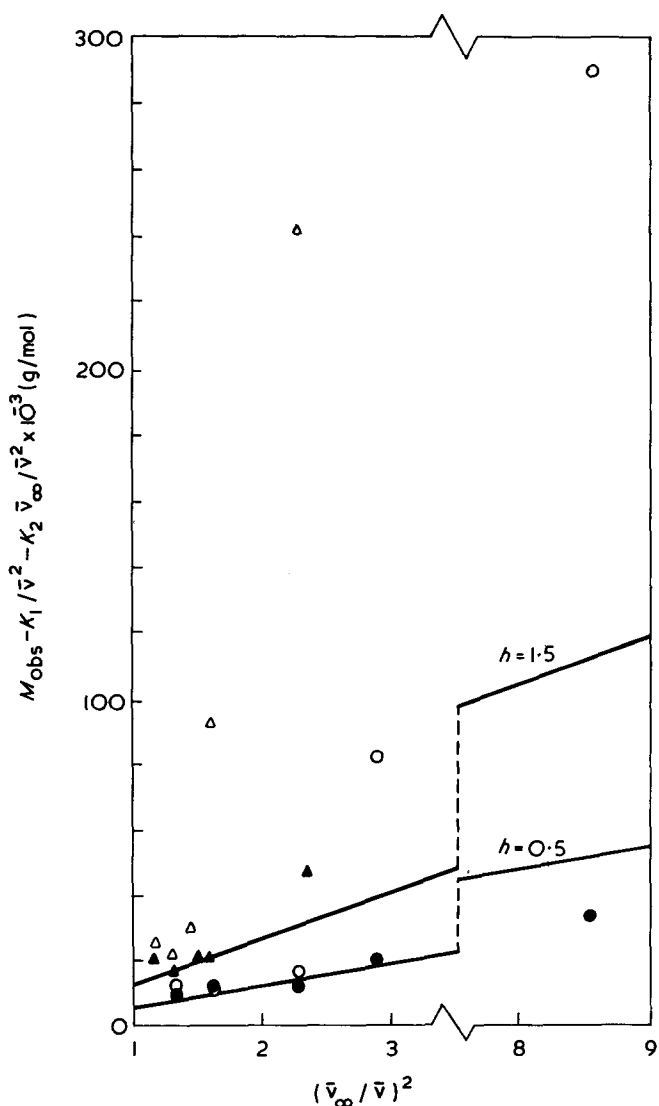


Figure 7  $M_{\text{obs}} - K_1/\bar{v}^2 - K_2\bar{v}_\infty/\bar{v}^2$  as a function of  $(\bar{v}_\infty/\bar{v})^2$ .  $\circ, \bullet$ ,  $h=0.5$  product;  $\Delta, \blacktriangle$ ,  $h=1.5$  product. Straight lines calculated from results in cyclohexane and equation (20). Open symbols:  $K_1=K_2=0$  (i.e., ordinate gives  $M_{\text{obs}}$ ). Solid symbols:  $K_1, K_2$  from Table 5

for  $\bar{M}_w$ . An alternative procedure is to note that  $\bar{M}_n$  and  $\bar{M}_n^*$  are nearly equal (Table 1), and that the correction terms for heterogeneity in equation (18) will be negligible in solvents with refractive indices far from the refractive index of the pure polymer<sup>24</sup>. The value of  $\bar{v}_\infty/\bar{v}$  approaches unity for solvents with refractive indices far from that of the polymer, and the convergence of  $M_{\text{obs}}$  in Figure 7 (open symbols) to a limit at small values of  $\bar{v}_\infty/\bar{v}$  indicates thus that the values of  $\bar{M}_w$  in cyclohexane calculated using equation (16) and listed in Table 3 are approximately correct. The terms containing  $R$  and those containing  $S$  in equation (18) cancel roughly and we expect that<sup>24</sup>  $\nu^A - \nu^B$  and  $\nu_\infty^A - \nu_\infty^B$  are nearly independent of the refractive index of the solvent. With these approximations, equation (18) becomes:

$$\bar{v}^2(M_{\text{obs}} - \bar{M}_n^*) - \bar{v}_\infty^2(\bar{M}_w - \bar{M}_n^*) = K_1 + K_2\bar{v}_\infty \quad (20)$$

where  $K_1 \approx Q(\nu_\infty^A - \nu_\infty^B)^2$ ,  $K_2 \approx 2P(\nu_\infty^A - \nu_\infty^B)$ . Least-square values for  $K_1$  and  $K_2$  are given in Table 5 for the products  $h=0.5$  and  $h=1.5$ . In Figure 7, the general agreement of values of  $M_{\text{obs}} - K_1/\bar{v}^2 - K_2\bar{v}_\infty/\bar{v}^2$  (solid symbols) with the straight lines  $\bar{M}_n^* + (\bar{M}_w - \bar{M}_n^*)(\bar{v}_\infty/\bar{v})^2$  indicates that

Table 5 Parameters of heterogeneity

Parameter	Mol H <sub>2</sub> O/mol Ti, $h$	
	0.5	1.5
$K_1$ , equation (20) (cm <sup>6</sup> g <sup>-1</sup> mol <sup>-1</sup> )	215	519
$\sigma(K_1)$ (cm <sup>6</sup> g <sup>-1</sup> mol <sup>-1</sup> )	32	44
$K_2$ , equation (20) (cm <sup>3</sup> mol <sup>-1</sup> )	-1430	-3310
$\sigma(K_2)$ (cm <sup>3</sup> mol <sup>-1</sup> )	270	380
Molecular weights $\times 10^{-3}$ :		
$\bar{M}_w^A$	14	30
$\bar{M}_w^B$	4.0	8.4
$\nu_\infty^A - \nu_\infty^B$ (cm <sup>3</sup> g <sup>-1</sup> )	-0.30	-0.32

equation (20) is a reasonable approximation. If  $\bar{M}_w^A/\bar{M}_w$  and  $\bar{M}_w^B/\bar{M}_w$  are the same for both products, the ratio of the two values of either  $K_1$  or  $K_2$  should be equal to 2.3 (the ratio of the two values of  $\bar{M}_w$ ), since  $w_A$  is very nearly constant (see Table 1). The ratios from Table 5 are 2.3,  $\sigma=0.2$  for  $K_1$  and 2.4,  $\sigma=0.2$  for  $K_2$ . The ratio  $K_1/K_2$  in cm<sup>3</sup>g<sup>-1</sup> is 0.30,  $\sigma=0.02$  for  $h=0.5$  and 0.31,  $\sigma=0.01$  for  $h=1.5$ , indicating that  $\bar{M}_w^A/\bar{M}_w^B$  is the same for each product.

Since  $K_2^2/4K_1 = P^2/Q$  is independent of  $\nu_\infty^A$  and  $\nu_\infty^B$ , values of this ratio can be used with equation (19), the values of  $w_A$  from Table 1, and the equation  $\bar{M}_w = w_A\bar{M}_w^A + w_B\bar{M}_w^B$  to calculate  $\bar{M}_w^A, \bar{M}_w^B$  and  $\nu_\infty^A - \nu_\infty^B$ . A quadratic equation is obtained for  $\bar{M}_w^A$ , and the solution is chosen that makes  $\bar{M}_w^A > \bar{M}_w^B$ . Values obtained by this method are given in Table 5. The uncertainties in the molecular weights are large, and difficult to estimate, but high weight-average molecular weights of one component seem to occur, possibly as a result of intermolecular condensation processes during hydrolysis, as discussed above. The values of  $\nu_\infty^A - \nu_\infty^B$  are abnormally large, and difficult to reconcile with the evidence from ultracentrifugation, where the refractive index increments for each component seem to be very similar. In addition, estimates of  $\nu_\infty^A - \nu_\infty^B$  based on the models in Figure 1 and on bond refractions give values about ten times smaller than those in Table 5. A recalculation of all the data for the  $h=0.5$  product, using a model consisting of a mixture of octamers with heterogeneous chains<sup>9</sup> containing both singly- and doubly-bridged octameric units, gave even more unreasonable values for  $\nu_\infty^A - \nu_\infty^B$ . However, light-scattering molecular weights are not very precise in solvents in which the refractive index increment is very small, and we do not consider that the values in Table 5 are more than order-of-magnitude estimates.

The second virial coefficients given in Table 3 depend on molecular weight as  $A_2\bar{M}_w = 2.0$ ,  $\sigma = 0.3$  cm<sup>3</sup>g<sup>-1</sup>. We postulate that, for  $h=0.1$ , interactions between Ti and O atoms on different molecules are large. As the degree of polymerization increases, these intermolecular interactions are decreased by removal of OSiMe<sub>3</sub> groups, and by the increase in intramolecular interactions, namely formation of titanoxane bonds and interactions between neighbouring octameric units. The virial coefficients therefore decrease rapidly with increasing molecular weight.

The model on which the above discussion is based gives, on the whole, a self-consistent picture of the properties of the titanium oxide trimethylsilyloxides in solution. A successful fractionation procedure would probably enable further progress to be made in the elucidation of the structure of these polymers and others of the same generic type.

## ACKNOWLEDGEMENTS

The research for this paper was supported, in part, by the Defence Research Board of Canada and the National Research Council of Canada. We wish to thank Professor D. C. Bradley for initiating this project and for his continued interest, Dr C. Prevedorou-Demas for advice on preparative and analytical techniques, Mrs C. MacDonald for assistance with some of the measurements, and Dr P. C. Fitz-James for making the ultracentrifuge available. We also wish to thank the Government of Ontario for a graduate fellowship to D. E. G. J. and the British Council for a travel grant to J. W. L.

## REFERENCES

- 1 Bradley, D. C. in 'Inorganic Polymers', (F. G. A. Stone and W. A. G. Graham, Eds), Academic Press, New York, London, 1962, Ch 7
- 2 Bradley, D. C. and Prevedorou-Demas, C. *Can. J. Chem.* 1963, **41**, 629
- 3 Bradley, D. C. and Prevedorou-Demas, C. *J. Chem. Soc.* 1964, p 1580
- 4 Bradley, D. C. and Prevedorou-Demas, C. *J. Chem. Soc. (A)* 1966, p 1139
- 5 Bradley, D. C., Lorimer, J. W. and Prevedorou-Demas, C. *Can. J. Chem.* 1971, **49**, 2310
- 6 Bradley, D. C. and Prevedorou-Demas, C. *J. Chem. Soc. (A)* 1967, p 43
- 7 Bradley, D. C., Lorimer, J. W. and Prevedorou-Demas, C. *Can. J. Chem.* 1969, **47**, 4113
- 8 Bradley, D. C. and Holloway, H. *Can. J. Chem.* 1962, **40**, 1176
- 9 Lorimer, J. W. and Jones, D. E. G. *Can. J. Chem.* 1969, **47**, 4101
- 10 Bradley, D. C., Gaze, R. and Wardlaw, W. *J. Chem. Soc.* 1955, p 721
- 11 Bradley, D. C. and Thomas, I. M. *J. Chem. Soc.* 1959, p 3404
- 12 Coumou, D. J., Mackor, E. L. and Hijmans, J. *Trans. Faraday Soc.* 1964, **60**, 1539
- 13 Sommer, L. H., Pietrusza, E. W. and Whitmore, F. C. *J. Am. Chem. Soc.* 1946, **68**, 2282
- 14 Bradley, D. C., Mehrotra, R. C. and Wardlaw, W. *J. Chem. Soc.* 1952, p 2027
- 15 Vofsi, D. and Katchalsky, A. *J. Polym. Sci.* 1957, **26**, 127
- 16 Hermans, J. J. and Ende, H. A. in 'Polymer Reviews' (B. Ke, Ed.), Interscience, New York, 1964, Vol 6
- 17 Cannon, M. R., Manning, R. E. and Bell, J. D. *Anal. Chem.* 1960, **32**, 355
- 18 Shedlovsky, T. and Brown, A. S. *J. Am. Chem. Soc.* 1934, **56**, 1066
- 19 Brice, B. A. and Halwer, M. *J. Opt. Soc. Am.* 1951, **41**, 1033
- 20 Tomimatsu, Y. and Palmer, K. J. *J. Polym. Sci.* 1959, **35**, 549
- 21 Huque, M. M., Jaworzyn, J. and Goring, D. A. I. *J. Polym. Sci.* 1959, **39**, 9
- 22 Maron, S. H. and Lou, R. L. *J. Phys. Chem.* 1955, **59**, 231
- 23 Hamilton, W. C. 'Statistics in Physical Science', Ronald Press, New York, 1964, Sections 4-1, 5-6
- 24 Lorimer, J. W. and Jones, D. E. G. *Polymer* 1972, **13**, 52
- 25 Barry, A. J., Daudt, W. H., Domenicone, J. J. and Gilkey, J. W. *J. Am. Chem. Soc.* 1955, **77**, 4248
- 26 Martin, R. L. and Winter, G. *J. Chem. Soc.* 1961, p 2947
- 27 Barry, A. J. and Beck, H. N., in 'Inorganic Polymers' (F. G. A. Stone and W. A. G. Graham, Eds), Academic Press, New York, London, 1962, pp 223, 264
- 28 Sprung, M. M. and Guenther, F. O. *J. Polym. Sci.* 1958, **28**, 17
- 29 Rossi, C., Bianchi, U. and Bianchi, E. *Makromol. Chem.* 1960, **41**, 31
- 30 Rossi, C. and Perico, A. *J. Chem. Phys.* 1970, **53**, 1217, 1223
- 31 Frisch, H. L. and Simha, R., in 'Rheology' (F. R. Eirich, Ed.), Academic Press, New York, 1956, Vol I, pp 569-570
- 32 Watenpaugh, K. and Caughlan, C. N. *Chem. Commun.* 1967, p 76
- 33 Pauling, L. 'The Nature of the Chemical Bond', Cornell University Press, Ithaca, 1960, 3rd edn, Sections 7.1, 7.2, 7.9, 13.3, 13.4
- 34 Takatani, T. *Bull. Chem. Soc. Japan* 1957, **30**, 705
- 35 Gmelins Handbuch der anorganischen Chemie, Verlag Chemie, Weinheim, 1951, 8th edn, Syst. no. 41
- 36 Bauer, N., Fajans, K. and Lewin, S. Z., in 'Physical Methods of Organic Chemistry', (A. Weissberger, Ed.), Interscience, New York and London, 1960, 3rd edn, Vol I, part 2, Ch 18, p 1166

# Refractive index increments of polymers in solution:

## 3. Dependence on concentration

J. W. Lorimer

*Department of Chemistry, University of Western Ontario,  
London 72, Ontario, Canada  
(Received 1 November 1971)*

The coefficient  $a_2$  in the empirical equation  $\Delta n/c_s = \nu + a_2 c_s$  for the refractive index increment of a polymer in solution is shown to be:

$$a_2 = (3n_1^2 - 2)\nu^2/2n_1(n_1^2 + 2) - (n_1^2 - 1)(n_1^2 + 2)(\partial\bar{v}_s/\partial c_s)/12n_1$$

where  $n_1$  is the refractive index of the solvent,  $\nu$  is the refractive index increment at infinite dilution,  $\partial\bar{v}_s/\partial c_s$  is the change in partial specific volume with concentration, and Lorenz-Lorentz refractivities have been used. Experimental values of  $a_2$  may be used to obtain  $\partial\bar{v}_s/\partial c_s$ , in favourable cases, and estimates of  $a_2$  itself can be made. The dependence of  $a_2$  on temperature and wavelength can also be found accurately from the above equation.

### INTRODUCTION

The refractive index  $n$  of a solution containing a polymer of concentration  $c_s$  (in mass per unit volume) depends on concentration as:

$$\Delta n/c_s \equiv (n - n_1)/c_s = \nu + a_2 c_s \quad (1)$$

where  $n_1$  is the refractive index of the solvent,  $\nu = (\partial n/\partial c_s)_{c_s=0}$  is the specific refractive index increment at infinite dilution,\* and  $a_2$  depends on wavelength and temperature. Experimental evidence in support of equation (1) has been summarized by Huglin<sup>1,2</sup>. The only deviations from equation (1) that occur appear to be connected with gross structural changes in the solution<sup>2,3</sup>.

The relation of the coefficient  $a_2$  to other optical and thermodynamic properties of the solution has not been investigated. In Part 1 of this series<sup>4</sup>, a general equation for the derivative  $\partial n/\partial c_s$  at any concentration was deduced, based on only two assumptions. The first assumption is that the specific refraction  $R_i$  of a component  $i$  in solution is given by:

$$R_i = f(n_i)v_i = K_i g_i(n_i, u_i) \quad (2)$$

where  $n_i$ ,  $v_i$ ,  $u_i$  are the refractive index, specific volume and molecular parameter<sup>4</sup> for each of the  $q$  pure com-

\* Partial derivatives without subscripts other than  $c_s=0$  indicate differentiation at constant temperature  $T$ , pressure  $P$  and wavelength  $\lambda$ . For derivatives such as  $\partial n/\partial c_i$ ,  $T$ ,  $P$ ,  $\lambda$  and all other concentrations are held constant

ponents of the solution,  $K_i$  is assumed to be independent of temperature and pressure, and  $f(n_i)$  and  $g_i$  are functions which may be empirical, but preferably are obtained from theories of polarizability. The second assumption is that, for the solution (component 1 is the solvent):

$$f(n) = \sum_{i=1}^q \phi_i f(n_i) \quad (3)$$

where  $\phi_i = V_i/V$  is the volume fraction of component  $i$ , defined as the ratio of the volume  $V_i$  of pure component  $i$  to the volume  $V$  of the solution. Additivity of volumes is not assumed. For the purposes of this paper, the Lorenz-Lorentz form of  $f(n_i)$ :

$$f(n_i) = (n_i^2 - 1)/(n_i^2 + 2) \quad (4)$$

with  $g_i = 1$ , is of sufficient accuracy, and the equation for  $\partial n/\partial c_s$  is<sup>4</sup>:

$$\begin{aligned} \partial f(n)/\partial c_s &= [\partial f(n)/\partial n][\partial n/\partial c_s] \\ &= \sum_{i=2}^q \beta_i v_i f(n_i) - \phi_1 \bar{v}_s f(n_1)/(1 - c_s \bar{v}_s) \end{aligned} \quad (5)$$

where  $\beta_i$  is the relative mass fraction of component  $i$  in the polydisperse solute, and  $\bar{v}_s$  is the partial specific of the polydisperse solute.

Equation (5) contains information on the dependence of  $n$  on concentration. In this paper, we express this dependence in the form of equation (1), and calculate an explicit equation for  $a_2$ .

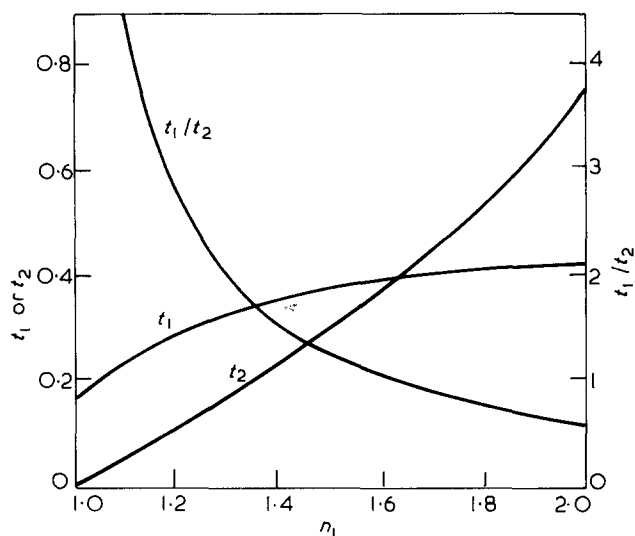


Figure 1 Terms  $t_1 = (3n_1^2 - 2)/2n_1(n_1^2 + 2)$ ,  $t_2 = (n_1^2 - 1)(n_1^2 + 2)/12n_1$  in equation (12) and the ratio  $t_1/t_2$  as a function of  $n_1$ , the refractive index of the solvent

## THEORY AND DISCUSSION

Expansion of  $n$  as a function of  $c_i$  ( $i=2, \dots, q$ ) about

$$c_s = \sum_{i=2}^q c_i = 0$$

in a Taylor series gives:

$$n = n_1 + \sum_{i=2}^q (\partial n / \partial c_i)_{c_i=0} c_i + \frac{1}{2} \sum_{i,j=2}^q (\partial^2 n / \partial c_i \partial c_j)_{c_i=c_j=0} c_i c_j \quad (6)$$

to terms in the square of the concentration, or, since  $\beta_i = c_i/c_s$  and

$$\nu = \sum_{i=2}^q \beta_i (\partial n / \partial c_i)_{c_i=0} \quad (7)$$

then

$$\begin{aligned} \Delta n / c_s &\equiv (n - n_1) / c_s \\ &= \nu + (1/2) \sum_{i,j=2}^q \beta_i \beta_j (\partial^2 n / \partial c_i \partial c_j)_{c_i=c_j=0} c_s \end{aligned} \quad (8)$$

However,

$$\begin{aligned} \partial^2 n / \partial c_s^2 &= \sum_{i,j=2}^q (\partial^2 n / \partial c_i \partial c_j) (\partial c_i / \partial c_s) (\partial c_j / \partial c_s) \\ &= \sum_{i,j=2}^q \beta_i \beta_j (\partial^2 n / \partial c_i \partial c_j) \end{aligned}$$

so that equation (8) becomes:

$$\Delta n / c_s = \nu + (1/2) (\partial^2 n / \partial c_s^2)_{c_s=0} c_s \quad (9)$$

The second derivative in equation (9) is evaluated by finding  $\partial^2 f / \partial c_s^2$  from equation (5), and equating the result to the second derivative of  $f(n) = (n^2 - 1)/(n^2 + 2)$  with respect to  $c_s$ . Since the  $\beta_i$  values are constants for a given polymer sample and<sup>4</sup>:

$$\partial \phi_1 / \partial c_s = \phi_1 \bar{v}_s / (1 - c_s \bar{v}_s) \quad (10)$$

the results of the differentiations give:

$$\begin{aligned} \partial^2 f / \partial c_s^2 &= 6n [\partial^2 n / \partial c_s^2 + \\ &\quad (2 - 3n^2) (\partial n / \partial c_s)^2 / n(n+2)] / (n^2 + 2)^2 \\ &= -\phi_1 f'(n_1) (\partial \bar{v}_s / \partial c_s) / (1 - c_s \bar{v}_s)^2 \end{aligned} \quad (11)$$

In the limit  $c_s \rightarrow 0$ , where  $\phi_1 \rightarrow 1$ ,  $n \rightarrow n_1$ , we have:

$$\begin{aligned} a_2 &= (1/2) (\partial^2 n / \partial c_s^2)_{c_s=0} \\ &= (3n_1^2 - 2) \nu^2 / 2n_1 (n_1^2 + 2) - \\ &\quad (n_1^2 - 1)(n_1^2 + 2) (\partial \bar{v}_s / \partial c_s) / 12n_1 \end{aligned} \quad (12)$$

where the derivative of  $\bar{v}_s$  is evaluated at infinite dilution. For a given mass of solvent, it is found readily that:

$$\partial \bar{v}_s / \partial c_s = (w_1 \bar{v}_1^2 / \bar{v}_1) (\partial^2 \bar{v}^E / \partial w_s^2) \quad (13)$$

where  $\bar{v}_1$  is the partial specific volume of the solvent,  $w_1$  the mass fraction of the solvent, and  $\bar{v}^E$  the excess specific volume of the solution. In the limit  $w_1 \rightarrow 1$ ,

$$\partial \bar{v}_s / \partial c_s = v_i \partial^2 \bar{v}^E / \partial w_s^2 \quad (14)$$

Thus, the derivative in equation (12) is a measure of the curvature of the excess volume-composition curve at  $c_s = 0$ .

Several features of equation (12) should be noted. Equation (12) contains no unknown averages, and will depend on molecular weight through the dependence of  $\nu$  and  $\partial \bar{v}_s / \partial c_s$  on molecular weight<sup>5</sup>. The dependence of  $a_2$  on  $n_1$ , the refractive index of the solvent, is illustrated in Figure 1, where the coefficients  $t_1 = (3n_1^2 - 2)/2n_1(n_1^2 + 2)$  and  $t_2 = (n_1^2 - 1)(n_1^2 + 2)/12n_1$  from equation (12) and the ratio  $t_1/t_2$  are given as functions of  $n_1$ . The ratio  $t_1/t_2$  becomes unity at  $n_1 = 1.628$ , while the coefficient  $t_1$  goes through a shallow maximum at  $n_1 = 2.076$ . For values of  $\nu^2$  and  $\partial \bar{v}_s / \partial c_s$  of the same magnitude, both terms in equation (12) are of importance at all practical values of  $n_1$ . In many cases,  $\partial \bar{v}_s / \partial c_s$  is probably much smaller in magnitude than  $\nu^2$ , so that  $a_2$  will be positive.

Differentiation of equation (12) with respect to temperature gives, at constant pressure  $P$  and wavelength  $\lambda$ ,

$$\begin{aligned} (\partial a_2 / \partial T)_{P, \lambda} &= (3n_1^2 - 2) \nu (\partial \nu / \partial T)_{P, \lambda} / n_1 (n_1^2 + 2) - \\ &\quad (n_1^2 - 1)(n_1^2 + 2) [\partial (\partial \bar{v}_s / \partial T) / \partial c_s]_{P, \lambda} / 12n_1 - \\ &\quad [(3n_1^4 - 12n_1^2 - 4) \nu^2 / (n_1^2 + 2)^2 + (3n_1^4 + n^2 + 2) \times \\ &\quad (\partial \bar{v}_s / \partial c_s) / 6] (\partial n_1 / \partial T)_{P, \lambda} / 2n_1^2 \end{aligned} \quad (15)$$

The derivative  $(\partial a_2 / \partial P)_{T, \lambda}$  is of the same form as equation (15), with  $P$  replacing  $T$ . The derivative  $(\partial a_2 / \partial \lambda)_{T, P}$  is also of the form of equation (15), with  $\lambda$  replacing  $P$  and  $\partial^2 \bar{v}_s / \partial c_s \partial \lambda = 0$ . The temperature and pressure derivatives of  $a_2$  involve the temperature and pressure coefficients of  $\bar{v}_s$  (the partial specific expansibility and partial specific compressibility, respectively). These coefficients are probably negligible in most polymer solutions compared to the terms involving the derivatives of  $\nu$  and of  $n_1$ .

Several illustrations of the use of equation (12) for  $a_2$  follow. For egg albumin<sup>6</sup>, a typical globular protein,  $n_1 \approx 1.33$ ,  $\nu = 0.190 \text{ cm}^3 \text{ g}^{-1}$ , and the maximum concentration investigated by Perlmann and Longworth<sup>6</sup> was  $c_s = 0.1 \text{ g cm}^{-3}$ . These values give a maximum  $a_2 c_s = 0.0012 \text{ cm}^3 \text{ g}^{-1}$ , if  $\partial \bar{v}_s / \partial c_s = 0$ , which is the same

order as the maximum spread (0.0009) and the standard deviation ( $0.0004 \text{ cm}^3 \text{ g}^{-1}$ ) of the experimental results. Variations of  $\nu$  with composition are thus expected to be of the same order as the experimental error.

For polystyrene and poly(methyl methacrylate) in various solvents,  $\partial \bar{v}_s / \partial c_s = 0$ . In toluene, with  $n_1 \sim 1.5$ , and a maximum  $c_s = 0.02 \text{ g cm}^{-3}$ , the maximum value of  $a_2 c_s$  is only  $10^{-4}$  for polystyrene and  $10^{-6}$  for poly(methyl methacrylate), compared to experimental errors<sup>8</sup> of about  $1 \times 10^{-4} \text{ cm}^3 \text{ g}^{-1}$  in  $\nu$ . No dependence of  $\nu$  on concentration is predicted, in agreement with experiment<sup>8</sup>.

For polydimethylsiloxane (PDMS) in toluene, experiment<sup>9</sup> gives  $a_2 = 0.104 \text{ cm}^6 \text{ g}^{-2}$  at 436 nm and at 15–35°C. The calculated value of  $a_2$  from the first term of equation (12) is  $0.004 \text{ cm}^6 \text{ g}^{-2}$ , giving  $\partial \bar{v}_s / \partial c_s = -0.339 \text{ cm}^6 \text{ g}^{-2}$ . At 546 nm, a similar calculation gives  $\partial \bar{v}_s / \partial c_s = -0.325 \text{ cm}^6 \text{ g}^{-2}$ , in good agreement. No measurements of  $\bar{v}_s$  as a function of concentration seem to have been reported for PDMS. However, measurements of osmotic second virial coefficients<sup>10</sup> suggest that PDMS molecules associate in solution, and the large negative value for  $\partial \bar{v}_s / \partial c_s$  probably reflects such association. In favourable cases, therefore, measurement of the concentration dependence of the specific refractive index increment can lead to information concerning the concentration dependence of the partial specific volume  $\bar{v}_s$ , just as measurements of  $\nu$  lead to information about  $\bar{v}_s$ <sup>4, 11</sup>. On the other hand, if  $\partial \bar{v}_s / \partial c_s$  and  $\nu$  can be estimated, equation (12) may be used to predict if  $\Delta n / c_s$  should vary measurably with concentration.

For a mean value  $\partial \bar{v}_s / \partial c_s = 0.33 \text{ cm}^6 \text{ g}^{-2}$  in toluene, and  $\partial^2 \bar{v}_s / \partial T \partial c_s = 0$ ,  $\partial n_1 / \partial T = 5.6 \times 10^{-4} \text{ K}^{-1}$ , equation (15) gives  $(\partial a_2 / \partial T)_{T, P, \lambda} = -1.15 \times 10^{-4} \text{ K}^{-1}$  for PDMS at 436 nm, which is outside the precision of the measurements of  $a_2$ , in agreement with experiment<sup>9</sup>. The observed dependence of  $\nu$  on  $\lambda$  is roughly linear<sup>9</sup>:

$$(\partial \nu / \partial \lambda)_{T, P} = 1.0 \times 10^3 \text{ cm}^2 \text{ g}^{-1}$$

With  $(\partial n_1 / \partial \lambda)_{T, P} = -1.55 \times 10^3 \text{ cm}^{-1}$ , equation (15) gives  $(\partial a_2 / \partial \lambda)_{T, P} = -4.4 \times 10^2 \text{ cm}^5 \text{ g}^{-2}$ . The observed value<sup>9</sup> is  $-4.5 \times 10^2 \text{ cm}^5 \text{ g}^{-2}$ , in excellent agreement. We conclude

that equation (12) gives  $a_2$  to sufficient accuracy under a wide variety of conditions.

Mächtle and Fisher<sup>12</sup> have used a form of equation (5) at infinite dilution to deduce the dependence of  $\nu$  on wavelength, and Heller<sup>11</sup> has used essentially the same equation<sup>4</sup> to discuss temperature coefficients of  $\nu$  and  $\bar{v}_s$ . Dependence of  $\nu$  on molecular weight has also been considered<sup>2, 5, 11</sup>. The equations given above for the dependence of  $\Delta n / c_s$  on concentration, along with the rigorous formulation<sup>4</sup> of the basic equations, complete the theoretical basis for estimation of refractive index increments at any given temperature and wavelength from the properties of the solvent and polydisperse solute, or, conversely, for the estimation of properties of the solute from measurements of  $dn/dc_s$ .

#### ACKNOWLEDGEMENTS

The research for this paper was supported, in part, by grants from the National Research Council of Canada and the Defence Research Board of Canada (grant no. 7583-04).

#### REFERENCES

- 1 Huglin, M. B. *J. Appl. Polym. Sci.* 1965, **9**, 3963
- 2 Huglin, M. B. *J. Appl. Polym. Sci.* 1965, **9**, 4003
- 3 Matsumoto, M. and Ohyanagi, Y. *J. Polym. Sci.* 1958, **31**, 225
- 4 Lorimer, J. W. *Polymer* 1972, **13**, 46
- 5 Lorimer, J. W. and Jones, D. E. G. *Polymer* 1972, **13**, 52
- 6 Perlmann, G. E. and Longworth, L. G. *J. Am. Chem. Soc.* 1948, **70**, 2719
- 7 Schulz, G. V. and Hoffmann, M. *Makromol. Chem.* 1957, **23**, 220
- 8 Bodmann, O. *Makromol. Chem.* 1969, **122**, 196
- 9 Nilsson, R. and Sundelöf, L.-O. *Makromol. Chem.* 1963, **66**, 11
- 10 Kuwahara, N. and Miyake, Y. *Kobunshi Kagaku* 1961, **18**, 153; *Chem. Abstr.* 1961, **55**, 22894g
- 11 Heller, W. *J. Polym. Sci. (A-2)* 1966, **4**, 209
- 12 Mächtle, W. and Fischer, H. *Angew. Makromol. Chem.* 1969, **7**, 147

# Gel permeation chromatography: the behaviour of polystyrenes with long-chain branching

J. Pannell

*Imperial Chemical Industries Limited, Plastics Division, Welwyn Garden City, Herts, UK  
(Received 18 November 1971)*

The gel permeation chromatography (g.p.c.) behaviour of a wide range of branched polystyrenes, in which the branching frequency and the branch length are varied, is described. It is found that, qualitatively, the separation of these branched polymers by g.p.c. does depend on size but contrary to other results reported in the literature, the hydrodynamic volume  $[\eta]M$  of the polymer molecules is not the appropriate size parameter to use. That is, a single plot of  $\log[\eta]M$  against elution volume embracing all the branched polystyrenes prepared and linear polystyrenes is not obtained. Because the mean square radii of gyration of these branched polystyrenes could not be measured directly no positive evidence as to the nature of the correct size-separation parameter was obtained. It is pointed out that, even if the correct size-separation parameter were known, g.p.c. could not be used to characterize branched polymers unambiguously.

## INTRODUCTION

Existing empirical evidence suggests that separation in gel permeation chromatography depends on the size of the polymer molecules, the most widely used measure of the size being the hydrodynamic volume  $[\eta]M$ , where  $[\eta]$  is the intrinsic viscosity and  $M$  the molecular weight. This was first shown to be the case by Benoit *et al.*<sup>1</sup> who obtained a single calibration curve of  $\log[\eta]M$  against elution volume not only for a number of chemically different linear polymers and copolymers in a common solvent, but for some star-shaped and comb-shaped branched polymers also. Since then single plots of  $\log[\eta]M$  against elution volume have been obtained by Drott and Mendelson<sup>2</sup> and by Wild and Guliana<sup>3</sup> for fractions of linear and branched polyethylene, by Johnson and Adams<sup>4</sup> for some linear and tetra-chain star-branched polybutadienes and by Berry<sup>5</sup> for some linear, star-shaped and comb-shaped polystyrenes. Similarly, single universal calibration plots of  $\log[\eta]M$  against elution volume have been obtained by Boni *et al.*<sup>6</sup> for fractions of linear polyethylene, polystyrene and polybutadiene, and by Coll and Gilding<sup>7</sup> for fractions of polystyrene, poly( $\alpha$ -methyl styrene) and polypropylene.

The use of the hydrodynamic volume of a polymer molecule as the correct size parameter to use in gel permeation chromatography (g.p.c.) has, however, been questioned by Dawkins<sup>8</sup>, who considers that separation depends on the mean square unperturbed radius of gyration,  $\langle S_0^2 \rangle$ , of the molecule. Support for this view was sought by examining linear polymers with appreciably different Mark-Houwink exponents in a common solvent, but it turns out that plots of  $\log[\eta]M$  and  $\log\langle S_0^2 \rangle$  against elution volume both give equally good correlations, i.e. g.p.c. elution data on linear polymers provides

no basis for choosing between  $[\eta]M$  or  $\langle S_0^2 \rangle$  as the correct size parameter for universal calibration.

The view has been expressed by Casassa and Tagami<sup>9</sup> that only by studying the elution behaviour of branched polymers might it be possible to decide which of the several possible size parameters is appropriate to separation in g.p.c. Although the results on star-shaped and comb-shaped branched polymers referred to earlier indicate that hydrodynamic volume is the correct size parameter, a much wider range of branched polymers needs to be studied to settle the issue. The aim of the work described in the present paper was to study the elution behaviour of a reasonably wide range of branched polystyrenes and to determine, if possible, which of the possible size parameters is appropriate to their separation by g.p.c. The difficulties of using g.p.c. to characterize branched polymers, even when the appropriate size parameter is known, are briefly discussed.

## EXPERIMENTAL

The linear and branched polystyrenes used in the present study were prepared anionically, and some details of their syntheses and properties are given elsewhere<sup>10</sup>. As prepared, each of the branched polymers was associated with a certain amount of a linear homopolymer, this being the branch precursor. Since no attempt was made to separate the linear and branched components by classical fractionation methods, information on the branched polymers was obtained by resolving the chromatograms of the mixtures into the two components. This resolution was readily achieved in all cases and was made possible by being able to obtain the chromatograms of the linear components separately (see Appendix). From the resolved



chromatograms the weight fraction of each component in the mixture was determined by area measurement (the composition of the mixtures were required in determining the intrinsic- and melt-viscosities of the branched polymers<sup>10</sup>) and the peak elution volumes of the branched polymers were measured. Typical chromatograms, showing the result of resolution, are reproduced in *Figure 1*, where it is seen that the component polymers have fairly narrow distributions.

All samples were injected into a Waters Associates gel permeation chromatograph at 293K using toluene as the solvent and a flow rate of about 1 cm<sup>3</sup> min<sup>-1</sup>. The polymer samples, at 1/4% concentration (w/w), were injected for 1 min. Concentration effects were found to be small. Four columns (each 4 ft long and 3/8 in. in diameter) containing Styragel were used in series and their characteristics are shown below:

Waters Associates column designation	Plate count per foot	Pressure drop across column (lb/in <sup>2</sup> )
10 <sup>7</sup> A	1190	28
10 <sup>5</sup> A	1123	40
10 <sup>4</sup> A	820	78
250 A	906	20
Combination	1241	

The plate count of each column, and that of the combination, was determined in the usual way by injecting a sample of tetrahydrofuran or *o*-dichlorobenzene. In the course of several months the calibration curve of log *M* against elution volume for the linear polymers did not shift appreciably showing that the column characteristics remained virtually unchanged over this period.

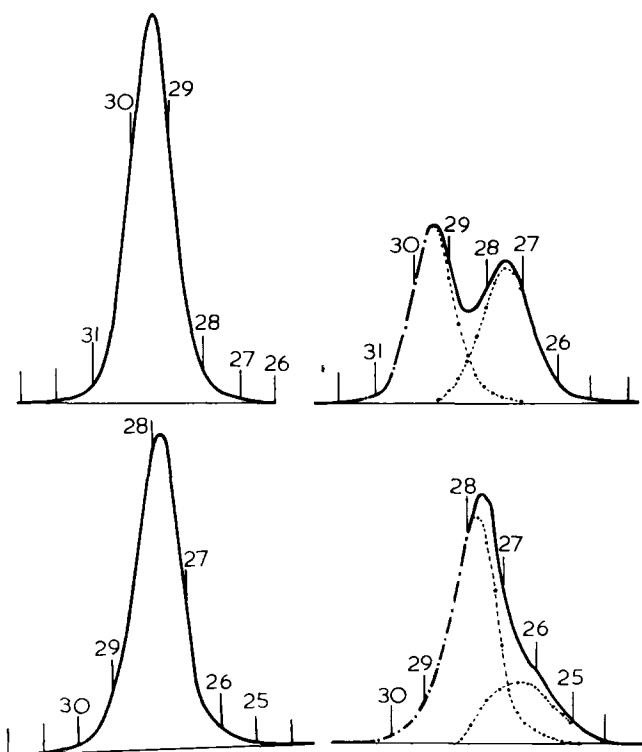


*Figure 1* Examples of the chromatograms obtained from the mixtures of branched and linear polystyrenes, prepared by reacting polystyryl potassium with chloromethylated polystyrene, and from the linear precursors (branches)

*Table 1* Intrinsic viscosities, molecular weights and peak elution volumes of linear polystyrenes

Sample	Intrinsic viscosity at 298 K [ $\eta$ ] <sub>TOL</sub> (dm <sup>3</sup> kg <sup>-1</sup> )	$\bar{M}_n \times 10^{-5}$	Peak elution volume/5 (cm <sup>3</sup> )
U26	21.3*	0.36	29.8
B114.L	28.2	0.465	29.5
B111.L	29.7	0.496	29.5
B112.L	28.8*	0.498	29.4
B110.L	35.6	0.567	29.3
B118.L	34.0	0.603	29.2
B107.L	41.8	0.783	29.1
B116.L	34.5	0.801	29.1
U18	37.6*	0.824	28.9
B105.L	48.4	0.946	28.6
B121.L	54.1	1.11	28.2
B123.L	52.0	1.14	28.25
U14	54.4*	1.17	28.6
U19	57.8*	1.18	28.2
U29	48.1	1.22	28.4
B108.L	63.0	1.36	28.0
B137.L	57.2*	1.42	28.1
U27	60.2*	1.55	27.9
B120.L	66.3	1.57	27.8
B130.L	69.4	1.75	27.7
U34	68.6	1.81	27.7
B131.L	69.8	1.96	27.7
B103.L	78.4	2.06	27.3
U33	72.8	2.12	27.5
B124.L	81.6	2.13	27.6
B122.L	104.7	2.42	27.0
B115.L	93.8*	2.66	27.05
B106.L	118	3.67	26.2
U25	105.2*	3.82	26.5
U28	105.2*	3.86	26.7
U17	113*	4.03	26.4
B104.L	117	4.18	26.3
U23	120.6*	4.77	26.2
U21	152*	6.59	25.4
U31	190*	9.32	25.0
U24	181*	8.91	25.1

\* Estimated from correlation plot of [ $\eta$ ]<sub>THF</sub> against [ $\eta$ ]<sub>TOL</sub>. Intrinsic viscosities in THF are given in *Table 3*, ref. 18

## RESULTS AND DISCUSSION

The complete results for the linear and branched polystyrenes examined in this work are given in *Tables 1* and *2* respectively. It may be seen from *Table 2* that four series of branched polymers were studied, each series being characterized by a particular branching frequency. In each series the branch length was varied. The results for some calibration samples of linear polystyrenes supplied by Waters Associates are given in *Table 3*. Because the branched polymers were not separated from the linear branch-precursor polymers, no direct measurements on them could be carried out. The molecular weights, intrinsic viscosities and unperturbed radii of gyration given in *Table 2* were therefore obtained indirectly<sup>10</sup>.

Plots of log *M* and log [ $\eta$ ]*M* against elution volume for the linear polystyrenes are shown in *Figures 2* and *3*, respectively. The majority of these linear polymers have narrow molecular weight distributions ( $\bar{M}_w/\bar{M}_n < 1.2$  in most cases<sup>18</sup>) so little error is introduced by assuming that the number-average molecular weight corresponds to the peak elution volume. Also shown in *Figure 2* are the results obtained for the narrow distribution polystyrenes supplied by Waters Associates. The intrinsic viscosities of some of the linear polymers in the g.p.c. solvent, toluene,

Table 2 Results for branched polystyrenes

Backbone* polymer	Parent mixture	Intrinsic viscosity† of branched component at 298 K [ $\eta$ ] <sub>TOL</sub> (dm <sup>3</sup> kg <sup>-1</sup> )	Molecular weight†		Unperturbed radius of gyration† $\langle S_0^2 \rangle \times b^{-2}$	Peak elution volume/5 (cm <sup>3</sup> )
			$M_n^B \times 10^{-5}$	$M_w^B \times 10^{-5}$		
U34 $\bar{p}=2.55$ $\lambda=682$	B1114	78	3.00	3.18	348	27.4
	B118	78	3.35	3.63	398	27.4
	B116.1	79	3.85	4.28	457	27.35
	B121	104	4.64	5.32	561	27.0
	B120	124	5.82	6.91	725	26.5
	B130	139	6.28	7.52	790	26.7
	B122	155	7.99	9.87	1040	25.8
	B115.1	151	8.59	10.7	1138	25.6
U29 $\bar{p}=5.78$ $\lambda=202$	B110.4	91	4.50	4.91	369	26.8
	B116.3	83	5.86	6.48	464	26.4
	B123	121	7.82	8.78	607	25.5
	B108.2	113	9.08	10.2	699	25.75
	B131	166	12.5	14.3	950	24.6
	B124.2	157	13.6	15.5	1030	25.0
U27 $\bar{p}=8.87$ $\lambda=168$	B115.2	191	16.6	19.0	1260	24.1
	B110.1	90	6.58	7.01	475	26.1
	B107.1	100	8.49	9.12	549	26.1
	B105	129	9.94	10.7	641	25.2
	B108.1	143	13.6	14.8	844	25.1
	B103	191	19.8	21.7	1147	23.7
	B106	268	34.1	37.6	1882	23.0
	B104	282	38.6	42.6	1979	23.1
U33 $\bar{p}=18.7$ $\lambda=109$	B111	90	4.40	4.66	446	26.3
	B112	104	11.4	12.1	521	25.3
	B107.5	116	16.8	17.4	647	25.0
	B108.4	150	25.6	26.8	955	24.2
	B115.4	219	51.9	54.1	1530	23.0

\* See Table 1 for results on linear backbone polymers.  $\bar{p}$  = average number of branches per backbone molecule

† Details of the determination of the intrinsic viscosities of the branched components and calculation of their molecular weights and theoretical unperturbed dimensions are given in ref. 10

Table 3 Data for the polystyrene calibration samples supplied by Waters Associates

Sample	Intrinsic viscosity at 298 K		$\bar{M}_n^*$	$\bar{M}_w^*$	Peak elution † volume/5 (cm <sup>3</sup> )
	$[\eta]_{\text{THF}}$	$[\eta]_{\text{TOL}}$ ‡			
25169	6.5	—	4 600	5 000	32.0
25171	9.1	—	9 700	10 300	31.1
4190039	15.5	15.7	19 650	19 850	30.5
25170	28.9	29.0	49 000	51 000	29.4
41995	46.8	46.2	96 200	98 200	28.6
41984	67.2	65.7	164 000	173 000	27.8
4190037	127.6	124.2	392 000	411 000	26.2
4190038	219	214	773 000	867 000	24.9
61970	380	—	1 780 000	2 145 000	23.8

\* Molecular weights are those quoted by the Pressure Chemical Company, Pittsburgh, USA, who supply the polymers to Waters Associates

† This is the average of the figures obtained at the beginning and the end of the period in which the work on polystyrenes was carried out

‡ Estimated from correlation plot of  $[\eta]_{\text{THF}}$  against  $[\eta]_{\text{TOL}}$  (see Table 1)

were not measured directly (see Table 1) but were estimated from a correlation plot of  $[\eta]_{\text{THF}}$  against  $[\eta]_{\text{TOL}}$  in order to calculate the hydrodynamic volume  $[\eta]M$  in toluene.

For the branched polystyrenes, plots of  $\log M$  and  $\log [\eta]M$  against elution volume are shown in Figures 4 and 5 respectively, where the molecular weight is given by  $M = M_{\text{peak}} = (M_n^B M_w^B)^{1/2}$ . (This is a better approximation

for these branched polymers, which have marginally wider distributions than the linear polymers because of the statistical spread in the number of branches.) Figure 4 shows that at a given molecular weight a branched polymer elutes later than a linear polymer, and this agrees qualitatively with the results from other g.p.c. studies on branched polymers<sup>1-7</sup>. Since a branched polymer molecule is smaller than a linear one of the same molecular weight, the result shows qualitatively that separation in g.p.c. depends on molecular size.

The plot shown in Figure 5 indicates that in the region where a comparison can be made with linear polymers, many of the branched polymers elute later than the corresponding linear polymers with the same hydrodynamic volumes  $[\eta]M$ , or, at a given elution volume most of the branched polystyrenes have larger hydrodynamic volumes in a good solvent (toluene) than the corresponding linear polymer. Thus if separation in g.p.c. depends on the size of the polymer molecules, then the hydrodynamic volume  $[\eta]M$  is not the appropriate size parameter for the branched polystyrenes considered here.

Since this result conflicts with results already made known in the literature<sup>1-7</sup>, it is worth examining the use of hydrodynamic volume and other possible size parameters in g.p.c.

The hydrodynamic volume of a polymer molecule is defined as the volume of an equivalent hydrodynamic sphere, impenetrable to solvent, which would exhibit the same frictional properties, or would enhance the viscosity by the same amount as the actual polymer molecule in

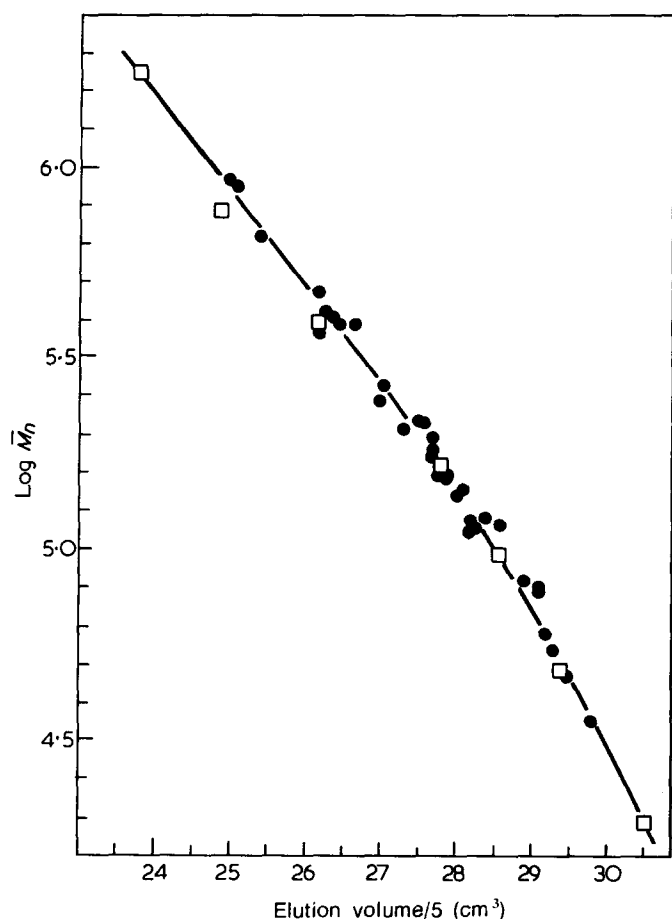


Figure 2 Plot of  $\log \bar{M}_n$  against elution volume for linear polystyrenes. ●, Polystyrenes prepared in this work (Table 1); □, polystyrenes supplied by Waters Associates (Table 3)

solution<sup>11</sup>; the concept of an equivalent hydrodynamic sphere is applicable to linear and branched polymers alike. Application of Stokes' Law and Einstein's viscosity relation to the equivalent sphere gives the result that its volume is proportional to the product  $[\eta]M$ . Although this definition does not imply that the hydrodynamic volume will be proportional to the actual size of the polymer molecule in solution, for linear polymer chains it is found to be so<sup>12</sup>, i.e.

$$[\eta]M = \Phi \langle S^2 \rangle^{3/2} = \Phi \alpha^3 \langle S_0^2 \rangle^{3/2} \quad (1)$$

where  $\Phi$  is a constant,

$\langle S^2 \rangle$  is the mean square radius of gyration of the polymer molecule in a good solvent,

$\langle S_0^2 \rangle$  is the mean square unperturbed radius of gyration,

and  $\alpha^3$  is the expansion factor in the good solvent.

Ptitsyn and Eizner<sup>13</sup> have shown that  $\Phi$  in equation (1) is not strictly a universal constant for all linear polymers, as assumed in the Fox-Flory theory, but depends on the Mark-Houwink exponent  $a$ :

$$\Phi = \Phi_0(1 - 2.63\epsilon + 2.86\epsilon^2)$$

where

$$\epsilon = (2a - 1)/3 = (\alpha^2 - 1)/(5\alpha^2 - 3)$$

and

$$\Phi_0 = 2.86 \times 10^{21}$$

Thus linear polymers with appreciably different Mark-Houwink exponents in a given solvent will have different values of  $\langle S^2 \rangle^{3/2}$  (and  $\langle S_0^2 \rangle^{3/2}$ ) for a particular value of the hydrodynamic volume, and *vice versa*. This suggests that in order to decide which of the size parameters  $[\eta]M$ ,  $\langle S^2 \rangle^{3/2}$  or  $\langle S_0^2 \rangle^{3/2}$  is the one most appropriate to separation in g.p.c., a study of linear polymers with markedly different Mark-Houwink exponents in a given solvent is required. This was first pointed out by Dawkins<sup>14</sup> but his studies on polystyrene and polydimethylsiloxane in *o*-dichlorobenzene at 411K show that the g.p.c. results cannot discriminate between the different size parameters in spite of the difference in the Mark-Houwink exponents for these two polymers in this solvent ( $a=0.70$  and  $0.57$  respectively). At present, therefore, the results obtained on linear polymers do not provide a basis for deciding which of the size parameters is appropriate to their separation in g.p.c.

For branched polymers there is no fundamental reason to suppose that their separation in g.p.c. should depend on the volumes of their equivalent hydrodynamic spheres. Unlike linear polymers, a direct proportionality between hydrodynamic volume and the actual molecular size in solution has not yet been demonstrated for all branched polymers. It is more natural to assume that the appropriate size-separation parameter for branched polymers is

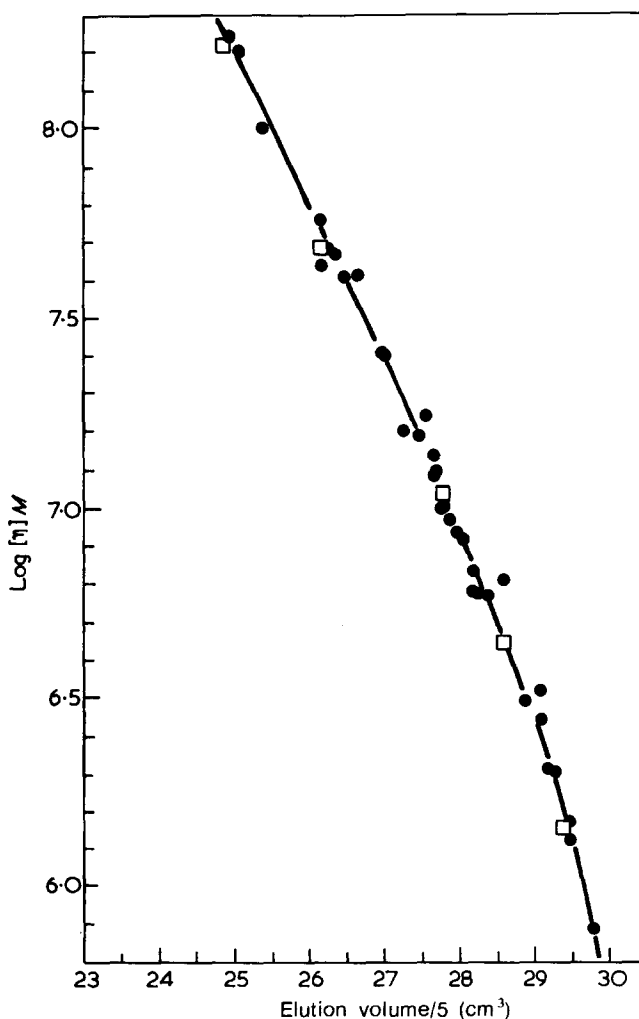


Figure 3 Plot of  $\log [\eta]M$  against elution volume for linear polystyrenes. Symbols as in Figure 2

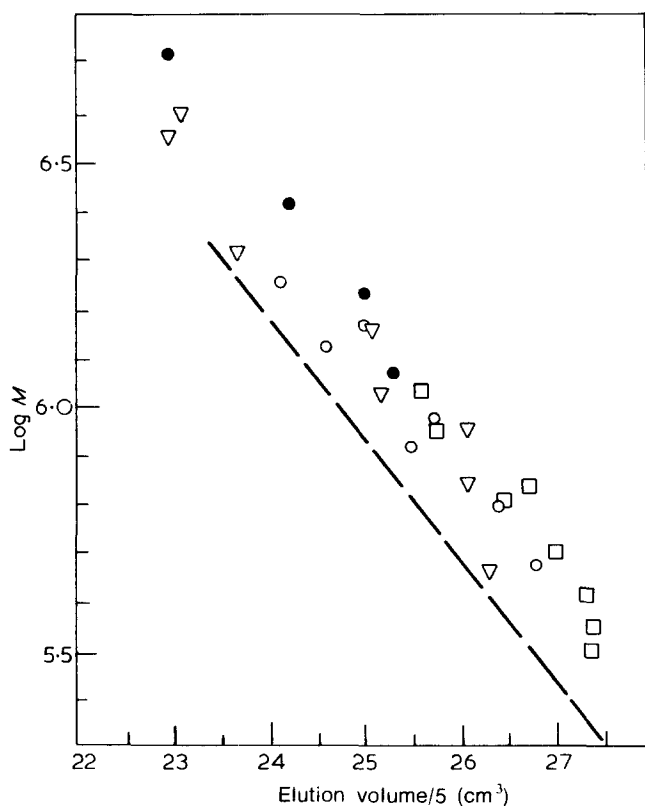


Figure 4 Plot of  $\log M$  against elution volume for branched polystyrenes, where  $M=(M_n \cdot M_w)^{1/2}$  (Table 2). The curve for linear polystyrenes is shown by the broken line. Each symbol denotes a series of polymers with a fixed branching frequency (conveniently expressed as  $\lambda$ =degree of polymerization of backbone/ $\bar{p}$ , see ref. 10) and variable branch length.  $\square$ ,  $\lambda=682$ ;  $\circ$ ,  $\lambda=202$ ;  $\nabla$ ,  $\lambda=168$ ;  $\bullet$ ,  $\lambda=109$ .

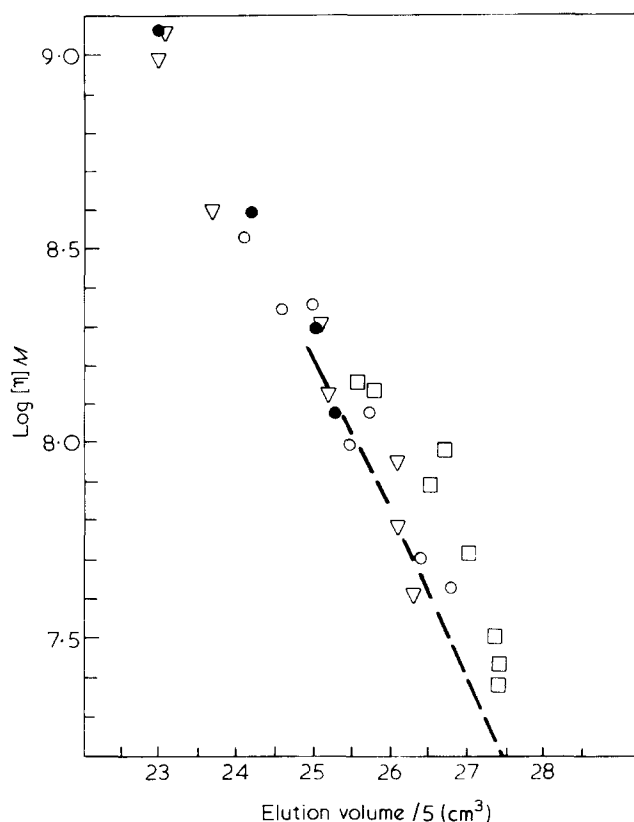


Figure 5 Plot of  $\log [\eta]M$  against elution volume for branched polystyrenes. The behaviour of linear polystyrenes is shown by the broken curve. Symbols are defined in the caption for Figure 4

$\langle S^2 \rangle^{3/2}$  rather than  $[\eta]M$ , although for some the two parameters may be interchangeable. Whether separation of the branched polystyrenes considered here depends on  $\langle S^2 \rangle^{3/2}$  could not be checked because it was not possible to make direct measurements of their mean square radii of gyration. It was possible, however, to calculate the mean square unperturbed radii of gyration,  $\langle S_0^2 \rangle$ , of these branched polystyrenes from the equation given by Orofino<sup>15</sup>, and the result of plotting  $\log \langle S_0^2 \rangle$  against elution volume is shown in Figure 6. Although Figure 6 shows that the elution behaviour of these branched polystyrenes does not correlate with their theoretical unperturbed dimensions, it is not known at present how close the theoretical values of  $\langle S_0^2 \rangle$  are to the actual  $\theta$ -point dimensions of these polymer molecules. Further studies of a wide range of branched polymers of known structures will be necessary before the question of the correct size parameter to use in g.p.c. is settled.

The empirical universal calibration plot of  $\log [\eta]M$  against elution volume obtained for linear polymers enables g.p.c. to be used to characterize these polymers, provided the Mark-Houwink equations for the polymers concerned are known. The question which of the size parameters is appropriate to separation of linear polymers is therefore largely academic. For branched polymers, even if the correct size-separation parameter were known, full characterization of an unknown branched polymer from the size-elution volume correlation will not be possible until the size parameter concerned can be related

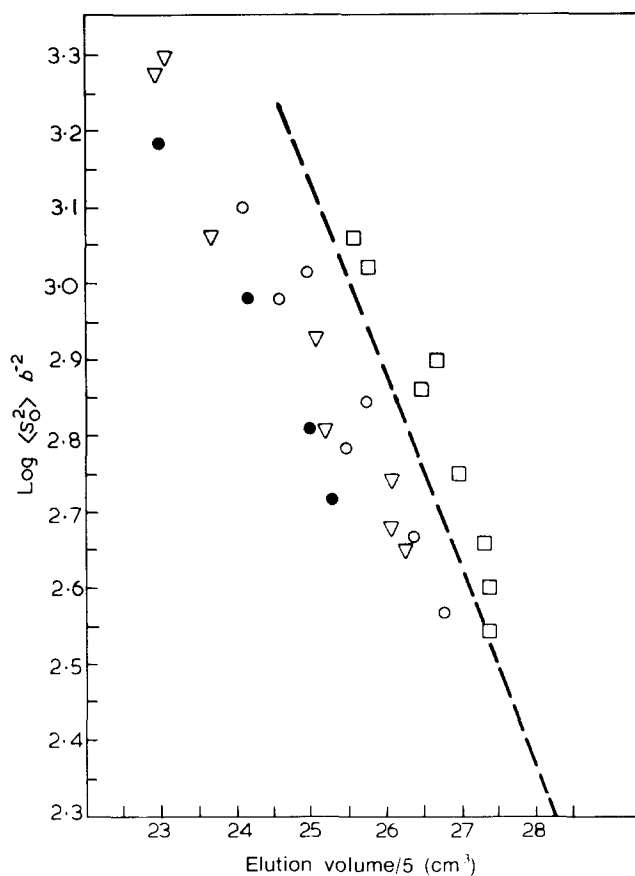


Figure 6 Plot of  $\log \langle S_0^2 \rangle b^{-2}$  against elution volume for branched polystyrenes, where  $\langle S_0^2 \rangle$  is the theoretical unperturbed radius of gyration<sup>15</sup> and  $b$  is the length of a single chain segment. The broken curve describes the behaviour of linear polystyrenes. Symbols are defined in the caption for Figure 4

unambiguously to structure as well as molecular weight. This will not be easy because of the wide range of branched polymers possible, a good many of them, of different structure and molecular weight, will have the same size and therefore the same elution volume. The sort of assumptions involved at present in using g.p.c. to characterize branched polymers, in particular to determine the degree of long-chain branching in low-density polyethylene, are to be found in papers by Drott and Mendelson<sup>2, 16, 17</sup>.

## REFERENCES

- 1 Benoit, H., Grubisic, Z. and Rempp, P. *J. Polym. Sci. (B)* 1967, **5**, 753
- 2 Drott, E. E. and Mendelson, R. A. Paper presented at 5th International GPC Seminar, London, May 1968
- 3 Wild, L. and Guliana, R. *J. Polym. Sci. (A-2)* 1967, **5**, 1087
- 4 Personal communication referred to in ref. 6
- 5 Berry, G. C. *J. Polym. Sci. (A-2)* 1971, **9**, 687
- 6 Boni, K. A., Sliemers, F. A. and Stickney, P. B. *J. Polym. Sci. (A-2)* 1968, **6**, 1579
- 7 Coll, H. and Gilding, D. K. *J. Polym. Sci. (A-2)* 1970, **8**, 89
- 8 Dawkins, J. V. *J. Macromol. Sci.* 1968, **B2**, 623
- 9 Casassa, E. F. and Tagami, Y. *Macromolecules* 1969, **2**, 14
- 10 Pannell, J. *Polymer* 1972, **13**, 2
- 11 Flory, P. J. 'Principles of Polymer Chemistry', Cornell University Press, 1953
- 12 Fox, T. G. and Flory, P. J. *J. Am. Chem. Soc.* 1951, **73**, 1904
- 13 Ptiitsyn, O. B. and Eizner, Yu. E. *Soviet Phys. (Tech. Phys.)* 1959, **4**, 1020
- 14 Dawkins, J. V., Maddock, J. W. and Coupe, D. *J. Polym. Sci. (A-2)* 1970, **8**, 1803
- 15 Orofino, T. A. *Polymer* 1961, **2**, 305
- 16 Drott, E. E. and Mendelson, R. A. *J. Polym. Sci. (B)* 1968, **6**, 795
- 17 Drott, E. E. and Mendelson, R. A. *J. Polym. Sci. (A-2)* 1970, **8**, 1361
- 18 Pannell, J. *Polymer* 1971, **12**, 547

## APPENDIX

### Resolution of the chromatograms of the mixtures of linear and branched polystyrenes

Provided there is no irreversible adsorption of polymer in the g.p.c. columns, the area under the chromatogram is proportional to the total weight of polymer introduced and the ordinate  $h_i$  at any value of elution volume  $V_i$  is proportional to the concentration  $C_i$  of polymer eluting at  $V_i$

$$\text{Total area} = \int_{V_0}^{V_\infty} h_i dV$$

The area under a portion of the chromatogram between elution volumes  $V_1$  and  $V_2$  is therefore a measure of the weight fraction  $W_{1,2}$  of polymer eluting between  $V_1$  and  $V_2$ , i.e.

$$W_{1,2} = \int_{V_1}^{V_2} h_i dV / \int_{V_0}^{V_\infty} h_i dV \quad (\text{A1})$$

In resolving the chromatograms of the mixtures it is assumed that the total ordinate  $h_i^M$  at a given elution volume  $V_i$  for the mixture is given by the sum of the contributions  $h_i^L$  and  $h_i^B$  from the linear and branched polymers, respectively, i.e.

$$h_i^M = h_i^B + h_i^L \quad (\text{A2})$$

Considering the known component (linear polymer) only

$$W_{1,2} = \int_{V_1}^{V_2} H_i^L dV / \int_{V_0}^{V_\infty} H_i^L dV = \int_{V_1}^{V_2} h_i^L dV / \int_{V_0}^{V_\infty} h_i^L dV \quad (\text{A3})$$

where  $H_i^L$  is the ordinate at elution volume  $V_i$  in the chromatogram of the linear polymer alone. When  $V_1$  and  $V_2$  are sufficiently close together,

$$\int_{V_1}^{V_2} H_i^L dV = H_i^L \Delta V \quad \text{and} \quad \int_{V_1}^{V_2} h_i^L dV = h_i^L \Delta V$$

where  $H_i^L$  and  $h_i^L$  are now averages in the range  $\Delta V$  of elution volume. Equation (A3) may now be re-written

$$\int_{V_0}^{V_\infty} h_i^L dV / \int_{V_0}^{V_\infty} H_i^L dV = h_i^L / H_i^L \quad (\text{A4})$$

For a given mixture the ratio on the left hand side of equation (A4) is fixed since the numerator is the area contributed by the linear component to the total area under the chromatogram of the mixture and the denominator is the area under the chromatogram of the linear component alone. The ratio  $h_i^L / H_i^L$  is therefore independent of the elution volume but can be determined only in that region of the chromatogram of the mixture where the linear component is not affected by overlap from the branched component. Such a region was found to exist in the chromatograms of all the mixtures examined here. Once the ratio  $h_i^L / H_i^L$  is known the height  $h_i^L$  at any elution volume may be computed knowing the corresponding values of  $H_i^L$ . Resolution of the chromatogram of the mixture into its two parts is then completed by making use of equation (A2). The ratio of the area contributed by each component to the total area under the chromatogram is equal to the weight fraction of that component in the mixture.

In this treatment the precise concentration of polymer in solution need not be known, but it does assume that the elution behaviour is independent of polymer concentration, i.e. no overloading occurs. Examples of this analysis of chromatograms of mixtures containing branched and linear polystyrenes are shown in *Figure 1* and the peak elution volumes obtained for the branched polymers after resolution are given in *Table 2*. Results obtained on mixtures of linear polymers show that the compositions determined from the chromatograms by this method agree to better than 7% with those given by direct weighing. The major part of this discrepancy is thought to arise from uncertainties introduced by an unsteady baseline, a characteristic defect of the (unmodified) instrument used.

### Note added in proof

Professor M. Nagasawa of Nagoya University, Japan has made it known in a personal communication to the author that he too has found that branched and linear polystyrenes in toluene do not give a universal calibration of  $\log [\eta]M$  against elution volume. His results, which will be published in full in due course, show that  $\langle S^2 \rangle^{3/2}$  is the correct size parameter to use, as suggested here.

# Influence of hydrogen bonding on crazing and cracking of amorphous thermoplastics

P. I. Vincent and S. Raha

*Imperial Chemical Industries Limited, Plastics Division, Welwyn Garden City, Herts, UK  
(Received 6 October 1971; revised 15 November 1971)*

The stress crazing and cracking of poly(methyl methacrylate), poly(vinyl chloride) and polysulphone in the presence of liquid environments have been examined. The results are found to be inexplicable solely in terms of the solubility parameters of the liquids. Hydrogen bonding is shown to be an important factor. A more effective representation of solution, crazing and cracking behaviour is obtained by considering the capacity of each liquid to hydrogen bond as well as its solubility parameter. This two-parameter representation is applied with success to the three polymers.

## INTRODUCTION

The phenomena of stress-crazing and stress-cracking of polymers in the presence of liquid environments have been extensively discussed in the literature<sup>1</sup>. They occur in both crystalline and amorphous materials. Recently, Bernier and Kambour<sup>2</sup> have attempted to rationalize the role of organic agents in the environmental stress failure of a non-crystalline (but crystallizable) polymer by studying the action of a range of liquids on poly(2,6-dimethyl-1,4-phenylene oxide) (PPO). They found a useful correlation between the solubility parameter of each liquid and its effectiveness in dissolving, crazing or cracking the polymer and proposed that the phenomena were determined by the closeness of the solubility parameter of the liquid to that of the polymer. A liquid would act as a solvent when its solubility parameter was identical to that of the polymer. When the difference between the two solubility parameters was small the liquid would promote cracking. When the difference was large, liquids would be crazing agents. Others have endeavoured to relate environmental stress-cracking to the molecular volume and surface tension properties of a liquid<sup>3</sup> but these relationships are not successful when extended to a wider range of polymers such as the polymers discussed below. As Bernier and Kambour have pointed out, such relationships are not in any case mutually exclusive since both surface tension and solubility parameter are dependent on the intermolecular forces present in the liquid.

Bernier and Kambour took care to exclude those liquids which were thought to interact via hydrogen bonding. It was of interest to us to extend their study to a range of polymers and to include liquids which could participate in hydrogen bonding.

## SAMPLES

Specimens of approximate length 90 mm and width 10 mm were cut from approximately 3 mm thick sheets of PMMA, PVC and polysulphone. The cut edges were milled to give a smooth machine finish. Crazing or cracking in

the subsequent tests was never initiated solely from these machined edges and additional polishing of the surfaces was felt to be unnecessary.

The samples of poly(methyl methacrylate) (PMMA) were from 'Perspex' and those of poly(vinyl chloride) (PVC) were from 'Darvic' 024, an unplasticized PVC. ('Perspex' and 'Darvic' are ICI trade marks.) The polysulphone samples were cut from 114 mm diameter injection moulded discs of Bakelite Polysulfone P1700. The discs were edge-gated and the specimens were cut so that their axes were perpendicular to the diameter through the gate.

## EXPERIMENTAL

The experimental technique was to subject a 90 mm by 10 mm strip of material to flexural deformation across a span length of 75 mm in the three-point bending jig shown in *Figure 1*, followed by immediate immersion of the sample in one of the test liquids. After immersion for one hour the sample was examined for evidence of crazing, cracking or dissolution. All experiments were at room temperature.

The jig consisted of a central spring loaded screw of pitch 1 mm attached to an anvil acting as a fulcrum. A graduated drum fixed to the end of the screw enabled measurement of the movement of the fulcrum to within 0.1 mm.

If the centre of the specimen of thickness  $t$  mm is deflected through a distance  $\delta$  mm over a span length of  $l$  mm (*Figure 1*) the maximum strain in the specimen  $\epsilon_{\max}$  is<sup>4</sup>:

$$\epsilon_{\max} = 6\delta t/l^2 \quad (1)$$

For strains of the order of 1% or less, the strain at a distance  $a$  mm from the fulcrum is:

$$\epsilon = (l-2a)\epsilon_{\max}/l \quad (2)$$

When crazing occurred, the density of crazes decreased as distance from the fulcrum increased. In accordance with equation (2) the critical strain for crazing  $\epsilon_c$  could be

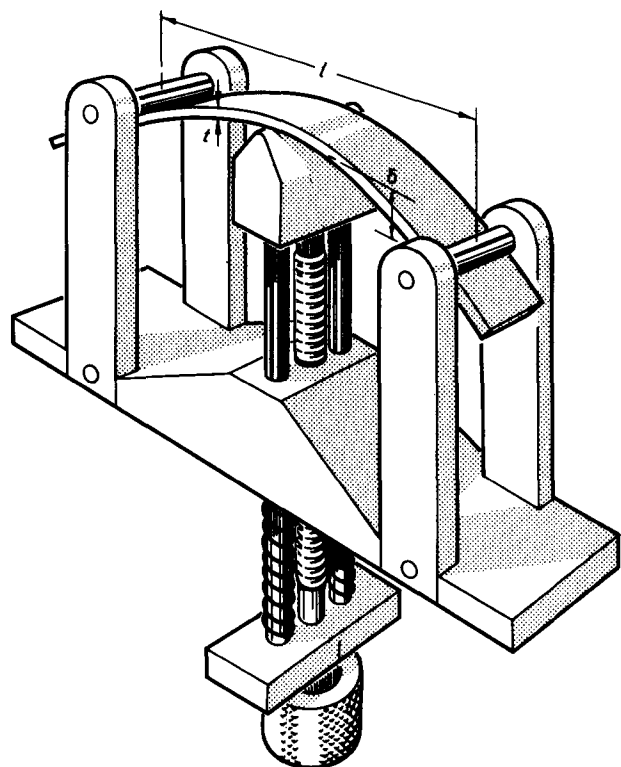


Figure 1 Three-point bending apparatus

determined by measuring the separation of the craze boundaries on either side of the fulcrum. If this is  $b$  mm then from equation (2):

$$\epsilon_c = (l - b)\epsilon_{\max}/l \quad (3)$$

The use of equation (3) is limited from its derivation to strains such that  $\delta$  is not larger than  $t$ ; that is, 1–2% strain for the sample thickness and experimental arrangement described. It is limited also by the presence of any stress concentrators or variations in specimen thickness. For these reasons it is important that, when determining  $\epsilon_c$ ,  $\epsilon_{\max}$  should be as close to  $\epsilon_c$  as possible. In practice  $\epsilon_c$  was estimated from an initial experiment. A strain close to  $\epsilon_c$  was then applied to a fresh specimen and the experiment was repeated until this condition was satisfied. In determining the craze boundaries, care was taken to exclude crazes at the edges of the specimen initiating from defects attributable to the milling process during sample preparation. Where cracking occurred, additional tests were performed in which successively lower strains were applied until cracking ceased.  $\epsilon_c$  does depend on the time under strain, particularly at short times, but the arbitrarily chosen time of one hour is sufficiently long so that the rate of change is unimportant.

## RESULTS

Solvents, cracking and crazing agents are listed in Table 1. The crazing agents have been classed into low-strain and high-strain crazing agents. Although the classification is arbitrary, there appeared to be a reasonable demarcation at a critical strain for crazing of about 0.6% for all three polymers. Liquids which did not cause crazing below this strain required considerably higher strains of 1% or greater before crazing occurred.

Solubility parameters of the liquids are from the data of

Hansen<sup>5</sup> and Crowley *et al.*<sup>6</sup>. Hydrogen bonding parameters are from the data of Crowley<sup>6</sup> and Nelson *et al.*<sup>7</sup>. The parameter is based on the work of Gordy and Stanford<sup>8</sup>, who measured the displacement of the OD infra-red absorption band in the 4  $\mu$ m range when different liquids were added to a solution of deuterated methanol (CH<sub>3</sub>OD) in benzene. The magnitude of this displacement, in wave numbers divided by ten, was defined as the hydrogen bonding parameter. Nelson's more recent data take into account the small hydrogen bonding capacity of benzene and use cyclohexane as a base of zero. Since the data are claimed to be more accurate than those of Gordy they have been used in preference to Gordy's or Crowley's wherever possible.

From Table 1 it is evident that correlation between crazing, cracking and solubility parameter is not good. Solvents for PMMA may have a solubility parameter between 8.5 and 13.3 (cal/cm<sup>3</sup>)<sup>1/2</sup> whilst cracking agents lie between 8.2 and 10.4. For the eight liquids of zero hydrogen-bonding parameter a plot of  $\epsilon_c$  against solubility parameter is similar to that of Bernier and Kambour<sup>2</sup> with a pronounced minimum in  $\epsilon_c$  close to the solubility parameter of the polymer. There are several indications that the behaviour of a more general range of liquids may be understood by considering specific interactions between the liquid and the polymer, particularly hydrogen bonding.

Solution theory is based on the thermodynamics of mixing of the components<sup>9</sup>. For intermolecular forces such as dispersion forces or polar forces in certain instances the assumptions of the theory remain approximately true and the theory may be applied with reasonable accuracy<sup>9</sup>. The complexity of type and strength of hydrogen bonding forces precludes rigorous analysis where such bonding occurs. Nevertheless, various attempts have been made to accommodate hydrogen bonding within a more general albeit empirical theory<sup>5-7</sup>.

Of these theories, that of Crowley *et al.*<sup>6</sup> appeared to offer most promise. They presented a three-parameter model incorporating solubility parameter, hydrogen bonding parameter and dipole moment to predict the solubility of cellulosic polymers in organic solvents. Solvents were found to be contained within a reasonably well defined volume of the three-dimensional plot.

The results on PMMA are plotted in Figure 2 as a function of solubility parameter and hydrogen bonding parameter using different symbols to distinguish solvents, cracking and crazing agents. Solvents for PMMA describe a definable region of the plot. This region of solubility is surrounded by cracking agents, low-strain crazing agents and, more remote from the region, high-strain crazing agents. The same is true for PVC and polysulphone (see Figures 3 and 4). For PVC it has been necessary to plot swelling agents since there are only a few good solvents with a listed hydrogen bonding parameter. Published hydrogen bonding parameters were not available for the cracking agents.

There is a large discrepancy in the hydrogen bonding parameter of dimethyl formamide (DMF) as determined by Gordy<sup>8</sup> and Nelson<sup>7</sup>. Gordy's figure of 11.7 puts DMF within the solvent region for PMMA, PVC and polysulphone whereas Nelson's result of 18.9 makes DMF anomalous for all three polymers. Significant differences between Hansen's data<sup>5</sup> for solubility parameters and Crowley's<sup>6</sup> occur for two of the liquids, 2-butoxyethanol and  $\gamma$ -butyrolactone. Crowley's value of 8.9 for the

Table 1 Properties of liquids and their effects on stressed polymers

Liquid	Solubility parameter (cal/cm <sup>3</sup> ) <sup>1/2</sup>	Hydrogen bonding parameter	Critical strain for crazing and other comments		
			PMMA	PVC	P1700
n-Pentane	7.0	0	0.90	1.23	High
Di-n-butyl ether	7.1	11.0	0.56	0.57	High
n-Hexane	7.3	0	0.79	—	—
n-Heptane	7.4	0	0.86	1.18	High
Diethyl ether	7.6	13.0	0.28	0.23	0.42
Methyl cyclohexane	7.8	0	0.92	0.73	High
Diocetyl phthalate	7.9	3.6	1.44	0.70	—
Cyclohexane	8.2	0	1.10	0.87	High
Ethyl benzoate	8.2	6.3	Crack	—	Crack
Methyl isobutyl ketone	8.4	10.5	S	Sw	—
Isoamyl formate	8.5	—	Crack	—	—
n-Butyl acetate	8.5	8.0	S	—	—
Carbon tetrachloride	8.7	0	0.31	0.69	Crack
1-Bromobutane	8.7	1.5	Crack	0.07	—
Tributyl amine	8.7	21.8	0.96	0.79	High
Ethyl benzene	8.8	4.2	Crack	0.19	Crack
Toluene	8.9	4.2	Crack	0.15 (Sw)	Crack
Butyl digol	8.9	13.0	0.19	0.21	Crack
2-Butoxyethanol	8.9	13.0	0.07	0.30	Crack
1,2-Dichloropropane	9.0	1.5	S	0.07	S
Ethyl acetate	9.1	8.4	S	—	Crack
Benzene	9.2	0	Crack	0.08 (Sw)	S
Chloroform	9.2	1.5	S	—	S
Mesityl oxide	9.2	12.0	S	S	—
Dibutyl phthalate	9.3	—	0.89	Crack	—
Methyl ethyl ketone	9.3	10.5	S	S or Sw	Crack
n-Butyl lactate	9.4	7.0	S	—	Crack
Tetrahydrofuran	9.5	12.0	S	—	—
Dimethyl aniline	9.5	14.3	Crack	—	—
1,1,2-Trichloroethane	9.6	1.5	—	—	S
Chlorobenzene	9.6	2.7	S	Sw	S
Acetophenone	9.7	—	S	—	—
Cyclohexanone	9.7	13.7	S	S	Crack
1,4-Dioxane	9.7	14.6	S	S	—
n-Octanol	9.7	18.7	0.48	> 0.60	—
Ethylene dichloride	9.8	1.5	—	—	S
Acetone	9.8	12.5	S	—	Crack
Methylene chloride	9.9	1.5	S	Sw	S
Dimethyl carbonate	9.9	4.9	—	—	Crack
2-Ethyl hexanol	9.9	18.7	0.37	—	0.81
o-Dichlorobenzene	10.0	—	S	0.26	—
Diethyl phthalate	10.0	—	0.39	Crack	—
Carbon disulphide	10.0	0	0.39	—	Crack
2-Nitropropane	10.0	4.0	S	—	S
Ethyl lactate	10.0	7.0	S	—	Crack
Butyronitrile	10.0	7.7	S	—	—
n-Heptanol	10.3	18.7	0.46	—	—
Acetic acid	10.4	—	0.12	0.31	—
1,2-Dibromoethane	10.4	—	Crack	—	—
Cyclopentanone	10.4	8.4	—	—	S
Nitrobenzene	10.6	2.8	S	S	S
Diethyl formamide	10.6	11.7	—	—	S
Pyridine	10.6	18.1	S	S (whitened)	S
Dimethyl phthalate	10.7	—	0.37	—	—
n-Hexanol	10.7	18.7	0.34	> 0.60	High
Acetyl acetone	10.8	8.4	—	—	S
Aniline	11.0	18.1	S	S	S
Nitroethane	11.1	2.5	S	—	—
n-Butanol	11.3	18.0	0.30	0.68	—
Isopropanol	11.5	16.7	0.26	0.79	—
n-Propanol	11.9	18.7	—	—	High
Dimethyl aniline	12.0	14.3	—	Sw	S
Dimethyl formamide	12.1	11.7	S	Sw (whitened)	S
Nitromethane	12.7	2.5	S	0.05	Crack
γ-Butyrolactone	12.8	9.7	S	Sw	S
Dimethyl sulphoxide	12.9	7.7	S	0.35	S
Ethanol	12.9	17.7	0.30	0.72	High
Propylene carbonate	13.3	4.9	S	—	Crack
Ethylene glycol	14.2	20.6	0.94	1.16	—
Methanol	14.3	19.8	0.31	0.68	—
Methyl formamide	16.1	12.0	0.04	0.19	0.50
Glycerol	21.1	—	1.40	1.36	—
Water	23.5	39.0	1.76	1.90	—

S=solvent; Sw=swelling agent; —=not known



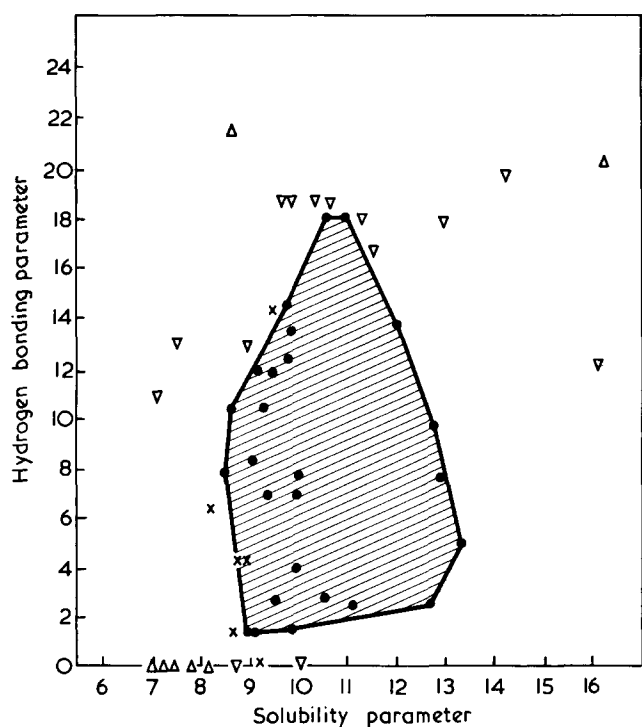


Figure 2 Solvents (●), cracking agents (x), low strain crazing agents (▽), and high strain crazing agents (△) for PMMA

solubility parameter of 2-butoxyethanol was more consistent with the bulk of the data on the three polymers than was Hansen's value of 10.3. In contrast, Crowley's value of 15.5 for  $\gamma$ -butyrolactone would be anomalous for these polymers and others that were tested whilst Hansen's value of 12.8 appears to be appropriate. In these three instances we have chosen the values which correlate most sensibly with the bulk of the results.

## DISCUSSION

It is evident from the results that a model considering solely the solubility parameter of liquids is inadequate to explain solution, crazing and cracking behaviour of a polymer in a general series of liquids. It is necessary to take account of other properties of the liquid. One such property appears to be the strength of hydrogen bonds between the liquid molecules themselves and between the molecules of the liquid and the polymer. Small<sup>10</sup> has shown the contribution to the heat of mixing that occurs due to the proton donating and attracting capabilities of the components of the mixture and has discussed how this affects solution.

A two-parameter model incorporating solubility parameter and hydrogen bonding parameter produces a more useful representation of solution, stress-cracking and crazing behaviour. The existence of a definite solvent region in Figures 2-4 with cracking agents adjacent to and crazing agents more remote from the region suggests that hydrogen bonding is indeed playing a part in these phenomena.

The distinction between solution or swelling and cracking is often diffuse, the predominating behaviour being determined by the applied strain and the time of immersion in the liquid. Thus, at lower strains and longer times an apparent cracking agent may evidently be a poor solvent or a swelling agent. In the light of this it appears

that the strain concentration at the crack tip permits more rapid local plasticization thus creating an instability favouring crack growth. Whether solution or cracking dominates will be determined by the rate of crack initiation and local plasticization which, in turn, will be a function of the applied strain.

PMMA, PVC and polysulphone each have sites capable of taking part in hydrogen bonding. The carbonyl oxygen of PMMA and the ether oxygen and sulphone group of polysulphone would be expected to be proton acceptors. The hydrogen atoms adjacent to the chlorine atoms in PVC could act as proton donors. Whether interaction will occur between these polymers and a particular liquid will depend on whether the liquid contains complementary proton donating or accepting ability.

It is interesting that, with the exception of tributyl amine and toluene, liquids which are solely proton donors or acceptors<sup>11</sup> are all solvents, swelling agents or cracking agents for the three polymers. Liquids which have a combination of donating and accepting ability or no hydrogen bonding properties at all tend to be crazing agents. The only exception to this was the polysulphone where carbon disulphide and carbon tetrachloride were cracking agents and benzene was a solvent.

This adds weight to our belief that hydrogen bonding is as crucial as solubility parameter in determining the solvent cracking or crazing properties of a liquid. The possibility of forming hydrogen bonds between liquid and polymer would energetically favour solution. As discussed above, cracking is closely allied to solution. In contrast, liquids which combine proton donating and accepting abilities have the alternative capacity to form intermolecular or intramolecular hydrogen bonds. In the former case, the breakdown of liquid-liquid bonds will disfavour solution. In the latter case the liquid will behave as if it had no hydrogen bonding property.

The solvent region for PMMA, PVC and polysulphone is bounded at a hydrogen bonding parameter of about 18 by points corresponding to the alcohols. Nelson *et al.*<sup>7</sup> have pointed out that the dilution of alcohols will cause

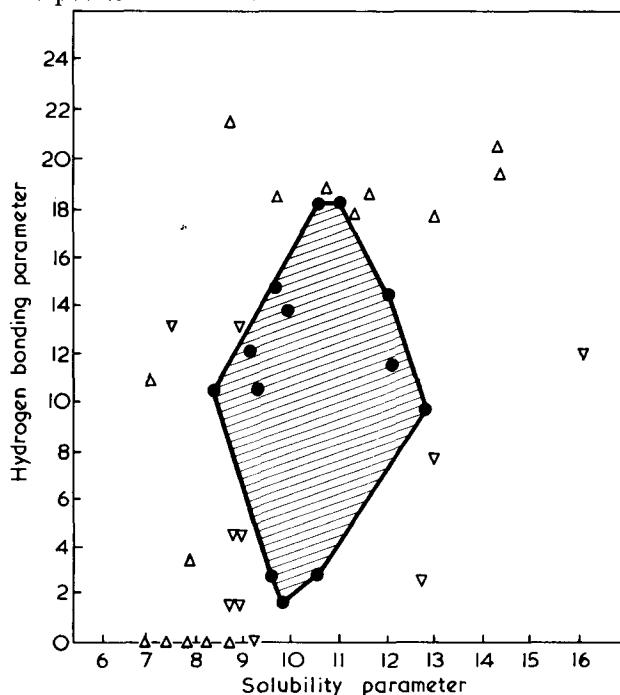


Figure 3 Solvents and swelling agents (●), low strain crazing agents (▽), and high strain crazing agents (△) for PVC

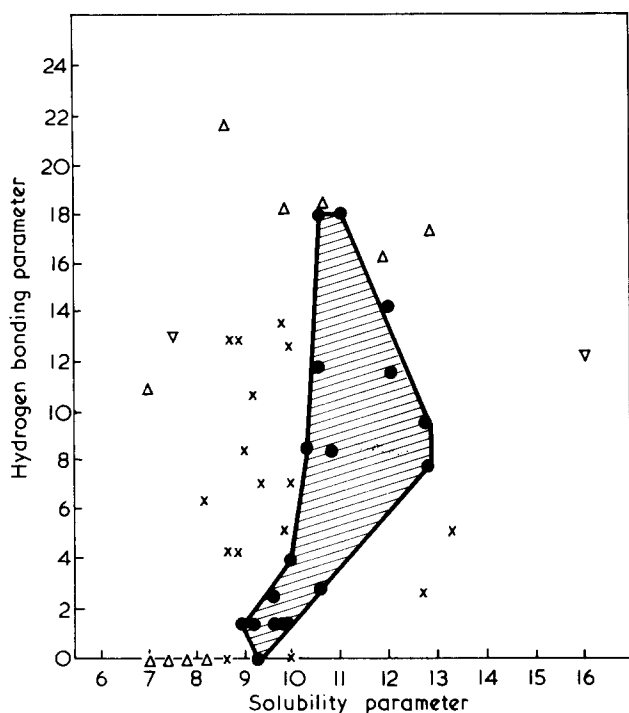


Figure 4 Solvents, cracking and crazing agents for polysulphone. Symbols are as in Figure 2.

hydrogen bonds to be broken. The energy required to do this may outweigh the energy of bonds formed between the alcohol and the polymer thus producing a condition disfavoured solution. For the particular case of the alcohols the values for the hydrogen bonding parameters may also be unrepresentative since the measurements were made using an alcohol, deuterated methyl alcohol, as the common liquid participating in hydrogen bonding with the liquids under test. Such a model liquid may be far removed from the complex situations present in polymers. More appropriate values might be obtained by using a better analogue of each polymer as the base liquid; for example, 2,4-dichloropentane for PVC.

Only proton accepting sites exist in PMMA and polysulphone and only a proton donating site in PVC. Since both proton accepting and donating liquids were effective as solvents for the three materials, factors other than hydrogen bonding parameter must be playing a contributory part. Each of the liquids is polar, as are the three polymers. It seems likely that dipolar interactions could be adding to the conditions favouring solution. Crowley successfully incorporated a third parameter accommodating the dipole moment of the liquids to explain the solution of cellulosic polymers. The same approach added no extra information to our results, possibly because the range of liquids we have used was not as extensive as Crowley's.

Other attempts at accounting for hydrogen bonding and dipole moment such as the data of Hay<sup>12</sup> and Hansen<sup>5</sup> were found to be unsuccessful when applied to the results on the polymers tested. In each case a scatter of apparently unrelated points was obtained.

For PMMA and PVC, weakly hydrogen bonded liquids of bonding parameter less than 1.5 are not solvents. For moderately hydrogen bonded liquids solubility extends over about four units of solubility parameter. As hydrogen bonding parameter increases further the solvent region narrows and terminates.

For the polysulphone the solvent region is more restricted than for PMMA and PVC. The shape of it is such as to suggest that for moderately hydrogen bonded liquids (up to a parameter of about 9) the apparent solubility parameter of the polymer increases. This is further illustrated by measurements by Nield (personal communication) to determine the solubility parameter of the polymer by the intrinsic viscosity method<sup>13</sup>. The intrinsic viscosity of solutions from solvents of different solubility parameters is measured. The maximum in the plot of intrinsic viscosity *versus* solubility parameter is taken as the solubility parameter of the solute. Using mixtures of two moderately hydrogen bonded liquids, chlorobenzene and propylene carbonate, Nield obtained a value of 10.3 for the solubility parameter of the polymer; a higher value than the figure of 9.2 for non-bonded liquids suggested by the data of Figure 4. Substituting a more strongly hydrogen bonded liquid, DMF, in place of propylene carbonate, the maximum viscosity moved to an even higher solubility parameter of 11.4.

## CONCLUSIONS

Solution, environmental stress crazing and cracking cannot be adequately explained solely by the solubility parameters of the liquids. There is considerable evidence that the hydrogen bonding properties of the liquids are playing a crucial role. A two-parameter model incorporating solubility parameter and hydrogen bonding parameter appears to be an effective means of representing the solubility, cracking and crazing properties of a polymer capable of participating in hydrogen bonding. The success in applying this model to the polymers discussed suggests that determination of the 'solvent region' for other amorphous polymers would be a rapid way of examining their likely behaviour in the presence of liquid environments.

## ACKNOWLEDGEMENTS

Thanks are due to Dr E. Nield who gave valuable advice during this project. The experimental work was performed by P. White, T. P. Mervyn and C. Toates.

## REFERENCES

- Howard, J. B. 'Engineering Design for Plastics', Reinhold, New York, 1964, p 742
- Bernier, G. A. and Kambour, R. P. *Macromolecules* 1968, **1**, 393
- Bergen, R. L. Jr. *SPE J.* 1968, **24** (8), 77
- Roark, R. J. 'Formulas for Stress and Strain', McGraw-Hill, New York, 1954
- Hansen, C. M. *J. Paint Tech.* 1967, **39**, 404
- Crowley, J. D., Teague, G. S. and Lowe, J. W. *J. Paint Tech.* 1966, **38**, 269
- Nelson, R. C., Hemwall, R. W. and Edwards, G. D. *J. Paint Tech.* 1970, **42**, 636
- Gordy, W. and Stanford, S. C. *J. Chem. Phys.* 1941, **9**, 204
- Morawetz, H. 'Macromolecules in Solution', Interscience, New York, 1965, p 33
- Small, P. A. *J. Appl. Chem.* 1953, **3**, 71
- Pimentel, G. C. and McClennan, A. L. 'The Hydrogen Bond', Reinhold, New York, 1960, p 39
- Hay, K. L. 'Tables of Solubility Parameters', Union Carbide Corporation, South Charleston, W. Va, July 1969.
- Cowie, J. M. G., Ranson, R. J. and Burchard, W. *Br. Polym. J.* 1969, **1**, 187

# Polymerization of vinyl chloride by the AlEt<sub>3</sub>/benzoyl-peroxide/Lewis-base system and the role of the Lewis base in initiation

E. B. Milovskaya, E. L. Kopp, O. S. Mikhailicheva,  
V. M. Denisov and A. I. Koltsov

*Institute of High Molecular Compounds, Bolshoi 31, Leningrad, USSR  
(Received 1 January 1971)*

Kinetics of polymerization of vinyl chloride under the influence of the AlEt<sub>3</sub>/benzoyl-peroxide initiation system in the presence of the complexing agents allyl acetate, dibutyl ether and pyridine have been studied. It follows from the kinetic dependences established (which were confirmed by infra-red and nuclear magnetic resonance spectroscopies) that the role of polar agents, irrespective of their complexing ability, is to reduce the initial concentration of aluminium alkyl. Free-radical formation proper occurs by the interaction of the uncomplexed form of AlEt<sub>3</sub> with peroxide. The process as a whole has S<sub>N</sub>1 kinetics. When the polar monomer vinyl acetate is used as a complexing agent, the complexed form of AlEt<sub>3</sub> participates in the initiation. A suggestion is put forward concerning the possibility of the occurrence of a quite different mechanism of interaction between the components of the initiation system in the presence of polar monomers.

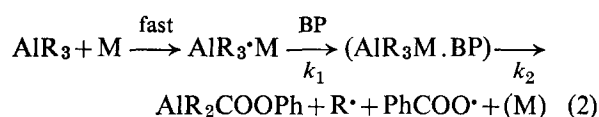
## INTRODUCTION

In recent years systems based on aluminium alkyls and acyl peroxides have been used to initiate the polymerization of the vinyl monomers—vinyl acetate (VA)<sup>1,2</sup>, methyl methacrylate (MMA)<sup>3</sup>, acrylonitrile (AN)<sup>4</sup> and vinyl chloride (VC)<sup>5,6</sup>. The process involves free-radical polymerization and can be carried out at much lower temperatures than the thermal decomposition of peroxide. The efficiency of these systems lies in the separation of the initiating system components by the polar agent or the monomer since direct reaction between AlR<sub>3</sub> and peroxide is explosive<sup>7,8</sup>. The electron-donating ability of such monomers as VA, AN and MMA proves to be sufficient for the development of polymerization. For all the systems investigated the same expression has been derived for the dependence of the overall rate of the process on the concentrations of the monomer and of the initiator components:

$$V = k[M]^{1.0-1.2}[AlR_3]^{0.5}[P]^{0.5} \quad (1)$$

where M is AN, MMA and VA, AlR<sub>3</sub> is AlEt<sub>3</sub> and Al(iBu)<sub>3</sub>, P is benzoyl peroxide (BP) and dicyclohexyl peroxidicarbonate (PC).

On the basis of the kinetic results and the fact that the monomer should participate in the initiation, the formation of free radicals has been represented as a series of reactions<sup>5</sup>:



Under the condition that  $k_1 \ll k_2$

$$V_{in} = k_{in}[AlR_3][BP] \quad (1a)$$

The effective polymerization of the monomer with low polarity (VC)\* could be carried out in the presence of the complexing agent (CA)—ester, ether and nitrile<sup>5,6†</sup>. To establish the mechanism of free-radical formation and the role of CA in VC polymerization, detailed kinetic investigations were made using the AlEt<sub>3</sub>-BP system in the absence and the presence of CA—ethyl acetate (EA)<sup>6</sup>. It was found that the expression for the dependence of the

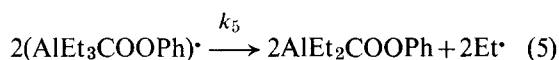
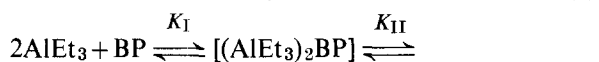
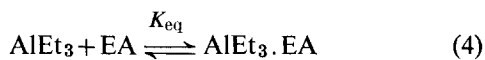
\* In this case, the term polarity means the electron-donating ability.  
† Polymerization of VC in the absence of CA can be carried out only over a very narrow range of concentrations of monomer (not lower than 7 mol/l) and initiator components ( $3 \times 10^{-3}$ – $5 \times 10^{-2}$  mol/l), but even under these conditions conversion does not exceed 5–7%<sup>6</sup>

overall rate of the process in the presence of catalytic amounts of EA on the concentrations of the monomer, EA, and the initiator components has the form:

$$V = k_3[VC]^{1.2} \left( \frac{[AlEt_3]}{[EA]} \right)^{0.5} [BP]^{0.25} \quad (3)$$

A similar dependence on the concentration of monomer and initiator components was shown for the case of VC polymerization without CA.

The mechanism for the initiation reactions is:



If the equilibria with  $K_I$  and  $K_{II}$  shifts to the left, the equilibrium of reaction (4) shifts to the right and the overall rate of interaction (5) is determined by  $k_5$ , the expression for the initiation reaction rate in the system with EA can be written:

$$V_{in} = k_{in} \frac{[AlEt_3]}{[EA]} [BP]^{0.5} \quad (3a)$$

From the results obtained, it follows that the role of EA is to reduce the initial concentration of aluminium alkyl by complex formation (equation 4); free-radical formation occurs by reaction of uncomplexed aluminium alkyl with peroxide (i.e., it occurs in the same manner as under model conditions<sup>7-9</sup>).

Comparison of the kinetic dependence for the polymerization of polar monomers (equation 1) with that found for VC polymerization in the presence of EA (equation 3), and comparison of reactions responsible for the initiation (reactions 2 and 4-5) both showed that EA did not simulate the polar monomer function in the initiation.

Further investigations were carried out to determine the true role of the polar monomer in initiation. It is clear that this problem cannot be solved under the conditions of the polymerization of the polar monomer; therefore, an artificial device was used, namely VC polymerization was studied in the presence of catalytic amounts of a polar monomer (VA).

On the other hand, it was interesting to establish to what extent the reactions for the EA system are valid for different classes of CA.

Our results allowed us to obtain general ideas about the mechanism of free-radical formation in the AlR<sub>3</sub>/acyl peroxide systems in the presence of electron-donors, including polar monomers.

## EXPERIMENTAL

Experiments were conducted in the absence of moisture and air. The solvents benzene and octane were purified in the usual way and then dried with calcium hydride and concentrated butyl lithium. The complexing agents were purified according to the methods<sup>10</sup> previously described and then dried with calcium hydride and distilled under vacuum.

VA was pre-polymerized with the Al(iBu)<sub>3</sub>-BP system. At low concentrations these compounds were used in octane solution. Commercial AlEt<sub>3</sub> was used without additional purification in octane solution. Its concentration was determined according to the method of Razuvaev and Graevsky<sup>11</sup>. The concentration of the solution of the complexing compound was determined from the AlEt<sub>3</sub> solution of a known concentration. Al(iBu)<sub>3</sub> was distilled under vacuum and the fraction boiling at 41°C (1 mmHg) was used. Benzoyl peroxide was purified from its chloroform solution, the active oxygen content being 98.5-99%. The BP-benzene solution was added. VC was carefully degassed, dried at -30°C over the concentrated butyl lithium, the polymerization being allowed to go to 3-5% conversion. VC was then pre-polymerized using the AlEt<sub>3</sub>-Bu<sub>2</sub>O-BP system. The purity of the monomer was checked chromatographically.

Polymerization was carried out in a single-cell dilatometer (with a magnetic stirrer) having a capacity of about 15 ml and with a capillary calibrated to 0.01 ml. The dilatometer, previously heated under vacuum, was filled with argon and the AlEt<sub>3</sub> and CA solutions and octane were introduced from Schlenk vessels supplied with a needle. The monomer was added in weighed amounts from the balloon through the needle. The order in which the components were added was always the same: CA, AlEt<sub>3</sub>, solvent, monomer. The temperature of the reaction mixture was thermostatically controlled to within ±0.1°C, and the BP solution was injected with a syringe. In the kinetic experiments the polymerization rate was calculated for a 3-5% conversion, this being estimated from contraction. The contraction coefficient was found as a mean value from several experiments on the basis of gravimetric measurements of the polymer yield.

Infra-red spectra were taken using a UR-10 spectrometer. Sealed cells of potassium bromide were used to protect the organo-aluminium compounds from moisture and air. The cell was carefully dried under vacuum and filled with the previously prepared solutions of the analysed components in octane.

The equilibrium constant ( $K_{eq}$ ) of reaction (4) was calculated from:

$$K_{eq} = \frac{[AlEt_3 \cdot EA]}{[EA][AlEt_3]} \quad (6)$$

The following expression was used to calculate the concentration of free EA  $[EA]$  from the 1752 cm<sup>-1</sup> band intensity:

$$[EA] = \frac{E_x[EA]_0}{E_0} \quad (7)$$

where  $[EA]_0$  is the initial EA concentration;

$E_0$  is the molar extinction coefficient of the absorption band of the EA carbonyl oxygen, equal to (562 ± 14) l mol<sup>-1</sup> cm<sup>-1</sup>;

$E_x$  is the extinction coefficient of the 1752 cm<sup>-1</sup> band in the spectra of the complex.

The concentration of the AlEt<sub>3</sub>·EA complex was determined as the difference between  $[EA]_0$  and  $[EA]$ , and the concentration of  $[AlEt_3]$  from  $\{[AlEt_3]_0 - [AlEt_3 \cdot EA]\}$ .

The preparation of samples for proton magnetic resonance (p.m.r.) and <sup>27</sup>Al nuclear magnetic resonance

Table 1 VC polymerization with the AlEt<sub>3</sub>-BP system in the absence and presence of CA. [VC]=8mol/l; solvents: octane, benzene; temperature=0°C

Exp. No.	CA*	Concentration × 10 <sup>2</sup> (mol/l)			Conversion (%)		
		AlEt <sub>3</sub>	CA	BP	1h	2h	4h
1	VA	1.0	16.0	1.0	11.8	15.6	18.1
2	EA	5.0	25.0	5.0	30.0	45.5	56.6
3	—	5.0	—	5.0	2.2	2.9	3.3

\* CA = complexing agent

(n.m.r.) study was carried out as follows: 10% benzene solutions of Al(iBu)<sub>3</sub> with a certain amount of added CA were placed into the sample tubes—5 mm and 18 mm outside diameter for p.m.r. and <sup>27</sup>Al-n.m.r., respectively—which had been dried at high temperature in vacuum. All operations including sealing the tubes were performed under vacuum. The samples were stored in liquid nitrogen and n.m.r. spectra were recorded (4–5 times) just after the samples had reached room temperature.

High resolution p.m.r. spectra were recorded with a YEOL YNM-3 spectrometer (40 MHz). No changes were observed in the spectra for one hour. Weak <sup>27</sup>Al-n.m.r. signals were observed with a RYa-2301 spectrometer (8 MHz) using phase detection techniques. The peak-to-peak line widths were measured allowing for over-modulation<sup>12</sup>. Modulation amplitude and frequency were equal to 1.5 gauss and 35 Hz, respectively. The speed of field sweep was equal to 50 mg/sec and response time was 20 sec.

RESULTS AND DISCUSSION

AlEt<sub>3</sub>/vinyl-acetate/benzoyl-peroxide system

In the presence of catalytic amounts of VA the AlEt<sub>3</sub>-BP system can be successfully used for VC polymerization. Table 1 shows the data obtained and gives the results for the system without CA and in the presence of EA. The reaction kinetics were studied at 0°C.

The rate was estimated gravimetrically from the polymer yield. When the ratio [VA]/[AlEt<sub>3</sub>] is equal to or greater than one, the rate practically coincides with the value calculated from the contraction. Figure 1 shows the rate dependence of the VA concentration, from which one can conclude that under the experimental conditions the composition of the complex resulting from the reaction between AlEt<sub>3</sub> and VA is 1 : 1



With the same concentration ratio of VA and AlEt<sub>3</sub> the rate is fixed by the initial concentration of AlEt<sub>3</sub>, from which it follows that the free-radical formation under given conditions is a result of the interaction between benzoyl peroxide and the AlEt<sub>3</sub>.VA complex. When the concentrations of VA are lower than those of AlEt<sub>3</sub> two processes occur simultaneously (with comparable rates): they result from the reaction of BP with free aluminium alkyl and with aluminium alkyl complexed with VA. The dependence in Figure 1 for the region of [VA]/[AlEt<sub>3</sub>] < 1 can be explained by the fact that the rate was estimated from the polymer yield and the interaction

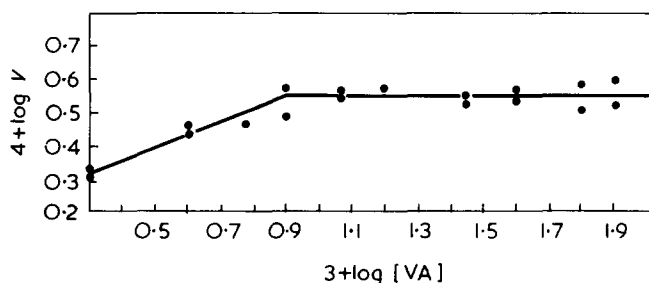


Figure 1 Dependence of the polymerization rate on the VA concentration with the system AlEt<sub>3</sub>-VA-BP in the solvents octane and benzene at 0°C. [VC]=4mol/l; [AlEt<sub>3</sub>]=1 × 10<sup>-2</sup> mol/l; [BP]=5 × 10<sup>-3</sup> mol/l

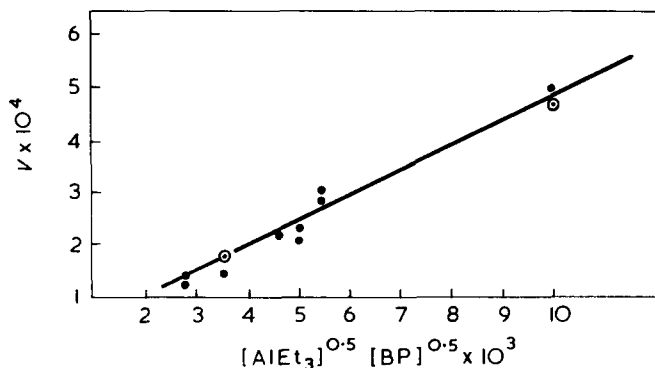


Figure 2 Dependence of the polymerization rate on the concentration of the initiator components in the system AlEt<sub>3</sub>-VA-BP in the solvents octane and benzene at 0°C. [VC]=4 mol/l; [VA]=5 × 10<sup>-2</sup> mol/l

of large amounts of free AlEt<sub>3</sub> with BP was followed by the formation of considerable amounts of oligomers<sup>6</sup>. In order to avoid the superposition of two effects, a further study of the kinetics was made in the concentration range 10 > [VA]/[AlEt<sub>3</sub>] > 1. (As noted, the region of low concentration ratios is characterized by appreciable oligomerization, whereas at large values one should take into account the copolymerization processes.)

Figure 2 demonstrates the rate dependence of the process on the concentration of the components of the initiation system. From these data, under conditions of bimolecular termination of growing chains, the expression for the initiation reaction rate may be written as follows:

$$V_{in} = k_9 [AlEt_3] [BP] \quad (9)$$

Figure 3 gives the dependence of the overall rate constant of the process on the inverse temperature from which E<sub>0</sub> is estimated to be 9.7 ± 1.2 kcal/mol, E<sub>in</sub> being 16.5 kcal/mol. In the calculation of E<sub>in</sub> we used the value (E<sub>p</sub> - ½ E<sub>t</sub>) = 1.5 kcal/mol for VC<sup>13, 14</sup>.

The kinetic results obtained enable the initiation in the AlEt<sub>3</sub>-VA-BP system to be represented as a sequence of reactions expressed by reaction (2). The similarity of the kinetic results (equations 1a and 9) and the E<sub>in</sub> value for the AlEt<sub>3</sub>-VA-BP system with the corresponding parameters, as established in the polymerization proper of VA<sup>1</sup>, is evidence that in both cases the free radicals are formed by the same mechanism. Thus, this work suggests that in the presence of a polar monomer (VA) the free radicals are formed as a result of reaction between the complexed form of aluminium alkyl with peroxide,

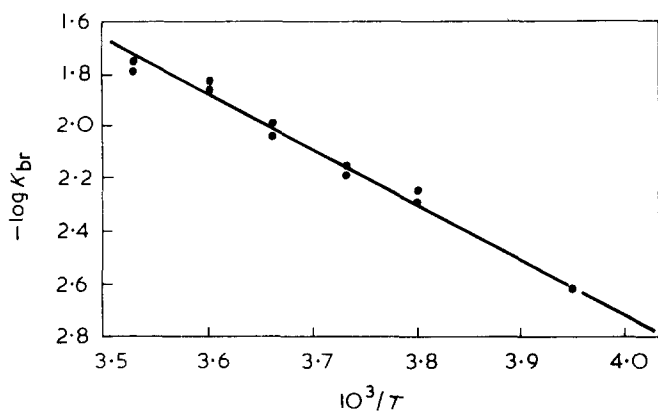


Figure 3 Dependence of the rate constant on the inverse temperature for the system  $\text{AlEt}_3$ -VA-BP

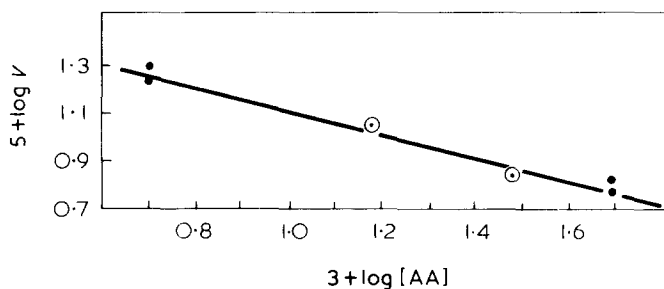


Figure 4 Dependence of the polymerization rate on the AA concentration with the system  $\text{AlEt}_3$ -AA-BP in the solvents octane and benzene at  $0^\circ\text{C}$ .  $[\text{VC}] = 4 \text{ mol/l}$ ;  $[\text{AlEt}_3] = [\text{BP}] = 5 \times 10^{-3} \text{ mol/l}$

whereas for EA this process is described by the reactions of the  $\text{S}_{\text{NI}}$  type.

#### $\text{AlEt}_3$ /allyl-acetate/benzoyl-peroxide system

The reason for the sharp difference in behaviour of compounds of similar structure was investigated. The complexing agent used was allyl acetate (AA), a compound combining all the structural features of EA and VA. AA itself is not polymerized under the influence of the  $\text{AlEt}_3$ -BP system, but its presence in catalytic amounts ensures the effective polymerization of VC. Thus, under conditions similar to those in Table 1 (experiment 2) the polymer yield is 25.3, 38.3 and 46.4%. The kinetics of VC polymerization with the  $\text{AlEt}_3$ -AA-BP system was studied at  $0^\circ\text{C}$ . Figure 4 shows the dependence of the rate of the process on the AA concentration; Figure 5 shows the same dependence on the concentration of the initiator components. On the basis of the above data the expression for the initiation reaction rate in this system can be written as:

$$V_{\text{in}} = k_{10} \frac{[\text{AlEt}_3]}{[\text{AA}]} [\text{BP}]^{0.5} \quad (10)$$

The overall constant of the process is  $1.18 \times 10^{-4} (\text{l mol}^{-1})^{0.25} \text{ sec}^{-1}$  at  $0^\circ\text{C}$ . The overall activation energy for the VC polymerization is estimated to be  $7.3 \pm 1.0 \text{ kcal/mol}$  (Figure 6), hence  $E_{\text{in}}$  is 11.6 kcal/mol.

From the equality of the expressions obtained for EA (equation 3a) and for AA (equation 10) it follows that the

free-radical formation in the systems with the participation of these CA is the result of the same reactions (4 and 5). As mentioned above, a similar mechanism of the interaction of the initiator components is also realized without CA. This permits one to calculate, from the kinetic data, the thermodynamic parameters for the complexing reaction of AA with  $\text{AlEt}_3$  (reaction of type 4), the equilibrium constant ( $K_{\text{eq}}$ ) and the enthalpy ( $\Delta H$ ).

$$k_0 = (2f)^{1/2} \frac{k_p}{k_t^{1/2}} \cdot k_{\text{in}}^{1/2} \text{ in the absence of CA}$$

and

$$k'_0 = (2f)^{1/2} \frac{k_p}{k_t^{1/2}} \cdot \left( \frac{k_{\text{in}}}{K_{\text{eq}}} \right)^{1/2} \text{ in the presence of CA}$$

Using the  $k_0$  values without CA equal to  $1.41 \times 10^{-2} (\text{l mol}^{-1})^{0.75} \text{ sec}^{-1}$  (corrected as compared with the value given in reference 6), and  $k'_0$  with AA as given above, the value of  $K_{\text{eq}}$  is obtained as  $1.4 \times 10^4 \text{ l mol}^{-1}$  at  $0^\circ\text{C}$ . (The assumption about the equality of  $f$  efficiencies of the initiation in the absence and presence of CA makes this calculation somewhat tentative.)

The value for the heat of complexing reaction is derived from:

$$E_{\text{in}} (\text{without CA}) = E_{\text{in}} (\text{with AA}) + \Delta H \quad (11)$$

Taking  $E_{\text{in}} (\text{without CA}) = 1.8 \text{ kcal/mol}$  (ref. 6) the value of  $\Delta H$  is  $-9.8 \text{ kcal/mol}$ .

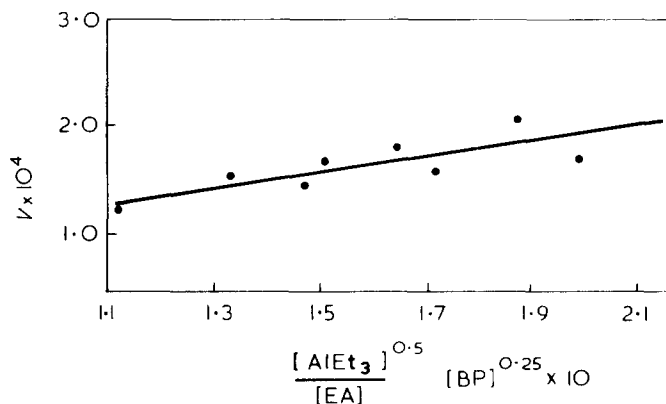


Figure 5 Dependence of the polymerization rate on the concentration of the initiator components in the system  $\text{AlEt}_3$ -AA-BP in the solvents octane and benzene at  $0^\circ\text{C}$ .  $[\text{VC}] = 4 \text{ mol/l}$ ; molar ratio  $\text{AA}/\text{AlEt}_3 = \text{constant} = 4$

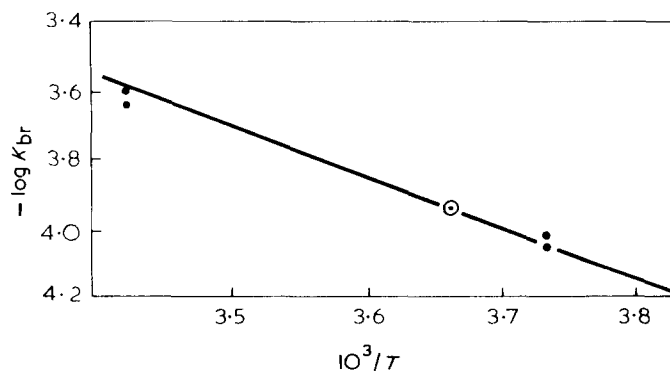


Figure 6 Dependence of the rate constant on the inverse temperature for the system  $\text{AlEt}_3$ -AA-BP

The values of the heat effect and the equilibrium constant of the complexing reaction of  $AlEt_3$  with AA practically coincide with the corresponding parameters established for EA ( $\Delta H = -9.2$  kcal/mol;  $K_{eq} = 1.5 \times 10^4$  l mol<sup>-1</sup> \*), which suggests a rather similar electron-donating ability for these compounds.

Infra-red spectra of CA complexes with  $AlEt_3$  were studied to check the conclusions, obtained from kinetic data, about reversibility and the stoichiometric relations of the complexing reaction of EA and AA with  $AlEt_3$  and also to find which oxygen atom of the ester group takes part in this interaction. Figures 7 and 8 compare the spectra of  $AlEt_3$ /EA and  $AlEt_3$ /AA complexes with those of the corresponding free CA. From the data obtained it follows that in the presence of  $AlEt_3$  the carbonyl-oxygen absorption band is split into two bands, one of which corresponds to the carbonyl oxygen of the free CA (1752 cm<sup>-1</sup>), the other one corresponding to the carbonyl oxygen of the CA in the complex with  $AlEt_3$  (1678 cm<sup>-1</sup>). The absorption band of the ether oxygen (1230 cm<sup>-1</sup>) is shifted towards higher frequencies (1320 cm<sup>-1</sup>), suggesting the absence of complexing between this group and  $AlEt_3$ , since such interaction would cause the reverse effect. The results obtained lead to the conclusion that the complexing between  $AlEt_3$  and the ester investigated occurs only with the carbonyl oxygen, and the shift in the absorption band of the ether oxygen is caused by this interaction. These facts agree with the information obtained from the study of the i.r. spectra of benzoic and caprylic esters complexes with  $AlEt_3$  <sup>15</sup>.

A quantitative study of the complexing reaction with i.r. spectroscopy was conducted with EA. The presence of the absorption band in the 1752 cm<sup>-1</sup> region with  $[EA]/[AlEt_3] \leq 1$  (Figures 9A and B) indicates the existence of non-complexed EA, i.e. the reversibility of the complexing reaction. The band intensity is low, which suggests a large value of  $K_{eq}$ . At  $[EA]/[AlEt_3] > 1$  a sharp increase in the intensity of this band occurs (Figure 9C). On this basis we can state that stoichiometry of the formation of the  $AlEt_3$ /EA complex corresponds to 1 : 1. We have estimated  $K_{eq}$  from the intensity of the free EA band using equation (6). The value of the constant obtained is  $7 \times 10^3$  l mol<sup>-1</sup> at 25°C. To compare the  $K_{eq}$  value obtained under model conditions (at 25°C) and in the kinetic experiments (at 0°C), it was calculated for 25°C. From the usual equations  $-RT \ln K_{eq} = \Delta H - T\Delta S$  (using  $\Delta H = -9.2$  kcal/mol and  $\Delta S = -14.8$  e.u.)  $K_{eq(25^\circ C)}$  was estimated to be  $2 \times 10^3$  l mol<sup>-1</sup>.

Sufficiently good agreement of the equilibrium constant obtained for the reaction of EA with  $AlEt_3$  by two independent methods confirms both the validity of the proposed kinetic scheme and shows that the kinetic data obtained can be used for the calculation of this value.

As may be expected, one of the reasons for different behaviour of EA and VA in the initiation is connected with a much larger stability of the  $AlEt_3$  complex with the polar monomer. This, in turn, could be due to chelate formation (with the participation of double bond). It is clear that such a possibility is also valid for the case of

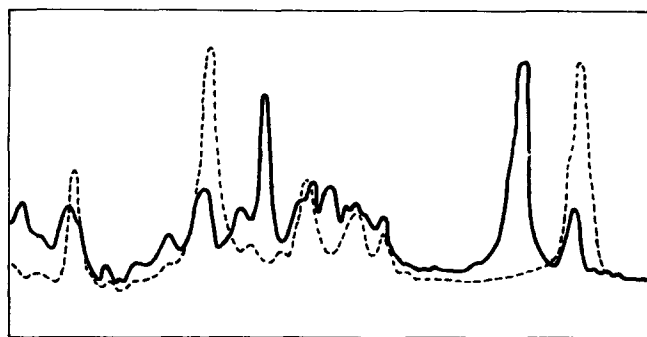


Figure 7 Infra-red spectra of EA complexed with  $AlEt_3$  (—) and of free EA (-----) in octane at 25°C

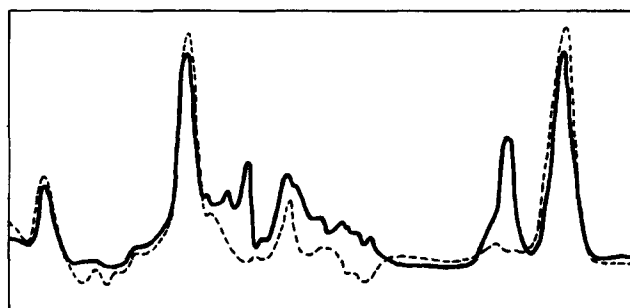


Figure 8 Infra-red spectra of AA complexed with  $AlEt_3$  (—) and of free AA (-----) in octane at 25°C

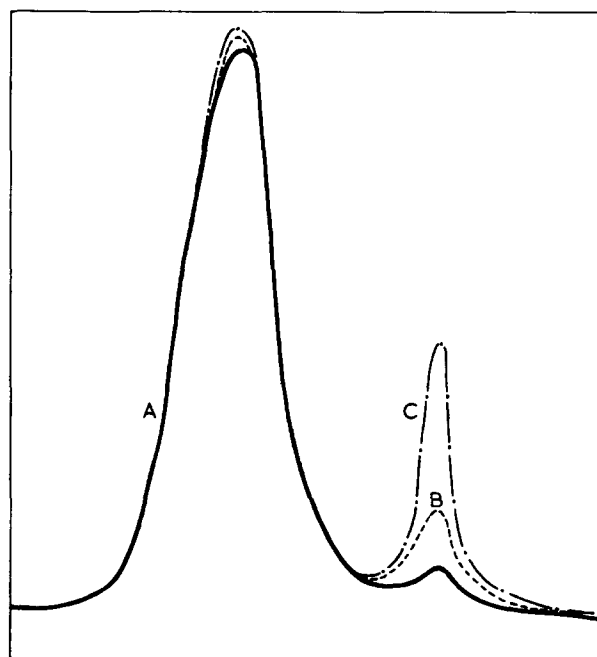


Figure 9 Infra-red spectra of the complex  $AlEt_3$ -EA (100 mol/l) in octane at 25°C. (A) Molar ratio  $[EA]/[AlEt_3] = 0.9$ ; EA = 7.4 mol/l (—). (B) Molar ratio  $[EA]/[AlEt_3] = 1.0$ ; EA = 8.0 mol/l (-----). (C) Molar ratio  $[EA]/[AlEt_3] = 1.1$ ; EA = 8.8 mol/l (---·---·)

\* For the calculation of  $K_{eq}$  the value  $k_o = 1.41 \times 10^{-2}$  (l mol<sup>-1</sup>)<sup>0.75</sup> sec<sup>-1</sup> was used, i.e. the same value as in the calculation of  $K_{eq}$  for AA. This led to a change in  $K_{eq}$  for EA compared to that given by Kopp and Milovskaya<sup>6</sup>

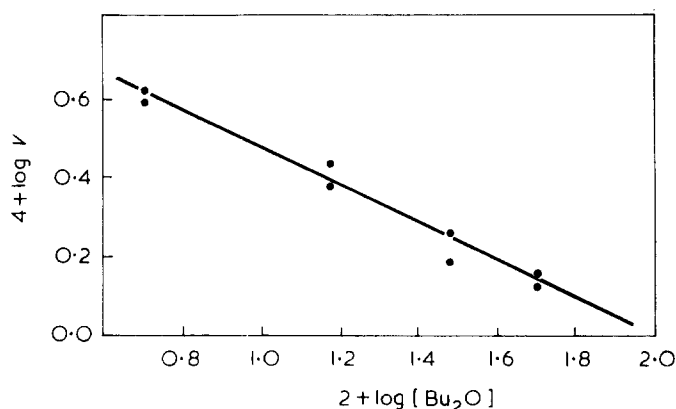


Figure 10 Dependence of the polymerization rate on the  $Bu_2O$  concentration with the system  $AlEt_3$ - $Bu_2O$ -BP in the solvents octane and benzene at  $0^\circ C$ .  $[VC]=8\text{ mol/l}$ ;  $[AlEt_3]=[BP]=1 \times 10^{-2}\text{ mol/l}$

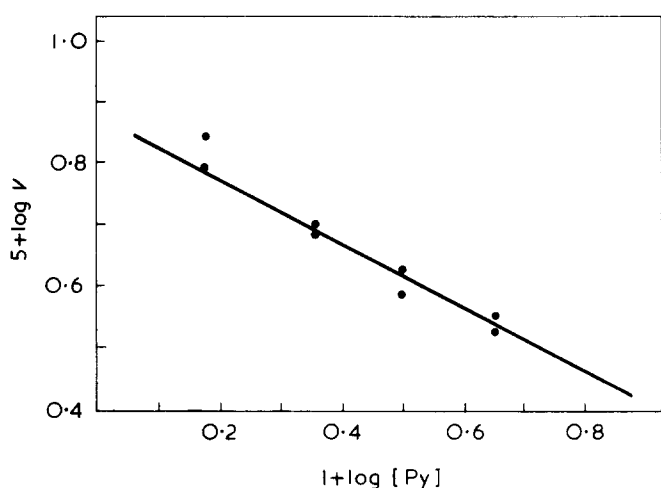


Figure 11 Dependence of the polymerization rate on the Py concentration with the system  $AlEt_3$ -Py-BP in the solvents octane and benzene at  $20^\circ C$ .  $[VC]=8\text{ mol/l}$ ;  $[AlEt_3]=[BP]=5 \times 10^{-2}\text{ mol/l}$

AA, but the kinetic studies showed that the initiation process is similar for EA and AA, which suggests that the chelate reaction cannot be responsible for the observed effect.

*$AlEt_3$ /pyridine/benzoyl-peroxide and  $AlEt_3$ /ether/benzoyl-peroxide systems*

In a further study, the complexing agents used were selected on the basis of the stability of the complexes formed. Pyridine (Py)<sup>16</sup>, whose complexes with  $AlR_3$  are among the most stable\* and dibutyl ether ( $Bu_2O$ ), whose complexes are much less stable, were chosen. A study of kinetics using these complexing agents was restricted to evaluating the dependence on the CA concentration. The process with  $Bu_2O$  participation was investigated at  $0^\circ C$ . The appreciable complexing ability of Py, as compared with other complexing agents, was shown by the fact that polymerization had a noticeable rate only at higher con-

\* Py unlike  $R_3N$  does not form a low temperature initiating system with BP<sup>17</sup>

centrations of the initiator components and of the monomer and at  $20^\circ C$ . (At  $0^\circ C$ , polymerization also occurs but, because of extremely low rates, the process cannot be studied over a sufficiently large range of pyridine concentrations.) It follows from the dependence of polymerization rates on the  $Bu_2O$  and Py concentrations (Figures 10 and 11) that the order for CA is  $-0.5$ , i.e. it corresponds to the same dependence as in the case of EA and AA. Hence we can affirm that for all the cases investigated the function of non-polymerized CA is uniform. Hence free-radical formation, i.e. the reaction proper between  $AlEt_3$  and BP, can be described by equation (5). On this basis and using equation (3), a calculation can be made of the overall rate constants ( $k_0'$ ) of the processes with  $Bu_2O$  and Py. These are  $5.03 \times 10^{-6} (\text{l mol}^{-1})^{0.25} \text{ sec}^{-1}$  and  $2.54 \times 10^{-4} (\text{l mol}^{-1})^{0.25} \text{ sec}^{-1}$  at  $0^\circ C$  for Py and  $Bu_2O$ , respectively.

The data necessary for the calculation of the overall activation energy of the VC polymerization with the  $AlEt_3$ -Py-BP and  $AlEt_3$ - $Bu_2O$ -BP systems are given in Figures 12a and b. The calculated values were  $8.9 \pm 0.8 \text{ kcal/mol}$  ( $Bu_2O$ ) and  $12.1 \pm 1 \text{ kcal/mol}$  (Py).

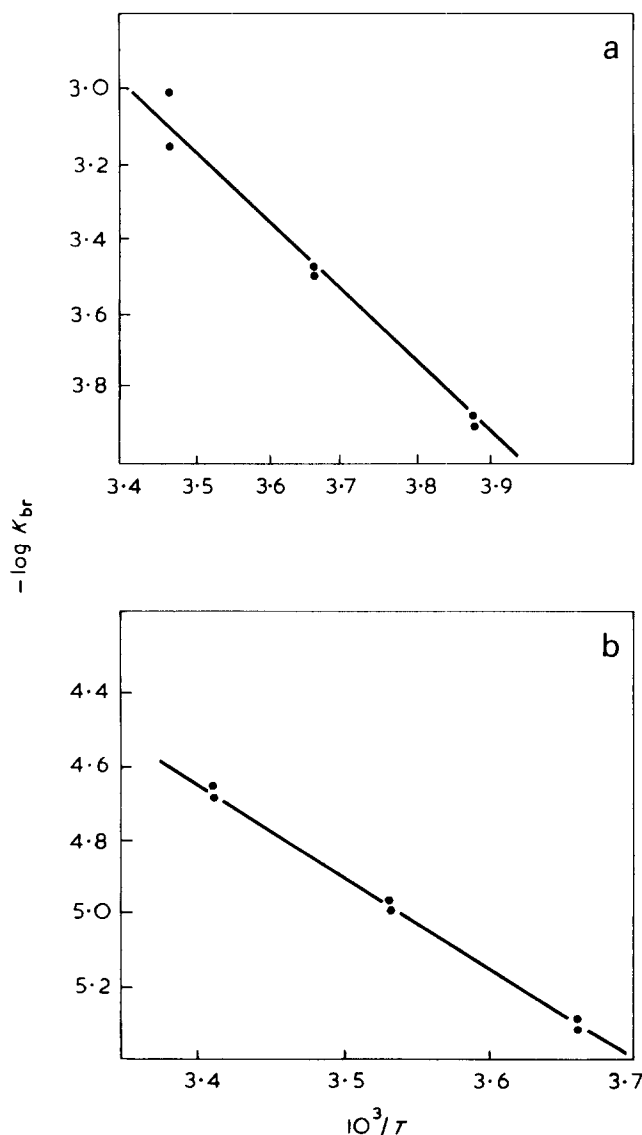


Figure 12 Dependence of the rate constant on the inverse temperature. (a)  $AlEt_3$ - $Bu_2O$ -BP; (b)  $AlEt_3$ -Py-BP



Table 2 Characteristics of the complexing reaction of EA, AA,  $Bu_2O$  and Py with  $AlEt_3$ 

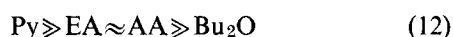
CA	$K_{eq} \times 10^{-3}$ at 0°C (mol <sup>-1</sup> )	$-\Delta H$ (kcal/mol)	$-\Delta S$ (e.u.)
EA	15	9.2	14.8
AA	14	9.8	17.0
$Bu_2O$	3	13.0	32.7
Py	5000	19.4	40.6

 Table 3 The line width ( $\delta H$ ) in the  $Al(iBu)_3 \cdot CA$  complexes  
 $\delta H$  of  $Al(iBu)_3 = 4.8$  gauss

CA	$\delta H$ (gauss)
$Bu_2O$	$6.5 \pm 0.4$
EA	$4.8 \pm 0.2$
AA	$5.2 \pm 0.2$
VA	$4.1 \pm 0.3$
$Bu_2O + EA$	$4.8 \pm 0.4$
$Bu_2O + AA$	$4.8 \pm 0.3$
EA + AA	$5.3 \pm 0.2$
$Bu_2O + VA$	$4.9 \pm 0.2$
EA + VA	$4.6 \pm 0.3$
AA + VA	$5.2 \pm 0.2$

The  $K_{eq}$  and  $\Delta H$  values of the complexing reaction for these complexing agents were calculated from kinetic parameters ( $k'_0$  and  $E_{1n}$ ) in the same manner as for the AA system. The thermodynamic values obtained are given in Table 2 which also presents, for comparison, the information about EA and AA.

Values for  $\Delta H$  of the reaction with  $Bu_2O$  and Py as estimated from kinetic data are in a good agreement with those obtained from calorimetric measurements under model conditions<sup>16, 18</sup>. Thus the  $\Delta H$  values of the complexing reaction of  $AlEt_3$  with EA and AA calculated in the same manner can be considered as valid; published data for these CA are unavailable. The  $K_{eq}$  values in Table 2 enable the electron donors studied to be arranged in the following series, according to the stability of their complexes:



To confirm the correctness of these suggestions we have studied the n.m.r. spectra on  $^{27}Al$  nuclei of  $AlR_3$  complexes with different Lewis bases.  $Al(iBu)_3$  was used as the organo-aluminium compound<sup>†</sup>. In n.m.r. spectroscopy on  $^{27}Al$  the complex formation leads to a change in the  $^{27}Al$  nuclear quadrupolar relaxation time and to the corresponding change in the line width<sup>19, 20</sup>.

In Table 3 peak-to-peak  $^{27}Al$  n.m.r. line widths ( $\delta H$ ) are presented for free  $Al(iBu)_3$  and for  $Al(iBu)_3$  with two moles of ligand added. (The line width depends only slightly on CA concentrations in the range 1–4 mol/mol  $Al(iBu)_3$ <sup>19</sup>.) In the same cases  $\delta H$  values are quite different and it is possible to compare the abilities of the two ligands,  $CA_1$  and  $CA_2$ , to compete for a place in the complex. In this case one can measure  $\delta H$  for the

<sup>†</sup> It is possible to extend the data obtained with  $Al(iBu)_3$  to the reactions of CA with  $AlEt_3$ , since it has been shown that aluminium alkyls behave in the same manner both in the polymerization process<sup>3, 5</sup> and under model conditions<sup>7, 8</sup>.

$Al(iBu)_3 + CA_1 + CA_2$  system. If a fast exchange takes place, the preference of the  $Al(iBu)_3 \cdot CA_1$  complex will be shown by the closeness of the  $\delta H$  values for the  $Al(iBu)_3 + CA_1 + CA_2$  and  $Al(iBu)_3 \cdot CA_1$  systems (Table 3).

The complexing agents studied can be arranged according to their complexing ability:



The established regularity agrees with that obtained in the polymerization process.

The kinetic investigation (the results of which are independently confirmed) showed that the mechanism of initiation by the  $AlEt_3$ -CA-BP systems, where CA is a non-polymerized polar compound, is always the same and does not depend on the complexing ability of the electron donor used. The function of the electron donor is to reduce the concentration of free aluminium alkyl: this prevents the polymerization from being instantaneous since the free-radical formation is a result of the interaction of the uncomplexed form of  $AlR_3$  with peroxide.

#### Role of polar monomers in the initiation

The reason for the different behaviour of non-polymerizable electron donors and the polar monomer (VA) remained unsolved. The difference in the kinetic schemes in the  $AlEt_3$ -BP and  $AlEt_3$ -VA-BP systems prevents estimation of  $K_{eq}$  of reaction (8) from kinetic data. The independence of the rate of VC polymerization initiated by the  $AlEt_3$ -VA-BP system (at  $[VA] > [AlEt_3]$ ) on the VA concentration (Figure 1) suggests a relatively high value for  $K_{eq}$  of reaction (8). An attempt to estimate this value by the i.r. method did not yield the desired data since under experimental conditions,  $T = 25^\circ C$ ,  $[VA] = [AlEt_3]$ , a comparatively rapid irreversible consumption of [VA] is observed. To find where VA comes in the established series of basicity of CA we have estimated the stability of its complex with  $Al(iBu)_3$  by  $^{27}Al$ -n.m.r. and by p.m.r. methods. The data from  $^{27}Al$ -n.m.r. (Table 3) showed that, by its complexing ability, VA is situated in the middle of the series (eqn. 13).

Additional data on the  $Al(iBu)_3$  behaviour in the presence of polar agents were obtained from p.m.r. High resolution p.m.r. spectroscopy shows complex formation from the shielding of  $Al(iBu)_3$  methylene protons, caused by electron donation to the aluminium atom from the ligand hetero-atom.

Figure 13 shows the dependence of the internal chemical shift of  $Al(iBu)_3$  ( $\Delta = \tau_{CH_2} - \tau_{CH_3}$ ) on the VA concentration. Almost identical plots were obtained for all the ligands studied: CA (EA,  $Bu_2O$ , AA) and the polar monomers (VA, MMA, AN). The data presented suggest the formation of a 1 : 1 type labile complex with a short life time ( $< 0.1$  sec). This is proved by the coalescence of the free and coupled  $Al(iBu)_3$  p.m.r. signals into one common signal with the averaged  $\Delta$  value. The same pattern was maintained for different ether- $AlR_3$  complexes<sup>21–23</sup>.

Another pattern is observed for Py. Here the p.m.r. signal coalescence does not take place owing to a more rigid complex formation with life time exceeding one second.

This information is consistent with published data on the behaviour of the complex of  $AlEt_3$ -Py<sup>21</sup>. The data suggest that the reason for the unusual behaviour of VA

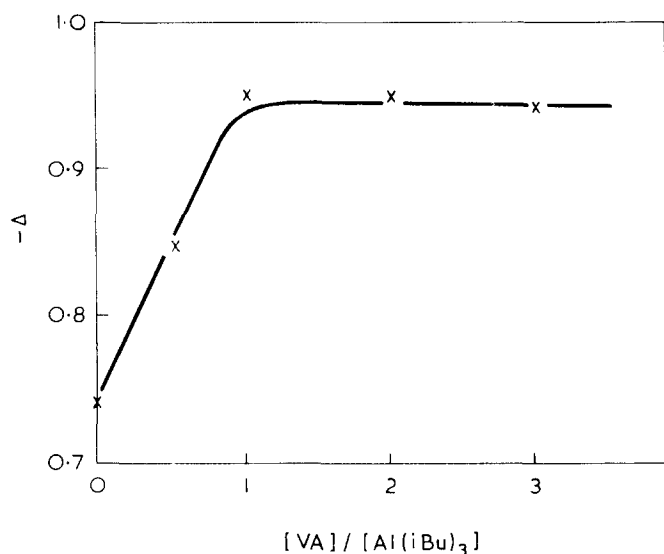


Figure 13 Dependence of the internal chemical shift for  $\text{Al}(\text{iBu})_3$  ( $\Delta = \tau_{\text{CH}_2} - \tau_{\text{CH}_3}$ ) on the molar ratio of the VA and  $\text{Al}(\text{iBu})_3$  concentrations. The concentration of  $\text{Al}(\text{iBu})_3$  is 10% by wt. in benzene

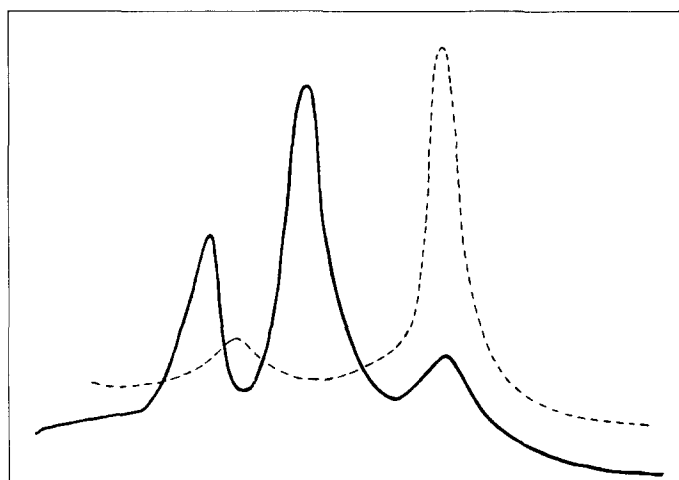


Figure 14 Infra-red spectra of MMA complexed with  $\text{AlEt}_3$  and of free MMA in octane at 25°C. Molar ratio  $[\text{MMA}]/[\text{AlEt}_3]=1$  (—);  $\text{MMA}=8 \times 10^{-2}$  mol/l; free MMA (-----)

in the initiation process is not connected with the stability of the complex.

The experimental data available indicate another possibility—a fundamentally different mechanism of interaction between  $\text{AlEt}_3$  and BP in the presence of a polar monomer<sup>3</sup>.

Both the information obtained under simulated conditions<sup>7, 8</sup> and the kinetic results (obtained in an earlier investigation and in the present research) show that stoichiometry of the BP reaction corresponds to 1 : 2, i.e. the interaction with both carbonyl oxygens is necessary for the rupture of the peroxide bond.

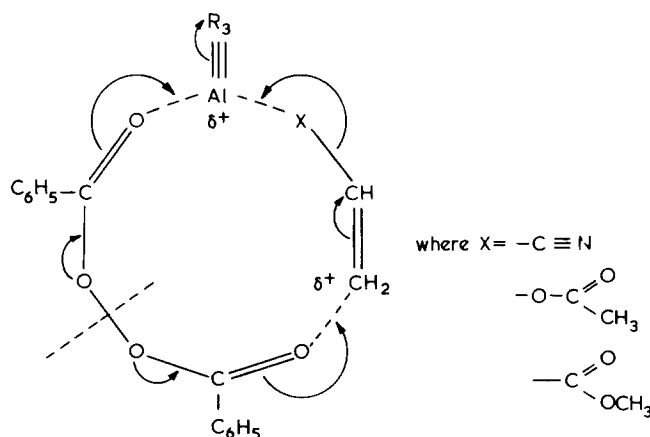
As already stated, the same expression was obtained for the initiation for all the polar monomers (equation 1a). This enables us to pass from a particular case of VA to the general analysis of the phenomenon\*. It is natural to

\* It is not possible to use other polar monomers (AN and MMA) in catalytic amounts in the VC polymerization with these systems because of a rather unfavourable ratio between the copolymerization constants of VC-AN and VC-MMA. Using the catalytic system with MMA a simultaneous occurrence of the initiation and inhibition was established

suppose that in the formation of the complex between  $\text{AlR}_3$  and the polar monomer a certain polarization of its double bond occurs followed by the electron cloud shift towards the electron acceptor, aluminium alkyl. This process is obviously feasible for the monomers having a direct conjugation between the double bond and the hetero-atom, i.e. for AN and MMA. In the VA molecule the movement of the double bond electron cloud can, obviously, occur through the uncoupled electron pair of the other oxygen (as an inductive effect).

The decrease in the electron density on the monomer double bond in the complex is shown by the example of MMA.  $\text{AlEt}_3$  using i.r. spectroscopy. Figure 14 gives a comparison of the i.r. spectral regions of MMA and the complex  $\text{AlEt}_3$ . MMA. It is established that the vibration band of the C=C double bond normally at  $1632 \text{ cm}^{-1}$  is shifted to lower frequencies ( $1624 \text{ cm}^{-1}$ ) in the complex. The distortion of the double-bond symmetry leads to a sharp increase in the intensity of the corresponding band. (With i.r. spectroscopy we failed to find a similar shift in the VA molecule: this might be connected with the difference in the structure of these monomers.)

Hence the complex  $\text{AlEt}_3 \cdot \text{M}$  is a kind of bifunctional compound in which the electron-deficient centres are represented by aluminium alkyl and the double bond of the complexing monomer. We may assume that in the subsequent reaction with BP (a bi-functional electron donor) this complex acts as a single bi-accepting compound. The transition state of the interaction can be schematically shown as follows:



Stoichiometry of this interaction corresponds to the experimentally established ratio  $\text{AlEt}_3 : \text{BP}$  equal to 1 : 1 (see equations 1a and 9).

In accordance with the proposed interaction scheme not only the alkyl radicals (the only radicals obtained under the experimental conditions<sup>9</sup>) but also benzoate radicals are formed. Occurrence of the latter was shown with PMMA<sup>3</sup> for which the chain transfer reaction to BP is known to be absent<sup>24</sup>, therefore the presence of terminal benzoate groups in the polymer must be entirely due to the initiation reaction.

The fact that the rate constant of the initiation reaction is strongly dependent on the nature of the medium provides a certain confirmation of the conception of the free-

radical formation resulting from the interaction between the highly polarized particles. Thus with a complete agreement of the kinetic orders for the initiator components (equations 1a and 9) and for the  $E_{in}$  values, the  $k_{in}$  values with the  $AlEt_3$ -BP system in the VC medium in the presence of catalytic amount of VA, and in the VA medium are  $7.25 \times 10^{-3} \text{ l mol}^{-1} \text{ sec}^{-1}$  and  $7.2 \times 10^{-5} \text{ l mol}^{-1} \text{ sec}^{-1}$  (ref. 1), respectively.

Since the systems studied are efficient as initiators for the low temperature polymerization, analogous systems based on other organometallic compounds might also be effective.

As was shown recently in similar experiments, the replacement of M-C bonds (where M is B, Al etc.) by M-O bonds is energetically favourable<sup>25, 26</sup>. The energetic gain must be still greater in the interaction between metal alkyls and acyl peroxide. In particular, in the interaction between aluminium alkyls and BP the driving force of the free radical's formation is the transformation of the covalent Al-C bond into the partly ionic bond Al-OCO<sup>-5</sup>. It is quite evident that the advantages of this process will be principally determined by the metallicity of the central atom. Thus it has been established that a trialkyl boron with BP does not yield a system of high activity<sup>27</sup>. No data exist about the use of organic compounds of Zn and Cd in this combination but we may assume that they will be less active than organo-aluminium compounds for the same reason.

Conversely, organic compounds of alkaline and alkaline earth metals can hardly be used with acyl peroxide as initiating systems. In this case the ionic contribution to the M-C bond is too great. For instance, this causes the interaction with BP to develop as a heterolytic process rather than a homolytic one<sup>28</sup>. Besides, we have found that the reaction of  $MgR_2$  with BP, even in the presence of a considerable excess of an electron donating compound (dioxan), occurs practically instantaneously. Thus this interaction cannot be a source of continuous formation of free radicals.

## REFERENCES

- 1 Milovskaya, E. B. and Zhuravleva, T. G. *Vysokomol. Soedin.* 1964, **6**, 1035
- 2 Milovskaya, E. B. and Zamoiskaja, L. W. *Vysokomol. Soedin.* 1965, **7**, 670
- 3 Milovskaya, E. B., Zamoiskaja, L. W. and Winogradova, S. I. *Eur. Polym. J.* 1970, **6**, 1589
- 4 Milovskaya, E. B. and Zhuravleva, T. G. *Vysokomol. Soedin. (A)* 1967, **9**, 1128
- 5 Milovskaya, E. B., Zhuravleva, T. G. and Zamoiskaja, L. W. *J. Polym. Sci. (C)* 1967, **16**, 899
- 6 Kopp, E. L. and Milovskaya, E. B. *Vysokomol. Soedin. (A)* 1969, **11**, 750
- 7 Milovskaya, E. B., Pokrovsky, E. I. and Fedorova, E. F. *Izv. Akad. Nauk S.S.S.R., Ser. Khim.* 1967, p 1093
- 8 Zamoiskaja, L. W., Milovskaya, E. B. and Orestova, W. A. *Izv. Akad. Nauk S.S.S.R., Ser. Khim.* 1970, p 2053
- 9 Kopp, E. L. and Milovskaya, E. B. *Izv. Akad. Nauk S.S.S.R., Ser. Khim.* in press
- 10 Weisberger, A. 'Organic Solvents', Interscience, New York, 1955, Vol VII
- 11 Razuvaev, G. A. and Graevsky, A. I. *Dokl. Akad. Nauk. S.S.S.R.* 1959, **128**, 309
- 12 Myers, O. and Pitzer, E. J. *Appl. Phys.* 1959, **30**, 1987
- 13 Danusso, F. and Sianesi, D. *Chim. Ind.* 1955, **37**, 695
- 14 Burnett, G. and Wright, W. *Proc. R. Soc.* 1954, **231**, 28
- 15 Pasynkiewicz, S. and Starowieyski, K. *Roczn. Chem.* 1967, **41**, 1139
- 16 Bonitz, E. *Chem. Ber.* 1955, **88**, 742
- 17 Margaritova, M. F. and Rysanova, K. A. *Vysokomol. Soedin. (A)* 1969, **11**, 2741
- 18 Emerson, W. and Ramirez, E. *Anal. Chem.* 1965, **37**, 806
- 19 Poole, C. P., Swift, H. E. and Itzel, Y. E. *J. Chem. Phys.* 1965, **42**, 2576
- 20 Swift, H. E., Poole, C. P. and Itzel, Y. E. *J. Phys. Chem.* 1964, **68**, 2509
- 21 Takashi, Y. *Bull. Chem. Soc. Japan*, 1967, **40**, 612
- 22 Takeshita, T. and Frankle, W. *Tetrahedron Lett.* 1968, 5913
- 23 Hatade, K. and Yuki, H. *Tetrahedron Lett.* 1968, p 213
- 24 Baysal, B. and Tobolsky, H. J. *J. Polym. Sci.* 1952, **8**, 529
- 25 Davies, A. and Roberts, B. *J. Organomet. Chem.* 1969, **19**, 17
- 26 Krusic, P. and Kochi, J. *J. Am. Chem. Soc.* 1969, **91**, 3942
- 27 Contreras, J., Grotewold, J., Lissi, E. and Rozas, R. *J. Polym. Sci. (A-1)* 1969, **7**, 2341
- 28 Lawesson, S. and Wang, W. *J. Am. Chem. Soc.* 1959, **81**, 4230

# Characterization of a cyclic oligomer of poly(pentamethylene terephthalamide)

H. K. Livingston\* and R. L. Gregory†

Department of Chemistry, Wayne State University, Detroit, Michigan 48202, USA  
(Received 24 November 1971; revised 24 January 1972)

Poly(pentamethylene terephthalamide) made by interfacial polycondensation contained 20% of a fraction that was more soluble in concentrated aqueous  $\text{H}_2\text{SO}_4$  solutions. The more soluble fraction was sublimable. It had the correct elemental analysis for  $(\text{C}_{18}\text{H}_{16}\text{O}_4)_n$  but the endotherm pattern on differential thermal analysis was quite different from that for the major fraction. The crystals formed on sublimation of the more soluble fraction were elongated lamella in which the polyamide units were probably hydrogen bonded parallel to the long crystal axis. Mass spectrometry of the crystals indicated a molecular weight of 464. This fact, combined with the evidence of the elemental analysis, indicates that the sublimable crystals are  $(\text{C}_{18}\text{H}_{16}\text{O}_4)_2$ , the cyclic dimer of pentamethylene terephthalamide.

The simultaneous occurrence of linear polymerization and oligomeric cyclization was recognized in 1930 by Carothers *et al.*<sup>1</sup> in their studies of polyesters. In polyamide synthesis it was first reported by Hoshino<sup>2</sup>, who observed the cyclic dimer of caprolactam in nylon-6. For nylon-*n,n*, the earliest report of cyclic oligomers was made simultaneously by Hermans<sup>3</sup> and by Brown *et al.*<sup>4</sup> working with nylon-6,6. Von Dietrich *et al.*<sup>5</sup> proved the structure of the cyclic dimer of nylon-6,6 by X-ray diffraction of a single crystal. Even earlier the presence of cyclic oligomers in aliphatic-aromatic polyesters was noted and the structure of the cyclic trimer of poly(ethylene terephthalate) was identified by Ross *et al.*<sup>6</sup>

The particular property of the cyclic oligomers that makes them easy to recognize is their volatility. As has been discussed elsewhere<sup>7</sup>, one of the most characteristic properties of a high polymer is that it has zero volatility. In contrast, the cyclic oligomers sublime out of the high polymers when they are heated, as was noted by Hoshino<sup>2</sup> for caprolactam dimer and Berr<sup>8</sup> for ethylene isophthalate dimer.

No reports of cyclic dimers in the aliphatic-aromatic polyamides have come to our attention. In our research with the aliphatic terephthalamides<sup>9</sup> it was noted that preparations of poly(pentamethylene terephthalamide), which is coded nylon-5T, could be separated into two distinct fractions. The sublimability of one fraction prompted some further investigation into its chemical composition and structure.

The nylon-5T was synthesized by a variation of the interfacial polycondensation method of Shashoua and Eareckson<sup>10</sup>. Freshly distilled pentamethylenediamine was dissolved in 0.1 M aqueous KOH and the mixture was diluted so that the final aqueous phase for the interfacial polycondensation was 0.012 M in diamine and 0.023 M in KOH. Terephthaloyl chloride was dissolved in  $\text{CH}_2\text{Cl}_2$ , the hydrolysed acid impurity was filtered out, and the filtered solution was further diluted to give a 0.036 M

$\text{CH}_2\text{Cl}_2$  solution. A 4 l Waring Blendor was charged with 55 ml of the organic phase and 500 ml of the aqueous phase, blended for a few minutes, and filtered on a medium-porosity sintered-glass filter. The precipitate was boiled in distilled water, filtered, boiled again, filtered, and dried in air for one hour at 100°C.

The nylon-5T was dissolved in concentrated  $\text{H}_2\text{SO}_4$ . On addition of a small amount of water, a high polymer, coded 5T<sub>1</sub>, precipitated out. Addition of more water led to the precipitation of a fraction coded 5T<sub>2</sub>. The peculiar behaviour of 5T<sub>2</sub> on heating was first suggested when an attempt was made to determine the melting point of unfractionated nylon-5T on a Kofler microscope hot stage. At about 330°C the nylon-5T appeared to begin to melt and needles of crystalline material formed out of the melt. The needles were birefringent and apparently single crystals. It was noticed that the crystals tended to form on the surface of the cover slip as if by condensation. Experiments in which the crystalline material was transferred from one surface to another by evaporation and condensation confirmed the crystals' tendency to sublime.

Terephthalic acid is known to sublime at about 300°C. Contamination by terephthalic acid from the hydrolysis of terephthaloyl chloride was immediately suspected and attempts were made to reproduce the same type of crystals with terephthalic acid and with partly hydrolysed terephthaloyl chloride. The attempts were not successful. Elemental analysis of 5T<sub>1</sub> and 5T<sub>2</sub> showed that both were similar to the expected condensation product and ruled out the possibility that the crystals were terephthalic acid (Table 1). The similarity of the infra-red spectra also indicated a similarity in chemical functionality.

Table 1 C : N ratios from elemental analysis

Sample	C : N found
5T <sub>1</sub>	5.60 : 1
5T <sub>1</sub>	5.56 : 1
5T <sub>2</sub>	5.55 : 1
5T <sub>2</sub>	5.48 : 1

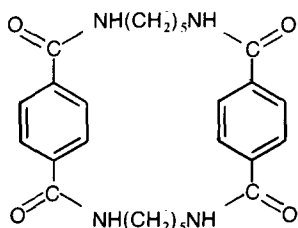
Theoretical C : N ratio for nylon-5T = 5.55 : 1

\* Now deceased.

† Present address: Ford Motor Company, PO Box 128, Mt. Clemens, Michigan 48043, USA.

The differential thermal analysis of the two fractions showed the 5T<sub>2</sub> melted at 407°C, compared with 322°C for 5T<sub>1</sub>. It was evident at this point that the 5T<sub>2</sub> was probably an oligomer but the physical properties indicated an unusual structure. The melting points of a series of fractions of a polymer would be expected to increase as the molecular weight increased and the solubility should decrease. The 5T<sub>2</sub> was the more soluble fraction and should then be expected to be lower in molecular weight and to have a lower melting point. This anomalous behaviour suggested the 5T<sub>2</sub> might be the cyclic oligomer. To test this hypothesis a purified sample of 5T<sub>2</sub> was prepared by condensing the sublimate *in vacuo*. The vacuum was necessary to avoid oxidation of the organic compound. The condensate was a white microcrystalline powder without visible signs of degradation.

This purified 5T<sub>2</sub> was run in a low resolution mass spectrograph at 200 and 260°C with an accelerating potential of 8 kV. The 200°C scan had peaks which gradually tapered off above mass 200. The 260°C scan had a well defined parent peak at mass 464. This would be the molecular weight of a cyclic dimer of nylon-5T:



The higher melting point of the dimer is consistent with the observations of Goodman and Nesbitt<sup>11</sup>, who studied the 2T polyester. They found the cyclic dimer of poly(ethylene terephthalate) to have a melting point of 314–316°C, compared to 267°C for the polymer.

The observation that there was 20% cyclic dimer in the polyamide was in line with Morgan's report<sup>12</sup> of 11% cyclic diamide in nylon-6,6 prepared by interfacial polycondensation. As Morgan points out, no truly systematic study has been made of the factors affecting cyclic oligomer formation in interfacial polycondensation. Where investigators have looked for such oligomers, they have usually found them.

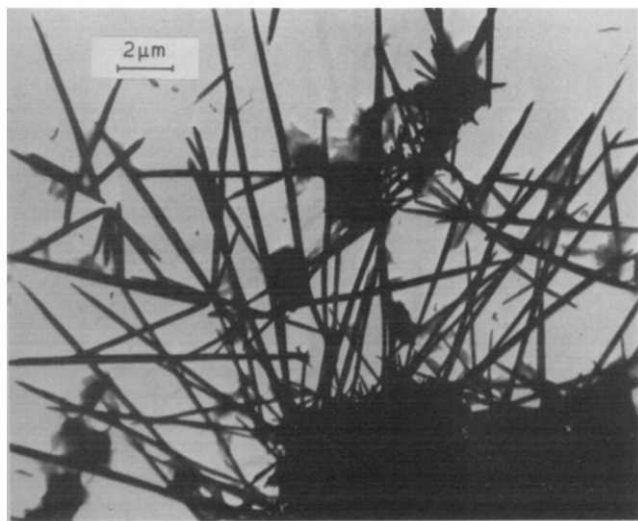


Figure 1 Electron photomicrograph of clusters of crystals formed from nylon-3T linear polymer



Figure 2 Electron photomicrograph of crystals formed by sublimation from the nylon-5T cyclic oligomer coded 5T<sub>2</sub>

The similarity under the optical microscope of the 5T<sub>2</sub> crystals to the nylon-3T single crystals that we have described previously<sup>9</sup> (Figure 1) led us to examine the 5T<sub>2</sub> crystals by electron microscope. Figure 2 shows some of the 5T<sub>2</sub> crystals. They are elongated lamellae, sometimes rolled laterally and tending to have ends which are fibrous. The larger crystals are on the order of 1 μm by 20 μm. The crystals differ from the nylon-3T crystals in their obvious lamellar habit, but are similar in that the ends are fibrous. Fractures in the crystals were observed to be parallel to the long axes. By analogy to fracture behaviour in other polyamides this would lead to the conclusion that the hydrogen bonding is parallel to the long crystal axes.

#### ACKNOWLEDGEMENT

The mass spectroscopy of the dimer was obtained through the cooperation of Professor D. C. DeJongh of our department and the electron microscopy with the help of Mr Ken Mikel of our medical school and Dr J. H. L. Watson of Henry Ford Hospital, Detroit.

#### REFERENCES

- Carothers, W. D., Arvin, J. A. and Dorough, G. L. *J. Am. Chem. Soc.* 1930, **52**, 3292
- Hoshino, K. *Bull. Chem. Soc., Japan* 1948, **21**, 63
- Hermans, P. H. *Nature* 1956, **177**, 126
- Brown, C. J., Hill, A. and Youle, P. V. *Nature* 1956, **177**, 128
- von Dietrich, H., Zahn, H. and Schmidt, F. *Acta Cryst.* 1957, **10**, 477
- Ross, S. D., Coburn, E. R., Leach, W. A. and Robinson, W. B. *J. Polym. Sci.* 1954, **13**, 406
- Livingston, H. K. *Inorg. Macromol. Rev.* 1970, **1**, 127
- Berr, C. E. *J. Polym. Sci.* 1955, **15**, 591
- Livingston, H. K. and Gregory, R. L. *J. Polym. Sci. (A-2)* 1971, **9**, 2081
- Shashoua, V. E. and Eareckson, W. M. *J. Polym. Sci.* 1959, **40**, 343
- Goodman, I. and Nesbitt, B. F. *Polymer* 1960, **1**, 384
- Morgan, P. W. 'Condensation Polymers by Interfacial and Solution Methods', Interscience, New York, 1965, p 453

# Note to the Editor

## Absence of free radical activity during reaction of organotin stabilizers with chlorohydrocarbons

G. Ayrey, R. C. Poller and I. H. Siddiqui

Queen Elizabeth College (University of London), Campden Hill Road, London W8 7AH, UK  
(Received 21 February 1972)

In a recent communication<sup>1</sup> it was observed that the most plausible mechanism for reaction of organotin stabilizers of the type  $R_2SnY_2$  ( $Y =$  mercaptide, thioglycollate or carboxylate) with tertiary or allylic chlorohydrocarbons was via ionic intermediates. A similar conclusion was reached for the reaction between cadmium carboxylates and allylic chlorides<sup>2</sup>. The precise details of the mechanisms require further definition, but the low Lewis acidity of tin in compounds of the types  $R_2Sn(SR^1)_2$  and  $R_2Sn(OCOR^1)_2$ <sup>3</sup> make the 6-coordinate intermediate proposed earlier<sup>4</sup> seem very unlikely. Though activation to nucleophilic attack of carbon bound to chlorine by weak coordination of the chlorine atom to the stronger Lewis acid  $Bu_2SnCl_2$  probably explains the catalytic effect<sup>1,5</sup> of the latter in promoting replacement of reactive chlorine atoms, an alternative view, that free radical intermediates are involved when cadmium or zinc carboxylates react with reactive chlorine atoms in PVC<sup>6</sup> has recently been supported in a study of thermal stabilization of PVC by Group II metal laurates<sup>7</sup>.

It is most important to clearly differentiate two modes of stabilization. The first involves prior reaction of a stabilizer with PVC to produce a thermally more stable polymer, whereas in the second mode a stabilizer intervenes in the degradation process and causes inhibition or retardation. Work with model compounds<sup>1,2,5</sup> has largely been directed at investigation of the first mode of stabilization and has proved that replacement of reactive chlorine atoms is of importance. However, there is an increasing body of evidence which, in various ways, implicates free radicals in the chain degradation of pure PVC and PVC copolymers<sup>8-12</sup>, and it may be that effective stabilizers should have free radical reactivity as well as the ability to replace reactive chlorine atoms. Indeed, a preliminary study has shown that some of the most effective organotin stabilizers do have some reactivity toward free radicals in methyl methacrylate polymerizations<sup>13</sup>.

So far as stabilization by replacement of reactive chlorines is concerned, we still favour ionic mechanisms and have now shown that neither a free radical acceptor (diphenyl disulphide) nor an effective inhibitor (2,5-di-*t*-butylhydroquinone) have any effect on the rates of reactions between organotin stabilizers and chlorohydro-

Table 1 Reaction of RCl (0.05 mol) with  $Bu_2SnY_2$  (0.005 mol) in the presence and absence of radical acceptors (0.0004 mol) at 180°C

RCl	Y	Reaction time (min)	Extent of reaction (%) in the presence of		
			No additive	Diphenyl disulphide	2,4-Di- <i>t</i> -butyl hydroquinone
3-Chloro-but-1-ene	-SCH <sub>3</sub>	37.5	72	68	70
3-Chloro-but-1-ene	-OCOCH <sub>3</sub>	180	40	48	44
<i>t</i> -Butyl chloride	-SCH <sub>3</sub>	30	88	90	90
<i>t</i> -Butyl chloride	-OCOCH <sub>3</sub>	52.5	80	74	78

carbons. Reactions were carried out in sealed tubes at 180°C as described previously<sup>1</sup>, and the results recorded in Table 1 show no evidence of retardation or inhibition. Thus, there is no evidence that free radical chains are involved in these reactions.

## REFERENCES

- 1 Ayrey, G., Poller, R. C. and Siddiqui, I. H. *J. Polym. Sci. (B)* 1970, **8**, 1; *J. Polym. Sci. (A-1)* 1972, **10**, 725
- 2 Anderson, D. F. and McKenzie, D. A. *J. Polym. Sci. (A-1)* 1970, **8**, 2905
- 3 Poller, R. C. 'The Chemistry of Organotin Compounds', Academic Press, London and New York, 1970, p 186
- 4 Frye, A. H., Horst, R. W. and Paliobagis, M. A. *J. Polym. Sci. (A)* 1964, **2**, 1765, 1785, 1801
- 5 Klemchuk, P. P. *Adv. Chem. Ser.*, 1968, **85**, 1
- 6 Baum, B. *SPE JI* 1961, **17**, 71
- 7 Deanin, R. D., Reynolds, H. H. and Ozcayir, Y. *J. Appl. Polym. Sci.* 1969, **13**, 1247
- 8 McNeill, I. C. and Neil, D. *Makromol. Chem.* 1968, **117**, 265
- 9 Bamford, C. H. and Fenton, D. F. *Polymer* 1969, **10**, 63
- 10 Ouchi, I. *J. Polym. Sci. (A)* 1965, **3**, 2685
- 11 Guyot, A., Bert, M., Michel, A. and Spitz, R. *J. Polym. Sci. (A-1)* 1970, **8**, 1596
- 12 McNeill, I. C., Neil, D., Guyot, A., Bert, M. and Michel, A. *Eur. Polym. J.* 1971, **7**, 453, 471
- 13 Ayrey, G., Head, B. C. and Poller, R. C. unpublished results

# Book Reviews

## Plastic deformation of polymers

Edited by A. Peterlin

Marcel Dekker, New York, 1971, 299 pp, \$17.50

This book consists of selected papers presented at the American Chemical Society Symposium on Plastic Deformation of Polymers held at New York in September 1969. It is essentially a hard back book consisting of the contents of the *Journal of Macromolecular Science (Physics)* 1970, **134**, No. 3.

The papers cover many aspects of the plastic deformation of polymers from structural studies by X-ray diffraction techniques, infra-red spectroscopy and electron spin resonance to phenomenological studies of linear and non-linear viscoelasticity and yield. This volume reflects the diversification of research in this area and provides an excellent cross-section of the different approaches. It has been edited by Dr Anton Peterlin, who has also contributed with his co-workers several articles of particular interest.

The book will be of value to research workers and postgraduate students in polymer science. Although it requires considerable knowledge of the subject if the reader is to gain full benefit, most of the papers are self contained and some of them such as that on the mechanical properties of isotactic polypropylene by R. J. Samuels, are comprehensive reviews of particular areas of the subject.

The book is well produced with a high standard of illustration, and appears to be reasonably priced. As will have been gathered from this review it contains much interesting material and can be recommended as initial reading in a complex and diverting subject.

I. M. Ward

## Biomedical polymers

Edited by A. Rembaum and M. Shen

Marcel Dekker, New York, 1971, 292 pp, \$17.50

This book is a valuable work. There is surprisingly up-to-date information about the areas covered and the papers are very comprehensive. The problem with this, as so often happens in books which are compiled as a collection of papers presented at a symposium, is a dual one. Firstly, there are differences in style in paper to paper. This means that the reader may enjoy one style in one paper and find that the next jars. But what is more important is that the contents have all the shortcomings of papers presented at a scientific meeting. They start off written in English and intelligible, and then lax almost immediately into scientific jargon, into mathematics and physical chemistry. This is both an advantage and disadvantage. It means that whatever level the reader is interested in, whether he wants a superficial review of the subject or whether he wants to know the latest details about the growing edge of the subject, it is there. However, other types of information retrieval systems may be necessary in the future, to allow people access to material according to the level at which their research is conducted. The criticisms which apply to this published symposium are common to all published symposia and apply less than usual to this one, which is well compiled and well produced. No self respecting bioengineer should be without it and it is important to remember that bioengineering by definition is engineering applied to biological problems, a fact which is frequently forgotten by contributors to this kind of symposium. What I would like to have seen would be for the two editors to have added a review chapter to the end of this book, cross referencing the reader to the papers within; then its readership would be so much wider it could be used by cardiac surgeons, by orthopaedic surgeons and in fact anyone considering implanting material using prosthesis or taking an interest in the subject. The tragedy is that books like this widen the gap between the general physician and the sophisticated bioengineering research projects, upon which their future practices will be based.

D. B. Longmore

## Physical chemistry of adhesion

D.H. Kaelble

Wiley — Interscience, New York, 1971, 507 pp, £13.00

Most adhesives in use today are polymers. Consequently a book on the physical chemistry of adhesion is, to a large extent, a book on polymeric materials. Now in general the theoretical determination of the properties of polymers, whether in solution, or existing as pure liquids or solids, involves considerable difficulties. Because of this, attempts to relate the surface chemistry, bonding, rheology or fracture of polymers to their molecular structures are either plausible extensions of similar relations derived for monomeric materials, or they are, in the last analysis, empirical relations for which some qualitative molecular interpretation is sought. Examples of both approaches are to be found here, and the modern physical chemist is unlikely to find them very satisfying.

The book is divided into three sections: surface chemistry (186 pages), rheology (130 pages), bonding and fracture (171 pages). In every section there are large quantities of experimental material requiring interpretation, and the range of subjects covered, from solubility parameters to the shear strengths of adhesive joints, is certainly very impressive. The character of the work can be judged from the section on surface chemistry. Here, in 55 pages devoted mainly to surface tension, Fowler's molecular theory, and numerical results obtained from it, are not mentioned. Indeed, the existence of a general molecular theory of fluids is only referred to once, and modern developments not at all. But the reason for these omissions is clear. Except perhaps in the field of solid-solid adhesion, fundamental ideas in chemistry and physics have had as yet, little impact on adhesion technology. It is better to bond muscovite mica with an  $\alpha$ -cyanoalkylacrylate adhesive than to rely on the many-body dispersion forces between the adherends.

T. B. Grimley

## Calendering of plastics

R. E. Elden and A. D. Swan

Iliffe Books, London, 1971, 106 pp, £2.40

Books on calenders and calendering processes for polymers are almost non-existent, the subject usually receiving only brief mention in most polymer reference works. This monograph commissioned by the Plastics Institute fills a very obvious gap and is most timely in appearance being essentially a practical work offering a wealth of sound advice concerning the calendering of thermoplastic materials in general and PVC in particular.

After a historical introduction to calendering by G. T. L. Griffin, the principles of PVC compounding for the calendering process are discussed in detail together with the pre-mixing and gelation processes necessary prior to feeding thermoplastic compounds to calenders. Subsequent chapters are devoted to calender design, ancillary equipment, post-calender processing operations, all illustrated clearly by simple line diagrams. Separate chapters cover processing faults and remedies, control testing of raw materials and finished sheet, all technical terms being explained by a separate glossary. An especially useful feature are frequent references throughout the text to production cum economic factors which dictate product sheet tolerances and machine design parameters. All chapters are supported by literature references which make detailed background reading possible.

This book is recommended reading for all engaged in polymer technology processes whether in the plastics or rubber fields but especially it should be useful to polymer technologists, production engineers and managers. It is of good quality, readable and produced at a modest price, thus being recommended as an essential addition to all polymer technology libraries. Further, students preparing for professional examinations will likely find this monograph an essential part of their reading lists.

C. Hepburn

# Ziegler–Natta catalysis:

## 1. A general kinetic scheme

D. R. Burfield, I. D. McKenzie and P. J. T. Tait

Department of Chemistry, University of Manchester Institute of Science and Technology, Manchester M60 1QD, UK

(Received 6 December 1971; revised 11 February 1972)

A kinetic scheme is postulated for Ziegler–Natta polymerization where propagation is considered to occur between adsorbed monomer and an active centre which has been formed by interaction of the metal alkyl with the transition metal halide. Chain transfer is considered to occur with adsorbed metal alkyl and also with adsorbed monomer. Rate, molecular weight and active centre dependencies are derived which are in qualitative agreement with the results of previous studies in Ziegler–Natta polymerization.

### INTRODUCTION

In recent years extensive kinetic studies of a wide spectrum of Ziegler–Natta systems have appeared in the literature, and a number of attempts have been made to derive kinetic schemes which have general application<sup>1,2</sup> as well as those which are restricted to individual systems<sup>3,4</sup>.

It is now some time since Eirich and Mark<sup>5</sup> pointed out that, since most Ziegler–Natta catalyst systems were of a heterogeneous nature, it was most likely that adsorption processes were involved in the reaction mechanism. These concepts were used by Saltman<sup>1</sup> in an attempt to derive a general kinetic scheme for the polymerization reaction. He thus proposed that monomer and metal alkyl were reversibly adsorbed onto the crystal surface of the transition metal halide and that propagation occurred between the adsorbed metal alkyl and monomer, either adsorbed or in solution.

At high metal alkyl concentrations the derived expression for the rate of propagation, assuming that propagation is with unadsorbed monomer, is given by:

$$R_p = k_p[M][S] \quad (1)$$

where [S] is the concentration of surface sites, [M] is the monomer concentration and  $k_p$  is the rate constant for propagation. This equation is similar to the expressions derived by Kern *et al.*<sup>6</sup> and Keii *et al.*<sup>7</sup>, for the polymerization of propylene by  $\text{TiCl}_3/\text{AlEt}_3$ .

These expressions do not have, however, general application for although they are consistent with the first order dependence of the overall rate of polymerization on monomer and consistent with the independence of rate at high metal alkyl concentrations<sup>6–8</sup>, they do not explain the maxima in rate observed by some authors as the metal alkyl concentration is increased. A maxima in rate has been observed in systems<sup>3, 9–11</sup> where it cannot be attributed to deactivation by reduction of the active species as has been suggested by Kern *et al.*<sup>6</sup>,

although this latter explanation is probably important for catalysts based on higher valence state transition metal halides, e.g.,  $\text{TiCl}_4$ .

Vesely *et al.*<sup>4</sup> on the other hand have proposed a kinetic scheme where propagation was considered to occur between adsorbed metal alkyl and adsorbed rather than unadsorbed monomer. In this case the rate of polymerization is of the form:

$$R_p = k_p \theta_M \theta_A S \quad (2)$$

where  $\theta_M$  and  $\theta_A$  are the fraction of surface covered by adsorbed monomer and metal alkyl respectively. This equation predicts a fall off in rate at high metal alkyl concentrations.

Reich and Stivala<sup>2</sup> set out to derive a comprehensive scheme which would resolve these apparent inconsistencies. They suggested that adsorbed metal alkyl constituted the active site, and that propagation occurred between adsorbed metal alkyl and neighbouring adsorbed or unadsorbed monomer. The subsequent derivations allowed qualitative agreement, a maxima in rate being observed if propagation were considered to occur with adsorbed monomer, whilst an independence of rate upon metal alkyl concentration was predicted if propagation occurred with unadsorbed monomer. However, it seems inconsistent to assume propagation with adsorbed monomer in one system and with unadsorbed monomer in another similar system merely in order to rationalize the experimental results. It might be possible to argue that in the case of ethylene which is the most reactive  $\alpha$ -olefin that this monomer reacts directly from solution without prior complexation whereas propylene and higher olefins undergo preliminary adsorption, but even this seems unlikely.

The above reaction schemes are based on the assumption that the active centre is an adsorbed metal alkyl species. On the other hand, Otto and Parravano<sup>3</sup> have proposed a scheme where propagation occurs between adsorbed monomer and an alkylated transition metal



entity, the concentration of which is proportional to the fraction of the surface covered by adsorbed metal alkyl. However, their derivations do not appear to have general application outside their own kinetic results.

Thus at the present time no kinetic scheme has been derived which fully explains all the kinetic results reported in the literature. A scheme is now proposed which adequately describes the extensive kinetic, molecular weight and active centre data obtained for the system  $VCl_3/AlR_3/4$ -methylpentene-1 and which appears to have fairly general application to a variety of systems. The scheme will be presented, and expressions derived for use and verification in subsequent papers.

## PROPOSED KINETIC SCHEME

### Propagation

In the proposed scheme propagation is considered to occur with an active centre formed by interaction of the metal alkyl with the transition metal halide, rather than with a metal alkyl molecule merely adsorbed onto the surface. The reason for this is that if propagation were to occur with adsorbed metal alkyl, then the active centre concentration ( $C_0$ ) would be proportional to the fraction of the surface covered by adsorbed monomeric metal alkyl ( $\theta_A$ ). It has, however, been found that this relationship does not hold for the system under study (Table 1). This is also supported by other kinetic data which shows that  $C_0$  can vary under conditions of constant  $\theta_A$ .

These observations indicate that the propagation reaction does not occur with aluminium alkyl merely adsorbed onto the surface of the vanadium trichloride. It may be similarly shown that propagation does not occur with adsorbed monomer and metal alkyl pairs as the polymerization rate is not proportional to the product of  $\theta_A$  and  $\theta_M$ .

The kinetic data are most adequately interpreted if propagation is considered to occur between an active centre and adsorbed monomer. The rate expression thus becomes:

$$R_p = k_p \theta_M C_0 \quad (3)$$

where  $k_p$  is the propagation rate constant with respect to adsorbed monomer, and  $\theta_M$  is the fraction of the surface covered by adsorbed monomer. The adsorption of monomer and metal alkyl onto the catalyst surface are considered to be described by the Langmuir-Hinshelwood isotherms, thus:

$$\theta_M = \frac{K_M[M]}{1 + K_M[M] + K_A[A]} \quad (4)$$

Table 1 Variation in the active centre concentration with  $\theta_A$

$[AlR_3] = 37.0$  mmol/l;  $[4\text{-MP-1}] = 2.0$  mol/l;  $[VCl_3] = 18.5$  mmol/l; solvent = benzene; temperature =  $30^\circ\text{C}$

Metal alkyl	$C_0 \times 10^4$ (mol/mol $VCl_3$ )	$\theta_A$	$C_0/\theta_A \times 10^9$
$Al(iBu)_3$	3.78	0.125	3.00
$AlEt_3$	6.10	0.445	1.37
$Al(nBu)_3$	3.30	0.090	3.65
$Al(nHex)_3$	2.30	0.110	2.10

Table 2 Some metal alkyl concentrations employed in Ziegler-Natta systems

System	Effect of increasing [A]	Range of [A] employed (mmol/l)	Ref.
$TiCl_3/AlEt_3$ for propylene	Maximum produced	10-200	4
	Independent	29-45	8
	Independent	5-30	7
	Independent	2-35	6

and

$$\theta_A = \frac{K_A[A]}{1 + K_M[M] + K_A[A]} \quad (5)$$

where  $[M]$  and  $[A]$  are the concentrations of monomer and metal alkyl, and  $K_M$  and  $K_A$  are the equilibrium constants for the respective adsorption equilibria.

It should be noted that where the metal alkyl is known to be dimeric  $K^{1/2}[A_2]^{1/2}$  should be substituted for  $[A]$ , where  $[A_2]$  is the concentration of metal alkyl dimer and  $K$  is the dissociation constant.

Thus the rate of propagation will be dependent upon the number of active centres and the value of  $\theta_M$ . Initially, as the metal alkyl concentration is raised the rate of polymerization will increase due to the formation of a greater number of active centres. The number of active centres should increase to a limiting value after which the polymerization rate would be expected to decrease, as the value of  $\theta_M$  is diminished by competitive adsorption of metal alkyl with monomer.

These predictions apparently do not fit the observations by some workers that the polymerization rate becomes independent of metal alkyl concentration at high concentrations. This discrepancy may, however, be simply explained. The authors who failed to observe a maximum in rate, although using similar ranges of catalyst component ratios, used much lower overall catalyst concentrations than those authors who do observe a rate maxima. This is significant since  $\theta_M$  depends on the actual concentration of the metal alkyl and not on the ratio of catalyst components. Clearly when the metal alkyl concentration is very low the term  $K_A[A]$  becomes insignificant, and  $\theta_M$  is more or less independent of the metal alkyl concentration. The results of different workers for the system  $TiCl_3/AlEt_3$ /propylene are summarized in Table 2.

When one notes that Vesely *et al.*<sup>4</sup> observed the maximum in rate at a concentration of 50 mmol/l of  $AlEt_3$ , it is not surprising that other workers did not detect this effect.

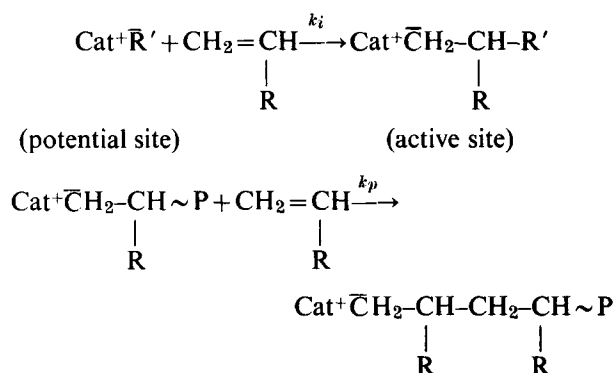
Thus the proposed theory is consistent with the results of those workers who do not observe a rate maxima but who use low catalyst concentrations, as well as those authors who observe a rate maxima when using higher catalyst concentrations. The kinetic scheme is also in accord with the findings of the majority of workers<sup>3, 8, 10, 11</sup> who observe that the polymerization rate is proportional to the metal halide concentration at a constant ratio of catalyst components. Hence from equation (3),  $R_p \propto C_0$ , and  $C_0$  in turn is a function of the metal halide concentration.

However, this scheme predicts a fall off in rate at very high catalyst concentrations, for as the metal alkyl concentration is increased, so as to maintain a

constant ratio of catalyst components, the value of  $\theta_M$ , and thus the rate, will decrease. This effect has in fact been observed in the present study above  $VCl_3$  concentrations of about 30 mmol/l, which is outside the range of concentrations employed by most previous workers. The scheme also predicts that the polymerization rate should be first order with respect to monomer, although at very high monomer concentrations the rate should become independent of the monomer concentration. Only the first of these effects has been observed, the latter effect occurring at monomer concentrations which cannot be realized experimentally.

### Initiation

Most authors<sup>12,13</sup> consider that the initiation and propagation of chain growth occur by the same type of mechanism, although the two steps are characterized by different activation energies<sup>14</sup>. Indeed there is a considerable amount of evidence that the rates of these two processes are very different, the rate of chain initiation being much lower than that of chain propagation<sup>14</sup>. Thus two types of active site may be envisaged as existing in these polymerization systems, viz., propagating sites of concentration,  $C_0$ , and potential sites of concentration,  $C_i$ . Potential sites are considered to be sites prior to initiation by monomer or sites arising from transfer reactions by either monomer or metal alkyl. Hence the following steps are distinguishable:



For a given concentration of metal halide there will be a maximum concentration of active sites,  $C_t$ , and if this is assumed to be constant then:

$$C_t = C_0 + C_i \quad (6)$$

The rates of initiation and propagation in a system where initiation and propagation are considered to occur with adsorbed rather than unadsorbed monomer and metal alkyl, are given by,

$$R_i = k_i C_i \theta_M \quad (7)$$

and

$$R_p = k_p C_0 \theta_M \quad (8)$$

Similarly, if chain transfer with adsorbed monomer and adsorbed alkyl are the major transfer steps then:

$$R_t = k_m C_0 \theta_M + k_a C_0 \theta_A \quad (9)$$

Under stationary state conditions:  $R_i = R_t$  and thus, on elimination of  $C_i$ :

$$C_0 = \frac{k_i C_t \theta_M}{k_i \theta_M + k_m \theta_M + k_a \theta_A} \quad (10)$$

Substitution for  $C_0$  in equation (8) gives the relationship:

$$R_p = \frac{k_p k_i C_t \theta_M^2}{k_i \theta_M + k_m \theta_M + k_a \theta_A} \quad (11)$$

At low monomer concentrations of metal alkyl and monomer,  $\theta_A = K_A[A]$  and  $\theta_M = K_M[M]$ ,

$$\therefore R_p = \frac{k_p k_i C_t K_M^2 [M]^2}{k_i K_M [M] + k_m K_M [M] + k_a K_A [A]} \quad (12)$$

and hence:

$$\frac{[M]}{R_p} = \frac{1}{k_p C_t K_M} \left( 1 + \frac{k_m}{k_i} \right) + \frac{1}{k_p C_t K_M} \left( \frac{k_a K_A [A]}{k_i K_M} \right) \frac{1}{[M]} \quad (13)$$

This derivation is somewhat analogous to that of Chirkov *et al.*<sup>15</sup>, Natta *et al.*<sup>16</sup> and Schindler<sup>17</sup> have also derived similar relationships but using different models.

A plot of  $[M]/R_p$  against  $1/[M]$  should therefore be linear with:

$$\text{slope/intercept} = \frac{k_a K_A [A]}{(k_i + k_m) K_M} \quad (14)$$

Such a plot may thus be used for the evaluation of  $k_i$  provided that only low concentrations of monomer are used.

### Chain transfer

The predominant chain transfer reactions for the system  $VCl_3/AlR_3/4\text{-MP-1}$  are considered to be: (a) transfer with adsorbed monomer; (b) transfer with adsorbed metal alkyl. Spontaneous termination is considered to be unimportant at 30–40°C, the temperature range employed in this study.

When transfer is with adsorbed metal alkyl, the rate of transfer is given by:

$$R_{ta} = k_a \theta_A C_0 \quad (15)$$

where  $k_a$  is the rate constant for chain transfer with metal alkyl. Similarly, for transfer with adsorbed monomer the rate of transfer is given by:

$$R_{tm} = k_m \theta_M C_0 \quad (16)$$

where  $k_m$  is the rate constant for transfer with adsorbed monomer.

The rate of spontaneous termination is given simply by:

$$R_{ts} = k_s C_0 \quad (17)$$

where  $k_s$  is the rate constant for spontaneous termination. This reaction is unimportant except at higher temperatures, and therefore will be omitted from the subsequent expressions for the number-average degree of polymerization.

### Molecular weight relationships

Where propagation occurs with adsorbed monomer, and chain transfer with adsorbed monomer and adsorbed metal alkyl then the number-average degree of polymerization, after time  $t$  is given by:

$$\bar{P}_n = \frac{\int_0^t k_p \theta_M C_0 dt}{C_0 + \int_0^t k_m \theta_M C_0 dt + \int_0^t k_a \theta_A C_0 dt} \quad (18)$$

Inverting, integrating and removing  $C_0$  gives:

$$\frac{1}{\bar{P}_n} = \frac{1 + k_m \theta_M t + k_a \theta_A t}{k_p \theta_M t} \quad (19)$$

Substituting for  $\theta_A$ ,  $\theta_M$  and simplifying yields:

$$\frac{1}{\bar{P}_n} = \frac{k_a K_A [A]}{k_p K_M [M]} + \frac{1}{k_p K_M [M] t} + \frac{K_A [A]}{k_p K_M [M] t} + \frac{(k_m + 1/t)}{k_p} \quad (20)$$

This equation predicts that the number-average degree of polymerization will be: (a) initially dependent on the duration of polymerization, but becoming independent at a later stage of the polymerization, i.e., when  $t$  is large; (b) reduced by increasing the metal alkyl concentration; (c) dependent on the monomer concentration; (d) altered by the nature of the metal alkyl compound; and (e) independent of the metal halide concentration.

These predictions are in general accord with the dependencies observed in other Ziegler-Natta catalyst systems and are in excellent agreement with those found in the present study, and which will be presented in subsequent papers.

#### Active centre concentration relationships

In a later paper the effect of various parameters on the concentration of metal-polymer bonds (MPB) in the system  $\text{VCl}_3/\text{AlEt}_3/4\text{-MP-1}$  will be presented, and it is useful at this stage to derive expressions for later interpretation.

*Variation of metal-polymer bond concentration with metal alkyl concentration.* The radioactive quench method enables measurement of the total concentration of MPB in the reaction mixture, i.e., both growing polymer chains bound to the active sites, and transferred polymer chains bound to the metal of the metal alkyl. Thus the MPB concentration at time  $t$  is given by:

$$[\text{MPB}]_t = C_0 + \int_0^t R_{ta} dt \quad (21)$$

The rate of transfer with metal alkyl can thus be measured in addition to  $C_0$ . If transfer is with adsorbed metal alkyl then:

$$R_{ta} = k_a \theta_A C_0 \quad (15)$$

Substitution for  $\theta_A$  and rearranging gives:

$$\frac{C_0}{R_{ta}} = \frac{1 + K_M [M]}{k_a K_A [A]} + \frac{1}{k_a} \quad (22)$$

Thus a plot of  $C_0/R_{ta}$  against  $1/[A]$ , or  $1/[A_2]^{1/2}$  for dimeric metal alkyls should be linear with:

$$\text{slope} = \frac{1 + K_M [M]}{k_a K_A} \quad (23)$$

or

$$= \frac{1 + K_M [M]}{k_a K^{1/2} K_A} \text{ for dimeric metal alkyls}$$

and

$$\text{intercept} = 1/k_a \quad (24)$$

Thus  $k_a$  may be evaluated.

*Variation of metal-polymer bond concentrations with monomer concentration.* The number-average degree of polymerization by tritium end group analysis  $(\bar{P}_n)_T$  is given by:

$$(\bar{P}_n)_T = \frac{\text{Monomer polymerized at time } t}{\text{Number of metal-polymer bonds}} \quad (25)$$

$$\therefore (\bar{P}_n)_T = \frac{\int_0^t R_p dt}{C_0 + \int_0^t R_{ta} dt} \quad (26)$$

Substitution for  $R_p$  and  $R_{ta}$  yields:

$$(\bar{P}_n)_T = \frac{\int_0^t k_p \theta_M C_0 dt}{C_0 + \int_0^t k_a \theta_A C_0 dt} \quad (27)$$

It should be noted that  $\theta_A$  is independent of time under the polymerization conditions employed, and although  $\theta_M$  varies with time, the polymerization runs for which these derivations were made were terminated at similar conversions, and hence would have similar values for the term  $\int \theta_M dt$ . Thus equation (27) becomes:

$$(\bar{P}_n)_T = B \times \frac{k_p \theta_M t}{1 + k_a \theta_A t} \quad (28)$$

where  $B$  is a constant.

The specific radioactivity of the polymer is proportional to  $1/(\bar{P}_n)_T$

$$\therefore \text{specific activity} = C \times \frac{(1 + k_a \theta_A t)}{k_p \theta_M t} \quad (29)$$

where  $C$  is constant. On substitution for  $\theta_A$  and  $\theta_M$  the following equation is obtained:

$$\text{specific activity} = D \left[ \frac{1 + K_M [M] + (1 + k_a t) K_A [A]}{K_M [M]} \right] \quad (30)$$

where  $D$  is the constant required after removing  $k_p$  and  $t$  from the denominator.

Hence a plot of activity versus  $1/[M]$  should be linear with:

$$\text{intercept} = D \quad (31)$$

and

$$\text{slope} = D \left[ \frac{1 + (1 + k_a t) K_A [A]}{K_M} \right] \quad (32)$$

The use of equation (30) affords a convenient method of checking the validity of the proposed scheme.

Equations (23) and (32) when used together enable values of  $K_M$  and  $K_A$  to be calculated.

*Variation of metal-polymer bond concentration with metal halide concentration.* It is generally accepted that  $C_0 \propto [\text{VCl}_3]$ . Now in this particular study the ratio  $[A]/[\text{VCl}_3]$  was kept constant, whilst the  $\text{VCl}_3$  concentration was varied. Therefore for this particular series under these conditions:

$$C_0 \propto [A] \text{ or } C_0 = P [A] \quad (33)$$

where  $P$  is a constant. Substitution for  $C_0$  and  $\theta_A$  in equation (21) gives:

$$[\text{MPB}]_t = P [A] + \frac{P k_a t K_A [A]^2}{1 + K_A [A] + K_M [M]} \quad (34)$$

However,  $K_A[A] \ll 1 + K_M[M]$  under the conditions employed, and thus the denominator may be assumed constant. Hence a plot of [MPB] versus  $([A] + Q[A]^2)$  should be linear and of slope  $P$ , where  $Q$  is a constant given by:

$$Q = \frac{k_{at}K_A}{1 + K_A[A] + K_M[M]} \quad (35)$$

and may be evaluated.

$C_0$  may now be calculated from equation (33) and compared with the value determined by extrapolation of the MPB versus conversion plot.

The experimental data shortly to be presented are found to conform to these derived expressions and confirm the validity of the proposed kinetic scheme for the polymerization system  $VCl_3/AlR_3/4-MP-1$ .

## CONCLUSIONS

The postulated kinetic scheme, where propagation is considered to occur between adsorbed monomer and an active centre, formed by interaction of metal alkyl with the transition metal halide, has been shown to be in qualitative agreement with the kinetic results observed for Ziegler-Natta polymerization. Quantitative cor-

relation with kinetic, molecular weight, and active centre data will be demonstrated in subsequent papers for the polymerization system  $VCl_3/AlR_3/4-MP-1$ .

## REFERENCES

- 1 Saltman, W. M. *J. Polym. Sci.* 1960, **46**, 375
- 2 Reich, L. and Stivala, S. S. *J. Polym. Sci. (A)* 1963, **1**, 203
- 3 Otto, F. D. and Parravano, G. *J. Polym. Sci. (A)* 1964, **2**, 5131
- 4 Vesely, K., Ambroz, J., Vilim, R. and Hamrik, O. *J. Polym. Sci.* 1961, **55**, 25
- 5 Eirich, F. and Mark, H. F. *J. Colloid Sci.* 1960, **46**, 375
- 6 Schnecko, H., Reinmoller, M., Weirauch, K. and Kern, W. *J. Polym. Sci. (C)* 1964, **4**, 71
- 7 Keii, T., Soga, K. and Saiki, N. *J. Polym. Sci. (C)* 1967, **16**, 1507
- 8 Natta, G. *J. Polym. Sci.* 1959, **34**, 21
- 9 Natta, G., Danusso, F. and Pasquon, I. *Colloq. Czech. Chem. Commun.* 1957, **22**, 191
- 10 Tait, P. J. T. and McKenzie, I. D. IUPAC Symposium on Macromolecular Chemistry, Budapest, 1969
- 11 McCarty, W. H. and Parravano, G. *J. Polym. Sci. (A)* 1965, **3**, 4029
- 12 Cossee, P. *Tetrahedron Lett.* 1960, **17**, 12
- 13 Natta, G. and Mazzanti, G. *Tetrahedron* 1960, **8**, 86
- 14 Novokshonova, L. A., Berseneva, G. P., Tsvetkova, V. I. and Chirkov, N. M. *Vysokomol. Soedin. (A)* 1967, **9**, 562
- 15 Novokshonova, L. A., Tsvetkova, V. I. and Chirkov, N. M. *Izv. Akad. Nauk. SSSR, Ser. Khim.* 1963, **7**, 1176
- 16 Natta, G., Pasquon, I., Svab, J. and Zambelli, A. *Chim. Ind. Milan* 1962, **44**, 621
- 17 Schindler, A. *J. Polym. Sci. (C)* 1963, **4**, 81

# Ziegler–Natta catalysis:

## 2. A kinetic investigation

I. D. McKenzie, P. J. T. Tait and D. R. Burfield

*Department of Chemistry, University of Manchester Institute of Science and Technology, Manchester M60 1QD, UK*

*(Received 6 December 1971; revised 11 February 1972)*

The kinetics of the polymerization of 4-methylpentene-1 by the Ziegler–Natta system  $VCl_3/AlR_3$  have been examined at 30°C and 40°C. The dependence of the overall rate of polymerization on the concentration of metal halide, aluminium alkyl concentration, monomer concentration, temperature, and nature of the aluminium alkyl has been established. The energy of activation of the overall polymerization process has been found to be 16.6 kcal/mol in benzene and 13.7 kcal/mol in heptane. The results have been examined in relation to a previously described kinetic scheme.

### INTRODUCTION

Although the recent literature contains several excellent studies of the physical properties of poly(4-methylpentene-1), very little has been published on the details of the kinetics of polymerization using Ziegler–Natta catalyst systems. A number of papers discuss in detail the solid and solution properties of this polymer<sup>1–4</sup> and various catalyst systems have been used for the preparation of these samples. Thus, Natta<sup>5</sup> described the preparation of a highly crystalline polymer using  $\alpha$ - $TiCl_3$  and  $AlEt_3$ . Campbell<sup>6</sup> reported on the preparation of polymer using a catalyst derived from  $TiCl_4$  and  $LiAl(C_{10}H_{21})_4$ , whilst others<sup>1,2</sup> have used  $\alpha$ - or  $\gamma$ - $TiCl_3$  with  $AlEt_2Cl$ . Descriptions of the polymerization processes have usually been limited to such details as the effect of catalyst composition on the polymer yields and characteristics<sup>7</sup>. In only two instances have any substantial kinetic data been reported for the polymerization of 4-methylpentene-1 by lower valence transition metal compounds<sup>8,9</sup>. Burnett and Anderson<sup>8</sup> studied the polymerization of this monomer by the catalyst system  $\alpha$ - $TiCl_3/AlEt_3$  in heptane, using a dilatometric technique. Ehrig *et al.*<sup>9</sup> have used the catalyst system  $\alpha$ - $TiCl_3/AlEt_2Cl$ . Similarly, relatively few kinetic investigations have been carried out using vanadium trichloride as the transition metal halide component of the catalyst, as the attention of research workers has been almost entirely directed towards catalysts based on titanium compounds.

The aim of this study has been to investigate the kinetics of the polymerization of 4-methylpentene-1 by the catalyst system  $VCl_3/AlR_3$ , and in particular the system using tri-isobutylaluminium as the alkyl-aluminium component of the catalyst. 4-Methylpentene-1 is a particularly convenient monomer for the laboratory study of Ziegler–Natta catalysts, for as a liquid, it offers

advantages in ease of handling and experimental convenience over gaseous monomers. The results of these experiments are discussed in terms of the kinetic scheme proposed in an earlier paper<sup>10</sup>. In this scheme chain propagation is considered to occur between adsorbed monomer molecules and active centres formed on the surface of the transition metal halide by its interaction with an aluminium alkyl.

### EXPERIMENTAL

#### *Reagents*

*4-Methylpentene-1 (4-MP-1)*. The monomer was kindly supplied by ICI Plastics Division, Welwyn Garden City, in a 99% pure state. Before each series of kinetic runs the monomer was dried over sodium wire and fractionally distilled. The middle fraction, boiling at 54°C at 1 atmosphere ( $\equiv 101.325 \text{ kN/m}^2$ ) pressure, was collected and stored over clean sodium wire until required.

*Benzene*. The Analar solvent was dried by heating under reflux with sodium wire for several hours. The solvent was then purified by fractional distillation. The middle fraction was then stored over sodium wire in a dry box.

*n-Heptane*. The Analar solvent was shaken with two portions of concentrated sulphuric acid and then with two portions of 5 N sodium hydroxide solution. This was followed by washing with distilled water until the washings were neutral to litmus. After drying over calcium chloride for 24 h, the solvent was refluxed over sodium wire and then fractionally distilled. The middle fraction was collected and stored over sodium wire in a dry box.

*Vanadium trichloride*. This compound was kindly supplied by Magnesium Elektron Ltd., Clifton Junction,

in a 99% pure state and was stored in an inert atmosphere in a dry box. The batch was analysed before delivery and the following results were quoted:  $V^{3+}$ , 31.8%;  $Cl^-$ , 67.2%;  $O^{2-}$ , 0.001%.

**Tri-isobutylaluminium.** The alkyl was kindly supplied by the Shell Chemical Co. Ltd, Carrington, and stored in an inert atmosphere in a dry box. Analysis, before delivery, yielded the following results:  $Al(iBu)_3$ , 91.2%;  $Al(iBu)_2H$ , 4.1%;  $Al(iBu)_2OBu$ , 4.7%.

**Diethylaluminium chloride.** This aluminium alkyl was also supplied by the Shell Chemical Co. Ltd, Carrington, and was reported to be 95.2% pure.

**Triethylaluminium.** Koch Light Limited supplied the alkyl and claimed a purity of better than 90%.

**Trimethylaluminium and tri-n-decylaluminium.** These were purchased from K & K Laboratories Inc., New York, who claimed their purity to be 95–99%.

**Tri-n-butylaluminium and tri-n-hexylaluminium.** Both these alkyls were obtained from Pfaltz and Bauer Inc., and were stated to be 95% pure.

#### Polymerization procedure

Polymerizations were carried out in special dilatometers as described previously<sup>11</sup>. All glassware used in polymerization experiments was thoroughly cleaned, dried at 150°C and finally flamed out under vacuum.

In order to obtain reproducible results it was considered essential to prepare polymerization mixtures in an identical manner; all components were made up in a similar manner and mixed in the same order. Quantities of vanadium trichloride were introduced into weighed stoppered tubes in a dry box. The filled tubes were then removed from the dry box and weighed, so that the accurate weight of vanadium trichloride was determined. A tube containing the required amount of vanadium trichloride was unstoppered in the dry box and dropped into the bulb of the dilatometer filler. Required amounts of benzene and aluminium alkyl solution were then added, in that order, by means of graduated syringes. The dilatometer filler was then quickly stoppered, removed from the dry box, attached to the high vacuum line, and degassed. The desired quantity of degassed monomer was then distilled in from a graduated tube. Finally, the dilatometer was sealed off and placed in a thermostat bath and allowed to warm up to the required temperature. The polymerization reaction was usually followed for 1.5–4 h using a cathetometer reading to  $\pm 0.01$  mm.

#### Reproducibility

It was found that all rates could be reproduced using the above procedure within  $\pm 4\%$ .

## RESULTS AND DISCUSSION

The polymerization reaction is characterized by an initial 'settling' period during which the rate increases followed by a much longer period in which the rate gradually decreases due to depletion in monomer concentration. Results for a typical polymerization are shown in Figure 1. After the initial 'settling' period the polymerization rate, corrected for decrease in monomer concentration, remains constant up to at least 55% conversion. This is confirmed

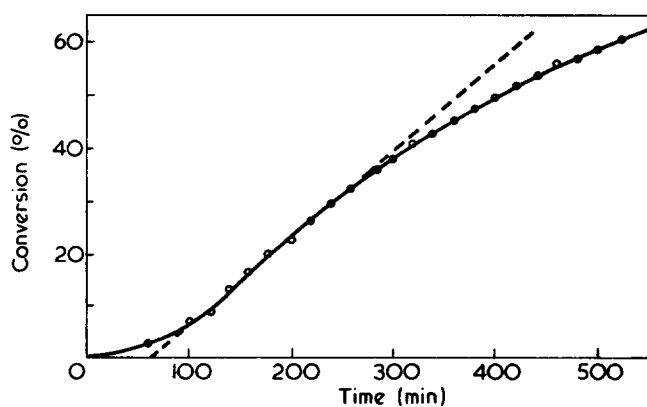


Figure 1 Plot of conversion versus time.  $[4-MP-1]=2.00$  mol/l;  $[VCl_3]=18.5$  mmol/l;  $[Al(iBu)_3]=37.0$  mmol/l; temperature = 30°C

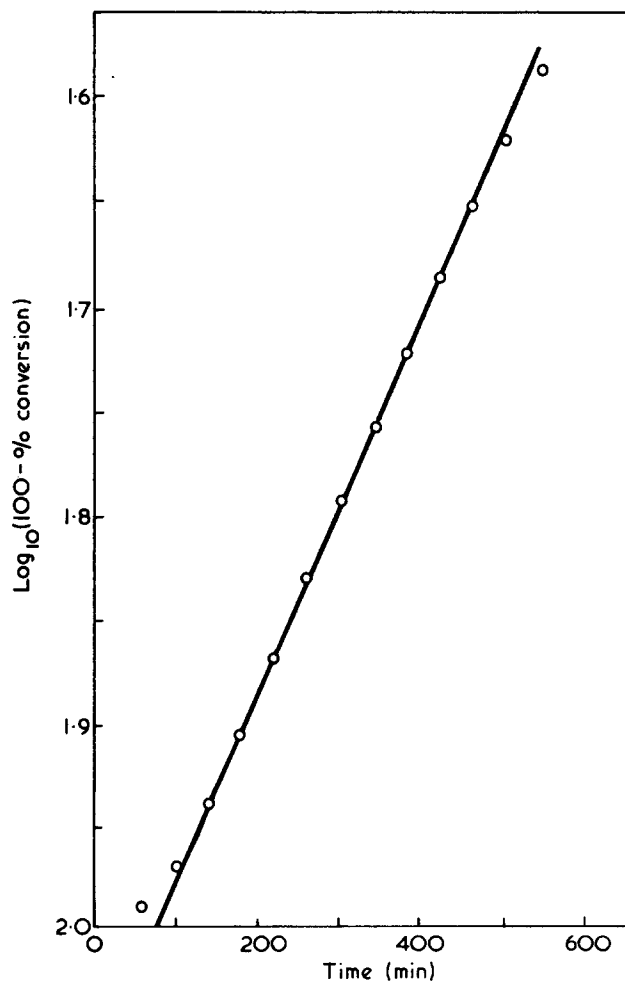


Figure 2 Plot of  $\log_{10}(100-\% \text{ conversion})$  versus time.  $[4-MP-1]=2.00$  mol/l;  $[VCl_3]=18.5$  mmol/l;  $[Al(iBu)_3]=37.0$  mmol/l; temperature = 30°C

in Figure 2 which also shows that the rate within a given polymerization run is first order with respect to monomer concentration. The settling period is found by extrapolation of the linear portion of the first order plot to zero conversion, as illustrated in Figure 2.

During polymerization the vanadium trichloride particles, which are initially finely dispersed, aggregate to form large clusters. As the polymerization proceeds these aggregates break up until the characteristic purple colour is present throughout the whole system. Finally the

polymerization mixture consists of a uniform dispersion of polymer coated catalyst particles, many times larger than their initial size.

#### Dependence of rate on catalyst concentration

The effect of increasing the catalyst concentration on the rate of polymerization was investigated at 30°C and 40°C. Whilst the monomer concentration and tri-isobutylaluminium to vanadium trichloride molar ratio were kept constant, the vanadium halide concentration was varied over a range of  $6.0 \times 10^{-3}$  to  $2.6 \times 10^{-1}$  mol/l at 30°C, and  $3.9 \times 10^{-3}$  to  $18.5 \times 10^{-3}$  mol/l at 40°C. The experimental results are given in *Tables 1* and *2* respectively.

*Table 1a* and *Table 2* show that the steady state rate, ( $R_p$ ), i.e., the rate after the 'settling' period is finished, varies linearly with the concentration of vanadium trichloride when the catalyst concentration is low, i.e., when the ratio [4-MP-1]/[Al(iBu)<sub>3</sub>] is high. Logarithmic plots of the catalyst concentrations versus steady state rates yield straight line plots of slope unity, indicating a first-order reaction with respect to catalyst concentration. These results indicate that, as is usual in Ziegler-Natta systems, the number of active centres is directly proportional to the concentration of the transition metal halide, i.e.

$$C_0 \propto [\text{VCl}_3] \quad (1)$$

and are in accordance with the kinetic scheme proposed earlier<sup>10</sup>.

However, under conditions where the ratio [4-MP-1]/[Al(iBu)<sub>3</sub>] is much lower, the steady state rate divided by the vanadium concentration decreases with increase in vanadium trichloride concentration, i.e., with increase in the ratio [Al(iBu)<sub>3</sub>]:[4-MP-1]. This is evident from an

*Table 1a* Effect of catalyst concentration on rate

[4-Methylpentene-1]=2.00 mol/l; Al(iBu)<sub>3</sub>:VCl<sub>3</sub>=2.0:1; solvent=benzene; polymerization temperature=30°C

[VCl <sub>3</sub> ] × 10 <sup>3</sup> (mol/l)	[4-MP-1] [VCl <sub>3</sub> ]	Steady state rate × 10 <sup>3</sup> (mol/l min)	Rate [VCl <sub>3</sub> ]
6.0	333 : 1	1.88	0.314
8.8	226 : 1	2.58	0.292
10.2	196 : 1	2.70	0.264
13.7	145 : 1	3.84	0.286
15.2	131 : 1	4.18	0.274
15.7	127 : 1	3.94	0.252
16.8	119 : 1	4.60	0.274
17.5	115 : 1	4.44	0.254
18.9	106 : 1	5.56	0.294
21.5	93 : 1	6.12	0.284
22.6	89 : 1	5.54	0.246

*Table 1b* Effect of catalyst concentration on rate

[4-Methylpentene-1]=2.00 mol/l; Al(iBu)<sub>3</sub>:VCl<sub>3</sub>=2.0:1; solvent=benzene; polymerization temperature=30°C

[VCl <sub>3</sub> ] × 10 <sup>2</sup> (mol/l)	[4-MP-1] [VCl <sub>3</sub> ]	Steady state rate × 10 <sup>3</sup> (mol/l min)	Rate [VCl <sub>3</sub> ]
4.8	42 : 1	9.16	0.190
5.8	35 : 1	9.48	0.164
10.3	19 : 1	10.84	0.106
11.0	18 : 1	13.30	0.122
12.6	16 : 1	12.12	0.096
17.6	11 : 1	14.76	0.084
25.5	8 : 1	18.86	0.074

*Table 2* Effect of catalyst concentration on rate

[4-Methylpentene-1]=2.00 mol/l; Al(iBu)<sub>3</sub>:VCl<sub>3</sub>=2.0:1; solvent=benzene; polymerization temperature=40°C

[VCl <sub>3</sub> ] × 10 <sup>3</sup> (mol/l)	[4-MP-1] [VCl <sub>3</sub> ]	Steady state rate × 10 <sup>3</sup> (mol/l min)	Rate [VCl <sub>3</sub> ]
3.9	519 : 1	2.34	0.606
4.8	414 : 1	3.38	0.698
7.4	272 : 1	4.72	0.642
7.4	270 : 1	4.80	0.648
7.5	268 : 1	4.70	0.632
8.7	229 : 1	5.64	0.646
11.2	178 : 1	7.04	0.628
14.7	137 : 1	8.90	0.608
18.4	109 : 1	12.30	0.668

examination of *Table 1b* and its significance will be discussed in the next section.

In experiments 1, 2, 4 and 5 in *Table 1a* a batch of vanadium trichloride was used which had been ball-milled for 2.5 h in an atmosphere of nitrogen. The surface area of this sample, as determined by the Brunauer-Emmett-Teller (B.E.T.) method using nitrogen, was found to be 5.3 m<sup>2</sup>/g, as opposed to 2.3 m<sup>2</sup>/g for the unground sample. As can be seen from *Table 1a* the steady state rate of polymerization was unaffected by the increased surface area of the vanadium trichloride. The duration of the settling period was, however, reduced as is shown in *Figure 3*. These effects have already been reported by Natta<sup>12</sup> for the polymerization of propylene using the catalyst system α-TiCl<sub>3</sub>/AlEt<sub>3</sub>.

#### Dependence of rate on tri-isobutylaluminium concentration

The concentration of monomer and vanadium trichloride were kept constant, whilst the tri-isobutylaluminium concentration was varied over the range  $9.22 \times 10^{-3}$  to  $5.58 \times 10^{-1}$  mol/l at 30°C, and  $4.42 \times 10^{-3}$  to  $2.82 \times 10^{-1}$  mol/l at 40°C.

In *Figure 4* the steady state rate per unit catalyst concentration has been plotted as a function of the aluminium to vanadium ratio. A distinct maximum in the rate of polymerization occurs at a molar ratio of catalyst

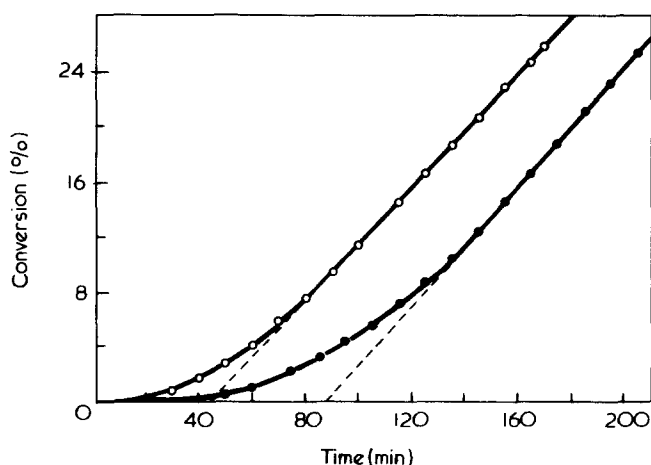


*Figure 3* Effect of using ground (○) and unground (●) vanadium trichloride at 30°C. Using ground VCl<sub>3</sub>: [4-MP-1]=2.00 mol/l; [VCl<sub>3</sub>]=15.2 mmol/l; [Al(iBu)<sub>3</sub>]=30.4 mmol/l. Using unground VCl<sub>3</sub>: [4-MP-1]=2.00 mol/l; [VCl<sub>3</sub>]=16.8 mmol/l; [Al(iBu)<sub>3</sub>]=33.6 mmol/l

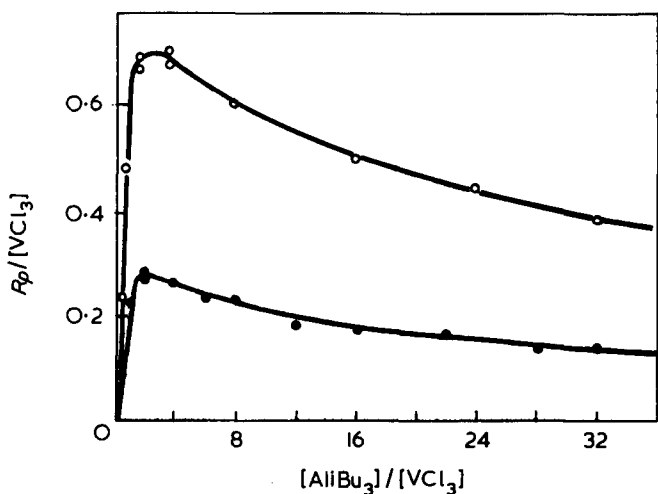


Figure 4 Rate of polymerization as a function of Al to V ratio at constant monomer and constant vanadium trichloride concentration.  $[4\text{-MP-1}] = 2.00 \text{ mol/l}$ ;  $[\text{VCl}_3] \approx 17.5 \text{ mmol/l}$  at  $30^\circ\text{C}$ ;  $[\text{VCl}_3] \approx 8.75 \text{ mmol/l}$  at  $40^\circ\text{C}$ . ●,  $30^\circ\text{C}$ ; ○,  $40^\circ\text{C}$

components of approximately 2 : 1 at each of the two temperatures. However, the actual number of moles of alkyl which combine with the vanadium trichloride in the formation of the active site does not necessarily correspond to the initial Al : V ratio, since the alkyl may assume several roles in the catalyst system<sup>10</sup>. The decline in the rate above this maximum may be attributed to the excess alkyl competing with the monomer molecules for active sites.

In order to determine the exact dependence of the rate of polymerization on the aluminium alkyl concentration, logarithmic plots of the steady state rates versus tri-isobutylaluminium concentrations were drawn for each of the two series of polymerizations. A typical plot is shown in Figure 5, and consists of two distinct linear parts (on either side of the maximum shown in Figure 4). At low aluminium alkyl concentrations the gradients of lines were  $1.07 \pm 0.17$  and  $0.92 \pm 0.08$  at  $30^\circ\text{C}$  and  $40^\circ\text{C}$ , respectively. For higher aluminium concentrations (above the maximum) the gradients had values of  $-0.33 \pm 0.02$  and  $-0.27 \pm 0.02$  respectively. The intercept of the two lines of these logarithmic plots provides a convenient method for determining the optimum catalyst ratio. This was calculated to be 2.32 : 1 at  $30^\circ\text{C}$  and 2.26 : 1 at  $40^\circ\text{C}$ .

A second series of polymerizations were carried out in which the concentration of vanadium trichloride was varied, whilst the amount of tri-isobutylaluminium was kept constant. This effectively changes the ratio of the catalyst components, but at the same time maintains a constant concentration of aluminium alkyl. It may be seen from Figure 6 that, under these experimental conditions, the steady rate (per unit catalyst concentration) increases to a limiting value as the concentration of vanadium trichloride is decreased, i.e., as the catalyst ratio Al : V is increased. Hence the fall off in rate described previously must be attributed to the increasing tri-isobutylaluminium concentration, and is not a consequence of the ratio of the catalyst components. Similar results were found for several other aluminium alkyls and are depicted in Figure 7.

If the active centre for the polymerization is an alkylated entity on the surface of the vanadium trichloride, such as  $\text{VCl}_2\text{R}$ , then the increase in the rate of polymerization at constant vanadium trichloride con-

centration with increasing tri-isobutylaluminium concentration in the region to Al : V = 2 : 1 can readily be explained by considering the following sequence of reactions:

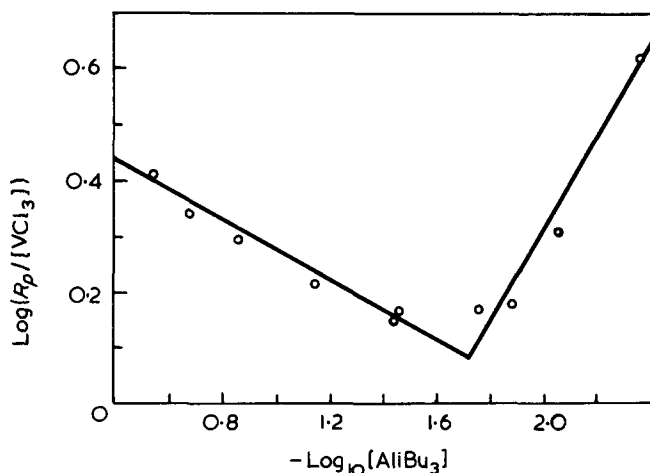
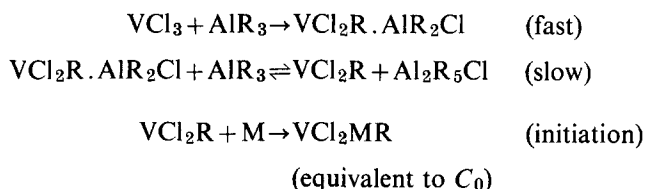


Figure 5 Plot of  $\log_{10}(\text{rate})$  versus  $\log_{10}[\text{Al}(\text{iBu})_3]$ .  $[4\text{-MP-1}] = 2.00 \text{ mol/l}$ ;  $[\text{VCl}_3] = 8.7 \text{ mmol/l}$ ; temperature =  $40^\circ\text{C}$

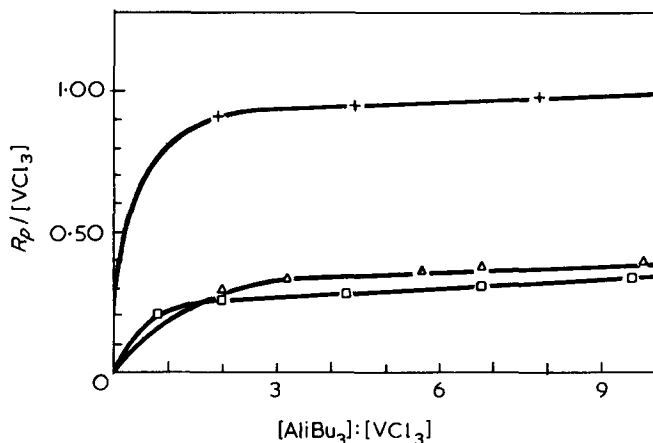


Figure 6 Rate of polymerization as a function of Al to V ratio at constant monomer and constant aluminium tri-isobutyl concentration.  $[4\text{-MP-1}] = 2.0 \text{ mol/l}$ ;  $[\text{Al}(\text{iBu})_3] = 37.0 \text{ mmol/l}$ . +,  $50^\circ\text{C}$ ; □,  $30^\circ\text{C}$ ; △,  $30^\circ\text{C}$  (aged catalyst)

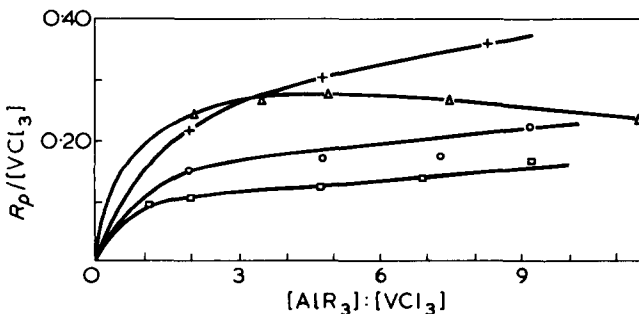
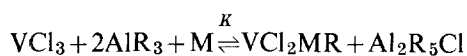


Figure 7 Rate of polymerization as a function of Al : V ratio at constant monomer and constant aluminium alkyl concentration for different aluminium alkyls at  $30^\circ\text{C}$ .  $[4\text{-MP-1}] = 2.00 \text{ mol/l}$ ;  $[\text{AlR}_3] = 37.0 \text{ mmol/l}$ . +,  $\text{Al}(\text{nBu})_3$ ; △,  $\text{AlEt}_3$ ; ○,  $\text{Al}(\text{nHex})_3$ ; □,  $\text{Al}(\text{nDec})_3$



Summing these equations and simplifying gives the overall reaction sequence as:



The concentration of growing polymer chains is then given by the equation:

$$[\text{VCl}_2\text{MR}] = \frac{K[\text{VCl}_3][\text{AlR}_3]^2[\text{M}]}{[\text{Al}_2\text{R}_5\text{Cl}]} \quad (2)$$

It would have been more accurate to use  $\theta_M$  and  $\theta_A$  instead of  $[\text{M}]$  and  $[\text{AlR}_3]$  in equation (2). Nevertheless equation (2) will give a good approximation for the concentration of growing polymer chains at the low concentrations under consideration in this section. Further



Substitution for  $[\text{Al}_2\text{R}_5\text{Cl}]$  in equation (2) gives the relation:

$$[\text{VCl}_2\text{MR}] = \frac{K_2[\text{VCl}_3][\text{AlR}_3][\text{M}]}{[\text{AlR}_2\text{Cl}]} \quad (3)$$

i.e., the concentration of growing polymer chains,  $C_0$  is given by:

$$C_0 \propto \frac{[\text{VCl}_3][\text{AlR}_3][\text{M}]}{[\text{AlR}_2\text{Cl}]} \quad (4)$$

Under the present experimental conditions the concentration of vanadium trichloride, and consequently the concentration of aluminium chloroalkyl is constant, and thus,

$$C_0 \propto [\text{AlR}_3][\text{M}] \quad (5)$$

Hence the initial increase in rate with increase in concentration of aluminium alkyl should be almost directly proportional to the concentration of aluminium alkyl since at these low concentrations,  $\theta_A \propto [\text{AlR}_3]$ . This is found to be the case (Figure 5).

It should be noted that  $C_0$  has a maximum value when the whole of the potential active centres have become growing chains. Consequently at higher concentrations when the formation of active centres is almost complete, the steady state rate will begin to fall because of the lower values of  $\theta_M$ . Above an Al : V ratio of 2 : 1 the rate of polymerization is given by the expressions derived in an earlier paper<sup>10</sup> viz.

$$R_p = k_p \theta_M C_0 \quad (6)$$

where

$$\theta_M = \frac{K_M[\text{M}]}{1 + K_M[\text{M}] + K_A[\text{A}]} \quad (7)$$

i.e.,

$$R_p = \frac{k_p K_M[\text{M}] C_0}{1 + K_M[\text{M}] + K_A[\text{A}]} \quad (8)$$

Without a prior knowledge of  $K_A$  and  $K_M$  it is not possible to predict exactly how  $R_p$  will vary with increase in aluminium alkyl concentration. From equation (8) the rate of polymerization would nevertheless be expected to decrease with increase in aluminium alkyl concentration above a ratio of Al : V > 2, as has been observed experimentally (Figure 4). A comparison between observed and predicted rates of polymerization will be detailed later<sup>13</sup>.

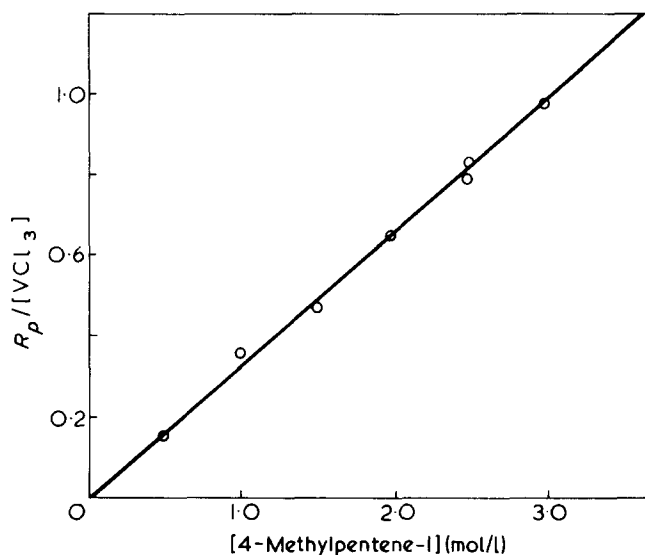


Figure 8 Variation in rate of polymerization with monomer concentration at 40°C.  $[\text{VCl}_3] = 8.8 \text{ mmol/l}$ ;  $[\text{Al}(\text{iBu})_3] = 17.6 \text{ mmol/l}$

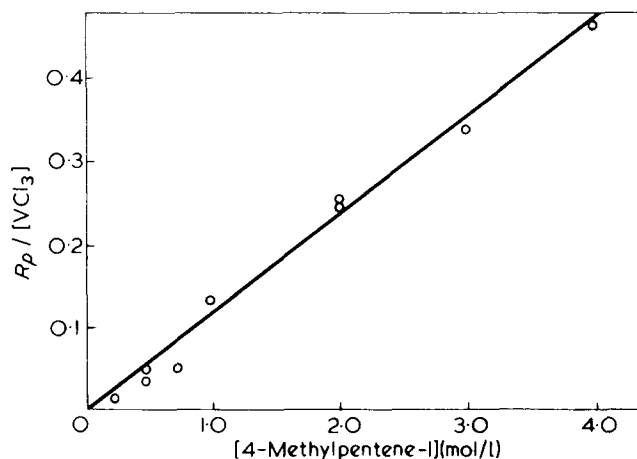


Figure 9 Variation in rate of polymerization with monomer concentration at 30°C.  $[\text{VCl}_3] = 17.8 \text{ mmol/l}$ ;  $[\text{Al}(\text{iBu})_3] = 35.6 \text{ mmol/l}$

#### Dependence of rate on 4-methylpentene-1 concentration

In this series of polymerizations the catalyst concentration and aluminium to vanadium ratio were kept constant whilst the monomer concentration was varied from 0.25 to 4.0 mol/l at 30°C, and from 0.5 to 3.0 mol/l at 40°C.

Polymerizations at 40°C gave a linear plot of steady state rate of polymerization as a function of monomer concentration (Figure 8). The order with respect to monomer concentration was shown to be  $1.04 \pm 0.03$ , and is thus in agreement with the results shown in Figure 2.

At 30°C, however, although the points above 1.0 mol/l lie on a straight line passing through the origin, points below this concentration deviate considerably from a first-order dependence (Figure 9). A logarithmic plot of the variation of steady state rate with monomer concentration is shown in Figure 10, and consists of two distinct linear parts. At low monomer concentrations the gradient is equal to  $1.78 \pm 0.04$ , whereas at concentrations above

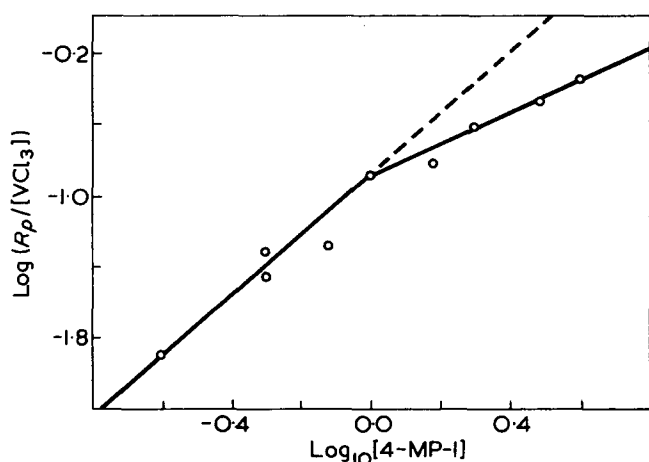


Figure 10 Plot of  $\log_{10}$  (rate) versus  $\log_{10}[4\text{-MP-1}]$  at  $30^\circ\text{C}$ .  $[\text{VCl}_3]=17.8\text{ mmol/l}$ ;  $[\text{Al}(\text{iBu})_3]=35.6\text{ mmol/l}$

1.0 mol/l the gradient changes to  $0.87 \pm 0.03$ . Thus, on reducing the monomer concentration the rate apparently changes from nearly first to nearly second order with respect to monomer concentration. This change of order of rate dependence on monomer concentration has also been observed in other Ziegler-Natta systems. Bier<sup>14</sup> has suggested that the slowly decreasing rates of propylene polymerization with the catalyst system  $\alpha\text{-TiCl}_3/\text{AlEt}_2\text{Cl}$  under polymer precipitating conditions were caused by diffusion control. Similar explanations were advanced by Burnett and Tait<sup>15</sup> for the depressed rates of styrene polymerization in heptane below styrene concentrations of 3.5 mol/l.

Another possible explanation of these depressed rates of polymerization at low concentrations emerges if the sequence proposed in an earlier paper is considered<sup>10</sup>. Two types of active site were envisaged as existing in these polymerization systems, viz., propagating sites of concentration  $C_0$ , and potential sites of concentration  $C_t$ . Potential sites were considered to be sites prior to initiation by monomer or sites arising from transfer reactions by either monomer or metal alkyl; under these conditions and when the concentration of monomer was low the following expression was shown to hold:

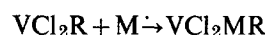
$$\frac{[\text{M}]}{R_p} = \frac{1}{k_p C_t K_M} \left(1 + \frac{k_m}{k_i}\right) + \frac{1}{k_p C_t K_M} \left(\frac{k_a K_A [\text{A}]}{k_i K_M}\right) \frac{1}{[\text{M}]} \quad (9)$$

If equation (9) applies to this system a plot of  $[\text{M}]/R_p$  should be linear. Such a plot is shown in Figure 11, and is indeed linear, indicating that the proposed sequence could be applicable in this instance. It should be noted that only values of  $[\text{M}] < 1$  have been used.

The fact that the depression in rate at low monomer concentrations is not observed at  $40^\circ\text{C}$  in the concentration range studies (0.5–3.0 mol/l) is explicable if it is assumed that the activation energy for chain initiation is greater than that for chain propagation. In the case of the polymerization of propylene by the catalyst system  $\text{VCl}_3/\text{Al}(\text{iBu})_3$  values of 21.0 and 12.9 kcal/mol have been reported for the activation energies of initiation and propagation respectively<sup>16</sup>.

Although explanations of this kind fit the observed depression of the rate of polymerization at low monomer concentrations reasonably well, the possibility of some diffusion control in these regions cannot be ruled out completely.

The apparent contradiction arising from the observations that while the rate of polymerization at  $30^\circ\text{C}$  is first order with respect to monomer concentration within a given polymerization (fixed initial monomer concentration, Figure 2) yet it has a variable order with respect to monomer concentration when the initial monomer concentration is varied, is believed to arise from the non-equilibrium nature of the slow initiation process which has been formulated as:



When chain initiation is slow (i.e., low monomer concentration at  $30^\circ\text{C}$ ) the maximum value of  $C_0$  has not been reached by the time the steady state rate has been recorded. During this period  $C_0$  is a function of the monomer concentration and hence:

$$R_p \propto [\text{M}]^2$$

Within a given polymerization (i.e., under the conditions and concentrations depicted in Figure 2) the value of  $C_0$  will be constant for any given initial concentration of monomer, and hence the rate of polymerization, determined as the polymerization reaction proceeds varies with remaining monomer concentration, and,  $R_p \propto [\text{M}]$ .

#### Dependence of rate on temperature

Plots of  $\log$  (rate) versus  $1/T$  for the polymerization in benzene solution consisted of two distinct linear parts. A typical plot is shown in Figure 12. The slope of the line up to  $47^\circ\text{C}$  gives an overall activation energy of  $16.6 \pm 1.0$  kcal/mol. This value compares favourably with the value of 15 kcal/mol found by Ehrig *et al.*<sup>9</sup> for the polymerization of 4-MP-1 by the catalyst system of  $\alpha\text{-TiCl}_3/\text{AlEt}_2\text{Cl}$  in heptane.

Above  $47^\circ\text{C}$  the rate decreases with further increase in temperature. This decrease in rate could be caused by either a reduction in the number of active centres or by viscous effects due to the dissolution of polymer at higher temperatures.

Figure 13, however, shows an Arrhenius plot for the polymerization in heptane, a much poorer solvent which does not swell the polymer as does benzene. The plot is

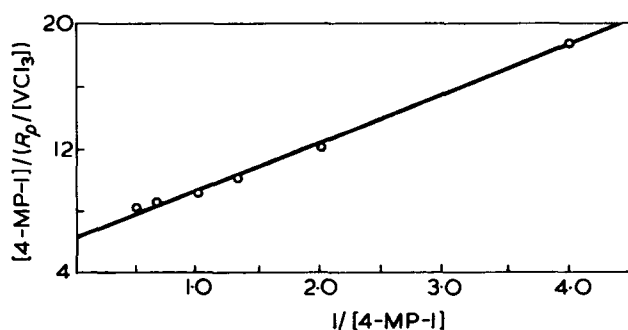


Figure 11 Plot of  $[4\text{-MP-1}]/\text{rate}$  versus  $1/[4\text{-MP-1}]$  at  $30^\circ\text{C}$ .  $[\text{VCl}_3]=17.8\text{ mmol/l}$ ;  $[\text{Al}(\text{iBu})_3]=35.6\text{ mmol/l}$

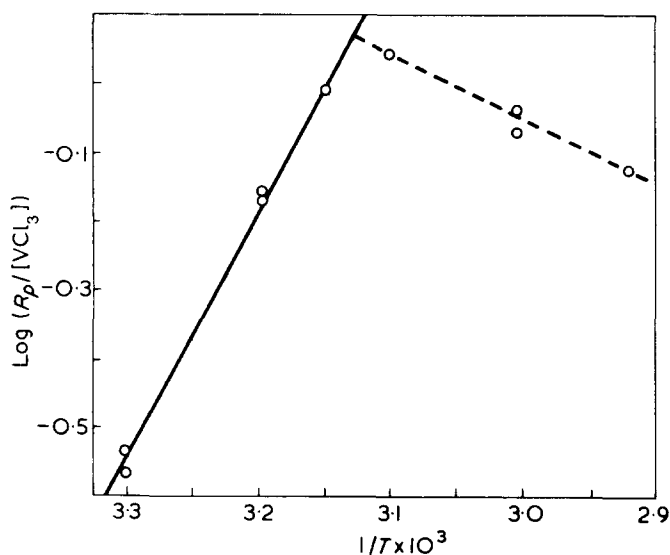


Figure 12 Plot of  $\log_{10}(\text{rate})$  versus  $1/T$  for polymerization in benzene.  $[4\text{-MP-1}] = 2.00 \text{ mol/l}$ ;  $[\text{Al}(\text{iBu})_3] : [\text{VCl}_3] = 2.0 : 1$

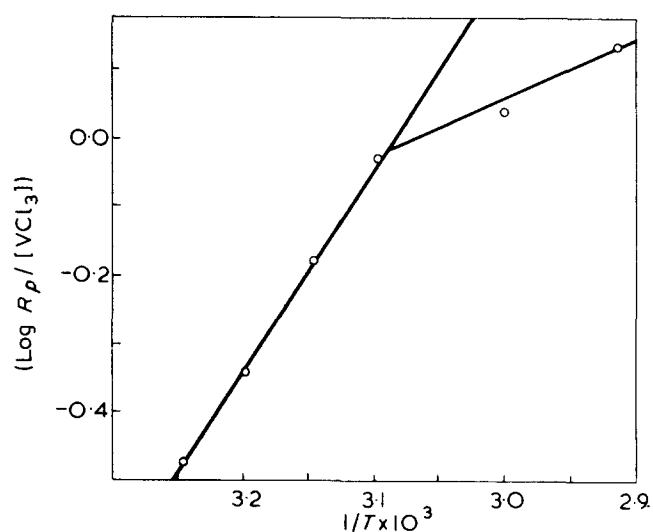


Figure 13 Plot of  $\log_{10}(\text{rate})$  versus  $1/T$  for polymerizations in n-heptane.  $[4\text{-MP-1}] = 2.00 \text{ mol/l}$ ;  $[\text{Al}(\text{iBu})_3] : [\text{VCl}_3] = 2.0 : 1$

similar to that in benzene in that it is composed of two distinct linear parts. The slope of the line up to  $50^\circ\text{C}$  gives an overall activation energy of  $13.7 \pm 0.5 \text{ kcal/mol}$ . In this case, however, the reaction rate does not decrease with further increase in temperature above  $50^\circ\text{C}$ , but continues to increase, though at a somewhat reduced rate. Also, the polymerization mixture was not found to be particularly viscous even at  $70^\circ\text{C}$ .

Furthermore, in Figure 14 are shown plots at  $30^\circ\text{C}$  and  $50^\circ\text{C}$  of  $\log(100 - \% \text{ conversion})$  against time using triisobutylaluminium as the metal alkyl. It will be observed that at  $50^\circ\text{C}$  the plot starts to deviate from linearity at a lower conversion than at  $30^\circ\text{C}$ .

These observations when taken together suggest that the catalyst system becomes less active above  $50^\circ\text{C}$ , possibly due to the reduction of the vanadium trichloride by the triisobutylaluminium compound to give the catalytically inactive vanadium dichloride<sup>17</sup>.

#### Dependence of the rate on different aluminium alkyl compounds

The results of using a series of aluminium alkyl compounds are summarized in Table 3. In this Table the rates quoted are the averages obtained at each of the two temperatures.

Table 3 Variation in rate with nature of aluminium alkyl

Aluminium alkyl	$R_p/[\text{VCl}_3]$ (mol/l min per mol $\text{VCl}_3$ )	
	$30^\circ\text{C}$	$40^\circ\text{C}$
Trimethyl	0.288	0.286
Tri-isobutyl	0.280	0.660
Triethyl	0.253	0.700
Tri-n-butyl	0.221	—
Diethylchloride	0.169	0.110
Tri-n-hexyl	0.149	—
Tri-n-decyl	0.107	0.240

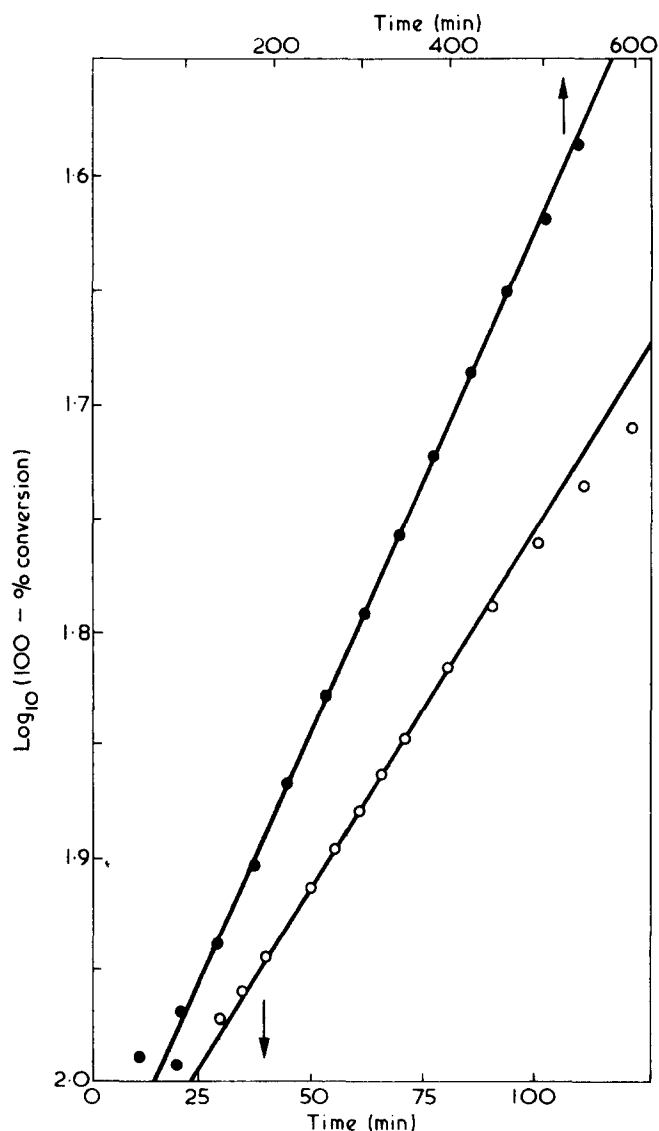


Figure 14 Plot of  $\log_{10}(100 - \% \text{ conversion})$  versus time at two different temperatures.  $\bullet$ ,  $30^\circ\text{C}$ ;  $\circ$ ,  $50^\circ\text{C}$ .  $[4\text{-MP-1}] = 2.00 \text{ mol/l}$ ;  $[\text{Al}(\text{iBu})_3] : [\text{VCl}_3] = 2.0 : 1$

It may be seen that at 30°C the aluminium alkyl compounds may be placed in the following order of decreasing catalytic activity:  $\text{AlMe}_3 \geq \text{Al}(\text{iBu})_3 > \text{AlEt}_3 > \text{Al}(\text{nBu})_3 > \text{AlEt}_2\text{Cl} > \text{Al}(\text{nHex})_3 > \text{Al}(\text{nDec})_3$ . However, the results at 40°C are somewhat different:  $\text{AlEt}_3 \geq \text{Al}(\text{iBu})_3 > \text{AlMe}_3 > \text{Al}(\text{ndecyl})_3 > \text{AlEt}_2\text{Cl}$ .

When trimethylaluminium is used as the aluminium alkyl component of the catalyst system, the vanadium trichloride particles remain as a fine dispersion throughout the polymerization, so that when the reaction mixture is precipitated, the polymer is obtained as a very fine white powder. During the polymerization small bubbles of gas are evolved probably due to reduction of the vanadium trichloride by the trimethylaluminium thus accounting for the low rate at 40°C.

When diethylaluminium chloride or tri-n-decylaluminium is used the vanadium trichloride particles are found to coagulate instantly into a few loosely held aggregates. As the polymerizations proceed these aggregates expand in size and slowly break up to give a fairly uniform dispersion of catalyst particles coated with polymer, but of a coarser nature than with trimethylaluminium. Triethylaluminium tends to behave in much the same way as trimethylaluminium in that the vanadium trichloride remains finely dispersed throughout the polymerization. Tri-isobutylaluminium, on the other hand, gives a fairly coarse dispersion of catalyst particles, though the particles do not coalesce as rapidly as they do with tri-n-decylaluminium and diethylaluminium chloride.

The catalyst systems based on  $\text{AlMe}_3$ ,  $\text{AlEt}_3$  and  $\text{Al}(\text{ndecyl})_3$  all exhibit the same type of kinetic behaviour as that using  $\text{Al}(\text{iBu})_3$  in that there is an initial 'settling' period, followed by a steady state period. The rate of polymerization, after the 'settling' period can be shown to be first order with respect to monomer concentration.

The kinetic behaviour of the catalyst system  $\text{VCl}_3/\text{AlEt}_2\text{Cl}$  is different from the other systems investigated, as the rate is found to increase rapidly to a maximum and then decrease after a short steady state period. This is best illustrated in Figure 15 in which  $\log_{10}(100 - \%$  conversion) is plotted as a function of time. Although the reaction initially appears to follow a first-order kinetic plot, the plot deviates from linearity after a short reaction time. This type of behaviour has also been reported for the polymerization of propylene by the catalyst system  $\text{TiCl}_3/\text{AlEt}_2\text{Cl}$ <sup>18</sup>. Also, on increasing the reaction temperature from 30°C to 40°C the rate of polymerization is found to decrease slightly.

## CONCLUSIONS

- (1) The rate of polymerization is proportional to the catalyst concentration.
- (2) The rate of polymerization is proportional to the tri-isobutylaluminium concentration up to an Al : V ratio of 2 : 1. Above this ratio the rate of polymerization decreases with further increase in the aluminium concentration at constant monomer concentration.
- (3) The rate of polymerization is proportional to the monomer concentration at 40°C and 30°C above a 4-MP-1 concentration of 1.0 mol/l. For monomer concentrations below 1.0 mol/l at 30°C the rate of poly-

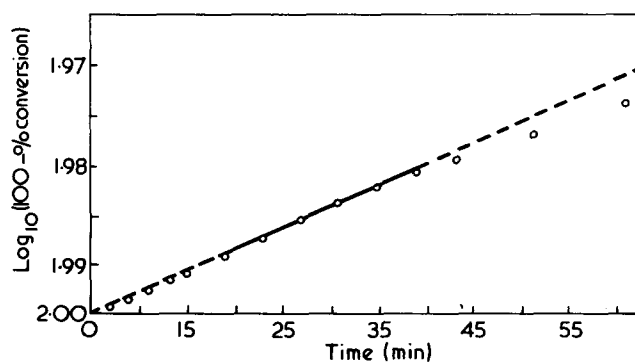


Figure 15 Plot of  $\log_{10}(100 - \%$  conversion) versus time using aluminium diethylchloride.  $[4\text{-MP-1}] = 2.00 \text{ mol/l}$ ;  $[\text{VCl}_3] = 9.00 \text{ mmol/l}$ ;  $[\text{Al}(\text{iBu})_3] = 18.00 \text{ mmol/l}$ ; temperature = 40°C

merization is approximately second order with respect to the monomer concentration.

(4) The rate of polymerization is slower in n-heptane solution than in benzene. The activation energies are 13.7 and 16.6 kcal/mol respectively.

(5) Catalyst systems based on  $\text{AlMe}_3$ ,  $\text{AlEt}_3$  and  $\text{Al}(\text{ndecyl})_3$  in conjunction with vanadium trichloride all exhibit the same type of kinetic behaviour as does the system using  $\text{Al}(\text{iBu})_3$ . The catalyst system  $\text{VCl}_3/\text{AlEt}_2\text{Cl}$  differs from the others in that it exhibits a decay type of polymerization.

(6) These general kinetic relationships are consistent with a polymerization scheme in which chain propagation proceeds between adsorbed monomer molecules and active centres formed on the surface of the solid vanadium trichloride by its interaction with aluminium alkyl.

## REFERENCES

- 1 Hewett, W. A. and Weir, F. E. *J. Polym. Sci. (A)* 1963, 1, 1239
- 2 Hoffman, A. S., Fries, B. A. and Condit, P. C. *J. Polym. Sci. (C)* 1963, 4, 109
- 3 Inone, M. *J. Polym. Sci. (B)* 1963, 1, 217
- 4 Litt, M. *J. Polym. Sci. (A)* 1963, 1, 2219
- 5 Natta, G. *Atti Accad. Naz. Lincei, Rend. Classe Sci. Fis. Mat. Nat.* 1955, 29, 397
- 6 Campbell, T. W. *J. Appl. Polym. Sci.* 1961, 5, 184
- 7 Watt, W. R. *J. Polym. Sci.* 1960, 45, 509
- 8 Burnett, G. M. *54th A. Meet. AIChE, New York* 1961, Preprint 12; Anderson, I. H. *PhD Thesis*, Aberdeen University, 1961
- 9 Ehrig, R. J., Godfrey, J. J. and Krishnamurthy, G. S. 'Elastomer Stereospecific Polymerisation', *Am. Chem. Soc. Symp. New Aspects of Elastomer Stereospecific Polymerization*, Chicago, 1964, p 105
- 10 Burfield, D. R., McKenzie, I. D. and Tait, P. J. T. *Polymer* 1972, 13, 302
- 11 Anderson, I. H., Burnett, G. M. and Tait, P. J. T. *J. Polym. Sci.* 1962, 56, 391
- 12 Natta, G. *J. Polym. Sci.* 1959, 34, 21
- 13 Burfield, D. R., Tait, P. J. T. and McKenzie, I. D. *Polymer* 1972, 13, 321
- 14 Bier, G. *Kunststoffe* 1958, 48, 35
- 15 Burnett, G. M. and Tait, P. J. T. *Polymer* 1960, 1, 151
- 16 Novokshonova, L. A., Berseneva, G. P., Tsvetkova, V. I. and Chirkov, N. M. *Vysokomol. Soedin (A)* 1967, 9 (3), 562
- 17 Natta, G., Mazzanti, G., De Luca, D., Giannini, V. and Bandini, F. *Makromol. Chem.* 1964, 76, 54
- 18 Caunt, A. D. *J. Polym. Sci. (C)* 1964, 4, 49

# Ziegler–Natta catalysis:

## 3. Active centre determination

D. R. Burfield and P. J. T. Tait

*Department of Chemistry, University of Manchester Institute of Science and Technology, Manchester M60 1QD, UK  
(Received 6 December 1971)*

The number of active centres in the polymerization system  $VCl_3/AIR_3/4\text{-MP-1}$  has been shown to lie in the range  $2.3\text{--}6.1 \times 10^{-4}$  mol/mol  $VCl_3$  for a series of aluminium alkyls, and to vary with the nature of the aluminium alkyl used. Chain transfer with aluminium alkyl has been demonstrated. The propagation rate constant has been evaluated and found to be independent of the nature of the metal alkyl. The location of, and nature of, the active centre is discussed. The validity of the tritium labelling procedure is tested by comparison of calculated and experimentally determined molecular weights.

### INTRODUCTION

In the area of Ziegler–Natta polymerization the actual value of the active centre concentration has been the focus of scientific investigation since shortly after the discovery of these systems. So far four distinct methods have been reported in the literature for these determinations:

(i) Kinetic methods. The active centre concentration is evaluated from rate and molecular weight data<sup>1–7</sup>.

(ii) Catalyst labelling. The number of radioactive endgroups introduced into the polymer chains is determined by using <sup>14</sup>C-labelled catalyst components, and related to the number of active centres in the catalyst system<sup>8, 9</sup>.

(iii) Quenching methods. The polymerization reaction is terminated by the addition of compounds which react quantitatively with the catalyst–polymer bonds, thus labelling the polymer molecules which were attached to the catalyst. The active centre concentration may then be evaluated from the number of labelled macromolecules<sup>10–25</sup>.

(iv) Electron microscopy. The number of active sites is estimated from observation of growing polymer chains<sup>26</sup>.

In a recent review of methods for active centre determinations Kern *et al.*<sup>10</sup> concluded that quenching techniques involving tritium labelling were probably the most reliable provided that care was taken in the application and interpretation of the results (see also Appendix). This latter method was used in this present study where the polymerization reaction mixture was quenched by the addition of excess tritium-labelled methanol.

### EXPERIMENTAL

#### Materials

Details of catalysts have already been published<sup>27</sup>.

*Tritium-labelled water.* This was purchased from

UKAEA, Radiochemical Centre, Amersham, at an activity of 5 Ci/cm<sup>3</sup> and was used as received.

*Tritium-labelled methanol.* This was prepared by exchanging small quantities of tritium-labelled water with dried inactive methanol in the presence of excess freshly prepared sodium methoxide. The labelled methanol was further purified by fractionation and used at a specific activity of about 0.7 Ci/mol.

*Tritium-labelled standards.* 1,2-<sup>3</sup>H-n-hexadecane was purchased from the Radiochemical Centre and had a certified specific activity of 2.27 Ci/g.

*Scintillation solutions.* The NE 221 scintillation gel was supplied by Nuclear Enterprises (G.B.) Ltd, Edinburgh, and was used for assaying the labelled polymer. A scintillation solution of 4 g/l PPO, 0.4 g/l POPOP in toluene was used for measuring the activity of the methanol.

#### Procedure

Polymerizations were carried out under high vacuum<sup>27</sup>. For the majority of these polymerizations the  $VCl_3$  addition was followed by the required quantities of monomer, benzene and aluminium alkyl in benzene in that order. This order of addition was found to give better reproducibility. Quench runs were performed in an all glass reaction vessel with an ampoule containing the labelled methanol sealed in a side-arm (*Figure 1*). The rate of polymerization was checked by comparison of the gravimetric yield at the quench time with that obtained by a dilatometric run under identical conditions. Rates of polymerization as checked by this method always agreed within  $\pm 4\%$ .

To ensure completeness of the quench reaction a 30 M excess of MeOH to  $AIR_3$  was used, under which conditions the violet coloured reaction mixture rapidly turned light-green probably due to the formation of the complex  $[VCl_2(MeOH)_4]^+Cl^-$ <sup>28</sup>. Addition of active methanol to the reaction mixture, after quenching with inactive methanol whilst still under high vacuum, gave rise to only

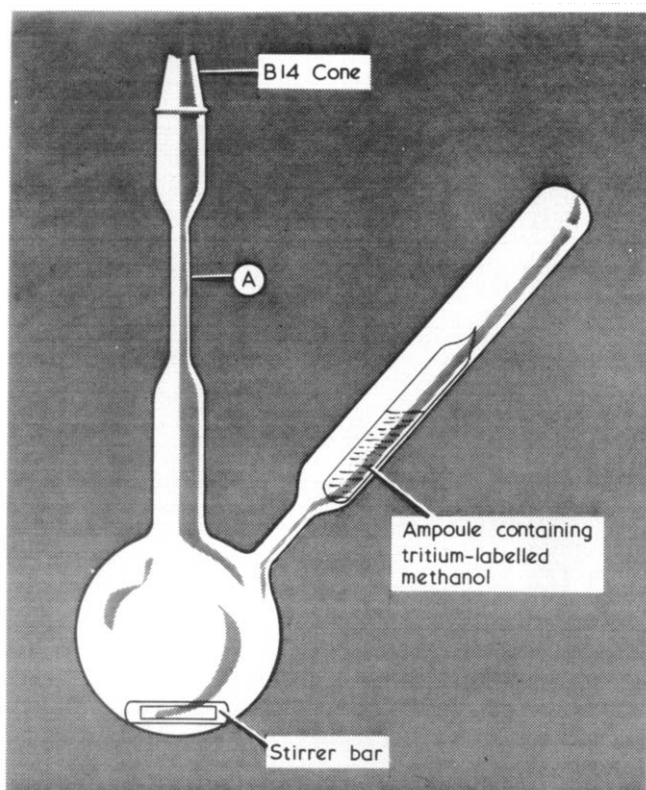


Figure 1 Reaction vessel used for quenched polymerization runs background activity in the polymer. This demonstrates that: (a) tritium is not incorporated into the polymer by exchange reactions; (b) the initial quench reaction is essentially complete; and (c) the decontamination procedure is effective.

Decontamination was accomplished by methanol/HCl precipitation of the reaction mixture, followed by Soxhlet extraction with inactive methanol and finally drying under high vacuum at 80°C for 48 hours. It was possible to show that this procedure gave rise to a negligible loss of labelled low molecular weight polymer, due to the high insolubility of the samples.

The activity of the polymer was determined by liquid scintillation counting. Samples were prepared for assay by dispersing about 100 mg of finely powdered polymer in 10 cm<sup>3</sup> of NE 221 gel scintillator. Sampling reproducibility was found to be within  $\pm 1\%$ . The efficiency of counting was determined as  $12.3 \pm 0.5\%$ . Background counts were always less than 5% of the total count, which was never less than 10 000 counts.

The tritium-labelled methanol was assayed in a scintillation solution previously specified, at an efficiency of  $22.2 \pm 0.2\%$ . All radioactive measurements were made with a Nuclear Chicago Model 725 liquid scintillation spectrometer.

#### Kinetic isotope effect

This effect arises due to the difference in reactivity between the oxygen-hydrogen and oxygen-tritium bonds. Tritium, the heavier isotope, has a smaller rate constant for bond rupture. In consequence the amount of tritium (T) incorporated into the polymer is smaller by a factor of  $k_H/k_T$  than the value expected if the reactivities were equal. Thus Feldman and Perry's derivation<sup>14</sup> includes the correction factor  $K$ , which must be experimentally determined.

Values of between 1 and 3.7 for this factor have been reported by different authors<sup>10, 14, 15, 17, 20</sup> for a variety of systems. Kern *et al.*<sup>10</sup> have shown that the value is dependent on the concentration of MeOH used in quenching, and on the nature of the monomer. They concluded that determination of the correction factor was mandatory for individual systems. In the present study the correction factor has been determined by comparison of the <sup>3</sup>H content of polymer quenched rapidly with an excess of tritiated methanol with the tritium content of polymer quenched by slow titration. A value of  $3.20 \pm 0.15$  has been determined at 30°C for the correction factor and found to be independent of the nature of the aluminium alkyl.

## RESULTS

The number of metal-polymer bonds (MPB) in the reaction mixture at the time of quenching was evaluated from the equation derived by Feldman and Perry<sup>14</sup>. Thus:

$$[\text{MPB}] = \frac{KAG}{a} \quad (1)$$

where  $[\text{MPB}]$  = MPB concentration (mol/l),  
 $K$  = correction factor for the isotope effect,  
 $A$  = specific activity of the polymer (dpm/g),  
 $G$  = polymer yield at time of quenching (g/l),  
 $a$  = specific activity of the methanol (dpm/mol).

Variation of the MPB concentration with time and with % conversion, at constant catalyst and monomer concentrations, was investigated for a series of aluminium alkyls. For Al(*i*Bu)<sub>3</sub> the MPB concentration was found to increase continuously with polymerization time and with % conversion, as indicated in Figures 2 and 3. It has been shown previously<sup>27</sup> that the rate of polymerization, corrected for decrease in monomer concentration, reaches a constant value by about 20% conversion, and thus it seems reasonable to suppose that the number of active centres has also reached a constant value. However, Figures 2 and 3 show a continued increase in the MPB concentration beyond this point, thus clearly

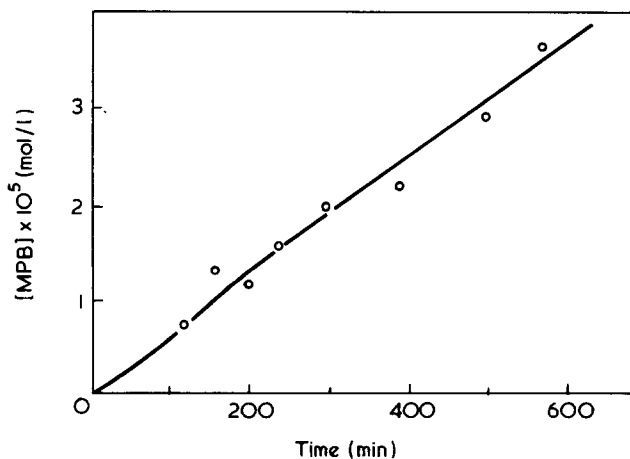


Figure 2 Variation of MPB concentration with time.  $[4\text{-MP-1}] = 2.00 \text{ mol/l}$ ;  $[\text{VCl}_3] = 18.5 \text{ mmol/l}$ ;  $[\text{Al}(\text{iBu})_3] = 37.0 \text{ mmol/l}$ ; temperature = 30°C

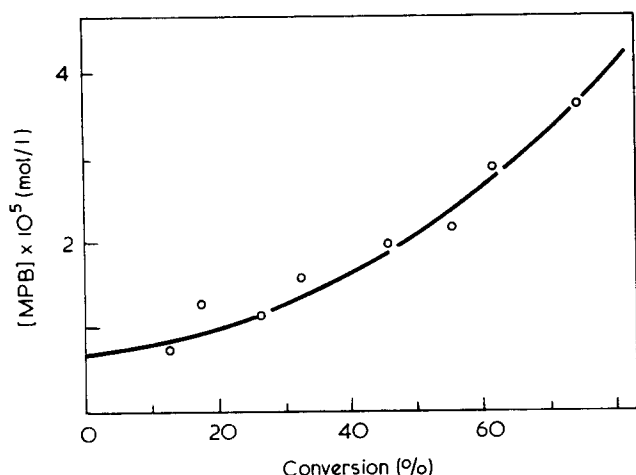


Figure 3 Variation of MPB concentration with % conversion. [4-MP-1]=2.00 mol/l; [VCl<sub>3</sub>]=18.5 mmol/l; [Al(iBu)<sub>3</sub>]=37.0 mmol/l; temperature=30°C

indicating the formation of a non-propagative metal-bonded species. This is indicative of chain transfer with metal alkyl as has been proposed by Natta<sup>4</sup>. Similar observations have been made by other workers<sup>11-17</sup> who also mainly interpret the continued increase in MPB concentration as the result of a chain transfer reaction.

Examination of Figure 2 shows an initial non-linear increase in the MPB concentration, corresponding to the initial formation of centres active in polymerization. This is followed by a long period of linear increase in the MPB concentration due to the transfer reaction. The slope of the linear portion of the graph is equal to the rate of transfer with aluminium alkyl ( $R_{ta}$ ), and is seen to remain constant over the range which was investigated.

As the polymerization is characterized by an initial settling period it was felt necessary to evaluate the active centre concentration ( $C_0$ ) from a plot of [MPB] versus conversion rather than time. The non-linearity of the [MPB] versus conversion plot is due to the depletion in monomer concentration with corresponding decrease in rate. However, extrapolation of this graph is simplified by use of the first order plot of  $\log_{10}(100 - \% \text{ conversion})$  versus time (which is shown in Figure 4) and which gives rise to a linear plot over the investigated range.  $C_0$  is evaluated from the value of the intercept at zero conversion.

Similar plots were obtained using AlEt<sub>3</sub>, Al(nBu)<sub>3</sub> and Al(nHex)<sub>3</sub> and are shown in Figures 5-7. It will be observed that the plot for AlEt<sub>3</sub> is non-linear. This effect is most likely to arise because of deactivation of the active centres. This was observed only in the case of AlEt<sub>3</sub>.

The active centre concentration was also obtained for Al(iBu)<sub>3</sub> at 50°C by a similar procedure.

All these results are summarized in Table 1.

## DISCUSSION

The number of active centres in the polymerization system 4-MP-1/VCl<sub>3</sub>/AlR<sub>3</sub> at 30°C was found to lie in the range  $2.3-6.1 \times 10^{-4}$  mol/mol VCl<sub>3</sub> for a series of aluminium alkyls. This compares with values of  $3-10 \times 10^{-3}$  mol/mol TiCl<sub>3</sub> found by several authors<sup>4,7,17</sup> for the system

$\alpha$ -TiCl<sub>3</sub>/AlEt<sub>3</sub>/propylene. Thus the values of  $C_0$  determined in this study are a factor of ten lower than those found by other workers. This discrepancy is outside the limits of experimental error which has been estimated at a maximum of  $\pm 12\%$ .

This disparity in the values of active centre concentration is capable of several explanations, the most important of these is probably concerned with differences in the transition metal halide used. Kern *et al.*<sup>3</sup> have shown that the number of active centres in the polymerization of propylene is dependent upon the method of preparation of the  $\alpha$ -TiCl<sub>3</sub>. It is quite conceivable that the number of active sites for VCl<sub>3</sub> would be less than for  $\alpha$ -TiCl<sub>3</sub> because of differences in crystal structure and in stabilities of the organo-transition metal species.

In addition it should be noted that several authors<sup>29-31</sup> observe that the rate of polymerization, and hence  $C_0$ , is dependent on the initial surface area of the transition metal halide. The initial surface area of the VCl<sub>3</sub> used in this study was 2.3 m<sup>2</sup>/g, as measured by the Brunauer-Emmett-Teller (B.E.T.) method, which is low compared with a value of about 7 m<sup>2</sup>/g for the  $\alpha$ -TiCl<sub>3</sub> used by other workers in active centre determination.

Kern *et al.*<sup>10</sup> have further shown that the number of active centres is dependent on the nature of the monomer, e.g.,  $C_0$  decreases from  $4.5 \times 10^{-3}$  to  $3.8 \times 10^{-3}$  mol/mol TiCl<sub>3</sub> on changing from propylene to butene-1. This reduction in  $C_0$  may reflect a 'steric restriction' at some of the sites. Hence, it is possible that the number of active sites in the polymerization of the bulky monomer 4-methylpentene-1 may be somewhat less than in the polymerization of propylene.

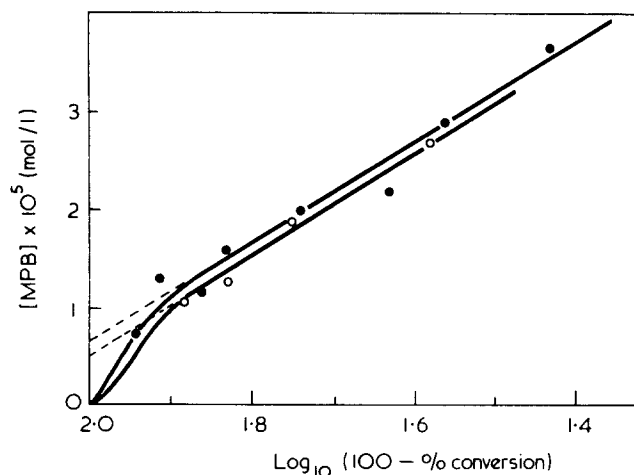


Figure 4 Variation of MPB concentration with  $\log_{10}(100 - \% \text{ conversion})$  for Al(iBu)<sub>3</sub>. [4-MP-1]=2.00 mol/l; [VCl<sub>3</sub>]=18.5 mmol/l; [Al(iBu)<sub>3</sub>]=37.0 mmol/l. ●, 30°C; ○, 50°C

Table 1 Variation in  $C_0$  and  $R_{ta}$  with aluminium alkyl

[4-MP-1]=2.0 mol/l; [VCl<sub>3</sub>]=18.5 mmol/l; [AlR<sub>3</sub>]=37.0 mmol/l; solvent=benzene

Aluminium alkyl	Temperature (°C)	$C_0 \times 10^4$ (mol/mol VCl <sub>3</sub> )	$R_{ta} \times 10^6$ (mol/l min VCl <sub>3</sub> )
AlEt <sub>3</sub>	30	6.10	17.2
Al(iBu) <sub>3</sub>	30	3.78	3.24
Al(iBu) <sub>3</sub>	50	2.90	12.8
Al(nBu) <sub>3</sub>	30	3.30	1.53
Al(nHex) <sub>3</sub>	30	2.30	0.87

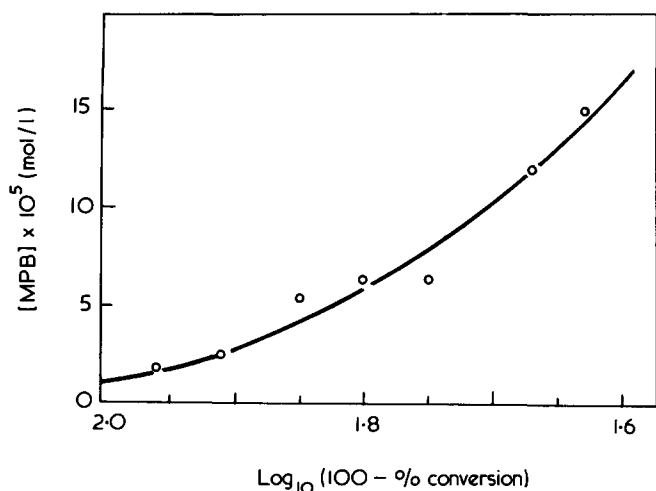


Figure 5 Variation of MPB concentration with  $\log_{10}$  (100-% conversion) for  $\text{AlEt}_3$ . [4-MP-1]=2.00 mol/l;  $[\text{VCl}_3]=18.0$  mmol/l;  $[\text{AlEt}_3]=36.0$  mmol/l; temperature=30°C

A reduction of about 23% in the active centre concentration is observed for the  $\text{VCl}_3/\text{Al}(\text{iBu})_3$  system, as the temperature is raised from 30 to 50°C. This decrease is most likely due to deactivation of the active sites by reduction at the higher temperature. Deactivation has been demonstrated with this system at 50°C in a previous paper<sup>27</sup>. Few investigations of the effect of temperature on the number of active centres have been made. Feldman *et al.*<sup>14</sup> and Chien<sup>9</sup> observe a decrease in active centres as the temperature is raised, whereas Kohn *et al.*<sup>15</sup> found the opposite effect.

#### Location of active sites

The location of the active sites on the crystal surface is by no means certain. Cossee<sup>32</sup> proposed that site formation occurred at chlorine vacancies on the lateral faces of the crystal, a suggestion which is apparently supported by electron microscopy<sup>21, 26</sup>. However, more recently Chirkov and Kissin<sup>7</sup> have suggested that active centres are also formed on the basal planes of the crystal lattice so as to cover the entire surface of the catalyst. The contradictory findings of electron microscopy are explained in terms of the 'artificial' conditions pertaining in the absence of solvents. Further, Rodriguez *et al.*<sup>33</sup> have shown that the use of  $\text{AlMe}_3$ , which is the metal alkyl employed in their electron microscopy studies, leads to inactive surface complexes on the basal planes, whereas the inactive compound formed by interaction with higher metal alkyls can decompose with formation of a chlorine vacancy which can then react with more metal alkyl to yield an active centre.

It is possible to calculate the maximum number of active centres for this system. Thus assuming that the cross-sectional area of a poly(4-methylpentene-1) molecule is about 70 Å<sup>2</sup>, i.e., the area likely to be taken up by a growing polymer chain, and also assuming that the surface area of the  $\text{VCl}_3$  is 2.3 m<sup>2</sup>/g, then the number of active sites corresponding to complete coverage of the crystal surface is about  $9 \times 10^{-4}$  mol/mol  $\text{VCl}_3$ , which is close to the maximum experimentally determined value of  $6.1 \times 10^{-4}$  mol/mol  $\text{VCl}_3$ . It must be emphasized that the calculation is based on the initial surface area of the  $\text{VCl}_3$  and does not allow a significant change in area through breakdown in particle size as suggested by Natta<sup>4</sup>.

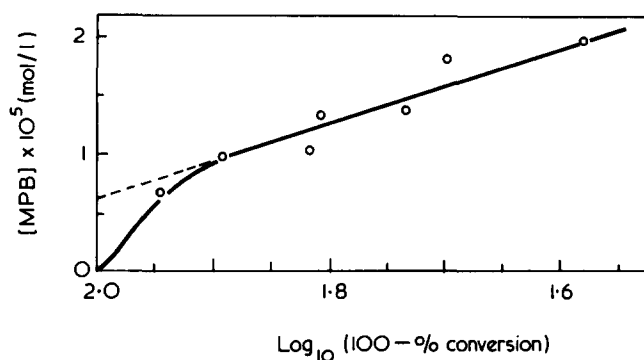


Figure 6 Variation of MPB concentration with  $\log_{10}$  (100-% conversion) for  $\text{Al}(\text{nBu})_3$ . [4-MP-1]=2.00 mol/l;  $[\text{VCl}_3]=18.5$  mmol/l;  $[\text{Al}(\text{nBu})_3]=37.0$  mmol/l; temperature=30°C

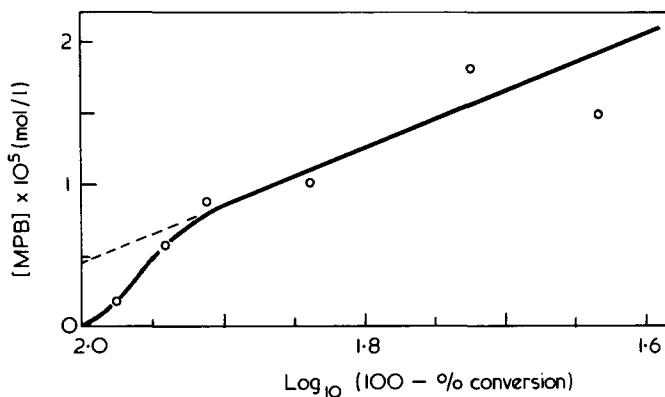


Figure 7 Variation of MPB concentration with  $\log_{10}$  (100-% conversion) for  $\text{Al}(\text{nHex})_3$ . [4-MP-1]=2.00 mol/l;  $[\text{VCl}_3]=18.5$  mol/l;  $[\text{Al}(\text{nHex})_3]=37.0$  mol/l; temperature=30°C

As the lateral faces of the  $\text{VCl}_3$  crystal may only comprise about 5% of the total surface area, a twenty-fold increase in surface area during polymerization would be necessary in order to accommodate all the active sites on the faces. An increase in surface area of this magnitude seems unlikely as several workers<sup>29-31</sup> have shown that the rate of polymerization is dependent upon the initial surface area of the transition metal halide. This finding argues against any significant increase in surface area during polymerization.

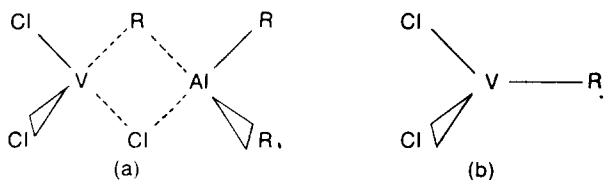
There is thus some uncertainty regarding the exact location of the active centres, and it is possible that active sites may be located on both the basal and lateral faces of the crystal lattice.

#### Nature of the active centre

From Table 1 it may be seen that the number of active centres is dependent upon the nature of the aluminium alkyl. The aluminium alkyls used in the present study may be placed in the following order of decreasing ability for active site formation:  $\text{AlEt}_3 > \text{Al}(\text{iBu})_3 > \text{Al}(\text{nBu})_3 > \text{Al}(\text{nHex})_3$ . This order is most likely the same as the order of decreasing alkylating ability, and hence the difference in the number of active sites may be considered to be due to the different reactivities of the aluminium alkyls which in turn govern the extent of reaction with the crystal surface.

The exact nature of the species active in polymerization has not been unequivocally established. Two main classes of active species are conceivable for the catalyst system  $\text{AlR}_3/\text{VCl}_3$ : (a) a bridge type complex, and (b) an alkylated vanadium species.





In the present study the polymerization rates<sup>27</sup> and active centre concentration have been determined for a series of different aluminium alkyls. If the active species were a bridge type complex then the rate constant for propagation,  $k_p$ , should be dependent on the nature of the aluminium alkyl, whereas  $k_p$  should be independent on the metal alkyl if chain growth only occurs at an alkylated vanadium entity.

Since propagation is considered to occur with adsorbed monomer<sup>34</sup> the overall rate of polymerization is given by:

$$R_p = k_p \theta_M C_0 \quad (2)$$

The value of  $\theta_M$  is, however, dependent on the nature of the metal alkyl, and consequently it is necessary to plot  $R_p$  against  $\theta_M C_0$  rather than against  $C_0$  alone. Numerical values for  $\theta_M$  are to be presented in a subsequent paper but are used here without further justification. An appropriate plot is shown in Figure 8 and is seen to be linear with slope,  $k_p$ , equal to  $(3.0 \pm 0.5) 10^3 \text{ min}^{-1}$ . It may be seen therefore that  $k_p$  is independent of the nature of the aluminium alkyl, a fact which strongly suggests that the species active in polymerization in the present study is an alkylated vanadium entity.

These conclusions are not completely unambiguous since the propagation rate constant might also be expected to be independent of the metal alkyl if the rate-determining step were the prior co-ordination of the monomer at the transition metal site, as has been suggested by some authors<sup>35, 36</sup>. However, Cossee<sup>37</sup> convincingly argues that the observed activation energy of 11–14 kcal/mol is unlikely to be associated with complexation of a neutral molecule into a vacant position on a crystal surface. This is in accordance with the observation that no stable complexes between  $\alpha$ -olefins and elements of the first half of the transition series have been found. Ingbermann *et al.*<sup>5</sup> from kinetic considerations also conclude that the rate-determining step is not prior complexation at the transition metal.

Further, the observation that the activation energy for initiation is very different from that of propagation<sup>6</sup> is not consistent with the idea that the rate-determining step is the prior complexation of the monomer. Initiation and propagation of chain growth are considered to occur by similar mechanisms<sup>38, 39</sup>, and if the rate-determining step were prior complexation of the monomer then the activation energies for initiation and propagation would be expected to be of a similar magnitude; this is not so since the activation energy of initiation is considerably higher.

Chirkov *et al.*<sup>6</sup> also show that the activation energy of initiation is dependent upon the nature of the substituent of the metal alkyl. Thus for the system  $\text{VCl}_3/\text{AlR}_3/\text{propylene}$ , the activation energy of initiation for  $\text{Al}(\text{iBu})_3$  and  $\text{AlEt}_3$  is found to be 21 and 14 kcal/mol respectively. This hardly allows the conclusion that the rate-determining step is prior complexation since if this were so the activation energy of initiation would be independent of the substituent group on the metal alkyl.

In addition it can be argued that if the active species were a bimetallic entity the bond strength of the initial

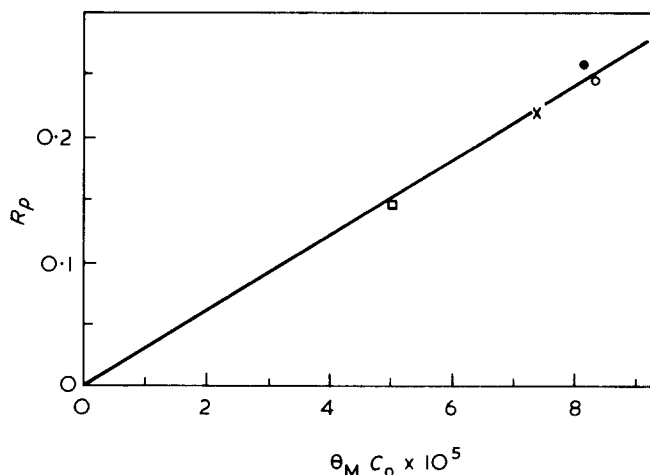


Figure 8 Dependence of  $k_p$  on the nature of the metal alkyl. [4-MP-1]=2.00 mol/l;  $[\text{VCl}_3]=18.5 \text{ mmol/l}$ ;  $[\text{AlR}_3]=37.0 \text{ mmol/l}$ ; temperature=30°C. ●,  $\text{Al}(\text{iBu})_3$ ; ○,  $\text{AlEt}_3$ ; ×,  $\text{Al}(\text{nBu})_3$ ; □,  $\text{Al}(\text{nHex})_3$

monomer  $\pi$ -complex should be affected by the nature of the metal alkyl bound to the transition metal atom. It has, however, been clearly demonstrated<sup>40, 41</sup> that the rate-determining step is independent of the metal and substituent groups of the metal alkyl. This latter independence is confirmed by this study. This strongly suggests that the entity active in polymerization is an alkylated vanadium species.

## CONCLUSIONS

The number of active centres in the polymerization system  $\text{VCl}_3/\text{AlR}_3/4\text{-MP-1}$  lies in the range  $2.3\text{--}6.1 \times 10^{-4} \text{ mol/mol VCl}_3$  for a series of aluminium alkyls. This number of active centres is somewhat lower than many previously observed values, and is probably explainable in terms of differences in the polymerization systems. The present study has shown that the number of active centres is dependent on the nature of the aluminium alkyl used in the polymerization system, and that these alkyls can be placed in the following order of decreasing activity for active site formation:  $\text{AlEt}_3 > \text{Al}(\text{iBu})_3 > \text{Al}(\text{nBu})_3 > \text{Al}(\text{nHex})_3$  which probably corresponds to the order of decreasing alkylating ability.

Chain transfer with metal alkyl has been demonstrated, and the variation in the rate of this transfer process with a number of different aluminium alkyls has been evaluated.

The propagation rate constant,  $k_p$ , has the value  $[3.0 \pm 0.5] \times 10^3 \text{ min}^{-1}$  at 30°C, and was found to be independent of the alkyl used.

The active species is most likely an organovanadium compound located on the basal planes and/or on the lateral faces of the crystal lattice. Complexation of the vanadium alkyl species with the metal alkyl must be allowed where the metal alkyl is known to have complexing abilities, although this is perhaps most likely to yield a complex which is inactive in polymerization.

## REFERENCES

- Grievson, B. M. *Makromol. Chem.* 1965, **84**, 93
- Tanaka, S. and Morikawa, H. *J. Polym. Sci. (A)* 1965, **3**, 3147
- Schnecko, H., Dost, W. and Kern, W. *Makromol. Chem.* 1969, **121**, 159
- Natta, G. and Pasquon, I. *Adv. Catalysis* 1959, **11**, 1

- 5 Ingberman, A. K., Levine, I. J. and Turbett, R. J. *J. Polym. Sci. (A-1)* 1966, **4**, 2781
- 6 Novokshonova, L. A., Berseneva, G. P., Tsvetkova, V. I. and Chirkov, N. M. *Vysokomol. Soedin. (A)* 1967, **9**, 562
- 7 Kissin, Yu. V., Mezhevikovsky, S. M. and Chirkov, N. M. *Eur. Polym. J.* 1970, **6**, 267
- 8 Natta, G. *J. Polym. Sci.* 1959, **34**, 21
- 9 Chien, J. C. W. *J. Polym. Sci. (A)* 1963, **1**, 425
- 10 Schnecko, H. and Kern, W. IUPAC Macromolecular Symposium, Budapest, 1969
- 11 Chien, J. C. W. *J. Am. Chem. Soc.* 1958, **81**, 86
- 12 Caunt, A. D. *J. Polym. Sci. (C)* 1964, **4**, 49
- 13 Schnecko, H., Lintz, W. and Kern, W. *J. Polym. Sci. (A-1)* 1967, **5**, 205
- 14 Feldman, C. F. and Perry, E. *J. Polym. Sci.* 1960, **46**, 217
- 15 Kohn, E., Schuurmans, H. J. L., Cavender, J. V. and Mendelson, E. A. *J. Polym. Sci.* 1962, **58**, 681
- 16 Cooper, E., Eaves, D. E., Owen, G. D. T. and Vaughan, G. *J. Polym. Sci. (C)* 1964, **4**, 211
- 17 Coover, R. W., Guillet, J. E., Combs, R. L. and Joyner, F. S. *J. Polym. Sci. (A-1)* 1966, **4**, 2583
- 18 Bawn, C. E. H., North, A. M. and Walker, J. S. *Polymer* 1964, **5**, 419
- 19 Boor, J. Jr and Youngman, E. A. *J. Polym. Sci. (B)* 1966, **4**, 913
- 20 Bier, G., Hoffmann, W., Lehmann, G. and Seydel, G. *Makromol. Chem.* 1962, **58**, 1
- 21 Rodriguez, L. A. M. and van Looy, H. M. *J. Polym. Sci. (A-1)* 1966, **4**, 1951
- 22 Childers, C. W. *J. Am. Chem. Soc.* 1963, **85**, 229
- 23 Cooper, W., Eaves, D. E. and Vaughan, G. *Makromol. Chem.* 1963, **67**, 229
- 24 Natta, G., Porri, L., Carbonaro, A. and Greco, A. *Makromol. Chem.* 1964, **71**, 207
- 25 Bresler, L. S., Poddubnyi, I. Ya. and Sokolov, V. N. *J. Polym. Sci. (C)* 1969, **16**, 4337
- 26 Guttman, J. Y. and Guillet, J. E. *Macromolecules* 1968, **1**, 461
- 27 McKenzie, I. D., Tait, P. J. T. and Burfield, D. R. *Polymer* 1972, **13**, 307
- 28 Casey, A. T. and Clark, R. J. H. *Inorg. Chem.* 1969, **8**, 1216
- 29 Vesely, K., Ambroz, J., Vilim, R. and Hamrik, O. *J. Polym. Sci.* 1961, **55**, 25
- 30 Keit, T. *Nature* 1964, **203**, 76
- 31 Kollar, L., Simon, A. and Kallo, A. *J. Polym. Sci. (A-1)* 1968, **6**, 937
- 32 Cossee, P. and Arlman, E. J. *J. Catalysis* 1954, **3**, 99
- 33 Rodriguez, L. A. M., van Looy, H. M. and Cabant, J. A. *J. Polym. Sci. (A-1)* 1966, **4**, 1905
- 34 Burfield, D. R., McKenzie, I. D. and Tait, P. J. T. *Polymer* 1972, **13**, 302
- 35 Schindler, A. *J. Polym. Sci. (B)* 1965, **3**, 147
- 36 Pasquon, I., Natta, G., Zambelli, A. and Maringangelli, A. *J. Polym. Sci. (C)* 1967, **16**, 2501
- 37 Cossee, P. 'The Stereochemistry of Macromolecules' (Ed. A. D. Ketley), Marcel Dekker, New York, 1967, p 156
- 38 Cossee, P. *Tetrahedron Lett.* 1960, **17**, 12
- 39 Natta, G. and Mazzanti, G. *Tetrahedron* 1960, **8**, 86
- 40 Pasquon, I. *Pure Appl. Chem.* 1967, **15**, 465
- 41 Carrick, W. L., Karol, F. J., Karapinka, G. L. and Smith, J. J. *J. Am. Chem. Soc.* 1960, **82**, 1502
- 42 Ayrey, G. *Adv. Polym. Sci.* 1969, **6**, 128
- 43 McKenzie, I. D. and Tait, P. J. T. *Polymer* in the press

## APPENDIX

Recently Ayrey<sup>42</sup> in a survey of the uses of radioactive-labelling techniques in polymer analysis has shown that for a meaningful result in tritium quench methods, the number of quench hydrogens per polymer molecule ( $N_q$ ) should be less than or equal to one. This can be checked by comparing experimentally determined number average molecular weights with those calculated from tritium data (Table 2).

Table 2 Comparison of molecular weights

[4-MP-1]=2.0 mol/l; [VCl<sub>3</sub>]=18.5 mmol/l; [AlR<sub>3</sub>]=37.0 mmol/l; solvent=benzene; temperature=30°C

Metal alkyl	Specific activity of polymer × 10 <sup>5</sup> (dpm/g)	( $\bar{M}_n$ ) <sub>T</sub>	$\bar{M}_n$ (exp.)
AlEt <sub>3</sub>	5.50	8.64 × 10 <sup>5</sup>	5.18 × 10 <sup>5</sup>
Al(iBu) <sub>3</sub>	1.50	4.15 × 10 <sup>6</sup>	8.91 × 10 <sup>5</sup>

Assuming that each labelled chain contains one tritium (T) atom, then:

$$(\bar{M}_n)_T = \frac{\text{Specific activity of quench methanol (dpm/mol)}}{\text{Specific activity of polymer (dpm/g)} \times K}$$

where  $K$  is the correction factor for the isotope effect.

The experimentally determined values of the number-average molecular weights are thus seen to be lower than those calculated from tritium data. This is to be expected as the latter determination ignores transfer with monomer, which is known to be important.

The number-average degree of polymerization may be defined by:

$$\bar{P}_n = \bar{M}_n / MW = \frac{\int_0^t R_p dt}{C_0 + \int_0^t R_{ta} dt + \int_0^t R_t dt} \quad (A1)$$

where  $R_{ta}$  and  $R_t$  refer to the rate of transfer with metal alkyl and the sum of the rates of all other transfer reac-

tions respectively, and where  $MW$  is the molecular weight of a monomeric unit.

From equation (A1), for 4-methylpentene-1:

$$\frac{1}{\bar{M}_n} = \frac{C_0 + \int_0^t R_{ta} dt + \int_0^t R_t dt}{84 \int_0^t R_p dt} \quad (A2)$$

Now, the tritium average molecular weight is given by:

$$\frac{1}{(\bar{M}_n)_T} = \frac{C_0 + \int_0^t R_{ta} dt}{84 \int_0^t R_p dt} \quad (A3)$$

By defining a term  $(\bar{M}_n)_R$  such that:

$$\frac{1}{(\bar{M}_n)_R} = \frac{\int_0^t R_t dt}{84 \int_0^t R_p dt} \quad (A4)$$

where  $R_t$  is the rate of chain transfer apart from transfer with metal alkyl we may write:

$$\frac{1}{\bar{M}_n} = \frac{1}{(\bar{M}_n)_T} + \frac{1}{(\bar{M}_n)_R} \quad (A5)$$

From the data in Table 2 it is possible to derive a value for  $(\bar{M}_n)_R$ , which should be similar for AlEt<sub>3</sub> and Al(iBu)<sub>3</sub> if the tritium-labelling procedure is valid, as the other transfer steps should be independent of the nature of the metal alkyl. Values of  $(\bar{M}_n)_R$  of 1.14 × 10<sup>6</sup> and 1.29 × 10<sup>6</sup> are found for Al(iBu)<sub>3</sub> and AlEt<sub>3</sub> respectively, which is fairly close agreement and within the limits of experimental error.

Using this procedure it is possible to evaluate the number-average molecular weights from tritium data obtained in a series of experiments. These are in excellent agreement with the molecular weight results which will be presented in a later paper<sup>43</sup> and confirm the validity and accuracy of this method for determining active centre concentrations in Ziegler-Natta systems.

# Ziegler–Natta catalysis: 4. Quantitative verification of kinetic scheme

D. R. Burfield, P. J. T. Tait and I. D. McKenzie

Department of Chemistry, University of Manchester Institute of Science and Technology, Manchester M60 1QD, UK

(Received 6 December 1971)

Chain transfer with adsorbed aluminium alkyl has been investigated for the system  $VCl_3/AlR_3/4$ -methylpentene-1, where adsorption of the metal alkyl onto the catalyst surface is described by a Langmuir type adsorption isotherm. Rate constants for chain transfer with metal alkyl and equilibrium constants for adsorption of a series of aluminium alkyls and 4-methylpentene-1 onto the transition metal halide surface have been determined. The activation energy for the chain transfer process with tri-isobutylaluminium has also been evaluated. The number of active centres is found to be reduced at low monomer concentrations probably because of slow initiation by monomer. Quantitative verification of a previously presented kinetic scheme has been effected.

## INTRODUCTION

In a previous paper in this series<sup>1</sup> the concentration of active centres was determined for the polymerization system  $VCl_3/AlR_3/4$ -methylpentene-1 by means of a quench technique. A further series of experiments are now reported in which the effect of variation of several parameters on the active centre concentration is examined. These investigations have led to the evaluation of transfer rate constants and equilibrium constants for the adsorption of monomer and metal alkyl onto the vanadium trichloride crystal surface. The experimental procedures have been described previously<sup>1,2</sup> and a number of expressions are used which have been derived in an earlier paper.

## RESULTS AND DISCUSSION

### Variation of metal–polymer bond concentration with metal alkyl concentration

This series of experiments was performed in an attempt to investigate the effect of the metal alkyl concentration on the number of active centres. However, it proved impossible to follow directly the variation of active centre concentration since any change was masked by the much larger change in the rate of chain transfer with metal alkyl.

These experiments were carried out to a constant reaction time of 300 min, whilst the concentration of metal alkyl was varied in separate polymerizations from 37 to 300 mmol/l at constant monomer and vanadium

trichloride concentrations. The results obtained using tri-isobutylaluminium are summarized in *Figure 1*. It is immediately apparent that the rate of formation of metal polymer bonds, and thus the rate of transfer with metal alkyl ( $R_{ta}$ ) is not directly proportional to the metal alkyl concentration in the solution. It is more likely, however, that transfer would be with adsorbed metal alkyl, where the concentration of adsorbed metal alkyl would be given by a Langmuir–Hinshelwood isotherm<sup>3</sup>. The rate of transfer with adsorbed metal alkyl is then given by:

$$R_{ta} = k_a \theta_A C_0 \quad (1)$$

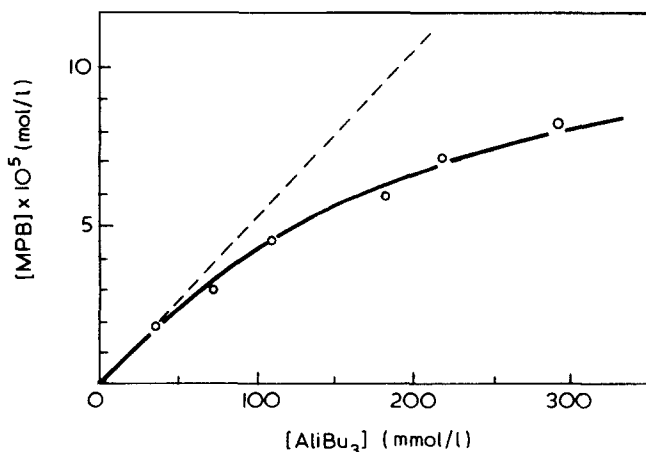


Figure 1 Dependence of [MPB] on  $[Al(iBu)_3]$ .  $[4-MP-1]=2.00$  mol/l;  $[VCl_3]=18.5$  mmol/l; temperature = 30°C

Rearrangement and substitution for  $\theta_A$  yields

$$\frac{C_0}{R_{ta}} = \frac{1}{k_a} \left( \frac{1 + K_M[M] + K_A[A]}{K_A[A]} \right) \quad (2)$$

Thus if the rate of transfer is with adsorbed metal alkyl then a plot of  $C_0/R_{ta}$  against  $1/[A]$  should be linear.

A problem associated in effecting such a plot is that in reality  $C_0$  is not constant throughout the duration of the polymerization reaction since there is an initial period during which the number of active centres increases to a limiting value. Consequently it is necessary to use the integral value of  $C_0$  ( $\int C_0$ ) over the reaction period.

The value of  $\int C_0$  over the reaction period may be evaluated from the area under the steady state rate of polymerization ( $R_p$ ) versus time plots. These plots are of the form shown in Figure 2.

$C_0$  under 'steady state' conditions, i.e., where  $R_p$  is constant, has been determined previously<sup>1</sup>, and  $\int C_0$  may now be simply derived by direct proportionality. Thus:

$$\int C_0 = C_0(\text{steady state}) \times \frac{\text{shaded area}}{\text{area ABCD}} \quad (3)$$

The steady state value of  $C_0$  was found to be  $7.0 \times 10^{-6}$  mol/l under the experimental conditions employed, at an Al : V ratio of 2 : 1. This corresponds to a value of  $\int C_0$  equal to  $4.85 \times 10^{-6}$  mol/l up to 300 min reaction.

One added complication, which is evident from experiments in which the Al : V ratio is increased by decreasing the vanadium trichloride concentration alone, is that the steady state rate increases as the Al : V ratio is increased. This is considered to be due to an increase in the concentration of propagating active centres ( $C_0$ )<sup>2</sup>.

The values of  $C_0$  for different Al : V ratios ( $C_{0(Al:V)}$ ) were thus calculated from the value of  $C_{0(2:1)}$  and the steady state values of the polymerization rates, i.e.

$$C_{0(Al:V)} = C_{0(2:1)} \times \frac{R_{p(Al:V)}/[VCl_3]}{R_{p(2:1)}/[VCl_3]} \quad (4)$$

The relevant steady state rate of polymerization versus time plots are shown in Figure 3.

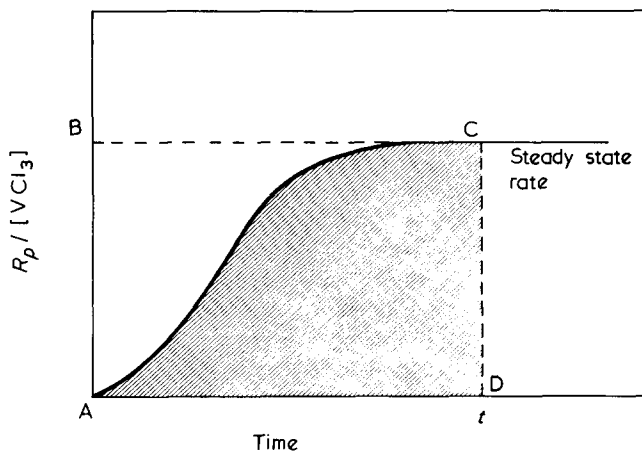


Figure 2 Typical plot of rate of polymerization as a function of time

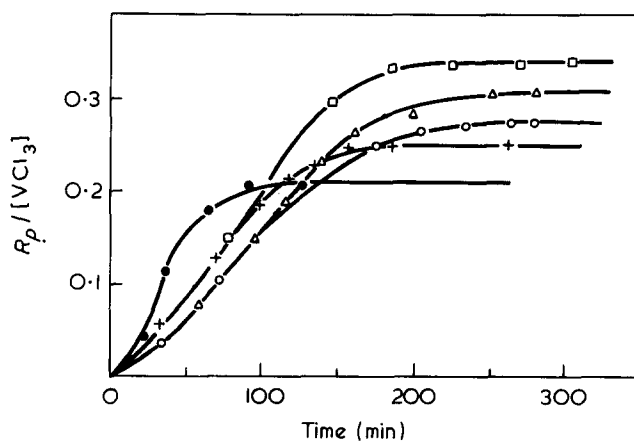


Figure 3 Variation of rate of polymerization with time for different  $VCl_3$  concentrations. [4MP-1]=2.00 mol/l; [Al(iBu)<sub>3</sub>]=37.0 mmol/l. Temperature=30°C. [ $VCl_3$ ] in mmol/l: □, 3.51; △, 5.44; ○, 8.61; +, 18.2; ●, 44.3

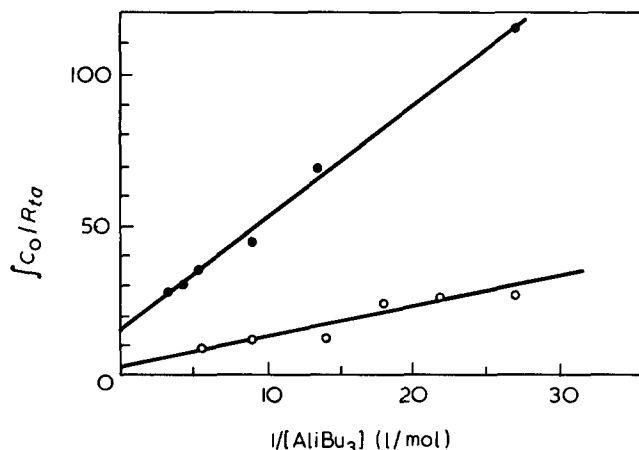


Figure 4 Langmuir plot for Al(iBu)<sub>3</sub>. [4-MP-1]=2.00 mol/l; [ $VCl_3$ ]=18.5 mmol/l. ●, 300 min; ○, 70 min

The rate of transfer using tri-isobutylaluminium at a catalyst ratio of 2 : 1 ( $R_{ta(2:1)}$ ) has been found previously<sup>1</sup> to be  $6.00 \times 10^{-8}$  mol/l min at an active centre concentration of  $7.00 \times 10^{-6}$  mol/l for the system  $VCl_3/Al(iBu)_3/4-MP-1$ . Thus the value of  $\int C_0$  equal to  $4.85 \times 10^{-6}$  mol/l, calculated for a catalyst ratio of 2 : 1, corresponds to an integral rate of transfer of  $4.16 \times 10^{-8}$  mol/l min.

The rates of chain transfer for other catalyst ratios were then found from the relationship:

$$R_{ta(Al:V)} = R_{ta(2:1)} \times \frac{[MPB]_{(Al:V)} - C_{0(Al:V)}}{[MPB]_{(2:1)} - C_{0(2:1)}} \quad (5)$$

where  $[MPB]_{Al:V}$  and  $[MPB]_{(2:1)}$  are the metal-polymer bond concentrations at  $t=300$  min at the respective catalyst ratios.

These derivations necessitate the assumption that the increase in rate observed<sup>2</sup> as the catalyst ratio is increased at constant monomer and metal alkyl concentrations, is due to an increase in the number of sites active in polymerization. This assumption is substantiated by the excellent plots obtained using these equations.

In Figure 4 the plot of  $\int C_0/R_{ta}$  against  $1/[Al(iBu)_3]$  is linear, with a positive intercept, thus confirming that

the adsorption of metal alkyl may be described by a Langmuir type isotherm.

Under these conditions<sup>3</sup>:

$$\text{intercept} = 1/k_a \quad (6)$$

$$\frac{\text{slope}}{\text{intercept}} = \frac{1 + K_M[M]}{K_A} \quad (7)$$

and thus  $k_a$  may be evaluated directly whilst  $K_A$  requires further data.

Similar linear plots were found by exactly analogous procedures for triethylaluminium, tri-*n*-butylaluminium and tri-*n*-hexylaluminium and are depicted in Figures 5 and 6. In these cases  $\int C_0/R_{ta}$  is plotted against  $1/[A_2]^{1/2}$ , since these aluminium alkyls are known to be at least partly dimeric in benzene solution.

In each case chain transfer is observed with adsorbed monomeric metal alkyl. The values of the chain transfer constants are recorded in Table 1.

Thus it may be seen that these aluminium alkyls may be placed in the following order of decreasing reactivity for chain transfer:  $\text{AlEt}_3 > \text{Al}(\text{iBu})_3 > \text{Al}(\text{nBu})_3 > \text{Al}(\text{nHex})_3$ , which is in the order of decreasing reactivity of the Al-C bond.  $\text{Al}(\text{iBu})_3$  occupies an anomalous position presumably connected with the branching at the  $\alpha$ -carbon atom which affects the reactivity of the metal-carbon bond.

#### Variation of the metal-polymer bond concentration with monomer concentration

This series of experiments was performed to investigate the effect of the monomer concentration on the number of active centres for the system  $\text{VCl}_3/\text{Al}(\text{iBu})_3/4\text{-MP-1}$ , and to provide further data for the evaluation of  $K_A$  and  $K_M$ . These experiments were performed at constant catalyst concentration using a range of monomer concentrations from 1 to 4 mol/l. The polymerizations were quenched after 200 min reaction time.

It would be expected that the concentration of metal-polymer bonds should be independent of the monomer concentration since:

$$[\text{MPB}]_t = C_0 + \int_0^t k_a \theta_A C_0 dt \quad (8)$$

and since the fraction of surface covered by adsorbed metal alkyl ( $\theta_A$ ) would vary only slightly over the investigated range. The results for this series are shown in Figure 7. It can be seen that the concentration of metal-polymer bonds falls sharply at low monomer concentrations.

Coover *et al.*<sup>4</sup> observed a similar effect for the polymerization system  $\text{Et}_2\text{AlCl}/\text{TiCl}_3/\text{propylene}$  in which the rate of formation of metal-polymer bonds was found to increase with monomer concentration during the *initial stages* of polymerization. This increase in rate of formation of metal-polymer bonds was interpreted as an increase in the rate of transfer with metal alkyl which was supposed to involve both monomer and metal alkyl.

However, it seems more likely that this effect is due to slow chain initiation by monomer which would effectively reduce the number of centres active in polymerization at low monomer concentrations. A corresponding reduction in the number of metal-polymer

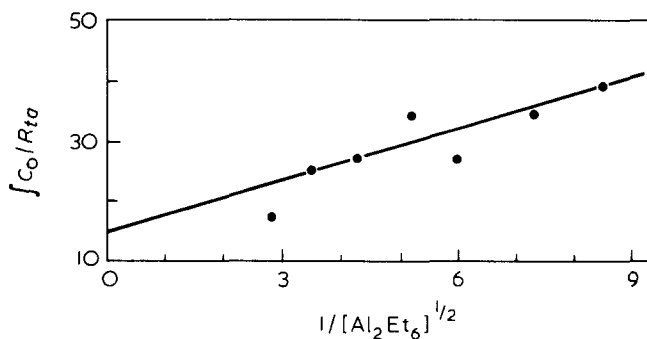


Figure 5 Langmuir plot for  $\text{AlEt}_3$ .  $[4\text{-MP-1}] = 2.00 \text{ mol/l}$ ;  $[\text{VCl}_3] = 18.0 \text{ mmol/l}$ ; temperature =  $30^\circ\text{C}$ ; time = 200 min

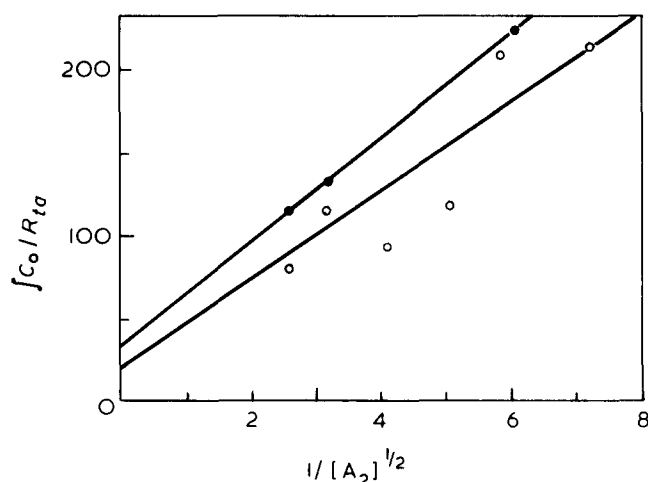


Figure 6 Langmuir plots for  $\text{Al}(\text{nBu})_3$  and  $\text{Al}(\text{nHex})_3$ .  $[4\text{-MP-1}] = 2.00 \text{ mol/l}$ ;  $[\text{VCl}_3] = 18.5 \text{ mmol/l}$ ;  $\circ$ ,  $\text{Al}(\text{nBu})_3$ , 270 min;  $\bullet$ ,  $\text{Al}(\text{nHex})_3$ , 360 min; temperature =  $30^\circ\text{C}$

Table 1 Chain transfer constants at  $30^\circ\text{C}$   
 $[4\text{-MP-1}] = 2.0 \text{ mol/l}$ ;  $[\text{VCl}_3] = 18.5 \text{ mmol/l}$ ;  
 solvent = benzene

Aluminium alkyl	$k_a$ ( $\text{min}^{-1}$ )
$\text{AlEt}_3$	$0.067 \pm 0.003$
$\text{Al}(\text{iBu})_3$	$0.067 \pm 0.003$
$\text{Al}(\text{nBu})_3$	$0.050 \pm 0.005$
$\text{Al}(\text{nHex})_3$	$0.033 \pm 0.001$

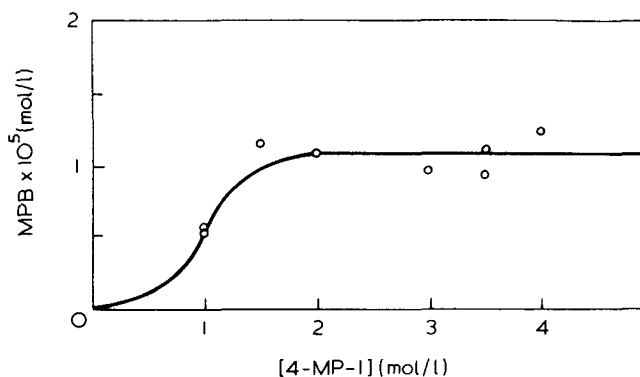


Figure 7 Variation of MPB concentration with monomer concentration.  $[\text{VCl}_3] = 18.5 \text{ mmol/l}$ ;  $[\text{Al}(\text{iBu})_3] = 37.0 \text{ mmol/l}$ ; temperature =  $30^\circ\text{C}$

bonds would then be expected according to equation (8).

This is in agreement with the observation<sup>2</sup> that the order of the polymerization rate with respect to monomer changes from one to nearly two at monomer concentrations below 1.0 mol/l. Similar observations have been made by other authors<sup>5-9</sup>.

Furthermore if the rate of transfer with metal alkyl was dependent on the monomer concentration as suggested by Coover, then the rate would be expected to decrease during the course of polymerization in step with decrease in the monomer concentration. It has been shown in the present study<sup>1</sup> that the rate of transfer with metal alkyl remains constant up to at least 75% conversion.

The results of these experiments may be interpreted to provide data for the evaluation of  $K_M$  and  $K_A$ . A graph of specific activity of polymer versus  $1/[M]$  should be linear<sup>3</sup> with a positive intercept. Such a plot for aluminium tri-isobutylaluminium is depicted in Figure 8, and for this plot:

$$\frac{\text{slope}}{\text{intercept}} = \frac{1 + (1 + k_{at})K_A[A]}{K_M} \quad (9)$$

Equation (7) can be used in conjunction with equation (9) to evaluate both  $K_M$  and  $K_A$ . The relevant values of slope/intercept can be obtained from Figure 4 and Figure 8 respectively. Both  $k_a$  and  $t$  are known together with the concentrations of monomer and tri-isobutylaluminium.

On solving equations (7) and (9) the following values for  $K_M$  and  $K_A$  are obtained:  $K_M = 0.164 \pm 0.020$  l/mol at 30°C;  $K_A = 5.12 \pm 0.20$  l/mol at 30°C. Using the value of  $K_M = 0.164$  the  $K_A$  or  $K^{1/2}K_A$  values<sup>3</sup> may be deduced for other aluminium alkyls from the data presented in the previous section. The values obtained are summarized in Table 2.

Thus, it can be seen that  $\text{AlEt}_3$  is very much more strongly adsorbed than the sterically hindered  $\text{Al}(\text{iBu})_3$ . It will be noticed also that  $K^{1/2}K_A$  for  $\text{Al}(\text{nBu})_3$  is smaller than for  $\text{Al}(\text{nHex})_3$ . This probably reflects the more complete dimerization of the n-butyl species, as the  $K_A$  values are likely to decrease with increasing size of the substituent group.

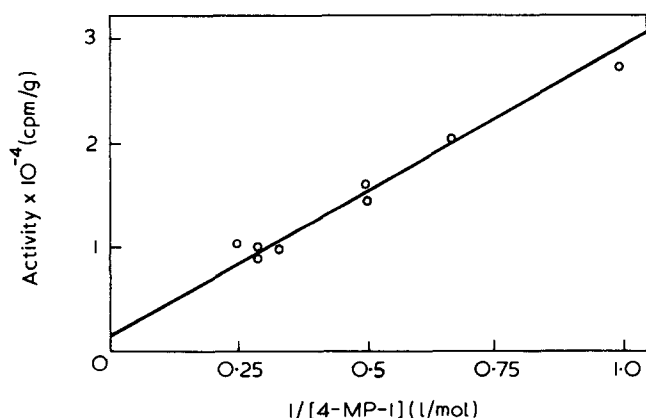


Figure 8 Plot of activity versus  $1/[4\text{-MP-1}]$ .  $[\text{VCl}_3] = 18.5$  mmol/l;  $[\text{Al}(\text{iBu})_3] = 37.0$  mmol/l; temperature = 30°C

Table 2 Values of  $K_A$  for some aluminium alkyls at 30°C

Aluminium alkyl	$K^{1/2}K_A$	$K_A$
$\text{Al}(\text{iBu})_3$	—	$5.12 \pm 0.20$
$\text{AlEt}_3$	$7.83 \pm 0.40$	$224^* \pm 10$
$\text{Al}(\text{nBu})_3$	$0.97 \pm 0.10$	—
$\text{Al}(\text{nHex})_3$	$1.21 \pm 0.06$	—

\* Pitzer<sup>10</sup> found a value of  $K^{1/2} = 0.035$  for  $\text{AlEt}_3$  in benzene

Unfortunately values of the dissociation constant for  $\text{Al}(\text{nBu})_3$  and  $\text{Al}(\text{nHex})_3$  could not be found in the literature. It seems likely, however, that these aluminium alkyls may be placed in the following order of decreasing 'strength' of adsorption:  $\text{AlEt}_3 > \text{Al}(\text{nBu})_3 > \text{Al}(\text{iBu})_3 > \text{Al}(\text{nHex})_3$ . The 'strength' of adsorption is probably largely governed by steric factors.

The value of  $K_M = 0.164 \pm 0.020$  l/mol for the adsorption of 4-methylpentene-1 onto  $\text{VCl}_3$  at 30°C compares with a value of 0.163 obtained by Vesely<sup>11</sup> for the adsorption of propylene onto  $\text{TiCl}_3$  at 50°C.

The value of  $K_A = 224 \pm 10$  l/mol for the adsorption of  $\text{AlEt}_3$  onto  $\text{VCl}_3$  at 30°C is much higher than the value of  $K_A = 21.2$  found by Vesely for the adsorption of  $\text{AlEt}_3$  onto  $\text{TiCl}_3$  at 50°C. Vesely's calculations did not allow, however, for the dimerization of  $\text{AlEt}_3$ , and recalculation of his results yields a value of  $K_A = 216$  which is in close agreement with the value obtained from this study.

#### Variation of metal-polymer bond concentration with the vanadium trichloride concentration

In this series the value of the metal-polymer bond concentration was determined as the catalyst concentration was varied. Experiments were carried out to a constant reaction time of 240 min, whilst the monomer concentration was kept constant, and the vanadium trichloride concentration was varied over a five-fold range from 4 to 23 mmol/l at a constant  $[\text{Al}(\text{iBu})_3]/[\text{VCl}_3]$  of 2 : 0. It has been shown that under these conditions the rate of polymerization is proportional to the vanadium trichloride concentration, and thus it seems likely that:  $C_0 \propto [\text{VCl}_3]$ . A plot of  $[\text{MPB}]_t$  versus  $[\text{VCl}_3]$  would be expected to be linear since:

$$[\text{MPB}]_t = C_0 + \int_0^t k_a \theta_A C_0 dt \quad (8)$$

The plot of  $[\text{MPB}]$  versus  $[\text{VCl}_3]$  is shown in Figure 9 and it is immediately apparent that the plot is not linear. This may be readily explained, however, because the value of  $\theta_A$  in equation (8) increases with increasing vanadium trichloride concentration, since the tri-isobutylaluminium concentration is simultaneously increased to maintain a constant ratio of catalyst components.

The present series should be described<sup>3</sup> by an equation of the form:

$$[\text{MPB}]_t = P[A] + \frac{Pk_{at}K_A[A]^2}{1 + K_A[A] + K_M[M]} \quad (10)$$

For the present case,  $t = 240$  min,  $k_a = 0.067$  min<sup>-1</sup>,  $K_A = 5.12$  l/mol and taking an average value for the expression  $(1 + K_A[A] + K_M[M])$  of 1.48 as this expression

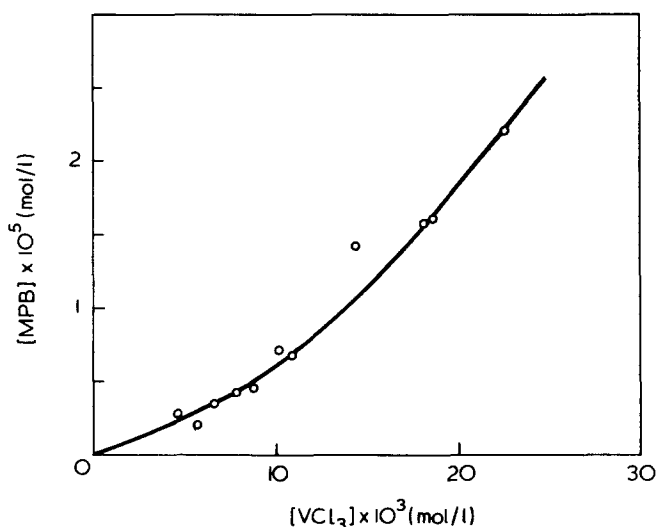


Figure 9 Variation of MPB concentration with  $VCl_3$  concentration.  $[4-MP-1]=2.00$  mol/l;  $[Al(iBu)_3] : [VCl_3]=2 : 1$ ; temperature =  $30^\circ C$

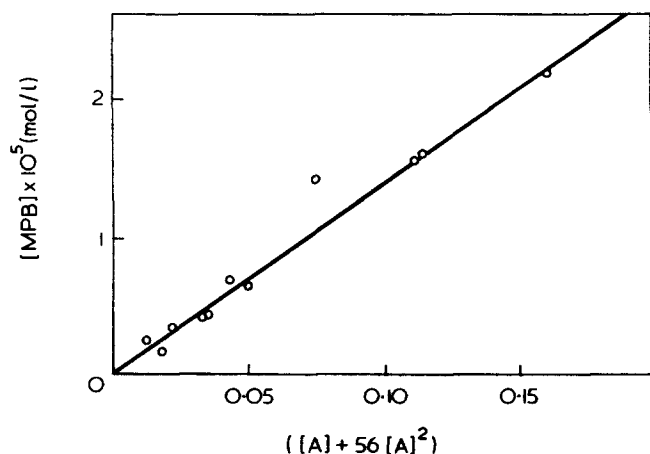


Figure 10 Plot of  $[MPB]$  versus  $([A] + 56[A]^2)$ .  $[4-MP-1]=2.00$  mol/l;  $[Al(iBu)_3] : [VCl_3]=2 : 1$ ; temperature =  $30^\circ C$ ; time = 240 min

remains approximately constant over the concentration range employed, equation (10) becomes:

$$[MPB]_t = P([A] + 56[A]^2) \quad (11)$$

A plot of  $[MPB]_t$  versus  $([A] + 56[A]^2)$  is shown in Figure 10 and is seen to be linear with slope of  $P$  equal to  $(1.37 \pm 0.03) \times 10^{-4}$ .

Now  $P$  was defined by the expression:

$$C_0 = P[A] \quad (12)$$

and for this series  $[A]=2[VCl_3]$ , thus  $C_0$  is equal to  $(2.74 \pm 0.06) \times 10^{-4}$  mol/mol  $VCl_3$ . This value of  $C_0$  compares with a value of  $(3.78 \pm 0.15) \times 10^{-4}$  mol/mol  $VCl_3$  measured previously<sup>1</sup>. The apparent discrepancy in values is easily explained as the former value is the integral value of  $C_0$  up to  $t$  equal to 240 min, whilst the latter value is measured under steady-state conditions. The integral value of  $C_0$ , calculated as described above, using the steady-state value of  $C_0$  of  $3.78 \times 10^{-4}$  mol/mol

$VCl_3$ , is found to be  $2.68 \times 10^{-4}$  mol/mol  $VCl_3$ , which value compares very closely to the value of  $2.74 \times 10^{-4}$  mol/mol  $VCl_3$  as determined above.

It is of interest to note that the specific activity of the polymer increases with increasing catalyst concentration, i.e., the molecular weight measured by tritium labelling decreases with increasing catalyst concentration. This merely reflects, in this instance, an increase in the rate of transfer with metal alkyl and not a transfer reaction with transition metal species as has been suggested previously<sup>12</sup>.

#### Variation of metal-polymer bond concentration with temperature

This series of experiments using tri-isobutylaluminium is exactly analogous to those already described above except that the polymerizations were carried out at the higher temperature of  $50^\circ C$ . This is of interest since if the adsorption of metal alkyl were to follow a Langmuir type dependence then the values of the equilibrium constant for adsorption ( $K_A$ ) should decrease with increasing temperature. Furthermore, the effect of temperature on the rate constant of chain transfer with metal alkyl ( $k_{ta}$ ) can also be observed.

These experiments were carried out to a constant reaction time of 70 min and at constant monomer and vanadium trichloride concentrations, whilst the concentration of tri-isobutylaluminium was varied in separate experiments from 37 to 180 mmol/l. The polymerization mixtures were cooled to  $30^\circ C$  before quenching so as to avoid the necessity of checking the value of the correction factor for the kinetic isotope effect.

A plot of  $\int C_0/R_{ta}$  against  $1/[A]$  is shown in Figure 11 and is seen to be linear. However, considerable experimental scatter is evident.

The value of  $K_A$  using optimized values of slope and intercept was found to be  $3.0 \pm 0.3$  l/mol at  $50^\circ C$  compared to a value of  $5.12 \pm 0.20$  l/mol at  $30^\circ C$ . This corresponds to a heat of adsorption of about  $-5.2$  kcal/mol. The decrease in value of the equilibrium constant for adsorption with temperature is in keeping with the proposed Langmuir adsorption scheme.

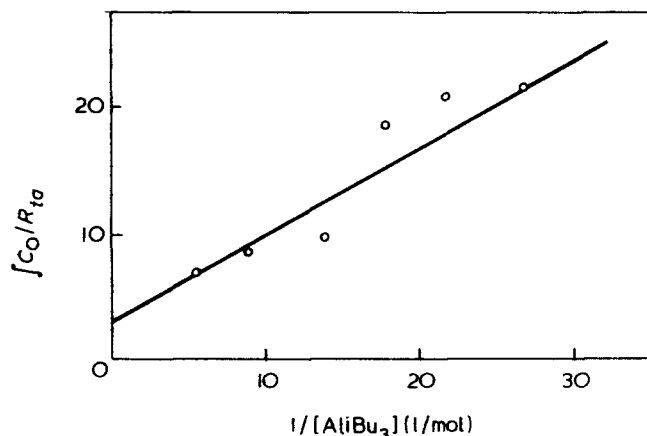


Figure 11 Langmuir plot for  $Al(iBu)_3$ .  $[4-MP-1]=2.00$  mol/l;  $[VCl_3]=28.0$  mmol/l; temperature =  $50^\circ C$ ; time = 70 min

The rate constant for chain transfer is found to increase, as would be expected, from  $0.067 \pm 0.003 \text{ min}^{-1}$  at  $30^\circ\text{C}$  to about  $0.36 \pm 0.03 \text{ min}^{-1}$  at  $50^\circ\text{C}$ . This corresponds to an activation energy of  $16.3 \text{ kcal/mol}$ .

#### Variation of rate of polymerization with alkyl concentration

It was suggested in an earlier paper<sup>2</sup> that the decrease in the steady-state rate observed with increase in metal alkyl concentration above an Al : V ratio of 2 : 1 was due to competitive adsorption of metal alkyl with monomer. Under these conditions the rate of polymerization was given by:

$$R_p = k_p \theta_M C_0 \quad (13)$$

where

$$\theta_M = \frac{K_M[M]}{1 + K_A[A] + K_M[M]} \quad (14)$$

whilst  $C_0$  may be determined at different catalyst ratios as described earlier. It is now possible to obtain quantitative verification of this hypothesis since the evaluation of  $K_A$  and  $K_M$  enables numerical values of  $\theta_M$  to be calculated.

The calculated and experimental results are reported in Table 3.

Table 3 Comparison of calculated and theoretical rates at  $30^\circ\text{C}$  [4-MP-1] =  $2.0 \text{ mol/l}$ ;  $[\text{VCl}_3]$  =  $18.5 \text{ mmol/l}$ ; solvent = benzene

[Al(iBu) <sub>3</sub> ] × 10 <sup>3</sup> (mol/l)	Experimental $R_p/[\text{VCl}_3]$ (mol/l min per mol $\text{VCl}_3$ )	$\theta_M$	$\frac{C_{0(\text{Al:V})}}{C_{0(2:1)}}$	Calculated $R_p/[\text{VCl}_3]$ (mol/l min per mol $\text{VCl}_3$ )
33.7	0.274	0.216	1.00	0.260
66.6	0.266	0.196	1.14	0.266
110	0.234	0.173	1.20	0.250
138	0.233	0.161	1.23	0.240
217	0.186	0.131	1.30	0.211
289	0.176	0.117	1.34	0.187
369	0.164	0.102	1.38	0.167
491	0.140	0.086	1.39	0.142
558	0.142	0.079	1.40	0.130

The agreement between the predicted and experimental values is good, deviations being within the limits of experimental error. Thus it can be seen that these results may be interpreted in terms of a kinetic scheme involving competitive adsorption of metal alkyl with monomer.

#### Variation of rate of polymerization with monomer concentration

The steady-state rate of polymerization has been described by the equation:

$$R_p = k_p \theta_M C_0 \quad (13)$$

and consequently, under conditions where  $C_0$  remains constant, the rate of polymerization should be directly proportional to  $\theta_M$ , i.e., a plot of  $R_p$  against  $\theta_M$  should be linear and pass through the origin. It is possible now

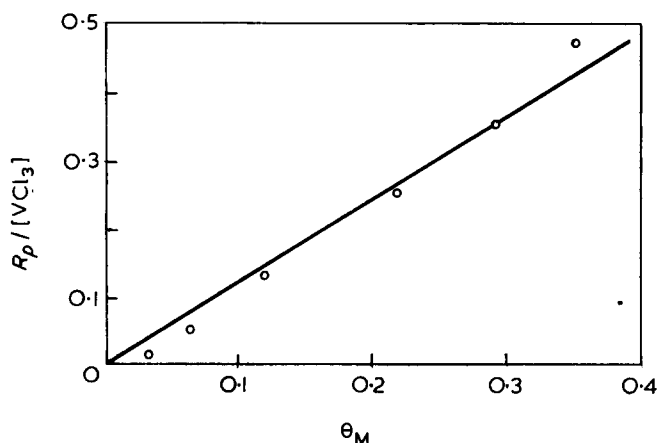


Figure 12 Variation in rate of polymerization with  $\theta_M$ . [4-MP-1] =  $0.25$  to  $4.00 \text{ mol/l}$ ;  $[\text{VCl}_3]$  =  $18.5 \text{ mmol/l}$ ;  $[\text{Al}(\text{iBu})_3] : [\text{VCl}_3]$  =  $2 : 1$ ; temperature =  $30^\circ\text{C}$

to evaluate  $\theta_M$  at varying monomer concentrations since both  $K_A$  and  $K_M$  are known. Figure 12 shows a plot of  $R_p$  against  $\theta_M$  as the monomer concentration is varied. The plot which shows some scatter, is a good straight line but deviates from linearity at low values of  $\theta_M$  (at low monomer concentrations). It has, however, been observed that the number of active centres is reduced at low monomer concentrations and consequently  $C_0$  is not constant in this region.

A value of  $k_p$  equal to  $3.10 \times 10^3 \text{ min}^{-1}$ , was obtained from the slope of the plot (for  $C_0$  equal to  $3.78 \times 10^{-4} \text{ mol/mol VCl}_3$ ). This value is in good agreement with the value previously determined<sup>1</sup>.

## CONCLUSIONS

This study has demonstrated the validity of the kinetic scheme proposed earlier<sup>3</sup> in which propagation was considered to occur between an alkylated vanadium species and adsorbed monomer, and in which chain transfer was considered to occur with adsorbed monomer and adsorbed metal alkyl.

## REFERENCES

- Burfield, D. R. and Tait, P. J. T. *Polymer* 1972, **13**, 315
- McKenzie, I. D., Tait, P. J. T. and Burfield, D. R. *Polymer* 1972, **13**, 307
- Burfield, D. R., McKenzie, I. D. and Tait, P. J. T. *Polymer* 1972, **13**, 302
- Coover, H. W., Guillet, J. E., Combs, R. L. and Joyner, F. B. *J. Polym. Sci. (A-1)* 1966, **4**, 2583
- Laputte, R. and Guyot, A. *Makromol. Chem.* 1969, **129**, 234
- McCarty, W. H. and Parravano, G. *J. Polym. Sci. (A)* 1965, **3**, 4029
- Burnett, G. and Tait, P. J. T. *Polymer* 1960, **1**, 151
- Novokshonova, L. A., Tsvethova, V. I. and Chirkov, N. M. *J. Polym. Sci. (C)* 1967, **16**, 2659
- Natta, G., Pasquon, I., Svab, J. and Zambelli, A. *Chim. Ind., Milan* 1962, **44**, 621
- Pitzer, K. S. and Gutowsky, H. S. *J. Am. Chem. Soc.* 1946, **68**, 2204
- Vesely, K. *Pure Appl. Chem.* 1962, **4**, 407
- Otto, F. D. and Parravano, G. *J. Polym. Sci. (A)* 1964, **2**, 5131



# Effect of chemical structure on crystallization rates and melting of polymers: Part 1. Aromatic polyesters

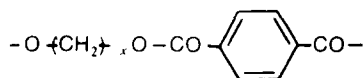
Marianne Gilbert and F. J. Hybart

Chemistry Department, The University of Aston in Birmingham, Birmingham B4 7ET, UK  
(Received 4 October 1971; revised 1 February 1972)

Crystallization rates of five aromatic polyesters have been measured using the Du Pont Differential Thermal Analyser fitted with the DSC cell. Poly(tetramethylene terephthalate) was used to show that consistent results were obtained by this method and by dilatometry. Heats of fusion have been determined for all the polymers and in three cases, spherulite growth rates could be measured. The difference in properties between the polymers has been discussed with respect to the variation in chemical structure.

## INTRODUCTION

Much work has been published concerning the crystallization kinetics of different polymers and the structural factors which allow crystallization. There have been no systematic studies of the effect of chemical structure on polymer crystallization rates and on morphology. The linear aromatic polyesters:



provide a convenient series for preparing polymers with small variations in the chemical structure. We have prepared and studied those polymers in which  $x$  is 2, 4, 5 and 6 to determine the effect of lengthening the aliphatic component and of having odd and even numbers of carbon atoms in it. With  $x=4$ , we have also prepared the polymer with isophthalic acid, to study the effect of symmetrical and non-symmetrical substitution in the benzene ring.

Isothermal crystallization rates were measured using the Du Pont Differential Thermal Analyser. The use of this instrument has not been reported previously. Chiu<sup>1</sup> used a double decker cell to measure crystallization half-times between 40 and 100 sec for polypropylene. Other workers<sup>2-4</sup> have used the Perkin Elmer Differential Scanning Calorimeter and obtained crystallization rates comparable to those measured by dilatometry.

## EXPERIMENTAL

### Materials

The polyesters (Table 1) were prepared<sup>5-7</sup> by heating the appropriate glycol with dimethyl terephthalate or dimethyl isophthalate and a catalyst under nitrogen for

2-3 h at temperatures between 140°C and 220°C as shown. Methanol was evolved. The reaction was completed by heating at the second stage temperature for another 2-3 h at a pressure of 0.1 mmHg (1 mmHg  $\equiv$  133.322 N/m<sup>2</sup>). Butyl titanate was not used as catalyst for poly(ethylene terephthalate) as it caused discoloration of the polymer<sup>5-7</sup>. The number-average molecular weight for each sample was measured using a Mechrolab Model 502 high speed membrane osmometer at 25°C with a 60/40 mixture of *o*-chlorophenol and tetrachloroethylene as solvent<sup>8</sup>.

### Differential thermal analysis (d.t.a.)

The Du Pont 900 Thermal Analyser, fitted with a DSC cell, was used to measure isothermal crystallization rates, and heats of fusion. 10-25 mg of each polymer were placed in a standard aluminium sample pan, and the lid was positioned while the sample was in a molten state, so that the polymer was in the form of a thin disc.

For crystallization rate measurements glass beads were used as reference. To record a crystallization trace the polymer was first melted for 20 min at the temperature shown (Table 2). This was chosen to be 30°C above the bulk melting temperature. The cell was then cooled quickly without overshooting, to the required crystallization temperature,  $T$ . At this stage the temperature was controlled using an external supply to the cell heater. This supply consisted of a stabilized voltage which could be varied from 0-60 V or 0-120 V to control the cell at the required temperature. The temperature could be controlled to  $\pm 0.1^\circ\text{C}$  below 100°C and to  $\pm 0.2^\circ\text{C}$  at higher temperatures, and was observed on an external recorder during the cooling and crystallization processes. The temperature difference between the sample and reference was recorded on a time base using a 1 mV integrating

Table 1 Preparation of the polyesters

Polymer	Repeat unit	Notation	Catalyst	$M_n$	Optical melting temperature (°C)	Polymerization temperature (°C)	
						Stage 1	Stage 2
Poly(ethylene terephthalate)	$-\text{O}(\text{CH}_2)_2\text{OOC}-\text{C}_6\text{H}_4-\text{CO}-$	2T	0.02% antimony acetate	12 200	276	160-216	276
Poly(tetra-methylene terephthalate)	$-\text{O}(\text{CH}_2)_4\text{OOC}-\text{C}_6\text{H}_4-\text{CO}-$	4T	0.1% butyl titanate	13 400	234	150-220	250
Poly(penta-methylene terephthalate)	$-\text{O}(\text{CH}_2)_5\text{OOC}-\text{C}_6\text{H}_4-\text{CO}-$	5T	0.1% butyl titanate	10 600	142	160-200	266
Poly(hexa-methylene terephthalate)	$-\text{O}(\text{CH}_2)_6\text{OOC}-\text{C}_6\text{H}_4-\text{CO}-$	6T	0.1% butyl titanate	11 800	156	200	280
Poly(tetra-methylene isophthalate)	$-\text{O}(\text{CH}_2)_4\text{OOC}-\text{C}_6\text{H}_4-\text{CO}-$	4I	0.1% butyl titanate	12 800	150	160-186	243

recorder. A typical trace and its integrated area is shown in Figure 1. Crystallization half times,  $t_{1/2}$ , were obtained. This method was used to measure crystallization rates for all the aromatic polyesters except 4I, which crystallized too slowly.

For the heat of fusion measurements, an empty sample pan was used as the reference. The cell was calibrated using pure metals. Each polymer sample was crystallized overnight at a temperature for which  $t_{1/2}$  was greater than 100 min. The melting of the sample was followed by differential thermal analysis when heating at  $5^\circ\text{C min}^{-1}$ . It was then allowed to cool below the temperature of maximum crystallization rate and reheated past the melting temperature. Heats of fusion after both the slow and the more rapid crystallization were calculated from the melting traces.

#### Dilatometry

Our dilatometric method for the measurement of crystallization rates has been described previously<sup>9</sup>. 0.15-0.20 g of polymer were just melted in the dilatometer at a pressure of approximately  $10^{-4}$  mmHg, to remove moisture. The polymer was cooled and mercury was then distilled into the dilatometer which was sealed. The melt conditions were as used for the differential thermal analysis measurements. After melting the polymer, the dilatometer was quickly transferred to a crystallization bath controlled at temperature  $T$ . The dilatometric height,  $h_t$ , at time  $t$  was plotted against  $1/t$ . The change in slope of this plot towards the end of the crystallization was assumed to occur at  $h_\infty$ , the end of the primary crystallization process. The time for half of the primary crystallization process could then be calculated. The  $h_t$  value for complete crystallization was obtained by extrapolating  $1/t$  to 0.

Table 2 Avrami values and crystallization rate constants for aromatic polyesters

Polyester	Melt temperature (°C)	$n$	Crystallization temperature (°C)	$K(\text{sec}^{-n})$			
2T <sup>a</sup>	295	2.0	228.3	$3.3 \times 10^{-6}$			
			230.2	$1.6 \times 10^{-6}$			
			232.6	$5.1 \times 10^{-7}$			
			233.7	$5.4 \times 10^{-7}$			
			234.6	$3.3 \times 10^{-7}$			
			236.8	$1.2 \times 10^{-7}$			
			237.2	$1.5 \times 10^{-7}$			
			239.8	$4.8 \times 10^{-8}$			
			4T <sup>a</sup>	260	2.6	208.8	$8.8 \times 10^{-8}$
						209.8	$2.8 \times 10^{-8}$
211.1	$7.4 \times 10^{-9}$						
212.0	$3.1 \times 10^{-9}$						
212.7	$1.5 \times 10^{-9}$						
212.9	$9.2 \times 10^{-10}$						
213.5	$5.6 \times 10^{-10}$						
4T <sup>b</sup>	260	2.8				210.1	$7.1 \times 10^{-9}$
						211.7	$2.1 \times 10^{-9}$
						212.1	$1.5 \times 10^{-9}$
			213.6	$3.7 \times 10^{-10}$			
			214.3	$2.6 \times 10^{-10}$			
			214.7	$1.5 \times 10^{-10}$			
			214.9	$8.9 \times 10^{-11}$			
			6T <sup>a</sup>	186	2.9	131.5	$1.2 \times 10^{-8}$
						132.7	$6.1 \times 10^{-9}$
						134.0	$1.4 \times 10^{-9}$
135.2	$5.3 \times 10^{-10}$						
136.6	$1.6 \times 10^{-10}$						
138.0	$3.1 \times 10^{-11}$						
4I <sup>b</sup>	185	2.5				78.0	$2.8 \times 10^{-11}$
						85.8	$4.1 \times 10^{-11}$
			90.7	$4.9 \times 10^{-11}$			
			95.3	$3.7 \times 10^{-11}$			
			98.6	$3.5 \times 10^{-11}$			
			102.0	$1.9 \times 10^{-11}$			
			105.3	$1.8 \times 10^{-11}$			
			109.7	$1.2 \times 10^{-11}$			

<sup>a</sup> Measured by d.t.a.

<sup>b</sup> Measured by dilatometry

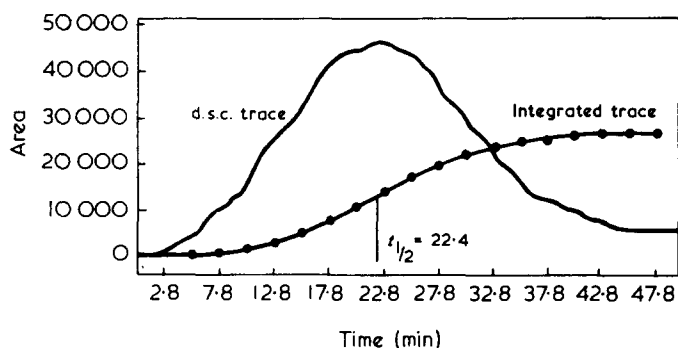


Figure 1 Typical d.s.c. trace, with the integrated trace and the method for the determination of  $t_{1/2}$

#### X-ray fibre diagrams

X-ray fibre diagrams were obtained for drawn samples of the 5T, 6T and 4I polyesters, using nickel filtered copper  $K_{\alpha}$  radiation supplied from a Solus-Schall X-ray generator with an accelerating voltage of 40 kV, and a cathode current of 20 mA. Rigid fibres were produced when the molten polymer was extruded from a glass syringe and then crystallized under tension at 80°C.

#### Microscopy

Spherulite growth rates were measured for the 4T, 5T and 4I polyesters using a hot stage microscope<sup>10</sup>. A small polymer sample (approximately 2 mg) was melted on the melting stage between two dust free cover slips, then transferred to the crystallization stage controlled to within  $\pm 0.2^{\circ}\text{C}$  of the required temperature. The diameters of spherulites were measured using a micrometer eyepiece. If possible the melting conditions used in crystallization rate experiments were used. In some cases the nucleation density observed was too high for growth rate measurements, and it was necessary to use higher melting temperatures. Plots of spherulite size against time were linear.

A second hot stage microscope was used to measure polymer melting temperatures. This microscope was used as an accessory for the Du Pont 900 Thermal Analyser. The temperature of the hot stage was recorded on the X-axis of the X-Y recorder; depolarized light intensity was detected by a photocell and recorded on the Y-axis. The polymer melting temperature was the temperature at which the last trace of birefringence disappeared. Samples were crystallized slowly (over a period of 16–72 h), and then reheated at  $\frac{1}{2}^{\circ}\text{C}/\text{min}$ . Melting temperatures are shown in Table 1.

## RESULTS

#### Crystallization rates

Crystallization half times for the series of aromatic polyesters were obtained from d.t.a. or dilatometry and plotted against  $\Delta T$ , the extent of supercooling where  $\Delta T = T_m - T$ , i.e. the difference between  $T_m$ , the melting temperature shown in Table 1 and  $T$ , the temperature at which the crystallization rates were measured (Figure 2). The variation between the different polymers was much greater than the differences that can be observed with one polymer because of changes in molecular weight, melt temperature or melt time. 4T and 6T polymers were closest in behaviour in this series. Figure 3 shows the

effect of varying the melting time, the melting temperature and the molecular weight on the crystallization half-times of the 4T polyester. Although there is some variation, it is less than the difference between 4T and 6T polyester samples studied under similar conditions and with almost the same molecular weights. The spherulite growth rates for polyesters 4T, 5T and 4I have been plotted against the extent of supercooling  $\Delta T$  (Figure 4).

For use in a computer programme the Avrami equation has been used in the form:

$$n = t \frac{dh_t}{dt} / \left[ (h_{\infty} - h_t) \log_e \left( \frac{h_{\infty} - h_0}{h_{\infty} - h_t} \right) \right]$$

for dilatometry where  $n$  is the Avrami integer,  $t$  is time, and  $h_0$ ,  $h_{\infty}$ , and  $h_t$  are the dilatometer height at the beginning, the end and at time  $t$  respectively,

$$\text{or } n = t \frac{dA_t}{dt} / \left[ (A_{\infty} - A_t) \log_e \left( \frac{A_{\infty} - A_0}{A_{\infty} - A_t} \right) \right] \text{ for d.t.a.}$$

where

$$A_{\infty} = \int_0^{\infty} T_a dt$$

and

$$A_t = \int_0^t T_a dt$$

where  $T_a$  = temperature difference between the sample and the reference during the crystallization. [ $A_0 = 0$  but

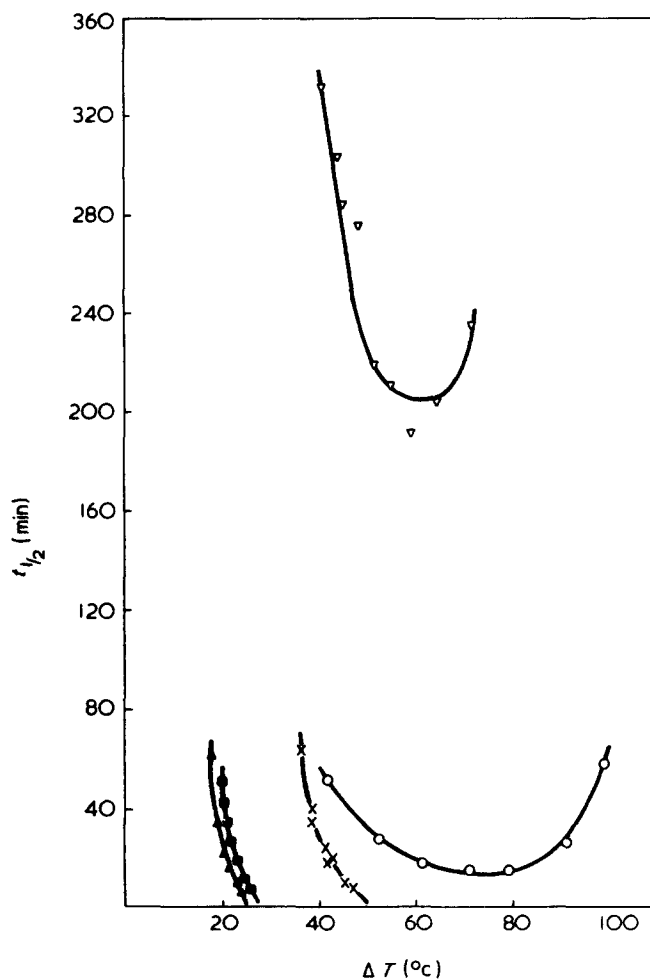


Figure 2 Crystallization half-times for aromatic polyesters. x, 2T; ■, 4T; ○, 5T; ▲, 6T; ▽, 4I

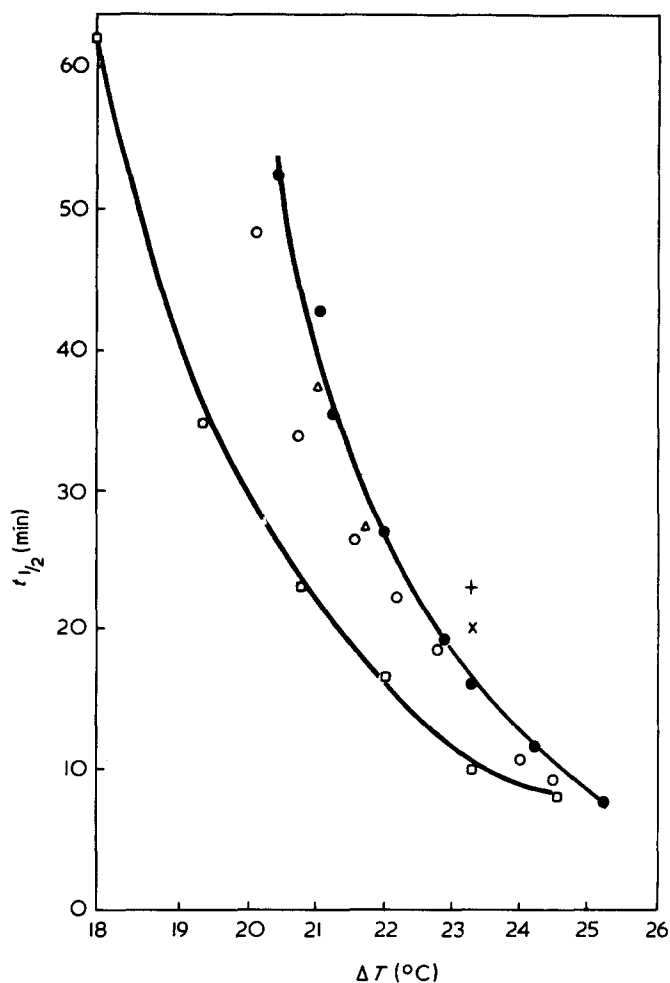


Figure 3 Crystallization half-times. ○, 4T ( $M_n$  13 400) melted at 260°C for 5 min; ●, 4T ( $M_n$  13 400) melted at 260°C for 20 min; △, 4T ( $M_n$  13 400) melted at 250°C for 20 min; ×, 4T ( $M_n$  11 100) melted at 260°C for 20 min; +, 4T ( $M_n$  9300) melted at 260°C for 20 min; □, 6T ( $M_n$  11 800) melted at 186°C for 20 min

was needed for the computer programme]  $n$  was calculated at different times from the appropriate equation. This programme assessed whether  $n$  was constant to within  $\pm 0.2$  for a major part of the crystallization. If  $n$  was constant for over 80% of the crystallization, it was averaged over the range for which it was approximately constant.

No systematic variation of  $n$  with temperature of crystallization was observed with any of these polymers. The calculated values of  $n$  at different temperatures were within  $\pm 0.2$  of the average quoted (Table 2). This average value was then used to calculate  $K$  the crystallization rate constant  $K = \log_2(t_{1/2})^{-n}$ .

A constant value of  $n$  over each crystallization was not obtained for the 5T polymer and the results are therefore not included in Table 2. Half times of crystallization, after melting the polymer at 165°C are shown (Figure 2).

The average value of 2.0 for  $n$  for the 2T polymer differs from values of 3 and 4 previously reported<sup>11</sup>. Morgan observed distinct spherulites but in this work, the nucleation density was high so that distinct spherulites could not be observed with the hot stage microscope even with severe melting conditions. In this case growth may not occur in three dimensions at an equal rate and hence a low Avrami value may be obtained.

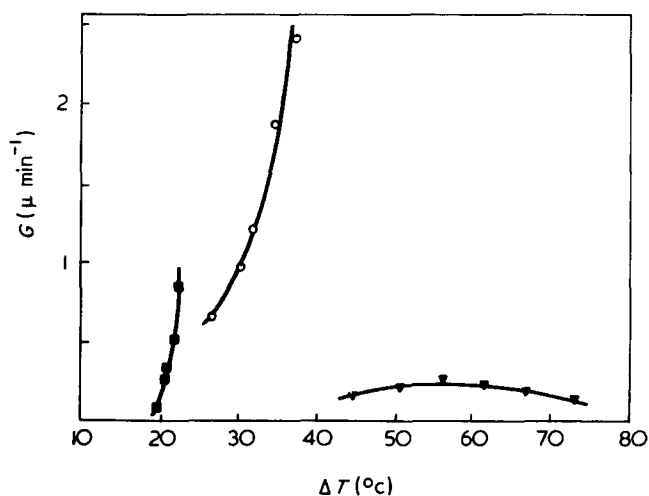


Figure 4 Spherulite growth rates for aromatic polyesters. ■, 4T; ○, 5T; ▼, 4I

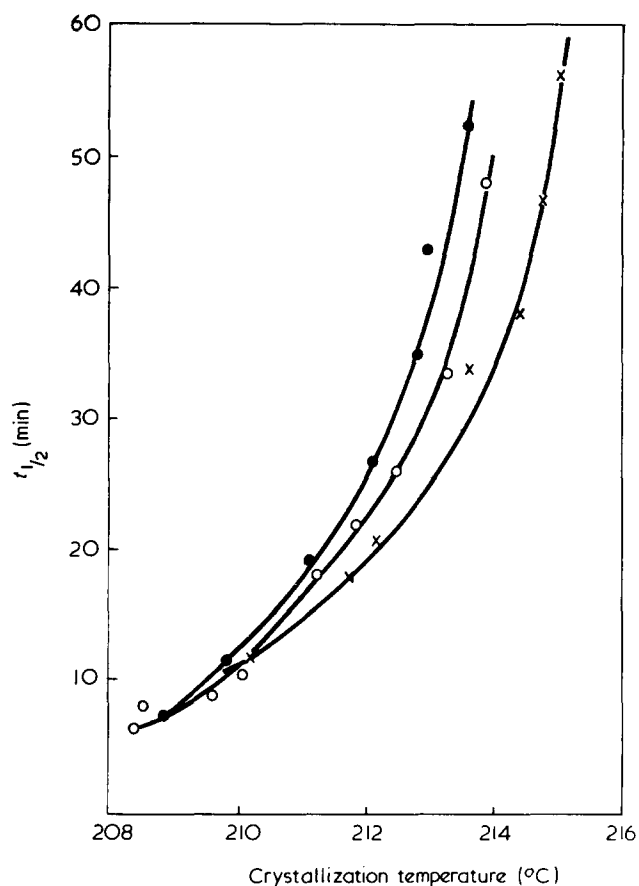


Figure 5 Comparison of crystallization half times for polyester 4T melted at 260°C by dilatometry and d.s.c. ○, measurement by d.s.c.: melt time 5 min; ●, measurement by d.s.c.: melt time 20 min; ×, measurement by dilatometry: melt time 20 min

For the 4T, 6T and 4I polyesters, a constant non-integer value of  $n$  was observed. The long secondary crystallization observed by dilatometry is not detected by the d.t.a. method.

Crystallization isotherms for polyester 4T have been obtained by dilatometry and by differential thermal analysis. A similar  $n$  value was computed and the isotherms are superimposable. There is a maximum discrepancy of 1.5°C in the crystallization temperature for a certain rate (Figure 5). It is thought that the d.t.a. method

Table 3 Heats of fusion and extents of crystallization of aromatic polyesters

Polyester	Annealed samples <sup>a</sup>					Rapidly crystallized samples <sup>b</sup>		
	$\Delta H^*$ (J g <sup>-1</sup> )	$\Delta H$ (J g <sup>-1</sup> )	Crystallinity (%)	D.t.a. peak temperatures (°C)	Crystallization temperatures (°C)	$\Delta H$ (MJ mg <sup>-1</sup> )	Crystallinity (%)	D.t.a. peak temperatures (°C)
2T	122·1 <sup>12</sup>	75·7	62	272	240	—	—	—
4T	144·6 <sup>13</sup>	56·4	39	228	215	40·5	28	218, 228
5T	—	36·4	—	136	100	—	—	—
6T	143·4 <sup>14</sup>	54·8	38	153	140	39·3	27	142, 153
4I	191·9 <sup>13</sup>	27·2	13	109, 131, 144	90	—	—	—

<sup>a</sup> Before fusion, samples were crystallized for 16 hours at the temperature shown

<sup>b</sup> These samples were rapidly crystallized during natural cooling in the d.s.c. cell

gives a better measurement of the temperature of the sample since the sensor is much closer to it. Both methods are valid for a comparison of crystallization data between the series of polyesters. We have chosen the d.t.a. method because of its greater convenience.

#### Heats of fusion

Percentage crystallinities of the aromatic polyesters after slow and fast crystallization are shown (Table 3). The heats of fusion ( $\Delta H^*$ ) for four of the fully crystallized polyesters have been reported<sup>12-14</sup>. In each case this quantity was determined from the depression of the melting point of the polymer when mixed with diluent. The peaks of the melting endotherms, recorded by d.t.a. were up to 5° lower than those observed by the optical method. Multiple peaks were observed in several cases. No crystallization and hence no melting peaks were observed when the 2T, 5T and 4I polyesters were cooled quickly.

#### X-ray fibre diagrams

Table 4 shows the identity periods that were measured for the 5T, 6T and 4I polymers and obtained from the literature for the 2T polymer<sup>15</sup>. The repeat distances have been calculated in each case and are also shown.

## DISCUSSION

It has been shown that similar isothermal crystallization rate data for the 4T polyester can be obtained using the DuPont Thermal Analyser fitted with the scanning calorimeter as is obtained by dilatometry. In this technique, unlike the Perkin Elmer DSC instrument, the difference in temperature between the crystallizing sample and the standard is measured against time. Booth and Hay<sup>2</sup> suggested that thermal analysis techniques could not be used to measure crystallization rates because the sample temperature may be changing during the crystallization. In this work, better temperature control and an increased sensitivity is achieved.

The half-times of crystallization for 2T, 4T and 6T polyesters have been plotted in Figure 2 as a function of the amount of supercooling. Although factors such as the average molecular weight, the melting time and temperature, affect the rates of crystallization, their effect is less than the difference shown between these three polyesters. The polymers containing the longer sections of aliphatic units, which would be expected to lead to more flexible chains, crystallize more readily.

Table 4 X-ray data for aromatic polyesters

Polyester	Measured identity period (nm)	Calculated repeat distance (nm)
2T	1·075 <sup>15</sup>	1·086
4T	—	1·337
5T	1·22 (this work)	1·462
6T	1·53 (this work)	1·588
4I	2·60 (this work)	1·358

However, lower extents of crystallinity were observed for the annealed samples of 4T and 6T than for 2T polyesters (Table 3). The extents of crystallization of 4T and 6T polyesters were very similar when measured after fast or slow crystallizations. In each case the extent of crystallinity rose from 27-28% to 38-39%. As has been reported previously (for example, in ref. 10) the melting point of the polymers decrease considerably on increasing the length of the aliphatic sequence between the aromatic rings in the chain.

Previously it has been shown<sup>15</sup> that 2T, 6T and 10T polyesters crystallize in the triclinic system and have one chemical repeat unit, slightly distorted, in each unit cell. Identity period measurements for the 2T and 4T were not obtained in this work but those for the 6T agreed with those obtained by Bateman *et al.* It is probable that the 4T polyester crystallizes in the same crystal class. The identity periods for the 4I polyester (2·60 nm) suggests a slightly distorted planar zigzag conformation with two chemical repeat units per unit cell. For 5T polyester there is a considerable discrepancy between the identity period (1·22 nm) and the calculated repeat distance (1·46 nm). For a fully extended planar zigzag conformation, the repeat distance would be expected to be close to the length of two chemical repeat units. It seems that in this case severe distortion of the chain occurs more readily than the alignment of the lengthy planar zigzag repeat distance.

5T polyester requires a great deal more supercooling for crystallization than the polyesters containing an even number of carbon atoms in the diol component. The maximum rate of crystallization was measurable for this polyester (Figure 2). The polymer has a lower crystalline melting point than 6T showing the odd even effect that has often been observed with polyesters and polyamides<sup>16</sup>. This polymer also failed to crystallize when cooled quickly in the Differential Thermal Analyser. Under isothermal conditions crystallization occurred. It was then possible to obtain a heat of fusion (Table 3) on reheating but the information is not available to calculate a percentage crystallinity. The heat of fusion suggests that it would be lower than that obtained with the 2T, 4T and 6T poly-

esters. Crystallization is obviously very much more difficult when the diol containing an odd number of carbon atoms is introduced into the polyester chain. The values for the Avrami integer  $n$  obtained for the 5T polymer varied considerably. For the 2T, 4T and 6T polymers constant non-integer values were obtained. The value of 2.0 obtained for the 2T polymer was quite different from that obtained by Morgan<sup>11</sup> and may arise from the high level of nucleation which prevented any measurements of spherulite growth rates for this polymer.

Samples of 4T and 6T polyesters crystallized quickly and when reheated in a d.t.a. experiment show two melting peaks. On melting samples that were crystallized slowly only one melting peak is observed. If two crystallization processes are occurring this could be an explanation of the fractional Avrami values.

The polyester 4I in which the *p*-substituted benzene ring of the 4T polymer is replaced with a ring with the two carboxyl groups in the *m*-positions, requires a great deal of supercooling and even then crystallizes very slowly. The annealed sample of this polymer is only 13% crystalline but shows three distinct melting peaks by differential thermal analysis.

Spherulite growth rates (Figure 4) could readily be measured for the 5T and 4I polymers which did not crystallize after preparation. After a first crystallization some nuclei in these polymers were not destroyed by remelting. For the 2T, 4T and 6T polymers the nucleating density was much higher, and many nuclei which were introduced on cooling after preparation were not subsequently removed even by severe melting conditions. For 4T it was possible to make spherulite growth rate measurements; for 2T and 6T the nucleation density was always too high.

Extremely slow growth rates at a very large degree of supercooling were found for the 4I polymer. Measurements for 4T and 5T polyesters were made over a limited temperature range but a given rate of growth was obtained at a lower extent of supercooling for 4T than for 5T.

#### ACKNOWLEDGEMENT

We are grateful to the Science Research Council for the award of a Research Studentship to M. G.

#### REFERENCES

- 1 Chiu, J. *Anal. Chem.* 1964, **36**, 2058
- 2 Booth, A. and Hay, J. N. *Polymer* 1969, **10**, 95
- 3 Hay, J. N. and Sabir, M. *Polymer* 1969, **10**, 203
- 4 Fatou, J. M. G. and Barrales-Rienda, J. M. *J. Polym. Sci. (A-2)* 1969, **7**, 1755
- 5 Smith, J. G., Kibler, C. J. and Sublett, B. J. *J. Polym. Sci. (A-1)* 1966, **4**, 1851
- 6 Goodman, I., personal communication
- 7 Br. Pat., 740,381
- 8 Gilbert, M. and Hybart, F. J. *J. Polym. Sci. (A-1)* 1971, **9**, 227
- 9 Hybart, F. J. and Pepper, B. *J. Appl. Polym. Sci.* 1967, **13** 2673
- 10 Harvey, E. D. and Hybart, F. J. *J. Appl. Polym. Sci.* 1970, **14**, 2133
- 11 Morgan, L. B. *Phil. Trans. R. Soc.* 1954, **A247**, 13
- 12 Roberts, R. C. *Polymer* 1969, **10**, 113
- 13 Conix, A. and van Kerpel, R. *J. Polym. Sci.* 1959, **40**, 521
- 14 Flory, P. J., Bedon, H. D. and Keefor, E. H. *J. Polym. Sci.* 1958, **28**, 151
- 15 Bateman, J., Richards, R. E., Farrow, G. and Ward, I. M. *Polymer* 1960, **1**, 63
- 16 Goodman, I. 'Synthetic Fibre Forming Polymers', RIC Lecture series No 3, London, 1967

# An investigation of the effect of chain geometry on the two-phase morphology of polystyrene/polyisoprene block copolymers

C. Price, A. G. Watson and Mei T. Chow

Department of Chemistry, University of Manchester, Manchester M13 9PL, UK  
(Received 14 December 1971)

Block copolymers having structures of the type A-B, (A-B)<sub>2</sub>X, (A-B)<sub>3</sub>Y and (A-B)<sub>4</sub>Z, where A is polystyrene, B is polyisoprene, and X, Y and Z are linking agents, have been synthesized by anionic polymerization. Electron microscopy of thin films cast from benzene solutions showed that all the polymers formed ordered arrays of regular domains. The inter-domain distances and domain radii of the two phase structures were not influenced by changes in chain geometry, provided the overall composition and the length of the A blocks remained constant. Some results are reported concerning the compatibility of polystyrene/polyisoprene and polystyrene/polybutadiene block copolymers.

## INTRODUCTION

Microphase separation in many block copolymers has been shown to give rise to ordered arrays of regular domains<sup>1,2</sup>. For the case of styrene-isoprene block copolymers Inoue *et al.*<sup>3</sup> showed that for solvent cast films the two-phase structure obtained is governed by the incompatibility between the A and B segments, the solvation of the segments in solution, the casting temperature, the total chain length of the block copolymer and the overall composition. The three types of domains most often observed were cylinders, spheres and lamellae. Supporting evidence can be drawn from the work of Matsuo *et al.*<sup>4</sup> on styrene-butadiene block copolymers and from a wide range of general studies carried out by Skoulios and his colleagues<sup>5</sup>. For the case of A-B block copolymers several theories have been put forward which attempt to establish an interrelationship between the type and size of domains and the important molecular, or thermodynamic, variables<sup>3,6</sup>. The relationships obtained have been found to provide a useful semi-quantitative understanding of the observed behaviour.

The theoretical problem clearly becomes more difficult if we move on to consider A-B-A and other multi-block systems. However, it has been tentatively suggested that simple changes in chain geometry (such as going from A-B to an A-B-A polymer whilst keeping the length of the A blocks and the overall composition constant) may not have a significant effect upon the tertiary structure, i.e. on the type, size and arrangement of the domains<sup>6</sup>. This does not mean that changes in chain geometry will not influence the mechanical behaviour of the polymer. Indeed it is well established that for polymers in which B is a long block of a rubbery polymer and A is a shorter block of a glassy polymer, the A-B-A system can have properties similar to a conventionally crosslinked elastomer (due to the formation of a continuous network) whilst the A-B system behaves like an uncrosslinked rubber.

In the present study we have prepared and characterized two series of styrene/isoprene block copolymers of the type A-B, (A-B)<sub>2</sub>X, (A-B)<sub>3</sub>Y and (A-B)<sub>4</sub>Z, where A is polystyrene, B polyisoprene and X, Y and Z

are short linking agents; the overall composition of each of the polymers was ~25% by weight of polystyrene, and within each series the lengths of the A blocks were the same. The overall aim of the work of which this paper constitutes the first report, is to investigate experimentally the influence of chain geometry on domain morphology and physical properties.

In recent times a considerable amount of research has been carried out in synthesizing and characterizing star-shaped homopolymers. Thus, tetra-chain star-type polystyrenes have been synthesized by the reaction of polystyryl lithium with silicon tetrachloride<sup>7</sup> and with 1,2,4,5-tetrachloromethyl benzene and by the reaction of polystyryl potassium with the latter<sup>8,9</sup>. Tri-chain polystyrenes have been prepared by the reaction of polystyryl lithium with 1,2,4-trichloromethyl benzene<sup>10</sup> and methyl trichlorosilane<sup>11</sup>. In the present study we used n-butyl lithium as the initiator in preparing an isoprenyl lithium-ended polystyrene-polyisoprene block copolymer and chose the series of silicon compounds, SiCl<sub>4</sub>, SiCl<sub>3</sub>CH<sub>3</sub>, SiCl<sub>2</sub>(CH<sub>3</sub>)<sub>2</sub> as linking agents.

## EXPERIMENTAL AND RESULTS

### Materials

*Styrene monomer.* Styrene (BDH, Laboratory Reagent Grade) was first dried over calcium hydride, and then degassed and distilled. The middle fraction (~75% by wt.) was collected and allowed to stand over lithium aluminium hydride for 48 h and then it was distilled in a vacuum system on to a freshly prepared sodium mirror. As soon as polymerization began to take place monomer was distilled off and sealed into ampoules.

*Isoprene monomer.* Isoprene (BDH, Laboratory Reagent Grade) was also dried over calcium hydride, degassed and distilled, and then the middle fraction allowed to stand over calcium hydride for 48 h. The monomer was next introduced into a small vacuum system consisting of a reservoir and a series of ampoules. n-Butyl lithium was added until the characteristic colour of poly(isoprenyl lithium) appeared. The ampoules were cleansed of reactive impurities by washing with the polymerizing mixture and rinsed by repeated distillation

of monomer from the reservoir. Finally known volumes of isoprene were distilled into the ampoules and these sealed off.

**Linking agents.** These were tetrachlorosilane, trichloromethylsilane and dichlorodimethylsilane. They were each distilled several times in a vacuum system before being introduced into ampoules attached to the main apparatus.

**Benzene.** This was dried over calcium hydride and fractionally distilled. After degassing on the vacuum line it was stored ready for use.

**n-Butyl lithium.** This was obtained as a 15% solution in hexane from the Koch-Light Chemical Co. and was used without further purification. The concentration of the n-butyl lithium solution was estimated using the method of Gilman and Haubein<sup>12</sup>.

#### Polymerizations

The technique used was somewhat similar to that developed by Bywater *et al.*<sup>13</sup>. Reactions were carried out in benzene solution at approximately 25°C in a sealed vacuum system. All glassware was first washed with a polystyryl lithium solution and rinsed by repeated distillation of solvent from a reservoir. So as not to employ greased joints extensive use was made of break seals.

The all glass reaction vessel is shown in *Figure 1*. Initially it was attached to the vacuum line at I, and ampoules G and H contained known volumes of styrene and isoprene. 400 cm<sup>3</sup> of benzene were distilled into bulb B, and the reaction vessel was sealed off at J.

About 1 cm<sup>3</sup> of styrene was introduced into the apparatus via serum cap K followed by n-butyl lithium until the characteristic red colour of polystyryl lithium persisted. The resulting solution was washed around the vessel and then run back into flask B. Repeated distillation of benzene from flask B to all the extremities of the apparatus served to rinse out any residual polystyryl lithium. The solution was then stirred for some time to ensure all the styrene had polymerized, after which benzene was distilled from flask B to flask A and flask B sealed off at the constriction L.

The styrene ampoule G was broken using a glass breaker, and a known quantity of catalyst injected through serum cap F to initiate polymerization. The serum cap was removed by sealing it off at the constriction and the solution, which gradually became orange-red in colour, was stirred for 4 h. At the end of this period a small sample was removed at M, and after it had been terminated with methanol, it was analysed by gel permeation chromatography (g.p.c.).

The next stage of the polymerization was started by breaking the isoprene ampoule H. The solution, which became immediately pale yellow in colour, was left to stir for 24 h. At the end of this period a sample of the styrene-isoprene block copolymer was removed (via ampoule N) terminated with methanol, and analysed by g.p.c.

Provided the g.p.c. analysis indicated a sharp molecular weight distribution, the remaining solution was divided as equally as possible between the graduated flasks C, D and E, and the flasks sealed off at the constrictions. To each of the flasks, via a break seal, was added one of the coupling agents SiCl<sub>4</sub>, SiCl<sub>3</sub>CH<sub>3</sub> and SiCl<sub>2</sub>(CH<sub>3</sub>)<sub>2</sub>. In each case it was arranged that the molar ratio isoprenyl lithium to silicone-chlorine bonds was 1:25. The mixtures were stirred for 4 days after which time any residual anions

were terminated by adding methanol, and the polymers were subjected to g.p.c. analysis.

#### Fractionation

The polymers were fractionated at 25°C using the method of successive liquid-liquid phase separation. Briefly successive quantities of methanol were added to dilute solutions of the polymer in benzene (~0.2% by wt. concentration). The liquid phases so obtained were equilibrated using the usual heating and cooling cycle and then separated by syphoning off the dilute phase. Approximately ten fractions were collected in each fractionation case and these were isolated from solution by freeze drying.

The number-average molecular weights of the fractions were determined using a 'Hi-Speed' C5M2 recording osmometer fitted with a Sartorius filter (pore size L 50 Å). The measurements were carried out in toluene solutions at 25°C; approximately an hour was required for each solution to reach equilibrium. The fractions (in tetrahydrofuran solution) were also analysed by gel phase chromatography using a Waters instrument. This technique was employed primarily to establish the homogeneity of fractions rather than to assess molecular weight. In *Figure 2* a g.p.c. trace for a fraction is compared with that for an unfractionated sample.

The fractionation technique outlined was found to provide a sharp fractionation of species on the basis of chain geometry. A typical set of data are given in *Table 1* for a polymer prepared using the tetrafractional linking agent. After completing such fractionation and molecular weight analysis the fractions corresponding to the dominant species were combined together, whilst the rest of the fractions were discarded. The number-average molecular weight of each of the polymer samples isolated by this procedure are recorded in *Table 2*.

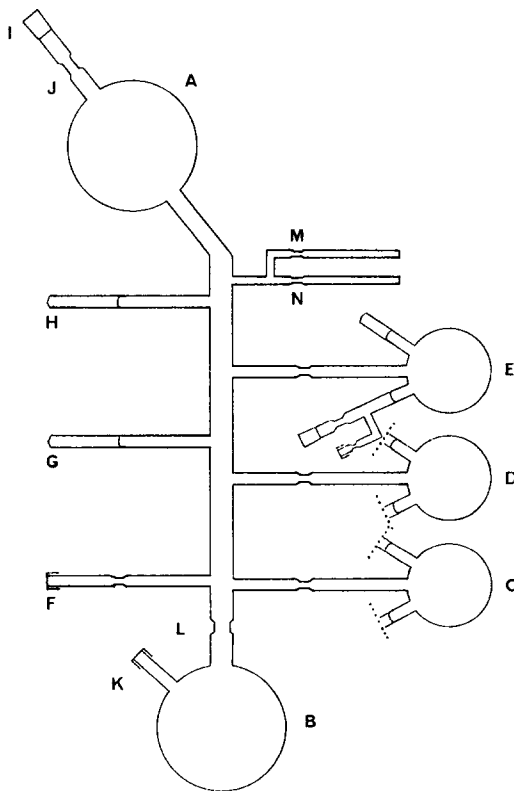


*Figure 1* Apparatus used in the synthesis of the block copolymers



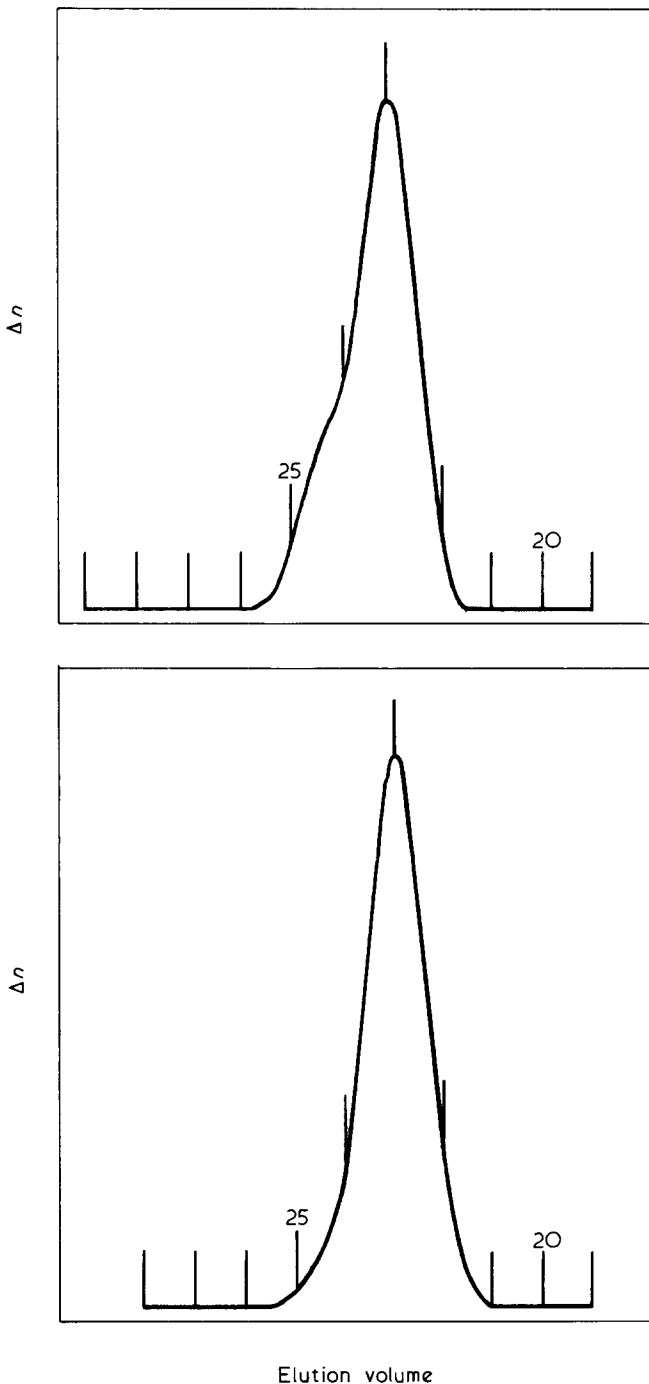


Figure 2 G.p.c. traces for sample 2P4 before (upper) and after (lower) fractionation

Table 1 Fractionation from benzene-methanol mixtures at 25°C of a copolymer synthesized by coupling an AB polymer with SiCl<sub>4</sub>

Fraction no.	Weight %	Vol. methanol		g.p.c. suggests	$M_n \times 10^{-4}$
		Vol. benzene			
1	39.04	0.452		(AB) <sub>4</sub> Z	18.8
2	9.13	0.465		(AB) <sub>4</sub> Z	18.6
3	29.17	0.475		(AB) <sub>4</sub> Z	18.8
4	9.50	0.482		(AB) <sub>3</sub> Y	14.2
5	0.89	0.491		(AB) <sub>3</sub> Y	
6	1.34	0.523		(AB) <sub>3</sub> Y	
7	5.49	0.576		AB, (AB) <sub>3</sub> Y	
8	5.41	Residue		A, AB, (AB) <sub>3</sub> Y	

The AB polymer isolated before the addition of SiCl<sub>4</sub> was found to have  $M_n = 48\,100$ . Fractions 1 and 2 were combined together and designated sample 1P4.

Table 2 Molecular weight and electron microscopy (EM) results for the two series of styrene/isoprene block copolymers

Sample	Type	$M_n \times 10^{-4}$	$D$ (nm)	$d_{int}$ (nm)	% Volume polystyrene	
					from EM assuming h.p.c.	from chain structure
Series 1						
1P1	AB	4.81	18.7	36.0	24.5	23.5
1P2	(AB) <sub>2</sub> X	9.8	17.0	33.7	23.1	23.0
1P3	(AB) <sub>3</sub> Y	14.2	18.1	33.7	26.2	23.9
1P4	(AB) <sub>4</sub> Z	18.8	18.6	34.1	27.0	24.0
$M_n$ of the A block = 12 500						
Series 2						
2P1	AB	9.6	26.9	48.1	28.4	22.9
2P2	(AB) <sub>2</sub> X	18.5	26.0	49.0	25.5	23.8
2P3	(AB) <sub>3</sub> Y	27.5	26.2	48.6	26.4	24.1
2P4	(AB) <sub>4</sub> Z	36.5	26.0	50.0	24.5	24.2

$M_n$  of the A block = 24 400

$D$  = domain diameter;  $d_{int}$  = interdomain distance; h.p.c. = hexagonally packed array of cylinders

### Electron microscopy

Electron micrographs of ultra-thin films were obtained using an AEI EM6G electron microscope. The instrument was operated at an accelerating voltage of 100 kV under which conditions the stated resolution was better than 1 nm. Ultra-thin films were prepared by carefully evaporating solutions of the polymers in benzene. The concentration of the solutions used was calculated to give a film thickness of 50 nm. The films were stained using osmium tetroxide, which selectively combines with the olefinic bonds of the polyisoprene chains. On using a fairly slow rate of evaporation and casting from mercury, each polymer gave regular hexagonal arrays of 'circular' domains of the type shown in Figure 3. At larger fields of view, grain structures were clearly visible. On varying the method of casting more irregular arrays of the type described previously by one of us<sup>13</sup> were observed, but in the present study they were not analysed. For the regular arrays the measured domain radii and inter-domain distances (i.e. nearest distance between centres) are given in Table 2.

### DISCUSSION

Let us first consider the evidence which will enable us to make assignments to the two-phase structures of the polymers we have studied. If we assume there is complete phase separation of the two components, the volume fraction of polystyrene may be calculated by two independent methods. Firstly we can calculate it from a knowledge of the chain geometry and block lengths, and secondly from measured area fractions assuming a particular domain structure (spheres, cylinders or lamellae). From such a comparison we conclude that the two-phase structures of all 8 polymers (listed in Table 2) are consistent with a model in which cylinders of polystyrene are hexagonally packed in a polyisoprene matrix. The data are given in Table 2.

For reasons we have discussed in detail previously the use of ultra-thin solvent cast films to investigate morphological features is not completely satisfactory<sup>14,15</sup>.

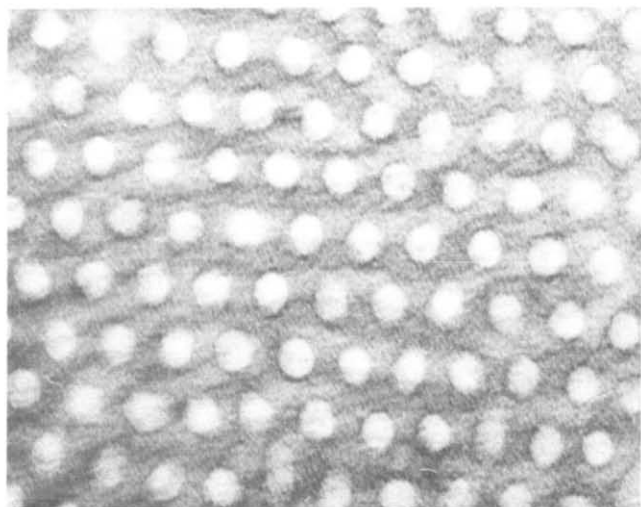


Figure 3 Electron micrograph of solvent cast film of sample 2P4

Nevertheless, provided a suitable solvent is chosen, information obtained by this method in the past has been found, in the light of more detailed studies involving low-angle scattering<sup>15</sup> and electron microscopy of ultramicrotomed sections<sup>16</sup>, to provide a very useful guide to the actual behaviour of the bulk polymer. For the purpose of the present investigation the main advantage of using solvent cast film is that the technique is simple to apply, and very reproducible. Hence any small differences in the two-phase behaviour of the samples could readily have been detected.

Examination of *Table 2* shows that within experimental error the cylindrical radii and inter-domain distances are independent of the changes in chain geometry we have made provided the polystyrene end-block lengths and the overall composition remain constant. This can be interpreted to mean that the configurational entropy of the matrix plays only a secondary role in determining the two-phase morphology. Each (A-B)<sub>4</sub>Z polymer molecule has the possibility of occupying by way of its four A end-blocks, from one to a maximum of four separate domains. In practice one would expect to find a statistical distribution. Each A-B polymer molecule on the other hand can only occupy one domain. Thus moving along the series from A-B to (A-B)<sub>4</sub>Z the degree of constraint on the rubbery chains is progressively increased. This increase can be expected to be quite marked in view of the fact that the large cylindrical domains will have a very much lower mobility than that normally associated with the low functionality chemical crosslink encountered in the case of rubbery vulcanizates. In spite of this very little change in structural behaviour is observed moving along a series.

#### Comparison with styrene/butadiene block copolymers

Listed in *Table 3* for comparison are results we obtained in a previous study for a (polystyrene)(polybutadiene)(polystyrene) block copolymer<sup>15</sup>, where  $M_n$  for this polymer is 84000 and for the polystyrene blocks 11000. Perhaps not surprising in view of the similar nature of polyisoprene and polybutadiene the domains are seen to compare closely with those observed for sample 1P2. In view of this similarity we decided to make up a 50% by wt. mixture of the two polymers, and then reinvestigate the structure. Because of the incompatibility problem we expected to observe the usual

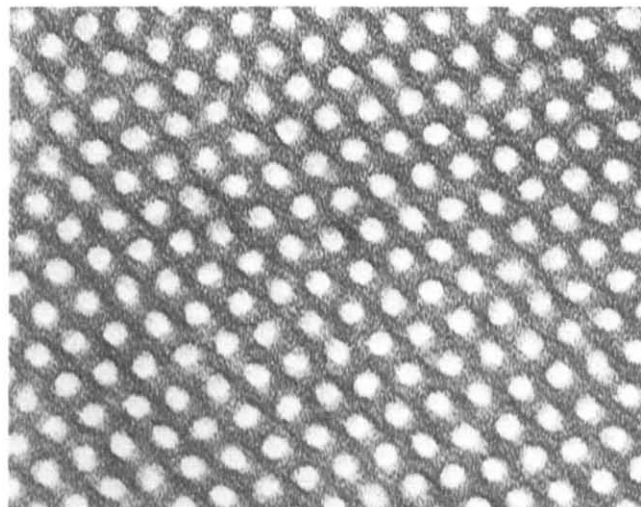


Figure 4 Electron micrograph of solvent cast film 50/50% by weight mixture of sample 1P4 and an SBS polymer

Table 3 Electron microscopy results

Sample	D (nm)	d <sub>int</sub> (nm)
1P2	17.0	33.7
SBS	20.0	43.0
1P2/SBS	18.2	34.5

macroscopic separation of the two polymers. However, under the conditions of our solvent casting technique the two polymers appear to blend together to form a single two-phase structure. If anything the ordering of the cylindrical domains was even more regular than for the case of the individual block copolymers (see *Figure 4*). The characteristic dimensions for the mixed polymer structure are given in *Table 3*. To what extent the polybutadiene and polyisoprene chains are blended together within the matrix has not yet been established by us, and is currently being subjected to a more detailed investigation.

#### ACKNOWLEDGEMENTS

We wish to acknowledge the assistance of the departmental glassblowers, Mr P. Le Pinnet and Mr D. Greenhalgh. During the course of investigation A.G.W. was supported by a grant from Dunlop Research Ltd and M.T.C. by SRC.

#### REFERENCES

- 1 Matsuo, M. *Japan Plastics* 1968, **19**, 6
- 2 Lewis, P. R. and Price, C. *Nature* 1969, **223**, 494
- 3 Inoue, T., et. al. *J. Polym. Sci. (A-2)* 1969, **7**, 1283
- 4 Matsuo, M., Sagal, S. and Asai, H. *Polymer* 1969, **10**, 79
- 5 Skoulios, A. *Adv. Colloid Interface Sci.* 1967, **1**, 3
- 6 Meier, D. J. *J. Polym. Sci. (C)* 1969, **26**, 81
- 7 Morton, M., Helminiak, T. E., Gadkary, S. D. and Beuche, F. *Conf. High Temperature Polymer Fluid Res.* 1962, **1**, 165
- 8 Altaras, T., et. al. *J. Polym. Sci. (A)* 1965, **3**, 4131
- 9 Yen, S.-P. S. *Polym. Preprints* 1963, **4**, 332
- 10 Wenger, F. and Yen, S.-P. S. *Polym. Preprints* 1962, **3**, 162
- 11 Zelinski, R. P. and Wofford, C. F. *J. Polym. Sci. (A)* 1965, **3**, 93
- 12 Gilman, H. and Haubein, A. H. *J. Am. Chem. Soc.* 1944, **66**, 1515
- 13 Worsfold, D. J. and Bywater, S. *Can. J. Chem.* 1960, **38**, 1891
- 14 Lewis, P. R. and Price, C. *Polymer* 1972, **13**, 20
- 15 Lewis, P. R. and Price, C. *Polymer* 1971, **12**, 258
- 16 Dlugosz, J. et. al. *Kolloid-Z.* 1970, **242**, 1125

# Mechanics and mechanism of environmental crazing in a polymeric glass

E. H. Andrews and L. Bevan

Department of Materials, Queen Mary College, London E1, UK  
(Received 18 October 1971)

The conditions have been studied for propagation of single discontinuities (cracks and crazes) in poly(methyl methacrylate) under the combined influence of stress and solvents. A series of aliphatic alcohols, water-alcohol mixtures and carbon tetrachloride were employed and temperature effects were investigated over the range 273K to 323K. Using a fracture mechanics approach, the minimum surface work  $\mathcal{F}_0$  required to propagate the discontinuity was estimated as a function of temperature for each solvent.  $\mathcal{F}_0$  varies with temperature in a consistent manner, decreasing rapidly as the temperature rises up to a characteristic temperature  $T_c$  and then remaining constant at some value  $\mathcal{F}_0^*$  for  $T > T_c$ . The value of  $\mathcal{F}_0^*$  is a smooth function of the difference  $(\delta_s - \delta_p)$  between the solubility parameters of the solvent and the polymer, both for pure solvents and water mixtures, reaching a minimum at  $(\delta_s - \delta_p) = 0$ . The critical temperature for pure solvents (but not solvent-water mixtures) decreases with increasing  $(\delta_s - \delta_p)$ , probably extrapolating to  $T_g$  for the plastic at  $(\delta_s - \delta_p) = 0$ . The behaviour of  $\mathcal{F}_0$  can be explained in terms of a cavitation criterion for craze formation and the necessary theory is developed. It attributes the temperature-independent value of  $\mathcal{F}_0^*$  to a polymer/solvent interfacial energy effect, and the variation of  $\mathcal{F}_0$  at  $T < T_c$  to a yield stress effect.

## INTRODUCTION

In the presence of chemically active environments, many materials undergo failure by cracking or crazing at stresses much lower than would otherwise be necessary to cause detectable damage. These effects are observed in materials as diverse as metals, glass and rubber and the chemistry of the causative process varies from system to system.

In spite of this, however, the *mechanics* of the phenomenon are similar in all cases. The cracks or crazes always propagate normal to the direction of major principal stress and require some threshold condition of stress or strain to be achieved. It is for this reason that fracture mechanics are applicable to these various phenomena and have been employed successfully in polymeric systems by Braden and Gent<sup>1-3</sup> and by Gent and Hirakawa<sup>4</sup> for vapour cracking in elastomers, and by Andrews and Bevan<sup>5</sup> and by Marshall *et al.*<sup>6</sup> for solvent stress cracking and crazing. These studies have established that both the threshold conditions and the propagation velocities for cracks or crazes are governed by fracture mechanics criteria rather than by overall stress or strain levels. An exception to this is the special case of a 'fully load bearing' craze for which, under some circumstances, a critical stress criterion becomes appropriate. It will be seen later, however, that an equivalent fracture mechanics criterion can be used even in this case, enabling us to unify the mechanical description of all such phenomena.

Polymeric glasses may 'fail' either by cracking or crazing and it is necessary to distinguish between these phenomena. Figure 1 shows schematically the structural

difference between a crack and a craze. Whereas a crack can be viewed as the separation of two adjacent layers of atoms, a craze must be viewed as the lateral expansion of a layer of polymer of finite thickness. For a craze of infinite area this expansion takes place by means of a uniaxial extension normal to the craze plane and under plane strain conditions, so that void formation is a natural consequence of volume conservation. The void volume provides a measure of the (plastic) strain suffered by the polymer in forming the craze, a void content of 50% indicating a uniaxial strain of unity and so on.

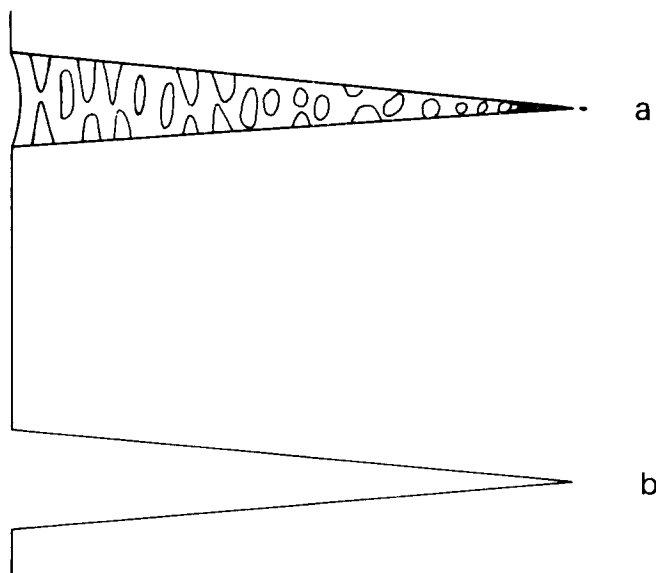


Figure 1 Structure of (a) a craze in comparison to (b) a crack

Since the opposing walls of a craze are connected by solid material, it does not follow that the stress distribution around a craze is the same as for a crack. In particular it can no longer be assumed that the stress normal to the craze wall is zero as in the case of a free boundary. In the general case of a loaded body partly 'severed' by a craze plane, the proportion of the load carried across the craze may lie anywhere between zero (as for a crack) and the value appropriate to the homogeneous solid (i.e. the craze is fully load-bearing). This will depend entirely on the relative elastic constants of the solid polymer and the craze matter; a very soft or rubberlike craze will exhibit a stress distribution very similar to that of a crack, whilst a strongly strain-hardened craze, even allowing for its void content, could be as stiff as the parent polymer itself causing a minimum perturbation in a homogeneous stress field. Even in the latter situation, however, the fact that the craze has grown at all indicates that a stress-field perturbation must be present at the tip. There must be a localized stress maximum on the craze axis at that point, otherwise transformation of polymer to craze would not occur there. The difference therefore between the stress distributions at a craze or a crack are not, in the vicinity of the tip, primarily qualitative but quantitative, the craze matter reducing the stress concentrating ability of the craze below that of a crack of similar geometry. The amount of this reduction will depend only on the elastic properties of the craze, though these properties may vary widely even in a given polymer. The elastic behaviour of the craze will, for example, be different for a dry polymer than for one infused with solvent. It will vary with temperature. Perhaps most important for the understanding of the present work is the fact that 'craze matter' displays severe mechanical hysteresis<sup>7</sup> so that, under load cycling, the stress carried by a craze at a given strain will vary strongly with the stress history of the specimen. For example, the application of a high load to the specimen followed by a reduction of load will leave the craze carrying much lower stresses than if the same final load had been achieved by monotonic increase from zero.

From this discussion it can be seen that crazes may behave *mechanically* in any manner from that of a crack to that of a fully load-bearing craze and that even a single craze may exhibit different behaviour under different circumstance.

For conciseness the term 'discontinuity' will be used to include cracks and crazes when it is not required to differentiate between them.

FRACTURE MECHANICS

Cracks

According to the theory of fracture mechanics the propagation behaviour of a crack is governed entirely by the stress-intensity factor *K* of linear fracture mechanics<sup>8</sup> or by the energy available for propagation from the elastic stress field,  $-\partial\mathcal{E}/\partial A$ , per unit area of crack<sup>9, 10</sup>. The latter formulation is necessary for solids not obeying linear elastic theory and will be employed here, although polymeric glasses at low stress are sufficiently Hookean for linear elastic theory to be safely used.

Propagation will occur when the available energy per area equals the energy requirement or surface work<sup>11</sup>,

i.e. when:

$$-\partial\mathcal{E}/\partial A = \mathcal{F} \tag{1}$$

where, in general,  $\mathcal{F}$  is a function of temperature and the propagation rate. There may exist a value of  $-\partial\mathcal{E}/\partial A$  below which no propagation occurs and this defines the minimum value  $\mathcal{F}_0$  of  $\mathcal{F}$  under the conditions obtaining.

For an edge crack of length *c* in a semi-infinite sheet of material (Figure 2):

$$-\partial\mathcal{E}/\partial A = kcW \tag{2}$$

where *k* is a constant and *W* the elastic stored energy density in the material remote from the crack. For a solid exhibiting Hookean behaviour in bulk and loaded in uniaxial tension:

$$kcW = \frac{\pi c \sigma^2}{2E} \tag{3}$$

where  $\sigma$  is the applied tensile stress and *E* is Young's modulus. There may, therefore, be a threshold value  $\sigma_c$  of  $\sigma$  below which no propagation occurs and given by:

$$\frac{\pi c \sigma_c^2}{2E} = \mathcal{F}_0 \tag{4}$$

If such a threshold value  $\sigma_c$  can be measured, a plot of  $\sigma_c^2$  against  $c^{-1}$  should be a straight line of slope  $2E\mathcal{F}_0/\pi$ .

In practice it is inconvenient to use very large sheets of material to fulfil the semi-infinite requirement and equation (4) can be modified to apply to a sheet of finite width *b*. The resulting equation is<sup>12</sup>:

$$\frac{c \sigma_c^2 Z^2}{2E} = \mathcal{F}_0 \tag{5}$$

where

$$Z = 1.99 - 0.41(c/b) + 18.70(c/b)^2 - 38.48(c/b)^3 + 53.85(c/b)^4 \tag{6}$$

Equation (5) has been used in all that follows,  $\mathcal{F}_0$  being evaluated from  $\sigma_c^2$  against  $(Z^2c)^{-1}$  plots.

Crazes

Since fracture mechanics as previously formulated relies upon the known stresses at a crack or, alternatively, upon the assumption that crack walls are free boundaries,

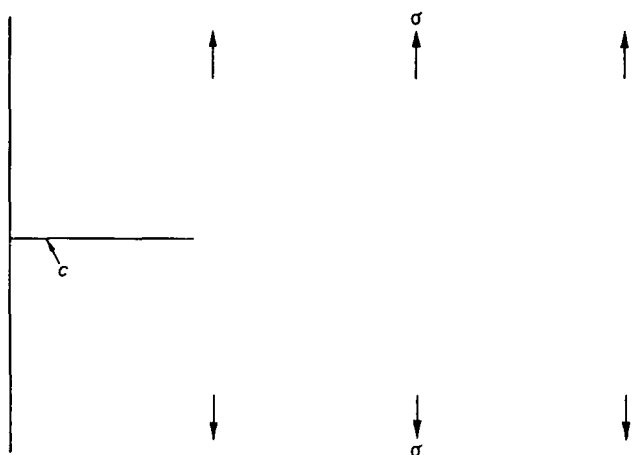


Figure 2 Edge crack in a semi-infinite sheet under a uniform tensile stress

the theory is not directly applicable to crazes. To extend the theory to crazes it is necessary either to determine analytically the stress distribution around a craze (a task requiring full knowledge of the elastic constants for the anisotropic craze material) or else to adopt some more general device. It is proposed to represent the craze mechanically by an 'equivalent' crack, i.e. a crack which produces the same degree of stress concentration at its tip as does the craze itself. It is not necessary that the equivalent crack should produce an identical stress distribution to that of the craze, but only that the maximum stresses, which are operative in causing propagation, should be replicated.

Figure 3 shows schematically several examples of discontinuities with their accompanying axial distributions of the major principal stress  $\sigma_y$  (normal to the discontinuity plane). Figure 3a shows the case of a crack and Figures 3b and 3c two possible distributions for a fully load-bearing craze. Figure 3d shows that for a bullet-shaped crack of length  $l$ , and since the tip stresses at a crack scale in proportion to the square root of its length<sup>8, 13</sup> it is evident that  $l$  can be chosen to provide 'equivalence' with the fully load-bearing craze. The particular attribute of the notional bullet-shaped crack is that it propagates in a uniform stress field without change in the stress intensity at its tip.

Figure 3e shows a further situation, previously discussed in the literature<sup>6, 14</sup> in which the craze is itself subject to cracking. As a result coplanar crack and craze coexist, with the craze tip some distance ahead of the crack tip. Providing this distance is large compared with  $l$ , this situation can be represented by an equivalent bullet-shaped crack propagating in the stress field of the true crack rather than in the uniform applied tensile field.

#### Limits of behaviour

It is clear from the foregoing discussion that the mechanical behaviour of a discontinuity may vary between the limits appropriate to a true crack of the same length,  $c$ , as the discontinuity and an equivalent crack of constant length  $l$ , where  $l \ll c$ . Intermediate behaviour will be found for craze material of high but non-infinite compliance and when the crack and craze co-exist (Figure 3e). Variable intermediate behaviour is expected if the craze is hysteretic and subject to load cycling.

The limits of behaviour can now be represented in fracture mechanics terms by reference to the  $\sigma_c^2$  against  $\{Z^2c\}^{-1}$  diagram (Figure 4), where  $c$  is the total length of discontinuity. For a crack of length  $c$ , propagation at a constant energy requirement will be represented by a straight line passing through the origin (behaviour I in Figure 4). This will apply whether it propagates as a crack or as an incipient craze (i.e. with a constant size craze region running ahead of the crack). For an equivalent crack of constant length  $l$ , the  $\sigma_c^2$  against  $\{Z^2c\}^{-1}$  plot will be a horizontal straight line (behaviour II) intercepting line I at the point  $l^{-1} = c^{-1}$ . Intermediate behaviour will give results lying within the shaded triangle.

Experimental data taking the form of Figure 4 are therefore capable in principle of providing values for (i) the minimum energy requirement  $\mathcal{F}_0$  for the propagation of cracks or for the formation of craze as the case

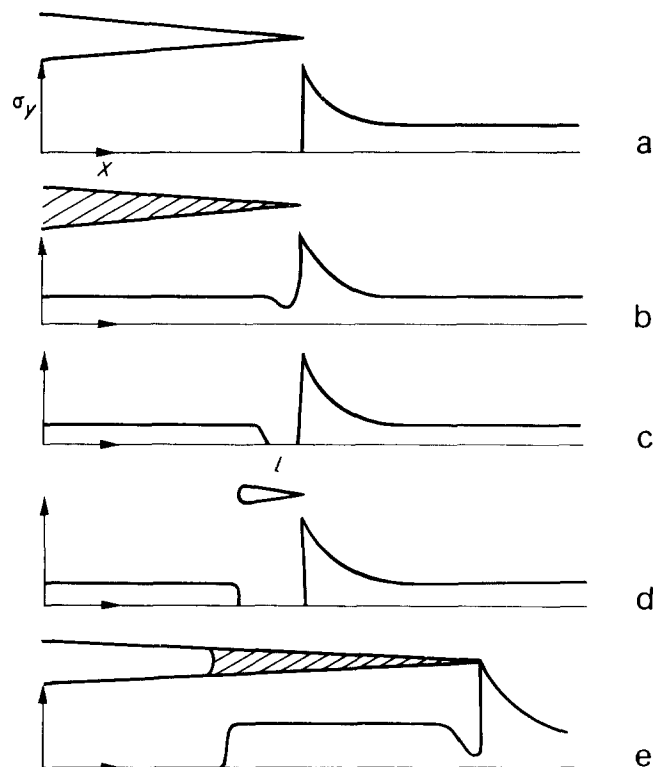


Figure 3 Stress distribution along discontinuities. (a) crack; (b) and (c) fully load-bearing craze; (d) bullet-shaped crack; (e) craze with crack

may be, and (ii) for the quantity  $l$ . The former is derived from the slope of the lower bound to experimental data and the latter from the intercept of lower and upper bounds.

It will be seen later than in some of the systems used propagation is crack-like, whilst in others a scatter of intermediate behaviour is found. This scatter almost certainly arises in cases where the craze matter is highly hysteretic as mentioned previously. The measurement of critical stresses inevitably requires load cycling (as will be seen) producing crazes with a variable load bearing capacity. Because of the load cycling, pure type II behaviour (Figure 4) was not observed in the main series of experiments, but has been found in further studies (Andrews and Levy, to be published) in which critical stresses were derived indirectly in steady-load experiments by extrapolating craze velocity against stress data to zero velocity. This strongly supports the view that the systems which display a wide scatter of critical stresses, do so because of mechanical hysteresis of the craze material combined with load cycling of the specimen. This anelasticity of the craze matter does not invalidate the elastic analysis implicit in the 'equivalent crack' concept since the latter involves only the untransformed bulk material. The role of the craze matter in this analysis is simply to provide a distributed load over the craze boundaries, this load reducing to zero in the case of a crack or infinitely soft craze.

#### EXPERIMENTAL

Experiments were carried out on cast sheets of poly-(methyl methacrylate) (PMMA) ('Perspex') 20 cm long, 0.1–0.3 cm thick and 8–10 cm wide. These were loaded

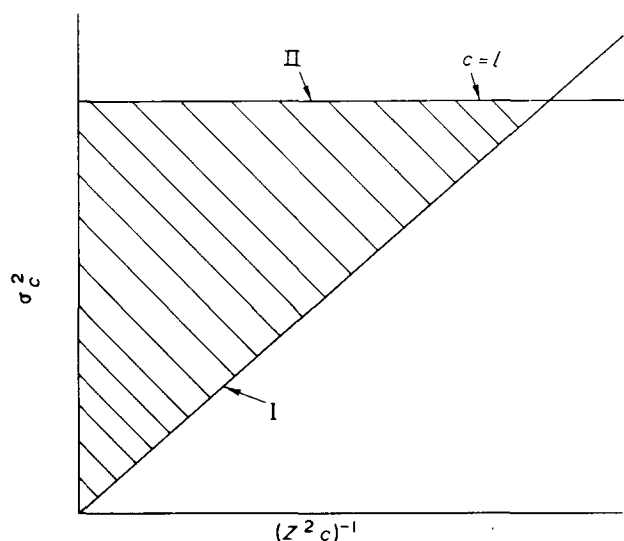


Figure 4 Limits of behaviour in a plot of critical stress squared against reciprocal of discontinuity length. I, pure cracking; II, fully load bearing craze

axially in simple tension by deflection of a stiff, simply supported beam whose displacement could be read by a sensitive dial gauge. This not only records the applied load but rapidly indicates any stress relaxation occurring in the specimen. Because of the low loads employed, no stress relaxation was observed over the time scale of the experiment except at the highest temperatures. Experiments revealing stress relaxation were abandoned. Precautions necessary to ensure uniform loading have been discussed previously<sup>5</sup>.

A central edge crack (Figure 2) of controlled length was introduced into the specimen in the following manner. A small saw cut was made to locate the crack and the cut edge of the sheet was immersed in liquid nitrogen to cause embrittlement. On removal from the coolant, the saw cut was immediately wedged open by a screw-driven jig, causing a brittle crack to run into the uncooled region of the sheet, where it arrested. The edge of the sheet was subsequently milled away to provide cracks of any desired length. Sharp, reproducible cracks are obtained by this method, although equally good results have been observed using high frequency fatigue cracks<sup>15</sup> and cracks produced rapidly by impact<sup>6</sup>.

Cracks and crazes were observed by travelling microscope using rear illumination of the specimen. Crack extensions of as little as  $10\ \mu\text{m}$  could be detected using an eyepiece graticule.

Specimen and loading assembly were placed within a double-walled thermostatically controlled solvent bath which contained windows for observation. Temperature control in the solvent, which was stirred continuously, was within  $\pm 0.5\text{K}$ .

Load was applied to the specimen and propagation established. The load was progressively diminished until growth ceased again, at which point the load and discontinuity length were recorded. Several of such critical measurements were usually made on the same discontinuity always providing that  $c < b/3$ , growth being arrested and re-started by manipulation of the load. This load-cycling is unavoidable if direct measurements of critical stress are to be made.

In all cases the length  $c_0$  of the starter crack was also recorded. From these measurements  $\sigma_c^2$  against  $\{Z^2 c\}^{-1}$

plots were made for different temperatures and solvents,  $\sigma_c$  being defined as the critical load divided by the specimen cross-section area, and  $c$  being the total discontinuity length.

Independent measurements were made, using an Instron testing machine, of Young's modulus  $E$  for the polymer at different temperatures and at an extension rate ( $10^{-4}\text{s}^{-1}$ ) chosen to approximate the long loading times used in the propagation measurements.

Solvent systems used in the present work were de-ionized water; various water/isopropyl alcohol mixtures; methanol; ethanol; methylated spirit; iso- and n-propyl alcohols; iso- and n-butyl alcohols, and carbon tetrachloride.

## RESULTS

### $\sigma_c^2$ against $\{Z^2 c\}^{-1}$ plots

Typical data are shown in Figures 5, 6 and 7 which illustrate respectively the behaviour for water, methylated spirit and isopropyl alcohol. Figures 5 and 6 reveal behaviour of a crack-like or type I nature (cf. Figure 4), in that all points lie within bounds which are straight lines through the origin. A statistical analysis of the data for methylated spirit at a given temperature gives a correlation between  $\sigma_c^2$  and  $\{Z^2 c\}^{-1}$  in the region of 0.9. In accordance with the earlier discussion, the lower bound is taken to provide a value for  $\mathcal{F}_0$  even in such cases, but the use of the lower bound will be considered further in the next section.

Type I behaviour predominates for methylated spirit, water and water/alcohol mixtures with high water content. Figure 7, in contrast, is typical of data for most of the pure solvents especially isopropyl alcohol. Both a lower bound (see next section), and possibly an upper horizontal bound, can be identified giving values for  $\mathcal{F}_0$  and, tentatively, for  $l$ . Estimates of the latter are given in Table 1.

### Use of the lower bound to define $\mathcal{F}_0$

Use of the lower bound to experimental points is based upon the arguments presented above. Briefly summarized these claim that the slope of the lower bound has special physical significance as giving the true surface work for the formation of craze at a propagating discontinuity tip. This corresponds to the case of a true crack with craze forming at its tip. If the discontinuity is not a true crack (or craze with zero load bearing propensities), its stress concentrating ability can only be lower than that of the true crack of similar length and the applied stress  $\sigma_c$  for arrest will therefore be artificially high. The critical stress  $\sigma_c$  for a given discontinuity length can never be artificially low so that its minimum value (which determines lower bound slopes) is the appropriate value to combine with the length  $c$  to obtain the true work of formation of craze.

The question then arises as to whether the experimental data do, in fact, reveal the existence of a lower bound or merely of a general scatter. Clearly this question can only be satisfactorily answered by having a much larger number of experimental points than in Figures 5, 6 and 7.

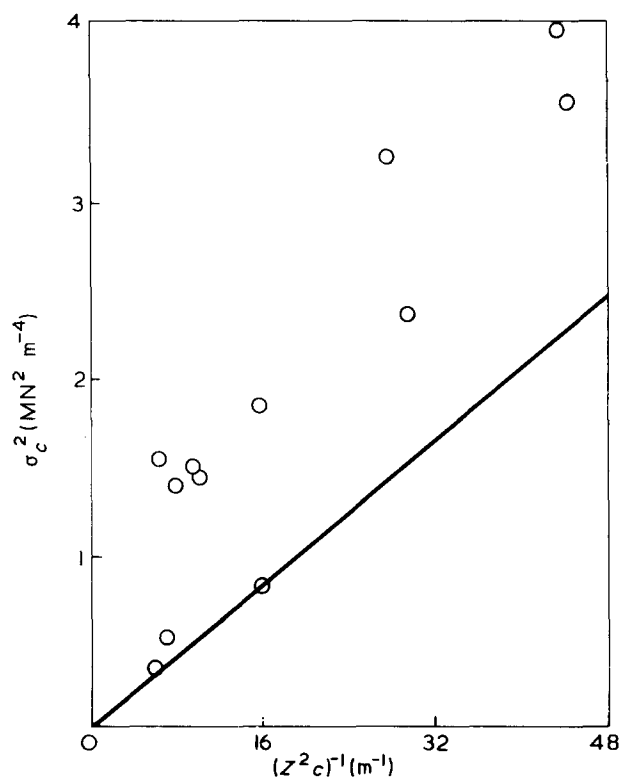


Figure 5  $\sigma_c^2$  against  $(Z^2c)^{-1}$  plot for PMMA and water. Line is lower bound to experimental points

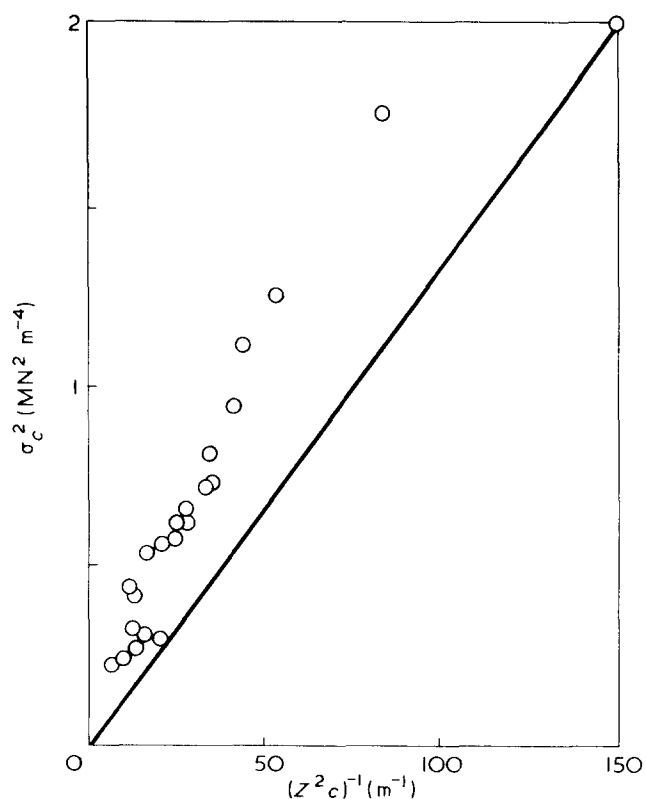


Figure 6  $\sigma_c^2$  against  $(Z^2c)^{-1}$  plot for PMMA and methylated spirit at 19°C. Line is lower bound to experimental points

Table 1 Estimated values of  $l$

Solvent	Temperature (°C)	$l$ (cm)
n-propanol	37	0.043
isopropanol	39	0.024
90% isopropanol/water	34	0.027
75% isopropanol/water	30	0.078

To collect enough data at each temperature for each system studied would have been prohibitive, but data taken at different temperatures can be superimposed to reveal the definite existence of a lower bound by the following device.

Lower bound values for  $\mathcal{F}_0$  are derived from data such as shown in Figures 5-7 and plotted against temperature. As will be seen below, a characteristic smooth dependence upon temperature was found. This fact in itself provides confidence in the lower bound concept. The  $\mathcal{F}_0$  values are next normalized by multiplying by a function of temperature such that  $\mathcal{F}_0 f(T) = \text{constant}$ ,  $f(T)$  being evaluated from the aforementioned plots of  $\mathcal{F}_0$  against temperature. The lower bounds of  $\sigma_c^2$  against  $(Z^2c)^{-1}$  plots at different temperatures, if they really exist, can now be brought into coincidence by plotting all data as  $\sigma_c^2 f(T)$  against  $(Z^2c)^{-1}$ . This has been done in two cases in Figures 8 and 9 which contain data for methylated spirit and isopropyl alcohol respectively. These normalized plots reveal unmistakable lower bounds. This does not, of course, prove categorically that lower bounds exist but only that their existence and a certain well defined form of temperature dependence are mutually consistent. It is inconceivable, however, that the temperature dependence and the lower bound in normalized plots could arise by a combination of chance fluctuations in data.

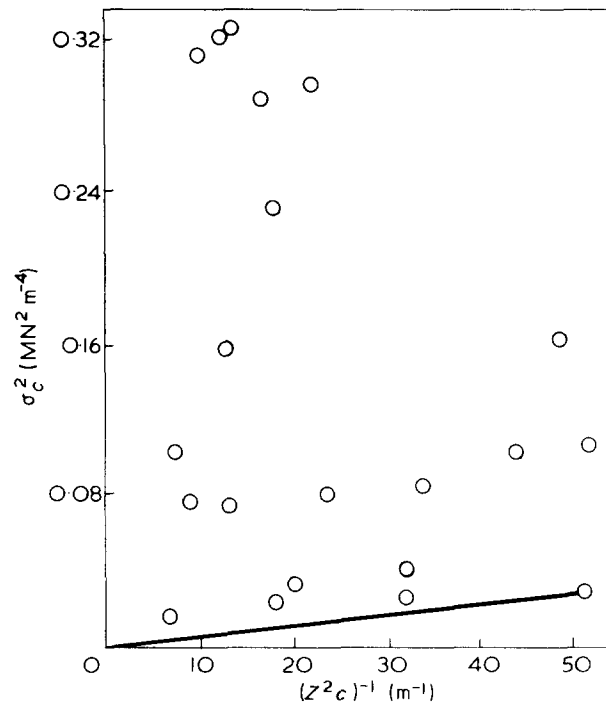


Figure 7  $\sigma_c^2$  against  $(Z^2c)^{-1}$  plot for PMMA and isopropyl alcohol. Line is lower bound to experimental points

#### Data for $\mathcal{F}_0$ and $T_c$

Values for  $\mathcal{F}_0$  obtained from lower-bound slopes are plotted against temperature in Figures 10a, b and c. Figures 10a and 10b show data for methanol, isobutanol, the propyl alcohols, ethanol and carbon tetrachloride whilst Figure 10c shows a wholly similar set of curves

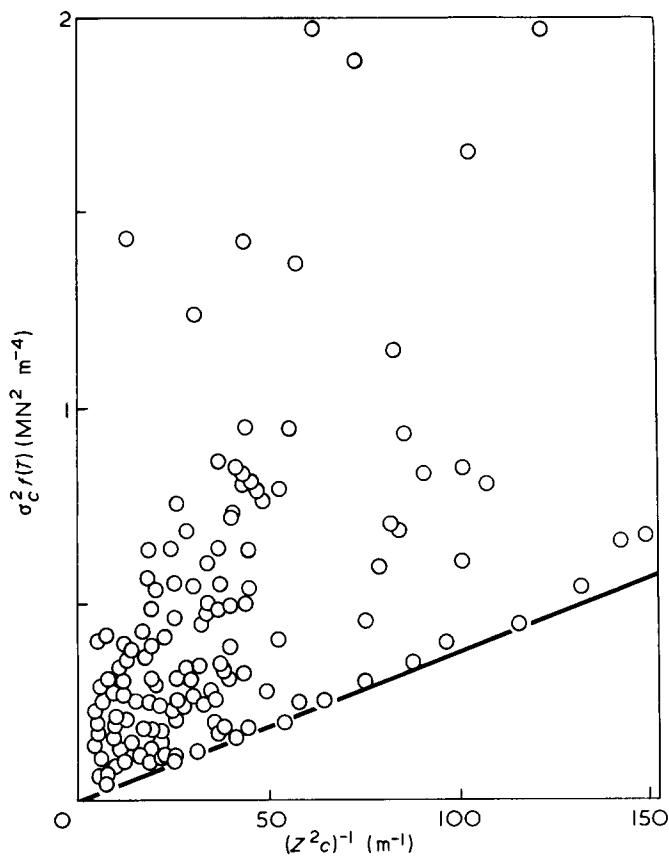


Figure 8 Normalized plots of data for methylated spirit from  $\sigma_c^2$  against  $(Z^2c)^{-1}$  diagrams

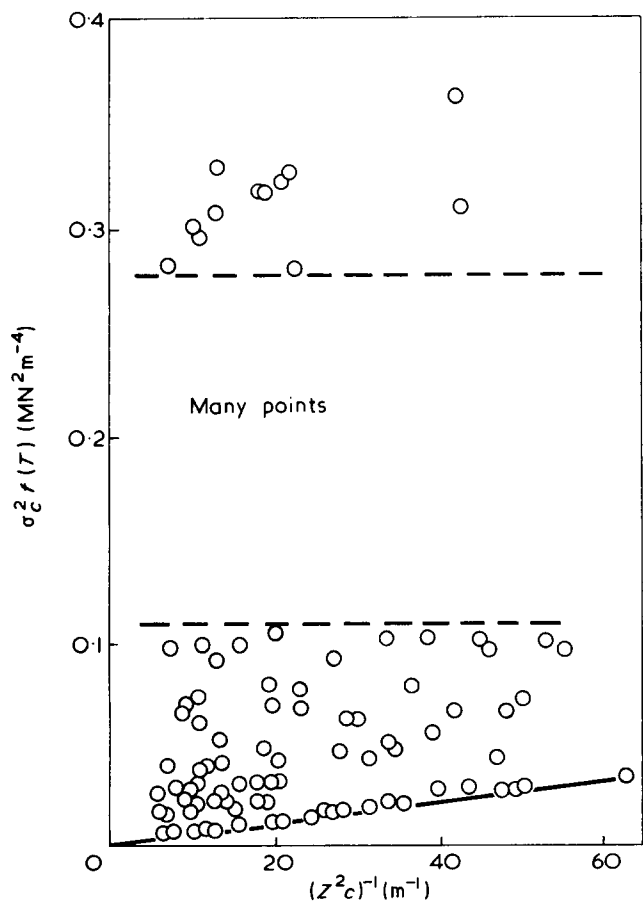


Figure 9 Normalized plots of data for isopropyl alcohol from  $\sigma_c^2$  against  $(Z^2c)^{-1}$  diagrams

using water-isopropanol mixtures. The data for water are given in Figure 11, the value of  $\mathcal{F}_0$  showing no obvious dependence upon temperature.

The characteristic form of the graphs is evident. It confirms the earlier findings of Andrews and Bevan<sup>5</sup> for methylated spirit, though the actual values of  $\mathcal{F}_0$  now reported are much lower than obtained previously.

As the temperature rises,  $\mathcal{F}_0$  decreases rapidly up to a characteristic temperature  $T_c$ , remaining constant thereafter at a value denoted  $\mathcal{F}_0^*$ . Both  $T_c$  and  $\mathcal{F}_0^*$  vary with the solvent, but their variation can be systemized by plotting these parameters against the solubility parameter  $\delta$  of the solvent as shown in Figures 12 and 13. Figure 12 shows that  $\mathcal{F}_0^*$  decreases rapidly as the solubility parameter of the solvent approaches that of the polymer to a broad minimum centred around

$$(\delta_s - \delta_p) = 0$$

Results for both pure solvents and mixtures lie on a single curve. This result is closely analogous to that of Bernier and Kambour<sup>16</sup>, who also found a minimum at  $(\delta_s - \delta_p) = 0$  when the critical strain for surface crazing was plotted against solubility parameter for poly-(phenylene oxide) (PPO). The measurements cannot be directly compared, however, since  $\mathcal{F}_0^*$  is the value above  $T_c$ , which differs according to solvent, whilst Bernier and Kambour's results were at constant temperature. Furthermore there is no direct relationship between  $\mathcal{F}_0$  and critical strain. It is not surprising, therefore, that the minimum for  $\mathcal{F}_0^*$  is broad in contrast to a very sharp minimum in the PPO results. If we plotted  $\mathcal{F}_0$  at a constant temperature against  $\delta$ , instead of  $\mathcal{F}_0^*$ , the characteristic temperature effect would lead to a much sharper minimum in our results also.

The behaviour of  $T_c$  for pure solvents is shown in Figure 13 where it is seen to increase with decreasing  $(\delta_s - \delta_p)$ . The increase is rapid and can be extrapolated to the glass transition of PMMA (383K) at  $\delta_s = \delta_p$ . The significance of this will emerge later. One interesting point is that  $T_c$  for water-alcohol mixtures (Figure 10c) does not behave in the same way. The point for 90% isopropanol fits on the pure solvent curve of Figure 13 and the point for 75% shows a tendency to do so, but thereafter  $T_c$  begins to rise again as  $(\delta_s - \delta_p)$  increases. The fact that mixtures and pure solvents behave similarly in respect of  $\mathcal{F}_0^*$  but not in respect of  $T_c$  is significant and will be referred to in the discussion.

### THEORETICAL

Most polymeric glasses are non-strain hardening, elastic-plastic solids at temperatures not too far below  $T_g$ . Even where macroscopically brittle behaviour prevails the material often yields on the small scale appropriate to a crack or craze tip. Consider therefore a crack or narrow slit perpendicular to a uniaxial stress field in an elastic-plastic solid with infinite extensibility. If plane stress conditions apply, as in a very thin sheet of material, propagation takes the form of a narrow axial plastic zone<sup>17</sup>, but in plane strain, e.g. in the centre of a thick sheet, the elastic constraint of the unyielded material prevents plastic deformation on the axis at any significant distance ahead of the crack tip. A symmetrical plastic zone, therefore, usually develops and grows until its diameter is commensurate with the sheet



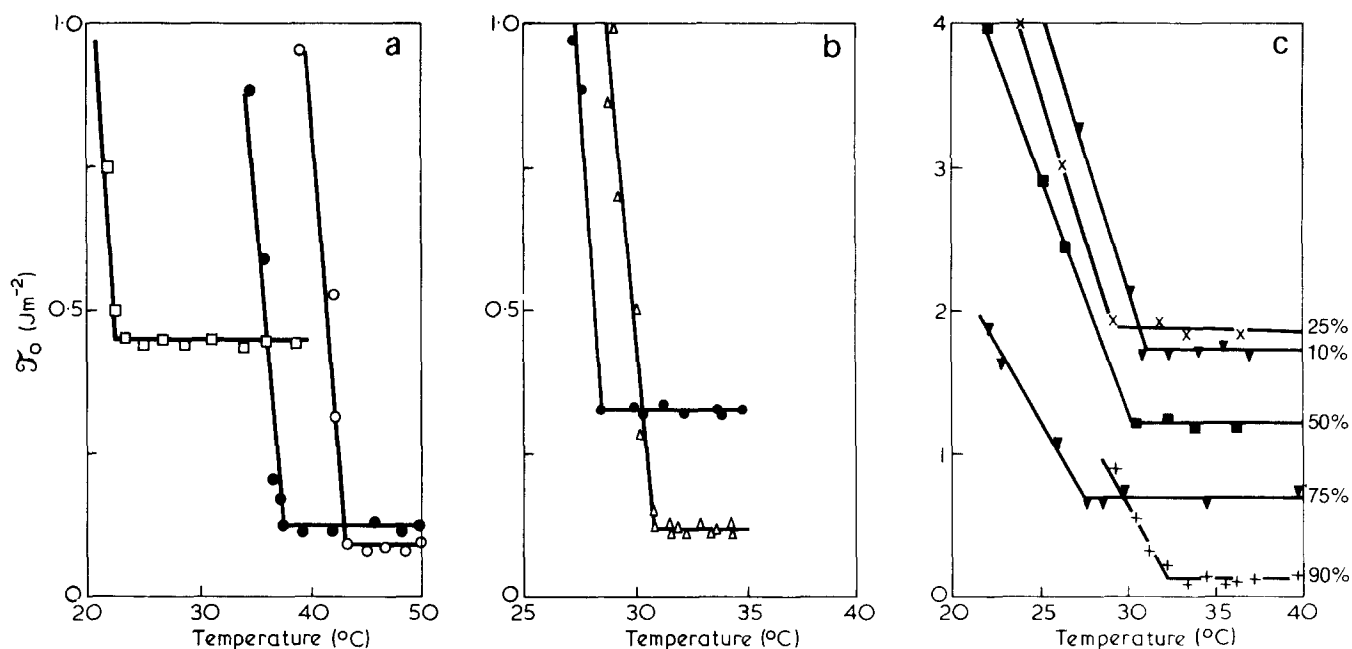


Figure 10  $\mathcal{T}_0$  as a function of temperature for PMMA in (a) methanol ( $\square$ ), isobutanol ( $\circ$ ), carbon tetrachloride ( $\bullet$ ), (b) ethanol ( $\bullet$ ), n-propyl and isopropyl alcohols ( $\triangle$ ) and (c) water/isopropanol mixtures (numbers give % isopropanol)

thickness, at which point the plane strain condition is relieved.

There is, however, one circumstance under which a narrow axial plastic zone can develop under plane strain conditions, viz. if cavitation can occur in the solid. Cavitation enables the highly stressed material to deform plastically (i.e. by large amounts) in the direction of the applied stress without requiring lateral contraction of the deforming mass. Since it is this lateral contraction which is normally prevented by elastic constraint under plane strain, the cavitation effectively restores a 'plane stress' situation, and a narrow axial plastic zone is again able to form, however thick the sheet.

The resulting propagation zone is therefore a narrow plastic zone of cavitated material coplanar with the starter crack, i.e. a craze.

The necessary condition for craze formation is therefore the ability of the material to undergo cavitation at stresses lower than are required to enlarge the plastic zone symmetrically. This criterion for craze formation will now be developed quantitatively.

#### Conditions for cavitation of an elastic-plastic solid

Consider an infinite elastic-plastic solid, with its boundaries subjected to a hydrostatic tensile stress,  $p$ , and containing a spherical cavity of radius,  $r$ . If the material is incompressible, the conditions for equilibrium are identical to those for the case where a positive pressure,  $p$ , acts within the cavity and the material is unstressed at infinity, since the transformation from one case to the other is accomplished by superposition of a uniform hydrostatic stress field.

Enlargement of the cavity by plastic flow under the pressure  $p$  is inhibited by: (i) the resistance to plastic flow, characterized by the tensile yield stress  $Y$ ; and (ii) by surface tension forces in the cavity wall. Neglecting surface tension effects, Hill<sup>18</sup> has shown that a cavity of radius  $r$  will grow continuously in an elastic-plastic solid under a constant internal pressure  $p$  providing that:

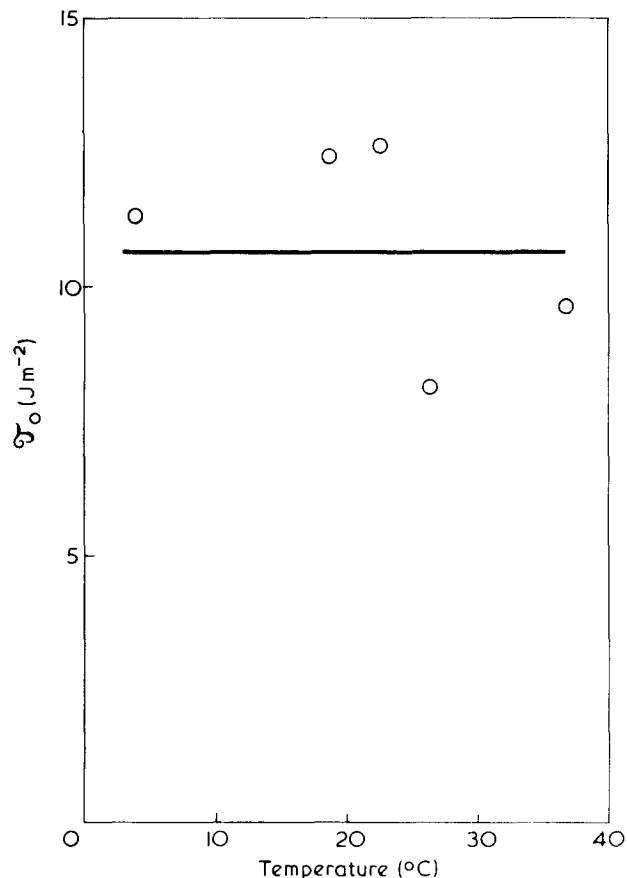


Figure 11  $\mathcal{T}_0$  as a function of temperature for PMMA in water

$$p > \frac{2Y}{3} \left\{ 1 + \ln \left( \frac{E}{3(1-\nu)Y} \right) \right\} \equiv \frac{2Y}{3} \psi \quad (7)$$

where  $\nu$  is Poisson's ratio. The variation of  $\psi$  with  $Y$  is slow, and  $\psi$  will be considered constant to a first approximation. The effect of this on the ensuing calculation is small and is discussed later. The surface tensional resistance is, of course,  $2\gamma/r$  where  $\gamma$  is the interfacial tension between the solvent in the void and the surrounding polymer, so that, at equilibrium:

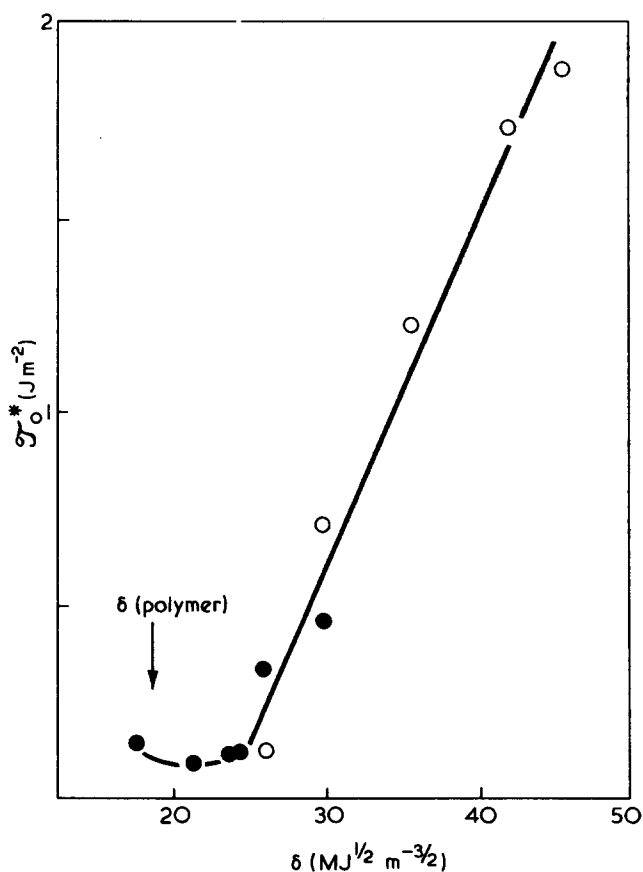


Figure 12 Variation of  $\mathcal{F}_0^*$  for PMMA with solubility parameter of the solvent. (●) pure solvents, (○) water/isopropanol mixtures

$$p = 2\gamma/r + 2Y\psi/3 \quad (8)$$

The work done by the internal pressure (or by the external hydrostatic tension) in enlarging the cavity from a volume  $v_0$  to a volume  $v$  is, under quasi-static conditions:

$$w = \int_{v_0}^v p dv = 3\gamma \left(\frac{4\pi}{3}\right)^{1/3} (v^{2/3} - v_0^{2/3}) + \frac{2Y\psi}{3} (v - v_0) \quad (9)$$

If  $v \gg v_0$

$$w = 4.84\gamma v^{2/3} + 0.67\psi v Y \quad (10)$$

Consider unit area of craze, of thickness  $h$  and void fraction  $f$ , containing a total of  $N$  uniformly sized voids. The total work of void formation within this region can then be expressed as:

$$Nw = 4.84\gamma Nv^{2/3} + 0.67\psi Nv Y \quad (11)$$

Or, since  $Nv = hf$ :

$$Nw = 4.84\gamma h^{2/3} f^{2/3} N^{1/3} + 0.67\psi hf Y \quad (12)$$

Assuming that the work of void formation forms the major contribution to the minimum surface work  $2\mathcal{F}_0$  per area of surface (two surfaces involved) we obtain:

$$\mathcal{F}_0 = 2.42\gamma(hf)^{2/3} N^{1/3} + 0.33 Y\psi hf \quad (13)$$

If  $\rho$  is the mean distance between void centres in the fully developed craze:

$$\left(\frac{N}{h}\right)^{1/3} \approx \rho^{-1}$$

since  $N/h$  is the number in unit volume, so that:

$$\mathcal{F}_0 = 2.42(h\gamma/\rho)f^{2/3} + 0.33 Y\psi hf \quad (14)$$

### DISCUSSION

Equation (14) is based on the following assumptions: (i) that the threshold or minimum surface work for crack or craze propagation is the quasi-static work of formation of the craze matter by cavitation; and (ii) that the material in the crazing region can be considered ideally elastic-plastic. Both of these assumptions are reasonable and a comparison of the equation with experimental data is thus in order. None of the quantities in the equation are unknown in an absolute sense, being susceptible of measurement, but it must be remembered that  $Y$  and  $E$  refer to the tip region which is probably plasticized by diffusion of the solvent under the high stresses obtaining there. Furthermore the interfacial tension  $\gamma$  will be that between plasticized polymer and solvent, since the latter will presumably fill, by diffusion, any cavities formed and little numerical data are available for such quantities. A precise quantitative test of the theory is therefore not possible at this stage, but a semi-quantitative evaluation shows a good fit with experimental data for reasonable values of the parameters.

### Temperature dependence of $\mathcal{F}_0$

The equation for  $\mathcal{F}_0$  contains two terms depending respectively upon  $\gamma$  and  $Y$ . The first of these will vary only slowly with temperature whereas the fall of yield stress with rising temperature in glassy plastics is well documented. The yield stress vanishes at the glass transition temperature, so that  $\mathcal{F}_0$  should be independent of temperature at  $T > T_g$ . It is proposed that

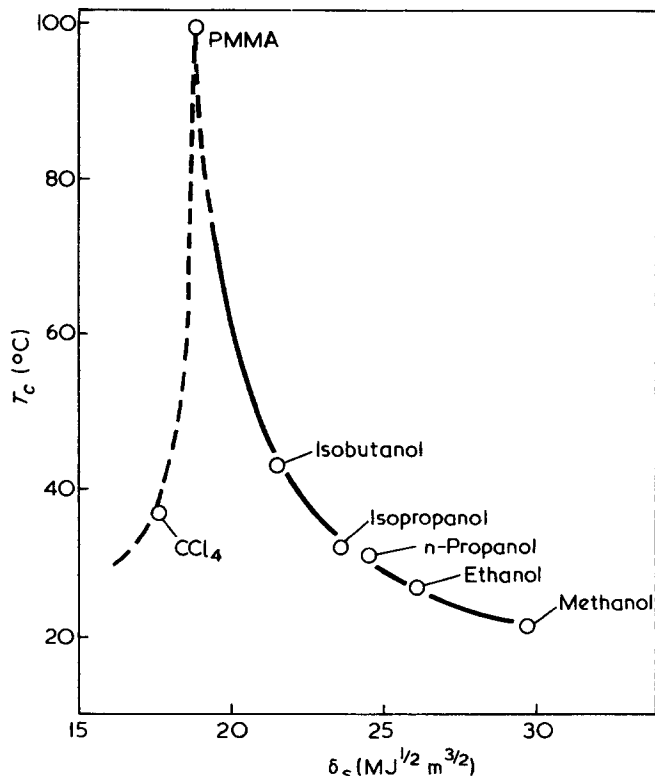


Figure 13 Variation of  $T_c$  with solvent solubility parameter

this effect gives rise to the 'characteristic temperature' phenomenon and that  $T_c$  is, in fact, the glass transition temperature of the solvated region at the tip of the discontinuity.

Depression of  $T_g$  by swelling with organic solvents is a well-known phenomenon, and subsidiary experiments on the yield stresses of swollen PMMA (refluxed in the alcohols used in this study) have shown that the swollen polymer has  $T_g$  values in the region of  $T_c$  (Andrews, Levy and Willis, to be published). Such data cannot be used uncritically, since (a) the tip region is under stress and may absorb more solvent than unstressed material, and (b) the solvent content of the tip region may be kinetically controlled and not achieve an equilibrium value.

In spite of these reservations there appear to be strong similarities between the plasticized bulk polymer and the material at the craze tip. Plots of  $T_g$  (defined by  $Y=0$ ) for plasticized PMMA in a given alcohol, against the characteristic temperature  $T_c$  obtained in the same solvent are shown in Figure 14 for a range of such solvents. Each plot relates to a given volume fraction  $\phi_2$  of polymer, and the curve for  $\phi_2=0.69$  gives a reasonably close fit to the condition  $T_c=T_g$ . Precise agreement can be obtained by allowing  $\phi_2$  to vary from 0.67 for methanol to 0.70 for n-propanol and about 0.80 for n-butanol.

Differentiation of equation (14), assuming  $d\gamma/dT=0$ , gives:

$$\frac{d\mathcal{F}_0}{dT} = 0.33hf \frac{dY}{dT} \psi + \frac{d\psi}{dT} Y \quad (15)$$

The term  $Y(d\psi/dT)$  is small, affecting results by only 10%, and will be ignored in what follows.

The value of  $dY/dT$  for appropriate  $\phi_2$  values can be obtained from the data already referred to. This gradient is constant, for a given solvent and  $\phi_2$  value, for temperatures below  $T_g$  except over the range  $0 < (T_g - T) < 3K$ . In this region  $dY/dT$  increases rapidly becoming infinite at  $T=T_g$ . The relevant value of  $dY/dT$  for comparison with  $d\mathcal{F}_0/dT$  values will be taken as the constant value measured in the range  $(T_g - T) > 3K$  which gives:

$$\frac{dY}{dT} \approx -0.5 \text{ MN m}^{-2} \text{ K}^{-1}$$

for all solvents and for  $\phi_2 \sim 0.6-0.8$ .

The parameters  $\psi$ ,  $h$  and  $f$  are also required to obtain a theoretical estimate of  $d\mathcal{F}_0/dT$ . The parameter  $\psi$  varies slowly with temperature, both for plasticized and unplasticized material and lies within the range  $3.8 < \psi < 5.0$  over the temperature interval 273K to 323K, and the mean value of 4.4 will be adopted.

The quantities  $h$  and  $f$  define the physical structure of the craze and are experimentally accessible. Kambour<sup>19</sup> has shown that the void fraction  $f$  for PMMA is some 0.4. Craze thickness  $h$  is less well defined and is known to vary widely as conditions change. In the present work, independent optical measurements of craze thickness were made under the appropriate conditions of load, temperature and solvent system. The craze appears as a fine black line in transmitted light and has a thickness near the craze tip of the order of 1  $\mu\text{m}$  or less, a limit to the measurement being set by the resolution of the microscope and by diffraction effects. The craze widens at larger distances from the tip, but since  $\mathcal{F}_0$

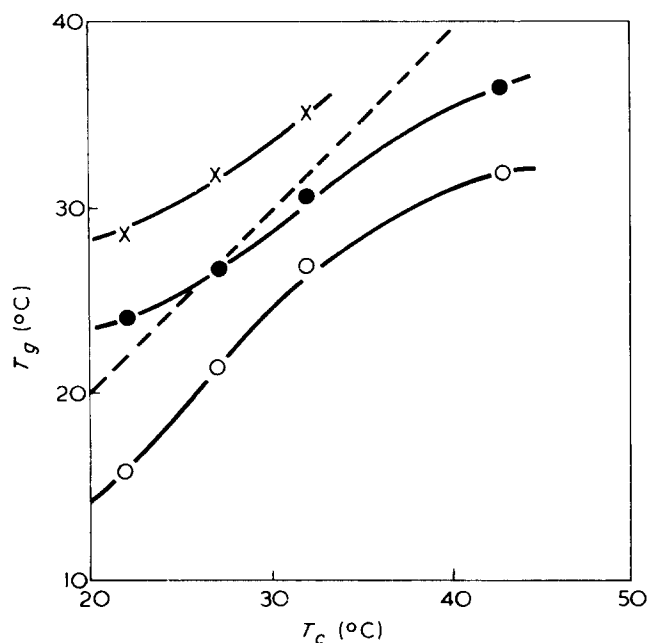


Figure 14 Plots of  $T_g$  (for a given fraction  $\phi_2$  of polymer) against  $T_c$ . ----, 1 : 1 relation. ○,  $\phi_2=0.62$ ; ●,  $\phi_2=0.69$ ; ×,  $\phi_2=0.79$

refers to incipient crazing, the appropriate value of  $h$  should be that close to the newly formed tip. Replicas of the specimen surface examined in the electron microscope show the craze width to be 0.85  $\mu\text{m}$  in this region.

Using  $h=0.85 \mu\text{m}$ , and the values adopted earlier for  $\psi$  and  $f$ , a theoretical value for  $d\mathcal{F}_0/dT$  of  $-0.48 \text{ J m}^{-2} \text{ K}^{-1}$  is obtained compared with  $-0.2$  to  $-0.4 \text{ J m}^{-2} \text{ K}^{-1}$  from experimental data. Considering the uncertainties in the values of  $h$  and  $\psi$ , this order-of-magnitude agreement is quite acceptable.

The temperature independent region  $\mathcal{F}_0 = \mathcal{F}_0^*$

Above  $T_c$  (i.e.  $T_g$  of the plasticized polymer),  $Y$  is zero and:

$$\mathcal{F}_0 = \mathcal{F}_0^* = 2.42(h\gamma/\rho)f^{2/3} \quad (16)$$

Using the quoted values for  $h$  and  $f$  this becomes

$$\mathcal{F}_0^* = 1.15 \times 10^{-6} \gamma/\rho$$

The mean distance between void centres,  $\rho$ , was not determined in the present work, but published data<sup>6, 20</sup> favour a value of the order of 0.1 to 0.25  $\mu\text{m}$ . These figures are almost certainly too high since they refer to the developed craze in which originally separate voids have coalesced. The relevant value for our purpose is the void separation during the early stages of the process of formation.

Kambour (personal communication) has obtained sections of crazes in various polymers which include the extreme tip region, and here the spacing of voids is something like half that in the developed craze, e.g. 0.05  $\mu\text{m}$ . We shall therefore use this lower figure, giving:

$$\mathcal{F}_0^* = 23\gamma \quad (17)$$

The results shown in Table 2 are then obtained for  $\gamma$  using the known  $\mathcal{F}_0^*$ .

Because both polar and dispersion forces operate at the interface between alcohols and PMMA, it is difficult to calculate a reliable theoretical value for  $\gamma$ , the interfacial tension between solvent and polymer. An upper value for  $\gamma$  is, of course, given by the Young equation:

$$\gamma = \gamma_s - \gamma_L \cos \theta$$

allowing  $\theta \rightarrow 0^\circ$ , where  $\gamma_s$ ,  $\gamma_L$  are the surface energies of the solid and liquid respectively, and such upper values are given in Table 2. Quite good agreement is obtained for the lower alcohols, but results for the more compatible solvents do not correlate. This can plausibly be attributed to the fact that the polymer is swollen, so that  $\gamma_s$  is not that for dry PMMA. As  $(\delta_s - \delta_p) \rightarrow 0$ , a decrease in  $\gamma$  would then be expected since both  $\gamma$  and  $(\delta_s - \delta_p)$  are measures of the intermolecular forces operating across the solvent/polymer interface.

It is now possible, finally, to explain why water-alcohol mixtures behave similarly to pure solvents in respect of  $\mathcal{T}_0^*$  but not in respect of  $T_c$ . The former parameter is governed, according to our theory, by the interfacial tension between the liquid and the swollen polymer and is thus expected to change progressively with  $(\delta_s - \delta_p)$  as observed. The characteristic temperature is, in contrast, controlled by the state of swelling of the polymer by the solvent, the latter being present as a molecular dispersion in the solid and not as a separate phase. The diffusion behaviour and compatibilities of alcohol and water in PMMA are quite disparate and only the former will penetrate the polymer in any significant quantity. The plasticizing effects of an alcohol-water mixture will therefore be mainly those of the alcohol and the depression of  $T_g$  caused thereby will be similar to that produced by the pure alcohol. A small amount of water can, of course, enter the polymer and this would explain why the mixtures with low water content agree with the pure solvent data.

## CONCLUSION

Although it is difficult to test the theory in a precisely quantitative manner, order-of-magnitude calculations establish that the theory is physically plausible whilst its qualitative predictions are in excellent agreement with observation. To summarize, therefore, the threshold conditions observed for craze formation are attributed to a cavitation criterion which involves both the work necessary to produce plastic yielding and that necessary to create the void interfaces. The first of these contributions is strongly temperature dependent whilst the latter is not and this gives rise to a characteristic shape for the curve of  $\mathcal{T}_0$  against temperature. An important step in the argument is the identification of the tip region as a solvent plasticized region, containing 60 to 80% polymer by volume, which is a precursor of the craze matter itself.

Table 2 Values of  $\gamma$  in different solvents

Solvent	$\gamma \times 10^{-3}$ (J m <sup>-2</sup> )	$\gamma_s - \gamma_L$
Methanol	19.7	17.4
Ethanol	13.8	17.2
Propyl alcohols	5.0	16.2
Butanol	3.5	15.4

The practical implications of this work are as follows: (i) temperature is a vitally important parameter in solvent-stress crazing and should be included as a variable in all tests for crazing behaviour; (ii) the crazing behaviour of a glassy polymer in solvents follows a pattern dictated by the difference  $(\delta_s - \delta_p)$  in solubility parameters and by the swelling propensities of the solvent for the polymer (affecting the yield stress of the solvated tip region).

These results are in good agreement with the conclusions of Bernier and Kambour<sup>16</sup> who studied the effects of solvent solubility parameter and interfacial energy up to the critical strain for crazing of poly(2,6-dimethyl-1,4-phenylene oxide). The present work goes considerably further, however, in investigating temperature dependence and in defining the actual mechanism of solvent induced crazing in glassy plastics.

## REFERENCES

- 1 Braden, M. and Gent, A. N. *J. Appl. Polym. Sci.* 1960, **3**, 90
- 2 Braden, M. and Gent, A. N. *J. Appl. Polym. Sci.* 1960, **3**, 100
- 3 Braden, M. and Gent, A. N. *J. Appl. Polym. Sci.* 1962, **6**, 449
- 4 Gent, A. N. and Hiraikawa, H. *J. Polym. Sci. (A-2)* 1968, **6**, 1481
- 5 Andrews, E. H. and Bevan, L. 'Physical Basis of Yield and Fracture', Institute of Physics, London, 1966, p 209
- 6 Marshall, G. P., Culver, L. E. and Williams, J. G. *Proc. R. Soc. (A)* 1970, **319**, 165
- 7 Kambour, R. P. *Polym. Eng. Sci.* 1968, **8**, 281
- 8 Irwin, G. R. *Eng. Fract. Mech.* 1968, **1**, 214
- 9 Griffith, A. A. *Phil. Trans. R. Soc. (A)* 1921, **221**, 163
- 10 Rivlin, R. S. and Thomas, A. G. *J. Polym. Sci.* 1953, **10**, 291
- 11 Andrews, E. H. 'Fracture in Polymers', Oliver and Boyd, London, 1968
- 12 Brown, W. E. and Srawley, J. E. *ASTM Spec. Tech. Publ.* 1967, p 410
- 13 Inglis, C. E. *Trans. Inst. Nav. Archit.* 1913, **55** (1), 219
- 14 Murray, J. and Hull, D. *Polymer* 1969, **10**, 451
- 15 Atkinson, J. R. and Faulker, P. G. *J. Appl. Polym. Sci.* 1971, **15**, 209
- 16 Bernier, G. A. and Kambour, R. P. *Macromolecules* 1968, **1**, 393
- 17 Dugdale, D. S. *J. Mech. Phys. Solids* 1960, **8**, 100
- 18 Hill, R. 'The Mathematical Theory of Plasticity', Oxford University Press, 1950, p 104
- 19 Kambour, R. P. *J. Polym. Sci. (A-2)* 1964, p 4159
- 20 Zhurkov, S. N., Kuksenko, V. S. and Slutsker, A. I. *Proc. 2nd Int. Conf. Fracture* 1969, p 531

# Elastic behaviour of rubber under small uniaxial extension and compression

F. P. Wolf\*

*Department of Chemistry, University of Manchester, Manchester M13 9PL, UK  
(Received 25 October 1971; revised 11 January 1972)*

An apparatus has been designed which allows measurement of the length of a lightly crosslinked rubber sample in relation to the acting force from the range of small uniaxial elongation to small uniaxial compression, passing through the undeformed length, in one experiment. Elongation ratios  $0.88 \leq \lambda \leq 1.18$  have been produced at 20°C and 40°C. An accurate determination of the unstrained length has been achieved. The results show Gaussian behaviour for this range without any discontinuity at  $\lambda=1$ . Some additional data at higher elongation continue the measurements up to  $\lambda=1.73$  and are in good agreement with those of other investigators. Mooney–Rivlin plots are linear for  $\lambda > 1.1$  but tend to flatten in the transition to compression.

## INTRODUCTION

In recent years a large amount of work has been done in investigating the relative energy contribution,  $f_e$ , to the retractive force,  $f$ , of rubber specimens stretched to various degrees. Considerable discrepancies appear frequently in the range of small elongations. These are caused by the difficulty in determining the unstrained length of the sample exactly. Therefore it seemed to be of interest to examine the elastic behaviour of rubber in the vicinity of the unstrained state, applying uniaxial extension as well as uniaxial compression.

Whereas there is ample documentation of extension measurements in the literature, very few compression experiments have been reported. One of the principal difficulties in performing one-dimensional compression is the tendency of the samples to buckle. Thus, if one end is rigidly fixed, the sample easily bends under the influence of a compressive force. If both ends are fixed, it tends to give way to one side, as has been shown for instance on testing the elastic stability of columns of rubber compression springs<sup>1</sup>. The onset of buckling depends upon the slenderness of the specimens. Therefore only relatively short, thick samples are suitable for compression measurements.

A sample with a diameter of more than twice its length has been compressed up to 32% by Forster<sup>2</sup>. In order to avoid friction between the surfaces of the sample and the pistons of the pressure apparatus, and thus to prevent the sample from assuming a barrel-like shape, a special lubrication system was used. The other way of dealing with the problem is to replace compression by two-dimensional extension, which is basically a similar type of deformation, as long as volume effects are negligible.

Rubber sheets have been inflated to form bubbles with a thickness equivalent to about 97% compression of their original dimension<sup>3–5</sup>. Both these types of experiments are unsuitable for extension measurements.

Treloar<sup>6</sup> points out that compression and extension data should fit one single curve of force against elongation. When converting the data of two-dimensional extension into one-dimensional compression, the experiments<sup>3–5</sup> give curves which show a slight shift against plots fitting one-dimensional extension data, although the slopes at zero coincide. An experiment covering both areas would therefore be of some interest.

The following report describes probably one of the first attempts to measure in one single experiment the relation between the length of a rubber sample and the acting force from the range of small extensive forces through zero to small compressive forces. The idea of the combined experiment was to couple the sample to a set of expanded metal springs. To keep it in the neutral position a force, counteracting the contractile force of the springs, had to be generated by appropriate weights. One-dimensional extension and compression of the sample resulted from changing the amount of weights.

## THEORY

### *Stored energy*

It is generally assumed that the changes of the free energy,  $F$ , of a macromolecular elastic body can be split into two terms<sup>7</sup>:

$$\Delta F = \Delta F_{liq}(T, V) + \Delta F_{el}(T, V, \lambda) \quad (1)$$

The first term accounts for liquid-like intermolecular interactions whereas the second one describes intra-

\* Permanent address: Fritz-Haber-Institut der Max-Planck-Gesellschaft, D1 Berlin 33 (Dahlem) Faradayweg 4-6, Germany.

molecular interactions, i.e. changes of the configurational energy of the macromolecules. To derive a relation between elastic force,  $f$ , absolute temperature,  $T$ , volume,  $V$ , and elongation ratio  $\lambda = L/L_0$  (actual length,  $L$ , divided by unstrained length  $L_0$ ) it is therefore sufficient to regard the term  $\Delta F_{e1}$  only.

There are two approaches which lead to an expression for the change of the free energy that accompanies the elastic deformation of a specimen. One of them uses Gaussian statistics of macromolecular networks and yields<sup>7</sup>:

$$\Delta F_{e1} = A_1(\lambda_1^2 + \lambda_2^2 + \lambda_3^2 - 3) + A_3 \ln(\lambda_1 \lambda_2 \lambda_3) \quad (2)$$

where the  $\lambda_i$  denote the elongation ratios of the specimen in the three principal directions.  $A_1$  and  $A_3$  are independent of the  $\lambda_i$ , and  $A_1$  is expressed as<sup>8</sup>:

$$A_1 = \frac{1}{2} NkT \frac{\langle r_i^2 \rangle}{\langle r_f^2 \rangle} \quad (2a)$$

Here  $N$  is the number of active chains in the network,  $k$  the Boltzmann constant and  $\langle r_i^2 \rangle / \langle r_f^2 \rangle$  the so called front-factor, which takes into account that the mean square end-to-end distance  $\langle r_i^2 \rangle$  of the macromolecules under the conditions of the actual experiment does not normally coincide with the mean value  $\langle r_f^2 \rangle$  for the free macromolecules under the conditions where crosslinking took place.  $A_3$  is regarded to be of similar shape to  $A_1$  despite a numerical factor.

An important assumption is that the mean square end-to-end distance of the crosslinked macromolecules varies according to the geometrical dimensions of the specimen<sup>8</sup>, which means in terms of the volume  $V_0$  of the undeformed specimen:

$$\langle r_i^2 \rangle \sim V_0^{2/3} \quad (2b)$$

The value  $\langle r_f^2 \rangle$  of free chains is implicitly assumed to depend on the temperature  $T$  only. Thermoelastic measurements therefore provide an insight into molecular properties by determining  $d \ln \langle r_f^2 \rangle / dT$ .

The other representation of the elastically stored energy is a function of the strain invariants<sup>9</sup>:

$$\Delta F_{e1} = B_1(\lambda_1^2 + \lambda_2^2 + \lambda_3^2 - 3) + B_2(\lambda_1^2 \lambda_2^2 + \lambda_2^2 \lambda_3^2 + \lambda_3^2 \lambda_1^2 - 3) + B_3(\lambda_1^2 \lambda_2^2 \lambda_3^2 - 1) \quad (3)$$

A comparison between equations (2) and (3) points to  $A_1 = B_1$ . Furthermore  $A_3$  and  $B_3$  are similar apart from a factor 2, as may be shown by expanding the relative volume into a power series:

$$\lambda_1 \lambda_2 \lambda_3 = \frac{V}{V_0} = 1 + \frac{\Delta V}{V_0} \quad (3a)$$

Since in the scope of this paper only uniaxial deformation is considered:

$$\lambda_1 = \lambda = L/L_0 \quad (3b)$$

$$\lambda_2^2 = \lambda_3^2 = \frac{1}{\lambda} \frac{V}{V_0} \quad (3c)$$

#### Force laws

According to thermodynamics infinitesimal changes of the free energy are given by:

$$dF = -SdT - p dV + f dL \quad (4)$$

with entropy  $S$ , pressure  $p$  and refractive force  $f$  of the deformed sample. Force laws are obtained therefore by differentiation of  $\Delta F_{e1}$  with respect to the actual length  $L$  so that Gaussian statistics lead to the force dependence:

$$f \simeq C(\lambda - \lambda^{-2}) \quad (5)$$

where the volume changes  $\Delta V/V_0$  on deformation, which are typically of the order of  $10^{-4}$ , are neglected and

$$C = \frac{NkT}{L_0} \frac{\langle r_i^2 \rangle}{\langle r_f^2 \rangle} \simeq f/(\lambda - \lambda^{-2}) \quad (5a)$$

From the approximation (2b) it follows that  $C$  is proportional<sup>10</sup> to  $V_0^{1/3}$ . Experimental support for this relationship comes from measurements on rubbers swollen by a solvent<sup>11,12</sup>.

Differentiating the series of strain invariants and neglecting the volume changes, the phenomenological Mooney-Rivlin equation is obtained:

$$f \simeq \left\{ C_1 + \frac{C_2}{\lambda} \right\} (\lambda - \lambda^{-2}) \quad (6)$$

Both the approximations (5) and (6) will be used in this paper for the evaluation of experimental data.

Expressions with the volume anisotropy  $\alpha$  instead of  $\lambda$  are quoted frequently, but since only  $\lambda$  is obtained directly in the experiments the approximation  $\alpha \simeq \lambda$  is used normally, which leads to the equivalent of equation (5) or (6). Conversions between different sets of variables are given for instance by Roe<sup>10</sup>.

In this paper theoretical calculations will be confined to the Gaussian approximation (5) of the force law. They are facilitated by an equation similar to that given by Gee<sup>8</sup>:

$$f = \frac{C}{L_0} \left\{ L - \frac{V}{L^2} \frac{L_0^3}{V_0} \right\} = c \left( L - \frac{qV}{L^2} \right) \quad (7)$$

Then  $c = c(T)$  depends on  $T$  only, and  $q$  is a constant, equal to one for cubic samples:

$$q = \frac{L_0^3}{V_0} = \frac{L_0^2}{A_0} \quad (7a)$$

$A_0$  being the cross-sectional area.

#### Young's modulus

If the tension  $\tau$  is calculated from the force  $f$  per unstrained cross-section  $A_0$  of the sample, Young's modulus  $E$  can be evaluated in the vicinity of the unstrained state according to the theory of infinitesimal deformations. Then with  $\lambda = 1 + \epsilon$  and Hooke's law:

$$E \simeq \frac{3C}{A_0} = \frac{3cL_0}{A_0} \quad (8)$$

In the limit  $\lambda = 1$  the shear modulus  $G$  is equal to one third of  $E$ , but since the deformation is mainly longitudinal, and since Poisson's ratio  $m$  in the relation  $E = 2G(1 + m)$  is equal to  $\frac{1}{2}$  only in this limit, the use of the shear modulus should be restricted. With increasing elongation  $m$  diminishes considerably<sup>13</sup>.

### Volume effects

The volume changes which accompany the uniaxial deformation of a sample can be determined on the basis of the force law (7) from

$$\left(\frac{\partial V}{\partial L}\right)_{p, T} = \left(\frac{\partial f}{\partial p}\right)_{T, L} = \frac{cq}{L^2} V \kappa_L \quad (9)$$

with the compressibility at constant length:

$$\kappa_L = -\frac{1}{V} \left(\frac{\partial V}{\partial p}\right)_{T, L} \quad (9a)$$

The compressibility  $\kappa_L$  has been found to be independent of the elongation  $\lambda$  for lightly crosslinked butyl rubber<sup>14</sup>. The same is the case for natural rubber.

Then

$$\left(\frac{\partial \ln V}{\partial \lambda}\right)_{p, T} = \frac{L_0 cq}{L^2} \kappa_L = \frac{\kappa_L}{A_0} \frac{f}{\lambda^3 - 1} \quad (9b)$$

or using the slope of the curve force against length:

$$\left(\frac{\partial f}{\partial \ln L}\right)_{p, T} \approx L \left(\frac{\partial f}{\partial L}\right)_{p, T} = \frac{c}{L^2} (L^3 + 2qV) \quad (9c)$$

$$\left(\frac{\partial \ln V}{\partial \lambda}\right)_{p, T} \approx \frac{\kappa_L}{A_0} \frac{1}{\lambda^3 + 2} \left(\frac{\partial f}{\partial \ln L}\right)_{p, T} \quad (9d)$$

The total amount of the volume change results from integration of equation (9) and yields:

$$\frac{\Delta V}{V_0} \approx \frac{\kappa_L}{A_0} \frac{f}{\lambda + 1 + \lambda^{-1}} \quad (10)$$

An equivalent equation has been given<sup>7, 15</sup>.

### Bulk expansion coefficient

The bulk thermal expansion coefficient at constant pressure and force:

$$\beta_f = \left(\frac{\partial \ln V}{\partial T}\right)_{p, f} \quad (11)$$

can be determined from the linear thermal expansion coefficient at zero force:

$$3\beta_{\ln}(f=0) = 3 \left(\frac{\partial \ln L}{\partial T}\right)_{p, f=0} = \beta_f \quad (11a)$$

where  $\beta_f$  is almost equal to the coefficient  $\beta_L$  measured at constant length:

$$\beta_L = \left(\frac{\partial \ln V}{\partial T}\right)_{p, L} \quad (11b)$$

The latter has been found to be constant<sup>16</sup> within the experimental error of  $\pm 1\%$  up to  $\lambda=2.2$ . Since the relative difference between  $\beta_f$  and  $\beta_L$  is of the order  $10^{-4}$  in the range of moderate elongations either of them can be regarded as being independent of  $\lambda$ .

## EXPERIMENTAL

### Apparatus

The apparatus (Figure 1) consisted of a metal frame (A) from which a metal plate (B) was suspended by means of four metal springs (C) from the upper end. In the centre

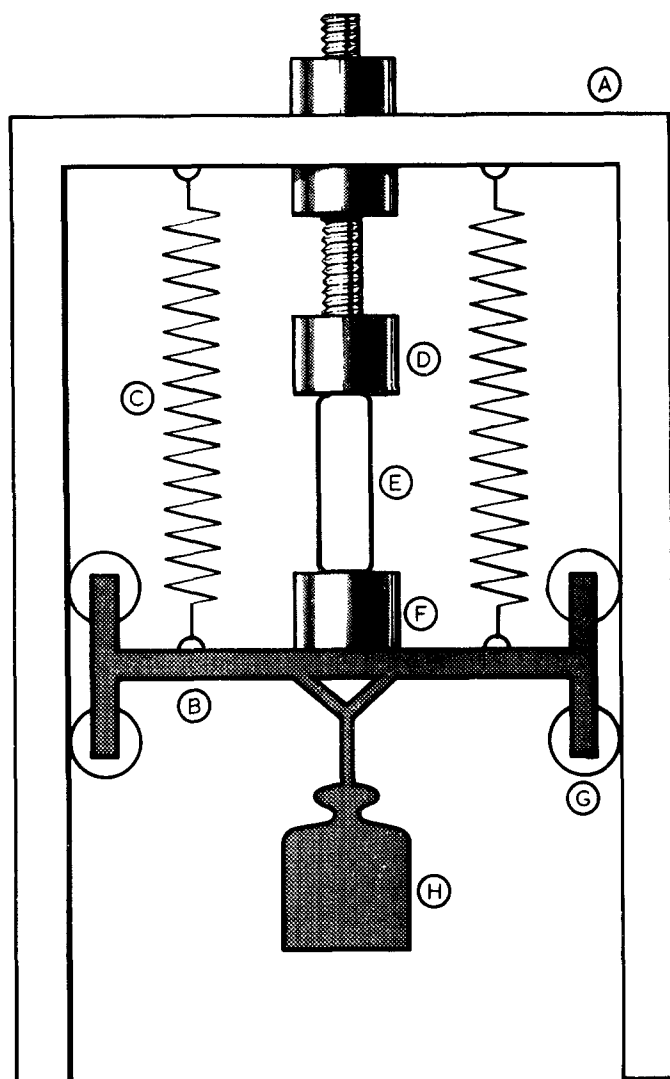


Figure 1 Apparatus with sample under compression

of the top of the frame an adjustable clamp (D) was provided to fix the upper end of the sample (E) rigidly in a vertical position. The lower end of the sample was clamped (F) to the centre of the metal plate, so that it could move in a vertical direction together with the plate. The latter was guided by ball bearings (G) which, to avoid mechanical friction, hardly touched the vertical parts of the frame, but prevented the plate from tilting. Furthermore, tilting would have produced a counteracting moment of the springs.

The sample was compressed by the contractile force of the springs to the maximum amount of uniaxial compression, which then could be decreased and even converted into uniaxial elongation by hanging weights (H) from a hook in the centre of the metal plate. The retractive force of the springs was calibrated against their length at different temperatures using reference marks on the clamps provided for the sample. Excellent linearity was obtained at each temperature, though the measurements were somewhat time-consuming due to hysteresis effects. When the sample was connected to the metal plate, these effects became negligible. The device of coupling the sample to a set of contractile springs produces a result

intermediate between creep and stress relaxation. In elongation for instance creep leads to an increase of the length of the sample, which automatically enlarges the contractile force of the springs and thus gradually reduces the acting force; in compression the effects are reversed. Thus smaller creep is achieved at the cost of some stress relaxation.

The frame with the sample was housed in an air thermostat made of expanded polystyrene with a double-glazed window. To minimize temperature differences in the thermostat, an air blower and heater, controlled by a contact thermometer, was provided.

To read the length of the sample a cathetometer was used. Its accuracy was improved by a number of minor additional devices, which amongst others prevented backlash. Thus measurements of any mark were reproducible with an error of less than  $\pm 0.001$  cm, which improved normal readings of that kind<sup>15, 17, 18</sup> considerably. Since lighting was found to increase the temperature of the sample, a low-voltage spot light, travelling together with the telescope of the cathetometer, was used to light up just a small area for the time necessary to take a reading.

### Sample

Lightly crosslinked natural rubber was used in the experiment. The curing conditions were 45 min at 140°C for dicumyl peroxide and the average molecular weight between crosslinks (as determined by swelling in benzene) was 7500<sup>11</sup>. The sample was a rod 1.27 cm in diameter and 4.2 cm in length, bonded to mild steel end-pieces to facilitate clamping<sup>17</sup>. All measurements were taken on this sample because of the difficulty of getting consistent values when using different samples<sup>19</sup>. At about 0.4 and 0.8 cm from either end reference marks were fixed to the sample in a way similar to that described by Mark and Flory<sup>18</sup>. The distance between the outer pair of marks was then about 3.4 cm in the undeformed state and between the inner pair about 2.6 cm. The arrangement of two sets of reference marks is useful because it helps to detect any appearance of inhomogeneous deformation caused by the rigid connection of the sample to the steel end-pieces. From observation it appeared that non-uniform deformation was limited to a portion of about 0.2 cm from either end in extension as well as in compression.

As mentioned before, only rather short, thick samples can be employed for compression measurements. The sample under investigation could be compressed without buckling to about 85% of its undeformed length. Therefore the range to be covered by measurements was limited to approximately 15% deformation in either direction.

Since the upper end of the sample was fixed to the frame, a force equal to half its weight was regarded as acting at its centre of gravity in addition to any other weight. This, together with the lower steel end-piece and a bolt amounted to 26.2 g.

### Measurements

The distances between both pairs of marks were measured directly by means of the cathetometer, which type of measurement was expected to yield a higher degree of accuracy than any transducer method, and to be preferable with regard to non-uniform deformations at the

ends of the sample. The position of each mark was first read three times while shifting the vernier each time and averaged if necessary. After the positions of all marks, including the reference marks for the elongation of the springs, had been read this way, the whole cycle was repeated. Thus 36 readings, taking about 15 min, led to the determination of three length differences: one for either set of marks and one for the elongation of the springs. The reproducibility of these lengths between both cycles was  $\Delta \leq 0.001$  cm.

The force was calculated from the weights suspended from the plate. 26.2 g were added as mentioned above, then the contractile force of the springs according to their actual length had to be subtracted. Maximum compression and elongation were achieved by forces of about  $\pm 2250$  g. The force was changed normally in steps of 200 g or less. Then at least 20 min were allowed to establish mechanical equilibrium. Readings were taken starting from zero force and from both maximum forces of either sign. In the vicinity of zero force more readings were taken changing the force in smaller steps than in the region of the maximum forces. After any direct change from zero force to one of the maximum forces or *vice versa* the sample was allowed to relax at least for one day. Extension and compression were produced alternately and at two different temperatures. All these measurements were reproducible to within less than 0.1%.

Except during the measurements the sample was kept at approximately zero force all the time. No chemical relaxation could be detected, which had been found to become important at temperatures above 80°C, but to account for the failure to reach equilibrium even at much lower temperatures<sup>20</sup>.

After the measurements at small deformations had been finished, the metal plate, which limited extension to about 18% was removed from the frame, and some single measurements were carried out at higher elongation ratios up to  $\lambda = 1.73$ . Since it becomes more difficult to reach mechanical equilibrium without the contractile springs, several hours up to one day were allowed for relaxation before any length was measured. Scattering between values read with increasing or decreasing load was found to be less than  $\pm 0.1$ %.

The temperature was read to 0.1°C from a thermometer, placed inside a dummy specimen. It was proved that the temperature could be held constant within  $\pm 0.1$ °C at the actual measuring temperatures 20° and 40°C.

## RESULTS

Altogether 115 data points of length against force were obtained for each pair of marks from the measurements made at 20°C. Similarly, 91 points were taken at 40°C. To fit them, 4th degree polynomials were calculated by a least-square method computer program. Since the range of  $\lambda$  for all these data was between 0.88 and 1.18 this will be called 'small deformations'. A similar method has been used<sup>21</sup> for data in the range  $1.1 < \lambda < 2.0$  to extrapolate the unstrained length, but even so a correction of about 1% had to be made for  $L_0$ . For the inner and outer pair of marks curves of almost identical shape were obtained. No points of inflection could be detected, which proved



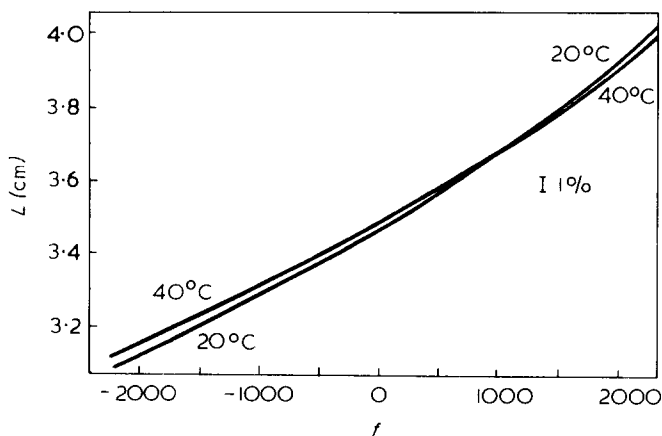


Figure 2 Length (*L*) between outer marks against force (*f*)

that there had been no buckling in the compression range.

Apart from these data for small deformations, single readings at higher elongation ratios were taken for 5 different forces at both temperatures. The lowest of these forces was chosen to be still in the range of small deformations. Excellent consistency between these values for 'moderate deformations' and those for small deformations was found.

The computer calculations showed that the standard deviation for a single measurement was about 0.03%. Hardly any point had a deviation of more than 0.1%. Since in the vicinity of zero force there were at least 10 data, the determination of  $L_0$  could be expected to be accurate to 0.01%. A change of  $\pm 0.1^\circ\text{C}$  in temperature, which would influence  $L_0$  to about  $\pm 0.002\%$  is implicitly contained in this assessment.

The curves for one pair of marks are shown in Figure 2. The following undeformed lengths in cm were calculated:

	Temperature	Inner marks	Outer marks
$L_1$	(20.0)	2.664 77 $\pm 0.01\%$	3.477 44 $\pm 0.01\%$
$L_2$	(40.0)	2.676 68 $\pm 0.01\%$	3.492 31 $\pm 0.01\%$

Whether the accuracy really is of that order can be tested by evaluating the bulk thermal expansion coefficient  $\beta_f$ . According to equation (11a) the coefficient  $\beta_f$  is obtained from:

$$\beta_f = 3\beta_{lin} = 3 \cdot \frac{L_2 - L_1}{10(L_2 + L_1)}$$

Even with the accuracy of the undeformed lengths the error in the difference ( $L_2 - L_1$ ) turns out to be about 3.2%. Thus the following  $\beta_f [\times 10^{-4} \text{ deg}^{-1}]$  are evaluated, which coincide within the limits of their experimental error:  $6.69 \pm 0.21$  for inner marks and  $6.40 \pm 0.21$  for outer marks. The average of  $\beta_f = 6.55 \times 10^{-4} \text{ deg}^{-1}$  is in excellent agreement with the value obtained by Allen, Bianchi and Price<sup>16</sup> for a similar rubber.

The polynomials  $L(f)$  were used to plot some graphs. Figure 3 reproduces the Gaussian plot of force against  $(\lambda - \lambda^{-2})$  at 20°C according to equation (5). As expected, this plot represents the elastic behaviour fairly closely in the range of small deformations  $0.88 < \lambda < 1.18$ . The data taken at moderate elongation fit the same curve but

deviate much more from the tangent to the curve at  $\lambda = 1$ . Figure 4 gives the Gaussian plot at 40°C for the range of small deformations on a larger scale.

From the slopes at  $\lambda = 1$  the following values of the factor  $C$  as in equation (5a) are obtained, where the data originating from the inner marks are given first and those from the outer marks in brackets:  $C(20^\circ) = 5804 [5765] \text{ g}$  and  $C(40^\circ) = 6119 [6065] \text{ g}$ . According to equation (8) Young's modulus amounts to:  $E(20^\circ) = 1.340 [1.349] \times 10^7 \text{ dynes/cm}^2$  and  $E(40^\circ) = 1.410 [1.422] \times 10^7 \text{ dynes/cm}^2$ . The difference between the results for either set of marks is less than 1%.

To represent the results of moderate elongations the Mooney-Rivlin plot is more appropriate. It is drawn for 20°C and 40°C in Figure 5. Since in the vicinity of zero force this plot is extremely sensitive to even minute errors in the length measurements, it is not surprising that the computer data for small deformations lead to curves rather than straight lines.

Another test of the experimental data comes from the evaluation of volume changes due to elastic deformation. The dilation coefficient at both temperatures as evaluated by means of equations (9b and d) is represented in Figure 6.

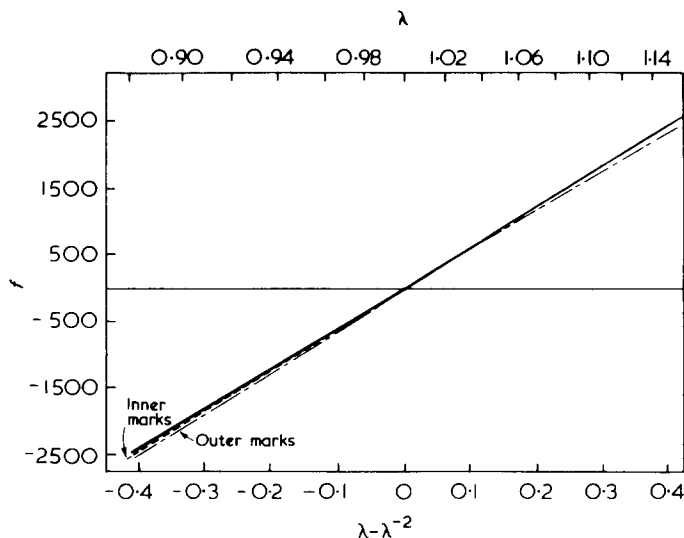


Figure 3 Force, *f* against  $(\lambda - \lambda^{-2})$  at 20°C

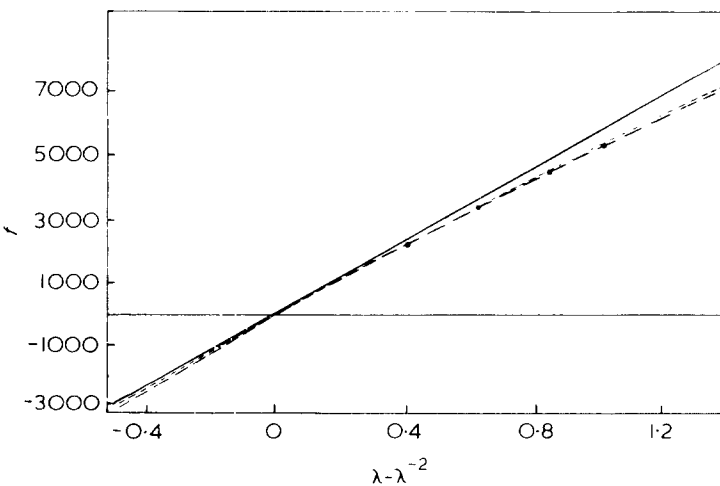


Figure 4 Force, *f* against  $(\lambda - \lambda^{-2})$  at 40°C

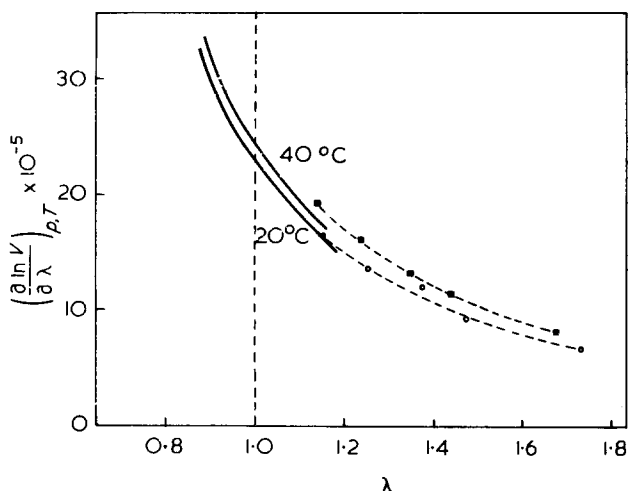


Figure 5  $f/(\lambda - \lambda^{-2})$  against  $1/\lambda$

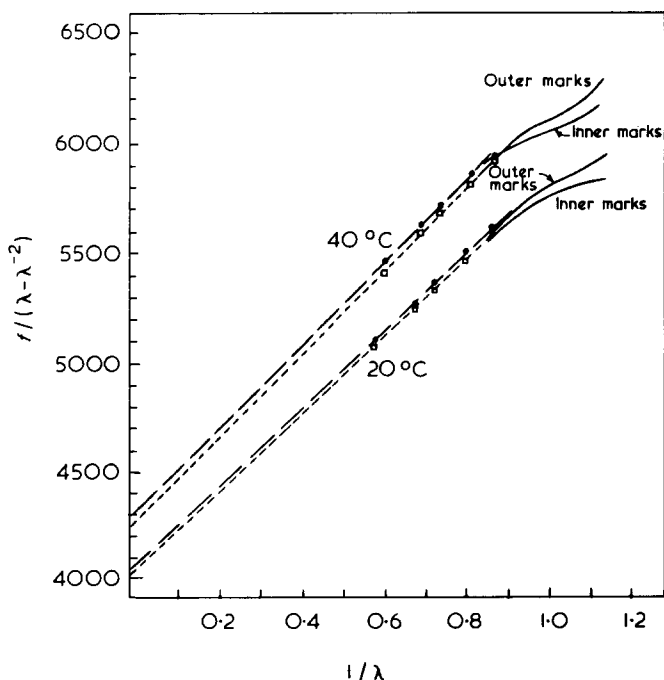


Figure 6 Volume dilation coefficient

It shows some scatter in the range of moderate elongations. The relative change of volume as calculated from equation (10) is given in Figure 7. The following values<sup>22</sup> of the isothermal compressibility were used:  $\kappa_T(20^\circ) = 5.0 \times 10^{-11}$  and  $\kappa_T(40^\circ) = 5.4 \times 10^{-11} \text{ cm}^2/\text{dyne}$ .

DISCUSSION

Length against force plot

The data of this relationship are represented by a monotonic function in Figure 2. The absence of a point of inflection in the compression area proves that no buckling occurred in the sample. The curves show no inconsistencies in the transition from elongation to compression. This is

hardly surprising, but it underlines the conclusion drawn from two dimensional extension experiments, that extension as well as compression data should fit the same curve.<sup>6</sup> Sheppard and Clapson<sup>4</sup> applied one-dimensional and two-dimensional extension, the latter subsequently referred to as 'quasi-compression', to the same rubber specimen. They found that the equivalent compression and elongation curves coincided fairly well, though the compression curve had to be shifted towards increasing force (tension) to go through zero. No data have been obtained in the interval  $0.91 < \lambda < 1.25$ .

The experimental device described here overcomes the difficulty of accurately determining the unstrained length  $L_0$  of a sample. This quantity is available with high accuracy, if extension and compression are carried out alternately. The range of compression, of course, is limited by the shape of the sample and by the maximum contractile force of the springs. For elongation there are no such well-defined limits of elastic stability, but it was thought that the range of deformation should be kept equivalent in both directions to have a similar scale of relaxation times. Another restriction comes from the fact that rigidly clamped, short, thick samples show the appearance of secondary tensions even in their centres when stretched too much. According to Sekiguchi *et al.*<sup>13</sup> this is the case for a sample with a length to diameter ratio  $L_0/b_0 = 1$  from  $\lambda = 2.2$  onwards and for  $L_0/b_0 = 3$  from  $\lambda > 4.6$ . Besides that the frame did not allow the metal plate to travel too far, because otherwise problems of a mechanical nature, like differences in the width of the frame, might have arisen. Therefore elongations higher than  $\lambda = 1.18$  could only be achieved after the plate had been removed.

Another important feature of the device is the 'negative characteristic' of the springs, which by reducing the creep of the sample improves the reproducibility of data read after different experimental cycles.

Gaussian plot

The Gaussian plots in Figures 3 and 4 also show no inconsistencies in the vicinity of zero force. They yield another check for the absence of buckling in the com-

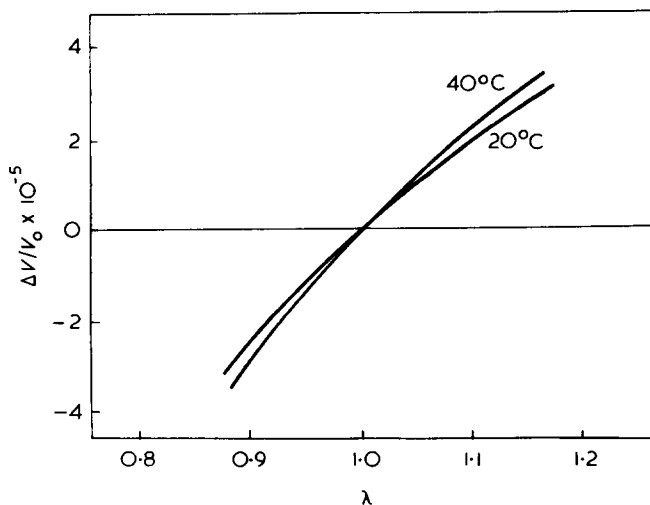


Figure 7 Volume changes

pression range in that there is no intersection of the actual curve with the tangent at the origin. This intersection would have shown, if  $\lambda$  had decreased under the influence of a constant force, the onset of buckling<sup>1</sup>.

The compression part of the curve obtained from the inner marks shows less deviation from the tangent at both temperatures and leads to the conclusion that some secondary effects may have occurred at the ends of the sample. Therefore the inner marks are thought to better represent undisturbed uniaxial compression.

The relative deviations  $\delta f$  from the tangents at 20° and 40°C are:

	$\lambda=0.88$	1.16	1.73
$\delta f$ (inner marks)	1%	3%	13%
$\delta f$ (outer marks)	3%	3%	13%

These deviations are of the same order as mentioned in other investigations, for instance,

Wood<sup>23</sup>: 4% deviation from the Gaussian plot for  $\lambda > 1.15$ , better coincidence in quasi-compression,

Forster<sup>2</sup>: good agreement with Gaussian theory for quasi-compression to  $\lambda=0.68$ , though slightly S-shaped curve,

Treloar<sup>5</sup>: good agreement with Gaussian theory for quasi-compression, but for elongation only to  $\lambda < 1.5$ .

An interesting point is to study the effects of time-dependent relaxation in the Gaussian plot. In elongation, creep leads to higher elongation and stress relaxation to lower force, so that there is a progressive deviation in the course of time from the tangent at the origin which represents ideal Gaussian behaviour. On the contrary, in compression creep produces more compression and stress relaxation smaller compressive force, so that the time-dependent relaxation processes tend to give data approaching ideal Gaussian behaviour. This may be the reason why better agreement with equation (5) is found in compression than in elongation.

The Gaussian plots regarded here represent the behaviour of samples under uniaxial compression in accordance with the findings of van der Hoff and Glynn<sup>24</sup> although their conclusions cannot be followed in all points. From equations (5a) and (8) they come to the definition of  $\tau/(\lambda - \lambda^{-2})$  as the shear modulus which will be called  $\bar{G}$  here. Then  $\bar{G}$  for any deformation is equivalent to the slope of the secant from the origin to the actual point on the Gaussian curve. Since the curve is monotonic any secant in the range of compression will yield a higher  $\bar{G}$  than in elongation. Their so-called 'initial modulus'  $G_{\text{comp}}$  in compression was determined at approximately  $\lambda=0.92 \dots 0.95$  and compared with  $G_{\text{ext}}$  in elongation at  $\lambda \approx 1.05 \dots 1.08$ . Therefore a ratio  $G_{\text{comp}}/G_{\text{ext}} > 1$  can be expected for lightly crosslinked natural rubber. The appearance of values less than one which they have found on *cis*-1,4-polybutadiene samples with low crosslink concentrations is not as easy to understand. It may, of course, be due to inaccuracies in the determination of the undeformed lengths in compression and/or in elongation which can be avoided by the combined experiment.

Then, there is no guarantee that time-dependent effects are equal on either side of  $\lambda=1$ . In any case it is likely that

the ratio  $G_{\text{comp}}/G_{\text{ext}}$  as measured by van der Hoff and Glynn is time dependent though both moduli decrease in the course of time. They quote a decrease of the compressive force (pressure) of 3–8% between measurements after 2 and 10 min relaxation respectively. Furthermore, shifts in the time dependency can be expected with varying crosslink concentration.

The comparison between elongation as one-dimensional and compression as two-dimensional extension of the molecules is useful to explain the dependency of  $\bar{G}$  on  $\lambda$ , but there is no reason why  $\bar{G}$  should have a bend or a jump for  $\lambda=1$ .

#### Mooney–Rivlin plot

The Mooney–Rivlin plot (Figure 5) shows no discontinuity in the vicinity of  $\lambda=1$ , but it is not linear there. Towards higher elongation straight lines are obtained for each set of marks at both temperatures. In compression the curves for the inner marks tend to flatten, whereas those for the outer marks show an upward trend.

The tendency to approach a horizontal line points towards better agreement with Gaussian theory. This, indeed, has been found for the inner marks in the compression region. Rivlin and Saunders<sup>3</sup> detected a similar behaviour in the area of quasi-compression, where their results between  $1/\lambda \approx 2$  and  $1/\lambda \approx 12$  showed an almost horizontal curve, slightly lower in the middle than towards either end. In elongation they obtained a straight line, but unfortunately no data for the intermediate range were quoted. The same applies to a Mooney plot for the compression range of lightly crosslinked natural rubber by van der Hoff and Glynn<sup>24</sup> which is almost a straight horizontal line from  $1/\lambda=1$  to 3 apart from a slight minimum in the range  $0.9 > \lambda > 0.7$ . This can probably be accounted for by uncertainties of the force (pressure) and  $L_0$  determinations.

The Mooney–Rivlin plot turns out to be extremely sensitive in the vicinity of  $\lambda=1$ . An estimation shows, that an experimental error of 0.1% in  $\lambda$  causes quite drastic relative changes  $\Delta$  of the quantity  $f/(\lambda - \lambda^{-2})$ :

$\lambda$	$\lambda - \Delta\lambda$	$\Delta$
1.01	1.0090	10.5%
1.10	1.0989	1.0%
1.50	1.4985	0.24%

Therefore it can be concluded that Figure 4 represents approximately the behaviour of a sample even in the region of very small deformations, and that in compression there is a trend towards smaller slopes.

An evaluation of the constants  $C_1$  and  $C_2$  in equation (6) from the straight portion of the elongation curves yields:

	$C_1$ (g)	$C_2$ (g)	$C_1/A_0$ (N/m <sup>2</sup> )	$C_2/A_0$ (N/m <sup>2</sup> )
20°	4040	1810	$3.13 \times 10^9$	$1.40 \times 10^9$
40°	4280	1920	$3.32 \times 10^9$	$1.49 \times 10^9$

The temperature dependence of  $C_1$  and  $C_2$  comes out to be similar in the small temperature interval of the

investigations. After dividing by the undeformed cross-section  $A_0$  of the sample and conversion of the units they compare fairly well with the values for sample *C* given by Allen *et al.*<sup>11</sup>, which had been cured in a similar way.

#### Volume dilation coefficient

The coefficient  $(\partial \ln V / \partial \lambda)_{p, T}$  as given in *Figure 6* has been calculated using equations (9d) for the range of small deformations and (9b) for moderate elongation ratios. The latter values show some statistical scatter. Good agreement exists with the curve for sample *C* in ref. 11 representing Gaussian behaviour, though experimental points in that plot tend to give higher values of the coefficient.

#### Volume changes

The volume changes  $\Delta V / V_0$  given in *Figure 7* agree with values by Christensen and Hoeve<sup>15</sup> for small elongations, whose experimental values deviated from the curve calculated on the basis of Gaussian theory for elongation ratios  $\lambda > 1.2$  only. Even though experiments<sup>11, 15</sup> yield higher volume effects than predicted by Gaussian theory, this approximation is valid in the range of small deformations. At elongation ratios  $\lambda < 1.5$  the volume change<sup>15, 16, 25, 26</sup> of rubbers of sufficiently high molecular weight remains  $\Delta V / V_0 < 10^{-4}$  and can therefore normally be disregarded.

#### CONCLUSIONS

The experimental device of coupling the sample to a set of metal springs allows the sample to be uniaxially stretched and compressed. It partly compensates for the tendency to creep of rubber specimens and provides the means for an accurate determination of their undeformed lengths. Gaussian theory is sufficient for the evaluation of data obtained in the range of small deformations.

Using Gaussian theory the relative energy contribution  $f_e$  to the retractive force  $f$  of deformed rubber samples can be calculated from the force against length data at different temperatures. The necessary theoretical considerations and the results will be reported in a subsequent paper.

#### ACKNOWLEDGMENTS

The author wishes to thank Professor G. Allen for suggesting these investigations and for stimulating discussions during their progress and completion. He thanks Professor G. Gee, Professor L. R. G. Treloar and Dr C. Price for discussing the results. Thanks are also due to the Science Research Council for granting a fellowship.

#### REFERENCES

- Gent, A. N. *Rubber Chem. Technol.* 1965, **38**, 415
- Forster, M. J. *J. Appl. Phys.* 1955, **26**, 1104
- Rivlin, R. S. and Saunders, D. W. *Phil. Trans. R. Soc. (A)* 1951, **243**, 251
- Sheppard, J. R. and Clapson, W. J. *Ind. Eng. Chem.* 1932, **24**, 782
- Treloar, L. R. G. *Trans. Faraday Soc.* 1944, **40**, 59
- Treloar, L. R. G. 'The Physics of Rubber Elasticity', Oxford University Press, 1958, p 86
- Flory, P. J. *Trans. Faraday Soc.* 1961, **57**, 829
- Gee, G. *Polymer* 1966, **7**, 373
- Krigbaum, W. R. and Roe, R. J. *Rubber Chem. Technol.* 1965, **38**, 1039
- Roe, R. J. *Trans. Faraday Soc.* 1966, **62**, 312
- Allen, G., Kirkham, M. J., Padget, J. and Price, C. *Trans. Faraday Soc.* 1971, **67**, 1278
- Gumbrell, S. M., Mullins, L. and Rivlin, R. S. *Trans. Faraday Soc.* 1953, **49**, 1495
- Sekiguchi, H., Kakiuchi, M., Morimoto, T., Fujimoto, K. and Yoshimura, N. *Rubber Chem. Technol.* 1969, **42**, 547
- Price, C., Padget, J., Kirkham, M. J. and Allen, G. *Polymer* 1969, **10**, 495
- Christensen, R. G. and Hoeve, C. A. J. *J. Polym. Sci. (A-1)* 1970, **8**, 1503
- Allen, G., Bianchi, U. and Price, C. *Trans. Faraday Soc.* 1963, **59**, 2493
- Price, C., Allen, G., de Candia, F., Kirkham, M. J. and Subramaniam, A. *Polymer* 1970, **11**, 486
- Mark, J. and Flory, P. J. *J. Am. Chem. Soc.* 1964, **86**, 138
- Tanaka, T., Yokoyama, T. and Yamaguchi, Y. *Rubber Chem. Technol.* 1971, **44**, 127
- Steiner, G. and Tobolsky, A. V. *Rubber Chem. Technol.* 1970, **43**, 1036
- Barrie, J. A. and Standen, J. *Polymer* 1967, **8**, 97
- Wood, L. A. and Martin, G. M. *Rubber Chem. Technol.* 1964, **37**, 850
- Wood, L. A. *J. Res. Natl. Bur. Stand.* 1958, **60**, 193
- Van der Hoff, B. M. E. and Glynn, P. A. R. *J. Macromol. Sci.* 1969, **A3**, 991
- Hewitt, F. G. and Anthony, R. L. *J. Appl. Phys.* 1958, **29**, 1411
- Gee, G., Stern, J. and Treloar, L. R. G. *Trans. Faraday Soc.* 1950, **46**, 1101

# Crystallization of high molecular weight fractions of poly(ethylene oxide) from dilute solution in ethanol

D. R. Beech\* and C. Booth

*Department of Chemistry, University of Manchester, Manchester M13 9PL, UK*

*(Received 11 January 1972)*

The kinetics of crystallization of high molecular weight poly(ethylene oxide) fractions from dilute solution in ethanol have been investigated by means of dilatometry. At low extents of crystallinity the crystallization isotherms are well represented by the free growth Avrami expression with exponent  $n=4$ . Crystallization rates increase with increasing molecular weight in the manner predicted from the established thermodynamic properties of polymers in dilute solution.

## INTRODUCTION

The kinetics of crystallization of fractions of high molecular weight polymers have been investigated previously by measurement of single crystal growth rates<sup>1</sup> and by dilatometry<sup>2</sup>. Other investigations have involved polymers of wide molecular weight distribution<sup>3</sup> or block copolymers of moderately low molecular weight<sup>4</sup>. Here we present the results of a dilatometric investigation of the crystallization kinetics of several high molecular weight fractions of poly(ethylene oxide) from dilute solutions in ethanol.

## EXPERIMENTAL

Polyox WSR-35 and WSR-205 (Union Carbide Ltd, Chemicals Division) were fractionated by precipitation from dilute solution in benzene by addition of iso-octane<sup>5</sup>. Intrinsic viscosities were measured in benzene at 25°C. Molecular weight distributions were studied by gel permeation chromatography by methods discussed earlier<sup>6</sup>. Viscosity-average molecular weights<sup>7</sup> and molecular weight ratios for the fractions are given in *Table 1*.

The dilatometers were similar in design to those used by Kovacs and Manson<sup>4</sup>. A poly(ethylene oxide) fraction (~0.4 g) was mixed with outgassed ethanol (~150 cm<sup>3</sup>) and the solution was further outgassed before being confined with mercury. A nail-in-glass stirrer was incorporated in the dilatometer to permit gentle stirring of the mixture prior to crystallization.

The poly(ethylene oxide) was dissolved at 55–60°C and the dilatometer was then transferred to a water bath held at the appropriate crystallization temperature (to

±0.001 deg.). Temperature equilibration took (with stirring) some 10–15 min. The contraction due to crystallization (of about 7 cm) was followed by means of a cathetometer (to ±0.04 mm). Since the dilatometer dimensions were such that a temperature drift of 0.01 deg. produced a change in meniscus height of 1 mm, an identical dilatometer containing pure ethanol was placed adjacent to the crystallization dilatometer and the meniscus height also measured.

## RESULTS AND DISCUSSION

### *Crystallization isotherms*

We have studied the crystallization from dilute solution (0.27 g/dl) in ethanol of the four fractions (*Table 1*) and a mixture of 27% fraction  $2 \times 10^6$  and 73% fraction  $2 \times 10^5$  (this mixture has a viscosity-average molecular weight of  $6 \times 10^{-5}$  and is denoted  $M : 6 \times 10^5$ ). Measurements were made within the temperature range 27 to 33°C. In all cases the termination of crystallization was abrupt, which is in contrast to the crystallization of high molecular weight fractions of poly(ethylene oxide) in bulk for which a slow increase in crystallinity is evident over a long period of time towards the end of the crystallization<sup>8</sup>. We also found that the total contraction (dilatometer meniscus height at zero time less that at completion) was practically independent of crystallization temperature whereas a marked increase with increasing crystallization temperature of the total contraction was noted for high molecular weight fractions crystallized in bulk<sup>8</sup>. These observations suggest that secondary processes (of crystal perfecting) are absent in the crystallization of poly(ethylene oxide) from dilute solution and also, within the molecular weight range encompassed by sample  $M : 6 \times 10^5$ , that the rejection of lower molecular weight species during the crystallization is unimportant.

\* Present address: Materials Science Unit, Turner Dental School, University of Manchester

Table 1 Molecular characteristics of poly(ethylene oxide) fractions

Fraction	Intrinsic viscosity (dl/g)	$\bar{M}_v$	$\bar{M}_w/\bar{M}_n$
$7 \times 10^4$	0.87	$7.4 \times 10^4$	1.2
$2 \times 10^5$	1.92	$2.4 \times 10^5$	1.2
$1 \times 10^6$	5.29	$1.0 \times 10^6$	1.2
$2 \times 10^6$	7.58	$1.7 \times 10^6$	1.2

The crystallinity at time  $t$  is defined in terms of dilatometer meniscus heights read at times 0,  $t$  and  $\infty$  (completion) by:

$$X = (h_0 - h_t)/(h_0 - h_\infty) \quad (1)$$

Crystallization isotherms ( $X$  versus  $\log t$ ) obtained for fraction  $1 \times 10^6$  at several crystallization temperatures are illustrated in Figure 1. These isotherms are not all the same shape; there is a noticeable attenuation of rate during the crystallizations carried out at the higher crystallization temperatures. This effect was noted in crystallizing other samples.

There is every indication in other work<sup>1-3</sup> that crystallization from dilute solution, at least in its early stages, meets the primary requirement of Avrami analysis<sup>9, 10</sup>, i.e. that the rate of growth of the crystalline entities is independent of the extent of crystallization. In bulk systems it is necessary to allow for impingement of growing crystalline bodies. In dilute solution, because of the mobility of the system, this is unnecessary and a form of the Avrami equation appropriate for free growth is best applied to our data. We have in fact used the simplest free growth approximation:

$$X = kt^n \quad (2)$$

which should hold over the initial part of the crystallization. It would in any event be inappropriate, since theory is lacking, to extend the analysis of the data to the later stages of the crystallization. In equation (2)  $k$  is the rate constant and the value of the exponent  $n$  is related to the mode of nucleation and the geometry of the growing crystalline entities in the usual way<sup>9, 10</sup>.

Experimental difficulties, principally of temperature equilibration, limited the number of crystallizations which

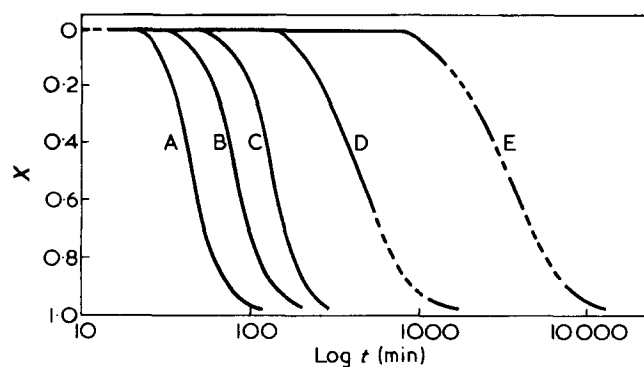


Figure 1 Crystallization isotherms for dilute solutions of fraction  $1 \times 10^6$  in ethanol. Crystallization temperatures: A, 29°C; B, 30.1°C; C, 31°C; D, 32°C; E, 33°C

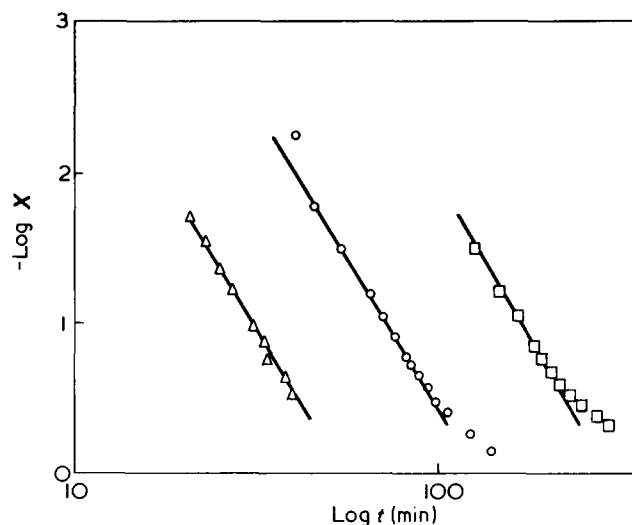


Figure 2 Free growth Avrami plots for dilute solutions of poly(ethylene oxide) fraction  $2 \times 10^6$  in ethanol. Lines are for equation (2) with  $n=4$ . Crystallization temperatures:  $\Delta$ , 29.8°C;  $\circ$ , 31°C;  $\square$ , 32°C

could be usefully analysed over the initial 15 to 25% of crystallinity. Plots of  $\log X$  versus  $\log t$  obtained for fraction  $2 \times 10^6$  are illustrated in Figure 2, and the reliable values of the Avrami exponent  $n$  obtained from such plots are given, to the nearest integer, in Table 2. The evidence predominantly favours a value of the Avrami exponent of 4, in agreement with the finding of Devoy and Mandelkern<sup>2</sup> for a fraction of polyethylene. We note that the attenuation in rate noted for fraction  $1 \times 10^6$  (Figure 1) is substantiated by a lower value (3) of the Avrami exponent. We find no changes in isotherm shape which are directly attributable to changes in molecular weight. Insofar as we test the effect of molecular weight distribution, by use of sample  $M : 6 \times 10^5$ , we find no differences in crystallization isotherms which can be attributed to this parameter.

An Avrami exponent of 4 points to a three-dimensional growth process. The lack of morphological information about crystals of high molecular weight poly(ethylene oxide) fractions grown from solutions of the concentration used here precludes further discussion of this finding. Nor would we, at this time, pursue an explanation of the lower  $n$  values observed at high crystallization temperatures. Such effects have been attributed<sup>11, 12</sup> to settling out of the crystalline phase during the long time periods covered by crystallization at high  $T_c$ . We were unable to observe this visually.

Table 2 Avrami exponents for crystallization of poly(ethylene oxide) fractions from dilute solution

Crystallization temperature	$7 \times 10^4$	$2 \times 10^5$	$M : 6 \times 10^5$	$1 \times 10^6$	$2 \times 10^6$
29.0	4	—	—	—	—
29.6	—	4	—	—	—
29.8	—	—	—	—	4
30.1	—	—	—	—	—
31.0	—	4	4	—	4
32.0	—	—	—	3	4

Table 3 Crystallization half-lives (min) of poly(ethylene oxide) fractions in dilute solution

Crystallization temperature	$7 \times 10^4$	$2 \times 10^5$	$M : 6 \times 10^5$	$1 \times 10^6$	$2 \times 10^6$
27.8	37	—	—	—	—
28.6	62	—	—	—	—
29.0	125	64	50	44	—
29.6	—	89	—	65	—
29.8	—	—	100	—	50
30.1	—	125	—	81	—
31.0	—	450	361	133	118
32.0	—	1200	—	446	308

## Effect of molecular weight on crystallization rate

Overall rates of crystallization are given in terms of crystallization half-life ( $t_{1/2}$ ) in Table 3. The rates increase with increasing molecular weight, even at molecular weights exceeding  $10^6$ . The molecular weight distribution, provided all molecules are within the high molecular weight region as in sample  $M : 6 \times 10^5$ , is unimportant. The effect of molecular weight is similar to that found by Holland and Lindenmeyer<sup>1</sup> who measured single crystal growth rates for polyethylene fractions in the molecular weight range  $10^4$  to  $1.2 \times 10^5$ . By contrast the crystallization rates of poly(ethylene oxide) fractions in bulk are independent of the molecular weight when this is high<sup>13</sup>.

In common with crystallization in bulk the temperature coefficient of crystallization rate is negative (Table 3). It is usual to discuss the rate-temperature relationship in terms of nucleation theory, suitably modified to apply to polymeric materials<sup>9,10</sup>. If it is assumed that the crystallization is controlled in rate by a single nucleation step then:

$$(1/t_{1/2}) = (1/t_{1/2})_0 \exp(-\Delta F^*/RT_c) \quad (3)$$

where  $(1/t_{1/2})_0$  is a constant (over the temperature range considered) and  $\Delta F^*$  is the activation free energy, i.e. the free energy of formation of a nucleus of critical size at the crystallization temperature  $T_c$ . If, as is possible, the rate-determining step is the formation of a monolayer nucleus then, for polymer of high molecular weight:

$$\Delta F^* = \frac{4\sigma_u\sigma_e T_m^e}{\Delta H_u(T_m^e - T_c)} \quad (4)$$

where  $\Delta H_u$  is the heat of fusion (per repeat unit),  $T_m^e$  is the equilibrium melting point of the polymer in the system, and  $\sigma_u$  and  $\sigma_e$  are the lateral and end interfacial free energies. For high molecular weight polymers in bulk  $T_m^e$  is equated with  $T_m^0$ , the thermodynamic melting point (that of a crystal of infinite dimensions composed of polymer of infinite molecular weight). For polymers in solution,  $T_m^e$  is equated with  $T_s^0$ , the dissolution tempera-

ture of a crystal of infinite dimensions composed of polymer of infinite molecular weight.

None of the variables in equation (4) (i.e.  $\sigma_u$ ,  $\sigma_e$ ,  $\Delta H_u$ ) seem likely to be significantly dependent on molecular weight when this is high, nor would we introduce any new parameters of significance if we considered nuclei other than monolayers. Consequently the insensitivity to molecular weight of the crystallization rates of high molecular weight fractions *in bulk* is readily explained.

Combination of equations (3) and (4) leads to

$$\log(t_{1/2}) = \log(t_{1/2})_0 + \frac{4\sigma_u\sigma_e T_m^e}{R\Delta H_u T_c \Delta T} \quad (5)$$

and so a plot of  $\log(t_{1/2})$  against  $T_m^e/T_c \Delta T$  should be a straight line provided the rate controlling step is the formation of a monolayer nucleus. For crystallization in bulk<sup>13</sup> plots of  $\log(t_{1/2})$  against  $T_m^0/T_c \Delta T$  for high molecular weight fractions of poly(ethylene oxide) lie on a single straight line the slope of which corresponds<sup>13</sup> to a value of  $\sigma_e = 1.7$  kcal/(mol of chains emerging)<sup>-1</sup> [when  $T_m^0 = 76^\circ\text{C}$ ,  $\Delta H_u = 2$  kcal/(mol of repeat units)<sup>-1</sup> and  $\sigma_u$  is taken to be  $0.2$  kcal/(mol of repeat units)<sup>-1</sup>]. It is necessary to know  $T_s^0$  in order to carry out this analysis for crystallization from dilute solution. The evaluation of  $T_s^0$  is difficult and we have not pursued the matter experimentally. Rather have we chosen  $T_s^0 = 50^\circ\text{C}$  as a reasonable value on the grounds that this leads to  $\sigma_e$  values (with  $\Delta H_u$  and  $\sigma_u$  as before) in the region  $1.5$  to  $2.0$  kcal/mol. Correspondence between the interfacial free energies for nuclei in crystallization from bulk and from dilute solution has been noted for polyethylene<sup>9,14</sup>.  $T_s^0 = 50^\circ\text{C}$  also leads to minimum curvature in plots according to equation (5). These plots are illustrated in Figure 3.

It is clear, from the nature of Figure 3, that the data for the various fractions cannot be brought into coincidence

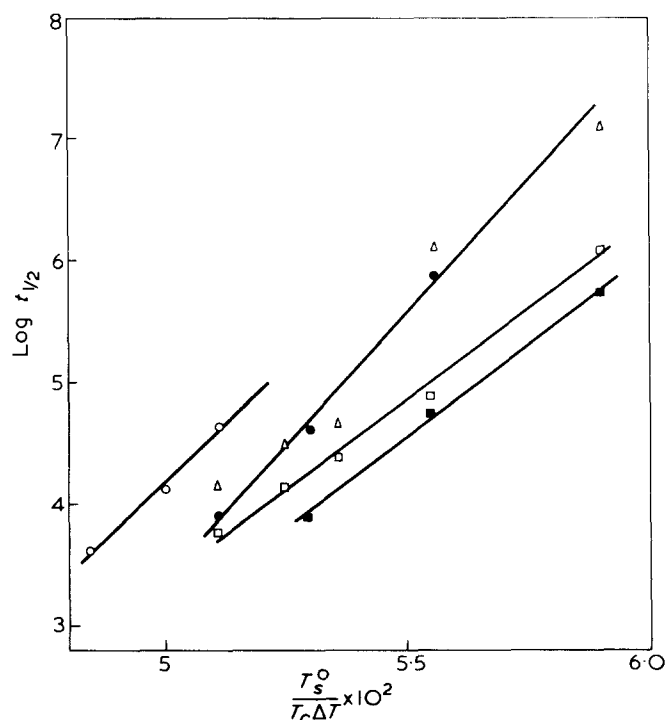


Figure 3 Temperature dependence of crystallization half-life, according to equation (5) with  $T_s^0 = 50^\circ\text{C}$ . Points are for samples:  $\circ$ ,  $7 \times 10^4$ ;  $\triangle$ ,  $2 \times 10^5$ ;  $\bullet$ ,  $M : 6 \times 10^5$ ;  $\square$ ,  $1 \times 10^6$ ;  $\blacksquare$ ,  $2 \times 10^6$

\* If the chemical potential of the solvent is given by:

$$\mu_1 - \mu_1^0 = RTV_1[(C_2/M_2) + A_2C_2^2]$$

where  $C_2$  = concentration of polymer,  $M_2$  = molecular weight of polymer,  $V_1$  = molar volume of solvent and  $A_2$  = second virial coefficient for the system, then use of the Gibbs-Duhem relation leads to the expression:

$$\mu_2 - \mu_2^0 = RT \ln (M_1 k_2 C_2 / M_2 \rho_2) + 2RTA_2 M_2 C_2$$

where  $M_1$  = molecular weight of solvent,  $\rho_2$  = density of liquid polymer, and  $k_2$  is the Henry's law constant for the system.

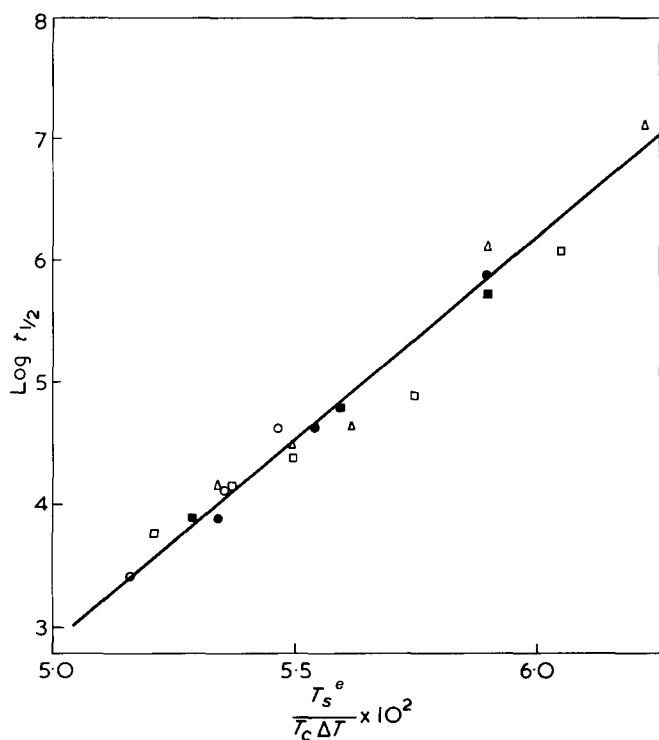


Figure 4 Temperature dependence of crystallization half-life, according to equation (5) with  $T_s^e$  adjusted to achieve superposition. Points are for samples:  $\circ$ ,  $7 \times 10^4$ ;  $\triangle$ ,  $2 \times 10^5$ ;  $\bullet$ ,  $M : 6 \times 10^5$ ;  $\square$ ,  $1 \times 10^6$ ;  $\blacksquare$ ,  $2 \times 10^6$

by changes in  $\sigma_e$  (or  $\sigma_u \sigma_e$ ) but only by changes in the dissolution temperature ( $T_s^e$ ) of the sample. In Figure 4 we plot  $\log(t_{1/2})$  against  $T_s^e/T_c \Delta T$  ( $\Delta T = T_s^e - T_c$ ) where  $T_s^e$  is chosen so as to bring all the data into approximate coincidence with that for fraction  $2 \times 10^6$ ; i.e.  $T_s^e = 50.0^\circ\text{C}$  for  $2 \times 10^6$ ,  $T_s^e = 49.5^\circ\text{C}$  for  $1 \times 10^6$ ,  $T_s^e = 49.0^\circ\text{C}$  for  $M : 6 \times 10^5$  and  $2 \times 10^5$ , and  $T_s^e = 48.5^\circ\text{C}$  for  $7 \times 10^4$ . The increase in  $T_s^e$  of some 1.5 deg. when the molecular weight varies from  $7 \times 10^4$  to  $2 \times 10^6$  is explained as follows.

The chemical potential of a polymer in solution ( $\mu_2$ ) is related to that of pure crystalline polymer ( $\mu_2^c$ ) by the equilibrium condition

$$\mu_2 = \mu_2^c \quad (6)$$

and to the free energy of fusion of pure crystalline polymer ( $\Delta G_f$ ) by:

$$\mu_2 - \mu_2^0 = \mu_2^c - \mu_2^0 = -\Delta G_f \quad (7)$$

where  $\mu_2^0$  is the chemical potential of pure liquid polymer. The quantity  $\mu_2 - \mu_2^0$  can therefore be determined by measuring the dissolution temperature ( $T_s^e$ ) since, to an acceptable degree of approximation

$$\Delta G_f = \Delta H_f [1 - (T_s^e/T_m^0)] \quad (8)$$

We have already referred to the lack of this kind of data for our system.

It has been suggested<sup>9</sup> that the chemical potential of polymer in dilute solution should be obtained from the chemical potential of the solvent by use of the Gibbs–Duhem relation. However, solvent activities covering the whole concentration range from pure liquid polymer to dilute solution are seldom available. Solvent activities within the dilute solution range are available from osmometry, light-scattering, etc., but conventional treatment of such data by the Gibbs–Duhem relation leads to

an expression for the chemical potential of solute involving the Henry's law constant for the system.\* Such an expression cannot be directly applied in equation (7) without independent assessment of the Henry's law constant, particularly of its dependence upon molecular weight.

Rather than introduce a theoretical estimate of the Henry's law constant it is simpler, and probably no less accurate in the present context, to use the Flory–Huggins equation<sup>15</sup> which gives an explicit expression for  $\mu_2 - \mu_2^0$ . In doing this we ignore the excluded volume effect. This effect will not be large in our system since ethanol is a poor solvent for poly(ethylene oxide). In any event we will relate our calculations to similar calculations in which the Flory–Huggins equation is applied to results for the chemical potential of the solvent and so compensate for the omission.

According to the Flory–Huggins formulation<sup>15</sup>:

$$\left( \frac{1}{T_s^e} - \frac{1}{T_m^0} \right) = \frac{R}{\Delta H_u} \frac{V_u}{V_1} \left[ -\frac{\ln \phi_2}{m} + \left( 1 - \frac{1}{m} \right) \phi_1 - \chi \phi_1^2 \right] \quad (9)$$

where  $m = xV_u/V_1$  ( $x$  being the number of chain units of molar volume  $V_u$  per polymer molecule),  $\phi_1$  and  $\phi_2$  are volume fractions of solvent and polymer, and  $\chi$  is the Flory–Huggins parameter. If we consider two polymers,  $A$  ( $M = 10^6$ ) and  $B$  ( $M = 10^5$ ) then the quantity  $\Delta T_S = T_{s,A}^e - T_{s,B}^e$  can be written:

$$\Delta T_S = \frac{RT_s^e T_m^0 V_u}{\Delta H_u V_1} \left[ (\phi_1 + \ln \phi_2) \left( \frac{1}{m_B} - \frac{1}{m_A} \right) - \phi_2 \Delta \chi \right] \quad (10)$$

where  $\Delta \chi = \chi_A - \chi_B$  and where it is assumed that  $\Delta T_S$  is small, i.e.  $T_{s,A}^e \sim T_{s,B}^e \sim T_s^e$ . The introduction of suitable values for the parameters into equation (10) (i.e.  $\Delta H_u = 2 \text{ kcal/mol}$ ,  $T_s^e = 323 \text{ K}$ ,  $T_m^0 = 349 \text{ K}$ ,  $V_u \sim 48^{16}$ ,  $V_1 \sim 59 \text{ cm}^3/\text{mol}$ ,  $\phi_2 = 0.003$ ) gives the equation:

$$\Delta T_S = -0.24 - 90(\chi_A - \chi_B) \quad (11)$$

Thus it is seen that a value of  $\Delta \chi$  of 0.01 will lead to a value of  $\Delta T_S$  of about 1 degree.

An increase in parameter  $\chi$  of 0.01 between molecular weights of  $10^6$  and  $10^5$  is entirely reasonable. We do not have data for the chemical potential of ethanol in dilute solutions of poly(ethylene oxide) fractions, but data are available for dilute solutions in methanol, a somewhat better solvent. The second virial coefficients for poly(ethylene oxide) fractions in methanol, as determined by light-scattering<sup>17</sup>, vary from  $10^{-3}$  to  $6 \times 10^{-4} \text{ cm}^3 \text{ g}^{-2} \text{ mol}$  as the molecular weight increases from  $10^5$  to  $10^6$ . Since, in the Flory–Huggins formulation, the second virial coefficient is given by:

$$A_2 = (\frac{1}{2} - \chi) / V_1 \rho_2^2$$

where  $\rho_2$  is the liquid polymer density, the difference in  $A_2$  of  $4 \times 10^{-4} \text{ cm}^3 \text{ g}^{-2} \text{ mol}$  corresponds to a difference in  $\chi$  of about 0.02.

We conclude that the rates of crystallization of high molecular weight fractions of poly(ethylene oxide) from dilute solutions in ethanol vary with molecular weight as expected from our knowledge of the properties of dilute polymer solutions. No special effects, such as adsorption or other molecular weight dependent surface effects<sup>1</sup>, need to be invoked in order to rationalize our data. In that the course of crystallization of poly(ethylene oxide) fractions from ethanol is similar to that found for the crystallization of a polyethylene fraction from several solvents<sup>2</sup> we



anticipate that our conclusion will have general application.

We have reported earlier<sup>5</sup> that the crystallization from dilute solution in ethanol (and other solvents) of samples of poly(ethylene oxide) of wide molecular weight distribution is accompanied by a fractionation effect in the sense that the lower molecular weight species precipitate most rapidly (provided the molecular weights are sufficiently high to preclude significant depression of the melting point by chain ends). This observation has been confirmed by use of our fractions. The present investigation of overall crystallization rates of fractions and mixtures of fractions sheds no new light upon the cause of this effect. It may well be that a model for crystallization of polymers from dilute solution which is properly founded on morphological information (such as that in ref. 1) will provide an explanation.

#### ACKNOWLEDGEMENTS

We thank Mr D. J. Roy for assistance with the characterization of the polymers. One of us (D. R. B.) acknowledges receipt of a Science Research Council Studentship.

#### REFERENCES

- 1 Holland, V. F. and Lindenmeyer, P. H. *J. Polym. Sci.* 1962, **57**, 589
- 2 Devoy, C. J., Mandelkern, L. and Bourland, L. *J. Polym. Sci. (A-2)* 1970, **8**, 869
- 3 Mandelkern, L. *Polymer* 1964, **5**, 637
- 4 Kovacs, A. J. and Manson, J. A. *Kolloid-Z.* 1966, **214**, 1
- 5 Booth, C. and Price, C. *Polymer* 1966, **7**, 85
- 6 Beech, D. R. and Booth, C. *J. Polym. Sci. (A-2)* 1969, **7**, 575
- 7 Allen, G., Booth, C., Hurst, S. J., Jones, M. N. and Price, C. *Polymer* 1967, **8**, 391
- 8 Beech, D. R., Booth, C., Dodgson, D. V. and Hillier, I. H. *J. Polym. Sci.* in press
- 9 Mandelkern, L. 'Crystallization of Polymers', McGraw-Hill, New York, 1964
- 10 Sharples, A. 'Introduction to Polymer Crystallization', Arnold, London, 1966
- 11 Turnbull, D. *Acta Metall.* 1953, **1**, 684
- 12 Devoy, C. J., personal communication
- 13 Beech, D. R., Booth, C., Hillier, I. H. and Pickles, C. J. *Eur. Polym. J.* in press
- 14 Hoffman, J. D., Lauritzen, J. I., Passaglia, E., Ross, G. S., Frolen, L. J. and Weeks, J. J. *Kolloid-Z.* 1968, **231**, 564
- 15 Flory, P. J. 'Principles of Polymer Chemistry', Cornell University Press, Ithaca, 1953
- 16 Booth, C. and Devoy, C. J. *Polymer* 1971, **12**, 309
- 17 Price, C., unpublished data

# Melting and annealing of oriented single crystal aggregates of *trans*-polydodecenamer

E. Martuscelli and V. Vittoria

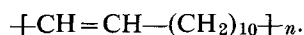
Laboratorio di Ricerche su Tecnologia dei Polimeri e Reologia, CNR,  
Via Toiano 2, Arco Felice, Napoli, Italy  
(Received 11 October 1971)

The annealing behaviour of single crystal aggregates of two samples of *trans*-polydodecenamer with a *trans* double bond content of 96 and 75% is examined. Quantities such as density, long spacing, apparent enthalpy of fusion and crystallinity are measured. Two different mechanisms of thickening of crystallites, are involved in the annealing process, corresponding to two different regions of temperature and long-spacing. The temperature and the long-spacing at which the transition occurs are dependent upon the configurational purity of the polymer increasing with the percentage of *trans* double bonds ( $T_A \simeq 63^\circ\text{C}$ ,  $L \simeq 111\text{\AA}$ ;  $T_A \simeq 67^\circ\text{C}$ ,  $L \simeq 137\text{\AA}$  for samples having *trans* double bond content of 75 and 96% respectively). The equilibrium melting points  $T_m^\circ$  and the surface free energy  $\sigma_e$  of the crystallites of the two samples of *trans*-polydodecenamer have been calculated thermodynamically by using the slope method. Values of 88 and  $80^\circ\text{C}$  for the thermodynamic temperature and of 20 and  $19\text{ erg/cm}^2$  for the end surface free energy are found for the two samples of *trans*-polydodecenamer with high and low *trans* double bond content respectively.

## INTRODUCTION

In preceding papers<sup>1, 2</sup> we described the crystallization and the morphological characterization of solution grown single crystals of *trans*-polydodecenamer and *trans*-polydecenamer as part of a study in which the single crystals of the polymers were subjected to oxidative attack by ozone and nitric acid. These studies were performed in an attempt to determine the number of double bonds in the crystals which are more accessible to the oxidative agents. The apparent rate of the reaction of the ozone on the double bonds in the case of *trans*-polydodecenamer was shown to be strongly dependent upon the percentage of *trans* double bonds in the chain.

In the present investigation we have studied the effect of heat treatment or annealing on the physical properties of samples of oriented chain folded single crystal aggregates of *trans*-polydodecenamer



The overall density, the apparent enthalpy of fusion and the overall crystallinity of the single crystal mats were measured and their values were correlated with the annealing temperature and the thickness of the crystallites. Using samples of polydodecenamer with different percentages of *trans* double bonds in the chain, we studied the effects of the configurational purity of the polymer on the annealing behaviour and on some

thermodynamic quantities such as the equilibrium melting point  $T_m^\circ$  and the free energy of folding  $\sigma_e$ .

We find these studies interesting, together with those previously reported, because the physical and technological properties of this kind of material are strictly dependent upon the configuration of the vinylene double bond. In fact, depending on the type of steric configuration assumed by the double bonds during polymerization, a thermoplastic crystalline polymer (high content of *trans* double bonds), or an amorphous elastomer at room temperature (low content of *trans* double bond) may be obtained.

Finally, we discuss briefly the mechanisms of thickening of the crystallites involved in the dry annealing of oriented single crystal mats.

## EXPERIMENTAL

As starting material, two samples of unfractionated polydodecenamer with *trans* double bond content of 96% and 75% were used. Henceforth, these samples will be called P12(a) and P12(b) respectively. Single crystals were prepared according to the method reported in a previous note by Keller and Martuscelli<sup>1</sup>. Some relevant characteristics, such as crystallization conditions and some thermodynamic quantities of the two samples of polydodecenamer are summarized in *Table 1*. After precipitation, the crystals

**Table 1** Molecular and thermodynamic properties of the two samples of *trans*-polydodecenamer. Crystallization conditions used to grow single crystals are reported

	Polymer	
	P12(a)	P12(b)
<i>trans</i> -double bond content <sup>a</sup> (%)	96	75
Melting point of bulk polymers (°C)	82	69
Fusion enthalpy <sup>b</sup> (cal/mol of repeating unit)	9700	8800
Concentration of the polymer used for crystallization, <i>n</i> -octane as solvent (wt. %)	0.10	0.12
Temperature of seeding (°C)	54	50
Temperature of crystallization (°C)	23	22

<sup>a</sup> *trans*-double bond content was determined by i.r. spectroscopy on 0.5% solution in CS<sub>2</sub>.<sup>21</sup>

<sup>b</sup> By diluent method using Flory's formula<sup>21</sup>

were filtered from the suspension at room temperature to form oriented crystal mats in which the lamella of the individual crystals lies essentially in the plane of the film. To minimize the possible effect of trapped solvent, the mats were first pumped down on a diffusion pump for several days. X-ray photographs taken with the beam parallel to the mat show fibre orientation over a wide angle. The fact that the reflections (110) and (200) are on the equator indicates that the molecular axes stand almost perpendicular to the film. Low-angle X-ray diffraction maxima are observed on the meridian.

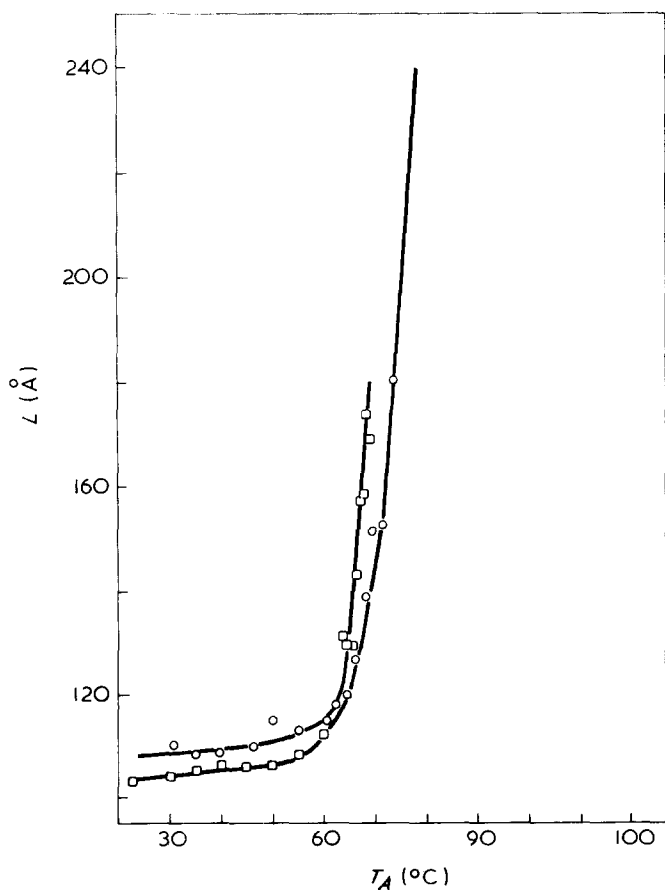


**Figure 1** Long spacing of *trans*-polydodecenamer single crystal aggregates as function of the annealing temperature. Annealing time 24 h. ○, P12(a): *trans* double-bond content 96%; □, P12(b): *trans* double-bond content 75%.

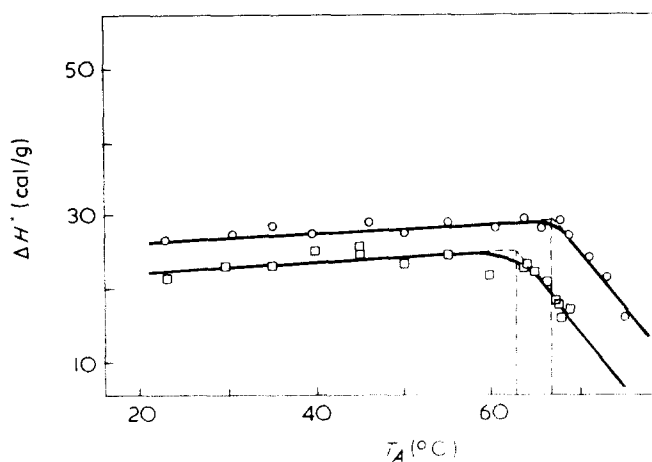


**Figure 2** Apparent enthalpy of fusion of *trans*-polydodecenamer single crystal aggregates as function of the annealing temperature. ○, P12(a): *trans* double-bond content 96%; □, P12(b): *trans* double-bond content 75%.

These films were used for the thermal experiments reported in the present note.

For the purpose of annealing, portions of the crystalline aggregates were wrapped in aluminium foil and placed in thin walled test-tubes. These tubes were first evacuated, then sealed, and finally placed in constant temperature baths for 24 hours. By evacuating the tubes it was hoped that any possible degradation of the samples would be avoided or at least reduced. The thickness of the lamellar crystals was calculated from their low-angle X-ray diffraction using Bragg's law. The small angle X-ray patterns were recorded at room temperature, by means of a pinhole collimated Rigaku Denki camera. A Perkin-Elmer differential scanning calorimeter DSC-1 was used to obtain melting points  $T_m$ , apparent heats of fusion  $\Delta H^*$  and crystallinities  $x_c$  of the polymer single crystal samples. For every measurement, 2-4 mg of weighed polymer were heated. Heating rates of 16 and 32 °C/min were used for P12(b) and P12(a) respectively. The calorimeter was calibrated in the temperature scale, at the scanning speed to be used, using substances with standard melting points. The peak maximum temperatures were assumed to correspond to the melting temperatures of the samples. They could be measured with a precision of  $\pm 0.5^\circ\text{C}$ . The apparent enthalpy of fusion  $\Delta H^*$  was computed by comparing the area under the fusion curve of the polymer samples with that obtained from a known weight of indium heated under the same conditions. Finally, the overall crystallinity was obtained as the ratio between  $\Delta H^*$  and the true enthalpy of fusion  $\Delta H$  whose values for the two polymers are reported in *Table 1*. Overall densities were measured at 23 °C by using a gradient column with isopropyl alcohol and ethylene glycol as miscible liquids. Results are accurate to  $\pm 0.001\text{g/cm}^3$ .

## RESULTS

In *Figures 1* and *2* the long period  $L$  and the apparent enthalpy of fusion  $\Delta H^*$  of P12(a) and P12(b) single crystal mats are shown as functions of the annealing temperature. The overall density of P12(b) versus the annealing temperature is plotted in *Figure 3*.

In order to discuss the data, it is appropriate to divide the relationship illustrated in *Figures 1 to 3* in two regions of high and low temperature sides. For convenience, the high temperature sides with a large slope are called region I and the low temperature sides with a small slope, region II. The annealing temperature corresponding to the transition from region II to region I is  $\approx 63^\circ\text{C}$  for P12(b) and  $\approx 67^\circ\text{C}$  for P12(a). Above these characteristic temperatures, the long spacing abruptly increases while the apparent enthalpy of fusion and the overall density (only density data of P12(b) are reported) sharply decrease falling below even their initial values at higher temperatures. In *Figures 4 to 6* the apparent enthalpy of fusion, the overall crystallinity and the overall density of samples of P12(a) and P12(b) single crystal mats are plotted *versus* the reciprocal of the long-spacing  $1/L$ . The quantities mentioned above at first increase with  $1/L$  up to a maximum value and then they begin to decrease. The fall off is more drastic in the case of P12(b) single crystal mats.

The long-spacing values relative to the inversion in the trend of the curves, henceforth called 'transition long-spacing', is  $\approx 137\text{ \AA}$  and  $\approx 111\text{ \AA}$  for P12(a) and P12(b) respectively.

The values of the crystallinity of the single crystal mats (ranging between  $\approx 30\%$  and  $\approx 50\%$ ) as determined by differential thermal analysis (d.t.a.) measurements, seem to be rather low especially if, as in the case of P12(b), the density of the samples can be compared with the crystallographic density value.

The crystallographic density of *trans*-polydodecenamer as deduced from X-ray analysis is  $1.001\text{ g/cm}^3$ . If the density of the amorphous polymer  $\rho_a$  is assumed equal to that of the completely amorphous polyethylene ( $0.85\text{ g/cm}^3$ ), then the mass crystallinity  $x_c$  of the unannealed single crystal mat of P12(b) ( $\rho = 0.952\text{ g/cm}^3$ ), calculated by using the expression:

$$x_c = \frac{(1/\rho_a) - (1/\rho)}{(1/\rho_a) - (1/\rho_c)}$$

turns out to be  $\approx 0.70$ .

This discrepancy, however, is not surprising and could be ascribed to either an overestimation of the true

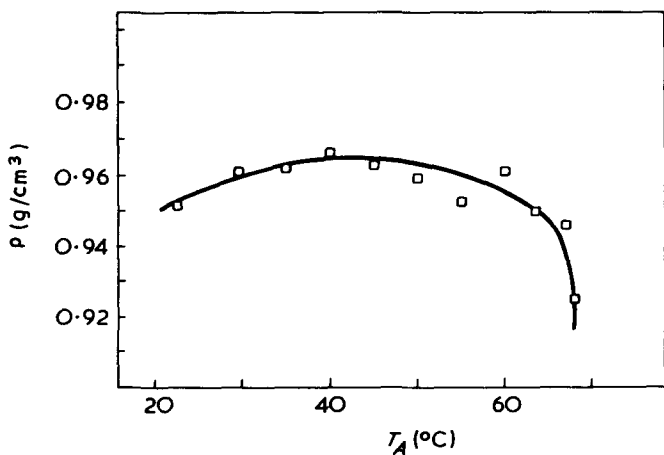


Figure 3 Overall density of *trans*-polydodecenamer single crystal aggregates of P12(b) sample as function of the annealing temperature

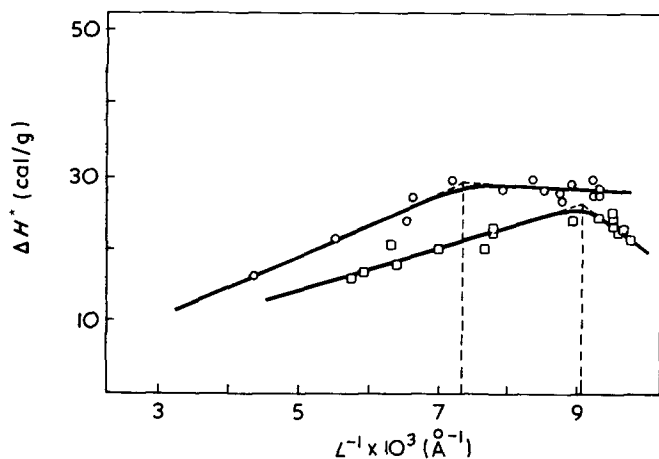


Figure 4 Apparent enthalpy of fusion of *trans*-polydodecenamer single crystal mats as function of the reciprocal of the long spacing.  $\circ$ , P12(a): *trans* double-bond content 96%;  $\square$ , P12(b): *trans* double-bond content 75%

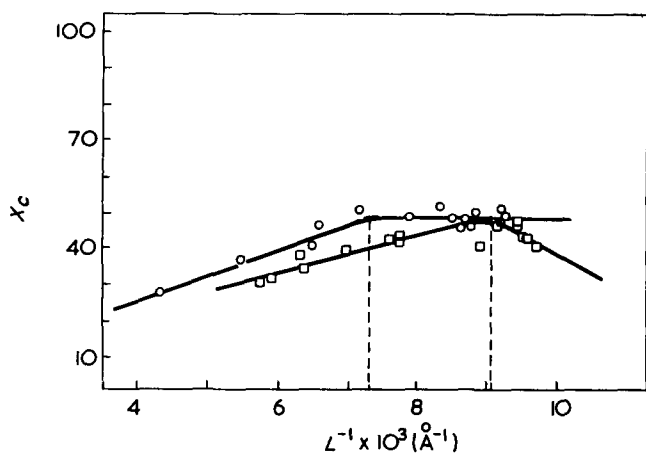


Figure 5 Crystallinity of *trans*-polydodecenamer single crystal mats (d.t.a. method) as function of the reciprocal of the long spacing

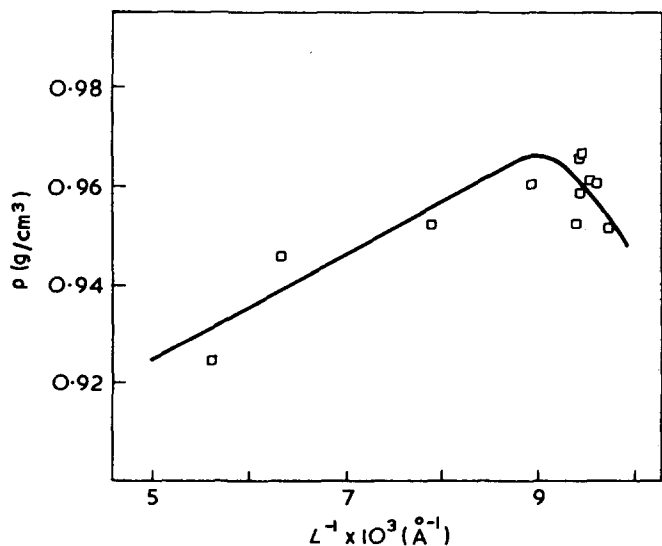


Figure 6 Density of *trans*-polydodecenamer single crystal mats (P12(b) sample) as function of the reciprocal of the long spacing

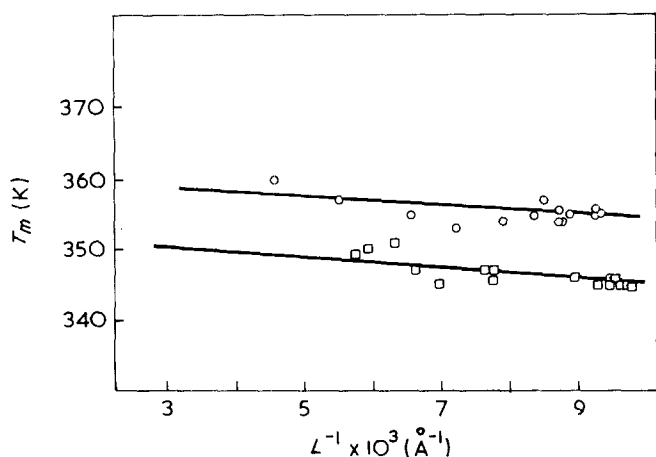


Figure 7 Melting temperature of trans-polydodecenamer single crystal aggregates as function of the reciprocal of the long spacing.  $\circ$ , P12(a): trans double-bond content 96%;  $\square$ , P12(b): trans double-bond content 75%

enthalpy of fusion  $\Delta H$  and/or to a systematic underestimation of the area of the d.t.a. endothermic peaks.

In Figure 7 the melting points are plotted against the reciprocal of the crystal thickness  $L$ . Good linear relationships are obtained for both polymers throughout the temperature range examined.

Finally, we wish to point out that the orientation of crystals determined by the X-ray method does not change drastically either before or after the heat treatment although a broadening of the low-angle reflection is observed in samples heated at higher temperatures.

## DISCUSSION

The experimental data reported in the previous section suggest that two mechanisms of thickening are involved in the annealing process of single crystal mats of P12(a) and P12(b). The corresponding temperature and long-spacing of transition can easily be deduced from the abrupt change in the trend of the plots of density, crystallinity, and apparent enthalpy of fusion versus the annealing temperature and the reciprocal of the long-spacing respectively (see Figures 1 to 6). This characteristic temperature and long-spacing, in the case of polydodecenamer, seems to be dependent upon the configurational purity of the polymer. As matter of fact, these values increase with the percentage of trans double bonds ( $T_A \approx 63^\circ\text{C}$ ,  $L \approx 111 \text{ \AA}$  for P12(b);  $T_A \approx 67^\circ\text{C}$ ,  $L \approx 137 \text{ \AA}$  for P12(a)) and thus with the melting point of the polymer.

A similar transition temperature located at about  $117^\circ\text{C}$  was found while annealing single crystal mats of polyethylene<sup>5,6</sup>. At this temperature the density, the tensile modulus, the solvent swelling capacity as well as the morphology suddenly changed. The morphological studies were performed by means of electron microscopic observations on cleft lamella of single crystals of linear polyethylene obtained by supersonic irradiation of the samples<sup>5</sup>.

On the other hand, in the annealing of bulk polyethylene the overall density continuously increases with the annealing temperature<sup>7</sup>. This implies a mechanism of thickening of crystallites in the bulk polymers different from that of a single crystal in oriented aggregates.

As far as the kind of mechanism involved in the low temperature region (region II) is concerned, it is likely that the thickening of the lamella, from between 10 and  $20 \text{ \AA}$ , proceeds through the motion of the polymer chains in the crystal along the backbone of the molecule according to the 'sliding diffusion mechanism' postulated by Hirai *et al.*<sup>8</sup> and by Peterlin<sup>9</sup>. Defects in the crystal, such as point dislocations of the type suggested by Reneker<sup>10</sup>, could contribute in lowering the energy barrier to the motions. The lamella retain their crystal lattice and individuality in the mat. The slight increase observed in the overall density, crystallinity and apparent enthalpy of fusion could mainly result from an improvement in the packing of lamella in the mat since the pre-existing holes can be filled by refolding chains. This, in effect, leads to a more intimate interlamellar contact. The possibility of the creation of an interlamellar link of the type postulated by Blackadder and Lewell<sup>6</sup> for polyethylene single crystal aggregates must also be taken into account when the mats of polydodecenamer are annealed at a temperature below that of transition.

Above the transition temperature the crystalline lattice is first destroyed, partly at least, and then reformed again, provided that the annealing time is sufficiently long. In other words, at higher temperatures the thickening proceeds through melting and recrystallization of the crystallites. A mechanism for that has been worked out by Kawai<sup>10</sup>. It is logical to conclude that during this process the lamella lose their individuality and the resulting material assumes a texture very similar to that of bulk polymers. This partial melting process is accompanied by a sharp decrease in crystallinity, overall density and apparent enthalpy of fusion.

It is interesting to point out that the apparent enthalpy of fusion and density of unannealed polyethylene single crystals, crystallized in a rather wide temperature range with the same morphology, increase linearly with the long spacing<sup>12,13</sup>.

This is a further indication that the transition observed while annealing single crystal aggregates is not an intrinsic property of the polymer single crystals but is chiefly due to the fact that the process of melting and recrystallization, in this case, leads to a rather abrupt change in the morphology of the material.

The initial lamellar single crystal texture of the mat is almost completely lost at higher temperatures of annealing and becomes similar to that of semi-crystalline bulk polymer although the orientation of the crystallites remains almost the same.

The equilibrium melting temperatures ( $T_m^\circ$ ) and the end surface free energies ( $\sigma_e$ ) were calculated for P12(a) and P12(b) by applying to the experimental data presented in Figure 7 Hoffman and Week's expression for the melting point lowering due to fold surface<sup>14</sup>:

$$T_m = T_m^\circ \left[ 1 - \frac{2\sigma_e}{\Delta H L} \right] \quad (1)$$

The equations of the straight lines interpolating the experimental points are:

$$T_m = 361 - 600 \frac{1}{L} \text{ for P12(a)}$$

$$T_m = 353 - 600 \frac{1}{L} \text{ for P12(b)}$$

Table 2 End surface free energy of the crystallites of series of polymers calculated according to the thermodynamic method

Polymer	$\sigma_e(\text{erg/cm}^2)$
Polyethylene:	
melt-crystallized	57 <sup>15</sup> ; 90 <sup>16</sup>
single crystals	89 <sup>11</sup> ; 70 <sup>17</sup>
Nylon-6:	
melt and solution crystallized	33 <sup>18</sup>
drawn filaments	42 <sup>19</sup>
trans-1,4-polyisoprene:	
single-crystals	
61% of LMF	47 <sup>20</sup>
29% of LMF	72 <sup>20</sup>
melt-crystallized	
100% of LMF	102 <sup>21</sup>
Polypropylene:	
melt-crystallized	175 <sup>22</sup>
trans-polydodecenamer	
96% of trans double bonds	20*
75% of trans double bonds	19*

\* Present paper

Consequently, the thermodynamic melting temperatures of P12(a) and P12(b) crystals are found to be 88 and 80°C respectively. Values of  $T_m^0$  of  $\approx 82$  and  $\approx 70^\circ\text{C}$  are obtained from interpolation of the plot published by Giannotti and Capizzi<sup>3</sup> of melting temperatures of polydodecenamers versus their trans double bond content. The method used by the above mentioned authors was Flory's method concerned with melting point decreases in the presence of diluents.

From the slopes of Figure 7, and by using the following crystallographic data<sup>4</sup>: monoclinic crystalline modification of the single crystals, *c*-axis period 14.85 Å with one structural unit in the period and 2 chains in the unit cell of volume 550.6 Å<sup>3</sup>, we obtain the values of 20 and 19 erg/cm<sup>2</sup> for the surface free energy  $\sigma_e$  of P12(a) and P12(b) crystallites. This finding seems to indicate that the configurational purity of the polymer has no appreciable effect on the  $\sigma_e$  of the crystallites. The values of  $\sigma_e$  found for the two samples of polydodecenamer are rather low if compared with the  $\sigma_e$  values of some other polymers (see Table 2) and could be accounted for by a more disordered crystallite surface. This finding is in agreement with oxidation and degradation studies performed by Keller and Martuscelli<sup>2</sup> on the single crystals of polyalkenamers. Most probably the surface disorder must be ascribed to the macrocyclic structure of these polymers<sup>23, 24</sup>. It is also noteworthy that, for the same thickness of the crystallites,

the values of the overall crystallinity and the apparent enthalpy of fusion of P12(b) are constantly lower than the corresponding values of P12(a) samples (see Figures 4 and 5). Assuming that when the long-spacing is the same, the relative mass amounts of the crystalline and amorphous phases are equal in the two polymers, we have to conclude that the deficiency in the overall crystallinity of P12(b) is principally due to the higher number of *cis* double bonds incorporated as defects in the crystalline lattice of this polymer.

## ACKNOWLEDGEMENTS

The authors wish to thank A. Botta, L. Araimo and C. Mancarella who helped in the experiments.

## REFERENCES

- Keller, A. and Martuscelli, E. *Makromol. Chem.* 1971, **141**, 189
- Keller, A. and Martuscelli, E. *Makromol. Chem.* 1972, **151**, 169
- Giannotti, G. and Capizzi, A. *Eur. Polym. J.* in the press
- Natta, G. and Bassi, J. W. *Eur. Polym. J.* 1967, **3**, 43
- Takayanagy, M. and Nagatoshi, F. *Mem. Fac. Eng., Kyushu Univ.* 1965, **24**, 2
- Blackadder, D. A. and Lewell, P. A. *Polymer* 1970, **11**, 125, 147, 659
- Kavesh, S. and Schultz, J. M. *J. Polym. Sci. (A-2)* 1971, **9**, 85
- Hirai, N., Yamoshita, Y., Matsuhata, T. and Tamusa, Y. *Rep. Res. Lab. Surface Sci. Okayama Univ.* 1961, **2**, 1
- Peterlin, A. *J. Polym. Sci. (B)* 1963, **1**, 279
- Reneker, D. H. *J. Polym. Sci.* 1962, **59**, 539
- Kawai, T. *Kolloid-Z. Z. Polym.* 1965, **201**, 104
- Roe, R.-J. and Bair, H. E. *Macromolecules* 1970, **3**, 454
- Fisher, E. W. and Lorenz, R. *Kolloid-Z. Z. Polym.* 1963, **189**, 97
- Hoffman, J. D. *SPE Trans.* 1964, **4**, 315
- Brown, R. G. and Eby, R. K. *J. Appl. Phys.* 1964, **35**, 1156
- Wunderlich, B. and Arakawa, A. *Tech. Rep. Rensselaer Politech. Inst. Troy, New York*, July 1963, No. 6
- Jackson, J. B., Flory, P. J. and Chiang, R. *Trans. Faraday Soc.* 1963, **59**, 1906
- Liberti, F. N. and Wunderlich, B. *J. Polym. Sci. (A-2)* 1968, **6**, 833
- Arakawa, T., Nagatoshi, F. and Arai, N. *J. Polym. Sci. (A-2)* 1969, **7**, 1461
- Keller, A. and Martuscelli, E. *Makromol. Chem.* 1972, **151**, 189
- Martuscelli, E. *Makromol. Chem.* 1972, **151**, 159
- Blais, J. J. B. P. and Manley, R. *St J. J. Macromol. Sci.* 1967, **B1** (3), 525
- Wasserman, E., Ben-Efraim, D. A. and Wolovsky, R. *J. Am. Chem. Soc.* 1968, **90**, 3286
- Scott, K. W., Calderon, N., Ofstead, E. A., Judy, W. A. and Ward, J. P. *Adv. Chem. Ser.* 1969, **91**, 399

# Rubber modified polystyrene: structural variation induced during pre-polymerization

G. F. Freeguard

*Department of Chemical Engineering, University of Nottingham, Nottingham NG7 2RD, UK  
(Received 13 March 1972)*

Different structures for the two phase system polystyrene-polybutadiene are shown to be produced at constant rubber concentration by varying the shear rate during the pre-polymerization stage in the bulk polymerization of styrene in the presence of dissolved rubber. Two distinct structural forms are identified: in one the dispersed phase is particulate with the overall aggregate particle size varying with the shear rate, whereas the other structure is in the form of a three-dimensional semi-regular network throughout the whole polymer.

## INTRODUCTION

The role of agitation in the production of high impact polystyrene (HIPS) during the bulk polymerization of a styrene solution of a butadiene rubber has been previously discussed in the knowledge that the system is non-Newtonian<sup>1</sup> and that there exists a minimum shear requirement for phase inversion<sup>2</sup>. The present paper describes in more detail how the final polymer structure can be related to the shear rate operating during the post-inversion period and links the observed structural variation with the previous hypothesis that at phase inversion the dispersed phase does not consist of simple droplets, but clusters or aggregates<sup>3</sup>. By adopting the design and operating procedure published previously<sup>3</sup> the phenomena of multiple inversion<sup>4</sup> is apparently suppressed and therefore an additional complication in this preliminary structural correlation is avoided. Thus this work is concerned with the particular case in which phase inversion apparently occurs at the earliest time that this is possible, due at that time to a favourable combination of thermodynamic, interfacial and rheological parameters. Unfortunately at present it would not appear possible to predict the phase volume ratio at inversion as a function of those parameters, since the mechanism is complex and not well understood. In a separate investigation a correlation between rheological properties and inversion point has been attempted together with a study of the effect of mass transfer, and these results will be discussed later in this series. For convenience therefore, the particular case considered is referred to as a 'smooth non-delayed inversion system'.

## EXPERIMENTAL

The polymerization conditions, apparatus and dimensions of the helical ribbon agitator were as previously described<sup>3</sup>. The polybutadiene rubber used in the investigation was Intene 55NFA, selected because of its

high initial solution viscosity, which increases considerably during pre-polymerization and thereby offers a wide choice of shear rate range for structural investigation. The rubber concentrations used were up to 10% wt/wt, because this gives a viscosity range within the limits of the design of the apparatus. The shear rate conditions were changed by varying the rev/min of the agitator either immediately after phase inversion or at some fixed interval of time, and then allowing an hour for the system to reach equilibrium before removing a representative sample. This was then polymerized in a glass tube at 100°C and subsequently a thin ultramicrotomed section used for structural analysis by electron microscopy using osmium tetroxide as fixing medium.

It is important to ensure that no polymerization occurs during the shear studies, since a relatively small additional conversion can lead to a large change in the apparent viscosity of the system. Two techniques were adopted and shown to give comparable results. More usually the polymerization was carried out at 70°C using benzoyl peroxide as catalyst to give a rate of 4% h<sup>-1</sup> to the required point, and then the polymerization was carefully inhibited by the addition of a minimum quantity of t-butyl catechol. Otherwise the reaction was carried out at 90°C under similar catalysed rate conditions to the required point, when the temperature was dropped to 70°C so that the conversion is insignificant during the shear rate variation period. The advantage of the second technique is that it is considerably easier to re-initiate the polymerization under controlled conditions for the final finishing stage for conversion to solid polymer.

## RESULTS AND DISCUSSION

Consider first the structure that exists at the phase inversion point. Rubber solution droplets will have been formed by a shearing action on what was the continuous

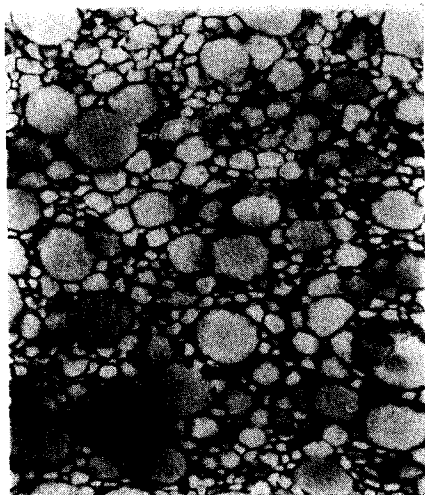


Figure 1 8% polybutadiene, shear rate 40 rev/min, agitation discontinued at inversion to give semi-regular network magnification.  $\times 7000$

phase, and it is likely that these droplets will account for approximately half the total volume of the system, and in size be of similar magnitude to the previous polystyrene droplets. Since these droplets are stabilized by graft copolymer<sup>5</sup> and do not readily coalesce, it is possible that on contact they exhibit a tendency to adhere, which is counteracted by the shearing force between droplets. At this stage in the process the continuous phase of swollen polystyrene and the dispersed phase of swollen rubber can be treated as separately polymerizing systems, particularly since the polymerization rate is lowered in the presence of dissolved rubber. Additionally, because of the viscous nature of the dispersed phase, transfer of styrene monomer from this phase to the continuous phase will be impeded, particularly if agitation is stopped. Thus on further polymerization there can be a volume reduction of the continuous phase which under controlled conditions is sufficient to cause the rubber solution droplets to touch in such a way that small volumes of polystyrene solution become trapped and there is no longer a truly continuous phase. Then the system consists of polystyrene solution and rubber solution as discrete volumes of comparable size separated by graft copolymer. During the polymerization of the rubber phase there will be an incompatibility of the forming polystyrene with the rubber present. When the polymerization rate is low there exists the possibility that diffusion of rubber molecules to the more compatible graft interfacial boundary can occur at a rate whereby the majority of the rubber then present is finally concentrated at the former phase boundary. The consequence of such a mechanism is the building up of a rubber-rich network through the whole polymer system, as shown in *Figures 1* and *2*. In one case shearing was discontinued before phase inversion was complete, so that some large polystyrene droplets survived until they eventually became incorporated into the network as large holes. However, it is generally not possible to assign which areas are continuous or dispersed phase in origin. Such a network can show remarkable stability to high

shearing action in the later stages of the polymerization, when the bulk viscosity has increased appreciably.

With sufficient shearing after phase inversion there is little tendency to form the network structure described; however, there is a marked tendency for rubber particles to aggregate and form large and complex clusters. At any time the size of such aggregates is a function of the shear rate and the system viscosity as is clearly demonstrated from the three sets of electron micrographs which comprise *Figures 3, 4* and *5*.

In these the effect of varying the shear rate is compared: (i) just after phase inversion, using 8% rubber (*Figure 3*); (ii) 1 h after phase inversion after a time interval when the viscosity of the system is higher due to an increase in polystyrene conversion (*Figure 4*); (iii) just after phase inversion but using 10% rubber to increase the system viscosity (*Figure 5*). In general it is seen that there is a correlation between aggregate size and shear rate and that the higher the system viscosity the lower the shear rate to produce a comparable aggregate structure. Furthermore because of the stability of the droplets it can be shown that once a required structure has been obtained, the shear level may be somewhat reduced to a level sufficient only to ensure good mixing and heat transfer without any further structural variation in aggregate particle size.

These findings may now be examined in relationship to the observations of other workers. Molau and Keskkula<sup>6</sup> have shown that the mechanism of rubber particle formation leads to two types of occlusions. Their type I is due to the formation of a multiple emulsion at the phase inversion point which survives the further polymerization, whereas the type II postulated is considered to be a consequence of polystyrene formed within droplets forming a separate phase because of incompatibility with the coexisting rubber.

Balova *et al.*<sup>7</sup> have observed that in systems of low viscosity, on discontinuation of stirring the rubber solution droplets adhere, and that on increasing conversion there is a size reduction due to a reduction in the rate of adhesion, until at high conversion and high viscosity the droplets do not adhere even without agitation. Unfortunately their microphotographs are at low magnification and do not show droplet structures in sufficient detail to fully support their argument.

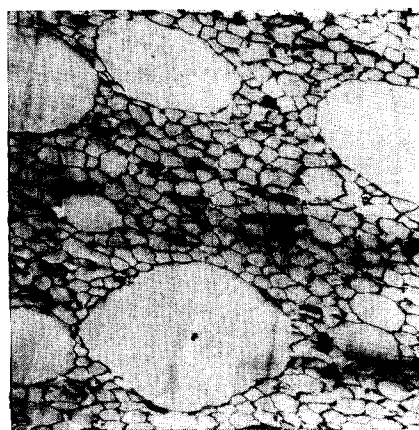


Figure 2 8% polybutadiene, shear rate 40 rev/min, agitation discontinued before inverted structure completed.  $\times 3500$



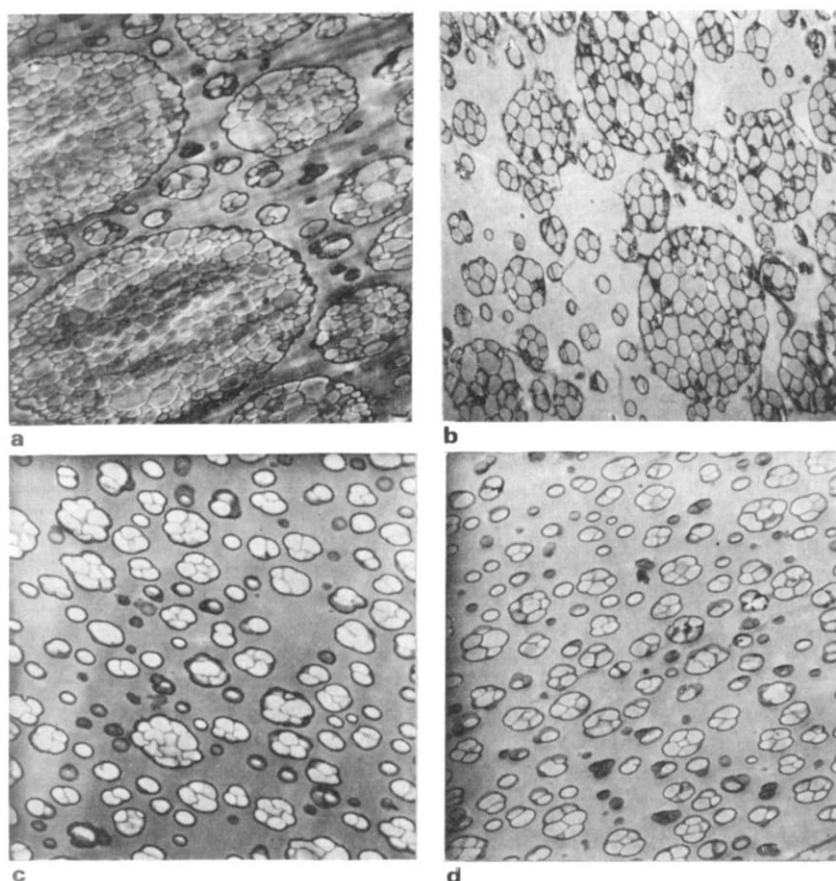


Figure 3 8% polybutadiene,  $\times 7000$ . Shear rate varied immediately after inversion. (a) 50 rev/min; (b) 80 rev/min; (c) 150 rev/min; (d) 200 rev/min

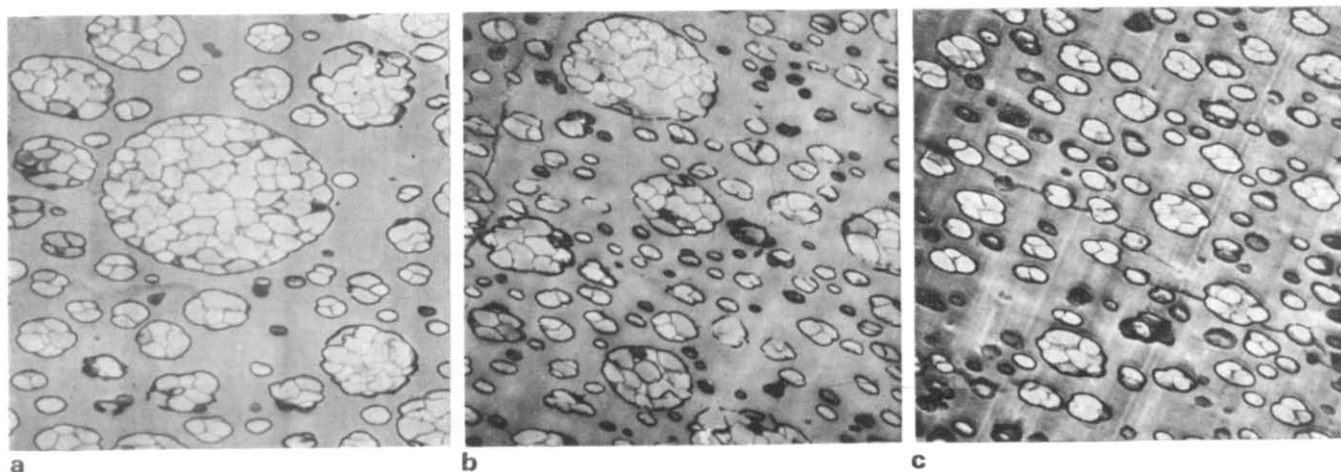


Figure 4 8% polybutadiene,  $\times 7000$ . Shear rate varied one hour after inversion. (a) 50 rev/min; (b) 110 rev/min; (c) 200 rev/min

Moore<sup>8</sup> varied rubber type, concentration and polymerization temperature at constant (but unquoted) shear rate using an anchor stirrer. He obtained a wide range of structures and concluded that final and overall particle size increased with viscosity of the initial rubber in styrene solution, provided that rubber type and concentration and pre-polymerization temperature were constant. However, Moore also concluded that the effect of these three variables could not be related to viscosity changes.

If these<sup>8</sup> micrographs are re-interpreted in terms of the findings of this investigation the variation in structure and particle size fit the pattern as previously discussed, since the effect shown is one of varying the system viscosity at roughly constant shear rate. Thus it would appear that a network structure with holes as shown with 10% Intene 55NFA at 60°C (see Fig. 9 of ref. 8) is a consequence of low shear, as shown here in Figure 1.

Similarly the complex particles shown for the lower rubber concentration of 5% (see Figs 5 and 6 of ref. 8)

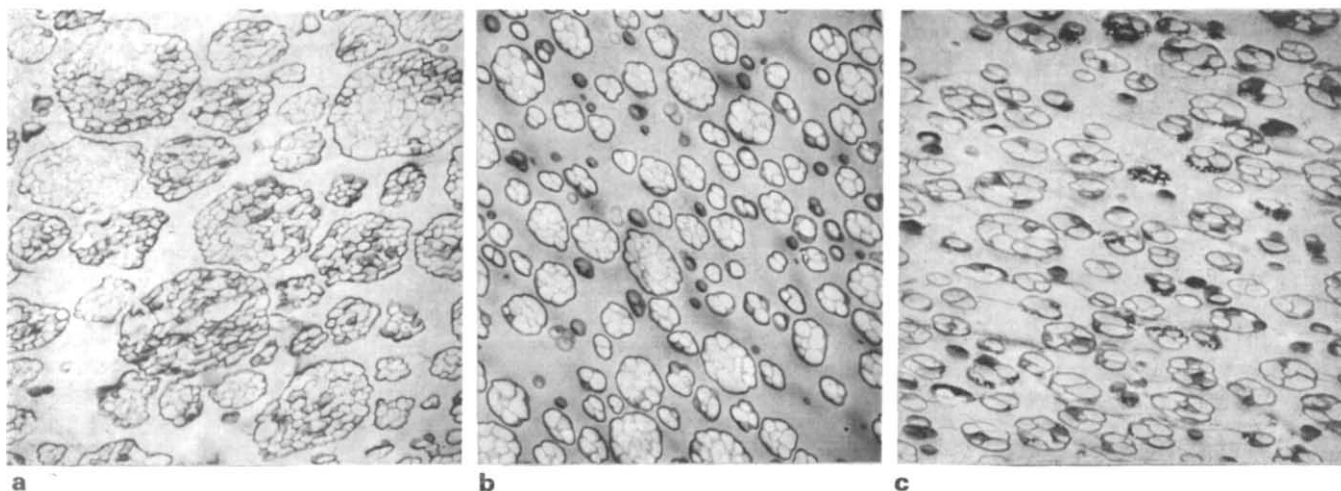


Figure 5 10% polybutadiene,  $\times 7000$ . Shear rate varied immediately after inversion. (a) 50 rev/min; (b) 120 rev/min; (c) 150 rev/min

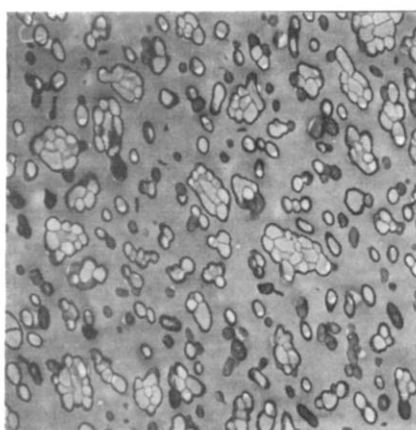


Figure 6 8% SBR rubber,  $\times 7000$ . Shear rate 40 rev/min 1 hour after inversion

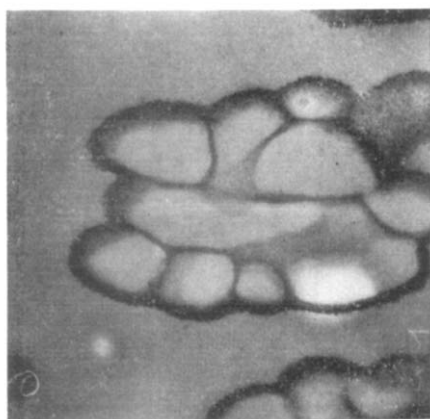


Figure 7 Aggregate rubber particle.  $\times 40\ 000$

It must, however, be noted that agitation conditions were apparently maintained constant to about 35% conversion<sup>8</sup>, so that the structural pattern to be compared is essentially that produced in the higher viscosity solution at the higher conversion level. Furthermore Moore has followed the industrial practice of conducting the polymerization in the presence of a chain transfer agent. In this way the system viscosity is lowered, and therefore illustrates a modified approach to varying the overall particle size, particularly in systems where there is a limit to the power available for agitation.

For comparison purposes the structure obtained with Duradene, a solution SBR containing  $\sim 25\%$  bound styrene and an  $\bar{M}_n$  of 130 000, is shown in Figure 6. The simple structure shown here is obtained at a lower shear rate than in the case of the polybutadiene system, and is in fact close to the minimum shear rate for a 'non-delayed' phase inversion of the system. This illustrates a difficulty that can arise if it is desired to obtain large complex particles in systems of low viscosity without a considerable delay in the phase inversion.

Consider next the detailed structure of the particles. It will be apparent that there is an implied presumption that Type I and II occlusions of Molau and Keskkula are absent from the structures shown, which are, however, interpreted as being formed by the aggregation of solution droplets. The evidence for this can be summarized as follows: (a) the electron micrographs presented in this paper can be interpreted as showing the breakdown of large complex particles to simpler particles by the application of increasing shear. In addition whereas the sub-particle size is somewhat dependent on rubber concentration it is apparently not dependent on shear rate: (b) some structures show evidence of coalescence within particles, particularly in systems of low viscosity (see Fig. 11 of ref. 3 and Figs 7 and 15 of ref. 8); (c) certain particles retain the appearance of aggregate droplets, as shown in Figure 7.

Slow polymerization rates should favour the concentration of the rubber phase in the droplet interface, particularly when the viscosity of the droplet is lowest since diffusion should occur more readily, and this will be the case in 'non-delayed' inversion systems.

are consistent with the structures shown in the present paper in Figures 3 and 5 for shear rates close to the minimum for phase inversion. For rubber solutions of much lower viscosity at phase inversion the less complex structural patterns are also shown, together with examples in low viscosity solutions of coalescence within particles.

## CONCLUSION

By adjusting the shear rate immediately after the phase inversion in the bulk polymerization of a rubber solution of styrene, the structure of the final polymer can be controlled. Several distinct structures have been identified, as follows.

1. Semi-uniform network, which may contain large holes.
2. Large composite particles which may contain several hundred sub-particles.
3. Medium composite particles of less than a hundred sub-particles.
4. Simple aggregate particles containing few sub-particles.
5. Highly sheared structures in which the sub-particles have either been coalesced or sheared to below the original sub-particle size.

Provided that a minimum shear requirement is met, multiple inversions and hence Type I occlusions of Molau and Keskkula may not generally be expected to be associated with these structures. Type II occlusions could be obtained superimposed on the structures shown, and would be most likely to occur when both solution viscosity and polymerization rate are high, since they originate from a diffusional problem.

Particle size control by the use of chain transfer agents

or mixtures of grafting/non-grafting catalyst systems are postulated as functioning by reducing the viscosity of the system primarily to obtain a desired shear profile in the reactor and secondary for promoting diffusion of the rubber to the interface under conditions of high rates of polymerization.

## ACKNOWLEDGEMENTS

Acknowledgement is made to the Science Research Council for their generous support of this work, to J.I.L. and H.M. for technical assistance and the International Synthetic Rubber Company for providing the samples of Intene and Duradene rubbers.

## REFERENCES

- 1 Freeguard, G. F. and Karmarkar, M. *J. Appl. Polym. Sci.* 1971, **15**, 1649
- 2 Freeguard, G. F. and Karmarkar, M. *J. Appl. Polym. Sci.* 1971, **15**, 1657
- 3 Freeguard, G. F. and Karmarkar, M. *J. Appl. Polym. Sci.* 1972, **16**, 69
- 4 Molau, G. E. *J. Polym. Sci. (A)* 1965, **3**, 1267
- 5 Molau, G. E. *J. Polym. Sci. (A)* 1965, **3**, 4235
- 6 Molau, G. E. and Keskkula, H. *J. Polym. Sci. (A)* 1966, **4**, 1595
- 7 Ballova, G. D., Bulatova, V. M., Vylegzhanina, K. A. *et al. Vysokomol. Soedin (A)* 1969 **11** (8), 1827
- 8 Moore, J. D. *Polymer*, 1971, **12**, 478

# Thermally stimulated conductivity of poly(vinyl fluoride)

A. R. McGhie, G. McGibbon, A. Sharples and E. J. Stanley

*Inveresk Research International, Inveresk, Musselburgh, Midlothian, Scotland, UK  
(Received 10 November 1971)*

A study has been made of thermally stimulated conduction processes in poly(vinyl fluoride), mainly with a view to providing information on the nature of trapping processes in polymers. Stored charge, injected by a previously applied field, was found to be released from this polymer in the form of a single peak at  $\sim 120^\circ\text{C}$ . It is deduced however, that the charge-carriers are not stored in discrete traps, but are simply slow-moving under ambient conditions. On raising the temperature, mobility is increased to give a detectable current, which increases with temperature to a peak at  $120^\circ\text{C}$  and then decays as the reservoir of charge is depleted. The peak temperature is thus determined not by a trap-depth, but by the activation energy of the mobility process. Two further thermally stimulated processes have also been observed. The first involves charge displacement (probably associated with dipole orientation) and results in a series of four current peaks, associated with second order transition processes. The second is a thermoelectric effect, arising from a temperature gradient formed across the sample on heating.

## INTRODUCTION

Over the past few years evidence has accumulated to indicate that the currents which can be detected in most polymers (including those such as polyethylene, polystyrene, and poly(ethylene terephthalate) which are normally considered as insulators) can be ascribed to the movement of electronic charge rather than of ions<sup>1-3</sup>. More recently still there have been indications that some quite simple vinyl polymers can show quite high dark currents, to an extent that they can no longer be considered as insulators<sup>4</sup>. Thus Viton (the copolymer of perfluoropropylene and vinylidene fluoride) gives a level of current seven orders greater in magnitude than polyethylene; and poly(vinyl fluoride) gives photocurrents of up to  $10^{-6}$  A.

The question thus arises as to the explanation for these differences in conductivity between different polymers. In particular it is of interest to know whether bulk physical or chemical structure is responsible; or whether impurity centres or defects are involved, acting as donors or traps. If the latter is the case, control over behaviour is possible in principle through the manipulation of impurity concentration.

The present paper explores the possible existence of traps, and uses the method of thermally stimulated conductivity to establish whether they are present in polymer films. In view of the fact that a considerable amount of information has been obtained on other aspects of the conduction process in poly(vinyl fluoride) this polymer is considered exclusively in this paper. The findings will be generalized in a later paper by studies using other polymers.

Thermally stimulated conductivity (t.s.c.) has been used as a technique for characterizing organic solids

fairly extensively and in the case of polymers it is now well established that multiple peaks are frequently observed in the t.s.c. spectrum<sup>5-14</sup>.

The present trend is to interpret these in terms of a number of discrete trapping levels. This conclusion is reasonable and of course well-accepted for the case of highly ordered materials such as silicon; but is somewhat surprising when applied to polymeric materials which invariably contain a significant fraction of a disordered component. This point is given particular consideration in the following reported study.

## EXPERIMENTAL

### *Materials*

The poly(vinyl fluoride) (PVF) samples used were Tedlar films, usually  $50\ \mu\text{m}$  in thickness, obtained from Du Pont. They contained a small amount of u.v. stabilizing additives, and are designated Type B (additive-containing) in another paper in this series<sup>15</sup>.

Electrodes in general were formed by evaporating silver onto each side of the polymer to form discs  $3.1\ \text{cm}^2$  in area. The electrical leads were attached to the electrodes by means of silver 'dag'.

### *Apparatus*

The thermally stimulated conductivity apparatus is shown diagrammatically in *Figure 1*. The instrument consisted of a cylindrical brass vacuum chamber and a stainless-steel cold finger, insulated thermally by an O ring and Tufnol annulus. The sample, which was clamped between two brass rings and held in contact with the finger, was  $\sim 3\ \text{mm}$  from a silica window. This window

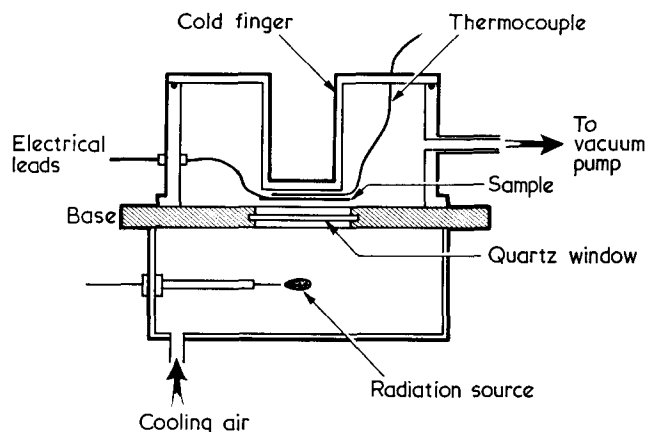


Figure 1 Apparatus for the determination of thermally and optically stimulated currents

allowed illumination of the sample from an MB/U lamp situated directly underneath.

The initial experiments in which the thermally stimulated conductivity plots were obtained had the top electrode of the polymer in contact with the bottom of the cold finger. This was done to ensure good thermal contact with the polymer sample.

**Heating system.** The temperature range with which the sample could be studied was from  $-196^{\circ}\text{C}$  to  $+200^{\circ}\text{C}$ . The low temperatures were obtained by the addition of liquid nitrogen to the cold finger and subsequent heating was effected by means of a Variac controlled, resistance wound heating element. This element gave an almost linear rate of temperature increase which could be varied over the range  $1\text{--}15^{\circ}\text{C}/\text{min}$ . The temperature of the sample was measured by means of a chromel-alumel thermocouple placed directly underneath the cold finger.

**Optical system.** The standard source of light used was a 125 W MB/U mercury lamp positioned  $\sim 5\text{ cm}$  underneath the sample. The overall intensity was  $50\text{ mW}/\text{cm}^2$  and since the outer envelope of the lamp was removed, the energy emission ranged from 185 nm to long wavelengths.

**Current measuring system.** Current was measured with a Vibron 33B2 vibrating reed electrometer by measuring the voltage drop across fixed resistors of values  $10^6$ ,  $10^8$ ,  $10^{10}$  ohms in a B33B current measuring unit. Difficulties were encountered during short-circuiting measurements, when the effective voltage generated became  $< 1\text{ V}$ ; and when the sample resistance fell below  $10^6$  ohm. This was an important potential source of experimental errors and arose because the voltage drop across the measuring resistor became comparable with that across the sample. The effect was apparent above  $100^{\circ}\text{C}$ . It was possible to check that the instrument was giving correct readings at temperatures below this point since there was some overlap on the scales used and consistency could be checked on switching from one measuring resistance to another. Above  $130^{\circ}\text{C}$ , however, meaningful results could not be obtained.

Measurements were made in a vacuum of less than  $10^{-3}\text{ mmHg}$  or in an atmosphere of nitrogen.

Voltage could also be determined using the electrometer, but only for values below 2 V. Unfortunately the

use of the Lindemann electrometer described later in connection with the measurement of higher steady voltages, was not possible for dynamic experiments.

### Methods

**Opposed electrodes.** Since the polymer was heated from one side only and the thickness of the sample of PVF was usually  $50\text{ }\mu\text{m}$  it is clear that a thermal gradient must exist across the film and this was the reason for the thermoelectric effect discussed later. This effect obscured the high temperature part of thermally stimulated conductivity plot and a system using split-opposed electrodes was used to minimize it. The electrodes were of the same total area ( $3.1\text{ cm}^2$ ) but consisted of two semi-circular electrodes separated by about 3 mm (Figures 2a and b). The diagonally opposite electrodes on either side were connected to each other so that current arising from the thermal gradient was counter-balanced. In order to prevent the two electrodes short-circuiting while in contact with the finger it was necessary to place an insulating layer of Teflon FEP ( $12.5\text{ }\mu\text{m}$  thick) between the finger and the sample.

Owing to the poor thermal conductivity of the Teflon FEP, a further temperature gradient was set up relative to the cold finger, which could only be overcome *in vacuo* by using a very slow heating rate. To reduce this effect a stainless-steel jacket was fitted over the end of the finger enclosing the sample between two layers of Teflon FEP (Figure 2c). An atmosphere of nitrogen was also used in these experiments to improve the heat transfer properties further. A control experiment with a sample of PVF with unopposed electrodes in contact with the finger showed no difference to that carried out under evacuated conditions.

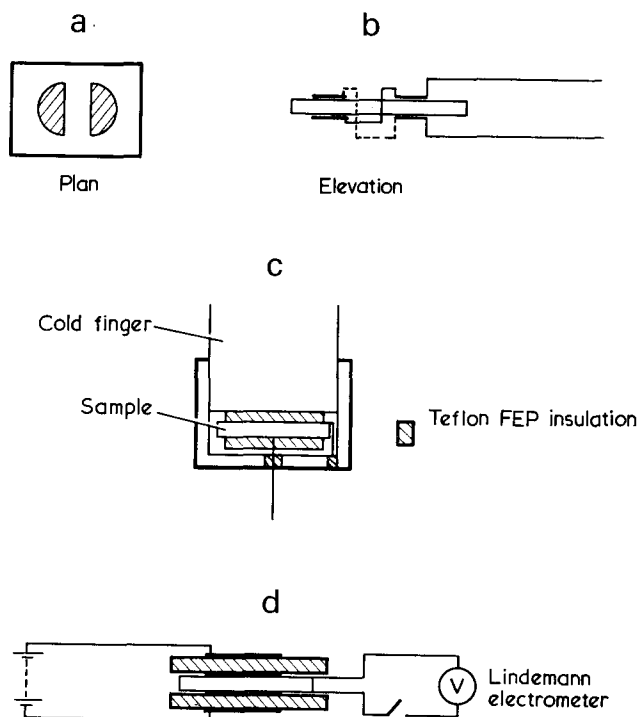


Figure 2 Use of split-opposed electrodes ((a) and (b)) and steel jacketting (c) to minimize the effects of thermal gradients. (d) Experimental set-up for measuring voltage drop across PVF with blocking electrodes

**Blocking electrodes.** In experiments where it was necessary to prevent injection of charge into the polymer films from the metal electrodes a system using blocking electrodes was devised. The blocking electrodes, made of 12.5  $\mu\text{m}$  thick Teflon FEP were pressed into contact with the PVF under a pressure of 20 000 lb (1 lb  $\approx$  0.45 kg) and at a temperature of 60°C for 30 min. This was to ensure good contact between the polymer and so improve heat conduction across the system. Silver electrodes were then evaporated onto the outside of the sandwich arrangement and the system was enclosed in the stainless-steel jacket in the same way as described previously.

A thermally stimulated conductivity control experiment using Teflon FEP was carried out and this showed that this polymer was thermally inert in that no measurable peaks in the range of temperatures used in the experiments were observed.

In order to keep the results comparable, a voltage of 320 V was applied across the sandwich equivalent to a voltage of 120 V across the PVF. This was checked using a Lindemann electrometer.

**Effect of heating rate on the thermally stimulated conductivity plots.** Experiments were carried out to determine the effect of heating rate on the positions and heights of the peaks of the thermally stimulated conductivity plots. The heating rate was varied between 2°C/min and 15°C/min and it was found that the positions of the peaks below room temperature were displaced towards a higher temperature with increasing rate, by an average value of 10°C. However, the charge calculated from the area under the current-time curves was constant at  $\sim 3 \times 10^{-8}$  coulombs.

At high heating rates ( $> 5^\circ\text{C}/\text{min}$ ) it was found difficult to obtain the high temperature peak unequivocally without experiencing the difficulties in current measurements which have been mentioned earlier.

Also inaccuracies arose in the blocking electrode and opposed electrode temperature measurements owing to the presence of the Teflon FEP layer between the thermocouple and the film sample.

Because of these inaccuracies and the difficulty with the high temperature peak it was decided to use a heating rate in the region of 3°C/min.

## RESULTS AND DISCUSSION

The study of thermally stimulated currents as a means of obtaining information on trapping levels is usually based on the following experimental procedure. A source of energizing radiation (e.g. ultra-violet light) is applied to the material at low temperature, in order to excite charge-carriers (e.g. electrons) either from the valence band or from donor centres to the conduction band. The carriers then migrate under the influence of an applied field or trapping centres where they are localized in the trapped state at low temperature. On removing the radiation and raising the temperature under short circuit conditions, the associated thermal energy is eventually sufficient to release the trapped carriers, and a current is observed corresponding to their movement to recombination centres. The current rises to a peak and then decays as the traps are thermally emptied. The temperature at which the peak occurs depends on the trap depth, and on the heating rate, but can be analysed to determine the value of the former.

In the present case with PVF, this type of effect was not observed. Thus although PVF shows evidence of photoeffects at room temperature, the application of u.v. or visible light at  $-196^\circ\text{C}$  to, for example, a 50  $\mu\text{m}$  film at 120 V, does not give rise to any detectable current when the sample is subsequently warmed under short circuit to  $+30^\circ\text{C}$ . Work reported elsewhere<sup>3,4</sup> has indicated that the explanation probably lies in the fact that PVF, and indeed most simple polymers, do not contain inherent charge-carriers. The currents observed in the dark and on optical stimulation in fact arise by injection of carriers from the external electrode. With this in mind an experimental sequence was used which did in fact give rise to thermally stimulated effects in a range of polymers, including PVF, polyethylene, poly(ethylene terephthalate) and Viton (a copolymer of perfluoropropylene and vinylidene fluoride). The results are least complicated below room temperature, and studies in this region are discussed first in relation to PVF, in the following section.

### Thermally stimulated current below room temperature

The following experimental sequence designated sequence I was applied to a 50  $\mu\text{m}$  PVF film, onto which had been evaporated silver electrodes. A voltage of 120 V was applied at 20°C *in vacuo* for  $10^4$  sec. The film was then cooled to  $-196^\circ\text{C}$ , and short circuited. On heating the sample at 2.5°C/min, the current-time relation shown in *Figure 3(I)* was obtained. It was argued that the application of a field at 20°C, which is known to give rise to detectable current ( $\sim 10^{-11}$  A/cm<sup>2</sup> in the above case), should result in the injection of charge-carriers, which may subsequently be trapped. By lowering the temperature to  $-196^\circ\text{C}$  with the field still applied, the charge may remain trapped on short-circuiting. It is thus possible that the peaks observed in *Figure 3(I)* correspond to the thermal release of the charge, and its subsequent return to its image charge on the electrode. The direction of the current in *Figure 3(I)* was in the correct direction (namely opposite) to that observed during the application of the field at 20°C. It might thus be deduced that there are at least three discrete trapping levels in PVF.

However, if this explanation were correct, it should follow that on applying a field at  $-196^\circ\text{C}$  to a fresh sample and then raising the temperature (sequence II), the current should increase progressively and that there should be no regions of decreasing current. Thus, no peaks should be observed in this type of experimental sequence. In fact the plot shown in *Figure 3(II)* was obtained, which is similar in shape but opposite in sign to *Figure 3(I)*.

An alternative explanation for these peaks which is consistent with the above results is that the application of a field at room temperature, or in sequence II, (*Figure 3*), displaces charge to a limited extent<sup>1,6</sup>; and that this charge returns to its original position on short circuiting, during sequence I (*Figure 3*). Such limited and reversible charge displacement is of course typified by dipole orientation, and the amount of charge displaced ( $3 \times 10^{-8}$  coulombs/cm<sup>3</sup>) is consistent with this explanation in the present case. If it is assumed that the dipoles are only partly oriented under the above conditions, the application of higher field strengths should result in higher current peaks in *Figure 3*, with the amount of charge associated with the area under the peaks, proportional

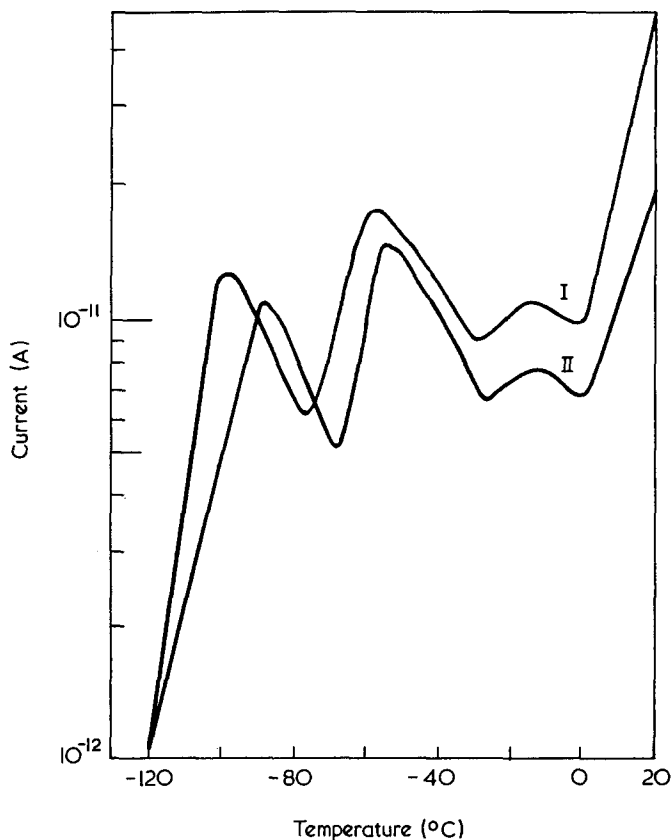


Figure 3 Thermally stimulated currents in PVF below room temperature

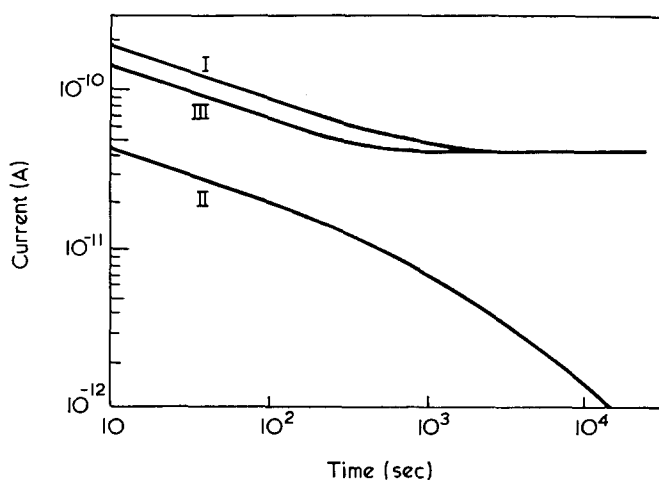


Figure 4 Current-time relationships in PVF film at 20°C: 120V across a 50  $\mu\text{m}$  film. (I), Silver electrodes evaporated onto PVF; (II), blocking contacts; (III), (I) and (II)

to (voltage)<sup>1.0</sup>. This was in fact found to be the case. The effects below room temperature thus do not involve the injection and trapping of a localized space charge, which would be expected to have a voltage dependence involving a square, or higher power.

In order to confirm this point, the experiments discussed above were repeated using a sample of PVF film which was sandwiched between two quartz plates, with the silver electrodes evaporated onto the quartz, and only in light contact with the PVF. A separately reported study<sup>15</sup> has shown that electrodes of this kind are not injecting (and this point is confirmed in the next section), but in spite of this fact identical plots to those shown in

Figure 3 were obtained. Hence, the charges involved in these thermally stimulated current experiments below room temperature cannot arise by injection, and are probably associated with dipole orientation. Their orientation or relaxation at three discrete temperatures is more likely to be associated with second order transitions, at which various radicals or chain-segments become mobile.

Various workers have in fact reported transitions in PVF, and a summary of these results are given in Table 1. The thermally stimulated current peaks at -60°C and -20°C are thus consistent with previously observed transition points. The lower peak at -100°C is below the range used by previous workers; while the second order transition work indicates that a further t.s.c. peak may be expected above room temperature. It should be appreciated that there is no absolute significance to be attached to the t.s.c. peak temperatures, which are strongly dependent on the experimental conditions, e.g. rate of heating.

Table 1 Comparison of thermally stimulated current peak temperatures with second order transitions in PVF

Method	Peak temperatures (°C)			
Present work (t.s.c.)	-100	-60	-20	+75
Dynamic <sup>17</sup>	—	—	-20	+41
Dynamic <sup>18</sup> 1Hz	—	-75	—	+45
Dielectric loss max <sup>12</sup>	—	-60	—	—
(mech. relax. at -100°C)				

#### Currents at room temperature

The application of a field at room temperature (120 V across a 50  $\mu\text{m}$  film of PVF for example) with evaporated silver electrodes results in a current-time relation of the form given in Figure 4(I). The existence of a steady-state current suggests that with evaporated electrodes charge carriers are being continually injected, and transported through the film. The use of silver on quartz electrodes lightly pressed against the polymer gives rise to a continually decreasing current, at a lower level. In this case injection is absent, and current is associated exclusively with the orientation of dipoles—a process which of course eventually terminates when the dipoles take up steady-state positions in the presence of the field. The area under this curve (II) is  $2.5 \times 10^{-8}$  coulomb, and the fact this corresponds quite closely to the combined areas of the peaks in Figure 3 ( $3 \times 10^{-8}$  coulomb) gives strong support to the conclusion that the low temperature t.s.c. peaks do not involve injection and trapping. With evaporated electrodes (I in Figure 4) the dipole orientation process is superimposed on the charge-injection process.

The short circuiting of the sample with pressed, non-injecting electrodes, gives rise to a current-time relation which is equal but opposite in sign to II. Thus the oriented dipoles return to their normal positions on short-circuiting at room temperature, although a period of some  $10^4$  sec is required. If the sample with evaporated electrodes is short-circuited after the application of a field, a plot similar to II is again obtained, indicating that the dipoles relax as might be expected; but that if any trapped charge is present, it is not released to any detectable extent.

The charge-injection process on application of the field can be separated from the dipole orientation process

by subtracting II from I to give III. The important feature of this plot is that it is still time-dependent in the early stages until a steady state has been set up, indicating that a detectable amount of charge is absorbed by the film. Insofar as this charge is probably located near to the injecting electrode, its effect in the external circuit will only be registered in proportion to the distance moved. Consequently the area under curve III, which is  $1 \times 10^{-8}$  coulomb (in a  $1.5 \times 10^{-2} \text{ cm}^3$  sample) only represents a lower limit for the injected charge. Nevertheless, the important point is that this charge is retained by the polymer on short-circuiting at room temperature, and so may be expected to be released at some higher temperature.

Thus from the above experiments, there are indications that a charge release peak may be observed above room temperature; and as there is known to be a major second order transition in this region it is also expected that a further dipole-orientation peak may be observed.

#### Thermally stimulated currents above room temperature

The two sequences involving applying a field at room temperature, cooling to  $-196^\circ\text{C}$ , short-circuiting and warming (I); and cooling under short-circuit to  $-196^\circ\text{C}$ , applying a field, and warming (II) were extended to the range above room temperature. In Figure 5 heating was in fact continued to  $100^\circ\text{C}$ . The low temperature peaks occur as before (slightly displaced owing to the use of different experimental conditions), and some new features are apparent above room temperature. Plots I and II in this region are no longer similar in contour although they are opposite in sign. In sequence I, a peak is apparent at  $75^\circ\text{C}$ , but this is swamped in sequence II (with field applied) by the normal conduction current, which becomes significant above  $-20^\circ\text{C}$ . This peak is of obvious interest, especially as it is in a region where it could reasonably be assigned to the main glass-to-liquid transition (Table I). However, it is followed by a region of further current increase even in sequence I (which uses short-circuit conditions), which tends to overlay the  $75^\circ\text{C}$  peak. This is of some concern in that it reaches the high current value of  $10^{-8} \text{ A}$  at  $120^\circ\text{C}$ , and decays only slowly from this value. The charge displaced during this period ( $10^{-4}$  coulomb in a  $1.5 \times 10^{-2} \text{ cm}^3$  sample) is far in excess of what might be reasonably ascribed to the release of trapped charge, and so an alternative explanation was sought.

In a separately reported study<sup>15</sup> on photoeffects in PVF it was observed that a photoelectric e.m.f. and current could be obtained. The current in the present case could thus be thermoelectric in origin, in view of the fact that the sample is not only heated, but is also subjected to a temperature gradient. If this is correct the effect should also be present in a fresh sample which has not previously been subjected to a field, and the consequent injection of charge. This was in fact found to be the case, and the direction of the current was consistent with the flow of electrons away from the higher temperature electrode. When the temperature gradient was reversed by heating the normally cooler electrode by a source of radiant heat, the direction of the current was similarly reversed. A further feature of the effect which indicated its thermoelectric origin was the associated voltage. The voltages associated with dipole orientation were too large to be recorded by the electrometer used but

were in excess of the figure of 2V (the experimental limit of the instrument). (These high values are consistent with the high voltages ( $>100 \text{ V}$ ) used to produce dipole orientation.) For the thermoelectric effect, however, a much lower voltage of  $\sim 100 \text{ mV}$ , was observed.

Thus the large persistent currents observed under short-circuit conditions at high temperatures are adequately explained. The effect also yields the useful piece of information that the charge-carriers involved are electrons rather than holes. It is of some inconvenience, however, in that it overlays the  $75^\circ\text{C}$  peak and so makes it difficult to decide whether this is a further dipole relaxation effect; or whether it is associated with the release of any injected charge in samples which have been subjected to previously applied field. It is, of course, the release of such charge, possibly from trapping centres, which is the main purpose of this study.

Two approaches were used to overcome these difficulties. In the first, use was again made of non-injecting electrodes. The thermoelectric effect depends on the displacement of charge across the polymer/electrode interface, to differing extents determined by the temperature gradient. The prevention of injection should thus eliminate the effect. Unfortunately the simple expedient of using pressed electrodes which is effective below room temperature, fails at higher temperatures because the softening of the polymer results in improved contact, so that injection becomes increasingly apparent. (This was confirmed in various ways including the determination of transferred static charge on separation of the polymer, and measurement of the steady-state current under an applied field.) Teflon FEP spacers of  $12.5 \mu\text{m}$  thickness were found to be effective, and a sandwich was constructed of silver-on-Teflon FEP/PVF/Teflon FEP on-silver.

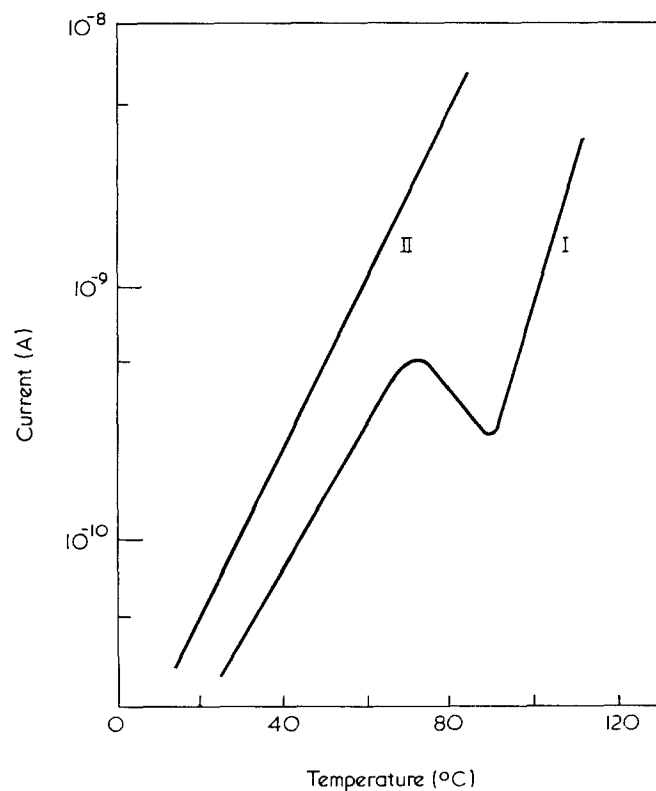


Figure 5 Thermally stimulated currents in PVF above room temperature using injecting electrodes



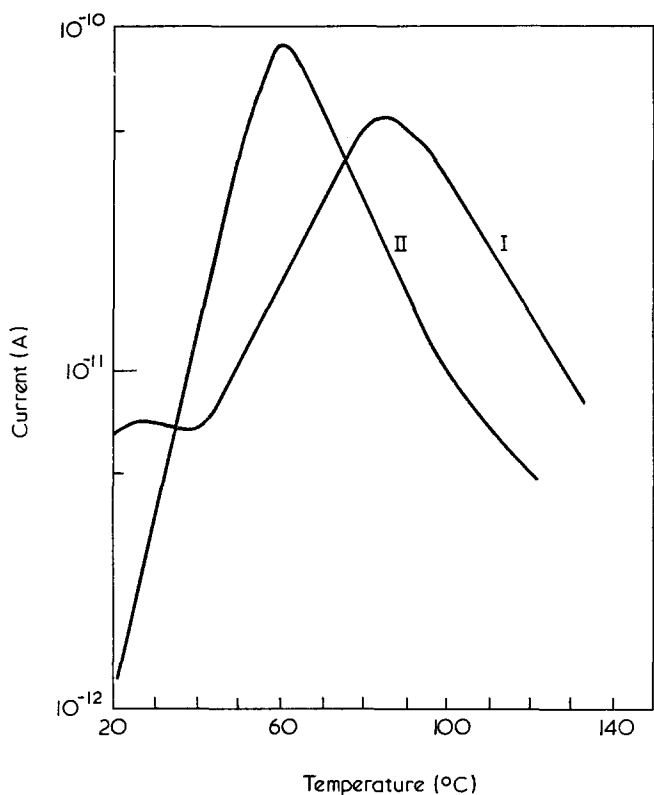


Figure 6 Thermally stimulated current in PVF above room temperature using non-injecting electrodes

From the equation:

$$\frac{V_1}{V_2} = \frac{d_1 \epsilon_2}{d_2 \epsilon_1}$$

where  $V$  and  $d$  represent voltage and distance, and  $\epsilon$  is the dielectric constant, it was calculated that a voltage across the sandwich of 320 V was necessary to provide a voltage drop of 120 V across the 50  $\mu\text{m}$  PVF film. The resulting current-time plots at 20°C, both on application of the voltage, and on subsequent short-circuiting, were identical with plot II in Figure 4, as would be expected.

On heating a fresh sample to 130°C no current was observed, indicating that the thermoelectric effect had been eliminated. With sequence I, involving heating a previously charged sample under short-circuit, the normal low temperature peaks were evident, and above room temperature one single peak was apparent (Figure 6) with no further effects at higher temperatures. The peak in fact was displaced slightly from that in Figure 5 owing to the different temperature measurement arising from the use of the insulating Teflon FEP layer. The peak temperature was 95°C. A similar peak was observed in sequence II, which gave a plot similar in contour, but opposite in sign to I. The charge associated with this peak,  $7.2 \times 10^{-8}$  coulomb, is slightly greater than that associated with the low temperature peaks under similar conditions ( $3 \times 10^{-8}$  coulomb).

It thus seems reasonable to ascribe this peak to the main glass-to-liquid transition, determined by mechanical methods to lie at 41–45°C (Table I), and to associate it with the displacement of dipoles.

The question thus still remains as to whether a peak corresponding to the release of trapped charge can be detected at higher temperatures. The second approach to minimizing the thermoelectric effect involved the use

of half-disc electrodes evaporated onto the PVF, and connected in opposition in order to cancel out the thermal gradient across the film (Figures 2a and b). Using this approach it was found that the thermoelectric current (observed using a fresh sample) was not in fact eliminated, but it was reduced to the level of  $\sim 10^{-11}$  A at 100°C, and this was considered to be sufficiently encouraging to look for the release of trapped charge.

In order to increase the chance of detecting a charge release peak, voltage was applied at higher temperatures, in the hope of injecting an increased amount of charge. When 120 V was applied to a 50  $\mu\text{m}$  thick film of PVF at 80°C, the current-time relation before a steady-state current was reached indicated that  $\sim 7 \times 10^{-5}$  coulomb is introduced—a significant increase over the amount introduced at 20°C. On cooling to room temperature and heating under short-circuit (sequence I) the normal 75°C peak was observed, but on raising the temperature further the current increased again, beyond the level expected for the residual thermoelectric effect. A further difficulty now arose in that above 90°C the effective resistance of the sample becomes less than that of the measuring resistor in the electrometer with the result that distorted current readings are obtained. In order to overcome this problem the temperature was held steady at 110°C, and the current measured (Figure 7). The current eventually started to decay after 600 sec, and approached the level associated with the residual thermoelectric effect. It was thus only possible to estimate the location of the peak on the temperature scale, and this estimated value was 120°C. The amount of charge estimated from the area under the peak was  $\sim 3 \times 10^{-5}$  coulomb.

It is thus established that a peak can be observed in the thermally stimulated spectrum of PVF which is not associated with the reversible displacement of internal charge (for example dipole orientation) as it does not appear when non-injecting electrodes are used. It can thus reasonably be ascribed to the release of charge, injected by the prior application of a field. Only one peak has been detected and this is located at 120°C.

The fact that charge can be injected and immobilized for long periods, and subsequently released by thermal (or as reported elsewhere optical) energy might indicate that the 120°C peak can be considered as a trap. However, this is not necessarily the case if a trap is defined as a localized centre, different in nature from the bulk of the polymer, and occurring only to a limited extent. This definition is important insofar as it involves the presence of physical or chemical defects in the overall structure; and if the latter is the case there exists the possibility of removing or neutralizing these impurities, and so obtaining control over behaviour. A simpler alternative explanation, however, is that the charge carriers after injection are slow-moving to an extent which is determined not by traps but by an inherently low-mobility process, such as hopping. The effect of increased temperature is thus to increase mobility and so to speed up the release of charge. When the half-life of this process becomes comparable with the time scale of the experimental method (determined in the present case by the rate of heating) discharge becomes measurable and gives rise to a current which first increases with increasing temperature, and then decays when the supply of charge is depleted. A peak is thus obtained which is no longer characteristic of a trapping energy level; but is determined by the current-

temperature relation for the polymer, and the experimental rate of heating.

In the former case the thermal energy would overcome the energy gap between the trapping level and that of the conduction level, which itself may involve a thermally activated mobility process. The situation is represented by *Figure 8(a)*. Provided that the rate of movement of charge-carriers in the conduction level is sufficiently rapid to be non-rate-limiting (which probably means that  $\Delta E_c$  should be less than  $\Delta E_t$ ) then the thermally stimulated current peak is determined by the trap depth  $\Delta E_t$ . In the second case, however, (*Figure 8(b)*), the peak is determined by the activation energy of the carrier mobility only ( $\Delta E_c$ ), and hence is an inherent characteristic of the material, rather than of any defects.

In order to distinguish these possibilities, a study was made of the steady state current-temperature relation in PVF.

#### Steady state current-temperature relation in PVF

The thermally stimulated current experiments (which yield current as a function of both temperature and time) have shown that two processes occur when a field is applied to a PVF film. There is a reversible displacement of charge, probably corresponding to the orientation of dipoles; and there is a time-dependent injection current, involving electrons injected from the electrode. It is obviously necessary to separate these two processes when attempting to study temperature dependence of the steady-state current.

In order to overcome this difficulty, the voltage was applied at a high temperature, and the steady-state current

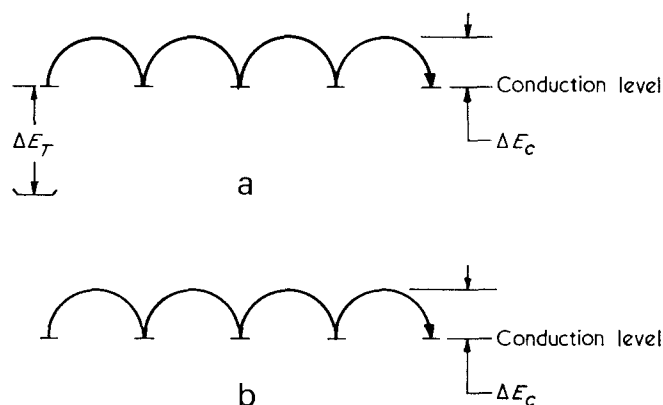


*Figure 8* (a) Thermally stimulated current arising from detrapping; (b) thermally stimulated current associated with the increased mobility of charge, which is effectively immobilized at lower temperatures

(after  $10^4$  sec) was determined at a series of decreasing temperatures. Using this sequence of events it was assumed that the dipoles would be oriented at the higher temperatures, and would remain so on passing through the second order transition point. The results given in *Figure 9* show that under these conditions there is a single value for the activation energy of 1.05 eV, between 150°C and 20°C.

If the explanation for the charge release peak at 120°C in *Figure 7* is one involving traps, then it is known that after  $10^4$  sec at 110°C (*Figure 7*) this charge is released, and hence that the traps must be empty. At room temperature, however, it is also known (*Figure 4*) that the injected charge persists for  $10^5$  sec under short-circuit conditions. Consequently in the steady-state current experiments, trapping would be expected to become evident between 80°C and 20°C, with the result that a discontinuity in the plot would be expected in this region. In fact no discontinuity was observed (*Figure 9*).

It thus follows that discrete traps, present in the polymer to only a limited extent, are not present.

#### CONCLUSIONS

Results from thermally stimulated current experiments using PVF are consistent with the picture that in the normal conduction process charge-carriers are not inherently generated from within the polymer, but are injected from the electrodes on the application of a field. On subsequent short-circuiting at room temperature the movement of these charge-carriers in the absence of a field is so slow that no detectable current is observed ( $< 10^{-15}$  A). The application of thermal energy, however, causes an increase in mobility with the result that the associated current at first increases, and then decreases as the reservoir of previously injected charge is depleted. The resulting current peak has typically a value of  $10^{-9}$  A at 120°C. The activation energy of the process (1.05 eV) is such that a five order decrease is expected in the magnitude of the mobility between 120°C and 20°C, which is the reason why no detectable currents are observed at room temperature on short-circuiting.

The charge is deduced to be inherently slow-moving at room temperature, rather than trapped at localized defects or impurities. The distinction is important in that it rules out the possibility of controlling conduction behaviour through the extraction or neutralization of

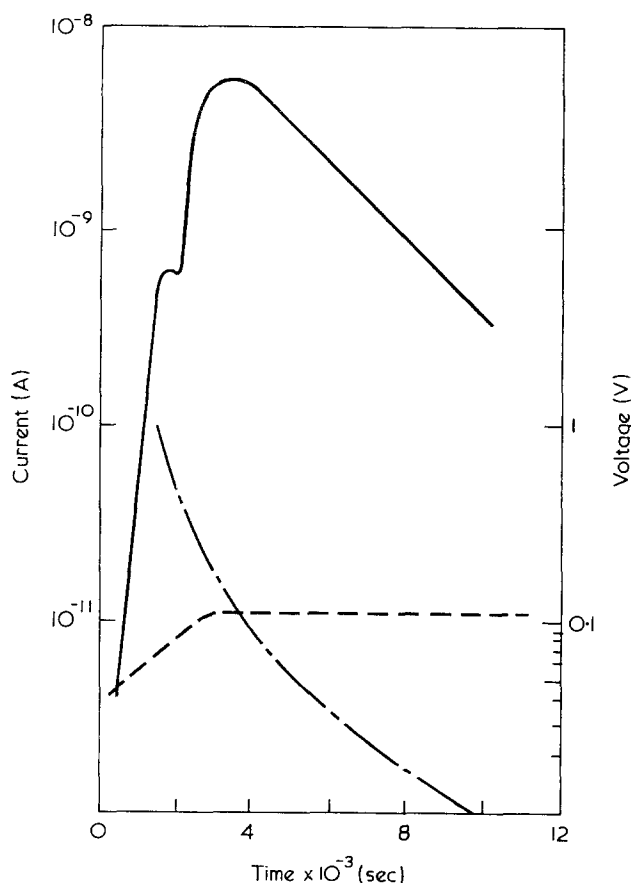


*Figure 7* Thermally stimulated current (—) and voltage (---) in PVF using split-opposed electrodes to minimize the thermoelectric effect (---)

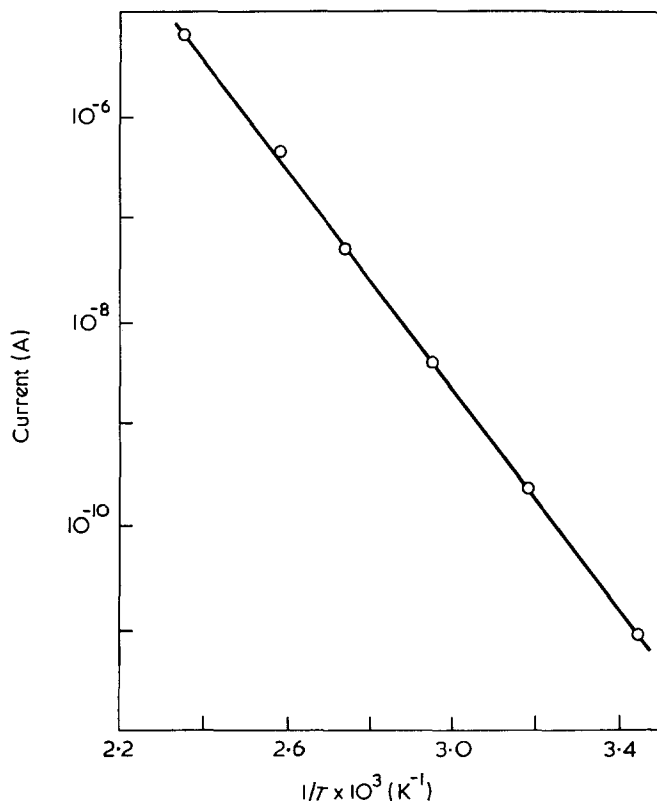


Figure 9 Steady state current vs. temperature in PVF film

impurity trapping centres. The mobility of the charge-carriers is thus an inherent characteristic of the bulk structure of PVF, and the fact that this polymer shows higher dark conduction levels than for example does polyethylene, is a function of this overall chemical structure rather than of the existence of a lower concentration of traps.

In any picture involving trapping, the location of a charge release peak is taken as a measure of trap depth, and can be interpreted quantitatively to give a value for the latter<sup>19</sup>. On the present picture, the peak temperature 120°C has a different significance. Two processes are involved. First the charge which has previously been injected by a field increases in mobility with temperature. This is determined by the value of the mobility at a given temperature ( $\mu_0$ ) and its temperature dependence (determined by the activation energy  $\Delta E_\mu$ ). The rising current thus depends on  $\mu_0$  and  $\Delta E_\mu$ , and also on the amount of charge previously injected. This in turn is a function of the field strength and time of application of the previously applied field. The second process involves the depletion of the previously injected charge with time, and this of course gives rise to a decreasing current with temperature. The result is that a peak is obtained, whose location in the temperature scale depends on the experimental conditions used (i.e. strength and time of application of previously applied field, and rate of heating during the t.s.c. experiment); but also on  $\mu_0$  and  $\Delta E_\mu$ .

The t.s.c. peak temperature (for a given set of experimental conditions) is thus determined by charge carrier mobility; to be more precise by  $\mu_0$  and  $\Delta E_\mu$ . If the currents in simple vinyl polymers can be considered generally to arise from injection and hence to involve space-charge-limited process, mobility is the only important parameter, and should be correlated with the peak temperature

when a range of polymers is considered. This point is considered in detail in a later paper, but it should be evident here that in lower conductivity polymers discharge can only be effected by raising the temperature of the charged material to a much higher temperature (than 120°C), and probably in some cases to the point where chemical decomposition occurs.

Two other thermal effects have been observed in this study, which can be distinguished from the charge release process through the use of blocking electrodes, and of split-opposed electrodes. In the first case, four discrete peaks can be observed, three below room temperature and one above, which are associated with the reversible and limited displacement of inert charge. The most likely explanation is that the orientation of dipoles is involved<sup>16</sup>, and that movement becomes possible progressively at various stages on an increasing temperature scale, as the sample passes through a series of second order transition points. There is a good correlation with previously observed transitions detected by mechanical methods for three of the peaks; but the fourth peak at -100°C has not previously been observed. Peaks of this type have been observed by previous workers, and ascribed to traps<sup>6, 8</sup>. This explanation is, however, definitely excluded for the reasons detailed above.

The second effect is that of a thermally generated e.m.f., arising from a thermal gradient across the sample. This gives rise to currents as high as  $10^{-8}$  A across a 50  $\mu\text{m}$  sample, and is in a direction such that electrons rather than holes are indicated as charge-carriers. The value of the e.m.f. is in the region of 100 mV for the conditions used.

There is reason to think that these effects and their interpretation are general in nature, and in a later paper results from other polymers are considered to support this contention.

## REFERENCES

- 1 Fowler, J. F. *Proc. R. Soc.* 1956, **236**, 464
- 2 McGubbin, W. L. and Gurney, I. D. *C. J. Chem. Phys.* 1965, **43**, 983
- 3 Binks, A. E., Campbell, A. G. and Sharples, A. *J. Polym. Sci. (A-2)* 1970, **8**, 529
- 4 McGibbon, G., Rostron, A. J. and Sharples, A. *J. Polym. Sci. (A-2)* 1971, **9**, 569
- 5 Kryszewski, M., Lagiewka, B. and Szymanski, A. *Proc. Int. Conf. Lum.* 1966, p 589
- 6 Lilly, A. C. Jr., Henderson, R. M. and Sharp, P. S. *J. Appl. Phys.* 1970, **41** (5), 2001
- 7 Lilly, A. C., Jr., Stewart, L. L. and Henderson, R. N. *J. Appl. Phys.* 1970, **41** (5), 200
- 8 Creswell, R. A. and Pearlman, M. M. *J. Appl. Phys.* 1970, **41** (6), 2365
- 9 Monteith, L. K. *J. Appl. Phys.* 1966, **37** (7), 2633
- 10 Seiwatz, H. and Brophy, J. J. *A. Rep. Conf. Electrical Insulation, NAS-NRC 1356* 1965
- 11 Lilly, A. C., Jr. and McDowell, J. R. *J. Appl. Phys.* 1968, **39**, 141
- 12 Sacher, E. *J. Polym. Sci. (A-2)* 1968, **6**, 1813
- 13 Ishida, Y. and Yamafuji, K. *Kolloid Z.* 1964, **200** (1), 50
- 14 Kosaki, K., Ohskima, M. and Ieda, M. *J. Phys. Soc., Japan* 1970, **29** (4), 1012
- 15 McGibbon, G., Sharples, A. and Stanley, E. J., to be published
- 16 Osaki, S., Uemura, S. and Ishida, Y. *J. Polym. Sci. (A-2)* 1971, **9**, 585
- 17 Schmeider, K. and Wolf, K. *Z. Colloid.* 1953, **134**, 172
- 18 Turley, S. J., Pettis, A. A. and Fritz, J. A. unpublished results quoted by Boyer, R. F. *J. Polym. Sci. (C)* 1966, **14**, 3
- 19 Garlick, G. F. J. and Gibson, A. F. *Proc. Phys. Soc.* 1948, **60**, 574

# Electron microscope investigation of poly(ethylene oxide) supermolecular particles in solution

Carla Cuniberti and R. Ferrando

*Istituto di Chimica Industriale, Università di Genova, 16132 Genova, Italy  
(Received 19 November 1971 ; revised 24 January 1972)*

Using freeze-drying methods, preparations are obtained which enable the state of polymer molecules in solution to be investigated by electron microscopy. With poly(ethylene oxide) in dimethylformamide and water evidence for supermolecular particles in the solutions was found. The sizes and size distributions for fractions of different molecular weights at various concentrations were determined. The results show that poly(ethylene oxide) molecules give rise to polydisperse aggregates in both solvents but that only in the crystallizing solvent (dimethylformamide) does a growth process follow the primary aggregation. Indications of the probable mechanism of growth have been obtained from the increase of the mean particle diameter with the concentration for the different molecular weights.

## INTRODUCTION

The possibility of direct, electron microscope observation of particles dissolved in solution has been repeatedly exploited in the past years for directly measuring the sizes of dissolved macromolecules<sup>1-4</sup> as an alternative method of molecular weight determination.

The basic difficulty involved is to preserve the original arrangement in solution on the surface.

The preparation processes for electron microscope examination in fact usually involve the removal of the solvent from drops of solution directly deposited onto Formvar or carbon supports. This procedure may cause secondary agglomeration of the dissolved particles, unless the original solution is extremely dilute<sup>4-6</sup>.

In order to prevent these artefacts, a combined spraying and freeze-drying technique may be used<sup>6-8</sup>. In this way, particles present in the solution, either single molecules or aggregates, will be preserved with the conformation they have in the sprayed droplets. Furthermore, if a low volatility solvent is employed, the conformation is that characteristic of the solution.

On the other hand, accurate size measurements are directly connected with the resolving power of the microscope and with the shadow-casting technique employed. A limiting size therefore exists beyond which questionable results are obtained<sup>9</sup>. However, the electron microscope is of particular interest for showing supermolecular structures in polymer solutions.

The present paper deals with poly(ethylene oxide) (PEO) solutions. The presence of supermolecular particles in dilute solutions has been observed in our laboratories<sup>10</sup> through light-scattering measurements, as well as by other authors<sup>11, 12</sup>. It is not quite clear whether they

are covalently bonded microgels, molecular clusters, or crystalline nuclei.

Poly(ethylene oxide) is a crystalline polymer with a melting point of 66–69°C<sup>13</sup>. Crystalline phase separation can therefore take place in dilute solution in certain solvents at lower temperatures.

The crystallization process follows a well identified path<sup>14</sup>, a nucleation process being involved in the initiation. Nucleation is initiated by transient structures brought about by thermal fluctuations, which lead to persistent clusters and eventually to entities with a solid-like configuration of molecules. The subsequent growth to macroscopic crystals can start only if such embryos exceed a certain critical size, thus acting as crystallization 'nuclei'.

It has been ascertained in a general way<sup>15</sup> that suspensions of polymer crystals give rise, above the clearing point, to solutions containing submicroscopic entities capable of nucleating single crystals on subsequent cooling. Such entities exist usually in a limited temperature range above the clearing point (10 to 15°C) well below the melting point of the bulk polymer. Their characterization has been attempted<sup>15</sup> for polyethylene but several uncertainties exist, especially regarding their polymolecularity and morphology. Furthermore it is uncertain if they are equilibrium entities. If this is the case they should also exist in a solution cooled to a temperature in the range reported from a temperature above the melting point of the bulk polymer. A study of such apparently homogeneous solutions would give useful direct information on the nucleation mechanism.

Electron microscope investigations on sprayed and freeze-dried solutions can be usefully employed to

ascertain the presence of supermolecular entities as well as to determine their sizes and shapes and their dependence on some solution parameters such as concentration or type of solvent, which may aid in elucidating the nucleation mechanism.

Direct evidence for the presence of large particles and their dimensions in visually homogeneously dispersed solutions of poly(ethylene oxide) in dimethylformamide and water are reported in this paper.

## EXPERIMENTAL

Poly(ethylene oxide) can be particularly useful when spraying solutions at room temperature owing to its low melting temperature. The spraying of a hot solution is in fact quite impracticable.

Dimethylformamide has been chosen as a solvent because the polymer is reported to crystallize from dilute solution<sup>13</sup> at a temperature around 10–12°C. Submicroscopic nuclei might therefore exist up to 20–25°C if the knowledge gained for polyethylene<sup>15</sup> can be directly applied to poly(ethylene oxide).

Water, on the other hand, does not give a crystalline phase separation; therefore, only single molecules or non-crystalline aggregates might be evidenced.

Both dimethylformamide and water have a sufficiently low vapour pressure to guarantee that at room temperature spraying is not accompanied by noticeable solvent evaporation thus avoiding molecule coalescence in the droplet<sup>4</sup>.

The highly crystalline character of poly(ethylene oxide) guarantees furthermore that, whatever the sublimation temperature in the freeze-drying apparatus, as long as this is lower than the melting point of the polymer, the freeze-dried particles do not collapse in subsequent heating to room temperature. This is a necessary condition if shapes and sizes of the particles detected on the micrographs have to be related to the particles present in the solution<sup>4</sup>. If the particles in solution are crystalline entities no problem exists. If they are amorphous only a contraction due to their crystallization will happen.

It is well known<sup>16</sup> that crystalline polymers quenched from the melt to a temperature lower than their  $T_g$  are amorphous, if their crystallization rate is not too high, but crystallize rapidly when raising the temperature above  $T_g$ .

The exact amount of the volume contraction will depend on the degree of crystallinity attained but will never exceed the limits of precision in particle size determination by electron microscope techniques.

For poly(ethylene oxide) the maximum contraction could be calculated assuming a liquid like configuration of molecules in the particle in solution and a crystalline arrangement in the particle on the support. This would involve the density to pass from a value of about 1.12 to 1.17 at 25°C<sup>9</sup> and consequently the measured diameter will be equal to the real diameter times a factor 0.985. The maximum error in the diameter evaluation will therefore be equal to about 1.5%.

### Materials and solutions

The PEO samples employed in this investigation were fractions obtained from a commercial Polyox by Union Carbide. A fractional precipitation procedure with

chloroform/n-hexane at 25°C was chosen for the fractionation.

Table 1 reports the molecular weights of the samples used in this study, as calculated from the intrinsic viscosity in benzene at 25°C by means of the equation<sup>17</sup>:

$$[\eta]_{C_6H_6}^{25} = 3.97 \times 10^{-4} M^{0.687}$$

Reagent grade dimethylformamide (DMF) was doubly distilled under high vacuum and twice-distilled water was used for the aqueous solutions.

Table 1 Intrinsic viscosities and molecular weights of poly(ethylene oxide) fractions employed in the electron microscope investigation

Sample	$[\eta]_{C_6H_6}$ (dl/g)	$M \times 10^{-5}$
PEO-F1	3.92	6.65
PEO-F2	2.48	3.40
PEO-F3	1.82	2.20

Since PEO does not dissolve in DMF at room temperature, a standard thermal treatment of 1 hour at 80°C was adopted both for DMF and water solutions in order to ensure that no crystalline residues were left in the solutions. Such a temperature is in fact 10–15°C higher than the melting point of the bulk samples and complete dissolution should be achieved.

Dimethylformamide solutions so obtained and cooled to room temperature are visually homogeneous and do not show crystal separation at any time. With a cooling rate of 5°C per hour separation of a crystalline phase is achieved at a temperature around 1°C for the more concentrated solution.

### Electron microscopy

The specimens for electron microscope examination were prepared by spraying the polymer solution through a home-made high pressure atomizer onto a cold carbon surface supported on a Formvar substrate, employing the freezing and drying technique indicated by Ruscher<sup>4</sup>.

A sublimation chamber connected to a trap, according to the description given by Horne<sup>8</sup> was employed as the freeze-drying unit. The chamber was cooled to the liquid nitrogen temperature before spraying.

Spraying was performed by using a nitrogen gas flux after flushing the chamber with nitrogen. A pumping time of 15–20 min was then applied. The cooling temperature was then raised to –70°C for DMF solutions and to –25°C for water solutions, a further pumping time of 8 to 10 hours being allowed. Care was taken to allow sufficient time for the sublimation chamber to attain room temperature before admitting air. The material deposited was shadow-casted with Au–Pd or Cr. Blank specimens were also prepared in order to check that the solvents left no residues.

All the electron micrographs were taken with a Hitachi H11 microscope.

## RESULTS AND DISCUSSION

Single molecules of polymers with molecular weights equal to those employed in this work would have, if considered as spherical particles with a density equal to

that of the bulk polymer at 25°C<sup>18</sup>, average diameters of 55 Å, 44 Å and 37 Å respectively.

If not tightly coiled the density would be lower and the diameters correspondingly appear larger. The radii of gyration of isolated coils with the molecular weights reported here may average<sup>19</sup> around 300 Å, 220 Å and 175 Å, corresponding to spherical particles with radii of 500 Å, 370 Å and 290 Å respectively. The very low density of such particles would presumably make them appear more like loosely coiled threads than like compact particles, though what conformation the isolated chains on a support may assume when taken to a temperature where flexibility is high can only be a matter of speculation. It will naturally also depend on the interactions between the molecule and the surface.

On the basis of such observations, observed compact particles larger than about 100 Å cannot be single chains and aggregates can be easily differentiated owing to their larger sizes and higher compactness. The technique used guarantees that, when particles appear on the micrographs, they derive from the solution, the crystalline character of the polymer preventing artefacts due to collapse of particles.

Figures 1 to 3 represent typical micrographs obtained for fractions PEO-F1 and PEO-F2 in DMF and for PEO-F3 in water at two different concentrations. The particles look more or less like flattened spheroids, much larger than molecular dimensions and not uniform in size. In order to obtain the aggregate size distribution only particles with a diameter larger than 100 Å were considered on each micrograph. Their linear dimensions were measured with a  $\times 10$  microscope-millimeter rule.

Table 2 Number average and most probable particle diameters for the systems PEO-F1 and PEO-F2 in DMF and PEO-F3 in water

System	<i>c</i> (g/dl)	$\langle D \rangle$ (Å)	$D_m$ (Å)
PEO-F1 in DMF	0.024	720	670
	0.105	940	900
	0.204	1620	1200-2080
PEO-F2 in DMF	0.018	320	260
	0.060	400	320
	0.090	475	400
PEO-F3 in H <sub>2</sub> O	0.048	500	400
	0.082	625	550
	0.120	450	400
	0.180	440	310

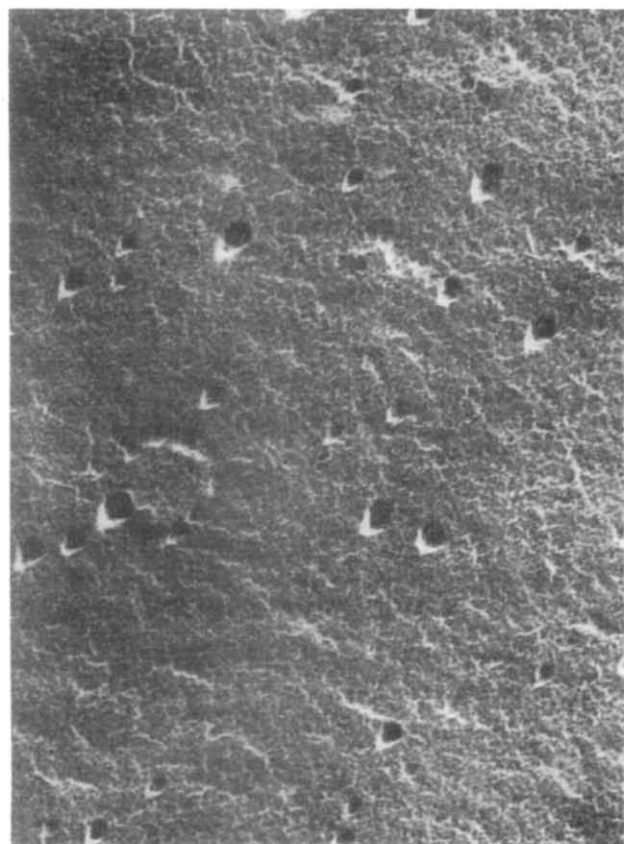
No attempt has been made to determine their thickness or their concentration in the solutions.

From the cumulative number *versus* particle diameter plots, the smoothed distribution curves shown in Figures 4 to 6 were obtained by graphical differentiation. When asymmetric sizes were observed, both the minor and major axes were measured and the geometric mean reported on the plots.

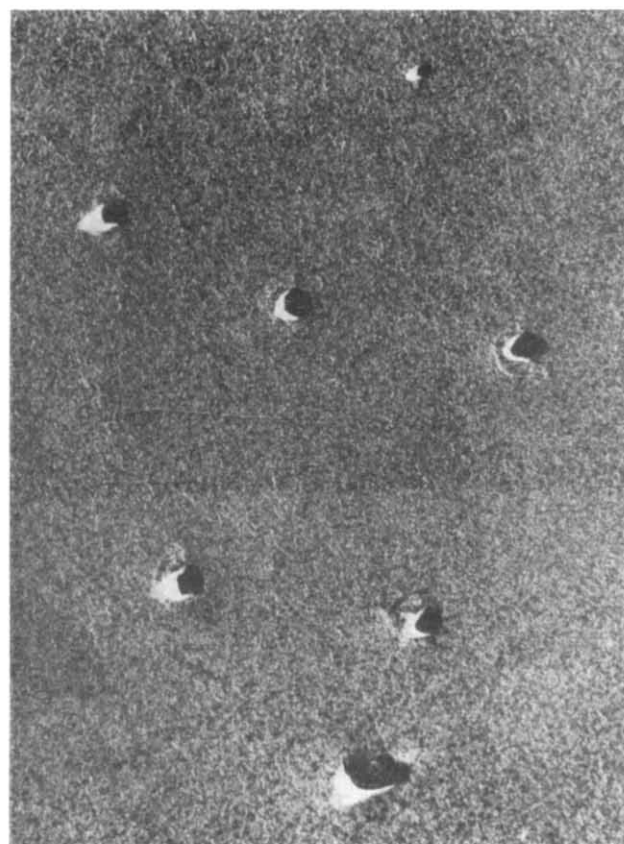
Each curve may be characterized by a number-average diameter,  $\langle D \rangle$ , and by a most probable diameter,  $D_m$ . The difficulty of discerning the particles boundaries with sufficient accuracy and shadow effects<sup>4</sup> do not allow precise *D* values to be obtained.

Table 2 shows  $\langle D \rangle$  and  $D_m$  values observed in solutions of increasing concentration for the systems indicated.

In Figure 7,  $D_m$  data are plotted against the concentration for each system. This representation has been

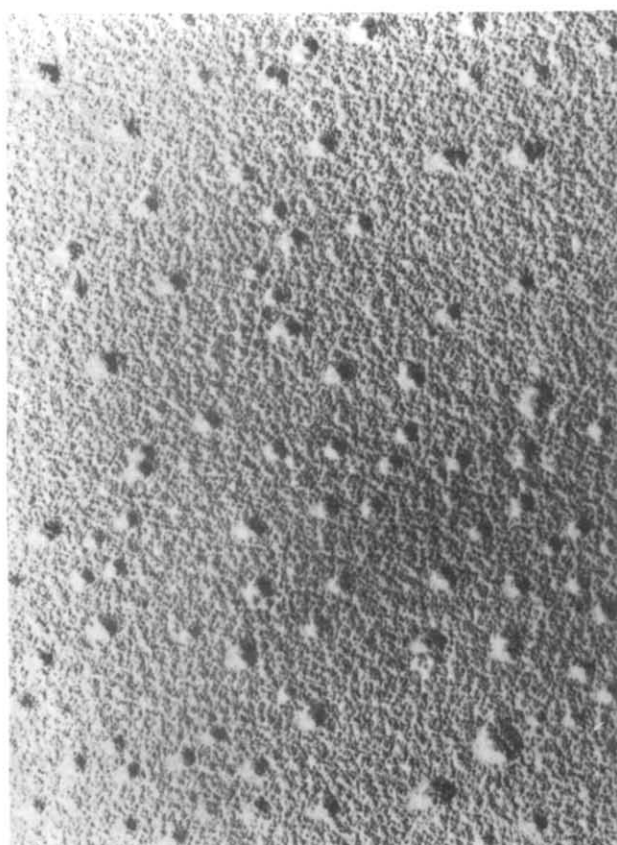


a

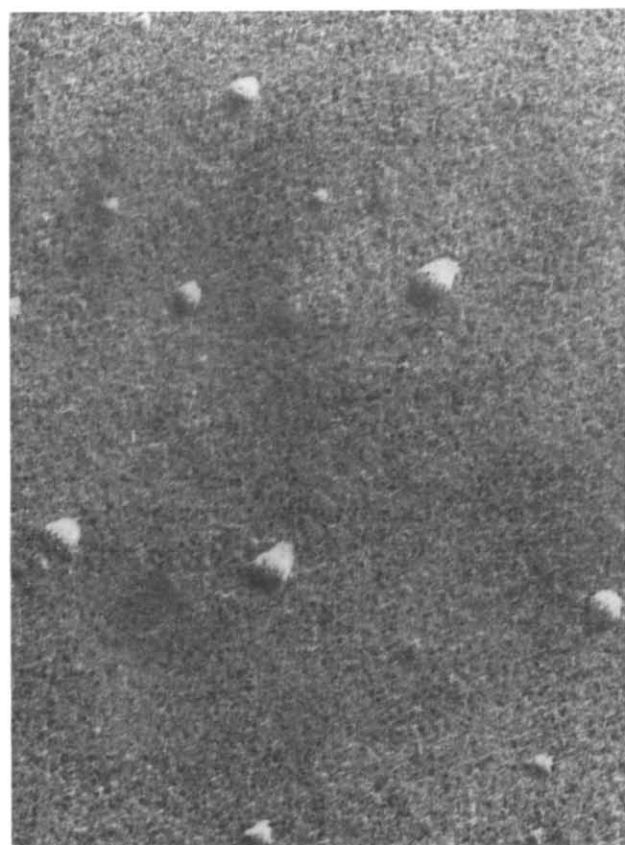


b

Figure 1 Electron micrographs of PEO-F1/DMF system: (a)  $c=0.105\%$ ,  $\times 32\,500$ ; (b)  $c=0.204\%$ ,  $\times 18\,500$

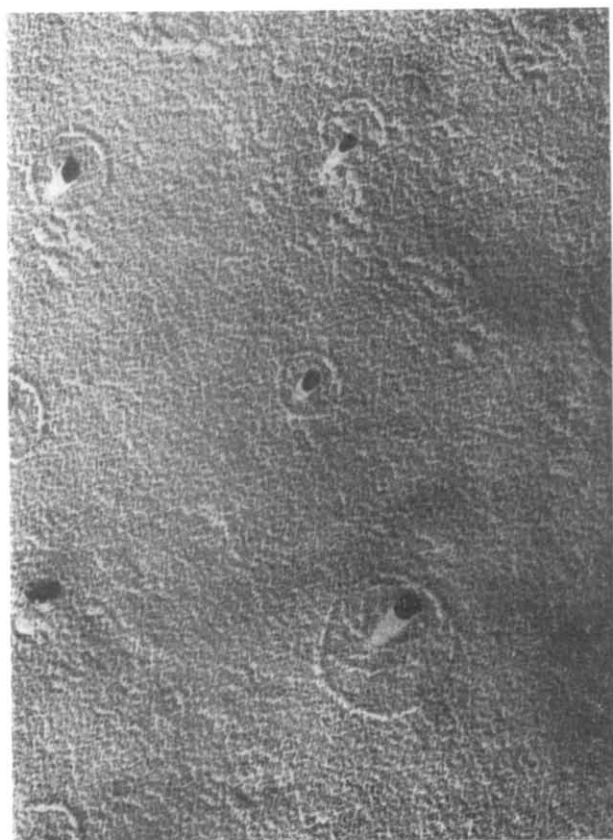


a

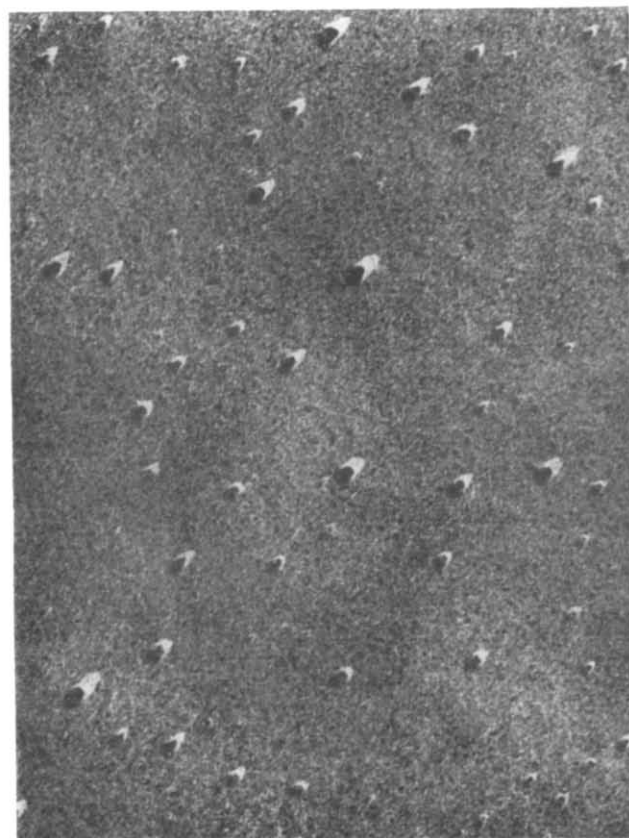


b

**Figure 2** Electron micrographs of PEO-F<sub>2</sub>/DMF system: (a)  $c=0.018\%$ ,  $\times 50\,000$ ; (b)  $c=0.06\%$ ,  $\times 50\,000$



a



b

**Figure 3** Electron micrographs of PEO-F<sub>3</sub>/H<sub>2</sub>O system: (a)  $c=0.082\%$ ,  $\times 32\,500$ ; (b)  $c=0.18\%$ ,  $\times 32\,500$

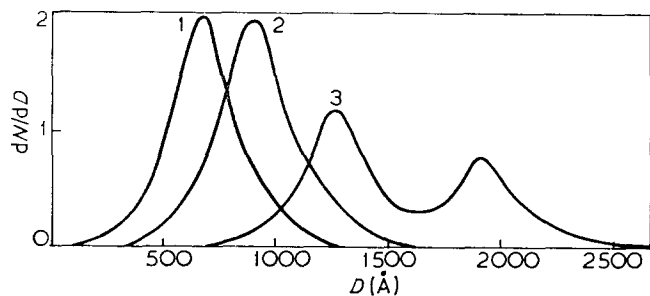


Figure 4 Size distribution curves of supermolecular particles in PEO-F1/DMF solutions: 1,  $c=0.024\%$ ; 2,  $c=0.105\%$ ; 3,  $c=0.204\%$

chosen because PEO-F1 in DMF at  $c=0.18\%$  shows a bimodal distribution (curve 3 in Figure 4); only  $D_m$  related to the lowest peak appears in the plot.

It is evident that particle sizes and size dispersions increase with both concentration and molecular weight in DMF; these findings cannot be explained by the presence in the solutions of microgels deriving from the solid polymer, since in this case uniformity in size would be expected<sup>3</sup>. A multi-steps association<sup>20</sup> would represent a better interpretation of the large polydispersity and of the concentration and molecular weight dependence.

The molecular weight and concentration dependence in DMF may also be employed to gain further insight in the mechanism of particle growth. The slope of the diameter-concentration relation may be written as:

$$\left(\frac{dD}{dc}\right)_{M_i} = \left(\frac{dD}{dM}\right)_c M_i \left(\frac{dn}{dc}\right)_{M_i} \quad (1)$$

where  $M_i$  is the molecular weight of the non-aggregated phase and  $n = M/M_i$  is the average aggregation number.

Equation (1) enables differentiation between particle shapes because it gives:

$$\left(\frac{dD}{dc}\right)_{M_i} = \frac{1}{3} \left(\frac{1}{6\pi N_A \rho}\right)^{-1/3} M_i^{1/3} \left(\frac{1}{n^{2/3}} \frac{dn}{dc}\right)_{M_i} \quad (2)$$

for spherical particles, and

$$\left(\frac{dD}{dc}\right)_{M_i} = \frac{1}{2} \left(\frac{1}{3\pi \rho N_A b}\right)^{-1/2} M_i^{1/2} \left(\frac{1}{n^{1/2}} \frac{dn}{dc}\right)_{M_i} \quad (3)$$

or

$$\left(\frac{dD}{dc}\right)_{M_i} = \left(\frac{2}{3\pi N_A b^2}\right)^{-1} M_i \left(\frac{dn}{dc}\right)_{M_i} \quad (4)$$

respectively for oblate and prolate ellipsoids with thickness,  $b$ , independent of the concentration.

By assuming that  $n$  and  $dn/dc$  do not change with concentration and  $M_i$ , and plotting  $(dD/dc)_{M_i}$  respectively against  $M_i^{1/3}$ ,  $M_i^{1/2}$  or  $M_i$  a straight line going through the origin should be expected only in one case, depending on what relation, among the three postulated, is obeyed.

In Figure 8 the slopes of the two lines for DMF shown in Figure 7 are plotted against  $M_i^{1/2}$ ; this is in fact the only case showing the expected linear dependence.

The particles grow therefore as oblate ellipsoids their average number of aggregation increasing according to the equation:

$$\frac{1}{n^{1/2}} \frac{dn}{dc} = \text{constant} \quad (5)$$

which means that  $n$  increases as the square of the concentration.

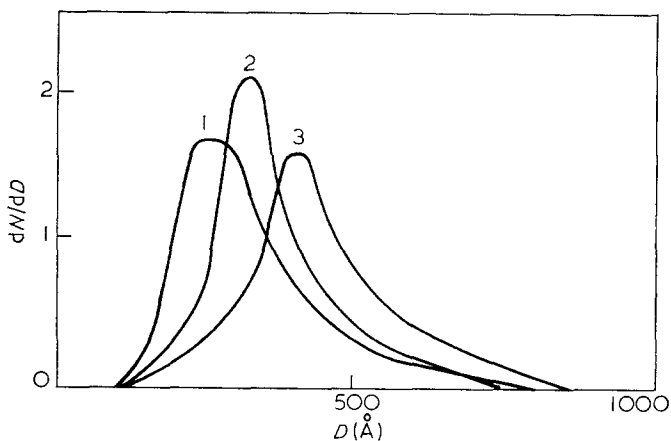


Figure 5 Size distribution curves of supermolecular particles in PEO-F2/DMF solutions: 1,  $c=0.018\%$ ; 2,  $c=0.06\%$ ; 3,  $c=0.09\%$

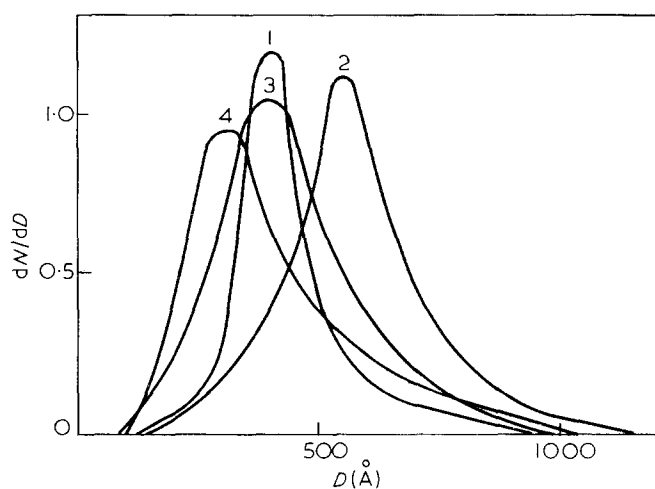


Figure 6 Size distribution curves of supermolecular particles in PEO-F3/H<sub>2</sub>O solutions: 1,  $c=0.048\%$ ; 2,  $c=0.082\%$ ; 3,  $c=0.12\%$ ; 4,  $c=0.18\%$

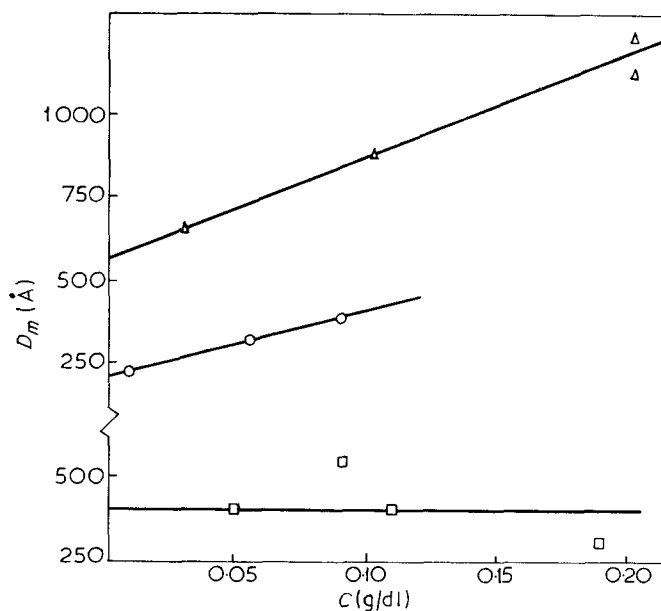


Figure 7 Most probable particle diameter,  $D_m$ , plotted against the concentration:  $\Delta$ , PEO-F1 in DMF;  $\circ$ , PEO-F2 in DMF;  $\square$ , PEO-F3 in water



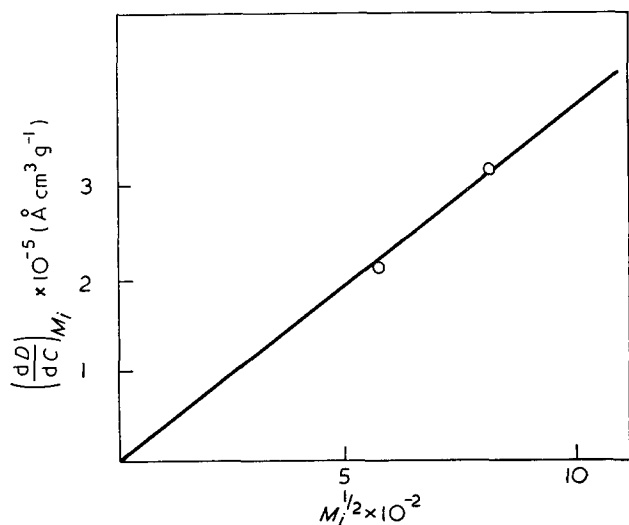


Figure 8 Dependence of the slopes of the lines of Figure 7, in DMF, on the sample's molecular weight

Numerical values of  $n$  have been omitted because such calculation would imply to assume a value for  $b$  and  $\rho$ , which would lie outside the limits of this paper. The growth is similar to that characteristic of polymer single crystals<sup>21</sup> and one is therefore compelled to conclude that DMF solutions should contain microcrystalline embryos that do not give rise to macroscopic crystals because they do not reach their critical size. This conclusion is also supported by the fact that no appreciable differences were detected in the size distribution curves obtained at different times.

However, aggregates are also evident on micrographs obtained from water solutions, where crystalline nuclei should not exist and only single molecules would be expected. On the basis of the molecular weight dependence in DMF, particle sizes in water should be smaller than the ones detected and have a  $(dD/dc)_M$  value quite near to that for PEO-F2 in DMF, which is well outside the experimentally detected constancy.

Consequently, the primary aggregation among poly(ethylene oxide) molecules seems to be determined by intermolecular interactions other than those involved in crystallization. Whether the aggregation process occurs at the dissolution temperature cannot be inferred from our results at room temperature. Presumably, however, in DMF at lower temperature a secondary nucleation superimposes on the primary aggregation.

## CONCLUSIONS

Our electron microscope investigation of poly(ethylene oxide) in dimethylformamide and water solutions shows

the presence, at room temperature, of particles much larger than the molecular dimensions.

The direct examination of the particle sizes for different molecular weights and concentrations eliminates the possible presence of covalently bonded microgels and indicates that a reversible association is involved.

Whether the particles observed represent molecular clusters or crystalline nuclei it is difficult to say. However, since PEO may separate as a crystalline phase from dilute DMF solutions at low temperature, while this does not happen in water, the presence of molecular clusters of unknown density seems to be the best representation of the aggregates.

From the data obtained from DMF solutions a tentative interpretation of the mechanism of growth in this solvent has been made, which allows speculation on the concentration dependence of the shape and average number of aggregation of the supermolecular particles.

## ACKNOWLEDGEMENT

The authors wish to thank Dr E. Pedemonte and Mr G. Dondero for their valuable assistance in the electron microscope work.

## REFERENCES

- Husemann, E. and Ruska, H. *Naturwissenschaften* 1940, **28**, 543
- Siegel, B. M., Johnson, D. H. and Mark, H. J. *J. Polym. Sci.* 1950, **5**, 111
- Heyn, A. N. J. *J. Polym. Sci.* 1959, **41**, 23
- Quayle, D. V. *Br. Polym. J.* 1969, **1**, 15
- Barnikol, J., Barnikol, W. K., Beck, A. et al. *Makromol. Chem.* 1970, **137**, 111
- Ruscher, C. J. *J. Polym. Sci. (C)* 1967, **16**, 2923
- Claesson, S., Boman, N. and Gellerstedt, N. *Makromol. Chem.* 1966, **92**, 51
- Horne, R. W. in 'Techniques for Electron Microscopy', Blackwell, Oxford, 1967, p 311
- Zingsheim, H. P. and Bachmann, L. *Kolloid-Z. Z. Polym.* 1971, **246**, 561
- Cuniberti, C. in press
- Strazielle C. *Makromol. Chem.* 1968, **119**, 50
- Delmas, G. J. *J. Appl. Polym. Sci.* 1968, **12**, 839
- Davidson, R. L. and Sittig, M. 'Water-Soluble Polymers', Reinhold, New York, 1968, p 192
- Waeton, A. G. in 'Nucleation', (Ed. A. C. Zettelmayer), Marcel Dekker, New York, 1969
- Blundel, D. J. and Keller, A. J. *Macromol. Sci.* 1968, **B2**, 301
- Fielding-Russel, G. S. and Pillai, P. S. *Makromol. Chem.* 1970, **135**, 263
- Allen, G., Booth, C., Hurst, S. J., Jones, M. N. and Price, C. *Polymer* 1967, **8**, 391
- Mandelkern, L., *J. Appl. Phys.* 1955, **26**, 443
- Braundrup, J. and Immergut, E. H. (Eds), 'Polymer Handbook', Interscience, New York, 1966
- Ginell, R. J. *J. Polym. Sci.* 1951, **7**, 413
- Geil, P. H. 'Polymer Single Crystals', Interscience, New York, 1963, p 79

# Equilibrium ring concentrations and the statistical conformations of polymer chains: Part 8. Calculation of small ring concentrations in polydihydrogensiloxane and polydimethylsiloxane equilibrates

M. S. Beevers and J. A. Semlyen

Department of Chemistry, University of York, Heslington, York YO1 5DD, UK  
(Received 7 December 1971)

Theoretical molar cyclization equilibrium constants  $K_x$  for small, unstrained cyclics  $[\text{H}_2\text{SiO}]_x$  ( $x=4-8$ ) and  $[(\text{CH}_3)_2\text{SiO}]_x$  ( $x=4-9$ ) in undiluted polydihydrogensiloxane and polydimethylsiloxane equilibrates are calculated using the Jacobson and Stockmayer theory, without assuming that the corresponding chain molecules obey Gaussian statistics. The statistical conformations of dihydrogensiloxane chains are described by a simple rotational isomeric state model with skeletal bonds assigned to *trans* ( $\phi=0^\circ$ ) and *gauche* ( $\phi=\pm 120^\circ$ ) states with equal probability; and the statistical conformations of dimethylsiloxane chains are described by Flory, Crescenzi and Mark's (FCM) rotational isomeric state model. Dihydrogensiloxane and dimethylsiloxane chains in undiluted equilibrates are assumed to be unperturbed by excluded volume effects, and the probabilities of intramolecular cyclization are calculated by simply computing the statistically weighted fractions of the total number of conformations defined by the rotational isomeric state models that have terminal atoms in juxtaposition for ring closure. The calculated  $K_x$  values for cyclic dihydrogensiloxanes are compared with the published experimental  $K_x$  values for the homologous cyclic hydrogenmethylsiloxanes and dimethylsiloxanes. The FCM rotational isomeric state model of polydimethylsiloxane gives theoretical molar cyclization equilibrium constants for the cyclics  $[(\text{CH}_3)_2\text{SiO}]_8$  and  $[(\text{CH}_3)_2\text{SiO}]_9$  in excellent agreement with the experimental values. However, it is shown that before the FCM model can be used to calculate the molar cyclization equilibrium constants for smaller dimethylsiloxane rings, it must be modified so that it takes into account the mutual interdependence of sequences of bond rotational states.

## INTRODUCTION

Up to the present time, the cyclic populations of polysiloxane equilibrates have been studied in greater detail than those of any other class of polymer. The molar cyclization equilibrium constants  $K_x$  for cyclics  $[\text{R}(\text{CH}_3)\text{SiO}]_x$  in equilibrated melts have been determined for  $\text{R}=\text{H}$ ,  $\text{CH}_3$ ,  $\text{CH}_3\text{CH}_2$ ,  $\text{CH}_3\text{CH}_2\text{CH}_2$ ,  $\text{CF}_3\text{CH}_2\text{CH}_2$  and  $\text{C}_6\text{H}_5$ . Furthermore, the effect of temperature, pressure and the nature and concentration of added diluent on the concentrations of cyclics in some of these systems has also been investigated<sup>1-6</sup>.

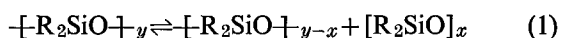
The Jacobson and Stockmayer<sup>7</sup> theory provides an expression for the molar cyclization equilibrium constants for large, unstrained cyclics in polysiloxane equilibrates.

In a previous study<sup>8</sup>, theoretical  $K_x$  values for cyclic dimethylsiloxanes  $[(\text{CH}_3)_2\text{SiO}]_x$  were computed using Flory, Crescenzi and Mark's<sup>9</sup> rotational isomeric state model to describe the statistical conformations of dimethylsiloxane chains. Chains of all lengths were assumed to obey the Gaussian expression for the probabilities of intramolecular cyclization and their terminal bonds were assumed to be randomly oriented. Theoretical and experimental  $K_x$  values were in agreement for cyclics with more than thirty chemical bonds and differences between the theoretical and experimental  $K_x$  values for the smaller cyclics were attributed to deviations shown by the corresponding chains from Gaussian statistics as well as to the neglect of correlations between the directions of the terminal bonds<sup>8</sup>.

In this paper, we report calculations of the molar cyclization equilibrium constants  $K_x$  for small cyclic dihydrogensiloxanes and dimethylsiloxanes by direct computational methods similar to those used to calculate cyclic oligomer concentrations in equilibrated melts of sulphur<sup>10-12</sup>, poly(ethylene terephthalate)<sup>13</sup> and sodium phosphate<sup>14</sup>. The results are compared with the published experimental  $K_x$  values for cyclics in polyhydrogenmethylsiloxane<sup>4</sup> and polydimethylsiloxane<sup>3</sup> equilibrates.

### THEORETICAL EXPRESSION FOR MOLAR CYCLIZATION EQUILIBRIUM CONSTANTS

The equilibrium between ring and chain molecules in a polydihydrogensiloxane (R=H) or polydimethylsiloxane (R=CH<sub>3</sub>) melt may be represented as follows:



The cyclic trimers  $[\text{R}(\text{CH}_3)\text{SiO}]_3$  (where R=H, CH<sub>3</sub>, CH<sub>3</sub>CH<sub>2</sub>, CH<sub>3</sub>CH<sub>2</sub>CH<sub>2</sub>, C<sub>6</sub>H<sub>5</sub>, CF<sub>3</sub>CH<sub>2</sub>CH<sub>2</sub>) have been found to be strained<sup>1-5</sup>, and in this paper attention will be confined exclusively to unstrained cyclics with  $x \geq 4$ .

It has been established that there is a most probable distribution of chain lengths in polysiloxane equilibrates<sup>4, 15</sup>, and a similar distribution would be expected for polydihydrogensiloxane equilibrates. Hence, the molar cyclization equilibrium constants  $K_x$  for cyclic dihydrogensiloxanes and dimethylsiloxanes should be related to the extent of reaction of functional groups in the chain polymers  $p$  by:

$$K_x = [\text{R}_2\text{SiO}]_x / p^x \quad (2)$$

For high molecular weight equilibrates ( $p \approx 1$ ), the  $K_x$  values for small rings will be approximately equal to their molar concentrations.

The Jacobson and Stockmayer theory yields the following expression for the  $K_x$  values (in mol/l) for cyclics formed by the forward step of equation (1) with zero enthalpy change<sup>7, 8</sup>:

$$K_x = \bar{\mathbf{W}}_x / 2N_A x \quad (3)$$

where  $\bar{\mathbf{W}}_x$  is the density of end-to-end vectors  $\mathbf{r}$  in the region  $\mathbf{r} \approx \mathbf{0}$  (in molecules/l) and  $N_A$  is the Avogadro constant. This is the expression that is required for the calculations to be described here.

In the derivation of equation (3), correlations between the directions of terminal bonds expected for chains undergoing intramolecular cyclization have been neglected. Favourable orientation of termini of short siloxane chains undergoing intramolecular cyclization reactions would be expected to result in increases in the molar cyclization equilibrium constants for small cyclic siloxanes because termini undergoing the competitive intermolecular condensation reaction should be randomly oriented<sup>8</sup>. However, in the absence of molecular structural information defining the solid angle within which the active termini of siloxane chains meet to form a chemical bond, no quantitative conclusions can be reached as to the magnitude of the corresponding changes in the  $K_x$  values.\*

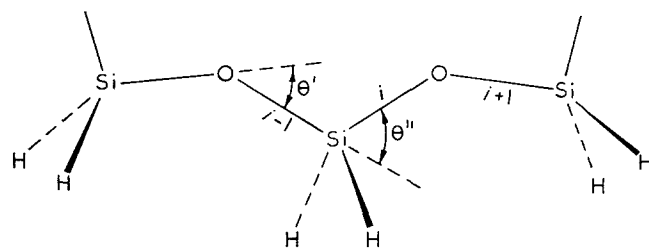


Figure 1 Section of the dihydrogensiloxane chain in the all-trans conformation. The structural parameters  $d_{\text{Si-O}}=1.64 \text{ \AA}$ ,  $\theta'=37^\circ$ ,  $\theta''=70^\circ$  are assumed to be the same as in polydimethylsiloxane<sup>9</sup> and  $d_{\text{Si-H}}=1.48 \text{ \AA}$

Experimental and theoretical studies have shown that chains in amorphous polymers and polymeric melts adopt random-coil conformations that are unperturbed by intramolecular interactions between atoms and groups remote in sequence along the chain<sup>16-18</sup>. Hence, in the calculations to be described, excluded volume effects are neglected and the dihydrogensiloxane and dimethylsiloxane chains are treated as if they are free to intersect themselves. The only intramolecular interactions that are considered are those between non-bonded atoms and groups, which are separated by only a few chemical bonds.

### CYCLIC DIHYDROGENSILOXANES

#### Rotational isomeric state model for polydihydrogensiloxane

Polydihydrogensiloxane is structurally the simplest polysiloxane. Although the polymer is readily oxidized and hydrolysed and has not yet been fully characterized, several oligomeric dihydrogensiloxanes have been isolated and identified<sup>19, 20</sup>. Furthermore, experimental information relating to the effect of hydrogen atoms on the statistical conformations of polysiloxane chains has been made available by the measurement of cyclic concentrations in polyhydrogenmethylsiloxane equilibrates<sup>4</sup>.

A section of the polydihydrogensiloxane chain is shown in Figure 1. Structural parameters of the chain were assigned using data provided by electron diffraction studies of two low molecular weight analogues. In disiloxane (H<sub>3</sub>Si)<sub>2</sub>O, the Si-O bond length  $d_{\text{Si-O}}=1.634 \pm 0.002 \text{ \AA}$ , the Si-H bond length  $d_{\text{Si-H}}=1.486 \pm 0.010 \text{ \AA}$  and the Si-O-Si bond angle is  $144 \pm 0.9^\circ$ <sup>21</sup>. In the tetrameric cyclic, prosiloxane [H<sub>2</sub>SiO]<sub>4</sub>,  $d_{\text{Si-O}}=1.628 \pm 0.004 \text{ \AA}$ ,  $d_{\text{Si-H}}=1.48 \pm 0.04 \text{ \AA}$ , the Si-O-Si bond angle is  $149^\circ$ , the O-Si-O bond angle is  $112^\circ$  and the arrangements of bonds about the silicon atoms are approximately tetrahedral<sup>22</sup>. The Si-O bond length and the Si-O-Si and O-Si-O bond angles in these hydrogensiloxanes are similar to those in octamethylcyclotetrasiloxane<sup>23</sup> and other methylsiloxanes<sup>24-26</sup>. Thus, with the exception of  $d_{\text{Si-H}}$ , the structural parameters of polydihydrogensiloxane shown in Figure 1 are the same as those assigned to polydimethylsiloxane by Flory, Crescenzi and Mark<sup>9</sup>.

Scott and his coworkers<sup>27</sup> have shown that the energy barriers restricting internal rotation about the Si-O bonds in hexamethyldisiloxane are very low; and the unusual physical properties of polysiloxanes are believed to result, at least in part, from the ease of rotation about the skeletal siloxane bonds<sup>28-30</sup>. Nonetheless, as Flory<sup>18</sup> has argued, the statistical conformations of polysiloxane chains should be adequately described by representing the

\* Correlation effects may be appreciable for very short siloxane chains, but they are expected to be negligible for the longest dihydrogensiloxane and dimethylsiloxane chains (with 15-17 skeletal bonds) considered in this paper.

continuum of rotational states about skeletal bonds by choice of a discrete number of rotational isomeric states. Following Flory, Crescenzi and Mark's<sup>9</sup> analysis of polydimethylsiloxane, skeletal bonds of polydihydrogensiloxane are assigned to *trans* ( $\phi=0^\circ$ ), *gauche+* ( $\phi=120^\circ$ ) and *gauche-* ( $\phi=240^\circ$ ) positions. Statistical weight matrices  $U'$  and  $U''$  are introduced to take account of the mutual interdependence of rotational states for pairs of bonds centred on silicon and oxygen atoms respectively. The elements of these matrices are Boltzmann factors  $\exp(-\Delta E/RT)$  where  $\Delta E$  is the difference in energy between its associated conformation and the all-*trans* conformation and  $R$  is the gas constant.

As a consequence of the small size of the hydrogen atoms, the wide bond angles at skeletal oxygen atoms and the long silicon-oxygen bonds, steric interactions involving substituent hydrogen atoms in polydihydrogensiloxane would be expected to have virtually no effect on the statistical conformations of the chains; and a detailed analysis of the steric and Coulombic interaction energies between pairs of non-bonded atoms has shown that the only intramolecular interactions of consequence are electrostatic interactions between skeletal silicon and oxygen atoms. Even these are relatively unimportant and if they are neglected, all the elements of the statistical weight matrices  $U'$  and  $U''$  can be taken as unity, so that

$$U' = \begin{matrix} & t_i & g_i^+ & g_i^- \\ \begin{matrix} t_{i-1} \\ g_{i-1}^+ \\ g_{i-1}^- \end{matrix} & \begin{bmatrix} 1 & 1 & 1 \\ 1 & 1 & 1 \\ 1 & 1 & 1 \end{bmatrix} \end{matrix}; \quad (4)$$

$$U'' = \begin{matrix} & t_{i+1} & g_{i+1}^+ & g_{i+1}^- \\ \begin{matrix} t_i \\ g_i^+ \\ g_i^- \end{matrix} & \begin{bmatrix} 1 & 1 & 1 \\ 1 & 1 & 1 \\ 1 & 1 & 1 \end{bmatrix} \end{matrix}$$

In this approximation, the characteristic ratio for polydihydrogensiloxane is given by the familiar relation for a polysiloxane chain with free rotation about its skeletal bonds<sup>16</sup>:

$$\frac{\langle r^2 \rangle_0}{nl^2} = \frac{(1 + \cos\theta')(1 + \cos\theta'')}{(1 - \cos\theta' \cos\theta'')} \quad (5)$$

where  $\langle r^2 \rangle_0$  is the mean-square end-to-end distance of the unperturbed chain of  $n$  bonds each of length  $l$  in the limit  $n \rightarrow \infty$ . Using the bond angle supplements  $\theta'$  and  $\theta''$  quoted in the caption to Figure 1,  $\langle r^2 \rangle_0/nl^2$  is calculated to be 3.3 at all temperatures.\*

#### Calculation of molar cyclization equilibrium constants for cyclic dihydrogensiloxanes

The distances between the terminal atoms of  $x$ -meric dihydrogensiloxane chains  $[-H_2SiO-]_x$  with  $x=4-8$  were calculated for all  $3^{2x-3}$  conformations defined by the three-state rotational isomeric state model, and the number of conformations of each chain with terminal silicon and oxygen atoms within 2, 3, 4, 5 Å are listed in

Table 1 Number of conformations of dihydrogensiloxane chains with terminal atoms in close proximity

Value of $x$ in acyclic $[-H_2SiO-]_x$	Number of conformations defined by the rotational isomeric state model, with bonds in <i>trans</i> , <i>gauche+</i> , <i>gauche-</i> positions, that have the centres of terminal silicon and oxygen atoms within the range $0-r$ Å				Total number of conformations
	$r=2$ Å	$r=3$ Å	$r=4$ Å	$r=5$ Å	
4	2	10	18	36	243
5	38	78	160	266	2 187
6	170	490	1332	2 260	19 683
7	1300	3 884	8938	16 736	177 147
8	9270	29 766	—	—	1 594 323

Table 1. Densities of end-to-end vectors  $r$  in the region  $r \approx 0$  were found by dividing the fraction of the total number of conformations for each  $x$ -meric chain with terminal atoms within a reaction distance  $r$  by the volume  $(4/3)\pi r^3$  (cf. the calculations in refs 10 and 13). Theoretical molar cyclization equilibrium constants  $K_4-K_8$  were calculated by equation (3) with  $r=3$  Å (a distance corresponding approximately to the sum of the van der Waals radii of the terminal atoms of the chains). In Figure 2, they are compared with the experimental  $K_x$

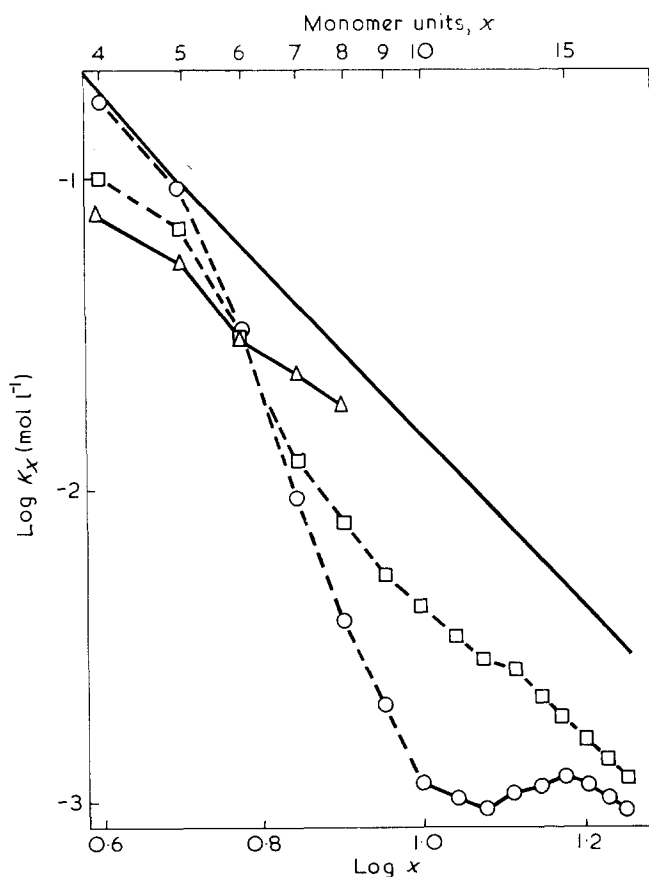


Figure 2 Theoretical molar cyclization equilibrium constants  $K_x$  for cyclic dihydrogensiloxanes ( $\Delta$ ) calculated by the direct computational method assuming a reaction distance  $r=3$  Å are compared with the experimental  $K_x$  values for cyclics  $[H(CH_3)_2SiO]_x$  at 273K ( $\square$ ) and  $[(CH_3)_2SiO]_x$  at 383K ( $\circ$ ). The unbroken line shows theoretical  $K_x$  values for cyclic dihydrogensiloxanes calculated assuming that the corresponding chain molecules obey Gaussian statistics (equation 6)

\* It is noted that when Carmichael and Kinsinger<sup>31</sup> calculated the molar cyclization equilibrium constants for  $[(CH_3)_2SiO]_3$  and  $[(CH_3)_2SiO]_4$ , they assigned skeletal siloxane bonds to *trans* ( $\phi=0^\circ$ ) and *gauche* ( $\phi=\pm 120^\circ$ ) positions with equal probability. Their rotational isomeric state model is identical to that represented by equation (4). Thus, it would be expected to provide a good representation of the statistical conformations of dihydrogensiloxane chains but not, of course, of dimethylsiloxane chains.

values for the homologous cyclic dimethylsiloxanes and hydrogenmethylsiloxanes, as well as with  $K_x$  values for cyclic dihydrogensiloxanes calculated by assuming that the corresponding chains obey Gaussian statistics so that<sup>7, 8</sup>:

$$\bar{W}_x \cong (3/2\pi \langle r_x^2 \rangle_0)^{3/2} \quad (6)$$

Unperturbed mean-square end-to-end distances  $\langle r_x^2 \rangle_0$  required by equation (6) were computed by the methods of Flory and Jernigan<sup>32, 33</sup> and the corresponding  $\bar{W}_x$  values were substituted into equation (3) to give  $K_x$  values shown as an unbroken line in Figure 2.

Although the  $K_x$  values for cyclic dihydrogensiloxanes have not yet been measured, the  $K_4$ – $K_8$  values calculated by the direct computational method are in accord with those expected by comparison with the experimental  $K_x$  values for the homologous cyclic dimethylsiloxanes and hydrogenmethylsiloxanes.

It is noted that in a more exact calculation, each discrete conformation defined by the rotational isomeric state model would be accorded a statistical weight based on a consideration of all the intramolecular interactions between non-bonded silicon, oxygen and hydrogen atoms. Furthermore, correlations between the directions of terminal bonds in the intramolecular cyclization reactions would also be taken into account. However, such refinements of the calculations must await more detailed molecular structural information pertaining to siloxane molecules than is available in the literature at the present time.

## CYCLIC DIMETHYLSILOXANES

Flory, Crescenzi and Mark's (FCM) rotational isomeric state model of polydimethylsiloxane<sup>9</sup>

The FCM rotational isomeric state model of polydimethylsiloxane was set up on the basis of a theoretical analysis of the polymeric chain using all the available molecular structural information<sup>9</sup>. In the model, each skeletal bond is assigned to either a *trans* ( $\phi=0^\circ$ ), *gauche+* ( $\phi=120^\circ$ ) or *gauche-* ( $\phi=240^\circ$ ) state and the mutual interdependence of adjacent pairs of bond rotational states is taken into account by means of two statistical weight matrices  $U'$  and  $U''$ . The matrix  $U'$  applies to rotational states about pairs of bonds centred on silicon atoms and the matrix  $U''$  applies to rotational states about pairs of bonds centred on oxygen atoms, thus:

$$U' = \begin{matrix} & t_i & g_i^+ & g_i^- \\ \begin{matrix} t_{i-1} \\ g_{i-1}^+ \\ g_{i-1}^- \end{matrix} & \begin{bmatrix} 1 & \sigma & \sigma \\ 1 & \sigma & 0 \\ 1 & 0 & \sigma \end{bmatrix} \end{matrix}; \quad (7)$$

$$U'' = \begin{matrix} & t_{i+1} & g_{i+1}^+ & g_{i+1}^- \\ \begin{matrix} t_i \\ g_i^+ \\ g_i^- \end{matrix} & \begin{bmatrix} 1 & \sigma & \sigma \\ 1 & \sigma & \delta \\ 1 & \delta & \sigma \end{bmatrix} \end{matrix}$$

The statistical weight parameters  $\sigma$  and  $\delta$  are assigned values so as to reproduce the experimental characteristic ratio  $\langle r^2 \rangle_0/nl^2$  of the linear polymer and the temperature coefficient  $d \ln \langle r^2 \rangle_0/dT$ . At 383 K, the temperature of the calculations to be described here, the values of the parameters are  $\sigma=0.327$  and  $\delta=0.082$ . As noted above, the

Table 2 Densities of end-to-end vectors  $\mathbf{r}$  in the region  $\mathbf{r} \cong \mathbf{0}$  for dimethylsiloxane chains calculated using statistical weights provided by the FCM model

Value of $x$ in acyclic $-(\text{CH}_3)_2\text{SiO}-)_x$	$\bar{W}_x \times 10^{-24}$ molecules/l calculated by eqn (9) for			
	$r=2\text{\AA}$	$r=3\text{\AA}$	$r=4\text{\AA}$	$r=5\text{\AA}$
4	0.00000	0.00044	0.00075	0.00894
5	0.00088	0.00089	0.00483	0.00675
6	0.00280	0.00178	0.00925	0.01210
7	0.01270	0.02090	0.01850	0.01410
8	0.03740	0.02990	0.02010	0.01760
9	0.01406	0.02242	—	—

structural parameters of the chain are:  $d_{\text{Si-O}}=1.64\text{\AA}$ ,  $\theta'=37^\circ$ ,  $\theta''=70^\circ$  (see legend to Figure 1).

## Calculation of molar cyclization equilibrium constants for cyclic dimethylsiloxanes

Molar cyclization equilibrium constants  $K_x$  for small cyclic dimethylsiloxanes  $[(\text{CH}_3)_2\text{SiO}]_x$  were calculated by computing the distances between the terminal silicon and oxygen atoms of the corresponding open chain molecules  $-(\text{CH}_3)_2\text{SiO}-)_x$  in all  $3^{2x-3}$  conformations, and using the FCM rotational isomeric state model to assign statistical weights to individual conformations. The densities of end-to-end vectors  $\mathbf{r}$  in the region  $\mathbf{r} \cong \mathbf{0}$  were calculated by dividing the sum  $Z_r$  of the statistical weights for all chain conformations with their terminal atoms separated by less than  $r\text{\AA}$ , by the volume  $(4/3)\pi r^3$  and by the total sum  $Z$  of the statistical weights of all  $3^{2x-3}$  conformations. The latter is simply the conformational partition function of the chain and is given by:

$$Z = [1 \quad 0 \quad 0] (\mathbf{U}' \mathbf{U}'')^{x-2} \mathbf{U}'' \begin{bmatrix} 1 \\ 1 \\ 1 \end{bmatrix} \quad (8)$$

so that

$$\bar{W}_x = Z_r / Z (4/3)\pi r^3 \quad (9)$$

Values for the probability densities  $\bar{W}_x$  of  $x$ -meric dimethylsiloxane chains with  $x=4-6$  calculated using the FCM model were found to be sensitive to the particular value chosen for  $r$  (see Table 2); and, when  $r$  is in the range  $2 < r < 5\text{\AA}$ , the corresponding  $K_4$ ,  $K_5$ ,  $K_6$  values were far lower than those found experimentally (see Figure 3 for  $K_x$  values calculated by equations (3), (7), (8) and (9) assuming  $r=3\text{\AA}$ ).

An explanation for the failure of the FCM model to yield meaningful theoretical values for  $K_4$ ,  $K_5$ ,  $K_6$  was given in a previous paper<sup>3</sup>. There it was pointed out that in order to calculate the molar cyclization equilibrium constants for small dimethylsiloxane rings it is necessary to take account of the mutual interdependence of bond rotational states further down the chain than in the FCM model. This is most clearly illustrated by considering steric and Coulombic interactions in the tetrameric acyclic  $-(\text{CH}_3)_2\text{SiO}-)_4$  when the five central skeletal bonds are in the following sequences of rotational states:  $\text{tg}^+\text{g}^-\text{g}^+\text{g}^-$  and  $\text{tg}^-\text{g}^+\text{g}^-\text{g}^+$ . There are no severe steric conflicts between non-bonded atoms or groups in these conformations, yet the FCM model accords them statistical weights of zero. In order to illustrate the effect of assigning such conformations more realistic statistical weights, pairs of  $\text{g}^+\text{g}^-$  and  $\text{g}^-\text{g}^+$  states centred on silicon atoms were given statistical

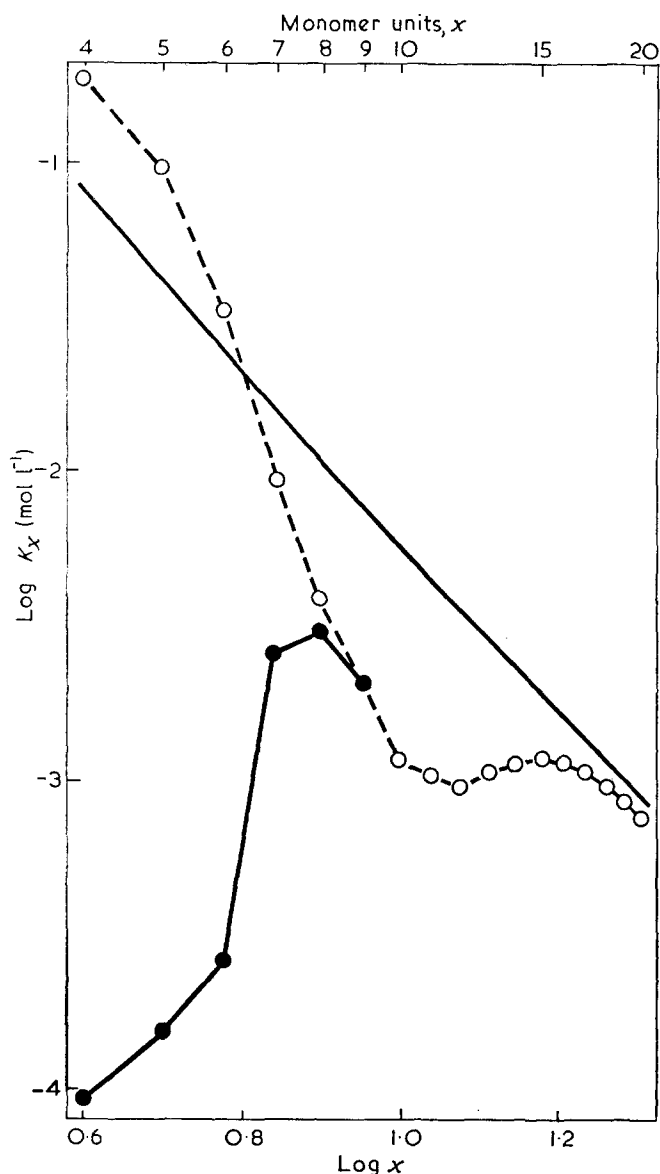


Figure 3 Theoretical molar cyclization equilibrium constants  $K_x$  for cyclic dimethylsiloxanes at 383K (●) calculated by the direct computational method, using the FCM model and assuming a reaction distance  $r=3\text{ \AA}$ . The corresponding experimental values<sup>3</sup> are denoted ○. The unbroken line shows  $K_x$  values calculated (using the FCM model) by assuming that the corresponding chains obey Gaussian statistics (equation 6)

weights of 20 (instead of zero) whenever the adjacent skeletal bonds were in *gauche* states of opposite sign. All other statistical weights were those provided by the FCM model. Thus, for example, at 383 K sequences of bond rotational states  $tg^+g^-g^+g^-t$  and  $tg^-g^+g^-g^+t$  in the acyclic  $\text{-(CH}_3)_2\text{SiO-}_x$  were given statistical weights of 0.044 relative to a statistical weight of unity for the all-*trans* conformation. The  $K_x$  values for small dimethylsiloxane cyclics were calculated as described above using the FCM model with this single modification. The densities of end-to-end vectors  $r$  in the region  $r \approx 0$  were found to be far less sensitive to the value chosen for  $r$  when  $2 < r < 5\text{ \AA}$  (see Table 3) and the  $K_4, K_5, K_6$  values were close to the experimental values (see Figure 4).

It is important to appreciate that it is only necessary to modify the FCM model for the calculation of the  $K_x$  values for cyclics corresponding to short dimethylsiloxane

Table 3 Densities of end-to-end vectors  $r$  in the region  $r \approx 0$  for dimethylsiloxane chains calculated using statistical weights provided by the modified FCM model (see text)

Value of $x$ in acyclic $\text{-(CH}_3)_2\text{SiO-}_x$	$\bar{W}_x \times 10^{-24}$ molecules/l calculated by eqn (9) for			
	$r=2\text{ \AA}$	$r=3\text{ \AA}$	$r=4\text{ \AA}$	$r=5\text{ \AA}$
4	0.480	0.251	0.118	0.086
5	0.687	0.371	0.195	0.118
6	0.055	0.110	0.112	0.139

chains. For longer chains, the FCM model can be used in its unmodified form. Thus, the FCM model yields probability densities of end-to-end vectors  $r$  for the octameric and nonameric acyclics that are relatively insensitive to the value of  $r$  provided it is small (see Table 2), and the theoretical molar cyclization equilibrium constants  $K_8$  and  $K_9$  (calculated using equations (3), (7), (8) and (9) by assuming a reaction distance  $r=3\text{ \AA}$ ) are in excellent agreement with the experimental values (see Figure 3).

In the future, it is hoped that the calculations described here may be extended to larger cyclic siloxanes. It will be interesting to discover whether the FCM model will yield theoretical molar cyclization equilibrium constants for cyclic dimethylsiloxanes with the characteristic minimum at  $x=12$  that was first reported by Brown and Slusarczuk<sup>2</sup>.

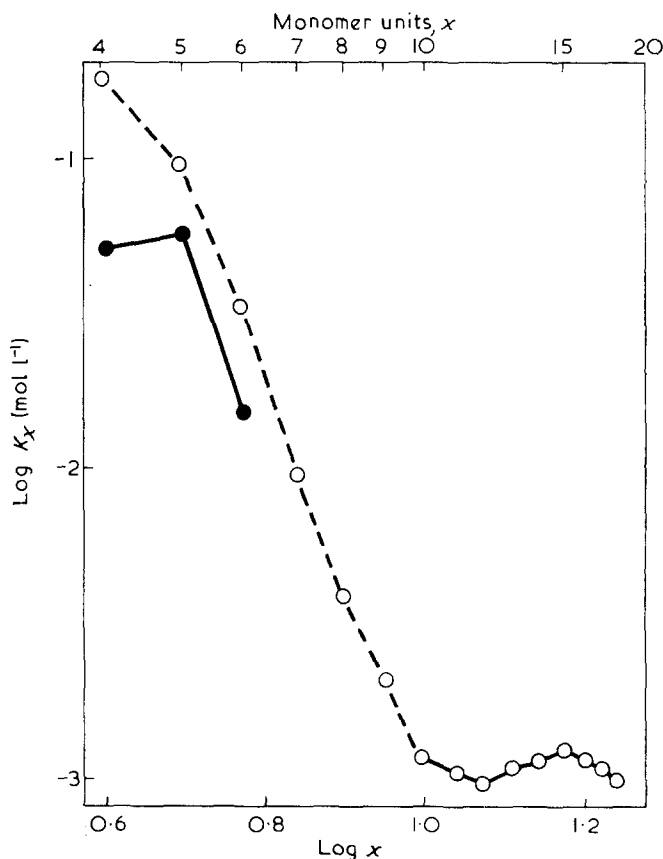


Figure 4 Theoretical molar cyclization equilibrium constants  $K_x$  for cyclic dimethylsiloxanes (●) calculated at 383K by the direct computational method by assuming a reaction distance  $r=3\text{ \AA}$  and using the FCM model modified so as to take account of the higher order interdependence of bond rotational states (see text). The corresponding experimental values are denoted ○

ACKNOWLEDGEMENTS

We are indebted to the Science Research Council for a Research Grant (to M.S.B.). We gratefully acknowledge computational facilities at the University of York.

REFERENCES

- 1 Carmichael, J. B. and Winger, R. *J. Polym. Sci. (A)* 1965, **3**, 971
- 2 Brown, J. F. and Slusarczuk, G. M. *J. Am. Chem. Soc.* 1965, **87**, 931
- 3 Semlyen, J. A. and Wright, P. V. *Polymer* 1969, **10**, 543
- 4 Wright, P. V. and Semlyen, J. A. *Polymer* 1970, **11**, 462
- 5 Beevers, M. S. and Semlyen, J. A. *Polymer* 1971, **12**, 373
- 6 Wright, P. V. *D.Phil. Thesis*, University of York, 1970
- 7 Jacobson, H. W. and Stockmayer, W. H. *J. Chem. Phys.* 1950, **18**, 1600
- 8 Flory, P. J. and Semlyen, J. A. *J. Am. Chem. Soc.* 1966, **88**, 3209
- 9 Flory, P. J., Crescenzi, V. and Mark, J. E. *J. Am. Chem. Soc.* 1964, **86**, 146
- 10 Semlyen, J. A. *Trans. Faraday Soc.* 1967, **63**, 2342
- 11 Semlyen, J. A. *Trans. Faraday Soc.* 1968, **64**, 1396
- 12 Semlyen, J. A. *Polymer* 1971, **12**, 383
- 13 Walker, G. R. and Semlyen, J. A. *Polymer* 1970, **11**, 472
- 14 Cooper, D. R. and Semlyen, J. A. *Polymer* 1972, **13**, in the press
- 15 Carmichael, J. B. and Heffel, J. *J. Phys. Chem.* 1965, **69**, 2218
- 16 Flory, P. J. 'Principles of Polymer Chemistry', Cornell University Press, Ithaca, 1953
- 17 Flory, P. J. in 'Lectures in Materials Science', W. A. Benjamin, New York, 1963
- 18 Flory, P. J. 'Statistical Mechanics of Chain Molecules', Interscience, New York, 1969
- 19 Petrov, A. D., Mironov, B. F., Ponomarenko, V. A. and Chernyshev, E. A. 'Synthesis of Organosilicon Monomers', Heywood, London, 1964
- 20 Campbell-Ferguson, H. J. *J. Inorg. Nucl. Chem.* 1965, **27**, 2121
- 21 Almenningen, A., Bastiansen, O., Ewing, V., Hedberg, K. and Traettenberg, M. *Acta. Chem. Scand.* 1963, **17**, 2455
- 22 Glidewell, C., Robiette, A. G. and Sheldrick, G. M. *Chem. Commun.* 1970, p 931
- 23 Steinfink, H., Post, B. and Fankuchen, I. *Acta Cryst.* 1955, **8**, 420
- 24 Larsson, K. *Ark. Kemi* 1960, **16**, 203
- 25 Damaschun, G. *Kolloid-Z.* 1962, **180**, 65
- 26 Yamasaki, K., Kotera, A., Yokoi, M. and Ueda, Y. *J. Chem. Phys.* 1950, **18**, 1414
- 27 Scott, D. W., Messerly, J. F., Todd, S. S. *et al. J. Phys. Chem.* 1961, **65**, 1320
- 28 Roth, W. L. *J. Am. Chem. Soc.* 1947, **69**, 474
- 29 Rochow, E. G. and LeClair, H. G. *J. Inorg. Nucl. Chem.* 1955, **1**, 92
- 30 Baney, R. H. and Haberland, G. G. *J. Organomet. Chem.* 1966, **5**, 320
- 31 Carmichael, J. B. and Kinsinger, J. B. *Can. J. Chem.* 1964, **42**, 1996
- 32 Flory, P. J. *Proc. Natl. Acad. Sci., Wash.* 1964, **51**, 1060
- 33 Flory, P. J. and Jernigan, R. L. *J. Chem. Phys.* 1965, **42**, 3509

# Accurate measurement of carboxyl and hydroxyl end-group concentrations in poly(ethylene terephthalate) film by infra-red spectroscopy

R. L. Addleman\* and V. J. I. Zichy\*

*Imperial Chemical Industries Limited, Plastics Division, Welwyn Garden City, Herts, UK  
(Received 13 December 1971; revised 2 February 1972)*

A new method which provides a rapid and reproducible quantitative determination of the alcoholic -OH and the carboxylic -OH end-group content of poly(ethylene terephthalate) film is described. The method is based on existing infra-red spectroscopic techniques and uses standard equipment. It may be applied over a wide range of film conditions. The previously unreported dichroism of various spectral features in the range of frequencies considered is established. A correlation is demonstrated between the dichroism of the hydroxyl and carboxyl absorption bands and birefringence in the visible spectrum.

## INTRODUCTION

The concept of using infra-red spectroscopy for the detection of hydroxyl and carboxyl end-groups in poly(ethylene terephthalate) (PET) film was originally demonstrated by Patterson and Ward<sup>1</sup>. The need to have a simple method of obtaining a quantitative measurement on a range of experimental films (which included amorphous, undrawn films, one-way and out-of-balance two-way drawn films, as well as films of various degrees of crystallinity) necessitated the development of this infra-red test.

The method is based on the measurement of the absorption bands at  $3542\text{cm}^{-1}$  and  $3256\text{cm}^{-1}$ , respectively attributed to the stretching vibration modes of alcoholic and carboxylic hydroxyl end-groups in poly(ethylene terephthalate). The method was calibrated with reference to both model systems and a chemical titration method.

In practice, this method of examination needs to be performed on a high resolution spectrophotometer. As these are usually grating instruments, there is a correspondingly high degree of instrument polarization involved<sup>2</sup>. The problems arising from this polarization effect are realized and overcome with this technique. There is also a marked correlation between the density of the sample and the apparent hydroxyl content ( $\pm 30\%$ ). This is accommodated by the adoption of a variable absorption coefficient, which is calibrated against the density of the film.

It is demonstrated that a correlation exists between birefringence at  $5896\text{Å}$  and the dichroism shown by the

absorption bands of both the -OH and the -COOH end-groups. This correlation could be demonstrated over a wide range of sample thickness ( $0.02\text{--}0.50\text{mm}$ ) because the absorption of PET in the relevant spectral range is low enough to permit the examination of thick films. During this work various dichroic features were observed, and these have been recorded.

## EXPERIMENTAL

### *Method*

The basic method is to obtain a plot of percentage transmittance against frequency in the range  $4000\text{cm}^{-1}$  to  $2380\text{cm}^{-1}$ . This may be carried out on any spectrophotometer with the necessary resolving power (for the experiments reported here a Grubb-Parsons Model DB3 was used<sup>3</sup>, see *Figure 1*). Because moisture strongly affects the spectrum obtained, samples have to be both thoroughly dried before testing and also prevented from taking up any moisture during examination. For this purpose a vacuum cell was specially designed (see *Figure 2*); it was equipped with a clamp to align the sample, and with alkali halide windows, so that the sample could be examined without being removed from the cell. The cell also had to be made small enough to fit easily into the sample beam of the spectrophotometer. A criterion for the 'dryness' of the sample also needed to be devised, and this was done (see below). The accurate determination of the density and thickness of a sample is also necessary for the numerical measurement of end-group content. These ancillary measurements together with the determination of the directions of the principal axes of the sample need to be completed before the sample is placed in the cell.

The directions of the principal axes are established by rotating the film between crossed polarizers until extinc-

\* The work described here has been carried out on a co-operative basis with the Dept. of Mechanical Engineering at Imperial College of Science and Technology, London SW7, UK.



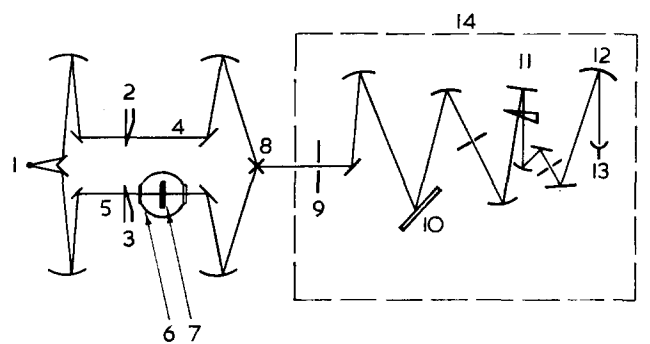


Figure 1 Spectrophotometer layout. 1, Nernst (infra-red source); 2, null-balance comb; 3, trimmer comb (zero adjust); 4, reference beam; 5, sample beam; 6, vacuum cell; 7, sample; 8, reciprocating mirror; 9, variable aperture slit; 10, diffraction grating; 11, Littrow mirror; 12, ellipsoid; 13, thermocouple (infra-red detector); 14, monochromator housing

tion is obtained. In this position the principal in-plane axes of the sample are aligned with the polarization directions of the polarizer and analyser. The density measurement is carried out using a gradient column, the method being that of Payne and Stephenson<sup>4</sup>. A column is set up with a gradient in the concentration of a solute in a solvent producing the required density gradient. For PET a solution of calcium nitrate in water is used to give a density range of 1.30–1.45 g/cm<sup>3</sup>. This method yields an accuracy of  $\pm 0.0003$  g/cm<sup>3</sup>. The thickness of the sample is measured with a dial gauge micrometer, and should lie between approximately 0.13 and 0.60 mm. This minimum thickness is dictated by three considerations: primarily samples below this thickness give absorbances at the frequencies of interest too small for accurate measurement; they also have a tendency to produce significant interference patterns superimposed on the spectrum; and finally the percentage error in thickness measurement can become significant on thinner samples. It is possible to use thinner films laminated to give specimens of the required thickness. This is done with the use of an immersion liquid which holds the layers together by its surface tension, suppresses the formation of interference fringes, and also reduces reflection and scattering losses at the interfaces. Care has to be taken that the optical axes of each of the layers are aligned with the others. The immersion liquid used for this purpose is pure dry liquid paraffin (BP grade). The sample is dried by keeping it in a vacuum of less than 0.013 kN/m<sup>2</sup> (absolute pressure = 0.1 mmHg) at room temperature for periods varying from 10 to 70 h depending on sample thickness and condition. The usual time necessary is about 18 h, the dryness of the sample being immediately apparent on taking the spectrum.

A few words should be said about the alignment of the sample. It is observed that if one of the principal axes is aligned with the direction of the instrument polarization then the absorbance measured at the frequencies used in this analysis significantly depends ( $\pm 10\%$  for carboxyl results) on which of the two in-plane axes is aligned. To overcome this effect one of two methods may be employed. Either two measurements can be made, one with each of the in-plane primary axes in line with the inherent instrument polarization direction, and the average of the results taken. Alternatively the well established method of using a single measurement with the film's principal in-plane axes at 45° to the direction of the instrument polarization may be adopted<sup>2, 5, 6</sup>. The difference in the

final numerical result is less than experimental scatter, and all results obtained by either method give excellent agreement with those obtained for carboxyl content by chemical titration (better than 3%). It proved possible to utilize fully the instrument polarization for the determination of the dichroism of weak spectral features.

To see if there is any correlation between birefringence and the difference in apparent end-group content with the sample in its different alignments, the refractive indices of all the samples were determined using an Abbé 60 refractometer<sup>7</sup> (which accurately measures the critical angle). The birefringences quoted are at 20°C, 5896 Å wavelength, and may be taken as accurate to 0.0005.

#### Measurement of spectra

A typical spectrum obtained from a dry PET sample is shown in Figure 3. The most important frequencies for the calculations concerned are designated A, B, C, D, E and F.

We will consider first the transmission peaks at A (3717 cm<sup>-1</sup>) and B (3663 cm<sup>-1</sup>). These are taken as the earlier mentioned criterion for dryness, as any moisture present absorbs at B. It was found that if the transmission at B is as great as or greater than that at A then the numerical results given by a specimen are unaltered with further drying (see Figure 4 which shows the alteration of this part of the spectrum with sample dryness, and also demonstrates the corresponding change in apparent hydroxyl content).

The tangent from B which is common to either E (2667 cm<sup>-1</sup>) or F (2457 cm<sup>-1</sup>) is taken as the transmission maximum base line. The tangent used is that which gives the highest background transmission (in Figure 3 the

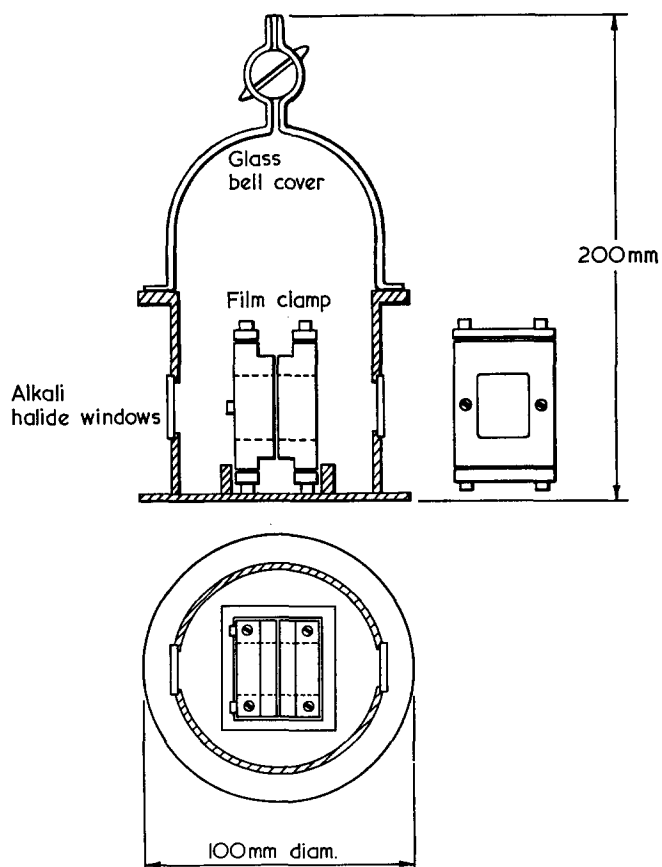


Figure 2 Vacuum cell

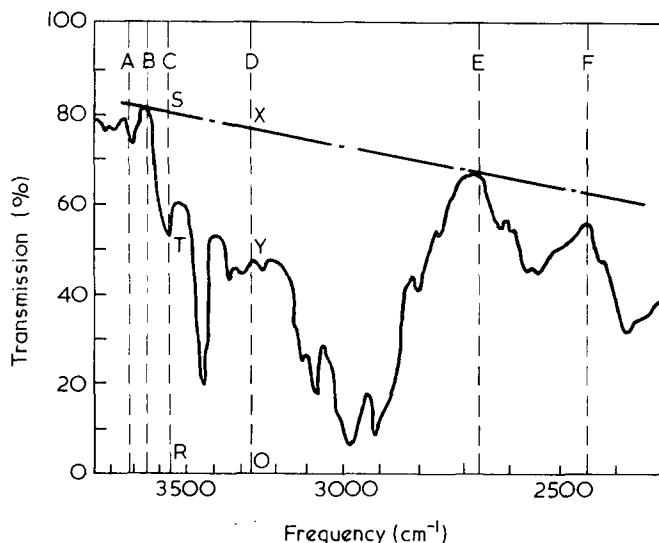


Figure 3 Typical spectrum of dry PET film where the B-E base line is used

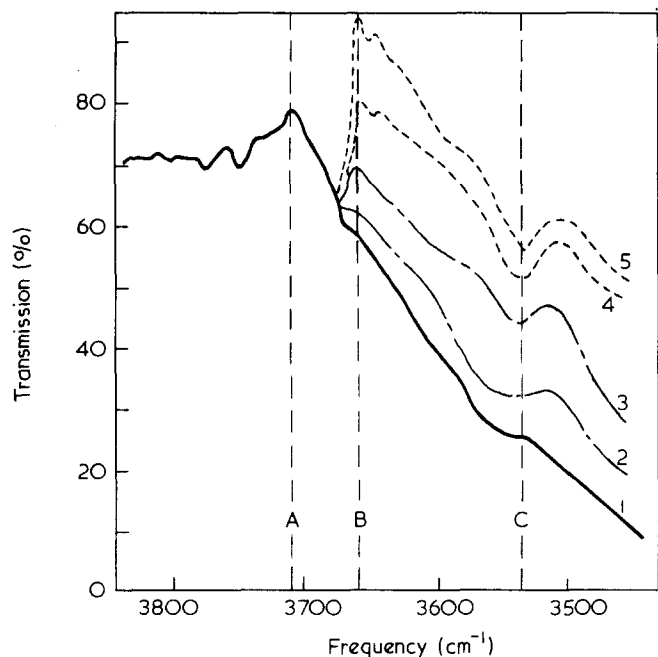


Figure 4 Effect of film dryness on the spectrum near the hydroxyl absorption band. 1, sample as received: measured  $N_{OH}=76$ ; 2, sample dried for 5h: measured  $N_{OH}=68$ ; 3, sample dried for 20h: measured  $N_{OH}=51$ ; 4, sample dried for 40h: measured  $N_{OH}=48.6$ ; 5, sample dried for 70h: measured  $N_{OH}=48.5$

tangent B to E is used, in Figure 5 the tangent to F is chosen). The 'base line' method is well established spectroscopic practice<sup>8</sup> and will not be justified here.

The quantities required for the numerical determination of end-group content are the absorbances at  $3256\text{ cm}^{-1}$  (carboxyl) and  $3542\text{ cm}^{-1}$  (hydroxyl). These absorbances need to be corrected in each case for the background absorbance of PET which contains no hydroxyl or carboxyl end-groups. These corrections were initially determined on deuterated samples using the same method as that of Patterson and Ward<sup>1</sup>. Dry amorphous PET film was immersed in heavy water in a dry nitrogen atmosphere for two weeks. This procedure replaced the  $-\text{COOH}$  and  $-\text{OH}$  end-groups by the corresponding  $-\text{COOD}$  and  $-\text{OD}$  groups (see Patterson and Ward for justification of this

statement). The absorption band from the  $-\text{COOH}$  end-groups at  $3256\text{ cm}^{-1}$  is replaced by that at  $2458\text{ cm}^{-1}$  for  $-\text{COOD}$ . Similarly the  $3542\text{ cm}^{-1}$  band due to the alcoholic  $-\text{OH}$  end-groups is eliminated and replaced by a band at  $2631\text{ cm}^{-1}$  arising from alcoholic  $-\text{OD}$  end-groups (see Figure 6). The spectrum of the dry deuterated film directly gives the background absorbances of dry PET at the frequencies used for the measurement of the end-group concentrations. The absorbance of deuterated PET film with no carboxyl end-groups was noted to be 0.142 per mm thickness of sample at  $3256\text{ cm}^{-1}$ . Similarly the absorbance at  $3542\text{ cm}^{-1}$  was noted to be 0.065 per mm of PET film. Thus if  $t$  is the thickness of film in mm, the corrected absorbance for the carboxyl end-group determination,  $(CA)_{\text{COOH}}$  is:  $\log(\text{OX}/\text{OY}) - 0.142t$ . Similarly the corrected absorbance for the hydroxyl end-group determination  $(CA)_{\text{OH}}$  is:  $\log(\text{RS}/\text{RT}) - 0.065t$  (see Figures 3 and 5). The number of carboxyl end-groups expressed in g equiv./ $10^6$  g of polymer is given by:

$$N_{\text{COOH}} = \frac{(CA)_{\text{COOH}} \times 10^4}{\rho \times t \times Q_1}$$

where  $\rho$  is the density in  $\text{g}/\text{cm}^3$  and  $Q_1$  is the extinction coefficient. The value of  $Q_1$  used in the experiments is 135. This was worked out by infra-red spectroscopy on a model system consisting of a series of solutions of *p*-cresoxy-acetic acid in di-*n*-butyl phthalate. The value was further verified by comparison with values obtained by accurate chemical titration methods and a tritium exchange method (derived from that of Chul-Yung Cha<sup>9</sup>).

The number of hydroxyl end-groups (g equiv./ $10^6$  g polymer) is given by:

$$N_{\text{OH}} = \frac{(CA)_{\text{OH}} \times 10^4}{\rho \times t \times Q_2}$$

where  $Q_2$  is the extinction coefficient for the hydroxyl band. It was found that  $Q_2$  was strongly influenced by the density of the sample, and using similar techniques to those described for the determination of  $Q_1$  (with a model of lauryl alcohol in di-*n*-butyl phthalate) it was established that  $Q_2=113$  for amorphous film of density 1.338. It was further established that  $Q_2=154$  for drawn and crystallized film of density 1.40. Assuming a direct proportionality between extinction coefficient and density we get the numerical relation:

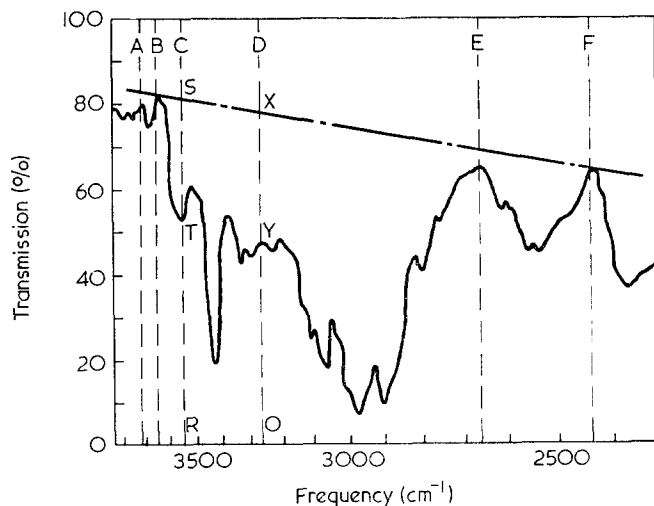


Figure 5 Typical spectrum of dry PET film where the B-F base line is necessary

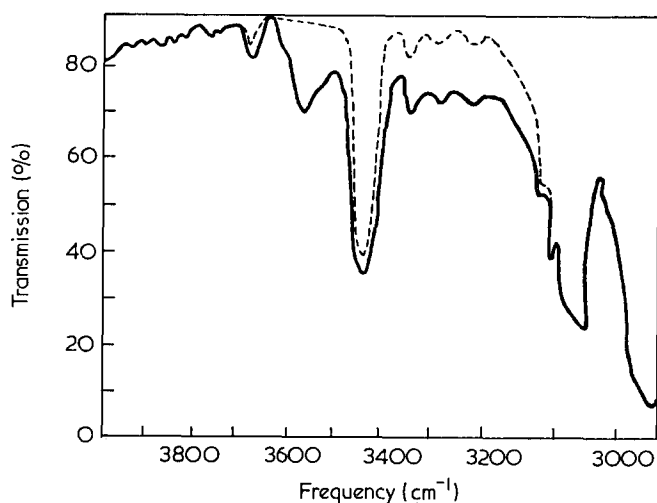


Figure 6 Effect of deuteration on the spectrum of dry PET film. —, sample, dried; ----, sample, deuterated for two weeks and dried. (Note the complete disappearance of the hydroxyl absorption band at 3542 cm<sup>-1</sup>)

$$Q_2 = 661.3\rho - 772$$

Thus:

$$N_{\text{OH}} = \frac{(CA)_{\text{OH}} \times 10^4}{\rho \times t \times (661.3\rho - 772)}$$

The assumption that  $Q_2$  is proportional to  $\rho$  is justified later in the paper.

Both end-group concentration results are calculated in units of g equiv./10<sup>6</sup> g of polymer. This may be converted to the more basic unit of absolute number per gramme of polymer by multiplying by Avogadro's Number and dividing by 10<sup>6</sup> (i.e. by multiplying  $N_{\text{COOH}}$  and  $N_{\text{OH}}$  by 6.023 × 10<sup>17</sup>).

#### Calibration technique

Four main calibrations are necessary to obtain a reliable end-group measurement technique: (1) the absorption resulting from the end-group vibrations; (2) the absorption resulting from the PET polymer chains at the frequencies where the end-groups absorb; (3) the effect of anisotropy; (4) the variation in absorption with conditions such as wetness and crystallinity of the film. Some of these calibrations have been mentioned already, but it was felt to be worthwhile to discuss these and others more fully.

Calibrations (1) and (2) have already been described. It is important that amorphous film be used for both of these calibrations, as the model solution used for the calibration is clearly amorphous. This also simplifies the calibration as  $A_0$ , the 'true' absorbance independent of molecular orientation, is directly measured.

The effect of anisotropy becomes important for drawn films. To ascertain the effect of this anisotropy two of the most out of balance films (4.0 × 1.0 one-way drawn uncrystallized film, and two-way drawn crystallized film) were tested in order to determine their absorbances with the plane of the electric vector in three mutually perpendicular directions, using Schmidt's<sup>15</sup> and Koenig's<sup>2</sup> technique. The results are given in Table 1.

Although the theoretically correct method is to calculate  $\frac{1}{3}(A_x + A_y + A_z)$  (which is the 'true' absorbance,  $A_0$ ), as may be seen, a good approximation of this is given

Table 1 Effect of film anisotropy on absorbance measured in each of three mutually perpendicular directions

	$A_x$	$A_y$	$A_z$	$\frac{1}{3}(A_x + A_y + A_z) = A_0$	$\frac{1}{2}(A_x + A_y)$
One-way drawn film:					
COOH	0.178	0.099	0.112	0.138	0.130
OH	0.079	0.106	0.100	0.093	0.095
Two-way drawn film:					
COOH	0.123	0.097	0.112	0.110	0.111
OH	0.084	0.109	0.087	0.092	0.090

by  $\frac{1}{2}(A_x + A_y)$ . This treatment is acceptable for these two absorption bands because they do not have a high degree of dichroism. As the average of the in-plane absorbances may be ascertained with a single measurement, whereas  $\frac{1}{3}(A_x + A_y + A_z)$  requires six measurements<sup>15</sup>, it is felt that a good enough approximation of the true absorbance is given by  $\frac{1}{2}(A_x + A_y)$ .

The effect of dryness has already been discussed. Using the absorption band of water as a measure of wetness, several films were dried until no numerical difference in absorbances at the end-group frequencies were discernable on further drying.

To gauge the effect of crystallinity, several drawn, crystallized dry films were tested. These films were then dried, quenched, redried and retested. It was found that the absorbance at the carboxyl end-group frequency had not changed at all. However, the absorbance at the hydroxyl end-group frequency had changed by more than 35%, a much greater amount than could possibly be explained in terms of re-orientation (see Table 1). It was also noticed that the absorption band resulting from the -OH end-groups tended to be narrower in the case of the crystalline material. As this technique measures the peak height intensity of an absorption band, rather than the area under the absorption band, a narrower band of greater peak height intensity, but of equal area to the amorphous band could explain the different values of the absorption coefficient,  $Q_2$ . A possible explanation of the fact that  $Q_2$  alters with crystallinity, and not  $Q_1$  may be that the -OH end-groups are small enough to be contained in the crystalline regions of the polymer, whereas the -COOH end-groups, because of their bulk, tend to remain in the amorphous regions.

#### Samples used

Three series of PET films were used. They were: (a) melt cast, (b) plant produced two-way drawn films, and (c) a series of one-way and two-way drawn films produced on the 'Long' stretcher<sup>10</sup> by one of us (R.L.A.) from the cast film (a).

The melt cast film (a) was approximately 0.6 mm thick. It showed complete extinction when viewed between crossed polarizers, whatever the alignment of the sample (showing that there is no in-plane orientation).

The plant produced two-way drawn films were standard 'off the shelf' unfilled polymer films, with thicknesses varying from 0.025 mm to 0.175 mm, and in-the-plane birefringences varying from 0.021 to 0.040. All these films were 'heat set' (Heffelfinger and Schmidt<sup>11</sup> define this term as used here) to a similar crystallinity. In the Tables they will be designated P1-P3.

Table 2 Film characteristics with numerical end-group results

Sample number	Draw ratio	Birefringence (in-plane) $ n_1 - n_2  \times 10^3$	Density (g/cm <sup>3</sup> )	Carboxyl				Hydroxyl		
				$\langle N \rangle = \frac{1}{2}(N_1 + N_2)$	$N_3$	$\frac{\Delta N}{ N_1 - N_2 }$	$N_T$	$\langle N \rangle = \frac{1}{2}(N_1 + N_2)$	$N_3$	$\frac{\Delta N}{ N_1 - N_2 }$
1	Cast	0.43	1.3446	49.5	49.6	0.1	50	49.5	49.5	0
2	Cast	0.39	1.3440	50.1	49.6	0.4	—	50.1	49.8	0.2
3	2.0 × 1.0	9.11	1.3452	49.2	—	1.5	—	51.2	—	0.4
4	2.5 × 1.0	63.07	1.3493	47.6	—	3.5	—	49.3	—	0.8
5	3.0 × 1.0	80.47	1.3673	47.9	47.8	5.8	—	50.0	49.8	0.8
6	3.5 × 1.0	81.40	1.3714	50.3	50.1	5.9	49	51.0	50.8	1.0
7	4.0 × 1.0	95.33	1.3730	48.7	48.4	6.2	49	50.7	50.6	0.9
8	3.0 × 2.0	32.79	1.3708	49.9	49.7	1.9	—	49.8	49.6	0.9
9	3.0 × 2.5	12.16	1.3741	49.8	—	1.3	—	48.6	—	0.3
10	3.0 × 3.0	0.67	1.3700	50.2	—	0.5	—	49.1	—	0.3
11	3.0 × 3.5	19.25	1.3709	51.7	—	4.8	52	51.7	—	0.9
12	3.0 × 4.0	36.87	1.3710	49.7	49.2	10.1	—	49.8	49.4	2.9
13	3.0 × 3.0 (s)	16.17	1.3726	48.9	48.8	1.4	—	49.9	49.9	0.4
P1	— (s)	21.05	1.4024	59.7	59.5	3.4	59	41.7	41.5	1.2
P2	— (s)	30.05	1.4012	60.3	60.0	6.1	59	47.0	46.6	2.0
P3	— (s)	40.06	1.4050	50.7	50.6	8.7	52	47.8	47.5	2.8

Table 3 Spectroscopic reproducibility

Sample no. with draw ratio	NOH (i)	NOH (ii)	NOH (iii)	NCOOH (i)	NCOOH (ii)	NCOOH (iii)
1 Cast	49.5	49.6	49.5	49.5	49.0	49.1
	49.6	49.6	49.5	49.6	49.0	49.3
	49.7	49.5	49.6	49.5	49.1	49.2
9 3.0 × 2.5	48.5	48.8	—	50.4	49.2	—
	48.4	48.9	—	50.3	49.1	—
	48.6	48.8	—	50.4	49.3	—

 $\bar{\sigma} \approx 0.05$ 

The samples produced on the 'Long' stretcher were all drawn under identical conditions as far as practically allowed. They were all drawn at a temperature of 95°C ( $\pm 1^\circ\text{C}$ ), and at a speed of 640% engineering strain per second ( $\pm 10\%$ /sec) [engineering strain = (length/initial length) - 1]. The samples were all heated for 120 sec before being drawn, and quenched by keeping them in a stream of air at 20°C for 90 sec (with all the machine heaters being turned off) before being removed. These samples were not heat set, and therefore have a wide range of crystallinity and density. They were one-way drawn at ratios of 2.0 : 1, 2.5 : 1, 3.0 : 1, 3.5 : 1 and 4.0 : 1, with the width being held constant. Two-way drawn samples were also prepared at ratios of 3.0 × 2.0, 3.0 × 2.5, 3.0 × 3.0, 3.0 × 3.5, 3.0 × 4.0. The process was controlled so that the draw speed in each direction was the same (640% strain/sec), and the draw in each direction was started at the same instant. A sequentially drawn 3.0 × 3.0 sample was also prepared to complete the series.

## RESULTS

As already stated most measurements were made with the plane of the electric vector in three directions relative to the film, and these should be defined: (1) this refers to one of the axes of draw on the 'Long' stretcher. It is the drawn direction for the one-way drawn film, the 3.0 (constant) draw direction for the two-way drawn film, and the primary draw direction for the sequentially drawn film. A similar criterion is applied for the cast and plant films; (2) at right angles to (1), in the plane of the film; (3) at 45° to both (1) and (2), in the plane of the film. The numerical results from the three sets of film are given in Table 2.

The postscript (s) in the draw ratio column refers to films which were sequentially drawn.  $N$  is the end-group concentration expressed in g equiv./10<sup>6</sup> g of polymer. Subscript 1 refers to a measurement with the direction of the electric vector being parallel to direction 1, with corresponding notation for subscripts 2 and 3. The birefringence as tabulated is 'in-plane' birefringence and is  $|n_1 - n_2|$  where  $n$  is the refractive index. Similarly  $\Delta N$  is  $|N_1 - N_2|$  and  $\langle N \rangle$  is  $\frac{1}{2}(N_1 + N_2)$ .  $N_T$  is the value of  $N$  given by chemical titration methods for certain carboxyl end-group tests.

The reproducibility of the spectroscopic process was ascertained by repeating the spectra on sample number 1 (cast) and sample number 9 (3.0 × 2.5) three times in each direction (giving 10 readings repeated three times). The sample was removed and replaced before each spectrum was recorded. The results are shown in Table 3.

## DISCUSSION

### End-group concentration

It is improbable on chemical grounds that any hydroxyl end-groups can be formed by chain scission. In addition to this, at the temperature of drawing (95°C in dry air) hydrolytic degradation (a well known mechanism of producing additional hydroxyl end-groups by degradation) is highly unlikely to occur. This means that for the experimental films a consistency of hydroxyl end-group concentration is required. This consistency is obtained when the absorption coefficient ( $Q_2$ ) is taken to be directly proportional to the film density. The combination of this consistency of results together with the known value of

$Q_2$  for amorphous films (obtained by a deuterium exchange method, tritium exchange method and analysis of model systems) both justifies the assumption of  $Q_2$  being proportional to density, and ensures numerical accuracy. In reality  $Q_2$  is obviously proportional to crystallinity and density is used only as a convenient measure of crystallinity which is adequate for unvoided samples such as are described here<sup>14-16</sup>.

Both the averaged hydroxyl and the averaged carboxyl end-group measurements vary by less than  $\pm 2$  end-groups over the entire range of experimental cast, one-way and two-way drawn films (which were all taken from the same cast sheet). The excellent repeatability of the test when applied to the same sample (better than  $\pm 0.2$  end-groups) would imply that the variation of  $\pm 2$  in end-group concentration is either due to lack of uniformity in the cast film itself, or due to variations in the ancillary measurements such as thickness. It is probably due to both, as in two cast samples there is a difference of 0.6 end-groups, and as thickness measurements from any one sample (experimental) can vary over the area used for the measurement. These variations appear to be random.

The agreement in results for carboxyl end-groups as given by chemical titration and infra-red spectroscopy is indeed very good. It must be remembered that whereas the spectroscopic test applies only to an area of about  $1 \text{ cm}^2$  (0.02 g of the polymer), the chemical titration needs 100 times the weight to get a value which can be considered meaningful. This means that the sample used for titration cannot be considered identical to that used in the spectroscopic test, even though it contains the spectroscopically analysed sample.

#### Effect of polarized radiation on absorption bands

As already shown dichroism of many of the spectral features was apparent with the radiation polarized only by the instrument optics. Although the fractional polarization could have been improved by inserting additional polarizing devices, this would have been at the expense of greatly reducing intensity and making the accurate measurement of weak bands more difficult due to the reduced signal-to-noise ratio. We will define the terms 'parallel' and 'perpendicular' dichroism as used in this context. Linearly polarized light with the unidirectional electric vector parallel to the polymer chain gives rise to strong absorbance by the parallel vibrational mode ( $\pi$ ) of dipoles, and less or no absorbance by the perpendicular ( $\sigma$ ) vibrational mode. The direction of inherent polarization of the instrument was confirmed by inserting a silver chloride pile-of-plates polarizer in the sample beam of the instrument.

The dichroism of various spectral features is shown in Figure 7, which gives a typical pair of spectra obtained in the test on a dry film. The previously unreported absorption bands are marked (i) to (x). They are listed in Table 4. On other major bands such as the carbonyl overtone (xi) and the highly dichroic region from  $3225 \text{ cm}^{-1}$  to  $2858 \text{ cm}^{-1}$ , which includes the C-H stretching modes, complete agreement was obtained with existing assignments (mainly taken from Liang and Krimm<sup>12</sup>, Tadakoro *et al.*<sup>13</sup> and Manley and Williams<sup>6</sup>). However, the hydroxyl end-group stretching band ( $3542 \text{ cm}^{-1}$ ) was observed to have weak  $\sigma$  dichroism (in agreement with Tadakoro *et al.* but contrary to Liang and Krimm, and Manley and Williams). This discrepancy may be due to

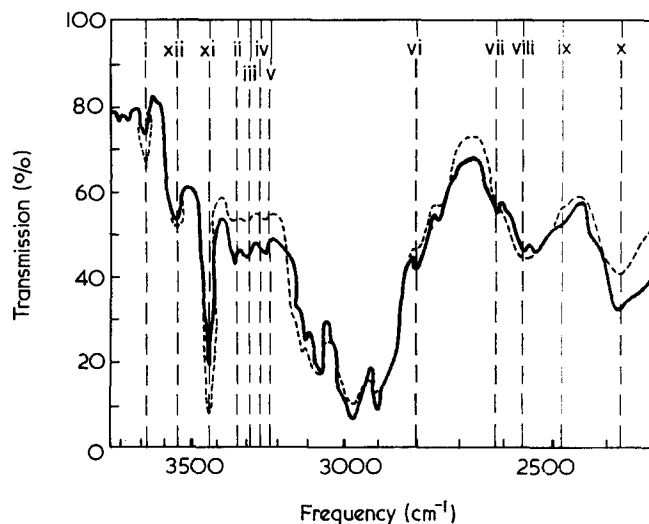


Figure 7 Typical spectra of a one-way drawn film. —, draw axis parallel to the direction of inherent polarization of the instrument; ---, draw axis perpendicular to the direction of inherent polarization of the instrument

the fact that samples containing various amounts of moisture could have been examined by these authors (and moisture strongly affects this region of the spectrum). Although the dichroism of the carboxyl absorption band cannot be observed directly because of interference from other absorption bands of PET, it can be conclusively deduced from Table 2 that it is a strong parallel band.

#### Correlation between birefringence and the numerical effect of polarization

The apparent intensity of the carboxyl group absorption band depends in most cases upon which of the primary axes of the sample was aligned with the direction of the inherent polarization of the spectrophotometer. The difference in apparent values of end-group concentrations,  $\Delta N_{\text{COOH}}$ , was directly related to the in-plane birefringence of the sample,  $P$ . The plot of  $\Delta N_{\text{COOH}}$  against  $P$  is given in Figure 8a. As can be seen, for the plant produced films considered,  $\Delta N_{\text{COOH}}$  varied from 3.4 to 7.7 over a range of typical plant film birefringences. It is of considerable interest that the plant films and the experimental films lie on the same curve. Furthermore, it is interesting that there are two distinct curves. The  $3 \times 3.5$ ,  $3 \times 4$  experimental films together with all the plant films have their values of  $\Delta N_{\text{COOH}}$  more strongly dependent on birefringence ( $P$ ) than all the other experimental films.

Table 4 Previously undetected absorption bands

Number in Figure 7	Wavelength ( $\mu\text{m}$ )	Wavenumber ( $\text{cm}^{-1}$ )	Polarization
(i)	2.71	3690	$\sigma$
(ii)	3.00	3333	$\pi$
(iii)	3.03	3300	$\sigma$
(iv) -COOH	3.07	3257	$\pi$
(v)	3.09	3236	$\pi$
(vi)	3.57	2801	$\pi$
(vii)	3.81	2625	$\pi$
(viii)	3.88	2577	$\sigma$
(ix)	4.03	2481	$\pi$
(x)	4.19	2387	$\pi$

$\sigma$  denotes perpendicular dichroism,  $\pi$  denotes parallel

For example a birefringence of 0.032 gives a  $\Delta N_{\text{COOH}}$  of 1.9 on the  $3 \times 2$  film, whereas  $P$  of 0.030 (P2) gives a  $\Delta N_{\text{COOH}}$  of 6.1. Four suggestions are put forward to explain this difference in the films: (a) high crystallinity made  $\Delta N_{\text{COOH}}$  more sensitive to birefringence; (b) the  $\Delta N_{\text{COOH}}$  was dependent on planar orientation [ $= (n_1 + n_2/2) - n_4$ , where direction (4) is perpendicular to the plane of the film]; (c) after a certain area increase the sensitivity increases; or (d) the sequentially drawn films have a greater  $d(\Delta N_{\text{COOH}})/dP$ . Theory (a) must be discarded as the densities (and hence percentage crystallinities<sup>14, 16</sup>) of the  $3 \times 2$ ,  $3.5 \times 1$ , and  $4 \times 1$  films are as great as those of the  $3 \times 3.5$  and  $3 \times 4$  films, whereas their  $\Delta N_{\text{COOH}}$  is much less. Theory (b) must also be discarded

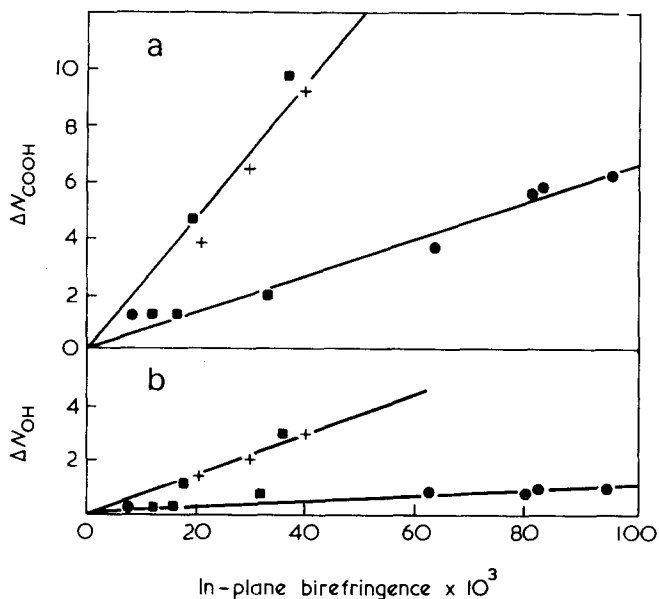


Figure 8 Birefringence:  $\Delta N$  correlation (a,  $\Delta N_{\text{COOH}}$ ; b,  $\Delta N_{\text{OH}}$ ). +, Plant samples; ●, one-way drawn experimental samples; ■, two-way drawn experimental samples

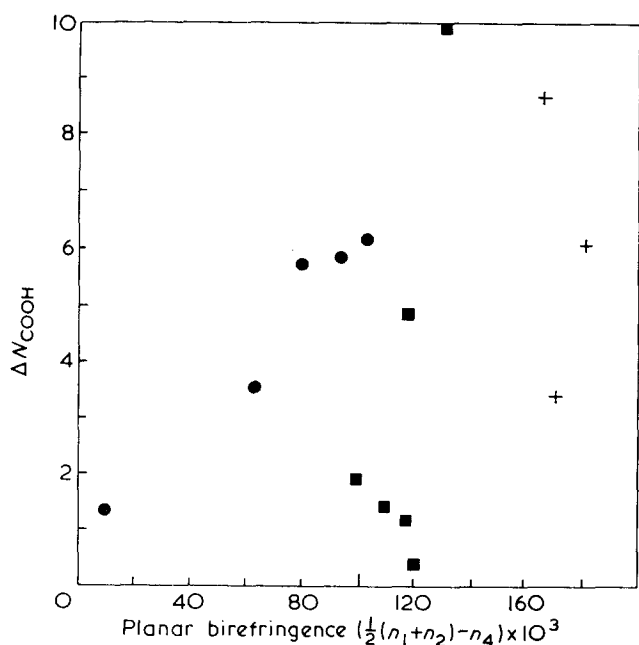


Figure 9  $[\Delta N_{\text{COOH}}]$ : planar birefringence lack of correlation. +, Plant samples; ●, one-way drawn experimental samples; ■, two-way drawn experimental samples. (Direction 4 is perpendicular to the plane of the film, and  $n_4$  uses the same notation as  $n_1$  and  $n_2$ )

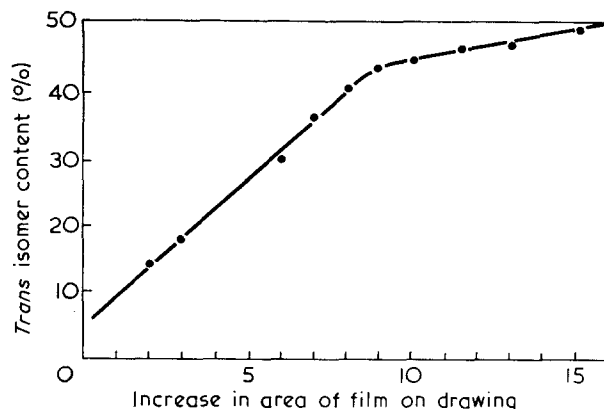


Figure 10 Percentage *trans* isomer content: area increase

as it is quite clear from Figure 9 that there is no obvious relationship between planar birefringence and  $\Delta N_{\text{COOH}}$ . Theory (d) must also be discarded, as some of the extra-sensitive films were simultaneously drawn (the experimental films). Theory (c) may certainly be possible, as all the extra-sensitive films have an in-plane area increase greater than 9, and all the other films have an in-plane area increase less than 9. At this specific area increase discontinuities can be observed in other quantities, such as the extended *trans* isomer content (see Figure 10). There may be further possible explanations, but as this paper is mainly to show a method of measuring end-group concentrations the niceties of physical structure which cannot easily be proved will not be dealt with here.

A similar trend in the apparent difference in hydroxyl end-group concentrations given,  $\Delta N_{\text{OH}}$ , may also be observed.  $\Delta N_{\text{OH}}$  plotted against  $P$  is given in Figure 8b. As may be seen the shape of the curve is similar to that for the carboxyl apparent differences, although the effect is clearly very much diminished, and the dichroism is perpendicular rather than parallel. It should be stressed that the numerical values of  $\Delta N_{\text{COOH}}$  and  $\Delta N_{\text{OH}}$  are also a function of the degree of polarization inherent in the spectrophotometer used for the measurements. It is assumed, however, that the form of relation shown in Figures 8a and b will be independent of degree of polarization.

## CONCLUSIONS

A quantitative infra-red method has been developed for the determination of the hydroxyl and carboxyl end-group concentrations in PET film. It can measure the carboxyl end-group concentration of a small sample with great accuracy and reproducibility (for a film of uniform thickness the infra-red method has an accuracy of about  $\pm 0.8$  end-groups, the normal titration method has an accuracy of about  $\pm 1.6$  end-groups). As this infra-red method does not involve the use of any of the toxic chemicals necessary for titration, or the radioactive liquids used for deuterium or tritium exchange methods, it is a very safe method. The infra-red test may be applied to almost any PET film, and can be used over a very wide range of thickness, in-plane birefringences ( $n_1 - n_2$ ), planar birefringences  $[(n_1 + n_2/2) - n_4]$ , densities, heat-set conditions and draw states without any prior knowledge of the polymer's history. It should be remembered, however, that this method is designed for use with films. The extension of the method for use with polymer in fibre or chip form may present difficulties. The photometric accuracy is better

than  $\pm 0.2\%$ , with a typical standard deviation of 0.05 end-groups in  $10^6$  g of polymer (although this is applied to only three repeats in this report, the standard deviation remains at this level with further repeats). The final accuracy in result is therefore dependent on the thickness and density uniformity of the sample combined with the numerical accuracy of these measurements.

The dichroism of ten unknown absorption bands has been ascertained and duly noted.

An unexpected form of relationship between in-plane birefringence and the dichroism shown by both the hydroxyl and carboxyl end-group absorption bands has been demonstrated, with various explanations as to its occurrence put forward. Much more work will need to be done on this phenomenon before any direct physical significance can be demonstrated.

#### ACKNOWLEDGEMENTS

The authors wish to convey their thanks to Mr H. A. Willis for useful discussions concerning the project. Dr G. A. Webster and Dr J. G. Williams of Imperial

College, London are also thanked for their support to, and encouragement of this work.

#### REFERENCES

- 1 Patterson, D. and Ward, I. M. *Trans. Faraday Soc.* 1957, **53**, 291
- 2 Koenig, J. L., Cornell, S. W. and Witenhafer, D. E. *J. Polym. Sci. (A-2)* 1967, **5**, 301
- 3 Sir Howard Grubb, Parsons and Co. Ltd, Walkergate, Newcastle-upon-Tyne
- 4 Payne, N. and Stephenson, C. E. *Mater. Res. Stand.* 1964, **4**, 3
- 5 Charney, E. *J. Opt. Soc. Am.* 1955, **45**, 980
- 6 Manley, T. R. and Williams, D. A. *Polymer* 1969, **10**, 339
- 7 Bellingham and Stanley Co, London
- 8 Willis, H. A. and Miller, R. G. J. 'Molecular Spectroscopy', Heywood and Co, London, 1961
- 9 Chul-Yung Cha, *J. Polym. Sci. (B)* 1964, **2**, 1069
- 10 T. M. Long Co, Inc., Sommerville, NJ, USA
- 11 Heffelfinger, C. J. and Schmidt, P. G. *J. Appl. Polym. Sci.* 1965, **9**, 2661
- 12 Liang, C. Y. and Krimm, S. *J. Mol. Spectrosc.* 1959, **3**, 554
- 13 Tadakoro, H., Tatsuka, K. and Murahashi, S. *J. Polym. Sci.* 1962, **59**, 413
- 14 Johnson, J. E. *J. Appl. Polym. Sci.* 1959, **2**, 205
- 15 Schmidt, P. G. *J. Polym. Sci. (A)* 1963, **1**, 1271
- 16 Cobbs, Jr., W. H. and Burton, R. L. *J. Polym. Sci.* 1953, **10**, 275

# Stress relaxation after steady-state shear flow in undilute polydisperse polymers\*

W. Conti and E. Sorta

*Snam Progetti L.M.-FIB, San Donato Milanese, Milan, Italy*  
(Received 6 August 1971; revised 22 March 1972)

The behaviour of stress relaxation after steady-state shear flow of polydisperse polymers was calculated starting from the experimental evidence that stress relaxation of a monodisperse polymer can be expressed by an *Erfc* function against  $\log t$ . The results of this analysis are: (a) stress relaxation curves for polydisperse polymers are *Erfc* functions, i.e. the experimental data plotted on log-probability paper lie on a straight line; (b) the slope of this straight line depends on the heterogeneity and probably also the position depends only on heterogeneity. These facts were experimentally confirmed and the following experimental conclusions were obtained: the mixing rule for the fractions is not linear; the relaxation time is not proportional to  $\eta M$ , its proportionality to  $\eta$  seems to be preferable than that to  $\eta/M$ ; both the slope and position of the relaxation curve, when plotted on log-probability paper, are linked with the heterogeneity ratio  $\bar{M}_w/\bar{M}_n$  in such a way that its determination from stress relaxation measurements is possible.

## INTRODUCTION

The Rouse-Bueche theory<sup>1,2</sup> predicts that the maximum relaxation time, for monodisperse polymers, is proportional to viscosity multiplied by molecular weight. On the basis of the Ferry, Landel and Williams extension of the theory<sup>3</sup> to the case of undiluted polymers, the maximum relaxation time is proportional to the 4.5 power of molecular weight. This conclusion was tested indirectly by means of non-Newtonian flow measurements. At first, good agreement was found<sup>4</sup>; however, as recent measurements indicate, the agreement is still better when a correction factor is introduced<sup>5</sup>. Tobolsky and coworkers<sup>6</sup> have performed measurements of the maximum relaxation time by means of stress relaxation after instantaneous deformation on monodisperse polymers. They found that maximum relaxation time is proportional to viscosity. Other authors<sup>7,8</sup> confirmed Tobolsky's result, remarking that it holds true only if the molecular weight is sufficiently high<sup>9</sup>. Williams<sup>10</sup> derived Tobolsky's result theoretically (although his theory does not apply to undiluted polymers and therefore the dependence of viscosity on molecular weight is not correct).

Graessley's theory<sup>11</sup> predicts, both for undiluted polymers and for concentrated solutions, that the maximum relaxation time is proportional to the ratio

of viscosity to molecular weight. West<sup>12</sup> confirmed experimentally Graessley's result by using stress relaxation after steady-state shear flow measurements.

As other authors pointed out, no theory predicts the molecular weight dependence of more than one rheological parameter (viscosity, relaxation time, etc.) correctly<sup>8</sup>; moreover, experimental data disagree with one another.

The results of all the theories and experiments just mentioned, can be summarized in an equation where a single parameter  $\rho$  takes into account different theories or experimental data. In fact if we put

$$\tau = K\eta \frac{M_c^{1-\rho} M^\rho}{dRT} \quad (1)$$

where  $\tau$  is the relaxation time,  $\eta$  the viscosity,  $M_c$  the critical molecular weight for entanglement formation,  $M$  the molecular weight,  $d$  the density,  $R$  the gas constant,  $T$  the absolute temperature and  $K$  a constant, we can see that when the parameter  $\rho$  takes the values  $-1, 0, 1$  we match all experimental and theoretical results.

In this paper we shall try to formulate the behaviour of stress relaxation after steady-state shear flow for polydisperse polymers in such a way that an experimentally based selection of the value for  $\rho$  can be obtained. This formulation, furthermore, will be made in an even more general manner, so that the experimental data will also determine the mixing rule of fractions and the molecular weight dependence of rheological parameters for fractions in the whole polymer.

\* Paper presented at the First Italian Congress of Rheology held in Siena, May 1971.



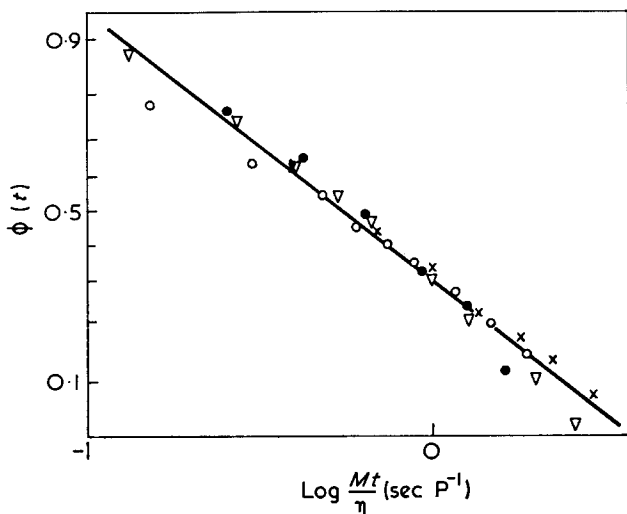


Figure 1 Stress relaxation after steady shear flow for monodisperse polystyrene with different molecular weights. ●, M4:  $M^* = 4.11 \times 10^5$ ; ×, M3:  $M^* = 2.60 \times 10^5$ ; ○, M2:  $M^* = 1.87 \times 10^5$ ; ▽, S111:  $M^* = 2.24 \times 10^5$

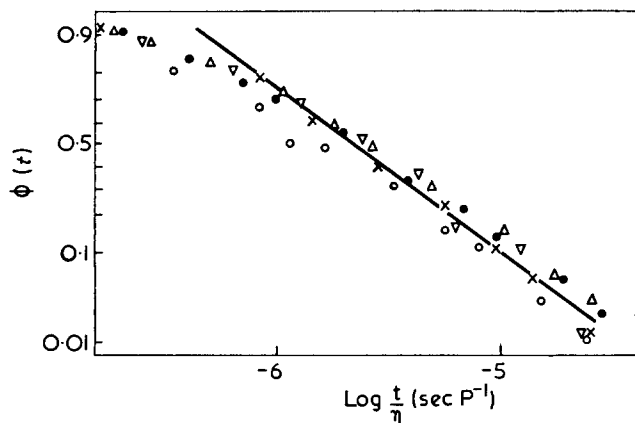


Figure 2 Stress relaxation of monodisperse polystyrene after steady shear flow calculated from Tobolsky's data<sup>6</sup> relative to stress relaxation after instantaneous deformation. ●, S111:  $M^* = 2.39 \times 10^5$ ; ○, S112:  $M^* = 8.00 \times 10^4$ ; ×, S103:  $M^* = 1.25 \times 10^5$ ; ▽, S108:  $M^* = 1.93 \times 10^5$ ; △, S109:  $M^* = 2.67 \times 10^5$

#### STRESS RELAXATION FOR MONODISPERSE POLYMERS

It is clear that a knowledge of the relaxation function for monodisperse polymers is the basis for its extension to polydisperse polymers. Since all theories show some deviation from experiment, we prefer to assume an empirical curve to describe the stress relaxation of monodisperse polymers. A few authors have studied, experimentally, stress relaxation after steady-state shear flow<sup>12, 13</sup>, but only one of them examined a small range of molecular weights<sup>12</sup>.

The stress relaxation of Giuliani and De Chirico was measured after steady flow with shear rate in the linear behaviour range where a substantially Newtonian viscosity was observed<sup>13</sup>. Besides West<sup>12</sup> points that, in the range of shear rate used, the shape of the relaxation curve is independent of shear rate.

The stress relaxation data of West and Giuliani-De Chirico<sup>12, 13</sup>, for monodisperse polymers, plotted on

log-probability paper versus the reduced variable suggested by West ( $tM/\eta$ ), yield a single straight line (Figure 1). So, in the shear range of Newtonian viscosity, we may write

$$\begin{aligned} \phi(t) &= \frac{\sigma(t)}{\eta\dot{\gamma}} = \frac{\sigma(t)}{\sigma_0} \\ &= \frac{1}{(\pi)^{1/2}} \int_{(1/h)\log t/\tau_0}^{\infty} \exp(-v^2) dv \equiv \text{Erfc}\left(\frac{1}{h} \log \frac{t}{\tau_0}\right) \quad (2) \end{aligned}$$

where  $\sigma(t)$  is the decaying shear stress,  $\eta$  the Newtonian shear viscosity,  $\dot{\gamma}$  the shear rate at which the steady-state shear flow was measured and  $h$  and  $\tau_0$  are two parameters. The  $h$  parameter is molecular weight independent, while the  $\tau_0$  parameter is the characteristic time proportional to  $\eta/M$ .

Since the West data cover a small range of molecular weights, in order to be sure that the  $h$  parameter is independent of molecular weight, we have examined Tobolsky's data on relaxation after instantaneous deformation for monodisperse polymers<sup>6</sup>. Tobolsky's data were transformed to stress relaxation after steady-state shear according to the linear theory of viscoelasticity<sup>14</sup> by means of the following equations:

$$\Phi(t) = \frac{1}{3\eta} \int_t^{\infty} E(t) dt; \quad \eta = \frac{1}{3} \int_0^{\infty} E(t) dt$$

where  $E(t)$  is the time dependent relaxation modulus in stress relaxation after instantaneous elongational deformation. The relaxation functions so obtained were plotted on log-probability paper versus the reduced variable suggested by Tobolsky ( $t/\eta$ ) and a straight line was obtained (Figure 2).

It can be seen from Figure 1 (West and Giuliani-De Chirico data) and from Figure 2 (from Tobolsky's data) that the  $h$  parameter is practically the same in both cases, but while in the former case  $\tau_0$  is proportional to  $\eta/M$ , in the latter it appears to be proportional to  $\eta$ .

This apparent conflict is irrelevant for our purposes since the formulation of the theory does not depend on an *a priori* choice of the molecular weight dependence of  $\tau_0$ . The experimental data will enable us to establish the type of correlation existing between  $\tau_0$  and  $M$ . It is important to note that the stress relaxation after steady-state shear calculated from Tobolsky's data confirms equation (2), where the  $h$  parameter is molecular weight independent.

It should be mentioned that the  $\tau_0$  parameter is proportional to relaxation time  $\tau$  and may be expressed by equation (1) owing to the presence of an unspecified constant  $K$ . It should be further pointed out that equation (2) describes the stress relaxation behaviour only in the rubbery flow region.

Narkis *et al.*<sup>15</sup> also obtained an empirical equation for stress relaxation which describes the stress relaxation behaviour in the rubbery flow region; this equation, however, is not so useful as equation (2) as the basis for an extension to polydisperse polymers owing to mathematical difficulties.

#### EXTENSION TO POLYDISPERSE POLYMERS

To perform this extension it is necessary, at first, to decide the mixing rule to be used, i.e. how each fraction, with weight fraction  $w_i$ , viscosity  $\eta_i$  and molecular

weight  $M_i$ , contributes to the whole polymer viscosity  $\eta_b$ .

At zero shear rate the mixing rule can be expressed by the following equation

$$\eta_b = \left( \sum_i w_i \eta_i^{1/\mu} \right)^\mu \quad (3)$$

where  $\mu$  is a constant which can assume the values 1 or 3.5 according to different authors<sup>16-20</sup>. We shall determine experimentally whether 1 or 3.5 is the best value.

Multiplying both sides of equation (3) by shear rate,  $\dot{\gamma}$ , we get the stress in steady flow

$$\sigma_0 = \left( \sum_i w_i \sigma_{0i}^{1/\mu} \right)^\mu \quad (3a)$$

where  $\sigma_{0i}$  is the contribution of the  $i$ th fraction to the total stress.

*A priori* equation (3a) cannot be supposed to hold at all times, so we shall put:

$$\sigma(t) = \left\{ \sum_i w_i \sigma_{0i}^{1/\mu} \left[ \frac{\sigma_i(t)}{\sigma_{0i}} \right]^{\nu/\mu} \right\}^\mu \quad (3b)$$

where  $\nu$  is a function of polydispersity to be determined, subject to the condition that it must be unity for monodisperse polymers. Substitution of equation (2) into equation (3b) yields:

$$\sigma(t) = \dot{\gamma} \left\{ \sum_i \eta_i^{1/\mu} w_i \left[ \phi \left( \frac{t}{\tau_i} \right) \right]^{\nu/\mu} \right\}^\mu \quad (4)$$

where  $\phi$  is given by equation (2) and  $\tau_i$  is the relaxation time for molecules with molecular weight  $M_i$  and viscosity  $\eta_i$ .

Another problem to be solved is the molecular weight dependence of stress relaxation time and viscosity for each fraction. First of all, we may observe that this dependence should be different for different fractions according to the value of the molecular weight compared to the critical molecular weight  $M_c$  for entanglement formation. We shall not take into account, for the moment, this aspect because it is insignificant for the polymers under consideration. This hypothesis will be justified *a posteriori*.

The dependence of relaxation time and viscosity on molecular weight for the  $i$ th fraction is not necessarily the same as that observed for the monodisperse polymer, and such quantities are completely independent of each other. Theories and experimental data on monodisperse polymers suggest that it is reasonable to assume that relaxation time and viscosity for each fraction are proportional to unknown powers of their molecular weight. The dependence of relaxation time and viscosity of each fraction on their own molecular weight should be such that it reduces itself to monodisperse behaviour when polydispersity becomes one. It is possible to express the above statements by writing the relaxation time and viscosity for the  $i$ th fraction in terms of whole polymer viscosity  $\eta_b$ . In fact, defining the following average molecular weight,

$$\bar{M}_\mu^\xi = \left( \sum_i w_i M_i^{\xi/\mu} \right)^\mu$$

and putting

$$\eta_i = \eta_b \frac{M_i^\gamma}{\bar{M}_\mu^\gamma}; \quad \tau_i = \eta_b \frac{K M_c^{1-\rho}}{dRT} \frac{M_i^{\alpha+\rho}}{\bar{M}_\mu^\alpha} \quad (5)$$

where  $\alpha$  and  $\gamma$  are two possible arbitrary values of  $\xi$ , we obtain equation (1) for a monodisperse polymer. Taking

a continuous molecular weight distribution, i.e. substituting a summation by an integral, we obtain for polydisperse polymer the following by means of equations (2), (4) and (5):

$$\phi(t) = \frac{\sigma(t)}{\eta_b \dot{\gamma}} = \left\{ \int_0^\infty \left( \frac{M^\gamma}{\bar{M}_\mu^\gamma} \right)^{1/\mu} w(M) \left[ \text{Erfc} \frac{1}{h} \times \log \left( \frac{dRT \bar{M}_\mu^\alpha}{K \eta_b M_c^{1-\rho} M^{\alpha+\rho} t} \right) \right]^{\nu/\mu} dM \right\}^\mu \quad (6)$$

where  $w(M)$  is the polymer weight fraction with molecular weight between  $M$  and  $M + dM$ .

It is quite easy to perform the integration of equation (6) if the molecular weight distribution (*MWD*) is log-probabilistic, that is:

$$w(M) dM = \frac{1}{(\pi)^{1/2}} \exp \left[ - \left( \frac{1}{\beta} \ln \frac{M}{M_0} \right)^2 \right] d \left( \frac{1}{\beta} \ln \frac{M}{M_0} \right) \quad (7)$$

where  $\beta$  and  $M_0$  are two distribution parameters linked to number ( $\bar{M}_n$ ) and weight ( $\bar{M}_w$ ) average molecular weights by the following equations:

$$Q = \frac{\bar{M}_w}{\bar{M}_n} = \exp(\beta^2/2); \quad \bar{M}_w = M_0 Q^{1/2}$$

This is the case for some polymers (linear polyethylene) but not for others [polystyrene, poly(methyl methacrylate)].

These last polymers have a Shulz<sup>21</sup> type *MWD*, i.e.

$$W(M) dM = \frac{1}{\Gamma(p+1)} (zM)^p e^{-zM} d(zM) \quad (8)$$

where  $\Gamma$  is the gamma function,  $z$  and  $p$  are two distribution parameters linked to the number ( $\bar{M}_n^*$ ) and weight ( $\bar{M}_w^*$ ) average molecular weights by the following equations:

$$z = \frac{p+1}{\bar{M}_w^*}; \quad Q^* = \frac{\bar{M}_w^*}{\bar{M}_n^*} = \frac{p+1}{p}$$

Henceforward, for convenience, we will use an asterisk (\*) for the average molecular weight and the heterogeneity ratio of polymers with a Shulz *MWD* and no asterisk for the corresponding quantities obtained by approximating with a log-probabilistic distribution. For polymers with log-probabilistic distribution the average molecular weight and heterogeneity ratio will also be without asterisks.

As long as the heterogeneity ratio remains lower than three in the polymers with a Shulz *MWD*, we can put without any significant error

$$\left( \frac{M^\gamma}{\bar{M}^{\nu/\mu}} \right)^{1/\mu} w(M) dM \simeq \frac{1}{(\pi)^{1/2}} \exp \left[ - \left( \frac{1}{m} \ln \frac{M}{M_x} \right)^2 \right] \times d \left( \frac{1}{m} \ln \frac{M}{M_x} \right) \quad (9)$$

where  $m$  and  $M_x$  are two suitable distribution parameters<sup>22</sup>. These parameters must be calculated imposing the second and the third coefficients to be zero in the Hermite's expansion of the left side of equation (9). *A posteriori* we shall give a justification of this simplification as means of  $\alpha$ ,  $\gamma$ ,  $\nu$  and  $\mu$  have been determined.

By means of equation (9) we have introduced a log-probabilistic distribution function characterized by  $\bar{M}_w$  and  $Q$  where  $\bar{M}_w$  and  $Q$  are connected with  $z$  and  $p$

Table 1 Molecular and rheological parameters calculated from published experimental data

Samples	Ref.	$\bar{M}_w \times 10^{-5}$	$\bar{M}_w^* \times 10^{-5}$	Q	Q*	$M_c \times 10^{-4}$ (ref. 14)	Temp. (°C)	$\eta \times 10^{-5}$ (P)	$\frac{t_{0.5}}{\eta} \times 10^6$ (sec P <sup>-1</sup> )	$\frac{t_{0.088}}{\eta} \times 10^5$ (sec P <sup>-1</sup> )	$\epsilon^2$
PS-M4	12		4.11		1.06	3.8	227	1.39	1.4	0.66	0.50
PS-M3	12		2.60		1.07	3.8	227	0.29	2.3	1.03	0.48
PS-M2	12		1.87		1.06	3.8	227	0.13	3.2	1.2	0.38
PS-P1	12		2.54		2.60	3.8	227	0.18	5.0	10.5	1.24
PS-S111	24		2.24		1.04	3.8	180	3.6	2.65	1.07	0.46
PS-B8	24		2.70		2.47	3.8	200	1.25	3.9	3.3	0.98
	24		2.70		2.47	3.8	180	5.4	4.8	4.1	0.97
PS-ST	24		2.24		2.40	3.8	150	120	3.7	4.9	1.40
	24		2.24		2.40	3.8	170	11	3.5	5.6	1.54
	24		2.24		2.40	3.8	190	2.3	3.6	5.0	1.46
PMMA	23		9.88		2.20	3.15	192	8.4	0.81	0.83	1.04
HDPE a	13	0.9		7.0		0.38	180	0.9	30	167	3.25
b	13	1.05		11.0		0.38	180	8.5	52	270	3.22
c	13	1.00		7.1		0.38	180	4.0	1.2	7.5	3.05
d	13	1.4		8.9		0.38	180	6.0	23	120	3.30
P	16	1.12		5.0		0.38	180	1.93	4.8	12.5	2.20

PS-M4, PS-M3, PS-M2, PS-S111=monodisperse polystyrene; PS-P1, PS-B8, PS-ST=polydisperse polystyrene; PMMA, poly(methyl methacrylate); HDPE, high density polyethylene

parameters which appear in the Shulz  $MWD$ , by the following equations:

$$Q = \exp \left[ \psi' \left( 1 + p + \frac{\gamma}{\mu} \right) \right] \quad (9a)$$

$$\bar{M}_w = \frac{1}{z} \exp \left[ \psi \left( 1 + p + \frac{\gamma}{\mu} \right) \right] Q^{1/2 - \gamma/\mu} \quad (9b)$$

where  $\psi$  and  $\psi'$  are the digamma and trigamma functions with the argument  $1 + p + (\gamma/\mu)$ .

It is possible to integrate equation (6) observing that we may put:

$$\left\{ \operatorname{Erfc} \frac{1}{a} \log x \right\}^{\xi} \simeq \operatorname{Erfc} \frac{1}{a \delta_{\zeta}} \log \frac{x}{f_{\zeta}} \quad (10)$$

With this approximation we do not introduce a significant error even if  $a$  and  $\zeta$  can vary in a broad range.  $\delta_{\zeta}$  and  $f_{\zeta}$  are two coefficients depending on  $\zeta$  and they can be mathematically determined (see Appendix).

After the integration of equation (6) we get

$$\phi(t) = \left\{ \frac{1}{(\pi)^{1/2}} \int_{(1/\epsilon) \log(t/t_0)}^{\infty} \exp(-v^2) dv \right\}^{\mu} \quad (11)$$

where

$$\epsilon^2 = h^2 \delta_{\nu/\mu} + \frac{2}{2.3} (\alpha + \rho)^2 \log Q \quad (12)$$

$$t_{\phi} = \frac{\eta_b \bar{M}_w^{\rho} M_c^{1-\rho}}{dRT} f_{\nu/\mu} Q^{(1/\mu)[(\alpha + \rho)\gamma - (\alpha^2/2)] - \rho/2} \quad (13)$$

$\delta_{\nu/\mu}$  and  $f_{\nu/\mu}$  depend on the ratio  $\nu/\mu$ .

Obviously for  $\mu=1$ ,  $\phi(t)$  of equation (11) is an  $\operatorname{Erfc}$  function. On the basis of equation (10) we may consider  $\phi(t)$  in equation (11) as an  $\operatorname{Erfc}$  function also for  $\mu=3.5$  with different expressions for the characteristic parameters  $\epsilon$  and  $t_{\phi}$ . So equation (12) assumes the form

$$\epsilon^2 = A + B \log Q \quad (12a)$$

where  $A$  is a function of  $\nu/\mu$  and  $\mu$ , and

$$B = 0.87(\alpha + \rho)^2 \quad \text{for } \mu = 1$$

$$B = 0.44(\alpha + \rho)^2 \quad \text{for } \mu = 3.5$$

As far as the meaning of the parameter  $t_{\phi}$  is concerned, we can observe that: (a) in the case  $\mu=1$  we have  $\Phi(t)=0.5$  when  $t=t_{\phi}$  so that  $t_{\phi}=t_{0.5}$  where  $t_{0.5}$  is the time when  $\Phi(t)$  assumes the value 0.5; (b) in the case  $\mu=3.5$  when  $t=t_{\phi}$  we have  $\Phi=(0.5)^{3.5}=0.088$  so that  $t_{\phi}=t_{0.088}$  where  $t_{0.088}$  is the time when  $\Phi(t)$  assumes the value 0.088.

Equation (13) may be written as follows:

$$\log \frac{dRT}{M_c^{1-\rho} \bar{M}_w^{\rho} \eta_b} t_{\phi} = C + D \log Q \quad (13a)$$

where  $C$  depends on the ratio  $\nu/\mu$  and  $\mu$ , and

$$D = \frac{1}{\mu} \left[ (\alpha + \rho)\gamma - \frac{\alpha^2}{2} \right] - \frac{\rho}{2}$$

In Table 1 all molecular ( $\bar{M}_w$ ,  $Q$ ,  $\bar{M}_w^*$ ,  $Q^*$ ,  $M_c$ ) and rheological ( $\eta$ ,  $\epsilon^2$ ,  $t_{0.5/\eta}$ ,  $t_{0.088/\eta}$ ) parameters, calculated by us from published experimental data, are reported.

The rheological parameters  $\epsilon^2$ ,  $t_{0.5/\eta}$ ,  $t_{0.088/\eta}$ , were calculated plotting the stress relaxation curves on log-probability paper versus time and recording the times when the stress assumes the values 0.5 or 0.088 of its initial value.  $\eta$  is the viscosity at very low shear rate where the flow behaviour can be considered still Newtonian.  $\eta$  is the  $\eta_b$  in the previous equations.

Figures 3 and 4 experimentally confirm that the stress relaxation after steady shear of polydisperse polymers may be represented by means of an  $\operatorname{Erfc}$  function. Only for poly(methyl methacrylate) (Figure 4) do we have a significant deviation from a straight line, on log-probability paper, but this occurs only when the stress is lower than 5% of the initial stress.

On the basis of the data of Table 1 it is possible to check the validity of equations (12a) and (13a).

As far as the polymers with log-probabilistic  $MWD$  are concerned, it is sufficient to perform the linear regression between  $\epsilon^2$  and  $\log Q$  and between  $\log(dRT t_{\phi}) / (M_c \bar{M}_w^{1-\rho} \eta)$  and  $\log Q$ , using the least squares method, for different values of  $\rho$  and  $\mu$ , namely  $\rho = -1, 0, 1$  and  $\mu = 1$  and  $\mu = 3.5$ . The index of correlation  $r$  could indicate which of the previous hypotheses is the most probable one. From  $B$  and  $D$  so determined it is possible to calculate  $\alpha$  and  $\gamma$ .

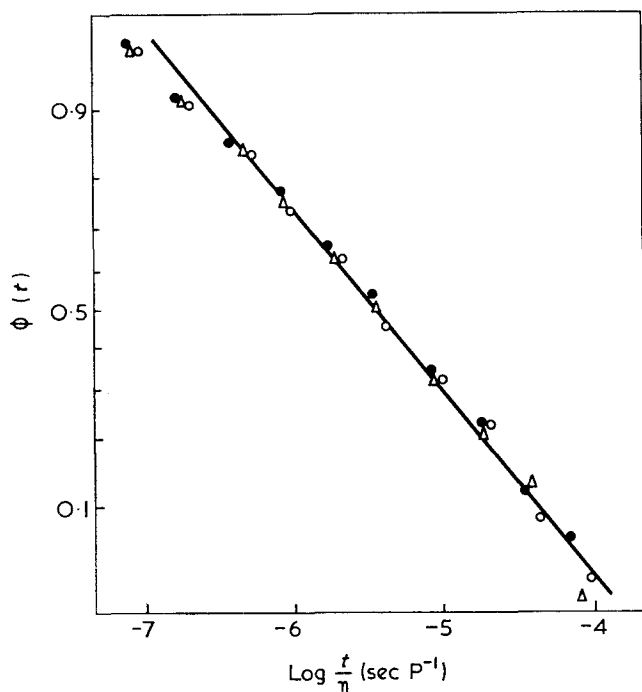


Figure 3 Stress relaxation for sample PS-ST at different temperatures (heterogeneous polystyrene<sup>24</sup>). ●, 150°C; ○, 170°C; ×, 190°C

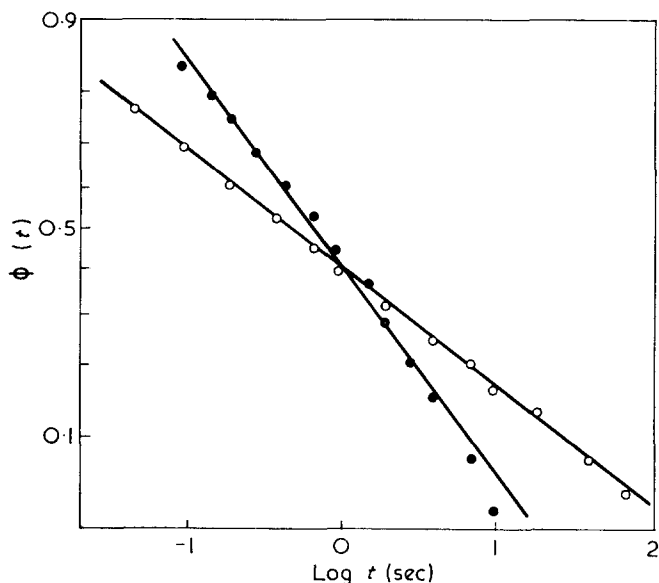


Figure 4 Stress relaxation for PMMA<sup>23</sup> (●) and for sample HDPE-c (○) (polyethylene<sup>13</sup>)

In the case of polymers with a Schulz  $MWD$  the situation is more complicated. In fact  $Q$  and  $\bar{M}_w$  can be calculated only if  $\gamma$  and  $\mu$  are known [see equations (9a) and (9b)].

In the hypothesis that  $\nu=1$ , by a method of trial and error, we looked for a value of  $\gamma$  equal to the one derived from the values of  $B$  and  $D$  obtained by the least squares method through experimental data, according to equations (12a) and (13a).

In Table 2 we report the results of these regressions.  $r_1$  and  $r_2$  are the indices of correlation relative to equations (12a) and (13a) respectively. It may be observed that  $r_1$  is very close to unity; therefore within this confidence

Table 2 Results of the regressions for the cases when  $\mu=1$  and  $\mu=3.5$  at  $\rho=-1, 0$  or  $+1$

	$\mu=1$			$\mu=3.5$		
	$\rho=-1$	$\rho=0$	$\rho=+1$	$\rho=-1$	$\rho=0$	$\rho=+1$
$r_1$	0.95	0.97	0.97	0.96	0.97	0.97
$A$	0.74	0.53	0.53	0.65	0.58	0.53
$B$	2.74	2.85	2.85	2.73	2.8	2.85
$\alpha$	3.22	0.81	0.81	3.5	2.52	1.54
$r_2$	0.97	0.61	0.72	0.98	0.96	0.89
$C$	1.28	0.42	1.41	1.27	0.45	1.48
$D$	4.29	0.68	1.23	3.86	2.67	2.35
$\gamma$	4.05	1.23	1.13	7.0	5.0	4.78
$\gamma/\mu$	4.05	1.23	1.13	2	1.43	1.37

limit  $A$  does not depend on  $Q$ . It follows that  $\nu=1$  also for polydisperse polymers.

In accordance with the values of  $r_2$ , the cases  $\mu=1$ ,  $\rho=0$ ;  $\mu=1$ ,  $\rho=1$ ;  $\mu=3.5$ ,  $\rho=1$ , show a confidence limit lower than the other three ones.

In order to get a better understanding of the previous results, we have plotted, in Figures 5 and 6,  $\epsilon^2$  versus  $\log Q$  and  $\log [(dRT/M_c\eta)t_{0.088}]$  versus  $\log Q$  for the case  $\rho=0$  and  $\mu=3.5$ . The straight line, on both figures, is the regression line.

#### Source of the data

In our analysis we took into account experimental data from different authors. To avoid the need to refer to the original papers we shall briefly summarize the experimental conditions under which the data were obtained.

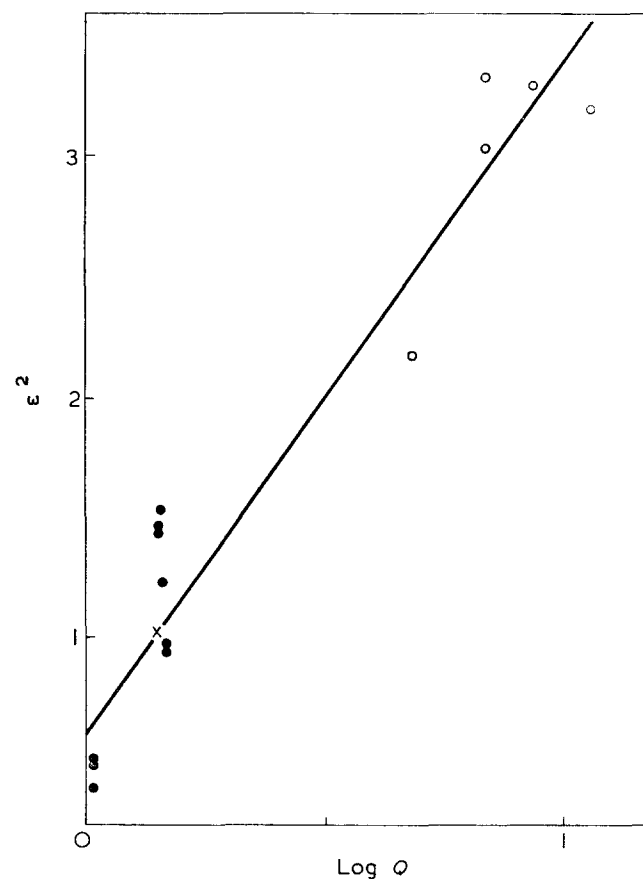


Figure 5  $\epsilon^2$  as a function of  $\log Q$  in the case  $\rho=0$ ,  $\mu=3.5$ . ○, HDPE; ●, polystyrene; ×, PMMA

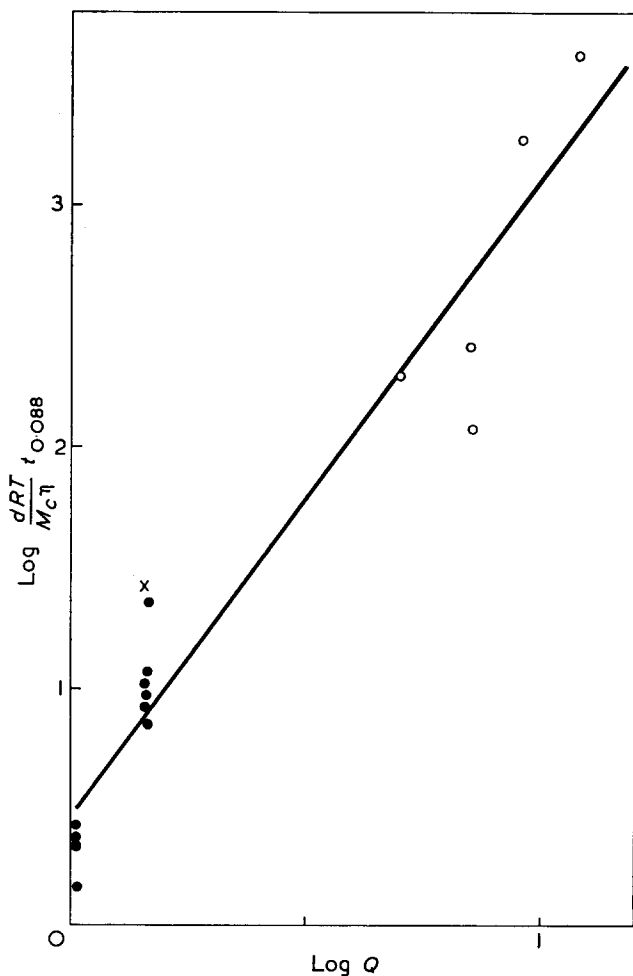


Figure 6  $\text{Log} \left( \frac{dRT}{M_c} t_{0.088} \right)$  as a function of  $\text{log } Q$ .  $\circ$ , HDPE;  $\bullet$  polystyrene;  $\times$ , PMMA.  $\rho=0$ ;  $\mu=3.5$

The stress relaxation after steady shear flow was obtained by means of different rheometers. West<sup>12</sup> performed his experiments at 223°C by using a Weissenberg Rheogoniometer after the imposition of a steady shear rate of 1.42 sec<sup>-1</sup>. The samples were monodisperse polystyrenes (M4, M3, M2) and polydisperse polystyrene (P1).

Giuliani did stress relaxation after cessation of steady-state flow experiments<sup>13, 24</sup> with a similar equipment imposing a steady shear rate in such a way to obtain Newtonian viscosity behaviour of the materials. He used different temperatures as shown in Table 1. Peticolas made similar experiments using an apparatus designed by Menefee<sup>16</sup> at 180°C. Ajroldi-Pezzin<sup>23</sup> data were obtained on a Képes rheometer at 180°C. In order to determine average molecular weight and molecular weight distribution all samples were characterized using gel permeation chromatography except sample P(16) which was characterized by column fractionation. All the data are summarized in Table 1.

## DISCUSSION

The published experimental data, used in the present paper, are not suitable to select the most probable values for  $\rho$  and  $\mu$ ; in fact the cases (a)  $\rho=1$ ,  $\mu=1$ , (b)  $\rho=-1$ ,  $\mu=3.5$ , (c)  $\rho=0$ ,  $\mu=3.5$  have the same confidence limits. This is mainly due to experimental errors and to a relatively low number of experimental data found. Moreover the

polyethylene samples, with different polydispersity, fall within a narrow molecular weight range and branching may be present. In all cases the Rouse-Bueche theory is not experimentally confirmed as many authors pointed out<sup>6-8</sup>. For all the cases where  $\rho \neq 1$ , the value of  $D$  is strongly dependent on the  $M_c$  value; in fact this is the only reason for which  $D$  increases when  $\rho$  changes from 0 to +1 (see Table 2).

We have chosen  $M_c$ , the critical molecular weight for entanglement coupling, because this critical molecular weight was previously connected with steady flow compliance<sup>8</sup>.

In any case the proper choice of the critical molecular weight is not essential as the other critical molecular weights, for instance the average molecular weight between coupling loci ( $M_e$ ), are roughly proportional and consequently do not affect the coefficient  $D$  but only the coefficient  $C$  which is not interesting at all.

Mills<sup>8</sup> found that the limiting value of the steady shear compliance  $J$  is independent of molecular weight and depends only on polydispersity. Mills performed his analysis not only taking into account his own experimental data but also published data<sup>7, 25</sup> relative to different polymers. This means that the case  $\rho=0$  is experimentally confirmed. As to the case  $\rho=0$  and  $\mu=3.5$ , it is useful to find the relation existing between the reduced steady flow compliance  $J' = (dRT/M_c)J$  and  $\text{log } Q$  in order to confirm Mills' results also from a quantitative standpoint.

The steady flow compliance may be calculated from stress relaxation after steady flow by means of the following equation (14):

$$J = \int_0^{\infty} t \Phi(t) dt$$

When  $\Phi(t)$  is an *Erfc* function with argument  $\text{log } t$  the integration of the previous equation yields:

$$J = \frac{t_{0.5}}{\eta} \exp \left[ \left( \frac{2}{2.3} \epsilon \right)^2 \right]$$

where  $\epsilon$  is the slope factor of the relaxation *Erfc* function (Table 1). In Figure 7 we have plotted  $\text{log } J'$  against  $\text{log } Q$ . The straight line is the regression line obtained by means of the least squares method with index of correlation  $r=0.94$ . So we can write

$$J' \propto Q^{3.65}$$

getting, for the exponent, the same value found by Mills<sup>8</sup>. It seems that the case  $\rho=0$  and  $\mu=3.5$  would be better than the other cases having the same probability.

In this case  $\epsilon^2$  and  $t_{0.088}$  are both only heterogeneity ratio ( $Q$ ) dependent. It is interesting to calculate  $Q$  from experimentally determined  $\epsilon^2$  and  $t_{0.088}$  according to equations (12a) and (13a) and compare the values with those obtained by means of a direct technique (Table 3).

In Table 3 the heterogeneity ratio  $Q$  for polymers with a Shulz *MWD* was calculated using equation (9a) from published  $Q^*$ ;  $\bar{Q}$  is the geometric mean of the  $Q$  values obtained from  $\epsilon^2$  and from  $t_{0.088}$ . Generally speaking the agreement is satisfactory.

From homogeneous polymers we obtained an heterogeneity ratio less than unity, but this value lies in the range of statistical errors.

To justify the substitution made in equation (9) we integrated numerically equation (6) for the particular case when  $\rho=0$ ,  $\mu=3.5$ ,  $\alpha=2.5$ ,  $\gamma/\mu=2$ , for a polymer

Table 3 Values of  $Q$  and  $\bar{Q}$  for polymers with a Schulz MWD

Sample	$Q$	$\bar{Q}$
M4	1.00	0.85
M3	1.00	0.89
M2	1.00	0.91
P1	1.48	1.93
S111	1.00	0.85
B8	1.47	1.37
PS-ST	1.46	1.86
PMMA	1.44	1.82
HDPE-a	7.0	7.3
HDPE-b	11.8	11.6
HDPE-e	7.1	5.6
HDPE-d	8.9	10.5
HDPE-P	5.0	4.3

PS-M4, PS-M3, PS-M2, PS-S111 = monodisperse polystyrene; PS-P1, PS-B8, PS-ST = polydisperse polystyrene; PMMA, poly(methyl methacrylate); HDPE, high density polyethylene

having  $Q^* = 3$ . In Figure 8 we plotted the results of the analysis (full points) and the straight line predicted by equation (11). From Figure 8 we can see that, when  $Q^* = 3$ , the approximation of equation (9) is justified and this will be *a fortiori* true when  $Q^* < 3$ .

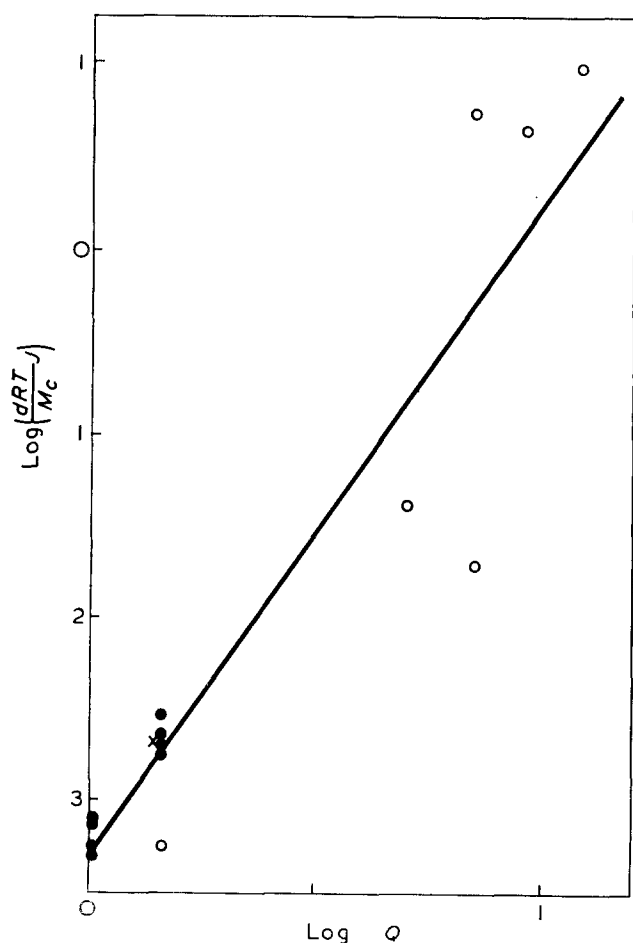


Figure 7  $\text{Log}\left(\frac{dRT}{M_c}\right)$  as a function of  $\text{log } Q$ .  $\circ$ , HDPE;  $\bullet$ , polystyrene;  $\times$ , PMMA.  $\rho = 0$ ;  $\mu = 3.5$

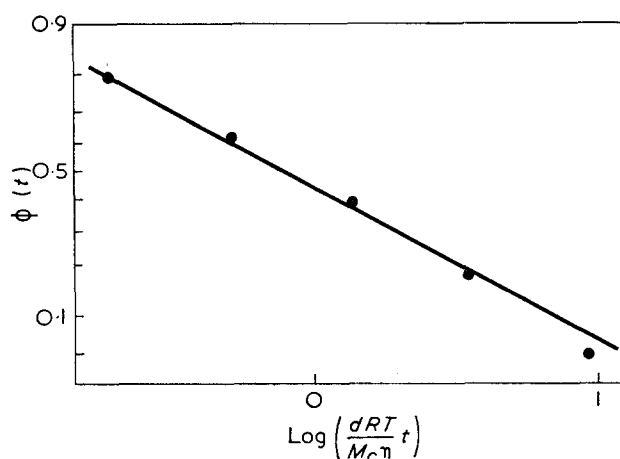


Figure 8 Stress relaxation for a polymer with a Schulz MWD for  $Q=3$  obtained as a numerical integration of equation (6) (points) compared with the straight line predicted by the theory.  $\mu = 3.5$ ;  $\alpha = 2.5$ ;  $\gamma/\mu = 2$

In equation (6) the lower limit of integration is assumed to be zero. This implies an overestimate of the influence of low molecular weight molecules ( $M < M_c$ ). At the initial time the influence of low molecular weight molecules on the stress relaxation is negligible; it will be even more negligible at higher times since  $\mu < \gamma$ .

We realize that an understanding of the stress relaxation and its dependence on weight average molecular weight and heterogeneity requires an additional series of tests on polymers with a large range of molecular weights and heterogeneity; but the current analysis made on available experimental data shows that the stress relaxation after steady-state shear flow can be expressed by means of an *Erfc* function.

#### REFERENCES

- 1 Rouse, P. E. *J. Chem. Phys.* 1953, **21**, 1272
- 2 Bueche, F. *J. Chem. Phys.* 1954, **22**, 603
- 3 Ferry, J. D., Landel, R. L. and Williams, H. L. *J. Appl. Phys.* 1955, **26**, 359
- 4 Middleman, S. 'The flow of High Polymers', Interscience, New York, 1968
- 5 Graessley, W. W. and Segal, L. *Macromolecules* 1969, **2**, 49
- 6 Tobolsky, A. V., Aklonis, J. J. and Akovali, G. *J. Chem. Phys.* 1965, **42**, 723
- 7 Akovali, G. *J. Polym. Sci. (A-2)* 1967, **5**, 875
- 8 Mills, N. *J. Eur. Polym. J.* 1969, **5**, 675
- 9 Prest, Jr., W. M. *J. Polym. Sci. (A-2)* 1970, **8**, 1897
- 10 Williams, M. C. *Am. Inst. Chem. Eng. J.* 1967, **13**, 534
- 11 Graessley, W. W. *J. Chem. Phys.* 1965, **43**, 2696
- 12 West, G. H. *Polymer* 1969, **10**, 751
- 13 Giuliani, G. and De Chirico, A. *J. Macromol. Sci.* 1971, **B5**, 429
- 14 Ferry, J. D. 'Viscoelastic Properties of Polymers', Wiley, New York, 1970
- 15 Narkis, M., Hopkins, I. L. and Tobolsky, A. V. *Polym. Eng. Sci.* 1970, **10**, 66
- 16 Peticolas, W. *J. Chem. Phys.* 1963, **39**, 3392
- 17 Menefee, E. and Peticolas, W. *J. Chem. Phys.* 1961, **35**, 946
- 18 Conti, W. and Gigli, I. *J. Polym. Sci.* 1966, **A14**, 1093
- 19 Conti, W. and Gigli, I. *Makromol. Chem.* 1967, **107**, 16
- 20 Fujita, H. and Ninomiya, K. *J. Polym. Sci.* 1967, **24**, 233
- 21 Shulz, G. *V. Z. Phys. Chem.* 1939, **B43**, 25
- 22 Milne, W. E. 'Numerical Calculus', Princeton University Press, 1949
- 23 Ayroldi, G. and Pezzin, G. *Symp. Adv. Rheology, Glasgow*, 1969
- 24 Giuliani, G. personal communication
- 25 Ueno, T. and Murakami, K. *J. Soc. Mat. Sci. Japan* 1967, **16**, 498

(APPENDIX over page)

APPENDIX\*

We will assume, for the moment, that:

$$\left[ \operatorname{Erfc} \frac{1}{a} \log x \right]^\zeta = \operatorname{Erfc} \frac{1}{a \delta_\zeta} \log \frac{x}{f_{a,\zeta}} \quad (\text{A1})$$

where  $\delta_\zeta$  and  $f_{a,\zeta}$  are two new parameters. Deriving equation (A1) and taking into account the values of equation (A1) and of its derivative when  $x=1$  we obtain the following equations for  $\delta_\zeta$  and  $f_{a,\zeta}$

$$\operatorname{Erfc} \left( -\frac{1}{a \delta_\zeta} \log f_{a,\zeta} \right) = 0.5 \quad (\text{A2})$$

$$\delta = \frac{(0.5)^{1-\zeta}}{\zeta} \exp \left( -\frac{1}{a \delta_\zeta} \log f_{a,\zeta} \right) \quad (\text{A3})$$

Observing equation (A2) we can see that  $(1/a \delta_\zeta) \log f_{a,\zeta}$  depends on  $\zeta$  and consequently  $f_{a,\zeta}$  depends on  $a$  and  $\zeta$  while  $\delta_\zeta$  only from  $\zeta$  (see equation (A3)).

In the present paper we have considered  $\zeta=1/3.5$  or  $\zeta=3.5$ ; in these cases we found  $\delta_{1/3.5}=1/\delta_{3.5}=1.5$  and  $f_{1/3.5,a}=1/f_{3.5,a}=10^{0.96a}$ .

As a proof of equation (A1) in Figure 9 we have plotted  $\operatorname{Erfc}[(1/a) \log x]$  and  $[\operatorname{Erfc}[(1/a) \log x]]^{3.5}$  in our limiting cases, i.e. for homogeneous polymers where  $\epsilon^2=0.59$  and therefore  $a^2=(1.4\epsilon)^2=1.18$  and for heterogeneous polymers with  $Q=12$  where  $\epsilon^2=3.61$  and therefore  $a^2=(1.4\epsilon)^2=7.2$ .

\* For interested readers a copy with the detailed mathematical development is available from the senior author

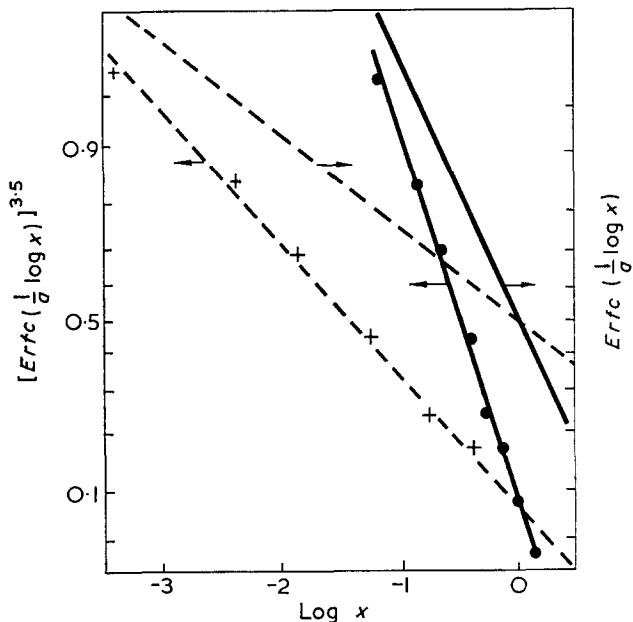


Figure 9  $\operatorname{Erfc}[(1/a) \log x]$  and  $\{\operatorname{Erfc}[(1/a) \log x]\}^{3.5}$  for the limiting values of  $a$ : —,  $Q=1$ ; - - - - -,  $Q=12$ . ● and + are the calculated points

The points ● and + in Figure 9 were calculated directly using the 3.5 power of the function  $\operatorname{Erfc}[(1/a) \log x]$ . Clearly equation (A1) is satisfied from the practical point of view.

# Effect of molecular weight on the rate of crystallization of polyethylene fractions at high undercooling

J. M. Barrales-Rienda and J. M. G. Fatou

*Division of Polymer Physics, Instituto de Plásticos y Caucho, Madrid 6, Spain  
(Received 13 July 1971)*

Isothermal crystallization of polyethylene fractions by calorimetry at high undercoolings has been studied for a wide range of molecular weights between  $1.55 \times 10^6$  and  $C_{36}H_{74}$ . The influence of molecular weight on crystallization rates as undercooling increases is very moderate. The crystallization temperature coefficient has been analysed according to three-dimensional nucleation theory and it has been shown that the crystallization is described by a unique function of the free energy required for nucleation when the change of the interfacial free energy with molecular weight is considered. The interfacial free energy reaches an asymptotic value at high molecular weights, decreases as the molecular weight is lowered and reaches an asymptotic value at the lower molecular weight.

## INTRODUCTION

The crystallization of polymers from the melt is characterized by a high negative temperature coefficient, which shows that nucleation of the system is the predominating factor in the transformation<sup>1,2</sup>, independently of the mechanism involved.

Moreover, the rate with which crystallization takes place from the melt can be obtained from the general expression for the kinetics of phase transformations<sup>3,4</sup> and for very low levels of transformation, it can be assumed that the critical free energy for nucleus growth is approximately the same as that required for nucleation, the overall crystallization rate depending on two energetic terms: the activation energy for transport and the critical free energy for forming a nucleus.

The latter can be calculated for finite molecular weights by the expressions developed by Mandelkern *et al.*<sup>5,6</sup> for tri- and bi-dimensional growth mechanisms and this treatment has recently been applied<sup>7,8</sup> to the analysis of spherulitic growth for different polymers, showing that independently of the molecular weight, the growth rate is a unique function of the free energy for nucleation and that the excess interfacial free energy in the (001) face of the crystal is a function of the molecular weight.

On the other hand, the variation in crystallization rate from the melted state at low undercoolings has been attributed to a transport effect so that, when the crystal-

lization temperature decreases and conditions for nucleation are less restricted, the viscosity of the medium is less important and there are no complicating effects by the energy of transport<sup>2,9</sup>.

The main purpose of this work is, therefore, to analyse polyethylene crystallization kinetics at high undercoolings and to study the temperature coefficient as a function of the molecular weight and of the thermodynamic parameters involved encompassing a molecular weight range from  $1.55 \times 10^6$  to  $1.8 \times 10^3$ .

The highly purified  $C_{36}H_{74}$  paraffin has been included in the analysis for comparative purposes.

## EXPERIMENTAL

Crystallization kinetics were studied using the calorimetric technique described in detail elsewhere<sup>9</sup>. Eight polyethylene fractions with the following molecular weights were used:  $1.55 \times 10^6$ ,  $4.25 \times 10^5$ ,  $1.0 \times 10^5$ ,  $2.0 \times 10^4$ ,  $12.5 \times 10^3$ ,  $5.3 \times 10^3$ ,  $3.3 \times 10^3$  and  $1.8 \times 10^3$ . These samples were obtained using a column fractionation technique already described<sup>10</sup>, using linear polyethylenes. A highly purified  $C_{36}H_{74}$  paraffin (Fluka, A.-G.) was the fraction with the lowest molecular weight.

The crystallization was studied with a Perkin-Elmer, DSC-1B differential scanning calorimeter. The method used is the same as described by us in a previous paper<sup>9</sup>. Briefly, it can be summarized as follows. The molten samples were undercooled at  $64^\circ\text{C}$  per minute until the



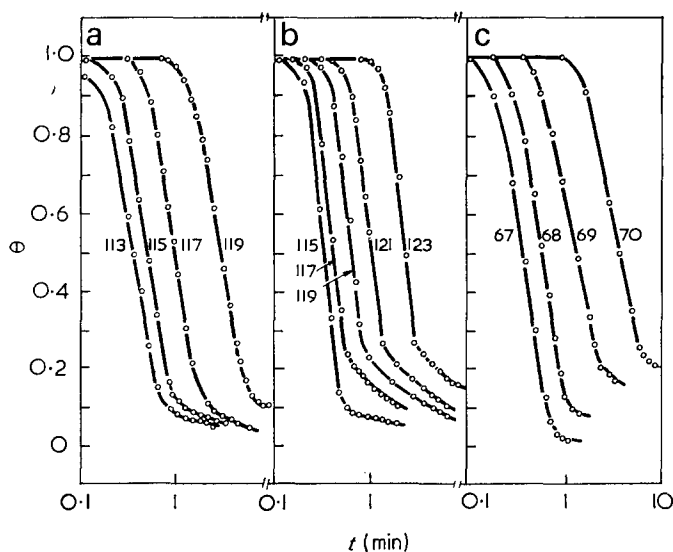


Figure 1 Typical isotherms for molecular weight fractions of (a) 3300, and (b) 20 000 linear polyethylene fractions and (c) paraffin ( $C_{36}H_{74}$ ) at high undercoolings. Temperature ( $^{\circ}C$ ) of crystallization is indicated for each isotherm

desired crystallization temperature was reached. Crystallization heat was recorded as a function of time until crystallization was complete or the heat evolved was small enough to be detected. The percentage crystallization was obtained in the usual way<sup>3</sup>.  $\Delta H_u = 6.8$  cal/g was used for the indium and  $\Delta H_u = (960/14)$  cal/g was used for the high molecular weight polyethylene fractions ( $\bar{M}_n = 2.0 \times 10^4$ ). The melting heat for the lowest molecular weights were calculated using the Flory and Vrij<sup>11</sup> equation modified for a value of  $\Delta H_u = 960$  cal/mol<sup>12</sup>,

$$\Delta H_u = 960 - \Delta C_p \Delta T - (2150/n) \quad (1)$$

where  $\Delta H_u$  is the melting enthalpy per  $-CH_2-$  unit and  $n$  is the chain length,  $\Delta T$  is the difference between the equilibrium melting temperature of an extended chain polyethylene crystal of infinite molecular weight in equilibrium, that is to say  $145.5^{\circ}C$ <sup>11, 13</sup> and the melting temperature for a chain with  $n$  methylene groups, and  $\Delta C_p$  is the difference between the heat capacity of extended chain polyethylene crystal<sup>14</sup> and amorphous polyethylene<sup>15</sup>. The melting heat of 30 900 cal/mol<sup>16, 17</sup> taken for the  $C_{36}H_{74}$  paraffin corresponds to melting enthalpy of  $\Delta H_u = 853.3$  cal/mol per  $-CH_2-$  group.

Thus, the functions  $(1 - \lambda_t)$  versus  $t$  were obtained for each undercooling. The value  $(1 - \lambda_t)_{\infty}$  was obtained by the usual method of taking the extrapolated value of the curve after two decades of time, because secondary crystallization was extremely slow. The usual form of the equation of Avrami  $\ln \theta = kt^n$  was obtained by calculating the function  $\theta$  from the following relation:

$$(1 - \lambda_t)_{\infty} \cdot (1 - \theta) = (1 - \lambda_t) \quad (2)$$

Isotherms thus obtained for two of the fractions and paraffin  $C_{36}H_{74}$  are shown in Figure 1.

## RESULTS AND DISCUSSION

The results of the crystallization rates, expressed in terms of time  $\tau_{0.5}$  for 50% of the transformation are given in Figure 2 for the various temperatures studied.

The most important fact noted is that at the highest crystallization temperatures ( $121-123^{\circ}C$ ) a maximum in the crystallization rate may be observed which corresponds as a minimum when plotting  $\tau_{0.5}$  against  $\bar{M}_n$ .

This minimum is not so well defined in each case and, as can be seen, as undercooling increases, it moves to much lower molecular weights and nearly completely disappears at the lowest undercooling. This minimum is more pronounced at the highest crystallization temperature, as may be noted for all crystallization temperatures used.

Furthermore, with any molecular weight, crystallization rate increases when crystallization temperature decreases. It is a well established fact that this indicates a nucleation process in the crystallization is occurring. Another important fact is that at the lowest crystallization temperatures and in the range of the highest molecular weight, crystallization rate only seems to be slightly dependent on molecular weight. The nucleation theories developed<sup>5, 6</sup> have shown that the free energy for stable nucleus formation is independent of molecular weight for chains with a molecular weight above  $10^5$  whatever the crystallization temperature and crystallization rate changes with molecular weight have been attributed to the transport term or rate of growth<sup>2</sup>. When the crystallization temperature decreases, the critical nucleation conditions diminish and the viscosity of the medium is not of important influence.

This has been shown in a previous work and it is strongly supported by our own results which cover a wider range of molecular weights.

Crystallinity, at the end of the transformation at a given crystallization temperature, is a function of the molecular weight and decreases as this increases. Figure 3 represents this variation after crystallization at  $115^{\circ}C$  for fractions of molecular weight between  $1.55 \times 10^6$  and  $1.8 \times 10^3$ . For these limits, crystallinity varies from 35% for the fraction of highest molecular weight up to 85% for the fraction of lowest molecular weight. Similar results were previously reported<sup>10</sup> after crystallization at low undercoolings.

On the other hand, the crystallization rate can be expressed as a function of time  $\tau_{0.1}$  in which 10% of the transformation takes place by the equation<sup>3, 4</sup>:

$$\ln(\tau_{0.1})^{-1} = \ln(\tau_{0.1})_0^{-1} - E_D/RT_c - \Delta F^*/RT_c \quad (3)$$

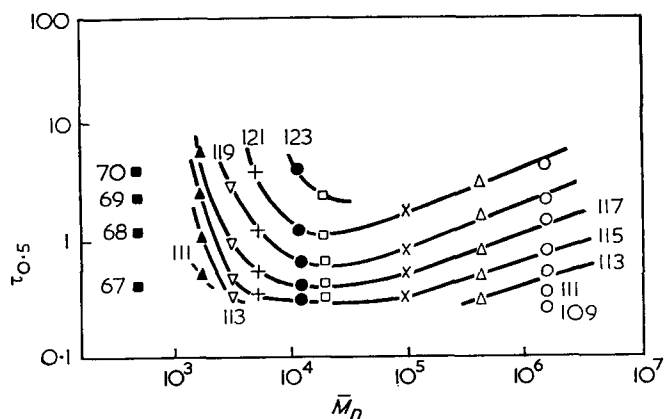


Figure 2 Double logarithmic plot of crystallization half-time,  $\tau_{0.5}$  (minutes) against number-average molecular weight. Isothermal crystallization temperatures ( $^{\circ}C$ ) indicated for each curve

where  $T_c$  is the crystallization temperature,  $\Delta F^*$  the free energy for forming a stable nucleus and  $E_D$  is the transport term.

From equation (3) it can be deduced that a representation of  $\ln(\tau_{0.1})^{-1}$  against  $\Delta F^*/RT_c$  should correspond to a straight line with a  $-1$  slope and independent of the molecular weight when the value of  $\Delta F^*$  is stipulated for the model of finite molecular weight in a tridimensional nucleation process.

For the case of a cylindrical nucleus, it has been shown that<sup>5</sup>:

$$\Delta F^* = \pi^{1/2} \xi^* \rho^* \sigma_u^2 \quad (4)$$

where  $\xi^*$  and  $\rho^*$  are the critical dimensions of the nucleus and  $\sigma_u$  the lateral interfacial free energy per structural unit.

For a finite chain with chain length  $x$ , the critical dimensions are related by the following expressions:

$$\begin{aligned} (\xi^*/2) [\Delta f_u - (RT_c/x) + (RT_c/x - \xi^* + 1)] = \\ 2\sigma_e - RT_c \ln [(x - \xi^* + 1)/x] \quad (5) \end{aligned}$$

and

$$\rho^* = 2\pi^{1/2} \sigma_u / [\Delta f_u - (RT_c/x) - (RT_c/x - \xi^* + 1)] \quad (6)$$

where  $\sigma_e$  is the interfacial free energy per unit in the basal plane and  $\Delta f_u$  is the free melting energy per repeating unit at  $T_c$  which is given by the approximation

$$\Delta f_u = \Delta H_u (T_m^0 - T_c) / T_m^0 \quad (7)$$

$\Delta H_u$  being the melting enthalpy per unit and  $T_m^0$  the equilibrium melting temperature.

In the limit of high molecular weights equations (4), (5) and (6) are reduced to the known expression:

$$\Delta F^* = 8\pi \sigma_e \sigma_u^2 (T_m^0)^2 / \Delta H_u^2 (T_m^0 - T_c)^2 \quad (8)$$

Analysis of the experimental data according to the above equations require exclusively the specification of  $T_m^0$ ,  $\Delta H_u$  and  $\sigma_e$ . In the case of polyethylene, Flory and Vrij<sup>11</sup> have developed the theoretical relationship between the molecular weight and the equilibrium melting temperature. This theoretical treatment and suggested extrapolations<sup>12, 13</sup> give an equilibrium melting temperature for infinite molecular weight polyethylene of 145.5°C. Melting enthalpy is known by independent measurements and for high molecular weights corresponds to 960 cal/mol<sup>12</sup>. If a value for  $\sigma_e$  is stipulated it is possible to calculate the ratio  $\Delta F^*/2\sigma_u^2 T_c$ . The value chosen was that of  $\sigma_e = 2400$  cal/mol, although the conclusions obtained do not depend on it if other values are selected.

The representation of  $\ln(\tau_{0.1})^{-1}$  against  $\Delta F^*/2\sigma_u^2 T_c$  is shown in Figure 4. All the analysed fractions give straight lines, with a common intersection, except those corresponding to the fraction of  $1.8 \times 10^3$  and paraffin  $C_{36}H_{74}$ , which are not included. The slopes of these lines vary with the molecular weight and the lower the molecular weight, the lower the slopes are. However, the straight lines can be extrapolated to a common intercept, i.e.  $\ln(\tau_{0.1})_0^{-1}$ . Similar results have been described in bidimensional analysis of the spherulitic growth of different polymers<sup>7, 8</sup>.

Considered literally, variations in the slopes in Figure 4 represent a change in the values of  $\sigma_e$  or  $\sigma_u$  or both, if  $\Delta H_u$  is a constant. If we assume that  $\sigma_u$  is constant and

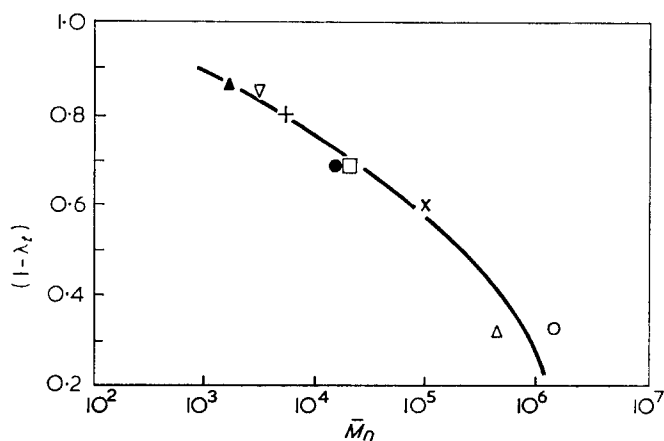


Figure 3 Degree of crystallinity ( $1 - \lambda_t$ ), as a function of molecular weight for linear polyethylene fractions after crystallization at 115°C

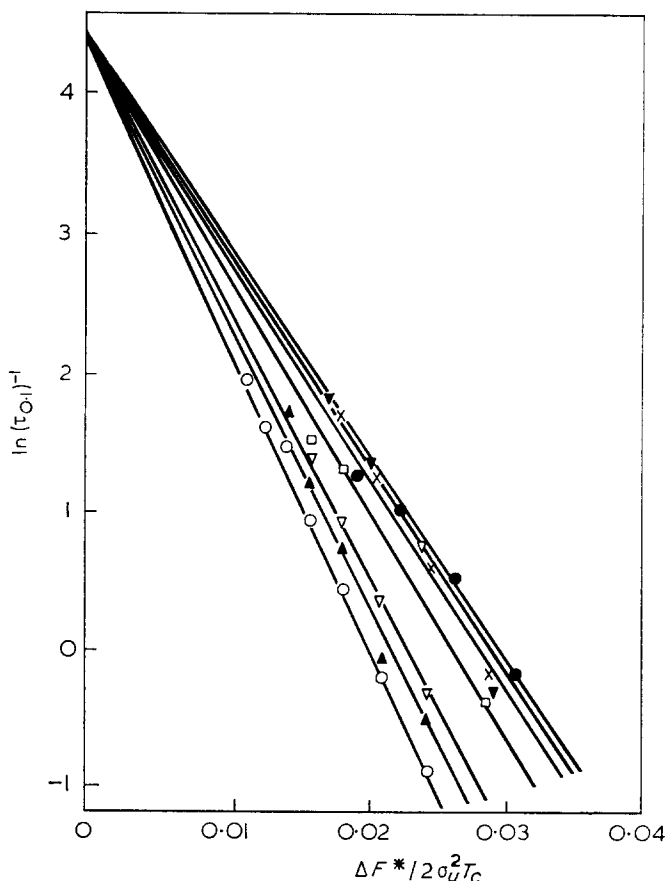


Figure 4 Plot of  $\ln(\tau_{0.1})^{-1}$  against  $\Delta F^*/2\sigma_u^2 T_c$  for linear polyethylene molecular weight fractions.  $\sigma_e = 2400$ ;  $T_m^0 = 145.5^\circ\text{C}$ . Number-average molecular weight of fractions:  $\blacktriangledown$ , 3300;  $\times$ , 5300;  $\bullet$ , 12 500;  $\square$ , 20 000;  $\nabla$ , 100 000;  $\blacktriangle$ , 425 000;  $\circ$ , 1 550 000

independent of the molecular weight, and a value of  $\sigma_e$  is established for the fraction of the highest molecular weight ( $\sigma_e = 2400$  cal/mol) and as a result  $\sigma_u = 15$  cal/mol, the value of  $\sigma_e$  can be determined for each molecular weight. These values are indicated in Figure 5, where  $\sigma_e$  has been represented against number-average molecular weight.

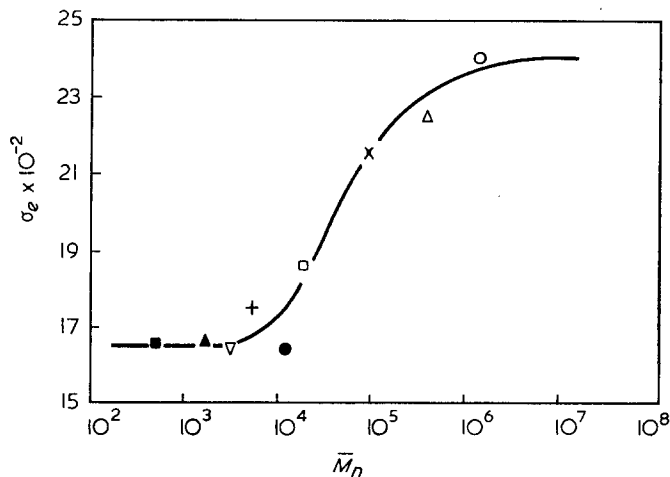


Figure 5 Plot of  $\sigma_e$ , interfacial free energy, against number-average molecular weight

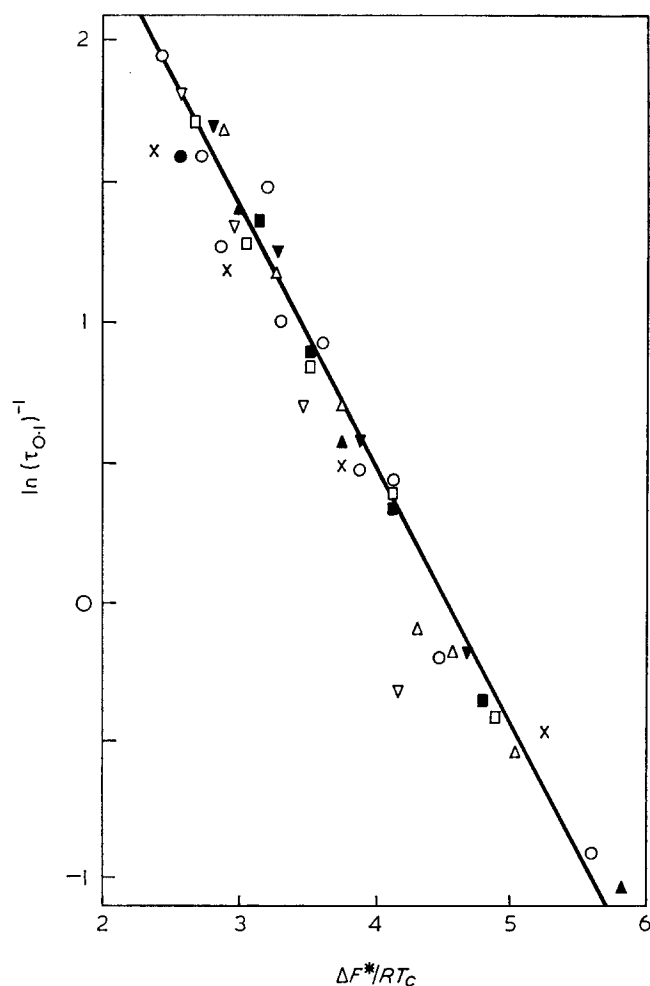


Figure 6  $\ln(\tau_{0.1})^{-1}$  against  $\Delta F^*/RT_c$  for samples studied utilizing interfacial free energies shown in Figure 5.  $\times$ ,  $C_{36}H_{74}$ ;  $\blacktriangle$ , 1800;  $\nabla$ , 3300;  $\blacktriangledown$ , 5300;  $\bullet$ , 12 500;  $\square$ , 20 000;  $\blacksquare$ , 100 000;  $\triangle$ , 425 000;  $\circ$ , 1 550 000

Representation of the data for the fraction of lower molecular weight ( $1.8 \times 10^3$ ) lead to a curve. A value of the slope can be estimated by extrapolation of this curve at the previously established value of  $\ln(\tau_{0.1})^{-1}$ . The value of the slope has been used analytically according to equations (5) and (6) for calculating  $\Delta F^*$ .

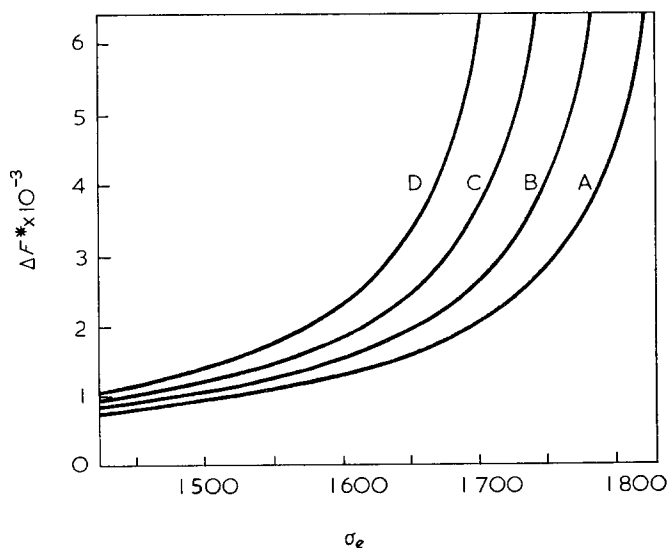


Figure 7 Plot of  $\Delta F^*$  against interfacial free energy,  $\sigma_e$ , at various temperatures for paraffin  $C_{36}H_{74}$ . A, 67°C; B, 68°C; C, 69°C; D, 70°C

The analysis of experimental data can now be made calculating  $\Delta F^*$  according to equations (4), (5) and (6) for each fraction and each crystallization temperature, with the corresponding  $\sigma_e$  values. The representation of  $\ln(\tau_{0.1})^{-1}$  vs.  $\Delta F^*/RT_c$ , as can be seen in Figure 6, give a unique straight line with slope  $-1$  according to equation (3).

The case of  $C_{36}H_{74}$  deserves special discussion. As has been pointed out, this paraffin presents three crystalline forms: monoclinic, orthorhombic and hexagonal with transition temperatures of 345.3°, 347.0° and 349.1°C respectively<sup>16-18</sup>. The melting energy corresponding to the monoclinic to liquid form is 30 900 cal/mol<sup>16-18</sup>. In the experimental crystallization conditions (341°, 342°, 343°, and 344°C), the most stable form corresponds to the monoclinic form, although as has been pointed out by Ohlberg<sup>19</sup> and subsequently by Atkinson and Richardson<sup>17</sup>, an intermediate component appears, as a precursor of the stable phase of high molecular weight paraffins.

Representation of kinetic parameters as a function of  $\Delta F^*/2\sigma_e^2 T_c$  leads to curves in the range of large values of this quantity when  $\sigma_e = 2400$  cal/mol is used. The extrapolation or determination of the slope at high undercoolings is experimentally impossible, owing to the high speed of crystallization, and analytically very risky.

The correct treatment corresponds to the analysis of equations (5) and (6) for different values of  $\sigma_e$ , for which these equations have real values. The variation of  $\Delta F^*$  as a function of  $\sigma_e$ , for  $\sigma_u = 15$  cal/mol is indicated in Figure 7, on condition that  $\rho^* = 1$ . For values of  $\sigma_e$  greater than those represented, the value of  $\Delta F^*$  tends towards infinity as  $T_m$ , melting temperature, is lower than crystallization temperature, and the solutions of equations (5) and (6) have values with no possible physical significance.

If a similar value is stipulated to that of the fraction of  $1.8 \times 10^3$ , that is,  $\sigma_e = 1660$  cal/mol,  $\xi^* = 32.05$  and  $\rho^* = 14.86$  for  $T_c = 343$  K, the values of  $\Delta F^*/RT_c$  are according to equation (3), as shown in Figure 6. Small

variations in the value assigned to  $\sigma_e$  do not alter this conclusion.

This excellent concordance shows the validity of the model of nucleation for finite molecular weights according to the theories of Mandelkern *et al.*<sup>5, 6</sup>.

The variation in  $\sigma_e$  with the molecular weight as shown in the analysis of the spherulitic growth<sup>7, 8</sup> corresponds fundamentally to the region in which there is a change in morphology in the crystal, of folded chains to extended chains.

The highest values of  $\sigma_e$  correspond to the areas of molecular weights where  $\xi^*$  is much less than  $x$ . When  $\xi^*$  is comparable to  $x$ , the value of  $\sigma_e$  is much smaller and also reaches a constant value. The region situated between these two asymptotic regions corresponds to the molecular weights in which there is a morphological change<sup>7, 8</sup> and the ratio  $\xi^*/x$  ranges in between the values of 0.001 and 0.900, where  $\xi^*$  has been taken for a constant crystallization temperature of 115°C for fractions and 70°C for paraffin C<sub>36</sub>H<sub>74</sub>.

The results described in this work show that the crystallization process of polymers is governed by the nucleation of the system and that when the variation in the interfacial energy in the (001) face of the crystal with the molecular weight is stipulated, the phase transformation is described by a unique function of the free energy required for nucleation.

## REFERENCES

- 1 Mandelkern, L. *Polym. Eng. Sci.* 1967, **7**, 232
- 2 Mandelkern, L., Fatou, J. M. G. and Ohno, K. *J. Polym. Sci. (B)* 1968, **6**, 615
- 3 Mandelkern, L. 'Crystallization of Polymers', McGraw-Hill, New York, 1964
- 4 Devoy, C., Mandelkern, L. and Bourland, L. *J. Polym. Sci. (A-2)* 1970, **8**, 869
- 5 Mandelkern, L., Fatou, J. M. G. and Howard, C. *J. Phys. Chem.* 1964, **68**, 3386
- 6 Mandelkern, L., Fatou, J. M. G. and Howard, C. *J. Phys. Chem.* 1965, **69**, 956
- 7 Devoy, C. and Mandelkern, L. *J. Polym. Sci. (A-2)* 1969, **7**, 1883
- 8 Lovering, E. G. *J. Polym. Sci. (A-2)* 1970, **8**, 747
- 9 Fatou, J. M. G. and Barrales-Rienda, J. M. *J. Polym. Sci. (A-2)* 1969, **7**, 1755
- 10 Fatou, J. M. G. and Mandelkern, L. *J. Phys. Chem.* 1965, **69**, 417
- 11 Flory, P. J. and Vrij, A. *J. Am. Chem. Soc.* 1963, **85**, 3548
- 12 Quinn, F. A. Jr. and Mandelkern, L. *J. Am. Chem. Soc.* 1958, **80**, 3178
- 13 Gopalan, M. R. and Mandelkern, L. *J. Phys. Chem.* 1967, **71**, 3833
- 14 Wunderlich, B. *J. Phys. Chem.* 1965, **69**, 2078
- 15 Wunderlich, B. *J. Chem. Phys.* 1962, **37**, 1203
- 16 Schaerer, A. A., Busso, C. J., Smith, A. E. and Skinner, L. B. *J. Am. Chem. Soc.* 1955, **72**, 2017
- 17 Atkinson, C. M. L. and Richardson, M. J. *Trans. Faraday Soc.* 1969, **65**, 1749
- 18 Atkinson, C. M. L., Larkin J. A. and Richardson, M. J. *J. Chem. Thermodyn.* 1969, **1**, 435
- 19 Ohlberg, S. M. *J. Phys. Chem.* 1959, **63**, 248

# Book Reviews

## **Principles of Polymerization**

*George Odian*

McGraw-Hill, New York, 1970, 652 pp. \$18.50

Many textbooks dealing with synthetic high polymers give broad coverage to their chemistry, physics and technology. This volume sets out to deal in much more detail with the chemistry of the synthetic processes which have been developed in recent years.

A very brief introduction serves to introduce the range of polymer types, the concepts of molecular weight and its distribution and the relationship between physical state and bulk properties. As might be expected a substantial proportion of the book is devoted to step polymerization of the condensation type and to free radical chain polymerization. Mechanisms for studying these processes are described in detail, together with the relationship of kinetic parameters to the physical characteristics of the product. The especially important emulsion polymerization is described separately but briefly and on the whole qualitatively. Ionic polymerization mechanisms are described also in a fairly general manner, but with numerous illustrations of individual systems.

The added complications of copolymerization are given considerable space and the mathematical description of the kinetics is clearly developed. Attention is also given to diffusion control, solvent effects and the 'penultimate' effect, for example.

Because of their recent importance, ring-opening polymerization mechanisms are dealt with separately and in some detail as is the stereochemistry of polymers where comment is made on naturally occurring polymers as well as synthetic. A final brief mention is made of reactions of polymer molecules such as grafting, cross-linking, vulcanization and halogenation to name but a few. This is, however, only a qualitative indication of what can be done by regarding a polymer as a reactive chemical.

The general impression of the book is very good, the type is bold, diagrams and illustrations are clear and numerous tables present the matter in an easily assimilable manner. Individual chapters are referenced to important key publications enabling the reader to follow up selected topics in more detail. This publication should be of value to any final year student of chemistry who is specializing in the field of high polymers and can be highly recommended to anyone who has need of being introduced to this important study. The relatively high cost of the book will no doubt restrict its sale to the more enthusiastic buyer.

*J. C. Robb*

## **Polyester fibres: chemistry and technology**

*Hermann Ludewig*

Wiley, New York, 1971, 476 pp. £8.00

This book is a translation of Polyesterfasern which was published in Germany by the Akademie-Verlag GmbH (Berlin) in 1965. It has been written in collaboration with chemists and engineers and for this reason is able to span the many scientific and technological areas involved in fibre production. The book begins with the chemistry of the raw materials and their transformation into poly(ethylene terephthalate), and leads on to the various processes involved in the production of fibres, e.g. melt spinning, drawing, etc. These aspects are then followed by textile processes involved in yarn preparation, e.g. twisting, winding, crimping, etc. The final chapters deal with the characteristics of polyester filaments, their processing, e.g. dyeing, and their end uses. The presentation is biased towards the technological aspects of the manufacture of polyester fibres. This side is comprehensive and well documented and much valuable information of the physical behaviour of fibres is included.

The scientific background, on the other hand, is not so well presented. Part of this criticism arises from the fact that the book was published some six years ago. One would have hoped to see, for example, some of the background of fibre structure discussed, or alternatively, the importance of oligomers in the context of heat setting and dyeing brought out. In this context, it would have been advantageous if the author had given more information on polyesters other than poly(ethylene terephthalate), in particular copolymers.

Nevertheless, with these provisos, the book gives an extremely comprehensive survey of the production and use of poly(ethylene terephthalate) fibres, and will undoubtedly be of great value to scientists and technologists in industry. On the academic side, the book is rather too specialist for an undergraduate, although many of the chapters would be of use for reference purposes. On the other hand, postgraduate students confronted with problems concerned with melt spinning would find this book a very good starting point for their investigations.

The book is well presented and written. It contains only a few curious turns of phrase which presumably have arisen in translation. For the information and in particular the number of references to relevant literature which it contains, the book is reasonably priced.

*R. H. Peters*

## **Toluene diisocyanate in industry: operating and medical codes of practice**

British Rubber Manufacturers Association Ltd,  
London, 1971, 52 pp. £2.00

This report of the Isocyanate Sub-Committee of the B.R.M.A. Health Advisory Committee arises from the workings of a panel representing research, production, trade union and medical interests concerned with the use of diisocyanates for products based on polyurethanes.

With the introduction of toluene diisocyanate and other isocyanates in the manufacture of foams, elastomers, adhesives, coatings, etc., there has rightly been much concern over the hazards associated with these extremely reactive intermediates which can produce distressing respiratory and dermatological effects unless correctly used. The scientific, technical and trade literature has over the years frequently drawn attention to these hazards and provided valuable advice but with the growth of the industry, particularly in large-scale production of flexible foams, the desirability of making available a comprehensive and authoritative guide was recognized by the B.R.M.A.

The present report deals with the equipment, plant, handling and storage (but not transport) problems associated with toluene diisocyanate and, to some extent, with other isocyanates. Many recommendations made relate to health factors and safe working, including the medical screening applicable to the selection of employees. It should be read and used by all responsible in places where isocyanates are used and the B.R.M.A. is to be congratulated in taking the initiative to produce this worthwhile publication.

*R. J. W. Reynolds*

## **Reviews of Macromolecular chemistry**

*Edited by G. B. Butler, K. F. O'Driscoll and M. Shen*

Marcel Dekker, New York, 1971, Vol 6, 490 pp. \$19.50

This book is Vol 6 of 'Reviews in macromolecular chemistry' and like the previous volumes contains reviews of special areas or topics written by experts in the various fields. The particular subjects covered in this volume are: 1. Proton magnetic resonance of molecular interactions in polymer solutions; 2. Preparation and polymerization of vinyl heterocyclic compounds; 3. Catalysis of isocyanate reactions; 4. Thermodynamics of polymerization. II. Thermodynamics of ring-opening polymerization; 5. Copolymers of naturally occurring macromolecules; 6. Molecular configuration and pyrolysis of phenolic novolaks; 7. Physical properties of ionic polymers; 8. Synthesis and properties of polyphenyls and polyphenylenes; 9. Dependence of flow properties on molecular weight, temperature and shear; and 10. Synthesis methods and properties of polyazoles. The chapters have been clearly selected to cover recent advances in macromolecular chemistry and although of most interest to the specialist the book is also of value to chemists wishing to obtain an authoritative account of the state of knowledge in a given area.

*C. E. H. Bawn*

# Equilibrium ring concentrations and the statistical conformations of polymer chains: Part 9. Sodium metaphosphates in Graham's salt

D. R. Cooper and J. A. Semlyen

Department of Chemistry, University of York, Heslington, York YO1 5DD, UK  
(Received 20 March 1972)

The molar cyclization equilibrium constants  $K_x$  for oligomeric metaphosphates  $(\text{NaPO}_3)_x$  in high molecular weight sodium phosphate melts at 1000K are calculated using a rotational isomeric state model to describe the statistical conformations of the corresponding open chain molecules. The model is based on a previously published analysis of the molecular structure of the polyphosphate chain. Each skeletal bond is assigned to one of three rotational states in *trans* ( $\phi=0^\circ$ ) and *gauche* ( $\phi=\pm 120^\circ$ ) positions, and the interdependence of adjacent pairs of bond rotational states is taken into account by assuming that only Coulombic interactions between charged non-bonded atoms of the chain separated by eight or fewer chemical bonds need to be considered. The probabilities that polyphosphate chains  $(\text{O-PO}_2)_x$  (with  $x=3-10$ ) will intramolecularly cyclize are calculated by computing the statistically weighted fraction of the  $3^{2x-3}$  conformations defined by the rotational isomeric state model that have their termini in close proximity for ring formation. Molar cyclization equilibrium constants calculated by this direct computational method are compared with experimental values deduced from data of Thilo and Schülke, as well as with values calculated assuming that the polyphosphate chains obey Gaussian statistics.

## INTRODUCTION

In his classic paper of 1833 entitled 'Researches on the arseniates, phosphates and modifications of phosphoric acid', Thomas Graham<sup>1</sup> described the preparation of a sodium phosphate glass with the empirical formula  $\text{NaPO}_3$ . This glass has since become known as Graham's salt. It may be prepared by heating sodium dihydrogen phosphate  $\text{NaH}_2\text{PO}_4$  above 923K for many hours and then chilling the melt rapidly between metal plates<sup>2, 3</sup>. The quenched water-soluble product has been the subject of many investigations<sup>4-7</sup> and it has been shown to consist of long linear polyphosphate chains terminated by hydroxyl groups<sup>8, 9</sup> together with about 10% cyclics  $(\text{NaPO}_3)_x$  with  $x=3-7$ <sup>10, 11</sup>. An equilibrium between ring and chain molecules is established in the melt and the average lengths of the chains have been found to be greater the higher the equilibration temperature and the lower the water vapour pressure in the surrounding atmosphere<sup>3, 12</sup>. Rapid quenching is required to freeze the equilibrium, as slow cooling results in the formation of sodium trimetaphosphate  $(\text{NaPO}_3)_3$ <sup>13, 14</sup>. The concentrations of oligomeric sodium metaphosphates  $(\text{NaPO}_3)_x$  in samples of Graham's salt have been measured by van

Wazer and his coworkers (for  $x=3-6$ )<sup>10, 15</sup> and by Thilo and Schülke (for  $x=3-7$ )<sup>11</sup>. Both groups used paper chromatography as their principal analytical technique.

In this paper, the concentrations of oligomeric metaphosphates in sodium melts at 1000K are calculated by a direct computational method that has recently been used to calculate the molar cyclization equilibrium constants for oligomeric dimethylsiloxane rings in undiluted polydimethylsiloxane equilibrates<sup>16</sup>. The statistical conformations of polyphosphate chains are described by a rotational isomeric state model that is based on a previously published analysis of the linear polymer<sup>17</sup>; and the probabilities that such chains will intramolecularly cyclize are calculated by computing the statistically weighted fraction of the total number of discrete conformations defined by the model that have terminal atoms in close proximity for bond formation.

## EXPERIMENTAL MOLAR CYCLIZATION EQUILIBRIUM CONSTANTS

Experimental studies<sup>18, 19</sup> have shown that there is a small degree of crosslinking in high molecular weight samples of Graham's salt. Nonetheless, for present

Table 1 Experimental molar cyclization equilibrium constants for cyclic metaphosphates in sodium phosphate melts

Value of $x$ in cyclic ( $\text{NaPO}_3$ ) $_x$	Graham's salt prepared by heating $\text{NaH}_2\text{PO}_4$ at 973K for 1½ days <sup>10</sup>		Graham's salt prepared by heating $\text{NaH}_2\text{PO}_4$ at 1073K for 24 hours <sup>11</sup>	
	Wt. %	$K_x$ (mol/l)	Wt. %	$K_x$ (mol/l)
3	3.9	0.28	4.3	0.31
4	2.5	0.14	2.6	0.14
5	0.75	0.032	0.8	0.035
6	0.5	0.018	1.0	0.036
7	—	—	0.5	0.015

purposes, chains in sodium phosphate melts may be assumed to be unbranched, so that the equilibrium between ring and chain molecules resulting from the interchange of phosphate linkages may be represented:



The molar cyclization equilibrium constants  $K_x$  for sodium metaphosphates formed by the forward step of equation (1) are given by:

$$K_x = \frac{[\text{HO}-(\text{NaPO}_3)_{y-x}-\text{H}][(\text{NaPO}_3)_x]}{[\text{HO}-(\text{NaPO}_3)_y-\text{H}]} \quad (2)$$

so the  $K_x$  values for oligomeric cyclics in high molecular weight sodium phosphate melts (where  $y \gg x$ ) may be obtained using the approximate relationship

$$K_x = [(\text{NaPO}_3)_x] \quad (3)$$

The experimental  $K_x$  values (in mol/l) for oligomeric metaphosphates in sodium phosphate melts at  $\sim 1000\text{K}$  are listed in Table 1. These values were calculated from the data of McCullough *et al.*<sup>10</sup> at 973K and of Thilo and Schülke<sup>11</sup> at 1073K, by using equation (3) and assuming that the density of the melt is 2.2g/ml at both temperatures<sup>2,20</sup>. There is good agreement between the  $K_3$ ,  $K_4$  and  $K_5$  values obtained by the two groups of workers, and the substantial difference between their  $K_6$  values is believed to be the result of the limited precision of the paper chromatographic technique used to measure the cyclic concentrations. The more recent  $K_6$  value of Thilo and Schülke will be assumed to be the correct experimental value.

It is noted that the experimental molar cyclization equilibrium constants for oligomeric sodium metaphosphates in sodium phosphate melts at 1000K are of the same order of magnitude as those for the analogous oligomeric cyclic dimethylsiloxanes in polydimethylsiloxane melts at 383K<sup>21</sup>, with the exception of  $K_3$  for the cyclic trimer. The presence of only small amounts of the cyclic trimers ( $\text{R}(\text{CH}_3)_2\text{SiO})_3$  (where  $\text{R} = \text{H}, \text{CH}_3, \text{CH}_3\text{CH}_2, \text{CH}_3\text{CH}_2\text{CH}_2, \text{CF}_3\text{CH}_2\text{CH}_2$  or  $\text{C}_6\text{H}_5$ ) in polysiloxane equilibrates<sup>22</sup> has been attributed to strain in the ring molecules associated with large deformations in the Si-O-Si bond angles<sup>23</sup>. The far higher concentrations of cyclic trimer in sodium phosphate melts suggest that  $(\text{NaPO}_3)_3$  is not subject to such strain; and this conclusion is supported by the fact that the P-O-P bond angles in sodium trimetaphosphate<sup>24</sup> are similar to the values found in open polyphosphate chains<sup>25</sup>.

\*  $\langle r^2 \rangle_0$  represents the mean-square distance between the ends of a chain of  $n$  skeletal bonds each of length  $l$  taken in the limit  $n \rightarrow \infty$ .

## ROTATIONAL ISOMERIC STATE MODEL OF THE POLYPHOSPHATE CHAIN

In common with other polyelectrolytes, polyphosphate chains are highly extended in aqueous solution as a result of long-range intramolecular electrostatic interactions between the negatively charged phosphate units<sup>19</sup>. However, Strauss and his coworkers<sup>26, 27</sup> have shown that in aqueous solutions of high ionic strength, long-range interactions may no longer be of consequence and  $\theta$ -point conditions may be realized. The characteristic ratio\*  $\langle r^2 \rangle_0/nl^2$  was found to be 6.6 for sodium polyphosphate in 0.415 M sodium bromide at 298 K<sup>26</sup> and 7.1 and 7.2 for two lithium polyphosphates in 1.80 M lithium bromide at the same temperature<sup>27</sup>. These values are typical of synthetic random-coil polymers, whose characteristic ratios commonly lie in the range  $4 < \langle r^2 \rangle_0/nl^2 < 10$  (see ref. 28).

In a paper published by Semlyen and Flory<sup>17</sup>, the unperturbed dimensions of the linear polyphosphate chain were found to be amenable to theoretical interpretation in terms of the molecular structure of the polymer using the rotational isomeric state theory of linear macromolecules. Structural parameters were assigned to the chain based on several X-ray crystallographic studies (see legend to Figure 1) and the continuum of rotational states about each skeletal bond was represented by assigning each bond to one of three rotational isomeric states in *trans* ( $\phi = 0^\circ$ ), *gauche+* ( $\phi = 120^\circ$ ) and *gauche-* ( $\phi = 240^\circ$ ) positions. Long-range intramolecular interactions were neglected in the analysis because they do not affect the dimensions of polymer chains under  $\theta$ -point conditions. The counter-ions were assumed to have a negligible effect on the statistical conformations of polyphosphate chains under  $\theta$ -point conditions and short-range intramolecular interactions were estimated using conventional semi-empirical expressions to calculate the steric and electrostatic attractive and repulsive energies between non-bonded phosphorus and oxygen atoms of the chains. Statistical weight matrices  $U'$  and  $U''$  were set up to take account of the interdependence of adjacent pairs of bond rotational states centred on phosphorus and oxygen atoms respectively, thus with reference to Figure 1:

$$U' = g_{i-1}^+ \begin{bmatrix} 1 & \sigma & \sigma \\ 1 & \alpha/\sigma & \beta/\sigma \\ 1 & \beta/\sigma & \alpha/\sigma \end{bmatrix}; \quad U'' = g_i^+ \begin{bmatrix} 1 & \sigma & \sigma \\ 1 & \gamma/\sigma & \delta/\sigma \\ 1 & \delta/\sigma & \gamma/\sigma \end{bmatrix} \quad (4)$$

The parameter  $\sigma$  depends on interactions arising from *gauche* rotations about a single skeletal bond with all other skeletal bonds remaining in *trans* positions. The parameters  $\alpha$ ,  $\beta$ ,  $\gamma$ ,  $\delta$  depend on interactions between non-bonded atoms arising from *gauche* rotations about adjacent pairs of skeletal bonds. All the parameters are related to conformational energy differences by Boltzmann factors. Thus, for example, the statistical weight parameter  $\sigma$  is given by:

$$\sigma = \exp[-(E_{tg^\pm} - E_{tt})/RT] \quad (5)$$

where  $R$  is the gas constant,  $T$  is the temperature and  $(E_{tg^\pm} - E_{tt})$  is the difference in conformational energy between a section of a polyphosphate chain with all the

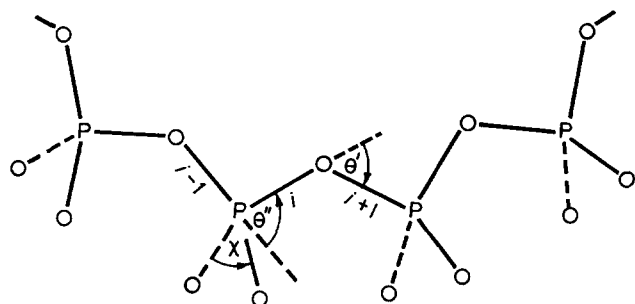


Figure 1 Section of a polyphosphate chain in the all-*trans* conformation. The structural parameters are those assigned in ref. 17, viz. 1.62 Å for the length of a skeletal P-O bond, 1.48 Å for the P-O bond joining a pendant oxygen to the backbone,  $\theta = 50^\circ$ ,  $\theta' = 78.5^\circ$  and  $\chi = 121^\circ$

skeletal bonds in *trans* positions and the energy  $E_{tg\pm}$  when one of the bonds is rotated into a *gauche* position. Analysis of the intramolecular interactions led to the conclusion that at 298K,  $\sigma$  is of the order of unity,  $\gamma$  is smaller but finite,  $\beta = 0$  and  $\alpha$  and  $\delta$  are close to zero. Strauss's value for the characteristic ratio of the polyphosphate chain ( $\langle r^2 \rangle_0/nl^2 \cong 7$ ) was calculated by Flory's<sup>28</sup> exact matrix algebraic methods by taking  $\sigma \cong 1$ ,  $\gamma = 0.1$  and  $\alpha = \beta = \delta = 0$ .

It is the purpose of this paper to describe calculations of equilibrium cyclic concentrations in sodium phosphate melts at 1000K. Although there have been no experimental studies of the statistical conformations of polyphosphate chains in the high-temperature melt, the chains would be expected to adopt random-coil conformations under these conditions<sup>29</sup> and the calculations of cyclic concentrations described below are based on this assumption. A similar rotational isomeric state model to that set up previously<sup>17, 28</sup> has been used to represent the statistical conformations of chains in sodium phosphate melts. However, it is important to note that the values of the statistical weight parameters of  $U'$  and  $U''$  would not be expected to be the same for chains in the melt at 1000K as for chains in  $\theta$ -solvents at 298K, both as a result of temperature differences and also because of differences in the polarities of the media. In order to calculate cyclic concentrations in sodium phosphate melts, the statistical weight parameters of  $U'$  and  $U''$  were estimated for chains in the melt at 1000K by similar methods to those used previously<sup>17</sup>. The counterions were assumed to have a negligible effect on the conformations of polyphosphate chains in sodium phosphate melts and partial charges of +0.9, -0.3 and -0.8 were assigned to phosphorus atoms, skeletal oxygen atoms and pendant oxygen atoms respectively. Intramolecular electrostatic energies were calculated by Coulomb's law. Thus, the energy  $Q_{ij}$  (in kJ/mol) between atoms  $i$  and  $j$  carrying partial charges  $q_i$  and  $q_j$  separated by  $r_{ij}$  Å was expressed by:

$$Q_{ij} = 1389 q_i q_j / \epsilon r_{ij} \quad (6)$$

The dielectric constants of sodium phosphate glasses have been found to lie in the range  $4 < \epsilon < 6$  (see ref. 2) and a fixed value of  $\epsilon = 5$  was taken as the dielectric constant of the melt at 1000K.

Chains in sodium phosphate melts should be unperturbed by excluded volume effects<sup>29</sup> and, as in the previ-

ous study<sup>17</sup>, intramolecular Coulombic interactions between non-bonded atoms were ignored if the atoms were separated by more than eight chemical bonds. *Gauche* rotations of opposite sign about bonds centred on phosphorus atoms result in severe steric repulsions between non-bonded oxygen atoms separated by six chemical bonds, so that the states  $g_{i-1}^+ g_i^-$  and  $g_{i-1}^- g_i^+$  must be accorded statistical weights of zero even at 1000K. Steric interactions between non-bonded atoms in all other combinations of bond rotational states are of far less importance than electrostatic interactions and they were ignored. The statistical weight parameters  $\sigma$ ,  $\alpha$ ,  $\gamma$ ,  $\delta$  were calculated using equation (6) with  $\epsilon = 5$  by including all the electrostatic interactions between pairs of non-bonded atoms separated by three, four, five, six, seven and eight chemical bonds. These calculations provided the following values of the statistical weight parameters of  $U'$  and  $U''$  at 1000K:  $\sigma = 0.60$ ,  $\alpha = 0.018$ ,  $\gamma = 0.27$  and  $\delta = 0.16$ . These values (together with  $\beta = 0$ ) were used to provide statistical weights for each discrete conformation of the polyphosphate chains.

The principal source of uncertainty in the values of the statistical weight parameters  $\sigma$ ,  $\alpha$ ,  $\gamma$ ,  $\delta$  is believed to arise from the procedure whereby all Coulombic interactions between non-bonded atoms separated by up to eight chemical bonds are included in their estimation and all longer-range interactions are excluded. The values of the parameters alter if longer-range electrostatic interactions are taken into account and to restrict consideration to interactions between atoms separated by three to eight chemical bonds (as in the earlier study<sup>17</sup>) is reasonable but arbitrary. Hence, the calculations of oligomeric cyclic concentrations in sodium phosphate melts described below must be regarded as illustrative only. Further experimental information relating to the conformations of polyphosphate chains in sodium phosphate melts is required before refinement of the model will be possible.

#### CALCULATION OF MOLAR CYCLIZATION EQUILIBRIUM CONSTANTS

Theoretical  $K_x$  values (in mol/l) for unstrained metaphosphates  $(\text{NaPO}_3)_x$  in sodium phosphate melts formed by the forward step of equation (1) were calculated using the rotational isomeric state model described above together with an expression obtained from the Jacobson and Stockmayer theory<sup>16, 30, 31</sup>:

$$K_x = \bar{W}_x / 2xN_A \quad (7)$$

where  $\bar{W}_x$  is the density of end-to-end vectors  $\mathbf{r}$  in the region  $r \cong 0$  (in molecules/l) and  $N_A$  is the Avogadro constant.

The rotational isomeric state model of the polyphosphate chain defines  $3^{2x-3}$  conformations for chains  $-(\text{O}-\text{PO}_2)_x$  containing  $x$  monomeric units. The densities  $\bar{W}_x$  of end-to-end vectors  $\mathbf{r}$  of such chains in the region  $r \cong 0$  were calculated by dividing the sum  $Z_r$  of the statistical weights for all chain conformations with their terminal phosphorus and oxygen atoms separated by less than  $r$  Å, by the volume  $(4/3)\pi r^3$  as well as by the total sum  $Z$  of the statistical weights of all  $3^{2x-3}$  conformations, thus

$$\bar{W}_x = Z_r / Z (4/3)\pi r^3 \quad (8)$$



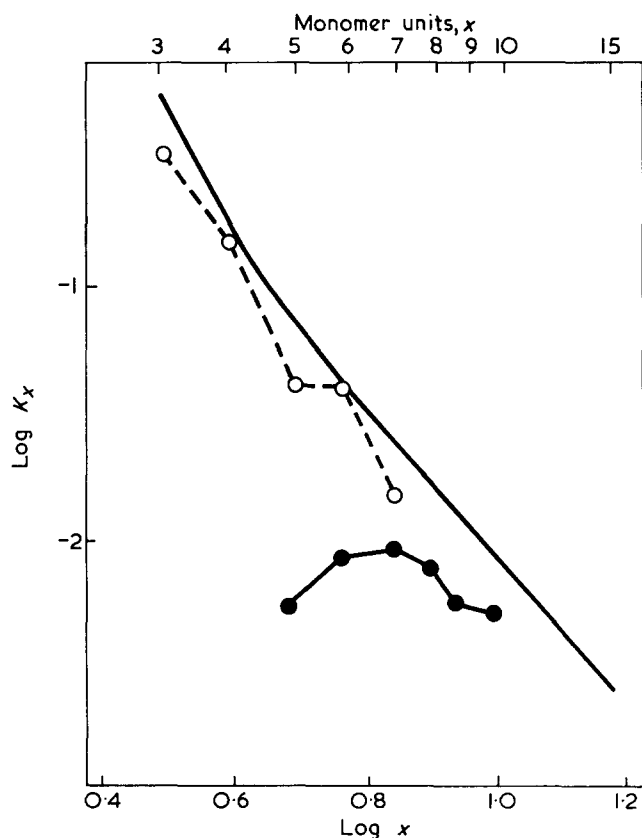


Figure 2 Theoretical molar cyclization equilibrium constants  $K_x$  (in mol/l) (denoted ●) for oligomeric sodium metaphosphates  $(\text{NaPO}_3)_x$  in sodium phosphate melts at 1000K (calculated by the direct computational method using equations (7), (8) and (9) with  $r=3 \text{ \AA}$ ) are compared with Thilo and Schülke's experimental values (denoted ○). The unbroken line shows theoretical  $K_x$  values calculated assuming that all the chains obey Gaussian statistics, so that  $K_x = (3/2\pi \langle r_x^2 \rangle_0)^{3/2} (1/2 \times N_A)$  [see equation (7)]. The required  $\langle r_x^2 \rangle_0$  values were obtained by the mathematical methods of Flory<sup>28</sup> using  $\sigma=0.60$ ,  $\alpha=0.018$ ,  $\beta=0$ ,  $\gamma=0.27$  and  $\delta=0.16$

The sum  $Z$  is the conformational partition function of the chain and it is given by:

$$Z = [1 \ 0 \ 0] (\mathbf{U}' \mathbf{U}')^{x-2} \mathbf{U}' \begin{bmatrix} 1 \\ 1 \\ 1 \end{bmatrix} \quad (9)$$

Probability densities  $\bar{W}_x$  for  $x$ -meric polyphosphate chains  $-(\text{O}-\text{PO}_2)_x$  calculated by equations (8) and (9) for values of  $r$  in the range  $2 < r < 5 \text{ \AA}$  are listed in Table 2. Theoretical  $K_x$  values obtained by substituting  $\bar{W}_x$  values (calculated with  $r=3 \text{ \AA}$ ) into equation (7) are compared with Thilo and Schülke's experimental values in Figure 2. The value of  $3 \text{ \AA}$  was chosen for  $r$  because it corresponds approximately to the sum of the van der Waals radii of the terminal phosphorus and oxygen atoms of the chains. Other small but finite values of  $r$  could have been used. As expected, the calculated  $K_x$  values become increasingly independent of the value chosen for  $r$  (provided it is small) as the lengths of the open chain molecules increase (see Table 2).

Theoretical molar cyclization equilibrium constants for the cyclic pentamer and hexamer are lower than the experimental values by factors of six and four respectively (see Figure 2). These differences between theory and experiment are believed to result from the failure of

Table 2 Densities  $\bar{W}_x$  of end-to-end vectors  $r$  in the region  $r \cong 0$  for polyphosphate chains in sodium phosphate melts calculated using the rotational isomeric state model with the statistical weight parameters:  $\sigma=0.60$ ,  $\alpha=0.018$ ,  $\beta=0$ ,  $\gamma=0.27$ ,  $\delta=0.16$

Value of $x$ in the chain conformations $-(\text{O}-\text{PO}_2)_x$ of the chain	Total number of discrete conformations	$\bar{W}_x \times 10^{-24}$ molecules/l calculated by equations (8) and (9) for			
		$r=2 \text{ \AA}$	$r=3 \text{ \AA}$	$r=4 \text{ \AA}$	$r=5 \text{ \AA}$
3	27	0.000	0.000	0.005	0.101
4	243	0.000	0.000	0.035	0.065
5	2 187	0.001	0.033	0.028	0.051
6	19 683	0.048	0.062	0.062	0.045
7	177 147	0.113	0.077	—	—
8	1 594 323	0.088	0.077	—	—
9	14 348 907	0.059	0.064	—	—
10	129 140 163	0.065*	0.063*	—	—

\* Assignment of a value of zero to  $\alpha$  (and not 0.018) was found to have a negligible effect on  $\bar{W}_x$  values for  $x=8, 9$  and  $\bar{W}_{10}$  was computed with  $\alpha$  set equal to zero. This approximation resulted in a considerable saving of computational time

the three-state rotational isomeric state model to provide reliable values for the probability density  $\bar{W}_x$  of end-to-end vectors  $r$  in the region corresponding to the close approach of chain ends ( $r \cong 0$ ),\* as well as to the neglect of favourable relative orientations of chain termini in the highly coiled conformations<sup>31</sup>. A favourable disposition of terminal non-bonded atoms and groups in the highly coiled conformations of short polyphosphate chains is believed to be the important factor in increasing small cyclic concentrations in sodium phosphate melts above the values predicted by simple application of the rotational isomeric state model described above. Jacobson and Stockmayer<sup>30</sup> showed that the molar cyclization equilibrium constants for unstrained ring molecules in polymeric equilibrates depend on the relative probabilities of intermolecular condensation and intramolecular cyclization reactions; and while reacting centres of polyphosphate chains will be randomly oriented in the intermolecular condensation reactions, this situation will only be approached in the intramolecular cyclization reactions of  $-(\text{O}-\text{PO}_2)_x$  chains for larger values of  $x$ . In this connection, it is of interest to note that the theoretical  $K_7$  value for the heptameric metaphosphate  $(\text{NaPO}_3)_7$  ( $K_7=9.2 \times 10^{-3} \text{ mol/l}$ ) is close to the value deduced from Thilo and Schülke's data ( $1.5 \times 10^{-2} \text{ mol/l}$ ). Furthermore,  $K_8$ ,  $K_9$  and  $K_{10}$  are calculated to be  $8.0 \times 10^{-3}$ ,  $5.9 \times 10^{-3}$  and  $5.3 \times 10^{-3} \text{ mol/l}$  respectively. These values are in accord with Thilo and Schülke's conclusion that there are only very small amounts ( $\sim 1.2\%$  by wt.) of cyclics with  $x \geq 8$  in samples of Graham's salt.

Molar cyclization equilibrium constants for cyclics in sodium phosphate melts were also calculated by assuming that the corresponding open chain molecules obey Gaussian statistics so that the densities  $\bar{W}_x$  of end-to-end vectors  $r$  in the region  $r \cong 0$  are given by<sup>29</sup>:

$$\bar{W}_x = (3/2\pi \langle r_x^2 \rangle_0)^{3/2} \quad (10)$$

\*  $\bar{W}_3$  and  $\bar{W}_4$  are calculated to be zero by equations (8) and (9) when  $r < 3 \text{ \AA}$  (see Table 2). However, finite values of  $\bar{W}_3$  and  $\bar{W}_4$  are obtained if rotational isomeric state models with six (or twelve) rotational states are employed. The results of calculations using such models will not be discussed here.

The mean-square end-to-end distances  $\langle r_z^2 \rangle_0$  of the unperturbed  $x$ -meric chain molecules required by equation (10) were computed by Flory's mathematical methods<sup>28</sup>. In Figure 2, molar cyclization equilibrium constants calculated by equations (7) and (10) are compared with those obtained by the direct computational method. The Gaussian formula should be obeyed by random-coil polyphosphate chains containing many skeletal bonds. Hence, the measurement of large ring concentrations in high molecular weight samples of Graham's salt would be expected to provide a direct measure of the average dimensions of chains in sodium phosphate melts.

#### ACKNOWLEDGEMENTS

We are indebted to the Science Research Council for a Research Scholarship (for D.R.C.). We gratefully acknowledge computational facilities at the University of York.

#### REFERENCES

- 1 Graham, T. *Phil. Trans. R. Soc.* 1833, **A123**, 253
- 2 van Wazer, J. R. 'Phosphorus and its Compounds', Interscience, New York, 1958, Vol 1
- 3 Thilo, E. in 'Advances in Inorganic Chemistry and Radiochemistry' (Eds H. J. Emeleus and A. G. Sharpe), Academic Press, New York, 1962, Vol 4
- 4 Lamm, O. and Malmgren, H. *Z. Anorg. Allgem. Chem.* 1940, **245**, 103
- 5 Samuelson, O. *Sven. Kem. Tidskr.* 1949, **61**, 76
- 6 van Wazer, J. R. *J. Am. Chem. Soc.* 1950, **72**, 639, 644, 647, 655, 906
- 7 Strauss, U. P., Smith, E. H. and Wineman, P. L. *J. Am. Chem. Soc.* 1953, **75**, 3935
- 8 Samuelson, O. *Sven. Kem. Tidskr.* 1944, **56**, 343
- 9 Treadwell, W. D. and Leutwyler, F. *Helv. Chim. Acta* 1937, **20**, 931
- 10 McCullough, J. F., van Wazer, J. R. and Griffith, E. J. *J. Am. Chem. Soc.* 1956, **78**, 4528
- 11 Thilo, E. and Schülke, U. *Z. Anorg. Allgem. Chem.* 1965, **341**, 293
- 12 Winkler, A. and Thilo, E. *Z. Anorg. Allgem. Chem.* 1959, **298**, 302
- 13 Graham, T. *Ann. Phys.* 1834, **32**, 33
- 14 Fleitmann, T. and Henneberg, W. *Ann. Phys.* 1848, **65**, 304
- 15 van Wazer, J. R. and Karl-Kroupa, E. *J. Am. Chem. Soc.* 1956, **78**, 1772
- 16 Beevers, M. S. and Semlyen, J. A. *Polymer* 1972, **13**, 385
- 17 Semlyen, J. A. and Flory, P. J. *Trans. Faraday Soc.* 1966, **62**, 2622
- 18 Strauss, U. P., Smith, E. H. and Wineman, P. L. *J. Am. Chem. Soc.* 1953, **75**, 3935
- 19 Strauss, U. P. and Smith, E. H. *J. Am. Chem. Soc.* 1953, **75**, 6186
- 20 Callis, C. F., van Wazer, J. R. and Metcalf, J. S. *J. Am. Chem. Soc.* 1955, **77**, 1468
- 21 Semlyen, J. A. and Wright, P. V. *Polymer* 1969, **10**, 543
- 22 Wright, P. V. and Semlyen, J. A. *Polymer* 1970, **11**, 462
- 23 Piccoli, W. A., Haberland, G. G. and Merker, R. L. *J. Am. Chem. Soc.* 1960, **82**, 1883
- 24 Ondik, H. M. *Acta Cryst.* 1965, **18**, 226
- 25 Jost, K.-H. *Acta Cryst.* 1963, **16**, 640
- 26 Strauss, U. P. and Wineman, P. L. *J. Am. Chem. Soc.* 1958, **80**, 2366
- 27 Strauss, U. P. and Ander, P. *J. Phys. Chem.* 1962, **66**, 2235
- 28 Flory, P. J. 'Statistical Mechanics of Chain Molecules', Interscience, New York, 1969
- 29 Flory, P. J. 'Principles of Polymer Chemistry', Cornell University Press, Ithaca, 1953
- 30 Jacobson, H. and Stockmayer, W. H. *J. Chem. Phys.* 1950, **18**, 1600
- 31 Flory, P. J. and Semlyen, J. A. *J. Am. Chem. Soc.* 1966, **88**, 3209

# Sequence peptide polymers: Part 1. Poly(leucyl-leucyl-aspartic acid- $\beta$ -benzyl ester)—synthesis and some conformational aspects in solutions\*

M. D'Alagni, P. Bemporad and A. Garofolo

*Istituto di Chimica delle Macromolecole, Nucleo di Roma, c/o Istituto di Chimica Fisica, Università di Roma, 00181 Roma, Italy*

*(Received 6 December 1971; revised 16 February 1972)*

A polypeptide containing ordered sequence of leucyl and  $\beta$ -benzyl-aspartyl residues has been synthesized via the *p*-nitrophenyl active ester method. Polymerization of the TFA H-Leu-Leu-Asp (OBzl) ONp was carried out in dimethyl sulphoxide and in chloroform by mixing the salt with triethylamine. The polymer obtained showed a relatively high  $[\eta]$  and  $\alpha$ -helical conformation in solution as well as in the solid state, as shown by optical rotatory dispersion and infra-red spectra, respectively.

## INTRODUCTION

The study of the forces responsible for the stability of the secondary structure of polypeptides and proteins has recently been the subject of much attention<sup>1, 2</sup>.

A general approach to this problem is to investigate the conformations adopted by polypeptides of known amino acid sequence by varying pH, temperature, solvent, etc. in order to clarify the factors controlling their conformational stability.

This research prompted us to prepare various copolymers, containing polar and non-polar amino acid residues in different proportions and different sequences and to investigate their behaviour in water.

We now report the synthesis and the study of some conformational aspects in organic solvents of an interesting intermediate of such copolymers, e.g. a sequential polypeptide containing an aspartyl- $\beta$ -benzyl ester residue, [Leu-Leu-Asp(OBzl)]<sub>n</sub> while the properties of the corresponding polyacid in water will be published later<sup>3</sup>.

## EXPERIMENTAL

### Materials

HCl.H-Leu-OBzl (Miles Corporation), Boc-Leu-OH (Fluka) and Boc-Asp-(OBzl).OH (Schwarz C.) were

\* The following amino acid abbreviations are used in this paper: Bzl = benzyl; Boc = *t*-butyloxycarbonyl; HONp = *p*-nitrophenol; DCC = dicyclohexylcarbodiimide; DCU = dicyclohexylurea; H-Asp(OBzl)-H = aspartic acid- $\beta$ -benzyl ester; H-Leu-OH = leucine; TEA = triethylamine; TFA = trifluoroacetic acid; DMS = dimethyl sulphoxide.

used in the synthesis of peptides without further purification.

All the solvents were purified and distilled over P<sub>2</sub>O<sub>5</sub> before use. The dimethyl sulphoxide was treated with molecular sieve 4 Å type, previously activated at 300°C, and vacuum distilled.

### Synthesis of peptides†

*Boc-Leu-Leu-OBzl*. HCl.H-Leu-OBzl (2.82 g, 11 mmol;  $[\alpha]_D^{25} = -8.22$ ;  $c = 2.0\%$  in 0.1 N HCl) was added to a solution of DCC (2.26 g, 11 mmol) in dichloromethane, cooled to  $-10^\circ\text{C}$ .

To the solution thus obtained, and kept under magnetic stirring, a cooled solution of Boc-Leu-OH (2.56 g, 11 mmol) and dry triethylamine (1.53 ml) in dichloromethane was added in portions. The reaction was kept at  $0^\circ\text{C}$ , being stirring magnetically and protected from moisture, for about 2 h, and then gradually allowed to reach room temperature. The reaction was followed by thin-layer chromatography (t.l.c.) on silica gel using chloroform-methanol (95 : 5 by vol.) as eluant. DCU was filtered off, the solvent was removed, and the dry residue was taken up in ethyl acetate. A crystalline solid, insoluble in ethyl acetate, was separated (1.2 g, m.p. 179–180°C) and identified by infra-red and t.l.c. analyses as Boc-leucyl-*N,N'*-dicyclohexylurea.

The ethyl acetate solution was washed with 5% aqueous sodium bicarbonate, water, 0.05 N HCl, water again, and dried over anhydrous sodium sulphate.

† All the elemental analyses reported were performed in the laboratory of Dr A. Bernhardt. Melting points were taken in a Kofler apparatus.

Removal of the solvent and fractional crystallization of the residue from ethyl acetate-hexane mixtures left a solid (needles) in 75% yield [m.p. 92–92.5°C;  $[\alpha]_D^{25} = -41.65$  ( $c = 1.06\%$  in chloroform)]. Calculated for  $C_{24}H_{38}N_2O_5$ : C = 66.35%; H = 8.75%; N = 6.45%. Found: C = 66.39%; H = 8.81%; N = 6.54%; and C = 66.23%; H = 8.88%; N = 6.41%.

**Boc-Leu-Leu-OH.** Boc-Leu-Leu-OBzl (1.5 g) was dissolved in a *t*-butanol-dioxane mixture (4 : 1 by vol.) with magnetic stirring. Nitrogen was bubbled into the solution for 15 min before and after the catalyst (Pd/C 10%, 0.1 g) was added. Hydrogen was then bubbled in for 15 h. Samples of the solution were collected every 5 h for t.l.c. analysis to detect the end of hydrogenolysis.

The reaction mixture was filtered on Celite, and after lyophilization, a chromatographically pure compound (dioxane-benzene-acetic acid 5 : 5 : 1 by vol. as eluant) was left that was used as such in the synthesis of the tripeptide Boc-Leu-Leu-Asp(OBzl)-ONp, as will be described later.

**Boc-Asp(OBzl)-ONp.** Boc-Asp(OBzl)-OH (7.0 g, 21.6 mmol) and HONp (3.0 g, 21.6 mmol) were dissolved in dry ethyl acetate (30 ml). The solution was added in portions, with magnetic stirring, to a cooled (–10°C) suspension of DCC (4.54 g) in ethyl acetate (100 ml). The reaction mixture was magnetically stirred at –10°C for about 2 h and then allowed to stand at room temperature for 5 h. A thin-layer chromatography control on silica gel showed that the reaction was almost complete (95% yield). The reaction mixture was filtered and the filtrate was evaporated to dryness. Crystallization of the residue from benzene-hexane mixture (7 : 5 by vol.) gave a chromatographically pure (chloroform-methanol 95 : 5 by vol. as eluant) crystalline product: m.p. 107.5–108°C;  $[\alpha]_D^{25} = -35.85$  ( $c = 1.97\%$  in DMF). Calculated for  $C_{22}H_{24}O_8N_2$ : C = 59.45%; H = 5.44%; N = 6.30%. Found: C = 59.57%; H = 5.51%; N = 6.45%.

**TFA. H-Asp(OBzl)-ONp.** Boc-Asp(OBzl) ONp (1.6 g) was dissolved in TFA (4.5 ml) in a flask protected from moisture and light. After 20 min excess TFA was removed under vacuum; the residue (oil) was treated twice with dry ether and a wax-like product was obtained. The whole treatment had to be repeated until all Boc-Asp(OBzl)-ONp had disappeared (thin-layer chromatography control). The obtained trifluoroacetate was washed with ether again, dried and crystallized from dichloromethane and ether: yield 80% (needles); m.p. 91.5–93°C;  $[\alpha]_D^{25} = 48.30$  ( $c = 1.588\%$  in  $CH_2Cl_2$ ).

**Boc-Leu-Leu-Asp(OBzl)-ONp.** TFA.H-Asp(OBzl)-ONp (2.06 g; 4.5 mmol) was added to a cooled (–5°C) stirred solution of DCC (0.935 g; 4.5 mmol) in freshly distilled dichloromethane. A solution containing Boc-Leu-Leu-OH (1.55 g; 4.5 mmol) and triethylamine (0.62 ml) in 50 ml of dichloromethane was added in portions over a period of 30 min to the suspension previously obtained. The reaction mixture was kept at –5°C, stirred and protected from moisture, for about 2 h. After the reaction mixture had slowly reached room temperature, DCU was filtered off (0.65 g); complete removal of the solvent left a very impure oil that after purification on a silica gel column and by crystallization from ethyl acetate-hexane mixtures

gave a compound in 45% yield: m.p. 146.5–152°C;  $[\alpha]_D^{25} = -46.43$  ( $c = 0.5944\%$  in methanol). I.r. spectrum (Nujol) showed bands at: 1763  $cm^{-1}$  (COONp); 1735  $cm^{-1}$  (COOBzl); 1680  $cm^{-1}$ ; 1640  $cm^{-1}$ ; 1540  $cm^{-1}$ ; 1527  $cm^{-1}$ ; 1390  $cm^{-1}$  (tBu). Calculated for  $C_{33}H_{44}N_4O_{10}$ : C = 60.88%; H = 6.91%; N = 8.35%. Found: C = 60.72%; H = 7.04%; N = 8.14%; and C = 60.76%; H = 7.09%; N = 8.22%.

**TFA. H-Leu-Leu-Asp(OBzl)-ONp.** Chromatographically pure Boc-Leu-Leu-Asp(OBzl)-ONp (0.6 g) was dissolved in TFA (10 ml) and allowed to stand at room temperature for about 30 min. Excess TFA was removed under vacuum (external bath at 25°C) and the residue (oil) was treated with anhydrous ether and dried under vacuum. The solid thus obtained was crystallized from acetonitrile and chromatographically controlled using chloroform-methanol (95 : 5 by vol.) as eluant.

**Poly-Leu-Leu-Asp(OBzl).** Chromatographically pure tripeptide trifluoroacetate (0.53 g) was dissolved in dimethyl sulphoxide (0.6 ml).

Anhydrous triethylamine (0.101 ml) was added at room temperature. After four days the wax-like product obtained was dissolved in 150 ml of chloroform. The polymer solution was washed several times with tris-hydroxymethyl aminomethane buffer (pH 7.2) and water and was dried with anhydrous sodium sulphate. Solvent was removed in vacuum (external bath at 26°C). The solid residue was extracted with dry ether to remove *p*-nitrophenol impurities, and then dried under vacuum. The white polymer obtained was dissolved in chloroform (50 ml), precipitated again with ether (500 ml), collected after centrifugation and dried under high vacuum at 80°C: yield 85%; m.p. 260°C. Calculated for  $C_{23}H_{33}N_3O_5$ : C = 64.01%; H = 7.70%; N = 9.73%. Found: C = 63.94%; H = 7.65%; N = 9.71%.

The obtained polymer is insoluble in acetonitrile, dioxane, trifluoroethanol, dimethyl sulphoxide, dimethylformamide, benzene, trimethylphosphate and hexafluoroacetone sesquihydrate, swells in *m*-cresol and is soluble in chloroform and dichloroacetic acid.

Polymerization was also carried out in chloroform, using the same ratio active ester/initiator. The polymer showed identical properties and the same  $[\eta]$  as that obtained in dimethyl sulphoxide.

#### Determination of optical purity of the polymer

The optical purity of the polymer, as polyacid, was checked by hydrolysis with 5 N hydrochloric acid at 106°C for 72 h in degassed sealed tubes.

By comparison of the optical rotation of the amino acids obtained from the hydrolysed polymer, whose concentrations were determined from the amino acid analyser, with that of the corresponding amino acids treated in the same way, the optical purity was found to be  $93 \pm 2\%$ . In connection with this result it must be taken into account that acid hydrolysis can give *per se* some racemization<sup>4</sup> in the sample which probably was absent in the starting material.

In a typical duplicate determination of the optical purity, the optical rotation of the mixture of amino acids obtained from the hydrolysed polymer in 5 N hydrochloric acid was  $[\alpha]_{265.3}^{25} = 262.5$ , whereas that of leucine was  $[\alpha]_{265.3}^{25} = 316.5$  and that of aspartic acid was  $[\alpha]_{265.3}^{25} = 212.3$ .

### Methods of characterization

Viscosity measurements have been carried out in the conventional way (0.3% solutions at 25°C).

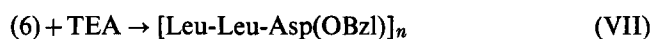
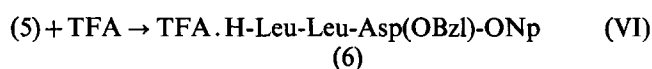
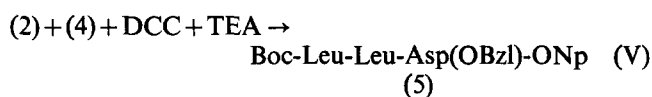
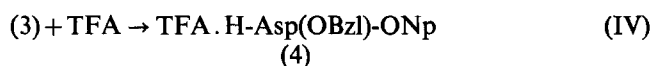
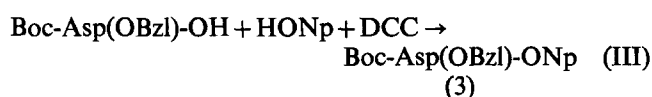
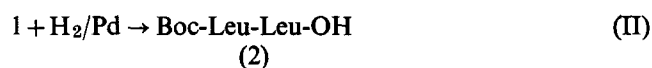
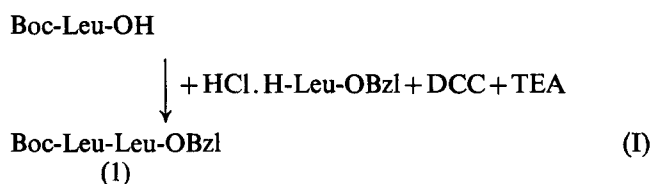
Optical rotatory dispersion curves were obtained using a Perkin-Elmer 141 M Spectropolarimeter at 25°C ( $c=0.2-0.3\%$ , in pure or mixed solvents).

Circular dichroism spectra were performed by a Cary 61 apparatus using 0.1 and 0.01 cm quartz cells.

Infra-red spectra were recorded by a Perkin-Elmer 157 or a Beckman I.R. 9 apparatus.

### RESULTS AND DISCUSSION

The synthesis of the tripeptide via the DCC method<sup>5, 6</sup> and of the corresponding polymer via the *p*-nitrophenylester<sup>7, 8</sup> is summarized in the following scheme:



The polymer so obtained shows a satisfactory optical purity and a high molecular weight, if compared with other sequential polypeptides<sup>9</sup>, as may be inferred from the data reported in *Table 1*. The results, as it may be clearly seen, are strictly dependent on the solvent.

The values of  $b_0$  shown in *Table 1* strongly indicate that the poly[Leu-Leu-Asp(OBzl)] exhibits an  $\alpha$ -helical con-

*Table 1* Properties of the tripeptide in various solvents

Solvent	$[\eta]^{25^\circ}$	$K'$	$b_0^{b,c}$	$[\theta]_{222} \times 10^{-3}^d$
Chloroform	5.3	0.47	-550	-47
Chloroform-dimethylformamide (0.5%)	2.89	1.2	—	-59.2
Chloroform-methylformamide (0.5%)	2.25	1.4	—	-55.2
Chloroform-formamide (0.5%)	2.04	0.69	-606	-45.6
Dichloroacetic acid <sup>a</sup>	0.69	—	-85	—

<sup>a</sup> Soon after dissolution.

<sup>b</sup> The optical rotatory dispersion in the range 589–302 nm.

<sup>c</sup> The refractive index at 589 nm has been used.

<sup>d</sup> The values are not corrected for the Lorentz factor.

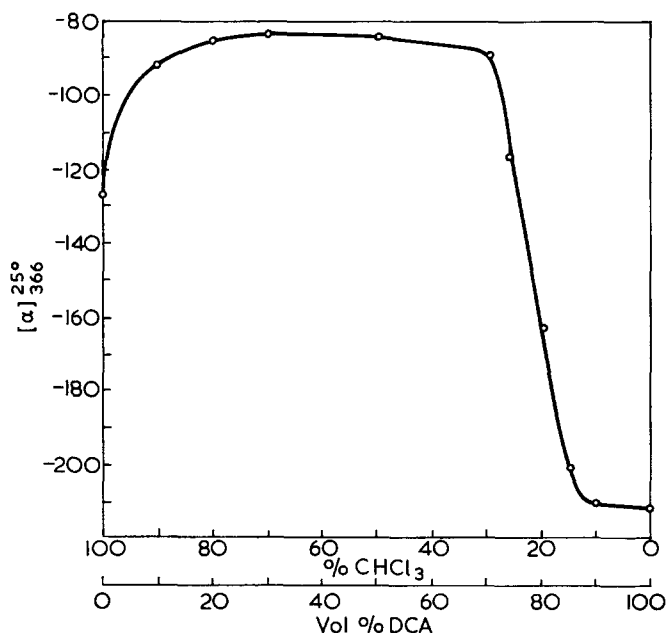


*Figure 1* Specific rotation,  $[\alpha]_{366}^{25}$  of poly[Leu-Leu-Asp(OBzl)], in chloroform-dichloroacetic acid solutions

formation in the presence of helicogenic solvents. These data are consistent with the results of circular dichroism spectra, which suggest a right handed  $\alpha$ -helical conformation in the polymer. From *Table 1* it may be noted that the poly[Leu-Leu-Asp(OBzl)] shows a very high intrinsic viscosity in chloroform. This fact may be accounted for by inter- and/or intra-molecular association phenomena, through the leucyl side-chains and aromatic-aromatic groups of the aspartyl-benzylester residues. However, the very low value of  $K'$  (the Huggins constant) suggests<sup>10</sup> that intramolecular interactions probably predominate.

The addition of a small amount of dimethylformamide, methylformamide or formamide in the chloroform solution, near their maximum solubility, gives rise to a remarkable decrease of the intrinsic viscosity.

Since the  $b_0$  and the ellipticity values do not show any substantial variation, upon such addition, the observed effect may be mainly ascribed to a change of the hydrodynamic behaviour of the macromolecule, rather than to conformational changes.

It is reasonable to consider in fact that the adsorption of the added solvents on the polymer through different types of polymer-solvent interactions, i.e. dipole-dipole interactions, hydrogen bond formations and/or screening of  $\pi$ - $\pi$  overlaps in the aromatic substituents by the solvent molecules, leads to a different array of the macromolecule in solution without any marked influence on the helical conformation.

An estimation of the stability of the poly[Leu-Leu-Asp(OBzl)]  $\alpha$ -helix in solution may be gained from *Figure 1*, where the dependence of  $[\alpha]_{366}^{25}$  on solvent composition, for mixtures of dichloroacetic acid and chloroform, is reported. A sharp change is observed at about 77% by vol. dichloroacetic acid, due to the helix random-coil transition.

This result strongly supports the idea that the  $\alpha$ -helix of the polymer investigated has a rather high stability<sup>11</sup>.

It seems reasonable to relate this property to the high content of leucine residues in an ordered array, together

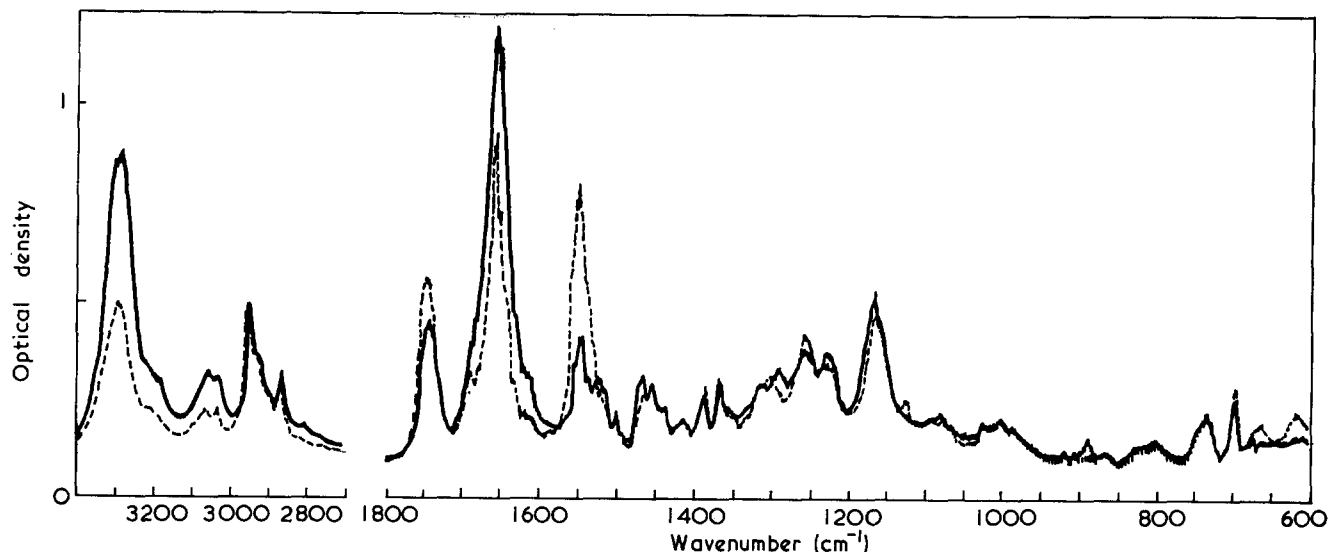


Figure 2 Polarized infra-red spectra of oriented film of poly[Leu-Leu-Asp(OBzl)]: (—) E vector parallel, (---) E vector perpendicular to the direction of orientation



Figure 3 X-ray diffraction pattern of film of poly[Leu-Leu-Asp(OBzl)], 5cm, flat camera

with a favourable arrangement of the phenyl groups capable to interact by  $\pi$ - $\pi$  overlaps.

Unfortunately, the very poor solubility of the poly[Leu-Leu-Asp(OBzl)] in solvents transparent below 220 nm made it impossible to extend the spectral investigation in the region of the amide Cotton effects.

Studies in the solid state clearly show that the polymer exhibits the  $\alpha$ -helical conformation. In fact i.r. investigations on an oriented film casted from chloroform (Figure 2) show that the amide A band at  $3300 \pm 2 \text{ cm}^{-1}$  and the amide I at  $1659 \pm 2 \text{ cm}^{-1}$  have a parallel dichroism, and the amide II at  $1553 \pm 2 \text{ cm}^{-1}$  is, consistently perpendicularly polarized. In addition the band relative to the side-

chain ester carbonyl groups ( $1744 \pm 2 \text{ cm}^{-1}$ ) shows a perpendicular dichroism.

Therefore<sup>12-15</sup> the poly[Leu-Leu-Asp(OBzl)] may be considered to be in  $\alpha$ -helical conformation.

Moreover, the X-ray diffraction pattern shows a high degree of crystallinity (Figure 3) that is a further support to the stereoregularity of the peptide sequences.

#### ACKNOWLEDGEMENT

This work has been sponsored by the Consiglio Nazionale delle Ricerche through the Istituto di Chimica delle Macromolecole, Milano.

#### REFERENCES

- 1 'Poly- $\alpha$ -aminoacids' (Ed. Fasman, G. D.), Marcel Dekker, New York, 1967
- 2 'Structure and Stability of Biological Macromolecules', (Eds Timasheff, S. N. and Fasman, G. D.), Marcel Dekker, New York, 1969
- 3 Carità Morelli, M. and D'Alagni, M. *Polymer* 1972, 13, in press
- 4 Bodanszky, M. and Ondetti, M. A. in 'Peptide Synthesis', (Ed. Olah, G. A.), Interscience, New York, 1966, p 154
- 5 Sheehan, J. C. and Hess, G. P. *J. Am. Chem. Soc.* 1955, 77, 1067
- 6 Khorana, H. G. *Chem. Ind.* 1955, p 1087
- 7 Goodman, M., Schmitt, E. E. and Yphantis, D. A. *J. Am. Chem. Soc.* 1962, 84, 1283
- 8 Stewart, F. H. C. *Aust. J. Chem.* 1964, 18, 887
- 9 De Los, F., De Tar, F., Fulton, F., Rogers, F. F. Jr. and Bach, H. *J. Am. Chem. Soc.* 1967, 89, 3039
- 10 Doty, P., Bradbury, J. H. and Holtzer, A. M. *J. Am. Chem. Soc.* 1956, 78, 947
- 11 'Poly- $\alpha$ -aminoacids' (Ed. Fasman, G. D.), Marcel Dekker, New York, 1967, Vol 1, p 514
- 12 Ambrose, E. J. and Elliott, A. *Proc. R. Soc.* 1951, A205, 47
- 13 Miyazawa, T., Fukuyshima, K., Sugano, S. and Masuda, Y. in 'Conformation of Biopolymers', (Ed. Ramachandran, G. N.), Academic Press, New York, 1967, Vol 2, p 557
- 14 Hashimoto, M. and Arakawa, S. *Bull. Chem. Soc. Japan* 1967, 40, 1698
- 15 Bradbury, E. M., Carpenter, B. G. and Stephens, R. M. *Biopolymers* 1968, 6, 905

# Crystallinity and crystallite size measurement in cellulose fibres: 1. Ramie and Fortisan\*

A. M. Hindeleh

*Department of Physics, University of Jordan, Amman, Jordan*

and D. J. Johnson

*Textile Physics Laboratory, Department of Textile Industries, University of Leeds, Leeds LS2 9JT, UK*

*(Received 21 February 1972; revised 25 May 1972)*

A new method for assessing crystallinity in cellulosic materials has been established after a rigorous computational analysis of X-ray diffraction traces from the highly crystalline fibrous forms of cellulose I and II, Ramie and Fortisan. The method involves resolution of the diffraction peaks into profiles which are part Gaussian ( $f$ ) and part Cauchy ( $1-f$ ); crystallinity is then a parameter dependent on  $f$ . A plot of the residual sum of squares gives a clear indication of the optimum  $f$  values, 0.7 for Ramie and 0.4 for Fortisan; in terms of the resolved profiles at these  $f$  values, Ramie has a crystallinity of 72% and Fortisan a crystallinity of 74%. Optimum crystallite sizes obtained from integral-breadth measurements are 53 Å for Ramie and 37 Å for Fortisan, and from peak-width measurements sizes are 64 Å for Ramie and 50 Å for Fortisan. The latter appear to overestimate the crystallite width when compared with fibrils observed in electron micrographs obtained at very high resolution with little phase-contrast enhancement; here electron-scattering units vary in width with mean values of around 50 Å for Ramie and 40 Å for Fortisan. There is no evidence for the concept that the elementary fibril in these celluloses is a discrete unit 35 Å in width.

## INTRODUCTION

Measurements of crystallinity and crystallite size in polymers and fibres have always been equivocal since they depend not only upon the experimental method employed but also upon the model of structure in vogue. Recent papers by Nieduszynski and Preston<sup>1</sup>, and Caulfield<sup>2</sup> have highlighted the controversy existing in the cellulose field especially with respect to crystallite width. Essentially the contention is that some workers report X-ray diffraction and electron microscope evidence for a fundamental fibrillar unit of cellulose in the 100 to 200 Å range, whereas another group, working mainly in electron microscopy, claim that elementary fibrils 35 Å in size are the fundamental unit. Since we have investigated methods for estimating both relative<sup>3</sup> and actual crystallinity<sup>4</sup> in cellulose triacetate, and since the latter method leads to accurate estimates of crystallite size, we decided to apply the method to the classical celluloses of high crystallinity, Ramie (cellulose I) and Fortisan (cellulose II). At the same time it was necessary to compare the results obtained from X-ray diffraction data with results obtained by high-resolution electron microscopy.

### *Crystallinity measurement by X-ray diffraction*

Although relative methods for assessing crystallinity, based upon the equivalence of the total X-ray scatter from standard specimens with maximum and minimum crystallinity, have been applied to cotton<sup>5</sup>, poly(ethylene

terephthalate)<sup>6</sup>, and cellulose triacetate<sup>3</sup>, it is not always possible to prepare standard specimens and consequently a method for estimating actual crystallinity is required. The classical procedure for crystallinity measurement assumes a two-phase crystalline-amorphous structure and involves drawing an arbitrary background to the diffraction trace, thus separating an arbitrary crystalline phase from an arbitrary amorphous phase. Because this method entirely neglects the overlap of adjacent diffraction maxima the amorphous, i.e. completely disordered, phase tends to be overestimated. In an attempt to account for the concept of lattice disorder or paracrystallinity, Ruland<sup>7</sup> has developed a method which involves a disorder function and integration over different intervals of the diffraction trace until a constant crystallinity is obtained. Ruland's method again requires the separation of peaks and background by drawing a line between the intensity minima and not surprisingly produces low values of crystallinity in polypropylene and polyamides, since paracrystalline distortions of the second kind<sup>8</sup> are precluded. Evidently we require a method which will account for both peak overlap and the effect of lattice distortion by means of procedures which fit suitable functions to the X-ray profile.

### *Crystallite size measurement by X-ray diffraction*

Since measurements of crystallite size are usually based upon peak broadening and require an estimate of the integral or peak breadth, valid measurements can only be made when interference peaks are resolved and separated from the background scatter. Clearly measurements made after the type of arbitrary separation dis-

\* A project supported in part by the Jordan Science Research Council, Amman.

cussed earlier must involve some error. Thus although Buchanan and Miller<sup>9</sup> have rigorously examined methods used to correct for experimental and distortion broadening, they again relied upon a graphical method for separating the diffraction peaks.

A method of profile fitting in terms of Cauchy functions has been carried out for celluloses<sup>10</sup>; more recently, with the aid of electronic computation, Cauchy and Gaussian functions have been fitted to the diffraction traces of silk<sup>11</sup> and nylon<sup>12</sup>. Although these methods were an advance on the earlier graphical methods they usually assume a background of straight-line form. We have developed a program which fits a designated function to the diffraction peaks and a polynomial function to the background; the overall fit is improved in an iterative process which commences by assuming zero-value parameters for the background<sup>13</sup>. We have reported the use of this program on cellulose triacetate<sup>4</sup>, a fibre with a very complex diffraction pattern; here the celluloses Ramie and Fortisan have much simpler patterns and the type of function used for each diffraction profile can be varied more easily. Since the peak-resolution procedure yields a mathematically fitted background, the area under the profiles serves as a measure of crystallinity which will be a parameter dependent upon the function chosen for the interference peaks.

#### Crystallite size measurement by electron microscopy

Compared with the problems involved in the correction of X-ray diffraction data, it might be thought that the interpretation of measurements from electron microscope images would be straightforward. Even if we consider a purely geometrical concept of image formation there is always the possibility that overlapping structures will lead to a size measurement only a fraction of the true value<sup>14</sup>, however, of greater fundamental importance is the effect of defocusing phase contrast, which gives enhanced contrast for a repeat  $r$  at a defocus  $\Delta f$  given by  $\Delta f = r^2/2\lambda$ , where  $\lambda$  is the electron wavelength and  $r$  is greater than 10 Å. These defocus effects have been shown to give rise to spurious periodic structures in negatively stained microfibrils<sup>15</sup>; in particular Fortisan fibrils at  $\Delta f = +2.5 \mu\text{m}$  give a phase contrast repeat of 45 Å, and hence appear to be composed of elementary units 35 Å wide with negative stain between them<sup>16</sup>. A more acceptable image at  $\Delta f = 0$  showed fibrils in the range 18 to 70 Å.

In general, phase-contrast images have much better contrast than images taken near to true focus, which have amplitude contrast only; it seems very likely that since phase-contrast images were chosen for measurement purposes by earlier workers, this might explain why the reported size of the fundamental fibril in cellulose fibres has diminished over the years as the resolving power of the electron microscope has improved. For the purpose of this investigation the only images regarded as valid for measurement purposes are those where the defocus enhances a repeat approximately one-quarter of the size measurement to be made.

#### EXPERIMENTAL

The Ramie fibres used in the experiment had been degummed and decorticated then boiled in 2% NaOH for 72 h; Fortisan fibres were extracted successively in

distilled water and ether. For electron microscope examination specimens were cut into short lengths and then dispersed by ultrasonic irradiation for periods of about 24 h; specimens were placed on carbon-coated grids, stained with uranyl formate, and examined in a Philips EM300 at a wide range of magnifications; specimen contamination was reduced by the use of an anticontamination trap.

Equatorial X-ray diffraction traces were recorded with a modified Hilger and Watts Y115 diffractometer and a Y90 constant-output generator; the diffractometer employs a scintillation counter whose output can be fed through a single-channel pulse-height analyser to a counter or, via a ratemeter, to a chart recorder. Corrections to the diffraction traces were made for air scatter, polarization, Lorentz factor and Compton scatter; they were then normalized to a convenient standard area. Corrected data for the three peaks in the range 2 to 30° (2θ) were analysed by the resolution program described earlier which fits the envelope to a function of the form:

$$Y = \sum_{i=1}^3 Q_i + R$$

where

$$Q_i = f A_i \exp \left\{ - \ln 2 \left( \frac{2(X - P_i)}{W_i} \right)^2 \right\} + (1 - f) A_i / 1 + \{ 2(X - P_i) / W_i \}^2$$

and

$$R = a' + b'X + c'X^2 + d'X^3$$

The peaks are defined by the parameters  $A_i$  the peak height,  $P_i$  the peak position, and  $W_i$  the width of the peak at half height; the background is defined by the parameters  $a'$ ,  $b'$ ,  $c'$ , and  $d'$ . For  $f=0$  we have a Cauchy distribution, and for  $f=1$  we have a Gaussian distribution. A detailed study by Warren<sup>17</sup> suggests that the size broadening component is of a Cauchy form and the distortion broadening of a Gaussian form. Here the profiles were resolved for  $f$  varying between 0 and 1; in each case the program outputs the best estimate of the peak and background parameters, the limiting sum of squares  $S$  between observed and calculated  $Y$  values, and the areas under the peaks and background. The combined area under the peaks expressed as a percentage of total area is also output; this is our measure of crystallinity.

In order to correct for line broadening due to the experimental conditions the diffraction trace from crystals of hexamethylenetetramine compacted at 85°C was recorded. The line breadths can be corrected by the approximations for the deconvolution procedure discussed by Jones<sup>18</sup>; they are:

$$\beta^2 = B^2 - b^2 \quad (\text{Gaussian})$$

and

$$\beta = B - b \quad (\text{Cauchy})$$

where  $\beta$  is the corrected breadth,  $B$  the observed breadth and  $b$  the instrumental breadth. Although it is often convenient to work in terms of peak width as defined by  $W_i$ , it is more correct to use the integral breadth, that is the area of the peak divided by  $A_i$ . When  $f$  lies between



0 and 1 we have also used the correction:

$$\beta = f(B^2 - b^2)^{1/2} + (1-f)(B-b)$$

In addition we have extracted the corrected profile by the Fourier transform method of Stokes<sup>19</sup> using the main peak from hexamethylenetetramine as the instrumental-broadening profile.

Low angle X-ray photographs of dry fibre specimens were recorded in a Luzatti-Baro type camera (Beaudouin) incorporating a double curved-crystal monochromator. Traces from photographs of rotated specimens were obtained by means of a Joyce-Loebl microdensitometer.

## RESULTS

### Crystallinity measurement by X-ray diffraction

Computed values of  $A$  the peak height,  $P$  the peak position, and  $W$  the peak width at half-height, are given for Ramie in Table 1 and for Fortisan in Table 2. Crystallinity, the total area under the peaks evaluated as a percentage, is given under  $C$ , the background area is under  $B$ . Peak profiles computed from the data in Tables 1 and 2, together with the background trace and the experimental envelope, are given in Figures 1 and 2. It is immediately apparent that the Cauchy function ( $f=0$ ) underestimates the background, especially for Ramie, and that the Gaussian function ( $f=1$ ) overestimates the background; this is a consequence of the longer tails of the Cauchy function.

In order to make a choice of the most appropriate  $f$  values, we must consider the operation of the peak-resolution program in more detail. This program modifies the peak and background parameters until a limiting sum of squares  $S$  is reached between the observed and calculated  $Y$  values, a process which involves around 1200 calculations. These  $S$  values have been plotted against  $f$  in Figure 3, and it can be seen that the points lie on smooth curves with well-defined minima around  $f=0.7$  for Ramie and  $f=0.4$  for Fortisan. These figures may be assumed to be the optimum or 'best-fit'  $f$  values for the particular samples under investigation. The  $C$  values, which are our measure of crystallinity by this method, are also plotted against  $f$  in Figure 3. From the minima on the  $S$  curves it is thus possible to obtain the 'best-fit'  $C$  values; these are 72% for Ramie and 74% for Fortisan.

A test run on the data from Ramie at  $f=0.7$ , and from Fortisan at  $f=0.4$  gave values of  $S$  and  $C$  close to those anticipated from the data in Figure 3. The values of  $S$  at the 'best-fit' of  $f$  correspond to relative error in the data points of 3.3 and 3.5% for Ramie and Fortisan, respectively.

### Crystallite width measurement by X-ray diffraction

Weight-average crystallite size measurements  $L(hkl)$  are given in Tables 3 and 4 as evaluated by the usual Scherrer equation:

$$L(hkl) = \frac{1}{\beta} = K\lambda / \cos\theta d(2\theta)$$

where  $K=1$  and  $d(2\theta)$  can be either the width of the peak, or more correctly, the integral breadth. Values of crystallite size normal to the diffracting planes ( $hkl$ ) are tabulated in terms of both the peak width ( $Lw$ ) and the integral breadth ( $Li$ ). These are uncorrected values but

Table 1 Resolved peak parameters and crystallinity for Ramie

$f$	Peak	$A$	$P$	$W$	$C$ (%)	$B$ (%)
0	101	21.3	14.6	2.01	107.4	-7.4
	10 $\bar{1}$	19.8	16.2	1.85		
	002	69.7	22.4	1.72		
0.1	101	21.3	14.6	1.98	101.1	-1.1
	10 $\bar{1}$	19.4	16.2	1.77		
	002	68.5	22.4	1.70		
0.2	101	21.2	14.6	1.96	95.3	4.7
	10 $\bar{1}$	19.0	16.2	1.69		
	002	67.3	22.4	1.69		
0.3	101	21.2	14.6	1.94	90.1	9.9
	10 $\bar{1}$	18.7	16.3	1.63		
	002	66.2	22.4	1.68		
0.5	101	21.1	14.6	1.92	80.6	19.4
	10 $\bar{1}$	18.0	16.3	1.52		
	002	64.1	22.4	1.67		
0.8	101	20.7	14.7	1.91	68.2	31.8
	10 $\bar{1}$	17.1	16.3	1.40		
	002	61.1	22.4	1.66		
1.0	101	20.4	14.7	1.92	60.9	39.1
	10 $\bar{1}$	16.5	16.3	1.33		
	002	59.2	22.4	1.66		

$f$ =function parameter for peak profile;  $A$ =peak height (arbitrary units);  $P$ =peak position ( $2\theta^\circ$ );  $W$ =peak width ( $2\theta^\circ$ );  $C$ =crystallinity, i.e. area under peaks;  $B$ =area under background

Table 2 Resolved peak parameters and crystallinity for Fortisan

$f$	Peak	$A$	$P$	$W$	$C$ (%)	$B$ (%)
0	101	9.1	11.6	1.99	88.8	11.2
	10 $\bar{1}$	39.2	19.5	1.92		
	002	39.7	21.5	1.83		
0.2	101	8.6	11.6	1.88	81.2	18.8
	10 $\bar{1}$	38.9	19.5	1.89		
	002	39.4	21.5	1.80		
0.3	101	8.4	11.6	1.84	77.7	22.5
	10 $\bar{1}$	38.8	19.5	1.88		
	002	39.2	21.5	1.79		
0.5	101	8.0	11.6	1.78	71.2	28.8
	10 $\bar{1}$	38.5	19.5	1.87		
	002	38.9	21.5	1.77		
0.8	101	7.5	11.6	1.72	62.2	37.8
	10 $\bar{1}$	38.1	19.5	1.85		
	002	38.4	21.5	1.75		
1.0	101	7.2	11.6	1.69	56.6	43.4
	10 $\bar{1}$	37.2	19.5	1.85		
	002	38.1	21.6	1.74		

$f$ =function parameter for peak profile;  $A$ =peak height (arbitrary units);  $P$ =peak position ( $2\theta^\circ$ );  $W$ =peak width ( $2\theta^\circ$ );  $C$ =crystallinity, i.e. area under peaks;  $B$ =area under background

it is evident that for Ramie  $Li(10\bar{1}) > Li(101)$  and that the crystallites are roughly tablet-shaped in cross-section; this confirms the evidence of Mukherjee *et al.*<sup>20</sup> that the (101) planes are parallel to the largest face of the section [the (101) and (10 $\bar{1}$ ) planes are approximately perpendicular]. In Fortisan  $Li(101) = Li(10\bar{1})$  and the crystallites appear to be square in cross-section.

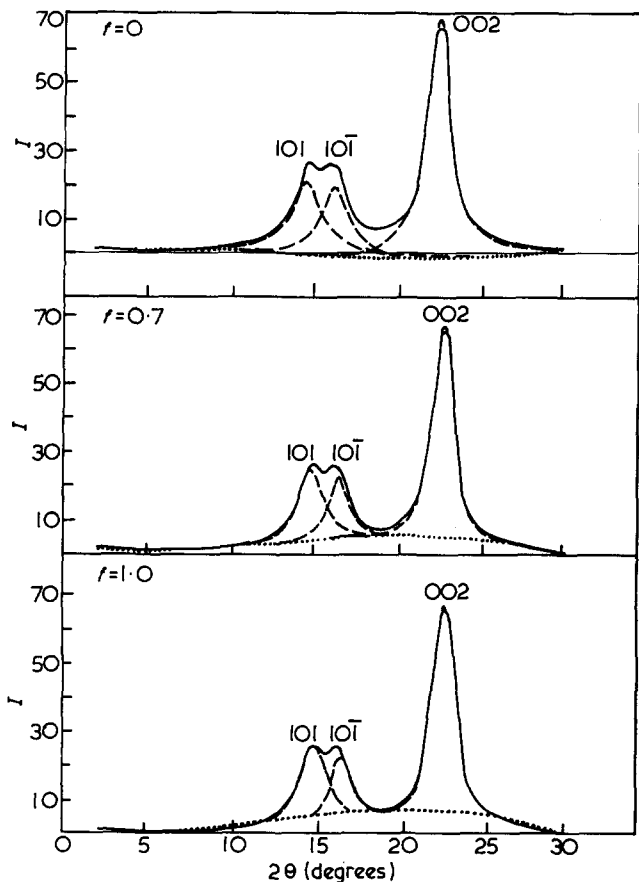


Figure 1 Peak resolution for Ramie. —, Experimental diffraction trace; ----, resolved peak profiles; ..... , computed background. (a)  $f=0$ , Cauchy profiles; (b)  $f=0.7$ , 0.7 Gaussian/0.3 Cauchy; (c)  $f=1$ , Gaussian profiles

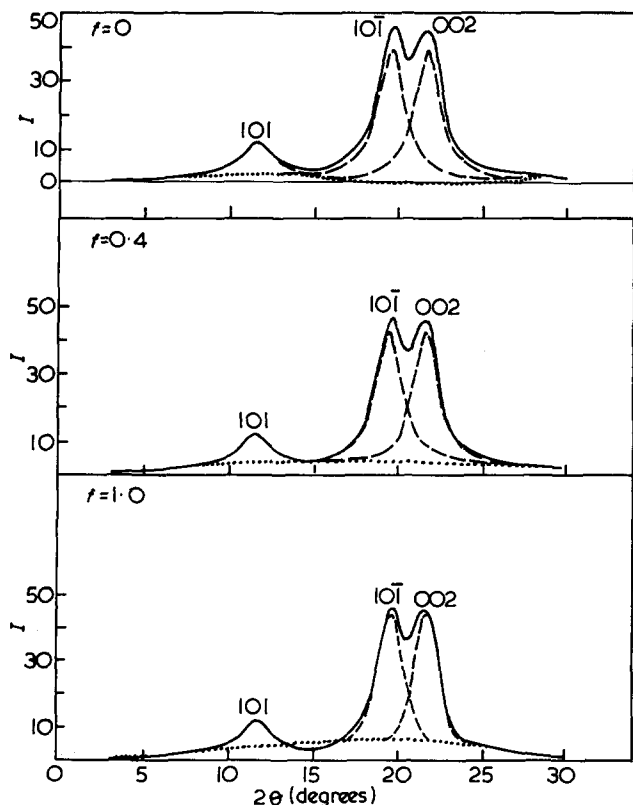


Figure 2 Peak resolution for Fortisan. —, Experimental diffraction trace; ----, resolved peak profiles; ..... , computed background. (a)  $f=0$ , Cauchy profiles; (b)  $f=0.4$ , 0.4 Gaussian/0.6 Cauchy; (c)  $f=1$ , Gaussian profiles

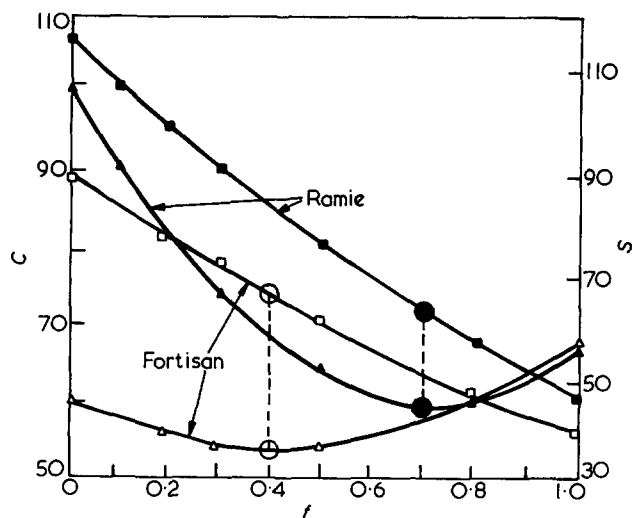


Figure 3 Crystallinity  $C$  and least sum of squares  $S$ , against the function parameter  $f$  for Ramie (solid symbols) and Fortisan (open symbols). The minimum  $S$  value gives the 'best-fit' estimate of crystallinity

Table 3 Crystallite size parameters ( $\text{\AA}$ ) for Ramie

$f$	Peak	$L_w$	$L_{wj}$	$L_{ws}$	$L_i$	$L_{ij}$	$L_{is}$
0	101	44.3	47.1	45.6	29.5	30.8	31.8
	101̄	48.2	51.6	49.8	32.1	33.5	34.4
0.2	101	45.5	47.8	46.7	32.2	33.3	34.6
	101̄	52.7	55.9	54.4	37.1	38.7	39.7
0.5	101	46.5	48.1	47.1	36.3	37.2	38.7
	101̄	58.7	61.2	60.3	45.4	46.9	48.1
0.7	101	46.5	47.6	47.2	39.2	39.9	41.0
	101̄	62.1	63.8	65.7	51.9	53.1	54.6
1.0	101	46.5	46.6	47.4	43.6	43.7	45.9
	101̄	66.9	67.2	68.6	63.1	63.3	66.6

$f$ =function parameter for peak profile;  $L_w$ =crystallite size from peak widths;  $L_{wj}$ = $L_w$  corrected by the Jones approximation;  $L_{ws}$ = $L_w$  corrected by the Stokes deconvolution procedure;  $L_i$ =crystallite size from integral breadths;  $L_{ij}$ = $L_i$  corrected by the Jones approximation;  $L_{is}$ = $L_i$  corrected by the Stokes deconvolution procedure

Table 4 Crystallite size parameters ( $\text{\AA}$ ) for Fortisan

$f$	Peak	$L_w$	$L_{wj}$	$L_{ws}$	$L_i$	$L_{ij}$	$L_{is}$
0	101	44.7	47.6	47.2	30.0	31.3	32.8
	101̄	46.8	50.0	48.2	31.4	32.8	33.1
0.2	101	47.3	49.9	48.6	33.5	34.8	35.9
	101̄	47.4	50.0	48.7	33.3	34.5	35.3
0.4	101	49.1	51.3	49.9	37.2	38.4	39.6
	101̄	47.8	49.8	49.0	36.2	37.3	38.1
0.8	101	51.7	52.5	52.8	45.0	45.6	46.6
	101̄	48.3	49.1	49.3	42.0	42.6	43.6
1.0	101	52.5	52.6	53.5	49.6	49.7	51.3
	101̄	48.5	48.6	49.2	44.9	45.0	46.3

$f$ =function parameter for peak profile;  $L_w$ =crystallite size from peak widths;  $L_{wj}$ = $L_w$  corrected by the Jones approximation;  $L_{ws}$ = $L_w$  corrected by the Stokes deconvolution procedure;  $L_i$ =crystallite size from integral breadths;  $L_{ij}$ = $L_i$  corrected by the Jones approximation;  $L_{is}$ = $L_i$  corrected by the Stokes deconvolution procedure

Although the Cauchy function has much larger tails than the Gaussian function, both have similar widths at half-maximum intensity for any particular peak, consequently there is only a small increase in  $Lw$  as  $f$  increases from 0 to 1. However, there is a pronounced increase in  $Li$  since the integral breadth takes into account the considerably greater area in the Cauchy profiles. If we consider the width of the  $10\bar{1}$  reflection alone, it is evident that the lowest uncorrected estimate of crystallite size would be 32 Å in Ramie and 31 Å in Fortisan ( $Li$  at  $f=0$ ); the highest estimate would be 67 Å in Ramie and 48 Å in Fortisan ( $Lw$  at  $f=1$ ). All the estimates of crystallite size are increased slightly on application of the corrections for instrumental broadening. Tables 3 and 4 therefore include size values based on peak-width and integral breadth data corrected by the Jones approximations ( $Lwj$  and  $Lij$  respectively), and by the full Stokes method ( $Lws$  and  $Lis$  respectively). The value of the instrumental breadth used for these corrections was  $0.12^\circ$  which gave an integral breadth of  $0.104^\circ$ .

The best estimates of crystallite size in Ramie will be the corrected values of the width normal to  $(10\bar{1})$  at the 'best-fit'  $f$  value of 0.7; these are  $Lwj=63.8$  Å,  $Lws=65.7$  Å,  $Lij=53.1$  Å, and  $Lis=54.6$  Å. Similar estimates for the width normal to  $(10\bar{1})$  in Fortisan at  $f=0.4$  are  $Lwj=49.8$  Å,  $Lws=49.0$  Å,  $Lij=37.3$  Å, and  $Lis=38.1$  Å. The Stokes correction should give the most accurate values since it operates on the whole profile; here the resolved profiles are necessarily symmetrical and the results of the simpler Jones corrections are always within 3% of the Stokes corrections. Perhaps the most important result is that use of the peak width instead of the integral breadth will always lead to relatively high values of crystallite size unless the  $K$  parameter in the Scherrer equation is adjusted. Here  $K$  would vary from about 0.65 to 0.95 for equivalence of  $Lw$  with  $Li$ , values which can be compared with Warren's estimate of  $K$  for peak width (0.89) assuming a Gaussian shape for the peak profile<sup>28</sup>. We may note, however, that distortions in the crystals will lead to further broadening of the diffraction peaks and hence an increase in the true crystallite size; unfortunately methods for the correction of distortion broadening are not practicable in this case since we cannot distinguish more than one order of reflection in the diffraction trace.

So far we have concentrated on the usual 'weight-average' crystallite size; the Stokes deconvolution procedure evaluates Fourier coefficients which can be used to provide information about the 'number-average' crystallite size, a parameter often derived in metallurgical analyses. Normalized Fourier coefficients obtained from the Stokes procedure are plotted in Figure 4 against the harmonic number  $t$  for the  $10\bar{1}$  peaks of Ramie resolved at  $f=0$ , 0.5, and 1.0. The Gaussian resolution ( $f=1$ ) gives a profile starting with the shape of the error curve and is considered by Warren and Averbach<sup>21</sup> to be an indication of the lattice distortion; the Cauchy function has a finite initial slope which is usually considered to be a measure of the 'number-average' crystallite size. From Figure 4, following Warren and Averbach's procedure, the straight line parts of the curves, give 'number-average' crystallite sizes which range from 36 Å at  $f=0$  to 54 Å at  $f=1$ ; these values compare favourably with the 'weight-average' crystallite sizes obtained from integral breadths. A similar analysis of Fortisan gave a 'number-average' crystallite size of 36 Å for both  $f=0$

and  $f=1$ , again comparable with 'weight-average' values obtained from integral breadths.

This Fourier transform approach suggests that the 'best-fit'  $f$  value for peak resolution could be considered as a measure of lattice distortion. When the hexamethylenetetramine peak is used as the instrumental-broadening standard, it might be expected that it would show negligible size or distortion broadening. In fact a subsidiary program determined the 'best-fit'  $f$  value as 0.725, a figure which must be a function of the collimator geometry in the diffractometer. Consequently we may assume that an analysis of peak profiles in fibrous specimens can give no useful information on lattice distortion. A similar conclusion was reached by Mitra<sup>22</sup> after an analysis of peak profiles from metallurgical specimens.

Finally in this section, we may note that there are no discrete interferences in the small-angle diffraction patterns of Ramie or Fortisan, hence no evidence for a unique elementary unit of structure. From Guinier plots of  $\log I$  against  $\theta^2$  the average size of scattering units can be estimated as 47 Å in Ramie and 42.5 Å in Fortisan. The results of Baltá-Calleja reported by Peterlin and Ingram<sup>23</sup> give a value of 55 Å for Ramie using the same method. The validity and interpretation of this method seems open to question but, after a more rigorous analysis, Heyn<sup>24</sup> found a value of 45 Å for Fortisan. Our low-angle estimates are of the same order of magnitude as those found by high-angle techniques, but the latter, despite their dependence on the form of the peak profile, must be considered the more reliable.

#### Electron microscopy

A general view of typical negatively stained Ramie fibrils is given in Figure 5a; there is a considerable overlap of fibrils in each ribbon but no evidence of single units greater than 65 Å in width. A ribbon composed of three individual fibrils is marked, the overall width is about 135 Å so that the average fibril width is 45 Å. Part of this ribbon is seen in greater detail in Figure 5b which was recorded at a higher magnification than Figure 5a. Both images making up Figure 5 are very close to focus and have little phase contrast. The variable width of the three fibrils in Figure 5b is evident, the individual fibril widths at the point indicated are 16 Å, 28 Å and 37 Å.

Without negative staining no fine structure can be seen in the ribbons, but with light staining we have the situation illustrated in Figure 6. Figure 6a, recorded at an instrumental magnification of  $\times 30\ 000$ , has phase contrast enhancing a repeat of about 35 Å ( $\Delta f \approx 1.5 \mu\text{m}$ ). Figure 6b, recorded at an instrumental magnification of  $\times 116\ 000$  has slight phase contrast enhancing a repeat of 7 Å ( $\Delta f \approx 0.8 \mu\text{m}$ ). Figure 6a gives very marked indication of a 35 Å repeating fibrillar unit because of the phase-contrast enhancement; however, in the more acceptable image, Figure 6b, a regular 35 Å repeat is not indicated and fibrils can be measured in the size range 30 to 75 Å.

A fibrillar ribbon with a considerable amount of stain is depicted in Figure 7a, recorded at  $\times 30\ 000$ , and in Figure 7b, recorded at  $\times 168\ 000$ . There is again phase contrast in Figure 7a to enhance a 30 Å repeat which is evident in the fibrils, the negative stain, and the supporting membrane. In the high-resolution image of Figure 7b there is almost no phase structure in

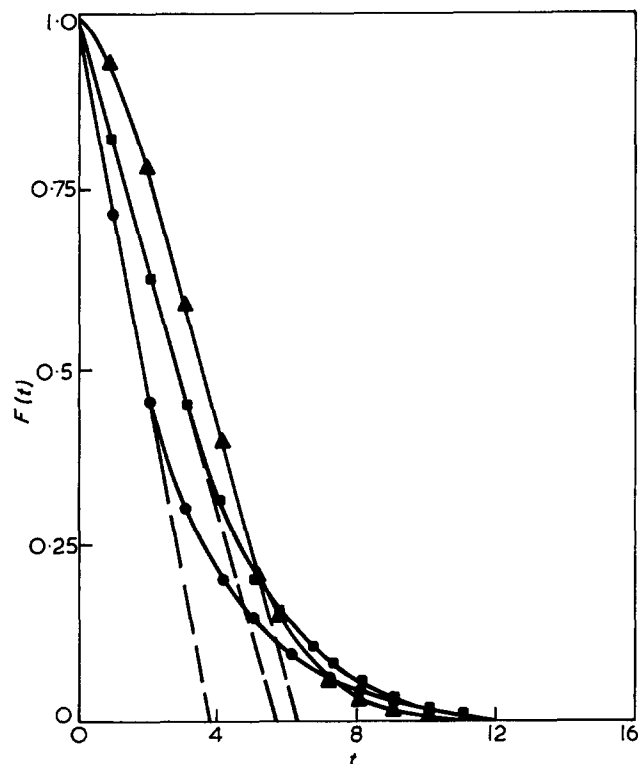


Figure 4 Normalized Fourier coefficients  $F(t)$  against the harmonic number  $t$  for the  $10\bar{1}$  peaks of Ramie at  $f=0$  (●),  $0.5$  (■) and  $1.0$  (▲)



Figure 5 Ramie dispersed by ultrasonic irradiation and negatively stained with uranyl formate; (a)  $\times 100\,000$ ; (b)  $\times 435\,000$

the fibrils or in the negative stain and the image is very close to true focus. At the point indicated by the arrow we have one fibril about  $60\text{ \AA}$  in width in the high resolution image and two 'fibrils'  $30\text{ \AA}$  in width in the phase-contrast image. The fibril is probably embedded in stain in this region so that the spurious periodicities can be anticipated by the phase contrast mechanism and are in fact seen over the entire micrograph of which Figure 7a is a part.

The danger of interpreting images taken at low magnification with phase-contrast enhancement is clearly illustrated. There is no doubt that in high-resolution images of Ramie, fibril widths can be measured in the range  $16$  to  $75\text{ \AA}$ ; however, there is no evidence for regular  $35\text{ \AA}$  elementary fibrils and although an average size of  $45$ – $50\text{ \AA}$  can be considered reasonable in the light of the above evidence, there is no suggestion that there is a well defined unit of exactly this dimension in Ramie. A similar analysis of Fortisan has already been made with micrographs illustrating phase contrast effects<sup>15</sup>. Again there was no evidence of regular elementary fibrils and Fortisan fibril widths were measured in the range  $18$  to  $70\text{ \AA}$  although there is an overall tendency for the fibrils to be slightly smaller than in Ramie.

#### DISCUSSION

We have shown that the best mathematical function for resolving the three main peaks in Ramie is  $0.7$  Gaussian and  $0.3$  Cauchy ( $f=0.7$ ), and for Fortisan is  $0.4$  Gaussian and  $0.6$  Cauchy ( $f=0.4$ ). The crystallinity of Ramie at  $f=0.7$  is found to be  $72\%$ , and for Fortisan at  $f=0.4$  is found to be  $74\%$ . Figure 3 clearly demonstrates that crystallinity as measured by this method is a parameter depending upon the function fitted to the peak profiles; nevertheless the 'best fit' is precisely determined and we believe that these crystallinity figures are based on a sound mathematical analysis which may be considered as a new method for determining this parameter. We may also point out that the best  $f$  value will probably vary for different specimens and for the same material examined under different experimental conditions.

The crystallinity value of  $72\%$  for Ramie agrees well with the infra-red measurement of Knight *et al.*<sup>25</sup>, and with the X-ray measurement of Smith *et al.*<sup>26</sup>, although this was made by an arbitrary method. The latter workers have obtained a figure of only  $39\%$  for Fortisan by the X-ray method, and a figure of  $58\%$  from an infra-red method. In contrast Kraessig and Kitchen<sup>27</sup> have obtained a crystallinity of  $82\%$  using a relative method. Our 'best-fit' value of  $74\%$  falls between the extremes of  $56.6$  and  $88.2\%$  obtained with the Gaussian and Cauchy functions used in the analysis.

If we concentrate on corrected 'best-fit' values of 'weight-average' crystallite size, we find that for Ramie the width normal to  $10\bar{1}$  is  $64\text{ \AA}$  from the resolved peak width and  $53\text{ \AA}$  from the resolved integral breadth; similar sizes for Fortisan are  $50\text{ \AA}$  and  $37\text{ \AA}$  respectively. Although we have seen that electron microscope images of the two specimens rarely differentiate single fibrillar entities in the interwoven fibrillar bundles, average widths are in the range  $45\text{ \AA}$  to  $50\text{ \AA}$  for Ramie and  $35\text{ \AA}$  to  $40\text{ \AA}$  for Fortisan. These values are in much greater agreement with X-ray diffraction data obtained from integral breadths than from peak widths; we may

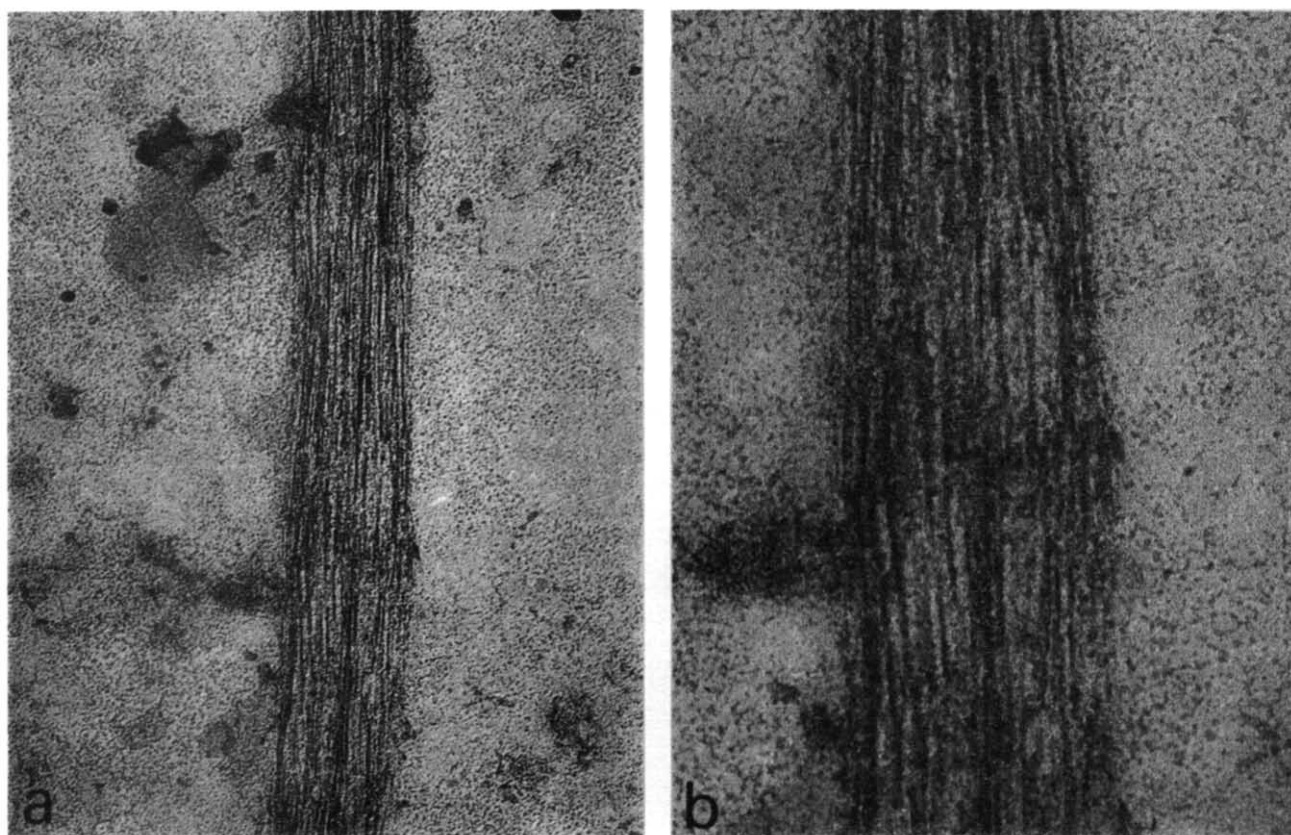


Figure 6 Ramie dispersed by ultrasonic irradiation and negatively stained with uranyl formate; (a)  $\times 150\,000$ ; (b)  $\times 350\,000$

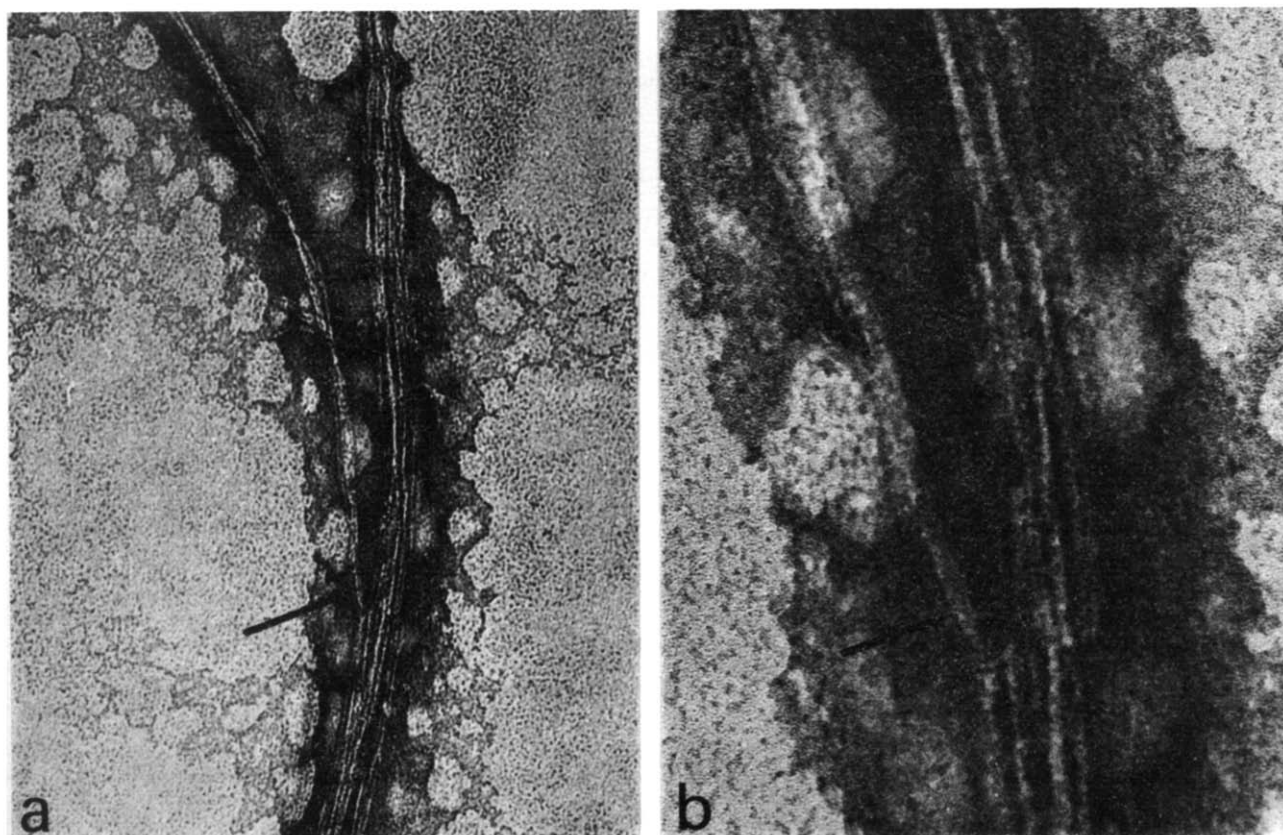


Figure 7 Ramie dispersed by ultrasonic irradiation and negatively stained with uranyl formate; (a)  $\times 150\,000$ ; (b)  $\times 500\,000$

therefore conclude that only size values obtained from integral breadths are valid. Certainly the effect of ignoring the tails of the peak profiles is to give inordinately high crystallite size values; for example, the size normal to  $10\bar{1}$  in Ramie at  $f=1$  is 67 Å from the peak width, and 33.5 Å at  $f=0$  from the integral breadth.

We conclude that the best estimates of average crystallite size are around 50 Å in Ramie and 40 Å in Fortisan; nevertheless the electron microscope evidence points to the existence of a variation in size over the range 20 to 70 Å. We have no evidence for the existence of a discrete 35 Å fundamental unit of structure nor is there any evidence in these specimens for organization at the 100 to 200 Å level.

#### REFERENCES

- 1 Nieduszynski, I. and Preston, R. D. *Nature* 1970, **225**, 273
- 2 Caulfield, D. F. *Text. Res. J.* 1971, **41**, 267
- 3 Hindeleh, A. M. and Johnson, D. J. *Polymer* 1970, **11**, 666
- 4 Hindeleh, A. M. and Johnson, D. J. *Polymer* 1972, **13**, 27
- 5 Wakelin, J. H., Virgin, H. S. and Crystal, E. *J. Appl. Phys.* 1959, **30**, 1654
- 6 Statton, W. O. *J. Appl. Polym. Sci.* 1963, **7**, 803
- 7 Ruland, W. *Acta Cryst.* 1961, **14**, 1180
- 8 Hosemann, R. and Bagchi, S. N. 'Direct Analysis of Diffraction by Matter', North Holland Publishing Co., Amsterdam, 1962, p 656
- 9 Buchanan, D. R. and Miller, R. L. *J. Appl. Phys.* 1966, **37**, 4003
- 10 Gjonnes, J., Norman, N. and Viervoll, H. *Acta Chem. Scand.* 1958, **12**, 489
- 11 Fraser, R. D. B. and Suzuki, E. *Anal. Chem.* 1966, **38**, 1770
- 12 Warwicker, J. O. *J. Soc. Dyers Colour.* 1970, **86**, 303
- 13 Hindeleh, A. M. and Johnson, D. J. *J. Phys. (D: Appl. Phys.)* 1971, **4**, 259
- 14 Preston, R. D. *J. Microsc.* 1971, **93**, 7
- 15 Johnson, D. J. *J. R. Microsc. Soc.* 1968, **88**, 39
- 16 Johnson, D. J. *Proc. 4th Eur. Conf. Electron Microsc., Rome* 1968, p 101
- 17 Warren, B. E. *Progr. Metal Phys.* 1959, **8**, 147
- 18 Jones, F. W. *Proc. R. Soc.* 1938, **A166**, 16
- 19 Stokes, A. R. *Proc. Phys. Soc.* 1948, **A61**, 382
- 20 Mukherjee, S. M., Sikorski, J. and Woods, H. J. *Nature* 1951, **167**, 821
- 21 Warren, B. E. and Averbach, B. L. *J. Appl. Phys.* 1950, **21**, 595
- 22 Mitra, G. B. *Br. J. Appl. Phys.* 1965, **16**, 77
- 23 Peterlin, A. and Ingram, P. *Text. Res. J.* 1970, **40**, 345
- 24 Heyn, A. N. *J. Appl. Phys.* 1955, **26**, 1113
- 25 Knight, J. A., Hicks, H. L. and Stephens, K. W. *Text. Res. J.* 1969, **39**, 324
- 26 Smith, J. K., Kitchen, W. and Mutton, D. B. *J. Polym. Sci. (C)* 1963, **2**, 499
- 27 Kraessig, H. and Kitchen, W. *J. Polym. Sci.* 1961, **51**, 123
- 28 Warren, B. E. 'X-Ray Diffraction', Addison Wesley, Reading, Mass., 1969, p 254

# Spin-lattice relaxation in substituted polysiloxanes

J. A. Barrie, M. J. Fredrickson\* and R. Sheppard

Physical Chemistry Department, Imperial College of Science and Technology,  
London SW7 2AY, UK  
(Received 11 February 1972)

Spin-lattice relaxation time ( $T_1$ ) measurements have been made over wide ranges of temperature for polydimethylsiloxane (DMS), polyphenylmethylsiloxane (PMS) and poly(3,3,3-trifluoropropylmethylsiloxane) (FMS) gums and an FMS oil. For all polymers two  $T_1$  minima were observed. Activation energies  $E_{T_1}$  of DMS, PMS and FMS were obtained for the high temperature process reflecting the effect of the bulky substituents on the segmental motion.  $T_1$  measurements were also made over a wide range of dilution for the same polymers in several solvents. For DMS both  $T_1$  and  $E_{T_1}$  were little affected by dilution over a wide range. For PMS and FMS,  $T_1$  increased steadily and  $E_{T_1}$  decreased on dilution. Long range (intersegmental) interactions do not appear to play a dominant role in the change of  $T_1$  with concentration.

## INTRODUCTION

The measurement of spin-lattice relaxation times ( $T_1$ ) in studies of molecular motion in polymer systems is well established and has been reviewed in some detail<sup>1-3</sup>. In this paper  $T_1$  measurements are reported for a polydimethylsiloxane gum (DMS), a polyphenylmethylsiloxane gum (PMS), a poly(3,3,3-trifluoropropylmethylsiloxane) gum (FMS) and a low molecular weight FMS oil. The DMS polymer has been studied previously in some detail<sup>4-7</sup> and a comparison with the PMS and FMS polymers is of interest. For the fluoro polymers both <sup>1</sup>H and <sup>19</sup>F resonances were employed.

Although  $T_1$  measurements have been made on a number of polymer-solvent systems<sup>8-10</sup>, by comparison they have not been investigated as extensively. The systems DMS-carbon tetrachloride, PMS-carbon tetrachloride, PMS-d<sub>6</sub>-acetone and FMS-methyl ethyl ketone have been investigated over a wide range of dilution. The changes in  $T_1$  on dilution are discussed in relation to the relative importance of long range ('intersegmental') and short range ('intra-segmental') interactions in these systems.

## EXPERIMENTAL

The polymer specimens were supplied by Midland Silicones Ltd, (UK). The PMS gum was prepared from an isomer of tetraphenyltetramethylcyclotetrasiloxane in which two pairs of adjacent phenyl groups lie respectively above and below the plane of the siloxane ring. A gel permeation chromatography (g.p.c.) analysis indicated the presence of a small amount of a low molecular fraction which was shown by n.m.r. and mass spectrometry to consist of cyclic tetramer and pentamer constituting approximately 3% by weight of the gum. Some physical properties of the materials are given in Table 1.

The number-average molecular weight  $\bar{M}_N$  was measured with a Mechrolab 502 osmometer. The glass transition temperature  $T_g$  and melting point  $T_m$  were recorded with a Du Pont differential Thermal Analyser. A weak minimum appeared at 272K on the differential thermal analysis (d.t.a.) trace for PMS indicative of some degree of melting. No melting transition was observed with FMS. Viscosities were measured on a Weissenberg Rheogoniometer at a shear rate of  $1.18 \times 10^{-3} \text{ s}^{-1}$ . The value for the FMS oil is that supplied by Midland Silicones Ltd. For the solutions Analar grade solvents were used. Methyl ethyl ketone was chosen for the FMS gum as it underwent extensive degradation in acetone over a period of a few weeks. The viscosity and relaxation behaviour of the gum reverted to that of the low molecular weight oil in this period<sup>11</sup>.

Spin-lattice relaxation times were measured with a Bruker-Physik A.G. pulsed n.m.r. spectrometer (B-KR

Table 1 Physical properties of the polymers

Polymer	$\bar{M}_N$	$\eta \times 10^5$ at 294K ( $\text{kg m}^{-1} \text{ s}^{-1}$ )	$T_g$ (K)	$T_m$ (K)
DMS	268 000	2	148	228
PMS	263 000	1.3	244	
FMS	—	10.0	201	
FMS oil	—	$\sim 3 \times 10^{-5}$	189	

304S) operating at 60 MHz, corresponding to an applied field of  $\sim 14\,000$  Gauss for <sup>1</sup>H resonance. The specimen temperature was controlled to within 1K in the range 99 to 493K with a conventional gas flow thermostat. A 90°, 90° pulse sequence with variable times between pulses was used and the spin-lattice relaxation was found to be satisfactorily represented by a single  $T_1$ . The samples were not outgassed as earlier measurements on DMS indicated this had little effect on  $T_1$ <sup>6</sup>.

\* BP Chemicals International Ltd, Epsom, Surrey, UK.

## RESULTS AND DISCUSSION

## Undiluted polymer systems

The temperature dependence of  $T_1$  for the gums is summarized in Figure 1 and in all cases two minima are present. The results for the FMS oil are similar to those for the gum. Values of the temperature  $T_{\min}$  at which minima occur and of  $(T_1)_{\min}$  the value of  $T_1$  at the minimum are given in Table 2. The low temperature minima are diffuse so that an exact location of  $T_{\min}$  is difficult. In particular, the values for the DMS and PMS gums are very approximate as measurements were not made at temperatures sufficiently low to establish the minima with a reasonable degree of accuracy.

**Low temperature minima.** The low temperature minima are generally ascribed to spin-lattice relaxation of methyl groups attached to the main chain<sup>2</sup>. The DMS gum is partly crystalline in this temperature range; even so the relaxation is described by a single  $T_1$ . Replacement of half of the methyl groups by the bulky phenyl group increases  $(T_1)_{\min}$  significantly. Earlier line-width and second moment studies<sup>7</sup> indicate that phenyl group rotations are frozen out at these low temperatures and so do not contribute to  $T_1$ . Replacement of a methyl by the trifluoropropyl group has less effect on  $(T_1)_{\min}$  and compared with phenyl it would appear that these group motions are not so effectively frozen out. It has been suggested that rotations of the trifluoropropyl group persist down to 77K<sup>7</sup>.

As the minima are not well defined it is not possible to decide whether the introduction of the bulky phenyl group results in steric interaction with the methyl groups so as to restrict the motion of the latter. For both <sup>19</sup>F and <sup>1</sup>H resonances  $T_{\min}$  for FMS gum is higher than for PMS. The <sup>19</sup>F minimum can only be associated with rotations of the trifluoropropyl group which clearly freeze out at temperatures much higher than for methyl rotation. For the

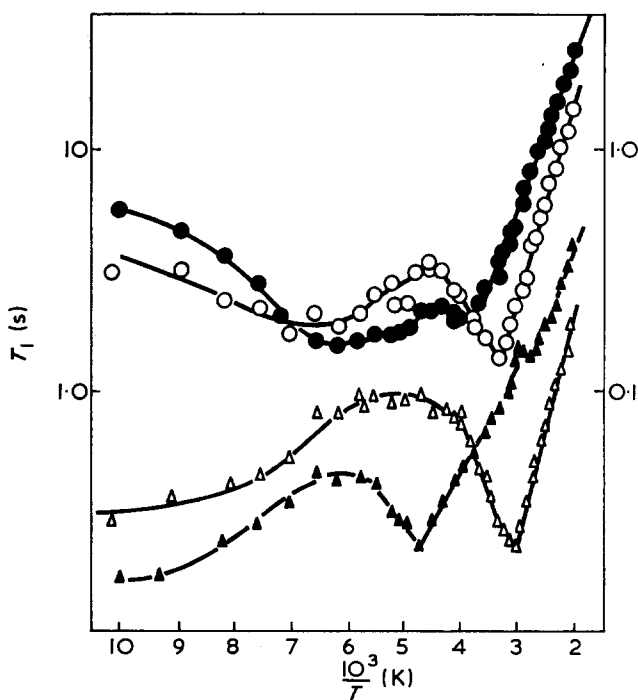


Figure 1 Temperature dependence of  $T_1$  for the undiluted polymers. Left-hand ordinate:  $\blacktriangle$ , DMS;  $\triangle$ , PMS; right-hand ordinate:  $\circ$ , FMS (<sup>1</sup>H);  $\bullet$ , FMS (<sup>19</sup>F)

Table 2  $T_{\min}$  and  $(T_1)_{\min}$  for high and low temperature minima

Polymer	Low temperature		High temperature	
	$T_{\min}$ (K)	$(T_1)_{\min} \times 10$ (s)	$T_{\min}$ (K)	$(T_1)_{\min} \times 10$ (s)
DMS	~100	~1.6	212	2.2
PMS	~100	~3.0	333	2.4
FMS ( <sup>1</sup> H)	153	2.0	298	1.4
FMS ( <sup>19</sup> F)	166	1.6	249	2.0
FMS oil ( <sup>1</sup> H)	143	1.6	270	1.8
FMS oil ( <sup>19</sup> F)	174	1.5	232	1.8

Table 3 Apparent energies of activation (kJ/mol)

Polymer	$E_{T_1}$	$E_{\tau_c}$	$E_D$
DMS	9	—	13(H <sub>2</sub> O) 13(C <sub>6</sub> H <sub>6</sub> )
PMS	18	—	
FMS ( <sup>1</sup> H)	16	—	17(H <sub>2</sub> O) 23(C <sub>6</sub> H <sub>6</sub> )
FMS ( <sup>19</sup> F)	13	14	
FMS oil ( <sup>1</sup> H)	16	18	
FMS oil ( <sup>19</sup> F)	13	15	

<sup>1</sup>H spin-lattice relaxation both methyl and trifluoropropyl groups will contribute and a broad minimum results lying between those of the methyl and trifluoropropyl. It is possible that interaction between the fluorine and hydrogen atoms on neighbouring groups raises the minimum of the methyl nearer to that of the trifluoropropyl to make resolution of the two motions difficult. As the low temperature minima are diffuse it is not possible to decide whether the difference in  $T_{\min}$  for the gum and oil are significant.

**High temperature minima.** These minima are much less diffuse and occur at 68, 69 and 97K above the  $T_g$  for DMS, PMS and FMS respectively. The  $(T_1)_{\min}$  are in the same order as the  $T_g$  for the series and probably reflect a similar spectrum of segmental motions as occur at the  $T_g$  but on a different time scale. For both the FMS gum and oil,  $T_{\min}$  is lower for the <sup>19</sup>F resonance and is more diffuse. As the low temperature minima tend to encroach on the high temperature minima it is likely that convolution effects are responsible. Alternatively some motion other than that of the main chain segments is contributing to the <sup>19</sup>F spin-lattice relaxation.

Apparent energies of activation  $E_a$  were calculated from the limiting slopes of  $\log T_1$  against  $1/T$  on the high temperature sides of the minima only. From the BPP formula, correlation times  $\tau_c$  of the motion were evaluated following Allen and Cowking<sup>8</sup> and Woessner and Snowdon<sup>9</sup> and activation energies obtained from plots of  $\log \tau_c$  against  $1/T$ . Values of  $E_a$  obtained by both methods are given in Table 3. For <sup>1</sup>H resonance with the three gums the plots of  $\log \tau_c$  against  $1/T$  were sigmoidal in shape and not sufficiently linear to enable accurate values of  $E_{\tau_c}$  to be calculated. The departure from linearity was particularly marked for DMS and was least for PMS. This may be a result of the BPP formula being a poor approximation for polymer systems or evidence that more than one correlation time is required to describe the motion.

In view of the possibility of a distribution of relaxation times the results of Table 3 are to be regarded as minimum values for  $E_{T_1}$  and  $E_{\tau_c}$ . These values are in fact smaller than activation energies obtained for small molecule diffusion in these systems which are included in Table 3 for comparison. It appears that  $T_1$  is associated with rela-



tively short range motions rather than with the longer range co-operative motions which accompany viscous flow<sup>3</sup>.

For DMS there is some indication of a small minimum around 360K above which  $E_T$  increases to  $\sim 16$  kJ/mol compared with a value of 9 below this temperature. Powles<sup>4,5</sup> observed an increase in the slope of  $\log T_1$  against  $1/T$  for this polymer but at the lower temperature of 286K. It was proposed that two types of motion were present in the amorphous phase, namely a short range 'link' motion which prevailed at the lower temperatures and was unaffected by crystallization, and a 'drift' motion comprising a larger number of chain units which became dominant above 286K. The DMS system was also studied by McCall *et al.*<sup>6</sup>, but they give no indication of any similar change in slope in the plot of  $\log T_1$  against  $1/T$ . Neither the PMS nor FMS gums exhibited this behaviour.

For the FMS gum and oil,  $T_{\min}$  is higher for the gum for both  $^1\text{H}$  and  $^{19}\text{F}$  resonance. This behaviour reflects the difference in the  $T_g$  of the two specimens.

#### Polymer solutions

The results for the polymer-solvent systems are shown in Figures 2, 3, 4 and 5. The addition of solvent causes the high temperature minimum to move to lower temperatures in a similar fashion to the  $T_g$  of the system. For the FMS-methyl ethyl ketone system a more limited temperature range was investigated and the behaviour of the minimum was not established. The shift of  $T_{\min}$  with dilution is relatively small for DMS but very marked for PMS which has the much higher  $T_g$ . This behaviour is paralleled by the change in  $T_g$  on dilution as measured by d.t.a. For the system DMS-carbon tetrachloride,  $T_g$  changes by little more than a few degrees whereas for PMS in carbon tetrachloride and  $d_6$ -acetone respectively changes of 100 and 170K are recorded. Any correlation of  $T_g$  with the volume fraction of polymer  $V_p$  is complicated by the fact that phase separation occurs in all systems at

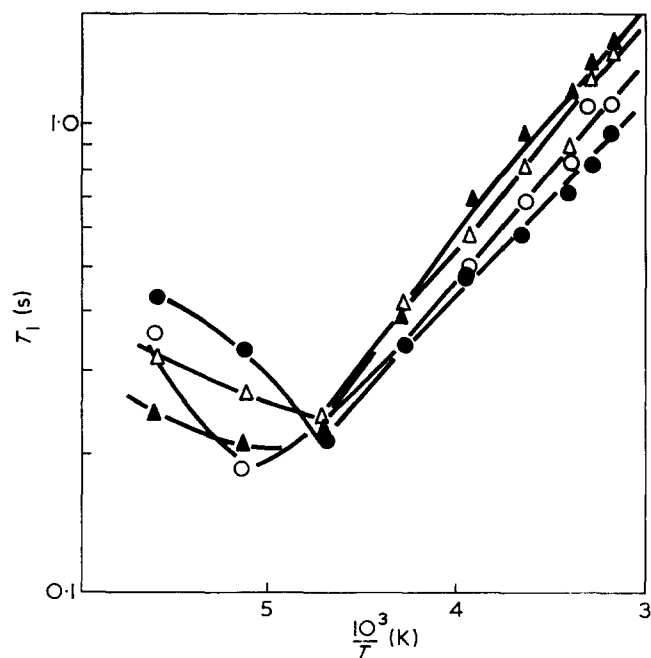


Figure 2 Temperature dependence of  $T_1$  for the DMS-carbon tetrachloride system.  $V_p=1.0$  (●); 0.8 (○); 0.6 (△); 0.4 (▲)

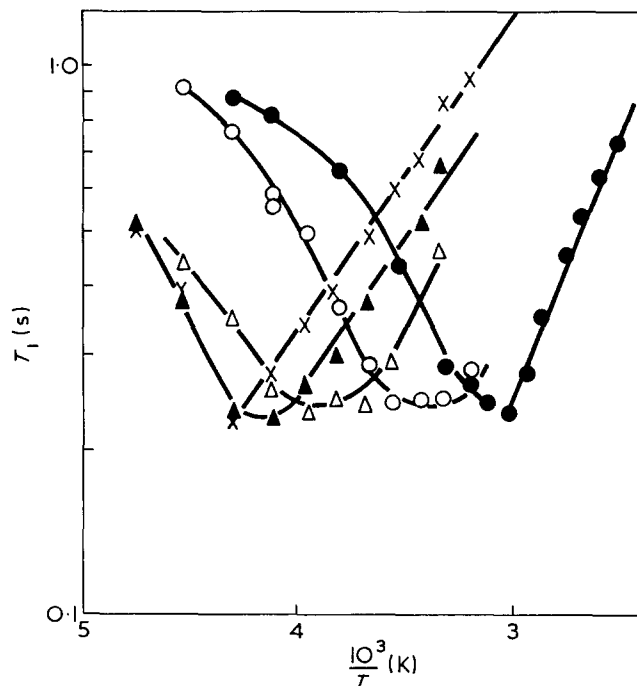


Figure 3 Temperature dependence of  $T_1$  for the PMS-carbon tetrachloride system.  $V_p=1.0$  (●); 0.89 (○); 0.57 (△); 0.37 (▲); 0.18 (×)

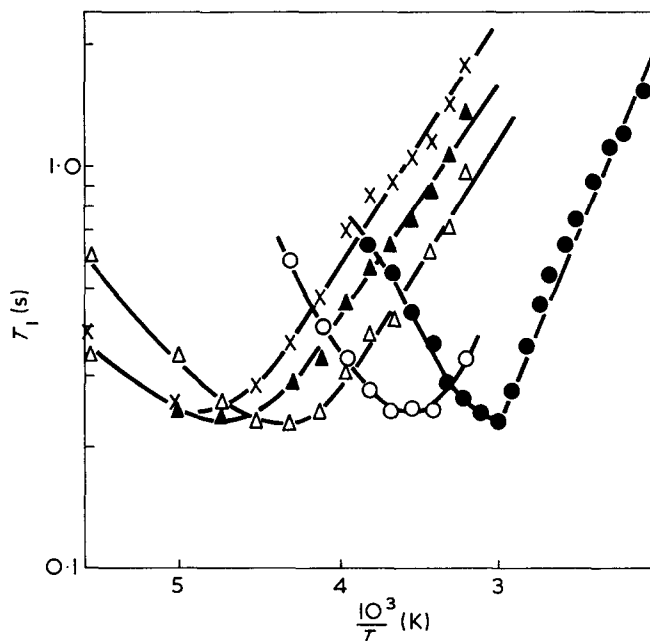


Figure 4 Temperature dependence of  $T_1$  for the PMS-acetone system.  $V_p=1.0$  (●); 0.88 (○); 0.57 (△); 0.37 (▲); 0.18 (×)

sufficiently low temperatures. For example, with the DMS-carbon tetrachloride the solid state solvent transition appears at 229K for  $V_p=0.37$  and the melting transition at 245K for  $V_p=0.37$ . For  $V_p \geq 0.59$  no solvent transitions were observed. The results for PMS in carbon tetrachloride are similar to those for DMS. With PMS in acetone the melting transition of the solvent appears at  $\sim 180$ K when  $V_p \leq 0.51$  but is absent for  $V_p \geq 0.54$  and with FMS-methyl ethyl ketone the solvent transition appears at  $\sim 183$ K for  $V_p \leq 0.57$  but not for  $V_p \geq 0.63$ . For both  $T_g$  and  $T_{\min}$  the change on dilution becomes significantly less in the region where phase separation occurs.

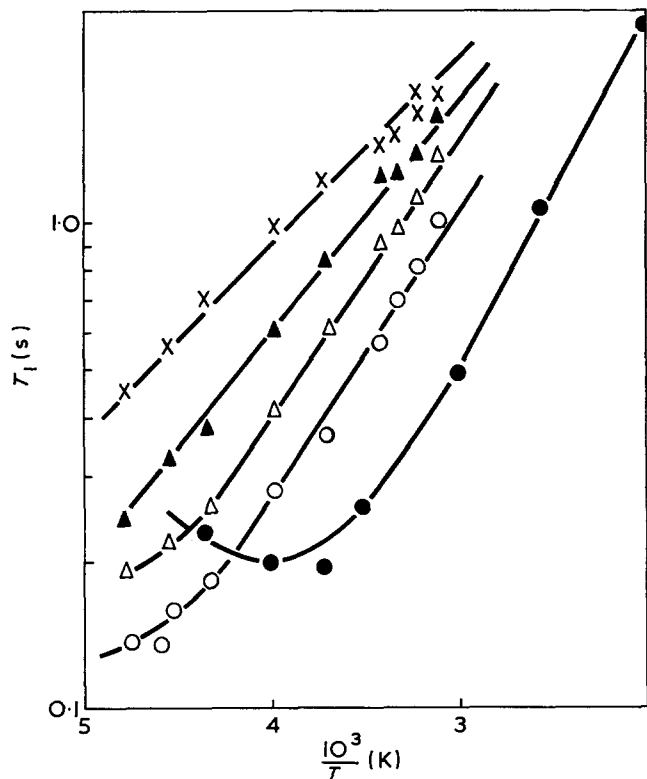


Figure 5 Temperature dependence of  $T_1$  for the FMS-methyl ethyl ketone system.  $V_p=1.0$  (●);  $0.8$  (○);  $0.6$  (△);  $0.4$  (▲);  $0.2$  (×)

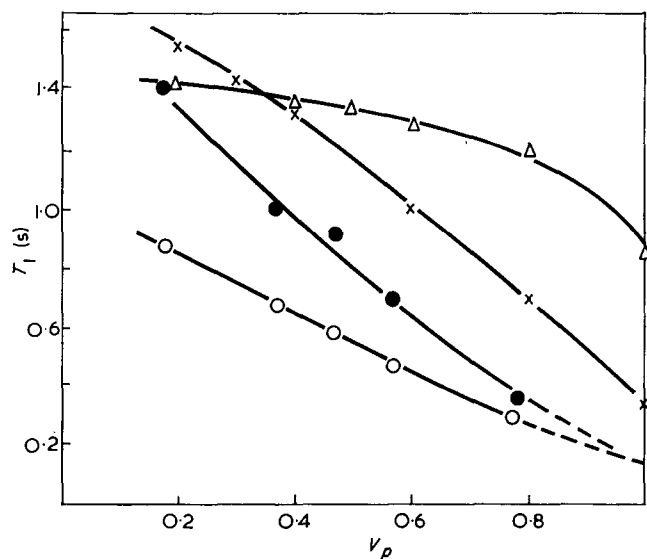


Figure 6 Concentration dependence of  $T_1$  for the polymer-solvent systems at 303K. △, DMS-carbon tetrachloride; ○, PMS-carbon tetrachloride; ●, PMS- $d_6$ -acetone; ×, FMS-methyl ethyl ketone

From plots of  $\log T_1$  against  $1/T$  on the high temperature side of the minimum, values of  $E_{T_1}$ , the apparent activation energy, were estimated. For DMS  $E_{T_1} \sim 9.0$  kJ/mol and was little affected by dilution while for PMS  $E_{T_1}$  varied from 18 to 11.0 kJ/mol and for FMS from 14 to 8.0 kJ/mol.

In Figure 6  $T_1$  at 303K is given as a function of  $V_p$ . For PMS the value of  $T_1$  for the dry polymer was obtained by extrapolation so that all  $T_1$  values relate to the high temperature side of the minimum. The results for DMS-carbon tetrachloride confirm the dilution behaviour

obtained in earlier studies<sup>9,10,13</sup> in that  $T_1$  changes but little over much of the concentration range with a relatively small change at high values of  $V_p$ . Estimates of  $\tau_c$ , the correlation time for the motion, based on the BPP equation<sup>12,13</sup> indicate that  $\tau_c$  changes from  $\sim 2$  to  $\sim 1 \times 10^{-10}$  s in the range of  $V_p$  from 1 to 0. For both PMS and FMS the changes on dilution are much more significant and for the former  $\tau_c$  changes on dilution from  $\sim 40$  to  $\sim 2 \times 10^{-10}$  s for carbon tetrachloride and to  $\sim 1 \times 10^{-10}$  s for  $d_6$ -acetone. The corresponding rise in  $T_1$  with dilution for both PMS and FMS may be interpreted as resulting from an increase in the rate of segmental motions associated with a reduction in the microscopic viscosity of the system. It is well established that for polymer systems  $T_1$  is not governed by the macroscopic viscosity. For example  $\eta(\text{polymer})/\eta(\text{solvent}) \sim 10^7$ , very much larger than either  $(T_1)_\infty/(T_1)_0$  or  $(\tau_c)_\infty/(\tau_c)_0$  where the subscripts refer to infinite and zero degree of dilution. The difference in behaviour of PMS in carbon tetrachloride and  $d_6$ -acetone can again be attributed to differences in the microscopic viscosities of the systems. Thus  $\eta(\text{carbon tetrachloride})/\eta(\text{acetone}) \sim 2.8$  so that  $(T_1)_\infty$  will on this basis be larger for acetone.

The rise in  $T_1$  on dilution may also be considered in terms of long range (intersegmental) interactions as opposed to short range (intra-segmental) interactions. If long range interactions contributed in a major sense to the relaxation process then dilution would result in a decrease in the number of these interactions and hence an increase in  $T_1$ . On this basis acetone would appear to be a better solvent than carbon tetrachloride for PMS. However, Connor and Blears<sup>8</sup> on the basis of BPP theory have shown that if long range ('intermolecular') interactions are dominant then  $(T_1)_{\min} \propto N^{-1}$  where  $N$  is the concentration of spins in the system. On this basis  $(T_1)_{\min}$  should increase on dilution whereas for both DMS and PMS it is virtually constant. It would appear therefore that intersegmental contributions to the relaxation process are not significant.

#### ACKNOWLEDGEMENTS

The authors thank Dr H. Pyszora, BP Chemicals International Ltd, Epsom for his assistance in establishing the structure of the PMS gum and Dr Cooper, University of Strathclyde, for fractionating the PMS sample.

#### REFERENCES

- 1 Powles, J. G. *Polymer* 1962, 1, 219
- 2 Slichter, W. P. *J. Polym. Sci. (C)* 1966, 14, 33
- 3 McCall, D. W. and Falcone, J. R. *Trans. Faraday Soc.* 1970, 66, 262
- 4 Powles, J. G., Hartland, A. and Kail, J. A. E. *J. Polym. Sci.* 1961, 55, 361
- 5 Kusumoto, H., Lawrenson, I. J. and Gutowsky, H. S. *J. Chem. Phys.* 1960, 32, 724
- 6 McCall, D. W., Douglas, D. C. and Anderson, E. W. *J. Polym. Sci.* 1962, 59, 301
- 7 Haberland, G. G. and Carmichael, J. B. *J. Polym. Sci. (C)* 1966, 14, 291
- 8 Connor, T. M. and Blears, D. J. *Polymer* 1965, 6, 385
- 9 Anderson, J. E., Liu, K. J. and Ullman, R. *Discuss. Faraday Soc.* 1970, 49, 257
- 10 Cuniberti, C. *J. Polym. Sci. (A-2)* 1970, 8, 2051
- 11 Fredrickson, M. *PhD Thesis* University of London, 1969
- 12 Allen, P. S. and Cowking, A. *J. Chem. Phys.* 1968, 49, 789
- 13 Woessner, D. E. and Snowden, B. S. *J. Chem. Phys.* 1966, 47, 378, 2361; *J. Phys. Chem.* 1967, 71, 952

# Solvent effects in free radical copolymerization of styrene and methacrylonitrile

G. G. Cameron and G. F. Esslemont\*

*Department of Chemistry, University of Aberdeen, Aberdeen AB9 2UE, UK*

*(Received 3 February 1972)*

The reactivity ratios for the free radical copolymerization at 60°C of methacrylonitrile ( $M_1$ ) and styrene have been determined in benzene, benzonitrile, acetonitrile and benzyl alcohol solutions. In the first three systems there is a minor solvent effect on  $r_1$  which may be attributable to changes in the dielectric constant of the solution. In benzyl alcohol there is a marked solvent effect, which has not been satisfactorily explained, on both  $r_1$  and  $r_2$ .

## INTRODUCTION

It is clear from a number of recently published papers<sup>1-3</sup> that, contrary to earlier reports<sup>4</sup>, the medium affects the reactivity ratios in some free radical copolymerizations. The influence of the medium must be on the propagation reactions and these observations may clarify the role of solvents in free radical homopolymerization<sup>5,6</sup>. Furthermore, 'The effect on the reactivity ratios of the change in the dielectric constant of the reaction mixture is of considerable interest because of its bearing on the causes of the alternating effect'<sup>7</sup>. The effect, however, may be small and easily obscured by a large experimental error. The criteria for minimizing errors in determining reactivity ratios are now well established<sup>8</sup> and these parameters should be determinable with increased precision particularly with improving analytical methods. In the present instance methacrylonitrile and styrene were chosen as monomers since it was comparatively easy to meet these criteria and to analyse the copolymers accurately. The reactivity ratios were calculated from composition-conversion data using the integrated form of the copolymer composition equation and also, in two cases, by the Fineman-Ross method<sup>9</sup>.

## EXPERIMENTAL

### *Materials*

Styrene and methacrylonitrile were purified by drying over activated  $MgSO_4$  followed by distillation through a 36 cm Vigreux column under nitrogen. Styrene distilled at 34°C at 7 mmHg and methacrylonitrile at 90°C at atmospheric pressure. In each case only the middle cut of distillate was collected. The monomers were then distilled on the high vacuum line into tubes, containing freshly

activated molecular sieves, where they were partly polymerized by exposure to a u.v. lamp. They were finally distilled under vacuum and stored in sealed tubes at -10°C.

The four solvents—benzene, benzonitrile, acetonitrile and benzyl alcohol—were purified by distillation at atmospheric pressure through the Vigreux column. Middle fractions, with boiling points in agreement with literature values, were collected. Benzene was stored over sodium and the other solvents over molecular sieves.

Laboratory grade methanol was filtered through a glass sinter (porosity 2) before use as a precipitant.

Benzoyl peroxide, the initiator in all polymerizations, was purified by recrystallization from light petroleum.

### *Polymerization and isolation of the copolymers*

Copolymerizations were conducted at 60°C in tubes containing 50% by vol. of solvents sealed under vacuum. The calculated amount of initiator dissolved in Analar acetone to give  $8 \times 10^{-2}$  mol/0.9–1.0 mol of total monomers was run into the tube. The acetone was then distilled off on the vacuum line. The required volumes of solvent and monomer were added to the tube and the mixture was degassed by successive freeze-pump-thaw cycles. For each solvent-comonomer system two different initial monomer mixtures (1:1 and 4:1 by vol. styrene:methacrylonitrile) were polymerized to four different conversions in the range 2–22% by wt.

In order to use the integrated form of the copolymer composition equation it is necessary to determine the conversion of monomers exactly. This is best done gravimetrically but requires that copolymers should be precipitated and recovered quantitatively. Styrene-methacrylonitrile copolymers can be recovered quantitatively and freed from monomer and solvent by the method previously described with benzene as solvent and methanol at -78°C as precipitant<sup>10</sup>. The purified copolymers were

\* Present address: Department of Chemistry, The University of Reading, Reading RG6 2AH, UK

dissolved in the minimum volume of benzene and freeze-dried, the last traces of benzene being removed in a vacuum oven at 60°C over 4–5 days before analysis.

For the determination of reactivity ratios by the Fineman–Ross method seven initial monomer ratios (from 9 : 1 to 1 : 3 by vol. styrene : methacrylonitrile) were employed for each solvent. In these cases the conversion was normally kept below 4% and never exceeded 5.5%.

#### Copolymer analysis

The monomer content of the copolymers was determined using a Varian 100 MHz nuclear magnetic resonance (n.m.r.) spectrometer. The n.m.r. method of copolymer analysis has been shown to be particularly advantageous for nitrile copolymers<sup>11</sup>. Spectra were recorded in 10% deuteriochloroform solution at 30°C. The phenyl protons of styrene absorb at 4.0 $\tau$ , and the aliphatic protons of styrene, together with the methylene and methyl protons of methacrylonitrile, absorb in the region 8–9.5 $\tau$ . Duplicate or triplicate integrals on these peaks were run to reduce errors from noise or stray signals. The phenyl proton integration was corrected for a small amount of hydrogen in the deuteriochloroform. Reproducibility was within 0.8%. Elemental analyses for carbon and nitrogen were also carried out on most of the copolymers but reproducibility was poor. Nitrogen estimations, by a micro-Kjeldahl technique, gave methacrylonitrile contents which were invariably lower than those from carbon or n.m.r. analyses. This effect has been reported previously<sup>11</sup>. For these reasons calculations of reactivity ratios are based entirely on n.m.r. analyses, carbon analyses being used simply as a rough check.

Table 1 Compositions (wt. fraction of methacrylonitrile  $M_1$ ) and conversions of copolymers of methacrylonitrile and styrene formed in various solvents at 60°C

Wt. fraction of $M_1$ in initial monomers	Wt. fraction of $M_1$ in copolymer from n.m.r. analyses	Wt. % conversion	Solvent
0.188	0.277	2.4	Benzene
	0.275	8.7	
	0.274	14.7	
	0.270	20.4	
0.483	0.415	10.9	Benzene
	0.418	14.6	
	0.419	20.3	
0.188	0.271	9.85	Benzonitrile
	0.270	12.7	
	0.267	21.8	
0.483	0.412	12.7	Benzonitrile
	0.411	17.7	
	0.417	21.5	
0.188	0.268	10.1	Acetonitrile
	0.269	12.4	
	0.264	16.2	
0.483	0.402	9.3	Acetonitrile
	0.404	14.5	
	0.405	15.7	
0.188	0.341	5.3	Benzyl alcohol
	0.340	10.25	
	0.339	12.7	
	0.337	15.3	
0.483	0.480	7.6	Benzyl alcohol
	0.479	10.0	
	0.480	12.35	

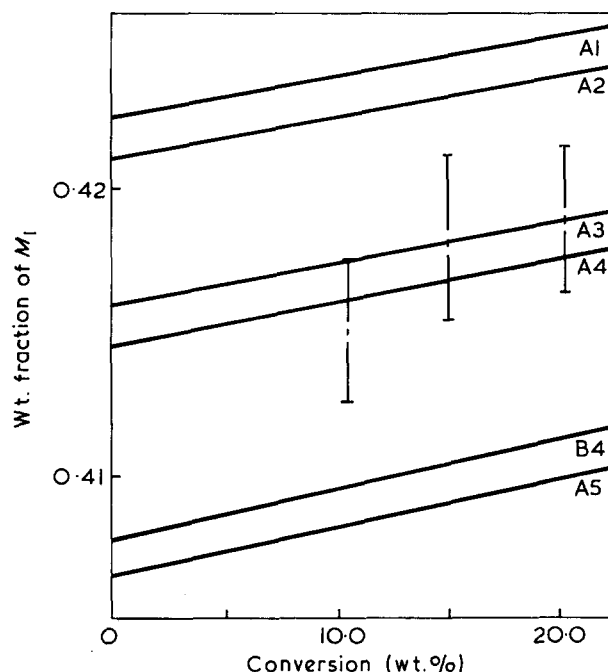


Figure 1 Composition-conversion data for copolymerization of methacrylonitrile ( $M_1$ ) and styrene ( $M_2$ ) in benzene solution at 60°C. Initial wt. fraction of  $M_1=0.483$ .  $r_1$  and  $r_2$  respectively in computed trial composition-conversion curves: A1, 0.245, 0.280; A2, 0.250, 0.300; A3, 0.226, 0.293; A4, 0.225, 0.300; A5, 0.205, 0.320; B4, 0.200, 0.300

#### Infra-red spectroscopy

The wavenumbers for the C=C stretching in styrene and methacrylonitrile and the C≡N stretching in methacrylonitrile were recorded with 4% solutions of monomers in sodium chloride microcells with a 1 mm path-length. A Perkin-Elmer 237 Grating i.r. spectrometer was used.

## RESULTS

#### Copolymer composition and determination of reactivity ratios

The copolymer compositions (as weight fraction of methacrylonitrile,  $M_1$ ) are shown in Table 1 with the corresponding weight % conversions. From these data  $r_1$  and  $r_2$  were calculated by the computer method based on the integrated form of the copolymer composition equation. This method, which is derived from that of Montgomery and Fry, has been discussed previously<sup>10</sup>. Briefly, the first programme produces values of  $r_1$  and  $r_2$  from pairs of points on the composition-conversion diagram while the second programme generates trial composition-conversion curves based on the average values of  $r_1$  and  $r_2$ . Using the second programme the experimental points can be enclosed in an envelope of composition-conversion curves. In this manner it is possible to select the curve to which the experimental points lie closest and to evaluate the experimental error in  $r_1$  and  $r_2$ . The use of two initial monomer compositions greatly increases the precision attainable by this bracketing process since the number of acceptable values of  $r_1$  and  $r_2$  is considerably reduced. This is illustrated by reference to Figures 1 and 2 which show some trial composition-conversion curves for selected values of  $r_1$  and  $r_2$ . In Figure 1 A3 and A4 are acceptable, and all the

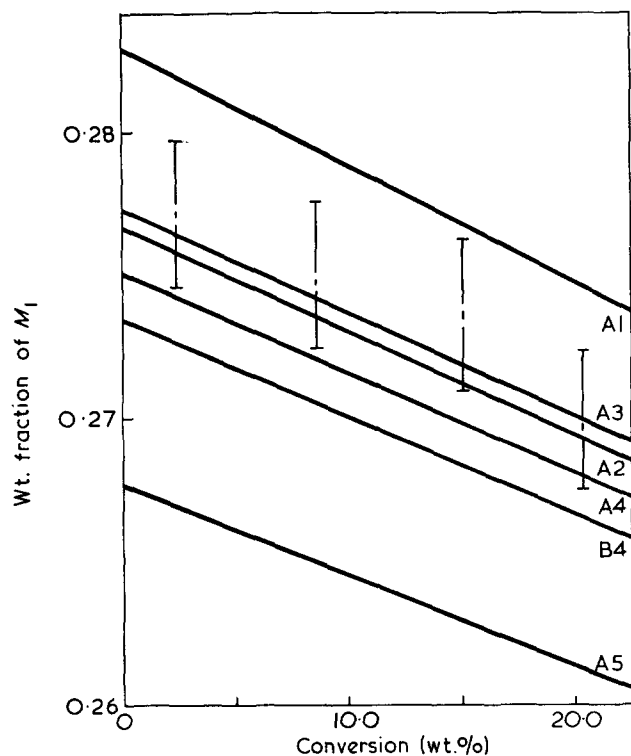


Figure 2 Composition-conversion data for copolymerization of methacrylonitrile ( $M_1$ ) and styrene ( $M_2$ ) in benzene solution at 60°C. Initial wt. fraction of  $M_1=0.188$ .  $r_1$  and  $r_2$  values in trial curves as in Figure 1

others can be rejected, while Figure 2 shows that A4 can also be rejected. The values of  $r_1$  and  $r_2$  shown in Table 3 were determined in this manner for the four comonomer-solvent systems. The error limits quoted are generous and can be regarded confidently as the maximum possible.

The analytical data on the copolymers used for determination of  $r_1$  and  $r_2$  by the Fineman-Ross method are shown in Table 2 and the corresponding plots are shown in Figure 3. The Fineman-Ross method is based on the differential version of the copolymer composition equation in the form:

$$\frac{F}{f}(f-1) = r_1 \frac{F^2}{f} - r_2$$

in which  $F$  represents the molar ratio of monomers  $M_1$  and  $M_2$  in the feed and  $f$  the molar ratio in the resulting copolymer. Thus, a plot of  $F(f-1)/f$  against  $F^2/f$  yields a straight line of slope  $r_1$  and intercept  $r_2$ . The values of  $r_1$  and  $r_2$  shown in Table 3 were calculated from the data in Table 2 by a computerized least-squares method. The errors were derived from the standard deviations in the slopes and intercepts in Figure 3, and are somewhat greater than the errors arising from composition-conversion calculations. Agreement between the values of  $r_1$  and  $r_2$  calculated by the two methods is good except for  $r_2$  in benzene, although in this case the two values still agree within the associated experimental errors.

The reactivity ratios in Table 3, apart from those in benzyl alcohol, are in good accord with most literature values although the latter show a wide variation and usually have a larger experimental error<sup>12</sup>.

## DISCUSSION

Table 3 shows a small effect, just outside experimental error, on the reactivity ratio  $r_1$  by the solvents benzene,

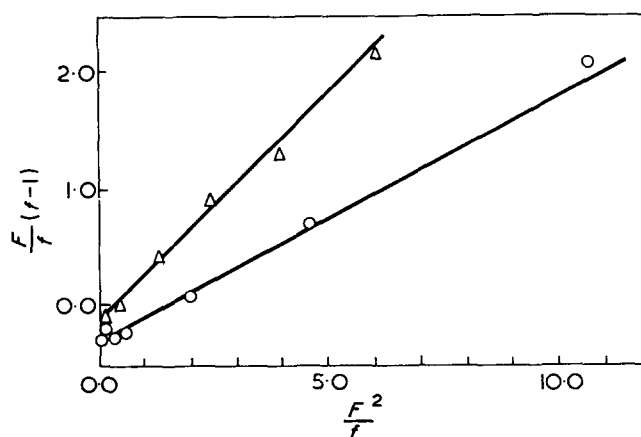


Figure 3 Fineman-Ross plots for copolymerization of methacrylonitrile ( $M_1$ ) and styrene ( $M_2$ ) at 60°C.  $\circ$ , benzene solution;  $\Delta$ , benzyl alcohol solution

Table 2 Monomer and copolymer compositions for the copolymerization of methacrylonitrile ( $M_1$ ) and styrene in solution at 60°C

Mol fraction of $M_1$ in initial monomers	Mol fraction of $M_1$ in copolymer from n.m.r. analyses	Wt. % conversion	Solvent
0.143	0.255	3.3	Benzene
0.257	0.379	2.5	
0.315	0.378	2.2	
0.394	0.4125	2.2	
0.595	0.511	2.0	
0.738	0.5745	1.3	
0.818	0.656	1.9	
0.133	0.334	5.1	Benzyl alcohol
0.257	0.426	5.3	
0.409	0.490	5.3	
0.581	0.588	4.6	
0.674	0.6385	3.8	
0.7335	0.660	2.4	
0.791	0.705	2.0	

Table 3 Reactivity ratios for copolymerization of methacrylonitrile ( $M_1$ ) and styrene at 60°C in various solvents

Solvent	$r_1$	$r_2$
Benzene	$0.23 \pm 0.01$ $0.23 \pm 0.03^a$	$0.29 \pm 0.01$ $0.35 \pm 0.07^a$
Benzonitrile	$0.21 \pm 0.01$	$0.30 \pm 0.01$
Acetonitrile	$0.18 \pm 0.01$	$0.30 \pm 0.01$
Benzyl alcohol	$0.39 \pm 0.01$ $0.40 \pm 0.02^a$	$0.14 \pm 0.005$ $0.16 \pm 0.07^a$

<sup>a</sup> From Fineman-Ross method

benzonitrile and acetonitrile while  $r_2$  is constant within experimental error. In benzyl alcohol, on the other hand, both reactivity ratios are strongly affected. It is noteworthy that the effect of the first three solvents on  $r_1$  is only observable because of the small experimental error.

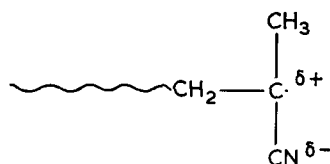
A solvent effect on  $r_1$  implies a change in the ratio  $k_{11}/k_{12}$  where  $k_{11}$  and  $k_{12}$  are the rate coefficients for addition of methacrylonitrile and styrene monomers respectively to the methacrylonitrile radical. In the case of the styrene-methyl methacrylate, styrene-acrylamide and

Table 4 Stretching frequencies (cm<sup>-1</sup>) from i.r. spectra of methacrylonitrile and styrene in various solvents

Solvent	Styrene	Methacrylonitrile	
	C=C	C=C	C≡N
Benzene	1636	1631	2236
Benzonitrile	1638	1630	2235
Acetonitrile	1637	1629	2236
Benzyl alcohol	1635	1630	2236
Liquid film of pure monomer	1637	1626	2235

methyl methacrylate-acrylamide systems solvent effects have been attributed to changes in the polarization of the carbonyl or amide groups in the monomers brought about by the different polarities of the solvents<sup>1,2</sup>. This suggestion has been supported by spectral measurements which showed differences in stretching frequencies of the double bonds of the monomers in solvents of different polarities. Such an explanation does not appear to be applicable to the present results. Table 4 shows that the stretching frequencies of the unsaturated groups in both monomers are unaffected even by benzyl alcohol which shows the greatest solvent effect.

Figure 4 shows  $r_1$  as a function of solvent dielectric constant  $D$ , and for benzene, benzonitrile and acetonitrile  $r_1$  decreases as  $D$  increases. From the spectroscopic evidence the change in  $r_1$  does not appear to be associated with a solvent effect on the monomers but it is possible that the polarity of the propagating methacrylonitrile radical is sensitive to its environment. The decrease in  $r_1$  could be due to a decrease in  $k_{11}$ , an increase in  $k_{12}$  or both. The growing methacrylonitrile end is polarized mainly by the electron-withdrawing nitrile group:



This polarization would be enhanced by increasing solvent polarity resulting in a relative decrease in reactivity towards methacrylonitrile monomer compared with that towards styrene. The product  $r_1 r_2$  for the styrene-methacrylonitrile system is  $\ll 1$  indicating a strong alternating tendency which would be enhanced by increased polarization of the methacrylonitrile radical. The effect of polar solvents on  $r_1$  can be illustrated by reference to the three-parameter  $Q$ - $e$  scheme which gives  $r_1$  as

$$r_1 = \frac{Q_1}{Q_2} \exp[-e_1^*(e_1 - e_2)]$$

where the subscript 1 refers to methacrylonitrile.  $Q$  denotes the general reactivity of the monomer and  $e$  its polar properties, while  $e^*$  refers to the polar properties of the adduct radical. The  $Q$  and  $e$  values respectively are 1.12 and 0.81 for methacrylonitrile, and 1.00 and -0.80 for styrene<sup>13</sup>. The positive  $e$  value for methacrylonitrile reflects the electron-withdrawing nature of the nitrile group. On this basis  $r_1$  is given by:

$$\log r_1 = \log 1.12 - \frac{e_1^* \times 1.61}{2.303}$$

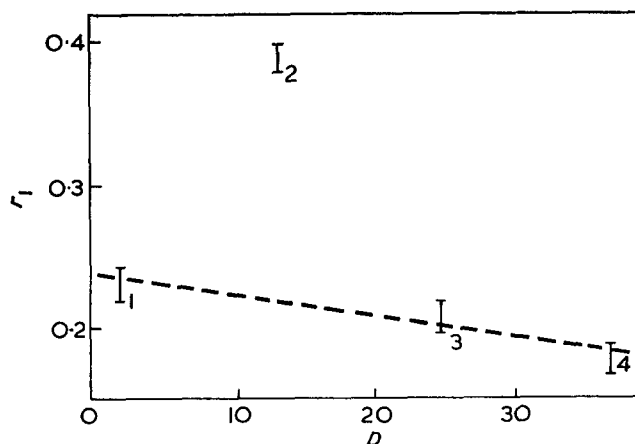


Figure 4 Reactivity ratio  $r_1$  for copolymerization of methacrylonitrile ( $M_1$ ) and styrene ( $M_2$ ) as a function of solvent dielectric constant. 1, benzene; 2, benzyl alcohol; 3, benzonitrile; 4, acetonitrile

Clearly as  $e_1^*$  increases  $r_1$  decreases. It is postulated here that as the polarity of the solvent increases,  $e_1^*$  also increases. If this interpretation is correct it predicts that in the homopolymerization of methacrylonitrile the propagation rate coefficient should decrease if the solvent is changed from benzene to acetonitrile. It would appear that as  $r_2$  is invariant within experimental error in benzene, benzonitrile and acetonitrile, the value of  $e_2^*$ , i.e. for the styrene radical, is relatively insensitive to the polymerization medium.

It is thus possible to account satisfactorily for the variation of  $r_1$  in benzene, benzonitrile and acetonitrile. The effect of benzyl alcohol on the reactivity ratios, however, cannot be accommodated satisfactorily in this manner and it is not apparent why the reactivity ratios should show such a large variation in this solvent. It may be significant that benzyl alcohol can form molecular aggregates in solution but precisely how these aggregates affect the copolymerization is not clear.

#### ACKNOWLEDGEMENTS

Grants from the Science Research Council and the University of Aberdeen are gratefully acknowledged.

#### REFERENCES

- Ito, T. and Otsu, T. *J. Macromol. Sci.* 1969, **A3**, 197
- Saini, G., Leoni, A. and Franco, S. *Makromol. Chem.* 1971, **144**, 235
- Saini, G., Leoni, A. and Franco, S. *Makromol. Chem.* 1971, **146**, 165
- Price, C. C. and Walsh, J. G. *J. Polym. Sci.* 1951, **6**, 259
- Bamford, C. H. and Brumby, S. *Makromol. Chem.* 1967, **105**, 122
- Burnett, G. M., Cameron, G. G. and Zafar, M. M. *Eur. Polym. J.* 1970, **6**, 823
- Bamford, C. H., Barb, W. G., Jenkins, A. D. and Onyon, P. F. 'The Kinetics of Vinyl Polymerization by Radical Mechanisms', Butterworths, London, 1958, p 162
- Mortimer, G. A. and Tidwell, P. W. *J. Macromol. Sci.* 1970, **C4**, 281
- Fineman, M. and Ross, S. D. *J. Polym. Sci.* 1950, **5**, 259
- Cameron, G. G., Kerr, G. P. and Russell, D. A. *Eur. Polym. J.* 1971, **7**, 1029
- Ritchey, W. M. and Ball, L. E. *J. Polym. Sci. (B)* 1966, **4**, 557
- Young, L. J. 'High Polymers—Copolymerization' (Ed. G. E. Ham) Interscience, New York, 1964, Vol XVIII, Appendix A, p 750
- Ibid.* Appendix B

# Solution properties of polysulphones of some 1,2-disubstituted alkenes

A. H. Fawcett\* and K. J. Ivin

Department of Chemistry, The Queen's University of Belfast, Belfast BT9 5AG, UK  
(Received 27 February 1972)

Fractions of poly(cyclohexene sulphone),  $\bar{M}_n=22\,500\text{--}324\,000$ , and poly(cyclopentene sulphone),  $\bar{M}_n=47\,200\text{--}571\,000$ , were prepared. Unlike poly(hex-1-ene sulphone) and poly(2-methylpent-1-ene sulphone), neither of these polymers, nor poly(but-2-ene sulphone) nor poly(hex-2-ene sulphone), showed any dielectric dispersion in solution over the frequency range  $2 \times 10^2$  to  $1.2 \times 10^7$  Hz. The dielectric increment was similar in magnitude to the high frequency value for poly(hex-1-ene sulphone) and poly(2-methylpent-1-ene sulphone), and was attributed entirely to distortion polarization. The absence of a permanent dipole indicates that in the polysulphones of 1,2-disubstituted alkenes the C-C bonds are all in the *trans* conformation, whether or not the alkene has a cyclic structure. Unperturbed dimensions were calculated from viscosity data and compared with those calculated for free rotation about the two C-S bonds in each repeat unit, the C-C bonds being assumed to be all in the *trans* conformation. The observed values are not greatly in excess of the free-rotation values.

## INTRODUCTION

The solution properties of poly(hex-1-ene sulphone) and poly(2-methylpent-1-ene sulphone) have been determined in a number of theta and non-theta solvents<sup>1-3</sup>. The dielectric behaviour is unusual in that the critical frequency is a strong function of molecular weight, indicating relaxation by overall motion rather than by segmental motion<sup>4</sup>; also the dipole moment is not exactly proportional to the square root of molecular weight<sup>5</sup>. The latter effect has been attributed to the unsymmetrical nature of the alkene unit, giving rise to a small cumulative dipole component running along the length of the chain. Such an effect should be absent in the polysulphone of a 1,2-symmetrically substituted alkene and this prompted us to make a study of such polymers. Most of the work was concerned with the polysulphone of cyclohexene. The polysulphones of cyclopentene and to a lesser extent of but-2-ene and hex-2-ene were also studied.

## EXPERIMENTAL

### Preparation of polymers

Peroxides were removed from the alkenes by refluxing over sodium in an atmosphere of nitrogen, followed by fractionation. Immediately before use the alkene was treated with iron(II) sulphate solution, washed with water and dried with calcium chloride. 20 ml alkene were mixed at  $-78^\circ\text{C}$  with sulphur dioxide (80 ml) and 4 ml of 20% *t*-butyl hydroperoxide in toluene were added. The mixture was allowed to warm to boiling point and further catalyst was added if necessary. With cyclopentene care was needed to prevent the reaction from becoming violent. The polymer was precipitated by pouring the reaction mixture into methanol (1 litre) containing a little hydrochloric acid to promote coagulation. Next day the polymer was filtered, washed and dried under vacuum.

\* Present address: Department of Chemistry, Makerere University, Kampala, Uganda.

### Fractionation of polymers

The polysulphones of cyclohexene and cyclopentene were fractionated by a procedure similar to that previously used for other polysulphones<sup>1-3</sup>. The solvents were benzene and dioxane respectively. The non-solvent was methanol in both cases. Altogether some 35 fractions were collected for each polymer. Some of these were combined and reprecipitated according to the method of Chipiro and Palma<sup>6</sup>.

### Osmotic and viscometric measurements

Osmotic measurements were made with a Hewlett-Packard High Speed Membrane Osmometer (model 501) operating at  $53.5^\circ\text{C}$  with dioxane as solvent for both polymers. It was found that working above room temperature increased the speed and reliability of the measurements.

Viscosities were determined with an Ubbelohde viscometer having a 0.4 mm i.d. capillary. Kinetic energy corrections were made when necessary. The magnitudes of the viscosities and the shear stress in the viscometer make it unlikely that the results were appreciably affected by shear.

Solvents were purified as previously described<sup>1-5</sup>.

### Dielectric measurements

These were made as previously described<sup>4, 5</sup>.

## RESULTS

### Osmotic data

Plots of  $(\pi/c)^{1/2}$  against  $c$  were linear, as shown in Figures 1 and 2. The intercepts gave number-average molecular weights  $\bar{M}_n$  ranging from 22 500 (H30) to 324 000 (H5) for poly(cyclohexene sulphone), and from 47 200 (P36) to 571 000 (P21) for poly(cyclopentene sulphone). The slopes of these lines are equal to  $0.5 A_2 \bar{M}_n$  and the second virial coefficient  $A_2$  showed the usual

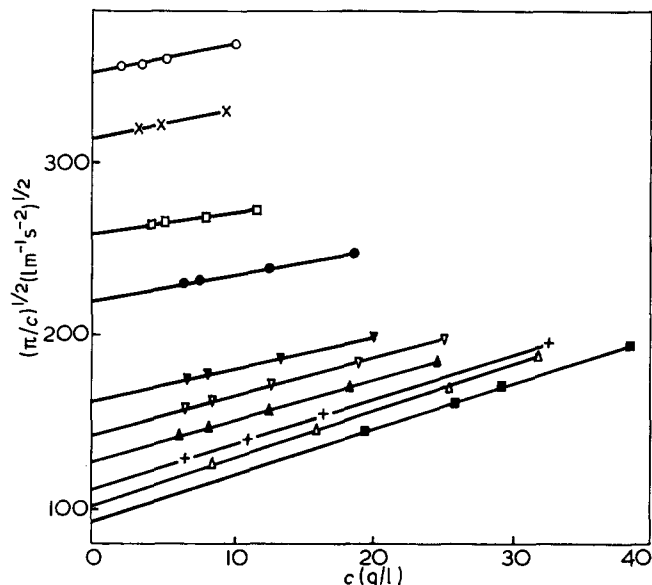


Figure 1 Osmotic data for fractions of poly(cyclohexene sulphone) in dioxane at 53.5°C. ■, H5; △, H7; +, H9; ▲, H11; ▽, H13; ▼, H16; ●, H25; □, H27; ×, H29; ○, H30

inverse dependence on molecular weight: for poly(cyclohexene sulphone)/dioxane at 53.5°C,  $A_2 = 4.2 \bar{M}_n^{-0.25} \text{ l mol kg}^{-2}$ ; for poly(cyclopentene sulphone)/dioxane at 53.5°C,  $A_2 = 3.9 \bar{M}_n^{-0.25} \text{ l mol kg}^{-2}$ . The exponent of  $-0.25$  is close to the value predicted ( $-0.23$ ) for flexible macromolecules in good solvents<sup>7</sup>.

#### Viscometric data

The results are arranged in Table 1 in order of decreasing solvent power. As an indication of the precision of the data two sets of results are plotted in Figure 3. For poly(cyclohexene sulphone) an attempt was made to achieve theta-conditions by adding the non-solvent cyclohexane to the solvent dioxane. It will be seen that this goal was not quite achieved, the exponent  $a$  being greater than 0.5 in the 59/41 mixture. On lowering the temperature of this mixture from 25°C to 13.6°C the limiting viscosity number of polymer increased by about 2%. It increased by a similar amount when the temperature was raised to 34.4°C. Hence the viscosity passes through a minimum somewhere between these two temperatures. Attempts to determine the theta-temperature for a benzene/toluene mixture by the Mandelkern-Flory<sup>10</sup> method failed, apparently because of the separation of solid polymer instead of a second liquid phase on cooling. For poly(cyclopentene sulphone) in dioxane the limiting

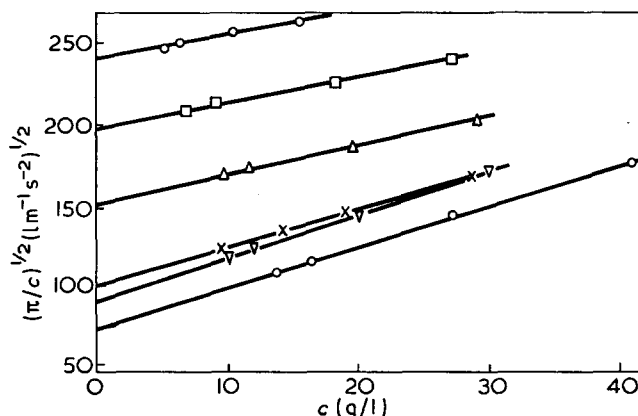


Figure 2 Osmotic data for fractions of poly(cyclopentene sulphone) in dioxane at 53.5°C. ○ (lower), P21; ▽, P26; ×, P27; △, P33; □, P35; ○ (upper), P36

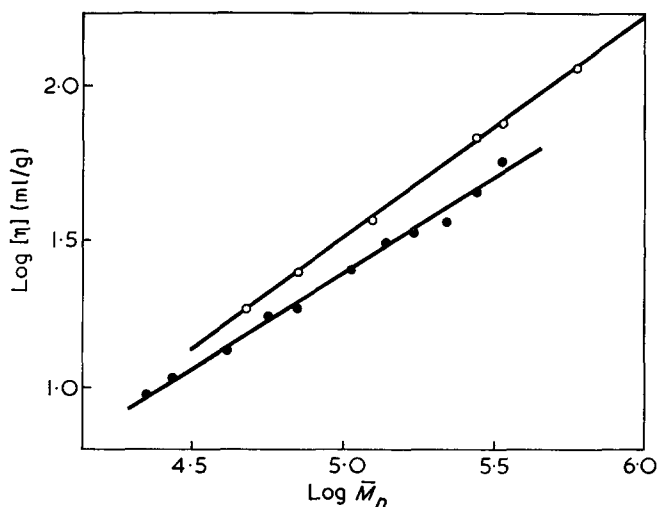


Figure 3 Viscosity data for poly(cyclohexene sulphone) in benzene (●) and for poly(cyclopentene sulphone) in dioxane (○) at 25°C

viscosity number decreased by about 0.25% per degree between 15° and 55°C.

Although it did not prove possible to obtain values of  $K_\theta$  by direct measurement at the theta-point, they could be found by one of the usual extrapolation procedures, as indicated in Table 1.

For both polymers the Huggins' constant was 0.40 for high molecular weights in good solvents. For lower molecular weights, particularly in poor solvents, the value rose to 1.0 or more. This behaviour is typical of random-coil polymers.

Table 1 Viscosity parameters  $K$  and  $a$  in the equation  $[\eta] = KM^a$ . The molecular weights for both polymers lie within the range 20 000–580 000 (see text)

Polymer	Number of fractions	Solvent*	Temp. (°C)	$10^2 K$ (ml/g)	$a$	$10^2 K_\theta$ (ml/g)	Reference to extrapolation method
Poly(cyclopentene sulphone)	6	Dioxane	25	0.53	0.76	$5.6 \pm 0.3$	8
						$5.3 \pm 0.3$	9
Poly(cyclohexene sulphone)	4	Dioxane	25	0.57	0.72	$5.1 \pm 0.3$	8
		Benzene	25	1.33	0.65	$5.1 \pm 0.3$	8
	8	Dioxane/cyclohexane (60/40)*	25	2.94	0.57	$5.5 \pm 0.2$	8
		Dioxane/cyclohexane (59/41)*	25	3.93	0.54	$5.56 \pm 0.06$	8

\* Proportions by volume



## Dielectric data

No dielectric dispersion was found in the frequency range  $2 \times 10^2$  to  $1.2 \times 10^7$  Hz for 1–3% solutions of any of the polymers shown in Table 2. With the same apparatus an unfractionated sample of poly(hex-1-ene sulphone) in benzene ( $[\eta] = 23$  ml/g in chloroform at 25°C) gave a substantial dispersion in the region of  $10^5$ – $10^6$  Hz, the limiting values of  $d\epsilon/dw_2$  being about 12 (at low frequency) and 2.4 (at high frequency), in agreement with previous results<sup>5</sup>. Measurements by Dr P. J. Phillips (University of Liverpool) using the slotted line technique<sup>11</sup> failed to detect any dielectric loss at higher frequencies ( $5$ – $20 \times 10^8$  Hz) either in poly(hex-1-ene sulphone) or poly(cyclohexene sulphone) solutions in benzene.

## DISCUSSION

The osmotic and viscometric measurements indicate that the poly(cyclo-alkene sulphones) are, like the poly(alk-1-ene sulphones), randomly coiled in solution. The most surprising feature of the present results was the complete absence of dielectric loss for any of the polymers shown in Table 2, in marked contrast to the behaviour of poly(hex-1-ene sulphone) and poly(2-methylpent-1-ene sulphone). For the latter polymers we have shown that it is possible to predict the critical frequency for overall rotation within a factor of 2, knowing  $[\eta]$ ,  $\bar{M}_n$  and the viscosity of the solvent<sup>4</sup>. On this basis we can be sure that had any of the systems in Table 2 shown a relaxation of this type it would have fallen within the experimental frequency range. There remains the possibility of segmental relaxa-

tion at a higher frequency to account for the small observed values of  $d\epsilon/dw_2$ . However, the fact that the values are very similar to the high frequency values for poly(hex-1-ene sulphone), which are 2.4 in benzene and 3.2 in dioxane, and for which no higher-frequency relaxation process was detected, make it very probable that the observed values of  $d\epsilon/dw_2$  are wholly accountable in terms of distortion polarization, i.e. that the polymers in Table 2 have negligible permanent net dipole.

For the polysulphone of a symmetrically substituted alkene the dipole associated with each sulphone group may be resolved into two equal components directed along the two C–S bonds. If the conformation about the C–C bonds is entirely *trans*, with the two C–S bonds parallel and opposed, then the net dipole of the whole molecule will be zero, apart from a negligible contribution from the two end-units. However, oscillations within the sulphone groups and about the C–C bonds in the main chain will make a significant contribution to the distortion polarization. There is a good deal of evidence to show that the atomic polarization part of distortion polarization can assume quite significant proportions in molecules that contain more than one substantial bond dipole. For example the apparent dipole moments of 1,4-dioxane (0.4 D)<sup>14</sup>, 1,4-cyclohexane dione (1.3 D)<sup>14</sup>, 1,4-dinitrobenzene (0.8 D)<sup>15</sup> and tetramethyl-1,3-cyclobutanedione (0.8 D)<sup>12, 15</sup> have all been attributed to atomic polarization. It is therefore not unreasonable to suppose that the values of  $d\epsilon/dw_2$  in Table 2, which correspond to apparent values of  $(\mu^2/z)^{1/2}$  of about 1.6 D ( $z$  = degree of polymerization), are also due to distortion polarization, especially in view of the large sulphone dipole (4.4 D).

We thus conclude that the solutions listed in Table 2 contain polymer molecules whose main-chain C–C bonds are solely in the *trans* conformation. The vicinal coupling constants in the n.m.r. spectrum of poly(propene sulphone) dissolved in dimethyl sulphoxide indicate that even in a polar solvent the main-chain C–C bonds adopt a predominantly *trans* conformation<sup>26</sup>. However, in poly(hex-1-ene sulphone) and poly(2-methylpent-1-ene sulphone) there are evidently sufficient non-*trans* conformations to give the molecules an appreciable overall dipole.

For poly(but-2-ene sulphone) and poly(hex-2-ene sulphone) the molecules are free to take up a preferential *trans* conformation about the main-chain C–C bonds, but in poly(cyclopentene sulphone) and poly(cyclohexene sulphone) this is not so because of the restriction imposed by the rings. In the latter two cases preferred *trans* conformations can only result from preferred *trans* addition at the time of formation of the polymer. With poly(propene sulphone) it is known that *trans* addition is

Table 2 Dielectric properties of polysulphones of some 1,2-disubstituted alkenes at 25°C

Polymer	Solvent	$[\eta]$ (ml/g)	$\frac{d\epsilon}{dw_2}$ ( $\pm 0.1$ )	$\frac{dn_D^2}{dw_2}$ ( $\pm 0.05$ )
Poly(cyclopentene sulphone)	Dioxane	36.5 (F)	2.9	-0.30
		24.7 (F)	2.8	
Poly(cyclohexene sulphone)	Dioxane	52 (F)	3.0	-0.27
		19 (F)	3.1	
		43.5 (F)	1.65	
Poly(but-2-ene sulphone)*	Dioxane	17.3 (F)	1.73	-0.18
		51 (U)	3.3	-0.25
Poly(hex-2-ene sulphone)†	Dioxane	34 (U)	2.7	-0.23
		Benzene	1.7	-0.06

\* Made from 100% *trans*-but-2-ene

† Made from 50/50 *cis/trans*-hex-2-ene

F=fractionated sample; U=unfractionated sample

$w_2$ =weight fraction of polymer;  $n_D$ =refractive index for sodium D line

Table 3 End-to-end distance parameters for some poly(alkene sulphones) in similar solvents.  $\sigma = (\langle r_{0f}^2 \rangle / \langle r_{0f}^2 \rangle)^{1/2}$

Alkene	Solvent*	Temp. (°C)	$\left\{ \frac{\langle r_{0f}^2 \rangle}{z} \right\}^{1/2}$ (Å)	$\left\{ \frac{\langle r_{0f}^2 \rangle}{z} \right\}^{1/2}$ (Å)	$\sigma$	Notes and ref.
Hex-1-ene	29.8/70.2 MEK/hexane	8.0	7.26	4.20	1.73	a 2
		20.5	7.75	4.20	1.85	a 3
2-Methylpent-1-ene	35.4/64.6 MEK/hexane	11.5	8.68	4.20	2.05	a 2
Cyclohexene	59/41 Dioxane/cyclohexane	25.0	7.34	5.91	1.24	b
Cyclopentene	Dioxane	25.0	6.94	5.91	1.17	b

\* MEK=methyl ethyl ketone. Solvent code is preceded by volume ratio

a  $\langle r_{0f}^2 \rangle$  values based on free rotation about all main-chain bonds and assuming tetrahedral angles

b  $\langle r_{0f}^2 \rangle$  values based on free rotation about all C–S bonds and assuming main-chain C–C bonds all in *trans* conformation

indeed preferred at  $-80^\circ$ , though not exclusively<sup>16</sup>. It is not unreasonable to suppose that radical addition to a cyclo-alkene involves a greater degree of specificity. With cyclohexene *trans* addition will result in a non-polar axial-axial structure which may be expected to be preferred over the polar equatorial-equatorial structure. With cyclopentene on the other hand although *trans* addition will result in an axial-axial structure the two C-S bonds will not be parallel unless the ring is distorted from a planar structure. The absence of a dielectric dispersion for poly(cyclopentene sulphone) indicates that such distortion must occur. This is not surprising since it is known that distortion requires relatively little energy<sup>17</sup> and this could easily be provided by the interaction between adjacent sulphone dipoles.

Finally we consider the values of the unperturbed dimensions of the polymers relative to those calculated for free rotation. It is evident that for the polysulphones of cyclohexene and cyclopentene we have to consider the special case of free rotation about the two C-S bonds, the C-C bonds being fixed in the *trans* conformation.

The unperturbed dimensions were calculated from:

$$\left(\frac{\langle r_0^2 \rangle}{z}\right)^{1/2} = \left[ \left[ \frac{K_\theta}{\Phi} \right]^{2/3} M_0 \right]^{1/2} \quad (1)$$

where  $\langle r_0^2 \rangle$  = mean-square end-to-end distance (cm),

$z$  = degree of polymerization,

$M_0$  = relative molecular mass of repeat unit,

$\Phi$  = Flory constant, taken<sup>18</sup> as  $2.5 \times 10^{23} \text{ g}^{-1}$ ,

$K_\theta = [\eta]_\theta / M^{1/2}$ , expressed in  $\text{cm}^3/\text{g}$ .

Values are given in Table 3.

The biggest uncertainty in the free rotation value,  $(\langle r_{0f}^2 \rangle / z)^{1/2}$  lies in the values assumed for the bond angles. Thus for free rotation about all three bonds in an infinite  $\text{-[C-C-S]-}$  chain, Huglin and Stepto<sup>19</sup> find  $(\langle r_{0f}^2 \rangle / z)^{1/2} = 4.02 \text{ \AA}$ , taking  $l_{\text{CS}} = 1.80 \text{ \AA}$ ,  $l_{\text{CC}} = 1.53 \text{ \AA}$ ,  $\text{C-S-C} = 98.97^\circ$ ,  $\text{S-C-C} = 112.5^\circ$ . Using their formulae but taking  $l_{\text{CS}} = 1.80 \text{ \AA}$ ,  $l_{\text{CC}} = 1.54 \text{ \AA}$ ,  $\text{C-S-C} = \text{S-C-C} = 109.5^\circ$  (tetrahedral angles), we find  $(\langle r_{0f}^2 \rangle / z)^{1/2} = 4.20 \text{ \AA}$ .

When the C-C bond is fixed in the *trans* conformation the distance between successive sulphur atoms  $l_{\text{SS}}$  is fixed and equal to  $4.36 \text{ \AA}$  (using the second set of bond lengths and angles), and the SS vector makes an angle  $\alpha$  of  $19.5^\circ$  with the two intermediate C-S bonds. The chain may then be replaced by a set of vectors SS, each vector being able to take up a limited number of positions with respect to the previous vector, as illustrated in Figure 4.  $\text{S}_0\text{S}_1$  represents a fixed vector lying in the plane of the paper at the angle  $\alpha$  to the C-S<sub>1</sub> bond. The next vector  $\text{S}_1\text{S}_2$  may lie on the surface of a cone of semi-angle  $\alpha$  which may rotate freely about the CS<sub>1</sub> axis. By chance the angle C-S<sub>1</sub>-S<sub>2</sub> in Figure 4 is exactly  $90^\circ$ . The average projection of  $\text{S}_1\text{S}_2$  on  $\text{S}_0\text{S}_1$  is readily calculated to be  $l_{\text{SS}} \cos^2 \alpha \sin \alpha = 0.296 l_{\text{SS}} = \beta l_{\text{SS}}$ . By following the procedure described by Flory<sup>20</sup> we find that  $\langle r_{0f}^2 \rangle / z l_{\text{SS}}^2 = (1 + \beta) / (1 - \beta) = 1.84$  which is a little less than the value of 2.00 for a chain of tetrahedrally linked identical atoms. Inserting the value of  $l_{\text{SS}}$  gives  $(\langle r_{0f}^2 \rangle / z)^{1/2} = 5.91 \text{ \AA}$ .

The values of  $(\langle r^2 \rangle / z)^{1/2}$  and appropriate ratios are summarized in Table 3. The values of  $\sigma$  for the first two polymers are 1% higher than those calculated previously by an approximate method<sup>2,3</sup>. The fact that  $\sigma$  is close to 1

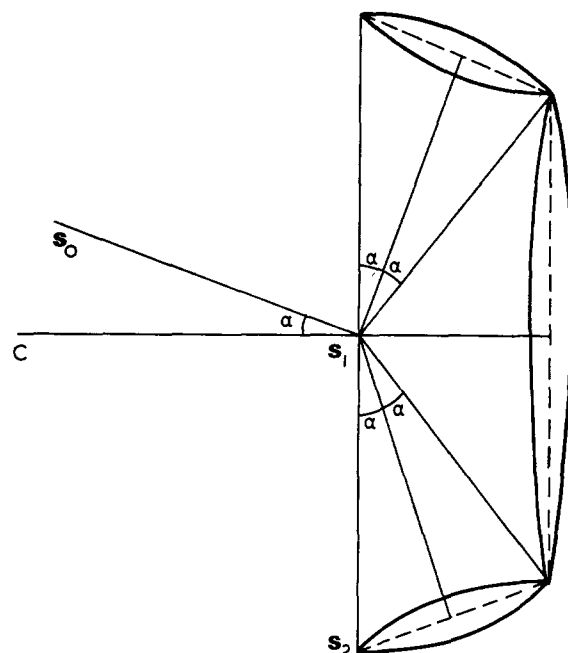


Figure 4 Diagram illustrating the relative positions which can be taken up by successive SS vectors

for the last two polymers does not necessarily mean that there is free rotation about the C-S bonds; rather it indicates that the energy levels for the three conformations about the C-S bonds are rather close together.

#### ACKNOWLEDGEMENTS

A.H.F. thanks the Science Research Council for the award of a maintenance grant. We gratefully acknowledge financial assistance from the Courtaulds Educational Trust Fund. We thank Dr F. J. Phillips, University of Liverpool, for making the high frequency measurements.

#### REFERENCES

- Ivin, K. J., Ende, H. A. and Meyerhoff, G. *Polymer* 1962, **3**, 129
- Bates, T. W., Biggins, J. and Ivin, K. J. *Makromol. Chem.* 1965, **87**, 180
- Bates, T. W. and Ivin, K. J. *Polymer* 1967, **8**, 263
- Bates, T. W., Ivin, K. J. and Williams, G. *Trans. Faraday Soc.* 1967, **63**, 1964
- Bates, T. W., Ivin, K. J. and Williams, G. *Trans. Faraday Soc.* 1967, **63**, 1976
- Chapiro, A. and Palma, G. *J. Appl. Polym. Sci.* 1966, **10**, 955
- Isihara, A. and Guth, E. *Adv. Polym. Sci.* 1967, **5**, 232
- Stockmayer, W. H. and Fixman, M. *J. Polym. Sci. (C)* 1963, **1**, 137
- Inagaki, H., Suzuki, H. and Kurata, M. *J. Polym. Sci. (C)*, 1966, **15**, 409
- Mandelkern, L. and Flory, P. J. *J. Polym. Sci.* 1952, **9**, 503
- North, A. M. and Phillips, P. J. *Trans. Faraday Soc.* 1967, **63**, 1537
- Cooper, I. E. and Sutton, L. E. *J. Chem. Soc.* 1938, p 1269
- Smith, C. P. 'Dielectric Behaviour and Structure', McGraw-Hill, London, 1955
- Mizushima, S. I. 'Structure of Molecules and Internal Rotation', Academic Press, New York, 1954
- Di Carlo, E. N., et al. R. E. *J. Phys. Chem.* 1968, **72**, 1517
- Ivin, K. J. and Navrátil, M. *J. Polym. Sci. (A-1)* 1970, **8**, 3373
- Hendrickson, J. B. *J. Am. Chem. Soc.* 1961, **83**, 4537
- Crescenzi, V. and Flory, P. J. *J. Am. Chem. Soc.* 1964, **86**, 141
- Huglin, M. B. and Stepto, R. F. T. *Makromol. Chem.* 1970, **132**, 225
- Flory, P. J. 'Principles of Polymer Chemistry', Cornell University Press, Ithaca, 1953, p 414

# Mechanical relaxation studies of the cure of epoxy resins: 1. Measurement of cure

R. G. C. Arridge

*H. H. Wills Physics Laboratory, University of Bristol, Bristol BS8 1TL, UK*

and J. H. Speake

*NDT Centre, AERE, Harwell, Didcot, Berks, UK  
(Received 22 February 1972; revised 4 April 1972)*

Studies are reported of the dependence of the low temperature secondary mechanical relaxation in amine-cured epoxy resins on the state of cure of the system. The shear modulus below the transition increases with increased crosslinking, while above the transition the reverse is true. The present study covers the range of cure temperatures from 20°C to 160°C and shows that the ratio of the values of the shear modulus above and below the transition may be used as a quantitative measure of cure, particularly above the gel point. The effects of time and temperature of cure on the value of this modulus ratio are reported, as are the effects of departure from the stoichiometric quantity of hardener. The phenomena observed are interpreted as being caused by a secondary chain relaxation hindered increasingly by steric effects resulting from the increased cure.

## INTRODUCTION

Many methods have been studied in order to find a technique which monitors, or can test cure in a practical structure. The majority of test methods, whether destructive or non-destructive, used for assessing cure are very sensitive up to the gel point (the early stages of crosslinking) but fail in the later stages. Yet many important changes take place in the resin after gelation as the reaction is continued. At the gel point about 70% of the reaction has been completed<sup>1</sup> but post curing has been shown to have a marked effect particularly on the mechanical properties of the resin so that monitoring of this solid state reaction is important.

Chemical measurements which are often used are equilibrium swelling, sol-gel analysis and solvent analysis. Equilibrium swelling measurements are done above the glass transition and entering into this region before the material is fully cured alters the state of cure. Sol-gel analysis is only satisfactory to the gel point and solvent analysis in the solid state is limited by the availability of a suitable solvent and the extent of reaction. For high degrees of cure long immersion times in the solvent are needed. Bell<sup>2</sup> has used this together with swelling and sol-gel analysis to determine the extent of cure and relative reaction rates of primary and secondary amine groups with epoxy.

Infra-red analysis provides an accurate, quick test to determine the extent of reaction but the chemistry of the curing process needs to be known as several competing reaction mechanisms often take place simultaneously.

Strecker *et al.*<sup>3,4</sup> came to the somewhat erroneous conclusion that far less than 100% of the chemical reaction took place in the system they studied, because they were unable to detect any further change in the infra-red spectrum after a certain degree of conversion.

Physical test methods are usually adopted after the gel point and one of the most widely used in the plastics industry is the heat distortion test<sup>5,6</sup>. However, there are two major deficiencies: (a) in a chemically reactive polymer the reaction proceeds as the specimen is heated so the measured distortion temperature is not the heat distortion temperature of the original specimen; (b) the heat distortion test is destructive. Examples of the confusing results of measuring heat distortion point on incompletely cured resins are given by Planer *et al.*<sup>7</sup>.

Surface hardness tests have been used as an empirical way of monitoring cure and Barcol hardness<sup>8,9</sup> and hot needle testing<sup>10</sup> have been used on phenolic, epoxy and polyester resins. Judd<sup>9</sup> compares hardness testing with water absorption and also with resistivity methods. However, resistivity above 10<sup>14</sup> ohmcm is not easy to measure, so that although the resistance method is much more sensitive than Barcol hardness or water absorption it presents difficulties at high resistivities. Chadwick<sup>11</sup> and Miller<sup>12</sup> have also used resistivity methods for studying filled systems.

Fava<sup>13</sup> using differential scanning calorimetry has investigated cure in an epoxy resin crosslinked with an amine-catalysed anhydride mixture and showed that after the gel point is reached further reaction requires tem-

peratures in excess of  $T_g$  and that such reaction ceases as soon as  $T_g$  reaches the cure temperature.

Dielectric studies by Haran *et al.*<sup>14</sup> confirm this for lower temperatures of cure. For filled systems, however, differential scanning calorimetry is less sensitive because of the presence of unreactive filler and dielectric methods may fail altogether because of Maxwell-Wagner effects.

Dilatometric methods have been used by Shimazaki<sup>15</sup> and Shito and Sato<sup>16</sup> to study epoxy resin/acid anhydride mixtures with different degrees of crosslinking.

All these methods tend to become more inaccurate as cure proceeds and may suffer from the disadvantage that the test is based on movement of  $T_g$  to higher temperatures and thus the very measurement affects the state of cure.

Dynamic mechanical properties, obtained over a wide range of temperatures and frequencies have been shown to be very sensitive to changes in molecular structure and do not suffer from the limitations listed above.

The dynamic mechanical spectrum of amine-cured epoxy resins is well known<sup>17-23</sup> and is characterized by four loss peaks labelled  $\alpha'$ ,  $\alpha$ ,  $\beta$  and  $\gamma$  in decreasing order of temperature. The  $\alpha'$  peak is associated with degradation and the  $\alpha$  peak is due to the glass transition. The  $\beta$  relaxation, which is large in under-cured resins and decreases as curing proceeds, has been shown<sup>19, 20</sup> to be an experimental artefact and is the glass transition which is reduced in temperature. The secondary relaxation, termed  $\gamma$ , has been postulated<sup>17-19</sup> to be due to mobility of the segment  $-\text{CH}_2-\text{CH}(\text{OH})-\text{CH}_2-\text{O}-$  and Pogany<sup>19</sup> has suggested that this group could rotate in the manner of a crankshaft as outlined by Schatzki<sup>24</sup>. Other workers<sup>25, 26</sup> have suggested alternative sources for this relaxation, but these will be discounted for reasons presented later.

Although it has been noted that the  $\gamma$  relaxation is dependent on the state of cure, there have been few controlled experiments to determine this dependence. Kline<sup>17</sup> showed that the peak at 240K (the  $\gamma$  peak) increased with increasing time of an elevated temperature cure, 70°C, for an amine-cured epoxy resin. The changes in modulus were stated to be 'very minor'. Pogany<sup>19</sup> showed that the effect of increased cure temperature on the  $\gamma$  peak was to increase the area under it, to increase its peak value and to increase the temperature of the maximum. Krehling and Kline<sup>21</sup> showed effects similar to these using post cures at 345, 375 and 400K, and for the first time demonstrated that there is a significant change in the modulus behaviour in the region of the  $\gamma$  peak as higher cure temperatures are used. Other studies<sup>20</sup> also showed changes in the  $\gamma$  relaxation as cure proceeds.

Our contribution has been to undertake a detailed examination of the  $\gamma$ -relaxation over a wider temperature range than before and to show that the dependence of the modulus on the state of cure is measurable with a high degree of reproducibility leading to the proposal that the ratio of moduli above and below the transition be used as a monitor of cure in amine-hardened epoxy resins.

## EXPERIMENTAL

The materials used in the investigation are listed in *Table 1*. Dynamic mechanical properties were determined over a range of frequencies by using a torsion pendulum operating at 0.67 Hz, an ultrasonic resonance technique covering a frequency range of 10 kHz to 100 kHz and an ultra-

sonic transit time technique operating between 200 kHz and 2 MHz. The torsion pendulum yielded loss tangent and shear modulus as a function of temperature and the ultrasonic techniques shear and Young's moduli. Unfortunately loss measurements were not recorded using the latter techniques owing to experimental difficulties which will not be discussed here.

Castings were prepared by carefully weighing both resin and the appropriate amount of hardener, thoroughly mixing, and then casting in one of a variety of moulds dependent on the test method to be adopted.

Initially three casts were prepared using the commercial diglycidyl ether of bisphenol A (DGEBA) and triethylene-tetramine (TETA). Although equal quantities of the constituents were used in each cast, the method of preparation was slightly different in each case. This was done to determine whether differences in experimental procedure produced any significant variation in the dynamic mechanical properties of systems which nominally were identical. Rather less than the stoichiometric quantity of curing agent was used because the agent is hydrophilic and by using less the chance of the agent having reacted at least at one site is greater and prevents the uptake of moisture which would alter the system. The conditions of preparation of these casts are listed in *Table 2*.

Three specimens were machined from each cast and the loss tangent and shear modulus were measured between -150°C and ambient using a torsion pendulum at ~1 Hz.

It was found that the variation between specimens from the same casting was insignificant compared with the variation between casts. The difference between casts can in part be attributed to the different temperatures at which each was prepared and the different experimental procedure adopted in the preparation.

## RESULTS

### *Effect of curing on $\tan\delta$*

The three casts, labelled C-1-1, C-1-2, C-1-3, were heated for 2 h at increasingly higher temperatures and it was assumed that an equilibrium state of cure was established after each anneal. The curing temperatures at which each cast was cured are shown in *Table 3*.

Measurements were made on each of the three specimens in each cast, so that for each state of cure three loss

*Table 1* Materials used

Trade name	Chemical name	Source of supply
MY750	Diglycidyl ether of bisphenol A (DGEBA)	Ciba
HY951	Triethylene-tetramine (TETA) Ethylene diamine (EDA)	Ciba BDH

*Table 2* Preparation conditions of casts

Cast	Time for which cast was stirred (min)	Time under vacuum (min)	Cure temp. (°C)
C-1-1	5	2	19.0
C-1-2	5	3	21.0
C-1-3	10	3	19.3

curves were obtained. The mean curve was plotted for each temperature of cure and the results are shown in Figure 1. Not all curves have been plotted, to preserve clarity. It is immediately apparent that as the state of cure increases, the following features are manifested: (i) the area under the  $\tan\delta$  curve increases; (ii) the peak value of  $\tan\delta$  increases; (iii) the temperature of  $\tan\delta_{\max}$  increases; (iv) the curve broadens more on the high temperature side; and (v) for curing temperatures of 149°C and 159°C the curve broadens but the peak value decreases.

Table 3 Curing temperature for each cast

Cast	Temperature (°C)
C-1-1	31.5
C-1-2	48.0
C-1-3	64.0
C-1-1	74.5
C-1-2	84.0
C-1-3	93.9
C-1-1	102.5
C-1-2	110.4
C-1-3	118.8
C-1-1	128.2
C-1-2	139.3
C-1-3	149.3
C-1-1	159.3

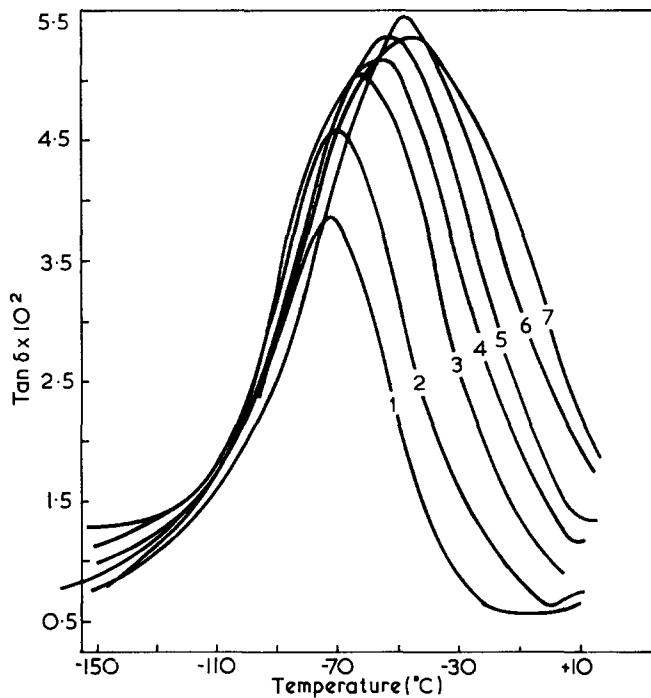


Figure 1 Change in  $\gamma$ -relaxation with cure

Curve number	Cast	Cure temp. (°C)
1	C-1-1	19.0
2	C-1-2	48.0
3	C-1-2	84.0
4	C-1-3	93.9
5	C-1-2	110.4
6	C-1-1	128.2
7	C-1-1	159.0

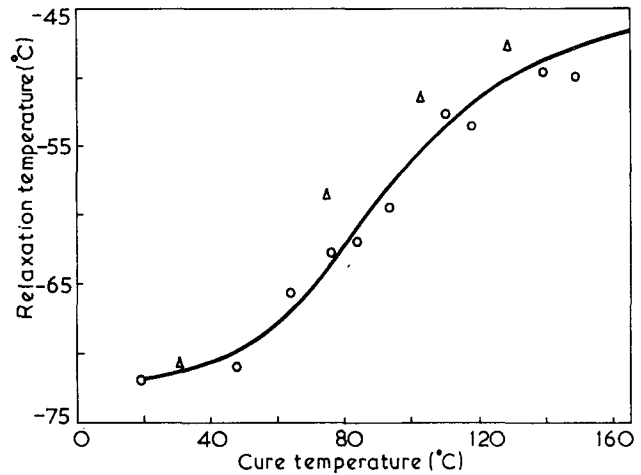


Figure 2 Temperature of  $\tan\delta_{\max}$  as a function of cure temperature.  $\Delta$ , C-1-1 specimens;  $\circ$ , C-1-2 and C-1-3 specimens

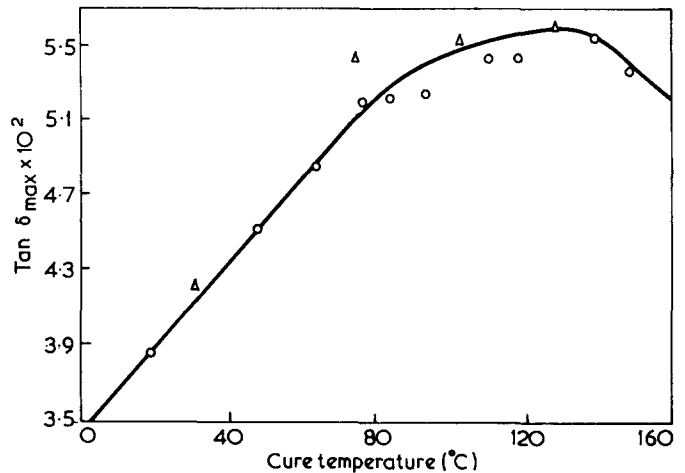


Figure 3 Peak value of  $\tan\delta$  as a function of cure temperature.  $\Delta$ , C-1-1 specimens;  $\circ$ , C-1-2 and C-1-3 specimens

The temperature of the  $\tan\delta$  peak increases from about  $-74^\circ\text{C}$  to  $-46^\circ\text{C}$  after a cure at  $159^\circ\text{C}$ . Figure 2 illustrates the relationship between the temperature of the  $\tan\delta$  peak and curing temperature. There are clearly three distinct stages in the movement of the peak. In stage 1 the peak temperature increases only slightly to a cure at  $48.0^\circ\text{C}$  but for cures between  $48.0^\circ\text{C}$  and about  $100^\circ\text{C}$  (stage 2) the movement is much more pronounced and for cures above  $100^\circ\text{C}$  (stage 3) there is only a small increase again.

Figure 3 shows the dependence of the peak  $\tan\delta$  value on curing temperature. For resins cured to  $80^\circ\text{C}$  there is a linear correlation between  $\tan\delta_{\max}$  and curing temperature, after which the value of  $\tan\delta_{\max}$  approaches a constant value and then decreases. This decrease is associated with the onset of degradation<sup>19</sup> caused by oxidation of the surface of the resin and possibly chain scission.

#### Effect of cure on the storage modulus $G'$

The shear modulus of the set of specimens previously discussed was also measured and the mean results are given in Figure 4. Not all the curves are shown in order to preserve clarity. The relaxation is manifested by a typical

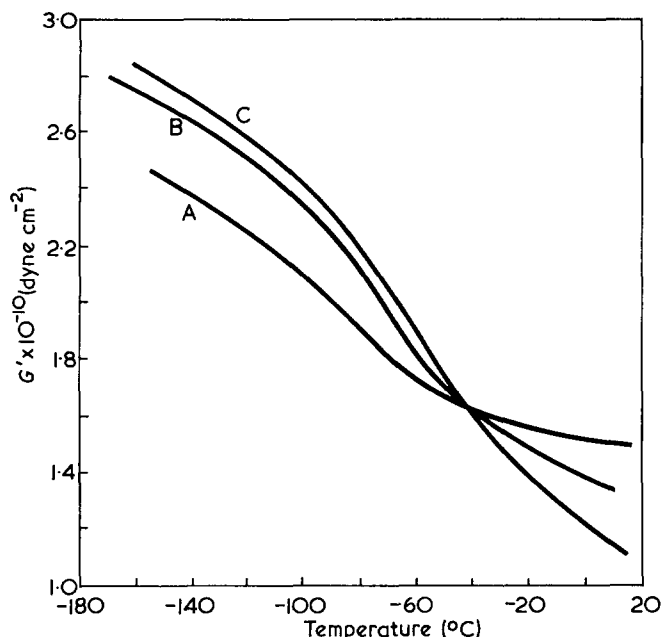


Figure 4 Shear modulus-temperature relation for varying cures. A, cast C-1-1, cure temp. 19°C; B, cast C-1-2, cure temp. 84°C; C, cast C-1-1, cure temp. 159°C

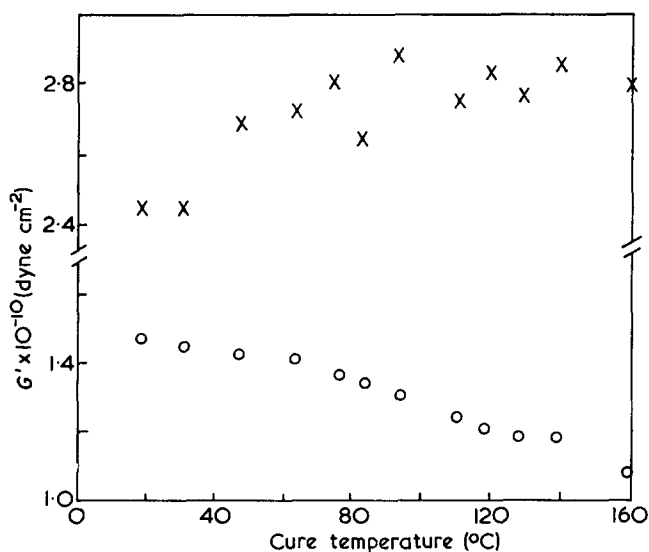


Figure 5 Shear modulus at  $-150^{\circ}\text{C}$  (x) and  $15^{\circ}\text{C}$  (o) as a function of cure temperature

sigmoidal modulus/temperature curve and the sigmoid becomes more pronounced as the degree of cure increases. The striking feature about this set of curves is that the modulus on the low temperature side of the relaxation increases with increasing cure, while the modulus at room temperature decreases. This is rather surprising since one would intuitively expect the modulus over this temperature range to increase with increasing density of crosslinking. The effect is discussed later.

The dependence of the storage modulus, measured at  $15^{\circ}\text{C}$  and  $-150^{\circ}\text{C}$ , on curing temperature is shown in Figure 5.  $G'(-150^{\circ}\text{C})$  shows quite a large scatter and the reason for this is not known. It is possible that ice formed on the surface of the specimen at low temperatures, the quantity formed being dependent on the relative humidity.

Certainly the greatest stresses are in the surface and any contamination, be it ice or an oxide layer, will affect the modulus measurement.  $G'(15^{\circ}\text{C})$  clearly shows a similar sigmoidal-shaped curve as shown in the plot of relaxation temperature against cure temperature in Figure 2. The magnitude of the changes in  $G'(-150^{\circ}\text{C})$  and  $G'(15^{\circ}\text{C})$  are about the same. It was suggested (McCrum, N. G., personal communication) that the ratio  $G'(15^{\circ}\text{C})/G'(-150^{\circ}\text{C})$  might be a convenient parameter for assessing the state of cure as this ratio reflected the magnitude of the relaxation. A plot of this ratio as a function of cure temperature is shown in Figure 6 where it is observed that a negative correlation exists between the ratio and extent of cure. It might be expected that the ratio would decrease to a constant value, this value indicating maximum cure in the system under investigation. The ratio parameter as an index for assessing cure and also for studying factors affecting cure is discussed later.

## DISCUSSION

### Features of the $\tan\delta$ curve

Intuitively the increase in area under the  $\tan\delta$  curve and the increase in its peak value are to be expected because the number of mobile segments increases with increasing cure. The curve (Figure 2) showing the relation between the temperature of the maximum  $\tan\delta$  value and the cure temperature shows three stages which can be interpreted in the following way; in stage 1 there exist in the network many epoxy and hardener chains reacted at one end only, so that mobility of a  $-\text{CH}_2-\text{CH}(\text{OH})-\text{CH}_2-\text{O}-$  segment is not influenced by neighbouring segments. However, as the density of crosslinking increases and stage 2 is reached, the resin and hardener become tied between crosslinks and mobility is restricted and possibly hindered by the surrounding crosslinked network. Finally, in stage 3 the majority of reactive sites have reacted and a further increase in crosslinking density is achieved only by increasing the thermal energy in the system. In the final stages it is envisaged that rearrangement of physical entanglements occurs and during this rearrangement the few unreacted sites will diffuse through the macromolecular structure until the meeting of another site allows further reaction. However, it is unlikely that complete reaction will ever occur. If the activation energy of the  $\gamma$ -relaxation were found in stage 1 then this energy would be the true activation energy of the relaxation and the difference between this energy and the energy necessary for relaxation in a highly cured system would represent the barrier arising as a result of network hindrance of

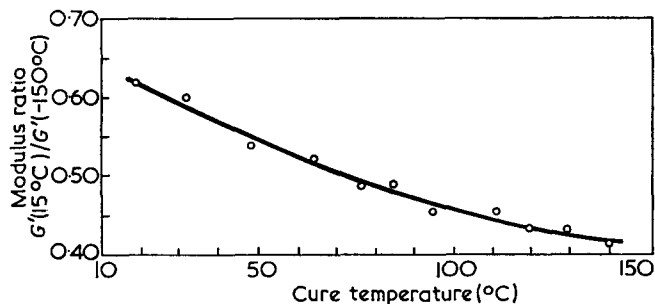


Figure 6 Change in modulus ratio with increasing cure temperature (30 min at each temperature)

the relaxation. This amounts to saying that the activation energy barrier for relaxation is increased due to the increased steric hindrance of the segments and this hindrance is only overcome by applying thermal energy to the system so that previously tied segments have sufficient energy and hence mobility to relax.

#### The modulus changes

The fact that the modulus on the high temperature side of the  $\gamma$ -relaxation decreases means that in this temperature region a highly crosslinked macromolecular network can accommodate more strain under a fixed stress than can a lightly crosslinked network. This is not altogether surprising because the curing process involves the disappearance of epoxy groups and the creation of flexible segments. Now the flexibility of the epoxy group must be very low and when the epoxy ring is opened there is a greater free volume for the resulting segments to relax into and it is envisaged that this increase in molecular mobility is the factor which allows the overall structure to become more flexible. This increase in mobility is reflected in the broadening of the  $\tan\delta$  curve on the high temperature side. At temperatures lower than the relaxation temperature, all mobility of the  $-\text{CH}_2-\text{CH}(\text{OH})-\text{CH}_2-\text{O}$ -segments will cease and an increase in crosslinking density will impede any other potentially flexible group, resulting in an overall increase in modulus. This again is in line with the  $\tan\delta$  data where a decrease in  $\tan\delta$  is observed for temperatures less than  $-100^\circ\text{C}$  reflecting a decrease in molecular mobility. Similar modulus behaviour has been reported by Starkweather<sup>27</sup> for the uptake of water in nylon.

#### MODULUS RATIO—A PROPOSED MONITOR OF CURE

##### Effects of time and temperature

Since a rapid and simple test of cure would be to measure the modulus at two temperatures only, it was decided to conduct experiments to measure the modulus at  $-196^\circ\text{C}$  and at room temperature. These tests were conducted using a torsion pendulum. The frequency of oscillation was measured at room temperature and at liquid nitrogen temperature using a fixed inertia, as the variation in modulus with very small changes of frequency was found to be negligible. Specimens were cured at three temperatures for varying periods of time and results are shown in Figure 7. This clearly shows that an optimum degree of cure is achieved at any one temperature and that this optimum quantity can only be increased by curing at a higher temperature. Whereas six hours at  $120.8^\circ\text{C}$  is sufficient to produce an optimum degree of crosslinking, the same curing time at  $132.8^\circ\text{C}$  has not produced an equilibrium extent of reaction. This is because  $T_g$  is about  $130^\circ\text{C}$ . For a temperature well above  $T_g$ , an equilibrium state of cure is achieved and it seems likely that the plateau is indicative of the maximum cure attainable in this system. As a consequence of these results it was decided to obtain more information on the roles of time and temperature in the curing process. A large number of specimens were prepared using the DGEBA/TETA system. The quantity of hardener was 11 parts per hundred parts of resin (phr), as before, which is less than the stoichiometric amount. Specimens were cured for varying periods of time at a series of temperatures. The results are shown

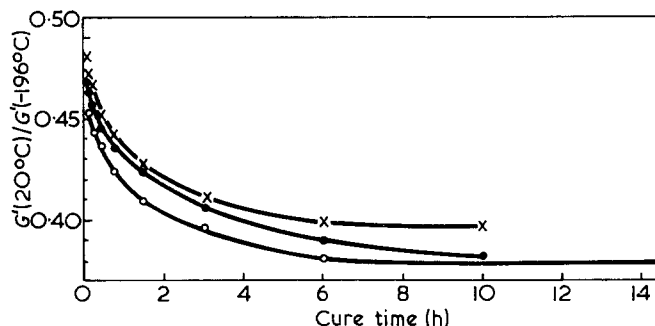


Figure 7 Modulus ratio as a function of cure time for three different cure temperatures:  $\times$ ,  $120.8^\circ\text{C}$ ;  $\bullet$ ,  $132.8^\circ\text{C}$ ;  $\circ$ ,  $145.6^\circ\text{C}$

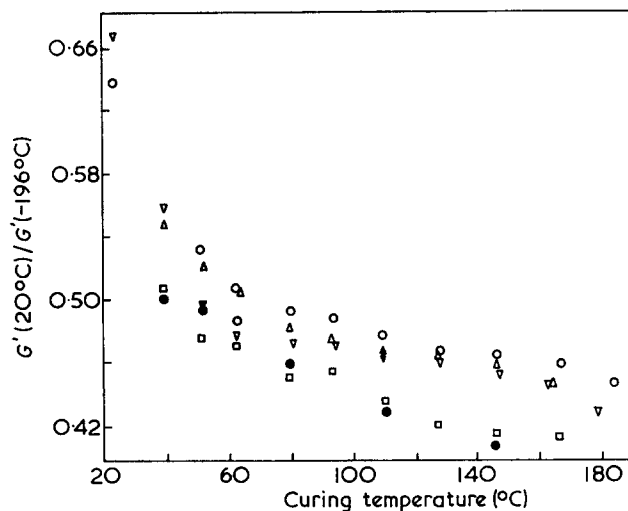


Figure 8 Change in modulus ratio as a function of cure temperature.  $\circ$ , 7 min at each temp.;  $\triangle$ , 15 min at each temp.;  $\nabla$ , 30 min at each temp.;  $\square$ , 60 min at each temp.;  $\bullet$ , 120 min at each temp.

in Figure 8. Each result was obtained using a particular specimen to avoid any cumulative effect in the curing process. There is some scatter in these results but nonetheless different degrees of cure arising from a change in cure schedule are easily observed. These results also demonstrate that at least one hour is required at any temperature for a maximum state of cure to be achieved. Unfortunately the results are not of sufficient accuracy to allow a correlation of time and temperature.

In view of the differences arising from different cure schedules, a check was made on the effect of cumulative curing. A specimen was cured for 30 min at increasingly higher temperatures and these results are illustrated in Figure 9 together with results using a batch of specimens in which each individual specimen was cured for 30 min only. Even allowing for batch variations the shape of the two curves is markedly different, illustrating that 30 min is insufficient time for an equilibrium state of cure to be achieved. Comparison of the curve showing cumulative curing with the 120 min curve in Figure 8 shows that a true equilibrium state is achieved in this case.

##### Non-stoichiometric effects

It is well known that any deviation from stoichiometry lowers  $T_g$  because a negative departure from stoichiometry results in a less densely crosslinked network, whilst an increase has a plasticizing effect. Similar behaviour might be expected for the  $\gamma$ -relaxation. However, this is

not completely analogous and plasticizing effects are only significant for quantities of hardener greatly in excess of the stoichiometric quantity. This is illustrated in *Figure 10* in which  $\tan\delta$  is plotted for various quantities of TETA hardener. For pure DGEBA resin the stoichiometric quantities for ethylene diamine (EDA) and triethylene-tetramine are 8.8 and 14.3 phr respectively, but for the commercial resin used in this investigation they are about 8.5 and 13.8 phr. The modulus ratio is plotted in *Figure 11*

and it is noted that hardener in excess of the stoichiometric ratio has little effect on the magnitude of the relaxation. This signifies that any change which occurs in the modulus ratio is due almost solely to changes in cross-linking density. It is interesting to note that specimens cured with EDA cure faster than ones cured with TETA in the region where less than the stoichiometric quantity is used. This is due to the greater mobility of the ethylene diamine molecule, leading to a less viscous mixture in the pre-gelation stage and hence a greater chance of reaction.

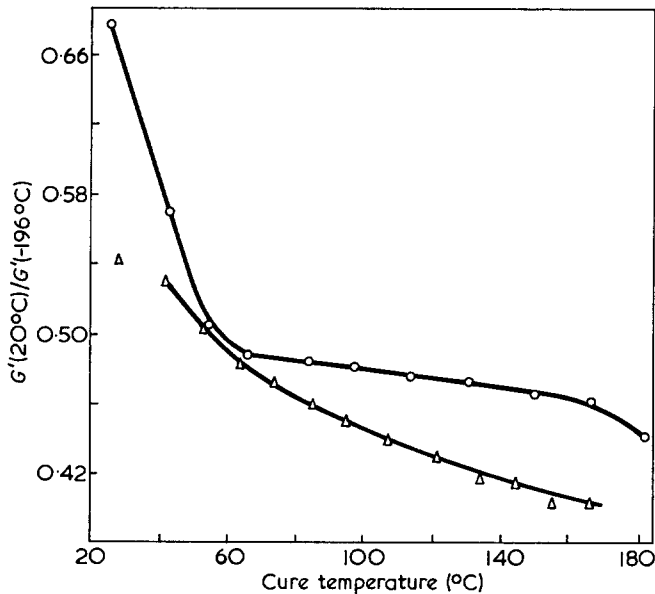


*Figure 9* Modulus ratio as a function of cure temperature for single and for successive cures. ○, Separate specimens, 30 min at each temp.; △, single specimen, 30 min at each temp.

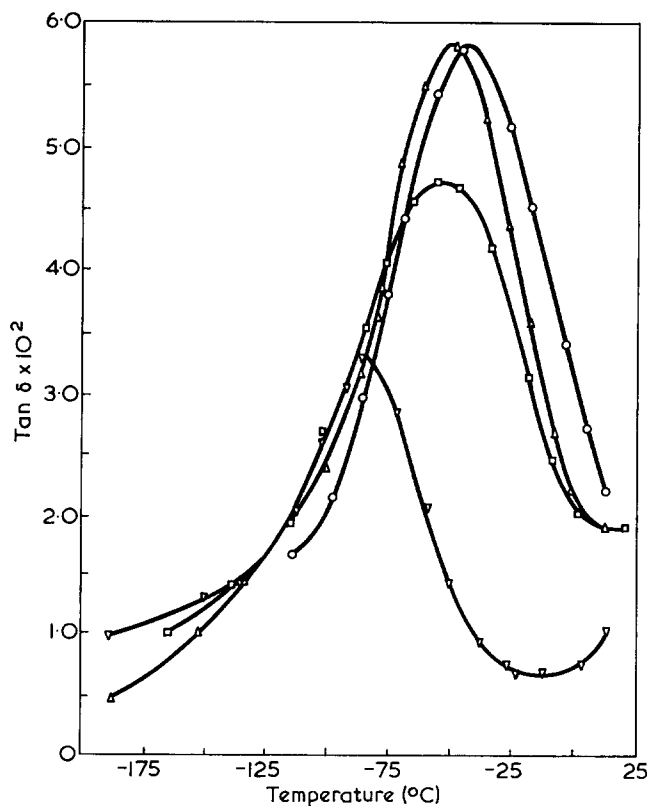


*Figure 10* Effect of non-stoichiometry on  $\tan\delta$ . Hardener content: △, 19 phr; ○, 15 phr; □, 11 phr; ▽, 8 phr. Cure: 141°C for 60 min

### Applications

It is clear that the modulus ratio test is a sensitive measure of cure in amine-cured epoxy resins particularly in stage 3 of the cure where other methods fail. We postpone discussion of the activation energy changes until Part 2 and discuss here possible ways in which the laboratory method could be extended. (i) Change of frequency. If the measurements below and above the  $\gamma$ -relaxation are to be a practical possibility then it would be better to perform them in a more suitable temperature range. Since the shift in temperature of a single relaxation-time process for 1 decade of frequency is given<sup>28</sup> by  $(\Delta H/R)[(1/T_1)-(1/T_2)]=2.303$  the  $\gamma$  process should be found at or near room temperature when ultrasonic frequencies are used. This is discussed more fully in Part 2. (ii) The change in slope of the modulus temperature curve above the  $\gamma$ -relaxation is most marked (see *Figure 4* above  $-40^\circ\text{C}$ ). Thus, from these curves  $[(dG/dT)]_0=0$  for specimens cured at  $19^\circ\text{C}$ , rising to 0.36 for specimens cured at  $84^\circ\text{C}$  and 0.90 for a  $159^\circ\text{C}$  cure. The corresponding modulus ratio values would be 0.59, 0.45, 0.40 so that the change of slope of the ( $G-T$ ) curve is also a very sensitive measure of cure. This suggests that measurement not by temperature but by frequency variation might be feasible.

In fact, for a single relaxation time model such as this the entire  $G-T$  curve shifts bodily in temperature as the frequency is changed. This is shown by *Figure 12* where superposition of curves taken at 1 Hz, 30 kHz and 1.25 MHz is nearly perfect.

Now, for a single relaxation-time process the relaxation time  $\tau = \tau_0 \exp(\Delta H/RT)$ . Substituting this value in the equation for the shear modulus:

$$G(\omega) = G(0) + \frac{[G(\infty) - G(0)]\omega^2\tau^2}{1 + \omega^2\tau^2}$$

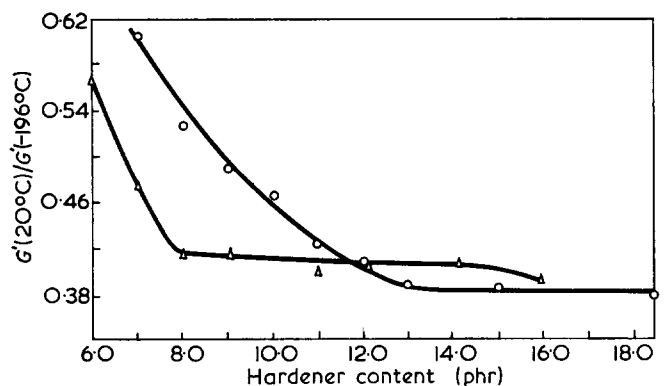


*Figure 11* Effect of non-stoichiometry on modulus ratio. ○, Triethylene tetramine (HY951); △, ethylene diamine. Cure: 141°C for 60 min



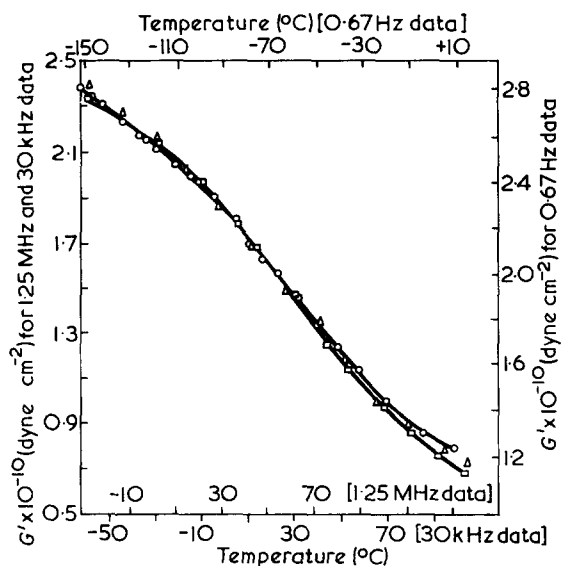


Figure 12 Shear modulus-temperature curves for three frequencies:  $\square$ , 0.67 Hz fully cured;  $\circ$ , 1.25 MHz fully cured;  $\triangle$ , 30 kHz fully cured

the relation:

$$\frac{dG}{d\omega} = \frac{R\tau^2}{\omega\Delta H} \frac{dG}{dT}$$

is obtained and we can measure the change of this quantity with cure by simple small scale change of frequency about a suitable mean value.

This and other ways of using the change of modulus at the  $\gamma$ -peak are now being studied.

#### ACKNOWLEDGEMENTS

We should like to thank the NDT Centre, AERE Harwell for providing facilities for part of the work and the Procurement Executive, Ministry of Defence for financial

support. The work was commenced at the Department of Engineering Science, University of Oxford, as part of a programme of research on amorphous polymers initiated by Dr N. G. McCrum, whose support and advice is gratefully acknowledged.

#### REFERENCES

- 1 Tanaka, Y. & Kakiuchi, H. *J. Appl. Polym. Sci.* 1963, 7, 1951
- 2 Bell, J. P. *J. Appl. Sci. (A-2)* 1970, 6, 417
- 3 French, D. M., Strecker, R. A. H. and Tompa, A. S. *J. Appl. Polym. Sci.* 1970, 14, 599
- 4 Strecker, R. A. H. *J. Appl. Polym. Sci.* 1969, 13, 2439
- 5 ASTM test D648-55T, American Society for Testing and Materials, Philadelphia
- 6 Horner, A. H., Cohen, M. and Kohn, L. S. *Mod. Plast.* 1957, (Sept.), p 184
- 7 Planer, G. V., Hall, R. H. and Christmas, M. *J. Appl. Mat. Res.* 1965 (Oct.), p 202
- 8 Robinson, A. K. *Br. Plast.* 1962, 35, 80
- 9 Judd, N. C. W. *4th Int. Reinf. Plast. Conf.* 1964
- 10 Bennett, J. H. and Avenell, C. E. *Chem. Ind.* 1952, 39, 936
- 11 Chadwick, G. F. *145th Meeting Am. Chem. Soc., New York* 1963
- 12 Miller, B. *J. Appl. Polym. Sci.* 1966, 10, 217
- 13 Fava, R. A. *Polymer* 1968, 9, 137
- 14 Haran, E. N., Gringas, H. & Katz, D. *J. Appl. Polym. Sci.* 1965, 9, 3505
- 15 Shimazaki, A. *J. Polym. Sci. (C)* 1968, 23, 555
- 16 Shito, N. and Sato, M. *J. Polym. Sci. (C)* 1967, 16, 1069
- 17 Kline, D. E. *J. Polym. Sci.* 1960, 47, 237
- 18 May, C. A. and Weir, F. E. *SPE Trans.* 1962 (July), p 207
- 19 Pogany, G. *DPhil Thesis Oxford University*, 1966
- 20 Kenyon, A. S. and Neilsen, L. E. *J. Macromol. Sci.* 1969, A3, 275
- 21 Krehling, R. P. and Kline, D. E. *J. Appl. Polym. Sci.* 1969, 13, 2411
- 22 Akimov, S. V. and Barkova, M. V. *Soviet Plast.* 1969, 12, 46
- 23 Kosuge *et al. Chem. High Polymers (Japan)* 1971, 28, 719
- 24 Schatzki, T. F. *J. Polym. Sci.* 1962, 57, 496
- 25 Cuddihy, E. F. and Moacanin, J. *J. Polym. Sci. (A-2)* 1970, 8, 1627
- 26 Delatycki, O., Shaw, J. G. and Williams, J. G. *J. Polym. Sci. (A-2)* 1969, 7, 753
- 27 Starkweather, H. W. *J. Macromol. Sci.* 1969, B3 (4), 727
- 28 Neilsen, L. E. 'Mechanical Properties of Polymers', Reinhold, New York, 1962

# Mechanical relaxation studies of the cure of epoxy resins: 2. Activation energy of the $\gamma$ -process in amine-cured epoxy resins

R. G. C. Arridge

*H. H. Wills Physics Laboratory, University of Bristol, Bristol BS8 1TL, UK*

and J. H. Speake

*NDT Centre, AERE, Harwell, Didcot, Berks, UK  
(Received 22 February 1972; revised 4 April 1972)*

Measurements are reported of the activation energy for secondary relaxation ( $\gamma$ -relaxation) in amine-cured epoxy resins. Good agreement was found between values determined from the area under the loss modulus/inverse absolute temperature curve and those derived from the shift of the  $\gamma$ -relaxation in temperature for different measuring frequencies. The energy was found to be dependent on the degree of cure, increasing from about 14 kcal/mol during the early stages of cure to higher values following post cure after gelation, eventually levelling out to a value characteristic of the hardener used (23 kcal/mol for triethylene tetramine, 26 kcal/mol for ethylene diamine). If less than the stoichiometric amount of hardener is used the activation energy is reduced (e.g. to 18 kcal/mol for 11phr TETA). The interpretation of the  $\gamma$ -relaxation as being due to 'crankshaft' rotation of the  $-\text{CH}_2-\text{CH}(\text{OH})-\text{CH}_2-\text{O}$  group with an activation energy of 14 kcal/mol is therefore modified on post curing to become an example of hindered rotation in a double potential well, the additional energy barrier being due to steric effects arising from the increase in crosslink density.

## INTRODUCTION

The secondary mechanical relaxation in amine-cured epoxy resins, known as the  $\gamma$ -relaxation, is generally thought<sup>1-4</sup> to be caused by a flexible segment  $-\text{CH}_2-\text{CH}(\text{OH})-\text{CH}_2-\text{O}$  formed during the curing process, although other hypotheses have also been suggested<sup>5, 6</sup>. The manner in which the glycidyl segment relaxes is not known but Pogany<sup>1</sup> has suggested that the group probably rotates in the manner of a crankshaft as outlined by Schatzki<sup>7</sup>. It is the purpose of this paper to present measurements of the activation energy of the  $\gamma$ -process for resins in various states of cure to partly elucidate the mechanism of this relaxation.

The usefulness of determining the activation energy of a mechanical relaxation is that it provides a quantitative measure of the magnitude of the relaxation and often an indication of the type and location of the molecular species giving rise to it.

There have been many determinations of the activation energy of the major transition but only Krehling and Kline<sup>8</sup> and Van Hoorn<sup>4</sup> have put forward any value for the  $\gamma$ -relaxation. The former found a value of 16 kcal/mol in a system consisting of diglycidyl ether of bisphenol A cured with metaphenylene diamine whereas the figure of

14 kcal/mol quoted by Van Hoorn is the average of a number of systems each containing the glycidyl ether segment.

## EXPERIMENTAL

The materials and measuring techniques used in this investigation were the same as previously reported<sup>9</sup> in which a commercial diglycidyl ether of bisphenol A (DGEBA) was crosslinked with either ethylene diamine (EDA) or triethylenetetramine (TETA). Varying degrees of cure were achieved by using less than the stoichiometric quantity of curing agent and also by heat treatment.

The methods of measurement were a torsion pendulum operating at 0.67 Hz which yielded both the real and imaginary parts of a complex shear modulus, and ultrasonic techniques. These were employed over the frequency range of 10 kHz to 2 MHz and only the real part of a complex shear modulus was measured.

## LOSS MODULUS

The loss modulus is the imaginary part of a complex modulus and is denoted  $G''$ . It is related to the storage modulus  $G'$  and the loss tangent,  $\tan\delta$ . The change in loss

modulus with cure is governed by the same factors as  $\tan\delta$  and indeed plots of  $G''$  as a function of temperature for a series of states of cure are similar to those of  $\tan\delta$  but occur at lower temperatures<sup>9</sup>. However, the usefulness of the loss modulus is in the determination of the activation energy of the relaxation. Read and Williams<sup>10</sup> have put forward a theory which allows the calculation of activation energy from the area beneath a  $G''$  versus  $1/T$  plot. Their theory showed that the relationship between area and activation energy is of the following form:

$$\int_0^\omega G'' \left( d\frac{1}{T} \right) = \frac{AR^2}{\Delta H^2} \left[ \frac{-\pi \ln \omega \tau_0}{2} \right] + \sum_{r=0}^{\infty} \frac{(-1)^r (\omega \tau_0)^{2r+1}}{(2r+1)^2} \quad (1)$$

where  $A$  = a constant,  $\Delta H$  = the activation energy,  $R$  = the gas constant,  $T$  = temperature in K,  $\omega$  = the measuring frequency,  $\tau$  = relaxation time at temperature  $T$  K,  $\tau_0$  = relaxation time at infinite temperature.

If the temperature of the maximum loss is denoted  $T(\max)$ , then

$$A = (G_R^{T(\max)} - G_U^{T(\max)}) T(\max)$$

and

$$\tau_{\max} = \tau_0 \exp \left( \frac{\Delta H}{RT(\max)} \right) \quad (2)$$

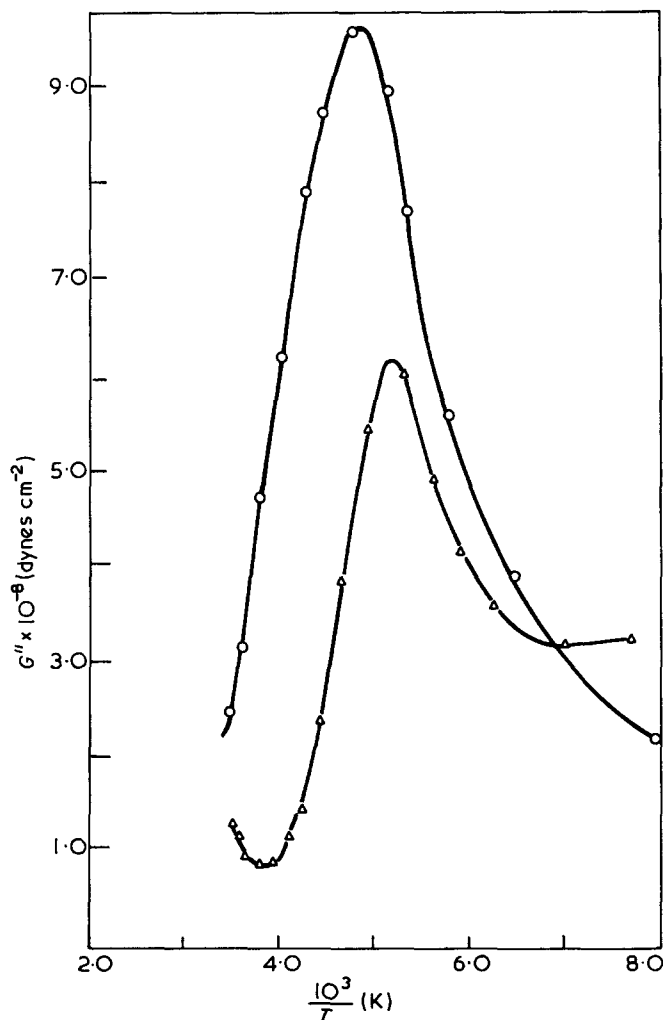


Figure 1 Loss modulus for two states of cure. O, 2h at 159°C; Δ, cured at room temperature

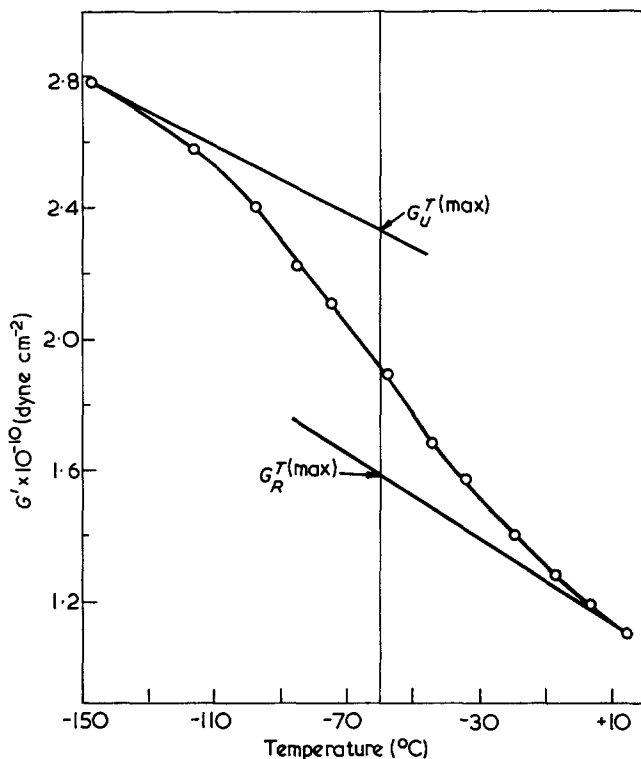


Figure 2 Evaluation of  $G_U^{T(\max)}$  and  $G_R^{T(\max)}$

$G_U$  and  $G_R$  are the unrelaxed and relaxed values of shear modulus respectively.

Schallamach<sup>11</sup> showed that  $\omega\tau_{\max}$  differs only slightly from unity, which is the value predicted by the single relaxation time model, and also that  $\omega\tau_0 \ll 1$  for the frequencies normally encountered, thus a combination of equations (1) and (2) leads to the following result:

$$\Delta H = [G_R^{T(\max)} - G_U^{T(\max)}] \frac{R\pi}{2 \int_0^\infty G'' d\left(\frac{1}{T}\right)} \quad (3)$$

Thus the area under the  $G''$  versus  $1/T$  curve and the extrapolated values of  $G_U$  and  $G_R$  at  $T(\max)$  are the only experimental quantities required.

Unfortunately equation (3) is limited in applicability. Two curves of loss modulus are shown in Figure 1 for a system of DGEBA hardened with 11 parts of TETA (by weight) per hundred parts of resin (phr). It is apparent that the curve representing 19°C cure has two widely differing values of loss modulus. This renders the construction of a baseline open to considerable conjecture and for curves of this form no activation energy was calculated. The area under the curve for 159°C cure is well defined and was measured. Measurements of area were made using a planimeter.  $G_U^{T(\max)}$  and  $G_R^{T(\max)}$  were found by extrapolation to  $T(\max)$  using values of  $G_U$  and  $G_R$  at temperatures at which the baseline of the  $G''$  versus  $1/T$  curve intersected  $G''$ , as shown in Figure 2.

## RESULTS

Values of activation energy are given in Table 1 for cure temperatures above 70°C, where the areas under the loss modulus curves are well defined.

Table 1 Activation energies for cure temperatures above 70°C

Cure temp. (°C)	Activation energy (kcal/mol)
76.3	15.2
93.9	17.9
118.0	18.3
159.0	17.3

The value obtained at a cure temperature of 159°C is lower than the one at 118.8°C and this is due to the onset of degradation<sup>12</sup>. The results would seem to suggest that the activation energy increases with increasing cross-linking density and this is borne out as shown in the following section.

Modulus/temperature curves were also obtained at differing frequencies and it was found that the temperature of the  $\gamma$ -relaxation, in a system of DGEBA cured to a true equilibrium state with 11 phr of TETA, moved from about -45°C when measured at 0.67 Hz to about 65°C when measured at 1.25 MHz. The good superposition of curves obtained at different frequencies signified that the activation energy of the  $\gamma$ -process does not depend on temperature in contrast to the glass/rubber transition where the activation energy is strongly dependent on temperature. Hence equation (2) can be rewritten to yield the activation energy by measuring the shift in temperature of the relaxation when observed at a different frequency. This is expressed as:

$$\Delta H = \frac{R}{\left(\frac{1}{T_1} - \frac{1}{T_2}\right)} \ln \frac{\omega_2}{\omega_1} \quad (4)$$

where  $\omega_1$ ,  $\omega_2$  are the measuring frequencies and  $T_1$ ,  $T_2$  are the temperatures of the  $\gamma$ -relaxation when observed at  $\omega_1$  and  $\omega_2$  respectively. Results are shown in Figure 3, the slope of which yields an activation energy of 17.9 kcal/mol. This is in very good agreement with the value found by the loss modulus analysis on the same resin system.

#### DEPENDENCE OF ACTIVATION ENERGY ON STATE OF CURE

The loss modulus analysis suggested that the activation energy decreased with decreasing degree of cure and a detailed investigation was therefore made on the relationship between activation energy and state of cure.

Curves of shear modulus as a function of temperature measured at 30 kHz were obtained on the system DGEBA cured with the stoichiometric quantity of TETA at various temperatures. Some of these curves are shown in Figure 4. The modulus and temperature were recorded at the point of inflection for each curve. A small section of the cylindrical specimen used in the resonance technique was then inserted into the transit time equipment operating at 1.25 MHz. The temperature was then altered until the measured velocity yielded a modulus value identical to that noted at the inflection point. Use of the Arrhenius relationship then allowed calculation of the activation energy.

Results are illustrated in Figure 5. It was tempting, although not justifiable, to draw a sigmoid through the points because apart from the results at 25°C and 80°C

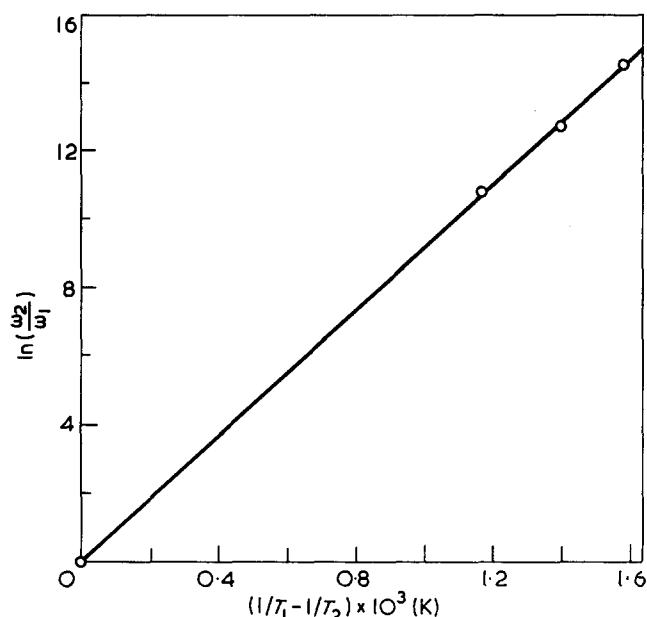
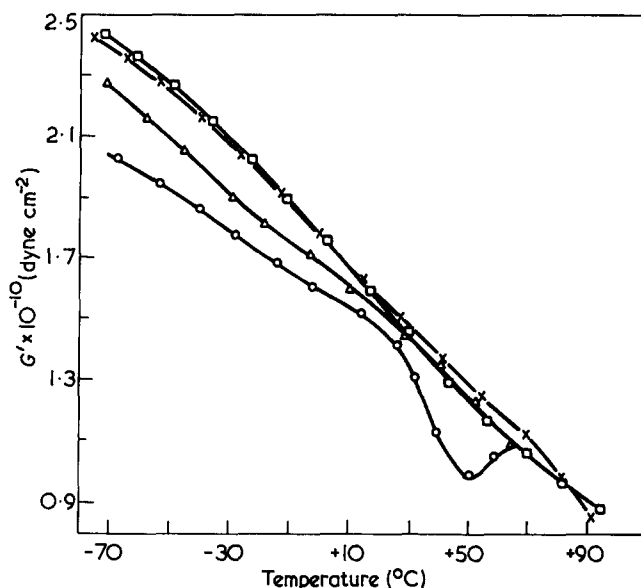
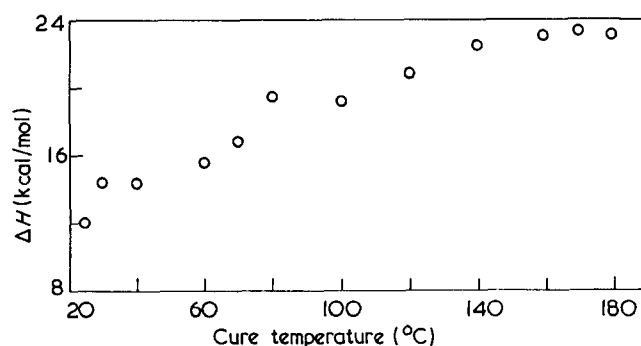


Figure 3 Determination of activation energy from data at four frequencies


 Figure 4 Shear modulus measured at 30 kHz for various states of cure. (The anomaly in the curve for room temperature cure is due to post cure during test.)  $\circ$ , Room temperature cure;  $\Delta$ , 65°C cure for 2h;  $\times$ , 100°C cure for 2h;  $\square$ , 130°C cure for 2h

 Figure 5 Activation energy of the  $\gamma$ -relaxation as a function of cure temperature. Cured 30 min at each temperature

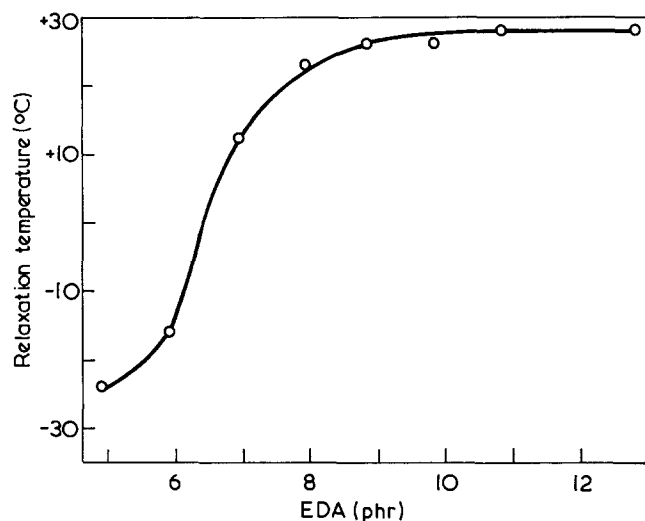


Figure 6 Temperature of the  $\gamma$ -relaxation for varying quantities of hardener

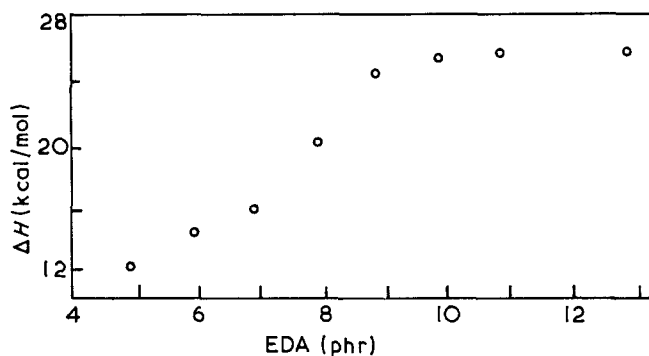


Figure 7 Activation energy of the  $\gamma$ -relaxation for different amounts of hardener

the others lie on a smooth sigmoidal-shaped curve. The determination of activation energies of resins with a small degree of crosslinking is more inaccurate than for fully cured material owing to the greater uncertainty in determining the temperature of inflection on the modulus/temperature curve. The upper value of about 23 kcal/mol for the fully cured resin is much higher than the value of 17.9 kcal/mol found using four frequencies and the reason for the difference is that a stoichiometric quantity of hardener was used in the former case whereas only 11 phr was used in the latter, resulting in a higher density of crosslinking. This was checked by measuring the activation energy in systems containing varying quantities of hardener in which an equilibrium state of cure has been achieved. EDA was used rather than TETA owing to the greater ease of preparation of specimens utilizing the former constituent. The temperature of the relaxation, determined by the inflection point, was plotted as a function of EDA concentration and is shown in Figure 6. These results are similar in form to those obtained using a torsion pendulum where  $\tan\delta_{\max}$  was plotted against cure temperature. The activation energy was determined and results are presented in Figure 7 where it is demonstrated that the activation energy for a resin cured with less than

the stoichiometric quantity is less than for resins cured with higher concentrations of hardener.

## DISCUSSION

The results lend striking support for the proposed mechanism of cure outlined in Part 1<sup>9</sup>. Here it was postulated that crosslinks are initiated at widely dispersed sites in the network but as the number increase, potentially reactive segments are sterically hindered from diffusing to other reactive sites and to overcome this barrier more thermal energy must be supplied to the network. This mechanism is certainly borne out by the results shown in Figure 5 in which the activation energy is seen to increase until a curing temperature of 140°C is attained when it becomes constant. These results illustrate the importance of knowing the state of cure when determining activation energies and the values of 16 kcal/mol reported by Krehling and Kline<sup>8</sup>, and of 14 kcal/mol by Van Hoorn<sup>4</sup> are not meaningful because these workers failed to realize that an increase in crosslinking density inhibits the  $\gamma$ -relaxation, thus increasing the apparent activation energy, and they do not stipulate the state of cure to which those energies refer. If Figure 5 is assumed to be sigmoidal, then the apparently constant value of about 14 kcal/mol for low degrees of cure must be indicative of the energy necessary for the glycidyl ether segment to relax and any value above this represents the extra energy needed to overcome the increasing steric hindrance as more crosslinks are formed. If a crankshaft-type relaxation mechanism is assumed then the lower value certainly agrees well with the value of 13 kcal/mol calculated by Schatzki<sup>7</sup> based on twice the butane potential barrier plus a van der Waals barrier determined from cohesive energy density. However, the relaxation temperature for methylene sequences is about -120°C when measured at 1 Hz and because the  $\gamma$ -relaxation in epoxy resin occurs at a higher temperature, owing to the hindrance of the pendant hydroxyl, the activation energy assuming a crankshaft model would be expected to be higher than the 13 kcal/mol proposed by Schatzki. Thus the crankshaft model does not seem to be realistic from energy considerations and it is suggested that the relaxation is governed by hindered rotation in a double potential well whose height above about 14 kcal/mol is determined by the extent of steric hindrance caused by an increase in crosslinking density. It is interesting to note that the form of the curves shown in Figures 6 and 7 is identical adding further weight to the proposed curing mechanism. Also apparent is the fact that the activation energy for the relaxation in a resin fully cured with the stoichiometric quantity of EDA is higher than one cured with TETA, i.e. 26 as compared with 23 kcal/mol. This would seem to signify that the stiffness of the hardener chain influences the relaxing segment. The EDA chain is about half the length of a molecule of TETA and probably less mobile although in both hardeners reactive hydrogen atoms are separated by two (CH<sub>2</sub>) units. Nonetheless the longer chain is expected to exhibit greater flexibility. Delatycki *et al.*<sup>5</sup> examined a series of epoxy-diamine networks using a low frequency torsion pendulum and found that the temperature of the  $\gamma$ -relaxation remained constant for diamines containing up to 12 methylene groups, although the height of the loss modulus/temperature curve decreased with increasing chain length. This suggests that the activation energy of the relaxation

decreased with increasing chain length. In view of the results presented in our paper it is surprising that the relaxation temperature remained constant because the change in steric hindrance arising from the change in crosslinking density when the hardener is varied might be expected to shift the relaxation along the temperature axis. This could be checked by employing an ultrasonic test method for measuring the loss modulus where any change in activation energy would be shown up by a spread of relaxation temperatures even though the temperature remained constant in the low frequency test.

#### CONCLUSION

The dependence of the activation energy of the  $\gamma$ -relaxation on the state of cure demonstrates the part played by steric hindrance on the relaxation mechanism. For low degrees of cure the activation energy of the  $\gamma$ -process is fairly constant and of the order of 13 kcal/mol. It must be remembered that this value is obtained in a system which has already undergone about 70% of the total crosslinking reaction. It is unlikely that 100% of the reaction is ever achieved and so the large part played by steric effects in the later stages is rather surprising. The limiting value of activation energy in a fully cured system

is determined by the crosslinking density and is found to be higher in systems where short chains are reacted.

#### ACKNOWLEDGEMENTS

This work was supported by the Procurement Executive, Ministry of Defence. We should also like to thank the NDT Centre, Harwell for providing the experimental facilities.

#### REFERENCES

- 1 Pogany, G. A. *Polymer* 1970, **11**, 66
- 2 May, C. A. and Weir, F. E. *SPE Trans.* 1962 (July) p 207
- 3 Kline, D. E. *J. Polym. Sci.* 1960, **47**, 237
- 4 Van Hoorn, H. J. *Appl. Polym. Sci.* 1968, **12**, 871
- 5 Delatycki, O., Shaw, J. C. and Williams, J. G. J. *Polym. Sci. (A-2)* 1969, **7**, 753
- 6 Cuddihy, E. F. and Moacanin, J. J. *Polym. Sci. (A-2)* 1970, **8**, 1627
- 7 Schatzki, T. F. *J. Polym. Sci.* 1962, **57**, 496
- 8 Krehling, R. P. and Kline, D. E. *J. Appl. Polym. Sci.* 1969, **13**, 2411
- 9 Arridge, R. G. C. and Speake, J. H. *Polymer* 1972, **13**, 443
- 10 Read, B. E. and Williams, G. *Trans. Faraday Soc.* 1961, **57**, 1979
- 11 Schallamach, A. *Trans. Faraday Soc.* 1946, **A42**, 495
- 12 Pogany, G. A. *DPhil Thesis* Oxford University, 1966

# Kinetics of epoxy cure: 2. The system bisphenol-A diglycidyl ether/polyamide

R. B. Prime

*IBM Systems Development Division, Monterey and Cottle Roads, San Jose, California 95114, USA*

and E. Sacher\*

*IBM Systems Development Division, PO Box 6, Endicott, NY 13760, USA*

*(Received 14 February 1972)*

Differential scanning calorimetry, infra-red absorption and d.c. conductivity were used to study the cure of the system bisphenol-A diglycidyl ether/polyamide in the range 23–110°C. At elevated temperatures, two reactions were found to occur subsequent to the cure reaction. In addition, glass transition data indicate that, where network mobility permits, large-scale reorganization of the network occurs subsequent to cure to give an 'equilibrium' glass.

## INTRODUCTION

This paper is part of a continuing study of the cure, structure and physical properties of several common epoxide/hardener systems. Previous work<sup>1</sup>, using *m*-phenylene diamine as hardener, showed that the cure of bisphenol-A diglycidyl ether occurred by only one reaction, network formation, which was diffusion controlled. Complete cure was obtained only at temperatures above the  $T_g$  of the cured epoxy; below the  $T_g$ , the extent of cure was governed by network rigidity, in not allowing reactants into proximity for further reaction.

The present study, using a polyamide hardener, was undertaken not only because polyamide constitutes one of the most popular hardeners in use today, but also to test the generality and applicability of the conclusions in the previous study. Polyamides are manufactured<sup>2,3</sup> from drying and semi-drying oils. Heating these oils causes the dioenic acids they contain to polymerize; partial reaction with a polyfunctional amine results in a mixture, each of whose molecules contains several primary and secondary amine groups. It is these groups which react with the epoxide.

The existence of several reactive groups on each polyamide molecule is a distinct advantage: since only two groups need react to include the molecule in the forming network, and only three for crosslinking, the epoxide/polyamide ratio may be varied over wide ranges<sup>3,4</sup>, resulting in epoxies varying from glassy to rubbery.

## EXPERIMENTAL

### Materials

The bisphenol-A diglycidyl ether (Dow DER 332) and polyamide (General Mills Versamid 140) were used

without further purification. Versamid 140 has an amine value ( $\equiv$  mg KOH equivalent to amine alkalinity in 1 g) of 385. Thus, in 1 g of polyamide there are 385 mequiv. amine  $\div$  56.01 mg KOH/mequiv. = 6.87 mequiv. KOH = 6.87 mequiv. amine. In terms of available amine hydrogens, there are 145.6 mg/mequiv.†

The physical properties of a polyamide appear to depend far less on the type of oil used in the manufacture than on the polyfunctional amine and reaction conditions employed<sup>2</sup>, suggesting that fluctuating market prices may determine the oil used at any given time. To avoid the possibility of batch-to-batch variations, a single batch of polyamide was used throughout. Both it and the epoxy were stored at  $-20^\circ\text{C}$ .

The epoxy was made as previously described<sup>1</sup>. Two epoxide/polyamide ratios were used: 2 g/5 g and 2 g/1.5 g, equivalent to a 300% excess of polyamide and a 10% excess of epoxide, respectively, calculated on a 1 : 1 basis. A fresh sample of epoxy was prepared each week.

### Instrumental procedures

Differential scanning calorimetry (d.s.c.), infra-red (i.r.) absorption and d.c. conductivity data, in the temperature range 23–110°C, were obtained as previously described<sup>1</sup>. Both d.s.c. and i.r. are more sensitive to the early stages of the reaction and were used to obtain data to about 70% of cure. Because there is little change in the d.c. conductivity prior to the gel point, which, in the present case was determined<sup>1</sup> to occur at about 50% reaction, this latter method was used to obtain data on the last 50% of cure.

---

† The authors wish to point up the uselessness of the term 'amine value', since it is just as simple for the manufacturer to carry the calculation a step further and indicate the mg of amine hydrogens available per mequiv. It is this latter value which must be compared with the epoxide value ( $\equiv$  mg epoxide/mequiv.) in calculating epoxide/hardener ratios.

---

\* To whom correspondence should be addressed.

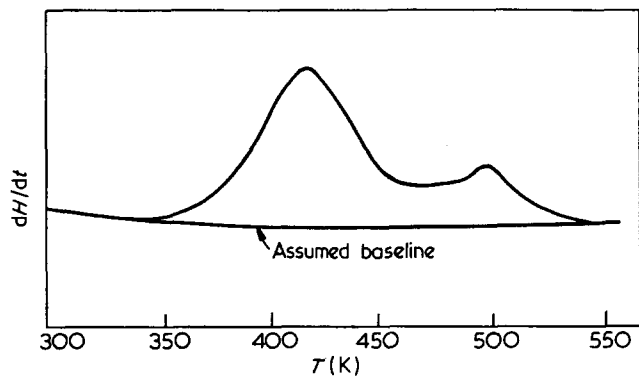


Figure 1 Dynamic d.s.c. trace, at 20°C/min, of the cure of the 2/1.5 epoxide/hardener ratio

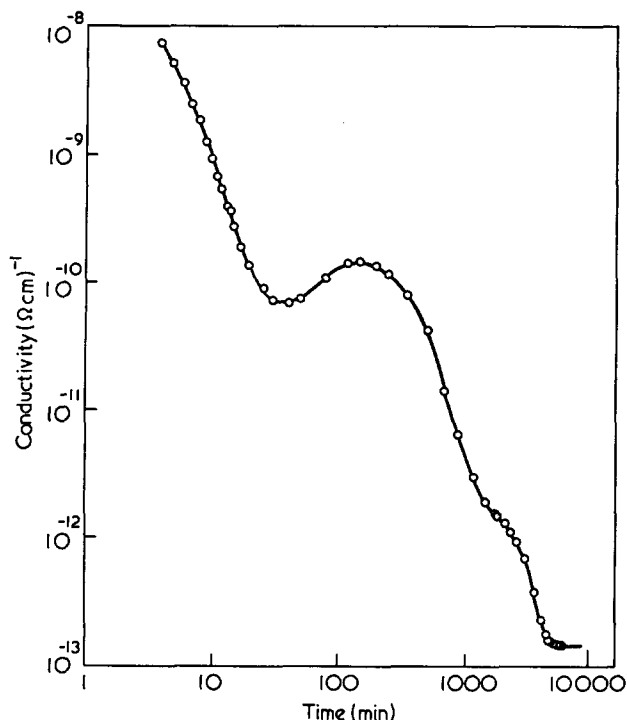


Figure 2 Isothermal d.c. conductivity plot, at 110°C, of the cure of the 2/1.5 epoxide/hardener ratio

#### Treatment of data

The various data were fitted to the equation<sup>5</sup>

$$\frac{d\alpha}{dt} = k(1-\alpha)^n \quad (1)$$

where  $\alpha$  is the fraction reacted at time  $t$ ,  $k$  is the overall rate constant and  $n$  is the overall reaction order.

Neither d.s.c. or i.r. showed an induction time, even at room temperature. Its absence is due to the presence of carboxylic acid and tertiary amine groups in the polyamide mixture, which are known catalysts<sup>6,7</sup>.

## RESULTS

At room temperature only one reaction occurs for both epoxide/hardener ratios. Raising the temperature to

Table 1 Changes in the i.r. spectrum at 40°C

Frequency (cm <sup>-1</sup> )	Direction	Preferred assignment <sup>a</sup>
3240	Increase	Bonded OH, NH stretch
1640	Increase	Carbonyl stretch
1025	Increase	OH stretch
909	Decrease	Oxirane ring

<sup>a</sup> Several peaks are composite. The preferred assignments were made after considering the positions and directions of the magnitude changes of all the peaks, and the reaction possibilities

70°C causes a second reaction to occur subsequent to the first; at 100°C, a third reaction occurs. These three reactions are seen in Figure 1, which shows a dynamic d.s.c. trace, and in Figure 2, which shows an isothermal d.c. conductivity plot.

It was found possible to separate the d.s.c. trace into its three components, using a DuPont 310 Curve Resolver, as seen in Figure 3. Significant changes in the i.r. spectrum at 40°C, a temperature at which only the first reaction occurs, are found in Table 1. Clearly, the first reaction is the expected attack of the epoxide by the hardener. For each epoxide/hardener ratio, Arrhenius plots of the d.s.c., i.r. and d.c. conductivity data all fit on the same straight line. For the 2/1.5 ratio (10% excess epoxide), giving a glassy cured material:

$$k (\text{sec}^{-1}) = 6.34 \times 10^5 \exp(-14.5 \text{ kcal mol}^{-1}/RT)^* \quad (2)$$

where  $R$  is the gas constant and  $T$  is the absolute temperature;  $n$  values ranged from 0.2 to 1.7. For the 2/5

\* 1 kcal mol<sup>-1</sup> = 4.1868 kJ mol<sup>-1</sup>.

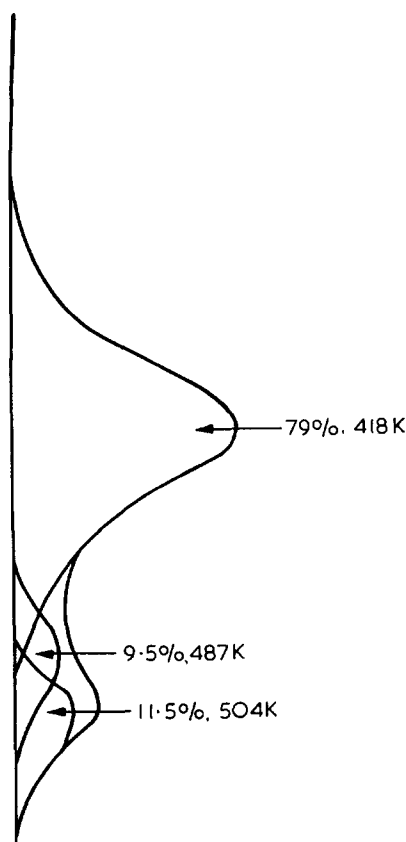


Figure 3 Curve resolution of the d.s.c. trace in Figure 1



Table 2 Changes in the i.r. spectrum at 80°C

Frequency (cm <sup>-1</sup> )	Direction	Preferred assignment <sup>a</sup>
3240	Increase	Bonded OH, NH stretch
1645	Increase	Carbonyl stretch
1290	Increase	Ester stretch
720	Decrease	Amide V

<sup>a</sup> See Table 1

ratio (300% excess polyamide), giving a rubbery cured material:

$$k(\text{sec}^{-1}) = 2.96 \times 10^6 \exp(-15.1 \text{ kcal mol}^{-1}/RT) \quad (3)$$

where  $n$  varied from 0.6 to 1.9.

The significant changes in the i.r. spectrum which occur on raising the temperature to 80°C, where the second reaction occurs, are found in Table 2. The data suggest that ester and amine are being formed at the expense of amide.

Infra-red data were not used in evaluating the kinetics of this second reaction because the spectrum consisted of a preponderance of broad, overlapping peaks, several of which were clearly composite in nature. D.c. conductivity data could not be used because a clear separation of the processes could not be established. Data were evaluated solely from a previously determined relationship<sup>8</sup> between the d.s.c. peak temperatures and the heating rates. For the 2/1.5 ratio:

$$k(\text{sec}^{-1}) = 1.6 \times 10^6 \exp(-18.0 \text{ kcal mol}^{-1}/RT) \quad (4)$$

and for the 2/5 ratio:

$$k(\text{sec}^{-1}) = 3.3 \times 10^6 \exp(-17.6 \text{ kcal mol}^{-1}/RT) \quad (5)$$

A comparison of the kinetics of the first reaction, calculated in this manner, with equations (2) and (3), and a similar comparison with the system using *m*-phenylene diamine as hardener<sup>1</sup>, indicated that the Kissinger method gives pre-exponentials which are consistently an order of magnitude too low and activation energies which are consistently 1.6 to 1.8 kcal mol<sup>-1</sup> too low. Thus, the pre-exponentials and activation energies in equations (4) and (5) should be considered as lower limits.

When the temperature is increased to 110°C, a third reaction occurs. Significant changes in the i.r. spectrum occurring at that temperature are found in Table 3, where the data indicate the loss of amide. Here, too, kinetics were necessarily evaluated solely from d.s.c. data, to which the same comments apply as previously. The kinetics could not be evaluated for the 2/5 ratio because the peaks were too low and too broad to obtain peak positions. For the 2/1.5 ratio:

$$k(\text{sec}^{-1}) = 4.4 \times 10^9 \exp(-26.5 \text{ kcal mol}^{-1}/RT) \quad (6)$$

Glass transitions were determined by d.s.c., using a temperature rise of 10°C/min. They are found in Table 4, where it is seen that the second reaction raises the  $T_g$  of the first reaction, and the third reaction introduces another transition at a lower temperature.

These glass transitions are for a system which is in a dynamic state of equilibration, as may be seen by the following: carrying out the cure at a temperature below which the subsequent reactions occur leads to the  $T_g$  values for reaction 1 found in Table 4. After several

Table 3 Changes in the i.r. spectrum at 110°C

Frequency (cm <sup>-1</sup> )	Direction	Preferred assignment <sup>a</sup>
1640	Decrease	Carbonyl stretch
1580	Decrease	NH deformation
1100	Decrease <sup>b</sup>	OH stretch
735	Decrease	Amide V

<sup>a</sup> See Table 1<sup>b</sup> Either no decrease or slight decrease

Table 4 Glass transition temperatures (°C)

Reaction	Epoxy/polyamide ratios	
	2/1.5	2/5
1	40	-10
2	85	20
3	30, 85	20 <sup>a</sup>

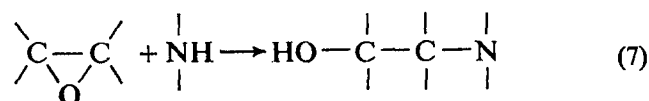
<sup>a</sup> No distinct  $T_g$  found below 20°C

hundred hours at room temperature, both  $T_g$  values were raised to 52°C and an endotherm was seen on the d.s.c. trace at 65°C, with no change in the subsequent reactions. That is, not only does structural equilibration occur, in the case of the 2/1.5 ratio it occurs substantially below the  $T_g$ .

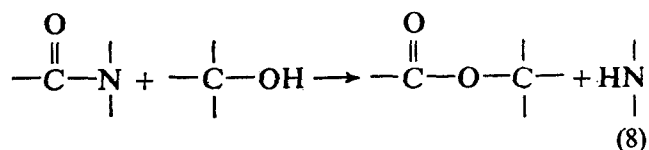
## DISCUSSION

The activation energies of many epoxy/hardener systems were previously noted<sup>1</sup> to be very close in magnitude, irrespective of whether monomeric<sup>9,10</sup> or polymeric systems<sup>9-13</sup> were being studied. These values generally fall in the range  $13 \pm 2 \text{ kcal mol}^{-1}$  and indicate that the forming network has little effect on the activation energy. The similarity of these values to the activation energy for self-diffusion in polymers<sup>14,15</sup> has prompted the suggestion<sup>1</sup> that the reaction is diffusion controlled.

In the present case, the cure appears to occur through three reactions, the first of which is the expected attack of the oxirane ring by the primary or secondary amine group:

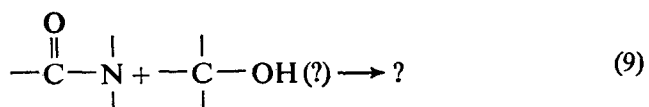


At sufficiently elevated a temperature, a subsequent reaction occurs, which our data suggest to be:



This reaction must occur subsequent to the first, since it uses the alcohol formed in that reaction. That equation (8) is not, however, complete is indicated by the fact that no reactions occur on heating either of the reactants separately, with added alcohol.

On raising the temperature still further, another reaction occurs, which appears to involve:



Equation (7) would be expected to have an activation energy comparable to those of the monomeric and polymeric systems previously mentioned. As seen in equations (2) and (3), this is the case; further, a change in polyamide content of over 300% has no effect on the activation energy. The change in the rate constant reflects solely the change in the pre-exponential. Because the pre-exponential increases in magnitude as the system becomes more rubbery, the magnitude of the pre-exponential (and the rate constant) appears to reflect the ease of motion of the reacting chain ends. It is to be noted, however, that a statistical analysis using a 95% confidence level<sup>1</sup> would indicate no difference in pre-exponentials.

The first of the subsequent reactions, equation (8), seems identically the same for both epoxide/polyamide ratios, as seen in equations (4) and (5). Although this identity suggests that large-scale motions of the epoxy network are not involved, the increases in both activation energy and  $T_g$  during this reaction, as well as a conductivity decrease, indicate a tightening of the network. This may be due to crosslinking, although it is just as likely to be due to the formation of an ester linkage which is less flexible than the reactant amide linkage. The absence of a similar reaction on heating polyamide and alcohol may be because the reaction depends on the tertiary structure of the system subsequent to the first reaction, much as in enzymic reactions.

The second of the subsequent reactions, equation (9) is clearly different for the two epoxide/polyamide ratios: kinetics are not available for the 2/5 ratio because of diffuse d.s.c. traces in that case, and it does not give rise to a second, lower temperature  $T_g$ . It may be that the larger amount of polyamide incorporated into the network during the first reaction offers some steric hindrance to this reaction, causing the reactants to be separated by some substantial distance or barrier. This would require a higher activation energy, as in equation (6), and would account for the lower enthalpy of reaction for the 2/5 ratio, as determined by d.s.c. Here, too, the accompanying conductivity decrease suggests a tightening of the network.

As with the previous study<sup>1</sup>, total cure occurred only at temperatures above the  $T_g$  of the totally cured system. At temperatures below the  $T_g$ , the maximum extent of cure was governed by the stiffness of the network.

For both ratios, the  $T_g$  values of the first reaction increased dramatically, subsequent to total cure, to the identical temperature of 52°C. This increase was accompanied by a d.s.c. endotherm at 65°C. Such behaviour is expected<sup>16,17</sup> when the rate of change of an adopted conformation cannot keep up with the heating rate. In the present case, this means that the non-equilibrium glass initially formed can, on heating, change conformation more rapidly than the 'equilibrium' glass.

It is interesting to note that, despite the fact that the two ratios differ in polyamide content, the 'equilibrium'  $T_g$  values are the same. Since the conformations of the two ratios must be different, because of the different amounts of polyamide in the networks, the temperature correspondence may be a coincidence of the two respective lowest energy conformations. Similar behaviour was not found with the *m*-phenylene diamine hardener<sup>1</sup>, implying a network too stiff to undergo large-scale reorganization.

For the 2/1.5 ratio, the second of the subsequent

reactions gives rise to a second, lower temperature  $T_g$  (Table 4), indicating that equation (9) involves the formation of a new linkage, rather than a linkage exchange as in equation (8), postulated for the first of the subsequent reactions. Its absence for the 2/5 ratio, as well as the lower enthalpy, indicate that the reaction does not proceed to any great extent, in this case.

This study has several important commercial applications. First, the cure at room temperature is not the same as the cure at another temperature. This is not only because the extents of cure may be different at the two temperatures, but because of the subsequent reactions occurring at elevated temperatures.

Second, the stiffness of the fully cured epoxy will increase with time, before finally levelling off, because of the reorganization of the amorphous network into a lower energy conformation.

## CONCLUSIONS

The cure of the system bisphenol-A diglycidyl ether/polyamide proceeds through three reactions in the temperature range 23–110°C. The first reaction, occurring at room temperature, is the expected attack of the oxirane rings of the epoxide by the reactive amine groups of the polyamide. At elevated temperatures, two reactions occur subsequent to the first; both involve amide linkages.

## ACKNOWLEDGEMENTS

The authors wish to thank M. A. Acitelli and F. J. Strock for help with some of the initial i.r. studies, and W. C. Hamm and D. G. Sedor for obtaining most of the experimental data reported herein.

## REFERENCES

- 1 Acitelli, M. A., Prime, R. B. and Sacher, E. *Polymer* 1971, **12**, 335
- 2 U.S. Pat. 2 450 940 (1948)
- 3 General Mills, Inc. U.S. Pat. 2 705 223 (1955)
- 4 Floyd, D. E., Peerman, D. E. and Wittkoff, H. *J. Appl. Chem.* 1957, **7**, 250
- 5 Piloyan, G. O., Ryabchikov, I. D. and Novikova, O. S. *Nature* 1966, **212**, 1229
- 6 Partansky, A. M. *Adv. Chem. Ser.* 1970, **92**, 29
- 7 Bowen, D. A. and Whiteside, R. C., Jr. *Adv. Chem. Ser.* 1970, **92**, 48
- 8 Kissinger, H. E. *Anal. Chem.* 1957, **29**, 1702
- 9 Horie, K., Hiura, H., Sawada, M., Mita, I. and Kambe, H. *J. Polym. Sci. (A-1)* 1970, **8**, 1357
- 10 Sokolnikova, I. N., Gurman, I. M., Sivergin, Yu. M. and Akutin, M. S. *Plast. Massy* 1967, **9**, 32
- 11 French, D. M., Strecker, R. A. H. and Tompa, S. A. *J. Appl. Polym. Sci.* 1970, **14**, 599
- 12 Jenkins, R. and Karre, L. *J. Appl. Polym. Sci.* 1966, **10**, 303
- 13 Gough, L. J. and Smith, I. T. *J. Appl. Polym. Sci.* 1960, **3**, 362
- 14 Rogers, C. E. 'Physics and Chemistry of the Organic Solid State', (Eds D. Fox, M. M. Labes and A. Weissberger), Interscience, New York, 1965, Vol II, p 509
- 15 Hollands, K. M. and Kalnin, I. L. *Adv. Chem. Ser.* 1970, **92**, 60 (see particularly Figure 1, where the data for 0% accelerator were used by the present writers to calculate an activation energy of 12 kcal mol<sup>-1</sup>)
- 16 Wunderlich, B., Bodily, D. M. and Kaplan, M. H. *J. Appl. Phys.* 1964, **35**, 95
- 17 Tonelli, A. E. *Macromolecules* 1971, **4**, 653

## Interpretation of melting data for low molecular weight poly(ethylene oxide)

P. C. Ashman and C. Booth

Department of Chemistry, University of Manchester, Manchester M13 9PL, UK  
(Received 19 May 1972)

Poly(ethylene oxide) fractions of low molecular weight ( $M_n \leq 10\,000$ ) show well defined melting transitions which can be assigned<sup>1,2</sup> to extended-, once-folded- or twice-folded-chain crystals. In interpreting these melting points account must be taken of the depression of melting point due to the finite lengths of the polymer chains as well as that due to the limited thickness of the lamellar crystals. Expressions for the melting points of lamellar crystals of finite chains have been published by Flory<sup>3</sup> and by Flory and Vrij<sup>4</sup>. Both theories assume that chain ends are excluded from the crystal lattice. The Flory<sup>3</sup> theory allows for chain ends which take up independent locations within the amorphous phase. The assumptions and approximations are such that this theory is most appropriately applied when crystalline sequences occupy only a small length of the polymer chain. By contrast the Flory-Vrij<sup>4</sup> theory is for chains which are completely crystalline and have their ends paired at the crystal surface. A modification<sup>4</sup> of the Flory-Vrij theory allows for partial melting, i.e. for chains only partially crystallized but with their ends localized in the interfacial layer.

In recent papers<sup>1,2</sup> we applied the Flory theory to the melting of crystals of low molecular weight poly(ethylene oxide). Here we apply the Flory-Vrij theory. In the notation used previously<sup>1,2</sup>, the melting point derived from the Flory-Vrij theory is:

$$T_m = T_m^0 [1 - (2\sigma_e / \Delta h \zeta)] / [1 - (RT_m^0 \ln I / \Delta h t \zeta)] \quad (1)$$

This is the melting point of a lamellar crystal of thickness  $\zeta$  chain units composed of chains which each traverse the crystal (on average)  $t$  times. The numerator of equation (1) is the familiar equation for lamellar crystals of infinite molecular weight. The denominator of equation (1)

Table 1 End interfacial free energies ( $\sigma_e$ ) of poly(ethylene oxide) crystals

$M_n$	$M_w/M_n$	$t$	$T_m$ (K)	$\sigma_e$ (kcal/mol)	
				Mono-disperse end-paired	Poly-disperse
1 000	1.05	1	312.3	1.4	1.7
1 500	1.05	1	322.2	1.5	1.9
2 000	1.05	1	327.0	1.6	2.1
3 300	1.10	1	333.4	1.9	2.7
3 700	1.10	1	334.5	2.0	2.8
4 000	1.05	1	334.6	2.2	3.0
4 300	1.10	1	334.9	2.4	3.3
6 000	1.20	1	337.3	2.9	4.0
3 700	1.10	2	332.1	1.3	1.8
4 300	1.10	2	333.3	1.4	2.0
6 000	1.20	2	334.2	2.1	2.7
10 000	1.20	2	338.4	2.6	3.3
10 000	1.20	3	337.5	1.9	2.2

contains the terms due specifically to the finite chain length.  $T_m^0$  is the thermodynamic melting point of the polymer,  $\Delta h$  is the enthalpy of fusion (per mol of chain units) and  $\sigma_e$  is the end interfacial free energy (per mol of chains which emerge from the end interface). Parameter  $I$  allows for the various possible states of order in the crystal. If chain ends are paired<sup>4</sup> then:

$$I = 1/x \quad (2)$$

where  $x$  is the chain length of a monodisperse polymer. Usually chain-ends are not paired, possibly because of partial melting<sup>4</sup> but certainly because of the chain length distribution in a real polymer fraction<sup>1</sup>. For a monodisperse polymer which forms a regularly folded-chain crystal  $I$  has the form\*:

$$I = (x - s\zeta + 1)/x \quad (3)$$

where  $s$  is the number of sequences chosen consecutively from a given molecule, and  $s\zeta \leq x$ . For a polydisperse polymer the requirement of high crystallinity<sup>5</sup> can be ensured by assuming that each chain folds to its maximum extent so that:

$$I = \sum_{s=1}^{\infty} \int_{s\zeta}^{(s+1)\zeta} w(x) [(x - s\zeta + 1)/x] dx \quad (4)$$

where  $w(x)$  is the weight fraction of molecules of chain length  $x$  units. We assume that  $w(x)$  is given by the Schulz-Zimm expression<sup>6</sup> with parameters defined by  $M_n$  and  $M_w/M_n$ .

We have used these equations to compute values of  $\sigma_e$  for crystals of low molecular weight poly(ethylene oxide), by comparison of calculated melting points with those observed<sup>1,2</sup>. Molecular weights, melting points and values of the folding parameter  $t$ , taken from earlier work<sup>1,2</sup>, are quoted in Table 1. We have taken  $\zeta = x_n/t$ , in order that direct comparison can be made between the results obtained assuming end-pairing of monodisperse polymers (equations (1) and (2) with  $\zeta = x = x_n$ ) and those obtained for the polydisperse fractions [equations (1) and (4)]. We have shown earlier<sup>1,2</sup> that for polydisperse polymers the exact choice of  $\zeta$  is not critical. We have also used, as earlier<sup>1,2</sup>,  $T_m^0 = 76^\circ\text{C}$  and  $\Delta h = 2$  kcal/mol.

End interfacial free energies so derived are listed in Table 1. The effect of allowing for polydispersity is significant, values of  $\sigma_e$  being as much as 30% higher when evaluated using equation (4) rather than equation (2). Values of  $\sigma_e$  calculated using the Flory-Vrij model

\* This equation differs from that used earlier<sup>2</sup> where all configurations of adjacent re-entry (including end-pairing at the surface) were included, and where all crystalline sequences of  $\zeta$  chain units were taken to be independent.

[equations (1) and (4)] are also higher (by about 20%) than those calculated earlier<sup>1,2</sup> using the Flory model. However, the conclusions of the earlier papers<sup>1,2</sup>, with regard to the variation of  $\sigma_e$  with molecular weight and with extent of chain-folding, are unaltered by the adoption of the Flory-Vrij model.

## ACKNOWLEDGEMENT

P.C.A. acknowledges receipt of a Science Research Council Studentship.

## Dynamic mechanical properties of poly(ethylene oxide)

Bruce Hartmann

Naval Ordnance Laboratory, Silver Spring, Maryland 20910, USA  
(Received 17 March 1972; revised 22 May 1972)

In their study of the dynamic mechanical properties of poly(ethylene oxide) (PEO), Wetton and Allen<sup>1</sup> found no maxima in the imaginary part of the shear modulus, but a replot of the data in terms of the loss tangent ( $\tan\delta$ ) showed a pronounced peak with a width of 15°C centred precisely on the melting point. Wetton and Allen were unable to explain the origin of this loss peak. Thus, it seemed worthwhile to investigate further the dynamic mechanical properties of PEO in the vicinity of the melting point.

There are many experimental difficulties in trying to make torsional pendulum measurements on a specimen at its melting point, but the torsional braid analyser<sup>2</sup> (TBA) is ideally suited to this type of problem. In the TBA, a multifilament glass braid is impregnated with a solution of the material to be tested followed by thermal removal of the solvent. In contrast to a torsional pendulum, the TBA permits investigation of materials which cannot support their own weight. A limitation of the TBA is that absolute values are not obtained, only relative values. The nominal frequency of this instrument is 0.1 Hz.

The PEO used for this study was WSR-301 (Union Carbide Corporation), which was supplied as a powder. A 0.5% solution of PEO in anhydrous isopropanol and water was used to impregnate the glass braid. Thermal removal of the solvent was done at 80°C in nitrogen.

The experimental results are shown in Figure 1. The relative rigidity is the relative value of the real part of the shear modulus,  $G'$ . The shape of the relative rigidity curve is in agreement with the  $G'$  curve of Wetton and Allen<sup>1</sup>. In particular, there is a slow decrease of modulus with temperature up to about 60°C, a rapid decrease of modulus from 60°C to the melting point, and a relatively constant modulus above the melting point.

The mechanical damping index shown in Figure 1 is the relative value of the loss tangent. In agreement with the results of Wetton and Allen, there is a relatively constant damping index below the melting point that increases to a higher value in the melt. This higher value is assumed to be due to viscous damping in the melt.

## REFERENCES

- 1 Beech, D. R., Booth, C., Dodgson, D. V., Sharpe, R. R. and Waring, J. R. S. *Polymer* 1972, **13**, 73
- 2 Beech, D. R., Booth, C., Pickles, C. J., Sharpe, R. R. and Waring, J. R. S. *Polymer*, 1972, **13**, 246
- 3 Flory, P. J. *J. Chem. Phys.* 1949, **17**, 223
- 4 Flory, P. J. and Vrij, A. *J. Am. Chem. Soc.* 1963, **85**, 3548
- 5 Arlie, J. P., Spegt, P. A. and Skoulios, A. E. *Makromol. Chem.* 1966, **99**, 160; *ibid.* 1970, **104**, 212
- 6 Schulz, G. V. *Z. Phys. Chem.* 1939, **B43**, 25; Zimm, B. H. *J. Chem. Phys.* 1948, **16**, 1093

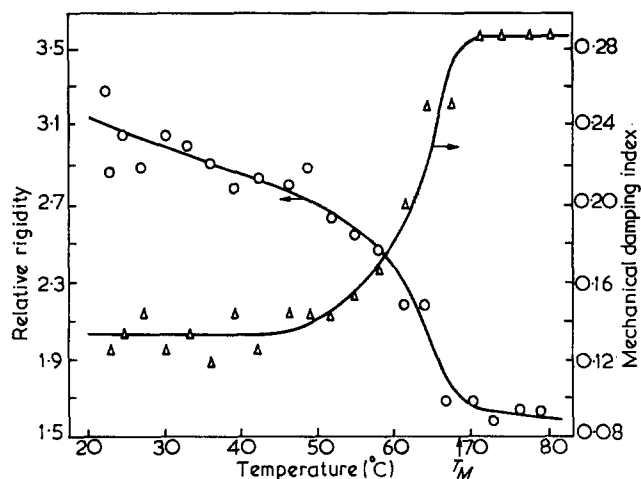


Figure 1 Torsional braid analyser results for poly(ethylene oxide)

Contrary to the results of Wetton and Allen, however, there is no evidence of a damping peak at the melting point indicated on Figure 1. Why a peak is observed using Wetton and Allen's equipment but not with a TBA is not clear, but further work is indicated to elucidate the dynamic mechanical properties of PEO at the melting point.

## ACKNOWLEDGEMENTS

Thanks are due to Mr Raymond T. Payne, Jr, for operating the experimental equipment and to Mr James V. Duffy for preparing the poly(ethylene oxide) solution.

## REFERENCES

- 1 Wetton, R. E. and Allen, G. *Polymer* 1966, **7**, 331
- 2 Lewis, A. F. and Gillham, J. K. *J. Appl. Polym. Sci.* 1962, **6**, 422

[equations (1) and (4)] are also higher (by about 20%) than those calculated earlier<sup>1,2</sup> using the Flory model. However, the conclusions of the earlier papers<sup>1,2</sup>, with regard to the variation of  $\sigma_e$  with molecular weight and with extent of chain-folding, are unaltered by the adoption of the Flory-Vrij model.

## ACKNOWLEDGEMENT

P.C.A. acknowledges receipt of a Science Research Council Studentship.

## REFERENCES

- 1 Beech, D. R., Booth, C., Dodgson, D. V., Sharpe, R. R. and Waring, J. R. S. *Polymer* 1972, 13, 73
- 2 Beech, D. R., Booth, C., Pickles, C. J., Sharpe, R. R. and Waring, J. R. S. *Polymer*, 1972, 13, 246
- 3 Flory, P. J. *J. Chem. Phys.* 1949, 17, 223
- 4 Flory, P. J. and Vrij, A. *J. Am. Chem. Soc.* 1963, 85, 3548
- 5 Arlie, J. P., Spegt, P. A. and Skoulios, A. E. *Makromol. Chem.* 1966, 99, 160; *ibid.* 1970, 104, 212
- 6 Schulz, G. V. *Z. Phys. Chem.* 1939, B43, 25; Zimm, B. H. *J. Chem. Phys.* 1948, 16, 1093

## Dynamic mechanical properties of poly(ethylene oxide)

Bruce Hartmann

Naval Ordnance Laboratory, Silver Spring, Maryland 20910, USA  
(Received 17 March 1972; revised 22 May 1972)

In their study of the dynamic mechanical properties of poly(ethylene oxide) (PEO), Wetton and Allen<sup>1</sup> found no maxima in the imaginary part of the shear modulus, but a replot of the data in terms of the loss tangent ( $\tan\delta$ ) showed a pronounced peak with a width of 15°C centred precisely on the melting point. Wetton and Allen were unable to explain the origin of this loss peak. Thus, it seemed worthwhile to investigate further the dynamic mechanical properties of PEO in the vicinity of the melting point.

There are many experimental difficulties in trying to make torsional pendulum measurements on a specimen at its melting point, but the torsional braid analyser<sup>2</sup> (TBA) is ideally suited to this type of problem. In the TBA, a multifilament glass braid is impregnated with a solution of the material to be tested followed by thermal removal of the solvent. In contrast to a torsional pendulum, the TBA permits investigation of materials which cannot support their own weight. A limitation of the TBA is that absolute values are not obtained, only relative values. The nominal frequency of this instrument is 0.1 Hz.

The PEO used for this study was WSR-301 (Union Carbide Corporation), which was supplied as a powder. A 0.5% solution of PEO in anhydrous isopropanol and water was used to impregnate the glass braid. Thermal removal of the solvent was done at 80°C in nitrogen.

The experimental results are shown in *Figure 1*. The relative rigidity is the relative value of the real part of the shear modulus,  $G'$ . The shape of the relative rigidity curve is in agreement with the  $G'$  curve of Wetton and Allen<sup>1</sup>. In particular, there is a slow decrease of modulus with temperature up to about 60°C, a rapid decrease of modulus from 60°C to the melting point, and a relatively constant modulus above the melting point.

The mechanical damping index shown in *Figure 1* is the relative value of the loss tangent. In agreement with the results of Wetton and Allen, there is a relatively constant damping index below the melting point that increases to a higher value in the melt. This higher value is assumed to be due to viscous damping in the melt.

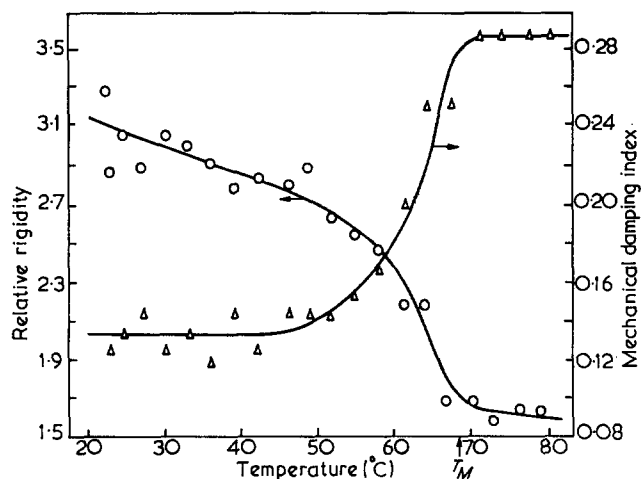


Figure 1 Torsional braid analyser results for poly(ethylene oxide)

Contrary to the results of Wetton and Allen, however, there is no evidence of a damping peak at the melting point indicated on *Figure 1*. Why a peak is observed using Wetton and Allen's equipment but not with a TBA is not clear, but further work is indicated to elucidate the dynamic mechanical properties of PEO at the melting point.

## ACKNOWLEDGEMENTS

Thanks are due to Mr Raymond T. Payne, Jr, for operating the experimental equipment and to Mr James V. Duffy for preparing the poly(ethylene oxide) solution.

## REFERENCES

- 1 Wetton, R. E. and Allen, G. *Polymer* 1966, 7, 331
- 2 Lewis, A. F. and Gillham, J. K. *J. Appl. Polym. Sci.* 1962, 6, 422

# High polymers of acrylic and methacrylic esters of *N*-hydroxysuccinimide as polyacrylamide and polymethacrylamide precursors

P. Ferruti, A. Bettelli and Angelino Feré

*Istituto di Chimica Industriale del Politecnico, Piazza Leonardo da Vinci 32, 20133 Milano, Italy*

(Received 4 February 1972)

High molecular weight poly(*N*-acryloxysuccinimide) and poly(*N*-methacryloxysuccinimide) were obtained by radical polymerization of the corresponding monomers, in turn prepared by coupling of acrylic or methacrylic acid with *N*-hydroxysuccinimide in the presence of dicyclohexylcarbodiimide. The new polymers proved to be good polyacrylamide or polymethacrylamide precursors, yielding essentially pure derivatives by reaction with primary or secondary aliphatic or cycloaliphatic amines. Linear polyvinyl-type poly(*N*-allylacrylamide), which cannot be directly prepared by polymerization of the corresponding monomer, could be obtained in this way.

## INTRODUCTION

Considerable interest is being focused on multifunctional high polymers, either as macromolecular catalysts<sup>1-3</sup> or as macromolecular drugs, e.g. against silicosis<sup>4-6</sup> or as antagonists of heparin<sup>7, 8</sup>; synthetic polymers purposely tailored are also being studied as antimetastase agents<sup>9</sup>.

A way to obtain macromolecules with specialized functions is to prepare polymers or copolymers of *N*-substituted acrylamides or methacrylamides, having the desired groups attached as substituents. This method, for example, has been used for the preparation of several tertiary amino polymers, some of which have been tested for their pharmacological activity<sup>5, 6, 9</sup>. The synthesis of the corresponding monomers, however, or their polymerization to linear high molecular weight polymers, is often difficult or even impossible, especially if complex structures are required.

In many cases these difficulties can be avoided if polymers or copolymers are synthesized with chemical functions in the side chain that can be transformed into amido groups by condensation with primary or secondary amines in a specific and quantitative way. In fact, amines with a suitable structure are generally easier to obtain than the corresponding acryloyl or methacryloyl derivatives.

The scope of this work was to provide suitable monomers for this purpose, as part of the research on the synthesis of multifunctional polymers to be used in a pharmaceutical or biomedical context<sup>5-9</sup>. Acryloylchloride and methacryloylchloride had formerly been studied for this reason<sup>10-13</sup>. They have, however, considerable disadvantages. They are aggressive substances,

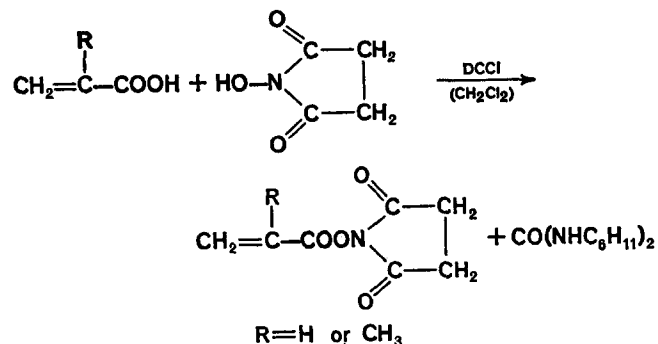
very sensitive to water, and cannot be copolymerized with many other functional monomers; furthermore, they often yield cyclized or crosslinked products when reacted with amines<sup>12, 13</sup>.

It is known that *O*-acyl derivatives of *N*-hydroxysuccinimide react smoothly with primary or secondary amino groups giving the corresponding amides; for this, they are extensively used in peptide synthesis<sup>14</sup>. This prompted us to study the synthesis and polymerization of *O*-acryloyl and methacryloyl derivatives of *N*-hydroxysuccinimide, together with the ability of the resulting polymers to subsequently give polyacrylamides or polymethacrylamides by modification of the amines.

## RESULTS

### Monomers

Coupling of acrylic or methacrylic acid with *N*-hydroxysuccinimide in the presence of dicyclohexylcarbodiimide<sup>15</sup> proved to be a suitable way to prepare the monomers:



In the case of *N*-methacryloxysuccinimide the yield was over 80%; *N*-acryloxysuccinimide was obtained in a lower yield (~45%) because of a partial polymerization during isolation, which could not be completely avoided by adding radical inhibitors to the reaction mixture. Both monomers are white solids, which are easily purified by recrystallization. They are freely soluble in many solvents such as dioxane, benzene, chloroform, etc., and do not appear to be very sensitive to atmospheric moisture. When crystalline, they may be stored for a long time in the cold.

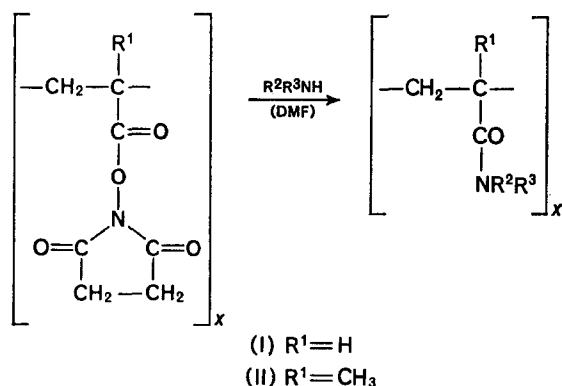
### Polymers

The polymerization of *N*-acryloxy- and *N*-methacryloxysuccinimide can be readily accomplished with radical initiators in dioxane or benzene solution. In both solvents, the polymers precipitate during the reaction. Their intrinsic viscosities and analytical data are given in Table 1.

Poly(*N*-acryloxysuccinimide) (I) and poly(*N*-methacryloxysuccinimide) (II) exhibit a similar behaviour towards solvents. In Table 2 some solubility data are reported. It may be observed that only highly polar solvents such as dimethylformamide or dimethylsulphoxide are able to dissolve both polymers. On the other hand, such solvents are known to be suitable for the reaction between *O*-acyl derivatives of *N*-hydroxysuccinimide and amines, as indicated by a number of peptide syntheses<sup>14</sup>.

### Reaction of the polymers with amines

We proved in two steps the ability of poly(*N*-acryloxysuccinimide) (I) and poly(*N*-methacryloxysuccinimide) (II) to react quantitatively with aliphatic or cycloaliphatic amines to give substantially homopolymeric polyacrylamides and polymethacrylamides:



First, the polymers I and II were allowed to react respectively with piperidine and *n*-butylamine, and the products were found by infra-red spectroscopy to be identical with authentic samples of poly(*N*-acryloyl-piperidine) and poly(*N*-*n*-butylmethacrylamide), prepared by radical polymerization of the corresponding monomers<sup>16, 17</sup>.

Secondly, the polymer (I) was allowed to react with allylamine, thus obtaining a soluble, and presumably linear polymer which gave a correct analysis as poly(*N*-allylacrylamide). It may be noted that *N*-allyl derivatives of acrylamides or methacrylamides are not expected to give linear, polyvinyl-type polymers by radical polymerization. They may either give crosslinked polymers, or cyclopolymerize giving soluble polymers whose structure is not basically polyvinyl<sup>18, 19</sup>.

Table 1 Intrinsic viscosity and analytical data of poly(*N*-acryloxysuccinimide) (I) and poly(*N*-methacryloxysuccinimide) (II)\*

Polymer	[ $\eta$ ] in DMF at 30°C (dl/g)	Found Calculated for	Analytical data
(I)	0.32	[C <sub>7</sub> H <sub>7</sub> NO <sub>4</sub> ] <sub>x</sub>	C: 49.51%; H: 4.25%; N: 8.11% C: 49.71%; H: 4.17%; N: 8.28%
(II)	0.16	[C <sub>8</sub> H <sub>9</sub> NO <sub>4</sub> ] <sub>x</sub>	C: 52.24%; H: 4.94%; N: 7.80% C: 52.46%; H: 4.95%; N: 7.65%

\* Samples obtained by polymerization of ~25% solution of the monomers in benzene, with 0.5% azodiisobutyronitrile, at 60°C

Table 2 Solubility data on poly(*N*-acryloxysuccinimide) (I) and poly(*N*-methacryloxysuccinimide) (II)\*

Solvents	Polymer (I)	Polymer (II)
Dioxane	sw (hot)†	i
Chlorobenzene	i	sw (hot)
Dimethylformamide	S	S
Dimethylsulphoxide	S	S
Acetonitrile	sw	i

\* Both polymers are insoluble in *n*-heptane, benzene, toluene, methanol, ethanol, acetone, 2-butanone, chloroform, methylene chloride and carbon tetrachloride

† S = soluble; i = insoluble; sw = swells

The reactivity towards primary or secondary amines is higher in the case of I. The completion of the reaction can be checked by i.r. spectroscopy, observing the disappearance of two bands at 5.65 and 5.8  $\mu\text{m}$ , which should correspond to the imidic CO, and of a band at 5.55  $\mu\text{m}$ , which should correspond to the ester CO. These bands are replaced by a strong band at about 6.05  $\mu\text{m}$  (amidic CO).

In the conditions we used, the reaction of I and II with aromatic amines does not seem to be substantially quantitative. Several attempts to obtain homopoly(*N*-phenylacrylamide) or homopoly(*N*-phenylmethacrylamide) by reacting I or II in DMF solution with aniline have not been successful so far. Further investigation is needed for this purpose; however, the inability of I and II to react quantitatively with aromatic amines represents a serious limit on their use as polyacrylamide or polymethacrylamide precursors. Even so, however, they may be considered valuable tools in the synthesis of multifunctional polymers.

## EXPERIMENTAL

### *N*-Acryloxysuccinimide

To a stirred solution of 17.26 g *N*-hydroxysuccinimide in 200 ml of dry dioxane, cooled at 5°C with an ice-bath, 10.81 g acrylic acid and 30.95 g *N,N'*-dicyclohexylcarbodiimide were added. The mixture was stirred at 0°C for 2 h, then 0.2 g of *t*-butylcatechol was added, the cooling bath was removed and the mixture was stirred for a further 2 h while it reached room temperature. The precipitated *N,N'*-dicyclohexylurea was then removed by

filtration and the solvent was evaporated *in vacuo*. The residue was extracted exhaustively with boiling n-heptane. The combined n-heptane extracts were cooled to 0°C; crystallization of the product, which at first often separates as an oil, was induced by rubbing. The product was then recrystallized from n-heptane, m.p. 67°C (hot plate). Yield: 11.33 g (44.7%). Found: C, 49.82%; H, 4.26%; N, 8.46%; calculated for C<sub>7</sub>H<sub>7</sub>NO<sub>4</sub>: C, 49.71%; H, 4.17%; N, 8.28%.

#### *N*-Methacryloxysuccinimide

The same procedure as in the previous case, starting from 12.9 g of methacrylic acid and the same quantities of *N*-hydroxysuccinimide, dicyclohexylcarbodiimide and solvent, immediately after evaporation gave 24.5 g (89.2%) of crystalline product which was directly recrystallized from n-heptane, m.p. 105°C (hot plate). Found: C, 52.29%; H, 5.05%; N, 7.48%; calculated for C<sub>8</sub>H<sub>9</sub>NO<sub>4</sub>: C, 52.46%; H, 4.95%; N, 7.65%.

#### *Poly(N-acryloxysuccinimide) (I) and poly(N-methacryloxysuccinimide) (II)*

To a solution of 2 g *N*-acryloxysuccinimide or *N*-methacryloxysuccinimide in 5 ml dry benzene, 10 mg of azodiisobutyronitrile were added, and after purging with nitrogen the mixture was kept at 60°C for 24 h under a nitrogen atmosphere. The polymers precipitated out and were collected by filtration, washed thoroughly with dry benzene and then with light petroleum ether (b.p. 30–50°C), and finally dried at 40°C and 0.1 mmHg. The yields ranged from 75 to 90%.

#### *Poly(N-acryloylpiperidine)*

To a solution of 0.17 g of (I) ( $[\eta]=0.32$  dl/g) in 2 ml dimethylformamide, a solution of 0.4 ml of piperidine in 1 ml of dimethylformamide (DMF) was added portionwise. An initial precipitate of polymer was formed, which redissolved by stirring. After some minutes, a crystalline precipitate was formed, which was probably a by-product of the reaction. This was water soluble and was not further investigated. The mixture was left at room temperature for 4 h, then it was diluted with 5 ml of water and dialysed against distilled water. The solution was then evaporated to dryness *in vacuo*, and the product was dissolved in chloroform or dimethylformamide and reprecipitated into an excess of ether and dried at 40°C and 0.1 mmHg to give an almost quantitative yield (apart from mechanical losses) of poly(*N*-acryloylpiperidine) having  $[\eta]=0.39$  dl/g (in DMF at 30°C) and whose i.r. spectrum was exactly superimposable to that of an authentic sample prepared as previously described<sup>16</sup>.

#### *Poly(N-n-butylmethacrylamide)*

To a solution of 0.1 g of II ( $[\eta]=0.16$  dl/g in DMF at 30°C) in 2 ml dimethylformamide, 0.5 ml of n-butylamine

was added. A precipitate was formed. The mixture was then gently heated with stirring until the precipitate gradually dissolved and a clear solution was obtained. The reaction mixture was then left at 60°C for 6 h, then it was poured into 30 ml of ether. The precipitate was collected and washed thoroughly with ether. It was then dissolved in methanol, reprecipitated into an excess of ether, and dried at 40°C and 0.1 mmHg to give an almost quantitative yield of poly(*N*-n-butylmethacrylamide) ( $[\eta]=0.37$  dl/g), whose i.r. spectrum was exactly superimposable to that of an authentic sample prepared by radical polymerization of the corresponding monomer<sup>17</sup>.

#### *Poly(N-allylacrylamide)*

The same procedure as in the case of poly(*N*-acryloylpiperidine), starting from 0.17 g (I), 0.4 ml allylamine and the same quantities of solvent, together with a trace of *t*-butylcatechol as radical inhibitor, gave an almost quantitative yield of poly(*N*-allylacrylamide), having  $[\eta]=1$  dl/g (in DMF at 30°C). Found: C, 64.65%; H, 8.04%; N, 12.46%; calculated for [C<sub>6</sub>H<sub>9</sub>NO]<sub>x</sub>: C, 64.84%; H, 8.14%; N, 12.60%.

#### REFERENCES

- Overberger, C. G. and Maki, H. *Macromolecules* 1970, **3**, 214
- Overberger, C. G., Sitaramaiah, S., St Pierre, T. and Yaroslavsky, S. *J. Am. Chem. Soc.* 1965, **87**, 3270
- Klotz, I. M., Royer, G. P. and Scarpa, I. S. *Proc. Natl. Acad. Sci. USA* 1971, **68**, 263
- Schlipkötter, H. W. and Broekhaus, A. *Fortschr. Int. Stablungen-taugung*, 3–5 April, Münster, p 397
- Natta, G., Vigliani, E. C., Danusso, F. et al. *Atti Accad. Naz. Lincei VIII* 1965, **39**, 498
- Vigliani, E. C. et al. *XV Congr. Int. Med. Trav. Wien* 1966, Vol II, p 665
- Marchisio, M. A., Sbertoli, C., Farina, G. and Ferruti, P. *Eur. J. Pharmacol.* 1970, **12**, 236
- Marchisio, M. A., Longo, T., Ferruti, P. and Danusso, F. *6th Congr. Eur. Soc. Exp. Surg., Hälsinhborg* 27–29 April, 1971, in press
- Ferruti, P., Franchi, G. Polentarutti, N., Danusso, F. and Garattini, S. *J. Med. Chem.* in the press
- Schulz, R. C., Elzer, P. and Kern, W. *Chimia* 1959, **13**, 235
- Schulz, R. C., Elzer, P. and Kern, W. *Makromol. Chem.* 1961, **42**, 197
- Boyer, S. and Rondeau, A. *Bull. Soc. Chim. France* 1958, p 240
- Blatz, P. E. *J. Polym. Sci.* 1962, **58**, 755
- Petitt, G. R. in 'Synthetic Peptides', Van Nostrand-Reinhold, New York, 1970, Vol 1
- Kurzer, F. and Douraghi-Zadeh, K. *Chem. Rev.* 1967, **67**, 107
- Perrod, J. and Ellés, J. C. R. *Hebd. Séanc. Acad. Sci.* 1956, **243**, 1040
- Koton, M. M., Sokolova, T. A., Savitskaya, M. N. and Kiseleva, T. H. *Zh. Obsch. Khim.* 1957, **27**, 2239; *Chem. Abstr.* 1957, **52**, 6228h
- Trossarelli, L., Guaita, M., Priola, A. and Saini, G. *Chim. Ind. Milan* 1964, **46**, 1173
- Kawai, W. *J. Polym. Sci. (A-1)* 1966, **4**, 1191

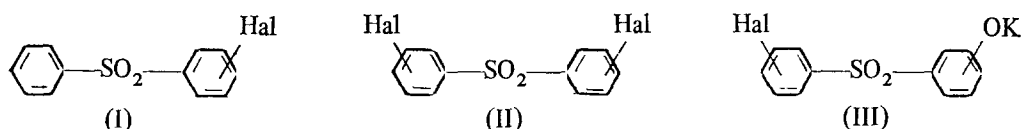


# Relative reactivities of the functional groups involved in synthesis of poly(phenylene ether sulphones) from halogenated derivatives of diphenyl sulphone

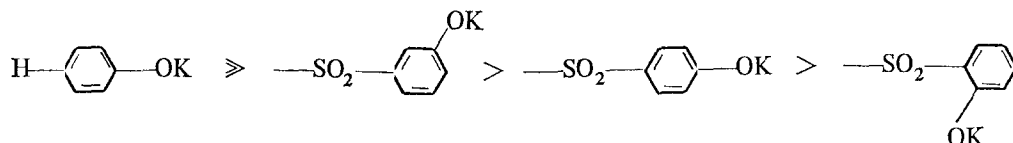
A. B. Newton and J. B. Rose

Imperial Chemical Industries Limited, Plastics Division, Welwyn Garden City, Herts, UK  
(Received 11 February 1972; revised 29 March 1972)

Rate constants have been measured for the displacement of halogen from certain halogenated derivatives of diphenyl sulphone (e.g. structures I, II and III) by hydroxyl ion or by certain phenoxide anions using dimethyl sulphoxide or a dimethyl sulphoxide/water mixture as solvent.



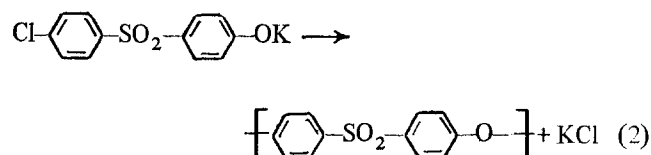
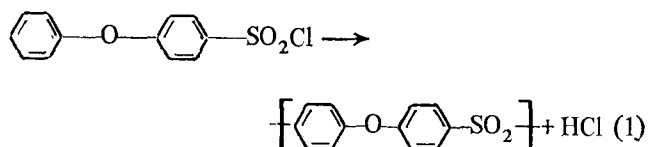
Initial rate constants for the self condensation of halogenophenoxides (III) in anhydrous dimethyl sulphoxide were also determined. The order of halogen reactivities found was  $F > Cl \sim Br$  with *p*-halogenophenyl sulphonyl groups showing greater reactivity than the *o*-isomers, while displacement from the *m*-halogeno sulphones was very slow and comparable with the rate of sulphone bond fission. Phenoxide reactivities were found to vary in the order:



The observed influence of substituents on reactivity is discussed in terms of direct effects, when the substituent is in the same ring as the reacting group, and 'bridge' effects where the substituents' influence is transmitted from an adjacent ring via the sulphone linkage. In polycondensations of halogenophenoxides (III) functional group reactivities increase with conversion owing to the operation of 'bridge' effects. Evidence is presented to indicate that in these polycondensations ether interchange probably occurs in a manner comparable to ester interchange in a polyesterification.

## INTRODUCTION

Two main routes to poly(arylene ether sulphones) have been reported; one employs polysulphonylation procedures to form sulphone linkages between aromatic nuclei, e.g. reaction (1), while the other is a polyether synthesis in which arylene ether linkages are formed by displacement of halogen from derivatives of diphenyl sulphone, e.g. reaction (2) (for reviews see refs. 1, 2 and 3). This paper is concerned with the second type of process and examines the effects of structural factors on the reactivity of the functional groups (halogen and phenoxide ion) involved.



Displacement of halogen from activated aryl halides by nucleophilic reagents such as phenoxide anions usually obeys a second order rate law and in this work reactivities were determined by measuring second order rate constants for the reactions involved. In comparing the reactivity of halogens in various diphenyl sulphone derivatives the nucleophilic reagent usually employed was the hydroxyl ion as we wished to combine this research with other work aimed at the synthesis of halogenophenoxides of the type employed for the polycondensation reaction (2). The use of dipolar aprotic solvents to enhance the rates of nucleophilic substitution reactions is well known<sup>4</sup> and in the present work the solvents were dry dimethyl sulphoxide (DMSO), when the reagent was a phenoxide anion, and a DMSO/water mixture containing 80.5 wt. % DMSO for reactions involving the hydroxyl ion.

## RESULTS

### Halogen reactivities

Second order rate constants,  $k_2$ , for the displacement of halogen from monohalogenodiphenyl sulphones by hydroxyl ion, reaction (3), and by the phenoxide anion, reaction (4), are given in Table 1.

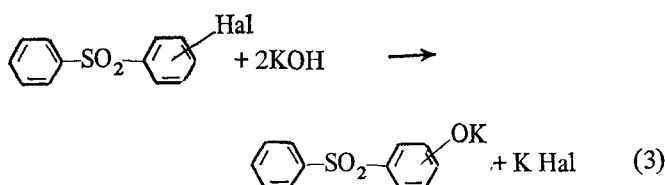
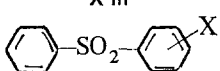
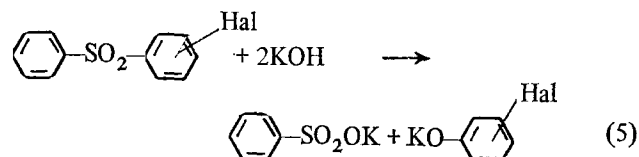
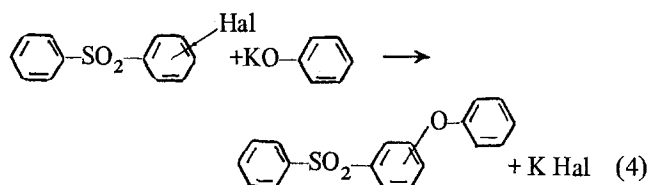


Table 1 Displacement of halogen from monohalogeno diphenyl sulphones

X in 	$k_2 \times 10^5$ for $\text{OH}^-$ <sup>a</sup> ( $\text{l mol}^{-1}\text{sec}^{-1}$ )	$k_2 \times 10^5$ for $\text{PhO}^-$ <sup>b</sup> ( $\text{l mol}^{-1}\text{sec}^{-1}$ )
<i>p</i> -F	14 300	—
<i>p</i> -Cl	112	3 024
<i>o</i> -Cl	23	100
<i>m</i> -Cl	4.5	10.5

a Measured at 120°C in 80.5 wt. % DMSO/water mixture as solvent  
b Measured at 120°C in anhydrous DMSO as solvent



The order of reactivities, *p*-chloro > *o*- > *m*-, is the same as that found by Oae and Khim<sup>5</sup> under different experimental conditions. A possible side reaction is cleavage of the sulphone linkage by attack at the sulphur to carbon bond, reaction (5); cleavage could not be detected with *para* and *ortho* halides but with the *meta* chloride  $k_2$  for cleavage by  $\text{OH}^-$  was  $0.9 \times 10^{-5}$  as compared with  $4.5 \times 10^{-5} \text{ l mol}^{-1} \text{ sec}^{-1}$  for displacement of chlorine.

The same general trends in reactivity are shown by the dihalogenodiphenyl sulphones listed in Table 2. Cleavage of the sulphone group was detected only when the halide was 3,3'-dichlorodiphenyl sulphone where it is the predominant mode of reaction. Comparison of the first column of rate constants in Table 2 (which are for reaction 6) with the second (for reaction 7) shows that five of these compounds are hydrolysed in two distinct stages, displacement of the first halogen to give a halophenoxide proceeding much more rapidly than formation of bisphenoxide by displacement of the second halogen. A plot of mol halide displaced/mol dichloride employed against time (see Figure 1) shows a marked diminution in slope at a point just beyond 50% reaction and the product at this stage is predominantly halophenoxide, little bisphenoxide having been formed. Thus, with the first four compounds

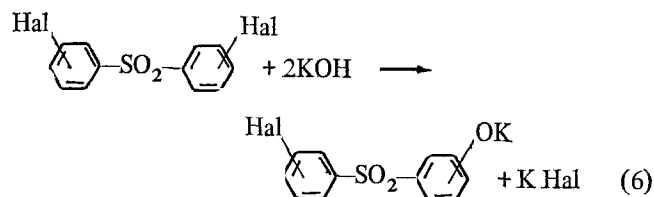
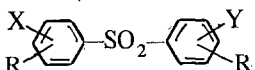
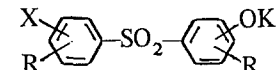
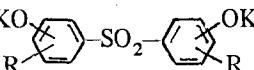
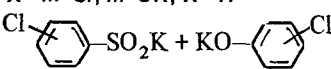
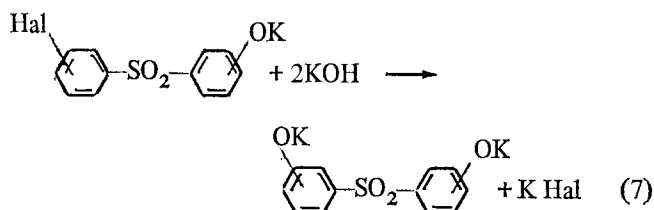


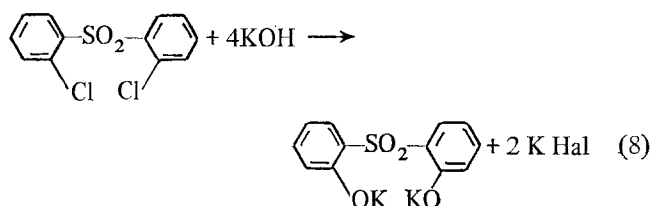
Table 2 Displacement of halogen from dihalogenodiphenyl sulphones by KOH  
Rate constants,  $k_2$ , are for reaction in 80.5% DMSO/water at 120°C, using 4 mol KOH per mol dihalide

Dihalide X, Y and R in 	$10^5 \times k_2$ ( $\text{l mol}^{-1}\text{sec}^{-1}$ )	Intermediate product(s) X, OK and R in 	$10^5 \times k_2$ ( $\text{l mol}^{-1}\text{sec}^{-1}$ )	Final product(s) OK and R in 
X, Y = <i>p</i> -F; R = H	Too fast to measure	X = <i>p</i> -F; <i>p</i> -OK; R = H	850	<i>p</i> -OK; R = H
X, Y = <i>p</i> -Cl; R = H	358	X = <i>p</i> -Cl; <i>p</i> -OK; R = H	3.24	<i>p</i> -OK; R = H
X, Y = <i>p</i> -Br; R = H	356	X = <i>p</i> -Br; <i>p</i> -OK; R = H	6.33	<i>p</i> -OK; R = H
X, Y = <i>p</i> -Cl; R = <i>m</i> -Me	71.5	X = <i>p</i> -Cl; <i>p</i> -OK; R = <i>m</i> -Me	~1.4	<i>p</i> -OK; R = <i>m</i> -Me
X = <i>o</i> -Cl; Y = <i>p</i> -Cl; R = H	110	X = <i>o</i> -Cl; <i>p</i> -OK; R = H	1.5	<i>p</i> -OK; <i>o</i> -OK; R = H
X = <i>p</i> -Cl; Y = <i>o</i> -Cl; R = H	26	X = <i>p</i> -Cl; <i>o</i> -OK; R = H		
X, Y = <i>m</i> -Cl; R = H	~4	X = <i>m</i> -Cl; <i>m</i> -OK; R = H		
X, Y = <i>m</i> -Cl; R = H	~13			
X, Y = <i>o</i> -Cl; R = H	Reaction does not stop halfway		52	<i>o</i> -OK; R = H
X, Y = <i>o</i> -Cl; R = <i>p</i> -Me	Reaction does not stop halfway		25	<i>o</i> -OK; R = <i>p</i> -Me



the hydrolysis can be run on a preparative scale (preferably with 2 mol KOH/mol dichloride) to give high yields of halophenoxides and this reaction provides a useful route to these polycondensation intermediates<sup>6,7</sup>. As would be expected from the data in Table 1, the chlorine atoms of 4,2'-dichlorodiphenyl sulphone are of unequal reactivities so that the intermediate product is a mixture of isomers.

2,2'-Dichlorodiphenyl sulphone and 2,2'-dichloro-4,4'-dimethyldiphenyl sulphone behave quite differently on hydrolysis. The rate of halide ion displacement does not slow down just beyond 50% reaction (see Figure 1) and the only products isolated in high yields were the corresponding bisphenoxides. Analysis of samples taken at 40% conversion from a hydrolysis of 2,2'-dichlorodiphenyl sulphone with two mol KOH showed the phenolic product to be ~80% bisphenoxide and 20% chlorophenoxide while the non-phenolic product was unreacted dichloride containing ~8% of the phenoxathiin dioxide (II). Kinetic analysis showed that a second order kinetic law was obeyed when the stoichiometry was taken as for equation (8) but not for equation (6).



Hydrolysis of II is known<sup>8</sup> to give the bisphenoxide (III) and we find that this reaction occurs rapidly with a second order rate constant  $k_2 = 700 \times 10^{-5} \text{ l mol}^{-1} \text{ sec}^{-1}$ , over 10 times greater than the rate constant for the overall reaction. Further investigation showed that hydrolysis of the chlorophenoxide obeyed a first order rate law and the rate of reaction was virtually independent of the hydroxyl ion concentration ( $k_1 = 63.9 \times 10^{-5} \text{ sec}^{-1}$  in

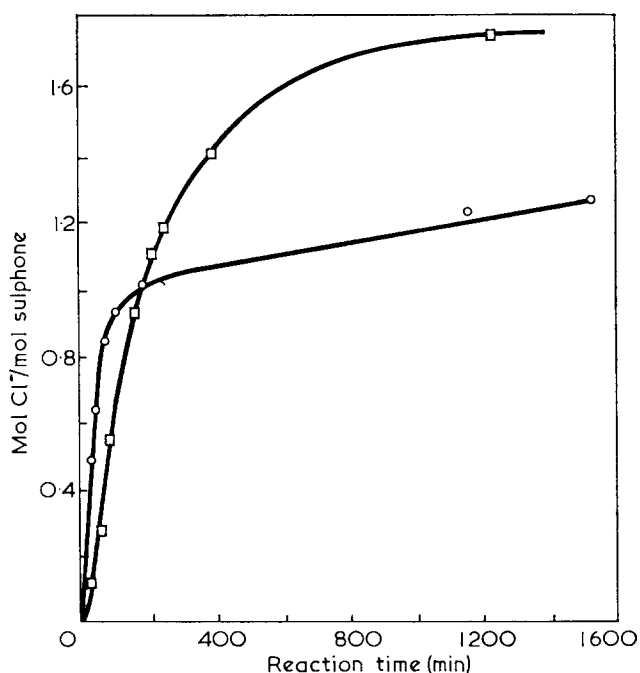


Figure 1 Hydrolysis of dichlorodiphenyl sulphones at 120°C in 80.5 wt. % DMSO/water (4 mol KOH). □, 2,2'-substituted; ○, 4,4'-substituted

absence of KOH and  $61.6 \times 10^{-5} \text{ sec}^{-1}$  at a KOH concentration of 0.195 mol/l). A hydrolysis mechanism consistent with these data is as indicated in reaction (9) where the rate determining step is formation of chlorophenoxide (I). This mechanism will give second order kinetics (stoichiometry as in reaction 8) provided that the rates at which I and II react do not limit the rate of the overall reaction. This is certainly the case for hydrolysis of II, but it is not obviously so for the formation of II from I, which obeys first order kinetics. However, in the kinetic experiments the initial concentration of KOH was 0.195 molar so that the initial overall rate of reaction at unit concentration of dichloride would be  $\sim 10 \times 10^{-5} \text{ mol l}^{-1} \text{ sec}^{-1}$  as compared with  $63 \times 10^{-5} \text{ mol l}^{-1} \text{ sec}^{-1}$  for the reaction of unit concentration of the chlorophenate. Thus, cyclization to give II is relatively fast and the overall reaction kinetics will be determined by reaction of the dichloride to give the chlorophenoxide (I).

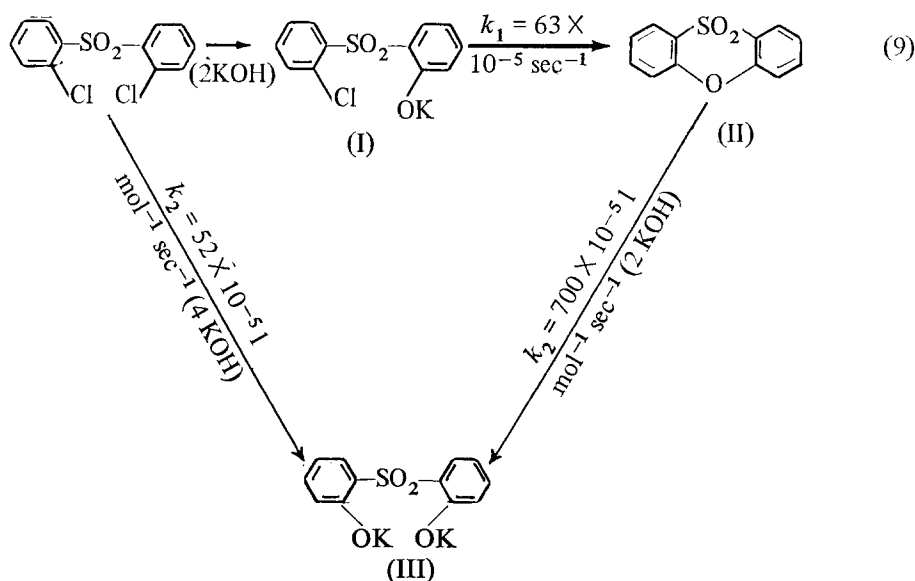


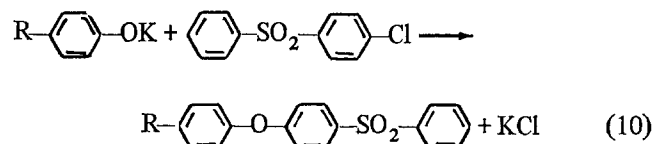
Table 3 Displacement of chlorine as chloride ion from tetrachlorodiphenylsulphones by KOH  
Rate constants are for reaction in 80.5% DMSO/water at 120°C using 4 mol KOH per mol sulphone

Tetrachlorosulphone X, Y and Z in	$10^5 \times k_2$ ( $l\ mol^{-1}\ sec^{-1}$ )	Intermediate product(s) X, Y and Z in	$10^5 \times k_2$ ( $l\ mol^{-1}\ sec^{-1}$ )	Final product(s) X, Y and Z in
X, Z = <i>m</i> -Cl; Y = H X = <i>m</i> -Cl; Y = <i>o</i> -Cl; Z = H	> 3000 > 5000	X, Z = <i>m</i> -Cl; Y = H X = <i>m</i> -Cl; Y = <i>o</i> -Cl; Z = H	180 8.2	X, Z = <i>m</i> -Cl; Y = H X = <i>m</i> -Cl; Y = <i>o</i> -Cl; Z = H
X, Z = <i>o</i> -Cl; Y = H	Reaction does not stop half way		~200	
X, Z = <i>o</i> -Cl; Y = H	500	X, Z = <i>o</i> -Cl; Y = H	—	X, Z = <i>o</i> -Cl; Y = H

Rate constants for the hydrolysis of three tetrachlorodiphenyl sulphones are given in Table 3. These are such that pure chlorophenoxides can be isolated without difficulty from the first two compounds tabulated, but hydrolysis of the third compound gives a complex mixture.

Phenoxide reactivities

Rate constants for displacement of chlorine from 4-chlorodiphenyl sulphone by several different phenoxides, reaction (10), are given in Table 4 and show that wide variations in reactivity occur, the more basic phenoxides (less acidic phenols) being the more reactive.



Polycondensations

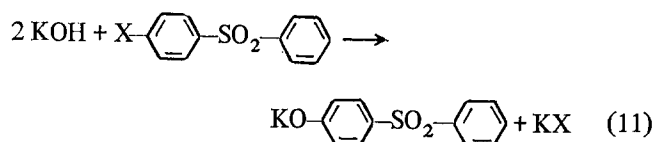
Second order rate constants for the initial rates at which the functional groups (halogen and KO-) react to form polyethersulphones are given in Table 5. None of these reactions obey second order kinetics indicating that the reactivity of the functional groups changes during the polycondensation process, and this effect has been observed previously by Schulze and Baron<sup>9</sup> for the polycondensation of dichlorodiphenyl sulphone with Bisphenate A (last system in Table 5). Curves for the extent of reaction against time (Figures 2 and 3) for several of these systems indicate that the single component (chlorophenoxide) systems show kinetics which are quite different from those of the dichloride plus bisphenoxide system.

Fission of ether linkages

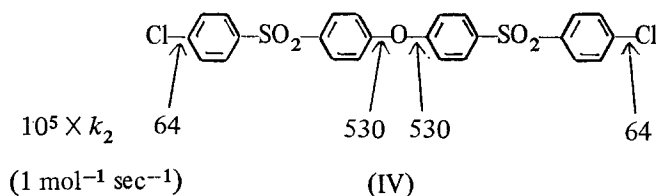
Diaryl ethers are normally very stable to attack by hydroxyl ions but as the ether linkages in polyethersulphones are activated by sulphone groups they may be labile. Data given in Table 6 show that ether bonds attached to the diphenyl sulphone grouping are labile (reaction 11), phenoxyl being displaced almost as rapidly as chlorine and 4-phenylsulphonyl-phenoxyl several times faster, the rate of displacement increasing with increasing stability of the phenoxide ion displaced.

Table 4 Displacement of halogen from 4-chlorodiphenyl sulphone by phenoxides  
Rate constants are for reaction in dry DMSO at 120°C using equimolar quantities of reactants

R in equation (10)	$10^5 \times k_2$ ( $l\ mol^{-1}\ sec^{-1}$ )
H	3024
	3740 per OK group
	1.08
	5.1 per -OK group



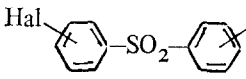




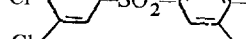
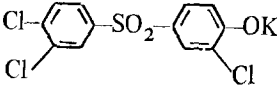
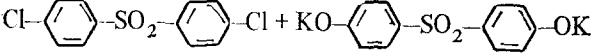
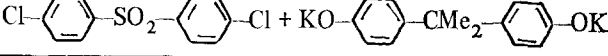
A further comparison of chlorine and 4-phenylsulphonyl phenoxyl as leaving groups is available from a kinetic and product composition study on the hydrolysis of IV with KOH where the rate constants for bond fission (under the condition of Table 6) are as indicated below:



DISCUSSION

It is accepted that the displacement of halogen from halogenophenyl sulphones by hydroxyl ion or by other nucleophilic reagents occurs via an intermediate complex V, and that the sulphone group, which is strongly electron accepting, aids reaction by stabilizing the complex via resonance hybrids such as VI. This effect operates when the halogen is positioned *ortho* or *para* to sulphone, but not when the orientation is *meta* so that the *m*-halogenophenyl sulphones are much less reactive (see Tables 1 and 2).

Table 5 Initial rate constants for polycondensations  
The rate constants,  $k_2$ , quoted are for the displacement of chlorine in dry DMSO

Compound(s) polycondensed	$10^5 \times k_2$ (l mol <sup>-1</sup> sec <sup>-1</sup> )	
	120°C	178°C
 <p><i>p</i>-F, <i>p</i>-OK</p>	1.45	—
 <p>” <i>p</i>-F, <i>o</i>-OK</p>	0.07	—
 <p>” <i>p</i>-Cl, <i>p</i>-OK</p>	0.0098	1.28
 <p>” <i>p</i>-Cl, <i>m</i>-OK</p>	0.58	—
 <p>” <i>p</i>-Cl, <i>o</i>-OK</p>	—	0.07
 <p>” <i>o</i>-Cl, <i>p</i>-OK</p>	—	0.13
	—	1.06
	16.0*	—
	6100*	—

\* For reaction of one chlorine with one phenoxide group

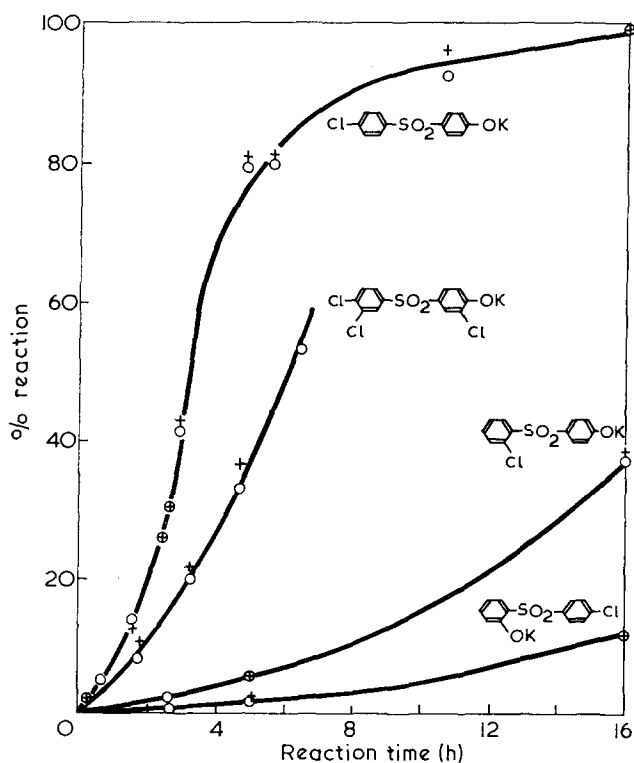


Figure 2 Polycondensation of potassium halophenates at 40 wt. % in DMSO at 178°C. +, determined by titration for alkali; o, determined by titration for chloride ion

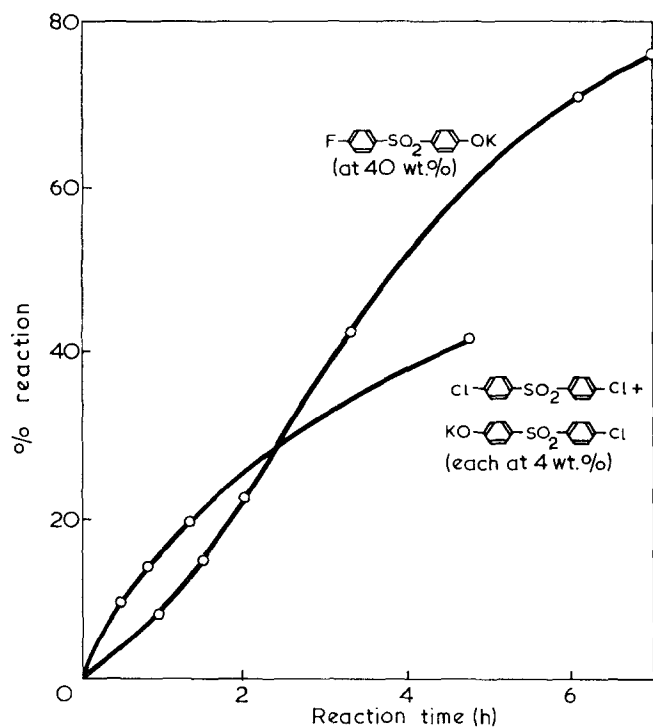


Figure 3 Polycondensations in DMSO at 120°C

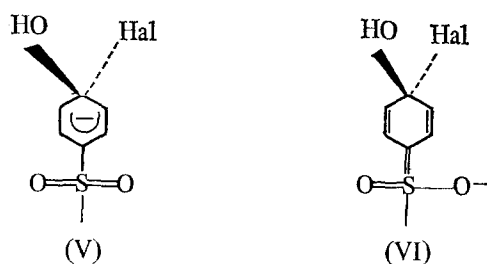
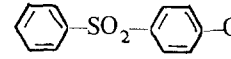
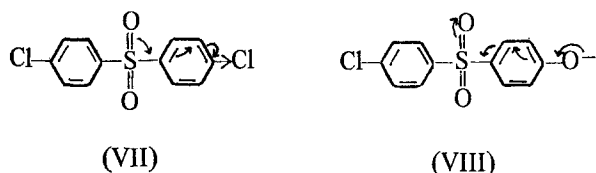


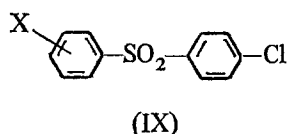
Table 6 Fission of ether linkages by  $\overline{\text{OH}}$   
Rate constants are for reaction in 80.5% DMSO/water at 120°C

X in equation (11)	$10^5 \times k_2$ (l mol <sup>-1</sup> sec <sup>-1</sup> )
Cl	112
MeO	33
PhO	100
	340 per ether bond

The introduction of other electron accepting groups such as chlorine into the same ring will stabilize the complex further and the increased reactivity shown by the tetrachlorodiphenyl sulphones (Table 3) results. Conversely groups such as methyl which donate electrons reduce reactivity as was found with 4,4'-dichloro-3,3'-dimethyldiphenyl sulphone (Table 2). The activating effect that sulphone has on displacement in one ring can be modified by substituents in the other, electron accepting groups enhancing the effect (by increasing the sulphone group's ability to accept electrons via displacements in the initial state such as in VII) while electron donating groups have the opposite effect as in VIII:

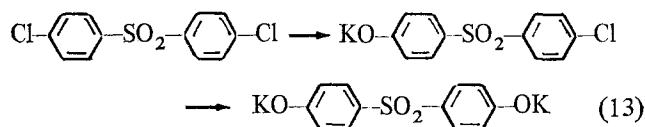
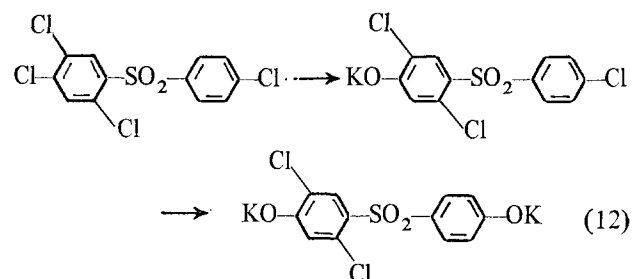


Thus, the electronic effects of a substituent in one ring are transmitted to the other via the sulphone linkage and the operation of this 'bridge' effect can be seen by comparing rate constants for the displacement of chlorine from compounds of structure IX (see Table 7).



Electron donation from a phenoxide anion occurs by both inductive (+I) and conjugative (+K) effects (ref. 10, p 291); therefore it occurs for all orientations of phenoxide but more strongly when phenoxide is in the *ortho* or the *para* rather than the *meta* position. For this reason, phenoxide oriented *ortho* or *para* to the sulphone groups (X = *o*-OK or *p*-OK in IX) reduces that group's ability to accept electrons from the reaction centre and leads to values for  $k_2$  40–50 times less than for the parent compound (IX where X = H) while the *meta*-oriented phenoxide group (X = *m*-OK in IX) deactivates to a lesser (~8 times) extent. Electron accession to halogen substituents in the benzene rings occurs via an inductive (-I) effect moderated by a conjugative (+K) effect in the opposite direction (ref. 10, p 294); therefore, it occurs for all orientations of chlorine but more strongly for the *meta* rather than *ortho* or *para* orientations. Thus, a chloro-substituent in any position should enhance the

activating effect of sulphone, and *meta*-Cl should be more effective than chlorine in either the *ortho* or *para* positions. The rate constants for displacement of one chlorine from 4,3'-dichlorodiphenyl sulphone (X = *m*-Cl in IX) and from the 4,4'-isomer (X = *p*-Cl in IX) are, as expected, 1.8 and 1.6 times greater than that for displacement from 4-chlorodiphenyl sulphone (X = H in IX), but the reactivity of the 4,2'-isomer (X = *p*-Cl in IX) is anomalous,  $k_2$  being almost the same as that for 4-chlorodiphenyl sulphone. However, this is not surprising as the 'bridge' effect of chlorine is small (a factor of 1.8 at most as compared with 8 for the phenoxide pole in the least active *meta*-orientation) and it is well known that the additivity of substituent effects often does not apply for *ortho*-substituents, as is evident from the fact that *ortho*-substituents do not conform to the Hammett relation (see ref. 10, p 1201).



The effect of a substituent operating through the sulphone bridge is not so great as the effect when the substituent is in the ring where displacement occurs, e.g.  $k_2$  for the first stage of reaction (12) is more than 25 times that for reaction of one chlorine atom in the first stage of reaction (13) (see Table 2) but the rate factor between the second stages of these reactions is less than 3 as the chloro substituents in the trichloro phenoxide must now act via the sulphone bridge. However, with highly polar substituents, e.g. phenoxide, the bridge effect can have an important influence on reactivity (compare  $k_2$  for the first compound in Table 7 with  $k_2$  for the last three).

As an approximate guide, the effect of a given substituent on the reactivity of a phenoxide group can be taken as opposite to that on halogen. This is because substituents such as -SO<sub>2</sub>- or -Cl which accept electrons delocalize the negative charge on oxygen and so reduce reactivity, while electron donating groups such as -CMe<sub>2</sub>- have the opposite effect. This can be very important, Bisphenate A being ~1000 times more reactive towards 4-chlorodiphenyl sulphone than is Bisphenate S (see Table 4). With sulphonyl phenoxide groups the orientation of phenoxide with respect to sulphone will be important and according to the above generalization, the expected order of reactivity would be *meta* > *ortho* > *para*. 'Bridge' effects can also alter phenoxide reactivities, e.g. each phenoxide in Bisphenate S activates the other so that  $k_2$  for reaction of either phenoxide group with 4-chlorodiphenyl sulphone is 5 times  $k_2$  for the reaction of this halide with the phenoxide from 4-hydroxydiphenyl sulphone (Table 4).

Table 7 Bridge effects in the displacement of chlorine from IX by OH<sup>-</sup>

Temperature = 80°C; solvent = 80.5 wt % DMSO/water

X in IX	$k_2 \times 10^5$
H	112
<i>p</i> -Cl	179 (for each Cl)
<i>m</i> -Cl	198
<i>o</i> -Cl	110
<i>p</i> -Me	76
<i>p</i> -Cl-C <sub>6</sub> H <sub>4</sub> -SO <sub>2</sub> -C <sub>6</sub> H <sub>4</sub> -O-	64 (for each Cl)
<i>p</i> -OK	3.2
<i>m</i> -OK	14.6
<i>o</i> -OK	2.0

Certain generalizations concerning the reaction of halogenophenyl sulphones with sulphonyl phenoxides to synthesize polyethersulphones can now be made. 4-Halogenophenyl sulphones are the preferred reagents for reaction with phenoxides, being substantially more reactive than their 2-chlorophenyl analogues ( $\sim 5$  times more reactive to  $\text{OH}^-$  and  $\sim 30$  times to  $\text{OPh}^-$  where steric hindrance will be more important—see *Table 1*), while the 3-chlorophenyl derivatives are unsuitable because the halogen in these compounds reacts so slowly that fission of the sulphone bond becomes significant. The relatively low reactivity of 2-chlorophenyl sulphones is well illustrated by the low initial rate of polycondensation shown by the potassium salt of 2-chloro-4'-hydroxy diphenyl sulphone as compared with that for the salt from the analogous 4-chloro-4'-hydroxy compound (*Table 5*). As is often found for the nucleophilic substitution reactions of activated aromatic halides<sup>11</sup> fluorides are more reactive than chlorides, and in the systems examined here the fluorophenyl sulphones are  $\sim 100$  times more reactive than the corresponding chloro derivatives, (cf.  $k_2$  for fluoride vs. chloride in *Tables 1, 2* and *5*). The tetrachlorodiphenyl sulphones in *Table 3* are all substantially more reactive than 4,4'-dichlorodiphenyl sulphone, but whereas the 3,3', 4,4'-tetrachloro compound is essentially bifunctional owing to the low reactivity of chlorine in the 3- and 3'-positions, the two other compounds are polyfunctional and their use is expected to give crosslinked products. Although the hydrolysis of 3,3', 4,4'-tetrachlorodiphenyl sulphone to the 3,3', 4-trichloro-4'-phenoxide is rapid compared with formation of the 4-chloro-4'-phenoxide by hydrolysis of 4,4'-dichlorodiphenyl sulphone, the two chlorophenoxides polycondense at comparable rates (see *Table 5*). Presumably activation of the 4-chlorophenylsulphonyl group by a 3-chloro substituent is balanced by a corresponding deactivation of the 4'-phenylsulphonyl phenoxide function by a chloro substituent in the 3'-position.

Deactivation of the phenoxide groups by the sulphone linkage in Bisphenate S leads to the low value of  $k_2$  for the initial rate of polycondensation of this compound with 4,4'-dichlorodiphenyl sulphone as compared with the polycondensation of the dihalide with Bisphenate A (*Table 5*). In practice this leads to the use of sulfolane at  $\sim 230^\circ\text{C}$  as the reaction medium for the polycondensation with Bisphenate S in contrast to dimethylsulphoxide at  $\sim 130^\circ\text{C}$  using Bisphenate A<sup>12</sup>.

A *m*-phenylsulphonyl phenoxide is expected to be more reactive than the corresponding *p*-grouping and this is probably the predominant effect leading to the observed rate factor of  $\sim 60$  between the initial rates of polycondensation for the potassium salt of 4-chloro-3'-hydroxydiphenyl sulphone and the isomeric 4-chloro-4'-phenoxide (*Table 5*). Application of the approximate guide that the effect of a substituent on phenoxide reactivity is opposite to that on halogen suggests (see *Table 1*) that the potassium salt of 4-chloro-2'-hydroxydiphenyl sulphone should polycondense faster than the 4-chloro-4'-phenoxide. In fact (see *Table 5*) the 4-chloro-2'-phenoxide is the less reactive, presumably due to steric hindrance by the *o*-sulphonyl group.

'Bridge' effects are important in several of the reactions leading to the synthesis of polyethersulphones. Stepwise hydrolysis of halogenodiphenyl sulphones (*Tables 2* and *3*) via halogenophenoxides occurs because the phenoxide group formed by displacement of one halogen atom

deactivates halogens present at other positions in the same ring directly, and halogen atoms in the adjacent ring by a 'bridge' effect. Thus, hydrolysis is stopped easily at the halogenophenoxide stage making these compounds readily available<sup>6,7</sup>. Halogenophenoxides are useful polycondensation intermediates<sup>6,13</sup> as they provide both functional groups in the same molecule, and their (mono) potassium salts are more soluble in the polycondensation solvent than the dipotassium salts of bisphenols. However, halogenophenoxides have a marked disadvantage in that the 'bridge' effect leads to lower halogen (due to phenoxide) and phenoxide (due to halogen) reactivities as compared with the corresponding dihalide plus bisphenoxide system, where the bridge effect enhances the reactivity of both functional groups. Thus the initial rate for the polycondensation of 4,4'-dichlorodiphenyl sulphone with Bisphenate S is  $\sim 10^3$  times greater than that for polycondensation of the corresponding chlorophenoxide (*Table 5*). As polycondensation proceeds the bridge effect operates to make this disadvantage disappear; as more of the (like) functional groups in the two-component system become separated by interposition of polymer repeat units the average reactivity of this system declines, while with the chlorophenoxide system the average reactivity of both functional groups is increased. Eventually both systems will have the same rate constant, the group acting via the sulphone linkage to modify the reactivity of all functional groups being the polymer repeat unit.

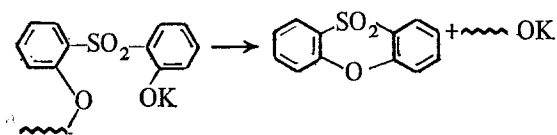
Increasing reactivity of the functional groups with conversion during the polycondensation of halophenylsulphonyl phenoxides is demonstrated by the conversion vs. time plots in *Figure 2*. It is seen that the slopes of these curves first increase with time, due to the increased reactivity of the functional groups, before decreasing as the reduction in functional group concentrations outweighs their increased reactivity. This situation is the opposite of that found by Schulze and Baron<sup>9</sup> for the polycondensation of 4,4'-dichlorodiphenyl sulphone with bisphenoxides, where the reaction rates drop off more rapidly than would be expected from the drop in functional group concentrations owing to a decrease in the reactivity of both functional groups.

The ether linkage in 4,4'-bis(4-phenylsulphonyl) diphenyl ether is labile to attack by  $\text{OH}^-$  (*Table 6*) and it may be estimated from the data given in this section that the rate constant for fission of the ether linkage in poly(diphenylene ether sulphone) by  $\text{OH}^-$  will be at least three times the rate constant for displacement of chlorine

*Table 8* Novel sulphones

Name	M.p. ( $^\circ\text{C}$ )	Criteria of purity
3,4'-Dichlorodiphenyl sulphone	110.5–112.5	i.r., n.m.r., g.l.c., t.l.c.
2,2',4,4'-Tetrachlorodiphenyl sulphone	196–197	i.r., n.m.r.
2,2'-Dichloro-4,4'-dimethyl-diphenyl sulphone	177–180	i.r., n.m.r., m.s., g.l.c.
4-Chloro-3'-hydroxydiphenyl sulphone	172–172.5	i.r., n.m.r.
2-Chloro-2'-hydroxydiphenyl sulphone	138.5–140	i.r., n.m.r., t.l.c.
4,4'-Bis(4-chlorophenylsulphonyl)-diphenyl ether	214–215	i.r., n.m.r., m.s., t.l.c.

from the end of a polymer chain by  $\overline{\text{OH}}$ . It is not possible to extrapolate from these data to the polycondensation system with any real confidence as the reactivity of a phenoxide group at the end of a polymer chain is very different from that of  $\overline{\text{OH}}$ . However, it appears likely that in polycondensations such as reaction (2) ether interchange will occur in a manner comparable to ester interchange in a polyesterification. For this reason the bisphenate of 2,2'-dihydroxydiphenyl sulphone is unlikely to be useful as a polycondensation intermediate for polyethersulphones because in such systems ether interchange could lead to elimination of repeat units as phenoxathiin dioxide:



## EXPERIMENTAL

### Starting materials

Dimethyl sulphoxide was fractionated under reduced pressure and a middle fraction b.p. 124.0°C at 100 mmHg was used. Aryl sulphones were prepared by methods described in the literature<sup>14</sup> and recrystallized to constant melting point. Several novel sulphones were employed and these are reported in Table 8.

The potassium phenoxide salts were prepared by neutralizing a methanolic solution of the corresponding phenol with the appropriate amount of aqueous potassium hydroxide. The solution was evaporated to dryness and the residue was dried under high vacuum at 120°C for 18 hours. These salts were protected from the atmosphere and prepared immediately before use.

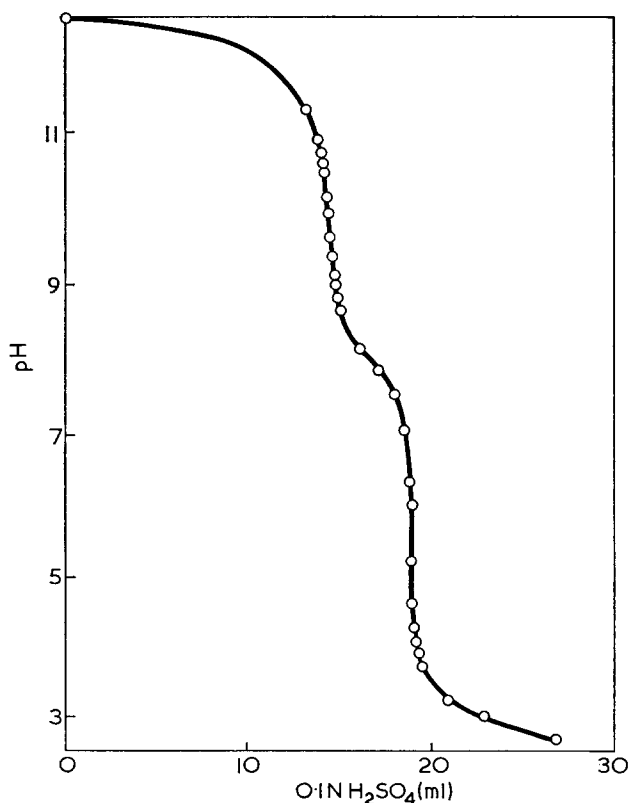


Figure 4 Hydrolysis of 4,4'-dibromodiphenyl sulphone at 120°C: titration of hydrolysate after 35 min reaction

### Hydrolysis technique

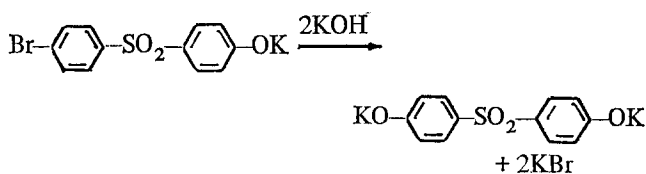
A DMSO/water system containing 80.5 wt. % DMSO, which boils at about 130°C, was chosen as reaction solvent because this system is homogeneous in sulphone and potassium halides both before and after reaction at room temperature. The reactions were conducted under nitrogen in an electrically heated, stainless-steel vessel (350 ml) fitted with a stirrer, a control thermocouple and a thermometer. A typical experiment is described in detail below.

### Hydrolysis of 4,4'-dibromodiphenyl sulphone

5.6414 g of 4,4'-dibromodiphenyl sulphone (15.00 mmol) were weighed into the reaction vessel and 225 ml of redistilled dimethyl sulphoxide were added. This system was stirred under nitrogen and made to thermostat at 120 ± 0.1°C. The hydrolysis was started by adding, as rapidly as possible, 60.0 ml of 1.000 N potassium hydroxide solution which had been preheated to 90°C. Under these conditions, owing to the considerable heat of dilution of dimethyl sulphoxide, a temperature of 120 ± 2°C was obtained which returned to 120 ± 0.1°C during the next 2–3 minutes. The total mass of the system is 317.0 g and occupies a volume of 307.5 ml at 120°C. Samples of hydrolysate were removed periodically using a syringe, rapidly cooled, weighed into beakers, diluted with water and titrated with 0.1 N sulphuric acid. The neutralization was followed using an EIL Model 23A pH meter fitted with a glass indicator electrode and a saturated sodium sulphate–mercurous sulphate reference electrode.

A typical neutralization curve is shown in Figure 4. The inflections at pH 9.5 and pH 5.5 were noted and the system was adjusted to pH 2.5 with more acid. The glass electrode was exchanged for one of silver and a potentiometric estimation of Br<sup>-</sup> using 0.02 N silver nitrate solution was then made.

In Table 9 all the results are tabulated. The inflection at pH 9.5 in Figure 4 is attributed to excess potassium hydroxide and the inflection at pH 5.5 to excess potassium hydroxide, monophenoxide and bisphenoxide. The rate at which the total concentration of base decreases is very close to the rate at which halide ion is produced, so that no significant amount of alkali is consumed in side reactions, e.g. sulphone cleavage. In Figure 5 the liberated bromide ion is plotted against time and clearly shows the tendency to 'half-way hydrolysis'. An extrapolation of the graph as indicated cuts the ordinate at 50% reaction and yields two curves. The curve ABC gives data on the formation of bisphenoxide:



and the difference between curve ABC and curve OBC gives data on the formation of monophenoxide:

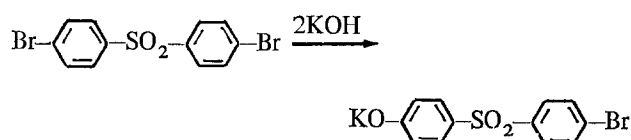




Table 9 Hydrolysis of 4,4'-dibromodiphenyl sulphone in aqueous dimethyl sulphoxide at 120°C using 4 equivalents KOH

Reaction time (min)	Mass sample (g)	Titration using 0.1 N H <sub>2</sub> SO <sub>4</sub>				Titration with 0.021 N Ag <sup>+</sup>	
		ml		equiv.		ml equiv. Br <sup>-</sup>	
		To pH 9.5	To pH 5.5	To pH 9.5	To pH 5.5		
2	12.430	21.55	22.90	3.650	3.880	4.05	0.1372
7	11.945	19.35	21.30	3.410	3.752	8.55	0.301
14	11.760	17.50	20.12	3.132	3.608	12.12	0.434
20	12.320	17.10	20.60	2.920	3.520	16.10	0.550
27	11.550	15.34	18.80	2.796	3.427	17.23	0.628
38	10.970	14.40	18.90	2.763	3.625	21.15	0.812
62	11.615	17.62	12.62	3.194	2.287	24.00	0.870
89	11.235	11.38	16.58	2.134	3.110	25.40	0.951
122	11.415	10.65	16.50	1.962	3.040	27.12	1.000
274	10.470	9.90	14.75	1.992	2.966	27.00	1.090
321	10.220	8.85	14.30	1.821	2.945	26.92	1.109
393	11.045	9.40	15.38	1.792	2.931	29.70	1.132
1061	11.750	770	15.40	1.380	2.759	35.80	1.282

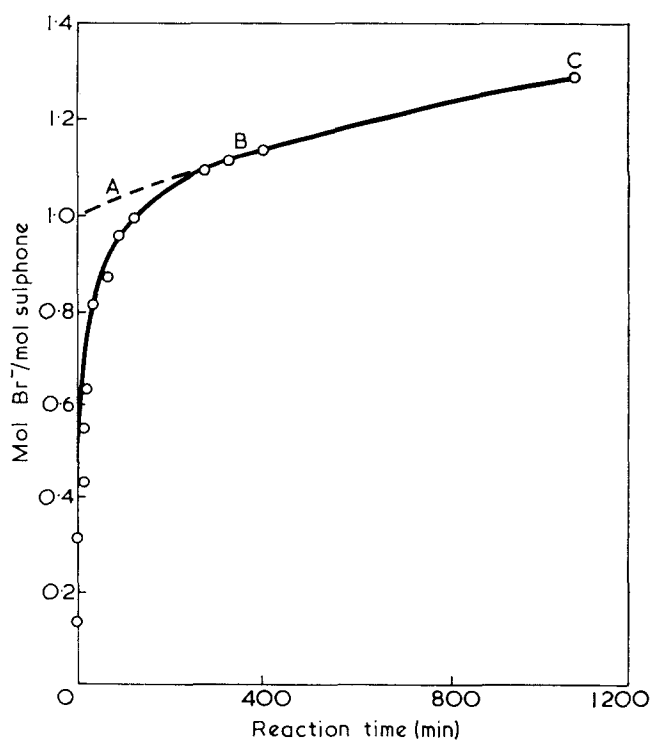
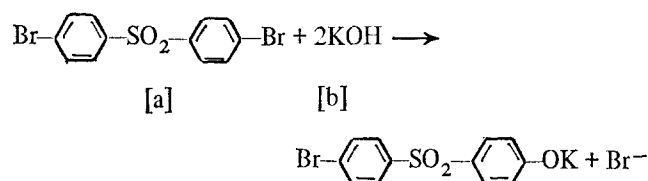


Figure 5 Hydrolysis of 4,4'-dibromodiphenyl sulphone at 120°C in 80.5 wt. % DMSO/water (4 mol KOH). A, B, C, see text

#### Calculation of rate constants

For each hydrolysis the reaction product was isolated and examined for structure and purity. Usually, this was a single substance formed in a clean reaction. From a knowledge of the stoichiometry, linear rate functions were calculated for different orders of reaction and these were plotted. As anticipated, the second order rate plots gave straight lines (over at least 80% of the reaction course) and the gradient of this line enabled the rate constant to be determined. Where insufficient data were available, approximate rate constants were obtained by estimation of the half-life of the reaction or by measuring the initial rate of reaction. In these cases it is necessary to assume the reaction order. With some compounds the rate at which halide ions was produced was less than the rate at which alkali was consumed, e.g. in the reactions with the 3-chloro and 3,3'-dichlorodiphenyl sulphones, and the difference between these rates was used to estimate the rate at which cleavage of the sulphone bond occurred.

#### Derivation of rate constant for 4,4'-dibromodiphenyl sulphone



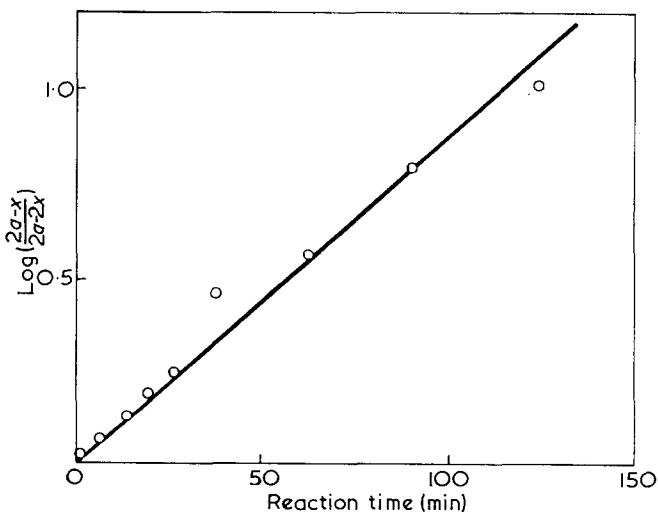
Let [a] and [b] be the concentrations of reactants in mol/l. If [x] mol/l of Br<sup>-</sup> is generated after a time *t* then for second order kinetics:

$$dx/dt = k_2(a-x)(b-2x)$$

where *k*<sub>2</sub> is the second order rate constant. Integration and writing *b*=4*a*, since 4 equivalents of potassium hydroxide were used, gives:

$$2ak_2t = \ln\left(\frac{2a-x}{2a-2x}\right)$$

This rate function is plotted in Figure 6, the value of *a* being 0.0488 mol/l at 120°C (15 mmol in 307.5 ml).


 Figure 6 Second order rate plot for 4,4'-dibromodiphenyl sulphone + 4 KOH at 120°C leading to bromophenoxide. Slope =  $0.9 \times 10^{-2} \text{ min}^{-1}$  ( $1.5 \times 10^{-4} \text{ sec}^{-1}$ );  $k_2 = 385 \times 10^{-9} \text{ l mol}^{-1} \text{ sec}^{-1}$

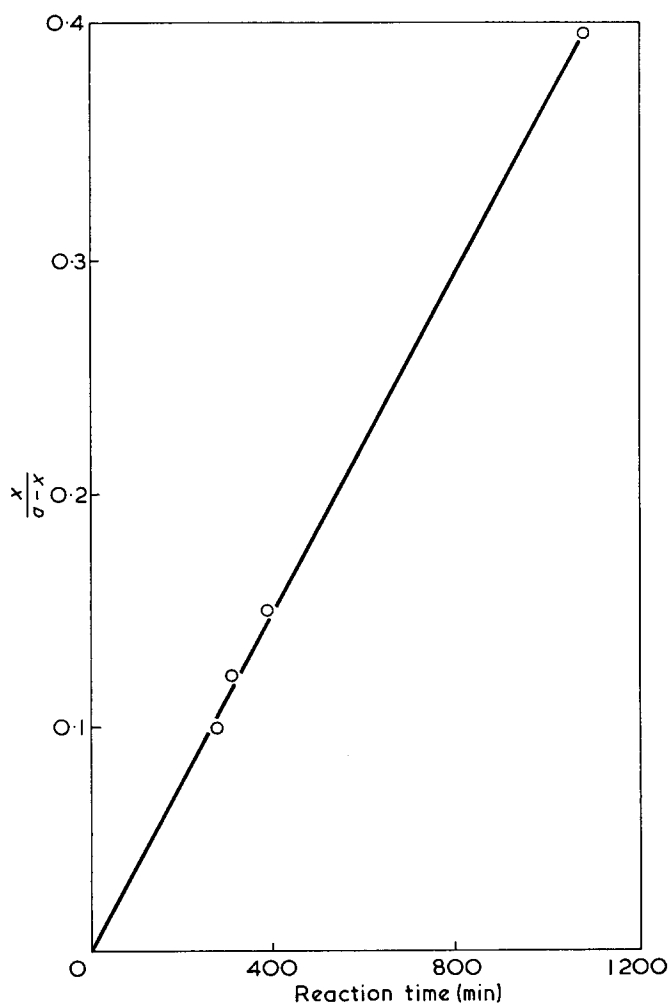


Figure 7 Second order rate plot for  $p\text{-KO}-(\text{C}_6\text{H}_4)\text{-SO}_2\text{-(C}_6\text{H}_4)\text{-p-Br} + 2\text{KOH}$  at  $120^\circ\text{C}$  leading to bisphenoxide. Slope  $= 0.371 \times 10^{-3} \text{ min}^{-1}$  ( $0.6183 \times 10^{-5} \text{ sec}^{-1}$ );  $k_2 = 6.33 \times 10^{-5} \text{ l mol}^{-1} \text{ sec}^{-1}$

Clearly, the reaction obeys second order kinetics with  $k_2 = 385 \times 10^{-5} \text{ l mol}^{-1} \text{ sec}^{-1}$ . For the formation of bisphenoxide:  $\frac{dx}{dt} = k_2^1(a-x)(2a-2x)$  which yields  $2k_2^1 t = \frac{x}{a-x}$ . This rate function is plotted in Figure 7 and as the data only extend over 28% of the reaction, second order kinetics must be assumed which gives  $k_2^1 = 6.33 \times 10^{-5} \text{ l mol}^{-1} \text{ sec}^{-1}$ .

#### Polycondensation of halophenoxides in anhydrous dimethyl sulphoxide

These reactions are much slower than the hydrolysis reactions and at  $120^\circ\text{C}$  with lengthy reaction periods, salt concentrations of 40 wt. % were necessary. These reactions were studied in evacuated, sealed, glass tubes which were thermostated for known reaction periods at  $120^\circ\text{C}$  and at  $178^\circ\text{C}$ . The tubes were then cooled, opened and analysed for residual phenoxide and potassium halide (which precipitate in this system). In all cases, the halide generated corresponded to the phenoxide consumed and no evidence for side reactions could be obtained. Initial rate constants were calculated from the slopes of the curves in Figure 2 at zero time.

#### Reaction of potassium phenoxide with halosulphones

These reactions were faster than the hydrolysis reactions and were studied in the stainless-steel apparatus described. The reactions were started by adding 10 mmol of the halosulphone to a thermostated solution of 10 mmol of pure potassium phenoxide in 250 ml of anhydrous DMSO at  $120^\circ\text{C}$ . Samples were removed periodically and estimated for residual phenoxide. Halide ion could not be determined with reliability because it is thrown out of solution. Using the phenoxide data, second order rate plots were made and second order rate constants were determined.

#### REFERENCES

- Rose, J. B. *Chem. Ind.* 1968, p 461
- Ivin, K. J. and Rose, J. B. 'Advances in Macromolecular Chemistry' (Ed. W. M. Pasika), Academic Press, London and New York, 1968, Vol 1, p 336
- Johnson, R. N. 'Kirk-Othmer Encyclopedia of Chemical Technology', 3rd edn, Wiley, New York, 1968, Vol 16, p 272
- Parker, A. J. *Q. Rev.* 1962, **16**, 163
- Oae, S. and Khim, Y. H. *Bull. Chem. Soc. Japan* 1967, **40**, 1716
- Rose, J. B. and Barr, D. A. Br. Pat. 1 153 035
- Johnson, R. N. and Farnham, A. G. *J. Polym. Sci. (A-1)* 1967, **5**, 2415
- Hawthorne, J. O., Mihelic, E. L. and Morgan, M. S. *J. Org. Chem.* 1968, **33**, 447
- Schulze, S. R. and Baron, A. L. *Adv. Chem. Ser.* 1969, **91**, 693
- Ingold, C. K. 'Structure and Mechanism in Organic Chemistry', 2nd edn, Bell, London, 1969
- Miller, J. 'Aromatic Nucleophilic Substitution', Elsevier, London, 1968, p 140
- Johnson, R. N. and Farnham, A. G. Br. Pat. 1 078 234
- Clendinning, R. A. Br. Pat. 1 177 183
- Suter, C. H. 'The Organic Chemistry of Sulfur', Wiley, New York, 1944, Ch VII

# Effect of end groups on the melting temperatures of low molecular weight poly(ethylene oxide)

C. Booth, J. Malcolm Bruce and M. Buggy

Department of Chemistry, University of Manchester, Manchester M13 9PL, UK  
(Received 27 March 1972)

Chloro- and phenoxy-ended poly(ethylene oxide) fractions of molecular weight 1000 and 1500 have been prepared. Their melting points are substantially (5–7 deg) lower than those of the corresponding hydroxy-ended poly(ethylene oxide) fractions. The differences in melting point correspond to an increase in end interfacial free energy ( $\sigma_e$ ) of 0.5 kcal/mol, relative to the hydroxy-ended polymers. The effect is explained in terms of a stabilization due to hydrogen bonding in the end interfacial layer of the crystals of the hydroxy-ended polymers.

## INTRODUCTION

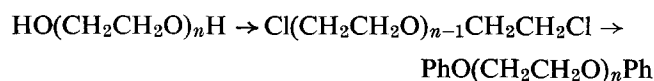
The properties (such as melting points, densities, crystallite morphologies, and crystallization rates) of low molecular weight fractions of poly(ethylene oxide) are usually interpreted in terms of molecular theories which assume exclusion of end groups from the crystalline phase, with the implication that the end groups are concentrated in the interfacial phase. Most experimental measurements have been made using hydroxy-ended samples of poly(ethylene oxide)<sup>1–10</sup>. Consequently it was of interest to investigate the effect of replacing hydroxy-ends by less polar groups. Here we report on the preparation of chloro- and phenoxy-ended poly(ethylene oxide)s of number-average molecular weights 1000 and 1500, and on their melting points.

## EXPERIMENTAL

### Preparation of materials

Hydroxy-ended poly(ethylene oxide) samples were obtained from Shell Chemical Co. Ltd (mol. wt. 1000 and 1500) or were prepared as described elsewhere<sup>5</sup> (mol. wt. 3300). Fractions, comprising about half the original sample, were obtained by addition of iso-octane to a dilute solution of the poly(ethylene oxide) in benzene, and were freeze-dried from benzene before use. Number-average molecular weights of the fractions (*Table 1*) were close to the nominal molecular weights given above.

Model experiments for the transformations



were carried out using diethylene glycol,



Diethylene glycol has previously been converted into bis(2-chloroethyl) ether by treatment with thionyl chloride either alone<sup>11</sup> (72% yield) or in the presence<sup>12</sup> of pyridine (62% yield). The latter mixture is often used<sup>13</sup> for the corresponding transformation of mono-

hydric alcohols, and it has also been employed<sup>14</sup> for higher poly(ethylene glycol)s, e.g.  $\text{HO}(\text{CH}_2\text{CH}_2\text{O})_n\text{H}$  with  $n=6, 18$  and  $42$  gave the corresponding dichloro-compounds in yields of, respectively, 77, 38.5 and 28%. We obtained the best yields (68–70%) of bis(2-chloroethyl) ether using the thionyl chloride/pyridine reagent in benzene as solvent; tetrahydrofuran was less effective than benzene, and yields were not improved by addition<sup>15</sup> of catalytic quantities of dimethylformamide.

Almost quantitative *O*-alkylation of phenols has been effected<sup>16</sup> using the sodium salt and a *n*-alkyl halide in dimethyl sulphoxide, and this method was used in the present work. The maximum yield of bis(2-phenoxyethyl) ether obtained was 80%.

Application of the above chlorination procedure to the polymers  $\text{HO}(\text{CH}_2\text{CH}_2\text{O})_n\text{H}$  with  $n=22$  (mol. wt. 1000) and  $n=34$  (mol. wt. 1500) failed to effect complete replacement of the hydroxy groups, but the dichloro-polymer could be separated from hydroxy-polymer by extraction with ether. Yields were about 20%. The method failed for  $n=74$  (mol. wt. 3300). Treatment of the dichloro-polymers with sodium phenoxide in dimethyl sulphoxide gave the corresponding diphenoxy-polymers in yields of about 60%.

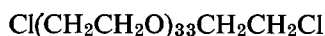
Thionyl chloride was distilled from quinoline and then from boiled linseed oil<sup>17</sup>. Pyridine was dried over and distilled from solid potassium hydroxide. Benzene was dried by distillation, and then distilled from lithium aluminium hydride. Dimethyl sulphoxide was dried over and distilled (reduced pressure) from calcium hydride. Diethylene glycol was distilled.

*Bis(2-chloroethyl) ether.* Thionyl chloride (9 g) was added dropwise during 40 min to a stirred, ice-cooled solution of diethylene glycol (4 g) and pyridine (8 g) in benzene (20 ml), and the mixture was then heated on a steam-bath for 1 h, cooled, and added to aqueous 5% sodium hydroxide (75 ml). The mixture was extracted with benzene (5 × 25 ml), and the combined extracts were washed with aqueous 20% sulphuric acid (2 × 5 ml)

and then with water (2 × 20 ml) and dried (CaCl<sub>2</sub>). Removal of the solvent and distillation of the residue gave the ether (4.5 g, 70%), b.p. 68–70°C at 15 mmHg (lit.<sup>12</sup> 65°C at 15–16 mmHg), identical (infra-red spectrum) with authentic<sup>18</sup> material.

*Bis(2-phenoxyethyl) ether.* Sodium hydride (1.05 g) was added portionwise to a solution of phenol (4 g) in dimethyl sulphoxide (100 ml) stirred under nitrogen at room temperature, and stirring was continued for 2 h. Bis(2-chloroethyl) ether (3.04 g) was then added, and the mixture was stirred at 60°C for 6 h, and then cooled and added to water (100 ml). The solution was acidified with 10% hydrochloric acid, and then extracted with benzene (6 × 50 ml), the combined extracts being washed with aqueous 10% sodium hydroxide (3 × 30 ml), then with water (4 × 20 ml), and dried (MgSO<sub>4</sub>). Removal of the solvent gave the ether (4.38 g, 80%), m.p. 63–65°C, identical (mixed m.p. and infra-red spectrum) with authentic<sup>19</sup> material (m.p. 64–65°C).

*Chloro-ended polymers.* Poly(ethylene oxide) (19 g, mol. wt. 1500) in a mixture of benzene (100 ml) and pyridine (50 ml) was added during 50 min to a stirred, ice-cooled, solution of thionyl chloride (4 ml) in benzene (100 ml) and stirring was continued at 0°C for 5 h, and finally under reflux for 30 min. Volatile materials were removed at 25–30°C and 20 mmHg, and the residual mixture of pyridine hydrochloride and polymer was extracted with dry benzene to remove the polymer, which was then recovered by freeze-drying. Continuous (Soxhlet) extraction of the crude product with dry ether for 24 h gave the chlorine-ended polymer, which was crystallized from dry ether (25 ml/g) and then freeze-dried from benzene to give an almost white solid (4 g, 20%) (Found: C, 52.6%; H, 8.9%; Cl, 4.9%;



requires C, 54.5%; H, 9.1%; Cl, 4.7%).

Polymer of mol. wt. 1000 was prepared analogously, but the scale was reduced to one-twentieth.

*Phenoxy-ended polymers.* Sodium hydride (0.15 g) was added portionwise to a stirred solution of phenol (0.6 g) in dimethyl sulphoxide (30 ml) at room temperature, and stirring was then continued for 2 h. The solution was heated to 60°C, and to it was added dropwise to a solution of chlorine-ended poly(ethylene oxide) (0.9 g, mol. wt. 1500) in dimethyl sulphoxide (10 ml), and the mixture was then stirred at 60°C for 24 h. The mixture was cooled, added to water (50 ml), and the solution was acidified with 10% hydrochloric acid and then extracted with benzene (6 × 30 ml). The combined extracts were shaken with sodium hydroxide pellets (10 g) for 30 min, separated and the solvent was removed, finally at 100°C and 20 mmHg, leaving phenoxy-ended polymer (~60% yield) contaminated with dimethyl sulphoxide. The polymer was purified by gel permeation chromatography (see below).

An analogous reaction was carried out with polymer of mol. wt. 1000, but residual dimethyl sulphoxide was removed by distillation at 100°C (bath) and 0.01 mmHg into a trap cooled in liquid nitrogen. The yield was 60%.

<sup>1</sup>H n.m.r. spectra of the phenoxy-ended polymers (in C<sub>6</sub>D<sub>6</sub>) showed only bands due to PhO-(τ 2.70–3.05) and -CH<sub>2</sub>O-(τ 6.50) groups, with the required intensities.

### Molecular weights

No degradation of molecular weight was observed in the preparations of chloro- and phenoxy-ended polymers. The relevant molecular weight data are given in *Table 1*. The intrinsic viscosity in benzene at 25°C of the chloro-ended 1500 polymer was identical (0.062 dl/g) with that of the hydroxy-ended polymer. Intrinsic viscosities of poly(ethylene oxide) samples are<sup>20</sup> insensitive to end-group when the molecular weight exceeds 1000. All fractions were characterized by gel permeation chromatography (tetrahydrofuran at 45°C, 2 ml injection of 0.25% solution, flow rate 1 ml/min, columns: maximum nominal pore sizes (Å) of 1.5 × 10<sup>5</sup>, 1.5 × 10<sup>4</sup>, 2 × 10<sup>3</sup>, 3.5 × 10<sup>2</sup>). Calibration was by means of hydroxy-ended poly(ethylene oxide) fractions covering the molecular weight range 1000 to 10 000. Correction for adventitious dispersion was made by the method of Aldhouse and Stanford<sup>21</sup>. Minor variations in the number-average molecular weights calculated from the gel permeation chromatographs are attributable to the overlap of impurity peaks with the low molecular weight tail of the distributions, and also to changes in the size and polarity of the end-group.

### Melting points

*Dilatometry.* Small samples (<200 mg), moulded in high vacuum, were placed in glass dilatometers, outgassed and confined with mercury. The dilatometers were immersed in boiling water for 15 min and their contents were then allowed to crystallize at room temperature. Melting was effected by placing the dilatometer in an oil bath held a degree or so below the melting point and then raising the temperature by 8 deg/h. Expansion was followed by means of a cathetometer. The melting point was taken to be that point at which detectable crystallinity (judged by volume) disappeared.

*Microscopy.* Small samples (<10 mg) were placed between slide and coverslip, melted near 80°C, and then allowed to crystallize at room temperature. The slide was viewed on the hot stage of a Reichert polarizing microscope, the temperature of which was raised at about 1 deg/min. The temperature at which birefringence disappeared was taken to be the melting point.

## RESULTS

Melting points were measured several times and mean values are given in *Table 2*. Reproducibility was about ±0.1 deg for dilatometry, ±0.5 deg for microscopy.

Values of the end interfacial free energy of lamellar crystals (σ<sub>e</sub>) have been calculated by comparison of the

*Table 1* Molecular characteristics of poly(ethylene oxide) fractions

Fraction	Hydroxy-ended		Chloro-ended		Phenoxy-ended			
	M <sub>n</sub>	[η] (dl/g)	M <sub>w</sub> /M <sub>n</sub>	M <sub>n</sub>	[η] (dl/g)	M <sub>w</sub> /M <sub>n</sub>		
1000	1000	—	1.06	1000	—	1.05	1000	1.05
1500	1500	0.062	1.05	1300	0.062	1.05	1500	1.05
3300	3300	0.110	1.08	—	—	—	—	—

Table 2 Melting points ( $T_m$ ) and end interfacial free energies ( $\sigma_e$ ) of poly(ethylene oxide) fractions

Fraction	End group	$T_m$ (°C)		$\sigma_e$ (kcal/mol)
		Dilatometry	Microscopy	
1000	-OH	39.1*	37.5	1.4
	-Cl	—	30.0	1.9
	-OPh	—	30.7	1.9
1500	-OH	48.5	48.9	1.5
	-Cl	43.6	43.9	2.0
	-OPh	—	43.0	2.0

\* Data reported earlier<sup>4</sup> for a similar fraction

measured melting points with those calculated for extended chain lamellar crystals of poly(ethylene oxide). The calculation, discussed in detail in an earlier paper<sup>4</sup>, is based on Flory's theory<sup>22</sup> of melting of crystals composed of polymer of finite molecular weight, which has been modified<sup>4</sup> to allow for the effect of molecular weight distribution. The appropriate equation for extended chain crystals is<sup>4</sup>:

$$T_m = T_m^0 [1 - (2\sigma_e / \Delta h \zeta)] / \{1 + (RT_m^0 / \Delta h) [(1/x_n) - (\ln I / \zeta)]\}$$

where  $T_m^0$ , the thermodynamic melting point of poly(ethylene oxide), is<sup>23</sup> 349K;  $\Delta h$ , the heat of fusion of bulk poly(ethylene oxide), is<sup>2, 24</sup> 2 kcal (mol chain units)<sup>-1</sup>;  $x_n$  is the number-average chain length (in chain units);  $\zeta$  is the lamellar crystal thickness (in chain units);  $I$  is given by:

$$I = \int_{\zeta}^{\infty} w(x) [(x - \zeta + 1) / x] dx$$

where  $w(x)$  is the weight distribution, which can be taken<sup>4</sup> to be given by a Schulz-Zimm<sup>25</sup> distribution.

The assumption  $\zeta = 0.9x_n$ , which is indicated by observations of lamellar thickness and density for crystals of hydroxy-ended poly(ethylene oxide), taken together with the values of  $x_n$  and  $M_w/M_n$  indicated by Table 1, leads to the values of  $\sigma_e$  given in Table 2. It has already been shown<sup>4</sup> that values of  $\sigma_e$  calculated in this way are not very sensitive to the choice of lamellar thickness.

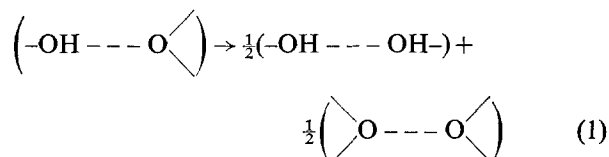
## DISCUSSION

As expected, the melting points of fractions 1000 are consistently lower than those of 1500 no matter what the end-group. However, the melting points of the hydroxy-ended poly(ethylene oxide) fractions are higher, by some 5-7 deg, than those of the fractions with non-polar end-groups, either chloro or phenoxy. Within the assumption that crystallites of all the samples are lamellae composed essentially of extended-chain molecules, the lowering of melting point observed when the hydroxy-ends are replaced by chloro- or phenoxy-ends corresponds to an increase in end interfacial free energy ( $\sigma_e$ ) of about 0.5 kcal (mol of chains emerging)<sup>-1</sup> irrespective of molecular weight. The alternative assumption, that  $\sigma_e$  is unchanged and that the lowering of melting point observed on replacing hydroxy-ends by non-polar-ends is due to a large decrease in lamellar thickness, is not attractive. A decrease in lamellar thickness to about half the extended chain length would be required in order to explain the observed changes in melting points,

and this would be possible at constant  $\sigma_e$  only if extensive chain-folding occurred<sup>5</sup>. A decrease in lamellar thickness whilst maintaining the extended-chain conformation of the polymer would result<sup>4</sup> in a large increase in  $\sigma_e$ .

The similarity of the effects found for chloro- and phenoxy-ended poly(ethylene oxide) fractions points to an explanation based on differences in end-group interactions rather than on differences in packing in the end interfacial layer. In particular there is the possibility of forming hydrogen bonds (hydroxy-hydroxy and hydroxy-ether) in systems involving hydroxy-ended polymers.

The end interfacial free energy of an extended chain crystal is the free energy change on transferring 1 mol of chain ends from the melt to the melt-crystal end interfacial layer. Measurements of the density of hydroxy-ended poly(ethylene oxide) of molecular weight near 1000 indicate a degree of crystallinity of about 80% so that exclusion of end-groups from the crystalline phase results in their concentration in the interfacial (interlamellar) layer, to mol% near 45 in the interfacial layer compared with 9 in the melt. Consequently the process of formation of the end interface will be accompanied by an interchange of hydroxy-ether for hydroxy-hydroxy hydrogen bonds which can be written:

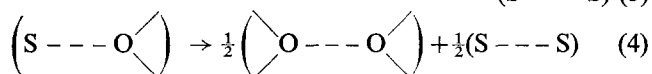
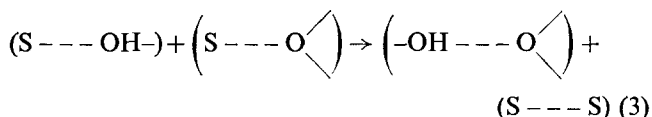
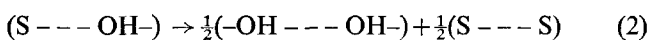


where -OH denotes a hydroxy end-unit and  $\text{O} \langle \rangle$  an ether chain-unit, and the intermolecular contacts are indicated by -OH ---  $\text{O} \langle \rangle$  and -OH --- OH- for

hydrogen bonding, and by  $\langle \rangle \text{O} \text{---} \langle \rangle \text{O}$  for van der

Waals interaction. If we assume, reasonably, that the interchange free energy for the end-unit and chain-unit contacts is near zero when the polymers are chloro- or phenoxy-ended, then our result is consistent with a free energy change for the interchange process (1) of not less than -0.5 kcal/mol, and equal to -0.5 kcal/mol if all hydroxy-groups are involved in the interchange process.

The thermodynamic properties of hydrogen-bonded species between alcohols and between alcohols and ethers have been discussed by Pimentel and McClellan<sup>26</sup>. Data are available<sup>26</sup> for processes of formation in inert solvents (S) which can be written:



and which provide a path [(2)+(4)-(3)] equivalent to the interchange process (1). Values of  $\Delta H$  and  $\Delta S$  for process (4), which involves interchange of van der Waals interactions, will be effectively zero. Values of  $\Delta H$  and  $\Delta S$  for processes (2) and (3) vary with the alcohol or ether under consideration, but place the value of  $\Delta G$

for process (1) between zero and  $-1$  kcal/mol in the temperature range used in this work. It would seem, therefore, that a very simple model for the crystallization in which hydroxy-hydroxy bonding is infrequent in the melt but predominant in the interfacial layer conforms with our experimental results.

#### ACKNOWLEDGEMENTS

We thank D. J. Roy and D. Rowlinson for assistance with the characterization of the polymers. M.B. acknowledges receipt of a Science Research Council Advance Course Studentship.

#### REFERENCES

- 1 Spegt, P. A., Terrisse, J., Gilg, B. and Skoulios, A. E. *Makromol. Chem.* 1967, **107**, 29
- 2 Braun, W., Hellwege, K. H. and Knappe, W. *Kolloid-Z.* 1967, **215**, 10
- 3 Hay, J. N., Sabir, M. and Stephen, R. L. T. *Polymer* 1969, **10**, 187, 203
- 4 Beech, D. R., Booth, C., Dodgson, D. V., Sharpe, R. R. and Waring, J. R. S. *Polymer* 1972, **13**, 73
- 5 Beech, D. R., Booth, C., Pickles, C. J., Sharpe, R. R. and Waring, J. R. S. *Polymer* 1972, **13**, 246
- 6 Arlie, J. P., Spegt, P. A. and Skoulios, A. E. *Makromol. Chem.* 1966, **99**, 160
- 7 Arlie, J. P., Spegt, P. A. and Skoulios, A. E. *Makromol. Chem.* 1967, **104**, 212
- 8 Spegt, P. A. *Makromol. Chem.* 1970, **140**, 167
- 9 Barnes, W. J., Luetzel, W. G. and Price, F. P. *J. Phys. Chem.* 1961, **65**, 1742
- 10 Mandelkern, L., Quinn, F. A. and Flory, P. J. *J. Appl. Phys.* 1954, **25**, 840
- 11 Kahane, E. and Rousseau, G. *Bull. Soc. Chim. France* 1939, p 647
- 12 Fakstorp, J., Christiansen, J. A. and Pedersen, J. G. A. *Acta Chem. Scand.* 1953, **7**, 134
- 13 Brooks, L. A. and Snyder, H. R. *Org. Synth.* 1945, **25**, 84; Frazer, M. J., Gerrard, W., Machell, G. and Shepherd, B. D. *Chem. and Ind.* 1954, p 931
- 14 Fordyce, R., Lovell, E. L. and Hibbert, H. *J. Am. Chem. Soc.* 1939, **61**, 1905
- 15 Bosshard, H. H., Mory, P., Schmid, M. and Zollinger, H. *Helv. Chim. Acta* 1959, **42**, 1653
- 16 Kornblum, N., Seltzer, R. and Haberfeld, P. *J. Am. Chem. Soc.* 1963, **85**, 1148
- 17 Vogel, A. I. 'A Text-book of Practical Organic Chemistry', Longmans, Green and Co., London, 1948, p 185
- 18 Kamm, O. and Waldo, J. H. *J. Am. Chem. Soc.* 1921, **43**, 2223
- 19 Mamedov, S., Mamedova, A. R. and Avanesyan, M. A. *Zh. Obshch. Khim.* 1963, **33**, 1451; *Chem. Abstr.* 1963, **59**, 12680g
- 20 Sadron, C. and Rempp, P. *J. Polym. Sci.* 1958, **29**, 127
- 21 Aldhouse, S. T. E. and Stanford, D. M. *5th Int. Gel Permeation Chromatog. Seminar, London* 1968
- 22 Flory, P. J. *J. Chem. Phys.* 1949, **17**, 223
- 23 Beech, D. R. and Booth, C. *J. Polym. Sci. (B)* 1970, **8**, 731
- 24 Beaumont, R. H. *et al. Polymer* 1966, **7**, 401; Booth, C., Gee, G. and Devoy, C. *J. Polymer* 1971, **12**, 327
- 25 Schulz, G. V. *Z. Phys. Chem.* 1939, **B43**, 25; Zimm, B. H. *J. Chem. Phys.* 1948, **16**, 1093
- 26 Pimentel, G. C. and McClellan, A. L. 'The Hydrogen Bond', Freeman, New York, 1960

# High temperature stability in fluorosilicone vulcanisates

D. K. Thomas

Materials Department, Royal Aircraft Establishment, Farnborough, Hants, UK  
(Received 20 March 1972)

Fluorosilicones are less heat stable than conventional methyl silicones because (a) they are more likely to revert to low molecular weight cyclic products, and (b) they are more susceptible to oxidation and free radical attack generally. Reversion is promoted by base catalyst residues from the polymerization process, but the effect can be minimized by a proper choice of compounding ingredients and vulcanizing reagents. Oxidation leads to crosslinking and in certain circumstances this can mask the effect of reversion.

## INTRODUCTION

Silicone rubbers are outstanding in their ability to resist the effects of high and low temperature. At present the best balance of properties in respect of mechanical strength and resistance to extremes of temperature is achieved in the methyl-vinyl silicones, but they lack resistance to a range of commercially important hydrocarbon based fluids.

The introduction of fluorosilicones provided silicone rubbers having an excellent resistance to non-polar fluids. In many other respects their properties are comparable with those of methyl-vinyl silicones, but in both the vulcanized and unvulcanized state they appear to be substantially less heat stable than the latter. For example, conventional oven ageing tests gave the following estimates for heat stability in the two vulcanisates<sup>1</sup>:

	Useful life in hours at high temperature		
	150°C	175°C	200°C
Fluorosilicone	20 000	5 000	4 000
Methyl-vinyl silicone	30 000	15 000	10 000

It has been shown, for methyl-vinyl silicones, that the type of organic peroxide used for vulcanization has a significant effect on vulcanisate stability<sup>2</sup> and that residual catalyst from the polymerization process can adversely affect heat stability<sup>3</sup>. It is also known that hydrolytic scission can be a major cause of structural change in methyl-vinyl silicones in confined or humid conditions at moderately high temperatures<sup>4</sup>, and that certain fine particle fillers have a considerable effect on heat stability.

The present work is concerned with establishing the principal causes of high temperature instability in vulcanisates produced from commercially available fluorosilicone gum stock. The effect on heat stability of the different curatives and fine silica powder used in practical formulations is also considered.

## EXPERIMENTAL

### Materials and processing

The polymers used were a commercially available methyl trifluoropropyl silicone (Dow-Corning LS.420) containing about 0.2 mol% of vinyl groups and a non-vinyl methyl trifluoropropyl silicone (not available commercially; supplied by Dow-Corning). The cross-linking reagents used were benzoyl peroxide (BzP), dichlorobenzoyl peroxide (DCBzP), dicumyl peroxide (DCP), and 2,5-dimethyl-2,5-di-*t*-butylperoxyhexane (VX). Filled compounds contained 20 parts by weight of fine fumed silica, Aerosil K3 (now known as Aerosil 200).

In all cases compounding was carried out on a 6 × 2 in laboratory roll mill and vulcanization was effected under pressure for 1 h at 160°C; no post-cure treatment was given.

### Equilibrium swelling measurements

The solubility and degree of swelling of fluorosilicone vulcanisates was determined in ethyl acetate at 28°C. About 0.2 g of rubber was weighed accurately and immersed in a large excess of ethyl acetate until it had reached an equilibrium swollen state (usually about 48 h). The rubber was then removed, surface dried, and weighed in a stoppered bottle. Finally the solvent was removed under reduced pressure at room temperature and the dry rubber was weighed. Solubility was calculated from the initial and final dry weights, and the volume fraction of rubber in the vulcanisate swollen to equilibrium ( $V_r$ ) was calculated using values of 1.30 and 0.90 for the densities of polymer and solvent respectively. The value of  $V_r$  is related to crosslink density or the number-average molecular weight between crosslinks ( $M_c$ ) by the Flory-Rehner equation<sup>5</sup>. In some instances the results of swelling measurements are expressed in terms of a swelling ratio (=equilibrium swollen weight/final dry weight); this is designated SR and the smaller it is the more highly crosslinked is the rubber.

Oven ageing experiments

Rubber specimens of thickness 0.50 mm were exposed to high temperature in air in a relaxed state. Heating was carried out in an oven having forced ventilation and changes in rubber network structure were followed by swelling measurements in ethyl acetate.

Stress-relaxation measurements

Continuous stress-relaxation measurements were made using the technique described previously<sup>6</sup>. Measurements were made on strips of rubber of dimensions 51 × 5.1 × 0.5 mm at a constant extension of about 25%. When 'moist' and 'dry' atmospheres were required the procedure described by Lewis and Turner<sup>7</sup> was adopted. The rate of flow of air through the relaxometer envelope was 0.76 l/min in all cases and the temperature was controlled to within ±0.2°C.

RESULTS AND DISCUSSION

Vulcanization of fluorosilicones

In methyl-vinyl silicones the crosslink density achieved on heating with organic peroxides is virtually controlled by the concentration of vinyl groups in the polymer<sup>2</sup>. The crosslink density rises sharply with increasing peroxide concentration and quickly reaches a maximum, the value of which is determined by the vinyl content of the material. In the fluorosilicones the situation appears to be different. In vinyl-containing fluorosilicones there is again a sharp rise in crosslink density at low peroxide concentration, but this is followed by a continuing upward trend in crosslink density with increasing peroxide concentration (see Figure 1). Furthermore experiments carried out with a non-vinyl fluorosilicone and curing agents BzP and DCBzP give results which are virtually coincident with those found for the vinyl containing polymer.

Apart from indicating the much greater susceptibility to free radical attack of the fluorosilicones by comparison with the methyl silicones, and the implications this has in terms of their ability to resist thermo-oxidative attack, these results suggest that the nature of the crosslinks may be rather different as between vinyl-fluorosilicones and methyl-vinyl silicones. It is also possible that unreacted vinyl groups may be present in press-cured vinyl-fluorosilicone rubber.

From equilibrium swelling measurements in ethyl acetate and a knowledge of the molar concentration of peroxide curing agent, it is possible to calculate the crosslinking efficiency of each peroxide in the vinyl-

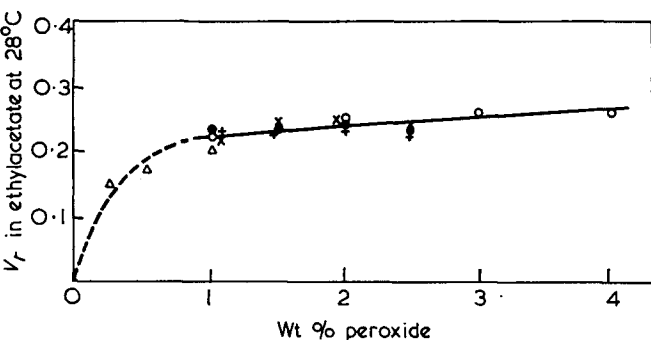


Figure 1 Crosslinking of fluorosilicone rubber. ●, VX; ○, BzP; ×, DCBzP; +, DCP; △, BzP in non-vinyl rubber

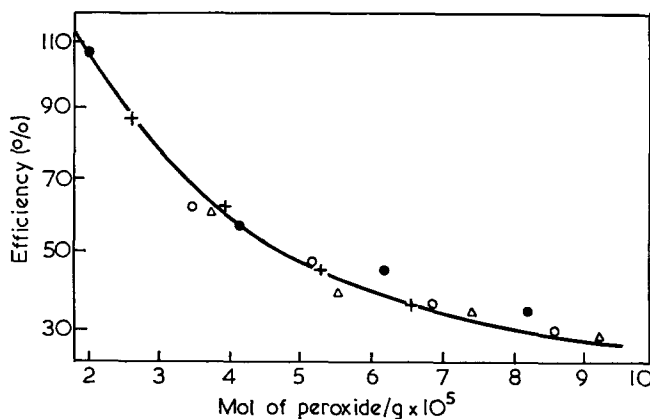
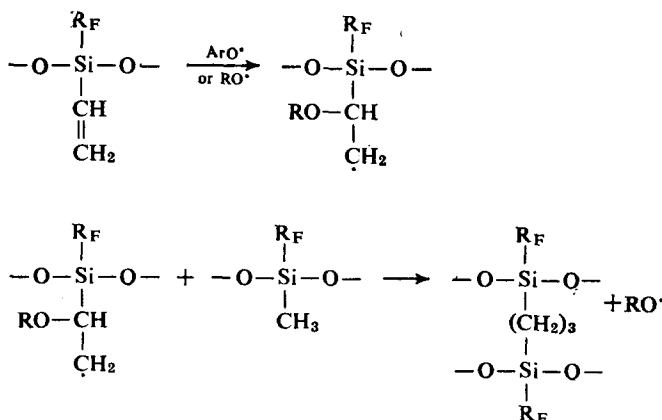


Figure 2 Crosslinking efficiency of organic peroxides in fluorosilicone. ●, BzP; ○, VX; +, DCBzP; △, DCP

fluorosilicone. The efficiency of all four peroxides appears essentially the same (see Figure 2), varying from 109% at the lowest concentration to 27% at the highest. The occurrence of efficiencies greater than 100% indicates that vinyl groups must be involved to some extent in the crosslinking reaction. Such high efficiencies would follow from the mechanism proposed for the vinyl group crosslinking reaction in which the primary aryloxy or alkoxy free radicals are regenerated.



In terms of ease of handling and crosslinking efficiency there is no apparent difference between the four peroxides used. However, in view of the ease with which BzP and DCBzP crosslink a non-vinyl fluorosilicone they are likely to leave significant amounts of rather involatile acidic residues in a vinyl-fluorosilicone vulcanisate. VX and DCP are cleaner reagents in that they produce volatile by-products which should be lost from the vulcanisate during press and post-cure treatment.

Network scission at high temperature

In a peroxide-cured vinyl-containing fluorosilicone there are four reactions which could lead to network scission during heating in air: (a) depolymerization or reversion to give low molecular weight cyclic products; (b) hydrolytic scission at siloxane bonds in the main chain polymer; (c) oxidative scission at crosslinks which are hydrocarbon in nature; (d) thermal scission of labile crosslinks, e.g. -Si-Si-. During long-term heating in the absence of air and moisture the main effect would be a reversion of the polymer to low molecular weight cyclic products, and this process will be accelerated in the



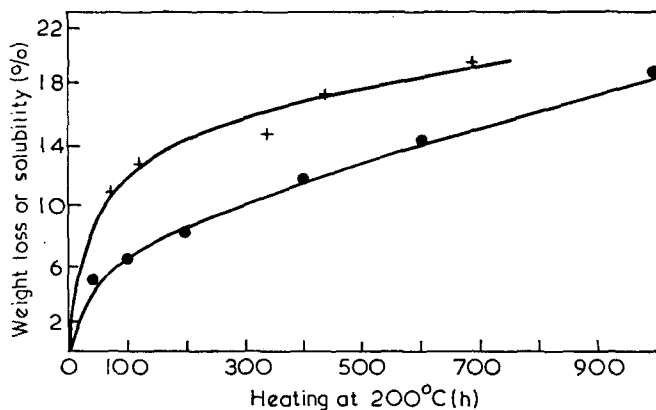
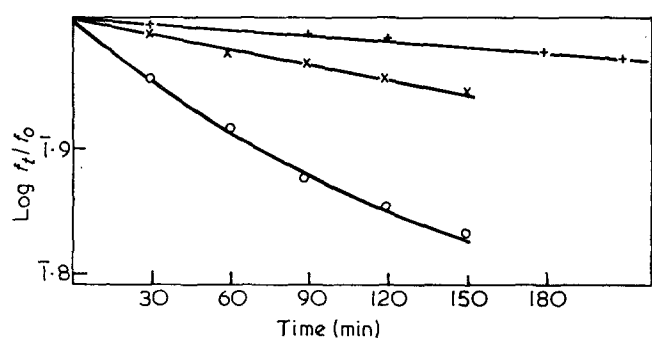
**Table 1** Loss of weight in vinyl-fluorosilicone gum vulcanisates during heating in air at 200°C

Curative	Loss in weight (%)				
	100h	200h	400h	600h	1000h
2.5% DCP	6.6	8.6	12.0	14.8	19.6
2.0% BzP	4.7	5.5	6.8	8.0	10.0
1.5% VX	4.0	4.6	6.4	7.5	—
1.5% DCBzP	3.8	4.1	4.8	5.4	6.8

presence of base catalyst residues<sup>3</sup>. These cyclic siloxanes, presumably trimer and tetramer, will be volatile at elevated temperatures and their formation will be evidenced by a progressive loss in weight during heating. The losses in weight observed on heating vinyl-fluorosilicone gum vulcanisates in air at 200°C are shown in *Table 1*, and there appear to be significant differences in stability between vulcanisates prepared with different peroxides.

In addition to a loss in weight there is also a considerable increase in the fraction of vulcanisate soluble in ethyl acetate. The results of solubility and weight loss measurements on a 2.5% DCP vulcanisate are shown together in *Figure 3*, and they indicate that reversion to volatile products is accompanied, or possibly preceded, by a scission reaction leading to the production of involatile but soluble main chain fragments. Such a reaction could be hydrolytic scission in the main chain which has previously been established as a cause of network scission in methyl-vinyl silicones<sup>4</sup>.

The best method of observing network scission in a rubber vulcanisate is by means of continuous stress-relaxation measurements. Experiments carried out on


**Figure 3** Effect of heating a fluorosilicone gum vulcanisate in air at 200°C. ●, Weight loss; +, solubility in ethyl acetate

**Figure 4** Continuous stress-relaxation in moist air at 200°C. ○, 3% BzP; ×, 2.5% VX; +, 2.5% DCBzP

**Table 2** Continuous stress-relaxation rate constants ( $k$ ) for vinyl-fluorosilicone gum vulcanisates

Wt.% of peroxide curative	$k$ in moist air at 200°C (min <sup>-1</sup> )			
	DCBzP	VX	BzP	DCP
1.0	—	—	$1.2 \times 10^{-3}$	—
1.5	—	—	$1.3 \times 10^{-3}$	—
2.0	$4.15 \times 10^{-4}$	—	$1.35 \times 10^{-3}$	Too unstable for measurement
2.5	$2.7 \times 10^{-4}$	$8.2 \times 10^{-4}$	—	—
3.0	—	—	$1.59 \times 10^{-3}$	—

**Table 3** Continuous stress-relaxation rate constants ( $k$ ) for silica-filled vinyl-fluorosilicone vulcanisates

Wt.% of peroxide curative	$k$ in 'moist' air at 200°C (min <sup>-1</sup> )			
	DCBzP	VX	BzP	DCP
1.0	$3.2 \times 10^{-4}$	$3.8 \times 10^{-4}$	$6 \times 10^{-4}$	—
1.5	—	—	$6.2 \times 10^{-4}$	—
2.0	$3.2 \times 10^{-4}$	$5.0 \times 10^{-4}$	$9.0 \times 10^{-4}$	—
2.5	$3.4 \times 10^{-4}$	$4.0 \times 10^{-4}$	—	$6.6 \times 10^{-4}$

**Table 4** Rates of network scission in filled vinyl-fluorosilicone vulcanisates in 'moist' and 'dry' air at 200°C

Curative	Continuous relaxation rate constant, $k$ (min <sup>-1</sup> )	
	In 'moist' air	In 'dry' air
2.5% DCP	$6.6 \times 10^{-4}$	$2.3 \times 10^{-4}$
2.5% DCBzP	$3.4 \times 10^{-4}$	$5.8 \times 10^{-6}$
2.5% VX	$4.0 \times 10^{-4}$	$8.2 \times 10^{-5}$

gum vulcanisates in 'moist' air at 200°C confirmed the order of stability given by the weight loss experiments, the DCP vulcanisate being so unstable that a meaningful value could not be obtained for the relaxation rate constant. A few continuous stress-relaxation curves are shown in *Figure 4* and the relaxation rate constants, expressed as slopes of the semi-log plots of relative stress ( $f_t/f_0$ ) versus time, are shown in *Table 2*.

The DCBzP gum vulcanisate is clearly the most resistant to network scission and the order of stability in moist air at 200°C is DCBzP > VX > BzP ≫ DCP. With an optimum amount of DCBzP or VX the resistance of fluorosilicone gum vulcanisates to network scission at 200°C can equal that of methyl-vinyl gum vulcanisates.

The incorporation of 20 parts by weight of fine silica improves vulcanisate stability in all cases, and it becomes possible to assign a relaxation rate constant to DCP vulcanisates. The results are shown in *Table 3* and it can be seen that although the addition of fine silica has gone some way towards smoothing out the differences between vulcanisates, those prepared with DCBzP and VX are still the most stable.

At 250°C the superior stability of DCBzP vulcanisates in moist air is also evident:

2.5% DCBzP	$k = 2.76 \times 10^{-3} \text{ min}^{-1}$
2.5% VX	$k = 4.54 \times 10^{-3} \text{ min}^{-1}$
1.5% BzP	$k = 5.03 \times 10^{-3} \text{ min}^{-1}$

As with methyl-vinyl silicones a change in environment from 'moist' to 'dry' air leads to a significant decrease

in the rate of network scission, presumably the same reaction, i.e. hydrolytic scission in the main chain polymer, is responsible for this difference in stability. The data in Table 4 illustrate the magnitude of the contribution of hydrolytic scission to network instability at 200°C.

The relatively small contribution made by oxidative reactions to the observed rate of continuous stress-relaxation is shown by the small change in rate on going from air to nitrogen. For example, for a 1.5% BzP unfilled vulcanisate the relaxation rate constant at 200°C was reduced from  $1.3 \times 10^{-3}$  to  $1.07 \times 10^{-3}$  on changing the environment from air to nitrogen.

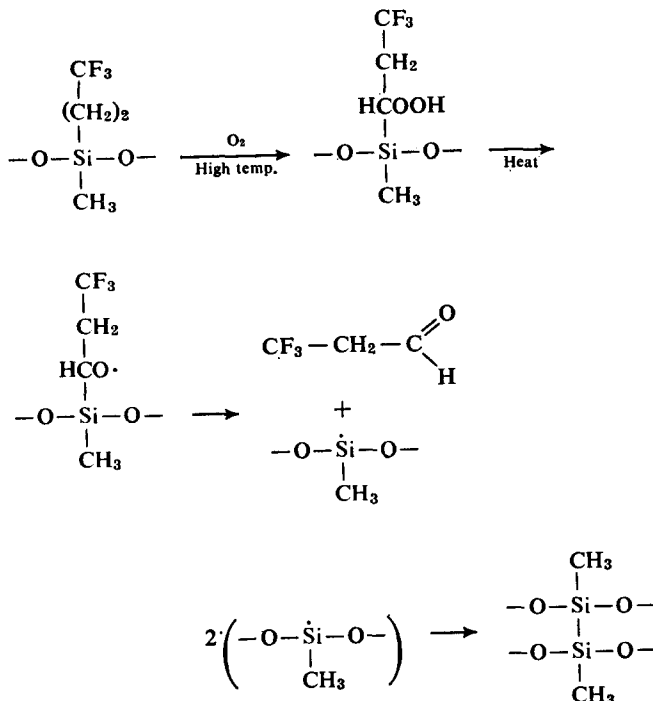
#### Crosslinking at high temperature

In general both scission and crosslinking occur during the heat ageing of rubbers in air; fluorosilicones are no exception. Preliminary experiments carried out in air at 250°C showed gross differences in behaviour between gum vulcanisates cured with different peroxides. Whereas DCBzP and VX vulcanisates embrittled rapidly, DCP and BzP vulcanisates became extremely soft and sticky. These changes occurred too quickly at 250°C for quantitative study but indicate that scission reactions predominate in DCP and BzP vulcanisates while crosslinking reactions predominate in DCBzP and VX vulcanisates.

In order to study the changes occurring during heat ageing in air more closely a series of experiments was carried out at 200°C on gum vulcanisates prepared with various concentrations of all four peroxides. Typical results are shown in Figure 5 as plots of relative swelling ratio in ethyl acetate against time of heating. The behaviour observed at 250°C is reproduced at 200°C but over a much longer time scale, i.e. DCBzP and VX vulcanisates eventually embrittle and DCP and BzP vulcanisates soften. An additional feature apparent in these results is that stability is sensitive to peroxide concentration. For example, the degree of softening in a 2.5% DCP vulcanisate is significantly greater than in a 1.5% DCP vulcanisate, and the rate of hardening in a 1.5% DCBzP vulcanisate is somewhat higher than that in a 2.5% DCBzP vulcanisate. The increases in swelling ratio shown in Figure 5 are always accompanied by an increase in the fraction of soluble material in the vulcanisate.

In oven ageing experiments the observed change in network chain concentration will be the overall change resulting from scission and crosslinking reactions. It might be expected that fluorosilicones would be more

susceptible to oxidative attack than methyl silicones because of their high content of methylene groups. Oxidative reactions at these groups could lead to crosslinking.



The extent to which oxidative crosslinking occurs is shown by a comparison of the overall changes in network chain concentration following heating in air and *in vacuo*. In a 2% DCP gum vulcanisate the value of the relative swelling ratio after 53 h heating in air was 1.43, the value after the same time *in vacuo* was 2.05. The much smaller decrease in network chain concentration evident after heating in air must be due to a high rate of oxidative crosslinking partly offsetting the effects of network scission.

It appears, therefore, that the fluorosilicone network, as represented by DCP gum vulcanisates, is extremely unstable at temperatures of 200°C and above. The stability observed in gum vulcanisates during oven ageing at these temperatures is not a genuine stability but merely reflects the extent to which oxidative crosslinking is countering the effects of scission due to hydrolysis and reversion. In a situation in which the vulcanisate is in a strained configuration the real instability should become evident.

The use of peroxides other than DCP can lead to vulcanisates of much greater stability, and the results of continuous stress-relaxation experiments together with those of oven ageing suggest that the principal effect of using VX, BzP, or DCBzP in place of DCP is to reduce substantially the rate of network scission. It is important at this stage to consider why stability in gum vulcanisates is so dependent upon the nature of the peroxide used.

#### Stability of DCBzP and BzP vulcanisates

The primary products of thermal decomposition of DCBzP and BzP are dichlorobenzoyloxy and benzoyloxy radicals respectively and in a hydrocarbon substrate they may abstract hydrogen and form dichlorobenzoic and benzoic acid. It is known that DCBzP and BzP can pro-

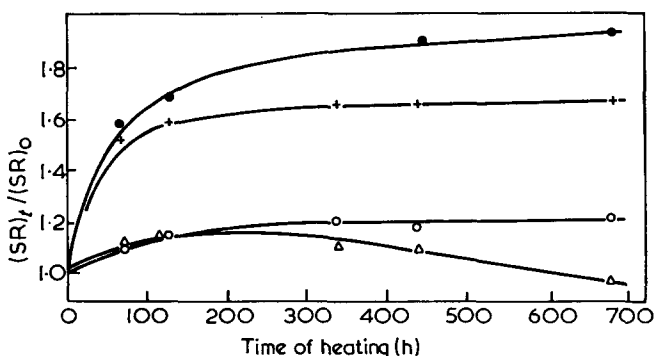


Figure 5 Oven ageing of fluorosilicone gum vulcanisates at 200°C. ●, 2.5% DCP; +, 1.5% DCP; ○, 2.5% DCBzP; △, 1.5% DCBzP

duce crosslinks in a polydimethylsilicone, albeit with very low efficiency, by abstraction of hydrogen from methyl side groups. The opportunities for hydrogen abstraction are much greater in a fluorosilicone, as evidenced by the ease with which both peroxides vulcanize a non-vinyl fluorosilicone, and there will undoubtedly be a considerable amount of hydrogen abstraction, and therefore production of free acid, during vulcanization of a vinyl-fluorosilicone with these peroxides. An alternative fate for the primary aryloxy radical would be rearrangement to give carbon dioxide and a phenyl radical, and a certain amount of this may also occur.

Tests showed the raw vinyl-fluorosilicone polymer to be alkaline to litmus, and this is due, presumably, to residual basic catalyst from the polymerization reaction. Since the presence of residual catalyst encourages reversion of the polymer to low molecular weight cyclic siloxanes at elevated temperature it is possible that the improved stability of DCBzP and BzP vulcanisates, relative to that of DCP vulcanisates, is due to a deactivation of base catalyst residues by free acid and/or by carbon dioxide formed during vulcanization. If neutralization by free acid were the principal cause of improved stability it should be possible to achieve the overall stability of a DCBzP gum vulcanisate by addition of free dichlorobenzoic acid to a DCP formulation before vulcanization. The crucial test of whether free acid stabilizes the rubber by reducing network scission lies in continuous stress-relaxation measurements rather than in oven ageing tests where the issue could be clouded by the occurrence of acid catalysed oxidative crosslinking.

The results of continuous stress-relaxation measurements on a DCP gum vulcanisate containing 0.2% by weight of free dichlorobenzoic acid are shown in Figure 6. The same vulcanisate without free acid was too unstable for measurements to be made at 200°C and it is evident, therefore, that the introduction of free acid has led to a large reduction in the rate of network scission. Increasing the concentration of free acid to 2.0% only produced a further 18% decrease in rate of network scission, and it would appear that addition of around 0.2% dichlorobenzoic acid is sufficient to neutralize the base catalyst residues in this particular batch of vinyl-fluorosilicone gumstock. The overall stabilization achieved by the addition of free acid is shown by the results of oven ageing tests in Figure 7. The effect is striking, and the similarity between a vulcanisate compounded with free acid and one in which acid is produced as a by-product of vulcanization is evident.

The increased stability of silica-filled vulcanisates over

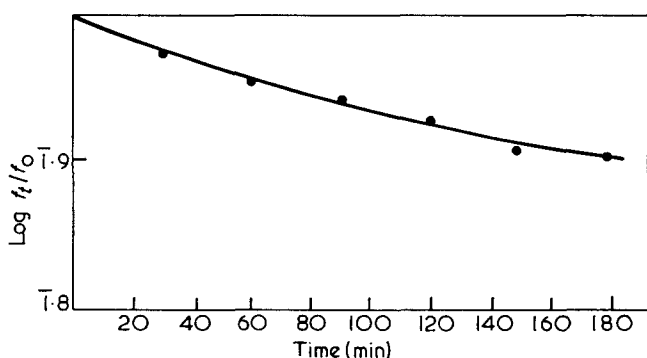


Figure 6 Continuous stress-relaxation of a fluorosilicone gum vulcanisate in moist air at 200°C (1.5% DCP + 0.2% free acid)

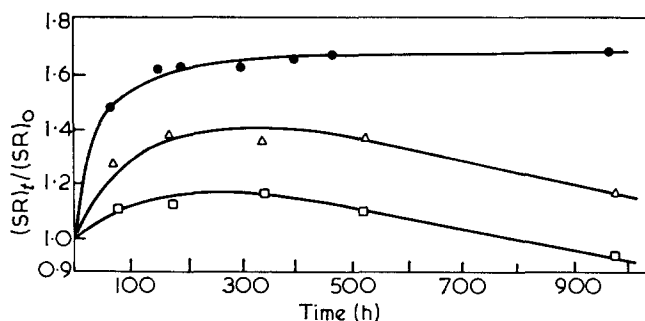


Figure 7 Oven ageing of fluorosilicone gum vulcanisates at 200°C. ●, 1.5% DCP; △, 1.5% DCP + 0.2% acid; □, 1.5% DCP + 1.0% acid

that shown by gum vulcanisates may also be connected with neutralization of base catalyst residues. The fine fumed silica normally used in silicone rubbers gives a strongly acidic reaction; a 10% by weight slurry of fine silica in water had a pH in the range 4.2–4.3. It is significant that the addition of silica had very little effect on the rate of network scission in DCBzP vulcanisates (see Tables 2 and 3) where it is proposed that free acid produced during cure is itself sufficient to neutralize base catalyst residues.

#### Differences in heat stability between VX and DCP vulcanisates

In silicone rubber technology both VX and DCP are regarded as vinyl specific reagents. They are both relatively unreactive towards the primary hydrogen atoms in a dimethyl silicone rubber and in an unreactive substrate they both give rise to methyl radicals by rearrangement of the primary alkoxy or aryloxy radical.

As far as reaction with the base fluorosilicone polymer is concerned the reagents should be closely similar; the gross difference in heat stability between their respective gum vulcanisates must derive from another source.

The DCP used in the present work was in pure crystalline form and was not diluted with inert powders or low molecular weight silicones, as is often the case with organic peroxides used in rubber processing. The VX was used as a 50:50 mixture with finely divided calcium carbonate. Under vulcanizing conditions, and at the temperatures used for evaluating heat stability a certain amount of carbon dioxide will be evolved and this is known to deactivate base catalyst residues in the polymer<sup>3</sup>. The stability of VX vulcanisates is due, therefore, to a reduction in the rate of base catalysed reversion, and it should be possible to achieve a similar stability in a DCP gum vulcanisate by the addition of calcium carbonate during compounding. The results of oven ageing experiments are shown in Figure 8 and the increase in stability is striking.

#### CONCLUSIONS

A fluorosilicone gum rubber, as represented by DCP vulcanisates, is very unstable at high temperatures. At 200°C in the presence or absence of air network scission proceeds at a high rate, and appears to be due to the additive effects of hydrolytic attack in the main chain polymer and reversion to low molecular weight cyclics. The rate of reversion is influenced by the presence

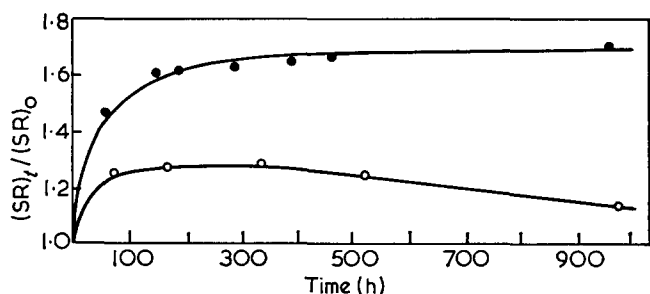


Figure 8 Oven ageing of fluorosilicone gum vulcanisates at 200°C. ●, 1.5% DCP; ○, 1.5% DCP+3% CaCO<sub>3</sub>

in the polymer of base catalyst residues from the polymerization process. It is proposed that the superior stability shown by DCBzP, BzP, VX, and all fumed silica-filled vulcanisates is due to a neutralization of these residues during vulcanization. Neutralization could be due to the free acid produced during vulcanization with DCBzP and BzP, to the acidic nature of the silica filler, or to the production of carbon dioxide from the calcium carbonate used as carrier for VX.

The advantages of using free acid or calcium carbonate when compounding polymer containing base catalyst residues are shown by the results of continuous stress-relaxation measurements and oven ageing tests. The use of free acid must be closely controlled since amounts in excess of that required to neutralize catalyst residues will

catalyse oxidative crosslinking and thereby lead to poor compression and tension set characteristics in the rubber. Fluorosilicones are susceptible to oxidative crosslinking at elevated temperatures and it is possible that further significant improvements in stability could be achieved by the use of suitable antioxidants.

When compounding fluorosilicones for maximum heat stability it would seem desirable first to determine the pH of the gum stock. If the polymer is basic it is possible to select the type and concentration level of peroxide curative and filler to neutralize the system and thereby stabilize the polymer against excessive reversion.

#### ACKNOWLEDGEMENTS

Crown copyright and published by permission of the Controller, Her Majesty's Stationery Office.

#### REFERENCES

- 1 Sinnott, R. Unpublished Procurement Executive Ministry of Defence Report
- 2 Thomas, D. K. *Polymer* 1966, 7, 243
- 3 Kücera, M. and Lanikova, J. *J. Polym. Sci.* 1961, 53, 301
- 4 Thomas, D. K. *Polymer* 1966, 7, 99
- 5 Flory, P. J. and Rehner, J. *J. Chem. Phys.* 1950, 18, 108
- 6 Atkinson, A. S. *RAE Tech. Note Chem.* 1393 1963 (January)
- 7 Turner, M. J. and Lewis, J. *Proc. 4th Rubber Technol. Conf., London, May 1962*

# Measurement of infra-red dichroism, stress and strain of elongated polymers

B. E. Read and D. A. Hughes

*Division of Materials Applications, National Physical Laboratory, Teddington, Middlesex TW11 0LW, UK*

and D. C. Barnes and F. W. M. Drury

*Measurement Group Equipment Services, National Physical Laboratory, Teddington, Middlesex TW11 0LW, UK*

*(Received 24 April 1972)*

A differential method is described for determining the difference of infra-red absorbance of an elongated polymer for radiation polarized parallel and perpendicular to the stretching direction, respectively. Measurements can be made at temperatures up to 200°C and the specimen tension and elongation can also be measured. In combination with conventional unpolarized measurements on undeformed samples the dichroic ratio, and its relationship to stress and strain, may be determined. The technique is similar to that reported by previous workers but differs in a number of detailed design features. Also, the sensitivity of the method is quantitatively discussed in relation to the sensitivity of conventional dichroism measurements. Correction procedures are proposed and analysed both for spectrometer resolution, and for the emission of radiation by the specimen at high temperatures.

## INTRODUCTION

For a uniaxially elongated polymer, the absorbance ( $A_{\parallel}$ ) of an infra-red peak measured with radiation polarized parallel to the stretching direction generally differs from the absorbance ( $A_{\perp}$ ) determined for radiation polarized perpendicular to this direction. This difference is a consequence of the orientation of the transition moment vectors of the absorbing molecular groups relative to the direction of extension<sup>1</sup>. If the angle between the transition moment vector and an axis of the absorbing group is known, then the dichroic ratio  $D = A_{\parallel}/A_{\perp}$  can be used to evaluate the average orientation of these axes<sup>1</sup>.

For crosslinked amorphous polymers in the rubberlike state, measurements of  $D$  for different absorption peaks can yield the preferential orientation of different conformational sequences within the polymer chain<sup>2,3</sup>. For partially crystalline polymers, dichroic measurements on peaks respectively associated with the crystalline and amorphous regions can provide information on the relative orientation of the two phases<sup>2</sup>. Additional measurements of stress and strain afford a means of relating the mechanical behaviour to the structural deformation on a molecular level.

In the conventional determination of the dichroic ratio, the oriented polymer and infra-red polarizer are each placed in the sample beam of a double beam spectrometer.  $A_{\parallel}$  and  $A_{\perp}$  are then successively determined with the polarizer inclined to transmit radiation polarized first parallel and then perpendicular to the direction of elongation. However, the magnitude of  $A_{\parallel} - A_{\perp}$  is frequently

small so that values of  $D$  are close to unity. In this case the determination of  $D$  from separate measurements of  $A_{\parallel}$  and  $A_{\perp}$  lacks sensitivity.

Methods have been proposed<sup>1,4</sup> for the direct determination of  $A_{\parallel} - A_{\perp}$  which are capable of increased sensitivity. Marrinan<sup>4</sup> and Tink<sup>1</sup> independently proposed a double beam method in which the sample is placed in the common beam and two polarizers are employed, one in the sample beam and the other in the reference beam. The polarizers are inclined to transmit radiation polarized parallel and perpendicular, respectively, to the sample orientation direction, or *vice versa*. This type of method was subsequently used by Le Grand<sup>5</sup> and by Gotoh and coworkers<sup>6-9</sup> and more recently by Wilkes and Stein<sup>10</sup>. The present method is similar to that reported by these authors but differs in a number of detailed design features. Also, the sensitivity of the method is quantitatively analysed, and correction procedures are proposed both for resolution and for the emission of radiation by the sample at high temperatures.

## CONSTRUCTION OF APPARATUS

A schematic diagram illustrating the arrangement of components is given in *Figure 1*. The existing spectrometer was a Grubb Parsons GS 2A or GS 3 instrument. The Nernst source (A) was moved back from its original location at the present sample space (D) to the position shown in *Figure 1*. Radiation from the source is reflected by a plane mirror (B) onto a concave mirror (C) and is

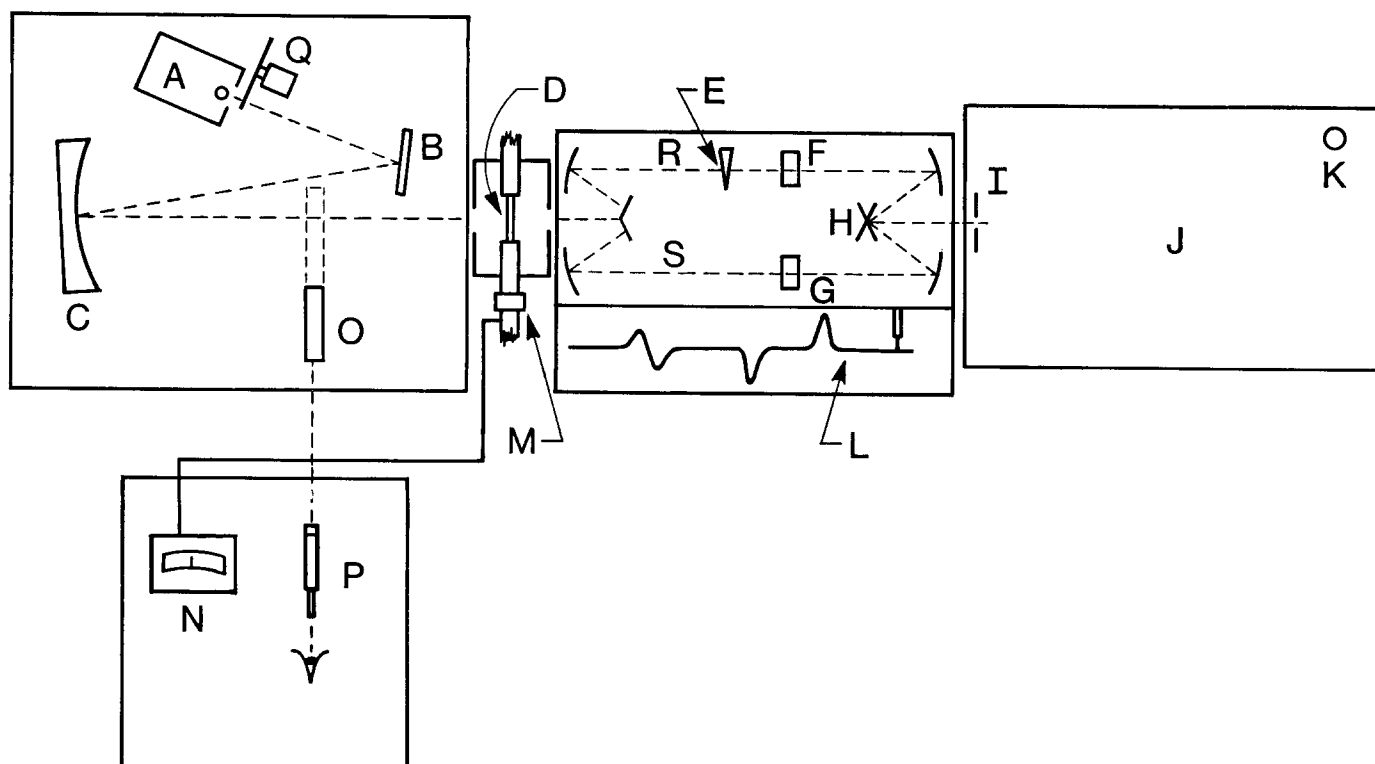


Figure 1 Schematic illustration of equipment

thereby focused on the sample (D) to give an image approximately the same size (25 mm high, 3 mm wide) as the Nernst source. The sample is clamped in a stretching device inclined at 45° to the (approximately) vertical monochromator components.

After passing through the sample, the infra-red beam enters the double beam unit where it is split into two components. The usual reference beam (R) is focused close to the comb attenuator (E) and then passes through a silver halide wire grid polarizer (F). The polarizer is held in a rotatable graduated mount which is set to transmit radiation polarized at 45° to the monochromator components. The usual sample beam (S) passes through a similar polarizer (G) whose polarization axis is perpendicular to that of polarizer F. Subsequently the two beams are alternately focused on the entrance slit (I) of the monochromator (J) by means of the 12.5 Hz reciprocating mirrors (H). After being dispersed by the monochromator the beams are received by the thermocouple detector (K) and the spectrometer then functions in the normal manner. At null balance, the trace obtained on the recorder (L) is the ratio of intensities transmitted by the sample and reference beam polarizers, respectively, as a function of wavelength.

In order to correct for the effects of sample radiation at high temperatures (see below), a rotating sector (Q) may be placed immediately in front of the Nernst source. This serves to reduce the intensity incident upon, and hence transmitted by, the specimen. Three rotating sectors have been constructed, and these reduce the incident intensity by 25, 50 and 75% respectively. The sector is rotated by a motor at about 130 Hz, which is a factor of about ten greater than the frequency of the reciprocating mirrors.

The sample elongation is determined from the change in the distance between lines which are vapour deposited on the sample surface. The distance between lines is measured with a cathetometer (P). The cathetometer receives light

from the sample via a reflecting mirror device (O) which may be inserted into a track on the optical bench between spectral measurements. The mirror system comprises two mirrors mounted one above the other in a Perspex frame. The lower mirror is located in line with the sample and its plane is inclined at 45° both to the horizontal and vertical planes. The plane of the upper mirror is perpendicular to the sample plane and 77.5° to the horizontal. This geometry yields a vertical image of the sample at the cathetometer having a 1 : 1 magnification. The lines on the sample thus appear horizontal.

The stretching device, shown in Figure 2, is designed to displace samples equally from both ends<sup>11</sup>. It incorporates a proof ring (M), the displacement of which is detected by a transducer (T) and recorded on the meter of an associated bridge (N, Figure 1). The proof ring displacement is calibrated against load, and thus yields the tension in the specimen. The sample is surrounded by an insulated enclosure (U) which may be heated electrically to 200°C. Temperature is controlled manually by a Variac transformer and measured with a chromel-alumel thermocouple (V) inserted through guide tubes at the top of the enclosure. Inlet tubes (W and W') allow the introduction of inert gas and a fan-shaft respectively. The enclosure contains KBr windows (X) which are held between silicone rubber gaskets within detachable mounts. The windows allow the transmission of the infra-red beam. For reducing the height of the beam at the sample when studying narrow specimens, collimating plates (Y) are attached to the ends of adjustable rods (Z) inserted through opposite sides of the enclosure.

Samples are vacuum moulded into dumbbell shapes having dimensions shown in Figure 3. This Figure also illustrates the positions of the surface lines used for elongation measurements. The effective lengths of the unextended samples between clamps of the stretcher is 50 mm. They can be extended to an effective length of up to 150 mm, equivalent to a maximum extension of 200%.

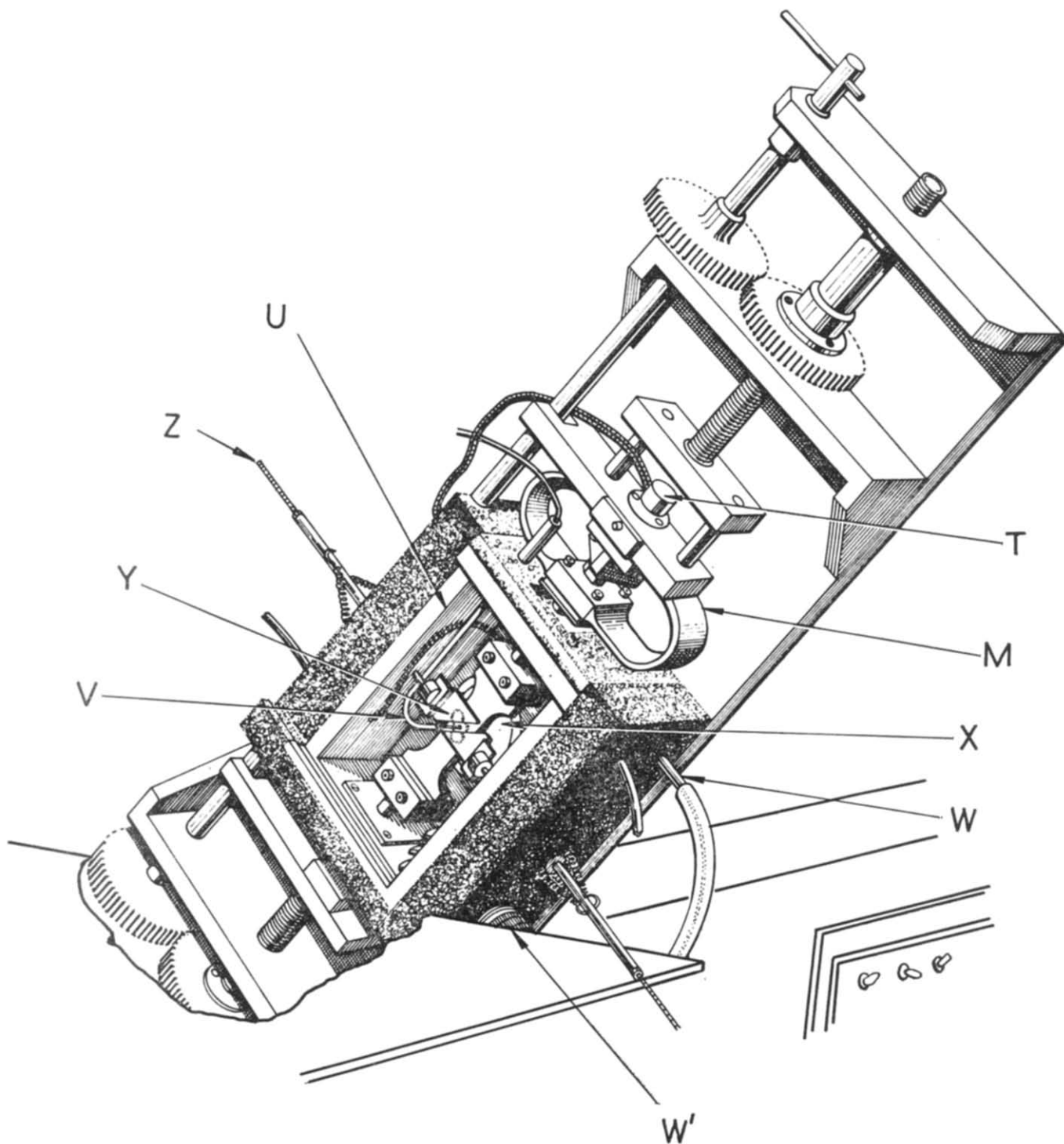


Figure 2 Stretcher unit and accessories

The percentage extension may be considerably increased by using shorter unextended samples.

The following aspects of the current design merit particular comment. (1) The  $45^\circ$  inclination of the sample and polarizers eliminates polarization effects subsequently introduced by the monochromator<sup>1</sup>. (2) The location of the sample in front of the double beam unit differs from most previous designs<sup>1, 4, 6-9</sup> in which the sample is placed in front of the monochromator entrance slit after the two beams have been recombined. Our arrangement was adopted since, with relatively minor modifications, it yielded greater space for, and accessibility to, the sample and accessories. Furthermore this arrangement eliminates

errors due to sample birefringence which may arise if the sample is located between polarizers and monochromator<sup>1</sup>. Relatively large local heating of the sample by the infra-red beam is encountered with the present arrangement, although this effect is no larger than that found with many modern infra-red instruments. (3) As noted above, the stretcher is designed to displace the sample equally from both ends. This design maintains the beam at the same part of the sample at all extensions and thus eliminates errors arising from non-uniformities of specimen thickness or orientation. (4) The wire grid polarizers are compact and yield a much higher degree of polarization than the tilted plate polarizers frequently

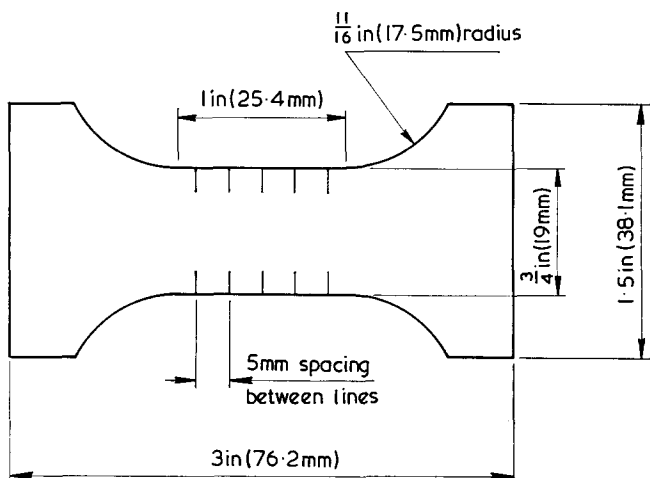


Figure 3 Sample dimensions and illustration of vapour deposited lines for strain measurement

employed. Errors due to polarizer inefficiency are thus negligible.

### THEORY

#### Determination of $A_{\parallel} - A_{\perp}$

For a normal infra-red absorption peak, obtained with both the sample and polarizer in the usual sample area of a double beam instrument, we define  $A_{\parallel}$  and  $A_{\perp}$  as follows:

$$A_{\parallel} = \log_{10}(I_{0, \parallel} / I_{\parallel}) \quad (1)$$

and

$$A_{\perp} = \log_{10}(I_{0, \perp} / I_{\perp}) \quad (2)$$

where  $I_{\parallel}$  and  $I_{\perp}$  are the intensities of transmitted radiation at the wavelength of maximum absorption for radiation polarized, respectively, parallel and perpendicular to the stretching direction.  $I_{0, \parallel}$  and  $I_{0, \perp}$  are the transmitted intensities corresponding to the baselines of the parallel and perpendicularly polarized spectra respectively. The above quantities are schematically illustrated in Figure 4a.

With the differential method, if the sample and reference beam polarizers are inclined to transmit radiation polarized parallel and perpendicular to the stretching direction respectively, then the intensity transmitted by the sample beam polarizer is, from equation (1):

$$I_{\parallel} = I_{0, \parallel} 10^{-A_{\parallel}} \quad (3)$$

Similarly, from equation (2), the radiation intensity transmitted by the reference beam polarizer is:

$$I_{\perp} = I_{0, \perp} 10^{-A_{\perp}} \quad (4)$$

As noted above, the spectrometer records directly the ratio of intensities transmitted by the sample and reference polarizers. From equations (3) and (4) this ratio is:

$$\frac{I_{\parallel}}{I_{\perp}} = \frac{I_{0, \parallel}}{I_{0, \perp}} 10^{-(A_{\parallel} - A_{\perp})} \quad (5)$$

Thus,

$$A_{\parallel} - A_{\perp} = \log_{10}(I_{0, \parallel} / I_{0, \perp}) - \log_{10}(I_{\parallel} / I_{\perp}) \quad (6)$$

The ratios  $I_{0, \parallel} / I_{0, \perp}$ , and  $I_{\parallel} / I_{\perp}$  correspond, respectively, to the baseline and the peak of the differential spectrum,

as indicated schematically in Figure 4b. In practice  $I_{0, \parallel}$  and  $I_{0, \perp}$  may differ slightly for a number of reasons including: (a) possible differences in scattering by the sample of the parallel and perpendicular components of the incident radiation; and (b) possible differences in transmission of the two polarizers. Generally, however, the ratio  $I_{0, \parallel} / I_{0, \perp}$  will be close to unity, as assumed by Gotoh and coworkers<sup>6</sup>. Differences between  $I_{0, \parallel}$  and  $I_{0, \perp}$  are, in any case, of no consequence in this method, since  $A_{\parallel} - A_{\perp}$  is determined from the measured ratios  $I_{0, \parallel} / I_{0, \perp}$  and  $I_{\parallel} / I_{\perp}$  according to equation (6).

If, in the differential method, the sample and reference beam polarizers are set to transmit radiation polarized perpendicular and parallel, respectively, to the stretching direction then equation (6) becomes:

$$A_{\parallel} - A_{\perp} = \log_{10}(I_{\perp} / I_{\parallel}) - \log_{10}(I_{0, \perp} / I_{0, \parallel}) \quad (7)$$

In this case the baseline and peak of the differential spectrum correspond to  $I_{0, \perp} / I_{0, \parallel}$  and  $I_{\perp} / I_{\parallel}$  respectively, as illustrated in Figure 4c, and  $A_{\parallel} - A_{\perp}$  is calculated according to equation (7).

It must be emphasized that the absorbances  $A_{\parallel}$  and  $A_{\perp}$ , and hence the difference  $A_{\parallel} - A_{\perp}$ , are proportional to the thickness  $d$  of the specimen in the infra-red beam. In order to eliminate the thickness variable, and obtain a number characteristic of a given material, the quantity  $(A_{\parallel} - A_{\perp}) / d$  could be evaluated. Similarly, if we define an extinction

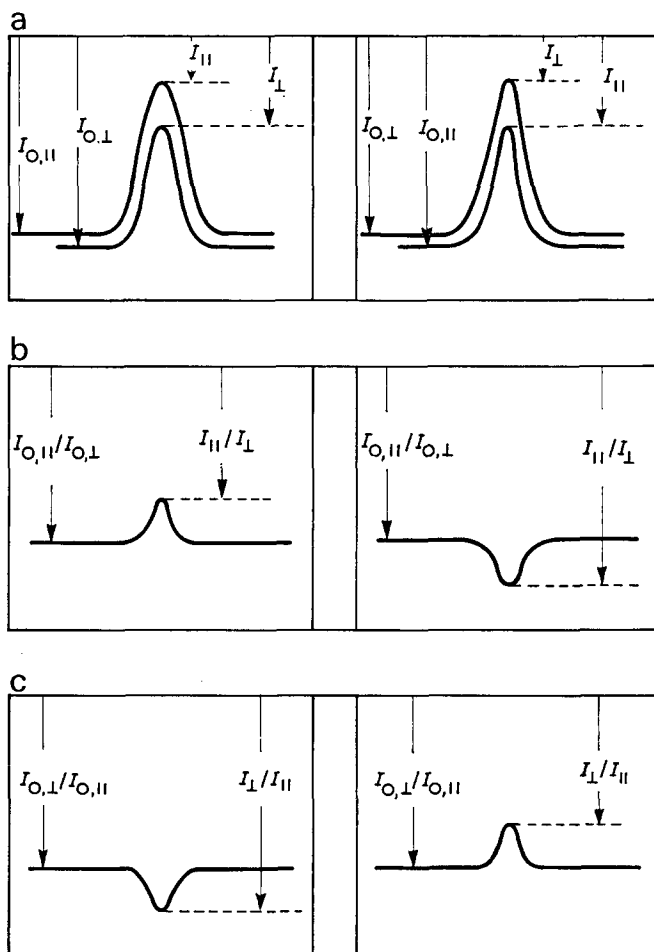


Figure 4 Schematic illustration of ordinary polarized spectra (a) and differential spectra with sample beam polarized  $\parallel$ , reference beam polarized  $\perp$  (b) and sample beam polarized  $\perp$ , reference beam polarized  $\parallel$  (c). Left and right hand diagrams correspond to positive and negative values of  $A_{\parallel} - A_{\perp}$  respectively



coefficient  $\epsilon$  by  $\epsilon = A/d\rho$ , where  $\rho$  is the sample density, then the difference in extinction coefficient for parallel and perpendicular radiation,  $\epsilon_{\parallel} - \epsilon_{\perp} = (A_{\parallel} - A_{\perp})/d\rho$  may be determined. Preferably, however, the dichroic ratio  $D = A_{\parallel}/A_{\perp} = \epsilon_{\parallel}/\epsilon_{\perp}$  should be obtained, since this quantity is both independent of specimen thickness and has been related theoretically to the average orientation of absorbing molecular groups. In the following section the determination of  $D$  from  $A_{\parallel} - A_{\perp}$  will therefore be considered.

#### Determination of the dichroic ratio from $A_{\parallel} - A_{\perp}$

Additional measurements of either  $A_{\parallel}$  or  $A_{\perp}$  enable the determination of  $D$  from  $A_{\parallel} - A_{\perp}$  since:

$$\frac{A_{\parallel} - A_{\perp}}{A_{\perp}} = D - 1 \quad (8)$$

or

$$\frac{A_{\parallel} - A_{\perp}}{A_{\parallel}} = 1 - D^{-1} \quad (9)$$

If the sample accessories and polarizer are sufficiently compact to fit into the usual sample space of the spectrometer, then the separate determination of  $A_{\parallel}$  or  $A_{\perp}$  can be effected in the conventional manner. However, with the present spectrometer, the usual sample area is too small to accommodate the stretcher, temperature enclosure and polarizer and  $A_{\parallel}$  or  $A_{\perp}$  are estimated from absorbance measurements on unextended samples. The method is based on the assumption, frequently valid to a good approximation, that the concentration of absorbing species is unaffected by the deformation. In this case  $A_{\parallel}$  and  $A_{\perp}$  are related to the average absorbance  $A_0$  for the unstrained polymer, measured with unpolarized radiation, by the equation:

$$A_{\parallel} + 2A_{\perp} = 3A_0 \frac{d\rho}{d_0\rho_0} = 3\epsilon_0 d\rho \quad (10)$$

where  $d_0$ ,  $\rho_0$  and  $\epsilon_0$  are the thickness, density and extinction coefficient, respectively, for the unextended specimen. From equation (10) it follows that:

$$A_{\parallel} = \frac{2(A_{\parallel} - A_{\perp}) + 3\epsilon_0 d\rho}{3} \quad (11)$$

and

$$A_{\perp} = \frac{3\epsilon_0 d\rho - (A_{\parallel} - A_{\perp})}{3} \quad (12)$$

Hence

$$D = \frac{2(A_{\parallel} - A_{\perp}) + 3\epsilon_0 d\rho}{3\epsilon_0 d\rho - (A_{\parallel} - A_{\perp})} \quad (13)$$

The determination of  $D$  from  $A_{\parallel} - A_{\perp}$  thus requires the additional knowledge of  $\epsilon_0$ ,  $d$  and  $\rho$ .  $\epsilon_0$  can be obtained from measurements of  $A_0$ ,  $d_0$  and  $\rho_0$ . The determination of  $A_0$  is straightforward and only requires the unstrained specimen in a small temperature enclosure to be accommodated in the usual sample area. Assuming negligible volume change on extension, and an equal contraction in thickness and width, then  $\rho = \rho_0$  and  $d$  can be calculated from measured values of  $d_0$  and elongation.

#### Sensitivity of measurement

It has been variously reported that the differential method increases the precision of dichroism measure-

ments by over a hundredfold<sup>4</sup> or tenfold<sup>9</sup> compared with the conventional method. In fact the relative sensitivity of the two methods depends on the magnitude of both the dichroic ratio  $D$  and the average absorbance  $A = (A_{\parallel} + 2A_{\perp})/3$ . We may note that  $D$  is related to the molecular orientation and is independent of the concentration of absorbing species. Conversely  $A$  is proportional to the concentration of absorbing species and sample thickness and, providing that these remain constant, is independent of orientation. In the following discussion  $D$  and  $A$  are thus taken as the independent variables.

For purposes of analysing the sensitivity of the differential technique, it is convenient to derive a few relevant relationships. Firstly, from the definition  $D = A_{\parallel}/A_{\perp}$  and equations (1) and (2) we have:

$$\log_{10}(I_{0,\parallel}/I_{\parallel}) = D \log_{10}(I_{0,\perp}/I_{\perp}) \quad (14)$$

Furthermore, from equation (14) we obtain:

$$\begin{aligned} A &= \frac{1}{3}(A_{\parallel} + 2A_{\perp}) \\ &= \frac{1}{3}[\log_{10}(I_{0,\parallel}/I_{\parallel}) + 2\log_{10}(I_{0,\perp}/I_{\perp})] \\ &= \frac{1}{3}(D + 2)\log_{10}(I_{0,\perp}/I_{\perp}) \end{aligned} \quad (15)$$

Hence,

$$\frac{I_{\perp}}{I_{0,\perp}} = 10^{-3A/(D+2)} \quad (16)$$

From equations (14) and (15):

$$A = \frac{1}{3}\left(\frac{D+2}{D}\right)\log_{10}(I_{0,\parallel}/I_{\parallel}) \quad (17)$$

Thus

$$\frac{I_{\parallel}}{I_{0,\parallel}} = 10^{-3DA/(D+2)} \quad (18)$$

The sensitivity of the differential technique depends on the magnitude of the observed peak height as a function of  $D$  and  $A$ . Considering the case in which the sample and reference polarizers are set in the parallel and perpendicular orientations, respectively, it is evident from *Figure 4b* that the peak height can be represented by:

$$\begin{aligned} H &= \left(\frac{I_{0,\parallel} - I_{\parallel}}{I_{0,\perp} - I_{\perp}}\right) \frac{I_{0,\parallel}}{I_{0,\perp}} \\ &= 1 - (I_{\parallel}/I_{0,\parallel}) / (I_{\perp}/I_{0,\perp}) \end{aligned} \quad (19)$$

Equations (16), (18) and (19) then yield,

$$H = 1 - 10^{-3A(D-1)/(D+2)} \quad (20)$$

*Figure 5* shows plots of  $H$  against  $D$  for different values of  $A$  according to equation (20). The sensitivity of measurement, as represented by the slopes of these curves, is seen to increase with increasing  $A$  and decreasing  $D$ . The slopes are given by the partial derivative:

$$\left(\frac{\partial H}{\partial D}\right)_A = \frac{2.303 \times 9A}{(D+2)^2} 10^{-3A(D-1)/(D+2)} \quad (21)$$

As  $D$  tends to unity equation (21) becomes

$$\left(\frac{\partial H}{\partial D}\right)_A \underset{D \rightarrow 1}{=} 2.303A \quad (22)$$

so that the sensitivity becomes proportional to  $A$ . According to equation (22) a dichroic ratio of 1.01 would yield peak heights of about 2.3% and 4.5% of a full-scale

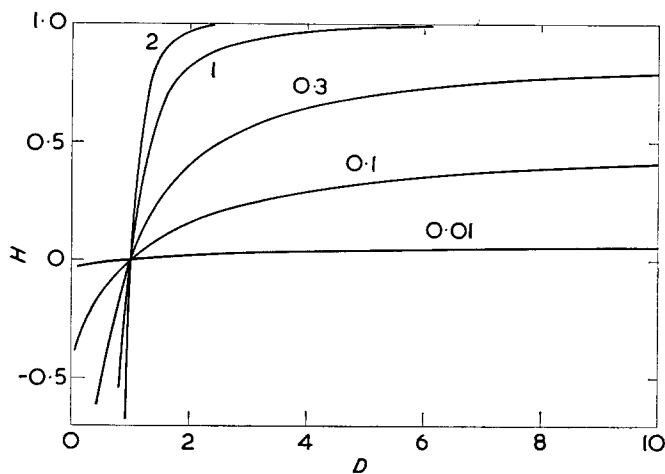


Figure 5 Differential peak height,  $H$ , plotted against  $D$  for various values of average absorbance,  $A$ , indicated on the curves

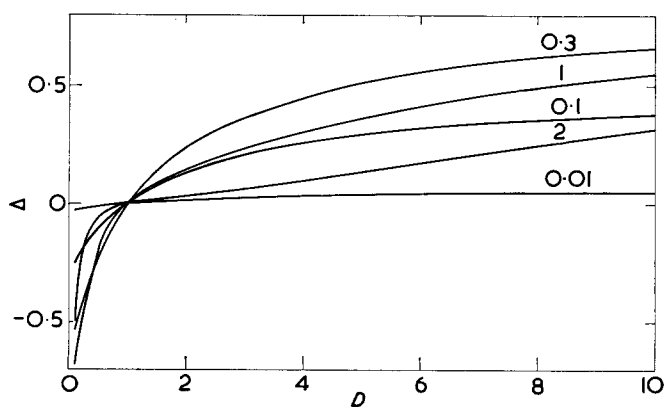


Figure 6 Plots of  $\Delta$  against  $D$  for different values of average absorbance,  $A$ , indicated on the curves

deflection for average absorbancies of 1 and 2, respectively. Dichroic ratios of the order of 1.01 probably represent the lowest dichroic effects which could be determined by the differential method.

The relationship between the differential and conventional methods is illustrated by recasting equation (19) in the form:

$$\begin{aligned}
 H &= \frac{(I_{\perp}/I_{0,\perp}) - (I_{\parallel}/I_{0,\parallel})}{(I_{\perp}/I_{0,\perp})} \\
 &= \frac{I_{0,\perp}}{I_{\perp}} \left[ \frac{(I_{0,\parallel} - I_{\parallel})}{I_{0,\parallel}} - \frac{(I_{0,\perp} - I_{\perp})}{I_{0,\perp}} \right] \\
 &= \frac{I_{0,\perp} \Delta}{I_{\perp}} \quad (23)
 \end{aligned}$$

Reference to Figure 4a shows that  $\Delta$  measures the difference between peak heights of the two spectra determined separately with parallel and perpendicularly polarized radiation, respectively. This quantity largely determines the sensitivity of the conventional method.

From equations (16), (18) and (23) it follows that:

$$\Delta = 10^{-3A/(D+2)} - 10^{-3DA/(D+2)} \quad (24)$$

Figure 6 shows plots of  $\Delta$  against  $D$  for different values of  $A$  according to equation (24). From the slopes of these curves we observe that the sensitivity passes through a

maximum at intermediate values of  $A$ . The slopes are given by:

$$\left( \frac{\partial \Delta}{\partial D} \right)_A = \frac{2.303 \times 3A}{(D+2)^2} [10^{3A/(D+2)} + 2 \times 10^{-3DA/(D+2)}] \quad (25)$$

which becomes:

$$\left( \frac{\partial \Delta}{\partial D} \right)_{D \rightarrow 1} = 2.303A10^{-A} \quad (26)$$

as  $D$  approaches unity.

The condition of maximum sensitivity is obtained by differentiating equation (26) with respect to  $A$ ,

$$\left[ \frac{\partial(\partial \Delta / \partial D)_A}{\partial A} \right]_{D \rightarrow 1} = 2.303 \times 10^{-A} (1 - 2.303A) \quad (27)$$

Equating equation (27) to zero we observe that the maximum slope at  $D=1$  occurs when  $A=1/2.303=0.434$ . At this value of  $A$

$$\left( \frac{\partial \Delta}{\partial D} \right)_{D \rightarrow 1} = 10^{-0.434} = 0.368 \quad (28)$$

which is less than the value of unity for  $(\partial H / \partial D)_A$ . The maximum sensitivity of the conventional method at intermediate  $A$  values is further evident from the appearance of maxima or minima in plots of  $\Delta$  against  $A$  at different  $D$  values. The maxima or minima occur at  $A$  values determined from:

$$\left( \frac{\partial \Delta}{\partial A} \right)_D = \frac{2.303 \times 3}{D+2} (D \times 10^{-3DA/(D+2)} - 10^{-3A/(D+2)}) = 0 \quad (29)$$

which yields

$$A = \frac{(D+2)}{3(D-1)} \log_{10} D \quad (30)$$

Comparison of Figures 5 and 6 shows that  $\Delta$  is considerably smaller than  $H$  except at very low  $A$  values. This result is best illustrated by considering the ratio  $H/\Delta$  which, from equations (16) and (23) is given by:

$$R = \frac{H}{\Delta} = \frac{I_{0,\perp}}{I_{\perp}} = 10^{3A/(D+2)}$$

or

$$\log_{10} R = 3A/(D+2) \quad (31)$$

The ratio  $R$  thus increases with increasing  $A$  and decreasing  $D$ . As  $D$  tends to unity  $\log_{10} R = A$  so that  $R$  is equal to 10 for  $A=1$  and is equal to 100 for  $A=2$ . As  $A$  tends to zero, the two methods approach equal sensitivity ( $R \rightarrow 1$ ), but at low  $A$  values each method lacks precision.

We conclude that, whereas the conventional method attains reasonable precision when average absorbancies are around 0.434, the differential method is always more sensitive. The relative sensitivity of the differential method is particularly high at low dichroic ratios and high average absorbancies. For high absorbancies, the main problem with the differential method concerns the decrease in available energy. Methods for increasing this energy are considered below.

## OPERATIONAL PROCEDURES AND CORRECTION OF ERRORS

With the differential method, many of the procedures for setting up and operating the instrument are the same as those required for normal infra-red measurements. These include, for example, the alignment of optical components and adjustments to the reference comb for linearity. Certain procedures, however, require particular consideration in the case of the differential technique and these are considered below. Correction procedures are also proposed and analysed for the major sources of error so far encountered.

### Orientation of polarizers and sample

Two methods have been jointly employed for setting the polarizers at the desired orientations of  $\pm 45^\circ$  to the (approximately) vertical monochromator components. In the first method, each polarizer is placed successively in the usual sample space and two angular settings are located which are separated by exactly  $90^\circ$  and which yield the same transmission. These angles correspond to the required  $\pm 45^\circ$  settings. The second method follows from the observation of a sharp change in polarization behaviour of the GS 2A and GS 3 monochromators in the wavelength range between  $9\ \mu\text{m}$  and  $10\ \mu\text{m}$ . This effect gives rise to a peak in transmission at about  $9.5\ \mu\text{m}$  when the polarizer setting differs from  $\pm 45^\circ$ . The required  $45^\circ$  setting is obtained by rotating the polarizer until the peak in the transmission-wavelength scan is eliminated. Each of the two methods yields the same polarizer settings to within the experimental error of  $0.5^\circ$ . The second method has been found particularly sensitive for final small adjustments to the two polarizer settings after they have been located in their respective positions in the sample and reference beams.

Having set the polarizers at their respective  $+45^\circ$  and  $-45^\circ$  orientations to the monochromator polarization direction, the  $45^\circ$  sample orientation is adjusted. Using an extended sample, this adjustment is effected by rotating the stretcher until the differential peak is maximized.

### Gain, slit width and scan speed settings

Concerning the question of energy availability, we have shown above that the sensitivity of the differential method increases as the average absorbance increases. Hence, to achieve sufficient sensitivity, it may frequently be necessary to increase the average absorbance by increasing the specimen thickness. However, with highly absorbing samples in the common beam, the available energy for operating the reference comb servo motor is considerably reduced. An increase in energy may be achieved by increasing the gain of the detector amplifier, but this method is limited by the increase in noise level.

The most useful method of increasing energy is to increase manually the monochromator slit width. When estimating the required slit width, account should be taken of the reference beam polarizer which transmits about 40% of the incident intensity. Hence, with a sample having an average peak absorbance of 1, corresponding to 10% transmission, the total energy at the wavelength of maximum absorption is only about 4% of that available under normal operating conditions. Since the energy is proportional to the square of the slit width, the slit width needs to be increased by a factor of five ( $25^{1/2}$ ) of its normal value if the normal gain setting is unaltered. By

similar reasoning, an average sample absorbance of 2, corresponding to 1% peak transmission, would require the slit width to be increased by a factor of about 16 ( $250^{1/2}$ ) for a given gain setting. These increases in slit width can be reduced, of course, by increasing the gain (providing that the noise increase is acceptable) and by using very slow wavelength scans, thereby reducing the energy necessary for the accurate recording of peaks.

### Selection of baseline

As discussed above, the determination of  $D$  from  $A_{\parallel} - A_{\perp}$  requires the measurement of the absorbance  $A_0$  for the undeformed specimen. This measurement is subject to errors arising from the overlap of neighbouring absorptions, which causes uncertainties in the choice of baseline and hence in the value of  $I_0$ . The problem could be approached by attempting to resolve the overlapping peaks although this procedure is laborious and generally somewhat arbitrary. The method so far adopted has been to select different baselines (*Figure 7* indicates schematically two types of selection), and to evaluate  $A_0$  as a function of sample thickness  $d_0$ . Since the absorbance should be proportional to thickness ( $A_0 = \epsilon_0 \rho_0 d_0$ ), the most suitable baseline corresponds to that which yields a plot of  $A_0$  against  $d_0$  which is both linear and passes through the origin.

The determination of  $A_{\parallel} - A_{\perp}$  from the differential spectrum is not subject to baseline uncertainties of the above type. In this case the baseline ( $I_{0, \parallel} / I_{0, \perp}$ ) is obtained independently from measurements with the unextended sample in the common beam.

### Corrections for insufficient resolution

Since the differential method often necessitates slit widths considerably larger than those employed for normal operation, it should be remembered that an increase in slit width causes a proportionate reduction in spectrometer resolution, and that corrections may thus be required to the observed  $A_{\parallel} - A_{\perp}$  values. For conventional unpolarized spectra, Ramsay<sup>12</sup> has computed theoretical correction factors for the observed peak absorbancies to account for insufficient spectrometer resolution. His calculations are based on the assumption that for *monochromatic* radiation the absorption band shape can be represented by a Lorentz curve:

$$\log_e \left( \frac{I_0}{I} \right)_{\nu} = \frac{a}{(\nu - \nu_0)^2 + b^2} \quad (32)$$

where  $\nu$  is the frequency in  $\text{cm}^{-1}$ ,  $\nu_0$  the frequency of the peak maximum and  $a$  and  $b$  are constants. It follows from equation (32) that the peak intensity is given by:

$$\log_e \left( \frac{I_0}{I} \right)_{\nu_0} = a/b^2 \quad (33)$$

and that the bandwidth at half peak intensity is,

$$\Delta \nu_{1/2} = 2b \quad (34)$$

Ramsay has further assumed that the wavelength band emerging from the exit slit can be represented by a triangular energy distribution function  $\rho(\nu, \nu')$ .  $\nu'$  is the frequency at which the spectrometer is set and is assumed to be the frequency of maximum energy. The energy distribution is also characterized by a half-energy spectral

slit width,  $s$ . The apparent values of  $I/I_0$  are then given by:

$$\left(\frac{I}{I_0}\right)_{\nu'}^a = \frac{\int \rho(\nu, \nu') \exp\left[\frac{-a}{(\nu - \nu_0)^2 + b^2}\right] d\nu}{\int \rho(\nu, \nu') d\nu} \quad (35)$$

Equation (35) was numerically integrated for various values of  $a$ ,  $b$  and the spectral slit width  $s$ , and the observed absorption peaks characterized by their apparent peak intensity,  $\log_e(I_0/I)_{\nu(\text{max})}^a$ , and apparent half-intensity width  $\Delta\nu_{1/2}^a$ . Ramsay has tabulated values of correction factors  $[\log_e(I_0/I)_{\nu(\text{max})}]/[\log_e(I_0/I)_{\nu(\text{max})}^a]$  for various values of the apparent peak intensity and the ratio  $s/\Delta\nu_{1/2}^a$ . These values could be used for estimating corrections to the observed  $A_0$  values.

In applying Ramsay's procedure to the differential spectra we assume that the parallel and perpendicularly polarized spectra, if measured separately with monochromatic radiation, can each be represented by Lorentz curves and have the same maximum frequency  $\nu_0$  and half-intensity bandwidth  $\Delta\nu_{1/2}$ . These assumptions seem reasonable for low degrees of orientation where the vibrational interactions are not highly anisotropic. The true differential peak may then be represented by:

$$\log_e\left(\frac{I_{0,\parallel}}{I_{\parallel}}\right)_{\nu} - \log_e\left(\frac{I_{0,\perp}}{I_{\perp}}\right)_{\nu} = \frac{a_{\parallel} - a_{\perp}}{(\nu - \nu_0)^2 + b^2} \quad (36)$$

which has a peak intensity equal to  $(a_{\parallel} - a_{\perp})/b^2$  and a half-intensity bandwidth of  $2b$ . In terms of the triangular slit function, the apparent differential peak is then given by:

$$\left(\frac{I_{\parallel}/I_{\perp}}{I_{0,\parallel}/I_{0,\perp}}\right)_{\nu'}^a = \frac{\int \rho(\nu, \nu') \exp\left[\frac{-(a_{\parallel} - a_{\perp})}{(\nu - \nu_0)^2 + b^2}\right] d\nu}{\int \rho(\nu, \nu') d\nu} \quad (37)$$

The right-hand sides of equations (35) and (37) become identical if we equate the parameters  $a$  and  $a_{\parallel} - a_{\perp}$ . Hence Ramsay's correction factors can be applied to the observed values of  $A_{\parallel} - A_{\perp}$  if the differential peak intensities are identified with his ordinary peak intensities. It should, however, be remembered that these factors are theoretically derived on the basis of a triangular slit function and Lorentz shaped curves for monochromatic radiation. Whilst these factors may serve as approximations to the corrections for a given  $s/\Delta\nu_{1/2}$  ratio, it would seem preferable to obtain independent experimental estimates of the required corrections.

One method involves the measurement of peak absorbance as a function of mechanical slit width for the ordinary unpolarized spectrum. As the slit width is decreased, the peak absorbance should attain, or approach, the true value corresponding to that for monochromatic radiation. The correction factor is thus obtained as the ratio of this limiting absorbance value to the observed absorbance at the slit width employed for the differential measurement. Repeated measurements with varying sample thickness should serve to establish if the correction factor depends on peak absorbance. This method is based, of course, on the above analysis [equations (35) and (37)] which suggests, with reasonable assumptions, that the ordinary and differential spectra are similarly dependent on resolution.

#### Corrections for sample radiation at high temperatures

The infra-red spectra of materials at high temperatures are subject to errors arising from the emission of radiation

by the sample itself. For highly absorbing samples placed close to a focus in the optical system, the intensity of sample radiation reaching the detector may become significant compared with the intensity of the transmitted beam. The intensity of the sample radiation, indicated by  $I_r$  in Figure 7, is given by the recorder trace obtained after blocking off the sample beam *prior* to entering the specimen. Since  $I_r$  adds to all intensities in the subsequently recorded spectrum, the sample radiation decreases the apparent height of the absorption peak. In general  $I_r$  will vary with wavelength, and the transmitted intensity  $I$  at the peak wavelength  $\lambda_{\text{max}}$  is obtained by subtracting  $I_{r,\text{max}}$  at this wavelength from the apparent intensity  $I_a$ ,

$$I = I_a - I_{r,\text{max}} \quad (38)$$

If a linear baseline is drawn between two points on the spectrum at wavelengths  $\lambda_1$  and  $\lambda_2$  (Figure 7), then  $I_0$  may be estimated by subtracting from the apparent intensity the mean value of  $I_{r_1}$  and  $I_{r_2}$  observed at  $\lambda_1$  and  $\lambda_2$  respectively:

$$I_0 = I_{0,a} - \left[ I_{r_s} - \frac{(I_{r_s} - I_{r_1})(\lambda_2 - \lambda_{\text{max}})}{(\lambda_2 - \lambda_1)} \right] \quad (39)$$

In the case of symmetrical peaks for which  $\lambda_2 - \lambda_1 = 2(\lambda_2 - \lambda_{\text{max}})$  then equation (39) reduces to:

$$I_0 = I_{0,a} - (I_{r_s} + I_{r_1})/2 \quad (40)$$

so that the proposed correction involves the subtraction of the arithmetic mean of  $I_{r_1}$  and  $I_{r_s}$ . Alternatively, if a horizontal baseline is drawn from the point on the spectrum at wavelength  $\lambda_2$  then  $I_0$  may be estimated from:

$$I_0 = I_{\lambda_s} - I_{r_s} \quad (41)$$

where  $I_{\lambda_s}$  is the total measured intensity at  $\lambda_2$ . The above corrections may be applied in the evaluation of  $A_0$ .

The emission of radiation by the sample can also reduce apparent peak intensities in the differential spectra, in addition to causing other spurious effects such as the appearance of small peaks on the baseline for an unextended sample. With the specimen located in the common beam, sample radiation may reach the detector via both the sample and reference paths, and if the intensities

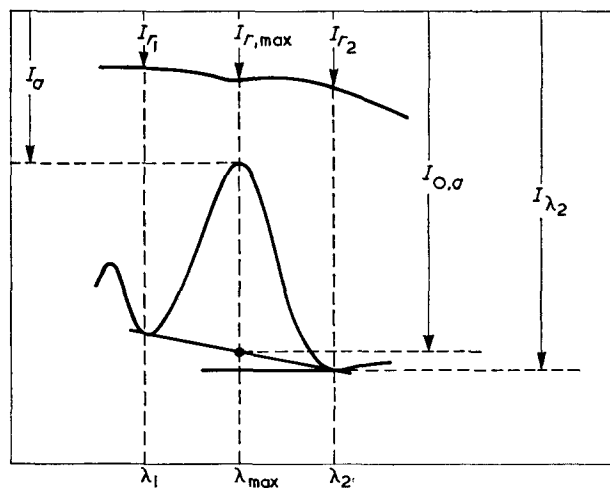


Figure 7 Illustration of the effect of sample emission on the ordinary unpolarized spectrum

of these two radiations become comparable with the transmitted intensities from the source, then the differential spectra will be affected. In order to investigate and, if necessary, correct for the effects of sample radiation, a method has been devised which involves the use of rotating sectors immediately in front of the source to successively reduce the source intensity. The technique is shown schematically in Figure 8.

If the source is completely blocked off in front of the sample, then the incident, and hence transmitted, intensities become zero. The spectrometer then records the ratio  $I_{Sr}/I_{Rr}$  (Figure 8) where  $I_{Sr}$  and  $I_{Rr}$  are the intensities of sample radiation reaching the detector through the sample and reference paths respectively. Although the ratio  $I_{Sr}/I_{Rr}$  will be independent of wavelength,  $I_{Sr}$  and  $I_{Rr}$  will individually vary with wavelength. In the following analysis it is assumed that these variations are negligible compared with the transmitted intensities over the wavelength range of a differential peak. Considering first the case in which the sample and reference beam polarizers have the parallel and perpendicular orientation, respectively, then the ratio of the observed baseline, with no rotating sector in front of the source, to  $I_{Sr}/I_{Rr}$  is given by (Figure 8a):

$$\frac{(I_{0,\parallel} + I_{Sr}) \cdot I_{Rr}}{(I_{0,\perp} + I_{Rr}) \cdot I_{Sr}} = C \quad (42)$$

It will be noted that  $C$  depends on the difference in partitioning between the sample and reference paths of the radiation transmitted by and radiated from the specimen, respectively. When the transmitted and radiated intensities are equally partitioned between the two paths

then  $C$  becomes unity. If we now consider the baseline observed when a rotating sector is employed which passes  $x\%$  of the source intensity, then from Figure 8a we have:

$$\frac{(xI_{0,\parallel} + I_{Sr}) \cdot I_{Rr}}{(xI_{0,\perp} + I_{Rr}) \cdot I_{Sr}} = C_x \quad (43)$$

From equations (42) and (43) we obtain:

$$\frac{I_{0,\parallel}}{I_{0,\perp}} = \frac{I_{Sr}}{I_{Rr}} \left[ \frac{C(C_x - 1) - xC_x(C - 1)}{(C_x - 1) - x(C - 1)} \right] \quad (44)$$

The recorded intensities at the peak maxima (Figure 8a) also yield the following ratios:

$$\frac{(I_{\parallel} + I_{Sr}) \cdot I_{Rr}}{(I_{\perp} + I_{Rr}) \cdot I_{Sr}} = K \quad (45)$$

$$\frac{(xI_{\parallel} + I_{Sr}) \cdot I_{Rr}}{(xI_{\perp} + I_{Rr}) \cdot I_{Sr}} = K_x \quad (46)$$

Equations (45) and (46) give

$$\frac{I_{\parallel}}{I_{\perp}} = \frac{I_{Sr}}{I_{Rr}} \left[ \frac{K(K_x - 1) - xK_x(K - 1)}{(K_x - 1) - x(K - 1)} \right] \quad (47)$$

and we finally obtain from equations (44) and (47):

$$\frac{I_{0,\parallel} I_{\perp}}{I_{\parallel} I_{0,\perp}} = \frac{[C(C_x - 1) - xC_x(C - 1)][(K_x - 1) - x(K - 1)]}{[(C_x - 1) - x(C - 1)][K(K_x - 1) - xK_x(K - 1)]} \quad (48)$$

Figure 8b illustrates the intensity ratios recorded when the sample and reference beam polarizers are set to transmit the perpendicular and parallel polarized components, respectively. By a procedure analogous to that used above, these intensity ratios yield:

$$\frac{I_{0,\parallel} I_{\perp}}{I_{\parallel} I_{0,\perp}} = \frac{[(C'_x - 1) - x(C' - 1)][K'(K'_x - 1) - xK'_x(K' - 1)]}{[C'(C'_x - 1) - xC'_x(C' - 1)][(K'_x - 1) - x(K' - 1)]} \quad (49)$$

in which

$$\frac{(I_{0,\perp} + I_{Sr}) \cdot I_{Rr}}{(I_{0,\parallel} + I_{Rr}) \cdot I_{Sr}} = C' \quad (50)$$

$$\frac{(xI_{0,\perp} + I_{Sr}) \cdot I_{Rr}}{(xI_{0,\parallel} + I_{Rr}) \cdot I_{Sr}} = C'_x \quad (51)$$

$$\frac{(I_{\perp} + I_{Sr}) \cdot I_{Rr}}{(I_{\parallel} + I_{Rr}) \cdot I_{Sr}} = K' \quad (52)$$

$$\frac{(xI_{\perp} + I_{Sr}) \cdot I_{Rr}}{(xI_{\parallel} + I_{Rr}) \cdot I_{Sr}} = K'_x \quad (53)$$

The absorbance difference  $A_{\parallel} - A_{\perp}$  is now obtained as the logarithm of the right-hand side of either equation (48) or (49). It will be noted that if the sample radiation is neglected the apparent value of  $A_{\parallel} - A_{\perp}$  is calculated as the logarithm of either  $C/K$  or  $K'/C'$ . When the sample radiation intensity is, in fact, negligible in comparison with the transmitted intensity then these ratios each become equal to  $I_{0,\parallel}/I_{0,\perp}$ , the logarithm of which yields the true value of  $A_{\parallel} - A_{\perp}$ .

Three points deserve comment in connection with the above analysis. Firstly, when using rotating sectors the spectrometer slit width should be the same as that employed in the absence of a sector, otherwise the differential peak height will be modified due to changes in

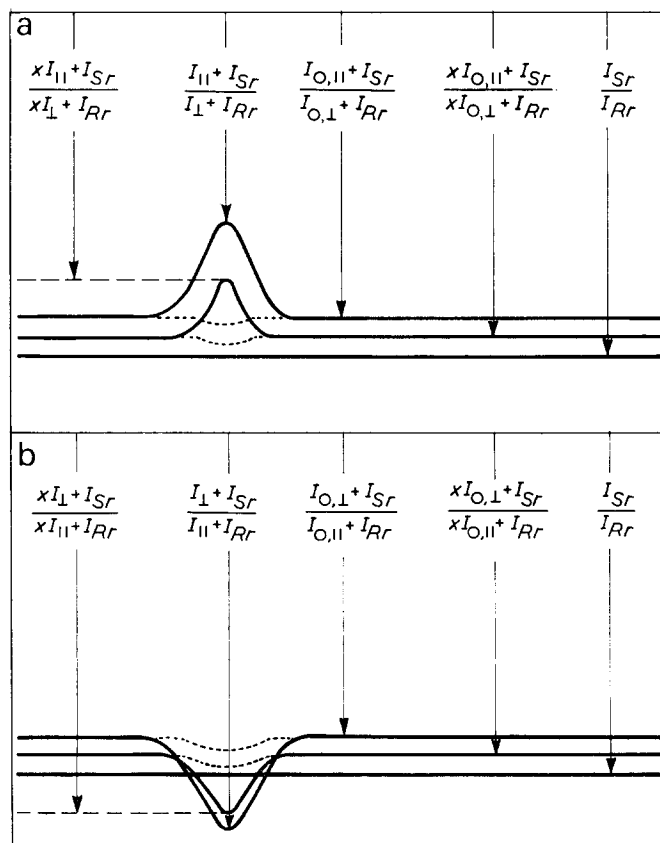


Figure 8 Illustration of the effects of sample radiation on the differential spectrum. Dotted lines indicate the baselines obtained with an unextended specimen

resolution. Secondly, when determining the baseline using an undeformed sample, the transmitted intensities pass through a minimum at the wavelengths of maximum sample absorption. Consequently the ratio of the intensities radiated by and transmitted through the sample, respectively, passes through a maximum. This effect may result in the appearance of small peaks on the baseline (Figure 8) which are not related to molecular orientation in the specimen (since it is unextended) and the direction (or sign) of which are thus independent of polarizer orientations. The peaks are generally small and may be ignored in the baseline determination. Thirdly, since the sample temperature is increased somewhat by the energy absorbed from the incident beam, the sample emission may be slightly reduced when a rotating sector is employed to decrease the source intensity. This effect may be compensated for by re-establishing the original sample temperature (by adjusting the enclosure temperature) subsequent to introducing the sector. Alternatively a range of sectors may be successively employed, corresponding to different  $x$  values in the above analysis, and the corrected values of  $I_{0, \parallel} I_{\perp} / I_{0, \perp} I_{\parallel}$  extrapolated to  $x=1$ , at which point the sample emission is unchanged.

#### *Other sources of error and order of corrections*

Additional sources of error have been discussed by Zbinden<sup>1</sup> and these arise from polarizer inefficiency, beam convergence, scattered light and spectral dilution. With the present apparatus, errors due to these factors should be small or negligible. The major sources of error so far encountered involve the choice of baseline for the ordinary unpolarized spectra, and the problems of resolu-

tion and sample radiation at high temperatures for the differential spectra. Ordinary spectra are first determined with various specimen thicknesses and spectrometer slit widths. After correcting for sample radiation (if recorded at high temperatures) these measurements enable the baseline to be selected and yield  $A_0$  (or  $\epsilon_0$ ) and the factors required for resolution corrections. With the differential spectra, corrections are first made for sample radiation, if necessary, and subsequently for resolution.

Results obtained with the present equipment, using the proposed correction methods, are discussed in a later paper<sup>13</sup>.

#### REFERENCES

- 1 Zbinden, R. 'Infrared Spectroscopy of High Polymers', Academic Press, New York, 1964
- 2 Read, B. E. and Stein, R. S. *Macromolecules* 1968, **1**, 116
- 3 Flory, P. J. and Abe, Y. *Macromolecules* 1969, **2**, 335
- 4 Stein, R. S. *J. Appl. Polym. Sci.* 1961, **5**, 96
- 5 Le Grand, D. G. *J. Polym. Sci. (A)* 1965, **3**, 301
- 6 Gotoh, R., Takenaka, T. and Hayama, N. *Kolloid Z.* 1965, **205**, 18
- 7 Gotoh, R., Takenaka, T., Umemura, J. and Hayashi, S. *Bull. Inst. Chem. Res., Kyoto Univ.* 1966, **44**, 286
- 8 Umemura, J., Takenaka, T., Hayashi, S. and Gotoh, R. *Bull. Inst. Chem. Res., Kyoto Univ.* 1968, **46**, 228
- 9 Takenaka, T., Shimura, Y. and Gotoh, R. *Kolloid Z.* 1970, **237**, 193
- 10 Stein, R. S. *Polym. Eng. Sci.* 1969, **9**, 320
- 11 Barnes, D. C., Drury, F. W. M., Hughes, D. A. and Read, B. E. *Mater. Appl. Rep. No. 15* National Physical Laboratory, Teddington
- 12 Ramsay, D. A. *J. Am. Chem. Soc.* 1952, **74**, 72
- 13 Read, B. E. and Hughes, D. A. *Polymer* 1972, **13**, 495

# Stress-dichroism studies of the 4.92 $\mu\text{m}$ band of amorphous crosslinked polyethylene

B. E. Read and D. A. Hughes

Division of Materials Applications, National Physical Laboratory, Teddington, Middlesex TW11 0LW, UK  
(Received 24 April 1971)

Using a differential method, measurements have been made of the dichroic ratio of the 4.92  $\mu\text{m}$  (2033  $\text{cm}^{-1}$ ) infra-red band during the elongation of crosslinked amorphous polyethylene at 170°C. Simultaneous measurements of stress and strain were also made. Corrections of the infra-red data for polarizer inefficiency were negligible, but the data required correcting both for resolution and for the effects of sample emission at high temperatures. From the data, second moment orientation functions are evaluated as a function of strain. Analysis of the results in terms of recent statistical calculations of Flory and Abe, suggests that the orienting units detected in measurements on the 4.92  $\mu\text{m}$  band comprise on average *trans* sequences of about 7 chain bonds.

## INTRODUCTION

The dichroic ratios of infra-red absorption peaks can yield valuable information on the relative orientation of different parts of a polymer structure when the material is deformed<sup>1</sup>. In the case of crosslinked rubberlike polymers, stress-dichroism data should complement stress-birefringence results<sup>2</sup> and provide more detailed information on the preferential orientation of different conformational sequences within the polymer chain<sup>1,3</sup>. Furthermore, the analysis of such data in terms of statistical calculations of polymer chain conformations<sup>3</sup> may aid in the assignments of infra-red bands of amorphous origin<sup>4</sup>.

In a previous report<sup>5</sup> equipment has been described for simultaneously determining the stress, strain and infra-red dichroic ratio of extended polymers. The purpose of this report is to present and discuss results obtained on the 4.92  $\mu\text{m}$  (2033  $\text{cm}^{-1}$ ) band of crosslinked amorphous polyethylene at 170°C.

## THEORY

For a uniaxially elongated material, the dichroic ratio  $D$  is defined as the ratio of the absorbance  $A_{\parallel}$ , measured with radiation polarized parallel to the stretching direction, to the absorbance  $A_{\perp}$  determined with perpendicularly polarized radiation:

$$D = \frac{A_{\parallel}}{A_{\perp}} = \frac{\log_{10}(I_{0,\parallel}/I_{\parallel})}{\log_{10}(I_{0,\perp}/I_{\perp})} \quad (1)$$

In equation (1),  $I_{\parallel}$  and  $I_{\perp}$  are the transmitted intensities at the wavelength of an absorption peak determined with parallel and perpendicularly polarized radiation, respectively.  $I_{0,\parallel}$  and  $I_{0,\perp}$  are the transmitted intensities at the baselines of the respective peaks.

The magnitude of  $D$  is determined by the average orientation of the transition moment vectors of absorbing molecular groups relative to the direction of extension.

If the angle  $\phi$  between the transition moment vector and an axis of the absorbing group is known<sup>6</sup>, then measurements of  $D$  yield the molecular second moment orientation function  $f_2$ ,

$$f_2 = \frac{1}{2}(3\overline{\cos^2\theta} - 1) = \frac{(D_0 + 2)(D - 1)}{(D_0 - 1)(D + 2)} \quad (2)$$

Here  $D_0 = 2\cot^2\phi$  and  $\theta$  is the angle between the axis of the absorbing group and the stretching direction. The quantity  $\overline{\cos^2\theta}$  is the value of  $\cos^2\theta$  averaged over all orienting groups.

For crosslinked amorphous polymers in the rubberlike state, Flory and Abe<sup>3</sup> have recently derived the following equation relating  $D$  to the extension ratio:

$$D - 1 \approx (3G_2^*/2n')(V/V_0)^{2/3}(\alpha^2 - 1/\alpha) \quad (3)$$

where  $V$  is the volume of the strained specimen and  $V_0$  a reference volume which may usually be taken as the unstrained volume. The extension ratio  $\alpha$  equals  $l/l_0$  where  $l$  is the extended sample length and  $l_0$  the unextended length referred to the same volume  $V$ . In practice the volume changes produced by extending rubbers is very small and the factor  $V/V_0$  has a value close to unity. The quantity  $n'$  represents the number of chain bonds or bond sequences eligible to assume the local conformation required for the specified absorption.  $G_2^*$  is a parameter describing the average correlation, per absorbing group, of the transition moment directions with respect to the chain end-to-end vector. From a detailed accounting of polymer chain statistics, Flory and Abe have evaluated  $G_2^*$  for a polymethylene chain for several conformational sequences and various axes referred to each conformation.

The corresponding stress-strain relationship for crosslinked rubbers is:

$$t = NkT(V/V_0)^{2/3}(\alpha^2 - 1/\alpha) \quad (4)$$

where  $t$  is the stress referred to the cross-sectional area of the extended specimen,  $N$  is the number of polymer

chains per unit volume between crosslink points,  $k$  is Boltzmann's constant and  $T$  the absolute temperature. The factor  $NkT$  in equation (4) may be written:

$$NkT = \frac{\rho RT}{M_c} = \frac{\rho RT}{nM_0} \quad (5)$$

where  $\rho$  is the sample density,  $R$  the gas constant and  $M_c$  the molecular weight of a network chain between crosslink points.  $n$  is the number of bonds or repeat units in the network chain and  $M_0$  the molecular weight of a repeat unit. Hence the slope of a plot of  $t$  against  $\alpha^2 - (1/\alpha)$  yields  $M_c$  or  $n$  providing that  $\rho$  and  $M_0$  are known and that  $V/V_0$  is either known or assumed equal to unity. Alternatively  $M_c$  or  $n$  can be estimated from the Young's modulus  $E$ , defined as the slope of the plot of  $t$  against  $\alpha$  at  $\alpha=1$ ,

$$E = \left( \frac{dt}{d\alpha} \right)_{\alpha=1} = \frac{3\rho RT}{M_c} = \frac{3\rho RT}{nM_0} \quad (6)$$

Combining equations (3), (4) and (5) we obtain:

$$\frac{D-1}{t} \approx \frac{3G_2^* n M_0}{2n' \rho RT} \quad (7)$$

When  $n$  is much greater than the number of chain bonds involved in the local absorbing sequence we assume that  $n \approx n'$  and equation (7) becomes:

$$\frac{D-1}{t} \approx \frac{3G_2^* M_0}{2\rho RT} \quad (8)$$

Equation (8) enables the determination of  $G_2^*$  from the measured ratio  $(D-1)/t$ . A comparison of measured values of  $G_2^*$  with values calculated for different local conformational sequences, provides a method for exploring the nature of the orienting chain unit, and additionally should aid in the assignment of the infra-red peak under investigation.

## EXPERIMENTAL

### Material

The polyethylene employed in this investigation was a linear high density grade obtained in fine powdered form from Hoechst Chemicals Ltd. It was designated Hostalen GUR and was reported<sup>7</sup> to have a weight-average molecular weight of  $1.5 \times 10^6$  and number-average molecular weight of  $10^5$ . Crosslinking was affected by adding 3 wt.% dicumyl peroxide to the polymer and vacuum moulding at 180°C for about 15 min. In order to incorporate the dicumyl peroxide into the polymer, it was dissolved in ethyl alcohol or acetone and the powdered polymer was suspended in the solution. Whilst stirring the suspension, the solvent was evaporated and the peroxide containing polymer was thoroughly dried at 60°C. The dimensions of the dumbbell shaped specimens and also the arrangement of vapour deposited lines used for strain determinations are given in a previous paper<sup>5</sup>.

### Measurement of sample density, thickness, extension ratio and stress

Samples were freely suspended in a silicone oil bath and their widths and lengths were measured with a cathetometer whilst cycling the temperature between 20°C and 190°C. Assuming isotropic expansion, the

results of these measurements were used to compute densities ( $\rho_0$ ), thicknesses ( $d_0$ ) and widths ( $b_0$ ) of unextended samples at 170°C from measured values at room temperature. The room temperature densities and thicknesses were measured with a density gradient column and micrometer, respectively. All room temperature dimensions were made after cycling to high temperatures, since the original dimensions were influenced by the pressure maintained on the mould during cooling.

Extension ratios ( $\alpha$ ) were calculated from the change in the distance between lines on the specimen surface<sup>5</sup>. Thicknesses ( $d$ ) and cross-sectional areas of extended samples were calculated from  $\alpha$ ,  $d_0$  and  $b_0$  values assuming a negligible volume change ( $\rho = \rho_0$ ) and an equal contraction in thickness and width on extension. Stresses ( $t$ ) were calculated from the measured tension<sup>5</sup> and extended cross-sections.

### Absorbance measurements on undeformed specimens

The extinction coefficient  $\epsilon_0$  for the undeformed sample at 170°C was determined from measurements of  $A_0$  ( $\epsilon_0 = A_0/\rho_0 d_0$ ) using unpolarized radiation. The sample was placed in the sample beam of the spectrometer in an evacuated, temperature controlled, enclosure obtained from RIIC Ltd. The temperature was measured with a chromel-alumel thermocouple resting lightly against the sample within the infra-red beam. After attaining temperature equilibrium at 170°C, the spectrum was scanned at 1  $\mu\text{m}/8$  min between 4.5  $\mu\text{m}$  and 5.5  $\mu\text{m}$ . Subsequently the sample beam was blocked off prior to entering the specimen, and the slight fall in sample temperature (about 4°C) compensated for by re-adjusting the temperature controller. The wavelength was then scanned in order to determine the intensity of emitted radiation from the sample reaching the detector. For purposes of exploring the most suitable baseline, and for obtaining correction factors for resolution, the above measurements were carried out for a range of specimen thickness (0.5 to 3 mm) and spectrometer slit width, respectively.

### Measurement of differential spectra

Details of the differential method for determining  $A_{\parallel} - A_{\perp}$  are presented in a previous paper<sup>5</sup>. The method consists, essentially, of extending the sample at a focus in the infra-red beam prior to splitting. After splitting, the beam passes through two polarizers, one in the usual sample beam and the other in the reference beam. The polarizers are of the wire grid type, corrections for inefficiency being negligible<sup>5</sup>. They are oriented to transmit parallel and perpendicularly polarized radiation, respectively, or *vice versa*. The spectrometer then records the ratio of intensities ( $I_S/I_R$ ) transmitted by the sample beam and reference beam polarizers, respectively. From this record  $A_{\parallel} - A_{\perp}$  can be evaluated<sup>5</sup>.

During the initial heating of the specimen to 170°C, and for all subsequent measurements, a slow stream of oxygen-free nitrogen was introduced into the sample enclosure to minimize thermal oxidation of the specimen. After establishing a steady temperature of 170°C, collimating plates<sup>5</sup> were first adjusted to ensure that the infra-red beam was fully contained within the sample area for both the unextended and extended sample. The sample beam comb was adjusted to give a suitable baseline level, and preliminary scans performed to establish



the gain, slit width and scan speed settings required for sufficient energy. A scan speed of  $1\ \mu\text{m}/4\ \text{min}$  was generally employed.

The wavelength was first scanned to determine the baseline for the unextended sample, both parallel/perpendicular and perpendicular/parallel orientations of the two polarizers being studied. These measurements were repeated after blocking off the source completely and again after introducing rotating sectors in front of the source which transmitted, respectively, 25% and 50% of the source intensity. The rotating sectors were introduced to correct, if necessary, for the effects of sample radiation reaching the detector<sup>5</sup>. After measuring the spacing between lines on the sample, and setting the force measuring bridge to zero, the sample was slowly extended in increments of about 12% strain.

At each extension, the differential spectrum was recorded for both parallel/perpendicular and perpendicular/parallel orientations of the two polarizers, both without and with rotating sectors and with the source completely blocked. Care was taken not to alter the spectrometer slit width or the sample comb position, thus maintaining the baseline at its original level. The force and elongation were also determined. Generally the differential spectra were recorded over the wavelength range  $4.5\ \mu\text{m}$  to  $5.5\ \mu\text{m}$ , but occasionally the range  $4\ \mu\text{m}$  to  $6\ \mu\text{m}$  was covered for purposes of more accurately defining the baseline.

Specimen thicknesses of about 1 mm, 2 mm and 3 mm were studied and the slit width was occasionally varied. These variations served as a check on stress determinations and on the procedures adopted for the correction of resolution and sample radiation. After cooling samples to room temperature at the completion of experiments, the KBr window mounts were detached and stored in a vacuum desiccator to avoid the absorption of atmospheric moisture by the windows.

## RESULTS

### Stress-strain data

The tensile stress  $t$  is plotted against extension ratio  $\alpha$  and  $\alpha^2 - (1/\alpha)$  in Figures 1a and 1b respectively. Good reproducibility is shown by the results on a number of

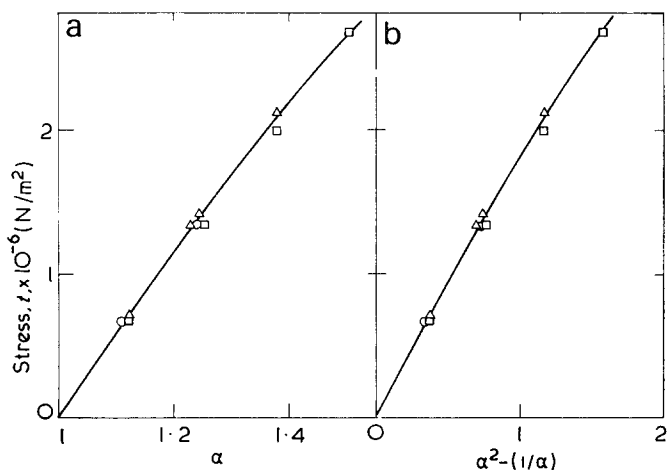


Figure 1 Plots of the tensile stress  $t$  at  $170^\circ\text{C}$  against (a) extension ratio  $\alpha$  and (b)  $\alpha^2 - (1/\alpha)$ . The different point symbols refer to samples of different thickness, each crosslinked with 3wt.% dicumyl peroxide. Unstrained sample thicknesses:  $\circ$ , 1.16 mm;  $\triangle$ , 2.27 mm;  $\square$ , 3.43 mm

samples (indicated by different point symbols in Figure 1) each crosslinked with 3 wt.% dicumyl peroxide. Figures 1a and 1b each deviate only slightly from linearity over the range of  $\alpha$  investigated. As  $\alpha$  tends to unity, they yield, from equations (6) and (4) respectively,  $E = 5.83 \times 10^6\ \text{N/m}^2$  and  $NkT = 1.94 \times 10^6\ \text{N/m}^2$ . Inserting the value of the measured density ( $\rho = 0.790\ \text{g/cm}^3$  at  $170^\circ\text{C}$ ) and the value  $M_0 = 14$  into equations (5) or (6) gives  $M_c = 1497$  and  $n = 107$ .

### Unpolarized spectra

Figures 2 and 3 illustrate the unpolarized spectra obtained with different sample thicknesses and spectrometer slit widths, respectively. The line labelled  $I_r$  in Figure 2b shows the trace obtained after blocking off the sample beam prior to entering the specimen, and arises from the emission of radiation by the sample itself. Owing to the overlap of the neighbouring peak at  $4.6\ \mu\text{m}$ , the choice of baseline for the  $4.92\ \mu\text{m}$  peak requires investigation, and Figure 2b shows three baselines A, B and C, respectively, which have been studied. Baselines B and C are horizontal lines drawn from minima at  $4.73\ \mu\text{m}$  and  $5.2\ \mu\text{m}$  respectively, and baseline A is the straight line connecting the two minima. Taking account

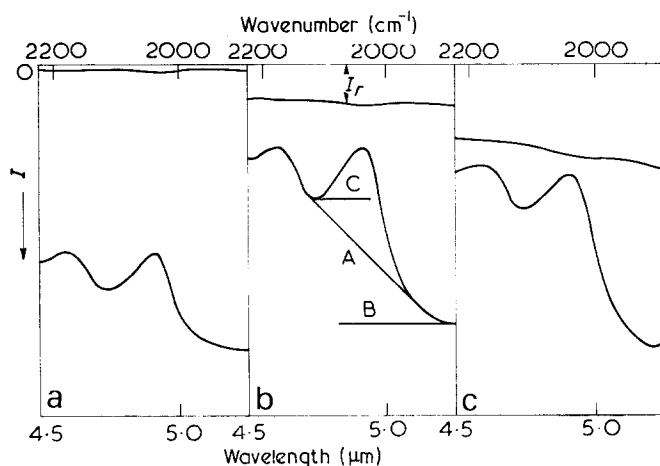


Figure 2 Ordinary unpolarized spectra at  $170^\circ\text{C}$  for three unextended samples using a mechanical slit width of 0.5 mm. Sample thicknesses: (a) 0.62 mm; (b) 2.30 mm; (c) 3.39 mm. Scan speed  $1\ \mu\text{m}/8\ \text{min}$

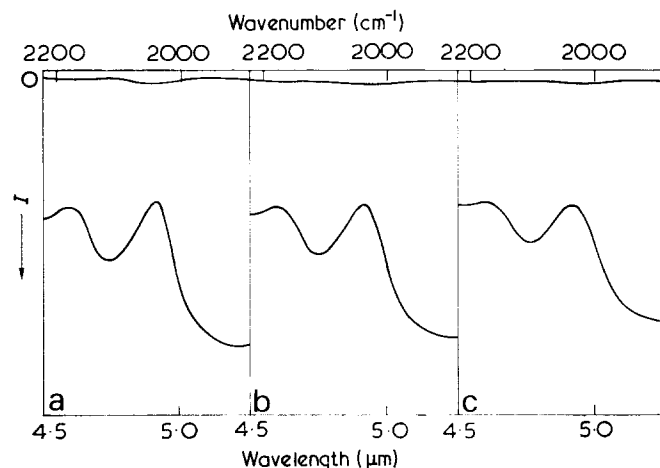


Figure 3 Unpolarized spectra for a 1.15 mm thick unstrained specimen. (a), (b) and (c) refer to mechanical slit widths of 0.5 mm, 1 mm and 1.5 mm, respectively. Scan speed  $1\ \mu\text{m}/8\ \text{min}$

of the sample radiation, absorbancies  $A_0 = \log_{10}(I_0/I)$  were evaluated for each of the three baselines by methods detailed previously<sup>5</sup>. According to the proposed methods, the transmitted intensity  $I$  at the peak maximum is obtained from:

$$I = I_a - I_{r,\max} \quad (9)$$

where  $I_a$  is the total measured intensity and  $I_{r,\max}$  the sample radiation intensity at the peak wavelength<sup>5</sup>. For baselines B and C the  $I_0$  values were calculated from

$$I_0 = I_{\lambda_1} - I_{r_1} \quad (10)$$

and

$$I_0 = I_{\lambda_2} - I_{r_2} \quad (11)$$

respectively. Here  $I_{\lambda_1}$  and  $I_{\lambda_2}$  are the total recorded intensities at wavelengths  $4.73 \mu\text{m}$  and  $5.2 \mu\text{m}$  respectively, and  $I_{r_1}$  and  $I_{r_2}$  the sample radiation intensities at these wavelengths. For baseline A,  $I_0$  was calculated from,

$$I_0 = I_{0,a} - (I_{r_1} + I_{r_2})/2 \quad (12)$$

where  $I_{0,a}$  is the apparent  $I_0$  value. Although strictly applicable to symmetrical peaks, equation (12) was found to be an adequate approximation for present purposes.

In Figure 4 the calculated values of  $A_0$ , obtained using a slit width of 0.5 mm, are plotted against specimen thickness. Baseline C yields a curved plot which extrapolates to give a positive intercept on the abscissa. Baselines A and B each yield linear plots within experimental error, although the points obtained from baseline B appear to extrapolate closer to the origin. For this reason, baseline B would seem to be the better choice, and will therefore be employed in the subsequent analysis. However, on account of the combined errors in the

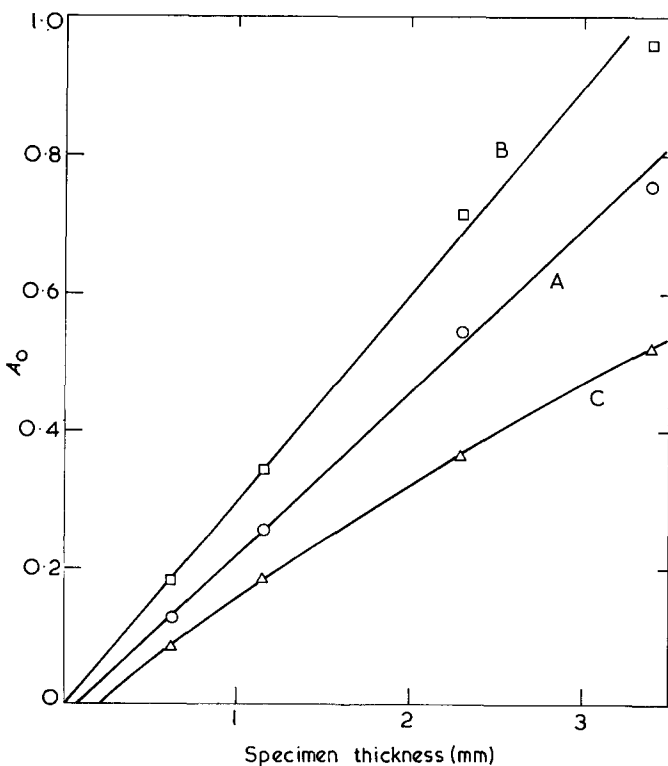


Figure 4 Average absorbance  $A_0$  of unstrained samples plotted against sample thickness. The three lines were obtained using baselines A, B and C, as indicated

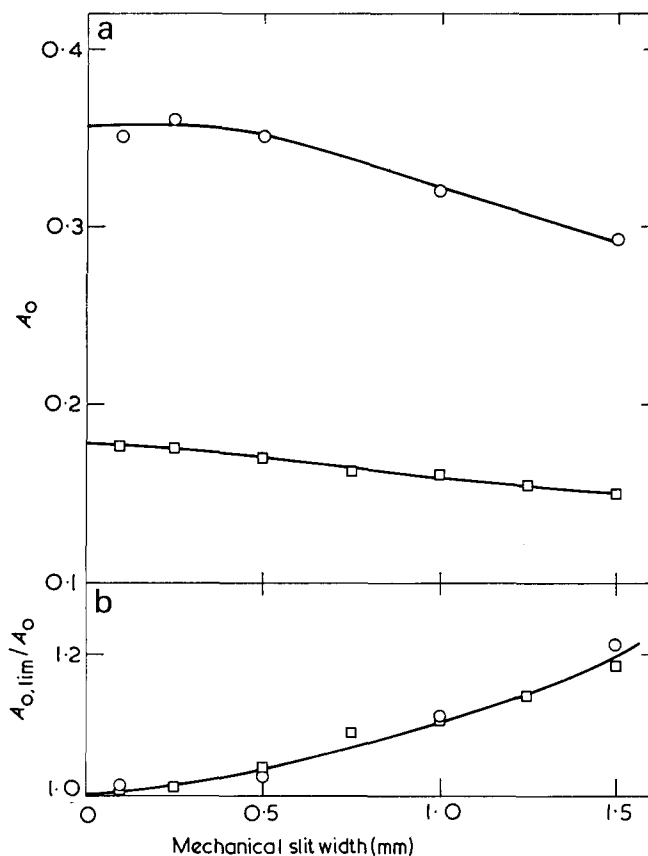


Figure 5 Variation of the absorbance  $A_0$  (a) and the ratio  $A_{0,\text{lim}}/A_0$  (b) with spectrometer slit width. Sample thicknesses:  $\circ$ , 1.15 mm;  $\square$ , 0.63 mm

measurement of  $A_0$  and thickness, and the consequent degree of uncertainty in the precise choice of baseline, final results evaluated according to baseline A will also be noted.

Figure 5a shows plots of  $A_0$ , calculated according to baseline B, against spectrometer slit width for two samples of thickness 1.15 mm and 0.63 mm respectively. Extrapolating these plots to zero slit width we obtain the limiting values  $A_{0,\text{lim}}$  of 0.356 and 0.178 respectively. The values of  $A_{0,\text{lim}}/A_0$  shown in Figure 5b were subsequently used as correction factors for insufficient resolution, as described earlier<sup>5</sup>. From the slopes in Figure 4 after multiplying by the  $A_{0,\text{lim}}/A_0$  value corresponding to a 0.5 mm slit width, we obtain the extinction coefficient  $\epsilon_0 = A_{0,\text{lim}}/d_0\rho_0$ . Baseline B yields  $\epsilon_0 = 389 \text{ mm}^2/\text{g}$  and, by a similar procedure, baseline A gives  $\epsilon_0 = 319 \text{ mm}^2/\text{g}$ .

#### Differential spectra

Figure 6 illustrates the differential spectra between  $4 \mu\text{m}$  and  $6 \mu\text{m}$  for a 2.92 mm thick specimen having an extension ratio of 1.379. The spectra obtained with the parallel/perpendicular and perpendicular/parallel polarizer orientations, respectively, are shown, together with the baselines obtained for the unextended sample. The effect of blocking off the source completely, and of introducing a rotating sector in front of the source which transmits 25% of the source intensity, is shown in Figure 7.

As proposed in ref. 5, the rotating sectors were employed to correct, if necessary, for the effects of radiation emitted from the sample. With the sample and

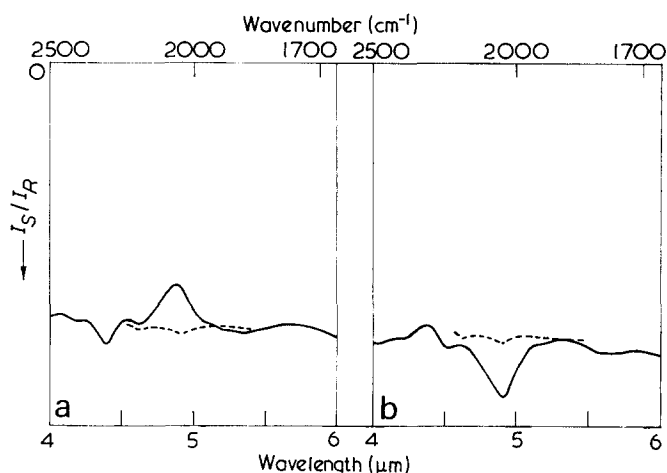


Figure 6 Differential spectra for a sample extended by 37.9% at 170°C, and having an unstrained thickness of 3.43mm. (a), Sample beam polarizer parallel, reference beam polarizer perpendicular; (b), sample beam polarizer perpendicular, reference beam polarizer parallel. Broken lines are the baselines for the unextended specimen. Slit width 1.5mm; scan speed 1 μm/4min

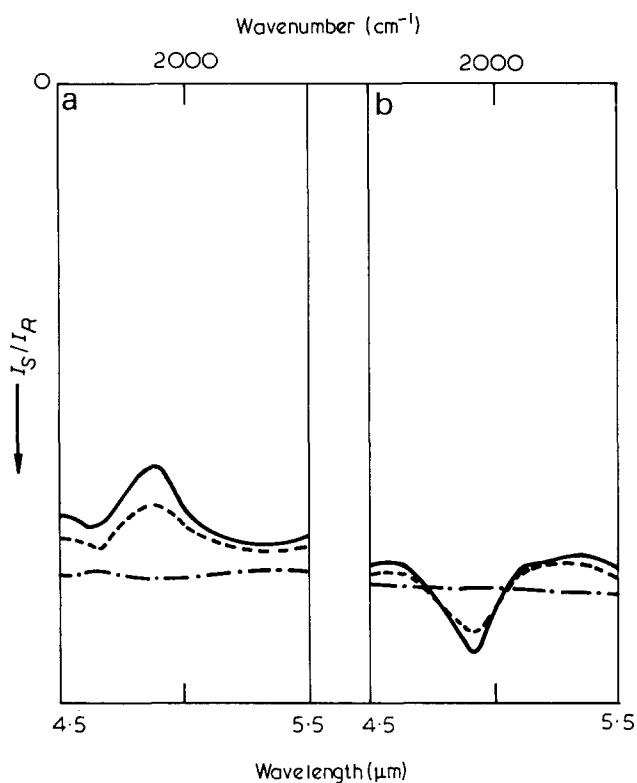


Figure 7 Change in the differential spectra of Figure 6 after blocking off the source (---) and after introducing a rotating sector which transmits 25% of the source intensity (....)

reference beam polarizers in the parallel and perpendicular orientations, respectively, we obtain<sup>5</sup>:

$$\frac{I_{0,\parallel}I_{\perp}}{I_{\parallel}I_{0,\perp}} = \frac{[C_1(C_x - 1) - xC_x(C_1 - 1)][(K_x - 1) - x(K_1 - 1)]}{[(C_x - 1) - x(C_1 - 1)][K_1(K_x - 1) - xK_x(K_1 - 1)]} \quad (13)$$

where

$$C_x = \frac{(xI_{0,\parallel} + I_{Sr}) \cdot I_{Rr}}{(xI_{0,\perp} + I_{Rr}) \cdot I_{Sr}} \quad (14)$$

$$K_x = \frac{(xI_{\parallel} + I_{Sr}) \cdot I_{Rr}}{(xI_{\perp} + I_{Rr}) \cdot I_{Sr}} \quad (15)$$

and  $C_1$  and  $K_1$  are the values of  $C_x$  and  $K_x$ , respectively, when  $x=1$ . Here  $x$  is the fraction of the source intensity

transmitted by the rotating sector.  $I_{Sr}$  and  $I_{Rr}$  are the sample radiation intensities reaching the detector via the sample and reference paths, respectively. The corresponding equations for the case in which the sample and reference beam polarizers are oriented in the perpendicular and parallel orientations, respectively, are:

$$\frac{I_{0,\parallel}I_{\perp}}{I_{\parallel}I_{0,\perp}} = \frac{[(C'_x - 1) - x(C'_1 - 1)][K'_1(K'_x - 1) - xK'_x(K'_1 - 1)]}{[C'_1(C'_x - 1) - xC'_x(C'_1 - 1)][(K'_x - 1) - x(K'_1 - 1)]} \quad (16)$$

in which

$$C'_x = \frac{(xI_{0,\perp} + I_{Sr}) \cdot I_{Rr}}{(xI_{0,\parallel} + I_{Rr}) \cdot I_{Sr}} \quad (17)$$

$$K'_x = \frac{(xI_{\perp} + I_{Sr}) \cdot I_{Rr}}{(xI_{\parallel} + I_{Rr}) \cdot I_{Sr}} \quad (18)$$

and  $C'_1$  and  $K'_1$  are the values of  $C'_x$  and  $K'_x$ , respectively, for  $x=1$ .

We note that the ratio  $I_{Sr}/I_{Rr}$  corresponds to the trace obtained when the source is completely blocked off, and it follows<sup>5</sup> from Figure 7 that this ratio is larger than either  $I_{0,\parallel}/I_{0,\perp}$  or  $I_{0,\perp}/I_{0,\parallel}$ . This result is responsible<sup>5</sup> for the small downward peaks observed on the baselines of Figure 6 at wavelengths of maximum absorption. The peaks are small and may be neglected in the determination of  $C_1$ .

Neglecting the effects of sample radiation, the apparent values of  $(I_{0,\parallel}I_{\perp})/(I_{\parallel}I_{0,\perp})$  are given by either  $C_x/K_x$  or  $K'_x/C'_x$ . These ratios have been calculated from the results of Figures 6 and 7 and are plotted as a function of  $x$  in Figure 8. Corrected values of  $(I_{0,\parallel}I_{\perp})/(I_{\parallel}I_{0,\perp})$  from equation (13) correspond to those obtained from equation (16) within the error limits indicated in Figure 8. However,

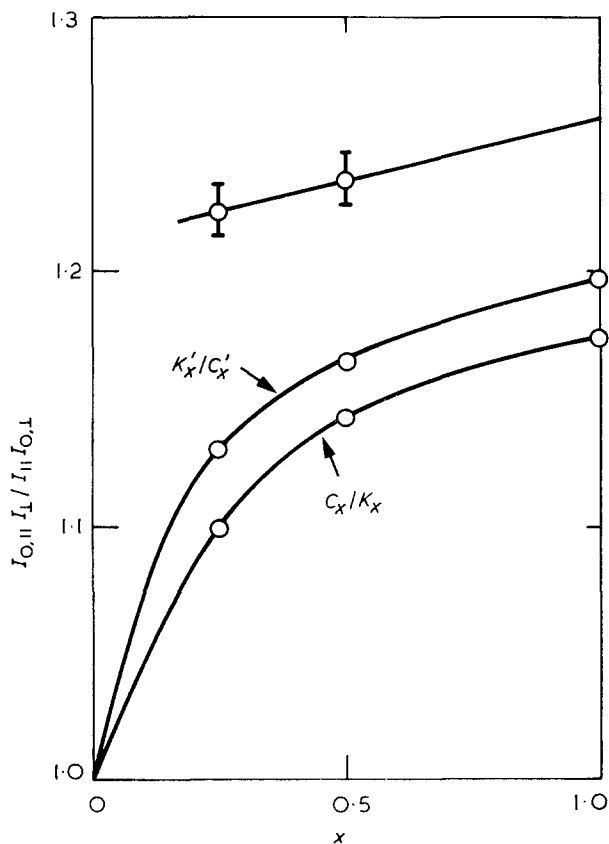


Figure 8 Plots of apparent values (O) of  $(I_{0,\parallel}I_{\perp})/(I_{\parallel}I_{0,\perp})$  and values corrected for sample radiation against the fraction  $x$  of source intensity transmitted by the rotating sector

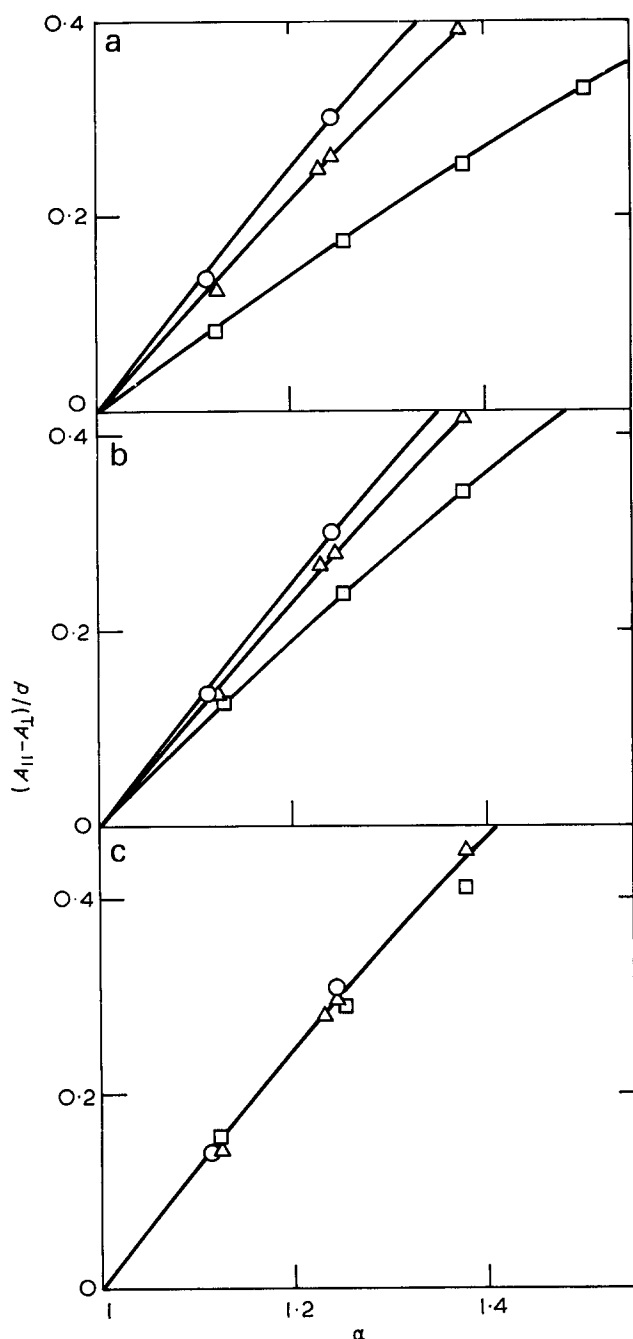


Figure 9 Calculated values of  $(A_{||} - A_{\perp})/d$  plotted against extension ratio for three samples having unstrained thicknesses of 1.16 mm (○), 2.27 mm (△) and 3.43 mm (□). (a), Uncorrected values; (b), values corrected for sample radiation; (c), values further corrected for resolution

a fairly general observation is that the corrected values tend to increase somewhat with increasing  $x$ . This effect probably arises from the fact that the sample temperature within the infra-red beam is decreased (by  $5^{\circ}\text{C}$  to  $10^{\circ}\text{C}$ ) when the source intensity is reduced by the rotating sectors. The sample radiation would be consequently reduced by an amount which increases with decreasing  $x$ . The effect could have been compensated for by restoring the sample to its original temperature subsequent to introducing the rotating sectors. However, with the present results we have estimated the correction for this effect by extrapolating the corrected values of  $(I_{0,||}I_{\perp})/(I_{||}I_{0,\perp})$  to  $x=1$  at which point the effect must vanish.

Values of  $(A_{||} - A_{\perp})/d$  were evaluated from the logarithm of  $(I_{0,||}I_{\perp})/(I_{||}I_{0,\perp})$  values both before and after correcting this ratio for the effects of sample radiation. Figure 9 shows the results of these calculations as a function of extension ratio. In Figure 9a the apparent values of  $(A_{||} - A_{\perp})/d$  were obtained from the arithmetic mean of the  $C_x/K_x$  and  $K'_x/C'_x$  values at  $x=1$  (Figure 8). The values shown in Figure 9b were obtained from the corrected values of  $(I_{0,||}I_{\perp})/(I_{||}I_{0,\perp})$  after extrapolating to  $x=1$ , as in Figure 8. It will be observed that the corrections for sample radiation were negligible in the case of the 1.16 mm thick sample. However for the 2.27 mm and 3.43 mm thick specimens, the corrections for sample radiation produced increases in the apparent  $(A_{||} - A_{\perp})/d$  values of about 7% and 33%, respectively. The increasing effect of sample radiation with increasing thickness results from the increased sample absorption, such that ratio of radiated to transmitted intensity increases.

The  $(A_{||} - A_{\perp})/d$  values in Figure 9c were obtained from the values in Figure 9b by multiplying by the correction factors for resolution shown in Figure 5b. Differential spectra occasionally obtained at different slit widths substantiated that these factors were applicable to the differential results. For the 1.16 mm, 2.27 mm and 3.43 mm thick samples, slit widths of 0.5 mm, 0.75 mm and 1.5 mm were employed, so that the correction factors for resolution increased with sample thickness. After applying these corrections for resolution the  $(A_{||} - A_{\perp})/d$  values for the three specimens correspond within about 5% (Figure 9c).

From the corrected values of  $A_{||} - A_{\perp}$ , and the measured value of  $\epsilon_0$  for the unstrained sample, the dichroic ratio was evaluated from<sup>5</sup>:

$$D = \frac{2(A_{||} - A_{\perp}) + 3\epsilon_0 d \rho}{3\epsilon_0 d \rho - (A_{||} - A_{\perp})} \quad (19)$$

Values of  $(D-1)/(D+2)$  using the  $\epsilon_0$  value obtained from baseline B are plotted against  $\alpha$  in Figure 10. Since the transition moment vectors are parallel to the chain axis for the  $4.92 \mu\text{m}$  band<sup>1a</sup> this plot represents the variation of the second moment orientation function  $f_2$

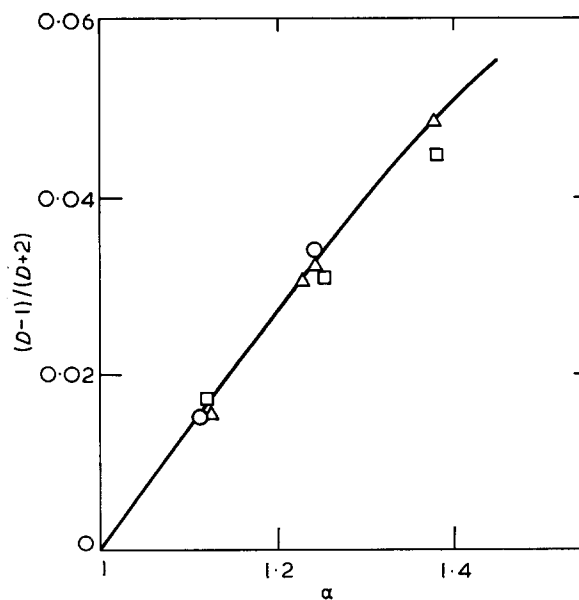


Figure 10  $(D-1)/(D+2)$  plotted against extension ratio. Results evaluated according to baseline B

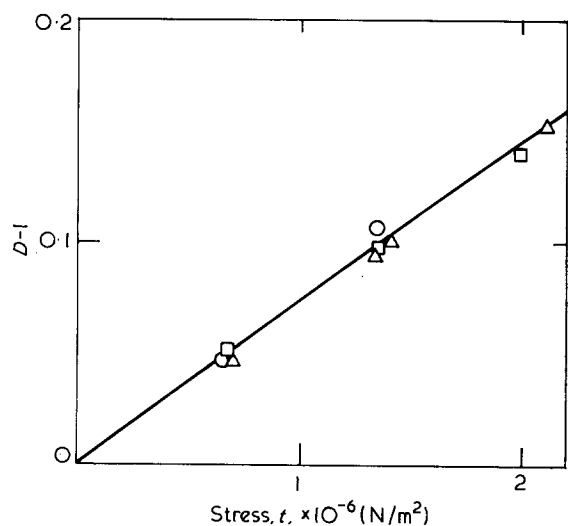


Figure 11 Variation of  $D-1$ , calculated from baseline B, with tensile stress,  $t$

with  $\alpha$  [equation (2) with  $D_0 = \infty$ ]. Values of  $(D-1)/(D+2)$  obtained according to baseline A are about 20% higher than those from baseline B.

A plot of  $D-1$ , evaluated using baseline B, against stress is shown in Figure 11. The plot is linear within experimental error and its slope gives  $(D-1)/t = 7.3 \times 10^{-8} \text{ m}^2/\text{N}$ . From equation (8) with  $M_0 = 14$ ,  $\rho = 0.790 \text{ g}/\text{cm}^3$  and  $T = 443 \text{ K}$  we thus obtain  $G_2^* = 10.1$ . A similar plot according to baseline A gives  $(D-1)/t = 9.1 \times 10^{-8} \text{ m}^2/\text{N}$  and  $G_2^* = 12.6$ .

## DISCUSSION

In discussing the above data we first note that, for partially crystalline polyethylene at room temperature, the band under investigation occurs at  $4.96 \mu\text{m}$  ( $2016 \text{ cm}^{-1}$ )<sup>1a</sup>. The slight shift of the band to shorter wavelengths ( $4.92 \mu\text{m}$ ) for the wholly amorphous polymer is thought to be mainly due to the elimination of the neighbouring crystalline peak at  $5.28 \mu\text{m}$  ( $1894 \text{ cm}^{-1}$ ) and the increasing influence of the overlapping peak at  $4.6 \mu\text{m}$ . The  $4.96 \mu\text{m}$  band has components due to both the crystalline and the amorphous regions of the polymer<sup>1a</sup> and has been assigned to a combination mode involving in part, the  $720 \text{ cm}^{-1}$  fundamental. This assignment, in conjunction with the observation that the amorphous orientation functions are higher for this band than for all other bands of amorphous origin, is responsible for the suggestion that extended sequences of more than four bonds in the *trans* conformation give rise to the amorphous component of the absorption<sup>1a, 3, 4</sup>.

As mentioned earlier, Flory and Abe have calculated the parameter  $G_2^*$  for a variety of local conformational sequences within the polyethylene chain and for different axes referred to each conformation. The value of  $G_2^*$  obtained from the present experiments is considerably larger (in absolute magnitude) than any of the values so far calculated<sup>3</sup>. This result suggests that relatively long extended sequences are responsible for the dichroism results on the  $4.92 \mu\text{m}$  band.

With regard to the assignment proposed above, Flory and Abe's calculations on *trans* sequences are based on the conformation and orthogonal axes reproduced in Figure 12. Since the transition moment vector for the

$4.92 \mu\text{m}$  band is parallel to the chain axis<sup>1a</sup>, the calculated values of  $G_2^*$  for the  $a'$  axis are relevant to the present discussion. However, two points should be mentioned about the values given in ref. 3. First, they refer to a temperature of  $140^\circ\text{C}$ , and depend on the parameters  $\sigma = \exp(-E_\sigma/RT)$  and  $\omega = \exp(-E_\omega/RT)$  where  $E_\sigma$  and  $E_\omega$  are conformational energies the most probable values for which are 500 and 2000 cal/mol, respectively<sup>3</sup>. At  $170^\circ\text{C}$ , the temperature used for the present measurements, these values of  $E_\sigma$  and  $E_\omega$  give  $\sigma = 0.567$  and  $\omega = 0.103$  which compare with the values  $\sigma = 0.544$  and  $\omega = 0.0874$  at  $140^\circ\text{C}$ . From the variation of the calculated  $G_2^*(a')$  values with  $\sigma$  and  $\omega$  (Tables I, II and III of ref. 3) we estimate that the  $G_2^*(a')$  values should decrease by less than 2% when the temperature increases from  $140^\circ\text{C}$  to  $170^\circ\text{C}$ . Secondly, the calculated values correspond to a chain with  $n = 515$  bonds compared with the effective value of  $n = 107$  estimated for the polymer studied in this work. From Fig. 3 of ref. 3 we find that this decrease in  $n$  yields an average decrease of about 4% in the  $G_2^*(a')$  values for the *trans* sequences.

Since the calculations of  $G_2^*(a')$  for *trans* sequences so far extend to sequences of only four chain bonds, we have plotted in Figure 13 values of  $\log G_2^*(a')$ , slightly reduced to account for differences in temperature and  $n$  value, against the number of bonds in the *trans* sequence. The calculated values give an approximately linear plot which we tentatively extrapolate to the values  $G_2^* = 10.1$  and  $G_2^* = 12.6$  obtained using baselines B and A, respectively. This extrapolation gives values of 6.6 and 7.8 for the average number of bonds in the orienting sequence, according to baselines B and A, respectively. An extension of the  $G_2^*$  calculations to longer chain sequences, and a

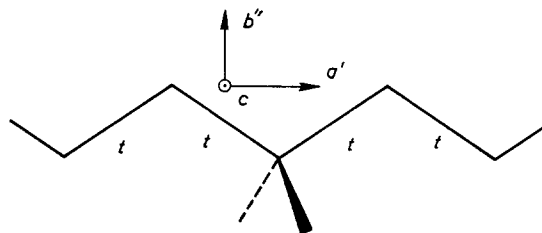


Figure 12 Illustration of the axes defined by Flory and Abe for the calculation of  $G_2^*$  for *trans* sequences in polyethylene.  $t$  represents a *trans* bond

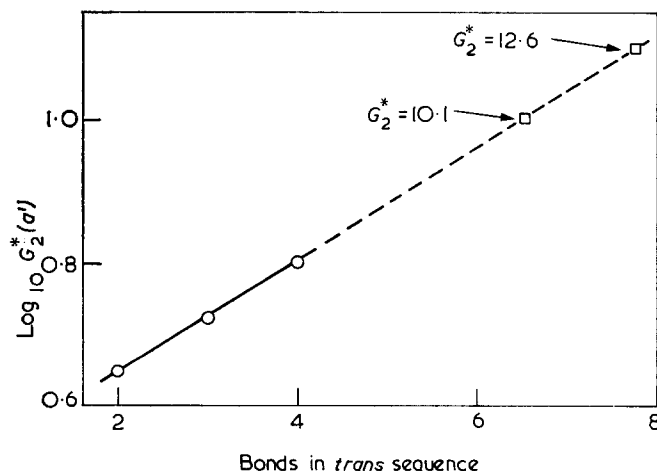


Figure 13 Logarithmic plot of  $G_2^*(a')$  against the number of bonds in the *trans* sequence. Experimental values of  $G_2^*$  are indicated

more precise baseline investigation (or resolution of the overlapping peaks), should yield a more accurate definition of the orienting unit.

Preliminary experiments have been carried out on a lower molecular weight grade of linear polyethylene (Hostalen GS), also crosslinked with 3 wt.% dicumyl peroxide. The measurements were made up to 80% extension, and for a given extension ratio both the stress and  $D-1$  values were about 7 times lower than the values obtained for Hostalen GUR. However, within experimental error the ratio of  $(D-1)/t$  was essentially unaffected. This result suggests that the orienting sequence is little affected by a reduction in the effective degree of crosslinking (as characterized by the modulus). More extensive investigations of the effects of degree of crosslinking and temperature, as have been made in stress-birefringence studies<sup>2</sup>, are envisaged.

No measurable dichroic effects have yet been observed at wavelengths above 4.92  $\mu\text{m}$ . This is due to a number

of factors including difficulties in obtaining samples of required thickness and sufficiently high degrees of orientation. The effects of sample emission become increasingly prominent at longer wavelengths and modifications to the equipment may be required to reduce this problem.

#### REFERENCES

- 1 (a) Read, B. E. and Stein, R. S. *Macromolecules* 1968, **1**, 116;  
(b) Glenz, W. and Peterlin, A. *J. Polym. Sci. (A-2)* 1971, **9**, 1191
- 2 Saunders, D. W., Lightfoot, D. R. and Parsons, D. A. *J. Polym. Sci. (A-2)* 1968, **6**, 1183
- 3 Flory, P. J. and Abe, Y. *Macromolecules* 1969, **2**, 335
- 4 Snyder, R. G. *J. Chem. Phys.* 1967, **47**, 1316
- 5 Read, B. E., Hughes, D. A., Barnes, D. C. and Drury, F. W. M. *Polymer* 1972, **13**, 485
- 6 Fraser, R. D. B. *J. Chem. Phys.* 1953, **21**, 1511
- 7 Pennings, A. J., van der Mark, J. M. A. A. and Booij, H. C. *Kolloid Z.* 1970, **236**, 99

# Note to the Editor

## Reverse osmosis properties of poly(*trans*-2,5-dimethylpiperazine fumaramide) films

L. Credali, A. Chiolle and P. Parrini

Montecatini Edison SpA, Ferrara Research Centre, Piazzale Privato Donegani, 44100 Ferrara, Italy  
(Received 11 April 1972; revised 12 June 1972)

### INTRODUCTION

Reverse osmosis is an interesting process for the desalination of brackish and sea water, and for water purification in general.

The application of cellulose acetate films in a reverse osmosis process, was described, for the first time in 1959 by Reid and Breton<sup>1</sup> and others<sup>2,3</sup>; successful preparation methods for high flux membranes, based on cellulose acetate, were developed<sup>4,5</sup> and it became possible to obtain an economically valid reverse osmosis process for water desalination. The application of different materials in reverse osmosis has been intensively studied in many laboratories, but today cellulose acetate remains the only material used for high flux membranes.

Nevertheless, cellulose acetate membranes have drawbacks, mainly due to the chemical structure of the polymer used in their fabrication. These drawbacks greatly limit the application of reverse osmosis in the treatment of water or in other separation processes. Among the various polymeric materials studied as substitutes for cellulose acetate, polyamides were found to be interesting. In fact, the hydrophilic nature of polyamides, together with a chemical structure which makes it possible to forecast greater resistance to chemical and bacteriological degradation, makes this class of polymers potentially useful for reverse osmosis.

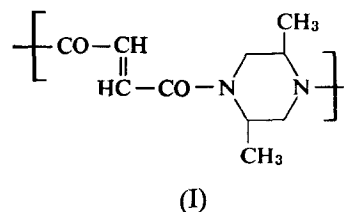
The possibility of changing the structure of the components of the polymer chain of polyamides, with a certain ease, may offer the opportunity of preparing high flux membranes with greater resistance to compaction. The use of polyamides in reverse osmosis has already been described in the literature<sup>1-3,6,7</sup>, but polyamides with reverse osmosis properties comparable to cellulose acetate have never been reported. During tests carried out in our laboratories, on the use of new materials in reverse osmosis, it was found that polyamides derived from piperazine presented properties of permeability to water and salt comparable to those of cellulose acetate<sup>8</sup>.

We believe that these polyamides are the first example of a class of polymers showing exceptionally high permeability to water and high salt rejection, comparable to cellulose acetate.

This paper describes the reverse osmosis properties of poly(*trans*-2,5-dimethylpiperazine fumaramide) films, which is one of the most interesting among the materials studied.

### EXPERIMENTAL

The polymer, *t*-2,5-DMPF (I), was prepared, according to a previously described method<sup>9</sup>, by condensation of fumaric acid dichloride with *trans*-2,5-dimethylpiperazine:



The samples of polymer used had an inherent viscosity of 2.2 (determined at a concentration of 0.5 g/100 ml of 98 wt.% H<sub>2</sub>SO<sub>4</sub>, at 30°C). The *t*-2,5-DMPF films were prepared by dry casting as described previously<sup>10</sup>, using formic acid or a chloroform-methanol mixture in the ratio of 88:12 parts, as casting solvents.

The water and salt fluxes were measured by direct osmosis (d.o.) using unsupported film of 2 cm diameter. The film is assembled in a cell formed of two Lucite blocks. The cell has two holes through which deionized water and a salt solution are introduced. Two magnetic stirrers, coated with Teflon, are placed as close as possible to the film in order to limit polarization phenomena.

The water flux is determined at two open glass capillaries, each with a diameter of about 0.1 cm; the salt flux is measured from the change in the electric conductivity of the initially salt-free solution, using two platinum electrodes placed within the cell. The reverse osmosis (r.o.) measurements were obtained using a laboratory test apparatus described previously<sup>11</sup>. The samples of the films tested in the reverse osmosis plant were rectangular in shape and had an area of 18 cm<sup>2</sup>. The pressure of the feed salt solution can be adjusted from 30 to 120 atm (1 atm ≡ 101.325 kN/m<sup>2</sup>). The measurements were made at temperatures of 25°C and 30°C.

The permeability to water and salt were calculated according to the method of Lonsdale *et al.*<sup>12</sup> from the equations:

$$J_1 = D_1 C_1 \bar{V}_1 (\Delta P - \Delta \pi) / RT \Delta X \quad (1)$$

$$J_2 = D_2 K \Delta \rho_2 / \Delta X \quad (2)$$

Note to the Editor

where  $D_1C_1=P_1$  is the permeability to water ( $\text{g cm}^{-1} \text{sec}^{-1}$ );  $D_2K=P_2$  is the permeability to salt ( $\text{cm}^2 \text{sec}^{-1}$ );  $J_1$  and  $J_2$  are respectively the water and the salt fluxes ( $\text{g cm}^{-2} \text{sec}^{-1}$ );  $\bar{V}$  is the partial volume of the water in the outer phase ( $\text{cm}^3/\text{mol}$ );  $(\Delta P - \Delta \pi)$  is the difference between the applied pressure and the osmotic pressure at the sides of the film (atm);  $\Delta X$  is the thickness of the film (cm);  $R$  and  $T$  are respectively the gas constant ( $\text{cm}^3 \text{atm mol}^{-1} \text{K}^{-1}$ ) and the absolute temperature (K) and  $\Delta \rho_2$  is the concentration difference of the solute in the solutions separated by the film ( $\text{g cm}^{-3}$ )<sup>12</sup>.

Equation (1) is reduced to equation (3) in direct osmosis measurements, when  $\Delta P=0$ .

$$J_1 = D_1 C_1 \bar{V}_1 \Delta \pi / RT \Delta X \quad (3)$$

The salt rejection in reverse osmosis experiment is defined as:

$$SR = \frac{\rho_2' - \rho_2''}{\rho_2} \quad (4)$$

where  $\rho_2'$  and  $\rho_2''$  are respectively the concentrations of the solute in the feed solution and in the product.

RESULTS

Figure 1 shows a typical flow of water and salt through a *t*-2,5-DMPF film in a d.o. measurement. In general, the flow of water and of salt is constant in time, about 30 min after starting the measurements. Table 1 reports the results of the direct osmosis measurements using 5% (w/v) NaCl solution on *t*-2,5-DMPF and cellulose acetate film (Eastman 398-3) used as reference.

The direct osmosis measurements were made on films cast from HCOOH and  $\text{CHCl}_3\text{-CH}_3\text{OH}$ . The films were generally equilibrated in water for 48 h before making the measurements. The effect of a heat treatment was examined on film treated in water at 100°C for 1 h.

Table 2 gives the results of reverse osmosis measurements at pressures of 50, 80 and 105 atm, with a 0.5% (w/v) NaCl feed solution. The measurements were made on *t*-2,5-DMPF film cast from HCOOH and  $\text{CHCl}_3\text{-CH}_3\text{OH}$  and on cellulose acetate film cast from acetone.

Table 3 gives the results of reverse osmosis measurements with a feed solution containing 1% (w/v) of  $\text{MgSO}_4$ .

In the r.o. tests the films were assembled in the plant

Table 1 Direct osmosis measurements on completely dry films of *t*-2,5-DMPF and cellulose acetate. 5% (w/v) NaCl solution; temperature = 25°C

Casting solvent	Treatment*	Thickness ( $\mu\text{m}$ )	$J_1 \times 10^5$ ( $\text{g cm}^{-2} \text{sec}^{-1}$ )	$J_2$ ( $\text{g cm}^{-2} \text{sec}^{-1}$ )	Membrane constant $\times 10^7$ ( $\text{g cm}^{-2} \text{sec}^{-1} \text{atm}^{-1}$ )	Water permeability, $P_1 \times 10^6$ ( $\text{g cm}^{-1} \text{sec}^{-1}$ )	NaCl permeability, $P_2$ ( $\text{cm}^2 \text{sec}^{-1}$ )	$P_1/P_2$ ( $\text{g cm}^{-3}$ )
<i>t</i> -2,5-DMPF:								
HCOOH	a	25	1.520	$3.98 \times 10^{-7}$	3.83	1.30	$1.99 \times 10^{-8}$	61.3
HCOOH	a	44	0.846	$3.10 \times 10^{-7}$	2.17	1.29	$2.78 \times 10^{-8}$	46.5
HCOOH	b	35	0.572	$0.74 \times 10^{-7}$	1.38	0.65	$0.49 \times 10^{-8}$	131.8
$\text{CHCl}_3/\text{CH}_3\text{OH}$	a	36	0.985	$2.68 \times 10^{-7}$	2.48	1.21	$1.94 \times 10^{-8}$	62.5
$\text{CHCl}_3/\text{CH}_3\text{OH}$	b	36	0.424	$0.35 \times 10^{-7}$	1.06	0.52	$0.25 \times 10^{-8}$	205.4
Cellulose acetate (E-398-3):								
Acetone	a	26	0.350	$7.00 \times 10^{-9}$	0.88	0.31	$3.64 \times 10^{-10}$	854.6
Acetone	a	24	0.394	$5.50 \times 10^{-9}$	0.98	0.32	$2.60 \times 10^{-10}$	1223.2

\* a= film conditioned 48 h in  $\text{H}_2\text{O}$  at room temperature (25°C)

b= film annealed 1 h at 100°C in  $\text{H}_2\text{O}$ , conditioned 48 h in  $\text{H}_2\text{O}$  at room temperature (25°C)

Table 2 Water flux and NaCl rejection of completely dry films of *t*-2,5-DMPF and cellulose acetate by reverse osmosis. Feed=0.5% (w/v) NaCl; temperature=30°C

Casting solvent	Thickness ( $\mu\text{m}$ )	Pressure (atm)	Water flux ( $\text{l/m}^2$ per day)	Product NaCl concentration (ppm)	Salt rejection (%)	Water permeability, $P_1 \times 10^6$ ( $\text{g cm}^{-1} \text{sec}^{-1}$ )	$P_1/P_2$ ( $\text{g cm}^{-3}$ )
<i>t</i> -2,5-DMPF:							
HCOOH	40*	50	9.8	440	91.2	1.4	320
$\text{CHCl}_3/\text{CH}_3\text{OH}$	30*	50	10.0	430	91.4	1.1	330
HCOOH	40*	80	12.0	295	94.1	1.0	287
HCOOH	36*	80	15.5	280	94.4	1.2	313
HCOOH	22*	80	24.0	345	93.1	1.1	243
HCOOH	13*	80	38.0	310	93.8	1.0	265
HCOOH	8.5†	80	64.3	195	96.1	1.2	468
HCOOH	40*	105	13.5	175	96.5	0.87	384
Cellulose acetate (E-398-3):							
Acetone	40*	80	2.4	70	98.6	0.21	1231

\* Films supported on filter paper Nagel-Co Duren-No 640

† Films supported on Millipore-VSWP 29300 membrane



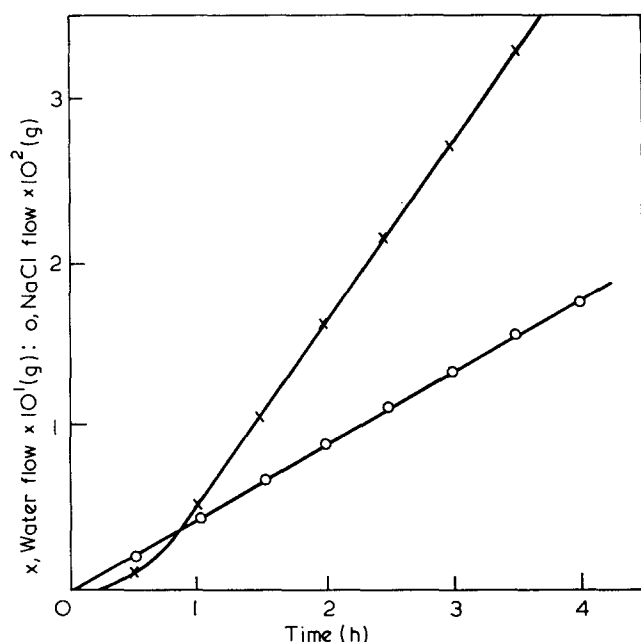


Figure 1 Extended water (x) and NaCl (o) flows through *t*-2,5-DMPF film, cast from CHCl<sub>3</sub>-CH<sub>3</sub>OH solution, thickness 36 μm, by d.o. measurement

Table 3 Water flux and MgSO<sub>4</sub> rejection by reverse osmosis measurements on completely dry films of *t*-2,5-DMPF. Feed = 1% (w/v) MgSO<sub>4</sub>; temperature = 30°C

Thickness (μm)	Casting solvent	Pressure (atm)	Water flux (l/m <sup>2</sup> per day)	Product MgSO <sub>4</sub> concentration (ppm)	MgSO <sub>4</sub> rejection (%)
22	CHCl <sub>3</sub> /CH <sub>3</sub> OH	50	12.0	28	99.7
28	HCOOH	50	14.7	20	99.8

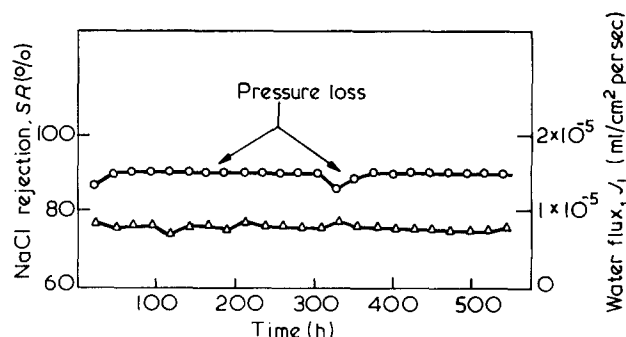


Figure 2 Water flux (Δ) and NaCl rejection (o) of *t*-2,5-DMPF film, cast from CHCl<sub>3</sub>-CH<sub>3</sub>OH solution, thickness 40 μm, in a long r.o. experiment. Pressure: 50 atm; temperature = 25°C; feed = 0.5 wt.% NaCl

DISCUSSION

The results of the d.o. tests on cellulose acetate film given in Table 1 are in good agreement with the values reported by Lonsdale<sup>12</sup> and by Bloch and Vieth<sup>13</sup>. The value of  $P_1$  calculated by us from the d.o. measurements is intermediate between the values of  $0.20$  and  $0.32 \times 10^{-6}$  g cm<sup>-1</sup> sec<sup>-1</sup> reported by Lonsdale<sup>12</sup>. Considering that the d.o. measurements were carried out using a more dilute NaCl solution, the Table 1 data can be compared to those given in the literature for cellulose acetate or other polymers.

The most important properties shown by *t*-2,5-DMPF films are: the high permeability to water  $P_1$  which is 4-5 times that of cellulose acetate measured under the same conditions (Tables 1 and 2); the good NaCl rejection exceeding 90%, demonstrated in the r.o. tests (Table 2); and the very high salt rejection, exceeding 99%, with regard to more steric hindered solutes such as MgSO<sub>4</sub> (Table 3).

The permselectivity of *t*-2,5-DMPF films has been indicated in Tables 1 and 2 as the ratio ( $P_1/P_2$ ) between the permeability to water and to salt<sup>14</sup>. This ratio has a relatively low value from the d.o. measurements, while it undergoes marked increase in the r.o. measurements. Nevertheless, it appears, comparing the values of Tables 1 and 2, that the effect of the pressure has more influence on reducing salt permeability than water permeability. This fact would appear to indicate marked compaction of the material at the pressures used in the r.o. tests. The  $P_1$  values from the d.o. measurements are comparable with those obtained at 50 and 80 atm during the r.o. measurements. For the same film 40 μm thick, the respective  $P_1$  values obtained at 50, 80 and 105 atm are:  $1.4 \times 10^{-6}$ ;  $1.0 \times 10^{-6}$ ;  $0.87 \times 10^{-6}$  (g cm<sup>-1</sup> sec<sup>-1</sup>). Annealing the films in hot water shows a marked improvement in semipermeability properties. As a consequence the  $P_1/P_2$  (Table 1) values approached the r.o. values for unheat-treated films.

It can be seen from the values of Table 2 that the reverse osmosis properties are retained when the thickness of the film is reduced, while there is a great increase in the water flux. A film 8.5 μm thick permits to obtain, at 80 atm, a flux of 64.3 l/m<sup>2</sup> per day with a 96.1% NaCl rejection; it should be pointed out that this film was supported on a Millipore membrane, as the filter paper used in the other tests was too coarse for such a fine film.

The general properties of *t*-2,5-DMPF were determined previously<sup>10,15</sup> and are given in Table 4. *t*-2,5-DMPF films look very similar to cellulose acetate films, they are transparent and shiny, with a high ultimate tensile strength, a high modulus of elasticity and low elongation.

Table 4 General properties of *t*-2,5-DMPF films prepared from HCOOH

Tensile strength (kg/cm <sup>2</sup> )	810
Elongation (%)	5
Modulus (kg/cm <sup>2</sup> )	$31 \times 10^3$
Density (g/cm <sup>3</sup> )	1.217
Resistivity (ohm-cm)	$2 \times 10^{-12}$
Dielectric strength (kV/25 μm)	1.0
Moisture regain (98% r.h.) (%)	16.6
Haze (%)	1.6
Luminous transmittance (%)	94-96
Gloss (%)	160

after conditioning them for 24 h at 25°C and 65% relative humidity. The results reported were obtained after 24 h operation. Reverse osmosis tests carried out for over 25 days on *t*-2,5-DMPF film did not reveal flux or salt rejection losses.

A r.o. test for a long time is given in Figure 2. During this test the r.o. plant was subjected to two drops in pressure at 192 h and 336 h. In both cases, when the pressure was returned to the original value, the properties of the membrane were re-established.

Table 5 Tensile properties\* of *t*-2,5-DMPF films after immersion in water<sup>15</sup>

Casting	Immersion time					
	24 h			720 h		
solvent	TS	E	TM	TS	E	TM
HCOOH	256	63	34	143	23	56
CHCl <sub>3</sub> /CH <sub>3</sub> OH	375	54	213	236	61	67

\* TS=tensile strength at break (kg/cm<sup>2</sup>); E=elongation at break (%); TM=tensile modulus (kg/cm<sup>2</sup> × 10<sup>-2</sup>)

The high moisture regain at 98% r.h. is in good agreement with the high permeability found in d.o. and r.o. measurements.

We have recently observed that *t*-2,5-DMPF films after equilibration in water, show a reduced ultimate tensile strength, a reduced modulus of elasticity and an increased elongation, as reported in Table 5<sup>15</sup>. This negative effect of water on the mechanical properties of *t*-2,5-DMPF films does not appear to have any effect on the mechanical resistance of the film in the reverse osmosis application, even in long time tests (Figure 2).

By contrast, the effect of the reduction of the modulus of elasticity is different. In fact, the compaction which the film undergoes in reverse osmosis conditions is justified only by the reduced modulus of the wet films.

In general, it may be believed that the reverse osmosis properties of *t*-2,5-DMPF films are particularly interesting for practical application: the high permeability to water, in comparison with cellulose acetate, makes this

material suitable for use in the preparation of composite membranes or hollow fibres.

#### ACKNOWLEDGEMENT

This work has been undertaken with a contribution from the Consiglio Nazionale delle Ricerche, Istituto Ricerca sulle Acque, Rome.

#### REFERENCES

- 1 Reid, C. E. and Breton, E. J. *J. Appl. Polym. Sci.* 1959, **1**, 133
- 2 Reid, C. E. and Koppers, J. R. *J. Appl. Polym. Sci.* 1959, **2**, 264
- 3 Reid, C. E. and Spencer, H. J. *J. Appl. Polym. Sci.* 1960, **4**, 354
- 4 Loeb, S. and Sourirajan, S. University of California, Los Angeles (Dept. Eng.) *Report No. 60-60* 1961
- 5 Manjikian, S. University of California, Los Angeles (Dept. Eng.) *Report No. 65-13* 1965
- 6 Lonsdal, H. K., Merten, U., Riley, R. L. and Vos, K. D. *Res. Develop. Progr. Rep. O.S.W.*, No. 150 1965
- 7 Capaccioli, T. and Sbroli, W. *Quad. Ric. Sci. (Roma)* 1968, **49**, 88
- 8 Credali, L., Chiolle, A. and Parrini, P. *CNR-Ist. Ric. Acque (Roma) Rep. No. 4* 1971, p 89
- 9 Mortillaro, L., Russo, M., Guidotti, V. and Credali, L. *Makromol. Chem.* 1970, **138**, 151
- 10 Credali, L., Parrini, P., Mortillaro, L., Russo, M. and Simonazzi, T. *Angew. Makromol. Chem.* 1971, **19**, 15
- 11 IRSA-CNR *Quad. Ric. Sci. (Roma)* 1969, **58**, 86
- 12 Lonsdale, H. K., Merten, U. and Riley, R. L. *J. Appl. Polym. Sci.* 1965, **9**, 1341
- 13 Bloch, R. and Vieth, W. R. *J. Appl. Polym. Sci.* 1969, **13**, 193
- 14 Lonsdale, H. K. in 'Desalination by Reverse Osmosis' (Ed. U. Merten), MIT Press, Cambridge, Mass. 1966, Ch 4
- 15 Credali, L. and Parrini, P. *Polymer* 1971, **12**, 717

# Book Reviews

## Penn's PVC technology

Edited by W. V. Titow and B. J. Lanham

Applied Science Publishers, Barking, 3rd Edn, 1971, 545 pp. £12.50

The late W. S. Penn's well established reference book 'PVC Technology' has been revised extensively and up-dated by Titow and Lanham. They have maintained the essential character of the earlier editions which have been valuable to the technologist in providing an easy reference source for commercial polymers, compounds, plasticizers, stabilizers, fillers and other compounding ingredients. Not only is the chemical identity of these products indicated but commercial names, grades and sources are given. The manifold processes for converting PVC to products are described lucidly.

A substantial rewriting of many chapters had added to the technological content. The pattern of presentation is such that there is an excellent balance between the discussion of the principles of technology and commercial details. Because of this the book well achieves the aims of the authors to present a reference source which can be read and utilized at several levels. The non-specialist has a useful guide to PVC technology whilst the student will have a well presented and readable textbook. For those who wish to read the subject in more detail there are ample references to original papers in each chapter.

The final chapter of the book reviews applications of PVC and is followed, appropriately, by an appendix which lists BS, ASTM, DIN and ISO standards relevant to PVC and its products. A second appendix includes units, conversions and definitions. The index, although not comprehensive is adequate.

The book is well produced and is strongly recommended to all who have an interest in PVC, its processing and its uses.

Finally one might comment that this publication is a fitting testimony to the valuable contributions which the late W. S. Penn made to education and plastics technology.

K. A. Scott

## Engineering principles of plasticating extrusion

Z. Tadmor and I. Klein

Van Nostrand, New York, 1970, 500 pp. £9.35

This is probably the first book to attempt to represent mathematically the performance of each section of the single-screw extruder—solid feed, melting, and melt pumping. It draws largely on previously published work by the authors and others, which should permit a lucid treatment of the overall behaviour of the complete machine. However, the sheer weight of mathematics seems to magnify trivial details and obscure the major effects, many of which have previously been represented, at least qualitatively, by simpler approximations.

The chapter on 'Basic flow concepts' reproduces the fundamental equations of continuity, motion, and energy (unfortunately with several errors\*) followed by a brief discussion including the effects of shear rate, temperature, and pressure. There is little adaptation to practical situations or indication of how the equations may be handled, since in most cases many factors are unknown. Equation 2.4 assumes constant density, which implies isothermal conditions, though this is not stated, nor is it clear whether thermal expansion has been ignored subsequently. Appendix C provides little viscometric data additional to that published in 1959 in 'Processing of thermoplastic materials' by Bernhardt. The chapter on 'Screw geometry' is an example of undue attention to detail, some of it inapplicable to screws as manufactured.

The feed section is treated by the method of Darnell and Mol, with some additional work by the authors covering the effects of flight width and pressure rise and of different coefficients of friction on the screw and barrel. The latter suggests that the temperature difference between screw and barrel in this section will have a profound influence on the rate of feeding, although no experimental data are presented on the variation of friction coefficient with temperature for commercial polymers. In practice the temperature conditions are rarely critical, providing cooling is applied to the feed section. Pressure rise is shown to be exponential and hence critically dependent on the initial pressure. However, factors influencing flow in the feed hopper and the filling of the screw, e.g. particle size distribution, degree of hopper filling, air entrainment, and geometry of the hopper and feed opening are not considered.

The melt pumping section is treated in a very long chapter (nearly 150 pages) similarly to a number of other computer analyses, where the equations are progressively developed from the Newtonian isothermal case to non-Newtonian non-isothermal with shear heating and channel curvature. The first 40 pages or so present the work of previous authors on the isothermal Newtonian case, but in what appears to be an unnecessarily obscure manner. In 'Polymer processing' McKelvey shows curves of output *versus* helix angle which clearly explain why the apparent optimum angle of 30° is not often used, yet these are not reproduced; the conditions for maximum pressure gradient (p 222) could be much more clearly described in terms of the dimensionless factor  $Q/Wbh$  or the pressure flow/drag flow ratio; there is much discussion of velocity profiles yet only one rough pressure profile (p 237), although these are used later in Section 8.3 as basis for comparison of theory and experiment. A section of seven pages of mathematics on the effect of flight clearance leads to the well-known correction  $(1 - \delta/H)$  to the drag flow, yet the much more significant effect on power input is not really tackled. Although given in great detail, the treatment is not critical as in 'Extruder screw design' by Fenner, and Fig. 6.43 is the only attempt to justify the additional computing time required for the more sophisticated solutions.

The key section of the book deals with the process of melting the solid polymer in the screw; this is based on work done by the authors and colleagues in the Western Electric laboratories. They are to be congratulated on deriving expressions with a minimum number of factors to be determined experimentally. However, some of the assumptions are surprising, e.g. that the molten film above the solid bed is of uniform thickness in the cross-channel

\* E.g. p 12, Table 2.2A: minus sign omitted before penultimate term and third denominator given as  $\partial x$  in place of  $\partial z$ . p 18, Table 2.6A: first denominator given as  $\partial x$  in place of  $\partial t_z$

## Multicomponent Polymer Systems

Advances in Chemistry Series 99

American Chemical Society, Washington, 1971, 588 pp. \$16.50

The above-mentioned book represents another in the well known *Advances in Chemistry Series* published by the American Chemical Society. It contains the series of thirty-seven papers given at a recent national ACS meeting.

The subject of the symposium, namely 'Multicomponent polymer systems', is one of the most topical subjects in polymer chemistry at this time. Essentially, it is the use of two or more polymeric components to produce a different species having certain improved properties over those of the original material. This area of research is truly 'applied' in that the goals are usually distinct, namely the improvement of properties using existing products. This area of research becomes even more important if we assume that few, if any, new *major* polymers will appear on the market in the foreseeable future. Instead, new polymeric species will be prepared by modification of polymerization conditions using existing monomers or by the modification of existing polymers. This last area is the one with which this series of papers is concerned.

The subjects covered in the symposium are extremely divergent and include topics such as simple polyblends, random block and graft copolymers, reinforced plastics and elastomers and fringe areas, such as surface coatings. It is within these confines that the polymer engineer, polymer physicist and polymer chemist find that their own particular disciplines merge into what could be loosely termed materials science.

With regard to the book itself, it is printed in a style which suits the reviewer. The diagrams and photographs are very clear and at \$16.50 for 588 pages it represents exceedingly good value for money. It can be thoroughly recommended to anyone with an interest in polymer science.

J. M. Locke

## Book Reviews

direction, that heat transfer from the barrel to the solid is by pure conduction through molten film, and that heat transfer between the solid polymer and the melt pool is negligible in spite of the high shear rates at this point. It is claimed that by this method it is possible to calculate reliably the melting length from physical and geometrical factors and so supply the principal missing factor, the effective length, for calculations of the melt pumping section. Considerable experimental evidence with a number of commercial polymers is presented in support of the theoretical predictions, but the range of screw diameters, profiles, and speeds is small, and the resulting melting lengths also vary over a comparatively small range of say 15–25 diameters. Although the authors' results show both temperature fluctuations and discrete unmolten regions towards the end of the melting section, they do not consider the mechanisms by which these are reduced further along the screw, and yet any practical extrusion technologist knows that it is these factors, as much as any, that lead to poor quality extrusion, especially as output is raised.

The overall performance of the extruder is given mathematically by a simple addition of the effects of the separate sections, with only the most trivial consideration of interactions between them. Some experimental results are compared with calculation; on p 365 it is stated, 'the only general conclusion that can be drawn from the results presented is that the better the melting conditions, the better is the agreement of theory to experiments'. While the theory predicts many features of the experimental pressure and temperature profiles, the reviewer feels the quantitative agreement is not shown to be reliable enough to justify the vast computational effort involved. The present theory fails to give any indication of instabilities such as surging, which frequently limit performance; a shorter chapter on 'Stability' discusses experimental data on fluctuations of temperature, pressure etc., but the only theory referred to is by previous workers.

This book is well produced, though with typographical errors. Its complexity makes it impossible to make general statements on the overall performance of the extruder, and the book will therefore be of little assistance to the process technologist. It would probably have been better to produce the original work in the form of a monograph covering the melting zone only.

M. J. Stevens

## IUPAC International Symposium on Macromolecules

Edited by M. J. Voorn

Butterworths, London, 1971, 282 pp. £7.75

This volume collects together the main lectures and the survey lectures presented at the IUPAC Symposium on Macromolecules held in Leiden in September 1970. The main lectures are a particularly powerful group of papers. Flory brings up to date the work described in detail in his book on the statistical mechanics of chain molecules, and Professor Hodgkin presents a synopsis of the current knowledge of the structure of insulin molecules in a way which will be appreciated by polymer scientists. The article by Vinogradov on the flow and rubber elasticity of polymeric materials presents a view which is not often seen in the West. There are also contributions by Katchalsky on polyelectrolytes and Fischer on X-ray scattering studies of phase transitions.

Among the eight survey lectures included in the volume, I would single out articles by Zerbi on defect induced infra-red absorption of polymers and Stockmayer *et al.* on local jump models for chain dynamics as papers illustrating the complexity and the difficulties faced by workers in these particular fields. A paper on the stiffness of polymers by Holliday and White collects together the results of macroscopic estimates of Young's modulus of crystals and compares them with estimates obtained from various forms of spectroscopy. Among the other lectures, workers in the field of polymeric characterization will be particularly interested to read the resumé by Strazielle and Benoit of the results of the molecular characterization of a series of commercial polymers by a number of laboratories. The conclusion is that the results are not much better than the ones obtained in a similar experiment by Atlas and Mark in 1961, but one has to remember that the present exercise was much more ambitious in that it included polymers having a wide variety of molecular weight distributions and polymers of complicated structure.

The book is priced at £7.75. It should certainly be on the shelves of all libraries and workers in special fields will wish to buy the volume for one or two outstanding individual papers.

G. Allen

### Conference Announcement

10 – 14 September 1973

The Chemical Society

## IUPAC International Symposium on Macromolecules

University of Aberdeen, Scotland

The programme will be arranged in the following two main sections, running in parallel throughout the Meeting: *Synthesis and Manufacture* and *Physical and Technological Aspects*. Emphasis will be given to the relationship between the science and technology of polymers. Each section will consist of a limited number of invited lectures and contributed papers.

The Programme Committee will consider contributed papers of special interest and novelty in relation to the following topics with major emphasis on Thermoplastic Polymers and Elastomers, and in particular the relationship between any of these topics: (1) The Manufacture of Polymers; (2) Synthesis of Polymers; (3) Science and Technology of Fluid Polymers; and (4) Science and Technology of Solid Polymers. Those wishing to present a paper should apply to Dr John F. Gibson, The Chemical Society, Burlington House, London W1V 0BN for the form of a submission of a communication, which should be returned together with the abstract not later than 1 January 1973.

Further details about registration, accommodation, travel, social and ladies' programme will be available in February 1973.

# Book Reviews

## Penn's PVC technology

Edited by W. V. Titow and B. J. Lanham

Applied Science Publishers, Barking, 3rd Edn, 1971, 545 pp. £12.50

The late W. S. Penn's well established reference book 'PVC Technology' has been revised extensively and up-dated by Titow and Lanham. They have maintained the essential character of the earlier editions which have been valuable to the technologist in providing an easy reference source for commercial polymers, compounds, plasticizers, stabilizers, fillers and other compounding ingredients. Not only is the chemical identity of these products indicated but commercial names, grades and sources are given. The manifold processes for converting PVC to products are described lucidly.

A substantial rewriting of many chapters had added to the technological content. The pattern of presentation is such that there is an excellent balance between the discussion of the principles of technology and commercial details. Because of this the book well achieves the aims of the authors to present a reference source which can be read and utilized at several levels. The non-specialist has a useful guide to PVC technology whilst the student will have a well presented and readable textbook. For those who wish to read the subject in more detail there are ample references to original papers in each chapter.

The final chapter of the book reviews applications of PVC and is followed, appropriately, by an appendix which lists BS, ASTM, DIN and ISO standards relevant to PVC and its products. A second appendix includes units, conversions and definitions. The index, although not comprehensive is adequate.

The book is well produced and is strongly recommended to all who have an interest in PVC, its processing and its uses.

Finally one might comment that this publication is a fitting testimony to the valuable contributions which the late W. S. Penn made to education and plastics technology.

K. A. Scott

## Engineering principles of plasticating extrusion

Z. Tadmor and I. Klein

Van Nostrand, New York, 1970, 500 pp. £9.35

This is probably the first book to attempt to represent mathematically the performance of each section of the single-screw extruder—solid feed, melting, and melt pumping. It draws largely on previously published work by the authors and others, which should permit a lucid treatment of the overall behaviour of the complete machine. However, the sheer weight of mathematics seems to magnify trivial details and obscure the major effects, many of which have previously been represented, at least qualitatively, by simpler approximations.

The chapter on 'Basic flow concepts' reproduces the fundamental equations of continuity, motion, and energy (unfortunately with several errors\*) followed by a brief discussion including the effects of shear rate, temperature, and pressure. There is little adaptation to practical situations or indication of how the equations may be handled, since in most cases many factors are unknown. Equation 2.4 assumes constant density, which implies isothermal conditions, though this is not stated, nor is it clear whether thermal expansion has been ignored subsequently. Appendix C provides little viscometric data additional to that published in 1959 in 'Processing of thermoplastic materials' by Bernhardt. The chapter on 'Screw geometry' is an example of undue attention to detail, some of it inapplicable to screws as manufactured.

The feed section is treated by the method of Darnell and Mol, with some additional work by the authors covering the effects of flight width and pressure rise and of different coefficients of friction on the screw and barrel. The latter suggests that the temperature difference between screw and barrel in this section will have a profound influence on the rate of feeding, although no experimental data are presented on the variation of friction coefficient with temperature for commercial polymers. In practice the temperature conditions are rarely critical, providing cooling is applied to the feed section. Pressure rise is shown to be exponential and hence critically dependent on the initial pressure. However, factors influencing flow in the feed hopper and the filling of the screw, e.g. particle size distribution, degree of hopper filling, air entrainment, and geometry of the hopper and feed opening are not considered.

The melt pumping section is treated in a very long chapter (nearly 150 pages) similarly to a number of other computer analyses, where the equations are progressively developed from the Newtonian isothermal case to non-Newtonian non-isothermal with shear heating and channel curvature. The first 40 pages or so present the work of previous authors on the isothermal Newtonian case, but in what appears to be an unnecessarily obscure manner. In 'Polymer processing' McKelvey shows curves of output *versus* helix angle which clearly explain why the apparent optimum angle of 30° is not often used, yet these are not reproduced; the conditions for maximum pressure gradient (p 222) could be much more clearly described in terms of the dimensionless factor  $Q/Wbh$  or the pressure flow/drag flow ratio; there is much discussion of velocity profiles yet only one rough pressure profile (p 237), although these are used later in Section 8.3 as basis for comparison of theory and experiment. A section of seven pages of mathematics on the effect of flight clearance leads to the well-known correction  $(1 - \delta/H)$  to the drag flow, yet the much more significant effect on power input is not really tackled. Although given in great detail, the treatment is not critical as in 'Extruder screw design' by Fenner, and Fig. 6.43 is the only attempt to justify the additional computing time required for the more sophisticated solutions.

The key section of the book deals with the process of melting the solid polymer in the screw; this is based on work done by the authors and colleagues in the Western Electric laboratories. They are to be congratulated on deriving expressions with a minimum number of factors to be determined experimentally. However, some of the assumptions are surprising, e.g. that the molten film above the solid bed is of uniform thickness in the cross-channel

\* E.g. p 12, Table 2.2A: minus sign omitted before penultimate term and third denominator given as  $\partial x$  in place of  $\partial z$ . p 18, Table 2.6A: first denominator given as  $\partial x$  in place of  $\partial t_z$

## Multicomponent Polymer Systems

Advances in Chemistry Series 99

American Chemical Society, Washington, 1971, 588 pp. \$16.50

The above-mentioned book represents another in the well known *Advances in Chemistry Series* published by the American Chemical Society. It contains the series of thirty-seven papers given at a recent national ACS meeting.

The subject of the symposium, namely 'Multicomponent polymer systems', is one of the most topical subjects in polymer chemistry at this time. Essentially, it is the use of two or more polymeric components to produce a different species having certain improved properties over those of the original material. This area of research is truly 'applied' in that the goals are usually distinct, namely the improvement of properties using existing products. This area of research becomes even more important if we assume that few, if any, new *major* polymers will appear on the market in the foreseeable future. Instead, new polymeric species will be prepared by modification of polymerization conditions using existing monomers or by the modification of existing polymers. This last area is the one with which this series of papers is concerned.

The subjects covered in the symposium are extremely divergent and include topics such as simple polyblends, random block and graft copolymers, reinforced plastics and elastomers and fringe areas, such as surface coatings. It is within these confines that the polymer engineer, polymer physicist and polymer chemist find that their own particular disciplines merge into what could be loosely termed materials science.

With regard to the book itself, it is printed in a style which suits the reviewer. The diagrams and photographs are very clear and at \$16.50 for 588 pages it represents exceedingly good value for money. It can be thoroughly recommended to anyone with an interest in polymer science.

J. M. Locke

## Book Reviews

direction, that heat transfer from the barrel to the solid is by pure conduction through molten film, and that heat transfer between the solid polymer and the melt pool is negligible in spite of the high shear rates at this point. It is claimed that by this method it is possible to calculate reliably the melting length from physical and geometrical factors and so supply the principal missing factor, the effective length, for calculations of the melt pumping section. Considerable experimental evidence with a number of commercial polymers is presented in support of the theoretical predictions, but the range of screw diameters, profiles, and speeds is small, and the resulting melting lengths also vary over a comparatively small range of say 15–25 diameters. Although the authors' results show both temperature fluctuations and discrete unmolten regions towards the end of the melting section, they do not consider the mechanisms by which these are reduced further along the screw, and yet any practical extrusion technologist knows that it is these factors, as much as any, that lead to poor quality extrusion, especially as output is raised.

The overall performance of the extruder is given mathematically by a simple addition of the effects of the separate sections, with only the most trivial consideration of interactions between them. Some experimental results are compared with calculation; on p 365 it is stated, 'the only general conclusion that can be drawn from the results presented is that the better the melting conditions, the better is the agreement of theory to experiments'. While the theory predicts many features of the experimental pressure and temperature profiles, the reviewer feels the quantitative agreement is not shown to be reliable enough to justify the vast computational effort involved. The present theory fails to give any indication of instabilities such as surging, which frequently limit performance; a shorter chapter on 'Stability' discusses experimental data on fluctuations of temperature, pressure etc., but the only theory referred to is by previous workers.

This book is well produced, though with typographical errors. Its complexity makes it impossible to make general statements on the overall performance of the extruder, and the book will therefore be of little assistance to the process technologist. It would probably have been better to produce the original work in the form of a monograph covering the melting zone only.

M. J. Stevens

## IUPAC International Symposium on Macromolecules

Edited by M. J. Voorn

Butterworths, London, 1971, 282 pp. £7.75

This volume collects together the main lectures and the survey lectures presented at the IUPAC Symposium on Macromolecules held in Leiden in September 1970. The main lectures are a particularly powerful group of papers. Flory brings up to date the work described in detail in his book on the statistical mechanics of chain molecules, and Professor Hodgkin presents a synopsis of the current knowledge of the structure of insulin molecules in a way which will be appreciated by polymer scientists. The article by Vinogradov on the flow and rubber elasticity of polymeric materials presents a view which is not often seen in the West. There are also contributions by Katchalsky on polyelectrolytes and Fischer on X-ray scattering studies of phase transitions.

Among the eight survey lectures included in the volume, I would single out articles by Zerbi on defect induced infra-red absorption of polymers and Stockmayer *et al.* on local jump models for chain dynamics as papers illustrating the complexity and the difficulties faced by workers in these particular fields. A paper on the stiffness of polymers by Holliday and White collects together the results of macroscopic estimates of Young's modulus of crystals and compares them with estimates obtained from various forms of spectroscopy. Among the other lectures, workers in the field of polymeric characterization will be particularly interested to read the resumé by Strazielle and Benoit of the results of the molecular characterization of a series of commercial polymers by a number of laboratories. The conclusion is that the results are not much better than the ones obtained in a similar experiment by Atlas and Mark in 1961, but one has to remember that the present exercise was much more ambitious in that it included polymers having a wide variety of molecular weight distributions and polymers of complicated structure.

The book is priced at £7.75. It should certainly be on the shelves of all libraries and workers in special fields will wish to buy the volume for one or two outstanding individual papers.

G. Allen

### Conference Announcement

10 – 14 September 1973

The Chemical Society

## IUPAC International Symposium on Macromolecules

University of Aberdeen, Scotland

The programme will be arranged in the following two main sections, running in parallel throughout the Meeting: *Synthesis and Manufacture* and *Physical and Technological Aspects*. Emphasis will be given to the relationship between the science and technology of polymers. Each section will consist of a limited number of invited lectures and contributed papers.

The Programme Committee will consider contributed papers of special interest and novelty in relation to the following topics with major emphasis on Thermoplastic Polymers and Elastomers, and in particular the relationship between any of these topics: (1) The Manufacture of Polymers; (2) Synthesis of Polymers; (3) Science and Technology of Fluid Polymers; and (4) Science and Technology of Solid Polymers. Those wishing to present a paper should apply to Dr John F. Gibson, The Chemical Society, Burlington House, London W1V 0BN for the form of a submission of a communication, which should be returned together with the abstract not later than 1 January 1973.

Further details about registration, accommodation, travel, social and ladies' programme will be available in February 1973.

# Ziegler–Natta catalysis: 5. A molecular weight investigation

I. D. McKenzie and P. J. T. Tait

Department of Chemistry, University of Manchester Institute of Science and Technology, Manchester M60 1QD, UK  
(Received 11 April 1972)

Molecular weight relationships in the polymerization of 4-methylpentene-1 by the Ziegler–Natta system  $VCl_3/AlR_3$  have been examined at 30°C and 40°C. The dependence of the number-average degree of polymerization on the concentration of metal halide, aluminium alkyl concentration, monomer concentration, temperature, and nature of the aluminium alkyl has been established. The results have been examined in relation to a previously described kinetic scheme, and the rate constant for chain transfer with adsorbed monomer has been evaluated.

## INTRODUCTION

An analysis of the molecular weight relationships which operate in Ziegler–Natta polymerization systems can yield important information concerning the nature of this complex polymerization process. That this is so has been clearly demonstrated for the polymerization of propylene<sup>1–7</sup> and ethylene<sup>8</sup> and for other systems as well. No comparable studies have been reported on the polymerization of 4-methylpentene-1 (4-MP-1) by the catalyst system  $VCl_3/AlR_3$ . The results reported in this paper form an integral part of a fairly comprehensive study on this particular polymerization system.

## EXPERIMENTAL

The polymerization procedures which are used have already been described<sup>9</sup>.

Owing to the insolubility of poly(4-methylpentene-1) it was necessary to carry out viscosity measurements in decalin at 135°C. A viscometer employing a vapour bath thermostat was used in these determinations, and was a modified Ubbelohde suspended level dilution viscometer of the Fitzsimon type<sup>10,11</sup>. The temperature of the viscometer was controlled within  $\pm 0.05^\circ\text{C}$ .

The relationship:

$$[\eta] = 1.94 \times 10^{-4} (M_n)^{0.81}$$

as derived by Hoffman *et al.*<sup>12</sup>, was used in the calculation of number-average molecular weights for this study.

## RESULTS

### *Effect of polymerization time on number-average molecular weight*

Polymerizations were carried out at 30°C and 40°C using a constant vanadium trichloride and monomer concentration and a constant Al:V ratio. Typical experimental details and results are shown in Figure 1. It may be seen that the molecular weight increases up to a

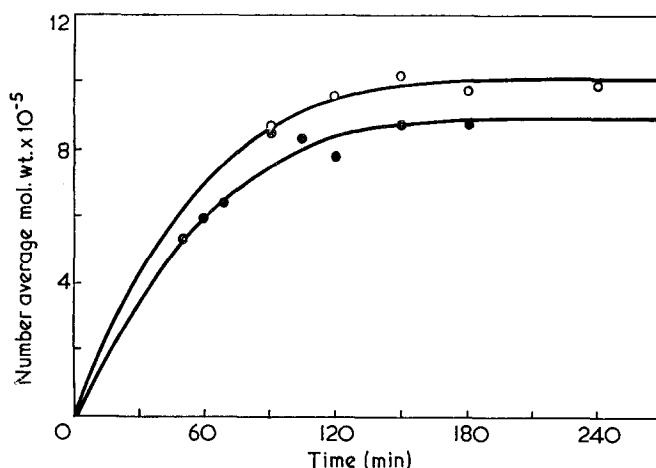


Figure 1 Plot of molecular weight versus time. [4-MP-1]=2.0 mol/l; Al:V ratio=2.0:1; solvent=benzene. ●: 30°C;  $[VCl_3]=18.5$  mmol/l; ○: 40°C;  $[VCl_3]=7.4$  mmol/l

limiting value with increase in reaction time. At 40°C the limiting value of the molecular weight is reached in  $\sim 100$  min. Other workers report similar results<sup>1, 8, 13</sup>.

The average lifetime ( $\tau$ ) of a growing polymer chain can be calculated from the variation in the number-average degree of polymerization ( $\bar{P}_n$ ) with reaction time, provided that  $C_0$  is independent of time, and provided that the molecular weight distribution remains constant, i.e.

$$\tau = \frac{d(1/\bar{P}_n) \bar{P}_n}{d(1/t)} \quad (1)$$

Some workers<sup>1, 8</sup> have used this equation to determine the average lifetime of a growing polymer chain. For the present system this relationship can only be used satisfactorily in the earlier stages of the polymerization as is seen in Figure 2. Use of equation (1) would, however, introduce serious errors into the calculation of  $\tau$ , since  $C_0$  is known not to be constant during the early stages of these polymerizations.

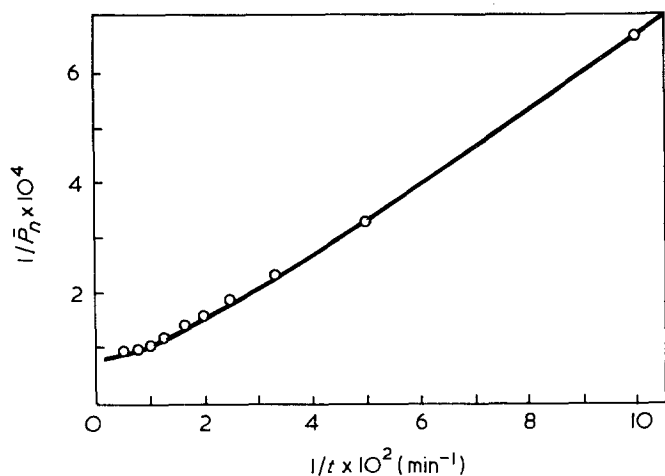


Figure 2 Plot of  $1/\bar{P}_n$  against  $1/t$  for 30°C. [4-MP-1]=2.0 mol/l; Al:V ratio=2.0:1;  $[\text{VCl}_3]$ =18.5 mmol/l

Table 1 Effect of catalyst concentration on number-average molecular weight at 40°C

Reaction time (min)	$[\text{VCl}_3] \times 10^3$ (mol/l)	$[\eta]$ (dl/g)	$\bar{M}_n \times 10^{-5}$
180	3.62	13.70	9.66
180	3.85	13.80	9.75
180	7.35	14.00	9.95
240	7.45	14.25	10.17
180	8.74	13.35	9.33
180	11.22	13.50	9.51
180	18.41	13.40	9.43

The average steady state value of  $\tau$  may, nevertheless, be calculated from the equation,

$$\tau = \frac{\bar{P}_n C_0}{R_p} \quad (2)$$

Use of equation (2) yields values for  $\tau$  of 14.8 min and 7–8 min at 30°C and 40°C respectively.

Values of 1–30 min have been reported<sup>14</sup> for  $\tau$  in the polymerization of propylene by the catalyst system  $\text{TiCl}_3/\text{Al}(\text{iBu})_3$ .

#### Effect of catalyst concentration on the number-average molecular weight

Molecular weight determinations were carried out on samples of polymers prepared at 40°C using a constant Al:V ratio, constant monomer concentration and constant duration of polymerization. The results of these experiments are shown in Table 1, and show quite clearly that the vanadium trichloride concentration has no effect on the number-average molecular weight of the polymer over the sixfold range of concentration investigated. These results appear to conflict with the results of Natta *et al.*<sup>1</sup> for the polymerization of propylene by the catalyst system  $\alpha\text{-TiCl}_3/\text{AlEt}_3$ . However, it is important to ensure that the duration of the polymerization reaction is fairly long (180 min in this case) owing to the somewhat long average chain lifetimes found in these systems.

#### Effect of tri-isobutylaluminium concentration on number-average molecular weight

Polymerizations were carried out at 40°C using constant vanadium trichloride and monomer concentrations,

but using differing concentrations of tri-isobutylaluminium. Typical results are shown in Figure 3, and show that the molecular weight initially increases slightly with the alkyl concentration up to a value which corresponds to an Al:V ratio of 2:1; above this ratio the molecular weight decreases with further increase in alkyl concentration. This complex behaviour should be compared with that observed for the rate dependence on the alkyl concentration described previously<sup>9</sup>.

Many authors<sup>3–6</sup> have reported that, in  $\text{MCl}_3/\text{AlR}_3$  catalyst systems, the molecular weight decreases as the ratio  $\text{AlR}_3/\text{MCl}_3$  is increased, and this has usually been interpreted as arising from chain transfer with aluminium alkyl.

Furthermore, chain transfer with adsorbed alkyl has already been demonstrated<sup>15,16</sup>.

#### Effect of monomer concentration on number-average molecular weight

All experiments were carried out at constant catalyst concentration, and were taken to constant conversion. In all cases the duration of polymerization was in excess of 200 min and so the polymer samples obtained were not in the time-molecular weight-dependent region. Typical results for 30°C and 40°C are shown in Figure 4. Inverse

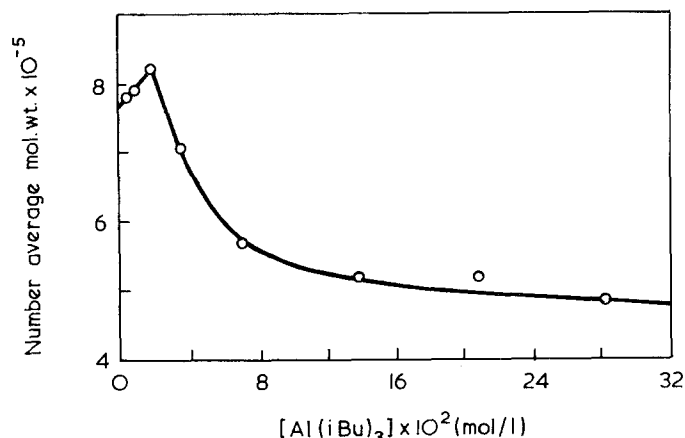


Figure 3 Plot of number-average molecular weight versus tri-isobutylaluminium concentration. [4-MP-1]=2.0 mol/l;  $[\text{VCl}_3]$ =8.7 mmol/l; temperature=40°C; solvent=benzene

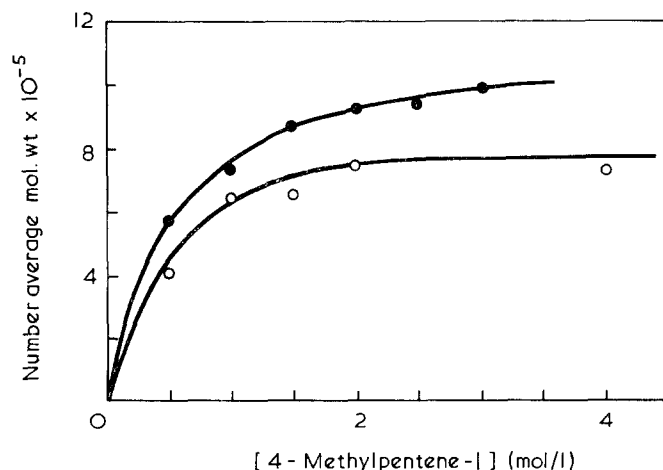


Figure 4 Plot of number-average molecular weight versus 4-methylpentene-1 concentration. Al:V ratio=2.0:1; solvent=benzene. ○: 30°C;  $[\text{VCl}_3]$ =18.0 mmol/l; ●: 40°C;  $[\text{VCl}_3]$ =8.8 mmol/l



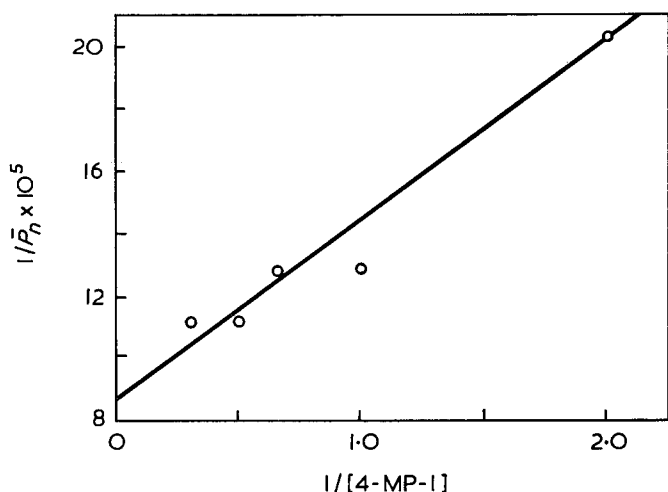


Figure 5 Plot of  $1/\bar{P}_n$  against  $1/[4\text{-MP-1}]$ . Al:V ratio=2.0:1;  $[\text{VCl}_3]=18.0\text{ mmol/l}$ ; temperature= $30^\circ\text{C}$ ; solvent=benzene

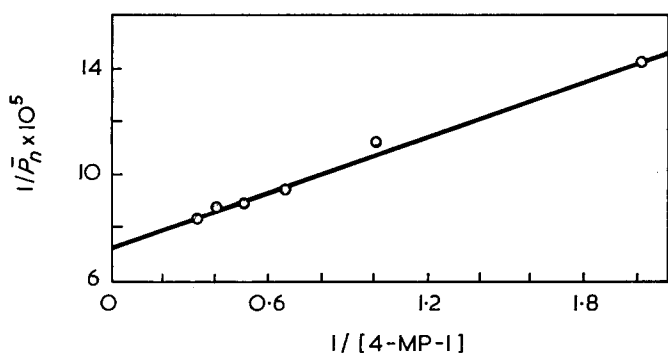


Figure 6 Plot of  $1/\bar{P}_n$  against  $1/[4\text{-MP-1}]$ . Al:V ratio=2.0:1;  $[\text{VCl}_3]=8.8\text{ mmol/l}$ ; solvent=benzene; temperature= $40^\circ\text{C}$

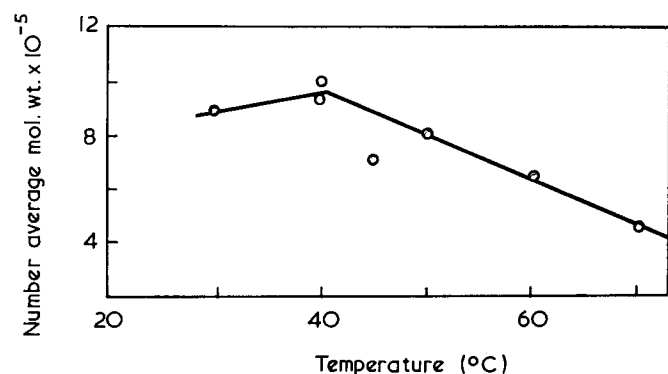


Figure 7 Plot of number-average molecular weight versus temperature.  $[4\text{-MP-1}]=2.0\text{ mol/l}$ ; Al:V ratio=2.0:1; solvent=benzene

plots of number-average degree of polymerization versus monomer concentration are linear, and the results obtained are shown in Figures 5 and 6.

From these results it is concluded that the monomer is involved in a chain transfer process with the growing polymer chain, a feature which is consistent with results obtained in many other Ziegler-Natta systems<sup>1, 2, 8</sup>.

#### Effect of temperature on the number-average molecular weight

The range of temperature investigated was  $30\text{--}70^\circ\text{C}$ . The Al:V ratio and monomer concentration were kept constant. The results obtained are plotted in Figure 7.

The molecular weight above a temperature of  $40^\circ\text{C}$  was found to decrease with increasing temperature, indicating that the activation energy of termination is greater than that of propagation. This is supported by the results of Chirkov *et al.*<sup>2</sup> who determined the activation energies of chain propagation and chain rupture to be 16.8 and 26.7 kcal/mol, respectively.

#### Effect of varying the nature of the aluminium alkyl compound on the number-average molecular weight

In all cases the Al:V ratio, monomer and vanadium trichloride concentrations and duration of the polymerization reaction were kept constant. The results of these experiments are shown in Table 2.

On the basis of these experiments the aluminium alkyl compounds can be placed in the following order of ability to reduce the molecular weight of the polymer:



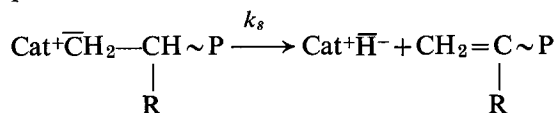
#### DISCUSSION

The relationships established above may be summarized as follows: (i) the molecular weight initially increases with reaction time, gradually becoming independent of the duration of polymerization after about 2 h; (ii) the molecular weight is independent of the vanadium trichloride concentration at a constant Al:V ratio of 2:1; (iii) the molecular weight decreases with increase in the triisobutylaluminium concentration above an Al:V ratio of 2:1; (iv) the molecular weight increases with increasing monomer concentration, such that an inverse relationship between the number-average molecular weight and the monomer concentration gives a linear plot; (v) the molecular weight decreases with an increase in the polymerization temperature; (vi) the molecular weight is dependent on the nature of the aluminium alkyl used.

It will be apparent that these relationships are in excellent qualitative agreement with those predicted on the basis of a kinetic scheme presented in a previous paper<sup>17</sup>.

The following termination and transfer reactions may now be formulated<sup>1</sup>:

#### (a) Spontaneous termination:

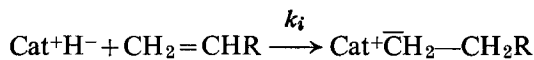


This reaction may be followed by realkylation of the resulting catalyst-hydride bond, so that there is no change

Table 2 Effect of varying the nature of the alkylaluminium compound on the number-average molecular weight  $[4\text{-MP-1}]=2.0\text{ mol/l}$ ;  $[\text{VCl}_3]=8.4\text{ mmol/l}$ ;  $\text{AlR}_3:\text{VCl}_3=2.0:1$ ; solvent=benzene; polymerization temperature= $40^\circ\text{C}$

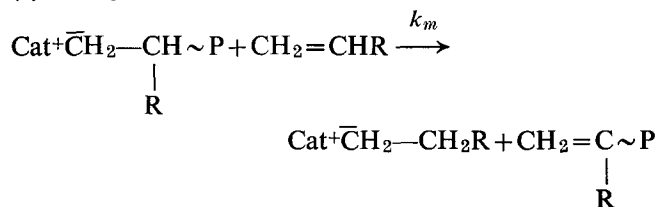
Alkylaluminium compound	Reaction time (min)	$[\eta]$ (dl/g)	$\bar{M}_n \times 10^{-5}$
Trimethyl	180	3.40	1.74
Triethyl	160	8.25	5.18
Diethylchloride	180	14.50	10.40
Tri-isobutyl	180	13.35	9.33
Tri-isobutyl	180	14.00	9.95
Tri-n-decyl	180	11.00	7.40

in the overall number of active centres, i.e.

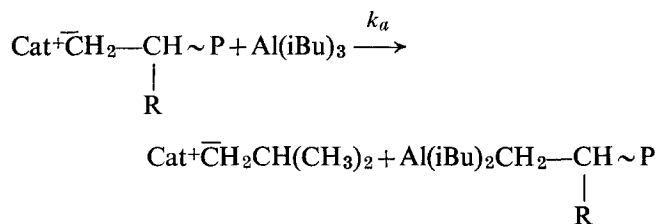


Such a spontaneous termination process is not considered to be important at temperatures between 30°C and 40°C.

(b) *Transfer to monomer:*



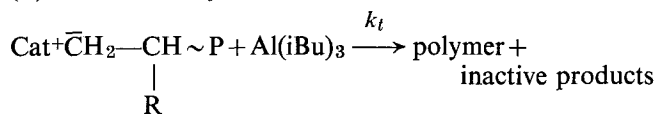
(c) *Transfer to tri-isobutylaluminium:*



It is emphasized that these equations are formulations only in which  $k_s$ ,  $k_m$  and  $k_a$  are rate constants for the spontaneous termination of growing chains, transfer with monomer and transfer with tri-isobutylaluminium.

In addition to these transfer steps it is possible that the tri-isobutylaluminium might be deactivating the active centres in some manner, i.e.

(d) *Termination of active centres:*



It is considered unlikely, nevertheless, that any true termination reactions are occurring in the catalytic system  $\text{VCl}_3/\text{Al}(\text{iBu})_3$  at 30°C, in view of the observed constancy, over long periods, of the rates of polymerization. However, at a temperature of 50°C when using  $\text{Al}(\text{iBu})_3$ , and at 30°C when using  $\text{AlEt}_3$ , the steady state rate gradually decreases with time<sup>9</sup>, indicating that some deactivation process, perhaps by reduction, is occurring.

If the propagation reaction were considered to occur between an adsorbed monomer molecule and an active centre, and if the transfer reactions are with adsorbed monomer and adsorbed aluminium alkyl then the following equations<sup>17</sup> are valid for the present system:

$$\bar{P}_n = \frac{\int_0^t k_p \theta_M C_0 dt}{C_0 + \int_0^t k_m \theta_M C_0 dt + \int_0^t k_a \theta_A C_0 dt} \quad (3)$$

Integration and inversion yields:

$$\frac{1}{\bar{P}_n} = \frac{k_a \theta_A}{k_p \theta_M} + \frac{1}{k_p \theta_M t} + \frac{k_m}{k_p} \quad (4)$$

Substitution for  $\theta_M$  and  $\theta_A$  gives:

$$\frac{1}{\bar{P}_n} = \frac{k_a K_A [A]}{k_p K_M [M]} + \frac{1/t}{k_p K_M [M]} + \frac{(1/t) K_A [A]}{k_p K_M [M]} + \frac{(1/t) + k_m}{k_p} \quad (5)$$

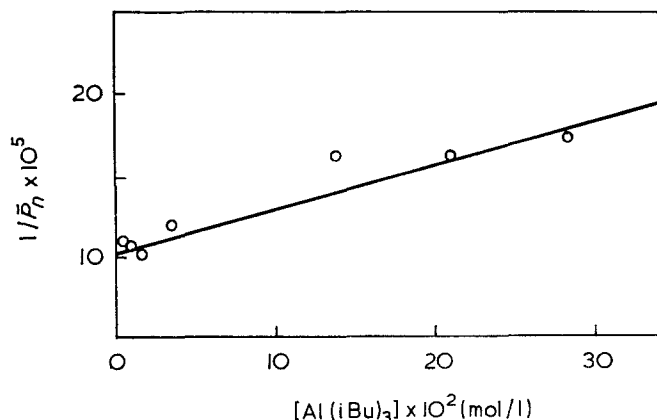


Figure 8 Plot of  $1/\bar{P}_n$  against  $[\text{Al}(\text{iBu})_3]$ .  $[\text{4-MP-1}] = 2.0 \text{ mol/l}$ ;  $[\text{VCl}_3] = 8.7 \text{ mmol/l}$ ; temperature = 40°C; solvent = benzene

Table 3 Values of transfer constant with monomer

Source	$k_m$ (min <sup>-1</sup> )	
	30°C	40°C
Molecular weight data (equation 6)	$0.26 \pm 0.06$	
Tritium data	$0.26 \pm 0.08$	
Molecular weight data (equation 6)		$0.49 \pm 0.10$
Molecular weight data (equation 7)		$0.70 \pm 0.15$

A plot of  $1/\bar{P}_n$  against  $1/[M]$  should thus be linear as has already been demonstrated in Figures 5 and 6 (see also Appendix).

It is now possible to evaluate the rate constant for chain transfer with adsorbed monomer ( $k_m$ ) since in accordance with equation (5) a plot of  $1/\bar{P}_n$  against  $1/[M]$  is linear with:

$$\text{intercept} = \frac{(1/t) + k_m}{k_p} \quad (6)$$

In addition, a plot of  $1/\bar{P}_n$  against  $[A]$  is also linear, as is shown in Figure 8, and in this case:

$$\text{intercept} = \frac{1/t}{k_p K_M [M]} + \frac{(1/t) + k_m}{k_p} \quad (7)$$

Using values of  $k_p = (3.18 \pm 0.05) \times 10^3 \text{ min}^{-1}$  at 30°C and  $(14.6 \pm 2.5) \times 10^3 \text{ min}^{-1}$  at 40°C, the values of  $k_m$  given in Table 3 can be calculated.

It is possible to check the value of  $k_m$  at 30°C since it has already been shown<sup>15</sup> using tritium end-group analysis that the ratio:

$$\frac{\text{rate of transfer with monomer}}{\text{rate of transfer with metal alkyl}} = \frac{(\bar{M}_n)_{T'}}{(\bar{M}_n)_R} \quad (8)$$

$(\bar{M}_n)_T$  and  $(\bar{M}_n)_R$  have already been defined and evaluated<sup>15</sup>.  $(\bar{M}_n)_{T'}$  is now defined for poly(4-methylpentene-1) as:

$$(\bar{M}_n)_{T'} = \frac{84 \int_0^t R_p dt}{\int_0^t R_{ta} dt} \quad (9)$$

$(\bar{M}_n)_T$  can thus be evaluated, and hence:

$$\frac{(\bar{M}_n)_{T'}}{(\bar{M}_n)_R} = \frac{5.78 \times 10^6}{1.14 \times 10^6} = 5.07 \quad (10)$$

However,

$$\frac{\text{rate of transfer with monomer}}{\text{rate of transfer with metal alkyl}} = \frac{k_m \theta_M C_0}{k_a \theta_A C_0} = \frac{k_m \theta_M}{k_a \theta_A} \quad (11)$$

On combining equations (8), (10) and (11) the following equation can be obtained:

$$k_m = \frac{5.07 \times k_a \times \theta_A}{\theta_M} \quad (12)$$

Using values of  $k_a = 0.067 \text{ min}^{-1}$ ,  $\theta_A = 0.125$  (assumed constant over the duration of the polymerization), and  $\theta_M = 0.162$  (average value up to 300 min), it is possible now to calculate  $k_m$  from equation (12):

$$k_m = (0.26 \pm 0.08) \text{ min}^{-1}.$$

This value for  $k_m$  compares exceptionally well with the value listed in Table 3.

Unfortunately a comparable check on the values of  $k_m$  at  $40^\circ\text{C}$  is not possible due to the absence of reliable numerical data for  $\theta_M$ ,  $\theta_A$  and  $k_a$  at this temperature.

For  $k_m = 0.49 \text{ min}^{-1}$  the activation energy,  $E_{tm}$ , is  $11.9 \text{ kcal/mol}$ , while for  $k_m = 0.70 \text{ min}^{-1}$   $E_{tm}$  has the value  $18.5 \text{ kcal/mol}$ . These  $E_{tm}$  values compare with  $E_p = 14.8 \text{ kcal/mol}$  and  $E_{ta} = 16.3 \text{ kcal/mol}$  which have already been determined for this system<sup>16</sup>. The value of  $11.9 \text{ kcal/mol}$  for  $E_{tm}$  is, however, more consistent with the data plotted in Figure 7. The decrease in molecular weight at temperatures greater than  $40^\circ\text{C}$  could then arise from the onset of spontaneous termination<sup>1, 3</sup>. Moreover, vanadium alkyl compounds are unstable at these higher temperatures.

In conclusion, the molecular weight results presented in this paper can be successfully interpreted using the proposed kinetic scheme, and are consistent with both active centre and kinetic investigations presented in earlier papers. In addition, an analysis of these results has afforded an evaluation of the rate constant,  $k_m$ , for chain transfer with adsorbed monomer, which process is found to be the predominant chain regulating process in this system.

#### ACKNOWLEDGEMENT

The authors are indebted to Dr D. R. Burfield for helpful discussion.

#### REFERENCES

- 1 Natta, G. *J. Polym. Sci.* 1959, **34**, 21
- 2 Novokshonova, L. A., Tsvetkova, V. I. and Chirkov, N. M. *Izv. Akad. Nauk SSSR Ser. Khim.* 1963, **7**, 1176
- 3 Novokshonova, L. A., Tsvetkova, V. I. and Chirkov, N. M. *Vysokomol. Soedin.* 1965, **7** (5), 898
- 4 Schnecko, H., Weirauch, K., Reinmoller, M., Bednjagin, V. and Kern, W. *Makromol. Chem.* 1965, **82**, 156
- 5 Boor, J. Jr *J. Polym. Sci. (C)* 1963, **1**, 237
- 6 Otto, F. D. and Parravano, G. *J. Polym. Sci. (A)* 1964, **2**, 5131
- 7 Chien, J. C. W. *J. Polym. Sci. (A)* 1963, **1**, 425
- 8 Grieveson, B. M. *Makromol. Chem.* 1965, **84**, 93
- 9 McKenzie, I. D., Tait, P. J. T. and Burfield, D. R. *Polymer* 1972, **13**, 307
- 10 Ubbelohde, L. *J. Inst. Petrol. Technol.* 1933, **19**, 376
- 11 Merrington, A. C. 'Viscometry', Arnold, London 1949, p 25
- 12 Hoffman, A. S., Frier, B. A. and Condit, P. C. *J. Polym. Sci. (C)* 1963, **4**, 109
- 13 Caunt, A. D. *J. Polym. Sci. (C)* 1964, **4**, 49
- 14 Feldman, C. F. and Perry, E. *J. Polym. Sci.* 1960, **46**, 219
- 15 Burfield, D. R. and Tait, P. J. T. *Polymer* 1972, **13**, 315
- 16 Burfield, D. R., Tait, P. J. T. and McKenzie, I. D. *Polymer* 1972, **13**, 321
- 17 Burfield, D. R., McKenzie, I. D. and Tait, P. J. T. *Polymer* 1972, **13**, 302

#### APPENDIX

If chain transfer were with unadsorbed monomer and adsorbed metal alkyl:

$$\frac{1}{\bar{P}_n} = \frac{k_a K_A [A]}{k_p K_M [M]} + \frac{1/t}{k_p K_M [M]} + \frac{(1/t) K_A [A]}{k_p K_M [M]} + \frac{1/t}{k_p} + \frac{k_m}{k_p K_M} + \frac{k_m [M]}{k_p} + \frac{k_m K_A [A]}{k_p [M]}$$

Since  $k_m [M]/k_p$  is a large term compared with the other terms, a plot of  $1/\bar{P}_n$  against  $1/[M]$  would be non-linear. A plot of  $1/\bar{P}_n$  against  $[A]$  should, however, be linear, but in this case;

$$\frac{\text{slope}}{\text{intercept}} = \frac{1/[M] \cdot \{k_a K_A (1 + 1/t)\} + k_m K_A}{(1/t)[M] + (K_M/t) + k_m + (k_m K_M [M])}$$

Solving this equation for  $k_m$  and using the relevant experimental values reveals that  $k_m$  has a negative value, clearly demonstrating that chain transfer is not with unadsorbed monomer.

# Sequence peptide polymers: Part 2. Poly(leucyl-leucyl-aspartic acid)— conformational aspects in water solution

M. Carità Morelli and M. D'Alagni\*

*Istituto di Chimica delle Macromolecole, Nucleo di Roma, c/o Laboratorio di Chimica Fisica,  
Istituto Chimico, Università di Roma, 00185 Roma, Italy  
(Received 1 March 1972; revised 13 April 1971)*

A new sequential peptide, poly(leucyl-leucyl-aspartic acid) has been synthesized and the conformational properties in water have been examined by spectroscopic methods at different degrees of neutralization of the  $\beta$ -carboxyls of the aspartate residues and by potentiometric measurements. The experimental data are in agreement with the presence of  $\alpha$ -helical segments stabilized by strong hydrophobic interactions. The calculation of the thermodynamic functions,  $\Delta G^0$ ,  $\Delta H^0$ ,  $\Delta S^0$  related to the transition uncharged random coil to uncharged  $\alpha$ -helical state, gives at 25°C the following values:  $\Delta G^0 = -1575$  cal/mol;  $\Delta H^0 = 6173$  cal/mol;  $\Delta S^0 = 26.0$  cal/deg mol. These values are expressed in cal/mol of repeating unit. The temperature dependence of the ellipticity and the function  $\text{pH} - \log[\alpha/(1-\alpha)]$  versus  $\alpha$ , allows us to analyse the conformational stability of poly(leucyl-leucyl-aspartic acid).

## INTRODUCTION

As is known, a number of factors influence the conformation of biological macromolecules in solution and it is difficult to determine quantitatively the predominance of one of these factors over the others. Although it is not difficult to propose contributing factors, a quantitative estimate of the thermodynamic functions for any biological macromolecule is a hard task. In fact, in many cases it is not yet known from experimental measurements whether the enthalpy and entropy terms are positive or negative.

The quantitative data available from models are inadequate either for the lack of theory or for the inaccuracy of the models. In addition, most of the factors, already computed in the chemistry of small molecules and of some polypeptides, cannot be transferred in proteins, so that they do not provide a firm basis for the quantitative analysis of the thermodynamics of folding.

Hydrophobic interactions<sup>1</sup> are very often introduced in discussing the conformation of biological macromolecules mainly in terms of their stabilizing effect. This is due to the important role which the solvent structure plays in determining the stability of the macromolecule, but more to the fact that hydrophobic forces are experimentally well supported because of the cooperativity of the interactions and which are, therefore, greatly perturbed by small variations of temperature, solvent composition, and pressure.

In order to gain a better understanding of the hydrophobic interactions involved in the conformation of biological macromolecules in water, it seemed meaningful

to study the behaviour in water of some sequential polypeptides containing non-polar and polar amino acid residues. These systems are more appropriate research model compounds than homopolypeptides, block and random copolypeptides, because it is generally accepted that the three-dimensional structure of a protein molecule is chiefly determined by the primary structure. In this paper we report an investigation on the conformational transition of poly(leucyl-leucyl aspartic acid) when the polypeptide is subjected to pH changes.

Zimm and Rice<sup>2</sup>, and Nagasawa and Holtzer<sup>3</sup> showed that the free-energy change of the helix-coil transition of an ionizable polypeptide could be obtained by analysing potentiometric titration data. This method has been repeatedly used for the estimation of the degree of stability of uncharged poly(L-glutamic acid)<sup>4-7</sup>, poly(L-lysine)<sup>5,8</sup>, as well as other ionizable poly( $\alpha$ -amino acids), and random copolymers<sup>9</sup> in aqueous media.

Applying this method to the poly(leucyl-leucyl-aspartic acid) at various temperatures, we obtained  $\Delta G^0$ ,  $\Delta S^0$ , and  $\Delta H^0$  for the repeating unit, characterizing the transition process.

The presence of  $\alpha$ -helical conformation is established for the poly(leucyl-leucyl-aspartic acid) when the  $\beta$ -carboxyls of the aspartate residues are in the uncharged state, by means of spectroscopic methods.

## EXPERIMENTAL

### *Synthesis of poly(leucyl-leucyl-aspartic acid) (PLLAA)*

PLLAA has been obtained by the removal of the benzyl groups from the corresponding poly(leucyl-leucyl-aspartic acid- $\beta$ -benzyl ester) (PLLAB), prepared as described in a previous paper<sup>10</sup>. The debenzilation was

\* To whom enquiries should be addressed.

accomplished according to the method of Fasman *et al.*<sup>11</sup>.

The detailed procedure used for the synthesis of PLLAA was the following. To a solution of the PLLAB ( $[\eta]^{25^\circ} = 2.04$  in  $\text{CH}_3\text{Cl}-\text{HCONH}_2$  (99.5:0.5%)) in anhydrous, freshly distilled chloroform (0.1 g in 30 ml), benzene (15 ml) was added. Dry gaseous HCl was bubbled for 0.5 h through the solution which remained perfectly clear. Then dry gaseous HBr was bubbled through for 2 h, and the deblocked polymer precipitated as a white powder. The mixture was left standing for 3 h. The polymer, recovered by filtration, was exhaustively washed with dry acetone and diethyl ether (Merck).

The polymer, after drying, was dissolved in dilute NaOH and dialysed. Dialysis was performed with a 4465-A2 dialysing tube (A. Thomas Co., Philadelphia) which retains materials with a molecular weight of 12 000 or higher.

Finally, the polymer was recovered by lyophilization and dried under vacuum over phosphorus pentoxide at 100°C; spectrophotometric controls allowed us to establish the accomplishment of the reaction.

#### Titration

Potentiometric titrations were carried out with a Radiometer titrator, pH meter 26, using a 2222 B glass electrode and a K 4112 calomel electrode in a thermostated vessel. The pH meter was initially standardized at several pH values with standard buffers (Radiometer). A flow of nitrogen,  $\text{CO}_2$  free, was used to prevent atmospheric  $\text{CO}_2$  from dissolving in solution during the experiment.

Some base (0.1 N  $\text{CO}_2$ -free NaOH) was added to obtain the PLLAA in solution.

The water used to make the solutions was doubly distilled and  $\text{CO}_2$  free. Each experiment was performed with 5 ml of solution at 0.03% in PLLAA concentration.

The polymer concentration of sample solutions were determined by amino acid analyses. The solutions were titrated with 0.1 N HCl by use of a micrometer syringe.

#### Amino acid analyses

The polymer concentrations of sample solutions were determined by amino acid analyses with a BioCal BC 200 automatic amino acid analyser. Hydrolysis of the polymer was carried out with 5 N HCl at 106°C in degassed sealed tubes for 72 h.

#### Circular dichroism and optical rotatory dispersion

The circular dichroism (c.d.) spectra were recorded on a Cary 61 apparatus using 0.1 and 0.01 cm quartz cells. The optical rotatory dispersion (o.r.d.) was measured with a Cary 60 spectropolarimeter.

C.d. and o.r.d. measurements on PLLAA solutions at various pH values were carried out from aliquots of a mother solution at a pH of 10.40, brought to the desired pH value by adding  $\text{HClO}_4$  at 8% or 3% (Merck) with a micrometer syringe.

It was not possible to carry out measurements on polymer solutions at pH lower than 4.00 because of polymer precipitation. In addition, c.d. spectra for aqueous solutions at two different pH values (4.57 and 6.96) were recorded as a function of temperature in the range 28–71°C. The data obtained are shown in Figures 1–3.

#### Infra-red (i.r.) spectra

I.r. spectra were performed on a Beckman IR 9 apparatus in  $\text{D}_2\text{O}$  solutions using 0.1 mm  $\text{BaF}_2$  cells or KBr pellets. We have not been able to obtain an oriented sample. Some characteristic spectra are shown in Figure 4.

#### RESULTS

The equation<sup>12</sup> describing the hydrogen ion titration of polyacids or polybases is:

$$\text{pH} - \log[\alpha/(1-\alpha)] = \text{p}K^0 + (0.434/RT)(\partial G(\text{ion})/\partial \alpha) \quad (1)$$

where  $\alpha$  is the dissociation degree,  $K^0$  is the intrinsic dissociation constant, and  $G(\text{ion})$  is the electrostatic and conformational free energy.

The value of  $\alpha$ , which corresponds to each pH, is the ratio of net mol of added base at this pH to mol of residue. The net mol of added base have been obtained by subtracting the amount of titrant used in the solvent blank from the total mol of base added to the solution.  $\text{p}K^0$  is determined by extrapolating to  $\alpha=0$  a plot of the experimentally determined function  $\text{pH} - \log[\alpha/(1-\alpha)]$  versus  $\alpha$ .

The change in free energy associated with the transition from uncharged coil to uncharged helix ( $\Delta G^0$ ) is related<sup>3, 5, 6</sup> to the area lying between this curve, obtained

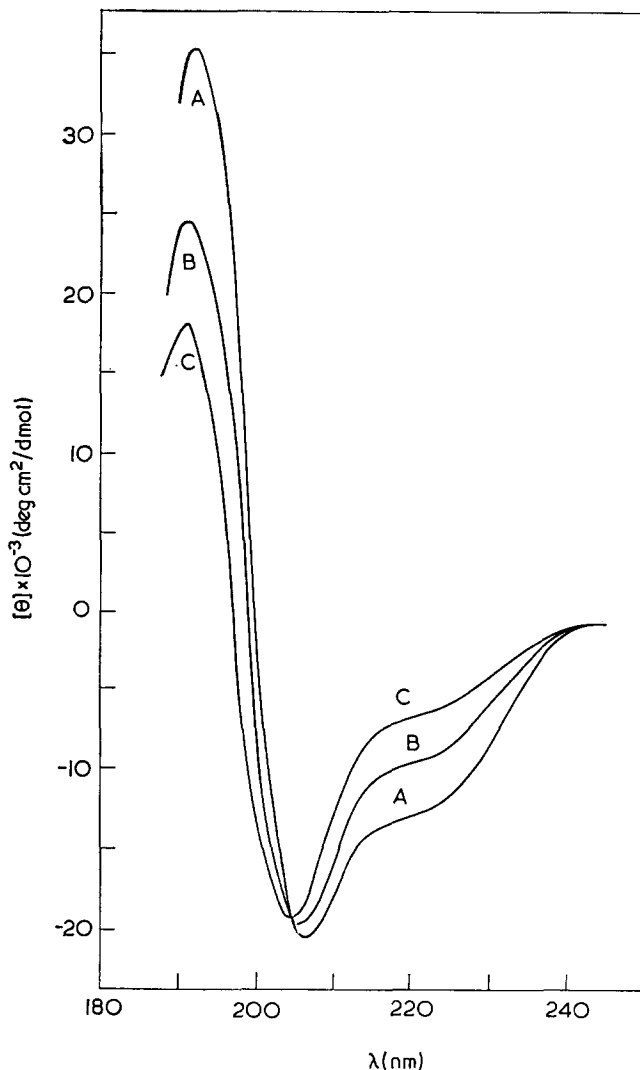


Figure 1 C.d. spectrum of PLLAA in water. A, at pH=4.20; B, at pH=6.37; C, at pH=10.40

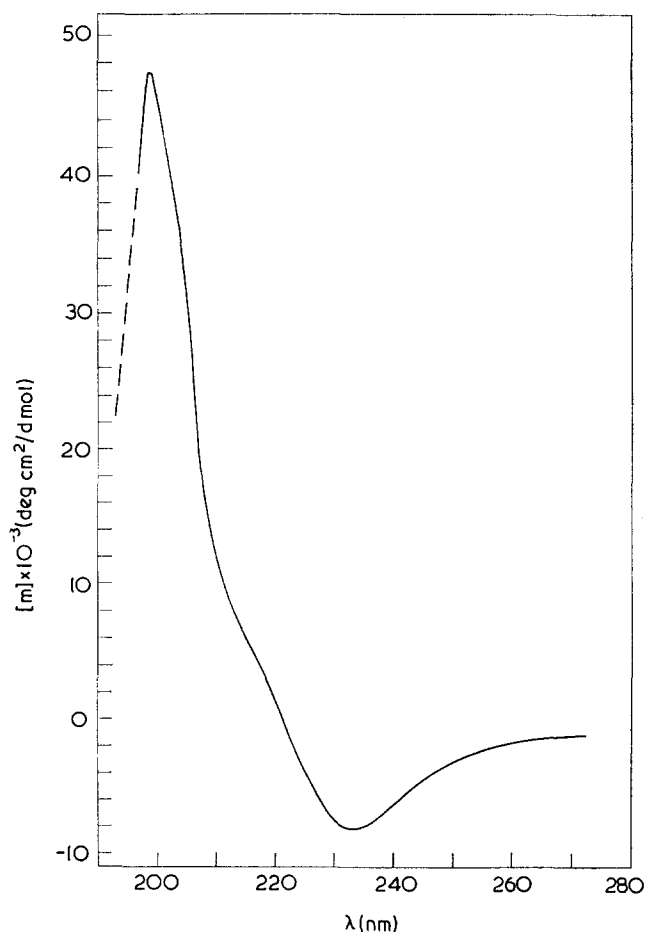
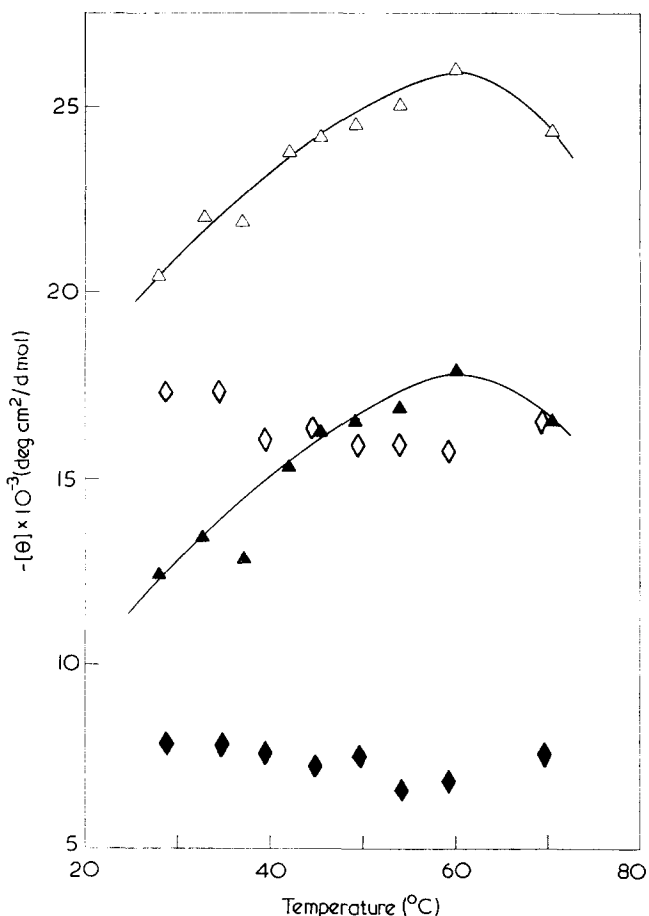
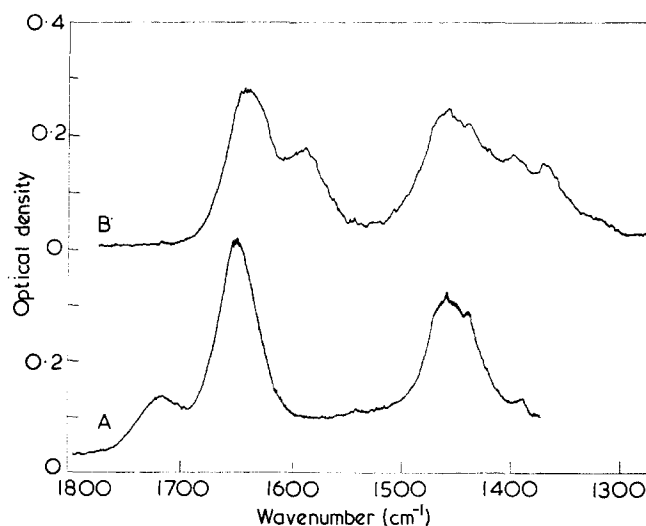
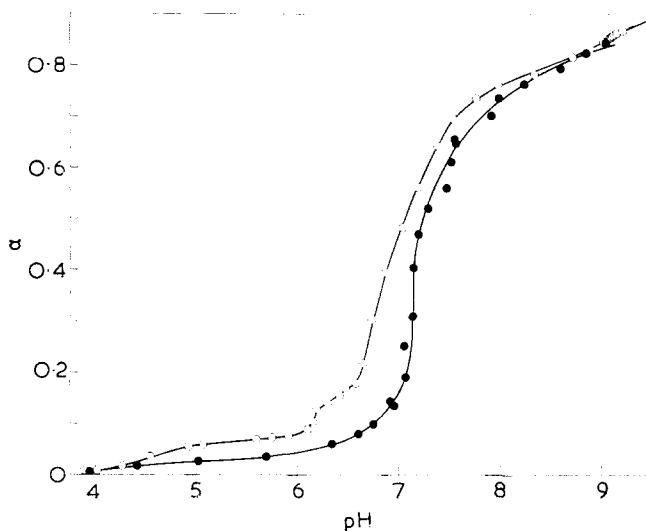


Figure 2 O.r.d. curve of PLLAA in water at pH=3.96


 Figure 3 Effect of temperature on the c.d. spectrum of PLLAA in water.  $\Delta$ ,  $\lambda=207$  nm and  $\blacktriangle$ ,  $\lambda=220$  nm at pH=4.58;  $\diamond$ ,  $\lambda=207$  nm and  $\blacklozenge$ ,  $\lambda=220$  nm at pH=6.96

 Figure 4 The infra-red spectra of PLLAA in  $D_2O$ : A, pH=4.15 ( $pD \approx 4.55$ ); B, pH=10.24 ( $pD \approx 10.64$ )

 Figure 5 Potentiometric titration curves of  $\alpha$  against pH, of PLLAA in water at two different temperatures:  $\circ$ , 25°C;  $\bullet$ , 45°C

from the experimental titration, and the corresponding hypothetical curve for the 'pure' random coil. This curve may be calculated by  $0.434 \Delta G^0/RTN$ , where  $\Delta G^0/N$  is the free energy change per residue.

Figure 6 shows the titration curves of PLLAA, plotted according to equation (1). Extrapolation to  $\alpha=0$  gives the intrinsic  $pK$  value,  $pK^0$ , of an aspartic acid residue, flanked with two leucine residues on each side, in an aqueous solution containing 0.012 M NaCl at the end of titration.  $pK^0$  does not depend on temperature within experimental error ( $\pm 0.02$  unit) for titrations between 25 and 45°C. It is well known<sup>5,6</sup> that the plots of Figure 6 offer some difficulties in determining by extrapolation the limit of the function  $pH - \log[\alpha/(1-\alpha)]$  at very low and very high  $\alpha$  values. The procedure used by us was to determine by trials, using a computer programme, the straight lines which best fitted the experimental points for the same value of  $pK^0$ .

The values of  $\Delta G^0$  against  $T$ , reported in Figure 7, were fitted with a straight line: its slope is  $-\Delta S^0$ , the standard entropy change of the transition from which is readily computed the enthalpy change.

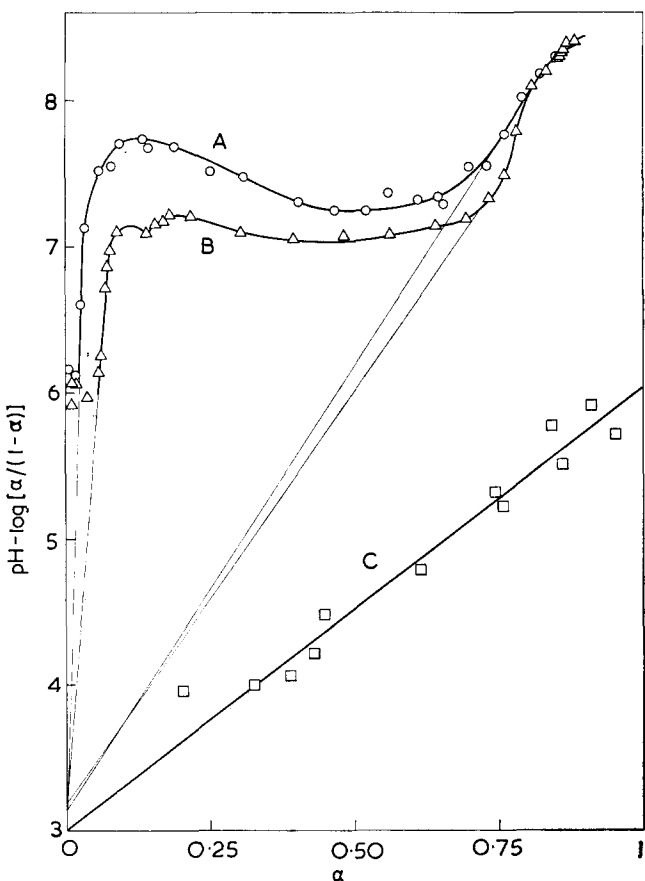


Figure 6 Titration data for PLLAA at three different temperatures, plotted in the manner of Zimm and Rice<sup>2</sup>. A, 45°C; B, 25°C; C, 55°C

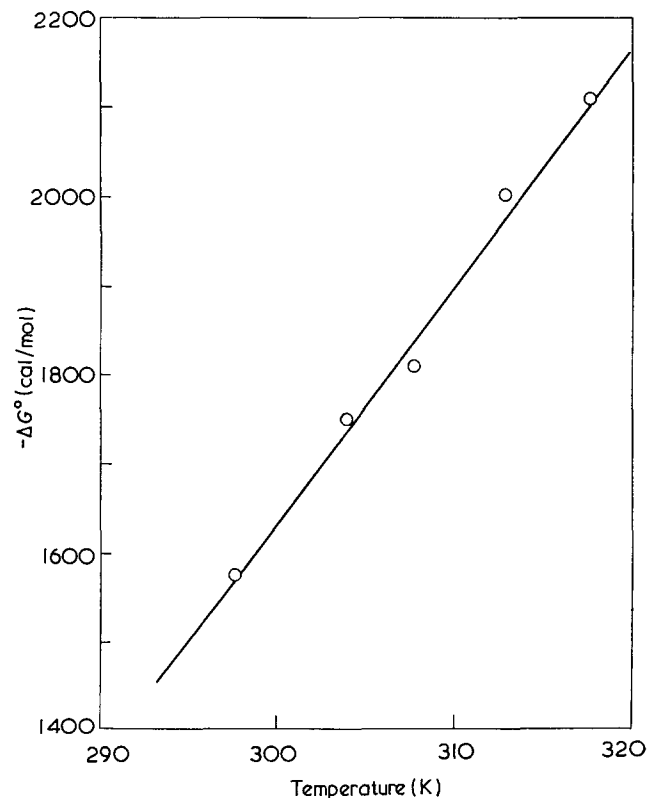


Figure 7 Standard free energies for the formation of the uncharged  $\alpha$ -helix from the uncharged random coil for PLLAA, as a function of temperature. Values are expressed in cal/mol of repeating unit

## DISCUSSION

It has been widely shown<sup>13, 14</sup> that helix-coil transitions can be brought about through pH change of the solutions for polypeptides with ionizable groups on the side-chain. In Figure 1 are shown the c.d. spectra of PLLAA obtained at three different pH values. The c.d. spectrum at pH=4.20, relative to the uncharged polymer is not characterized for any pure conformational state reported in the literature<sup>15</sup>. However, the 192 nm, 207 nm and 222 nm bands together with their signs and intensities point to the presence at least of segments in a right-handed  $\alpha$ -helical structure. In agreement with this interpretation is the o.r.d. curve of PLLAA obtained for the same uncharged state. In fact, the o.r.d. spectrum reproduced in Figure 2 exhibits, in addition to the negative Cotton effect (through at 233 nm), a crossover at 222-223 nm, a shoulder near 215 nm, and a peak at 199 nm, supporting the identification of a right-handed  $\alpha$ -helical conformation<sup>16</sup>.

Curve C in Figure 1 shows a peculiar behaviour of the PLLAA in the random state. The c.d. spectrum is quite different compared to those obtained for random homopolyamino acids<sup>17</sup>. In fact, the observed spectrum does not show the positive dichroic band near 218 nm and the same band shift for the minimum located at 207 nm, as in the case of the completely ionized form of poly(glutamic acid) and polylysine in water<sup>18</sup>. We do not have an explanation for this difference, but we wish to point out that similar behaviour has been already noted<sup>17</sup> for several proteins (myoglobin, ribonuclease,  $\beta$ -lactoglobulin, chymotrypsinogen, and lysozyme) in random conformation.

To clarify this interesting feature it is necessary to analyse other sequential polypeptides; that investigation may further improve the use of circular dichroism for the evaluation of protein conformation.

Support for the interpretation of c.d. and o.r.d. results is obtained by inspection of the i.r. spectra. A comparison of spectra A and B in Figure 4 shows the presence of two different conformational states corresponding to the almost uncharged and charged PLLAA: curve A, recorded in D<sub>2</sub>O at pH=4.15 (pD=4.55), gives the amide I band at about 1652 cm<sup>-1</sup>, consistent<sup>15, 19, 20</sup> with the predominance of an  $\alpha$ -helical conformation; curve B, measured at pH=10.24 (pD  $\approx$  10.64), exhibits the same amide I band at 1643 cm<sup>-1</sup>, leading to the assignment of a random conformation for the PLLAA in its charged state.

Figures 5 and 6 show the titration data of PLLAA reported in two different manners. The plots of  $\alpha$  versus pH and the modified ones of Zimm and Rice<sup>2</sup> are drawn at some peculiar temperatures. From inspection of Figure 5 two features can be pointed out: the shift of pH transition towards a higher value by temperature increase; and the presence of a small plateau for the titration at 25°C between pH 6.2 and 6.6, the physical meaning of which is dubious.

The pH transition shift can be related to the need of a larger amount of titrant, when temperature increases, to reach the necessary charge density on the macromolecule for the transition to occur. A high degree of co-operativity in this process can be inferred from the experimental curves.

$\Delta G^0$  values of the reaction uncharged random coil to uncharged  $\alpha$ -helix, for PLLAA, though large, are in

agreement with the data reported<sup>4</sup> for a leucine residue in random copolymers of leucine and glutamic acid.

The value of the characteristic thermodynamic functions for repetitive units at 25°C are as follows:  $\Delta G^0 = -1575$  cal/mol;  $\Delta H^0 = 6173$  cal/mol, and  $\Delta S^0 = 26.0$  cal/deg mol. These figures are completely in disagreement with the values expected for a process involving only hydrogen bond formation. The high positive value of  $\Delta S^0$ , accounting for the presence of hydrophobic interactions due to the non-polar side-chains of the leucine residues and mainly determined by changes in the water structure, should be noted.

The final state of the transition has an unfavourable enthalpy of formation, much higher than that found by application of the Lifson-Roig theory for leucine residues in block copolymers of L-leucine and DL-lysine in water<sup>21</sup>. As is known from the literature<sup>22-24</sup>, hydrophobic forces become stronger with increasing temperature, in some cases up to about 60°C. This assertion is supported for PLLAA by the lowering of  $\Delta G^0$  as the temperature increases. Curve C in Figure 6 clearly determines an upper limit of 55°C to the existence range of the hydrophobic state. On the other hand, at pH = 4.57 the  $\alpha$ -helix content of PLLAA shows a maximum at 60°C (see Figure 3).

This behaviour may be ascribed to the presence of intra-helical hydrophobic interactions which further stabilize the  $\alpha$ -helix. Similar evidence, indicating stabilization of the helical conformation upon heating over a limited temperature range, has been already reported<sup>25</sup> for random copolymers of glutamic acid and leucine, and explained in terms of hydrophobic interactions.

The endothermic nature of hydrophobic interactions may be related to the van der Waals forces by being temperature-dependent. In this respect it is noticeable<sup>26, 27</sup> that in lipid-water systems the van der Waals forces increase with temperature by means of microwave and infra-red contribution, whereas the electromagnetic fluctuations at ultra-violet frequencies are negligible. Therefore, the low-frequency proton fluctuations<sup>28</sup> and the permanent dipole-dipole interactions may be important for some macromolecules in water, since the free energy of the lipid-water mixture resembles that available by hydrophobic systems.

It is our opinion that the simple method developed by Parsegian and Ninham<sup>26, 27</sup> to calculate van der Waals forces in condensed media by applying the Lifshitz<sup>29</sup> theory can be successfully extended to the study of biological systems. Moreover, these authors point out that the energy values, computed as a sum of pairwise interactions in solution, are wrong and this result must lead to further consideration of some of the data obtained in the literature.

No relevant change in the  $\alpha$ -helix content is observed in the c.d. spectra recorded at pH = 6.96 (Figure 3). This equilibrium situation probably arises from a competitive effect between the attractive hydrophobic and the repulsive electrostatic forces. In fact, the intramolecular

coulombic interactions, which are opposed to  $\alpha$ -helix formation, are obviously stronger than at pH = 4.57. The lack of a sufficient charge density prevents the breakdown of the helix in a large temperature range.

In conclusion, the results obtained in the present work seem promising for the explanation of some physico-chemical properties of proteins, and have prompted us to progress further in this direction.

Further work is now contemplated on sequential polypeptides containing ionizable cationic groups in various ratios with non-polar amino acid residues.

#### ACKNOWLEDGEMENT

The authors are grateful to Professor E. Giglio for stimulating discussions and helpful suggestions.

#### REFERENCES

- Némethy, G. *Angew. Chem. (Int. Edn)* 1967, **6**, 195
- Zimm, B. H. and Rice, S. A. *J. Mol. Phys.* 1960, **3**, 391; Rice, S. A. and Nagasawa, M. in 'Polyelectrolyte Solutions', Academic Press, New York, 1961, Section 7.7
- Nagasawa, M. and Holtzer, A. *J. Am. Chem. Soc.* 1964, **86**, 538
- Miller, W. G. and Nylund, R. E. *J. Am. Chem. Soc.* 1965, **87**, 3542
- Hermans, J. J. *J. Phys. Chem.* 1966, **70**, 510
- Olander, D. S. and Holtzer, A. *J. Am. Chem. Soc.* 1968, **90**, 4549
- Ptitsyn, O. B. *J. Polym. Sci. (C)* 1970, **30**, 615
- Gourke, M. J. and Gibbs, J. H. *Biopolymers* 1971, **10**, 795
- Sugiyama, H. and Noda, H. *Biopolymers* 1970, **9**, 459
- D'Alagni, M., Bemporad, P. and Garofolo, A. *Polymer*, 1972, **13**, 419
- Fasman, G. D., Idelson, M. and Blout, E. R. *J. Am. Chem. Soc.* 1961, **83**, 709
- Tanford, C. in 'Physical Chemistry of Macromolecules', Wiley, New York, 1961, p 550
- Blout, E. R. and Idelson, M. *J. Am. Chem. Soc.* 1956, **78**, 497
- Doty, P., Wada, A., Yang, J. T. and Blout, E. R. *J. Polym. Sci.* 1957, **23**, 851
- Timasheff, S. N. *et al.* in 'Conformation of Biopolymers' (Ed. G. M. Ramachandran), Academic Press, London, 1967, Vol I, p 173
- Yang, J. T. in 'Poly- $\alpha$ -Amino Acids' (Ed. G. D. Fasman), Marcel Dekker, New York, 1967, Vol I, p 239
- Dearborn, D. G. and Wetlaufer, D. B. *Biochem. Biophys. Res. Commun.* 1970, **39**, 315
- Myer, Y. P. *Macromolecules* 1969, **2**, 624
- Ambrose, E. J. and Elliott, A. *Proc. Roy. Soc. (A)* 1951, **205**, 47
- Elliott, A., Hanby, W. E. and Malcolm, B. R. *Discuss. Faraday Soc.* 1958, **25**, 167
- Ostroy, S. E., Lotan, N., Ingwall, R. T. and Scheraga, H. A. *Biopolymers* 1970, **9**, 749
- Némethy, G. and Scheraga, H. A. *J. Phys. Chem.* 1962, **66**, 1773
- Scheraga, H. A., Némethy, G. and Steinberg, I. *Z. J. Biol. Chem.* 1962, **237**, 2506
- Némethy, G. and Scheraga, H. A. *J. Phys. Chem.* 1963, **67**, 2888
- Fasman, G. D., Lindblow, C. and Bodenheimer, E. *Biochemistry* 1964, **3**, 155
- Parsegian, V. A. and Ninham, B. W. *Biophys. J.* 1970, **10**, 664
- Parsegian, V. A. and Ninham, B. W. *J. Colloid Interface Sci.* 1971, **37**, 332
- Kirkwood, J. G. and Shumaker, J. *Proc. Nat. Acad. Sci. USA* 1952, **38**, 863
- Lifshitz, E. M. *Zh. Eksp. Teor. Fiz.* 1955, **29**, 95



# N.m.r. and u.v. spectra of 2'-deoxyadenosine in water/dimethyl sulphoxide mixtures

C.-G. Jang\*, P. Bartl† and T. Williams

Chemical Research Department, Hoffmann-La Roche Inc.,  
Nutley, New Jersey 07110, USA

(Received 20 March 1972)

Nuclear magnetic resonance spectra of 2'-deoxyadenosine (dA) were measured at several solute concentrations in binary solvent mixture (D<sub>2</sub>O/dimethyl sulphoxide) varying in composition from 0% to 100% by vol. D<sub>2</sub>O. One type of upfield shift of the C<sub>2</sub> and C<sub>8</sub> protons of the base moiety was found to be dA concentration dependent. In the range of dA concentrations studied, this upfield shift, due to base stacking interactions, decreases with decreasing D<sub>2</sub>O proportion until it vanishes at about 40–50% of D<sub>2</sub>O; this is near the concentration found to induce RNA denaturation. On the other hand, the other type of upfield shift, in water concentration decreasing below 40%, was found to be dA concentration independent and is interpreted, with corroboration from ultra-violet spectral measurements, as due to the hydration of dA.

## INTRODUCTION

Some organic solvents may serve as reaction media and/or denaturing agents for nucleic acids. Dimethyl sulphoxide (DMSO) particularly has been used in studies of nucleic acids denaturation<sup>1–3</sup>, base pair formation<sup>4–6</sup> and interaction of nucleoside bases with the solvent<sup>7</sup>. In nuclear magnetic resonance (n.m.r.) studies on stacking interaction abnormal shifts of the nucleoside protons were detected<sup>8</sup>.

In this paper an attempt is made to determine the reason for such abnormal chemical shifts ( $\delta$  values) of aromatic proton signals in n.m.r. spectra of 2'-deoxyadenosine (dA) in D<sub>2</sub>O/DMSO mixtures as well as to elucidate the mechanism of denaturation of nucleic acid in the same system. Ultra-violet (u.v.) difference spectra of some of these solutions are also discussed.

## MATERIALS AND METHODS

Crystalline 2'-deoxyadenosine monohydrate (P.L. Biochemicals, Inc.), D<sub>2</sub>O and DMSO with all six hydrogen atoms substituted with deuterium (DMSO-d<sub>6</sub>) (Merck, Sharp and Dohme of Canada, Ltd) and DMSO spectrophotometric grade (Mann Research Laboratories) were commercial products and were used without further purification. DMSO, DMSO-d<sub>6</sub> and non-aqueous solutions in these solvents were stored over molecular sieve 5A (W. R. Grace & Co.).

In determinations of dA concentrations the molar extinction coefficient  $\epsilon_{260}^{1\text{cm}} = 15.4 \times 10^3$  was used<sup>9</sup>. Samples in pure DMSO were also kept over molecular

sieves and care was taken to prevent water absorption from the air during experiments.

The n.m.r. spectra were measured at 100 MHz on a Varian HA-100 spectrometer in the frequency sweep mode. The probe ambient temperature was 31°C. A tetramethylsilane (TMS) capillary was used as an external reference. For very dilute solutions, repeated scans were accumulated on a Varian C-1024 accessory in order to enhance the signal-to-noise ratio.

Ultra-violet difference spectra of 10<sup>-3</sup>M dA in D<sub>2</sub>O/DMSO mixtures were recorded on a Cary 15 Spectrophotometer using 1 mm optical path cells in tandem arrangement against an aqueous solution of dA.

## RESULTS AND DISCUSSION

Dependence on solute concentration of the upfield shift of the C<sub>2</sub> and C<sub>8</sub> protons of the base moiety of dA was measured in ten D<sub>2</sub>O/DMSO mixtures (0 to 100% by vol. of D<sub>2</sub>O). The dependence of the upfield shift on dA concentration decreases with decreasing D<sub>2</sub>O content and finally vanishes at 30 to 40% D<sub>2</sub>O (Figure 1).

The increased upfield shift of signals of base protons with increasing solute concentration in aqueous solutions has been attributed to stacking interactions<sup>10,11</sup>. Our results indicate that stacking interactions decrease with increasing DMSO content. Actually the disappearance of concentration dependence of the upfield shift at 50–60% DMSO in D<sub>2</sub>O is near to conditions found to denature RNA<sup>1</sup>.

In Figure 2, chemical shifts of C<sub>1'</sub>, C<sub>2</sub> and C<sub>8</sub> proton signals at different dA concentrations were plotted as dependent on D<sub>2</sub>O in DMSO content. The magnitude of the chemical shift clearly increases with molar concentrations of dA in solutions containing  $\geq 40\%$  D<sub>2</sub>O. The slope of the individual curves has a positive value and is much steeper for 0.1 M dA than for 0.01 M dA.

\* Present address: Department of Chemistry, Princeton University, Princeton, N.J. 08540, USA.

† To whom requests for reprints should be addressed. Present address: Roche Institute of Molecular Biology, Nutley, N.J. 07110, USA.

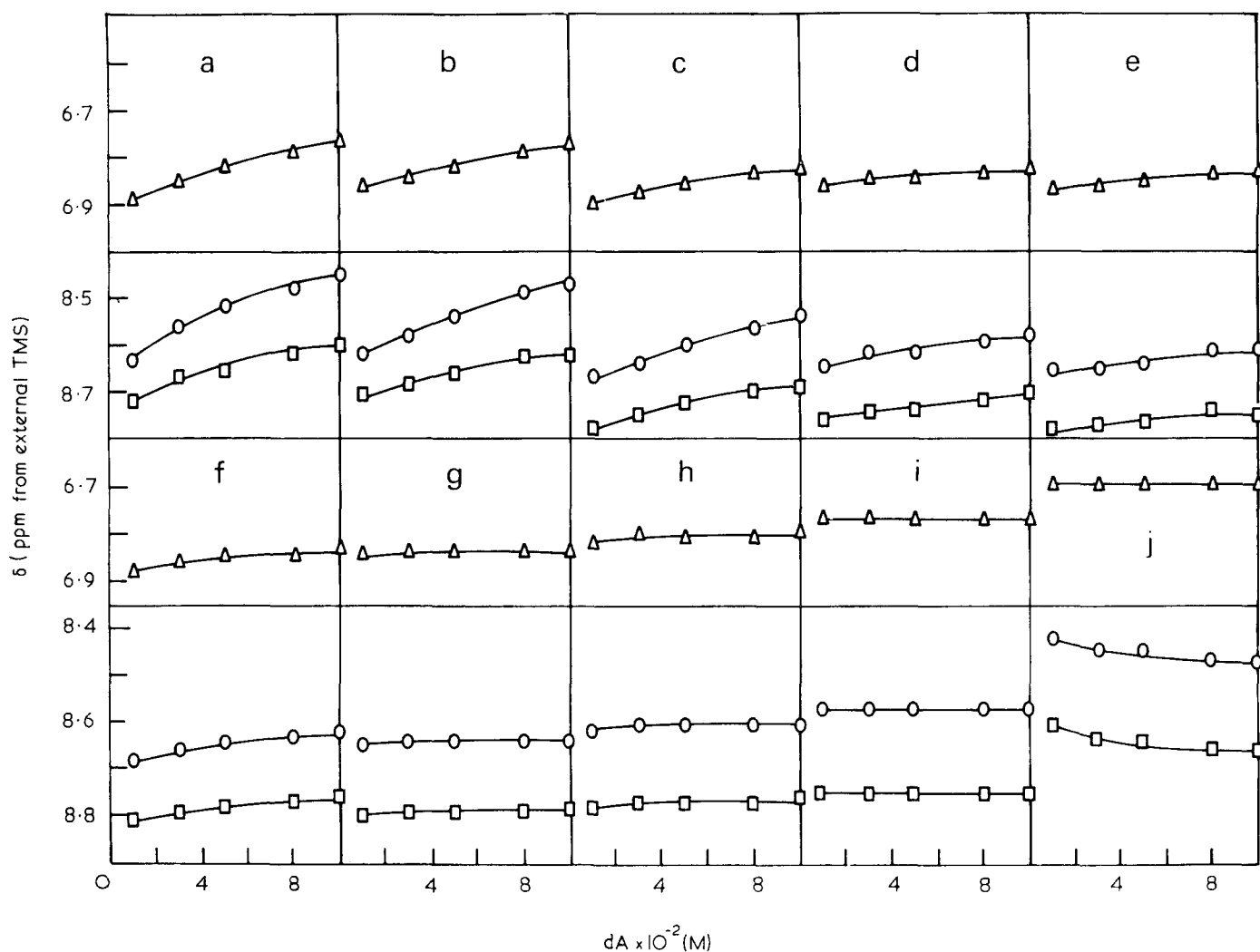


Figure 1 Dependence of chemical shift,  $\delta$ , of C<sub>1'</sub> ( $\Delta$ ), C<sub>2</sub> ( $\circ$ ), and C<sub>8</sub> ( $\square$ ) proton signals on dA molarity and D<sub>2</sub>O content (% by vol.) in D<sub>2</sub>O/DMSO mixtures; temperature=31°C. (a) 100:0; (b) 90:10; (c) 80:20; (d) 70:30; (e) 60:40; (f) 50:50; (g) 40:60; (h) 30:70; (i) 20:80; (j) 0:100% by vol. D<sub>2</sub>O: DMSO.

Again, this can be interpreted as an indication of stacking interactions. On the other hand, the dependence of  $\delta$  values on dA concentration is negligible for solutions containing  $\leq 40\%$  D<sub>2</sub>O. The slope of the curves in this range is almost identical and negative with respect to increasing water proportion in D<sub>2</sub>O: DMSO mixtures. This can be attributed partly to bulk magnetic susceptibility difference<sup>8</sup> and partly to hydrogen bonding of some (C<sub>8</sub>H) dA protons to water molecules<sup>12</sup>. Results similar to ours were obtained previously by Hruska *et al.*<sup>7</sup> for a related system.

In order to distinguish between magnetic susceptibility and other contributions to the observed chemical shift values, the n.m.r. spectra of 0.03 M dA were redetermined (Figure 3) in 0% to 50% D<sub>2</sub>O in DMSO with 2% of 1-pentanol as internal standard (CH<sub>3</sub> proton of 1-pentanol). After correction for magnetic susceptibility the curves show an overall trend similar to those obtained in previous experiments with an external standard (Figure 2). This may be interpreted as an indication that the observed negative slope of the upfield shift (shielding effect) curve, in the range of 0% to 40% D<sub>2</sub>O in DMSO, is mainly due to the solvent-solute interaction in terms of hydration of solute.

If such an interpretation is correct, one should be able to observe changes in u.v. spectra of dA in solvents of various H<sub>2</sub>O content. It has been suggested<sup>13-15</sup> that adenine may be expected to have  $n-\pi^*$  transition in

the 280 nm region. Such transition could be suppressed by hydration.

By measuring difference spectra of dA in DMSO/water against dA in water (Figure 4) we were able to detect a shoulder near 280 nm which gradually disappeared with increasing content of water in the solvent system. In agreement with the interpretation of changes in circular dichroism (c.d.) spectra of oligo-dA this indicates that  $n-\pi^*$  transition is suppressed by hydration. The results of u.v. spectra measurements are in agreement with Bush and Scheraga's<sup>16</sup> interpretation of changes in c.d. spectra of oligo-dA.

From the results of our experiments we conclude that the experimental curve, exhibiting a minimum, results from two types of interaction of dA in D<sub>2</sub>O/DMSO mixtures: (1) at higher D<sub>2</sub>O concentrations solute-solute or base stacking interactions predominate; whereas (2) at low D<sub>2</sub>O concentrations the experimental results may be attributed to solute-solvent interactions (hydration).

At present, however, we are unable to determine the shielding mechanism of the protons in question due to hydration. Several possibilities may be considered (individually or together):

1. Hydrogen bond formation between water protons and the lone pair of electrons of the base nitrogen atoms or oxygen atoms of the sugar moiety. Both types of hydrogen bonds would result in a decrease of electron density around the measured protons.

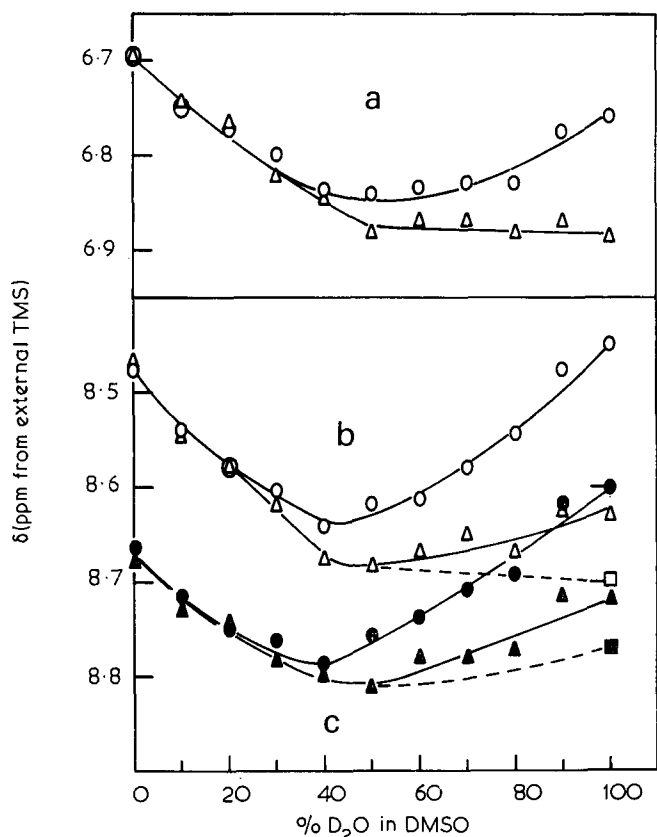


Figure 2 Dependence of chemical shift,  $\delta$ , of (a) C<sub>1'</sub>, (b) C<sub>2</sub> and (c) C<sub>8</sub> proton signals on D<sub>2</sub>O content (% by vol.) in D<sub>2</sub>O/DMSO mixtures for three different dA concentrations: O,  $\bullet$ , 0.1 M dA;  $\Delta$ ,  $\blacktriangle$ , 0.01 M dA;  $\square$ ,  $\blacksquare$ , 0.002 M dA

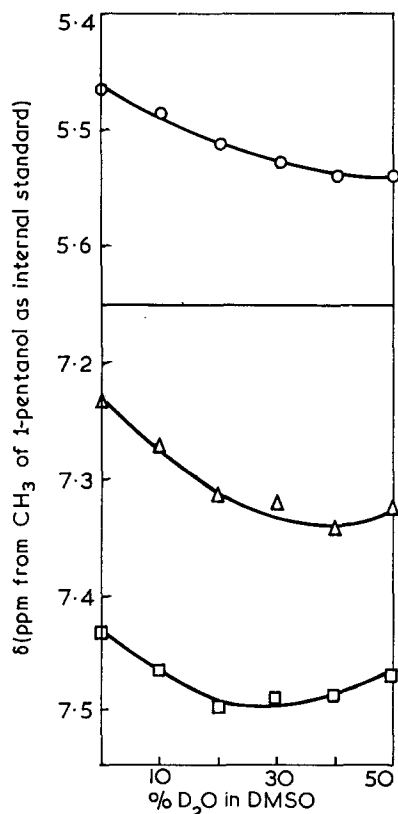


Figure 3 Upfield chemical shift,  $\delta$ , of C<sub>1'</sub> (O), C<sub>2</sub> ( $\Delta$ ) and C<sub>8</sub> ( $\square$ ) proton signals measured at one dA concentration (0.03M) with CH<sub>3</sub> proton of 2% l-pentanol as internal standard

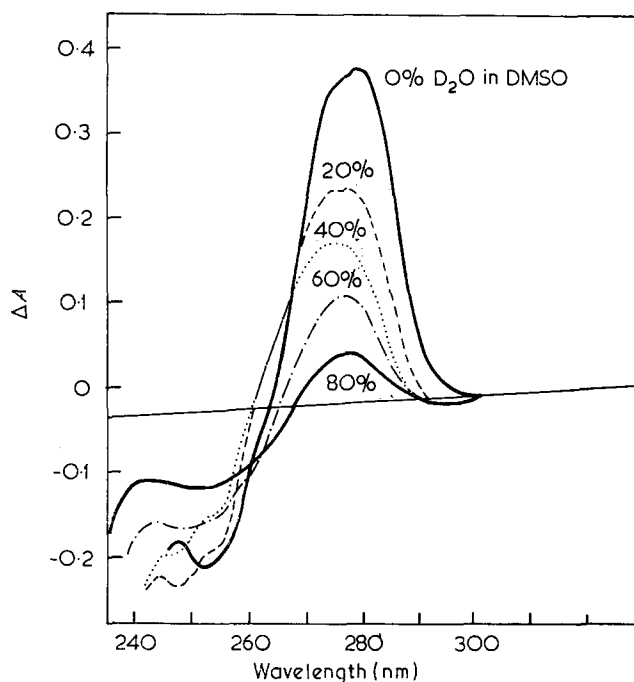


Figure 4 Ultra-violet difference spectra of  $9.8 \times 10^{-4}$  M dA in different D<sub>2</sub>O/DMSO mixtures (% by vol.) measured in 1mm cells in tandem arrangement.  $\Delta A = (\text{O.D. in D}_2\text{O/DMSO}) - (\text{O.D. in D}_2\text{O})$

- Hydrogen bond formation between water protons and the  $\pi$ -electron system of the base.
- Hydrogen bonding between protons of the base and oxygens of water molecules<sup>7</sup>.

Hydration detected on monomer level may play an important role in maintaining the native structure of nucleic acid molecules<sup>17</sup> since it has been suggested that a polynucleotide has various sites of hydration besides phosphate groups<sup>18</sup>.

#### ACKNOWLEDGEMENTS

Critical remarks of visiting Professor V. Sasisekharan from the University of Madras, India and Professor R. Langridge, Department of Biochemical Science, Princeton University, Princeton, are gratefully acknowledged.

#### REFERENCES

- Strauss, Jr, J. H. et al. *Bio-polymers* 1968, **6**, 793
- Helmkamp, G. K. and Ts'o, P. O. P. *J. Am. Chem. Soc.* 1961, **83**, 138
- Katz, L. and Penman, S. *Biochem. Biophys. Res. Commun.* 1961, **23**, 557
- Katz, L. and Penman, S. *J. Mol. Biol.* 1966, **15**, 220
- Newmark, R. A. and Cantor, C. R. *J. Am. Chem. Soc.* 1968, **90**, 5010
- Katz, L. *J. Mol. Biol.* 1969, **44**, 279
- Hruska, F. E. et al. *Biochemistry* 1968, **7**, 3721
- Ts'o, P. O. P. et al. *J. Am. Chem. Soc.* 1969, **91**, 5625
- Ness, R. K. and Fletcher, Jr, H. G. *J. Am. Chem. Soc.* 1960, **82**, 3434
- Broom, A. D. et al. *Chem. Soc.* 1967, **89**, 3612
- Jardetzky, O. *Biopolymers* 1964, Symposia 1, p 501
- Danyluk, S. S. and Hruska, F. E. *Biochemistry* 1968, **7**, 1038
- Rich, A. and Kasha, M. *J. Am. Chem. Soc.* 1960, **82**, 6197
- Stewart, R. F. and Davidson, N. *J. Chem. Phys.* 1963, **39**, 255
- Voelter, W. et al. *J. Am. Chem. Soc.* 1968, **90**, 6163
- Bush, C. A. and Scheraga, H. A. *Biopolymers* 1969, **7**, 395
- Langridge, R. et al. *J. Mol. Biol.* 1960, **19**
- Lewin, S. *J. Theor. Biol.* 1967, **17**, 181

# Equilibrium ring concentrations and the statistical conformations of polymer chains: Part 10. Cyclics in a polymeric paraffin-siloxane

M. S. Beevers and J. A. Semlyen

Department of Chemistry, University of York, Heslington, York YO1 5DD, UK  
(Received 22 May 1972)

Cyclic oligomers  $[(\text{CH}_3)_2\text{Si}-(\text{CH}_2)_4-(\text{CH}_3)_2\text{Si}-\text{O}]_x$  with  $x=2-10$  were found to be present in poly(2,2,7,7-tetramethyl-1-oxa-2,7-disilacycloheptane) samples prepared by monomer-polymer equilibrations using concentrated sulphuric acid as catalyst. The molar cyclization equilibrium constants,  $K_x$ , for cyclics  $[(\text{CH}_3)_2\text{Si}-(\text{CH}_2)_4-(\text{CH}_3)_2\text{Si}-\text{O}]_x$  with  $x=1-6$  were measured for undiluted equilibrates at 298, 333, 383 and 423K. Apart from  $K_1$  for the monomer, the  $K_x$  values were found to be independent of the temperature of equilibration. Experimental molar cyclization equilibrium constants  $K_x$  for the cyclics with  $x \geq 3$  were close to theoretical values calculated by the Jacobson-Stockmayer theory, using a rotational isomeric state model to describe the statistical conformations of chains in the undiluted equilibrates and assuming that the chains obey Gaussian statistics.

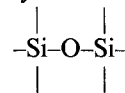
## INTRODUCTION

The conventional experimental methods for investigating the average dimensions of polymer chains in random-coil conformations (viz. light-scattering, viscometry and ultracentrifugation techniques) are applicable only to high molecular weight polymers in very dilute solution<sup>1</sup>. At the present time, we are investigating a new method for studying the statistical conformations of linear molecules based on the precise measurement of the concentrations of cyclics in polymeric systems in which there is a chemical equilibrium between ring and chain molecules. Equilibrium cyclic concentrations are determined by gas-liquid chromatography (g.l.c.) or gel permeation chromatography (g.p.c.), and the Jacobson and Stockmayer<sup>2</sup> theory is used to relate these concentrations to the statistical conformations of the corresponding acyclics. A wide range of linear molecules should be amenable to study by this method under a variety of experimental conditions.

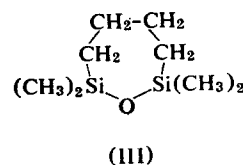
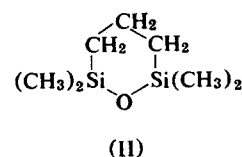
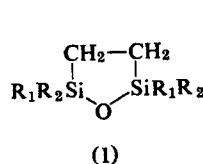
The equilibrium cyclic concentration method for investigating the statistical conformations of chain molecules differs from the well-established light-scattering and viscometric methods in that it may be applied to investigate the structures of polymeric melts and concentrated polymer solutions. Furthermore, it can provide detailed information relating to the statistical conformations of chain molecules containing only a few, to as many as fifty or more, skeletal bonds. The method is unique in providing an estimate of the lower limit of chain length above which an homologous series of chain molecules obeys the Gaussian relationship for

the probability of intramolecular cyclization, and it can be used to measure the average dimensions of chain molecules that are too short to be amenable to investigation by the conventional techniques of polymer science<sup>3-7</sup>.

Here, we report the results of an application of the equilibrium cyclic concentration method to the study of the statistical conformations of chain molecules in bulk equilibrates of a polymeric paraffin-siloxane. The paraffin-siloxanes contain methylene residues  $-(\text{CH}_2)_n-$  connected by siloxane linkages



and polymers of this type containing two, three and four methylene groups respectively, can be prepared from cyclic monomers first synthesized by Picolli *et al.*<sup>8</sup> (I, with either methyl or phenyl substituents), Kumada and Habuchi<sup>9</sup> (II) and Sommer and Ansul<sup>10</sup> (III):



It is with the cyclic populations of polymeric equilibrates derived from III that this paper is concerned.

Samples of poly(2,2,7,7-tetramethyl-1-oxa-2,7-disilacycloheptane) were equilibrated at different temperatures using concentrated sulphuric acid to catalyse skeletal bond interchange between the siloxane linkages. The equilibrates were prepared on a smaller scale than in previous closely related studies<sup>5-7</sup>, so that the total weight of cyclics  $[(\text{CH}_3)_2\text{Si}-(\text{CH}_2)_4-(\text{CH}_3)_2\text{Si}-\text{O}]_x$  with  $x=2-6$  in each equilibrate was only  $\sim 0.3$  g. Nonetheless, it was still found possible to measure individual molar cyclization equilibrium constants  $K_x$  with an experimental uncertainty estimated as being less than  $\pm 10\%$ , by adding suitable internal standards to the undiluted equilibrates prior to the separation and gas-liquid chromatographic analysis of the cyclic oligomers.

In the latter part of this paper, experimental  $K_1-K_6$  values are compared with theoretical values calculated by the Jacobson-Stockmayer<sup>2</sup> theory, using a rotational isomeric state model to describe the statistical conformations of the corresponding open chain molecules.

## EXPERIMENTAL

### Preparation of the monomer

The seven-membered cyclic monomer (2,2,7,7-tetramethyl-1-oxa-2,7-disilacycloheptane) was prepared from 1,4-dibromobutane and trimethylchlorosilane by the synthetic route described by Sommer and Ansul<sup>10</sup>. The monomer was fractionally distilled and its purity was established by g.l.c.

### Equilibration reactions

5g samples of cyclic monomer were equilibrated at temperatures in the range 298–423 K by the addition of small quantities of concentrated sulphuric acid ( $\sim 0.01\%$  w/w). The samples were left to equilibrate for several days and g.l.c. and g.p.c. were used to establish that equilibrium conditions had been attained. The equilibria were quenched by rapid cooling, followed by the addition of small quantities of ammonia. The densities of the equilibrates were determined separately. The equilibrates at 298 K and 333 K were colourless but the equilibrates at 383 K and 423 K were light brown in colour. This colour is believed to result from traces of side-product formed during the equilibration reactions.

### Analysis of the equilibrates

Each quenched equilibrate was analysed using g.l.c. and g.p.c. instruments described elsewhere<sup>5,6</sup>. The following analytical procedure was adopted. Internal standards (n-hexadecane and 2,6,10,15,19,23-hexamethyl-tetracosane) were added to the equilibrate, which was then dissolved in diethyl ether at a concentration of less than 1% w/w. The solution was washed with water and dried over anhydrous calcium chloride. Sufficient methanol was then added under reflux to produce a permanent turbidity. The solution was allowed to cool and left to stand at 278 K for 12 h. The supernatant liquid was decanted off and the residual polymer was extracted again in the same way. The extracts containing the cyclic oligomers were combined and most of the diethyl ether and methanol was removed by distillation. The concentrations of individual oligomers in the

concentrated cyclic extract were determined by g.l.c. Response factors for the cyclics  $[(\text{CH}_3)_2\text{Si}-(\text{CH}_2)_4-(\text{CH}_3)_2\text{Si}-\text{O}]_x$  with  $x=1-6$  were measured relative to the internal standards using either samples of individual cyclics or sharp fractions obtained by the molecular distillation of mixtures of cyclic oligomers.

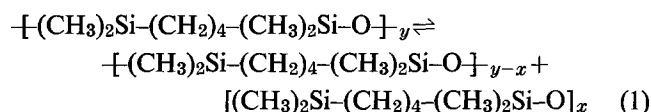
The average molecular weights of the linear polymers produced in the equilibration reactions were estimated from g.p.c. tracings using the universal calibration procedure recommended by Dawkins and his co-workers<sup>11,12</sup>.

Infra-red spectroscopy and proton nuclear magnetic resonance spectroscopy were used to confirm that all the cyclic oligomers and linear polymers contained the repeat unit  $(\text{CH}_3)_2\text{Si}-(\text{CH}_2)_4-(\text{CH}_3)_2\text{Si}-\text{O}$ .

## RESULTS AND DISCUSSION

### Experimental molar cyclization equilibrium constants

In the presence of small amounts of concentrated sulphuric acid, equilibria between ring and chain molecules are established in undiluted samples of poly(2,2,7,7-tetramethyl-1-oxa-2,7-disilacycloheptane) over a range of temperatures. Such equilibria may be represented as follows:



Cyclics  $[(\text{CH}_3)_2\text{Si}-(\text{CH}_2)_4-(\text{CH}_3)_2\text{Si}-\text{O}]_x$  with  $x=2-10$  were identified in oligomeric extracts from quenched equilibrates by their g.l.c. retention times. They represented approximately 6% w/w of each equilibrate, and their molar concentrations were found to decrease monotonically with increase in  $x$ .

Gas-liquid chromatographic response factors for individual cyclics were only obtained up to  $x=6$ , so the molar cyclization equilibrium constants for the larger cyclics were not measured. Gel permeation chromatographic tracings showed that the linear polymers formed in the equilibrates were of high molecular weight, and that their molecular weight distributions corresponded to those expected for a most probable distribution of chain lengths. Hence, the molar cyclization equilibrium constants  $K_x$  for the individual cyclic oligomers [formed by the forward step of equation (1)] were assumed to be equal to their molar concentrations. Experimental  $K_x$  values for  $x=1-6$  obtained at 298, 333, 383 and 423 K are listed in Table 1.

Table 1 Molar cyclization equilibrium constants  $K_x$  for cyclics  $[(\text{CH}_3)_2\text{Si}-(\text{CH}_2)_4-(\text{CH}_3)_2\text{Si}-\text{O}]_x$  in undiluted equilibrates

Number of monomeric units $x$ in cyclic	Molar cyclization equilibrium constants $K_x$ (in mol/l) for cyclics in undiluted equilibrates at different temperatures, $T$ . The density of each equilibrate is quoted below the corresponding temperature			
	$T=298$ K (0.87 g/ml)	$T=333$ K (0.85 g/ml)	$T=383$ K (0.81 g/ml)	$T=423$ K (0.79 g/ml)
1	0.128	0.139	0.196	0.179
2	0.0419	0.0396	0.0356	0.0423
3	0.0240	0.0231	0.0210	0.0239
4	0.0101	0.0104	0.0097	0.0106
5	0.0063	0.0064	0.0061	0.0067
6	0.0037	0.0037	0.0038	0.0038

## Theoretical molar cyclization equilibrium constants

The Jacobson and Stockmayer<sup>2</sup> equilibrium theory of macrocyclization provides the following expression for the molar cyclization equilibrium constants  $K_x$  for large, unstrained cyclics formed by the forward reaction of equation (1):

$$K_x = (3/2 \pi \langle r_x^2 \rangle)^{3/2} (1/2 N_A x) \quad (2)$$

where  $\langle r_x^2 \rangle$  represents the mean-square end-to-end distance of  $x$ -meric chains and  $N_A$  is the Avogadro constant. This expression is based on the assumptions that chains in undiluted equilibrates of poly(2,2,7,7-tetramethyl-1-oxa-2,7-disilacycloheptane) obey the Gaussian expression for the probability density  $W_x(\mathbf{r})$  of end-to-end vectors  $\mathbf{r}$  in the region  $\mathbf{r}=\mathbf{0}$ , and that the termini of chains undergoing intramolecular cyclization reactions are randomly oriented<sup>13, 14</sup>.

Theoretical molar cyclization equilibrium constants for cyclics in the polymeric paraffin-siloxane equilibrates were calculated using equation (2). Mean-square end-to-end distances  $\langle r_x^2 \rangle$  of chains in the undiluted equilibrates were identified with their unperturbed values  $\langle r_x^2 \rangle_0$  and computed by the exact mathematical methods of Flory and Jernigan<sup>15, 16</sup> using the following rotational isomeric state model to describe the statistical conformations of the polymeric chains.

The model is based on an analysis of the molecular structure of the linear polymer, a section of which is shown in Figure 1 in the all-*trans* conformation. Structural parameters of the chain are listed in the legend to this Figure. They were assigned using published molecular structural data for *n*-paraffins<sup>17</sup> and dimethylsiloxanes<sup>18</sup>. By analogy with the rotational isomeric state treatments of polyethylene<sup>19, 20</sup>, polydimethylsiloxane<sup>18</sup> and other linear polymers<sup>14</sup>, each skeletal bond within the paraffin-siloxane chain is assigned to one of three rotational isomeric states in *trans* ( $\phi=0^\circ$ ), *gauche+* ( $\phi=120^\circ$ ) and *gauche-* ( $\phi=240^\circ$ ) positions; and the mutual interdependence of adjacent pairs of bond rotational states is taken into account by means of seven statistical weight matrices  $U_i$  ( $i=1-7$ ). The elements of each matrix  $U_i$  are indexed on the rows and columns by the *trans* (t), *gauche+* (g<sup>+</sup>) and *gauche-* (g<sup>-</sup>) states of pairs of skeletal bonds  $i-1$  and  $i$ , as shown in Figure 1. Following the notation adopted by Flory<sup>14</sup>, the elements of the matrices are defined as Boltzmann factors:

$$u_{\zeta\eta, i} = \exp(-E_{\zeta\eta, i}/RT) \quad (3)$$

where  $R$  is the gas constant,  $T$  is the temperature and  $\zeta\eta$  may be tt, tg<sup>+</sup>, tg<sup>-</sup>, g<sup>+</sup>t, g<sup>+</sup>g<sup>+</sup>, g<sup>+</sup>g<sup>-</sup>, g<sup>-</sup>t, g<sup>-</sup>g<sup>+</sup> or g<sup>-</sup>g<sup>-</sup>. The energy  $E_{\zeta\eta, i}$  is the difference between the conformational energy of a section of the chain when bonds

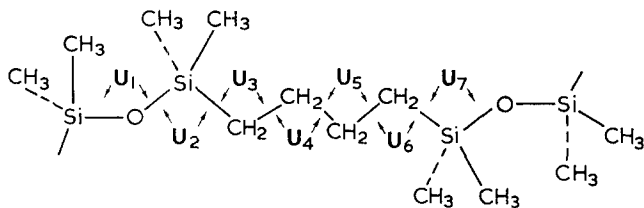


Figure 1 Section of poly(2,2,7,7-tetramethyl-1-oxa-2,7-disilacycloheptane) in the all-*trans* conformation. Bond lengths and bond angles were assigned as follows:  $d_{\text{Si-O}} = 1.64 \text{ \AA}$ ,  $d_{\text{Si-C}} = 1.90 \text{ \AA}$ ,  $d_{\text{C-C}} = 1.53 \text{ \AA}$ ,  $d_{\text{C-H}} = 1.10 \text{ \AA}$ ,  $\text{Si-O-Si} = 143^\circ$ ,  $\text{O-Si-C} = 110^\circ$ ,  $\text{C-Si-C} = 110^\circ$ ,  $\text{C-C-C} = 112^\circ$ ,  $\text{C-C-Si} = 112^\circ$ . The statistical weight matrices  $U_1-U_7$  take account of the mutual interdependence of rotational states about the pairs of bonds shown.

$i-1$  and  $i$  are in rotational states  $\zeta$  and  $\eta$  (and all other bonds are *trans*), and the conformational energy of the same section when all the skeletal bonds are in *trans* states.

There are insufficient molecular structural data available in the literature to provide reliable values for all the conformational energy differences  $E_{\zeta\eta, i}$  ( $i=1-7$ ), and so a simple 'hard-sphere' model was adopted for the calculation of the unperturbed dimensions of poly(2,2,7,7-tetramethyl-1-oxa-2,7-disilacycloheptane) chains. Attractive forces between non-bonded atoms of the chain were neglected, and all the statistical weight parameters were set equal to unity except those that corresponded to bond rotations which resulted in a large steric overlap of non-bonded atoms. The latter were set equal to zero. This procedure yielded the following statistical weight matrices  $U_1-U_7$ :

$$U_1 = \begin{bmatrix} 1 & 1 & 1 \\ 1 & 1 & 1 \\ 1 & 1 & 1 \end{bmatrix} \quad (4)$$

$$U_2 = \begin{bmatrix} 1 & 1 & 1 \\ 1 & 1 & 0 \\ 1 & 0 & 1 \end{bmatrix} \quad (5)$$

$$U_3 = \begin{bmatrix} 1 & 0 & 0 \\ 1 & 0 & 1 \\ 1 & 1 & 0 \end{bmatrix} \quad (6)$$

$$U_4 = \begin{bmatrix} 1 & 1 & 1 \\ 1 & 1 & 0 \\ 1 & 0 & 1 \end{bmatrix} \quad (7)$$

$$U_5 = \begin{bmatrix} 1 & 0 & 0 \\ 1 & 0 & 0 \\ 1 & 0 & 0 \end{bmatrix} \quad (8)$$

$$U_6 = \begin{bmatrix} 1 & 1 & 1 \\ 1 & 0 & 1 \\ 1 & 1 & 0 \end{bmatrix} \quad (9)$$

$$U_7 = \begin{bmatrix} 1 & 1 & 1 \\ 1 & 1 & 0 \\ 1 & 0 & 1 \end{bmatrix} \quad (10)$$

Using this model, the characteristic ratio  $\langle r_x^2 \rangle_0 / 7x\bar{l}^2$  of polymeric 2,2,7,7-tetramethyl-1-oxa-2,7-disilacycloheptane chains, containing  $7x$  skeletal bonds of mean-square length  $\bar{l}^2$  in the limit  $x \rightarrow \infty$ , was calculated to be 4.0 at all temperatures. This value may be compared with the ratio of 2.4 calculated by assuming that each rotational state is equally probable (so that all the elements of  $U_1-U_7$  are set equal to unity).

## Comparison of experiment with theory

Experimental molar cyclization equilibrium constants  $K_x$  for cyclics  $[(\text{CH}_3)_2\text{Si}-(\text{CH}_2)_4-(\text{CH}_3)_2\text{Si-O}]_x$  in an undiluted poly(2,2,7,7-tetramethyl-1-oxa-2,7-disilacycloheptane) equilibrate at 298 K are plotted as  $\log K_x$  against  $\log x$  in Figure 2. They are compared with theoretical values calculated by equation (2) using the rotational isomeric state model described above.

The agreement between the experimental and theoretical  $K_x$  values is close for cyclics with 21 or more skeletal bonds, and it is concluded that the densities  $W_x(\mathbf{r})$  of end-to-end vectors  $\mathbf{r}$  in the region  $\mathbf{r}=\mathbf{0}$  of

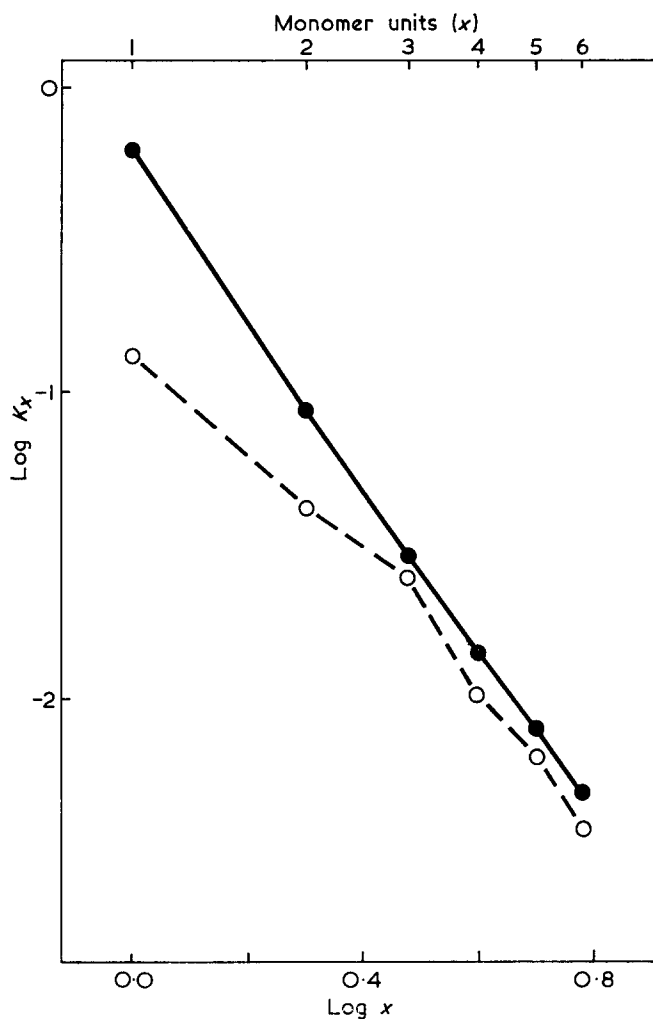


Figure 2 Experimental molar cyclization equilibrium constants  $K_x$  (in mol/l) for cyclics  $[(\text{CH}_3)_2\text{Si}-(\text{CH}_2)_4-(\text{CH}_3)_2\text{Si}-\text{O}]_x$  in an undiluted equilibrium at 298 K (○) are compared with theoretical values calculated by the Jacobson and Stockmayer theory (●) using the rotational isomeric state model described in the text.

the corresponding open chain molecules  $\text{-(CH}_3)_2\text{Si}-(\text{CH}_2)_4-(\text{CH}_3)_2\text{Si}-\text{O-}_x$  (with  $x \geq 3$ ) are closely approximated by the Gaussian expression:

$$W_x(\mathbf{0}) = (3/2 \pi \langle r_x^2 \rangle)^{3/2} \quad (11)$$

It is noteworthy that the experimental and theoretical  $K_2$  values for the 14-membered cyclic dimer  $[(\text{CH}_3)_2\text{Si}-(\text{CH}_2)_4-(\text{CH}_3)_2\text{Si}-\text{O}]_2$  differ by a factor of only two.

By contrast, the experimental  $K_2$  value for the 14-membered cyclic dimer  $[\text{NH}(\text{CH}_2)_5\text{CO}]_2$ , present in melt equilibrates of nylon-6, is lower than the theoretical value (predicted by assuming Gaussian statistics) by a factor of about six<sup>4</sup>.

Finally, it is noted that there are no detectable changes in the  $K_x$  values for the cyclic dimer and larger cyclics in poly(2,2,7,7-tetramethyl-1-oxa-2,7-disilacycloheptane) equilibrates over the temperature range of 125 K. The changes in the molar cyclization equilibrium constant  $K_1$  for the monomer  $[(\text{CH}_3)_2\text{Si}-(\text{CH}_2)_4-(\text{CH}_3)_2\text{Si}-\text{O}]$  suggest that this cyclic must be strained, although the results shown in Table 1 suggest that the strain energy is small ( $\sim 4 \text{ kJ mol}^{-1}$ ).

#### ACKNOWLEDGEMENTS

We are indebted to the Science Research Council for a Research Grant (for M.S.B.). We gratefully acknowledge computational facilities at the University of York.

#### REFERENCES

- 1 Flory, P. J. 'Principles of Polymer Chemistry', Cornell Univ. Press, Ithaca, 1953
- 2 Jacobson, H. and Stockmayer, W. H. *J. Chem. Phys.* 1950, **18**, 1600
- 3 Semlyen, J. A. and Wright, P. V. *Polymer* 1969, **10**, 543
- 4 Semlyen, J. A. and Walker, G. R. *Polymer* 1969, **10**, 597
- 5 Wright, P. V. and Semlyen, J. A. *Polymer* 1970, **11**, 462
- 6 Beevers, M. S. and Semlyen, J. A. *Polymer* 1971, **12**, 373
- 7 Andrews, J. M. and Semlyen, J. A. *Polymer* 1972, **13**, 142
- 8 Piccoli, W. A., Haberland, G. G. and Merker, R. L. *J. Am. Chem. Soc.* 1960, **82**, 1883
- 9 Kumada, M. and Habuchi, A. *J. Inst. Polytech. Osaka City Univ.* 1952, **3** (C), 65
- 10 Sommer, L. H. and Ansul, G. R. *J. Am. Chem. Soc.* 1955, **77**, 2482
- 11 Dawkins, J. V. *J. Macromol. Sci. (B)* 1968, **2**, 623
- 12 Dawkins, J. V., Maddock, J. W. and Coupe, D. *J. Polym. Sci. (A-2)* 1970, **8**, 1803
- 13 Flory, P. J. and Semlyen, J. A. *J. Am. Chem. Soc.* 1966, **88**, 3209
- 14 Flory, P. J. 'Statistical Mechanics of Chain Molecules', Interscience, New York, 1969
- 15 Flory, P. J. *Proc. Natl. Acad. Sci., USA* 1964, **51**, 1060
- 16 Flory, P. J. and Jernigan, R. L. *J. Chem. Phys.* 1965, **42**, 3509
- 17 Abe, A., Jernigan, R. L. and Flory, P. J. *J. Am. Chem. Soc.* 1966, **88**, 631
- 18 Flory, P. J., Crescenzi, V. and Mark, J. E. *J. Am. Chem. Soc.* 1964, **86**, 146
- 19 Hoeve, C. A. J. *J. Chem. Phys.* 1961, **35**, 1266
- 20 Nagai, K. and Ishikawa, T. *J. Chem. Phys.* 1962, **37**, 496

# Dielectric relaxation in polymaleimide and *N*-substituted polymaleimides

H. Block, R. Groves and S. M. Walker

Department of Inorganic, Physical and Industrial Chemistry,  
University of Liverpool, PO Box 147, Liverpool L69 3BX, UK  
(Received 16 May 1972)

We report a study on the dielectric relaxation of polymaleimide and selected *N*-alkyl and *N*-aryl polymaleimides covering the frequency range  $10^{-5}$  to  $10^6$  Hz and the temperature range  $-80^\circ$  to  $+230^\circ$  C. In most instances three relaxations are observable and these have been assigned to the glass to rubber transition, a local chain motion and an in-plane deformation of the maleimide ring. Activation energies for these processes are reported. Secondary factors such as crystallinity and, in polymaleimide and poly(*N*-methyl maleimide), thermal reactions are demonstrated to affect the individual relaxations.

## INTRODUCTION

The measurement of dielectric loss ( $\epsilon''$ ) and relative permittivity ( $\epsilon'$ ) as functions of frequency and temperature is a well established method of detecting molecular motions in macromolecules, particularly in the solid state<sup>1</sup>. The mode of movement may involve whole molecule rotation, motion in the backbone, or simple side-chain rearrangements, but must in all such cases involve a realignment of the dipole in order to be dielectrically active. Such a dielectrically active relaxation process will manifest itself by changes in the complex permittivity ( $\epsilon^* = \epsilon' - i\epsilon''$ ), with variation of either the frequency, or temperature of measurement. In favourable circumstances the molecular movement causing the observed relaxation can be identified, and in this way dielectric (and other) relaxation techniques provide an insight into motional behaviour.

It has become established practice in the polymer relaxation field, to label relaxations  $\alpha$ ,  $\beta$ ,  $\gamma$  etc., in the sequence in which they occur from the lowest to highest frequency at constant temperature (frequency plane) or highest to lowest temperature at constant frequency (temperature plane). Assignment then requires deductive reasoning often based in part on ancillary evidence. For example, the  $\alpha$ -relaxation usually corresponds to the glass-rubber process, occurring at the glass transition temperature ( $T_g$ ), and a dielectric study provides a sensitive method for the detection of the glass-rubber

transition. As illustrated below, environmental factors such as the presence of crystalline regions may also manifest themselves by influencing particular relaxation processes.

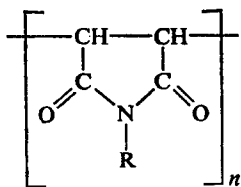
Polymaleimides have not previously been studied dielectrically. They possess facets of interest since these materials (I) possess dipole moments at right angles to the chain direction, have considerable chain rigidity, (as evidenced by their high  $T_g$  and melting points), and have been reported<sup>2</sup> to possess regions of ordered structure. Variation in the side chain R (and thus in dipole moment and side chain bulk) is synthetically relatively simple. Further evidence as to the molecular modes involved in polymaleimides can be obtained by comparative studies into its copolymers with styrene<sup>3</sup> and by studying the monomers in isolation in a polystyrene matrix<sup>4</sup>.

Below we report on the dielectric relaxation behaviour of solid samples of polymaleimide and various *N*-alkyl- and *N*-aryl-substituted polymaleimides in the temperature range  $-80^\circ$  to  $+230^\circ$  C and frequency range  $10^{-5}$  to  $10^6$  Hz. Three common relaxation processes ( $\alpha$ ,  $\beta$  and  $\gamma$ ) are observed and assigned to polymer modes.

## EXPERIMENTAL

### Monomers

Maleimide, supplied by Eastman-Kodak was twice crystallized from benzene. *N*-phenyl and *N*-*ortho*-chlorophenyl maleimides were supplied by courtesy of ICI Ltd. The former was recrystallized from ethanol prior to use. *N*-*meta*-chlorophenyl maleimide and *N*-*para*-chlorophenyl maleimide were prepared by the method of Nield<sup>5</sup>; both were recrystallized from benzene-petroleum ether (b.p.  $60-80^\circ$  C); m.p.  $86^\circ$  C and  $112^\circ$  C respectively. *N*-*n*-dodecyl maleimide was prepared from a sample of *N*-*n*-dodecyl maleamic acid. The latter (250 g), obtained by condensing<sup>5</sup> *N*-*n*-dodecylamine with



In the report presented R = H, CH<sub>3</sub>, C<sub>2</sub>H<sub>5</sub>, *n*-C<sub>5</sub>H<sub>11</sub>, *n*-C<sub>7</sub>H<sub>13</sub>, *n*-C<sub>12</sub>H<sub>23</sub>, cyclo-C<sub>6</sub>H<sub>11</sub>, C<sub>6</sub>H<sub>5</sub>, *o*-C<sub>6</sub>H<sub>4</sub>Cl, *m*-C<sub>6</sub>H<sub>4</sub>Cl and *p*-C<sub>6</sub>H<sub>4</sub>Cl.



maleic anhydride, was cyclized by refluxing in toluene (500 cm<sup>3</sup>) using orthophosphoric acid (10 cm<sup>3</sup>) as a catalyst. A Dean-Stark tube was incorporated and the reflux was discontinued after the extraction of water had ceased (several hours). After cooling and filtering, *in vacuo* removal of solvent yielded crude *N*-*n*-dodecyl maleimide. Purification was achieved by crystallization from aqueous ethanol; m.p. 51°C, lit.<sup>6</sup> 56–57°C.

*N*-methyl, *N*-ethyl, *N*-*n*-amyl, *N*-*n*-heptyl and *N*-cyclohexyl maleimides were prepared from malic acid and the appropriate amine by the method of Lukes and Pergal<sup>7</sup>. This method resulted in larger yields (~40%) than methods employing maleic anhydride such as that of Mehta *et al.*<sup>8</sup> (yields ~10%). *N*-methyl (m.p. 96°C) and *N*-ethyl (m.p. 44°C) maleimide were crystallized from benzene; *N*-*n*-amyl, *N*-*n*-heptyl (m.p. 35°C) and *N*-cyclohexyl (m.p. 81°C) maleimides were fractionated under reduced pressure.

#### Preparation of polymers

The polymers were prepared by free radical polymerization of monomers in a suitable solvent (see Table 1) using either azodiisobutyronitrile or benzoyl peroxide as initiators. Respective initiators were purified by recrystallization from ethanol and chloroform. Polymerizations were carried out under vacuum in sealed tubes (to exclude oxygen) essentially as described for polymaleimide by Touvy<sup>9</sup> and substituted polymaleimides by Cubbon<sup>2</sup>. However, conditions were modified in the light of subsequent mechanistic information<sup>10, 11</sup>. Details of charge, temperature of polymerization and reaction time are shown in Table 1. After completion of the reaction, the polymers had generally precipitated and were isolated by filtration, washed with ethanol and vacuum dried. Poly(*N*-*n*-amyl maleimide), poly(*N*-*n*-heptyl maleimide) and poly(*N*-*n*-dodecyl maleimide) did not precipitate from the reaction mixture, and were isolated by precipitation into a ten-fold excess of methanol, following which they were filtered, washed and dried.

#### Characterization of polymers

Number-average molecular weights were determined for the toluene-soluble members: viz. poly(*N*-*n*-amyl maleimide) and poly(*N*-*n*-dodecyl maleimide), with a Hewlett Packard 502 High Speed Membrane Osmometer. For the remaining toluene-insoluble polymers, molecular weights were estimated viscometrically at 30°C, using *N,N*-formdimethylamide as solvent, and the relation:

$$[\eta] = 6.45 \times 10^{-3} \bar{p}_n^{0.701} \quad (1)$$

Relation (1) is based on the approximation that polymaleimide<sup>11</sup> and substituted polymaleimides of equal number-average degree of polymerization ( $\bar{p}_n$ ) exhibit identical intrinsic viscosities ( $[\eta]$ ) in *N,N*-formdimethylamide. Table 2 shows estimates of the molecular weight so obtained (since  $\bar{M}_n = \bar{p}_n \times \text{residue weight}$ ): that viscometric studies provide only an order of magnitude result [owing to the approximations in relation (1)] can be seen by comparison of the results for poly(*N*-*n*-amyl maleimide), estimated viscometrically and measured osmotically. Poly(*N*-*n*-heptyl maleimide) was insoluble in all solvents examined; hence its molecular weight could not be determined.

The thermal behaviour of polymaleimides was studied in the range 30° to 230°C using a Perkin-Elmer differential scanning calorimeter (DSC-1B). A scan rate of 16°C min<sup>-1</sup> enabled  $T_g$  to be established for most polymers. The values so obtained are shown in Table 2.

Polymer crystallinity was investigated by a study of X-ray powder photographs. The equipment used for all polymers, except poly(*N*-*meta*-chlorophenyl maleimide), was a Phillips X-ray generator with a PW 1030 flat plate camera, using X-rays from a chromium target (vanadium filtered) to give monochromatic radiation of wavelength  $2.291 \times 10^{-10}$  m. The poly(*N*-*meta*-chlorophenyl maleimide) samples, were submitted to X-ray investigation by Yarsley Research Laboratories Ltd using a Metropolitan-Vickers Raymax 100 unit with a Unicam 9 cm powder camera. Radiation from a copper target ( $K_\alpha$ ) filtered with a nickel filter was used. Exposures of twelve

Table 1 Conditions of polymer synthesis

R	Sample No.	Monomer charge (g)	Solvent* (cm <sup>3</sup> )	Initiator† charge (g)	Polymerizing temperature (°C)	Polymerizing time (h)
H	1	30.0	90M	0.3B	60	6
H	2	30.0	90M	0.3B	60	6
H	3	43.6	10W+90A	2.3B	75	6
H	4	40.7	100M	2.2B	90	21
H	5	36.9	110M	0.4B	60	6
H	6	47.0	141M	0.5B	70	6
CH <sub>3</sub>	—	25.3	200B	0.015A	70	18
C <sub>2</sub> H <sub>5</sub>	—	32.1	200B	0.019A	70	18
<i>n</i> -C <sub>5</sub> H <sub>11</sub>	—	44.8	200B	0.020A	70	10
<i>n</i> -C <sub>7</sub> H <sub>15</sub>	—	16.4	100B	0.010A	70	10
<i>n</i> -C <sub>12</sub> H <sub>25</sub>	—	28.3	100B	0.3B	70	8
cyclo-C <sub>6</sub> H <sub>11</sub>	—	28.5	150M	0.3B	70	8
C <sub>6</sub> H <sub>5</sub>	1	40.6	100M	1.2B	90	22
C <sub>6</sub> H <sub>5</sub>	2	31.0	200B	0.014A	85	15
<i>o</i> -C <sub>6</sub> H <sub>4</sub> Cl	1	44.3	110M	0.3B	90	6
<i>o</i> -C <sub>6</sub> H <sub>4</sub> Cl	2	32.3	100B	0.015A	100	15
<i>o</i> -C <sub>6</sub> H <sub>4</sub> Cl	3	45.3	150B	0.021A	70	10
<i>m</i> -C <sub>6</sub> H <sub>4</sub> Cl	—	30.0	100B	0.1A	80	6
<i>p</i> -C <sub>6</sub> H <sub>4</sub> Cl	—	30.0	100B	0.1A	80	6

\* Solvent code: M = methanol; A = acetone; W = water; B = benzene

† Initiator code: A = azodiisobutyronitrile; B = benzoyl peroxide

Table 2 Characteristic data for polymaleimides

R	Sample No.	$[\eta]$	$10^{-4}\bar{M}_n$	$T_g$ ( $^{\circ}\text{C}$ )
H	1	0.172	1.1	reaction
H	2	0.245	1.7	reaction
H	3	0.151	0.9	reaction
H	4	0.138	0.75	reaction
H	5	0.238	1.7	reaction
H	6	0.209	1.4	reaction
CH <sub>3</sub>	—	0.250	2.0	reaction
C <sub>2</sub> H <sub>5</sub>	—	0.128	0.9	180
n-C <sub>5</sub> H <sub>11</sub>	—	0.288	3.8 (8.6 ± 0.3a)	160
n-C <sub>7</sub> H <sub>13</sub>	—	—	b	130
n-C <sub>12</sub> H <sub>23</sub>	—	—	1.7 ± 0.1a	110
cyclo-C <sub>6</sub> H <sub>11</sub>	—	0.078	0.6	not observed
C <sub>6</sub> H <sub>5</sub>	1	0.104	0.9	—
C <sub>6</sub> H <sub>5</sub>	2	0.258	2.8	145
o-C <sub>6</sub> H <sub>4</sub> Cl	1	0.194	2.7	—
o-C <sub>6</sub> H <sub>4</sub> Cl	2	0.211	3.0	—
o-C <sub>6</sub> H <sub>4</sub> Cl	3	0.155	1.9	170
m-C <sub>6</sub> H <sub>4</sub> Cl	—	0.166	1.3	170
p-C <sub>6</sub> H <sub>4</sub> Cl	—	0.134	1.6	170

a Osmometric value in toluene

b No estimate because of polymer insolubility

hours were required for the Phillips system; the Metropolitan-Vickers assembly required exposure times in the region of 10–25 min.

#### Dielectric measurements

For all dielectric measurements polymers were formed into discs (5.08 cm diameter, 0.1 cm nominal thickness) by pressing powdered polymer in a dye. Pressures of around  $3 \times 10^6 \text{ N m}^{-2}$  were applied by an Ajax 4454 hydraulic press, fitted with thermostatically controlled heating plates to allow forming temperatures in the range, ambient to 250°C.

The a.c. bridge method was used for determining resistances and capacitances as a function of frequency (range 105 to  $10^6$  Hz) in the temperature range  $-80^{\circ}$  to  $+90^{\circ}\text{C}$ . The faces of specimens were first coated with a thin layer of petroleum jelly (purified by passage in the melt through an alumina column at 100°C) and

then covered with tinfoil to provide good electrical contact<sup>12</sup>. The specimens were then placed in a General Radio 1690-A two-terminal micrometer electrode capacitor contained in a small dry-box. Temperature control was effected by a stream of preheated (or cooled) dry air passing through the dry-box and acting as a thermostating medium. A thermocouple attached to the electrode at ground potential monitored the temperature and indicated a stability of  $\pm 0.5^{\circ}\text{C}$  over the range  $-80^{\circ}$  to  $90^{\circ}\text{C}$ . Two bridge assemblies were used to cover the frequency range 105– $10^6$  Hz. From 105 Hz to 20 kHz a Wayne-Kerr B221 transformer ratio-arm bridge, energized externally by a Venner 635/2 wide range oscillator and matching transformer, was used, null detection being achieved with a Tinsley 5710 frequency sensitive detector amplifier. In the frequency range 100 kHz to 1 MHz recourse was made to a Wayne-Kerr B601 bridge and SR 268 combined source-detector unit.

For low frequency measurements ( $10^{-5}$  to  $10^{-1}$  Hz) the transient step-response technique was employed. Specimen discs were placed in a three-terminal capacitance cell (the guard ring of which carried a thermocouple). Since electrode contact through tinfoil would cause shorting of the guard ring to one electrode, contact between sample and electrodes was made directly. The cell had an externally wound electric element for temperature variation, the heater being powered and regulated by an Advance TCN4 temperature controller. Temperatures in the range 25–300°C, controlled to  $\pm 0.1^{\circ}\text{C}$  were achieved.

After an initial charging time ( $> 10^3$  s) from batteries to a voltage in the range 6–500 V, current-time data for discharge were obtained by measuring the voltage drop across a standard resistance (order  $10^8 \Omega$ ), by means of a Wayne-Kerr M141 electrometer (equivalent time constant 0.2 s).

The electrometer and capacitance cell were shielded by enclosing them in a grounded metal box. Voltage data were automatically sampled every 1.095 s by externally pulsing a LM1620 Solartron Digital Voltmeter at this rate. Numerical Fourier inversion of

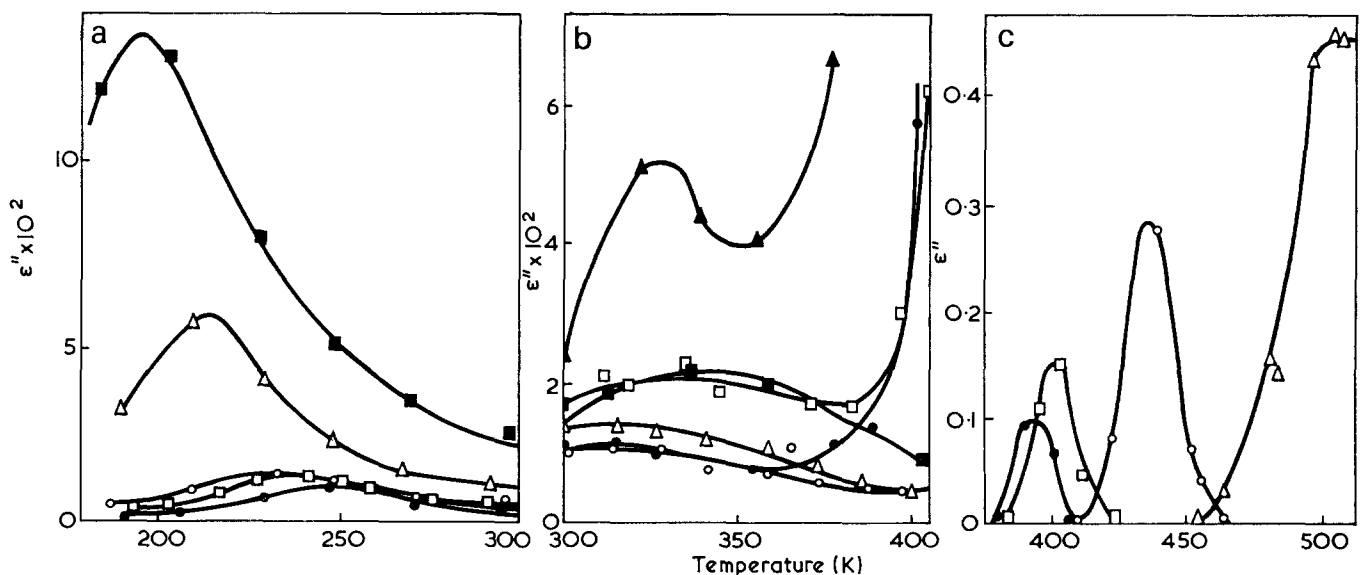


Figure 1 Loss curves for poly(*N*-alkylmaleimides).  $\blacktriangle$ , R=H (sample No. 6);  $\blacksquare$ , R=CH<sub>3</sub>;  $\triangle$ , R=C<sub>2</sub>H<sub>5</sub>;  $\circ$ , R=n-C<sub>5</sub>H<sub>11</sub>;  $\square$ , R=n-C<sub>7</sub>H<sub>13</sub>;  $\bullet$ , R=n-C<sub>12</sub>H<sub>23</sub>. (a) At  $10^8$  Hz showing the  $\gamma$  process; (b) at  $10^{-2}$  Hz showing the  $\beta$  process; (c) at  $7 \times 10^{-5}$  Hz showing the  $\alpha$  process

current-time data was undertaken by the computer-based procedure described elsewhere<sup>13</sup>, using the University of Liverpool KDF 9 computer. This analysis makes no *a priori* assumption of the functionality of the current-decay curve.

The accuracies of  $\epsilon'$  and  $\epsilon''$  measurements were estimated to be within  $\pm 1.5\%$  and  $\pm 5\%$  respectively, when bridge techniques were used, and such estimates of error were confirmed by comparison with literature values<sup>14</sup> for test discs of polystyrene and poly(methyl methacrylate). The accuracy of  $\epsilon''$  in the frequency range  $10^{-5}$  to  $10^{-1}$  Hz depends on the frequency chosen<sup>13</sup>; over most of the range the error is  $\pm 5\%$ , but near the high frequency limit this increases to  $\pm 20\%$ . For this reason the temperature, rather than frequency plane was generally chosen to locate the positions of the loss maxima.

RESULTS AND DISCUSSION

Figures 1 to 4 illustrate the dependence of  $\epsilon''$  and  $\epsilon'$  on temperature for representative samples of polymaleimide and substituted polymaleimides. With the exception of poly(*N*-cyclohexyl maleimide) (two relaxations) three distinct dielectric relaxation regions were generally observed. Following the established convention, these will be referred to as the  $\alpha$ ,  $\beta$  and  $\gamma$  relaxations. As a group, poly(*N*-aryl maleimides) show variations in relaxation behaviour, particularly in changes of the  $\gamma$  loss peak (Figure 4), which are dependent on the thermal history of the sample. The magnitudes of the loss peaks due to these processes were all in the order  $\alpha > \gamma > \beta$  and the proximity of the small loss peak of the  $\beta$  process to the  $\alpha$ -peak renders the detection of the former difficult in many cases, particularly with poly(*N*-aryl maleimides).

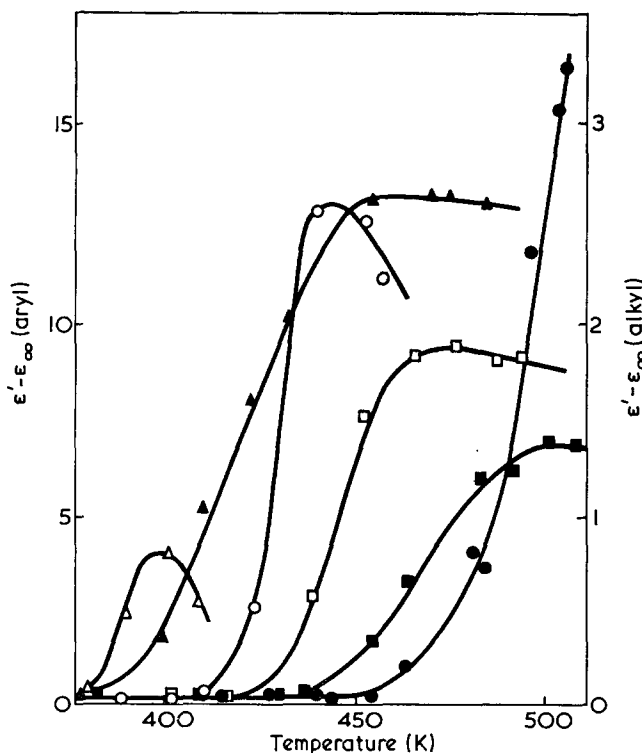


Figure 2 Relative permittivity of the  $\alpha$ -process in some poly(*N*-alkyl maleimides) and poly(*N*-aryl maleimides). Frequency  $7 \times 10^{-5}$  Hz.  $\bullet$ , R=C<sub>2</sub>H<sub>5</sub>;  $\circ$ , R=n-C<sub>5</sub>H<sub>11</sub>;  $\Delta$ , R=n-C<sub>12</sub>H<sub>25</sub>;  $\blacktriangle$ , R=C<sub>6</sub>H<sub>5</sub>;  $\blacksquare$ , R=o-C<sub>6</sub>H<sub>4</sub>Cl;  $\square$ , R=m-C<sub>6</sub>H<sub>4</sub>Cl

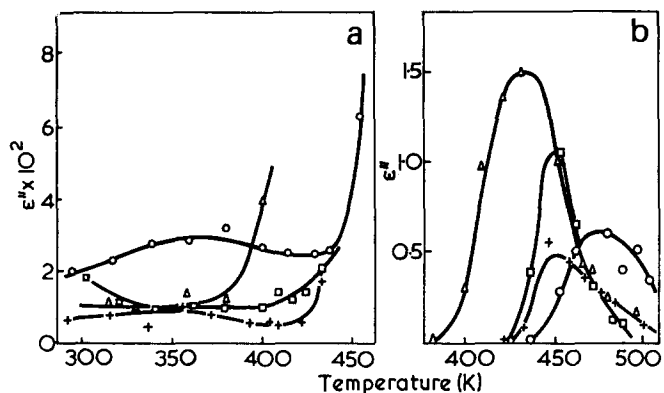


Figure 3 Loss curves for the  $\alpha$  and  $\beta$  processes in poly(*N*-aryl maleimides). (a)  $10^{-2}$  Hz; (b)  $7 \times 10^{-5}$  Hz.  $\Delta$ , R=C<sub>6</sub>H<sub>5</sub> (sample No. 2);  $\circ$ , R=o-C<sub>6</sub>H<sub>4</sub>Cl (sample No. 3);  $\square$ , R=m-C<sub>6</sub>H<sub>4</sub>Cl;  $+$ , R=p-C<sub>6</sub>H<sub>4</sub>Cl

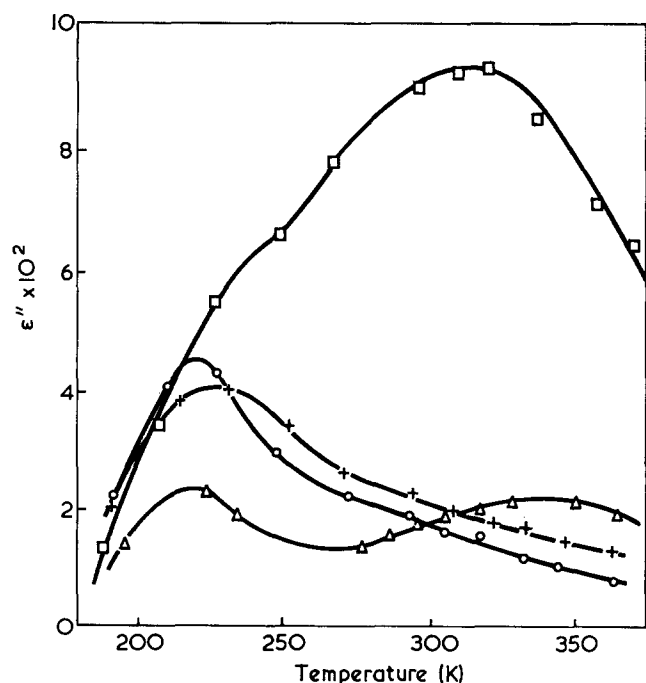


Figure 4 The  $\gamma$ -process in poly(*N*-aryl maleimides) at a frequency of  $10^3$  Hz.  $\Delta$ , R=C<sub>6</sub>H<sub>5</sub> (sample No. 1);  $\circ$ , R=o-C<sub>6</sub>H<sub>4</sub>Cl (sample No. 3);  $\square$ , R=m-C<sub>6</sub>H<sub>4</sub>Cl;  $+$ , R=p-C<sub>6</sub>H<sub>4</sub>Cl

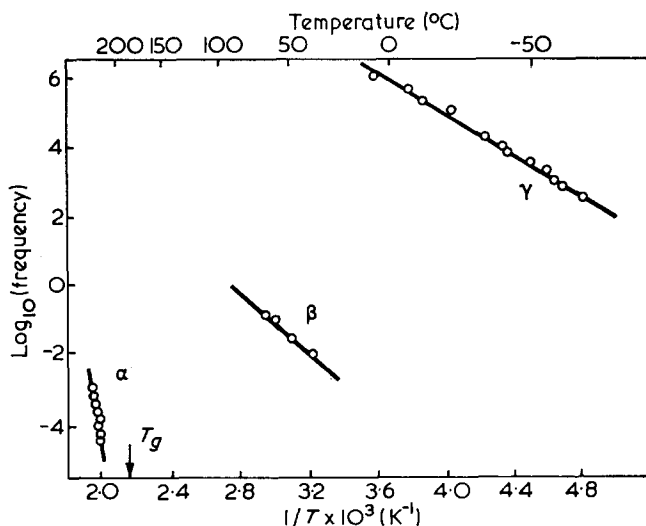


Figure 5 Temperature dependencies of relaxation processes in poly(*N*-methyl maleimide)

Three polymers, viz. unsubstituted polymaleimide, poly(*N*-methyl maleimide) and poly(*N*-cyclohexyl maleimide) all showed aspects of complex behaviour, which was absent in other *N*-alkyl and *N*-aryl polymaleimides. For clarity, discussion of the behaviour of polymaleimide, its *N*-methyl and *N*-cyclohexyl derivatives, will be deferred until the end of this section.

*N*-ethyl, *N*-*n*-amyl, *N*-*n*-heptyl and *N*-*n*-dodecyl polymaleimides all exhibited resolved  $\alpha$ ,  $\beta$  and  $\gamma$  processes (Figures 1 and 2). The temperature (K) dependence of the critical frequencies (obtained from  $\epsilon''$  against  $T$  data) for these processes are shown in Figures 5 to 8 in the form of Arrhenius plots; the corresponding activation energies are shown in Table 3. The onset of the  $\alpha$ -process is closely related to the appropriate  $T_g$  (indicated in Table 2 and Figures 5 to 8). This correspondence, together with the magnitudes of the

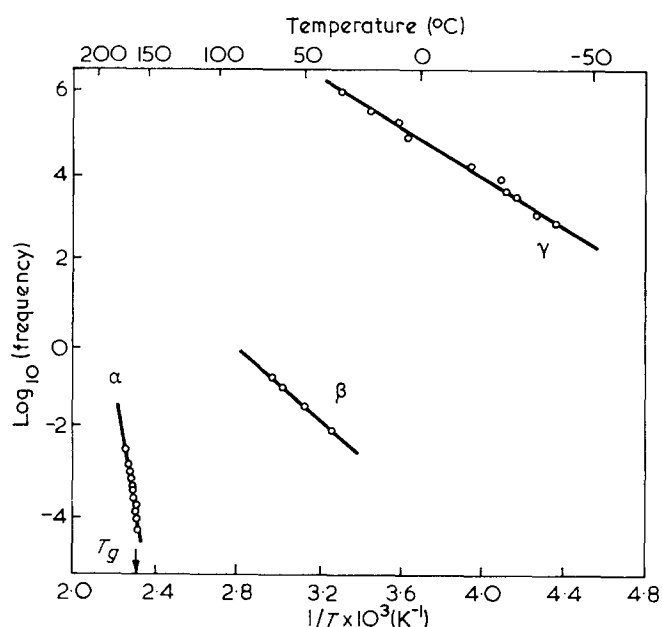


Figure 6 Temperature dependencies of relaxation processes in poly(*N*-*n*-amyl maleimide)

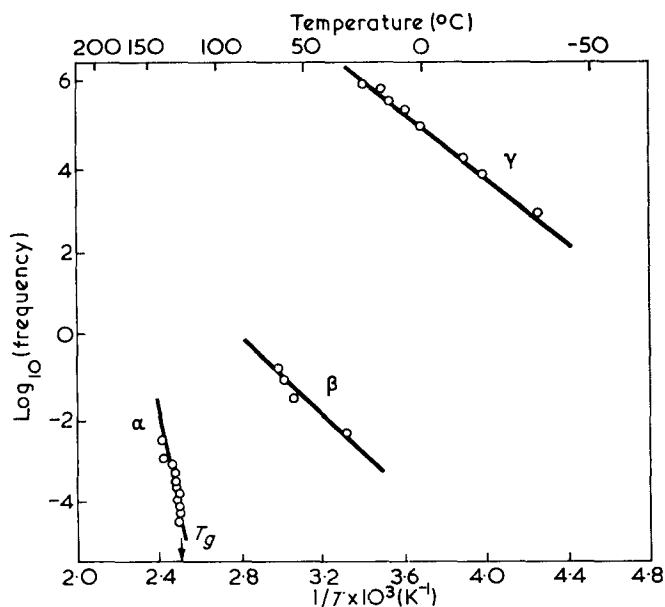


Figure 7 Temperature dependencies of relaxation processes in poly(*N*-*n*-heptyl maleimide)

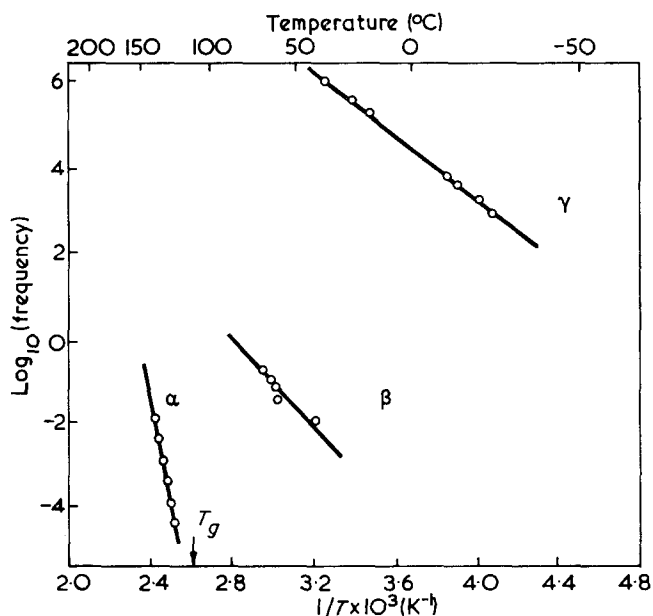


Figure 8 Temperature dependencies of relaxation processes in poly(*N*-*n*-dodecyl maleimide)

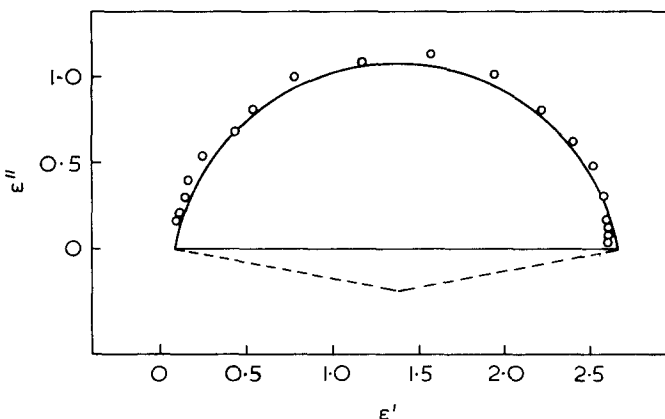


Figure 9 Cole-Cole diagram for poly(*N*-*n*-amyl maleimide)

activation energies involved, strongly support the assignment of the  $\alpha$ -process to the second-order glass-rubber transition. The loss peaks for the  $\alpha$ -process are generally sharp, show good symmetry in the Cole-Cole<sup>15</sup> plots (for the amyl substituted polymer see Figure 9) and have  $\beta$  values  $\sim 0.9$ . It follows that the  $\alpha$ -process does not have a wide distribution of relaxation times (thus of processes) and that the various molecular chain movements which occur at the glass transition are, by and large, equally facile. The effect of substitution is to lower the relaxation time for the  $\alpha$ -process with increasing substituent chain length. Such easing of chain movement by a substituent, acting as self-plasticizer<sup>16</sup>, is a well established phenomenon.

Activation energies (Table 3) for the  $\alpha$ -process also reflect the greater ease of relaxation with increasing chain length of aliphatic substituents.

Excluding the cyclohexyl derivative all the *N*-alkyl and *N*-aryl polymaleimides (including polymaleimide itself) exhibit a  $\beta$  relaxation which appears as a substantially resolved shoulder on the low temperature side of the  $\alpha$ -peak (e.g. Figures 1 and 3). In all cases its intensity is considerably less than that of the  $\alpha$ -peak. The dependence of critical frequency on reciprocal

Table 3 Activation energies (kJ)

R	Code No.	$\alpha$	$\beta$	$\gamma$ (amorphous)	$\gamma$ (crystalline) <sup>a</sup>
H	1	—	—	—	100
H	2	—	—	—	95
H	3	—	—	—	55
H	4	—	—	—	70
H	5	—	—	—	100
H	6	—	170	—	80
CH <sub>3</sub>	—	—	150	55	—
C <sub>2</sub> H <sub>5</sub>	—	710	90	56	—
n-C <sub>5</sub> H <sub>11</sub>	—	530	80	53	—
n-C <sub>7</sub> H <sub>13</sub>	—	400	80	70	—
n-C <sub>12</sub> H <sub>23</sub>	—	400	110	73	—
C <sub>6</sub> H <sub>5</sub>	1	—	—	55	110
C <sub>6</sub> H <sub>5</sub>	2	240 (260 <sup>q</sup> )	—	57 (48 <sup>q</sup> )	95
<i>o</i> -C <sub>6</sub> H <sub>4</sub> Cl	1	—	—	—	110
<i>o</i> -C <sub>6</sub> H <sub>4</sub> Cl	2	—	—	—	100
<i>o</i> -C <sub>6</sub> H <sub>4</sub> Cl	3	400 (350 <sup>q</sup> )	100	53 (53 <sup>q</sup> )	75
<i>m</i> -C <sub>6</sub> H <sub>4</sub> Cl	—	370 (380 <sup>q</sup> )	—	80	120 (120 <sup>q</sup> )
<i>p</i> -C <sub>6</sub> H <sub>4</sub> Cl	—	320 (350 <sup>q</sup> )	100	50 (45 <sup>q</sup> )	80

<sup>a</sup> Partly crystalline as evidenced by the presence of X-ray reflections from the powder

<sup>q</sup> Samples treated by heating above  $T_g$  and rapid quenching below  $T_g$

temperature for the representative poly(*N*-alkyl maleimides) is shown in Figures 5 to 8, and the corresponding activation energies are given in Table 3. It will be seen that the process involved for these polymers, has an activation energy which is generally little influenced by the nature of the substituent. The exceptions consist of the two anomalous polymers: R=H and CH<sub>3</sub>. Losses ( $\epsilon''$ ) for the  $\beta$  processes are of relatively low magnitude indicating that the processes involve either a mode with small dipole change, or that only a small fraction of the responsible dipoles are able to relax by the  $\beta$ -mode, or that both factors are involved. Since any dielectrically active relaxation requires significant polarization changes (such as the movement or change of magnitude of a dipole), the  $\beta$  process cannot involve a side-chain mode. There remain the possibilities of either a local chain motion involving the inclination of one amide ring relative to its neighbours, or a conformational change of the amide ring itself. Evidence for assigning the latter mode to the  $\gamma$ -process is given below, so that the assignment of the former mode to the  $\beta$ -process is proposed. Some confirmatory evidence has been adduced from studies of substituted maleimide-styrene copolymers<sup>3</sup> and a styrene-maleic anhydride copolymer<sup>4</sup> where more facile (higher frequency-lower temperature)  $\beta$  processes occur. The spatial reorganization proposed for the  $\beta$  process is shown in Figure 10, which also reproduces a computer-based estimation of activation energy for local chain rotations (based on selected atomic interaction potentials after the method of Gotlib *et al.*<sup>17</sup>). The value of 97 kJ mol<sup>-1</sup> for the lowest rotational energy barrier agrees well with the activation energies (Table 3) found for the  $\beta$  processes.

The  $\gamma$  process, which has been detected in the majority of the polymaleimides investigated (the exception being the *N*-cyclohexyl substituted polymer), occurs as a simple structureless relaxation with the *N*-alkyl substituted members. Loss curves for these processes are shown in Figure 1. It is noticeable that the intensity of the  $\epsilon''$  peak decreases with the length of chain substituent. Further, the temperatures (at 10<sup>3</sup> Hz) for peak maxima lie fairly close together, a situation which is a reflection of the relatively minor changes in activation

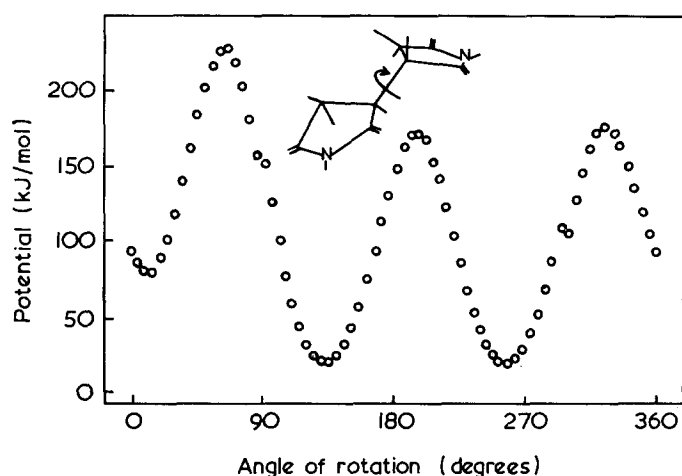


Figure 10 Calculated potential energy diagram for local mode chain rotation. The rotation illustrated corresponds to that proposed for the  $\beta$ -process

energy between the different members (Table 3). The  $\gamma$ -process has been assigned by us to an out-of-plane deformation of the substituted succinimide ring. This implies non-planarity of this system with the nitrogen atom lying above or below the carbon framework plane. Such a hypothesis is consistent with the presence of a  $\gamma$  relaxation in the styrene-*N*-substituted maleimide copolymers<sup>3</sup>, styrene-maleic anhydride copolymer<sup>18</sup> and a very similar (in activation energy and peak position) relaxation process in the monomer dispersed in a polystyrene matrix<sup>4</sup>.

This conclusion is supported by some structural evidence as to the non-planarity of *N*-*para*-bromophenyl succinimide<sup>19</sup>. It also agrees well with a small but definite change in activation energy for the  $\gamma$ -process with substituent chain length; the longer chain members reducing the ease of nitrogen inversion.

The reproducible, very simple, relaxation behaviour of the typical *N*-alkyl substituted polymaleimides described above, becomes more involved in the *N*-aryl substituted members. Both the  $\alpha$  (Figure 3) and  $\gamma$  (Figure 4) relaxations have, to a greater or lesser extent, more structure

than is shown by the *N*-alkyl members; in some cases such structure in the  $\gamma$  peaks being partly resolved into two relaxations. The relative magnitudes of the two components (occasionally reflected only in the width of the relaxation peak) was found to depend on the thermal history of the sample. Thus, the low frequency-high temperature component of both the  $\alpha$  and  $\gamma$  relaxations could generally be removed, or considerably reduced, by heating the sample above the appropriate glass transition temperature and then quenching it. The implication that the doublet character of the  $\alpha$  and  $\gamma$  absorptions are a reflection of crystallinity is clear; (a high frequency-low temperature amorphous peak, plus a low frequency-high temperature crystalline peak). Confirmation of this view was obtained by comparing X-ray powder photographs of polymers with their dielectric behaviour. The poly(*N*-aryl maleimides), when

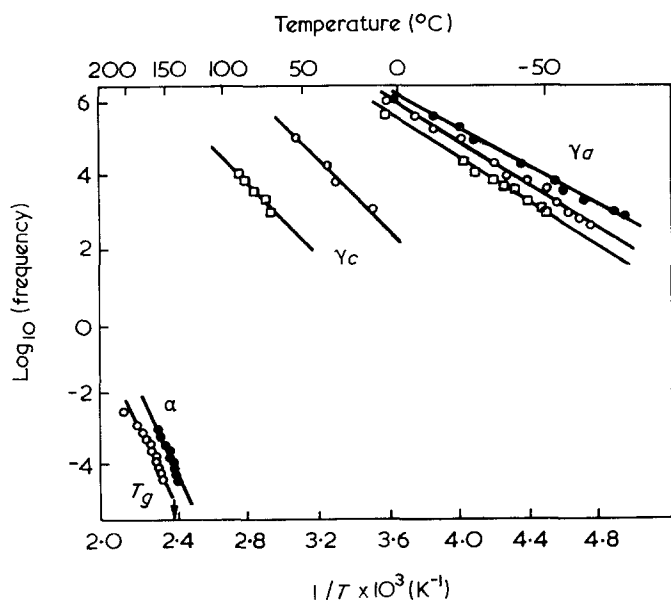


Figure 11 Temperature dependencies of relaxation processes in poly(*N*-phenyl maleimides).  $\square$ , Sample No. 1;  $\circ$ , sample No. 2;  $\bullet$ , sample No. 2 after quenching treatment

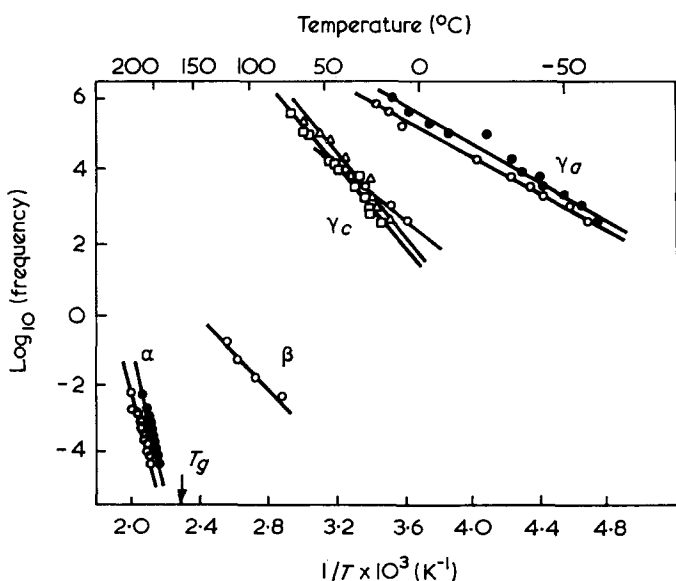


Figure 12 Temperature dependencies of relaxation processes in poly(*N*-ortho-chlorophenyl maleimides).  $\triangle$ , Sample No. 1;  $\square$ , sample No. 2;  $\circ$ , sample No. 3;  $\bullet$ , sample No. 3 after quenching treatment

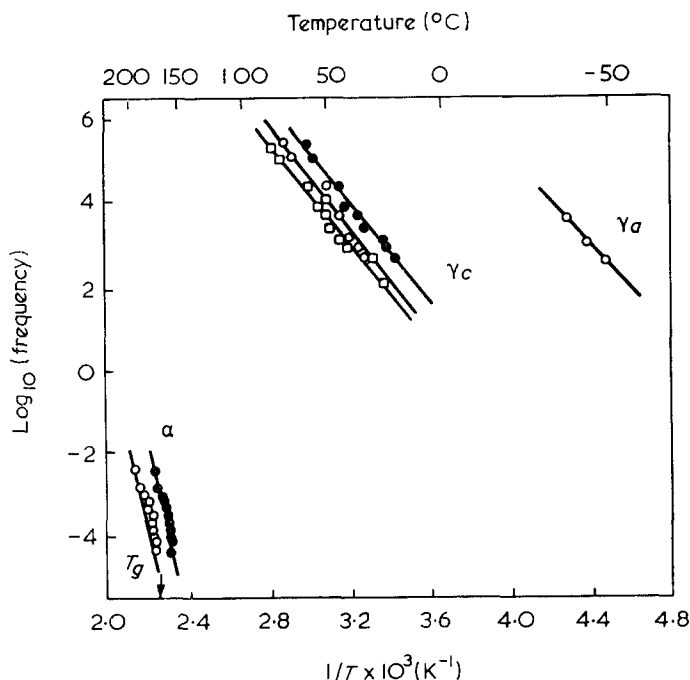


Figure 13 Temperature dependencies of relaxation processes in poly(*N*-meta-chlorophenyl maleimides).  $\circ$ , Unquenched sample;  $\square$ , after single quenching treatment;  $\bullet$ , after two quenching treatments

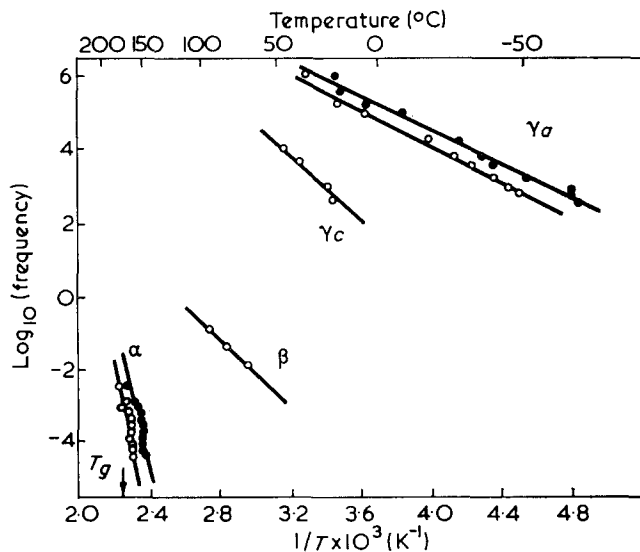


Figure 14 Temperature dependencies of relaxation processes in poly(*N*-para-chlorophenyl maleimides).  $\circ$ , Unquenched sample;  $\bullet$ , after single quenching treatment

partly crystalline all exhibit the reflection first reported by Cubbon<sup>2</sup> and ascribed by him to a helical chain structure. We have found qualitative agreement between the intensity of this X-ray band and the intensity of the crystalline loss peak. Resolution of the doublet character of both the  $\alpha$  and  $\gamma$  relaxations can in some cases be achieved by working over a suitable temperature range and this fact is a reflection of small differences in the activation energies for these processes, which depend on the environment. This situation is illustrated in Figures 11 to 14 which show Arrhenius plots for the  $\alpha$ ,  $\beta$  and  $\gamma$  processes: the corresponding activation energies are given in Table 3.

In conclusion we discuss the anomalous behaviour of polymaleimide, poly(*N*-methyl maleimide) and poly-

(*N*-cyclohexyl maleimide). Although the first two materials exhibited  $\alpha$ ,  $\beta$  and  $\gamma$  relaxations, the thermal conditions necessary to observe the  $\alpha$ -relaxation caused a continuous upward shift of this absorption in the temperature plane. After such heat treatment the polymer samples were found to have become insoluble (polymaleimide) or difficultly soluble [poly(*N*-methyl maleimide)] in *N,N*-formdimethylamide, and it is presumed that, particularly in the former, crosslinking had occurred. Some confirmatory evidence of a thermal decomposition was evidenced by the infra-red observation of the appearance of water in heated polymaleimide. In polymaleimide it is probable that the crosslinking process involves the N-H group in a dehydrating reaction. The nature of the crosslinking or other thermal changes in poly(*N*-methyl maleimide) remains unknown, as is the factor which distinguishes these polymers from other homologous members which are free of this effect. The presence of crosslinks also affects the  $\beta$  and  $\gamma$  relaxations in that much higher activation energies (Figure 15 and Table 3) are observed for both processes

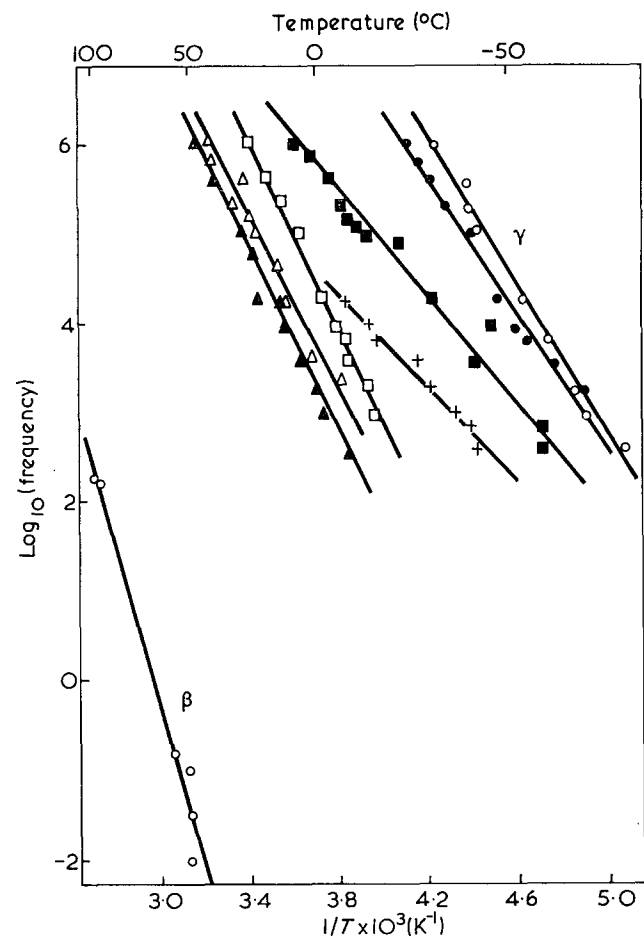


Figure 15 Temperature dependencies of relaxation processes in samples of polymaleimides

Sample No.	Symbol
1	▲
2	△
3	□
4	●
5	○
6	○
5 quenched	+

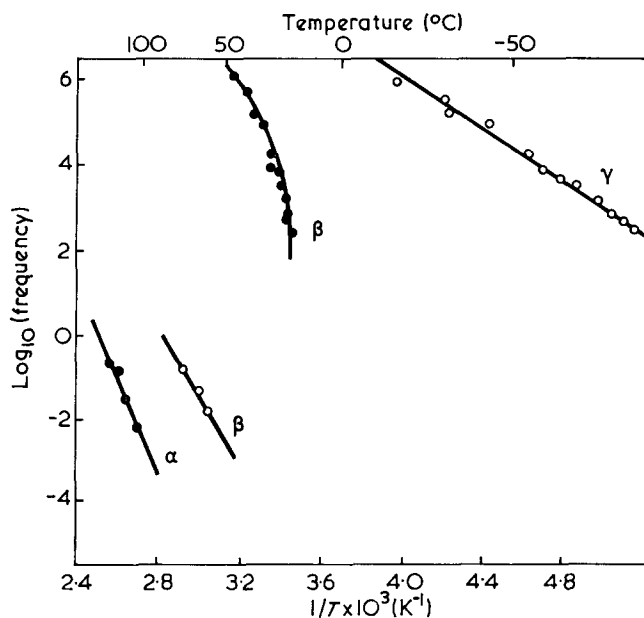


Figure 16 Temperature dependencies of relaxation processes in poly(*N*-methyl maleimide) (○) and poly(*N*-cyclohexyl maleimide) (●). The processes are labelled according to convention and should not be taken to imply similar molecular interpretations

in poly(*N*-methyl maleimide) and the  $\gamma$  process in polymaleimide. The latter also shows a variation of critical frequency with thermal history (even with differing polymerization temperatures). Similar, but not so extensive effects of thermal history, were found with poly(*N*-methyl maleimide) (Figure 16).

Poly(*N*-cyclohexyl maleimide) differs from all the other polymaleimides studied in that only two relaxations are observed. Further, the low temperature relaxation is anomalous in that  $\log f_{max} - 1/T$  dependence shows considerable curvature (Figure 16). This introduces uncertainty into estimates of the activation energy for the process but the average value of 200 kJ suggests a hindered relaxation. The high temperature process shows no such anomaly but is also accompanied by a high activation energy (270 kJ). The nature of these processes or the reason why further relaxations are absent, is not at hand. One possibility is that this polymer has an inherently different structure. A suggestion is that chain growth in polymerization proceeds to give a different back-bone structure by a polymerization mechanism involving transfer of the tertiary cyclohexyl hydrogen atom to the normal radical site; a similar transfer is known in the polymerization of maleimide<sup>10, 11</sup>.

#### ACKNOWLEDGEMENTS

We wish to thank the Science Research Council for a grant in support of this research and for a studentship for one of us (R.G.). Thanks are due to ICI Ltd, for the gift of certain monomers; to Yarsley Research Laboratories Ltd, and the Department of Materials Science, University of Liverpool for X-ray facilities, and to colleagues in the Polymer Characterization Unit of this Department for molecular weight measurements. We would like to thank Professor C. E. H. Bawn for his continued interest and encouragement.

REFERENCES

- 1 McCrum, N. G., Read, B. E. and Williams, G. 'Anelastic and dielectric effects in polymeric solids', Wiley, London, 1967
- 2 Cubbon, R. C. P. *Polymer* 1965, **6**, 419
- 3 Block, H., Lord, P. W. and Walker, S. M. in preparation
- 4 Block, H., Groves, R. and Walker, S. M. in preparation
- 5 Br. Pat. 1 041 027 (1966)
- 6 U.S. Pat. 2 444 536 (1948)
- 7 Lukes, R. and Pergal, M. *Coll. Czech. Chem. Commun.* 1962, **27**, 1387
- 8 Mehta, N. G., Phillips, A. P., Lui, F. F. and Brooks, R. E. *J. Org. Chem.* 1960, **25**, 1012
- 9 Fr. Pat. 1 248 700 (1960)
- 10 Nakayama, Y. and Smets, G. *J. Polym. Sci. (A)* 1967, **5**, 1619
- 11 Bamford, C. H., Bingham, J. F. and Block, H. *Trans. Faraday Soc.* 1970, **66**, 2612
- 12 ASTM Designation D150-65T, 1965
- 13 Block, H., Groves, R., Lord, P. W. and Walker, S. M. *J. Chem. Soc., Faraday Trans. II* in the press
- 14 Mikhailov, G. P. and Borisova, T. I. *Soviet Phys. Tech. Phys.* 1958, **3**, 120; Saito, S. and Nakajima, T. *J. Appl. Polym. Sci.* 1959, **2**, 93
- 15 Cole, R. H. and Cole, K. S. *J. Chem. Phys.* 1941, **9**, 341
- 16 Immergut, E. H. and Mark, H. F. *Adv. Chem. Ser.* 1965, **48**, 1
- 17 Gotlib, Yu. Ya. and Darinskii, A. A. *Polym. Sci. USSR* 1965, **7**, 1914
- 18 Block, H., Collinson, M. A. and Walker, S. M. in preparation
- 19 Hargreaves, M. K., Pritchard, J. G. and Dare, H. R. *Chem. Rev.* 1970, **70**, 439



# Effects of long-chain branching on distribution of degree of polymerization

P. A. Small

*Imperial Chemical Industries Limited, Plastics Division, Welwyn Garden City, Herts, UK  
(Received 6 April 1971)*

The method of generating functions is used to calculate the number fraction of molecules having any specified degree of polymerization and number of long branches for polymers produced under conditions in which the probabilities of chain propagation and of branching on a monomer unit incorporated in the polymer are both constant; termination by combination is assumed absent. Expressions are given for the moments of degree of polymerization and the first two moments of branch number. It is shown that all moments of degree of polymerization are finite, for this model. An asymptotic expression for the number distribution at very high degrees of polymerization is obtained. The way in which the average number of branches per monomer unit varies with degree of polymerization is studied.

## INTRODUCTION

The effects of long-chain branching on the distribution on degree of polymerization ( $DP$ ) of free-radical polymers have been considered by a number of authors, amongst whom Beasley<sup>1</sup>, Nicolas<sup>2</sup>, and Mullikin and Mortimer<sup>3</sup> (MM) must be particularly mentioned. The last named have recently presented some calculations relating to a model definable by several conditions: (1) the probability of chain propagation, i.e. the probability that a polymer radical adds at least one more monomer unit, is constant,  $p$ ; (2) a monomer unit incorporated in a polymer chain has a number of sites,  $\alpha$ , for radical attack leading to long-chain branching; the probability that a branch is formed at the  $r$ th such site is constant,  $b_r$ , and depends neither upon the occurrence of branches at other sites nor on the history of the polymer molecule; (3) the initiator radicals are univalent and termination by combination is excluded.

In this paper, the method of generating functions<sup>4,5</sup> will be used to study this model, which will be called the Mullikin and Mortimer model, in more detail. Their results plus many new ones will be obtained by this method. It is likely that it is possible to extend this model so as to include the effects of termination by combination by means of this method, but this has not yet been done.

As the aim of this paper is to present general results for the MM model, i.e. to give analytical expressions for the various quantities calculated as functions of the parameters of the model, numerical methods will not be used.

No particular kinetic scheme will be assumed here. The calculations presented below apply to any kinetic scheme consistent with the conditions stated above; the probabilities in question can then be expressed in terms of the rate constants and reactant concentrations, for the kinetic scheme concerned.

MM do not formulate very clearly the kinetic scheme assumed in their treatment. The reaction is said to take place in a well-stirred continuous reactor; under such conditions, the mean residence time in the reactor, as

polymer, of the later-added branches of a polymer molecule must be shorter than that of the earlier-added branches, and the probability of radical attack on any monomer unit in them must be lower. The assumption of constant branching probabilities for these conditions, therefore, involves an approximation, the validity of which will not be examined here. It is, however, an assumption that makes the problem of calculating the distribution on  $DP$  and branching, and various statistical parameters, a fairly tractable one. It is thus of interest to consider the MM model in some detail.

Short-chain branching, due to a unimolecular 'back-biting' reaction, as in ethylene polymerization, does not affect the distribution on  $DP$  except insofar as, by introducing tertiary C-H groups, it affects the probability of long-chain branching. It will therefore not be considered here.

The case of unequal branching probabilities at the various potential branching sites on a monomer unit was considered by MM, but will not be dealt with here in detail; the method given can be applied to it without difficulty but leads to rather complicated expressions. A few results relating to this case will be stated. Normally the  $\alpha$  branching probabilities  $b_r$  will be taken as equal, and the symbol  $b$  will be used for any of them. This symbol, and  $p$ , have the same significance here as in Mullikin and Mortimer's paper, but  $\langle m^i \rangle$  is used for the moments of  $DP$  in place of their  $M_i$ . For any quantity  $x$ ,  $\langle x \rangle$  is the average of  $x$  over the number distribution  $N(m, q)$ .

In cases of practical interest  $1-p$  and  $b$  (or  $b_r$ ) are small, and  $1-p-\alpha b$  (or  $1-p-\sum_r b_r$ ) is small but positive.

## GENERATING FUNCTIONS

The use of generating functions ( $GF$ ) facilitates calculations of the effects of branching and crosslinking distribution of  $DP$ <sup>4,5</sup>. The Laplace transform method<sup>4,6</sup> is equivalent, and is advantageous when the  $DP$  is

regarded as a continuous rather than a discrete variable.

Generating functions owe their use in probability theory<sup>7</sup> to the fact that the *GF* for the sum of  $n$  independent random variables is the product of their  $n$  *GF*'s; if they have the same probability distribution it is the  $n$ th power of the *GF* of any of them.

For the number distribution function  $N(m, q)$ :

$$\sum_m \sum_q N(m, q) = 1 \quad (1)$$

The two complex variables  $u$  and  $z$  are introduced to carry respectively the *DP*,  $m$ , and the number of branches in the polymer molecule,  $q$ ; when the latter is not of interest  $z$  may be set equal to unity. The *GF*  $G(u, z)$  is defined by the double series:

$$G(u, z) = \sum_{m=1}^{\infty} u^m \sum_{q=0}^{m-1} z^q N(m, q) \quad (2)$$

The summation over  $q$  does not go beyond  $q=m-1$  as a molecule with  $q$  branches must have at least  $q+1$  monomer units, since the first monomer unit can never constitute a branch, though any later-added unit may do so.

Comparison of the series (2) with that of equation (1) shows that (2) converges at least over the region,  $|u| \leq 1$ ,  $|z| \leq 1$  of the two variables. It is also obvious that  $G(1, 1) = 1$ .

The function defined by the series (2) is one branch, which will be called the main branch, of a multi-valued function. The symbol  $G$  or  $G(u, z)$  will be used for any branch of this function; the context will show which is intended. Any of the three quantities  $G$ ,  $u$  and  $z$  may be regarded as a function of the other two. Partial differentiation of one of these with respect to a second implies the constancy of the third; however,  $\ln u$  and  $\ln z$  may be used in place of  $u$  or  $z$ .

If moments  $\langle m^i q^j \rangle$  exist, defined by:

$$\langle m^i q^j \rangle = \sum_{m=1}^{\infty} m^i \sum_{q=0}^{m-1} q^j N(m, q) \quad (3)$$

they are given by:

$$\langle m^i q^j \rangle = \left\{ \partial^{i+j} G(u, z) / \partial (\ln u)^i \partial (\ln z)^j \right\}_{u=1, z=1} \quad (4)$$

Conversely, if all these moments exist, so do all the derivatives of  $G$  with respect to  $u$  and  $z$  at  $u=z=1$  and  $G$  is analytic with respect to both variables there, as well as within the region  $|u| < 1$  and  $|z| < 1$ .

The moments of *DP* can be written:

$$\langle m^i \rangle = \left\{ d^i G(u, 1) / d (\ln u)^i \right\}_{u=1} \quad (5)$$

#### DERIVATION OF THE *GF* AND NUMBER DISTRIBUTION FUNCTION

A polymer molecule having  $q$  branches has  $q+1$  monomer units (one at the end of the primary chain and one at the end of each branch) that have not added any further units by the propagation reaction, though they may be branched. Thus, as stated above, it must contain  $q+1$  monomer units at least and in general contains more. Because of the conditions stated above, it has also a unique end consisting of a radical (here called the starting radical) derived from the initiator, or from transfer with monomer or chain transfer agent, or produced by scission of the growing radical; it thus has  $q+2$  ends in all. The starting radical will not here be counted as a

monomer unit, and it will be assumed that it does not form branches; this assumption is not essential but is made for simplicity. MM assumed that the starting radical is equivalent to a monomer unit and that it has the same branching probability as a monomer unit; this assumption gives the same results as that made here and is equivalent to it.

Any polymer molecule may be divided into two portions between the starting radical and the first monomer unit, or between any two monomer units. One portion will contain the starting radical, the other will not; the former may be regarded as a generalized starting radical for the latter. The distribution  $N(m, q)$  is assumed independent of the nature of the starting radical; any reasonable kinetic scheme will give this result.  $N(m, q)$  is therefore the distribution for the latter part of the molecule not containing the starting radical, no matter where the cut is made; that is, the probability that any growing radical that adds at least one monomer unit will add  $m$  more units containing  $q$  branches is  $N(m, q)$  irrespective of its size or nature. In particular, this is the distribution and  $G(u, z)$  is the *GF* for any branch together with all its sub-branches.

Consider primary chains having  $n$  monomer units that grow exactly  $r$  branches, which may branch further. The *GF* for such molecules will be:

$$u^n z^r [G(u, z)]^r \quad (6)$$

The probability that a primary chain of  $n$  units grows  $r$  branches is:

$$(\alpha n)! (1-b)^{z n - r} b^r / (\alpha n - r)! r! \quad (7)$$

so that the *GF* for all molecules derived from primary chains of  $n$  units is:

$$\sum_{r=0}^{\alpha n} (\alpha n)! (1-b)^{z n - r} b^r u^n z^r G^r / (\alpha n - r)! r! \quad (8)$$

This is:

$$u^n (1-b + bzG)^{\alpha n} \quad (9)$$

The probability that a primary chain has  $n$  monomer units is:

$$(1-p)p^{n-1} \quad (10)$$

so that the *GF* for molecules derived from primary chains of any size is:

$$G = \sum_{n=1}^{\infty} (1-p)p^{n-1} u^n (1-b + bzG)^{\alpha n} \quad (11)$$

This summation converges for  $|pu(1-b + bzG)^\alpha| < 1$ , to give:

$$G = (1-p)u(1-b + bzG)^\alpha / [1 - pu(1-b + bzG)^\alpha] \quad (12)$$

Since, for  $|u| \leq 1$  and  $|z| \leq 1$ ,  $G \leq 1$  by equations (1) and (2), and  $p < 1$ , the series (11) will converge over at least these regions of  $u$  and  $z$ . Since  $G(1, 1) = 1$ , this series converges at  $u=1, z=1$ , to unity, as it should. A further check on equation (12) can be obtained by setting  $b=0$ , when equation (12) reduces to the *GF* for the distribution (10), which is:

$$(1-p)u / (1-pu) \quad (13)$$

If the branching probabilities are unequal, the expression

$(1-b+bzG)^\alpha$  in equation (12) must be replaced by:

$$\prod_{r=1}^{\alpha} (1-b_r+b_rzG) \quad (14)$$

Equation (12) is rearranged to give:

$$u = G/(1-p+pG)(1-b+bzG)^\alpha \quad (15)$$

Thus  $u$  is a single-valued function of  $G$  and  $z$  but  $G$  is a many-valued function of  $u$  and  $z$ . For  $\alpha=1$ , equation (15) gives an easily soluble quadratic equation for  $G$ ; for  $\alpha=2$  or 3 the resulting equations are too complex to be useful, and for  $\alpha \geq 4$  no algebraic solutions exist.

There can be only one expansion of the main branch of  $G$  as a series of positive powers of  $u$ , and this is given by the Lagrange inversion formula<sup>9</sup> applied to equation (15) as:

$$G = \sum_{m=1}^{\infty} \frac{u^m}{m!} \left\{ \left( \frac{d}{dx} \right)^{m-1} (1-p+px)^m (1-b+bzx)^{\alpha m} \right\}_{x=0} \quad (16)$$

Picking out the coefficient of  $z^q$  in equation (16) and performing the indicated differentiation gives:

$$N(m, q) = \frac{(\alpha m)!(m-1)!p^{m-q-1}(1-p)^{q+1}b^q(1-b)^{\alpha m-q}}{(\alpha m-q)!q!(m-q-1)!(q+1)!} \quad (17)$$

Summing equation (17) over  $q$  or setting  $z=1$  in equation (16) before differentiating leads to:

$$N(m) = \sum_q N(m, q) = (\alpha m)!(m-1)! \times \sum_{q=0}^{m-1} \frac{p^{m-q-1}(1-p)^{q+1}b^q(1-b)^{\alpha m-q}}{(\alpha m-q)!q!(m-q-1)!(q+1)!} \quad (18)$$

Values of  $N(m, q)$  calculated from equation (17) for some low values of  $m$  and  $q$ , and of  $N(m, 0)$ , agree with values that can be calculated directly.

### ASYMPTOTIC RELATIONS

In considering branched polymers, the amount and degree of branching of the high  $DP$  tail of the distribution are of particular interest. Asymptotically valid relations can be obtained by expressing the quantities of interest as complex contour integrals and approximating these by the method of steepest descents<sup>8, 9</sup>.

It can be shown that the general function  $G(u, 1)$  given by equations (12) or (15) with  $z=1$  has two branch points on the positive real axis of  $u$ , at  $u_1$  and  $u_2$  say, with  $u_1 < u_2$ . If  $\alpha > 1$ , there is also a branch-point at  $u=0$  except on the main branch of  $G$ . The branch-points are located by solving the equation:

$$du/dG(u, 1) = 0 \quad (19)$$

If  $G(u_1, 1)$  be denoted by  $G_1$ , the condition (19) gives:

$$G_1 = \{(1-\alpha)(1-p)b + [(1-\alpha)^2(1-p)^2b^2 + 4\alpha pb(1-p)(1-b)]^{1/2}\} / 2\alpha pb \quad (20)$$

The negative sign of the root gives  $G(u_2, 1)$ . Insertion of  $G_1$  into equation (15), with  $z=1$ , gives  $u_1$ . In the special case  $\alpha=1$  the expression for  $u_1$  is simple:

$$u_1 = \{(p+b-2pb) - 2[pb(1-p)(1-b)]^{1/2}\} / (p-b)^2 \quad (21)$$

the positive sign of the root giving  $u_2$ . Otherwise, the

expression for  $u_1$  is rather complicated. It is important to note that since the series (2) converges at  $u=1$  for  $z=1$ ,  $u_1$  must exceed 1 by some finite amount so that  $u_1^n \rightarrow 0$  as  $n \rightarrow \infty$ . As the branch-point at  $u_1$  is of order 2, the main branch of  $G(u, 1)$  may be written in the vicinity of  $u=u_1$  in the form:

$$G(u, 1) = G_1 - \delta(u_1 - u)^{1/2} + O(u_1 - u) \quad (22)$$

If the positive sign is taken for the root, this gives another branch of  $G$ . It is found on evaluation that:

$$\delta = \left\{ \frac{2(1-p+pG_1)(1-b+bG_1)^2}{\alpha b u_1 [2p(1-b+bG_1) + (\alpha-1)b(1-p+pG_1)]} \right\}^{1/2} \quad (23)$$

The value of

$$N(m) \equiv \sum_q N(m, q)$$

is the coefficient of  $u^m$  in the series expansion of the main branch of  $G(u, 1)$  about the origin of  $u$ . This is given by a complex contour integral:

$$N(m) = \frac{1}{2\pi i} \int_C \frac{G(u, 1) du}{u^{m+1}} \quad (24)$$

along a contour  $C$  enclosing the point  $u=0$  in the positive sense but no other singularity of the integrand; in particular not enclosing the points  $u_1$  or  $u_2$ .

The integrand of equation (24) has a saddle-point on the real axis of  $u$ , at which its first derivative is zero and its second derivative positive, at a point  $u=u_s$ ; and as  $m \rightarrow \infty$ ,  $u_s \rightarrow u_1$ . The integrand may be expanded in the vicinity of this saddle-point using equation (22) and the contour of integration may be replaced by the line  $u=u_s+it$ ,  $-\infty < t < \infty$ . Details will be omitted here for brevity; the standard method of approximation of such integrals gives:

$$N(m) \sim (u_1/\pi)^{1/2} (\delta/2) u_1^{-m} m^{-3/2} \quad (25)$$

This can be written in the form:

$$N(m) \sim \text{const. exp}(-m \ln u_1) m^{-3/2} \quad (26)$$

An asymptotic expression of the same form was found<sup>4</sup> for the weight distribution (rather than the number distribution) of crosslinked polymers.

### MOMENTS OF DP

These are obtainable in principle from  $N(m)$ , as given by equation (18), but more readily by applying equation (5). It is, however, preferable to express the derivatives of  $G$  with respect to  $\ln u$  in terms of the derivatives of  $\ln u$  with respect to  $G$ , which are readily obtainable. Equation (15) gives:

$$\ln u = \ln G - \ln(1-p+pG) + \alpha \ln(1-b+bzG) \quad (27)$$

It is convenient to use the notation:

$$(-1)^r \partial^r \ln u / \partial G^r = \lambda_r(u, z) \quad (28)$$

Then:

$$\lambda_r = (r-1)! [1/G^r - p^r / (1-p+pG)^r - \alpha b^r z^r / (1-b+bzG)^r] \quad (29)$$

so that:

$$\lambda_r(1, 1) = (r-1)! (1-p^r - \alpha b^r) \quad (30)$$

Then it is found that:

$$\left. \begin{aligned} \partial G/\partial \ln u &= 1/\lambda_1 \\ \partial^2 G/\partial (\ln u)^2 &= \lambda_2/\lambda_1^3 \\ \partial^3 G/\partial (\ln u)^3 &= -\lambda_3/\lambda_1^4 + 3\lambda_2^2/\lambda_1^5 \\ \partial^4 G/\partial (\ln u)^4 &= \lambda_4/\lambda_1^5 - 10\lambda_2\lambda_3/\lambda_1^6 + 15\lambda_2^3/\lambda_1^7 \end{aligned} \right\} (31)$$

and generally:

$$\partial^i G/\partial (\ln u)^i = \sum_{j=i}^{2i-2} \frac{(-1)^j j!}{\lambda_1^{j+1}} \sum_{k, P_k} \prod \frac{1}{P_k!} \left(\frac{\lambda_k}{k!}\right)^{P_k} (32)$$

The second summation is taken over all sets of values of  $k$  and  $P_k$  such that:

$$k \geq 2; P_k \geq 1; \sum_k P_k = j+1-i; \sum_k k P_k = j (33)$$

Equations (5), (31), and the values (30) for  $\lambda_r(1, 1)$  give:

$$\left. \begin{aligned} \langle m \rangle &= 1/(1-p-\alpha b) \\ \langle m^2 \rangle &= (1-p^2-\alpha b^2)/(1-p-\alpha b)^3 \\ \langle m^3 \rangle &= -2(1-p^3-\alpha b^3)/(1-p-\alpha b)^4 + \\ &\quad 3(1-p^2-\alpha b^2)^3/(1-p-\alpha b)^5 \\ \langle m^4 \rangle &= 6(1-p^4-\alpha b^4)/(1-p-\alpha b)^5 - \\ &\quad 20(1-p^2-\alpha b^2)(1-p^3-\alpha b^3)/(1-p-\alpha b)^6 + \\ &\quad 15(1-p^2-\alpha b^2)^3/(1-p-\alpha b)^7 \end{aligned} \right\} (34)$$

Higher moments can be obtained from equations (5), (30) and (32), but the expressions obtained are complicated.

In the case where branching probabilities are different,  $\alpha b^i$  in equations (30) and (34) must be replaced by

$$\sum_{r=1}^{\infty} b_r$$

The expressions (34) agree with those given by MM for the first and second moments of  $DP$  in their Table 1, and with their conjectured generalizations, which are thus confirmed.

It is easily seen from the general expression (32) that not only the first and second moments, but all the moments, must be finite. The numerators of all the terms in expression given involve the  $\lambda_r$ , which are necessarily finite at  $u=z=1$ , from (30). The denominators are powers of  $\lambda_1$ , which at  $u=z=1$  is  $1-p-\alpha b=1/\langle m \rangle$ . Now  $\langle m \rangle$  cannot become infinite, because it is the ratio of the finite number of molecules of monomer consumed to the number of molecules of dead polymer produced, both these numbers relating to the same volume and time. The latter can never be zero as long as a mutual termination reaction occurs. Though attack on dead polymer by growing radicals may start any given polymer molecule growing again, it does not change the total rate of formation of dead polymer molecules. Hence  $1-p-\alpha b$  must be positive. MM give a more detailed kinetic argument to demonstrate this. Equation (5) shows that there exists an expansion of  $G(u, 1)$  in the vicinity of  $u=1$  in the form:

$$G(u, 1) = \sum_{r=0}^{\infty} \frac{\langle m^r \rangle (\ln u)^r}{r!} (35)$$

whence:

$$\langle m^r \rangle = \frac{r!}{2\pi i} \int_C \frac{G(u, 1) d \ln u}{(\ln u)^{r+1}} (36)$$

The contour is about the origin of  $\ln u$ . The method of steepest descents applied to this yields the asymptotic expression for  $\langle m^r \rangle$  as  $r \rightarrow \infty$ :

$$\langle m^r \rangle \sim r!(u_1 \ln u_1 / \pi)^{1/2} (\delta/2) (\ln u_1)^{-r} r^{-3/2} (37)$$

so that though  $\langle m^r \rangle$  increases with  $r$  without limit, it remains finite.

The fact that all moments are finite implies that all the usual averages of the  $DP$ , which are the ratios of pairs of successive moments, also remain finite for the MM model. This contrasts with the results of Beasley<sup>1</sup>, who implicitly assumed termination by combination to be absent, as in the MM model, but nevertheless found that  $\langle m^2 \rangle$ , and even  $\langle m \rangle$  became infinite under certain conditions. His calculation tacitly assumes that the time for the growth of a branch is negligible in comparison with the time required for the initiation of a new branch, but this cannot be true in the limit of very high degree of polymerization.

#### MOMENTS OF BRANCHING DISTRIBUTION

The  $\langle q^i \rangle$  are more difficult to obtain, as differentiation with respect to  $z$  yields complicated expressions. Thus:

$$\partial G/\partial \ln z = \alpha b z G/\lambda_1(1-b+bzG) (38)$$

and hence from equation (4):

$$\langle q \rangle = \alpha b/(1-p-\alpha b) = \alpha b \langle m \rangle (39)$$

This is the expected result, since  $\alpha b$  is the mean number of branches per monomer unit. Evaluation of  $\partial^2 G/\partial (\ln z)^2$  gives:

$$\langle q^2 \rangle = \alpha^2 b^2 \langle m^2 \rangle + 2\alpha^2 b^2 (1-b) \langle m \rangle^2 + \alpha b (1-b) \langle m \rangle (40)$$

A quantity of interest is the degree of branching,  $\rho = q/m$ ; this is the ratio of the number of branches to the number of monomer units in the polymer molecule. It is to be expected that  $\rho$  will vary with molecular size, since those molecules that happen to have a high degree of branching will grow larger than the others: it is easy to see that for  $m=1$ ,  $\rho=0$ . The dependence of  $\rho$  on  $m$  is difficult to investigate directly, but it is possible to average  $\rho$  over the distribution in various ways which weight the contribution from the higher  $DP$  differently. These give the same kind of information as the different average of  $DP$ . The number, weight,  $z$ , and  $z+1$  averages of  $\rho$  are respectively  $\langle \rho \rangle$ ,  $\langle \rho m \rangle/\langle m \rangle$ ,  $\langle \rho m^2 \rangle/\langle m^2 \rangle$ ,  $\langle \rho m^3 \rangle/\langle m^3 \rangle$ . Since  $\rho = q/m$ , these are also  $\langle m^{-1}q \rangle$ ,  $\langle q \rangle/\langle m \rangle$ ,  $\langle mq \rangle/\langle m^2 \rangle$  and  $\langle m^2q \rangle/\langle m^3 \rangle$ , respectively. If  $\rho$  increases with molecular size, these averages will increase in this order.

The number-average value of  $\rho$ ,  $\langle m^{-1}q \rangle$ , is obtained as follows:

$$\langle m^{-1}q \rangle = \int_0^1 \frac{du}{u} \left[ \frac{\partial G(u, z)}{\partial z} \right]_{z=1} (41)$$

$$= \int_0^1 \alpha b G dG/(1-b+bG) (42)$$

$$= \alpha [1 + (1-b) \ln(1-b)/b] (43)$$

$$= \alpha b \left[ 1/2 + \sum_{r=1}^{\infty} \frac{b^r}{(r+1)(r+2)} \right] (44)$$

The weight-average value of  $\rho$ ,  $\langle q \rangle/\langle m \rangle$  is:

$$\langle q \rangle/\langle m \rangle = \alpha b (45)$$

The weight-average is the average that weights each monomer unit equally. Since, as pointed out above, a molecule having  $q$  branches must contain at least  $q+1$  monomer units, there is an upper limit to the value of  $\alpha b$ . The most highly branched polymer permitted by the MM model is one for which  $p=0$  and every monomer unit added beyond the first constitutes a branch. In this case  $\langle q \rangle$ , the number-average value of  $q$ , which is the weight-average value of  $\rho$ , is  $\langle m \rangle - 1$ , and the maximum value of  $\alpha b$  is  $\alpha b = \langle q \rangle / \langle m \rangle = 1 - 1/\langle m \rangle$ . This is also obtained by setting  $p=0$  in the expression (34) for  $\langle m \rangle$ . Thus  $\alpha b$  can certainly not exceed 1 and  $b$  cannot exceed  $1/\alpha$ , in the MM model, because of the topological implications of the defining conditions. This limitation does not significantly affect the generality of this model.

Using equation (4), one obtains for the  $z$  and  $z+1$  averages of  $\rho$ :

$$\langle m^z q \rangle / \langle m^z \rangle = \alpha b [1 + (1-b) \langle m \rangle^z / \langle m^z \rangle] \quad (46)$$

$$\langle m^{z+1} q \rangle / \langle m^{z+1} \rangle = \alpha b [1 + 3(1-b) \langle m \rangle \langle m^z \rangle / \langle m^{z+1} \rangle - 2b(1-b) \langle m \rangle^3 / \langle m^{z+1} \rangle] \quad (47)$$

These may be written in terms of number, weight, and  $z$  average  $DP$ , which are:

$$\left. \begin{aligned} \bar{P}_N &= \langle m \rangle \\ \bar{P}_W &= \langle m^2 \rangle / \langle m \rangle \\ \bar{P}_Z &= \langle m^3 \rangle / \langle m^2 \rangle \end{aligned} \right\} \quad (48)$$

and the  $z$  and  $z+1$  averages of  $\rho$  become:

$$\langle m^z q \rangle / \langle m^z \rangle = \alpha b [1 + (1-b) \bar{P}_N / \bar{P}_W] \quad (49)$$

$$\langle m^{z+1} q \rangle / \langle m^{z+1} \rangle = \alpha b [1 + 3(1-b) \bar{P}_N / \bar{P}_Z - 2b(1-b) \bar{P}_N^2 / \bar{P}_W \bar{P}_Z] \quad (50)$$

Thus, though the weight-average  $\rho$  is approximately twice the number-average value, the next few averages are not very much greater, as  $\bar{P}_Z \gg \bar{P}_W \gg \bar{P}_N$  when there is much branching.

### ASYMPTOTIC DEGREE OF BRANCHING

It is of interest to investigate the degree of branching  $\bar{\rho}(m)$  for very high  $DP$ . It is possible to show that:

$$\bar{q}(m)N(m) = \alpha b m N(m) + b(1-b) \partial N(m) / \partial b \quad (51)$$

the derivative with respect to  $b$  referring to constant  $m$ ,  $p$  and  $\alpha$ . That is:

$$\bar{\rho}(m) = \alpha b + [b(1-b)/m] \partial \ln N(m) / \partial b \quad (52)$$

From equation (26):

$$(1/m) \partial \ln N(m) / \partial b \sim - \partial \ln u_1 / \partial b \quad (53)$$

and it is found that:

$$\partial \ln u_1 / \partial b = - \alpha (G_1 - 1) / (1 - b + bG_1) \quad (54)$$

Thus the degree of branching is asymptotically given by:

$$\bar{\rho}(m) \sim \alpha b [1 + (1-b)(G_1 - 1) / (1 - b + bG_1)] \quad (55)$$

which can be rearranged to give:

$$\bar{\rho}(m) \sim \alpha b G_1 / (1 - b + bG_1) \quad (56)$$

The degree of branching does not, therefore, increase indefinitely with  $m$ , but levels out. From equation (20), for small  $b$ :

$$G_1 \approx [(1-p)(1-b)/\alpha p b]^{1/2} \quad (57)$$

and the asymptotic value of  $\rho(m)$  is then approximately:

$$\bar{\rho}(m) \sim [\alpha b(1-p)/p(1-b)]^{1/2} \quad (58)$$

which for small  $b$  exceeds the weight-average value of  $\rho$ , i.e.  $\alpha b$  (45). Saito *et al.*<sup>10</sup> have recently shown (for a

rather different model however) that the average number of branch points,  $\bar{q}(m)$  in the present notation, increases at first as the square of the  $DP$  and ultimately linearly with  $DP$ . This behaviour is similar to that found here.

### CONCLUSIONS

When the conditions stated in the Introduction hold, or can be regarded as a reasonable approximation, calculation of the number distribution and the moments of  $DP$  by the generating function method is fairly straightforward. The moments are all finite and so are all the usual averages of  $DP$  for the model used. The degree of branching, defined as the ratio of the number of branches to the number of monomer units, increases at first with  $DP$  but eventually levels out.

MM have compared the results obtained with their model with those obtained by Beasley<sup>1</sup> and Nicolas<sup>2</sup>, and have presented curves showing the relation between  $\bar{P}_W/\bar{P}_N$  and  $b$  for various values of  $\bar{P}_N$ ; it is not necessary therefore to do this here.

### NOMENCLATURE

$\alpha$	Number of potential branching sites per monomer unit
$b_r, b$	Probability of branching at one site
$G \equiv G(u, z)$	Generating function for $N(m, q)$
$G_1 \equiv G(u_1, 1)$	
$\lambda_r = (-1)^{r-1} \partial^r \ln u / \partial G^r$	
$m$	Degree of polymerization ( $DP$ )
$\langle m^j \rangle, \langle m^j q^k \rangle, \langle q^k \rangle$	Averages of $m^j, m^j q^k, q^k$ over the distribution $N(m, q)$ ; i.e. moments
$N(m, q)$	Number fraction of polymer molecules with $m$ monomer units and $q$ branches
$N(m) = \sum_q N(m, q)$	Number fraction of $m$ -mer
$p$	Probability that a polymer radical adds at least one monomer unit
$\bar{P}_N, \bar{P}_W, \bar{P}_Z$	Number, weight, and $z$ averages of $DP$
$q$	Number of (long) branches in a polymer molecule
$\bar{q}(m)$	Average value of $q$ for $m$ -mers
$\rho = q/m$	Degree of branching; average number of branches per monomer unit
$\bar{\rho}(m)$	Average value of $\rho$ for $m$ -mers
$u$	Variable of transformation for $m$
$u_1, u_2$	Branch-points of $G(u, 1)$
$z$	Variable of transformation for $q$

### REFERENCES

- 1 Beasley, J. K. *J. Am. Chem. Soc.* 1953, **75**, 6123
- 2 Nicolas, L. *J. Chim. Phys.* 1958, **55**, 185
- 3 Mullikin, R. V. and Mortimer, G. A. *J. Macromol. Sci.* 1970, **A4** (7), 1495
- 4 Small, P. A. *J. Polym. Sci.* 1955, **18**, 431
- 5 Gordon, M. *Proc. R. Soc.* 1962, **A268**, 240
- 6 Bamford, C. H. and Tompa, H. *Trans. Faraday Soc.* 1954, **50**, 1097
- 7 Feller, W. 'Probability Theory and Its Applications', Wiley, New York, 1950, Vol 1
- 8 Jeffreys, H. 'Asymptotic Approximations', Oxford University Press, Oxford, 1962
- 9 De Bruin, N. G. 'Asymptotic Methods in Analysis', 2nd edn, Noordhoff, Groningen, 1961
- 10 Saito, O., Nagasubramanian, K. and Graessley, W. W. *J. Polym. Sci. (A-2)* 1969, **7**, 1937

# Correlation between molecular parameters and some bulk properties of a plasticized highly crosslinked unsaturated polyester–styrene polymer system:

## 2. Some general rheological properties of the plasticized system

D. Katz and I. Steg

Scientific Department, Israel Ministry of Defence, PO Box 7063, Tel Aviv, Israel  
(Received 6 September 1971; revised 30 March 1972)

A highly crosslinked polyester–styrene system, preswollen and plasticized with different amounts of dioctyl phthalate was investigated. Transition temperatures  $T_c$ , which seem to be very close to the glass transition  $T_g$  of the polymers, were measured in compression, and a numerical relation between the lowering of  $T_c$  with the increasing amount of plasticizer up to 12% by weight was found. A new type of master curve, expressing the stress relaxation of the polymers in the system at a certain temperature as a function of their plasticizer weight fraction content, was suggested.

### INTRODUCTION

Much work has been carried out in the field of plasticized polymers<sup>1–8</sup>, but only a little of it has been reported on highly crosslinked preswollen systems<sup>9</sup>. This investigation was undertaken in order to find the correlation between some molecular parameters of a highly crosslinked unsaturated polyester–styrene system polymerized in the presence of different amounts of plasticizer (preswollen) and a few bulk properties of the final polymer.

### EXPERIMENTAL

#### Materials

The materials used in this work were: Laminac 4116 (American Cyanamid Co.), an unsaturated polyester of the maleic type dissolved in about 30% by wt. of styrene; dioctyl phthalate (DOP) (Fluka A.-G.); Lupersol DDM (Wallace and Tiernan Inc.), a solution of 60% of methyl ethyl ketone peroxide in dimethyl phthalate.

#### Polymer preparation

Proper amounts of Laminac 4116 and DOP were mixed in a closed vessel and degassed for 30 min under decreased pressure (15 mmHg); afterwards, the corresponding amount of Lupersol was added and mixing continued for an additional 5 min. The mixed prepolymeric system was cast into aluminium moulds with Teflon-coated internal walls and cured for 3 h at 60°C and for 3 more hours at 100°C. At the end of the curing period the moulds with the polymer were cooled slowly (5°C/h) to room temperature, opened and polymer blocks of 15 × 8 × 8 cm were obtained for preparation of testing samples.

#### Determination of the degree of crosslinking

In order to determine the degree of crosslinking of the polymers with different amounts of plasticizer the method suggested by Cluff *et al.*<sup>10</sup>, and based on the measurement of equilibrium compression moduli at very small deformations of swollen samples was used.

Cylindrical samples of diameter 10 mm and length 4 mm, made by machining from polymer blocks, were swollen in toluene at 35°C to equilibrium during one week. The samples were placed in a Haake consistometer equipped with an adjustment that made possible compression of the swollen samples between parallel plates, and with a linear variable differential transformer showing deformations with an accuracy of 0.01 mm. Different stresses were applied to the swollen samples and the equilibrium strains were recorded; the stresses applied were small enough to ensure only very small deformations of the swollen samples (up to a few %). The degree of crosslinking for the average network chain length was found by the use of the equation<sup>10</sup>:

$$M_c = \frac{3\rho A_0 R T}{h_0 S} \left[ \frac{V_r}{V_r + V_a} \left( 1 - \frac{V_a}{V_r + V_a + V_s} \right) \right]^{1/3} \quad (1)$$

where  $\rho$  is the polymer density,  $A_0$  the unswollen cross-sectional area,  $h_0$  the height of the unswollen sample,  $R$  the gas constant,  $T$  the absolute temperature,  $S$  the slope of the line expressing the correlation between the force applied and deflection of the swollen sample, and  $V_r$ ,  $V_a$  and  $V_s$  are respectively the volumes of polymer, additives and solvent in the sample.

*Determination of the transition temperature  $T_c$*

Cylindrical samples of diameter 10 mm and length 8 mm, made by machining from polymer blocks, were compression tested in a Haake consistometer under a load of 10 kg. The 10 sec modulus of the samples was determined as a function of temperature, while a steady increase of the sample temperature  $2^\circ\text{C}/\text{min} \pm 0.2^\circ$  was obtained by use of a heating system containing a precise programming and controlling unit. A plot of the compression modulus as a function of temperature showed the characteristic S-shaped curve with the glassy, transition and rubbery regions. The point obtained from the intersection of the straight tangential lines to the glassy and transition region was defined as the transition temperature  $T_c$  of the investigated polymers, a temperature which seems to be very close to their glass transition temperatures  $T_g$ .

*Stress-relaxation experiments*

The stress-relaxation experiments were carried out by compression of cylindrical samples of diameter 6 mm and length 20 mm machined from polymer blocks. Strain gauges of the type K-A1-3 made by Kiowa (Japan) were glued on each sample and on a second dummy sample (in order to compensate for temperature changes) and the terminal leads of the two strain gauges were connected to a Bruel and Kjar strain indicator. The stress relaxation was measured by use of a UG type load cell made by BLH (USA), and connected to a 860 Hewlett-Packard recorder. Thermostatic conditions of the experiment were ensured by immersion of the sample in silicone oil in a glass heat-exchanger connected to a Haake thermostat and equipped with automatic controllers; the accuracy of the

temperature control achieved by this arrangement was about  $0.2^\circ\text{C}$ .

The preset strain was applied to the sample by use of a Hegentogler apparatus to which all the other elements were attached and which consists basically of a table that can be moved up automatically at a controlled speed. The samples were prestrained to a value of 0.1% in all experiments. The assembly for stress-relaxation experiments is shown in Figure 1.

RESULTS AND DISCUSSION

*Degree of crosslinking*

The results of calculation of the degree of crosslinking of the investigated polymers based on the Cluff-Gladding-Pariser method are expressed as the average network chain length between two consecutive points of crosslinking ( $M_c$ ) in Table 1.

It is to be expected that with the increase of crosslink density of the polymer,  $M_c$  should decrease, but the results obtained show, that in spite of the increase of the plasticizer content in the investigated polymers there is no significant change in their degree of crosslinking. It can even be observed, that with the addition of small percentages of DOP the degree of crosslinking slightly increased. Such behaviour can be probably attributed to the decrease of steric hinderance in the system during polymerization due to plasticization, this effect compensating the decrease of the degree of crosslinking occurring as a result of dilution of the system because of the plasticizer addition. A similar behaviour, an increase of the degree of crosslinking, was reported also by Shen<sup>11</sup> in his work on

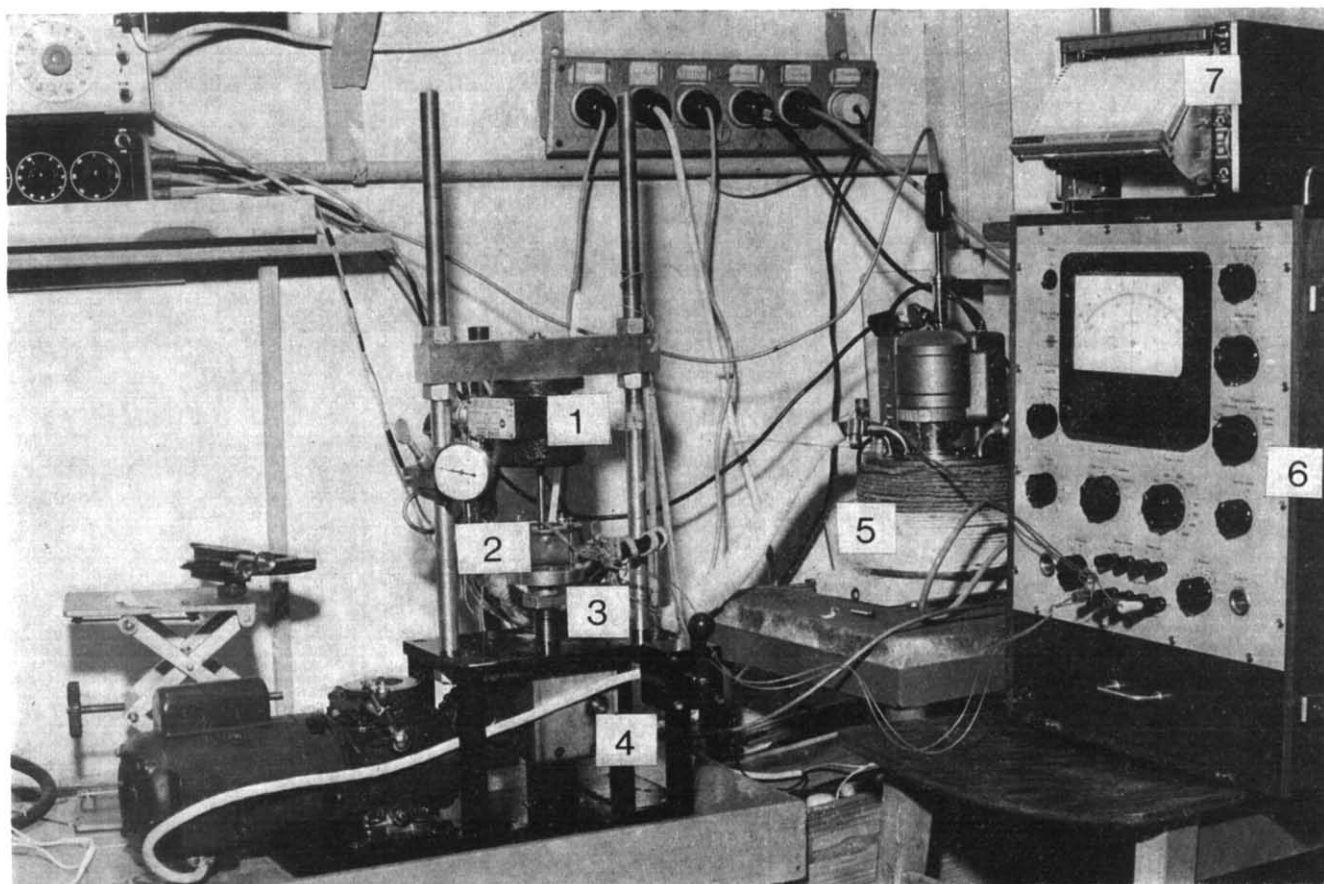
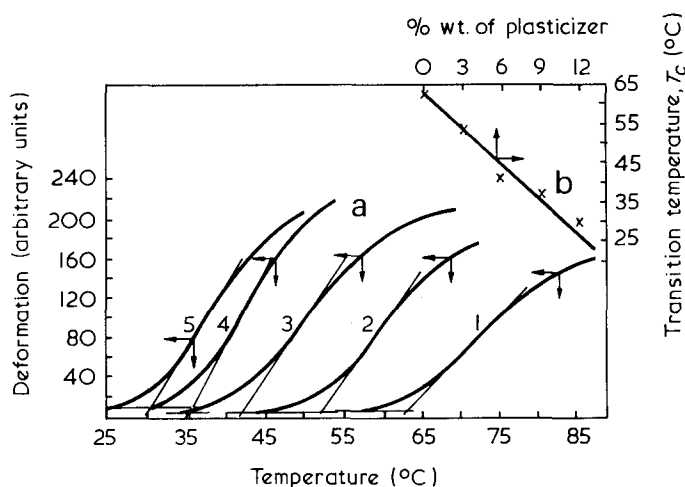


Figure 1 Assembly for stress-relaxation experiments: 1, load cell; 2, conditioning chamber; 3, moving table; 4, gear; 5, thermostat; 6, strain indicator apparatus; 7, recorder

Table 1 Degree of crosslinking of Laminac 4116 plasticized with dioctyl phthalate

DOP (wt.%)	$M_c$	
	At 70°C	At 80°C
0	807	770
3	647	657
6	708	730
9	820	850


 Figure 2 Transition temperatures  $T_c$  of DOP plasticized L-4116 polymers. (a) Determination of  $T_c$ ; (b)  $T_c$  as a function of the plasticizer content. 1, 0% DBP; 2, 3% DBP; 3, 6% DBP; 4, 9% DBP; 5, 12% DBP

slightly crosslinked polymeric systems containing small additions of plasticizers.

#### Lowering of glass transition temperature due to diluent addition

It is well known<sup>11-15</sup> that plasticizer addition depresses the glass transition temperature of thermoplastic polymers linearly at small weight percentages of the additive according to the relation:

$$T_g = T_{g(0)} - kw \quad (2)$$

where  $T_g$  and  $T_{g(0)}$  are glass transition temperatures of the plasticized and unplasticized polymers, respectively,  $w$  is the weight fraction of the diluent and  $k$  is a coefficient which varies for different diluents (e.g. for polystyrene from  $-220$  to  $-560$  K<sup>4</sup>).

When data for the transition temperatures of the polymers investigated in our work, were plotted against percentage of plasticizer, a linear relation was obtained for compositions with diluent content up to 10-12% by wt. (Figure 2b). The following numerical expression can be written for this relation

$$T_c = 335 - 2.7P \quad (3)$$

where  $T_c$  and 335 are the transition temperatures in K of the plasticized and unplasticized polymers, respectively, 2.7 is the average value of the coefficient and  $P$  is the weight fraction of the diluent. An interesting observation can be made, that the same general relation that was found for corresponding weight fractions of diluents in thermoplastic systems described by other investigators, is valid also in the case of the crosslinked polyester polymers.

The transition temperatures for our plasticized systems

( $T_c$ ) were also calculated by use of the relation based on the iso free volume theory and suggested by Bueche<sup>16</sup> for calculation of  $T_g$ :

$$T_c = \frac{\alpha_p V_p T_{kp} + \alpha_d V_d T_{gd}}{\alpha_p V_p + \alpha(1 - V_p)} \quad (4)$$

where  $\alpha$  is the difference between the coefficient of thermal expansion above and below the glass transition,  $V$  is the volume fraction and the indices  $p$  and  $d$  refer to the polymer and diluent respectively. The agreement between the calculated and measured values of  $T_c$  for the different polymers was good as can be seen in Table 2.

#### Time-temperature superposition in plasticized systems

Plots obtained in stress-relaxation experiments for the investigated systems at different temperatures, were reduced to 55°C, shifted along the log time coordinate and master curves were obtained for the systems with different amounts of plasticizer (Figure 3). The possibility of applications of the Williams-Landel-Ferry (WLF) equation<sup>17</sup>:

$$\log a_T = \frac{-C_1(T - T_0)}{C_2 + (T - T_0)} \quad (5)$$

was investigated, and as reference temperatures  $T_0$  the measured transition temperatures ( $T_c$ ) for the different systems were used. The coefficients  $C_1$  and  $C_2$  were obtained from the graphic representation of the relation  $(T - T_c)/\log a_T$  against  $T - T_c$ . The results obtained for  $C_1$  and  $C_2$  are tabulated in Table 3, and as they are reasonably close it seems to us that average values for  $C_1$  and  $C_2$  can be used, and the WLF equation can be applied in its general form.

Although the determination of transition temperatures,  $T_c$ , was done in a rather arbitrary way, the agreement between experimental values and the ones calculated by application of relations characteristic for the glass transition temperature was good. It seems to us reasonable therefore to assume, that the data obtained by the method used for determination of the transition temperatures of the investigated polymers were close to the true glass transition temperatures,  $T_g$ , of the polymers.

 Table 2 Calculated and measured values of  $T_c$  for the investigated polymer system

Plasticizer (wt.%)	$T_c$ measured (°C)	$T_c$ calculated (°C)
0	62	62.0
3	53	51.5
6	45	44.8
9	38	35.5
12	29	28.5

 Table 3 Coefficients  $C_1$  and  $C_2$  in the general form of the WLF equation for plasticized polyester systems

Plasticizer (wt.%)	$T_c$ (°C)	$C_1$		$C_2$	
		Experimental	Average	Experimental	Average
0	62	-4.45		14.5	
3	53	-5.4		11.9	
6	45	-5.72	-5.82	11.2	13.7
9	38	-7.15		14.3	
12	29	-5.6			
15	24	-6.6		16.5	



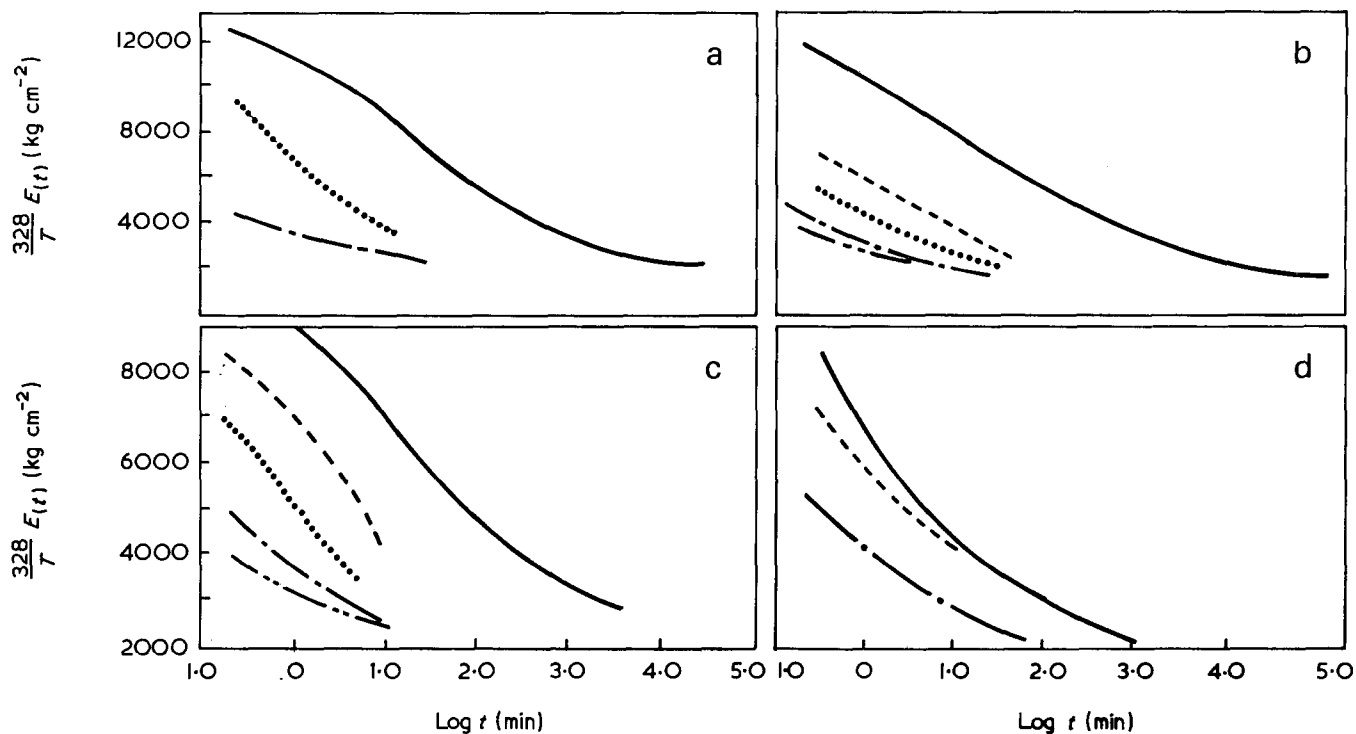


Figure 3 Stress relaxation of L-4116 polymers plasticized with DOP at different temperatures and their master curves reduced to 55°C: (a) 0% DOP; (b) 3% DOP; (c) 6% DOP; (d) 12% DOP. —, 55°C; ---, 65°C; ·····, 75°C; - · - · - ·, 85°C; - - - - - , 90°C [(d) only]; - · - · - · - ·, 95°C

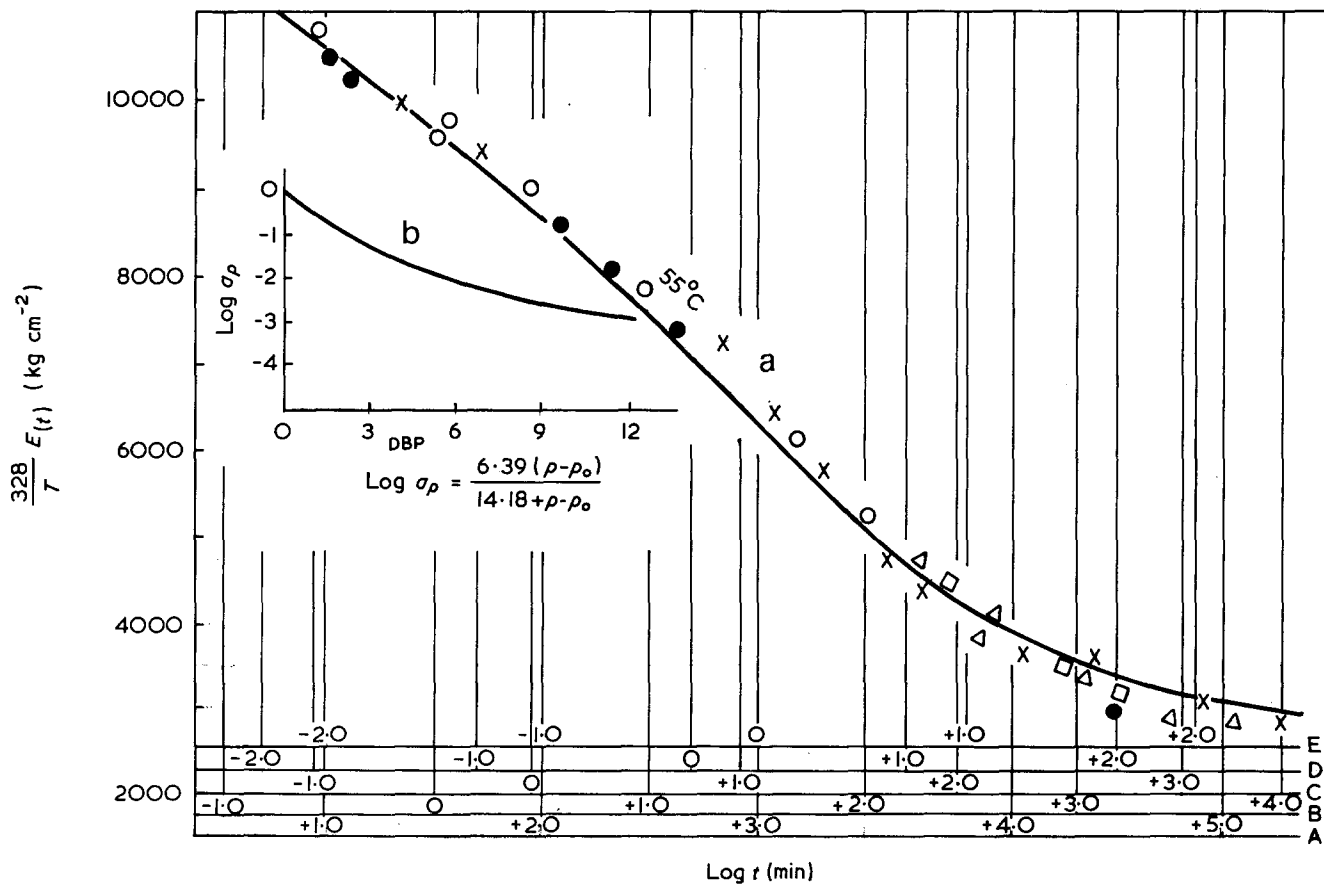


Figure 4 Stress relaxation of the system at 55°C as a function of the DOP weight fraction. (a) General stress relaxation master curve built from master curves each representing the stress relaxation of the same basic system with a different degree of plasticization: A, 0% DOP (O); B, 3% DOP (●); C, 6% DOP (x); D, 9% DOP (Δ); E, 12% DOP (□). (b) Shift factor  $\log a_p$  against DOP content

As in many other cases mentioned in the literature, when  $C_1$  and  $C_2$  were obtained for  $T_0 = T_g$ , the experimental values of  $C_1$  and  $C_2$  in our system differ from  $C_1$  and  $C_2$  in the original WLF equation ( $C_1 = 17.44$ ,  $C_2 = 51.6$ ) and the time-temperature relation characteristics can be represented by:

$$\log a_T = \frac{-5.82(T - T_c)}{13.68 + T - T_c} \quad (6)$$

By use of equation (3) the above relation can be presented in a form that takes into consideration the plasticizer weight fraction in the polymer  $P$ , and:

$$\log a_T = \frac{-5.82[T - (335 - 2.7P)]}{13.68 + T - (335 - 2.7P)} \quad (7)$$

#### Time-diluent fraction superposition

When the master curves, obtained from stress-relaxation measurements at different temperatures and reduced to the same arbitrary temperature,  $T_0 = 55^\circ\text{C}$ , were shifted horizontally along the  $\log$  (time) axis, they superimposed and a new kind of master curve was obtained. This curve represents the stress relaxation of the investigated system at a certain temperature as a function of the plasticizer (diluent) weight fraction (Figure 4). The new correlation can be explained by assuming that the activation energies of flow of chain segments in the polymers are very close, as it has been also found in Part 1 of our work<sup>12</sup>, and by the experimental evidence that crosslink density of the systems is practically unaffected by the amount of plasticizer addition in the investigated range. The shift factor,  $\log a_P$ , expressing the shift of the isothermal master curves for different percentages of plasticizer along the  $\log t$  axis in order to obtain a single curve, can be plotted against the percentage of plasticizer and a hyperbolic curve, very similar to the one representing the relation between  $\log a_T$  and  $T$ , is obtained. The relation between  $\log a_P$  and  $P$  can be expressed by an equation of the WLF type:

$$\log a_P = \frac{C_1^{(P_0)}(P - P_0)}{C_2^{(P_0)} + P - P_0} \quad (8)$$

where  $\log a_P$  is the shift factor due to the diluent content,  $P_0$  is the percentage reference plasticizer and  $C_1^{(P_0)}$  and  $C_2^{(P_0)}$  are coefficients. The two coefficients  $C_1^{(P_0)}$  and  $C_2^{(P_0)}$  can be found from the graphic representation of the

relation  $(P - P_0)/\log a_P$  against  $P - P_0$  as explained earlier, and in this work they are 6.39 and 14.18, respectively.

According to Tobolsky, the time-temperature superposition can be defined by the general equation:

$$\frac{T_0}{T} E_{t, T}(t) = E_{t, T} \left( \frac{t}{a_T} \right) \quad (9)$$

where  $E_t$  is the modulus of relaxation,  $a_T$  is the shift factor,  $T_0$  is the reference temperature and  $t$  is the time of the experiment. Based on our observations, that the diluent (plasticizer) addition has a similar effect on stress relaxation of the polymer as an increase in temperature, we suggest a slightly different form for the previous equation, that takes also into consideration the effect of the diluent (plasticizer):

$$\frac{T_0}{T} E_{t, T, P}(t) = E_{t, T_0, P_0} \left( \frac{t}{a_T + a_P} \right) \quad (10)$$

where  $a_T$  is the shift factor due to temperature changes and  $a_P$  is the shift factor connected with the diluent concentration.

#### REFERENCES

- 1 Aiken, W., Alfrey, T. and Mark, H. *J. Polym. Sci.* 1947, **2**, 178
- 2 Boyer, R. F. and Spencer, S. *J. Polym. Sci.* 1947, **2**, 157
- 3 Jones, H. *J. Soc. Chem. Ind.* 1948, **67**, 415
- 4 Nielsen, L. E., Buchdahl, R. and Lavreault, R. *J. Appl. Polym. Sci.* 1950, **21**, 607
- 5 Doolittle, A. K. 'The Technology of Solvents and Plasticizers', Wiley, New York, 1954
- 6 Mellan, I. 'The Behavior of Plasticizers', Pergamon Press, New York, 1961, Part 3
- 7 Thinius, K. 'Chemie, Physik and Technologie der Weichmacher', Verl. Technik, Berlin, 1960
- 8 Nielsen, L. 'Mechanical Properties of Polymers', Pergamon Press, New York, 1963
- 9 Shen, M. C. *PhD Thesis*, Princeton University, Princeton, 1963
- 10 Cluff, E. F., Gladding, E. K. and Pariser, R. *J. Polym. Sci.* 1960, **45**, 341
- 11 Shen, M. C. and Tobolsky, A. V. *J. Appl. Polym. Sci.* 1965, **3**, 629
- 12 Steg, I. and Katz, D. *J. Appl. Polym. Sci.* 1969, **13**, 2621
- 13 Zhurkov, S. V. and Lehrman, R. I. *Dokl. Acad. Nauk USSR* 1945, **47**, 106
- 14 Jenkel, E. and Heusch, R. *Kolloid Z.* 1953, **130**, 89
- 15 Ferry, J. D. 'Viscoelastic Properties of Polymers', Wiley, New York, 1961, Ch 16
- 16 Bueche, F. 'Physical Properties of High Polymers', Interscience, New York, 1962, Ch 5
- 17 Williams, M. L., Landel, R. F. and Ferry, J. D. *J. Am. Chem. Soc.* 1955, **77**, 3701

# Correlation between molecular parameters and some bulk properties of a plasticized highly crosslinked unsaturated polyester–styrene polymer system:

## 3. Some mechanical properties of the plasticized system

I. Steg and D. Katz

*Scientific Department, Israel Ministry of Defence, PO Box 7063, Tel Aviv, Israel  
(Received 6 September 1971; revised 30 March 1972)*

Some additional rheological properties of a highly crosslinked polyester–styrene (Laminac 4116) polymer preswollen and plasticized with dioctyl phthalate were investigated. The breaking stress and time to break under tensile load at a constant rate of strain were determined as a function of temperature and plasticizer content for the investigated system, and a numerical relation between the different parameters was found.

### INTRODUCTION

In Part 2 of this work a few general rheological properties of a highly crosslinked unsaturated polyester–styrene system polymerized in the presence of different amounts of plasticizer (preswollen) were described<sup>1</sup>. The lowering of the transition temperature measured in compression which is close to the glass transition temperature of the different polymers due to the addition of diluent, the influence of the plasticizer addition on the degree of crosslinking of the system, and the time–temperature superposition principle, were studied. A new type of master curve was suggested expressing the stress relaxation of the polymer system at a certain temperature as a function of the plasticizer (diluent) weight fraction.

More work, reported herewith, was done in a further attempt to correlate some bulk properties of the investigated system with its microstructure. The breaking stress and time to break under tensile load were determined as a function of the temperature and plasticizer content.

The creep and creep recovery behaviour of the system was described earlier<sup>2</sup>.

### EXPERIMENTAL

#### *Materials*

The materials used in this work were: Laminac 4116 (American Cyanamid Co.), an unsaturated polyester of the maleic type dissolved in about 30% by wt of styrene; dioctyl phthalate (DOP) (Fluka A.-G.); Lupersol DDM (Wallace and Tiernan Inc.), a solution of 60% of methyl ethyl ketone peroxide in dimethyl phthalate.

#### *Polymer preparation*

Polymer preparation was described in Part 2 of this work<sup>1</sup>.

#### *Tensile strength measurements*

Specimens for tensile strength measurements were prepared in the form of ‘dumbbells’, with a circular cross-section diameter of 4 mm and length 20 mm, by machining from polymer blocks. The heads of the specimen were held in the grips of a modified Haake consistometer and mechanical arrangements were made in the apparatus in order to assure good alignment during the tensile experiment. The test sample was closed in a conditioning chamber, and strain and time to failure under constant stress at constant temperature were measured by use of linear variable differential transformer connected to a Mosley 860 recorder.

### RESULTS AND DISCUSSION

#### *Time to break under tensile load*

The relation between the log (time to break) or durability of the polymeric samples and the following parameters was studied: stress imposed on the sample, temperature of the experiment and percentage of plasticizer in the polymer.

#### *Durability–stress correlation*

The durability ( $T$ ) of the unplasticized and plasticized samples stressed at different temperatures to break is shown in *Figure 1*. Each set of curves shows the results of experiments carried out with samples of the same composition at different temperatures, and as it can be seen that each family of lines, when extrapolated, intersects in a single point. The equation for each family of lines as suggested by Bartenyev and Zuev<sup>3</sup> is:

$$\sigma - \sigma_0 = S \log(\tau - \tau_0) \quad (1)$$

where  $\sigma_0$  and  $\tau_0$  are the coordinates of the point intersection, and  $S$  is the slope of the line. When the right side

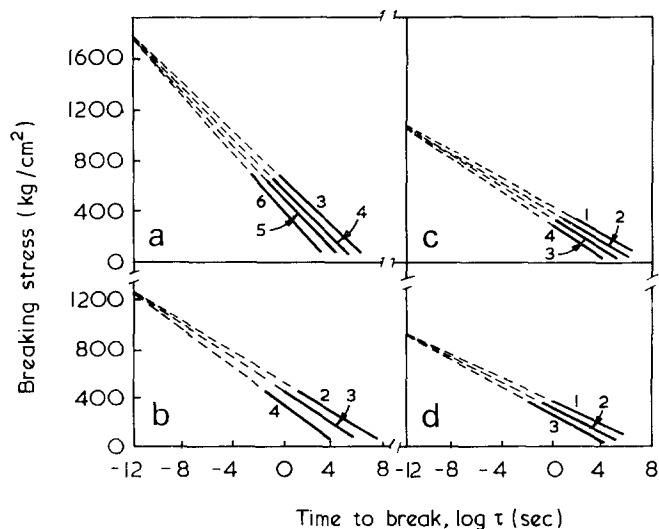


Figure 1 Durability against breaking stress of unplasticized and plasticized L-4116 at different temperatures. (a) 0% DOP; (b) 3% DOP; (c) 6% DOP; (d) 9% DOP. 1, 30°C; 2, 35°C; 3, 40°C; 4, 50°C; 5, 60°C; 6, 70°C

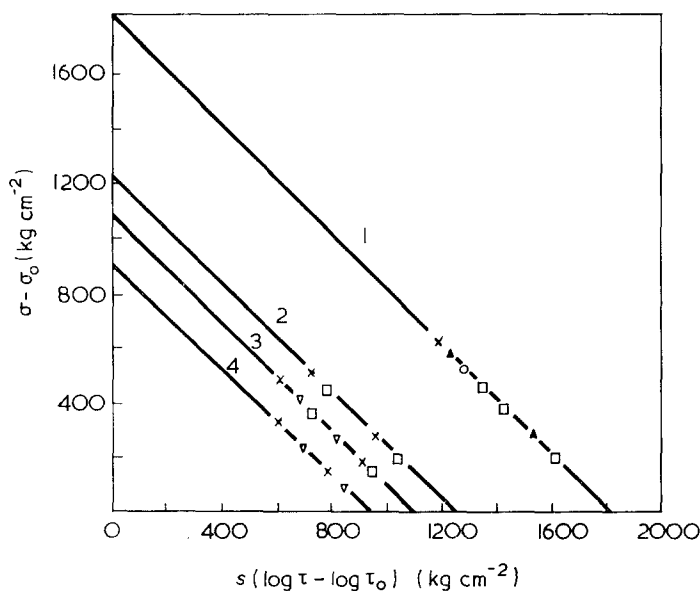


Figure 2 Master curves of durability against tensile breaking stress of the investigated L-4116/DOP polymers. 1, 0% DOP; 2, 3% DOP; 3, 6% DOP; 4, 9% DOP. ▽, 30°C; ×, 40°C; □, 50°C; ○, 60°C; ▲, 70°C

of equation (1) is substituted by  $\Theta$ , the equation can be presented in the simple form:

$$\Theta = \sigma - \sigma_0 \quad (2)$$

and linear master curves based on data from isothermic experiments are built representing the relation between the durability and the tensile breaking strength of a given composition (Figure 2).

In order to construct a master curve, that makes possible the prediction of time to break of a polymer at a temperature  $T_2$  as a function of any stress, the knowledge of durability behaviour of the polymer at one temperature  $T_1$  and one experiment at  $T_2$  are necessary. By some more elaboration and shifting, the master curves representing the durability of the investigated plasticized polyester systems at different temperatures could be shown in the form of one generalized curve with some additional data

for the new shift factor, but from the practical point of view the picture will become too complicated.

#### Durability-plasticizer content correlation in isothermal experiments

When  $\log$  (time to break) of the investigated polymers in isothermal experiments was plotted against breaking stress, a family of straight lines intersecting in one point was obtained for each temperature (Figure 3) and the value of  $\tau_0$  characteristic for the point of intersection

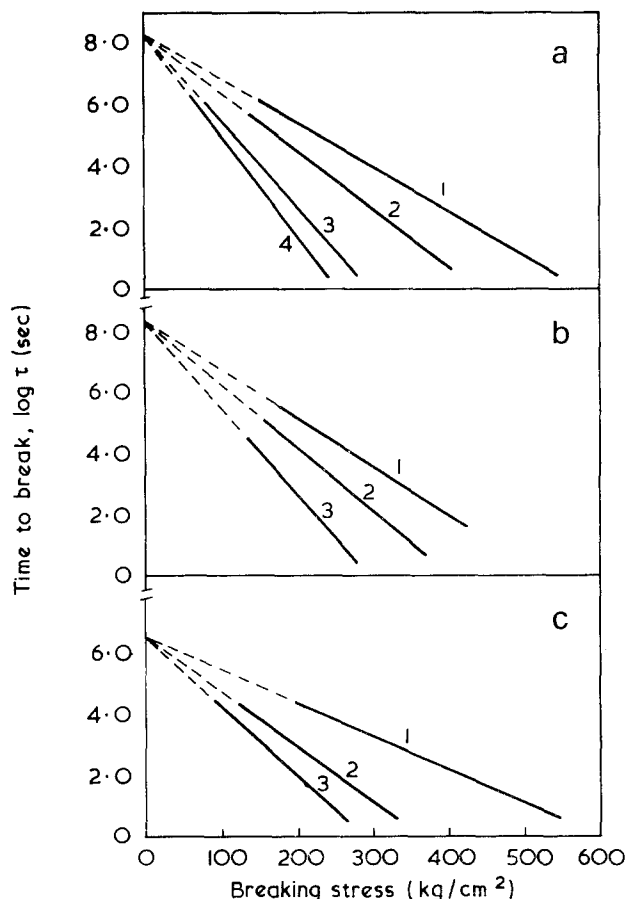


Figure 3 Durability against breaking stress of L-4116 with DOP at (a) 35°C, (b) 40°C, and (c) 60°C. 1, 0% DOP; 2, 3% DOP; 3, 6% DOP; 4, 9% DOP

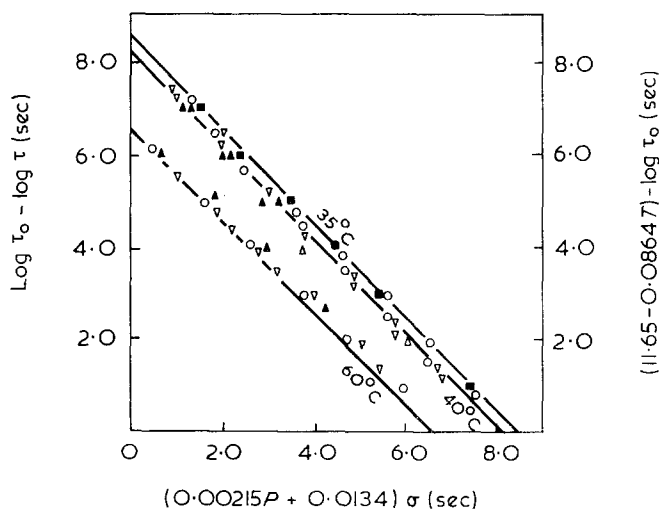


Figure 4 Master curves of durability against  $B\sigma$  for the investigated L-4116/DOP systems;  $B$  is related to wt.% DOP. —, equation (7); ▲, 0% DOP; ○, 3% DOP; ▽, 6% DOP; ■, 9% DOP

decreased with the rise of the temperature of the experiments. A similar general picture was obtained as a result of durability investigation of plasticized viscose fibres<sup>4</sup>. Based on the experimental results an equation for each series of isothermal experiments with different degrees of plastification can be written as follows:

$$\log \tau_0 - \log \tau = B_i \sigma_i \quad (3)$$

where  $B_i$  expresses the inclination of  $\log \sigma$ . As a result of further analysis of the experimental results, equation (3) can be presented in a more general form that takes into consideration the percentage of plasticizer  $P$  in each polymeric system:

$$\log \tau_0 - \log \tau = (mP + q)\sigma \quad (4)$$

and in which

$$B = 0.00215P + 0.0134 \quad (5)$$

The plot of  $\log \tau_0 - \log \tau$  against  $B\sigma$  is shown in *Figure 4*. Because the value of  $\tau_0$  of the polymer changes with temperature, and the experimental relation between  $\log \tau_0$  and temperature can be expressed as:

$$\log \tau_0 = 11.65 - 0.0864T \quad (6)$$

equations (1), (2) and (3) can be presented in a combined form:

$$11.65 - 0.0864T - \log \tau_b = (0.00215P + 0.0134)\sigma \quad (7)$$

and consequently,

$$\log \tau_b = 0.0864T - (0.00215P + 0.0134)\sigma - 11.65 \quad (8)$$

This empirical treatment, which takes into consideration the relation between temperature, percentage of plasticizer and durability, seems to be applicable for the investigated polyester system mainly in its transition region and for plasticizer content up to 10%. Deviations from linear relations are growing with the departure from the transition region in both directions either to the glassy or to the rubbery region.

#### REFERENCES

- 1 Katz, D. and Steg, I. *Polymer* 1971, 13, 541
- 2 Steg, I. and Katz, D. *J. Appl. Polym. Sci.* 1969, 13, 2621
- 3 Bartenyev, G. M. and Zuev, Yu. S. 'Strength and Failure of Viscoelastic Materials', Pergamon Press, Oxford, 1968, p 89
- 4 Zhurkov, S. N. and Abasov, S. A. *Vysokomol. Soedin.* 1961, 3, 430

# Copolymerization of phenylethyne with maleic anhydride

H. Block, M. A. Cowd and S. M. Walker

Department of Inorganic, Physical and Industrial Chemistry,  
University of Liverpool, PO Box 147, Liverpool L69 3BX, UK  
(Received 22 May 1972)

We report the successful free radical copolymerization of phenylethyne with maleic anhydride to give a high molecular weight (up to  $\sim 10^5$ ), alternating copolymer. Some of the chemical and physical properties of this material are described. The possibility of converting this and allied copolymers to conjugated polymers is discussed.

## INTRODUCTION

There have been a number of reports<sup>1-13</sup> on the polymerization of phenyl and allied ethynes. It is the general experience of workers that such homopolymerizations produce polyethynes of low molecular weight, in comparison to the molecular weights frequently realized in vinyl polymerization. Variation in the initiating system has not been really fruitful in improving this situation, although thermal<sup>1, 2, 6</sup>, free radical<sup>3, 4</sup>, radiation<sup>5</sup> and Ziegler-Natta type catalysts<sup>7-13</sup> have been tried.

As materials, polyethynes are of interest owing to the possibilities of semi-conduction. Indeed, polyphenylethyne and its homologues have been shown to possess semi-conducting character<sup>4, 13</sup>, even in those members of limited chain-length. Semi-conduction, as a property, is likely to be enhanced by an increase in the conjugation of the system. It is with this motivation that the described investigation was undertaken.

The cause of the low molecular weights attained in the free radical homopolymerization of phenylethyne has been clarified by the kinetic studies of Berlin and coworkers<sup>3</sup>. Two factors, the decreasing reactivity of the propagating radical with chain length due to conjugation, and the ease of hydrogen atom transfer from phenylethyne, combine to produce short chains in polymerization. To overcome these conflicting factors it would seem that radical activity must be increased, and polymerizing conditions chosen so as to minimize chain transfer. One method of increasing radical activity is to remove the conjugation in the growing polymer chain, by introducing an ethene as comonomer. This would cause breaks in the conjugation of the radical by introducing fully saturated units. There have been reports on the copolymerization of phenylethyne with vinyl comonomers. However, because of the high reactivity of vinyl monomers *vis-à-vis* ethynes, the resulting copolymers have only a low phenylethyne content, and would, in general, not be likely precursors to highly conjugated systems. The choice of comonomer for the present purpose should be one in which its homopolymerization does not override the insertion of the unreactive phenylethyne. Maleic anhydride is an obvious choice, particularly in view of its propensity for forming

alternating copolymers with vinyl monomers<sup>14</sup>. Alternation of phenylethyne and maleic anhydride along the chain would probably confer an increased facility for subsequent conjugation. The situation is shown in *Figure 1*. Case (a) refers to a simple vinyl polymer [for example, poly(vinyl chloride), poly(vinylidene chloride) or polyacrylonitrile] which may be partly conjugated by removal of HX. As illustrated, removal of HX out of sequence along the chain can (and does) lead to retention of tetragonal carbon atoms which break the conjugation. Case (b) schematically illustrates the possible advantages in an ethyne-ethene alternating copolymer (such as phenylethyne-maleic anhydride copolymer). Unsaturation of units, whether by dehydrogenation as shown or by other means, would not lead to an out-of-sequence formation of double bonds.

We report below the synthesis and characterization of a high molecular weight (up to  $\sim 10^5$ ) alternating copolymer of phenylethyne and maleic anhydride. Preliminary reports on some of the chemistry of this polymer are also given. Work on conjugative reactions of this and similar copolymers is in progress.

## EXPERIMENTAL

### Materials

Phenylethyne (Fluka, technical grade) was fractionated, the middle cut (60°C at  $\sim 1$  torr) being collected.

Maleic anhydride was crystallized from chloroform and stored in a desiccator over silica-gel.

The initiator, azodiisobutyronitrile, was crystallized from ethanol.

Only dried solvents and precipitating media were used (acetone, ethyl acetate and but-2-one: molecular sieve; diethyl ether, tetrahydrofuran and petroleum ether: sodium wire). Acetophenone was fractionated under reduced pressure, the middle cut (70°C at  $\sim 1$  torr) being collected.

### Instrumentation

Thermal analysis was undertaken using a Perkin-Elmer DSC/1B differential scanning calorimeter at a heating rate of 16°C min<sup>-1</sup>. Viscosities were measured with

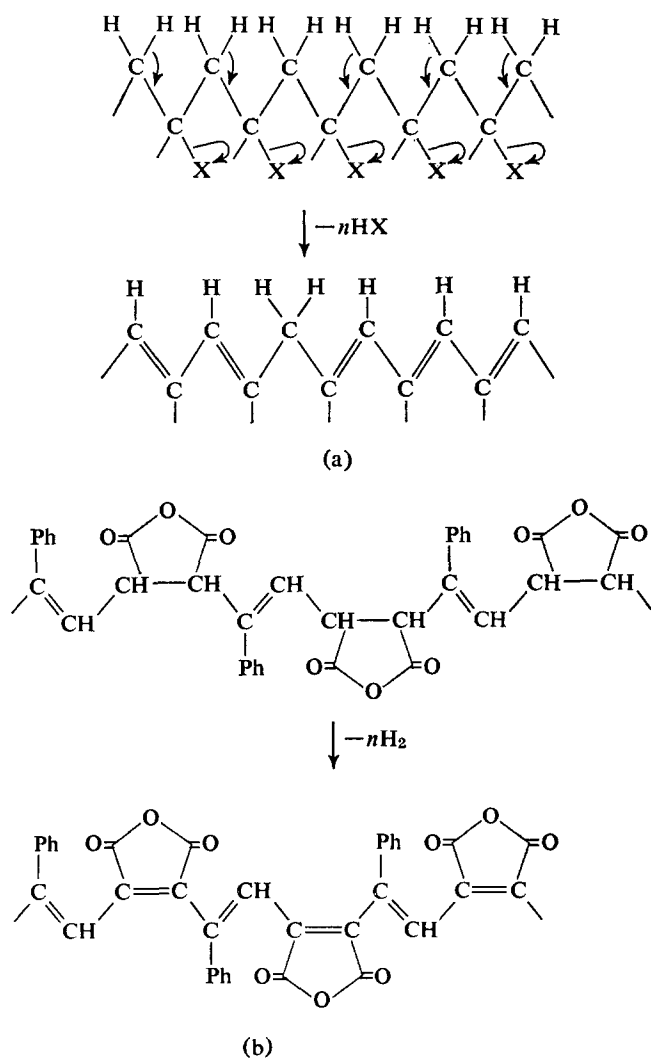


Figure 1 Alternative schemes for the conjugation of a polymer. (a) Method leading to isolated  $sp^3$  carbon; (b) present projected approach

U-tube dilution viscometers at a temperature of  $29.6^\circ \pm 0.1^\circ\text{C}$ . Osmometry and gel permeation chromatography were carried out by the courtesy of the Rubber and Plastics Research Association.

Spectroscopic information was obtained using the following instruments: i.r.—Unicam SP200 spectrophotometer, e.s.r.—Varian E4 spectrometer, n.m.r.—Varian A60 spectrometer.

## COPOLYMERIZATIONS

Mixtures of phenylethyne and maleic anhydride, in equimolar proportions, were subject to free radical *in vacuo* polymerization. This was achieved by initiation with azodiisobutyronitrile, either thermally, or photochemically by irradiation with the 365 nm line of a mercury arc. Details of charge, mode of initiation, solvent, temperature, time of reaction and yield are shown in Table 1. Some thermal initiations were carried out in the absence of solvent. Under such conditions the reaction mixture was heterogeneous, but polymer formation, by consuming maleic anhydride, decreased the bulk of the solid phase as the reaction proceeded. Because elevated temperatures increased the solubility of maleic anhydride, and thermal polymerization in a diluent at  $60^\circ\text{C}$  produced very little polymer,  $98^\circ\text{C}$  was selected for thermal initiation. Polymer was isolated in all experiments by precipitating the reaction mixture into a large excess of dry light petroleum ether (b.p.  $100\text{--}120^\circ\text{C}$ ) and subsequently well washed with anhydrous ether. All polymer samples were vacuum dried and stored over anhydrous silica gel.

Yields with thermal initiator were largest in the absence of a diluent; absence of initiator resulted in no polymer production at  $60^\circ\text{C}$  but some polymer was produced at  $98^\circ\text{C}$ . Photochemical initiation produced polymer in both the absence and presence of azodiisobutyronitrile; however, lower yields were obtained in the former case.

Intrinsic viscosities ( $[\eta]$ ) in acetophenone indicated that photoinitiation produced polymer of higher molecular weight than thermal initiation. Further, a reduced reaction temperature during photoinitiation generally favoured the production of high molecular weight material. These observations are consistent with the view that radical transfer (probably to phenylethyne) occurs<sup>3</sup>. This reaction which produces low molecular weight material, would be expected to have a higher activation energy than propagation; reduction of reaction temperature would then favour propagation rather than transfer. Thus photoinitiation is the preferable synthetic method of initiation.

## COPOLYMER PROPERTIES

Table 2 shows the intrinsic viscosities obtained for a series of copolymers and estimates of number average molecular weight ( $\bar{M}_n$ ) obtained osmotically in

Table 1 Conditions for copolymerization of phenylethyne with maleic anhydride

Sample No.	Maleic anhydride (g)	Phenylethyne ( $\text{cm}^3$ )	Initiator (g azodiisobutyronitrile)	Solvent ( $\text{cm}^3$ )	Polymerizing temperature ( $^\circ\text{C}$ )	Reaction time (h)	Yield (%)
1	4.50	5.0	0.0262 (T)	23 (A)	98	6.5	8
2	4.50	5.0	0.0262 (T)	—	98	6.5	23
3	4.50	5.0	0.0262 (T)	—	98	3	4
4	22.50	25	0.131 (T)	—	98	6.5	30
5	8.83	10.0	0.0163 (T)	—	98	10	20
6	8.83	10.0	0.0295 (T)	—	98	10	22
7	6.24	7.0	0.0109 (P)	11.2 (B)	ambient	9	17
8	6.24	7.0	0.0123 (P)	11.5 (B)	4–6	5	13
9	6.25	7.0	0.0110 (P)	11.5 (B)	ambient	14.5	20
10	6.25	7.0	0.0106 (P)	11.5 (B)	ambient	5	12
11	1.79	2.0	— (T)	—	98	10	21
12	0.37	0.5	— (P)	1.2 (B)	ambient	5	11

T=thermal initiation; P=photochemical initiation; A=acetophenone as solvent; B=but-2-one as solvent

tetrahydrofuran as solvent. For thermally initiated polymer, reliable  $\bar{M}_n$  values were unobtainable because of the diffusion of low molecular weight material across the osmometer membrane. On the basis of photo-initiated polymer the relation:

$$[\eta] = 6.15 \times 10^{-3} \bar{M}_n^{0.80} (\text{cm}^3 \text{g}^{-1})$$

was established for acetophenone at 29.6°C. Polymers were also investigated by gel permeation chromatography with the results indicated in Figure 2. Thermally initiated polymer was found to possess two distinct molecular weight fractions, the lower of which has an estimated  $\bar{M}_n \sim 700$ ; undoubtedly this material is the cause of the diffusion problems in osmometry. The differing nature in thermal polymer of the low molecular weight material from the high molecular weight portion of any) has not been established. However, we discount the possibility that it is a homopolymer of phenylethyne

Table 2 Some properties of a series of copolymers of phenylethyne with maleic anhydride

Sample No.	Intrinsic viscosity (cm <sup>3</sup> g <sup>-1</sup> )	10 <sup>4</sup> $\bar{M}_n$	Analysis <sup>b</sup> (%)	
			C	H
1	—	0.96 <sup>a</sup>	69.7	4.9
3	—	—	70.4	4.7
4	—	—	72.0	4.5
5	19.0	~0.07+5.0 <sup>c</sup>	—	—
6	17.0	~0.07+5.0 <sup>c</sup>	—	—
7	42.0	6.5	—	—
8	53.0	9.1	—	—
9	33.0	5.0	—	—
10	—	—	69.7	4.9

<sup>a</sup> Determined osmotically in acetophenone at 65°C

<sup>b</sup> C<sub>12</sub>H<sub>8</sub>O<sub>3</sub> requires C: 72.0%; H: 4.0%. <sup>c</sup> Estimates from gel permeation data which showed a double peaked distribution

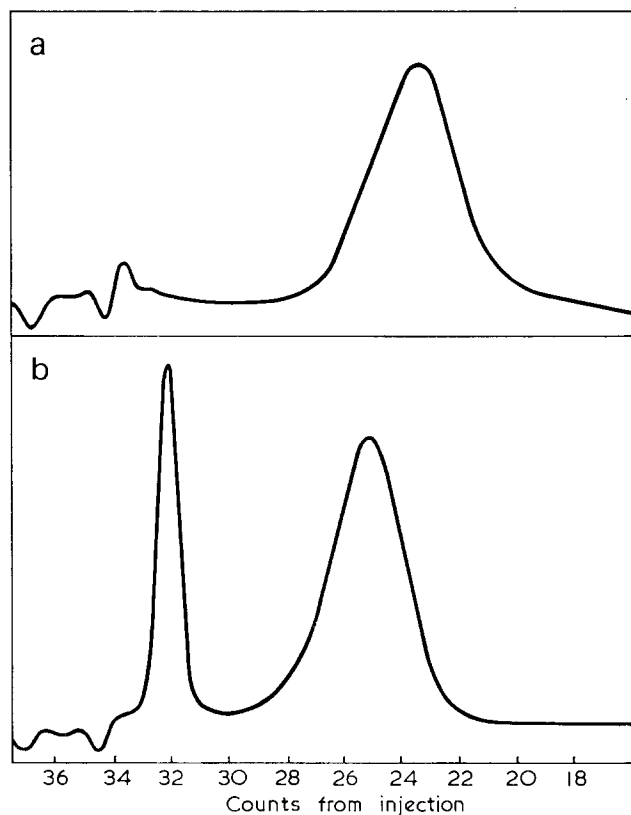


Figure 2 Gel-permeation chromatograms for (a) polymer No. 9 (photoinitiated) and (b) polymer No. 6 (thermally initiated)

on the grounds that no e.s.r. signal or u.v. spectrum due to a polyene<sup>1, 2, 4, 5</sup> could be observed in the bulk polymer sample, nor could the material be extracted from the bulk polymer by benzene or chloroform, both solvents for polyphenylethyne (Farmer, D. B., personal communication). The high molecular weight component peak in the thermal polymer, and the single peak obtained from photoinitiated polymer, show the characteristic, rather broad distribution of a polymer obtained from free radical polymerization taken to significant conversion.

The composition of the copolymers corresponds in both thermal and photochemically initiated systems, to a 1 : 1 phenylethyne-maleic anhydride uptake (Table 2). This ratio strongly suggests alternation of monomers in the copolymer. The chemical analysis (Table 2) is confirmed by infra-red spectra which has anhydride absorption at 1860(m), 1775(s) and 1220(s)cm<sup>-1</sup>, aromatic bands at 1075(w) and 1010(w)cm<sup>-1</sup>, a CH band at 930(s)cm<sup>-1</sup>, and a —C=C— band at 1620(w)cm<sup>-1</sup>. N.m.r. of a photoinitiated copolymer in d<sub>6</sub>-acetone provided a broad band spectrum with a multiplet at 2.95  $\tau$  (5H, phenolic) and absorptions at 4.6  $\tau$  (1H, =CH), 6.6  $\tau$  and 7.7  $\tau$  (both 1H, —CH).

All the polymer samples were found to dissolve unchanged in tetrahydrofuran, acetone, but-2-one, acetophenone, ethyl acetate and *N,N*-formdimethylamide, provided these were pure and dry. Toluene, benzene, aliphatic hydrocarbons, chlorinated alkanes and diethyl ether, were non-solvents for the polymer. The copolymers react with ethanol and rapidly with water to give the half ester and di-acid respectively. (For the di-acid C, 65.6%; H, 4.6%; C<sub>12</sub>H<sub>10</sub>O<sub>4</sub> requires C, 66.1%; H, 4.6%). The latter reaction occurs readily, even in moist air.

Differential scanning calorimetry indicated that the copolymers had a glass-rubber transition at 220° ± 5°C and melted at 260–266°C with decomposition.

#### ACKNOWLEDGEMENTS

The authors wish to thank the Science Research Council for support in this work and for a studentship (M. A. C.). Thanks are due to the staffs of the Polymer Characterization Unit, University of Liverpool and of the British Rubber and Plastics Research Association for osmometric measurements and gel permeation chromatograms, and to the staff of the Department of Organic Chemistry, University of Liverpool for micro-analysis.

#### REFERENCES

- Berlin, A. A. *et al. Vysokomol. Soedin.* 1959, **1**, 1361
- Shantarovich, P. S. and Shlyapnikova, I. A. *Vysokomol. Soedin.* 1961, **3**, 1495
- Barkalov, I. M. *et al. Vysokomol. Soedin.* 1963, **5**, 368
- Hankin, A. G. and North, A. M. *Trans. Faraday Soc.* 1967, **63**, 1525
- Barkalov, I. M. *et al. Vysokomol. Soedin.* 1960, **2**, 1103
- Korshak, V. V. *et al. Vysokomol. Soedin.* 1960, **2**, 1246
- Natta, G. *et al. G. (Montecatini) Ital. Pat.* 530 753 (1955)
- Natta, G. *et al. (Montecatini) Ital. Pat.* 536 899 (1955)
- Berlin, A. A., Cherkashin, M. I. and Kisilitsa, P. P. *Izv. Akad. Nauk SSSR, Ser. Khim.* 1965, p 1875
- Cordischi, D. *et al. Gazz. Chim. Ital.* 1971, **101**, 526
- Berlin, A. A. *et al. Vysokomol. Soedin.* 1964, **6**, 1773
- Berlin, A. A. *et al. Vysokomol. Soedin. (A)* 1967, **9**, 1835
- Berlin, A. A., Cherkashin, M. I. and Chernysheva, I. P. *Izv. Akad. Nauk SSSR, Ser. Khim.* 1967, p 55
- Cubbon, R. C. P. *J. Polym. Sci. (C)* 1967, **16**, 387



# Notes to the Editor

## Flocculation property of the hydrolysis products of carbamoylated polyethylenimine

Norio Ise and Tsuneo Okubo

Department of Polymer Chemistry, Kyoto University, Kyoto, Japan  
(Received 15 August 1972)

In previous papers<sup>1, 2</sup>, the preparation of carbamoylated polyethylenimine (carb.PEI) and its flocculation ability on inorganic suspension have been recorded. In a continuation of our work on polymer flocculants, we describe here briefly the results of exploratory work on the flocculating ability of the hydrolysis products of carb.PEI (HCPEI). From the analogy with the hydrolysis products of polyacrylamide, which is reported to have excellent flocculation properties<sup>3</sup>, it was thought interesting to test the HCPEI.

Polyethylenimine (Separane C-120 of Dow Chemicals, molecular weight about  $10^5$ ) was mixed with dilute aqueous hydrochloric acid solution and with sodium cyanate to obtain carb.PEI. The degrees of carbamoylation were 50% and 100% on the basis of the secondary and primary amine groups. 13% aqueous solutions of these carb.PEI were made alkaline with NaOH, the final concentration being about 4 N. These solutions were heated at 80°C for 8 hours. The hydrolysed polymer salted out and was dried at 50°C under reduced pressure. The degree of hydrolysis, determined by the conductometric titration, was found to be practically unity. The hydrolysis products (hygroscopic white powder), designated as HCPEI (50 : 100) and HCPEI (100 : 100), were obtained at yields of 90 and 83%, respectively. The infra-red (i.r.) spectra showed absorptions at  $1610 \sim 1550 \text{ cm}^{-1}$  and  $1400 \text{ cm}^{-1}$  due to carboxylate groups.

Table 1 gives flocculation properties of HCPEI, carb.PEI and PEI. For experimental details of the determination of the flocculation velocity, the transparency of the supernatant liquid and the precipitate volume, the paper by Ise *et al.*<sup>1</sup> should be consulted.

It is seen that the flocculation velocity by HCPEI is larger than that by carb.PEI, and HCPEI is much more effective than PEI and Sumifloc FC, which are quite inefficient for the system studied. Furthermore, HCPEI (50 : 100) gives a slightly larger velocity than HCPEI (100 : 100).

In most cases, HCPEI gives higher transparency than carb.PEI and especially more so than PEI. At small quantities, HCPEI (50 : 100) gives higher transparency than HCPEI (100 : 100).

The precipitate volume is larger with HCPEI than with carb.PEI and PEI.

Similar experiments were carried out with kaolin and bentonite suspensions. Usually, the hydrolysis increased the flocculation velocity and increased or did not affect the transparency. With these suspensions, also, the flocculation velocity was increased in comparison with PEI. Furthermore, the precipitate volume was smaller with carb.PEI than with PEI.

Table 1 Flocculation properties of HCPEI, carb.PEI, PEI and Sumifloc FC<sup>a</sup> at 23°C  
[Suspension: diatomaceous earth (1%)/H<sub>2</sub>O]

pH	Flocculant	Quantity of flocculant (ppm)	Flocculation velocity (cm min <sup>-1</sup> )	Transparency <sup>b</sup> (%)	Precipitate volume <sup>c</sup> (ml)
5.5	HCPEI (100 : 100)	0.25	19	70	11.8
		0.5	16	78	14.0
		1.5	14	82	13.8
		3.5	14	76	13.0
	HCPEI (50 : 100)	0.25	12	80	11.5
		0.5	19	86	11.2
		1.5	16	73	12.7
	carb.PEI (100)	1.5	12	77	12.2
		PEI	1.5	7	70
	9.0	Sumifloc FC <sup>a</sup>	1.5		No flocculation
1.5				No flocculation	
HCPEI (100 : 100)		2.5	12	60	12.7
		5	13	72	12.0
		15	14	68	12.0
		25	12	64	12.0
HCPEI (50 : 100)		1	19	81	13.1
		2.5	16	82	12.1
		5	12	71	11.2
carb.PEI (100)		5	9	61	9.8
	PEI	5	Very slow	22	8.0
10.2	Sumifloc FC <sup>a</sup>	5-40		No flocculation	
		5-40		No flocculation	
	HCPEI (100 : 100)	2.5	9	50	9.0
		10	9	74	12.0
		25	9	53	10.7
	HCPEI (50 : 100)	1.5	14	58	10.5
		2.5	14	70	10.7
		10	10	67	11.1
	carb.PEI (100)	5	Very slow	31	5.5
		PEI	10	Very slow	31
Sumifloc FC <sup>a</sup>	100		No flocculation		
	100		No flocculation		

<sup>a</sup> A cationic derivative of polyacrylamide.

<sup>b</sup> Measured at 660nm after 8 min of mixing.

<sup>c</sup> Measured after 8 min of mixing.

A detailed account of this work will be published shortly.

### REFERENCES

- Ise, N., Moritani, H. and Okubo, T. *Polymer* 1972, **13**, 187
- Ise, N. and Okubo, T. *Symp. Water-Soluble Polymers* 164th ACS National Meeting, New York, 1972
- Michaels, A. S. and Morelos, O. *Ind. Eng. Chem.* 1955, **47**, 1801

# Gel permeation chromatography: column packing method for polystyrene gels

J. V. Dawkins and M. Hemming

Imperial Chemical Industries Limited, Corporate Laboratory, PO Box 11,  
The Heath, Runcorn, Cheshire WA7 4QE, UK  
(Received 21 July 1972)

Since their introduction by Moore<sup>1</sup>, crosslinked polystyrene gels have been widely used for polymer fractionation by gel permeation chromatography. Techniques for packing these gels into columns have not been reported extensively in the literature. A brief summary of the principles involved can be found in the review article by Altgelt and Moore<sup>2</sup>. A packing technique has been described in detail by Peaker and Tweedale<sup>3</sup>, who obtained columns having plate counts in the range 700–1300 plates per foot (ppf) for polystyrene gels covering the porosity range  $2 \times 10^3$  to  $5 \times 10^6$  Å. Their technique involves balancing the gel in a mixture of acetone and perchloroethylene and then pumping the gel slurry into a column at pressures up to 550 lbf/in<sup>2</sup> with tetrahydrofuran. Acetone, a non-solvent for polystyrene, is used because it opposes the swelling effect of perchloroethylene. Nevertheless, the gel is partly swollen to an extent depending on the crosslink density. In this communication, we describe a packing technique employing a balancing mixture in which both components are non-solvents for linear polystyrene. The crosslinked polystyrene gel is then not swollen by the balancing mixture.

The column packing apparatus is basically similar to that described by Peaker and Tweedale<sup>3</sup> (we thank Dr Peaker for providing details of his technique). Four grades of polystyrene gel, Styragel 10<sup>3</sup>, 10<sup>4</sup>, 10<sup>5</sup> and 10<sup>6</sup> Å, were obtained from Waters Associates. Coarse and fine gel particles were removed according to the recommendations of Peaker and Tweedale<sup>3</sup>. For method A, their balancing and pumping technique was followed except for the use of toluene as pumping fluid instead of tetrahydrofuran. In method B, non-swelling agents were used during balancing and pumping. The sized gel (100 ml), after washing with acetone and drying, was added to 2-chloroethanol (80 ml). (*Caution*: this liquid is extremely toxic and should always be handled in a fume cupboard.) Separate additions of acetone and 2-chloroethanol were made until the gel neither floated nor sank on centrifuging for 2 min at 1500 rev/min. Degassed cyclohexane was placed in the solvent store. After first pumping at 1 ml/min, the rate was gradually raised until the pressure gauge registered at least 1000 lbf/in<sup>2</sup>. Columns obtained by methods A and B were placed in a Waters model 200 gel permeation chromatograph using chloroform as solvent at 35°C. Plate counts were determined by injecting 1% solutions of toluene in chloroform for 15 sec at a flow rate of 1 ml/min. Chromatograms of narrow molecular weight distribution polystyrene standards (Pressure Chemical Co., Pittsburgh) were obtained by injecting 0.25% solutions for 2 min at the same flow rate.

The plate count measurements in *Table 1* indicate a pronounced increase in plate count for 10<sup>3</sup> and 10<sup>4</sup> Å gels with method B. These low porosity gels are not as

*Table 1* Dependence of plate count on packing method

Styragel (Å)	Plate count (ppf)	
	Method A	Method B
10 <sup>3</sup>	680	1100
10 <sup>4</sup>	700	1150
10 <sup>5</sup>	1050	1230
10 <sup>6</sup>	1100	1180

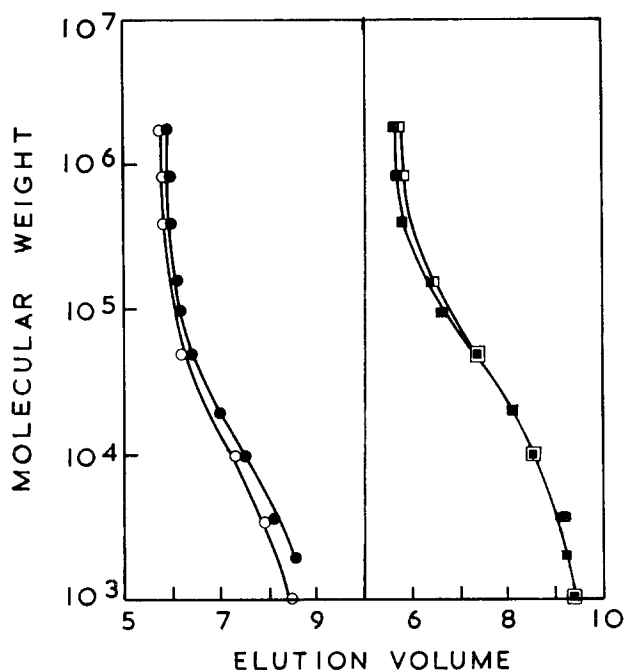


*Figure 1* Molecular weight versus elution volume (counts) calibration for polystyrene. ○, 10<sup>3</sup> Å Styragel; □, 10<sup>4</sup> Å Styragel; open symbols, method A; solid symbols, method B

densely crosslinked as those of higher porosity, and are swollen by good solvents for linear polystyrene. The weight of gel (measured dry) forced into a column by method B is greater than that by method A (about 50% more for 10<sup>3</sup> Å Styragel). The increase in weight of gel packed and plate count are not accompanied by an increase in pressure drop across a column. Since plate count alone is not sufficient for assessing the column resolution of polymers<sup>4,5</sup>, we show, in *Figure 1*, polystyrene calibration curves for columns packed by both methods. These curves indicate that separation power is not greatly changed when method B is employed. Chromatograms for polystyrene samples, representative of the three sections of the 10<sup>4</sup> Å calibration curve, are illustrated in *Figure 2* and indicate that peak-spreading is less for columns packed by method B. Similar observations have been made on columns packed with the

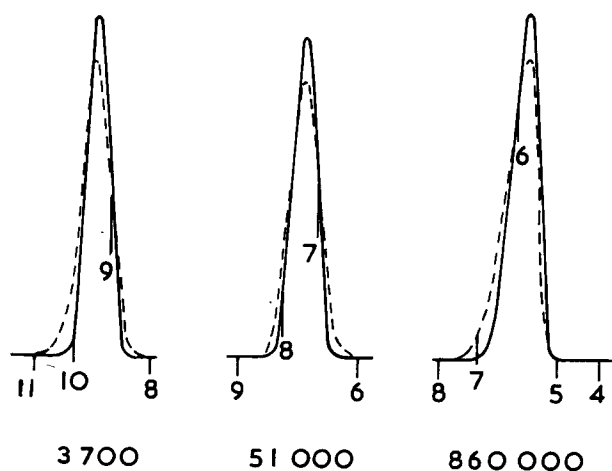


Figure 2 Chromatograms obtained on  $10^4 \text{ \AA}$  Styragel of polystyrenes having peak molecular weights of 3700, 51 000 and 860 000. ----, method A; —, method B

$10^3$ ,  $10^5$  and  $10^6 \text{ \AA}$  gels, but the improvement is most marked for the  $10^3$  and  $10^4 \text{ \AA}$  gels.

In conclusion, method B with non-swelling liquids gives plate counts of 1000 ppf. This technique will be useful when elutions with non-solvents for linear polystyrene are required, e.g. trifluoroethanol<sup>6,7</sup> and acetone<sup>8</sup>. Low porosity polystyrene gel packed by method A will deswell when placed in contact with such non-solvents. Results of gel permeation chromatograph

fractionations with cyclohexane and decalin as theta solvents for linear polystyrene will be reported shortly.

#### ACKNOWLEDGEMENTS

The authors thank Professor J. C. Bevington of Lancaster University for helpful discussions. This work was undertaken as part of the Research Student Community Scheme at the Corporate Laboratory, Runcorn, and as part of a programme to develop gel permeation chromatography for polymer characterization. Techniques and apparatus arising from this programme are being developed commercially by Applied Research Laboratories Ltd, Luton, under licence from ICI Ltd.

#### REFERENCES

- 1 Moore, J. C. *J. Polym. Sci. (A)* 1964, **2**, 835
- 2 Altgelt, K. H. and Moore, J. C. in 'Polymer Fractionation', (Ed. Cantow, M. J. R.), Academic Press, New York, 1967, Ch B4
- 3 Peaker, F. W. and Tweedale, C. R. *Nature* 1967, **216**, 75
- 4 Bly, D. D. *J. Polym. Sci. (C)* 1968, **21**, 13
- 5 Smith, W. V. and Feldman, G. A. *J. Polym. Sci. (A-2)* 1969, **7**, 163
- 6 Dark, W. A., Levangie, R. F. and Bombaugh, K. J. *Proc. 6th Int. Semin. Gel Permeation Chromatography, Miami Beach* 1968, p 414
- 7 Provder, T., Woodbrey, J. C. and Clark, J. H. *Sep. Sci.* 1971, **6**, 101
- 8 Meyerhoff, G. *Makromol. Chem.* 1970, **134**, 129

#### ERRATA

'The thermodynamic properties of liquids, including solutions: Part 2. Polymer solutions considered as ditonic systems', by Maurice L. Huggins, *Polymer* 1971, **12**, 389-399.

Page 395, 4 lines and 3 lines from bottom:  
for  $K=0.74$  read  $K=1.54$  and for  $\epsilon_{\Delta}=2.68$  read  $\epsilon_{\Delta}=268$

We apologize for these errors, resulting from mistyping from an earlier version of the manuscript.

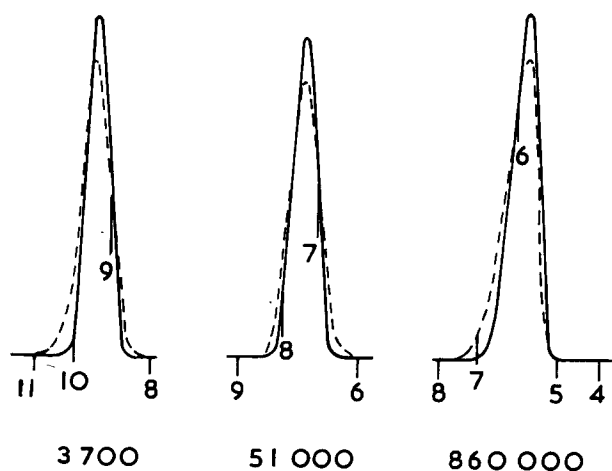


Figure 2 Chromatograms obtained on  $10^4 \text{ \AA}$  Styragel of polystyrenes having peak molecular weights of 3700, 51 000 and 860 000. ----, method A; —, method B

$10^3$ ,  $10^5$  and  $10^6 \text{ \AA}$  gels, but the improvement is most marked for the  $10^3$  and  $10^4 \text{ \AA}$  gels.

In conclusion, method B with non-swelling liquids gives plate counts of 1000 ppf. This technique will be useful when elutions with non-solvents for linear polystyrene are required, e.g. trifluoroethanol<sup>6,7</sup> and acetone<sup>8</sup>. Low porosity polystyrene gel packed by method A will deswell when placed in contact with such non-solvents. Results of gel permeation chromatograph

fractionations with cyclohexane and decalin as theta solvents for linear polystyrene will be reported shortly.

#### ACKNOWLEDGEMENTS

The authors thank Professor J. C. Bevington of Lancaster University for helpful discussions. This work was undertaken as part of the Research Student Community Scheme at the Corporate Laboratory, Runcorn, and as part of a programme to develop gel permeation chromatography for polymer characterization. Techniques and apparatus arising from this programme are being developed commercially by Applied Research Laboratories Ltd, Luton, under licence from ICI Ltd.

#### REFERENCES

- 1 Moore, J. C. *J. Polym. Sci. (A)* 1964, **2**, 835
- 2 Altgelt, K. H. and Moore, J. C. in 'Polymer Fractionation', (Ed. Cantow, M. J. R.), Academic Press, New York, 1967, Ch B4
- 3 Peaker, F. W. and Tweedale, C. R. *Nature* 1967, **216**, 75
- 4 Bly, D. D. *J. Polym. Sci. (C)* 1968, **21**, 13
- 5 Smith, W. V. and Feldman, G. A. *J. Polym. Sci. (A-2)* 1969, **7**, 163
- 6 Dark, W. A., Levangie, R. F. and Bombaugh, K. J. *Proc. 6th Int. Semin. Gel Permeation Chromatography, Miami Beach* 1968, p 414
- 7 Provder, T., Woodbrey, J. C. and Clark, J. H. *Sep. Sci.* 1971, **6**, 101
- 8 Meyerhoff, G. *Makromol. Chem.* 1970, **134**, 129

#### ERRATA

'The thermodynamic properties of liquids, including solutions: Part 2. Polymer solutions considered as ditonic systems', by Maurice L. Huggins, *Polymer* 1971, **12**, 389-399.

Page 395, 4 lines and 3 lines from bottom:  
for  $K=0.74$  read  $K=1.54$  and for  $\epsilon_{\Delta}=2.68$  read  $\epsilon_{\Delta}=268$

We apologize for these errors, resulting from mistyping from an earlier version of the manuscript.

# Book Reviews

## Fillers for plastics

*Edited by W. C. Wake*

Iliffe Books, London, 1971, 152 pp. £3.75

Many of the characteristic properties of rubbers and plastics are achieved by the incorporation of fillers, either in particulate or fibre form. This book brings together much valuable information on these materials and includes many useful tables on their properties. Essentially, the book may be regarded as a short work of reference and from this point of view will be of considerable value to technologists in the rubber, plastics, paint and allied chemical industries. A student of polymer technology will also find it a very useful source of information.

The book, after an introductory chapter on interfacial phenomena, comprises some eight chapters authoritatively written by authors from industry, universities and the Rubber and Plastics Research Association. The subject matter is devoted to the sources and preparation of particulate and fibrous materials as well as their chemical and physical structure. Of particular interest perhaps, are the chapters on fibres (cellulose, glass and asbestos); included in these is one on paper, felts and non-woven fabrics. No attempt has been made to discuss in detail the effects produced by fillers or their mode of action, except in the case of carbon black when some differentiation of the properties of these fillers is made.

The book is well written, well presented and well documented. It certainly succeeds in its objective, namely that of a source of reference. The price is moderate.

*R. H. Peters*

## Polyimide manufacture

*M. W. Ranney*

Noyes Data Corporation, Park Ridge, New Jersey, 1971, 243 pp. \$35

This paper-bound volume, No. 54 of the Chemical Process Reviews series issued by the publishers during the past four years, provides information on polyimides by way of a review of relevant US patents which have appeared since 1962. In all, detailed synopses are given of 103 patents relating to: amide acids, imide esters and imide-amide condensates through which polyimides are prepared; intermediates, condensing and crosslinking agents; processing techniques; special modifications including the introduction of fluorocarbon, silicone and sulphone groupings; fabrication methods; and the use of the products in films, cellular mouldings, electrical insulation, adhesives, and photosensitive compositions.

Over the past decade there has been considerable research and development activity in polyimides and related condensates, particularly in the USA, resulting in the commercial exploitation of a number of heat-resistant polymers for mouldings, coatings and unsupported films, but the actual products used and processes adopted commercially are difficult to relate directly to the examples and methods set out. The title would suggest that industrially established processes are discussed and readers may find the book disappointing in this respect. 'Polyimide Preparation' rather than 'Manufacture' would have been more appropriate.

Dr Ranney deals only with patent specifications and does not attempt to relate any particular disclosures with known commercial practice nor does he include any critical discussion of the processes claimed or of the many patent examples extensively detailed. As an extended summary of US patents on polyimides, the volume will be acceptable but there are limitations to what it offers. No references are made to the non-patent literature (where there are many papers which have a direct bearing on the subject) nor to recent text books dealing with heat-resisting polymers.

The book is essentially of a specialist nature for, while throwing considerable light on the chemistry and processes involved in forming heat-stable polymers of this nature, it can but appeal to

a limited number of people. To those working in the field it provides a convenient method for recourse to this particular facet of the technical literature and may be worth the price of \$35. To others it provides interesting and useful reading on findings arising out of preparative and process research and on some polymer properties and applications although only so far as these relate to results which are presented in US patent specifications.

*R. J. W. Reynolds*

## Polymer networks

*Edited by A. J. Chomppff and S. Newman*

Plenum Press, New York, 1971, 493 pp. \$30.80

This volume is a collection of independent papers, based on the proceedings of an American Chemical Society symposium held in 1970. As would be expected from the title, most of the contributions are connected with the properties of elastomers, though glassy polymers receive some consideration.

While it is difficult to summarize the contents, the general emphasis is on a more detailed theoretical and experimental examination of the mechanical properties of network-type polymers, going beyond the simple statistical theory. The methods brought to bear on these topics include thermoelasticity, swelling, light-scattering and birefringence, as well as the analysis of the form of the stress-strain relations. The processes of network breakdown and rupture also receive attention.

As is usual in collections of this kind the connection between the various papers is rather loose, and the title is not intended to indicate a systematic—much less a comprehensive—treatment of the subject. The reproduction is direct from typescript, with wide variations in style. The collection will be useful for those who can afford the luxury, but one cannot help feeling that the general reader would have been better served by the publication of these papers in the regular journals.

*L. R. G. Treloar*

## Advances in polymer science, Vol. 8

*Edited by H.-J. Cantow et al.*

Springer-Verlag, Berlin, 1971, 237 pp. \$25.50

'Advances in Polymer Science' has been a source of useful and timely reviews for the past eight years. The present volume, which contains four articles, is no exception.

A lengthy review (90 pp) by R. B. Bird, H. R. Warner, Jr. and D. C. Evans of dumb-bell kinetic theory will be useful to a chemist who seeks a molecular interpretation of shear or elongational flow in polymer solutions. The model of polymers in dilute solution which has proved most useful in the interpretation of flow phenomena is the 'string of beads' model. The simplest possible such model is the rigid dumb-bell, which occupies a place polymer solution theory similar to the hard sphere model in the theory of low molecular weight fluids, in that it permits of analytical solutions to problems while retaining a degree of realism which makes these solutions useful in interpretation and prediction. This review is comprehensive and is illustrated by comparison of theory with experimental data or with the corresponding phenomenological theory.

Equally comprehensive in its way is a review (83 pp) by G. Kraus of reinforcement of elastomers by carbon black. Here the problem is not so much the explanation of the elastomeric, rheological and ultimate properties of carbon black filled elastomers in terms of adequate models as the establishment of suitable models in the first place. Appropriately then the earlier sections of this review are devoted to characterization of the systems: the structure and morphology of carbon blacks, the interactions between carbon blacks and elastomers, and the effect of carbon black upon chain stiffness. The rest of the review is concerned with a description and discussion of the properties of carbon black filled elastomers.

## Book Reviews

The predominance of phenomenological interpretation over molecular explanation in this part of the review is a measure of the scope for further study in this area.

More specialized in approach, but of interest to a wide readership, is the review (46 pp) by G. L. Wilkes of the measurement of molecular orientation in solid polymers. Wide-angle X-ray diffraction, birefringence, linear dichroism, sonic behaviour and polarized fluorescence are discussed. These methods are somewhat complimentary and the application of more than one technique to orientation problems is recommended. Costs are given.

The remaining article is a brief (18 pp) critique by P. H. Plesch of cationic polymerization, with particular emphasis on the determination of propagation rate constants ( $k_p$ ). This is a field of study fraught with dangers for the novice because of the complexities of the systems. Criteria by which determinations (past and future) of  $k_p$  may be judged are discussed. It is regrettable, though not surprising, that the list of values of  $k_p$  which survive scrutiny is so short.

C. Booth

### Physicochemical characteristics of oligonucleotides and polynucleotides

Borek Janik

Plenum Press, New York, 1971, 213 pp. \$16.24

This is not a book on the physical chemistry of nucleic acids; it is, instead, a list of acid/base dissociation constants, absorptivities and 'melting temperatures' of synthetic oligo- and poly-nucleotides. These have been culled from 289 papers published over the last decade or so up to the end of 1970. The preface makes it clear that the collection is only representative and that the author has not attempted to include every published and relevant measurement. To fill certain gaps, attention is drawn to other similar compilations that are readily available.

Relevant experimental conditions of solvent composition, temperature etc. have been recorded in the tables, for without

these, the properties and parameters listed for these polyelectrolytes would be virtually meaningless. On the other hand, there has been little attempt to critically assess the data listed; in many cases several discordant values of the same parameter, measured under similar conditions are given and it is anybody's guess as to which is the better. It is striking that in but very few cases, there is no listed estimation of the uncertainty of the various parameters though random checks suggest that this is the fault of the original authors rather than the compiler of this volume. For these reasons it is possible that research workers in the field of physical biochemistry to whom this book appears to be addressed will find it more useful as a guide to the literature than as a source of precise and useful data.

The introductions to the three sections which explain the tables are terse, not always clear and sometimes ambiguous. For instance it may be satisfactory to define the  $pK$  of a simple monovalent acid as the negative logarithm of the dissociation constant (thermodynamic or practical?) but what exactly is the apparent  $pK_a$  of a polyelectrolyte? The reader's attention is brought to bear on the distinction between thermal, residual and total hypochromicity but it is not always clear which of these is listed in the tables; moreover it should be noted that the magnitude of thermal hypochromicity is rarely adequately defined since a completely denatured state can rarely be attained in aqueous solution below 100°C. The values of mean residue absorptivities quoted are sometimes based on analysis for phosphate and sometimes on concentration measurements obtained from the absorbance of a hydrolysate; the latter values, of course, depend on the values assumed for the standard absorptivities on the hydrolysis products; there are three currently used sets of standard absorptivities which are not fully concordant; this is glossed over in these tables.

The book is well bound in hard covers and the text is reproduced from a typescript. Random sampling detected no errors except a few numbers that had obviously crept into the wrong column. Individual purchasers may however feel that \$16.24 is a lot to pay for a collection of literature references; no doubt libraries will wish to acquire it.

E. G. Richards

### Conference Announcement

10 - 14 September 1973

The Chemical Society

## IUPAC International Symposium on Macromolecules

University of Aberdeen, Scotland

The programme will be arranged in the following two main sections, running in parallel throughout the Meeting: *Synthesis and Manufacture* and *Physical and Technological Aspects*. Emphasis will be given to the relationship between the science and technology of polymers. Each section will consist of a limited number of invited lectures and contributed papers.

The Programme Committee will consider contributed papers of special interest and novelty in relation to the following topics with major emphasis on Thermoplastic Polymers and Elastomers, and in particular the relationship between any of these topics: (1) The Manufacture of Polymers; (2) Synthesis of Polymers; (3) Science and Technology of Fluid Polymers; and (4) Science and Technology of Solid Polymers. Those wishing to present a paper should apply to Dr John F. Gibson, The Chemical Society, Burlington House, London W1V 0BN for the form of a submission of a communication, which should be returned together with the abstract not later than 1 January 1973.

Further details about registration, accommodation, travel, social and ladies' programme will be available in February 1973.

# Book Reviews

## Fillers for plastics

*Edited by W. C. Wake*

Iliffe Books, London, 1971, 152 pp. £3.75

Many of the characteristic properties of rubbers and plastics are achieved by the incorporation of fillers, either in particulate or fibre form. This book brings together much valuable information on these materials and includes many useful tables on their properties. Essentially, the book may be regarded as a short work of reference and from this point of view will be of considerable value to technologists in the rubber, plastics, paint and allied chemical industries. A student of polymer technology will also find it a very useful source of information.

The book, after an introductory chapter on interfacial phenomena, comprises some eight chapters authoritatively written by authors from industry, universities and the Rubber and Plastics Research Association. The subject matter is devoted to the sources and preparation of particulate and fibrous materials as well as their chemical and physical structure. Of particular interest perhaps, are the chapters on fibres (cellulose, glass and asbestos); included in these is one on paper, felts and non-woven fabrics. No attempt has been made to discuss in detail the effects produced by fillers or their mode of action, except in the case of carbon black when some differentiation of the properties of these fillers is made.

The book is well written, well presented and well documented. It certainly succeeds in its objective, namely that of a source of reference. The price is moderate.

*R. H. Peters*

## Polyimide manufacture

*M. W. Ranney*

Noyes Data Corporation, Park Ridge, New Jersey, 1971, 243 pp. \$35

This paper-bound volume, No. 54 of the Chemical Process Reviews series issued by the publishers during the past four years, provides information on polyimides by way of a review of relevant US patents which have appeared since 1962. In all, detailed synopses are given of 103 patents relating to: amide acids, imide esters and imide-amide condensates through which polyimides are prepared; intermediates, condensing and crosslinking agents; processing techniques; special modifications including the introduction of fluorocarbon, silicone and sulphone groupings; fabrication methods; and the use of the products in films, cellular mouldings, electrical insulation, adhesives, and photosensitive compositions.

Over the past decade there has been considerable research and development activity in polyimides and related condensates, particularly in the USA, resulting in the commercial exploitation of a number of heat-resistant polymers for mouldings, coatings and unsupported films, but the actual products used and processes adopted commercially are difficult to relate directly to the examples and methods set out. The title would suggest that industrially established processes are discussed and readers may find the book disappointing in this respect. 'Polyimide Preparation' rather than 'Manufacture' would have been more appropriate.

Dr Ranney deals only with patent specifications and does not attempt to relate any particular disclosures with known commercial practice nor does he include any critical discussion of the processes claimed or of the many patent examples extensively detailed. As an extended summary of US patents on polyimides, the volume will be acceptable but there are limitations to what it offers. No references are made to the non-patent literature (where there are many papers which have a direct bearing on the subject) nor to recent text books dealing with heat-resisting polymers.

The book is essentially of a specialist nature for, while throwing considerable light on the chemistry and processes involved in forming heat-stable polymers of this nature, it can but appeal to

a limited number of people. To those working in the field it provides a convenient method for recourse to this particular facet of the technical literature and may be worth the price of \$35. To others it provides interesting and useful reading on findings arising out of preparative and process research and on some polymer properties and applications although only so far as these relate to results which are presented in US patent specifications.

*R. J. W. Reynolds*

## Polymer networks

*Edited by A. J. Chomppff and S. Newman*

Plenum Press, New York, 1971, 493 pp. \$30.80

This volume is a collection of independent papers, based on the proceedings of an American Chemical Society symposium held in 1970. As would be expected from the title, most of the contributions are connected with the properties of elastomers, though glassy polymers receive some consideration.

While it is difficult to summarize the contents, the general emphasis is on a more detailed theoretical and experimental examination of the mechanical properties of network-type polymers, going beyond the simple statistical theory. The methods brought to bear on these topics include thermoelasticity, swelling, light-scattering and birefringence, as well as the analysis of the form of the stress-strain relations. The processes of network breakdown and rupture also receive attention.

As is usual in collections of this kind the connection between the various papers is rather loose, and the title is not intended to indicate a systematic—much less a comprehensive—treatment of the subject. The reproduction is direct from typescript, with wide variations in style. The collection will be useful for those who can afford the luxury, but one cannot help feeling that the general reader would have been better served by the publication of these papers in the regular journals.

*L. R. G. Treloar*

## Advances in polymer science, Vol. 8

*Edited by H.-J. Cantow et al.*

Springer-Verlag, Berlin, 1971, 237 pp. \$25.50

'Advances in Polymer Science' has been a source of useful and timely reviews for the past eight years. The present volume, which contains four articles, is no exception.

A lengthy review (90 pp) by R. B. Bird, H. R. Warner, Jr. and D. C. Evans of dumb-bell kinetic theory will be useful to a chemist who seeks a molecular interpretation of shear or elongational flow in polymer solutions. The model of polymers in dilute solution which has proved most useful in the interpretation of flow phenomena is the 'string of beads' model. The simplest possible such model is the rigid dumb-bell, which occupies a place polymer solution theory similar to the hard sphere model in the theory of low molecular weight fluids, in that it permits of analytical solutions to problems while retaining a degree of realism which makes these solutions useful in interpretation and prediction. This review is comprehensive and is illustrated by comparison of theory with experimental data or with the corresponding phenomenological theory.

Equally comprehensive in its way is a review (83 pp) by G. Kraus of reinforcement of elastomers by carbon black. Here the problem is not so much the explanation of the elastomeric, rheological and ultimate properties of carbon black filled elastomers in terms of adequate models as the establishment of suitable models in the first place. Appropriately then the earlier sections of this review are devoted to characterization of the systems: the structure and morphology of carbon blacks, the interactions between carbon blacks and elastomers, and the effect of carbon black upon chain stiffness. The rest of the review is concerned with a description and discussion of the properties of carbon black filled elastomers.

## Book Reviews

The predominance of phenomenological interpretation over molecular explanation in this part of the review is a measure of the scope for further study in this area.

More specialized in approach, but of interest to a wide readership, is the review (46 pp) by G. L. Wilkes of the measurement of molecular orientation in solid polymers. Wide-angle X-ray diffraction, birefringence, linear dichroism, sonic behaviour and polarized fluorescence are discussed. These methods are somewhat complimentary and the application of more than one technique to orientation problems is recommended. Costs are given.

The remaining article is a brief (18 pp) critique by P. H. Plesch of cationic polymerization, with particular emphasis on the determination of propagation rate constants ( $k_p$ ). This is a field of study fraught with dangers for the novice because of the complexities of the systems. Criteria by which determinations (past and future) of  $k_p$  may be judged are discussed. It is regrettable, though not surprising, that the list of values of  $k_p$  which survive scrutiny is so short.

C. Booth

### Physicochemical characteristics of oligonucleotides and polynucleotides

Borek Janik

Plenum Press, New York, 1971, 213 pp. \$16.24

This is not a book on the physical chemistry of nucleic acids; it is, instead, a list of acid/base dissociation constants, absorptivities and 'melting temperatures' of synthetic oligo- and poly-nucleotides. These have been culled from 289 papers published over the last decade or so up to the end of 1970. The preface makes it clear that the collection is only representative and that the author has not attempted to include every published and relevant measurement. To fill certain gaps, attention is drawn to other similar compilations that are readily available.

Relevant experimental conditions of solvent composition, temperature etc. have been recorded in the tables, for without

these, the properties and parameters listed for these polyelectrolytes would be virtually meaningless. On the other hand, there has been little attempt to critically assess the data listed; in many cases several discordant values of the same parameter, measured under similar conditions are given and it is anybody's guess as to which is the better. It is striking that in but very few cases, there is no listed estimation of the uncertainty of the various parameters though random checks suggest that this is the fault of the original authors rather than the compiler of this volume. For these reasons it is possible that research workers in the field of physical biochemistry to whom this book appears to be addressed will find it more useful as a guide to the literature than as a source of precise and useful data.

The introductions to the three sections which explain the tables are terse, not always clear and sometimes ambiguous. For instance it may be satisfactory to define the  $pK$  of a simple monovalent acid as the negative logarithm of the dissociation constant (thermodynamic or practical?) but what exactly is the apparent  $pK_a$  of a polyelectrolyte? The reader's attention is brought to bear on the distinction between thermal, residual and total hypochromicity but it is not always clear which of these is listed in the tables; moreover it should be noted that the magnitude of thermal hypochromicity is rarely adequately defined since a completely denatured state can rarely be attained in aqueous solution below 100°C. The values of mean residue absorptivities quoted are sometimes based on analysis for phosphate and sometimes on concentration measurements obtained from the absorbance of a hydrolysate; the latter values, of course, depend on the values assumed for the standard absorptivities on the hydrolysis products; there are three currently used sets of standard absorptivities which are not fully concordant; this is glossed over in these tables.

The book is well bound in hard covers and the text is reproduced from a typescript. Random sampling detected no errors except a few numbers that had obviously crept into the wrong column. Individual purchasers may however feel that \$16.24 is a lot to pay for a collection of literature references; no doubt libraries will wish to acquire it.

E. G. Richards

### Conference Announcement

10 - 14 September 1973

The Chemical Society

## IUPAC International Symposium on Macromolecules

University of Aberdeen, Scotland

The programme will be arranged in the following two main sections, running in parallel throughout the Meeting: *Synthesis and Manufacture* and *Physical and Technological Aspects*. Emphasis will be given to the relationship between the science and technology of polymers. Each section will consist of a limited number of invited lectures and contributed papers.

The Programme Committee will consider contributed papers of special interest and novelty in relation to the following topics with major emphasis on Thermoplastic Polymers and Elastomers, and in particular the relationship between any of these topics: (1) The Manufacture of Polymers; (2) Synthesis of Polymers; (3) Science and Technology of Fluid Polymers; and (4) Science and Technology of Solid Polymers. Those wishing to present a paper should apply to Dr John F. Gibson, The Chemical Society, Burlington House, London W1V 0BN for the form of a submission of a communication, which should be returned together with the abstract not later than 1 January 1973.

Further details about registration, accommodation, travel, social and ladies' programme will be available in February 1973.



# A correlation between critical tensile strength and polymer cross-sectional area

P. I. Vincent

Imperial Chemical Industries Limited, Plastics Division, Welwyn Garden City, Herts, UK  
(Received 26 July 1972)

The brittle point of un-notched specimens occurs when the tensile yield stress is equal to a critical value of the tensile breaking stress. This critical tensile strength correlates well with the molecular cross-sectional area as calculated from crystallographic data or models. This finding accounts for some apparent anomalies found when trying to relate impact behaviour with dynamic mechanical data.

## INTRODUCTION

Heijboer<sup>1</sup> has reviewed the possibility that there is a useful correlation between the positions of mechanical damping peaks and the tough-brittle transitions of un-notched specimens in impact for a range of thermoplastics. He concluded that 'a dynamic mechanical damping peak is not always accompanied by a transition in the impact strength' and conversely that 'a large increase in the impact strength can occur without the presence of a pronounced damping peak'.

The author has pointed out previously<sup>2</sup> that the brittle point of un-notched specimens can be defined as the temperature at which the tensile yield stress equals the tensile brittle strength. The brittle point therefore depends partly on the temperature-dependence of the yield stress and it is possible to argue<sup>2</sup> that this accounts for many of the apparent relations between dynamic mechanical properties and impact behaviour. However, the temperature of the tough-brittle transition also depends on the brittle strength, which is not related to dynamic mechanical loss processes. The object of this paper is to show that the brittle strength of thermoplastics is dependent on the effective cross-sectional area of the molecule and that this dependence can explain some of the apparent anomalies reported by Heijboer<sup>1</sup>. A note on the results of this work has been published previously<sup>3</sup>.

## CRITICAL TENSILE STRENGTH

Figure 1 shows the results of some tensile tests performed by a method described elsewhere<sup>4</sup>. The tensile yield stress is plotted above the brittle point and the tensile brittle strength is plotted below the brittle point. These brittleness temperatures were +50°C for poly(methyl methacrylate) (PMMA) and -100°C for the oxymethylene copolymer (POM). This difference between the brittle points of un-notched specimens of these two polymers can be partly explained by their different trends of tensile yield stress with temperature. However, it is also important to note that the critical stress at which ductile fracture changes to brittle fracture is about three times higher for POM than for PMMA. If POM became brittle at the

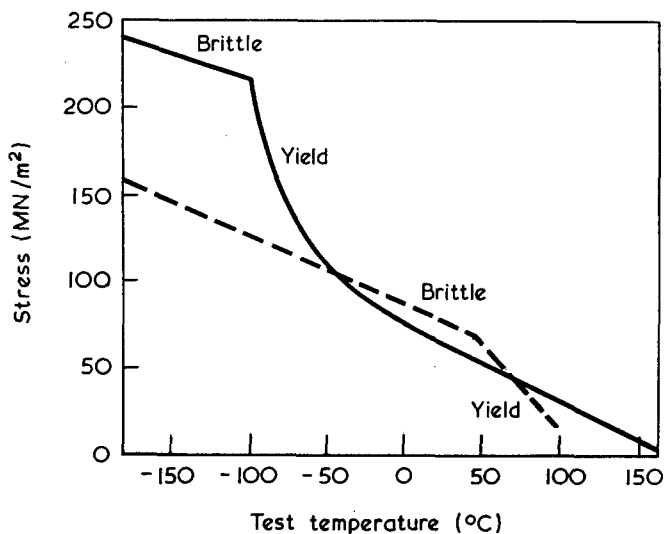


Figure 1 Yield stress and brittle strength in tension for samples of polyoxymethylene (—) and poly(methyl methacrylate) (---) as functions of test temperature

same stress as PMMA, its brittle point would be about +15°C instead of -100°C. It is therefore essential, when trying to relate the brittle point of polymers to their chemical constitution, to take account of the factors affecting the critical tensile brittle strength.

It is known<sup>2,4</sup> that the brittle strength is affected by changes in molecular weight, molecular orientation and the presence of defects. Therefore, when measuring the critical tensile strength, it is necessary to take certain precautions:

(1). The average molecular weight of the sample should be sufficiently high so that further increase does not significantly increase the brittle strength.

(2). The sample should be sufficiently nearly isotropic so that tests in different directions give essentially the same results. Particular care is needed with injection moulded tensile specimens, when the melt flow is along the extension direction, since the resulting anisotropy can give a false measure of the brittle strength of isotropic specimens.

Table 1 Estimated critical tensile brittle strengths

Polymer	Abbreviation	Critical stress (MN/m <sup>2</sup> )	Temperature (°C)
Poly(4-methyl pentene-1)	P4MP	53	-30
Poly(methyl methacrylate)	PMMA	68	+60
Poly(pentene-1)	PPe	58	-60
Poly(butene-1)	PB	81	-100
Polypropylene	PP	98	-120
Poly(vinyl chloride)	PVC	142	-80
Polytetrafluoroethylene	PTFE	117	-196
Polycarbonate of Bisphenol A	PC	145	-140
Polyethersulphone	PES	148	-180
Poly(ethylene terephthalate) <sup>5</sup>	PET	155	-100
Polyethylene	PE	160	-196
Poly(hexamethylene adipamide)	Ny	179	-100
Polyoxymethylene	POM	216	-100

(3). The specimens should be free of any obvious defects such as poorly machined surfaces, contamination, holes or cracks, which might tend to reduce the brittle strength.

During the last eight years, tensile tests over wide temperature ranges have been performed on samples of many thermoplastics for a variety of reasons. The records of the results of these tests have been re-examined and the highest yield stress obtained for each polymer has been taken as a lower limiting estimate of the critical tensile strength. For polyethylene and polytetrafluoroethylene it is probable that the estimates are too low because good, high molecular weight, isotropic specimens were ductile at -196°C which was the lowest test temperature used. With this reservation, the estimated critical tensile strength and the relevant test temperature are given in Table 1 for thirteen polymers. Stearne and Ward<sup>5</sup> have carried out a detailed study of the tensile behaviour of poly(ethylene terephthalate) and their value of the critical stress has been included in Table 1.

#### MOLECULAR CROSS-SECTIONAL AREA

It has been pointed out previously<sup>2</sup> that polymers with bulky inflexible side groups, such as polystyrene, poly(cyclohexyl methacrylate) and poly(*N*-vinyl carbazole) have lower brittle strengths than polymers without such side groups. These polymers are not included in Table 1 because it has not been found possible to obtain a tensile yield stress of isotropic specimens. For example, a sample of polystyrene was brittle at +95°C and very soft at +100°C.

In order to discover whether this principle can be applied more generally, it is necessary to estimate the average cross-sectional area of a molecule, perpendicular to the chain axis. The formula used for this purpose was:

$$\text{Molecular cross-sectional area} = \frac{\text{Weight of repeat unit}}{\text{Sample density} \times \text{length of repeat unit}}$$

Where possible, the length of the repeat unit was obtained from the crystallographic data tabulated by Miller<sup>6</sup>. The value for polycarbonate of Bisphenol A (PC) was taken from the work of Prietzschk<sup>7</sup>. The value for polyethersulphone was measured on a molecular model in the most extended conformation. Table 2 gives the relevant data for polystyrene (PS) and the thirteen polymers of Table 1. The

reciprocal of the molecular cross-sectional area is listed under the heading bonds/nm<sup>2</sup> in the last column of Table 2.

#### CORRELATION

Figure 2 shows graphically the dependence of critical tensile strength on bonds/nm<sup>2</sup> for the thirteen polymers

Table 2 Molecular cross-sectional area

Polymer	Repeat unit molecular weight	Density (g/cm <sup>3</sup> )	Repeat unit length (10 <sup>-10</sup> m)	Molecular area × 10 <sup>-20</sup> (m <sup>2</sup> )	Bonds/nm <sup>2</sup>
PS	104	1.06	2.21	74.1	1.35
P4MP	84	0.83	1.98	85.4	1.17
PMMA	100	1.19	2.11	66.5	1.50
PPe	70	0.90	2.16	60.2	1.66
PB	56	0.90	2.17	47.9	2.09
PP	42	0.91	2.17	35.5	2.82
PVC	62.5	1.39	2.55	29.4	3.40
PTFE	100	2.17	2.60	29.6	3.38
PC	254	1.20	10.75	32.9	3.04
PES	232	1.37	10.4	27.2	3.68
PET	192	1.37	10.77	21.8	4.60
PE	28	0.96	2.53	19.3	5.19
Ny	226	1.14	17.3	19.2	5.22
POM	30	1.41	1.92	18.5	5.41

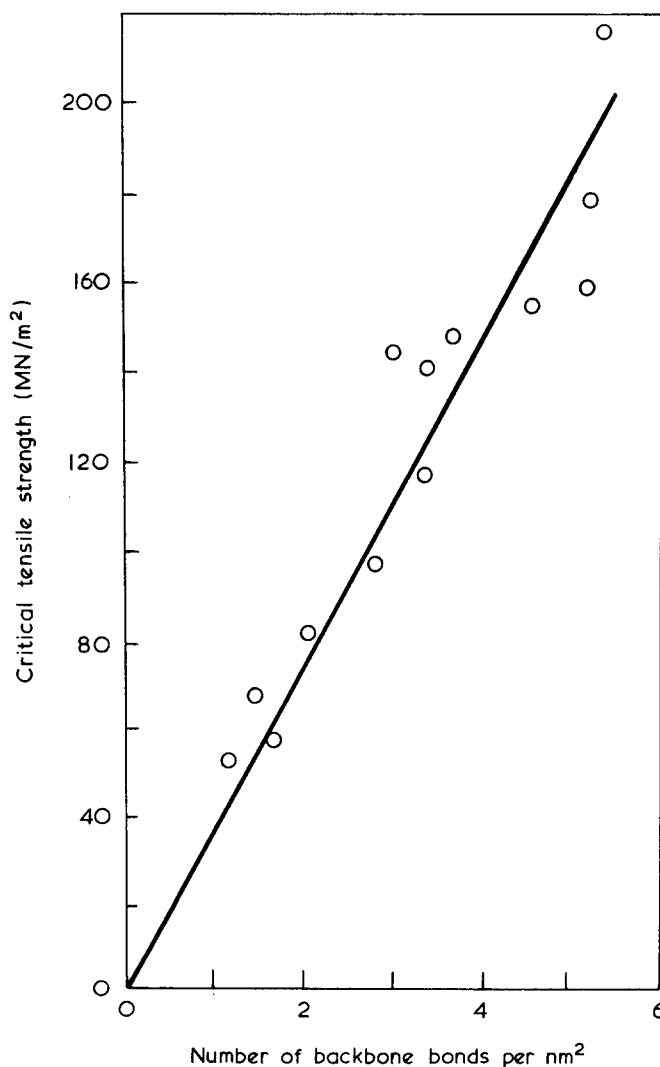


Figure 2 Critical tensile strength and number of bonds/nm<sup>2</sup> for thirteen polymers

for which both quantities are known. It is clear that there is a good correlation and this is confirmed by statistical analysis. The correlation coefficient is 0.949 and for thirteen results this corresponds to an extremely high level of significance. The best straight line was fitted to the results but the intercept was not statistically significant. Accordingly, the best straight line through the origin was fitted and is shown in *Figure 2*. The regression equation is:

$$\text{Critical strength (MN/m}^2\text{)} = 36.8 \times \text{number of backbone bonds per nm}^2.$$

It may be taken as established that the critical tensile strength of thermoplastics is dependent on the cross-sectional area of the molecule.

In the simplest calculation of the theoretical tensile strength of polymers, the load to break a carbon-carbon bond (given by Kelly<sup>8</sup> as  $6.1 \times 10^{-9}$  N) is divided by the molecular cross-sectional area. This theory leads to a relation between critical strength and bonds/nm<sup>2</sup> of the experimentally established form but with a coefficient of 6100 instead of 36.8. This discrepancy may be a consequence of the assumption in the theory that all the molecules are oriented in the direction of the applied stress whereas the experimental results apply to isotropic specimens.

## DISCUSSION

The establishment of this correlation throws new light on the effect of chemical constitution on brittle fracture. It is necessary to distinguish between two different ways in which changes in chemical constitution can affect the impact behaviour of un-notched specimens:

(1). An increase in the strength of the intermolecular forces, whether through hydrogen bonding or polarity or for steric reasons, will tend to increase the moduli and yield stresses and therefore, other things being equal, to reduce the impact strengths. It is probably for this reason that PMMA is more brittle than polypentene-1 and that nylon has a higher brittleness temperature than polyethylene.

(2). A decrease in the effective strength of the backbone bonds, because of increasing molecular cross-sectional area, will have an insignificant effect on the moduli and yield stresses. However, it decreases the brittle strength and the critical tensile strength and thereby reduces the impact strengths. It is probably for this reason that poly(4-methyl pentene-1) is more brittle than high density polyethylene and that PVC has a higher brittle point (un-notched) than polyoxymethylene.

It is conceivable that dynamic mechanical moduli and low loss processes could give useful information about the strength of intermolecular forces and therefore about the first type of effect of chemical constitution on brittle fracture. Indeed the partial correlations between dynamic mechanical properties and impact strength reported by Heijboer<sup>1</sup> and others are probably explicable in these terms. On the other hand, it would not be expected that dynamic mechanical properties could give information about the effective strength of backbone bonds. Consequently, a trend in brittle point caused by a change in molecular cross-sectional area would not correlate with

the loss processes. This line of thought can explain some of the apparent anomalies noted by Heijboer<sup>1</sup>:

(1). A copolymer of methyl methacrylate with cyclohexyl methacrylate had a much lower impact strength than PMMA in spite of the presence of a damping peak at  $-80^\circ\text{C}$  and 1 Hz. This may now be seen as a consequence of the increased average molecular cross-sectional area when the bulky cyclohexyl groups are included.

(2). A copolymer of methyl methacrylate with acrylonitrile had higher impact strength than PMMA in spite of the absence of an additional damping peak. This may now be seen as a consequence of reduced average molecular cross-sectional area. Polyacrylonitrile has 3.45 bonds/nm<sup>2</sup> compared with 1.50 for PMMA. The impact strength of un-notched specimens of random acrylonitrile-styrene copolymers increases as the molar ratio of acrylonitrile to styrene increases from 0 to 4<sup>9</sup>. Again, molecular cross-sectional area provides a reasonable explanation though the drop in toughness for molar ratios above 6 requires consideration of the difficulty of fabricating good samples.

(3). Poly(2,6-dimethyl-*p*-phenyleneoxide) (PPO) showed up well in Heijboer's<sup>1</sup> tests, in comparison with the polycarbonate of Bisphenol A, in spite of the fact that the latter has a substantial low temperature loss process whereas the former does not. It seems significant that the molecular cross-sectional areas are not very different—2.70 bonds/nm<sup>2</sup> for PPO, assuming that alternate ether oxygen atoms are on opposite sides of the chain, compared with 3.04 bonds/nm<sup>2</sup> for PC. A fuller explanation of the impact behaviour of un-notched specimens of these two polymers would have to take account of, and explain, the trends of yield stress with temperature.

So far this discussion has centred on the behaviour of un-notched specimens. For the more brittle materials this is sufficient to provide reasonable understanding of behaviour in the practically important region around normal ambient temperatures. For the tougher materials, it is necessary to consider the behaviour of notched specimens of various notch tip radii<sup>10</sup>. The impact strengths of notched specimens are more difficult to relate to molecular parameters; although molecular cross-sectional area and the strength of secondary bonds may both play a part, it seems likely that additional considerations will be necessary.

## ACKNOWLEDGEMENTS

This work would not have been possible without the co-operation of many of my colleagues.

## REFERENCES

- 1 Heijboer, J. *J. Polym. Sci. (C)* 1968, **16**, 3755
- 2 Vincent, P. I. *Polymer* 1960, **1**, 425
- 3 Vincent, P. I. *Nature (Phys. Sci.)* 1971, **233**, 104
- 4 Vincent, P. I. in 'Encyclopedia of Polymer Science and Technology', John Wiley, New York, 1967, Vol 7, p 292
- 5 Stearne, J. M. and Ward, I. M. *J. Mater. Sci.* 1969, **4**, 1088
- 6 Miller, R. L. 'Polymer Handbook' (Eds J. Brandrup and E. H. Immergut), John Wiley, New York, 1966, III-1
- 7 Prietzschk, A. *Kolloid-Z.* 1958, **156**, 9
- 8 Kelly, A. 'Strong Solids', Clarendon Press, Oxford, 1966
- 9 Br. Pat. 1 185 305
- 10 Vincent, P. I. 'Impact Tests and Service Performance of Thermoplastics', Plastics Institute, London, 1971

# Broadline nuclear magnetic resonance studies of some poly(*N*-substituted maleimides)

J. Bailey and S. M. Walker

Department of Inorganic, Physical and Industrial Chemistry, University of Liverpool, PO Box 147, Liverpool L69 3BX, UK

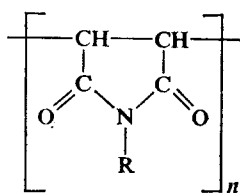
(Received 2 May 1972; revised 1 June 1972)

Broadline nuclear magnetic resonance studies have been carried out on a number of poly(*N*-substituted maleimides) and compared with existing dielectric relaxation information. In general, the results have confirmed the existence of a ring deformation relaxation mode in these polymers and, in addition, dielectrically inactive motion involving the non-polar nitrogen substituent has been detected. Apparent activation energies have been calculated for all the transitions and have been modified to include relaxation time distributions where the necessary information exists.

## INTRODUCTION

Low resolution or broadline nuclear magnetic resonance (n.m.r.) studies form a useful method for observing molecular motions in solid polymers<sup>1-3</sup>. This technique has often been complemented<sup>4,5</sup> by other relaxation methods—dielectric, mechanical and viscoelastic—which are also used in this type of investigation. In particular n.m.r. measurements may be sensitive to microscopic motions which do not involve rotation of a dipole, or which are on too small a scale to produce any appreciable change in the mechanical properties of the material.

There is current interest in the development and study of the physico-chemical properties of thermally stable polymers. In this laboratory various methods are being used to study molecular motion in one such class of material, the poly(*N*-substituted maleimides):



This paper reports the results of broadline n.m.r. experiments which have been carried out on several polymers of this type with both *n*-alkyl and aryl substituents at the nitrogen atom. Attempts have been made to correlate the n.m.r. results with some of the dielectric data which have been obtained in a concurrent investigation<sup>6</sup>.

## EXPERIMENTAL

Details of the methods of preparation and of the dielectric experiments are given in another paper<sup>6</sup>.

The samples consisted of the powdered polymer contained in a 0.5 cm diameter glass tube which was pumped for several hours before sealing off. The single coil broadline spectrometer was operated at around 22 MHz using a Newport Instruments 4 in. electromagnet and type P magnetometer. Phase-sensitive detection was employed

with a Brookdeal lock-in amplifier. A gas flow system was utilized for temperature variation. About seven spectra were recorded for each polymer sample at each temperature in the range 140 to 500K. Below 140K the spectra became so broad that the signal to noise ratio was too small for accurate recordings.

The second moment and line width of the spectra were derived using a computer programme which fits the best Gaussian curve to the spectrum. For a few of the polymers the transitions gave rise to pronounced double spectra (cf. *Figure 1*). Such behaviour is attributed by us to the onset of molecular motion at different rates in the amorphous and crystalline regions of the polymer. In these cases it was sometimes possible to fit the spectra to two superimposed Gaussian curves, and to determine separate line widths and second moments for the amorphous and crystalline processes.

It should be pointed out that other types of curve fitting procedures were used in addition to the Gauss fit. These were semi-empirical, involving no *a priori* assumptions about the line shape. In few cases did these methods give rise to results which were significantly different from the Gaussian curve. At higher temperatures (> 370K), the several experimental spectra at each temperature were found to have line widths and second moments agreeing

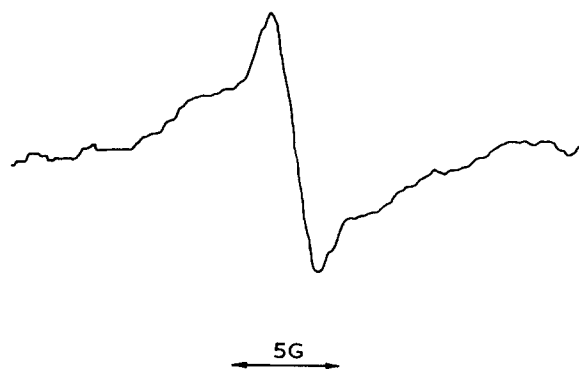


*Figure 1* Spectrum of polymaleimide at 40°C, showing the broad (crystalline) and narrow (amorphous) components

to  $\pm 3\%$ . However, this spread of values increased markedly at the lower temperatures, when it was occasionally as high as  $\pm 15\%$ .

The plots of line width *versus* temperature in the transition region were fitted to a cubic curve, and the mean values of  $\delta H$  at each temperature were calculated in this way. This technique gives an accurate and less arbitrary picture of the line width and second moment variation as a function of the temperature in the region of a transition.

## RESULTS AND DISCUSSION

The n.m.r. spectrum of a solid amorphous polymer usually consists of a single broad resonance peak<sup>1</sup>, which is the result of almost every proton existing in a magnetically different environment. The shape of the peak may often be approximated to that of a Gaussian or truncated Lorentzian curve. Two parameters associated with the spectrum are of some importance. The line width  $\delta H$  is defined by

$$\delta H = H_a - H_b$$

where  $H_a$ ,  $H_b$  are values of the field  $H$  such that  $d^2\xi/dH^2=0$ , and  $\xi(H)$  is a function which represents the shape of the resonance signal.

$\delta H$  is important because of its relation to  $T_2$ , the transverse relaxation time. For a Gaussian line shape,

$$T_2 = \frac{2^{3/2}}{\gamma\delta H} \quad (1)$$

and  $T_2$  is related to the correlation time  $\tau_c$  for molecular motion in the sample by the Kubo and Tomita expression<sup>7</sup>.

$$\frac{1}{T_2''} = \left(\frac{1}{T_2''}\right)^2 \frac{2}{\pi} \tan^{-1}\left(\frac{2^{1/2}\tau_c}{\pi T_2''}\right) \quad (2)$$

where  $T_2''$  is the rigid lattice relaxation time (with line width  $\delta H''$ ).

The second moment of the spectrum  $\Delta H_2$  is defined by:

$$\Delta H_2 = \frac{\int_{\text{line}} \xi(H)(H-H_c)^2 d(H-H_c)}{\int_{\text{line}} \xi(H) d(H-H_c)}$$

where  $H_c$  is the centre of the spectrum. In fact the second moment is a fundamental molecular quantity in that its magnitude derives from the interaction of all the magnetic nuclei in the sample<sup>1</sup>.

In the region of a line width transition there is onset of molecular motion, and the line width falls from one constant value to another as the temperature increases. The behaviour can be shown more quantitatively by substituting a relation of the form:

$$\tau_c = A \exp(E^*/RT)$$

into equation (2). Values of  $\tau_c$  may be obtained at any temperature where  $\delta H$  is known, and the activation energies  $E^*$  may be calculated. The second moment of the spectrum usually also falls in the transition temperature range, although there are some cases<sup>8</sup> where this quantity remains constant in accordance with strict theoretical requirements<sup>1</sup>.

For polymeric systems, the activation energies which are obtained by the above method are generally found to be very low when compared to the corresponding dielectric data<sup>1</sup>. These discrepancies are believed to be due

to the neglect in equation (2) of the distribution of relaxation times which is nearly always found for dielectric relaxation in polymers. The precise effect of the distribution on equation (2) is complex, but the general conclusion<sup>1</sup> is that one can obtain a single, fairly accurate value of  $\tau_c$  where the  $\delta H$  curve shows the point of inflection which is when  $\delta H \approx \delta H''/2$ . It is not difficult to show that  $\nu_c$  is approximately  $10^4$ – $10^5$  s<sup>-1</sup> in this region<sup>9</sup>. Results obtained from  $\delta H$  values removed from the point of inflection, however, are markedly sensitive to the distribution effect.

When the n.m.r. and dielectric relaxations arise from the same molecular motion, then it will be possible to observe the correlation between the two processes on an Arrhenius diagram. This is usually done by plotting all the dielectric relaxation frequencies on a  $\ln f_r$  *versus*  $1/T$  graph. The single most accurate n.m.r. correlation frequency (obtained at the temperature of the point of inflection of the  $\delta H$  graph) may then appear to lie on one of the dielectric lines. In general, of course, polymers may exhibit more than one type of relaxation process.

If a correlation of this nature is obtained, then a more realistic estimate of the activation energy for the nuclear spin process may be obtained by multiplying the apparent activation energy by  $\beta^{-1}$  where  $\beta$  is a parameter which describes the width of the distribution of dielectric relaxation times<sup>10</sup>. This procedure is subject to certain disadvantages, which are described elsewhere<sup>11</sup>.

An approach of this kind should strictly only be applied when using  $T_1$  and not  $T_2$  data for the n.m.r. information. We adopt the view that the applicability of the method is justified by the good agreement obtained between the n.m.r. and dielectric activation energies.

### Polymaleimide

Polymaleimide itself showed a single line-width transition extending over the temperature range 213 to 333K and centred on 263K. The transition was accompanied by a marked change in second moment, as indeed were all the transitions discussed in this paper. The measurements on this polymer were particularly interesting because it was found possible to separate the spectra into broad and narrow components over a wide range of temperature. *Figure 2* shows the results of this analysis. At 263K, the correlation frequencies in the amorphous and crystalline regions are  $8.0 \times 10^4$  and  $7.5 \times 10^4$  s<sup>-1</sup>

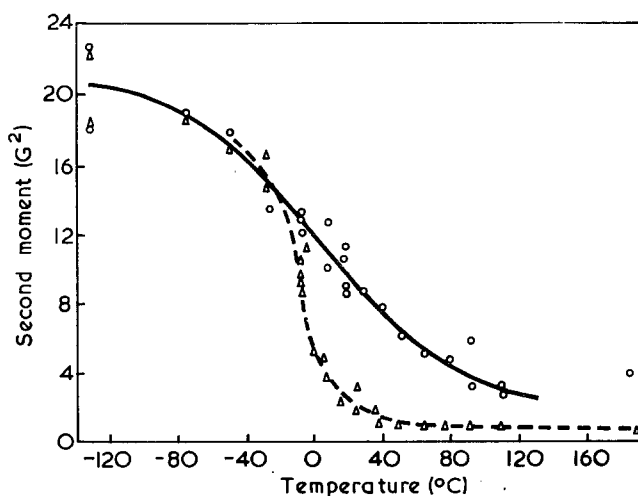


*Figure 2* Second moment data for polymaleimide.  $\Delta$ , Narrow component;  $\circ$ , broad component

respectively and the corresponding activation energies are 25 and 9 kJ mol<sup>-1</sup>.

Figure 3 shows the results of the dielectric investigation on this polymer. The single n.m.r. correlation frequency ( $\nu_c = 8.0 \times 10^4 \text{ s}^{-1}$  at 263K) in the amorphous region is seen to lie very close to the amorphous  $\gamma$  (i.e. highest frequency) dielectric relaxation process. Now the Fuoss-Kirkwood distribution parameter for this process has been found by computation to be equal to 0.24, so that the true n.m.r. activation energy is 104 kJ mol<sup>-1</sup>. This is excellent evidence that the n.m.r. and dielectric methods are observing the same kind of molecular motion, since the activation energy for the dielectric process is found to be 100 kJ mol<sup>-1</sup>.

The dielectric process in all the maleimide polymers has been assigned<sup>6</sup> to an out-of-plane deformation of the substituted succinimide ring involving nitrogen inversion. It would really be expected that this mechanism would be more facile in the amorphous than in the crystalline regions of the polymer, but this does not appear to be the case. The activation energy of the narrow (amorphous) line appears to be higher than that of the broad (crystalline) line. However, the close similarity of the n.m.r. correlation frequencies and transition temperatures in the two phases lends weight to the supposition that the same molecular mechanism is responsible for the relaxations.

It is also noteworthy that the change in second moment observed for the polymaleimide transition ( $\sim 18 \text{ G}^2$ ) is the largest such change recorded in these measurements. This observation is again surprising when it is considered that a rather small degree of molecular motion is involved.

#### N-ethyl, N-amyl and N-dodecyl polymaleimides

All of these polymers showed a single line width transition, the correlation frequencies being  $2.3$ ,  $1.8$  and  $1.4 \times 10^4 \text{ s}^{-1}$  at 313, 293 and 278K for the N-ethyl, N-amyl and N-dodecyl derivatives, respectively. Figure 4 shows the dielectric relaxation data for these polymers. It can be seen that the n.m.r. transition appears to coincide with the Arrhenius line for the dielectric  $\gamma$  process in poly(N-dodecyl maleimide) but the corresponding points for the

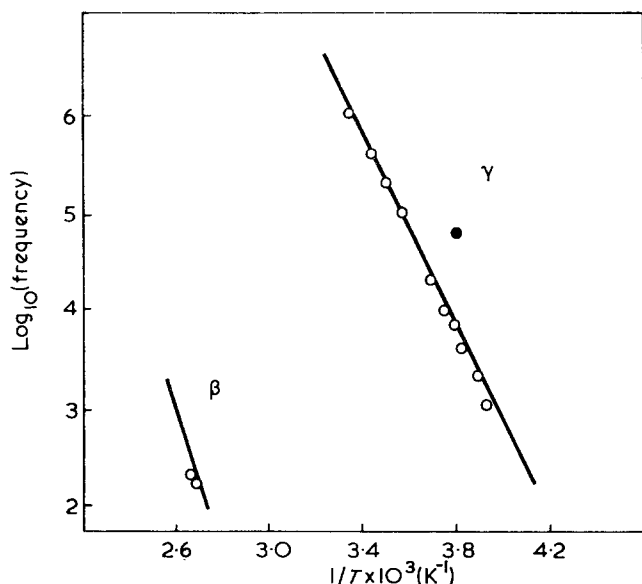


Figure 3 Dielectric and n.m.r. relaxation data for polymaleimide.  $\circ$ , Dielectric relaxation frequencies;  $\bullet$ , n.m.r. correlation frequency

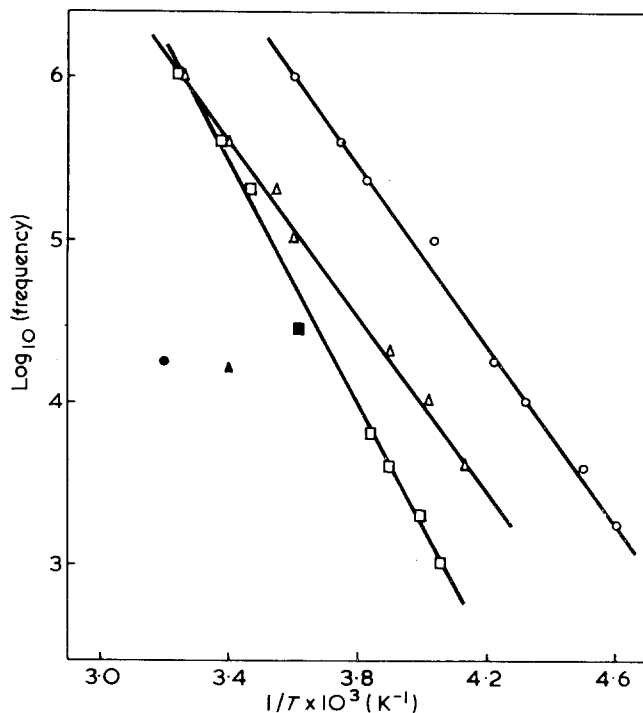


Figure 4 Dielectric (open symbols) and n.m.r. (solid symbols) relaxation data for the poly(N-alkyl maleimides).  $\circ$ ,  $\bullet$ , Poly(N-ethyl maleimide);  $\Delta$ ,  $\blacktriangle$ , poly(N-amyl maleimide);  $\square$ ,  $\blacksquare$ , poly(N-dodecyl maleimide)

N-amyl and N-ethyl polymaleimides appear several decades below the  $\gamma$  line at the same temperatures.

Considering the case of poly(N-dodecyl maleimide) in more detail, one can compare the activation energies for nuclear spin and dielectric relaxation using a knowledge of the Fuoss-Kirkwood  $\beta$  value for the  $\gamma$  relaxation. This parameter was found to be 0.30, which gives a true n.m.r. activation energy of 48 kJ mol<sup>-1</sup>, compared to 73 kJ mol<sup>-1</sup> for the dielectric  $\gamma$  process. Hence it would appear that in the N-dodecyl derivative also, these two processes do not appear to have the same molecular origin, in spite of the apparent frequency correlation.

The molecular motion responsible for nuclear spin relaxation in the poly(N-alkyl maleimides) must therefore be one which does not involve re-orientation of a dipole. It seems obvious that some mechanism involving motion of the alkyl side chain (probably rotation about the carbon-carbon bonds) is occurring in these polymers. The transition temperature, and hence the activation energy, appears to decrease as the alkyl side chain becomes longer, but in the absence of distribution parameters it is not possible to put a quantitative estimate on this effect. Presumably a longer side chain creates for itself a larger free volume in which it is able to move. This theory would seem reasonable if, for example, the kind of rotation were of the 'crankshaft' type as suggested by Schatzki<sup>12,13</sup> and Boyer<sup>14</sup>. Furthermore the activation energy calculated by these authors, around 52 kJ mol<sup>-1</sup>, is in very favourable agreement with the experimental values if a  $\beta$  of 0.3 is assumed.

It is interesting to note that these N-alkyl derivatives are the only polymers in the series which do not show a parallel between the nuclear spin relaxation process and the dielectric  $\gamma$  process. It is obvious that the motion of many protons in the alkyl substituents is much more efficient in relaxing nuclear spin energy than the com-

paratively small proton movement which results from the partial twist of the maleimide ring.

*Poly(N-cyclohexyl maleimide)*

It was hoped that this polymer would reveal some effects of the well known chair-chair interconversion of the cyclohexyl ring. The experimental measurements showed the existence of only one very sharp transition centred close to 273K, with an apparent activation energy of 40 kJ mol<sup>-1</sup>. When compared with the dielectric relaxation data for this polymer, the transition ( $\nu_c = 2.5 \times 10^4 \text{ s}^{-1}$  at 273K) is seen to lie close to, but at a higher frequency than, the line corresponding to the dielectric  $\gamma$  process (Figure 5). However, the dielectric  $\gamma$  line is observed to be markedly curved, indicating that the activation energy varies by as much as a factor of two over the temperature range 280-310K. At the higher end of this temperature range, the activation energy for dielectric relaxation was found to be 106 kJ mol<sup>-1</sup>, with a Fuoss-Kirkwood distribution factor of 0.39. The true n.m.r. activation energy is therefore  $40/0.39 = 102 \text{ kJ mol}^{-1}$ , which is in remarkably good agreement with the dielectric value. Nevertheless, the uncertainty in the dielectric measurements, and the comparatively poor frequency correlation, give grounds for considerable suspicion as to whether the dielectric and n.m.r. methods are observing the same molecular process. It could well be that a co-operative motion between the twisting of the maleimide ring and the chair-chair interconversion of the cyclohexyl ring make varying contributions to the total observable behaviour depending on the type of relaxation study.

*Poly(N-phenyl maleimide)*

Three distinctly separate transitions were observed in this polymer sample. The transition temperatures, the corresponding correlation frequencies and the apparent

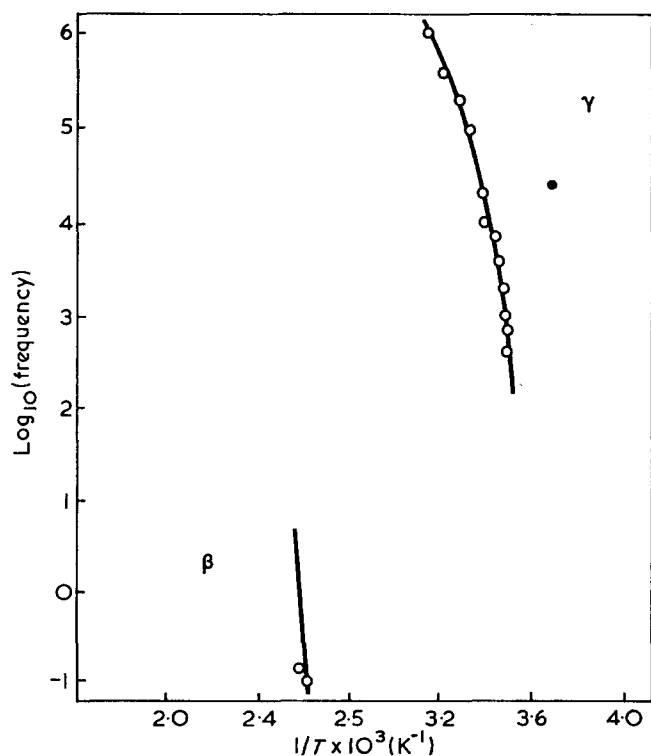


Figure 5 Dielectric and n.m.r. relaxation data for poly(N-cyclohexyl maleimide). O, Dielectric data; ●, n.m.r. correlation frequency

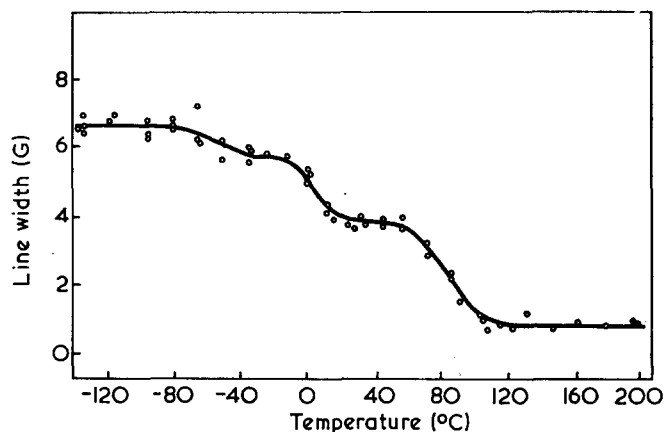


Figure 6 Line width data for poly (N-phenyl maleimide)

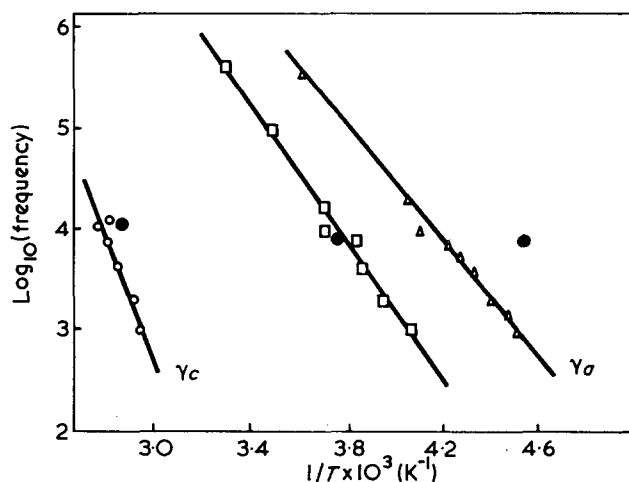


Figure 7 Dielectric and n.m.r. relaxation data for poly(N-phenyl maleimide). O, Δ, Dielectric relaxation frequencies; ●, n.m.r. correlation frequencies; □, dielectric behaviour of monomer trapped in a polystyrene matrix

activation energies were (220K,  $0.82 \times 10^4 \text{ s}^{-1}$ , 14.1 kJ mol<sup>-1</sup>) (270K,  $0.86 \times 10^4 \text{ s}^{-1}$ , 27.8 kJ mol<sup>-1</sup>) and (350K,  $1.1 \times 10^4 \text{ s}^{-1}$ , 31.1 kJ mol<sup>-1</sup>). Approximately equal line width changes were associated with each transition (Figure 6).

The transition at 220K is undoubtedly associated with the dielectric  $\gamma$  relaxation. Reference to Figure 7 shows that it lies close to the Arrhenius line for the  $\gamma$  process. Furthermore the dielectric distribution parameter was found to be 0.15, which makes a more realistic n.m.r. activation energy to be 94 kJ mol<sup>-1</sup> a value which compares very favourably with the 110 kJ mol<sup>-1</sup> found for the dielectric  $\gamma$  process itself.

Interestingly, the 270K n.m.r. transition in poly(N-phenyl maleimide) coincides almost exactly with the frequency and temperature found for dielectric relaxation of N-phenyl maleimide monomer which is trapped in a polystyrene matrix (cf. Figure 7). Therefore the process involved here would appear to be localized to the N-phenyl maleimide monomer unit, and could be some co-operative motion of the maleimide and phenyl rings.

The 350K transition has no parallel in the dielectric relaxation results, and it is concluded that this transition arises from motion of a non-polar group in the material. The most probable explanation is a restricted torsional rotation of the phenyl group itself. The apparent activa-

tion energy is 31 kJ mol<sup>-1</sup>. Since the distribution parameter will be close to unity for this type of 'local' process, the activation energy is probably very similar to the 38 kJ mol<sup>-1</sup> found by Yano and Wada<sup>15</sup> for torsional oscillations of the phenyl groups in polystyrene.

#### Poly (*N*-monochlorophenyl maleimides)

All three monochlorophenyl maleimide derivatives were examined. In every case a transition corresponding to the dielectric  $\gamma$  (crystalline) process was observed, the frequency correlations being indicated in Figure 8 and the activation energy comparisons in Table 1. Poly(*N*-*para*-chlorophenyl maleimide) was exceptional in that the measurements revealed the existence of two further transitions centred at 223 and 463K, the  $\gamma$  (crystalline) process itself being centred on 313K (cf. Figure 8). Comparison with the dielectric data shows that the 223K

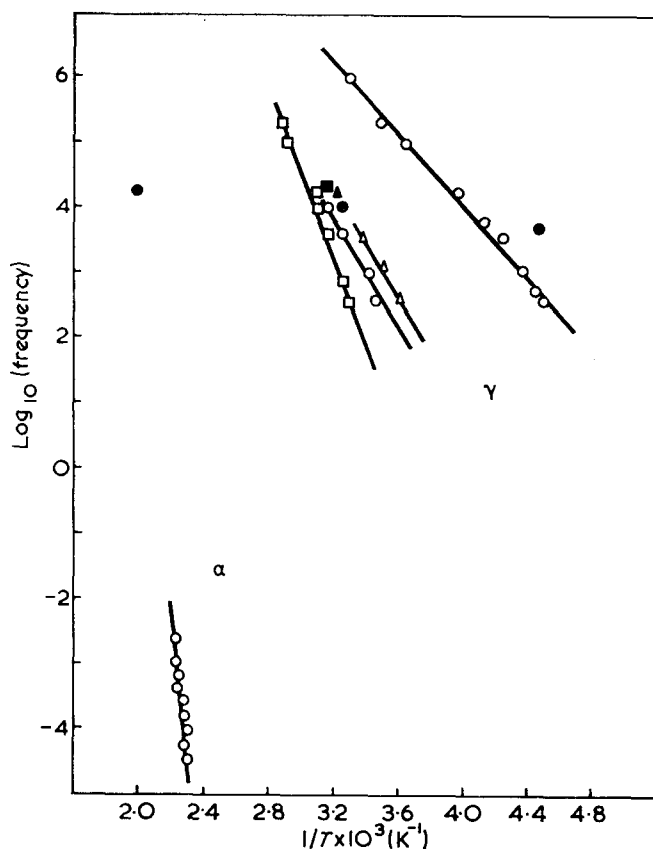


Figure 8 Dielectric (open symbols) and n.m.r. (solid symbols) relaxation data for the poly(*N*-monochlorophenyl maleimides).  $\Delta$ ,  $\blacktriangle$ , Poly(*N*-*ortho*-chlorophenyl maleimide);  $\square$ ,  $\blacksquare$ , poly(*N*-*meta*-chlorophenyl maleimide);  $\circ$ ,  $\bullet$ , poly(*N*-*para*-chlorophenyl maleimide)

Table 1 Activation energy correlations for the  $\gamma$  process in the poly(monochlorophenyl maleimides)

Derivative	Apparent n.m.r. activation energy (kJ mol <sup>-1</sup> )	Dielectric $\beta$ value	Absolute n.m.r. activation energy (kJ mol <sup>-1</sup> )	Dielectric activation energy for $\gamma$ process (kJ mol <sup>-1</sup> )
<i>o</i>	17.6	0.21	84	75
<i>m</i>	25.1	0.22	114	117
<i>p</i> *	22.6	0.41	55	49

\* Data given for  $\gamma$  (amorphous).

Table 2 Second moment changes for those polymaleimides exhibiting the  $\gamma$  process

Derivative	Second moment change (G <sup>2</sup> )
R=H	18.0
cyclohexyl	10.0
phenyl	8.5
<i>o</i> -chlorophenyl	8.0
<i>m</i> -chlorophenyl	8.0
<i>p</i> -chlorophenyl	7.5

transition corresponds to the dielectric  $\gamma$  process also, but is associated with the maleimide ring twist in the amorphous rather than the crystalline region of the polymer. Here it is noted that the rates of molecular motion are so different in the two phases that they give rise to two separate line width transitions rather than to a separation of the line into broad and narrow components as occurred for polymaleimide. In addition, in the case of this polymer, the transition temperature in the amorphous region is lower than that in the crystalline region, indicating the more normal situation of a lower activation energy where the material is more disordered.

The transition in poly(*N*-*para*-chlorophenyl maleimide) observed at 463K would appear to correspond to the glass transition in the polymer, observed by differential scanning calorimetry to be at 450K, and as the dielectric  $\alpha$  process at 435K at 10<sup>-4</sup> Hz. This is the only case where the glass transition was observed by the n.m.r. technique in this series of polymers.

No evidence for a transition corresponding to phenyl group rotation was seen in any of the chlorophenyl derivatives. It is recalled that this transition was seen at 350K in poly(*N*-phenyl maleimide) itself. This could be because the polymers have been shown by X-ray studies to be rather more crystalline than other members of the series.

#### CONCLUSIONS

In most of the poly(*N*-substituted maleimides) nuclear spin relaxation has been shown to occur by a mechanism which is analogous to the dielectric  $\gamma$  process, viz. a torsional twist of the maleimide ring. A comparison of the changes in second moment for each of the polymers where this type of relaxation is observed is shown in Table 2. With the exception of polymaleimide the second moment changes are rather similar, as would be expected. In polymaleimide this very large change in second moment over the transition region may reflect a large change in magnetic environment for the N-H proton. Molecular models of the known helical structure of polymaleimide reveal that the N-H protons point outwards from the axis of the helix, hence interchain interactions may be the most important contributor to the second moment. In longer alkyl chains, larger changes in environment may be masked by compensating changes in the configuration of the pendant alkyl chain.

#### ACKNOWLEDGEMENTS

We wish to thank the SRC for assistance towards equipment costs. One of us (J.B.) thanks the Leverhulme Trust for the award of a fellowship during this period.



REFERENCES

- 1 Powles, J. G. *Polymer* 1960, **1**, 220
- 2 Roshchupkin, V. P., Lyubovskii, R. B., Kochervinskii, V. V. and Roshchupkina, O. S. *Polym. Sci. USSR* 1970, **11**, 2848
- 3 Merrill, L. J. *Diss. Abstr.* 1965, **26**, 728
- 4 Illers, K. H. *Kolloid-Z.* 1969, **231**, 622
- 5 Slichter, W. P. *J. Polym. Sci. (C)* 1966, **14**, 33
- 6 Block, H., Groves, R. and Walker, S. M. *Polymer* 1972, **13**, 527
- 7 Kubo, R. and Tomita, K. *J. Phys. Soc. Japan* 1954, **9**, 888
- 8 Bergmann, K. and Novotky, K. *Chem. Soc. Spec. Publ. No. 20* 1965, p 135
- 9 McCall, D. W. *Acc. Chem. Res.* 1971, **4**, 223
- 10 Connor, T. M. *J. Polym. Sci. (A-2)* 1970, **8**, 191
- 11 Bailey, J., Cowden, D. R. and Walker, S. M. in preparation
- 12 Schatzki, J. F. *J. Polym. Sci.* 1962, **57**, 496
- 13 Schatzki, J. F. *Polym. Preprints* 1965, **6**, 646
- 14 Boyer, R. F. *Rubb. Rev.* 1963, **3**, 1303
- 15 Yano, O. and Wada, Y. *J. Polym. Sci. (A-2)* 1971, **9**, 669

# Morphology of nascent polyethylene prepared with the catalyst $\text{VOCl}_3/(\text{C}_2\text{H}_5)_2\text{AlCl}$

T. Georgiadis and R. St John Manley

*Department of Chemistry and Pulp and Paper Research Institute,  
McGill University, Montreal, Canada  
(Received 23 March 1971; revised 8 March 1972)*

The catalyst  $\text{VOCl}_3/(\text{C}_2\text{H}_5)_2\text{AlCl}$  was used to prepare polyethylene under various conditions of polymerization. The nascent polymer samples were examined by optical and electron microscopy, fuming nitric acid oxidation and differential scanning calorimetry. It was observed that the samples consisted of lamellar as well as fibrillar crystals. Examination of catalyst preparations by light-scattering photometry revealed the presence of a colloidal dispersion besides the soluble catalyst complex. It is proposed that the lamellar and fibrillar crystals have different origins. The lamellar crystals are formed by intramolecular crystallization of polymer chains generated from the soluble catalyst complex, whereas the fibrils are the product of intermolecular crystallization of polymer chains growing from adjacent active sites residing on the surface of the colloidal particles. The degree of chain extension in the fibrillar crystals is dependent on the conditions of polymerization.

## INTRODUCTION

In a recent paper we showed that the nascent crystalline polyethylene, prepared with the soluble Ziegler–Natta catalyst bis(cyclopentadienyl)titanium dichloride/dialkylaluminum chloride, has a lamellar morphology<sup>1</sup>. The lamellar morphology was observed in samples prepared under both quiescent and stirred conditions, provided that the polymerization is carried out below the dissolution temperature of the polymer. Similarly, it was reported several years ago<sup>1a</sup> that folded-chain lamellar crystals were formed when ethylene is polymerized using a soluble catalyst system based on vanadium salts<sup>2</sup>.

In contrast to the above polymers, the nascent polymers prepared with heterogeneous Ziegler–Natta catalysts have a characteristic fibrillar morphology. In the polymerization of ethylene, for example, depending on the experimental conditions, the nascent polymer is composed either of extended chain structureless fibrils<sup>3</sup>, or of fibrils consisting of a central filament and folded-chain lamellae arranged transversely to the filament axis<sup>4, 5</sup>. Other polyolefins synthesized with heterogeneous Ziegler–Natta catalysts are likewise fibrous<sup>4</sup>. Although these nascent polymers morphologically resemble the fibrillar crystals obtained in polymer crystallizations from solution under shear<sup>6</sup>, the fact that the nascent polymer has a fibrillar habit even in polymerizations conducted under quiescent conditions<sup>4</sup> suggests that external stress is not essential for fibril formation. It seems more probable that in heterogeneous Ziegler–Natta polymerizations the organization of the polymer molecules into fibrils is related to the catalyst itself. The formation of the extended chain filaments requires the intermolecular nucleation of many polymer chains which have a common orientation. The surface of a

solid catalyst with many active sites in close proximity provides the conditions for the growth of such filaments. On the other hand, in a soluble catalyst system where each active site exists in isolation only intramolecular nucleation leading to lamellar structures is possible. Boor<sup>7</sup> has suggested that if the apparent relation between the physical state of the catalyst and the morphology of the nascent polymer proves to be of general applicability, then it would be possible to use the study of morphology as a means of differentiating between heterogeneous and homogeneous Ziegler–Natta catalysts. It has recently been reported, however, that certain soluble vanadium-based catalyst systems can also generate fibrillar nascent polyethylene<sup>8, 9</sup>. To account for the formation of fibrils in this system it has been proposed that fibrous growth by intermolecular nucleation may be possible at high catalyst concentrations by the lateral aggregation of many adjacent growing chains, whereas at low catalyst concentrations the active sites would be sufficiently separated to only allow the individual polymer chains to crystallize intramolecularly by chain folding<sup>9</sup>. This suggestion is at variance with our own observations with the system bis(cyclopentadienyl)titanium dichloride/dialkylaluminum chloride which invariably yielded folded chain lamellar crystals over a wide range of catalyst concentrations. Because of this inconsistency in our knowledge of the morphology of nascent polyethylene prepared with soluble catalyst systems it was considered of interest to extend our investigation to the soluble vanadium-based catalysts.

In the present paper we examine the morphology of nascent polyethylene prepared with the catalyst system vanadium oxytrichloride/diethylaluminum chloride, one of the reported soluble vanadium catalysts<sup>8</sup>. Polymer

samples were prepared under various experimental conditions and studied by electron microscopy, nitric acid oxidation and thermal analysis. The state of dispersion of the catalyst in the polymerization medium was examined by light-scattering photometry in the absence of monomer.

## EXPERIMENTAL

### Materials

Vanadium oxytrichloride (Stauffer Chemical Co.) was used as a dilute solution in cyclohexane. The solution was stored in a sealed bottle under nitrogen and measured aliquots were transferred to the reaction vessel with a hypodermic syringe. Diethylaluminium chloride (Ethyl Corp.) was used as received, or as a molar solution in cyclohexane. Nitrogen and CP grade ethylene (Matheson Co.) were purified before use by passing through tubes containing calcium chloride and magnesium perchlorate and then bubbling through a 50% solution of triethylaluminium in kerosene. Reagent grade hydrocarbons were refluxed and distilled over sodium shortly before use.

### Polymerizations

All polymerizations were conducted in a conventional reactor<sup>10</sup> and strict precautions were taken to ensure anaerobic and anhydrous conditions. The reactor was first charged with about 500 ml of solvent and the system was purged with nitrogen. The appropriate amount of diethylaluminium chloride was then added, nitrogen flow was stopped and ethylene was allowed to enter the system. When the catalyst vanadium oxytrichloride was added, the colourless reaction mixture developed a characteristic pink colour in accordance with the expected behaviour of soluble vanadium catalysts<sup>11-16</sup>. Polymerization started immediately as evidenced from the appearance of solid polymer in the reaction mixture. The reactor was thermostated to within  $\pm 0.5^\circ\text{C}$ . To stop the reaction the catalyst was poisoned with a small amount of isopropanol.

Gentle stirring (about 50 rev/min) with a Teflon paddle was generally used to ensure adequate mixing. However, in some cases the reaction was carried out under quiescent conditions; the ethylene was then introduced into the reactor through an orifice placed well above the surface of the solution. The ethylene dissolved in the reaction mixture by diffusion through the gas-liquid interface and the polymerization occurred without mechanical disturbance of the reaction mixture.

Table 1 summarizes the experimental conditions under which the various samples were prepared.

### Polymer recovery and purification

The precipitated polymer was separated from the reaction mixture by centrifugation or filtration. Samples prepared at high temperature were filtered at the polymerization temperature in order to avoid contamination with dissolved polymer which would crystallize on cooling. After separation, the samples were first washed with aliquots of fresh solvent; they were then purified of catalyst residues by washing in a 10% solution of

Table 1 Experimental conditions of polymerizations with the catalyst system  $\text{VOCl}_3/(\text{C}_2\text{H}_5)_2\text{AlCl}$

Sample	Catalyst concentration $\text{VOCl}_3$ (mmol/l)	Molar ratio Al : V	Solvent	Polymerization temperature ( $^\circ\text{C}$ )	Molecular weight, $\bar{M}_w$
PE-1	0.1	50	cyclohexane	25	750 000
PE-2a	0.1	50	cyclohexane	25	
PE-3	0.02	50	cyclohexane	25	
PE-4	0.2	50	cyclohexane	25	960 000
PE-5	0.1	50	cyclohexane	35	
PE-6a	0.1	50	cyclohexane	35	
PE-7	0.1	50	cyclohexane	65	
PE-9	0.1	50	toluene	25	
PE-10a	0.1	50	toluene	25	
PE-11	0.2	50	toluene	25	
PE-12	0.1	50	toluene	55	
PE-13	0.1	50	toluene	65	

a Polymerization conducted under quiescent conditions

hydrochloric acid in isopropanol and finally stored resuspended under toluene. The X-ray diffraction patterns of all nascent samples were identical to the diffraction pattern of crystalline polyethylene.

### Microscopy

Preliminary observations of the morphology of the nascent polyethylene samples were made by optical microscopy. For more detailed information, the specimens were examined with a JEM 6A transmission electron microscope using the double condenser system and an accelerating voltage of 80 kV. The samples were observed by direct transmission or by the use of replicas using a method described earlier<sup>1</sup>.

### Fuming nitric acid treatment

Selected polyethylene samples were treated with fuming nitric acid. Weighed samples were placed in glass tubes containing 90% fuming nitric acid (about 0.4 g of polyethylene in 100 ml acid) and the tubes were suspended in an oil bath at  $73 \pm 0.5^\circ\text{C}$ . After a specified time of treatment, the sample was left for one day or more in distilled water, filtered, washed with distilled water and acetone, and finally dried under vacuum.

### Differential scanning calorimetry

The melting behaviour of the nascent samples was studied with a Perkin-Elmer differential scanning calorimeter, model DSC-1B.

Measurements were performed in the manner described earlier<sup>1</sup>. Each sample was melted, recrystallized from the melt by cooling in the instrument, and remelted. Thus the endotherms of the sample in its original and melt-recrystallized state were compared.

The temperature scale of the calorimeter was calibrated with pure compounds of known melting points.

### Viscometry

Viscosities of the samples were measured at  $135^\circ\text{C}$  in decalin containing 0.2% *N*-phenyl-2-naphthylamine using a Cannon-Ubbelohde viscometer. Average molecular weights were calculated from the viscosity values using the relation<sup>17</sup>:

$$[\eta] = 6.2 \times 10^{-4} \bar{M}_w^{0.70}$$

where  $\bar{M}_w$  is the weight average molecular weight, and  $[\eta]$  is the intrinsic viscosity.

#### Light scattering

Light-scattering measurements were carried out on the catalyst system (vanadium oxytrichloride/diethylaluminium chloride dissolved in cyclohexane or toluene) using a Brice-Phoenix photometer operating at a wavelength of 5460 Å. The measurements were made in a cylindrical cell under nitrogen atmosphere. The cell was fitted with a Plexiglass cap provided with inlet and outlet tubes for nitrogen flow and a puncture seal rubber stopper through which the solvent and catalyst components were introduced using a hypodermic syringe.

The scattering cell was first purged with nitrogen and the solvent (cyclohexane or toluene) was added. The nitrogen flow was continued for about 0.5 h to completely remove traces of atmospheric oxygen. The catalyst components were then added in the same order as in the polymerization reaction. During the preparation of the catalyst the solution was continuously agitated with a magnetic stirrer. The intensity of the light scattered by the pure solvent and the catalyst solutions were measured at 45, 90 and 135°C.

## RESULTS

### Microscopy

Examination of the nascent polymer samples by optical and electron microscopy showed that the morph-

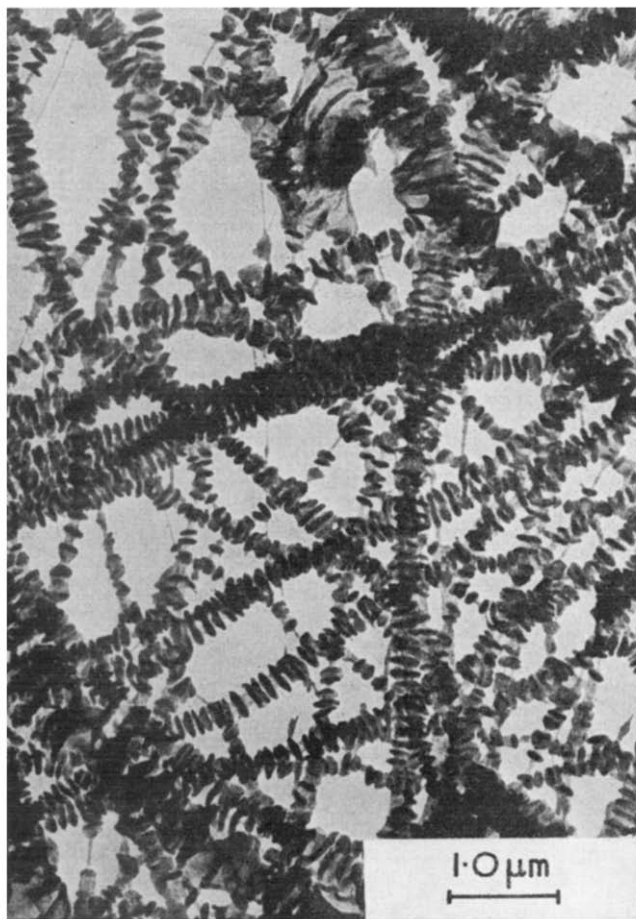


Figure 1 'Shish-kebab' fibrils prepared in a quiescent polymerization in cyclohexane at 25°C. Sample PE-2. Electron micrograph, unshaded



Figure 2 Smooth fibrils prepared in a stirred polymerization in cyclohexane at 25°C. Sample PE-1. Electron micrograph (replica). Pt shadowed. The proportion of the smooth fibrils decreases with increasing polymerization temperature

ology varies somewhat with the solvent used in the polymerization, but is independent of the catalyst concentration over the range 0.02–0.2 mmol/l.

Observations in the optical microscope showed that samples prepared in cyclohexane were predominantly composed of birefringent fibres admixed with a smaller amount of polymer having an apparently granular texture. Detailed examination in the electron microscope showed that most of the fibres have a 'shish-kebab' microstructure (Figure 1) and thus are similar to those formed during the polymerization of  $\alpha$ -olefins with heterogeneous Ziegler-Natta catalysts<sup>4</sup>.

A small fraction of the fibrous polymer consisted of fibrils whose texture is illustrated in the replica shown in Figure 2. The fibrils are devoid of lamellar overgrowth and thus appear to be smooth and featureless. Presumably these fibrils have a structure similar to the central filament of the 'shish-kebab'.

A representative electron micrograph of the non-fibrillar portion of the polymer is shown in Figure 3. Evidently this material consists of irregularly shaped particles which are probably compact aggregates of small lamellae.

The morphology of the polymer samples prepared in toluene is illustrated in Figures 4 and 5. The samples were composed of aggregates of globular particles, fibrillar material and lamellar crystals. Because of excessive sample thickness a detailed examination of the globular particles by direct transmission electron microscopy was not possible. Therefore, in order to obtain



Figure 3 Representative electron micrograph (replica) of non-fibrillar polyethylene prepared in a stirred polymerization in cyclohexane at 25°C; sample PE-1

more information about the structure of the particles the samples were replicated. Figure 6 shows the surface replica of a sample composed chiefly of globular particles. From the general appearance of the replica it is evident that the constitution of the particles is not revealed in an unambiguous manner. However, on careful examination, certain areas of the replica give the impression of being composed of fine, structureless fibrils. It is therefore tempting to suggest that the globular particles are composed of fine filaments which are tightly wound together.

The inference that seems to emerge from the foregoing observations is that the nascent polymer has a dual morphology being composed of fibrillar as well as lamellar crystals. The possible origin of these two morphological forms will be discussed later in terms of the state of dispersion of the catalyst in the polymerization medium.

#### Nitric acid oxidation

In order to obtain further information on the structure of the nascent polymer, observations were made on samples digested with fuming nitric acid. Electron microscope observations showed that the extent of the oxidative effect on the fibrillar polymer depended on the duration of the treatment. Short oxidation times, in general up to 10 hours, had no perceptible effect on the fibrillar crystals. Samples oxidized for periods exceeding 10 hours showed a progressive decrease in

the number and length of the fibrils in comparison with the original unoxidized sample. Beyond approximately 50 hours of treatment only lamellar debris remained in the oxidized samples. It is known that 'shish-kebab' fibrils prepared in stirred crystallizations have an extended-chain central filament which withstands even prolonged treatment with fuming nitric acid<sup>5, 18</sup>. The ease of disintegration of the nascent 'shish-kebabs' obviously indicates that the central filament of the fibrils is easily oxidized and cleaved under the action of the nitric acid. In this regard the behaviour of the nascent fibrils is very similar to that of fibrillar polyethylene crystals prepared with heterogeneous Ziegler-Natta catalysts<sup>5</sup>. It is a reasonable inference that the susceptibility of the central filament of the nascent fibrils is due to crystal defects, probably chain folds, which are the sites of the nitric acid oxidation.

As expected, the lamellar portion of the polymer was readily attacked by fuming nitric acid. After short times of treatment, aggregates as those shown in Figure 3 were no longer present in the oxidized samples. Instead, the samples contained a fine debris of irregular lamellae which apparently originated from the disintegration of the aggregates.

The samples prepared in toluene were not significantly affected even after 80 hours of treatment with fuming

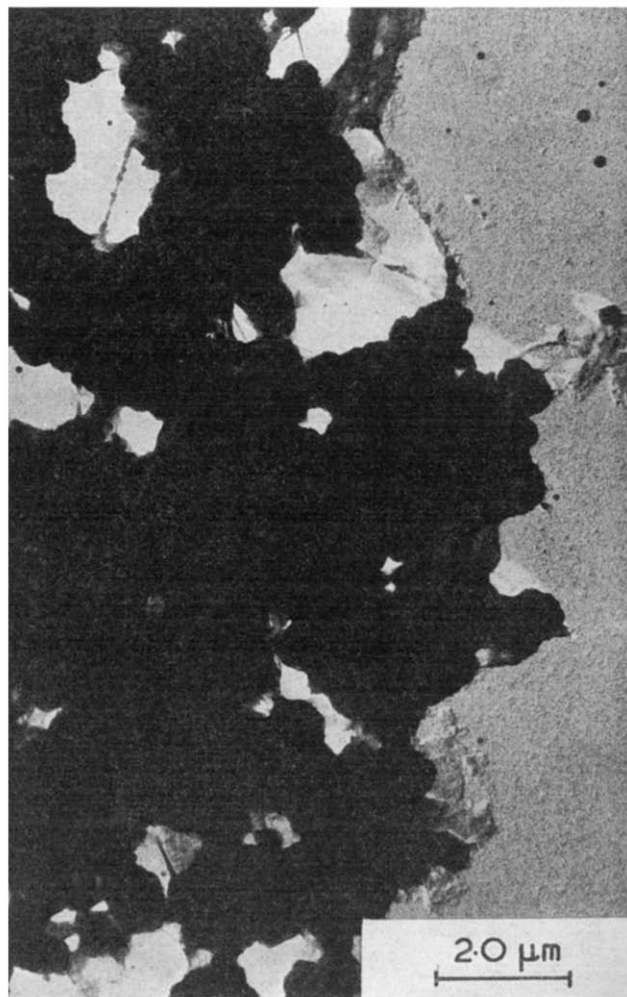


Figure 4 Aggregates of globular particles obtained in a stirred polymerization in toluene at 25°C. Sample PE-9. Electron micrograph, Pt shadowed. Sample PE-10 prepared at the same temperature under quiescent conditions has similar morphology

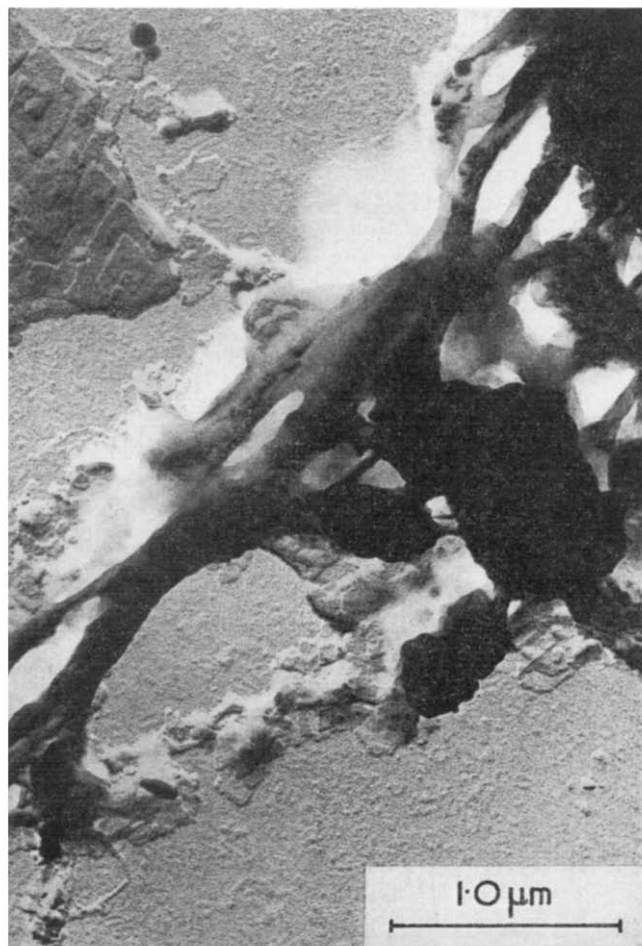


Figure 5 Electron micrograph showing lamellar crystals and fibrils connecting globular particles prepared in a stirred polymerization in toluene at 55°C; sample PE-12

nitric acid. The globular particles retained their original texture and were still aggregated in clusters, despite the fact that macroscopically the oxidized polymer became brittle. As already indicated, the electron microscope observations suggest that the globular particles are composed of fine structureless filaments. The observation that the globular particles retain their original constitution even after prolonged exposure to fuming nitric acid suggests that these filaments are more resistant to nitric acid digestion and, therefore, have a greater crystal perfection than the central filaments of the 'shish-kebabs'. This means that the filaments of the globular particles have a higher degree of chain extension than the central filaments of the 'shish-kebabs'. As will be shown below this interference is supported by the thermal behaviour of the polymer samples.

#### Thermal analysis

The following observations were made when the melting behaviour of the nascent polyethylene samples was examined with a differential scanning calorimeter in the manner described above.

Figure 7 shows a typical melting curve of a sample prepared in cyclohexane together with the melting curve of the same sample recrystallized from the melt by cooling in the calorimeter. It can be seen from the position of the melting peak on the temperature scale that the samples melt at relatively low temperatures which are comparable to those of folded-chain crystals,

and that the endotherm has a rather sharp return to the base line. The low melting temperature of the sample indicates that the bulk of the polymer consists of folded-chain crystals.

The melting behaviour of the polyethylene samples prepared in toluene is illustrated in Figure 8. The most notable characteristic of these samples is that a major fraction of the polymer melts at temperatures higher than expected for folded-chain polyethylene crystals. (Polyethylene crystals having a folded-chain structure usually melt at 136°C or lower temperatures<sup>19</sup>.) Such high melting points are usually associated with polyethylene crystals having an extended conformation of molecular chains<sup>20-23</sup>. Melting points of similar magnitude have also been reported for certain nascent polyethylene samples for which an extended-chain structure was postulated<sup>3, 24, 25</sup>. Accordingly, a predominantly extended-chain structure is also postulated for the present polyethylene samples in order to account for their high thermodynamic stability. On second melting, after recrystallization from the melt by cooling in the calorimeter, the melting peak of the polymer occurs at a position 7°C lower than that of the nascent sample. Obviously the polymer on recrystallization from the melt develops a spherulitic morphology and now melts at temperatures commensurate with a folded-chain structure<sup>22-24</sup>.

#### Light scattering

The foregoing observations show that part of the nascent polymer has a fibrillar morphology. If the



Figure 6 Replica of the surface of globular particles obtained from the same preparation as those shown in Figure 4. Electron micrograph, Pt shadowed

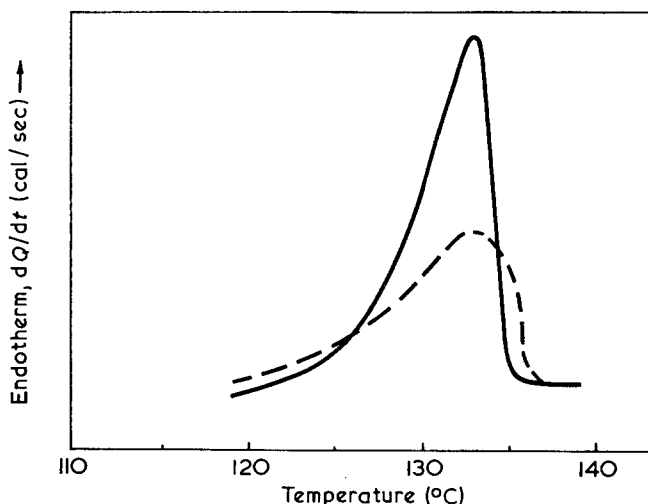


Figure 7 D.s.c. melting curves for a sample prepared in cyclohexane at 25°C (PE-1). —, Original sample; ---, recrystallized from the melt in the calorimeter. Heating rate, 5°C/min

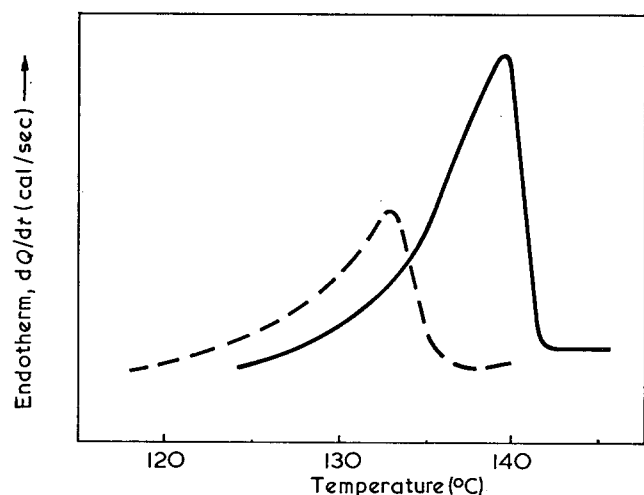


Figure 8 D.s.c. melting curves for a sample prepared in toluene at 25°C (PE-9). —, Original sample; ---, recrystallized from the melt in the calorimeter. Heating rate, 5°C/min

catalyst is truly homogeneous, it is difficult to envisage the mechanism by which the fibrillar crystals grow. It was therefore of interest to investigate the state of catalyst dispersion in the polymerization medium.

Catalyst preparations in toluene or cyclohexane containing 0.02, 0.1 and 0.2 mmol/l of  $\text{VOCl}_3$  were tested in the photometer. The molar ratio of  $(\text{C}_2\text{H}_5)_2\text{AlCl}$  to  $\text{VOCl}_3$  was 50 or 200. In all cases, even with the most dilute preparations, the scattering ratios of the catalyst solutions far exceeded that of the pure solvent. For the lowest catalyst concentration tested,

$$[\text{VOCl}_3]=0.02 \text{ mmol/l, } [\text{Al}]/[\text{Ti}]=50,$$

the scattered intensity of the catalyst solution was 6 times higher than the intensity of the  $(\text{C}_2\text{H}_5)_2\text{AlCl}$  solution and 20 times higher than that of the  $\text{VOCl}_3$  solution. The difference between the scattered intensities of the catalyst solutions, and solutions of each of the two catalyst components alone, became greater at higher catalyst concentrations. These observations clearly indicate that the catalyst solutions were not truly homogeneous but instead contained some kind of heterogeneity, probably in the form of colloidal particles.

Furthermore, the observation that the scattering power of the catalyst solution is many times stronger than that of the individual catalyst components, shows that the heterogeneity is due to reaction products formed in the preparation of the catalyst.

The dependence of scattering power on the age of catalyst was examined in agitated and quiescent systems. When the catalyst solution was agitated by stirring, the scattered intensity did not show any significant change over a 2 h period. On the other hand, when the solution was left undisturbed a gradual decrease of scattering with time was noticed. The decrease of scattering for a catalyst preparation in cyclohexane containing 0.1 mmol/l  $\text{VOCl}_3$  and 5 mmol/l  $(\text{C}_2\text{H}_5)_2\text{AlCl}$  is illustrated in Figure 9. Similar behaviour was observed with other catalyst preparations, although the rate of scattering decrease for the catalyst preparation containing 0.02 mmol/l  $\text{VOCl}_3$  was significantly slower. On the other hand, the scattered intensity of solutions containing one of the catalyst components alone remained constant with time both under quiescent and under stirred conditions. The decline of the scattering power of the undisturbed catalyst solutions is probably due to a gradual sedimentation of the colloidal particles which serve as scattering centres. The rate of scattering decrease, and hence of particle sedimentation, implies that the size of the particles must be substantial. That this is the case is also indicated from the dissymmetry ratios of the catalyst solutions which were found to vary between 3.5 and 4.

In conclusion, the light-scattering measurements provide strong evidence that besides the soluble active species associated with the pink colour of the solution, the catalyst preparations also contain colloidal particles which originate from the interaction of the catalyst

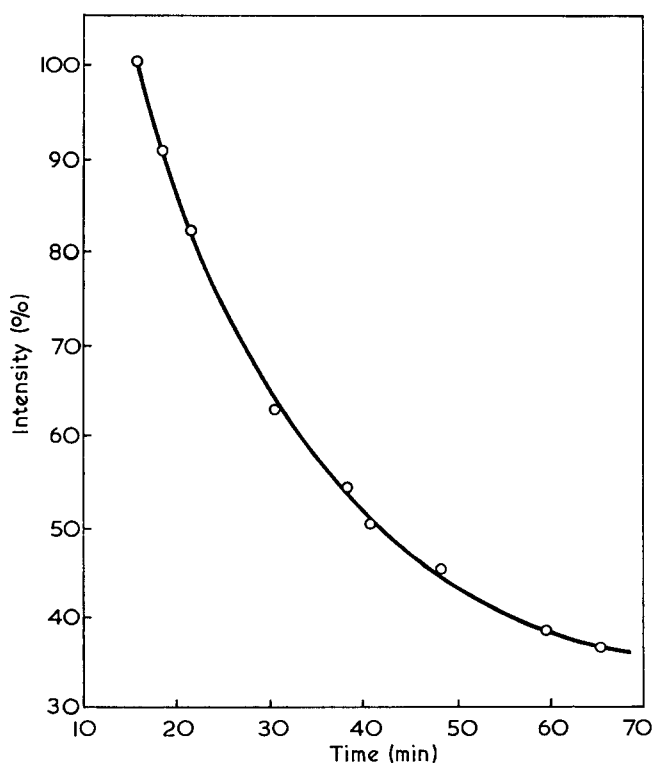


Figure 9 Percentage decrease of light-scattering intensity as a function of time for an undisturbed catalyst preparation in cyclohexane containing 0.1 mmol/l  $\text{VOCl}_3$  and 5 mmol/l  $(\text{C}_2\text{H}_5)_2\text{AlCl}$ .  $t=0$  is taken as the time of mixing of the catalyst components

components. The possible implications of these observations as regards the morphology of the nascent polymer will now be discussed.

## DISCUSSION

The optical and electron microscopic examination of the polymer revealed the presence both of fibrillar and of lamellar crystals. As mentioned earlier, it is believed that the morphology of the as-polymerized polyethylene prepared with Ziegler-Natta catalysts is determined by the state of the catalyst dispersion. Polyethylene prepared with a soluble catalyst has a folded-chain lamellar structure, whereas almost all cases of fibrillar crystal formation involved heterogeneous catalysts<sup>3-5</sup>. The difference in crystal morphology results from the different nucleation mechanism of the crystalline polymer prepared with the two polymerization systems. Since in the soluble catalyst systems the active sites exist independently of one another, only intramolecular nucleation is possible and folded-chain lamellar crystals are formed. On the other hand, with heterogeneous systems aggregation of active sites on the catalyst surface promotes the intermolecular nucleation of polymer chains growing from adjacent sites and leads to fibrillar growth. Given that the present catalyst system is considered homogeneous the presence of fibrillar crystals in the polymer is contrary to the suggested mechanism of fibrillar growth. However, the light-scattering measurements provide the answer to the apparent contradiction. It is believed that with the present catalyst system the active sites exist in the polymerization medium in a dual form, i.e., as soluble complex and in a colloidal dispersion. The presence of the soluble complex is demonstrated by the pink colour of the solution which develops on mixing the two catalyst components and decreases in intensity with catalyst deactivation during polymerization. The formation and chemical nature of the soluble complex<sup>14, 26-28</sup> have been the subject of several investigations and do not directly concern the present study. Suffice it to say that it is recognized that each soluble complex involves one active site which generates one molecular chain at a time. Besides the soluble portion of the catalyst there exists in the polymerization medium a colloidal dispersion whose presence was revealed with the light-scattering measurements. The real nature of the colloidal particles is unknown and is presently only a matter of speculation. However, it is suspected that the micelles are active in the polymerization of ethylene and are in fact the sites of formation of the fibrillar crystals.

Accordingly, the formation of the crystal forms observed in the polymer samples may be explained in terms of the dual catalyst composition as follows. The lamellar crystals and the platelets grown epitaxially on the central filament of the 'shish-kebabs' are formed by intramolecular crystallization of polymer chains generated from the soluble active sites. The central filament of the 'shish-kebabs' and the structureless fibrils, on the other hand, are the product of intermolecular crystallization of polymer chains emanating from adjacent active sites residing within a given area of the catalyst micelle.

The true nature of ostensibly soluble catalyst preparations has been the subject of speculation in the past<sup>29</sup>, and recently, the presence of colloidal particles has been confirmed by light-scattering measurements in the case of dilute catalyst solutions prepared by mixing (Ti/acac)<sub>3</sub>

and (C<sub>2</sub>H<sub>5</sub>)<sub>2</sub>AlCl<sup>30</sup>. Increase of the catalyst concentration in this system above a certain point results in the appearance of visible precipitates. There is, therefore, a maximum catalyst concentration which marks the transition point between catalyst preparations containing visible precipitates and those which appear clear but which, nevertheless, contain colloidal particles. It appears that there is a parallel between the behaviour of the above catalyst and that of the catalyst employed in the present study. The catalyst system VOCl<sub>3</sub>/(C<sub>2</sub>H<sub>5</sub>)<sub>2</sub>AlCl under the conditions of catalyst concentration and Al/V molar ratio used in the present study has been reported to be soluble<sup>8</sup>. Our observations with light scattering, however, revealed the presence of colloidal particles despite the apparent homogeneity of the catalyst solutions. Furthermore, earlier works report that with the present and other similar vanadium catalysts the extent of catalyst solubility depends on the concentration of the catalyst components and the Al/V molar ratio. Decrease of catalyst concentration and increase of Al/V molar ratio result in higher catalyst proportions remaining in solution<sup>14, 31-34</sup>. It is evident, therefore, that the physical state of the catalyst in the polymerization medium is determined by its concentration and the Al/V molar ratio.

On the basis of the above observations it may be assumed that at sufficiently low concentrations and optimum Al/V ratios completely soluble catalyst preparations, devoid of colloidal particles, could be obtained. Such catalyst preparations are expected to produce polyethylene composed only of folded-chain lamellar crystals. They may be used, therefore, to test our proposition that the fibrillar crystals originate from the colloidal particles. However, at very low catalyst concentrations the polymer yield, especially in quiescent polymerizations, is so low that, even if catalyst solutions free of micelles exist, it would be difficult to test the hypothesis.

The above mechanism of fibril growth is based on the concept of aggregation of active sites on the surface of the micelles and the consequential intermolecular crystallization of polymer chains growing from the sites. However, the possibility that the fibrils are flow-induced should not be left without further consideration. It is conceivable that the formation of fibrils could be due to the external stirring of the polymerization medium or to convection currents generated by the dissipation of the heat of polymerization. That the growth of fibrils was not effected by the action of stirring is indicated from the presence of fibrils in quiescent polymerizations. The electron microscope observations showed that polymer samples prepared under identical polymerization conditions except stirring of the polymerization medium had the same morphology. On the other hand, the proposition that the formation of fibrils may be induced by convection currents in the polymerization medium is not substantiated from the behaviour of other soluble catalyst systems. As has been shown elsewhere<sup>1</sup> polyethylene prepared with the soluble catalyst system (C<sub>5</sub>H<sub>5</sub>)<sub>2</sub>TiCl<sub>2</sub>/R<sub>2</sub>AlCl in stirred or quiescent polymerizations always consisted of folded-chain lamellar crystals. Since, therefore, in homogeneous polymerizations even external stirring of the polymerization medium is not effective in inducing fibrillar growth, it is rather improbable that in the present case the much weaker convection currents could have any



effect. Excluding, therefore, the possibility of flow-induced growth, the fibril formation may be accounted for most reasonably in terms of an intermolecular crystallization of polymer chains growing from clusters of active sites residing on the surface of the observed colloidal particles.

Perhaps these considerations may also apply to the reported case of growth of fibrillar polyethylene crystals with a supposedly soluble catalyst system<sup>9</sup>. Thus, the catalyst preparation although free of any visible precipitate, probably contained some kind of colloidal dispersion which gave rise to the observed fibrillar crystals.

## CONCLUSIONS

It has been shown that polyethylene prepared with the soluble catalyst system  $\text{VOCl}_3/(\text{C}_2\text{H}_5)_2\text{AlCl}$  has a dual morphological structure, i.e., it consists of folded-chain lamellar crystals and fibrillar crystals, the degree of chain extension in the latter depending on the experimental conditions of polymerization. These two crystal forms grow by two different crystallization mechanisms. Folded-chain lamellar crystals are formed by intramolecular crystallization whereas fibrillar crystals are formed by intermolecular crystallization. On the basis of these observations, and excluding the possibility that intermolecular crystallization has been flow-induced, it is postulated that in addition to the soluble part of the catalyst, clusters of active sites exist in the system which give rise to the fibrillar crystals. This postulate is supported by light-scattering measurements which revealed the presence of a colloidal dispersion that is apparently the locus of the active site aggregates.

These observations also suggest that the study of morphology of nascent polyethylene, apart from its inherent interest, may have some implications regarding the study of the catalyst itself. Thus, it may indeed be possible, as suggested by Boor<sup>7</sup>, to differentiate between truly homogeneous and colloidally dispersed catalysts on the basis of the nascent morphology of the polymer.

## REFERENCES

- 1 Georgiadis, T. and Manley, R. *St J. Kolloid-Z. Z. Polym.* 1972, **250**, 557
- 2 Carrick, W. L. *et al. J. Am. Chem. Soc.* 1960, **82**, 3883
- 3 Ingram, P. and Schindler, A. *Makromol. Chem.* 1968, **111**, 267
- 4 Blais, P. and Manley, R. *St J. J. Polym. Sci. (A-1)* 1968, **6**, 291
- 5 Wikjord, A. G. and Manley, R. *St J. J. Macromol. Sci.* 1968, **B2**, 501
- 6 Pennings, A. J. *Proc. Int. Conf. on Crystal Growth, Boston*, Pergamon Press, Oxford, 1967, p 389
- 7 Boor, J. Jr., in 'Macromolecular Reviews', (A. Peterlin, *et al.*, Eds) Interscience, New York, 1967, Vol 2, p 137
- 8 *Product Licensing Index* 1967, **40**, 25
- 9 Keller, A. and Willmouth, F. M. *Makromol. Chem.* 1969, **121**, 42
- 10 Sorenson, W. R. and Campbell, T. W. 'Preparative Methods of Polymer Chemistry', (2nd edn), Interscience, New York, 1968
- 11 Carrick, W. L. *J. Am. Chem. Soc.* 1958, **80**, 6455
- 12 Carrick, W. L., Chasar, A. G. and Smith, J. J. *J. Am. Chem. Soc.* 1960, **82**, 5319
- 13 Kelly, R. J., Garner, H. D., Haxo, H. E. and Bingham, W. R. *Ind. Eng. Chem. Prod. Res. Develop.* 1962, **1**, 210
- 14 de Liefde Meijer, H. J., van den Hurk, J. W. G. and vander Kerk, G. J. M. *Rec. Trav. Chim.* 1966, **85**, 1018
- 15 Cunningham, R. E. *J. Polym. Sci. (A)* 1965, **3**, 3157
- 16 W. R. Grace & Co., Br. Pat. 917,439
- 17 Chiang, R. *J. Phys. Chem.* 1965, **69**, 1645
- 18 Willmouth, F. M., Keller, A., Ward, I. M. and Williams, T. *J. Polym. Sci. (A-2)* 1968, **6**, 1627
- 19 Wunderlich, B., Cormier, C. M., Keller, A. and Machin, M. J. *J. Macromol. Sci.* 1967, **B1**, 93
- 20 Wunderlich, B. and Arakawa, T. *J. Polym. Sci. (A)* 1964, **2**, 3697
- 21 Arakawa, T. and Wunderlich, B. *J. Polym. Sci. (C)* 1967, **16**, 653
- 22 Kardos, J. L., Baer, E., Geil, P. H. and Koenig, J. L. *Kolloid-Z.* 1965, **204**, 1
- 23 Rees, D. V. and Bassett, D. C. *Nature* 1968, **219**, 368
- 24 Wunderlich, B. *et al. Kolloid-Z.* 1965, **204**, 125
- 25 Chanzy, H., Day, A. and Marchessault, R. H. *Polymer* 1967, **8**, 567
- 26 Phillips, G. W. and Carrick, W. L. *J. Polym. Sci.* 1962, **59**, 401
- 27 de Liefde Meijer, H. J., van den Hurk, J. W. G. and van der Kerk, G. J. M. *Rec. Trav. Chim.* 1966, **85**, 1025
- 28 Lehr, M. H. *Macromolecules* 1968, **1**, 178
- 29 Natta, G. *et al. Makromol. Chem.* 1964, **77**, 114
- 30 Watt, W. R., Fry, F. H. and Pobiner, H. J. *J. Polym. Sci. (A-1)* 1968, **6**, 2703
- 31 Junghanns, E., Gumboldt, A. and Bier, G. *Makromol. Chem.* 1962, **58**, 18
- 32 Bier, G., Gumboldt, A. and Schleitzer, G. *Makromol. Chem.* 1962, **58**, 43
- 33 Obloj, J., Uhnat, M. and Nowakowska, M. *Vysokomol. Soedin.* 1965, **7**, 939; *Polym. Sci. USSR* 1965, **7**, 1040
- 34 United States Rubber Company, Br. Pat. 886,368
- 35 Wunderlich, B. *Angew. Chem. (Int. Edn. Engl.)* 1968, **7**, 912

# Surface areas of fillers in polymers by small-angle X-ray scattering

D. S. Brown, F. P. Warner and R. E. Wetton

Department of Chemistry, University of Technology, Loughborough, Leics LE11 3TU, UK  
(Received 12 June 1972)

The surface areas of Aerosil silicas in air and dispersed in a silicone rubber have been determined by analysing small-angle X-ray data according to the methods of Porod and Debye. Broad agreement with the manufacturers' BET (Brunauer–Emmett–Teller) area values is obtained. The silica surface area and basic state aggregation are not measurably modified by milling into the rubber.

## INTRODUCTION

The electron microscope has been used extensively to study dispersion and agglomeration of fillers in rubbers of colloidal dimensions. Unfortunately, with the small particle, high structure fillers, ultra-thin sectioning is required and it is difficult to obtain quantitative results representative of the bulk material. Studies of filler in fracture or other surfaces, similarly, are unlikely to be representative of the bulk. Small-angle X-ray scattering (SAXS) provides a useful alternative technique as thick samples (~1 mm) are employed without modification and the results apply to a statistically large number of particles.

A silica/silicone rubber system was selected for study in the first instance as fine particle silica fillers exert an enormous influence on mechanical properties. A knowledge of the *in situ* filler surface area, degree of aggregation and the randomness of the system is essential before proper interpretation of the mechanical properties can be made, yet this evidence is largely lacking. There is a large difference in reinforcement properties between silica with silanol surface groups and silica of similar particle size but with more lyophobic surface groups<sup>1</sup> and good evidence was sought on relative dispersions in these systems.

For a two-phase system, the surface area per unit mass of dispersed phase,  $S_1$ , may be obtained from the relationship<sup>2-4</sup>:

$$S_1 = \frac{8\pi\phi_2 \lim [\tilde{I}(\theta)\theta^3]}{d_1\lambda\bar{Q}} \quad (1)$$

where

$\phi_2$  is the volume fraction of the continuous phase;

$d_1$  is the density of the dispersed phase;

$\lambda$  is the wavelength of the X-rays;

$\bar{Q}$  is an invariant, which for slit collimation is given by  $\bar{Q} = \int_0^\infty \tilde{I}(\theta)\theta \, d\theta$ , where  $\theta$  is the scattering angle (twice the 'Bragg' angle) and  $\tilde{I}(\theta)$  is the slit-smearred observed intensity at an angle  $\theta$ ;

$\lim [\tilde{I}(\theta)\theta^3]$  represents the limiting constant value at high angles of  $\tilde{I}(\theta)\theta^3$  as predicted by Porod's law<sup>2, 3</sup>.

This method of estimating surface areas should, in principle, be applicable to all truly two-phase systems, but requires documentation of the scattering curve over as wide an angular range as possible. Even then, extrapolations are required at the low and high angle regions of the scattering in order to evaluate  $\bar{Q}$ . An alternative method of estimating  $\bar{Q}$  is available if the absolute intensity of the primary beam can be determined using, for example, a Kratky standard sample<sup>5-7</sup> when

$$\bar{Q} = kP_s t \phi_1 \phi_2 \Delta\rho^2 \quad (2)$$

where

$$k = 4.55 \times 10^{21} \lambda^3 \text{ mol}^{-2} \text{ cm}^5,$$

$P_s$  is the sample attenuated intensity of the whole primary beam,

$t$  is the sample thickness,

$\phi_1$  and  $\phi_2$  are the volume fractions of the dispersed and continuous phases respectively,

$\Delta\rho$  is the electron density difference between the two phases.

Equation (2) may also be used with the experimentally determined value of  $\bar{Q}$ , to determine the electron density difference between the phases.

A second approach to the determination of surface areas from small-angle scattering data is from the slope of the correlation function<sup>8</sup> at zero distance. According to Debye *et al.*<sup>9</sup> a *completely random* two-phase system has an exponential correlation function. For slit-smearred intensities:

$$\tilde{I}(\theta) = \frac{A}{\left(1 + \frac{4\pi^2}{\lambda^2} \theta^2 c^2\right)^{3/2}} \quad (3)$$

where  $A$  is a constant, and  $c$  is a constant related to surface area ( $S_1$ ) by

$$S_1 = \frac{4\phi_2}{cd_1} \quad (4)$$

Hence  $c$  may be evaluated by a plot of  $\tilde{I}(\theta)^{-2/3}$  versus  $\theta^2$ , where

$$c = \frac{\lambda}{2\pi} \left( \frac{\text{slope}}{\text{intercept}} \right)^{1/2}$$

Agreement between surface areas determined by Debye's method and those determined from Porod's law indicates that the system is likely to be both random and two-phase. Porod's law is not obeyed when there are more than two phases present, although corrections can be made to take into account diffuse interphase boundaries or electron density fluctuations within phases<sup>10</sup>. Debye's method is erroneous when applied to systems which are not completely random.

The two methods, outlined above, have been applied to surface area determination of some silicone rubbers filled with colloidal silica.

### EXPERIMENTAL

Three different Degussa Aerosil silicas were examined. Aerosils 130 and 300 were hydrophilic systems with one silanol group per 30 Å<sup>2</sup> of surface and nominal surface areas (in m<sup>2</sup>/g) given by the code numbers. The third silica, R972, is surface treated with dimethyl dichlorosilane which is believed to react with 80% of the original silanol groups to give a hydrophobic surface. The systems were investigated as uncompacted powders in air and as filler dispersed in a silicone rubber (ICI, E351). This polymer is predominantly polydimethylsiloxane, but contains a small fraction of phenyl and vinyl groups. The powders for X-ray examination were contained in exactly calibrated 1 mm diameter glass capillary tubes. The polymer-filler systems were produced by milling the silica into the polymer on a two roll mill until good optical clarity was obtained. This normally took approximately 10 min.

Small-angle X-ray scattering data were obtained using slit-collimated nickel filtered Cu radiation in a Rigaku-Denki goniometer (2202). Detection was by means of a scintillation counter (NaI) and the pulses were pulse-height analysed before being fed into a ratemeter and chart recorder unit.

The absolute intensity of the primary beam was estimated with a Kratky standard Lupolen sample.

### RESULTS

Surface areas of the silica-air and silica-rubber interfaces were determined by both Porod's and Debye's methods. Evaluation of the invariant  $\tilde{Q}$  required extrapolations both at low and high angles where experimental measurements are impossible. Figure 1 shows a plot of  $\tilde{I}(\theta)\theta$  versus  $\theta$  for R972 coated aerosil in silicone rubber, used in the Porod surface area determination. The low angle extrapolation to the origin is indicated by a dotted line. It is clear that the area below this line is small, compared with the total area under the curve and hence extrapolation errors here will not cause appreciable error in the ensuing surface area determination. Above point A the relationship  $\tilde{I}(\theta) \propto 1/\theta^3$  is obeyed, and the high angle extrapolation was effected by integration of this expression to infinity. Intensities are very low in the high angle region but the precision of these measurements affects both  $\tilde{Q}$  and the limiting value of  $\tilde{I}(\theta)\theta^3$ . Figure 2 shows a typical plot of  $\tilde{I}(\theta)^{-2/3}$  versus  $\theta^2$  for R972 aerosil in silicone rubber, used in the Debye surface area determination.

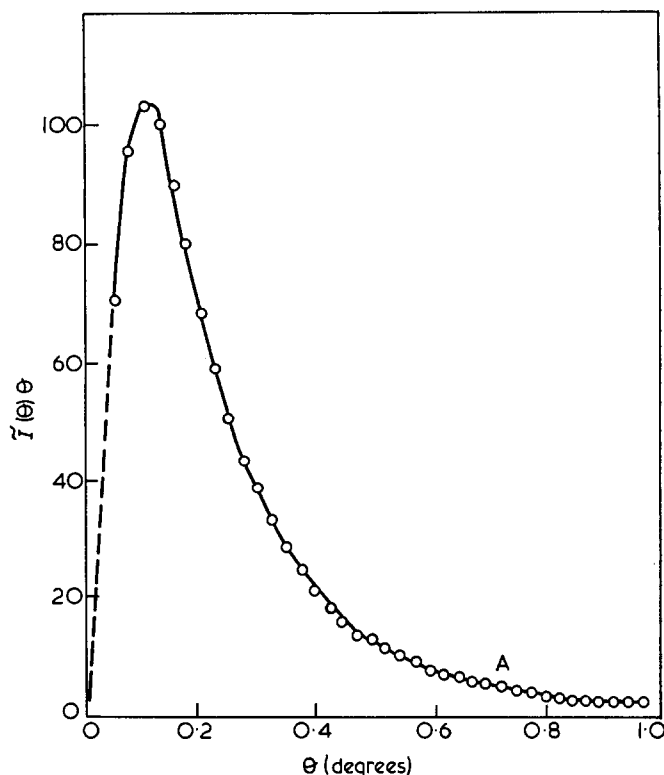


Figure 1 Plot of  $\tilde{I}(\theta)\theta$  versus  $\theta$  to determine the invariant  $\tilde{Q}$  for R972 coated aerosil in silicone rubber. Above point A the relationship  $\tilde{I}(\theta) \propto 1/\theta^3$  is obeyed

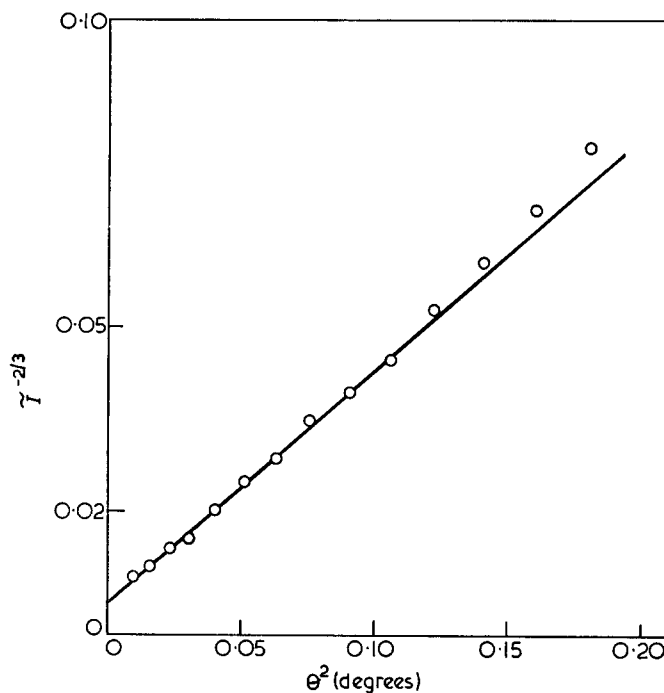


Figure 2 Debye plot for R972 in silicone rubber

tion. Slopes and intercepts were always determined from the first (linear) part of the curve. Absolute intensities were used to calculate the electron density difference between phases in the silica-rubber systems.

The results are presented in Table 1. The determined surface areas, expressed as m<sup>2</sup>/g of dispersed phase are compared with the manufacturers' quoted BET (Brunauer-Emmett-Teller) surface area values for the materials.

Table 1 Surface areas of Aerosil silicas in air and dispersed in silicone rubber

Sample	$\phi_1$	$t$ (mm)	$S_1$ (Debye) (m <sup>2</sup> /g)	$S_1$ (Porod) (m <sup>2</sup> /g)	$S_1$ (BET) (m <sup>2</sup> /g)	$\Delta\rho$ (mol cm <sup>-3</sup> )
Aerosil 300-air	0.0296	1.26	244	218	300 ± 30	
300-rubber	0.123	1.14	264	202		0.552
130-air	0.0452	0.93	114	112	130 ± 25	
130-rubber	0.165	1.01	140	97		0.515
R972-air	0.0210	1.11	136	122	120 ± 30	
R972-rubber	0.165	0.87	136	102		0.557
Estimated standard error			± 7%	± 9%		

## DISCUSSION

The data in *Table 1* show immediately that the silica/air and silica/silicone rubber systems are very amenable to study by the low angle X-ray diffraction method. There are two dramatically obvious conclusions. One is the general agreement of surface areas determined by the two X-ray methods with the BET gas adsorption value. Considering the completely different premises of the BET and X-ray methods this is certainly good confirmation of the exactness in an absolute sense of each method. The second clear conclusion is that the silica surface area and basic state of aggregation is not modified by milling into the rubber.

Turning attention now to finer details of the results it is seen that the Debye results are self consistent in a rubber or air matrix to within ± 10% of mean values and the Porod results are self consistent to within about the same tolerance, but in each case the Porod result is slightly lower. The results are broadly in line with the manufacturer's BET specification except for the nominal 300 m<sup>2</sup>/g sample, which should be about 250 m<sup>2</sup>/g for this material. The BET results quoted are of course not determined on the individual batches of silica used in this work, but are the manufacturer's nominal specifications. X-ray diffraction techniques measure all particle surfaces whether internal or external and the broad agreement between these techniques and BET values indicates that these silica particles are free of internal voids and small pores inaccessible to gas. The Debye and Porod values for each silica/air system agree within our estimates of random error. This gives confidence in the exactness of the methods and the data manipulative operations employed. Conversely, for the silica/silicone rubber systems the Porod result is systematically lower than both the Debye result and the result with the same silica in air.

There is little reason to suspect systematic errors in the volume fraction terms or  $\bar{Q}$  values in equation (1) as these lead to the correct  $\Delta\rho$  terms via equation (2) as discussed later. The only reasonable explanation for the slightly low Porod's law values is the  $\bar{I}(\theta)\theta^3$  limit at high angles. Because of low intensities in the continuously scanned system employed in this work the limit of reasonable accuracy occurred at an angle of about 1°. In the silica/air system with a relatively high average particle separation this was clearly high enough to satisfy the Porod condition. In the silica/rubber system the average particle spacings are much lower and hence will give normal interparticle scattering to higher angles with the Porod condition possibly not being fully satisfied even at the 1° angle<sup>11</sup>. It may be pointed out, however, that tests of Porod's law applicability in this region were always made and always seemed to give agreement. The reasons for the slightly low Porod's law values in the rubber system are thus not fully understood.

The data can be used to evaluate the electron and hence mass density difference between phases. The average electron density difference between the phases in *Table 1* is 0.541 mol electrons cm<sup>-3</sup> and as the measured mass density of the unfilled rubber is 0.965 g cm<sup>-3</sup> the mass density of the silica is calculated to be 2.12 g cm<sup>-3</sup>. This is within our error limits of the manufacturer's quoted density of 2.2 g cm<sup>-3</sup>.

The Debye method assumes a model in which the density variations (i.e. phase positions) are random in all directions. In the present work the applicability of this method indicates that both the silica/air and silica/rubber systems are random by this criterion. Electron micrographs of similar Aerosil materials indicate spherical particles with a rather large distribution of particle size. The present results show that these particles show no great regularity of arrangements such as chain structures or clusters. Recent measurements in these laboratories indicate that the applicability of the Debye method is very dependent upon randomness of structure. For example, a sample of Spheron 6 containing *very regular* spheres of graphite, suggested a particle diameter of 350 Å when Porod's method was applied, in good agreement with electron microscopy, but the Debye method gave a negative intercept on the  $\bar{I}^{-2/3}$  versus  $\theta^2$  plot, which is meaningless. Similar results have been obtained on other systems containing some order. However, if the system is such that the Debye method *is* applicable, it has the great advantage that the complete scattering curve need not be documented. In particular, it may not be necessary to acquire data at the high angle (low intensity) end of the scattering curve.

It is well known that the modulus of rubber systems filled with 'high structure' fillers is not very amenable to treatment by relations of the Einstein type or even the more refined equations taking account of neighbouring particle perturbations. To give any sort of agreement with more general relations of the type derived by Guth<sup>12</sup>:

$$E = E_0(1 + 0.67f\phi + 1.62f^2\phi^2)$$

enormously high values of the shape factor  $f$  are required. Bueche<sup>13</sup> quotes values of  $f$  up to 110, but concludes that the model is wrong, and that basically a network is set up which modifies  $E_0$ . The present results show that there is no reason to invoke high  $f$  values on the grounds of particle structures in the bulk rubber and that rubber network theories therefore represent a better approach to the modulus problem.

## ACKNOWLEDGEMENT

We are indebted to Mr D. Southwart (Dunlop Ltd) for the provision of samples, and we thank the Science Research Council for financial support and for a maintenance grant to one of us (F.P.W.).

REFERENCES

- 1 Chahal, R. S. and St Pierre, L. E. *Macromolecules* 1969, **2**, 193
- 2 Porod, G. *Kolloid Z.* 1951, **124**, 83
- 3 Porod, G. *Kolloid Z.* 1952, **125**, 51
- 4 Kahovec, L., Porod, G. and Ruck, H. *Kolloid Z.* 1953, **133**, 16
- 5 Kratky, O., Pilz, I. and Schmidt, P. *J. Colloid Sci.* 1966, **21**, 24
- 6 Pilz, I. and Kratky, O. *J. Colloid Sci.* 1967, **24**, 211
- 7 Pilz, I. *J. Colloid Sci.* 1969, **30**, 140
- 8 Debye, P. and Bueche, A. M. *J. Appl. Phys.* 1949, **20**, 518
- 9 Debye, P., Anderson, H. R. and Brumberger, H. *J. Appl. Phys.* 1957, **28**, 679
- 10 Ruland, W. *J. Appl. Cryst.* 1971, **4**, 70
- 11 Renouprez, A. 'IUPAC Conf. Surface Area Determination', Butterworths, London, 1970, p 361
- 12 Guth, E. *J. Appl. Phys.* 1945, **16**, 20
- 13 Bueche, A. M. *J. Polym. Sci.* 1957, **24**, 139

# Electron spin resonance study of the role of calcium in the fibrinogen-fibrin reaction

C. Earland, J. H. Keighley\*, D. B. Ramsdent† and R. L. Turner

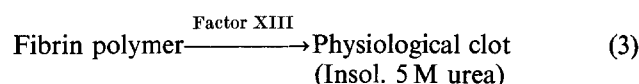
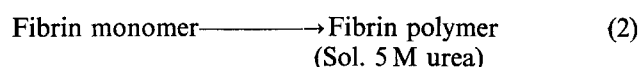
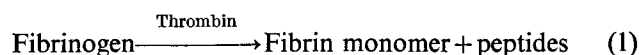
Postgraduate School of Studies in Medical and Surgical Sciences, University of Bradford, Bradford BD7 1DP, UK

(Received 22 May 1972; revised 26 July 1972)

For the first time a study has been made of the fibrinogen-fibrin conversion using electron spin resonance spectroscopy. Marked differences in spectra of the fibrin were observed with increasing calcium content of the clotting media. A model is proposed for the environment of the calcium in fibrin which involves either glutamic or aspartic acid residues in addition to histidine and tyrosine residues. The model proposed would explain the accelerating effect calcium ions have on the conversion of monomeric fibrin to urea-soluble polymeric fibrin and the essential role they play in the formation of the insoluble physiological clot.

## INTRODUCTION

The clotting of fibrinogen involves a long complex series of biochemical processes, the key reactions of which may be summarized as follows:



Fibrinogen molecules contain tyrosine and histidine residues and it has been shown<sup>1</sup> that nine intermolecular hydrogen bonds may be formed between such groups per molecule from the possible nineteen sites available<sup>2,3</sup>. The polymerization of fibrin monomer (reaction 2) proceeds by the formation of such hydrogen bonds, whilst the conversion of the urea-soluble fibrin polymer to the final physiological clot which is insoluble in 5 M urea (reaction 3) is the result of the formation of intermolecular isopeptide links between the  $\gamma$ -carbonyl groups of glutamine residues and the  $\epsilon$ -amino groups of lysine residues of adjacent molecules<sup>4,5</sup>. A proposed mechanism for this crosslinking by Lorand and Ong<sup>6</sup> involves reactive thiol groups in the fibrin stabilizing factor (Factor XIII or FSF).

Little work has thus far been reported on the precise role calcium ions play in these reactions, although it is known that they catalyse reaction (2) and are essential for reaction (3). Godal<sup>7</sup>, however, has reported that fibrinogen is able to bind calcium ions within its structure and X-ray diffraction studies<sup>8</sup> have indicated that the metal is

bonded to the fibrin in such a manner that its position is determined by the orientation of the protein molecules.

In the present work, electron spin resonance (e.s.r.) spectroscopy has been used for the first time to study the role calcium ions play in the polymerization of fibrin and its subsequent stabilization by factor XIII, and from these studies a possible mode of incorporation of the metal in the fibrin structure is suggested.

## MATERIALS AND METHODS

### Preparation of non-calcified fibrin

0.04 g of fibrinogen (Kabi Pharmaceuticals Ltd, L grade Human, 95% clottable) was dissolved in 5 ml of de-ionized distilled water and to this solution was added 0.10 ml of thrombin solution (1 NIH unit/ml Koch Light, human lyophilized). Clotting was allowed to proceed for 30 min. After removing excess water by allowing the clot to drain on nylon gauze placed on filter paper, it was finally freeze-dried.

### Preparation of calcified fibrin

Four solutions were prepared containing similar amounts of fibrinogen and thrombin to that described previously with the addition of 0.0002 g, 0.080 g, 0.30 g and 3.00 g of calcium chloride ( $\text{CaCl}_2 \cdot 6\text{H}_2\text{O}$ ) respectively. Clotting was allowed to proceed for 17 h, after which the clots were dried as before. The solution containing the maximum quantity of calcium chloride did not produce a clot and the whole was freeze-dried.

### Electron spin resonance spectroscopy

Samples of the original fibrinogen and fibrin clotted in the absence and presence of calcium were redried *in vacuo* over phosphorus pentoxide for 24 h. They were then placed in a Spectrosil high purity quartz tube and irradiated for 2 h with either 50 kV  $\text{CuK}\alpha$  X-rays or the radiation from a  $^{60}\text{Co}$  source to produce free radicals in the protein structure. The only exception was sample (f)

\* Department of Textile Industries, University of Leeds, Leeds LS2 9JT, UK.

† Present address: Clinical Research Centre, Watford Road, Harrow, Middlesex, HA1 3UJ, UK.

which was irradiated for 4h. During this period the samples were maintained under vacuum. E.s.r. studies were then carried out using a Hilger and Watts Microspin spectrometer with a modified magnet system and 100 kHz modulation having ascertained that the Spectrosil tube gave no signal after exposure to radiation. All measurements were made under the same conditions of time constant, amplifier gain, modulation current and microwave power level at the sample, except for sample (f) where a higher gain was used. Measurements were carried out at 20°C which was also the temperature used for irradiation. For some practical and theoretical aspects of e.s.r. spectroscopy an article by Keighley<sup>9</sup> should be consulted.

## RESULTS

The e.s.r. spectra of fibrinogen and fibrin formed in the presence and absence of calcium ions are given in *Figure 1*. The state of the clots and the interpretation of the spectra are summarized in *Table 1*.

## DISCUSSION

### Fibrinogen

This is an  $\alpha$ -protein of the k.m.e.f. (keratin-myosin-epidermin-fibrinogen group which has a similar infra-red spectrum to that of wool keratin. The molecules contain

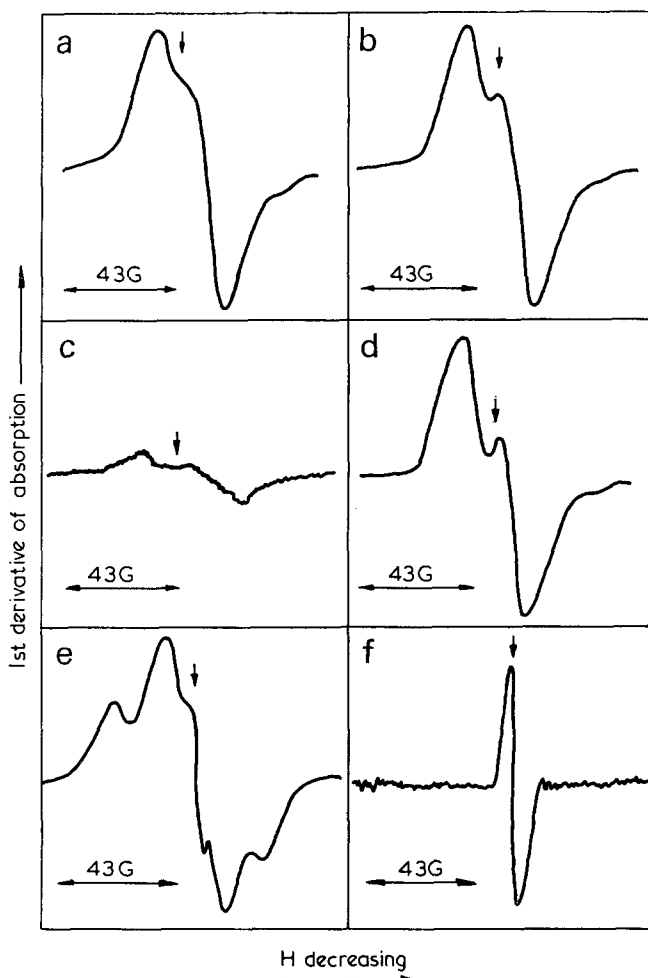


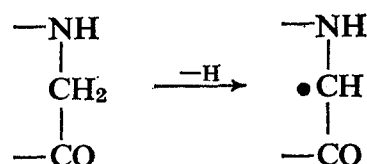
*Figure 1* E.s.r. spectra of fibrinogen and fibrin formed in the presence of different amounts of calcium. (a) Fibrinogen (no Ca); (b) fibrin (no Ca); (c) fibrin (0.0002g  $\text{CaCl}_2 \cdot 6\text{H}_2\text{O}$ ); (d) fibrin (0.080g  $\text{CaCl}_2 \cdot 6\text{H}_2\text{O}$ ); (e) fibrin (0.30g  $\text{CaCl}_2 \cdot 6\text{H}_2\text{O}$ ); (f) fibrin (3.0g  $\text{CaCl}_2 \cdot 6\text{H}_2\text{O}$ )

*Table 1* Properties of fibrinogen and fibrin clots formed in the presence of different amounts of calcium

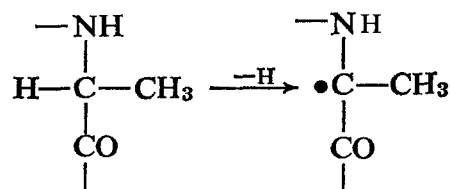
Sample	Calcium present ( $\text{CaCl}_2 \cdot 6\text{H}_2\text{O}$ ) (g)	State of clot	E.s.r. spectrum
(a) Fibrinogen	—	Unclothed	Unresolved doublet Quartet Singlet
(b) Non-calcified fibrin	—	Opaque gel soluble in 5M urea	Unresolved doublet Quartet Singlet
(c) Calcified fibrin	0.0002	Opaque gel insoluble in 5M urea	Unresolved doublet (low radical yield)
(d) Calcified fibrin	0.080	Opaque fibrous clot insoluble in 5M urea	Unresolved doublet
(e) Calcified fibrin	0.30	Clear gel insoluble in 5M urea	Triplet Singlet
(f) Calcified fibrin	3.0	No clot formed	Singlet (very low intensity)

clusters of negatively charged groups in fibrinopeptide residues and are hence mutually repellent.

The e.s.r. spectrum arises from three different radical species which produce a doublet, a quartet and a singlet, all superimposed (see *Figure 2*) to produce the spectrum shown in *Figure 1a*. This spectrum is similar to that obtained from chemically modified wool samples<sup>9</sup> and the interpretation of fibrinogen and fibrin spectra has been facilitated by previous experience with this fibrous protein. The separation of the two peaks of the doublet is of such a value that it is clear that the absorptions arise from the interaction of an unpaired electron with a single proton. Such a radical arises from the loss of a proton from a glycine residue:



The spacing and intensity ratios of the peaks in the quartet are such that the electron is interacting equally with three protons and this can only arise from an alanine radical:



The origin of the singlet, however, is not clear and may be associated with a conjugated system, aromatic group or an atom which has zero nuclear spin (e.g. an oxygen atom). In view of the nature of the molecular system and from a consideration of previous results<sup>10,11</sup> it is possible that radicals have been formed on tyrosine residues.

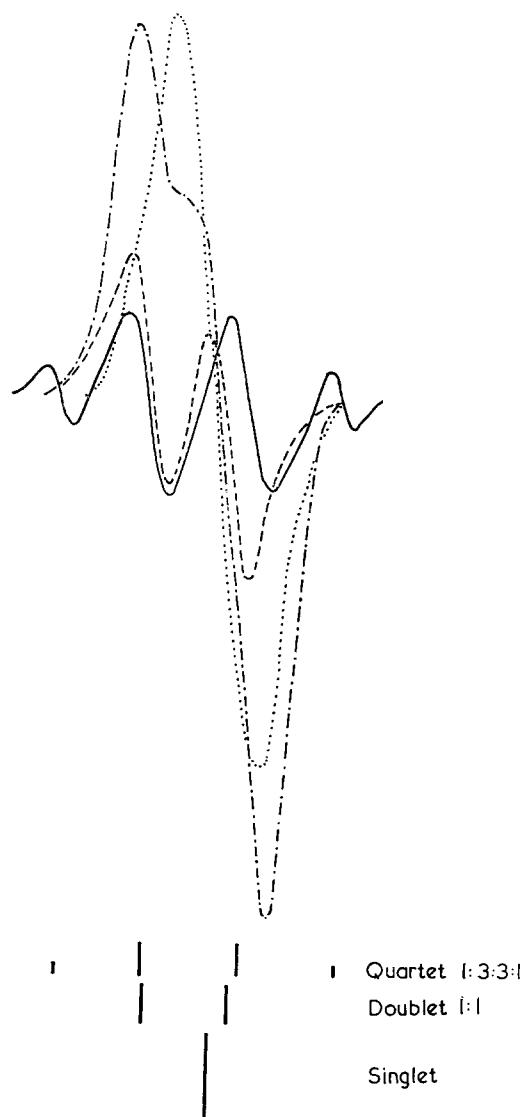


Figure 2 Diagrammatic representation of spectrum 1(a). —, Quartet; - - - -, doublet; ·····, singlet; - · - · -, resultant

In view of the complex nature of the structure of proteins of this type and the presence of many different amino acids, the detection of only a small number of different radical species is a surprising result. It has been shown by previous workers, however, that similar results are obtained when proteins in general are irradiated<sup>12</sup> and the small number of different radical species has been used to illustrate the presence of electronic conduction bands in proteins. This is the basis of a self stabilizing system in which charge migrates within the molecule to leave it in a condition of minimum energy. It has been proposed by Gordy and Shields<sup>13</sup> that certain amino acid residues are able to donate electrons to the system leaving an 'electron hole' of the lowest energy. Such residues are, for example, cystine, glycine and alanine in a probable order of decreasing stability. It has been shown by Keighley<sup>9</sup> that electronic conduction bands extend to the ends of main chains and side chains of a protein and that this is directly associated with chemical reactivity. It has also been found that chemical modification of the structure of proteins change the type of radical produced and in particular, when such changes involve groups attached to the ends of main chains and side chains, the specific types of radicals formed on irradiation are changed also.

#### Fibrin (non-calcified, non-crosslinked)

When fibrinogen is converted to fibrin by the action of thrombin, fibrinopeptides are released and the fibrin molecules aggregate by the formation of hydrogen bonds between the phenolic groups of tyrosine residues and the imidazole groups of histidine residues<sup>2,3</sup>. The e.s.r. spectrum of fibrin (Figure 1b) is similar to that of fibrinogen but the quartet is of lower intensity suggesting the loss of alanine residues in the above transformation. This is in agreement with the facts since alanine residues are lost as *N*-terminal residues of the fibrinopeptide during the fibrinogen-fibrin conversion. The newly formed *N*-terminal groups are glycine residues which may account for the glycine doublet absorption.

#### Fibrin (calcified, low calcium concentration)

The spectra obtained from fibrin samples containing small concentrations of calcium (Figures 1c and d) are unresolved doublets. In the presence of trace quantities of calcium the yield of radicals from interaction with a given dose of radiation is low possibly due to high water content resulting from difficulties encountered in the freeze-drying process. As in the sample spectra already discussed, the characteristics of the doublet lead to the suggestion that glycine radicals are present. It is interesting to note that the spectra of samples (a) to (d) all contain a contribution from glycine radicals and that the chemical treatments carried out have affected the formation of the other radical species determined in the original irradiated fibrinogen. This would suggest that the glycine residue responsible for the unresolved doublet absorption is the same throughout and is the *N*-terminal glycine residue of fibrin. That these residues represent a site of high electron density even in the intact fibrinogen would account for the specificity of thrombin severing these particular arginine-glycine bonds as opposed to the numerous others present in the molecule.

It has already been shown that the extent of a conduction band may be influenced by other factors (e.g. charged groups) and it is therefore concluded that the electronic conduction bands in the fibrin proteins have been conditioned by the crosslinking produced by hydrogen bonding in the structure. Since tyrosine residues have been shown to be included in this crosslinking system, this evidence may be regarded as additional support for the assignment of the singlet absorption in Figures 1a and b to the tyrosine residue.

#### Fibrin (higher concentration of calcium)

The spectrum is shown in Figure 1e. The presence of such a concentration of calcium ions dramatically changes the radical entities formed and it is clear that this spectrum is composed of a triplet absorption with a superimposed singlet centred near free spin (see Figure 3). The singlet in this case is much narrower than previously observed and this can be explained in terms of a radical in a well ordered region of the structure. The characteristic shape of the triplet, i.e. broad lines, peak to peak separation and relative heights in the ratio 1 : 2 : 1, indicates that this arises from the interaction of an unpaired electron with two protons. This can arise from two possible sources (i) from an alanine residue or (ii) from a break in the protein chain. In considering the former of these two possibilities, it is necessary to envisage the circumstances in which



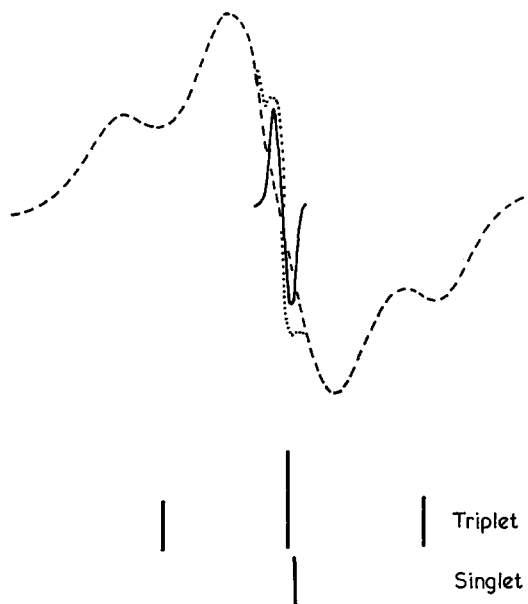
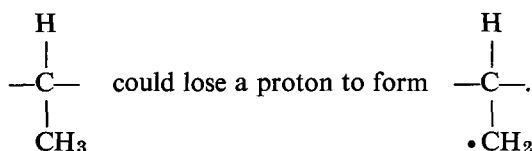


Figure 3 Diagrammatic representation of spectrum 1(e). —, Singlet; - - - -, triplet; ·····, resultant



Calculations by Gordy and Shields<sup>13</sup> showed that for the alanine residue, the proton from the  $\alpha$ -carbon atom will be lost in preference to a proton from the methyl group. From the results of Eaton and Keighley<sup>14</sup> on keratin, it is unlikely that the triplet can arise from an alanine residue, since this will occur in the crystalline regions of the structure, and hence the radical must be formed by a break in the main protein chain or side chain. Since the presence of larger concentrations of calcium ions in the structure changes the radical entities formed on irradiation, it is clear that this is the result of the formation of a new structural group and it can be concluded that the structure formed during the crosslinking process is such that electrons can be donated from this region to the structure to leave electron vacancies with lower energies than when calcium is not present in such quantities. The structural group formed involving the calcium includes the ends of chains and side chains and since electron transfer can occur from such positions in the structure, the detected radicals are formed near the ends of such chains since the transfer of electronic charge along polymer chains has been found to be limited<sup>15</sup>.

E.s.r. studies of poly(L-tyrosine)<sup>16</sup> have shown that the observed singlet arises from an oxygen radical on the phenolic oxygen atom and it is proposed that the origin of the singlet observed in the presence of higher calcium concentrations lies with this radical since tyrosine groups are involved in the fibrin crosslinking. The formation of an ordered region by the inclusion of calcium ions into the structure<sup>8</sup> will narrow the resonance from that observed in Figures 1a and b<sup>17, 18</sup>. It is concluded that radiation-induced electron ejection in the molecular vicinity of the tyrosine residue will be replaced by electron donation by the tyrosine hydroxyl to form an oxygen radical.

It is notable from a comparison of Figures 1b, 1c, 1d

and 1e that the latter spectrum is markedly different and it is clear from this and the properties of the clot formed that the corresponding molecular structure differs also. The presence of calcium in the clotting solution accelerates clot formation and imparts the property of insolubility in 5M urea solution. Nine tyrosine and histidine residues are involved in hydrogen bonding during clotting, and since the total calcium concentration in samples (c) and (d) is low, whereas the concentration of this ion in sample (e) is sufficient to allow the presence of  $\text{Ca}^{2+}$  at each hydrogen bonding and covalent crosslinking site, it is concluded that the metal ions are bonded in the structure. X-ray diffraction data support these conclusions<sup>8</sup>.

In view of the fact that tyrosine and histidine residues in fibrin are joined by hydrogen bonds<sup>1</sup> it was considered possible that the experimental data were consistent with a structure in which only the phenolic oxygen atom of the tyrosine and the tertiary nitrogen atom of the histidine co-ordinate to the calcium ion. Such a structure would, however, be unlikely since it is known that only loose complexes are possible when  $\text{N} \rightarrow \text{Ca}$  co-ordination is involved and, furthermore, ions exemplified by  $\text{Ca}^{2+}$  usually co-ordinate with six ligands. Such a complex is therefore unlikely to be highly stable.

It is suggested that the structure shown in Figure 4 in which the carboxylic acid groups of either aspartic or glutamic acid residues also complex with the calcium ion is more likely to be correct. Such a structure is electrically neutral and additional stabilization will be imparted to the histidine  $\rightarrow \text{Ca}^{2+}$  co-ordination by virtue of the extra hydrogen bond formed. Since this structure involves hexaco-ordination from four amino acid residues, no stability or static problems will arise from this structure which is in conformity with the recent findings of Marguerie *et al.*<sup>19</sup> that carboxyl groups are involved in the binding of the calcium ions. The projection shown in Figure 4 has been constructed from atomic models and it has been found by measurement that in the histidine-tyrosine hydrogen bond,  $-\text{O}-\text{H} \dots \text{N}-$ , the O-N distance is about 2.3 Å and the  $\text{Ca} \rightarrow \text{O}$  co-ordinate bond length is about 1.7 Å. Stereochemically, therefore, the proposed structure is sound.

In the light of this proposal, it is suggested that the triplet will be formed as a consequence of decarboxylation resulting from electron transfer processes. It is possible for the structure shown in Figure 4 to undergo electron withdrawal from a glutamic acid side chain

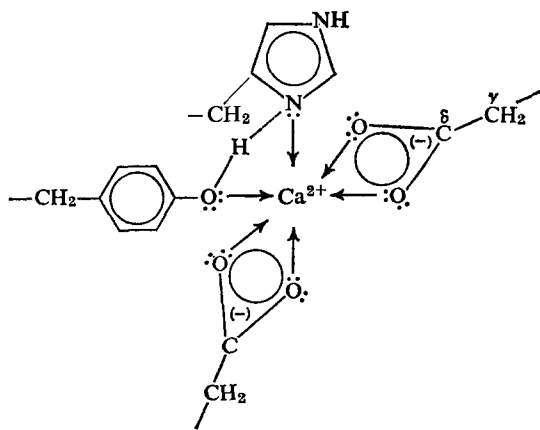


Figure 4 Incorporation of calcium in the fibrin structure

resulting from the co-ordination and when such a side chain donates an electron to the protein structure to replace that removed by irradiation, the result will be a rupture of the  $\gamma$ - $\delta$  carbon-carbon bond with an unpaired electron left associated with the  $\delta$ -carbon.

The unpaired electron left associated with the  $\gamma$ -carbon atom and two equivalent protons will produce the triplet recorded from sample (e). It is also clear that such a radical can be formed from either glutamic or aspartic acid residues so that it is not possible to distinguish further the nature of the co-ordinated groups.

Such a structure as proposed in *Figure 4* would also explain the catalytic effect or, more precisely, the accelerating effect of calcium ions on the polymerization or monomeric fibrin<sup>20</sup>, by reducing the repulsion associated with negative charges near the hydrogen bonding sites. It would also explain the difference in the structure of clots<sup>1</sup> between those which do and those which do not possess calcium, the former being more fibrous and tightly structured, the latter being more gel like.

In the presence of higher concentrations of calcium ions, no clot is formed (sample f). It is suggested that one ion combines with each half of the hydrogen bonding system thus creating repulsion between now two positively charged entities.

#### REFERENCES

- 1 Scheraga, H. A. 'Protein Structure', Academic Press, New York, 1961
- 2 Mihalyi, E. *J. Biol. Chem.* 1954, **209**, 723
- 3 Sturtevant, J. M., Laskowski, M., Donnelly, T. H. and Scheraga, H. A. *J. Am. Chem. Soc.* 1955, **77**, 6168
- 4 Maticic, S. and Loewy, A. G. *Biochem. Biophys. Res. Commun.* 1968, **30**, 356
- 5 Pisano, J. J., Finlayson, J. S. and Peyton, M. P. *Science* 1968, **160**, 892
- 6 Lorand, L. and Ong, H. H. *Biochemistry* 1966, **5**, 1747
- 7 Godal, H. C. 'Precipitation and Coagulation of Fibrinogen', Oslo University Press, 1961
- 8 Blakey, P. R., Byfield, P. G. H., Earland, C. and Turner, R. L. personal communication
- 9 Keighley, J. H. *J. Text. Inst.* 1968, **59**, 470
- 10 Windle, J. J. *Text. Res. J.* 1962, **32**, 963
- 11 Dunlop, J. I. and Nicholls, C. H. *Photochem. Photobiol.* 1965, **4**, 881
- 12 Kenny, P. and Nicholls, C. H. *Proc. 3rd Int. Wool Text. Res. Conf., Paris* 1965, Sect 2, p 99
- 13 Gordy, W. and Shields, H. *Bull. Acad. R. Belg. Cl. Sci.* 1961, **33**, 191
- 14 Eaton, W. C. and Keighley, J. H. *Proc. 4th Int. Wool Text. Res. Conf.; Appl. Polym. Symp.* 1971, **18**, 263
- 15 Truby, F. K. *J. Chem. Phys.* 1962, **36**, 2227
- 16 Drew, R. C. and Gordy, W. *Radiation Res.* 1963, **18**, 552
- 17 Assenheim, H. M. 'Introduction to Electron Spin Resonance', Hilger and Watts, London, 1966, p 105
- 18 Eaton, W. C. and Keighley, J. H. *J. Text. Inst.* 1969, **60**, 556
- 19 Marguerie, G., Hudry, G. and Hollard, D. *Thromb. Diath. Haemorrh.* 1970, **24**, 373
- 20 Lorand, L. and Konishi, K. *Arch. Biochem. Biophys.* 1964, **105**, 58

# Annealing of high density polyethylene for very long times at low supercooling under vacuum

D. A. Blackadder and J. S. Keniry

*Department of Chemical Engineering, University of Cambridge, Pembroke Street, Cambridge CB2 3RA, UK*

and M. J. Richardson

*National Physical Laboratory, Teddington, Middlesex TW11 0LW, UK  
(Received 3 July 1972)*

Unfractionated high density polyethylene has been annealed under vacuum for periods of up to two years, the temperature being raised slowly to a final value of 135.8°C. After annealing, specimens were characterized by density and fusion measurements. Material obtained by very long term annealing proved to be similar to that produced by high pressure crystallization or annealing of the same polyethylene. Nevertheless, interesting differences in melting behaviour were also observed.

## INTRODUCTION

The crystallization and annealing of polyethylene at low supercoolings under pressures of several kilobars has been widely investigated<sup>1, 2</sup>. Highly crystalline material is obtained, consisting of molecules which are either fully extended or which contain only a few folds. In these circumstances crystal growth is considered<sup>1</sup> to be a two-stage process. The first step is the transition of a molecule from the melt to a metastable folded chain configuration in the nucleus or crystal. This is followed by a change in the solid state which involves thickening of the crystal to a longer fold length.

The mechanism may apply to the corresponding process at low pressures. Until now, however, experiments at low pressures have failed to produce polyethylene of the highest crystallinity, a failure attributed to the very slow rate of crystal thickening at ordinary pressure. The applicability of the mechanism has now been checked by experiments in which Rigidex 50 polyethylene was annealed under vacuum for very long periods under low supercoolings.

## EXPERIMENTAL

Rigidex 50 polyethylene was recrystallized from a 5% (w/v) *p*-xylene solution at 25°C. The solids were filtered off, washed with acetone and vacuum dried at 40°C for two weeks. Crystals grown and dried under comparable conditions had a residual *p*-xylene content of less than 0.001% as estimated by vapour phase chromatography. One gramme samples of the resulting powder were sealed into Pyrex glass tubes under high vacuum, melted at 145°C for 4 hours, and crystallized for two days in an oil thermostat set at 120 ± 0.05°C. The temperature of the

thermostat was gradually raised to 135.8°C over a period of two years. Increments of only 0.2°C were used at temperatures above 130°C.

A sample tube was withdrawn at intervals and cooled from the bath temperature to 118°C at the rate of 1°C/day, and from 118°C to room temperature at 10°C/hour. The cooled tube was then opened and the polymer was analysed for density, specific viscosity and fusion characteristics. The density was measured in a gradient column operating at 25°C, while the viscosity of a 0.25% (w/v) solution in decalin was measured at 135°C.

To provide a basis for interpreting the properties of samples prepared by long annealing at low supercoolings under vacuum it was necessary to obtain material crystallized (HPC) or annealed (HPA) under high pressure. A piston cylinder apparatus was used with the same polyethylene, Rigidex 50. The polymer specimen was encapsulated in gold foil to protect it from the pressure transmitting fluid, and was cooled at 0.5°C/min before the pressure was lowered to atmospheric.

Fusion measurements were made on all the samples using a Perkin-Elmer Model 1B Differential Scanning Calorimeter. The enthalpy change,  $H_{a2} - H_1$ , between one steady temperature,  $T_1$ , and another  $T_2$ , was found by operating the calorimeter in the 'specific heat mode'<sup>3</sup>. (The subscript *a* refers to an amorphous or molten state.) Full details of the enthalpy and temperature calibrations are given elsewhere<sup>4</sup>. The heat of fusion at  $T_1$ ,  $\Delta H(T_1)$ , was found by subtracting the enthalpy change of the supercooled melt<sup>5</sup>,  $H_{a2} - H_{a1}$ , from  $H_{a2} - H_1$ .

$$\Delta H(T_1) = (H_{a2} - H_1) - (H_{a2} - H_{a1}) = (H_{a1} - H_1)$$

This result assumes that  $T_2$  is above the melting point,  $T_m$ , and in practice it was convenient to make  $T_2 \geq T_m + 15$

to overcome the problem of superheating effects in the vicinity of  $T_m$ .

For a given heating rate the shapes of differential scanning calorimeter (d.s.c.) traces, and the location of peaks thereon, are very dependent on the packing, geometry and size of the specimen. Several milligrammes were used for each determination of  $H_{a2} - H_1$ , but peak temperatures were obtained from less than 0.1 mg of polymer. For such small samples there was a linear relationship between peak temperature and heating rate in the range 1 to 16°C/min. Melting points obtained by extrapolation to zero rate of heating were checked by increasing the temperature stepwise, by 1°C or less, allowing a steady state to be reached before the next increment. The completion of fusion was easily monitored in this way, and additional 'annealing' during the d.s.c. melting experiments was negligible following the prolonged high temperature annealing. The procedure would not be valid for quenched films.

## RESULTS AND DISCUSSION

The results are shown in *Table 1*, and some specific heat curves, derived from d.s.c. traces, appear in *Figure 1*. The d.s.c. runs were made at a rate of 16°C/min using small samples (0.1 mg), and a comparison of the major peak temperatures on the Figure with the  $T_m$  data in the Table shows that the curves are displaced 4–5°C for this heating rate. The viscosity data indicate that degradation of the polymer was successfully avoided.

The properties listed in the first part of the Table beside a particular total annealing time and maximum annealing temperature,  $T_a$ , do not necessarily represent equilibrium values. Even the final values are likely to change further on prolonged annealing at still higher temperatures. Important conclusions may be drawn, however, especially from a comparison of the data in the two parts of the Table.

The highest density reached, 0.989 g/cm<sup>3</sup>, exceeds by about 1% the highest values previously reported for crystallization<sup>1</sup> or annealing<sup>6</sup> of unfractionated polyethylene at low pressures. Indeed the density of 0.989 g/cm<sup>3</sup> is only slightly lower than the 0.991 g/cm<sup>3</sup> achieved by Gruner *et al.*<sup>7</sup> by annealing at 240°C and 5 kbar pressure.

Heats of fusion show the expected increase with density. Comparison with the weight fraction crystallinity,  $x_V$ , must be made at room temperature since there was not enough material available to measure  $x_V$  at higher temperatures. A meaningful comparison can be made by calculating two crystallinities,  $x_V$  and  $x_H$ , defined by

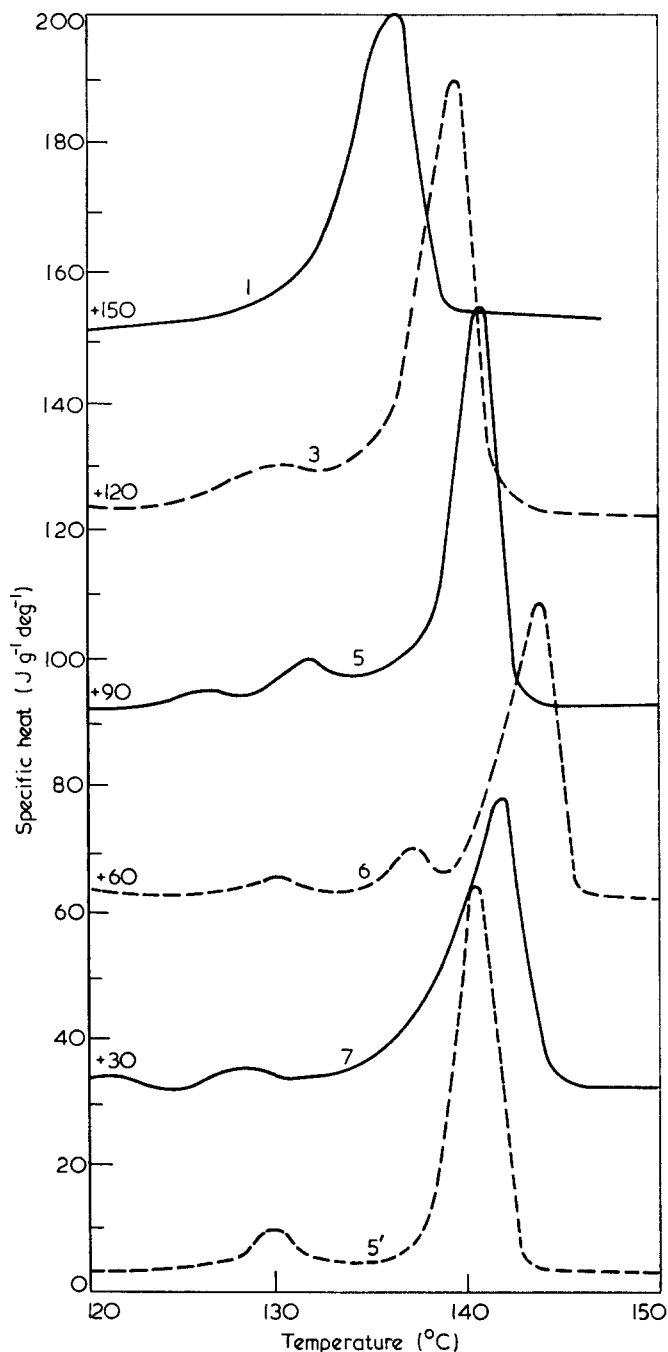


*Figure 1* Specific heat/temperature curves for polyethylene specimens. Data based on d.s.c. measurements with a heating rate of 16°C/min. 1, 3, 5, 6 and 7 refer to samples in *Table 1*; +30, +60 etc. indicate displacement of ordinate; curve 5' is sample 5 (curve 5) after being held at 133°C for 20 min and cooled to 90°C at 0.5°C/min before being re-run

*Table 1* Properties of high density samples of polyethylene

Sample	Preparative conditions		Specific viscosity	Density at 25°C (g/cm <sup>3</sup> )	Heat of fusion at 25°C (J/g)	Crystallinity at 25°C		Melting point (°C)
	Time (weeks)	Max. temp. (°C)				$x_V$	$x_H$	
1	0	120.0	0.387	0.979	242	0.882	0.869	133.6
2	5	128.5	0.387	0.980	—	0.886	—	—
3	38	132.0	—	0.986	247	0.922	0.913	135.5
4	68	134.1	0.385	0.988	—	0.932	—	135.7
5	96	135.8	0.389	0.989	249	0.940	0.920	136.6
	Pressure (kb)	Temp. (°C)						
6	4.8 (HPC)	226 (8h)	—	0.992	257	0.956	0.950	139.4
7	5.9 (HPA)	252 (3h)	—	0.991	254	0.951	0.938	136.6

$x_X = \Delta X / \Delta X_\infty$ , where  $\Delta X = X_a - X$  and  $\Delta X_\infty = X_a - X_c$ . Here  $X$  is either specific volume,  $V$ , or enthalpy,  $H$ , the subscripts referring to amorphous,  $a$ , or perfectly crystalline material,  $c$ , and the actual sample measurement having no subscript. Values for  $V_a$  and  $V_c$  have been given earlier<sup>8,9</sup>, and  $\Delta H_\infty$  was obtained by extrapolation of n-alkane data<sup>10</sup>. Table 1 shows that  $x_H$  is about 1–2% less than  $x_V$ , in agreement with earlier work<sup>11</sup> on samples of lower crystallinity. Crystallinities at higher temperatures were calculated using the expression for  $\Delta H_\infty$  published previously<sup>11</sup>.

On heating samples 3–7 there was first a slow fall in crystallinity to a value of about 0.65 at 133°C, followed by a rapid drop to zero at the melting point. This varied from 135.5°C to 139.4°C (see Table 1), and melting was therefore sharper for samples having lower values of  $T_a$ . It would be difficult to reach even qualitative conclusions of this kind from conventional d.s.c. curves. The crystallinity at 133°C can be obtained only by means of the 'enthalpy change' technique used here. Although initially surprising, the sharper melting associated with lower values of  $T_a$  is understandable for unfractionated polymer. Even at 132.0°C, the highest annealing temperature experienced by sample 3, the shortest molecules would be close to melting<sup>12</sup>, and there must have been appreciable fusion prior to the disappearance of the largest crystals formed by annealing at the highest temperature of 135.8°C (sample 5). It is noteworthy that sample 5 had the same melting point, 136.6°C, as the material briefly annealed under high pressure (sample 7). This melting point agrees well with the value of 137.0°C obtained dilatometrically by Chiang and Flory<sup>13</sup> who crystallized Marlex 50 at 131.3°C for 40 days. The significantly higher melting point observed here for the specimen *crystallized* under high pressure (sample 6) appears to be genuine. Certainly the stepwise melting technique adopted for the d.s.c. does not appear to have been in error, and the melting point of the pressure crystallized sample may be compared with a value of 138.7°C obtained dilatometrically by Arakawa and Wunderlich for pressure crystallized linear polyethylene.

The high pressure conditions were chosen to give samples with similar densities at room temperature and atmospheric pressure (samples 6 and 7). Despite the similarity of the densities there are important differences in other details, notably the low  $T_m$  of HPA relative to that of HPC and the temperature range over which peaks occur in the d.s.c. (curves 6 and 7 in Figure 1).

A remarkable feature of the d.s.c. traces for long annealed samples was the development of fine structure, a well-known effect for pressure crystallized material attributed to the separation of low molecular weight fractions<sup>15</sup>. Because of the temperatures involved, these fractions must have formed in the present experiments on cooling from  $T_a$  to room temperature, and they were detected only because of the very slow cooling (1°C/day) after long term annealing. When samples were heated in the d.s.c. to temperatures above those of the minor peaks (but below the onset of the major peak), cooled at 0.5°C/

min and subsequently reheated, only a single sub-peak was found (curve 5'). This example clearly demonstrates the difficulty of achieving equilibrium conditions in whole polymer. High temperature annealing is essential to ensure the development of the most perfect crystals, yet the process is thereby made very slow, the rate being a function of the supercooling. Corresponding treatment at progressively decreasing temperatures is necessary to accommodate all the lower molecular weight material in good crystals, since it is unable to crystallize at the higher temperatures.

Striking changes were observed in the mechanical properties of the various long annealed samples. The originally tough ductile material showed signs of brittleness at a density of 0.986 g/cm<sup>3</sup> and this became increasingly marked. At the highest density of 0.989 g/cm<sup>3</sup> the sample could be crushed between the fingers, as found for pressure crystallized material.

## CONCLUSIONS

The properties of the sample annealed under vacuum for two years, coupled with the manner in which properties changed with long term annealing, provides evidence of a striking similarity to samples obtained by crystallization or annealing under high pressure. In addition to underlining the very close similarity between the final effects of high and low pressure annealing the results are compatible with the most recent discussion<sup>16</sup> of crystallization and annealing mechanisms under pressure.

## ACKNOWLEDGEMENTS

Pressure treated samples were kindly made available by N. G. Saville (NPL).

One of us (J.S.K.) is indebted to the Colonial Sugar Refining Company Ltd of Sydney for financial support.

## REFERENCES

- 1 Wunderlich, B. and Davidson, T. *J. Polym. Sci. (A-2)* 1969, **7**, 2043
- 2 Rees, D. V. and Bassett, D. C. *J. Polym. Sci. (A-2)* 1971, **9**, 385
- 3 Wunderlich, B. *J. Phys. Chem.* 1965, **69**, 2078
- 4 Richardson, M. J. *J. Polym. Sci. (C)* 1972, **38**, in press
- 5 Atkinson, C. M. L., Larkin, J. A. and Richardson, M. J. *J. Chem. Thermodyn.* 1969, **1**, 435
- 6 Mandelkern, L. *Rubber Chem. Technol.* 1959, **32**, 1392
- 7 Gruner, C. L., Wunderlich, B. and Bopp, R. C. *J. Polym. Sci. (A-2)* 1969, **7**, 2099
- 8 Richardson, M. J., Flory, P. J. and Jackson, J. B. *Polymer* 1963, **4**, 221
- 9 Swan, P. R. *J. Polym. Sci.* 1962, **56**, 403
- 10 Atkinson, C. M. L. and Richardson, M. J. *Trans. Faraday Soc.* 1969, **65**, 1749
- 11 Atkinson, C. M. L. and Richardson, M. J. *Trans. Faraday Soc.* 1969, **65**, 1764
- 12 Prime, R. B. and Wunderlich, B. *J. Polym. Sci. (A-2)* 1969, **7**, 2073
- 13 Chiang, R. and Flory, P. J. *J. Am. Chem. Soc.* 1961, **83**, 2857
- 14 Arakawa, T. and Wunderlich, B. *J. Polym. Sci. (C)* 1967, **16**, 653
- 15 Prime, R. B., Wunderlich, B. and Melillo, L. *J. Polym. Sci. (A-2)* 1969, **7**, 2091
- 16 Bassett, D. C. *et al. Nature (Phys. Sci.)* 1972, **239**, 106

# Crosslinked polyethylene at elevated temperatures

T. R. Manley and M. M. Qayyum

*Department of Materials Science, Newcastle upon Tyne Polytechnic,  
Newcastle upon Tyne NE1 8ST, UK*

*(Received 21 May 1971; revised 8 June 1972)*

The behaviour of crosslinked polyethylene has been studied by differential thermal analysis (d.t.a.) up to 150°C, by stress relaxation up to 240°C and by thermogravimetry (t.g.) up to 350°C. No single technique is sufficient to characterize the polymer. D.t.a. gives a very rapid indication of the crystalline portion of the crosslinked polyethylene; t.g. shows the loss of degradation products some of which may be associated with crosslinking; stress relaxation gives information on crosslinking and degradation but is time consuming and does not provide absolute values. The results obtained agree with earlier work that showed marked differences between the properties obtained with low and high amounts of peroxide.

## INTRODUCTION

In this paper the effect of heat on crosslinked linear polyethylene has been studied. The methods used are differential thermal analysis (d.t.a.), thermogravimetry (t.g.) and stress relaxation at different temperatures. D.t.a. shows the melting point and heat of fusion of the polymer and gives an indication of the previous thermal history. Thus it shows the amount of crystallinity in the polyethylene. T.g. gives an indication of the thermal stability of a polymer and stress relaxation gives the combined effect of stress and temperature.

Crosslinked polyethylene deforms easily above the crystalline melting point and this deformation can be fixed by cooling. On reheating it recovers to its original shape. This heat shrinkage or memory effect may be put to practical use particularly in the packaging industry.

The effect of variations in the amount of peroxide used on certain physical and mechanical properties of crosslinked linear polyethylene, e.g. density, gel content, tensile strength, elongation and shear modulus of cross-linked polyethylene has been reported previously<sup>1</sup>.

## EXPERIMENTAL

Details of the material used and the extrusion techniques were given in an earlier paper<sup>1</sup>.

Lupolen 5261 Z (BASF) density 0.95 to 0.953 and melt flow index 1.7 to 2.3 were extruded with a peroxide solution containing 100 parts of di-t-butyl peroxide, 100 parts of hydrocarbon solvent (special boiling point spirit No. 4, Shell Mex and BP) and 40 parts of MS 550 (Midland Silicones).

The percentages of peroxide given refer to pure di-t-butyl peroxide. The extruder pressure chamber, pin and die were at 130°C, 110°C and 200 to 210°C respectively. The design pressure of the chamber was 150 000

lbf/in<sup>2</sup> ( $1.034 \times 10^9$  N/m<sup>2</sup>) as in the previous work<sup>1</sup>.\* Different rates of extrusion were used.

### *Differential thermal analysis*

The DuPont 900 was used with a d.s.c. head in still air, the reference cell being empty. The heat of melting of the indium used for standardization was taken as 6.79 cal/g (1 cal = 4.18 J). Results are shown in *Table 1*.

### *Thermogravimetry*

A Stanton HT-SM thermobalance was used to measure the weight losses when samples were heated from room temperature to 350°C at a heating rate of  $\frac{1}{3}$ °C/min in still air at atmospheric pressure. The samples in the form of chips of 100 mg were put in shallow aluminium pans.

A Mark IIB, CI Electronic thermobalance was also used to study degradation at a rate of 2°C/min in still air under atmospheric pressure. Samples of 50–70 mg weight were taken in small aluminium pans. Results are given in *Table 2*.

### *Stress relaxation*

Continuous and intermittent stress relaxation were measured at 175°C, 220°C, 230°C and 240°C, in air using a Shawbury Agestester (H. Wallace Ltd). All samples were held for 15 min at the experimental temperature before any stress was applied. The ratio of  $f(t)/f(0)$ , where  $f(t)$  is the force at time  $t$  and  $f(0)$  the initial force, was plotted against time. The results are summarized in *Table 3*.

## RESULTS AND DISCUSSION

### *Differential thermal analysis*

No exothermic peak near the melting point was observed showing that no unreacted peroxide was

\* Please note erratum (*Polymer* 1971, 12, 177, 6 lines from bottom): for lbf/cm<sup>2</sup> read lbf/in<sup>2</sup>.

Table 1 Differential thermal analysis of crosslinked linear polyethylene

Sample number	Peroxide (%)	Gel (tetralin) (%)	1st heating cycle <sup>a</sup>		Cooling cycle <sup>b</sup>		2nd heating cycle <sup>a</sup>	
			$T_m$ (°C)	$\Delta H_f$	$T_c$ (°C)	$-\Delta H_c$	$T_m$ (°C)	$\Delta H_f$
1	Nil	Nil	140.0	35.8	123.0	33.7	145.0	33.0
2	0.140	45.84	138.5	34.6	121.0	31.8	140.0	33.0
3	0.223	67.74	131.0	23.6	114.0	22.8	133.0	23.3
4	0.263	68.06	134.0	23.4	111.0	22.5	134.0	23.5
5	0.266	69.25	134.5	23.2	113.5	22.2	134.5	23.7
6	0.393	67.84	132.0	24.0	113.5	21.2	134.5	22.8
7	0.436	70.12	137.0	25.7	120.0	26.3	138.0	27.6
8	0.543	71.05	135.0	22.4	113.8	22.3	135.5	23.2
9	0.585	73.81	133.0	21.8	114.0	25.5	134.0	25.9
10	0.693	75.69	125.0	21.7	110.0	23.2	126.0	23.5

$T_m$ =Crystalline melting point;  $\Delta H_f$ =heat of fusion;  $\Delta H_c$ =heat of crystallization;  $T_c$ =maximum crystallization point

<sup>a</sup> Heating rate 2°C/min; <sup>b</sup> cooling rate 2°C/min

present. From Table 1 it can be seen that the crystalline melting point decreases with the increase in the amount of peroxide used up to 0.22%. Above this figure there is little change in the gel constant or the melting point until the final sample at 0.69%. The same is true for the heat of fusion, the heat of crystallization and the temperature at which crystallization occurs on cooling. This is in agreement with previous results where density<sup>1,2</sup> and X-ray<sup>3</sup> techniques were used to study crystallinity.

The processing conditions have a significant effect on both the crystallinity and crosslinking of polyethylene. In this process polyethylene is crosslinked whilst molten, thus inducing a high crosslink density with the result that the molecules have difficulty in rearranging themselves and forming crystals<sup>1</sup>. By contrast when samples are crosslinked by irradiation at ambient temperature<sup>4</sup> there is no drop in the crystalline melting point. The samples were cooled with air in the d.t.a. apparatus at 2°C/min and then reheated. The second heating gives slightly higher readings indicating a small increase in the degree of crystallinity, as is also suggested by the heat of fusion. During the controlled cooling cycle the molecules have more time for the growth of crystals to take place.

The difference in crystalline melting point between the heating cycles correlates with the gel content (Table 1).

The temperature at which these transitions occur in crystalline polymers is necessarily dependent on the heating rates. 2°C is a convenient compromise between a very slow rate that would induce higher crystallinity and a fast heating rate where the melting point results obtained appear to be up to 10°C higher. Figure 1 shows the d.t.a. trace for sample No. 4. All the melting temperatures quoted are taken at the peak B. It is more usual in thermoanalytical studies to quote the temperature at A, where the tangents to the curves meet but for comparative purposes B is more convenient.

#### Thermogravimetry

Two reactions could be distinguished by thermogravimetry (Figure 2) in crosslinked polyethylene. The temperature at which the first reaction takes place decreases with the increase in peroxide content (Table 2). This first reaction is attributed to breaking of weak links rather than loss of solvent (b.p. 145°C) as the polymer has already been heated at 200°C. These weak links, which are mainly hydroperoxide and peroxides, could give rise to low molecular weight hydrocarbons, e.g. butane, hexane etc. depending on their situation in the polymer chain. Once these weak links are broken, the thermal stability of the material rises with the increase in the peroxide content.

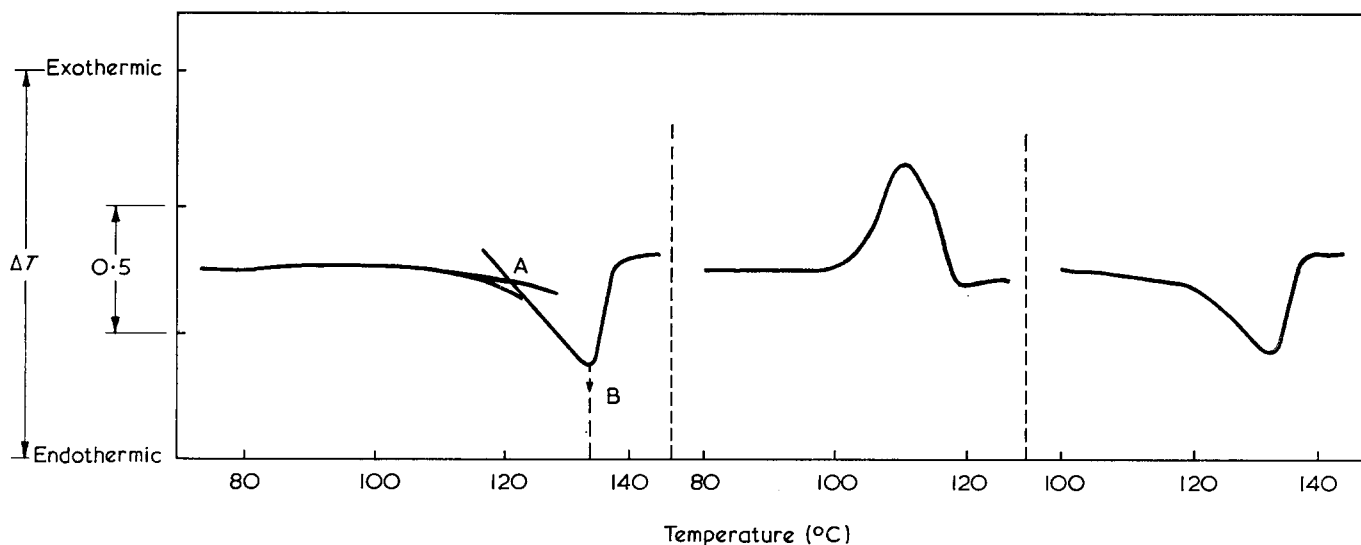


Figure 1 Differential thermal analysis trace for crosslinked linear polyethylene (sample No. 4)

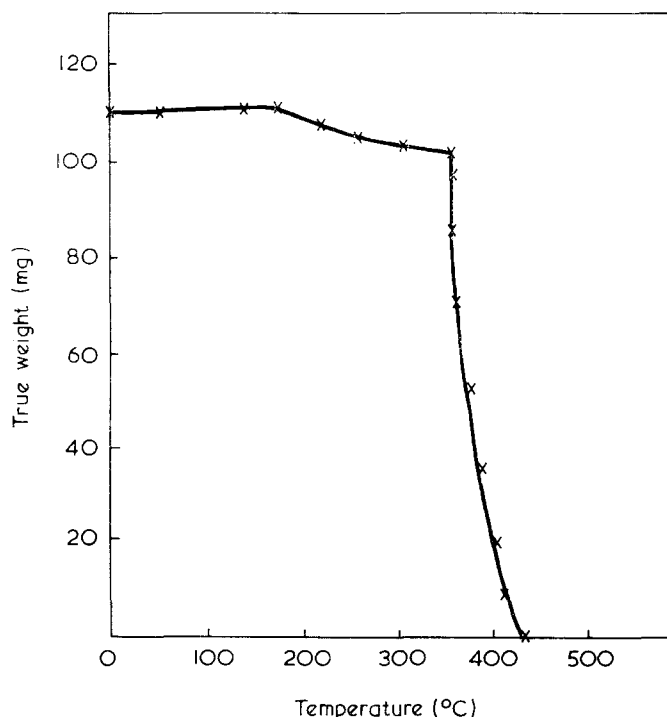


Figure 2 Thermogravimetric trace of crosslinked linear polyethylene (sample No. 2, Stanton balance)

Table 2 Initial temperature and activation energies of the decomposition of crosslinked polyethylene from thermogravimetry

Peroxide (%)	Gel (tetralin) (%)	1st reaction (°C)	2nd reaction (°C)		Comparative (activation energy) 1st reaction (kcal/mol)
			CI	Stanton	
—	—	200	307	330	8.9
0.140	45.84	175	307	346	33.73
0.223	67.74	170	320	350	33.65
0.263	68.06	170	323	350	29.99
0.266	69.25	165	338	362	65.99
0.393	67.84	165	311	362	69.45
0.436	70.12	162	345	360	67.12
0.543	71.05	162	310	358	62.56
0.585	73.81	160	356	358	71.00
0.693	75.69	158	366	375	70.70

Stanton thermobalance: heating rate  $\frac{1}{3}$ °C/min; CI Electronic Mk IIB thermobalance: heating rate 2°C/min

The first reaction was not observed when the CI balance was used either in still air or *in vacuo*. This is attributed to the faster heating rate as it was not possible to control this balance below 1°C/min. The first reaction was also absent when the Stanton furnace was heated at 6°C/min. In the latter experiment, the temperature of the inception of the second reaction was 15°C higher than when a rate of  $\frac{1}{3}$ °C/min was used.

In spite of the higher heating rate in the CI balance the second reaction apparently occurs at a lower temperature than when the Stanton was used. This is caused by differences in the location of the thermocouple.

The Stanton thermocouple is near to the furnace wall whilst in the CI balance the thermocouple is above, and much closer to the sample and thus the latter gives a lower reading than the Stanton.

The error in reading the weight of the t.g. curve in the Stanton thermobalance cannot be neglected<sup>5</sup>. The recording chart can only be read to  $\pm 5^\circ\text{C}$ .

Activation energies were calculated for the first reaction assuming a first order reaction<sup>6</sup>. Because of the experimental variations these values are far from exact. They do, however, serve for purposes of comparison. The term 'comparative activation energy' is therefore employed lest anyone might put more reliance on the figures than is warranted.

It is evident, however, that three distinct mechanisms are involved in the case of pure polyethylene, polyethylene with lower content of peroxide and polyethylene with high concentrations of peroxide respectively. This is shown by the differences in the comparative activation energy (Table 2).

The uncrosslinked polyethylene at 200°C is presumably beginning to oxidize. The comparative activation energy (8.9 cal/mol) is probably affected by the rate of diffusion of the oxygen into the polymer, but for our present purpose it is sufficient to note that this reaction is different from those occurring in the crosslinked polymer.

In the case of specimens with lower amounts of peroxide further crosslinking is taking place with the concomitant loss of small molecular weight fragments ( $E_{\text{comp}}=33$ ). Finally, the highly crosslinked materials are beginning to break down at the crosslinks already formed or at the backbone of the polymer. In both cases comparatively large molecules are broken off. There is no correlation between gel content and activation energies but there is an indication that activation energy is affected by extrusion rate as is shown by elongation at room temperature<sup>1</sup>. This is to be further investigated.

The second reaction which occurs for all materials over a narrower range is a catastrophic breakdown for which it is difficult to calculate the activation energy because of the large amount of material lost (over 90%) and is clearly due to oxidation of all hydrocarbons present.

#### Stress relaxation

Stress relaxation methods<sup>7</sup>, both continuous and intermittent, were used to investigate the further degradation and crosslinking reactions occurring above 175°C. In the continuous technique the specimen is extended throughout the experiment at a fixed elongation and the stress is measured as a function of time, whereas in the intermittent method the specimen is maintained in a relaxed, unstretched condition and at specific time intervals the sample is suddenly stretched to a fixed elongation, the equilibrium stress is rapidly measured and the sample is immediately returned to its unstretched length. It is assumed that a continuous fall in the stress supported shows degradation while crosslinking is indicated by a rise in the stress supported. Where both reactions occur simultaneously the intermittent mode is more favourable to crosslinking which is illustrated by the difference between the curves for the two modes. The results in Tables 4 and 5 were obtained using the equipment as supplied by the manufacturer. At 220°C and above, however, the specimens were able to support the stress applied only for a short time. The spring in the apparatus was therefore replaced by a rubber band that produced less strain and thus enabled measurement to be performed at higher temperatures. The results at 175°C therefore are not directly comparable with those at 220°C, 230°C and 240°C.



Table 3 Summary of stress relaxation results for crosslinked polyethylene at various temperatures

Temperature (°C)	Mode of stress	Sample number									
		2	3	4	5	6	7	8	9	10	
175	Continuous	D, D	D, D	D, D	D, D	D, D	D, D	D, D	D, D	D, D	D, D
	Intermittent	X, D	X, D	X, D	X, D	X, D	X, D	X, D	X, D	X, D	X, D
220	Continuous	D, D	D, X	D, D	D, D	D, D	D, X	D, D	D, D	D, D	D, D
	Intermittent	X, D	X, D	X, D	X, D	D, D	D, X	D, D	D, X	D, X	D, X
230	Continuous	D, D	D, D	D, D	D, D	D, D	D, D	D, D	D, D	D, D	D, D
	Intermittent	X, D	X, D	X, D	X, D	X, D	X, D	X, D	X, D	X, D	X, D
240	Continuous	D, X	D, X	D, X	D, X	D, X	D, X	D, X	D, X	D, X	D, X
	Intermittent	X, D	X, D	X, D	X, D	X, D	X, D	X, D	X, D	X, D	X, D

D=degradation; X=crosslinking

The results for crosslinked polyethylene at various temperatures are summarized in Table 3. At 175°C and above a fast chemical reaction occurs. The intermittent stress measurements reflect the combined effect of degradation and crosslinking whereas the continuous relaxation curve shows degradation in practically all cases except at 240°C where the dependency of the continuous curve on degradation only no longer holds (*vide infra*).

Results at 175°C. In both continuous and intermittent experiments at 175°C the stress decays sharply from the start of the experiment (Tables 4 and 5). If only degradation were occurring, then the continuous and intermittent stress relaxation curves should be similar. The stress supported in the continuous experiment, is less than that in the intermittent case (apart from sample 6). The difference in these two curves indicates that crosslinking is occurring. No relationship could be found

between the amount of peroxide used and the time-dependent stress decay.

Results at 220°C. At 220°C when the stress is applied continuously there is a sharp initial fall in the stress that can be supported by the specimen; after between four and six hours the curves level out (Figure 3). This initial drop in stress indicates that the specimen is being degraded but that the reaction soon slows down. There is apparent evidence of crosslinking (shown by a slight rise in the stress supported) in the case of samples 3 and 7 that will be discussed later.

A more complex pattern appears when intermittent stress is applied. Specimens 2-5 which have lower amounts of peroxide crosslink initially and then rapid degradation occurs while specimens 6-10 which have greater amounts of peroxide are initially degraded and then level off. Sample 9 is anomalous in being further degraded after 4h. There is again some apparent cross-

Table 4 Variation in stress relative to initial stress, [f(t)/f(0)]. Continuous operation at 175°C

Sample No.	Peroxide (%)	Gel (tetralin) (%)	Time (min)											
			0	20	45	60	120	180	240	360	480	600	720	840
1	—	Nil	—	—	—	—	—	—	—	—	—	—	—	—
2	0.140	45.84	1	0.65	0.47	0.39	0.31	0.28	0.26	0.25	0.23	0.22	0.22	0.21
3	0.223	67.74	1	0.85	0.70	0.57	0.37	0.33	0.29	0.28	0.26	0.25	0.24	0.23
4	0.263	68.06	1	0.61	0.50	0.43	0.35	0.31	0.28	0.27	0.25	0.24	0.24	0.24
5	0.266	69.25	1	0.80	0.66	0.46	0.20	0.17	0.16	0.14	0.11	0.10	0.09	0.08
6	0.393	67.84	1	0.62	0.59	0.57	0.38	0.27	0.26	0.23	0.22	0.21	0.20	0.19
7	0.436	70.12	1	0.45	0.34	0.27	0.20	0.17	0.16	0.15	0.13	0.12	0.11	0.10
8	0.543	71.05	1	0.50	0.37	0.34	0.30	0.28	0.26	0.25	0.23	0.22	0.20	0.19
9	0.585	73.81	1	0.30	0.25	0.20	0.07	0.06	0.05	0.05	0.05	0.05	0.05	0.05
10	0.693	75.69	1	0.40	0.26	0.24	0.18	0.17	0.15	0.13	0.12	0.12	0.11	0.10

Table 5 Variation in stress relative to initial stress, [f(t)/f(0)]. Intermittent stress operation at 175°C

Sample No.	Peroxide (%)	Gel (tetralin) (%)	Time (min)												
			0	20	45	60	120	180	240	300	360	480	600	720	840
1	—	Nil	—	—	—	—	—	—	—	—	—	—	—	—	
2	0.140	45.84	1	0.98	0.94	0.91	0.87	0.85	0.79	0.22	0.21	0.20	0.19	0.18	
3	0.223	67.74	1	0.97	0.92	0.89	0.75	0.60	0.35	0.20	0.18	0.17	0.16	0.15	
4	0.263	68.06	1	0.96	0.89	0.80	0.63	0.60	0.58	0.54	0.51	0.50	0.48	0.47	
5	0.266	69.25	1	0.92	0.81	0.75	0.54	0.46	0.43	0.41	0.40	0.36	0.34	0.31	
6	0.393	67.84	1	0.75	0.54	0.45	0.34	0.30	0.22	0.18	0.17	0.17	0.16	0.15	
7	0.436	70.12	1	0.68	0.55	0.42	0.33	0.32	0.30	0.28	0.18	0.18	0.17	0.16	
8	0.543	71.05	1	0.74	0.59	0.50	0.34	0.31	0.30	0.30	0.29	0.29	0.28	0.27	
9	0.585	73.81	1	0.97	0.96	0.92	0.74	0.63	0.60	0.58	0.44	0.42	0.18	0.17	
10	0.693	75.69	1	0.95	0.81	0.76	0.65	0.61	0.60	0.59	0.57	0.57	0.57	0.56	

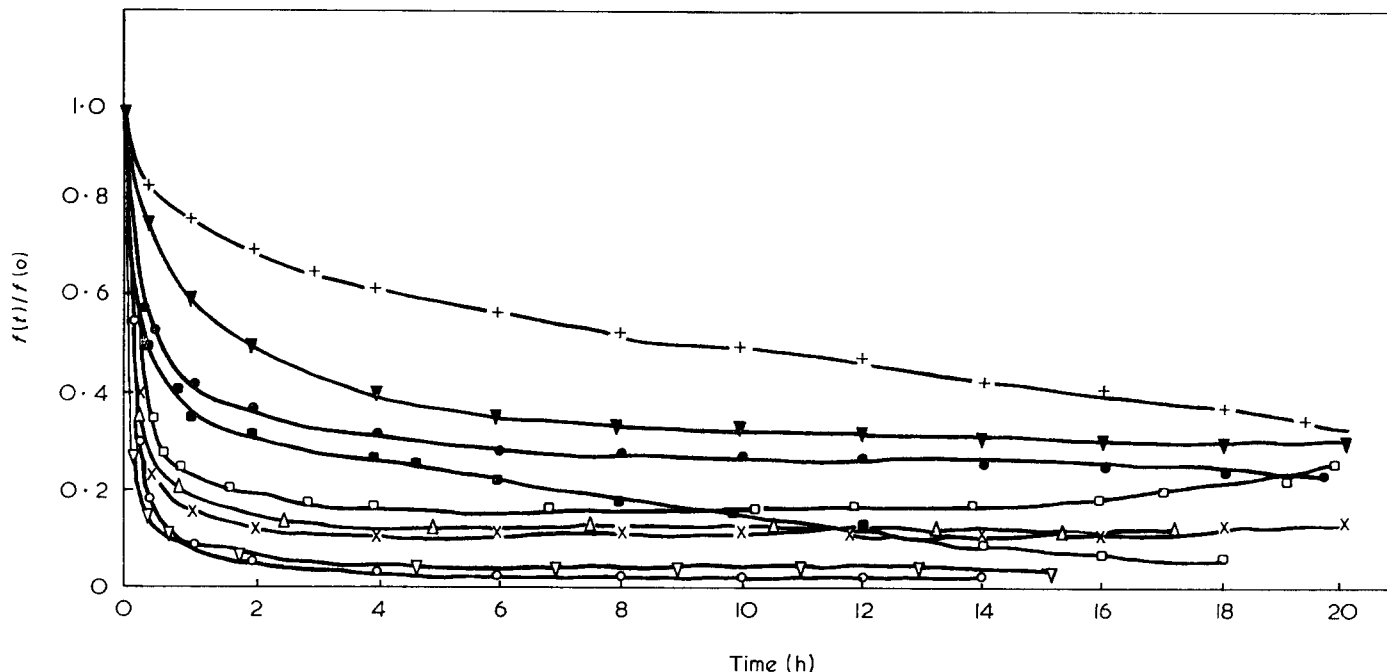


Figure 3 Continuous stress relaxation curves for crosslinked polyethylene at 220°C. ■, (2), 0.140; ×, (3), 0.223; ○, (4), 0.263; △, (5), 0.266; ▽, (6), 0.393; □, (7), 0.436; +, (8), 0.543; ●, (9), 0.585; ▼, (10), 0.693

linking in the case of specimens 7 and 10 shown by a rise in the stress supported (Figure 4).

At 220°C as already mentioned<sup>1</sup> the samples with high peroxide are heavily crosslinked and further linkages do not show significant increases in the crosslink density, many being 'redundant'. With less peroxide, on the other hand, significant crosslinking can still occur.

By the same token the probability of degradation is higher in the case of the specimens with high peroxide and the results do in fact show this to occur.

**Results at 230°C.** Under continuous load at 230°C there is a rapid drop in the stress in all the specimens indicating degradation. After this initial drop in stress the curves flatten out as shown in Figure 3.

Under intermittent load a rapid initial rise in the curve for sample 2 shows a significant increase in crosslinking. All the other specimens show a slight rise in

stress attributed to a minor degree of crosslinking; then further degradation occurs as is seen from the subsequent fall in the stress supported. For clarity Figure 5 shows only a representative selection of the results.

**Results at 240°C.** Under intermittent load the curves show an initial slight rise followed by a sharp fall; the curves are similar to those of Figure 3 for 230°C. In this instance, there is no anomaly in the results for sample 2.

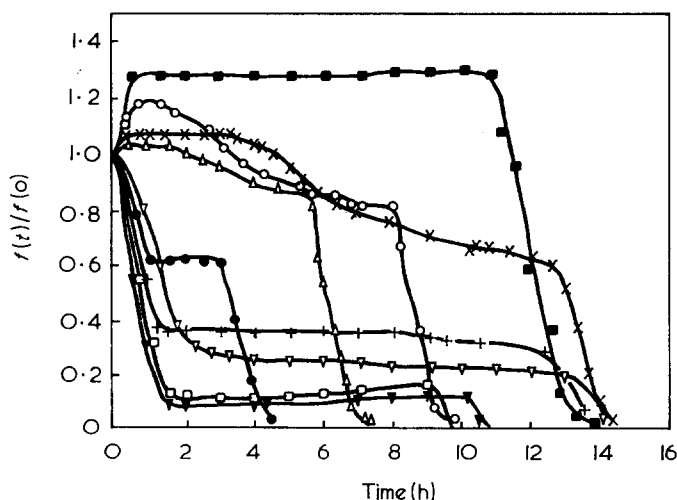


Figure 4 Intermittent stress relaxation curves for crosslinked polyethylene at 220°C. ■, (2); ×, (3); ○, (4); △, (5); ▽, (6); □, (7); +, (8); ●, (9); ▼, (10)

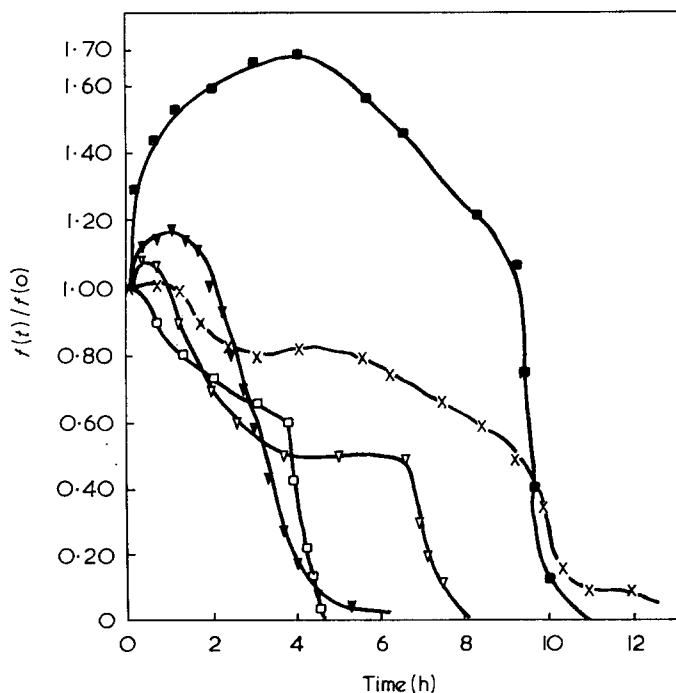


Figure 5 Intermittent stress relaxation curves for some crosslinked polyethylene samples at 230°C. ■, (2); ×, (3); □, (7); ▽, (6); ▼, (10)

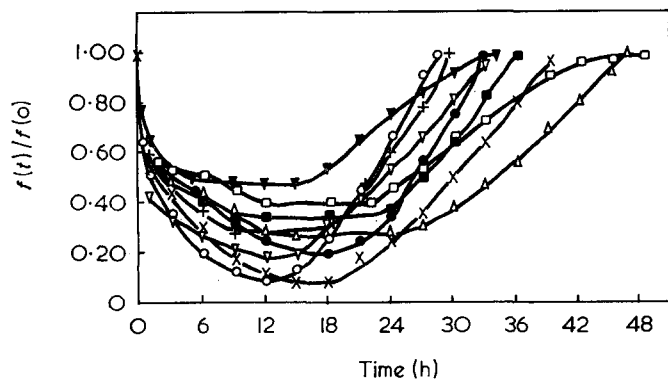


Figure 6 Continuous stress relaxation curves for crosslinked polyethylene at 240°C. ■, (2); ×, (3); ○, (4); △, (5); ▽, (6); □, (7); +, (8); ●, (9); ▼, (10)

Under continuous load at 240°C the stress curve falls sharply at the beginning and then shows a steady rise (Figure 6). This normally indicates an initial degradation followed by crosslinking.

These results appear to contradict the statement made earlier that crosslinking is favoured by conditions of intermittent stress. In fact, the results are not strictly comparable because the intermittent experiment ceased after 8 h. (In all cases specimens fail sooner under intermittent conditions as the repeated sharp application of a load is more severe than a continued stress.) Up to this point the results indicate that there was some crosslinking in the intermittent specimens whilst the 'continuous' specimens show degradation only.

The t.g. curves of all specimens show that the rate of loss at 240°C is high (Figure 2). In view of the long time (16 h) before the rise occurred the normal interpretation of the stress analysis curve is not valid in this case. The contraction of the specimen may be caused by cyclization but we have no direct evidence of this. A similar effect was found with low density polyethylene<sup>8</sup>.

*Summary of stress relaxation results.* No correlation could be obtained between the relaxation results at 175°C and the amount of peroxide used. In the extrusion process the polymer reaches a maximum of 210°C and that for only a short period (~30 sec). The results at 175°C therefore show that further heating is required to complete the crosslinking reaction. At 220°C peroxide contents are directly related to intermittent stress behaviour and give good correlation with the gel content. The initial rise in stress in low peroxide content polyethylene is due to new links formed while any redundant link between two already linked molecules does not

support this stress and reduction in stress takes place. After some time, the stress increases in a few specimens indicating that new crosslinks are being formed.

At 230°C degradation occurs as before in the continuous experiments and commences sooner in the intermittent ones. At 240°C the intermittent pattern is similar but the anomalous results of the continuous experiment show that the technique is no longer valid.

Because of the evidence of crosslinking in the stress relaxation experiments several samples were examined by differential thermal analysis in air and in argon but no evidence of an exotherm due to crosslinking could be found.

## CONCLUSIONS

D.t.a. is a rapid technique for measuring crystallinity and gives good correlation with gel content. It is a useful quality control method. It does not, of course, measure crosslinking density but the crystalline melting point of crosslinked polyethylene can be used for comparative purposes.

Thermogravimetry is a straightforward technique for the evaluation of the effects of crosslinks and other additives on the stability of polyethylene. Although activation energies are only comparative it is clear that three different reactions occur depending on whether the amount of peroxide in the polyethylene is low, high or zero.

Stress relaxation is a useful technique for following reactions in elastomers at high temperature but it is difficult to obtain absolute values.

## ACKNOWLEDGEMENTS

We thank Mr C. W. Evans for his continued interest in this work, Mr J. Hood for useful discussions and Dunlop Ltd for permission to publish.

## REFERENCES

- 1 Manley, T. R. and Qayyum, M. M. *Polymer* 1971, **12**, 176
- 2 Danneberg, E. N., Jordan, M. E. and Cole, H. M. *J. Polym. Sci.* 1958, **31**, 127
- 3 Narkis, M. and Milts, J. *Israel J. Chem.* 1970, **8**, 7
- 4 Brenner, W., Alder, A., Oswald, H. J. and Turi, E. A. *J. Appl. Polym. Sci.* 1969, **13**, 2689
- 5 Manley, T. R. and Martin, C. G. *Acta Chim. Acad. Sci., Hung.* 1971, **67** (4), 443
- 6 Reich, L. *J. Polym. Sci. (B)* 1966, **4**, 423
- 7 Tobolsky, A. V. 'Properties and Structure of Polymers', Wiley, New York, 1960
- 8 Narkis, M. and Tobolsky, A. V. *J. Appl. Polym. Sci.* 1969, **13**, 22, 57

# Polymerization of hexachlorotriphosphonitrile, (NPCl<sub>2</sub>)<sub>3</sub>

J. Emsley and P. B. Udy

Department of Chemistry, University of London King's College, London WC2R 2LS, UK  
(Received 10 May 1972)

The discovery that the acidity of the walls of the glass reaction tube markedly affects the polymerization of (NPCl<sub>2</sub>)<sub>3</sub> is reported. The effects of temperature and time on the nature of the products are also discussed. An alternative cationic polymerization mechanism is proposed.

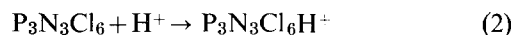
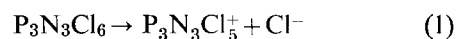
A good deal of research has been carried out into the polymerization of the cyclic hexachlorotriphosphonitrile, (NPCl<sub>2</sub>)<sub>3</sub>, to high linear polymers. However, there seems to be little correlation of the results obtained by different workers. The products of the bulk polymerization of pure (NPCl<sub>2</sub>)<sub>3</sub> depend very much on the temperature and time, and varying ratios of the benzene soluble component [linear (NPCl<sub>2</sub>)<sub>n</sub>] and a benzene insoluble component [crosslinked (NPCl<sub>2</sub>)<sub>n</sub>] can be obtained. At about 250°C polymerization takes about two days and the linear material predominates. At 300°C polymerization times are of the order of minutes and after about 1 h crosslinked product is formed<sup>1</sup>.

Even with pure (NPCl<sub>2</sub>)<sub>3</sub>, standard apparatus, and good temperature control reproducible results are the exception rather than the rule, suggesting that some unsuspected factor is influencing or catalysing the reaction. In the past suspicion has fallen on oxygen<sup>2</sup>, traces of water<sup>3</sup>, and the make of glassware used for the reaction tube<sup>4</sup>. Nevertheless high vacuum conditions, rigorous drying and the use of standard reaction tubes have failed to achieve consistent results.

That many compounds will act as catalysts is well known. In particular metals and oxygen-containing organic compounds (ethers, ketones, alcohols and carboxylic acids) are capable of acting in this capacity<sup>5</sup>. Benzoic acid in particular has been singled out for intensive investigation<sup>6</sup>. Catalysed polymerization takes place at 210°C and here reproducibility of results is high.

Basically there are only three variables which can affect the uncatalysed polymerization of a given sample of pure (NPCl<sub>2</sub>)<sub>3</sub>: temperature, time and the surface of the containing vessel. Assuming a reaction which is highly sensitive to all three variables the conditions chosen for study were temperatures 240° and 260°C, times 40 and 48 h, and pretreatment of the glass reaction tubes by primary washing with alkali or acid. The results of 8 experiments with all possible combination of these variables are given in *Table 1*, and show the sensitivity of the polymerization to all three variables.

The relationship of crosslinking and temperature is obvious and the effect of time and the acidity of the glass also play a part. The sensitivity of the polymerization to time and temperature is not unexpected<sup>3</sup> but just as important is the acidity of the surface of the glass, especially at the lower temperature. As a result of these experiments it is clear that the polymerization is catalysed by surface components and in particular H<sup>+</sup>. The results are consistent with a cationic polymerization mechanism, but unlike the more usually postulated loss of Cl<sup>-</sup> as the initial step (1), there is addition of a proton (2):

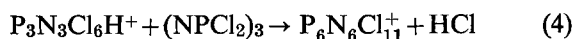
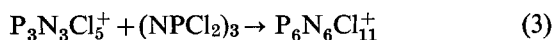


In the former the P<sup>+</sup> centre now attacks a nitrogen atom on another ring (3) with either a prior or concurrent ring opening step. In the latter case the proton presumably attaches itself to a nitrogen atom which then attacks

Table 1 Bulk polymerization of pure (NPCl<sub>2</sub>)<sub>3</sub> (17.4 g, 0.05 mol samples)

Glass surface	Temp. (°C)	Time (h)	Composition of products					
			Low polymers and (NPCl <sub>2</sub> ) <sub>3</sub>		High linear polymer		Crosslinked polymer	
			g	%	g	%	g	%
Acid	240	40	11.8	68	6.6	32	0	0
	240	48	6.5	37	10.9	63	0	0
Alkali	240	40	15.4	89	2.0	11	0	0
	240	48	14.2	82	3.2	18	0	0
Acid	260	40	4.5	26	1.3	8	11.6	66
	260	48	2.1	12	0.8	5	14.5	83
Alkali	260	40	5.0	28	1.7	10	10.7	62
	260	48	2.7	16	1.8	11	12.9	73

a phosphorus on another ring with elimination of HCl (4) and formation of the same cation as in reaction (3):



The new mechanism would explain the presence of HCl which is invariably produced in the polymerization of  $(NPCl_2)_3$  no matter how careful the drying process.

Crosslinking can be imagined as occurring via a similar proton mechanism.

## EXPERIMENTAL

The  $(NPCl_2)_3$  was purified by distillation under reduced pressure and crystallization from light petrol (b.p. 60–80°C) to a sharp m.p. of 113°C. Polymerizations were performed on samples (17.4 g, 0.05 mol) in sealed Pyrex tubes (1.8 × 12 cm) which had been pretreated by washing with NaOH or HNO<sub>3</sub> solution, as required, followed by repeated rinsing with distilled water and drying at >350°C under pumping. The sample of  $(NPCl_2)_3$  was admitted and degassed by melting and pumping *in situ* prior to sealing the tube. The tubes were heated by means of a fluidized sand bath which was capable of maintaining temperatures of 240° and 260° ± 2°C indefinitely in a closed room. After the requisite time the tubes were opened and the contents were extracted with dry benzene (300 cm<sup>3</sup>) for two days. At the end of this period any benzene-swollen crosslinked product was milled to break up its bulk and extracted for a further period. The mixture was filtered and solvent was removed from both soluble and swollen product.

The linear product and unreacted starting material were refluxed with a calculated weight of sodium octanoate, NaOC<sub>8</sub>H<sub>17</sub>, in benzene for 48 h; this gave the substituted polymer,  $[NP(OC_8H_{17})_2]_n$  and  $[NP(OC_8H_{17})_2]_3$ . The NaCl was filtered off and the solvent was removed. A sample of the product was transferred to a rubber sac (surgeon's finger stall), suspended in a Soxhlet apparatus and dialysed for 12 h with light petrol (b.p. 40–60°C). The undialysed material was dried and weighed and represented the yield of high molecular weight polymer. This was a white resin. The dialysed product consisted of oligomers and  $[NP(OC_8H_{17})_2]_3$ .

The high polymer was tested as a viscosity improver but showed little effect in this capacity.

## ACKNOWLEDGEMENTS

The authors wish to acknowledge the help of J. S. Elliott and I. H. R. Crail and thank the Burmah Oil Trading Co. Ltd for a grant.

## REFERENCES

- 1 Allcock, H. R., Kugel, R. L. and Valan, K. J. *Inorg. Chem.* 1966, **5**, 1709
- 2 Patat, F. *Angew. Chem.* 1953, **65**, 173
- 3 MacCallum, J. R. and Werninck, A. J. *J. Polym. Sci. (A-1)* 1967, **5**, 3061
- 4 Gimblett, F. G. R. *Plastic Inst. (London) Trans. J.* 1960, **28**, 65
- 5 Konecny, J. O. and Douglas, C. M. *J. Polym. Sci.* 1959, **36**, 195
- 6 Gimblett, F. G. R. *Polymer* 1960, **1**, 418

# Note to the Editor

## A universal relationship for the crystallization kinetics of polymeric materials

A. Gandica

Department of Chemical Engineering, University of Pittsburgh, Pittsburgh, Pa 15213, USA

and J. H. Magill

Department of Metallurgical and Materials Engineering, University of Pittsburgh, Pittsburgh, Pa 15213, USA

(Received 14 August 1972; revised 4 September 1972)

Over the last decade or two, there has been a real effort to obtain relations capable of characterizing the crystallization of materials<sup>1-6</sup>. Most of these formalisms have had limited applicability. Recently, from an extensive study of crystallization data, we have derived a model which appears to be universal. This new corresponding states relation has a phenomenological basis. Furthermore, it does not invoke any biased selection of a nucleation mechanism or activation energy for transport.

In this communication, we briefly present how it is effective in providing a master curve for describing polymeric materials. Figure 1 shows spherulitic growth rate data for a wide variety of polymers. Not only is a wide span of temperature covered in this plot, but different modes of crystallization are included, viz., from the glassy state and from the melt. In addition, fractionated polymers and polymer mixtures are included. Moreover, tacticity effects are also illustrated here as well as the results of widely different molecular weight polymers. Selenium, of high purity, is also featured on this plot.

The corresponding states plot shown in Figure 2, clearly brings all experimental results into coincidence. The maximum rate of crystallization (from Figure 1) is denoted by  $G_x$ ,  $T_m$  is the thermodynamic melting temperature usually obtained by an extrapolation procedure<sup>5</sup> (see also Figure 2, ref. 7).  $T_\infty$  is generally about 50°C below the glass temperature,  $T_g$ , and is also arrived at by extrapolation or other methods<sup>4-6</sup>. All the data used in this analysis were available in the referenced literature. The master curve produced peaks at about  $0.63 \pm 0.01$  and tends to zero at  $T_\infty$  and  $T_m$  respectively in the dimensionless relation:

$$\ln(G/G_x) = f(T - T_\infty)/(T_m - T_\infty)$$

Bulk crystallization plots of polymers have also been examined in a similar manner. Monomeric materials (or small molecules) follow a similar pattern of behaviour except that the reduced plot peaks at about  $0.84 \pm 0.01$  instead of at 0.63. Any change from monomeric (0.84) to polymeric (0.63) behaviour can be examined by means of this corresponding states relation and information on the size of the segmental unit participating in the growth process should be indicated. Interestingly, the polymeric character of selenium is clearly evidenced here, since it belongs to the polymeric species of Figure 2 and not to the low molecular weight materials which have maxima at a much higher value.

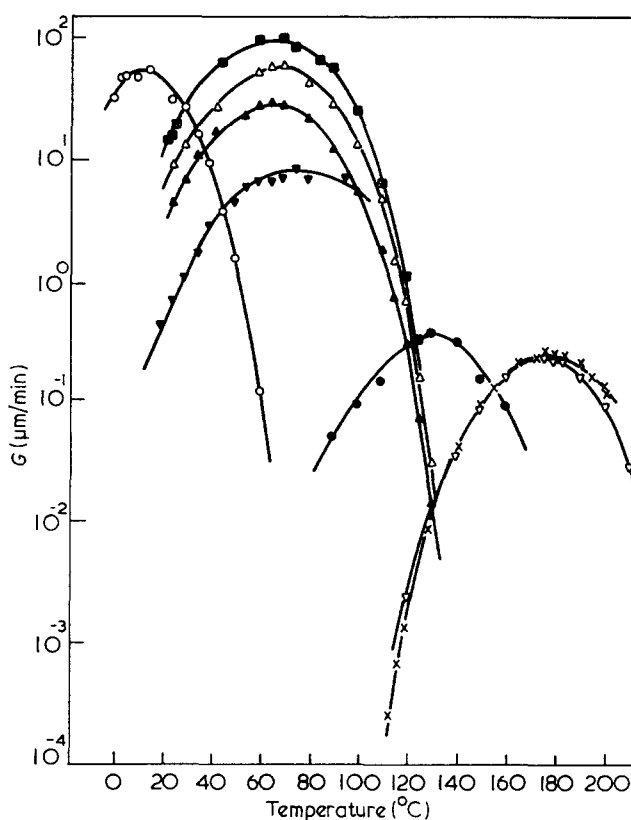


Figure 1 Logarithm of the spherulitic growth rate,  $G$ , against temperature,  $T$ , for a variety of polymers. ●, Selenium<sup>7</sup> (99.999%); ○, 1-poly(propylene oxide)<sup>8</sup> ( $M_n = 1.03 \times 10^4$ ); ×, isotactic polystyrene<sup>9</sup> ( $M_v = 2.2 \times 10^6$ ); ▲, poly(tetramethyl-*p*-silphenylene siloxane) mixture<sup>10</sup> ( $M_n = 1.09 \times 10^5$ ); △, poly(tetramethyl-*p*-silphenylene siloxane) mixture<sup>10</sup> ( $M_n = 2.7 \times 10^4$ ); ▼, poly(ethylene terephthalate) from the glassy state<sup>11</sup> ( $M_v = 1.9 \times 10^4$ ); ■, poly(tetramethyl-*p*-silphenylene siloxane)<sup>12</sup> ( $M_v = 1 \times 10^4$ ); □, poly(tetramethyl-*p*-silphenylene siloxane)<sup>13</sup> ( $M_v = 1.4 \times 10^6$ ); ▽, poly(ethylene succinate)<sup>14</sup> ( $M_n = 5.98 \times 10^3$ )

The approach described here has the advantage of correlating new data as reduced variable plots. At the same time, it provides a check on internal consistency with other data on polymer systems and suggests a means of extrapolating values from limited available information. The dependence of growth rate on molecular weight is also accounted for in this relation [see for example the data on poly(tetramethyl-*p*-silphenylene siloxane), which reduce to a single curve]. The product of the crystallite 'surface'

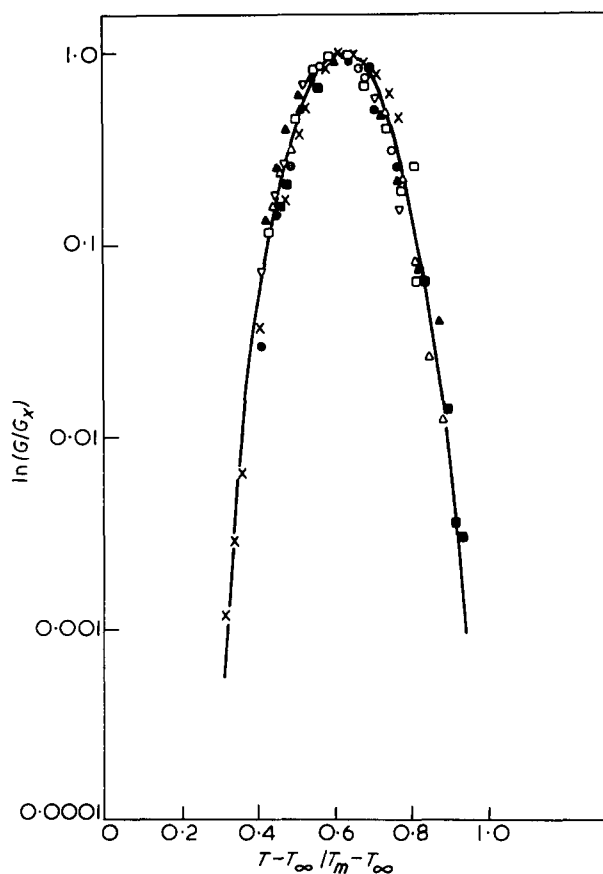


Figure 2 A corresponding states plot for the data of Figure 1.  $G_x$  is the maximum growth rate in Figure 1;  $T_m$  is the melting point;  $T_\infty$  is the temperature where polymer chain segmental transport tends to zero

energies ( $\sigma\sigma_e$ ) can also be deduced from this equation and polymer growth rate equations<sup>15-17</sup>.

Plots of another related corresponding states function  $\ln(G/G_x) = f(T - T_g)/(T_m - T_g)$  are also valuable although those obtained using  $T_\infty$  seem more meaningful. Here  $T_g$  is the glass temperature of the polymer, and it is related to  $T_\infty$  referred to above. A more extensive report of our analysis is being prepared for publication.

#### ACKNOWLEDGEMENT

Financial support from the Natural Science Foundation is gratefully acknowledged.

#### REFERENCES

- 1 Bunn, C. W. in 'Fibres from Synthetic Polymers', (Ed. R. Hill) Elsevier, London, 1953, Ch 12
- 2 Kim, H. and Mandelkern, L. *J. Polym. Sci. (A-2)* 1968, **6**, 695
- 3 Mandelkern, L., Jain, N. L. and Kim, H. *J. Polym. Sci. (A-2)* 1968, **6**, 165
- 4 Boon, J., Challa, G. and van Krevelen, D. W. *J. Polym. Sci. (A-2)* 1968, **6**, 1791
- 5 Hoffman, J. D. *SPE Trans.* 1964, **4**, 315
- 6 Magill, J. H. *Polymer* 1965, **6**, 367
- 7 Crystal, R. G. *J. Polym. Sci. (A-2)* 1970, **8**, 1755, 2153
- 8 Magill, J. H. *Makromol. Chem.* 1965, **86**, 283
- 9 Suzuki, T. and Kovacs, A. *J. Polymer J.* 1970, **1**, 82
- 10 Magill, J. H. *Bull. Am. Phys. Soc.* 1972, 27-30 March, Atlantic City
- 11 van Antwerpen, F. *Doctoral Thesis* Delft Technical University, 1971
- 12 Magill, J. H. *J. Appl. Phys.* 1964, **35**, 3249
- 13 Magill, J. H. *J. Polym. Sci. (A-2)* 1967, **5**, 89
- 14 Takayanagi, M. and Kusumoto, N. *J. Chem. Soc. Japan (Ind. Sect.)* 1959, **62**, 587
- 15 Price, F. P. *J. Chem. Phys.* 1961, **35**, 1884
- 16 Frank, F. C. and Tosi, M. *Proc. R. Soc.* 1961, **A263**, 323
- 17 Hoffman, J. D. *et al. Kolloid-Z. Z. Polym.* 1968, **231**, 386

# Book Reviews

## Handbook of plastics test methods

G. C. Ives, J. A. Mead and M. M. Riley  
Iliffe Books, London, 1971, 476 pp. £10.00

This Plastics Institute monograph is an extremely comprehensive review of plastics test methods, covering standards used in Great Britain, the USA and Germany as well as some useful methods not as yet standardized. In addition, the many literature references cited throughout make this book invaluable as a general handbook.

An excellent introductory chapter is particularly useful to students of plastics technology, discussing the significance of testing, and its relevance. The following chapter describes the function and structure of some Standards Issuing Bodies including the International Standards Organisation (ISO), and an appendix provides addresses of all national standard organizations, so giving access to any standard required. Another appendix lists all British Standards and ISO recommendations for plastics available up to June 1970.

Several chapters discuss preliminaries to actual plastics testing, including preconditioning, characterization of polymer structure, measurement of density and specimen dimensions, tests on materials before moulding, and the preparation of test specimens.

The remainder of the book describes in detail tests for all types of mechanical, electrical and thermal properties, and some for ageing and optical properties. Limitations of the tests are stressed. Certain unrelated properties are grouped as 'non-destructive' tests. Many of these are rather specific (for example birefringence and ultrasonic testing) and are mentioned briefly since they do not justify detailed description in the context of general testing, although useful references are given. A final chapter discusses specific tests for foams, pipes and tubes, film and sheet, and laminates.

For most properties standard tests are given in detail and important non-standardized methods are also considered. In some instances (e.g., mechanical and electrical testing) valuable details of test equipment are given, but in other cases information is restricted to a list of tests with variations and test-piece dimensions. These are available in the standard cited, and some details or comment concerning results obtained would be informative.

In view of the current change to SI units the practice of quoting units directly from each reference is perhaps unfortunate, particularly where alternative units, with tolerances have been given. While this is acceptable in standards and reference material, it tends to destroy the continuity if the monograph is to be used as a textbook. This is, however, only a minor feature of a handbook which is highly recommended both to those involved in plastics testing, and to those interested in its study and practice.

M. Gilbert

## Textbook of polymer science

Fred W. Billmeyer, Jr.,  
Wiley-Interscience, New York, 2nd edn, 1971,  
598 pp. £7.50 (paper, £4.30)

The 1962 edition of this book, like its predecessor *Textbook of polymer chemistry*, gained a deservedly wide readership among students, teachers and general practitioners of the polymeric arts, because it provided them with an accurate and clearly presented conspectus of the principles and applications of the subject, and yet it was sufficiently comprehensive to satisfy most needs up to the specialist level. The task of adequately encompassing such a large field within 600 pages was a notable achievement at that time; today it is one that might be considered almost impossible.

Professor Billmeyer, nevertheless, has succeeded in giving us a new edition which is right up to date while preserving the essential form and spirit of his earlier books. Some details of lesser importance have had to be sacrificed in order to keep the price of the book within reasonable bounds; the effect of this is seen mainly in the part dealing with the properties of commercial polymers, which has been rearranged and reduced in length from seven chapters to four. The sections on polymer solutions, crystalline polymers, polymer structure and properties, have been extensively revised and expanded. Other revisions and additions of new material have been made throughout,

principally to the chapters on molecular weight measurement, analysis and testing, and ionic and co-ordination polymerization.

The most obvious change from the first edition is that almost all the literature references have been selected from specialist monographs and review articles, the titles in each case being given in full, so that the reader is immediately directed to the most profitable secondary sources of information. There are about one thousand of these references, of which approximately half were published between 1966 and 1970. This feature adds materially to the usefulness of the revised version.

The only criticism that can be made—perhaps an unfair one in view of the purpose of the book—is that a few of the topics of more recent interest are given only fleeting mention; but the balance between the main divisions of the subject is nicely judged, and the inclusion of more detail would probably serve only to impair the overall effect of a remarkably clear and direct exposition, the style itself being a worthy example for students to follow. For them, and also for many others seeking a modern survey of the whole field, one can continue unreservedly to recommend 'Billmeyer' as the best there is. No misprints were noted.

P. F. Onyon

## Solvents

T. J. Durrans (revised by E. H. Davies)  
Chapman and Hall, London, 8th edn, 1971,  
267 pp. £2.50

Every scientist and technologist has near to hand a few books which are well-used sources of information and many who are concerned with polymer research and development, manufacture and applications will have had occasion to refer to Durrans' 'Solvents' in its various editions, so that it is of some interest to see now the eighth edition make its appearance.

As before, the subject matter is presented in two parts, the first of which (81pp) deals generally with solvent action and balance, plasticizing solvents, viscosity, vapour pressure and rates of evaporation, inflammability and, very important, toxicity aspects and legal requirements regarding storage and handling. The 175 pages of Part II include manufacture, standard specifications, properties and solvent action of many types of solvents ranging from hydrocarbons, alcohols, ketones and esters to glycols, chlorinated compounds, furan derivatives and plasticizers. The appendices provide a source of information on trade names, solubility behaviour and plasticizer proportions.

This revised edition takes note of some developments since the last edition of 14 years ago. Some new solvents appear in the lists but although the solubility tables give extensive coverage of natural resins and gums, no new polymers are included—indeed these tables are very much as before and in many ways the text shows evidence of its early ancestry, with marked emphasis on cellulose ester lacquers. There is no direct lead, for example, to a solvent for a polyamide or a copolyester, while the table on plasticizer proportions still deals specifically with cellulose nitrate and acetate films. Some new entries such as polyurethane lacquers and PTFE are to be found in the index but these receive little attention in the text except where there is mention under some particular solvent heading.

It is a pity that in this edition greater care was not taken to eliminate printing errors (e.g. the headings of the tables on p 57 and p 258 require attention as does the formula for dipentene on p 96) and to avoid the use of different, and sometimes imprecise, names for the same or related polymers: thus we have methyl methacrylate 'resin' and Perspex; poly(vinyl chloracetate) and poly(vinyl acetochloride); glyceryl phthalate, glyptal, alkyd; bakelite, bakelite A, rezyl, phenol-formaldehyde; GRN, nitrile, hycar, perbunan—all appearing in a haphazard manner. Indeed some of the terms now seem a little archaic, e.g. 'polymerized alcohol' (p 5) and 'the manufacture of art silk' (p 187), while some references could well be updated.

However, despite these criticisms the book contains much useful information, especially regarding the individual solvents; it will continue to serve, as did the earlier editions, as a volume for consultation, especially on physical properties and solvent action, is well bound and offered at a reasonable price.

R. J. W. Reynolds



**Polyolefins : modifications of structure and properties**

A. G. Sirota (Translated by J. Schmorak)  
Israel Program for Scientific Translations,  
Jerusalem, 1971, 120 pp. £5.00

The modification of polymer properties by copolymerization, grafting, reticulation, and the introduction of novel chemically reactive sites is of profound importance and its intensive study over many years has generated much fundamental knowledge on the reactivity of macromolecules on the one hand, and a wealth of novel and useful industrial products on the other. Because of their ready availability and cheapness, and also through a desire to surpass certain inherent properties limitations, the polyolefins have been particularly deeply investigated in this respect with successes well known through such diverse products as high density, sulphochlorinated and peroxide-cured polyethylenes, ethylene-propylene copolymer elastomers, ethylene-vinyl acetate copolymer resins, emulsions and adhesives, and the ionomers. The present slender volume, originally published in Russian in 1969, aims to present a synoptic view of the methods and application of these ideas.

The book commences with a short account of polymers formed by different catalytic methods from ethylene, propylene and the higher  $\alpha$ -olefins and proceeds to a description of the copolymers of ethylene with other  $\alpha$ -olefins with polar monomers. The third chapter deals with graft and block copolymers of  $\alpha$ -olefins and the fourth covers chemical modifications by halogenation, sulphochlorination, phosphorylation, oxidation and thermal degradation. This chapter together with the fifth, which is concerned with chemical, photochemical and radiation-induced methods of crosslinking, form the most interesting and best-written parts of the book. The final chapter gives a cursory survey of additional approaches based on compounding and formulation.

It is difficult to discern the intended readership. The subject is over-specialized for beginners in polymer science and technology, yet the treatment is too shallow for anyone requiring to pursue the topic in depth. The book (which lacks indexes) appears to have been assembled mainly by the scissors-and-paste method as a series of factual statements with little attempt to compare and critically evaluate the various methods and results. The approach is also uneven. To give a few examples: (a) the spectroscopic analysis of ethylene-vinyl acetate copolymers is discussed in detail but no mention is made of their established technical uses; (b) ethylene-propylene copolymers are discussed from an academic standpoint over about 17 pages of text but the notably important EPT elastomers occupy less than one; (c) phosphorylation reactions, which whilst interesting have little practical significance, receive three separate treatments and six times the space given to the modification of polyolefins for dyeability—a critical problem in the development of polypropylene as a textile material. Comment must also be made on the lack of definition of many test parameters cited from Russian investigations; thus, low temperature properties are given qualitatively as 'resistant to frost', and there is repeated mention of unclassified surfactants used in stress-cracking tests.

In this reviewer's opinion the book, which is not cheap even by present-day standards, does not give a satisfactorily balanced appreciation of the problems or the achievements of the subject. It might be held to have some value as a compilation of data and literature references, but intending readers should be advised that three-quarters of the 617 citations are to Western literature which is probably already available on their shelves.

I. Goodman

**Mechanical properties of solid polymers**

I. M. Ward  
Wiley, New York and London, 1971, 375 pp. £7.00

The subject of the mechanical properties of polymers is so extensive that the task of presenting a reasonably comprehensive account of it poses formidable problems of selection and of systematic presentation. In the work under review the treatment, while giving an adequate background in terms of molecular concepts of the structure of polymers, is more concerned with the engineering type of approach than has been customary in this field. A good example is in the treatment of elasticity, which starts from the classical theory and then leads

on to the general formulation of the elastic properties of rubber-like materials. The molecular theory of rubbers is introduced later and shown to fit in neatly with the more general formulation. The classical theory also provides the basis for the presentation of the properties of anisotropic materials, such as drawn polymers, fibres, etc., and for the broadening out into the theory of linear and non-linear viscoelastic properties. The treatment of viscoelastic properties, including relaxation-time spectra, is extremely well done, both from the theoretical and from the experimental standpoints. It is clear that in the case of crystalline polymers particularly we are still a long way from achieving a complete molecular interpretation of the various relaxation processes encountered.

A later chapter on the processes of yielding includes a thorough critical discussion of the applicability of the various engineering-type criteria to the prediction of yielding, which brings out the importance of the hydrostatic pressure component of the stress. The final chapter, on fracture properties, includes a consideration of the application of the Griffith theory to glassy polymers, and the mechanism of crazing.

Although the theoretical sections are necessarily somewhat mathematical in character, the author does not in this respect go beyond what is essential for the proper understanding of the subject, and the physical significance of the mathematical formulation is always kept clearly in view. The book has an original quality, and owes much to the author's own contributions to many aspects of his subject. It is clearly written and reliable, and should prove extremely valuable for advanced students and research workers in polymers or allied branches of materials science.

L. R. G. Treloar

**Magnetic resonances in biological research**

Edited by C. Franconi  
Gordon and Breach, New York, 1971, 400 pp. £10.20

This volume represents the proceedings of a conference held in Cagliari, Italy in the summer of 1969 on magnetic resonance spectroscopy in biology. There are 38 separate contributions. Since that time there has been another meeting under the same general heading (Oxford, 1970), but the proceedings have not been published and this therefore represents the latest summary of the field.

Books resulting from conferences not infrequently resemble the curate's egg for a number of reasons. Firstly, the actual participants may not include all those active in the field and secondly those that do speak may not write up their contributions as fully as many would-be readers might like.

Nevertheless, a predominant topic often emerges from a general title and this is true in this case since a fair proportion of the papers deal with the study of iron-casting proteins, largely by means of e.s.r. Particularly noteworthy in this respect are chapters by Ingram, Blumberg and Kotani devoted largely to haemoglobin. There are 5 other contributions devoted to haem proteins and although 3 of them are concerned with n.m.r. studies, e.s.r. nevertheless is much the more prominent technique of the two in this volume: reflecting perhaps the fact that it was the earlier to be applied to biological problems. In the chapters on haem proteins lies the book's main merit. The remainder (~70%) is a varied collection of the latest (1969) findings from a number of laboratories throughout the world given in outline form. Noteworthy among the reports on n.m.r. work are those by Raftery on lysozyme, Craig on cyclic polypeptides, McLauchlan on collagen and Bothner-By on  $^{25}\text{Mg}$  resonance. Important topics under the broad title of the book that are little covered include the n.m.r. of enzymes (save for a summarized report of 3 pages by Jardetzky), membranes (save for a short paper from the Unilever laboratory), spin labelling (save for a useful note by Piette on  $\alpha$ -chymotrypsin) and proton relaxation enhancement. The book is introduced by two worthwhile chapters not on resonance work but having as common theme the effect of ligand binding on protein conformation, particularly in cases of sub-unit structure. Attention is paid in both articles to relating empirical binding curves to models of cooperative subunit interaction.

The book is a must for all research groups actively engaged on resonance work in biological systems, but is unlikely to be worth the rather stiff price for anyone else. The preparation and the quality of the diagrams are quite adequate, there being no unnecessarily lavish expenditure on glossy paper or elaborate type to further inflate the price.

C. Crane-Robinson

# Classified Contents

- Acrylic and methacrylic esters of *N*-hydroxysuccinimide as polyacrylamide and polymethacrylamide precursors, 462
- Adamantane polymer, thermally stable fibres from, 85
- AlEt<sub>3</sub>/benzoyl-peroxide/Lewis-base system, polymerization of vinyl chloride by, and the role of the Lewis base in initiation, 288
- Annealing of high density polyethylene for very long times at low supercooling under vacuum, 584
- Birefringence of plastically deformed poly-(methyl methacrylate), 174
- Bisphenol-A diglycidyl ether/polyamide system, 455
- Block copolymers, polystyrene/polyisoprene, investigation of the effect of chain geometry on the two-phase morphology of, 333
- Block polymers, sym-SBS, electron microscopy of, 20
- Calcium, role of, in the fibrinogen-fibrin reaction, electron spin resonance study, 579
- Cellulose fibres, Ramie and Fortisan, crystallinity and crystallite size measurement, 423
- Cellulose, sorbed water on, pulsed n.m.r. study of molecular motion and environment, 259
- Cellulose triacetate, heat-treated, peak resolution and X-ray crystallinity determination in, 27
- Chain geometry on the two-phase morphology of polystyrene/polyisoprene block copolymers, investigation of the effect, 333
- Characterization of a cyclic oligomer of poly(pentamethylene terephthalate), 297
- Chloroprene, preparation and properties of networks containing, 57
- Conformational properties of isotactic poly( $\alpha$ -olefins) in solution, calculation of, 232
- Conformational studies of poly(L-tyrosine) in solvent mixtures of dimethylsulphoxide with water and trimethylphosphate, 33
- Conformation and dimensions of polymethylene and polypropylene in solution, 218
- Copolymerization behaviour of some *N*-vinyl monomers, 149
- Copolymerization, free radical, of styrene and methacrylonitrile, solvent effects, 435
- Copolymerization of phenylene with maleic anhydride, 549
- Crazing, environmental, mechanics and mechanism in a polymeric glass, 337
- Critical tensile strength and polymer cross-sectional area, a correlation between, 558
- Crystallinity and crystallite size measurement in cellulose fibres: 1. Ramie and Fortisan, 423
- Crystallization kinetics of polymeric materials, universal relationship, 595
- Crystallization of high molecular weight fractions of poly(ethylene oxide) from dilute solution in ethanol, 355
- Crystallization of polyethylene fractions at high undercooling, effect of molecular weight on rate, 407
- Crystallization rates and melting of polymers, effect of chemical structure on: Part 1. Aromatic polyesters, 327
- Degree of polymerization, effects of long-chain branching on distribution of, 1536
- 2'-Deoxyadenosine, n.m.r. and u.v. spectra of, in water/dimethyl sulphoxide, 520
- Dielectric relaxation in polymaleimide and *N*-substituted polymaleimides, 527
- Dimethylsulphoxide solvent mixtures with water and trimethylphosphate, conformational studies of poly(L-tyrosine) in, 33
- Dynamic mechanical properties of poly-(ethylene oxide), 460
- Elastic behaviour of rubber under small uniaxial extension and compression, 347
- Electron microscope investigation of poly-(ethylene oxide) supermolecular particles in solution, 379
- Electron microscope study of freeze-etched polystyrene latex, 226
- Electron microscopy of sym-SBS block polymers, 20
- Electron spin resonance studies of spin-labelled polymers: Part 2. Preparation and characterization of spin-labelled polystyrene, 89
- Electron spin resonance study of the role of calcium in the fibrinogen-fibrin reaction, 579
- Epoxy cure, kinetics of: 2. The system bisphenol-A diglycidyl ether/polyamide, 455
- Epoxy resins, mechanical relaxation studies of the cure: 1. Measurement of cure, 443:2. Activation energy of the  $\gamma$ -process in amine-cured epoxy resins, 450
- Equilibrium ring concentrations and the statistical conformations of polymer chains: Part 7. Cyclics in poly(1,3-dioxolane), 142
- Part 8. Calculations of small ring concentrations in polydihydrogensiloxane and polydimethylsiloxane equilibrates, 385
- Part 9. Sodium metaphosphates in Graham's salt, 414
- Part 10. Cyclics in a polymeric paraffin-siloxane, 523
- Etch method for microscopy of rubber-toughened plastics, 115
- Fibrinogen-fibrin reaction, electron spin resonance study of the role of calcium in, 579
- Filler reinforcement in silicone polymers, 109
- Flocculation property of the hydrolysis products of carbamoylated polyethylenimine, 552
- Fluorosilicone vulcanisates, high temperature stability, 479
- Free radical activity during reaction of organotin stabilizers with chlorohydrocarbons, absence of, 299
- Gel permeation chromatography: column packing method for polystyrene gels, 553
- Gel permeation chromatography: the behaviour of polystyrenes with long-chain branching, 277
- Glass transition temperatures of poly(methyl methacrylate), effect of stereostructure, 94
- Graham's salt, sodium metaphosphates in, 414
- Hexachlorotriphosphonitrile, (NPCl<sub>2</sub>)<sub>3</sub>, polymerization of, 593
- Hexa-1,4-diene, *cis-trans* isomerism in Ziegler-catalysed terpolymerization with ethylene and propylene, 242
- Hydrogen bonding on crazing and cracking of amorphous thermoplastics, influence of, 283
- N*-Hydroxysuccinimide, high polymers of acrylic and methacrylic esters of, as polyacrylamide and polymethacrylamide precursors, 462
- Infra-red dichroism, stress and strain of elongated polymers, measurement, 485
- Infra-red spectroscopy, accurate measurement of carboxyl and hydroxyl end-group concentrations in poly(ethylene terephthalate) film by, 391
- Interchain force field and elastic constants of polytetrafluoroethylene, 40
- Interfacial free energy of crystals of low molecular weight poly(ethylene oxide), 246
- Interfacial technique, production of organometallic polymers by: 24. Kinetics of polycondensation and thermal properties of poly[oxy(dicyclopentadienylzirconium)oxycarbonylferrocenylcarbonyl], 153
- cis-trans* Isomerism in Ziegler-catalysed terpolymerization of hexa-1,4-diene with ethylene and propylene, 242
- $\alpha$ -Keratin, reduced and silver-stained, low angle X-ray diffraction studies, 63
- Kinetics, crystallization, of polymeric materials, universal relationship, 595
- Kinetics of epoxy cure: 2. The system bisphenol-A diglycidyl ether/polyamide, 455
- Laser-Raman spectrum of polyethylene: Part 1. Structure and analysis of the polymer, 104
- Light-scattering, and refractive index increments in polydisperse systems of low molecular weight, 52
- Linear, high molecular weight poly(2-alkyl-4-vinyl-6-(dialkylaminomethyl) phenols) and poly(2,6-bis-(dialkylaminoethyl)-4-vinyl phenols), 184
- Long-chain branching, behaviour of polystyrenes with, 277
- Long-chain branching, effects of, on distribution of degree of polymerization, 536
- Long-chain branching, polymers with, 2
- Low angle X-ray diffraction studies of reduced and silver-stained  $\alpha$ -keratin, 63
- Maleic anhydride, copolymerization of phenylene with, 549
- Maleic anhydride, terpolymerizations involving, 249
- Manganese carbonyl + halide systems, after-effects in polymerizations photo-initiated by, 208
- Mechanical relaxation studies of the cure of epoxy resins: 1. Measurement of cure, 443
2. Activation energy of the  $\gamma$ -process in amine-cured epoxy resins, 450

## Classified Contents

- Mechanics and mechanism of environmental crazing in a polymeric glass, 337
- Melting and annealing of oriented single crystal aggregates of *trans*-polydodecener, 360
- Melting and transition phenomena in some polyester-urethanes, 133
- Melting characteristics, and thermal history, of high density polyethylene, 13
- Melting data for low molecular weight poly(ethylene oxide), interpretation, 459
- Melting of low molecular weight poly(ethylene oxide), 73
- Melting temperatures of low molecular weight poly(ethylene oxide), effect of end groups on, 475
- Methylene groups, orientation in poly(ethylene terephthalate), 69
- Methyl group motion in poly(propylene oxide), polypropylene and poly(methyl methacrylate), 157
- Molecular motion and environment of sorbed water on cellulose, pulsed n.m.r. study, 259
- Molecular orientation in drawn poly(vinyl chloride) by broad line nuclear magnetic resonance, 145
- Molecular parameters and some bulk properties of a plasticized highly crosslinked unsaturated polyester-styrene polymer system: 2 and 3, 541, 546
- Morphology of nascent polyethylene prepared with the catalyst  $\text{VOCl}_3/(\text{C}_2\text{H}_5)_2\text{AlCl}$ , 567
- N.m.r. and u.v. spectra of 2 deoxyadenosine in water/dimethyl sulphoxide mixtures, 520
- Nuclear magnetic resonance, broad line, measurement of molecular orientation in drawn poly(vinyl chloride), 145
- Nuclear magnetic resonance studies, broadline, of some poly(*N*-substituted maleimides), 561
- Peak resolution and X-ray crystallinity determination in heat-treated cellulose triacetate, 27
- Peptide polymers, sequence: Part 1. Poly(leucyl-leucyl-aspartic acid- $\beta$ -benzyl ester)-synthesis and some conformational aspects in solutions, 419
- Part 2. Poly(leucyl-leucyl-aspartic acid)-conformational aspects in water solution, 515
- Phenolic cosolutes, interaction with poly(vinyl pyrrolidone), 119
- Phenylene, copolymerization of, with maleic anhydride, 549
- Phosphazene copolymers: Part 1. Synthesis and bulk properties, 253
- Phosphorus pentoxide in dimethyl sulphoxide, polysaccharide synthesis from mono- and oligo-saccharides by the action of, 190
- Plasticized highly crosslinked unsaturated polyester-styrene polymer system, molecular parameters and some bulk properties: 2 and 3, 541, 546
- Plastics, rubber-toughened, an etch method for microscopy of, 115
- Poly(2-alkyl-4-vinyl-6-(dialkylaminomethyl)phenols) and poly(2,6-bis(dialkylaminomethyl)-4-vinylphenols), linear, high molecular weight, 184
- Polydihydrogensiloxane and polydimethylsiloxane equilibrates, calculations of small ring concentrations in, 385
- Poly(*trans*-2,5-dimethylpiperazine fumaramide) films, reverse osmosis properties, 503
- Poly(1,3-dioxolane), cyclics in, 142
- trans*-Polydodecener, melting and annealing of oriented single crystal aggregates, 360
- Polyesters, aromatic: effect of chemical structure on crystallization rates and melting of, 327
- Polyester-urethanes, melting and transition phenomena in some, 133
- Polyethylene, amorphous crosslinked, stress-dichroism studies of the 4.92  $\mu\text{m}$  band, 495
- Polyethylene, crosslinked, at elevated temperatures, 587
- Polyethylene fractions, effect of molecular weight on the rate of crystallization at high undercooling, 407
- Polyethylene, high density, annealing of for very long times at low supercooling under vacuum, 584
- Polyethylene, high-density: thermal history and melting characteristics, 13
- Polyethylene, laser-Raman spectrum: Part 1. Structure and analysis of the polymer, 104
- Polyethylene, nascent, morphology of, prepared with the catalyst  $\text{VOCl}_3/(\text{C}_2\text{H}_5)_2\text{AlCl}$ , 567
- Poly(ethylene oxide), crystallization of high molecular weight fractions from dilute solution in ethanol, 355
- Poly(ethylene oxide), dynamic mechanical properties, 460
- Poly(ethylene oxide), low molecular weight, effect of end groups on melting temperatures, 475
- Poly(ethylene oxide), low molecular weight, interfacial free energy of crystals, 246
- Poly(ethylene oxide), low molecular weight, interpretation of melting data, 459
- Poly(ethylene oxide), melting of low molecular weight, 73
- Poly(ethylene oxide) supermolecular particles in solution, electron microscope investigation, 379
- Poly(ethylene terephthalate) film, accurate measurement of carboxyl and hydroxyl end-group concentrations in, by infra-red spectroscopy, 391
- Poly(ethylene terephthalate), orientation of the methylene groups, 69
- Polyethylenimine, carbamoylated, flocculation property of the hydrolysis products, 552
- Polyethylenimine, carbamoylated, preparation and flocculation property, 187
- Polymaleimide and *N*-substituted polymaleimides, dielectric relaxation in, 527
- Polymerization of hexachlorotriphosphonitrile,  $(\text{NPCl}_2)_3$ , 593
- Polymerization of vinyl chloride by the  $\text{AlEt}_3$ /benzoyl-peroxide/Lewis-base system and the role of the Lewis base in initiation, 288
- Polymerizations, after-effects in, photo-initiated by manganese carbonyl + halide systems, 208
- Polymethylene and polypropylene in solution, conformation and dimensions, 218
- Poly(methyl methacrylate), birefringence of plastically deformed, 174
- Poly(methyl methacrylate), effect of stereostructure on glass transition temperatures, 94
- Poly(methyl methacrylate), poly(propylene oxide) and polypropylene, methyl group motion in, 157
- Poly( $\alpha$ -olefins), isotactic, calculation of the conformational properties in solution, 232
- Polyolefin solutions, temperature scanning studies, 78
- Poly[oxy(dicyclopentadienylzirconium)oxycarbonylferrocenylcarbonyl], kinetics of polycondensation and thermal properties, 153
- Poly(pentamethylene terephthalate), characterization of a cyclic oligomer of, 297
- Poly(*m*-phenylene adamantane-1,3-dicarboxamide) fibres, modifications to the morphology, 43
- Poly(phenylene ether sulphones), relative reactivities of the functional groups involved in the synthesis from halogenated derivatives of diphenyl sulphone, 465
- Poly(propylene oxide), polypropylene and poly(methyl methacrylate), methyl group motion in, 157
- Polysaccharide synthesis from mono- and oligo-saccharides by the action of phosphorus pentoxide in dimethyl sulphoxide, 190
- Polysiloxanes, substituted, spin-lattice relaxation, 431
- Polystyrene gels, column packing method: gel permeation chromatography, 553
- Polystyrene latex, freeze-etched, electron microscope study, 226
- Polystyrene/polyisoprene block copolymers, investigation of the effect of chain geometry on the two-phase morphology of, 333
- Polystyrene, rubber modified: structural variation induced during pre-polymerization, 366
- Polystyrene, spin-labelled, preparation and characterization: electron spin resonance studies, 89
- Polystyrenes of known structure: Part 3. Polymers with long-chain branching, 2
- Polystyrenes with long-chain branching, behaviour, 277
- Poly(*N*-substituted maleimides), broadline nuclear magnetic resonance studies of, 561
- Polysulphones of some 1,2-disubstituted alkenes, solution properties, 439
- Polytetrafluoroethylene, interchain force field and elastic constants, 40
- Poly(trimethylsiloxanotitanoxanes) (titanium oxide trimethylsiloxides), solution properties, 265
- Poly(L-tyrosine), conformational studies in solvent mixtures of dimethylsulphoxide with water and trimethylphosphate, 33
- Polyurethane elastomers, branched, tensile failure properties, 169
- Poly(vinyl chloride), measurement of molecular orientation by broad line nuclear magnetic resonance, 145
- Poly(vinyl fluoride), thermally stimulated conductivity, 371
- Poly(vinyl pyrrolidone), interaction with phenolic cosolutes, 119
- Precipitation chromatographic column: theory, critique and method of design, 124
- Refractive index increments of polymers in solution: 1. General theory, 46
2. Refractive index increments and light-scattering in polydisperse systems of low molecular weight, 52
3. Dependence on concentration, 274
- Reverse osmosis properties of poly(*trans*-2,5-dimethylpiperazine fumaramide) films, 503

- Rubber cylinder in torsion, swelling of:  
Part 1. Theory, 195  
Part 2. Experimental, 203
- Rubber, elastic behaviour under small uniaxial extension and compression, 347
- Rubber modified polystyrene: structural variation induced during pre-polymerization, 366
- Segregation and conformational transition in triblock copolymers: Part 2. Light-scattering studies, 97
- Silicone polymers, filler reinforcement in, 109
- Solution properties of polysulphones of some, 1,2-disubstituted alkenes, 439
- Solution properties of poly(trimethylsiloxanotitanoxanes) (titanium oxide trimethylsiloxides), 265
- Solvent effects in free radical copolymerization of styrene and methacrylonitrile, 435
- Spin-lattice relaxation in substituted polysiloxanes, 431
- Stabilizers, organotin, absence of free radical activity during reaction with chloro-hydrocarbons, 299
- Stress-dichroism studies of the 4.92  $\mu\text{m}$  band of amorphous crosslinked polyethylene, 495
- Stress relaxation after steady-state shear flow in undilute polydisperse polymers, 399
- Surface areas of fillers in polymers by small angle X-ray scattering, 575
- Swelling of a rubber cylinder in torsion:  
Part 1. Theory, 195  
Part 2. Experimental, 203
- Synthesis of poly(phenylene ether sulphones) from halogenated derivatives of diphenyl sulphone, relative reactivities of the functional groups involved, 465
- Temperature scanning studies of polyolefin solutions, 78
- Tensile failure properties of some branched polyurethane elastomers, 169
- Tensile strength, critical, and polymer cross-sectional area, a correlation between, 558
- Terpolymerizations involving maleic anhydride, 249
- Thermally stable fibres from an adamantane polymer, 85
- Thermally stimulated conductivity of poly(vinyl fluoride), 371
- Thermoplastics, amorphous, influence of hydrogen bonding on crazing and cracking of, 283
- Transient scattering from absorbing solutions, 164
- Triblock copolymers, segregation and conformational transition in: Part 2. Light-scattering studies, 97
- Vinyl chloride, polymerization by the  $\text{AlEt}_3$ /benzoyl-peroxide/Lewis-base system and the role of the Lewis base in initiation, 288
- N*-Vinyl monomers, copolymerization behaviour, 149
- Vulcanisates, fluorosilicone, high temperature stability, 479
- X-ray crystallinity, and peak resolution, determination in heat-treated cellulose triacetate, 27
- X-ray diffraction studies, low angle, of reduced and silver-stained  $\alpha$ -keratin, 63
- X-ray scattering, small angle, surface areas of fillers in polymers by, 575
- Ziegler-catalysed terpolymerization of hexa-1,4-diene with ethylene and propylene. *cis-trans* isomerism, 242
- Ziegler-Natta catalysis:
1. A general kinetic scheme, 302
  2. A kinetic investigation, 307
  3. Active centre determination, 315
  4. Quantitative verification of kinetic scheme, 321
  5. A molecular weight investigation, 510

# Author Index

- Addleman, R. L. and Zichy, V. J. I.: Accurate measurement of carboxyl and hydroxyl end-group concentrations in poly(ethylene terephthalate) film by infra-red spectroscopy, 391
- Allen, G.: *see* Higgins, J. S., Allen, G. and Brier, P. N.
- Allen, G. and Mortier, R. M.: Phosphazene copolymers: Part 1. Synthesis and bulk properties, 253
- Andrews, E. H. and Bevan, L.: Mechanics and mechanism of environmental crazing in a polymeric glass, 337
- Andrews, J. M. and Semlyen, J. A.: Equilibrium ring concentrations and the statistical conformations of polymer chains: Part 7. Cyclics in poly(1,3-dioxolane), 142
- Arridge, R. G. C. and Speake, J. H.: Mechanical relaxation studies of the cure of epoxy resins:  
1. Measurement of cure, 443  
2. Activation energy of the  $\gamma$ -process in amine-cured epoxy resins, 450
- Ashman, P. C. and Booth, C.: Interpretation of melting data for low molecular weight poly(ethylene oxide), 459
- Ashworth, J., Bamford, C. H. and Smith, E. G.: Preparation and properties of networks containing chloroprene, 57
- Ayrey, G., Poller, R. C. and Siddiqui, I. H.: Absence of free radical activity during reaction of organotin stabilizers with chlorohydrocarbons, 299
- Bailey, J. and Walker, S. M.: Broadline nuclear magnetic resonance studies of some poly(*N*-substituted maleimides), 561
- Bamford, C. H.: *see* Ashworth, J., Bamford, C. H. and Smith, E. G.
- Bamford, C. H. and Paprotny, J.: After-effects in polymerizations photo-initiated by manganese carbonyl + halide systems, 208
- Bandyopadhyay, P. and Rodriguez, F.: Interaction of poly(vinyl pyrrolidone) with phenolic cosolutes, 119
- Barlow, J. R.: *see* Reed, R. and Barlow, J. R.
- Barnes, D. C.: *see* Read, B. E., Hughes, D. A., Barnes, D. C. and Drury, F. W. M.
- Barrales-Rienda, J. M. and Fatou, J. M. G.: Effect of molecular weight on the rate of crystallization of polyethylene fractions at high undercooling, 407
- Barrie, J. A., Fredrickson, M. J. and Shepard, R.: Spin-lattice relaxation in substituted polysiloxanes, 431
- Bartl, P.: *see* Jang, C.-G., Bartl, P. and Williams, T.
- Beech, D. R. and Booth, C.: Crystallization of high molecular weight fractions of poly(ethylene oxide) from dilute solution in ethanol, 355
- Beech, D. R., Booth, C., Dodgson, D. V., Sharpe, R. R. and Waring, J. R. S.: Melting of low molecular weight poly(ethylene oxide), 73
- Beech, D. R., Booth, C., Pickles, C. J., Sharpe, R. R. and Waring, J. R. S.: Interfacial free energy of crystals of low molecular weight poly(ethylene oxide), 246
- Beevers, M. S. and Semlyen, J. A.: Equilibrium ring concentrations and the statistical conformations of polymer chains: Part 8. Calculations of small ring concentrations in polydihydrogensiloxane and polydimethylsiloxane equilibrates, 385. Part 10. Cyclics in a polymeric paraffin-siloxane, 523
- Bemporad, P.: *see* D'Alagni, M., Bemporad, P. and Garofolo, A.
- Benoit, H. C.: *see* Dondos, A., Rempp, P. and Benoit, H. C.
- Bettelli, A.: *see* Ferruti, P. and Bettelli, A.
- Bettelli, A.: *see* Ferruti, P., Bettelli, A. and Feré, Angelino
- Bevan, L.: *see* Andrews, E. H. and Bevan, L.
- Bevington, J. C. and Nicora C.: Terpolymerizations involving maleic anhydride, 249
- Blackadder, D. A., Keniry, J. S. and Richardson, M. J.: Annealing of high density polyethylene for very long times at low supercooling under vacuum, 584
- Blakey, P. R.: *see* Montgomery, D. E., Tregonning, K. and Blakey, P. R.
- Block, H., Cowd, M. A. and Walker, S. M.: Copolymerization of phenylene with maleic anhydride, 549
- Block, H., Groves, R. and Walker, S. M.: Dielectric relaxation in polymaleimide and *N*-substituted polymaleimides, 527
- Booth, C.: *see* Ashman, P. C. and Booth, C.
- Booth, C.: *see* Beech, D. R. and Booth, C.
- Booth, C.: *see* Beech, D. R., Booth, C., Dodgson, D. V., Sharpe, R. R. and Waring, J. R. S.
- Booth, C.: *see* Beech, D. R., Booth, C., Pickles, C. J., Sharpe, R. R. and Waring, J. R. S.
- Booth, C., Bruce, J. Malcolm and Buggy, M.: Effect of end groups on the melting temperatures of low molecular weight poly(ethylene oxide), 475
- Bowden, P. B.: *see* Raha, S. and Bowden, P. B.
- Bradbury, E. M., Crane-Robinson, C., Giancotti, V. and Stephens, R. M.: Conformational studies of poly(L-tyrosine) in solvent mixtures of dimethylsulphoxide with water and trimethylphosphate, 33
- Brier, P. N.: *see* Higgins, J. S., Allen, G. and Brier, P. N.
- Brown, D. S., Warner, F. P. and Wetton, R. E.: Surface areas of fillers in polymers by small angle X-ray scattering, 575
- Bruce, J. Malcolm: *see* Booth, C., Bruce, J. Malcolm and Buggy, M.
- Bucknall, C. B., Drinkwater, I. C. and Keast, Wendy E.: An etch method for microscopy of rubber-toughened plastics, 115
- Buggy, M.: *see* Booth, C., Bruce, J. Malcolm and Buggy, M.
- Bullock, A. T., Cameron, G. G. and Smith, P.: Electron spin resonance studies of spin-labelled polymers: Part 2. Preparation and characterization of spin-labelled polystyrene, 89
- Burfield, D. R.: *see* McKenzie, I. D., Tait, P. J. T. and Burfield, D. R.
- Burfield, D. R., McKenzie, I. D. and Tait, P. J. T.: Ziegler-Natta catalysis: 1. A general kinetic scheme, 302
- Burfield, D. R. and Tait, P. J. T.: Ziegler-Natta catalysis: 3. Active centre determination, 315
- Burfield, D. R., Tait, P. J. T. and McKenzie, I. D.: Ziegler-Natta catalysis: 4. Quantitative verification of kinetic scheme, 321
- Bywater, S. and Toporowski, P. M.: Effect of stereostructure on glass transition temperatures of poly(methyl methacrylate), 94
- Cameron, G. G.: *see* Bullock, A. T., Cameron, G. G. and Smith, P.
- Cameron, G. G. and Esslemont, G. F.: Solvent effects in free radical copolymerization of styrene and methacrylonitrile, 435
- Carità Morelli, M. and D'Alagni, M.: Sequence peptide polymers: Part 2. Poly(leucyl-leucyl-aspartic acid)—conformational aspects in water solution, 515
- Carraher, C. E., Jr. and Reimer, J. T.: Production of organometallic polymers by the interfacial technique: 24. Kinetics of polycondensation and thermal properties of poly(oxy(dicyclopentadienylzirconium)oxycarbonylferrocenylcarbonyl), 153
- Child, T. F.: Pulsed n.m.r. study of molecular motion and environment of sorbed water on cellulose, 259
- Chiolle, A.: *see* Credali, L., Chiolle, A. and Parrini, P.
- Chow, Mei T.: *see* Price, C., Watson, A. G. and Chow, Mei T.
- Conti, W. and Sorta, E.: Stress relaxation after steady-state shear flow in undilute polydisperse polymers, 399
- Cooper, D. R. and Semlyen, J. A.: Equilibrium ring concentrations and the statistical conformations of polymer chains: Part 9. Sodium metaphosphates in Graham's salt, 414
- Cowd, M. A.: *see* Block, H., Cowd, M. A. and Walker, S. M.
- Crane-Robinson, C.: *see* Bradbury, E. M., Crane-Robinson, C., Giancotti, V. and Stephens, R. M.
- Credali, L., Chiolle, A. and Parrini, P.: Reverse osmosis properties of poly(*trans*-2,5-dimethylpiperazine fumaramide) films, 503
- Cudby, M. E. A.: *see* Gall, M. J., Hendra, P. J., Peacock, C. J., Cudby, M. E. A. and Willis, H. A.
- Cuniberti, C. and Ferrando, R.: Electron microscope investigation of poly(ethylene oxide) supermolecular particles in solution, 379
- D'Alagni, M.: *see* Carità Morelli, M. and D'Alagni, M.
- D'Alagni, M., Bemporad, P. and Garofolo, A.: Sequence peptide polymers: Part 1. Poly(leucyl-leucyl-aspartic acid- $\beta$ -benzyl ester)—synthesis and some conformational aspects in solutions, 419
- Dawkins, J. V. and Hemming, M.: Gel permeation chromatography: column packing method for polystyrene gels, 553
- Denisov, V. M.: *see* Milovskaya, E. B., Kopp, E. L., Mikhailicheva, O. S., Denisov, V. M. and Koltsov, A. I.
- Dickinson, M.: *see* Loke, K. M., Dickinson, M. and Treloar, L. R. G.
- Dodgson, D. V.: *see* Beech, D. R., Booth, C., Dodgson, D. V., Sharpe, R. R. and Waring, J. R. S.
- Dondos, A., Rempp, P. and Benoit, H. C.: Segregation and conformational transition in triblock copolymers: Part 2. Light-scattering studies, 97
- Drinkwater, I. C.: *see* Bucknall, C. B., Drinkwater, I. C. and Keast, Wendy E.

- Drury, F. W. M.: *see* Read, B. E., Hughes, D. A., Barnes, D. C. and Drury, F. W. M.
- Dyson, E., Montgomery, D. E. and Tregonning, K.: Thermally stable fibres from an adamantane polymer, 85
- Earland, C., Keighley, J. H., Ramsden, D. B. and Turner, R. L.: Electron spin resonance study of the role of calcium in the fibrinogen-fibrin reaction, 579
- Emsley, J. and Udy, P. B.: Polymerization of hexachlorotriphosphonitrile, (NPCl<sub>2</sub>)<sub>3</sub>, 593
- Esslemont, G. F.: *see* Cameron, G. G. and Esslemont, G. F.
- Fatou, J. M. G.: *see* Barrales-Rienda, J. M. and Fatou, J. M. G.
- Fawcett, A. H. and Ivin, K. J.: Solution properties of polysulphones of some 1,2-disubstituted alkenes, 439
- Feldman, D.: *see* Negulescu, I., Feldman, D. and Simionescu, Cr.
- Feré, Angelino: *see* Ferruti, P., Bettelli, A. and Feré, Angelino
- Ferrando, R.: *see* Cuniberti, C. and Ferrando, R.
- Ferruti, P. and Bettelli, A.: Linear, high molecular weight poly(2-alkyl-4-vinyl-6-(dialkylaminomethyl)phenols) and poly(2,6-bis(dialkylaminomethyl)-4-vinylphenols), 184
- Ferruti, P., Bettelli, A. and Feré, Angelino: High polymers of acrylic and methacrylic esters of *N*-hydroxysuccinimide as polyacrylamide and polymethacrylamide precursors, 462
- Fredrickson, M. J.: *see* Barrie, J. A., Fredrickson, M. J. and Sheppard, R.
- Freeguard, G. F.: Rubber modified polystyrene: structural variation induced during pre-polymerization, 366
- Gall, M. J., Hendra, P. J., Peacock, C. J., Cudby, M. E. A. and Willis, H. A.: Laser-Raman spectrum of polyethylene: Part 1. Structure and analysis of the polymer, 104
- Gandica, A. and Magill, J. H.: A universal relationship for the crystallization kinetics of polymeric materials, 595
- Garofolo, A.: *see* D'Alagni, M., Bemporad, P. and Garofolo, A.
- Georgiadis, T. and Manley, R. St John: Morphology of nascent polyethylene prepared with the catalyst VOCl<sub>3</sub>/(C<sub>2</sub>H<sub>5</sub>)<sub>2</sub>AlCl, 567
- Giancotti, V.: *see* Bradbury, E. M., Crane-Robinson, C., Giancotti, V. and Stephens, R. M.
- Gilbert, Marianne and Hybart, F. J.: Effect of chemical structure on crystallization rates and melting of polymers: Part I. Aromatic polyesters, 327
- Gregory, R. L.: *see* Livingston, H. K. and Gregory, R. L.
- Groves, R.: *see* Block, H., Groves, R. and Walker, S. M.
- Hall, I. H.: Orientation of the methylene groups in poly(ethylene terephthalate), 69
- Harland, W. G., Khadr, M. M. and Peters, R. H.: High-density polyethylene: thermal history and melting characteristics, 13
- Hartmann, Bruce: Dynamic mechanical properties of poly(ethylene oxide), 460
- Heatley, F.: Conformation and dimensions of polymethylene and polypropylene in solution, 218
- Hemming, M.: *see* Dawkins, J. V. and Hemming, M.
- Hendra, P. J.: *see* Gall, M. J., Hendra, P. J., Peacock, C. J., Cudby, M. E. A. and Willis, H. A.
- Higgins, J. S., Allen, G. and Brier, P. N.: Methyl group motion in poly(propylene oxide), polypropylene and poly(methyl methacrylate), 157
- Hindeleh, A. M. and Johnson, D. J.: Crystallinity and crystallite size measurement in cellulose fibres: 1. Ramie and Fortisan, 423
- Peak resolution and X-ray crystallinity determination in heat-treated cellulose triacetate, 27
- Hirano, Shigehiro; Kashimura, Naoki; Kosaka, Noboru; and Onodera, Konoshin: Polysaccharide synthesis from mono- and oligo-saccharides by the action of phosphorus pentoxide in dimethyl sulphoxide, 190
- Hughes, D. A.: *see* Read, B. E.
- Hughes, D. A.: *see* Read, B. E., Hughes, D. A., Barnes, D. C. and Drury, F. W. M.
- Hybart, F. J.: *see* Gilbert, Marianne and Hybart, F. J.
- Ise, Norio; Moritani, Hiroyuki; and Okubo, Tsuneo: Preparation of carbamoylated polyethylenimine and its flocculation property, 187
- Ise, Norio and Okubo, Tsuneo: Flocculation property of the hydrolysis products of carbamoylated polyethylenimine, 552
- Ivin, K. J.: *see* Fawcett, A. H. and Ivin, K. J.
- Jang, C.-G., Bartl, P. and Williams, T.: N.m.r. and u.v. spectra of 2'-deoxyadenosine in water/dimethyl sulphoxide mixtures, 520
- Jennings, B. R. and Schweitzer, J.: Transient scattering from absorbing solutions, 164
- Johnson, D. J.: *see* Hindeleh, A. M. and Johnson, D. J.
- Jones, D. E. G.: *see* Lorimer, J. W. and Jones, D. E. G.
- Jones, D. E. G. and Lorimer, J. W.: Solution properties of poly(trimethylsiloxanotitanoxanes) (titanium oxide trimethylsilyloxides), 265
- Kashimura, Naoki: *see* Hirano, Shigehiro; Kashimura, Naoki; Kosaka, Noboru; and Onodera, Konoshin
- Kashiwagi, M. and Ward, I. M.: The measurement of molecular orientation in drawn poly(vinyl chloride) by broad line nuclear magnetic resonance, 145
- Katz, D.: *see* Steg, I. and Katz, D.
- Katz, D. and Steg, I.: Correlation between molecular parameters and some bulk properties of a plasticized highly crosslinked unsaturated polyester-styrene polymer system: 2. Some general rheological properties of the plasticized system, 541
- Keast, Wendy E.: *see* Bucknall, C. B., Drinkwater, I. C. and Keast, Wendy E.
- Keighley, J. H.: *see* Earland, C., Keighley, J. H., Ramsden, D. B. and Turner, R. L.
- Keniry, J. S.: *see* Blackadder, D. A., Keniry, J. S. and Richardson, M. J.
- Khadr, M. M.: *see* Harland, W. G., Khadr, M. M. and Peters, R. H.
- Koltsov, A. I.: *see* Milovskaya, E. V., Kopp, E. L., Mikhailicheva, O. S., Denisov, V. M. and Koltsov, A. I.
- Kopp, E. L.: *see* Milovskaya, E. B., Kopp, E. L., Mikhailicheva, O. S., Denisov, V. M. and Koltsov, A. I.
- Kosaka, Noboru: *see* Hirano, Shigehiro; Kashimura, Naoki; Kosaka, Noboru; and Onodera, Konoshin
- Lewis, P. R. and Price, C.: Electron microscopy of sym-SBS block polymers, 20
- Livingston, H. K. and Gregory, R. L.: Characterization of a cyclic oligomer of poly(pentamethylene terephthalamide), 297
- Loke, K. M., Dickinson, M. and Treloar, L. R. G.: Swelling of a rubber cylinder in torsion: Part 2. Experimental, 203
- Lorimer, J. W.: Refractive index increments of polymers in solution: 1. General theory, 46
3. Dependence on concentration, 274
- Lorimer, J. W.: *see* Jones, D. E. G. and Lorimer, J. W.
- Lorimer, J. W. and Jones, D. E. G.: Refractive index increments of polymers in solution: 2. Refractive index increments and light-scattering in polydisperse systems of low molecular weight, 52
- Luisi, P. L.: Calculation of the conformational properties of isotactic poly( $\alpha$ -olefins) in solution, 232
- McGhie, A. R., McGibbon, G., Sharples, A. and Stanley, E. J.: Thermally stimulated conductivity of poly(vinyl fluoride), 371
- McGibbon, G.: *see* McGhie, A. R., McGibbon, G., Sharples, A. and Stanley, E. J.
- McKenzie, I. D.: *see* Burfield, D. R., McKenzie, I. D. and Tait, P. J. T.
- McKenzie, I. D.: *see* Burfield, D. R., Tait, P. J. T. and McKenzie, I. D.
- McKenzie, I. D. and Tait, P. J. T.: Ziegler-Natta catalysis: 5. A molecular weight investigation, 510
- McKenzie, I. D., Tait, P. J. T. and Burfield, D. R.: Ziegler-Natta catalysis: 2. A kinetic investigation, 307
- McLean, Donald L. and White, James L.: The precipitation chromatographic column: theory, critique and method of design, 124
- Magill, J. H.: *see* Gandica, A. and Magill, J. H.
- Manley, R. St John: *see* Georgiadis, T. and Manley, R. St John
- Manley, T. R. and Qayyum, M. M.: Crosslinked polyethylene at elevated temperatures, 587
- Martuscelli, E. and Vittoria, V.: Melting and annealing of oriented single crystal aggregates of *trans*-polydodecenamer, 360
- Mikhailicheva, O. S.: *see* Milovskaya, E. B., Kopp, E. L., Mikhailicheva, O. S., Denisov, V. M. and Koltsov, A. I.
- Milovskaya, E. B., Kopp, E. L., Mikhailicheva, O. S., Denisov, V. M. and Koltsov, A. I.: Polymerization of vinyl chloride by the AlEt<sub>3</sub>/benzoylperoxide/Lewis-base system and the role of the Lewis base in initiation, 288
- Montgomery, D. E., Tregonning, K. and Blakey, P. R.: Modifications to the morphology of poly(*m*-phenylene adamantane-1,3-dicarboxamide) fibres, 43

## Author Index

- Montgomery, D. E.: *see* Dyson, E., Montgomery, D. E. and Tregonning, K.
- Moore, B. B.: *see* Thomas, D. K. and Moore, B. B.
- Moritani, Hiroyuki: *see* Ise, Norio; Moritani, Hiroyuki; and Okubo, Tsuneo
- Mortier, R. M.: *see* Allen, G. and Mortier, R. M.
- Negulescu, I., Feldman, D. and Simionescu, Cr.: Copolymerization behaviour of some *N*-vinyl monomers, 149
- Newton, A. B. and Rose, J. B.: Relative reactivities of the functional groups involved in synthesis of poly(phenylene ether sulphones) from halogenated derivatives of diphenyl sulphone, 465
- Nicora, C.: *see* Bevington, J. C. and Nicora, C.
- Okubo, Tsuneo: *see* Ise, Norio; Moritani, Hiroyuki and Okubo, Tsuneo
- Okubo, Tsuneo: *see* Ise, Norio and Okubo, Tsuneo
- Onder, K., Peters, R. H. and Spark, L. C.: Melting and transition phenomena in some polyester-urethanes, 133
- Onodera, Konoshin: *see* Hirano, Shigehiro; Kashimura, Naoki; Kosaka, Noboru; and Onodera, Konoshin
- Pannell, J.: Gel permeation chromatography: the behaviour of polystyrenes with long-chain branching, 277
- Polystyrenes of known structure: Part 3. Polymers with long-chain branching, 2
- Paprotny, J.: *see* Bamford, C. H. and Paprotny, J.
- Parrini, P.: *see* Credali, L., Chiolle, A. and Parrini, P.
- Peacock, C. J.: *see* Gall, M. J., Hendra, P. J., Peacock, C. J., Cudby, M. E. A. and Willis, H. A.
- Peters, R. H.: *see* Harland, W. G., Khadr, M. M. and Peters, R. H.
- Peters, R. H.: *see* Onder, K., Peters, R. H. and Spark, L. C.
- Pickles, C. J.: *see* Beech, D. R., Booth, C., Pickles, C. J., Sharpe, R. R. and Waring, J. R. S.
- Poller, R. C.: *see* Ayrey, G., Poller, R. C. and Siddiqui, I. H.
- Price, C.: *see* Lewis, P. R. and Price, C.
- Price, C., Watson, A. G. and Chow, Mei T.: An investigation of the effect of chain geometry on the two-phase morphology of polystyrene/polyisoprene block copolymers, 333
- Prime, R. B. and Sacher, E.: Kinetics of epoxy cure: 2. The system bisphenol-A diglycidyl ether/polyamide, 455
- Qayyum, M. M.: *see* Manley, T. R. and Qayyum, M. M.
- Raha, S.: *see* Vincent, P. I. and Raha, S.
- Raha, S. and Bowden P. B.: Birefringence of plastically deformed poly(methyl methacrylate), 174
- Ramsden, D. B.: *see* Earland, C., Keighley, J. H., Ramsden, D. B. and Turner, R. L.
- Read, B. E. and Hughes, D. A.: Stress-dichroism studies of the 4.92  $\mu\text{m}$  band of amorphous crosslinked polyethylene, 495
- Read, B. E., Hughes, D. A., Barnes, D. C. and Drury, F. W. M.: Measurement of infra-red dichroism, stress and strain of elongated polymers, 485
- Reed, R. and Barlow, J. R.: Electron microscope study of freeze-etched polystyrene latex, 226
- Reimer, J. T.: *see* Carraher, C. E., Jr. and Reimer, J. T.
- Rempp, P.: *see* Dondos, A., Rempp, P. and Benoit, H. C.
- Richardson, M. J.: *see* Blackadder, D. A., Keniry, J. S. and Richardson, M. J.
- Rodriguez, F.: *see* Bandyopadhyay, P. and Rodriguez, F.
- Rose, J. B.: *see* Newton, A. B. and Rose, J. B.
- Sacher, E.: *see* Prime, R. B. and Sacher, E.
- Schreiber, H. P.: Temperature scanning studies of polyolefin solutions, 78
- Schweitzer, J.: *see* Jennings, B. R. and Schweitzer, J.
- Semlyen, J. A.: *see* Andrews, J. M. and Semlyen, J. A.
- Semlyen, J. A.: *see* Beevers, M. S. and Semlyen, J. A.
- Semlyen, J. A.: *see* Cooper, D. R. and Semlyen, J. A.
- Sharpe, R. R.: *see* Beech, D. R., Booth, C., Dodgson, D. V., Sharpe, R. R. and Waring, J. R. S.
- Sharpe, R. R.: *see* Beech, D. R., Booth, C., Pickles, C. J., Sharpe, R. R. and Waring, J. R. S.
- Sharples, A.: *see* McGhie, A. R., McGibbon, G., Sharples, A. and Stanley, E. J.
- Sheppard, R.: *see* Barrie, J. A., Fredrickson, M. J. and Sheppard, R.
- Siddiqui, I. H.: *see* Ayrey, G., Poller, R. C. and Siddiqui, I. H.
- Simionescu, Cr.: *see* Negulescu, I., Feldman, D. and Simionescu, Cr.
- Skinner, G. A., Viney, M. and Wallis, S. R.: *Cis-trans* isomerism in Ziegler-catalysed terpolymerization of hexa-1,4-diene with ethylene and propylene, 242
- Small, P. A.: Effects of long-chain branching on distribution of degree of polymerization, 536
- Smith, E. G.: *see* Ashworth, J., Bamford, C. H. and Smith, E. G.
- Smith, P.: *see* Bullock, A. T., Cameron, G. G. and Smith, P.
- Sorta, E.: *see* Conti, W. and Sorta, E.
- Spark, L. C.: *see* Onder, K., Peters, R. H. and Spark, L. C.
- Speake, J. H.: *see* Arridge, R. G. C. and Speake, J. H.
- Stanley, E. J.: *see* McGhie, A. R., McGibbon, G., Sharples, A. and Stanley, E. J.
- Steg, I.: *see* Katz, D. and Steg, I.
- Steg, I. and Katz, D.: Correlation between molecular parameters and some bulk properties of a plasticized highly crosslinked unsaturated polyester-styrene polymer system: 3. Some mechanical properties of the plasticized system, 546
- Stephens, R. M.: *see* Bradbury, E. M., Crane-Robinson, C., Giaccotti, V. and Stephens, R. M.
- Tait, P. J. T.: *see* Burfield, D. R., McKenzie, I. D. and Tait, P. J. T.
- Tait, P. J. T.: *see* Burfield, D. R. and Tait, P. J. T.
- Tait, P. J. T.: *see* Burfield, D. R., Tait, P. J. T. and McKenzie, I. D.
- Tait, P. J. T.: *see* McKenzie, I. D. and Tait, P. J. T.
- Tait, P. J. T.: *see* McKenzie, I. D., Tait, P. J. T. and Burfield, D. R.
- Thomas, D. K.: High temperature stability in fluorosilicone vulcanisates, 479
- Thomas, D. K. and Moore, B. B.: Filler reinforcement in silicone polymers, 109
- Toporowski, P. M.: *see* Bywater, S. and Toporowski, P. M.
- Tregonning, K.: *see* Dyson, E., Montgomery, D. E. and Tregonning, K.
- Tregonning, K.: *see* Montgomery, D. E., Tregonning, K. and Blakey, P. R.
- Treloar, L. R. G.: Swelling of a rubber cylinder in torsion: Part 1. Theory, 195
- Treloar, L. R. G.: *see* Loke, K. M., Dickinson, M. and Treloar, L. R. G.
- Turner, R. L.: *see* Earland, C., Keighley, J. H., Ramsden, D. B. and Turner, R. L.
- Twisleton, J. F. and White, J. W.: Interchain force field and elastic constants of polytetrafluoroethylene, 40
- Udy, P. B.: *see* Emsley, J. and Udy, P. B.
- Vincent, P. I.: A correlation between critical tensile strength and polymer cross-sectional area, 558
- Vincent, P. I. and Raha, S.: Influence of hydrogen bonding on crazing and cracking of amorphous thermoplastics, 283
- Viney, M.: *see* Skinner, G. A., Viney, M. and Wallis, S. R.
- Vittoria, V.: *see* Martuscelli, E. and Vittoria, V.
- Walker, S. M.: *see* Bailey, J. and Walker, S. M.
- Walker, S. M.: *see* Block, H., Cowd, M. A. and Walker, S. M.
- Walker, S. M.: *see* Block, H., Groves, R. and Walker, S. M.
- Wallis, S. R.: *see* Skinner, G. A., Viney, M. and Wallis, S. R.
- Ward, I. M.: *see* Kashiwagi, M. and Ward, I. M.
- Waring, J. R. S.: *see* Beech, D. R., Booth, C., Dodgson, D. V., Sharpe, R. R. and Waring, J. R. S.
- Waring, J. R. S.: *see* Beech, D. R., Booth, C., Pickles, C. J., Sharpe, R. R. and Waring, J. R. S.
- Warner, F. P.: *see* Brown, D. S., Warner, F. P. and Wetton, R. E.
- Watson, A. G.: *see* Price, C., Watson, A. G. and Chow, Mei T.
- Wetton, R. E.: *see* Brown, D. S., Warner, F. P. and Wetton, R. E.
- White, James L.: *see* MacLean, Donald L. and White, James L.
- White, J. W.: *see* Twisleton, J. F. and White, J. W.
- Whittaker, R. E.: Tensile failure properties of some branched polyurethane elastomers, 169
- Williams, T.: *see* Jang, C. -G., Bartl, P. and Williams, T.
- Willis, H. A.: *see* Gall, M. J., Hendra, P. J., Peacock, C. J., Cudby, M. E. A. and Willis, H. A.
- Wilson, G. A.: Low-angle X-ray diffraction studies of reduced and silver-stained  $\alpha$ -keratin, 63
- Wolf, F. P.: Elastic behaviour of rubber under small uniaxial extension and compression, 347
- Zichy, V. J. I.: *see* Addleman, R. L. and Zichy, V. J. I.

## UK EDITORS

**C. H. Bamford** PhD, ScD, FRS  
Campbell Brown Professor of Industrial  
Chemistry, University of Liverpool,  
P. O. Box 147, Liverpool L69 3BX

**C. E. H. Bawn** CBE, FRS  
Grant Brunner Professor of Inorganic and  
Physical Chemistry, University of Liverpool,  
P. O.Box 147, Liverpool L69 3BX.

**E. M. Bradbury** PhD  
Head of Biophysics Section,  
Portsmouth Polytechnic,  
Park Road, Portsmouth PO1 2DZ

**Geoffrey Gee** CBE, FRS  
Sir Samuel Hall Professor of Chemistry,  
University of Manchester,  
Manchester M13 9PL

**R. J. W. Reynolds** PhD, FPI  
Professor and Director,  
Institute of Polymer Technology,  
Loughborough University of Technology,  
Loughborough LE11 3TU

Annual subscription including postage  
UK £20; USA \$56 (surface mail)  
Airmail USA \$84; Japan £36  
Rates for other countries available on request

Published monthly by IPC Science and Technology  
Press Ltd, IPC House, 32 High Street,  
Guildford, Surrey, England  
Telephone: Guildford (0483) 71661  
Telegrams and Telex: Bisnespres 25137 London

Reprints (minimum quantity usually 100) of papers  
may be ordered from the publishers. Write to the  
Reprints Dept, IPC Science and Technology Press  
Ltd, at the above address

American Representatives: IPC (America) Ltd,  
205 East 42nd Street, New York, NY 10017, USA

© IPC Business Press Ltd, 1972

## OVERSEAS EDITORS

**H. C. Benoit** PhD  
Professor, Faculty of Science,  
University of Strasbourg  
Director, Centre de Recherche  
sur les Macromolecules,  
6, Rue Boussingault,  
67 Strasbourg, France

**S. Bywater** PhD  
Head, Polymer Section,  
National Research Council,  
Ottawa KIA OR9, Canada

**F. Danusso** PhD  
Professor of Macromolecular Chemistry,  
Istituto Chimica Industriale del Politecnico,  
Piazza Leonardo da Vinci 32,  
20133 Milano, Italy

**M. Szwarc** PhD  
State University Polymer Research Center,  
Syracuse University, Syracuse,  
NY 13210, USA

## MANAGING EDITOR

**J. A. G. Thomas** PhD

## ASSISTANT EDITOR

**C. J. Rawlins** BSc